SCHOLARLY PUBLICATIONS

A CURRENT AWARENESS BULLETIN
OF RESEARCH OUTPUT

@DTU

(114th Edition)

JUNE 2022

BY: CENTRAL LIBRARY

DELHI TECHNOLOGICAL UNIVERSITY
(FORMERLY *DELHI COLLEGE OF ENGINEERING)*
GOVT. OF N.C.T. OF DELHI
SHAHBAD DAULATPUR, MAIN BAWANA ROAD
DELHI 110042

PREFACE

This is the **One Hundred Fourteenth** Issue of Current Awareness Bulletin started by Delhi Technological University, Central Library. The aim of the bulletin is to compile, preserve and disseminate information published by the faculty, students and alumni for mutual benefits. The bulletin also aims to propagate the intellectual contribution of Delhi Technological University (DTU) as a whole to the academia.

The bulletin contains information resources available in the internet in the form of articles, reports, presentations published in international journals, websites, etc. by the faculty and students of DTU. The publications of faculty and student which are not covered in this bulletin may be because of the reason that the full text either was not accessible or could not be searched by the search engine used by the library for this purpose.

The learned faculty and students are requested to provide their uncovered publications to the library either through email or in CD, etc. to make the bulletin more comprehensive.

This issue contains the information published during **June, 2022**. The arrangement of the contents is alphabetical. The full text of the article which is either subscribed by the university or available in the web is provided in this bulletin.

Central Library

CONTENTS

1. A Comparative Analysis of Deep Learning Algorithms for Skin Cancer Detection, ***3.Priya Singh***, ***8.Mayand Kumar*** and ***8.Aman Bhatia***, Software Engineering, DTU

2. A Comparative Study of Machine Learning Based Image Captioning Models, ***3.Priya Singh***, ***8.Piyush Gupta*** and ***8.Hardik Jain***, Software Engineering, DTU

3. A comparative study of Naive Bayes Classifiers with improved technique on Text Classification, ***6.Chingmuankim*** and ***3.Prof.Rajni Jindal***, CSE, DTU

4. A Comparison of Apriori Algorithm and Apriori with Hashing Algorithm, ***8.Arjun Malik***, ***8.Mihir Agarwal*** and ***3.Sonika Dahiya***, Software Engineering, DTU

5. A Compendious Research on Big Data File Formats, ***8.Arnav Gohil***, ***8.Anshul Shroff***, ***8.Arnav Garg*** and ***3.Shailender Kumar***, CSE, DTU

6. A first-principles Study of Electronic, Thermoelectric, and Optical Properties of Sulfur Doped c-HfO2, ***3.Rajesh Kumar***, Ramesh Kumar, Ankush Vij and ***3.Mukhtiyar Singh***, Applied Physics, DTU

7. A Literature survey based on DBSCAN algorithms, ***8.Harsh Vardhan Singh***, ***8.Ashwin Girdhar*** and ***3.Sonika Dahiya***, Software Engineering, DTU

8. A Novel ES-RwCNN Based Finger Vein Recognition System with Effective L12 DTP Descriptor and AWM-WOASelection, ***3.Ajai Kumar Gautam*** and ***3.Rajiv Kapoor***, Electronics, DTU

9. A Review on Center-Less Recess Grinding and Its Applications, ***8.Rohan Sharma***, ***8.Rohan Chopra***, ***8.Rohan Singh*** and ***3.Dr. Ak Madan***, Mechanical, DTU

10. A Review on GAN based Image Dehazing, ***3.Kavinder Singh***, ***8.Vishruth Khare***, ***8.Vishwas Agarwal*** and ***8.Sourabh***, CSE, DTU

11. A Survey on Deep Learning Techniques for COVID-19 Detection using Medical Imaging, ***8.Harsh Jain***, ***8.Bhanu Pratap Singh***, ***8.Aryan Rana*** and ***3.Aruna Bhat***, CSE, DTU

12. A tree classifier based network intrusion detection model for Internet of Medical Things, Karan Gupta, Deepak Kumar Sharma, Koyel Datta Gupta and ***7.1.Anil Kumar***, CSE, DTU

13. A Two Stream Convolutional Neural Network with Bi-directional GRU Model to Classify Dynamic Hand Gesture, ***3.Bindu Verma***, IT, DTU

14. Adaptive Social Acceleration Constant Based Particle Swarm Optimization, Jyoti Jain, ***3.Uma Nangia*** and ***3.N. K. Jain***, Electrical, DTU

15. AI Techniques in Imaging Data, Detecting & Monitoring Symptoms of COVID-19, ***8.Imane Elouaghzani*** and ***6.Deepak Kumar Mishra***, CSE, DTU

16. An adaptive rejuvenation of bacterial foraging algorithm for global optimization, ***6.Tejna Khosla*** and ***3.Om Prakash Verma***, CSE and Electronics, DTU

17. An empirical study of knowledge environment and suitability of performance measures of a civil organization for a knowledgebased military force, Mukesh ***6.Kumar Singh*** and ***3.Vikas Gupta***, DSM, DTU

18. An era of new future wireless 5G technology and its aspects: a review, ***8.Akhilesh Verma*** and ***3.Srinivasa Nallanthighal Raghava***, Electronics, DTU

19. Analysis of Road Traffic Accidents & Review of Ridesafe (Motorcycle Crash Detection & Alert System), ***8.Afzal Hannan***, ***Bhavit Yadav*** and ***8.Chirag Yadav***, CSE, DTU

20. Antitumor Activity of Choerospondias axillaris Fruit Extract by Regulating the Expression of SNCAIP and SNCA on MDA-MB-231 Cells, Sonia Mann1, Ashish Sarkar, Ankita Sharma, ***3.Rajinder K Gupta*** and Sagarika Biswas, Applied Chemistry, DTU

21. Applications of Flexible Manufacturing Systems in Industry: A Review, ***6.Mayank Chugh***, ***6.Jitesh Jassi***, ***6.Mohd Zaid*** and ***3.Dr. A.K. Madan***, Mechanical, DTU

22. Automated detection of COVID-19 from chest Xrays using CNN, ***8.Surbhi Anand***, ***8.Nilesh Nishant*** and ***8.Tanyam Singal***, CSE, DTU

23. Bohr–Rogosinski Phenomenon for $S*(\psi)$ and $C(\psi)$, ***6.Kamaljeet Gangania*** and ***3.S. Sivaprasad Kumar***, Applied Mathematics, DTU

24. CBFDR- Context-Based Fake News Detection and Reporting using Blockchain and Machine Learning, Himani Mishra, Dr Amita Jain and ***6.Ankur Tayal***, DSM, DTU

25. Characteristics assessment of local scour encircling twin bridge piers positioned side by side (SbS), ***6.GEETA DEVI*** and ***3.MUNENDRA KUMAR***, Civil, DTU

26. Characterization of Residual Stresses in Conventional Forming and Hydroforming of Tailor Welded Blanks, Amit Kumar, Ravi Kumar Digavalli, ***3.Vijay Gautam***, and Hariharan Krishnaswamy, Mechanical, DTU

27. Communication between immune system and mycobiota impacts health and disease, ***7.Gunjan Sachdeva*** and ***3.Asmita Das***, Biotechnology, DTU

28. Comparative Analysis of Forecasting Models for Air Quality Index Prediction, ***3.Dr. Shailender Kumar***, ***8.Abhay Lodhi***, ***8.Abhi Chauhan*** and ***8.Amrit Kumar***, CSE, DTU

29. Comparative Study of Supervised Learning Algorithms for Fake News Classification, ***8.Tejas Harish Borkar*** and ***8.Tushar Ahuja***, CSE, DTU

30. Comparison between Information Theoretic Measures to Assess Financial Markets, ***6.Luckshay Batra*** and ***3.Harish Chander Taneja***, Applied Mathematics, DTU

31. Complaint and Severity Identification from Online Financial Content, Apoorva Singh, ***8.Rohan Bhatia*** and Sriparna Saha, DTU

32. CONCEPT OF GROUP TECHNOLOGY AND IT'S IMPLEMENTATION IN THE FIELD OF MOBILE PRODUCTION SYSTEMS, ***3.Dr. Ak Madan***, ***8.Aditya Atul Gupta*** and ***8.Aman Kumar Kaushik***, Mechanical, DTU

33. Control of DSTATCOM in Distribution Systems by Artificial Intelligence based Controller, ***8.Pooja Meena***, ***8.Piyush Dua***, ***8.Nilayan Maji*** and ***3.Ankita Arora***, Electrical, DTU

34. Corporate Governance and M&A Performance: A Systematic Review of Literature, ***6.Harsh Gautam***, ***3.Archana Singh*** and ***3.Girish Chandra Maheshwari***, DSM, DTU

35. Covid Prevention using machine learning and blockchain technology, Rajat Goel, Tulika Aggarwal, Kancharla Sai, Naga Devulapalli, Venkata Mudunuru and ***6.Ashish Kumar***, IT, DTU

36. Credit Card Fraud Detection using Deep and Machine Learning, ***8.Sahil Negi***, ***8.Sudipta Kumar Das*** and ***8.Rigzen Bodh***, CSE, DTU

37. Cryogenic Grinding, ***8.Roshan Kumar***, ***8.Sachin Malik***, ***8.Saksham Verma*** and ***3.AK Madan***, Mechanical, DTU

38. Customer Market Segmentation using Machine Learning Algorithm, ***8.Swesh Raj Regmi***, ***3.Jasraj Meena***, ***8.Utkarsh Kanojia*** and ***8.Vishesh Kant***, IT, DTU

39. Design and analysis of a compact asymmetrical CPW fed stubs loaded hook-shaped patch antenna for upper 5G- and data collection applications, ***6.Karteek Viswanadha*** and ***3.N.S.Raghava***, Electronics, DTU

40. Design and Analysis of Circular Microstrip Patch Antenna for White Space TV Band Application, ***3.Richa Sharma***, ***3.N. S. Raghava*** and ***3.Asok De***, ECE, DTU

41. DESIGN AND ANALYSIS OF KINETIC ENERGY RECOVERY SYSTEM FOR BICYCLE, ***3.Dr. Ashok Madan***, ***8.Sarthak Jain***, ***8.Tushar Gupta*** and ***8.Abhay Singh***, Mechanical, DTU

42. Design and Analysis of wide bandwidth Quad 'e' mirror-shaped metamaterial for Wi-Fi and Satellite Applications, ***6.Ankit***, ***3.Kamal Kishor*** and ***3.Ravindra Kumar Sinha***, Applied Physics, DTU

43. DESIGN OF MULTI-PURPOSE DRONE CAPABLE OF SURFICIAL AND AERIAL MOVEMENT, ***3.Dr. Ak Madan***, ***8.Aakash***, ***8.Abhay Dharia***, ***8.Aayush Kumar***, ***8.Abhishek Verma*** and ***8.Ashwin Rao***, Mechanical, DTU

44. Detecting malicious transactions in database using hybrid metaheuristic clustering and frequent sequential pattern mining, ***3.Rajni Jindal*** and ***3.Indu Singh***, CSE, DTU

45. Detection of hatefulness in Memes using unimodal and multimodal techniques, ***3.Aruna Bhat***, ***8.Vaibhav Varshney***, ***8.Varun Bajlotra*** and ***8.Vishesh Gupta***, CSE, DTU

46. Dielectric Insertion effect on Frequency Selective Surfaces for Band Pass Filter design, ***6.Sanjeeta Dhegaya*** and ***3.Lavi Tanwar***, Electronics, DTU

47. Disease Prevention and Treatment Using β-Carotene: the Ultimate Provitamin A, ***7.Raksha Anand***, ***7.Lalit Mohan*** and ***3.Navneeta Bharadvaja***, Biotechnology, DTU

48. Dleep Learning based Regularization as defense against Clean Label Targeted Data Poisoning, ***3.Anil Singh Parihar***, ***8.Jushaan Singh Kalra*** and ***8.Abhinav Java***, CSE, DTU

49. Driver Drowsiness Detection System using Convolutional Neural Network, ***8.Mohammad Elham Walizad***, ***8.Mehreen Hurroo*** and ***3.Divyashikha Sethia***, Software Engineering, DTU

50. Effect of post-treatment methods and nanoparticles on the conformation of silk fibroin and their impact on electrical properties, ***6.Reetu Yadav*** and ***3.Roli Purwar***, Applied Chemistry, DTU

51. Electromyography data recorded from orbicularis oculi muscle during a novel grasping pilot study, ***3.Mohd Rizwan Jafar***, Mechanical, DTU

52. Energy efficient cluster-based routing protocol for Wireless Sensor Network using Nature Inspired Algorithm, ***6.Rashmi Mishra*** and ***3.Rajesh K. Yadav***, CSE, DTU

53. Enhancing Spam Detection on SMS performance using several Machine Learning Classification Models, ***8.Tarandeep Singh***, ***8.Tushar Anupam Kumar*** and ***3.Prashant Giridhar Shambharkar***, CSE, DTU

54. ENVIRONMENTAL MANAGEMENT IN THE WORLD'S LARGEST MASS GATHERING KUMBH MELA 2019 AT CONFLUENCE OF RIVER GANGA AND YAMUNA AT PRAYAGRAJ, INDIA, ***7.1.Ayushi Raghav***, ***3.S.K. Singh*** and ***7.Twinkle Bhatia***, Environmental, DTU

55. Evaluation of water quality using water quality index, synthetic pollution index, and GIS technique: a case study of the river Gomti, Lucknow, India, ***8.Amit Krishan***, Anwar Khursheed and ***3.Rajeev Kumar Mishra***, Environmental, DTU

56. Exploring relationships between service quality dimensions and customers satisfaction: empirical study in context to Indian logistics service providers, Anchal Gupta, Rajesh Kumar Singh, K. Mathiyazhagan, ***3.Pradeep Kumar Suri*** and Yogesh K. Dwivedi, DSM, DTU

57. Factors Influencing Piezoelectric Response of Horizontally and Vertically Embedded PZT Patch in Confined Granular Fills, ***6.Nisha Kumari*** and ***3.Ashutosh Trivedi***, Civil, DTU

58. Financial feasibility of concentrated solar power with and without sensible heat storage in hot and dry Indian climate, ***8.Naman Goyal***, ***8.Akshansh Aggarwal***, ***3.Anil Kumar***, Mechanical, DTU

59. GenGen: Analysing the Performance of Transformer-based Encoder-Decoder in a General Natural Language Generation Paradigm, ***8.Angad Sethi***, ***8.Aman Kumar Gond***, ***8.Abhishek Kumar Singh*** and ***3.Prashant Giridhar Shambharkar***, CSE, DTU

60. iCACD: an intelligent deep learning model to categorise current affairs news article for efficient journalistic process, Sachin Kumar, Shivam Panwar, ***3.Jagvinder Singh***, Anuj Kumar Sharma and Zairu Nisha, DSM, DTU

61. Importance of Human Gait Analysis in Biometric Recognition using Machine Learning: A Review, ***7.Shipra Shand*** and ***3.Rahul***, Software Engineering, DTU

62. Industrial AI in Manufacturing, ***8.Amulya Tiwari***, ***8.Tanishk Verma*** and ***3.Dr. A.K Madan***, Mechanical, DTU

63. INDUSTRY 4.0: IMPACT ON FUTURE OF WORK, ***6.Aman Jha*** and ***3.Dr. Ashok Madan***, Mechanical, DTU

64. Influence of Nano-Sized Al2O3 Nanoparticles and Multipass FSW on Microstructure and Mechanical Characteristics of Dissimilar Welded Joints of AA6061 and AA5083, ***6.Preety Rani*** and ***3.Radhey Shyam Mishra***, Mechanical, DTU

65. Influence of process parameters in synergic MIG welding of 304L stainless steel using response surface methodology, Shanti Lal Meena, ***3.Ravi Butola***, ***6.Muhsin Ahmad Khan***, R.S Walia and ***3.Qasim Murtaza***, Mechanical, DTU

66. License Plate Image Super Resolution Using Generative Adversarial Network(GAN), ***8.Bickey Kumar Shah***, ***8.Anshul Yadav*** and ***8.Ashutosh Kumar Dixit***, CSE, DTU

67. Managing resilience of micro, small and medium enterprises (MSMEs) during COVID-19: analysis of barriers, ***6.1.Anchal Gupta*** and Rajesh Kumar Singh, DSM, DTU

68. Maneuvering Control of Autonomous Underwater Vehicle (AUV) by Simulated Annealing and Moth Flame Optimization Tuned Controllers, ***3.Sudarshan K.Valluru*** and ***8.Hitesh Thareja***, Electrical, DTU

69. Mapping of glacial lakes and glacial lake outburst flood in Kinnaur district, Himachal Pradesh using remote sensing and GIS, ***6.Gopinadh Rongali***, ***3.K. C. Tiwari*** and ***6.Poonam Vishwas***, Geoinformatic, DTU

70. Modeling of variable speed compressor vapour compression refrigeration system using ecofriendly refrigerants and nano refrigerants and water cooled condenser-evaporator with experimental validation, ***3.Radhey Shyam Mishra***, Mechanical, DTU

71. Multi-label Classification Methods and Challenges, ***8.Raghav Agrawal*** and ***8.Rohit Sah***, Applied Mathematics, DTU

72. Optimal Sizing of Hybrid Energy System Using Random Exploratory Search-Centred Harris Hawks Optimizer with Improved Exploitation Capability, Priyanka Anand, Vikram Kumar Kamboj, Muhannad Alaraj, ***3.Mohammad Rizwan*** and Isaka J. Mwakitalima, Electrical, DTU

73. OTA Based Fractional-Order Oscillator With Controlled Phase Difference, ***6.Garima varshney***, ***3.Neeta Pandey*** and ***3.Rajeshwari Pandey***, ECE, DTU

74. Pressure-induced topological phase transition in XMR material YbAs: a first-principles study, ***3.Mukhtiyar Singh***, ***6.Ramesh Kumar*** and Ramesh K. Bibiyan, Applied Physics, DTU

75. Real Time Drowsiness Detection System based on ResNet-50, ***8.Ankit Kumar Yadav***, ***8.Ankit*** and ***3.Dr. Abhilasha Sharma***, Software Engineering, DTU

76. Recent advancements over a decade for organic light-emitting diodes: from structural diversity, role of layers, colour emission, material classification, performance improvement, fabrication to applications, ***6.SUGANDHA YADAV***, ***3.POORNIMA MITTAL*** and SHUBHAM NEGI, Electronics, DTU

77. Recognition of multi-cognitive tasks from EEG signals using EMD methods, Akshansh Gupta, ***3.Dhirendra Kumar***, Hanuman Verma, M. Tanveer, Andreu Perez Javier, Chin-Teng Lin and Mukesh Prasad, Applied Mathematics, DTU

78. Residual stress investigation in the metallic coating approach of micro-sized particles on the substrate: cold spray additive manufacturing, Abdul Faheem, Ankit Tyagi, Faisal Hasan, Abid Ali Khan, ***3.Qasim Murtaza*** and Kuldeep K Saxena, Mechanical, DTU

79. Review based on Variations of DBSCAN algorithms, ***8.Ankit Bhardwaj***, ***8.Ankit Pandey*** and ***3.Sonika Dahiya***, Software Engineering, DTU

80. Review of development and advancement in Flexible Manufacturing System, ***8.Ritvik Maliya***, ***8.Rohan Gupta*** and ***3.Ak Madan***, Mechanical, DTU

81. Sentiment Analysis on Online Reviews using Machine Learning and NLTK, ***3.Shailender Kumar***, ***8.Nazir Ahmad Jailani***, ***8.Abhinav Raj Singh*** and ***8.Shubham Panchal***, CSE, DTU

82. Smart Beta Investing : An Alternative Investment Paradigm in Emerging Indian Equity Market, ***8.Reema Monga***, ***3.Deepti Aggrawal*** and ***3.Jagvinder Singh***, USME, DTU

83. Software Change Prediction using Ensemble Learning on Object Oriented Metrics, ***8.Nikhil Khanna***, ***8.Ojas Agarwal*** and ***3.Rahul***, Software Engineering, DTU

84. STUDY OF FAVORABLE SURFACE ROUGHNESS IN MILLING MACHINE AND ITS OPTIMIZATION, ***3.Dr. A.K. Madan***, ***8.R. Maheshwari***, ***8.R.R. Thakur***, Mechanical, DTU

85. STUDY THE SLIDER CRANK MECHANISM, ***8.Chander Mohan Aggarwal***, ***8.Bhavya Dhanwaria***, ***8.Ashish Kudiyal*** and ***3.Dr.Sushila Rani***, Mechanical, DTU

86. TECHNICAL ANALYSIS OF POWER GENERATION USING VERTICAL AXIS WIND TURBINES ON METRO TRACKS, ***8.MD Zia Arzoo***, ***8.Mozammil Hassan***, ***8.David Simeon*** and ***3.Dr. Pushpendra Singh***, Mechanical, DTU

87. Toxicity and Challenges of Nanomaterials and Their Impact on the Environment, ***7.Sakshi Awasthi*** and ***3.Jai Gopal Sharma***, Biotechnology, DTU

88. Ultrasensitive Dual-Band Terahertz Metasurface Sensor Based on All InSb Resonator, ***6.Pooja Agarwal***, ***3.Kamal Kishor*** and ***3.Ravindra Kumar Sinha***, Applied Physics, DTU

89. Underwater Image Enhancement with Feature Preservation using Generative Adversarial Networks (UIEFP GAN), ***3.Dr. Aruna Bhat***, ***8.Yogesh Narang*** and ***8.Yogesh Goyal***, CSE, DTU

90. Using AI to Improve India's Logistic Conditions, ***8.Sanskar Jethi***, ***8.Madhav Rathi*** and ***Dhiraj Kumar Pal***, DTU

91. VLSI Layout: Concept to Realization, ***3.Malti Bansal***, ***8.Riyanshi Arora*** and ***8.Ritvik Bharti***, Electronics, DTU

1. *Vice Chancellor*
2. *Pro Vice Chancellor*
3. *Faculty*
4. *Teaching-cum-Research Fellow*
5. *Asst. Librarian*
6. *Research Scholar*
7. *PG Scholar*
8. *Undergraduate Student*

1.1. *Ex Vice chancellor*
2.1. *Ex Pro Vice Chancellor*
3.1. *Ex Faculty*
4.1. *Alumni*
5.1 *Others*
6.1. *Ex Research Scholar*
7.1. *Ex PG Scholar*
8.1. *Ex Undergraduate Student*

Proceedings of the Sixth International Conference on Intelligent Computing and Control Systems (ICICCS 2022)
IEEE Xplore Part Number: CFP22K74-ART; ISBN: 978-1-6654-1035-9

A Comparative Analysis of Deep Learning Algorithms for Skin Cancer Detection

Priya Singh
Department of Software Engineering
Delhi Technological University
Delhi, India
priya.singh.academia@gmail.com

Mayand Kumar
Department of Software Engineering
Delhi Technological University
Delhi, India
mayandkumar10@gmail.com

Aman Bhatia
Department of Software Engineering
Delhi Technological University
Delhi, India
aman.b25@hotmail.com

2022 6th International Conference on Intelligent Computing and Control Systems (ICICCS) | 978-1-6654-1035-9/22/$31.00 ©2022 IEEE | DOI: 10.1109/ICICCS53718.2022.9788197

***Abstract*— In the current world, machine learning and computing techniques are being used in every industry. One of these involves the healthcare and medical industry. Already due to intensive research and analysis huge leaps have been taken in strengthening the existing system. One area in the research is Skin Cancer Detection. Skin Cancer is diagnosed when damaged DNA cells start to multiply uncontrollably. This makes the detection in the preliminary stages highly essential. This is an area where machine learning or deep learning algorithms can help in the development of models which accurately predict the onset of diseases in early stages. Some research has been done in this area but high accuracy results haven't been produced. Therefore, the focus of this research work is to compare between four deep learning techniques RNN (Recurrent Neural Networks), CNN (Convolutional Neural Networks), ResNet50, and Xception to conclude which algorithm works the finest in successfully predicting the disease with high accuracy. The dataset used for the purpose of this research is the HAM10000 which is available on Kaggle. The empirical results demonstrate that the accuracy by using CNN, RNN, ResNet50, and Xception was 72%, 69%, 79%, and 93% respectively with Xception performing the best.**

***Keywords*— RNN, CNN, ResNet50, Xception, Data augmentation, Skin Cancer**

I. INTRODUCTION

Skin is the largest organ present on the human body. It consists of three layers known as the epidermis and dermis meaning the upper and lower layer of the skin and the subcutaneous tissue. The epidermis is the layer which is present on the top. It is made up of three cells which are squamous, basal and melanocytes. The flat cells present on the top are known as the squamous cells. Underneath them lie round cells which are known as the basal cells. The cells present in the lower epidermis are known as the melanocytes cells. These are responsible for producing melanin which is the pigment that gives it colour. The primary function of the outer layer which is the epidermis is to act as a barrier from the outside world.

Cancer has taken its place as one of the deadliest and most widespread diseases in the world. Skin cancer is a type of cancer which also is the fifth most common type of cancer to affect both men and women. Cancer of the basal and squamous are the most common types of skin cancer [3]. These types of cancers are known to be usually cured however usually leave a disfiguring impact and are also expensive to treat. The third type of cancer originates in the melanocytes and is also known as melanoma. Among the three, melanoma is known to be the most deadly due to its tendency to spread to other organs of the body. Skin cancer is caused by overexposure with UV lights. These interactions can happen through direct contact with the sun or by tanning beds and sun lamps. These rays cause damage to the skin cells and in the long run may even lead to cancer.

Skin cancer can however, if diagnosed early be treated and has a high recovery rate [2]. This is where the importance of increasing development in artificial intelligence comes into play. Skin cancer can be detected using imaging techniques. The skin lesion can be run through tests and with effective algorithms it can be detected. For this we propose a computer aided diagnosis which is also known as CAD. In this system various techniques using computer vision, deep learning and imaging an analysis or detection can be performed. We propose a CAD system for this paper using different deep learning techniques.

In our study we perform a comparative analysis between the following deep learning algorithms: RNN, CNN, ResNet50, and Xception. CNN is one of the oldest and most popular techniques which provides decent results in image classification according to by Zilong Hu in their paper [2]. RNN has been previously used for Skin Cancer detection on a different dataset which was performed by Mh. Sahim Ali [5]. ResNet50 and Xception have little research in the field of Skin Cancer detection however, due to their refined architecture they have provided accurate results for image classification as described by Feng Zeng [6] and hence are being explored. The current study aims to compare the performance of the four models viz CNN, RNN, ResNet and Xception to predict which model works well for skin cancer detection.

The dataset used for this study is the HAM10000 dataset published on Kaggle Repository [16]. It consists of 10015 dermatoscopic images collected with the purpose of providing realistic images for training and testing of machine learning and deep learning models [8].

Authorized licensed use limited to: DELHI TECHNICAL UNIV. Downloaded on June 15,2022 at 11:20:06 UTC from IEEE Xplore. Restrictions apply.

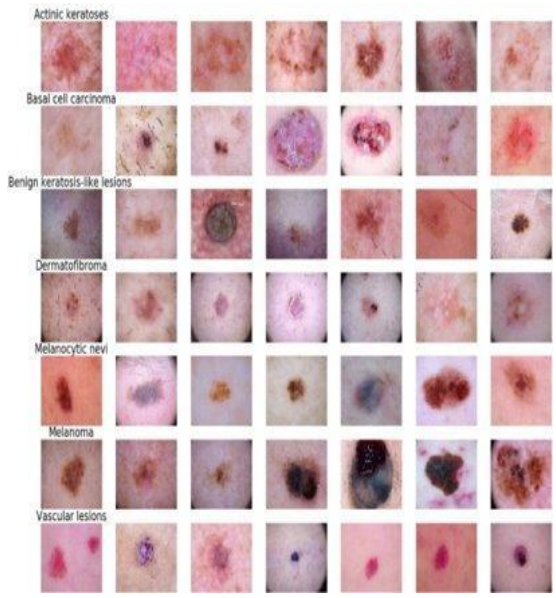

Fig. 1. Skin Lesion images from HAM10000 Dataset.

II. LITERATURE SURVEY

Over a few years, there has been tremendous advancement in the research field of skin cancer detection. Now with the development in this field, cancer can be diagnosed at an early stage. Various methods and techniques are used, from (CAD) Computer-Aided Diagnosis systems to ML algorithms like SVM, Decision tree, Bayesian Learning [7], and CNN. Numerous other methods are also used, like the ensemble of deep learning models and the aggregation of various models' features [15]. Significant changes were observed in the classification of images due to development in models and fields like regularization, data augmentation, and other hyper-parameters.

After analyzing and comparing various deep learning algorithm's performances over a period of time, it was concluded that nearly every other model was focused on already existing models of deep learning. The first deep learning model, which provided better results than pre-existing models, consisted of a two-stage framework of DRN and FCRN. Several methods were proposed, and this paper will provide a comparative study of four such deep learning algorithms.

III. METHODOLOGY

Data collection is one of the integral parts of exploring or visualizing the data. One crucial thing is collecting specific data that is vital, relevant, and fulfills the research needs. Edge or extreme cases and various possible scenarios should be present in the dataset so that the model can perform well for all the conditions and give more precise and realistic results. The bedrock of the research is the data collected, so it should be done very carefully.

For this research, we decided to design the dataset which contains both images and MNIST. Therefore, in the dataset, we have 10015 dermatoscopic images in the training set, which can be used to train our model. All the diagnostic categories have been included in the dataset in pigmented lesions, such as intraepithelial carcinoma / Bowen's disease or Actinic keratoses (akiec), pyogenic granulomas and hemorrhage, vasc), dermatofibroma (df), basal cell carcinoma (bcc), vascular lesions (angiomas, angiokeratomas, benign keratosis-like lesions (solar lentigines / seborrheic keratoses and lichen-planus like keratosis, bkl), and melanoma (mel), melanocytic nevi (nv). Histopathology or histo is used in 50% cases to confirm the lesions, rest of the cases are confirmed with follow-up examination, specialist consensus or either by in-vivo confocal microscopy [4].

When we explored the dataset as provided in Fig. 2, It is observed that data is unbalanced across different categories. And as stated most of the time cancer was diagnosed in histo.

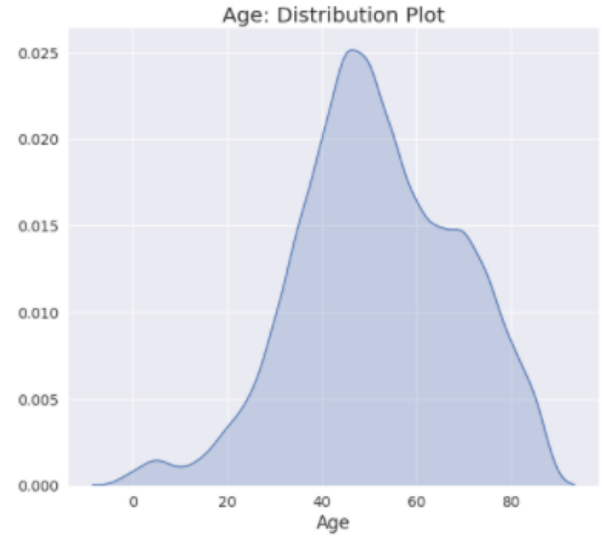

(a)

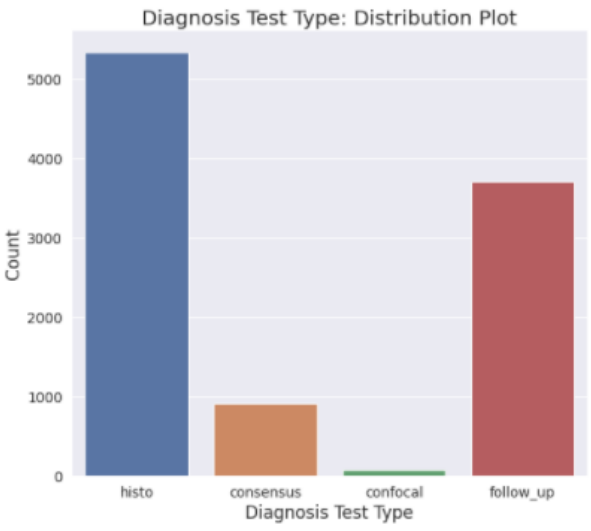

(b)

Fig. 2. (a) Age and Probability of Cancer

Authorized licensed use limited to: DELHI TECHNICAL UNIV. Downloaded on June 15,2022 at 11:20:06 UTC from IEEE Xplore. Restrictions apply.

(b) Type of Skin Cancer

A) Loading and Pre-processing of Dataset

To work on the dataset, we imported and explored the dataset for cancer detection. The key insights during visualization were that there were some missing values, the dataset came out to be balanced between Males and Females, approximately 67% of the dataset was of a single class Melanocytic nevi which can give biased result, Samples are of patients whose age is between 35 to 60 years [16]. An example sample for each category of lesion is shown in Figure 3.

As discussed earlier that the dataset is unbalanced across categories, the class with least number of samples in the dataset were Dermatofibroma lesions and Vascular Skin lesions with 115 and 142 samples respectively [9].

Only one type of malignant skin lesion is present in the dataset, i.e, Malignant Melanoma, rest is of benign type.
From Figure 4,we can recognize the cluster within the age of 45 to 70. Lower, upper, and back areas of the body is where melanoma commonly occurs [10]. But between the ages of 50 to 70m, it is noticed that the face, trunk, chest, and abdomen have higher frequency.

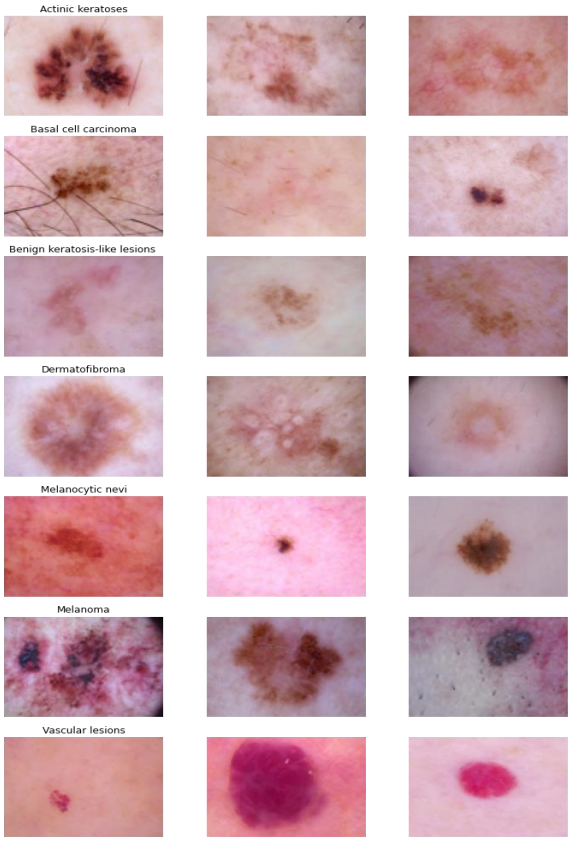

Fig. 3. Images present in the dataset.

B) Data Augmentation

Without Data augmentation there was overfitting. So, In order to increase the size of the dataset, Data Augmentation is one of the methods. This method creates a variety in the dataset. We can generate more data from a single image data. The main motivation behind increasing the dataset size is to avoid overfitting [12]. ImageDataGenerator module has been used to implement data augmentation which includes rotation of images by 90 degrees, horizontal and vertical shift by 0.1, randomly zooming the image, and horizontal and vertical flips.

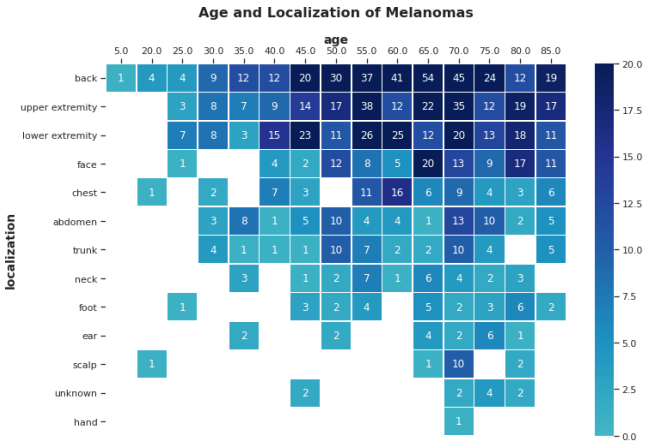

Fig. 4. Age and Localisation of Melanomas

C) Model Building

Models are built using the functions from the Keras library. We used conv2d, max pooling, average pooling, and various other functions. Moreover, there was use of dropout and batch normalization to avoid overfitting. The models used to analyse and solve the problem are discussed below.

a. CNN Model

In deep learning, CNN is a model which is initialized as a sequence of layers. passing of data takes place from input to hidden to output layer. In CNN, Convolution is the mathematical operation used to identify the features from the image using a kernel or feature detector and store them in a feature map. Spatial relationship is maintained by the map between pixels. Initializing the model is the basic step towards building a CNN model. The CNN is an ideal neural network for the data that can be represented in the form of a grid. As images can be easily perceived in the form of 2D matrix, CNN is commonly used for image recognition tasks [11].

In this paper, we have used 7 conv2d layers along with average pooling, batch normalization, dropout, and 1 flatten layer. During the trials, average pooling performed better than max pooling layer [13]. Furthermore to avoid

Authorized licensed use limited to: DELHI TECHNICAL UNIV. Downloaded on June 15,2022 at 11:20:06 UTC from IEEE Xplore. Restrictions apply.

overfitting every hyper parameter was taken into consideration and introduction of batch normalization layer and dropout layer was done. ReLu activation function (Figure 4) has been used between the convolution layers to increase the non-linearity in the cost function.

In the basic CNN model, we have average pooling as it is performing much better than the max pooling layer. Average pooling takes the whole object into consideration or smoothens the whole image for processing whereas max pooling considers only brighter pixels and retains only 1/4th of the image.

In the end, we have taken the Softmax activation (1) function to classify the cancer [14]. We could have used the *Sigmoid* function but as we know it performs better only for classification between 2 classes. Here, softmax makes certain that the sum of probabilities of all classes sums to 1.

$$\sigma(\vec{z})_i = \frac{e^{z_i}}{\sum_{j=1}^{K} e^{z_j}} \quad (1)$$

Where,
σ= softmax
z= Input Vector
e^{z_i}= Input vector's standard exponential function
K= Count of classes in multi class classifier
e^{z_j}= Output vector's standard exponential function

b. RNN Model

RNN also known as Recurrent Neural Networks are networks in which the output from previous layers is remembered and used as input for the next layer. They are generally used for natural language processing and predictive analysis. However, RNN also helps in constructing strong classification models. For the sake of our study we chose an algorithm to perform classification on the input images [12].

In our paper, we used the tensorflow library to create our own RNN model. For this model the input image size used is 28 x 28. The model is built with an input layer of shape 28 x 28 x 3. The model is then connected to hidden layers. The hidden layers are as follows: 2 layers of Conv2D and BatchNormalization. The Conv2D layer has 32 filters of size 3 x 3 with the activation function as relu. These are then connected to a MaxPooling layer of size 2 x 2 and a Dropout layer of factor 0.2. This architecture is repeated with Convolutions of 64 and 128 of the same size. The connection between the hidden layer and the output layer has the following architecture: A GlobalMaxPooling layer is connected to a Flattening layer. After these 2 layers of Dense and Dropout layers with the activation functions ReLu and softmax being used (Figure 6).

c. Xception Model

Xception is a deep learning model which is based on CNN. It stands for extreme inception and in a way that is what the algorithm tries to achieve. The architecture it uses is to apply the filters for each of the depth wise depth maps and then introduce a convolution of 1x1.
For our model we built an architecture in order to achieve higher performance along with better accuracy. In order to achieve that we used a combination of four layers - dense, dropout, normalization and activation. The kernel initialization used is "he_uniform". Along with that batch normalization is used and "ReLu" function is used for the activation layer. This architecture is repeated with different values for the dense and dropout layers. Finally for the output layer *Softmax* function was used.

The hyperparameters set for our model were as follows: learning rate for the model has a value of 0.1 whereas the batch size is set to 256 and the number of epochs were 20. The reason a higher value was not chosen is to avoid overfitting of the model.

Furthermore, in order to have a more consolidated and robust algorithm we added Xgboost along with the build algorithm. Xgboost is a gradient boosted decision tree in our model we use the gradient descent tree. It can have other parameters like stochastic and regularized gradient boosting however, for the purpose of our project we choose the gradient boosting parameter. The reason behind this was to consolidate the algorithm without making it inefficient as Xception is already a complex algorithm.

The base_score for the model was set to 0.5 while other hyperparameters remained the same as the ones used above.

d. ResNet Model

ResNet models are known as Residual Machine Learning models. The algorithm was introduced to solve the problem of complex deep neural networks which begin to lean towards overfitting with addition of more layers or attributes. The layers which are stacked together produce an output which are added to the outputs of the connections, which perform identity mapping. This solves two problems, it makes the algorithm easily optimizable and also increases the accuracy as the depth of the model is increased without leading to excessive overfitting.
In our project we used the ResNet50 model with some modification compared to before. Ti included two skipping levels which represent a shortcut connection. However, for the sake of this study we implemented the same with three skip layers with convolutions of size 1x1. This structure is followed for the remaining depth of the ResNet50 model we have implemented.. The architecture uses 50 layers comprising of an input layer connected to 9 layers of convolution size 1x1 with kernel 64 followed by 12 layers of convolution size 1x1 with kernel size 128 and finally 18 layers of kernel size 1,256. Finally the output layer is connected to the model with *Softmax* as the activation function. This architecture helped in building a rigorous model which was trained over 20 epochs. The results are discussed in the next section.

C) Independent and Dependent Variables

Authorized licensed use limited to: DELHI TECHNICAL UNIV. Downloaded on June 15,2022 at 11:20:06 UTC from IEEE Xplore. Restrictions apply.

The number of images the dataset contains is considered as an independent variable and the weight of pixels as well. Feature map obtained from convolution operation performed, and the amount of map which is fed to the next input layer is considered as a dependent variable.

D) Parameters and Hyper Parameters

Feature detector size, step of a detector, numbers of kernels, size of the kernel, padding, average and max pooling are parameters.
Number of epochs, learning rate value, rate of dropping neurons, batch size are considered to be hyperparameters.

E) Performance Measure

The perfection of the model is evaluated with the help of performance measures. In this paper, we are using Accuracy, AUC Score, Precision, Recall, and F1 Score to evaluate our model's performance [16].

F) Validation Method

Holdout validation technique has been used in this paper to validate the model. The dataset has 10,015 samples of which 20% is put in the testing set. The dataset is then divided into validation and training datasets. Validation set contains 10% of the training set. In the end, the proposed model's performance is evaluated based on the predictions made by it on the test set. To assess the performance of our model, We are using earlier stated performance metrics.

IV. RESULTS AND ANALYSIS

After performing the above experimentation using the all four algorithms which are CNN, RNN, Xception, and ResNet50 the results obtained are shown in Table 1. Xception outperformed the rest of the algorithms in almost all aspects. It can be seen that Xception has achieved the best results with accuracy of 93% and AUC Score of 90.58%, and recall of 93%, while ResNet50 gave a recall of 89%. Therefore, based on this comparative study it can be concluded that the Xception algorithm can be used for better image classification of skin lesions to detect skin cancer between target classes. In situations where deadly diseases like cancer have to be predicted with it is required the model to have a high success rate. Bold text in Table 1 signifies the best value for the given metric.

Table 1. Performance Measure values for different algorithms.

Measure	CNN	RNN	Xception	ResNet50
Accuracy	0.72	0.69	**0.93**	0.79
Recall	0.72	0.88	**0.93**	0.89
Precision	0.87	0.72	**0.89**	**0.89**
F1 Score	0.85	0.81	**0.93**	0.87
AUC	0.8988	0.8836	**0.9058**	0.73

One of the reasons for a lower accuracy can be that the dataset was unbalanced in which the Melanocytic Nevi class dominated the samples present in the training and testing data. In situations like these, accuracy is not considered to be an accurate measure for analysing the performance of the model. In such cases other metrics like auc score should be used.

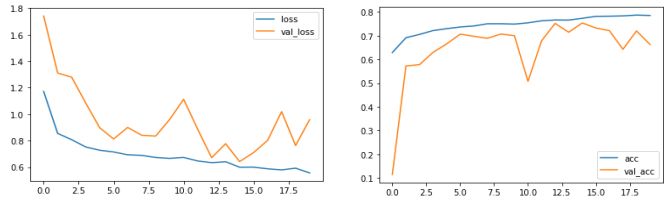

Fig. 5. Accuracy and loss evolution of RNN

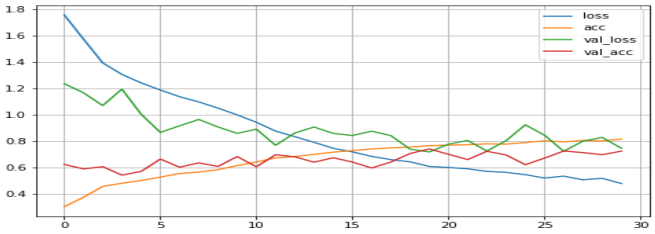

Fig. 6. Accuracy and loss evolution of CNN

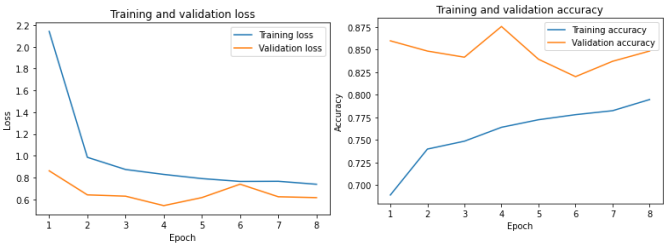

Fig. 7. Accuracy and loss evolution of ResNet50

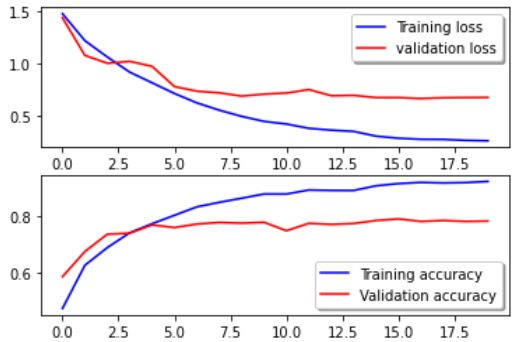

Fig. 8. Accuracy and loss evolution of Xception + XGboost.

Authorized licensed use limited to: DELHI TECHNICAL UNIV. Downloaded on June 15,2022 at 11:20:06 UTC from IEEE Xplore. Restrictions apply.

Moreover, further information can be analysed by developing a confusion matrix for the models as shown in the figure. The main aim for generating the matrix is to analyse how the models are predicting the Melanoma samples. It can be observed that a rather large amount of input samples were wrongly classified. A model which classifies samples which are malign as benign cannot be used in order to predict cancer accurately. In sensitive situations like these, false negatives can cause problems and lead to dangerous outcomes. Therefore, utmost care should be taken to reduce the number of false negatives and keep them as low as possible.

As it can be seen, accuracy is not an accurate measure for such studies as it does not show the true picture. A model with high accuracy but with high false negative rates is detrimental for the situation. Hence, we also calculated the AUC scores of the models. The AUC Score for CNN, RNN, Xception, and ResNet50 are 88.36%, 89.8%, 90.58%, and 73% respectively. This means that the models are able to distinguish between the classes.

Figure 5-8 shows the accuracy and loss evolution of each model, and after observing each graph, we can conclude that Xception has better performance in every aspect.

V. CONCLUSION AND FUTURE WORK

As it has been discussed above, the models provide a good baseline for the classification of skin cancer types, however they are not yet ready for the industry standard. In order to reduce the false negative rates we propose the following improvements and developments:

In order to have better optimization methods which not only result in better data augmentation but also help in providing a more accurate set of hyperparameters. For this study, Grid search was used, however it isn't the best technique to determine the hyperparameters for training the models. As discussed the dataset was imbalanced. Therefore more data should be extracted and collected in order to have a more complete and balanced dataset. GAN can be used in order to provide the training phase with more samples and in turn also helps in improving the generalisation of the model. Lastly, for increasing the performance or accuracy of the models, other techniques like ensemble methods can be used. They can provide a better method of predicting and help in improving the performance.

REFERENCES

[1] M.M. Mijwil Skin cancer disease images classification using deep learning solutions. *Multimed Tools Appl* vol. 80, pp. 26255–26271 (2021).

[2] Z. Hu, J. Tang, Z. Wang, K. Zhang, L. Zhang, Q. Sun, Deep learning for image-based cancer detection and diagnosis − A survey, Pattern Recognition, vol. 83, 2018, pp. 134-149

[3] A. A. AbuSamra and A. M. R. Al-Madhoun, "Applying Deep Learning and Natural Language Processing in Cancer: A Survey," 2021 Palestinian International Conference on Information and Communication Technology (*PICICT*), 2021, pp. 103-115, doi: 10.1109/PICICT53635.2021.00030.

[4] T. Saba,Recent advancement in cancer detection using machine learning: Systematic survey of decades, comparisons and challenges,Journal of Infection and Public Health, vol 13, no. 9, 2020, pp. 1274-1289

[5] M. S. Ali, M. S. Miah, J. Haque, M. M. Rahman, and M. K. Islam, "An enhanced technique of skin cancer classification using deep convolutional neural network with Transfer Learning Models," *Machine Learning with Applications*, vol. 5, p. 100036, 2021.

[6] F. Zeng, X. Li, X. Deng, L. Yao, and G. Lian, "An image classification model based on transfer learning for ulcerative proctitis," *Multimedia Systems*, vol. 27, no. 4, pp. 627–636, 2021.

[7] Deepti and S. Ray, "A survey on application of machine learning algorithms in cancer prediction and Prognosis," *Data Management, Analytics and Innovation*, pp. 349–361, 2020.

[8] S. Gilmore, R. Hofmann-Wellenhof, and H. P. Soyer, "A support vector machine for decision support in melanoma recognition," *Experimental Dermatology*, vol. 19, no. 9, pp. 830–835, 2010.

[9] M. Kumar, P. Gupta, R. K. Jha, A. Bhatia, K. Jha and B. K. Shah, "Sign Language Alphabet Recognition Using Convolution Neural Network," 2021 *5th International Conference on Intelligent Computing and Control Systems (ICICCS),* 2021, pp. 1859-1865,doi:10.1109/ICICCS51141.2021.9432296.

[10] A. Bhatia, V. Kedia, A. Shroff, M. Kumar, B. K. Shah and Aryan, "Fake Currency Detection with Machine Learning Algorithm and Image Processing," 2021 *5th International Conference on Intelligent Computing and Control Systems (ICICCS),* 2021, pp. 755-760, doi: 10.1109/ICICCS51141.2021.9432274.

[11] Y. Li, X. Wang, W. Liu and B. Feng, "Pose Anchor: A Single-Stage Hand Keypoint Detection Network," in IEEE Transactions on *Circuits and Systems for Video Technology*, vol. 30, no. 7, pp. 2104-2113, July 2020, doi: 10.1109/TCSVT.2019.2912620.

[12] X. Shen and F.-L. Chung, "Deep Network embedding for graph representation learning in signed networks," *IEEE Transactions on Cybernetics*, vol. 50, no. 4, pp. 1556–1568, 2020.

[13] Y. Zhu, M. Liao, M. Yang, and W. Liu, "Cascaded segmentation-detection networks for text-based traffic sign detection," *IEEE Transactions on Intelligent Transportation Systems*, vol. 19, no. 1, pp. 209–219, 2018.

[14] Z. Yu, X. Jiang, F. Zhou, J. Qin, D. Ni, S. Chen, B. Lei, and T. Wang, "Melanoma recognition in dermoscopy images via aggregated deep convolutional features," *IEEE Transactions on Biomedical Engineering*, vol. 66, no. 4, pp. 1006–1016, 2019.

[15] N. C. Codella, Q.-B. Nguyen, S. Pankanti, D. A. Gutman, B. Helba, A. C. Halpern, and J. R. Smith, "Deep Learning Ensembles for melanoma recognition in Dermoscopy Images," *IBM Journal of Research and Development*, vol. 61, no. 4/5, 2017.

[16] R. Maiti, P. Agarwal, R. R. Kumar and A. Bhat, "Detection Of Skin Cancer Using Neural Architecture Search with Model Quantization," 2021 *5th*

Authorized licensed use limited to: DELHI TECHNICAL UNIV. Downloaded on June 15,2022 at 11:20:06 UTC from IEEE Xplore. Restrictions apply.

International Conference on Intelligent Computing and Control Systems (ICICCS), 2021, pp. 1807-1814, doi: 10.1109/ICICCS51141.2021.9432190.

Authorized licensed use limited to: DELHI TECHNICAL UNIV. Downloaded on June 15,2022 at 11:20:06 UTC from IEEE Xplore. Restrictions apply.

Proceedings of the Sixth International Conference on Trends in Electronics and Informatics (ICOEI 2022)
IEEE Xplore Part Number: CFP22J32-ART; ISBN: 978-1-6654-8328-5

A Comparative Study of Machine Learning Based Image Captioning Models

Priya Singh
Department of Software Engineering
Delhi Technological University
Delhi,India
priya.singh.academia@gmail.com

Piyush Gupta
Department of Software Engineering
Delhi Technological University
Delhi, India
piyush.gupta1811@gmail.com

Hardik Jain
Department of Software Engineering
Delhi Technological University
Delhi, India
hardik187468@gmail.com

Abstract— **Automated image captioning is a crucial concept for numerous real-world applications as it is useful in robotics, image indexing, self-driving vehicles and greatly helpful for impaired eyesight people. An image provided in real-time can be converted into text using image captioning models developed by machine learning algorithms. Understanding an image mostly depends on the features of the image. Machine learning techniques are widely used for image captioning tasks. This research study has performed a comparative analysis on three Machine Learning (ML) algorithms, i.e. k-Nearest Neighbor (KNN), Convolution Neural Network (CNN) with Long Short Term Memory (LSTM) and Attention Based LSTM. In addition, an improved KNN algorithm with reduced time complexity and an improved CNN with LSTM and Attention Based LSTM model with an added beam search method is proposed to improve the underlying approaches further. The performance of the three selected models are empirically evaluated using BLEU, ROUGE and METEOR scores on the widely used flickr8k dataset, and the experimental results demonstrate the supremacy of the Attention Based LSTM over the other two approaches. Finally, the current study's findings help guide the researchers and practitioners in selecting the appropriate approach for Image Captioning with empirical evidence in terms of standard evaluation metrics.**

Keywords— Image Captioning (IC), Attention Based Model, Long-Short Term Memory (LSTM), k-Nearest Neighbor (KNN), Convolutional Neural Network (CNN).

I. INTRODUCTION

Every day, a person encounters different images from sources like the internet, articles, news, and advertisements. These images do not have descriptions, but the human interprets and understands them without any caption. However, machines need some Image captioning (IC) methods to describe the image. IC is the process of creating words that describes an image. It requires extracting relevant information from a photograph and interpreting it into natural language. IC is not to be confused with image classification. It helps both in recognizing things in the image and conveying information in natural language about the objects in the image. IC is a type of machine translation for which an image is converted into a written description. It is difficult because it demands both computer vision and natural language processing expertise. IC systems are divided into two categories, whether they provide novel captions. Some IC algorithms choose an appropriate caption from their database that best describes the test image. Other ways generate unique captions by constructing a description of the image. The Nearest Neighbor approach to IC is an example of the first type. In contrast, the Neural Image Caption generator is an example of the second group of innovative caption generators [1-2], [18] and [22-23].

In the past few years, a lot of research in the field of IC has been done [1-4], [14], [17-19] and [22-25]. The Nearest Neighbor approach can be used to find the best caption from the training dataset which is nearest to the specific image [2]. This means selecting general caption from all of the available captions that can be applied to various photos nearest to the given test image. Captions are created by combining visually comparable photographs from the test set. The consensus caption can then be used to describe the test image, which is intuitive. If the dataset is diverse, the chosen caption for the test image will arrive to be more common; for example- 'a cat', if the dataset is comparable, a more precise caption would be chosen like 'black cat'. In such a case, when one has to develop new captions for the test image employing a neural network will be a good choice. This method employs the LSTM Recurrent Neural Network (RNN) architecture, which is highly suited for sequential data, such as captions in this case [5], [18] and [22]. The model is trained on the dataset to get the best negative log likelihood of probability (S/I), where I is image used as the input and S is a sequential list of generated caption words present in the dictionary that sufficiently represents the image. The image is initially fed into a CNN, specifically Inception-V3 [8]. On the ImageNet database, Inception-V3 is an image classification model that has been shown to achieve higher than 78.1 per cent accuracy [8].

One more approach is to use an attention-based gated recurrent unit which uses the previous word and the next crucial part of the image to predict the next word in the caption thus, the decoder use only a region of the image to predict the caption [14]. Global attention is computationally costly as it focuses on all input words for all keywords. Thus, local attention is used, which focuses on the tiny subset of the encoder's hidden layer.

Based on these different encoding and decoding methods, we have selected three machine learning-based IC models for the paper: Nearest Neighbor Approach, CNN-LSTM Based and Attention Based LSTM method. We have improved the KNN approach by sorting and selecting a subset of captions and using the beam search method to improve the performance of CNN with LSTM and Attention Based LSTM model.

2022 6th International Conference on Trends in Electronics and Informatics (ICOEI) | 978-1-6654-8328-5/22/$31.00 ©2022 IEEE | DOI: 10.1109/ICOEI53556.2022.9777153

Authorized licensed use limited to: DELHI TECHNICAL UNIV. Downloaded on June 03,2022 at 06:27:51 UTC from IEEE Xplore. Restrictions apply.

II. LITERATURE SURVEY

Research in the field of image captioning is quite prevalent [1-4]. The early image captioning approaches mainly relies on the template-based methods that have to be predefined with the results of the object detection and their attributes and relationships [6-7]. Inspired by recent development in image captioning approaches [17-19], [22-25], they can be divided based on distance-based matching or encoder-decoder models. Jacob Devlin et al. [2] suggested a baseline technique that is Nearest Neighbor, based upon a distance learning classifier. The approach uses all the training dataset for finding the best suitable caption for the image. The Nearest Neighbor approach can be used for finding the annotations based on different objects in the image with similar meanings to produce more accurate captions [24].

There are two basic steps in the encoder-decoder approach. First, the CNN encoder extracts the image's visual features into a fixed-length embedding vector. Second, Recurrent Neural Network (RNN), especially LSTM, is used as a decoder to generate the sequential caption as proposed by [18] and [22-23].

Y. Chu et al. [18] developed the probability-based encoder-decoder model, which uses ResNet50 [26] for feature extraction and gated LSTM decoder. The predicted caption is generated using a sequence of words produced by the softmax function, which contains the probabilities of all the words present in the vocabulary.

Inspired by the encoder-decoder model, many of the current states of art models of image captioning used an attention-based encoder-decoder model to produce better captions [4], [14], [17] and [24-25]. Kelvin Xu et al. [4] developed a model that concentrates on the important region of the image. Sai Siddarth Yv et al. [14] suggested an attention-based encoder-decoder model using an extra layer of a gated recurrent unit in the classical CNN with LSTM model. The attention mechanism works by giving weights to the different objects in the image and using the relevant parts of the image at a given timestamp.

Instead of going in one direction into the LSTM network, S. Takkar et al. [19] suggested a bidirectional LSTM network to extract the image features. We can divide the image region into a grid of bounding boxes containing different objects in the image using the Yolo model as suggested by M. A. Al-Malla et al. [17] to improve the model's accuracy. O. Sargar et al. [13] proposed a Generative Adversarial Networks (GAN) and a soft attention layer to enhance the performance of the model. The Flickr8k, Flickr30k and MS COCO are the major datasets used by these research papers to improve the results produced by their proposed methods.

By now, it is evident that many researchers have proposed approaches for image captioning tasks. In the current study, we are conducting a comparative study for the three selected ML approaches, namely CNN with LSTM, Attention Based LSTM and KNN, by empirically accessing their performances on BLEU, METEOR and ROGUE measures. We also proposed the improvements of the selected approaches to improve the performance further. To the best of our knowledge, there is no study yet that empirically evaluates the selected approaches for image captioning and provides similar improvements over the selected approaches.

III. METHODOLOGY

A. Dataset Description

For evaluating the performance of the three selected models, namely CNN with LSTM, Attention Based LSTM and KNN, we have chosen the widely used Flickr8k benchmark dataset available for download at [15]. It contains 8092 images depicting various scenes and situations and contains respective descriptions. Out of all the images, 6000 images are selected for training and the rest for testing. Each image has five captions, as shown in Fig. 1, and the total captions are 40460.

Fig. 1. Flickr8k dataset sample

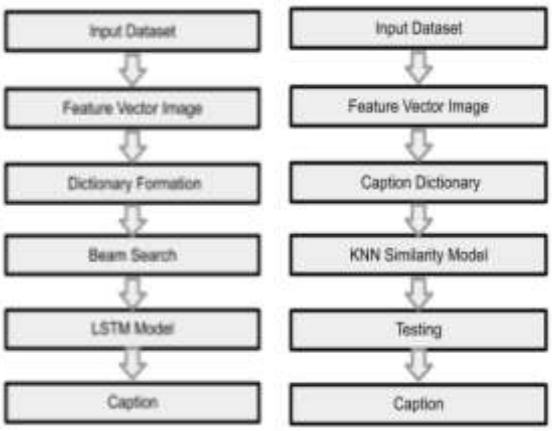

Fig. 2. Architecture of CNN with LSTM

Fig. 3. Architecture of KNN

B. Implementation Details

In this section three image captioning models are discussed that are CNN with LSTM, KNN and Attention Based LSTM. The CNN with LSTM and Attention Based LSTM models are implemented with proposed methodology of beam search that is based upon the maximum probability theory to improve the quality of captions. The proposed KNN model uses a similarity function to reduce the exponential time complexity.

Authorized licensed use limited to: DELHI TECHNICAL UNIV. Downloaded on June 03,2022 at 06:27:51 UTC from IEEE Xplore. Restrictions apply.

1) Implementation of CNN with LSTM

The image to text generation is a combined study of locating the critical regions in the image and sequentially rearranging them so that they give a meaningful sentence. A combined CNN can be used for locating the objects in the image and LSTM for sequential text generation. Thus CNN with LSTM is the most intuitive approach for the IC solution.

The model for the IC has two parts, an encoder and decoder. The encoder part is used to extract the feature vector of the image, which is the second last layer of the CNN model and a decoder part for generating the sequence caption describing the image. The CNN model used above is Inception v-3 or formerly googlenet trained on the imagenet database. The LSTM model has been used as the decoder part of the model. The LSTM is a more advanced RNN as the ordinary RNN has a problem of vanishing gradients. The LSTM contains a memory cell that stores the important values for a long period of time. Gates are used to control the update time of the state of the cell [5].

The result generated by the final layer of LSTM is the probability of the unique words present in the dataset that can give meaning to the next word in the sequence using the feature vector and the sequence of partial captions. The first partial caption is the start token (< startseq >), and the remaining caption is generated using this start token, and the caption ends with the end token (< endseq >). The model has been trained using categorical cross entropy as the loss function and adam optimizer as the optimizer to minimize the loss [12].

The preprocessing of the dataset is completed before training the model. The dictionary keeps track of every word with more than five occurrences. GloVe embedding is used to convert the words to a vector representation [21]. Words are translated into a meaningful space in which semantic similarity is related to the distance between them.

To enhance the performance of the model, we used the beam search method of variable k, where k is the number of chosen captions taken during the generation of the caption using softmax probabilities [20]. The captions are generated using beam search, which considers k most possible sentences. It is further improved using length normalization. Since the probabilities are small numbers, multiplying them forms even smaller numbers approaching zero. Therefore we use the logarithm of probabilities. The sentence with the highest probability will have the highest log probability. We can also say that it will have the most negligible negative log probability.

Fig. 2 shows the basic steps to implement the CNN with LSTM model. Higher values of k may provide better results theoretically, but it also increases the complexity. Simple naïve beam search assign greater probabilities to the sentences with a shorter length than sentences with a longer length. The solution is to perform length normalization on the probabilities during sorting and selecting the k most probable partial sentences.

2) Implementation of KNN model

The nearest neighbor approach is one of the machine learning approaches, which is very popular and easy to use because of its simplicity of implementation and understanding. Thus KNN can be used for IC problems and give better results if the dataset has comparable images with the test image. As there is no training in the KNN the images during testing use all the training dataset to find the suitable caption. This method uses the cosine similarity measure to determine the closest k photos for the image in the training dataset using one feature space. The caption set consists of 5*k captions because each k photo has five captions. Then the selected caption c* is the one with the highest value given by equation (1):

$$c* = argmax \ \sum Sim(c,c') \quad (1)$$

The selected caption is the caption that has the most significant similarity score with all the captions in the set.

Further, to reduce noise due to outliers, the solution is to evaluate the similarity score over only a subset of the set of candidate captions instead of the entire set of candidate captions. So the consensus caption after noise reduction is given by equation (2):

$$c* = argmax \ max \ \sum Sim(c,c') \quad (2)$$

So for every caption, it is required to evaluate the inner summation for all possible Size-M subsets of the set of candidate captions. We proposed the algorithms to compute the consensus caption below efficiently.

Fig. 3 shows the basic steps to implement the KNN model. To evaluate the consensus caption c*, we are required to evaluate the similarity scores of a given caption c with all possible M sized subsets of the N candidate caption we have. Our program will have an exponential time complexity using the brute force algorithm to evaluate the consensus caption. No computer or supercomputer will successfully execute the program in any reasonable time. Then we proposed an algorithm to reduce the time complexity to O (N*N logN).

a) The Brute Force Algorithm.

We generated all possible M-sized subsets of the N candidate captions set, and then for every caption c, we will calculate the similarity score for c. Once we have calculated the similarity scores for all the captions, we choose the caption that achieves the maximum consensus score. As discussed, the time complexity for the algorithm is exponential.

b) Proposed optimized KNN Algorithm.

This algorithm has an asymptotic runtime complexity of O (N*N logN) under the assumption that SIM (i, j) which is BLEU-1 score can be evaluated in constant time.

i. First, arbitrarily number the captions from 1 to N.
ii. Choose the ith caption :
iii. Evaluate the values SIM(i, j) where j goes from 1 to N
iv. Among the N values evaluated, choose the M largest values.
v. Sum the selected M values to get the score for the i^{th} caption.

Do this for all the N captions and choose the consensus caption that gets the highest score.

Authorized licensed use limited to: DELHI TECHNICAL UNIV. Downloaded on June 03,2022 at 06:27:51 UTC from IEEE Xplore. Restrictions apply.

3) Attention Based LSTM Model

The shortcoming of the CNN with LSTM model is that when this model is generating the next word of the caption, the model is not using the input image effectively. The attention mechanism helps overcome this problem by focusing on the image part that describes the next target word.

The CNN with LSTM based IC model would decode the input image with the already trained convolutional neural network inception V-3 in a hidden state (Hj). Then, using LSTM decodes the hidden state and generates a caption. The outputs from previous elements and new sequence data are used as inputs for subsequent target words.

However, as RNNs are computationally costly, it is not easy to analyze the whole input image by picking the important segment from the input image. This problem can be overcome. The image is first partitioned into n pieces with an attention method, and with CNN, we compute the representation of each piece. When the LSTM generates the next target word, the attention mechanism uses the relevant part of the image so that LSTM does not become computationally costly.

Only a few resource positions are focused on local attention compared with global attention, which is very costly as it focuses on all the input parts of the image. Local attention focuses only on the part of the CNN hidden layer per next word to compensate for this shortcoming. Local attention uses a centre point and calculates the attention weights in the left-hand right region of the centre point into the context vector. We have also used the beam search method to improve the model's performance.

The score for local attention is mentioned below in equation (3).

$$f_{ATT} = V_{attn}^{T} * \tanh\left(U_{attn} * h_j + W_{attn} * s_t\right) \quad (3)$$

where,

$$V_{attn}^{T} \in R^{d}, U_{attn} \in R^{d*d}, W_{attn} \in R^{d*d}, s_{t-1} \in R^{d}, h_j \in R^{d}$$

The importance of this segment is given by equation (4)

$$e_{jt} = f_{ATT}(s_{t-1}, h_j) \quad (4)$$

where,

- s_{t-1} is the prior state of decoder.
- The encoder state is h_j.
- The feed forward neural network f_{ATT} is a linear input transformation.

The Attention Based LSTM model is made up of four logical parts:

i. Encoder: Because the pre-trained Inception model already has done the picture encoding, the Encoder here is pretty basic. It includes a linear layer that transfers pre-encoded picture characteristics to the next part.

ii. Sequence Decoder: This is a recurrent neural network which has a gated recurrent unit. After travelling via an Embedding layer, the captions are provided in as inputs.

iii. Attention: As the Decoder creates each word in the output sequence, the attention module assists it in focusing on the most important region of the image for that phrase.

iv. Sentence Generator: This module is made up of a few linear layers. It uses the decoder's result to generate probabilities for each word in the corpus and each location in the expected sequence. The beam search applied in this module takes k candidate words with maximum probability, where k is the beam size. The end result is the output of the given test image having the highest summation of probability.

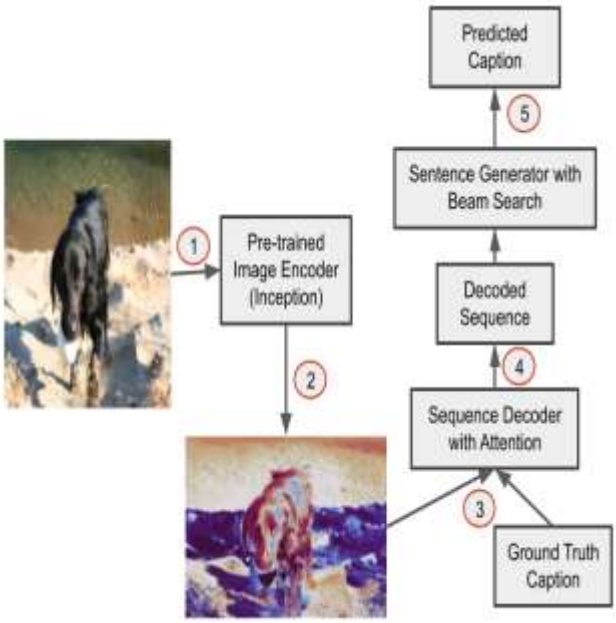

Fig. 4. Working of Attention Based LSTM model

IV. RESULTS AND DISCUSSIONS

For evaluating the performance of the three models- LSTM with CNN, KNN and Attention-based network, we have selected the following metrics:

a) BLEU: BLEU is Bilingual evaluation understudy which is a well-known performance metric for comparing the similarity of several references with a consensus text [9]. It gives a number between 0 and 1. One indicates that the reference sentence and the delivered sentences are comparable. Attention Based LSTM model with beam size of 7 outperforms KNN and CNN with LSTM model with a BLEU-4 score of 32.21, as shown in Table 1, Table 2 and Table 3.

b) ROUGE: ROUGE is Recall oriented understudy. It is selected as an evaluation performance metric because it

Authorized licensed use limited to: DELHI TECHNICAL UNIV. Downloaded on June 03,2022 at 06:27:51 UTC from IEEE Xplore. Restrictions apply.

evaluates recall of the reference sentence with the given summary [11]. It estimates the candidate's and reference's longest common subsequence, which is useful for assessing the generated caption. Our architecture for the Attention Based LSTM with beam size of 7 showed the best ROUGE-L score of 46.41 as shown in Table 5 and outperforms KNN and CNN with LSTM model.

c) METEOR: METEOR is Metric for evaluation for translation with explicit ordering and used for evaluating the translation generated by machine [10]. The issue with BLEU is that it uses a candidate caption identical to the reference caption in length. The METEOR solves this by replacing the BLEU precision and recall calculation with a weighted F-score. Our architecture for the Attention Based LSTM with beam size of 7 showed the best METEOR score of 28.86 as shown in Table 4 and outperforms KNN and CNN with LSTM model .

The above results depict that Attention-Based LSTM with a beam size of 7 gives better results than the other two models and can produce good quality image captions.

The above metrics were assessed on the Flickr8k dataset using the Nvidia K80 GPU provided by Kaggle [16]. The findings of different variations of the neural network-based model are presented. These versions are then compared. We compared greedy search and beam search on the CNN with LSTM and KNN with different k and M, where k is the number of images and M is the number of captions.

Then we try to improve the LSTM model by including the local attention layer to the model and different beam sizes. Finally, we compared all three models based on ROUGE-1, ROUGE-2, ROUGE-L, BLEU-1, BLEU-4 and METEOR performance measures.

We investigated various model versions and reported findings for:

i. CNN with LSTM-based neural network model with different beam sizes of 1,3,5, and 7
ii. KNN model with value of M = 40, 50 and k = 20, 30, 40.
iii. Attention Based LSTM with various beam sizes of 1,3,5, and 7
iv. METEOR Score of different Models
v. ROUGE Score of different Models

TABLE 1. BLEU SCORES FOR CNN WITH LSTM OF VARIOUS SIZE OF BEAMS

Beam Size	BLEU-1	BLEU-4
1(Greedy)	58.05	15.45
3	**59.04**	15.90
5	58.88	**15.97**
7	58.85	15.90

TABLE 2. BLEU SCORES FOR KNN

KNN	BLEU-1	BLEU-4
k=20,M=40	52.62	10.92
k=30,M=50	53.49	11.01
k=40,M=50	**55.24**	**11.87**

TABLE 3. BLEU SCORES FOR ATTENTION BASED LSTM MODEL

Beam Size	BLEU-1	BLEU-4
1(Greedy)	58.72	28.36
3	59.16	29.26
5	59.86	31.12
7	**62.34**	**32.21**

TABLE 4. METEOR SCORES FOR DIFFERENT MODELS

Model	Meteor
CNN with LSTM (Beam=5)	27.5
KNN (k=40,M=50)	27.3
Attention Based LSTM (Beam=7)	**28.6**

TABLE 5. ROUGE SCORES FOR DIFFERENT MODELS

	CNN with LSTM (BEAM-5)	KNN (k=40,M=50)	Attention Based LSTM (BEAM-7)
ROUGE-1	34.6	35.4	**48.27**
ROUGE-2	10.4	4.0	**11.42**
ROUGE-L	32.4	31.9	**46.41**

(a)

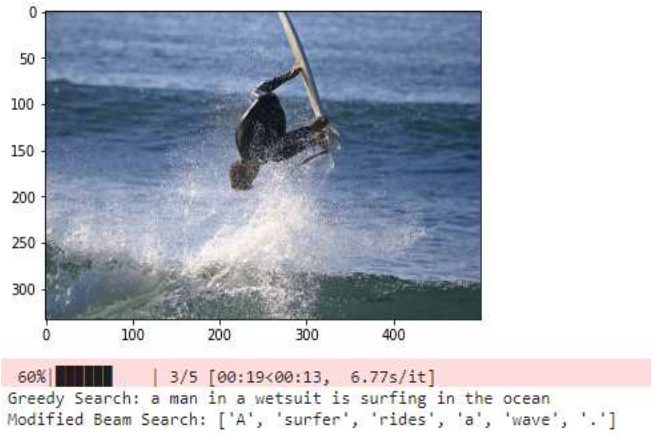

(b)

Fig. 5. Results showing Generation of Caption

Authorized licensed use limited to: DELHI TECHNICAL UNIV. Downloaded on June 03,2022 at 06:27:51 UTC from IEEE Xplore. Restrictions apply.

V. CONCLUSION AND FUTURE WORK

In the current study, we have empirically evaluated three models- CNN with LSTM, KNN and Attention Based LSTM for IC on the Flickr8k public dataset. Further, three performance metrics- BLEU, METEOR and ROGUE are selected to compare the results.

As it has been discussed above, the Attention Based LSTM model showed better results than KNN and CNN with LSTM models on all three performance measures. The proposed KNN algorithm also helps in reducing the time complexity without compromising the final result. We have added the beam search algorithm, which helps in improving the performance of the CNN with LSTM and Attention Based LSTM. The BLEU-4 score of Attention Based LSTM with a beam size of 7 is 32.21, which is much better than the greedy search score of 28.36 and also CNN with LSTM model performance with a beam size of 5 is 15.97, which is better than the greedy search BLEU-4 score of 15.45.

Every approach has its own set of limits and advantages, such as the KNN model which perform best when the dataset is huge. At the same time, the beam search proves to be an essential method to improve the quality of captions.

Also, there are a few limitations in the current study. Firstly, the alignment and dimensional relationships of the features are not considered by CNN. It is tough to assess the results of natural language generation systems. Secondly, the Attention Based LSTM is best compared to other models on the selected metrics, which may not be the case for other metrics selected. Further, we have evaluated results only on the Flickr8k dataset. There may be a possibility of the models not performing well on other datasets.

In the future, it would be intriguing to analyze the performance on hybrid models, models based on reinforcement learning and multi-directional RNN. One more future direction could be to explore the models on much larger datasets like MS COCO and Flickr30k. A larger dataset implies more data for training, which can help the suggested models perform better. Finally, the performance over other valuable metrics like CIDER and SPICE can be explored.

In the end, we conclude that the findings of the comparative study for IC are significant for researchers and practitioners.

REFERENCES

[1] O. Vinyals, A. Toshev, S. Bengio, and D. Erhan, "Show and tell: A neural image caption generator," in *2015 IEEE Conference on Computer Vision and Pattern Recognition (CVPR)*, 2015.

[2] J. Devlin, S. Gupta, R. Girshick, M. Mitchell, and C. L. Zitnick, "Exploring nearest neighbor approaches for image captioning," *arXiv [cs.CV]*, 2015.

[3] G. Ding, M. Chen, S. Zhao, H. Chen, J. Han, and Q. Liu, "Neural image caption generation with weighted training and reference," *Cognit. Comput.*, vol. 11, no. 6, pp. 763–777, 2019, doi: 10.1007/s12559-018-9581-x.

[4] K. Xu et al., "Show, attend and tell: Neural image caption generation with visual attention," *arXiv [cs.LG]*, 2015.

[5] S. Hochreiter and J. Schmidhuber, "Long short-term memory," *Neural Comput.*, vol. 9, no. 8, pp. 1735–1780, 1997, doi: 10.1162/neco.1997.9.8.1735.

[6] G. Kulkarni et al., "Babytalk: Understanding and generating simple image descriptions," *IEEE Transactions on Pattern Analysis and Machine Intelligence*, vol. 35, no. 12, pp. 2891–2903, 2013.

[7] M. Ivasic-Kos, M. Pobar, and S. Ribaric, "Two-tier image annotation model based on a multi-label classifier and fuzzy-knowledge representation scheme," *Pattern Recognit.*, vol. 52, pp. 287–305, 2016.

[8] C. Szegedy, V. Vanhoucke, S. Ioffe, J. Shlens, and Z. Wojna, "Rethinking the inception architecture for computer vision," in *2016 IEEE Conference on Computer Vision and Pattern Recognition (CVPR)*, 2016, doi: 10.1109/cvpr.2016.308.

[9] K. Papineni, S. Roukos, T. Ward, and W.-J. Zhu, "BLEU: A method for automatic evaluation of machine translation," in *Proceedings of the 40th Annual Meeting on Association for Computational Linguistics - ACL '02*, 2001, doi: 10.3115/1073083.1073135.

[10] Banerjee, Satanjeev and A. Lavie, ". METEOR: An automatic metric for MT evaluation with improved correlation with human judgments," *ACL workshop on intrinsic and extrinsic evaluation measures for machine translation and/or summarization*, pp. 65–72, 2005.

[11] Lin, Chin-Yew, and F. J. Och, ". Looking for a few good metrics: ROUGE and its evaluation," *4th NTCIR Workshops*, 2004.

[12] A. Mustapha, L. Mohamed, and K. Ali, "Comparative study of optimization techniques in deep learning: Application in the ophthalmology field," *J. Phys. Conf. Ser.*, vol. 1743, no. 1, p. 012002, 2021.

[13] O. Sargar and S. Kinger, "Image captioning methods and metrics," in *2021 International Conference on Emerging Smart Computing and Informatics (ESCI)*, pp. 522–526, 2021.

[14] S. S. Yv, Y. Choubey, and D. Naik, "Image captioning with attention based model," in *2021 5th International Conference on Computing Methodologies and Communication (ICCMC)*, 2021, doi: 10.1109/iccmc51019.2021.9418347.

[15] Machine Learning Mastery, *glass.csv at d20fcb6402ae34e653d4513b00f39257bb37ed7f · jbrownlee/Datasets*.

[16] "Kaggle: Your machine learning and data science community," *Kaggle.com*. [Online]. Available: https://www.kaggle.com/. [Accessed: 05-Mar-2022].

[17] M. A. Al-Malla, A. Jafar, and N. Ghneim, "Image captioning model using attention and object features to mimic human image understanding," *J. Big Data*, vol. 9, no. 1, 2022.

[18] Y. Chu, X. Yue, L. Yu, M. Sergei, and Z. Wang, "Automatic image captioning based on ResNet50 and LSTM with soft attention," *Wirel. Commun. Mob. Comput.*, vol. 2020, pp. 1–7, 2020.

[19] S. Takkar, A. Jain, and P. Adlakha, "Comparative study of different image captioning models," in *2021 5th International Conference on Computing Methodologies and Communication (ICCMC)*, pp. 1366–1371, 2021.

[20] "9.8. Beam Search — Dive into Deep Learning 0.16.1 documentation." Available: https://d2l.ai/chapter_recurrent-modern/beamsearch.html [Accessed 13-Mar-2021].

[21] J. Pennington, R. Socher, and C. Manning, "Glove: Global vectors for word representation," in *Proceedings of the 2014 Conference on Empirical Methods in Natural Language Processing (EMNLP)*, 2014.

[22] C. Amritkar and V. Jabade, "Image caption generation using deep learning technique," in *2018 Fourth International Conference on Computing Communication Control and Automation (ICCUBEA)*, pp. 1–4, 2018.

[23] A. Puscasiu, A. Fanca, D.-I. Gota, and H. Valean, "Automated image captioning," in *2020 IEEE International Conference on Automation, Quality and Testing, Robotics (AQTR)*, pp. 1–6, 2020.

[24] *Applsci-11-10176-v2.pdf*. [Online]. Available: http://applsci-11-10176-v2.pdf. [Accessed: 17-Mar-2022].

[25] I. Azhar, I. Afyouni, and A. Elnagar, "Facilitated deep learning models for image captioning," in *2021 55th Annual Conference on Information Sciences and Systems (CISS)*, pp. 1–6, 2021.

[26] K. He, X. Zhang, S. Ren, and J. Sun, "Deep residual learning for image recognition," in *2016 IEEE Conference on Computer Vision and Pattern Recognition (CVPR)*, 2016.

Authorized licensed use limited to: DELHI TECHNICAL UNIV. Downloaded on June 03,2022 at 06:27:51 UTC from IEEE Xplore. Restrictions apply.

TechRxiv
Powered by IEEE

A comparative study of Naive Bayes Classifiers with improved technique on Text Classification

This paper was downloaded from TechRxiv (https://www.techrxiv.org).

LICENSE

CC BY 4.0

SUBMISSION DATE / POSTED DATE

28-05-2022 / 31-05-2022

CITATION

Naulak, Chingmuankim (2022): A comparative study of Naive Bayes Classifiers with improved technique on Text Classification. TechRxiv. Preprint.
https://www.techrxiv.org/articles/preprint/A_comparative_study_of_Naive_Bayes_Classifiers_with_improved_tec

DOI

10.36227/techrxiv.19918360.v1

A comparative study of Naive Bayes Classifiers with improved technique on Text Classification

Chingmuankim and Prof.Rajni Jindal

***Abstract*— Naive Bayes classifier is a linear classifier based on Bayesian theorem that make use of conditional probabilities where the class of the comments in the dataset are decided by the result obtained from the product of prior probability and likelihood of the class. These textual features are represented into a vector form using different feature extraction techniques of Natural Language Processing such as BagOfWords and TermFrequency-InverseDocumentFrequency for the purpose of computation. Naive Bayes is also known as eager learner due to its quick capability to learn. It has been widely used for classification of text. One of the well-known limitation of this classifier is the independence assumption of features which creates a possibility for the occurrence of redundant features. Moreover, the significance of semantics is completely ignored. Despite these limitation, these classifier has performed very well. Earlier research has been conducted on comparision between two models of Naive Bayes, namely Bernoulli and Multinomial Naive Bayes, distribution of the datasets, errors such as system level error and weight error has been analysed. The objective of this work is to test imbalance dataset on the three types of Naive Bayes Model, compare the performance result and see the impact it has on the model by applying our improved technique that combines TF-IDF with n-gram language modelling. In this paper, we will discuss in detail about the experimental results and the methodology used for carrying out this research. Our experimental result shows a 2-3% increase in the accuracy than the old model.**

***Index Terms*—BagofWords, Naive Bayes, TF-IDF**

I. INTRODUCTION

Earlier before the emergence of Machine Learning, the task of text annotation was done manually by humans. As data grew larger with the passage of time, it will consume a lot of time and become harder to manage these big data manually. Therefore, such task needs to be automated using Machine Learning Algorithms and one such is Naive Bayes algorithm which is a supervised machine learning algorithm based on Bayesian theorem with the assumption that there is no dependency among the features. Due to this naive assumption, there is a possibility of the occurrence of redundant features within the data and it has no regard for the importance of semantics. Another drawback of Naive Bayes is the problem with zero probability where the product turns zero if any of the terms of the product is zero which in practical is impossible because there is no guarantee that the absence of word in a particular comment determines the non-occurrence of word in another comment.

These textual datas can be represented in a vector space using TF-IDF (TermFrequency-InverseDocumentFrequency) when dealing with Machine Learning algorithms. Various researchers have addressed the challenge that Naive Bayes has concerning the conditional independence assumption of features. Some of these are Augmented Naive Bayes, Chain Augmented (CAN), and Tree Augmented Naive Bayes Classifier (TAN). To be precise, CAN is a model which is developed by combining the Augmented Naive Bayes with the language model n-gram, while the simply augmented Naive Bayes is a Markov Chain model with dependency of attributes to the parent class and TAN is a tree like structure where the observed variables depend on the structure of the tree. Naive Bayes can be categorized into three types. These are GNB (Gaussian Naive Bayes), BNB (Bernoulli Naive Bayes) and MNB (Multinomial Naive Bayes). GBN follows Gaussian normal distribution and is suitable for a continuous data. While BNB follows a Bernoulli distribution and work with Boolean and discrete data. Like BNB, MNB is suitable for discrete data and follows multinomial distribution.

Naive Bayes can be applied in Real-time predictions such as disease diagnosis, making decision about treatment process and classification of RNA sequence. The paper is further categorized into different sections. The following section comprises of Literature Review, Methodology, Performance evaluation, Experimental Result and Conclusion.

II. LITERATURE REVIEW

[1]A descriptive paper on the different terminologies for classification based task using Non-Linear model. It provides different NLP techniques that are necessary for having a good model. Their study stated that "On comparing two different model of Naive Bayes, basically Multinomial model and Bernoulli model, the multinomial model tends to outperform the later in the case of a large vocabulary size. Moreover they have mentioned that the performance also depends upon the appropriate choice of features.

[2]A short survey on Naïve Bayes highlighting the shortcomings of Naïve Bayes such as the Naïve assumption and the zero conditional probability problem. One solution for the conditional independence is to increase its structure by adding more dependency among attributes, also known as Augmented Naïve Bayes Network and Laplacian correction for zero conditional probability problem.

[3]This is an empirical study where the authors studied the different factors that can effect the performance of Naive Bayes. They used Monte-Carlo simulation for examining the accuracy of the classifier on multiple classes of randomly generated problem. Some of the factors they have considered includes distribution entropy, completely independent features, functionally dependent features. Considering these factors, they have observed a good performance with low-entropy feature

distribution on Naive Bayes Classifier. Similarly they have observed the same for the features which are completely independent and functionally dependent which is unexpected. According to their findings, the classifier has no direct co-relation with the amount of dependency of features. They concluded that the amount of the lost information about the class could be a better predictor of the classifier due to its conditional assumption.

[4]Descriptive paper about the mathematical computation of the two types of Predictive Classifier, namely Bernoulli and Multinomial Naive Bayes. In this, they have discussed about the application of Bag of Words technique for the two models. Under their discussion, there are two types of counts of BoW. They have used Binary count representation for BNB and Absolute count for MNB.

[5]Performed an experiment on a large dataset using Multinomial Naive Bayes. These large dataset is processed using MapReduce function by dividing the large dataset into smaller pieces on which key value pairs are assigned to each datas and are further processed by performing tokenization, data cleaning, counting and aggregating counts. Final input gets stored in Hadoop Distributed File System (HDFS). On doing so, it has a good impact on the performance of the model with better accuracy result, good scalability, and extensibility for large-scale text classification.

[6]Proposed an auxiliary feature method by using the existing feature selection methods to select the auxiliary features. They have adjusted the corresponding probability of the selected auxiliary feature to improve Naive Bayes Classifier's performance. They have obtained the datasets from CCERT, where 45396 are junks and 18314 are normal. 30000 and 10000 mails respectively from the junk and normal classes are used for experimentation. They have performed three test cases. They have observed 96, 152, and 217 auxiliary features respectively with 1000 1500 and 2000 feature representation. The experiment was conducted five times, with a cross validation of 10-fold using Naïve Bayes algorithm.

[7]Performs simulation using GNB model which is based on clustering. The objective task is to recognise and classify the unseen continuous data that contains large number of Non-priori knowledge within a short time. They have performed feature extraction on the sample using Information entropy measure. The class labels and the data are mapped using Gaussian Naive Bayes algorithm. Increasing the sample size significantly improved the model accuracy, and the use of Information entropy ensures the accuracy of classification algorithm but also controls the overall small size of training dataset.

[8]They have used a multinomial Naive Bayes model for classifying a News dataset. According to their study, Multinomial Naive Bayes is not completely Bayesian, therefore they prepared a Bayesian Version of the classifier. Combination of Multinomial Naive Bayes Classifier with suitable Dirichlet hyper-parameters shows same result for MNB classifier.

[9]Proposed a text classification framework for Sentiment analysis using Multinomial Naive Bayes with TF-IDF. Thus accuracy is improved greatly with 89%.

[10]Comparision based task for Sentiment analysis of News articles. Text classification was performed on Multinomial and Bernoulli Naïve Bayes model and the performance are compared. The experiment was performed on News articles where they are classified as positive or negative classes. On analysing the performance of the model, Multinomial model outperforms Bernoulli Naive Bayes model. Total number of features taken into consideration is 15000. Performance metrics used for this experiment is Confusion matrix. Accuracy of 73.404% is obtained.

[11]Performs experimental work on Turkish document using N-gram features. The Turkish documents were classified into five categories using Naive Bayes algorithm. They have calculated Precision score, Recall, Accuracy and F-measure and the test result shows a success rate of 92%.

[12]Proposed a model known as Chain Augmented Naive Bayes which is developed with the combination of the traditional model with a language model i.e. n-gram to solve the limitations of the classifier. According to their study, CAN model is a better classifier than the Tree Augmented one. This was done by simplifying the Tree Augmented Naive Bayes model by limiting the dependency observed among the attributes to form a chain like Markov model instead of a tree. They further addressed the zero probability issue by applying smoothing techniques from the Statistical Language Modelling. This technique gives a better estimate than the Laplace Smoothing.

[13]Discussed about the n-gram based word-level text classification using a combination of Multinomial Naive Bayes Classifier and a classification based on hierarchy to restrict and improve the misclassification that occurs at the initial level and filtration of content-based model. They have also suggested an approach to lessen the time execution requirements for calculating the probabilities.

[14]Proposed a model to address the challenges of Unigram based model such as BOW model. Such models do not consider the word set that co-occur in a document level. The new model propose a new approach to incorporate the features that are co-occurring to the Bag of Words model. The method is analysed and it displays better result in classification of text. Co-occurrence may be a good indexes in Information Retrieval.

[15]Discuss about the experimental result of text classification using BagofWords model. The categories for classification are angry, bored, enthusiasm, fun, happiness, hate, neutral etc. The highest percentage of sentiment expressed by the authors in the dataset for neutral is more. The second highest is "happiness" and "angry" has the lowest class distribution.

[16] addressed the issue with Bag of Word model containing the negligence of co-relation among words, the traditional Bag of Words model was improved by proposing a new model called network based BOW model. These model collect the words that have high level structure and semantics. The result of the analysis showed that the new method performs the best with high efficiency in comparision to the existing one. They also concluded that dynamic network is better than the static/hybrid network.

[17]Proposed an improved TF-IDF algorithm to perform text classification. Previous research has seen challenges with the traditional text classification such as negligence of the importance of links of context-based semantics and unique vocabularies. In this work, they have represented the feature words as a vector using word2vec and its weight is calculated

using the proposed model by multiplying the word vector and its weight. The result of the analysis shows that the proposed model outperformed the traditional TF-IDF model.

[18]This paper proposes a text classification technique using TF-IDF along with Next word negation. They have conducted their experiment on three datasets such as movie review of IMDB, product review of Amazon and SMS Spam detection dataset. Analysis was performed on these datasets using the proposed technique. They have used cross validation technique of 10-fold to find out the average accuracy. The test result shows a good increase in the accuracy level of 89.91%, 88.86% and 96.83% respectively for the considered datasets.

There are various methods with which the efficiency of model can be improved. Research has been conducted with Augmented Naive Bayes, Multinomial Naive Bayes using Bag of Words, combination of Naïve Bayes classifier with Map Reduce, Naive Bayes with auxiliary feature etc to improve the performance of the model. It has also been stated by a researcher that "Deeper understanding of the characteristics of the data can improve the model's performance". Based on these reviews, we would like to experiment our data using n-gram language model on the three types of Naive Bayes classifiers and observe the impact it has on the performance of the model using Confusion matrix. We would also like to discover the other parameters that can affect the accuracy of the model.

III. METHODOLOGY

The following diagram shows the workflow of the proposed work. Each stages are discussed in detail at the later part.

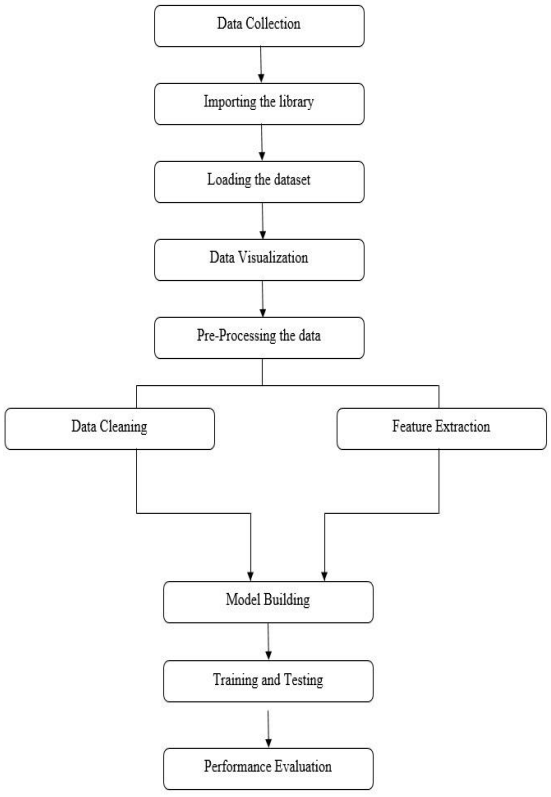

Fig. 1. Workflow of Proposed work

A. Data Collection

For every NLP related tasks, data-collection is the first step towards building any type of model, followed by importing the required libraries. We have collected our data from Kaggle, prepared by a collection of different datasets created for the purpose of text analysis.

B. Import the Libraries

Libraries such as numpy, pandas, seaborn, matplotlib, wordcloud, nltk, string, stopwords, countvectorizer, tfidfVectorizer and Confusionmatrix are used in performing our research.

C. Load the dataset

After importing the required libraries, the raw dataset are loaded to the program. The dataset comprises of tweet comments which are annotated with positive and negative labels using the tag 0 and 1. In this work, positive comments are annotated with 0 and negative comments with 1. The dataset has a dimension of 33086 rows and 3 columns as shown below.

	label	tweet
0	0	@user when a father is dysfunctional and is so...
1	0	@user @user thanks for #lyft credit i can't us...
2	0	bihday your majesty
3	0	#model i love u take with u all the time in ...
4	0	factsguide: society now #motivation
...	...	...
33081	1	@FercanY @BenjaminHarvey Rip Heath Ledger :(
33082	1	no more of being 'high all the time' :(((((((...
33083	1	@RealKrisTravis it came crashing down and it h...
33084	1	Now if only it had an app... Stupid Apple, not...
33085	1	i can't be there for you anymore & i'm sor...

33086 rows × 2 columns

Fig. 2. Raw Dataset

D. Data Exploration and Visualization

The dataset is further explored and are visualised using the library called wordcloud. When using the wordcloud library, all the comments in the dataset are first required to be concatenated into one string. Thereafter, the library can be used to visualize the words that frequently occurred in both the positive and negative classes.

1) **Data Exploration**

The data is explored to see the details of the dataset.

	label	tweet	Character_Count	Word_Count
0	0	@user when a father is dysfunctional and is so...	101	18
1	0	@user @user thanks for #lyft credit i can't us...	122	19
2	0	bihday your majesty	19	3
3	0	#model i love u take with u all the time in ...	84	14
4	0	factsguide: society now #motivation	38	4
...	...	...	...	...
33081	1	@FercanY @BenjaminHarvey Rip Heath Ledger :(	44	6
33082	1	no more of being 'high all the time' :((((((((...	63	13
33083	1	@RealKrisTravis it came crashing down and it h...	60	10
33084	1	Now if only it had an app... Stupid Apple, not...	87	17
33085	1	i can't be there for you anymore & i'm sor...	91	19

33086 rows × 4 columns

Fig. 3. Details of Dataset

Character and Word Count: Character count is the count of the letters present in each word of the comment excluding the white-spaces. While the Word count is the count of the chunk of words present in the comment excluding the white-spaces.

Shortest, Medium and Longest Comment: The maximum, medium and minimum length of the comment can be viewed by count of characters and words as shown below.

```
[ ] tweets_df[tweets_df['Character_Count'] == 11]['tweet'].iloc[0]

'shut up rat'
```

```
tweets_df[tweets_df['Word_Count'] == 3]['tweet'].iloc[0]

'bihday your majesty'
```

Fig. 4. Shortest comment

Frequency Table: Frequency Table displays the non-redundant words that are in the dataset alongwith its count. There are 46684 non-redundant words in the dataset. The image below shows the frequency count after cleaning the data.

	Word	Frequency
0	user	17472
1	the	10345
2	to	10052
3	a	6563
4	i	6179
...	...	...
46679	channelfriend	1
46680	polling	1
46681	germansandtheirbread	1
46682	ðõðâðï	1
46683	realkristravis	1

46684 rows × 2 columns

Fig. 5. Frequency Table

2) **Data Visualization**

Data Visualization is a technique to see the details and characteristics of the data.

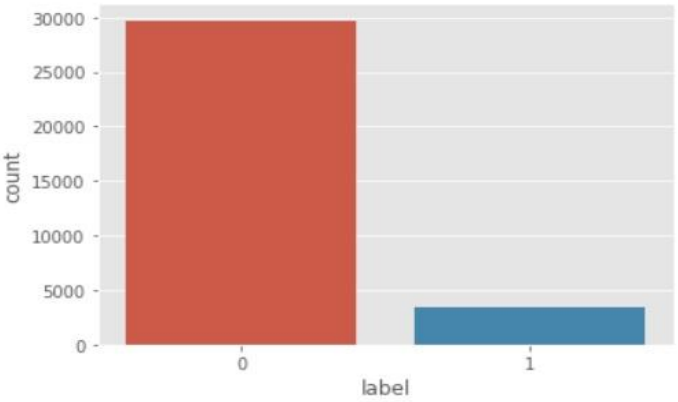

Fig. 6. Frequency Distribution of classes

As it can be seen in Fig 6, there are around 29720 comments with label 0, and 3366 comments with label 1 which represents the positive and negative classes.

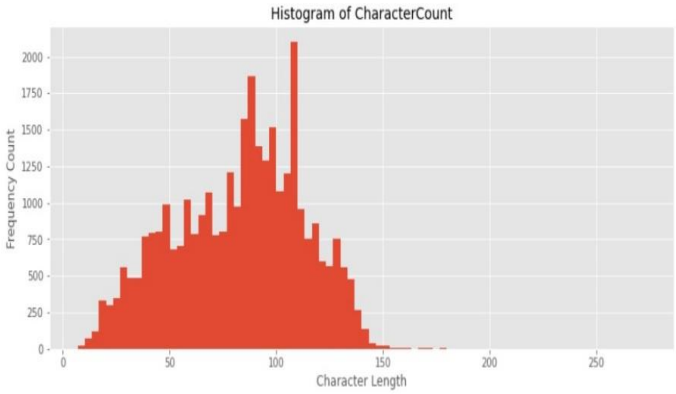

Fig. 7(a). Character Count

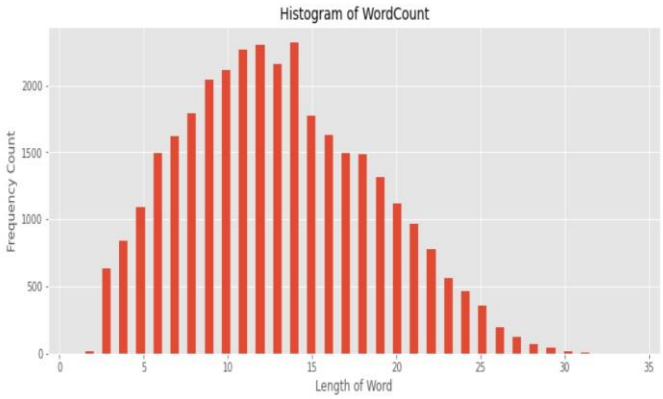

Fig. 7 (b). Word Count

The above two figures shows the frequency distribution of character and words. As it can be observed, they both are skewed towards the right.

E. Pre-Processing the Data

Data Pre-processing is the most crucial part of any Text analysis task. These stage can be further categorized into two steps:

1) Data Filtering: Data Filtering is a pre-processing technique where trivial datas are removed for better and smooth processing of the data. The raw data contains features that are not significant for the purpose of analysis. Therefore, such datas are first removed before feeding them to the model. In this work, we have performed the following:

- Removing the handle such as the symbol '@' that separates the username from the domain name.
- Removing punctuation such as exclamatory marks, commas, full stops etc.
- Removing stopwords which are frequently used in textual data such as 'a', 'an', 'the' etc but have no significance towards text analysis. Python has a list of stopwords that are stored in the pre-defined library.
- Lowercasing by converting all uppercases to lowercase
- Tokenization which is the process of dividing the comments into chunk of words.

user_removed	clean_tweet
when a father is dysfunctional and is so self...	[father, dysfunctional, selfish, drags, kids, ...
thanks for #lyft credit i can't use cause th...	[thanks, lyft, credit, cant, use, cause, dont,...
bihday your majesty	[bihday, majesty]
#model i love u take with u all the time	[model, love, u, take, u, time]
factsguide: society now #motivation	[factsguide, society, motivation]

Fig. 8. Cleaned Data

2) Feature Extraction

Feature extraction is the technique of narrowing the data dimension by dividing the cleaned raw data to a more manageable group without losing any relevant data. This technique can help improve the learning speed of the model and yields better performance. Two techniques of feature extraction are:

- **BagofWords:** BoW is a technique of representing words into feature vector. This is done by creating a vocabulary that contains a Non-redundant set of data with its word count. There are two types of word count in BOW model. These are Binary and Absolute count. In Binary count, the words that occur in the tweet comments has a feature vector of 1 and 0 otherwise. While Absolute count is the count of how frequently the word occur in the dataset. These technique is often used by previous researchers.
- **TF-IDF:** TF-IDF is a feature representation technique that represents the comment in the dataset by a feature vector whose value is the frequency of that word in the comment. This technique addressed the limitation of Bag of Words by finding semantics of the data and is preferred for the purpose of text classification. TF-IDF prioritize the context and semantics of words and evaluates the score of its relevance in the comment. Mathematically, it can be computed as:

$$TF = \frac{No.\,of\ words\ repeated\ in\ a\ document}{Total\ no.\,of word\ in\ a\ comment}$$

$$IDF = log\left(\frac{Total\ no.\,of comments\ in\ the\ dataset}{No.\,of commentscontainingthecorrespondingword}\right)$$

TF-IDF=TF*IDF

The quantitative data generated after calculating TF-IDF shows related datas. This is determined by the closeness of the corresponding score of the words. Higher score indicates higher relevance of data. Each word may have different score in every comment based on the context. In this work, we have augmented n-gram and TF-IDF for improving the accuracy of our model.

F. Model Building

The pre-processed data are then trained and tested on the three variants of Naive Bayes classifier. These classification models are:

a. Gaussian Naive Bayes:

GNB is a Naive Bayesian model that follows a Normal distribution. Before training a large dataset on Gaussian Naive Bayes, we first convert the sparse data to dense which generates a matrix data. Thereafter, it is feeded to the classification model. Gaussian Naive Bayes works with continuous data. Mathematically, the likelihood is calculated as:

$$P\left(\frac{Wt}{Cn}\right) = \frac{1}{\sqrt{2\pi\sigma 2Cn}} e - \frac{(x-\mu Cn)^2}{2\sigma^2 Cn}$$

where μ is the sample mean and σ is the standard deviation.

b. Bernoulli Naive Bayes:

Bernoulli, also known as Multi-variate Bernoulli Naive Bayes is a statistical technique that make use of binary count. It generates a Boolean value as its output. This type of classifier works with discrete data. Mathematically, using the improved technique, likelihood and prior probability can be calculated as:

$$P(\frac{Wt}{Cn}) = \frac{\eta n(Wt)}{Ndn}$$

$$P(Cn) = log\left(\frac{N}{Nn}\right)$$

$$TF\text{-}IDF = P\left(\frac{Wt}{Cn}\right) * P(Cn)$$

where $\eta n(Wt)$ is the count of word occurrence in a comment, N_{dn} represents total number of words in a document of class 'n', N_n denotes count of comment that contains the corresponding word of class 'n' and N is the amount of comments in a dataset

c. Multinomial Naive Bayes:

MNB is a probabilistic model that make use of absolute count and predicts the comment in the dataset by acknowledging the frequency of a specified word in the text document. This type of classifiers work well on discrete data. Unlike Bernoulli, absence of word in the dataset have no impact on the probability. Mathematically, likelihood and its prior probability will be calculated as:

$$P\left(\frac{Wt}{Cn}\right) = \frac{\eta n(Wt)}{\overset{v}{_1}\in \eta n(Ws)}$$

$$P(Cn) = log\left(\frac{N}{Nn}\right)$$

$$TF\text{-}IDF = P\left(\frac{Wt}{Cn}\right) * P(Cn)$$

where $\eta n(Wt)$ is the count of word occurrence in a comment and $\eta n(Ws)$ is the total word count in a comment of class 'n', N_n denotes count of comment that contains the corresponding word of class 'n' and N is the sum of all the comments in a dataset. V is dimension of the vocabulary.

G. Training and Testing

We fit the pre-processed data to the model for training and testing using a pre-defined library called train_test_split. 5)

H. Performance Evaluation

We have used Confusion matrix for evaluating the performance of the model by feeding the test dataset for which the true and false values are known. This evaluation technique estimates the number of times the model generates the right and wrong output and its type. There are four possible outcomes with this metrics.

a. **True Positive (TP)**
value of the test data correctly predicted as an actual positive
b. **False Positive (FP)**
misclassified negative values as positive.
c. **False Negative (FN)**
misclassified positive values as negative.
d. **True Negative (TN)**
Value of the test data correctly predicted as an actual negative.

Accuracy: ratio of the correctly classified data and total of all possible outcomes.

$$\frac{TP + TN}{TP + TN + FP + FN}$$

Precision: score of the number of correctly classified positive samples.

$$Precision = \frac{\text{TP}}{\text{TP} + \text{FP}}$$

Recall: score of the amount of samples that might have been missed out.

$$\text{Recall} = \frac{\text{TP}}{\text{TP} + \text{FN}}$$

F1-score: score that measures the balance between Precision and Recall.

$$\text{F1} - \text{Score} = 2 * \frac{\text{Precision} * \text{Recall}}{\text{Precision} + \text{Recall}}$$

Higher the score of precision, more the number of relevant results are returned by the algorithm than irrelevant ones, and high recall means that an algorithm returns most of the relevant results. Therefore, we can conclude that higher the value of precision and recall, better is the result.

IV. ALGORITHM

1) Create a vocabulary V, that contains the mapping of word frequency with Term Frequency.
2) Count the following parameters from the training dataset
   - Sum of the comments in the dataset, denoted by N
   - Count of comments labelled with class n for n=1,2……n
   - Count of comments of class n, containing word w_t for class n=1…n and t=1…|v|
3) Estimate the likelihood probability $P(W_t/C_n)$ for the three models.
4) Estimate the prior probability $P(C_n)$ for Bernoulli and Multinomial model.

5) In case of Gaussian Naive Bayes, prediction of class is done by substituting the parameters in the likelihood probabilities with new values, whereas in the case of Bernoulli and Multinomial model, using TF-IDF technique, the class is predicted by the maximum score of the posterior probability.

V. EXPERIMENTAL RESULT

The figure below shows the automatic layout of our confusion matrix generated at first iteration for one of the Naive Bayes model evaluation.

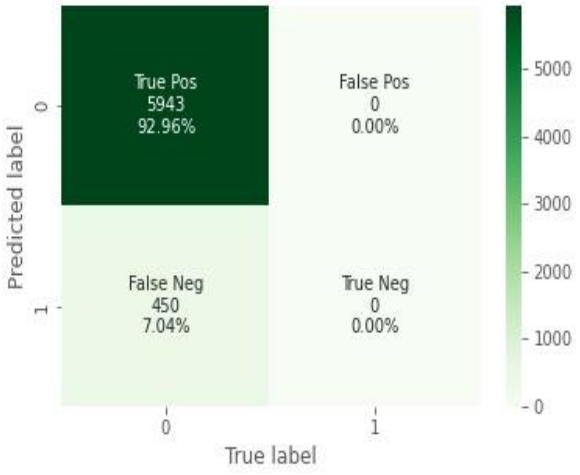

Fig. 9. Confusion matrix

The table below displays the comparative results of the existing model and proposed model on experimenting with 33086 dataset.

TABLE I
RESULT OF OLD MODEL

	GNB using BOW	BNB using BOW	MNB using BOW
Accuracy	✕	89.9%	90.2%
Precision	✕	95%	95%
Recall	✕	100%	100%
F1-score	✕	90%	90%
Support	✕	5950	5950

Since we are working on a large dataset, accuracy could not be calculated in the case of Gaussian Naive Bayes. However, this model can work will smaller data. On experimenting with smaller data of around 1166 comments, this model gives a really low accuracy below 50% in both the cases.

TABLE II
RESULT OF PROPOSED MODEL

	GNB (ngram and TF-IDF)	BNB (ngram and TF-IDF)	MNB (ngram and TF-IDF)
Accuracy	✕	92%	93%
Precision	✕	96%	97%
Recall	✕	100%	100%
F1-score	✕	93%	93%
Support	✕	5943	5943

The above table data record are the best score obtained after 'n' number of iterations of the experiment. It can be concluded from the observation table that our proposed model outperforms the old model. As shown in the table, our proposed model can accurately classify 92% and 93% of the positive comments for each classifiers, but poorly classifies the negative comments. This behavior of the data is expected as we are experimenting on imbalanced dataset that contains more number of positive comments. That is the reason why the model has been able to properly classify most of the positive comments. The table also displays the classification report of the precision, recall and F1 scores for better understanding the results. From the classification report we see similar results. The F1 score shows that the classifier is able to classify the positive comments very well, but the ability to classify the negative comments is really low. This can be further improved by upsampling the amount of negative comments in the data or also by trying out a whole different classifier.

VI. CONCLUSION & FUTURE SCOPE

Finally, we can conclude that the performance of the model can be improved by applying TF-IDF and n-gram language model. We observed a 2-3% accuracy higher than the old model. Our analysis result shows that the proposed model can accurately classify most of the test data. TF-IDF is more preferable than BOW due to its inability to understand semantics of the textual data, which is obsolete in the real word. It is expected that increasing the amount of data and exploring its characteristics may contribute towards getting a higher accuracy. Future work is to explore balanced dataset, and see the impact it can have on the model.

VII. REFERENCES

[1] S. Raschka, "Naive Bayes and Text Classification I - Introduction and Theory," pp. 1–20, 2014.

[2] P. Kaviani and S. Dhotre, "International Journal of Advance Engineering and Research Short Survey on Naive Bayes Algorithm," *Int. J. Adv. Eng. Res. Dev.*, vol. 4, no. 11, pp. 607–611, 2017.

[3] I. Rish, "An Empirical Study of the Naïve Bayes Classifier An empirical study of the naive Bayes classifier," *Cc.Gatech.Edu*, no. January 2001, pp. 41–46, 2014.

[4] G. Sanguinetti, "Text Classification using Naive Bayes = Learning only

=," no. February, 2012.
[5] H. Chen and D. Fu, "An Improved Naive Bayes Classifier for Large Scale Text," vol.146, no. Icaita, pp. 33–36, 2018, doi: 10.2991/icaita-18.2018.9.
[6] W. Zhang and F. Gao, "An improvement to naive bayes for text classification," *Procedia Eng.*, vol. 15, pp. 2160–2164, 2011, doi: 10.1016/j.proeng.2011.08.404.
[7] Z. Bi, Y. Han, C. Huang, and M. Wang, "Gaussian Naive Bayesian Data Classification Model Based on Clustering Algorithm," vol. 168, no. Masta, pp. 396–400, 2019, doi: 10.2991/masta-19.2019.67.
[8] S. Xu, Y. Li, and Z. Wang, "Bayesian multinomial naïve bayes classifier to text classification," *Lect. Notes Electr. Eng.*, vol. 448, no. May, pp. 347–352, 2017, doi: 10.1007/978-981-10-5041-1_57.
[9] M. Abbas, K. Ali, A. Jamali, K. Ali Memon, and A. Aleem Jamali, "Multinomial Naive Bayes Classification Model for Sentiment Analysis," *IJCSNS Int. J. Comput. Sci. Netw. Secur.*, vol. 19, no. 3, p. 62, 2019, doi: 10.13140/RG.2.2.30021.40169.
[10] G. Singh, B. Kumar, L. Gaur, and A. Tyagi, "Comparison between Multinomial and Bernoulli Naïve Bayes for Text Classification," *2019 Int. Conf. Autom. Comput. Technol. Manag. ICACTM 2019*, no. May 2020, pp. 593–596, 2019, doi: 10.1109/ICACTM.2019.8776800.
[11] M. Baygin, "Classification of Text Documents based on Naive Bayes using N-Gram Features," *2018 Int. Conf. Artif. Intell. Data Process. IDAP 2018*, no. 1, p. 940, 2019, doi: 10.1109/IDAP.2018.8620853.
[12] F. Peng and D. Schuurmans, "Combining naive Bayes and n-gram language models for text classification," *Lect. Notes Comput. Sci. (including Subser. Lect. Notes Artif. Intell. Lect. Notes Bioinformatics)*, vol. 2633, pp. 335–350, 2003, doi: 10.1007/3-540-36618-0_24.
[13] J. Shah, "Performance evaluation of applying n-gram based naïve bayes classifier for hierarchical classification," *Proc. 3rd Int. Conf. Comput. Methodol. Commun. ICCMC 2019*, no. Iccmc, pp. 92–98, 2019, doi: 10.1109/ICCMC.2019.8819751.
[14] S. George K and S. Joseph, "Text Classification by Augmenting Bag of Words (BOW) Representation with Co-occurrence Feature," *IOSR J. Comput. Eng.*, vol. 16, no. 1, pp. 34–38, 2014, doi: 10.9790/0661-16153438.
[15] N. V M and D. A. Kumar R, "Implementation on Text Classification Using Bag of Words Model," *SSRN Electron. J.*, no. May, pp. 241–248, 2019, doi: 10.2139/ssrn.3507923.
[16] D. Yan, K. Li, S. Gu, and L. Yang, "Network-Based Bag-of-Words Model for Text Classification," *IEEE Access*, vol. 8, pp. 82641–82652, 2020, doi: 10.1109/ACCESS.2020.2991074.
[17] H. Zhou, "Research of Text Classification Based on TF-IDF and CNN-LSTM," *J. Phys. Conf. Ser.*, vol. 2171, no. 1, pp. 218–222, 2022, doi: 10.1088/1742-6596/2171/1/012021.
[18] B. Das and S. Chakraborty, "An Improved Text Sentiment Classification Model Using TF-IDF and Next Word Negation," 2018.

Proceedings of the Sixth International Conference on Intelligent Computing and Control Systems (ICICCS 2022)
IEEE Xplore Part Number: CFP22K74-ART; ISBN: 978-1-6654-1035-9

A Comparison of Apriori Algorithm and Apriori with Hashing Algorithm

Arjun Malik
Student
Dept. of Software Engineering,
Delhi Technological University,
Rohini,Delhi,110042.
arjunmalik_2k18se036@dtu.ac.in

Mihir Agarwal
Student
Dept. of Software Engineering,
Delhi Technological University,
Rohini,Delhi,110042.
mihiragarwal_2k18se082@dtu.ac.in

Sonika Dahiya
Assistant Professor
Dept. of Software Engineering,
Delhi Technological University,
Rohini,Delhi,110042.
sonika.dahiya@dtu.ac.in

2022 6th International Conference on Intelligent Computing and Control Systems (ICICCS) | 978-1-6654-1035-9/22/$31.00 ©2022 IEEE | DOI: 10.1109/ICICCS53718.2022.9788238

***Abstract*—Data mining helps us in finding a pattern or some information that can help us relate different items even in a very big dataset. Association mining rules is one of the best applications of data mining that helps us in finding frequent itemsets [1]. Apriori algorithm is an algorithm that helps us find these similarities between different items using concepts of lift, support and confidence. This paper discusses about apriori algorithm, how it works, what are its advantages, disadvantages and how it can be made better and efficient with the help of data structure hash map [4].**

Keywords—Apriori algorithm, lift, support, confidence, data mining

I. INTRODUCTION

Data mining is a very powerful field that helps us in finding similarities and patterns between different items in huge databases [13] . The main aim is to discover the pattern and convert it into an understandable form so that it can be used for various purposes. Many things are considered here like preprocessing the data, considering time complexities of various algorithms etc. So we can say that process of scanning through our dataset to discover some relationship between various itemsets is the basic concept of data mining. The main challenge we have to face is that we need well worked and efficient methods/algorithms for different type of datasets like the ones that contain noise. Data mining is widely used in various fields like education, banking, e-commerce sites, social networking sites, stock markets, communication and transportation departments etc.

Association rule mining which is a branch of data mining helps us exactly in finding these "if-then" type relations i.e. it tells us about the chances of "if the x item occurs then there is a certain probability of finding the y item as well in the dataset" [7]. Apriori algorithm is a popular algorithm for association rule learning in our data. It is a bottom up and a bfs(breadth-first-search) technique which starts with taking all items individually to taking all these elements one by one in sets and this process goes on till we don't have any more successful sets that can yield the result we want. It uses the concepts of lift support and confidence to eliminate unsuccessful sets which have less probability of being found together in dataset one by one in each scan [5]. Some important terms that are used with apriori algorithm are:-

1)**SUPPORT**:- Support ({A}->{B}) mathematically can be calculated by dividing the number of transactions that has both A and B by the total number of transactions. So if Support ({d}->{c}) > Support({g}->{h}), then we can say that probability of finding c and together is higher than that of finding g and h together in our database. So basically we set a threshold support for our dataset. Suppose we set a threshold support of 0.04, this means that we will allow only those sets to go in next round have which occur more than 4 out of 100 times in our dataset. If an itemset has less support, it implies that we can't find it a lot in our dataset and so it cannot be used in forming association rules.

2) **CONFIDENCE:-** Confidence({X}->{Y}) mathematically can be calculated by dividing the number of transactions that contain both X and Y by the transactions that contain only X. Theoretically speaking it tells us what percentage of itemsets that had X also contain Y in them.

3) **LIFT:-** Lift ({A}->{B}) mathematically can be calculated by dividing Confidence ({A}->{B}) by Support (B). Theoretically it can be defined by how much more can we find A with B than the transactions without B.

II. APRIORI ALGORITHM

Here in this section we will discuss how apriori algorithm works and what are the steps needed to find association rules using apriori algorithm [2] :-

STEP I

The support of each individual item is computed as the first stage of the procedure. This essentially boils down to calculating the number of transactions for each product.

STEP II

We'll use the support for each of the various items to filter out some of the products that aren't used very often. To do so, we must first establish a threshold_support.

STEP III

The individual products which have a support less than threshold_support will not be chosen in our next steps. Only those items with support>=threshold_support will be chosen.

STEP IV

This step is kind of similar to the previous step. Here the only difference from previous step is that instead of taking 1 item at a time we take pair of all those products that were chosen is step III. Now the more the itemsets in dataset, the larger will be the number of pairs of items. And now we will count how many times all these pairs occur together in dataset (Remember: none of these pairs should contain even one of those items that were rejected in step III). And again only those pairs will be chosen for the next step whose support is greater than the threshold_support [3].

Authorized licensed use limited to: DELHI TECHNICAL UNIV. Downloaded on June 15,2022 at 11:17:18 UTC from IEEE Xplore. Restrictions apply.

STEP V

We will now just do the same thing we did in step III and step IV but now with sets containing 3 items. We'll continue this till we reach a point where it is not even possible to continue it any further.

STEP VI

What we will be having now are largest itemsets that occur together. Association rules can now be listed in this template: Item A -> Item B, which tells that if A occurs there's a huge probability that B also occurs with it.

STEP VII

Now final step is to calculate lift of these itemsets. The higher the lift value, the more the item on right side will be dependent on the one present on left side.

Let us take an example where we have some transaction_ids that contains items W,X,Y,Z,K and from these we'll choose which elements are eligible for association rules [11]. So let us assume the minimum or threshold_support =2

Trans_id	Itemsets
T_1	W,X
T_2	X,Z
T_3	X,Y
T_4	W,X,Z
T_5	W,Y
T_6	X,Y
T_7	W,Y
T_8	W,X,Y,K
T_9	W,X,Y

Now as explained in procedure, first we will count the occurrence of each individual item in transaction ids.

Items	Support
W	5
X	6
Y	5
Z	3
K	1

Now all those that cross the threshold_support are coupled with each other and their supports are calculated from dataset.

Itemsets	Support
W,X	4
W,Y	4
W,Z	1
X,Y	4
X,Z	2
Y,Z	0

All the items that crossed the threshold_support again are grouped in groups of three items and their supports are calculated now.

Itemsets	Support
W,X,Y	2
X,Y,Z	0
W,Y,Z	0
W,X,Z	1

From here we can see that only W,X,Y cross the threshold_support,so association rules will be formed on basis of these three elements only.

Some advantages of apriori algorithm:-

a) The algorithm is very easy to understand because it can be understood with basic concepts like support lift and confidence which are all basic probability terms.

b) This algo works well on unlabeled data

Drawbacks of apriori algorithm:-

The biggest drawbacks of the apriori algorithm is that this algorithm is very slow specially in the scenarios listed below-

1) If there are lot of unique itemsets in a single dataset.
2) If the minimum support is very low, which means more item will surpass that iteration.
3) More time and space will be needed to hold the itemsets after every iteration.

So basically,

a)It is slow.

b)Inefficient when used with large volumes of datasets.

Therefore apriori algorithm is not helpful when we take large datasets.
It basically scans the database many times and with every iteration, this algorithm becomes more and more expensive in terms of the time it takes [3].

So to avoid these problems and increase the efficiency of algorithm, we will improve apriori algorithm by using apriori with hashing algorithm

III. APRIORI WITH HASHING ALGORITHM

Given that the apriori algorithm has some weaknesses in reducing the promotional value of k sets, the Ck hashing method is used. Our use of Apriori-based hash, uses data structure that directly communicates with the hash table. Especially the two itemsets, as that is a way to improve performance. This calculation uses a hash-based process to reduce the number of applicant item sets created in the first pass. It is ensured that the number of C2-set objects produced using hashing can be reduced to a minimum, so that the output required to determine the L2 is very efficient [12].

Authorized licensed use limited to: DELHI TECHNICAL UNIV. Downloaded on June 15,2022 at 11:17:18 UTC from IEEE Xplore. Restrictions apply.

For example, when we scan everything in our database to create Frequent1-itemsets, L1, from candidate-1 objects in C1, we can produce most of the two itemset in all the actions, hash into a variety bucket of the table structure, and increase the corresponding number of buckets. The value of the corresponding buckets in the hash table below the min_sup limit cannot be specified and therefore must be lowered from the candidate set [9]. The hash-based apriori therefore reduces the set number of the k object.

Steps involved in Apriori with hashing algorithm-

1) The data structure which we used is hash table.

2) First iteration is required to count support of each itemset.

3) From second iteration, efforts have been made to enhance the execution of Apriori algorithm by utilizing the hash table concept.

4) Basically in hash-based techniques, hash table minimizes the number of itemset generated in the second iteration.

5) In the second iteration i.e. 2-itemset generation, for every combination of two items, we map them into the diverse bucket of hash table structure and increment the bucket count.

6) If count of bucket is less than the minimum support count, we basically remove them from the candidate sets.

TID	Items_List
T1	I1,I2,I3
T2	I2,I3
T3	I3,I4
T4	I1,I3
T5	I1,I2,I4
T6	I2,I3,I4
T7	I1,I2,I3,I4

Minimum Support Count=3

Order of items:-

I1=1
I2=2
I3=3
I4=4

Itemset	Support Count
I1	3
I2	3
I3	2
I4	2

Hash function :-

H(a,b) = ((Order of First)*10 + (Order of Second))mod7

Hash function

Itemset	Count	Hash Function
I1,I2	3	5
I1,I3	3	6
I1,I4	2	0
I2,I3	4	2
I2,I4	2	3
I3,I4	3	6

Minimum support count given is 3, so we basically need to pick up the buckets which satisfy the minimum support criteria. So here only these buckets get qualified :-

1)Bucket Address - 2

2)Bucket Address – 5

3)Bucket Address – 6

Because the bucket count of these buckets are greater than or equal to our minimum support count i.e. 3.

Advantages:-

1) It reduces the number of scan because of the hashing function that we used in the algorithm
2) Remove all the large candidates that cause high input cost and high output cost.
3) In initial iteration, it requires less space.

Bucket Address	Bucket Count	Bucket Contents	L2
0	2	(I1-I4) -> 2	No
1	-	-	No
2	4	(I2-I3) -> 4	Yes
3	2	(I2-I4) -> 2	No
4	-	-	No
5	3	(I1-I2) -> 3	Yes
6	6	(I1-I3) -> 3 (I3-I4) ->3	Yes

Authorized licensed use limited to: DELHI TECHNICAL UNIV. Downloaded on June 15,2022 at 11:17:18 UTC from IEEE Xplore. Restrictions apply.

IV. COMPARISON OF ALGORITHMS

So we'll basically compare the Apriori Algorithm and Apriori with Hashing Algorithm on the basis of these 5 factors/parameters:-

1) Storage structure
2) Technique
3) Memory Utilization
4) Databases
5) Time

Parameter	Apriori Algorithm	Apriori with Hashing Algorithm
Storage structure	Array based	Array based
Technique	Use Apriori property and join and prune method.	Use hash table as a data structure for finding frequent itemset.
Memory Utilization	It needs more space because of more number of candidate itemset are produced.	In initial iteration, it needs less memory space but when we go to the later stages, it also needs more space.
Databases	Apriori Algorithm works better in both datasets i.e. dense and sparse datasets.	Apriori with hashing algorithm is only suitable for the datasets with medium size.
Time	After every iteration, time is consumed in producing the candidate therefore execution time is more.	In small databases, time takes in execution is less as compared to Apriori Algorithm.

V. RESULT

We basically used three datasets which are large in size. The datasets we used are:-

1)Laptop
2)Laptop_Bag
3)Mouse

The table given below basically shows that three different datasets and their sizes. The dataset size is in the term of transaction.

Dataset	Size	Time taken by Apriori (in sec)	Time taken by Apriori with hashing
Laptop	7835	0.324	0.218
Laptop_Bag	38247	0.647	0.589
Mouse	38247	0.539	0.471

As shown in the above table, we basically did the comparative analysis of both the algorithms i.e. Apriori and Apriori with Hashing Algorithm on the basis of their execution time [6].

We basically performed our algorithm on these three large datasets and compared their results. The result proves that Apriori with Hashing Algorithm provides a better result in all of the three datasets as it takes lesser time when compared to normal apriori algorithm

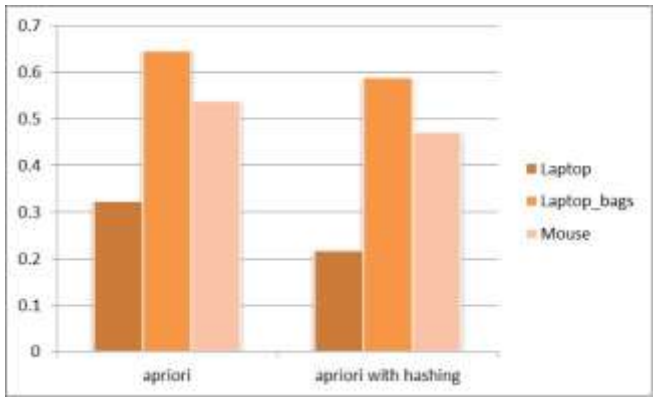

The graph above represents execution time of both our algorithms and that too with respect to all the three

Authorized licensed use limited to: DELHI TECHNICAL UNIV. Downloaded on June 15,2022 at 11:17:18 UTC from IEEE Xplore. Restrictions apply.

databases. We can clearly see apriori with hashing is easily better than normal apriori algorithm for larger databases.

VI. CONCLUSION

One of the most important aspects in data mining is determining frequent things [3]. The memory utilization of Apriori with Hashing Algorithm is lower than that of the Apriori algorithm. It is well known that the way candidates are defined has a significant impact on the amount of time it takes to complete tasks and the amount of memory required.

Experiment results showed that the Apriori with Hashing Algorithm consistently outperforms Apriori Algorithm. Apriori with Hashing Algorithm is one of the most efficient algorithm for creating frequent itemsets especially when compared with Apriori [7]. Apriori with Hashing Algorithm provides better result in less amount of time as compared to the Apriori Algorithm because in Apriori with Hashing we basically reduce the number of scans after every iteration [12].

In future, we will try to reduce the time complexity even more with more accurate results as well in order to improve the efficiency of the apriori algorithm using this map concept.

VII. REFERENCES

[1] Han J,Kamber M.Data Mining : Concepts and Techniques.Higher Education Press,2001..
[2] Surbhi K.Solanki ,Jalpa T .Patel"Survey on association rule",(2015),212 – 216
[3] Aggrawal R, Imielinksi.t, Swami.A."Mining Association Rules between Sets of Items in Large Databases".In Proc. Int'1 Conf. of the 1993 ACM SIGMOD Conference Washington DC, USA.
[4] Park J.S, M.S. Chen ,P.S. Yu."An effective hash-based algorithm for mining association rules".In Proc. ACM -SIGMOD Int'1 Conf.Management of Data (SIGMOD) , San Jose , CA , May 1995 , pages 175 – 186.
[5] Warnia Nengsih "A Comparative Study On Market Basket Analysis And Apriori Association Technique" Politeknik Caltex Riau – Indonesia 2015 IEEE
[6] Rupali, Gaurav gupta"Apriori Based Algorithms And their Comaprisons".ISSN : 2278-0181.
[7] R.Agarwal , R.Srikant, " Fast algorithms for mining association rules",Proceedings of the 20th Very Large Databases Conference (VLDB'94),Santiago de Chile,Chile,1994,pp. 487-499.
[8] Jiawei Han, M.Kamber , "Data Mining-Concepts and Techniques",Morgan kanufmann Publishers ,Sam Franciso ,2009.
[9] Dongme Sun , Shaohua Teng, Wei Zhang, Haibin Zhu. " An Algorithm to Improve the Effectiveness of Apriori".In Proc. Int'1 Conf. on 6th IEEE Int. Conf. on Cognitive Informatics(ICCI'07),2007.
[10] A. Savasere, E. Omiecinski, and S.Navathe. " An efficient algortihm for mining association rules in large databases".In Proc. Int'1 Conf. Very Large Data bases (VLDB),Sept .1995,pages 432-443.
[11] Ashish Shah " Association Rule Mining with Modified Apriori Algorithm using Top down Approach" – 2016 IEEE.
[12] Kaushal vyas,Shipa sherasiya "Modified apriori algorithm using hash based technique".IJARIIE-ISSN(0) – 2395 – 4396.
[13] F.H. AL-Zawaidah, Y.H. Jbara, and A.L. Marwan , " An Improved Algorithm for Mining Association Rules in Large Databases,"Vol.1,No.7 ,311-316,2011

Authorized licensed use limited to: DELHI TECHNICAL UNIV. Downloaded on June 15,2022 at 11:17:18 UTC from IEEE Xplore. Restrictions apply.

Proceedings of the Sixth International Conference on Intelligent Computing and Control Systems (ICICCS 2022)
IEEE Xplore Part Number: CFP22K74-ART; ISBN: 978-1-6654-1035-9

A Compendious Research on Big Data File Formats

Arnav Gohil
Department of Computer Engineering
Delhi Technological University
Delhi, India
arnavgohil_2k18co088@dtu.ac.in

Anshul Shroff
Department of Computer Engineering
Delhi Technological University
Delhi, India
anshulshroff_2k18co079@dtu.ac.in

Arnav Garg
Department of Computer Engineering
Delhi Technological University
Delhi, India
arnavgarg_2k18co087@dtu.ac.in

Shailender Kumar
Department of Computer Engineering
Delhi Technological University
Delhi, India
shailenderkumar@dce.ac.in

2022 6th International Conference on Intelligent Computing and Control Systems (ICICCS) | 978-1-6654-1035-9/22/$31.00 ©2022 IEEE | DOI: 10.1109/ICICCS53718.2022.9788141

***Abstract*— In modern times, the net amount of data generated is significantly higher than in previous times, and such data is enormous, complex and hard to manage. The field which deals with such kind of data is known as Big Data. Big Data has helped people understand and get a much better grasp of such complex data. It has also helped extract and analyse information from such data. Big Data is a prominent and promising field, and the three essential factors of big data are volume, variety, and velocity. Big data can be stored in different file formats. File formats play a vital role in big data, influencing the two most essential factors, volume and velocity. The file formats have to be chosen very carefully as they have a domino effect over the speed or velocity of the particular tasks that have to be carried out on the big data. So, a comprehensive study of the following formats CSV (Comma-Separated Values), JSON (JavaScript Object Notation), Avro, Parquet, ORC (Optimized Row Columnar) and XML (Extensible Markup Language), has been carried out. The quantitative analysis has been carried both on premise and on the cloud.**

Keywords— Big Data, File Formats, CSV, JSON, ORC, Avro, Parquet, File Compression, Compression Codecs, PySpark, Amazon Web Services (AWS)

I. Introduction

The 'chicken or egg' conundrum has captivated the curiosity of many philosophers, thinkers and scholars since it was first proposed in Ancient Greece. It is a paradox that applies to scenarios where a fine line separates cause and effect. A digitally relevant extrapolation of this concept would be to ask 'Which came first, big data or the internet?'. Technical advances in big data and the internet have skyrocketed each other's growth over the past few decades [1]. We are at a point where it is impossible to talk about both of them as independent concepts. For the uninitiated, the internet seems to have come first. However, it is big data that precedes the internet. The Internet was developed to facilitate the transfer of big data across various systems connected to the internet. Call it coincidence, but the first data to be accessed through the internet was the massive collection of scientific data and research papers stored in systems at CERN.

Simply put, Big Data deals with enormous volumes of information which is complex and hard to manage [2]–[5]. Research and development in this field have majorly revolved around managing, comprehending and extracting actionable insights from such data [6], [7]. It has found tremendous application in social welfare, industrial progression and technological breakthroughs [3], [7]–[13].

Big Data qualifies as a virtual commodity today, and the internet is its trade route. Data is quantifiable [14], [15]. It can be extracted through 'data mining' and can be traded in online marketplaces [1]. Like oil is measured and stored in standard containers called 'barrels', data is also stored in containers. Each container is known as a 'file', and various types of containers available for storage are 'file formats'. File formats influence vital factors such as velocity and volume, making or breaking these data supply chains. Velocity measures the speed at which operations such as data upload, data download, and data transfer occurs. Volume measures the space required by data to be stored, usually measured in bytes [7], [8], [11], [12], [16]. Specific file formats have specific characteristics [17]. Hence, they have to be chosen in a deliberate manner as they have a domino effect over the velocity and volume of the tasks that have to be carried out on data.

Owing to the fundamental nature of file formats in dictating how efficiently and conveniently data can be accessed and stored, we have undertaken a comprehensive study of staple file formats such as Comma-Separated Values (CSV), JavaScript Object Notation (JSON), Avro, Parquet, Optimized Row Columnar (ORC) and Extensible Markup Language (XML) [16], [18]. These formats have been chosen considering their significance and relevance in the field of big data. Both qualitative and quantitative analysis has been performed on premise and on the cloud. We will talk more about our approach in the upcoming sections.

II. Literature Review

The qualitative analysis of big data file formats has been done several times before. We reviewed some of the literature that has been published before. The publications [4], [18], [19] and [20] have been a great source of information regarding the qualitative analysis of these big data file formats. This section will dissect the characteristics of our shortlisted file formats based on their inherent properties, such as how data is read, written and stored.

A. CSV

CSV or Comma-Separated Values is a text-based file format. Tabular data is represented in this format using plain text. In a CSV file, data is stored in rows where each row indicates a separate data record. The enter key separates consecutive rows. Usually, the first row contains a list of field names and is followed by the data rows. Within each row, field-specific data is separated by commas.

Advantages: CSV is a human-readable and editable file format. Moreover, it is simple, lightweight, easy to implement

Authorized licensed use limited to: DELHI TECHNICAL UNIV. Downloaded on June 15,2022 at 11:23:48 UTC from IEEE Xplore. Restrictions apply.

and parse. It can be used with a wide variety of applications and languages. Also, it has a good compression ratio.

Disadvantages: CSV format has slow read and write speeds. It does not support schema specification. Hence there is no difference between numeric and textual columns. It does not support block-level compression, and compressible files are not splitable. Finally, there is a lack of a universal standard, and each application has its rendition.

B. JSON

JSON or JavaScript Object Notation is a text-based file format. It supports many data structures such as integer, Boolean, array, string, character, object, etc., and stored data can take any of these forms. JSON has recently become a staple in web technologies and network communication.

Advantages: JSON is a lightweight file format. It is both human and machine-readable. Being a simple text format, it is accessible via any text editor. It supports the storage of data in a hierarchical format. This allows the documentation of complex relationships and related data in a single file. It also supports future schema evolutions. JSON has built-in functionality for serialisation and deserialization. Data stored in JSON is compressible, and it can be used as an intermediate format for data exchange. Moreover, JSON is compatible with a wide array of online tools, applications and databases.

Disadvantages: JSON format has slow read and write speeds. It does not support block-level compression, and compressible files are not splitable. Moreover, JSON files lack indexing.

C. XML

XML or Extensible Mark-up Language is also a text-based file format. Although with a verbose syntax, XML establishes a standard, intermediate file format for data exchange operations. Major corporations have historically used XML to store their data. However, most ancient data is being stored in newer formats, and XML's presence decreases over time.

Advantages: XML is a lightweight file format. It supports the storage of hierarchical data and schema evolution. It has a higher compression ratio due to the verbose nature of its syntax.

Disadvantages: XML format has slow read and write speeds. XML files are usually larger than JSON files due to the redundant nature of their syntax. They are not splitable since the syntax contains start and end tags. This prohibits processing from taking place at any point in between those tags. XML files also encounter parsing issues due to the problematic nature of XML namespaces.

D. AVRO

Avro was released by Hadoop as Apache Avro. It is a row-based file format. Naturally, it is considered to be the best file format for Hadoop-based requirements. Internally, Avro stores the schema in JSON format and the data in binary format. This feature allows minimal file sizes, maximum efficiency and provides a bunch of functionality. It can be used for permanent data storage, data transfers and data processing.

Advantages: The most significant upside of Avro is the way it supports the storage of hierarchical data and schema evolution. It supports the independent updating of components at different times. Schema is stored in a self-describing, human-readable JSON file header, making it highly convenient for developers to comprehend. It is designed to be highly splitable by implementing synchronisation markers to separate blocks. It is also compressible. This makes Avro files fast, compact and efficient for performing analytics queries. It can perform serialisation and deserialization owing to its native JSON implementation. This additionally allows it to be read and parsed easily. Moreover, new data can be easily added as it is a row-based format.

Disadvantages: Avro format requires schema definition to be able to perform read and write operations [21]. Its syntax is not human readable. Moreover, all programming languages do not have integration for Avro.

E. PARQUET

Parquet is a column-based open-source file format for Hadoop [16], [22]. Parquet stores data in a binary format. Metadata related to its contents are stored at the end of each file which allows Spark to access information such as data types, column names, compression metrics, encoding, etc. This allows for fast, one-pass writing. Parquet is optimised for the paradigm Write Once Read Many (WORM). It means that file generation takes relatively more time, but the process of reading it is extremely fast. It works best for use cases where a subset of all columns need to be accessed for performing queries.

Advantages: Parquet files are ideal to use for analytics and business intelligence related use cases. Arranging data in columns provides high compression (up to 75%) due to the homogeneity of data. The files are also splitable and support schema evolution.

Disadvantages: Parquet format is only machine-readable. Hence, it is difficult for developers to comprehend information stored just by looking at it. Moreover, the whole file needs to be recreated in case additional data is to be added. This means that Parquet files are immutable.

F. ORC

ORC or Optimised Row Columnar is a column-oriented file format. ORC files store data in the form of stripes which are essentially groups of row data. By default, the memory allocated to a stripe is 250MB. This large stripe size allows for efficient reads from HDFS [21]. A file footer contains some auxiliary information and a postscript holds compression parameters at the end of the file.

Advantages: ORC files offer up to 75% compression on top of original data. This feature makes it extremely useful for analytics and business intelligence related use cases. It enhances overall performance by accelerating reading, writing and processing in Hive.

Disadvantages: ORC requires recreation of the whole file if new data has to be added. Apache Impala doesn't support ORC format. It also lacks support for schema evolution.

III. Quantitative Analysis

The qualitative characteristics are an essential yet theoretical measure of these file formats. In this section, extensive quantitative analysis has been carried out using a combination of datasets, file formats and metrics. Metrics to quantify volume and velocity have been recorded for these file formats. PySpark is integral for our study as it helps us analyse our data to attain the required metrics. PySpark is an interface for Apache Spark in Python [6], [16].

Authorized licensed use limited to: DELHI TECHNICAL UNIV. Downloaded on June 15,2022 at 11:23:48 UTC from IEEE Xplore. Restrictions apply.

Two datasets have been used for the study. Sales Dataset is used for Small Data Analysis sub-section which contains 1 million records across 14 fields. HR Dataset is used for Big Data Playoffs sub-section which contains 30 million records across 37 fields. These datasets have good diversity and replicate industrial use cases.

The first sub-section focuses on general space-time metrics for file conversion from one format to the other. Metrics pertaining to time taken to run six different queries on premise (local system) and on the cloud (Amazon Web Services) have also been included in this section. Moreover, similar metrics are computed for the different compression codecs of these file formats.

Furthermore, the most efficient file formats from small data analysis along with their compression codecs were advanced into Big Data Playoffs, which is discussed in the next sub-section.

SMALL DATA ANALYSIS

The dataset used for this section is the Sales Dataset. This dataset contains exactly one million records across 14 fields. The dataset schema is shown in *Table 1*.

SALES SCHEMA	
FIELD	**TYPE**
Region	String
Country	String
Item Type	String
Sales Channel	String
Order Priority	String
Order Date	String
Order ID	Integer
Ship Date	String
Units Sold	Integer
Unit Price	Float
Unit Cost	Float
Total Revenue	Float
Total Cost	Float
Total Profit	Float

Table 1. Sales dataset schema

A. Space Analysis

As we have learned, the sizes of these files would vary due to the different characteristics of different file formats. A bar graph (*Fig 1*) has been plotted to show the difference between the sizes of various file formats containing the same data.

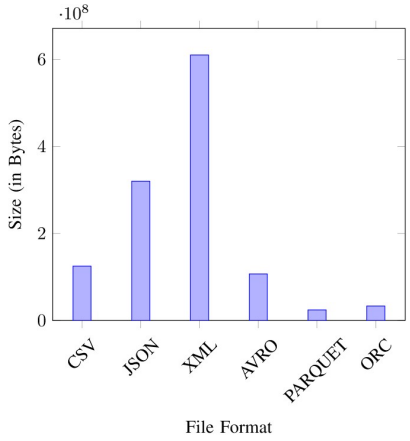

Fig 1. Sales file schema

B. Time Analysis for File Conversion

PySpark has been used to convert one sales file format into other file formats. The data was loaded into a Spark Dataframe from a particular file format and then written into various file formats. This was repeated for all the file formats.

The time taken for the writing process has been recorded and showcased using a conversion matrix and a timeline depicted in *Table 2* and *Fig 2*, respectively.

SALES FILE CONVERSION (LOCAL)						
FROM ↓ TO →	CSV	JSON	AVRO	PARQUET	ORC	XML
CSV	13.51885152	10.2919898	12.34335041	11.55880809	10.7998147	23.14989924
JSON	9.985178471	10.31562376	12.66678739	9.055528164	11.00577784	22.06493068
AVRO	7.926030159	6.679044485	9.187671423	5.126942396	7.120844603	17.71659112
PARQUET	5.871648073	5.664584637	8.181026936	4.328885078	6.041726828	16.84336877
ORC	6.035595894	5.364570856	7.233012199	3.540044069	5.644069433	16.14217901
XML	77.0146575	73.37705278	75.37257385	72.48771501	74.36798954	86.99630713

Table 2. File Conversion Matrix (all metrics are in seconds)

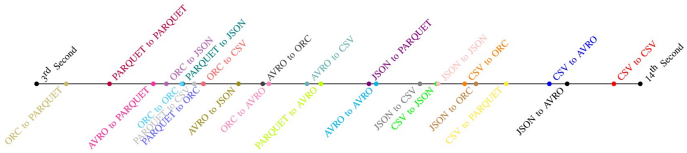

Fig 2. File Conversion Timeline

C. Sales Data Local Metrics

Various metrics of the sales dataset were recorded and analysed on premise. Metrics such as file size, the time taken to load the data into a data frame from the local system and several different queries ranging from basic read query to complex analytics oriented queries were executed. These queries were executed using Spark Dataframe as well as Spark SQL.

The metrics gathered are as follows:

- File Size: The initial file sizes of all the different file formats of the same sales data (refer *Fig 1*).
- Local Storage to Dataframe using inferSchema: The datasets are loaded to a Spark Dataframe along with inferSchema. When inferSchema is set to true, spark reads the whole data and then decides the data type allotted to each column (refer *Table 3*).

READ TIMES (SEC)		
FILE	With inferSchema	Using Own Schema
CSV	9.123762369	0.06096744537
JSON	5.020658493	0.03609251976
AVRO	0.1667802334	0.08683800697
PARQUET	0.4473392963	0.02285385132
ORC	0.1079375744	0.02748060226
XML	253.5850906	0.01080107689

Table 3. Time taken to load files

- Queries: Various queries such as analytical queries and counting queries were formulated which resembles queries used in the real world. They were executed to analyse runtime using Spark Dataframe and Spark SQL [18], [22]. The queries are as follows:

Authorized licensed use limited to: DELHI TECHNICAL UNIV. Downloaded on June 15,2022 at 11:23:48 UTC from IEEE Xplore. Restrictions apply.

A. Search random data: The query collected all the specific records with the country specified as India or Djibouti.

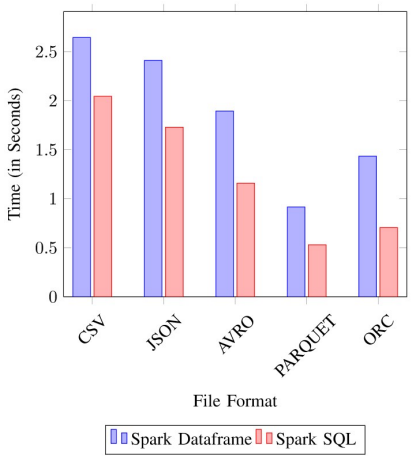

Fig 3A. Query A

B. Find the sum of total profit: The query calculated and returned the aggregated sum of Total Profit.

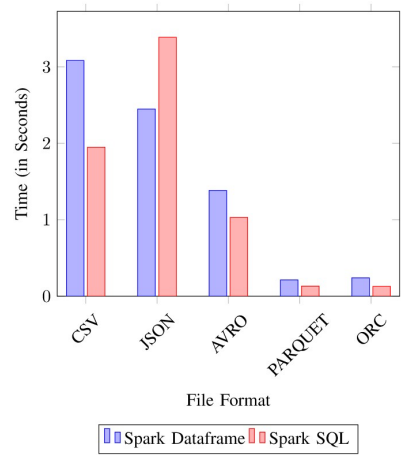

Fig 3B. Query B

C. Find the record with max total revenue and min country: Here, we sorted the data according to maximum total revenue and minimum country lexicologically and returned the first record.

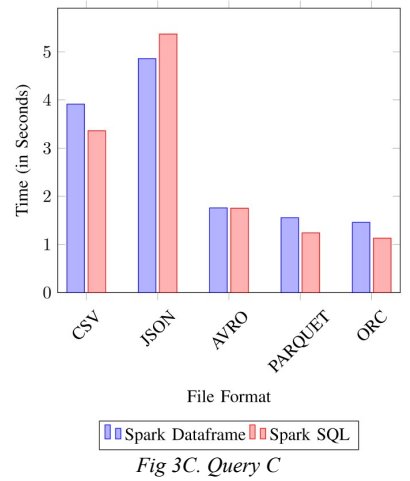

Fig 3C. Query C

D. Region-wise average units sold: This is a complex aggregation query that returns the average units sold in each region.

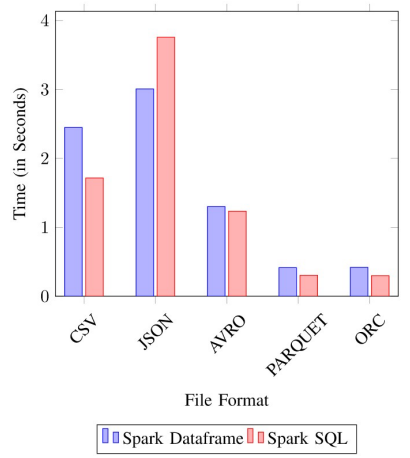

Fig 3D. Query D

E. Count entries with a total cost between 10k-25k: The query returned the count of records having a total cost between 10k and 25k.

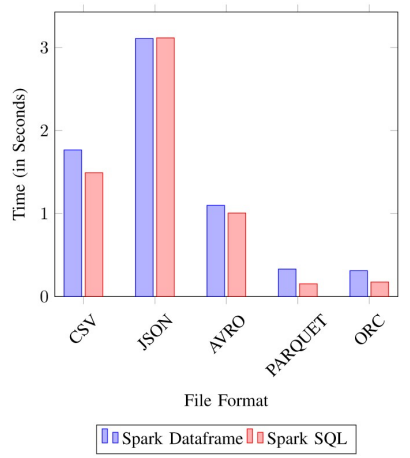

Fig 3E. Query E

F. Total distinct records: Trivial to its name, the count of unique records was attained.

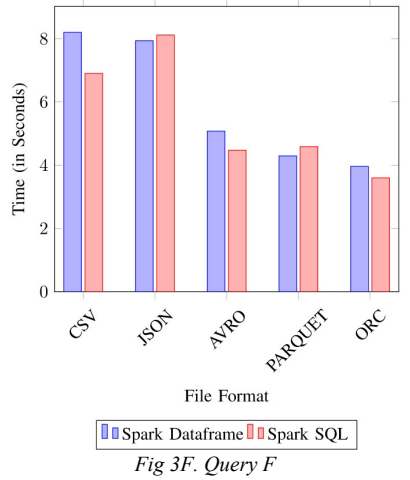

Fig 3F. Query F

XML file format has been exempted from the graphs due to extremity in metric values as compared to other file formats.

Authorized licensed use limited to: DELHI TECHNICAL UNIV. Downloaded on June 15,2022 at 11:23:48 UTC from IEEE Xplore. Restrictions apply.

The following observations were made from the above graph plots:

- When the data is loaded to Spark Dataframe with the inferSchema set to true, Avro, Parquet and ORC take very little time as they have a schema already associated with them.
- When reading a file, read times are faster when own schema is provided rather than inferSchema.
- The Spark Dataframe method of executing queries generally consumed more time than the Spark SQL except JSON file format. However, the first query in JSON file format took more time for Spark SQL method to complete.
- Overall, Parquet and ORC file formats were head to head for the pole position.

D. Sales Data Cloud Metrics

Cloud computing has become one of the world's most common and reliable technologies [2]. It has excellent availability, accessibility and has a very diverse and expansive range of consumers [23]. Cloud technology has been a game-changer for big data as it is handy for storing such big data on cloud platforms [8]. The ease of access and the reliable characteristics of cloud platforms have also made it very successful. Here, we used Amazon Web Services (AWS) cloud platform. AWS provides modules to integrate various AWS services with Apache Hadoop and Spark.

A storage container, i.e., a Simple Storage Service (S3) bucket in AWS, was created. The files were stored in the S3 bucket instead of keeping it on-premise. Metrics such as reading, writing and executing various queries (similar to that of the local storage) were recorded directly from the AWS S3 bucket without downloading them. *Fig 4A* and *Fig 4B* are plots depicting the AWS bucket's write and read operations, respectively. *Fig 5A* to *Fig 5F* are the plots for various queries similar to the ones executed in local storage. In these plots, Avro and XML file formats have been exempted due to extreme values.

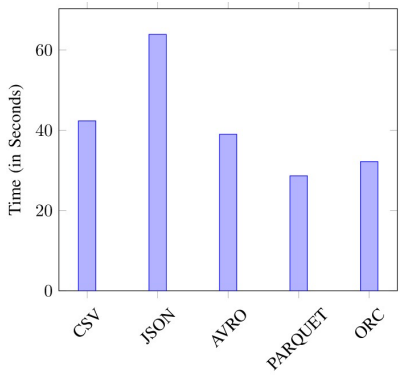

Fig 4A. Write time to AWS

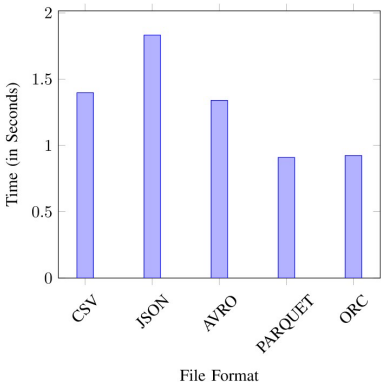

Fig 4B. Read time from AWS

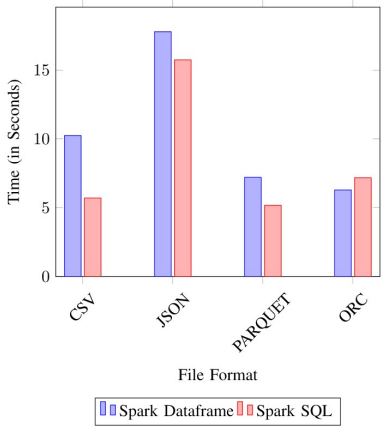

Fig 5A. Query A

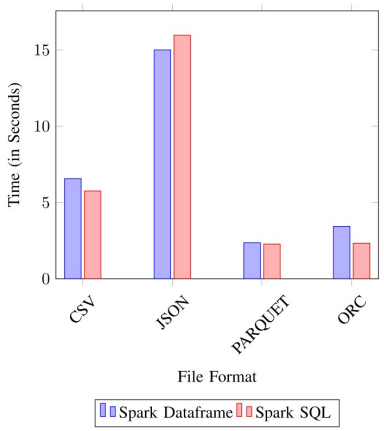

Fig 5B. Query B

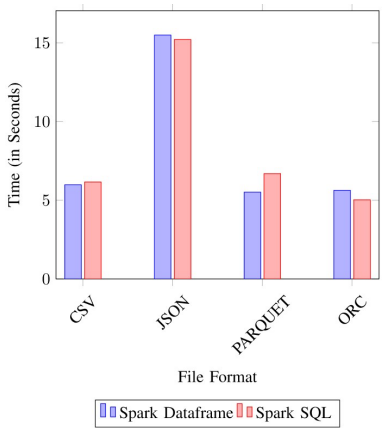

Fig 5C. Query C

Authorized licensed use limited to: DELHI TECHNICAL UNIV. Downloaded on June 15,2022 at 11:23:48 UTC from IEEE Xplore. Restrictions apply.

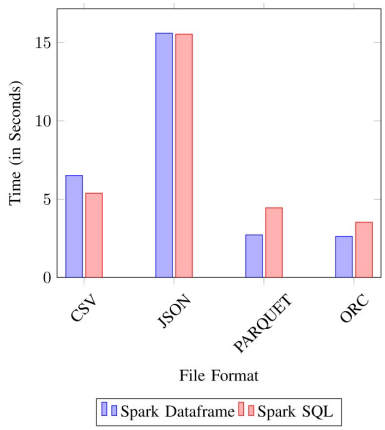

Fig 5D. Query D

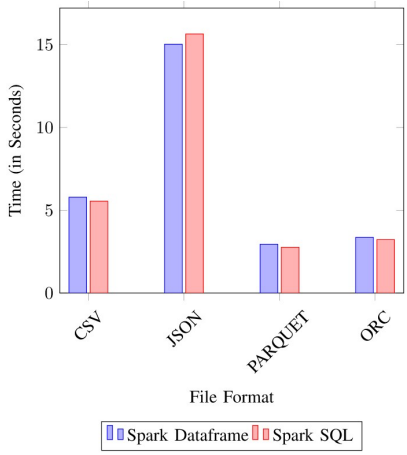

Fig 5E. Query E

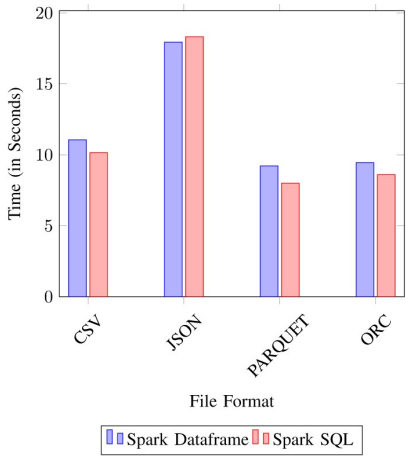

Fig 5F. Query F

The following observations were made from the above graph plots of queries executed on AWS:

- Execution time of queries holds similar pattern as executed on local, though the execution time increased in AWS.
- Surprisingly, the execution time for AVRO file format was elevated by many folds compared to the local execution.

BIG DATA PLAYOFFS

A. Dataset

An HR dataset was generated containing 30 million records with 37 fields, which makes it highly complex. This dataset was used with the shortlisted file formats for quantitative analysis. The schema of this data is shown below.

HR SCHEMA			
FIELD	**TYPE**	**FIELD**	**TYPE**
Emp ID	Integer	Month Name of Joining	String
Name Prefix	String	Short Month	String
First Name	String	Day of Joining	Integer
Middle Initial	String	DOW of Joining	String
Last Name	String	Short DOW	String
Gender	String	Age in Company	Float
E Mail	String	Salary	Integer
Father Name	String	Last Hike	String
Mother Name	String	SSN	String
Mother Maiden Name	String	Phone No	String
Date of Birth	String	Place Name	String
Time of Birth	String	County	String
Age in Yrs	Float	City	String
Weight in Kgs	Integer	State	String
Date of Joining	String	Zip	Integer
Quarter of Joining	String	Region	String
Half of Joining	String	User Name	String
Year of Joining	Integer	Password	String
Month of Joining	Integer		

Table 6. HR File Schema

B. File Format Compression

Compression in the context of file formats reduces the file size while not having any information loss. Every file format supports some specific compression codecs exclusively [19]. The idea behind analysing the compressed file formats is to reduce the volume of the file. The different available compression codecs for these file formats are listed below in *Table 4.*

COMPRESSION CODECS	
FORMAT	**CODECS**
CSV	`None, BZIP2, DEFLATE, GZIP, LZ4`
JSON	`None, BZIP2, DEFLATE, GZIP, LZ4`
AVRO	`None, BZIP2, DEFLATE, Snappy, XZ, ZSTD`
PARQUET	`None, GZIP, LZ4, Snappy, ZSTD`
ORC	`None, GZIP, LZ4, LZO, Snappy, ZLIB, ZSTD`
XML	`None, BZIP2, DEFLATE, GZIP, LZ4`

Table 4. Supported Compression Codecs

The time and the size taken to compress the file format were recorded in *Table 5A* and *Table 5B* respectively.

SALES FILE COMPRESSION (TIME)						
FROM ORC	CSV	JSON	AVRO	PARQUET	ORC	XML
None	9.132000923	4.821396828	7.751652002	5.639073133	6.723463774	19.38986826
bzip2	29.22816873	85.15369964	27.95273137	-	-	187.6701438
deflate	10.67995548	11.33607697	11.19948363	-	-	-
gzip	11.1234014	11.64954138	-	4.326918602	-	25.7945354
lz4	4.677136898	4.689693928	-	3.759133577	5.729939938	16.35944772
lzo	-	-	-	-	5.765543938	-
snappy	-	-	7.359685183	3.643456221	5.640215397	-
xz	-	-	105.5594587	-	-	-
zlib	-	-	-	-	6.767996788	-
zstd	-	-	8.253209352	3.681014776	6.613604784	-

Table 5A. File Compression Matrix – Time (seconds)

Authorized licensed use limited to: DELHI TECHNICAL UNIV. Downloaded on June 15,2022 at 11:23:48 UTC from IEEE Xplore. Restrictions apply.

SALES FILE COMPRESSION (SIZE)						
	CSV	JSON	AVRO	PARQUET	ORC	XML
None	121973661	320011381	106878330	24186437	33192946	610011456
bzip2	26430906	27607469	33033907	-	-	28745634
deflate	38526383	49445530	39425518	-	-	-
gzip	38526395	49445542	-	22654914	-	54853409
lz4	67019994	83870107	-	24248198	28012470	100386887
lzo	-	-	-	-	27205609	-
snappy	-	-	51313705	24145188	28501220	-
xz	-	-	35058231	-	-	-
zlib	-	-	-	-	24258157	-
zstd	-	-	41107781	22856868	24104065	-

Table 5B. File Compression Matrix - Size (bytes)

C. File Formats

Fig 6 represents a space vs. time plot for file format compression codecs discussed in the previous subsection. Specific region has been selected from this plot. This region represents those file formats which support most efficient compression. This allows them to be ideal candidates for Big Data Analysis as compressibility is a key requirement for handling big data along with the results from the small data section. The shortlisted codecs are NONE, SNAPPY, LZO, LZ4, ZSTD, GZIP, ZLIB codecs for Parquet and ORC file formats. These file formats are analysed with big data in this section.

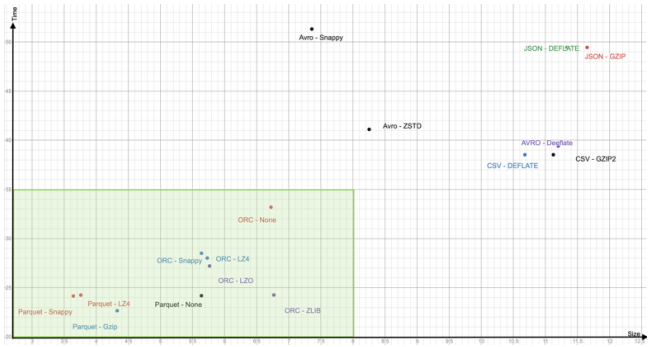

Fig 6. Time v/s Size for File Format Compression

D. Metrics

The evaluation of metrics was done after converting the dataset in the shortlisted file formats. The following metrics were evaluated:

- File Size: The initial file sizes of all the different file formats of the same HR data (*Fig 7)*.

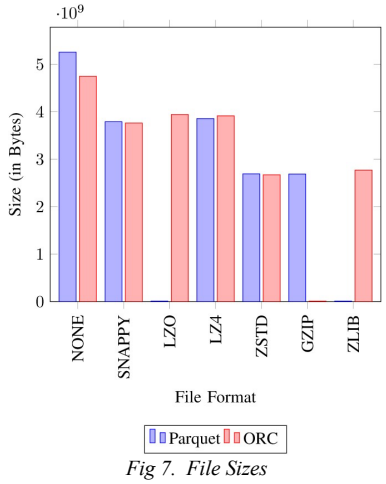

Fig 7. File Sizes

- Queries: Several queries were formulated and executed to analyse these datasets using Spark SQL as they executed queries faster. The graphs showcase the query execution times. The queries are as follows:

A. Search random data: The query collected all the specific records where the State is Alabama or Texas.

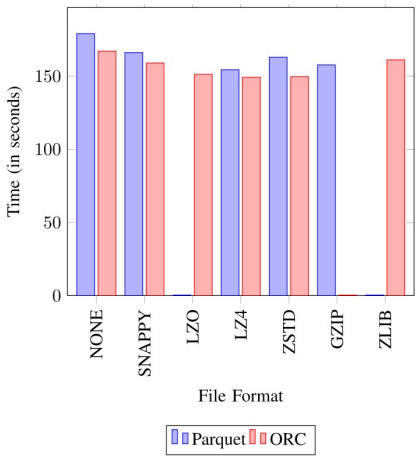

Fig 8A. Query A

B. Find the sum of total salary: The query calculated and returned the aggregated sum of salaries of all the employees.

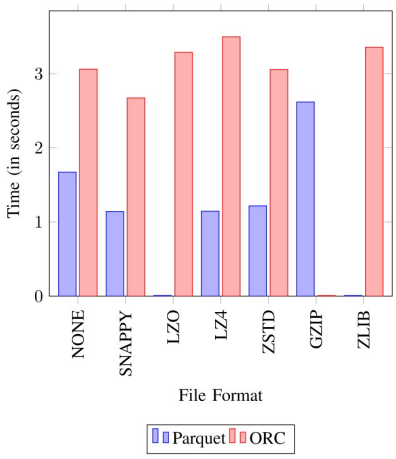

Fig 8B. Query B

C. Find the record with max date of joining and minimum age in years: Here, we sorted the data according to the most recent date of joining and minimum age of the employee and returned the first record.

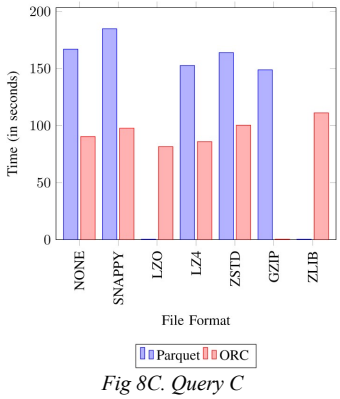

Fig 8C. Query C

Authorized licensed use limited to: DELHI TECHNICAL UNIV. Downloaded on June 15,2022 at 11:23:48 UTC from IEEE Xplore. Restrictions apply.

D. Region-wise average age in the company: A complex aggregation query that returns the average age of the employee in the company in each region.

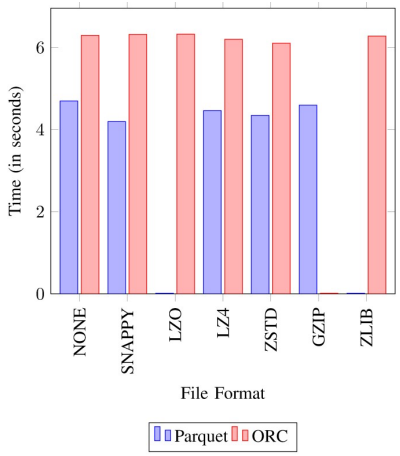

Fig 8D. Query D

E. Count entries with a weight between 72kg-150kg: This query returned the count of employees who weigh between 72kg and 150kg.

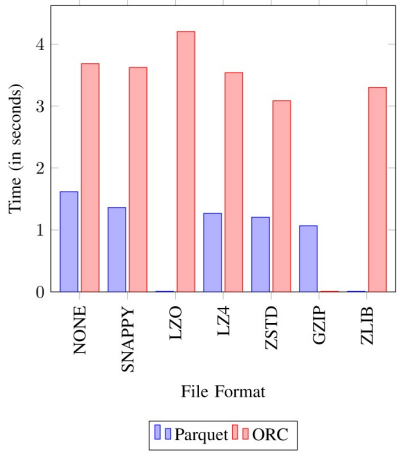

Fig 8E. Query E

F. Total distinct records: The count of distinct records from the whole data was attained.

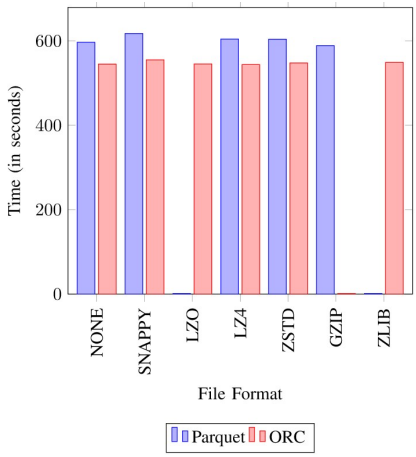

Fig 8F. Query F

From the above figures, the following inference was derived:

- From Query 3 and 6, it can be said that ORC executes operations more efficiently when the complete data has to be read.
- From Query 2, 4 and 5, it was imminent that analytical queries performed better for Parquet file format.
- Parquet and ORC file formats with zstd compression codec, ORC with zlib codec and Parquet with gzip codec were the most space-efficient of the lot.
- ORC with lzo compression codec was the most time-efficient, closely contested by ORC with lz4, none and ztsd compression codecs.

IV. Further Discussion

Parquet vs ORC Standoff

Parquet and ORC files are column-based formats and consume the least space out of the bunch [19]. We conducted further research by taking into consideration random numeric data of varying rows and columns [24]. Another integral part of the random data which we varied was the schema. If a schema is not provided, the default data type is assigned, the string data type. Then we recorded the file size after its conversion and compared it to the file size where the schema was specified. We observed that generally, we attained a file that consumed lesser space if the schema was specified. When we carried out further tests on decimal type data, we noticed an astonishing behaviour between parquet and orc file sizes. The results have been depicted in *Table 7*.

PARQUET VS ORC COMPARISON				
TYPE	SCHEMA	DATATYPE	PARQUET	ORC
1M Rows 6 Columns	Without Schema	Strings	53357302	32037057
	With Schema	Integer	24020216	18043140
1M Rows 12 Columns	Without Schema	Strings	106714377	64074208
	With Schema	Integer	48040213	36085239
30M Rows 12 Columns	Without Schema	Strings	789693341	635566900
	With Schema	Integer	439681297	421367128
1M Rows 6 Columns	Without Schema	Strings	70632900	50303258
	With Schema	Float	24020203	24027816
		Double	48022705	48027972
1M Rows 12 Columns	Without Schema	Strings	141275220	100614599
	With Schema	Float	44036838	44050128
		Double	96045169	96055931
1M Rows 30 Columns	Without Schema	Strings	353190674	251530963
	With Schema	Float	120100163	120136722
		Double	240119389	240141955
30M Rows 30 Columns	Without Schema	Strings	848763184	756818480
	With Schema	Float	530125128	1081223812
		Double	890556476	2163386151

Table 7. Parquet vs ORC Comparison

When the data is stored as strings or no schema is provided, ORC files consume less space than Parquet. A similar conclusion can be derived for the integer data type. Whereas in the case of decimal data types, Parquet files outperformed ORC files in terms of the file size.

V. Findings and Conclusions

Big Data file formats have been a revelation and are quickly becoming a staple in the industry. This paper aimed at conducting a comprehensive analysis of such file formats. Extensive qualitative and quantitative inspection has led us to the following findings:

Authorized licensed use limited to: DELHI TECHNICAL UNIV. Downloaded on June 15,2022 at 11:23:48 UTC from IEEE Xplore. Restrictions apply.

- As seen in the file conversion matrix, writing of files to Parquet file format is the fastest.
- Reading data from ORC file format consumes less time as compared to other file formats.
- During the research, it was found that when the schema was specified before writing a file, the obtained file was space-efficient compared to that of a file written without schema.
- ORC handled integer and string data types efficiently in terms of space, whereas Parquet handled decimal type data better.
- Avro file format was drastically poor when queries were executed by reading the data from AWS.
- We can conclude from the queries executed above that analytical queries were more efficient with Parquet file format.
- When Parquet files were compressed with different compression codecs, minimal changes in the size of compressed files were observed.

VI. Future Scope

Big Data is ever-expanding and ever-evolving. The development of cutting-edge technologies such as Cloud Computing, Machine Learning, and Artificial Intelligence hinged on big data technology evolution. With file formats forming the backbone of big data, breakthroughs in the former will undoubtedly reinforce perpetual advancements in the latter.

This research paper can be expanded to encompass further qualitative and quantitative research on advanced file storage systems like Delta Lake, Apache Hudi, Apache Iceberg, Apache Hive, and similar file systems. Moreover, it can help future researchers develop a profound cognisance of how the technical design of file formats affect their qualitative and quantitative properties. This can form the basis for designing more efficient and performance-intensive formats in the future. Finally, our paper provides a generalised framework for choosing specific file formats for specific jobs. This framework can find future applications in several industries where choosing appropriate file formats can be crucial.

References

[1] S. Sakr, A. Liu, and A. G. Fayoumi, “The family of mapreduce and large-scale data processing systems,” *ACM Comput. Surv.*, vol. 46, no. 1, pp. 1–44, 2013, doi: 10.1145/2522968.2522979.

[2] I. Mavridis and H. Karatza, “Performance evaluation of cloud-based log file analysis with Apache Hadoop and Apache Spark,” *J. Syst. Softw.*, vol. 125, pp. 133–151, 2017, doi: 10.1016/j.jss.2016.11.037.

[3] A. Siddiqa, A. Karim, and A. Gani, “Big data storage technologies: a survey,” *Front. Inf. Technol. Electron. Eng.*, vol. 18, no. 8, pp. 1040–1070, 2017, doi: 10.1631/FITEE.1500441.

[4] S. Ahmed, M. Usman, J. Ferzund, M. Atif, A. Rehman, and A. Mehmood, “Modern Data Formats for Big Bioinformatics Data Analytics,” *Int. J. Adv. Comput. Sci. Appl.*, vol. 8, no. 4, pp. 366–377, 2017, doi: 10.14569/ijacsa.2017.080450.

[5] W. A. Bhat, “Bridging data-capacity gap in big data storage,” *Futur. Gener. Comput. Syst.*, vol. 87, no. 2018, pp. 538–548, 2018, doi: 10.1016/j.future.2017.12.066.

[6] S. Salloum, R. Dautov, X. Chen, P. X. Peng, and J. Z. Huang, “Big data analytics on Apache Spark,” *Int. J. Data Sci. Anal.*, vol. 1, no. 3–4, pp. 145–164, 2016, doi: 10.1007/s41060-016-0027-9.

[7] F. Cappa, R. Oriani, E. Peruffo, and I. McCarthy, “Big Data for Creating and Capturing Value in the Digitalized Environment: Unpacking the Effects of Volume, Variety, and Veracity on Firm Performance*,” *J. Prod. Innov. Manag.*, vol. 38, no. 1, pp. 49–67, 2021, doi: 10.1111/jpim.12545.

[8] C. Yang, Q. Huang, Z. Li, K. Liu, and F. Hu, “Big Data and cloud computing: innovation opportunities and challenges,” *Int. J. Digit. Earth*, vol. 10, no. 1, pp. 13–53, 2017, doi: 10.1080/17538947.2016.1239771.

[9] Shakya, Subarna & Smys, Smys. (2021). Big Data Analytics for Improved Risk Management and Customer Segregation in Banking Applications. Journal of ISMAC. 3. 235-249. 10.36548/jismac.2021.3.005.

[10] D. Chong and H. Shi, “Big data analytics: a literature review,” *J. Manag. Anal.*, vol. 2, no. 3, pp. 175–201, 2015, doi: 10.1080/23270012.2015.1082449.

[11] Y. Chen, H. Chen, A. Gorkhali, Y. Lu, Y. Ma, and L. Li, “Big data analytics and big data science: a survey,” *J. Manag. Anal.*, vol. 3, no. 1, pp. 1–42, 2016, doi: 10.1080/23270012.2016.1141332.

[12] E. Nazari, M. H. Shahriari, and H. Tabesh, “BigData Analysis in Healthcare: Apache Hadoop , Apache spark and Apache Flink,” *Front. Heal. Informatics*, vol. 8, no. 1, p. 14, 2019, doi: 10.30699/fhi.v8i1.180.

[13] G. Wróbel and M. D. Wikira, “Overview of Big Data platforms,” *J. Comput. Sci. Inst.*, vol. 13, pp. 283–287, 2019, doi: 10.35784/jcsi.1296.

[14] E. Shahverdi, A. Awad, and S. Sakr, “Big stream processing systems: An experimental evaluation,” *Proc. - 2019 IEEE 35th Int. Conf. Data Eng. Work. ICDEW 2019*, no. 1, pp. 53–60, 2019, doi: 10.1109/ICDEW.2019.00-35.

[15] V. Chauhan and M. Sabharwal, “Systematic Review : Progression study on BIG DATA articles,” no. May, pp. 7979–7983, 2019.

[16] V. Belov, A. N. Kosenkov, and E. Nikulchev, “Experimental characteristics study of data storage formats for data marts development within data lakes,” *Appl. Sci.*, vol. 11, no. 18, 2021, doi: 10.3390/app11188651.

[17] Á. A. Isla, “HDFS File Formats: Study and Performance Comparison,” 2018.

[18] V. Belov, A. Tatarintsev, and E. Nikulchev, “Choosing a data storage format in the apache hadoop system based on experimental evaluation using apache spark,” *Symmetry (Basel).*, vol. 13, no. 2, pp. 1–20, 2021, doi: 10.3390/sym13020195.

[19] T. Ivanov and M. Pergolesi, “The impact of columnar file formats on SQL-on-hadoop engine performance: A study on ORC and Parquet,” *Concurr. Comput. Pract. Exp.*, vol. 32, no. 5, pp. 1–31, 2020, doi: 10.1002/cpe.5523.

[20] V. Belov, A. Tatarintsev, and E. Nikulchev, “Comparative Characteristics of Big Data Storage Formats,” *J. Phys. Conf. Ser.*, vol. 1727, no. 1, 2021, doi: 10.1088/1742-6596/1727/1/012005.

[21] R. F. Munir, A. Abelló, O. Romero, M. Thiele, and W. Lehner, “A cost-based storage format selector for materialized results in big data frameworks,” *Distrib. Parallel Databases*, vol. 38, no. 2, pp. 335–364, 2020, doi: 10.1007/s10619-019-07271-0.

[22] S. Lee, J. Y. Jo, and Y. Kim, “Survey of Data Locality in Apache Hadoop,” *Proc. - 2019 IEEE/ACIS 4th Int. Conf. Big Data, Cloud Comput. Data Sci. BCD 2019*, pp. 46–53, 2019, doi: 10.1109/BCD.2019.8885148.

[23] I. A. T. Hashem, I. Yaqoob, N. B. Anuar, S. Mokhtar, A. Gani, and S. Ullah Khan, “The rise of ‘big data’ on cloud computing: Review and open research issues,” *Inf. Syst.*, vol. 47, pp. 98–115, 2015, doi: 10.1016/j.is.2014.07.006.

[24] D. Plase, L. Niedrite, and R. Taranovs, “A Comparison of HDFS Compact Data Formats: Avro Versus Parquet,” *Moksl. - Liet. ateitis*, vol. 9, no. 3, pp. 267–276, 2017, doi: 10.3846/mla.2017.1033.

[25] M. Ragab, F. M. Awaysheh and R. Tommasini, "Bench-Ranking: A First Step Towards Prescriptive Performance Analyses For Big Data Frameworks," 2021 IEEE International Conference on Big Data (Big Data), 2021, pp. 241-251, doi: 10.1109/BigData52589.2021.9671277.

[26] V. Belov, A. Tatarintsev, and E. Nikulchev, “Choosing a Data Storage Format in the Apache Hadoop System Based on Experimental Evaluation Using Apache Spark,” Symmetry, vol. 13, no. 2, p. 195, Jan. 2021, doi: 10.3390/sym13020195

[27] A. K. Sandhu, "Big data with cloud computing: Discussions and challenges," in Big Data Mining and Analytics, vol. 5, no. 1, pp. 32-40, March 2022.

Authorized licensed use limited to: DELHI TECHNICAL UNIV. Downloaded on June 15,2022 at 11:23:48 UTC from IEEE Xplore. Restrictions apply.

Physica Scripta

ACCEPTED MANUSCRIPT

A first-principle study of electronic, thermoelectric, and optical properties of sulfur doped *c*-HfO_2

To cite this article before publication: Rajesh Kumar *et al* 2022 *Phys. Scr.* in press https://doi.org/10.1088/1402-4896/ac7678

Manuscript version: Accepted Manuscript

Accepted Manuscript is "the version of the article accepted for publication including all changes made as a result of the peer review process, and which may also include the addition to the article by IOP Publishing of a header, an article ID, a cover sheet and/or an 'Accepted Manuscript' watermark, but excluding any other editing, typesetting or other changes made by IOP Publishing and/or its licensors"

This Accepted Manuscript is **© 2022 IOP Publishing Ltd**.

During the embargo period (the 12 month period from the publication of the Version of Record of this article), the Accepted Manuscript is fully protected by copyright and cannot be reused or reposted elsewhere.
As the Version of Record of this article is going to be / has been published on a subscription basis, this Accepted Manuscript is available for reuse under a CC BY-NC-ND 3.0 licence after the 12 month embargo period.

After the embargo period, everyone is permitted to use copy and redistribute this article for non-commercial purposes only, provided that they adhere to all the terms of the licence https://creativecommons.org/licences/by-nc-nd/3.0

Although reasonable endeavours have been taken to obtain all necessary permissions from third parties to include their copyrighted content within this article, their full citation and copyright line may not be present in this Accepted Manuscript version. Before using any content from this article, please refer to the Version of Record on IOPscience once published for full citation and copyright details, as permissions will likely be required. All third party content is fully copyright protected, unless specifically stated otherwise in the figure caption in the Version of Record.

View the article online for updates and enhancements.

This content was downloaded from IP address 14.139.251.98 on 13/06/2022 at 07:54

A first-principles Study of Electronic, Thermoelectric, and Optical Properties of Sulfur Doped *c*-HfO_2

Rajesh Kumar[1], Ramesh Kumar[2], Ankush Vij[3], and Mukhtiyar Singh[1*]

[1]Department of Applied Physics, Delhi Technological University, Delhi-110042, India

[2]Department of Physics, Guru Jambheshwar University of Science & Technology, Hisar-125001, India

[3]Department of Physics, University of Petroleum and Energy Studies (UPES), Uttarakhand-248001, India

*Corresponding author: msphysik09@gmail.com, mukhtiyarsingh@dtu.ac.in

Abstract

In the present work, using first-principles calculations, we systematically investigated $HfO_{2-x}S_x$ (x = 0, 0.03, 0.06 doping concentrations) and demonstrated the enhancement in the thermoelectric and optical properties with sulfur (S)-doping. The thermodynamical stability of the studied concentrations is confirmed using convex hull formalism and also verified by phase stability diagram. The different exchange- correlation functionals are used to calculate the band gaps. It is found that using Tran-Blaha modified Becke-Johnson (TB-mBJ) functional, the estimated value of the band gap for pristine cubic-HfO_2 is 5.82 eV which is in good agreement with experimentally reported value (5.80 eV). For x = 0.03 and 0.06, the band gap value reduces to 4.88 eV and 4.18 eV, respectively. The Seebeck coefficient is 248.79 μV/K at 300 K for x = 0.03 and slightly increases to 294.39 μV/K at 400 K for x = 0.06 due to the creation of new states in the conduction band region, which is further confirmed by the increase in effective mass with doping concentration. The calculated Seebeck coefficient for $HfO_{2-x}S_x$ showed p-type behaviour over the entire temperature range for all doping concentrations. A significant reduction in the electronic thermal conductivity was observed with S-doping. This further results in a high figure of merit (ZT_e) ~ 0.77 and 0.82 for x = 0.03 and 0.06, respectively, at 800 K. The low value of the static dielectric constant for x = 0.03 makes it compatible for electron transport. The optical properties with doping suggest an enhancement in the UV absorption range and a decrease in reflectivity in the visible and near infrared regions of the electromagnetic spectra.

Accepted Manuscript

Keywords: *c*-HfO_2; DFT; Thermoelectric Properties; Optical Properties; TB-mBJ

1. Introduction

The continuous depletion of conventional energy resources leads to extensive research in renewable energy resources and the development of novel techniques for energy storage and conversion [1-3]. Thermoelectric (TE) energy conversion has become a hot area of research in recent times. Many materials with high TE energy conversion efficiency have been reported so far, including semiconductors [4-5] and different layered metal monochalcogenides [6-8]. An excellent TE material should have a high value of figure of merit i.e., ZT ($=\sigma S_\alpha^2 T/K$), which measures its TE efficiency [3]. This efficiency can be maximized by high electrical conductivity (σ), high Seebeck coefficient (S_α), and low thermal conductivity (K) [6]. But as these three parameters are correlated with each other, it is a challenging task to optimize them to achieve high ZT. Numerous efforts have been made to reduce the thermal conductivity [9-10], including lowering the dimensions of the materials [11] and strengthening of phonon scattering [12-14].

Despite the remarkable properties such as high melting point, and high thermal and chemical stability of metal oxides, the TE power generation in these materials is still in its early stage [15-17]. It is reported that a highly efficient doping mechanism can lead to a high power factor in these materials [18-19]. Hafnium Oxide (HfO_2), owing to its wide band gap and high thermal stability, has emerged as a most promising host for band engineering [20-21] and high temperature application [22], respectively. It exists in the monoclinic (m) phase at 1200 ^oC [23], cubic (c) phase at 2800 ^oC [24]. However, the stability at lower temperatures has been achieved in pristine and yttrium doped *c*-HfO_2 [25-26]. Also, the pressure study has shown its stability up to 26.2 GPa [27]. The applicability of this phase is identified in industrial applications like fuel cells [28], laser mirrors [29], random access memory devices [30], gas sensing [31], optical and protective coatings [32]. The hafnium's high density leads to the low value of lattice thermal conductivity (0.49 to 0.95 W/m-K) which has been observed in HfO_2 thin film [33]. Different doping mechanisms have been explored to enhance its TE and optical properties via various transition metal elements [34-36]. Besides the doping of transition metals, efforts of

Accepted Manuscript

anionic (S, N, F, and C) doping have been made in the recent past to enhance various physical and chemical properties of metal oxides [38-39]. Cao et al. have shown the enhancement in TE and optical properties of C-doped *c*-HfO_2 [37]. It has been shown that doping of S in HfO_2 thin film results in more S concentration which leads to improving its durability and response behaviour [40-42]. Zhang et al. have reported that the effect of co-doping of C and F can improve the optical properties of *c*-HfO_2 [43]. Various experimental and theoretical studies of S-doping are existing in literature which demonstrated the enhancement in stability and reduction in band gap of TiO_2 and ZrO_2 [44-48]. Motivated by these studies, we have examined S-doped *c*-HfO_2 for its electronic, structural, thermoelectric, and optical properties by using first-principles calculations. We have explored these properties with varying concentration of S in $HfO_{2-x}S_x$ (x = 0, 0.03, 0.06). We are highly optimistic that the new incites can be achieved by incorporating S-doping in *c*-HfO_2. To the best of our knowledge, no such study is yet reported.

2. Theoretical Methodology

Density Functional Theory (DFT) based WIEN2K program package [49] was used to carry out calculations for structural, electronic, and optical properties. WIEN2K is based on the full-potential linearized augmented plane wave method. Various available exchange- correlation (XC) functionals i.e., generalized gradient approximation (GGA) [50] of Perdew-Burke-Ernzerhof (PBE), PBE0 [51], TB-mBJ [52] and HSE06 [53] were tested vis-à-vis the available experimental result of *c*-HfO2. The TB-mBJ functional was found to be best amongst all which reproduce the true experimental band gap value. The validity of TB-mBJ was already tested on several wide and small band gap materials like SnO_2, LiCl, GeO_2, NiO, FeO, MgO etc. and the obtained value of band was found to be in agreement with the experimental results [52]. The muffin tin radii were chosen to be non-overlapping, and a strict energy convergence criterion (0.0001 Ry/cell) was used to get more realistic results. The $R_{MT}K_{max} = 7$ was used for plane wave cut-off, and the core and valance state cut-off energy were set to -6.0 Ry. To achieve well converged results, we were used a 20×20×20 k mesh which generated 256 k points in the irreducible Brillouin zone (IBZ). For PBE0 calculation a 10×10×10 k mesh was used. The HSE06 functional [53] was employed using Vienna ab initio simulation package (VASP) [54]. The plane wave cutoff energy

Accepted Manuscript

was set to 560 eV and a 10×10×10 Gamma-centred k-point mesh was used. For simulating various S-doping concentrations, a dense supercell of 2×2×2 dimensions which comprised of 96 atoms, were used. The temperature dependent thermoelectric properties were estimated within semiclassical Boltzmann transport theory under constant relaxation time approximation [55] as implemented in BoltzTrap code. A denser k-mesh (34×34×34) was used for these calculations. The optical properties were estimated using optic program as built in the WIEN2K package [56].

3. Results and discussion

3.1 Structural Properties

The HfO_2 crystallizes in cubic phase having space group $Fm\bar{3}m$ with Hf atom positioned at (0, 0, 0) and O atoms positioned at (0.25, 0.25, 0.25) and (0.75, 0.75, 0.75), respectively. The obtained optimized equilibrium lattice parameter for *c*-HfO_2 (5.09 Å) is in fair agreement with other theoretical and experimental reports [35,37,25]. The doped structures, $HfO_{1.97}S_{0.03}$ and $HfO_{1.94}S_{0.06,}$ are obtained by replacing two and four O-atoms with S-atoms, respectively, in the supercell as shown in Figure 1.

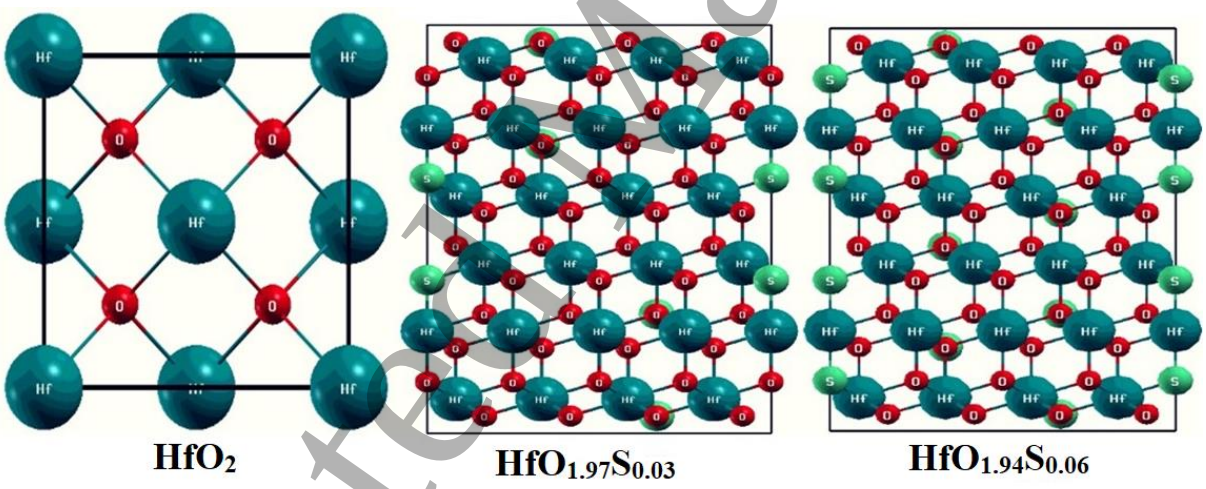

Figure 1. Crystal structures of $HfO_{2-x}S_x$ (x = 0, 0.03, 0.06)

It is vital to check the thermodynamical stability of both the doping concentrations as these are not experimentally synthesized yet. We have used the convex hull formalism and phase stability diagram [57-60,61] to ascertain their thermodynamical stability. The formation energies (E_{for}) are obtained using [34] following equation:

$$E_{for} = \frac{\{E_{Total} - n(E_{Hf\,atom} + E_{O\,atom} + E_{S\,atom})\}}{N} \quad (1)$$

Accepted Manuscript

where, E_{Total} is the pristine or doped supercell total energy, n is the number of atoms of specific species, N is the total number of atoms in the cell, E_{Hf}, E_O and E_s is the isolated Hf, O and S atom energies, respectively. The obtained value of formation energy is listed in Table 1.

Table 1: Calculated formation energy for $HfO_{2-x}S_x$ (x= 0,0.03,0.06,0.12,0.25,0.50,0.75) and HfS_2 in units of eV/atom.

	$HfO_{2-x}S_x$							HfS_2
	x = 0	x = 0.03	x =0.06	x =0.12	x = 0.25	x = 0.50	x = 0.75	
E_{for} (eV/atom)	-3.66	-9.82	-9.78	-9.40	-8.50	-6.91	-5.31	-2.55

If E_{for} is negative it shows that the particular material will not phase separated in to its elemental components but it does not guarantee its thermodynamical stability. However, convex hull is a reliable tool to check the thermodynamic stability of materials [60]. We have presented the convex hull of formation energies referenced to the elemental standard states as shown in Figure 2. It can be seen that $HfO_{1.97}S_{0.03}$ and $HfO_{1.94}S_{0.06}$ are lies on the convex hull line which shows that these doping concentrations are thermodynamically stable. We have also analysed few more hypothetical doping concentrations such as $HfO_{1.88}S_{0.12}$, $HfO_{1.75}S_{0.25}$, $HfO_{1.50}S_{0.50}$, $HfO_{1.25}S_{0.75}$ and found that these are lying above the convex hull line which shows their instability. The decomposition energy, ΔE_d, is equal to the vertical distance in formation energy space between the particular material and the hull line [60] and $\Delta E_d = 0$ is a signature of stability. The value of ΔE_d for $HfO_{1.88}S_{0.12}$, $HfO_{1.75}S_{0.25}$, $HfO_{1.50}S_{0.50}$ and $HfO_{1.25}S_{0.75}$ is 0.18 eV/atom, 0.55 eV/atom, 1.2 eV/atom and 1.79 eV/atom, respectively.

Accepted Manuscript

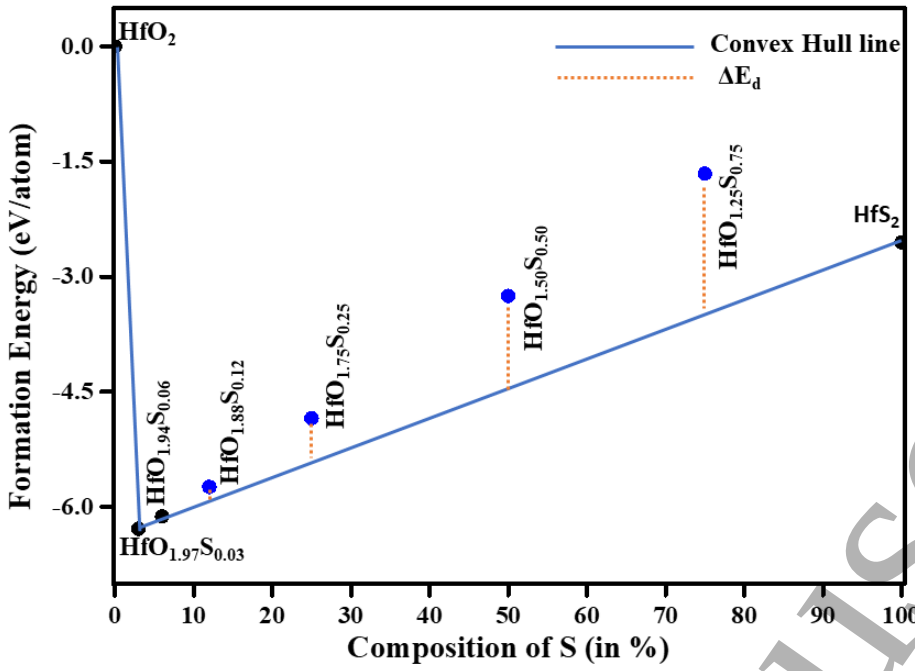

Figure 2. A schematic convex hull of $HfO_{2-x}S_x$ at different composition of S (in %). ΔE_d is given by the vertical distance in formation energy space between the particular material and the hull line.

Further, the phase stability diagram [61] of both doping concentrations is also plotted (Figure 3). The points located in the ABCD region shows the stability of various possible structures. The point C lies on the oxygen rich environment line and point D lies on the Hf rich environment line. The points A (HfS_2) and B (SO_2) limits the chemical potential region for $HfO_{2-x}S_x$ above the line BD and below AC. This describe that the formation energy of $HfO_{2-x}S_x$ can be tuned in the large region. The obtained points positioned at x_1 and x_2 shows the formation of stable 3% and 6% S doped HfO_2. The chemical potentials of $HfO_{1.97}S_{0.03}$ (x_1) and $HfO_{1.94}S_{0.06}$ (x_2) lie in the ABCD region which shows that these are the stable phases. Moreover, the dynamical stability of c-HfO_2 has been already reported through phonon band diagram [62-63].

Accepted Manuscript

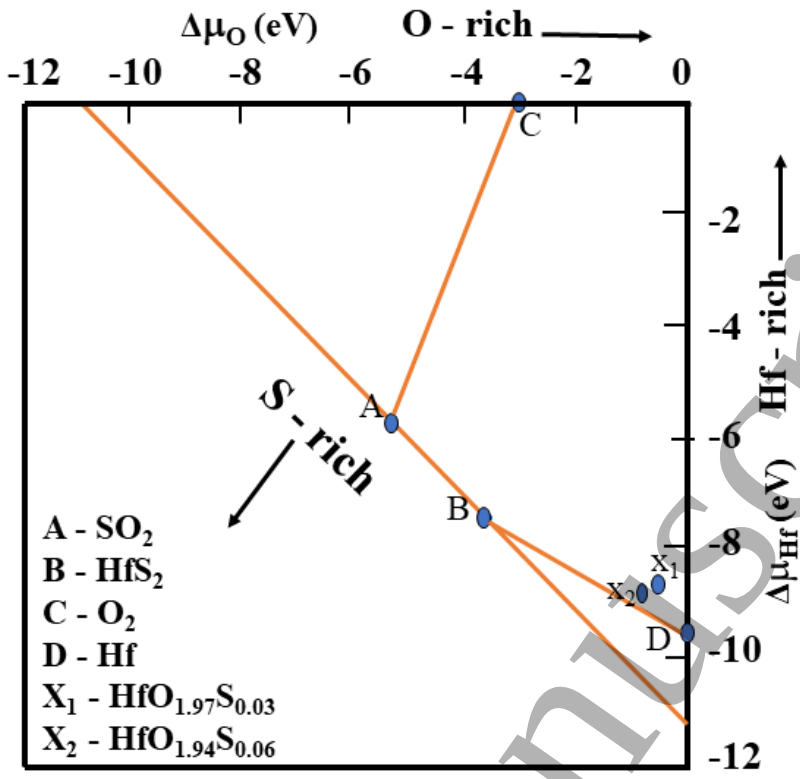

Figure 3. Phase stability diagram of S-doped HfO_2.

3.2 Electronic Properties

The band structure calculations are performed using the PBE0, HSE06, and TB-mBJ functionals. The obtained values of band gaps are given in Table 2. We find that using TB-mBJ functional accurately predicts the true band gap and agrees quite well with the earlier reported theoretical and experimental results [25,37,64,65] and therefore all the further calculations are performed in the framework of TB-mBJ functional. To gain more insights of electronic structure, the density of states (DOS) is plotted along with band structure (Figure 4), which clearly shows the dominant contribution of O-states over Hf-states in the valance band (VB), whereas Hf-states are dominant over O-states in the conduction band (CB).

Accepted Manuscript

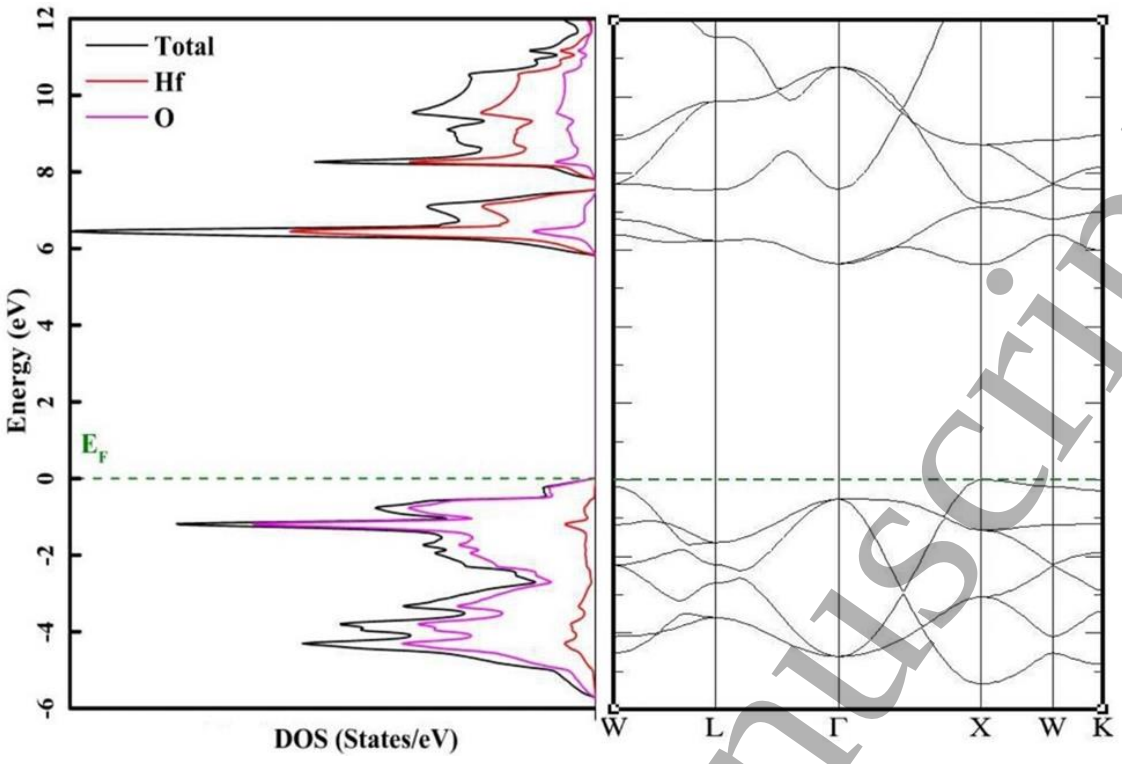

Figure 4. Band structure and Density of states (DOS) of pristine *c*-HfO_2

Next, we have analysed the electronic structure of S-doped *c*-HfO_2. At x = 0.03 and 0.06 doping, the obtained value of band gap along *Γ–H–N–Γ–P* high symmetry K points is 4.88 eV and 4.18 eV, respectively, which is in line with previous studies showing a reduction in band gap by S-doping [45, 47-48]. Both doping concentrations show a direct band gap with flat band curvature along *Γ–Γ* as represented in Figure 5. The reduction in band gap with doping can be ascribed to the fact that S ions have lower electronegativity than O ions, so the sulfurized oxides ($HfO_{2-x}S_x$) would tend to have lower energy which costs transferring an electron from the VB (S-3*p* or O-2*p*) to CB (Hf-5*d*) leading to the reduction in band gap.

Accepted Manuscript

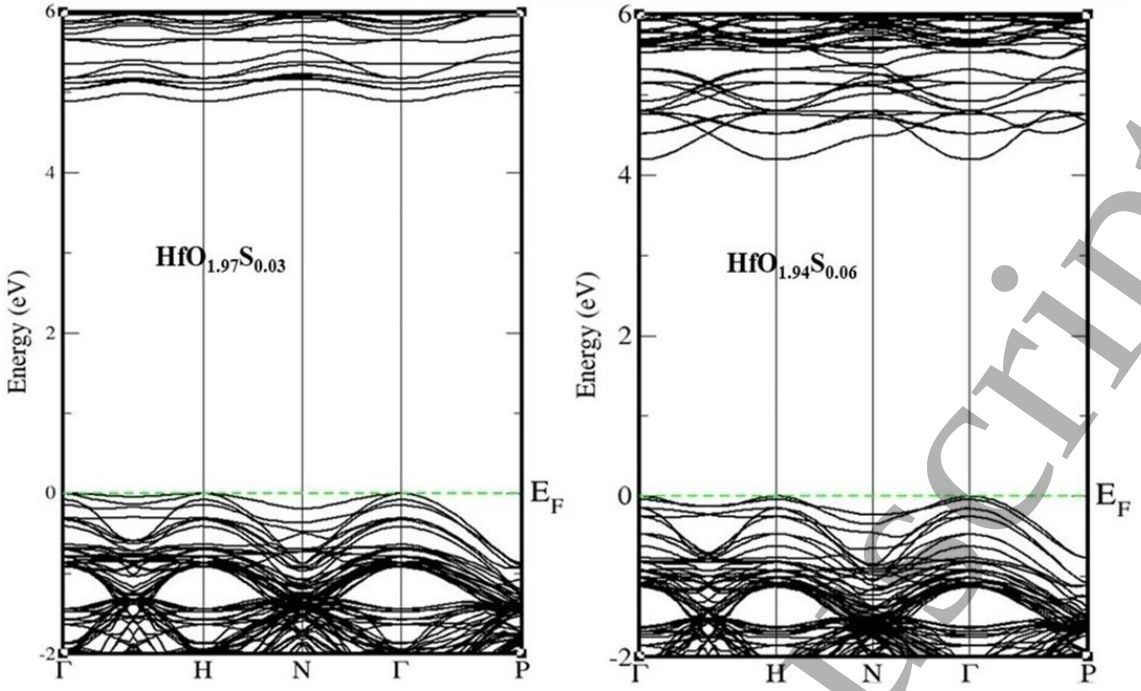

Figure 5. Band structures of $HfO_{2-x}S_x$ (x = 0.03, 0.06) using TB-mBJ approach

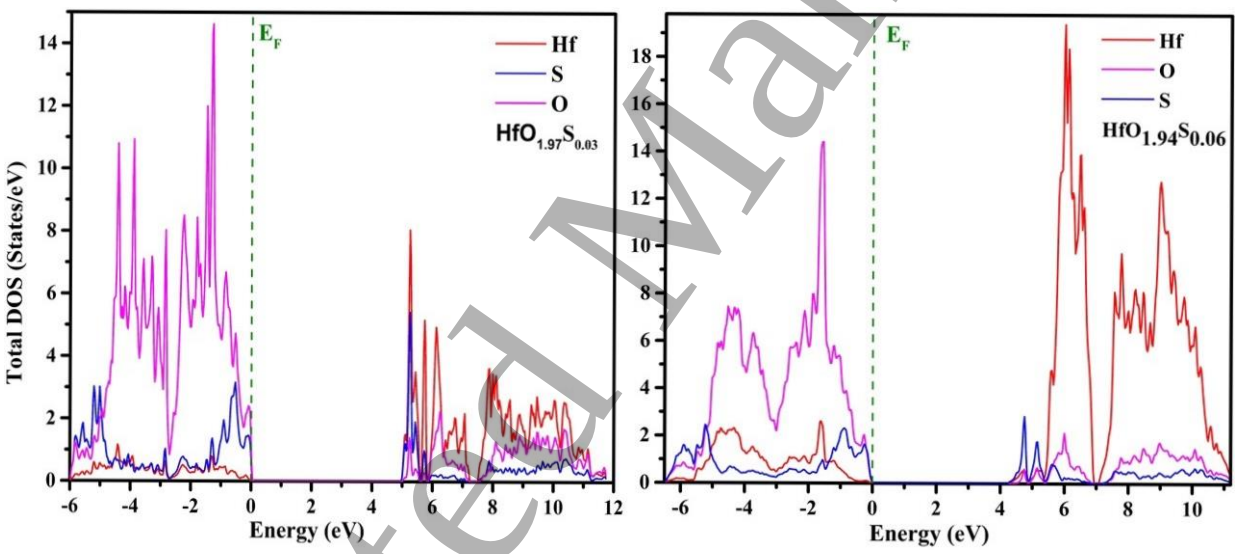

Figure 6. Density of states (DOS) of $HfO_{2-x}S_x$ (x = 0.03, 0.06) (Fermi energy set to 0 eV)

In Figure 6, the doping concentrations are examined to study the effect of various atomic species on the electronic structures. In VB, O-states have dominance over the S- states and Hf-states, whereas S-states are induced in lower CB (~ 4 eV – 6 eV), and Hf-states dominate in higher energy regions. A good extent of hybridization is observed between Hf-, S-, and O-states.

Accepted Manuscript

Table 2: Comparison of band gaps of $HfO_{2-x}S_x$ (x = 0, 0.03, 0.06) using different exchange-correlation functional (PBE, TB-mBJ, PBE0, and HSE06) and with available experimental data.

	PBE	TB-mBJ	PBE0/HSE06	Experimental
HfO_2	3.78 eV	5.82 eV	5.70 eV/5.55 eV	5.80 eV [65], 5.88 eV [25]
$HfO_{1.97}S_{0.03}$	3.25 eV	4.88 eV	–	–
$HfO_{1.94}S_{0.06}$	2.73 eV	4.18 eV	–	–

3.3 Thermoelectric Properties

The precise band gap description is critical for the analysis of a material for its TE properties. To achieve the precise TE property of $HfO_{2-x}S_x$ (x = 0, 0.03, 0.06) for comparison with future experiments, our first-principles calculation combined with TB-mBJ potential gave us a precise band gap. The S_α, σ, and K of the material are the most important quantities that influence TE performance. As a result, we have examined all of these variables in relation to temperature variations.

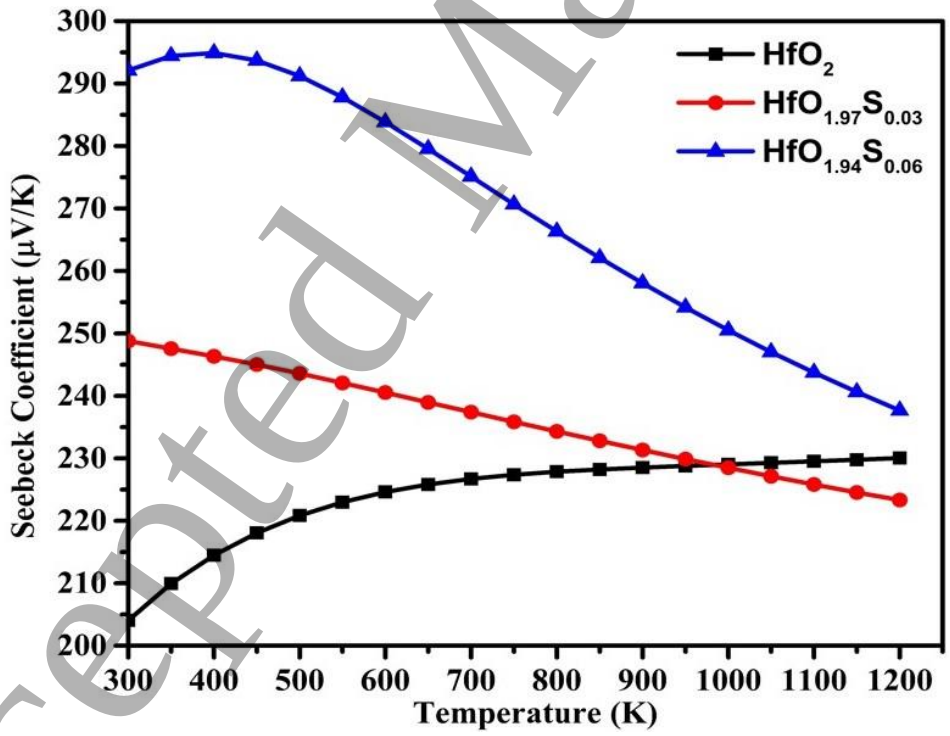

Figure 7. Seebeck coefficient of $HfO_{2-x}S_x$ (x = 0, 0.03, and 0.06)

The temperature dependence of S_α for $HfO_{2-x}S_x$ (x = 0, 0.03, 0.06) is shown in Figure 7. As the temperature increase from 300 K to 1200 K, the increase in value of S_α for x = 0 is observed, while for

Accepted Manuscript

doping concentrations (x = 0.03 and 0.06), S_α decreases with the increase in temperature. The calculated value of S_α at 300 K is found to be 214.48 μV/K, 248.79 μV/K, 292.10 μV/K, whereas, for 1200 K, the value is 230.03 μV/K, 223.32 μV/K, 237.66 μV/K for x = 0, 0.03, 0.06 concentrations, respectively. The observed value of S_α for pristine *c*-HfO_2 shows good agreement with previously reported results [34,35,37]. With an increase in the doping concentration, the enhancement in value of S_α may be due to an increase in DOS near the fermi level. The response of S_α depends on the orientation of bands in VB, with doping flat bands appearing in VB that results in high S_α value and low mobility, which leads to low electrical conductivity [6,34,66,67]. To confirm this, the effective mass (m^*) is calculated, and it was found that as S-doping concentration increases, the value of m^* increases (listed in Table-3). S-doping at O sites introduces large mass fluctuation due to significant differences in atomic masses and ionic radii. The positive value of S_α in the studied temperature range shows p-type behaviour of $HfO_{2-x}S_x$, indicating mobility of carriers is due to holes.

Table 3. Calculated effective mass (m^*) of $HfO_{2-x}S_x$ (x= 0, 0.03, and 0.06)

	$HfO_{2-x}S_x$		
	x = 0	**x = 0.03**	**x = 0.06**
Effective Mass m^* (at CBM)	0.73 m_e	1.11 m_e	3.03 m_e
Effective Mass m^* (at VBM)	0.28 m_e	1.70 m_e	2.01 m_e

The effect of temperature on electrical conductivity (σ/τ) and electronic thermal conductivity (K_e/τ) is shown in Figure 8a and 8b, respectively. σ/τ show almost linearly increasing trend with increase in temperature. The calculated value of σ/τ at room temperature is found to be 0.058 x 10^{20} $\Omega^{-1}m^{-1}s^{-1}$ [34,37], 0.017 x 10^{20} $\Omega^{-1}m^{-1}s^{-1}$, 0.006 x 10^{20} $\Omega^{-1}m^{-1}s^{-1}$, whilst for 1200 K the values are 0.32 x 10^{20} $\Omega^{-1}m^{-1}s^{-1}$ [34,37], and 0.129 x 10^{20} $\Omega^{-1}m^{-1}s^{-1}$, 0.089 x 10^{20} $\Omega^{-1}m^{-1}s^{-1}$, for x = 0, 0.03, 0.06 concentrations, respectively. The slight decrease in the value of σ/τ is may be due to decrease in mobility within rise in doping concentration. The electronic thermal conductivity results are consistent with Wiedemann-Franz law ($K_e = L\sigma T$, where L is Lorentz number and T is temperature). The calculated value of K_e/τ at 300 K is found to be 0.10 x 10^{15} W/mKs [34,37], 0.043 x 10^{15} W/mKs, 0.020 x 10^{15} W/mKs, and for 1200 K,

Accepted Manuscript

2.78 x 10^{15} W/mKs, 0.64 x 10^{15} W/mKs, and 0.53 x 10^{15} W/mKs, for x = 0, 0.03, 0.06 concentrations, respectively. It is evident that doping of sulfur is more significant to obtain lower K_e/τ as compared to C-doping [37].

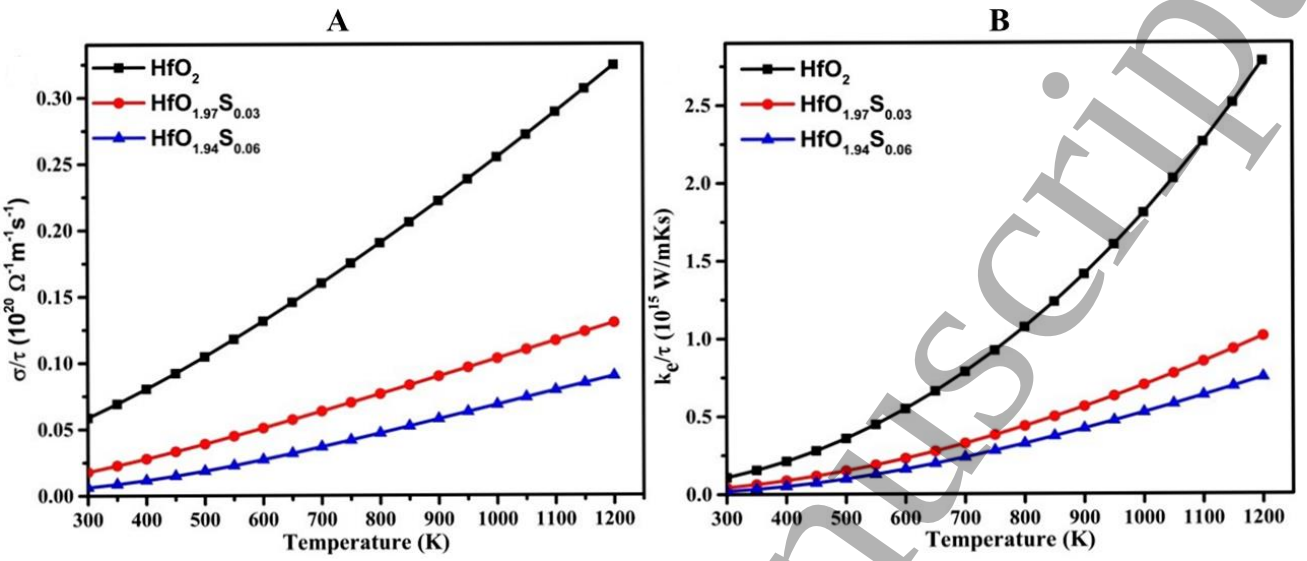

Figure 8. (A) Electrical conductivity and **(B)** Electronic thermal conductivity of $HfO_{2-x}S_x$ (x = 0, 0.03, and 0.06)

The power factor (PF) increases with temperature in pristine *c*-HfO_2. The observed value of PF at room temperature is 0.24 x 10^{12} W/mK^{2}s, and at 1200 K, this value increases to 1.71x 10^{12} W/mK^{2}s, which are in fair agreement with previously reported results [34,35,37]. At room temperature, a small deviation in the value of PF is observed in doped structures, as shown in Figure 9 (a). The observed value in the case of x = 0.03 and 0.06 doped structures are 0.11 x 10^{12} W/mK^{2}s and 0.053 x 10^{12} W/mK^{2}s, whilst at 1200 K values are 0.64 x 10^{12} W/mK^{2}s and 0.53 x 10^{12} W/mK^{2}s, respectively. The variation of PF clearly signifies that it depends on the S_α and σ/τ.

The value of ZT_e increases with an increase in temperature for c-HfO_2. The observed value of ZT_e at room temperature is 0.67 and increases to 0.74 at 1200 K, which is as per the previous studies [34,37]. We obtained a relatively higher value of ZT_e for doped structures. These values are 0.76 and 0.77 for x = 0.03 and 0.06, respectively at room temperature. At 1200 K, these values are 0.76, and 0.81, for x = 0.03 and 0.06, respectively. The variation of ZT_e with temperature is depicted in Figure 9 (b). The maximum value of ZT_e (0.82) is observed at 800 K for x = 0.06. This due to the lowest value of K_e/τ at this concentration among all structures. We have chosen the lower doping concentrations for this study

Accepted Manuscript

because it has been tested that at lower doping Ti doped HfO_2 shows good ZT_e [34], and also these doping concentrations are experimentally feasible. A similar enhancement has been observed in figure of merit in $(SnSe)_{1.16}NbSe_2$ (0.03) [68], $Cu_2SnSe_{3-x}S_x$ (0.66) [69], and BiOCuSe (0.30) [70] with S-doping. In our study, the S-doping leads to a high figure of merit at lower doping concentrations along with the wide band gap in $HfO_{2-x}S_x$, which opens new avenues for its uses in TE applications in a range of temperature.

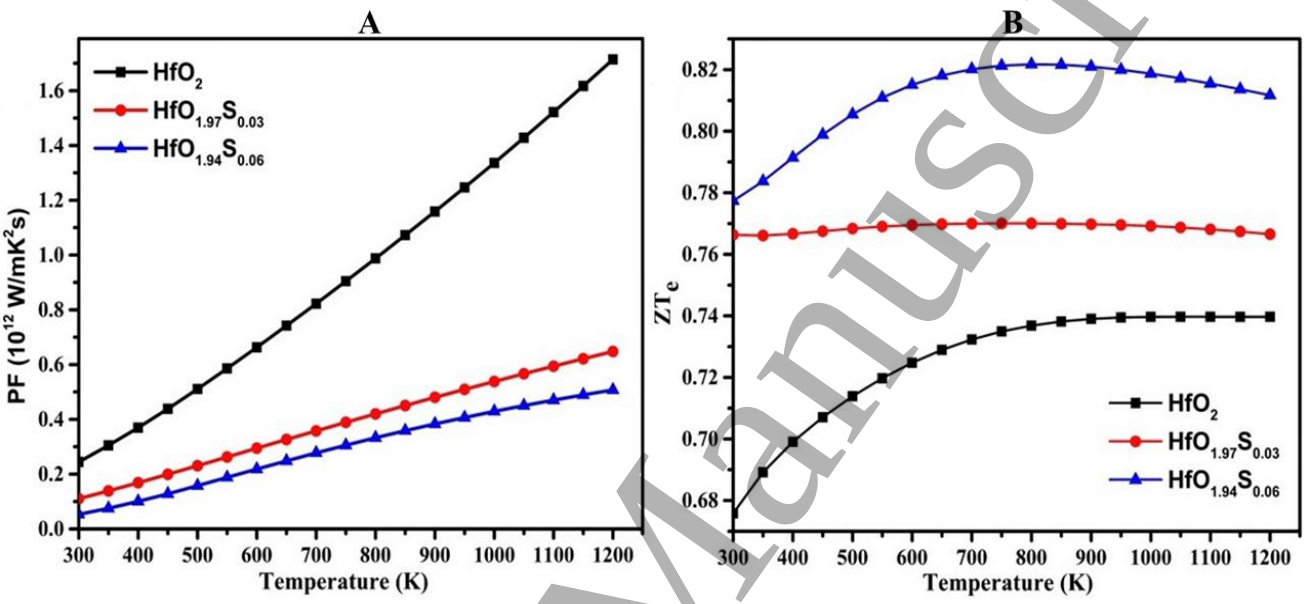

Figure 9. (A) Power factor (PF) and **(B)** Figure of merit (ZT_e) of $HfO_{2-x}S_x$ (x = 0, 0.03, and 0.06)

3.4 Optical properties

Optical properties are based upon Random phase approximation (RPA) which is an independent particle approximation [56]. We have also studied the optical response of *c*-HfO_2 under the effect of S-doping on O sites. To analyse how electromagnetic (EM) radiations interacts with a material, it is necessary to analyse the dielectric function:

$$\varepsilon(\omega) = \varepsilon_1(\omega) + i\varepsilon_2(\omega) \quad (2)$$

where the symbol $\varepsilon_1(\omega)$ and $\varepsilon_2(\omega)$ are real and an imaginary component of the dielectric function. The $\varepsilon_1(\omega)$ and $\varepsilon_2(\omega)$ components are associated with intraband transitions and interband transitions for a metallic and a semiconductor material, respectively. The Kramers-Kroning transformation is used to obtain the real component, $\varepsilon_1(\omega)$ [71], which is given by:

$$\varepsilon_1(\omega) = 1 + \frac{2p}{\pi}\int \frac{\omega'\varepsilon_{2(\omega')}}{(\omega'^2-\omega^2)}d\omega' \quad (3)$$

Accepted Manuscript

where p denotes the momentum matrix. The calculated value of static dielectric constant $\varepsilon_1(0)$ is given as 3.86 for pristine *c*-HfO_2; for doped structure, the observed value of $\varepsilon_1(0)$ slightly changes to 3.50, 3.72 at x = 0.03 and 0.06, respectively as shown in Figure 10 (a). With the increase in photonic energy, after 8 eV, the value of $\varepsilon_1(\omega)$ shows decreasing trend due to Maxwell-Wagner interfacial polarization [69 - 72]. At low incident photon energy, for x = 0 the $\varepsilon_1(\omega)$ has a higher value shows the greater ability of polarization and high value of the refractive index as compared to x = 0.03 and 0.06. Real component $\varepsilon_1(\omega)$ exhibits a maximum at 7.06 eV for pristine *c*-HfO_2 showing fair agreement with previous reported results [36, 71] and 8.04 eV, 7.94 eV for x = 0.03, and 0.06, respectively. As we move toward higher incident photon energy, the $\varepsilon_1(\omega)$ show negative value in range of 11.88-14 eV for pristine, 10.63-14.79 eV for x = 0.03, and 10.57-14.62 eV for x = 0.06. In the energy interval (10.57-14.62 eV), the material behaves as metallic, and EM radiations are reflected by the material owing to anomalous dispersion [73]. The imaginary component $\varepsilon_2(\omega)$ can be calculated from transitions between VB to CB states and related to electronic structure and the absorption of the incident EM wave as:

$$\varepsilon_2(\omega) = \frac{2\pi e^2}{\Omega \varepsilon_o} \sum |\Psi_k^c| u.r |\Psi_k^v|^2 \delta(E_k^c - E_k^v - E) \quad (4)$$

where $\Psi_k^c and\ \Psi_k^v$ are the wave function related with the CB and VB at *k* point, *u* represents the electric field component, Ω represents the unit cell volume, and *e* represents the charge.

As shown in Figure 10 (b), the observed value of optical band gap is 5.9 eV, 4.45 eV and 4.06 eV for x = 0, 0.03, 0.06, respectively. Above the value of the optical band gap, a sharp increment in the value of $\varepsilon_2(\omega)$ is observed, and it reaches the highest absorption peak at 11eV for x = 0 [36, 60], for x = 0.03, the observed values of highest absorption peak lie in the range of 9.71-10.19 eV, and for x = 0.06 lies at 9.83 eV. This shows the electron transitions between the S-3*p* and O-2*p* states to Hf-5*d* states. The optical band gap and shifting of the transition peaks of imaginary part is validated by the DOS results.

Accepted Manuscript

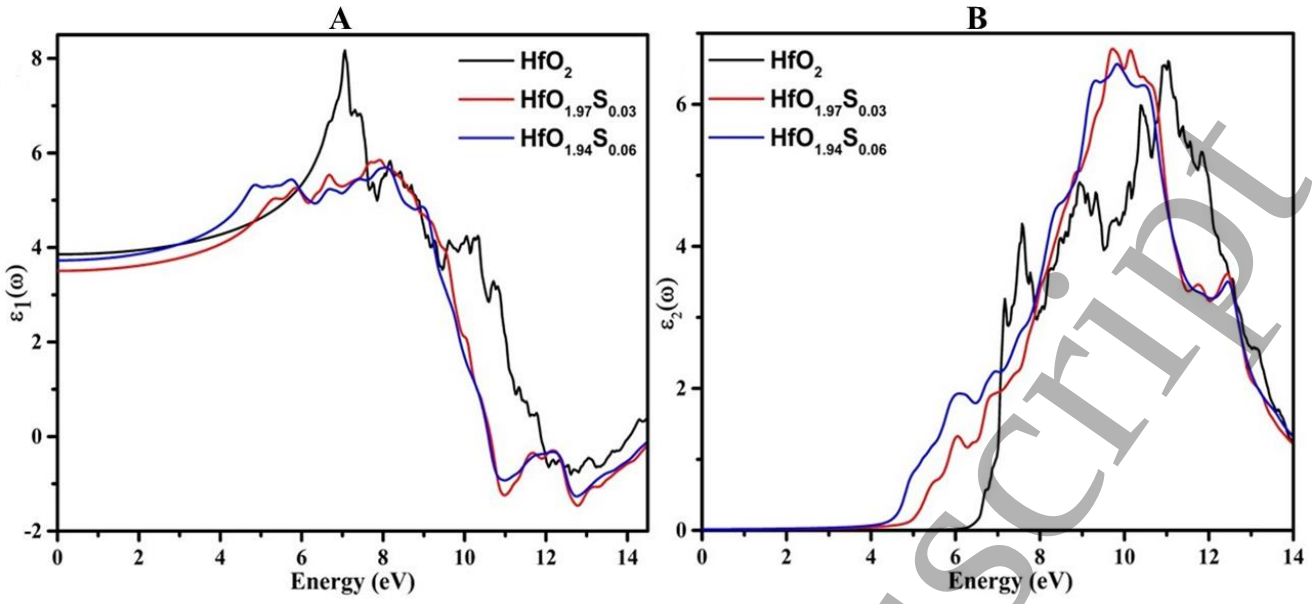

Figure 10. (A) Real part and **(B)** imaginary part of dielectric constant $HfO_{2-x}S_x$ (x = 0, 0.03, and 0.06)

The refractive index $n(\omega)$ and extinction coefficient $k(\omega)$ are related with the real and imaginary components as expressed below:

$$n(\omega) = \sqrt{\frac{|\varepsilon(\omega)| + \varepsilon_1(\omega)}{2}} \quad (5)$$

$$k(\omega) = \sqrt{\frac{|\varepsilon(\omega)| - \varepsilon_1(\omega)}{2}} \quad (6)$$

Figure 11 (a) shows that the value of $n(0)$ is 1.96 for pristine *c*-HfO_2 showing fair agreement with previous reported results [36, 71], and 1.87, 1.93 for x = 0.03 and 0.06 doping concentration. These values for S-doped structure are less as compared to Ti-doped HfO_2 [34]. Doping of x = 0.03 has the least value of $n(\omega)$, which will lead to enhancing the speed of incident EM radiations when it passes through the material. As $\varepsilon_1(\omega)$ decreases after 8 eV, the decrement is observed in the value of $n(\omega)$ is due to the optical dispersion behaviour of the material [73]. The Refractive index below unity shows the nature of medium changes from linear to non-linear.

The value of extinction coefficient $k(\omega)$ is shown in Figure 11 (b), which follows the same trend as the $\varepsilon_2(\omega)$. The highest observed value of $k(\omega)$ is 11.80 eV for pristine *c*-HfO_2, which show fair agreement with previously reported results [36, 71], and for x = 0.03 and 0.06, its value lies between 10.09 eV to 10.83 eV. In the high energy region, $k(\omega)$ shows large fluctuations this is may be due to different rates of excitation of the electron.

Accepted Manuscript

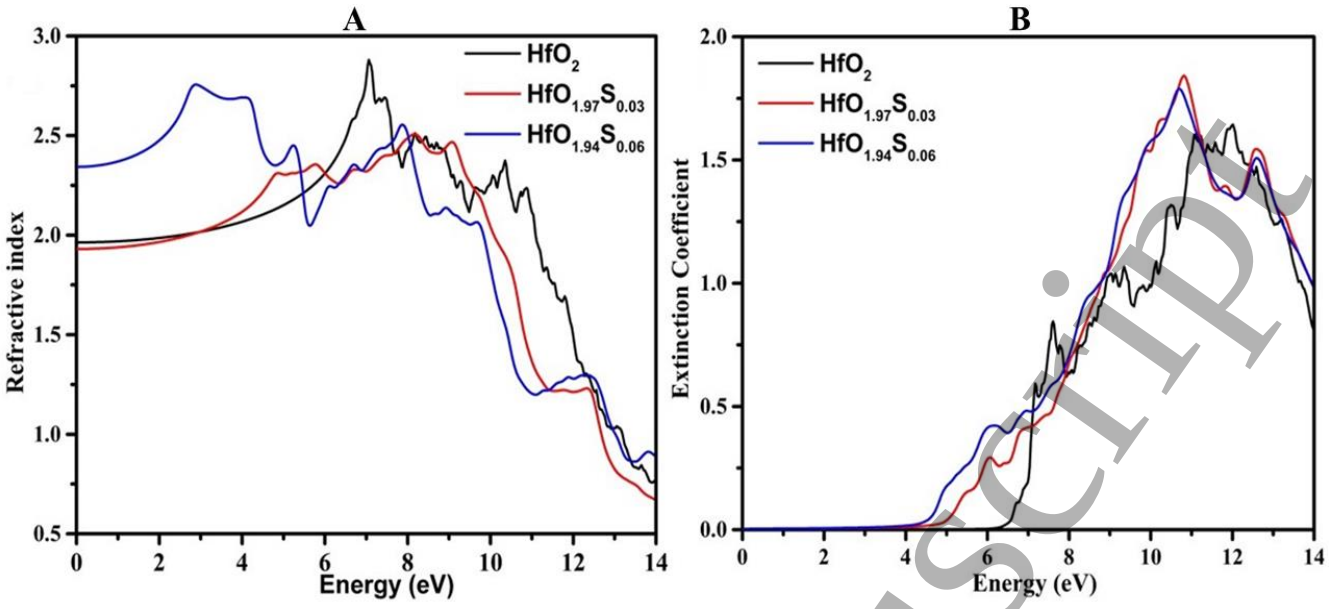

Figure 11. (A) Refractive index and **(B)** Extinction Coefficient of dielectric constant $HfO_{2-x}S_x$ (x = 0, 0.03, and 0.06)

The Reflectivity (Figure 12) defines the material's ability to reflect the incident photons from its surface and is given by:

$$R(\omega) = \frac{(n-1)^2+k^2}{(n+1)^2+k^2} \quad (7)$$

The calculated value of $R(0)$ is 0.105 for pristine *c*-HfO_2 showing fair agreement with previous reported results [36, 71], and 0.092, 0.10 for x = 0.03 and 0.06 doping concentrations, respectively. It is observed that there is a lower value of reflectivity in the visible and near IR region; hence this can be used as a suitable material for antireflective coating.

Accepted Manuscript

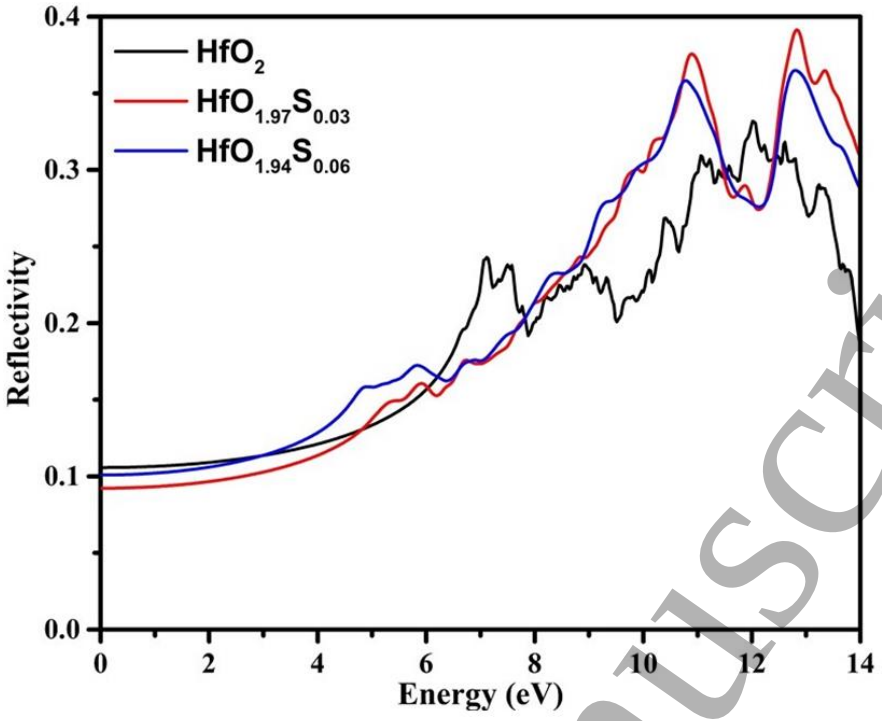

Figure 12. Reflectivity of $HfO_{2-x}S_x$ (x = 0, 0.03, and 0.06)

The absorption coefficient $\alpha(\omega)$ depends on $k(\omega)$, which is presented in Figure 13 (a); this shows the capacity of a material to absorb the incident light, which can be expressed by the relation:

$$\alpha(\omega) = \frac{2\omega k}{c} \quad (8)$$

The observed value of $\alpha(\omega)$ is 6.09, 4.88, 4.36 for x = 0, 0.03, and 0.06, respectively. The $\alpha(\omega)$ value fluctuations are owing to a different rate of excitations of the electron. The high absorption in the UV range and low absorption in the infrared and visible range makes $HfO_{2-x}S_x$ an efficient material to make UV based optical devices.

The optical conductivity is dependent on the imaginary component and can be expressed as:

$$\sigma(\omega) = \frac{\omega}{4\pi} Im\, \varepsilon\,(\omega) \quad (9)$$

The response of optical conductivity of the $HfO_{2-x}S_x$ is the same as the response of absorption and extinction coefficient, as depicted in Figure 13 (b). The highest peaks of optical conductivity are observed in the range of 9 eV to 11eV. The highest observed value is in the range where the value of $\varepsilon_1(\omega)$ is negative, which indicates that optical conductivity is high in the metallic region.

Accepted Manuscript

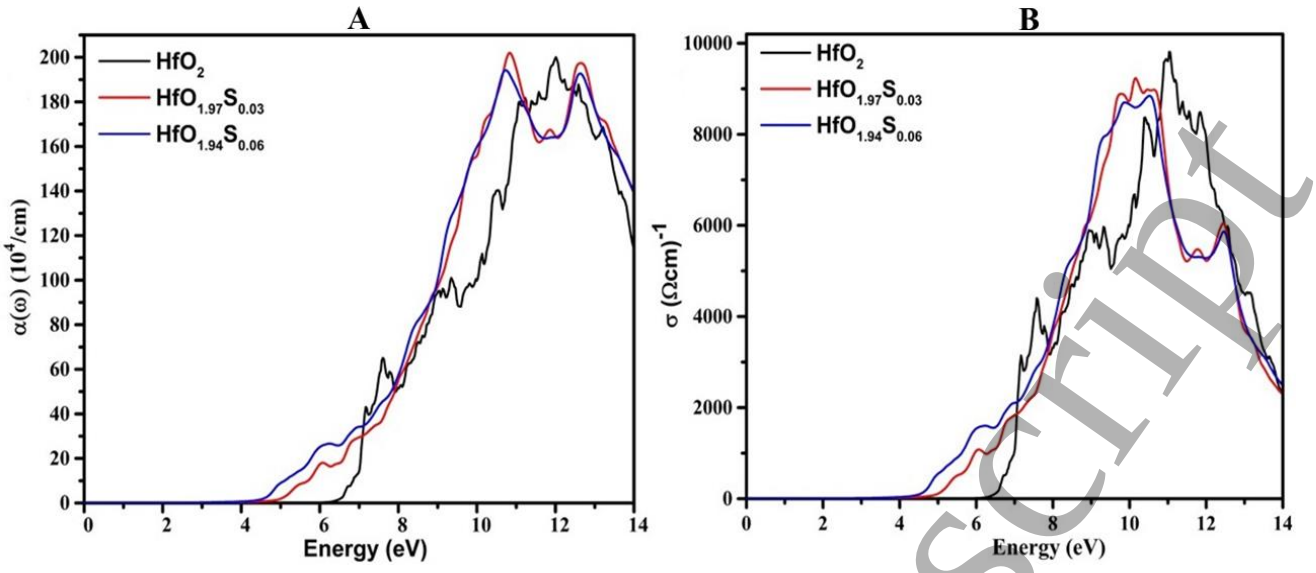

Figure13. (A) Absorption Coefficient and **(B)** Optical conductivity of $HfO_{2-x}S_x$ (x = 0, 0.03, and 0.06)

4. Conclusion

We have systematically presented the structural, electronic, thermoelectric, and optical properties of $HfO_{2-x}S_x$ (at x = 0, 0.03, 0.06) based on a first-principles methods. The thermodynamical stability of the studied concentrations has been ascertained using convex hull formalism and phase stability diagram. A comparative studied of band gap using different exchange-correlation functionals has been performed and found that the TB-mBJ functional gives true value of band gap for pristine cubic-HfO_2 which agrees well with experiments. The S-doping has led to lowering in the value of band gap and created new states in the conduction band. The maximum value of Seebeck coefficient has found to be 248.79 μV/K at room temperature for x = 0.03 and 294.89 μV/K at 400 K for x = 0.06. The creation of new states originated by S-doping decreased electronic thermal conductivity and increased the Seebeck coefficient, which has been further confirmed by an increase in effective mass with doping. This further helps to increase the figure of merit (ZT_e) ~ 0.82 for x = 0.06 and ~ 0.77 for x= 0.03 at 800 K. The optical properties have been evaluated to anticipate the use of $HfO_{2-x}S_x$ in optoelectronic applications. The decrease in reflectivity near the infrared and visible range of electromagnetic spectra makes the $HfO_{2-x}S_x$ suitable for the anti-reflective coating layer in night vision devices. The high value of absorption coefficient in the UV range makes it an appropriate material for UV-based opto-electronic devices. Our findings have shown that TE efficiency can be enhanced by tunning the key parameters such as σ/τ, k_e/τ,

Accepted Manuscript

S_α. Similarly, the suggested doping mechanism can be used to enhance the required and relevant optical properties.

Conflict of Interest

The authors declare that they have no conflict of interest.

References

[1] Lukai G, Qing L 2017 *Renew. Sustain. Energy Rev*. **72** 761–773

[2] Xie L, Song W, Ge J, Tang B, Zhang X, Wu T, Ge Z 2021 *Nano Energy* **82** 105770

[3] Zhang X, Zhao L D 2015 *J. Mater*. **1** 92–105

[4] Jiang Y, Zhang Y, Xing J, Hu Y, Yang X, Zhang J, Guo K, Luo J 2021 *J. Solid State Chem.* **299** 122169

[5] Jaishi D R, Ghimire M P 2021 *J. Mater. Today Commun*. **29** 102896

[6] Snyder G J, Toberer E S 2008 *Nat. Mat.* **7** 105-114

[7] Moshwa R, Liu W D, Shi X L, Wang Y P, Zou J, Chen Z G 2019 *Nano Energy* **65** 104056

[8] Qin B, Hu X, Zhang Y, Wu H, Pennycook S J, Zhao L D 2019 *Adv. Electron Mater*. **5** 1900609

[9] Deng L, Ni J, Qin J M, Ma H A, Jia X P 2018 *J. Solid State Chem*. **258** 397-400

[10] Wang Y, Zhang X 2021 *Superlattice Microst.* **160** 107057

[11] Dresselhaus M S, Chen G, Tang M Y, Yang R G, Lee H, Wang D Z, Ren Z F, Fleurial J P, Gongna P 2007 *Adv. Mater*. **19** 1043-1053

[12] He R, Kim H S, Lan Y, Wang D, Chen S, Ren Z 2014 *RSC Adv*. **4** 64711

[13] Chen S, Ren Z F 2013 *Mater. Today* **16** 387

[14] Jie Q, Wang H, Liu W, Wang H, Chen G, Ren Z 2013 *Phys. Chem. Chem. Phys*. **15** 6809-6816

[15] Liu C, Miao L, Zhou J, Huang R, Fisher A J, Tanemura S 2013 *J. Phys. Chem. C* **117** 11487-11497

[16] Kikuchi A, Okinaka N, Akiyama T 2010 *Scr. Mater*. **63** 407-410

[17] Feng Y, Jiang X, Ghafari E, Kucukgok B, Zhang C, Ferguson I, La N 2018 *Adv. Compos. Hybrid Mater*. **1** 114-126

[18] M. Ohtaki M, K. Araki K, K. Yamamoto K 2009 *J. Electron. Mater*. **38** 1234-1238

Accepted Manuscript

[19] Tsubota T, Kobayashi S, Murakami N, Ohno T 2014 *J. Electron. Mater*. **43** 3567 -3573

[20] Dehury T, Kumar S, Rath C 2021 *Mater. Lett.* **302** 130413

[21] Zhu H, Ramanath G, Ramprasad R 2013 *J. Appl. Phys*. **114** 114310

[22] Nie X, Ma D, Ma F, Xu K 2017 *J. Mater. Sci*. **52** 11524–11536

[23] Kumar R, Vij A, Singh M 2021 *Optik* **248** 168121

[24] Rauwel P, Rauwel E, Persson C, Sunding M F, Galeckas A 2012 *J. Appl. Phys*. **112** 102107

[25] Kumar N, George B P A, Abrahamse H, Parashar V, Ray S S, Ngila J C 2017 *Sci. Rep*. **7** 9351

[26] Liang H, Xu J, Zhou D, Wang X, Liu X, Chu S, Liu X 2017 *Mater. Des*. **120** 376-381

[27] Irshad K A, Srihari V, Kumar D S, Ananthasivan K, Jena H 2020 *J. Am. Ceram. Soc.* **103** 5374-5381

[28] Liu H 2015 *RSC Adv*. **5** 62891–62898

[29] Lu C H, Raitano J M, Khalid S, Zhang L, Chan S W 2008 *J. Appl. Phys.* **103** 124303

[30] Gritsenko V A, Perevalov T V, Islamov D R 2016 *Phys. Rep*. **613** 1–20

[31] Al-Kuhaili M F, Durrani S M A, Khawaja E E 2004 *J. Phys. D: Appl. Phys.* **37** 1254–1261

[32] Lauria A, Villa I, Fasoli M, Niederberger M, Vedda A 2013 *ACS Nano* **7** 7041–7052

[33] Panzer M A, Shandalov M, Rowlette J A, Oshima Y, Chen Y W, McIntyre P C, Goodson K E 2009 *IEEE Electron Device Lett*. **30** 1269-1271

[34] Kumar R, Vij A, Singh M 2022 *J. Solid State Chem.* **307** 122829

[35] Sharma R, Dar S A, Srivastava V 2021 Phys. Lett. A **411** 127559

[36] Khera E A, Ullah H, Imran M, Niaz N A, Hussain F, Khalil R M A, Rasheed U, Sattar M A, Iqbal F, Mahta C, Rana A M, Kim S 2020 *Optik* **212** 164677

[37] Cao Z, Fan T, Hou X, Niu J, Kumar R, Dar S A 2019 *Int. J. Energy Res.* **44** 1-14

[38] Zhu Y, Liu X, Jin S, Chen H, Lee W, Liu M, Chen Y 2019 *J. Mater. Chem. A* **7** 5875-5897

[39] Liu Y, Wang W, Xu X, Veder J P M, Shao Z 2019 *J. Mater. Chem. A* **7** 7280

[40] Jin H S, Seok T J, Chob D Y, Park T J 2019 *Appl. Surf. Sci.* **491** 83-87

[41] Zhang Z, Wang F, Hu K, She Y, Song S, Song Z, Zhang K 2021 *Materials* **14** 3330

[42] Kang H K, Kang Y S, Baik M, Jeong K S, Kim D K, Song J D, Cho M H 2018 *J. Phys. Chem. C* **122** 7226–7235

Accepted Manuscript

[43] Zhang YF, Ren H, Hou ZT 2015 *J. Magn. Magn. Mater*. **375** 61-64

[44] Malyi O I, Chen Z, Shu G G, Wu P 2011 *J. Mater. Chem.* **21** 12363-12368

[45] Idrissi S, Ziti S, Labrim H, Bahmad L 2021 *Mater. Sci. Eng. B* **270** 115200

[46] Andersson J R, Kleinke H, Franzen H F 1997 *J. Alloys Compd.* **259** L14 - L18

[47] Umebayashi T, Yamaki T, Itoh H, Asai K 2002 *Appl. Phys. Lett.* **81** 454

[48] Tian G, Pan K, Fu H, Jing L, Zhou W 2009 *J. Hazard Mater*. **166** 939–944

[49] Blaha P, Schwarz K, Madsen G K H, Vasnicka D K, Luitz J 2001 *wien2k An Augment Plane Wave+ Local Orbitals program for calculating crystal properties, User's Guide* ISBN 3-9501031-1-2

[50] Perdew P, Burke S, Ernzerhof M 1996 *Phys. Rev. Lett.* **77** 3865

[51] Heyd J, Scuseria G E 2003 *J. Chem. Phys*. **118**, 8207

[52] Tran F, Blaha P 2009 *Phys. Rev. Lett.* **102** 22640(1-4)

[53] Janesko B G, Henderson T M, Scuseria G E 2009 *Phys. Chem. Chem. Phys.* **11** 443–454

[54] Kresse G, Furthmüller J 1996 *Phys Rev B* **54** 11169–11186

[55] Madsen G K, Singh D J 2006 *Comput. Phys. Commu.* **175** 67-71

[56] Ambrosch-Draxl C, Sofo J O 2006 *Comput. Phys. Commu.* **175** 1-14

[57] Faiza-Rubab S, Naseem S, Alay-e-Abbas S M, Zulfiqar M, Zhao Y, Nazir S 2021 *Phys. Chem. Chem. Phys.* **23** 19472-1948

[58] Sun W, Dacek S T, Ong S P, Hautier G, Jain A, Richards W D, Gamst A C, Persson K A, Ceder G 2016 *Sci. Adv*. **2** e1600225

[59] Kirklin S, Saal J E, Meredig B, Thompson A, Doak J W, Aykol M, Rühl S, Wolverton C 2015 *npj Computational Materials*, 1, 15010

[60] Bartel C J 2022 *J. Mater. Sci*. https://doi.org/10.1007/s10853-022-06915-4

[61] Alay-e-Abbas S M, Nazir S, Noor N A, Amin N, Shaukat A, 2014 *Phys. Chem. C* **118** 19625–19634

[62] Ö. ÇĐFTCĐ Y, ERGÜN A H, ÇOLAKOĞLU K, DELĐGÖZ E 2014 GU J. Sci. **27** 627-636

[63] Goyal M, Kaur T, Sinha M M 2020 AIP Conference Proceedings **2220**, 130075

[64] Sharma R, Dar S A, Mishra A K 2019 *J. Alloys Compd.* **791** 983-993

Accepted Manuscript

[65] Lim S G, Kriventsov S, Jackson T N 2002 J. Appl. Phys. **91**, 4500

[66] Dutta M, Ghosh T, Biswas K 2020 *APL Mater.* **8** 040910

[67] Pei Y, Wang H, Snyder G J 2012 *Adv. Mater.* **24** 6125-6135

[68] Jood P, Ohta M 2016 *RSC Adv.* **6** 105653-105660

[69] Ma R, Liu G, Li Y, Li J, Chen K, Han Y, Zhou M, Li L 2018 *J. Asian Ceram. Soc.* **6** 13-19

[70] Han M K, Jan Y S, Yu B K, W. Choi W, You T S, Kim S J 2016 *J. Mater. Chem. A* **4** 13859-13865

[71] Mazumder J T, Mayengbam R, Tripathy S K 2020 *Mater. Chem. Phys.* **254** 123474

[72] Singh A, Chatterjee R, Mishra S K, Krishna P S R, Chaplot S L 2012 *J. Appl. Phys.* **111** 014113

[73] Sharma P, Katyal S C 2007 *J. Phys. D: Appl. Phys.* **40** 2115-2120

Accepted Manuscript

Proceedings of the Sixth International Conference on Intelligent Computing and Control Systems (ICICCS 2022)
IEEE Xplore Part Number: CFP22K74-ART; ISBN: 978-1-6654-1035-9

A Literature survey based on DBSCAN algorithms

Harsh Vardhan Singh
Student
Dept. of Software Engineering,
Delhi Technological University,
Shahbad Daulatpur Village,
Rohini, Delhi, 110042.
harshvardhansingh_2k18se065@dtu.ac.in

Ashwin Girdhar
Student
Dept. of Software Engineering,
Delhi Technological University,
Shahbad Daulatpur Village,
Rohini, Delhi, 110042.
ashwingirdhar_2k18se043@dtu.ac.in

Sonika Dahiya
Assistant Professor
Dept. of Software Engineering,
Delhi Technological University,
Shahbad Daulatpur Village,
Rohini, Delhi, 110042.
sonika.dahiya@dtu.ac.in

2022 6th International Conference on Intelligent Computing and Control Systems (ICICCS) | 978-1-6654-1035-9/22/$31.00 ©2022 IEEE | DOI: 10.1109/ICICCS53718.2022.9788440

***Abstract*—Data clustering is set of techniques for analyzing data. Data mining comes in handy when tried to find patterns and attributes from a large amount of data. There have been various clustering algorithms that are used for this purpose. Clustering is an unsupervised learning technique that groups similar points together. The points in a single cluster are similar to one another and dissimilar to the points in other clusters. There are various of clustering such as partitioning clustering, density-based clustering, hierarchical clustering, etc. In this paper, researchers have tried to cover one of the density-based clustering algorithms which is Density Based Spatial Clustering of Application with Noise (DBSCAN) algorithm. The main concept of density-based clustering is to form the clusters on basis of dense and non-dense regions. DBSCAN is density-based clustering that is used for spatial clustering on noise and outlier points. It performs well on outliers and noise making it a very efficient algorithm. But it has also many disadvantages: - 1) Performs poorly when there is varied density in a dataset 2) Large data as its complexity is higher 3) Its output is dependent on user parameters which is an undesirable trait for any algorithm. RNN-DBCAN, Grid DBSCAN, MR DBSCAN, TSF DBSCAN, KNN DBSCAN, µDBSCAN algorithms are all attempts to improve the basic DBSCAN algorithm in order to address these shortcomings. In this paper, researchers look at the various DBSCAN algorithms that have been suggested so far. These modifications are analyzed rigorously, and their drawbacks are stated.**

Keywords—DBSCAN, clustering, partitioning, density, data

I. INTRODUCTION

A. Overview

Data mining is the process of finding hidden and interesting patterns or traits from very big databases and applying them to decision-making and future behaviour prediction. As a result, more efficient and effective analytic methods are required to make use of this data. Clustering is one of the jobs, which involves dividing a set of objects into several clusters with the intra-cluster similarity maximized and the inter-cluster similarity minimized. Generally, these algorithms have high complexity so are not suitable for large dataset. So, there is huge demand to improvise on previous clustering algorithm. There are various types of clustering algorithm such as: - Partitioning, hierarchal, grid-based, density-based, model-based, and constraint-based methods are some of the strategies available. PAM, CLARA, and CLARANS are examples of partitioning techniques. These algorithms divide data into k groups, with the user supplying the value of k. CURE and CHEMELEON are two well-known hierarchical category algorithms [1]. Density-based clustering algorithms such as DBSCAN, DENCLUE, and OPTICS are widely employed. COBWEB and SOM are two examples of model-based clustering methods. The best match between the available data and a mathematical model is optimized using these procedures. Constraint-based clustering approaches look for clusters that meet a user's desire or constraint. The algorithms suggested in each of these areas attempt to solve clustering problems involving vast amounts of data in massive databases. None of them, however, are really effective. If a clustering technique meets the following criteria, it is deemed good: (a) Minimal domain expertise is required to establish the values of its input parameters, which is a critical issue, particularly for huge data sets. (b) Clusters of any shape can be discovered. (c) High efficiency while working with huge data sets. The density-based clustering techniques are effective for discovering clusters in datasets of any shape and size. Typically, these techniques cluster as dense clusters of points in the data space divided by low-density regions. The first density-based clustering technique is DBSCAN. A density-based connectivity study is used to grow clusters. In this work, have looked at the many DBSCAN upgrades that have been proposed so far. These are suggested as DBSCAN modifications and enhancements for successful clustering analysis of the underlying datasets. These modified DBSCAN techniques include Reverse Nearest Neighbour-DBSCAN (RNN-DBCAN), Grid DBSCAN, MapReduce-based DBSCAN (MR DBSCAN), Temporal Streaming Fuzzy DBSCAN (TSF DBSCAN), k-nearest Neighbour DBSCAN (KNN DBSCAN), µDBSCAN.

B. Motivation

The template The DBSCAN is a very good algorithm as discussed below but it has various disadvantages as well: -

1. It has been observed that it performs poorly on varied density databases because of reasons which are discussed later in this paper. If the density distributions are the same this algorithm works very well but when it comes to different densities of clusters in most cases it creates wrong clusters
2. It incurs some computational overhead which sometimes doesn't go well with large data sets
3. It is highly depended on user as it takes 2 input values from them that are eps and minPts. Generally, user don't have in-depth knowledge of data which results in wrong clusters,

There are numerous numbers of researches available on the DBSCAN algorithm which solves this problem and are

Authorized licensed use limited to: DELHI TECHNICAL UNIV. Downloaded on June 15,2022 at 11:29:17 UTC from IEEE Xplore. Restrictions apply.

specific to some applications in various fields. By doing review work on various DBSCAN algorithms one can a give fresh perspective about which algorithm can be used best in which scenario.

II. DBSCAN ALGORITHM

Density-Based Spatial Clustering of Applications with Noise also known as DBSCAN is a density-based clustering algorithm used to cluster data of any shapes in presence of outliers and noises from a large amount of data. As shown in Fig. 1 the major advantage of the DBSCAN algorithm over partitioning and hierarchical clustering algorithm is: -

1. DBSCAN algorithm can be used for any arbitrary shapes rather than only spherical or convex-based shapes. This makes it much more valuable than k-means and other clustering algorithms.
2. The major advantage of this algorithm as its name suggests is it is also effective in the presence of noise and outliers. The other algorithms perform poorly in noise which makes DBSCAN an effective algorithm.(Noise and outlier are points which are different/extra than the actual point) By taking Minpts in the clusters it ensures noise and outlier is not included)

These are the major pros over other clustering algorithms but it has more specific benefits over k-means algorithm such that one don't need to specify the value of k that is the number of clusters, so the number of the clusters can be arbitrary depending upon the data which makes the clusters more prominent and accurate.

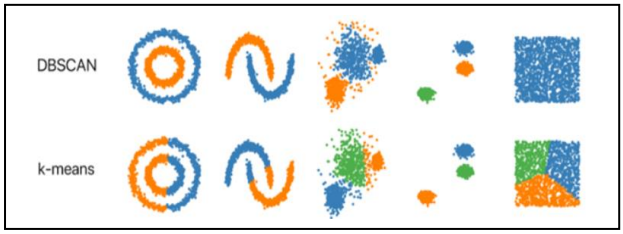

Fig. 1. DBSCAN vs k-means [16]

A. About DBSCAN

DBSCAN is designed to discover the clusters and the noise in a spatial database. Researchers need to know the parameters Eps and MinPts of each of the cluster along with minimum one point from the cluster. After that, it could find all those points which are density-reachable from the given known point using the correct parameters [2]. The DBSCAN forms the cluster using 2 main parameters eps and minPts: -

- eps(ε): - This is the radius around the point which is checked for other points in its proximity. It is used to determine the density of region. If large eps value is chosen, there will be low density clusters.
- minPts: - This is the number of points present in the surrounding (eps distance from the point) to form a cluster. For a good algorithm the minPts should not be very low.

After completion of DSCAN algorithm on any dataset researcher mainly get 3 types of points (Fig. 2): -

1. Core — If different clusters are made this is the point from which there are at least k number of points in r distance of radius.
2. Border — This can be any point that has one or more core points within r distance of radius.
3. Noise – Any point which is neither a core and a border and has at least k number of points in r distance of radius.

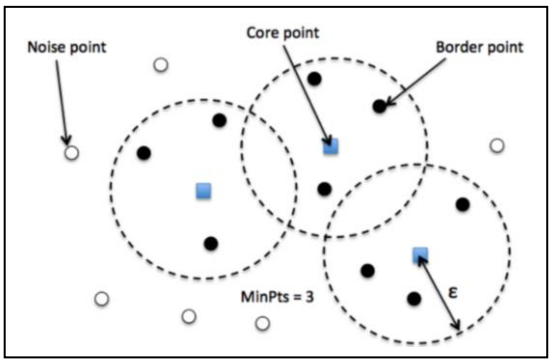

Fig. 2. About DBSCAN [16]

Fig. 3 represents the steps of DBSCAN algorithm. Fig. 4 represents DBSCAN results on a generated 750 spherical training data points with corresponding labels [16]: -

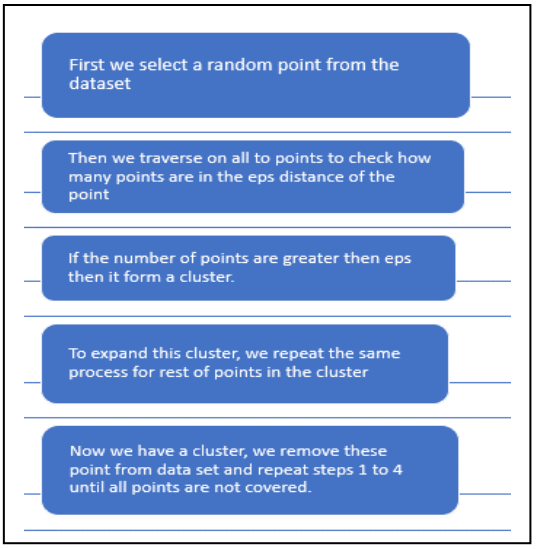

Fig. 3. Steps to perform DBSCAN

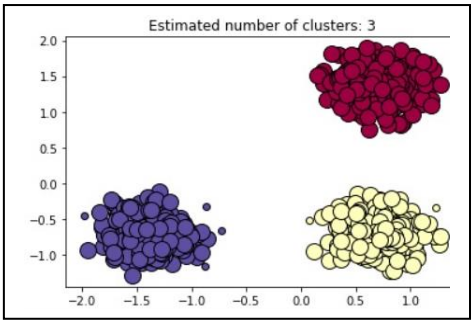

Fig. 4. DBSCAN result on a generated dataset [16]

Authorized licensed use limited to: DELHI TECHNICAL UNIV. Downloaded on June 15,2022 at 11:29:17 UTC from IEEE Xplore. Restrictions apply.

III. LITERATURE REVIEW

A. *KNN-DBSCAN*

About: -

1. As discussed, advantages of the DBSCAN algorithm over KNN(k-nearest neighbour) algorithm but it takes to input parameter eps and MinPts which makes it user-dependent(and perform poorly when user don't have domain knowledge).
2. To overcome these problems KNN-DBSCAN was invented, which only requires a single user input parameter "K" where the algorithm is not affected by the value of K [3]. So the main aim of this algorithm is to achieve a parameter-free clustering technique [3].
3. The simple algorithm is to find the cluster kernels through KNN and use DBSCAN to expand these clusters.

Algorithm: -

KNN part

1. Create a 2d matrix of distance between each point.
2. Keep the first k edges (on the basis of distance) for each point and remove the rest.
3. Now check for strongly connected components and remove the remaining edges.
4. Take the strongest connected components(the node which has the highest edges) as the cluster kernel.

DBSCAN part

5. Used MinPts as 3 (for 2-D data) and $Eps = \max_{p \in C} ||p,p_3||_2$ which is the maximum distance of first three nearest neighbours.
6. Expanded the cluster similar to the DBSCAN algorithm.
7. After getting the cluster, removed all these points from the dataset.
8. Repeat steps from 1 to 7 till all points are covered.

Complexity: -

After finding the distance between each point to another point it takes O(n^2) where n is the number of points in the dataset. So, The complexity of the algorithm is O(n^2) [3].

Disadvantages: -

The algorithm solves the problem of user-defined parameters but the complexity of the algorithm is large. So can't be applied to large datasets.

Applications: -It has been used in image segmentation process by using this algorithm. It improved the performance of the image with better segmentations. The amount of noise is also highly reduced [4].

Result: -

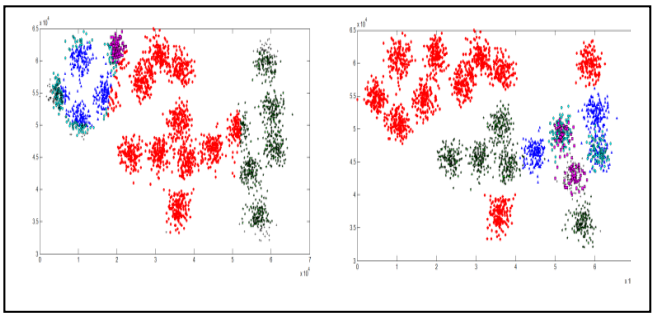

Fig. 5. Comparision of DSets-DBSCAN and KNN-DBSCAN [3]

Fig. 5 shows the comparison of DSets-DBSCAN and KNN-DBSCAN over A1 Dataset.

B. *RNN-DBSCAN*

RNN-DBSCAN is reverse nearest neighbor DBSCAN algorithm. There are many advantages of this algorithm. Instead of 2 input parameters, it uses only a single parameter which makes it less user-dependent (Fig. 6 represents an example for this). Other than this DBSCAN had a problem of performing poorly on varied density datasets but RNN-DBSCAN performs extremely on heterogenous density [5].

Algorithm: -

1. Traverse through the data points.
2. If any point is a core point is not yet part of any clusters then it is added to new cluster.
3. Then the cluster is expanded by BFS to unclustered points.

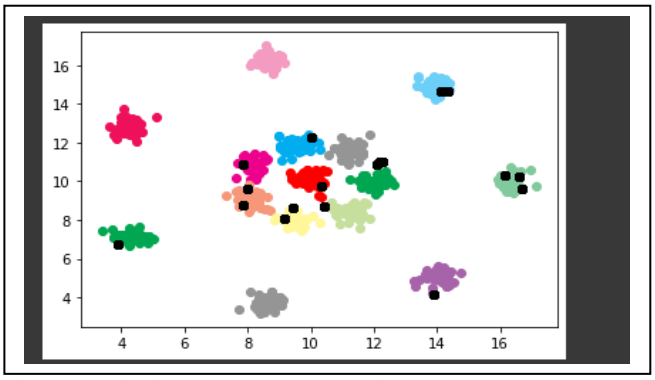

Fig. 6. Result of RNN-DBSCAN on R15 dataset

Complexity: -

In the traditional DBSCAN approach, the radius of the circle is fixed for finding the neighborhood but in RNN-DBSCAN it changes according to the value of k nearest neighbor. So, the complexity of the naive solution is O(n^2).

Application: -

1. Efficient Accessibility in Cloud Database of Health Networks [6].
2. Human Mobility predictions are some of the works where RNN-DBSCAN has been used [7].

Authorized licensed use limited to: DELHI TECHNICAL UNIV. Downloaded on June 15,2022 at 11:29:17 UTC from IEEE Xplore. Restrictions apply.

C. *µDBSCAN*

About: -

DBSCAN has been one the most popular algorithm used in various domains. It works in 2 steps, 1st step is neighbourhood query execution which takes o(n^2) time in worst case and 2nd step is cluster formation in which algorithm go through all the points in line, so it can't execute this step parallelly[8]. In today's era the size of the data is increasing exponentially. so expensive cost for neighbourhood query and non-parallel access of data makes it unsuitable [8].

To solve this problem , µDBSCAN can be used. It creates micro-clusters by breaking the sequential data into small clusters[8]. It totally solves the neighbourhood query problem and also it makes it scalable for high dimensity data. It also provides exactly same DBSCAN clusters so it solves the problem without getting affected for the results.

Algorithm: -

1. It first scans through all the data points in dataset to form micro-clusters.
2. It builds hierarchical based structure also known as µR-Tree (Fig. 7).

   µR Tree-It is a level tree in which micro-clusters(MC) are stored. The leaf of the R-tree stores the root of micro-clusters and it is the root of AuxR-tree[8]. A union-find is used to merge the clusters if possible.
3. These micro-clusters are then processed to get the resulting clusters.

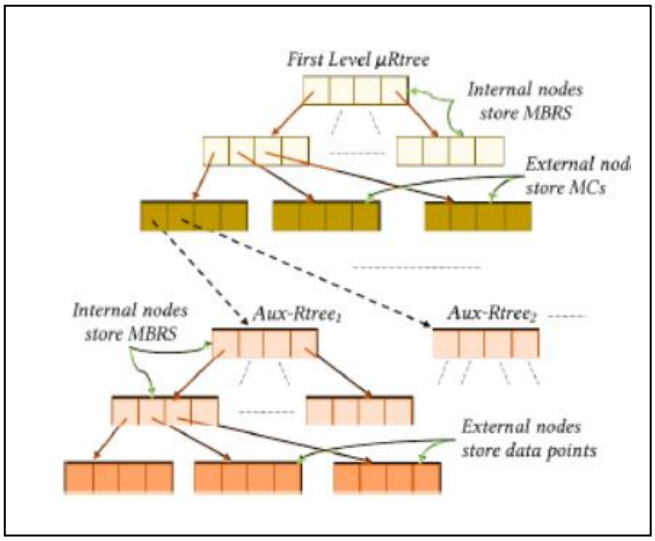

Fig. 7. µR-Tree structure [8]

Complexity: -

The time complexity for an average data is O(a log b+ a log c) where a is number of data points in dataset [8], b is number of micro clusters formed and c is average number of data points in a micro-cluster. There can be added complexity for merging these clusters.

Disadvantage: -

The algorithm has no such big disadvantages . It has a peak memory consumption little higher than other algorithm which generally does not affect much. In redemption its performance is excellent so memory addition is not much of problem [8].

Result: -

In conclusion it is excellent algorithm with results similar to DBSCAN but in terms of performance it has more efficient on large dataset and works in parallel which makes it one of the best algorithm.

D. *Grid-DBSCAN*

About: -

This variation of DBSCAN that is Grid-DBSCAN algorithm can be used to cluster the dataset of point objects based on both types of datasets that includes geographical and non-geographical ones. The idea of an object's neighborhood in the GDBSCAN method can be utilized if the clusters present in the neighborhood of current object's cluster are based on binary predicate [9]. In addition, rather than merely counting items in the vicinity of an object, one can utilize other measurements, such as non-geographical qualities such as the average salary of employees in an organization to determine its "cardinality" [9].

Algorithm: -

```
def GDBSCAN(SetOfObjects,Npred,MinCard,wCard):
    //SetOfObjects is UNCLASSIFIED
    ClusterId=nextId(NOISE)
    for i from 1 to SetOfObjects.size DO:
        Object=SetOfObjects.get(i)
        if Object.ClId=UNCLASSIFIED THEN:
            if ExpandClusters(SetOfObjects,Object,ClusterId,Npred,MinCard,wCard) THEN
                ClusterId=nextId(ClusterId)
            end if
        end if
    end for
end GDBSCAN
```

Fig. 8. GDBSCAN Algorithm [9]

1. Initially start with a random object say p and get all reachable points from this object according to NPred and MinWeight (Fig. 8).
2. If there isn't an object reachable from p then it is considered as NOISE in database.
3. Then proceed this until every object in dataset is marked visited.
4. Using the above algorithm, one can find weighted cardinality of each set that are marked differently.
5. Then use global density parameters which are NPred and MinCard along with wCard function which returns cardinality of object passed to it.
6. After some steps in this algorithm, the total number of set objects of the given dataset is known. So, each cluster is associated with different Id which is countable as it is in integer form.
7. And, next Id provides the Id of next cluster while running the algorithm on dataset. For a NOISE data it is marked as UNCLASSIFIED.
8. To get any element say x from set it is maintained in a structure and use a function to retrieve it.

Authorized licensed use limited to: DELHI TECHNICAL UNIV. Downloaded on June 15,2022 at 11:29:17 UTC from IEEE Xplore. Restrictions apply.

Complexity: -

In below Table I, complexities for various cases have been presented.

TABLE I. RUNTIME COMPLEXITY OF GDBSCAN [9]

Runtime Complexity of	*A single neighborhood*	*GDBSCAN algorithm*
Without index	O(n)	O(n^2)
With spatial index	O(log n)	O(n * log n)
With direct access	O(1)	O(n)

Advantages: -

The technique is unaffected by difficult-to-predict input characteristics like the number and shape of items in given dataset. The algorithm can easily beat DBSCAN in terms of time complexity by making use of the sensor's sample density (an increase of app. 40-70 percent). By incorporating Doppler and amplitude information, the method achieves an even better result than DBSCAN (unitless distance criteria) [9]. Also using this algorithm, one can handle spatial as well as non-spatial attributes. Also, the fuzziness present in given dataset can be dealt easily using this variation of DBSCAN algorithm [10].

Application: -

Using the GDBSCAN algorithm objects and spatially extended objects can be group points on the basis of both spatial and nonspatial properties. The usefulness and efficiency of this algorithm on large geographical datasets were demonstrated in an analytical and experimental performance evaluation.

E. MR-DBSCAN

About: -

MR-DBSCAN is a MapReduce-based scalable DBSCAN algorithm. All the important sub-procedures in this algorithm are fully parallelized. As a result, sequential processing does not pose a performance bottleneck [11]. It is a novel data partitioning approach based on computation cost estimation. Since its introduction in 2003, MapReduce has become the most popular parallel processing paradigm in shared-nothing environments in the field of large data research. MapReduce offers a streamlined programming model that hides the tangle of parallelism specifics. Most significantly, MapReduce gracefully handles a variety of errors. It accomplishes this by breaking down a work into smaller pieces and materializing the intermediate results. When a failure occurs, just the tasks that were affected must be re-run [12]. As a result, MapReduce can expand to tens of thousands of commodity devices, with regular errors. Data partitioning, local clustering, and global merging are the three steps of MR-DBSCAN. In the first stage, the entire dataset is divided into smaller divisions based on their spatial proximity. Each partition is clustered separately in the second stage. The component clustering findings are then combined in the final stage to produce global clusters [13].

Advantages: -

As this DBSCAN algorithm is a parallel programming paradigm and also due to its simplicity, MR-DBSCAN can be used for large number of datasets. In this researcher just need to write mapping and reducing functions.

Disadvantage: -

Not suitable for different indexing models, complicated spatial objects, high dimensional data and graph mining.

Complexity: -

Time complexity in this algorithm is O(N*m) where N represents total number of coordinates and m represents cost of getting neighborhood [11].

Result: -

It is an excellent algorithm for parallel programming paradigm but in terms of performance it has more efficient on large datasets and works in parallel which makes it one of the best algorithms.

F. TSF-DBSCAN

About: -

TSF-DBSCAN (Temporal Streaming Fuzzy) is a variation of DBSCAN which is an extension of SF-DBSCAN (Streaming Fuzzy). Algorithm in Fig. 9. In TSF-DBSCAN, fuzziness is widely used to detect uncertainty in distance threshold which is defined by the object's present neighborhood. Using this variation, the clusters present with overlapping fuzzy edges can be detected easily. This algorithm can easily adopt to changing data streams. Because of this advantage it can be used widely in live data where there are continuous variations in datasets. Minimum and maximum threshold distance along with MinWeight parameters can be easily changed according to the need and data to get desirable outcomes. These values can be determined in practical implementations using heuristic approaches during a warmup iteration on beginning portion of the data stream [14].

For the study of data streams, TSF-DBSCAN combines density-based clustering, fuzzy set theory and forgetting algorithms [15].

Algorithm: -

```
p #new object
pList #list of valied arrived objects
p.kernel, p.shell=fuzzyQuery(eps_min, eps_max, p, pList)
for k in p.kernel do:
  k.kernel=k.kernel ∪ {p}
for s in p.shell do:
  s.shell=s.shell ∪ {p}
add p to pList
if p.t % T_offline==0 then:
  offline-FDBSCAN(plist,p.t)
```

Fig. 9. TSF-DBSCAN Algorithm [15]

Advantage: -

It can take advantage of any aging algorithm and thus provides good performance on evolving or unbounded data.

Complexity: -

The overall time complexity for TSF-DBSCAN algorithm is O(n * (k+s)) [15].

Authorized licensed use limited to: DELHI TECHNICAL UNIV. Downloaded on June 15,2022 at 11:29:17 UTC from IEEE Xplore. Restrictions apply.

IV. CRITICAL REVIEW

As the amount of data is increasing exponentially, the necessity of data analytics is increasing to find patterns, enhance decision making etc. Clustering is a widely used concept to group the data in different clusters.

Density-Based algorithms have come in handy for data analytics which is based on forming clusters that are based on density distribution. DBSCAN is one of the most significant density-based clustering algorithms which works in presence of outliers and noise and can be used for any arbitrary shape clusters. Fig. 10 and Fig. 11 shows results of K-means and DBSCAN algorithm on R15 datasets respectively. Here is the benefit of DBSCAN over K-means.

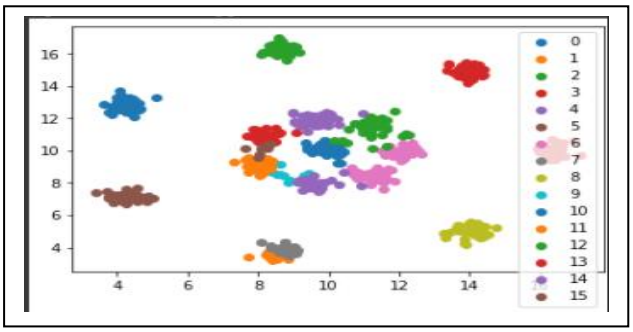

Fig. 10. K means clustering on R15 dataset

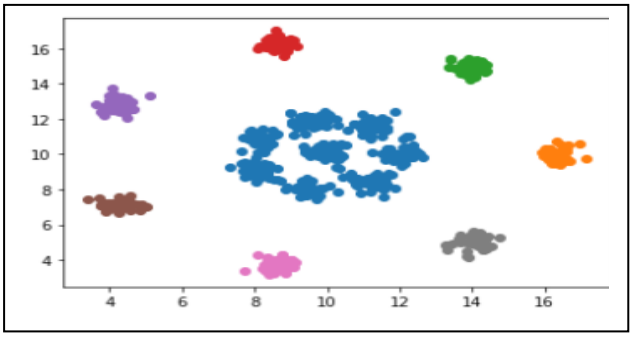

Fig. 11. DBSCAN clustering on R15 dataset

Clearly, DBSCAN has outperformed. DBSCAN is one of the best algorithm but it has its own disadvantage like it requires 2 user input parameters, for less dependency on eps and minPts or high performance on varied density datasets one should use KNN-DBSCAN or RNN-DBSCAN.

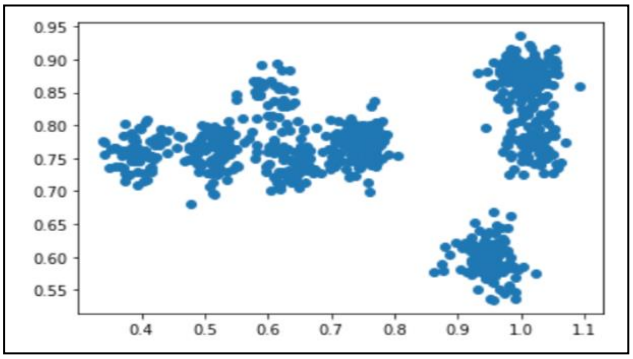

Fig. 12. DBSCAN Algorithm on A1 dataset

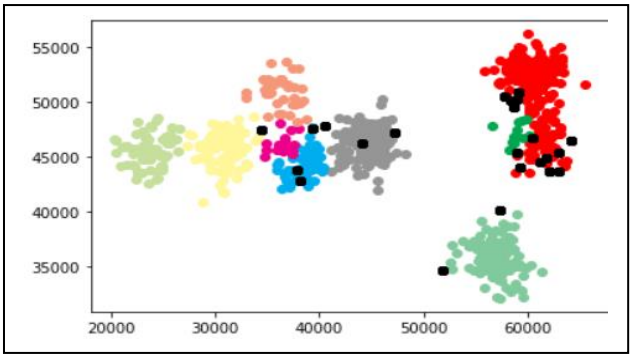

Fig. 13. RNN-DBSCAN Algorithm on A1 dataset

Clearly, we can see from Fig. 12 and Fig. 13 that RNN-DBSCAN performs better than DBSCAN algorithm.

µDBSCAN is one the best algorithm at it is completely parameters-free and have less time complexity.

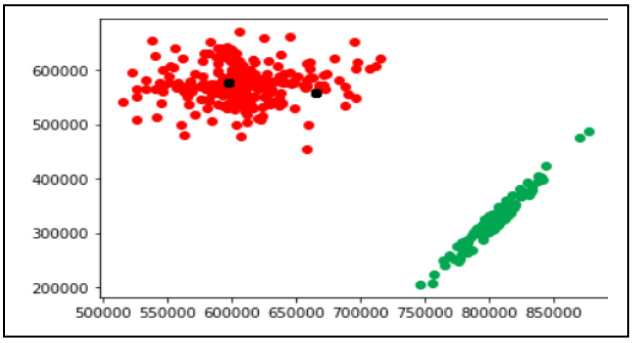

Fig. 14. DBSCAN Algorithm on S1 dataset

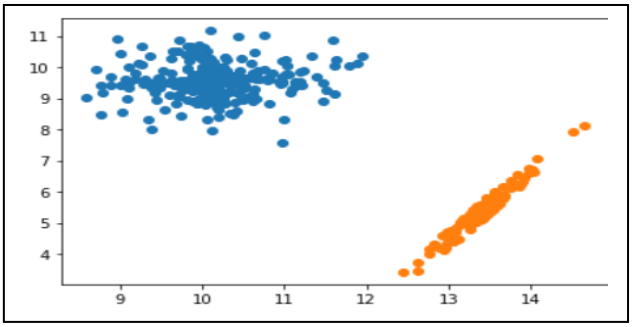

Fig. 15. µDBSCAN Algorithm on S1 dataset

Here it can be clearly seen from Fig. 14 and Fig. 15 that both DBSCAN and µDBSCAN have the same clusters but µDBSCAN is parameter-free and much faster.

For solving the problem of complexity and running it on a large dataset one should prefer using Grid-based clustering or TSF clustering.

V. RESULTS

Researchers have studied various variations of DBSCAN algorithms rigorously which overcome the problems faced by DBSCAN algorithm. But these algorithms have its own limitations. Depending on the problem these algorithms can be used accordingly. This work also portrays a critical evaluation in which comparison and contrast have been used to demonstrate the similarities and differences between the works of other authors. The following Table II shows the review of all the variations covered in this paper, which will give provide idea about which algorithm to use accordingly: -

Authorized licensed use limited to: DELHI TECHNICAL UNIV. Downloaded on June 15,2022 at 11:29:17 UTC from IEEE Xplore. Restrictions apply.

TABLE II. COMPARISION OF ALL VARIATIONS

S.NO	Algorithm	Complexity	Advantage	Disadvantage	About	eps and minPts
1)	KNN-DBSCAN	O(n^2)	It provides a parametric free algorithm (no user input value of eps and MinPts)	The complexity of the algorithm is still very high which is unsuitable for large dataset.	It uses KNN to find the core points and DBSCAN to expand the cluster around core point.	Determined on the basis of dataset (user free inputs, it takes k as input which does not affect much to the algorithm)
2)	RNN-DBSCAN	O(n^2)	It also provides parametric free algorithm. Other than this it performs well on heterogenous density data.	The complexity of the algorithm is still very high which is unsuitable for large dataset.	It uses RNN technique to add a core point into a cluster.	Determined on the basis of dataset (user free inputs, it takes k as input which does not affect much to the algorithm)
3)	μDBSCAN	O(n log n)	It is parametric free, significantly reduces the neighbourhood queries complexity and is good for high dimensional data.	It has no major disadvantage. It has small tweak that it has high peak memory consumption	It creates micro-clusters from the dataset and then uses it to create final clusters.	Determined on the basis of dataset.
4)	Grid	O(n)	The technique is unaffected by difficult-to-predict input characteristics like the number and shape of available items. The algorithm can easily beat DBSCAN in terms of time complexity by making use of the sensor's sample density (an increase of app. 40-70 percent)	Hierarchical clustering is not possible. only limited to one-level clustering. Also, heuristics to determine the parameters for GDBSCAN can't be calculated.	One can utilize any idea of an object's neighbourhood in the GDBSCAN method if the neighbourhood coordinates are based on a reflexive and symmetric binary predicate.	Determined using neighbourhood k-distance.
5)	MR	O(N*m)	As this DBSCAN algorithm is a parallel programming paradigm and also due to its simplicity, one can use MR-DBSCAN for large number of datasets. In this one just need to write mapping and reducing functions.	This is algorithm is not fir for height mentioned datasets and there are variety of indexes.	It is a new algorithm to distribute n partition. The data bits are based on execution time simulation.	Varying on the basis of geometric sequences and shifts in datasets.
6)	TSF	O(n*(k+s))	It can take advantage of any aging algorithm and thus provides good performance on evolving or unbounded data.	It does not have any major disadvantage.	In TSF-DBSCAN, fuzziness is widely used to detect uncertainty in distance threshold which is defined by the object's present neighbourhood. Using this variation, the clusters present with overlapping fuzzy edges can be detected easily.	Determined by fuzzy borders present in neighbourhood.

Authorized licensed use limited to: DELHI TECHNICAL UNIV. Downloaded on June 15,2022 at 11:29:17 UTC from IEEE Xplore. Restrictions apply.

REFERENCES

[1] Khan, Kamran, et al. "DBSCAN: Past, present and future." The fifth international conference on the applications of digital information and web technologies (ICADIWT 2014). IEEE, 2014.

[2] Ester, Martin, et al. "A density-based algorithm for discovering clusters in large spatial databases with noise." kdd. Vol. 96. No. 34. 1996.

[3] Sharma, Ankush, and Amit Sharma. "KNN-DBSCAN: Using k-nearest neighbor information for parameter-free density based clustering." 2017 International Conference on Intelligent Computing, Instrumentation and Control Technologies (ICICICT). IEEE, 2017.

[4] Kurumalla, Suresh, and P. Srinivasa Rao. "K-nearest neighbor based dbscan clustering algorithm for image segmentation." Journal of Theoretical and Applied Information Technology 92.2 (2016): 395.

[5] Bryant, Avory, and Krzysztof Cios. "RNN-DBSCAN: A density-based clustering algorithm using reverse nearest neighbor density estimates." IEEE Transactions on Knowledge and Data Engineering 30.6 (2017): 1109-1121.

[6] Haifeng, Zheng, Yan Yajie, and Zhang Ningbo. "Human Mobility Prediction Based on DBSCAN and RNN." 2021 IEEE 4th International Conference on Computer and Communication Engineering Technology (CCET). IEEE, 2021.

[7] Wadnare, Rupali J., Swati S. Sherekar, and Vilas M. Thakare. "Efficient Accessibility in Cloud Databases of Health Networks with Natural Neighbor Approach for RNN-DBSCAN." Cloud Computing Technologies for Smart Agriculture and Healthcare. Chapman and Hall/CRC, 2021. 217-232.

[8] Sarma, Aditya, et al. "μDBSCAN: an exact scalable DBSCAN algorithm for big data exploiting spatial locality." 2019 IEEE International Conference on Cluster Computing (CLUSTER). IEEE, 2019.

[9] Ali, Tariq, Sohail Asghar, and Naseer Ahmed Sajid. "Critical analysis of DBSCAN variations." 2010 international conference on information and emerging technologies. IEEE, 2010.

[10] Koteshwariah, Ch Bala, N. Raghu Kisore, and V. Ravi. "A fuzzy version of generalized DBSCAN clustering algorithm." Proceedings of the Second ACM IKDD Conference on Data Sciences. 2015.

[11] He, Yaobin, et al. "MR-DBSCAN: a scalable MapReduce-based DBSCAN algorithm for heavily skewed data." Frontiers of Computer Science 8.1 (2014): 83-99.

[12] Dai, Bi-Ru, and I-Chang Lin. "Efficient map/reduce-based dbscan algorithm with optimized data partition." 2012 IEEE Fifth international conference on cloud computing. IEEE, 2012.

[13] Leutenegger, Scott T., Mario A. Lopez, and Jeffrey Edgington. "STR: A simple and efficient algorithm for R-tree packing." Proceedings 13th international conference on data engineering. IEEE, 1997.

[14] Hahsler, Michael, and Matthew Bolaños. "Clustering data streams based on shared density between micro-clusters." IEEE Transactions on Knowledge and Data Engineering 28.6 (2016): 1449-1461.

[15] Bechini, Alessio, Francesco Marcelloni, and Alessandro Renda. "TSF-DBSCAN: a novel fuzzy density-based approach for clustering unbounded data streams." IEEE Transactions on Fuzzy Systems (2020).

[16] Chauhan, N., 2022. DBSCAN Clustering Algorithm in Machine Learning - KDnuggets. [online] KDnuggets. Available at: <https://www.kdnuggets.com/2020/04/dbscan-clustering-algorithm-machine-learning.html> [Accessed 23 May 2022].

Authorized licensed use limited to: DELHI TECHNICAL UNIV. Downloaded on June 15,2022 at 11:29:17 UTC from IEEE Xplore. Restrictions apply.

A Novel ES-RwCNN Based Finger Vein Recognition System with Effective L12 DTP Descriptor and AWM-WOA Selection

Ajai Kumar Gautam*, Rajiv Kapoor

***Abstract*—Fingerprints, faces, and also irises are Biometrics, which are extensively utilized in several recognition applications comprising door access control, automatic teller machines, personal authentication for computers, Internet banking, along with border-crossing controls with recent augments in security necessities. The unique patterns of finger veins (FV) are utilized by Finger vein recognition (FVR) for detecting individuals at a high-level accuracy. However, on account of the existence of artifacts, irregular shading, distortions, etc., precise FV detection is a difficult task. A framework for identifying FV is created by the work to offer a precise biometric authorization utilizing Enhanced Sigmoid Reweighted based Convolutional Neural Network (ES-RwCNN). The image is initially pre-processed by the framework via executing rotation, cropping, resizing, and normalization for avoiding unwilling distortions. Utilizing Trapezoid Membership Function-Based Contrast Limited Adaptive Histogram Equalization (TMF-CLAHE), the pre-processed image is followed with contrast enhancement (CE) that intensifies the image by evading irregular shading and vein posture deformation along with upgrades the accuracy rate. After that, utilizing the Local 12 direction texture pattern (L_{12}DTP) and Canny Edge method, knowledgeable textural and edge features (EF) are extracted. For attaining the most informative features, an Adaptive Weight Mutated Whale Optimization Algorithm (AWM-WOA) technique is formed by the work that enhances the model's accuracy and decreases the computational complexity (CC). Finally, for identifying the authorized person, the chosen features are presented to ES-RwCNN. The work attains a low information loss by achieving a 0.971 correlation betwixt the pre-processed image and the original image (OI), as shown by the experimental analysis. Classification accuracy (CA) of 97.05% is attained by the framework. It avoids misclassification by acquiring a 3.53% False Positive Rate (FPR) and 2.35% False Rejection Rate (FRR). It continues to be comparatively efficient analogized to the existing methods.**

***Index Terms*—Authorization, Biometric, Finger Vein Recognition (FVR), Trapezoid Membership Function-Based Contrast Limited Adaptive Histogram Equalization (TMF-CLAHE), Local 12 direction texture pattern (L12DTP), Adaptive Weight Mutated Whale Optimization Algorithm (AWM-WOA), Enhanced Sigmoid Reweighted based Convolutional Neural Network (ES-RwCNN).**

Manuscript received June 03, 2021; revised April 07, 2022.

Ajai Kumar Gautam is an Assistant Professor in Electronics & Communication Engineering Department at Delhi Technological University, Delhi, India. (phone: +919868244926; e-mail: ajaikumargautam.dtu@gmail.com).

Rajiv Kapoor is a Professor in Electronics & Communication Engineering Department at Delhi Technological University, Delhi, India. (e-mail: rajivkapoor@dce.ac.in.)

I. Introduction

The method of recognizing a person centered upon one's unique physiological or behavioral attributes is called Biometrics [1]. Biometric recognition (BR) approaches are generally categorized into 2 types: (i) extrinsic biometric features like iris, palm print, fingerprint, face, and also (ii) Intrinsic biometric features like palm vein, hand vein, and FV. Extrinsic Biometrics is more vulnerable to faked input, which results in security problems. Since intrinsic modalities are hidden beneath the skin, they are hard to be faked, therefore, safer [2, 3].

Face recognition, fingerprint recognition, along palm print recognition are several BR techniques utilized recently. But, the methods were most susceptible to faked input, spoof attacks, external damages, and impersonation, which produced security issues [5, 6]. For resolving such issues, FVR technology is broadly utilized for human verification. Therefore, owing to its unique identification along with proper authentication, the FVR technology is a suitable BR method [7].

The minute blood vessels inside our fingers that are distinctive to each individual are FV [8]. The blood vessels with hemoglobin are recognizable as a sequence of dark lines while passing infrared images [9]. Only from a living body, FV images could be captured; therefore, if the person is dead, it is impossible to steal the identity. Furthermore, FVR is not influenced by weather or age in the skin. It is comparatively secure and more steady [10]. But, the Computer-Aided Diagnosis (CAD) is utilized for the enhancement of accuracy with a decrease of time in interpreting the images.

Image acquisition (IA), feature extraction (FE), pre-processing, along with matching are the disparate stages for recognizing the FV images in CAD [11]. An Infrared LED light is transmitted via the finger together with attains a higher contrast image in the IA phase [12]. By conducting a few operations, like resizing, scaling, and CE, the information (unnecessary) in the image (input) is eliminated in a pre-processing stage. The major stage in FVR is the FE. Here, as of the image (pre-processed), the most informative features are extracted. For recognizing individuals, it is basically utilized [13]. The final step is matching; here, for checking whether the image (input) is authentic or not, the input's likeness and the enrolled templates are contrasted [14]. But, the FVR was more precise along with it possesses lower FRR along with False Acceptance Rate. It also presents a few drawbacks concerning extracting the FV

patterns from low contrast finger images. It also possesses an image classification issue [15].

For conquering such challenges, Zone-centered Minutia Matching [16], Support Vector Machine and also neural network (NN) method [17], Convolutional NN (CNN) [18], Lightweight CNN (L-CNN) [19], and also Deep learning (DL) methods are the several methods that are presented. Because of poor image restoration, information loss during FE, and reduction, the CA was not efficiently addressed by the scheme, although the prevailing methods possess a higher degree of privacy and higher recognition rate (RR). It also exhibits different problems like a deficit of training data's availability, uncertain image portrayal, misalignment, restricted CE, need high storage space for large templates along with noise amplification [20]. For overcoming such drawbacks, an ES-RwCNN is formed by the work for executing the user data's FV authentication.

This paper is categorized as Section II reviews the different top-notch methods in the FVR. Section III elucidates the proposed work. Section IV demonstrates the results and a discussion aimed at the proposed method centered on performance metrics. Lastly, section V presents the conclusion with future scope.

II. Literature Review

Wenhao You et al. [21] presented a bilayer restoration technique that dealt with skin scattering along with enhancing the FV image's visibility. The inherent factors were also examined that caused the FV image's degradation. Hence, the scheme enhanced the blurred image's clarity, enhanced the venous network, and was more dependable in FV image restoration. Concerning robustness and restoration performance, the method had surpassed the other techniques, as shown by the investigational outcomes. However, it possessed a noisy data drawback.

CihuiXie et al. [22] presented a method intended for the FV authentication centered on CNN and also supervised discrete hashing (SDH). The SDH's inclusion as of a CNN had attained the most precise performance, which utilized the triplet-centered loss function. Superior outcomes over other deemed CNN architecture were attained by means of the proposed work and also proffered a considerably decreased template size. However, low accuracy rates were shown by the scheme.

Tong Liu et al. [23] introduced a Direction-Variance-Boundary Constraint Search model and reinstated the broken FV patterns. Broken branches of FV patterns were not only effectively restored by the scheme but also enhanced the FVR's performance drastically. The scheme decreased the FVR's error rate from 0.57% to 0.29%, as exhibited by the investigational outcome, but it had a drawback of time consumption.

Ismail Boucherit et al. [24] formed an enhanced deep network called Merge CNN that utilized numerous CNN with shorter paths. The augmented RR with more precise identification was the method's major aim. The scheme competed with top-notch methods with a 99.56% RR, as shown by the experimentation outcome. However, it had a drawback of lower image quality.

Weili Yang et al. [25] developed a lightweight CNN named the FVR and Anti Spoofing Network (FVRAS-Net), which incorporated the recognition task together with the anti-spoofing task on a merged CNN by the Multi-Task Learning approach's usage. The more instructive image for FV identification was automatically chosen by the scheme, which efficiently enhanced the recognition performance. Furthermore, greater security along with strong real-time performance was attained by the scheme. Therefore, outstanding performance in recognition and also anti-spoofing tasks was attained by the technique as illustrated by the experiments. But, there prevailed a data scaling drawback.

Tao Zhan et al. [26] created a scheme centered on FV patterns, which utilized block uniform local binary patterns along with block 2 directional 2 dimensions principal component analysis technique. Thus, the data redundancy was efficiently decreased by the scheme, along it was more feasible. A RR over 99% was attained by the scheme, as shown by the investigational findings; however, the system needed higher computational power.

III. Proposed Finger Vein Authentication of The User Data

An effective biometric method that recognizes individuals utilizing their unique FV patterns is FVR. Amongst these, FVR possesses the subsequent advantages: (1) FV identification makes it complicated to falsify or steal identification since veins are concealed within the body and are mainly unseen to the naked eye; (2) both convenience and also cleanliness are ensured by the non-invasive along with contactless capture, thereby the system is created more apt for the user. But, FV identification is impacted by performance degradation resulting from illumination variations, information loss produced during feature pattern extraction, as well as reduction and misclassification error upon image capture. For addressing the above issues, an ES-RwCNN is created by the work for executing the user data's FV authentication, as exhibited in Fig 1.

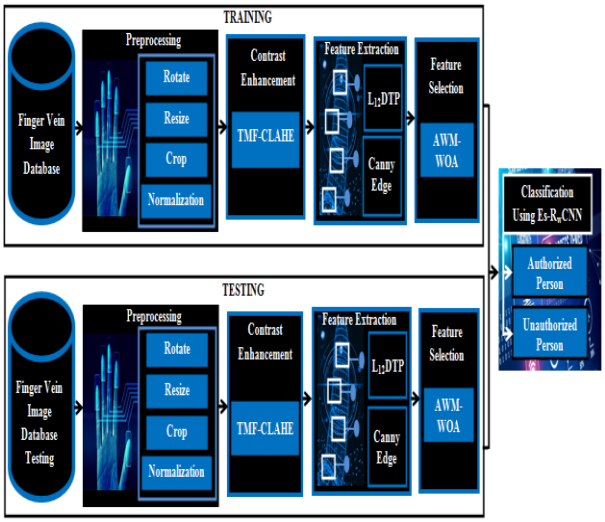

Fig 1: Proposed ES-RwCNN to perform the finger vein authentication of the user data

A. TRAINING PHASE AND TESTING PHASE

Utilizing the developed classification model namely ES-RwCNN for recognizing the FV, various sampled images

are separated into trained and tested images and processed. Disparate phases of processing namely pre-processing, CE, FE, along with feature selection (FS), is undergone by the compilation of split-sample trained and tested images for improvising the classification outcome to identify the FV.

Pre-processing

By addressing the challenges faced on account of the unwilling distortions, the image's image rotation (P_1^{rot}), resizing (P_2^{resize}), cropping (P_3^{crop}), along normalization ($\mathrm{P}_4^{normalize}$) are executed by pre-processing. The error chances are evaded by pre-processing and improvising the RR.

$$\mathrm{P}_1^{rot} = \Re_{i,j}^{rot}\left[\Gamma_{i,j}\right] \quad (1)$$

$$\mathrm{P}_2^{resize} = \Re_{i,j}^{resize}\left[\Gamma_{i,j}\right] \quad (2)$$

$$\mathrm{P}_3^{crop} = \Re_{i,j}^{crop}\left[\Gamma_{i,j}\right] \quad (3)$$

$$\mathrm{P}_4^{normalize} = \Re_{i,j}^{normalize}\left[\Gamma_{i,j}\right] \quad (4)$$

Wherein $\Gamma_{i,j}$ implies the input image, $\Re_{i,j}^{rot}$ $\Re_{i,j}^{resize}$ $\Re_{i,j}^{crop}$ along with $\Re_{i,j}^{normalize}$ demonstrates the pre-processing functions that execute rotation, resizing, cropping, and normalization.

Contrast Enhancement

The information's perception in the image is enhanced through the CE phase. A superior result is offered by arresting the uneven shading along with vein posture deformation that degrades the FV authentication accuracy. An enhancement technique called TMF-CLAHE is created by the work. Trapezoid Membership Function (TMF) is applied by the TMF-CLAHE method for automatic determination of clipping-parameter that restricts the contrast level in an image, therefore, causing an enhanced image (EI). For attaining the EI, the proposed TMF-CLAHE comprises the subsequent steps:

Step1: Firstly, convert the OI intensity level into the contextual regions, which don't overlap. This region is called an image tile of dimension $\mathrm{A}\times\mathrm{B}$.

Step2: By creating the textual region's histogram in the dimensional space $\mathrm{A}\times\mathrm{B}$, the respective region is assessed.

Step3: The contextual region is gauged along with restricted with a *CL* (clipped limit) value-centered upon the histogram, such as

$$\mathrm{B}_{avg} = \frac{(\mathrm{B}_\Gamma x \times \mathrm{B}_\Gamma y)}{\mathrm{B}_{grey}} \quad (5)$$

Wherein B_{avg} indicates the pixel's average number, B_{grey} symbolizes the grey levels in the contextual region, $\mathrm{B}_\Gamma x$ and $\mathrm{B}_\Gamma y$ signifies the pixel values along the x and also y directions inside the contextual regions. Now, utilizing the TMF, the images' over enhancement along with under enhancement is lessened by establishing the predetermined clip limit, which was a primary challenge whilst fixing a pre-fixed clip limit. Therefore, the clipping parameter attained is disparate as of the image upon which TMF-CLAHE is implemented that is presented as:

$$\vartheta_\Gamma(\mathrm{B}_{CL}) = \begin{cases} 0 & if\ (\mathrm{B}_{CL} \le a)\ o\ (\mathrm{B}_{CL} \ge d) \\ (\mathrm{B}_{CL} - a)/(b-a) & if\ \mathrm{B}_{CL} \in (a,b] \\ 1 & if\ \mathrm{B}_{CL} \in (b,c] \\ (d - \mathrm{B}_{CL})/(d-c) & if\ \mathrm{B}_{CL} \in (b,d] \end{cases} \quad (6)$$

Wherein $\vartheta_\Gamma(\mathrm{B}_{CL})$ signifies the image's clipping parameter, which is dependent, (a,b,c,d) shows the trapezoidal membership function (T_F) 's coordinates.

Hence, the clip limit is measured by the TMF, and the computed clip limit is changed on the predefined crisp clip limit. Now, the actual CL is specified as:

$$\mathrm{B}_{CL} = \mathrm{B}_{Clip} \times \mathrm{B}_{avg} \quad (7)$$

Here, by specific conditions, the pixel's clipping is decided; that are, the corresponding pixels get clipped if B_{CL} is lesser than a number of pixels in a specific limit of array [0, 1]. Now, that pixel's average location is decided as $\mathrm{B}_{\sum clip}$, and for every gray-level, the remaining pixel's average is distributed as:

$$\mathrm{B}_{avggray} = \frac{\mathrm{B}_{\sum clip}}{\mathrm{B}_{gray}} \quad (8)$$

The subsequent statements present the theory of trimming histograms:

$$\begin{aligned} &if \aleph_{region}(i) = \mathrm{B}_{CL} \\ &\aleph_{region_{clip}}(i) = \mathrm{B}_{CL} \\ &Else\ if\left(\aleph_{region}(i) + \mathrm{B}_{avggray}\right) > \mathrm{B}_{CL} \\ &\aleph_{region_{clip}}(i) = \mathrm{B}_{CL} \\ &else\ \aleph_{region_{clip}}(i) + \aleph_{region}(i) = \mathrm{B}_{CL} \end{aligned} \quad (9)$$

Whereas $\aleph_{region}(i)$ and $\aleph_{region_{clip}}(i)$ symbolizes the original grey-level histograms along with trimmed histograms of every region at i^{th} gray-level.

Step5: The remaining pixels are rearranged until every pixel has been allotted. The pixel step's rearrangement is proffered by: $step = \mathrm{B}_{gray} / \mathrm{B}_{remain}$

B_{remain} implies the remaining number of clipped pixels. The steps are repeated till every pixel gets distributed uniformly. The vein's important selection is offered by the TMF-CLAHE CE, where the ridges are observable and

distinguishable to each other along with deeming it the ROI of FV image.

Feature Extraction

For offering the FV's knowledge to the classification model, the features (relevant) are extracted via FE. For decreasing the CC, FE assists the model along with helping for precise personal identification systems. Utilizing L_{12}DTP and also Canny edge techniques, textural and EFs are extracted as of the EI by the proposed work. The developed extraction technique can extract both local and also global features comprising micro-patterns.

a. Local 12 direction texture pattern (L_{12}DTP)

Using L_{12}DTP, the texture-centered feature is extracted that separates the image into 13x13 regions. The divided region is measured along with the numerous directions, like 0°, 15°, 30°, 45°, 60°, 75°, 90°, 105°, 120°, 135°, 150°, and 165° centered upon the magnitude along with sign. Therefore, the center pixel's 12 diagonal directions in an image are formed by the pixel value. Then, by contrasting each pixel with the nearest neighboring pixel within the same direction, the 13 × 13 regions are assessed for sign operation (T_{θ_i}) as signified below

$$\mathrm{T}_{\theta_i}=\sum_{k=0}^{k-2}\mu\left(\chi_p-\chi_{p+1}\right)2^k k \tag{10}$$

$$\theta_i=0^{\bullet},15^{\bullet},30^{\bullet},45^{\bullet},60^{\bullet},75^{\bullet},90^{\bullet},105^{\bullet},120^{\bullet},135^{\bullet},150^{\bullet},165^{\bullet}$$

$$\mu(\Gamma^*)=\begin{cases}1, & \Gamma^*\geq 0\\ 0, & otherwise\end{cases} \tag{11}$$

Wherein, k symbolizes the number of neighbors and θ_i characterizes the 12 directions.

Then, by analyzing the nearby absolute differences values and a global threshold, the magnitude (M_{θ_i}) is estimated. The magnitude mathematical formulation is presented below:

$$M_{\theta_i}=\sum_{k=0}^{k-2}\mu\left(\left|\chi_p-\chi_{p+1}\right|-\alpha\right)2^k \tag{12}$$

$$\theta_i=0^{\bullet},15^{\bullet},30^{\bullet},45^{\bullet},60^{\bullet},75^{\bullet},90^{\bullet},105^{\bullet},120^{\bullet},135^{\bullet},150^{\bullet},165^{\bullet}$$

$$\alpha=\frac{1}{k-1}\sum_{k=0}^{k-2}\mu\left(\chi_p-\chi_{p+1}\right). \tag{13}$$

The entire image is signified by creating a histogram after calculating T_{θ_i} and M_{θ_i} as

$$hist(\mathrm{T}_{\theta_i}(l))=\sum_{i=1}^{A}\sum_{j=1}^{B}F_2\left(\mathrm{T}_{\theta_i}(i,j),l\right) \tag{14}$$

$$l\in\left[0,\left(2^k-1\right)\right] \tag{15}$$

$$hist(M_{\theta_i}(l))=\sum_{i=1}^{A}\sum_{j=1}^{B}F_2\left(M_{\theta_i}(i,j),l\right) \tag{16}$$

$$F_2(\Gamma_i,\Gamma_j)=\begin{cases}1 & \Gamma_i=\Gamma_j\\ 0 & otherwise\end{cases} \tag{17}$$

Wherein $\mathrm{A}\times\mathrm{B}$ symbolizes the input image's size and k represents the total neighbors. Lastly, the concatenation of two histograms and extraction of features is done.

$$hist_{concat}=\left[hist(\mathrm{T}_{\theta_i}(l));hist(M_{\theta_i}(l))\right] \tag{18}$$

b. Canny Edge

Different features linked to edges or boundaries are measured by Canny Edge Detector. An extra advantage is offered by EF via enhancing the FVR detection with huge accuracy.

Firstly, for removing the unnecessary details, the image is processed in a Gaussian filter, i.e., provided as:

$$e\left(\Gamma_i,\Gamma_j\right)=E\left(\Gamma_i,\Gamma_j\right)*F\left(\Gamma_i,\Gamma_j\right) \tag{19}$$

$$E=\frac{1}{\sqrt{2\pi\alpha^2}}\exp\left(-\frac{\Gamma_i^2+\Gamma_j^2}{2\alpha^2}\right) \tag{20}$$

Then, the gradient is measured for gradient operations:

$$G\left(\Gamma_i,\Gamma_j\right)=\sqrt{\kappa_i^2(\Gamma_i,\Gamma_j)+\kappa_j^2(\Gamma_i,\Gamma_j)} \tag{21}$$

$$\theta\left(\Gamma_i,\Gamma_j\right)=\tan^{-1}\left[\kappa_i\left(\Gamma_i,\Gamma_j\right)/\kappa_j\left(\Gamma_i,\Gamma_j\right)\right] \tag{22}$$

After that, for suppressing every noisy data as of the selected edge data, a threshold value is estimated.

$$G_T\left(\Gamma_i,\Gamma_j\right)=\begin{cases}G(\Gamma_i,\Gamma_j), & if\ G(\Gamma_i,\Gamma_j)>T\\ 0, & otherwise\end{cases} \tag{23}$$

Wherein T implies the selection in which every edge element are kept whilst numerous noise is repressed.

Next, for attaining a thin edge ridge, the chosen edge data G_T is suppressed. By checking whether each non-zero $G(\Gamma_i,\Gamma_j)$ is larger contrasted to its 2 neighbors along the gradient direction $\theta\left(\Gamma_i,\Gamma_j\right)$, each edge is assessed for thinning the edges. If so, it is kept unchanged otherwise, fix it to 0.

For obtaining 2 binary images ς_1 and ς_2, two disparate thresholds are fixed τ_1 and also τ_2 for the preceding result. There exists less noise and also fewer false borders while ς_2 is contains a larger threshold τ_2 but has a limitation of wide edge tolerance as analogized to ς_1 with a smaller threshold τ_1 .

Numerous features are calculated centered upon the edge. Therefore, a collection of features, i.e. the textural and also EF, is saved within the data frame.

Feature Selection

The most significant and informative features are extracted by the FS, which enhances the improved performance in FVR. AWM-WOA has been formed by the work for better FS. The CC is effectively mitigated by the created algorithm. Thus, the classification model's accuracy is improved with limited time and cost. The optimal solution

(OS) is attained by the AWM-WOA grounded on the developed objective function that chooses the more informative feature that is offered by a sum of disparate features and forms a sole objective function formulated as:

$$\xi_{objective}(\Gamma_E^*) = \xi_1(\Gamma_1^*) + \xi_2(\Gamma_2^*) + \xi_3(\Gamma_3^*) + ...+ \xi_n(\Gamma_n^*) \quad (24)$$

Wherein $\xi_1, \xi_2, ...\xi_n$ symbolizes the constant value that provides the polarity of the features $\Gamma_1^*, \Gamma_2^*, \Gamma_3^* \ldots\ldots \Gamma_n^*$.

Step 1: Firstly, the present best search agent's position is presumed as an optimum point. The other search agents update their position centered upon the best search agent-centered on the optimum point. This equation is provided as:

$$\vec{\vartheta} = \left|\vec{k}.\overrightarrow{\Gamma_n^{\chi}}(t) - \overrightarrow{\Gamma_n^*}(t)\right|, \quad (25)$$

$$\overrightarrow{\Gamma_n^*}(t+1) = \overrightarrow{\Gamma_n^{\chi}}(t) - \vec{\alpha}.\vec{\vartheta}, \quad (26)$$

Where t symbolizes the existing iteration, $\overrightarrow{\Gamma_n^{\chi}}$ implies the best solution's n^{th} position vector, $\overrightarrow{\Gamma_n^*}$ implies the n^{th} position vector of every agent along with $\overrightarrow{\Gamma_n^*}(t+1)$ symbolizes the updated position. $\vec{\alpha}$ along with's coefficients are gauged as

$$\vec{\alpha} = 2.\vec{a}.r - \vec{a} \quad (27)$$

$$\vec{k} = 2r \quad (28)$$

Where, a is slowly reduced as of 2 to 0 and r signifies a random number at the interval [0, 1].

Step 2: The exploitation assures the searching of OS inside the limited space in this step. Further, two disparate phases are undergone by the exploitation process that is described below:

Phase 1: $\vec{\alpha}$ implies a random value within the interval $[-a, a]$ in, which a reduces as of 2 to 0 over the iterations in this phase. The new search agent position could be stated betwixt the position (original) together with the agent's updated position by setting the arbitrary values for $\vec{\alpha}$ within the interval [-1, 1]. The best OS is not attained because the updated solution gets converged over the local optimal search space. For balancing this, the whale optimization merges with the Adaptive weight factor, which is dynamically modified with iteration number that sustains the global along with local searchability. The adaptive search scope grounded on the inertia weight function w is articulated as:

$$\begin{cases} \Lambda = w \times \vec{\vartheta} \times (rand(0,1) - 0.5) \\ w = \exp(-x_1 \times (I / I_m)^{x_2}) \end{cases} \quad (29)$$

Wherein, x_1 along with x_2 in the gamut of [1, 30] are the predefined constants for modifying the search scope, present iteration, together with the maximum iteration, is indicated as I and I_m correspondingly.

Phase 2: A spiral equation is formed betwixt the whale and also prey's position that is offered as

$$\overrightarrow{\vartheta^t} = \left|\overrightarrow{\Gamma_n^{\chi}}(t) - \vec{\Gamma}_n^*(t)\right| \quad (30)$$

$$\overrightarrow{\Gamma_n^*}(t+1) = \overrightarrow{\vartheta^t} e^{gl}.\cos(2\pi l) + \overrightarrow{\Gamma_n^{\chi}}(t) \quad (31)$$

Where the distance betwixt the whale along with prey is signified as ϑ^t, g implies a constant that signifies the logarithmic shape, l denotes a random value within the interval [-1, 1].

The spiral model movement is simulated throughout the algorithm's iterations that are proffered as.

$$\overrightarrow{\Gamma_n^*}(t+1) = \begin{cases} \overrightarrow{\Gamma_n^{\chi}}(t) - \vec{\alpha}.\vec{\vartheta} & if \quad p < 0.5; \\ \vec{\vartheta} e^{gl}.\cos(2\pi l) + \overrightarrow{\Gamma_n^{\chi}}(t) & if \quad p \geq 0.5, \end{cases} \quad (32)$$

(32))

Wherein, p implies a random number in [0, 1].

Step 3: The exploration stage is conducted, which assures the searching of the OS in a broad variety of areas in step 3. The exploration stage is contrary to the exploitation stage. In step 2 $\vec{\alpha}$ is presumed as a random value that is larger analogized to 1 or smaller than -1 in an interval [-1, 1]. The search agent's position might remain distant from the whale together with its position is updated utilizing the novel mutation operator. The new offspring's diversity is enhanced by this application and assists WOA to jump out of local optima. The searching process continues from the existing solution $\overrightarrow{\Gamma_n^*}(t)$ to its nearest solution Γ_{SN} centered on the novel mutation operator.

$$\overrightarrow{\Gamma_n^*}(t) = \overrightarrow{\Gamma_n^*}(t) + \phi_t(\overrightarrow{\Gamma_n^*}(t) - \Gamma_{SN}) \quad (33)$$

Where $t \in \{1,2,3.....,SN/2\}$ signifies a random index, SN implies the populace size, and $\phi_{i,j}$ signifies a random integer $[-1,1]$.

The updated solution's position is formulated as:

$$\vec{\vartheta} = \left|\vec{k}.\overrightarrow{\Gamma_n^*}(t) - \overrightarrow{\Gamma_n^*}\right| \quad (34)$$

$$\overrightarrow{\Gamma_n^*}(t+1) = \overrightarrow{\Gamma_n^*}(t) - \vec{\alpha}.\vec{\vartheta} \quad (35)$$

Wherein Γ_n^* is an updated position vector.

In the objective solution, the attained solution is substituted; the top solution is elected as the most instructive feature. Thereafter, it is kept in a set as stated below:

$$\xi(\Gamma_E^*) = \left\{\Gamma_1^* + \Gamma_2^* + \Gamma_3^* + ... + \Gamma\right\}_n^* \quad (36)$$

B. CLASSIFICATION

For detecting precisely whether the finger-vein is authorized or unauthorized, classification is useful. Generally, for attaining a superior classification score, the NN is mostly utilized. Whilst performing back-propagation, a vanishing gradient (VG) takes place that causes slow-down learning and also decreases the classification rate. For solving this issue, an Es-RwCNN is formed by the work for enhancing the CA for FVR.

Over the chosen features, the developed ES-RwCNN gets trained. Afterward, they are tested to compute the classification score for identifying finger veins. For obtaining training and attaining the recognition, that is if the person is authorized or not, the sample features are processed inside numerous layers. The convolution layer (CL), relu layer, pooling layer (PL), and also fully connected layer (FCL) are the layers.

1) Convolutional Layer: A set of two-dimensional convolutions betwixt the input features Γ_m^l is executed by the CL, where l and m symbolizes the levels and map indexes and the kernel filter K_m^l, i.e. provided as $\left[\Gamma_m^l\right]\times \mathrm{K}_m^l$. After filtration, the n^{th} output map $\mathfrak{\lambda}_n^l$ attained by the CL is measured as

$$\mathfrak{\lambda}_n^l = \sum_{i=0}^{n}\sum_{j=0}^{n} w_{i,j}^l \Gamma_{i,j}^l + \mathrm{B}_{i,j}^l \quad (37)$$

(37

Wherein i, j indicates rows and also columns that signify the features, $w_{i,j}^l$ signifies the weight at the respective interval of l, $\mathrm{B}_{i,j}^l$ implies the bias of interval of l

2) ReLU: For studying the features, an activation function (AF) that decides which neurons must be trained or activated is Relu (act_{relu}). It supports the system's nonlinearity, and the VG issue is decreased. It enables the network's quicker training without sacrificing accuracy. The ReLU activation is proffered as:

$$f\left(\Gamma_m^l\right) = \max\left[0, \Gamma_m^l\right] \quad (38)$$

This layer is united with the CL and deals with augmenting the model's nonlinear properties and also the total network without influencing the receptive fields of the CL i.e.

$$\mathfrak{\lambda}_n^l = act_{relu}\left(\sum_{i=0}^{N}\sum_{j=0}^{N} w_{i,j}^l \Gamma_{i,j}^l + \mathrm{B}_{i,j}^l\right) \quad (39)$$

(39)

3) Pooling: An approach aimed at down sampling the feature map is presented by the PL by summarizing a feature's existence in patches of the feature map. By decreasing dimensionality, the calculation power needed for processing the data is lessened. Whilst efficiently preserving the model's training, it is employed for extracting invariant dominant rotational and positional features.

$$\lambda_n^p = \forall_{layers}^{+}\left(\left|\Gamma_m^l\right|\right) \quad (40)$$

Wherein $\forall_{layers}^{+}$ might symbolize disparate PLs, like maximum PL, minimum PL, average PL, etc. For improvising the image's quality, the PL is helpful.

A CNN's i^{th} layer is formed by the CL and the PL. For capturing the low-level information much more depending upon the image's complexity, the number of such layers could be augmented. Therefore, the output from the CL is flattened and further preceded.

$$\aleph_3^{pooling}(F_{Flatten}) = \left[\Im_1, \Im_2, \Im_3, \Im_4, ... \Im_n\right] \quad (41)$$

4) Fully Connected Layer: An N-dimensional vector is generated, where N implies the total classes that the program has to select as of the flattened features. For categorizing the image (input) affiliated to a particular label, a Sigmoid AF (act_σ) is normally utilized. In FCL, the VG's drawback is possessed by the sigmoid function that generally occurred during the back-propagation method causing slow-down learning and also a reduction in classification rate. By mitigating saturation to lessen the VG issue within the network, Enhanced Sigmoid (ES) AF is designed overcome this issue. It attains superior results for classification. Let Γ_m implies the m^{th} input map of the output layer Θ_m^l. Next, the linear combination Θ_m^l is specified as:

$$\Theta_m^l = act_\sigma\left(\sum_{i=1}^{n} w_i \Im_{i,j} + \mathrm{B}_{i,j}\right) \quad (42)$$

$$\dot{f}_m'(\Gamma_m) = \begin{cases} \beta\left(\Gamma_m - a\right) + act_{E\sigma}(a) & \Gamma_m >= a \\ act_{E\sigma}(a) & -a < \Gamma_m < a \\ \beta\left(\Gamma_m + a\right) + act_{E\sigma}(a) & \Gamma_m \le -a \end{cases} \quad (43)$$

$$\dot{f}_m''(\Gamma_m) = \begin{cases} \beta & \left|\Gamma_m\right| >= a \\ act_{E\sigma}'(\Gamma_m) & \left|\Gamma_m\right| < a \end{cases} \quad (44)$$

Where, $\dot{f}_m'(\Gamma_m)$ signifies the ES function, $\dot{f}_m''(\Gamma_m)$ represents the derivative function, and where a indicates the threshold and β signifies the slope, both parameters are preset.

The classification result is proffered by the FCL. Thereafter, for obtaining a precise result, the loss function (LF) is calculated. The LF is assessed betwixt the actual value (Γ_i) and the predicted value ($\hat{\Gamma}_i$) that is provided as:

$$\lambda_n^{loss} = \sum\left(\Gamma_i - \hat{\Gamma}_i\right)^2 \quad (45)$$

For the optimization of weight function, the re-weighted LF is measured that is offered as:

$$w_n^{(t+1)} = w_n^t + \frac{\eta\nu}{mn}\sum_{i=1}^{m}\sum_{j=1}^{n} \forall_{\phi_j}\wp_{v_j} \forall_{\phi}\wp_i \left(a\lg\left(\theta, D_i^S\right)\right)^T \quad (46)$$

(4

Wherein, $w_n^{(t+1)}$ signifies the updated weights, w_n^t implies the current weights, η is a meta objective step size, ν is the weight update step size, $\forall_{\phi_j}\wp_{v_j}$ symbolizes the training feature's validation, $\forall_{\phi}\wp_i$ indicates the validation of the

tested features, $a\lg(\theta, D_i^S)$ demonstrates the weight's gradient descent.

Finally, the misclassification error is lessened by the reweighted loss for the CA enhancement aimed at FVR. Hence, Fig 2 exhibits the proposed ES-RwCNN's overall outline in pseudo-code.

Input: Extracted features $F_{EXT}^{'} = \left[\xi_1^+, \xi_2^+, \xi_3^+, \xi_4^+, \ldots, \xi_N^+\right]$

Output: Finger Vein Recognition (authorized person or unauthorized person)

Begin

Initialize the kernel (K_m^l), bias $(B_{i,j}^l)$, pooling layer $(\forall_{layers}^+)$, weights $w_{i,j}^l$

For κ features in dataset

Evaluate the convolution operation using,

$$\lambda_n^l(\kappa) = \sum_{i=0}^{n}\sum_{j=0}^{n} w_{i,j}^l \Gamma_{i,j}^l + B_{i,j}^l$$

Compute the convolution layer with activation function

$$\lambda_n^l = act_{relu}\left(\sum_{i=0}^{N}\sum_{j=0}^{N} w_{i,j}^l \Gamma_{i,j}^l + B_{i,j}^l\right)$$

Generate pooling layer,

$$\lambda_n^p = \forall_{layers}^+\left(\Gamma_m^l\right)$$

Evaluate the fully connected layer using,

$$\Theta_m^l = act_{Z\sigma}\left(\sum_{i=1}^{n} w_i \Im_{i,j} + B_{i,j}\right)$$

If $\left(\sum\left(\Gamma_l - \hat{\Gamma}_l\right)^2 = 0\right)$

Accurate finger vein recognition

If $\left(\hat{\Gamma}_i > 0.5\right)$

Output as Authorized person

Else

Output as Unauthorized person

End if

Else

Update weights using,

$$w_n^{(i+1)} = w_n^l + \frac{\eta\nu}{mn}\sum_{i=1}^{m}\sum_{j=1}^{n} \forall_{\phi_i}\varphi_{\nu_j}\forall_{\phi_j}\varphi_i\left(a\lg\left(\theta, D_i^S\right)\right)^T$$

End if

End for

End begin

Fig 2: Pseudo-code for proposed ES-RwCNN

IV. Results

Centered on different performance metrics for the FVR, the complete analysis of the proposed framework's final outcome with prevailing methods is elucidated here. For stating the proposed method's efficiency, both the performance analysis and also comparative analysis are executed. The proposed technique is implemented in MATLAB with machine configuration of Intel core i7 processor, 3.20 GHz CPU Speed, windows 7 OS. The data are amassed from the openly accessible dataset.

A. Performance Analysis

Centered upon different evaluation metrics, the proposed work's brief analysis was executed. Besides, a comparative review is also conducted. For the pre-processing model TMF-CLAHE and also the classification model ES-RwCNN, the analysis is executed.

1. Performance Analysis of Proposed Preprocessing Technique

Concerning disparate performance metrics, like Correlation, Image Quality Index (IQI), and Spearman Rank Correlation (SRC) with different prevailing methods like CLAHE, Histogram Equalization (HE), and Bi-lateral filtering method, the proposed TMF-CLAHE's performance analysis is validated. Next, to illustrate its efficiency, a comparative study was conducted. Table I tabulates the metric's evaluation.

TABLE I
Performance analysis of proposed TMF-CLAHE based on Correlation, Image Quality Index, and Spearman Rank Correlation

Performance metrics/Techniques	Correlation	Image Quality Index	Spearman Rank Correlation
Proposed TMF-CLAHE	0.971	0.799	0.998
CLAHE	0.940	0.583	0.939
Histogram Equalization	0.850	0.036	0.888
Bi-lateral Filtering	0.941	0.000	0.940

The performance analysis concerning the proposed TMF-CLAHE's correlation, IQI, and also SRC with different existent techniques, namely CLAHE, HE, and Bi-lateral filtering technique, is assessed in Table I. The similarities betwixt the EI and the OI are denoted by correlation. The similarities betwixt the EI and the OI with minimum information loss are denoted by the higher correlation rate. As per that, 0.971 correlations betwixt the images are attained by the proposed TMF-CLAHE, while the existing method obtains a 0.91 average correlation, which is moderately less as analogized to the existent techniques.

Furthermore, the SRC is also deemed. The degree of association betwixt the EI and the OI is quantified by the SRC. The higher Spearman correlation characterizes the better model and also vice versa. Thus, a higher SRC of 0.998 is displayed by the TMF-CLAHE proposed, but the prevailing methods acquire an average of 0.922 SRC, which is moderately less when weighted against the proposed one. Therefore, the proposed TMF-CLAHE is more effectual, together with the image is delivered at the higher-quality index at the rate of 0.799, whilst 0.583, 0.036, and 0.000 are attained by the prevailing techniques, like CLAHE, HE, and also Bi-lateral filtering technique correspondingly. Therefore, a quality image with no distortion is offered by the proposed TMF-CLAHE.

Fig 3 demonstrates the proposed TMF-CLAHE's graphical analysis with different existing methods, namely CLAHE, HE, and the Bi-lateral filtering technique. It is obviously known from figure 3 that a greater range of correlation, IQI, and SRC is attained by the TMF-CLAHE. The proposed method's high correlation is shown in figure 3 (a); thus, the uneven detection could be effortlessly rectified. Fig 3 (b) exhibits the IQI, which assists in clear image delivery. The SRC is exhibited in Fig 3 (c), which offers a precise association rate. These metrics measure the proposed TMF-CLAHE's effectiveness. Thus, the proposed TMF-CLAHE surpasses the existing technique.

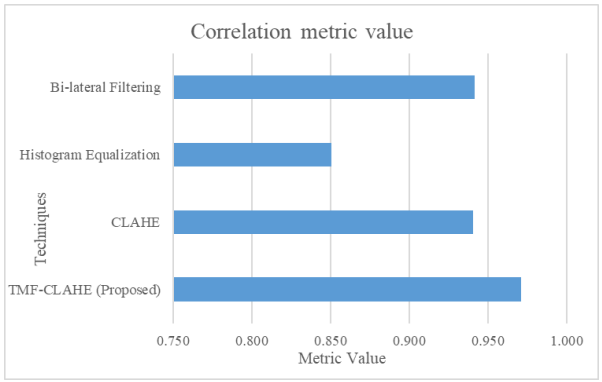

(a)

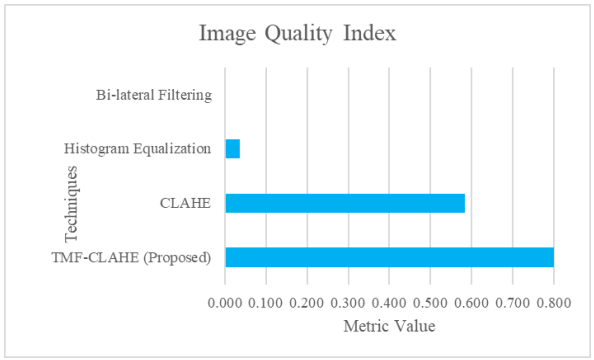

(b)

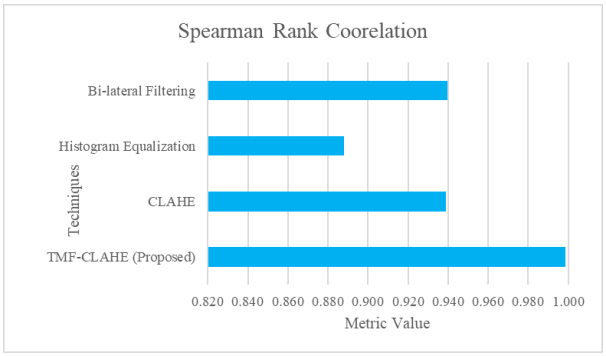

(c)

Fig 3: Graphical Demonstration of proposed TMF-CLAHE based on (a) Correlation, (b) Image Quality Index and (c) Spearman Rank Correlation.

B. Performance Analysis of Proposed Classification Technique:

Concerning disparate performance metrics, namely specificity, sensitivity, accuracy, Negative Predictive Value (NPV), recall, precision, F-Measure, Matthews Correlation Coefficient (MCC), FPR, and FRR, the proposed ES-RwCNN's performance analysis is validated. Afterward, a comparative study is conducted with prevailing methods, like Deep NN (DNN), Convolutional DNN (CDNN), along with Artificial NN (ANN). Tables II, III, and also IV tabularizes the metric's evaluation.

Table II:
Performance analysis of proposed ES-RwCNN based on sensitivity, specificity, accuracy, and NPV

Performance metrics/Techniques	Sensitivity	Specificity	Accuracy	NPV
Proposed ES-RwCNN	97.64	96.46	97.05	97.61
DNN	88.21	84.67	86.44	87.78
CDNN	90.57	91.75	91.16	90.68
ANN	69.81	42.22	56.01	58.31

Table II illustrates the different performance metrics' analysis, like specificity, NPV, accuracy, and also the sensitivity of the ES-RwCNN proposed with the various prevailing techniques, like DNN, CDNN, and ANN. The evaluation metrics must stand with a greater metrics rate for alleviating the VG issue within the network. According to that, the ES-RwCNN proposed attaining the sensitivity, specificity, accuracy, and NPV at the rate of 97.64%, 96.46%, 97.05%, and 97.61%, correspondingly, which overall ranges betwixt 96.46% to 97.64%. However, the metrics' value that overall ranges between 42.22%-91.75% are attained by the prevailing techniques, like DNN, CDNN, and ANN, which is relatively low when weighted against the proposed ES-RwCNN. Hence, the authorized along with the unauthorized person are efficiently distinguished by employing the proposed ES-RwCNN in the FVR.

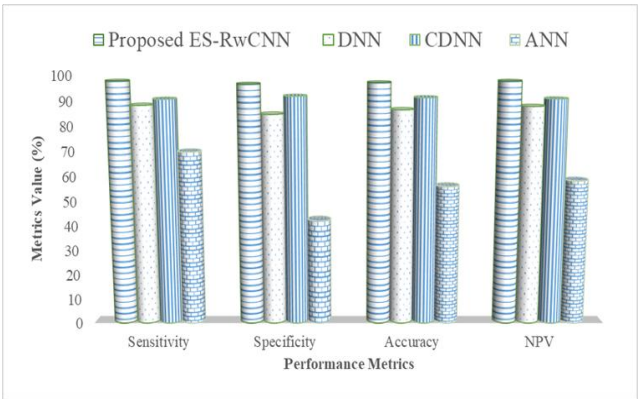

Fig 4: Graphical representation of the proposed ES-RwCNN based on sensitivity, specificity, accuracy, and NPV

Fig 4 exhibits the graphical depiction of the proposed ES-RwCNN's performance analysis with the disparate prevailing techniques, namely DNN, CDNN, and ANN. It is evidently known as of the figure that a superior performance metrics value is gained by means of the proposed one. Thus, the proposed ES-RwCNN surpasses several prevailing ones and offers precise FVR in disparate situations.

TABLE III
Performance analysis of proposed ES-RwCNN based on precision, recall and F-Measure

Performance metrics/Techniques	Precision	Recall	F-Measure
proposed ES-RwCNN	96.5	97.64	97.07
DNN	85.19	88.21	86.67
CDNN	91.65	90.57	91.1
ANN	54.71	69.81	61.35

Grounded upon the metrics of precision recall, along with F-Measure, Table III exhibits the proposed ES-RwCNN's evaluation. These metrics are mainly significant in the LF's prediction. The misclassification error is lessened by the LF for the CA enhancement for FVR. It is detected as of the table that 96.5% precision, 97.64% recall, and 97.07% F-Measure are attained by the ES-RwCNN proposed, which is relatively larger analogized to the prevalent technique. Thus, the existent method, like DNN, CDNN, and ANN attains the metrics' value that overall ranges from 54.71%-91.65%. Therefore, the FV is detected by the proposed one by overcoming the uncertainties along with a reduced error rate as contrasted to the prevailing model.

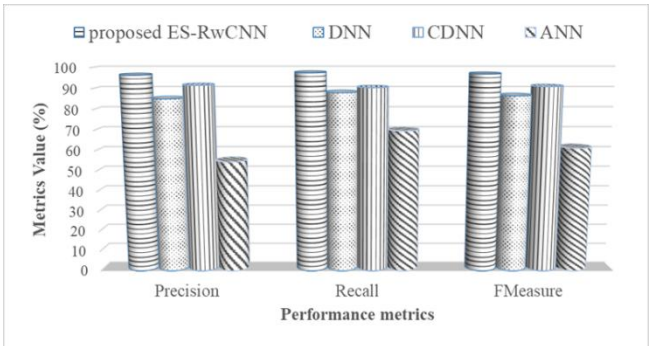

Fig 5: Graphical representation of the proposed ES-RwCNN based on precision, recall, and F-Measure.

The graphical illustration, which relatively examines the proposed ES-RwCNN with the prevailing methods, say DNN, CDNN, and ANN, is exhibited in Fig 5. The proposed ES-RwCNN is more effectual when contrasted to the prevalent methods, as stated by the comparative study. Hence, the uncertainties with the decreased error rate are effectively addressed by the proposed ES-RwCNN whilst the existing technique failed to manage such uncertainties.

TABLE IV
Evaluation of proposed ES-RwCNN based on MCC, FPR, and FRR

Performance metrics/Techniques	MCC	FPR	FRR
Proposed ES-RwCNN	94.11	3.53	2.35
DNN	72.92	15.33	11.79
CDNN	82.32	8.25	9.43
ANN	12.51	57.78	30.18

Centered upon the metrics of MCC, FPR, and FRR, Table IV depicts the proposed ES-RwCNN's performance analysis. The misclassification or miss-prediction error that happens in the FV's recognition is efficiently rejected by the lesser value of FPR and FRR. As per that, 3.53% FPR and 2.35% FRR are attained by the proposed one correspondingly. Contrarily, the high prediction rate is attained by the existing technique like DNN, CDNN, and ANN. FPR and FRR's average is 27.12% and 17.13%, correspondingly. Besides that, centered on MCC, the proposed ES-RwCNN is also deemed. The model's success is signified by a higher MCC score. Thus, the high MCC score of 94.11% is attained by the ES-RwCNN proposed, whilst the prevailing technique acquires the MCC score at an average of 60%. Hence, the slow convergence of triplet loss is conquered by the ES-RwCNN proposed and also assured the full usage of information with labels.

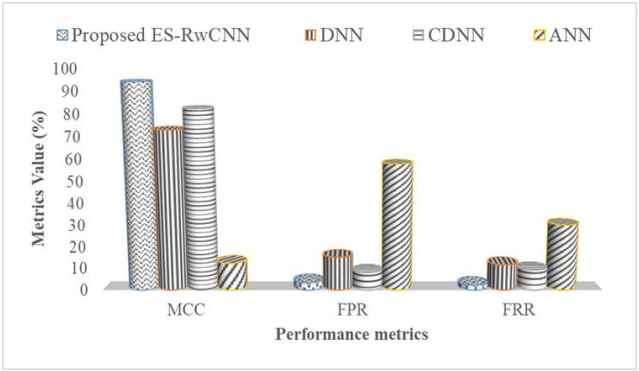

Fig 6: Graphical analysis of the proposed ES-RwCNN based on MCC, FPR, and FRR

The proposed ES-RwCNN's detailed analysis with different existing techniques, namely DNN, CDNN, and ANN is proffered in Fig 6. The best model is proffered by the illustration via examining the false prediction values. The false prediction is lessened by the proposed one and improvises the classification rate by evading misclassification and stays effective against the prevalent methods. Therefore, by attaining lower false prediction values and higher MCC scores, the proposed ES-RwCNN surpasses the prevailing methods.

V. Conclusion

A framework for detecting FV is formed by the work for safe authorization utilizing ES-RwCNN. Vein recognition is improved by the proposed framework via managing the challenge of unwilling distortions, diagonal pixel information, image variants, etc. In the TMF-CLAHE technique, the FV gets improved that concentrates upon irregular shading along with vein posture deformation and enhances the framework's accuracy. After that, utilizing the L_{12}DTP and also Canny Edge methods, relevant textural and EFs are extracted. Furthermore, AWM-WOA was applied by the work for removing the most knowledgeable feature which enhances accuracy along with lessens the CC. For identifying FV as an authorized or unauthorized person, the training along with testing is performed for the developed ES-RwCNN classification model. A low information loss is attained by the framework by attaining a 0.971 correlation betwixt the processed image and OI along with categorizes the FV with 97.05% accuracy, 97.64% sensitivity as shown by the experimental outcomes. The misclassification is evaded by employing the classification model via obtaining an FPR and FNR of 3.53% and 2.35%, correspondingly, and stays effective when weighted against the prevailing top-notch method.

References

[1] Antonio Iula, "Biometric recognition through 3D ultrasound hand geometry", Ultrasonics, vol. 111, pp. 1-24, 2021.
[2] Hui Ma and Zhang S. Y, "Contactless finger-vein verification based on oriented elements feature", Infrared Physics & Technology, vol. 97, pp. 149-155, 2019.
[3] Raid Rafi Omar Al-Nima, Mohammed AM Abdullah, Musab TS Al-Kaltakchi,Satnam Singh Dlay, WaiLok Woo and Jonathon A. Chambers, "Finger texture biometric verification exploiting multi-scale sobel angles local binary pattern features and score-based fusion", Digital Signal Processing, vol. 70, pp. 178-189, 2017.
[4] Yihua Shi Yang and GuiminJia, "Finger-vein image matching based on adaptive curve transformation", Pattern Recognition, vol. 66, pp. 34-43, 2017.
[5] Jian-DaWu and Chiung-Tsiung Liu, "Finger-vein pattern identification using principal component analysis and the neural network technique", Expert Systems with Applications, vol. 38, no. 5, pp. 5423-5427, 2011.
[6] ShirongQiu, Yaqin Liu, Yujia Zhou, Jing Huang and YixiaoNie, "Finger-vein recognition based on dual-sliding window localization and pseudo-elliptical transformer", Expert Systems with Applications, vol. 64, pp. 618-632, 2016.
[7] Huafeng Qin, Xiping He, Xingyan Yao and Hongbing Li, "Finger-vein verification based on the curvature in Radon space", Expert Systems with Applications, vol. 82, pp. 151-161, 2017.
[8] Kun Su, Gongping Yang, Bo Wu, Lu Yang, Dunfeng Li, Peng Su and Yilong Yin, "Human identification using finger vein and ECG signals", Neurocomputing, vol. 332, pp. 111-118, 2019.

[9] EuiChul Lee and Kang Ryoung Park, "Image restoration of skin scattering and optical blurring for finger vein recognition", Optics and Lasers in Engineering, vol. 49, no. 7, pp. 816-828, 2011.
[10] Shuyi Li, Bob Zhang, LunkeFei and Shuping Zhao, "Joint discriminative feature learning for multimodal finger recognition", Pattern Recognition, vol. 111, pp. 1-11, 2021.
[11] Kun Su, Gongping Yang, Lu Yang, Dunfeng Li, Peng Su and Yilong Yin, "Learning binary hash codes for finger vein image retrieval", Pattern Recognition Letters, vol. 117, pp. 74-82, 2019.
[12] Haiying Liu, Gongping Yang, Lu Yang and Yilong Yin, "Learning personalized binary codes for finger vein recognition", Neurocomputing, vol. 365, pp. 62-70, 2019.
[13] Fei Liu, Gongping Yang, Yilong Yin and Shuaiqiang Wang, "Singular value decomposition based minutiae matching method for finger vein recognition", Neurocomputing, vol. 145, pp. 75-89, 2014.
[14] Wenxiong Kang, Xiaopeng Chen and Qiuxia Wu, "The biometric recognition on contactless multi-spectrum finger images", Infrared Physics & Technology, vol. 68, pp. 19-27, 2015.
[15] Rama VasanthaAdiraju, Kranthi Kumar Masanipalli, Tamalampudi Deepak Reddy, RohiniPedapalli, SindhuChundru and Asisa Kumar Panigrahy, "An extensive survey on finger and palm vein recognition system", Materials Today: Proceedings, vol. 44, pp. 1-5, 2020.
[16] XianjingMeng, JinwenZheng, Xiaoming Xi, Qing Zhang and Yilong Yin, "Finger vein recognition based on zone-based minutia matching", Neurocomputing, vol. 423, pp. 1-16, 2021.
[17] Jian-Da Wu and Chiung-Tsiung Liu, "Finger-vein pattern identification using SVM and neural network technique", Expert Systems with Applications, vol. 38, no. 11, pp. 14284-14289, 2011.
[18] Dongdong Zhao, Hui Ma, Zedong Yang, Jianian Li and WenboTian, "Finger vein recognition based on lightweight CNN combining center loss and dynamic regularization", Infrared Physics & Technology, vol. 105, pp. 1-10, 2020.
[19] Yuxun Fang, Qiuxia Wu and Wenxiong Kang, "A novel finger vein verification system based on two-stream convolutional network learning", Neurocomputing, vol. 290, pp. 100-107, 2018.
[20] Mohsin A. H, Zaidan A. A, Zaidan B. B, Albahri O. S, Albahri A. S, Alsalem M. A and Mohammed K. I, "Based blockchain-PSO-AES techniques in finger vein biometrics: A novel verification secure framework for patient authentication", Computer Standards & Interfaces, vol. 66, pp. 1-25, 2019.
[21] Wenhao You, Weikang Zhou, Jing Huang, Feng Yang, Yaqin Liu and Ziyu Chen, "A bilayer image restoration for finger vein recognition", Neurocomputing, vol. 348, pp. 1-31, 2019.
[22] CihuiXieand Ajay Kumar, "Finger vein identification using convolutional neural network and supervised discrete hashing", In Deep Learning for Biometrics, Springer, Cham,vol. 119, pp. 1-31, 2017.
[23] Liu, Tong, JianbinXie, Wei Yan, Peiqin Li, and Huanzhang Lu, "Finger-vein pattern restoration with direction-variance-boundary constraint search", Engineering Applications of Artificial Intelligence, vol. 46, pp. 131-139, 2015.
[24] IsmailBoucherit, Mohamed OuldZmirli, HamzaHentabli and BakhtiarAffendiRosdi, "Finger vein identification using deeply-fused Convolutional Neural Network", Journal of King Saud University-Computer and Information Sciences, vol. 33, pp. 1-11, 2020.
[25] Weili Yang, Wei Luo, Wenxiong Kang, Zhixing Huang and Qiuxia Wu, "FVRAS-Net: an embedded finger-vein recognition and anti-spoofing system using a unified cnn", IEEE Transactions on Instrumentation and Measurement, vol. 69, no. 11, pp.1-12, 2020.
[26] Na Hu, Hui Ma and Tao Zhan, "Finger vein biometric verification using block multi-scale uniform local binary pattern features and block two-directional two-dimension principal component analysis", Optik, vol. 208, pp. 1-16, 2020.

WWW.IJRPR.COM

International Journal of Research Publication and Reviews

Journal homepage: www.ijrpr.com ISSN 2582-7421

A Review on Center-Less Recess Grinding and Its Applications

Rohan Sharma[1], Rohan Chopra[2], Rohan Singh[3] and Dr. Ak Madan[4]

[1, 2, 3] Student, Mechanical Engineering, Delhi Technological University, New Delhi
[4]Professor, Mechanical Engineering department, Delhi Technological University, New Delhi
DOI: https://doi.org/10.55248/gengpi.2022.3.5.11

ABSTRACT

The review manages extraordinary center less grinding process utilizing different strategies, especially the center less recess grinding technique. The aftereffects of estimating the surface harshness of front facing and cylindrical shaped regions and the roundness of the round and hollow surface of the work piece are displayed in the paper. Subjective boundaries of the machined surfaces are enhanced by the way of the grinding system. The alteration looking like the work piece causes the adjustment of the place of the work piece during the activity in the work zone.

KEYWORDS: Quality Parameters, The grinding process& Center-less Grinding

INTRODUCTION

The standard of every technique for grinding is withdrawal of material by abrasive grain. Abrasive grain is a cutting wedge with irregular math and direction. While grinding, the workpiece material is eliminated by a hard stone grinding wheel at high cutting rates. Centerless grinding is utilized for grinding smooth tube shaped parts, which are embedded between two discs. One of them is a grinding haggle other a managing wheel. Workpiece pivots at a fringe speed of the turning controlling wheel.

CENTERLESS RADIAL GRINDING

Recess grinding is utilized for machine parts that have a recess, formed or tapered surfaces, or, where proper, more coaxial barrel shaped surfaces without centers. Work pieces are embedded into the screen between the grinding and managing wheels, with parallel axes.

SPECIFIC FEATURES OF CENTERLESS RECESS GRINDING

Explicit elements of center less grinding recess strategy are:
1. Development (feed) of one of the plates in the spiral bearing of grinding. Toward the finish of this development (feed), the work piece gets the last aspect.
2. Hub of the wheels are lined up with the outer layer of the main slide.
3. Smooth method, since there is no hub development of the work piece.

Be that as it may, in the genuine method, the managing wheel shapes brief point (0.5°) with the outer layer of the main slide. This plan, which is ordinary for this strategy, is here to forestall the work piece from swaying in the pivotal bearing. The slanted hub of the directing wheel is squeezed against the front of the piece fence. Wheels are joining either physically or consequently. In this technique, we can crush the pieces of different shapes to a specific length and l max ≤ H, where l max is the greatest length of the piece of ground. Work pieces are embedded and taken out physically or by utilizing tanks. Grinding cycle is generally done with a surface of the work piece squeezed to surface of the main slide and managing wheel. The difference looking like the work piece in grinding prompts the difference in the area of this work piece in the work zone.

METHODOLOGY

RECESS GRINDING PROCESS

In Fig. 1 is a plan of moment situating the work piece during a solitary transformation when in-feed grinding? The apparatus way feed rate is checked t. assuming stipend is taken with specific pieces of the surface, the work piece diminishes and is moved to the directing wheel.
Fig. 1 (b). Consequently, the work piece doesn't have a right round and hollow shape after one unrest, in light of the fact that the profundity of grinding over the turn changes.

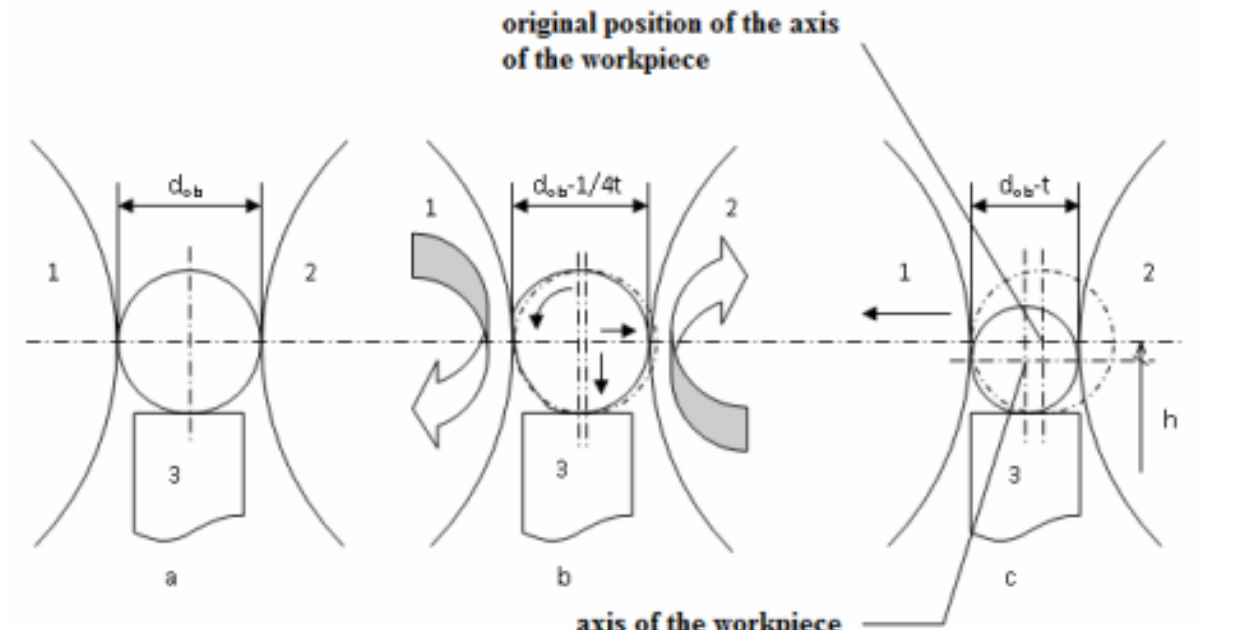

Fig. 1. Plan of moment situating of the work piece when in-feed grinding (a. beginning the interaction; b. transitional place of the work piece; c. position after one unrest of the work piece; 1. grinding wheel; 2. directing wheel; 3. driving slide).

To get the work piece of an exact round shape, it should be continued to turn without horizontal feed. While grinding, the mathematical hub of the work piece position is continually changing while at the same time staying lined up with its underlying position.

Fig. 1 (c). The property of center work piece uprooting is considered while setting the processors. It ought to be noticed that with expanding h, contrast dob - dob.o is additionally developing quickly. Line level h not entirely settled from the mathematical connections. Also, this applies to center less grinding through way, yet the idea of the work piece development is substantially more intricate. Work piece is pivoted and in this way its hub stops to be lined up with its unique position. These developments in the piece-through grinding lead to lessening the work piece width around by factor t, which was recently set up in the grinding machine. With a similar arrangement in center grinding, the work piece width would diminish by 2t. In centerless grinding, the variable-through dob - dob.o is generally called the profundity of cut. A twofold profundity of cut for grinding center is shown t, individually 2t. To abstain from misconception, variable t, which must be respected a momentary profundity of cut will called recompense of point.

CHANGE PROFILE AND QUALITATIVE PARAMETERS SURFACES WORKPIECES

To decide the effect of in-feed center less grinding on a roundabout profile and the boundaries of the surface (roundness and surface harshness), we did a progression of investigations inside which the parts displayed in figure were produced. Parts were made of ST 37 - 2K. Their distance across was ø 9.96-0.01 (measurement of semi-item prior to grinding ø10.04+0.06). Grinding was made on MULTIMAT 208 machine while utilizing the grinding wheel 400x30x203 99BA/96A 60N7V (STROH level precious stone), managing wheel 300x30x127 A120RL152R7 and it was directly to lead slide. Grinding machine's working time was 9.8s.

APPLICATIONS

- Carried pins
- Transmission bushings
- Ceramic shafts for circulator pumps utilized in home warming
- Ceramic shafts for circulator pumps utilized in valve seal embeds
- Earthenware shafts for circulator pumps utilized in aviation latches
- Ceramic shafts for circulator pumps utilized in dowel pins

CONCLUSION

The investigations demonstrated that the middle less dive grinding works on the boundaries of round profile and surface unpleasantness. Be that as it may, there are situations where grinding can demolish a subjective boundary. It concerns especially an exact common situating of the work piece surfaces. For instance, in a way through center less grinding of external surfaces (particularly with a little of length/width proportion of a part, for example ring-moulded parts) no uprightness of the round and hollow surface of the work piece with respect to its face can be a piece greater. This won't occur with plunge grinding. Every one of the techniques for center less grinding might cause that the external (grinding) surfaces and the inward surfaces of the work piece are not actually in arrangement. Coaxiality of surfaces is changed by go through grinding along the length of the work piece.

This is generally viewed as an arbitrary deviation. Truth be told, this peculiarity is brought about by unambiguous elements of center less grinding and it very well may be impacted. On the off chance that the processor is appropriately changed, a bigger measure of machine is utilized and the ideal recompense of grinding is held, accomplishing the precision to the degree of the endorsed resistances subsequent to grinding is conceivable.

FUTURE SCOPE

Assuming the test is to machine huge amounts of long as well as flimsy, round parts made of malleable or fragile materials, then there is essentially no option in contrast to centerless external width grinding. Moreover, center less grinding is the main procedure to offer grinding wheel sets which permit various assignments - for example roughing and getting done - to be acted in a solitary pass (picture shows Wendt camshaft and wheel set). The machining system itself compares to the next round and hollow grinding procedures like the ones previously shrouded in the segment "Outside measurement grinding" - even without centeres the interaction actually includes plunge grinding and through taking care of methods. Nonetheless, not having any centeres offers various benefits: - As the straight formed help for the work piece forestalls huge bowing burdens and torsional loads, even flexible or fragile materials can be machined with enormous grinding powers with no deformity. - Exceptionally short set-up times - no arrangement of the work piece is expected for clasping or for transmission of the rotational development (no wellsprings of blunders in the wake of centering, re-bracing). - Work piece changes are direct and simple to mechanize. - In consistent longitudinal grinding cycles there is no margin time for work piece changes. - Even very lengthy parts can be machined with minimal machines. - Out-of-roundness blunders and out-of-cylindricity mistakes are diminished to under 1µm and are subsequently around half as much as the same qualities for grinding between centeres.

REFERENCES

[1] KOCMAN, K., PROKOP, J. Machining technology. Brno: Academic publishing CERM. ISBN 80-214-3068-0

[2] SLONIMSKIJ, V. I. Theory and practice of centerless grinding second edition. Moscow: National Scientific and technical literature publishing machine, 1952.

[3] STN EN ISO 1101: 2006, Geometrical product specifications (GPS). Geometrical tolerancing. Tolerances on shape, orientation, location and runout (ISO 1101: 2004).

[4] DOVICA, M., KAŤUCH, P., KOVÁČ, J., PETRÍK, M. Metrology in engineering. 1. Edition. Košice: Series of scientific and technical literature – Faculty of Mechanical Engineering TU Košice. Tlač: EMILENA s.r.o., Košice, 2006. 351 p. ISBN 80 – 8073 – 407 – 0.

[5] PERNIKÁŘ, J., TYKAL, M. Engineering metrology II. 1. Edition. Brno: Publisher: University of Technology in Brno, Faculty of mechanical engineering. Publishing: ACADEMIC PUBLISHING CERM, s.r.o., 2006. 180 p. ISBN 80–214–3338–8

Proceedings of the Sixth International Conference on Intelligent Computing and Control Systems (ICICCS 2022)
IEEE Xplore Part Number: CFP22K74-ART; ISBN: 978-1-6654-1035-9

2022 6th International Conference on Intelligent Computing and Control Systems (ICICCS) | 978-1-6654-1035-9/22/$31.00 ©2022 IEEE | DOI: 10.1109/ICICCS53718.2022.9788377

A Review on GAN based Image Dehazing

Kavinder Singh
Dept. of Computer Science
Delhi Technological University
New Delhi, India
Kavinder85@gmail.com

Vishruth Khare
Dept. of Computer Science
Delhi Technological University
New Delhi, India
vishruthkhare3@gmail.com

Vishwas Agarwal
Dept. of Computer Science
Delhi Technological University
New Delhi, India
agarwalvishu6300@gmail.com

Sourabh
Dept. of Computer Science
Delhi Technological University
New Delhi, India
sourabhlathwal.dtu@gmail.com

***Abstract*—The improvement of deep learning facilitated the evolution of computer vision methods. Image dehazing is one of the challenging tasks in computer vision. Haze is a very common phenomenon arising due to bad weather, poor lighting, pollution, etc. Haze poses the problem of poor visibility in images under extreme circumstances. Several deep learning-based methods have been used to overcome haze-oriented problems. Generative networks (GANs) focus on the distribution of the normal images to remove the haze from a hazy image. The methods enhance the performance of computer vision under hazy conditions. This paper focuses on discussing a few important techniques, specially GANs, to solve the problem of dehazing. Various techniques have been qualitatively analyzed and the merits and demerits of the respective models have been discussed. Finally, some light is thrown upon the real-world applications and significance of dehazing.**

***Index Terms*—Generative Adversarial Network, Dehaze, Neural networks, Deep learning**

I. INTRODUCTION

Haze in images can be attributed to fog, mist, bad weather, pollution, etc. The main cause of Haze is Light and inactive fine particles. When Light encounters dust, some of it gets absorbed while the remaining gets scattered. During fog, mist, the number of particles increases, and so does the absorption and scattering of light, thereby reducing the contrast and visibility of the image that gets captured [1].

Factors such as the gradient of the image, distance of the observer, etc., also come into play when considering dehazing from a larger perspective. A significant context of the image is preserved while capturing images that have haze in them, which can be efficiently extracted by using advanced algorithms. An interactive approach involves using the Depth Heuristics wherein the dehazing is done using the heuristics of scene depth, thereby eliminating the need for accurate physical depth of the image [9]. Also, with the conventional de-weathering (de-hazing) algorithm [9,12], the relationship between Transmission Map, Scene radiance, and the image under consideration can be established by:

$$I(x) = J(x)t(x) + A(1 - t(x)) \quad (1)$$

I(x): Hazy Image can be parameterized via the J(x): clean image and the transmission map t(x). Given I(x) and J(x) during the training of the data, values of t(x) and A are estimated that facilitate the construction of the model. Some dehazing models also make use of visual cues to get an abstract estimation of t(x) and A. But, as we see some of the earlier results that use features like polarisation [13], these visual cues aren't enough as there is a weighted average of factors that need to be considered while coming up with a one-stop solution to achieve high quality of haze removal. The value of t(x) can be estimated by:

$$t(x) = e^{-\beta d(x)} \quad (2)$$

where β: extinction coefficient, and d(x): scene depth of x.

However, estimation of t(x) from a hazy image is not an efficient solution. Many successful approaches rely on an accurate estimation of the transmission map t(x), for example, the Dark-Channel Prior [5] and Non-local Color Prior [7]. But these priors are inconsistent with the practice leading to inaccurate estimations. Some methods do not hold for similarities to the natural light leading to unsatisfied dehazing quality for bright objects. Some of them fail in scenes where the sunlight is significantly brighter than the image creating a selectivity bias. Filters are used to better realise the transmission map. But they have high computation time and suffer from gradient reversal artefacts.

We are presenting a qualitative analysis of GAN based image dehazing methods. This paper has been structured as: Section 2 gives an overview of GANs. A general framework of Image dehazing techniques is discussed in Section 3. Section 4 entails the qualitative review of GANs based dehazing techniques. The most commonly used Dataset for image dehazing is described in Section 5. Section 6 covers Applications of Image Dehazing in real-world scenarios. We perform a Comparative analysis based on the merits, limitations and applications of different techniques in Section 7. Section 8 presents the conclusion of our observations.

II. GENERATIVE ADVERSARIAL NETWORK

Generative adversarial networks (GANs) are the new problem solver for most of the computer vision problems [14-20]. GANs are generally referred to as a way for generating images based on the requirements of a problem by repetitive modelling with the help of a convolutional neural network (CNN) and other learning-based mechanisms. GANs belong to the field of unsupervised learning, which focuses on studying the underlying structure of the data with no specified target value. Generative Adversarial Networks are growing at a very fast pace in this ever-changing turf and aim at building and

Authorized licensed use limited to: DELHI TECHNICAL UNIV. Downloaded on June 15,2022 at 11:24:33 UTC from IEEE Xplore. Restrictions apply.

enhancing the models' capability to produce practical illustrations. With the increased usage of data and the advancements in Deep Learning, data-augmentation has increased more than ever. GANs play a significant role in augmenting the data and thereby increasing the robustness of the model. GANs' ability to develop enhanced models and self cooperation also helps in reducing the loss by developing unique instances from the data provided and updating the Generator-Discriminator loss.

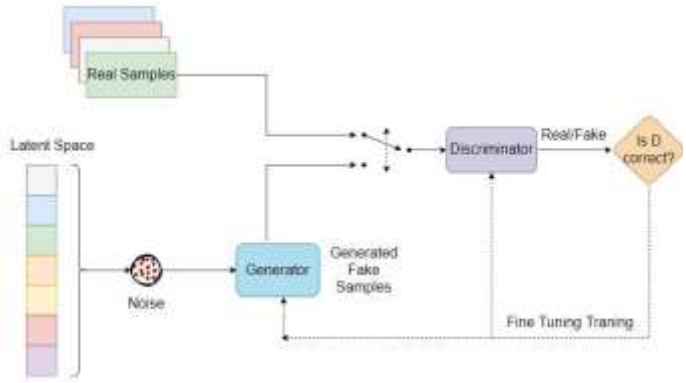

Fig. 1. Working of GAN

From Fig. 1, we can see how GANs actually work. The Generative networks routinely find the patterns and understand the habits in the dataset to generate the solutions. The generator model is often used as a sub-routine to produce some fabricated outputs, which further gets added to the input, behaving as a self-learning model. GANs are an intelligent method for guiding a generative mould essentially behaving as a supervised learning technique with two sub-routine models. The first model is known as the generator model, which is trained to produce fake or fabricated instances that look like authentic outputs. The second model is called the discriminator model, and its purpose is to classify samples as real (i.e., from the dataset) or fake (i.e., generated by generator).

A facet that makes the use of GANs more innovative and important is that whenever the field/domain is complex, or the data that has to be trained is present in a limited amount, generative modelling can pave the way for increasing the dataset for training. GANs can model data with high-dimension and can even graciously handle the missing data, thereby offering a multimodal yield. Fields or tasks that require GAN's ability to generate new examples are many. Some of the few hot topics are: Super-resolution of images, translation from one image to another, producing creative arts, etc. One of the main reasons GANs have gained so much popularity among researchers and developers is that they can develop pictures in such a genuine manner that it has become impossible for humans to differentiate them from the real ones.

III. Techniques Of Image Dehazing

For the purpose of training the models, the most commonly used dataset is the RESIDE standard's ITS (Indoor Training Set) [28]. RESIDE is an acronym for Realistic Single-Image De-hazing. It contains a large set of fabricated and genuine world images, which have proved to be constructive for complete learning along with the assessment of existing de-hazing models. RESIDE-Standard's Indoor Training Set (ITS) is a part of 5 subsets of RESIDE, all having distinct functionalities. Moreover, it comprises pictures without haze (1399) and equivalent hazy pictures and trans pictures (13990 each). For outdoor classification, RESIDE-OTS is generally used by all the models. It has 72135 haze free images. The assessment of the model is carried out on Synthetic-Objective Testing Set (SOTS), which is a part of RESIDE-standard. It has around 500 pairs of hazy and ground truth images for indoor purposes and same for outdoor purposes.

The most commonly used Validation Metric on the basis of which the model are quantitatively compared are:

SSIM Score: Structural Similarity Index is a perceptual metric that quantifies image degradation caused by processing such as data compression or by losses in data transmission

PSNR Score: Peak signal-to-noise ratio is an expression for the ratio between the maximum possible value (power) of a signal and the power of distorting noise that affects the quality of its representation.

With the advancements in Deep Neural Networks, the image dehazing problem has started gaining attention. Early research which used conventional methods for image dehazing couldn't give satisfactory results as they were primarily focused on transmission map estimation and the corresponding atmospheric light component of the haze [2,3,4]. Deep learning approaches always perform superior to the classical approaches as they extract the relevant features rather than being feduser-estimated features. Hence, many approaches have been formulated for the problem of haze removal in the images. Hodges et al. [6] created a model that is built on two separate networks: a dehazing network and a discriminator network. 1) The main usage of the structure is to create an abstract measure of the dehazing model's performance, which via feedback mechanism helps in improving the weights of the input parameters.

Hodges et al. [6] created a model that is built on two separate networks: a dehazing network and a discriminator network.

1) The main usage of the structure is to create an abstract measure of the dehazing model's performance, which via feedback mechanism helps in improving the weights of the input parameters.
2) Their model initially estimates the transmission map. Consequently, by fitting in the formula of dehazing, the initial haze-free image is obtained. The second network in their case is a discriminator and helps in fine-tuning the earlier weights obtained.
3) Both the CNN1 and CNN2 models help in faster execution, a higher level of dehazing as compared to conventional methods of using statistical analysis and a lower value of loss function.

Goncalves et al. [8] model also employ a similar kind of 2 CNN based model except they do not make use of any dimension

Authorized licensed use limited to: DELHI TECHNICAL UNIV. Downloaded on June 15,2022 at 11:24:33 UTC from IEEE Xplore. Restrictions apply.

1) They use Inception-ResNet-v2 architecture with 16 feature maps as input and 16 feature maps as output. Their model was quick (0.055 sec by TitalX GPU) to dehaze a 224x224 image and may find application in haze removal of live-stream data due to low latency.
2) The model successfully dehazes small-range to mid-range images but the drawback is in dehazing of large depth images such as drone shots, distant objects.

Cai et al. [11] key contributions to developing dehazing patterns in the DehazeNet system include a model that computes a relation between hazy image patches and medium transmission; and Bilateral ReLU that improves convergence and restoration. The limitation of the model is dehazing large grey-white regions because it is sensitive to white colour.

Suarez et al. [10] formulate a haze imaging model and images are integrated even before they are being fed into the model.

1) They use CNNs to learn both transmission priors and dark channel for single image dehazing. Using hand-crafted priors, their model can estimate iteratively better values of the Transmission map.
2) Their results as compared to DCP, CAP, MSCNN, DehazeNet, AOD-Net were of higher contrast, better resolution. An extension of their work includes haze removal for the underwater image; the success of which is yet to be determined for which there needs to be a dataset that needs to be synthesized.

IV. GANs For Dehazing

After the outstanding performance of Generative Adversarial Networks, introduced by Goodfellow et al. , on computer vision tasks such as image classification, translation and image denoising, researchers have started focusing their attention on applying GANs on the problem of haze removal in the images. Many promising GAN based image de-hazing models have been proposed in the past few years which have successfully closed the gap between hazed and de-hazed images.

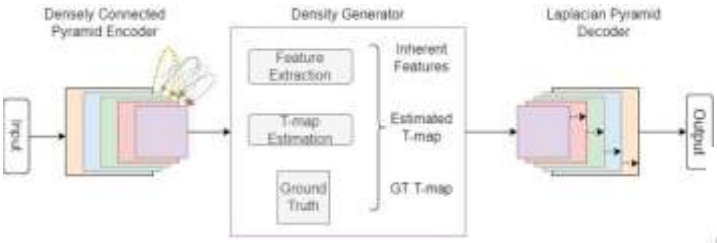

Fig. 2. Architecture of HDDNet

Zhang et al. [14] (Fig 2.) proposed a hierarchical density-aware dehazing network (HDDNet), consisting of :

1) a densely connected pyramid encoder to map input hazy images to feature representation. Different from the conventional encoders, the proposed encoder concatenates the downsampled features from the previous layers to the subsequent layers, thereby exploiting the multiscale features and capturing the global information of the hazy input.
2) a density generator to estimate haze concentration in the hazy input. Instead of evaluating the transmission maps on full resolution, the proposed density generator uses low resolution images for transmission map estimation.
3) a Laplacian pyramid decoder for progressive reconstruction of the dehazed images. Multiscale GANs are used at each pyramid level in order to improve the quality of dehazing. Six discriminators are trained to classify the image as fake or real so as to obtain realistic image textures at subsequent levels.

This model incorporated density estimation but subsided the need for atmospheric parameters and in turn provided superior results for synthetic as well as real world dataset against state-of-the-art models. However, this model has not yet been trained with a wider range of real world hazy images.

Qu et al. [15] presented a network for image dehazing, Enhanced Pix2pix GAN (EPDN). The model uses an enhancer for real-like image dehazing on fine-scale. The EPDN framework contains:

1) a generator (multi-resolution) that generates an image in coarse-to-fine manner. Two sub generators are employed; the first sub-generator works on coarse scale to generate an image, and the second sub-generator works on fine scale.
2) a discriminator (multi-scale) which helps in generation of realistic haze-free images. It consists of two discriminators to guide the generator having similar architecture, one to guide on the coarse scale and the other to guide on the fine scale.
3) an enhancer with two enhancing blocks to reinforce the generated image on the aspects of colour and details. The enhancing block focuses a receptive-field model for feature extraction on distinct levels.

The EPDN model does not rely on transmission map and atmospheric light for image dehazing. EPDN developed an image-to-image translation model for image dehazing. The model performs well for light hazed images but fails to retrieve the sharpness of edges in case of heavily hazed images.

Li et al. [16] (Fig 3.) established an encoder and de-

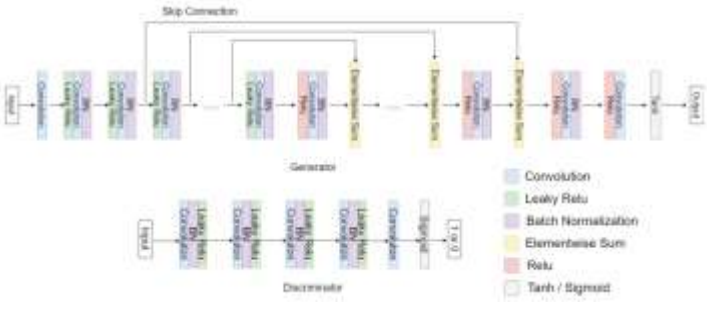

Fig. 3. Network structure of conditional GAN

coder architecture in conditional GAN along with a custom

Authorized licensed use limited to: DELHI TECHNICAL UNIV. Downloaded on June 15,2022 at 11:24:33 UTC from IEEE Xplore. Restrictions apply.

loss function based on pre-trained VGG features and L1-regularised gradient prior. The architecture consists of:

1) the generator consists of an encoding process and a decoding process. Encoding process provides feature maps to the symmetric layer of the decoding process and is based on up-sampling operations whereas the decoding process is based on down-sampling operations and uses a non-linear space transfer.
2) The discriminator used has a classic architecture with a batch of a convolutional layer followed by a batch normalisation layer and leaky Relu activation layer. Sigmoid activation layer is used as the final layer so as to limit the probability score to a range of [0,1].

The proposed model is robust to image noise and performs well against real world hazy images. However, the model has not been trained against an exhaustive dataset and hence it doesn't perform well for light hazy and night hazy images.

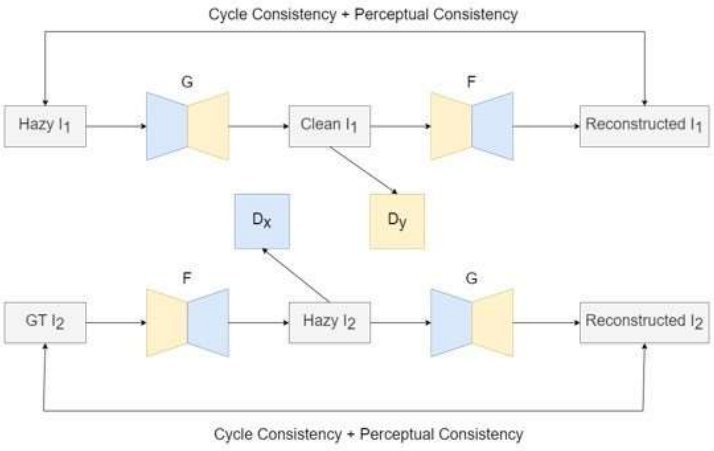

Fig. 4. Architecture of cycleDehaze network with G and F as Generators and D_x and D_y as Discriminators

Engin et al. [17] proposed an enhanced CycleGAN called CycleDehaze by combining cycle consistency and perceptual losses in order to preserve the textural information of the dehazed images. The major highlights of the proposed method are:

1) Cyclic perceptual-consistency loss to preserve the details and structures of the original image by taking into consideration the combination of high and low level features extracted from the VGG16 pooling layers.
2) Laplacian upscaling to preserve the resolution and edge details of high resolution hazy images. This process boosts the SSIM value during the upscaling level.
3) For high resolution input images bicubic downscaling was used and then Laplacian pyramid was used to upscale the low resolution outputs to their original resolution. The model performed superior to the state-of-the-art models but for outdoor conditions image sharpness was compromised.

Shao et al. [18] presented quite an innovative method for facilitating dehazing of real world images by including an image translation module along with 2 dehazing modules. In Fig-4 the representation is split into: haze to clean, and clean to hazy image. Image translation has been done using CycleGAN with the motive of presenting real world images as synthetic input images to the dehazing modules and this process has been termed as domain shift.

1) The image translation module consists of two translators, first, to convert real world to synthetic image and second, to convert synthetic to real world image. Since depth information is a key component of image dehazing, it is provided to the translator as an input in order to produce images with similar haze distribution.
2) The depth information is incorporated into the translation network by adopting the spatial feature transform (SFT) layer which can fuse features from depth map and synthetic image effectively.
3) Experimental results favoured the proposed model in dehazing real world images.

Yang et al. [19] illustrated a Disentangled Dehaze Network for generating dehazed images which are visually pleasing to the viewers rather than obtaining the original image. In the proposed method, the input hazy images are disentangled into three factors namely the transmission map, the scene radiance and the global atmospheric light using three generators. These three components are then composited using the haze function (eq 1) to reconstruct the original input. The research established that the difference between synthetic and real world images is that the synthetic or the forged image will definitely contain only haze whereas real world images may appear hazy but they might contain some heterogeneous components too which need not be removed. The proposed method introduces a physical-model based disentanglement and reconstruction mechanism along with multi-scale adversarial training to generate visually pleasing haze free images.

Dong et al. [20] proposed an innovative GAN based image dehazing method which uses a Fusion discriminator to guide the generator for producing more visually pleasing and realistic images along with a custom training dataset to improve the performance. The proposed model presented to major novelties:

1) A Fusion discriminator to guide the generator. Additional priors in terms of high frequency and low frequency characteristics are fed to the discriminator which further enhances its ability to compare textural and color differences between hazy and de-hazed images. Low frequency components such as smooth regions are extracted using Gausian filter whereas High frequency components such as fine details and sharp edges are determined using Laplace operator.
2) A custom training dataset consisting of various outdoor and indoor hazy images. Using this dataset for training the proposed model the authors emphasized on the fact that the performance of a learning based dehazing algorithm critically depends on the dataset quality. The proposed model performs better than many state-of-the-

Authorized licensed use limited to: DELHI TECHNICAL UNIV. Downloaded on June 15,2022 at 11:24:33 UTC from IEEE Xplore. Restrictions apply.

art methods to produce more visually pleasing de-hazed images with less color and textural distortion.

V. Applications of Image Dehazing

There has been a tremendous usage of newly developed observation techniques. Most of the new studies are focused on capturing images from the comfort of a safe environment like an office or observatory and utilizing them in various different important activities like surveillance and data analysis. However, often, it is observed that the degraded quality of the atmospheric conditions leads to the low-quality pictures, which are mostly of no use to the scientists or analysts, which in turn could have drastic effects. Various ways of dehazing have been already discussed in the paper till now, and now we can shed light on how they can be utilized and employed to generate a better quality of images so that they can have some plausible usage.

- **Photography in Water**

Clicking images in the water has been on the rise in the last few years. This may be to monitor pollution in the oceans, rivers, or lakes in the form of plastics or other pollutants. Along with this, it could be employed to monitor wildlife species or to discover new terrains inside the ocean, or maybe just for fun to create memories of a holiday. However, taking photographs inside water has never been an easy task and has its own set of challenges, like a failure of equipment and unclear photos. Former is primarily due to sprinkles and cast issues. Unclear images are a result of haze effects taking place when light reproduced from sight is scattered numerous times by water particles. This would consequently lead to a blurred image and would make it hard for anyone to recognize anything in it.

It has been observed that recently optimistic steps are being taken on this particular topic to reinstate the quality of the image and counter the issues caused by water. Many techniques are proving to be really effective in this cause. Progress here would lead to numerous benefits for underwater lives and geographical purposes.

- **Transportation Systems**

Every year lots of traffic-related issues come to the horizon and create havoc in the transportation system. It has been noted that most of the time, weather is not suitable for driving vehicles on the road because of fog, smoke or smog which causes huge traffic problems and results in decrements of efficiency of overall city life. Thousands of hours are wasted in the form of jams. Due to this, it would be a drastic shortcoming if they were not provided with clear and precise streaming. But recently, a lot of governments have taken this into consideration and are investing hugely to find solutions. If the drivers could be provided with a clear image of what is ahead of them on roads, the efficiency would boost up. Dehazing techniques could prove to be a plausible solution to this. However, as the vehicles move at high speeds, a faster image dehazing solution shall be required.

We often don't consider clear weather to be a problem for air transportation. However, this is not the case. Haze due to smoke, dust particles, or other suspended matter causes significant difficulties in takeoff and landing. Now, these being the most important aspects of a flight, require the utmost attention and precision. Numerous flights get postponed due to the low visibility of the runway and sky. For that reason, dehazing processes could prove to be useful to handle this issue.

The railways are among the worst affected due to weather, and they are the least advanced in tackling this issue as they have not installed any new instrument to mitigate the risks or any initiative to provide a better view for the locomotive driver. Numerous trains get postponed due to the low visibility of the track and a smog-filled environment, especially in winters. Governments are also least concerned about this situation. Better streaming of the tracks could have drastic effects on the timings and efficiency of the complete railway system. For that reason, dehazing processes could prove to be useful in handling this issue. The only issue in this process would be to provide a high-speed dehazing system (just as in roadways) to make it feasible in real-time situations. We are hopeful that in the coming years, GANs will help greatly in the transport systems as well.

- **Gathering of Evidence**

With the advancement of technologies and surveillance systems like CCTVs, crime rates have decreased. But a true change will only be seen if they provide a clear and recognizable image as evidence. Most of the cameras are able to show the activities in the background but are not able to depict the person in the foreground. This might be due to hardware limitations, but sometimes it is also because of bad atmospheric conditions. In those circumstances dehazing the image to process it for better quality will surely increase the reliability of evidence. Not only will it help to identify the accused in a situation, but it may also allow to nab him if he escapes. Along with this, it could also be really useful in the identification of cars at traffic signals which break the signal or speed limit. Therefore outdoor evidence in many cases can be improved.

- **Celestial Observation**

Astronomers face a lot of difficulties in observing the sky and capturing critical data for analysis in urban areas. Metropolitan cities are mostly covered with a dense haze due to various reasons. This makes it difficult for scientists to work. Captured images of astronomical objects can be improved drastically with dehazing methods. This will allow scientists to gather information without moving to remote locations and will also improve the quality of images previously captured.

VI. Comparative Analysis

Table 1 provides a comprehensive analysis of some of the most prominent image dehazing techniques proposed in recent years. The analysis is performed by taking several parameters into consideration such as computation complexity

Authorized licensed use limited to: DELHI TECHNICAL UNIV. Downloaded on June 15,2022 at 11:24:33 UTC from IEEE Xplore. Restrictions apply.

TABLE I
COMPARATIVE ANALYSIS

Method	Paper	Merits	Limitations	Applications
Multiscale GAN with Laplacian pyramid decoder	Zhang et al. [14]	Low computation time and memory	synthetic images are used for training	To preserve fine details in the image.
Pix2pix GAN followed by an enhancer	Qu et al. [15]	Doesn't rely on transmission map and atmospheric light estimations	not very robust for heavily hazy scene	To generate more realistic image in terms of colours and details
Modified Conditional GAN	Li et al. [16]	Good results in extreme hazy conditions	Restriction on the input size	To Dehaze extensively hazed images
CycleDehaze - An Enhanced Cycle GAN	Engin et al. [17]	Paired sample of ground truth and hazy images not required.	Reduced image sharpness in outdoor conditions	To dehaze high resolution images.
Cycle GAN based image translation module and two dehazing module	Shao et al. [18]	Real world images are used in training the dehaze module.	During training, input images are cropped randomly to make their size 256x256	Domain shift and to generate visually pleasing images
Disentangled Dehaze Network for generating dehazed images	Yang et al. [19]	The model can be trained using only unpaired supervision.	Unable to generate completely haze-free images	Usage on layered image, deraining and image matting
Densely connected Encoder-Decoder with a novel Fusion discriminator trained on a custom dataset.	Dong et al. [20]	Generate results that are more visually pleasing with less colour and textural distortion.	High inference time for higher resolution inputs	To Dehaze heavily hazed images as well as to produce visually pleasing de-hazed images.

and time, quality of the dataset, i.e., whether trained on a real or synthetic dataset, input image resolution, paired or unpaired training dataset, etc. This analysis gives sufficient information on the merits, demerits, and suitable applications of each proposed method. A multi-scale GAN with a Laplacian pyramid decoder required low computation time and memory, but the practice was limited to the use of a synthetic dataset. Pix-2-pix GAN doesn't rely on transmission map estimation but still generates more realistic images for lightly hazed images. A modified conditional GAN gives good results in extreme haze conditions, but there is a heavy restriction on the input size of the image. A cycle dehaze, which is an enhanced cycle GAN, can be used to dehaze high-resolution images. A disentangled dehaze network can be trained only using unpaired supervision but the problem still persists that it is not able to generate a completely haze free image.

VII. CONCLUSION

In this paper, we discussed various image dehazing methods on a number of viewpoints, including but not limited to theoretical models, equations involving mathematical fluency, and then we evaluated the predicted outcomes on various matrices. The study of many types of research provided a perspective on the advantages and limitations of the methods. We differentiated the techniques used in research before and after the GAN era. The way of approaching a dehazing problem saw a significant change after the introduction of generative adversarial networks. Generative adversarial networks are achieving good results in image dehazing. However, there is a further scope of improvement in image dehazing, which can be achieved by combining the knowledge of GANs and image dehazing. Further, it can be concluded that one method is not sufficient to deal with all types of weather in an image, i.e., one method can perform effective dehazing under certain conditions only. Thus, researchers are now aiming to combine multiple methods simultaneously, though deciding the order of the techniques still remains a very hot topic of discussion.

REFERENCES

[1] He, J., Gong, S., Zhou, C., Lu, S., Wu, L., Chen, Y., ... Yin, C. (2018). Analyses of winter circulation types and their impacts on haze pollution in Beijing. Atmospheric Environment, 192, 94-103.
[2] Fattal, R. (2008). Single image dehazing. ACM transactions on graphics (TOG), 27(3), 1-9. Chicago
[3] Ren, W., Liu, S., Zhang, H., Pan, J., Cao, X., Yang, M. H. (2016, October). Single image dehazing via multi-scale convolutional neural networks. In European conference on computer vision (pp. 154-169). Springer, Cham.
[4] Silberman, Nathan, Derek Hoiem, Pushmeet Kohli, and Rob Fergus. "Indoor segmentation and support inference from rgbd images." In European Conference on Computer Vision, pp. 746-760. Springer, Berlin, Heidelberg, 2012
[5] He, K., Sun, J., Tang, X. (2010). Single image haze removal usingdark channel prior. IEEE transactions on pattern analysis and machine intelligence, 33(12), 2341-2353.
[6] Hodges, C., Bennamoun, M., Rahmani, H. (2019). Single image dehazing using deep neural networks. Pattern Recognition Letters, 128, 70-77.
[7] Lefkimmiatis, S. (2017). Non-local color image denoising with convolutional neural networks. In Proceedings of the IEEE conference on computer vision and pattern recognition (pp. 3587-3596).
[8] Goncalves, L. T., Gaya, J. D. O., Drews, P., Botelho, S. S. D. C. (2017, October). Deepdive: An end-to-end dehazing method using deep learning. In 2017 30th SIBGRAPI Conference on Graphics, Patterns and Images (SIBGRAPI) (pp. 436-441). IEEE.
[9] Narasimhan, S. G., Nayar, S. K. (2003, October). Interactive (de) weathering of an image using physical models. In IEEE Workshop on color and photometric Methods in Computer Vision (Vol. 6, No. 6.4, p. 1). France.
[10] Suárez, P. L., Sappa, A. D., Vintimilla, B. X., Hammoud, R. I. (2018). Deep learning based single image dehazing. In Proceedings of the IEEE Conference on Computer Vision and Pattern Recognition Workshops (pp. 1169-1176).
[11] Cai, B., Xu, X., Jia, K., Qing, C., Tao, D. (2016). Dehazenet: An end-to-end system for single image haze removal. IEEE Transactions on Image Processing, 25(11), 5187-5198.

Authorized licensed use limited to: DELHI TECHNICAL UNIV. Downloaded on June 15,2022 at 11:24:33 UTC from IEEE Xplore. Restrictions apply.

[12] Sato, A., Yamaguchi, Y., Singh, G., Park, S. E. (2011). Four-component scattering power decomposition with extended volume scattering model. IEEE Geoscience and Remote Sensing Letters, 9(2), 166-170.
[13] Schechner, Y. Y., Narasimhan, S. G., Nayar, S. K. (2001, December). Instant dehazing of images using polarization. In Proceedings of the 2001 IEEE Computer Society Conference on Computer Vision and Pattern Recognition. CVPR 2001 (Vol. 1, pp. I-I). IEEE.
[14] Zhang, J., Ren, W., Zhang, S., Zhang, H., Nie, Y., Xue, Z., Cao, X. (2021). Hierarchical Density-Aware Dehazing Network. IEEE Transactions on Cybernetics.
[15] Qu, Y., Chen, Y., Huang, J., Xie, Y. (2019). Enhanced pix2pix dehazing network. In Proceedings of the IEEE/CVF Conference on Computer Vision and Pattern Recognition (pp. 8160-8168)
[16] Li, R., Pan, J., Li, Z., Tang, J. (2018). Single image dehazing via conditional generative adversarial network. In Proceedings of the IEEE Conference on Computer Vision and Pattern Recognition (pp. 8202-8211).
[17] Engin, D., Genç, A., Kemal Ekenel, H. (2018). Cycle-dehaze: Enhanced cyclegan for single image dehazing. In Proceedings of the IEEE Conference on Computer Vision and Pattern Recognition Workshops (pp. 825-833).
[18] Shao, Y., Li, L., Ren, W., Gao, C., Sang, N. (2020). Domain adaptation for image dehazing. In Proceedings of the IEEE/CVF Conference on Computer Vision and Pattern Recognition (pp. 2808-2817).
[19] Yang, X., Xu, Z., Luo, J. (2018, April). Towards perceptual image dehazing by physics-based disentanglement and adversarial training. In Proceedings of the AAAI Conference on Artificial Intelligence (Vol. 32, No. 1).
[20] Dong, Y., Liu, Y., Zhang, H., Chen, S., Qiao, Y. (2020, April). FD-GAN: Generative adversarial networks with fusion-discriminator for single image dehazing. In Proceedings of the AAAI Conference on Artificial Intelligence (Vol. 34, No. 07, pp. 10729-10736).
[21] Bhowmik, A., Kumar, S. Bhat, N. Evolution of automatic visual description techniques-a methodological survey. Multimed Tools Appl 80, 28015–28059 (2021).
[22] Mallik, A., Khetarpal, A. Kumar, S. ConRec: malware classification using convolutional recurrence. J Comput Virol Hack Tech (2022).
[23] Kumar, S., Kumar, M. (2019). Predicting Customer Churn Using Artificial Neural Network. In: Macintyre, J., Iliadis, L., Maglogiannis, I., Jayne, C. (eds) Engineering Applications of Neural Networks. EANN 2019.
[24] Bhowmik, A., Kumar, S., Bhat, N. (2019). Eye Disease Prediction from Optical Coherence Tomography Images with Transfer Learning. In: Macintyre, J., Iliadis, L., Maglogiannis, I., Jayne, C. (eds) Engineering Applications of Neural Networks. EANN 2019.
[25] Singh K., Parihar A.S. (2021), Variational optimization based single image dehazing, Journal of Visual Communication and Image Representation, (Vol. 79).
[26] Parihar, A.S., Singh, K, Rohilla, H, Asnani, G. Fusion-based simultaneous estimation of reflectance and illumination for low-light image enhancement. IET Image Process. 2021; 15: 1410– 1423.
[27] Parihar A.S., Gupta Y. K., Singodia Y., Singh V. and Singh K., "A Comparative Study of Image Dehazing Algorithms," 2020 5th International Conference on Communication and Electronics Systems (ICCES), 2020, pp. 766-771.
[28] B. Li et al., "Benchmarking single-image dehazing and beyond," IEEE Trans. Image Process., vol. 28, no. 1, pp. 492–505, Jan. 2019.
[29] Hamdan, Yasir Babiker. "Construction of Statistical SVM based Recognition Model for Handwritten Character Recognition." Journal of Information Technology 3, no. 02 (2021): 92-107.

Authorized licensed use limited to: DELHI TECHNICAL UNIV. Downloaded on June 15,2022 at 11:24:33 UTC from IEEE Xplore. Restrictions apply.

Proceedings of the Sixth International Conference on Intelligent Computing and Control Systems (ICICCS 2022)
IEEE Xplore Part Number: CFP22K74-ART; ISBN: 978-1-6654-1035-9

A Survey on Deep Learning Techniques for COVID-19 Detection using Medical Imaging

Harsh Jain
Department of Computer Engineering
Delhi Technological University
New Delhi, India
harshjain_2k18co140@dtu.ac.in

Bhanu Pratap Singh
Department of Computer Engineering
Delhi Technological University
New Delhi, India
bhanupratapsingh_2k18co109@dtu.ac.in

Aryan Rana
Department of Computer Engineering
Delhi Technological University
New Delhi, India
aryanrana_2k18co097@dtu.ac.in

Aruna Bhat
Department of Computer Engineering
Delhi Technological University
New Delhi, India
aruna.bhat@dtu.ac.in

2022 6th International Conference on Intelligent Computing and Control Systems (ICICCS) | 978-1-6654-1035-9/22/$31.00 ©2022 IEEE | DOI: 10.1109/ICICCS53718.2022.9788355

***Abstract*— Covid-19 has disrupted lives throughout the world. It has spread all over the world and detection of the virus is an imperative step in beating the virus. Methods such as the RTPCR and Rapid antigen tests are not only time consuming but also complex and expensive. Since the virus attacks the lungs, the Xray images of the chest can be used for the detection of coronavirus. This paper summarizes as well as gives a detailed study of the research and various techniques used for this subject. Methods used for COVID-19 detection using medical imaging using Chest X-Ray (CXR) and CT scan images as well as role and usage of GANs in tackling this problem have been summarized.**

Keywords*— *Deep Learning, GANs, COVID-19 detection, CNN, Medical Imaging

I. INTRODUCTION

The year 2020 saw the rise of COVID-19 cases around the world and deaths of millions of people all around the globe, ways to identify patients has become a problem gathering a lot of interest. Since machine learning and deep learning have been used to tackle problems in the area of healthcare in recent times, such methods have also been applied to the problem of detection of COVID-19. Most approaches focus on medical imaging to help detect COVID-19. These mainly include use of CXR or chest CT-scan images.

Since the problem of COVID-19 is fairly recent, the amount of patient data available is low which can become a restraint for deep learning models which usually require high amounts of data for getting stable results. Problems like this have been tackled by use of Generative Adversarial Networks (GANs) and deep learning techniques to help generate data to supplement existing datasets by generating synthetic data.

Convolutional neural networks (CNN) have been used extensively for the purpose of detection of COVID -19 using medical images as they operate fast and are able to capture features from images efficiently. Using deep convolutional neural networks, high accuracies have been achieved. As stated earlier, due to low availability of patient data, these accuracies may not be stable as the models might have overfit to smaller datasets.

II. USE OF CNN FOR COVID-19 DETECTION

Convolutional neural networks (CNN) have been used for working with medical images since they make use of convolutional images which work with kernels to deduct spatial information from images. CNNs are faster than other types of models when working on images and also provide better results as the convolutional layers are designed to manipulate images. Deep learning models require a large amount of data to train, and since COVID-19 pandemic is recent, the amount of CXR and CT scan images are low in number. This affects both the training and reliability of deep learning models. In [1] the authors review the effect of occlusion in images and how they can affect classification and mention techniques to alleviate the effects of occlusions in these images. [2] sheds light toward the difficulty of prediction of COVID-19 from chest CT scans due to boundary blurring and proposes a data driven framework to counter the same thus making an unbiased learning model.

In [3] the authors use deep learning to tackle the problem of COVID-19 detection. They use the EfficientNet model on chest CT scan images. They used fixed, cyclic as well as learning rate reduced on plateau strategy to fine tune their model where the plateau strategy performed best on their testing model with an accuracy of 89.7% followed by the cyclic learning rate which achieved an accuracy of 86% while a constant learning rate yielded 83% accuracy on their test set.

In [4] the authors use chest CT scan images to detect COVID-19 by using the LeNet-5 CNN architecture. They used data augmentation techniques to improve on the size of the dataset as there is lower availability of CT scan images of COVID-19 positive patients. They Converted all images to grayscale before feeding them to the model. They achieved 86.06% accuracy with this technique. In [5] the authors use low-dose chest CT images to detect COVID. The low-dose CT scan reduces the radiation exposure to the patients which is a safer method. They use a deep CNN for the classification process and conclude that the dosage can be reduced up to 89% while still keeping most of the information intact. [6] has a CNN for multiclass classification in which they combine numerous datasets to accumulate 10,200 chest CT images which include normal,COVID-19 positive as well as lung cancer patients and perform conversion so that the data is standardized. They got an accuracy of 94% with this model.

In [7], the authors propose a newer approach for recognition of COVID-19 from CT-scans based on deep learning. The authors employ CNN architectures with multi-task strategy for classification of the CT-scans into Normal,

Authorized licensed use limited to: DELHI TECHNICAL UNIV. Downloaded on June 15,2022 at 11:18:18 UTC from IEEE Xplore. Restrictions apply.

COVID-19 or community acquired pneumonia (CAP) classes defined by the authors. For the patient-level classification stage, the authors divided the CT-scans based on their number of slices, and used the models they trained previously on the slices of each group. Using this approach, they achieved an overall accuracy of 87.75%.

In [8], a two-stage CNN based framework is proposed by the authors for the classification of chest CT - scans in order to detect COVID-19 or Community Acquired Pneumonia. The dataset used by the authors is the SPGC Dataset, containing chest CT-scans of healthy, COVID-19 and CAP classes. The first stage is concerned with the detection of an infection of either COVID-19 or CAP using the DenseNet architecture. For the second stage, the authors employ a fine-grained multiclass classification using an EfficientNet architecture. Using this two stage approach, the authors managed to achieve a 94% accuracy at the slice level classification into COVID-19 or CAP, while the three-way classification reached an accuracy of around 89.3% into the classes of COVID-19, CAP or healthy for their validation set.

In [9] the authors have used a hybrid method of using a CNN and the Histogram of Oriented Gradients to introduce a model to help classify the CXR images as covid positive or negative. Image augmentation techniques were also used in order to expand the dataset. The results indicated that the most efficient results were obtained when all the features of the CNN and HOG were combined together, resulting in a 99.67% testing accuracy.

In [10], the authors propose an AI model which would classify an X-Ray image into four classes, namely COVID-19 , CAP or healthy CXR images. The system works in two stages. The first stage classifies the image as pneumonia or non-pneumonia. If stage 1 classifies the image as pneumonic, then stage 2 classifies it into COVID-19 positive or negative. The dataset used in this paper was acquired from SIRM and ESR. Stage 1 achieved a maximum accuracy of 96.5% and stage 2 classification had an accuracy of 98.31%.

In [11] the authors use transfer learning for COVID-19 detection using 3D Resnet50. Instead of training on just 2D images, this technique uses volumetric analysis for a multiclass classification for normal, pneumonial and COVID positive classes. The data was full volumetric chest CT scans for the patients rather than just a single slice from it. They use a novel preprocessing technique for this data which includes resampling, pulmonary segmentation as well as volume range selection to extract salient features from the slices. They achieved an accuracy of 85.56%.

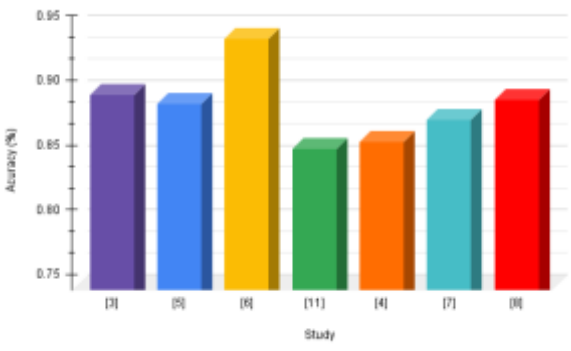

Fig. 1. Accuracy comparison of CNN on chest CT scan

Figure 1 shows the comparison of the accuracies of the CNNs developed in various research articles. In [12] the authors present a model to predict COVID-19 using a deep convolutional neural network called CheXNet from chest x-ray images. CheXNet consists of 121 layers, and helps in detection of COVID-19 by producing a heatmap which helps in the localization of the area which indicates high chances of symptoms for diseases with another metric of prediction probability. For the model proposed, the authors built a CheXNet model by using a pre-trained model of DenseNet121. The authors used the chestXray14 dataset for training their model, and achieved an accuracy of 99.9% in classifying images in binary classes (normal and COVID-19). They discuss implementing the model for real-time scenarios with further developments and working with a bigger dataset for better results. [13] introduces COVID-MobileXpert, which is a lightweight deep neural network based mobile application. This app can scan CXR images for Covid-19 Screening. The deep neural network was a fine-tuned Resident Fellow network for classification of the image into COVID-19 positive or negative, pneumonia or no pneumonia followed by a lightweight medical student network. They concluded from the experiments and results that the MobileNetV2 based COVID-19 app was resource hungry and had higher accuracy as compared to the SqueezeNet based mobile app which was not as resource hungry but also compromised on the accuracy of the app. This means that the MobileNetV2 based app could be used in high performance devices whereas the SqueezeNet is more suited for low end mobile devices. In [14] the authors propose a method based on deep learning. The purpose of the model is detection and localisation of pneumonia in CXR scans. “Pneumonia Ratio” is the metric calculated from the localization maps which is then used to calculate the severity of pneumonia. The backbone of this deep learning model was ResNet50. A localization head fused the intermediate layers of ResNet to form a localization prediction. A detection head was integrated for detecting pneumonia. The RSNA Pneumonia Detection challenge dataset, the Covid19 Image data collection dataset as well as the COVID19 Chest Xray Dataset were used in different combinations for model training. The model achieved accuracies ranging from 0.86 to 0.95, the minimum when just the RSNA Pneumonia Detection challenge dataset was used and the maximum when all the datasets were leveraged.

[15] explains the use of an ensemble model for detection of COVID and uses ensemble and deep learning techniques to mitigate the using snapshots of the models proposed in [16] and a weighted average type ensembling technique taking care of the different sensitivities of the models. [17] uses the VGG-16 based model for COVID-19 detection. [18] proposes a novel CNN architecture which has accuracy of 99.02%. It made use of X-Ray images for the detection of COVID.

In [19] the authors make use of Rmsprop and SGD optimizers for faster computational performance. The purpose was to make a real time COVID-19 detection system. They were able to speed up the time required for training and testing using these optimizers which results in faster classification thus more people can be classified early and the rate of spread of pandemic can be lowered. In [20] the authors use CLAHE to enhance the images to improve performance and also compare their CNN using CLAHE against a VGG-16 with transfer learning and show its

Authorized licensed use limited to: DELHI TECHNICAL UNIV. Downloaded on June 15,2022 at 11:18:18 UTC from IEEE Xplore. Restrictions apply.

superior performance where the CLAHE enhanced model receives 98% while using VGG16 with transfer learning gives only about 50% accuracy rate. In [21], the paper discusses how the current research for Pneumonia diagnosis focuses on only a single modality of

TABLE I. A BRIEF SUMMARY OF SOME OF THE ARTICLES AND THEIR METHODOLOGIES

Study	Approach	Classification	Accuracy (%)
[12]	CheXNet	Binary Classification on CXR (Healthy or COVID-19)	99.9%
[21]	Concatenation of ResNet50 and VGG16	Binary Classification on CXR and CT scan (Healthy or COVID-19)	98% For CT scans 98.93% for X ray Images
[7]	CNN Architectures	Multiclass classification on CXR (Healthy, COVID-19 and Cap Classes)	87.75%
[8]	Two Stage CNN	Multiclass classification on CXR (Healthy, COVID-19 and Cap Classes)	89.3%
[14]	ResNet50	Multiclass classification on CXR (Healthy, COVID-19 and Pneumonia)	Ranging from 86% to 95%, depending on the combination of the datasets used.
[13]	COVID-MobileXpert	Multiclass classification on CXR (Healthy, COVID-19 and Pneumonia)	MobileNetV2 and SqueezeNet were used. Concluded that MobileNetV2 is more resource hungry than SqueezeNet along with higher accuracy.
[10]	2 Stage AI Model, Stage 1: Pneumonia / no Pneumonia Stage 2: Covid / Non Covid	Multiclass classification on CXR (Healthy, COVID-19 and Pneumonia)	Stage 1: 96.5% Stage 2: 98.31%
[9]	Hybrid Model: CNN and Histogram of Oriented Gradients	Binary Classification on CXR (Healthy and COVID-19)	CNN + HOG: 99.67%
[4]	LeNet-5 CNN	Binary Classification on CXR (data aug: grayscale images) (Healthy and COVID-19)	86.06

data such as CT Scans or X-rays or some other modality. The authors discuss how different biomarkers may be able to provide information for detection of COVID-19. Following this, the authors propose the concatenation of two transfer learning models for which they use an open-source dataset, divided into binary classes of COVID-19 Pneumonia and Normal. By concatenating different transfer learning models, the authors get great accuracy, achieving the highest accuracy of 99.87% by concatenating ResNet50 and VGG16 networks.

Table 1 summarises the Articles reviewed in this paper. The approach, type of classification and the accuracies achieved are tabulated as shown. [12] has the best accuracy for binary classification as opposed to [4] which does not have a very high accuracy.

Authorized licensed use limited to: DELHI TECHNICAL UNIV. Downloaded on June 15,2022 at 11:18:18 UTC from IEEE Xplore. Restrictions apply.

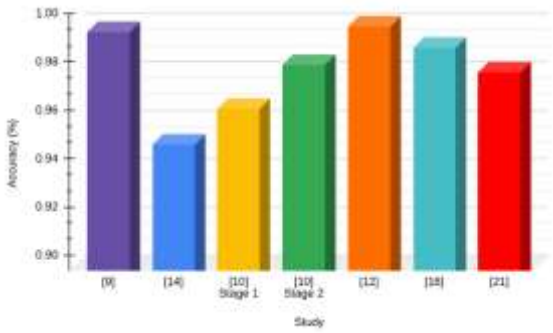

Fig. 2. Accuracy comparison of CNN on CXR images

They also managed to achieve a 98.00% accuracy for single modality CT-scan images with the ResNet50 network. An accuracy of 98.93% was achieved for X-Ray images with VGG16 networks.

Figure 2 visualises the comparison of the CNNs developed in some more research articles.

III. Limitations of Existing Work

Most of the work done in COVID-19 up until now, has been done on datasets of relatively smaller size, which makes the results of these papers unreliable, and thus unfit for practical purposes in real life situations. Thus, the unavailability of bigger datasets for COVID-19 is the major limiting factor for most researches related to COVID-19.

IV. Use of GANs For Covid-19 Detection

GANs or generative Adversarial networks utilize two models, a generator and a discriminator. For generating synthetic images, the generator tries to model fake images from noise while the discriminator tries to judge whether the image it received was generated by the generator or it came from a dataset with real images. This allows the generator to train as it tries to maximize the discriminator's loss. GANs have been used to generate images to supplement existing datasets as COVID-19 datasets generally do not have enough images themselves to be able to effectively train deep learning networks.

A. Background: GANs in Healthcare

[22] employs deep adversarial learning for segmentation of mammograms, using a fully convolutional network. [23] uses GANs for converting an image to another, the authors introduce a GAN capable of translating a PET image into a CT-Scan, in addition to this it is also capable of reducing noise in MRI image as well as PET image denoising. [24] uses a GAN model implemented using a variational autoencoder to supplement MRI images generated using a new ASL technique. In [25] the authors propose a GAN implementation which treats low and high quality images differently and also constrains the structure and illumination of the images to enhance them. [26] uses two different GANs to generate and supplement a dataset to improve performance of a CNN used to detect liver lesion in images. [27] works on denoising CT scan images using GAN, the authors use Wasserstein distance for this implementation. In [28], the authors implement a combination of two GANs to improve the resolution of low quality images for better performance on deep learning networks and test it on medical ultrasound images. In [29] the authors use a DC- GAN to generate COVID-19 positive chest CT scan images to supplement available datasets.

B. GANs for COVID-19 Detection

In [30] the authors use an auxiliary classifier GAN to help supplement datasets with synthetic CXR images and improve performance of a CNN by supplementing using these synthetic images. [31] uses Edge cloud computing with GANs in which they have local GANs which share data with each other over the cloud and this is combined to make a better performing global GAN. [32] undertakes training of a model that employs deep learning to classify COVID-19 cases using a GAN and generic data augmentation methods on CXR images, this helps make the model robust, they also compare this model to widely used CNN models such as ResNet and DenseNet. [33] uses a teacher student model as well as transfer learning GAN to generate realistic CXR images that improves the performance of not only a binary classifier but also multi class classifiers similar to [2] and [34] which also detect pneumonia.

GANs have also been used to generate and supplement chest CT-scan data such as in [35] where the authors display the risks of collecting CT scans from infected patients for medical staff and how the safer GAN route can thus outperform those images. In [36], the authors implement image to image translation by using a GAN to transform normal CXR images to COVID-19 positive CXR images to help generate more data and remove imbalances in the datasets. [37] proposes a GAN model for a reverse effect where they generate normal CT scans from COVID-19 CT scans and employ a novel method to make the realism of the GAN generated synthetic COVID-19 data more effective, by this they try to learn the localization mappings used for classification to assist classification systems.

V. Proposed Methodology

Use of deep learning techniques for COVID-19 detection has shown promising results, also shown by other methods mentioned in [38]. They can be applied in the real world in conjunction with other techniques such as RT-PCR tests currently, and with stable models and enough data, we might be able to use such models independently. Since the amount of training data is low, the models may have overfit and the results may not be stable so using only these techniques would not be viable since it is a matter of health care. Thus, we propose that by supplementing datasets with GAN generated images and making models more stable, these problems may be alleviated a little.

We propose a system that might be able to produce more stable models with the help of GANs
The system also uses data from multiple sources to increase volume since deep learning models are more stable if they have a large quantity of data to train on and have less chance of overfitting.

The first step is to gather data from various sources such as available datasets as well as hospitals and medical institutions to create a combined dataset for training the

Authorized licensed use limited to: DELHI TECHNICAL UNIV. Downloaded on June 15,2022 at 11:18:18 UTC from IEEE Xplore. Restrictions apply.

models. Since these images are from different sources we can use preprocessing techniques like resizing, cropping as well as contrast equalization to make a more homogenous dataset.

Since the amount of COVID-19 positive medical images are low, we could use a GAN to synthesize fake COVID-19 positive images similar to the ones present in our dataset and use them to supplement our bigger dataset.

We could then train CNN models or other deep learning models on these supplemented datasets which should improve overall accuracy of detection

$$Accuracy = \frac{Number\ of\ Correct\ Predictions}{Total\ Number\ of\ Predictions} * 100\% \quad (1)$$

VI. Conclusion And Future Scope

There is a lot of scope for deep learning for this task and with increase in the amount of available data as well as GAN usage we might see better and stable results with newer techniques. This will increase the accuracy of existing models not only on existing datasets but also larger amounts of newer data that the models have not seen before.

Data can be handpicked from the datasets which are available as of now and then a GAN model can be trained on this handpicked, high-quality data. Handpicking high quality data would ensure that the GAN model trained would give results which are as close to the real images as possible. An augmented dataset can hence be created with the help of using the GAN generated images. This dataset can then in turn be used to train various classifiers which can then be used, at scale, to detect and identify COVID-19 from Chest X Ray Scans.

References

[1] B. Udawat, A. Santani and S. Agrawal, "Occlusion Detection for COVID-19 Identification: A Review," 2021 7th International Conference on Advanced Computing and Communication Systems (ICACCS), 2021, pp. 298-301, doi: 10.1109/ICACCS51430.2021.9441749.

[2] Y. Yang et al., "Towards Unbiased Covid-19 Lesion Localisation And Segmentation Via Weakly Supervised Learning," 2021 IEEE 18th International Symposium on Biomedical Imaging (ISBI), 2021, pp. 1966-1970, doi: 10.1109/ISBI48211.2021.9433806.

[3] T. Anwar and S. Zakir, "Deep learning based diagnosis of COVID-19 using chest CT-scan images," 2020 IEEE 23rd International Multitopic Conference (INMIC), 2020, pp. 1-5, doi: 10.1109/INMIC50486.2020.9318212.

[4] M. R. Islam and A. Matin, "Detection of COVID 19 from CT Image by The Novel LeNet-5 CNN Architecture," 2020 23rd International Conference on Computer and Information Technology (ICCIT), 2020, pp. 1-5, doi: 10.1109/ICCIT51783.2020.9392723.

[5] I. Shiri et al., "Deep Residual Neural Network-based Standard CT Estimation from Ultra-Low Dose CT Imaging for COVID-19 Patients," 2020 IEEE Nuclear Science Symposium and Medical Imaging Conference (NSS/MIC), 2020, pp. 1-3, doi: 10.1109/NSS/MIC42677.2020.9507847.

[6] Y. Saad, A. Mustapha and A. Cherry, "Automatic classification between COVID-19 pneumonia, lung cancer and normal lung tissues on chest CT Scans," 2021 Sixth International Conference on Advances in Biomedical Engineering (ICABME), 2021, pp.197-201, doi:10.1109/ICABME53305.2021.9604860.

[7] F. Bougourzi, R. Contino, C. Distante and A. Taleb-Ahmed, "CNR-IEMN: A Deep Learning Based Approach to Recognise Covid-19 from CT-Scan," ICASSP 2021 - 2021 IEEE International Conference on Acoustics, Speech and Signal Processing (ICASSP), 2021, pp. 8568-8572, doi: 10.1109/ICASSP39728.2021.9414185.

[8] S. Chaudhary, S. Sadbhawna, V. Jakhetiya, B. N. Subudhi, U. Baid and S. C. Guntuku, "Detecting Covid-19 and Community Acquired Pneumonia Using Chest CT Scan Images With Deep Learning," ICASSP 2021 - 2021 IEEE International Conference on Acoustics, Speech and Signal Processing (ICASSP), 2021, pp. 8583-8587, doi: 10.1109/ICASSP39728.2021.9414007.

[9] Aleka Melese Ayalew, Ayodeji Olalekan Salau, Bekalu Tadele Abeje, Belay Enyew,Detection and classification of COVID-19 disease from X-ray images using convolutional neural networks and histogram of oriented gradients,Biomedical Signal Processing and Control,Volume 74, 2022, 103530, ISSN 1746-8094,https://doi.org/10.1016/j.bspc.2022.103530.

[10] M. Mishra, V. Parashar and R. Shimpi, "Development and evaluation of an AI System for early detection of Covid-19 pneumonia using X-ray (Student Consortium)," 2020 IEEE Sixth International Conference on Multimedia Big Data (BigMM), 2020, pp. 292-296, doi: 10.1109/BigMM50055.2020.00051.

[11] S. Xue and C. Abhayaratne, "Covid-19 Diagnostic Using 3d Deep Transfer Learning for Classification of Volumetric Computerised Tomography Chest Scans," ICASSP 2021 - 2021 IEEE International Conference on Acoustics, Speech and Signal Processing (ICASSP), 2021, pp. 8573-8577, doi: 10.1109/ICASSP39728.2021.9414947.

[12] D. Haritha, M. K. Pranathi and M. Reethika, "COVID Detection from Chest X-rays with DeepLearning: CheXNet," 2020 5th International Conference on Computing, Communication and Security (ICCCS), 2020, pp. 1-5, doi: 10.1109/ICCCS49678.2020.9277077.

[13] X. Li, C. Li and D. Zhu, "COVID-MobileXpert: On-Device COVID-19 Patient Triage and Follow-up using Chest X-rays," 2020 IEEE International Conference on Bioinformatics and Biomedicine (BIBM), 2020, pp. 1063-1067, doi: 10.1109/BIBM49941.2020.9313217.

[14] M. Frid-Adar, R. Amer, O. Gozes, J. Nassar and H. Greenspan, "COVID-19 in CXR: From Detection and Severity Scoring to Patient Disease Monitoring," in IEEE Journal of Biomedical and Health Informatics, vol. 25, no. 6, pp. 1892-1903, June 2021, doi: 10.1109/JBHI.2021.3069169.

[15] S. Tang et al., "EDL-COVID: Ensemble Deep Learning for COVID-19 Case Detection From Chest X-Ray Images," in IEEE Transactions on Industrial Informatics, vol. 17, no. 9, pp. 6539-6549, Sept. 2021, doi: 10.1109/TII.2021.3057683.

[16] Wang, L., Lin, Z.Q. & Wong, A. COVID-Net: a tailored deep convolutional neural network design for detection of COVID-19 cases from chest X-ray images. Sci Rep 10, 19549 (2020). https://doi.org/10.1038/s41598-020-76550-z

[17] Y. -C. Chang, A. -S. Liu and W. -C. Chu, "Using Deep Learning Algorithms in Chest X-ray Image COVID-19 Diagnosis," 2021 IEEE 3rd Eurasia Conference on Biomedical Engineering, Healthcare and Sustainability (ECBIOS), 2021, pp. 74-76, doi: 10.1109/ECBIOS51820.2021.9510393.

[18] E. Irmak, "A Novel Deep Convolutional Neural Network Model for COVID-19 Disease Detection," 2020 Medical Technologies Congress (TIPTEKNO), 2020, pp. 1-4, doi: 10.1109/TIPTEKNO50054.2020.9299286.

[19] M. Fradi and M. Machhout, "Real-Time Application for Covid-19 Class Detection based CNN Architecture," 2021 IEEE International Conference on Design & Test of Integrated Micro & Nano-Systems (DTS), 2021, pp. 1-6, doi: 10.1109/DTS52014.2021.9498055.

[20] disB. K. Umri, M. Wafa Akhyari and K. Kusrini, "Detection of Covid-19 in Chest X-ray Image using CLAHE and Convolutional Neural Network," 2020 2nd International Conference on Cybernetics and Intelligent System (ICORIS), 2020, pp. 1-5, doi: 10.1109/ICORIS50180.2020.9320806.

[21] N. Hilmizen, A. Bustamam and D. Sarwinda, "The Multimodal Deep Learning for Diagnosing COVID-19 Pneumonia from Chest CT-Scan and X-Ray Images," 2020 3rd International Seminar on Research of Information Technology and Intelligent Systems (ISRITI), 2020, pp. 26-31, doi: 10.1109/ISRITI51436.2020.9315478.

[22] Zhu, Wentao & Xiang, Xiang & Tran, Trac & Hager, Gregory & Xie, Xiaohui. (2018). Adversarial Deep Structured Nets for Mass Segmentation from Mammograms. IEEE International Symposium on Biomedical Imaging (ISBI).

Authorized licensed use limited to: DELHI TECHNICAL UNIV. Downloaded on June 15,2022 at 11:18:18 UTC from IEEE Xplore. Restrictions apply.

[23] Armanious, Karim & Jiang, Chenming & Fischer, Marc & Küstner, Thomas & Hepp, Tobias & Nikolaou, Konstantin & Gatidis, Sergios & Yang, Bin. (2019). MedGAN: Medical image translation using GANs. Computerized Medical Imaging and Graphics. 79. 101684. 10.1016/j.compmedimag.2019.101684.

[24] Li, Feihong & Huang, Wei & Luo, Mingyuan & Zhang, Peng & Zha, Yufei. (2021). A new VAE-GAN model to synthesize arterial spin labeling images from structural MRI. Displays. 70. 102079. 10.1016/j.displa.2021.102079

[25] Y. Ma et al., "Structure and Illumination Constrained GAN for Medical Image Enhancement," in IEEE Transactions on Medical Imaging, doi: 10.1109/TMI.2021.3101937.

[26] Frid-Adar, Maayan & Diamant, Idit & Klang, Eyal & Amitai, Marianne & Goldberger, Jacob & Greenspan, Heather. (2018). GAN-based Synthetic Medical Image Augmentation for increased CNN Performance in Liver Lesion Classification. Neurocomputing. 321. 10.1016/j.neucom.2018.09.013.

[27] Yang, Qingsong & Yan, Pingkun & Zhang, Yanbo & Yu, Hengyong & Shi, Yongyi & Mou, Xuanqin & Kalra, Mannudeep & Zhang, Yi & Sun, Ling & Wang, Ge. (2017). Low-Dose CT Image Denoising Using a Generative Adversarial Network With Wasserstein Distance and Perceptual Loss. IEEE Transactions on Medical Imaging. PP. 10.1109/TMI.2018.2827462.

[28] Y. Zhu, Z. Zhou, G. Liao and K. Yuan, "Csrgan: Medical Image Super-Resolution Using A Generative Adversarial Network," 2020 IEEE 17th International Symposium on Biomedical Imaging Workshops (ISBI Workshops), 2020, pp. 1-4, doi: 10.1109/ISBIWorkshops50223.2020.9153436.

[29] P. Mann, S. Jain, S. Mittal and A. Bhat, "Generation of COVID-19 Chest CT Scan Images using Generative Adversarial Networks," 2021 International Conference on Intelligent Technologies (CONIT), 2021, pp. 1-5, doi: 10.1109/CONIT51480.2021.9498272.

[30] A. Waheed, M. Goyal, D. Gupta, A. Khanna, F. Al-Turjman and P. R. Pinheiro, "CovidGAN: Data Augmentation Using Auxiliary Classifier GAN for Improved Covid-19 Detection," in IEEE Access, vol. 8, pp. 91916-91923, 2020, doi: 10.1109/ACCESS.2020.2994762.

[31] D. C. Nguyen, M. Ding, P. N. Pathirana, A. Seneviratne and A. Y. Zomaya, "Federated Learning for COVID-19 Detection with Generative Adversarial Networks in Edge Cloud Computing," in IEEE Internet of Things Journal, doi: 10.1109/JIOT.2021.3120998.

[32] S. Sakib, T. Tazrin, M. M. Fouda, Z. M. Fadlullah and M. Guizani, "DL-CRC: Deep Learning-Based Chest Radiograph Classification for COVID-19 Detection: A Novel Approach," in IEEE Access, vol. 8, pp. 171575-171589, 2020, doi: 10.1109/ACCESS.2020.3025010.

[33] S. Menon et al., "Generating Realistic COVID-19 x-rays with a Mean Teacher + Transfer Learning GAN," 2020 IEEE International Conference on Big Data (Big Data), 2020, pp. 1216-1225, doi: 10.1109/BigData50022.2020.9377878

[34] A. Shankar, Y. Sonar and K. A. Sultanpure, "Detection of COVID-19 using Chest X-Ray Scans," 2020 IEEE Bangalore Humanitarian Technology Conference (B-HTC), 2020, pp. 1-6, doi: 10.1109/B-HTC50970.2020.9297910.

[35] Y. Jiang, H. Chen, M. Loew and H. Ko, "COVID-19 CT Image Synthesis With a Conditional Generative Adversarial Network," in IEEE Journal of Biomedical and Health Informatics, vol. 25, no. 2, pp. 441-452, Feb. 2021, doi: 10.1109/JBHI.2020.3042523.

[36] Z. Liang, J. X. Huang, J. Li and S. Chan, "Enhancing Automated COVID-19 Chest X-ray Diagnosis by Image-to-Image GAN Translation," 2020 IEEE International Conference on Bioinformatics and Biomedicine (BIBM), 2020, pp. 1068-1071, doi: 10.1109/BIBM49941.2020.9313466.

[37] Z. Yang, L. Zhao, S. Wu and C. Y. -C. Chen, "Lung Lesion Localization of COVID-19 From Chest CT Image: A Novel Weakly Supervised Learning Method," in IEEE Journal of Biomedical and Health Informatics, vol. 25, no. 6, pp. 1864-1872, June 2021, doi: 10.1109/JBHI.2021.3067465.

[38] Sachin and A. Bhat, "A Survey on COVID-19 Detection from X-ray Images using Deep Learning," 2021 12th International Conference on Computing Communication and Networking Technologies (ICCCNT), 2021, pp. 1-6, doi: 10.1109/ICCCNT51525.2021.9580164.

Authorized licensed use limited to: DELHI TECHNICAL UNIV. Downloaded on June 15,2022 at 11:18:18 UTC from IEEE Xplore. Restrictions apply.

Computers and Electrical Engineering 102 (2022) 108158

Contents lists available at ScienceDirect

Computers and Electrical Engineering

journal homepage: www.elsevier.com/locate/compeleceng

A tree classifier based network intrusion detection model for Internet of Medical Things☆

Karan Gupta [a], Deepak Kumar Sharma [b,*], Koyel Datta Gupta [c], Anil Kumar [d]

[a] Department of Information Technology, Netaji Subhas University of Technology, New Delhi, India
[b] Department of Information Technology, Indira Gandhi Delhi Technical University for Women, Delhi, India
[c] Department of Computer Science and Engineering, Maharaja Surajmal Institute of Technology, New Delhi, India
[d] Data Science Research Group, School of Computing, DIT University, Dehradun, India

ARTICLE INFO

Keywords:
Internet of Medical Things
Intrusion detection
Tree classifier
Security
Estimator

ABSTRACT

Healthcare is one of the key areas of prospect for the Internet of Things (IoT). To facilitate better medical services, enormous growth in the field of the Internet of Medical Things (IoMT) is observed recently. Despite the numerous benefits, the cyber threats on connected healthcare devices can compromise privacy and can also cause damage to the health of the concerned patient. The massive demand for IoMT devices with seamless and effective medical facilities for the large-scale population requires a robust secured model to ensure the privacy and safety of patients in this network. However, designing security models for IoMT networks is very challenging. An effort has been made in this work, to design a tree classifier-based network intrusion detection model for IoMT networks. The proposed system effectively reduces the dimension of the input data to speed up the anomaly detection procedure while maintaining a very high accuracy of 94.23%.

1. Introduction

Revolutionary progress of IoT in different fields including healthcare has made the dispense of services a lot more effective and expedient. Remote patient monitoring systems using sensors have made the medical treatment convenient and precise without requiring the presence of medical practitioners at the site [1,2]. The IoMT technology has empowered the medical community to provide several facilities like early disease diagnosis, increased productivity, remote monitoring of health parameters to a large number of population. The early detection of diseases using IoMT devices can save several lives and even reduce the medical costs also. The patient information collected through the medical devices can also be saved in the IoMT cloud database for future use. However, cyber-attacks are posing serious threats to digital healthcare monitoring and record keeping.

The security breach in IoMT devices and networks can cause interference in disease diagnosis, delayed communication and also cause loss of patients' private information. The security threats related to IoMT devices and connections are escalating owing to the expertise of the hackers. Manipulation of medical devices and unauthorized access of health records through internet can be caused by diverse malicious malwares. The mode and nature of such attacks are changing rapidly and the existing procedures are not adequate for malware identification and respective analysis. Most of the cyber attacks result in Distributed denial of service

☆ This paper is for special section VSI-aihc. Reviews were processed by Guest Editor Dr. Deepak Gupta and recommended for publication.

* Corresponding author.
E-mail addresses: karankg1997@gmail.com (K. Gupta), dk.sharma1982@yahoo.com (D.K. Sharma), koyel.dg@msit.in (K. Datta Gupta), dahiyaanil@yahoo.com (A. Kumar).

https://doi.org/10.1016/j.compeleceng.2022.108158
Received 31 January 2022; Received in revised form 30 May 2022; Accepted 2 June 2022
Available online 17 June 2022
0045-7906/© 2022 Elsevier Ltd. All rights reserved.

(DDoS), denying access of devices or data to legitimate users. Hence, it is extremely important to identify any kind of unauthorized invasion in the IoMT system.

Several security mechanisms have been developed in past to protect IoT system including authentication, encryption and intrusion detection [3–5]. An intrusion detection system (IDS) [6] can identify an attack by examining system variables and possible attack signs or by detecting deviation from normal behaviour. Malicious activities can steal or modify health data either by intercepting the information during transmission in wireless medium or by accessing the cloud servers in an unauthorized manner. Attackers may also intervene with the diagnosis procedure. All these security breaches have a deep and long-lasting impact on the IoMT environment. This requires designing of a time efficient accurate IDS for the IoMT system.

In recent times researchers have been focusing specifically on Machine Learning (ML) techniques for detecting intrusions judiciously. In spite of several existing data analysis and statistical techniques for IDS, identifying new malicious activities is difficult. However, ML algorithms has the ability to recognize the dynamic changes in these activities' signatures. Machine Learning based models can be deployed in IDS for determining both network level and host level intrusions. Models equipped with ML can even identify unforeseen activities and classify the already detected malicious activities. In this paper, a novel lightweight model is proposed for effectively identifying intrusions in IoMT systems using anomaly detection. The model consists of a dimension reduction phase followed by an anomaly detection successively followed by a classification process. The main contributions of this work are mentioned below:

1. The input dataset is balanced by data augmentation to ensure sufficient availability of data for both normal and anomalous category.
2. IoMT datasets consists of vast amount of data with many features. Some features might not have much impact on the detection mechanism. To ensure that the model is able to determine the outcome within a short span of time, dimension reduction is applied.
3. A model based on random forest technique combined with Grid Search CV is followed by best estimator built, to determine anomalous data.
4. In addition, the model is evaluated with deranged datasets having large number of normal data or large number of anomalous data.

The remaining part of this paper is organized as follows. Section 2 comprises of related work followed by proposed work in Section 3. Experimentation and Results are provided in Section 4, and discussions in Section 5. Finally, Section 6 concludes the work.

2. Related work

In recent work throughout the years, numerous approaches have been proposed for building an Intrusion Detection system, and the following are some of the past work which has been done on IoMT Networks. Rani [7], proposed a cloud-based healthcare system, where authorization was given to only valid users. The system uses Support Vector Machine based model to determine a patient's condition and expected disease. This system uses ML-based approach for data mining and discoveries. This work not only gives an objective about malicious activities but also introduced an approach to merge the network flow metric with bio-metric data. Chakraborty [8] proposes a healthcare system design using blockchain technology. Blockchain technology is known to assure security, but the authors have not investigated the framework or tested it to present any benchmark result. Hady [9], proposed a new healthcare model for study in the area of Internet of Medical Things. The authors have introduced a wustl-ehms-2020 dataset using Enhanced Healthcare Monitoring System (EHMS) testbed. The proposed dataset was built on man-in-the-middle-attacks. The dataset combines the network flow metrics with patient biometrics. The authors in [10,11] uses K-Nearest Neighbour method as a base for cyber security research. Rao [10], used an Indexed Partial Distance search k-Nearest Neighbour(IKPDS) to test different types of attacks, which results in 99.6% accuracy. Shapoorifard [11] mainly focus on reducing the false alarm rate and show the accuracy of 85.2%. The above-discussed research uses an enhanced version of KDD Dataset but the dataset is being used since 1999 and the malicious attack signatures used are old. Further, Some recent studies have been done and compared with the current ones for providing a better approach in IoMT Security research and are mentioned in Table 1.

3. Proposed work

3.1. Motivation

The massive demand for IoMT networks to provide seamless effective medical facilities to a large scale population requires a robust secured model to ensure the privacy and safety of patients. However, designing security models for IoT networks is very challenging. An IoMT network typically involves sensor enabled medical devices, intermediate fog nodes, and cloud-based data servers which are connected via a wireless network. The indiscreet connection and dynamic nature of the network make it more vulnerable to attackers. Developing a security model for IoMT also requires the handling of huge data in a distributive manner. To address these challenges, a lightweight anomaly detection model is required for the IoMT network. This anomaly detection model can be used to protect the sensor data from cyber-attacks which can preserve the privacy and safety of the patients in real-time. As new IoMT Sensors are being introduced in wired or wireless mode, these models can be used to make these networks more robust from attacks using both network and biometric data. To represent the above challenge a new model has been introduced using both the metric data i.e., network and biometric.

Table 1
Related work summary.

Author	Dataset	Method	Results	limitations
Hady [9]	wustl-ehms- 2020	Used four different methods RF, KNN, SVM and ANN. ANN performed better on the dataset.	Training Accuracy = 88.75% Testing Accuracy = 90.42% AUC = 93.42	Requires hyperparameter tuning, prediction time is high, feature scaling was not performed.
Sarhan [12]	UNSW- BN 15 BoT-Iot ToN-IoT CSE-CIC- IDS2018	Used the standard dataset, generalize them into universal feature dataset, using n Probe Tool. Used extra tree classifier to bench mark the dataset. Derived NF-UQ-NIDS-V2 and Bench marked it with NF-UQ-NIDS-V1 with 43 Feature in Common Netflow.	Weighted Average = 96.93% F1 Score= 0.97 Prediction Time(μs) = 25.67	False Acceptance Rate (FAR) is higher. Takes more time in prediction. No other Algorithms have been considered for classification.
Sarhan [13]	UNSW- BN 15 BoT-Iot ToN-IoT CSE-CIC- IDS2018	Used the standard dataset, generalize them into universal feature dataset, using n Probe Tool. Used extra tree classifier to bench mark the dataset. Derived NF-UQ-NIDS-V1 and Bench marked it with 9 Feature in Common Netflow.	Weighted Average = 70.81% F1 Score = 0.79 Prediction Time(μs) = 14.67	Accuracy, FAR rate is higher. Takes more time in prediction. No other algorithms have been considered for classification.
Farhan [14]	CSE-CIC- IDS2018	Proposed a Deep Neural Network Model for classifying the attacks.	Accuracy = 90% Precision = 0.65 Recall = 0.59	No other Algorithms have been considered for classification, Dataset is not relevant for IoMT Purpose, Low precision and recall values.
Hussain [15]	CICIDS2017 CTU-13 IoT-23	Introduced the Universal Feature Set Concept. Common feature was selected using their frequency count. NB, KNN, RF, LR were used in Classification process.	Accuracy = 89.00% Precision = 81.64%	Dataset was not combined for universal classification process. Model was complex resulting in higher prediction time. Hyper-parameter tuning was not performed.
Kumar [16]	ToN-IoT	A Combination of ensemble learning and fog-cloud architecture-driven cyber-attack. The ensemble combines decision tree, naïve bayes , and random forest as first-level individual learners. Used IaaS on cloud side and Saas on fog side.	Accuracy = 96.35% Detection Rate = 99.98% FAR = 5.56	High FAR rate. Lack of Sensor Data. Not Lightweight.
Rathore [17]	Data obtained from Physionet	Used Supervised learning using Long Short-Term Memory model for preventing of stimulation strategies attacks on Deep brain simulators.	Multiple low Loss Value	Accuracy was not mentioned and the simulated attacks were not real.

3.2. Assumptions

The following assumptions have been made related to the system model:

1. The data contains both network and biometric information.
2. The cyber-attacks are initiated by the nodes placed outside a given network.
3. The model is trained and tested for Man-in-the-middle attacks (Data Spoofing and Alteration).

3.3. System design

The Framework proposed in this work Fig. 1 is a lightweight model designed for intrusion detection. The model uses a benchmarked Dataset [9] for the training model. The main goal is to achieve a model with less time in prediction and less FAR which is later explained in Sections 5.1, 5.2 and 5.4. The framework includes a data pre-processing phase which involves Analysis, Pre-processing and Feature Selection & Dimensional Reduction and an anomaly detection model. The anomaly detection model is based on Random Forest with Hyper-parameter tuning to achieve the best estimator which classifies for anomalies and normal samples.

3.4. Dataset description

The Dataset introduced by [9], is a combination of both network flow metric and bio-metric flow of the patients. The attack proposed in the dataset set is the Man in the Middle (MITM). The attack is described as when the attacker pretends to be a kind of router to get the packet first. Further two sub-types of MITM were considered by the researchers [9] as Spoofing attacks and Data Alteration. The dataset [9] has been built using a health monitoring sensor board that collects data from several healthcare sensors

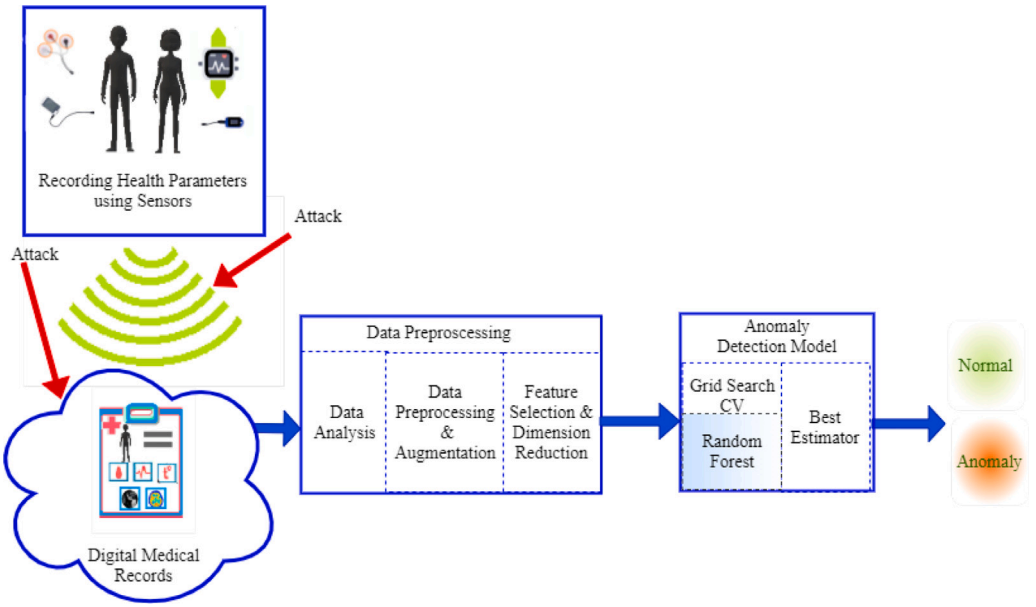

Fig. 1. Proposed framework.

Metric	Description	Metric Type	Metric Datatype	Metric	Description	Metric Type	Metric Datatype
Flgs	Flags Used in Network	Flow Metric	Object	Rate	Number of Packets per Second	Flow Metric	float64
SrcAddr	Source Address	Flow Metric	Object	SrcMac	Source Mac-address	Flow Metric	Object
DstAddr	Destination Address	Flow Metric	Object	DstMac	Destination Mac-address	Flow Metric	Object
Sport	Source Port	Flow Metric	int64	Packet_num	Packet Number	Flow Metric	int64
Dport	Desination Port	Flow Metric	int64	SIntPkt	Source Inter Packets	Flow Metric	float64
SrcBytes	Source Bytes	Flow Metric	float64	DIntPkt	Destination Inter Packets	Flow Metric	float64
DstBytes	Destination Bytes	Flow Metric	float64	SIntPktAct	Source Active Inter Packets	Flow Metric	float64
SrcLoad	Source Load	Flow Metric	float64	Dur	Duration	Flow Metric	float64
DstLoad	Destination Load	Flow Metric	float64	Trans	Aggregated Packet Counts	Flow Metric	int64
SrcGap	Source Missing Bytes	Flow Metric	float64	TotPkts	Total Packet Counts	Flow Metric	float64
DstGap	Destination Missing Bytes	Flow Metric	float64	TotBytes	Total Packet Bytes	Flow Metric	float64
DIntPktAct	Destination Active Inter Packets	Flow Metric	float64	Loss	Retransmitted or Dropped Packet	Flow Metric	int64
SrcJitter	Source Jitter	Flow Metric	float64	pLoss	Percentage of Retransmitted or Dropped Packet	Flow Metric	float64
DstJitter	Destination Jitter	Flow Metric	float64				
sMaxPktSz	Source Maximum Transmitted Packets	Flow Metric	int64	pSrcLoss	Percentage of Source Retransmitted or Dropped Packet	Flow Metric	float64
dMaxPktSz	Destination Maximum Transmitted Packets	Flow Metric	int64	pDstLoss	Percentage of Destination Retransmitted or Dropped	Flow Metric	float64
sMinPktSz	Source Minimum Transmitted Packets	Flow Metric	int64	Temp	Packet Temperature	Biometric	float64
dMinPktSz	Destination Minimum Transmitted Packets	Flow Metric	int64				
SpO2	Peripheral Oxygen Saturation	Biometric	int64	Load	Load	Flow Metric	float64

Fig. 2. Dataset description.

which are placed on a patient's body. The board was attached to a window-based system using the USB port. The software was developed using the C++ language. The system acts as a gateway where the transferring of data was done using TCP/IP protocol through Wi-Fi over the server. The testbed used Argus to collect all the network traffic flows and patient data between the gateway and server. It is open-source software that is used for monitoring the network flow traffic in real-time. The features used in dataset are mentioned in Fig. 2. Table 2 represents the number of samples in the dataset.

The number of samples in dataset are described in Table 2.

3.5. Data pre-processing

The Dataset was pre-processed before the Grid search process. The Pre-process Phase contains the Data Analysis, Data Pre-Processing and Augmentation, Feature Selection and Dimensional Reduction.

Table 2
No. of samples in the dataset [9].

Number of samples	Value
Normal samples	14,272
Attack samples	2,046
Total number of samples	16,318

3.5.1. Data analysis

The Data analysis part contains the study of features and their relationships. There are two parts of Data analysis which are mentioned below.

Count Analysis: It gives an idea about the data in feature such as total count, uniqueness, top value in feature and its frequency. Other than that, Count Analysis also provides the count for each value in the feature set which is to be explored. To build the relationship between the different features like number of attack samples which contains a particular flag number of the protocol in the network.

Variable analysis: It tells about the nature of the feature. The nature of the feature is related to datatype as object datatype will be equivalent to count analysis, but on the other hand in the int64 and float64 will give us some statistical observation about the feature. These observations include mean, standard deviation, min. value, max. value and three quartile values (1st, 2nd, and 3rd). If the same process is used continuously, these values play a significant role in building the model.

3.5.2. Data pre-processing and augmentation

This phase contains two steps namely Data Pre-Processing and Data Augmentation. In this phase, it is observed that there are some changes needed to be done in the dataset such as converting the related feature to relevant datatype, removal of irrelevant features which can create noise in classification and label encoding of the relevant feature. To scale the dataset the statistical feature was used such as quartile 1 and 3 in Robust scaler.

The main goal for robust scaling is to scale features using statistics that are robust to outliers. The scaler removes the median and scales the data according to the quartile range. Default range value is provided using 1st quartile and 3rd quartile.

$$X_{FeatureScaled} = \frac{X_{FeatureCurrentValue} - Q_1(X_{Feature})}{Q_3(X_{Feature})) - Q_1(X_{Feature})} \tag{1}$$

The first quartile (Q_1) is defined as the middle number between the smallest number (minimum) and the median of the data set. It is also known as the lower or 25th empirical quartile, as 25% of the data is below this point. The third quartile ($Q3$) is the middle value between the median and the highest value (maximum) of the data set. It is known as the upper or 75th empirical quartile, as 75% of the data lies below this point.

Other than that, two other scalers were used namely MinMax Scaler and Standard Scaler, they are explained as below.

Min–Max Scaler is also known as normalization and considered as the simplest scaling. The value range for this scaling is between 0 to 1. The feature value is obtained by subtracting the min value and divided by the max value minus min value.

$$X_{FeatureScaled} = \frac{X_{FeatureCurrentValue} - min(X_{Feature})}{max(X_{Feature}) - min(X_{Feature})} \tag{2}$$

Standard Scalar scaling technique uses mean and standard deviation to scale the feature. Standard scalar is not dependent upon any particular range. The main goal of this feature is to keep the mean equal to 0 and the standard deviation to 1 because it distributes all the feature values in the similar distribution.

$$X_{FeatureScaled} = \frac{X_{FeatureCurrentValue} - mean(X_{Feature})}{stdev(X_{Feature})} \tag{3}$$

In above Eqs. (1)–(3) $X_{FeatureScaled}$ represents a scaled feature value after scaling has been processed, $X_{FeatureCurrentValue}$ represents current feature value without any modifications, $X_{Feature}$ represents whole feature columns from the dataset, $Q_1()\&Q_3()$ represents a quartile function ranging from 0 to 100 but in the proposed work defaults were used i.e, 25 and 75, min() and max() represent minimum and maximum functions to retrieve the respective values from each feature of the dataset, mean() represents mean for each feature and stdev() represents standard deviation for the feature.

Data augmentation in data analysis is a technique used to increase the amount of data by adding slightly modified copies of already existing data or newly created synthetic data from existing data. It acts as a regularizer and helps reduce overfitting when training a machine learning model [18]. Oversampling in data analysis is a technique used to adjust the class distribution of a data set (i.e., the ratio between the different classes/categories represented). These terms are used both in statistical sampling, survey design methodology and in machine learning. There are a number of methods available to oversample a dataset used in a typical classification problem. The most common technique is known as SMOTE: Synthetic Minority Over-sampling Technique [19]. This technique was used to resample the dataset in the work. The below mentioned algorithm 1 in Section 3.8 was used to achieve the resampling of the dataset [9].

3.5.3. Feature selection and dimensional reduction

Feature selection is a technique of obtaining a subset of the features from the original feature set without any transformation on the dataset. On the other hand, Dimensional reduction is referred to same as Feature Selection but some transformation is applied to transform the higher dimension to the lower dimension in the dataset. A study of mean, standard deviation, 1st quartile, 3rd quartile and count analysis were considered to select various features from the original feature set of the dataset.

3.6. Anomaly detection model

In this phase, the model development is presented using Random Forest [20,21], GridSearchCV [22], and Best Estimator [21,22]. Here, other algorithms such as Logistic Regression [21,23], Decision Tree [24] and Extremely Randomized Tree [25] have also been considered. The various parts of this phase are described as below.

3.6.1. Grid search

In this section, a popular hyperparameter optimization technique called grid search is used, which helps in improvising the performance of classifier by finding optimal combination of hyperparameter values. Grid Search is a brute-force exhaustive search paradigm where a list of various values are defined for different hyperparameters to be initialized [22,24]. A grid search algorithm must be guided by some performance metric, typically measured by cross-validation on the training set or evaluation on a held-out validation set. After the training is completed on training data, the best estimator can be used which is result of best parameter from exhaustive search.

3.6.2. Logistic regression

It is a parametric classification algorithm which is very simple in use and implementation. It efficiently works on linear separable classes. It classifies both binary and multi-class problems using OvR(One-vs-Rest) Method [24]. Logistic Regression uses Sigmoid function for classification.

3.6.3. Decision tree

It is a non-parametric classification and regression algorithm and even multioutput tasks. These are very powerful algorithms so that this makes them capable of fitting the complex dataset. These trees are fundamentals for the random forest. To split the nodes, the use of most informative features is done like an objective function is defined as Informative Gain. Generally, binary decision tree is implemented to reduce the combinatorial search space [24]. There are three impurity measures or splitting criterion which are considered Gini Entropy (I_G), entropy (I_H) and classification error (I_E).

3.6.4. Random forest

A Random Forest [20] is known as ensemble of various Decision Trees, they are trained using bagging method. The intuition idea behind developing random forest was to get average multiple (deep) decision trees in which the individual suffer from high variance, to build more robust model having a better generalization performance and it is less susceptible to over-fitting.

3.6.5. Extra tree

An Extremely randomized Trees ensemble [25] is technique which trades more bias for a lower variance. It makes Extra-Trees much faster to train than regular forests, because finding the best possible threshold for each feature at every node is one of the most time-consuming tasks of growing a tree.

3.7. Proposed framework

The work aimed to design a lightweight intrusion detection model that deploys the feature scaling technique with the random forest model. The proposed model shown in Fig. 3 identifies an intrusion by classifying the input data as ‘intrusion’ and ‘normal’ data. The model is considered lightweight, since it uses feature selection and dimension reduction technique which reduces the number of features to be processed and also the overall detection time. To select the proper category of the input sample, hyperparameter tuning is used to attain a best estimator. The model can function with low resources and can be appropriately used both at the node and the network level of an IoMT system.

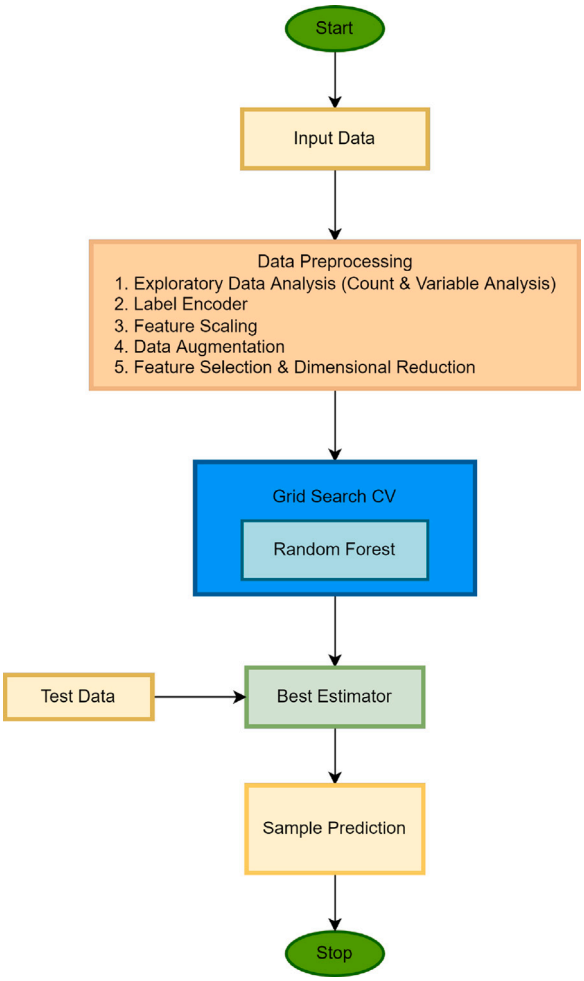

Fig. 3. Proposed model.

3.8. Algorithms

Algorithm 1 - Performs data augmentation in the dataset by making the number of samples equal to majority and minority class. The notations used in the algorithms are specified in Table 3.

Algorithm 1 Data Augmentation()

1: **Input: Dataset** DS
2: **Output:** DS'
3: **Begin**

i Initialization: $DS' = Data_Augmentation$(DS)
ii Data_Augmentation(DS)

(a) DS_{temp} = call SMOTE(DS)
(b) **return** (DS_{temp})

4: **End**

Algorithm 2 - It Computes the ratio between majority and minority classes in the dataset. This ratio is passed in classification algorithms as a parameter which will be explained later.

Algorithm 2 Compute Class Weight()

1: **Input: Training Classes** TC
2: **Output: ClassWeightMap**
3: **Begin**
4: **Initialization:** $Classes_Array$ = Number of Classes in the Array available.
5: **Call** $Compute_Class_Weight()$ function with parameter as **Balanced** ratio, $Classes_Array$, $Training_Classes$.
6: **Map** the weight ratio array with classes.
7: **return** (ClassWeightMap)

Algorithm 3- It perform a feature scaling using Eq. (1). Robust scaler function has two attributes scale_ and center_ which specifically returns an array of median values and quartile ranges for each feature.

Algorithm 3 Robust Scaler()

1: **Input: Training Dataset** TD
2: **Output:** TD'**,** $center_value_array$**,** $scale_array_1$
3: **Begin**

i Initialization: TD', $center_value_array$, $scale_array_1$ = Scaling(TD)
ii Scaling(TD)

(a) TD_{new} = call RobustScaler(TD) using Eq. (1).
(b) $center_value_array$ = call RobustScaler(TD).center_attribute
(c) $scale_array_1$ = call RobustScaler(TD).scale_attribute
(d) ***return*** (TD_{new} , $center_value_array$, $scale_array_1$)

4: **End**

Algorithm 4- It perform a feature scaling using Eq. (2). MinMax scaler function has two attributes data_min_ and data_max_ which specifically returns an array of minimum and maximum values for each feature.

Algorithm 4 MinMax Scaler()

1: **Input: Training Dataset** TD
2: **Output:** TD'**,** min_value_array**,** max_value_array
3: **Begin**

i Initialization: TD', min_value_array, max_value_array = Scaling(TD)
ii Scaling(TD)

(a) TD_{new} = call MinMaxScaler(TD) using Eq. (2).
(b) min_value_array = call MinMaxScaler(TD).data_min_attribute
(c) max_value_array = call MinMaxScaler(TD).data_max_attribute
(d) ***return*** (TD_{new} , min_value_array, max_value_array)

4: **End**

Algorithm 5- It perform a feature scaling using Eq. (3). Standard scaler function has two attributes mean_ and scale_ which specifically returns an array of mean and standard deviation values for each feature.

Algorithm 5 Standard Scaler()

1: **Input: Training Dataset** TD
2: **Output:** TD'**,** $mean_value_array$**,** $scale_array_2$
3: **Begin**

i Initialization: TD', $mean_value_array$, $scale_array_2$ = Scaling(TD)
ii Scaling(TD)

(a) TD_{new} = call StandardScaler(TD) using Eq. (3).
(b) $mean_value_array$ = call StandardScaler(TD).mean_attribute
(c) $scale_array_2$ = call StandardScaler(TD).scale_attribute
(d) ***return*** (TD_{new} , $mean_value_array$, $scale_array_2$)

4: **End**

Algorithm 6- This Algorithm uses Logistic regression. The *Param_grid* contains C parameter which is inverse of regularization strength. Scoring method and CV for algorithms 6, 7, 8 and 9 were accuracy and 10 folds respectively.

Algorithm 6 GridSearchCV + LogisticRegression()

1: **Input: Training Features and Classes**
2: **Output: Hyper-tuned Logistic Regression Classifier**
3: **Begin**
4: **Training**

i Initialize the *Param_grid* for Logistic regression.
ii Call the GridSearchCV estimator (with class weight if available) and input the *Param_grid*.
iii Fit the grid estimator with scaled training features and labelled classes.
iv Retrieve the best parameters for the classifier.
v Initialize the classifier using GridSearchCV Best Estimator as the input.
vi Fit the classifier with scaled training features and labelled classes.
vii Obtain the classifier.

5: **Testing**

i Predict class of each testing feature until all the features are processed and store prediction time for each prediction.
ii Evaluate the classifier using Evaluation Metrics such as Accuracy, Detection Rate, False Acceptance Rate, AUC Score, F1-Score, Precision and Prediction Time.

6: **End**

Algorithm 7, 8 and 9- These Algorithm uses Decision Tree, Random Forest and Extra Tree. The below parameters were used in random forest for getting better results and The *Param_grid* contains following ranges also:

1. Criterion - It is function to measure the quality of split i.e, Gini and Entropy.
2. min_samples_split - It is minimum number of samples required to split an internal node. Minimum Sample Split ranges from 10 to 100 at an interval of 10.
3. n_estimators(only for algorithms 8 and 9) - The number of trees to build the forest that ranges from 10 to 30 at an interval of 2.

Algorithm 7 GridSearchCV + DecisionTree()

1: **Input: Training Features and Classes**
2: **Output: Hyper-tuned Decision Tree Classifier**
3: **Begin**
4: **Training**

i Initialize the *Param_grid* for Decision Tree.
ii Call the GridSearchCV estimator (with class weight if available) and input the *Param_grid*.
iii Fit the grid estimator with scaled training features and labelled classes.
iv Retrieve the best parameters for the classifier.
v Initialize the classifier using GridSearchCV Best Estimator as the input.
vi Fit the classifier with scaled training features and labelled classes.
vii Obtain the classifier.

5: **Testing**

i Predict class of each testing feature until all the features are processed and store prediction time for each prediction.
ii Evaluate the classifier using Evaluation Metrics Accuracy, Detection Rate, False Acceptance Rate, AUC Score, F1-Score, Precision and Prediction Time.

6: **End**

Algorithm 8 GridSearchCV + RandomForest()

1: **Input: Training Features and Classes**
2: **Output: Hyper-tuned Random Forest Classifier**
3: **Begin**
4: **Training**

i Initialize the *Param_grid* for Random Forest.
ii Call the GridSearchCV estimator (with class weight if available) and input the *Param_grid*.
iii Fit the grid estimator with scaled training features and labelled classes.
iv Retrieve the best parameters for the classifier.
v Initialize the classifier using GridSearchCV Best Estimator as the input.
vi Fit the classifier with scaled training features and labelled classes.
vii Obtain the classifier.

5: **Testing**

i Predict class of each testing feature until all the features are processed and store prediction time for each prediction.
ii Evaluate the classifier using Evaluation Metrics Accuracy, Detection Rate, False Acceptance Rate, AUC Score, F1-Score, Precision and Prediction Time.

6: **End**

Algorithm 9 GridSearchCV + ExtraTreeClassifier()

1: **Input: Training Features and Classes**
2: **Output: Hyper-tuned Extra Tree Classifier**
3: **Begin**
4: **Training**

i Initialize the *Param_grid* for Extra Tree.
ii Call the GridSearchCV estimator (with class weight if available) and input the *Param_grid*.
iii Fit the grid estimator with scaled training features and labelled classes.
iv Retrieve the best parameters for the classifier.
v Initialize the classifier using GridSearchCV Best Estimator as the input.
vi Fit the classifier with scaled training features and labelled classes.
vii Obtain the classifier.

5: **Testing**

i Predict class of each testing feature until all the features are processed and store prediction time for each prediction.
ii Evaluate the classifier using Evaluation Metrics Accuracy, Detection Rate, False Acceptance Rate, AUC Score, F1-Score, Precision and Prediction Time.

6: **End**

4. Experimentation and results

To evaluate the proposed model, rigorous experimentation has been performed using the dataset [9].

4.1. Data augmentation and class weight ratio

After the Data Pre-processing, Class weight ratio algorithm 2 has been used on original dataset to adjust the class importance in classification. In addition, algorithm 1 has also been used to balance the dataset. The description of the number of samples and their class weight ratio in presented in Tables 4 and 5. The class weight ratio is a parameter in the classifier which will make an assumption of a balanced classification by assigning a ratio to the minority class in the process. To obtain these values, algorithms 1 and 2 are applied on the dataset.

Scaled dataset is for the classification algorithms under hyper-parameter tuning. The scaled feature dataset are Original Dataset and Data Augmented Dataset. Before that, only relevant features from the dataset i.e., 34 out of 44 are considered using variable analysis. All the bio-metric features in the classification process have been used.

4.2. Classification algorithms and hyper-parameter tuning

The algorithms 6, 7, 8 and 9 in Section 3.8 are executed with the original dataset, augmented dataset and variation of original dataset with class weight ratio. However, the class weight ratio is not calculated for augmented dataset as augmented dataset is already balanced.

Table 3
Notations used for the essential parameters.

Symbol	Details.
DS	Original Dataset.
DS'	Augmented Dataset.
DS_{temp}	Store the augmented dataset.
TD	Training Dataset.
TD'	Scaled Training Dataset.
TD_{new}	Store the scaled dataset.
$center_value_array$	Array to Store/Return quartile ranges for each feature in training dataset.
$scale_array_1$	Array to Store/Return median value for each feature in training dataset.
min_value_array	Array to Store/Return minimum value for each feature in training dataset.
max_value_array	Array to Store/Return maximum value for each feature in training dataset.
$mean_value_array$	Array to Store/Return mean value for each feature in training dataset.
$scale_array_2$	Array to Store/Return standard deviation for each feature in training dataset.
Scoring	Strategy to evaluate the performance of the cross-validated model on the test set.
$param_grid$	Parameter list for the classifiers.
CV	Cross-Validation splitting strategy

Table 4
Number of samples with and without data augmentation.

Number of samples	Without augmentation	With augmentation
Training samples	13,054	22,383
Testing samples	3,264	5,709
Total samples	16,138	28,544

Table 5
Class weight ratio.

Types of samples	Weight ratio
Normal samples	0.57134104
Attack samples	4.00429448

The result of each test is given in terms of accuracy (% of correctly classified instances). The evaluation metrics is been calculated using following measurements.

True Positives (TP)- Correctly classified as Attack Sample.

True Negatives (TN)- Correctly classified as Normal Sample.

False Positive (FP)- Classified a Normal data as Attack Sample.

False Negatives (FN)- Classified as Normal Sample but actually it is an Attack Sample.

Accuracy is calculated from True Positives(TP) and True Negatives(TN) for binary classification using Eq. (4):

$$Accuracy = \frac{TP + TN}{TP + TN + FP + FN} \times 100 \tag{4}$$

In order to measure performance, evaluation metrics like Precision, Recall/Detection Rate, FAR, F1-score and AUC are calculated in terms of positives and negatives :

Precision – It represents the number of correct positive prediction in total number of positive predictions and defined by Eq. (5):

$$Precision = \frac{TP}{TP + FP} \times 100 \tag{5}$$

Recall/Detection Rate – It represents the number of correct Positive prediction in total number of positive observations and defined by Eq. (6):

$$Recall/DR = \frac{TP}{TP + FN} \times 100 \tag{6}$$

False Acceptance Rate/False Positive Rate (FAR/FPR) – It represents number of False Positive Prediction in total number of False attempts and defined by Eq. (7):

$$FAR/FPR = \frac{FP}{TN + FP} \tag{7}$$

False Negative Rate (FNR) – It represents number of False Negative Prediction in total number of True Attempts and defined by Eq. (8):

$$FNR = \frac{FN}{TN + FN} \tag{8}$$

Table 6
Comparison with existing model.

Evaluation metrics	Hady [9]	Proposed model
10-Fold Training Accuracy	88.75%	92.85%
10-Fold Testing Accuracy	90.04%	94.23%
AUC Scores	93.42	90.68

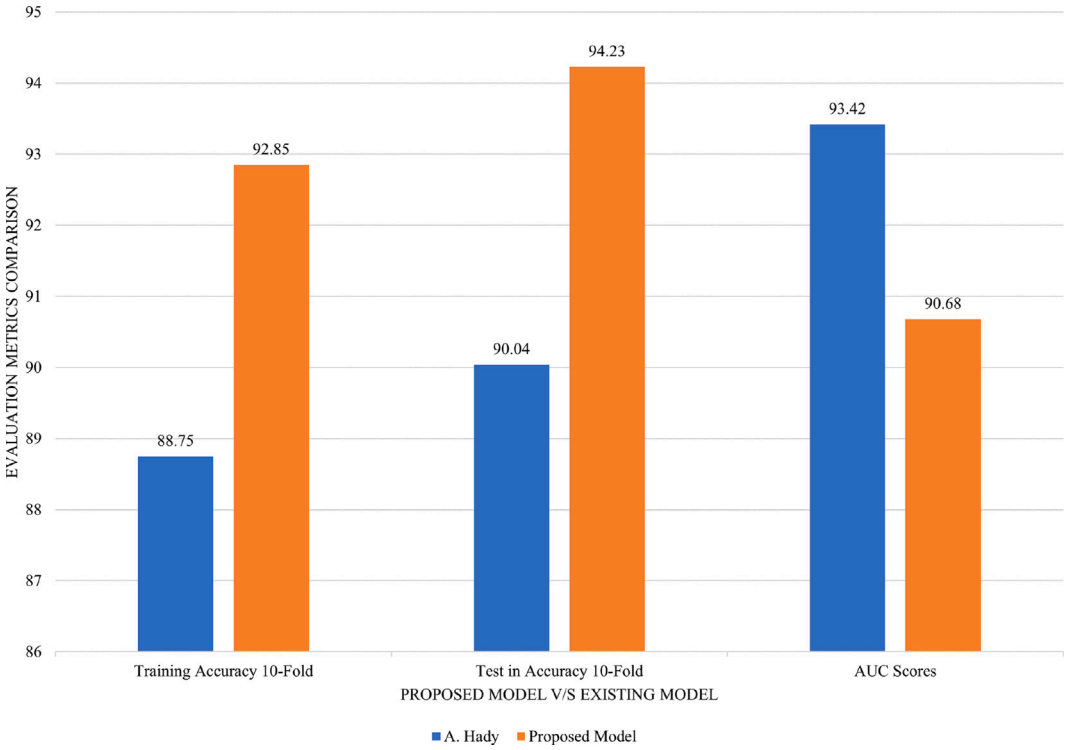

Fig. 4. Accuracy of the proposed model.

F1-Score - It is the harmonic mean of the Precision and the Recall. This evaluation metric is very useful to study imbalanced learning problems. To overcome this issue, algorithm 2 is used which is defined by Eq. (9):

$$F1 - Score = 2 \times \frac{PrecisionX\,Recall}{Precison + Recall} \times 100 \tag{9}$$

Prediction Time (μs) - The time is shown as prediction per sample.

ROC-AUC (Area under the Receiver Operator Characteristic Curve) - Receiver Operating characteristic(ROC) graph is a useful tool to choose models based on its performance for classification with respect to FPR and TPR [24]. The computation is recorded using a threshold decision which is shifted by the classifier. A classifier is said to be perfect when the top left corner of the graph lies with TPR of 1 and FPR of 0 [24]. The AUC value measures the correlation between the actual attacks that occurred during an event w.r.t number of flows that are classified as attacks but are not.

The results are obtained for the proposed model and compared with the other existing models along side with many variations of the dataset with different classifiers.

Table 6 compares 10-Fold Training, Testing Accuracy and AUC scores of Artificial Neural Network proposed by [9] and our proposed approach with combination of above-mentioned algorithms 1, 3, and 8.

The comparison of the existing model [9] and the proposed model is presented in Fig. 4. In the proposed work, four well recognized algorithms are considered Logistic Regression, Decision Tree, Random Forest and Extra Tree Classifier. The techniques are combined with various feature scaling techniques such as Robust Scaler, Standard Scaler and MinMax Scaler. Furthermore, to solve imbalanced learning problem class weight ratio parameter and data Augmentation are deployed. The combination of the Robust Scalar, Data Augmentation and Random Forest has significantly outnumbered the current existing work in terms of the training and testing accuracy for Intrusion Detection in IoMT with the values of 92.85% and 94.23% respectively.

Tables 7–15 and their subsequent Figs. 5–13 describe the evaluation metrics namely — Training Accuracy (%), Testing Accuracy (%), Detection Rate (%), AUC (%), False Acceptance Rate (only in tables), F1-score (%), Precision (%) and Time (μs).

Table 7
Comparison with other algorithms.

Model	Training accuracy (%)	Testing accuracy (%)	DR (%)	AUC (%)	FAR	F1-Score (%)	Precision (%)	Time (μs)
RF–Data augmentation (Proposed model)	92.85	94.23	93.72	90.68	0.06	93.8	93.45	3.5
LR–Data augmentation	75.13	74.89	55.98	75.14	0.05	69.30	90.94	57.10
DT–Data augmentation	90.55	92.56	89.55	90.81	0.07	90.7	92.06	82
ET–Data augmentation	88.86	89.01	93.25	89.09	0.06	88.54	84.45	3.6

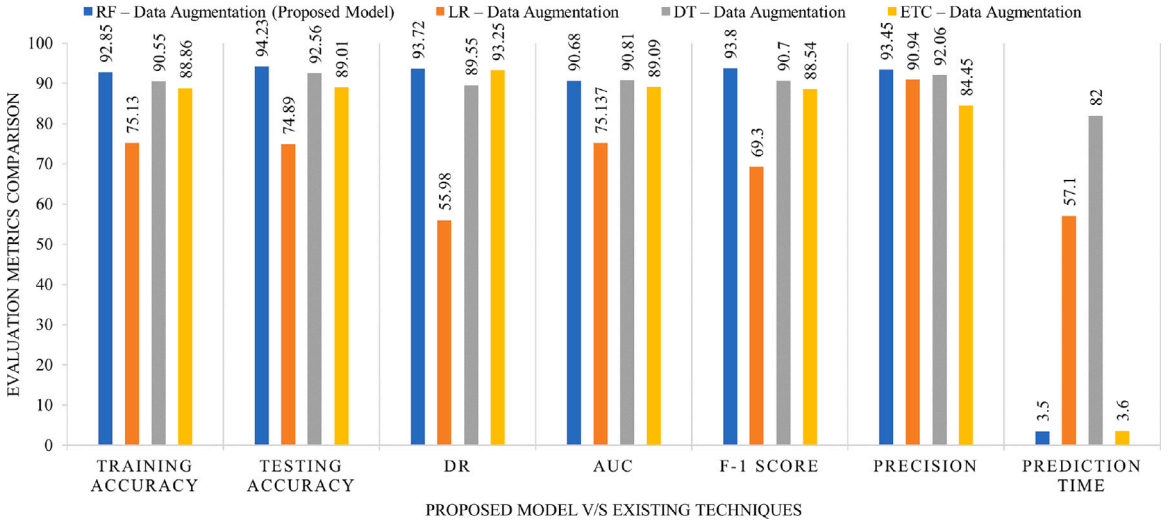

Fig. 5. Performance metrics of the proposed model using Robust Scalar.

Table 8
Comparison with other algorithms having class weight and Robust Scalar.

Model	Training accuracy (%)	Testing accuracy (%)	DR (%)	AUC (%)	FAR	F1-Score (%)	Precision (%)	Time (μs)
RF–Data augmentation (Proposed model)	92.85	94.23	93.72	90.68	0.06	93.8	93.45	3.5
LR–Class weight	89.88	89.00	55.52	74.70	0.06	56.27	57.03	42
DT–Class weight	89.71	91.81	89.90	91.00	0.07	73.69	62.43	41
RF–Class weight	92.58	91.85	67.78	81.57	0.04	67.95	68.11	0.39
ET–Class weight	92.45	92.95	59.61	78.72	0.02	68.31	80.00	4.7

The evaluation metrics are calculated using Eq. (4)–(9). From the results, it is evident that the proposed model based on the Data Augmentation and Random Forest, performed better than the other techniques, since random forest along with feature scaling, performs better than the other techniques specifically for large dataset with categorical data.

The next comparison is done with the other algorithms 6, 7 and 9 using Data Augmentation Algorithm 1 and Robust Scaler Algorithm 3 and the results are shown in Table 7 and Fig. 5.

In the next set of experimentation, class weight algorithm 2 and Robust Scaler Algorithm 3 are used to compare the proposed model with the other techniques. The results are shown in Table 8 and Fig. 6

In the next analysis only Robust Scaler is used for the comparison and shown in Table 9 and Fig. 7.

In the next comparison, Standard Scaler Algorithm 5 is only considered and corresponding results are in Table 10 and Fig. 8.

Table 11 and Fig. 9 depicts the next comparison of the other techniques with the proposed model using class weight ratio and Standard Scaler Algorithms.

In the next experimentation, a combination of Data Augmentation and Standard Scaler Algorithms are used. The results are shown in Table 12 and Fig. 10.

The results in Table 13 and Fig. 11 shows the performance of the proposed model using MinMax Scaler. Then the MinMax Scaler is combined with the Class Weight and the results are presented in Table 14 and Fig. 12.

In the last set of experimentation MinMax is combined with the Data Augmentation technique and the comparative results are shown in Table 15 and Fig. 13.

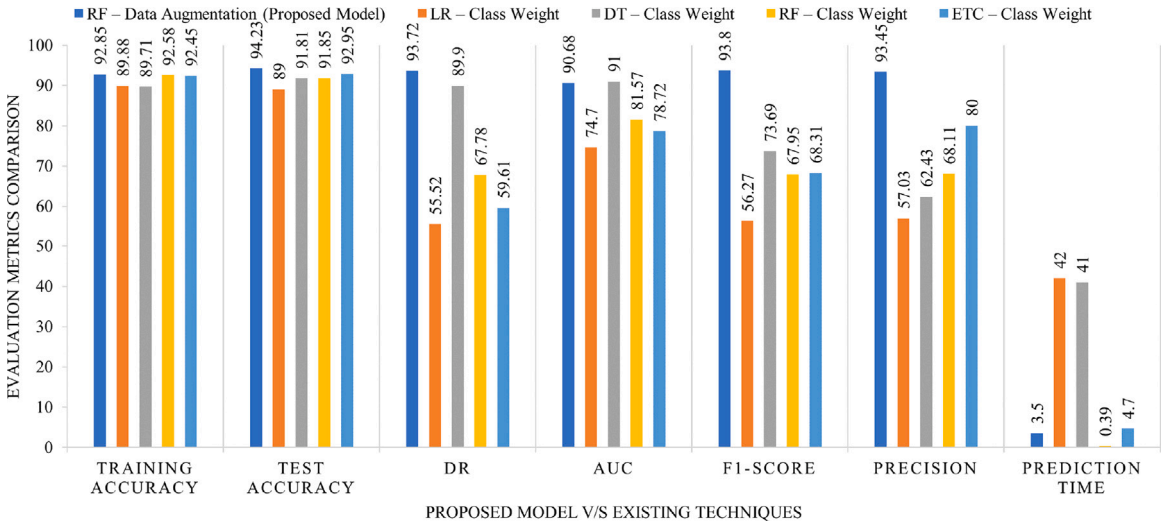

Fig. 6. Performance metrics of the proposed model using Robust Scalar with class weight ratio.

Table 9
Comparison with other algorithms using Robust Scaler.

Model	Training accuracy (%)	Testing accuracy (%)	DR (%)	AUC (%)	FAR	F1-Score (%)	Precision (%)	Time (μs)
RF–Data augmentation (Proposed model)	92.85	94.23	93.72	90.68	0.06	93.8	93.45	3.5
LR	93.4	93.32	50.48	75.02	0.00	65.82	94.59	27
DT	94.87	93.90	63.94	81.11	0.01	72.78	84.45	48
RF	94.10	93.71	51.20	75.56	0.00	67.93	100	0.13
ET	93.97	93.71	51.20	75.56	0.00	67.51	99.06	0.62

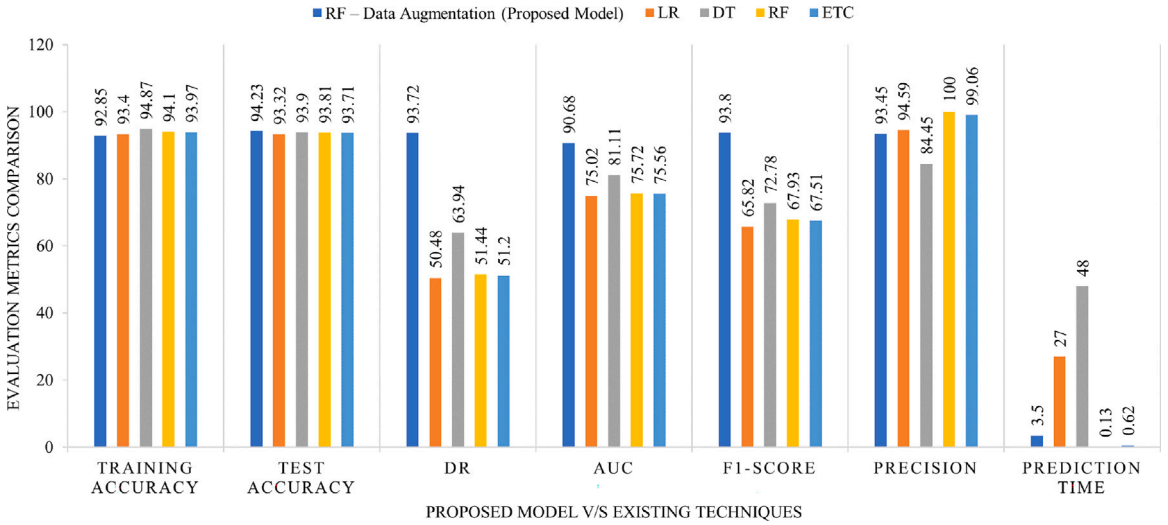

Fig. 7. Performance metrics of the proposed model using Robust Scalar with data augmentation.

5. Discussions

5.1. Confusion matrix for proposed model

Table 16 represents the confusion matrix for the proposed model. The False Positive Rate is 6.07% and the false Negative rate is 5.84% after classification on the augmented dataset.

Table 10
Comparison of proposed model with other algorithms using Standard Scaler only.

Model	Training accuracy (%)	Testing accuracy (%)	DR (%)	AUC (%)	FAR	F1-Score (%)	Precision (%)	Time (µs)
RF–Data augmentation (Proposed model)	92.85	94.23	93.72	90.68	0.06	93.8	93.45	3.5
LR	93.06	92.95	44.95	72.45	0.00	61.92	99.46	20.3
DT	95.02	93.90	63.90	81.11	0.01	72.77	84.45	32.19
RF	94.09	93.81	51.44	75.72	0.00	67.93	100	2.9
ET	93.97	93.75	50.96	75.48	0.00	67.51	100	1.77

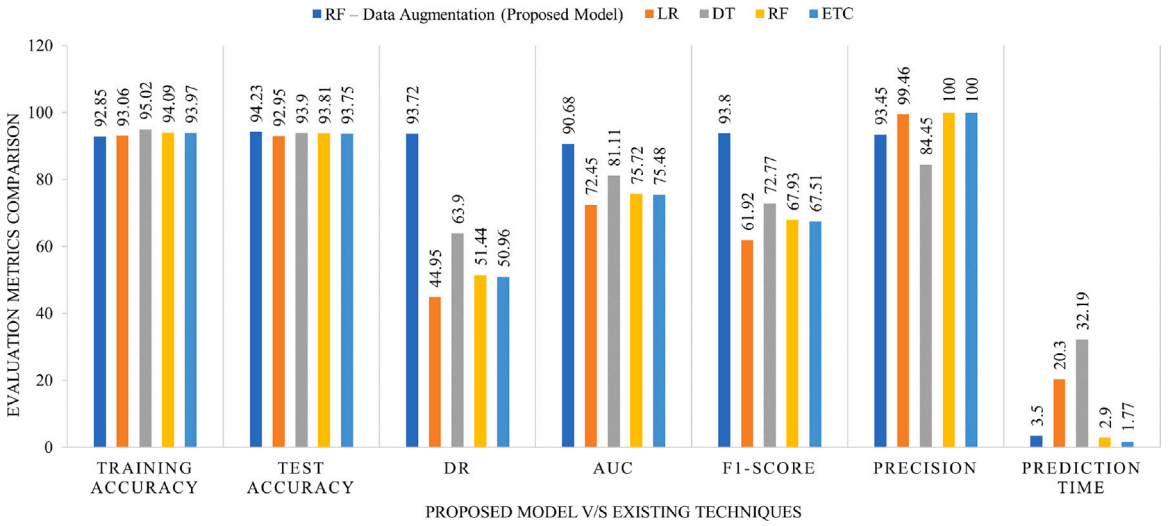

Fig. 8. Performance metrics of the proposed model using standard scalar.

Table 11
Comparison of proposed model with other algorithms using Standard Scaler and class weight ratio.

Model	Training accuracy (%)	Testing accuracy (%)	DR (%)	AUC (%)	FAR	F1-Score (%)	Precision (%)	Time (µs)
RF–Data augmentation (Proposed model)	92.85	94.23	93.72	90.68	0.06	93.8	93.45	3.5
LR-Class weight	89.49	89.062	57.211	75.42	0.06	57.14	57.07	33.84
DT-Class weight	89.80	91.85	90.14	91.12	0.07	73.81	62.50	2.73
RF-Class weight	92.85	91.81	67.30	81.35	0.04	67.30	68.12	26.41
ET-Class weight	92.50	93.07	58.41	78.27	0.01	68.25	82.09	5.02

Table 12
Comparison of proposed model with other algorithms using Standard Scaler and data augmentation.

Model	Training accuracy (%)	Testing accuracy (%)	DR (%)	AUC (%)	FAR	F1-Score (%)	Precision (%)	Time (µs)
RF–Data augmentation (Proposed model)	92.85	94.23	93.72	90.68	0.06	93.8	93.45	3.5
LR-Data augmentation	94.94	73.78	53.80	74.02	0.05	67.50	90.56	70
DT-Data augmentation	90.5	90.8	89.58	90.87	0.07	90.8	92.1	86.5
RF-Data augmentation	90.22	90.78	87.88	90.82	0.06	90.61	93.51	4.9
ET-Data augmentation	88.81	90.2	85.00	90.32	0.04	89.83	95.26	7.5

5.2. Role of data augmentation in classification

Initially, the dataset used to develop this model contained fewer attack samples. After data augmentation, better results were obtained in terms of Testing Accuracy, Detection Rate, AUC Score, F1-Score, and Precision. To achieve better results robust scaling algorithm 3 was used. The result are shown in Table 17.

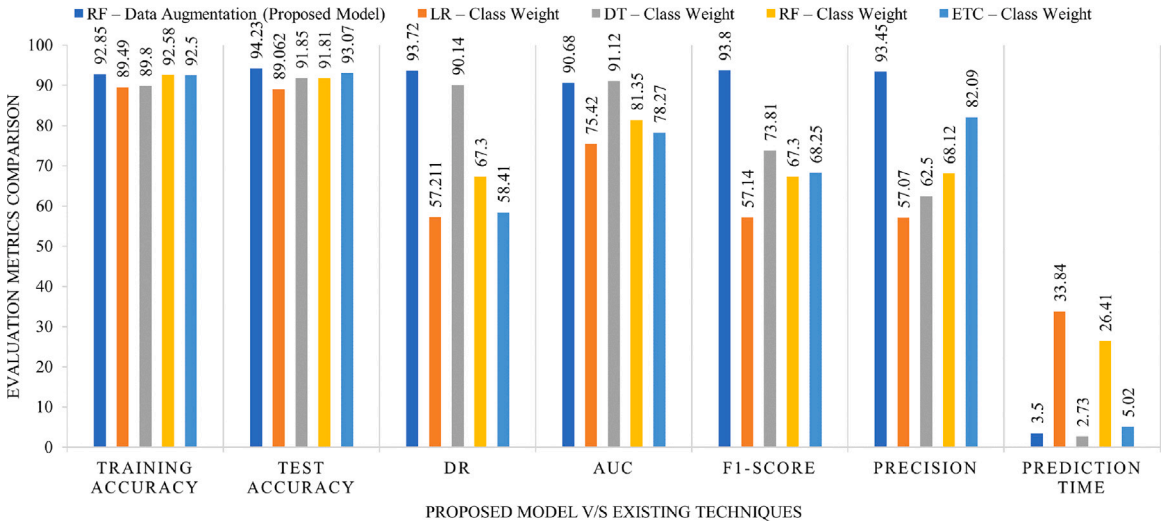

Fig. 9. Performance metrics of the proposed model using standard scalar with class weight ratio.

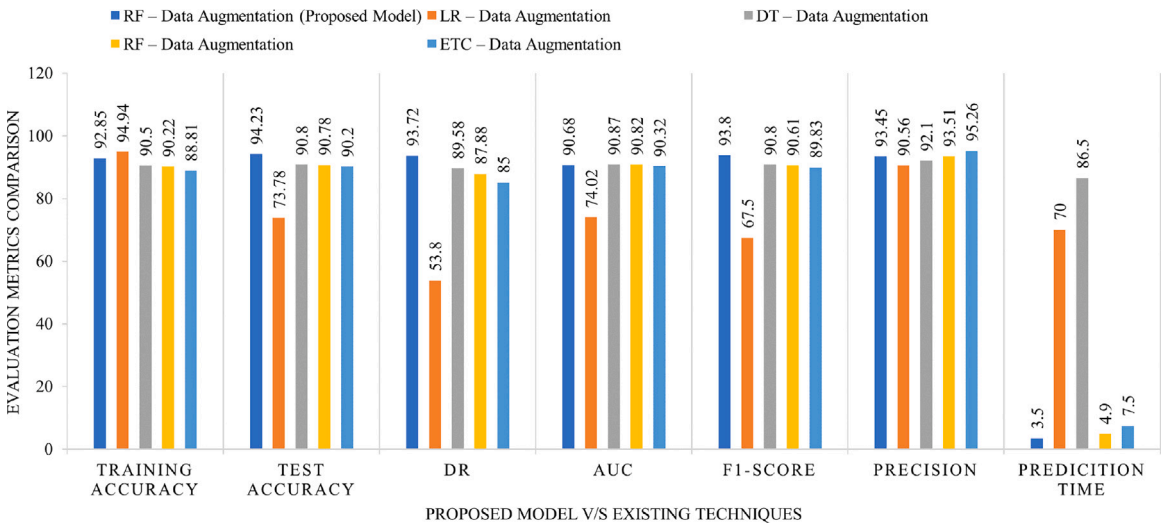

Fig. 10. Performance metrics of the proposed model using standard scalar with data augmentation.

Table 13
Comparison of proposed model with other algorithms using MinMax Scaler only.

Model	Training accuracy (%)	Testing accuracy (%)	DR (%)	AUC (%)	FAR	F1-Score (%)	Precision (%)	Time (μs)
RF–Data augmentation (Proposed model)	92.85	94.23	93.72	90.68	0.06	93.8	93.45	3.5
LR	93.31	92.98	44.95	72.47	0.00	62.03	100	25.8
DT	95.11	94.33	66.10	82.29	0.01	74.82	86.62	67.03
RF	94.11	93.81	51.44	75.72	0.00	67.94	100	2.87
ET	93.97	93.78	51.20	75.60	0.00	67.72	100	2.62

5.3. Prediction time

The Prediction time is reduced by data cleaning processes such as scaling, removal of irrelevant features, label encoding, and feature selection based on the mean and standard deviation. It is also reduced by choosing an appropriate algorithm, to show the further investigation the results are compiled in Table 18. The Prediction time is also relatable to the system specification on which

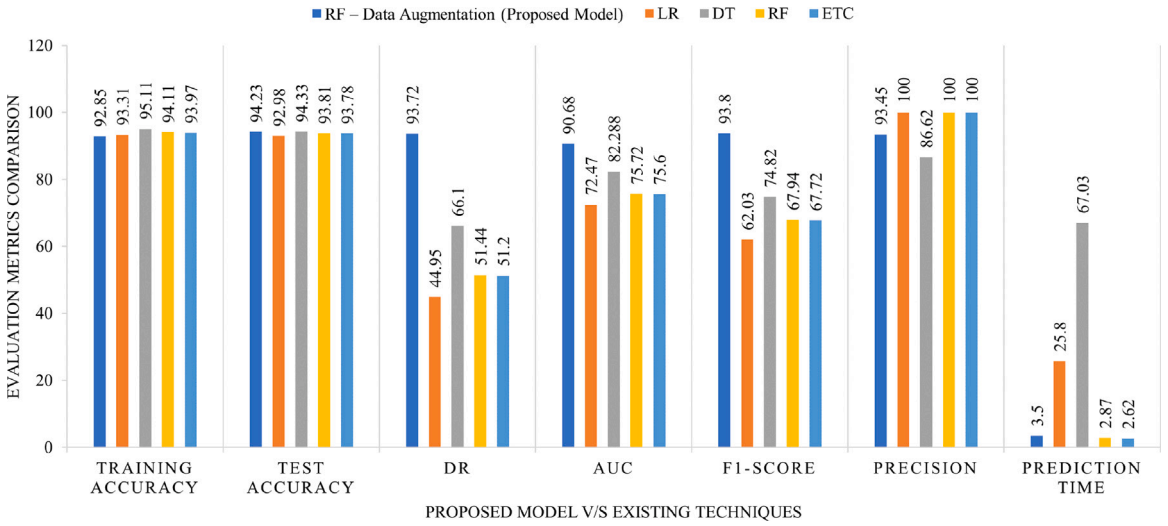

Fig. 11. Performance metrics of the Proposed Model using MinMax scalar.

Table 14
Comparison of proposed model with other algorithms using MinMax Scaler and class weight.

Model	Training accuracy (%)	Testing accuracy (%)	DR (%)	AUC (%)	FAR	F1-Score (%)	Precision (%)	Time (μs)
RF–Data augmentation (Proposed model)	92.85	94.23	93.72	90.68	0.06	93.8	93.45	3.5
LR-Class weight	90.98	90.53	49.27	72.339	0.034	57.00	68.65	33.67
DT-Class weight	90.33	92.21	92.66	90.92	0.03	95.40	98.32	50
RF-Class weight	92.66	92.31	69.71	82.66	0.04	69.79	69.87	2.7
ET-Class weight	92.50	93.04	59.13	78.56	0.02	68.42	81.18	2.25

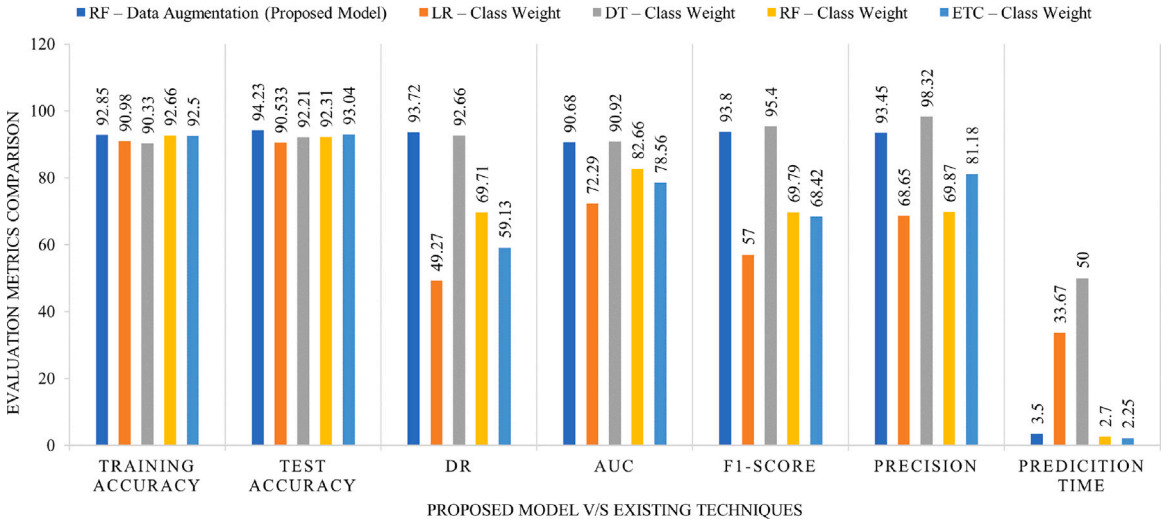

Fig. 12. Performance metrics of the proposed model using MinMax scaler with class weight ratio.

the model is being trained and tested. The proposed model is being constructed using system specification Intel Core i7-9750H @ 2.6 GHz Frequency and 16 GB RAM. The Table 18 represents the justified results.

Table 15
Comparison of proposed model with other algorithms using MinMax Scaler and data augmentation.

Model	Training accuracy (%)	Testing accuracy (%)	DR (%)	AUC (%)	FAR	F1-Score (%)	Precision (%)	Time (μs)
RF–Data augmentation (Proposed model)	92.85	94.23	93.72	90.68	0.06	93.8	93.45	3.5
LR–Data augmentation	72.72	73.02	48.33	73.33	0.01	0.64.46	96.74	65.6
DT–Data augmentation	90.83	90.48	89.02	90.50	0.02	90.4	91.77	58.46
RF–Data augmentation	90.31	90.79	93.75	90.08	0.06	90.93	88.27	3.3
ET–Data augmentation	88.95	90.05	95.77	90.121	0.04	90.48	85.74	3.1

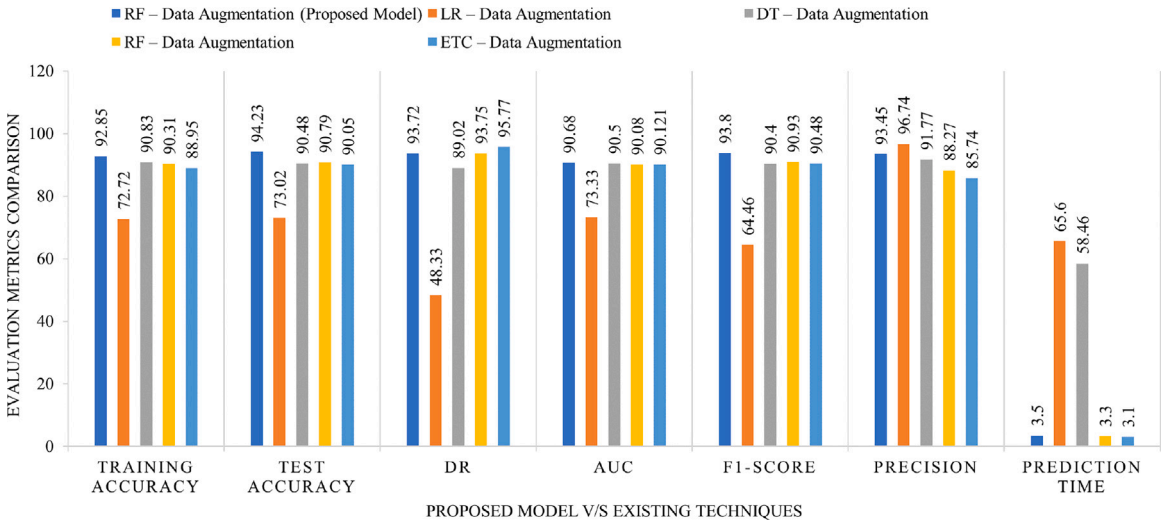

Fig. 13. Performance metrics of the proposed model using MinMax scalar with data augmentation.

Table 16
Confusion matrix of proposed model.

		True labels	
		0 (Normal)	1 (Attack)
Predicted labels	0(Normal)	2737 (TN)	177 (FP)
	1(Attack)	170 (FN)	2623 (TP)

Table 17
Comparison of proposed model with and without data augmentation.

Dataset status	Type of sample	Number of samples	Training accuracy (%)	DR (%)	AUC (%)	F1-Score (%)	Precision (%)
Without data augmentation	Benign	14,272	93.81	51.44	75.22	67.93	100
	Malignant	2046					
With data augmentation	Benign	14,272	94.23	93.72	90.68	93.80	93.8
	Malignant	14,272					

5.4. Effect of data size on DR

Without data augmentation i.e., with imbalanced dataset, the True Positive values were less which resulted in a poor Detection Rate i.e., is 51.44%. After performing the Data Augmentation there was an increase in data size which resulted in a good detection rate i.e., 93.72%. The following results are available in Table 19.

5.5. Limitations

The Dataset only focuses on two attacks of Man in the Middle Attack i.e., Data Alteration and Data Spoofing. In addition, the model has been simulated in a restricted network environment, which provided a combination of network and biometric data as an input to the model.

Table 18
Comparison of proposed model with other algorithms using MinMax Scaler and data augmentation.

Model	Training accuracy (%)	Testing accuracy (%)	DR (%)	AUC (%)	F1-Score (%)	Precision (%)	Time (μs)
Robust Scaler + RF + Data augmentation (Proposed model)	92.85	94.23	93.72	90.68	93.8	93.45	3.5
Robust Scaler + LR + Class weight ratio	89.88	89.00	55.52	74.70	5672	57.03	42
Robust Scaler + DT + Class weight ratio	89.71	91.81	89.90	91.00	73.69	62.43	41
Standard Scalar + RF + Class weight ratio	92.85	91.81	67.30	81.35	67.30	68.12	26.41

Table 19
Effect of data size on detection rate.

Data size	True negative	False positive	False negative	True positive	Benign samples	Malignant samples	Detection rate(%)
Without data augmentation	2848	0	202	214	14272	2046	51.44
With data augmentation	2737	177	170	2623	14727	14727	93.72

6. Conclusion and future work

The increase in the demand for IoMT services and the massive rise in the number of users requires robust security measures to counter any malicious activity. The security model for such distributive networks also needs a detection mechanism to identify if the data in the network has been tampered with by an intruder. The proposed model combines the random forest algorithm with the proper feature scaling method i.e, robust scaling. The model efficiently handles large and complex categorical data and effectively performs the classification in Intrusion Detection for IoMT networks. The methodology is highly appropriate for e-healthcare systems which deal with a vast amount of data. The proposed framework reduces the feature dimension and number of instances efficiently to improve the time of the classification process without compromising accuracy. The model reported an average accuracy of 94.23% and an F1-score of 93.8%. The performance of the proposed model has been analysed with the other ML based classification techniques namely logistic regression, decision tree and extra tree classifier. The results also infer that there is a significant reduction in the classification time. The reduction in time is achieved by processes involving scaling, elimination of extraneous features, encoding, and feature selection.

In future work, consideration for more attacks may be included. In addition, lightweight modelling of deep neural networks can be used for the development of the Intrusion Detection System for IoMT, to possibly improve the detection rate and AUC Score for better stability of the model. The work also has a scope of reducing the feature space using a combination of more than one dimension reduction algorithm.

Declaration of competing interest

No author associated with this paper has disclosed any potential or pertinent conflicts which may be perceived to have impending conflict with this work. For full disclosure statements refer to https://doi.org/10.1016/j.compeleceng.2022.108158.

References

[1] Gatouillat A, Badr Y, Massot B, Sejdić E. Internet of medical things: A review of recent contributions dealing with cyber-physical systems in medicine. IEEE Internet Things J 2018;5(5):3810–22. http://dx.doi.org/10.1109/JIOT.2018.2849014.

[2] Yanambaka VP, Mohanty SP, Kougianos E, Puthal D. PMsec: Physical unclonable function-based robust and lightweight authentication in the internet of medical things. IEEE Trans Consum Electron 2019;65(3):388–97. http://dx.doi.org/10.1109/TCE.2019.2926192.

[3] Sharma M, Pant S, Kumar Sharma D, Datta Gupta K, Vashishth V, Chhabra A. Enabling security for the Industrial Internet of Things using deep learning, blockchain, and coalitions. Trans Emerg Telecommun Technol 2021;32(7):e4137. http://dx.doi.org/10.1002/ett.4137, arXiv:https://onlinelibrary.wiley.com/doi/pdf/10.1002/ett.4137. URL https://onlinelibrary.wiley.com/doi/abs/10.1002/ett.4137.

[4] Thamilarasu G, Odesile A, Hoang A. An intrusion detection system for internet of medical things. IEEE Access 2020;8:181560–76. http://dx.doi.org/10.1109/ACCESS.2020.3026260.

[5] Goel A, Sharma DK, Gupta KD. LEOBAT: Lightweight encryption and OTP based authentication technique for securing IoT networks. Expert Syst 2021;n/a(n/a):e12788. http://dx.doi.org/10.1111/exsy.12788, arXiv:https://onlinelibrary.wiley.com/doi/pdf/10.1111/exsy.12788. URL https://onlinelibrary.wiley.com/doi/abs/10.1111/exsy.12788.

[6] Butun I, Morgera SD, Sankar R. A survey of intrusion detection systems in wireless sensor networks. IEEE Commun Surv Tutor 2014;16(1):266–82. http://dx.doi.org/10.1109/SURV.2013.050113.00191.

[7] Baburaj E, Rani AAV. Secure and intelligent architecture for cloud-based healthcare applications in wireless body sensor networks. Int J Biomed Eng Technol 2019.

[8] Chakraborty S, Aich S, Kim H-C. A secure healthcare system design framework using blockchain technology. In: 2019 21st International Conference on Advanced Communication Technology. 2019, p. 260–4. http://dx.doi.org/10.23919/ICACT.2019.8701983.

[9] Hady AA, Ghubaish A, Salman T, Unal D, Jain R. Intrusion detection system for healthcare systems using medical and network data: A comparison study. IEEE Access 2020;8:106576–84. http://dx.doi.org/10.1109/ACCESS.2020.3000421.
[10] Rao BB, Swathi K. Fast kNN classifiers for network intrusion detection system. Indian J Sci Technol 2017;10(14):1–10.
[11] Shapoorifard H, Shamsinejad P. Intrusion detection using a novel hybrid method incorporating an improved KNN. Int J Comput Appl 2017;173:5–9.
[12] Sarhan M, Layeghy S, Moustafa N, Portmann M. Towards a standard feature set of NIDS datasets. 2021, ArXiv abs/2101.11315.
[13] Sarhan M, Layeghy S, Moustafa N, Portmann M. NetFlow datasets for machine learning-based network intrusion detection systems. 2020, ArXiv abs/2011.09144.
[14] Farhan RI, Maolood AT, Hassan NF. Performance analysis of flow-based attacks detection on CSE-CIC-IDS2018 dataset using deep learning. Indones J Electr Eng Comput Sci 2020;20:1413–8.
[15] Hussain FB, Abbas SG, Fayyaz UU, Shah GA, Toqeer A, Ali A. Towards a universal features set for IoT botnet attacks detection. 2020, ArXiv abs/2012.00463.
[16] Kumar P, Gupta GP, Tripathi R. An ensemble learning and fog-cloud architecture-driven cyber-attack detection framework for IoMT networks. Comput Commun 2021;166:110–24. http://dx.doi.org/10.1016/j.comcom.2020.12.003, URL https://www.sciencedirect.com/science/article/pii/S0140366420320090.
[17] Rathore H, Al-Ali AK, Mohamed A, Du X, Guizani M. A novel deep learning strategy for classifying different attack patterns for deep brain implants. IEEE Access 2019;7:24154–64. http://dx.doi.org/10.1109/ACCESS.2019.2899558.
[18] Shorten C, Khoshgoftaar TM. A survey on image data augmentation for deep learning. J Big Data 2019;6:1–48.
[19] Chawla N, Bowyer K, Hall LO, Kegelmeyer WP. SMOTE: Synthetic minority over-sampling technique. J Artificial Intelligence Res 2002;16:321–57.
[20] Ho TK. Random decision forests. In: Proceedings of 3rd international conference on document analysis and recognition. vol. 1, 1995, p. 278–82. http://dx.doi.org/10.1109/ICDAR.1995.598994.
[21] Gron A. Hands-on Machine Learning with Scikit-Learn and TensorFlow: Concepts, Tools, and Techniques To Build Intelligent Systems. 2nd ed.. O'Reilly Media, Inc.; 2020.
[22] Claesen M, Moor BD. Hyperparameter search in machine learning. 2015, ArXiv abs/1502.02127.
[23] Hosmer Jr DW, Lemeshow S, Sturdivant RX. Applied Logistic Regression. vol. 398, John Wiley & Sons; 2013.
[24] Raschka S, Mirjalili V. Python Machine Learning. 2nd ed.. Birmingham, UK: Packt Publishing; 2017.
[25] Geurts P, Ernst D, Wehenkel L. Extremely randomized trees. Mach Learn 2006;63:3–42.

Karan Gupta is currently pursuing his master's degree in technology at the Netaji Subhas University of Technology. During his Master's programme, he focused in the field of Mobile Computing and Security. Before that, he obtained his B.Tech degree in Computer Science and Engineering from S.R.M. University, Haryana.

Deepak Kumar Sharma is working as an Associate Professor in the Department of Information Technology, Indira Gandhi Delhi Technical University for Women (IGDTUW), Delhi, India. Earlier, he has worked as Assistant Professor at Netaji Subhas University of Technology (formerly N.S.I.T.), Delhi. His research interests include opportunistic networks, wireless ad hoc and sensor networks, Software Defined Networks and IoT Networks

Koyel Datta Gupta is a gold medalist in M.Tech (Computer Technology) from Jadavpur University, Kolkata (2007). She received her Doctorate in 2015 from Jamia Milia Islamia, New Delhi. Her areas of research include Network Security, Digital Signal Processing, Pattern Recognition and Machine Learning. She is currently working as Associate Professor in Maharaja Surajmal Institute of Technology (MSIT) (under the GGSIP University), New Delhi.

Anil Kumar is currently working as a Professor CSE, Accreditation Coordinator, and Head-Data Science Research Group, DIT University. He received his M.Tech from Delhi College of Engineering, Delhi, and Ph.D. from Manipal Group. He has more than 24 years of teaching and industrial experience. His research interests include Image processing algorithms, Cryptography, Artificial Intelligence, Signal and System, Neural Systems, and Genetic algorithms.

Journal Pre-proof

A two stream convolutional neural network with bi-directional GRU model to classify dynamic hand gesture

Bindu Verma

PII: S1047-3203(22)00090-6
DOI: https://doi.org/10.1016/j.jvcir.2022.103554
Reference: YJVCI 103554

To appear in: *J. Vis. Commun. Image R.*

Received date : 11 September 2021
Revised date : 10 April 2022
Accepted date : 4 June 2022

Please cite this article as: B. Verma, A two stream convolutional neural network with bi-directional GRU model to classify dynamic hand gesture, *J. Vis. Commun. Image R.* (2022), doi: https://doi.org/10.1016/j.jvcir.2022.103554.

This is a PDF file of an article that has undergone enhancements after acceptance, such as the addition of a cover page and metadata, and formatting for readability, but it is not yet the definitive version of record. This version will undergo additional copyediting, typesetting and review before it is published in its final form, but we are providing this version to give early visibility of the article. Please note that, during the production process, errors may be discovered which could affect the content, and all legal disclaimers that apply to the journal pertain.

© 2022 Elsevier Inc. All rights reserved.

Journal Pre-proof

A Two Stream Convolutional Neural Network with Bi-directional GRU Model to Classify Dynamic Hand Gesture

Bindu Verma

[a]*Assistant Professor, Department of Information Technology, Delhi Technological University, New Delhi, India*

Abstract

Dynamic hand gesture recognition is still an interesting topic for the computer vision community. A set of feature vectors can represent any hand gesture. A Recurrent Neural Network (RNN) can recognize these feature vectors as a hand gesture that analyses the temporal and contextual information of the gesture sequence. Thus, we proposed a hybrid deep learning framework to recognize dynamic hand gestures. In the Hybrid model GoogleNet is pipelined with a Bidirectional GRU unit to recognize the dynamic hand gesture. Dynamic hand gestures consist of many frames, and features of each frame need to be extracted to get the temporal and dynamic information of the performed gesture. As RNN takes input as a sequence of feature vectors, we extract features from videos using pretrained GoogleNet. As Gated Recurrent Unit is one of the variants of RNN to classify the sequential data, we created a feature vector that corresponds to each video and passed it to the bidirectional GRU (BGRU) network to classify the gestures. We evaluate our model on four publicly available hand gesture datasets. The proposed method performs well and is comparable with the existing methods. For instance, we achieved 98.6% accuracy on Northwestern University Hand Gesture(NWUHG), 99.6% on SKIG, 99.4% on Cambridge Hand Gesture (CHG) datasets respectively. We performed our experiments on

*Bindu Verma
Email address: bindu.cvision@gmail.com (Bindu Verma)

Journal Pre-proof

Journal Pre-proof

DHG14/28 dataset and achieved an accuracy of 97.8% with 14-gesture classes and 92.1% on 28-gesture classes. DHG14/28 dataset contains skeleton and depth data, and our proposed model used depth data and achieved comparable accuracy.

Keywords: `Dynamic Hand Gesture`, `Gated Recurrent Unit`, `Convolutional Neural Network`, `Recurrent Neural Network`

1. Introduction

Hand gestures are a natural non-verbal form of communication between human-human and human-machine. Automated hand gesture recognition enables a natural way of communication between humans and machines. The dynamic hand gesture recognition finds application in many fields such as human-computer interaction, sign language recognition, robotic surgery, virtual reality, gaming, navigation and medical fields etc. Due to the small size of the gesturing hand, varied hand shape, illumination and background clutter make hand detection and tracking challenging. Moreover, partial hand detection and tracking lead to low classification accuracy. In the early age of hand gesture recognition system, the traditional method focuses on detection and tracking of the hand followed by feature extraction then classification [1] [2] [3] [4]. Our objective is to track the movement of the hand irrespective of the shape, size and colour of the hand. Thus, an optical flow video is created corresponding to each RGB/Depth video that captures the motion information of the moving hand.

To extract the features of hand gestures, one needs to segment the hand, then track the hand across the frames and then perform the feature extraction. Deep learning-based methods provide a plausible way to automatically learn multi-level features, overcoming the hand-crafted feature learning. Dynamic hand gesture recognition requires spatio-temporal information, and a recurrent neural network considers both spatial and temporal information. RNN faces the vanishing gradient problem due to back propagation. To solve the vanishing gradient issue, Long Short Term Memory (LSTM) and Gated Recurrent Unit

Journal Pre-proof

(GRU) were introduced with cell memories and gates to learn the long-term dependencies. Therefore, this paper presents a bi-directional GRU (BGRU) network to learn the spatio-temporal features and classify the gestures using the SoftMax function with cross-entropy loss. A two-stream hybrid model has been proposed in which features are extracted using a GoogleNet and BGRU used to learn the Spatio-temporal features. Inspired from work presented in paper [5] optical flow from RGB/Depth video is calculated and created as an optical flow video(OFV) that removes the unnecessary background.

The main motivation of this study is to propose a model that does not require detection and tracking of the gesturing hand. Thus, the calculation of optical flow videos removes unnecessary information, focuses on the movement of the gesturing hand, and captures the temporal information. Feature extraction from the RGB frames is not sufficient enough to classify the dynamic gestures due to the lack of temporal information. Thus fusion of the RGB and Optical flow features gives a better accuracy compared to the single modality. Due to the less training sample, deep learning models may underfit and require a data augmentation, while our proposed BGRU model performs well on the fewer training samples.

The main contribution of the paper is as follows:

- We proposed a two-stream hybrid model: Features are extracted from RGB data using a pre-trained GoogleNet model in one model stream. Features are extracted from an optical flow video(OFV) in the second stream. Finally, the features obtained from both streams are fused at the decision level using the average fusion technique.
- Novelty of our work lies in using a deeply coupled hybrid pipeline in which RGB data is passed to extract the spatial features in one pipeline. Similarly, dense optical flow data is passed to extract the temporal features in the second pipeline. Then, later on, the output of the SoftMax layer was averagely fused to get the final prediction.
- We evaluate the comprehensive review of the BLSTM and BGRU model

Journal Pre-proof

with different batch sizes. Similarly, we have shown model accuracy on different input types such as RGB videos, Optical flow videos, and fusion of both. Experimental results show that the BGRU model with optical flow and RGB videos performs better than state-of-the-art.

The rest of the paper is organized as follows: A detailed description of previous work discussed in section 2. Section 3 discussed the proposed methodology with a detailed explanation of the gated recurrent unit. Section 4 has a detailed explanation of the experimental analysis. Experiments were performed in different conditions, such as different batch sizes with different training epochs. Finally we conclude in section 5 with future directives.

2. Related Work

Movement of dynamic hand gestures can be captured by optical flow [5], motion history images [6] and dynamic image network [7]. These methods capture the motion of moving objects without the requirement of segmentation of gesturing hand. However, feature extraction is also an important step to recognize the dynamic hand gesture. Most traditional feature extraction methods demand a prior knowledge of the hand performing the gesture, thus segmenting the hand from the background in a video sequence. It is challenging to segment out the gesturing body part for more cluttered, complex, or changing background due to image resolution, clothing, or illumination variation. Authors Verma et.al [1] used depth data to segment the gesturing hand, and then hand trajectories are formed, and geometrical features are extracted. Then Grassmann discriminant analysis framework was proposed to recognize the gestures. In another work, verma et.al [3] extracted hand-crafted features using a 3D histogram of oriented gradient and then classified the gestures using Grassmann discriminant analysis by representing the feature vector as a subspace on the manifold. Similarly, to represent the hand pose, Smedt et.al [8] utilized the Shape of Connected Joints, a hand skeleton data descriptor. Then next they use a Gaussian Mixture Model (GMM) and a support vector machine (SVM) classifier to encode

Journal Pre-proof

each descriptor using a Fisher vector representation and classify the gesture. In another paper, Cheng et.al [9] proposed Image-to-Class Dynamic Time Warping (I2C-DTW) to recognize 3D static images and 3D hand trajectory. Yang et.al [10] proposed a key frame extraction algorithm using a multi-channel gradient magnitude frequency histogram (HGMF-MC) to represent the high-level features.

Deep learning-based methods performing tremendously in many area such as multi-modal face pose estimation [11], image retrieval [12], fine-grained image recognition [13], human pose recovery [14], locality-sensitive sparse retrieval [15] and hand gesture recognition [16] [5]. Several authors proposed a different deep learning framework that directly takes raw data, extracts the features deeply, and classifies the gesture with high accuracy. Mujahid et.al [16] proposed a lightweight model for gesture recognition based on YOLO (You Only Look Once) V3 and DarkNet-53 convolutional neural networks that do not require additional pre-processing, picture filtering, or image enhancement. Author Lai et.al [17] and Chen et.al [18] both uses skeleton data and bidirectional recurrent neural network (RNN) to classify the performed gesture. A different combination of RNN and LSTM is proposed in the literature. Li et.al [19] uses bi-directional LSTM to recognize the gestures. Chunyong et.al [20] proposed a hand gesture classification framework nested interval unscented Kalman filter (UKF) with long short-term memory (NIUKF-LSTM) using sequential hand gesture data. Authors Ameur et.al [21] used a Hybrid Bidirectional Unidirectional LSTM (HBU-LSTM) as a final prediction network in forward and backward pass to recognize the dynamic hand gesture. Hou et.al [22] used an attention mechanism to extract the keyframes and then Spatial-Temporal Attention Residual Temporal Convolutional Network (STA-Res-TCN) to recognize the dynamic hand gesture. Juan et.al [23] used Convolutional Neural Network (CNN) and a Long Short-Term Memory (LSTM) recurrent network for activity and hand gesture recognition. Chen et.al [24] proposed dynamic graph-based spatial-temporal attention (DG-STA) using skeleton data. Authors Lei et.al [25] proposed Spatio-temporal network for skeleton-based dynamic hand gesture recognition. Zhang

Journal Pre-proof

et.al [26] used Multiple extractions and Multiple predictions (MEMP) in which features of hand gestures are extracted and predicted multiple times. 3D deep learning models are also proposed in the field of hand gesture recognition. Liu et.al [27] proposed 3DCNN model combined with Hidden Markov Model using skeleton-based hand gesture data. Similarly, Zhang et.al [28], extract Spatio-temporal using 3DCNN and ConvLSTM to classify the gestures. Molchanov et al. [29] used the 3D recurrent convolutional model to detect and classify the hand gesture from multi-modal data.

In recent years, bi-stream work has achieved the attention of the researchers in computer vision areas such as salient object detection [30], hand gesture recognition [31]. Author Zhenyu et.al [30] proposed a bi-stream network using ResNet50 and VGG16 to detect salient objects for a small training sample. Author Chen et.al [32] used a supervised convolutional neural network to improve the performance of video saliency detection using long-term spatio-temporal information. In another paper, author chen et.al [33] proposed a selective class activation mapping (SCAM) to convert video audio semantic category tags to pseudo fixations. Sharma et.al [5] proposed 2D-CNN to extract features from optical flow motion template and 3D-CNN to extract the features from RGB sequences. Then in the last, before the classification layer, features are fused to boost the classification accuracy. Zhang et.al [34] used two-stream graph convolutional neural network to extract the pose and motion features using graph convolutional neural network. Similarly, Author Li et.al [35] proposed a two-stream graph-based convolutional to extract the short term and long term temporal information. Author Li et.al [36] proposed a spatial perception stream (SP-Stream) where skeleton image is encoded using the convex hull of the hand and a temporal perception stream (TP-stream) that captures the motion of the hand.

The key difference between the existing method and our method is that we have created optical flow videos rather than optical flow templates, which have constraints that performed gestures have to be in the plane perpendicular to the camera. Another difference is that our proposed model can work on RGB and

Journal Pre-proof

depth data. Many two-stream networks use the skeleton data to extract the temporal information, which is sensor-dependent. Third and foremost difference is that the inclusion of two different feature streams using BGRU increases the accuracy and is computationally efficient. It can also work on less number of training samples. DeepGRU [31] also performed well in the field of gesture recognition and activity recognition. The author used skeleton data as an input and trained to GRU model with an attention mechanism and achieved good accuracy. Inspired by DeepGRU [31] paper, we have used BGRU, but input to the BGRU model is a feature vector extracted from RGB and OFV videos.

3. Proposed Approach

The overall architecture of the proposed approach is shown in Figure 1. The proposed approach is pipelined in two streams and executed parallelly. In the first stream, the RGB/Depth frame sequence of each video is passed to the GoogleNet, and in the second stream, dense optical flow video (OFV) is passed to the GoogleNet. The advantage of calculating optical flow is that it captures motion in each frame and removes the stationary background. Moreover, dense optical flow can be calculated on RGB or depth data, so there is no dependency on any particular sensor type. Figure 3 shows detailed explanation of GoogleNet architecture. We have used a pre-trained GoogleNet model to extract the features from RGB videos and dense OFV videos. Features are stored in a sequence vector corresponding to each frame. Then these features vector work as an input layer in the sequence learning architecture where two bidirectional gated recurrent unit layer is used. Although LSTM work well but the use of BGRU over LSTM reduces the computation time, and BGRU can work on fewer training samples [31]. The output of GRU is flattened at the fully connected layer, and then SoftMax is applied to get the probability score. Now the output of the SoftMax layer of both the stream is averagely fused to get the final prediction.

Journal Pre-proof

Journal Pre-proof

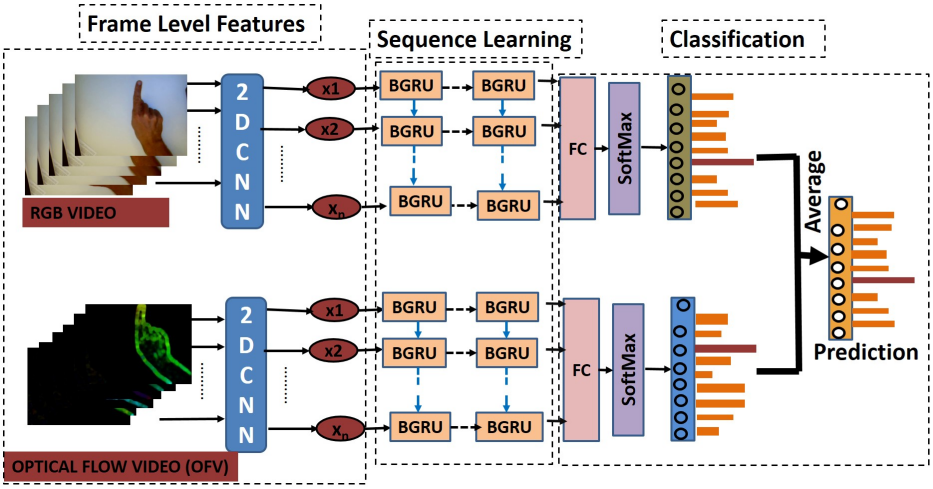

Figure 1: Shows proposed two pipe-line CNN and BGRU model. (a) Frame level features: RGB and dense optical flow sequence is passed in separate 2DCNN simultaneously to extract the frame features of each videos. (b) Sequence learning: An input layer is used to pass sequential frame features. Then bidirectional gated recurrent unit (BGRU) used to learn the sequential features. (c) Classification: Both network is terminated by fully connected layer followed by SoftMax. The classification score of both the network is fused to predict the final score.

3.1. Dense Optical Flow

Optical flow is used to capture the motion of the moving hand and create an optical flow video. The use of Optical flow videos adds an advantage to our proposed model to increase the recognition accuracy as shown in Figure 9. In our work, we have used Gunnar Faneback's method to calculate the dense optical flow videos corresponding to each RGB/Depth video, and the results are shown in the figure 2. Figure 2 (a) shows few RGB frames of a video and figure 2 (b) shows corresponding optical flow frames. As we can see, the background part is removed, and only the moving object is captured in the optical flow video. Let's assume that $I(x, y, t)$ is a pixel in the image and x, y are pixel coordinates at time t. Pixel I moves by $(\triangle x, \triangle y)$ in the next frame after $\triangle t$ time. We can

Journal Pre-proof

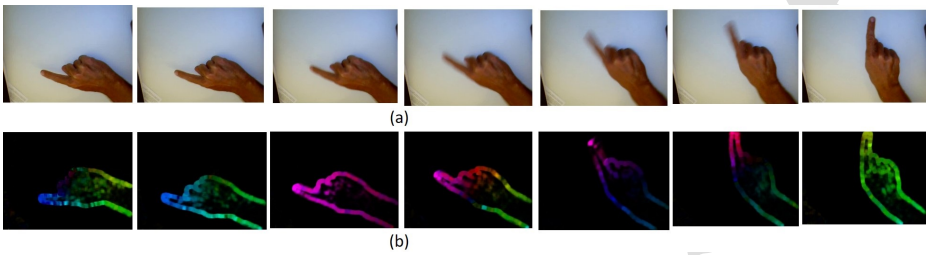

Figure 2: An example of the RGB and optical flow streams from the Northwestern University Hand Gesture dataset [2]. It can be seen, that for the stationary frames RGB provides better representation while optical flow provides better representation for the dynamic frames.(a) shows RGB frames (b) shows corresponding optical flow frames.

write the displacement as:

$$I(x, y, t) = I(x + \triangle x, y + \triangle y, t + \triangle t) \tag{1}$$

By doing Taylor approximation on the right side Equation 1 can be written as:

$$\frac{\triangle I}{\triangle x}\delta x + \frac{\triangle I}{\triangle y}\delta y + \frac{\triangle I}{\triangle t}\delta t = 0 \tag{2}$$

Dividing above equation by $\triangle t$ can be written as:

$$\frac{\triangle I}{\triangle x}w + \frac{\triangle I}{\triangle y}z + \frac{\triangle I}{\triangle t} = 0 \tag{3}$$

where w, z called as flow vector and $w = \frac{\delta x}{\delta t}$, also $\frac{\triangle I}{\triangle x}$ is a image gradient along the horizontal axis, and $z = \frac{\delta y}{\delta t}$, also $\frac{\triangle I}{\triangle y}$ is a image gradient along the vertical axis and $\frac{\triangle I}{\triangle t}$ along with time.

Flow vector w and z can be calculated as:

$$\begin{bmatrix} w \\ z \end{bmatrix} = \begin{bmatrix} \sum_i f_{x_i}^2 & \sum_i f_{x_i} f_{y_i} \\ \sum_i f_{x_i} f_{y_i} & \sum_i f_{y_i}^2 \end{bmatrix}^{-1} \begin{bmatrix} \sum_i f_{x_i} f_{t_i} \\ \sum_i f_{y_i} f_{t_i} \end{bmatrix} \tag{4}$$

where $f_x = \frac{\triangle I}{\triangle x}$ and $f_y = \frac{\triangle I}{\triangle y}$ are the image gradient of all the point in the image.

We got the flow vector (w, z) and calculate the magnitude and direction. We color code the image for better visualization where direction corresponds to Hue value of the image and magnitude corresponds to value plane in the HSV image

Journal Pre-proof

space. Thus, corresponds to each RGB video we calculate the dense optical flow video and pass to the 2DCNN to calculate the frame level features.

3.2. Convolutional Neural Network : GoogleNet

The pretrained convolutional network that is GoogleNet is used to extract the features. It has a total of 22 layers. In frame-level feature extraction, we pass the frames of each video to the GoogleNet model, and features of the average pooling layer are extracted and stored in the featured vector. Lets assume for any gesture sequence G having frames $\{f_1, f_2, f_3, f_4, ..., f_n\}$ passed to GoogleNet one by one. Then features at average pooling layer are extracted and stored in features vector $\{X_v = x_1, x_2, x_3, x_4, ..., x_n\}$. Thus, the dimension of feature vector X_v passed to the initial layer in a BGRU model is $1024 \times n$, where n is the number of frames in an OFV video. Likewise, we extracted the features of

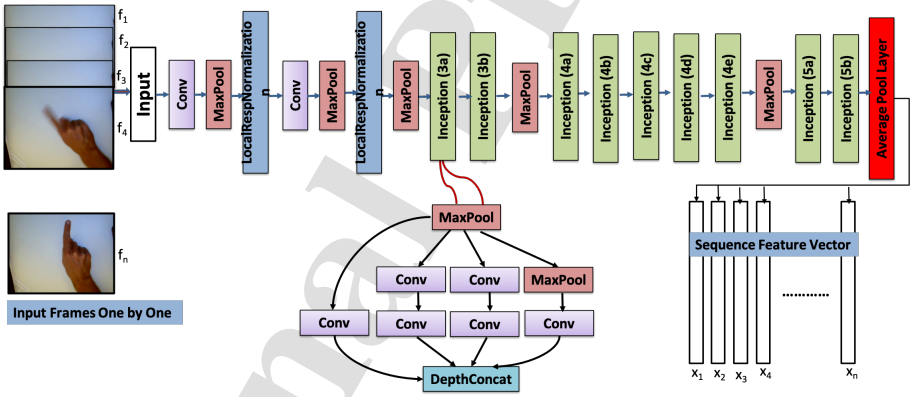

Figure 3: (a) Architecture of 2DCNN: GoogleNet

all the gestures and stored them in a sequence matrix. Then this matrix is used as an input to the input layer in a BGRU unit.

3.3. Gated Recurrent Unit (GRU)

GRU is a variant of recurrent neural networks to solve the problem of vanishing gradients that occurs in a traditional recurrent neural network. It uses

Journal Pre-proof

an update and reset gate and uses the hidden state to transfer the information. Update gate decides what to add and what information to discard. Reset gate decides how much past information to forget. GRU has fewer addition and multiplication operations, making it faster and easier than LSTM. Figure 4 illustrates the primary block of the gated recurrent unit (GRU). A horizontal line h_{t-1} at the top is previously hidden layer output passed as an input. This first gate represented in the square box is an update gate(u_t) that can add or remove information. This gate consists of a sigmoid neural layer that can process the data using point-wise multiplication. In the starting update gate u_t decide what

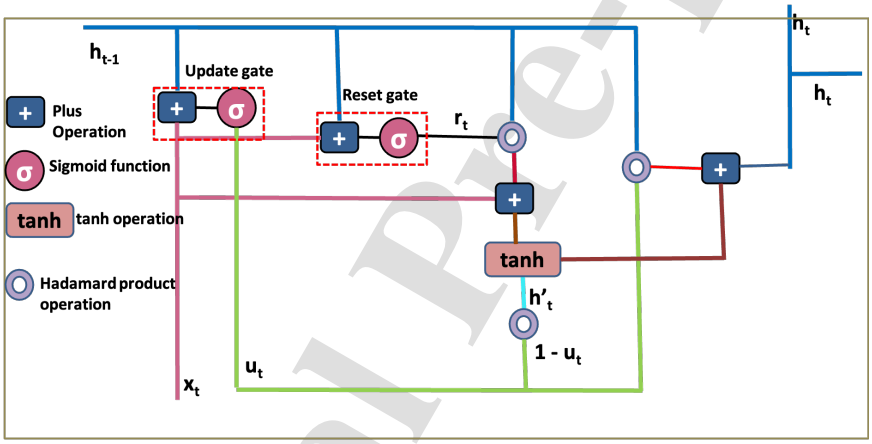

Figure 4: Shows GRU Architecture

information need to pass further and what information need to discard using equation 5.

$$u_t = \sigma((W^{(u)}x_t + b^u) + (Q^{(u)}h_{t-1} + b^u)) \tag{5}$$

In equation 5 x_t is current input and plugged into network unit and multiplied by its own weight $W^{(u)}$ and biases is added, similarly, h_{t-1} is a information of previous time stamp $t-1$ and multiplied with own weight $Q^{(u)}$ and biases. Both results are added together, and sigmoid σ activation is applied to get the final information to be passed on.

On the next step reset gate r_t decide how much information to forget from the

Journal Pre-proof

past information and can be calculated using equation 6.

$$r_t = \sigma((W^{(r)}x_t + b^r) + (Q^{(r)}h_{t-1} + b^r)) \tag{6}$$

In the next steps memory content $h_t^{'}$ is calculated using the reset gate r_t to get the relevant information from the past using Equation 7.

$$h_t' = tanh((Wx_t + b) + r_t \odot (Qh_{t-1} + b)) \tag{7}$$

where, input x_t is multiply with own weights and biases and $\odot$ is a hadamard product between reset gate r_t and previous hidden state $h_t - 1$. This will determine what to remove from previous steps. Then, both the results are summed up and *tanh* activation is applied.
In the last step h_t is calculated that holds the current information and pass it down in the network.

$$h_t = u_t \odot h_t - 1 + (1 - u_t) \odot h_t^{'} \tag{8}$$

where, u_t multiplied element wise with $h_t - 1$ to determine what information need to collect from previous step. Similarly, $(1 - u_t)$ is multiplied element wise with $h_t^{'}$ to get the information from current memory content. Then both results are summed up to get the final output h_t.

With a bi-directional structure, GRU can learn information from past and subsequent data to deal with the current data. The design of the BGRU model is shown in Figure 5. The BGRU model is based on the state of two GRUs that are unidirectional towards one another [37]. The forward-moving GRU begins from the start, and the backward-moving GRU begins from the end of the data sequence.

$$\overrightarrow{h_t} = GRU_{fwd}\left(x_t, \overrightarrow{h_{t-1}}\right) \overleftarrow{h_t} = GRU_{bwd}\left(x_t, \overleftarrow{h_{t+1}}\right) h_t = \overrightarrow{h_t} \oplus \overleftarrow{h_t} \tag{9}$$

where $\overrightarrow{h_t}$ is the state of the forward GRU, $\overleftarrow{h_t}$ is the state of the backward GRU, $\oplus$ indicates the operation of concatenating two vectors.

Journal Pre-proof

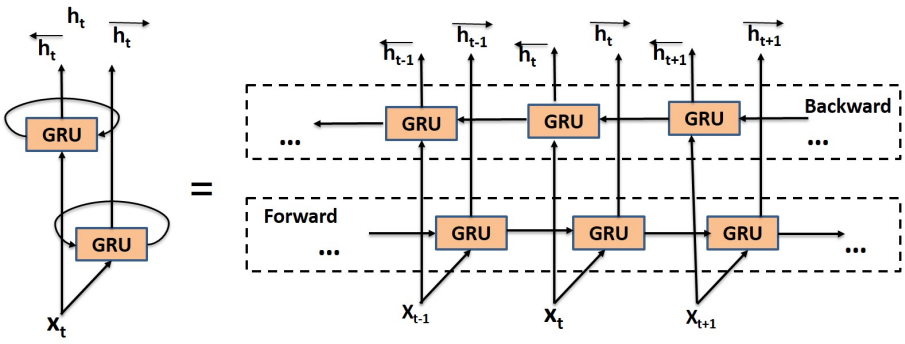

Figure 5: Shows Structure of a bidirectional GRU (BGRU) model

3.4. Training

For training, the complete network is trained with sequence features extracted from the GoogleNet network. Both stream networks are trained separately and parallelly. The initial layer of the BGRU network takes input as a sequence of the feature vector for a gesture G. At timestamp, t the input is a column vector $x_t \in R^N$, where N is the dimensionality of the feature vector. The feature vector extracted from GoogleNet is of size 1024. Thus, the input data of the entire temporal sequence of a single gesture sample is the matrix $x \in R^{1024 \times L}$, where L is the length of the sequence in time steps. Various gestures have different timestamps, and the entire sequence is used without clipping or down sampling. BGRU layer has 512 hidden nodes, and training is performed with 80% and 20% split.

The final layer of our model consist of one fully connected layer (FC) with ReLU activation followed by softmax layer. Output of BGRU layer is passed to the FC layer produce the probability distribution of the class labels using a softmax classifier.

$$\hat{y} = avg(softmax(FC(ReLU(O_{gru1}))) + softmax(FC(ReLU(O_{gru2})))) \quad (10)$$

SoftMax layer output of both the stream network is averagely fused to get the final prediction as shown in equation 10. During the training process, we

Journal Pre-proof

minimize the cross-entropy loss to reduce the difference between predicted class label $\hat{y}$ and the actual class label y.

4. Experimental Analysis and Discussions

To evaluate the performance of our proposed model, we performed a set of experiments on different types of dynamic hand gesture datasets such as Northwestern University Hand Gesture (NWUHG) dataset [2], Cambridge Hand Gesture dataset [38], SKIG dataset [39], DHG2016 dataset [8]. These datasets contain many variations, such as the same gesture performed by different hand shapes, lighting conditions, illuminations, and variations in the performed gesture. We have tested our model on the dataset mentioned above and reported average accuracy in terms of percentage.

4.1. Experimental Setup

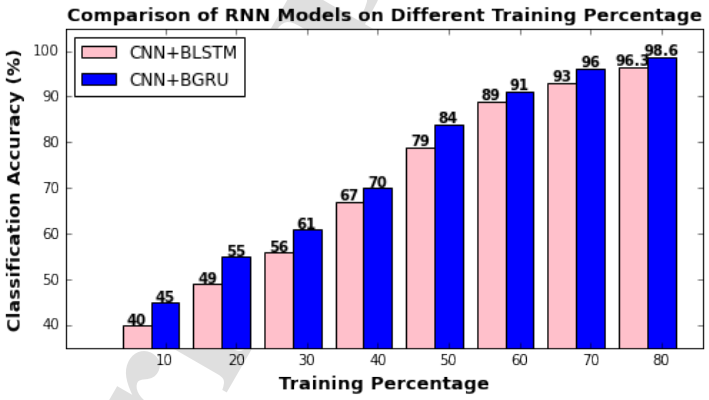

Figure 6: Shows accuracy of CNN + BLSTM and CNN+BGRU model on different training percentage over Northwestern University Hand Gesture dataset [2].

Experiments are conducted on Intel Core i7-7500U CPU @ 2.70GHz with 8GB RAM and GeForce 940MX GPU. In the proposed model, pretrained GoogleNet is used to extract the features. Then extracted features are passed to the BGRU network for a sequence to sequence learning. Adam is used as an optimizer with

Journal Pre-proof

varying batch sizes to perform the experiments. We have shown results on different batch sizes and found that the best batch size is 16 to perform the experiments. The learning rate is 0.0001, and training is completed after executing all the epochs and iterations. Details of hyper parameters is shown in Table 1. To show the effectiveness and performance of percentage of training examples, experiments on different training sample sizes are performed and reported the accuracy in Figure 6. In Figure 6 it is clear that when the total sample is divided into 80% for training and 20% for testing gives the best results. We performed training of BGRU model at different epochs and reported

Name	Details
Epochs	120
Batch Size	16
Learning Rate	0.0001
Optimizer	Adam
Loss	Cross Entropy

Table 1: Hyper Parameters of the BGRU Model

the training and testing accuracy in Figure 7 and loss accuracy in Figure 8. When we train the model around $120 - 140$ epochs, got best results. In the proposed two stream pipelined network, features are extracted from two types of data sequence i.e RGB/depth videos and OFV videos. To reduce the over fitting problem due to fewer training samples and low computation cost we have used BGRU network to train the model and classify the dynamic gestures. We have chosen different size of training examples with different type of network such as training with CNN + BLSTM and CNN + BGRU. When there are less training examples BGRU still performs better than all other network. As the results are experimented it shows that BGRU performs better than BLSTM as shown in Figure 9.

Accuracy is shown on different data inputs such as RGB data only, OFV only, and fusion of RGB and OFV data on CNN + LSTM model and CNN + BGRU model. The best accuracy of 98.6 is achieved with OFV and RGB data using the CNN + BGRU model on NWUHG dataset. The proposed model is trained

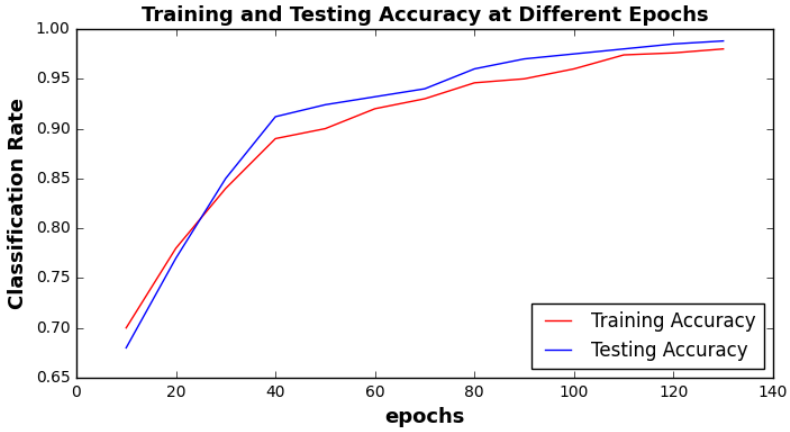

Figure 7: Training and testing accuracy of the proposed CNN + BGRU model over Northwestern University Hand Gesture dataset [2] dataset

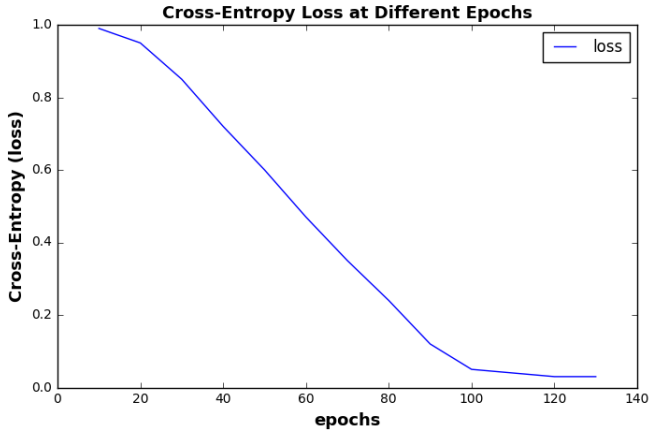

Figure 8: Cross entropy loss of the proposed CNN + BGRU model over Northwestern University Hand Gesture dataset [2] dataset:

on varying batch sizes such as $8, 16, 32, 64$ with 80% of training data over the NWUHG dataset. As in Figure 10, when batch size is 16 model performs better, having training and testing accuracy higher than in other cases where batch

Journal Pre-proof

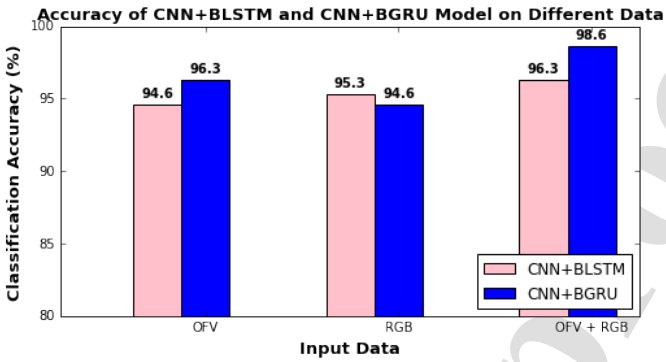

Figure 9: Shows accuracy of CNN + BLSTM and CNN + BGRU model on different input data on Northwestern University Hand Gesture dataset [2].

sizes are in $8, 32, 64$. Similarly, in the case of larger batch size, the training and testing loss is higher. Also, a cross-entropy loss is lower when the batch size is 16.

4.2. Experiments on different datasets

According to the discussion in Section 4.1 we have chosen 16 as a batch size with ADAM optimizer, 0.0001 learning rate and 120 epochs on different datasets and reported the accuracy in Figure 11, 12. Figure 11 shows the accuracy of the CNN + BLSTM and CNN + BGRU model on all the hand gesture datasets. In all the datasets, CNN + BGRU outperforms in terms of cost and training time than CNN + BLSTM. Both BLSTM and BGRU have nearly identical properties, but BGRU has fewer tensor operations and is computationally more efficient. Moreover, traditional RNN networks learn the representations from previous time sequences, which is a major issue. In contrast, bidirectional networks learn the representations from future time steps, resulting in a better understanding of context and eliminating data gaps. In addition, in the GRU cell, update and reset gates are employed in a hidden state layer in RNNs, which is more computationally efficient than an LSTM network due to a reduction in the number of gates, but still is at the same level of performance as LSTM.

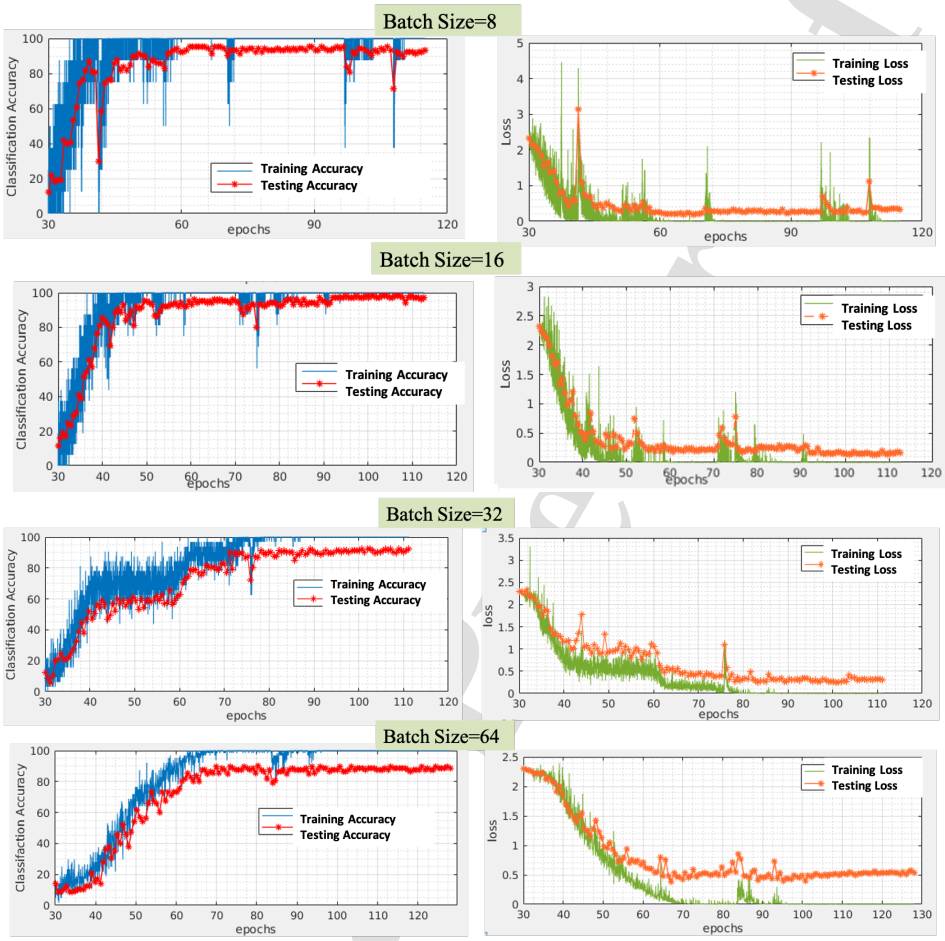

Figure 10: Shows training and testing accuracy and loss with varying batch sizes over Northwestern University Hand Gesture dataset [2].

We tested accuracy on different inputs such as RGB data only, OFV data, then fusion of RGB + OFV data. The best accuracy is when RGB + OFV data is used as an input with CNN + BGRU model as shown in Figure 12. Using only single stream also model gives good accuracy and comparable with the literature but fusion of both improves the accuracy.

Journal Pre-proof

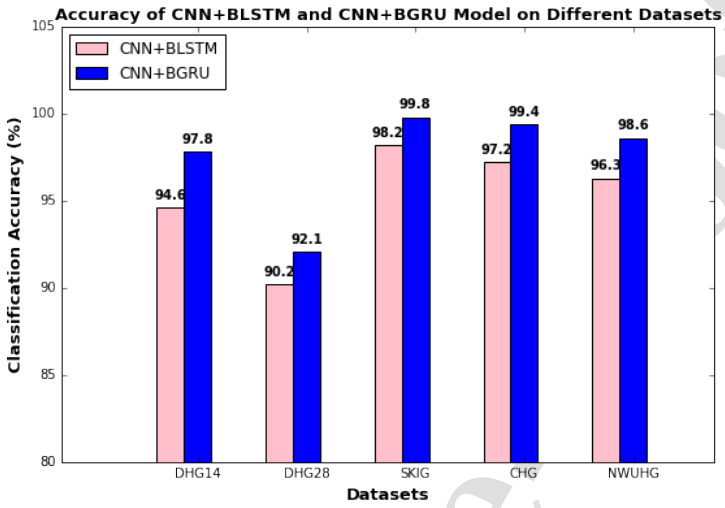

Figure 11: Shows accuracy of CNN+BLSTM and CNN+BGRU model on DHG14, DHG28, SKIG, CHG and NWUHG datasets. The best accuracy we achieved using CNN + BGRU model on SKIG dataset of 99.8%.

4.2.1. Experiments on DHG14/28 dataset [8]

DHG14/28 dataset contains depth and skeleton data having 14 coarse and fine dynamic gestures performed by 20 subject using 2 hand shapes and 5 times each. The gesture inventory contains coarse gestures are "Tap", "Swipe Right", "Swipe left","Swipe Up","Swipe Down","Swipe X", "Swipe V", "Swipe +", "Shake" and fine gestures are "Grab", "Expand", "Pinch", "Rotation Clock Wise", "Rotation Counter Clock Wise". Moreover, the shape of the performing hand changes as the gesture is performed, and therefore, the gestures are more complex. This dataset contains depth video and skeleton data only. Depth videos are preprocessed to increase the intensity of videos to calculate the OFV videos. Then, depth videos are used to extract the features from GoogleNet, and optical flow videos are created from depth videos. Then, optical flow video is used to extract the features, and both features are passed into a separate BGRU model. Finally, SoftMax scores are averagely fused to get the final prediction, and the average accuracy of 97.8% is shown in Figure 12. DHG gestures are

Journal Pre-proof

performed in two ways using the whole hands and using only one finger. In DHG14, we consider a gesture belongs to the same class performed by whole and single fingers and, in this case, got average accuracy of 97.8%. Similarly, in DHG28, we consider a gesture performed by the whole hand, and a single finger belongs to the different classes. In that case, it got lower accuracy of 92.1% because the gesture is same; only the shape of the hand is different.

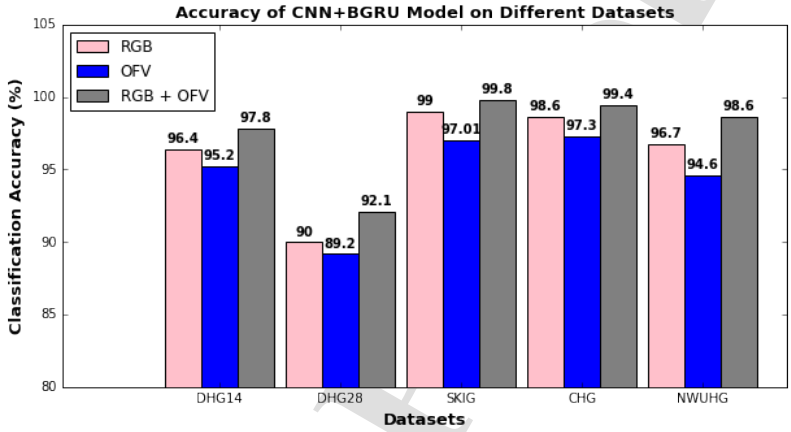

Figure 12: Shows accuracy of proposed model on DHG14, DHG28, SKIG, CHG and NWUHG datasets.The best accuracy we achieved using CNN + BGRU model on SKIG dataset of 99.8% with RGB + OFV

4.2.2. Experiments on Cambridge Hand Gesture(CHG) dataset [38]

CHG [38] has 900 image sequences for 9 classes of hand gestures, each of which is made up of 3 primitive shapes and 3 primitive motions. Each class has 100 images (5 different illuminations × 10 arbitrary motions of 2 subjects). RGB videos are used to extract the features from CNN and optical flow videos created from RGB video. Then, optical flow video is used to extract the features, and both features are passed into a separate BGRU model. Finally, softMax scores are averagely fused to get the final prediction, and the average accuracy of 99.4% is shown in Figure 12. In Figure 12 we can see that individual modality also gives good accuracy more than 97% using RGB or OFV videos.

Journal Pre-proof

4.2.3. Experiments on SKIG dataset [39]

SKIG dataset [39] contains RGB and depth videos of dynamic hand gesture that have 10 different kind of hand gestures performed by 6 subjects. Each subject performed the gesture using 3 different shapes having 3 backgrounds with 2 illumination conditions. Thus, each gesture have total $6 \times 3 \times 3 \times 2 = 108$ video sequences. We created optical flow videos of the RGB data and passed both the video into the google net model to extract the features. Gesture inventory of SKIG hand gesture datasets contains simple and complex gesture sequences such as "line", "Cross", "Circle", "Z", "Triangle", "Wave" are simple gesture and complex "Up-down", "Come-Here", "Turn around", and "Pat" gestures are complex gesture. RGB videos are used to extract the features from CNN and OFV videos created from RGB videos and used to extract features. Then, both features are passed into a separate BGRU model. Finally, the SoftMax score is averagely fused to get the final prediction and got average accuracy of 99.6% as shown in Figure 12.

We also calculated the accuracy of the proposed model when only depth data is available. OFV videos are calculated using depth data, and in one stream only depth data is passed, and in second stream, OFV videos are passed to calculate the features. Then BGRU model is used to train and classify the gestures. Average accuracy of 98.2% as shown in Figure 13 shows that the proposed model can work well if only depth data is available and the achieved accuracy is close to the RGB data accuracy.

4.2.4. Experiments on Northwestern University Hand Gesture Dataset [2]

Northwestern University Hand Gesture dataset [2] contains 10 dynamic hand gestures with 7 different postures performed by 15 subjects. Thus for each gesture $7 \times 15 = 105$ video sequence are available. The gesture inventory contains RGB videos such as "move right"," move left", "rotate up", "rotate down", "move down-right", "move right-down", "clockwise circle", "counter- clockwise circle", "Z", and "cross". We have used RGB video sequence to find the optical flow of moving object. In the NUHG total of 1050 samples are there, 840 samples

Journal Pre-proof

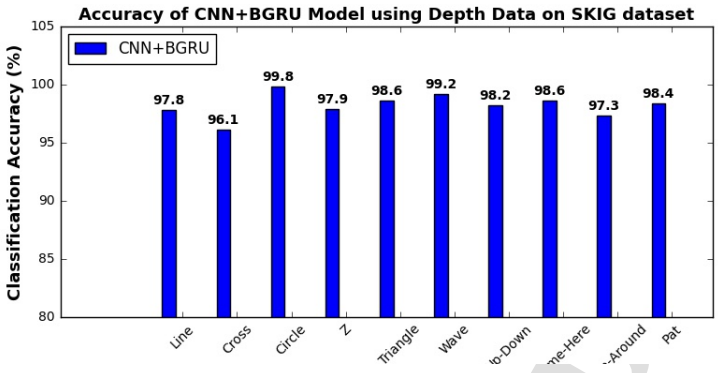

Figure 13: Shows accuracy of proposed model on SKIG dataset where input to the model is depth data.

used for training, and the remaining 210 sample used for testing. RGB videos are used to extract the features from CNN, and optical flow video created from RGB video is used to extract the features, and both features are passed into a separate GRU model. Finally, the softmax score is averagely fused to get the final prediction, and the average accuracy of 98.6% is shown in Figure 12.

4.3. Comparison with State-of-the-art

We perform an experimental comparison with state-of-the-art on DHG14/28, CHG, SKIG, and NWUHG data sets. The results are discussed and discussed below:

4.3.1. Comparison with state-of-the-art on DHG14/28 dataset [8]:

Table 2 compares proposed CNN+BGRU model with existing handcrafted and deep learning-based methods. As given in Table 2 proposed method outperforms all the handcrafted SOTA methods in 14-gesture classes as well as in 28 gesture class and comparable result with the paper [42]. However, in 28-gesture classes proposed method outperform all the SOTA methods except paper [35]. The reason is that when same gesture performed by two different hand shape (whole hand, one finger) considered as two different classes, then in both classes

Journal Pre-proof

Table 2: Comparison results of classification accuracies (%) on the DHG14/28 dataset with state-of-the-art with 720 samples for training and 180 for testing

Methods	14-**Gesture (%)**	28-**Gesture(%)**
SoCJ + HoHD + HoWR [8]	83.1	80.0
STA-Res-TCN[22]	89.2	85.0
CNN+LSTM [23]	85.6	81.1
ST-TS-HGR-NET [40]	94.2	89.4
HPEV-Net+HMM-Net [27]	92.5	88.8
DG-STA [24]	91.9	88.0
Motion Features+RNN [18]	84.6	80.3
NIUKF-LSTM [20]	84.9	80.4
MHI+VGG16 [41]	93.5	85.8
DeepGRU [31]	94.5	91.4
Leap Motion+RNN [42]	97.6	91.4
SAGCN+RBi-IndRNN [35]	96.3	**94.0**
DSTA-Net [25]	93.8	90.9
CNN+BGRU+OFV	95.2	89.2
CNN+BGRU+RGB	96.4	90
CNN+BGRU+RGB+OFV	**97.8**	92.1

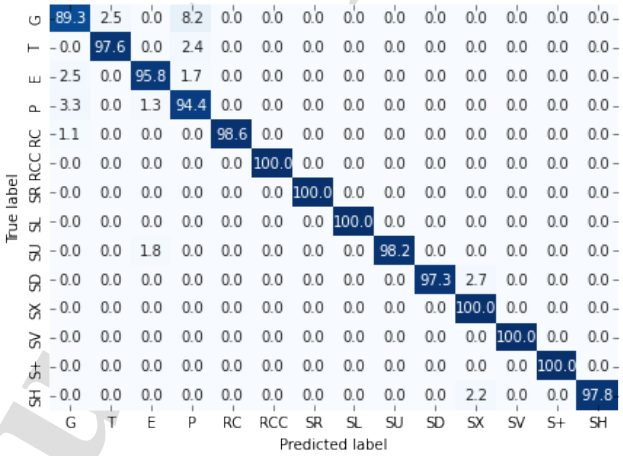

Figure 14: Shows confusion matrix of the 14-gesture classes.

Journal Pre-proof

Journal Pre-proof

we might get similar optical flow video (OFV) thus, reducing the accuracy. In the OFV video, we are capturing the motion of the moving hand and the same gesture performed by the whole hand or single finger; we get a similar track for both the classes in a few gestures. A confusion matrix is shown in Figure 14, 15 and from the confusion matrix, we can see that grab pinch and expand gestures are misclassified mostly. Grab gestures performed by a single finger or the whole hand are confused with each other and also confused with the pinch due to the similar track. Similarly, a tap gesture performed by a single or whole hand will have the same motion movement. These minor details are still challenging, and we would like the explore in the future.

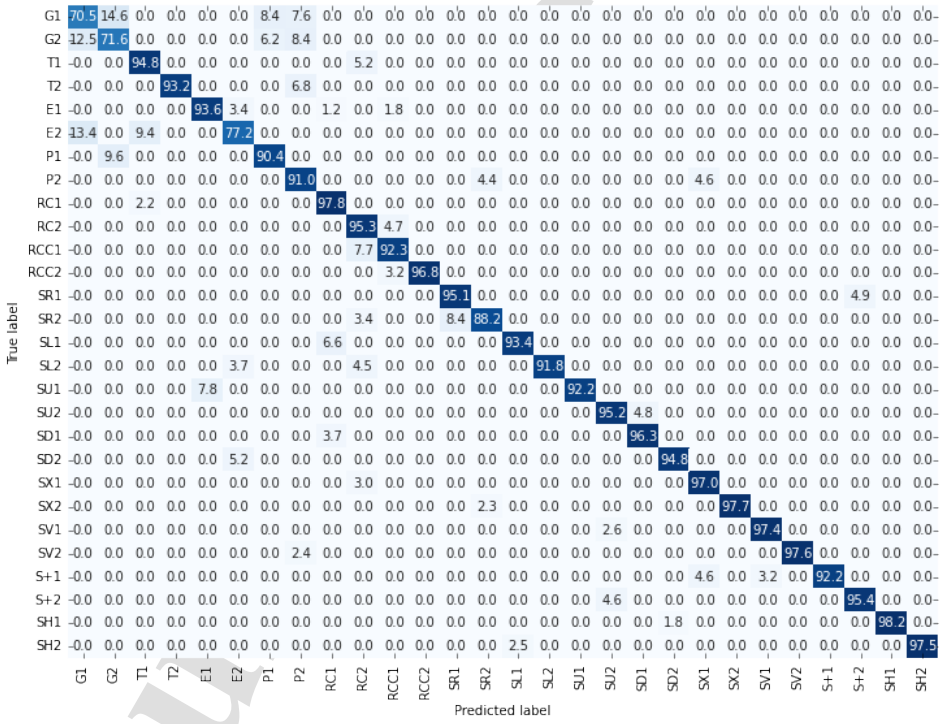

Figure 15: Shows confusion matrix of the 28-gesture classes.

Journal Pre-proof

4.3.2. Comparison with state-of-the-art on Cambridge Hand Gesture(CHG) dataset [38]

Table 3 shows the comparative analysis with existing methods and achieved 99.4% accuracy. Though training samples are less, but proposed system performs better than the literature without any data augmentation technique. We achieved 99.4% accuracy that is comparable to the paper [43] in which they used key frame extraction and fusion to classify the gestures. As shown in Table 3 accuracy of single modality is also more than all the existing SOTA methods except paper [43].

Table 3: Comparison results of classification accuracies (%) on the Cambridge Hand Gesture(CHG) dataset with state-of-the-art

Methods	**Accuracy (%)**
Key Frames + Feature Fusion [43]	99.1
TCCA + k-NN [38]	85.5
2D-DWT-PH [10]	90
Approximate Nearest Neighbor (ANN)	94.6
3DHOG+GGDA [3]	89.7
3DTensor+Manifold Learning [44]	91.0
Dense Trajectories + Hand Segmentation [45]	94.0
CNN+BGRU+OFV	97.3
CNN+BGRU+RGB	98.6
Ours CNN+BGRU+RGB+OFV	**99.4**

4.3.3. Comparison with state-of-the-art on SKIG dataset [39]

Table 4 shows a comparison of our proposed method with several other competing methods on the SKIG dataset. Proposed model achieved better accuracy with all the hand crafted methods [46], [1] and comparable with the deep learning methods [26], [19], [28], [47]. Paper [47] and our proposed method are very close in accuracy where the have used multi 3DCNN and we used BGRU that simple and computationally efficient.

Journal Pre-proof

Table 4: Comparison results of classification accuracies (%) on the SKIG dataset

Methods	Accuracy (%)
HOG+LBP [46]	97.3
Geometric Features + GGDA [1]	98.1
3DCNN + LSTM [48]	98.6
MEMP [26]	99.02
BLSTM [19]	99.07
ConvLSTM [28]	99.53
MultiD-CNN [47]	99.72
R3DCNN [29]	98.6
CNN+BGRU+OFV	97.01
CNN+BGRU+RGB	99
Ours CNN+BGRU+RGB+OFV	**99.8**

4.3.4. Comparison with state-of-the-art on Northwestern University Hand Gesture Dataset [2]

The performance of our proposed method on the Northwestern University Hand Gesture (NWUHG) dataset with several other competitive methods that were conducted on this dataset is shown in Table 5. A different hand-crafted method for NWUHG hand gesture classification achieved quite a reasonable accuracy. Using CNN and BGRU model, we achieved around 98.6% accuracy comparable with state-of-the-art methods.

Table 5: Comparison results of classification accuracies (%) on the Northwestern University Hand Gesture (NWUHG) dataset

Methods	Accuracy (%)
Key Frames + Feature Fusion [43]	97.9
Genetic Programming [49]	96.1
Maximum Stable Extremal Regions (MSER) [2]	97.62
CNN+BGRU+OFV	94.6
CNN+BGRU+RGB	96.7
Ours CNN+BGRU+RGB+OFV	**98.6**

Journal Pre-proof

Journal Pre-proof

4.4. Time Analysis

We have proposed a bidirectional gated recurrent unit (BGRU) model. Optical flow videos are calculated in OpenCV, and it takes 0.6 sec to process one video. Each video contains an average of 40 frames. Then frame-wise features are extracted using a pre-trained GoogleNet model parallelly for RGB and optical flow video, and it takes 0.5 seconds for one video. Then after extracting the features, features are passed into a sequence BGRU model that takes 7-8 hours training over 4500 videos. While testing the trained models takes 1 sec to classify the given gestures. Testing time depends on the length of the video. If the video has a lesser number of frames or normalized the video length or only key frames are extracted, this testing time can be reduced to some milliseconds.

5. Conclusions

To build a fast and robust hand gesture recognition system, we proposed a bidirectional gated recurrent unit (BGRU) model that is computationally efficient and can work on fewer training samples. The creation of optical flow videos and fusion of RGB and optical flow video features makes our model stronger with efficient accuracy and may be suitable for real-time applications. Moreover, our proposed framework can calculate optical flow on either RGB videos or depth videos, making the sensor independent. Experimental results on four publicly available datasets having an accuracy of more than 98% on SKIG, CHG, and NWUHG datasets and 97.8% on DHG14/28 dataset outperform better than state-of-the-art methods.

As a future directional, we would like to work on skeleton data. We would also like to propose some key features extraction techniques so that only required information should be processed for gesture recognition. We would like to propose a model that can be combined with a skeleton and RGB-D data to recognize the dynamic hand gesture with high accuracy.

Journal Pre-proof

Journal Pre-proof

Acknowledgements

The author would like to acknowledge Department of Information Technology, Delhi Technological University, New Delhi, India for providing me necessary resources to carry out the research.

References

[1] B. Verma, A. Choudhary, Grassmann manifold based dynamic hand gesture recognition using depth data, Multimedia Tools and Applications 79 (3) (2020) 2213–2237.

[2] X. Shen, G. Hua, L. Williams, Y. Wu, Dynamic hand gesture recognition: An exemplar-based approach from motion divergence fields, Image and Vision Computing 30 (3) (2012) 227–235.

[3] B. Verma, A. Choudhary, Framework for dynamic hand gesture recognition using grassmann manifold for intelligent vehicles, IET Intelligent Transport Systems 12 (7) (2018) 721–729.

[4] B. Verma, A. Choudhary, Unsupervised learning based static hand gesture recognition from rgb-d sensor, in: International Conference on Soft Computing and Pattern Recognition, Springer, 2016, pp. 304–314.

[5] D. Sarma, V. Kavyasree, M. K. Bhuyan, Two-stream fusion model for dynamic hand gesture recognition using 3d-cnn and 2d-cnn optical flow guided motion template, arXiv preprint arXiv:2007.08847.

[6] B. Verma, A. Choudhary, Affective state recognition from hand gestures and facial expressions using grassmann manifolds, Multimedia Tools and Applications 80 (9) (2021) 14019–14040.

[7] H. Bilen, B. Fernando, E. Gavves, A. Vedaldi, Action recognition with dynamic image networks, IEEE transactions on pattern analysis and machine intelligence 40 (12) (2017) 2799–2813.

Journal Pre-proof

[8] Q. De Smedt, H. Wannous, J.-P. Vandeborre, Skeleton-based dynamic hand gesture recognition, in: Proceedings of the IEEE Conference on Computer Vision and Pattern Recognition Workshops, 2016, pp. 1–9.

[9] H. Cheng, Z. Dai, Z. Liu, Y. Zhao, An image-to-class dynamic time warping approach for both 3d static and trajectory hand gesture recognition, Pattern recognition 55 (2016) 137–147.

[10] H. Yang, Q. Tian, Q. Zhuang, L. Li, Q. Liang, Fast and robust key frame extraction method for gesture video based on high-level feature representation, Signal, Image and Video Processing 15 (3) (2021) 617–626.

[11] C. Hong, J. Yu, J. Zhang, X. Jin, K.-H. Lee, Multimodal face-pose estimation with multitask manifold deep learning, IEEE transactions on industrial informatics 15 (7) (2018) 3952–3961.

[12] J. Yu, D. Tao, M. Wang, Y. Rui, Learning to rank using user clicks and visual features for image retrieval, IEEE transactions on cybernetics 45 (4) (2014) 767–779.

[13] J. Yu, M. Tan, H. Zhang, D. Tao, Y. Rui, Hierarchical deep click feature prediction for fine-grained image recognition, IEEE transactions on pattern analysis and machine intelligence.

[14] C. Hong, J. Yu, J. Wan, D. Tao, M. Wang, Multimodal deep autoencoder for human pose recovery, IEEE transactions on image processing 24 (12) (2015) 5659–5670.

[15] C. Hong, J. Yu, X. Chen, Image-based 3d human pose recovery with locality sensitive sparse retrieval, in: 2013 IEEE international conference on systems, man, and cybernetics, IEEE, 2013, pp. 2103–2108.

[16] A. Mujahid, M. J. Awan, A. Yasin, M. A. Mohammed, R. Damaševičius, R. Maskeliūnas, K. H. Abdulkareem, Real-time hand gesture recognition based on deep learning yolov3 model, Applied Sciences 11 (9) (2021) 4164.

Journal Pre-proof

[17] K. Lai, S. N. Yanushkevich, Cnn+ rnn depth and skeleton based dynamic hand gesture recognition, in: 2018 24th International Conference on Pattern Recognition (ICPR), IEEE, 2018, pp. 3451–3456.

[18] X. Chen, H. Guo, G. Wang, L. Zhang, Motion feature augmented recurrent neural network for skeleton-based dynamic hand gesture recognition, in: 2017 IEEE International Conference on Image Processing (ICIP), IEEE, 2017, pp. 2881–2885.

[19] D. Li, Y. Chen, M. Gao, S. Jiang, C. Huang, Multimodal gesture recognition using densely connected convolution and blstm, in: 2018 24th International Conference on Pattern Recognition (ICPR), IEEE, 2018, pp. 3365–3370.

[20] C. Ma, A. Wang, G. Chen, C. Xu, Hand joints-based gesture recognition for noisy dataset using nested interval unscented kalman filter with lstm network, The visual computer 34 (6) (2018) 1053–1063.

[21] S. Ameur, A. B. Khalifa, M. S. Bouhlel, A novel hybrid bidirectional unidirectional lstm network for dynamic hand gesture recognition with leap motion, Entertainment Computing 35 (2020) 100373.

[22] J. Hou, G. Wang, X. Chen, J.-H. Xue, R. Zhu, H. Yang, Spatial-temporal attention res-tcn for skeleton-based dynamic hand gesture recognition, in: Proceedings of the European Conference on Computer Vision (ECCV) Workshops, 2018, pp. 0–0.

[23] J. C. Nunez, R. Cabido, J. J. Pantrigo, A. S. Montemayor, J. F. Velez, Convolutional neural networks and long short-term memory for skeleton-based human activity and hand gesture recognition, Pattern Recognition 76 (2018) 80–94.

[24] Y. Chen, L. Zhao, X. Peng, J. Yuan, D. N. Metaxas, Construct dynamic graphs for hand gesture recognition via spatial-temporal attention, arXiv preprint arXiv:1907.08871.

Journal Pre-proof

[25] L. Shi, Y. Zhang, J. Cheng, H. Lu, Decoupled spatial-temporal attention network for skeleton-based action-gesture recognition, in: Proceedings of the Asian Conference on Computer Vision, 2020.

[26] X. Zhang, X. Li, Dynamic gesture recognition based on memp network, Future Internet 11 (4) (2019) 91.

[27] J. Liu, Y. Liu, Y. Wang, V. Prinet, S. Xiang, C. Pan, Decoupled representation learning for skeleton-based gesture recognition, in: Proceedings of the IEEE/CVF Conference on Computer Vision and Pattern Recognition, 2020, pp. 5751–5760.

[28] L. Zhang, G. Zhu, P. Shen, J. Song, S. Afaq Shah, M. Bennamoun, Learning spatiotemporal features using 3dcnn and convolutional lstm for gesture recognition, in: Proceedings of the IEEE International Conference on Computer Vision Workshops, 2017, pp. 3120–3128.

[29] P. Molchanov, X. Yang, S. Gupta, K. Kim, S. Tyree, J. Kautz, Online detection and classification of dynamic hand gestures with recurrent 3d convolutional neural network, in: Proceedings of the IEEE conference on computer vision and pattern recognition, 2016, pp. 4207–4215.

[30] Z. Wu, S. Li, C. Chen, A. Hao, H. Qin, A deeper look at image salient object detection: Bi-stream network with a small training dataset, IEEE Transactions on Multimedia.

[31] M. Maghoumi, J. J. LaViola, Deepgru: Deep gesture recognition utility, in: International Symposium on Visual Computing, Springer, 2019, pp. 16–31.

[32] C. Chen, G. Wang, C. Peng, X. Zhang, H. Qin, Improved robust video saliency detection based on long-term spatial-temporal information, IEEE transactions on image processing 29 (2019) 1090–1100.

[33] G. Wang, C. Chen, D.-P. Fan, A. Hao, H. Qin, From semantic categories to fixations: A novel weakly-supervised visual-auditory saliency detection ap-

Journal Pre-proof

proach, in: Proceedings of the IEEE/CVF Conference on Computer Vision and Pattern Recognition, 2021, pp. 15119–15128.

[34] W. Zhang, Z. Lin, J. Cheng, C. Ma, X. Deng, H. Wang, Sta-gcn: two-stream graph convolutional network with spatial–temporal attention for hand gesture recognition, The Visual Computer 36 (10) (2020) 2433–2444.

[35] C. Li, S. Li, Y. Gao, X. Zhang, W. Li, A two-stream neural network for pose-based hand gesture recognition, arXiv preprint arXiv:2101.08926.

[36] Y. Li, D. Ma, Y. Yu, G. Wei, Y. Zhou, Compact joints encoding for skeleton-based dynamic hand gesture recognition, Computers & Graphics 97 (2021) 191–199.

[37] C. Xiong, S. Merity, R. Socher, Dynamic memory networks for visual and textual question answering, in: International conference on machine learning, PMLR, 2016, pp. 2397–2406.

[38] T.-K. Kim, S.-F. Wong, R. Cipolla, Tensor canonical correlation analysis for action classification, in: 2007 IEEE Conference on Computer Vision and Pattern Recognition, IEEE, 2007, pp. 1–8.

[39] L. Liu, L. Shao, Learning discriminative representations from rgb-d video data, in: Twenty-third international joint conference on artificial intelligence, 2013.

[40] X. S. Nguyen, L. Brun, O. Lézoray, S. Bougleux, A neural network based on spd manifold learning for skeleton-based hand gesture recognition, in: Proceedings of the IEEE/CVF Conference on Computer Vision and Pattern Recognition, 2019, pp. 12036–12045.

[41] B. Verma, A. Choudhary, Dynamic hand gesture recognition using convolutional neural network with rgb-d fusion, in: Proceedings of the 11th Indian Conference on Computer Vision, Graphics and Image Processing, 2018, pp. 1–8.

Journal Pre-proof

[42] D. Avola, M. Bernardi, L. Cinque, G. L. Foresti, C. Massaroni, Exploiting recurrent neural networks and leap motion controller for the recognition of sign language and semaphoric hand gestures, IEEE Transactions on Multimedia 21 (1) (2018) 234–245.

[43] H. Tang, H. Liu, W. Xiao, N. Sebe, Fast and robust dynamic hand gesture recognition via key frames extraction and feature fusion, Neurocomputing 331 (2019) 424–433.

[44] Y. M. Lui, J. R. Beveridge, M. Kirby, Action classification on product manifolds, in: 2010 IEEE Computer Society Conference on Computer Vision and Pattern Recognition, IEEE, 2010, pp. 833–839.

[45] L. Baraldi, F. Paci, G. Serra, L. Benini, R. Cucchiara, Gesture recognition in ego-centric videos using dense trajectories and hand segmentation, in: Proceedings of the IEEE Conference on Computer Vision and Pattern Recognition Workshops, 2014, pp. 688–693.

[46] R. Azad, M. Asadi-Aghbolaghi, S. Kasaei, S. Escalera, Dynamic 3d hand gesture recognition by learning weighted depth motion maps, IEEE Transactions on Circuits and Systems for Video Technology 29 (6) (2018) 1729–1740.

[47] A. Elboushaki, R. Hannane, K. Afdel, L. Koutti, Multid-cnn: A multi-dimensional feature learning approach based on deep convolutional networks for gesture recognition in rgb-d image sequences, Expert Systems with Applications 139 (2020) 112829.

[48] G. Zhu, L. Zhang, P. Shen, J. Song, Multimodal gesture recognition using 3-d convolution and convolutional lstm, Ieee Access 5 (2017) 4517–4524.

[49] L. Liu, L. Shao, Synthesis of spatio-temporal descriptors for dynamic hand gesture recognition using genetic programming, in: 2013 10th IEEE International Conference and Workshops on Automatic Face and Gesture Recognition (FG), IEEE, 2013, pp. 1–7.

- The paper presented a two-stream hybrid model that uses a convolutional neural network to extract the frame-level features and used a BGRU to classify the dynamic hand gesture.
- Novelty of our work lies that we used a deeply coupled hybrid pipeline in which in one pipeline RGB data is passed to extract the spatial and temporal features. Similarly, in the second pipeline, dense optical flow data is passed to extract the spatial features.
- The paper presented a comprehensive review of the BLSTM and BGRU model with different batch sizes.
- Experimental results shows that the BGRU model with optical flow and RGB videos performs better than state-of-the-art.

Journal Pre-proof

Journal Pre-proof

Declaration of interest: None

☒ The authors declare that they have no known competing financial interests or personal relationships that could have appeared to influence the work reported in this paper.

☐The authors declare the following financial interests/personal relationships which may be considered as potential competing interests:

Bindu Verma
Assistant Professor
Department of Information Technology
Delhi Technological University,
Rohini, New Delhi, 110042

Journal Pre-proof

I. J. Mathematical Sciences and Computing, **2022, 2, 28-36**
Published Online June 2022 in MECS (http://www.mecs-press.org/)
DOI: 10.5815/ijmsc.2022.02.03

Adaptive Social Acceleration Constant Based Particle Swarm Optimization

Jyoti Jain
Maharaja Surajmal Institute of Technology, Electrical and Electronics Engineering Department , Delhi, 110058, INDIA
E-mail: jyotieee@msit.in

Uma Nangia
Delhi Technological University/Electrical Engineering, Delhi, 110042, INDIA
E-mail: uma_nangia@rediffmail.com

N. K. Jain
Delhi Technological University/Electrical Engineering, Delhi, 110042, INDIA
E-mail: vnarender84@yahoo.com

Received: 25 November 2021; Accepted: 01 January 2022; Published: 08 June 2022

Abstract: In this paper, an attempt has been made to develop an Adaptive Social Acceleration Constant based PSO (ASACPSO). ASACPSO converge faster in comparison to basic PSO. The best value has been selected based on the minimum number of kounts required to minimize the function. Adaptive Social Acceleration Constant based PSO (ASACPSO) has been developed using the best value of adaptive social acceleration constant. The Adaptive Social Acceleration Constant has been searched using three formulations which led to the development of three algorithms-ALDPSO, AELDPSO-I and AELDPSO-II. All three were implemented on Rosenbrock function to get the best value of adaptive social acceleration constant. Similarly it has been implemented on seven mathematical benchmark functions and its performance has been compared to Basic Particle Swarm Optimization (BPSO). ASACPSO was observed to converge faster and give better accuracy. Results show that Kounts required for convergence of mathematical function is lesser for ASACPSO in comparison to basic PSO.ASACPSO reduces the computational time to optimize the function.

Index Terms: Convergence, Inertia weight, Optimization, Population, Particles, Social acceleration constant.

1. Introduction

The concept of Particle Swarm Optimization (PSO) was introduced by [1] Eberhart and Kennedy. PSO is based on five basic principles- proximity, quality, diversity, stability, and adaptability. An overview of particle swarm optimization was suggested by [2] Riccardo poli *et* al. References [3,4] suggested reviews on PSO. Reference [5] suggested application of PSO in the Engineering and Computer science. Reference [6] represents the studies of the variants of PSO like constant inertia weight, linear inertia reduction, limit on maximum velocity, constriction factor, dynamic inertia and maximum velocity reduction. The authors observed that constriction and dynamic inertia weight both affect reliability and cost. Reference [7] proposed modification of PSO using simultaneous perturbation optimization algorithm. The technique proposed had good global search and effective local search capability. [8] Zhi-Xiang – hou developed an adaptive Particle Swarm Optimization algorithm and claimed this to be more effective and highly accurate. [9] Md. Sakhawat Hossen *et al.* also suggested an adaptive Particle Swarm Optimization based on behaviour of spider. They presented a comparison with traditional PSO and suggested methods to improve the performance of adaptive PSO. In references [10,11] N.K.Jain *et al.* has developed PSO based on initial selection of particles and applied on mathematical benchmark functions and on Economic load dispatch problem. Reference [12] N.K.Jain *et al.* has suggested application of PSO for Multi-objective Economic Load dispatch problem. Reference [13] shows the application of PSO to solve MELD Problem. Reference [14] shows the application of ASACPSO to solve Economic Load Dispatch Problem. Reference [15] shows the Impacts of PSO Parameters on its Convergence. Reference [16] suggested improved model of PSO to give steady convergence and a better . Reference [17] shows the Self-Adaptive Acceleration Constants based PSO. In this both the constants have been adaptive and giving execution time slightly higher than others technique.

Copyright © 2022 MECS

In this paper, an Adaptive Social Acceleration Constant based PSO (ASACPSO) has been developed. The best value of social acceleration constant has been searched and selected based on the minimum number of kounts required to minimize the function. Adaptive Social Acceleration Constant based PSO (ASACPSO) has been developed using the best value of adaptive social acceleration constant.Three formulations have been used to search the best adaptive social acceleration constant which is selected based on minimum number of kounts required to minimize the function. Kount is the number of function evaluations, i.e. how many times a function has been evaluated. To check the performance of ASACPSO has been tested on seven mathematical benchmark functions and compared with basic PSO (BPSO). ASACPSO has been found to perform better in terms of convergence and accuracy.

1.1 Basic Particle Swarm Optimization (Bpso)

BPSO is a population based self-adaptive, stochastic optimization technique. Its basic idea is mathematical modelling and simulation of food searching activities of a swarm of birds (particles). In the multidimensional space where the optimal solution is sought, each particle in the swarm is moved towards the optimal point. At each iteration, the particle moves towards the optimum solution, through its personal best solution obtained by itself and global best solution obtained by all the particles until they find food (optimum solution). In an n-dimensional search space, position and velocity of particle j is represented by vectors X_j=(X_{j1} , X_{j2},…… X_{jn}.) and V_{j1}=(V_{j1} V_{j2} ,… V_{jn}) respectively. Let X_{pbest} and X_{gbest} be the personal and global best position of particle j. The modified velocity and position of each particle can be calculated using current velocity and distance from X_{pbest} and X_{gbest} as follows:

$$V_{ij}^{k+1}=W * V_{ij}^{k}+C_p r_p(X_{pbestij}^{k}-X_{ij}^{k})+ C_g r_g(X_{gbestij}^{k}-X_{ij}^{k}) \qquad \text{i=1,2,…..N} \quad \text{j=1,2…..p} \tag{1}$$

Velocities are updated by eq. (1) and position of each particle is updated using (2)

$$X_{ij}^{k+1}=X_{ij}^{k}+V_{ij}^{k+1} \tag{2}$$
$$\text{i =1, 2….N;} \quad \text{j=1,2…..p}$$

Where
W: Inertia Weight.
K:teration Count
V_{ij}^{k+1} Velocity of j^{th} particle of i^{th} variable at k^{th} iteration.
X_{ij}^{k} Position of j^{th} particle of i^{th} variable at k^{th} iteration.
C_p: Cognitive acceleration coefficients.
$X_{pbestij}^{k}$: Personal best position of j^{th} particle of i^{th}variable in k^{th} iteration.
X_{gbesti}^{k} : Global best position of i^{th} variable until k^{th} iteration.
N: Total number of variables.
p : Number of particles in swarm.s
r_p, r_g : Two separately generated uniformly distributed random numbers.
F: Function value.

2. Development of Adaptive Social Acceleration Constant Based Pso (Asacpso)

In this paper, an adaptive social acceleration constant based PSO (ASACPSO) has been developed. Cg regulates the maximum step size in the direction of the global best particle. In basic PSO, C_p and C_g is fixed to 1.0, whereas in Adaptive Social Acceleration Constant based PSO (ASACPSO), Cg is searched adaptively and is named as adaptive social acceleration constant Csg. The adaptive social acceleration based constant Csg has been formulated using following three functions:

1. Linearly decreasing function

$$\text{Csg1= cgmax-(i*(Cgmax-Cgmin) / it)} \tag{3}$$

2. Exponential of linearly decreasing function

$$\text{Csg2 = exp((-1)* (Cgmax-(i*(Cgmax-Cgmin)) / it))} \tag{4}$$

3. Exponential decreasing function consisting of exponential of constant multiplied by linearly decreasing function.

$$\text{Csg3 = exp((-0.34)*(cgmax-(i*(cgmax-cgmin)/it)));} \tag{5}$$

Copyright © 2022 MECS

Where,
IT: Maximum number of iterations
I: Current iteration
Cgmax: Maximum value of Social acceleration constant
Cgmin: Minimum value of Social acceleration constant
Csg: Adaptive social acceleration constant
Csg1: Social acceleration constant based on linearly decreasing function
Csg2: Social acceleration constant based on exponential of linearly decreasing function
Csg3: Social acceleration constant based on exponentially decreasing function consisting of exponential of constant multiplied by linearly decreasing function.

2.1 Methodology

PSOs based on Csg1, Csg2, and Csg3 have been named as Adaptive Linearly decreasing PSO (ALDPSO), Adaptive Exponential Linearly Decreasing PSO (AELDPSO-I) and Exponential decreasing function consisting of constant multiplied by linearly decreasing function is called as Adaptive Exponential linearly decreasing PSO -II (AELDPSO-II) respectively.

All the three algorithms have been implemented to minimize the Rosenbrock function. The best value of Adaptive–Social acceleration constant Csg is searched by applying equation (3), (4) and (5) after second, third, fourth and upto seventh iteration. When these equations are applied after seventh iteration, there was no improvement in the results. The results of ALDPSO, AELDPSO- I, and AELDPSO- II are shown in Table 1, 2 and 3 respectively. The best value of Csg is selected based on minimum number of kounts required to minimize the function. Adaptive Social Acceleration Constant based PSO (ASACPSO) is then developed using the best value of Csg.

Kount is number of function evaluations, i.e. how many times a function has been evaluated. This is taken as the measure of computational time. The measure of computational time in seconds or minutes will depend on the technology, i.e. the type of computer being used. Therefore, the time has been measured in terms of function evaluations.

All the three algorithms are using following fixed value of parameters as follows:
Cgmax=1
Cgmin=0
IT=Maximum number of Iterations=1000
Population Size=40
Results for Mathematical Rosenbrock function using ALDPSO are shown in Table 1.

Table 1. Results Of Rosenbrock Function Using Aldpso

Condition for implementation of Csg1 (1)	**Results (2)**	**Itr (3)**	**Kount (4)**	**Csg1 (5)**
Iter>2	Sucess	45	1840	0.955
Iter>3	Sucess	46	1880	0.954
Iter>4	Sucess	42	1720	0.958
Iter>5	Sucess	**40**	**1640**	**0.96**
Iter>6	Sucess	48	1960	0.952
Iter>7	Sucess	44	1800	0.956

Column (1) of Table 1 shows the number of iterations after which Csg1 (defined by equation (3)) has been implemented. Column (2) shows the result of Rosenbrock function for defined condition of column (1). Column (3) and (4) represent number of iterations and number of kounts required respectively to optimize the function . Column (5) shows value of Csg1 searched for Rosenbrock function. When linear decreasing function Csg1 implemented after second iteration kounts required to optimize the function is 1840 and an adaptive social acceleration constant value is 0.955 as shown in row(2) of Table 1.

By observing column (4) of Table 1 minimum kount is obtained when adaptive Csg has been searched after five iterations and its value is 0.96. It has been highlighted in the Table 1. When this strategy is applied after 8^{th} iteration, no improvement has been observed in results.

Results for Mathematical Rosenbrock function using AELDPSO-I is shown in Table 2.

Table 2. Results of Rosenbrock Function Using Aeldpso-I

Condition for implementation of Csg2 (1)	Results (2)	Itr (3)	Kount (4)	Csg2 (5)
Iter>2	Failure	1000	40040	0
Iter>3	Sucess	68	2760	0.3428
Iter>4	Sucess	54	2200	0.348
Iter>5	Sucess	62	2520	0.345
Iter>6	Sucess	64	2600	0.3443
Iter>7	Sucess	**44**	**1800**	**0.956**

Column (1) of Table 2 shows the number of iterations after which Csg2 (defined by equation (4)) has been implemented. Column (2) shows the result of Rosenbrock function for defined condition of column (1). Column (3) and (4) represents number of iterations and number of kounts required respectively to optimize the function. Column (5) shows value of Csg2 searched for Rosenbrock function. By observing column (4) of Table-2 minimum kount is obtained when adaptive Csg2 is searched after seven 7^{th} iterations and its value is 0.956.The row corresponding to this has been highlighted. When this strategy is applied after 8^{th} iteration, no improvement has been observed in results.

Results for Mathematical Rosenbrock function using AELDPSO-II are shown in Table-3.

Table 3. Results of Rosenbrock Function For Aeldpso-Ii

Condition for implementation of Csg3 (1)	Result (2)	Itr (3)	Kount (4)	Csg3 (5)
iter>2	Sucess	33	1360	0.688
iter>3	Sucess	33	1360	0.79
iter>4	Sucess	36	1480	0.688
iter>5	Sucess	**30**	**1240**	**0.788**
iter>6	Sucess	32	1320	0.793
iter>7	Sucess	40	1640	0.7154

Column (1) of Table 3 shows the number of iterations after which Csg3 (defined by equation (5)) has been implemented. Column (2) shows the result of Rosenbrock function for defined condition of column (1). Column (3) and (4) represent number of iterations and number of kounts required respectively to optimize the function. Column (5) shows value of Csg3 searched for Rosenbrock function. When Csg3 implemented after five iteration kounts required optimizing the function is 1240 and an adaptive social acceleration constant value is 0.788 as shown in row (4) of Table 3. By observing column (4) of Table 3 minimum kount is obtained when adaptive Csg has been searched after five iterations and its value is 0.788. It has been highlighted in the Table 3. When this strategy is applied after 8^{th} iteration, no improvement has been observed in results.

Comparison of results of ALDPSO, AELDPSO-I and AELDPSO-II are shown in Table 4.

Table 4. Comparison of Results of Aldpso, Aeldpso-I And Aeldpso-Ii

	ALDPSO		AELDPSO-I		AELDPSO-II	
Condition for implementation of Csg (1)	Csg1 (2)	Kount (3)	Csg2 (4)	Kount (5)	Csg3 (6)	Kount (7)
iter>2	0.955	1840	0	40040	0.688	1360
iter>3	0.954	1880	0.3428	2760	0.79	1360
iter>4	0.958	1720	0.348	2200	0.688	1480
iter>5	**0.96**	**1640**	**0.345**	**2520**	**0.788**	**1240**
iter>6	0.952	1960	0.3443	2600	0.793	1320
iter>7	0.956	1800	0.956	1800	0.7154	1640

A column (1) of Table 4 represents the number of iterations after which Csg is implemented. Column (2), (4) and (6) represent the adaptive social constants Csg1, Csg2 and Csg3 achieved by ALDPSO, AELDPSO-I, and AELDPSO-II respectively for each condition of implementation shown in column 1. Column (3), (5) and (7) represent the kounts required to minimize the function. It is observed that AELDPSO-II requires least kounts as compared to ALDPSO and AELDPSO-I for all conditions of column (1). It is further observed from Table 4 that for case of Iter>5, minimum kounts are required by AELDPSO-II. For this condition of Csg implementation, the kounts required by three algorithms are :

ALDPSO: 1640
AELDPSO-I: 2520
AELDPSO-II: 1240

This row has been highlighted. The value of an adaptive social acceleration constant is achieved by AELDPSO-II and is taken as social acceleration constant for PSO which leads to the development of ASACPSO.

3 Results and Discussions on Implementation of Basic Pso, Aeldpso-Ii and Asacpso on Different Mathematical Benchmark Functions:

The Experimentation has been done on following seven mathematical benchmark functions using Basic PSO, AELDPSO-II and ASACPSO.

1. Rosenbrock function
2. Beale Function
3. Booth Function
4. Hyper Ellipsoid Function
5. Ackley function
6. Schwefel function
7. Three Hump Function

Following parameters are taken for basic PSO (BPSO).

1. $r_p = C_g = r_g = C_p = 1$
2. W=0.6
3. Population size=40

These parameters have been selected merely for comparison of the results obtained by the proposed algorithms. Initially Basic PSO (BPSO) has been applied for 40 particles. Then the best social acceleration constant was searched using AELDPSO-II. Then this best value of social constant worked as Csg for ASACPSO. All the three algorithms BPSO, AELDPSO-II and ASACPSO have been implemented on seven mathematical benchmark functions and their results have been compared in Table 5 to 11. For all types of PSOs Cognitive acceleration coefficient is kept fixed i.e. Cp=1.

1. Rosenbrock function:

Mathematically, it is defined as

$$f=100*(x_1^2 - x_2)^2+(1 - x_1)^2$$

f (1,1)=0 Range: $x_1 \geq 0, x_2 \leq 1$

Table 5. Results for Rosenbrock Function

PSOs (1)	x1 (2)	x2 (3)	f (4)	Cg/Csg (5)	Kount (6)	Itr (7)
BPSO	0.99	0.99	1.9e-9	1	1600	39
AELDPSO-II	0.99	0.99	5.9e-10	0.788	1240	30
ASACPSO	0.99	0.99	1.79e-8	0.788	1320	32

Column (1) of Table 5 shows the type of PSO being implemented on Rosenbrock function. Column (2) and (3) represents two variables of Rosenbrock function. Column (4) represents the corresponding function value. Column (5) represents Cg for BPSO and Csg for AELDPSO-II and ASACPSO. Column (6) and (7) represents Kounts and iteration required respectively to optimize the function.

2. Beale Function:

Mathematically Beale function defined as

$$f=(1.5 - 1 + x_1x_2)^2+(2.25 - x_1 + x_1x_2^2)^2+\ldots(2.625 - x_1 - x_1x_2^3)^2$$

f (3,0.5)=0. Range $x_1 \geq -4.5$, $x_2 \leq 4.5$

Table 6. Results For Beale Function

PSOs (1)	x1 (2)	x2 (3)	F (4)	Cg/Csg (5)	Kount (6)	Itr (7)
BPSO	2.99	0.5	5.4e-10	1	1800	44
AELDPSO-II	3	0.5	9.42e-10	0.8071	1440	35
ASACPSO	3	0.49	1.1e-8	0.8071	1000	24

3. Booth Function:

Mathematically, it is defined as

$$f=(x_1 + 2x_2 - 7)^2+(2x_1 + x_2 - 5)^2$$

f(1,3)=0 Range x1≥ -10, x_2<10

Table 7. Results for Booth Function

PSOs (1)	x1 (2)	x2 (3)	F (4)	Cg/Csg (5)	Kount (6)	Itr (7)
BPSO	1	3	2.06e-13	1	2000	49
AELDPSO-II	1	2.99	5.9e-10	0.7358	1320	32
ASACPSO	0.99	2.99	6.32e-8	0.7962	1280	31

4. Axis Parallel Hyper Ellipsoid Function:

Mathematically, it is defined as

$$f=\sum_{i=1}^{n} i\, x_i^2$$

f(x)=0 at i =1: n here n=2 Range $-5.2 \leq x_i \leq 5.12$

Table 8. Results for Axis Parallel Hyper Ellipsoid Function

PSOs (1)	x1 (2)	x2 (3)	f (4)	Cg/Csg (5)	Kount (6)	Itr (7)
BPSO	-1.165e-5	-7.33e-9	3.8e-11	1	1880	46
AELDPSO-II	-2.5e-6	-6.12e-6	8.15e-12	0.669	1680	41
ASACPSO	6.3e-5	6.3e-9	1.8e-9	0.669	1160	28

5. Ackley Function:

Mathematically, it is defined as

f(x1, x2)= -20exp(-0.2 √(0.5(x1^2)+x2^2))

f(0,0)=0 Range $-5.0 \leq x_i \leq 5.0$

Table 9. Results for Ackley Function

PSOs (1)	x1 (2)	x2 (3)	f (4)	Cg/Csg (5)	Kount (6)	Itr (7)
BPSO	-1.64e-11	-8.15e-12	5.204e-11	1	3920	97
AELDPSO-II	-1.40e-9	1.286e-9	5.3902e-9	0.725	2360	58
ASACPSO	6.09e-6	-2.692e-6	1.88e-5	0.725	2240	55

6. Schwefel Function:

Mathematically, it is defined as

f(x)=418.9829-x1*sin($\sqrt{abs}$(x1))

f(x)=0; at x=(420.9687)

Range $-500.0 \leq x_i \leq 500.0$

Table 10. Results for Schwefel Function

PSOs (1)	x1 (2)	x2 (3)	F (4)	Cg/Csg (5)	Kount (6)
BPSO	420.968	1.222e-5	1	3600	89
AELDPSO-II	420.965	1.4392e-5	0.7242	40	51
ASACPSO	6.09e-6	1.27e-5	0.7242	40	53

Copyright © 2022 MECS

7. Three Hump Camel Function:

Mathematically, it is defined as

$$f(x1,x2)=2x1^2-1.05x1^4+x1^6/6+x1*x2+x2^2$$
$$f(0,0)=0$$

Table 11. Results for Three Hump Camel Function

PSOs (1)	x1 (2)	x2 (3)	F (4)	Cg/Csg (5)	Kount (6)	PSOs (1)
BPSO	-1.8062e-6	2.20e-6	7.40e-12	1	1800	44
AELDPSO-II	-2.236e-6	1.42e-5	1.82e-10	0.719	1320	32
ASACPSO	-2.1779e-6	-4.07e-7	1.27e-5	0.719	1000	24

Comparison of kounts for all the functions optimized by BPSO, ALDPSO-II and ASACPSO are shown in Table 12

Table 12. Comparison of Kounts For Mathematical Functions

S.No. (1)	Functions (2)	BPSO (Kounts) (3)	AELDPSO-II (Kounts) (4)	ASACPSO (Kounts) (5)
1	Rosenbrock	1600	1240	1320
2	Beale	1800	1440	1000
3	Booth	2000	1320	1280
4	Axis Parallel hyper ellipsoid	1880	1680	1160
5	Ackley Function	3920	2360	2240
6	Schwefel function	3600	40	40
7	Three Hump Camel function	1800	1320	1000

It is observed that minimum kounts are required for ASACPSO except in case of Rosenbrock function in which case kounts required for AELDPSO-II are minimum.

Table 13 shows the % saving in kounts obtained using ASACPSO and compared to BPSO

Table 13. Results of Bpso and Asacpso And Saving In % Of Kount

S. No. (1)	Functions (2)	BPSO (3)	ASACPSO (4)	Saving in % of Kount
1	Rosenbrock	1600	1320	17.5
2	Beale	1800	1000	44.5
3	Booth	2000	1280	36
4	Axis Parallel hyper ellipsoid	1880	1160	38.29
5	Ackley	3920	2240	42.85
6	Schwefel	3600	40	97.8
7	Three Hump Camel function	1800	1000	44.5

It has been observed that every function converged for lesser iterations and lesser kounts for ASACPSO in comparison to basic PSO (BPSO). Minimum saving in kount for Rosenbrock function and maximum saving in kount for Schwefel function has been found as shown in Table 13.

A saving of 44.5% has been achieved in Beale function. The saving has been calculated by following formula. Saving in kount %=[100*(Kounts for 40 particles (with cg=1) – kounts for 40 particles with Csg1)] / kounts for 40 particles(with cg=1).

Comparison of kounts for different functions for BPSO & ASACPSO are shown in Fig.1.

Copyright © 2022 MECS

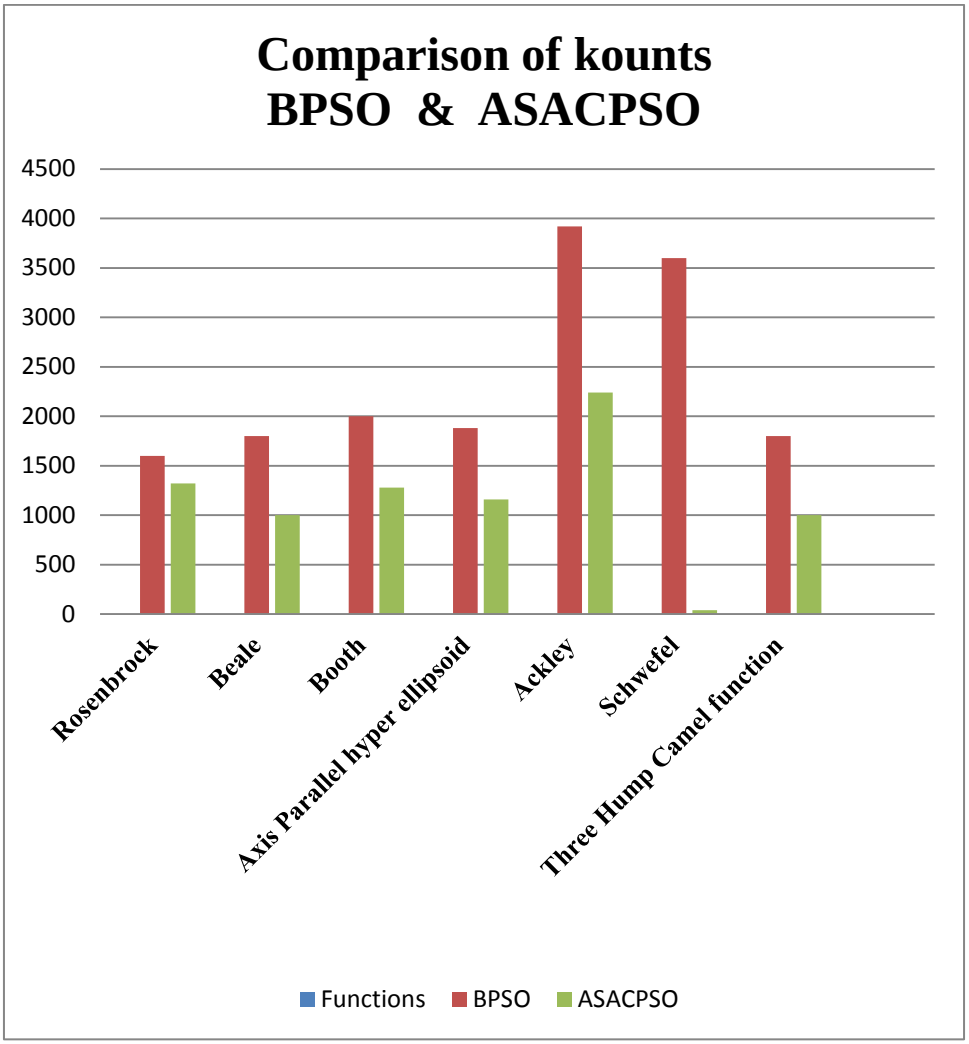

Fig. 1. Comparison of kounts for different functions for BPSO & ASACPSO.

4. Conclusions

1. In this paper ALDPSO, AELDPSO-I, AELDPSO-II have been developed and were applied to Rosenbrock Function. It was observed from the results of Rosenbrock function that AELDPSO-II minimized the function in less kount in comparison to ALDPSO and AELDPSO-I.
2. ASACPSO was developed using best value of Social Acceleration Constant obtained by AELDPSO-II .
3. ASACPSO was applied to the seven mathematical benchmark functions.
4. It was observed that AELDPSO-II and ASACPSO converge faster in comparison to basic PSO.
5. It has also been observed that saving in kounts is obtained for all the functions. Maximum saving of 97.6% in kounts is obtained for Schwefel function. However, for Rosenbrock function minimum saving of 17.5% kounts is achieved.

References

[1] J. Kennedy and R. Eberhart, "Particle swarm optimization", Proc. IEEE International Conference on Neural networks (Perth, Australia), 1995, IEEE Service Center, Piscataway, NJ, pp. 1942-1948.
[2] R. Poli, J. Kennedy, and T. Blackwell, "Particle swarm optimization. An overview," Swarm Intelligence, vol. 1, no. 1, pp. 33–57, 2007.
[3] Dian Palupi Rini, Siti Mariyam Shamsuddin, and Siti Sophiyati Yuhaniz, "Particle Swarm Optimization: Technique System and Challenges", International Journal of Computer Applications (0975-8887) Vol-14 – January 1, 2011.
[4] Jain N.K., Nangia Uma, Jyoti Jain, "A Review of Particle swarm optimization", Journal of The Institution of Engineers (India): Series B, August, 2018, 99(4), pp.407-411. ISSN 2250-2106, DOI 10.1007/s40031-018-0323-y.
[5] Russell C. Eberhart, and yuhui shi, "Particle Swarm Optimization: Developments, Applicationsand Resources"Evolutionary Computation,2001 Proceeding of the 2001 Congress on IEEE,1(2001),pp.81-86

Copyright © 2022 MECS

[6] Jaco F. Schutteand Albert A.Groenwold, "A Study of Global Optimization Using Particle Swarms", Journal of Global Optimization, Vol. 31, Springer 2005, pp. 93-108.
[7] yitaka Maeda and Naoto Matsushita , "Empirical Study of Simultaneous Perturbation Particle Swarm Optimization", SICE Annual Conference, August 20-22, 2008, pp. 2545-2548.
[8] Zhi-Xiang Hou, "Wiener model identification based on adaptive particle swarm optimization", Proceedings of the Seventh IEEE International Conference on Machine Learning and Cybernetics, Kunming, 12-15 July 2008, pp. 1041-1045.
[9] Md. Sakhawat Hossen, Fazle Rabbi, and Md. Mainur Rahman, "Adaptive Particle Swarm Optimization(APSO) for multimodal function optimization", International Journal of Engineering and Technology, Vol.1, No. 3,2009, pp. 98-103.
[10] N.K.Jain, Uma Nangia, Jyoti Jain "An improved PSO based on initial selection of particles (ISBPSO) for Economic Load Dispatch" Proceedings of 1st IEEE International Conference on Power Electronics, Intelligent Control and Energy Systems(ICPEICES 2016),4-6 july ,2016.
[11] N.K.Jain, Uma Nangia, Jyoti Jain, "An improved PSO based on initial selection of particles (ISBPSO)", Proceedings of 1st IEEE International Conference on Power Electronics, Intelligent Control and Energy Systems(ICPEICES 2016),4-6 july ,2016.
[12] N.K.Jain, Uma Nangia, Ashwary jain "PSO for Multiobjective Economic Load Dispatch(MELD) for minimizing Generation Cost and Transmission Losses", journal of the Institution of Engineers (India):series B,2015.
[13] Jain N.K., Nangia Uma, Jyoti Jain, "Multiobjective Economic Load Dispatch Studies in 2-D and 3-D Space by Particle Swarm Optimization Technique", February, 2019, Journal of The Institution of Engineers (India): Springer Series B, DOI : 10.1007/s40031-019-00386-z.
[14] Jain N.K., Nangia Uma, Jyoti Jain, " Economic load Dispatch using Adaptive Social Acceleration Constant based Particle Swarm Optimization", Journal Of Institution Of Engineers (India): Series B, October 2018, 99(5), 431-439, ISSN 2250-2106, DOI 10.1007/s40031-018-0322-z.
[15] N. K. Jain, Uma Nangia, Jyoti Jain, "Impacts of PSO Parameters on its Convergence" IEEE second International Conference on Power Electronics, Intelligent Control and Energy Sysytems (ICPEICES-2018), Delhi, pp.1-5, (22-24 October, 2018).
[16] Shengli Song, Li Kong and Jingjing Cheng, A Novel Particle Swarm Optimization Algorithm Model with Centroid and its Application, I.J. Intelligent Systems and Applications, 2009, 1, 42-49 October 2009 in MECS(http://www.mecs-press.org/)
[17] Sudip Mandal, " A Modified Particle Swarm Optimization Algorithm based on Self-Adaptive Acceleration Constants" I.J. Modern Education and Computer Science, 2017, 8, 49-56 Published Online August 2017 in MECS (http://www.mecs-press.org/) DOI: 10.5815/ijmecs.2017.08.07

Authors' Profiles

Dr. Jyoti Jain, is from Delhi. She has completed Ph.D. from Delhi Technological University Delhi. She is working in the field of solution of Multiobjective and Single objective optimization problems using Intelligent Techniques. She has 28 years teaching experience. She is working as an Associate professor at Maharaja Surajmal Institute of Technology (MSIT) Delhi.

She is a senior member of IEEE and Chapter Advisor of IEEE PES Student branch Chapter MSIT. She has received outstanding Engineer Award from IEEE PES IAS Delhi Chapter in 2021.

Dr. Uma Nangia and Dr. N.K. Jain are working as a Professor at Electrical Engineering Department of Delhi Technological University. They are working in the field of Optimization of Economic Load Dispatch, Reactive Power and Power Systems.

How to cite this paper: Jyoti Jain, Uma Nangia, N. K. Jain," Adaptive Social Acceleration Constant Based Particle Swarm Optimization ", International Journal of Mathematical Sciences and Computing(IJMSC), Vol.8, No.2, pp. 28-36, 2022. DOI: 10.5815/ijmsc.2022.02.03

EasyChair Preprint

№ 8011

AI Techniques in Imaging Data, Detecting & Monitoring Symptoms of COVID-19

Imane Elouaghzani and Deepak Kumar Mishra

EasyChair preprints are intended for rapid dissemination of research results and are integrated with the rest of EasyChair.

May 22, 2022

AI Techniques in Imaging Data, Detecting & Monitoring Symptoms of COVID-19

Imane Elouaghzani
Department of Computer Engineering
Delhi Technological University
Delhi, India
Imanecodeblack@gmail.com

Deepak Kumar Mishra
Department of Computer Engineering
Delhi Technological University
Delhi, India
deepakkumarmishra_2k21phdco03@dtu.ac.in

Abstract— **Coronavirus 2019 (COVID-19) has developed into a pandemic with severe clinical symptoms, including death. A major epidemic, such as COVID-19, poses significant challenges to the global health system. It causes damage to vulnerable people and poses a serious threat to global communities. In 2019, the most common result of coronavirus infection is a lung infection or pneumonia (COVID-19). Photographic imaging, such as X-rays and CT scans, positron emission tomography-CT (PET / CT), lung ultrasonography, and MRI, are vital to this global debate. Newly developed Artificial intelligence (AI) technology enhances the capabilities of digital cameras. This test will look at allowing technologies and programs to deal with the COID-19 epidemic.**

Keywords- Artificial Intelligence, Covid-19, Imaging, Telemedicine, Monitoring, Wearable devices

I. INTRODUCTION

Coronavirus 2019 infection (COVID-19), caused by SARS-CoV-2, has spread to more than 210 countries worldwide. More than 7.6 million people have been infected, and more than 427,000 have died from the virus. COVID-19 patients often show fever, respiratory symptoms, pneumonia, low white blood cell count (WBC), and low lymphocyte count. Even if the results of RT-PCR from a suspected patient do not have, SARS-CoV-2 infection will not be completely eliminated.

The COVID-19 epidemic has introduced significant barriers to global health care systems. It has the potential to quickly replenish health care systems, reducing their ability to provide services. Studies from epidemics in China, Italy, and the United States reveal that they may limit the effectiveness of a health care system.

Follow-up CT scans are frequently conducted on COVID-19 patients to monitor disease progression or improvement. Quantitative follow-up can also help radiologists recognise imaging features. This section focuses on CT manifestations at various phases, as well as the quantitative CT metric changes related to these stages.

The rest of the paper is structured as follows: Section 3 provides a comprehensive evaluation of wearable equipment and invisible sensor technology that can monitor the early symptoms of COVID-19 and other prevalent health problems. It also introduces a telehealth framework for diagnostic and diagnostic tests, as well as the most important research areas of the future. Section 4 examines the most relevant COVID-19 study based on the medical model until March 31, 2020. In the following sections, we will first describe the smart imaging systems before summarizing them. Section 5 provides a comprehensive evaluation of the role of photography in the identification and management of COVID-19 and is now required, Following the conclusion of Section 6.

II. AN OVERVIEW OF WEARABLE DEVICES & TELEHEALTH IN COVID-19

A. Wearable Technology for Health Monitoring COVID-19

Wearable items can play an important role in early warning of COVID-19 infections by combining important symptoms with clinical signs, diagnosing people who may be diagnosed, and experiencing any sudden decline in people who are isolated, living alone, or in the clinic. a downpour unit, especially those that do not have symptoms, and remotely monitor non-COVID-19 patients in order to prioritize the use and distribution of resources and to reduce infection

Other problems, such as heart damage, can develop in people who do not have lower heart disease. Therefore, it is important to check for respiratory, and cardiovascular monitoring, and other symptoms such as fever and cough to diagnose and diagnose any suspicious situations.

(i) Wearable Devices for Respiratory Assessment

SARS-CoV-2 directs the respiratory tract by attaching its extra nail-containing proteins to angiotensin-converting enzyme 2 (ACE2) receptors in healthy cells. The lungs may become inflamed, leading to dyspnea and rapidly growing ARDS. It can cause pneumonia, an infection of the alveoli within the lungs.

Wearable devices can allow for routine and continuous testing and monitoring of the patient's respiratory functions or parameters such as SpO2, RR, and lung sounds.

- ***Oxygen Saturation*:** Photoplethysmography, which analyses variations in light absorption, is used in pulse oximetry devices. Devices can be either reflective or transmissive in nature and can be worn in a number of positions on the body. Yokota et al.

used organic photodetectors to demonstrate a polymer LED-based pulse oximeter.

Figure 1: Commercially available wearable pulse oximeters

- *Respiratory Rate:* (RR) is an essential indicator of tracking the course of the disease. It is the first, measurable indicator of physical conditions such as hypoxia and hypercapnia. It has also been shown to be a powerful predictor of difficult events such as cardiac arrest.
- *Lung Sounds:* Respiratory rate (RR) is an essential metric for assessing illness progression. It is a detectable early indication of physiological problems including hypoxia and hypercapnia. It has also been demonstrated to be an excellent predictor of acute events such as cardiac arrest.

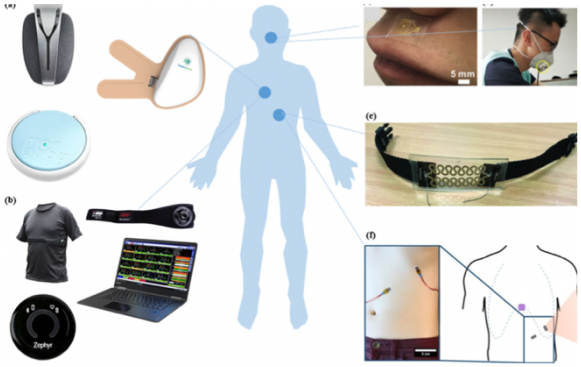

Figure 2: Wearable RR monitor product

(ii) Wearable Devices for Cardiovascular Evaluation

Cardiovascular comorbidities are a well-known risk factor for SARS-CoV-19, and CVD is one of the most common diseases in the world, especially among the elderly. Monitoring of cardiovascular indicators can help diagnose patients at high risk of SARS CoV-2 and may provide early warning of any heart failure

- *Electrocardiogram for Monitoring CVD and COVID-19 Patients*: The electrocardiogram (ECG) is a standard diagnostic procedure for assessing the electrical and muscular function of the heart. ECG abnormalities.

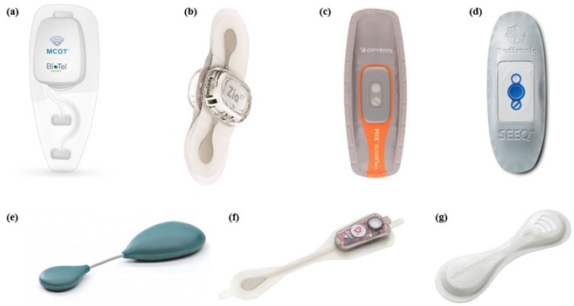

Figure 3: Commercial ECG patches used in clinical trials and in COVID- 19

- *Continuous Blood Pressure Monitoring:* A wristwatch, a sleeping pillow, or even a skin-like patch can be used to monitor your blood pressure continuously. The accuracy of many apps is still poor, particularly when used to track pharmacological effects. The technique for gathering energy from the human body should be enhanced and integrated with BP monitoring devices.

(iii) Wearable Devices for Clinical Symptom Monitoring

The most common clinical manifestations of COVID-19 are fever (90% or more), cough (approximately 75%), and dyspnea (up to 50%). These three symptoms are also important clinical indicators used to diagnose suspected individuals, as well as epidemiologic risks.

- Temperature: The wearable temperature monitor can detect a rise in body temperature before normal monitoring. The wearable nerves can be attached to the skin or worn on a specific area of the body. Han et al. studied the method of dual temperature fluctuations and developed wearable thermometry with a measurement error of less than 0.1 ° C.
- Cough Monitoring: Continuous cough monitoring assists inCOVID-19screeningandclinical diagnosis. Cough signals are frequently collected utilising oral or mechanical sensors able to detect the coughing motion or vibration. Imran et al. developed an app that identifies coughing based on 2-second cough audio and a combination of deep learning and classic machine learning approaches.

(iv) Unobtrusive Sensing for Physiological and Symptomatic Monitoring of COVID-19

Invisible sensory technology may enable the unaffected form to collect health information for one or more users for use at home or in public places. Sensors of this type may be concentrated in objects such as beds, toilets, and weight scales. It is a non-communicative way of measuring important signals in public places (e.g., airports).

One of the most obscure technologies used in the COVID-19 epidemic hot infrared camera is used to identify any patients with the flu at a hospital door or in public places such as airports. Video hearing is one of the most common ways to monitor important signals that no one can touch.

The nerves may be used to monitor vital signs in real-time in patients with minimally invasive health care facilities. They can also be used in the large screening of patients who may be infected in public places such as airports, which is important in reducing the spread of COVID-19.

(v) Multi-Parameter Physiological Monitoring Using Wearable and Unobtrusive sensors for Covid-19

BSN may be established to enable continuous monitoring and analysis of parameters of many organisms such as SpO2, RR, ECG, HR, BP, and other health data. Wireless BSNs, when connected to the hospital information system with mHealth technology, allow medical professionals to monitor remotely the patient's condition.

This section will look at mHealth wear-based technologies and telemedicine that allow you to monitor health everywhere. These technologies have the potential to improve and enhance health care systems while also improving the well-being of people affected by COVID-19.

B. Mobile Health and Telemedicine Technology For Tracking, Monitoring, Diagnosing and treating COVID-19

The rapid spread of COVID-19 has placed an enormous strain on healthcare systems. To address this catastrophe, we require an immediate digital transformation of the analogue healthcare system. Telemedicine and eHealth can help to address the problem by causing a paradigm change in health care.

(i) Mobile Health Monitoring of COVID-19

mHealth is a public health platform that is accessible via mobile devices. It may be used to monitor, diagnose, and treat a wide range of physiological and medical problems. Individuals with suspected or proven COVID-19, as well as those in need of other conventional clinical services, can receive aid and treatment.

- *Contact Tracing Technology:* A contact tracking system that builds a library of nearby links and quickly informs well-to-do contacts can help contain the epidemic. Yasaka et al. have developed a peer-to-peer contact tracking tool that uses an anonymous interaction network to track contacts.
- *Remote Physiological Monitoring:* Mobile sensors or monitors that may be used for remote health monitoring include smartwatches, pulse oximeters, and thermometers. During the pandemic, mobile ECG was one of the most often used health monitors for remotely monitoring patients' arrhythmia problems.

III. DIVERS METHOD FOR TREATING AND TRACKING COVID-19

A. Telemedicine Technology for COVID-19

Telemedicine is the use of communication to help treat illness. It can help with outpatient treatment, monitor critically ill patients in the ICU, and keep records of individuals who have been discharged from the hospital. In this section, we will look very closely at three applications of tele medication in the care of COVID-19 patients.

- Tele-imaging: Medical imaging is critical in the monitoring and diagnosis of illnesses. Tele- imaging can improve picture quality while lowering radiation exposure and speeding up patient throughput. During the COVID-19 pandemic in Wuhan, distant CT scans were sent to the West China Hospital in Sichuan Province using 5G connectivity.
- Tele-ICU: A tele-ICU is a fully integrated ICU platform that enables real-time electronic communication of health information between the central and satellite units. Off-site physicians can keep an eye on the patient's condition and consult with bedside staff about diagnostic and treatment options. Remote care delivery is preferable in order to reduce the presence of personnel at the bedside.
- Tele-Rehabilitation: The provision of treatment via a communication technology that connects patients with a centralised healthcare professional team is known as pulmonary telerehabilitation. Prompt pulmonary rehabilitation can enhance COVID-19 patients' respiratory function and quality of life. Rehabilitation therapies should be performed on a regular basis as part of standard therapeutic care.
- Other Telemedicine Technologies: Telemedicine can help improve the practice of long-distance health care. The COVID-19 test can be made available to the general public by locating test sites in easily accessible locations. The results may be linked to forums such as social networking and phone tracking systems, which can help prevent the transmission of the virus.
- Telerobotic: COVID-19 testing may be accessible to the general public by installing testing booths in publicly accessible locales. The results might be connected to platforms such as contract monitoring and tele triage systems. Despite all of these advantages, great attention should be paid to the potential hazards of telerobotic.

B. AI Empowered Contactless Imaging Workflows

Because of the high risk of infection in the workplace, health workers are at high risk. Photographers and specialists are given priority so that any possible contact with the virus is avoided. Additionally personal protective equipment, one must consider areas dedicated to photography and processes, which are important in reducing risks and saving lives.

- *Conventional Imaging Workflow:* X-rays and computed tomography (CT) scans are commonly used in the evaluation and diagnosis of COVID-19. Communication between specialists and patients is inevitable in normal images. This draws professionals

closer to patients, which increases the risk of infection. To minimize interaction, a touch-free and automatic recording method are required.

- *AI Empowered Imaging Workflow:* During the COVID-19 epidemic, these devices aid in the implementation of a contactless scanning methodology. With AI-powered visual sensors, a typical scanning parameter may be approximated. Scan range may be determined by recognising the subject's anatomical joints in the pictures. Artificial intelligence (AI) can deduce critical facts about the digital human body. Based on dynamic multi-modal inference, it can learn a model that can be used across numerous such applications. AI may also infer other crucial factors, such as ISO-centering.
- ***Applications in COVID-19:*** Several critical routines were built during the COVID-19 epidemic, including improved patient access and flexible installation. An automated scanning process based on a mobile CT platform is a prominent example. The mobile platform is self-contained and includes an AI-powered pre-scan and diagnosis system.

C. AI aided Image Segmentation

Photographic classification is an important phase in image processing and analysis to evaluate and measure COVID-19. It describes areas of interest (ROIs), including the lungs, lobes, bronchopulmonary segments, and infected or malignant

- Segmentation of Lung Regions and Lesions: The search for COVID-19 applications can be split into two types. Lung-focused techniques require the separation of ulcers (or metal objects moving in the lungs) in the lungs. Because sores or bumps may be small and have a wide variety of forms and textures, locating them is necessary.
- *Segmentation Methods:* In COVID programs, U-Net is a frequently used method of distinguishing lung areas and lung ulcers. It uses a fully flexible network with symmetric signal coding and recording methods. Shortcut links connect layers of the same level in two ways. A number of U-Net variants have been developed, which bring the acceptable results of separation into COVID-19 systems. Newly developed attention spans can learn the most discriminating part of network traits. This procedure is necessary to separate the lesions and lung lumps in medical imaging. Training an effective partition network requires a large amount of labelled data. Adequate training data for the separation of COVID-19 images are generally not available because diagnostics are time-consuming. The human-in-the-loop method incorporates the input of radiologists into network training.
- *Applications in COVID-19:* COVID-19 segmentation can be utilised in a variety of applications. In a multi-centre investigation, Li et al. employ U-Net for lung segmentation. Image segmentation is also used for quantification in a variety of medical applications.

D. AI-Assisted Differential Diagnosis of COVID-19

In epidemic regions, patients who may have had COVID-19 require prompt diagnosis and treatment. Medical imaging, particularly CT images, contains hundreds of pieces that take radiologists a long time to diagnose. The second table highlights the most current modern works on this topic.

(i) X-ray Based Screening of COVID-19

For patients with COVID-19, the standard first-line imaging modality is X-ray. According to a recent study, X-rays are normal in early or mild illnesses. The findings of the experiments reveal that Bayesian inference improves detection accuracy from 85.7% to 92.9%. Narin et al. offer three deep learning models for detecting COVID-19 infection in X-ray pictures. When compared to InceptionV3 and Inception-ResNetV2, the ResNet50 model obtains the greatest classification performance with 98.0% accuracy.

The photos are mostly from two internet databases, each of which has just 70 photographs of COVID- 19 patients. This little dataset is insufficient to assess the robustness of the approaches. Furthermore, the severity of the individuals is unknown; future research might focus on early diagnosis.

(ii) CT-based Screening and Severity Assessment of COVID-19

Radiological patterns in COVID-19 chest CT scans have been documented and summarised in four phases. GGO might be seen unilaterally or bilaterally subpleural in the lower lobes. These radiological patterns serve as critical evidence for CT-based categorization and severity evaluation.

a. Classification of COVID-19 from non-COVID-19

A number of investigations are being conducted to distinguish COVID-19 patients from non-COID- 19 participants (that include common pneumonia subjects and non-pneumonia subjects). With the aid of AI findings, radiologists' reading time is reduced by 65 %.

b. Classification of COVID-19 from Other Pneumonia

Pneumonia, particularly viral pneumo- nia, exhibits radiological features similar to COVID-19. On manually delineated area patches, proposes a 2D CNN model. The model is trained using chest CT scans from 99 individuals. Song et al. employ 2D slices with lung regions segmented by OpenCV. Each 3D chest CT image yields 15 slices of complete lungs. For pneumonia categorization, the model gets results with an accuracy of 86.0% (COVID-19).

The picture is segmented into the left/right lung, 5 lung lobes, and 18 pulmonary segments using a 3D VB-Net. The experimental findings suggest that distinguishing COVID-19 has a sensitivity of 90.7%, a specificity of 83.3 %, and an accuracy of 87.9%

c. Severity Assessment of COVID-19

A number of studies for CT-based COVID-19 diagnosis have been proposed, with generally encouraging findings. Screening research might aid in early detection, reducing radiologists' diagnostic uncertainty. Furthermore, the prediction of severity is critical since it might aid in the calculation of ICU events or clinical treatment planning decisions.

IV. Imaging Modalities in Diagnosis of COVID-19

Medical imaging can be used in addition to RT-PCR testing to help diagnose COVID-19. COVID-19 individuals have typical imaging features, particularly CT characteristics. In the sections that follow, we will discuss the use of CT and other imaging modalities in the diagnosis of COVID-19.

A. CT Characteristics in Diagnosis of COVID-19

(i) CT Characteristics of typical COVID-19

This diagram shows the typical CT features of four COVID-19 patients. GGO, nodules, pleural changes such as pleural rupture or pleural thickening, and other abnormalities such as linear blindness with a crazy compression pattern are examples of this.
The most common detection of COVID-19 in the CT chest is GGO, which appears to be a growing pulmonary embolism with the preservation of bronchial and vascular boundaries. In the middle stage of the disease, GGO often develops into multifocal consolidative opacities and septal thickening.
Another commonly found radiologic chest CT scan is patchy shadowing of two countries. CU scans for ICU patients often reveal multiple lobular and subcutaneous regions of incorporation. People with COVID-19 often have multiple sores and a crazy paved pattern.

(ii) CT Characteristics in Asymptomatic COVID-19

Screening for people with invisible or abnormal presentations is an important aspect of managing COVID-19. CT can also be used to diagnose patients with no atypical symptoms and signs. To diagnose these people with no symptoms of COVID-19, a combination of CT imaging of the chest, RT-PCR, and complete follow-up should be performed. Hu et al. found that seven people with normal CT results and no symptoms were significantly younger than the others.

(iii) Use of CT Characteristics for Discriminating COVID-19 pneumonia from other pneumonia

The use of CT findings to identify COVID-19 pneumonia from other types of pneumonia has garnered a lot of interest. Patients with the syndrome are more likely to experience peripheral distribution, vascular thickening, and the reverse halo sign. They had a lower risk of central- peripheral distribution, pleural effusion, and lymphadenopathy.

(iv) Other Imaging Techniques

Additionally to chest CT, additional imaging modalities, such as positron emission tomography - CT (PET / CT), lung ultrasonography, and magnetic resonance imaging, are used to add chest CT to the diagnosis of COVID-19 (MRI). A brief overview of these photography methods is provided in the following sections.

- **PET/CT***:* CT findings of differentiating COVID-19 pneumonia from pneumonia have received considerable attention. Patients suffering from this condition are more prone to the peripheral circulation, vascular congestion, and the opposite halo mark. They are less likely to have central-peripheral, pleural effusion, or lymphadenopathy.
- **Lung Ultrasound:** Lung ultrasonography (LUS) enables low-risk individuals to be screened at home and suspected cases to be diagnosed. LUS can lower the risk of infection among affected patients and health care professionals. LUS might be used by obstetricians and gynaecologists to do lung examinations.
- **MRI:** MRI is a radiation-free imaging tool that is extremely effective for analysing soft tissues. However, owing of the longer scanning time and higher cost when compared to CT and LUS, it is not commonly utilised for COVID-19 diagnosis. Nonetheless, a non-invasive MRI may be useful in assessing COVID-19 in children and pregnant women. SARS-CoV-2 is mostly identified in the lungs, but three minimally invasive autopsies demonstrated that the virus also affects the heart, arteries, liver, kidney, and other organs. Because of its better performance in imaging structural and functional information of many soft organs, MRI might be used to assess the vulnerability of various organs.

(v) AI-Based Image Analysis of COVID-19

Self-diagnosis in CT images necessitates a significant amount of manual work and time. Computer-assisted diagnostic techniques have been developed using in-depth research or machine learning technologies. The software was tested on 1,136 instances (723 COID-19 positives) from five hospitals.
An in-depth study approach based on an in-depth study may accelerate the identification of COVID- 19. The proposed in-depth study model achieved 94.98% accuracy, with an AUC of 97.91%, and 95.06% sensitivity among 1,255 independent experimental conditions.
Zheng et al. used UNet to divide the lung area before splitting it again using 3DResNet. There were 3,506 patients in the trial (468 with COVID-19, 1,551 with Community-Acquired Pneumonia (CAP), and 1,303 with non-pneumonia). Recent research has shown that AI demonstrates efficacy in the rapid diagnosis of COVID-19. With the help of AI, doctors can be separated from patients to avoid infection. Using AI and CT

imaging does not add up to the cost of healthcare professionals.

V. Conclusion

We concluded that Intelligent medical imaging was important in combating COVID-19. This study explains how Artificial Intelligence (AI) can deliver safe, accurate, and efficient solutions. To demonstrate the effectiveness of a powerful AI medical image, two imaging modes are used, X-ray and CT. Screening of suspected and symptomatic patients allows for immediate diagnosis and treatment. Remote monitoring and treatment may reduce communication between medical staff and patients. The goal of this program is to create portable devices and platforms based on highly advanced, inexpensive, flexible, and flexible sensors. Identifying and resolving ethical concerns, privacy threats, and potential security threats through the use of wearable devices, invisible sensors, and telemedicine.

References

[1] X. Ding et al., "Wearable Sensing and Telehealth Technology with Potential Applications in the Coronavirus Pandemic," in IEEE Reviews in Biomedical Engineering, vol. 14, pp. 48-70, 2021, doi: 10.1109/RBME.2020.2992838.

[2] F. Shi et al., "Review of Artificial Intelligence Techniques in Imaging Data Acquisition, Segmentation, and Diagnosis for COVID-19," in IEEE Reviews in Biomedical Engineering, vol. 14, pp. 4-15, 2021, doi: 10.1109/RBME.2020.2987975.

[3] D. Dong et al., "The Role of Imaging in the Detection and Management of COVID-19: A Review," in IEEE Reviews in Biomedical Engineering, vol. 14, pp. 16-29, 2021, doi: 10.1109/RBME.2020.2990959.

[4] 2020, [online] Available: https://covid19.who.int/.

[5] H. Yh et al., "The respiratory sound features of COVID-19 patients fill gaps between clinical data and screening methods", *medRxiv*, 2020.

[6] I. D. Apostolopoulos and T. Bessiana, "COVID-19: Automatic detection from X-ray images utilizing transfer learning with convolutional neural networks", 2020.

[7] J. Zhao, Y. Zhang, X. He and P. Xie, "COVID-CT-dataset: A CT scan dataset about COVID-19", 2020.

[8] S. Jin et al., "AI-assisted CT imaging analysis for COVID-19 screening: Building and deploying a medical AI system in four weeks", 2020.

[9] C. Zheng et al., "Deep learning-based detection for COVID-19 from chest CT using weak label", 2020.

Multimedia Tools and Applications
https://doi.org/10.1007/s11042-022-13313-0

An adaptive rejuvenation of bacterial foraging algorithm for global optimization

Tejna Khosla[1] · Om Prakash Verma[2]

Received: 1 August 2021 / Revised: 15 January 2022 / Accepted: 30 May 2022
© The Author(s), under exclusive licence to Springer Science+Business Media, LLC, part of Springer Nature 2022

Abstract
Bacterial foraging algorithm (BFA) is a novel nature-inspired algorithm that mimics the social foraging behavior of *E. coli*. Bacteria. However, it gets stuck in the local optima trap and yields poor convergence in complex landscapes. To improve the exploration-exploitation balance and achieve the global optima quickly, this paper proposes a novel hybrid called the Bacterial foraging algorithm-firefly algorithm (BFA-FA). In this work, two strategies namely adaptive strategy and leadership strategy are applied on conventional BFA. The performance is examined on standard, non-linear and CEC_2017 benchmark functions over several evaluation parameters. The results on benchmark functions show that BFA-FA provides accurate solutions, avoids local optima, works well on multimodal and multidimensional landscapes, and converges faster. It also shows the statistically significant difference among other algorithms. The proposed algorithm is applied on two classical engineering problems to validate its robustness and applicability.

Keywords Adaptation · Bacterial foraging algorithm · Firefly algorithm · Hybridization · Optimization

1 Introduction

Global optimization involves finding the global optimal values for the objective functions that contains local optima. The optimization algorithms search the entire input space and get closer to the function extrema to give the accurate value. Among these optimization algorithms, swarm-based

✉ Tejna Khosla
patoditejna@gmail.com

Om Prakash Verma
opverma.dce@gmail.com

[1] Department of Computer Science and Engineering, Delhi Technological University, Delhi, India

[2] Department of Electronics and Communication Engineering, Delhi Technological University, Delhi, India

Published online: 14 June 2022

algorithms have gained a lot of importance over the years in solving global optimization problems. They are extensively used to solve engineering and scientific problems. Some swarm-based algorithms are Particle Swarm Optimization (PSO) [17], Bacterial Foraging Optimization (BFA) [26], Salp Swarm Algorithm (SSA) [28], etc. Among these bio-inspired optimization algorithms, BFA is based on the *Escherichia Coli* (*E. Coli*) bacteria's foraging behavior i.e., the food-seeking and reproductive behavior. The bacteria search in the nutrient medium to increase the energy per unit time. It is a random searching algorithm that finds the global optimum value using the process of chemotaxis, reproduction, and elimination & dispersion. In the computational community, BFA has received great attention due to its exceptional performance in finding global optima. It was successfully applied on optimal control [19], machine learning [5], transmission loss reduction [37], harmonic estimation [1], multi- objective optimization problems [31], image enhancement [13] and edge detection [39–42], optimal multi-level thresholding [36], vehicle routing problems [35], numerical optimization [14], optimal placement of distributed generation [23], and so many other areas. However, BFA has poor convergence over multimodal and rough landscape problems as compared to other swarm-based algorithms [2]. This is because they follow the local search through the chemotaxis movement. To improve the performance of BFA, a lot of modifications have already been taken which can be broadly categorized in Hybridization and Self-adaptation. Hybridization means the fusing of two independent algorithms with their unique set of characteristics to form a better version of the algorithm. Self-adaptation means the setting of control parameters of the algorithm to improve the performance and balance the exploration-exploitation.

Many hybrids of BFA were developed to enhance the convergence characteristics and had given good results. In [29], fuzzy bacterial foraging for harmonic estimation was used, where Takagi-Sugeno fuzzy scheme was considered as the cost function. The algorithm worked well on estimation problems that had multimodal landscapes. Khodabakhshian et al in [18] proposed smart BFA where tumble was done using a smart unit of length and the new cost function would specify the direction of movement after the tumble. The performance of smart BFA was superior to conventional BFA over different optimization functions. In [20], a hybrid of GA and BFA was developed by incorporating mutation and crossover phenomena in BFA. The algorithm was very effective when tested on benchmark functions, and the application was done on PID parameter tuning. In [21], a simple hybrid of BFA and PSO was proposed where BFA performed the local search, and PSO performed the global search over the search domain. Due to accuracy and good convergence, the hybrid was used for detecting bundle branch blocks from the ECG patterns. The chemotaxis movement of BFA was incorporated in the exploitation process of Artificial Bee Colony (ABC) [24]. The hybrid was validated on benchmark functions and was found superior as compared to its classical counterparts in terms of convergence rate. Differential Evolution (DE) was hybridized with BFA and was named chemotactic DE. The equation of DE was used as the mutation operator in BFA to improve its efficiency [11]. The algorithm was applied to calculate similarity between two indexes. In [30], exploration ability of spiral dynamics and exploitation ability of BFA was utilized to make a novel hybrid. The authors had given a simple structure, and could achieve better performance on the benchmark models in lesser function evaluations. Gravitational search strategy and swarm search strategy was introduced in BFA to enhance exploration-exploitation ability As far as the impact of adaptation is concerned, Chen and Zhu [3] had stated that in chemotaxis step, if the step size was too big, bacteria would reach the vicinity of the optimum point very quickly and the precision was low. On the contrary, if the step size was too small, a lot of steps would be required to reach the convergence, and so the performance decreased. So, it was concluded that step size was an important parameter to determine convergence and error in the output. In this regard, a lot of researchers have explored this area where the key parameter for

adaptation was step size. The principle of adaptive delta modulation was proposed by Tanumay et al [10] to control the step size in BFA. It was successfully applied on the problem of null steering and synthesizing patterns. Another version of adaptive BFA was introduced by Majhi et al [27] where the cost function or the fitness value was used to change the step size value after each iteration. It was successfully applied in a stock prediction model, however there were a lot of parameters involved in the execution of the algorithm. In [9], adaptive step size was introduced based on the mathematical analysis of the fitness function of the bacteria. The main aim of the proposed algorithm was to accelerate the convergence of the bacteria to the global optimum value and avoid oscillation around it. It was tested against other state-of-art methods and proved effective due to no additional computations in terms of function evaluations. Tong [47] introduced roulette wheel selection in the reproduction step of BFA along with the adaptive change of step size during the chemotaxis movement. To enhance the quality of convergence results, serial heterogeneous cooperative search techniques were applied on BFA where different BFA algorithms run sequentially and the output of one algorithm works as the input for the other algorithm with lesser step size value [4]. The results were much better than other comparative algorithms and proved superior. To enhance the exploration-exploitation ability, two chaotic search strategies namely chaotic initialization and chaotic local search were incorporated in BFA along with the shrinking strategy [52], and the convergence rate was high in most of the cases. The quality of results was enhanced using gravitational search strategy and swarm search strategy in the equations of BFA [53]. The resultant algorithm was extensively tested on benchmark functions and the performance was quite good in terms of exploration and exploitation of search space.

Although the above-mentioned literature had improved the BFA but they were effective in specific problems and lacked universality. As observed, there were still many open problems that were required to be addressed. They can be defined as follows.

1. It was learnt from the literature that some algorithms involved too many control parameters to balance exploration-exploitation, which made the problem more complex. There was a need for improving the convergence using lesser parameters, and achieving effective parameter-tuning based on adaptation. Till now, all the adaptation strategies are based only on fitness values of bacteria or the iteration number.
2. In multimodal or any other complex landscapes where the search space is rough having multiple local optima, the algorithm got stuck in local optima trap and gave poor results.
3. From the related works, it was observed that mostly, very few evaluation parameters like convergence rate, multi-dimensional landscape, Wilcoxon rank test etc. were used for proving the superiority of the algorithm. There was a dire need for extensive analysis of the algorithm with other comparative algorithms to prove the quality of the results.

In addition, Wolpert et al. [45] had mentioned about the no free lunch theorem where no algorithm was better on all problems, and so there was always a scope for a new algorithm that outperforms other algorithms. These above-mentioned points are the motivation of this paper to optimize real-world problems. Unlike other works mentioned in the literature, this paper proposes the adaptation of step size based on the success rate of the swarm. Also, the leadership strategy is proposed in BFA for the first time to update positions of weak bacteria and move towards the strong bacterium.

The main aim of this paper is to improve the BFA for solving real- world problems. For this purpose, two novel improvements are proposed in conventional BFA, namely adaptation and hybridization. In adaptation, the dynamic step size is proposed using the success percentage of the

swarm of bacteria. A higher value of success means the swarm is moving closer to the optimum, whereas a lower value of success means the swarm is far from the optima. This step prevents the user-based initialization of key parameters; hence the algorithm is free of parameter-tuning. It leads to better exploration- exploitation balance, prevention of local optima trap, and works well even on complex optimization problems. In hybridization, the leadership strategy is proposed where the bacterium with the least fitness value (most healthy) is the leader and the other bacteria in the swarm follow the leader using the FA position equation. This leadership approach is used instead of the elimination and dispersion step. In this way, the weak bacteria are not eliminated, rather they are moved to a position of a high food source that is close to the best bacteria resulting in the rejuvenation of the population of bacteria. FA [48] has a fast convergence rate and involves fewer computations; hence it is most appropriate to hybridize FA with BFA and improve its convergence speed. It is interesting and promising to study the capability of leadership strategy and success percentage of the swarm in optimizing results. BFA-FA is tested against classical, single peak, multi peak and noisy nonlinear benchmark functions and CEC_2017 benchmark functions and compared to other well- established and recent metaheuristics. The scalability analysis is done by testing the algorithm in a multidimensional environment. The significance of the algorithm is validated using Wilcoxon rank-sum and Friedman rank test. The results are verified by addressing the two classical engineering problems (Cantilever beam design and three-bar truss design).

The paper is organized as follows. The summarized review of traditional BFA and FA is presented in Section 2. The proposed method is presented in Section 3. In Section 4, the experimental results are discussed qualitatively as well as quantitatively. Section 5 gives the application of the proposed algorithm in the field of Structural design and Section 6 gives the conclusions of this work.

2 Review of classical bacterial foraging algorithm and firefly algorithm

BFA is an Evolutionary Algorithm (EA) technique, which works on the foraging nature of *Escherichia coli* abbreviated as *E. Coli* bacteria. It is designed to handle complex objective functions that are non-differentiable and non-gradient optimization problems. The four main mechanisms, viz, chemotaxis step, reproduction step, swarming, and elimination dispersal step are as follows:

1. *Chemotaxis*

Two basic locomotive operations involved in chemotaxis are: Swim and tumble. The bacteria tumble when the flagella rotate clockwise. In this motion, there is the least displacement and after completion, the bacteria are aligned along a random direction. On the other hand, the bacteria swim in a counter-clockwise rotation. In this motion, bacteria move forward in a particular direction. Let us consider the q^{th} chemotactic step for p^{th} bacteria of r^{th} reproduction step of the k^{th} elimination-dispersion of BFA. After each movement, the bacteria change their position according to Equation (1) as given below.

$$pos(p, q+1, r, k) = pos(p, q, r, k) + C\frac{\Delta(p)}{\sqrt{\Delta^T(p)\Delta(p)}} \tag{1}$$

where $\Delta(p)$ is the direction vector of the p^{th} bacterium movement in the current chemotactic step, and C is the step size in each chemotactic swim or tumble.

2. *Reproduction*

In this step, the healthy bacteria sustain whereas the least healthy

bacteria die. The global fitness value is updated in each reproduction step. Each bacterium that survives splits into two so that the total number of bacteria remains constant. The criteria for deciding the bacteria that will survive is decided by calculating the total health compared to the preceding reproduction, given by Equation (2) below.

$$J_{health} = F\,(p, q, r, k) \tag{2}$$

where $F\,(p, q, r, k)$ is the fitness value of p^{th} bacteria for q^{th} chemotactic step, r^{th} reproduction step of the k^{th} elimination-dispersion step. The bacteria with minimum accumulated health function get selected for elimination.

3. *Elimination and dispersion*

This step occurs after a predefined number of reproduction steps with the intent of improving the global search. In this step, the bacteria are eliminated and dispersed in random positions to avoid getting trapped in the local optima. This happens according to the probability N_{eldis} , probability of elimination and dispersion.

4. *Swarming*

It has been noticed that several bacteria species including E.Coli form a stable spatiotemporal ring-shaped swarm in the presence of a semi-solid nutrient medium. The E.Coli cells when stimulated by a high level of succinate release an attractive called aspartate that helps them aggregate in such groups. This cell-cell attraction can be mathematically represented as the Equation (3) below.

$$\begin{aligned} J_{cc}(pos) &= \sum_{p=1}^{s} J_{cc}(pos(p,q,r,k)) \\ &= \sum_{p=1}^{s} \left(-d_{attractant} * \exp\left(-w_{attractant} \sum_{d=1}^{D} \left(pos_d - pos(p,q,r,k)_d \right)^2 \right) \right) \\ &+ \sum_{p=1}^{s} \left(h_{repellant} * \exp\left(-w_{repellant} \sum_{d=1}^{D} \left(pos_d - pos(p,q,r,k)_d \right)^2 \right) \right) \end{aligned} \tag{3}$$

where $J_{cc}(pos)$ is the fitness offset in the q^{th} chemotaxis or the cost function that is added to the original cost function; $d_{attractant}$, $w_{attractant}$, $h_{repellant}$, $w_{repellant}$ are the coefficients which determine the depth and width of attrac- tant and height and width of repellant, which are to be selected properly; D is the number of dimensions; pos_d means the population coordinates in d-dimension; $pos(p, q, r, k)_d$ means the p^{th} bacterium coordinates in d-dimension.

The Firefly Algorithm is a successful nature-inspired optimization algorithm where the fireflies get attracted to each other, independent of their sex, and the attractiveness is directly proportional to its brightness. The movement takes place from less bright firefly to brighter

firefly. The distance between any two Fireflies i and j whose positions are x_i and x_j respectively for the dimensions D is given by the Cartesian distance as Equation (4).

$$dist_{ij} = \left\| x_i - x_j \right\| = \sqrt{\sum_{k=1}^{D} \left(x_{i,k} - x_{j,k} \right)^2} \tag{4}$$

The Firefly's attractiveness is proportional to the intensity of light seen by the adjacent firefly. The attractiveness is determined as below Eq. (5):

$$B(r) = \beta_0 e^{-\gamma dist^2} \tag{5}$$

where β_0 means the attractiveness at $dist = 0$ and γ is the light absorption coefficient at the source. The movement of a Firefly i to another more attractive Firefly j is determined by Equation (6).

$$x_i^{new} = x_i^{current} + \beta_0 e^{-\gamma dist_{ij}^2} \left(x_i^{current} - x_j \right) + \alpha \left(rand - \frac{1}{2} \right) \tag{6}$$

where the second term is due to attraction and the third term is due to randomization, $\alpha = [0, 1]$ being the randomization parameter, rand is a random generator of uniform distribution between 0 and 1, x^{new} is the new position of firefly x_i, and $x^{current}$ is the current position of firefly x_i. In this paper, we set the light absorption coefficient $\gamma = 1$ and $\beta_0 = 1$.

3 The proposed algorithm

The proposed algorithm introduces two novel improvements in BFA, namely adaptation and hybridization, to improve the convergence and accuracy, avoiding local optima, and to make the algorithm free from parameter tuning.

3.1 Adaptation

In the chemotaxis step of classical BFA, step size C is a constant parameter and determines the amount of movement. However, it is observed that if there is a dynamic change in step size the convergence is affected greatly. In this paper, we dynamically determine the chemotactic step size during a run, to strike a balance in their exploration and exploitation behavior. The bacterium with a small step size has the capability of exploitation and one with a large step size has the capability of exploration. The large value of step size accelerates the bacteria's movement towards the optimal point, while the small value of step size slows down the bacteria to converge to the optimal point.

To achieve the adaptation, the situation of the swarm is first determined at each iteration for which the success percentage is introduced in this paper. If the success percentage is high, it means the swarm of bacteria is converging towards the global optimum. On the contrary, the low value of success percentage means there is not much improvement in the bacteria.The steps of adaptation are as follows:

1. The success of p^{th} bacteria at the q^{th} chemotactic step and r^{th} repro- duction step is defined in a minimization problem according to Eq. (7)

$$success_count(p) = \begin{cases} 1 & if\ F(p,q,r) < F_{last} \\ 0 & if\ F(p,q,r) \geq F_{last} \end{cases} \tag{7}$$

where $F(p, q, r)$ is the fitness function to be optimized and F_{last} is the best fitness value of the bacteria obtained so far.

2. The success percentage of the bacteria using the success values is computed as follows:

$$PS(p) = \frac{\sum_{p=1}^{s} success_count(p)}{s} \tag{8}$$

where s is the total number of bacteria, PS is the percentage of p^{th} bacteria that had an improvement in their fitness value during the last iteration.

3. A linear function is used to map PS values to the possible range of step size as shown in Eq. (9).

$$C = (Cmax - Cmin)PS(p) + Cmin \tag{9}$$

To determine the range of C , multiple values between 0 and 1 were tried experimentally. It was found that the values of C between 0.2 to 0.5 give good results. So, the lower range of C, C_{min} is taken to be 0.2 and the upper range C_{max} to be 0.5.

In this way, the step size is regulated and adaptively changed from high value (exploration) to low value (exploitation) to reach the global optimum. This ensures the best possible exploration-exploitation balance. This way, user interference is avoided to initialize the key parameter; hence the algorithm is free from key parameter-tuning. Since the situation of the swarm is considered at every step, and not the single bacterium, therefore, the chances of local optima trap are reduced significantly. This makes it perform better in rough landscapes also, like in the case of multimodal optimization algorithms. To the best of our knowledge, the success rate of the swarm of bacteria to determine the step size is used for the first time in BFA.

3.2 Hybridization

In the conventional elimination and dispersion stage, every bacterium is mapped to a random value between 0 and 1. If the random value is less than N_{eldis} , the bacterium is eliminated. An equal number of fresh bacteria are introduced at random locations to maintain the total count. However, in this event, the biological diversity is lost and a potential optimal bacterium can be killed. This paper proposes a new strategy to overcome this situation. The standard elimination and dispersion step is avoided altogether for this. To achieve this, the steps are as follows:

1. The bacteria are sorted in descending order, according to their health. The health of bacteria is calculated using Eq. (2).

$$\begin{aligned}
&For\ p = 1, \ldots, s \\
&Let\ J^{p}_{health} = \sum_{j=1}^{N_c+1} F(p, q, r)\ be\ the\ health\ of\ bacterium\ p \\
&end\ for \\
&Sort\ bacteria\ with\ J_{health}\ in\ descending\ order
\end{aligned}$$

2. The bacterium with the least fitness value is considered most healthy (for minimization problems) and is termed as Lead.

$$Lead = Last\ bacterium\ of\ the\ sequence$$

3. The positions of the weaker set of bacteria (first half of the sorted population) are then modified using the position update equation of the Firefly Algorithm, where the weaker bacteria move towards the strongest bacterium.

$$\begin{aligned} &for\ i = 1, 2\ldots, {}^{s}/_{2} \\ &pos(i, q+1, r) = pos(i, q+1, r) + \beta_0 e^{-\gamma dist_{iLead}^2}(pos(i, q+1, r) - Lead) \\ &\qquad + \alpha\left(rand - \frac{1}{2}\right) \\ &end\ for \end{aligned}$$

where $dist_{iLead}$ is the distance between i^{th} bacterium and Lead bacterium and is calculated using Equation (4); N_c is the number of chemotactic steps.

By introducing the randomness in the position of weak bacteria, we diversify the search space. In this way, exploration is improved several times. So, rather than killing the weak bacteria, an attempt to make them closer to nutrients is done by changing their position and rejuvenating them. Since we know that fire flies change position when they get attracted to brighter firefly, in our case, the weak bacteria (followers) are attracted to the strongest bacterium (Leader), which is most close to the nutrient medium, and update their positions accordingly. The strategy of leadership to find the best food resource works excellent [43, 54]. In this way, search efficiency (or convergence) is improved greatly and diversity is also achieved leading to better exploration. The chances of missing the global optimal solution are reduced. As compared to other nature-inspired algorithms, FA gives quick convergence in fewer computations, hence it is most suitable to fuse with BFA and reduce the total runtime and give good results with quick convergence. From the literature, it is seen that other swarm-based optimization algorithms were used for hybridization with BFA; however, FA is used for hybridization with BFA for the first time.

The overall structure of the novel BFA-FA algorithm with adaptation and hybridization is shown in Algorithm 1. The population is randomly initialized and all the parameters are set. During the chemotaxis movement (swim or tumble), the step size is dynamically adjusted according to the success percentage of the swarm. The bacteria moves ahead and the new fitness value of the entire swarm is evaluated. If the current fitness value of the bacteria at the new position is smaller than the previous value, the bacteria update its position. For reproduction process, the health of the bacterium is determined. In the proposed algorithm, the elimination and dispersion step is not used. So, the bacterium with the best health (least value of fitness), which is determined in the reproduction step, is defined as the Lead, and rest of the bacteria become the followers and update their position according to the firefly equation and moves towards the healthy bacteria. So, the overall number of bacteria remains constant. Once the bacteria move closer to the Lead, the health (fitness value) of the bacteria is improved. In this way, the potentially strong bacteria are not eliminated, and the biological diversity is increased. The overall health of the swarm is also improvised. The flow chart of the proposed BFA-FA is shown in Figure 1.

Algorithm 1. The Proposed BFA-FA Algorithm

Parameter definition:

(a) BFA parameters

D: the dimension of search space; s: population of bacteria; N_c: number of chemotactic steps; N_s: number of swims after tumble; N_{re}: number of reproductive steps; pos: position of each member in the population of s bacteria; C: step size; C_{min}: minimum step size; C_{max}: maximum step size; PS: Success percentage

(b) FA parameters

α: randomization parameter; β: attractiveness; γ: light absorption coefficient

1. Initialize all the parameters defined above
2. $success_count = 0$, $PS = 0$
3. Reproduction Loop: ***While*** $r < N_{re}$
4. Chemotaxis Loop: ***While*** $q < N_c$
   a. $PS = \frac{success_count}{s}$
   b. $C = (C_{max} - C_{min})PS + C_{min}$
   c. ***For*** $p = 1, \ldots, s$
   d. Compute Fitness cost, $F(p,q,r)$
   e. $F(p,q,r) = F(p,q,r) + J_{cc}(pos)$, where $J_{cc}(pos)$ is calculated using Equation (3)
   f. $F_{last} = F(\mathrm{p},\mathrm{q},\mathrm{r})$
   g. Tumble: Generation of a random vector $\Delta(p) \in R^D$ with each element $\Delta_d(p)$, $d = 1,2,\ldots D$, a random number $[-1,1]$ where R is a real number

   Computing pos for $p = 1,2\ldots,s$ (number of bacteria)

$$pos(p,q+1,r) = pos(p,q,r) + C\frac{\Delta(p)}{\sqrt{\Delta^T(p)\Delta(p)}}$$

   h. Swim:

   Set swim length counter, $m = 0$

   i. ***While*** $m < N_s$
   j. ***If*** $F(p,q+1,r) < F_{last}$ (if there is any improvement)
   k. $success_count = success_count + 1$
   l. $PS = \frac{success_count}{s}$
   m. $C = (C_{max} - C_{min})PS + C_{min}$
   n.
   o. let $F_{last} = F(p,q+1,r)$
   p. $pos(p,q+1,r) = pos(p,q,r) + C\frac{\Delta(p)}{\sqrt{\Delta^T(p)\Delta(p)}}$
   q. Use $pos(p,q+1,r)$ to calculate the new fitness function $F(p,q,r)$
   r. ***Else***
   s. $m = N_s$
   t. ***End If***
   u. $m = m + 1$
   v. ***End while***
   w. ***End For***

5. **End While** (Chemotaxis loop closes)
6. Reproduction:
   a. For given r, and ***For*** $p = 1, \ldots, s$
   b. $Let\ J^p_{health} = \sum_{j=1}^{N_c+1} F(p,q,r)$ be the health of the bacterium
   c. ***end For***
   d. $Sort\ bacteria\ with\ J_{health}\ in\ descending\ order$
   e. $Select\ Lead = Last\ bacterium\ of\ the\ sequence$
   f. computing new positions of follower bacteria using firefly algorithm:
   g. ***For*** $i = 1,2\ldots, {}^{S}/_{2}$
   h. $pos(i,q+1,r) = pos(i,q+1,r) + \beta_0 e^{-\gamma dist^2_{iLead}}(pos(i,q+1,r) - Lead) + \alpha\left(rand - \frac{1}{2}\right)$
   i. ***end For***
7. ***End While*** (Reproduction loop closes)

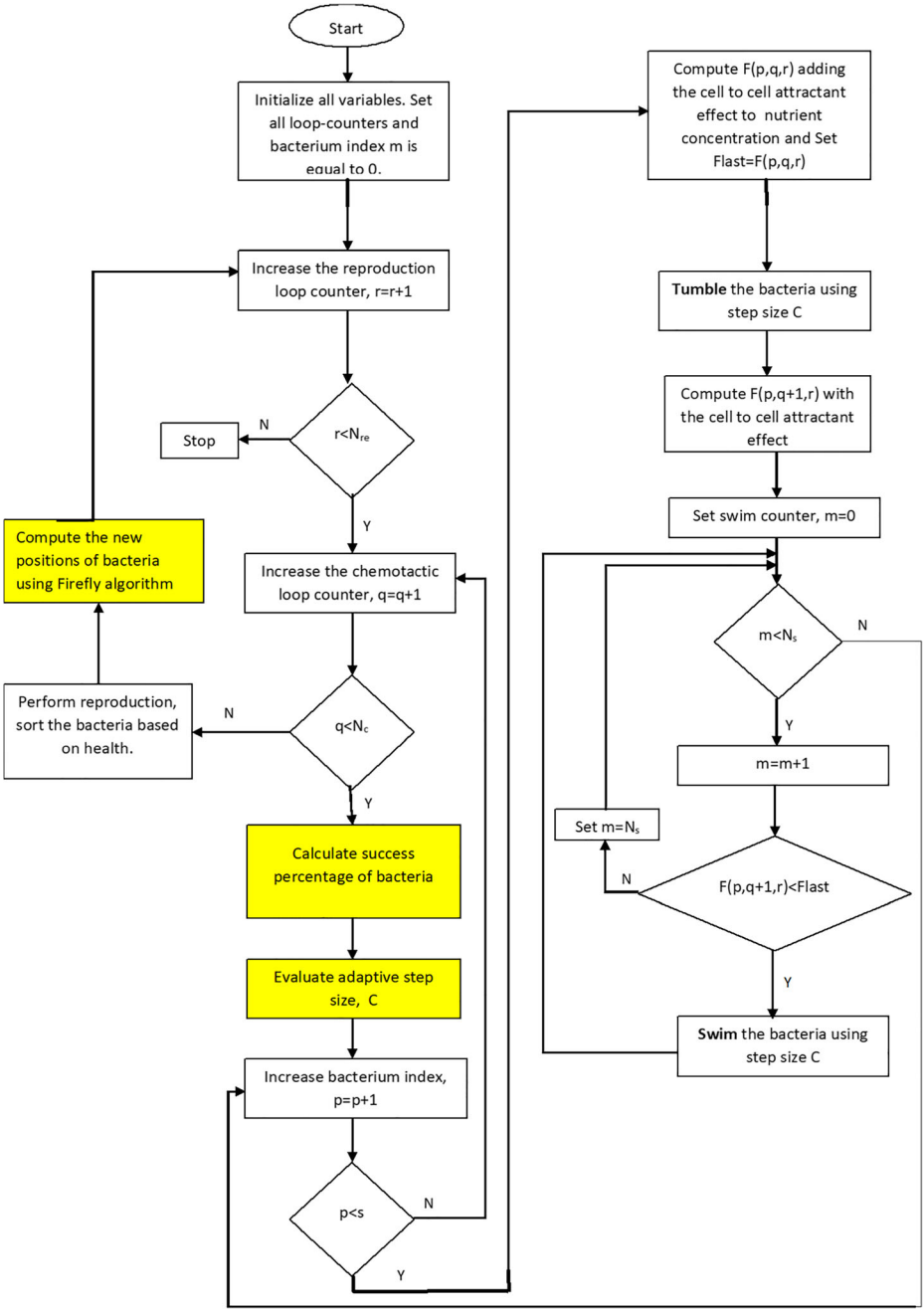

Fig. 1 The flow chart of the proposed BFA-FA algorithm

4 Experimental evaluation

4.1 Experimental setup

An experimental analysis of the proposed approach is done using MATLAB R2010a on 64-bit Windows to validate its performance. The classic benchmark functions, including unimodal, multimodal, and composite functions are used from [49] for testing the proposed algorithm. Along with standard benchmark functions, the experimental analysis is done on single peak, multi peak [25], noisy nonlinear benchmark functions [32] and modern numerical optimization problems from IEEE CEC_2017 [7, 46]. The CEC_2017 functions have features such as shifting, rotating, expanding the basic functions, or a variant of these. To verify the results of the proposed BFA-FA algorithm, it is compared with some well-established and recent metaheuristic algorithms. The well-established algorithms include BFA [26], FA [48], Artificial Bee Colony (ABC) [16], and the recent algorithms used are Monarch Butterfly Optimization (MBO) [44], SSA [28], Hybrid BFA and PSO (BF-PSO) [22]. In all the experiments, the population size is set to 50, the number of iterations to 100, and the evaluation is taken for 30 different runs. The best or optimal results are highlighted in bold. The parameters for the proposed approach are set as follows: $s = 50$; $N_c = 100$; $N_s = 4$; $N_{re} = 4$; $C_{min} = 0.2$; $C_{max} = 0.5$; $\gamma = 1$; $\beta_0 = 1$; $\alpha = 1$. The rest of the parameters of other algorithms used in the comparison are the same as those used in the literature .The performance is evaluated as follows:

1. Qualitative Analysis Analyzing the convergence curves of the proposed method and other algorithms.
2. Quantitative Analysis Validating the proposed method against other comparing algorithms by evaluating the fitness function over classic, noisy nonlinear, single peak, multi peak, and modern CEC benchmark functions, comparing the time complexity, performing the scalability analysis, and performing Wilcoxon statistical analysis at a 5% significance level, and Friedman rank test.

4.2 Qualitative results and discussion

The first set of experiments was performed by observing the convergence curve of the proposed approach and comparing it with the convergence curves of other metaheuristic algorithms. The main aim of conducting this experiment was to observe the behavior of BFA-FA qualitatively. The benchmark functions used are listed in Appendix A, where *Dim* shows the dimension of the function, *Range* is the boundary of the search space, and f_{min} value gives the optimal value.

Figure 2 shows the 2D versions of the benchmark functions that are used in this paper for testing purposes. These minimization functions can be simply categorized as unimodal, multimodal, multimodal (fixed dimension). Studying the pattern of the proposed algorithm on these functions helps to generalize the results for other unimodal and multimodal functions as well. Exploitation can be benchmarked using unimodal benchmark functions (f_1 to f_5). In contrast, multimodal functions (f_6 to f_{11}) have a lot of local optima, which can benchmark exploration. From f_{12}, which is a composite function, the capability of exploration and exploitation can be simultaneously benchmarked, along with the capability of local optima avoidance. The convergence curves of the proposed algorithm and various other metaheuristic algorithms are depicted in Fig. 3, for all the benchmark functions. From the convergence

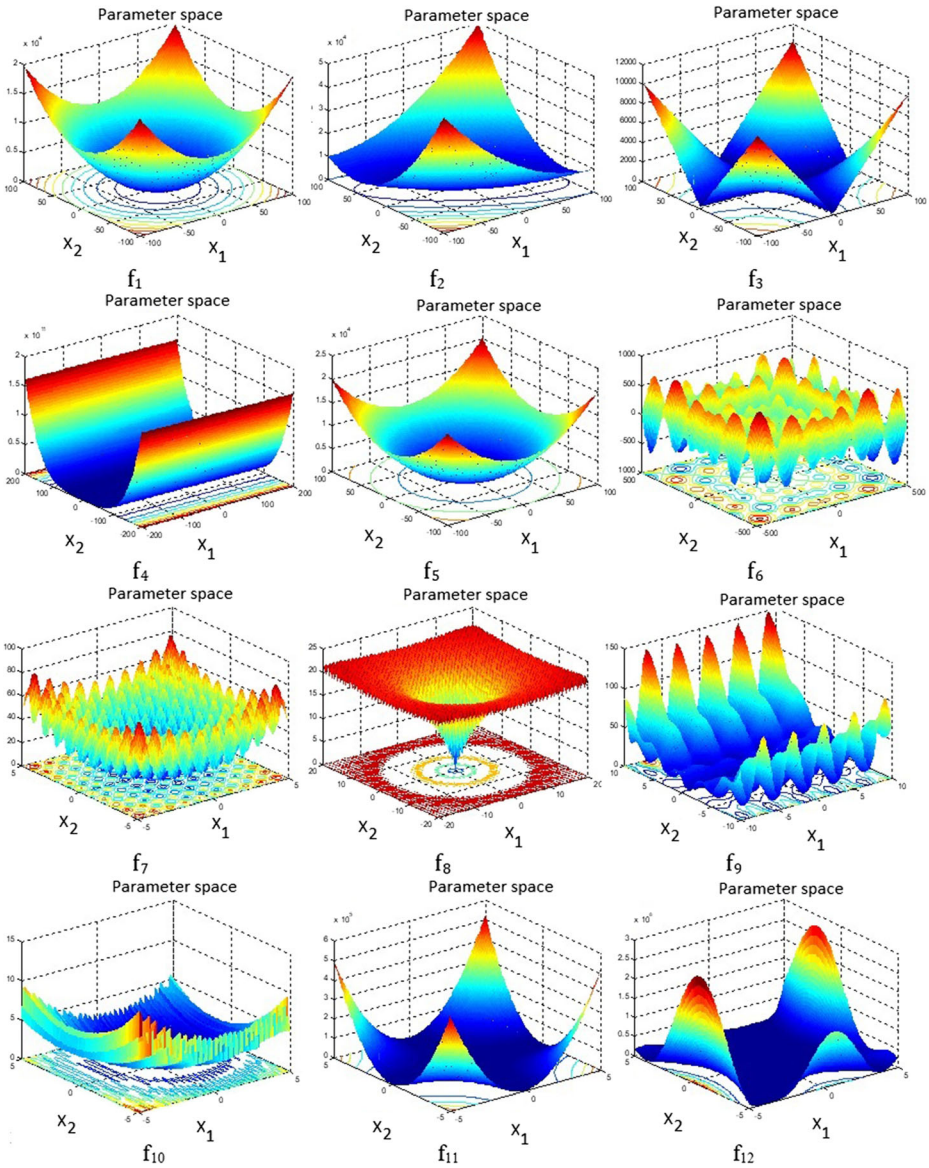

Fig. 2 2-D versions of the unimodal and multimodal benchmark functions

curves, it is clear that BFA-FA performs well over other metaheuristic algorithms in terms of convergence speed. For most of the unimodal functions (except f_3), BFA-FA shows significant results which means that they have merit in exploitation. As per the curves for the function f_7 to f_{11} (except f_6), BFA-FA gave superior results which makes it capable of good exploration, although BF-PSO gave competitive performance. It can be derived that BFA-FA performs well on multimodal optimization functions, and at the same time ensures quick convergence. The proposed approach is fairly competitive to other algorithms in terms of convergence speed for composite function as well, showing a good balance between

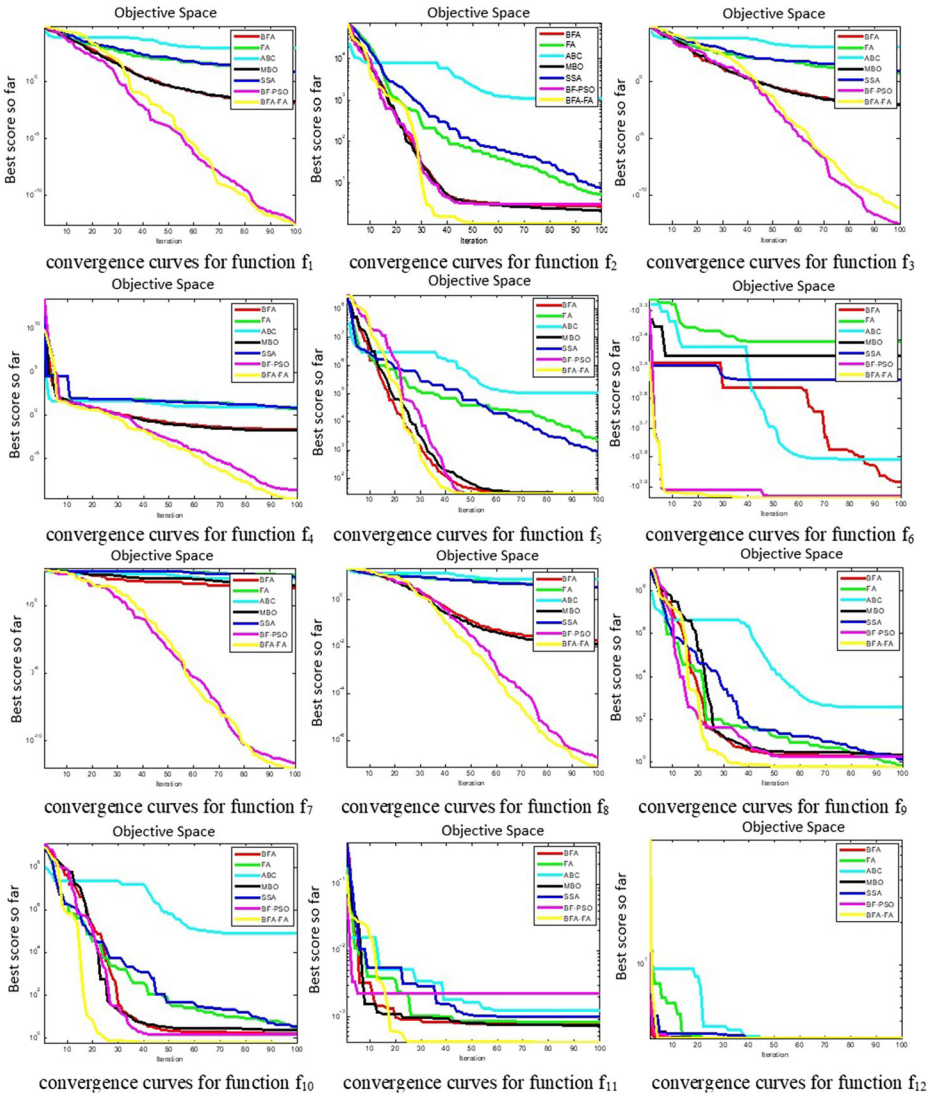

Fig. 3 Convergence curves of the proposed BFA-FA and other algorithms on the benchmark functions

exploration and exploitation. From the convergence trend, it can be further noticed that BFA-FA is better than its individual counterparts BFA and FA. The convergence of BFA is superior to FA, however, the convergence of BFA-FA outperforms both of them. For most cases, convergence was slow at the initial iterations in the exploration phase, however, it picks up the speed and converges faster at a later stage. This may be possible due to adaptation which ensures efficiency in search space during exploration, and acceleration in convergence later. The fusion of FA into BFA assists in ensuring fast convergence in few computational steps and reaches global optimum solution, which is validated in the quantitative analysis section.

4.3 Quantitative results and discussion

The second experiment was based on evaluating the fitness value, mean standard deviation, root mean square, mean absolute error, mean absolute percentage error, normalized root mean square error, and convergence time obtained by the proposed approach and comparing it with BFA, FA, ABC, MBO, SSA, Hybrid BF-PSO. The unimodal, multimodal, and composite benchmark functions used are already described in Appendix A. Along with standard benchmark functions, the experimental analysis was done on single peak, multi peak [25], noisy nonlinear functions [32] as well as modern numerical optimization problems from IEEE CEC 2017 [7, 46]. These functions have features such as shifting, rotating, expanding the basic functions, or a variant of these. The comparison is done over 30 different runs of the algorithms.

To achieve best results for any optimization problem, the control parameters of the algorithm should be tuned appropriately. This could provide more robustness and adaptability when solving a general set of problems. For our algorithm, the range of step-size C was selected using the Design of Experiments approach. The sensitivity of the algorithm was analyzed by trying various ranges of C between 0 and 1, and then performing the experiment. The values varied until a decent solution was obtained. The analysis was done on benchmark functions f_1, f_8, f_{12}, CEC_2017 function C_1, noisy nonlinear function NL_1. Each function was solved for 30 different runs. The results of some of the ranges of step-sizes are shown in Table 1. From the sensitivity analysis done in Table 1, it is evident that too small or too large difference between the range of step size gives inaccurate results, and the performance is much better for a reasonable range when tested for 30 independent runs. Hence C_{min} was taken as 0.2 and C_{max} was taken as 0.5.

Table 2 shows the evaluation results of optimal values for different algorithms. The best results of the global optima are highlighted in bold. The evaluation parameter here was the fitness function values obtained by the various algorithms over 30 different runs. As discussed, the functions f_1–f_5 benchmarks exploitation, it can be observed from the table that BFA-FA outperformed all comparative algorithms in almost all the functions except f_5. The results for the function f_5 were slightly better given by BFA and MBO. For the function f_1, BFA-FA as well as BF-PSO gave the same results which shows that these two algorithms are competitive. It can therefore be generalized that BFA-FA can solve unimodal optimization functions and with nearly accurate global optimum values. So, the proposed algorithm exhibits good exploitation capability. The functions f_7-f_{11} are suitable to benchmark exploration since these are multimodal in nature and have multiple local optima. From the table, it was observed that for the functions f_7, and f_8, BFA-FA showed competitive performance with BF-PSO. However, the results were outperformed for all other functions which showed that BFA-FA was able to reach the global optimum solutions for almost all multimodal functions. In this manner, the proposed algorithm exhibits good exploration capability as well. The balance of

Table 1 Fitness values of functions using different range of step size

Range of step size C		f_1	f_8	f_{12}	C_1	NL_1
C_{min}	C_{max}					
0.1	0.3	0.0055e+00	3.6200e−11	3.2400e+00	1.8892e-15	1.982
0.2	**0.5**	**8.8818e-16**	**0.0000e+00**	**3.0000e+00**	**0.0000e+00**	**1.4789**
0.3	0.8	4.8743e-02	1.59239e-01	3.6183e+00	5.3847e-20	12.9137
0.4	0.9	4.8021e-01	1.2365e-01	3.6900e+00	3.8473e-44	13.8373

Table 2 Fitness function f(.) evaluation on various optimization functions

Function	Optimum Value, f(.)						
	BFA	FA	ABC	BF-PSO	MBO	SSA	Proposed BFA-FA
f_1	0.4021e+00	0.0066e+00	0.0065e+00	**8.8818e-16**	5.7119e−05	4.8613e-06	**8.8818e-16**
f_2	1.9645 e+00	8.1553e-04	0.9986e+00	8.8818e-16	3.6200e−11	5.4306e-07	**0.0000e+00**
f_3	1.4950e-09	9.8998e-06	1.0276e-05	1.3298e-32	5.6500e-09	1.8418e-14	**1.4998e-34**
f_4	0.1471e+00	3.0002e-02	1.0044e-07	5.0339e-04	3.0012e-08	1.0018e-03	**3.0076e-09**
f_5	0.0000e+00	1.5393e-04	0.0122e+00	1.4998e-32	**0.0000e+00**	3.8327e-04	0.0067e+00
f_6	-1.1260e+03	−5.8275e+07	−7.2783e+04	−4.0327e+03	**−7.3423e+03**	−5.4306e+04	−6.0024e+03
f_7	0.1100e+00	7.8730e-06	2.6951e-05	**0.0000e+00**	**0.0000e+00**	3.2110e−14	**0.0000e+00**
f_8	0.1680e+00	4.7375e-07	4.2123e-08	**0.0000e+00**	**0.0000e+00**	3.1326e-07	**0.0000e+00**
f_9	−1.0020e+00	2.5908e-06	9.1240e-06	8.8818e−16	4.1240e−11	3.2110e−14	**0.0000e+00**
f_{10}	1.3584e-02	0.9999e-07	0.8110e-06	8.8395e−17	−1.0000e+00	8.7289e-01	**8.8261e-30**
f_{11}	-1.8074e+00	-1.6633e+00	-1.3860e+00	-1.5660e+00	−1.7309e+00	−1.5819e+00	**−1.0230e+00**
f_{12}	3.0300e+00	3.9285e+00	3.3700e+00	6.3890e+00	3.8013e+00	3.6400e+00	**3.0000e+00**

Table 3 Performance of BFA-FA and other algorithms when applied on nonlinear benchmark functions in terms of processing time (in sec)

Function	Proposed BFA-FA	FA	ABC	BF-PSO	MBO	SSA	BFA
NL1	**51.47**	51.49	51.74	51.68	52.68	51.53	51.87
NL2	**52.73**	52.63	52.81	52.17	52.79	52.74	52.65
NL3	**52.39**	52.39	52.73	52.94	53.04	53.02	53.23
NL4	**53.23**	53.23	56.24	56.34	53.48	54.28	54.29
NL5	**53.11**	53.58	53.82	53.67	53.18	53.12	54.23
NL6	**54.01**	54.85	54.26	54.83	54.94	54.23	54.39
NL7	**51.93**	52.43	52.23	51.98	52.49	51.99	52.95

exploration and exploitation was tested when a composite function was solved using all algorithms. Here, BFA- FA proved to be the best optimizer for solving the function f_{12}. So, it can be concluded that BFA-FA is able to establish exploration-exploitation balance and give nearly accurate values of global optima.

Another benchmarking model used to test the performance of BFA-FA was noisy nonlinear benchmark functions. The functions are described in Appendix A. The evaluation parameter was the processing time (in seconds) for solving the function through the mentioned comparative algorithms. The results of the algorithms when applied over noisy nonlinear functions are shown in Table 3. It is quite clear from the results that BFA-FA seems to solve the noisy functions in less time, hence it is potentially more powerful in solving nonlinear functions. The proposed method was used to benchmark single peak and multi peak functions, described in Appendix A. The accuracy index parameters for evaluation were the mean absolute error (MAE), mean absolute percentage error (MAPE), root mean square error (RMSE), and the normalized root mean square (NRMSE) . These parameters are evaluated as follows:

Table 4 Accuracy indexes of BFA-FA and other algorithms on single peak and multi peak functions

Algorithm	Benchmark functions	MAE	MAPE	RMSE	NRMSE
BFA	SP1	52.237	3.9621	71.231	0.0748
FA	SP1	57.328	4.2886	75.965	0.0748
BFA-FA	SP1	**50.013**	**3.1385**	**59.893**	**0.0367**
BFA	SP2	62.434	4.3892	65.937	0.0447
FA	SP2	64.329	5.9327	60.332	0.0632
BFA-FA	SP2	**57.047**	**4.2037**	**60.023**	**0.0334**
BFA	MP3	80.328	9.3208	90.328	0.0932
FA	MP3	99.327	8.3289	110.094	0.0863
BFA-FA	MP3	**71.943**	**6.2647**	**85.392**	**0.0632**
BFA	MP4	89.394	6.3727	98.438	0.0847
FA	MP4	65.048	5.6304	74.731	0.0743
BFA-FA	MP4	**60.322**	**4.6533**	**69.329**	**0.0614**
BFA	MP5	75.348	9.4389	79.439	0.0463
FA	MP5	74.243	8.4663	74.482	0.0623
BFA-FA	MP5	**74.0127**	**7.0456**	**71.958**	**0.0418**
BFA	MP6	92.473	9.3921	75.923	0.0958
FA	MP6	89.431	8.3947	73.042	0.0963
BFA-FA	MP6	**87.839**	**8.2894**	**73.385**	**0.0762**

$$MAE = \frac{\sum_{i=1}^{s} |y_i - f_i|}{s}$$

$$RMSE = \sqrt{\frac{\sum_{i=1}^{s} (y_i - f_i)^2}{s}}$$

$$NRMSE = \sqrt{\frac{s\sum_{i=1}^{s} (y_i - f_i)^2}{\sum_{i=1}^{s} y_i^2}}$$

where s is the total population, y_i is the obtained fitness value, f_i is the actual fitness value for the i^{th} iteration. The results of comparative analysis are shown in Table 4. It can be learnt from the table that BFA-FA gives smaller values for MAE, MAPE, RMSE, and MRMSE as compared to its classical algorithms BFA and FA. This proved the stability of the proposed technique since the error percentage is quite less. The strategy of adaptation and leadership in BFA-FA contribute in improving the performance in terms of accuracy, since the results of BFA-FA are outperforming BFA.

To test the robustness, effectiveness and stability of the proposed BFA-FA, the algorithms were compared over modern IEEE CEC_2017 Benchmark functions, since it is quite a challenging test suite and involves unimodal, multimodal, composite and hybrid functions. The description of benchmark functions in detail is mentioned in Appendix A. The comparison among algorithms is taken over 30 independent runs for all the algorithms. The average and standard deviation are used as performance measures. The evaluation results are shown in Table 5. It can be observed that BFA-FA showed improved average results in comparison to other algorithms for modern benchmark functions. The average scores by BFA-FA were better than other comparative algorithms for the functions C01, C02, C05, C07, C08, C10, C13, C16, C18, C19, C22, and C23. The functions C05, C8, and C10 were solved accurately using BFA- FA, BF-PSO, and SSA. The second rank was achieved by BF-PSO for its good performance over 9 CEC functions, followed by BFA. Also, another interesting observation was that the standard deviation of BFA-FA is least for most of the CEC functions. It can be learnt that the algorithm is quite stable in solving the problems, besides being stochastic in nature. These observations proved the superiority of the algorithm.

The third experiment was comparing the time complexities of the proposed approach with respect to the standard classical counterparts, i.e., BFA and FA. Table 6 shows the time complexity of BFA-FA, BFA, and FA. The convergence rate tells the time taken by the algorithm to reach the global optima. From the table, it was concluded that BFA-FA converges faster as compared to BFA and FA in most cases except the functions f_2, f_7, f_9, and f_{10}, where FA performed better than BFA-FA. Another observation was that for the composite function f_{12}, BFA-FA outperformed BFA and FA. It is important to note the performance on such functions since most of the algorithms fail or face difficulty in optimizing the composite functions on time. Hence, BFA-FA can be used to give optimal results for composite functions in lesser time. It is interesting to note that generally after the hybridization process, the time taken generally increases due to additional function evaluations, however the time taken by BFA-FA is less or comparable. This is because the elimination and dispersion step were removed in BFA-FA. This step in classical BFA involved the complexity of eliminating some part of the swarm of bacteria and dispersing some other part of the swarm to a random location. But in BFA-FA, when BFA is hybridized with FA, which has a randomness component, the overall function evaluations are less compared to classical BFA.

The fourth experiment was performed by testing the scalability in the multi- dimensional environment. Sometimes, it is observed that the algorithms per- form well in lower dimensions,

Table 5 Fitness function f(.) evaluation on CEC 2017 Benchmark Functions over 30 independent runs

Function	Proposed BFA-FA		BFA		FA		ABC		BF-PSO		MBO		SSA	
	Mean	Std	Mean	Std	Mean	Std	Mean	Std	Mean	Std	Mean	Std	Mean	Std
*C*01	0.00e+00	0.00e+00	6.03e-01	1.00e+00	1.08e-01	5.47e-01	6.05e-01	1.00e+00	0.00e+00	0.00e+00	3.52e-01	5.69e-02	5.82e-03	2.84e-03
*C*02	0.00e+00	0.00e+00	3.36e-01	2.15e-01	2.73e-01	3.68e-02	3.50e-01	1.59e-01	0.15e+00	0.03e+00	3.48e-01	1.90e-01	0.01e-01	0.83e-02
*C*03	3.60e+04	5.13e+04	3.00e+05	2.41e+04	8.73e+03	6.90e+03	3.52e+04	3.00e+04	1.23e+03	4.32e+02	5.35e+03	6.83e+03	5.34e+04	7.23e+03
*C*04	1.30e+01	5.40e-02	4.59e-02	6.30e-03	2.67e+01	9.57e+00	1.57e+01	6.74e-01	4.77e+01	1.23e-01	4.66e+01	5.67e-03	1.94e+01	1.20e-01
*C*05	0.00e+00	0.00e+00	1.52e-01	2.00e-03	0.00e+00	0.00e+00	6.79e-01	8.30e-01	0.00e+00	1.10e-01	4.56e-01	1.40e-01	0.00e+00	4.00e-03
*C*06	6.02e+02	1.08e+02	7.01e+02	1.01e+02	1.10e+03	2.89e+02	7.59e+03	4.35e+03	4.23e+02	7.90e+03	4.56e+03	5.18e+02	8.03e+02	5.03e+02
*C*07	4.25e+01	2.64e+01	5.32e+01	2.91e+01	5.63e+01	3.84e+01	6.13e+03	1.50e+01	6.40e+01	2.37e+01	5.43e+01	2.77e+01	6.78e+01	3.42e+01
*C*08	0.00e+00	0.00e+00	0.72e+00	0.02e-01	0.03e+00	0.14e-02	7.24e-02	7.50e-03	0.00e+00	0.00e+00	3.48e-02	4.50e-03	0.00e+00	5.60e-04
*C*09	4.00e-01	2.40e-03	3.20e-01	3.12e-01	7.34e-01	5.60e-03	8.30e-02	7.56e-03	2.43e-01	5.60e-03	7.83e-01	5.20e-02	6.40e-01	2.34e-04
*C*10	0.00e+00	8.80e-16	0.16e-01	1.03e-02	2.67e-01	7.82e-07	4.58e-02	3.14e-02	0.00e+00	9.50e-14	3.40e-13	9.91e-11	0.00e+00	9.24e-03
*C*11	2.30e-02	2.57e-17	1.32e-01	3.00e-07	5.67e-02	7.34e-01	8.36e-01	2.71e-01	6.70e-03	4.57e-12	5.67e-01	5.60e-01	3.10e-01	2.90e-10
*C*12	5.90e-12	2.53e-10	6.60e-12	4.63e+01	7.16e-01	0.00e+00	5.80e-02	7.87e-01	3.62e-01	7.56e-11	6.46e-21	6.50e-09	6.00e-10	5.00e-12
*C*13	0.00e+00	0.00e+00	3.20e-01	2.30e+00	1.17e-01	6.75e-02	4.16e-02	1.58e-01	1.20e-01	0.00e+00	5.60e-01	6.70e-01	0.00e+00	5.00e-03
*C*14	2.00e-20	5.60e-22	4.30e-30	2.30e-22	7.35e-02	4.76e-02	4.23e-14	1.26e-20	1.23e-03	7.82e-15	6.00e-12	4.65e-05	4.20e-18	4.00e-20
*C*15	7.12e+00	1.34e+00	1.92e+01	1.23e+01	1.87e+01	1.08e+01	8.12e+00	6.35e+00	4.12e+00	9.23e+00	8.34e+00	7.98e-01	8.34e+00	2.77e+00
*C*16	3.05e+00	8.09e-08	1.60e+01	5.00e-05	2.57e+01	5.68e-01	5.64e+00	3.60e+00	5.12e+00	3.23e-05	1.25e+01	9.89e+00	5.06e+00	9.03e-07
*C*17	9.67e-01	6.34e-20	1.18e+00	3.24e+00	5.65e-01	4.59e-01	8.53e-01	4.63e-03	4.50e-01	3.54e-17	4.70e-01	7.20e-10	1.40e+00	5.23e-18
*C*18	2.61e+03	1.63e+03	2.67e+05	5.27e+04	5.84e+07	8.75e+04	5.48e+05	5.69e+03	2.32e+04	1.42e+01	4.66e+04	1.23e+03	3.21e+03	2.57e+03
*C*19	0.00e+00	0.00e+00	0.36e-05	0.84e-06	4.37e-01	4.50e-01	0.00e+00	0.00e+00	0.00e+00	8.30e-01	4.49e-03	1.20e-04	0.91e+00	0.31e-01
*C*20	9.50e-02	5.40e-03	3.23e-03	7.33e-01	6.78e-01	6.79e-02	1.67e-01	2.55e-03	3.19e-01	6.23e-02	4.70e-03	7.50e-03	1.62e-01	6.70e-03
*C*21	3.90e+00	0.00e+00	1.25e-01	6.33e-01	2.86e+01	4.54e+00	1.02e+01	1.90e-01	2.90e+00	3.20e-01	8.56e+00	4.50e-03	4.70e+00	0.00e+00
*C*22	3.17e-01	4.56e-01	5.27e-01	7.29e-01	5.87e-01	4.37e-01	4.25e-01	2.30e-01	6.72e-01	9.45e-01	9.46e-01	6.50e-01	6.53e-01	3.79e-01
*C*23	4.32e-01	2.53e-01	5.74e+00	2.64e-01	6.75e+01	4.56e+01	6.75e+00	1.20e-03	7.43e+00	6.78e-01	1.56e+01	1.20e-01	6.73e+00	5.60e-01
*C*24	3.46e+01	2.34e-15	0.00e+00	5.27e-01	6.86e+01	4.55e+01	4.28e+01	1.25e-01	6.76e+01	8.56e-15	6.77e+01	3.40e-13	4.62e+01	5.60e-13
*C*25	2.92e+01	7.34e-01	7.98e+02	4.56e+00	7.46e+01	5.06e+01	6.12e+00	1.12e+00	1.24e+01	1.48e+01	8.47e+01	1.20e-03	3.54e+01	8.95e-01
*C*26	4.70e-01	3.20e-01	6.50e-01	6.40e-01	5.68e-01	3.64e-01	1.65e-01	4.32e-01	7.46e-01	6.45e-01	5.67e-01	6.00e-01	5.80e-01	7.85e-01
*C*27	2.13e+03	1.22e+03	2.35e+05	4.21e+03	5.90e+04	6.87e+03	3.24e+05	4.23e+02	6.22e+05	1.23e+03	4.59e+00	5.33e+03	3.12e+03	2.48e+03
*C*28	1.39e+01	8.37e+00	4.23e+02	6.70e+01	1.68e+01	6.67e+00	1.54e+01	6.87e-01	2.30e+01	9.15e+00	2.79e+00	9.12e+00	1.48e+01	9.43e+00

Table 6 Convergence Time (in sec) of BFA-FA compared to traditional BFA and FA

Function	Time (sec)		
	BFA	FA	Proposed BFA-FA
f_1	58.44	56.58	**56.36**
f_2	57.49	**57.45**	57.78
f_3	58.69	56.97	**56.32**
f_4	57.82	56.85	**56.21**
f_5	57.58	58.75	**55.63**
f_6	58.68	57.45	**56.67**
f_7	56.69	**55.22**	57.40
f_8	56.25	57.08	**53.44**
f_9	59.04	**57.42**	57.83
f_{10}	59.62	**56.22**	56.49
f_{11}	58.41	52.36	**52.12**
f_{12}	55.87	59.53	**55.40**

but give an absurd performance in higher dimensions. To test the performance of BFA-FA over higher and lower dimensions, a comparison of BFA-FA was done with BFA and FA over 20, 30, 50, and 100 dimensions in Table 7. The results demonstrate that BFA-FA outperforms the other two algorithms and offers feasible results for 20, 30 and 50 dimensions. For 100-D, the results are slightly improved giving a scope for more improvement in future. However, they are still better than the traditional BFA and FA for the optimization functions taken.

The fifth experiment was performed by testing the significance of the results (Wilcoxon rank-sum test at 5% significance level and Friedman rank test) [15, 50]. Wilcoxon test is a non-parametric statistical test that verifies whether or not both sets of solutions are significant. It

Table 7 Experimental results with higher dimensions and their comparison with conventional algorithm

Optimization function	Dimensions	Optimum Value, f(.)		
		BFA	FA	BFA-FA
f_1	20-D	9.887e-01	1.4833e-04	**7.1293e-16**
	30-D	0.1582e-01	2.9127e-03	**8.8004e-06**
	50-D	0.9923e-02	3.3939e-01	**1.7175e-03**
	100-D	2.4123e-01	2.0834e-01	**5.7119e-02**
f_5	20-D	0.3478e-01	1.8241e-01	**0.01604e-04**
	30-D	0.8432e+00	2.9127e+00	**0.1184e+00**
	50-D	0.5461e+00	2.2342e+00	**0.1427e+00**
	100-D	0.6923e+00	0.8982e+00	**0.3133e+00**
f_8	20-D	5.237e-05	1.3421e-07	**6.3287e-18**
	30-D	0.5933e-04	1.1284e-03	**0.4438e-10**
	50-D	0.2321e-01	0.8756e02	**0.455e-05**
	100-D	7.8673e+00	6.9223e+00	**5.4312e+00**
$f10$	20-D	9.3735e-11	2.4833e-13	**5.133e-30**
	30-D	0.01258e-08	0.8762e-10	**0.3622e-18**
	50-D	0.3552e-05	2.2398e-06	**1.1732e-11**
	100-D	2.7724e-01	2.8923e-01	**1.7193e-02**
$f12$	20-D	3.03e+00	3.9230e+00	**3.0000e+00**
	30-D	3.9730e+00	4.1730e+00	**3.7600e+00**
	50-D	**4.1277e+00**	4.2873e+00	4.1700e+00
	100-D	4.8123e+00	4.7662e+00	**4.6124e+00**

returns a p-value that defines the degree of significance. If the p- value is less than 0.05, an algorithm is statistically significant. This is done by choosing the best algorithm in each run and comparing it with other algorithms independently. Also, since the best algorithm cannot be compared to itself, hence N/A (Not Applicable) is written. Since the metaheuristic algorithms are stochastic, therefore it is required to test the significance. The Wilcoxon test results are shown in Table 8. It can be observed from the table that BFA-FA algorithm was able to perform well for the test functions C01, C02, C04, C06, C07, C09,C11, C14, C15, C17, C20, C21, C22, C24, C25, and C28. After BFA-FA, the algorithms BF-PSO and SSA were ranked second since they gave good performance on three test functions each. From the statistical results, it can be said that BF-PSO and SSA were able to give good results and outperform other algorithms, however, BFA-FA gave outstanding performance and proved superior. Friedman test is also a non-parametric test, which is based on the average ranked value. If the p-value level of significance) is less than or equal to 0.05, then the null hypothesis is rejected. This means that the statement that all the algorithms perform equally good, is not true. This verifies that the proposed algorithm performs statistically significant than other algorithms or not. The average rankings of all the algorithms used in this study on the test suites unimodal, multi modal, composite and CEC_2017 functions using Friedman rank test are shown in Table 9. The statistical value of the test came out to be 108.10, and the p-value of BFA-FA was 4.923E-06 which proved that there was significant difference between BFA- FA and other algorithms. BFA-FA was clearly followed by BF-PSO , SSA, MBO, BFA, FA, and

Table 8 Statistical Analysis using P-values obtained from the Wilcoxon rank sum test

CEC Functions	BFA	FA	ABC	BF-PSO	MBO	SSA	Proposed BFA-FA
C01	4.380e-04	1.089e-03	7.260e-02	5.4002e-01	7.182e-03	3.251e-04	**N/A**
C02	1.145e-03	4.513e-03	1.0528e-04	3.14292e-01	1.674e-06	6.180e-04	**N/A**
C03	3.022e-02	4.506e-03	1.748e-11	**N/A**	9.668e-02	4.603e-03	4.502e-03
C04	1.592e-03	3.886e-03	1.083e-04	2.6104e-04	2.2121e-10	6.219e-02	**N/A**
C05	8.126e-03	1.091e-03	5.138e-01	**N/A**	1.868e-03	5.4725e-02	1.093e-03
C06	2.566e-02	4.084e-02	7.410e-05	7.837e-05	9.437e-02	5.218e-15	**N/A**
C07	4.001e-01	3.0614e-01	0	7.13e-03	3.424e-02	7.85e-03	**N/A**
C08	1.110e-16	**N/A**	2.887e-15	0	4.273e-02	4.60e-03	7.74e-03
C09	1.568e-02	4.281e-02	0	8.089e-02	0	0	**N/A**
C10	9.83e-02	**N/A**	2.162e-04	7.332e-02	9.915e-02	7.832e-02	4.325e-02
C11	3.234e-02	0	8.862e-02	1.996e-08	0	6.6e-04	**N/A**
C12	1.243e-02	6.31e-03	0	8.184e-02	**N/A**	9.977e-02	9.960e-02
C13	6.6502e-01	3.3162e-05	4.160e-02	0	1.65e-03	**N/A**	6.745e-02
C14	3.214e-02	0	1.197e-04	0	0	6.523e-02	**N/A**
C15	3.4e-04	6.320e-02	3.226e-02	2.36e-03	6.3e-04	2.260e-02	**N/A**
C16	4.672e-02	6.4e-03	3.54e-02	0	7.3e-04	**N/A**	6.320e-02
C17	1.372e-02	8.376e-01	1.026e-02	0	0	0	**N/A**
C18	1.026e-02	5.412e-02	5.0685e-12	**N/A**	9.732e-02	5.408e-02	1.026e-02
C19	**N/A**	8.672e-02	9.069e-02	8.4095e-01	6.6e-04	9.977e-02	9.960e-02
C20	1.231e-02	6.968e-02	4.441e-16	0	0	0	**N/A**
C21	2.172e-02	8.278e-13	6.472e-13	0	1.716e-08	0	**N/A**
C22	3.423e-02	4.500e-02	1.903e-02	5.012e-01	2.9089e-01	2.21e-03	**N/A**
C23	**N/A**	0	1.981e-04	0	1.112e-16	0	5.001e-02
C24	3.428e-02	0	2.0096e-02	0	0	0	**N/A**
C25	2.133e-02	0	1.009e-02	0	2.01e-03	2.276e-05	**N/A**
C26	5.323e-02	4.367e-02	5.306e-01	8.96e-03	2.411e-02	**N/A**	7.400e-02
C27	**N/A**	1.112e-15	0	0	2.348e-02	9.985e-06	2.722e-02
C28	4.382e-02	2.018e-13	4.008e-01	5.792e-02	3.023e-02	1.009e-02	**N/A**

Table 9 Average rankings of algorithms using Friedman's test

Algorithm	standard functions f1-f12	CEC_2017 functions
BFA-FA	**1.894735**	**2.30**
BFA	5.284942	3.63
FA	5.928479	4.29
ABC	6.023848	3.49
BF-PSO	2.024725	4.20
MBO	3.928472	5.80
SSA	3.283682	4.78

ABC. The results show the superior and significant performance of BFA-FA over others for most of the functions. Hence, the proposed approach can solve problems efficiently, and stood at the first rank for this benchmark suite.

By observing the discussions and findings, it is evident that BFA-FA edged over most algorithms taken in this study in terms of efficiency, significance, and attaining global optima results. The convergence curve showed a smooth transition from exploration to exploitation within the search space. As compared to its classical part-and-parcels, the proposed approach BFA-FA possesses superior convergence capability for all optimization problems. The results for multimodal functions are superior when solved by BFA-FA, hence local optima avoidance is ensured to a much larger extent. The time taken by PSO-BOA is comparable and not more than its components, i.e., BFA and FA. The proposed algorithm is significantly better and stands on a better rank than other algorithms taken in this study.

5 Real world applications

This section applies the proposed BFA-FA algorithm to solve two structural design problems: The Cantilever beam design problem and the Three-bar truss design problem. The below section will show the best-obtained design and the function evaluations required to achieve it, during 10 runs.

5.1 Cantilever beam design problem

A Cantilever beam [8] consists of five elements that are hollow and have a square- shaped cross-section. As shown in Fig. 4, there are 5 structural parameters, each element being defined by a variable. Node 1 is rigidly supported and a vertical load is applied on Node 6. The optimization problem is formulated as follows:

$$\text{(Consider) } \overrightarrow{x} = [x_1\ x_2\ x_3\ x_4\ x_5]$$
$$\text{(Minimize) } f\left(\overrightarrow{x}\right) = 0.0624(x_1 + x_2 + x_3 + x_4 + x_5)$$
$$\text{Subject to } g\left(\overrightarrow{x}\right) = \frac{61}{x_1^3} + \frac{27}{x_2^3} + \frac{19}{x_3^3} + \frac{7}{x_4^3} + \frac{1}{x_5^3} - 1 \leq 0,$$
$$\text{Variable range } 0.01 \leq x_1, x_2, x_3, x_4, x_5 \leq 100.$$

Table 10 shows the solution to the problem using the proposed approach and its comparison with other techniques like Symbiotic Organisms Search (SOS) [6], Cuckoo search (CS) [12], Method of Moving Asymptotes (MMA) [51], Generalized Convex Approximation (GCA) first

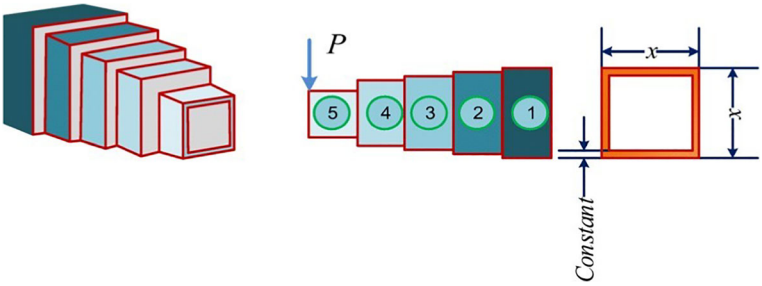

Fig. 4 Cantilever beam design problem

and second derivatives- GCA I [8], GCA II [8], ABC [16], MBO [44], SSA [28]. The optimum weights given by the algorithms SOS, ABC, MBO, and SSA was similar, however BFA-FA gave lesser value, which give an edge to its performance. Similarly, it can be seen that the functions evaluations required to reach the global optimum was optimum in case of BFA-FA, followed by SSA, MBO, ABC, and SOS. CS gave the output in least function evaluations i.e., 2500, but the optimal weight was higher. So, BFA-FA proves to a good optimizer that delivers optimal value in reasonable function evaluations.

5.2 Three-bar truss design problem

The three-bar truss design problem [8] is a highly constrained problem where one has to minimize its weight. The problem is formulated as follows:

$$\text{(Consider) } \overrightarrow{x} = [x_1\ x_2] = [A_1\ A_2],$$
$$\text{(Minimize) } f\left(\overrightarrow{x}\right) = \left(2\sqrt{2}x_1 + x_2\right) * l$$
$$\text{Subject to } g_1\left(\overrightarrow{x}\right) = \frac{\sqrt{2}x_1 + x_2}{\sqrt{2x_1^2 + 2x_1x_2}} P - \sigma \leq 0,$$
$$g_2\left(\overrightarrow{x}\right) = \frac{x_2}{\sqrt{2}x_1 + 2x_1x_2} P - \sigma \leq 0,$$
$$g_3\left(\overrightarrow{x}\right) = \frac{1}{\sqrt{2}x_2 + x_1} P - \sigma \leq 0,$$
$$\text{Variable range } 0 \leq x_1, x_2 \leq 1,$$
$$\text{(Where) } l = 100\ cm,\ P = 2\ KN/cm^2,\ \sigma = 2KN/cm^2$$

Table 10 Results for Cantilever design problem using proposed approach and other algorithms

Algorithm	Optimal Value for variables					Optimum weight	Max. function evaluations
	×1	×2	×3	×4	×5		
BFA-FA	6.014752	5.30716	4.48352	3.49965	2.15327	**1.33995**	12,000
SOS	6.01878	5.30344	4.49587	3.49896	2.15564	1.33996	15,000
CS	6.0089	5.3049	4.5023	3.5077	2.1504	1.33999	2500
MMA	6.0100	5.3000	4.4900	3.4900	2.1500	1.3400	NA
GCA I	6.0100	5.3000	4.4900	3.4900	2.1500	1.3400	NA
GCA II	6.0100	5.3000	4.4900	3.4900	2.1500	1.3400	NA
ABC	6.01812	5.31142	4.48836	3.49751	2.158329	1.33996	14,000
MBO	6.011674	5.31297	4.48307	3.50279	2.16333	1.33996	13,000
SSA	6.01523	5.3093	4.49532	3.5014262	2.1527879	1.339956	12,500

The three-bar truss is shown in Fig. 5, and the solution is shown in Table 11, which shows the solution using the proposed approach and other techniques. The other techniques used are Differential evolution with dynamic stochastic selection (DEDS) [51], BF-PSO [22], Mine blast algorithm (MBA) [34], Ray and Sain [33], Tsa [38], CS [12], ABC [16], MBO [44], and SSA [28]. It is clear from the results that BFA-FA stood first in optimizing the three-bar truss problem with minimum weight. The function evaluations were also reasonably less. Between ABC and BFA-FA, although the function evaluations were lower for ABC but the global optimum value was better delivered by BFA-FA. CS gave the optimal value in least function evaluations but the value was little higher. Over all, a good deal would be to get the minimum optimization value in reasonable function evaluations. Although BFA-FA was competitive to other state-of-art techniques, but its over-all performance was better.

6 Conclusions

This paper proposes two novel improvements in the conventional BFA for solving multi-modal optimization problems and convex landscapes with fast convergence, more scalability, and efficiency, and in less time. Also, the main goal is to achieve the global optimum value while balancing exploration as well as exploitation. To achieve this, firstly, a self-adaptive strategy is proposed where the step size of the bacteria is dynamically changed using the success percentage of bacteria and examining their state after each iteration, to reach the global optima. It leads to better exploration-exploitation balance, improved convergence time, accuracy close to the global optimal value, and good results for multimodal optimization problems. Secondly, in place of elimination and dispersion step, the leadership strategy is applied where the bacterium with the least fitness value (most healthy) is the leader and the other bacteria in the swarm follows the leader using the firefly algorithm position equation. It leads to lesser time complexity, fewer computations, and fast convergence since FA is known for its ability to converge faster. Also, therefore there is no addition of newer calculations, so it leads to decreased time complexity.

To benchmark the performance of the proposed algorithm, a series of tests were conducted. The convergence curves were studied and compared with other algorithms. The proposed algorithm was tested on 12 standard, 7 nonlinear, 2 single peak, 4 multi peak, as well as 28 CEC 2017 benchmark functions and compared to the classic as well as recent nature-inspired algorithms to validate its performance. For this several evaluation parameters were used like

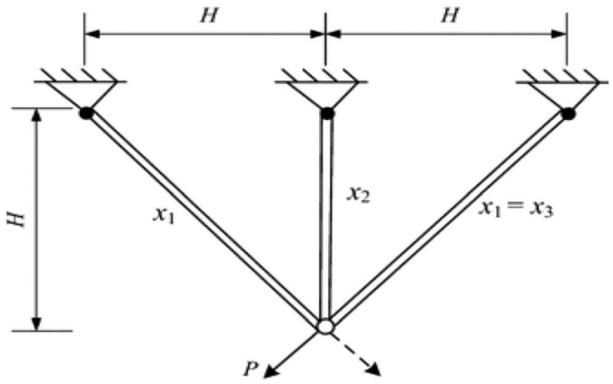

Fig. 5 Three-bar truss design problem

Table 11 Results for Three-bar truss design problem using proposed approach and other algorithms

Algorithm	Optimal value for variables		Optimum Weight	Max. Function evaluations
	x_1	x_2		
BFA-FA	0.7886715	0.4084389	**263.89582382**	12,000
DEDS	0.78867513	0.40824828	263.8958434	15,000
BF-PSO	0.7886751	0.4082482	263.8958433	17,600
MBA	0.7885650	0..4085597	263.8958522	20,000
Ray and Sain	0.795	0.395	264.3	NA
Tsa	0.788	0.408	263.68	NA
CS	0.78867	0.40902	263.9716	15,000
ABC	0.7886628160 00317	0.408283133832901	263.8958434	11,800
MBO	0.788897555578973	0.407619570115153	263.895881496069	13,000
SSA	0.788665414258065	0.408275784 4 44,547	263.8958434	12,500

optimal value, mean, standard deviation, processing time, MAE, MAPE, RMSE, NRMSE. The performance was tested on multi-dimensional landscape as well to test its scalability. The significance of the results was determined under Wilcoxon Statistical as well as Friedman rank test analysis at a 5% significance level. The over-all result was that BFA-FA performed better than other well-known algorithms in the literature, were able to converge quickly, exhibited stability, gave good results on multi-modal functions, were scalable in multi-dimensional cases, and statistically significant. BFA-FA was applied on two classical engineering problems (Cantilever design problem and three-bar truss design problem) and the results were compared to other algorithms that are efficient in solving the problem. The results proved that BFA-FA can solve real-world problems also with lesser function evaluations.

The main contributions of the proposed BFA-FA are as follows:

1. To increase the convergence and establish exploration-exploitation balance, a novel hybrid of BFA and FA is proposed, where adaptive strategy and leadership strategy are implemented.
2. The proposed method has been extensively tested on benchmark functions (standard, single peak, multi peak, noisy non-linear, and CEC_2017). The results outperform the other competitive algorithms in terms of convergence speed, time, mean absolute error, mean square error, mean, standard deviation, and other related parameters. It works well in multi- dimensional and multi-modal environments.
3. The algorithm has been successfully implemented on real-world engineering problems, and the results are better than other optimization algorithms.

To summarize, BFA-FA finds a better solution without getting trapped in local optima. Due to its stochastic nature, they can search a complicated and uncertain area as well. FA improves the search strategy of BFA and makes it more reliable to provide global optima within reasonable computation time and with better exploration. The performance of the proposed approach is proved to be better than some of the well-established and recent metaheuristic algorithms and can be generalized for other metaheuristics in the literature. In the future, BFA-FA may be developed for multi-objective, constrained as well as binary problems. Moreover, extending BFA-FA to the oppositional based or chaotic approach can be another interesting direction. The application of BFA- FA can be extended to solving real-world optimization problems in different nonlinear models like biotechnology, risk management, process control, environmental management.

Appendix A

Standard benchmark functions used are as follows:

Type of Function	Function	Dim	Range	f_{min} value
Unimodal benchmark functions	$f_1(x) = \sum_{i=1}^{s} x_i^2$	30	[−100,100]	0
	$f_2(x) = \sum_{i=1}^{s} \lvert x_i \rvert + \prod_{i=1}^{s} \lvert x_i \rvert$	30	[−10,10]	0
	$f_3(x) = \sum_{i=1}^{s} \left(\sum_{j=1}^{i} x_j \right)^2$	30	[−100,100]	0
	$f_4(x) = max_i\{\lvert x_i \rvert, 1 \le i \le s\}$	30	[−100,100]	0
	$f_5(x) = \sum_{i=1}^{s} ([x_i + 0.5])^2$	30	[−100,100]	0
Multimodal benchmark functions	$f_6(x) = \sum_{i=1}^{s} -x_i \sin\left(\sqrt{\lvert x_i \rvert}\right)$	30	[−500,500]	-418.9829 *X* 5
	$f_7(x) = \sum_{i=1}^{s} [x_i^2 - 10\cos(2\pi x_i) + 10]$	30	[−5.12,5.12]	0
	$f_8(x) = -20\exp\left(-0.2\sqrt{\frac{1}{s}\left(\sum_{i=1}^{s} x_i^2\right)}\right) - \exp\left(\frac{1}{s}\sum_{i=1}^{s} \cos(2\pi x_i)\right) + 20 + e$	30	[−32,32]	0
	$f_9(x) = \frac{\pi}{s}\{10\sin(\pi y_1) + \sum_{i=1}^{s-1} (y_i - 1)^2 [1 + 10sin^2(\pi y_{i+1})] + (y_s - 1)^2\} + \sum_{i=1}^{s} u(x_i, 10, 100, 4)$ $y_i = 1 + \frac{x_i + 1}{4}$ $u(x_i, a, k, m) = \begin{cases} k(x_i - a)^m & x_i > a \\ 0 & -a < x_i < a \\ k(-x_i - a)^m & x_i < -a \end{cases}$	30	[−50,50]	0
	$f_{10}(x) = 0.1\{sin^2(3\pi x_1) + \sum_{i=1}^{s} (x_i - 1)^2 [1 + sin^2(3\pi x_i + 1)] + (x_s - 1)^2 [1 + sin^2(2\pi x_s)]\} + \sum_{i=1}^{s} u(x_i, 5, 100, 4)$	30	[−50,50]	0
	$f_{11}(x) = \left[e^{-\sum_{i=1}^{s} (x_i/\beta)^{2m}} - 2e^{-\sum_{i=1}^{s} x_i^2} \right] \cdot \prod_{i=1}^{s} cos^2(x_i), m = 5$	30	[−20,20]	−1
fixed dimension multimodal benchmark function	$f_{12}(x) = [1 + (x_1 + x_2 + 1)^2 (19 - 14x_1 + 3x_1^2 - 14x_2 + 6x_1 x_2 + 3x_2^2)] \times [30 + (2x_1 - 3x_2)^2 \times (18 - 32x_1 + 12x_1^2 + 48x_2 - 36x_1 x_2 + 27x_2^2)]$	2	[−2,2]	3

CEC_2017 optimization functions are as follows:

Function Type	Function Number	Function Name
Unimodal function	C01	Shifted and Rotated Bent Cigar
	C02	Shifted and Rotated Sum of Different Power
	C03	Shifted and Rotated Zakharov
Simple Multimodal function	C04	Shifted and Rotated Rosenbrock
	C05	Shifted and Rotated Rastrigin
	C06	Shifted and Rotated Expanded Schaffer F6
	C07	Shifted and Rotated Lunacek Bi-Rastrigin
	C08	Shifted and Rotated Non-Continuous Rastrigin
	C09	Shifted and Rotated Levy
	C10	Shifted and Rotated Schwefel
Hybrid function	C11	Zakharov; Rosenbrock; Rastrigin
	C12	High-conditioned Elliptic; Modified Schwefel; Bent Cigar
	C13	Bent Cigar; Rosenbrock; Lunacek bi-Rastrigin
	C14	High-conditioned Elliptic; Ackley; Schaffer F7; Rastrigin
	C15	Bent Cigar; HGBat; Rastrigin; Rosenbrock
	C16	Expanded Schaffer F6; HGBat; Rosenbrock; Modified Schwefel
	C17	Katsuura; Ackley; Expanded Griewank plus Rosenbrock; Schwefel; Rastrigin
	C18	High-conditioned Elliptic; Ackley; Rastrigin; HGBat; Discus
	C19	Bent Cigar; Rastrigin; Griewank plus Rosenbrock; Weierstrass; Expanded Schaffer F6
	C20	HappyCat; Katsuura; Ackley; Rastrigin; Modified Schwefel; Schaffer F7
Composite functions	C21	Rosenbrock; High-conditioned Elliptic; Rastrigin
	C22	Rastrigin; Griewank; Modified Schwefel
	C23	Rosenbrock; Ackley; Modified Schwefel; Rastrigin
	C24	Ackley; High-conditioned Elliptic; Griewank; Rastrigin
	C25	Rastrigin; HappyCat; Ackley; Discus; Rosenbrock
	C26	Expanded Schaffer F6; Modified Schwefel; Griewank; Rosenbrock; Rastrigin
	C27	HGBat; Rastrigin; Modified Schwefel; Bent Cigar; High-conditioned Elliptic; Expanded Schaffer F6
	C28	8 Ackley; Griewank; Discus; Rosenbrock; HappyCat; Expanded Schaffer F6

Noisy non-linear functions used are as follows:

Type of Function	Function
Four Peak Function	$NL1(x,y) = e^{-(x-4)^2-(y-4)^2} + e^{-(x+4)^2-(y-4)^2} + 2\left[e^{-x^2-y^2} + e^{-x^2-(y+4)^2}\right]$
Parabolic Function	$NL2(x,y) = 12 - {\left(x^2+y^2\right)}\Big/{100}$
Camelback Function	$NL3(x,y) = 10 - \log\left(x^2 - \left(4 - 2.1x^2 + \left(\frac{1}{3}\right)x^4\right)\right) + xy + 4y^2\left(y^2 - 1\right)$
Styblinski Function	$NL4(x,y) = 275 - \left[\left(\frac{x^4-16x^2+5x}{2}\right) + \left(\frac{y^4-16y^2+5y}{2}\right) + 3\right]$
Goldstein-Price Function	$NL5(x,y) = 10 + \log\left[\frac{1}{\left\{\left(1+(1+x+y)^2\left(19-14x+3x^2-14y+6xy+3y^2\right)\right)\right\}} * \frac{1}{\left(30+(2x-3y)^2\left(18-32x+12x^2+48y-36xy+27y^2\right)\right)}\right]$
Rosenbrock Function	$NL6(x,y) = 70\left[\frac{\left[\left[20 - \left\{\left(1-\frac{x}{7}\right)^2 + \left(\left(\frac{y}{6}\right) + \left(\frac{x}{7}\right)^2\right)^2\right\}\right] + 150\right]}{170}\right] + 10$
Rastrigin Function	$NL7(x,y) = 80 - [20 + x^2 + y^2 - 10(\cos(2\pi x) + \cos(2\pi y))]$

Single peak and multi peak functions used are as follows:

Type of Function	Function name	Function	Range	Fitness Value
Single Peak	Needle-in-haystack	$SP1xy = 30.05 + x2 + y22 + x2 + y22$	$x, y\epsilon(5,-5)$	3600
Single Peak	Branin	$SP2xy = ax2-bx12 + cx1-r2 + s1-tcosx1 + s$	$x1\epsilon-510, x2\epsilon015, a = 1, b = 5.14\pi2, c = 5\pi, r = 6, s = 10, t = 18\pi$	0.397887
Multi peak	Extended Beale	$MP3xy = \sum i = 1n21.5-x2i-1-x2i2 + 2.25-x2i-11-x2i22$	$x\epsilon[-4.5,4.5]$	$f(x*)=0$, $x* =(3,0.5,\ldots,3,0.5)$
Multi peak	Griewank	$MP4xy = 14000\sum i = 1nxi2-\prod i = 1ncosxii + 1$	$x\epsilon(300,-300)$	$f(x*)=0$, $x* =(0,\ldots,0)$
Multi peak	MCCORMICK	$MP5xy = \sum i = 1n-1-1.5xi + 2.5xi + 1 + 1 + xi + 1 + xi2 + sinxi + 1 + xi$	$x_0=[1,1,\ldots,1]$	$f(x*)=-1.9133$, $x* =(-0.54719, -1.54719,\ldots, -0.54719,-1.54719)$
Multi peak	Drop-Wave	$MP6xy = 1 + cos12x12 + x220.5x12 + x22 + 2$	$x\epsilon[-5.12,5.12]$	$f(x*)=-1$, $x* =(0,\ldots,0)$

Declarations

Conflict of interest The author and co-author have no conflict of interest. This work is original and has not been published elsewhere nor it is currently under consideration for publication elsewhere.

References

1. Banerjee S, Chaudhuri SS (2021) Bacterial foraging-fuzzy synergism-based image dehazing. Multimed Tools Appl 80(6):8377–8421
2. Biswas A, Dasgupta S, Das S, Abraham A (2007) Synergy of pso and bacterial foraging optimization a comparative study on numerical benchmarks. In: Innovations in hybrid intelligent systems, Springer. pp. 255–263
3. Chen H, Zhu Y, Hu K (2008) Self-adaptation in bacterial foraging optimization algorithm. In: 2008 3rd International Conference on Intelligent System and Knowledge Engineering, IEEE. vol. 1, pp. 1026–1031
4. Chen H, Zhu Y, Hu K (2009) Cooperative bacterial foraging algorithm for global optimization. In: 2009 Chinese control and decision conference, IEEE. pp. 3896–3901
5. Chen H, Zhang Q, Luo J, Xu Y, Zhang X (2020) An enhanced bacterial foraging optimization and its application for training kernel extreme learning machine. Appl Soft Comput 86:105884
6. Cheng MY, Prayogo D (2014) Symbiotic organisms search: a new metaheuristic optimization algorithm. Comput Struct 139:98–112
7. Cheng R, Li M, Tian Y, Zhang X, Yang S, Jin Y, Yao X (2017) Benchmark functions for cec2017 competition on evolutionary many-objective optimization. In: Proc. IEEE Congr. Evol. Comput., pp. 1–20
8. Chickermane H, Gea HC (1996) Structural optimization using a new local approximation method. Int J Numer Methods Eng 39(5):829–846
9. Dasgupta S, Das S, Abraham A, Biswas A (2009) Adaptive computational chemotaxis in bacterial foraging optimization: an analysis. IEEE Trans Evol Comput 13(4):919–941
10. Datta T, Misra I, Mangaraj B, Imtiaj S (2008) Improved adaptive bacteria foraging algorithm in optimization of antenna array for faster convergence. Prog Electromagn Res C 1:143–157
11. Fuad MMM (2014) A hybrid of bacterial foraging and differential evolution-based distance of sequences. Procedia Computer Science 35:101–110
12. Gandomi AH, Yang XS, Alavi AH (2013) Cuckoo search algorithm: a metaheuristic approach to solve structural optimization problems. Eng Comput 29(1):17–35
13. Hanmandlu M, Verma OP, Kumar NK, Kulkarni M (2009) A novel optimal fuzzy system for color image enhancement using bacterial foraging. IEEE Trans Instrum Meas 58(8):2867–2879
14. Hern'andez-Ocana B, Mezura-Montes E, Pozos-Parra P (2013) A review of the bacterial for- aging algorithm in constrained numerical optimization. In: 2013 IEEE congress on evolutionary computation, IEEE. pp. 2695–2702
15. Hollander M, Wolfe DA, Chicken E (2013) Nonparametric statistical methods, vol. 751. John Wiley & Sons
16. Karaboga D, Basturk B (2008) On the performance of artificial bee colony (abc) algorithm. Appl Soft Comput 8(1):687–697
17. Kennedy JR (1995) A new optimizer using particle swarm theory. In: MHS'95. Proceedings of the Sixth International Symposium on Micro Machine and Human Science, IEEE. pp. 39–43
18. Khodabakhshian A, Daryabeigi E, Moazzami M (2013) A new optimization approach for multi-machine power system stabilizer design using a smart bacteria foraging algorithm. Simulation 89(9):1041–1055
19. Kim DH, Cho JH (2005) Adaptive tuning of pid controller for multivariable system using bacterial foraging based optimization. In: International Atlantic Web Intelligence Conference, Springer. pp. 231–235
20. Kim DH, Abraham A, Cho JH (2007) A hybrid genetic algorithm and bacterial foraging approach for global optimization. Inf Sci 177(18):3918–3937
21. Kora P, Kalva SR (2015) Hybrid bacterial foraging and particle swarm optimization for detecting bundle branch block. Springer Plus 4(1):1–19
22. Kora P, Abraham A, Meenakshi K (2020) Heart disease detection using hybrid of bacterial foraging and particle swarm optimization. Evol Syst 11(1):15–28
23. Kowsalya M et al (2014) Optimal size and siting of multiple distributed generators in distribution system using bacterial foraging optimization. Swarm Evol Comput 15:58–65
24. Li L, Zhang F, Liu C, Niu B (2015) A hybrid artificial bee colony algorithm with bacterial foraging optimization. In: 2015 IEEE International Conference on Cyber Technology in Automation, Control, and Intelligent Systems (CYBER), IEEE. pp. 127–132
25. Li MW, Wang YT, Geng J, Hong WC (2021) Chaos cloud quantum bat hybrid optimization algorithm. Nonlinear Dynamics 103(1):1167–1193

26. Liu Y, Passino K (2002) Biomimicry of social foraging bacteria for distributed optimization: models, principles, and emergent behaviors. J Optim Theory Appl 115(3):603–628
27. Majhi R, Panda G, Majhi B, Sahoo G (2009) Efficient prediction of stock market indices using adaptive bacterial foraging optimization (abfo) and bfo based techniques. Expert Syst Appl 36(6):10097–10104
28. Mirjalili S, Gandomi AH, Mirjalili SZ, Saremi S, Faris H, Mirjalili SM (2017) Salp swarm algorithm: a bio-inspired optimizer for engineering design problems. Adv Eng Softw 114:163–191
29. Mishra S (2005) A hybrid least square-fuzzy bacterial foraging strategy for harmonic estimation. IEEE Trans Evol Comput 9(1):61–73
30. Nasir ANK, Tokhi MO, Abd Ghani N, Ahmad MA (2012) A novel hybrid spiral-dynamics bacterial-foraging algorithm for global optimization with application to control design. In: 2012 12th UK Workshop on Computational Intelligence (UKCI), IEEE. pp. 1–7
31. Niu B, Wang H, Wang J, Tan L (2013) Multi-objective bacterial foraging optimization. Neurocomputing 116:336–345
32. Pal SK, Rai C, Singh AP (2012) Comparative study of firefly algorithm and particle swarm optimization for noisy non-linear optimization problems. Int J Intell Syst Appl 4(10):50
33. Ray T, Saini P (2001) Engineering design optimization using a swarm with an intelligent information sharing among individuals. Eng Optim 33(6):735–748
34. Sadollah A, Bahreininejad A, Eskandar H, Hamdi M (2013) Mine blast algorithm: a new population-based algorithm for solving constrained engineering optimization problems. Appl Soft Comput 13(5):2592–2612
35. Tan L, Lin F, Wang H (2015) Adaptive comprehensive learning bacterial foraging optimization and its application on vehicle routing problem with time windows. Neurocomputing 151:1208–1215
36. Tang K, Xiao X, Wu J, Yang J, Luo L (2017) An improved multilevel thresholding approach based modified bacterial foraging optimization. Appl Intell 46(1):214–226
37. Tripathy M, Mishra S, Lai LL, Zhang Q (2006) Transmission loss reduction based on facts and bacteria foraging algorithm. In: Parallel Problem Solving from Nature-PPSN IX, Springer. pp. 222–231
38. Tsai JF (2005) Global optimization of nonlinear fractional programming problems in engineering design. Eng Optim 37(4):399–409
39. Verma OP, Parihar AS (2016) An optimal fuzzy system for edge detection in color imagesusing bacterial foraging algorithm. IEEE Trans Fuzzy Syst 25(1):114–127
40. Verma OP, Hanmandlu M, Kumar P, Chhabra S, Jindal A (2011) A novel bacterial for- aging technique for edge detection. Pattern Recogn Lett 32(8):1187–1196
41. Verma OP, Sharma R, Kumar D (2012) Binarization based image edge detection usingbacterial foraging algorithm. Procedia Technology 6:315–323
42. Verma OP, Hanmandlu M, Sultania AK, Parihar AS (2013) A novel fuzzy system for edgedetection in noisy image using bacterial foraging. Multidim Syst Sign Process 24(1):181–198
43. Wang D, Qian X, Liu K, Ban X, Guan X (2018) An adaptive distributed size wolf pack optimization algorithm using strategy of jumping for raid (september 2018). IEEE Access 6:65260–65274
44. Wang GG, Deb S, Cui Z (2019) Monarch butterfly optimization. Neural Comput Appl 31(7):1995–2014
45. Wolpert DH, Macready WG (1997) No free lunch theorems for optimization. IEEE Trans Evol Comput 1(1):67–82
46. Wu G, Mallipeddi R, Suganthan PN (2017) Problem definitions and evaluation criteria for the cec 2017 competition on constrained real-parameter optimization. National University of Defense Technology, Changsha, Hunan, PR China and Kyungpook National University, Daegu, South Korea and Nanyang Technological University, Singapore, Technical Report
47. Ya-lin T (2015) Bacteria foraging optimization algorithm based on self-adaptative method. Value Engineering p. 11
48. Yang XS (2010) Nature-inspired metaheuristic algorithms. Luniver press
49. Yao X, Liu Y, Lin G (1999) Evolutionary programming made faster. IEEE Trans Evol Comput 3(2):82–102
50. Zhang Z, Hong WC (2021) Application of variational mode decomposition and chaotic grey wolf optimizer with support vector regression for forecasting electric loads. Knowl-Based Syst 228:107297
51. Zhang M, Luo W, Wang X (2008) Differential evolution with dynamic stochastic selection for constrained optimization. Inf Sci 178(15):3043–3074
52. Zhang Q, Chen H, Luo J, Xu Y, Wu C, Li C (2018) Chaos enhanced bacterial foraging optimization for global optimization. IEEE Access 6:64905–64919
53. Zhao W, Wang L (2016) An effective bacterial foraging optimizer for global optimization. Inf Sci 329:719–735
54. Zhou Q, Zhou Y (2013) Wolf colony search algorithm based on leader strategy. Appl Res Comput 30(9): 2629–2632

Publisher's note Springer Nature remains neutral with regard to jurisdictional claims in published maps and institutional affiliations.

The current issue and full text archive of this journal is available on Emerald Insight at:
https://www.emerald.com/insight/0368-492X.htm

An empirical study of knowledge environment and suitability of performance measures of a civil organization for a knowledge-based military force

Received 13 January 2022
Revised 30 March 2022
Accepted 2 May 2022

Mukesh Kumar Singh and Vikas Gupta
Delhi School of Management, Delhi Technological University, Delhi, India

Abstract

Purpose – This study aims to empirically analyze the significance of various knowledge management (KM) elements to the environment in a military organization and establish the efficacy of performance indicators of civil organizations for a military organization.

Design/methodology/approach – The research methodology includes the development of a research model based on a comprehensive literature review. A sample of 454 Indian Air Force Veterans was obtained and structural equation modeling (SEM) analysis using statistical package for the social sciences (SPSS) analysis of moment structures (AMOS) was conducted to test the hypotheses. The study first employed exploratory factor analysis (EFA) for redefining the theoretical constructs and then confirmatory factor analysis (CFA) to test the hypotheses.

Findings – The study empirically establishes the significance of various KM elements on the knowledge environment that creates, stores, transfers and applies knowledge to achieve military objectives. Findings indicate the complexity of KM in a military setup while applying the performance measures used in the civil organization.

Research limitations/implications – The study expects to expand the scope of the KM literature to the militaries of developing countries and provide a methodology to the leaders and practitioners in the military organizations, and to study the available KM practices, models and tools in the civil world.

Originality/value – To the best of the authors' knowledge, the present research is one of the first to generate empirical insights into a knowledge environment in military organizations and test its relation with parameters used in civil organizations. The paper would significantly contribute to the underexplored area of KM in military organizations and infuse a theoretical rigor into the KM literature.

Keywords Organizational structures, Knowledge management, Military organization

Paper type Research paper

1. Introduction

Success stories of knowledge management (KM) in a commercial enterprise have been highly acknowledged in the literature (Scuotto *et al.*, 2022; Vătămănescu *et al.*, 2021; Rezaei *et al.*, 2021; Carayannis *et al.*, 2018; Del Giudice *et al.*, 2010). Like any other organization, the requirement of an effective KM in a contemporary military cannot be ruled out (Singh and Gupta, 2021). Rapid changes in military technologies have resulted in complex warfare dynamics, and the success of military tactical or strategic actions highly relies on the accuracy and pace of information availability and knowledge superiority over adversaries. Therefore, in the 21st century, it has almost become obligatory for the military organizations to recognize and adopt KM practices holistically and evolve the role of their employees into that of a knowledge worker to remain current and relevant (McIntyre *et al.*, 2003).

Xu *et al.* (2011) says combat effectiveness of military can be improved by using KM. Realizing the significance of a knowledge-based force, most of the world's contemporary military forces have reorganized their policies and doctrines to include KM at the core. The United States (U.S.), Army Knowledge Management memorandum emphasizes KM strategy

Kybernetes
© Emerald Publishing Limited
0368-492X
DOI 10.1108/K-01-2022-0050

involving people, culture, process and technology to transform the Army into a network-centric–knowledge-based force (Lepak, 2009). The Air Force Instruction, U.S. specifies integration of knowledge workers and processes, enabled by technology to facilitate the exchange of expertise and operational information (Martin, 2014). A similar KM approach can also be found in a few other military organizations like Canada, Israel, United Nations and North Atlantic Treaty Organisation (Jabłoński and Lis, 2012; Marzukhi *et al.*, 2018; Lepak, 2009; Ariely, 2008; Mcintyre, 2002; Singh and Gupta, 2021; Boe, 2014). Though the literature establishes the significance of various KM elements such as people, culture, process and strategies in creating a knowledge environment that captures, stores, shares and applies knowledge to meet the organizational objectives, there lacks an empirical study that establishes the relation between these KM elements and knowledge environment in a military organization. Also, despite the widely acknowledged potential of KM, it was rare to find any significant KM study in the militaries of the developing countries, including India (Singh and Gupta, 2020).

According to the Global Firepower, the Indian military is the world's fourth-largest military after US, Russian and Chinese militaries with a total strength of approximately 2.9 million active, reserve and paramilitary personnel (Bielawski, 2021). The Indian Army (IA), India Air Force (IAF) and Indian Navy (IN) constitute the main fighting arms of the Indian military establishments (Ganguly, 2015). With the expansion of operational area and subconventional warfare taking center stage and the cutting-edge technologies involved, the Indian military organization needs to progress beyond the simple network-centric force to a network-centric–knowledge-enabled force and embrace KM in a big way. Toward this, the Indian military organization must assess the significance of their people, process, culture and strategies in creating an environment that creates, stores, transforms and applies knowledge to meet its military objectives, as well as improves the organization's performance. However, to the best of the author's knowledge, no literature could be found that empirically establishes the significance of these KM elements to the environment of any military organization.

Researchers in various civic organizations and commercial enterprises have documented the benefits of KM in improving organizations' performance and have specified multiple measures of performance such as cost and time saving, boosting innovations, increasing market share and profits, enhancing efficiency and customer satisfaction, and providing competitive edge (Zaied *et al.*, 2012; Massingham, 2018; Meher and Mishra, 2019; Santoro *et al.*, 2019; Scuotto *et al.*, 2017, Thomas, 2021). It was rare to find any such measures of performance to ascertain the success of KM initiatives in a military organization. Authors believe that defining such performance indicators for a military organization is intricate, as the military's primary objective is to safeguard the integrity of their country, and therefore, their success can only be measured during the war or hostilities. However, to facilitate the authorities in the military organization to assess the efficacy of their knowledge environment during the peacetime and routine military operations, this study chooses certain measures of performance in civil organizations like competitive advantage, information and decision superiority, innovation, expertise, efficiency, cost and time, learning curve, and morale and tries to establish the correlation between these performance indicators with the knowledge environment of a military organization.

The literature on the topic is rare and fragmented. The study aims to fill this significant gap in the literature and generate empirical insights into a knowledge environment in military organizations and test its relation with parameters used in civil organizations. The study expects to expand the scope of the KM literature to the militaries of developing countries and provide a template to the leaders and practitioners in military organizations, and to study the available KM practices, models and tools in the civil world. To examine the hypothesis, the model was empirically tested through the structural equation modeling (SEM) on a sample of 454 veterans from the Indian Air Force (IAF). Since the objectives and

structure of all the three fighting arms of the Indian military are the same, the term military organization has been used in the study to indicate generalization.

2. Literature review and hypotheses

2.1 Elements of KM

KM is a complex process with many factors influencing its implementation. These factors, also known as KM elements or enablers, are the key ingredients in creating, transferring, sharing and using knowledge, thereby creating a positive knowledge environment in an organization (Yeh *et al.*, 2006). These are the organizational mechanisms for fostering knowledge consistently; they can stimulate knowledge creation, protect knowledge and facilitate knowledge sharing in an organization (Ichijo *et al.*, 1998). Knowledge elements are the driving force in forming a positive knowledge environment. They do not just create knowledge in the organization but also motivate the group members to share their knowledge and experiences, allowing organizational knowledge to grow concurrently and systematically. Nagendra and Morappakkam (2016) present a list of enablers from various literature and identified organization culture, people and leadership as the key element for a closed environment like a military organization. Davenport (1997) identified eight success factors that linked KM to economic performance. Shah and Kant (2018) listed 46 enablers from 148 literature and articles. A broad range of knowledge elements or enablers for a KM environment identified in the literature is presented in Table 1.

Based on the literature review, the key KM elements that have been frequently referred to in military organizations are people, culture, processes and strategy and therefore chosen for the study.

2.1.1 People. KM is about people and exists only because of people. Del Giudice *et al.* (2013) say the right knowledge can be created by sharing tacit knowledge among people. People are the core of creating organizational knowledge because it is the people who create and share knowledge, and therefore, it is crucial to manage those who are willing to create and share their knowledge (Thomas and Gupta, 2021; Gupta and Thomas, 2019). Davenport (1999) highlights the relevance of the human dimension necessary for developing an effective knowledge environment. Through proper management of human resource, a culture that encourages the free flow of knowledge for meeting organizational needs can be created. Therefore, an essential element for an enterprise to successfully push for a conductive knowledge environment is to encourage people to communicate and share their knowledge with others (Mathi, 2004; Novak, 2017). Similarly, the role of the human element in creating a sustainable knowledge environment in a military organization cannot be undermined. Bryant (2002) says the armed forces are about soldiers or people, and it is the skill and competencies of these soldiers which govern the outcome of the war. Militaries need to provide a proper environment for the soldiers to hone their skills and knowledge so that they improve their value to the forces and the nation. Orhan (2015) emphasizes the importance of human capital in military organizations as they have a considerable amount of tacit knowledge acquired by experience. Situational awareness and decision making by the soldiers are the two most fundamental factors that affect modern warfare, and they rely heavily on knowledge more than ever. Walsh (2015) states that people in the military are trained to deal with stressful and unpredictable situations. Their experience, competence, and skills to handle stress and work with people, develop strategies and deal with uncertainties, each of which requires knowledge that applies in many areas of individual and organizational life. Their lifetime experience, indepth knowledge of the environment, culture, attitude to understand complex issues, and aptitude to integrate and correlate knowledge is of utmost importance for organization sustenance (Singh and Gupta, 2020). The military environment is volatile, uncertain, complex and ambiguous. It is, therefore, essential that in this environment warfighters share and exploit the knowledge contained within their organizations (Walsh, 2015). Soldiers are the core of

Literature support	KM enablers
Davenport and Prusak (1998)	Top management support
	Clear expression and promotion of KM activities
	Multiple channels of knowledge transfer
	Motivational rewards for users of KM
	Standard and flexible knowledge structure
	Strong technical and organizational infrastructure
	Knowledge friendly culture
Liebowitz (1999)	KM strategy
	KM infrastructure
	Knowledge repositories
	KM systems and tools
	Supportive culture
Chait (2000)	Content
	Culture
	Processes
	Infrastructure
Gold *et al.* (2001)	Technology
	Structure
	Culture
	KM processes
Forcadell and Guadamillas (2002)	KM strategy
	Culture
	Structure
	Individual
	Leadership method
	KM tools
Bartczak (2002)	Culture
	Leadership
	Technology
	Organizational adjustments
	Evaluation of KM activities
	Knowledge resources
	Employee motivation
	External Factors
Allard and Holsapple (2002)	Organizational structure
	Technological infrastructure
Lee and Choi (2003)	Collaboration
	Trust
	Learning
	Centralization
	Formalization
	Information technology
Chourides *et al.* (2003)	Strategy
	Human resource
	Information technology
	Quality
Gloet and Terziovski (2004)	Human resource management practices
	Information technology practices
Mathi (2004)	People
	Processes
	Technology
Wong (2005)	Management and leadership support
	Culture
	Information technology
	Strategy
	Organizational infrastructure
	Processes
	Training
	HRM

Table 1.
Summary of KM elements

(*continued*)

Literature support	KM enablers
Marques and Simón (2006)	Continuous learning
	Understanding of organization
	R&D
	Individual
Han and Anantatmula (2007)	Organization culture
	Practice
	Trust
	Technology
	Learning
	Leadership
Zack *et al.* (2009)	Customer intimacy
	Product leadership
	Operational excellence
Zheng *et al.* (2010)	Culture
	Structure
	Strategic
Mills and Smith (2011)	Organizational structure
	Knowledge application
	Technology
	Knowledge conversion
	Processes
Wang *et al.* (2012)	Core employee – value and uniqueness
	Core competence – organizational capabilities
Novak (2017)	Technology
	Culture
	Structure
Gupta and Chopra (2018)	Technology
	Structure
	Culture
	Knowledge processes
	People
	Knowledge strategy
	KM leadership
	Resource for KM
Agrawal (2020)	Knowledge creation
	Knowledge capture
	Knowledge organization
	Knowledge application

Source(s): Compiled by Authors

Table 1.

the human element in a military organization, and therefore, the term "Soldiers" has been used in the paper instead of people or human element to evoke the specificities of the military environment and avoid any generalization with the noncombatant staff of the military organization. Based on the literature, this study proposed the following hypothesis:

H1. Soldiers have a significant effect on the knowledge environment in a military organization.

2.1.2 Culture. Del Giudice *et al.* (2012) define culture as the combination of shared values, norms, beliefs, assumptions and implicit attitudes that the members of an organization possess. Rubenstein-Montano *et al.* (2001) believe that culture plays a key role in shaping assumption about knowledge and creating the context for the social interaction associated with knowledge sharing and influencing the creation of new knowledge. Many researchers believe organizational culture is the crucial influence on the knowledge environment and is significantly related to organizational performance (Gaur and Gupta, 2021; Sin and Alan, 2000; Holsapple and Joshi, 2004; Davenport, 1997; Zheng *et al.*, 2010). Schein (2010) defined organizational culture in the military organization at three-level composing of artefact (visual dimension of culture like

structure, process and practice), espoused beliefs and values (strategic goals and philosophies) and the underlying assumptions (unconscious elements that comprise perceptions, thought and feelings). Gupta and Govindarajan (2000) say that in the organization like police and armed forces, culture and its associated beliefs, values and attitude can be viewed as either a facilitator or barrier to the success of KM initiatives and commitment to knowledge sharing practices. The key ingredients to the success of an organizational KM are due to a supportive culture whereas the rigid processes, standard operating procedures, hierarchy and leadership style in a closed environment could act as a barrier for free flow of knowledge across the military organization. Tefft (2002) advocates transforming armed forces culture so that the identification, collection, dissemination and use of knowledge is a strategic priority and universally shared value. Fountain (2007) states that while armed forces have always prioritized teamwork, a profound culture shift must be realized from traditional information sharing to knowledge sharing. An efficient strategic KM requires the creation of a suitable organizational environment and culture. A precondition for KM in the military organization is the creation of a friendly, open and noncompetitive environment (Rhem, 2016). Therefore, building a culture with easily accessible knowledge is necessary for management in establishing a positive knowledge environment. Based on the previous reviews, this study proposed the following hypothesis:

H2. Culture has a significant effect on the knowledge environment in a military organization.

2.1.3 Process. KM processes are interrelated sets of various business processes developed in an organization and primarily consist of acquisition, collecting, conversion, application, storage and protection of knowledge (Mills and Smith, 2011). The literature suggests knowledge process improves organizational processes such as innovation, collaborative decision making, and individual and collective learning and is considered as an imperative antecedent for building an overall positive knowledge environment in an organization (Gold *et al.*, 2001; Chait, 2000; Forcadell and Guadamillas, 2002). In the case of a military organization, Bryant (2002) emphasizes armed forces to set a goal to integrate the KM and best business practices into the military routine process. This facilitates information sharing across boundaries and innovative thinking to achieve greater performance and enterprise cohesion in army activities. Considering the sensitive operations of the military organization, the KM process should not only embed knowledge assets in standard operating procedures and provide access to the needy across the enterprise but also protect and secure information and knowledge assets (Lepak, 2009). Van Laar *et al.* (2020) list out the five-step KM process and its activities that are integrated into various staff and organizational processes used in the preparation and conduct of military operations. This integration facilitates the transfer and exchange of knowledge both formally through established processes and procedures, and informally through collaboration and dialogue between and among individuals and organizations. Similarly, Wiig (1997) emphasizes value-creating processes such as organization structure, management practices, system procedures and the information technology infrastructure in the military setup. Bryant (2002) states that to form an environment of knowledge creation and sharing, the military organization needs to overcome the process challenges that fall into the area of abilities, tools, connectivity, geographical separation, access to knowledge and trust. For instance, if abilities or tools are not readily available to share knowledge, the process becomes too difficult to function smoothly. It would be hard to capture or codify the knowledge if it is perceived as an additional burden instead of a byproduct or normal process. The KM process provides the right processes and systems that enable a knowledge environment (Wong, 2005). Based on the studies noted above, this study proposes the following hypothesis:

H3. Process has a significant effect on the knowledge environment in a military organization.

2.1.4 Strategy. Theriou *et al.* (2011) say that an effective KM begins with a proper strategy. Knowledge strategy is a crucial element that affects the successful implementation of KM. Rezaei *et al.* (2021) defined KM strategy as the approaches an organization employs to align its knowledge resources and capabilities to the rational requirement of its organization's strategy. KM strategy determines the needs, means and activities for building a comprehensive knowledge environment to accomplish organizational objectives. The objective is to manage, share and create relevant knowledge assets that will help meet tactical and strategic requirements (Gamble and Blackwell, 2001). Wiig (1997) states that most organizations pursue five basic knowledge-centered strategies to achieve the best business values from their existing knowledge-based asset or create new competitive knowledge-related assets. These strategies include creating knowledge strategy as a business strategy to provide the best possible available knowledge and intellectual asset management strategy to manage assets such as patent technologies, operational and management practices, personal knowledge strategy that emphasizes on effective use and sharing of knowledge, and encouraging innovations and competitiveness, knowledge creation strategy that promotes organizational learning, and the knowledge transfer strategy to promote a systematic approach to transfer knowledge to those in need. Literature states that KM strategy should be integrated with the organizational business strategy to develop a positive knowledge environment to enhance organizational performance (Zack *et al.*, 2009; Cook and Brown, 1999; Maier and Remus, 2002). In a military organization, Nagendra and Morappakkam (2016) says that the primary strategy for KM is to evolve into a knowledge and network-based organization. A wisely articulated KM strategy in the military environment would result in a rational decision in operations and logistics including aid to civil authorities. Militaries need to develop KM strategies wherein they need to train KM leaders, reward people for knowledge sharing and make every interaction an opportunity to acquire and share knowledge (Elder, 2008). The organizational environment in the military must provide acceptance of and the opportunity for exchange, use and reuse of knowledge (Pettersson, 2009). Based on the studies noted above, this study proposes the following hypothesis:

H4. Strategy has a significant effect on the knowledge environment in a military organization.

2.2 Measures of organizational performance

Organizational performance can be defined as company performance compared to goals and objectives (Massingham, 2018). Improving organization performance by using KM is a kind of investment that most organizations are willing to invest in to gain a competitive advantage. KM facilitates an organization to be faster, efficient, and more innovative; therefore, effective KM is considered valuable due to its consequences to firm performance. Researchers have used various methods and tools to measure the organizations' performance ranging from the use of measurement index, balanced scorecards, and maturity models (Tseng and Lee, 2014; Marr and Schiuma, 2003; Gupta and Chopra, 2018; Vanini and Bochert, 2015; Miller *et al.*, 2014). Measures of organizational performance in the past were mostly restricted to financial measures like net profit, sales growth, return on investment, income, and market share; however, other non-financial measures have gained equal importance over a while. This includes multiple criteria, for example, operational efficacy, product quality, marketing effectiveness, value addition, innovation, customer satisfaction, etc (Zaied *et al.*, 2012). So, to ascertain success in the implementation of KM practices, continuous measurement of performance-related measures is essential. Tseng and Lee (2014) says that for an organization to succeed at enhancing its performance, it is crucial to establish a comprehensive measurement index that provides managers and staff with clear directions

and goals set by the enterprise. Table 2 lists various measures of performance for a civil organization as identified in the literature.

To the best of the author's knowledge, no specific measures of KM performance could be found for any military organization or a military force of a developing country to be specific. Motsenigos and Young (2002) also claims absence of suitable measure to the importance and success of KM. Vanini and Bochert (2015) described various maturity models used in industries to examine the effectiveness of KM. On similar lines, the US Army developed a tailored KM Maturity Model with unique components, area, methodology, delivery, and metrics for organization performance to measure its use of KM practices and techniques for optimal knowledge flown increased efficiency and enhanced decision making (Van Laar *et al.*, 2020). Lecocq and Gauvin (2006) studied KM in Canadian Armed Forces Environment and listed various KM benefits to the organization under the three categories comprising of knowledge-creation (efficiency, resource optimization improved decision, improved focus and vision, mission success, and good communication), learning (motivation, adaptability, problem-solving, satisfaction and recognition), and collaboration (trust, leadership, common goal, achieving objectives, reduced duplication, knowledge sharing, and efficiency). Vanini and Bochert (2015) say KM measurement parameters should be tailored to the type of organization. Similarly, Van Laar *et al.* (2020) state that a one-size-fits-all approach to KM would not work for the armed forces, as the military organization has unique processes and procedures that are unparallel outside the military. Therefore, the militaries need to develop models to account for these differences. In the absence of any specific measures of performance for the military force of a developing country like India, the authors shortlisted the most common measures of performance used in the civil organization and the parameters used to measure the effectiveness of KM on the performance of the US Army by Van Laar *et al.* (2020), the Canadian Armed Force Environment by Lecocq and Gauvin (2006) and the KM effects highlighted in the Air Force Instructions 33–396 of the US Air force (2014). The parameters were further discussed with the senior officers of the IAF, who have been associated with the organization for over 30 years to finalize the most suitable measure which may have a significant effect on the performance of a military organization in the Indian context. The key measures used in the study were a competitive advantage, information and decision superiority, innovation, expertise, efficiency, cost and time, learning curve, and morale. Based on the studies noted above, this study proposes the following hypothesis:

H5a. Competitive Advantage is a significant measure of organizational performance.

H5b. Information and Decision Superiority is a significant measure of organizational performance.

H5c. Innovation is a significant measure of organizational performance.

H5d. Expertise is a significant measure of organizational performance.

H5e. Efficiency is a significant measure of organizational performance.

H5f. Cost and Time is a significant measure of organizational performance.

H5g. Learning Curve is a significant measure of organizational performance.

H5h. Morale is a significant measure of organizational performance.

2.3 Knowledge environment and organizational performance

Organizational performance measures are the means to measure the extent to which organizational goals and objectives can be achieved or the level at which a firm conducts its strategic goals. This includes multiple criteria such as profitability, operational efficacy,

Literature support	Organization performance measures
Davenport (1997)	Organizational effectiveness
	Survival
	Improvement
	Innovation
Bender and Fish (2000)	Expertise
	Information Technology
	Advance Communication
Gold *et al.* (2001)	Knowledge infrastructure capability
	Knowledge processes
Thomas and Keithley (2002)	Improved ability to attract, train, develop, and retain an employee
Sher and Lee (2004)	Operating costs, shorten lead time, and differentiate products
Marques and Simón (2006)	Continuous learning
	Understanding of organization
	Innovative culture
	Competence development
Wu and Lin (2009)	Improving coordination efforts
Ho (2009)	Factor strategy
	Leadership
Aujirapongpan *et al.* (2010)	Expertise
	Learning
	Information
	Technology
	Structure
	Culture
	Efficiency
	Adaptability
	Innovativeness
Alwis (2011)	Financial measures (return on equity, return on investment)
	Operational measures (market share, sales growth, and, profit growth)
Mills and Smith (2011)	Organizational structure
	Knowledge application
Zaied *et al.* (2012)	Market share
	Profitability and growth rate
	Innovativeness
	Customer satisfaction
	Sales growth
	Efficiency and Effectiveness
	Return on investment
	Productivity
	Competitiveness
Argote (2012)	Learning Curve
	Organization Learning
Tseng and Lee (2014)	Dynamic Capabilities
	Individual level- job satisfaction, achieved goals
	Group level- morale, cohesion, efficiency and productivity
	Organization level- profit, productivity, turnover rate and adaptability
Amir and Parvar (2014)	Sustainable Competitive Advantage
	Information Availability
	Increasing Learning Curve
	Commitment and Loyalty
	Sustaining Mission Critical Knowledge
	Learning Lesson and solving recurrent problems
	Better Decision Making
	Benchmarking and Improving Performance
	Productivity
	Efficiency

(*continued*)

Table 2. Measures of performance in civil organization's

Literature support	Organization performance measures
Massingham and Massingham (2014)	Learning Curve- Accelerated time to competence
	Experience Curve- Sharing of experience
	Strategic Alignment- Decreases Capability Gap
	Connectivity- Search Cycle efficiency
	Risk Management- Increased work output
	Value Management- Improved Perception
	Psychological Contract- Staff Morale and Productivity
Becerra-Fernandez *et al.* (2014)	Effectiveness and degree of innovation of organizational processes
Novak (2017)	Financial performance
	Innovation performance
	Growth performance
	Operational performance
	Competitive advantage
	Value creation
Abuaddous *et al.* (2018)	Well-constructed culture
Meher and Mishra (2019)	Organization structure
	Organization culture
	Innovative capabilities
	Organization learning
	Knowledge integration
	Knowledge sharing
	Employee commitment
Rezaei *et al.* (2021)	Structure
	Strategy
	Technology
	Culture
	Leadership
	Trust

Table 2. **Source(s):** Compiled by Authors

innovation, customer satisfaction, market shares, etc (Zaied *et al.*, 2012; Gupta and Chopra, 2018). A knowledge environment in an organization indicates a conducive atmosphere to create, transfer, share and use knowledge (Yeh *et al.*, 2006). KM elements are the driving force in forming a positive knowledge environment; they motivate the group members to share their knowledge and experiences, allowing organizational knowledge to grow concurrently and systematically (Ichijo *et al.*, 1998). A broad range of literature in civil organizations and commercial enterprises indicates a significant direct relationship between a knowledge environment and organizational performance (Abuaddous *et al.*, 2018; Wu and Chen, 2014; Sinha *et al.*, 2012, 2015; Zack *et al.*, 2009; Mills and Smith, 2011; Novak, 2017). Defining such a performance indicator for a military organization is intricate, as the primary objective of a military is to safeguard the integrity of their country and therefore their success can only be measured during the war or hostilities (Singh and Gupta, 2020). Few researchers have tried to correlate the relation between KM in armed forces and private/business organizations. Van Laar *et al.* (2020) state military and business communities have similarities in the use of terms knowledge flow, knowledge creation, and innovation for increased organizational performance and competitive advantage. Whereas, the two differ in the outcome desired from the active KM. The armed forces aim for operational advantage coupled with decision making and improved efficiencies with organizational learning and mission accomplishment as the end state. The business community is concerned about creating business value for the organization through market share, shareholder value, and profit as the end state. Sullivan (2011) compared KM in US Army and Corporate KM and established that company have traditional hierarchy and quick methods of passing information from top to bottom and vice-versa which understandably is not acceptable process for the US army. Bartczak (2002) says military organization differs from large public and private sector organizations in many

aspects including culture, mission, and environment. For instance, civil culture promotes liberty and individuality, military culture emphasizes discipline and self-sacrifice. The mission and environment of the military are indeed unique in fighting a war to humanitarian relief and operating in an unusual complex environment. Plant (2000) studied KM in Australian Defence Forces and recognized that the military is a complex organization/environment for KM implementation. Similarly, Command (2008) also identified that cultural, technical, and structural aspects of the military organizations are unique and require special deliberation while implanting KM. However, to facilitate the authorities in the military organization to assess the efficacy of their knowledge environment during the peace-time and routine military operations, this study aims to establish a correlation between performance indicators specified in literature for the civil organization with the knowledge environment of a military organization. Based on the literature support, this study proposes the following hypothesis.

H6. The knowledge environment in a military organization has a significant relation with measures of performance used by civil organizations.

3. Research model

The study argues that various KM elements comprising people, culture, processes, and strategy are significantly related to a military organization's knowledge environment. The knowledge environment is significantly associated with an organization's performance measures used in civil organizations. Based on the hypotheses proposed, this study established the research framework shown in Figure 1.

4. Methodology

The Structural Equation Modelling was used to study the relationship among the latent constructs indicated by multiple measures and verify the hypothesized model empirically

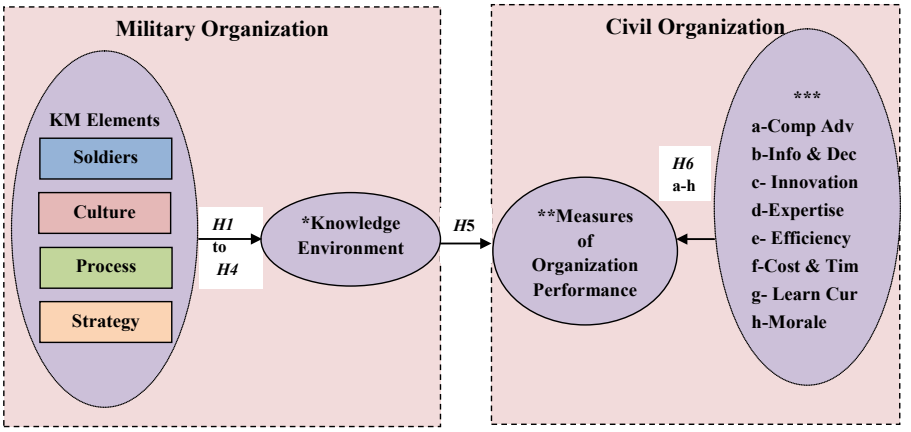

Note(s): *: Knowledge Environment, **: Measures of Organization Performance
***: a-Competitive Advantage, b-Information and Decision Superiority, c-Innovation, d-Expertise, e-Efficiency, f-Cost and Time, g-Learning Curve, h-Morale
Source(s): Author

Figure 1.
Research framework

(Simmering *et al.*, 2015). The questionnaire was designed based on Gold *et al.* (2001), De Grosbois (2011), Rasula *et al.* (2012), Liao *et al.* (2010), as placed in Table A1. Some modifications have been made to fit the current research, as most studies are primarily restricted to civil organizations. Veterans from the IAF were randomly selected as samples. The majority of the chosen sample includes veterans of more than 40 years of age (59%) and more than 20 years of service length (84%), indicating adequate seniority. The education level of the majority of respondents was graduation and above (90%). The demographic distribution of respondents does not affect the study as all have served across the country throughout their service life and no distinction in job profile exists in IAF based on the individual demographic profile (Singh and Gupta, 2020). Perez and Strizhko (2018) says there is no difference in the desired outcome due to the demographic variation of soldiers in a military organization. The culture in the military organizations emphasizes group unity and the prioritizing of the mission above individual characteristics and goals. The armed forces depend on cohesion, organizational identification, and group commitment and the soldiers who have internalized this culture see past individual differences such as minority and majority, gender, and race and identify others in the unit as fellow soldiers primarily.

Content and expert validity were conducted to measure content's adequacy, inclusiveness, and richness. The study invited 12 experts with over 30 years of experience in IAF to review and revise the questionnaire item by item to ascertain appropriate content validity. The experts were selected from all three branches of the IAF (operations, maintenance, and administration) and had adequate experience in policymaking, projects, HR, and management. Drawing from the literature and recommendations of Weijters *et al.* (2021), the variables were measured using a 5-point Likert scale, with one denoting strong agreement and five indicating strong disagreement. Data were collected by administering questionnaires in both online and offline mode. Approximately 1,120 questionnaires were distributed and 584 responses were received with a response rate of 52.14%, out of which 454 were used for study, 130 incomplete data could not be used. The study uses IBM SPSS 23 and AMOS 23 software as major tools to analyze the collected data.

5. Data analysis and results

5.1 Common Method Bias (CMB)

To obviate the issue of CMB, respondents were assured of the anonymity and confidentiality of the study, and reverse items were also added. However, since questionnaires were self-reported and data was collected from the same participants, there could be CMB due to emotions, personality styles, attitudes, consistency motifs, transient mood, etc (Podsakoff and Organ, 1986). Therefore, a comprehensive marker technique was employed to study CMB (Simmering *et al.*, 2015; Williams *et al.*, 2010). The comparison of data between Baseline vs Model-C to check the effect of Marker Variable on loadings concludes that Method Biasness is not present ($p > 0.05$). The results of the test are presented in Table 3.

Table 3. Results of common method bias test

Model	CMIN	DF	CFI	GFI	RMSEA	Comparison	Null hypothesis	*p*-value
Initial Model	851.785	322	0.904	0.887	0.06			
Baseline Model	875.803	335	0.902	0.883	0.06			
Model-C	875.545	334	0.901	0.883	0.06	Baseline vs Model-C	There is no Impact of Marker Var on Items	0.611

5.2 Measurement model testing

Exploratory factor analysis is used to explore the possible underlying factor structure of a set of observed variables without imposing a preconceived structure on the outcome, whereas Confirmatory factor analysis (CFA) is used to verify the factor structure of a set of observed variables based on prior theories. Few researchers have suggested using EFA and CFA to assess construct validity (Farrell, 2010; Marsh *et al.*, 2014). All the theoretical concepts used in the present research were taken from the existing studies, which provided a theoretical rationale for the existence of these concepts. However, since we have used items from multiple studies restricted to civil and commercial organizations and testing these concepts for the military organization, we first used EFA to redefine the theoretical constructs and then CFA to test the hypotheses.

5.2.1 Exploratory factor analysis. Principle component analysis with Varimax rotation was used to identify the set of uncorrelated factors. Six clear factors were identified in Rotated Component Matrix. KMO value of 0.814 indicated the adequacy of data. Bartlett's test of Sphericity was found to be significant for <0.05, indicating a good correlation between the variables. Total Variance Explained obtained was found to be good at 63.161% (Treiblmaier and Filzmoser, 2010; Reio Jr and Shuck, 2015).

5.2.2 Confirmatory factor analysis. The measurement model was found to be a good fit for the sample data as shown in Table 4.

Reliability, convergent validity, and discriminant validity of the scale were further examined using CFA. Values of Composite Reliability (CR), Average Variance Extracted (AVE), and Maximum Shared Variance (MSV) for each construct are indicated in Table 5.

Cronbach's alphas, of the reliability test in this study, are found to be higher than 0.7, indicating fair stability and consistency (Cronbach, 1951).

Convergent Validity, all standardized factor loading was found to be significant ($p < 0.01$).

Composite Reliability (CR), was found to be in the range of 0.746–0.899, above the recommended limit of 0.5 for factor loading, indicating an adequate relationship between the statements.

Average Variance Extracted (AVE), values for all the constructs exceed the suggested threshold value of 0.50, thereby confirming the convergent validity of the scale (Hair *et al.*, 2006; Fornell and Larcker, 1981).

Discriminant Validity, the square root of the AVE from the various dimensions in this study was found to be greater than the correlation between each pair of latent variables (MSV). Hence, the discrimination validity was also found to be adequate (Fornell and Larcker, 1981; Hair *et al.*, 2006).

Since the measurement model cleared all the checks for reliability and validity, the study moved forward to check the path coefficients of the structural model.

Index	Goodness of fit standards	Scholars	Measurement model estimate	Structural model estimate	Conclusion
χ^2/df	Between 1 and 3	Tabachnick and Fidell (2007), Hu and Bentler (1999), Byrne (2008)	2.645	2.654	Good Fit
GFI	>0.90		0.887	0.900	Acceptable
CFI	>0.90		0.904	0.917	Good Fit
SRMR	<0.08		0.059	0.061	Good Fit
RMSEA	<0.06		0.060	0.060	Good Fit

Note(s): χ^2/df – Chi-squared divided by degree of freedom, GFI – goodness of fit index, CFI- Comparative Fit Index, SRMR-standardized root mean square residual, RMESA-root mean square error of approximation

Table 4. Model fit measures for measurement model and structural model

Table 5.
Results of Reliability and Validity checks

	Cronbach alpha	CR	AVE	MSV	OrgPerf	Soldiers	Strategy	Culture	**IM	Process
*OrgPerf	0.798	0.9	0.5	0.03	*0.709*					
Soldiers	0.803	0.75	0.5	0.33	−0.065	*0.708*				
Strategy	0.838	0.84	0.58	0.22	−0.024	0.464	*0.758*			
Culture	0.803	0.79	0.55	0.33	0.034	0.573	0.421	*0.745*		
IM	0.804	0.81	0.52	0.03	0.173	−0.103	−0.061	−0.135	*0.721*	
Process	0.751	0.79	0.56	0.16	−0.016	0.331	0.292	0.404	−0.13	*0.746*

Note(s): **IM-is the Ideal Marker used for testing of Common Method Bias
OrgPerf = Organization Performance

5.2.3 Structural model and hypotheses testing. Like the measurement model, the structural model was also a good fit for the specified indexes, as shown in Table 4. SEM was carried out to test the relationship between different variables. The results of the path analysis coefficient and verification of the research hypotheses of the structural model are presented in Table 6. The results show that out of a total of thirteen hypotheses, twelve hypotheses were supported by the data.

6. Discussion

The result of the hypotheses and path analysis of structural mode is presented in Figure 2.

The results on the relation between the soldiers and the knowledge environment of military organizations, i.e. *H1 ($\beta = 0.725$, $t = 6.593$, p value $= 0.000$)*, is strongly supported. Data indicates that the soldiers in the military organization understand KM and are willing to accept and learn from experts and share their knowledge with those in need. They always try to find and use existing knowledge in the organization, rather than re-inventing the wheel. The comprehension gained by the soldiers through study, experience, practice, and human interaction provides the basis for expertise and skilled judgment (Orhan, 2015). By virtue of shifts in ranks and places, the military leaders become continuous learners. The knowledge acquired by them including self-discipline, information gathering, situational assessment, communication, and institution can prove highly valuable to the organization (Walsh, 2015). Therefore, the soldiers must understand and practice KM to enable military organization to be learning organization. The finding is augmented by the literature that supports people's role in an organization for building a knowledge environment that facilitates the creation, storage, transfer, and application of knowledge to achieve organizational aims (Lee and Choi, 2003; Wu and Chen, 2014; Marques and Simón, 2006; Novak, 2017; Thomas and Gupta, 2021).

Bartczak (2002) defines culture in a military organization as the combination of shared history, expectations, unwritten rules, and social traditions that affects common behavior and

Hypothesis			Beta	T	p	Supported
H1	Soldiers	Knowledge Environment	0.725	6.593	***	S
H2	Culture	Knowledge Environment	0.811	6.241	***	S
H3	Process	Knowledge Environment	0.479	6.593	***	S
H4	Strategy	Knowledge Environment	0.555	6.196	***	S
H5a	Competitive advantage	Measures of Organization Performance	0.484	9.527	***	S
H5b	Information and Decision Superiority	Measures of Organization Performance	0.615	13.220	***	S
H5c	Innovation	Measures of Organization Performance	0.712	15.643	***	S
H5d	Expertise	Measures of Organization Performance	0.838	16.405	***	S
H6e	Efficiency	Measures of Organization Performance	0.828	18.278	***	S
H5f	Cost and time	Measures of Organization Performance	0.676	14.745	***	S
H5g	Learning curve	Measures of Organization Performance	0.794	18.278	***	S
H5h	Morale	Measures of Organization Performance	0.699	17.342	***	S
H6	Knowledge Environment	Measures of Organization Performance	–0.048	–0.719	0.472	NS

Note(s): Significant*** at $p < 0.05$: S= Supported, NS= Not supported

Table 6. Results of Path Analysis and verification of research hypotheses

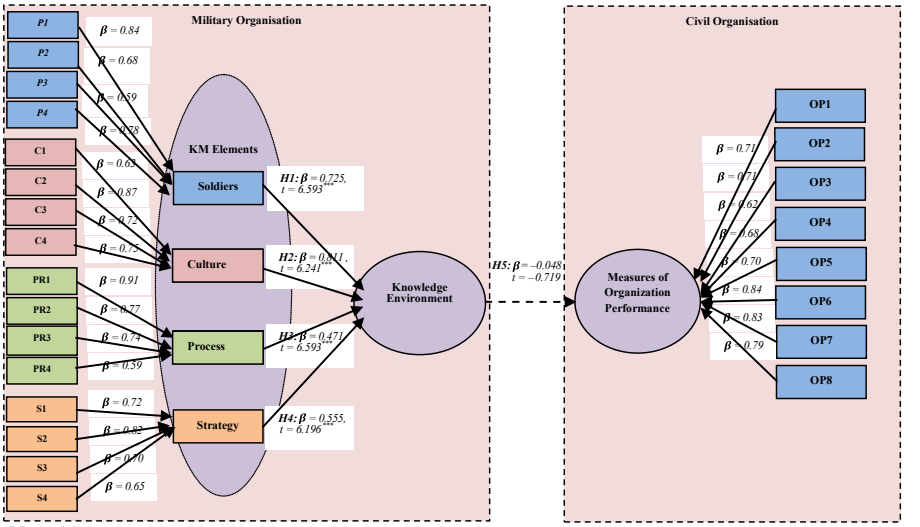

Note(s): Significant
Non-Significant
Source(s): Author

Figure 2.
A path analysis of the structural model

therefore most potent and difficult to alter. Janiszewski (2011) says a military organization that creates a culture that encourages collaboration and knowledge sharing with formal KM principles is more likely to achieve success in the operational environment. From the results, culture in a military organization has emerged as a strong positive influencer of all the elements to the knowledge environment, significantly proving *H2* ($\beta = 0.811$, $t = 6.241$, *p value* $= 0.000$). Data indicates, culture in a military organization actively supports KM activities. People in the Indian military establishment are recognized and rewarded for sharing their knowledge. They are recognized and rewarded for good work and innovation. Military organizations have a team-oriented approach and people trust, cooperate, and help each other. Leadership in the organization sees knowledge as a strategic asset. Findings are supported by many researchers who believe organizational culture is the key influence on the knowledge environment and are significantly related to organizational performance (Wong, 2005; Sin and Alan, 2000; Gold *et al.*, 2001; Zheng *et al.*, 2010). The organizational culture influences the way people interact, create, and ultimately share their knowledge, and the findings of the study empirically indicate a culture in a military organization that supports a knowledge environment.

The process in the organization should provide the right mechanism to share information and knowledge. The large organizations like militaries, people may not know each other and a lack of personal relationships would make it difficult to determine the validity and accuracy of knowledge received. Therefore, military organizations need to create an environment of trust and connectivity to exploit the power of the collective intellect of the entire organization. Connectivity must allow knowledge to be transferred to whoever needs it when they need it, where they need it, and how they need it (Bryant, 2002). The results show the relationship between process and the knowledge environment in a military organization to be significant thereby proving *H3* ($\beta = 0.555$, $t = 6.593$, *p value* < 0.01). Though military organizations have a strict rule with little tolerance for error and a rigid hierarchal structure, the study indicates that routine processes in the Indian military organization support creation, storage,

sharing, and application of knowledge. All the processes and procedures are explicitly defined and maintained up to date in the form of standard operating procedures and guidelines throughout the organization. Soldiers share knowledge using both formal (project, reports, meetings, briefings, publication, etc) and informal procedures (social gathering, cafe, group chats, etc). Findings are in line with literature that establishes process as a significant factor in the organization to enable and facilitate the creation, sharing, and use of knowledge for the benefit of the organization (Mills and Smith, 2011; Lee and Choi, 2003; Chait, 2000; Wong, 2005). Knowledge process improves organizational processes such as innovation, collaborative decision making, and individual and collective learning and is considered an important antecedent for overall organizational effectiveness. The findings of the study empirically substantiate the relation between culture and knowledge environment in a military organization.

Wiig (1997) says most of the organizations dovetail different KM strategies to match with their culture, priorities, and capabilities and derive the best business value from their existing knowledge-based assets or try to create new competitive knowledge-related assets. The organizations, therefore, need to develop KM strategies for managing both implicit and explicit knowledge and the processes associated with the transfer between these types of knowledge. The results indicate a significant relationship between the strategy and the knowledge environment in a military organization supporting *H4* ($\beta = 0.479$, $t = 6.196$, *p value* < 0.01). The study indicates that the Indian military organization has comprehensive and documented KM strategies. Policies in the organization support the proper management of individual and organizational knowledge. The military organization has a well-defined strategy for training, education, and skill up-gradation of the soldiers. The leadership support use of KM tools for sharing and application of knowledge such as knowledge portals, best practices, peer assist, lesson learned, storytelling, and mentoring. O'dell and Grayson (1998) says the KM strategy for armed forces should be aimed at getting the right knowledge to the right people at the right time and helping people share and put knowledge into action in ways to improve an organization's performance, and the study supports the same for the military organization of a developing nation. The findings of the relationship are supported by various literature in civil organizations (Zheng *et al.*, 2010; Novak, 2017; Gamble and Blackwell, 2001).

KM efforts or practices in an organization need to be assessed to understand its efficacy towards organizations performance, and requirement for modification in the existing practices or adoption of new practices as per the changing environment, role, and objectives of the organization. Researchers and practitioners have adopted various methods and tools to measure the organizations' performance, ranging from the use of measurement index, balanced scorecards, and maturity models (Tseng and Lee, 2014; Marr and Schiuma, 2003; Gupta and Chopra, 2018; Vanini and Bochert, 2015; Miller *et al.*, 2014). In the absence of any specific measures of performance for militaries of a developing country, the authors shortlisted a few measures commonly used in the civil organization and studied their correlation as a measure of organizational performance. These measures were subsequently used to correlate with the knowledge environment of a military organization. The results from the study indicate that selected measures had a high degree of correlation as a measure of organization performance. In the present scenario of network-centric-warfare, the degree of dominance for a military organization depends on the ability to acquire, control and exploit information and knowledge. Capturing and preserving mission-critical organizational knowledge provides organization a sustainable competitive advantage against adversaries (*H5a*: $\beta = 0.484$, $t = 9.527$, *p value* < 0.01). Active KM feeds data and information, ideas of its people, and concepts leading to deeper and richer tacit and explicit knowledge-bases. Proper management of information and knowledge provides current, relevant, and structured data and information that facilitate commanders to make better-informed decisions (*H5b:*

β = 0.615, t = 13.220, p value < 0.01). The new age military organizations are converted into learning organizations focusing on innovation where knowledge is the key. A knowledge-sharing culture that celebrates knowledge, rewards, and provides recognition for creating new ideas and sharing knowledge, promotes innovations *(H5c: β = 0.712, t = 15.643, p value < 0.01)*. The practice of KM tools like Peer assists, Community of Practice, and best practices facilitate expertise build-up, improvement in maintenance quality, and reduction in equipment downtime *(H5d: β = 0.838, t = 16.405, p value < 0.01)*. Using KM tools can help in classifying the various knowledge repositories based on their sensitivity, mission criticality, and access levels. KM tools like data mining and analysis, knowledge taxonomy, portals, best practices, peer assistance, etc, enhance the efficiency and effectiveness of the soldiers and the organization *(H5e: β = 0.828, t = 18.405, p value < 0.01)*. Proper storage, taxonomy, transfer, and application of information and knowledge eliminate the costs associated with duplicated effort and wasted time *(H5f: β = 0.676, t = 14.745, p value < 0.01)*. Use of KM tools like lessons learned, after-action reviews, storytelling, mentoring, etc, increases the learning curve of the employees *(H5g: β = 0.794, t = 18.278, p value < 0.01)*. A conducive KM environment that has collaborating organization culture, open communication, trust, and sharing; increases the loyalty, commitment, and morale of employees *(H5a: β = 0.699, t = 17.342, p value < 0.01)*. The measures of performance used in the study like competitive advantage, information and decision superiority, innovation, expertise, efficiency, cost and time, learning curve, and morale have been recognized in various literature highlighted in Table 2

The results in the study show that there is no significant relationship between the knowledge environment of a military organization and measures of organizational performance used in a civil organization, indicating the hypothesis H5 "Knowledge environment in a military organization has a significant relation with measures of performance used by civil organizations" was not confirmed *(β = −0.048, t = −0.719, p value > 0.01)*. A broad range of literature in civil, commercial, public, or private organizations indicates a significant direct relationship between a knowledge environment and organizational performance (Abuaddous *et al.*, 2018; Wu and Chen, 2014; Zack *et al.*, 2009; Mills and Smith, 2011; Novak, 2017; Thomas *et al.*, 2020). Van Laar *et al.* (2020) state that a one-size-fits-all approach to KM would not work for the armed forces, as the military organization has unique processes and procedures that are unparallel outside the military. Military organizations have a unique structural and cultural attributes, managerial resources, and environmental factors that influence KM and therefore require an indebt study (Bartczak, 2002). Findings indicate the KM in a military setup is a complex issue and the KM measurement parameters therefore should be tailored to the requirement of military organization in line with the suggestion from Van Laar *et al.* (2020).

7. Conclusion

Although research on KM is expanding, formal research focused exclusively on efforts in the military is lacking. The relevance of KM for the enhancement of organizational performance in various public and private has been widely acknowledged. However, only limited literature, mostly specific to the United States Armed Forces highlights the significance of active KM for the military organizations. The paper attempts to present a long due study of KM in the military forces of developing country. The findings are welcoming and it is revealed that various elements of KM like soldiers, culture, process, and strategy are significantly related to creating a positive knowledge environment in the military organization of the developing country. A key element for an enterprise to be successful is to encourage people to communicate and share their knowledge with others and the current study empirically establishes the same for a military organization. Soldiers are the repository

of knowledge acquired through training, experience, exercise, environment, and job rotation. Preservation, transfer, and reuse of this knowledge is the key to the success of any military operations. The culture that promotes sharing and use of the knowledge between individuals and organizations promotes a positive knowledge environment. The routine processes need to dovetail the KM process of acquisition, storage, transfer, and use of knowledge without creating an extra burden on the individuals. The military organizations need to build up a KM strategy that aligns with their role and objectives. Coordination of people and processes dovetailed with a far-reaching KM strategy through a collaborative and knowledge-sharing culture will create a knowledge environment that will help the military organization in achieving success in the operational environment. Various measures of organizational performance have been specified in the literature. In the absence of any such measures for the military organization, the study also attempted to study the correlation between the selected measures from the civil organization and the KM environment of the military organization. However, the results indicated no correlation between them. The findings are in the line with Van Laar *et al.* (2020) who state that a one-size-fits-all approach to KM would not work for the armed forces, as the military organization has unique processes and procedures that are unparallel outside the military. Therefore, the militaries need to develop models to account for these differences. The military environment is volatile, uncertain, complex, and ambiguous. The study made an effort to study the nuance of KM in such an environment without adequate support from the relevant literature, especially for the military organization of the developing countries. Finding would definitely the critical gap in the literature and would encourage the practitioners and leaders in the armed forces to encourage more such studies. Military organizations need to take a holistic approach and remove the organizational knowledge barriers to create a positive knowledge environment that originates from the organizational culture, from the organization structure, and the process (Kern *et al.*, 2008).

8. Implications

8.1 Theoretical implications

Bartczak (2002) states that though the research on KM is growing at a fast pace, very little has yet focused exclusively on efforts in the military. There is a lack of formal research in the military organization. To the best of authors knowledge, this study is unique and the first to generate empirical insights into a knowledge environment in military organizations and test its relation with parameters used in civil organizations. The findings of the study have made a significant contribution to preceding literature in various ways:

The first is in terms of the research gap. Literature on the topic is scarce and fragmented. Studies on KM are mostly restricted to civil organizations or a few contemporary western military organizations. The study hopes to fill the gaps in the literature and expand the scope of KM literature to the other militaries around the globe.

Secondly, the studies conducted in a military organization have been generally theoretical in nature, highlighting the significance of KM. This study is unique in empirically testing various aspects of KM in a military organization. The results have empirically established a significant relationship between the people, culture, process, and strategy to a knowledge environment that creates, stores, transfers and applies knowledge towards achieving military objectives.

Thirdly, the findings on the relation between the knowledge environment in a military organization and the performance measure used in civil organizations indicated that study on a military organization is a complex issue. The KM theories, models, and tools established for the civil organization cannot be directly applied to a military organization considering its vividness and therefore requires a more in-depth and holistic study. The study provides an opportunity to research scholars to explore the hidden insights of the various aspects of KM in a military organization.

8.2 Practical implications

The findings of the study are likely to make various practical implications:

First, the literature review establishes that KM is a force multiplier for the military organizations; however, formalized KM practices are restricted to a few contemporary militaries. Empirical findings in the study would encourage military organizations of the developing countries, including India, to create an environment for effective management of their organizational knowledge and institute KM policies and practices to capitalize on their knowledge assets.

Second, considering that most military organizations' objectives and structures are almost similar. The current study on IAF could be reasonably generalized for other military setups in the world.

9. Limitation and future research

Even though this study attempts to be rigorous and objective to the extent possible, some limitations can add more substance to the study if addressed in future studies. The scope of the study was limited to data and discussion of non-classified and non-sensitive nature in a military organization; therefore, getting more detailed insight was not possible. The research has been piloted on a single organization (IAF) that is one of the fighting arms of the Indian military setup. A comprehensive study involving other military arms may provide a better generalization. To the best of the author's knowledge, no literature could be found that had empirically examined the relationship between variables and constructs used in the study in any of the other military organizations of the world; therefore, findings could not be adequately augmented by the relevant literature. Future researchers may conduct a study on a few more military organizations and may explore various studies on KM in the civil world and perform correlation studies or compare their efficacy in complex military organizations. More set of performance measure utilized by various public and private institution could be studied to explore the best fit for the military context.

References

Abuaddous, H.Y., Al Sokkar, A.A. and Abualodous, B.I. (2018), "The impact of knowledge management on organizational performance", *International Journal of Advanced Computer Science and Applications*, Vol. 9, pp. 204-208.

Agrawal, N. (2020), "Modeling enablers of knowledge management process using multi criteria decision making approach", *VINE Journal of Information and Knowledge Management Systems*, Vol. 51 No. 3, pp. 389-417.

Allard, S. and Holsapple, C.W. (2002), "Knowledge management as a key for e-business competitiveness: from the knowledge chain to KM Audits", *Journal of Computer Information Systems*, Vol. 42, pp. 19-25.

Alwis, L. (2011), "Knowledge management and organizational performance".

Amir, R. and Parvar, J. (2014), "Harnessing knowledge management to improve organisational performance", *International Journal of Trade, Economics and Finance*, Vol. 5, p. 31.

Argote, L. (2012), *Organizational Learning: Creating, Retaining and Transferring Knowledge*, Springer Science & Business Media, Berlin.

Ariely, Gil (2008), "Operational knowledge management in the military", *Dans Knowledge Management: Concepts, Methodologies, Tools, and Applications*, IGI Global, pp. 2376-2386.

Aujirapongpan, S., Vadhanasindhu, P., Chandrachai, A. and Cooparat, P. (2010), "Indicators of knowledge management capability for KM effectiveness", *Vine*, Vol. 40 No. 2, pp. 183-203.

Bartczak, S.E. (2002), *Identifying Barriers to Knowledge Management in the United States Military*, Auburn University, Alabama.

Becerra-Fernandez, I., Leidner, D. and Leidner, D. (2014), "On knowledge, knowledge management, and knowledge management systems: an introduction", *Knowledge Management, Routledge*, Vol. 25 No. 1, pp. 107-137.

Bender, S. and Fish, A. (2000), "The transfer of knowledge and the retention of expertise: the continuing need for global assignments", *Journal of Knowledge Management*.

Bielawski, R. (2021), "Contemporary indicators of security. An attempt to measure the level of security", *Przegląd Nauk o Obronności*, Vol. 2020 No. 10, pp. 78-93.

Boe, O. (2014), "Changing knowledge management strategy in the Norwegian armed forces: a discussion of effects-based thinking as an alternative method in the planning and execution of military joint operations", *Proceeding of Knowledge Management International Conference (KMICe)*, Malaysia, 12th–15th August, Vol. 2.

Bryant, J.J. (2002), *Army Knowledge Management (AKM): Challenges Ahead*, Army War Coll Carlisle Barracks Pa.

Byrne, B.M. (2008), *Testing for Multigroup Equivalence of a Measuring Instrument: A Walk through the Process*, Psicothema, pp. 872-882.

Carayannis, E., Dagnino, G.B., Alvarez, S. and Faraci, R. (2018). "Entrepreneurial ecosystems and the diffusion of startups", doi: 10.4337/9781784710064.

Chait, L.P. (2000), "Creating a successful knowledge management system", *IEEE Engineering Management Review*, Vol. 28, pp. 92-95.

Chourides, P., Longbottom, D. and Murphy, W. (2003), "Excellence in knowledge management: an empirical study to identify critical factors and performance measures", *Measuring Business Excellence*, Vol. 7 No. 2, pp. 29-45.

Command, M. (2008), "Challenges in developing a knowledge management strategy: a case study of the air force", in *Selected Readings on Strategic Information Systems*, Vol. 76.

Cook, S.D. and Brown, J.S. (1999), "Bridging epistemologies: the generative dance between organizational knowledge and organizational knowing", *Organization Science*, Vol. 10 No. 4, pp. 381-515.

Cronbach, L.J. (1951), "Coefficient alpha and the internal structure of tests", *Psychometrika*, Vol. 16, pp. 297-334.

Davenport, T.H. (1997), "Ten principles of knowledge management and four case studies", *Knowledge and Process Management*, Vol. 4, pp. 187-208.

Davenport, T.H. (1999), "Knowledge management and the broader firm: strategy, advantage, and performance", *Knowledge Management Handbook*, Vol. 2, pp. 1-2.

Davenport, T.H. and Prusak, L. (1998), *Working Knowledge: How Organizations Manage what They Know*, Harvard Business Press, Boston, Massachusetts.

De Grosbois, J.F.P. (2011), *The Impact of Knowledge Management Practices on Nuclear Power Plant Organization Performance*, Carleton University.

Del Giudice, M., Della Peruta, M.R. and Carayannis, E. (2010), *Knowledge and the Family Business*, Springer, New York, NY.

Del Giudice, M., Della Peruta, M.R. and Carayannis, E.G. (2012), *Cross-cultural Knowledge Management: Fostering Innovation and Collaboration inside the Multicultural Enterprise*, Springer, New York.

Del Giudice, M., Della Peruta, M.R. and Maggioni, V. (2013), "The 'right' knowledge and spin–off processes: an empirical analysis on knowledge transfer", *Journal of the Knowledge Economy*, Vol. 4 No. 2013, p. 304.

Elder, D. (2008), "Operational knowledge management: a soldier's guide for implementing knowledge management in army organizations" (accessed 29 January 2011).

Farrell, A.M. (2010), "Insufficient discriminant validity: a comment on Bove, pervan, Beatty, and shiu 2009", *Journal of Business Research*, Vol. 63, pp. 324-327, doi: 10.1016/j.jbusres.2009.05.003.

Forcadell, F.J. and Guadamillas, F. (2002), "A case study on the implementation of a knowledge management strategy oriented to innovation", *Knowledge and Process Management*, Vol. 9, pp. 162-171.

Fornell, C. and Larcker, D.F. (1981), "Evaluating structural equation models with unobservable variables and measurement error", *Journal of Marketing Research*, Vol. 18, pp. 39-50.

Fountain, D.D. (2007), *Knowledge Management in an Information Age Army*, Army War Coll Carlisle Barracks Pa.

Gamble, P.R. and Blackwell, J. (2001), *Knowledge Management: A State of the Art Guide*, Kogan Page, London.

Ganguly, R. (2015), "Indian military transformation in the twenty-first century", *The Evolution of Military Power in the West and Asia*, Routledge.

Gaur, N. and Gupta, V. (2021), "Devising a knowledge culture", *Journal of Contemporary Issues in Business and Government*, Vol. 27 No. 1, pp. 1587-1623.

Gloet, M. and Terziovski, M. (2004), "Exploring the relationship between knowledge management practices and innovation performance", *Journal of Manufacturing Technology Management*, Vol. 15 No. 5, pp. 402-409.

Gold, A.H., Malhotra, A. and Segars, A.H. (2001), "Knowledge management: an organizational capabilities perspective", *Journal of Management Information Systems*, Vol. 18, pp. 185-214.

Gupta, V. and Chopra, M. (2018), "Gauging the impact of knowledge management practices on organizational performance—a balanced scorecard perspective", *VINE Journal of Information and Knowledge Management Systems*, Vol. 48 No. 1, pp. 21-46.

Gupta, A.K. and Govindarajan, V. (2000), "Knowledge management's social dimension: lessons from Nucor Steel", *MIT Sloan Management Review*, Vol. 42, p. 71.

Gupta, V. and Thomas, A. (2019), "Fostering tacit knowledge sharing and innovative work behaviour: an integrated theoretical view", *International Journal of Managerial and Financial Accounting*, Vol. 11, pp. 320-346.

Hair, J.F., Black, W.C., Babin, B.J., Anderson, R.E. and Tatham, R.L. (2006), *Multivariate Data Analysis*, 6th ed., Prentice-Hall, New Jersey.

Han, B.M. and Anantatmula, V.S. (2007), "Knowledge sharing in large IT organizations: a case study", *Vine*, Vol. 37 No. 4, pp. 421-439.

Ho, C.-T. (2009), "The relationship between knowledge management enablers and performance", *Industrial Management and Data Systems*, Vol. 109, pp. 98-117.

Holsapple, C.W. and Joshi, K.D. (2004), "A knowledge management ontology", in Holsapple, C.W. (Ed.), *Handbook on Knowledge Management 1. International Handbooks on Information Systems*, Springer, Berlin, Heidelberg, Vol. 1, doi: 10.1007/978-3-540-24746-3_6.

Hu, L.T. and Bentler, P.M. (1999), "Cutoff criteria for fit indexes in covariance structure analysis: conventional criteria versus new alternatives", *Structural Equation Modeling: A Multidisciplinary Journal*, Vol. 6, pp. 1-55.

Ichijo, K., Krough, G. and Nonaka, I. (1998), "Knowledge enablers", in Krogh, G. and Roos, J. (Eds), *Knowing in Firms*, Sage, London, pp. 173-203.

Jabłonski, J. and Lis, A. (2012), "Lessons learned system as a tool of managing organisational knowledge: the case of military organisations", *Business and Non-profit Organizations Facing Increased Competition and Growing Customers' Demands*, Vol. 18, p. 163.

Janiszewski, J.T. (2011), *Knowledge Management: A Model to Enhance Combatant Command Effectiveness*, Army War Coll Carlisle Barracks Pa.

Kern, E.-M., Koch, M., Fiechter, C. and Richter, A. (2008), "Knowledge barriers in CD&E projects in the German Federal armed forces", *Proc. Intl. Conf. on Knowledge Management and New Media Technology*.

Lecocq, R. and Gauvin, M. (2006), "Cross-analysis of data collected on knowledge management practices in Canadian forces environments", *Transformational Science and Technology for the Current and Future Force: (With CD-ROM)*, World Scientific.

Lee, H. and Choi, B. (2003), "Knowledge management enablers, processes, and organizational performance: an integrative view and empirical examination", *Journal of Management Information Systems*, Vol. 20, pp. 179-228.

Lepak, J.J. (2009), *Creating a Knowledge Management Strategy*, Army War Coll Carlisle Barracks Pa.

Liao, C., Wang, H.-Y., Chuang, S.-H., Shih, M.-L. and Liu, C.-C. (2010), "Enhancing knowledge management for RD innovation and firm performance: an integrative view", *African Journal of Business Management*, Vol. 4, pp. 3026-3038.

Liebowitz, J. (1999), "Key ingredients to the success of an organization's knowledge management strategy", *Knowledge and Process Management*, Vol. 6, pp. 37-40.

Maier, R.K. and Remus, U. (2002), "Defining process-oriented knowledge management strategies", *Knowledge and Process Management*, Vol. 9, pp. 103-118, 31.

Marques, D.P. and Simón, F.J.G. (2006), "The effect of knowledge management practices on firm performance", *Journal of Knowledge Management*, Vol. 10 No. 3, pp. 143-156.

Marr, B. and Schiuma, G. (2003), "Business performance measurement–past, present and future", *Management Decision*, Vol. 41 No. 8, pp. 680-687.

Marsh, H.W., Morin, A.J.S., Parker, P.D. and Kaur, G. (2014), "Exploratory structural equation modeling: an integration of the best features of exploratory and confirmatory factor analysis", *Annual Review of Clinical Psychology*, Vol. 10, pp. 85-110, doi: 10.1146/annurevclinpsy-032813-153700.

Martin, M.T. (2014), "The air force records management program: a paradigm shift from compliance to guiding principles in an ever-changing information environment".

Marzukhi, S., Mohammad Daud, N.H., Zainol, Z. and Zakaria, O.B. (2018), "Framework of knowledge-based system for united Nations peacekeeping operations using data mining technique", in *2018 Fourth International Conference on Information Retrieval and Knowledge Management (CAMP)*, pp. 1-6.

Massingham, P.R. (2018), "Measuring the impact of knowledge loss: a longitudinal study", *Journal of Knowledge Management*, Vol. 22 No. 4, pp. 721-758, doi: 10.1108/JKM-08-2016-0338.

Massingham, P.R. and Massingham, R.K. (2014), "Does knowledge management produce practical outcomes?", *Journal of Knowledge Management*, Vol. 18 No. 2, pp. 221-254.

Mathi, K. (2004), *Key Success Factors for Knowledge Management*, Lindau, Germany.

Mcintyre, S. (2002), *Knowledge Management in Defence R&D Canada*, Defence Research And Development Canadaottawa, Ontario.

McIntyre, S.G., Gauvin, M. and Waruszynski, B. (2003), "Knowledge management in the military context", *Canadian Military Journal*, Vol. 4 No. 1, pp. 35-40.

Meher, J.R. and Mishra, R.K. (2019), "Assessing the influence of knowledge management practices on organizational performance", *VINE Journal of Information and Knowledge Management Systems*, Vol. 49 No. 3, pp. 440-456.

Miller, C.W., Orban, G.A., Partida, B., Stroud, A. and Leavitt, P. (2014), "American productivity and quality center best practices study: using open innovation to generate ideas", *Open Innovation: New Product Development Essentials from the PDMA*, pp. 319-338.

Mills, A.M. and Smith, T.A. (2011), "Knowledge management and organizational performance: a decomposed view", *Journal of Knowledge Management*, Vol. 15 No. 1, pp. 153-171.

Motsenigos, A. and Young, J. (2002), *KM in the US Government Sector*, Vol. 11, KM World.

Nagendra, A. and Morappakkam, S. (2016), "Knowledge management enablers and barriers in the army: an interpretive structural modeling approach", *Indian Journal of Science and Technology*, Vol. 9, pp. 1-12.

Novak, A. (2017), "Knowledge management and organizational performance–Literature review", *Management Challenges in a Network Economy: MakeLearn and TIIM International Conference*, 2017, pp. 433-440.

O'dell, C. and Grayson, C.J. (1998), "If only we knew what we know: identification and transfer of internal best practices", *California Management Review*, Vol. 40, pp. 154-174.

Orhan, S.Ş.A.K.M. (2015), "Knowledge management in military organizations: applications of knowledge creation and knowledge transfer", *Military and Security Studies*, Vol. 2015, p. 20.

Perez, A.L. and Strizhko, T.V. (2018), "Minority representation, tokenism, and well-being in army units", *Military Psychology*, Vol. 30, pp. 449-463.

Pettersson, U. (2009), "Success and Failure factors for KM: the utilization of knowledge in the Swedish armed forces", *Journal of Universal Computer Science*, Vol. 15, pp. 1735-1743.

Plant, T. (2000), "Introducing knowledge management into complex organization", Australian Defense Force Academy, School of Computer Science, University College, University of New South Wales, Unpublished manuscript.

Podsakoff, P.M. and Organ, D.W. (1986), "Self-reports in organizational research: problems and prospects", *Journal of Management*, Vol. 12, pp. 69-82.

Rasula, J., Vuksic, V.B. and Stemberger, M.I. (2012), "The impact of knowledge management on organisational performance", *Economic and Business Review for Central and South-Eastern Europe*, Vol. 14, p. 147.

Reio, T.G. and Shuck, B. (2015), "Exploratory factor Analysis: implications for theory, research, and practice", *Advances in Developing Human Resources*, Vol. 17 No. 1, pp. 12-25, doi: 10.1177/1523422314559804.

Rezaei, F., Khalilzadeh, M. and Soleimani, P. (2021), "Factors affecting knowledge management and its effect on organizational performance: mediating the role of human capital", *Advances in Human-Computer Interaction*, Vol. 2021 No. 1, pp. 1-16.

Rhem, A.J. (2016), *Knowledge Management in Practice*, Auerbach Publications, New York.

Rubenstein-Montano, B., Liebowitz, J., Buchwalter, J., Mccaw, D., Newman, B., Rebeck, K. and Team, T.K.M.M. (2001), "A systems thinking framework for knowledge management", *Decision Support Systems*, Vol. 31, pp. 5-16.

Santoro, G., Thrassou, A., Bresciani, S. and Del Giudice, M. (2019), "Do knowledge management and dynamic capabilities affect ambidextrous entrepreneurial intensity and firms' performance?", *IEEE Transactions on Engineering Management*, Vol. 68 No. 2, pp. 378-386.

Schein, E.H. (2010), *Organizational Culture and Leadership*, John Wiley & Sons, San Francisco.

Scuotto, V., Del Giudice, M., Bresciani, S. and Meissner, D. (2017), "Knowledge-driven preferences in informal inbound open innovation modes: an explorative view on small to medium enterprises", *Journal of Knowledge Management*, Vol. 21 No. 3, pp. 640-655, doi: 10.1108/JKM-10-2016-0465.

Scuotto, V., Lemaire, S.L., Magni, D. and Maalaoui, A. (2022), "Extending knowledge-based view: future trends of corporate social entrepreneurship to fight the gig economy challenges", *Journal of Business Research*, Vol. 139, pp. 1111-1122, doi: 10.1016/j.jbusres.2021.10.060.

Shah, H.G. and Kant, R. (2018), "Knowledge management enablers: metadata analysis for KM implementation", *Journal of Information and Knowledge Management*, Vol. 17 No. 4, pp. 1-29.

Sher, P.J. and Lee, V.C. (2004), "Information technology as a facilitator for enhancing dynamic capabilities through knowledge management", *Information and Management*, Vol. 41, pp. 933-945.

Simmering, M.J., Fuller, C.M., Richardson, H.A., Ocal, Y. and Atinc, G.M. (2015), "Marker variable choice, reporting, and interpretation in the detection of common method variance: a review and demonstration", *Organizational Research Methods*, Vol. 18 No. 3, pp. 473-511.

Sin, L.Y. and Alan, C. (2000), "How does marketing effectiveness mediate the effect of organizational culture on business performance? The case of service firms", *Journal of Services Marketing*, Vol. 14 No. 4, pp. 295-309.

Singh, M.K. and Gupta, V. (2020), "Critical types of knowledge loss in military organisations", *VINE Journal of Information and Knowledge Management Systems*, Vol. 51 No. 4, pp. 618-635.

Singh, M.K. and Gupta, V. (2021), "IAF transition towards a network-centric-knowledge based force", *Journal of the United Service Institution of India*, Vol. CLI No. 623, January–March 2021, pp. 93-100.

Sinha, N., Kakkar, N.K. and Gupta, V. (2012), "Uncovering the secrets of the twenty-first-century organisation", *Global Business and Organizational Excellence*, Vol. 31 No. 2, pp. 49-56, doi: 10.1002/joe.21414.

Sinha, N., Kakkar, N.K. and Gupta, V. (2015), "Harnessing the power of knowledge management for innovation", *International Journal of Knowledge and Learning*, Vol. 10 No. 2, pp. 124-146, doi: 10.1504/IJKL.2015.071623.

Sullivan, P.K. (2011), *The Difference that Makes a Difference: Distinguishing between Knowledge Management and Information Management in the US Army*, Army Command And General Staff Coll Fort Leavenworth Ks School of Advanced . . ..

Tabachnick, B. and Fidell, L. (2007), *Using Multivariate Statistics*, 5th ed., Allyn & Bacon, New York, NY, Google Scholar.

Tefft, R. (2002), "Army medical department knowledge management", *Army AL&T*, Vol. 2, pp. 10-11.

Theriou, N.G., Maditinos, D. and Theriou, G. (2011), "Knowledge management enabler factors and firm performance: an empirical research of the Greek medium and large firms", *European Research Studies*, Vol. 15 No. 2, pp. 97-134.

Thomas, A. (2021), "Business beyond COVID-19: towards open innovation", *Globalization, Deglobalization, and New Paradigms in Business*, Palgrave Macmillan, Cham, pp. 189-212.

Thomas, A., Cillo, V., Caggiano, V. and Vrontis, D. (2020), "Drivers of social capital in enhancing team knowledge sharing and team performance: moderator role of manager's cultural intelligence", *International Journal of Managerial and Financial Accounting*, Vol. 12 Nos 3-4, pp. 284-303.

Thomas, A. and Gupta, V. (2021), "The role of motivation theories in knowledge sharing: an integrative theoretical reviews and future research agenda", *Kybernetes*, Vol. 51 No. 1, pp. 116-140.

Thomas, D. and Keithley, T. (2002), "Knowledge management improves performance", *AACE International Transactions*, No. 2002, PM171.

Treiblmaier, H. and Filzmoser, P. (2010), "Exploratory factor analysis revisited: how robust methods support the detection of hidden multivariate data structures in IS research", *Information and Management*, Vol. 47 No. 4, pp. 197-207, doi: 10.1016/j.im.2010.02.002.

Tseng, S.-M. and Lee, P.-S. (2014), "The effect of knowledge management capability and dynamic capability on organizational performance", *Journal of Enterprise Information Management*, Vol. 27 No. 2, pp. 158-179.

US Air Force (2014) *Air Force Instructions. 33-396,* Department of Air Force, USA.

Vătămănescu, E.-M., Mitan, A., Andrei, A.G. and Ghigiu, A.M. (2021), "Linking coopetition benefits and innovative performance within small and medium-sized enterprises networks: a strategic approach on knowledge sharing and direct collaboration", *Kybernetes*, Vol. 51 No. 7, pp. 2193-2214.

Van Laar, D.M., Kitchens, M.E. and Koskey, J.T. (2020), "Measuring knowledge management maturity in US Army headquarters", *Knowledge and Process Management*, Vol. 27, pp. 311-321.

Vanini, U. and Bochert, S. (2015), "Maturity levels in knowledge management–a case study approach", *Leading Issues in Knowledge Management*, Vol. Two, p. 186.

Walsh, A.V. (2015), *Information Sharing between the US Department State and the US Army: Using Knowledge Management Technology and Tools to Bridge the Gap*, Army Command And General Staff College Fort Leavenworth Ks.

Wang, K.-L., Chiang, C. and Tung, C.-M. (2012), "Integrating human resource management and knowledge management: from the viewpoint of core employees and organizational performance", *International Journal of Organizational Innovation (Online)*, Vol. 5, p. 109.

Weijters, B., Millet, K. and Cabooter, E. (2021), "Extremity in horizontal and vertical Likert scale format responses. Some evidence on how visual distance between response categories influences extreme responding", *International Journal of Research in Marketing*, Vol. 38 No. 1, pp. 85-103, 2021, ISSN 0167-8116, doi: 10.1016/j.ijresmar.2020.04.002.

Wiig, K.M. (1997), "Integrating intellectual capital and knowledge management", *Long Range Planning*, Vol. 30, pp. 399-405.

Williams, L.J., Hartman, N. and Cavazotte, F. (2010), "Method variance and marker variables: a review and comprehensive CFA marker technique", *Organizational Research Methods*, Vol. 13 No. 3, pp. 477-514.

Wong, K.Y. (2005), "Critical success factors for implementing knowledge management in small and medium enterprises", *Industrial Management and Data Systems*, Vol. 105 No. 3, pp. 261-279.

Wu, I.-L. and Chen, J.-L. (2014), "Knowledge management driven firm performance: the roles of business process capabilities and organizational learning", *Journal of Knowledge Management*, Vol. 18 No. 6, pp. 1141-1164, doi: 10.1108/JKM-05-2014-0192.

Wu, C. and Lin, C. (2009), "Case study of knowledge creation facilitated by Six Sigma", *International Journal of Quality and Reliability Management*, Vol. 26, pp. 911-932.

Xu, Y., Gao, P., Liu, Z. and Xu, P. (2011), "Armed forces knowledge management risk evaluation based on FNN", in *2011 IEEE 18th International Conference on Industrial Engineering and Engineering Management*, IEEE, pp. 1833-1837.

Yeh, Y., Lai, S. and Ho, C. (2006), "Knowledge management enablers: a case study", *Industrial Management and Data Systems*, Vol. 106 No. 6, pp. 793-810, doi: 10.1108/02635570610671489.

Zack, M., Mckeen, J. and Singh, S. (2009), "Knowledge management and organizational performance: an exploratory analysis", *Journal of Knowledge Management*, Vol. 13, pp. 392-409.

Zaied, A.N.H., Hussein, G.S. and Hassan, M.M. (2012), "The role of knowledge management in enhancing organizational performance", *International Journal of Information Engineering and Electronic Business*, Vol. 4, p. 27.

Zheng, W., Yang, B. and Mclean, G.N. (2010), "Linking organizational culture, structure, strategy, and organizational effectiveness: mediating role of knowledge management", *Journal of Business Research*, Vol. 63, pp. 763-771.

Appendix

Table A1.
Variable names and questionnaires

Variable name	Items
People	
P1	People in my organization understand about Knowledge Management (KM)
P2	People are always willing to accept and learn from the knowledge of the peers and experts
P3	People are always willing to share their knowledge with their co-workers
P4	People always try to find and use existing knowledge in the organization, rather than re-inventing the wheel
Culture	
C1	People are seen as the organization's most valued asset.
C2	People are recognized and rewarded for good work and innovation
C3	There is a team-oriented approach throughout the organization, i.e. various departments and people trust, cooperate and help each other
C4	Leadership in the organization sees knowledge as a strategic asset.

(*continued*)

Variable name	Items
Process	
PR1	Knowledge creation, sharing, and use are a natural part of the organization's normal work processes
PR2	The processes and procedures to perform a job have scope for creativity and initiative
PR3	All the processes and procedures are explicitly defined and maintained upto date
PR4	Employees share knowledge using both formal (project, reports, meetings, briefings, publication, etc) and informal procedures (social gathering, cafe, group chats, etc)
Strategy	
S1	The organization has comprehensive and documented KM strategies
S2	Organization has a well-defined strategy for training, education and skill up-gradation of the employees
S3	Policies in the organization support the proper management of individual and organizational knowledge
S4	Top leadership supports the use of KM tools for sharing and application of knowledge such as knowledge portals, best practices, peer assist, lesson learned, storytelling, and mentoring
Measures of organization performance	
OP1	*Competitive advantage*: KM helps in capturing and preserving mission-critical knowledge and provides the organization a sustainable competitive advantage against adversaries
OP2	*Creativity and Innovation*: KM practices like celebrating knowledge, rewards, and recognition for creating new ideas and sharing knowledge, promote innovations
OP3	*Information and Decision Superiority*: KM helps in providing current, relevant, and structured data and information that facilitate commanders to make better-informed decisions
OP4	*Situational Awareness*: Sharing and exchange of information and knowledge increase situational awareness of the employees
OP5	*Efficiency and Effectiveness*: Proper data mining, use of knowledge taxonomy, portals, best practices, peer assistance, etc, enhances the efficiency and effectiveness of the employees
OP6	*Cost and time*: Proper storage, transfer, and application of information and knowledge eliminate the costs associated with duplicated effort and wasted time
OP7	*Learning curve*: KM tools like lessons learned, after-action reviews, storytelling, mentoring, etc, increase the learning curve of the employees
OP8	*Morale*: A conducive KM environment that has collaborating organization culture, open communication, trust, and sharing; increases the loyalty, commitment, and morale of employees

Table A1.

About the authors

Mukesh Kumar Singh is an Aeronautical Engineer by profession. He has Bachelor of Engineering (E&E), Masters of Business Administration (IT), and Master of Technology (Signal Processing) from the prestigious Indian Institute of Technology, Roorkee. He is pursuing Ph.D. from the Delhi School of Management. He has 21 years of experience in the field of defence forces, training and HR management. He has few publications into national and International journals to his credit.

Dr. Vikas Gupta is a Gold Medalist (MBA) and has more than 20 years of experience. He is currently working as an Assistant Professor, Delhi School of Management, Delhi Technological University (Former Delhi College of Engineering). He has many research papers and articles in his credit which are published in Scopus, SCI, SSCI and ABDC listed Journals. His research interests are in the area of knowledge management, innovation, and corporate social responsibility. He has been awarded the Best Faculty Award in the area of management. He has also been associated with many consultancy projects. Vikas Gupta is the corresponding author and can be contacted at: vikasguptadtu@gmail.com

For instructions on how to order reprints of this article, please visit our website:
www.emeraldgrouppublishing.com/licensing/reprints.htm
Or contact us for further details: **permissions@emeraldinsight.com**

ResearchGate

See discussions, stats, and author profiles for this publication at: https://www.researchgate.net/publication/357793208

An era of new future wireless 5G technology and its aspects: a review

Article *in* International Journal of Systems Control and Communications · January 2022

DOI: 10.1504/IJSCC.2022.10044268

CITATIONS
0

READS
88

2 authors:

Akhilesh Verma
Delhi Technological University
20 PUBLICATIONS **31** CITATIONS
SEE PROFILE

Raghava Nallanthighal
Delhi Technological University
44 PUBLICATIONS **72** CITATIONS
SEE PROFILE

Some of the authors of this publication are also working on these related projects:

please forward the paper to nsraghava@gmail.com View project

All content following this page was uploaded by Akhilesh Verma on 23 May 2022.

The user has requested enhancement of the downloaded file.

An era of new future wireless 5G technology and its aspects: a review

Akhilesh Verma* and
Srinivasa Nallanthighal Raghava

Electronics and Communication Engineering,
Delhi Technological University,
Delhi 110042, New Delhi, India
Email: akhilesh.verma6388@gmail.com
Email: nsraghava@dtu.ac.in
*Corresponding author

Abstract: In this paper, various wireless technologies and methods to achieve 5G requirements and challenges have been studied. A surge in mobile data demand worldwide has more and more in demand to get speedy next-generation 5G mobile vices. The telecom industries are surprising because 5G is enough to restructure the previous wireless technology. It's not only escalating the speed of the network but the capacity of the network will also be enhanced too. This paper discussed a different type of works on 5G, which has been done by many researchers. Many modulation techniques used in 5G wireless technology are studied. The mm-wave and massive MIMO technology have drawn attention to implementing 5G wireless technology. The signal transmission is the main challenging task at mm-wave, which has been studied. The different security aspects applied to 5G are presented in this review.

Keywords: 5G; IM; MIMO; MM-Wave; modulation; OFDM; QAM; security.

Reference to this paper should be made as follows: Verma, A. and Raghava, S.N. (2022) 'An era of new future wireless 5G technology and its aspects: a review', *Int. J. Systems, Control and Communications*, Vol. 13, No. 3, pp.193–217.

Biographical notes: Akhilesh Verma received his undergraduate degree in Electronics and Communication Engineering in 2010 from Uttar Pradesh Technical University, Lucknow, India. He received his Master's in Electronics and Communication Engineering from the National Institute of Technical Teachers' Training and Research, Chandigarh, India in 2014. He has worked as a Lecturer in Hermes College of Engineering and Management, Roorkee, Uttarakhand from 2010 to 2012. He worked as an Assistant Professor in Tula's Institute (The College of Engineering and Management) from 2014 to 2015. He has been working toward his PhD degree at Delhi Technological University, Delhi, since 2016. He has authored or co-authored more than 12 articles in peer reviewed journals and conference proceedings. He has also published one Indian patent. His research interests include mm-wave antennas, beamforming networks, passive phase shifters, SIW for mobile terminals and base stations.

Srinivasa Nallanthighal Raghava is working as a Professor in Electronics and Communication Engineering Department (HOD) in Delhi Technological University, India. He has authored or co-authored more than 80 articles in peer reviewed journals and conference proceedings. He has also published two

Copyright © 2022 Inderscience Enterprises Ltd.

Indian patents. His area of specialisation is antenna and propagation, microwave engineering, digital communication, wireless comm., cloud computing, and information security.

1 Introduction

With the fast improvement of wireless communication, remote correspondence has improved over the years due to the implementation of advanced heterogeneous systems (Su et al., 2010). After 4G communication, the next generation of wireless communication has drawn attention called the fifth generation, i.e., 5G. The next generation of wireless technology will be advanced as compared to previous generations that are first introduced commercially in 2009. As compared to 4G whose speed is up to 100 mbps, 5G speeds that could reach 10 gigabits per second. With this high-speed network, high definition (HD) movies of more than 1 GB can be downloaded easily. The transmission speed, as well as the bandwidth of the 5G network, increases, which will be needed to, accommodates added demand from the 'internet of things' (Huang, 2018; Calin, 2015). 5G will provide a direct link between many devices and services like user experience continuity, mission-critical services (PPP, 2015). The multiband smart antenna is the prior condition for 5G applications. It is categorised by an adaptive array that changes the pattern of the beam according to the user and interference movements. For the direction of arrival (DOA), estimation null enforcement, digital beamforming are used (Ohishi et al., 2005; Ban et al., 2016; Rawat et al., 2012). Advanced generation systems are introduced to overcome the limitations of previous generations such as high speed, bandwidth, capacity, quality digital video conferencing, online gaming, and availability of the network all the time at any place (Cisco, 2015). The evolution of cellular technology over the previous versions is shown in Figure 1. First generation communication was introduced in 1980 and is popularly known as advanced mobile phone system (AMPS). It utilises a frequency re-use concept supporting 5 to 10 times more users than that of IMTS (Improved mobile telephone system). But, 1st generation systems are prone to hindrances like insecurity and full duplex analogue mode of communication. Some of the limitations of 1st generation were overcome by the 2nd generation communication systems which were launched in 1990 utilising GSM standard (global system for mobile communication). 2G systems are digitally encrypted and more efficient on the spectrum. They have paved the way to text messaging services. It is introduced in 1995 which was an amalgamation of packet switch network and GSM is possessing data rates up to 160 Kbps. This technology is usually referred to as 2.5G. The Evolution (EDGE) uses 8 PSK modulation which indeed provides fast internet services as the e-services were becoming more prevalent during this phase.

1.1 How 5G innovation will help to control an associated world

While past ages, 1G to 4G of remote systems empowered human to human and human to machine cooperation, 5G will see machines speaking with machines. The up and coming age of agriculturists makes them energise the times ahead. Envision a carrier flying over sections of land of farmland. Ultra top quality cameras on the aircraft watch out for the product maladies, what's more, send a status answer to the agriculturist.

Figure 1 Evolution of cellular technology (see online version for colours)

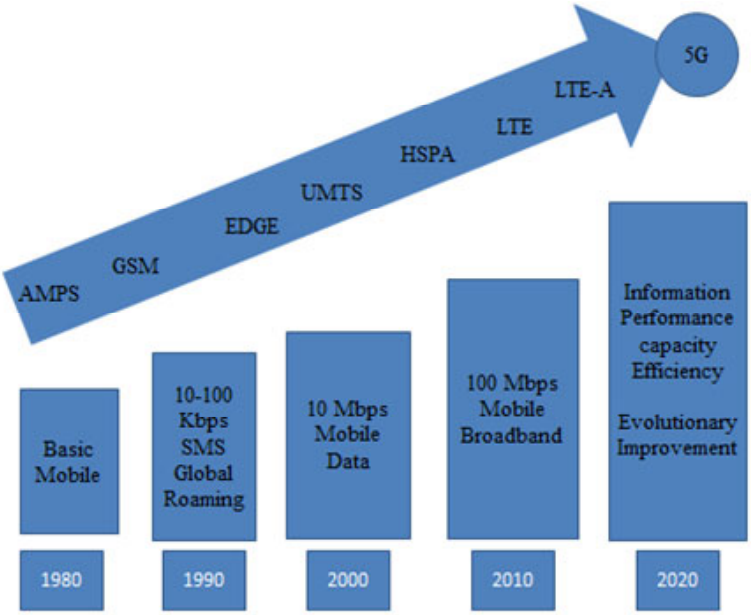

The rancher sees this data, including soil status, dampness, and temperature, because of shrewd sensors set in the homestead on a tablet and requests an automaton to get in on the activity. The automaton takes off and showers synthetic compounds and pesticides over the products to keep them solid. This is only a look at the eventual fate of correspondence, where human mediation will be the absolute minimum. The key component here is 5G, the up and coming age of versatile web networks (Hansen, 2017).

2.5G is the base to make an associated world work out. The coordinated effort will be a critical piece of this: working with the administration, the scholarly community, and industry. For one, the usage of 5G will lessen the idleness or slack in information transmission. The reaction time in 4G is around 50 ms. With 5G, inactivity is relied upon to come down to 1 ms. The client will have the capacity to download video records as large as 500–600 megabytes in only five to six seconds. In greater situations, similar to shrewd urban communities, '5G City' inside the advanced city to show this. CCTV cameras, computerised signages, and IOT (web of things) sensors are associated through 5G, Wi-Fi and Bluetooth, and so forth. This grows the system limit and permits a progressively precise method for observing a movement. In the city, CCTV cameras and video programming identify the speed of vehicles and screen for people on foot jaywalking. In a crisis, a warning springs up on the screens at a focal direction focus (Krishnamoorthy and Mathi, 2012).

Samsung additionally exhibited how 5G systems will change everything from our homes and roads. The utilisation of 5G as a business arrangement is gathering force all around. Samsung, as of now gives 4G and 5G answers for telecom administrators in the USA and South Korea, and as indicated by the Ericsson versatility report June 2018, one billion 5G gadgets for upgraded portable broadband are relied upon to be associated worldwide by 2023 (Firdaus and Indarto, 2016).

2 The expected spectrum of 5G

To meet the future expectations of advanced new coming wireless technology, i.e., 5G, more spectrums need to explore for 5G services. As shown in Figure 2, to deliver wide coverage for 5G, 6 GHz, and above is also an interesting frequency range. For the many initial services of 5G, 3.3–3.8 GHz is the expected range. The frequency range of 1–6 GHz offers a large capacity and support widespread coverage. For 5G communication, 28 GHz, 38 GHz, 60 GHz bands are also considered. The 28 GHz band has been allowed by the United State while it is analysed by Japan, Korea, for 5G use (Pirinen, 2014). Millimetre waves are usually prone to scattering and diffraction losses. Path loss models like close-in (CI) free space reference distance model, floating intercept model (FI), and the alpha-beta-gamma (ABG) model are proposed to calculate attenuation for 5G communication systems. In this research work, the CI model is used for evaluating path loss. The experimental result of path loss exponent less than 1.4 and attenuation values less than 9.7 dB are achieved (Al-Samman et al., 2016).

Figure 2 5G spectrum (see online version for colours)

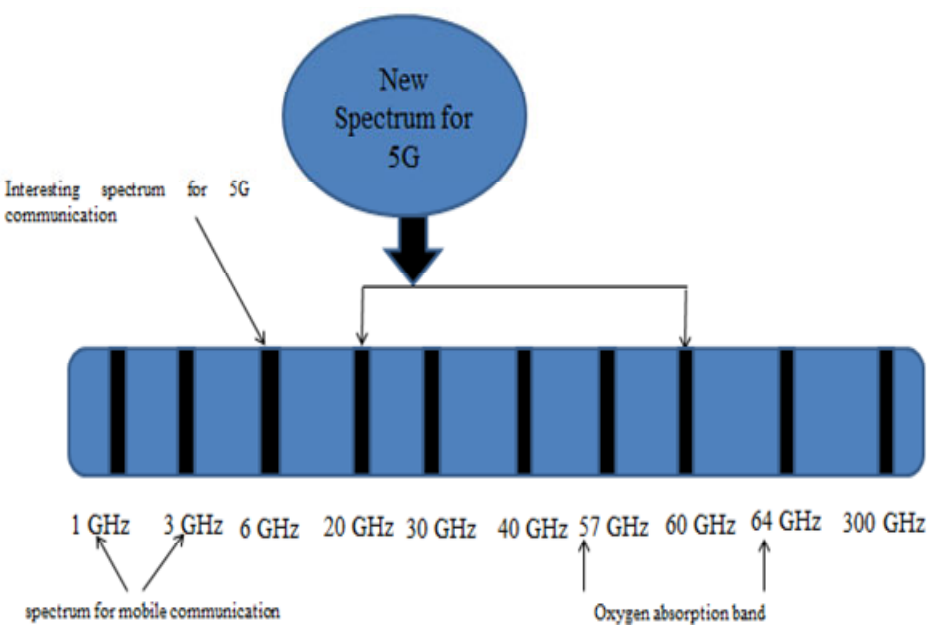

2.1 Expected features of 5G

1 Multi-gigabit per second (Gbps) data rates is ten times higher than existing LTE.

2 Ability to support higher data traffic growth.

3 Latency will be very less around 1ms which makes it 10 times faster as compared to 4G.

4 Wide bandwidth of 5 GHz and more to support large a number of connected devices.

5 It will provide mobile networks everywhere.

6 Low power consumption.

7 High efficiency (GSMA Intelligence, 2014).

2.2 Architecture of 5G

The excessive use of smartphones increases more multimedia traffic. For 88% of total mobile data, a load on the mobile network is due to the 26% smartphone users. Figure 3 shows the exploration of 5G services like the internet of things (IoT), device to device (D2D) communications, internet of vehicles (IOV), and machine to machine (M2M) communications. The latest changes in the architecture connected with the radio access network (RAN), smart antennas, mm-wave physical layer technology, design of the directional antenna, beamforming algorithms, and massive multiple-input-multiple-output (MIMO) technologies have been reviewed. The author has also discussed and reviewed MAC layer protocol and multiplexing schemes like SDMA, IDMA to support a new physical layer with energy and cost efficiencies involved during the implementation of 5G. Further, the author has shown the unused high-frequency mm-wave spectrum possibility for 5G in the 3–300 GHz band. The requirements of 5G are gigabit data rates, high bandwidth, low latency, full coverage, and high energy efficiency (Agival et al., 2016; Rappaport et al., 2014).

Figure 3 5G network architecture (see online version for colours)

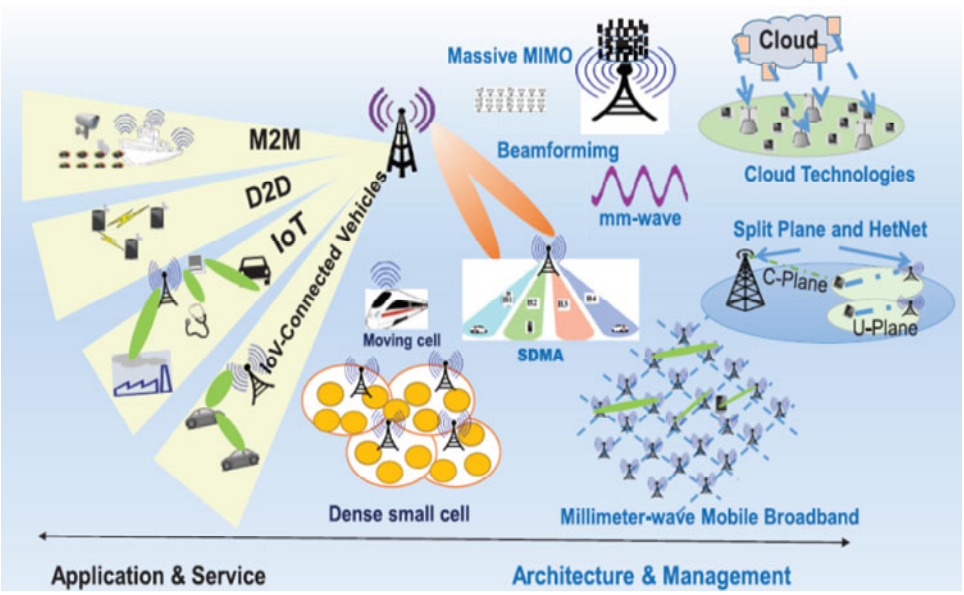

3 5G requirements

According to 5G technology, the high-speed trains will also have high-speed data whose desired value of downlink will be 200,000 devices/km^2, and user throughputs are DL: 50 Mbps, UL: 25 Mbps. The latency for the high-speed train would be 5 ms which is very less as compared to previous wireless technologies. The network should be available at any place and all time in emergency communication and battery life should be at least for one week which is also the basic requirement of 5G communication. The most attractive feature of 5G communication will contribute to the smart city in which user throughput desired values are DL: 300 Mbps, UL: 60 Mbps and traffic density 700 Gbps/km^2, Connection density is 200,000 devices/km^2.

Table 1 Some of the most requirements of 5G

Use cases	*Requirements*	*Desired value*
High-speed trains	Traffic density	Downlink:100 Gbps/km^2
	User throughput	Downlink:100 Gbps/km^2
	Mobility	500 kmph
	Latency	10 ms
Autonomous vehicle	Latency	5 ms
Control	Availability	99 %
	Reliability	99 %
Emergency	Availability	99 %victim discovery rate
Communication	EE	One-week battery life
Smart City	User throughput	DL: 350Mbps, UL: 80Mbps
	Traffic density	700 Gbps/km^2
	Connection density	Connection density 200,000
	200,000 devices/km^2	devices/km^2
Broadband to home	CD	5,000 devices/km^2
	Traffic density	60 Gbps/km^2
Zero-second switching	Switching time	10 ms
Zero latency and response times	Delay	< 1 ms

Source: Osseiran et al. (2016) and ICT-317669 METIS Project (2013)

4 Methods to achieve 5G requirements

Due to limited bandwidth at the existing spectrum, network providers are looking for mm-waves at which a huge unused spectrum ranging from 3–300 GHz is available to use for 5G communications. The expected aspects, as well as limitations of the millimetre waves, are considered properly before to implement in 5G. The mm-wave keep the size of the antenna miniaturised through which a large number of small antennas are located to increase the directivity as well as data on the network (Agival et al., 2018).

Table 2 5G security and challenges

Reference	*Security issues*	*Challenges*	*Method*
Maurer (1993)	Problem to generate a shared secret key	Implementation of cryptographic systems on given noisy communication channels.	Cryptographic coding error-control coding should be combined
Ulltveit-Moe et al. (2011)	Privacy of the network	Mobile devices will store more important information and transactions	Location-aware mIPS architecture
Li et al. (2011)	DOS attack	Security and prevention of DoS attack	Adaptive frequency hopping QoS physical layer parameter estimation
Shiu et al. (2011)	Security of information transfer through wireless networks	At the physical layer, jamming and eavesdropping are two primary attacks	Theoretical secure capacity, channel coding power, and signal detection
Yan et al. (2012)	Theoretical secure capacity, channel coding power, and signal detection	Smart grid communication security	Pervasive computing and sensing technologies heterogeneous network
Yang et al. (2015)	Physical layer security	High data rate, ultra-low latency, ultra wide coverage	Massive MIMO, mm-wave
Ghanem and Ara (2015)	Physical layer security	has to increase the secrecy rates in wireless clouds	D2D cooperation with adaptive and distributed algorithms
Trappe (2015)	Physical layer security	Confidentiality and authentication of physical layer	Channel need to be dynamic
Dabbagh et al. (2015)	Network Security	Forwarding plane attacks and counter measures, Packet Encryption and Tunnel Bypassing, Replay attacks, DDoS attack	SDN gives the following advantages, global network self-healing mechanism, additional control capabilities
Abd-Elrahman et al. (2015)	D2D communications security	Efficient encryption, decryption, encrypted information retrieval, attribute-based encryption, Attacks on available bands, reliability, and integrity of identities	Using IBE, introduced a secure group communication mechanism
Deng et al. (2015)	Physical layer security	Safeguarding massive MIMO HetNets	Linear zero-forcing beamforming (ZFBF), BS deployment density
Wang et al. (2016b)	Physical layer security	In the presence of multiple eavesdroppers, downlink secure transmission	Massive MIMO HetNets, BS deployment density

Table 2 5G security and challenges (continued)

Reference	*Security issues*	*Challenges*	*Method*
Luo et al. (2015)	Physical layer security	Physical layer security of D2D link	Stackelberg game frame to model D2D
Fan et al. (2015)	RFID security, privacy security	One application RFID tag	Revocation scheme in multi-application RFID, this scheme provides a higher level of security
Schneider and Hor (2015)	Security for 5G mobile	Potential security requirements, flexible security	Usage of virtual network functions (VNFs)
Dubrova et al. (2015)	5G security	without increasing bandwidth, detection of random and Malicious errors	New cryptographically secure CRC
Farhang et al. (2015)	Physical layer security	physical layer location privacy issues	To provide a decentralised algorithm for access point selection a matching game framework is established, to the mobile user, differentially private and distributed matching algorithm has been developed
Liyanage et al. (2015)	5G security	Security for software-defined networking (SDN), Network function virtualisation (NFV), cloud computing	Host Identity Protocol (HIP), IPSec tunnelling, leverage software-defined monitoring, data collection
Wang et al. (2016a)	Physical layer security in multi-tier HCN	Evaluate secrecy performance in HCNs	Access threshold-based secrecy mobile association policy which provides maximum truncated average received signal power
Abualhaol and Muegge (2016)	Physical layer security in multi-tier HCN	Evaluate secrecy performance in HCNs	Access threshold-based secrecy mobile association policy which provides maximum truncated average received signal power
Sedidi and Kumar (2016)	Physical layer security in multi-tier HCN	Evaluate secrecy performance in HCNs	Access threshold-based secrecy mobile association policy which provides maximum truncated average received signal power
Xu et al. (2016)	IOT communication security enhancement	Security against eavesdropping	To enhance the secrecy, relay transmission has been used
Nguyen et al. (2016)	Secure 5G wireless Communication transmission	Energy harvesting, enhance security performance	Multiple DF relays and multiple antennas to enhance security performance and energy harvesting

Table 2 5G security and challenges (continued)

Reference	*Security issues*	*Challenges*	*Method*
Qin et al. (2016)	Physical layer security	Enhancing secrecy performance	NOMA protocol in large-scale networks
Duan and Wang (2016)	Secure context information transformation	5G heterogeneous network security (HetNets), difficulty in small cell security key management small cells.	Authentication and its help to overcome frequent handover, in order to enhance authentication accuracy, it is applied in Neyman Pearson (NP) hypothesis test
Liyanage et al. (2016)	Mobile network security	Security is only at the perimeter, lack of adaptation, Lack of interoperability, vulnerability to various attacks, lack of visibility	SDN provides network function virtualisation (NFV), common device standards
Zappone et al. (2016)	Secure transmission in 5G	Energy efficient resources allocation	Artificial noise with statistical channel state information (CSI) maximising secrecy ee
Bernardo and de Leon (2016)	Physical layer security, Massive MIMO efficiency	Eavesdropping channel state information	Heterogeneous with massive MIMO technology which minimise the total power consumption with physical layer security, deployed multiple low powered small cell
Wang et al. (2016c)	Physical layer security	Jamming, interference cancellation, co-channel	introduced new technology ultra dense network provide security of physical layer, eavesdropping
Yan et al. (2015)	5Gsecurity issues	Security frame for VN and software defined network (SDN)	NFVI, SF as a service, trust functions as a service
Tian et al. (2017)	Cloud radio access network security	Eavesdropping, CR node impersonation attack wireless channel threats, MAC layer attack, Common control channel threats	Authentication
Chen et al. (2016)	SDN security	mobile network security problem, SDN, NFV security issues, decoy attacks, centralised control mode, programmability, APP authorisation	classification of SDMN is achieved by STRIDE method
Ericsson (2018)	5G security	communication security, resilience	SNOW 3G, AES-CTR, and ZUC and IA based on SNOW 3G, AES-CMAC and ZUC

Table 3 Modulation schemes and techniques for 5G technology

Sr. no.	*Type of modulation*	*Modulation scheme*	*Complexity*	*Compatibility with Massive MIMO/MM-wave*
Xu et al. (2016b)	WDM-FDM bidirectional	QPSK, 16QAM, 64QAM	High	Yes
Femenias et al. (2017)	OFDM	FBMC/OQAM	Low	MIMO-OFDM, MIMO-FBMC/OQAM
Patcharamaneepakorn et al. (2016)	Spatial modulation	Space-shift keying (SSK)	-	Massive MIMO
Takahashi et al. (2017)	TDD	CP-OFDM	-	MIMO
McCune and Delft (2018)	OFDM	-	-	MM-wave
Nagul (2018)	OFDM	FBMC, UFMC, GFDM,	High	MIMO
Song et al. (2017)	Spatial modulation	SM MIMO/MM-wave	-	MIMO/MM-wave
Ortega-Ortega et al. (2017)	OFDMA	M-QAM+LDPC codes+IFDMA	Low	-
Cheng et al. (2018)	Index modulation	IM-OFDM, MIMO-OFDM-IM, IM (OFDM-IQ-IM)	Low/high	MIMO
Basar (2016a)	Index modulation	IM spatial modulation and OFDM, IM-GSM-ESM QSM	Low	MIMO
Mrkic et al. (2017)	Index modulation	IM-OFDM, dual hop OFDM-IM-SM	Low	MIMO
Cai et al. (2017)	OFDM	OFDM with OMA, non-orthogonal MA	Low	MIMO
Gong et al. (2017)	OFDM	Green OFDMA-PONS	Low	MIMO
Aivazyan et al. (2016)	OFDM	-	-	MM-wave
Banelli et al. (2014)	OFDM/OFDMA	SC-FDMA, FBMC, FBMC-QAM	-	MIMO/MM-wave
Ayanoglu (2016)	OFDM	FQAM, NOMA, CE-OFDM, FQAM	-	MIMO
Majeed et al. (2018)	3D modulation	Used beam hoping	-	MIMO

Table 3 Modulation schemes and techniques for 5G technology (continued)

Sr. no.	*Type of modulation*	*Modulation scheme*	*Complexity*	*Compatibility with Massive MIMO/MM-wave*
Djordjevic et al. (2017)	Multidimensional coded modulation	OAM based, LDPC-coded, multidimensional signalling schemes	-	-
Basar (2016b)	OFDM-IM	MIMO-OFDM-IM	Low	MIMO
Fan et al.(2017)	Spatial modulation	SM-MIMO	-	MIMO
Altabas et al.(2017)	NOMA	NOMA-multi-CAP	Low	-
Correia and Carvalho (2018)	High order backscatter modulation	OFDM, bank of band pass filter, QAM	-	-
Hazareena and Mustafa (2018)	OFDM	FBMC, UFMC, GFDM, F-OFDM	Moderate	MIMO
Hadani et al. (2017)	Orthogonal time frequency space modulation (OTFS)	Windowing-inverse SFFT	-	-
Patcharamaneepakorn et al. (2018)	Quadrature space	QSM	-	MM-wave/MIMO
Ashour et al. (2017)	Hybrid modulation	Hybrid M-QAM/L-FSK (4/16 HQFM)	-	-
Öztürk et al. (2016)	Spatial modulation	SM-MIMO-GFDM	Low	MIMO
Browning et al. (2017)	UF-OFDM	UF-OFDM-GFDM with PAM-4 signal	-	-

Table 4 Companies working on 5G technology

Sr. no.	*Company name*	*Work*
1	Huawei	World's first 5G network with Deutche Telecom in Germany
2	Samsung	several 5G trials by Samsung has completed across Seoul
3	Intel	5G trial using (FGPA) circuits and Core i7 processors
4	Nokia	To deploy 5G network, Nokia using RAN, massive MIMO smart antennas started in 2017
5	Ericsson	With the help of FDD-Massive MIMO, it is launched 5G NR radio
6	ZTE	OFDMA, MUSA, MIMO, UFS, smooth virtual cell (SVC) is the new technologies which are developed by ZTE to implement 5G network which is based on SDN and network function virtualisation (NFV) technology respectively
7	Qualcomm	Qualcomm is working on 5G technology and trying to bring it in 2019 in collaboration with many other companies, Qualcomm will use X50 modem for 5G in devices

The propagation loss at mm-wave is calculated by Friss transmission equation is shown below:

$$L_{FSL} = 32.4 + 20\log_{10} f + 20\log_{10} R \tag{1}$$

where LFSL free space loss in dB, f is the resonant frequency in GHz and R is the distance between transmitter and receiver (Khan et al., 2012).

The attenuation of the signal propagated between 20 and 40 GHz is very low at around 0.012 dB, 0.016 dB within 200 m. The attenuation for 60 GHz is very high around 4 dB, which is due to oxygen absorption at high frequency. The impact of the rain on the signal is very high at mm-wave. The attenuation of signals is 0.9 dB/ km at the rate of light rainfall is 1mm/h and at 55 mm/h rainfall rate, the attenuation value is increased to 18.4 dB/km. The propagation losses of the signal at millimetre waves whose link possess very narrow beams could be overcome by locating a large antenna array with high gain and narrow beams (Ichkov et al., 2017).

In this section, different researchers' work has been reviewed to achieve 5G requirements using mm-waves and massive MIMO technology respectively.

4.1 Literature review on millimetre wave

In 2017, Park and Park proposed LHCP and RHCP polarised SIW antenna resonating at 28 GHz band for mm-wave applications. For 5G communication, millimetre wave antenna is an attractive topic. In this paper, the author designed an antenna array of 8 elements in which each antenna element is stacked with four layers and a feeding network mounted on substrate integrated waveguide to achieve gains of 13.09 dBi and 13.52 dBi respectively. In 2016, Shorbagy et al. proposed the different designs of the antenna to achieve 5G objectives. In the first design, slots have been introduced on a patch to get a dual-band of 28 GHz and 38 GHz, respectively. The proposed antenna is circularly polarised and utilised a single microstrip feed line for excitation. The proposed design achieved a high gain through the array to overcome the propagation loss in mm-wave. In 2nd design, a slim PIFA antenna is designed to increase the gain and obtain wide bandwidth and more efficiency with a single layer dielectric load of a superstrate,

furthermore, a slim planar inverted-F antenna is designed through a single superstrate layer with a dielectric load to improve the gain, impedance bandwidth, and efficiency. PIFA is mostly used for the miniaturisation of the antenna because of its low profile. In further design, the author has used a T-shaped patch antenna to operate in the mm-wave range. In 2016a, Xu et al. further proposed a millimetre-wave antenna for 5G applications. This design has been used as the amalgamation of tapered open-ended rectangular waveguide working as the probe antenna and patch antenna array resonating at 28 GHz to meet the requirements of 5G technology. The array of 4 × 4 elements using the structure edge coupled parasitic patch for wireless personal area network (WPAN) at 60 GHz has been designed by Lee and Yoon (2017). In the proposed design, the coplanar waveguide (CPW) feed network is used to obtain wide bandwidth. In 2011, Pi and Khan analysed the suitability of different mm-wave frequencies for mobile communication. The millimetre-wave range in the band of 3–300 GHz can conceivably give the transmission capacity required for portable broadband applications. Millimetre broadband transmission (MMB) has narrow beamwidth so that the interference among MMB base stations is very less than the traditional cellular systems. Millimetre-wave correspondence frameworks that can accomplish multigigabit information rates with the existing separation up to a couple of kilometres as of now for the point-to-point communications. In 2015, Qiao et al. discussed the scope of millimetre-wave communication technology for the 5G cellular network to provide ultra-high data for the cell phone. He has also introduced a mm-wave in the direction of the 4G system architecture with TDMA based on MAC structure. The D2D communications are used to provide direct connections between the two wireless devices in the conventional mobile network. In 2014, Roh et al. demonstrated that the mm-wave band is the best candidate for 5G cellular systems. He has presented the simulation results of a novel hybrid beamforming scheme and its link. He has measured the performance parameters of a patch antenna and antenna array of the same physical size at 3 GHz and 30 GHz by placing them at the ends of the anechoic chamber. The demonstration showed the same propagation loss is observed when a single patch and antenna array are used at the transmitter and receiver sides respectively. It is also observed that the measured received power is 20 dB higher in the case of the antenna array at 30 GHz than that of a patch antenna at 3 GHz while using these antennae at the transmitter and receiver ends respectively. The advanced hybrid beamforming algorithm in the analogue and digital domain for high directionality of the signal is described. In 2017, an antenna for millimetre-wave communications using SIW is designed (Passia et al., 2017). The proposed design is implemented using complementary split-ring resonators (CSRR) adjacently inside the cavity and a radiating slot is etched on its wall considering the antenna an option for mm-wave and 5G.

In 2017, for upcoming wireless technology, i.e., 5G smartphone applications, the Stanley et al. (2017) designed a millimetre-wave phased array antenna. The proposed planar inverted-F antenna with an open slot on FR4 substrate covers the 26–32 GHz bands and achieved a wide band of 6 GHz. In 2017, Zhang et al. discussed issues involved in the mm-wave band to design an antenna for 5G applications in which the shape of the antenna elements can be crossed, circles, or hexagon. To achieve more cover of mm-wave communication, distributed antenna systems along with antenna for implementing mm-wave cellular networks, network security, path loss is also discussed. The beamforming technologies are widely used for mobile communications at mm-wave for the reduction of path loss. In this paper, the author has used different arrays to

evaluate the radiation pattern of all array structure. The four types of antenna arrays are used to study the 5G requirements. It is also observed that the circular shaped array achieves higher gain and directivity as compared to other array structures. In Rappaport et al. (2013) the discussion on the shortage of the global bandwidth for wireless carriers and utilisation of the mm-wave spectrum for future generation 5G has been carried out. In this research paper, the authors have conducted propagation measurements at 28 GHz and 38 GHz and penetration of the mm-wave in building and reflection characteristics in the urban environments. These surveys show that when the base station is having 200 metres cell radius, the unchanged coverage can be achieved. Due to the nature of the denser urban environment, it is also observed that the reflection coefficients were higher. The value of reflection coefficients for tinged glass is 0.896 and clear non-tinged glass is 0.740. In the New Delhi city, the penetration losses for outdoor materials were higher so that the propagation of the signals cannot be properly through the materials on the outside of the building. Because of this, repeaters, data shower, access points need to be installed at the entrance of the buildings for proper propagation without any loss of the signals. In 2017, Yao et al. have proposed an array of antennas which is a diametric curvedly tapered slot antenna. The substrate integrated waveguide is used to feed the antipodal curvedly tapered slot antenna (ACTSA) which gives a circularly polarised field. The substrate integrated waveguide is used to feed the antipodal curved tapered slot antenna generating the circularly polarised field. With the help of two metal sheets on two sides of the rectangular substrate, the circular polarisation is achieved. In this research work, a CP 16-element antenna array of high gain has been designed which covers the frequency band from 81 GHz to 95 GHz with a high gain of 18.5 × 1.3 dBi which is suitable for 5G upper E band W band, respectively.

4.2 Massive MIMO

Massive MIMO means a group of an antenna array located in a small area to increase the directivity, data rate and to serve many terminals that are connected to it. Massive MIMO technology multiplies the capacity of the wireless spectrum without using more spectrum. Nowadays, massive MIMO becomes the key to deploy the next future generation beyond present 4G, i.e., 5G (Ghadyani and Shahzadi, 2018; Panwar et al., 2016).

Figure 4 Massive MIMO antenna arrays connected to many terminals (see online version for colours)

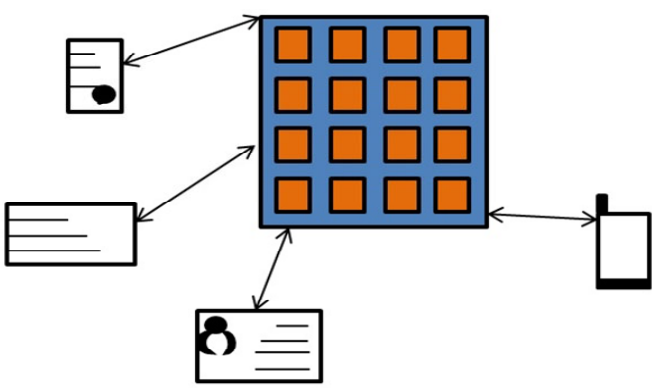

4.2.1 Benefits of massive MIMO

1 Superior spectral efficiency: At the same time, frequency resource, high spectral efficiency can be obtained by spatial multiplexing of many terminals. Different terminals require channels for efficient spectral efficiency. The massive MIMO work in the line of sight as well as in a rich scattering environment.

2 Efficient energy efficiency: By increasing the large array, it reduces the radiated power but through linear processing achieves excellent efficiency (Marzetta et al., 2016; Rajoria et al., 2018).

4.2.2 Characteristics of massive MIMO

1 Fully digital processing: Fully digital signal processing along with the improvement in performance and energy efficiency get much better. The signals from all antennas are processed digitally and it measures the complete channel response on the uplink channel and removes the erroneous signals.

2 The OFDM and single-carrier transmission is used for massive MIMO technology. The low-cost pre-coding/decoding algorithms used for the zero-forcing method are also known as conjugate beamforming. As the base station antennas increases, the gain of the antenna also increases. The phenomenon of channel hardening that happens in MIMO if the number of antennas or base stations in massive MIMO increases then the number of single-antenna user terminals increase. With the same basic effect, the correlation matrix becomes a diagonal matrix (Buzzi and D'Andrea, 2016; Nordrum, 2016; Larsson et al., 2014; Björnson et al., 2016; Abuibaid and Aldirmaz Çolak, 2017) increasingly.

4.2.3 Literature review on massive MIMO technology

In 2014, Larsson et al. have presented an overview of massive MIMO and its potential, limiting factors, and the concept for the next future generation. Massive MIMO is a technology that uses large antenna arrays to serve a large number of terminals at the same time. To increases the capacity of the network, spatial multiplexing is used in massive MIMO. The concept of massive MIMO is that using large antenna arrays focuses all of its energy with extreme sharpness in small space regions. The conventional MIMO uses expensive ultra-linear 50-watt amplifiers which are replaced by 100-watt inexpensive amplifiers output power ranging only a few milliwatts. The massive MIMO technology offers a lot of benefits over conventional MIMO in terms of se, ee, and low cost. In 2016, Yaacoub et al. investigated different configurations like rectangular, circular, and cylindrical for the massive MIMO scheme for 5G. It is observed that planar antenna arrays obtain directivity that leads to an enhanced gain in the desired direction and thereby creating low side lobes in the undesired direction. Planar configurations of the arrays are formed with linear arrays placed parallel to each other. The cylindrical configuration of the arrays is formed with the help of placing circular arrays, one above the other, i.e., stacking which formed linear arrays in the vertical direction. The circular stacking in cylindrical arrays increased the directivity and gain. In 2016, Obara et al. conducted the experiment of 28 GHz band for 5G super wideband transmission. The trial of this experiment is used to calculate the effectiveness of 28 GHz band with a bandwidth

of 800 MHz for 5G mobile communication systems. As we know that at a higher frequency, path loss increases and to compensate for this higher path loss, spatially multiplexed massive MIMO is the promising technology to achieve large capacity. In 2014, Andrews et al. discussed the definition of 5G, requirements, challenges, and expected spectrum that may be used in 5G. The key technologies to get 1,000 times data rate is achieved through:

a highly densification and offloading to improve the area spectral efficiency

b moving towards into mm-wave spectrum through which the bandwidth is increased.

c by using massive MIMO, spectral efficiency increased.

In 2017, Hussain et al. proposed an existing 4G and the latest coming 5G technology. The proposed design is used multiple-input-multiple-output (MIMO) antenna. The two reactive loaded monopoles are used in MIMO. In 2016, Li et al. designed dual-polarised hybrid eight antenna arrays using multi-input-multi-output (MIMO) which operates in 2.6 GHz bands which meet the requirements of 5G applications. The two different four antenna array, i.e., C-shaped coupled-fed and L-shaped monopole slot which gives orthogonal polarisation by placing the antenna array symmetrically on the corner of the substrate. In Haraz et al. (2015), the proposed design consists of three elements operated in 28 GHz band at millimetre-wave (mm-wave) and for the future 5th generation wireless communications. In this design, the author has used MIMO PIFA operating at three bands. The proposed antenna has achieved 807 MHz bandwidth. For frequencies in millimetre waves, there is high losses are observed, but using PIFAs substrate with lower relative permittivity in the air these losses may reduce that is the main reason to choose PIFA for designing an antenna to meet the requirements of 5G. In Khan and Singh (2018), a new algorithm sparse channel estimation has been proposed for massive MIMO on the basis of discrete fourier transform (DFT) channel estimation to separate channel tabs from the noise space and thereby reducing the minimum mean square error at the receiving end. In Chinnadurai et al. (2017), a robust beamforming design is proposed using joint user clustering and power allocation (JUCPA) algorithm which shows good performance as compared to an already existing non-orthogonal multiple access (NOMA) and conventional orthogonal multiple access (OMA) schemes. In 5G wireless communications, weighted sum-rate maximisation (WSRM) fails for multicell multiple input multiple outputs (MIMO) and non-orthogonal multiple access (NOMA) downlink system. This has solved the proposed robust beamforming design. The generalised frequency division multiplexing (GFDM) is another multiplexing scheme that is serving an alternate option for 5G communications. But for the GFDM system, the synchronisation problem which is caused by the carrier frequency offset (CFO) is very crucial. In 2018, Chang and Ueng have been proposed a turbo receiver to overcome the problem of carrier frequency offset (CFO). It is also observed in this research work, GFDM system with index modulation (IM) has achieved better performance. In 2018, Zhang et al. have proposed a block Bayesian matching pursuit (BBMP) based channel estimation which resolved the problem of taking more pilot overhead for downlink CSI acquisition in a frequency division duplex system. Massive MIMO is the key technology to implement 5G wireless communications which is a large number of antennas located in a small area to increase spectral efficiency and gain. In 2016, Tiwari and Rao have proposed a 60 GHz planar switched beam antenna array using the butler matrix feed network. In this research work, the proposed antenna is fabricated using a substrate

integrated waveguide (SIW), which has a low cost and provides the planar design. In 2016, Yang et al. proposed a butler matrix on SIW technology which achieves beam steering, a gain of 17.5 dBi and return loss, isolation less than –10 dB at 60 GHz respectively. The butler matrix has the capability of beamforming and scanning property which is used to design phased array antenna and with SIW technology using slot arrays, it improves the performance of the antenna at millimetre wave for 5G communications.

5 Li-Fi technology towards 5G communication

Li-Fi is the latest technology for fast transmission of the signal which uses a light emitting diode (LEDs) called wireless optical network technology. For optical data transmission, Li-Fi, LED bulbs are used which has a chip that modulates the light inconspicuous. It uses the concept of visible light communication (VLC) in the visible light spectrum to obtain secured high-speed wireless communication. The single LED source has 8 Gbps data rate which is obtained in 2016. The single point to point wireless communication created by VLC between LED light source and receiver uses the photodetection device like photodetector. The data rate increases up to 10 Gbps with a strong LED source. The data rate depends on types of light technology like phosphor coated blue LED, RGB LED, GaN micro-LED, RGB lasers. The different light colours of LED were created with the help of the combination of three primary colours red, blue, green. The white LED is considered as the source of next future wireless technology which is created by mixing these primary colours. As compared to other LEDs, white LED has more efficiency, and power consumption is low, low voltage, long lifetime respectively (Haas, 2018; Komine and Nakagawa, 2004).

Figure 5 Indoor wireless networking using the Li-Fi attocell networks concept (see online version for colours)

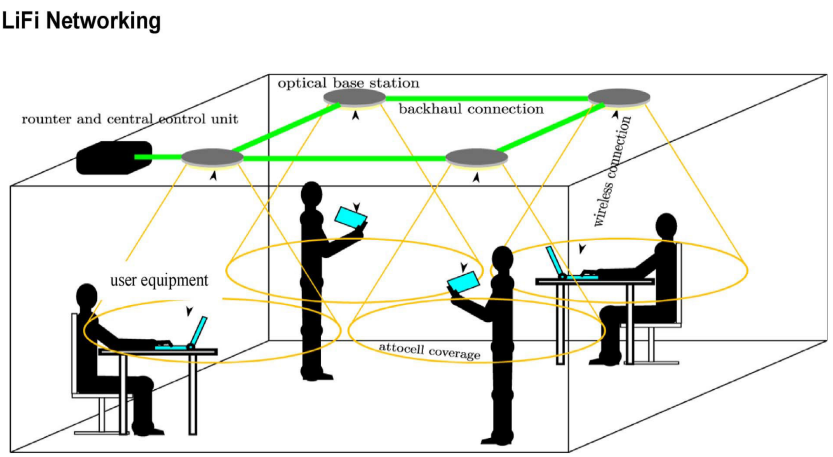

Source: Haas (2018)

In Bao et al. (2014), the VLC-OFDMA network model is proposed which consists of M VLC hotspots, LTE, one access point (AP) to resolve multi-users access problems. As VLC has the limitations of the limited range of the communication, the author has

investigated the different light source, merits, and demerits of the VLC systems as compared to RF communication. The visible light communication seems like a boon for 5G communication in respect of high speed, highly efficient transmission of the signals without any attenuation. Radio frequency communication has the limitation of the limited spectrum and it is almost allocated, therefore visible light communication also known as optical wireless communication came into the picture for replacement of RF communication, which may be a better option for indoor communication as it is free from interference which reduces the need of high power from the base station. The spectrum in the visible range is fully unused from 428 to 750 THz, which has the availability of very high bandwidth which gives high definition video, very high-speed file transfer and these are the basic requirements of 5G communication. The mobility of VLC is very low due to the narrow beamwidth of the light source. For a wide range of communication, the white LEDs are more suitable which determines the signal to noise ratio (SNR) (Wu et al., 2014).

6 Challenges to achieve 5G requirements

As millimetre-wave signals are prone to high path loss, it will be a challenge to achieve high efficiency. At mm-wave, the hardware design is not an easy task as compared to hardware design at low-frequency ranges. To achieve 5G requirements, one has to implement more antennas within less space called massive MIMO, which could increase the cost and complexity of the antenna fabrication, and at the same time, it is sensitive to beam alignment. Usually, the ultra-narrow beam is sensitive to the orientation of the antennas.

7 Conclusions

The summary of all the research that is going to deploy 5G beyond 2020 is studied in this paper. Different modulation schemes, as well as techniques, have been studied like SM MIMO/MM-wave, M-QAM+LDPC codes+IFDMA, IM spatial modulation, and OFDM, MIMO-OFDM-IM, BMC/OQAM which increases spectral efficiency and coverage of the network at any time and place. It is also observed from this literature, modulation techniques performed well as compared to conventional OFDM. The security issues are the problem with all existing wireless technologies, as different authors proposed many algorithms to secure the 5G network, which has been studied in this literature. The security of the physical layer, D2D communication, 5G mobile network, cloud radio access radio, SDN is the challenging task in 5G wireless technology. Moreover, security and privacy are the key focus, so 5G will have extra abilities to ensure that customer information is protected and harder to hack. Many researchers looking for technologies like the mm-wave spectrum are carrying out many experiments on the E and W bands to achieve wide bandwidth and massive MIMO is one of the most interesting technology in which a large number of antenna arrays are used for high spectrum efficiency in implementing in the future mobile broadband communications with low cost and latency.

8 Future scope

As all over the countries working on 5G technology, which will be deployed in 2020. Europe and the U.S. are going to launch new generation mobile technology in 2019-2020. With the help of this new technology, users can feel ultra-high speed internet. Different methods and requirements to implement 5G wireless communications technology are studied in this article. It can be concluded that 5G technology needs more work on low-efficiency problems at millimetre waves and massive MIMO consume more power because of huge antenna arrays located in less space. It is also observed that substrate integrated waveguide improves the efficiency as well as gain at the 5G spectrum. A group of Finland researchers is working on a new wireless technology called 6G which will be better than 5G. It can be seen as new possibilities with artificial intelligence, virtual reality and IOT. A group of Nokia research and development centre working on 5G at present and in the future they will start work on 6G technology. The University of Oulu is working on a 5G test network with 60 groups. 5GTN may be called the first 6G network. 6G will provide 1Tbps internet network speed and the latency will be improved with the help of artificial intelligence.

References

Abd-Elrahman, E., Ibn-Khedher, H. and Afifi, H. (2015) 'D2D group communications security', *Proc. Int. Conf. Protocol Eng. (ICPE)*, July, pp.1–6.

Abualhaol, I. and Muegge, S. (2016) 'Securing D2D wireless links by continuous authenticity with legitimacy patterns', *Proc. 49th Hawaii Int. Conf. Syst. Sci. (HICSS)*, January, pp.5763–5771.

Abuibaid, M.A. and Aldirmaz Çolak, S. (2017) 'Energy-efficient massive MIMO system: exploiting user location distribution variation', *AEU-International Journal of Electronics and Communications*, Vol. 72, pp.17–25.

Agival, M., Roy, A. and Saxena, N. (2016) 'Next generation 5G wireless networks: a comprehensive survey', *IEEE Communications Surveys and Tutorials*, February, Vol. 18, No. 3, pp.1617–1655.

Agival, M., Saxena, N. and Roy, A. (2018) 'Ten commandments of emerging 5G networks', *Wireless Personal Communication*, Vol. 98, No. 3, pp.9591–2621.

Aivazyan, M., Avetisyan, H., Grigoryan, L. and Babayan, A. (2016) 'Waveform modulation for the 5G mobile telecommunication systems', *IEEE East-West Design & Test Symposium (EWDTS)*.

Al-Samman, A.M., Rahman, T.A., Azmi, M.H. and Hindia M.N. (2016) 'Large-scale path loss models and time dispersion in an outdoor line-of-sight environment for 5G wireless communications', *AEU-International Journal of Electronics and Communications*, September, Vol. 70, No. 11, pp.1515–1521.

Altabas, J.A., Rommel, S., Puerta. R., Izquierdo. D., Garces, J.I., Lazaro, J.A., Olmos, V. and Tafur Monroy, I. (2017) 'Nonorthogonal multiple access and carrierless amplitude phase modulation for flexible multiuser provisioning in 5G mobile networks', *Journal of Lightwave Technology*, Vol. 35, No. 24, pp.5456–5463.

Andrews, J.G., Suzzi, B., Choi, W., Hanly, S.V., Lozano, A., Anthony, C. and Zhang, J.C. (2014) 'What will be 5G', *IEEE Journal on Selected Areas in Communications*, Vol. 32, No. 6, pp.1065–1082.

Ashour, A.F., ElAttar. H. and Aboul Dahab, M. (2017) 'Efficiency improvement using adaptive hybrid modulation/coding/frequency selection scheme for future 5G wireless network', *IEEE 17th International Conference on Communication Technology (ICCT)*, pp.1392–1396.

Ayanoglu, E. (2016) '5G today: modulation technique alternatives', *International Conference on Computing, Networking and Communications (ICNC)*, pp.1–5.

Ban, L., Li. C., Sim, C.Y., Wu, G. and Wong, L. (2016) '4G/5G multiple antennas for future multi-mode smartphone applications', *IEEE Access*, June, Vol. 4 pp.2981–2988.

Banelli, P., Buzzi, S., Colavolpe. G., Modenini, A., Rusek, F. and Ugolini, A. (2014) 'Modulation formats and waveforms for 5G networks: who will be the heir of OFDM?: An overview of alternative modulation schemes for improved spectral efficiency', *IEEE Signal Processing Magazine*, Vol. 31, No. 6, pp.80–93.

Bao, X., Zhu, X., Song, T. and Ou, Y. (2014) 'Protocol design and capacity analysis in hybrid network of visible light communication and OFDMA systems', *IEEE Transactions on Vehicular Technology*, Vol. 63, No. 4, pp.1770–1778.

Basar, E. (2016a) 'Index modulation techniques for 5G wireless networks', *IEEE Communications Magazine*, Vol. 54, No. 7, pp.168–175.

Basar, E. (2016b) 'On multiple-input multiple-output OFDM with index modulation for next generation wireless networks', *IEEE Transactions on Signal Processing*, Vol. 64, No. 15, pp.3868–3878.

Bernardo, N.I. and de Leon, F. (2016) 'On the trade-off between physical layer security and energy efficiency of massive MIMO with small cells', *Proc. Int. Conf. Adv. Technol. Commun. (ATC)*, pp.135–140.

Björnson, E., Larsson, G. and Marzetta, T.L. (2016) 'Massive MIMO: ten myths and one critical question', *IEEE Communications Magazine*, Vol. 54, No. 2, pp.114–123.

Browning, C., Farhang. A., Saljoghei, A., Marchetti, N., Vujicic, V., Doyle, L.E. and Barry, L.P. (2017) '5G wireless and wired convergence in a passive optical network using UF-OFDM and GFDM', *IEEE International Conference on Communications Workshops (ICC Workshops)*.

Buzzi, S. and D'Andrea, C. (2016) 'Are mmwave low-complexity beamforming structures energy-efficient? Analysis of the Downlink MU-MIMO', *IEEE Globecom Workshops*.

Cai, Y., Qin, Z., Cui, F., Li, G. and McCann, A.J. (2017) 'Modulation and multiple access for 5G networks', *IEEE Communications Surveys & Tutorials*, Vol. 20, No. 1, pp.629–646.

Calin, D. (2015) 'Technologies for future broadband wireless evolution', *IEEE 14th Canadian Workshop on Information Theory (CWIT)*, July, pp.58–61.

Chang, Y. and Ueng, F.B. (2018) 'A novel turbo GFDM-IM receiver for MIMO communications', *AEU-International Journal of Electronics and Communications*, Vol. 87, pp.22–32.

Chen, M., Qian, Y., Mao, S., Tang, W. and Yang, X. (2016) 'Software-defined mobile networks security', *Mobile Networks and Applications*, October, Vol. 21, No. 5, pp.729–743.

Cheng, X., Zhang, M., Wen, M. and Yang, L. (2018) 'Index modulation for 5G: striving to do more with less', *IEEE Wireless Communications*, Vol. 25, No. 2, pp.126–132, May.

Chinnadurai, S., Selvaprabhu, P., Jeong, Y., Sarker, A.L. and Lee, M. (2017) 'User clustering and robust beamforming design in multicell MIMO-NOMA system for 5G communications', *AEU-International Journal of Electronics and Communications*, Vol. 78, pp.181–191.

Cisco (2015) *Visual Networking Index*, White paper [online] https://www.Cisco.com.

Correia, R. and Carvalho, N.B. (2018) 'OFDM-like high order backscatter modulation', *IEEE MTT-S International Microwave Workshop Series on 5G Hardware and System Technologies (IMWS-5G)*.

Dabbagh, M., Hamdaoui, B., Guizani, M. and Rayes, A. (2015) 'Software-defined networking security: pros and cons', *IEEE Communications Magazine*, Vol. 53, No. 6, pp.73–79.

Deng, Y., Wang, L., Wong, K., Nallanathan, A., Elkashlan, M. and Lambotharan, S. (2015) 'Safeguarding massive MIMO aided HetNets using physical layer security', *Proc. Int. Conf. Wireless Commun. Signal Process. (WCSP)*, 1–5 October.

Djordjevic, I.B., Zhang, S. and Wang, T. (2017) 'Multidimensional coded modulation for wireless communications beyond 5G', *13th International Conference on Advanced Technologies, Systems and Services in Telecommunications (TELSIKS)*, pp.293–299.

Duan, X. and Wang, X. (2016) 'Fast authentication in 5G HetNet through SDN enabled weighted secure-context-information transfer', *Proc. IEEE Int. Conf. Commun. (ICC)*, 1–6 May.

Dubrova, E., Näslund, M. and Selander, G. (2015) 'CRC-based message authentication for 5G mobile technology', *Proc. IEEE Trust-com/BigDataSE/ISPA*, August, pp.1186–1191.

Ericsson (2018)*5G Security-Enabling a Trustworthy 5G System*, White paper.

Fan, K., Gong, Y., Du. Z., Li. H. and Yang, Y.P (2015) 'RFID secure application revocation for IoT in 5G', *Proc. IEEE Trustcom/BigDataSE/I*SPA, August, pp.175–181.

Fan, S., Xiao, Y., Lei, X., Shi, R., Deng, K. and Li, S. (2017) 'Multi-user detection for spatial modulation toward 5G wireless communications', *China Communications*, Vol. 14, No. 12, pp.100–110.

Farhang, S., Hayel, Y. and Zhu, Q. (2015) 'PHY-layer location privacy-preserving access point selection mechanism in next-generation wireless networks', *Proc. IEEE Conf. Commun. Netw. Secur. (CNS)*, September, pp.263–271.

Femenias, G., Riera-Palou, F., Mestre, X. and Olmos, J. (2017) 'Downlink scheduling and resource allocation for 5G MIMO-multicarrier: OFDM vs FBMC/OQAM', *IEEE Access*, July, Vol. 5, pp.13370–13786.

Firdaus, A.A. and Indarto E. (2016) 'Optical network design for 4G long term evolution distribution network in Sleman', *IEEE International Seminar on Application for Technology of Information and Communication (ISEMANTIC)*, August, pp.332–335.

Ghadyani, M. and Shahzadi, A. (2018) 'Compressive sensing power control for interference management in D2D underlaid massive MIMO systems', *AEU-International Journal of Electronics and Communications*, June, Vol. 90, pp.79–87.

Ghanem, S. and Ara, M. (2015) 'Secure communications with D2D cooperation', *International Conference on Communications, Signal Processing, and their Applications*, February, pp.1–6.

Gong, X., Guo, L. and Zhang, Q. (2017) 'Joint allocation of time, virtual subcarrier and modulation for 5G green OFDMA-PONs', *IEEE Global Communications Conference*.

GSMA Intelligence (2014) *Understanding 5G: Perspectives on future technological advancements in mobile*, White paper.

Haas, H. (2018) 'LiFi is a paradigm-shifting 5G technology', *Review in Physics*, Vol. 3, pp.26–31.

Hadani, R., Rakib, S., Molisch, A.F., Ibars, C., Monk, A., Tsatsanis, M., Delfeld, J, Goldsmith, A. and Calderbank, R. (2017) 'Orthogonal time frequency space (OTFS) modulation for millimeter-wave communications systems', *IEEE MTT-S International Microwave Symposium (IMS)*, pp.681–683.

Hansen, J.A.E. (2017) *5G and its Economic Aspects-Literature Review and Selection of a Connection Portfolio Under Risk*, Master's thesis, NTNU.

Haraz, O.M., Ashraf. M. and Alshebeili, S. (2015) 'Single-Band PIFA MIMO antenna system design for future 5G wireless communication applications', *IEEE 11th International Conference on Wireless and Mobile Computing, Networking and Communications (WiMob)*, pp.608–612.

Hazareena, A. and Mustafa, A. (2018) 'A survey: on the waveforms for 5G', *Second International Conference on Electronics, Communication and Aerospace Technology (ICECA)*.

Huang, H. (2018) 'Overview of antenna designs and considerations in 5G cellular phones', *International Workshop on Antenna Technology (iWAT)*, March.

Hussain, R., Alreshaid, A.T., Podilchak, S.K. and Sharawi, M.S. (2017) 'Compact 4G MIMO antenna integrated with a 5G array for current and future mobile handsets', *IET Microwaves, Antennas and Propagation*, Vol. 11, No. 2, pp.271–279.

Ichkov, A., Atanasovski, V. and Gavrilovska, L. (2017) 'Potentials for application of millimeter wave communications in cellular networks', *Wireless Personal Communication*, January, Vol. 92, No. 1, pp.279–295.

ICT-317669 METIS Project (2013) *Scenarios, Requirements and KPIs for 5G Mobile and Wireless System*, Deliverable D1.1.

Khan, F., Pi, Z. and Rajagopal, S. (2012) 'Millimeter-wave Mobile Broadband with Large Scale Spatial processing for 5G mobile communication', *50th Annual Allerton Conference on Communication, Control, and Computing (Allerton)*, pp.1517–1523.

Khan, I. and Singh. D. (2018) 'Efficient compressive sensing based sparse channel estimation for 5G massive MIMO systems', *AEU-International Journal of Electronics and Communications*, Vol. 89, pp.181–190.

Komine, T. and Nakagawa, M. (2004) 'Fundamental analysis for visible-light communication system using LED Lights', *IEEE Transactions on Consumer Electronics*, Vol. 50, No. 1, pp.100–107.

Krishnamoorthy, V. and Mathi, S. (2012) 'Security enhancement of handover key management based on media access control address in 4G LTE networks', *Computational Intelligence and Computing Research (ICCIC)*, December.

Larsson, E.G., Edfors, O., Tufvesson, F. and Marzetta, T.L. (2014) 'Massive MIMO for next generation wireless systems', *IEEE Communications Magazine*, February, Vol. 52, No. 2, pp.186–195.

Lee, B. and Yoon, Y. (2017) 'Low profile, low cost, broadband millimeter-wave antenna array for high data rate WPAN systems', *IEEE Antennas and Wireless Propagation Letters*, Vol. 99, pp.1957–1960.

Li, M.Y., Ban, Y.L., Xu, Z.Q., Wu, G., Chow-Yen-Desmond, S.I.M., Kang, K. and Yu, Z-F. (2016) 'Eight-port orthogonally dual-polarized antenna array for 5G smartphone applications', *IEEE Transactions on Antennas and Propagation*, Vol. 64, No. 9, pp.3820–3830.

Li, Y., Kaur, B. and Andersen, B. (2011) 'Denial of service prevention for 5G', *Wireless Pers. Commun.*, Vol. 57, No. 3, pp.365–376.

Liyanage, M., Abro, A.B., Ylianttila, M. and Gurtov, A. (2016) 'Opportunities and challenges of software-defined mobile networks in network security', *IEEE Security Privacy*, Vol. 14, No. 4, pp.34–44.

Liyanage, M., Ahmed. I., Ylianttila. M., Llorente Santos, J., Kantola Aaltom R., Perez, O., Itzazelaia, M., de Oca, E. and Valtierra, A. (2015) 'Security for future software defined mobile networks', *9th International Conference on Next Generation Mobile Applications, Services and Technologies*, September, pp.256–264.

Luo, Y., Cui, L., Yang, Y. and Gao, B. (2015) 'Power control and channel access for physical-layer security of D2D underlay communication', *Proc. Int. Conf. Wireless Commun. Signal Process. (WCSP)*, 1–5 October.

Majeed, E., Youssef, Z., Dominik Mueck M., Karls, I., Drewes. C., Bruck, G. and Jung, P. (2018) 'Concept design of three-dimensional modulation using beam hopping for 5G network', *IEEE Wireless Communications and Networking Conference (WCNC)*.

Marzetta, T., Larsson, E.G., Yang, H. and Ngo, Q. (2016) *Fundamentals of Massive MIMO*, Cambridge University Press, Cambridge.

Maurer, U.M. (1993) 'Secret key agreement by public discussion from common information', *IEEE Trans. Inf. Theory*, May, Vol. 39, No. 3, pp.733–742.

McCune, E. and Delft, T.U. (2018) '5G-nr bandwidth efficient modulation options for efficient link operation that are compatible with mmW transistor nonlinearities', *IEEE 5G World Forum (5GWF)*, July, pp.289–293.

Mrkic, J., Kocan, E. and Pejanovic-Djurisic, M. (2017) 'Index modulation techniques in OFDM relay systems for 5G wireless networks', *40th International Conference on Telecommunications and Signal Processing (TSP)*, pp.208–211.

Nagul, S. (2018) 'A review on 5G modulation schemes and their comparisons for future wireless communications', *Conference on Signal Processing and Communication Engineering Systems, (SPACES)*, January, pp.72–76.

Nguyen, N., Duong, T., Ngo. H., Hadzi-Velkov, Z. and Shu, L. (2016) 'Secure 5G wireless communications: a joint relay selection and wireless power transfer approach', *IEEE Access*. Vol. 3, pp.3349–3359.

Nordrum, A. (2016) '5G researchers set new world record for spectrum efficiency', *IEEE Spectr*., May [online] http://spectrum.ieee.org/techtalk/telecom/wireless/5gresearchers-achieve-new-spectrum-efficiency-record.

Obara, T., Inoue, Y., Aoki, Y., Suyama, S., Lee, J. and Okumurav, Y. (2016) 'Experiment of 28 GHz Band 5G super wideband transmission using beamforming and beam tracking in high mobility environment', *IEEE 27th Annual International Symposium on Personal, Indoor, and Mobile Radio Communications (PIMRC)*, pp.1–5.

Ohishi, T., Oodachi, N., Sekine, S. and Shoki, H. (2005) 'A method to improve the correlation coefficient and the mutual coupling for diversity antenna', *IEEE Propag. Soc. Int. Symp. Dig*., July, pp.507–510.

Ortega-Ortega, L., Andrés, F. and Bravo-Torres, J. (2017) 'Combining LDPC codes, M-QAM modulations, and IFDMA multiple-access to achieve 5G requirements', *International Conference on Electronics, Communications and Computers (CONIELECOMP)*.

Osseiran, A., Monserrat, F. and Marsch, P. (2016) *5G Mobile Wireless Communications Technology*.

Öztürk, E., Basar, E. and Çırpan, H.A. (2016) 'Spatial modulation GFDM: a low complexity MIMO-GFDM system for 5G wireless networks', *IEEE International Black Sea Conference on Communications and Networking.*

Panwar, N., Sharma, S. and Singh, A.K. (2016) 'A survey on 5G: The next generation of mobile communication', *Physical Communication*, March, Vol. 18, pp.64–84.

Park, S. and Park, O. (2017) 'LHCP and RHCP substrate integrated waveguide antenna arrays for millimeter-wave applications', *IEEE Antennas and Wireless Propagation Letters*, July, Vol. 16, pp.601–604.

Passia, M-T., Nitas, M. and Yioultsis, T.V. (2017) 'A fully planar antenna for millimeter-wave and 5G communications based on a new CSRR-enhanced substrate-integrated waveguide', *IEEE International Workshop on Antenna Technology: Small Antennas, Innovative Structure and Applications (iWAT)*, March.

Patcharamaneepakorn, P., Wang, C., Fu, Y., El-Hadi. M. Aggoune, M., Alwakeel, M., Tao, X. and Ge, X. (2018) 'Quadrature space-frequency index modulation for energy-efficient 5G wireless communication systems', *IEEE Transactions on Communications*, Vol. 66, No. 7, pp.3050–3064.

Patcharamaneepakorn, P., Wu, S., Wang, C-X., el-Hadi, M., Aggoune, M., Alwakeel, M., Xiaohu, G. and Di Renzo, M. (2016) 'Spectral, energy, and economic efficiency of 5G multicell massive MIMO systems with generalized spatial modulation', *IEEE Transactions on Vehicular Technology*, Vol. 65, No. 12, pp.9715–9731.

Pi, Z. and Khan, F. (2011) 'An introduction to millimeter-wave mobile broadband systems', *IEEE Communication Magazine*, June, Vol. 49, No. 6, pp.101–107.

Pirinen, P. (2014) 'A brief overview of 5G research activities', *IEEE International Conference on 5G for Ubiquitous Connectivity (5GU)*, November, pp.17–22.

PPP, G. (2015) '5G vision (the next generation of communication networks and services)', The 5G infrastructure public private partnership [online] https://5g-ppp.eu/wpcontent/uploads/2015/02/5G-Vision-Brochure-v1. pdf.

Qiao, J., Shen, X., Mark. J.W., Shen. Q., He, Y. and Lei, L. (2015) 'Enabling device-to-device communications in millimeter-wave 5G cellular networks', *IEEE Communications Magazine*, January, Vol. 53, No. 1, pp.209–215.

Qin, Z., Liu. Y., Ding, Z., Gao, Y. and Elkashlan, M. (2016) 'Physical layer security for 5G non-orthogonal multiple access in large-scale networks', *Proc. IEEE Int. Conf. Commun. (ICC)*, 1–6 May.

Rajoria, S., Trivedi, A. and Godfrey, W. (2018) 'A comprehensive survey: small cell meets massive MIMO', *Physical Communication*, February, Vol. 26, pp.40–49.

Rappaport, T.S., Roh, T. and Cheun, K. (2014) 'Wireless engineers long considered high frequencies worthless for cellular systems. They couldn't be more wrong', *IEEE Spectr.*, September, Vol. 51, No. 9, pp.34–58.

Rappaport, T.S., Sun, S., Mayzus, R., Zhao, H., Azar, Y., Wang, K., Wong, G., Schulz, J.K., Samimi, M. and Gutierrez, F. (2013) 'Millimeter wave mobile communications for 5G cellular: it will work', *IEEE Access*, May, Vol. 1, pp.335–349..

Rawat, A., Yadav, R. and Shrivastava, S.C. (2012) 'Neural network applications in smart antenna arrays: a review', *AEU-International Journal of Electronics and Communications*, March, Vol. 66, No. 11, pp.903–912.

Roh, W., Seol, J-Y., Park, J., Lee, B., Lee, J., Kim, Y., Cho, J., Cheun, K. and Aryanfar, F. (2014) 'Millimeter-wave beamforming as an enabling technology for 5G cellular communications: theortical feasibility and prototype results', *IEEE Communications Magazine*, February, Vol. 52, No. 2, pppp.106–113.

Schneider, P. and Horn, G. (2015) 'Towards 5G security', *Proc. Trustcom/BigDataSE/ISPA*, August, pp.1165–1170.

Sedidi, R. and Kumar, A. (2016) 'Key exchange protocols for secure device-to device (D2D) communication in 5G', *Proc. Wireless Days (WD)*, March, pp.1–6.

Shiu, Y.S., Chang, S.Y., Wu, H.C., Huang, S.C.H. and Chen, H.H. (2011) 'Physical layer security in wireless networks: a tutorial', *IEEE Wireless Commun.*, April, Vol. 18, No. 2, pp.66–74.

Shorbagy, M.E., Shubair, R.M., AIHajri, M.I. and Mallat, N.K. (2016) 'On the design of millimetre-wave antennas for 5G', *IEEE Microwave Symposium (MMS)*.

Song, J., He, L. and Wang. J. (2017) 'Reducing RF resource for 5G communication networks: a spatial modulation motivated approach', *Asia-Pacific Conference on Communications (APCC)*, December.

Stanley, M., Huang, Y., Loh, T., Xu, Q., Wang. H. and Zhou, H. (2017) 'A high gain steerable millimeter-wave antenna array for 5G smartphone applications', *IEEE 11th European Conference on Antennas and Propagation (EUCAP)*, March.

Su, W., Liu, Q., He, H. and Hang, H. (2010) 'A new context awareness scheme for multi-mode mobile terminals in mobile internet', *Proc. IET 3rd Int. Conf. IET Wireless, Mobile Multimedia Network*, September, pp.95–98.

Takahashi, Y., Inoue, Y., Yoshioka, S., Kishiyama, Y., Suyama, S., Mashino, J., Okumura, Y., Haruna, T., Tanaka, T., Splett, A. and Liljeström, H. (2017) 'Field experimental evaluation of higher rank MIMO in quad-directional UE antenna configuration for 5G radio access system', *The 20th International Symposium on Wireless Personal Multimedia Communications (WPMC)*, pp.542–546.

Tian, F., Zhang, P. and Yan, Z. (2017) 'A survey on C-RAN security', *IEEE Access*, June, Vol. 5, pp.13372–13386.

Tiwari, N. and Rao, T.R. (2016) 'A switched beam antenna array with butler matrix networkusing substrate integrated waveguide technology for 60 GHz wireless communications', *AEU-International Journal of Electronics and Communications*, Vol. 70, pp.850–856.

Trappe, W. (2015) 'The challenges facing physical layer security', *IEEE Commun. Mag.*, Vol. 53, No. 6, pp.16–20.

Ulltveit-Moe, N., Oleshchuk, V.A. and Køien, G.M. (2011) 'Location-aware mobile intrusion detection with enhanced privacy in a 5G context', *Wireless Pers Commun.*, Vol. 57, No. 3, pp.317–338.

Wang, H.M., Zheng. T.X., Yuan. J., Towsley. D. and Lee, M.H. (2016a) 'Physical layer security in heterogeneous cellular networks', *IEEE Trans. Commun.*, Vol. 64, No. 3, pp.1204–1219.

Wang, L., Wong, K.K. and Elkashlan, M. (2016b) 'Secrecy and energy efficiency in massive MIMO aided heterogeneous C-RAN: a new look at interference', *IEEE Journal of Selected Topics in Signal Processing*, Vol. 10, No. 8, pp.1375–1389.

Wang, Y., Miao, Z. and Jiao, L. (2016c) 'Safeguarding the ultra-dense networks with the aid of physical layer security: a review and a case study', *IEEE Access*, Vol. 4, pp.9082–9092.

Wu, S., Wang, H. and Youn, C.H. (2014) 'Visible light communications for 5G wireless networking systems: from fixed to mobile communications', *IEEE Network*, Vol. 28, No. 6, pp.41–45.

Xu, B., Helander, J., Ericsson, A., Ying, Z., He, S., Gustafsson, M. and Sjöberg, D. (2016a) 'Investigation of planar near-field measurement of millimeter-wave antenna for 5G application', *IEEE International Symposium on Antennas and Propagation (ISAP)*, pp.600–601.

Xu, M., Yan, J.H., Zhang, J., Lu, F., Wang, J., Cheng, L., Guidotti, D. and Chang, G.K. (2016b) 'Bidirectional fiber-wireless access technology for 5G mobile spectral aggregation and cell densification', *IEEE/OSA Journal of Optical Communications and Networking*, December, Vol. 8, No. 12, pp.104–110.

Xu, Q., Ren, P., Song, H. and Du, Q. (2016c) 'Security enhancement for IoT communications exposed to eavesdroppers with uncertain locations', *IEEE Access* Vol. 4, pp.2840–2853.

Yaacoub, E., Husseini, M. and Ghaziri, H. (2016) 'An overview of research topics and challenges for 5G massive MIMO antennas', *IEEE Middle East Conference on Antennas and Propagation (MECAP)*, pp.1–4.

Yan, Y., Qian, Y., Sharif, H. and Tipper, D. (2012) 'A survey on cyber security for smart grid communications', *IEEE Commun. Surveys Tuts.*, Vol. 14, No. 4, pp.998–1010.

Yan, Z., Zhang, P. and Vasilakos, A.V. (2015) 'A security and trust framework for virtualized networks and software-defined networking', *Secur. Commun. Netw.*, Vol. 9, No. 16, pp.3059–3069.

Yang, N., Wang. L., Geraci, G., Elkashlan, M., Yuan, J. and Di Renzo, M. (2015) 'Safeguarding 5G wireless communication networks using physical layer security', *IEEE Commun. Mag.*, Vol. 53, No. 4, pp.20–27.

Yang, Q.L., Ban, Y.L., Kang, K., Chow-Yen-Desmond, S.I.M. and Wu, G. (2016) 'SIW multibeam array for 5G mobile devices', *IEEE Access*, Vol. 4, pp.2788–2796.

Yao, Y., Cheng. X., Wang. C., Yu. J. and Chen. X. (2017) 'Wideband circularly polarized antipodal curvedly tapered slot antenna array for 5G applications', *IEEE Journal on Selected Areas in Communications*, July, Vol. 35, No. 7, pp.1539–1549.

Zappone, A., Lin, P. and Jorswieck. E. (2016) 'Artificial-noise-assisted energy-efficient secure transmission in 5G with imperfect CSIT and antenna correlation', *IEEE 17th International Workshop on Signal Processing Advances in Wireless Communications (SPAWC)*.

Zhang, J., Ge. X., Li, Q., Guizani, M. and Zhang, Y. (2017) '5G millimeter-wave antenna array: design and challenges', *IEEE Wireless Communications*, April, Vol. 2, No. 2, pp.106–112.

Zhang, R., Zhang, J., Gao, Y. and Zhao, H. (2018) 'Block Bayesian matching pursuit based channel estimation for FDD massive MIMO system', *AEU-International Journal of Electronics and Communications*, Vol. 93, pp.296–304.

Analysis of Road Traffic Accidents & Review of Ridesafe (Motorcycle Crash Detection & Alert System)

Afzal Hannan, Bhavit Yadav, Chirag Yadav

Abstract— This research paper deals with motorcycle road accidents and show how certain simple technologies such as a mobile application and a small hardware setup can improve and enhance overall response time over critical situations such as a crash or an accident through communication which leads to prompt medical treatment for the injured. Presents study of Ridesafe, an Android Mobile Application that provides a platform for motorcycle riders to inform their contacts about the crash so that there is information of the potential accident scenario even after the crash took place. This highlights that an automated crash emergency information mobile application is better than the traditional way of information communication of crash. The conclusion is validated by data.

Index Terms—crash detection & alert system, first aid, mobile android application, road traffic accidents(RTA).

1 INTRODUCTION

This paper is intended to search for all the available information which might help to validate the fact that a road accidents deaths are preventable if given prompt medical attention to the wounded or injured. Deaths caused by road accidents are due to increase in number of vehicles, disobeying of traffic rules and risky attitude while driving. This information has been gathered from newspaper articles. Websites, journals, databases and some government websites for an overview of recent years. [4]

The number of vehicles are increasing day by day and so are accidents, resulting in large numbers of deaths due to them. Two wheeler vehicles are among the most affected. Most of such accidents causes deaths due to lack of immediate medical help can be observed on urban roads, rural roads and highways.

A system that detects an accident and alerts the knowns can help in faster medical aid, thus comes the idea of a motorcycle crash detection and alert system that detects potential accidents and sends a message to given saved contacts about it. The system will check for an accident with the help of a hardware setup and via a mobile application will send the location using a google maps link of the area of the accident to three contacts via SMS.

The proposed system provides a low cost solution to two vehicle wheeler riders to avoid delay in communications in case of a potential accident.

To lower fatality rate number an improved motorcycle crash detection and alert system is presented. The system consists a gyroscope and an Android based mobile device along with a Bluetooth module HC06 for connectivity purposes of the hardware and mobile application.

The previous work regarding vehicle safety instrument was a complete hardware model which could be fixed in the vehicle without the use of any smartphone. It contained a SIM card module share location and had an integrated accelerometer to measure the speed of the vehicle, whereas our model uses a Bluetooth device to share data and uses the accelerometer present in our modern day smartphones. Our vehicle safety instrument is derived from this model and has the following advantages over its predecessor:

- Reduced assembly time: An additional accelerometer and SIM module increases the assembly time. Thus our model takes less assembly time.
- Accessibility: A mobile phone is mundanely available thus increasing accessibility.
- Features: A smartphone also has a better computing power, storage and other sensors thus adding onto more features such as creating an accident database, checking location with nearby accidents, noting down accident prone areas, etc. All such features can be added easily with an Android application.
- Cost: Cost is significantly reduced as we don't use a different SIM Card (and a telecom plan) and accelerometer. The SIM Card and accelerometer are both present in a modern day smartphone. We use a Bluetooth device to connect the smartphone with our model.
- Chances of failure: SIM card module is hard to manage as it is a very small component and might lose in an accident, thus failing the model. However, usually a smartphone is very well taken care of.

- *Afzal Hannan is currently pursuing B.Tech degree program in Computer Engineering at Delhi technological University, Delhi, PH-+91 8447192604. E-mail: Afzal.hannan@gmail.com*
- *Bhavit Yadav is currently pursuing B.Tech degree program in Computer Engineering at Delhi technological University, Delhi, PH-+91 8588039271. E-mail: bhavit.yadav@gmail.com*
- *Chirag Yadav is currently pursuing B.Tech degree program in Computer Engineering in Delhi technological University, Delhi, PH-+91 7838021768. E-mail: cyadav015@gmail.com*

2 Road Traffic Accidents (RTA)

This section examines the recent road traffic accidents scenario of our country in an overview by comparing fatality rates & injuries with respect to year 2016-2017.

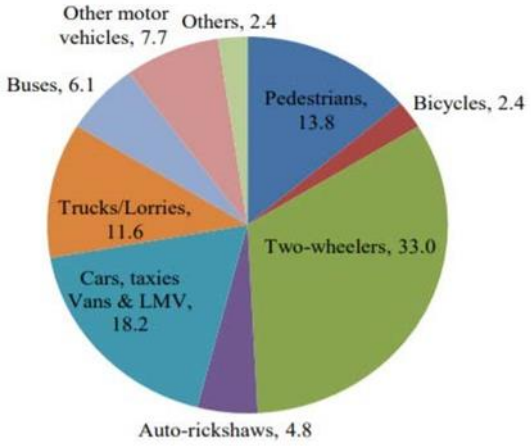

Figure 1: Share of different vehicles in road accidents (year 2017 and 2016)

Road traffic accident (RTA) is a nationwide concern and also one of the vital avoidable public health tie-up and is increasing which can be linked to increase in the number of vehicles (especially 2-wheelers) and enlarging lifestyle development and risky mindset. A total of 4,64,910 road accidents have been reported by States and Union Territories (UTs) in the year 2017, which took 1,47,913 lives and caused injuries to 4,70,975 persons. Among vehicle categories involved in road accidents, two-wheelers accounted for the highest share (33.9%) in total accidents and according to 'Global status report on road safety 2013' it is on the eighth place and expected to be at the fifth place by 2030 if trends continue at the same pace (1, 7). In developing countries mortality due to RTA is projected to rise by fatalities (29.8%) in 83% provided stringent measures are not taken. 2017.

The fatality rate due to RTA in South Asia was 10.2/100,000 persons in the year 2000 which is predicted to rise to 18.9/100,000 persons by the year 2020 (predicted to change by:

Table 1: Depicts deaths by various vehicles for years 2017 and 2016

Road-user category	Persons killed 2016	Persons killed 2017
Pedestrian	15,746 *(10.5)*	20,457 *(13.8)*
Bicycles	2,585 *(1.7)*	3,559 *(2.4)*
Two-wheelers*	52,500 *(34.8)*	48,746 *(33.0)*
Auto-Rickshaws	7,150 *(4.7)*	7,167 *(4.8)*
Cars, Taxis, Vans & LMVs	26,923 *(17.9)*	26,869 *(18.2)*
Trucks/Lorries	16,876 *(11.2)*	17,158 *(11.6)*
Buses	9,969 *(6.6)*	9,069 *(6.1)*
Other Motor Vehicles (including e-rickshaw)	15,988 *(10.6)*	11,410 *(7.7)*
Others (Animals drawn vehicle, cycle rickshaws, hand carts, & other persons)	3,048 *(2.0)*	3,479 *(2.4)*
Total	**1,50,785**	**1,47,913**

*Two-wheelers include motor cycles, scooters, mopeds and scooty.

144 %) lower and upper middle class account for 91% of the global mortality due to RTA although these countries have only about 50% of the world's vehicles [8].

Given below are some of the adverse effects:

1. Economic: RTAs cost US $518 billion globally. In developing nations a loss of about $100 billion/year occurs because of accidents. As a result of RTAs, the affected families have to put up with the cost of extended medical care, bear the loss of wage earner take additional care of the disabled which ultimately leads them to poverty because the expenses are borne exclusively by the family of the disabled .In India itself the gross domestic product lost due to RTAs was 1-3% in the year 200809 . RTAs also contributes to the massive burden on the health sector (e.g. pre hospital and acute care as well as rehabilitation). Lack of road safety leads to spending of 20 billion/year in India which corresponds to food requirements of half of the countries malnourished children [2]
2. Physical health: Around 30-50 million people are injured or disabled in an accident. More than three fifth of brain injuries was caused by RTAs. Head and neck injuries leads to major spinal and brain damage.
3. RTAs also effect on the psychological and social well-being aspect of a person along with his/her family.

3 Prompt Medical Help in RTA

The world health organization states that 50% of deaths in accidents can be prevented by prompt medical care if given with 30-60 minutes of the accident. First aid is the initial care given to the injured before a proper medical treatment begins. The first aid can be the difference between life and death if a person receives it before a medical help and also helps the wounded to recover faster.

Critical four minutes: When a person meets with an accident, after the impact when the air supply is blocked there is loss of oxygen that can cause death. Therefore the first four minutes becomes crucial.

The 'golden hour': The person has a greater chance of survival if first aid is given within an hour of an injury.

The first aid in emergency situations involves techniques that enhance the preparedness and trigger immediate response to health emergencies. Evidence proves that first aid are the life saving measures when given to person immediately enhances the chance of survival an even reduced consequences of injuries.

If information like location and time of such accidents or injuries can be communicated to the right contact at the right time and prompt medical help is provided it might help change the fatality rate of such accidents in our country.

4 Review of RideSafe

RideSafe is a system consists of an android mobile application as well as a small hardware setup. To overcome fatality rate number an improved bike accident detection and alert system is presented. The system consists of two modules namely an accelerometer cum gyroscope and GPS (Global Positioning System) cum GSM (Global system for Mobile) module of the

mobile device are used along with a Bluetooth module.
The main target is to make accident detection and alert detection for two wheeler vehicles as they are most vulnerable to accidents. The system detects the crash and sends the location of the driver in the form of a small message along with a link of location. There is no delay in communication and the medical help can reach the person faster even if the person is unable to communicate the information. Notification of such occurrence place and important role in analysis of the situation and better response time. The time of occurrence of the accident and the time of arrival of the medical health is an indicator to most of the survival cases. [5]
In the proposed system, biomechanics of the bike such as lean angle and data of various sensors such as accelerometer and gyroscope from the hardware and mobile device sensor (accelerometer) are integrated and studied to identify potential accident scenario. The same model can be applied to cycling, skiing and running etc. Features:

4.1 Architecture of the System

The proposed system consists of a crash detection hardware setup and an android mobile application on a smartphone. Sensors will constantly monitor the two wheeler vehicles orientation and as soon as bikes posture changes abnormally it sends an alert message to the synced contacts via SMS and location using GPRS of the mobile device.[1]

4.2 Accident Detection System

The MPU-650 sensor is a calibrated gyroscope cum accelerometer that is connected to the arduino uno. Further arduino is connected to a bluetooth module (HC06). As the vehicle falls or there is a potential crash the readings of the sensors would change abruptly the arduino signals bluetooth to communicate to the android application to send the alert SMS with location. [1]

4.3 Bluetooth Connection with Smartphone

The android mobile application and the hardware have independent bluetooth modules. Hardware has HC06 module and mobile application uses the bluetooth of the inbuilt mobile device. The information flow between the hardware setup and the mobile device take place by a bluetooth as it is efficient for small range connectivity. 4) Mobile Android Application
An Android application is used to communicate with the Bluetooth device and this Android application will send messages with the GPS location of the accident to the three synced contacts. Android Studio is used to develop the Android application. Android Studio for Android is an open-source web application provided by Google.
Purpose:
Accelerometer and gyroscope sensor are used to determine whether an accident had occurred. The communications between the modules are done by using Bluetooth. The smart phone with the android app will send a message to the friends and family of the victim through message. Crash detection and alert systems are highly relevant in these days and this project aims at developing a low cost solution for the same for the benefit of the society.

5 Fabrication of Components

5.1 Arduino and MPU-6050

- The MPU6050 supports only I2C Communication and hence, it must be connected only to the I2C Pins of the Arduino. The I2C pins of Arduino are multiplexed with the analog input pins A4 and A5 i.e. A4 is SDA and A5 is SCL.
- Coming to the MPU6050, we have used a normal breakout board that provided eight pins. The above image shows the schematic representation of the MPU6050 Breakout board.
- In this, we will be using the SCL, SDA and the INT pins to connect with Arduino.
- Hence, the SCL Pin of the Arduino (A5) is connected to the SCL Pin of the MPU6050. Similarly, the SDA Pin of the Arduino (A4) is connected to the SDA Pin of the MPU6050 board.
- Additionally, we will be using the Interrupt feature of the MPU6050 to indicate (or interrupt) Arduino when the 1024 Byte FIFO buffer is full. So, connect the INT pin of the MPU6050 to the external interrupt 0 (INT0) pin of Arduino UNO i.e. Pin 2.
- In I2C Communication, the MPU-6050 always acts as a slave.[3]

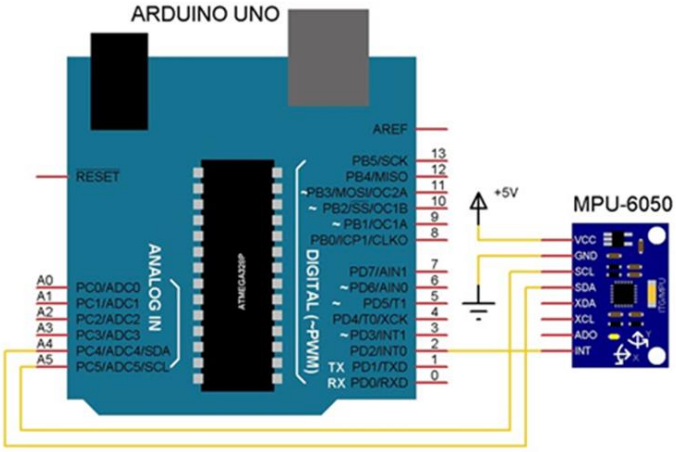

Figure 2: Connection between Arduino and MPU 6050

5.2 Arduino and HC-05 Bluetooth Module

- HC-05 is a serial port module which makes it very easy to use. If you see the pin configuration of HC-05, there are total 6 but we only need 4 middle ones for our set-up. o Connect VCC with 3.3V of Arduino, please do not connect it with 5V as that can cook the module
- Connect GND with any GND of Arduino
- Connect Rx pin with Tx of Arduino

- Connect Tx pin with Rx of Arduino

Now power-up the Uno using USB cable, a red light LED on HC-05 will start blinking, means we are ready to go forward.

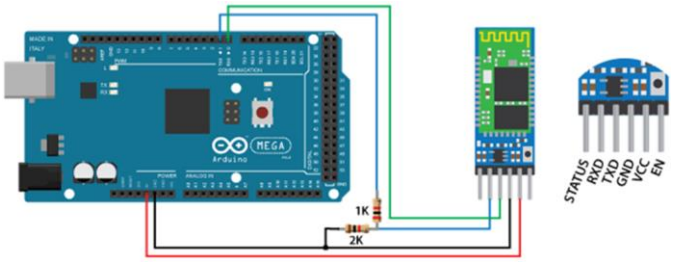

Figure 3: Connection between Arduino and HC-05 Module

5.3 How the hardware is working?

MPU-6050 Orientation Tracking – 3D Visualization
Next, in order to make the 3D visualization example we just need accept this data the Arduino is sending through the serial port in the Processing development environment. We read the incoming data from the
Arduino and put it into the appropriate Roll, Pitch and Yaw variables. In the main draw loop, we use these values to rotate the 3D object; in this case that's a simple box with a particular color and text on it. See figure to understand the Yaw, Pitch and Roll.

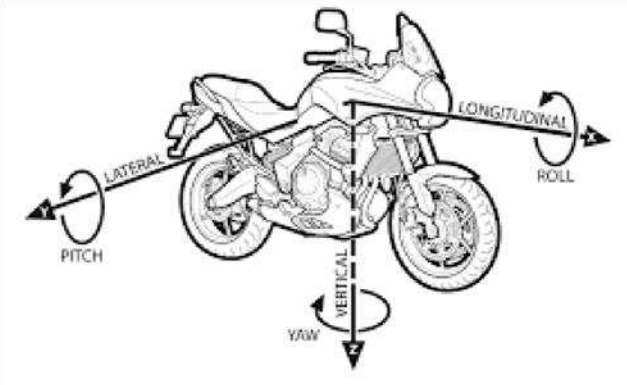

Figure 4: Yaw, Pitch and Roll variable

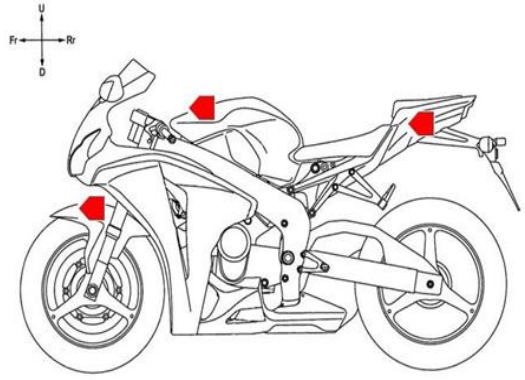

Figure 5: Bike along with sensors

The only down side is that the Yaw will drift over time because we cannot use the complementary filter for it. For improving this we need to use an additional sensor. That's usually a magnetometer which can be used as a long-term correction for the gyroscope Yaw drift. However, the MPU-6050 actually has a feature that's called Digital Motion Processor which is used for onboard calculations of the data and it's capable of eliminating the Yaw drift. below shows how sensor can be placed to get the accurate data about the orientation of the bike.

5.4 Android Application

The name of the android App is "RideSafe". The android app is a medium to read the values collected from the sensor and make a decision to send out the help message to trusted contact The Text message contains the location of the user where accident took place in the form of link which opens the Google Map.

Figure 6: Screenshot of the Android Application

6 CONCLUSION

This paper clearly depicts that fatality rate has increased globally as well as in India. Most of which are two wheeler Vehicles. Result of this analysis and review is intended to provide an insight on road traffic accidents and give an overview of recent year's scenario and how a motorcycle crash detection and alert device can benefit the person. The result of the analysis clearly shows a relationship between fatality rate and prompt medical help and how it can help reduce death numbers of accident and is validated with data. Ridesafe, Motorcycle Crash detection and Alert system performs it functionality. In addition, further works on test cases for various scenarios and improvement on accident data recording system is required and its integration with current motorcycle crash detection and alert system is recommended.

7 REFERENCES

[1] 2017 International Conference on Computer Communication and Informatics (ICCCI -2017), Jan. 05 – 07, 2017, Coimbatore, INDIA Intelligent Accident Detection and Alert System for Emergency Medical Assistance

[2] Indian Journal of Community Health 27(2):191-6 · June 2015 Road safety in India: A Public Health Concern

[3] ROAD ACCIDENTS IN INDIA – 2017 MINISTRY OF ROAD TRANSPORT & HIGHWAYS TRANSPORT RESEARCH WING NEW DELHI

[4] Civil Engineering Dimension, Vol. 12, No. 2, September 2010, 106-112 ISSN 14109530 print / ISSN 1979-570X online Factors on Motorcycle Fatal Accidents using Logistic Regression (Case Study: Denpasar-Bali) Factors on Motorcycle Fatal Accidents using Logistic Regression (Case Study: Denpasar-Bali)

[5] Vol 5, No 1 (2018) Bike Accident Detection and Alert System Minnu Maria Joseph, Thushara G., Pujari Sowmya, Xavier Arockiaraj S

[6] Kanchan T, Kulkarni V, Bakkannavar SM, Kumar N, Unnikrishnan B. Analysis of fatal road traffic accidents in a coastal township of South India. J Forensic Leg Med. 2012 Nov;19(8):448-51. doi: 10.1016/j.jflm.2012.02.031. Epub 2012 Mar 10. PubMed PMID: 23084306.[PubMed]

[7] World Health Organization. Global Status Report on Road Safety 2013: Supporting a decade of action, 2013. Available from: http://www.who.int/violence_injury_prevention/road_safety_status/2013/en/

[8] Ruikar M. National statistics of road traffic accidents in India. J Orthop Traumatol Rehabil. 2013;6(1):1. Available from: http://www.jotr.in/article.asp?issn=09757341;year=2013;volume=6;issue=1;spage=1; epage=6;aulast=Ruikar

[9] Chapter 1. Accidental Deaths in India. Available from: ncrb.nic.in/ADSI2010/accidental-deaths10.pdf

[10] Kengen Y, Renard A. Road safety in India: Insights and Analysis. India transport portal 2012. Available from: http://indiatransportportal.com/wpcontent/uploads/2012/11/Road_safety_2012.pdf

[11] Das A, Botticello AL, Wylie GR, Radhakrishnan K. Neurologic disability: a hidden epidemic for India. Neurology. 2012 Nov 20;79(21):2146-7. doi: [11].1212/WNL.0b013e3182752cdb. Review. PubMed PMID: 23170012; PubMed Central PMCID: PMC3511929.[PubMed].

[12] Farooqui JM, Chavan KD, Bangal RS, Syed MM, Thacker PJ, Alam S, Sahu S, Farooqui AA, Kalakoti P. Pattern of injury in fatal road traffic accidents in a rural area of western Maharashtra, India. Australas Med J. 2013 Sep 30;6(9):476-82. doi: 10.4066/AMJ.2013.1839. eCollection 2013. PubMed PMID: 24133540; PubMed Central PMCID: PMC3794418.[PubMed]

[13] Barffour M, Gupta S, Gururaj G, Hyder AA. Evidence-based road safety practice in India: assessment of the adequacy of publicly available data in meeting requirements for comprehensive road safety data systems. Traffic Inj Prev. 2012;13 Suppl 1:17-23. doi: 10.1080/15389588.2011.636780. PubMed PMID: 22414124.[PubMed]

[14] Pathak SM, Jindal AK, Verma AK, Mahen A. An epidemiological study of road traffic accident cases admitted in a tertiary care hospital. Med J Armed Forces India. 2014 Jan;70(1):32-5. doi: 10.1016/j.mjafi.2013.04.012. Epub 2013 Aug 30. PubMed PMID: 24623944; PubMed Central PMCID: PMC3946410.[PubMed]

[15] Rajasekaran S. The Alarming Facts of Road Accidents in India. Indian Orthopaedic Association. Available from: http://ioaindia.org/ROADTRAFFICACCIDENTS.pdf

[16] Mundi R, Chaudhry H, Flores-Miranda N, Puthukudy N, Petrisor B, Schemitsch EH, Bhandari M. Roads in India: safety and knowledge cross-sectional evaluation. J Orthop Trauma. 2014;28 Suppl 1:S30-2. doi: 10.1097/BOT.0000000000000115. PubMed PMID: 24857995.[PubMed].

[17] Krishnan M. India has the highest number of road accidents in the world. Deutsche Welle.

[18] National Crime Record Bureau. Annual Report on Road Accidents; 2010.

[19] Nantulya VM, Reich MR. The neglected epidemic: Road traffic injuries in developing countries. BMJ 2002;324:1139-41.

[20] Lagarde E. Road traffic injury is an escalating burden in Africa and deserves proportionate research efforts. PLoS Med 2007;4:e170. [PUBMED]

RESEARCH ARTICLE

Editorial Process: Submission:07/20/2021 Acceptance:05/19/2022

Antitumor Activity of *Choerospondias axillaris* Fruit Extract by Regulating the Expression of SNCAIP and SNCA on MDA-MB-231 Cells

Sonia Mann[1], Ashish Sarkar[1], Ankita Sharma[1], Rajinder K Gupta[2], Sagarika Biswas[1]*

Abstract

Objective: Cancer is a huge problem of disease globally. Today, the percentage of people die from cancer is more than a combination of various diseases. In females, most common types of malignancies that occur are breast and cervical. The present focus has been shifted on medicinal plants as a form of therapy and there is a constant need to identify new therapeutic agents. *Choerospondias axillaris* (*C. axillaris*), an underutilized fruit, has been used in the remedy of various diseases. In the present communication, we evaluated the molecular mechanism of *C. axillaris* methanol extract in regulating cell death in human breast cancer cells (MDA-MB-231). **Methods:** Methanol extract of *C. axillaris* was prepared and compounds were screened by Gas chromatography-mass spectrometry. The effect of fruit extract was determined on MDA-MB-231 cells by MTT ((3-(4, 5-dimethylthiazol-2-yl)-2, 5-diphenyltetrazolium bromide) assay and to analyse the molecular mechanism of human breast cancer cells after treating with fruit extract, protein profiling study was performed by two-dimensional gel electrophoresis. **Results:** A total 9 differentially expressed proteins were identified by matrix-assisted laser desorption/ionization-time of flight mass spectrometry (MALDI-TOF-MS/MS) analysis. Among 9 identified proteins, synphilin-1 protein was found to be significantly downregulated, validated by western blot and RT-qPCR analysis. Possible interacting partners of synphilin-1 (SNCAIP) were analyzed for their possible role in cancer by the in-silico method. **Conclusion:** Our data implicate that the presence of bioactive compound(s) in *C. axillaris* fruits might play an important role in inhibiting the proliferation of breast carcinoma cells and Synphilin-1 protein may play a role of apoptotic function.

Keywords: *Choerospondias axillaris*- Phytochemicals- GC-MS- proteomics- protein-protein interaction

Asian Pac J Cancer Prev, **23 (5)**, 1577-1586

Introduction

Breast cancer ranks second to cervical cancer in women, according to the National Cancer Registry Program (Mathur et al., 2020). It is the most frequently diagnosed malignant tumours and reported to have the largest number of deaths due to breast cancer in India and worldwide [Ayob et al., 2014, Chimplee et al., 2019). Nearly 80% population worldwide relies on traditional medicine (Oyebode et al., 2016) for their primary health care. Efforts have always been focused on discovering new anti-cancerous agents from medicinal plants and have been successfully resulted in several experimental models using natural products for the treatment (Basri et al., 2016, Mann et al., 2015, Khan et al., 2020). Therefore, traditional medicine knowledge was used to discover novel anticancer drugs (Figueroa et al., 2012). Plant-based anticancer compounds may play a significant role in cancer therapy (Abdullah et al., 2014) and has been considered to be safe with fewer side effects in comparison to the available synthetic anticancer agents (Lichota and Gwozdzinsk, 2018).

Present paper has been focused on investigating an underutilized fruit *Choerospondias axillaris* (Anacardiaceae) for its anticancer property. It is commonly known as Lupsi or Lapsi and is available in North-East India from October to January and is a native of India, China, Japan and other Asian countries. The bark of *C. axillaris* tree is used for treating secondary burns (Nguyen et al., 1996). Recently, we have reported that *C. axillaris* fruit possesses anti-oxidant and anti-inflammatory properties (Mann et al., 2020). Earlier, total flavonoid content of *C. axillaris* was reported to have therapeutic potential for treating myocardial ischemia (Li et al., 2013). Tsantan Sumtag, a traditional Tibetan medicine also consists of *C. axillaris* (Roxb.) Burtt et Hill along with other ingredients, has been reported to be used as a folk medicine for cardiovascular diseases and heart

*[1]CSIR-Institute of Genomics & Integrative Biology, Mall Road, Delhi-110007, India. [2]Department of Applied Chemistry, Delhi Technological University, New Delhi-110042, India. *For Correspondence: sagarika.biswas@igib.res.in*

failure (Dang et al., 2020).

The aim of the study was to evaluate the metabolic profile using Gas chromatography-mass spectrometry (GC-MS) and cytotoxic activities of methanol extract of *C. axillaris* fruits on human breast cancer cells and its mode of action.

Materials and Methods

Chemicals and reagents

Dulbecco's modified Eagle medium (DMEM), 3-(4,5-dimethylthiazol-2-yl)-2,5-diphenyltetrazolium bromide (MTT), 95% ethanol, methanol, dimethyl sulphoxide (DMSO), fetal bovine serum (FBS), phosphate buffer saline (PBS), antibiotics, trypan blue dye solution and trypsin ethylenediaminetetra acetic acid (EDTA) were purchased from Sigma-Aldrich (St. Louis, MO, USA).

Raw materials and preparation of crude extract

C. axillaris fruits were purchased from a local market in Kalimpong (West-Bengal), India and was recognized by a Botanist and voucher specimen from the Council of Scientific and Industrial Research (CSIR)- National Institute of Science Communication and Information Resources, Delhi, India. Fresh fruits of *C. axillaris* (100g) were washed, deseeded, grounded and 200ml methanol was added. The solution was centrifuged for 24h at 150rpm at 45˚C in an incubator shaker and filtered. The supernatant was recovered, dried under vacuum and stored at -20˚C for further analysis (Mann et al., 2016). *C. axillaris* fresh fruits were also extracted with a range of solvents depending upon the polarity (petroleum ether, n-hexane, dichloromethane, and methanol). Optimum results were obtained in methanol extract; hence only methanol extract was preceded for the present study (Mann et al., 2020).

Gas chromatography - mass spectrometry (GC-MS) analysis

Compounds present in the crude methanol extract of *C. axillaris* were identified by Agilent 6890 GC and 5975B MSD (Agilent Technologies#51832037). The extract was diluted in acetone and 1µl of the extract was injected into split injection (1:20) at 280˚C. Fused silica HP-5 ms capillary column was used for chromatographic separation. EI mode was used for eluents detection with ionization energy of 70eV. All the peaks of identified compound were compared with the spectra from the National Institute of Standards and Technology library (NIST'05) (Satpathy et al., 2011).

In vitro assay-MTT (3-(4, 5-dimethylthiazol-2-yl)-2, 5-diphenyltetrazolium bromide)

MDA-MB-231 cell line was obtained from the National Centre for cell science (NCCS), Pune, India. Cells were cultured in Dulbfecco's Modified Eagle's medium (DMEM), supplemented with 10% FBS and 1% antibiotics in an incubator at 37˚C with 5% CO_2. Cells were seeded in a 96-well plate having density 2×10^4 cells/well for 2h (Tominaga et al., 2015), incubated with various concentrations of methanol extract of the *C. axillaris* fruit (1,3,5,7,9 mg/ml) in triplicate at 37˚C in a CO_2 environment for 24h with not more than 1% final concentration of DMSO . The negative control was performed using growth medium with DMSO (1,3,5,7,9 mg/ml), while brucine (1,2,3,4,5 mg/ml) was used as the positive control. MDA-MB-231 cells without any treatment were used as control. Additionally, trauma cells (non-cancerous) were served as a healthy control (Makrane et al., 2018) generated from the tissues of trauma patients. Briefly, trauma tissues were chopped and transferred to DMEM containing collagenase (1mg/mL) and incubated for 12h at 37˚C in an incubator shaker. Cells were then transferred to T-flask after passing the digested tissues from the cell strainer of pore size-100µm and subcultured as per the needs. MTT solution (20µl) having a concentration 5mg/mL was added to each well and incubated again for 4h. After discarding the medium, solubilisation buffer was added to dissolve the formazan precipitate. The absorbance was recorded using a microtiter plate reader at 570 and 630nm (background) and the viability of the cells were determined as the percentage of live cells compared to control cells. The half-maximal inhibitory concentration (IC_{50}) of each treatment was estimated via dose-response curve.

Two-Dimensional Gel Electrophoresis (2-DE)

Protein estimation was performed by standard Bradford method. Protein (80µg) from cell lysate (*C. axillaris* treated cells and untreated cells) was solubilised for 30min with rehydration buffer (7M urea, 2M thiourea, 1% zwitterionic detergent ASB-14, 40mM Tris) and kept for 2h at room temperature (RT). The rehydrated sample was loaded on 7cm (Bio-Rad, USA) immobilized pH gradient (IPG) strip (pH- 4-7 NL strips) and kept for another 1h at RT followed by an overlay of mineral oil (Bio-Rad, USA) on the strip and overnight incubation. Proteins were then focused according to the isoelectric point using Protean Isoelectric focusing (IEF) System (Bio-Rad, USA), with the program: 250V rapid voltages ramping for 30min, 10,000V slow voltages ramping for 60min, and 10,000V rapid voltages ramping for 50KVh. After IEF, the strips were incubated for 20min in an equilibration buffer I (6M urea, 20% glycerol, 2% sodium dodecyl sulfate (SDS), 2% Dithiothreitol (DTT), and 0.375M Tris, pH 8.8) at RT followed by incubation in equilibration buffer II for an additional 20min by adding 2% iodoacetamide instead of DTT in the equilibration buffer I. The strips were then loaded onto 12% Sodium Dodecyl Sulfate Polyacrylamide Gel Electrophoresis (SDS-PAGE) and run in Mini protein gel assembly (Bio-Rad, USA) at 50V for 2.5h. A molecular standard was used to estimate the relative mass (Biswas et al., 2013). More than 3 sets of gel were run and silver stained.

Silver staining

After running 2-DE, gels were rinsed with water, followed by silver staining (Biswas et al., 2013) for spot visualization. Briefly, gels were fixed in fixative (50% methanol and 12% acetic acid) for 1h and then treated with 50% and 30% ethanol separately for 30min each. Gels were sensitized with freshly prepared sodium sulphite

(Na2S2O3) for 1min, washed with Milli Q and stained with 1M silver nitrate solution under dark. Again, gels were washed with Milli Q, and developed with sodium carbonate (60g/lt Na2CO3, 500µl/lt HCHO & 40µl//lt Na2S2O3). Once the spots appeared, further reactions were stopped by adding stop solution (6% acetic acid in MQ) (Biswas et al., 2013). All the sets of gel were silver stained and the three best sets of gel were used to make a master gel for each experimental group. The master gels were analyzed using "PDQuest" 2-D Analysis software (Bio-RAD) and significant differential protein spots with $p \leq 0.05$ were selected for further processing.

In-gel digestion and Matrix-Assisted laser Desorption/ Ionization-Time of Flight Mass Spectrometry (MALDI-TOF-MS/MS) analysis

In gel digestion was carried out according to the method of Biswas et al., 2013. The screened and selected protein spots were subjected to in-gel protein digestion and proceeded for MALDI TOF MS/MS analysis as follows. Briefly, protein spots were excised manually, washed with distilled water and then destained with 30mM potassium ferricyanide (50µl of 1:1 solution) and sodium thiosulphate (100mM). The gel pieces were further washed and dehydrated with 40µl of 1:1 acetonitrile (ACN)/water for 15min, washed with 40µl of ACN, equilibrated with 100mM ammonium bicarbonate (50µl) followed by the addition of 50µl ACN for 15min. Gel pieces were then dried using vacuum centrifugation and then digested by incubating with trypsin (10µl; 0.1µg/µl trypsin) for 45min. After incubation, 25-60µl of trypsin digestion buffer was added (5µl of 1M $CaCl_2$, 25µl of 1M NH_4CO_3) and incubated again at 37˚C overnight. The collected supernatant was then dried in a vacuum centrifuge. Extraction of peptides from the gel pieces were carried out by altering ACN and trifluoroacetic acid (TFA) concentration, sonicated for 30min in a water bath, followed by drying in speed-vac to remove TFA/ACN. The peptides were then stored at -20˚C till further use.

MALDI-TOF MS/MS (Applied Biosystems, Life Technologies, USA) was used for the determination of the molecular mass of polypeptides. Peptides (1µl) were dissolved with 1µl sinapinic acid matrix onto the MALDI target plate and dried. Spectra of MS/MS were found to be distributed within 10,000–20,000Da mass range in reflector positive mode having an intensity of 5600 laser shots. For the MS/MS precursor selection, minimum S/N (signal/noise) filter was set at 25 with an exclusion list for α-Cyano-4-hydroxycinnamic acid (CHCA) matrix peaks. Identifications of proteins were accepted with a statistically significant probability based Mowse score ($p \leq 0.05$). The protein score above 45 was considered a threshold score, having at least 2 unique peptide matches (Millares et al., 2012). However, a protein having a lower score was further validated using other technique such as Western-Blot and immunohistochemistry (IHC) (Llombart et al., 2017).

Western Blot Analysis

Protein (50µg) from cell lysate (*C. axillaris* treated cells and untreated cells) was run in 10% SDS gel using Mini protein gel assembly (Bio-Rad, USA) and transferred to the nitrocellulose membrane (NC) using Transblot semi-dry (Bio-Rad, USA). NC membrane was blocked with 5% BSA overnight. The membrane was washed 3 times with PBST (0.05% tween 20 in 1X PBS) for 10min each and then incubated for 3h with primary antibody Synphilin 1; 1:3,000 (monoclonal antibody, Santa Cruz Biotechnology; sc-365741). After washing again (3 times), the secondary antibody (polyclonal, Horseradish Peroxidase (HRP) conjugated anti-mouse (Jackson, USA)) was added in 1:5000 ratio and incubated for 1h. The immunoreactive bands were then visualized using enhanced chemiluminesc=-0980-nce (ECL) reagent (G-Biosciences). The densitometric analysis was carried out using Chemi Doc (BioRad, Image Lab 5.1).

Total RNA extraction and RT-qPCR

RNA was extracted from MDA-MB-231 cells (treated with 5mg/ml of *C. axillaris* methanol extract and untreated) using TRIzol reagent (G-Biosciences) and quantified using a nanodrop (Thermo Scientific, Nanodrop 1000). First strand cDNA was synthesised using kit (G-Biosciences) following the manufacturer's instructions. The sequences of the primers used for the RTPCR are shown in Table 1. The reverse transcription conditions were as follows 95°C for 5min for RT inactivation. The amplification was performed using the following conditions: 15s at 95°C for denaturation, 15s at 60°C for annealing, 15s at 72°C for extension.

Prediction of interacting partners

Interacting partners of SNCAIP (Synphilin-1) were identified using STRING database (http://string-db.org/). This database gives physical and functional protein-protein interaction network that may exhibit functional association of these partners with synphilin-1 (Khairon et al., 2016). The string network analysis was set at medium confidence (0.400). Proteins were linked to each other grounded on various criteria such as neighbourhood, gene fusion, co-occurrence, text mining, co-expression, experimental evidence, existing databases and protein homology (Khairon et al., 2016).

Results

In order to investigate anti-cancer property of *C. axillaris* fruit, following assays were conducted.

Bioactive Compound analysis via GC-MS

Eight bioactive compounds have been identified in the methanol extract of *C. axillaris* fruit by GC-MS analysis. Retention time, % area, molecular formulae and functions of these identified compounds has been shown in Table 2. The anti-cancerous property of *C. axillaris* extract has been investigated in this study by in-vitro experiments and protein profiling study by proteomic analysis.

Cytotoxic effect of methanol extract on control and cancer cells

The antiproliferative activity of methanol extract of *C. axillaris* fruit was evaluated against breast cancer cells

Table 1. Primer Sequences of RT-qPCR.

Gene	Forward Primer	Reverse Primer
SNCA	GGAGTGGCCATTCGACGAC	CCTGCTGCTTCTGCCACAC
SNCAIP	CATCAGGGGGACGCAGGTTT	TGTGGAGGTCCGCTGGAGAG
Bax	CCCGAGAGGTCTTTTTCCGAG	CCAGCCCATGATGGTTCTGAT
BCl2	TTGCCAGCCGGAACCTATG	CGAAGGCGACCAGCAATGATA
Caspase-3	CATGGAAGCGAATCAATGGACT	CTGTACCAGACCGAGATGTCA
Caspase-8	TAGGGACAGGAATGGAACACACTT	GAGAGGATACAGCAGATGAAGCAGT
ACTIN	CATCCGCAAAGACCTGTACG	CCTGCTTGCTGATCCACATC

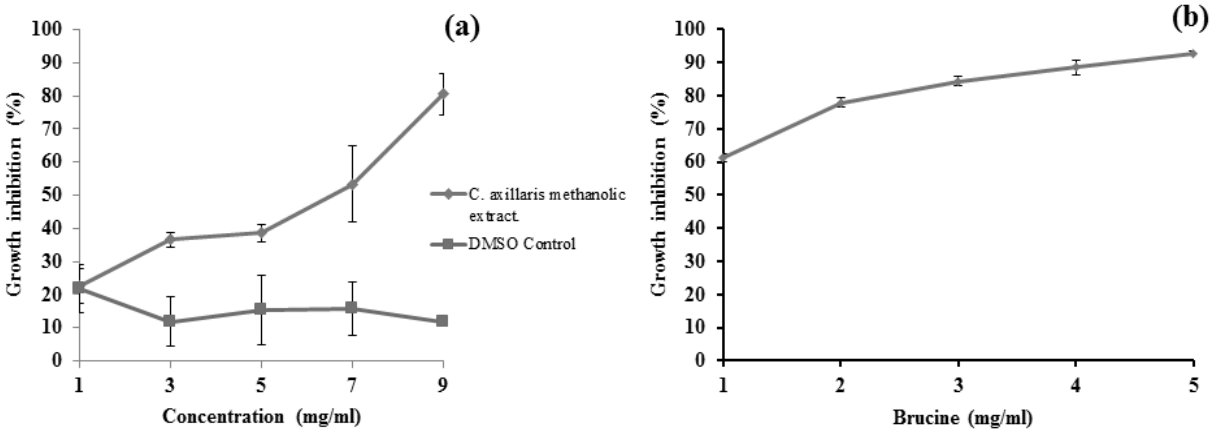

Figure 1. Cytotoxicity of (a) Methanol Extract of *C. axillaris* Fruit and DMSO Control on MDA-MB-231 Cells and (b) standard Brucine, seeded in 96 well plate (10,000 cells/well). Independent experiment was repeated thrice. Results are presented as mean ± S.D.

by MTT assay. MTT assay is a sensitive, quantitative and reliable colorimetric technique, most commonly used to determine cell viability (Ogbole et al., 2017). The human breast carcinoma cell line was used, which are estrogen receptor negative (ER-) MDA-MB-231 cells to determine the cytotoxicity of *C. axillaris* fruit extract. The MDA-MB-231 cell line is commonly used to model breast cancer (Conn 2013). The survival of the cells was determined after 24h treatment (*C. axillaris* extract, brucine and DMSO treatment). Brucine was used as a standard positive control whereas DMSO as negative control. The response of MDA-MB-231 cells with increasing concentrations of the methanol extract of *C. axillaris* fruit and DMSO has been shown in Figure 1a, and brucine has been shown in Figure 1b. Results showed that the proliferation of the cells (MDA-MB-231) were decreased significantly when treated with a methanol extract of *C. axillaris*, p-value ≤ 0.039 and when treated

Table 2. Secondary Metabolite Composition in *C. axillaris* Methanol Extract

RT	*Cas#	Compound Name	Molecular formula	**% Area	Function	Reference
6.194	000616-02-4	Succinic anhydride	C4H4O3	40.52	--	
8.605	000823-82-5	2,5-Furandicarboxaldehyde	C6H4O3	3.93	Antimicrobial, Preservative	[26]
9.805	028564-83-2	4H-Pyran-4-one	C5H4O2	4.15	Antimicrobial, Anti-inflammatory, Antiproliferative	[26]
11.274	000067-47-0	2-Furancarboxaldehyde, 5-hydroxymethyl	C6H6O3	29.73	Antimicrobial, Preservative	[26]
15.435	140224-88-0	6-Methyl benzobicyclo [2.2.1] heptenone-5	C12H12O	2.86	--	
16.545	001860-39-5	Hexanal	C6H12O	10.38	--	
19.932	000112-39-0	Hexadecanoic acid	C16H32O2	1.14	Antioxidant, Hypercholesterolemic, Lubricant, Pesticide, Antiandrogenic, Flavor, Hemolytic 5 alpha reductase inhibitor, Nematicide	[25]
21.637	000301-00-8	9,12,15-Octadecatrienoic acid	C18H30O2	0.68	Hepatoprotective, nematicide, insectifuge antihistaminic, antiarthritic, anticoronary, antieczemic antiacne,	[25]

*Chemical Abstracts Service (Identify the Chemical compound); ** % Matching with NIST library (mean 'Q value' is 91± 5.12%, n=3); RT Retention time of the compound, in minute; "area (%)" the percentages of the area of the total ion chromatogram represented by the peaks of each of the compounds identified. (+) means presence and (-) means absence

Table 3. Differentially Expressed Proteins on Treatment with *C. axillaris* Methanol Extract

Spot No.	Name of protein	Up/Down regulated in treatment	Protein Score	Theoretical mass (Da)	Experimental Mass (Da)	PI value*	Function**
1	Synphilin-1e-protein	↓	16	7744	7911	4.38	Cell death
2	HCG 1781285	↑	27	-	7247	6.31	-
3	General transcription factor IIB	↓	22	34833	25543	8.53	Gene expression
4	Cystic fibrosis transmembrane conductance regulator	↓	20	168142	4688	8.9	Transmembrane transport
5	Polyamine- modulated factor 1 isoform 3	↑	29	23339	20673	8.8	Chromosome segregation, mitotic nuclear division
6	Putative truncated protein	↓	19	-	15542	5.9	-
7	Interlukin 1 receptor like 1 isoform 2	↓	22	-	7807	6.1	Immune/inflammatory disorders; Upregulation in several conditions like inflammation, asthma, RA
8	HCG 2000618	↓	27	-	8853	4.75	-
9	Sodium channel type V alpha subunit	↓	26	226940	2018	6.02	Cellular response to calcium ion

↑, Up regulated; ↓, Down regulated; * Iso Electric Point; **, http://www.rcsb.org/

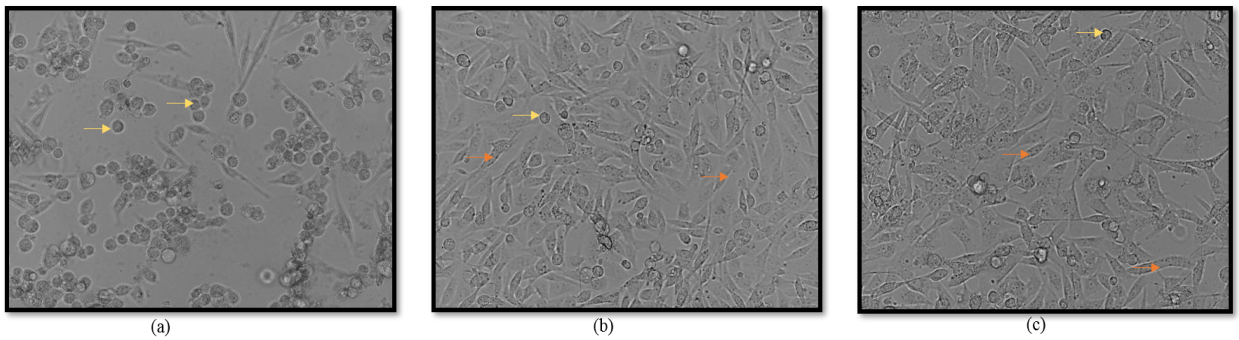

Figure 2. Representative Images of MDA-MB-231 Cells Showing; (a) MDA-MB-231 cells treated with methanol extract of *C. axillaris*, (b) DMSO treated MDA-MB-231 cells, (c) Healthy MDA-MB-231 cells at 10x resolution under inverted microscope (Nikon ECLIPSE TE2000-s). Dead cells are indicated with yellow colour arrows and viable cells with red arrows.

with standard brucine (p-value ≤ 0.0001), indicating that the results were statistically significant (Figure 1). DMSO treated cells were observed to have non-significant results as p-value ≥ 0.05. Brucine is a natural plant alkaloid that was reported to have IC_{50} at 116.4µM concentration against MDA-MB-231 cells (Habli et al., 2017, Serasanambati et

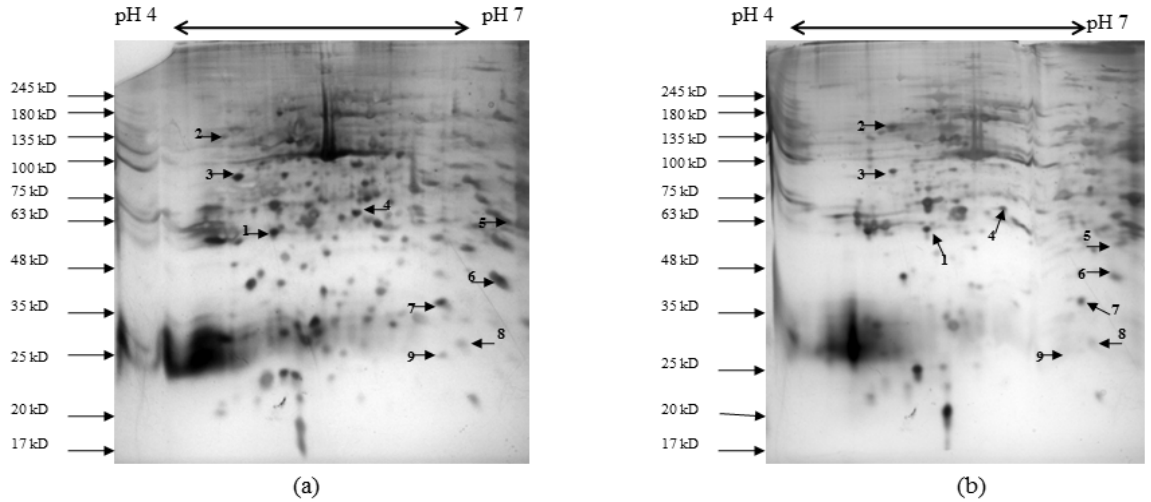

Figure 3. A Representative 2D Image of (a) MDA-MB-231 control cells without treatment and (b) cells treated with *C. axillaris* methanol extract (5 mg/ml); showing differentially expressed proteins.

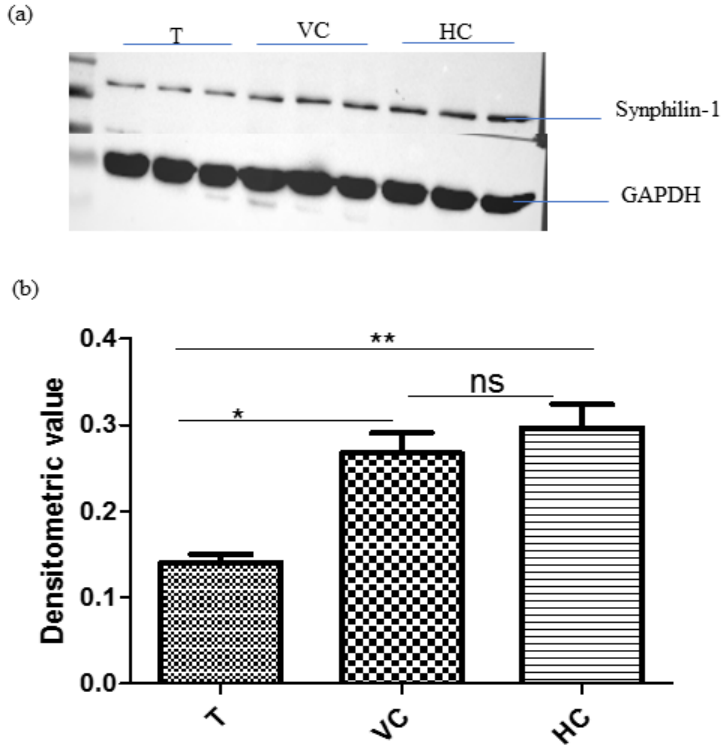

Figure 4. Western Blot Analysis (a) Representative image of protein expression level of Synphilin-1e. MDA-MB-231 cells were treated with 5mg/ml of *C. axillaris* methanol extract for 24h. (b) Densitometric analysis of Synphilin-1e protein over expression revealed 2.1fold change with $p<0.04$ after normalization with loading control GAPDH. T=Treated cells of MDA-MB-231 with 5mg/ml of *C. axillaris* methanol extract, VC=Vehicle control and HC=Control MDA-MB-231 cells without any treatment.

al., 2014). The IC50 value of *C. axillaris* extract was found to be 6.1±0.49mg/ml as compared to brucine (0.83mg/ml) indicating that *C. axillaris* extract possesses less cytotoxic property then brucine. Brucine being a pure compound may be highly active and hence may be more cytotoxic than the crude methanol extract. Similar results were also observed when an extract of Allium atroviolaceum flower was used to treat cells (MDA-MB-231) and was reported to have an anti-cancer property (Khazaei et al., 2017). Thus, to confirm our cytotoxic results, morphological

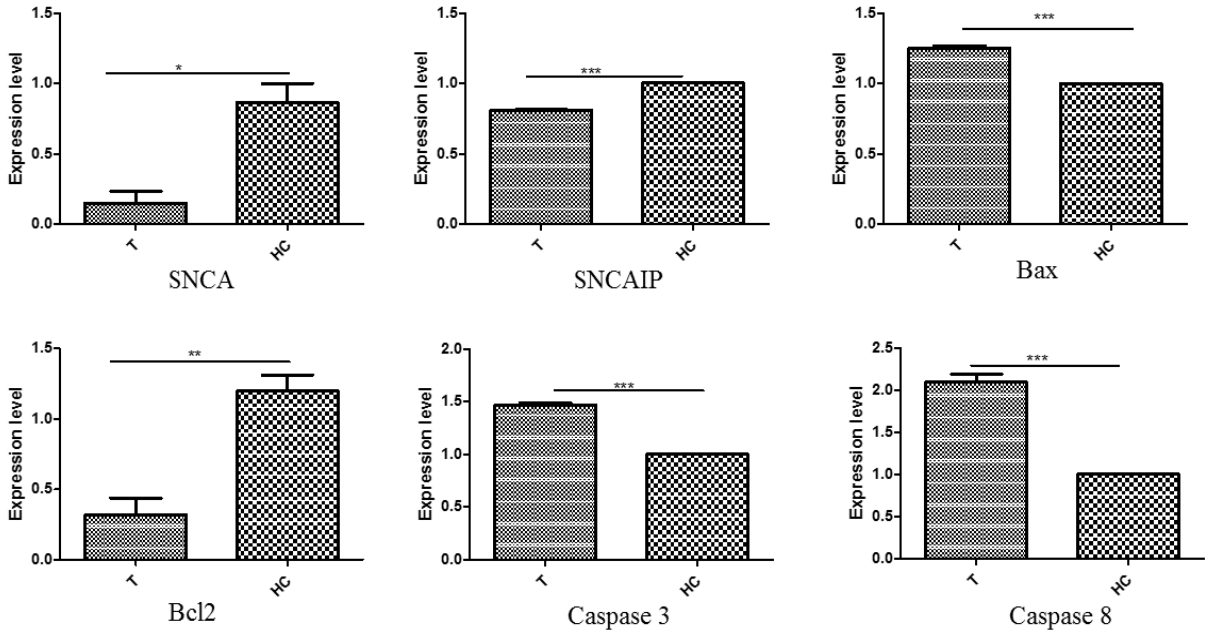

Figure 5. Effect of *C. axillaris* Methanol Extract on Apoptosis-Related Gene Expression in MDA-MB-231 Cells as Determined by RT-qPCR. T =Treated cells of MDA-MB-231 with 5mg/ml of *C. axillaris* methanol extract and HC=Control MDA-MB-231 cells without any treatment. * = Pvalue ≤ 0.0455, ** = Pvalue ≤0.0064, *** = Pvalue ≤ 0.0001.

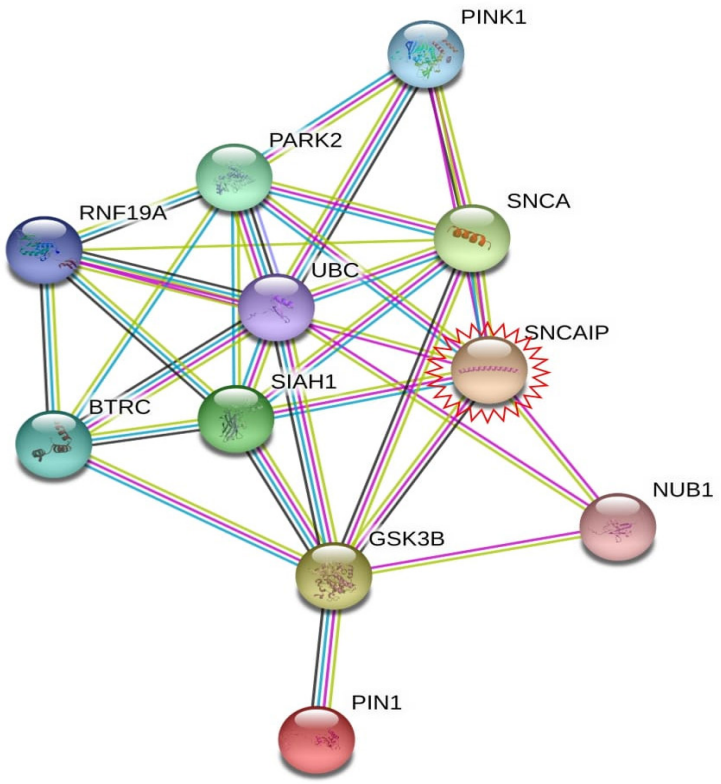

Figure 6. Interacting Partners of Synphilin-1 Protein (STRING network). Alpha-synuclein (SNCA), Glycogen Synthase Kinase 3 Beta (GSK3B), seven in absentia homolog (SIAH1), Ubiquitin C (UBC) and NEDD8 ultimate buster 1 (NUB1) showed close association with synphilin-1.

changes of cells (MDA-MB-231) were observed under an inverted microscope (Nikon ECLIPSE TE2000-s) at 10x magnification. Untreated and DMSO treated cells were observed to grow uniformly in high density monolayer with inherent morphology (Figure 2b and 2c). Whereas, treated (*C. axillaris* methanol extract treated) cells were observed to show the features of apoptosis such as shrinking, irregular nuclei and nuclear fragments (Figure 2a) than untreated cells, indicating that the treated cells were affected by cytotoxic property of extract (*C. axillaris*).

Further, experiments were conducted using additional control of human cells, generated out of trauma patients. The results revealed that there was no statistically significant (p-value ≤ 0.7231) cell death amongst control trauma cells (Supplementary Figure 1s, Figure 2s).

Proteomic analysis

In order to check the effect of the extract on the protein profile of cells (MDA-MB-231), total protein was extracted after the treatment of cells with methanol extract of *C. axillaris* fruit (5mg/ml). Nine proteins were identified after the differential protein profile analysis of control and experimental cells (Table 3, Figure 3). Proteins were well separated within the range of 10-70kDa and isoelectric points between pH 4 and 7.

Synphilin-1 protein was selected further among all identified proteins to study the effect on breast cancer. To further strengthen our studies, validation of Synphilin-1 protein was carried out by western blot analysis and 2.1 fold higher expression of Synphilin-1 protein was revealed in *C. axillaris* treated cells as compared to control cells ($p<0.005$) (Figure 4).

RT-PCR analysis of apoptosis related genes

Compared to untreated cells, the expression of Bax, Caspase-3 and Caspase-8 increased while the expression of BCl-2 decreased significantly in treated cells ($p<0.05$). Expression of SNCA and SNCAIP was also found to be decreased significantly ($p<0.05$) in treated cells as compared to untreated cells (Figure 5).

STRING analysis

Additionally, to elucidate more cancer-related roles, interacting partner study of SNCAIP (Synphilin-1) was carried out using the STRING database. The analysis revealed that this protein has 10 interacting partners (Figure 6).

Discussion

Breast cancer is the most frequent cancer among women in the world. There is a constant rising demand for new therapies to treat cancer because of toxicity of conventional drugs. Report shows that the naturally-derived compounds has less toxic side effects compared to presently available chemotherapy treatments at low cost (Greenwell and Rahman, 2015). Bioactive compound occurs in less quantity in fruits and vegetables, and provide various health benefits beyond nutrition (Singh et al., 2016). It also possesses therapeutic potential such as reducing inflammation, oxidative stress

and metabolic disorders (Singh et al., 2016). Amongst all the eight identified compounds via GC-MS in methanol extract of *C. axillaris*, 4H-Pyran-4-one was reported to have antiproliferative activity (Mahdavia et al., 2018) and other identified compounds (2,5-Furandicarboxaldehyde, hexadecanoic acid and 5-hydroxymethyl) were reported to have antimicrobial, anti-inflammatory and antioxidant activity (Tyagi et al., 2017, Ramalakshmi et al., 2011). Herbal/natural medicinal plants are producing secondary metabolites that are playing a role in the prevention and treatment of cancer (Greenwell and Rahman, 2015). Earlier studies also demonstrated the use of total flavonoid content (possessing good antioxidants) of *C. axillaris* extract for the treatment of cardiovascular diseases in clinic (Li et al., 2013). Studies have also reported the use of *C. axillaris* in aquaculture over drugs and antibiotics as the drug causes several side effects to the consumer (Shakya and Labh, 2019). The methanol extract of *C. axillaris* has been demonstrated to have good cytotoxic activity against breast cancer cells, suggesting that the extract might have great potential as an anti-cancer agent. To strengthen our results further, proteomic analysis was carried out.

Functional analysis indicated that the majority of the identified proteins were related to binding and transport mechanisms. The cell surface proteins are mainly phosphoproteins (DAVID Bioinformatics Resources, 6.7) and are playing various roles in different pathways. Amongst several differential proteins, dysfunctional cystic fibrosis transmembrane conductance regulator (CFTR) was found to be responsible for increased blood adenosine 5′-triphosphate (ATP) concentration in mice and in cystic fibrosis (CF) patients. Increased extracellular ATP concentration was demonstrated to inhibit tumor growth (Qiaoa et al., 2008). The upregulation of human chorionic gonadotropin (HCG) was observed in breast cancer. Studies reported that the overexpression of HCG decreases the proliferation and invasion of breast cancer (Toprak et al., 2017). Further, we have identified the synphilin-1 protein as a downregulated protein compared to control, in breast cancer cells after treatment with methanol extract of *C. axillaris*. But the role of this protein in disease pathogenesis has not been documented well, negligible reports are available. Literature report shows that the expression of α-synuclein (SNCA) was observed to have a close relationship with Synphilin-1 (SNCAIP), which has been reported to be related with various tumors. Downregulation of SNCA demonstrated potential tumor suppressor function and has a role in regulation of p53 gene, showing defects in case of cancer (Li et al., 2018, Szargel et al., 2009). Studies have also reported that knocking out SNCA in melanoma cells suppresses tumor growth (Shekoohi et al., 2021). As, SNCA and Synphilin-1 are significantly corelated, it can suggest that the protein (Synphilin-1) might control the growth of cancer cells, hence decreased cell proliferation.

Apoptosis is a gene related cell death process known as programmed cell death. Two types of signalling pathways lead to apoptosis i.e. extrinsic and intrinsic (Jang et al., 2020). The extrinsic pathway follows caspase cascade which finally leads to cell death, whereas intrinsic pathway is mitochondria-dependent and responds to various stress conditions, such as cytosolic calcium, genetic damage, and oxidative stress (Adams and Cory, 2007, Jonges et al., 2001, Llambi and Green, 2011, Liang et al., 2011). In the regulation of cell apoptosis Bcl-2 family plays an important role, which includes a sequence of antiapoptotic and proapoptotic markers. Apoptotic signalling pathway via Bcl-2 further stimulates the apoptotic pathway through various intercellular and intracellular signals. Bax is a proapoptotic protein which falls in the Bcl family, and it enhances apoptosis by activating caspases. On the contrary, Bcl-2 is an antiapoptotic protein, and it prevents apoptosis by inhibiting the mitochondrial apoptogenic factors release into the cytoplasm. Apoptosis is controlled by the comparative concentration of Bax and Bcl-2. Loss of MMP occurs when there is an imbalance of Bax and Bcl-2 proteins, which leads to release of cytochrome C, and activation of Caspase-3 and further results in apoptosis. SNCA and SNCAIP were also found to be significantly decreased as compared to untreated group, and studies have reported that downregulation/knocking out of SNCA supressed tumor growth (Shekoohi et al., 2021). As, SNCA and SNCAIP are positively corelated (Li et al., 2018) and in present study *C. axillaris* methanol extract treated cells have shown downregulation of SNCA and SNCAIP which might indicate that downregulation of Synphilin-1(SNCAIP) also helps in tumor suppression.

String analysis revealed 10 interacting partners of Synphilin-1, beta-transducing repeat containing E3 ubiquitin protein ligase (BTRC), Glycogen Synthase Kinase 3 Beta (GSK3B) and NEDD8 ultimate buster 1(NUB1) showed a close association with synphilin-1. BTRC was found to be involved in ubiquitination of protein, whereas GSK3B, is an anti-apoptotic protein, playing an important role in p53 binding (Jacobs et al., 2012). This protein phosphorylates Mucin 1(MUC1) and interferes in the interaction of Catenin beta-1(CTNNB1) in breast cancer cells (Adams and Cory, 2007). Another partner NUB1 includes tumour suppressor that includes growth arrest and apoptosis (Yang et al., 1999, Hosono et al., 2010). Results obtained from our analysis implicate that synphilin-1 may exhibit its antiproliferative function in association with identified interacting partners and presence of various bioactive compounds. Further studies are required to understand the effect of interacting partners on synphilin-1 function to use *C. axillaris* in the regulation of apoptosis during the cancerous conditions.

In conclusion, the investigation of our research towards the health beneficial properties of underutilized (*C. axillaris*) fruits may contribute to enhance its utilization. The findings of the present study indicated that *C. axillaris* fruit has various bioactive compounds that exhibit anti-oxidant, anti-microbial, and anti-inflammatory activities. The methanol extract of *C. axillaris* fruit also exhibit anti-cancerous property and the down-regulation of Synphilin-1 protein. Synphilin-1 protein may play a role in apoptotic function along with various protein interacting partners. Thus, this study implicates that *C. axillaris* fruit extract may be considered for the design and development of novel drug for treating cancer in the near future.

Author Contribution Statement

SM: work design, experimental and manuscript writing; AS and AS: Experimental and writing; RKG: data analysis and SB: data analysis, manuscript writing and overall approval of the work.

Acknowledgements

We acknowledge Council of Scientific and Industrial Research (CSIR) and Indian Council of Medical Research (ICMR), Government of India, New Delhi, India for providing fellowship to SM (Ref. No. 3/1/2/90/2018-Nut).

Availability of data and materials

The authors confirmed that the data supporting the findings of this research are available within the article.

Conflict of interest

The authors declare no conflict of interest, financial or otherwise.

References

Abdullah AS, Mohammed AS, Abdullah R, Mirghani ME Al-Qubaisi M (2014). Cytotoxic effects of Mangifera indica L. kernel extract on human breast cancer (MCF-7 and MDA-MB-231 cell lines) and bioactive constituents in the crude extract. *BMC Complement Altern Med*, **25**, 199.

Ayob Z, Bohari SPM, Samad AA, Jamil S (2014). Cytotoxic activities against breast cancer cells of local Justicia gendarussa crude extracts. *J Evid Based Complementary Altern Med*, **2014**, 1-12.

Basri DF, Alamin ZAZ, Chan KM (2016). Assessment of cytotoxicity and genotoxicity of stem bark extracts from Canarium odontophyllum Miq. (dabai) against HCT 116 human colorectal cancer cell line. *BMC Complement Altern Med*, **29**, 36.

Biswas S, Sharma S, Saroha A, et al (2013). Identification of novel autoantigen in the synovial fluid of rheumatoid arthritis patients using an immunoproteomics approach. *PLoS One*, **8**, e54246.

Chimplee S, Graidist P, Srisawat T, et al (2019) Anti-breast cancer potential of frullanolide from Grangea maderaspatana plant by inducing apoptosis. *Oncol Lett*, **17**, 5283-91.

Conn PM (2013). Animal models for the study of human disease. Oregon Health & Science University, Beaverton, Oregon, USA, 1108.

Dang Z, Su S, Jin G, et al (2020). Tsantan Sumtang attenuated chronic hypoxia-induced right ventricular structure remodeling and fibrosis by equilibrating local ACE-AngII-AT1R/ACE2-Ang1-7-Mas axis in rat. *J Ethnopharmacol*, **250**, 112470.

Figueroa AC, Soria EA, Cantero JJ, Sanchez MS, Goleniowski ME (2012). Cytotoxic activity of Thelesperma megapotamicum organic fractions against MCF-7 human breast cancer cell line. *J Cancer Ther*, **3**, 103-9.

Greenwell M, Rahman PKSM (2015). Medicinal plants: Their use in anticancer treatment. *Int J Pharm Sci Res*, **6**, 4103-12.

Habli Z, Toumieh G, Fatfat M, Rahal ON, Muhtasib HG (2017). Emerging cytotoxic alkaloids in the battle against cancer: overview of molecular mechanisms. *Molecules*, **22**, 250.

Hosono T, Tanaka T, Tanji K, Nakatani T, Kamitani T (2010). NUB1, an interferon inducible protein, mediates anti-proliferative actions and apoptosis in renal cell carcinoma cells through cell-cycle regulation. *Br J Cancer*, **102**, 873-82.

Jacobs KM, Bhave SR, Ferraro DJ, et al (2012). GSK-3β: A Bifunctional Role in Cell Death Pathways. J Cell Bio, 1-11.

Jang DK, Lee IS, Shin HS, Yoo HM (2020). 2α-Hydroxyeudesma-4,11(13)-Dien-8β,12-Olide isolated from inula britannica induces apoptosis in diffuse large B-cell lymphoma cells. *Biomolecules*, **10**, 1-16.

JM, Cory S (2007). The Bcl-2 apoptotic switch in cancer development and therapy. *Oncogene*, **26**, 1324-37.

Jonges LE, Nagelkerke JF, Ensink NG, et al (2001). Caspase-3 activity as a prognostic factor in colorectal carcinoma. *Lab Investig*, **81**, 681-8.

Khairon R, Zin NM, Rahman MA, Basri DF (2016). Comparative proteomic analysis of differential proteins in response to aqueous extract of Quercus infectoria Gall in Methicillin-Resistant Staphylococcus aureus. *Int J Proteomics*, **37**, 4029172.

Khan T, Ali M, Khan A, et al (2020). Anticancer plants: A review of the active phytochemicals, applications in animal models, and regulatory aspects. *Biomolecules*, **10**, 1-30.

Khazaei S, Abdul Hamid R, Ramachandran V, et al (2017). Cytotoxicity and proapoptotic effects of Allium atroviolaceum flower extract by modulating cell cycle arrest and caspase-dependent and p53-independent pathway in breast cancer cell lines. *Evid Based Complement Alternat Med*, **2017**, 1-16.

Li C, He J, Gao Y, et al (2013). Preventive Effect of Total Flavones of Choerospondias axillaries on Ischemia/Reperfusion-Induced Myocardial Infarction-Related MAPK signalling pathway. *Cardiovas Toxicol*, **14**, 145-52.

Li YX, Yu ZW, Jiang T, et al (2018). SNCA, a novel biomarker for Group 4 medulloblastomas, can inhibit tumor invasion and induce apoptosis. *Cancer Sci*, **109**, 1263-75.

Liang H, Gu MN, Yang CX, et al (2011). Sevoflurane inhibits proliferation, induces apoptosis, and blocks cell cycle progression of lung carcinoma cells. *Asian Pac J Cancer Prev*, **12**, 3415-20.

Lichota A, Gwozdzinsk K (2018). Anticancer activity of natural compounds from plant and marine environment. *Int J Mol Sci*, **19**, 3533.

Llambi F, Green DR (2011). Apoptosis and oncogenesis: give and take in the BCL-2 family. *Curr Opin Genet Dev*, **21**, 12-20.

Llombart V, Trejo SA, Bronsoms S, et al (2017). Profiling and identification of new proteins involved in brain ischemia using MALDI-imaging-mass-spectrometry. *J Proteomics*, **152**, 243-53.

Mahdavia SM, Habibia A, Dolatia H, et al (2018). Synthesis and antimicrobial evaluation of 4H-Pyrans and schiff bases fused 4H-Pyran derivatives as inhibitors of Mycobacterium bovis (BCG). *Iran J Pharm Res*, **17**, 1229-39.

Makrane H, Messaoudi ME, Melhaoui A, et al (2018). Cytotoxicity of the aqueous extract and organic fractions from Origanum majorana on human breast cell line MDA-MB-231 and human colon cell line HT-29. *Adv Pharmacolo Sci*, **2018**, 1-9.

Mann S, Satpathy G, Gupta RK (2016). Evaluation of nutritional and phytochemical profiling of Baccaurea ramiflora Lour. syn. Baccaurea sapida (Roxb.) Mull. Arg. Fruits. *Ind J Trad Know*, **15**, 135-42.

Mann S, Sharma A, Biswas S, Gupta RK (2015). Identification and molecular docking analysis of active ingredients with medicinal properties from edible Baccaurea sapida. *Bioinformation*, **11**, 437-43.

Mann S, Sharma A, Sarkar A, et al (2020). Evaluation of anti-inflammatory effects of Choerospondias axillaris fruit's methanol extract in synoviocytes and CIA rat model. *Curr Pharm Biotechno*, **21**, 596-604.

Mathur P, Sathishkumar K, Chaturvedi M, et al (2020). Cancer

statistics, 2020: report from national Cancer registry programme, India. *JCO Glob Oncol*, **6**, 1063-75.
Millares P, LaCourse EJ, Perally S, et al (2012). Proteomic Profiling and Protein Identification by MALDITOF Mass Spectrometry in Unsequenced Parasitic Nematodes. *PLoS One*, **7**, e33590.
Nguyen DD, Nguyen NH, Nguyen TT, et al (1996). The use of water extract from the bark of Choerospondias axillaris in the treatment of second degree burns. *Scand J Plast Reconstr Hand Surg*, **30**, 139-44.
Ogbole OO, Segun PA, Adeniji AJ (2017). In vitro cytotoxic activity of medicinal plants from Nigeria ethnomedicine on Rhabdomyosarcoma cancer cell line and HPLC analysis of active extracts. *BMC Complement Altern Med*, **17**, 494.
Oyebode O, Kandala NB, Chilton PJ, Litford RJ (2016). Use of traditional medicine in middle-income countries. *Health Policy Plan*, **31**, 984-91.
Qiaoa D, Yib L, Huaa L, et al (2008). Cystic fibrosis transmembrane conductance regulator (CFTR) gene 5T allele may protect against prostate cancer: A case-control study in Chinese Han population. *J Cyst Fibros*, **7**, 210-214.
Ramalakshmi S, Muthuchelian K (2011). Analysis of Bioactive constituents from the Ethanolic leaf extract of Tabebuia rosea (Bertol.) DC by Gas Chromatography – Mass Spectrometry. *Int J Chemtech Res*, **3**, 1054-9.
Satpathy G, Tyagi Y, Gupta RK (2011). Preliminary evaluation of nutraceutical and therapeutic potential of raw Spondias pinnata K., an exotic fruit of India. *Food Res Int*, **44**, 2076-2087.
Serasanambati M, Chilakapati SR, Vangavaragu JR, Chilakapati DR (2014). Inhibitory effect of gemcitabine and brucine on MDA MB-231human breast cancer cells. *Int J Drug Deliv*, **6**, 133-9.
Shakya SR, Labh SN (2019). Ethanol extract of Choerospondias axillaris fruit pulp enhances haematological parameters in Oncorhynchus mykiss cultured in Nepal. *Nepal J Biotechnol*, **7**, 21-9.
Shekoohi S, Rajasekaran S, Patel D, et al (2021). Knocking out alpha-synuclein in melanoma cells dysregulates cellular iron metabolism and suppresses tumor growth. *Sci Rep*, **11**, 5267.
Singh JP, Kaur A, Shevkani K, Singh N (2016). Composition, bioactive compounds and antioxidant activity of common Indian fruits and vegetables. *J Food Sci Technol*, **53**, 4056-66.
Szargel R, Rott R, Eyal A, et al (2009). Synphilin-1A inhibits seven in absentia homolog (SIAH) and modulates alpha-synuclein monoubiquitylation and inclusion formation. *J Biol Chem*, **284**, 11706-16.
Tominaga N, Kosaka N, Ono M, Katsuda T, et al (2015). Brain metastatic cancer cells release microRNA-181ccontaining extracellular vesicles capable of destructing blood-brain barrier. *Nat Commun*, **6**, 6716.
Toprak SS, Treeck O, Ortmann O (2017). Human Chorionic Gonadotropin and Breast Cancer. *Int J Mol Sci*, **18**, 1587.
Tyagi T, Agarwal M (2017). Phytochemical screening and GC-MS analysis of bioactive constituents in the ethanolic extract of Pistia stratiotes L. and Eichhornia crassipes (Mart.) solms. *J Pharmacogn Phytochem*, **6**, 195-206.
Yang SZ, Kohno N, Kondo Ket al (1999). Adriamycin activates E-cadherin-mediated cell-cell adhesion in human breast cancer cells. *Int J Oncol*, **15**, 1109-15.

This work is licensed under a Creative Commons Attribution-Non Commercial 4.0 International License.

iJRASET
International Journal For Research in Applied Science and Engineering Technology

INTERNATIONAL JOURNAL FOR RESEARCH

IN APPLIED SCIENCE & ENGINEERING TECHNOLOGY

Volume: 10 **Issue:** IV **Month of publication:** April 2022

DOI: https://doi.org/10.22214/ijraset.2022.41925

www.ijraset.com

Call: 08813907089 | E-mail ID: ijraset@gmail.com

International Journal for Research in Applied Science & Engineering Technology (IJRASET)
ISSN: 2321-9653; IC Value: 45.98; SJ Impact Factor: 7.538
Volume 10 Issue IV Apr 2022- Available at www.ijraset.com

Applications of Flexible Manufacturing Systems in Industry: A Review

Mayank Chugh[1], Jitesh Jassi[2], Mohd Zaid[3], Dr. A.K. Madan[4]
[1, 2, 3]*Research Scholar, Department of Mechanical Engineering, Delhi Technological University, Delhi*
[4]*Professor, Department of Mechanical Engineering, Delhi Technological University, Delhi*

Abstract: ***FMS and its adoption is a nuanced cradle technology in India and sees a limited implementation of its innovative technology and concepts. Our world today is a technologically sophisticated world, only characterized as fictional a few years ago. A lot today has transformed smart and technologists are striving to bring home new and innovative devices, homes, factories, and even cities. Scientifically proven is that these advanced technologies and concepts can boost an organization's overall performance. Many corporations, researchers, and institutions agree that automation and robotic systems are the foundation of industrial production and a key factor of the Industrial 4.0 revolution. There is an ongoing demand for increased output and manufacturing quality, as well as an urgent requirement to improve overall efficiency in manufacturing systems to withstand competitive pressure. Flexible Manufacturing Systems has added these advantages to organizations, due to its capabilities, capacity and advantages. The work of extensive research presented highlights the importance of FMS adoption and acceptance of various industrial automation technologies and techniques, as well as FMS potential.***
Keywords: Flexible Manufacturing Systems, Manufacturing, Industry 4.0, Industrial Production, Automation.

I. INTRODUCTION

The manufacturing industry is essential to a nation's economy. It remains vital as a key driver of growth and development. The sectoral focus is on manufacturing, increasing value proposition through the transformation of materials into products. Advanced technical advances in production and manufacturing are the goal of the next age industries, in which there is a thriving market and room for growth. Robots, NC machines, automation, CNC machines, and other new dynamic concepts, such as FMS, are pushing companies to develop these technical capabilities [1, 17]. Flexible Manufacturing Systems (FMS) is described as an interconnected complicated system controlled by the computer software for automation of material handling network and numerically controlled machinery that can handle small volumes of a variety of part types simultaneously [1]. A system capable of producing a broad variety of things by integrating a number of programmed machine tools integrated by an automated material management system [19]. The manufacturing technologies that comprise flexible manufacturing systems include computer or numerically controlled machines, conveyor systems (including roller, motorised roller), robotic systems, computers, automated guided vehicles and programmable electronic microcontrollers, among other things, are examples of numerical control or direct numerical control centres [2]. Flexible manufacturing can be understood as non-repeated mass production of multi-purposes due to changing client and market demand, production of different functions within the same period of the means of production made. Flexible manufacturing systems, providing macro operations planning and control with integrated control systems are computer-based systems and are capable of producing a wide range of goods or services quickly. Nowadays, flexibility entails developing competitively priced customized high-quality items that can be supplied to consumers promptly.

There is a vital significance and need to improve India's manufacturing efficiency and competitiveness. India's liberalization, globalization and privatisation strategies have mostly resulted in severe competition in the Indian sector. In contrast, the relative contribution of the manufacturing industry in general, as well as the sub-areas in particular, to India's overall GDP has remained dormant during the previous few decades. As a result, stakeholders and decision-makers are taking industrial competitiveness extremely seriously [2].

II. LITERATURE REVIEW

The acceptance of flexible manufacturing systems as an emerging technology has also been highlighted by Suresh et al. [3] in their presented work. The application of flexible manufacturing systems as an element of medium capacity, fairly diversified medium variety manufacturing has also been acclaimed. An attempt has also been made to describe FMS as a unified manufacturing facility comprising functional numerical controlled manufacturing units integrated with automatic material handling systems.

© IJRASET: All Rights are Reserved |

Flexibility within the systems is not a product of the capabilities of the equipment alone as argued by Gupta et al. [4]. It's really the result of multiple elements, including physical characteristics and functional decisions, consolidation of information, management approaches, etcetera. The effectiveness of flexibility in manufacturing process systems is quintessential under different operating environments. The vitality of advanced flexible manufacturing technology is also confirmed by Hammel [5]. Presented in his work is the capability of flexible manufacturing systems to increase system efficiencies, process flexibility and viability, and an end to end integration. It was also an observation that absolute transparency throughout the process chain at each stage can be achieved due to the ability of the systems to connect various departments and units together.

Bennett et al. [6] has further presented in their work aid to the development of impactful and efficient flexing manufacturing technology by virtue of critically important elements and attributes in literature.

Outlook	Definition of Flexibility
Manufacturing	➢ The capability of producing different parts without major retooling requirements. ➢ A measure of how swiftly the organization converts its processes from an old product line to a new one. ➢ The potential to change a production schedule to modify a component or handle multiple components.
Functional	➢ The ability to efficiently produce exceedingly customized and unique products.
Client	➢ The ability to utilize dimensions of delivery rate.
Strategic	➢ The ability of an organization to extend a diverse range of products to its customers.
Capability	➢ The ability to swiftly escalate or deescalate the production levels or rapidly switch the capacity from one product or service to the other.

Fig. 1 The flexibility concepts and diverse approaches

Additionally, Pandey et al. [7] analyzed the performing capabilities of flexible manufacturing technology in the context and setup of the manufacturing sector. The outcome provided the required evidence bringing to light the associated benefits including enhanced output and reduced lead times.

Dolage et al. [8] also considered the effects of the implementation of flexible manufacturing technology on the economic margins and synthesized that a significant relationship is present between both as per the research which makes it favourable for the organizations to adopt flexible manufacturing technologies at large.

Discussing the future trends of research, it was acclaimed by Chan et al. [9] that the advanced procedures on smart and intelligent flexible technologies will be critical in influencing research.

Fernandez et al. [10] presented the future of flexibility in manufacturing technologies in combination well with the industry's next-generation ready manufacturing areas. It was agreed that for supporting the next-gen manufacturing in an Industry 4.0 setup, the internet of things, cloud, and cyber systems are foundational blocks for advanced manufacturing activities to occur worldwide. These enhanced capabilities will be swift in scaling operations of production and will be attained with the help of emerging technology in material handling equipment, sensing, and integrating abilities.

It will therefore be equally important to consolidate the two dimensions of workspace namely virtual and physical in order to concentrate the required operational effectiveness of manufacturing as highlighted by Tao et al. [11].

It has also been agreed upon through the work presented by Tamimi et al. [12] that for elements of future research, it will be helpful to analyze flexible manufacturing technology through the use of models simulating the manufacturing systems as ascertained by measurement of performance of flexible systems in the carried out research.

Furthermore, the capabilities, limitations, and nuances of advancing and developing flexible systems and their utilization is a subject to be taken up for research in the near future as presented by Malhotra et al. [13] in his research. These avenues of research remain much less explored especially in the context of the Indian subcontinent. It has also been elucidated that the advancement and development of flexible manufacturing systems should be conforming with the ability to meet the demands while further boosting the manufacturing capability.

© IJRASET: All Rights are Reserved |

Blockchain technology assigns a unique identification to each part, allowing manufacturers to detect problems earlier and determine the source of the problem. Blockchain, for example, can track expiry dates, storage temperatures, and shipment information in the food business. Rather than recalling all of the merchandise, the food company may just remove the food that was affected in the one truck where the refrigeration system failed. The product may be recalled before it reaches to the customers [23, 26].

It is therefore clearly evident that the application of flexible manufacturing systems in the Indian scenario has a long way to go and is limited by a variety of influencing factors such as lacking advanced aspects considered essential for the success of these systems and also necessarily required in flexible cells and systems as mentioned by Rao et al. [14].

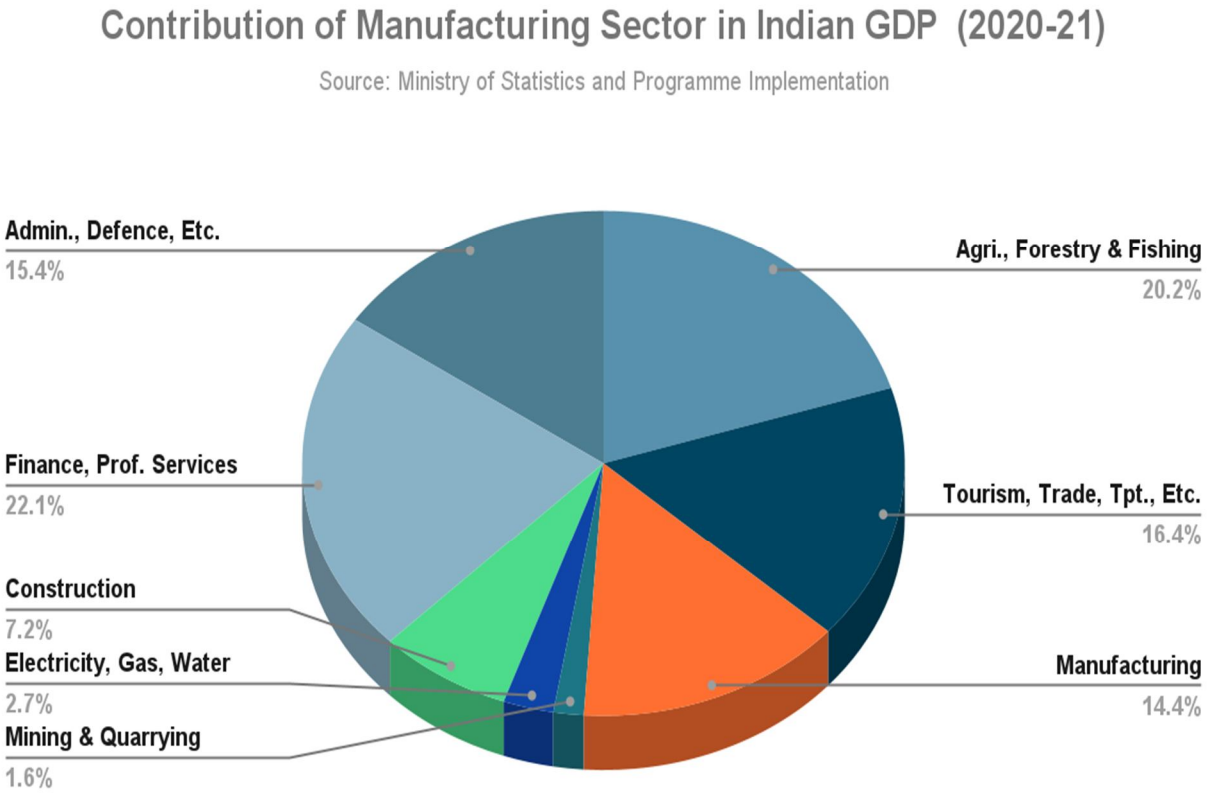

Fig. 2 The contribution of the manufacturing sector to Indian GDP (2020-21)

III. ACCEPTANCE AND IMPLEMENTATION CHALLENGES OF FLEXIBLE TECHNOLOGY IN THE INDIAN INDUSTRY

The fundamental stage in which the major crucial challenges are faced by flexible systems before any significant advancements can be initiated is the stage of design.

Not all the components that enter production can be suitably manufactured with flexible systems as the process might not be optimal. Therefore, it becomes essential to carefully select the components to be manufactured based on the potential of the system in terms of capacity, operational requisites, equipment, integration etcetera.

A conjunctional challenge is the amount of flexibility that is provided to each flexible system. Such a challenge arises because of the presence of a diverse set of requirements from each flexible unit due to variable operations purposes. An automated arm's flexibility and freedom in fabricating a mechanical component is an example of the challenge posed. Thus, design considerations have to be prioritized to eliminate the issue [16].

It also becomes important to address the ambiguity in the capability of each system for material handling including but not limited to roller conveyors, guided vehicles, tow trucks and tuggers, lifts, and robots at the fundamental stage.

At the early stage of design, blueprints of the factory floor highlighting the placement of each cell or unit aids the ultimate purpose of increasing the flexibility of the system through enhanced efficiency and effectiveness. The elements of such an objective would typically include and address queuing, vacant spaces, lead time optimization, congestion and traffic management etcetera.

© IJRASET: All Rights are Reserved | SJ Impact Factor 7.538 | ISRA Journal Impact Factor 7.894 |

An aspect closely related to computer-aided and integrated manufacturing is placing the control of the systems structurally considering the needs of multi-system and multi-element interaction. The decision pertaining to these elements such as control layout, equipment management, and production planning are needed to be taken at this point.

What follows the preliminary stages of design is the planning. Certain issues have been observed as a component of planning and essentially require resolution before the process of production starts.

It is an operational challenge to ascertain the components to be selected for the initiation of manufacturing of components. The decision of selection is based on a diverse range of factors that are determined.

The planning stage also includes the classification of the operations that need to be performed on the job on the numerical control machines using tools and equipment. Furthermore, the challenge is also to classify the machines to reduce lead times and the effectiveness of the flexible manufacturing systems.

As we now advance to the stage of scheduling, the challenges associated with sequencing and scheduling occur and are dealt with in real-time or instantaneously in flexible manufacturing systems. It demands ascertaining the right chain or set of events to be executed in the perfect order through advanced smart techniques of employing procedures or algorithms.

The performance of the entire flexible manufacturing system is also a function of the correct material handling systems put in place, hence the heedful selection of jigs, fixtures, conveyors, tuggers, trucks, lifts and pallets as per the requirements and capability of the systems is necessary.

As discussed earlier, each system operates under a set of constraints that limit its operation and performance. Thus, the system enjoys unique flexibility of operations including numerical control-related limitations, production capability related limitations etcetera. A flexible manufacturing system should, therefore, be considerate of the possibilities while operating [30].

Once the system is up and running, the process needs to be controlled and monitored, as a part of the control stage. It involves meticulous and strict adherence to the manufacturing schedule. Any errors or challenges that occur, such as those related to equipment and computer control, are dealt with by SOPs in place. It also involves periodic maintenance of systems underuse.

IV. APPLICATIONS OF FLEXIBLE MANUFACTURING SYSTEMS

A significant amount of literature has been researched and compiled on the use of flexible systems. The state and extent of its utilization and application in the real scenario differ and are also based on the industrial landscape and technological prowess of various nations and their individual sectors.

Hence, it becomes a tedious and challenging task to say with exactness quantitatively. Also, it can not be denied blatantly that the application and the extent to which these systems are put to use are constant across, therefore it becomes important to highlight the increase in difficulty in measuring and presenting statistics. However, attempts are being made to acing the challenge resolution [21].

Through means of research, it has been concluded that flexible systems are much more likely to thrive in the Indian industrial environment when the mentioned factors are predominantly present.

The systems and their performance should be backed by an adequately positive economic scenario. An absence can result in inferiority, high failures, and low confidence [23]. Also, some areas do struggle with inadequate capabilities to satisfy the requirements of the production of certain units or components in the Indian scenario due to varied reasons [25, 30].

A complete transformation in terms of the organization's composition and arrangement is required by a complete overhaul to make sure that it meets the standards of flexible systems under all encounterable conditions.

The synergy between the operating and functional components of the entire flexible ecosystem in various domains including but not limited to technology is of the essence.

The organization's stakeholders pay heed to the idea of flexible manufacturing which is deficient and imperfect without the presence of the right shareholder outlook, quality and performance measures, capital expenditure, and skill application, hence, remains the most critical aspect of the application of flexible systems in India. Moreover, data from complex manufacturing processes and systems may be examined and used to improve existing goods, processes, and services while also developing fresh offers [41,48].

Thus, in the manufacturing and production business, technologies such as data analytics, big data, and IIoT may be employed to assure quality, boost performance and efficiency, decrease costs, streamline supply chains and enhance flexible manufacturing systems [21, 27, 45, 50].

© IJRASET: All Rights are Reserved |

Influential Parameters	Indian Scenario
1. Market & Scenario a. Tough competition. b. Significant product diversity and differentiation. c. Induced confidence in high quality products.	a. Positive competition. b. Rich quality products are widely demanded. c. Positive market. d. Favorable tax regulations.
2. Governmental Policies a. Liberalized economy & policies. b. Technological reinforcement & assurance. c. Unhindered resource support. d. Liberal trade policies. e. Equity foreign participation.	a. Technological prowess present. b. Duty exemptions on certain products. c. Governmental financial aid. d. Foreign equity participation limited to 51%.
3. Investment Prospects a. Huge capital availability. b. Long term borrowing & low interest rates. c. Subsidized industrial inputs.	a. Capital raising prospects through markets. b. Governmental financial aid. c. Favorable governmental initiatives.
4. Resource Availability a. Unhindered resource support. b. Cheap & skilled workforce. c. Uninterrupted power availability.	a. Availability of skilled & cheap workforce b. Duty exemptions on certain products. c. Unhindered supply of certain resources.
5. Management Objectives a. Inventory minimization. b. Manufacturing cost reduction. c. Lead time reduction. d. Labor cost reduction. e. Rich quality products. f. Diverse product range.	Management Objectives are framed and maintained by individual organizations based on the organization's own interests.

Fig. 3 The scenario of flexible systems and their application in the Indian scenario

V. CONCLUSION

Flexible manufacturing systems are an integration of parts and processes. An essential component that finds its important mention is the computer or the process control unit which commands the operations involved. These flexible systems have changed the nature of manufacturing with limited human involvement and interference and huge production potential in today's world servicing and catering to swiftly evolving needs. This instils much-required confidence in the system. Such systems have thus claimed a special position in the global manufacturing industry. The work presented also highlights the scenario of limited contribution and adoption of flexible technological systems in Asia in contrast with the global scenario. It also stands by the fact that the utilization of this technology in the Indian subcontinent is also limited. However, owing to the fact that the adoption of smart and flexible technologies record performance enhancement in manufacturing, steps need to be taken towards its acceptance.

Furthermore, the future aspects of work regarding flexible systems need to be explored to incubate these systems out of their current nascent stage. Artificial Intelligence, Machine Learning, Deep Learning, Data Science, additive manufacturing technologies, and smart application of data will lead the way in research. With adequate evolution of these elements, we will be in a better position to embrace flexible manufacturing technology perfectly.

VI. ACKNOWLEDGEMENT

It gives us enormous pleasure to present this review paper on "Applications of Flexible Manufacturing Systems in Industry". We have put forth numerous efforts in building this project. Nonetheless, it would not have been possible without the caring support and help of numerous individuals and organizations. We might want to stretch out our sincere gratitude to each one of them. We are highly obliged to Dr. A.K. Madan for his instruction and consistent direction and for giving essential information concerning the project and his support in finishing the paper. We need to thank our parents for their benevolent cooperation and encouragement, which helped us complete this project. Our thanks and appreciation likewise go to our colleagues in building up the project and individuals who have readily helped us out with their abilities.

© IJRASET: All Rights are Reserved |

REFERENCES

[1] Chandra R, Dr. Subhash & Mandal, Dr. Arup Kumar. (2016). A Strategic and Hierarchical Approach to Implement a Flexible Manufacturing System (FMSs), its Scope and Applications: An Overview. International Journal of Science and Research (IJSR). 5. 905-911.
[2] P K, Manoj. (2019). Competitiveness of Manufacturing Industry in India: Need for Flexible Manufacturing Systems. International Journal of Innovative Technology and Exploring Engineering. 8. 10.35940/ijitee.K2452.1081219.
[3] Kumar, S., & Sridharan, R. (2007). Simulation modeling and analysis of tool sharing and part scheduling decisions in single-stage multi-machine flexible manufacturing systems. Robotics and Computer-Integrated Manufacturing, 23, 361–370.
[4] Gupta, D., Buzacott, JA, 1989. A framework for understanding flexibility of manufacturing systems. J. Manuf. Syst. 8 (2), 89–97.
[5] Hammel, O. "Three key benefits of a Modern flexible manufacturing system." https://www.linkedin.com/pulse/three-key-benefits-modern-flexible-manufacturing-system-hammel-oliver/
[6] Bennett, D., Forrester, P., Hassard, J., 1992. Market-driven strategies and the design of flexible production systems: evidence from the electronics industry. Int. J. Oper. Prod. Manag. 12 (2), 25–43.
[7] Pandey, R., A. S. T. and Sharma, N. "Performance Evaluation of Flexible Manufacturing Systems," Institute of Electrical and Electronics Engineers Transactions on Systems, Man, and Cybernetics 2(4), 2016, pp. 606–617.
[8] Dolage, D. A. R. and Sade, A. B. "The Impact of Adoption of Flexible Manufacturing Technology on Price Cost Margin of Malaysian Manufacturing Industry," Technology and Investment, 3(1), 2012, pp. 26–35.
[9] Chan, F. T. S. and Chan, H. K. "A comprehensive survey and future trend of a simulation study on FMS scheduling," J. Intell. Manuf., 15(1), 2004, pp. 87–102.
[10] Fernandez-Carames TM, Fraga-Lamas P. A Review on Human-Centered IoT-Connected Smart Labels for the Industry 4.0. IEEE Access. 2018;6:25939–57.
[11] Tao F, Zhang M. Digital Twin Shop-Floor: A New Shop-Floor Paradigm Towards Smart Manufacturing. IEEE Access. 2017;5:20418–27.
[12] El-Tamimi, A. M., Abidi, M. H., Mian, S. H. and Aalam, J. "Analysis of performance measures of flexible manufacturing system," Journal of King Saud University Engineering Sciences 24(2), 2012, pp. 115–129.
[13] V. Malhotra, T. Raj, and A. Arora, Excellent techniques of manufacturing systems: RMS and FMS, International Journal of Engineering Science and Technology, vol.2, no. 3, King's College London, pp.137–142, 2010.
[14] Rao, K.V. Sambasiva; and Deshmukh G.; "Strategic Framework for implementing manufacturing systems in India", International Journal of Operations and Production Management, Vol. 14, No. 4, MCB University Press Limited, USA., 1994, pp. 50 – 63.
[15] Zhang, Q., Vonderembse, M. A., & Cao, M. (2006, June 1). Achieving flexible manufacturing competence: The roles of Advanced Manufacturing Technology and Operations Improvement Practices. International Journal of Operations & Production Management.
[16] Batra, A., Rawat, A., & Khanapuri, V.B. (2018). Challenges in Flexible Manufacturing Systems : A Review.
[17] Bahrin, Mohd & Othman, Fauzi & Azli, Nor & Talib, Muhamad. (2016). Industry 4.0: A review on industrial automation and robotic. Jurnal Teknologi. 78. 10.11113/jt.v78.9285.
[18] Radziwon, Agnieszka & Bilberg, Arne & Bogers, Marcel & Madsen, Erik. (2014). The Smart Factory: Exploring Adaptive and Flexible Manufacturing Solutions. Procedia Engineering. 69. 10.1016/j.proeng.2014.03.108.
[19] Goyal, S.K., Mehta, K., Kodali, R. And Deshmukh, S.G. (1995). Simulation for analysis of scheduling rules for a flexible manufacturing system. Integrated manufacturing system, 6(5), pp 21-26.
[20] Fofana, S. B., Nyarko, . F. K. A. ., & Takyi, . G. (2021). Towards Flexible Manufacturing Systems in Africa (A review). Nigerian Journal of Technology, 40(6), 1048–1062. Retrieved from https://www.nijotech.com/index.php/nijotech/article/view/2750
[21] Cronin, Con & Conway, Andrew & Walsh, Joseph. (2019). Flexible manufacturing systems using IIoT in the automotive sector. Procedia Manufacturing. 38. 1652-1659. 10.1016/j.promfg.2020.01.119.
[22] Mishra, S. Rath, B. and Tripathy, A. "Analysis and Modelling of Flexible Manufacturing System," International Research Journal of Engineering and Technology, 2018, pp. 2439.
[23] Singholi, A. Chhabra, D. and Ali, M. "Towards improving the performance of flexible manufacturing system: A case study," Journal of Industrial Engineering and Management, 3(1), 2010, pp. 87–115.
[24] Qin, J. Liu, Y. and Grosvenor, R. "A Categorical Framework of Manufacturing for Industry 4.0 and beyond," in Elsevier, 52, 2016, pp. 173–178.
[25] Díaz-Reza, J. R., Mendoza-Fong, J. R., Blanco-Fernández, J., Marmolejo-Saucedo, J. A. and García-Alcaraz, J. L. "The role of advanced manufacturing technologies in production process performance: A causal model," Applied Science., 9(18), 2019.
[26] Bahga, A. and Madisetti, V. K. "Blockchain Platform for Industrial Internet of Things," Journal of Software Engineering and Application, 9(10),2016, pp. 33–546.
[27] Boyes, H., Hallaq, B., Cunningham, J. and Watson, T. "The industrial internet of things (IIoT): An analysis framework," Computers in Industry, 101, 2017, pp. 1–12.
[28] Margherita, E. G. and Braccini, A. M. "Industry 4.0 Technologies in Flexible Manufacturing for Sustainable Organizational Value: Reflections from a Multiple Case Study of Italian Manufacturers," Information Systems Frontiers Journal, 2020.
[29] Berry, W.L. and Cooper, M.C. (1999), "Manufacturing flexibility: methods for measuring the impact of product variety on performance in process industries", Journal of Operations Management, Vol. 17 No. 2, pp. 163-78.
[30] Bessant, J. and Francis, D. (1999), "Developing strategic continuous improvement capability", International Journal of Operations & Production Management, Vol. 19 No. 11, pp. 1106-19.
[31] Cagliano, R. and Spina, G. (2000), "Advanced manufacturing technologies and strategically flexible production", Journal of Operations Management, Vol. 18 No. 2, pp. 169-90.
[32] Cleveland, G., Schroder, R.G. and Anderson, J.C. (1989), "A theory of production competence", Decision Sciences, Vol. 20, pp. 655-68.
[33] Co, H., Patuwo, B. and Hu, M. (1998), "The human factor in advanced manufacturing technology adoption: an empirical analysis", International Journal of Operations & Production Management, Vol. 18 No. 1, pp. 87-106.

© IJRASET: All Rights are Reserved |

[34] Cooney, R. (2002), "Is „lean" a universal production system? Batch production in the automotive industry", International Journal of Operations & Production Management, Vol. 22 No. 10, pp. 1130-47.
[35] De Toni, A. and Meneghetti, A. (2000), "Traditional and innovative paths towards time-based competition", International Journal of Production Economics, Vol. 66 No. 3, pp. 255-68.
[36] Dixon, J.R. (1992), "Measuring manufacturing flexibility: an empirical investigation", European Journal of Operational Research, Vol. 60 No. 2, pp. 31-43.
[37] Small, M.H. and Chen. I. J.; "Economic and strategic justification of AMT. Inferences from industrial practices", International Journal of Production Economics, Vol. 49, 1997, pp. 65-75.
[38] Klahorst, T.H,; "Flexible Manufacturing Systems: Combining Elements to Lower Costs. Add Flexibility", Industrial Engineering, Vol. 32, No. 11, 1981, pp. 112-117.
[39] Huang, P.Y., and Sakurai, M., "Factory Automation: The Japanese Experience", IEEE Transaction on Engineering Management, Vol. 37, No. 2, 1999, pp. 102-108.
[40] Darrow, W. P.; "International Comparison of Flexible Manufacturing System Technology", Interfaces, Vol. 17, No. 6, November-December 1987, p. 88
[41] Ali, M., &Wadhwa, S. (2005). Performance analysis of partial flexible manufacturing systems. Global Journal of Flexible Systems Mgt, 6(1), 9-19.
[42] Duffie, Neil A. and Rex S. Piper, "Nonhierarchical Control of Manufacturing Systems," Journal of Manufacturing Systems, vol. 5 No.2, pp. 137139, 1986.
[43] Houshyar, A., and White, B., 1993, "Exact optimal solution for facility layout: Deciding which pairs of locations should be adjacent", Computers and Industrial Engineering, Vol. 24, No. 2, pp. 177-187.
[44] Konak, A. Konak, S.K. and Azizoglu, M. (2008). Minimizing the number of tool switching instants in Flexible Manufacturing Systems. International journal of production economics. 116, pp 298-307.
[45] Priore P, Fuente D, Gomez A and Puente J. (2001) A Review of Machine Learning in Dynamic Scheduling of Flexible Manufacturing Systems. Artificial Intelligence for Engineering Design, Analysis and Manufacturing, 15(3), pp. 251 – 263.
[46] Ketokivi, M. (2006). Elaborating the contingency theory of organizations: the case of manufacturing flexibility strategies. Production & Operations Management, 15, pp 215-28
[47] Mehrjerdi, Y. (2009) A decision-making model for flexible manufacturing system, Assembly Automation, 29(1), pp 32-40.
[48] J. Varsaluoma et al., "Usage Data Analytics for Human-Machine Interactions with Flexible Manufacturing Systems: Opportunities and Challenges," 2017 21st International Conference Information Visualisation (IV), 2017, pp. 427-434, doi: 10.1109/iV.2017.38.
[49] Heragu, S. S., and Kusiak, A, 1990, "Machine layout: an optimization and knowledge based approach", International Journal of Production Research, Vol. 28, No. 4, pp. 615-635.
[50] Venkatesh, K., and Ilyas, M., 1993, "Modeling, controlling and simulation of local area networks for flexible manufacturing systems using Petri Nets", Computers and Industrial Engineering, Vol.25, Nos. 1-4, pp. 155-158.

© IJRASET: All Rights are Reserved |

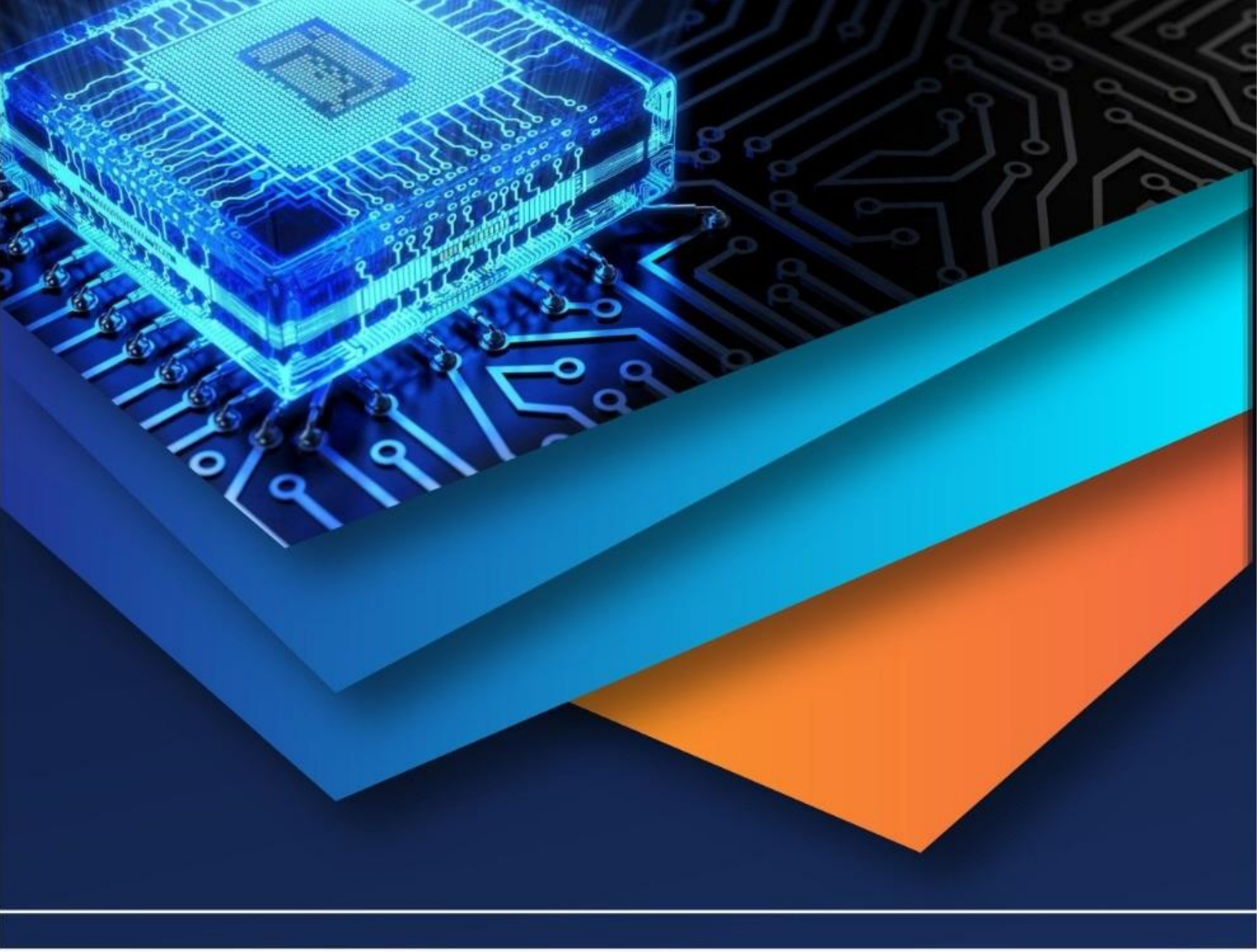

10.22214/IJRASET

45.98

IMPACT FACTOR: 7.129

IMPACT FACTOR: 7.429

INTERNATIONAL JOURNAL FOR RESEARCH

IN APPLIED SCIENCE & ENGINEERING TECHNOLOGY

Call : 08813907089 (24*7 Support on Whatsapp)

Proceedings of the Sixth International Conference on Intelligent Computing and Control Systems (ICICCS 2022)
IEEE Xplore Part Number: CFP22K74-ART; ISBN: 978-1-6654-1035-9

2022 6th International Conference on Intelligent Computing and Control Systems (ICICCS) | 978-1-6654-1035-9/22/$31.00 ©2022 IEEE | DOI: 10.1109/ICICCS53718.2022.9788336

Automated detection of COVID-19 from chest X-rays using CNN

Surbhi Anand
Computer Science Department
Delhi Technological University
New Delhi, India
surbhianand_2k18co365@dtu.ac.in

Nilesh Nishant
Computer Science Department
Delhi Technological University
New Delhi, India
nileshnishant_2k18co235@dtu.ac.in

Tanyam Singal
Computer Science Department
Delhi Technological University
New Delhi, India
tanyamsingal_2k18co371@dtu.ac.in

***Abstract*— The novel coronavirus (COVID-2019) , which first arrived in the Chinese city of Wuhan in December 2019, unrolled like a wind around the arena and brought into an epidemic and declared as a worldwide pandemic by WHO in march,2020. Agriculture, building, manufacturing, trade, lifestyle, tourism, and the global economy all suffer as a result of this disease .Consequently, it's very crucial to diagnose and treat the disease as soon as possible. According to radiology imaging methodologies radiological imaging techniques may aid in appropriately diagnosing and treating the condition with less response time . The utilization of raw chest X-ray pictures has been used to introduce a new model for the automatic detection of COVID-19 in this investigation .In this work we have built a binary classifier to detect covid-19 by deploying the deep learning technique –CNN on dataset collected from repository of JHU CSSE 2019 and was supported by JHU APL and transfer learning techniques has also been utilized to enhance the dataset. The best classification accuracy achieved by our model on chest X-ray dataset is 98.3%.We have also analyzed and compared the model in other research papers with our model.**

Keywords— Coronavirus,Convolutional Neural Network, COVID-19, Deep learning, Transfer learning.

I. INTRODUCTION

The Coronavirus pandemic has spread tremendously across the globe since 2019 December, originating from China, specifically from Wuhan. It is caused by "Severe Acute Respiratory Syndrome Coronavirus 2" (SARS-CoV-2). It drastically spreads across the world with lakhs of positive cases and fatalities. There have also been developed various variants of coronavirus such as alpha, beta ,delta ,Omicron, Florona but these variants possess less severe effects on the health of people as people got vaccinated and the government is also arranging booster shots as well . At the time of writing this research paper according to Worldometer there have been around 434,979,168 confirmed positive cases and 5,963,946 confirmed deaths worldwide. The time and cost required for RT-PCR toolkit to diagnose this illness is high.Artificial intelligence and deep learning have initiated to support doctors to treat this illness. The virus can only be stopped from further identification if the COVID positive person is identified at the early stage and avoids public gathering . This would help in breaking the chain of virus transmission. As, COVID-19 affects the respiratory system, chest radiography scans are a valuable diagnostic for early detection technique. In our research, we advocated the use of chest X-rays of patients for classifying patients having coronavirus or not .We have adopted the Deep learning neural network for the implementation of our project more specifically Convolutional Neural Networks.

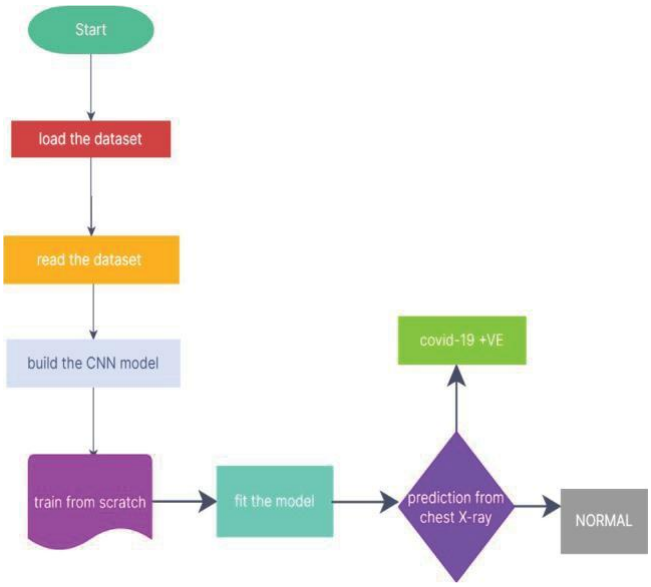

Fig-1. flowchart of our work

II. RELATED WORK

This section's preparation is crucial to the research process as it outlines a comprehensive strategy for conducting academic research.

Cohen[1] gathered radiological pictures from a range of COVID-19 case sources in order for researchers to construct an appropriate model for diagnosing the condition. The majority of the research in this area of the article has used COVID- 19 picture data as a source, although in certain cases, such as Non-COVID- 19, photographs have been gathered from a range of public sources. COVIDX-Net was presented by Hemdan et al. as a way to diagnose COVID-19 in X-ray pictures. Using 25 COVID-19 photos and 25 reference images, they achieved a 90% accuracy rate. COVID-Net, a research-based model for COVID-19, was created by Wang and Wong. With a total of 16,756 radiographic pictures obtained from various open data sources, COVIDNet achieved a 92.4 percent success rate. Loannis et al used Five hundred four normal radiological pictures were utilized in this study, 224 allowed COVID-19, 700 cases of pneumonia, and 224 licensed COVID-19. They found that category 2 issues performed at 98.75 per cent, whereas 3-class difficulties performed at 93.48 per cent. Narin et al. recruited three distinct CNN models using COVID-19 chest X-ray photos supplied by Cohenand 50 normal photographs obtained from Kaggle's shop (ResNet50, InceptionV3, and InceptionResNetV2). Non-COVID photos of children aged one to five years were utilized in this

Authorized licensed use limited to: DELHI TECHNICAL UNIV. Downloaded on June 15,2022 at 11:27:37 UTC from IEEE Xplore. Restrictions apply.

investigation. Researchers also combined a number of models and approaches. Sethy and Behera used CNN models with the SVM separator to extract visual components. The accuracy was 95.38 percent in this experiment using ResNet50 and SVM in conjunction with 50 photographs. Using CT scans. Using an in-depth Inception (M-Inception) model created using CT imaging, Wang et al. achieved 82.9 percent phase correctness. Zheng et al and Xu et al proposed a model having accuracy of 90.8 and 86.7 percent respectively. Xu et al. obtained an 86.7 percent. The bulk of previous research did not have enough data to build models. All these research paper are summarized in table-1 stating author, method adopter and accuracy attained.

Table-1 summary of research papers

Author	Method adopted	Accuracy
Ioannis et. al.[2]	VGG-19	93.48
Wang and Wong[3]	COVID-19	92.4
Sethy and Behra[4]	RESNET50+SVM	95.38
Hemdan et. al.[5]	COVIDX-NET	90.0
Narin et. al.[6]	Deep CNN RESNET-50	98
Ying et. al.[7]	DRE-Net	86
Wang et. al.[8]	M.Inception	82.9
Zheng et. al.[9]	UNet+3D network	90.8
Xu et. al.[10]	Resnet+location attention	86.7

III. OUR PROPOSED WORK

In this section, we first introduce the dataset utilized in our investigation. We then discuss our methodology adopted ,how we trained our model and how transfer learning has been adopted to enhance our dataset which will also improvise our research over large dataset

A. Dataset

A total of 284 photos (142 COVID-19 cases and 142 normal cases) were used to test the suggested algorithm's performance. It is made up of 120 female photos and 160 male photographs. The collection comprises the most photos from the 50-60 year old age group. These images are collected from the repository of JHU CSSE 2019 and was supported by JHU APL. In the given figure,(a) represents some sample x-rays of Covid patients and b represents some sample x-rays of normal (non-Covid) patients.

B. Methodology

(a) Convolutional neural networks

The aim of this domain is to enable machines to view and think the world just like humans do, perceive it in a similar manner and even use the knowledge for a multitude of tasks such as Image & Video recognition, Image Analysis & Classification, Media Recreation, Recommendation Systems, Natural Language Processing, etc. The advancements in Computer Vision with Deep Learning has been constructed, primarily over one particular algorithm known as a **Convolutional Neural Network**.

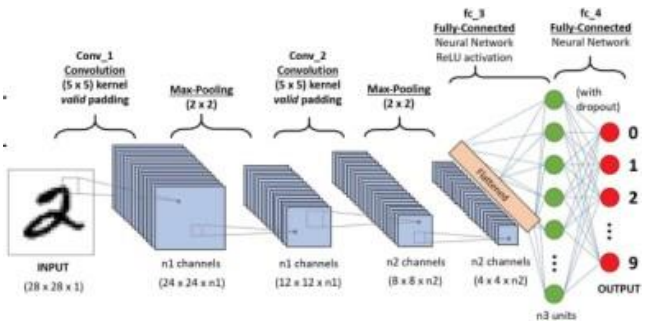

Fig-2. Generalized architecture of convolutional neural network source:

A convolutional neural network is a deep learning algorithm. This algorithm requires less number of preprocessing as compared to other classification algorithms. It is analogous to human brain neuron system and is inspired by visual cortex.

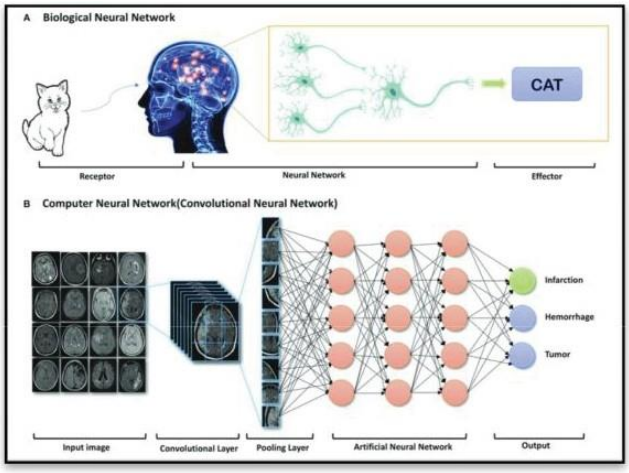

Fig-2-A. Comparison of the working of human brain to CNN Source:

The convolutional neural network consists of two fileds feature extraction and classification.
Convolution Layer- Convolution is the first layer to eliminate features from an embedded image. It encodes the intensities of the image pixel into input neurons.It's a mathematical function that accepts two inputs, such as an image matrix and a kernel or filter. as output: -5 x 5. multiplied by a 3 x 3 filter matrix called "Feature M Different filters can be used to execute operations such as sharpening, blurring and edge detection on images.

Strides: Stride is how far the filter moves in every step along one direction.

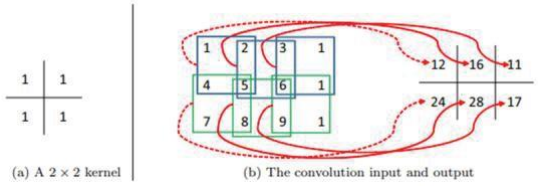

Fig-2-B. Strides

Authorized licensed use limited to: DELHI TECHNICAL UNIV. Downloaded on June 15,2022 at 11:27:37 UTC from IEEE Xplore. Restrictions apply.

Activation functions: The function of activation function is to decide whether the neuron should be activated or not.

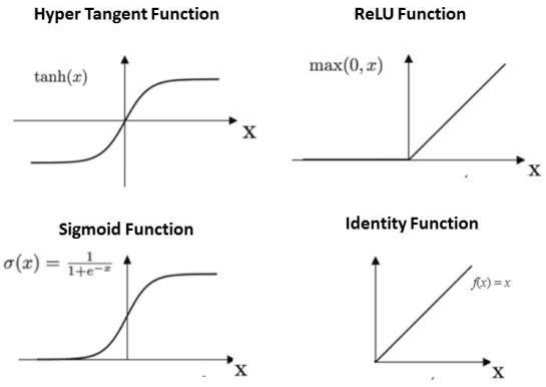

Fig-3. Activation functions

Padding: Occasionally, the applied filter does not perfectly match the input images. As a result, there are two options for dealing with the circumstance. fit. As a result, it only preserves the picture part that is allowed, which is referred to as Legitimate padding.

Pooling Layer: The downgrading of size of maps though maintaining necessary information is called Spatial pooling or sometimes referred as subsampling downsampling. The pooling layer could lower parameters if the photographs are large. Spatial pooling reduces the size of each map while keeping critical information. Spatial pooling can be divided into numerous types as well.

(b) Utilized architecture in our work

This is named after the mathematical operator convolution. A flexible layer collects features from the filters they employ, an integration layer to reduce computer size, and a fully linked layer, which is a neural network, are all part of the typical CNN architecture Using References from previously successful models, we created a Modified Model from the ground up. The output of this model comes from the Average Pool and softmax layers. Finally, a detailed model with several layers is created, which is required for the removal of a feature for real-time object capture. We ran into a few issues in this study, such as distinguishing photos from concealed data, but they were all resolved. Various models that incorporate similar principles and processes, such as the ResNets or ResNext model, should have a framework that can catch and learn minor variations rather than the deeper ones. The suggested model has five layers that are divided into Sequential and Neural Networks, which is an in-depth Learning method that can capture the inserted image, give value (readable weight and bias) to the various elements in the image, and distinguish one from the other. When compared to other partitioning techniques, ConvNet requires extremely little initial processing. Filters used to be constructed by hand in the old days. ConvNets has the ability to read these filters / symbols with proper training. For each layer, 2 2 combinations were regarded as a top layer, as well as 2 dense layers. To make working across all layers easier, a Flatten and Dense Functional layer has been created.Flatten is used to transform a Multidimensional Array into a Single Dimensional Array in order to convert Convolutional layers to Fully integrated layers, allowing Binary features to continue to exist as an important component of the project's operation. Also, unlike the TANH and SIGMOID functions, the ReLU activation function is widely utilised because it returns 0 if the input is negative but any positive input returns that value and is simple to use. The major reason we pick the sigmoid function is that it provides values in the range of (0 to 1). As a result, it's mainly employed in models where we need to forecast outbound opportunities (Binary). Given that opportunities only exist between grades 0 and 1, sigmoid is the best option.

```
[ ] model = Sequential()
    model.add(Conv2D(32,kernel_size=(3,3),activation="relu",input_shape=(224,224,3)))

    model.add(Conv2D(64,(3,3),activation="relu"))
    model.add(MaxPooling2D(pool_size = (2,2)))
    model.add(Dropout(0.25))

    model.add(Conv2D(64,(3,3),activation="relu"))
    model.add(MaxPooling2D(pool_size=(2,2)))
    model.add(Dropout(0.25))

    model.add(Conv2D(128,(3,3),activation="relu"))
    model.add(MaxPooling2D(pool_size=(2,2)))
    model.add(Dropout(0.25))

    model.add(Conv2D(128,(3,3),activation="relu"))
    model.add(MaxPooling2D(pool_size=(2,2)))
    model.add(Dropout(0.25))

    model.add(Flatten())
    model.add(Dense(64,activation="relu"))
    model.add(Dropout(0.5))

    model.add(Dense(1,activation="sigmoid"))

    model.compile(loss=keras.losses.binary_crossentropy,optimizer = "adam",metrics=["accuracy"])
```

Fig-4. Layers of our model

Table-2 Training our neural network

EPOCH	VAL_LOSS	VAL_ACCURACY
EPOCH 1	0.6927	0.5000
EPOCH 2	0.6181	0.8500
EPOCH 3	0.5284	0.8500
EPOCH 4	0.5509	0.9833
EPOCH 5	0.3462	0.9667
EPOCH 6	0.1182	0.8750
EPOCH 7	0.0733	0.9833
EPOCH 8	0.3499	0.8667
EPOCH 9	0.0001	0.9833
EPOCH 10	0.0485	1.000

BI. PERFORMANCE MEASURES USED

Performance measures are the measures that help to determine the effectiveness of the machine learning classification model. We are using Accuracy, Recall, Precision, F1 value as the performance measures.

To calculate the performance we need some other values that are popularly showcase in confusion matrix which are.

Authorized licensed use limited to: DELHI TECHNICAL UNIV. Downloaded on June 15,2022 at 11:27:37 UTC from IEEE Xplore. Restrictions apply.

- True-Negative (TN): Total number of truly predicted rows of negative class.
- False-Positive (FP): Total number of falsely predicted rows of positive class.
- False-Negative (FN): Total number of falsely predicted rows of negative class.
- True-Positive (TP): Total number of truly predicted rows of positive class.

Accuracy: The ratio of correctly classified news both fake and true over total number of classifications.

$$A = (TP + TN)/ \text{Total Where Total} = (TP + TN+FP+FN) \quad (1)$$

Recall: The ratio of correctly predicted true news over sum of correctly predicted true news and incorrectly predicted fake news.

$$r = TP / X \text{ Where } X = (TP+ FN) \quad (2)$$

Precision: The ratio of correctly predicted true news over the sum of correctly predicted true news and incorrectly predicted true news.

$$p = TP / (TP+ FP) \quad (3)$$

F1 value: It is equal to twice the division of product recall and precision over the sum of recall and precision.

$$F1\text{-value} = 2*(p.r)/(p+r) \quad (4)$$

IV. EXPERIMENTAL RESULTS

We used a feed forward neural network with variable duration development, which is a very efficient and important procedure for in-depth learning and machine learning. It combines the Adaptive Gradients and Root Mean Square Propagation modes of stochastic gradient reduction. Instead of using the entire set of data to calculate the actual slope, this optimization algorithm creates stochastic estimates using a randomly selected portion of data. We utilized binary cross entropy as the loss function since itcompares the projected odds to the actual class output of 0 or. Every 2 Epochs, we trained the model for a total of 10 Epochs. Val accuracy was 98.33% .The loss is very less and the accuracy is on point. We have also adopted the following performance metrics in our proposed work.

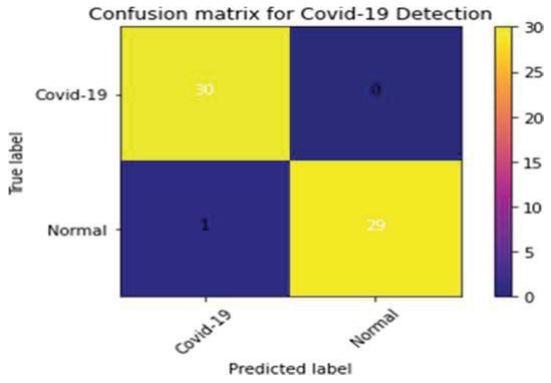

Fig-5. Confusion matrix for COVID-19 detection

Limitation of our approach

The dataset used in our research study is very small and limited. We have done data augmentation in order to maximize the dataset. It is a binary classifier in future we will investigate multiple classifier.

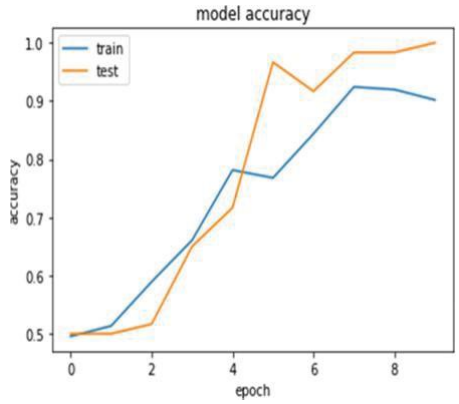

Fig-6. Model accuracy

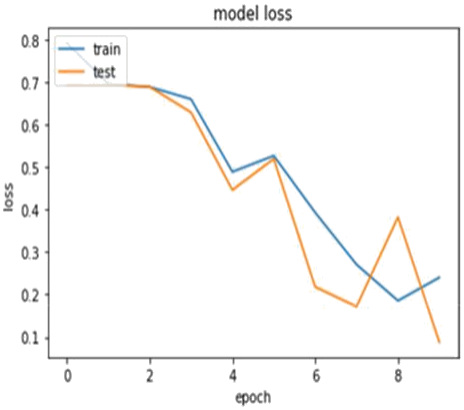

Fig-7. Model loss

Table-3 Classification report

type	accuracy	precision	recall	f1-score
Micro.avg	0.98	0.98	0.96	0.96
Macro.avg	0.98	0.97	0.97	0.97

V. CONCLUSION

The WHO, the European Center for Disease Prevention and Control, the European Union Agency, and other official websites around the world were used to compile the material of the coronavirus document. GitHub and Kaggle were used to gather chest X-ray pictures for modeling purposes. We suggested a Binary study-based phase model for identifying and distinguishing Covid-19 instances from common situations in X-RAY pictures in this study. Our sophisticated algorithm is capable of performing Binary class jobs with a 98.3% accuracy. This technique can be used to alleviate the scarcity of radiologists in remote parts of countries affected by COVID- 19.The use of Limited pictures is the only restriction here. Using a large number of such photos from local hospitals, we hope to strengthen and improve our model, thereby making the dataset very vast. The finding of COVID-19 in chest X-ray pictures is critical for both doctors and patients in terms of reducing diagnostic time and expenses. Images of the activities being taught can be detected using intelligence and in-depth learning skills. In future we will try to enhance the accuracy of our model compared with other performance measures as well. We will try to implement it with more advanced techniques in future by collecting more images.

Authorized licensed use limited to: DELHI TECHNICAL UNIV. Downloaded on June 15,2022 at 11:27:37 UTC from IEEE Xplore. Restrictions apply.

REFERENCES

[1] Boudrioua, M., 2020. COVID-19 Detection from Chest X-Ray Images Using CNNs Models:Further Evidence from Deep Transfer Learning. SSRN Electronic Journal.

[2] Communications in Mathematical Biology and Neuroscience, 2020. Detection of COVID - 19 chest X-ray using support vector machine and convolutional neural network.

[3] Elkorany, A. and Elsharkawy, Z., 2021. COVIDetection-Net: A tailored COVID-19 detection from chest radiography images using deep learning.

[4] Elkorany, A. and Elsharkawy, Z., 2021. COVIDetection-Net: A tailored COVID-19 detection from chest radiography images using deep learning.

[5] KORKMAZ, A. and ATİLA, Ü., 2021. Detection Of Covid-19 From Chest X-ray Images Using Deep Learning Techniques. Artificial Intelligence Studies

[6] Mohamed, A. and Abdelhady, A., 2021. DEEP LEARNING (CNN) MODEL FOR COVID-19 DETECTION FROM CHEST XRAY IMAGES. International Journal of Engineering Applied Sciences and Technology ,Shorfuzzaman, M. and Masud, M., 2020. On the Detection of COVID-19 from Chest X-Ray Images Using CNN-based Transfer Learning. Computers, Materials & Continua

[7] Waheed, M. Goyal, D. Gupta, A. Khanna, F. Al-Turjman, and P. R. Pinheiro, "CovidGAN: data augmentation using auxiliary classifier GAN for improved covid-19 detection," IEEE Access

[8] S. Rajaraman, J. Siegelman, P. O. Alderson, L. S. Folio, L. R. Folio, and S. K. Antani, "Iteratively pruned deep learning ensembles for COVID-19 detection in chest X-rays," IEEE Access

[9] S. Ying, S.Zheng, L. Li et al., "Deep learning enables accurate diagnosis of novel coronavirus (COVID-19) with CT images," IEEE/ACM Transactions on Computational Biology and Bioinformatics,

[10] Shelke, M. Inamdar, V. Shah et al., "Chest X-ray classification using deep learning for automated COVID-19 screening," SN Computer Science

[11] T. Rahaman, in COVID-19 Radiography Database, Kaggle, San Francisco, CA, USA, 2020, https://www.kaggle.com/tawsifurrahman/covid19-radiography-database. 12. S. Saha, "A comprehensive guide to convolutional neural networks — the ELI5 way," Medium, 2021.

[12] Worldometers Website. [Online]. Available: https://www.worldometers. info/coronavirus/ 2021.

[13] Yasin, R., Gouda, W.," Chest X-ray findings monitoring COVID-19 disease course and severity," Egypt J Radiol Nucl Med 51, 193 (2020). https://doi.org/10.1186/s43055-020-00296-x

[14] J. Zhang, Y. Xie, Y. Li, C. Shen, and Y. Xia, "Covid-19 screening on chest x-ray images using deep learning based anomaly detection," arXiv preprint arXiv:2003.12338, 2020.

[15] https://www.happiestminds.com/insights/convolutional-neural-networks-cnns/

[16] K. Simonyan and A. Zisserman, "Very deep convolutional networks for large-scale image recognition," 2014, arXiv:1409.1556. [Online]. Available: http://arxiv.org/abs/1409.1556.

[17] Y. Li, X. Zhang and D. Chen, "CSRNet: Dilated Convolutional Neural Networks for Understanding the Highly Congested Scenes," 2018 IEEE/CVF Conference on Computer Vision and Pattern Recognition, Salt Lake City, UT,

[18] M. J. Horry et al., "COVID-19 Detection Through Transfer Learning Using Multimodal Imaging Data," in IEEE Access, vol. 8, pp. 149808- 149824, 2020, doi: 10.1109/ACCESS.2020.3016780.

[19] West, C. P., Montori, V. M., & Sampath Kumar, P. (2020). "COVID19 Testing: The Threat of False-Negative Results," Mayo Clinic proceedings, 95(6), 1127-1129. https://doi.org/10.1016/ j.mayocp.2020.04.004

[20] C.-F. Yeh, H.-T. Cheng, A. Wei, K.-C. Liu, M.-C. Ko, P.-C. Kuo, R.-J. Chen, P.-C. Lee, J.-H. Chuang, C.-M. Chen et al., "A cascaded learning strategy for robust covid-19 pneumonia chest x-ray screening," arXiv preprint arXiv:2004.12786, 2020.

[21] H. Pratt, F. Coenen, D. M. Broadbent, S. P. Harding, and Y. Zheng, "Convolutional neural networks for diabetic retinopathy," Procedia Computer Science, vol. 90, pp. 200–205, 2016.

[22] https://www.worldometers.info/coronavirus/

[23] https://covid19.who.int/

[24] J. Deng, A. C. Berg, K. Li, and L. Fei-Fei, "What does classifying more than 10,000 image categories tell us?" in European conference on computer vision. Springer, 2010, pp. 71–84.

[25] X. Xu, X. Jiang, C. Ma, P. Du, X. Li, S. Lv, L. Yu, Y. Chen, J. Su, and G. Lang, "others," deep learning system to screen coronavirus disease 2019 pneumonia,"," arXiv preprint arXiv:2002.09334, 2020

[26] I. D. Apostolopoulos and T. A. Mpesiana, "Covid-19: automatic detection from x-ray images utilizing transfer learning with convolutional neural networks," Physical and Engineering Sciences in Medicine, p. 1, 2020

[27] https://towardsdatascience.com/a-comprehensive-guide-to-convolutional-neural-networks-the-eli5-way-3bd2b1164a53

[28] https://towardsdatascience.com/a-comprehensive-guide-to-convolutional-neural-networks-the-eli5-way-3bd2b1164a53

[29] https://www.analyticsvidhya.com/blog/2021/05/convolutional-neural-networks-cnn/

[30] https://www.geeksforgeeks.org/convolutional-neural-network-cnn-in-machine-learning/

[31] L. Li, L. Qin, Z. Xu, Y. Yin, X. Wang, B. Kong, J. Bai, Y. Lu, Z. Fang, Q. Song et al., "Artificial intelligence distinguishes covid-19 from community acquired pneumonia on chest ct," Radiology, p. 200905, 2020.

[32] https://en.wikipedia.org/wiki/Convolutional_neural_network

Authorized licensed use limited to: DELHI TECHNICAL UNIV. Downloaded on June 15,2022 at 11:27:37 UTC from IEEE Xplore. Restrictions apply.

Mediterr. J. Math. (2022) 19:161
https://doi.org/10.1007/s00009-022-02074-7
© The Author(s), under exclusive licence to Springer Nature Switzerland AG 2022

Mediterranean Journal of Mathematics

Bohr–Rogosinski Phenomenon for $\mathcal{S}^*(\psi)$ and $\mathcal{C}(\psi)$

Kamaljeet Gangania and S. Sivaprasad Kumar

Abstract. In Geometric function theory, occasionally, attempts have been made to solve a particular problem for the Ma-Minda classes, $\mathcal{S}^*(\psi)$ and $\mathcal{C}(\psi)$ of univalent starlike and convex functions, respectively. Recently, a popular radius problem generally known as Bohr's phenomenon has been studied in various settings; however, a little is known about Rogosinski radius. In this article, for a fixed $f \in \mathcal{S}^*(\psi)$ or $\mathcal{C}(\psi)$, the class of analytic subordinants $S_f(\psi) := \{g : g \prec f\}$ is studied for the Bohr–Rogosinski phenomenon in a general setting. Its applications to the classes $\mathcal{S}^*(\psi)$ and $\mathcal{C}(\psi)$ are also shown.

Mathematics Subject Classification. 30C45, 30C50, 30C80.

Keywords. Subordination, radius problem, Bohr radius, Bohr–Rogosinski radius.

1. Introduction

Let $\mathcal{A}$ denote the class of analytic functions of the form $f(z) = z + \sum_{k=2}^{\infty} a_k z^k$ in the open unit disk $\mathbb{D} := \{z : |z| < 1\}$. Using subordination [23], Ma and Minda [22] (also see [17]) introduced the unified class of univalent starlike and convex functions defined as follows:

$$\mathcal{S}^*(\psi) := \left\{ f \in \mathcal{A} : \frac{zf'(z)}{f(z)} \prec \psi(z) \right\}$$

and

$$\mathcal{C}(\psi) := \left\{ f \in \mathcal{A} : 1 + \frac{zf''(z)}{f'(z)} \prec \psi(z) \right\},$$

where ψ is analytic and univalent with $\Re\psi(z) > 0$, $\psi'(0) > 0$, $\psi(0) = 1$, and $\psi(\mathbb{D})$ is symmetric about real axis. Note that $\psi \in \mathcal{P}$, the class of normalized Carathéodory functions. Also, when $\psi(z) = (1+z)/(1-z)$, $\mathcal{S}^*(\psi)$ and $\mathcal{C}(\psi)$

K. Gangania would like to thank University Grant Commission, New-Delhi, India for providing Junior Research Fellowship under UGC-Ref. No.:1051/(CSIR-UGC NET JUNE 2017).

Published online: 21 June 2022

reduce to the standard classes $\mathcal{S}^*$ and $\mathcal{C}$ of univalent starlike and convex functions.

In GFT, radius problems have a rich history which is being followed till today; see the recent articles [9,10,13,15–17,19,31]. In 1914, Harald Bohr [8] proved the following remarkable radius problem related to the power series:

Theorem 1. (Bohr's Theorem, [8]) *Let $g(z) = \sum_{k=0}^{\infty} a_k z^k$ be an analytic function in $\mathbb{D}$ and $|g(z)| < 1$ for all $z \in \mathbb{D}$, then*

$$\sum_{k=0}^{\infty} |a_k||z|^k \leq 1, \quad \text{for} \quad |z| \leq \frac{1}{3}.$$

Bohr actually proved the above result for $r \leq 1/6$. Further Wiener, Riesz, and Shur independently sharpened the result for $r \leq 1/3$. Presently, the Bohr inequality for functions mapping unit disk onto different domains, other than unit disk is an active area of research. For the recent development on Bohr phenomenon, see the articles [2,3,6,7,11,24–26] and references therein. The concept of Bohr phenomenon in terms of subordination can be described as follows.

Definition 1. (Muhanna, [24]) Let $f(z) = \sum_{k=0}^{\infty} a_k z^k$ and $g(z) = \sum_{k=0}^{\infty} b_k z^k$ are analytic in $\mathbb{D}$ and $f(\mathbb{D}) = \Omega$. For a fixed f, consider a class of analytic functions $S(f) := \{g : g \prec f\}$ or equivalently $S(\Omega) := \{g : g(z) \in \Omega\}$. Then, the class $S(f)$ is said to satisfy Bohr phenomenon, if there exists a constant $r_0 \in (0, 1]$ satisfying the inequality $\sum_{k=1}^{\infty} |b_k| r^k \leq d(f(0), \partial\Omega)$ for all $|z| = r \leq r_0$ and $g \in S(f)$, where $d(f(0), \partial\Omega)$ denotes the Euclidean distance between $f(0)$ and the boundary of $\Omega = f(\mathbb{D})$. The largest such r_0 is called the Bohr radius.

In 2014, Muhanna et al. [26] proved the Bohr phenomenon for $S(W_\alpha)$, where $W_\alpha := \{w \in \mathbb{C} : |\arg w| < \alpha\pi/2, 1 \leq \alpha \leq 2\}$, which is a Concave-wedge domain (or exterior of a compact convex set) and the class $R(\alpha, \beta, h)$ defined by $R(\alpha, \beta, h) := \{f \in \mathcal{A} : f(z) := g(z) + \alpha z g'(z) + \beta z^2 g''(z) \prec h(z), g \in \mathcal{A}\}$, where h is a convex function (or starlike) and $R(\alpha, \beta, h) \subset S(h)$. In 2018, Bhowmik and Das [6] proved the Bohr phenomenon for the classes: $S(f) = \{g \in \mathcal{A} : g \prec f \text{ and } f \in \mu(\lambda)\}$, where $\mu(\lambda) = \{f \in \mathcal{A} : |(z/f(z))^2 f'(z) - 1| < \lambda, 0 < \lambda \leq 1\}$ and $S(f) = \{g \in \mathcal{A} : g \prec f \text{ and } f \in \mathcal{S}^*(\alpha), 0 \leq \alpha \leq 1/2\}$, where $\mathcal{S}^*(\alpha)$ is the well-known class of starlike functions of order α.

In the aforesaid work, the role of the sharp coefficient's bound of f was prominent to achieve the respective Bohr radius for the class $S(f)$; see [3,17,18]. However, in general, the sharp coefficient's bounds for functions in a given class are not available; for example, see [9,15–17,31]; thus, certain power series inequalities are needed. In this direction, Bhowmik and Das obtained the following important inequality to achieve the Bohr radius for the class $S(f)$, where $f \in \mu(\lambda)$ and $\mathcal{S}^*(\alpha), 0 \leq \alpha \leq 1/2\}$ respectively:

Lemma 1 [6]. *let $f(z) = \sum_{n=0}^{\infty} a_n z^n$ and $g(z) = \sum_{k=0}^{\infty} b_k z^k$ be analytic in $\mathbb{D}$ and $g \prec f$. Then*

$$\sum_{k=0}^{\infty} |b_k| r^k \leq \sum_{n=0}^{\infty} |a_n| r^n, \quad \text{for} \quad |z| \leq \frac{1}{3}.$$

Motivated by the class $S(f)$, Kumar and Gangania in [18, Sec. 5] (also see [11]) further used the above Lemma 1 in the absence of the sharp coefficient's bounds of f to study the Bohr phenomenon for the class $S_f(\psi)$, which eventually holds for the class $\mathcal{S}^*(\psi)$

Definition 2. Let $f \in \mathcal{S}^*(\psi)$ or $\mathcal{C}(\psi)$ be fixed. Then, the class of subordinants functions g is defined as

$$S_f(\psi) := \left\{ g(z) = \sum_{k=1}^{\infty} b_k z^k : g \prec f \right\}.$$

Definition 3. (Koebe radius) Let $f \in \mathcal{S}^*(\psi)$. Then, either f is a rotation of f_0 or

$$\{w \in \mathbb{C} : |w| \leq r_* = -f_0(-1) \subset f(\mathbb{D})\},$$

where $r_* = \lim_{r\to 1}(-f_0(-r))$. Equality holds for the function

$$f_0(z) = z \exp \int_0^z \frac{\psi(t) - 1}{t} dt.$$

Theorem 2 [18, Theorem 5.1]. (also see [11]) *Let r_* be the Koebe radius for the class $\mathcal{S}^*(\psi)$, $f_0(z)$ be given by Eq. (2) and $g(z) = \sum_{k=1}^{\infty} b_k z^k \in S_f(\psi)$. Assume $f_0(z) = z + \sum_{n=2}^{\infty} t_n z^n$ and $\hat{f}_0(r) = r + \sum_{n=2}^{\infty} |t_n| r^n$. Then, $S_f(\psi)$ satisfies the Bohr phenomenon*

$$\sum_{k=1}^{\infty} |b_k| r^k \leq d(f(0), \partial\Omega), \quad \text{for } |z| = r \leq r_b,$$

where $r_b = \min\{r_0, 1/3\}$, $\Omega = f(\mathbb{D})$ and r_0 is the least positive root of the equation

$$\hat{f}_0(r) = r_*.$$

The result is sharp when $r_b = r_0$ and $t_n > 0$.

Again, if we look at the classical Bohr inequality in Theorem 1 and try to replace the initial coefficients $a_k, (k = 0, 1)$ by $|f(z)|$ and $|f'(z)|$, and further z by some suitable choice of functions $\omega(z)$, such that $|\omega(z)| < 1$. Or replace the Taylor coefficients a_k completely by the higher order derivatives of f. Then, the combinations obtained lead us to the new inequalities, which are usually called Bohr-type inequalities. We now mention a few such combinations: Suppose that $f(z) = \sum_{k=0}^{\infty} a_k z^k$ be analytic in $\mathbb{D}$ and $a = |a_0|$ and $||f_0||_r^2 = \sum_{k=1}^{\infty} |a_{2k}| r^{2k}$, where $f_0(z) = f(z) - a_0$.

(*i*) $|f(z)|^n + \sum_{k=1}^{\infty} |a_k| r^k$, $n = 0$ or 1

(*ii*) $|f(z)| + |f'(z)||z| + \sum_{k=2}^{\infty} |a_k| r^k$

(*iii*) $|f(z)| + \sum_{k=N}^{\infty} \left| \frac{f^{(k)}(z)}{k!} \right| r^k$

(*iv*) $|f(\omega(z))| + \sum_{k=1}^{\infty} |a_k| r^k + \frac{1+ar}{(1+a)(1-r)} ||f_0||_r^2$.

For some important work in this direction, we refer to see [12,21].

Note that Muhanna et al. [27] recently discussed the Bohr-type inequalities for the kth section of the analytic functions $f(z) = \sum_{n=0}^{\infty} a_n z^n$ using the Bohr Operator

$$M_r(f) = \sum_{n=0}^{\infty} |a_n||z^n| = \sum_{n=0}^{\infty} |a_n| r^n.$$

Paulsen and Singh [28] using this operator provided a simple elementary proof of the Bohr's Theorem 1 and extended it to the Banach algebras (for the basic important discussion, see [27,28]). Now, for the simplicity and further discussion, we define the following basic operator for f, where $S^N(f(z)) = \sum_{n=N}^{\infty} a_n z^n$:

$$M_r^N(f) = \sum_{n=N}^{\infty} |a_n||z^n| = \sum_{n=N}^{\infty} |a_n| r^n,$$

and thus, the following observations hold for $|z| = r$ for each $z \in \mathbb{D}$:

(*i*) $M_r^N(f) \geq 0$, and $M_r^N(f) = 0$ if and only if $f \equiv 0$
(*ii*) $M_r^N(f+g) \leq M_r^N(f) + M_r^N(g)$
(*iii*) $M_r^N(\alpha f) = |\alpha| M_r^N(f)$ for $\alpha \in \mathbb{C}$
(*iv*) $M_r^N(f.g) \leq M_r^N(f).M_r^N(g)$
(*v*) $M_r^N(1) = 1$.

Using this operator, we now can get similar results as obtained by Muhanna et al. [27] for the interim kth sections $S_k^N(f(z)) = \sum_{n=N}^{k} a_n z^n$ and the function $S^N(f(z))$.

In analogy with Bohr's Theorem, there is also the notion of Rogosinski radius; however, a little is known about Rogosinski radius as compared to Bohr radius, which is defined as follows, also see [20,29,30]:

Theorem 3 [Rogosinski Theorem] *If* $g(z) = \sum_{k=0}^{\infty} b_k z^k$ *with* $|g(z)| < 1$, *then for every* $N \geq 1$, *we have*

$$\left| \sum_{k=0}^{N-1} b_k z^k \right| \leq 1, \quad \textit{for} \quad |z| \leq \frac{1}{2}.$$

The radius $1/2$ *is called the Rogosinski radius.*

Kayumov et al. [14] considered a new quantity, called Bohr–Rogosinski sum, which is described as follows:

$$|g(z)| + \sum_{k=N}^{\infty} |b_k||z|^k, \quad |z| = r.$$

For the case $N = 1$, note that this sum is similar to the Bohr's sum, where $g(0)$ is replaced by $|g(z)|$. We also refer the readers to see [1,4]. Now, we say the family $S(f)$ has Bohr–Rogosinski phenomenon, if there exists $r_N^f \in (0,1]$, such that the inequality

$$|g(z)| + \sum_{k=N}^{\infty} |b_k||z|^k \leq |f(0)| + d(f(0), \partial\Omega)$$

holds for $|z| = r \leq r_N^f$. The largest such r_N^f is called the Bohr–Rogosinski radius. Authors [14] also proved the following interesting results:

Theorem 4 [14, Theorems 5–6]. *Let $g \in S(f)$, where f is univalent in $\mathbb{D}$. Then, for each $m, N \in \mathbb{N}$, the inequality*

$$|g(z^m)| + \sum_{k=N}^{\infty} |b_k||z|^k \leq |f(0)| + d(f(0)\partial\Omega)$$

holds for $|z| = r \leq r_{m,N}^f$, where $r_{m,N}^f$ is the smallest positive root of

$$4r^m - (1-r^m)^2 + 4r^N(N(1-r)+r)\left(\frac{1-r^m}{1-r}\right)^2 = 0.$$

The radius is sharp for the Koebe function $z/(1-z)^2$. Moreover, if f is convex (univalent) in $\mathbb{D}$, then $r_{m,N}^f$ is the smallest positive root of

$$3r^m - 1 + 2r^N\left(\frac{1-r^m}{1-r}\right) = 0.$$

The radius is sharp for the convex function $z/(1-z)$.

Motivated by the above work, let us now introduce the Bohr–Rogosinski phenomenon for the class of analytic subordinants $S_f(\psi)$:

Definition 4. The class $S_f(\psi)$ has a Bohr–Rogosinski phenomenon, if there exists an $0 < r_0 \leq 1$, such that for each $g \in S_f(\psi)$

$$|g(z)| + \sum_{k=N}^{\infty} |b_k||z|^k \leq d(f(0), \partial\Omega)$$

for $|z| = r \leq r_0$, where $N \in \mathbb{N}$, $\Omega = f(\mathbb{D})$ and $d(f(0), \partial\Omega)$ denotes the Euclidean distance between $f(0)$ and the boundary of Ω.

Note that $\mathcal{S}^*(\psi) \subset \bigcup_{f\in\mathcal{S}^*(\psi)} S_f(\psi)$. Furthermore, the connection between the Bohr–Rogosinski and Bohr phenomenon can be seen through Definition 4, if we replace $|g(z)|$ by $|g(z^m)|$, where $m \in \mathbb{N}$, and then consider the special case by taking $m \to \infty$ with $N = 1$. In Sect. 2, for a fixed $f \in \mathcal{S}^*(\psi)$ or $\mathcal{C}(\psi)$, the class of subordinants $S_f(\psi) := \{g : g \prec f\}$ is studied for the Bohr–Rogosinski phenomenon in general settings along with its applications to the standard classes of univalent starlike and convex functions.

2. Bohr–Rogosinski Phenomenon

The following fundamental result is an extension of the Lemma 1.

Lemma 2. *Let $f(z) = \sum_{n=0}^{\infty} a_n z^n$ and $g(z) = \sum_{k=0}^{\infty} b_k z^k$ be analytic in $\mathbb{D}$ and $g \prec f$, then*

$$\sum_{k=N}^{\infty} |b_k| r^k \leq \sum_{n=N}^{\infty} |a_n| r^n \tag{1}$$

for $|z| = r \leq \frac{1}{3}$ and $N \in \mathbb{N}$.

Proof. Since $g \prec f$, we have $g(z) = f(\omega(z))$, where ω is a Schwarz function. For the case $\omega(z) = cz$, $|c| = 1$, the function g is a rotation of f or $g = f$, and the inequality (1) easily holds. Therefore, consider the case: $\omega(z) \neq cz$, $|c| = 1$. Now, the coefficient b_k of the function g is given by: for any $k \geq N \in \mathbb{N}$

$$b_k = \sum_{n=N}^{k} a_n {\beta_k}^{(n)},$$

where the tth power of the analytic function ω is represented as $\omega^t(z) = \sum_{l \geq t} {\beta_l}^{(t)} z^l$, $t \in \mathbb{N}$. Now, we see that

$$\begin{aligned} \sum_{k=N}^{m} |b_k| r^k &= \sum_{k=N}^{m} \left| \sum_{n=N}^{n} a_n {\beta_k}^{(n)} \right| r^k \\ &\leq \sum_{k=N}^{m} \sum_{n=N}^{n} |a_n| |{\beta_k}^{(n)}| r^k \\ &= \sum_{n=N}^{m} |a_n| {M_m}^{(n)}(r), \end{aligned}$$

where ${M_m}^{(n)}(r) = \sum_{k=n}^{m} |{\beta_k}^{(n)}| r^k$ and $m \in \mathbb{N}$. Since $|\omega^n(z)/z^n| < 1$ for any $n \geq 1$, using Bohr's Theorem 1, we have

$$\sum_{k=n}^{m} |{\beta_k}^{(n)}| r^{k-n} \leq \sum_{k=n}^{\infty} |{\beta_k}^{(n)}| r^{k-n} \leq 1, \quad r \leq \frac{1}{3},$$

that is, ${M_m}^{(n)}(r) \leq r^n$ holds for $r \leq 1/3$. Hence, for any $m \geq N \geq 1$ and $r \leq 1/3$

$$\sum_{k=N}^{m} |b_k| r^k \leq \sum_{n=N}^{m} |a_n| r^n.$$

The result now follows by taking $m \to \infty$. □

Proof. (Alternate proof of the Lemma 2) Since $g(z) = f(\omega(z))$, where ω is the Schwarz function, we have

$$\begin{aligned} M_r^N(g) &= M_r^N \left(\sum_{k=N}^{\infty} a_k (\omega(z))^k \right) \\ &\leq \sum_{k=N}^{\infty} |a_k| \left(M_r(\omega(z)) \right)^k \\ &\leq \sum_{k=N}^{\infty} |a_k| |z|^k \end{aligned}$$

for $|z| = r \leq 1/3$. □

Remark 1. In Lemma 2, taking $N \to 1$ and the fact the $g(0) = f(0)$, we obtain Lemma 1.

Moreover, the following results are obtained using the properties of the operator $M_r^N(f)$ and Lemma 2:

Corollary 1. *Let the analytic functions f, g, and h satisfy $g(z) = h(z)f(\omega(z))$ in $\mathbb{D}$, where ω is the Schwarz function. Assume $|h(z)| \leq \tau$ for $|z| < \tau \leq 1$. Then*

$$M_r^N(g) \leq \tau M_r^N(f), \quad 0 \leq |z| = r \leq \frac{\tau}{3}.$$

Corollary 2. *Let $\tau = 1$ in Corollary 1. Then*

$$M_r^N(g) \leq M_r^N(f), \quad 0 \leq |z| = r \leq \frac{1}{3}.$$

We need the following lemma for our next result.

Lemma 3. [22] *Let $f \in \mathcal{S}^*(\psi)$ and $|z_0| = r < 1$. Then, $f(z)/z \prec f_0(z)/z$ and*

$$-f_0(-r) \leq |f(z_0)| \leq f_0(r).$$

Equality holds for some $z_0 \neq 0$ if and only if f is a rotation of f_0, where $zf_0(z)/f_0(z) = \psi(z)$, such that

$$f_0(z) = z \exp \int_0^z \frac{\psi(t) - 1}{t} dt. \tag{2}$$

Our next results discuss Bohr–Rogosinski phenomenon for the classes $S_f(\psi)$ and $\mathcal{S}^*(\psi)$, respectively.

Theorem 5. *Let r_* be the Koebe radius for the class $\mathcal{S}^*(\psi)$, $f_0(z)$ be given by Eq. (2) and $f(z) = z + \sum_{n=2}^{\infty} a_n z^n \in \mathcal{S}^*(\psi)$. Assume $f_0(z) = z + \sum_{n=2}^{\infty} t_n z^n$ and $\hat{f}_0(r) = r + \sum_{n=2}^{\infty} |t_n| r^n$. If $g \in S_f(\psi)$. Then*

$$|g(z^m)| + \sum_{k=N}^{\infty} |b_k||z|^k \leq d(0, \partial\Omega) \tag{3}$$

holds for $|z| = r_b \leq \min\{\frac{1}{3}, r_0\}$, where $m, N \in \mathbb{N}$, $\Omega = f(\mathbb{D})$ and r_0 is the unique positive root of the equation

$$\hat{f}_0(r^m) + \hat{f}_0(r) - p_{\hat{f}_0}(r) = -f_0(-1), \tag{4}$$

where

$$p_{\hat{f}_0}(r) = \begin{cases} 0, & N = 1; \\ r, & N = 2 \\ r + \sum_{n=2}^{N-1} |t_n| r^n, & N \geq 3. \end{cases}$$

The result is sharp when $r_b = r_0$ and $t_n > 0$.

Proof. Let $g(z) = \sum_{k=1}^{\infty} b_k z^k \prec f(z)$, where $f \in \mathcal{S}^*(\psi)$. Now, by Lemma 2, for $r \leq 1/3$, we have

$$\sum_{k=N}^{\infty} |b_k| r^k \leq \sum_{n=N}^{\infty} |a_n| r^n.$$

Again applying Lemma 2 on $f(z)/z \prec f_0(z)/z$ (Lemma 3), we get that

$$\sum_{k=N}^{\infty} |b_k| r^k \leq \sum_{n=N}^{\infty} |a_n| r^n \leq \sum_{n=N}^{\infty} |t_n| r^n, \quad r \leq \frac{1}{3}. \tag{5}$$

Now, $g \prec f$ implies that $g(z) = f(\omega(z))$, which using the Lemma 3 yields

$$|g(|z| \leq r)| = |f(\omega(|z| \leq r))| \leq \max_{|z|=r} |f(|z| \leq r)| \leq f_0(r),$$

that is

$$|g(z)| = |f(\omega(z))| \leq f_0(r)$$

for $|z| = r$, where ω is a Schwarz function. Moreover, replacing z by z^m in the above inequality along with the definition of $\hat{f}_0$ gives

$$|g(z^m)| \leq \hat{f}_0(r^m). \tag{6}$$

Also, by letting r tends to 1 in Lemma 3, we obtain the Koebe radius $r_* = -f_0(-1)$. Therefore, the open ball $\mathbb{B}(0, r_*) \subset f(\mathbb{D})$, which implies that for $|z| = 1$

$$r_* \leq d(0, \partial\Omega). \tag{7}$$

Now, using Eqs. (5), (6), and (7), we have

$$\begin{aligned} |g(z^m)| + \sum_{k=N}^{\infty} |b_k||z|^k &\leq \hat{f}_0(r^m) + \sum_{n=N}^{\infty} |t_n| r^n \\ &= \hat{f}_0(r^m) + \hat{f}_0(r) - p_{\hat{f}_0}(r) \\ &\leq r_* \\ &\leq d(0, \partial\Omega) \end{aligned}$$

holds whenever $|z| = r \leq \min\{\frac{1}{3}, r_0\}$, where r_0 is the smallest positive root of the equation

$$G(r) := \hat{f}_0(r^m) + \hat{f}_0(r) - p_{\hat{f}_0}(r) - r_* = 0.$$

Note that $G(0) < 0$, and since $\hat{f}_0(1) \geq |f_0(1)| \geq r_*$ (see Lemma 3), we see that

$$2\hat{f}_0(1) - \sum_{n=1}^{N-1} |t_n| - r_* = (\hat{f}_0(1) - \sum_{n=1}^{N-1} |t_n|) + (\hat{f}_0(1) - r_*) > 0,$$

where $t_1 = 1$, which implies $G(1) > 0$. Clearly, for $0 \leq r \leq 1$

$$G'(r) = \hat{f}'_0(r^m) + (\hat{f}'_0(r) - p'_{\hat{f}_0}(r)) > 0,$$

which implies that G is a continuous increasing function in $[0, 1]$. Thus, $G(r) = 0$ has a root in the interval $(0, 1)$. Let us take $g = f = f_0$, then the sharpness follows for the function f_0 with the equality in (3) as

$$f_0({r_b}^m) + \sum_{n=N}^{\infty} t_n {r_b}^n = r^* = d(0, \partial\Omega)$$

when $r_b = r_0$ and $t_n > 0$. □

Remark 2. Let $\psi(z) = (1 + z)/(1 - z)$, then Theorem 5 reduces to [14, Theorem 5].

Remark 3. Observe that if we take $m \to \infty$ and $N = 1$, then Theorem 5 reduces to [18, Theorem 5.1].

Corollary 3. *Let r_* be the Koebe radius for the class $\mathcal{S}^*(\psi)$; $f_0(z)$ be given by Eq. (2). Assume $f_0(z) = z + \sum_{n=2}^{\infty} t_n z^n$ and $\hat{f}_0(r) = r + \sum_{n=2}^{\infty} |t_n| r^n$. If $f(z) = z + \sum_{n=2}^{\infty} a_n z^n \in \mathcal{S}^*(\psi)$. Then*

$$|f(z^m)| + \sum_{n=N}^{\infty} |a_n||z|^n \leq d(0, \partial\Omega) \tag{8}$$

holds for $|z| = r_b \leq \min\{\frac{1}{3}, r_0\}$, where $m, N \in \mathbb{N}$, $\Omega = f(\mathbb{D})$ and r_0 is the unique positive root of the equation

$$\hat{f}_0(r^m) + \hat{f}_0(r) - p_{\hat{f}_0}(r) = -f_0(-1),$$

where $p_{\hat{f}_0}$ is as defined in Theorem 5. The radius is sharp for the function f_0 when $r_b = r_0$ and $t_n > 0$.

Corollary 4. *Let $\psi(z) = 1 + \frac{4}{3}z + \frac{2}{3}z^2$, $f_0(r) = r \exp\left(\frac{4}{3}r + \frac{r^2}{3}\right)$ and $m = 1$. If $g \in S_f(\psi)$, then the inequality (3) holds for $|z| = r \leq r_N$, where $N \in \mathbb{N}$ and $r_N (< 1/3)$ is the unique positive root of the equation*

$$2r \exp\left(\frac{4}{3}r + \frac{r^2}{3}\right) - p_{f_0}(r) - \exp(-1) = 0,$$

where $p_{f_0} = p_{\hat{f}_0}$ is as defined in Theorem 5 with $|t_n| = t_n = {f_0}^n(0)/n!$. Moreover, if $f \in \mathcal{S}^*(\psi)$, then the inequality (8) also holds for $r \leq r_N$. The radius r_N is sharp.

Remark 4. In Corollary 4, we observe that the radius r_N approaches $r_0 = 0.25588\cdots$ for large value of N, where r_0 is the unique positive root of

$$r \exp\left(\frac{4}{3}r + \frac{r^2}{3}\right) - \exp(-1) = 0.$$

Moreover, if $m \geq 2$, then the inequalities (3) and (8) hold for $r \leq 1/3$.

Corollary 5. *Let $\psi(z) = 1 + ze^z$ and $m = 1$. If $g \in S_f(\psi)$, then the inequality (3) holds for $|z| = r \leq r_N = \{r_0, 1/3\}$, where $N \in \mathbb{N}$ and r_0 is the unique positive root of the equation*

$$2r \exp(e^r - 1) - T(r) - \exp(e^{-1} - 1) = 0,$$

where

$$T(r) = \begin{cases} 0, & N = 1; \\ r, & N = 2; \\ \sum_{n=1}^{N-1} \frac{B_{n-1}}{(n-1)!} r^n, & N \geq 3 \end{cases}$$

and B_n are the bell numbers, such that $B_{n+1} = \sum_{k=0}^{n} \binom{n}{k} B_k$. Moreover, if $f \in \mathcal{S}^*(\psi)$, then the inequality (8) also holds for $r \leq r_N$. The radius $r_N < 1/3$ is sharp for $N \leq 3$.

Corollary 6. *Let* $\psi(z) = 1 + \frac{z}{k}\left(\frac{k+z}{k-z}\right)$ *with* $k = \sqrt{2}+1$. *If* $g \in S_f(\psi)$, *then the inequality* (3) *holds for* $|z| = r \le r_b = \min\{1/3, r_0\}$, *where* $N \in \mathbb{N}$ *and* r_0 *is the unique positive root of the equation*

$$\frac{r^m}{e^{r^m}}\left(\frac{k}{k-r^m}\right)^{2k} + \frac{r}{e^r}\left(\frac{k}{k-r}\right)^{2k} - p_{f_0}(r) - e\left(\frac{k}{k+1}\right)^{2k} = 0,$$

where $p_{f_0} = p_{\hat{f}_0}$ *is as defined in Theorem* 5 *and* $t_n = |t_n|$ *are the Taylor coefficients of the function* $f_0(r) = \frac{r}{e^r}\left(\frac{k}{k-r}\right)^{2k}$. *Moreover, if* $f \in \mathcal{S}^*(\psi)$, *then the inequality* (8) *also holds for* $r \le r_b$. *The radius* r_b *is sharp when* $m = 1$ *and* $N \le 4$.

Since all the Taylor coefficients of the function $1+\sin z$ are not positive, $\hat{f}_0 \neq f_0$. Therefore, we consider the radius r_N up to three decimal places only, which also reveals the connection of positive coefficients of ψ to the sharp Bohr–Rogosinski radius.

Corollary 7. *Let* $\psi(z) = 1+\sin z$ *and* $m = 1$. *If* $g \in S_f(\psi)$, *then the inequality* (3) *holds for* $|z| = r \le r_N$, *where* $N \in \mathbb{N}$ *and* $r_N (< 1/3)$ *is the unique positive root of the equation*

$$2r\exp(Si(r)) - \exp(Si(-1)) - p_{f_0}(r) = 0,$$

where $f_0(r) = r\exp(Si(r))$, *where* $Si(x)$ *is the Sin Integral defined as*

$$Si(x) := \int_0^x \frac{\sin(x)}{x}dx = \sum_{n=0}^{\infty}\frac{(-1)^n x^{2n+1}}{(2n+1)(2n+1)!}.$$

Moreover, if $f \in \mathcal{S}^*(\psi)$. *Then, the inequality* (8) *also holds for* $r \le r_N$.

Remark 5. In Corollary 7, the numerical computations reveal that the Bohr–Rogosinski radius $r_N \approx 0.290 * \cdots < 1/3$ for any $N > 4$, where $* = 6$ or 7. Also, $r_N < 1/3$ for $N \le 4$. Moreover, as $N \to \infty$, the required radius $r_0 \approx 0.290 * \cdots$ is the unique positive root of

$$r\exp(Si(r)) - \exp(Si(-1)) = 0.$$

Next, we discuss the Bohr–Rogosinski phenomenon for the celebrated Janowski class of univalent starlike functions. For this, we first need the following: for simplicity, write $\mathcal{S}^*((1+Dz)/(1+Ez)) \equiv \mathcal{S}[D,E]$, where $-1 \le E < D \le 1$.

Lemma 4. [5, Theorem 3] *If* $f(z) = z + \sum_{n=2}^{\infty} a_n z^n \in \mathcal{S}[D,E]$. *Then, for* $n \ge 2$, *the following sharp bounds occur:*

$$|a_n| \le \prod_{k=0}^{n-2}\frac{|E-D+Ek|}{k+1}.$$

Theorem 6. *Let* $\psi(z) = (1+Dz)/(1+Ez)$, $-1 \le E < D \le 1$. *If* $f(z) = z + \sum_{n=2}^{\infty} a_n z^n \in \mathcal{S}^*(\psi)$, *then*

$$|f(z^m)| + \sum_{n=N}^{\infty}|a_n||z|^n \le d(0,\partial\Omega) \tag{9}$$

holds for $|z| = r \leq r_0$, *where* $m, N \in \mathbb{N}$, $\Omega = f(\mathbb{D})$ *and* r_0 *is the unique positive root of the equations*

$$r^m(1+Er^m)^{\frac{D-E}{E}} + A(r) + \sum_{n=N}^{\infty}\prod_{k=0}^{n-2}\frac{|E-D+Ek|}{k+1}r^n - (1-E)^{\frac{D-E}{E}} = 0, \quad \text{if } E \neq 0,$$

where $A(r) = r$ *for* $N = 1$ *and* 0 *otherwise, and*

$$r^m e^{Dr^m} + re^{Dr} - J(r) - e^{-D} = 0, \quad \text{if } E = 0,$$

where

$$J(r) = \begin{cases} 0, & N = 1; \\ r, & N = 2; \\ \sum_{n=2}^{N-1}\prod_{k=0}^{n-2}\frac{D}{k+1}r^n, & N \geq 3. \end{cases} \tag{10}$$

The radius r_0 *is sharp.*

Proof. Let us consider the function f_0, such that $zf_0'(z)/f_0(z) = (1+Dz)/(1+Ez)$, which is given by

$$f_0(z) = \begin{cases} z(1+Ez)^{\frac{D-E}{E}}, & E \neq 0; \\ ze^{Dz}, & E = 0. \end{cases} \tag{11}$$

Now, using Lemmas 3 and 4, we have

$$|f(z^m)| \leq f_0(r^m), \quad r_* = -f_0(-1)$$

and

$$\sum_{n=N}^{\infty}|a_n||z|^n \leq \sum_{n=N}^{\infty}\prod_{k=0}^{n-2}\frac{|E-D+Ek|}{k+1}r^n, \quad N \geq 2.$$

Now, proceeding as in Theorem 5, for r_0 as defined in the statement, the result follows. To prove the sharpness of the radius r_0, we see that at $|z| = r = r_0$ and $f = f_0$ given in (11)

$$\begin{aligned} &|f(z^m)| + \sum_{n=N}^{\infty}|a_n||z|^n \\ &= \begin{cases} (r_0)^m(1+E(r_0)^m)^{\frac{D-E}{E}} + A(r_0) + \sum_{n=N}^{\infty}\prod_{k=0}^{n-2}\frac{|E-D+Ek|}{k+1}(r_0)^n, & E \neq 0; \\ (r_0)^m e^{D(r_0)^m} + (r_0)e^{Dr_0} - J(r_0), & E = 0. \end{cases} \\ &= \begin{cases} (1-E)^{\frac{D-E}{E}}, & E \neq 0; \\ e^{-D}, & E = 0. \end{cases} \\ &= -f_0(-1) \\ &= d(0, \partial\Omega), \end{aligned}$$

where $J(r)$ is as defined in (10), and $A(r) = r$ for $N = 1$ and 0 otherwise for the case $E \neq 0$. □

Remark 6. Taking $m \to \infty$ and $N = 1$ in Corollary 6, we obtain the Bohr radius for the class $\mathcal{S}[D, E]$, which covers many classical cases.

In Theorem 6, putting $D = 1 - 2\alpha$ and $E = -1$, where $0 \leq \alpha < 1$, we get the result for the class of univalent starlike functions of order α, that is, $\mathcal{S}^*(\alpha)$:

Corollary 8. *If $f(z) = z + \sum_{n=2}^{\infty} a_n z^n \in \mathcal{S}^*(\alpha)$, then the inequality (9) holds for $|z| = r \leq r_0$, where $m, N \in \mathbb{N}$, $\Omega = f(\mathbb{D})$ and r_0 is the smallest positive root of the equations*

$$\frac{r^m}{(1-r^m)^{2(1-\alpha)}} + A(r) + \sum_{n=N}^{\infty} \prod_{k=0}^{n-2} \frac{k + 2(1-\alpha)}{k+1} r^n - \frac{1}{4^{1-\alpha}} = 0,$$

where $A(r) = r$ for $N = 1$ and 0 otherwise. The radius r_0 is sharp.

Putting $\alpha = 0$ in Corollary 8, we get the following:

Corollary 9. *If $f(z) = z + \sum_{n=2}^{\infty} a_n z^n \in \mathcal{S}^*$, then the inequality (9) holds for $|z| = r \leq r_0$, where $m, N \in \mathbb{N}$, $\Omega = f(\mathbb{D})$ and r_0 is the smallest positive root of the equations*

$$4r^m - (1-r^m)^2 + 4r^N (N(1-r) + r) \left(\frac{1-r^m}{1-r} \right)^2 = 0.$$

The radius r_0 is sharp.

To proceed further, we need to recall the following fundamental result:

Lemma 5. [22] *Let $f \in \mathcal{C}(\psi)$. Then $zf''(z)/f'(z) \prec zl_0''(z)/l_0'(z)$ and $f'(z) \prec l_0'(z)$. Also, for $|z| = r$, we have*

$$-l_0(-r) \leq |f(z)| \leq l_0(r),$$

where

$$1 + zl_0''(z)/l_0'(z) = \psi(z). \tag{12}$$

Furthermore, $r_* = -l_0(-1) = \lim_{r \to 1}(-l_0(-r))$ is the Koebe radius for the class $\mathcal{C}(\psi)$.

Now, we discuss the results for the convex analogue $\mathcal{C}(\psi)$ of $\mathcal{S}^*(\psi)$.

Theorem 7. *Let r_* be the Koebe radius for the class $\mathcal{C}(\psi)$, $l_0(z)$ be given by Eq. (12) and $f(z) = z + \sum_{n=2}^{\infty} a_n z^n \in \mathcal{C}(\psi)$. Assume $l_0(z) = z + \sum_{n=2}^{\infty} l_n z^n$ and $\hat{l}_0(r) = r + \sum_{n=2}^{\infty} |l_n| r^n$. If $g \in S_f(\psi)$, then*

$$|g(z^m)| + \sum_{k=N}^{\infty} |b_k||z|^k \leq d(0, \partial\Omega) \tag{13}$$

holds for $|z| = r_b \leq \min\{\frac{1}{3}, r_0\}$, where $m, N \in \mathbb{N}$, $\Omega = f(\mathbb{D})$ and r_0 is the unique positive root of the equation

$$\hat{l}_0(r^m) + \hat{l}_0(r) - p_{\hat{l}_0}(r) = -l_0(-1),$$

where

$$p_{\hat{l}_0}(r) = \begin{cases} 0, & N = 1; \\ r, & N = 2; \\ r + \sum_{n=2}^{N-1} |l_n| r^n, & N \geq 3. \end{cases}$$

The result is sharp when $r_b = r_0$ and $l_n > 0$.

Proof. Let $g(z) = \sum_{k=1}^{\infty} b_k z^k \prec f(z)$, where $f \in \mathcal{C}(\psi)$. From the Alexender relation, it is known that $f \in \mathcal{C}(\psi)$ if and only if

$$zf'(z) = \tilde{g}(z), \quad \text{or equivalently} \quad f(z) = \int_0^z \frac{\tilde{g}(t)}{t} dt$$

for some $\tilde{g} \in \mathcal{S}^*(\psi)$. Now, by Lemma 2, for $r \leq 1/3$, we have

$$\sum_{k=N}^{\infty} |b_k| r^k \leq \sum_{n=N}^{\infty} |a_n| r^n = \sum_{n=N}^{\infty} \frac{|\tilde{b}_n|}{n} r^n, \tag{14}$$

where $\tilde{b}_n$ are the Taylor coefficients of $\tilde{g}$. Again, applying Lemma 2 on $f'(z) \prec l_0'(z)$ (Lemma 5), we get that

$$M_{\tilde{g}}(r) - p_{\tilde{g}}(r) \leq M_h(r) - p_h(r), \quad r \leq \frac{1}{3}, \tag{15}$$

where $Mg(x) := \sum_{k=1}^{\infty} |b_k| x^k$, and h is given by the relation $zl_0'(z) = h(z)$. Now, using Eqs. (14) and (15), we have for $r \leq 1/3$

$$\begin{aligned} \sum_{k=N}^{\infty} |b_k||z|^k &\leq \sum_{n=N}^{\infty} \frac{|\tilde{b}_n|}{n} r^n \\ &= \int_0^r \frac{M_{\tilde{g}}(t) - p_{\tilde{g}}(t)}{t} dt \\ &\leq \int_0^r \frac{M_h(t) - p_h(t)}{t} dt = \sum_{n=N}^{\infty} |l_n| r^n \\ &= \hat{l}_0(r) - p_{\hat{l}_0}(r). \end{aligned} \tag{16}$$

Now, $g \prec f$ implies that $g(z) = f(\omega(z))$, which using the Lemma 5 yields

$$|g(|z| \leq r)| = |f(\omega(|z| \leq r))| \leq \max_{|z|=r} |f(|z| \leq r)| \leq l_0(r),$$

that is

$$|g(z)| = |f(\omega(z))| \leq l_0(r)$$

for $|z| = r$, where ω is a Schwarz function. Moreover, replacing z by z^m gives

$$|g(z^m)| \leq \hat{l}_0(r^m). \tag{17}$$

Also, by letting r tends to 1 in Lemma 5, we obtain the Koebe radius $r_* = -l_0(-1)$. Therefore, the open ball $\mathbb{B}(0, r_*) \subset f(\mathbb{D})$, which implies that for $|z| = 1$

$$r_* \leq d(0, \partial\Omega). \tag{18}$$

Hence, using the inequalities (16), (17) and (18), we have

$$\begin{aligned} |g(z^m)| + \sum_{k=N}^{\infty} |b_k||z|^k &\leq \hat{l}_0(r^m) + \hat{l}_0(r) - p_{\hat{l}_0}(r) \\ &\leq r_* \\ &\leq d(0, \partial\Omega) \end{aligned}$$

holds whenever $|z| = r \leq \min\{\frac{1}{3}, r_0\}$, where r_0 is the smallest positive root of the equation

$$H(r) := \hat{l}_0(r^m) + \hat{l}_0(r) - p_{\hat{l}_0}(r) - r_* = 0.$$

Clearly, H is continuous and $H'(r) > 0$ for $0 \leq r \leq 1$. Note that $H(0) < 0$, and since $\hat{l}_0(1) \geq |l_0(1)| \geq r_*$ (see Lemma 5), we see that

$$2\hat{l}_0(1) - \sum_{n=1}^{N-1} |l_n| - r_* = (\hat{l}_0(1) - \sum_{n=1}^{N-1} |l_n|) + (\hat{l}_0(1) - r_*) > 0,$$

which implies that $H(1) > 0$. Thus $H(r) = 0$ has a root in the interval $(0, 1)$. The sharpness follows for the function l_0 by taking $g = f = l_0$ with the equality in (13) as:

$$l_0(r_b^m) + \sum_{n=N}^{\infty} l_n r_b^n = r_* = d(0, \partial\Omega)$$

when $r_b = r_0$ and $l_n > 0$. □

Remark 7. Let $\psi(z) = (1 + z)/(1 - z)$, then Theorem 7 reduces to [14, Theorem 6].

Remark 8. Let $g \in S_f(\psi)$, where $f \in \mathcal{C}(\psi)$. In (14), if we use the Rogosinski's well-known result: "If $g \prec f$ and f is a normalized convex function, then $|b_n| \leq 1$ for $n \geq 1$", then we can remove the role of Lemma 2 in the proof of Theorem 7 and get

$$\sum_{k=N}^{\infty} |b_k| r^k \leq \sum_{n=N}^{\infty} r^k = \frac{r^N}{1 - r}, \quad r \in (0, 1). \tag{19}$$

Further combining (19) and the inequality (17)

$$|g(z^m)| \leq \hat{l}_0(r^m),$$

we get

$$|g(z^m)| + \sum_{k=N}^{\infty} |b_k| r^k \leq \hat{l}_0(r^m) + \frac{r^N}{1 - r}, \quad r \in (0, 1).$$

Thus, the inequality (13) follows for $|z| = r \leq r_0$, where r_0 is the smallest positive root of

$$\hat{l}_0(r^m) + \frac{r^N}{1 - r} + l_0(-1) = 0. \tag{20}$$

Also, the radius r_0 cannot be improved follows if we choose:

$$g(z) = f(z) = \frac{z}{1 - z} = l_0(z).$$

Note that if the coefficients of ψ are positive, then $\hat{l}_0 = l_0$, and in this case, (20) reduces to

$$l_0(r^m) + \frac{r^N}{1 - r} + l_0(-1) = 0.$$

Moreover, taking $N = 1$ and $m \to \infty$, we get the result obtained by Hamada [11, Theorem 4.1].

The following result is explicitly for the class $\mathcal{C}(\psi)$.

Corollary 10. *Let r_* be the Koebe radius for the class $\mathcal{C}(\psi)$, $l_0(z)$ be given by Eq. (12). Assume $l_0(z) = z + \sum_{n=2}^{\infty} l_n z^n$ and $\hat{l}_0(r) = r + \sum_{n=2}^{\infty} |l_n| r^n$. If $f(z) = z + \sum_{n=2}^{\infty} a_n z^n \in \mathcal{C}(\psi)$, then*

$$|f(z^m)| + \sum_{n=N}^{\infty} |a_n||z|^n \leq d(0, \partial\Omega) \tag{21}$$

holds for $|z| = r_b \leq \min\{\frac{1}{3}, r_0\}$, where $m, N \in \mathbb{N}$, $\Omega = f(\mathbb{D})$ and r_0 is the unique positive root of the equation

$$\hat{l}_0(r^m) + \hat{l}_0(r) - p_{\hat{l}_0}(r) = r_*,$$

where $p_{\hat{l}_0}$ is as defined in Theorem 7. The radius is sharp for the function l_0 when $r_b = r_0$ and $l_n > 0$.

Remark 9. The special case of taking $m \to \infty$ and $N = 1$ in Theorem 7 and Corollary 10 establishes the Bohr phenomenon for the classes $S_f(\psi)$ and $\mathcal{C}(\psi)$, respectively.

After some little computations when $\psi(z) = (1+z)/(1-z)$, the Corollary 10 yields:

Corollary 11. *If $f(z) = z + \sum_{n=2}^{\infty} a_n z^n \in \mathcal{C}$, then the inequality (21) holds for $|z| = r \leq r_0$, where $m, N \in \mathbb{N}$, $\Omega = f(\mathbb{D})$ and r_0 is the unique positive root of the equations*

$$3r^m - 1 + 2r^N \left(\frac{1 - r^m}{1 - r}\right) = 0.$$

The radius r_0 is sharp.

Corollary 12. *Let $\psi(z) = 1 + ze^z$ and $m = 1$. If $g \in S_f(\psi)$, then the inequality (13) holds for $|z| = r \leq r_N$, where $N \in \mathbb{N}$ and $r_N (< 1/3)$ is the unique positive root of the equation*

$$2r(1 + re^r)\exp(e^r - 1) - H(r) - (1 - e^{-1})e^{e^{-1}-1} = 0,$$

where

$$H(r) = \begin{cases} 0, & N = 1; \\ r, & N = 2; \\ \sum_{n=0}^{N-1} \binom{(n+1)B_n}{n!} r^{n+1}, & N \geq 3, \end{cases}$$

and B_n are the bell numbers, such that $B_{n+1} = \sum_{k=0}^{n} \binom{n}{k} B_k$. Moreover, if $f \in C(\psi)$, then the inequality (21) also holds for $r \leq r_N$. The radius r_N is sharp.

Acknowledgements

We would like to thank the Editor and the Reviewers for their valuable suggestions to improve this manuscript.

Declarations

Conflict of interest The authors declare that they have no conflict of interest.

Publisher's Note Springer Nature remains neutral with regard to jurisdictional claims in published maps and institutional affiliations.

References

[1] Aizenberg, L.: Remarks on the Bohr and Rogosinski phenomena for power series. Anal. Math. Phys. **2**(1), 69–78 (2012)

[2] Ali, R.M., Barnard, R.W., Solynin, AYu.: A note on Bohr's phenomenon for power series. J. Math. Anal. Appl. **449**(1), 154–167 (2017)

[3] Ali, R.M., Jain, N.K., Ravichandran, V.: Bohr radius for classes of analytic functions. Results Math. **74**(4), Paper No. 179 (2019)

[4] Alkhaleefah, S.A., Kayumov, I.R., Ponnusamy, S.: Bohr–Rogosinski inequalities for bounded analytic functions. Lobachevskii J. Math. **41**(11), 2110–2119 (2020)

[5] Aouf, M.K.: On a class of p-valent starlike functions of order α. Int. J. Math. Math. Sci. **10**(4), 733–744 (1987)

[6] Bhowmik, B., Das, N.: Bohr phenomenon for subordinating families of certain univalent functions. J. Math. Anal. Appl. **462**(2), 1087–1098 (2018)

[7] Boas, H.P., Khavinson, D.: Bohr's power series theorem in several variables. Proc. Am. Math. Soc. **125**(10), 2975–2979 (1997)

[8] Bohr, H.: A theorem concerning power series. Proc. Lond. Math. Soc. (2) **13**, 1–5 (1914)

[9] Cho, N.E., Kumar, V., Kumar, S.S., Ravichandran, V.: Radius problems for starlike functions associated with the sine function. Bull. Iran. Math. Soc. **45**(1), 213–232 (2019)

[10] Gangania, K., Kumar, S.S.: On Certain Generalizations of $\mathcal{S}^*(\psi)$. Comput. Methods Funct. Theory (2021). https://doi.org/10.1007/s40315-021-00386-5

[11] Hamada, H.: Bohr phenomenon for analytic functions subordinate to starlike or convex functions. J. Math. Anal. Appl. **499**(1), Art. 125019 (2021)

[12] Huang, Y., Liu, M.S., Ponnusamy, S.: Refined Bohr-type inequalities with area measure for bounded analytic functions. Anal. Math. Phys. **10**(4), 1–21 (2020)

[13] Janowski, W.: Extremal problems for a family of functions with positive real part and for some related families. Ann. Polon. Math. **23**, 159–177 (1970/71)

[14] Kayumov, I.R., Khammatova, D.M., Ponnusamy, S.: Bohr–Rogosinski phenomenon for analytic functions and Cesáro operators. J. Math. Anal. Appl. **496**(2), 124824 (2021)

[15] Kumar, S., Ravichandran, V.: A subclass of starlike functions associated with a rational function. Southeast Asian Bull. Math. **40**(2), 199–212 (2016)

[16] Kumar, S.S., Kamaljeet, G.: A cardioid domain and starlike functions. Anal. Math. Phys. **11**(2), 54 (2021)

[17] Kumar, S.S., Kamaljeet, G.: On geometrical properties of certain analytic functions. Iran. J. Sci. Technol. Trans. A Sci. (2020). https://doi.org/10.1007/s40995-021-01116-1

[18] Kumar, S.S., Kamaljeet, G.: On certain generalizations of $\mathcal{S}^*(\psi)$. (2020). arXiv:2007.06069v1

[19] Gangania, K., Kumar, S.S.: $\mathcal{S}^*(\psi)$ and $\mathcal{C}(\psi)$-radii for some special functions. Iran. J. Sci. Technol. Trans. A Sci. (2022). https://doi.org/10.1007/s40995-022-01313-6. arXiv:2008.13499v1

[20] Landau, E., Gaier, D.: Darstellung und Begründung einiger neuerer Ergebnisse der Funktionentheorie, 3rd edn. Springer, Berlin (1986)

[21] Liu, M.S., Shang, Y.M., Xu, J.F.: Bohr-type inequalities of analytic functions. J. Inequal. Appl. Art. 345 (2018)

[22] Ma, W.C., Minda, D.: A unified treatment of some special classes of univalent functions. In Proceedings of the Conference on Complex Analysis (Tianjin, 1992), 157–169, Conference Proceedings Lecture Notes Analysis, I, International Press, Cambridge (2018)

[23] Miller, S.S., Mocanu, P.T.: Differential Subordinations, Monographs and Textbooks in Pure and Applied Mathematics, 225. Marcel Dekker Inc, New York (2000)

[24] Muhanna, Y.A.: Bohr's phenomenon in subordination and bounded harmonic classes. Complex Var. Elliptic Equ. **55**(11), 1071–1078 (2010)

[25] Muhanna, Y.A., Ali, R.M.: Bohr's phenomenon for analytic functions into the exterior of a compact convex body. J. Math. Anal. Appl. **379**(2), 512–517 (2011)

[26] Muhanna, Y.A., Ali, R.M., Ng, Z.C., Hasni, S.F.M.: Bohr radius for subordinating families of analytic functions and bounded harmonic mappings. J. Math. Anal. Appl. **420**(1), 124–136 (2014)

[27] Muhanna, Y.A., Ali, R.M., Lee, S.K.: The Bohr operator on analytic functions and sections. J. Math. Anal. Appl. **496**(2), 124837 (2021)

[28] Paulsen, V.I., Singh, D.: A simple proof of Bohr's inequality. arXiv:2201.10251

[29] Rogosinski, W.: Über Bildschranken bei Potenzreihen und ihren Abschnitten. Math. Z. **17**(1), 260–276 (1923)

[30] Schur, I., Szegö, G.: Über die Abschnitte einer im Einheitskreise beschränkten Potenzreihe, Sitz.ber. Preuss. Akad. Wiss. Berl. Phys.-Math. Kl. 545–560 (1925)

[31] Sharma, K., Jain, N.K., Ravichandran, V.: Starlike functions associated with a cardioid. Afr. Mat. **27**(5–6), 923–939 (2016)

Kamaljeet Gangania and S. Sivaprasad Kumar
Department of Applied Mathematics
Delhi Technological University
Delhi 110042
India
e-mail: gangania.m1991@gmail.com

S. Sivaprasad Kumar
e-mail: spkumar@dce.ac.in

Received: June 2, 2021.
Revised: September 12, 2021.
Accepted: May 22, 2022.

Research Square

Preprints are preliminary reports that have not undergone peer review.
They should not be considered conclusive, used to inform clinical practice,
or referenced by the media as validated information.

CBFDR- Context-Based Fake News Detection and Reporting using Blockchain and Machine Learning

Himani Mishra
Netaji Subhas University of Technology(NSUT)
Amita Jain (amita.jain@nsut.ac.in)
Netaji Subhas University of Technology(NSUT)
Ankur Tayal
Delhi Technological University (DTU)

Research Article

Keywords: Amazon web services (AWS) , Fake News Detection, RNN-LSTM, XG-Boost, Smart contract, Blockchain, Proof of evidence (PoE)

Posted Date: June 2nd, 2022

DOI: https://doi.org/10.21203/rs.3.rs-1696196/v1

License: This work is licensed under a Creative Commons Attribution 4.0 International License.
Read Full License

Noname manuscript No.
(will be inserted by the editor)

CBFDR- Context-Based Fake News Detection and Reporting using Blockchain and Machine Learning

Himani Mishra[1] · Dr Amita Jain[2] · Ankur Tayal[3]

Abstract

Cases of fake news are increasing at a high pace, especially through social media portals. Even though there are various fact checker websites and portals that distinguish news from real or fake news and ongoing research have been done to stop the propagation of fake new. The major setback is timely detection, prevention and reporting of fake news. The proposed model CBFDR (Context-Based Fake News Detection and Reporting) first analyzes the domain of the given news through Amazon web services (AWS) Comprehend, secondly detects the fake news through RNN-LSTM (Recurrent neural network – Long short term memory & XG -Boost algorithm (extreme gradient) and thirdly includes a set of domain- experts who analyze the set of fake news as well as report in Block-chain (using smart contract and proposed algorithm Proof of Evidence (PoE)) to stop the propagation of fake news at an early stage. The given paper has shown the highest success rate of 98% using RNN-LSTM and 93% using the XG-Boost algorithm for fake news detection. This paper covers detection, prevention and reporting in one application with an average 60-70% faster and more accurate than the existing models.

Keywords Amazon web services (AWS) , Fake News Detection, RNN-LSTM, XG-Boost, Smart contract, Blockchain, Proof of evidence (PoE)

1 Introduction

Fake news has always been there, but now it's been exploited at a tremendous rate through various social media platforms or unauthorized news websites. Even though there are fact-checkers available these fake users can still spread false news without any fear due to multiple unauthorized accounts that enable them to spread without being accountable.

Today billions of users are using social media platforms actively using social media platforms which is growing each day Buster (5). Looking at the above statistics , the rate at which fake news is consumed by users around the world each day is undoubtedly alarming Thus in order to stop this fake news from spreading consumption asset further this paper proposes a novel approach to detecting and reporting fake news using blockchain and machine learning.

Based on the latest survey for the news consumption in the range of social media, news consumption between the age ranges (18 to 44) is the highest approx. 45% which is quite high. As per the Statista Srivastava et al. (2019) almost 80% of fake news was spread between 2020-2021 on COVID19 on social media which 70-75% contained false remedies, death rates and vaccine side effects.

1.1 Importance of Fake News Detection and Reporting

Fake news has created havoc, especially since the rise of various social media platforms. For Example, 2021 according to The Print media was "2021 was the year of fake news" , as quoted by the news headlines 141 (6). The misinterpreted news leads to havoc situations such as fights within or outside the community, hatred among the groups, affects the unity between the society, and health problems such as anxiety, depression etc. are some of the scenarios which may be seen as the after-effects of fake news.

Those who generate this news have their reasons such as to create terror among the people, ruin others' names or things, greed, for pleasure, generate hatred in one another and so on and forth. The question arises at the end of the day: how do we differentiate between real or fake news. The proposed solutions will be discussed in the following sections to generate awareness of fake news and create a safer platform.

Himani Mishra
himani500@gmail.com

Amita Jain
amita.jain@nsut.ac.in

Ankur Tayal
ankurtayal3@gmail.com

1 Netaji Subhas University of Technology,Delhi,India

2 Netaji Subhas University of Technology,Delhi,India

3 Delhi Technological University (DTU) , Delhi, India

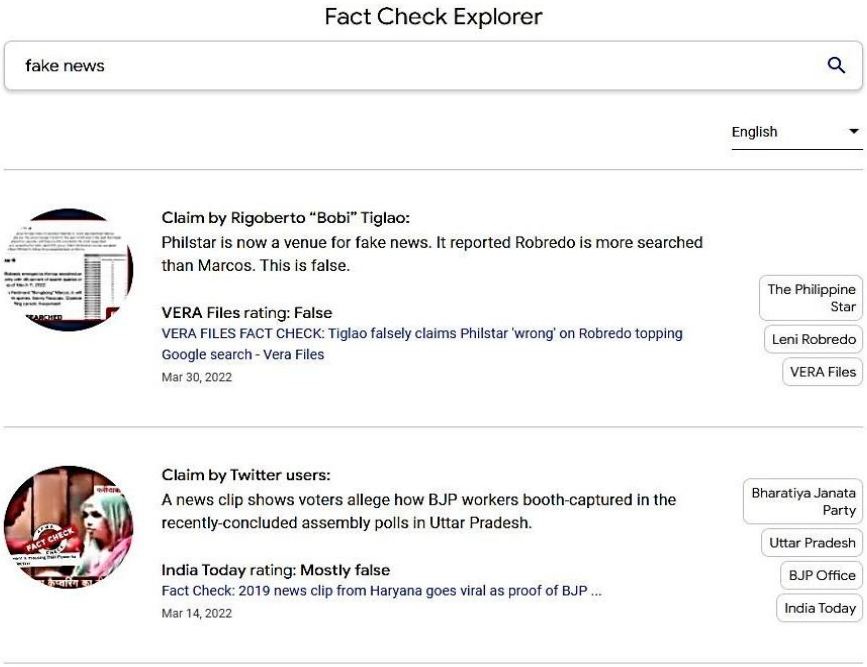

Fig 1 Snippet from Google tool fact news checker on fake news

On National Press Day, which is 16th November 2021, itcame to light during the parliament session that fake news

Should be curbed strictly and ethical principles of journalism should be abided due to the steep increase in fake news.

The given paper proposes a solution to compact the fake news with the help of blockchain, natural language processing and machine learning. New terminology has been slated for the false news or fake news is "infodemic" used to rise in misleading data or information in all modes of the news.

WHO (World Health Organization) has been actively participating in taking actions against the info- demic which caused due to fake news 141 [1].

According to the news, through proper certified channels go through intensive research and collaborations by the various prestigious reporters, authorizes and novel researchers who are well - versed in the given field domain.

But even though the news in today's day is prone to falsehood on a large scale, various digital platforms are equipped with the facilities of the wide-area network, which helps in spreading any kind of fake news. Regardless of any strict actions which may take place on them or the platform but due to lack of traceability, they are never caught which gives them more power to post fake news.

Still , there are a few possible ways by which one can figure out if the news is fake news which is as follows: -

- ➢ The given news is written in poor language and context.
- ➢ Fake accounts on social media with a fake identity that looks legitimate.
- ➢ Usually hold no proper background study and statics/data in order to prove their point.
- ➢ Biased over a specific context only.
- ➢ Certainly, created to trigger without any bases such

as remedies to heal or deaths in coronavirus during the pandemics in waves 1 and 2 were prevalent.
Besides the above-stated points, there are other ways to

check whether a news is fake or not such as fact-checking websites or tools such as google fact-checkers, a new checker.in etc. which are widely available 141 [5]

Even though there are comprehensive solutions yet there is a rise in fake news which can be seen especially after the introduction of various social media platforms where counterfeit accounts are made to post fake news and circulate them effortlessly bots are also set up which is certainly quite concerning 141.

In the years 2020-2021, many cyber threats and cyber-attacks have occurred which made the importance of a decentralized system more critical and to be precisely equipping a secure and authorized platform is the need of the hour in order to fulfill the CIA (Confidentiality, Integrity and Availability) triad for the user's safety.

In order to do so, this paper proposes a decentralized Context Based Fake News Detection and Reporting CBFDR framework that aims in detect and report fake news in order to stop the propagation of fake news.

This paper focuses on creating a decentralized platform for reporting fake news using machine learning and blockchain technology.

This paper proposes an automated system with the help generating the domain and sentiment analysis of the given news article along with a brief report which the subject review experts could consider on the given news domain during the decision making whether the given news is real or fake.

Using blockchain for its decentralized technology makes it more secure against cyberattacks such as single point failure, a man in the middle attack etc.

A decentralized platform would be created using blockchain technology where experts can review the news using the brief report and their expert review using the Proof of Evidence (PoE) algorithm.

Section II gives brief literature on the blockchain and past work fake news reports. Section III explains the proposed methodology of the given blockchain, smart contract and proof of Evidence (PoE) algorithm. Section IV focuses on implementation, Section V Implementation and discussion and Section VI Conclusion and Future work on the proposed paper.

1.2) Contribution

The model for the proposed paper is divided into three phases which are as follows –

- The proposed model focuses on early-stage detection and reporting of fake news in order to stop the propagation of fake news.
- Even though there are various prevention, detection and reporting fake news Research solutions are available, still the given proposed CBFDR model ensures all the three aspects listed above along with the CIA (Confidentiality, Integrity and Availability) triad of security under one application which makes it distinct and unique from the existing solution.
- The primary focus of the proposed model is to detect, prevent and report fake news through safe channels for which machine learning and block chain have been used.
- This paper focuses on three main aspects: prevention, detection and reporting of fake news using the help of blockchain and machine learning.
- Domain Detection of fake news using amazon web services (AWS) comprehend to analyze and categorize a given set of news in there subject domain blocks in the blockchain.
- On an average 60-70% faster and more accurate as compared to the existing models.
- Fake News Detection using RNN-LSTM and XG-Boost algorithm are used for fake news detection aft
- Reporting of fake news using the domain experts based on proposed Proof of Evidence (PoE) gives the evidence of the given reported information which provides clarity and adds points to the respective expert's wallet for their service each time.

2 Related Research

The literature survey explains the various studies done over time by various prestigious researchers. A researcher recently proposed "An incentive- aware blockchain-based solution for internet of fake media things" , published by Qian Chena et all.[22]

The Facebook algorithm has been the subject of speculation, especially since one of the whistleblowers exposed the algorithm's role in spreading false information during the US 2020 election [7]

Fake news has taken over the world through deceptive articles and news that have no basis, resulting in cyberbullying, hostility, and riots against communities that require strong regulation.

According to Song, Kim, Hwang, and Lee (2019), most people have access to content-creation software and applications.

Furthermore, false information spreads exponentially on social media because users are more likely to spread false news farther, faster, and more profound than accurate news through their social networks (Vosoughi & Roy, 2018).

Regardless of national, cultural, and political differences between governments, most agencies are now attempting to combat, both jointly and separately, the misuse of information published and distributed on a large scale.

According to current events, It has become easier to be posted on various social media platforms without any authorized body monitoring the system from time to time has become the need of the hour and understanding.[48]

The vast majority of research in this field is centered on the idea that social media plays a significant role in the spread of fake news. The concept of decentralized was integrated with Ethereum smart contracts in Paul's work, as well as a Breadth-First Search algorithm to calculate a user's closeness (Singh, Parizi, Zhang, Choo, & Dehghantanha, 2020). (2019). The blockchain now includes social networks.

Validators provide reviews as time passes and days pass in the media. As a result, the News will be presented to users with a rating that represents the correctness/authenticity of specific news (with multiple veracity levels) and is followed by a weight-based validation method in which validators in the same area are assigned the same peak weight

The Byzantine Fault Tolerance method was used in another research on a blockchain algorithm.Alfandi, Otoum, and Jararweh (2020; Alfandi, Otoum, and Jararweh, 2020; Alfandi, Otoum, and Jararweh, 2020; Alfandi, Otoum, and Jararweh, 2020; Alfandi, Otoum, and Jararweh.

Muhammed Saad and colleagues, (2019). Similarly, the authors of Song, Kim, Hwang, and Lee (2019) proposed a blockchain-powered social media notarization service. The article aims to complement the work done by Qayyum, Qadir, Janjua, and Sher (2019) to combat the spread of Fake News.

Smart Contracts are frequently used to simplify news registration and publication (Qayyum et al., 2019). Requests from news publishers are accepted into the scheme .After a preliminary check in the current mapping, the publisher is given a public key and secret pair with the status of the verified or unsourced publisher, as well as an initial credibility score that will evolve based on the news published. Even though various researchers have given great viewpoints on the detection and prevention of fake news but keeping in mind today's demand, it has been seen that the requirement of

immediate detection and reporting can help in curbing the fake news. Given that the data is present in a large amount the manual method is not accurate and thus needs an automated process that could generate.

Thus in order to prevent it from propagating further. Understand the current ways by which fake news is being detected to improve the scope of the given method further and come up with a new method for detecting and preventing the fake news in the given scenario of fake news.

Due to the gaps in the study of the given papers , we have proposed fake news detection and prevention using blockchain or available technology machine learning methods , which is still the future.

3. Proposed Approach

The proposed solution focuses on categorizing each news in the blockchain using Amazon Web Services comprehend, early fake news detection using RNN-LSTM and XG-Boost algorithm, and reporting fake news based on severity level using domain-based news experts in blockchain-based on proposed proof of evidence (PoE).
The main reason for combining the human mind, automation, and security monitoring, as well as transaction, is to employ machine learning and blockchain.

Online news is generated in bulk through various mediums such as social media platforms, blogs, websites and various other anonymous sites thus in order to timely detection and reporting of fake news has become an enormous task. Even if there are tools like fact news checkers that can determine whether a story is fake or not, the need for real-time detection and reporting in a secure setting is critical if fake news is to be stopped.

3.1 Proposed Architecture Model Overview

This section covers a brief overview of the proposed architecture model.The proposed model CBFDR is based on one of the machine learning parameters which is part of deep learning called Recurrent Neural Network- Long-short term memory (RNN-LSTM) and uses blockchain-based technology. The following section will cover the implementation of the dataset from various platforms [11],[12],[13] on fake news.

The figure gives an overview of the architecture diagram of the proposed CBDFR model. The experts in the given model are registered using smart contracts, which are the rules and conditions that every expert on the platform must adhere to in order to keep the

network safe, secure, and accurate news.The expert once registered are added to the blockchain where they are given a unique address along with the facility to report fake news based on their domain expertise and wallet in which they would be rewarded if and only if the evidence provided by them was correct

and the news was accurately categorized as fake or real depending upon the news the integrity of the news from wide domains and areas. Once the news is collected, it goes through domain detection which is performed using the amazon web services feature amazon web services comprehend.

The domains were extracted from the given set of news which was further categorized in the given blocks based on their respective domains in the blockchain.[47]
The experts would pick news from the block in the given blockchain. Once the news is selected they would be redirected to give their review based on the following category which is:-

Table I Score Grading for the Evidence Score

Sno.	Score Category	Points
1.	Real News	+5
2.	Fake News	-5
3.	Re-Review required	-6
4.	Not Defined	-8

Once the review score is determined, each expert will be given a score and an amount will be credited to their wallet for their services based on their performance. The subsection will be divided into three sections 3.1) Domain Detection of fake news using amazon web services comprehend., 3.2) Fake News Detection using RNN-LSTM and XG-Boost algorithm and 3.3) Reporting of fake news using the domain experts based on proposed Proof of Evidence (PoE).

3.1) Domain Detection of fake news using amazon web services comprehend

Each news has its domain associated with it which makes it fall under a specific category of news, likewise the given section covers the domain analysis of news using one of the features of Amazon web services that is amazon comprehends. Using the amazon comprehend will help in extracting the domains of each news which will further help in categorizing it into various domain-based blocks in the blockchain. The following steps were performed-

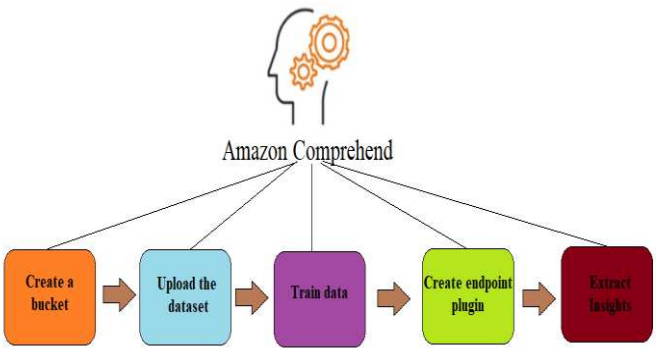

Fig 2 Steps used to perform domain detection using amazon comprehend

The given feature fetches the data using the amazon web s3 bucket where the dataset was uploaded. Once the data is stored in the s3 bucket it is prepared to train the dataset based on the amazon comprehend feature. This feature contains a variety of facilities such as domain detection, sentiment detection and so on which allows the user's to get more significant insights into the big data within a few minutes.

Domain detection using for amazon web services comprehend

Step 1 : Create a **bucket** in **->** (news-report-1) using aws services.

Step 2 : Import the dataset in the s3 bucket while creating an instance **->** (news-report-data)

Step 3 : Console aws comprehend to train the dataset (news-report-train) curated

an **endpoint ->** (news-report-endpoint) to connect the jupyter notebook with the trained dataset.

Fig 3 Steps used to perform domain detection using amazon web services to comprehend

The data is trained using Amazon Web Services, which took 30-35 minutes to process for the given dataset, before passing through the endpoints that are linked to the notebook to infer the information using the Amazon Web Service libraries boto3 and seaborn to plot the domain-specific news that was analysed along with word cloud to generate the set of words for the true dataset as shown above in the figure.

3.2) Fake News Detection using RNN-LSTM and XG-Boost algorithm

The gradient boosted trees technique's XGBoost (eXtreme Gradient Boosting) version is a popular and efficient open-source implementation. [5]

Because of its robust handling of a wide range of data kinds, relationships, and distributions, as well as the diversity of hyperparameters that can be fine-tuned, the XGBoost approach does well in machine learning competitions.

XGBoost can be used to solve regression, classification (binary and multiclass), and ranking problems.

RNN-LSTM (Recurrent Neural Network – Long Short Term Memory) is a type of RNN.LSTM solves the vanishing gradient problem in backpropagation.The news is collected from various sites in order to check the It uses a gating mechanism that controls the memory structure. [4].A sigmoid function was used to keep results between (0 and 1).

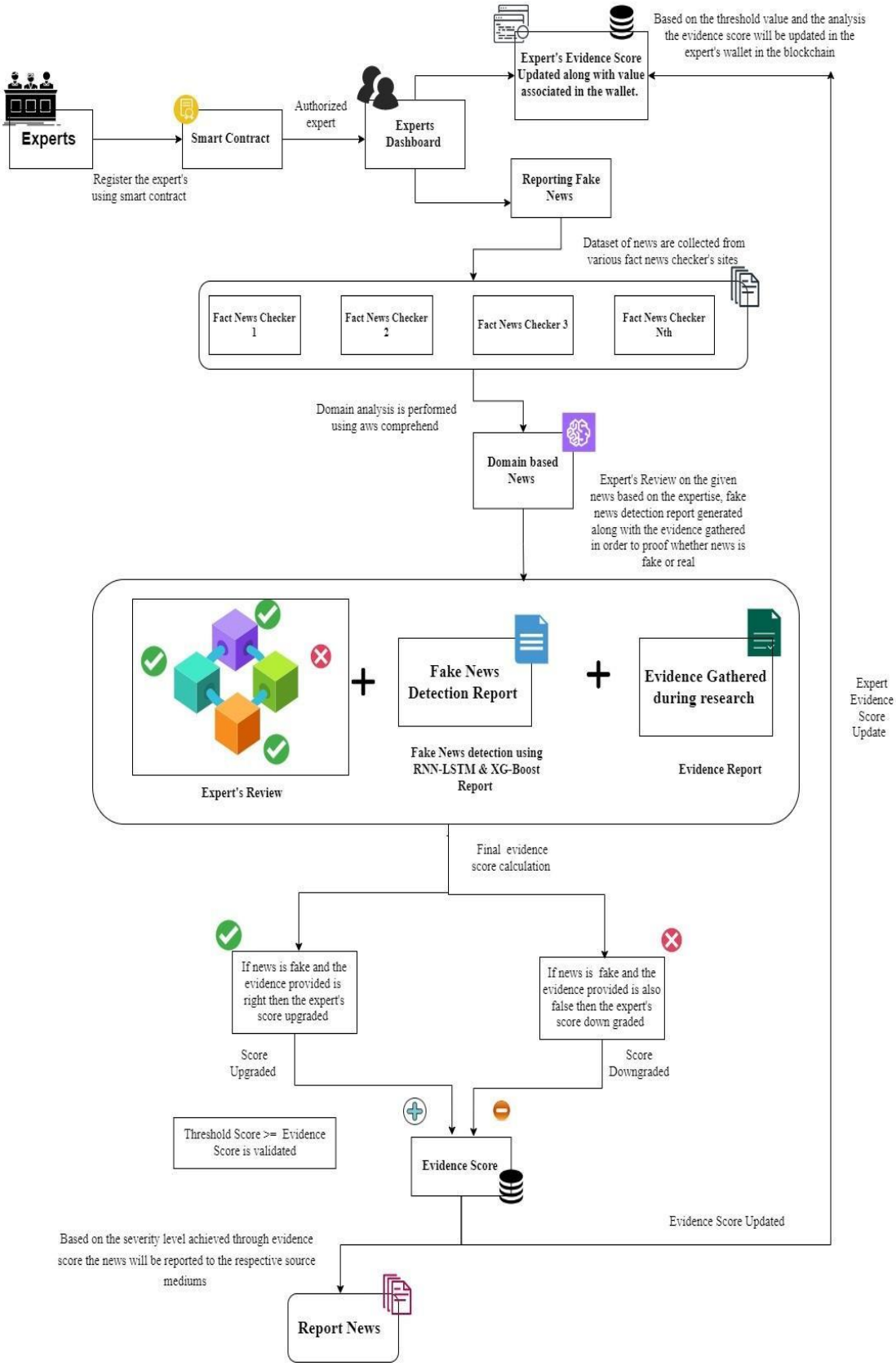

Fig 4 Architecture Flow diagram of the Context-Based Fake News Detection and Reporting using Blockchain

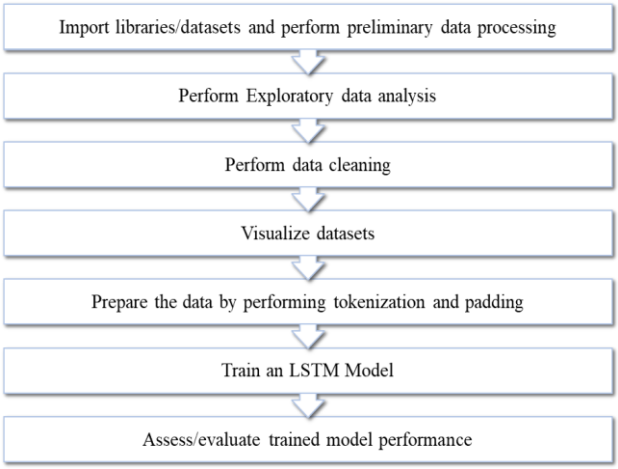

Fig 5 Steps to perform fake news detection using RNN-LSTM

Algorithm 1 CBFDR using Proof of Evidence

Input: fact check news, expert review, Output: Report of news

1. Extract data from the fact news checker websites.
2. Concatenate the news datasets and create one dataset.
3. Load the dataset in the AWS s3 bucket.
4. **Bucket name = news_dataset_1**
5. Uploading the news dataset in the AWS comprehend
6. **S3=news_dataset_1**
7. Let the trained dataset be called: news_dataset_trained,
8. Trained dataset linked to AWS Sagemaker for domain analysis.
9. Trained_dataset = news_dataset_trained
10. Creating an endpoint to join trained_dataste with the AWS Sagemaker with the nearest region end_point= news_dataset_endpoint
11. **region=asia_mumbai3**
12. Classifying the domain of the dataset using the AWS comprehend libraries in AWS Sagemaker
13. Batch_Detect :{ news_dataset_trained:
14. **Domain_Entitie = news_dataset_trained}**
15. Downloading the classified dataset in s3 bucket
16. Result=news_dataset_domain
17. Exporting this dataset to the private blockchain
18. Export = news_dataset_trained Private_blockchain news_dataset_trained
19. Domain-based blocks created contain the various fact news check data results.
20. Expert's Review based on their domain speculation along with news_dataset_trained will be taken into consideration during PoE(Proof of Evidence)
21. Calculating the News accuracy based on PoE (Proof of Evidence)
22. **Final_Result_News (%) = news_dataset_trained+ Domain_Expert_Review * 100**
23. **Output :** Report will be sent to social media platforms with the data such as news accuracy, source of news etc. in order to take action against such fake accounts and news timely.

Fig 6: Algorithm of Repo-Fake Framework and implementation of Proof of Evidence PoE

3.3) Reporting of fake news using the domain experts based on proposed Proof of Evidence (PoE).

The Repo-Fake Framework works on the private blockchain network. Various well-known and widely available fact-checking tools, such as Google's fact-checking tool, PIB's fact-checking tool, and others, can be integrated into this framework. Additionally, with the fact news check review, there would be an expert news review community based on their domain that would give a review based on the novel Proof of Evidence (PoE) that would check the province of the news and based on which the score for the given news piece would be given. (Figure 1)

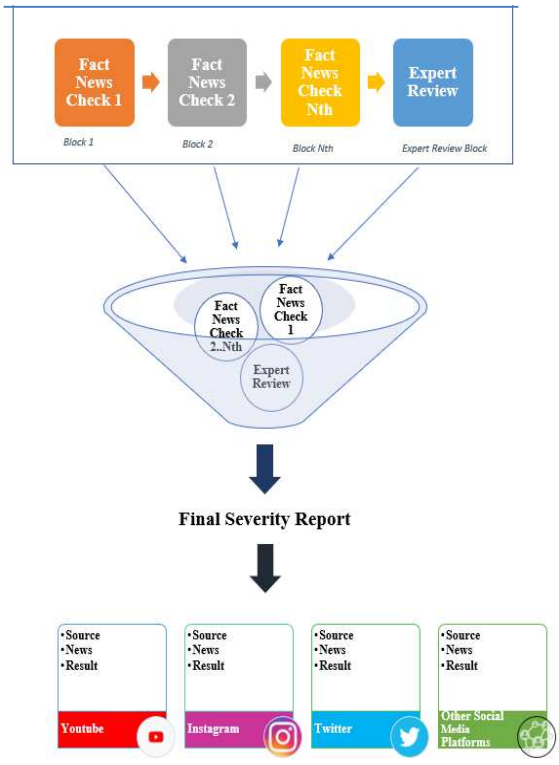

Fig 7 : CBFDR Fake News Detection and Reporting

4) Results and Evaluation

This sections covers The above experiments are performed using Python 3.0, Processor Intel(R) Core(TM) i5-10210U CPU @ 1.60GHz, 2112 Mhz, 4 Core(s), 8 Logical Processor(s) with 12 GB RAM. The dataset on which the experiment is performed is taken from Kaggle [2][3]. Dataset 1:PoliFact Fake News Dataset[11], 2: Covid19 Fake News, Dataset [12] 3: Fake and True News Dataset [13].

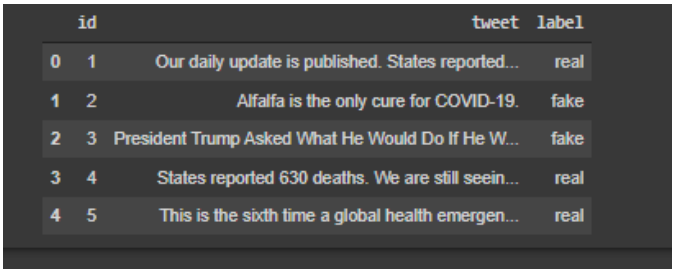

	id	tweet	label
0	1	Our daily update is published. States reported...	real
1	2	Alfalfa is the only cure for COVID-19.	fake
2	3	President Trump Asked What He Would Do If He W...	fake
3	4	States reported 630 deaths. We are still seein...	real
4	5	This is the sixth time a global health emergen...	real

Fig 8 Dataset snapshot of the dataset.

Table 2 Accuracy achieved through RNN-LSTM AND XG-Boost algorithm

Sno.	Dataset	Algorithm	Accuracy
1.	Dataset 1	XG boost	76.7%
		RNN-LSTM	87%
2.	Dataset 2:	XG-Boost	80.1%
		RNN-LSTM	82.2%
3.	Dataset 3	XG-Boost	93.6%
		RNN-LSTM	98%

The proposed model was trained in the three datasets given above using the RNN-LSTM algorithm for fake news detection reports and analysis. For domain analysis, amazon web services (AWS) were used to comprehend which is based on natural language processing and domain analysis of each news. The accuracy of the given dataset of the given model with build in available evaluation metrics.

The dataset is divided into training and testing sets in 70:30 ratio respectively for the dataset analysis purpose

The accuracy achieved was best by implementing of the RNN-LSTM algorithm for the given dataset. It was observed that using RNN-LSTM better accuracy as well as the performance of fake news detection was seen with the highest of 98% from all the given datasets. The XG-Boost has shown better performance for dataset three as compared to others with an accuracy of 93%. In the political news fact check dataset, there was a significant difference of 10.3% between both the RNN-LSTM and XG-Boost algorithms with accuracy was 87% and 76.7% respectively.

On the other hand, there was very a slight difference in the accuracy

When the RNN-LSTM method was used to implement dataset two, the results were 80.1 percent using XG Boost and 82.2 percent using the RNN-LSTM technique.

When both algorithms were used, the RNN-LSTM approach produced the best results in terms of fake news identification accuracy.

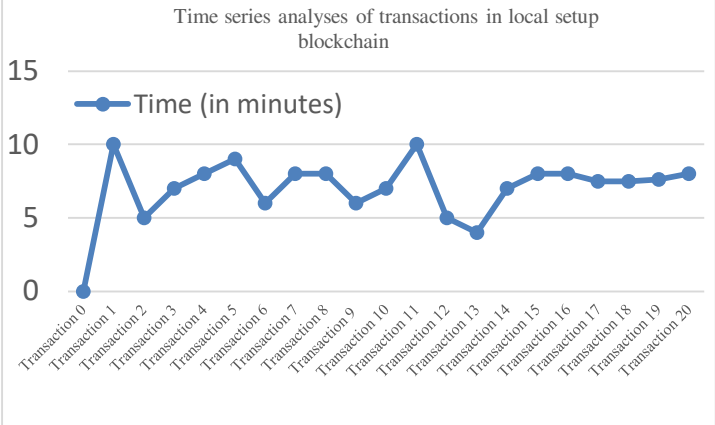

Fig 9 Time series analyses of transactions in local setup blockchain

In order to perform transactions , a local setup of blockchain was performed using javascript programming.
The formation of the first block as shown in the figure took **approx. 10 minutes** which gradually concerning time and the transaction.

Table III Specifications of local setup

Domain	**Specifications**
Processor	Intel Core(TM) i5-10210U
CPU Logical Processor(s)	1.60GHz, 2112 Mhz 4 Core(s), 8
Ram Memory	12 GB RAM

On average, each transaction took **approx. 6-7 minutes** which is good in terms of performance for small transactions **(20-50 transactions**).

Demerits areas the level of transactions grew the performance started to decline and computation time increased to **12-15 minutes after every 11th transaction.**
Thus, in order to improve usability, the Remix platform was employed, which provides wallets, plugins, transactions, and a considerably faster transaction rate.

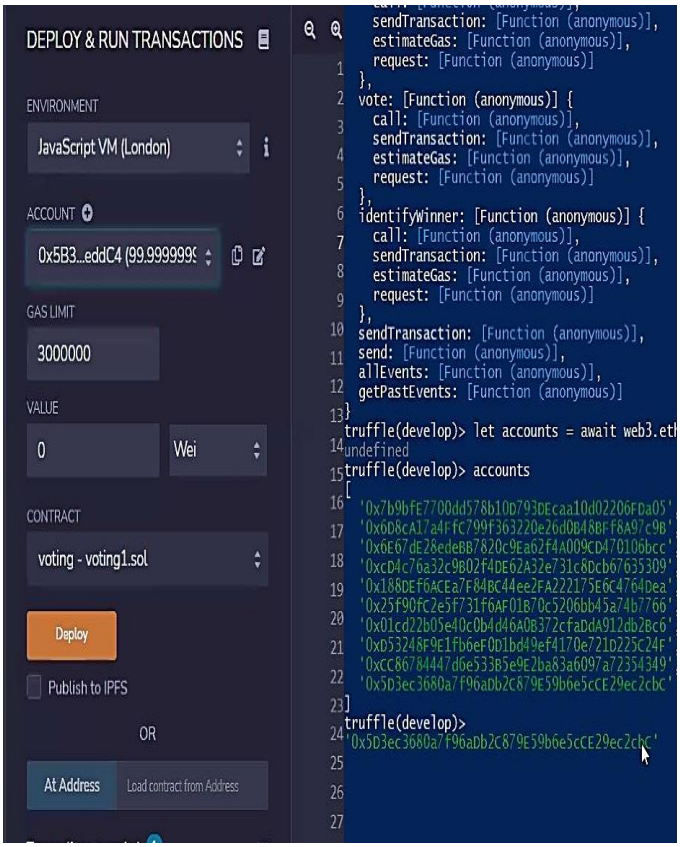

Fig 10 Voting authorized experts through blockchain

The initial transaction through the remix platform **took approx. 20 seconds to form the first block.**On average, it took about 12-14 seconds, which is over 60-70 percent faster than the old local setup technique

Table IV Specification of the remix platform

Sno.	Domain's	Specifications
1.	Coding Platform	Remix-IDEI v0.11.0
2.	Solidity Version	pragma solidity <0.7.0;
3.	Program Language	Solidity 0.5.7
4.	Extension	.sol

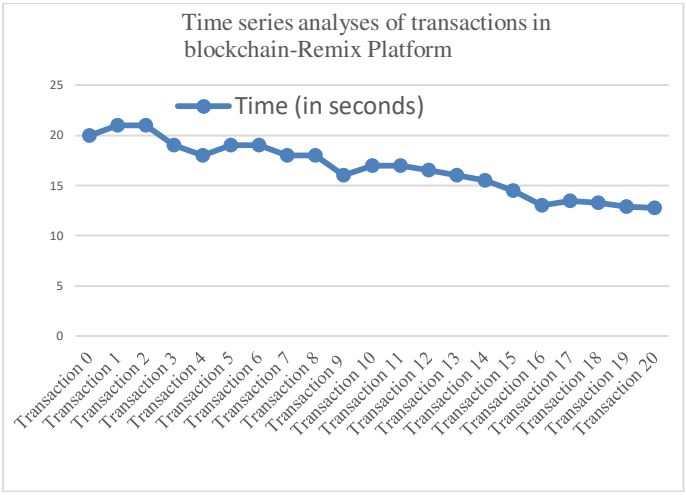

Fig 11 Time series analyses of transactions in blockchain-Remix Platform

.
Remix provides 100 free accounts with the provision of the plugin with the add on plugin of metamask and ganache.
Branch formation:-
--Expert Review.sol
|---Contract.sol
|---Vote.sol

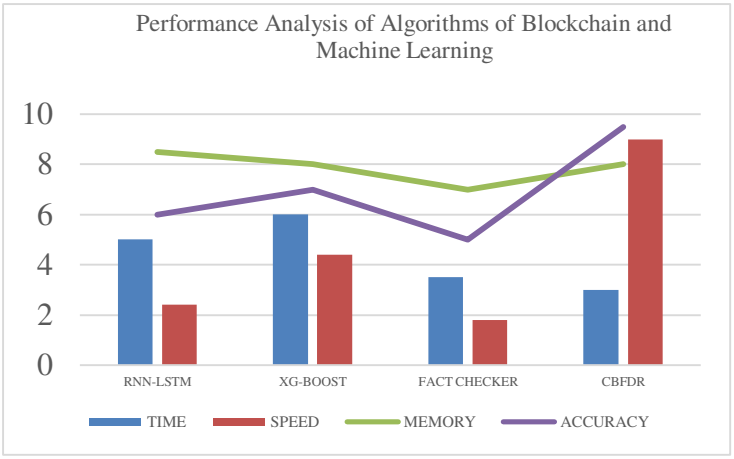

Fig 12 Performance Analysis of Algorithms of Blockchain and Machine Learning

Fake news is an ever-growing area, and fresh fake news is reported every day, therefore in order to raise awareness and comprehend the gravity of it, the supplied proposed paper will try to improve in order to protect the integrity of the information and keep the news safe from manipulation.

The news posted on various platforms which are not authorized could be reported and a list of which could be maintained in order to verify users based on which platforms they have earlier worked on is not matching with the unauthorized list

5) Conclusion and Future Work

This paper successfully gives a novel CBFDR model for detection , prevention and reporting fake news using blockchain and machine learning. The decentralized platform allows experts across the world to interact and give their expert reviews along with giving a platform to report the severity of the news at the level mentioned using the novel algorithm PoE (Proof of evidence). The domain detection performed through AWS Comprehend was using The best performance for fake news detection was shown using RNN-LSTM compared to XG-Boost for fake news detection achieved 98% (highest compared to another dataset in RNN-LSTM only) while XG-Boost achieved 93% highest compared to another dataset in XG-Boost only). In comparison to the local system, the remix platform achieved a 60-70 percent increase on blockchain consensus speed, implying that transactions in the blockchain took an average of 10-14 seconds.

Further future work papers can be elaborated on and can be enhanced with more security checks. Currently the given model focuses on the textual data and is constrained to the English language in the future it could be expanded to video and audio news as well as other languages such as Spanish, Hindi, French etc can be added for a broader range of audiences. In the future, different machine learning algorithms, such as fuzzy logic, can be used to compare the efficiency of fake news.

Declaration

Ethical Approval and Consent to participate: Not applicable

Human and Animal Ethics: Not Applicable

Consent for Publication: The participant has consented to the submission of the research paper to the journal.

Availability of supporting data: As per request

Competing interests: The authors have no competing interests to declare that are relevant to the content of this article.

Funding: No funding was received to assist with the preparation of this manuscript

Authors' contributions: Himani Mishra (the first author) carried out the literature review, studied the concepts and design, implemented the fake news detection using Machine Learning and Blockchain, analysed and interpreted data, and drafted the manuscript. Dr Amita Jain (the second author) have suggested and conceptiualised the idea for given manuscript along with the guidance.Ankur Tayal (third author) have conducted a literature survey, refining and editing the manuscript. All authors contributed to manuscript revision. All authors read and approve the final manuscript.

Acknowledgments: This work of Himani Mishra was conducted under the guidance of Dr Amita Jain .This paper and the research behind it would not have been possible without the exceptional support of my supervisor, Dr Amita Jain and Ankur Tayal for his support.

References

1 NCRB data: 214% rise in cases relating to fake news, rumours https://indianexpress.com/article/india/214-rise-in-cases-relating-to-fake-news-rumours-7511534

2 Fake News Buster: Cupping doesn't remove vaccine from body https://bangaloremirror.indiatimes.com/bangalore/others/fake-news-buster-cupping-doesnt-remove-vaccine-from-body/articleshow/86763513.cms

3 South Korea puts proposed 'fake news law' on ice after backlash https://www.thedrum.com/news/2021/10/04/south-korea-puts-proposed-fake-news-law-ice-after-backlash

4 An incentive-aware blockchain-based solution for internet of fake media things" published by Qian Chena, Gautam Srivastava,, Reza M. Parizic, Moayad, Aloqaily, Ismaeel Al Ridhawie in Elsevier.(2021)

5 India reported 11.8% rise in cybercrime in 2020; 578 incidents of 'fake news on social media: Datahttps://www.thehindu.com/news/national/india-reported-118-rise-in-cyber-crime-in-2020-578-incidents-of-fake-news-on-social-media-data/article36480525.ece

6 How to build data literacy to help students navigate misinformation https://universitybusiness.com/build-data-literacy-students-navigate-misinformation/

7 Facebook Algorithm Fuelled Spread of Misinformation Over Factual News During 2020 US Elections:Studyhttps://gadgets.ndtv.com/social-networking/news/facebook-fake-news-misinformation-more-clicks-read-user-2020-us-elections-twitter-google-2529546

8 Eishvak Sengupta1, Renuka Nagpal,Deepti Mehrotra1 and Gautam Srivastav ProBlock: a novel approach for fake news detection (2021)

9 Alim Al Ayub Ahmed ,Ayman Aljarbouh,Praveen Kumar Donepudi and Myung Suh Choi Detecting Fake News using Machine Learning: A Systematic Literature Review https://arxiv.org/ftp/arxiv/papers/2102/2102.04458.pdf

10 Iftikhar Ahmad ,Muhammad Yousaf,1 Suhail Yousaf ,and Muhammad Ovais Ahmad. Fake News Detection Using Machine Learning Ensemble Methods.

11 Nakamoto, S A peer-to-peer electronic cash system. https://bitcoin.org/bitcoin.pdf. (2008)

12 Aloqaily, M., Boukerche, A., Bouachir, O., Khalid, F., & Jangsher, S. An energy trade framework using smart contracts: Overview and challenges. IEEE Network, 34(4), 1–7. https://doi.org/10.1109/MNET.011.190057 (2020)

13 Srivastava, G., Parizi, R. M., Dehghantanha, A., & Choo, K.-K. R. (2019).

14 Yazdinejad, A., Parizi, R. M., Dehghantanha, A., & Choo, K.-K. R. (2020). P4-to-blockchain: 88, 101629. A secure blockchain-enabled packet parser for software-defined networking. Computers & Security,Wikipedia (2019).

15 Yazdinejad, A., Parizi, R. M., Dehghantanha, A., & Choo, K. R. (2019). IEEE Transactions on Network Science and Engineering. https://doi.org/10.1109/TNSE.2019.2937481 1–1 Blockchain-enabled authentication handover with efficient privacy protection in SDN-based 5g networks. (2019)

16 Yazdinejad, A., Srivastava, G., Parizi, R. M., Dehghantanha, A., Choo, K. R., & Aledhari, M. Decentralized authentication of distributed patients in hospital networks using blockchain. IEEE Journal of Biomedical and Health Informatics(2020)

17 Le Glaz A, Haralambous Y, Kim-Dufor D, Lenca P, Billot R, Ryan TC, Marsh J, DeVylder J, Walter M, Berrouiguet S, Lemey C Machine Learning and Natural Language Processing in Mental Health: Systematic Review (2019)

18 Natural Language Processing(NLP) for Machine Learning Https://towards datascience.com/natural-language-processing-nlp-for-machine-learning-d44498845d5b

19 Haber, S., Stornetta, W.S. How to time-stamp a digital document. J. Cryptology 3, 99–111. https://doi.org/10.1007/BF00196791(1991)

20 M. Dabbagh, M. Sookhak and N. S. Safa, "The Evolution of Blockchain: A Bibliometric Study," in IEEE Access, vol. 7, pp. 19212-19221, 2019, DOI: 10.1109/ACCESS.2019.2895646.(2019)

21 B. Bhutani, N. Rastogi, P. Sehgal and A. Purwar, "Fake News Detection Using Sentiment Analysis," Twelfth International Conference on Contemporary Computing (IC3), pp. 1-5, DOI: 10.1109/IC3.2019.8844880.(2019)

22 Sengupta, E., Nagpal, R., Mehrotra, D. et al. ProBlock: a novel approach for fake news detection. Cluster Comput 24, 3779–3795 https://doi.org/10.1007/s10586-021-03361-(2021).

23 2021 was the year of fake news and misinformation on social media. It's going to get worsehttps://theprint.in/opinion/2021-was-the-year-of-fake-news-and-misinformation-on-social-media-its-going-to-get-worse/792585/(2021)

24 On national press day, netas call to curb fake news, sensationalism https://timesofindia.indiatimes.com/india/on-national-press-day-netas-call-to-curb-fake-news-sennationalism/articles how/87747487.cm

25 Rocha, Yasmim Mendes et al. "The impact of fake news on social media and its influence on health during the COVID-19 pandemic: a systematic review." Zeitschrift fur Gesundheitswissenschaften = Journal of public health, 1-10. 9 Oct. 2021, doi:10.1007/s10389-021-01658-z https://www.ncbi.nlm.nih.gov/pmc/articles/PMC8502082/ (2021)

26 PoliticalNews Fact Checker Data Kaggle , Real and Fake Dataset https://www.kaggle.com/shivkumarganesh/politifact-factcheck-data,https://www.kaggle.com/datasets/clmentbisaillon/fake-and-real-news-dataset

27 Twitter revamps misinformation warning labels to curb fake news menacehttps://www.financialexpress.com/industry/technology/twitter-revamps-misinformation-warning-labels-to-curb-fake-news-menace/2370728/

28 A secure blockchain-enabled packet parser for software defined networking. Computers & Security,Wikipedia (2019). Fake news. https://en.wikipedia.org/wiki/Fake_news. Yazdinejad, A., Parizi, R. M., Dehghantanha, A., & Choo, K.-K. R. (2020). P4-to-blockchain: 88, 101629. https://doi.org/10.1016/j.cose.2019.101629

29 Onik, Md Mehedi Hassan & Miraz, Dr. (2019). Performance Analytical Comparison of Blockchain-as-a-Service (BaaS) Platforms. 3-18. 10.1007/978-3-030-23943-5_1.

30 Z. Shahbazi et al "Fake Media Detection Based on Natural Language Processing and Blockchain Approaches," in IEEE Access, vol. 9, pp. 128442-128453 doi: 10.1109/ACCESS.2021.3112607(.https://ieeexplore.ieee.org/document/9536745) (2021)

31 LSTMhttps://towardsdatascience.com/illustrated-guide-to-lstms-and-gru-s-a-step-by-step-explanation-44e9eb85bf21

32 Haumahu, J & Permana, Silvester & Yaddarabullah, Y. Fake news classification for Indonesian news using Extreme Gradient Boosting (XGBoost). IOP Conference Series: Materials Science and Engineering. 1098. 052081. 10.1088/1757-899X/1098/5/052081. (2021)

33 Tianqi Chen, Carlos Guestrin XGBoost: A Scalable Tree Boosting System , https://arxiv.org/abs/1603.02754 (2016)

34 Survey of popular platforms of news consumptions in US by February 2022 https://www.statista.com/statistics/717651/most-popular-news-platforms/(2022)

35 Ghatkopar: Fake Negative COVID-19 Certificate Scam Unearthed https://www.mumbailive.com/en/crime/fake-negative-covid19-certificate-scam-unheartened-71665 (2020)

36 WHO (World Health Organization) https://covid19.who.int/table

37 Population Statics https://www.populationu.com/india-population#:~:text=India%20population%20in%202021%20is,1.39%20Billion%20(139%20Crores).

38 Data sharing and privacy for patient IoT devices using blockchain. International conference on smart city and informatization. Springer Singapore334–348. (2021)

39 Anup Kumar Paul, Xin Qu & Zheng Blockchain–a promising solution to internet of things: A comprehensive analysis, opportunities, challenges and future research issues Wen Peer-to-Peer Networking and Applications (2021)

40 Robustness against fraudulent activities of a blockchain-based online review system Tanakorn Karode & Warodom Werapun Peer-to-Peer Networking and Applications volume 15, pages92–106 (2022)

Authors' information:

Himani Mishra is currently pursuing Masters in Technology (MTech) in Information Security. Received her Bachelors In Technology (B.Tech) degree in computer science from Sharda University.Her interests are in Information Security,Blockchain, Machine Learning, and Software Development.

Dr. Amita Jain has done her B.E.(CSE), M. Tech. (IT) and PhD (Natural Language Processing) from Jawaharlal Nehru University, New Delhi. She is having 20 years teaching and research experience. She has published more than 90 research papers in highly reputed International Journals and conferences including ACM Transactions, IEEE, Elsevier, Springer etc. She is the Associate Editor of International Journal of Forensic Software Engineering, Inderscience. She is also a reviewer on the panel of journals of IEEE, ACM, Elsevier etc. She has organized and delivered many talks in International Conferences, Seminars and Workshops etc. She supervised two Ph.D. students and four students are working under her guidance. She is extensively working in natural language processing and possesses Google H-Index Score of 16.0.

Ankur Tayal has done her B.Tech (Civil) , M.B.A. (Marketing and sales) , M. Tech. and Pursuing PhD (Industry Revolution 4.0 and Supply Chain) from Delhi School Of Management , Delhi Technological University, New Delhi. He is having 8 years teaching and research experience. He has published 10 research papers in reputed International and National Journals . He is the Associate Member of Institution Of Engineers (IEI) . His Research Interests include Supply Chain Management , Industry Revolution 4.0 and Technologies , Circular Economy and Logistics Management.

Sādhanā (2022)47:109
https://doi.org/10.1007/s12046-022-01877-4
© Indian Academy of Sciences

Characteristics assessment of local scour encircling twin bridge piers positioned side by side (SbS)

GEETA DEVI* and MUNENDRA KUMAR

Delhi Technological University, New Delhi 110042, India
e-mail: geeta_phd2k17@dtu.ac.in; munendrakumar@dtu.ac.in

MS received 28 August 2021; revised 24 January 2022; accepted 28 March 2022

Abstract. In the case of multiple pier arrangements, commonly used manuals still suggest using methods for an isolated pier, irrespective of the spacing between the pier and the factors influencing the pairs of the pier. The present study is an experimental investigation for assessing maximum scour depth (MSD) characteristics around the twin piers installed in side-by-side (SbS) positioning. Twenty-seven experimental conditions were evaluated for three sets of the rate of flow. The Acoustic Doppler Velocimeter (ADV) was used to precisely measure flow intensity under the clear water condition. Center-to-center (C2C) spacing between the piers was varied from 1.5, 2, 2.5, 3, 3.5, 4, 4.5 to 5 times pier diameter (D). In the vortex region higher amount of turbulence is perceived owing to a stronger horseshoe vortex forming between the piers. This turbulence resulted from various factors influencing the MSD, and these parameters are assessed and formulated by dimensional analysis. The findings of the study demonstrate the effect of Froud number, the effect of dimensional parameters, the effect of sediment deposition, and the effect of C2C spacing between the piers on the pattern of MSD for the two piers. During the comparison of the experimental data with the semi-empirical equations, the best value root mean square and maximum absolute percentage error was observed as 0.97 and 1.5%, respectively, for the Larsen and Toch equation. Bridge pier constitutes numbers of piers, this study will impart new light on mutual interference between the two piers and its effect on the local scouring evolved in the propinquity of the pier, so that the current engineering equations can be modified for the accurate prediction of scouring.

Keywords. Bridge piers; Local scour; Piers-flow interaction; Maximum scour depth; River hydraulics; Side-by-side positioning; Sediment transport.

1. Introduction

As traffic volumes increased in many nations due to fast economic growth, more and more bridges over the rivers and canals have been constructed. The presence of bridge piers affects the local flow field, often leading to the creation of small scouring holes that might harm the corresponding bridge components [1]. Sediment transport is a common phenomenon during flooding. When significant lift force on suspended particles is available to overcome the frictional grips between the particles, sediment suspension will be generated due to the turbulence in the flow [2]. Scour is one of the main problems for efficient management of water resources. Local scour has the potential to cause hydraulic structures like bridge piers, spur dikes, and abutments to collapse [3]. The major source of chorography changes resulting in land loss, exceeding sediment output, and consequent water quality degradation is the scouring processes in water bodies [4]. Owing to the flexibility of the fluid flow structure, the local scouring across the bridge structure is very hard to trace. A precise prediction of bridge MSD prevents bridge failure and effectively reduces overestimated building costs unnecessarily [5]. This is partly responsible for the flow through the piers and their interplay with the sediments in the bed. For over a half-century, several types of research studies have been made to discover scouring around the single pier [6–19]. However, no conflict with any other structure present in the encircling area was considered in such experiments.

In addition, two or three bridge piers placed in close proximity have drawn the interest of hydraulic engineers for the safety of the bridge piers. For this concern, some studies were conducted on a group of piers such as [20–26], these studies concluded that if the ratio of pier spacing is 0.25, the resultant scour in SbS arrangement is greater than 50% compared with the single pier. For a ratio of pier spacing less than 0.25, both the piers can be presumed as a single pier. In addition to the above, experimental research on the pier group to examine the spacing impact and countermeasures in scouring depth was conducted by Heidarpour M, Afzalimehr H, Izadinia E, 2010 [27]. Their study concluded that as the distance between the piers

*For correspondence
Published online: 08 June 2022

expands, the region between the piers without protection is washed away, resulting in deeper scour holes at the upstream side of the piers. Behzad and Beheshti [28] investigated the interference between the piers relies on the angle of attack, the geometry of the pier model, and the C2C spacing of piers. The Behzad and Beheshti [28] also investigated the local scour processes in piers with various configurations and distances. Results of work conducted shows that as the C2C spacing between the piers increases, the depth of the scour increases. To explore the flat, protected, and rough bed WU Peng, hirshfield Faye, SUI Jueyi in research work [29] have conducted fifty-four flume tests for evaluating the local scour across the single pier in the open channel. These studies reveal essential information about the behavior of the bridge single and two piers, but they also show that there is not a unified approach for predicting the scour depth for closely placed pier models and the role of pier spacing in the scour depth estimation. Considering these gaps, this research has been scheduled and carried out. The pier spacing (1.5–5 D) was varied with an interval of 0.5 D in order to consider the effect of C2C separation between piers. For assessment of MSD, different equations were used, and results of the equations were validated with the experimental data.

2. Experimental methodology

Testing was carried out in the hydraulic laboratory at Delhi Technological University. The 14 m length and 1.10 m width recirculating flume is fitted with ADV velocimeter and the Venturi meter and has a depth of 0.80 m, represented in figure 1. Venturi meter and ADV, were used to measure the velocity of the flume section. At a distance of 5 m from the inlet tank, a sand recess or working section of 5 m was prepared. The total length of the working section was 5 m which were located at 5 meters from the upstream of the flume. Two cylindrical piers made up of acrylic pipes of diameter D, 5 cm, were used as pier models. These piers were positioned at the center of the working section, which was 7.5 m from the upstream of the flume. The C2C spacing between the piers was 1.5, 2, 2.5, 3, 3.5, 4, 4.5, and 5 times the diameter of the pier. Experimental work was conducted in three sets by increasing the flow rate (0.0295, 0.0428, and 0.0537) m^3/sec under clear water conditions. The working section was prepared with Yamuna sand, with the mean particle size, D_{50}, being 0.60 mm, specific gravity S_g, 2.62, and uniformity coefficient, C_u, is 2, and then curvature coefficient, C_c, is 1. If $C_u < 6$ and $1 < C_c < 3$ for sand, then it will be taken into consideration as uniformly graded [18]. All the flow parameters and experimental conditions are described in table 2. The experimental run time was set to 480 minutes for each experiment, as the scour depth developed after 360 minutes was considered equilibrium scour depth. As per the research work conducted by Setia [30] time needed to achieve an equilibrium scour depth of around 90% was initial 300 minutes, and researchers like [8, 15] have also concluded that maximum scour takes place in the initial 180–240 minutes of the experimental run. Keeping in view the laboratory facilities, the experiment run duration of 480 minutes was fixed for carrying out all the experiments.

Scour depth around the piers was observed every 10 minutes for the initial one hour, and after that, observations were done after every 30 minutes for the next seven hours. The water pump was turned off, and the flume water was drained at the end of each test run. The final bed level measurements were then taken with a vernier point gauge with ± 0.1 mm accuracy. The scour depth was measured on the piers peripheral encircle (upstream, right, left, and

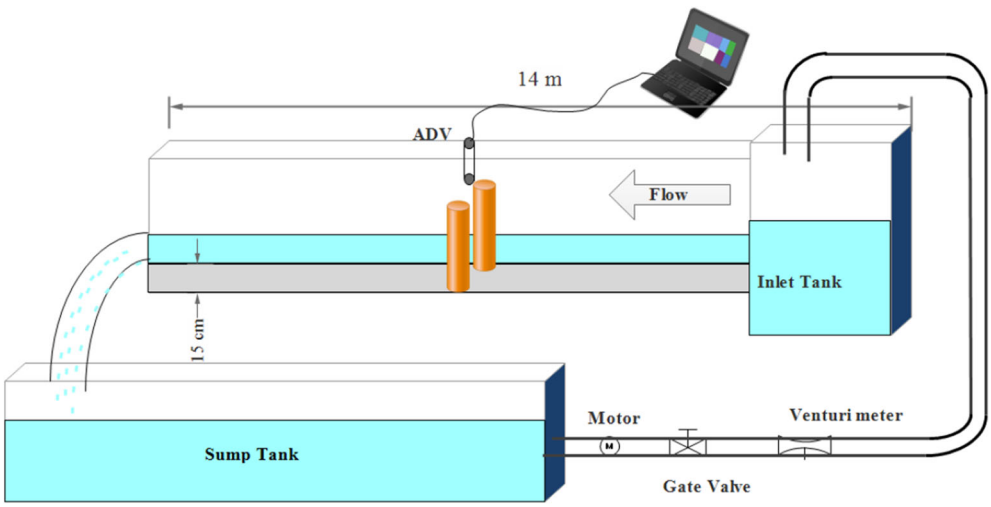

Figure 1. Experimental set up for SbS positioned bridge piers.

downstream). Scour profile was measured at about 20 mm away from the pier along the axis of symmetry as shown in figure 2. It was observed that no significant changes in scouring depth and scouring hole equilibrium depth were found after a lapse of 8 hours. The universal criteria proposed by Melville in his research work [16] need to be satisfied for the experimental conditions such as (a) the ratio of the bed width of the channel, B, to the diameter of a pier, D, should not be less than 6.5 for no channel wall effect or contraction effect, the ratio is equal to 110/5= 22; (b) the ratio of flow depth, H, to the pier diameter, D, should be greater than 3 for independent scour depth, the ratio is equal to 16/5 = 3.2 and (c) the ratio of pier diameter, D, to the mean particle size of sand, D_{50} should be greater than 50 for sediment particle effect, the ratio is equal to 50/0.60 = 83.33 (figure 2).

2.1 *ADV functioning*

The instantaneous 3-D velocity measurement was conducted by utilizing SonTek 16 MHz MicroADV. ADV is a single-point current meter that accurately measures the 3-Dimensional velocity components of water velocity in both high and low flow conditions. The specifications of the ADV are presented in table 1. Velocities are measured in a sampling volume located at a distance away from the probe head. The probe head was made up of a single transmitter located in the center of the probe head. The transmitter generates an acoustic pulse narrow beam that is projected through the water. The reflection of these pulses from the particles or "scatterers" is reflected and received by the ADV receiver. The intersection of the receiver axes designates the location of the sampling volume. There are four types of ADV probes: (i) 3-D down-looking probe, (ii) 3-D up-looking probe, (iii) 3-D side looking probe, and (iv) 2-D side-looking probe. Among these four types of probes, 3-D down-looking probe is employed for this study. In the present study, the x-axis of the down-looking probe indicates the velocity in the direction of flow, downward direction being positive; the y-axis indicates the transverse flow and the z-axis down-flow, downward direction being positive.

SonTek 16 MHz MicroADV with 5 cm distance to Sampling Volume, which had a maximum sampling rate of 50 Hz and volume of 0.09 cc was employed. In our study, the sampling rate for the data collection was selected as 25 Hz. The output data from the ADV were filtered by neglecting the negative values. Depending on the turbulence intensity, the sampling durations were 5 minutes in order to have a statistically time-independent average velocity. The ADV readings were taken at four vertical lines upstream and downstream of the pier and the inlet and outlet at the working section. Each vertical line consists of three horizontal points where ADV reading was recorded at bed level, surface level, and at 0.6 h (average velocity). However, the vertical resolution of the measurements was higher above the scour hole. As a general rule, the velocity range should always be set as small as possible. If, for example, the maximum expected velocity is 8 cm/sec, the velocity range should be set to 10 cm/sec. This is because the noise in the data increases with increasing velocity range and hence loses precision at high sampling rate [31]. In the present study, SonTek's HorizonADV software (v1.20) was utilized for the data collection.

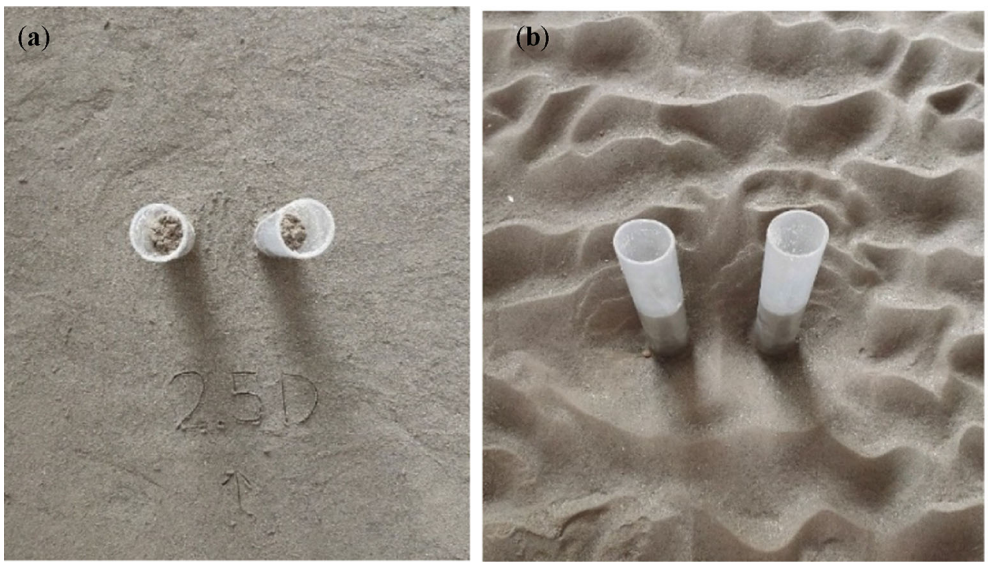

Figure 2. Experimental setup of two piers positioned at 2.5 D spacing in SbS (**a**) before equilibrium scour depth achieved; (**b**) after equilibrium scour depth achieved.

Table 1. ADV specifications.

Sampling Rate	0.1–50 Hz
Sampling Volume	0.09 cc
Distance to Sampling Volume	5 cm
Resolution	0.01 cm/s
Programmed velocity range	3, 10, 30, 100, 250 cm/s
Accuracy	1% of measured velocity, 0.25 cm/s
Maximum Depth	60 m
Temperature Sensor	0.1°C
Compass/Tilt Sensor-Heading, Pitch, Roll Resolution	0.1°
Compass/Tilt sensor-Heading Accuracy	± 2°
Compass/Tilt Sensor-Pitch, Roll Accuracy	± 1°
Pressure Sensor Strain Gauge-Accuracy	0.1%
Resonance Pressure Transducer (RPT)-Accuracy	0.01%
Input Power	12–24 VDC
Typical Power Consumption	2.5–4 W operating

3. Dimensional formulation for the factors affecting MSD around twin piers

For a particular discharge, the scour depth due to the presence of a bridge pier over time reaches a static depth, which is called equilibrium scour depth. The depth of the scour generally associated with the sediment movement with the flow [32]. Overall, the scouring depth across bridge columns depends on different parameters that have been grouped as flow parameters, material bed parameters, and channel geometry parameters. The scour depth can be described by equation (1).

$$\begin{aligned} Y_s = & f_1(\text{Flow parameters}(\rho, \mu, g, V, h, t, t_e)), \\ & f_2(\text{Bed material } (V_c, D, V, d_{50}, \rho_s)), \\ & f_3(\text{Channel geometry } (L, B, H)) \end{aligned} \tag{1}$$

where, variables of function f_1 are, ρ is water density, μ is dynamic viscosity, V is the velocity of flow, h is water depth above the sediment bed, g is the acceleration due to gravity, t is a time of the experimental run, t_e is a time of equilibrium scour depth; variable of function f_2 are, D_{50} is mean particle size, ρ_s density of soil particle, V_c is critical velocity, and variables of function f_3 are, D is the diameter of a pier, L is the length of the channel, B is the width of the channel, H is a depth of the channel (table 2).

From Vaschy Buckingham π theorem, we get:

$$Y_s = f_1\left[\frac{\rho v h}{\mu}, \frac{v^2}{gh}, \frac{t}{t_e}\right], f_2\left[\frac{v_c d_{50}}{v}, \frac{D}{d_{50}}\right], f_3\left[\frac{L}{B}, \frac{H}{B}\right] \tag{2}$$

The term Reynold number ($\frac{\rho V h}{\mu}$) and flow intensity ($\frac{V_c d_{50}}{V}$) are basic parameters considered for bed load. But due to entirely turbulent flow, the effect of the pier Reynolds number and flow intensity on the present study was considered in three sets for varying pier spacing. Thus, for each set of experiments, these two variables are ignored. So, the relative scour depth is a function of the degree of vorticity, $\frac{V^2}{gh}$; relative roughness, $\frac{D}{d_{50}}$; and non-dimensional parameters ($\frac{t}{t_e}$, $\frac{L}{B}$, $\frac{H}{B}$) as given in equation (3).

$$Y_s = f\left[\frac{V^2}{gh}, \frac{t}{t_e}, \frac{D}{d_{50}}, \frac{L}{B}, \frac{H}{B}\right] \tag{3}$$

4. Experimental findings and discussion

4.1 *Effect of the Froude number on the MSD for two piers placed in SbS positioning*

Figure 3 shows the temporal evolution of the scour depth for a single pier as the Froude number increases under the clear-water conditions. These curves shows the dependency of the scour depth on the experimental time, rate of flow and water depth. After the attainment of the dynamic equilibrium scour depth, the scour evolution stopped, but very low transportation of sediment from upstream of the pier to the downstream of the pier still takes place at a very low rate. In the present study, equilibrium state was achieved after 360 minutes. After 360 minutes of experimental run, scour depth approximately becomes constant as presented in figure 3.

Table 2. Flow parameters and experimental conditions.

Set No.	D (mm)	D_{50} (mm)	H (m)	V (m/sec)	Q (m^3/sec)	F_r	R_e	V_c	V/V_c
1	50	0.60	0.120	0.224	0.0295	0.206	30100	0.308	0.72
2	50	0.60	0.149	0.262	0.0428	0.217	43700	0.317	0.83
3	50	0.60	0.163	0.300	0.0537	0.237	54800	0.321	0.93

D = pier diameter; D_{50}= mean particle size; H = flow depth; Q = rate of flow; F_r = Froude number; R_e = Reynolds's number; V_c = Critical Velocity.

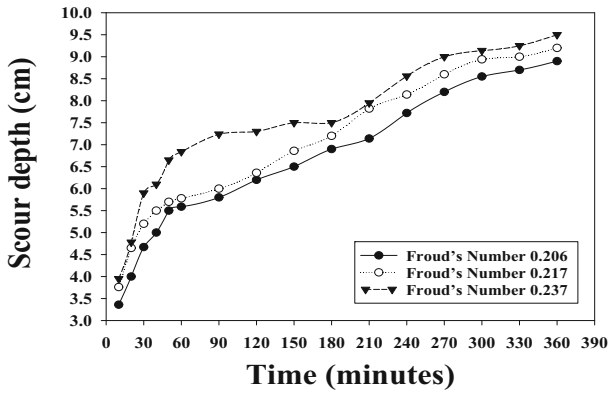

Figure 3. Temporal evolution of MSD across the single pier.

Table 3. Values of Equilibrium time calculated via using equation (3) and equilibrium scour depth extent.

Experimental Set	*h/D*	V/V_c	t_e	Y_t
1	2.4	0.72	2.74	0.9436
2	2.98	0.83	3.33	0.9189
3	3.26	0.93	3.66	0.8975

t_e is the Equilibrium time calculated using equation 3, Y_t is the equilibrium scour depth extent.

An equilibrium time t_e can be provisioned in two ways: firstly, for the last section of the experimental run, at the stage of development and mean scour depth attainment, the equilibrium time was determined. Secondly, equations proposed by Melville and Chiew [12] were opted for forecasting the equilibrium scour depth Y_t. The time factor is defined as the ratio of the scour depth (Y_s) achieved at a time interval t to the equilibrium scour depth upstream of the pier (Y_t) at time t_e. The expression for Y_t is expressed as:

$$\mathrm{Y_t} = \exp\left\{-0.03\left|\frac{\mathrm{V_c}}{\mathrm{V}}\ln\left(\frac{\mathrm{t}}{\mathrm{t_e}}\right)\right|^{1.6}\right\} \tag{4}$$

where $\mathrm{t_e}$ is given as:

$$\mathrm{t_e(days)} = 48.26\frac{\mathrm{D}}{\mathrm{V}}\left(\frac{\mathrm{V}}{\mathrm{V_c}} - 0.4\right) \text{ for } \frac{Y_s}{\mathrm{D}} > 6,\ \frac{\mathrm{V}}{\mathrm{V_c}} > 0.4 \tag{5}$$

$$\mathrm{t_e(days)} = 30.89\frac{\mathrm{D}}{\mathrm{V}}\left(\frac{\mathrm{V}}{\mathrm{V_c}} - 0.4\right)\left(\frac{Y_s}{\mathrm{D}}\right)^{0.25} \text{ for } \frac{Y_s}{\mathrm{D}} < 6, \frac{\mathrm{V}}{\mathrm{V_c}} > 0.4 \tag{6}$$

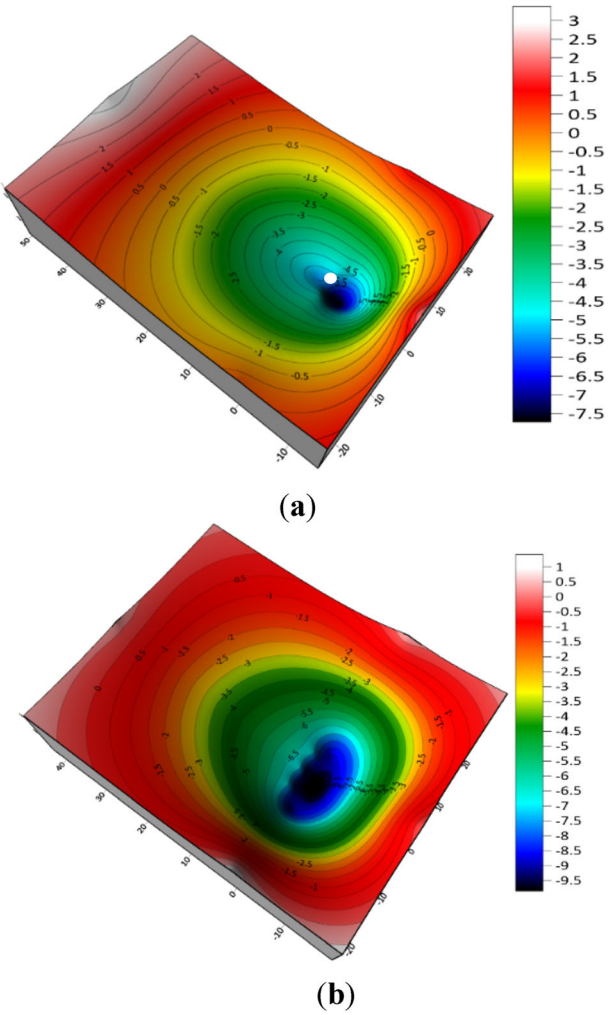

Figure 4. Contours after the equilibrium scour depth (**a**) single pier; (**b**) two piers in SbS positioning.

Here, $y_s/D < 6$, therefore equation (3) opted. For the present study, the values of time factor $\mathrm{Y_t}$ (8 hours) are represented in table 3; the meantime factor was calculated as 92% for the equilibrium scour depth.

The temporal evolution of the MSD for a single pier and twin piers located in SbS positioning with the C2C spacing (1.5D, 2D, 2.5 D, 3D, 3.5D, 4D, 4.5D, and 5D) was tracked. The representation of the temporal evolution of scour depth is shown in figure 3. Figure 3 shows that the scour depths $\mathrm{Y_t}$ were established speedily during the initial 480 minutes period and about 92 percent of overall scour depth was attained.

The higher the Froude number more significant will be the corresponding MSD. The dimensionless shear pressure increases with the Froude number [33]. Therefore, the finer the sediment of the river bed, lower will be the dimensional shear stress resulting in sediment movement. Due to this

reason scouring depths will be greater for increasing Froude numbers.

4.2 *Effect of sediment deposition patterns on MSD for two piers*

The amount of the sediment transported from the upstream of the piers gets deposited on downstream of the pier in the form of a deposition mound. The depth of the scour hole upstream, and the interaction of horseshoe and wake vortices influence the deposition of silt on the mound of bridge piers. Results showed that the greater the mound height downstream of the pier, the rate of flow between two piers would also be more pronounced. Owing to the existence of a scour hole and the reverse vector magnitudes, the relationship between the shear layers weakens in the wake of the pier. For each pier on the downstream side, wake vortices does not overlap with each other. For validation of this flow, visualization experiments [25] were conducted for instantaneous and average velocity, vorticity, and Reynold stress contour and streamline topology using PIV technologies. The experimental results show that the behavior of the cylinders is asymmetrical at a slight gap ratio due to the jet-like circulation between the cylinders in this side-by-side arrangement. The free surface and scour depth inside the scour hole for each pier also show independence of wake vortices [21]. As the initial surface level is lowered from its original bed level, this increases the flow space of water. The existence of a scour hole starts speeding up the flow into the scouring hole by reducing the frictional effect. This affects the movement of the sediments between the two piers. The findings demonstrate that the maximum scour depths have been found on the upstream side of the bridge piers. The upstream downflow of the pier is similar to a vertical jet that erodes an area facing the pier [34].

The wake vortex works like a vacuum cleaner, which collects sediment materials from the horseshoe vortex and deposits the sediment downstream the pier. Sediment is deposited on the bridge piers in the shape of a mound of deposit. The scour hole depth is visible in the contour plot as shown in figure 4 on the front of the bridge piers. At the stage of equilibrium scour, most of the flow passes through

Table 4. Experimental results on the upstream side of the pier for the side-by-side arrangement.

Run No.	Q	(C_s)	(Y_{su})	(Y_{sul})	(Y_{sur})	(Y_{sul}/Y_{su})	(Y_{sur}/Y_{su})
1	0.0295	0	89				
2	0.0428	0	92				
3	0.0537	0	95				
4	0.0295	1.5 D		81	80.8	0.91	0.91
5	0.0295	2 D		80	79	0.90	0.89
6	0.0295	2.5 D		81	80	0.91	0.90
7	0.0295	3 D		78	77.8	0.88	0.87
8	0.0295	3.5 D		72	72.5	0.81	0.81
9	0.0295	4 D		70.4	71.2	0.79	0.80
10	0.0295	4.5 D		69	70.5	0.78	0.79
11	0.0295	5 D		68.4	69	0.77	0.78
12	0.0428	1.5 D		83.5	83.6	0.91	0.91
13	0.0428	2 D		82	81.6	0.89	0.89
14	0.0428	2.5 D		83	83	0.90	0.90
15	0.0428	3 D		80	80.2	0.87	0.87
16	0.0428	3.5 D		74.7	74.2	0.81	0.81
17	0.0428	4 D		72.3	72.25	0.79	0.79
18	0.0428	4.5 D		70	70.4	0.76	0.77
19	0.0428	5 D		67.4	67.3	0.73	0.73
20	0.0537	1.5 D		85.6	85.5	0.90	0.90
21	0.0537	2 D		82	83	0.86	0.87
22	0.0537	2.5 D		85.4	85.2	0.90	0.90
23	0.0537	3 D		84	84.2	0.88	0.89
24	0.0537	3.5 D		80.7	80.4	0.85	0.85
25	0.0537	4 D		74	73.2	0.78	0.77
26	0.0537	4.5 D		71	70.8	0.75	0.75
27	0.0537	5 D		70	69.6	0.74	0.73

C_s is the clear space between the piers in mm, Y_{su} is the Scour depth upstream for the single pier in mm, Y_{sul} is the Scour depth on the upstream of the left pier in mm, Y_{sur} is the Scour depth on the upstream of the right pier in mm.

Table 5. Experimental results on the downstream side of the pier for the side-by-side arrangement.

Run NO.	Q	(C_s)	(Y_{sd})	(Y_{sdl})	(Y_{sdr})	(Y_{sdl}/Y_{sd})	(Y_{sdr}/Y_{sd})
1	0.0295	0	68				
2	0.0428	0	73				
3	0.0537	0	76				
4	0.0295	1.5 D		46	45.2	0.68	0.66
5	0.0295	2 D		48	49	0.71	0.72
6	0.0295	2.5 D		42.4	42	0.62	0.62
7	0.0295	3 D		40.3	40.2	0.59	0.59
8	0.0295	3.5 D		36	35.2	0.53	0.52
9	0.0295	4 D		34.1	33.8	0.50	0.50
10	0.0295	4.5 D		32.4	32.8	0.48	0.48
11	0.0295	5 D		30.8	30.1	0.45	0.44
12	0.0428	1.5 D		54.5	54.5	0.75	0.75
13	0.0428	2 D		62	62	0.85	0.85
14	0.0428	2.5 D		53.7	54.5	0.74	0.75
15	0.0428	3 D		51.7	50	0.71	0.68
16	0.0428	3.5 D		50.3	50.1	0.69	0.69
17	0.0428	4 D		48.7	49	0.67	0.67
18	0.0428	4.5 D		47	47	0.64	0.64
19	0.0428	5 D		45	45	0.62	0.62
20	0.0537	1.5 D		67	67.4	0.88	0.89
21	0.0537	2 D		68.5	68.3	0.90	0.90
22	0.0537	2.5 D		62.4	62.3	0.82	0.82
23	0.0537	3 D		60.4	60.2	0.79	0.79
24	0.0537	3.5 D		54	52.1	0.71	0.69
25	0.0537	4 D		53	53.2	0.70	0.70
26	0.0537	4.5 D		52	51.4	0.68	0.68
27	0.0537	5 D		50	50.2	0.66	0.66

C_s is the Clear Space between the piers in mm, Y_{sd} is the Scour depth downstream for the single pier in mm, Y_{sdl} is the Scour depth downstream of the left pier in mm, Y_{sdr} is the Scour depth on downstream of the right pier in mm

the piers near the actual bed, and the deflection of flow outside the piers was reduced. During the initial experimentation stage, the water flow between the piers acts as a water jet. These jet stars erode the sediment from the pier spacing region and deposit this on the downstream side. After the evolution of the equilibrium scour hole, this rate of erosion and transportation in the pier spacing region gets reduced. The resultant equilibrium scour hole for MSD has been presented in figure 4. The existence of jet flow between the two piers partially reduces when the equilibrium scour depth achieved. The flow divergence around the piers on the outer region of scour hole becomes negligible at equilibrium state, and that is represented in figure 4(a) and (b).

In both cases, the maximum negative z value (intensive downflow) was located upstream of the pier, but the maximum scour depth was achieved for the twin pier placed at 1.5 D, as shown in figure 4(b). These values are higher upstream and are linked to the influence of the inside scour hole. Upward flow is noticed at the wake of the pier, and the flow is then directed to the bed on the sides of the pier and the wake region for continuity of the flow. There was a heavier drop in the scour between the two piers than on the outside of the piers [21].

4.3 *Effect of spacing between the piers on the scour pattern around the two piers*

The experimental results of SbS positioned for MSD are tabulated below. Table 4 represents the MSD outcomes on the upstream side, and table 5 illustrates the MSD on the downstream side of the pier. Tables 4 and 5 also illustrate the non-dimensional scour depth findings for the upstream and downstream of the pier, respectively.

The evolution of the scour hole near the pier results from the sediment transportation phenomenon and 3-D characteristic flow. Firstly, due to the water flow around the piers undergoing 3-D separation. After that, individual shear layers start revolving around the pier and initiate the vortex formation upstream of the pier. This vortex formation is known as horseshoe vortex as it appears like a horseshoe from the top view. Due to the forming of horseshoe vortex and down flow near the pier, sediment transportation rate and shear stress increases. This led to the evolution of scour holes around the pier, and consequently, variation in flow pattern was observed, resulting in a decrease of shear stress and sediment transportation [35]. The MSD depends on the strength of the horseshoe vortex; the strength of the horseshoe vortex is dependent on flow turbulence so, flow

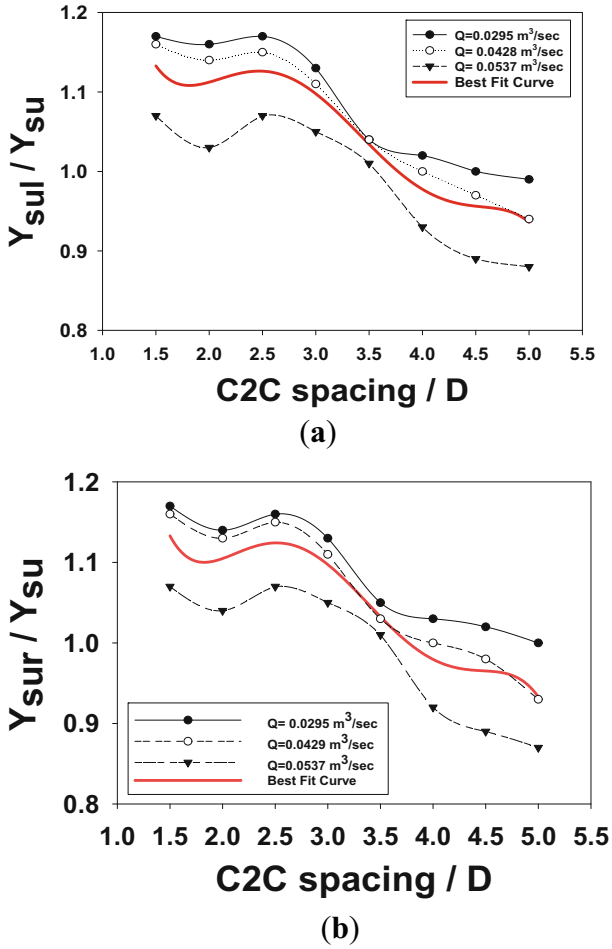

Figure 5. Normalized scour depth on the upstream of piers versus normalized C2C spacing between piers (**a**) left pier and (**b**) Right pier.

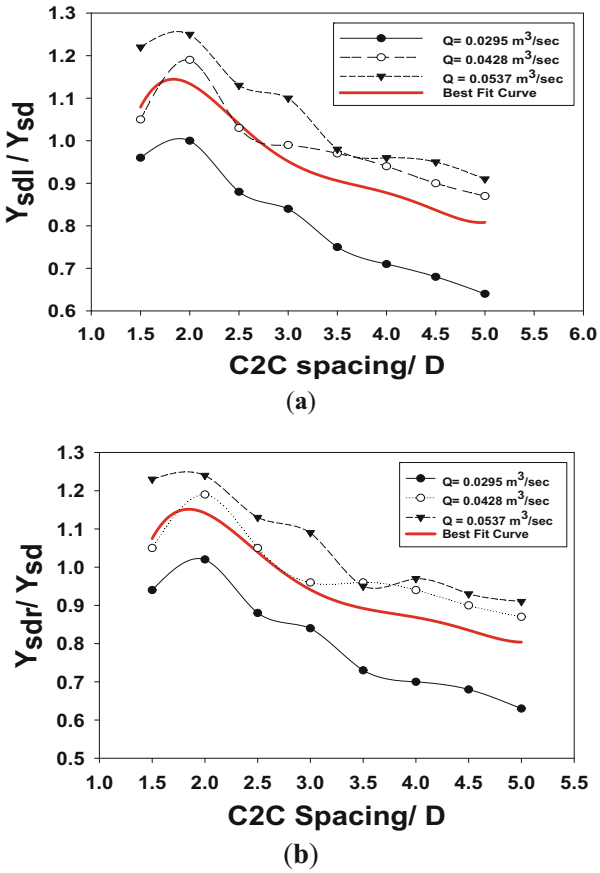

Figure 6. Normalized scour depth on the downstream of piers versus normalized C2C spacing between piers (**a**) left pier and (**b**) Right pier.

turbulence is directly dependent on the Reynolds number (R_e). Hence as a result of this correlation, the intensity of the horseshoe vortex is directly proportional to the Reynolds number of the pier (R_e). The resulting MSD decreases with an increase in the C2C pier spacing, and the intensity of horseshoe vortexes decreases. Thus, greater the pier spacing C2C spacing lower will be turbulence and enormous will be the horseshoe vortices, resulting into the growth of scour hole.

The pattern of the MSD on the upstream side of both the left and right piers is pretty similar, and evidence is represented in figure 5. Figure 5(a) and (b) represent normalized scour depth against the normalized C2C spacing between the left and right pier, respectively. The trend of both the curves is similar, and it shows that as we increase the C2C spacing, the mutual interdependence of the piers is reduced. Similarly, with the increase in the flow discharge, the depth of scouring is increased. This trend is projected as a rational 2nd-degree quadratic equation in equation (7) for the best fit curve with global goodness of fit R^2 for the left pier curve is 0.994. Similarly, equation (8) represents the best fit curve with global goodness of fit R^2 for the right pier curve is 0.9877.

$$Y_{sul} = \frac{a_1 + b_1 x + c_1 x^2}{1 + d_1 x + e_1 x^2} \tag{7}$$

where values of constants in equation (7) are such as: a_1 =1.0781, b_1= −0.5481, c_1= 0.0793, d_1= −0.5225, e_1 = 0.0780

$$Y_{sur} = \frac{a_2 + b_2 x + c_2 x^2}{1 + d_2 x + e_2 x^2} \tag{8}$$

where values of constants in equation (8) are such as: a_2 = 1.0693, b_2 = −0.5590, c_2 = 0.0828, d_2 = −0.5370, e_2 = 0.0819

The trend for the upstream side of piers is similar for both the piers, similar trend was perceived on the downstream of both the piers represented in figure 6. Figure 6(a) and (b) represent normalized scour depth against the normalized C2C spacing between the left and right pier, respectively. Both the piers behaved identically for three sets of experimental runs and curves plotted for the

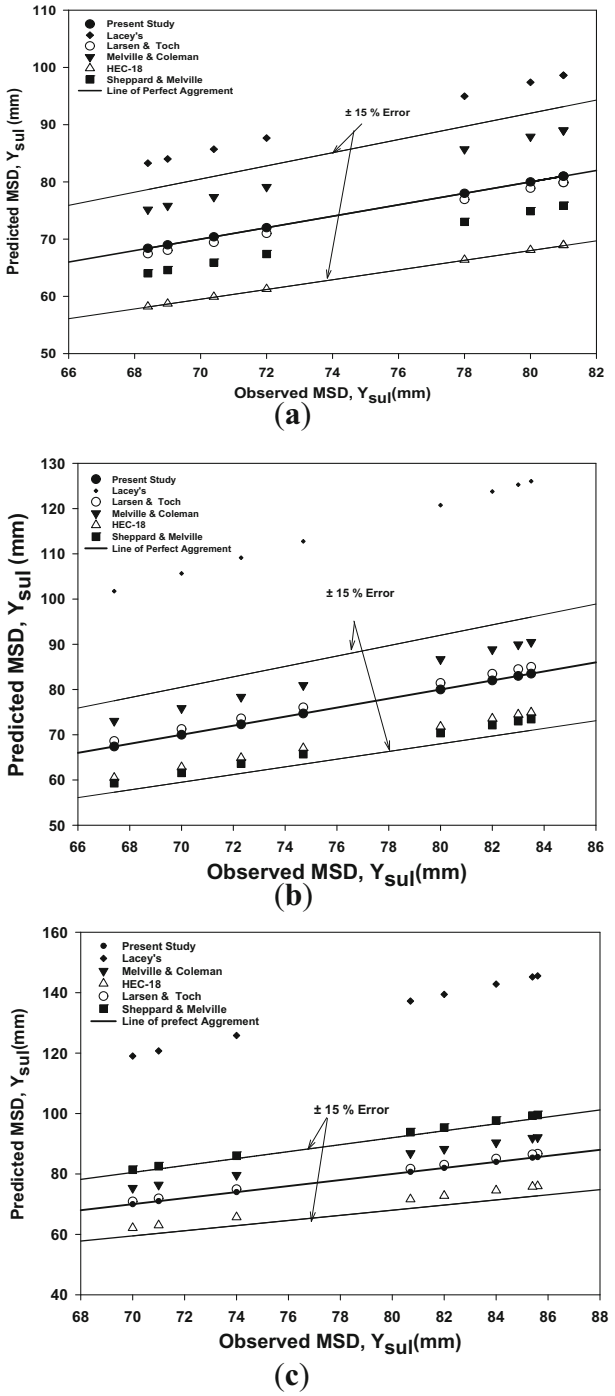

Figure 7. Observed versus predicted MSD on upstream of the left pier for Froude number (**a**) 0.206, (**b**) 0.217 and (**c**) 0.237.

normalized scour depth against the normalized C2C spacing between the piers and best-fitted curves represented. This trend is projected similarly as opted for upstream side, and concerned equations are represented. Equation (9) represents the best-fit curve for the left pier on the downstream side with global goodness of fit R^2 = 0.9605. Similarly, equation (10) represents the best fit curve with global goodness of fit R^2 for the right pier curve is 0.9475.

$$Y_{sdl} = \frac{a_3 + b_3 x + c_3 x^2}{1 + d_3 x + e_3 x^2} \tag{9}$$

where values of constants in equation (9) are such as: a_3 =1.4423, b_3 = −0.6195, c_3= 0.0035, d_3 = −0.2713, e_3 = −0.0647

$$Y_{sdr} = \frac{a_4 + b_4 x + c_4 x^2}{1 + d_4 x + e_4 x^2} \tag{10}$$

where values constants in equation are such as: a_4 =1.5107, b_4 = −0.5773, c_4 = −0.0100, d_4 = −0.1851, e_4 = −0.0852.

The curves presented in figure 6 shows a gradual decline in the scour depth with the increase in clear spacing between the piers and scour depth increases with the increases in the rate of flow. The two piers behave identically when they are placed side-by-side with each other and, when placed in very close proximity,they behave like one pier of larger diameter size, and as a result, the scour depth for the close spacing was higher than the single pier. C2C was more significant when the spacing was three times the diameter of the pier. At C2C, spacing equal to 3D piers started behaving individually, and scour depth decreased. Minimum scour depth was attained at the maximum C2C spacing that is 5D.

4.4 *Evaluation of MSD using semi-empirical equations*

For predicting the MSD across the bridge pier, the observed scour depth was multiplied by the spacing factor. The experimental scour depth across the piers was not the same as predicted values, which undoubtedly increases the difficulty of scour prediction. Therefore, a factor of pier spacing is defined as (P_s). P_{sul} and P_{sur} are the pier spacing factors for the left and right pier, respectively, for an upstream side of piers.

$$Y_{sul} = P_{sul} Y_s \tag{11}$$

$$Y_{sur} = P_{sur} Y_s \tag{12}$$

The observed experimental results of equilibrium scour depth at the upstream and downstream for all the pier arrangements were compared with the predicted results from semi-empirical equations.

Scour depth at the upstream of both the piers was calculated using the above expressions of the results of the traditional equations. Figure 7(a), (b), and (c) represent the MSD for the experimental results versus the predicted results of five well-known equations for the left pier. These plots concluded that the prediction ability of the IRC equation was almost double than the observed MSD as the factor of safety is very high. It can be used for structures where a higher factor of safety is needed. For accurately predicting the scour depth, these equations are lined as the

Table 6. List of semi-empirical equations used in the present study.

	Expression
Melville and Coleman	$Y_s = K_{yb}K_1K_dK_sK_\theta K_gK_t$ where, Y_s = Local scour depth below the bed level (m), K_{yb} = Factor of pier size for flow depth, K_1 = Factor of flow Intensity, K_d = Factor of sediment size, K_s = Factor of foundation shape, K_θ = Factor of foundation alignment, K_g = Factor of approach channel geometry, K_t = Factor of time.
HEC-18 Federal Highway Administration (FHwA)	$\frac{Y_s}{h_u} = 2.0k_1k_2k_3k_w\left(\frac{D}{h_u}\right)^{0.65} F^{0.43}$ where: Y_s = Scour depth (m), h_u = Head of flow on upstream of the pier (m), D = Diameter of pier (m), K_1, K_2, K_3 and K_w = Factors of correction, F = Froude number, g = Acceleration due to gravity, V = Mean velocity of flow (m/s).
IRC (1998 &2000):	$Y_s = 0.473\left(Q/f\right)^{1/3}, \quad when \frac{L}{B} \geq 1$ $Y_s = 1.34\left(q^2/f\right)^{1/3}, \quad when \frac{L}{B} \leq 1$ where; Q = Design discharge (m^3/sec), Y_s = Scour depth (m), q = Intensity of discharge (m^3/s/m), Q/L & f = Silt factor given by Lacey's equation, L = Clear waterway (m), and B = Mean width of channel (regime width) (m).
S/M Equation or Sheppard and Melville equation	$\frac{y_s}{D} = 2.5f_1f_2f_3 \quad for\ 0.4 \leq \frac{V}{V_c} \leq 1.0$ $\frac{y_s}{D} = f_1\left[2.2\left(\frac{\frac{v}{v_c}-1}{\frac{v_{IP}}{v_c}-1}\right) + 2.5f_3\left(\frac{\frac{v_{IP}}{v_c}-\frac{v}{v_c}}{\frac{v_{IP}}{v_c}-1}\right)\right] \quad for\ 1 \leq \frac{V}{V_c} \leq \frac{V_{Ip}}{V_c}$ $\frac{Y_s}{D} = 2.2f_1 \quad for\ \frac{V}{V_c} > \frac{V_{IP}}{V_c}$ where, Y_s = Scour depth below the bed level (m), D = Diameter of pier (m), f_1, f_2, f_3 = S/M's coefficients, V = Mean velocity of flow (m/s), V_c = Critical Velocity of flow (m/s), V_{IP} = Live bed peak velocity of flow (m/s).
Larsen and Toch	$Y_s = 1.35\ D^{0.7}\ h^{0.3}$ where Y_s = Scour depth below the bed level (m), D = Diameter of the pier (m), and h = Head of flow (m)

S/M equation, Larsen and Toch equation, Melville and Coleman, HEC-18, and IRC (Lacey's equation). The MSD prediction trend for the left and right pier for the side-by-side arrangement was observed similar to each other. Out of five semi-empirical equations Larsen and Toch and S/M equation were observed as the best suitable equation for the present study (table 6).

Figures 8(a), (b), and (c) represent the MSD for the observed experimental results versus predicted results by using the five well-known equations for the right pier. The trends of MSD around the right pier were similar to the left pier, and the prediction ability of equations was also similar. The best suitable equation for the present experimental data was Larsen and Toch and S/M equation. Maximum predicted scour depth was calculated using equations (11) and (12), and the results were compared with the experimental scour depth in order to find out the statistical errors. All the equations, with the exception of the Lacey equation, agreed with the experimental findings within the ± 15% Normalized Root Mean Square Error (NRMSE) range presented in table 7.

4.5 *Error statistics*

In addition to the experimental data, statistical parameters such as Normalized Root Mean Square Error (NRMSE), Mean Absolute Percentage Error (MAE), and R square Correlation for all the equations are presented in table 7. The method/equation with the least total error and under-prediction is the best performer. A mathematical study of the observed and predicted data was performed to determine the best equation. According to statistical analysis, the Larsen and Toch Equation is the best performing equation that provides the most precise local scour depth. Except for the IRC (Lacey's) equation, the rest of the four equations are lying under ± 15 % error bars, which is an acceptable range as proposed by the author in [36], so these equations can be considered for predicting the MSD around the twin piers placed in the transverse direction of flow. Use of Larsen and Toch, HEC-18, and Melville and Coleman Equations are highly recommended based on error statistics for the precise prediction of the MSD around the two piers placed in the transverse direction of flow despite varying spacing between the piers.

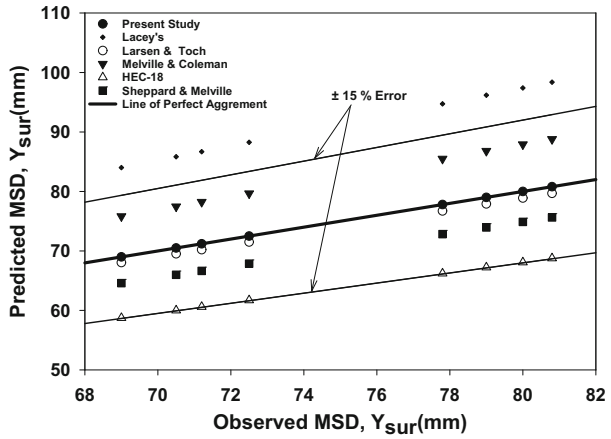

(**a**)

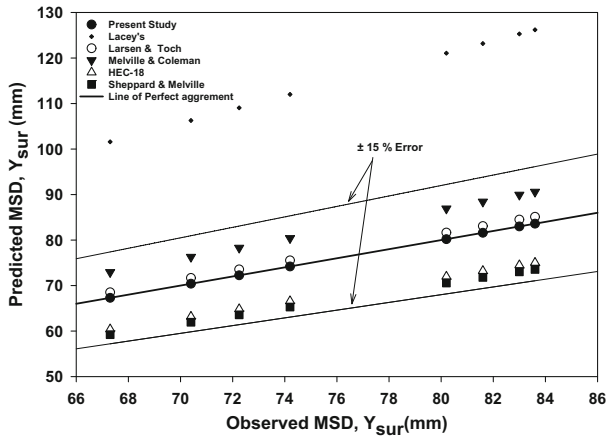

(**b**)

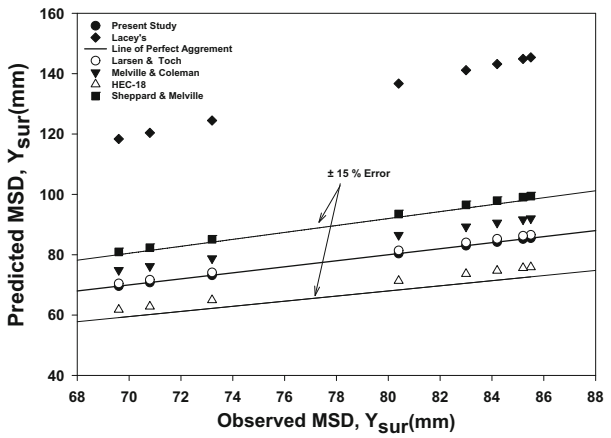

(**c**)

Figure 8. Observed versus predicted MSD on upstream of the right pier for Froude number (**a**) 0.206, (**b**) 0.217 and (**c**) 0.237.

4.6 *Discussion*

In this analysis, the effects of a flow pattern of the piers in the SbS positioning are comparable to the behavior of the twin pier, which changes with the C2C between the piers. We may conclude from the results of this study that the mutual interference among the pier has a direct relationship with the Froude Number and Reynolds number. The horseshoe vortex is extended deeper by the two piers on the upstream side. The flow intensity between the two piers is always higher, and the scouring hole developed is more extensive, so longitudinal and circumferential movement between the piers is impacted. The scour pattern, including the contracted flow and interference between horseshoe vortices, played an essential part in producing and forming a higher scouring depth between the two piers. The existence of the two piers directly impacts the behavior of vortices. The findings are graphically represented, and few mathematical equations have been chosen to validate the experimental results. Experimental results and Larsen and Toch's predicted results are ideally suited for the present study. The experimental results of this study can validate any numerical modeling and computational modeling methods. These experimental results can be in the future for validating any CFD tools.

Table 7. Statistical errors for the side-by-side arrangement.

Arrangement	Analysis results	NRMSE	MAPE	R^2
U/s scour for left pier	IRC	0.525	47.6	0.446
	Melville and Coleman	0.087	8.6	0.988
	HEC-18	0.123	12.1	0.933
	Larsen and Toch	0.015	1.5	0.973
	S/M equation	0.125	11.6	0.437
U/s scour for right pier	IRC	0.525	47.6	0.434
	Melville and Coleman	0.087	8.6	0.987
	HEC-18	0.123	12.1	0.93
	Larsen and Toch	0.015	1.5	0.972
	S/M equation	0.125	11.6	0.431

5. Conclusion

A series of experiments evaluated the effect of mutual interference between the two piers situated in the transverse direction of the flow. This study presents the principal conclusions and are given as follows.

- The extent of scouring at the upstream and downstream sides of the left and right piers was approximately similar. In the case of a SbS arrangement, both the piers behaved were identical. By increasing the spacing between the piers strength of the horseshoe vortices decreases, hence mutual interference will be reduced; this reduction concludes that for larger spacing between the piers, small will be the scour depth and vice versa. The smaller the spacing between the piers, the more enormous will be the interference and scour depth between the piers.

- Piers behaved as a single pier when they were placed in close proximity to each other for spacing less than 2.5D. Scouring at the upstream side increased due to these pier interactions. For the left and right pier, the maximum upstream scour was observed for the C_s = 2.5–3 times D. The minimum scour depth was evaluated for the C_s = 4.5 times D. Scour depth on the downstream side of the pier for both left, and a right pier was maximum for C_s = 1.5 times D and minimum for the C_s = 4.5 times D.
- There is a larger, substantial upflow in the separation between the two piers (especially in the downstream portion of the gap), but a smaller transverse-deflection is formed in contrast to the zone behind the single pier. The flow rate reaching the downstream pier near the bed reduces to 0.2–0.3 V. In the scouring hole at the base of the piers, the highest downflow was observed. The downflow intensity, vertical turbulence, shear stress, and kinetic energy between piers are greater than across the piers.F
- To assess variables impacting MSD, dimensional analysis using the theorem Buckingham π was conducted. So, the parameters that play a vital role in the MSD assessment are: degree of vortices, relative roughness, equilibrium scour depth time, and flow section.
- Five traditional equations were used for predicting the scour depth accurately. Comparison with observed experimental results was made with the ultimate asymptotic scour depth forecast by the suggested equations. Among the five equations used, Larsen and Toch and Sheppard and Melville, HEC-18 and Melville equations predict the scour depth for the mean absolute error percentage of less than 15%. IRC recommended equation overestimated MSD. This equation may be considered for the design in case of a high degree of freedom.

List of symbols

B	Width of the channel
C_c	Curvature coefficient
C_s	Clear space between the piers
C_u	Uniformity coefficient
D	Pier diameter
d_{50}	Mean particle size
F_r	Froude number
g	Acceleration due to gravity
H	Head of water flows over the sand bed
L	Length of the channel
P_{suL}	Pier spacing factors for the left
P_{suR}	Pier spacing factors for the right pier
Q	Rate of flow
R_e	Reynolds number
S_g	Specific gravity
t	Time of the experimental run
t_e	Time at which equilibrium scour depth attained
V	Velocity of flow
V_c	Critical velocity
Y_s	Scour depth
Y_{sd}	Scour depth downstream for the single pier
Y_{sdl}	Scour depth downstream of the left pier
Y_{sdr}	Scour depth on downstream of the right pier
Y_{su}	Scour depth upstream for the single pier
Y_{sul}	Scour depth on the upstream of the left pier
Y_{sur}	Scour depth on the upstream of the right pier
Y_t	Equilibrium scour depth
μ	Dynamic viscosity
ρ	Water density
ρ_s	Density of soil particle

Acknowledgements

This research was funded by the Delhi Technological University, New Delhi, India. Data availabilityThe data used in this research article is experimental data conducted in the Hydraulics Laboratory of the Civil Engineering Department, Delhi Technological University New Delhi, India.

References

[1] Tang H-W, Ding B, Chiew Y-M and Fang S-L 2009 Protection of bridge piers against scouring with tetrahedral frames. *Int. J. Sedim. Res.* 24: 385–399

[2] Pu J H, Wallwork J T, Khan M, Pandey M, Pourshahbaz H, Satyanaga A, Hanmaiahgari P R and Gough T 2021 Flood suspended sediment transport: Combined modelling from dilute to hyper-concentrated flow. *Water (Switzerland)* 13: 1–24

[3] Pandey M, Jamei M, Karbasi M, Ahmadianfar I and Chu X 2021 Prediction of maximum scour depth near spur dikes in uniform bed sediment using stacked generalization ensemble Tree-based frameworks. *J. Irrig. Drain. Eng.* 147: 04021050

[4] Pandey M, Valyrakis M and Qi M *et al.* 2021 Experimental assessment and prediction of temporal scour depth around a spur dike. *Int. J. Sedim. Res.* 36: 17–28

[5] Reza Namaee M and Sui J 2019 Local scour around two side-by-side cylindrical bridge piers under ice-covered conditions. *Int. J. Sedim. Res.* 34: 355–367

[6] Laursen E M and Arthur T 1956 Scour around bridge piers and abutments. Iowa Highway Research Board, Ames

[7] Breusers H N C, Nicollet G and Shen H W 1977 Local scour around cylindrical piers. *J. Hydraul. Res.* 15: 211–252

[8] Yanmaz A M and Altinbilek H D 1991 Study of time-dependent local scour around bridge piers. *J. Hydraul. Eng.* 117: 1247–1268

[9] Kothyari U C and Kumar A 2010 Temporal variation of scour around circular bridge piers. *ISH J. Hydraul. Eng.* 16: 35–48

[10] Melville B W 1997 Pier and abutment scour: Integrated approach. *J. Hydraul. Eng. ASCE* 123(2): 125–136
[11] Martfn-Vide J P, Hidalgo C and Bateman A 1998 Local scour at piled bridge foundations. *J. Hydraul. Eng.* 124: 439–444
[12] Melville B W and Chiew Y 1999 Time scale for local scour at bridge piers. *J. Hydraul. Eng.* 125(1): 59–65
[13] Richardson E V and Davis S R 2001 *Evaluating scour at bridges*
[14] Oliveto G and Hager W H 2002 Temporal evolution of clear-water pier and abutment scour. *J. Hydraul. Eng.* 128(9): 811–820
[15] Mia M F and Nago H 2003 Design method of time-dependent local scour at circular bridge pier. *J. Hydraul. Eng.* 129: 420–427
[16] Chang W, Lai J, Yen C and Asce F 2004 Evolution of scour depth at circular bridge piers. *J. Hydraul. Eng.* 130(9): 905–914
[17] Melville B W 2007 Local scour at bridge abutments. *J. Hydraul. Eng.* 118: 615–631
[18] Arneson L A, Zevenbergen L W, Lagasse P F and Clopper P E 2012 *Evaluating scour at bridges*
[19] Jain R, Lodhi A S, Oliveto G and Pandey M 2021 Influence of cohesion on scour at piers founded in clay–sand–gravel mixtures. *J. Irrig. Drain. Eng.* 147: 04021046
[20] Coleman S E 2005 Clearwater local scour at complex piers. *J. Hydraul. Eng.* 131(4): 330–334
[21] Ataie-Ashtiani B and Aslani-Kordkandi A 2012 Flow field around side-by-side piers with and without a scour hole. *Eur. J. Mech. B/Fluids* 36: 152–166
[22] Amini D, Ataie-ashtiani B and Beheshti A 2018 Prediction of current-induced local scour around complex piers: Review, revisit, and integration. *Coast. Eng.* 133: 43–58
[23] Muzzammil M and Gangadhariah T 2010 The mean characteristics of horseshoe vortex at a cylindrical pier. *J. Hydraul. Res.* 41: 285–297
[24] Muzzammil M, Alama J and Danish M 2015 Scour prediction at bridge piers in cohesive bed using Gene Expression Programming. In: *International conference on water resources, coastal and ocean engineering: Aquatic Procedia*. Elsevier B.V., pp 789–796
[25] Akilli H, Akar A and Karakus C 2004 Flow characteristics of circular cylinders arranged side-by-side in shallow water. *Flow Meas. Instrum.* 15: 187–197
[26] Sumner D, Wong S S T, Price S J and Païdoussis M P 1999 Fluid behaviour of side-by-side circular cylinders in steady cross-flow. *J. Fluids Struct.* 13: 309–338
[27] Heidarpour M, Afzalimehr H and Izadinia E 2010 Reduction of local scour around bridge pier groups using collars. *Int. J. Sedim. Res.* 25: 411–422
[28] Behzad A-A and Beheshti A A 2006 Experimental investigation of clear-water local scour at pile groups. *J. Hydraul. Eng.* 132(10): 1100–1104
[29] Peng W U, Faye H and Jueyi S U I *et al*. 2014 Impacts of ice cover on local scour around semi-circular bridge abutment. *J. Hydrodyn.* 26: 10–18
[30] Setia B 2008 Equilibrium scour depth time. In: *3rd IASME / WSEAS Int. Conf. on Water Resources, Hydraulics & Hydrology (WHH '08),* University of Cambridge, UK,. pp 114–117
[31] Sarker A 1998 Flow measurement around scoured bridge piers using Acoustic-Doppler Velocimeter (ADV). *Flow Meas. Instrum.* 9: 217–227
[32] Coleman B S E and Melville B W 2001 Case study: New Zealand bridge scour experiences. *J. Hydraul. Eng.* 127: 535–546
[33] Wu P, Hirshfield F and Sui J 2015 Armour layer analysis of local scour around bridge abutments under ice cover. *River Res. Appl.* 31: 736–746
[34] Hafez Y I 2016 Mathematical modeling of local scour at slender and wide bridge piers. *J. Fluids* 2016: 1–19
[35] Pandey M, Zakwan M, Khan M A and Bhave S 2020 Development of scour around a circular pier and its modelling using genetic algorithm. *Water Sci. Technol. Water Supply* 20: 3358–3367
[36] Qi M, Li J and Chen Q 2018 Applicability analysis of pier-scour equations in the field: Error analysis by rationalizing measurement data. *J. Hydraul. Eng.* 144: 04018050

JMEPEG
https://doi.org/10.1007/s11665-022-07020-y
©ASM International
1059-9495/$19.00

TECHNICAL ARTICLE

Characterization of Residual Stresses in Conventional Forming and Hydroforming of Tailor Welded Blanks

Amit Kumar, Ravi Kumar Digavalli, Vijay Gautam, and Hariharan Krishnaswamy

Submitted: 14 September 2021 / Revised: 16 March 2022 / Accepted: 4 May 2022

Residual stresses in sheet metal components depend on the forming technique and the history of load path changes during the process. Characterization of residual stresses in the case of tailor welded blanks (TWBs) is challenging due to the differences in thickness and/or plastic deformation behavior within the blank. In the present work, the forming outcome is evaluated based on the final residual stress distribution in the formed TWB specimens. The methodology is demonstrated by biaxial stretching of TWBs of interstitial-free (IF) steel and draw quality (DC01) steel under two different processing routes (conventional forming and hydroforming). The numerically predicted residual stresses are observed to be lower and more uniformly distributed in the case of hydroforming when compared to conventional forming. The negligible residual stresses (or less tensile near the weld zone) in the hydroformed parts can be advantageous in the automotive industry leading to an improved life. The weld zone properties play an insignificant role in the distribution of predicted residual stress in biaxial stretching of TWBs. The numerically predicted results are validated experimentally using the x-ray diffraction technique. The agreement between numerical and experimental results is better in hydroforming than in the case of conventional forming.

Keywords finite element simulation, hydroforming, residual stress, sheet metal forming, tailor welded blanks

1. Introduction

Residual stresses play a vital role in determining the life span of sheet metal components, especially in the automotive applications. During a deformation process, the residual stresses in a component are the resultant internal stresses that arise due to stored elastic energy upon the removal of deforming loads or temperature gradients. The service life of a component depends upon the residual plastic strain retained in the component post-forming (Ref 1, 2). The tensile residual stresses in the component are pernicious when subjected to static or dynamic loads and can result in its early failure (Ref 3, 4). On the other hand, compressive residual stresses are beneficial for the components subjected to fluctuating stresses since the fatigue failure initiates at the locations of high shear and tensile stresses. Therefore, researchers engineered ways to impart the compressive residual stresses into the mechanical components (Ref 5-7).

Residual stresses resulting from sheet metal forming have been reported by several researchers. Hariharan et al. (Ref 8) reported that the forming stresses were relieved in the central zone of the formed low carbon steel samples due to the release of elastic energy during springback in biaxial stretching. Barlat's 1989 yield criterion predicted the residual stresses more accurately than Hill's 1948 yield criterion. Bruni et al. (Ref 9) determined springback and residual stresses in hydroformed parts made using TRIP800 steel and FeP04 steel sheets of thickness 1.5 mm. Higher pressure, friction and lower corner radius increased the plastic strain at the die corners with a drop in springback. Krux et al. (Ref 10) determined the residual stresses at the bottom of the deep-drawn cup formed using hydroforming of a low carbon steel sheet of thickness 1 mm. High residual stresses (compressive in nature) were observed at the exterior layer of the cup bottom. Kleiner et al. (Ref 11) studied the effect of fluid pressure on residual stresses at the sidewall as well as at the bottom of the cup drawn by the hydroforming process. Higher values of pressure led to lower axial and tangential residual stresses in the sidewall of the workpiece but there was no significant change in residual stress values at the bottom of the cup. Bedan et al. (Ref 12) performed incremental forming experiments on an aluminum alloy sheet and analyzed the influence of forming depth and rotating speed of the tool on residual stresses in the part. The residual stresses in the part increased with the depth and became more uniform with increase in the rotational speed. Tanaka et al. (Ref 13) conducted numerical studies on residual stresses in the sheet component manufactured by incremental stretch forming. During forming, when the deforming ball-tool slides on the sheet, tensile residual stress is induced in the upper layer and compressive in the lower layer. It was also observed that the tip radius of the forming tool has a significant influence on the induced residual stress.

As discussed above, most of the work on characterization of residual stresses in the formed parts is limited to monolithic blanks and literature on residual stresses in components

Amit Kumar and **Ravi Kumar Digavalli**, Department of Mechanical Engineering, Indian Institute of Technology Delhi, New Delhi 110016, India; **Vijay Gautam**, Department of Mechanical Engineering, Delhi Technological University, New Delhi 110042, India; and **Hariharan Krishnaswamy**, Department of Mechanical Engineering, Indian Institute of Technology Madras, Chennai 600036, India. Contact e-mails: amitk3551@gmail.com, dravi@mech.iitd.ac.in, vijaygautam@dce.ac.in, hariharan@iitm.ac.in.

Published online: 31 May 2022

manufactured from tailor welded blanks (TWBs) is scarce. A TWB consists of multiple blanks of different thickness and/or properties joined by laser welding prior to forming. TWBs are widely used in automotive sheet metal stamping due to the flexibility in design and the potential for reducing weight, cost and forming operations.

Characterization of residual stresses in aluminum alloy sheets joined by friction stir welding has been reported (Ref 14, 15). With the increase in welding speed, the peak residual stress increased due to a steeper thermal gradient during welding and lesser time for stress relaxation to occur (Ref 16). Clapham et al. (Ref 17) determined residual stresses in a laser-welded blank of dissimilar thickness (0.9 mm and 1.5 mm). The residual stresses were measured inducing uniaxial tensile pre-strains of 0.5%, 3% and 7%. Residual stress in the component along the weld zone was lower on 0.9 mm thick side and higher on 1.5 mm thick side of the welded blank due to the reduced force constraint on the thinner side of the weld zone. Costa et al. (Ref 18) determined the residual stresses on the surface as well as in the joints of two hot working tool steel sheets of thickness 4 mm with the help of x-ray diffraction and incremental hole drilling techniques. The tensile residual stresses were not completely relieved after grinding but were substantially reduced by heat treatment after the welding process. Anand et al. (Ref 19) performed fatigue tests on TWBs prepared using ultra-low carbon steel with and without zinc coating. The TWBs with zinc coating exhibited lower fatigue life than TWBs without zinc coating because of the intergranular cracking caused by the penetration of zinc into the surface of the sheet. The tensile residual stresses were present on the top surface of the sheets because of the solidification of the molten zinc on it. This could also be one of the possible reasons for the lower fatigue life of the coated TWBs. With the increase in the required amount of stress to cause the deformation, the residual stresses slow down the failure in the material (Ref 16). The complex stress state due to geometry and deformation path does not allow complete release of the stored energy in some sheet metal parts resulting in residual stresses. For instance, Padmanabhan et al. (Ref 20) extracted a split ring from a deep-drawn cup made of TWB combining DP600 steel and DC04 steel. They reported that springback of 10-mm-wide split ring was more than that of 20-mm-wide ring. Similarly, Gautam et al. (Ref 21) showed that the residual stresses during V-bending is sensitive to the punch radius.

It may be inferred that the accuracy of residual stress prediction is closely related to the accuracy of springback prediction. The springback prediction is influenced by the choice of yield criteria and hardening models, chord modulus and contact friction. The above effects are further complicated in a TWB. The earlier studies (Ref 22, 23) showed that the effect of considering the weld zone properties in the material model on the overall formability prediction of steel sheets was minimal. However, the prediction of residual stresses with and without weld zone properties in the case of TWBs subjected to unconventional forming techniques such as hydroforming has not been reported in the literature.

The objective of the present work is to critically evaluate residual stresses in a TWB forming process. In order to minimize the influence of geometry and strain path on the accuracy of springback prediction, a simple hemispherical cup shape has been used in the present work. Due to growing importance of unconventional forming techniques in manufacturing, the efficiency of hydroforming process in the distribution of residual stresses in a TWB is evaluated and is compared with the conventional forming. The numerical simulation was performed using a commercially available finite element code. The stress distribution post-springback is assumed to be the residual stress and is validated using the experimental data measured using the x-ray diffraction method.

2. Selection of Materials, Fabrication of TWBs and Mechanical Properties

In the present study, TWBs were prepared from interstitial-free (IF) steel sheets of four different thicknesses—0.7, 0.8, 1.2 and 1.4 mm and draw quality (DC01) steel sheets of three thicknesses—0.5, 1.0, and 1.5 mm due to their applications in the automotive industry for the fabrication of the vehicle body components. The flow curves and the mechanical properties of the parent sheets of IF steel and DC01 steel were determined by uniaxial tensile tests and reported in the earlier work (Ref 24, 25), respectively, and they are used in the present work. The average uniaxial tensile properties and Lankford coefficients of IF steel and DC01 steel sheets were also reported in Ref 24, 25, respectively.

The preparation of the TWBs of IF steel sheets of three different thickness combinations (0.8-0.8, 0.8-1.2 and 0.7-1.4 mm) and DC01 steel sheets of two different thickness combinations (0.5-1.0 mm and 0.5-1.5 mm) has already been reported by Kumar et al. (Ref 25, 26), respectively. In both the cases, the weld integrity was checked by conducting uniaxial tensile tests on the specimens with the weld zone perpendicular to the longitudinal direction. The obtained results were analyzed, and it was observed that the failure occurred on the thinner side of the joint indicating sound weld integrity.

The weld zone properties of welded blanks of IF steel of all the three thickness combinations were determined using a miniaturized tensile specimen by Gautam et al. (Ref 21) and Kumar et al. (Ref 26), and the same properties are used in the present work. However, the tensile properties of TWBs of DC01 steel are determined in the present work. To determine the tensile properties of the weld zone of TWBs of DC01 steel, specimens with a special geometry as proposed by Cheng et al. (Ref 27) were used (shown in Fig. 1). The specimen width in the gauge portion is 1.5 mm. Since the width of the weld zone is 1.5-2.0 mm, this specimen geometry ensures that the properties of the weld zone alone are obtained from these tests. Cutting of the specimens was done using a CO_2 laser of power 3 kW. Three tensile specimens were tested for each thickness combination to confirm repeatability of results. Initial

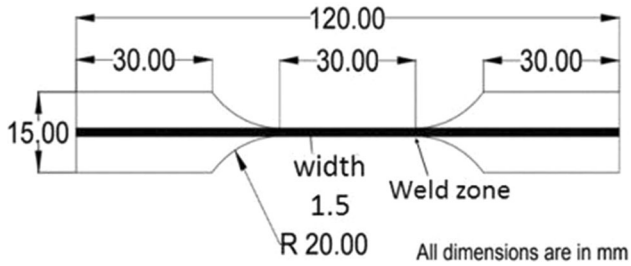

Fig. 1 Tensile specimen used for testing weld zone properties of laser-welded DC01 steel sheet (Ref 27)

and final lengths of the specimen were measured using vernier caliper of least count 0.01 mm to find out the total% elongation.

The flow curves for weld zone of both the TWBs of DC01 steel, shown in Fig. 2, are fitted using power law of strain hardening $\sigma = K\varepsilon^n$ (σ-true stress and ϵ-true strain, n-strain hardening exponent and K-strength coefficient), and the tensile properties are tabulated in Table 1. The low% elongation and n-values of the weld zone specimens of both the steels indicate that they have lower ductility and strain hardening ability when compared to the parent sheets. It was observed that yield strength (YS) and ultimate tensile strength (UTS) of the welded specimens are higher when compared to the parent sheets indicating that the material is stronger in the weld zone.

3. Prediction of Residual Stresses by Finite Element Analysis in Stretch Forming of TWBs

Numerical investigation of stretch forming of TWBs of IF and DC01 steels was carried out using a FEM software, DYNAFORM-LS-DYNA. Two strategies were used to model the weld zone: (i) a simplified weld zone representation by constraining the overlapping nodes of both the plates along the weld line (Ref 25) and (ii) a separate weld zone of finite width with an independent constitutive relation for mechanical behavior (shown in Fig. 3). In the preprocessor of the software, in order to ignore the elastic deformation of the tools-die and blank holder, they were modeled as rigid bodies. A stepped blank holder was modeled to ensure complete contact of the TWB blank in both the sides of weld line. In the simulation of conventional forming, a cylindrical punch of radius 25 mm with a hemispherical top was modeled. The welded blanks of dimensions 110 mm × 110 mm were meshed using Belytschko–Tsay shell elements. The mesh element size was taken as 2 mm, and the thickness of the elements was taken as the thickness of the parent sheets. Nine integration points were considered in modeling the TWB. The through thickness stress distribution is not linear, and often more number of integration points is required to simulate springback accurately. Wagoner et al. (Ref 28) used up to 51 through thickness integration points for spring back analysis. Nguyen et al. (Ref 29) showed that around 7 through thickness integration points are sufficient for simpler shapes. In the present work, 9 through thickness integration points were considered in modeling the TWB. The weld region thickness was taken to be the mean thickness of the parent sheets. The width of the weld region was taken to be 1.5 mm. The thickness difference between the joining blanks in butt configuration reflected on one side of the TWB, the other side remained flat.

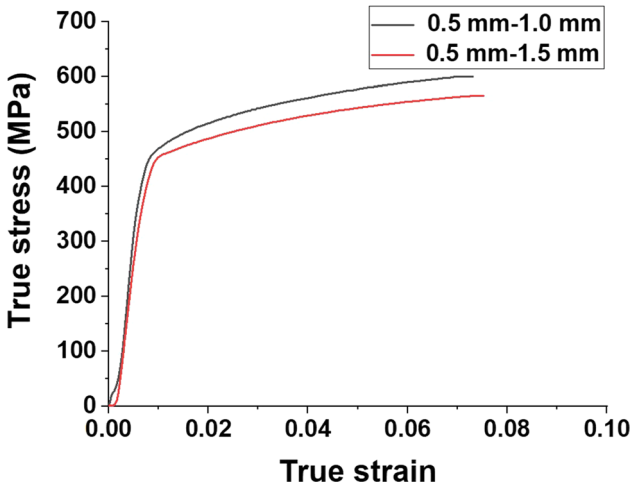

Fig. 2 Flow curves of the weld region of TWBs of DC01 steel sheets of thickness combinations—0.5-1.0 mm and 0.5-1.5 mm

The coefficient of friction of 0.04 (Ref 30) was assumed between the punch and the welded blank in conventional forming. The present analysis assumes constant coefficient of friction. The friction coefficient, however, is sensitive to applied pressure and velocity. The influence of friction coefficient on residual stresses needs further work and is beyond the scope of present manuscript. A blank holding force in the range of 80 to 100 kN was applied to prevent draw-in during forming. In hydraulic bulging, a clamping force in the range of 360 to 400 kN was defined. The optimum clamping force was iteratively arrived based on trial experiments. In simulations of hydraulic bulging, the pressure vs time path was defined linearly. In order to define a specific region on the blank for application of fluid pressure, masking was done over this particular region of the welded blank while defining the boundary conditions. As shown in Fig. 3, the area within the circular boundary line (shown in black color) was subjected to fluid pressure.

The constitutive behavior of the material is modeled assuming Barlat's Yld89 yield criterion (Ref 31) and Hollomon hardening law. To represent the strain hardening behavior of the parent sheets and the weld zones of IF steel and DC01 steel, the power law of strain hardening $\sigma = K\varepsilon^n$ was used and the experimentally determined n and K values were given as input to define the flow curves. Simulations were carried out up to a dome height of 12.50 mm for IF steel and 11.50 mm for DC01 steel to keep the deformation of the central region of the welded blanks in the uniform deformation zone for all the cases.

3.1 Springback Prediction in Stretch Forming of Tailor Welded Blanks

To numerically predict the components of the residual stresses on the outer surface of the deformed TWB in DYNAFORM software, the springback simulations of deformed TWBs were performed. The top layer of the deformed TWB was selected and at different points perpendicular to the weld region, and residual stresses were determined. Barlat 89 yield criterion with isotropic hardening was used for springback prediction (Ref 32). The springback process involves strain path change that might require complex isotropic-kinematic hardening models. However, it was shown by Lee et al (Ref 33) that apart from hardening models, there are multiple factors such as chord modulus, friction coefficient that might influence the results. It was also shown that the error due to isotropic hardening assumption is not significant. Therefore, the present work adopted the basic isotropic hardening assumption. Nevertheless, the methodology proposed in the present work is independent of the constitutive equation and can be deployed for any other complex models. Displacement constrained was imposed on eight locations in the flange region away from the deformed portion as shown in Fig. 4(a). The biaxially formed TWBs were unloaded, and the residual stresses were predicted after the springback at the weld zone and on either side of the

Table 1 Uniaxial tensile properties of weld region of TWBs of DC01 steel

Thickness combination, mm-mm	Yield strength, YS, MPa	Ultimate tensile strength, UTS, MPa	Total elongation, %	Strain hardening exponent, n	Strength coefficient, K, MPa
0.5-1.0	341±19	490±31	11.8±1.6	0.15±0.02	788±30
0.5-1.5	429±18	521±3	10.9±0.9	0.10±0.01	851±31

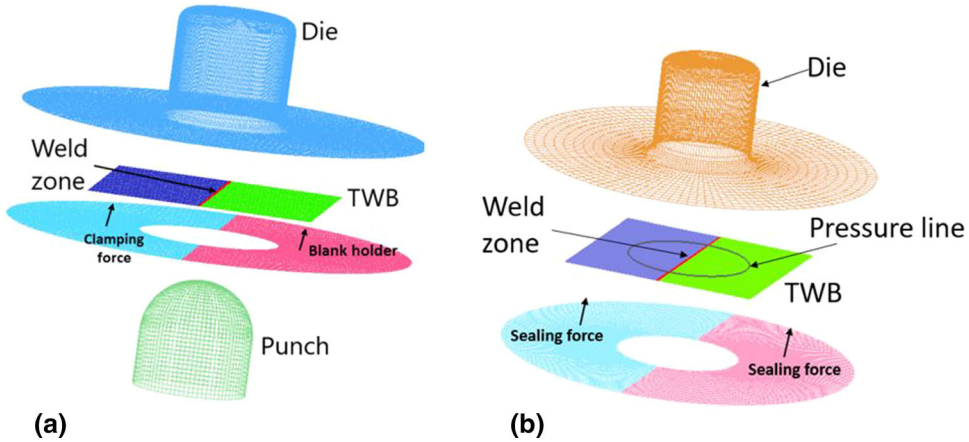

Fig. 3 FE model of the upper die, blank holder, and tailor welded blank (with weld zone) in the simulation of (a) conventional stretch forming and (b) hydraulic bulging

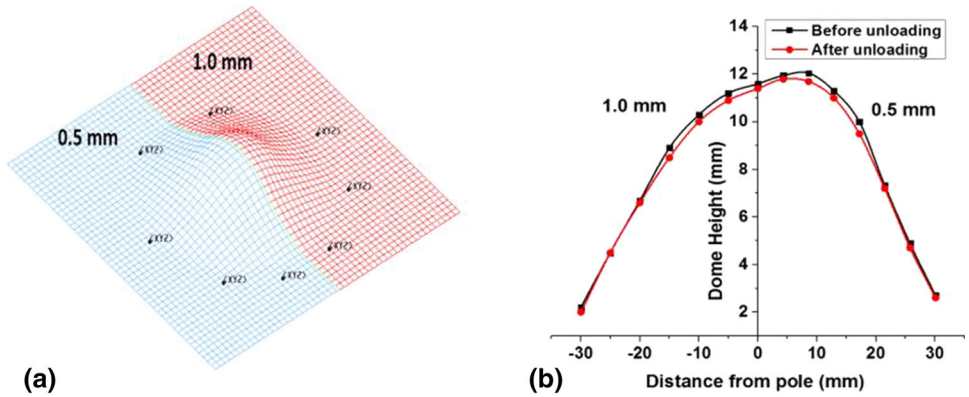

Fig. 4 (a) Nodal constraints on a deformed TWB 0.5-1.0 mm in springback simulation and (b) profiles of a deformed TWB 0.5-1.0 mm before and after unloading

weld zone. The profiles of a deformed TWB before and after unloading are shown in Fig. 4(b).

4. Stretch Forming Experiments

The conventional stretch forming and hydraulic bulge tests on TWBs of IF steel and DC01 steel sheets of all the thickness combinations were conducted to validate the predicted values in FE simulations. Figure 5(a) shows the experimental setup used for carrying out the conventional stretch forming experiments. The setup comprises of die, blank holder and hemispherical bottom cylindrical punch of diameter 50 mm. Initially, a circular grid pattern of 2.5 mm diameter was marked on the surface of the welded blanks with the help of a laser grid marking machine. The welded blank was kept between the upper die (blank holder) and the lower die along with the thin shim (placed on thinner side) so that the blank holder makes the uniform contact on either side of the weld zone. In order to reduce the friction between the punch and the welded blank, Teflon sheet of thickness 0.5 mm thickness was used. The blank holding force applied in conventional forming experiments was in the range of 80 to 100 kN. In order to maintain uniformity in all the conventional forming experiments, a punch speed of 2 mm/min was used. After a few trial experiments, the tests were successfully stopped at the predetermined dome heights. The dome height was measured by using an vernier height gauge with a least count of 0.01 mm.

Figure 5(b) shows the setup for carrying out hydroforming experiments on the welded blanks. The setup comprises of a die (with a cavity radius of 25 mm), a blank holder and a pressure amplifier for producing high fluid pressure in order to

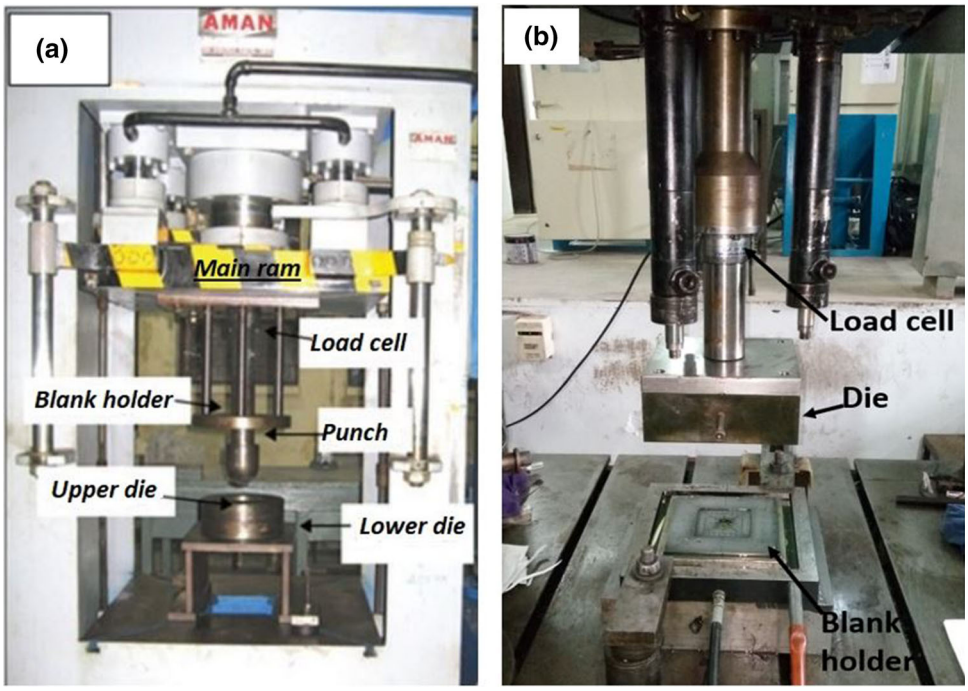

Fig. 5 Experimental setup of (a) conventional forming with a hemispherical punch of radius 25 mm and (b) hydraulic bulging

plastically deform the TWBs. The hydraulic press has been integrated with a data acquisition (DAQ) system in order to capture the pressure versus time plots by using LabVIEW software.

During the experiments, the fluid pressure was controlled between 14 and 17 MPa and a constant sealing force of 360 to 400 kN was applied. Time for complete cycle for which the fluid pressure remains was in the range of 12-15 s. In order to find the peak fluid pressure needed for all the thickness combinations to achieve a predetermined dome height, a few trial experiments were conducted. At this instant, the peak fluid pressure for DC01 steel TWBs of both the combinations was found to be 14.7 MPa (for 0.5-1.0 mm) and 15.1 MPa (for 0.5-1.5 mm) and the peak fluid pressure for IF steel TWBs of all the combinations was found to be 15.9 MPa (for 0.8-0.8 mm), 16.5 MPa (for 0.8-1.2 mm) and 14.8 MPa (for 0.7-1.4 mm).

4.1 Residual Stress Measurement

The residual stress measurements were carried out in the transverse direction after conventional and hydroforming of the TWBs using the x-ray diffraction technique using cos α method on the top surface of the specimens. This technique was used in the current study because of its ability to capture an entire Debye ring in one go with the help of the two-dimensional detector, thus neglecting the need of the multiple sample tilts (Ref 34). When an x-ray beam falls on the top surface of a specimen, it gets diffracted from all the crystals orientated in different directions. The diffracted beam forms a cone or a ring on a photographic plate (Ref 35). In this method, a set of four strains, ε_{α}, $\varepsilon_{\pi+\alpha}$, $\varepsilon_{-\alpha}$ and $\varepsilon_{\pi-\alpha}$ are determined for each α. Two subtractions of strains are used to calculate the following two strain parameters.

$$\varepsilon_{\alpha 1} = [(\varepsilon_{\alpha-}\varepsilon_{\pi+\alpha}) + (\varepsilon_{-\alpha} - \varepsilon_{\pi-\alpha})]/2 \quad \text{(Eq 1)}$$

$$\varepsilon_{\alpha 2} = [(\varepsilon_{\alpha-}\varepsilon_{\pi+\alpha}) - (\varepsilon_{-\alpha} - \varepsilon_{\pi-\alpha})]/2 \quad \text{(Eq 2)}$$

It has to be noticed that the above two parameters are calculated using the relative difference of radii. They are not dependent on the stress-free value of the radii and that makes it very important to reduce errors in stress determination. For the case of in-plane biaxial stresses, i.e., $\sigma_z = 0$, the first strain parameter at the rotation angle $\psi_0 = 0$ is given by following equation (Ref 36),

$$\varepsilon_{\alpha 1} = \frac{-1+v}{E}\sigma_x \sin 2\psi_0 \sin 2\eta \cos\alpha \quad \text{(Eq 3)}$$

where E is elastic modulus, v is the Poisson's ratio, 2η is the angle made by the incident ray with the diffracted ray, ψ_0 is the angle made by incident x-ray with the surface normal to the specimen, and $\varepsilon_{\alpha 1}$ is the strain at azimuthal angle α. All the angles are shown in Fig. 6.

Along the perpendicular direction to the weld zone, residual stress (in MPa) was measured by using Eq 4 (Ref 36).

$$\sigma_x = -\left(\frac{E}{1+v}\right)\left(\frac{1}{\sin 2\eta \sin\psi_0}\right)\left(\frac{\partial\varepsilon_{\alpha 1}}{\partial\cos\alpha}\right) \quad \text{(Eq 4)}$$

where $\frac{\partial\varepsilon_{\alpha 1}}{\partial\cos\alpha}$ is the slope of the linear relation between $\varepsilon_{\alpha 1}$ and cosα.

In order to eliminate the manufacturing history effect on the experimental results, the residual stress measurements were also carried out on as-welded TWBs and the x-component of the residual stress was determined. The difference would give the evolution of residual stress due to the forming process. The setup used for carrying out the residual stress measurements comprises of a sensor unit, and a small specimen holder to keep the welded specimen as shown in Fig. 7(a). A welded specimen before and after deformation is shown in Fig. 7(b) with the transverse direction in which the measurement of residual stresses was carried out.

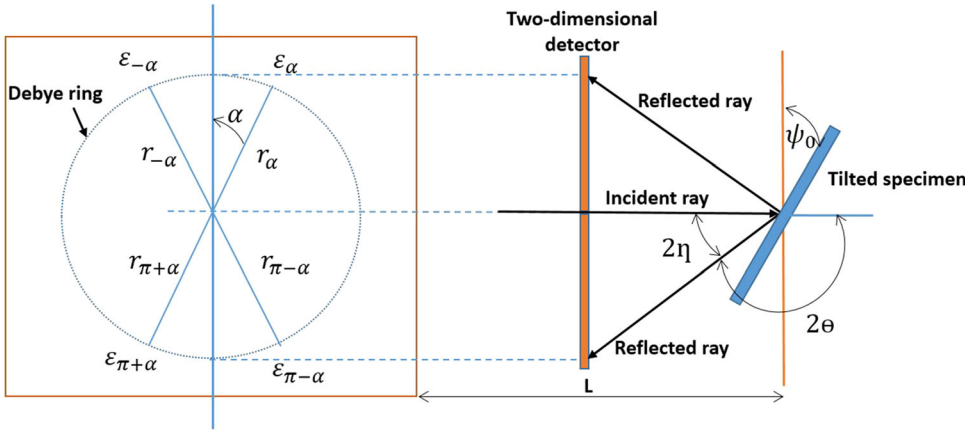

Fig. 6 Measurement of strains using Debye ring

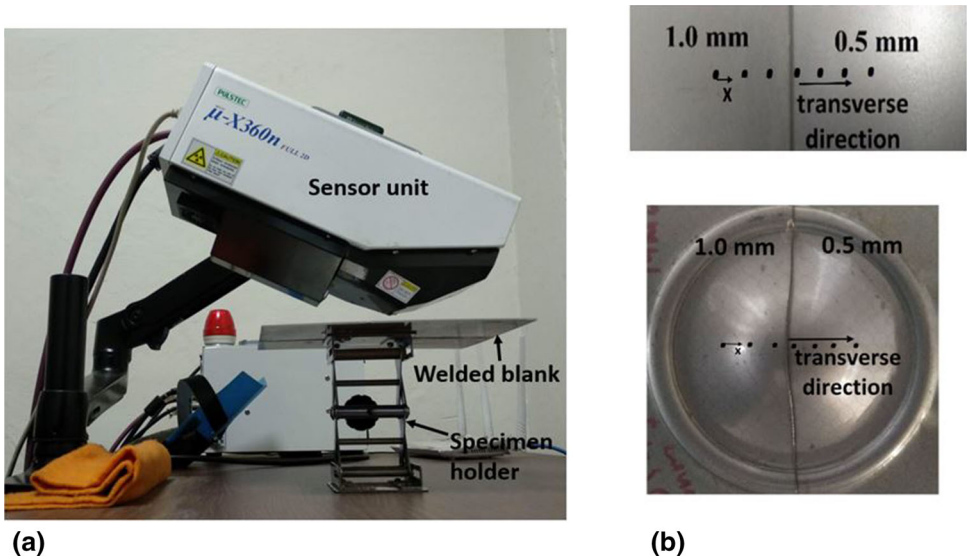

Fig. 7 (a) The experimental setup used for measurement of stresses in welded blanks before and after forming and (b) as-welded and deformed TWB samples

The sensor unit consists of an x-ray tube that produces the x-rays by utilizing a voltage of 30 kV and a current of 1 mA. A beam of wavelength 2.29 A^0 was used, and the target material in x-ray tube was chromium. The time taken for the measurement of the residual stress at each point was 90 s. For each thickness combination, three samples were considered for the measurement and the stresses were measured at an interval of 5 mm. On each sample, at seven different points, the residual stresses were measured (one at the weld zone and three points each on both sides of the weld region). At each point, three readings were taken and the average values were reported.

5. Results and Discussion

5.1 Residual Stresses in As-Welded Blanks

The pattern of the residual stresses in as-welded blanks of IF steel with respect to distance from the weld region on either side of TWB are already presented in (Ref 26), and they are not shown in this research paper. The pattern of the residual stresses in as-welded blanks of DC01 steel with respect to distance from the weld region on either side of TWB are shown in Fig. 8. The residual stress data represent an x-component of stress (perpendicular to the weld line). In the case of welded blanks of dissimilar thickness combinations, the residual stress pattern is asymmetrical with respect to the weld line. The residual stress on the thicker side is found to be higher in comparison with the thinner side of the welded blank, as expected from the trend reported previously in the literature. The higher residual stress on thicker side is due to the larger restrictions provided by the thicker side to the contraction of the molten weld pool during its solidification (Ref 17). Tensile residual stress is observed near the weld zone. The weld zone or near to the weld zone is subjected to heating and cooling during the joining of the blanks of the similar or dissimilar thickness. During solidification, tensile residual stresses are induced due to shrinkage of the weld region (Ref 17). With increase in the distance from the weld region, the residual stress (tensile) decreased, thus balancing the high tensile residual stress near the weld region (Fig. 8). The residual stresses were not measured at the weld region because the diffracted rays from the weld region give

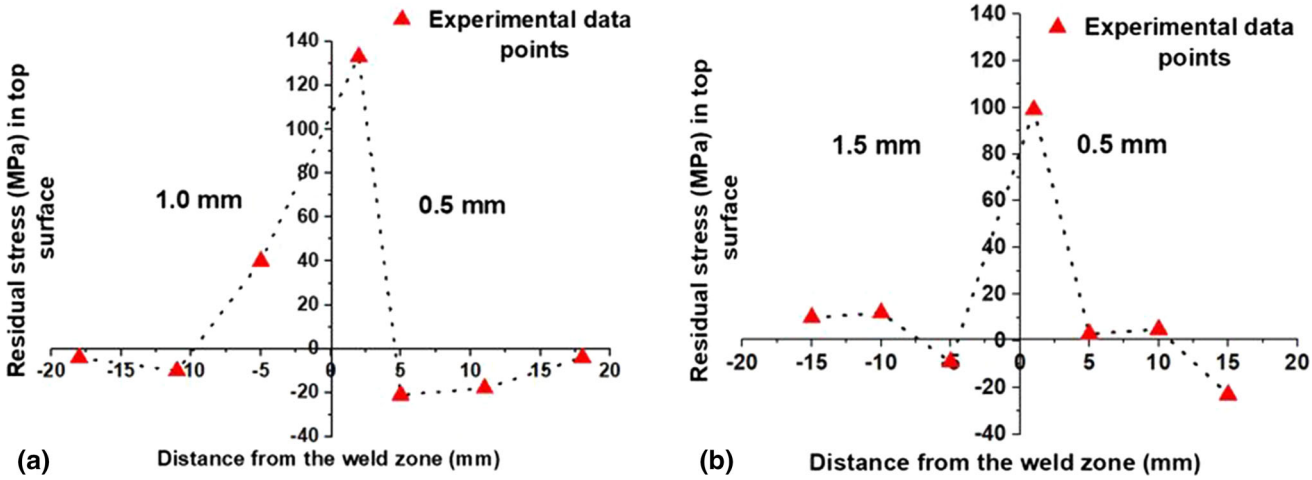

Fig. 8 Residual stress plots in TWBs of DC01 steel with thickness variation (a) 0.5-1.0 mm and (b) 0.5-1.5 mm

very low-intensity peaks (Ref 17). The residual stresses in DC01 steel are higher at and near the weld zone when compared to stresses in IF steel, and it could be because of the larger yield strength and ultimate tensile strength of DC01 than in the case of IF steel (Ref 24, 25). The maximum residual stress near the weld zone decreased from 130 MPa in the case of 0.5-1.0 mm to 100 MPa in the case of 0.5-1.5 mm (i.e., a decrease of 23%).

5.2 Residual Stresses in Deformed Welded Blanks of IF Steel and DC01 Steel

The residual stress patterns predicted by FE simulations after springback in stretch formed samples of IF steel by both conventional and hydroforming are shown in Fig. 9 for TWBs of similar and dissimilar thickness combinations, respectively. The residual stress patterns predicted in stretch formed samples of IF steel by conventional forming are already presented in Ref 26. For comparison, the predicted stress patterns before springback are also shown in the figures. In all these results, weld zone properties have been incorporated in the simulations. In the case of the same thickness combination, it can be observed in Fig. 9(a) and (b) that the stresses (before unloading) are comparable on either side of the weld region because of which deformation on both sides was observed to be equal. However, in the case of dissimilar thickness combinations, the stresses (before unloading) are observed to be higher on the thinner side of the welded blanks because of thinner side deformed largely as compared to the thicker side in both conventional forming and hydroforming as shown in Fig. 9(c)–(f). In the case of DC01 steel, the results for welded blanks of dissimilar thickness variation are shown in Fig. 10. The springback releases the stored elastic energy due to which residual stresses are generated in the weld region and on either side of the weld region (Ref 14). In FE predictions of conventional stretch forming of TWBs, it has been observed that, in the central region of the dome, the residual stresses are tensile and decreased with an increase in the distance from the weld zone and became nearly zero or compressive near the edges. In the case of hydroforming, the predicted residual stresses are more uniform and lower than in the case of conventional forming and in some locations, they are negligible or zero, especially in the central portion of the dome, and they became slightly compressive with an increase in the distance from the weld zone. It is also observed that the stresses (after unloading) are almost equal on either side of the weld region because of the constraint at the weld region provided by thicker side on the thinner side. At final stage of the conventional forming of TWB, there is a nonuniformity in stress distribution over the top surface of the dome. However, in hydroforming, the stresses have been observed to be more uniform due to the uniform hydrostatic pressure applied during the process. The nonuniformity of the stresses in conventional forming is because of the friction involved between the welded blank and the tool. Hence, after the springback, more nonuniformity is observed in the residual stresses in the case of conventional forming when compared to hydroforming. The uniform and negligible residual stresses (or less tensile near the weld zone) in hydroformed parts can be advantageous in the automotive industry leading to improved fatigue life.

Prediction of the stresses in FE analysis of stretch forming of welded blanks without considering the weld zone showed a similar trend to those obtained with considering the weld zone properties with only a marginal change in the values as shown in Fig. 11 for the TWBs with dissimilar thickness combinations. In the case of DC01 steel, the predicted results are shown in Fig. 12. Overall, it can be said that the consideration of the weld zone properties has only a marginal effect on the predicted values of the stresses before and after springback in FE analysis of biaxial stretching of welded blanks.

In the case of FE analysis of conventional forming of IF steel TWBs, it has been observed that, with an increase in the thickness ratio from 1 (0.8-0.8 mm) to 1.5 (0.8-1.2 mm) and 2 (0.7-1.4 mm), the residual stresses values in weld region have slightly increased. This could be because of the larger constraint imposed in weld region by the thicker zone on the thinner zone in the case of welded blank with a higher thickness ratio. However, the influence of thickness ratio on the stresses after springback has been found to be smaller in the hydroforming of TWBs. The influence of thickness ratio on stresses after springback is not visible in the case of DC01 steel, and it could be because of the larger variation of the mechanical properties among the sheets of different thicknesses of DC01 than in the case of IF steel.

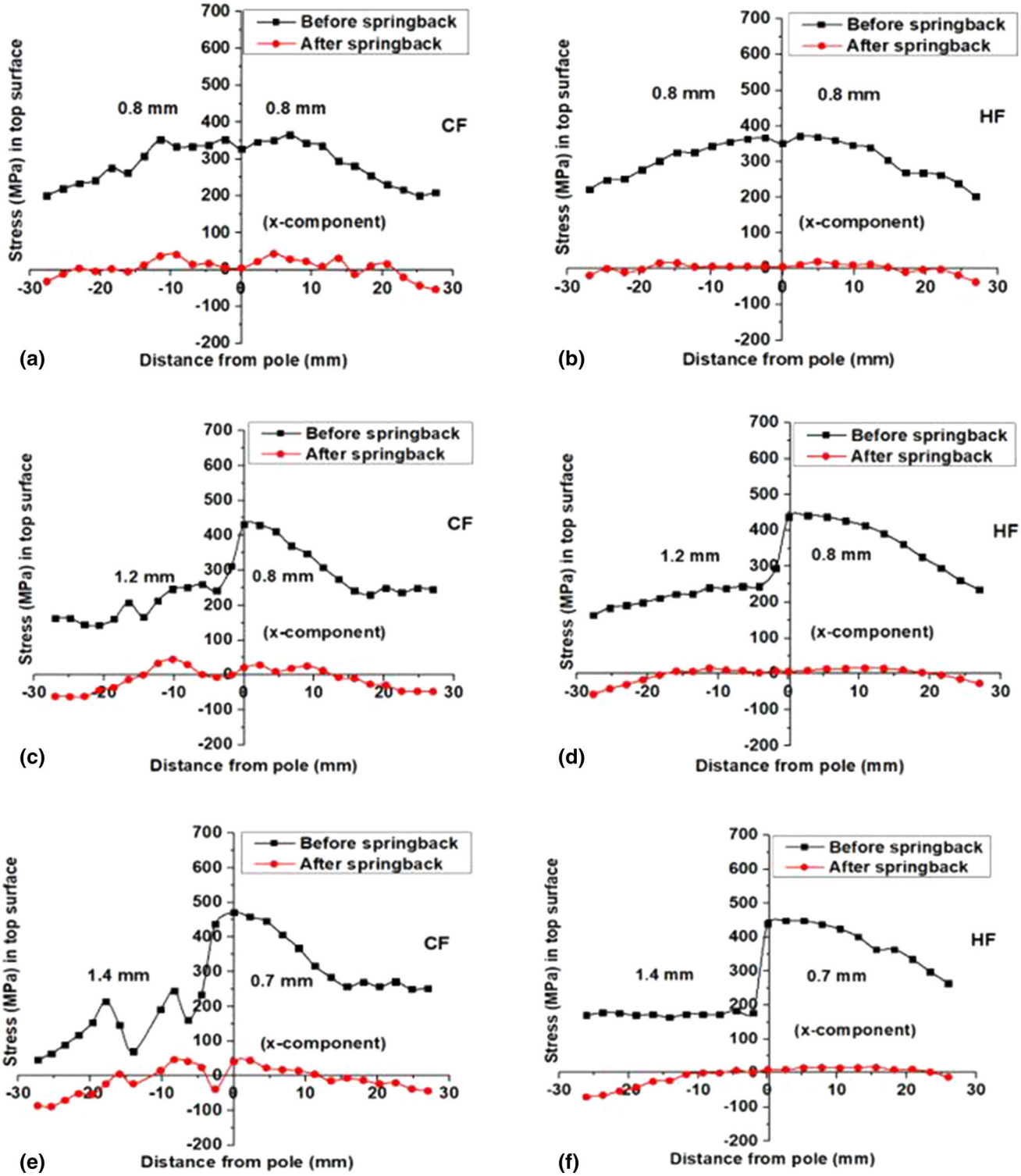

Fig. 9 Predicted stress patterns (x-component) in stretch forming of TWBs of IF steel considering the weld zone at a dome height of 12.50 mm: (a) CF (0.8-0.8 mm) (Ref 26), (b) HF (0.8-0.8 mm), (c) CF (0.8-1.2 mm) (Ref 26), (d) HF (0.8-1.2 mm), (e) CF (0.7-1.4 mm) (Ref 26) and (f) HF (0.7-1.4 mm). CF-conventional forming; HF-hydroforming

5.3 Comparison of Predicted and Experimental Residual Stresses

The residual stresses have been determined experimentally in the transverse direction in TWBs of both the materials for validation of the predicted values, and a comparison is presented for all the thickness combinations of IF steel in Fig. 13. Experimental results are compared with simulation results with and without considering the weld zone. The experimental results for DC01 steel are shown in Fig. 14. The residual stresses that arose pose conventional forming, as

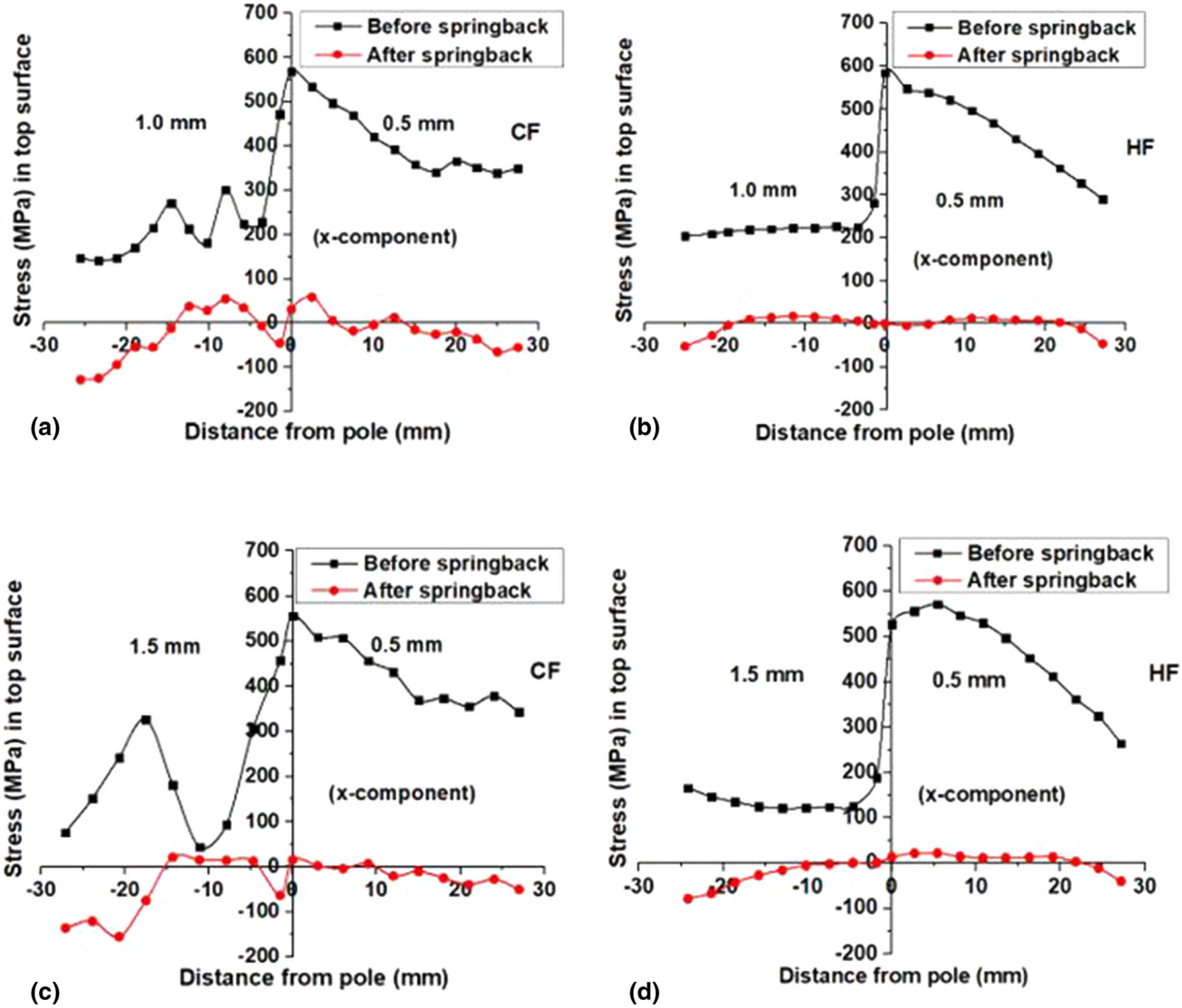

Fig. 10 Predicted stress patterns (x-component) in stretch forming of TWBs of DC01 steel considering the weld zone at a dome height of 11.50 mm: (a) CF (0.5-1.0 mm), (b) HF (0.5-1.0 mm), (c) CF (0.5-1.5 mm) and (d) HF (0.5-1.5 mm). *CF* conventional forming; *HF* hydroforming

expected was nonuniform against the relatively uniform and lower value of residual stresses post-hydroforming.

The predicted residual stresses, in general, have matched well with the experimental data but in hydroforming, the agreement is better than in the case of conventional forming. The better agreement in hydroforming could possibly be due to the absence of friction between the punch and blank. In the case of conventional forming, the assumed value of average friction coefficient can induce nonuniform stress distribution and subsequently influence the residual stresses. In both the steels, the maximum difference between the experimental and the predicted residual stress values is observed in the central portion of the dome.

The role of weld line modeling (merging of interface nodes or an explicit weld zone region) on the predictive capability of residual stresses needs attention to enable best practices of FEA modeling. In order to compare the weld zone representation, the predicted residual stresses are plotted against the experimental results in Fig. 15. A line of slope equivalent to unity is superposed in the scatter plot. The deviation from the unit slope line quantifies the accuracy of prediction. Following the above discussion, the scatter plot indicates that the deviation of residual stress prediction in conventional forming is higher than that of hydroforming. However, it is important to note that either in conventional forming or in hydroforming, the modeling of weld region did not play a significant role. Both

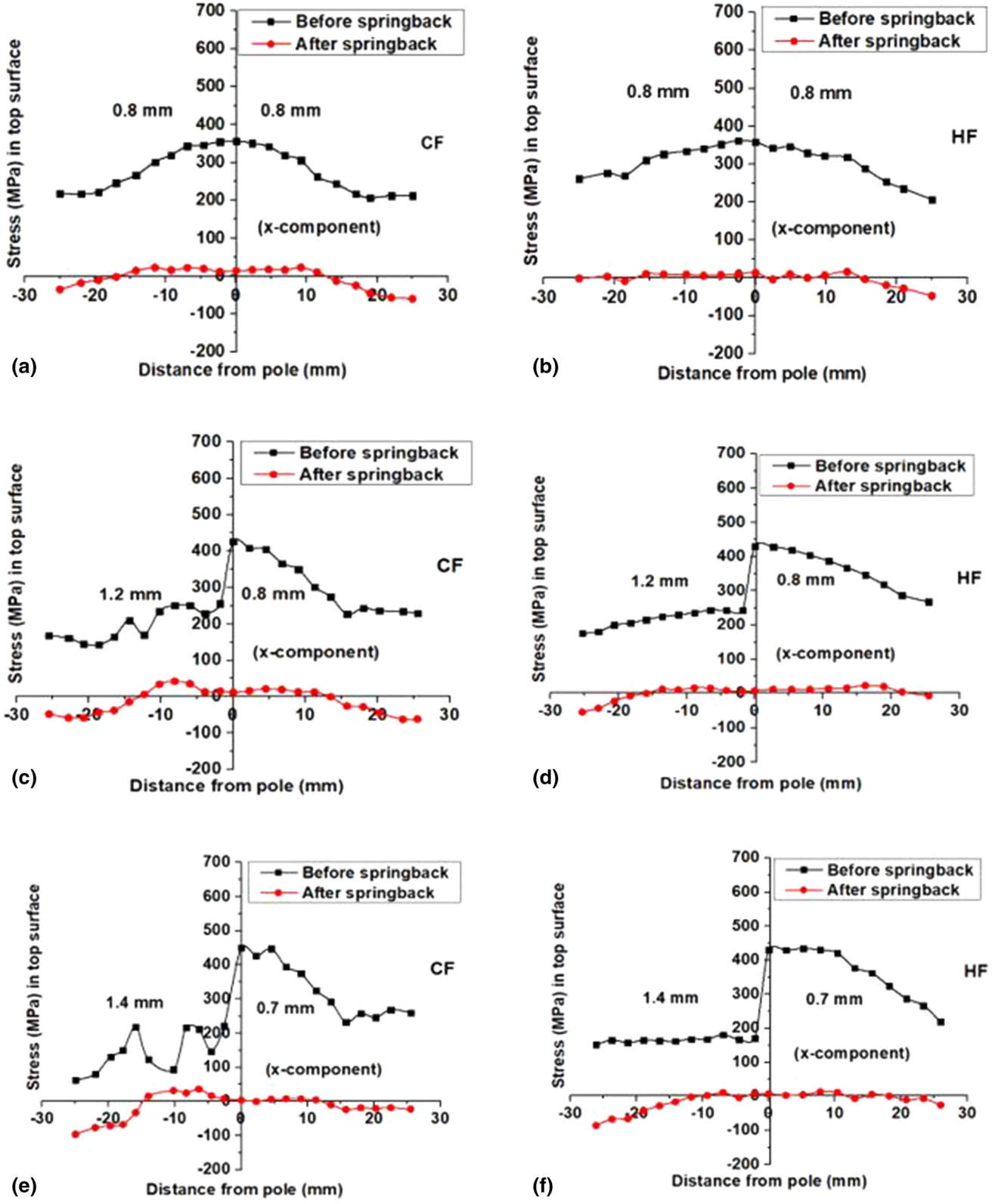

Fig. 11 Predicted stress patterns (x-component) in stretch forming of TWBs of IF steel without considering the weld zone at a dome height of 12.50 mm: (a) CF (0.8-0.8 mm), (b) HF (0.8-0.8 mm), (c) CF (0.8-1.2 mm), (d) HF (0.8-1.2mm), (e) CF (0.7-1.4 mm) and (f) HF (0.7-1.4 mm). *CF* conventional forming; *HF* hydroforming

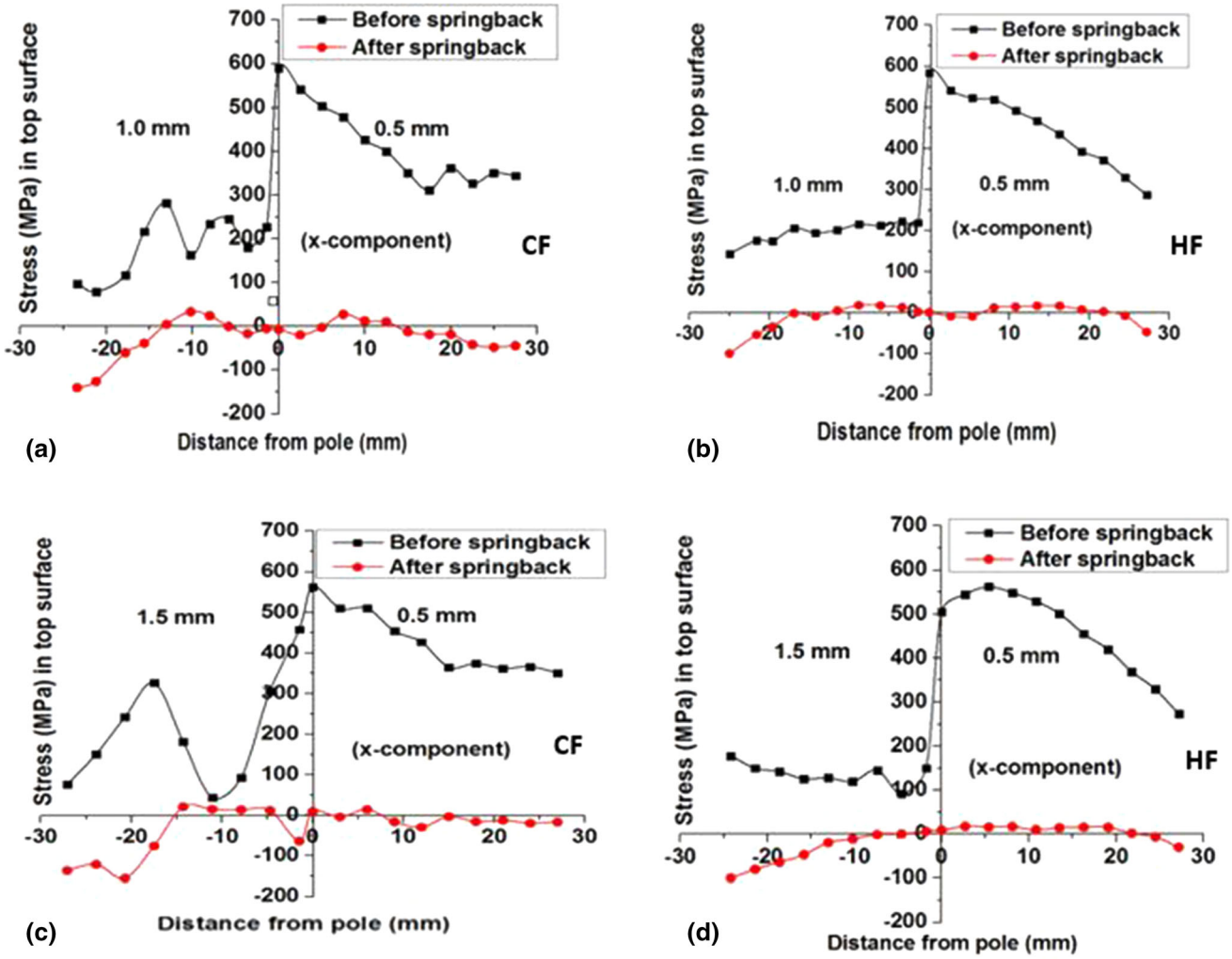

Fig. 12 Predicted stress patterns in stretch forming of TWBs of DC01 steel without considering the weld zone at a dome height of 11.50 mm: (a) CF (0.5-1.0 mm), (b) HF (0.5-1.0 mm), (c) CF (0.5-1.5 mm) and (d) HF (0.5-1.5 mm). *CF* conventional forming; *HF* hydroforming

the simplified rigid merge of common nodes and an explicit model of weld region showed similar scatter from the experiment in all the conditions. Therefore, based on the geometries and material properties analyzed in the present work, it is concluded that a simplified weld representation is sufficient for predicting residual stresses in TWB.

The better agreement between the prediction and experiments for TWB processed through two different processing routes gives confidence to adapt the residual stresses as a qualifying criterion for sheet components instead of empirically defined maximum reduction in thickness. It is proposed in future to develop qualifying criteria using residual stresses to match the functional requirements for each component.

The real benefit of hydroforming over conventional forming of TWBs can be further analyzed by studying the difference in the residual stresses between these two routes, as shown in Fig. 16. The difference is obtained by subtracting the residual stress post-hydroforming from in the corresponding values in conventional forming. The difference is positive in the central region of dome, in most of the cases (both DC and IF) indicating that the hydroformed TWBs exhibited least residual stress post-forming. The difference is maximum in the TWBs with thickness ratio equivalent to unity. As the thickness ratio (higher: smaller) increased, the difference in the residual stresses decreased. The distribution of the difference is asymmetrical from the center. In the case of dissimilar thickness, the difference is higher on the thicker side than the thinner side. This stems from the nonuniform distribution of residual stress in conventional forming as compared to hydroforming (shown in Fig. 13 and 14). Unlike hydroforming which attempts to induce uniform strain distribution in both thinner and thicker side, the thicker side in conventional forming resists plastic deformation in conventional forming resulting in nonuniform residual stresses (Fig. 13 and 14). Thus for a wider range of thickness ratio and two different steel grades, the hydroforming processes not only induce relatively lower residual stresses, but also improve the homogeneity of residual stress distribution.

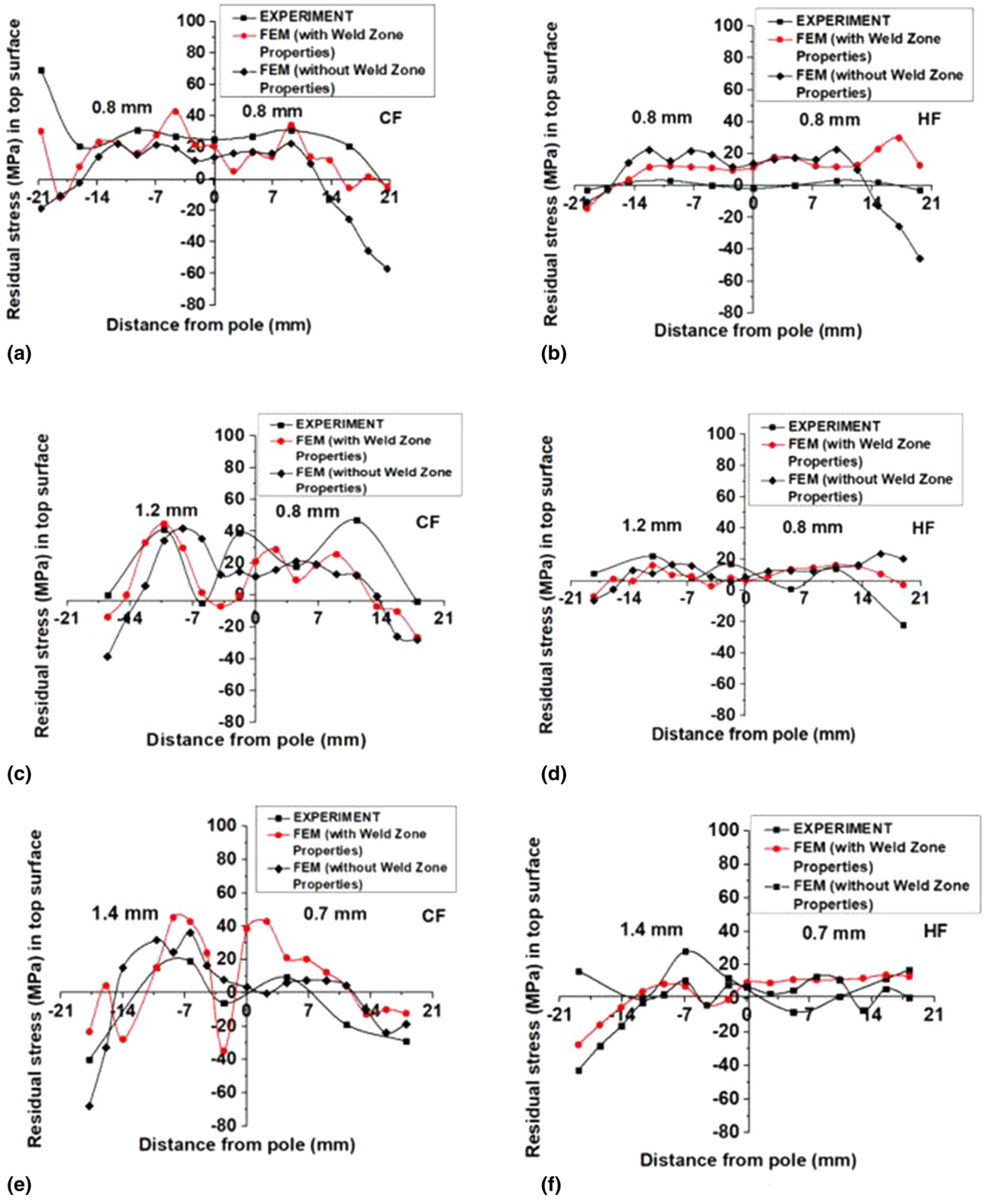

Fig. 13 Comparison of predicted and experimental residual stress patterns in TWBs of IF steel at a dome height of 12.50 mm: (a) 0.8-0.8 mm (CF), (b) 0.8-0.8 mm (HF), (c) 0.8-1.2 mm (CF), (d) 0.8-1.2 mm (HF), (e) 0.7-1.4 mm (CF) and (d) 0.7-1.4 mm (HF). CF-conventional forming; HF-hydroforming

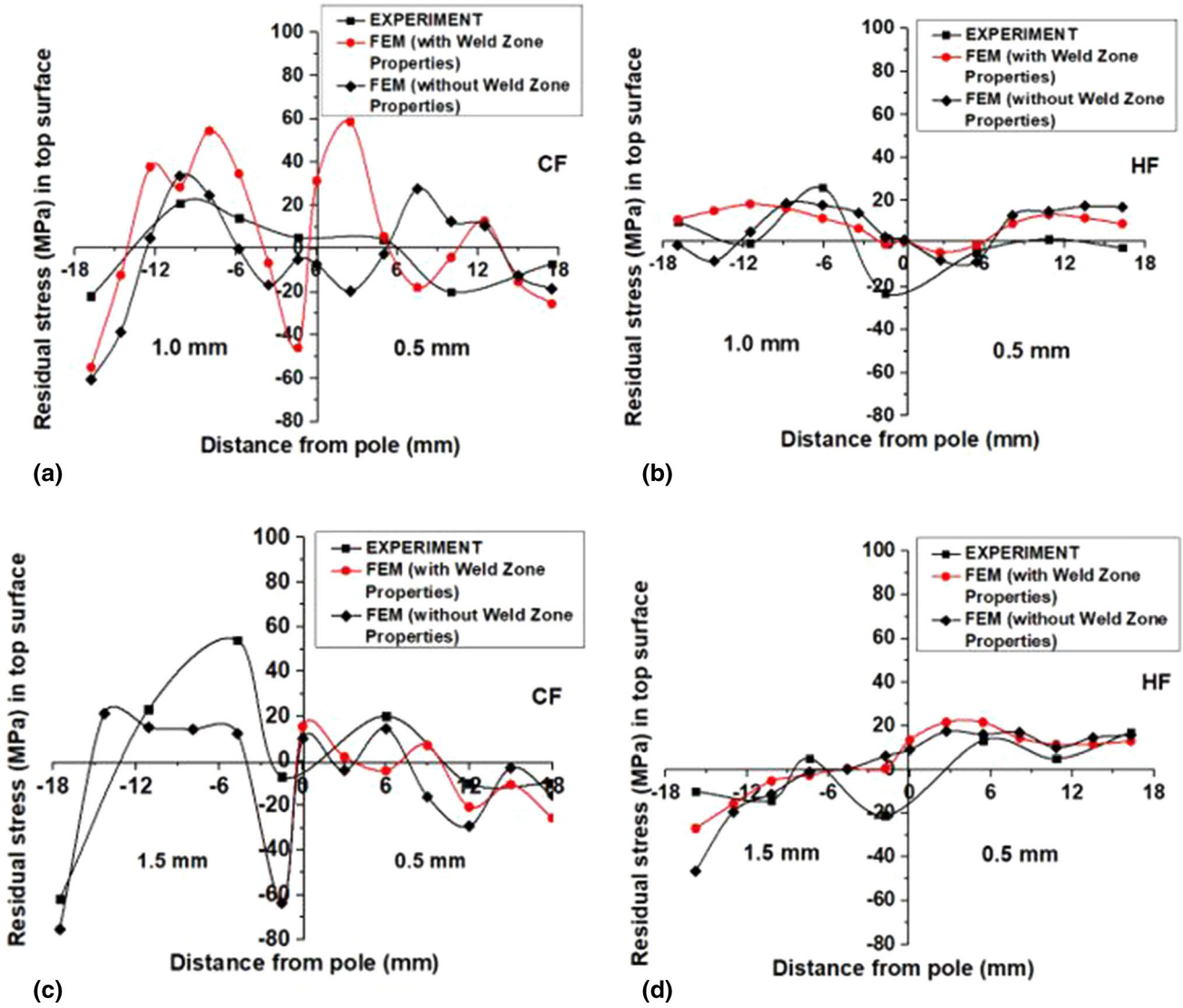

Fig. 14 Comparison of predicted and experimental residual stress patterns in TWBs of DC01 steel at a dome height of 11.50 mm: (a) 0.5-1.0 mm (CF), (b) 0.5-1.0 mm (HF), (c) 0.5-1.5 mm (CF) and (d) 0.5-1.5 mm (HF). *CF* conventional forming; *HF* hydroforming

6. Conclusions

The following are the main findings from the present work:

1. In the initial TWBs of same thickness combination (prior to forming), tensile residual stress is observed near the weld line and it changed to compressive away from the weld zone. In the case of TWBs of different thickness combination, the residual stress on the thicker zone is higher as compared to the thinner zone of the welded blank.
2. In the numerical analysis of stretch forming of TWBs, tensile residual stress has been observed in the central region of the dome and decreased with the distance from the weld zone and became nearly zero or compressive near the edges. In hydroforming, the predicted residual stresses have been found to be more uniform and lower than in the case of conventional forming. The uniform and negligible residual stresses (or less tensile near the weld zone) in hydroformed parts can be advantageous in the automotive industry leading to improved fatigue life.
3. The simplified rigid merge of common nodes and an explicit model of weld region showed similar scatter from the experiments in all the conditions. Therefore, it is concluded that a simplified weld representation is sufficient for predicting residual stresses in TWBs.
4. The agreement between the predicted and experimental residual stresses is better in hydroforming than in the

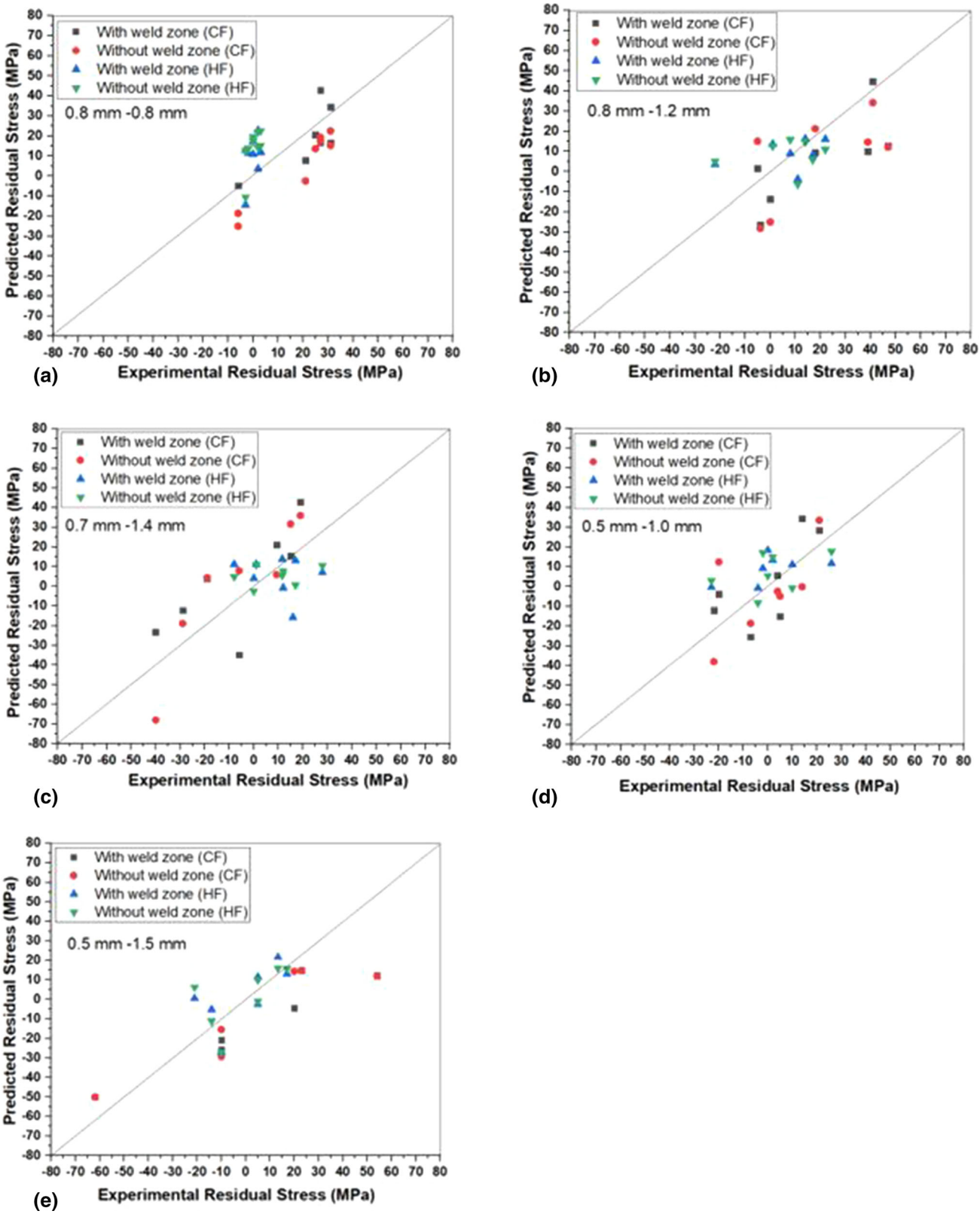

Fig. 15 Comparison between the experimental and the predicted residual stress values in conventional and hydroforming (with and without weld zone) for the TWBs (a) 0.8-0.8 mm (IF), (b) 0.8-1.2 mm (IF), (c) 0.7-1.4 mm (IF), (d) 0.5-1.0 mm (DC01) and (e) 0.5-1.5 mm (DC01)

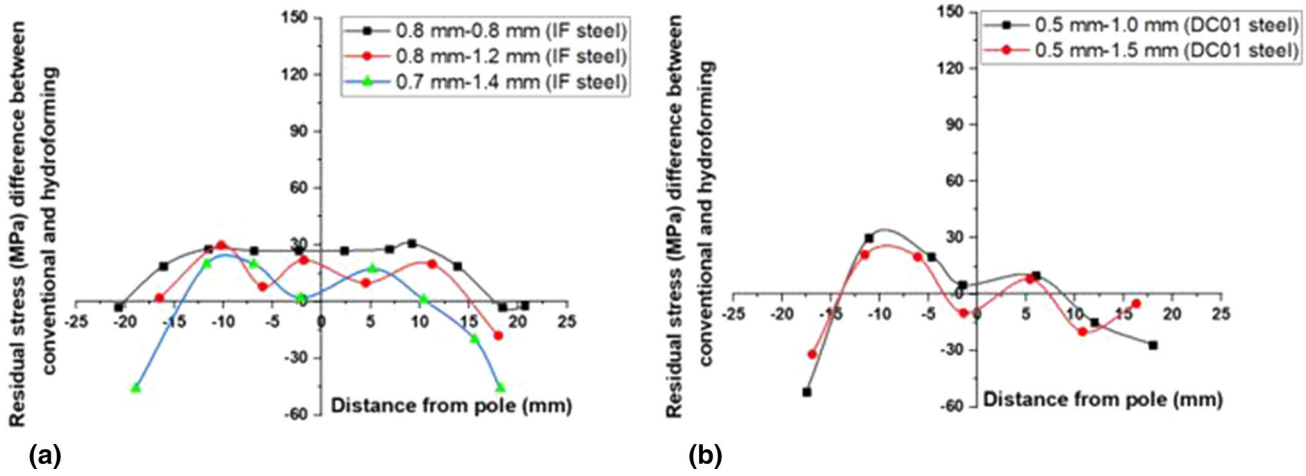

Fig. 16 Experimental residual stress difference between the conventional and hydroforming processes for the TWBs of (a) IF steel and (b) DC01 steel

case of conventional forming. For TWBs of low carbon steel with difference in thickness and grade, the hydroforming process not only induces relatively lower residual stresses, but also improves the homogeneity of residual stress distribution.

Funding

The first author would like to acknowledge the assistantship received from the Ministry of Human Resource Development (MHRD), Government of India, for his research work.

Conflict of interest

The author(s) declared no potential conflicts of interest concerning the research, authorship and/or publication of this article.

References

1. K. Hariharan and R.V. Prakash, Integrating Effect of Forming in Fatigue Life Prediction: review of Present Scenario and Challenges, *Proc. Inst. Mech. Eng. Part B: J. Eng. Manuf.*, 2012, **226**(6), p 967–979
2. A.M. Paradowska, J.W. Price, T.R. Finlayson, R.B. Rogge, R.L. Donaberger and R. Ibrahim, Comparison of Neutron Diffraction Residual Stress Measurements of Steel Welded Repairs with Current Fitness-for-Purpose Assessments, *Pressure Vessels and Piping Conference*, 2008, The American Society of Mechanical Engineers, p 603–612
3. V. Gautam, D.R. Kumar and S. Konar, Experimental and Numerical Characterization of Residual Stresses in Tailor Welded Blanks After Springback, *Advances in Simulation, Product Design and Development*. M. Shunmugam, M. Kanthababu Ed., Springer, Singapore, 2020, p 79–92
4. R. Kumar, G. Kumar, V. Gautam and S. Konar, Experimental and Numerical Assessment of Residual Stresses in AA6061 After Surface Treatment by Deep Cold Rolling, *Advances in Computational Methods in Manufacturing*. R.G. Narayanan, S.N. Joshi, U.S. Dixit Ed., Springer, Singapore, 2019, p 95–108
5. A. Kromm, J. Dixneit and T. Kannengiesser, Residual Stress Engineering by Low Transformation Temperature Alloys-State of the Art and Recent Developments, *Weld. World*, 2014, **58**(5), p 729–741
6. W.M. Sim, Residual Stress Engineering in Manufacture of Aerospace Structural Parts, *Technical Report of COMPACT Project 6th European Framework Programme*, Airbus SAS, Filton, UK, 2009
7. J. Altenkirch, A. Steuwer, P. Withers, S. Williams, M. Poad and S. Wen, Residual Stress Engineering in Friction Stir Welds by Roller Tensioning, *Sci. Technol. Weld. Join.*, 2009, **14**(2), p 185–192
8. K. Hariharan, R.V. Prakash, M.S. Prasad and G.M. Reddy, Evaluation of Yield Criteria for Forming Simulations Based on Residual Stress Measurement, *Int. J. Mater. Form.*, 2010, **3**(4), p 291–297
9. C. Bruni, M. Celeghini, M. Geiger and F. Gabrielli, A Study of Techniques in the Evaluation of Springback and Residual Stress in Hydroforming, *Int. J. Adv. Manuf. Technol.*, 2007, **33**(9–10), p 929–939
10. R. Krux, M. Kleiner, and W. Homberg, Residual Stress distribution in the Workpiece Bottom in High Pressure Sheet Metal Forming, *Proceedings. 8th ESAFORM Conference in Material Forming*, 2005, p 459–462
11. M. Kleiner, R. Krux and W. Homberg, Analysis of Residual Stresses in High-Pressure Sheet Metal Forming, *CIRP Ann. – Manuf. Technol.*, 2004, **53**(1), p 211–214
12. A.S. Bedan, S. Mohammed and M. Kamal, The Effects of Process Parameters on Residual Stresses in Single Point Incremental Forming of A1050 Aluminium Using ANOVA Model, *Eng. Technol. J.*, 2017, **35**(1), p 41–48
13. S. Tanaka, T. Nakamura, K. Hayakawa, H. Nakamura, and K. Motomura, Residual Stress in Sheet Metal Parts Made by Incremental Forming Process, *AIP Conference Proceedings: American Institute of Physics*, 2007, p 775–780
14. P. Staron, M. Kocak, S. Williams and A. Wescott, Residual Stress in Friction Stir-Welded Al Sheets, *Physica B*, 2004, **350**(1–3), p 491–493
15. M. Peel, A. Steuwer, M. Preuss and P.J. Withers, Microstructure, Mechanical Properties and Residual Stresses as a Function of Welding Speed in Aluminium AA5083 Friction Stir Welds, *Acta Mater.*, 2003, **51**(16), p 4791–4801
16. P.J. Withers and H. Bhadeshia, Residual Stress. Part 1–Measurement Techniques, *Mater. Sci. Technol*, 2001, **17**(4), p 355–365
17. L. Clapham, K. Abdullah, J.J. Jeswiet, P.M. Wild and R. Rogge, Neutron Diffraction Residual Stress Mapping in Same Gauge and Differential Gauge Tailor-Welded Blanks, *J. Mater. Process. Technol.*, 2004, **148**(2), p 177–185
18. J.M. Costa, J.T.B. Pires, F. Antunes, J.P. Nobre and L.P. Borrego, Residual Stresses Analysis of ND-YAG Laser Welded Joints, *Eng. Fail. Anal.*, 2010, **17**(1), p 28–37
19. D. Anand, D.L. Chen, S.D. Bhole, P. Andreychuk and G. Boudreau, Fatigue Behaviour of Tailor (Laser)-Welded Blanks for Automotive Applications, *Mater. Sci. Eng. A*, 2006, **420**, p 199–207
20. R. Padmanabhan, M.C. Oliveira, H. Laurent and J.L. Alves, Study on Springback in Deep Drawn Tailor Welded Blanks, *Int. J. Mater. Form.*, 2009, **2**(1), p 829–832

21. V. Gautam and D.R. Kumar, Experimental and Numerical Investigations on Springback in V-Bending of Tailor Welded Blanks of Interstitial Free Steel, *Proc. Inst. Mech. Eng. Part B: J. Eng. Manuf.*, 2017, **232**(12), p 2178–2191
22. K.M. Zhao, B.K. Chun and J.K. Lee, Finite Element Analysis of Tailor Welded Blanks, *Finite Elem. Anal. Des.*, 2001, **37**(2), p 117–130
23. F.I. Saunders and R.H. Wagoner, Forming of Tailor Welded Blanks, *Metall. Mater. Trans. A*, 1996, **27**, p 2605–2616
24. A. Kumar, V. Gautam and D.R. Kumar, Maximum Bulge Height and Weld line Displacement in Hydroforming of Tailor Welded Blanks, *J. Manuf. Sci. Eng.*, 2017, **140**(3), p 031005
25. A. Kumar and D.R. Kumar, Formability Prediction of Tailor Welded Blanks in Hydraulic Bulging using Flow Curves from Biaxial Tensile Tests, *Proc. Inst. Mech. Eng. Part L: J. Mater: Des. Appl.*, 2020, **235**(4), p 853–867
26. A. Kumar, V. Gautam, and D.R. Kumar, Prediction of Residual Stresses in Biaxial Stretching of Tailor Welded Blanks by Finite Element Analysis, *IOP Conf. Ser.: Mater. Sci. Eng.*, 2019, **651**, p 1–8
27. C.H. Cheng, M. Jie, L.C. Chan and C.L. Chow, True Stress-Strain Analysis Weldment of Heterogeneous Tailor Welded Blanks: A novel Approach for Forming Simulation, *Int. J. Mech. Sci.*, 2007, **49**(2), p 217–229
28. R.H. Wagoner and M. Li, Simulation of Springback: Through-Thickness Integration, *Int. J. Plast.*, 2006, **23**, p 345–360
29. V.T. Nguyen, Z. Chen and P.F. Thomson, Prediction of Springback in Anisotropic Sheet Metals, *J. Mech. Eng. Sci.*, 2004, **218**(6), p 651–661
30. S.A. Anup and M.T. Shete, Formability Analysis of Deep Drawing Process by Finite Element Simulation, *Int. J. Sci. Res.*, 2012, **3**(6), p 2153–2156
31. F. Barlat and K. Lian, Plastic Behaviour and Stretchability of Sheet Metals. Part I: A Yield Function for Orthotropic Sheet under Plane Stress Conditions, *Int. J. Plast.*, 1989, **5**, p 51–66
32. J.W. Lee, M.G. Lee and F. Barlat, Finite Element Modelling using Homogeneous Anisotropic Hardening and Application to Springback Prediction, *Int. J. Plast.*, 2012, **29**, p 13–41
33. J.W. Lee, F. Barlat and M.G. Lee, Constitutive and Friction Modelling for Accurate Springback Analysis of Advanced High Strength Steel Sheets, *Int. J. Plast.*, 2015, **71**, p 113–135
34. S. Taira, K. Tanaka and T. Yamasaki, A Method of X-Ray Microbeam Measurement of Local Stress and its Application to Fatigue Crack Growth Problems, *J. Soc. Mater. Sci.*, 1978, **27**(294), p 251–256
35. N. Kamura, T. Fujita and T. Sasaki, Evaluation of Rolling Contact Fatigue by X-ray Diffraction Ring, *NTN Tech. Rev.*, 2015, **83**, p 67–74
36. K. Tanaka, X-ray Measurement of Triaxial Residual Stress on Machined Surfaces by the cos α Method using a Two-Dimensional Detector, *J. Appl. Crystallogr.*, 2018, **51**(5), p 1329–1338

Publisher's Note Springer Nature remains neutral with regard to jurisdictional claims in published maps and institutional affiliations.

Proceedings of the Indian National Science Academy
https://doi.org/10.1007/s43538-022-00082-5

REVIEW ARTICLE

Communication between immune system and mycobiota impacts health and disease

Gunjan Sachdeva[1] · **Asmita Das**[1]

Received: 31 March 2022 / Accepted: 7 June 2022
© Indian National Science Academy 2022

Abstract
Fungi are the organisms present universally in the environment from ancient times. Being regarded as an essential part of human mycobiome either as commensals or as opportunistic pathogens they hold a spectacular place in our lives. Mycobiome is growing as a field of interest, but some questions still remain lurking like how fungi exactly modulate health and disease. Most of the studies focus on the interactions of the immune system with the bacterial and viral community rather than highlighting the communication with mycobiota. Crosstalk between the immune system and mycobiota have been found to be highly necessary for maintaining homeostasis, preventing susceptibility towards diseases, inducing immune tolerance, modulating microbial communities and generating signal responses by interacting with fungal molecular patterns. We are highlighting the latest advancement regarding the relationship of innate and adaptive branches of immunity with mycobiota, their role ranging from simple commensals to opportunistic pathogens and more importantly therapies designed to overcome fungal infections in this review.

Keywords Mycobiome · Commensals · Opportunistic pathogens · Immune system · Homeostasis · Therapeutic approaches

Introduction

Robert Urich quoted "*the health outside starts from inside*", which highlights the importance of all processes that take place inside a human body and account for a huge impact on their lives. Human body is a reservoir of a large number of microorganisms, their genomes, enzymes, and metabolites clubbed together and referred to as "Microbiome", which is further housed in various human organs. Whenever one hears about the microbiome, only bacteria are often picturized because, since long, they have occupied the centre of research**.** However, the microbiome doesn't only revolve around bacteria, it also consists of fungal, protozoan, parasitic, archaeal, and viral species that play significant roles even after staying behind curtains. *Mycobiome* (first voiced in 2009) "the fungal population" acquires only 0.1% of the total microbiome — counterbalance the number of bacterial species by being larger in size. (Qin et al. 2010) (Sam et al. 2017). They regulate health and disease significantly.

✉ Asmita Das
asmitadas1710@dce.ac.in

[1] Department of Biotechnology, Delhi Technological University, Delhi, India

Table 1 highlights the distribution of commensal and pathogenic fungi across various body sites, including skin, oral cavity, intestine, etc. Initially, fungal diversity was evaluated by culture-dependent methods, but the inability to culture most fungal species created a major barrier. However, Internal transcribed spacer (ITS) sequencing-based method (a culture-independent method) replaced conventional ones for identifying fungi. These ITS regions are fungal rDNA sequences that are highly divergent among different fungal species in terms of length and sequence, helps to categorize fungi at the species level (Underhill and Iliev 2014). Studies have documented that *maternal inheritance* has also been observed in the case of mycobiota apart from bacteriome. An infant's birth mode influences the prevalence of site-specific mycobiome: vaginally born infants have higher levels of *Candida albicans* on their skin, whereas those delivered by caesarean-section have *Candida orthopsilosis* dominantly in their oral cavity (Schei et al. 2017) (Ward et al. 2018). According to the observations, mycobiome is transmitted vertically to infants from mother. Infant mycobiota, on the other hand, can also be altered by nutrition; research are in progress to understand more about human milk mycobiome composition, as *C. albicans* has been reported in the breast milk of mothers suffering from mammary candidiasis (Ward et al. 2017).

Published online: 23 June 2022

Table 1 Mycobiota across different body sites

Mycobiota	Fungal microorganisms	Nature of fungal microorganisms
Oral mycobiota	***Candida spp.****	Commensal, opportunistic pathogen
	Cladosporium spp.	Commensal, opportunistic pathogen
	Aspergillus spp.	Commensal
	Saccharomyces spp.	Commensal
	Fusarium spp.	Commensal, opportunistic pathogen
	Aureobasidium spp.	Commensal, opportunistic pathogen
	Penicillium spp.	Commensal
	Pichia spp.	Commensal
	Cryptococcus spp.	Pathogen
Lung mycobiota	*Aspergillus spp.*	Commensal, opportunistic pathogen
	Candida spp.	Commensal, opportunistic pathogen
	Clavispora spp.	Commensal, opportunistic pathogen
	Cladosporium spp.	Commensal
	Pneumocystis spp.	Obligate lung commensals
	Wallemia spp.	Commensal
Intestinal mycobiota	***Candida spp.****	Commensal, opportunistic pathogen
	Saccharomyces spp.*	Commensal
	Fusarium spp.	Commensal, opportunistic pathogen
	Debaromyces	Rare fungal pathogen
	Penicillium spp.	Commensal
	Pichia spp.	Commensal
	Cladosporium spp.	Commensal
	Malassezia spp.	Commensal, opportunistic pathogen
	Cyberlindnera jadinii	Commensal
	Aspergillus	Commensal, opportunistic pathogen
Skin mycobiota	***Malassezia spp.****	Commensal, opportunistic pathogen
	Aspergillus spp.	Commensal, opportunistic pathogen
	Candida spp.	Commensal, opportunistic pathogen
Vaginal mycobiota	***Candida spp.****	Commensal, opportunistic pathogen
	Cladosporium spp.	Commensal
	Pichia spp.	Commensal
	Aspergillus spp.	Commensal, opportunistic pathogen
	Rhodotorula spp.	Commensal, opportunistic pathogen

*Bold text shows the abundancy of the particular fungi

Notably, Colonization of fungi in early life develops homeostasis and susceptibility towards diseases. For example, *Cladosporium* colonization generates a state of protection against allergies, but in contrast colonization of *C. albicans*, *Aspergillus*, and *Rhodotorula spp.* are associated with the risk of childhood atopy (Speakman et al. 2020). Altogether, more studies should be conducted to deduce the relationship between mycobiome inheritance and its persistence.

Identification of fungal microbes

In general, *Fungal Pathogen-Associated Molecular Patterns* (PAMPs), consists of several layers of carbohydrates (β-glucans, chitins, and mannans) that vary in proportion among numerous fungal species. Immune response can be developed by human pattern-recognition receptors (PRRs) after encountering microbe specific molecules (Gow et al. 2017) (Erwig and Gow 2016). Numerous studies quoted 3 important PAMPs— chitin's (polymers of N-acetylglucosamine) the size of which is significantly more important in *S. cerevisiae* to elicit an immunological response. Precisely, medium-sized chitin particles can induce IL-17 and TNFα production in the host. Alternatively, the small size chitin particles can induce anti-inflammatory responses (Da Silva et al. 2009). On the other hand, researches have shown that β-glucans (glucose polymers), specifically, β-1,3-glucans can interact with dectin-1 receptor which can further provoke an immune response against glucans. So far, no receptor for β-1,6-glucans (branches) has been recognized

in the host. In case of Mannans (chains of mannose residues linked to fungal proteins via N-linkage or O-linkage) that are identified by host dectin-2, and mincle receptors to control fungi in numbers (Borriello et al. 2020). Overall, fungal PAMPs are the main elicitors of immunity, any failure in their recognition can be a potential cause of disease.

Fungi and morphology

Fungi often cycle amid yeast and hyphal morphologies (dimorphism). Various resources have proven that the conversion occurs either due to variation in temperature, pH or oxygen concentration of the host that drives fungi to their pathogenic state. Specifically, authors highlighted that macrophages can induce phagocytosis on encountering *C. albicans* yeast form, but subsequent CO_2 production in macrophages promotes the transition to hyphal form**,** which eventually kills macrophages and ultimately disrupts the immune reactions (Hernández-Chávez et al. 2017). While in case of *Malassezia,* yeast form can survive as facultative intracellular parasite in keratinocytes by causing inhibition of inflammatory responses. However, sebaceous gland hyperactivity can induce morphological conversion *Malassezia* to hyphal form in *vivo*, which serves as an crucial basis for the development biofilms (Brand 2012). Meanwhile a study emphasizes that fungal morphology apart from inducing pathogenicity also governs T helper cell differentiation. For example, *C. albicans* yeast form, in *vivo,* induces TH17 responses while filamentous form induces the TH1 response. Contrastingly, in *vitro*, yeast form of *C. albicans,* via IL-12 induces TH1 response while hyphal form via IL-23 induces TH17 response (Speakman et al. 2020). Hence, these studies concluded that different morphologies are employed by fungal microbes in order to remain viable or pathogenic in host, but immune system keeps them in check.

Mycobiome and immunity

As discussed previously, Human body harbors various microorganisms, which maintains the human ecosystem through numerous interactions with the host. Fungal microbes are present all over the gut, lungs, skin etc., to maintain dynamics of host. In this part we will discuss about the receptors of host that communicate with fungi, crosstalk between immune cells and fungal species, other than that we will also examine the process of immune tolerance induced via mycobiota.

It is well documented that PRRs initiate an immune response after recognizing PAMPs of both pathogens and commensal microorganisms. C-type lectin receptors (CLRs), an antifungal PRR through Carbohydrate Recognition Domain (CRD) in the presence of calcium identify carbohydrate moiety (β-glucans, mannans) on fungal cells (Netea et al. 2015). Further, elicit innate immune response through integral immunoreceptor tyrosine-based activation motif (ITAM) or through FcRγ (Drickamer and Taylor 2015). Dectin-1 *(gene ClEC7A*), appears as an important CLR displayed on macrophages, mast cells, and dendritic cells which interacts with β-glucans present on fungal species (Saijo et al. 2010). Of utmost importance, Dectin-1 stimulates the release of cytokines associated with TH17, IL-22 which has anti-inflammatory as well as pro-inflammatory properties (A. et al. 2012). Evidences through studies disclosed that Dectin-1 gene polymorphism could increase the possibility of development of fungal diseases in patients who had undergone chemotherapy for acute myeloid leukemia. But more studies are required to refine about the relation of Dectin-1 gene with numerous fungal diseases (Fischer et al. 2016).

Dectin-2 *(gene CLEC6A),* another CLR expressed on dendritic cells, macrophages that recognize α-mannans in fungal cell wall and accelerates the release of cytokines through FcRγ and Syk-CARD9-NFκB signaling pathway. Clinical studies confirmed the presence of severe *C. albicans* infections in Dectin-2 knockout mice against the wild one. However, the response of dectin-2 deficient mice towards *C. neoformans* is normal indicating that mechanism of host defense is distinctive among different fungi. Another study by Saijo et al., validated that dectin-2 deficiency can enhance fungal load in kidney and subsequently lead to the development of hydronephrosis condition (Saijo et al. 2010). Apart from these, Cryptococcosis and aspergillosis are prominently reported in the individuals having dectin-2 polymorphism (Patin et al. 2019). Taken together, all these researches stress upon the significance of dectin-2 receptor in fungal infections.

Macrophage inducible C-type lectin (Mincle), distinctively recognizes mannans on fungal cell wall. Although they are not present on inactive macrophages rather their expression is stimulated by Macrophage C-type lectin (MCL) (Miyake et al. 2015). A study demonstrated that mincle can recognize *Malassezia spp*., *C. albicans* and potentiate the release of chemokines and cytokines against fungi. Their deficiency is often associated with *C. albicans* infections (Patin et al. 2019).

Toll-like Receptor (TLRs), another PRR serve as signaling receptor, are composed of two domains: N-terminal and C-terminal domain. Former one constitutes about 16–28 leucine-rich repeats, which recognize PAMPs while the latter one commences downstream signaling (Saijo et al. 2010). Multiple studies highlight distinctive functions of TLRs in recognition of fungus specific molecules, for example, TLR2 mainly recognizes fungal β-glucans and *C. albicans* phospholipomannans (PLMs) (Bourgeois and Kuchler 2012).

Moreover, they are also responsible for monocyte-mediated apoptosis of *C. albicans* through caspase 3 and caspase 8 (Dreschers et al. 2016). On the other hand, TLR4 interacts with *C. neoformans* glucuronoxylomannan (GXM) and *C. albicans* mannans (O-linked). However, *C. albicans* can cause systemic infections in TLR4 knockout mice by impairing neutrophil recruitment and chemokine responses. All apart, TLR6 overcome fungal species by inducing TH17 antifungal response. Furthermore, it has been demonstrated that any polymorphism in TLR-4, TLR-6 can cause aspergillosis (Skevaki et al. 2015). Meanwhile, other TLRs are also concerned with fungal genome detection like TLR-7 gets activated by single-stranded fungal RNA, while TLR3 interacts with double-stranded fungal RNA and TLR-9 recognizes the unmethylated fungal DNA (CpG) (Bourgeois and Kuchler 2012). Overall, TLRs had displayed their potential function in revealing the identity of fungal microbes and initiates various mechanisms to break the chain of fungal evasion.

Involvement of Nod-like receptors (NLRs) is required to detect internalized microbial components of PAMPs and to further induce inflammatory caspases, along with cytokines IL-1β and IL-18 (Pathakumari et al. 2020). Recent research indicates that *C. albicans's* morphological transition can activate both NLRP-3 and IL-1β. However, the authors also stated that NLRP-3 polymorphism can impair IL-1β production, which triggers the development of vulvovaginal candidiasis. Additionally, NLRP -/- mice had shown susceptibility towards *C. albicans* and *C. neoformans* infections (M. et al. 2017).

RIG-I-like Receptors (RLR), regarded as a cytosolic sensor, also shown to have a minor role in fungal recognition. It has 3 major receptors out of which MDA5 (Melanoma differentiation-associated gene 5) receptor altered expression is generally found in the case of chronic mucocutaneous candidiasis, owing to its crucial role in antifungal defense (M. et al. 2017).

Crosstalk between immune cells and fungal species

A latest study by de Zuani et al. confirmed that BMMCs (Bone marrow-derived mast cells) come into play after the detection of *C. albicans* and secrete some soluble factors to enhance the crawling movement of macrophages toward fungi. Additionally, ROS responses are also generated by BMMCs to overcome *C. albicans* population. Interestingly, When Dectin-1 knockout BMMCs are exposed to *C. albicans* (both hyphal and yeast forms), cytokine release is reduced but not totally suppressed, indicating that Dectin-1 is not the single receptor present on mast cells responsible for *C. albicans* identification. (De Zuani et al. 2018).

Macrophages (phagocytes derived from blood monocytes), a member of antigen presenting cells (APCs) that perform fungal phagocytosis and effectively generate reactive nitrogen intermediates and reactive oxygen species (antimicrobic components). Through research, it was concluded that on encounter with fungi, macrophages differentiate to M1 (classical activated macrophages) and M2 (alternative activated macrophages)**.** Specifically, M1 macrophages generate anti-inflammatory responses, while M2 macrophages generate pro-inflammatory responses against fungi (Reales-Calderón et al. 2014). More studies can be performed to highlight the specific relationship between macrophages and mycobiota.

Dendritic cells (DCs) are effectual APCs, in general two types of DCs are prominent in host for combating fungal infections**:** Myeloid dendritic cells (mDCs) that offer fungal PAMPs to naïve T cells transforming them to TH1 cells. In contrast, plasmacytoid dendritic cells (pDCs), another subset of DCs, differentiate naïve T cells to TH2 cells and potentially generate IFN-α, TNF-α which inhibits hyphal growth of *A. fumigatus.* However, previous studies have reported that any imbalance in between pDCs and mDCs levels can increase the incidence of fungal infections among individuals (Pathakumari et al. 2020).

Natural killer cells (NK) constitute about 5–10% of the total lymphocytes but their role remains endless regarding the dialogue with mycobiome. A number of sources have proven that they utilize different receptors to crosstalk with fungi. For instance, through NKp30 activating receptor they elicit perforin degranulation of *C. albicans*, *C. neoformans* and further through NKp46 receptor they mediate destruction of *C. glabrata* (Li et al. 2013) (Schmidt et al. 2017). Nevertheless, they also induce cytokine response against pathogenic fungi as in case where neutrophils are activated by IFN-γ and GM-CSF (Granulocyte–macrophage colony stimulating factor) to overcome C. *albicans* infection in host. Many clinical trials have shown that mice without NK cells are more prone to aspergillosis and candidiasis. (Schmidt et al. 2017) (Bär et al. 2014).

Neutrophils are the initial line of defense against infections. According to the literature, neutrophils inhibit the morphological transition of *C. albicans* and kill them via production of neutrophil extracellular traps (NET) (Wheeler et al. 2017). Meanwhile, they also produce IL-17, besides TH17, to overcome pulmonary aspergillosis infection (Werner et al. 2011). As per preliminary research, neutropenia (a lack of neutrophils) and GI mucosal breaching enhance the risk of fungal infections (aspergillosis, candidiasis) and mortality.(Wheeler et al. 2017). However, neutropenia has not been identified as a concern in the case of cryptococcosis (Hirai et al. 2011).

T Cells

T cells have been widely investigated for their interaction with the fungal community. Specifically, TH1 cells are responsible for production of TNF, IFN-γ and GM-CSF which promotes phagocytosis, affects APC function and further, stimulates the discharge of antibodies from B-cells against fungal pathogens (Pathakumari et al. 2020) (Kroetz and Deepe 2012). The function of GM-CSF has been observed in GM-CSF knockout mice, where the levels of TH1 and TH2 cytokines drastically decrease upon encountering *C. neoformans* (Chen et al. 2007). However, in normal mice, GM-CSF promotes ROS response via macrophages by sequestering Zn through upregulation of Zn exporters. Zn deficiency decreases fungal proliferation, inhibits immune cell responses, and further restricts the growth of intracellular yeast in mice (Subramanian Vignesh et al. 2013).

It is well known that TH2 subclass obstructs the protective TH1 cell responses and reduces pro-inflammatory cytokine synthesis (Pathakumari et al. 2020). Prior research suggests that equilibrium amid TH2 and TH1 responses are worthy to safeguard against fungal pathogens. For instance, increased GATA-3 (TH2 cell transcription factor) expression can suppress IFN-γ production and develop the risk of systemic candidiasis. Furthermore, TH2 CD4 + T cells can compromise the function of lungs and subsequently cause allergic bronchopulmonary aspergillosis (ABPA). Overall, prevalent TH2 responses produced during fungal infections are deleterious and fatal (van de Veerdonk and Netea 2010). TH2 responses, on the other hand, can help retain humoral immunity and protect against helminthic infections by producing interleukins (IL-4, IL-5, and IL-13).(Nakayama et al. 2017).

TH17 cells get activated via MYD88, mannose receptor or by SYK-CARD9 signaling pathways induced by macrophages and dendritic cells (Romani 2004). Park et al. discovered that γδ T cells in the dermal region of skin produce IL-17 cytokine after confronting with *C. albicans* and after 7 days they switch to αβ TH17 effector T cells. Further, it is observed that after 30 days, these TH17 CD4 + resident memory T cells (TRM) predominate against *C. albicans* more rapidly than migratory memory CD4 T cells (Park et al. 2018). This research indicates that substitution of γδ T cells with αβ T cells holds importance for generation of protective immunity against fungi. Additionally, it is well documented that mice with a genetic mutation in IL-17A gene, could impair IL-17 pathway and thereby increase fungal burden (Sparber et al. 2019).

Regulatory T-cells (T_{reg}) are regarded as the potent regulators of immune responses because they control inflammation via blocking the host tissue damage (Romani and Puccetti 2007). Two major T_{reg} cells have been seen during fungal infections — natural (thymus derived-nTreg, CD4 + CD25 +), that release IL-10 and CTLA-4 cytokines at the initial stage of infection by *A. fumigatus,* to control inflammation triggered by neutrophils in the lungs. While another subset is induced under infection- (iT_{reg}) that readily suppress the immune response mediated by TH2 at the later stage of aspergillosis (Montagnoli et al. 2006). Similarly, study by Whibley et al. highlighted that Forkhead box P3 (Foxp3 +) nT_{reg} cells can induce TH17 and inhibit TH1, TH2 responses in systemic candidiasis infection (Whibley et al. 2014). Taken together, T_{reg} cell subsets can control both arms of immunity to balance immune tolerance and inflammation in a coordinated manner during fungal infections (Romani and Puccetti 2007) (Fig. 1).

Immune tolerance and mycobiota

Tryptophan (Trp) is an essential amino acid procured from diet, which promotes synthesis of proteins and biogenic amines. Numerous studies have revealed that indoleamine 2,3-dioxygenase 1 (IDO1), promotes oxidation of Trp through kynurenine pathway, which holds a vital position in generation of immune tolerance to fungi. Neutrophils, macrophages, tolerogenic DCs, epithelial cells express IDO1 and regulate immune homeostasis by mounting Kyn-mediated Treg cells through Aryl hydrocarbon Receptor (AhR) and repress inflammation by decreasing the Trp levels and finally controlling the growth of pathogen (Romani et al. 2014) (de Araújo et al. 2017). It is well documented that catabolism of Trp to L-kynurenine is mediated by IDO1 after interaction with fungal microbes, promote the transcription of FOXP3 and dampen the transcript formation of RAR-related orphan receptor gamma (RORγ-t), in order to suppress the host immunity and promote the persistence of fungi, finally contributing to immune tolerance through Treg cells. However, TH17 cells inhibit Trp catabolism and favors pathology (de Araújo et al. 2017). Overall, during fungal infections, IDO1 holds the responsibility to maintain a level amid TH17 and Treg cells so as to generate a state of suppressed inflammation and immune tolerance to prevent tissue damage. Conversely, Fungi can obstruct the tolerogenic state of host, thus contributing in either commensalism or persistence of fungi.

Diseases caused by mycobiota

There has been growing concern in recent years regarding the role of fungi in the development of human diseases. Dysbiosis (an imbalance in which harmful microorganisms outweigh beneficial microbes) frequently causes fungal infections, disrupting the fungus-immune system balance, which can be lethal if ignored. Thus, in this section we will examine various mycobiota that have become causative

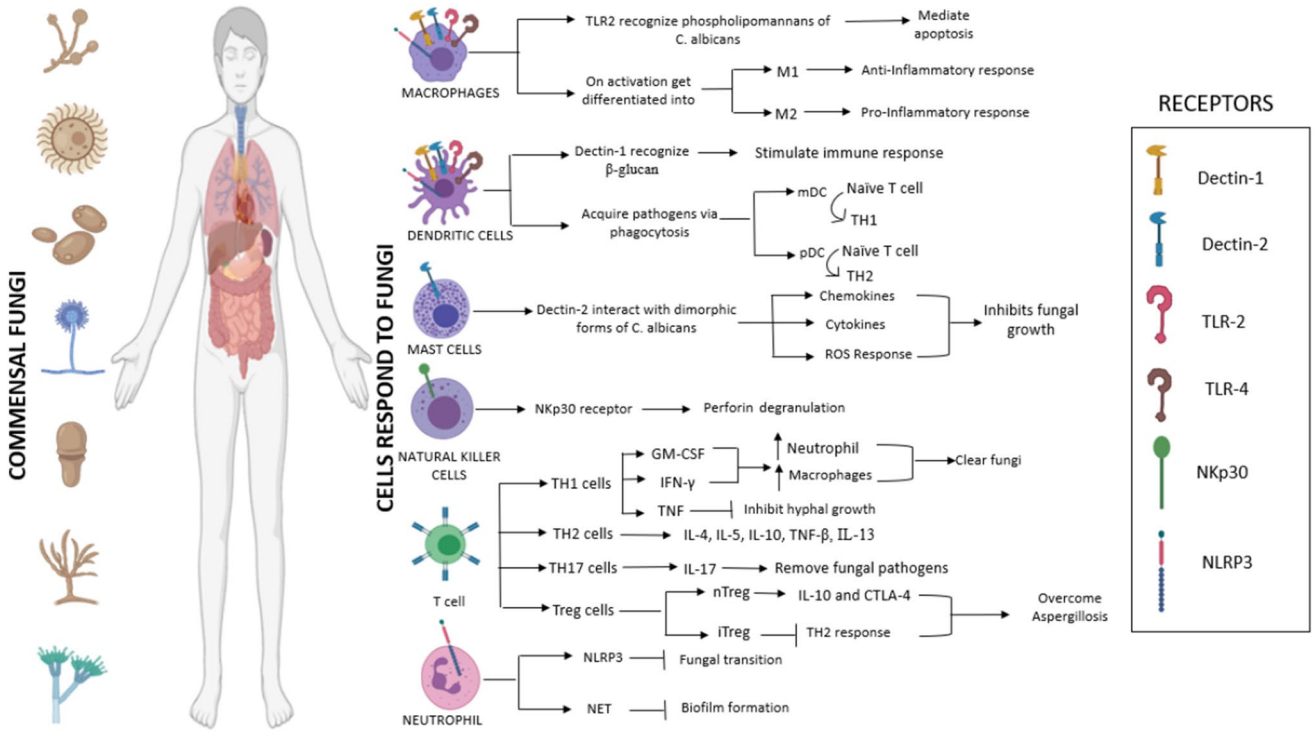

Fig. 1 Immune response to commensal fungi. Upon encountering fungi, modulation of immune cells stimulates several mechanisms to facilitate more effective response towards opportunistic fungi. **Citation**: Biorender and MS PowerPoint

agents of disease. Table 2 illustrates fungal diseases and their antifungal therapies.

Candidiasis

Candida spp. are natural inhabitants of human mycobiome, and it is evident from studies that the morphological transition can promote their conversion from commensals to pathogens, causing mucocutaneous, oral, and invasive infections. Specifically, invasive candidiasis results due to persistence of *C. albicans* in blood (candidemia) or peritonitis, or in osteomyelitis (deep-seated organ infections). From the findings, except *C. albicans* different species of *Candida* can also cause candidiasis in humans— *C. glabrata*, *C. krusei, C. tropicalis*, *C. guilliermondii* and *C. parapsilosis*, which differ in virulency. *Candida spp*. prevails in the body due to several reasons. First of which is extensive application of broad-spectrum antibiotics causing dysbiosis of bacterial species and flare up fungal species, second: cytotoxic chemotherapy-induced mucositis that ruptures GI and cutaneous layers, third being the presence of central venous catheters through which fungus can gain entry in the circulating blood and span to different regions (Pappas et al. 2018). A novel study conducted on murine model showed that kidney suffers from major candidiasis because of late initiation of innate immune response, minimal immune cells residing followed by their gradual enrollment (Hebecker et al. 2016). Meanwhile, recent study had documented a link between candidiasis and COVID-19, for example, it has been testified that due to prolonged ICU stays intrusive yeast infections have higher frequencies, especially the one's which are caused by *C. albicans*, *C. auris, C. glabrata,* and *C. parapsilosis* were observed in patients with COVID-19 (Arastehfar et al. 2020).

Aspergillosis

Aspergillosis, the most prevalent cause of mortality across the globe, caused by ten different species. Some of which are *Aspergillus fumigatus, Aspergillus flavus, Aspergillus niger, Aspergillus terreus, Aspergillus versicolor*, etc. (Vivek-Ananth et al. 2018). Overall, these fungal microbes pave their way into the host via inhalation and can prove to be fatal if sustained in the host. For instance, *Aspergillus* conidial spores in case of immunocompromised patients operate as opportunistic pathogens while in heathy individual's alveolar macrophages engulf and remove conidial spores effectively (Guerra et al. 2017). Subsequently, a study by Sainz et al. reported that patients with neutropenia, dectin-1 polymorphism, or who had received transplants (hematopoietic stem cell) had a higher chance of invasive aspergillosis (Sainz et al. 2012). Recently a study reported that ICU

Table 2 Fungal diseases and their antifungal therapies

Causative agent	Disease	Treatment strategies
Candida Spp	Vulvovaginal candidiasis Candidemia Chronic mucocutaneous infections (Skin, Oral, Nails) Pneumonia Intestinal oedema Meningitis	**Antifungal drugs**: Itraconazole and FLZ, thymol, nystatin, compound 61,894,700, caspofungin, micafungin, Anidulafungin **Immunotherapy**: IFN- γ immunotherapy **Vaccines***: rAls3p-N (Clinical Phase II trial), Recombinant secretory aspartyl proteinase 2 (Sap2), Crf (*A. fumigatus* cell wall glucanase), Fba *(C. albicans* wall protein fructose-bisphosphate aldolase), rHyr1p-N (*C. albicans* cell surface protein Hyr1), Laminarin Vaccine **NPs**: Silver nanoparticles along with FLZ and nystatin
Aspergillus spp.	Aspergilloma Pneumonia Influenza-associated pulmonary aspergillosis Allergic bronchopulmonary aspergillosis	**Antifungal Drugs:** Voriconazole, isavuconazole, echinocandin, liposomal AmB **Immunotherapy**: IFN- γ immunotherapy, CAR T cell technologies **Vaccines***: Asp f 16 vaccine, Subcutaneous Heat Killed *S. cerevisiae*, Laminarin Vaccine, Crf **NPs**: Silver nanoparticles along with fluconazole and nystatin
Malassezia Spp	Pityriasis Versicolor Atopic eczema	**Antifungal drugs**: Ketoconazole, Itraconazole, FLZ, Terbinafine, Zinc pyrithione, Pramiconazole **NPs:** FLZ loaded on solid nanoparticles topical gel
Fusarium spp.	Fusariosis	**Antifungal Drugs:** AmB, Voriconazole, Posaconazole **Immunotherapy**: Growth factors (G-CSF or GM-CSF) or granulocyte transfusions **Surgery**: Debride necrotic tissue
Cryptococcus Spp	Cryptococcosis Pneumonia Cryptococcal meningitis	**Antifungal Drugs**: AmB, Flucytosine, APX001 (prodrug of APX001A), FLZ **Immunotherapy:** IFN- γ immunotherapy, SDZ/PYR and SMX/TMP, 18B7, Mycograb (Clinical Phase II trial), **Vaccine***: PA- GalXM conjugate

*There are no licensed fungal vaccines; all vaccines are in different clinical phase studies

FLZ (Fluconazole); AmB (Amphotericin); SMX/ TMP (trimethoprim/sulfamethoxazole); SDZ/PYR (sulfadiazine–pyrimethamine); 18B7 (anti-capsular polysaccharide monoclonal antibody); Mycograb (anti-fungal heat shock protein 90 (Hsp90) recombinant human antibody)

patients with influenza can develop influenza-associated pulmonary aspergillosis (IAPA). Furthermore, this study in patients with serious SARS-CoV-2 infection can give rise to the probability of COVID-19-associated pulmonary aspergillosis (CAPA) (Verweij et al. 2020). In this context, further research is needed to assess the impact of aspergillosis in patients with viral infections.

Cryptococcosis

Cryptococcosis, a widespread invasive fungal infection, responsible for 20–70% mortality across the globe. *Cryptococcus* is a pathogenic fungus that gains entry into human body through inhalation but in an immunocompromised state the immune system is inefficient to remove them and thus, *C. neoformans* and *C. gatti* become predominant and cause cryptococcosis (Iliev and Underhill 2013). Emerging studies indicate the presence of different types of cryptococcosis depending upon the site of infection which includes: cutaneous, peripheral, disseminated, and cerebral cryptococcosis. Among these, cerebral cryptococcosis has been reported as invasive opportunistic infection that can cause meningoencephalitis in HIV-infected patients (Pathakumari et al. 2020) (Iliev and Underhill 2013). Meanwhile, another study indicates that cell wall polysaccharides of *Cryptococcus* namely GXM, glucuronoxylomannogalactan and melanin, can alter the activity of macrophages in circulation (oxidative burst) (Pathakumari et al. 2020). Also, *C. neoformans* produce giant cells (titan) that subsequently decrease the phagocytic activity of macrophages thus, promoting survival of *C. neoformans* (Zaragoza and Nielsen 2013).

Fungal Biofilms

Generally, packed fungal communities organize themselves in biofilms—shielded by extracellular matrix (ECM) to promote their adherence to the surfaces and protect them against host immune responses. Such fungal biofilms can colonize mucosal surfaces like oral and vaginal areas as well as on implanted medical equipments like catheters, dentures, etc. (Kernien et al. 2018). Notably, *Cryptococcus* biofilms originate from surface attachment taken over by microcolonies, ECM production and eventually get mature (R. et al. 2015).

Studies demonstrated that shedding of polysaccharide capsules (GXM, galactoxylomannans, and mannoproteins) by *C. neoformans* can enhance ECM production. Additionally, presence of GXM in biofilm matrix provides resistance against NET, antifungals and further reduces the phagocytic response

of macrophages. But still, it is unclear that whether the phagocytic response is sufficient enough to overcome *Cryptococcus* biofilms or not. Meanwhile, *Candida* biofilms can also inhibit the release of NET and ROS and altogether promote the growth of biofilms. Surprisingly, IL-17A has proven to induce the formation of *C. albicans* biofilms. While in contrast to *Cryptococcus and Candida* biofilms, *Aspergillus* biofilms have distinct ECM composition including: galactosaminogalactan (GAG) and galactomannan as core matrix polysaccharides. It is evident from studies that absence of GAG can reduce the probability of biofilm formation by *A. fumigatus* (Kernien et al. 2018).

Fusariosis

Another fungal species found in the environment, Fusarium that exists in mold form. Out of 70 species that are known, only 3 species (*F. solani* species, *F. dimerum* species, and *F. oxysporum* species) can cause disseminated (fusariosis) and superficial infections in transplant recipients, immunocompromised and diabetic patients (Guarro 2013) (Short et al. 2013) (Batista et al. 2020). Studies have documented that fusarium when penetrates via skin can generate multiple erythematous papules that further disseminates to whole body and proves to be fatal for immunocompromised patients. Additionally, Fusarium can also invade through contact lenses, which results in development of keratitis. The only therapy to eradicate fusariosis to date is Combination therapy (Batista et al. 2020).

Pityriasis versicolor (PV)

Malassezia is responsible for Pityriasis Versicolor (tinea versicolor), a common skin disease. The preliminary study concluded that the morphological transformation of *Malassezia* along with other factors such as hormonal imbalance, excessive use of antibiotics and high temperature can promote the susceptibility towards disease. Another study suggests that Pityriasis Versicolor (PV) triggers the development of hyperpigmentation or hypopigmented skin lesions (Dyląg et al. 2020). Specifically, in hypopigmented PV, *Malassezia* releases azelaic acid and malassezin that promotes apoptosis of melanocytes and subsequently halts the synthesis of melanin (Dolenc-Voljč 2017). However, the treatment of PV is possible through antifungal drugs, but results won't appear spontaneously due to persistence of dead fungal cells on the skin (Dyląg et al. 2020).

Therapies against fungal infections

Fungal infections are more prominent worldwide and cause mortality with unacceptable high rates which shows a need for therapies to overcome fungal infections. In this section, we will discuss about some existing therapies and shortcomings associated with therapies.

Immunotherapy

Currently, immunotherapy is one of the remarkable strategies to overcome fungal infections in which GM-CSF with IFN- γ protect against invasive aspergillosis. Precisely, GM-CSF can enhance antifungal ability and IFN- γ clears the pathogenic fungi in transplant recipients who had developed systemic fungal infections (Armstrong-James et al. 2017). A study by Jarvis et al. highlighted that adjunctive IFN- γ immunotherapy can eradicate *C. neoformans* from HIV-1 infected patient's cerebrospinal fluid much faster than conventional therapies (Jarvis et al. 2012). Additionally, by restoring immunological function, adjunctive IFN-γ immunotherapy can be beneficial to individuals infected with invasive *Candida* or *Aspergillus* infections (Delsing et al. 2014). Although IFN- γ therapy have shown positive results in numerous studies but still more trials are needed to ensure its worth. Apart from these, PRR agonists and antagonists can also stimulate an immune response against fungi by subsequently limiting inflammation. For instance, conjugation of β-glucan laminarian with diphtheria toxoid (CRM 1197) can promote the development of antibodies against β-glucan in mice with systemic candidiasis (Armstrong-James et al. 2017) (Patin et al. 2019). Furthermore, researchers have employed CAR T cell technologies to produce cytotoxic T cells (Tc Cells) against pathogenic fungi. This research has given positive results in halting the growth of *A. fumigatus* hyphae after recognizing β-glucans moieties (Patin et al. 2019).

Antifungal drugs

Presently, antifungal drugs exist in three classes for the therapy of systemic fungal infections which includes azoles inhibiting ergosterol biosynthesis, echinocandins target fungal cell wall biosynthesis, and polyenes facilitate cell lysis (Revie et al. 2018)**.** In a recent clinical study, antifungal drug posaconazole has proven to reduce the occurrence of invasive fungal infections in immunocompromised patients**.** Nevertheless, this drug is often linked with some side effects like nausea, vomiting, and malfunctioning of liver (Wong et al. 2020). Another study by Pierce et al. reported that compound 61894700 can halt the development of C. albicans filament and biofilms but is unable to inhibit the overall planktonic growth (Pierce et al. 2015). Additionally, two antifungal drugs had been developed namely sulfadiazine–pyrimethamine (SDZ/PYR) and sulfamethoxazole-trimethoprim (SMX/TMP) that repress growth and biofilm formation of *C. gatti* and C. *neoformans* (de Aguiar Cordeiro et al. 2013). Meanwhile, many researchers have repurposed

some old drugs like tamoxifen, Cox2 inhibitors that had shown positive results against fungal infections. In addition to this, combinations of antifungal drugs are currently being employed to increase their efficacy, where the synergistic combinations make it effective even at low doses and reduce the resistance (Spitzer et al. 2017).

Vaccines

Vaccines act as potential weapons against fungal infections. For instance, live-attenuated fungal vaccines had given appreciating results during preclinical studies, but these are not approved for immunocompromised patients (Santos and Levitz 2014). A study by Spellberg et al. observed that the rAls3p-N (adhesion protein associated with *C. albicans* cell wall) based vaccine would protect against disseminated, mucosal, and vulvovaginal candidiasis, and are under phase-II trials (Spellberg et al. 2006). Apart from that, recombinant protein Asp f 16 (association with unmethylated CpG oligodeoxynucleotides) based vaccines also proved to be effective against invasive aspergillosis (Bozza et al. 2002).

Nanotechnology

Nanotechnology has been actively researched as a low-cost, one-of-a-kind approach for developing novel antifungals and vaccines (Souza and Amaral 2017). Antifungal chemotherapy employs nanoparticles (NPs) to deliver intrinsic antifungal effects with the objective of decreasing the medication concentration required for the treatment. NPs can be utilized to increase the stability and immunogenicity of antigens like peptides in the vaccine formulation (Zhao et al. 2014). Furthermore, silver nanoparticles demonstrated increased antifungal efficiency against *C. albicans* ATCC 10,231 and *A. brasiliensis* ATCC 16,404 after conjugation with nystatin (NYT) and fluconazole (Hussain et al. 2019). Another study discovered that combining posaconazole-derived compounds with PEG-imidazole modified G5 dendrimers produced a soluble and potent posaconazole conjugate, which seems to be a new and effective antifungal medication. However, in vivo studies are necessary before nanoparticles are to be used for medical purposes (Tang et al. 2021).

Shortcomings of therapies

Antifungal drugs that are commercially available are limited and their extensive use has resulted in the development of resistance, which is a major rising health concern. Genetic variations in the cellular target, upregulation of the target molecules, and antifungal efflux pump extrusion are all factors that trigger azole resistance (A. and B. 1999). For example, mutations in drug target genes, as observed in the case of ERG11, promote their overexpression and increase the azole resistance against *C. albicans* infections. Furthermore, mutation in the ERG3 gene encoding for Δ-5,6- desaturase enzyme Erg3 can accumulate ergosterol and further develop resistance against azoles and polyenes (Revie et al. 2018). However, resistance to polyenes is primarily caused by sterol modification, which occurs as a result of decrease in the cell's ergosterol content, substitution of the sterol with the one that has lower affinity for polyenes, or reorientation of ergosterol that sterically inhibits polyene binding (A. and B. 1999). Apart from that, echinocandin resistance develops after therapy as a result of amino acid alterations in the 1,3-D-glucan synthase, coded by the FKS1 and FKS2 genes, that diminish the enzyme's susceptibility to medications (Perlin 2015). Thus, all these studies emphasize on necessitating the creation of new drugs to tackle antifungal resistance.

Although vaccination serves as an important strategy to overcome fungal infections, but to date no vaccine is sanctioned to treat fungal infections. Besides this, there is still considerable uncertainty about whether fungal vaccines could generate herd immunity or not (Santos and Levitz 2014).

Fungal probiotics

When given in the proper dosage, probiotics (live microorganisms) are helpful to the host. As an example, *Saccharomyces boulardii*, the major fungal probiotic used for the treatment of several diseases like bacterial diarrhea, acute GI diseases, also exhibits positive results against *Clostridium difficile* infections (Kelesidis and Pothoulakis 2012) (Sen and Mansell 2020). Other than that, they also boost immunity and improve gut microflora specifically in IBD (Inflammatory Bowel Disease). Also, it helps in restoring the tight junctions in enterocytes and regulate the expression of p120 through E-cadherin (Sen and Mansell 2020) (Abbas et al. 2014) (Terciolo et al. 2017). Although *S. boulardii* is genetically similar to *S. cerevisiae* but certain characteristics adds advantage to their extensive use such as non-sporulating nature, survival at acidic pH, viability around 55 °C and ability to metabolize different carbon sources (Sen and Mansell 2020). However, safety concerns are associated with the use of fungal probiotics for immunocompromised patients.

Conclusion and future perspective

Recently, the World Health Organization (WHO) conducted a poll to establish the first fungal priority pathogen list for public health relevance in order to define R&D priorities. The selection of fungal pathogens was based on six criteria:

mortality, transmission, community burden, treatability, health-care burden, and prevalence of medication resistance. For this reason, WHO has approached experts and individuals active in antifungal healthcare delivery and research for this purpose. Multi-criteria decision analysis (MCDA) was utilized in this approach, which combines scientific data and expert opinion. There are currently six fungal pathogens on the list: *Candida auris*, other azole-resistant *Candida spp.*, azole-resistant *A. fumigatus, C. neoformans*, *C. gatti*, *Pneumocystis jirovecii*, and Mucormycetes. More fungal pathogens and criteria will be added, as recommended by the expert panel.

From this review, it is clear that both arms of immunity are crucial for maintaining a healthy human mycobiome. However, if the balance between the two is disturbed for any reason, it can manifest as a deadly disease. Nonetheless, research to discover the obscurity of the mycobiome should be continued. Further research is needed to investigate whether mycobiome alterations reported in a number of disorders either reflect disease pathogenesis or are a consequence of the disease process. New therapeutic approaches like the use of nanoparticles need to be adopted to treat fungal complications and, hence, potentiation of the immune system that helps in maintaining the fungi in commensal mode can serve as a lesson for devising better therapeutic strategies and preventing the development of drug resistance. Moreover, cross-reaction between auto-antigens of humans with commensal fungi can offer new insight into the role of commensal fungi, particularly in autoimmune disorders. In addition to this, how does interaction between numerous fungal communities across different body sites affect humans can be brought to light by future studies only.

Declarations

Conflict of interest The authors declare no conflict of interest. The work has been performed with funding from Delhi Technological University to Dr. Asmita Das. No animal or human materials have been used, and all ethical norms of the university have been adhered to.

References

Abbas, Z., Yakoob, J., Jafri, W., Ahmad, Z., Azam, Z., Usman, M.W., Shamim, S., Islam, M.: Cytokine and clinical response to Saccharomyces boulardii therapy in diarrhea-dominant irritable bowel syndrome: a randomized trial. Eur J Gastroenterol Hepatol **26**(6), 630–639 (2014)

Arastehfar, A., Carvalho, A., Nguyen, M.-H., Hedayati, M., Netea, M., Perlin, D., Hoenigl, M.: COVID-19-associated Candidiasis (CAC): an underestimated complication in the absence of immunological predispositions? J Fungi J (2020). https://doi.org/10.3390/jof6040211

Armstrong-James, D., Brown, G.D., Netea, M.G., Zelante, T., Gresnigt, M.S., van de Veerdonk, F.L., Levitz, S.M.: Immunotherapeutic approaches to treatment of fungal diseases. Lancet Infect Dis **17**, 393–402 (2017). https://doi.org/10.1016/S1473-3099(17)30442-5

Bär, E., Whitney, P.G., Moor, K., Reis e Sousa, C., LeibundGut-Landmann, S.: IL-17 regulates systemic fungal immunity by controlling the functional competence of NK cells. Immunity **40**, 117–127 (2014). https://doi.org/10.1016/j.immuni.2013.12.002

Batista, B.G., de Chaves, M.A., Reginatto, P., Saraiva, O.J., Fuentefria, A.M.: Human fusariosis: an emerging infection that is difficult to treat. Rev Soc Bras Med Trop **53**, e20200013 (2020). https://doi.org/10.1590/0037-8682-0013-2020

Borriello, F., Zanoni, I., Granucci, F.: Cellular and molecular mechanisms of antifungal innate immunity at epithelial barriers: the role of C-type lectin receptors. Eur J Immunol **50**, 317–325 (2020). https://doi.org/10.1002/eji.201848054

Bourgeois, C., Kuchler, K.: Fungal pathogens-a sweet and sour treat for Toll-like receptors. Front Cell Infect Microbiol **2**, 142 (2012). https://doi.org/10.3389/fcimb.2012.00142

Bozza, S., Gaziano, R., Lipford, G.B., Montagnoli, C., Bacci, A., Di Francesco, P., Kurup, V.P., Wagner, H., Romani, L.: Vaccination of mice against invasive aspergillosis with recombinant Aspergillus proteins and CpG oligodeoxynucleotides as adjuvants. Microbes Infect **4**, 1281–1290 (2002). https://doi.org/10.1016/S1286-4579(02)00007-2

Brand, A.: Hyphal growth in human fungal pathogens and its role in virulence. Int J Microbiol **2012**, 517529 (2012). https://doi.org/10.1155/2012/517529

Chen, G.-H., Olszewski, M.A., McDonald, R.A., Wells, J.C., Paine, R., Huffnagle, G.B., Toews, G.B.: Role of granulocyte macrophage colony-stimulating factor in host defense against pulmonary Cryptococcus neoformans infection during murine allergic bronchopulmonary mycosis. Am J Pathol **170**, 1028–1040 (2007). https://doi.org/10.2353/ajpath.2007.060595

Da Silva, C.A., Chalouni, C., Williams, A., Hartl, D., Lee, C.G., Elias, J.A.: Chitin is a size-dependent regulator of macrophage TNF and IL-10 production. J Immunol **182**, 3573–3582 (2009). https://doi.org/10.4049/jimmunol.0802113

Dambuza, I.M., Levitz, S.M., Netea, M.G., Brown, G.D.: Fungal recognition and host defense mechanisms. Microbiol Spectrum **5**(4), 5–4 (2017)

de Aguiar Cordeiro, R., Mourão, C.I., Rocha, M.F.G., de Farias Marques, F.J., Teixeira, C.E.C., de Oliveira Miranda, D.F., Neto, L.V.P., Brilhante, R.S.N., de Jesus Pinheiro Gomes Bandeira, T., Sidrim, J.J.C.: Antifolates inhibit Cryptococcus biofilms and enhance susceptibility of planktonic cells to amphotericin B. Eur J Clin Microbiol Infect Dis **32**, 557–564 (2013). https://doi.org/10.1007/s10096-012-1774-8

de Araújo, E.F., Loures, F.V., Feriotti, C., Costa, T., Vacca, C., Puccetti, P., Romani, L., Calich, V.L.G.: Disease tolerance mediated by phosphorylated indoleamine-2,3 dioxygenase confers resistance to a primary fungal pathogen. Front Immunol **8**, 1522 (2017). https://doi.org/10.3389/fimmu.2017.01522

De Zuani, M., Paolicelli, G., Zelante, T., Renga, G., Romani, L., Arzese, A., Pucillo, C., Frossi, B.: Mast cells respond to *Candida albicans* infections and modulate macrophages phagocytosis of the fungus. Front Immunol (2018). https://doi.org/10.3389/fimmu.2018.02829

Delsing, C.E., Gresnigt, M.S., Leentjens, J., Preijers, F., Frager, F.A., Kox, M., Monneret, G., Venet, F., Bleeker-Rovers, C.P., van de Veerdonk, F.L., Pickkers, P., Pachot, A., Kullberg, B.J., Netea, M.G.: Interferon-gamma as adjunctive immunotherapy for invasive fungal infections: a case series. BMC Infect Dis **14**, 166 (2014). https://doi.org/10.1186/1471-2334-14-166

Dolenc-Voljč M (2017) Diseases caused by Malassezia species in human beings. In: Kon K, Rai Soft Tissue, Bone and Joint Infections MBT-TM of S (eds) Clinical microbiology: diagnosis,

treatments and prophylaxis of infections. Academic Press, New York, pp 77–91

Dreschers, S., Saupp, P., Hornef, M., Prehn, A., Platen, C., Morschhäuser, J., Orlikowsky, T.: Reduced PICD in monocytes mounts altered neonate immune response to *Candida albicans*. PLoS ONE **11**, e0166648 (2016). https://doi.org/10.1371/journal.pone.0166648

Drickamer, K., Taylor, M.E.: Recent insights into structures and functions of C-type lectins in the immune system. Curr Opin Struct Biol **34**, 26–34 (2015). https://doi.org/10.1016/j.sbi.2015.06.003

Dyląg, M., Leniak, E., Gnat, S., Szepietowski, J.C., Kozubowski, L.: A case of anti- pityriasis versicolor therapy that preserves healthy mycobiome. BMC Dermatol **20**, 9 (2020). https://doi.org/10.1186/s12895-020-00106-x

Erwig, L., Gow, N.: Interactions of fungal pathogens with phagocytes. Nat Rev Microbiol (2016). https://doi.org/10.1038/nrmicro.2015.21

Fischer, M., Spies-Weisshart, B., Schrenk, K., Gruhn, B., Wittig, S., Glaser, A., Hochhaus, A., Scholl, S., Schnetzke, U.: Polymorphisms of Dectin-1 and TLR2 Predispose to Invasive Fungal Disease in Patients with Acute Myeloid Leukemia. PLoS ONE **11**, e0150632–e0150632 (2016). https://doi.org/10.1371/journal.pone.0150632

Gessner, M.A., Werner, J.L., Lilly, L.M., Nelson, M.P., Metz, A.E., Dunaway, C.W., Chan, Y.R., Ouyang, W., Brown, G.D., Weaver, C.T., Steele, C.: Dectin-1-dependent interleukin-22 contributes to early innate lung defense against *Aspergillus fumigatus*. Infect Immunity **80**(1), 410–417 (2012)

Ghannoum, M.A., Rice, L.B.: Antifungal agents: mode of action, mechanisms of resistance, and correlation of these mechanisms with bacterial resistance. Clin Microbiol Rev. **12**(4), 501–17 (1999)

Gow, N., Munro, C., Latge, J.-P.: The fungal cell wall: structure, biosynthesis, and function. Microbiol Spectr (2017). https://doi.org/10.1128/microbiolspec.FUNK-0035-2016

Guarro, J.: Fusariosis, a complex infection caused by a high diversity of fungal species refractory to treatment. Eur J Clin Microbiol Infect Dis **32**, 1491–1500 (2013). https://doi.org/10.1007/s10096-013-1924-7

Guerra, E., Lee, C., Specht, C., Yadav, B., Huang, H., Akalin, A., Huh, J., Mueller, C., Levitz, S.: Central role of IL-23 and IL-17 producing eosinophils as immunomodulatory effector cells in acute pulmonary aspergillosis and allergic asthma. PLOS Pathog **13**, e1006175 (2017). https://doi.org/10.1371/journal.ppat.1006175

Hebecker, B., Vlaic, S., Conrad, T., Bauer, M., Brunke, S., Kapitan, M., Linde, J., Hube, B., Jacobsen, I.D.: Dual-species transcriptional profiling during systemic candidiasis reveals organ-specific host-pathogen interactions. Sci Rep **6**, 36055 (2016). https://doi.org/10.1038/srep36055

Hernández-Chávez MJ, Pérez-García LA, Niño-Vega GA, Mora-Montes HM (2017) Fungal Strategies to Evade the Host Immune Recognition. J. fungi (Basel, Switzerland) 3

Hirai, Y., Ainoda, Y., Shoji, T., Fujita, T., Yoshinaga, K., Shiseki, M., Mori, N., Teramura, M., Totsuka, K., Motoji, T.: Disseminated cryptococcosis in a non-hodgkin's lymphoma patient with late-onset neutropenia following rituximab-CHOP chemotherapy: a case report and literature review. Mycopathologia **172**, 227–232 (2011). https://doi.org/10.1007/s11046-011-9423-9

Hussain, M.A., Ahmed, D., Anwar, A., Perveen, S., Ahmed, S., Anis, I., Shah, M.R., Khan, N.A.: Combination therapy of clinically approved antifungal drugs is enhanced by conjugation with silver nanoparticles. Int Microbiol **22**, 239–246 (2019). https://doi.org/10.1007/s10123-018-00043-3

Iliev, I.D., Underhill, D.M.: Striking a balance: fungal commensalism versus pathogenesis. Curr Opin Microbiol **16**, 366–373 (2013). https://doi.org/10.1016/j.mib.2013.05.004

Invitation to participate in survey to establish the first WHO fungal priority pathogens list (https://www.who.int/news-room/articles-detail/invitation-to-participate-in-survey-to-establish-the-first-who-fungal-priority-pathogens-list-(fppl)

Jarvis, J.N., Meintjes, G., Rebe, K., Williams, G.N., Bicanic, T., Williams, A., Schutz, C., Bekker, L.-G., Wood, R., Harrison, T.S.: Adjunctive interferon-γ immunotherapy for the treatment of HIV-associated cryptococcal meningitis: a randomized controlled trial. AIDS **26**, 1105–1113 (2012). https://doi.org/10.1097/QAD.0b013e3283536a93

Kelesidis, T., Pothoulakis, C.: Efficacy and safety of the probiotic *Saccharomyces boulardii* for the prevention and therapy of gastrointestinal disorders. Ther Adv Gastroenterol **5**, 111–125 (2012). https://doi.org/10.1177/1756283x11428502

Kernien, J.F., Snarr, B.D., Sheppard, D.C., Nett, J.E.: The Interface between fungal biofilms and innate immunity. Front Immunol **8**, 1968 (2018). https://doi.org/10.3389/fimmu.2017.01968

Kroetz, D.N., Deepe, G.S.: The role of cytokines and chemokines in Histoplasma capsulatum infection. Cytokine **58**, 112–117 (2012). https://doi.org/10.1016/j.cyto.2011.07.430

Li, S.S., Kyei, S.K., Timm-McCann, M., Ogbomo, H., Jones, G.J., Shi, M., Xiang, R.F., Oykhman, P., Huston, S.M., Islam, A., Gill, M.J., Robbins, S.M., Mody, C.H.: The NK receptor NKp30 mediates direct fungal recognition and killing and is diminished in NK cells from HIV-infected patients. Cell Host Microbe **14**, 387–397 (2013). https://doi.org/10.1016/j.chom.2013.09.007

Miyake, Y., Oh-hora, M., Yamasaki, S.: C-type lectin receptor mcl facilitates mincle expression and signaling through complex formation. J Immunol **194**, 5366–5374 (2015). https://doi.org/10.4049/jimmunol.1402429

Ml, R., Arturo, C., Mahmoud, G., Matthew, P., Marvin, W., Pranab, M.: Biofilm formation by *Cryptococcus neoformans*. Microbiol Spectr (2015). https://doi.org/10.1128/microbiolspec.MB-0006-2014

Montagnoli, C., Fallarino, F., Gaziano, R., Bozza, S., Bellocchio, S., Zelante, T., Kurup, W.P., Pitzurra, L., Puccetti, P., Romani, L.: Immunity and tolerance to *Aspergillus* involve functionally distinct regulatory T cells and tryptophan catabolism. J Immunol **176**, 1712–1723 (2006). https://doi.org/10.4049/jimmunol.176.3.1712

Nakayama, T., Hirahara, K., Onodera, A., Endo, Y., Hosokawa, H., Shinoda, K., Tumes, D.J., Okamoto, Y.: Th2 cells in health and disease. Annu Rev Immunol **35**, 53–84 (2017). https://doi.org/10.1146/annurev-immunol-051116-052350

Netea, M.G., Joosten, L.A.B., van der Meer, J.W.M., Kullberg, B.-J., van de Veerdonk, F.L.: Immune defence against Candida fungal infections. Nat Rev Immunol **15**, 630–642 (2015). https://doi.org/10.1038/nri3897

Pappas, P.G., Lionakis, M.S., Arendrup, M.C., Ostrosky-Zeichner, L., Kullberg, B.J.: Invasive candidiasis. Nat Rev Dis Prim **4**, 18026 (2018). https://doi.org/10.1038/nrdp.2018.26

Park, C.O., Fu, X., Jiang, X., Pan, Y., Teague, J.E., Collins, N., Tian, T., Oalley, J.T., Emerson, R.O., Kim, J.H., Jung, Y., Watanabe, R., Fuhlbrigge, R.C., Carbone, F.R., Gebhardt, T., Clark, R.A., Lin, C.P., Kupper, T.S.: Staged development of long-lived T-cell receptor αβ TH17 resident memory T-cell population to Candida albicans after skin infection. J Allergy Clin Immunol **142**, 647–662 (2018). https://doi.org/10.1016/j.jaci.2017.09.042

Pathakumari, B., Liang, G., Liu, W.: Immune defence to invasive fungal infections: A comprehensive review. Biomed Pharmacother **130**, 110550 (2020). https://doi.org/10.1016/j.biopha.2020.110550

Patin, E.C., Thompson, A., Orr, S.J.: Pattern recognition receptors in fungal immunity. Semin Cell Dev Biol **89**, 24–33 (2019). https://doi.org/10.1016/j.semcdb.2018.03.003

Perlin, D.S.: Mechanisms of echinocandin antifungal drug resistance. Ann N Y Acad Sci **1354**, 1–11 (2015). https://doi.org/10.1111/nyas.12831

Pierce, C.G., Chaturvedi, A.K., Lazzell, A.L., Powell, A.T., Saville, S.P., McHardy, S.F., Lopez-Ribot, J.L.: A novel small molecule inhibitor of Candida albicans biofilm formation, filamentation and virulence with low potential for the development of resistance. NPJ Biofilms Microbiomes **1**, 15012 (2015). https://doi.org/10.1038/npjbiofilms.2015.12

Qin J, Li R, Raes J, Arumugam M, Burgdorf KS, Manichanh C, Nielsen T, Pons N, Levenez F, Yamada T, Mende DR, Li J, Xu J, Li S, Li D, Cao J, Wang B, Liang H, Zheng H, Xie Y, Tap J, Lepage P, Bertalan M, Batto J-M, Hansen T, Le Paslier D, Linneberg A, Nielsen HB, Pelletier E, Renault P, Sicheritz-Ponten T, Turner K, Zhu H, Yu C, Li S, Jian M, Zhou Y, Li Y, Zhang X, Li S, Qin N, Yang H, Wang J, Brunak S, Doré J, Guarner F, Kristiansen K, Pedersen O, Parkhill J, Weissenbach J, Consortium M, Bork P, Ehrlich SD, Wang J (2010) A human gut microbial gene catalogue established by metagenomic sequencing. Nature 464:59–65. https://doi.org/10.1038/nature08821

Reales-Calderón JA, Aguilera-Montilla N, Corbí ÁL, Molero G, Gil C (2014) Proteomic characterization of human proinflammatory M1 and anti-inflammatory M2 macrophages and their response to Candida albicans. Proteomics 14:1503–1518. https://doi.org/10.1002/pmic.201300508

Revie NM, Iyer KR, Robbins N, Cowen LE (2018) Antifungal drug resistance: evolution, mechanisms and impact. Curr Opin Microbiol 45:70–76. https://doi.org/10.1016/j.mib.2018.02.005

Romani, L.: Immunity to fungal infections. Nat Rev Immunol **4**, 11–24 (2004). https://doi.org/10.1038/nri1255

Romani, L., Puccetti, P.: Controlling pathogenic inflammation to fungi. Expert Rev Anti Infect Ther **5**, 1007–1017 (2007). https://doi.org/10.1586/14787210.5.6.1007

Romani, L., Zelante, T., Luca, A., Ianniti, R., Moretti, S., Bartoli, A., Aversa, F., Puccetti, P.: Microbiota control of a tryptophan-AhR pathway in disease tolerance to fungi: highlights. Eur J Immunol (2014). https://doi.org/10.1002/eji.201344406

Saijo, S., Ikeda, S., Yamabe, K., Kakuta, S., Ishigame, H., Akitsu, A., Fujikado, N., Kusaka, T., Kubo, S., Chung, S., Komatsu, R., Miura, N., Adachi, Y., Ohno, N., Shibuya, K., Yamamoto, N., Kawakami, K., Yamasaki, S., Saito, T., Akira, S., Iwakura, Y.: Dectin-2 recognition of alpha-mannans and induction of Th17 cell differentiation is essential for host defense against *Candida albicans*. Immunity **32**, 681–691 (2010). https://doi.org/10.1016/j.immuni.2010.05.001

Sainz, J., Muñoz, C.B., Segura-Catena, J., Vázquez, L., Ríos Tamayo, R., Oyonarte, S., Hemminki, K., Försti, A., Jurado, M.: Dectin-1 and DC-SIGN polymorphisms associated with invasive pulmonary aspergillosis infection. PLoS ONE **7**, e32273 (2012). https://doi.org/10.1371/journal.pone.0032273

Sam, Q.H., Chang, M., Chai, L.: The fungal mycobiome and its interaction with gut bacteria in the host. Int J Mol Sci **18**, 330 (2017). https://doi.org/10.3390/ijms18020330

Santos, E., Levitz, S.M.: Fungal vaccines and immunotherapeutics. Cold Spring Harb Perspect Med **4**, a019711 (2014)

Schei, K., Avershina, E., Øien, T., Rudi, K., Follestad, T., Salamati, S., Ødegård, R.A.: Early gut mycobiota and mother-offspring transfer. Microbiome **5**, 107 (2017). https://doi.org/10.1186/s40168-017-0319-x

Schmidt, S., Tramsen, L., Lehrnbecher, T.: Natural killer cells in antifungal immunity. Front Immunol **8**, 1623 (2017). https://doi.org/10.3389/fimmu.2017.01623

Sen, S., Mansell, T.J.: Yeasts as probiotics: mechanisms, outcomes, and future potential. Fungal Genet Biol **137**, 103333 (2020). https://doi.org/10.1016/j.fgb.2020.103333

Short, D.P.G., O'Donnell, K., Thrane, U., Nielsen, K.F., Zhang, N., Juba, J.H., Geiser, D.M.: Phylogenetic relationships among members of the *Fusarium solani* species complex in human infections and the descriptions of *F. keratoplasticum* sp. Nov. and *F. petroliphilum* stat. nov. Fungal Genet Biol **53**, 59–70 (2013). https://doi.org/10.1016/j.fgb.2013.01.004

Skevaki, C., Pararas, M., Kostelidou, K., Tsakris, A., Routsias, J.G.: Single nucleotide polymorphisms of Toll-like receptors and susceptibility to infectious diseases. Clin Exp Immunol **180**, 165–177 (2015). https://doi.org/10.1111/cei.12578

Souza, A.C.O., Amaral, A.C.: Antifungal therapy for systemic mycosis and the nanobiotechnology era: improving efficacy. Biodistribution and toxicity. Front Microbiol **8**, 336 (2017). https://doi.org/10.3389/fmicb.2017.00336

Sparber, F., De Gregorio, C., Steckholzer, S., Ferreira, F.M., Dolowschiak, T., Ruchti, F., Kirchner, F.R., Mertens, S., Prinz, I., Joller, N., Buch, T., Glatz, M., Sallusto, F., LeibundGut-Landmann, S.: The skin commensal yeast malassezia triggers a type 17 response that coordinates anti-fungal immunity and exacerbates skin inflammation. Cell Host Microbe **25**, 389–403 (2019). https://doi.org/10.1016/j.chom.2019.02.002

Speakman, E.A., Dambuza, I.M., Salazar, F., Brown, G.D.: T cell antifungal immunity and the role of C-type lectin receptors. Trends Immunol **41**, 61–76 (2020). https://doi.org/10.1016/j.it.2019.11.007

Spellberg, B.J., Ibrahim, A.S., Avanesian, V., Fu, Y., Myers, C., Phan, Q.T., Filler, S.G., Yeaman, M.R., Edwards, J.E., Jr.: Efficacy of the anti-candida rAls3p-N or rAls1p-N vaccines against disseminated and mucosal candidiasis. J Infect Dis **194**, 256–260 (2006). https://doi.org/10.1086/504691

Spitzer, M., Robbins, N., Wright, G.D.: Combinatorial strategies for combating invasive fungal infections. Virulence **8**, 169–185 (2017). https://doi.org/10.1080/21505594.2016.1196300

Subramanian Vignesh, K., Landero Figueroa, J.A., Porollo, A., Caruso, J.A., Deepe, G.S.: Granulocyte macrophage-colony stimulating factor induced Zn sequestration enhances macrophage superoxide and limits intracellular pathogen survival. Immunity **39**, 697–710 (2013). https://doi.org/10.1016/j.immuni.2013.09.006

Tang, S., Chen, J., Cannon, J., Cao, Z., Baker, J.R., Jr., Wang, S.H.: Dendrimer-based posaconazole nanoplatform for antifungal therapy. Drug Deliv **28**, 2150–2159 (2021). https://doi.org/10.1080/10717544.2021.1986605

Terciolo, C., Dobric, A., Ouaissi, M., Siret, C., Breuzard, G., Silvy, F., Marchiori, B., Germain, S., Bonier, R., Hama, A., Owens, R., Lombardo, D., Rigot, V., André, F.: *Saccharomyces boulardii* CNCM I-745 Restores intestinal barrier integrity by regulation of E-cadherin recycling. J Crohn's Colitis **11**, 999–1010 (2017). https://doi.org/10.1093/ecco-jcc/jjx030

Underhill, D.M., Iliev, I.D.: The mycobiota: interactions between commensal fungi and the host immune system. Nat Rev Immunol **14**, 405–416 (2014). https://doi.org/10.1038/nri3684

van de Veerdonk, F.L., Netea, M.G.: T-cell subsets and antifungal host defenses. Curr Fungal Infect Rep **4**, 238–243 (2010). https://doi.org/10.1007/s12281-010-0034-6

Verweij, P.E., Rijnders, B.J.A., Brüggemann, R.J.M., Azoulay, E., Bassetti, M., Blot, S., Calandra, T., Clancy, C.J., Cornely, O.A., Chiller, T., Depuydt, P., Giacobbe, D.R., Janssen, N.A.F., Kullberg, B.-J., Lagrou, K., Lass-Flörl, C., Lewis, R.E., Liu, P.W.-L., Lortholary, O., Maertens, J., Martin-Loeches, I., Nguyen, M.H., Patterson, T.F., Rogers, T.R., Schouten, J.A., Spriet, I., Vanderbeke, L., Wauters, J., van de Veerdonk, F.L.: Review of influenza-associated pulmonary aspergillosis in ICU patients and proposal for a case definition: an expert opinion. Intensive Care Med **46**, 1524–1535 (2020). https://doi.org/10.1007/s00134-020-06091-6

Vivek-Ananth, R.P., Mohanraj, K., Vandanashree, M., Jhingran, A., Craig, J.P., Samal, A.: Comparative systems analysis of the

secretome of the opportunistic pathogen *Aspergillus fumigatus* and other *Aspergillus* species. Sci Rep **8**, 6617 (2018). https://doi.org/10.1038/s41598-018-25016-4

Ward, T.L., Knights, D., Gale, C.A.: Infant fungal communities: current knowledge and research opportunities. BMC Med **15**, 30 (2017). https://doi.org/10.1186/s12916-017-0802-z

Ward, T.L., Dominguez-Bello, M.G., Heisel, T., Al-Ghalith, G., Knights, D., Gale, C.A.: Development of the human mycobiome over the first month of life and across body sites. mSystems **3**, 40–17 (2018). https://doi.org/10.1128/mSystems.00140-17

Werner, J.L., Gessner, M.A., Lilly, L.M., Nelson, M.P., Metz, A.E., Horn, D., Dunaway, C.W., Deshane, J., Chaplin, D.D., Weaver, C.T., Brown, G.D., Steele, C.: Neutrophils produce interleukin 17A (IL-17A) in a Dectin-1- and IL-23-dependent manner during invasive fungal infection. Infect Immun **79**, 3966–3977 (2011). https://doi.org/10.1128/IAI.05493-11

Wheeler, M.L., Limon, J.J., Underhill, D.M.: Immunity to commensal fungi: detente and disease. Annu Rev Pathol Mech Dis **12**, 359–385 (2017). https://doi.org/10.1146/annurev-pathol-052016-100342

Whibley, N., MacCallum, D.M., Vickers, M.A., Zafreen, S., Waldmann, H., Hori, S., Gaffen, S.L., Gow, N.A.R., Barker, R.N., Hall, A.M.: Expansion of Foxp3+ T-cell populations by Candida albicans enhances both Th17-cell responses and fungal dissemination after intravenous challenge. Eur J Immunol **44**, 1069–1083 (2014). https://doi.org/10.1002/eji.201343604

Wong, T.Y., Loo, Y.S., Veettil, S.K., Wong, P.S., Divya, G., Ching, S.M., Menon, R.K.: Efficacy and safety of posaconazole for the prevention of invasive fungal infections in immunocompromised patients: a systematic review with meta-analysis and trial sequential analysis. Sci Rep **10**, 14575 (2020). https://doi.org/10.1038/s41598-020-71571-0

Zaragoza, O., Nielsen, K.: Titan cells in Cryptococcus neoformans: cells with a giant impact. Curr Opin Microbiol **16**, 409–413 (2013). https://doi.org/10.1016/j.mib.2013.03.006

Zhao, L., Seth, A., Wibowo, N., Zhao, C.-X., Mitter, N., Yu, C., Middelberg, A.P.J.: Nanoparticle vaccines. Vaccine **32**, 327–337 (2014). https://doi.org/10.1016/j.vaccine.2013.11.069

Proceedings of the Sixth International Conference on Intelligent Computing and Control Systems (ICICCS 2022)
IEEE Xplore Part Number: CFP22K74-ART; ISBN: 978-1-6654-1035-9

Comparative Analysis of Forecasting Models for Air Quality Index Prediction

Prof. (Dr.) Shailender Kumar
Computer Science Department
Delhi Technological University
Delhi, India
shailenderkumar@dce.ac.in

Abhay Lodhi
Computer Science Department
Delhi Technological University
Delhi, India
abhaylodhi3@gmail.com

Abhi Chauhan
Computer Science Department
Delhi Technological University
Delhi, India
abhichauhan5682@gmail.com

Amrit Kumar
Computer Science Department
Delhi Technological University
Delhi, India
amritx8@gmail.com

2022 6th International Conference on Intelligent Computing and Control Systems (ICICCS) | 978-1-6654-1035-9/22/$31.00 ©2022 IEEE | DOI: 10.1109/ICICCS53718.2022.9788302

***Abstract*— Air pollution is a significant hazard to human life in India. The LSTM Model (Long Short-Term Memory, a robust deep learning approach), SARIGMA model, and Facebook Prophet model have been used in this work to forecast AQI. Root Mean Square Error (RMSE) is a statistic used to assess the effectiveness of prediction all the models. The Sub-Index Calculation is used in LSTM model for AQI calculation.**

The suggested methodology raises awareness about the degree of air pollution in India and notifies people to take preventative measures to save their lives. Furthermore, the comparative analysis helps to formulate a better model for AQI Prediction Model among various prediction models.

Keywords—AQI, LSTM, Forecasting, Prediction, Seasonality

INTRODUCTION

50% of the world's population is exposed to increasing air pollution. The World Health Organization estimated that around 4.2 million deaths annually are due to fine particulate matter or PM2.5. Coal, fireplaces, natural gases, road dust, car engines, tiny bits, materials are released into the air by applying crushing operation on particle PM10. PM 2.5 particles are tiny enough to bypass your lung's defense and enter the bloodstream. In high cases, they can cause serious illnesses and even death. Cities with high PM 2.5 levels have higher mortality rates.

Air quality forecasts are critical in reducing the adverse effects of severe weather on people's health. Air quality forecasting is to estimate future air quality metrics based on a region's historical meteorological and air pollutant concentration data. The primary role of air pollution early warning systems is to notify appropriate authorities when the air quality meets the early warning threshold. A robust pollution warning system considers the pollutant, the resource, and the extent of the effect. In this work, our target is to build a robust system that can forecast air quality so people living there are warned beforehand and so they can take precautions.

In the 90s physical models were used to predict air quality, long complex equations were used to create these models. To carry out a large number of iterations these algorithms required high-speed computers with enormous memory and still, accuracy was not significant. Recent development in machine learning has shown significant accuracy in air quality predictions. Recent studies have focused on sophisticated statistical learning methods for evaluating air quality and predicting air pollution. ML prediction methods like SVM (Support Vector Machine), Random Forest, Adaptive Boosting, Artificial Neural Network, Linear Regression, Stacking Ensemble. The Pre-eminent result obtained by the researcher using random forest is between 70 and 90 %, the extra tree is about 85.3 %, Extreme Learning Machine is 75.5%. Deep learning has more significant results as compared to machine learning algorithms. Artificial Neural Network has prediction performance of 0.16 MRE with benzene pollutants. Deep Belief Network has an error percentage of 1.6 % with PM2.5 pollutants.

Particulate matter under 10 micrometers in measurement (PM10), the particulate matter under 2.5 micrometers in width (PM2.5), carbon monoxide (CO), ammonia (NH3), nitrogen dioxide (NO2), and ozone are the six major contaminants in India.

Figure 1: Air Quality Index Categorization

RELATED WORK

Determines the PM2.5 concentration by devising a method called the "photograph-based method". By observation, the saturation maps are very sensitive to the quality of air, under high and low PM2.5 concentrations it shows different appearances. It uses the Weibull Distribution function to match the saturation maps and obtain a value to calculate the color information. Then, the image's PM2.5 concentration can be evaluated via combining the two features above, followed by the procedure called non-linear mapping. It's not sufficient for the Photographic method to estimate PM2.5, and it uses only one pollutant of concentration. This work is based on only a single variable "PM2.5" and to get extra monitoring information from different cities to validate the generalization of our project and other factors, e.g., geomorphic conditions. It can't thereby entirely determine the consistency of air pollutant data and obtain more precise prediction results.[1]

Presented the severe effects of polluted air on regular admissions in hospital for breathing and lung illness in Poisson regression analysis of day-by-day tallies of hospital confirmations, modifying for impacts of pattern, occasional and other recurrent variables, day of the week, occasions, flu pestilence, temperature, dampness, and auto-connection. Major variables of pollution were particulates ozone, SO2, and nitrogen dioxide, which delayed 0 to 3 days.[2]

Presented Data cleaning for data quality. Nowadays data is being generated rapidly through the internet every instance, and hence proposing any decisions has become a huge time-consuming. For achieving more benefits in business, for decision-makers,

Authorized licensed use limited to: DELHI TECHNICAL UNIV. Downloaded on June 15,2022 at 11:26:08 UTC from IEEE Xplore. Restrictions apply.

knowledge plays a key role. The data which is fetched from many sources possibly have a dummy and dirty data. Hence, cleaning of data should be done prior to the data being loaded into the warehouse in order to provide quality data. When the data has been cleaned while applying data mining, it will create exact outcomes. Hence consistent data is very essential as well as reliable for decision making. We have proposed an algorithm that comes with a Decision for every trait, and qualities that are missing are to be supplanted with leaf node values by which we can accomplish excellent and accurate quality.[3]

Proposed a huge repository of TB of data is created every day from modern computers and digital technologies such as Cloud Computing and IoT. Therefore, analysis of Big Data is the most prominent area of R&D (research and development). The primary goal of this paper is to observe the possible effect of Big Data challenges, issues in open research. It opens new ways for specialists to build up the solutions and the open research problems. This paper provides significant insights on big data and the philosophy behind its analysis, which is a major factor for this project because of the large size of the sample data being used to provide conclusions.[4]

Recognition Urban air poison mainly focuses on controlling a flood of huge ecologic checking data and complex changes of air toxins. It requires feasible expectation methods to improve forecast precision and turn away genuine contamination occurrences. In this paper, a new method named contamination fixation forecast has been proposed dependent on huge measures of all the natural data and intense deep learning procedures. The proposed method incorporates massive data utilizing two sorts of networks of deep systems.[5]

In Chengdu city, air contamination is a significant and prevalent point on account of its severe effect on the health of human beings and wellbeing. Nitrogen dioxide, Sulphur dioxide, and particulate matter are the significant air contaminants brought about by the utilization of petroleum derivatives, etc. In this investigation, the spatial circulation fluctuation of the significant air poisons over the principal city region of Chengdu was broken down and analyzed in 2010. So as to get the attributes, two spatial addition strategies dependent on Inverse Distance Weighted Interpolation, Geographic Information System, and Ordinary Kriging, were picked and looked at. The outcomes showed that the OK strategy was smarter to produce the forecast maps of toxin fixations than the IDW technique. High spatial descent variety of NO2, SO2 and PM10 focuses existed, particularly in the east-west course. Between the six principal locales in Chengdu city, Chenghua District was dirtied all the most truly in 2010.Inspired by these works we aim to develop an effective traffic sign detection framework.[6]

Angel Elenkov and Desislava Ivanova utilized the Raspberry Pi platform. It is with the Multilayer Perceptron technique of machine learning to successfully forecast an air pollutant. The main challenge of the classification, which is used for regression, discrete, and values which are used for continuous values, are conveyed by multilayer perceptron. Because this author employs discrete values and a multilayer perceptron with backpropagation, the input does not pass to the activation function, resulting in a zero or one showing the size of the discrepancy between the predicted and actual value. The resultant coefficient of determination (R2) is better; however, it may be increased further by increment feeding.[7]

Zhang and other suggested the wavelet neural network (WNN) are a resilient approach for estimating the number of air pollutants, however, it lacks the necessary wavelet function and the number of adequate hidden layers needed in their research, resulting in incorrect air pollution prediction.[8]

In their research, they used a neural network with an embedded sensor to provide correct levels of air contaminants, but it was costly since it required all of the data training set and can't operate with data that isn't a complete set.[9]

MODEL

1) LSTM

The LSTM network is a special type of RNN that can learn long-term dependencies. Hoch Reiter & Schmid Huber (1997) established it, and numerous individuals developed and popularized it in subsequent work. They are now widely used and perform well in a wide range of settings. (LSTM) is a recurrent neural network (RNN) architecture that is extensively employed in deep learning. Unlike normal feedforward neural networks, LSTM contains feedback connections. LSTM can analyze both single data points, such as pictures, and whole data sequences, such as voice or video. An input gate, a cell, an output gate, and a forget gate make up a basic LSTM unit. The cell holds values across arbitrary time periods and controls the flow of information in and out of the cells via three gates. classifying, analyzing, and generating predictions based on time-series data are all possible using LSTM networks. In a time, series, there may be delays of uncertain duration between real events. LSTM was created to solve the problem of vanishing gradients that might occur while training standard RNNs.

2) SARIGMA

We know the ARIGMA Model which is one of the most popular and widely used statistical methods for time series forecasting. An extension to ARIMA that supports the direct modelling of the seasonal component of the series is called SARIMA.

“AR” is autoregressive, which says we want to predict the time series values based on some periods in the past.

“I” is integrating, which is an upward or downward trend and to get rid of it, we use differencing.

“MA” is moving average, which is informing the errors from the previous period to the next period.

“S” is the new thing which is seasonality.

Whenever there is a W-type pattern is repeating, it indicates seasonality

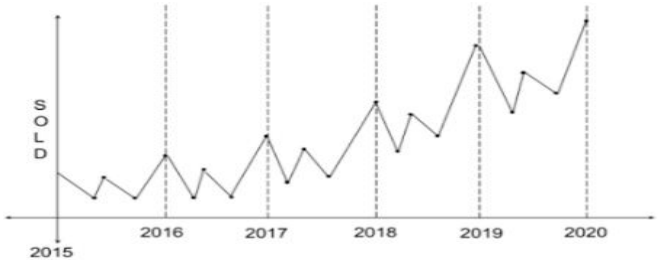

Figure 2: Illustration of seasonality in dataset.

Hence, the seasonal ARIMA(SARIMA) model is an ideal choice.

3) Facebook prophet

The Facebook prophet library was created by Facebook. It is an open-source library based on decomposable(seasonality+trend+holidays) models released by Facebook. It allows us to construct

accurate time-series predictions using very simple straightforward parameters. Also, it allows us to account for the influence of specific seasonality and holidays.

When any forecasting model fails to deliver as expected, we try to fine-tune the parameters of the technique to fit the unique scenario at hand.

Tuning these strategies necessitates a detailed understanding of the tuned time series models that underpin them. A typical analyst would have no idea how to change these instructions to avoid the

Authorized licensed use limited to: DELHI TECHNICAL UNIV. Downloaded on June 15,2022 at 11:26:08 UTC from IEEE Xplore. Restrictions apply.

behavior, and this is the kind of knowledge that is difficult to acquire and scale.

The package of Prophet has user-friendly parameters that are quite simple to adjust. Anyone with no prior experience with forecasting models can easily use this to produce accurate predictions for plenty of business situations.

The Prophet Model of Prediction:

We employ a three-part decomposable time series model: trend, holidays, and, seasonality.

In the equation, they are combined:

For modelling, g(t) is a logistic growth or piecewise linear curve. time-series with changes that are non-periodic.

s(t): regular changes (For example, weekly or yearly seasonality).

h(t): the effects of holidays (specified by the user) on schedules that are irregular.

(t): error term responsible for any unexpected changes which do not account for the model.

The prophet is attempting to fit numerous linear as well as non-linear time functions as

components using time as a regressor. Seasonality is modelled as an additive component, similar to how exponential smoothing is used in the Holt-Winters

technique. Instead of directly focusing on each observation which is time-based inside a time series, we are effectively framing the forecasting problem as a curve-fitting exercise.

METHODOLOGY

1) Dataset

We have used the dataset from Kaggle named "Air Quality Data in India (2015 - 2020)". It is specific to levels of many pollutants, including the Air Quality Index (AQI) across many states of India from 2015 to 2020. AQI is considered as an overall scheme that reconstructs weighted values of different air parameters related to pollution like CO, SO2, etc. AQI is beneficial for any person to understand the air quality in a simpler way.

Our dataset consists of City, Date, PM2.5, NH3, NO, CO, SO2, PM10, NO2, NOx, O3, Toluene, Xylene, Benzene, and AQI columns. It has AQIs of all the days from 2015 to 2020 of most of the cities of India. It also has significant data related to many contributors to air pollution. There are many missing values in the dataset, so working on the data pre-processing is a necessity, which will help us gain accuracy.

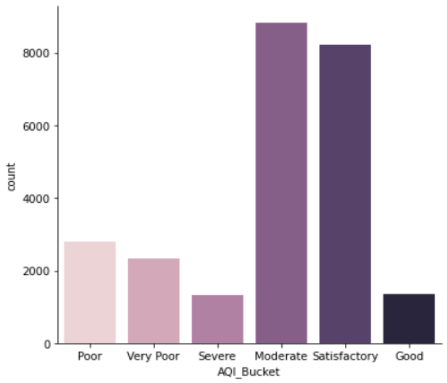

Figure 3: AQI categorization of dataset.

2) *Data Analysis*

This table indicates the number of missing values for all columns of the dataset along with their percentages. Here, Xylene has the most missing values around 61 per cent and Carbon Monoxide (CO) has the least missing values around 6 per cent.

	No of missing values	% of missing values
Xylene	18109	61.320000
PM10	11140	37.720000
NH3	10328	34.970000
Toluene	8041	27.230000
Benzene	5623	19.040000
AQI	4681	15.850000
AQI_Bucket	4681	15.850000
PM2.5	4598	15.570000
NOx	4185	14.170000
O3	4022	13.620000
SO2	3854	13.050000
NO2	3585	12.140000
NO	3582	12.130000
CO	2059	6.970000

Table 1: Percentage of missing values of following particulates.

Correlation is a metric that measures the linear connection between two or more variables. We can predict one variable based on the other using correlation. The reasoning for applying correlation to pick features is that the desirable variables are significantly associated with the target. As per the below data PM10, CO, PM2.5 is highly correlated with AQI.

PM10	0.80
CO	0.68
PM2.5	0.65
NO2	0.53
SO2	0.49
NOX	0.48
NO	0.45
Toluene	0.27
NH3	0.25
O3	0.19
Xylene	0.16
Benzene	0.04

Table 2: Correlation values of following particulates

3. Data Pre-processing

We can see that there are a lot of missing numbers, which can lead to inaccurate predictions and inferences. Taking a closer look, we see that only the Delhi dataset is full for the AQI column, with the remaining cities having missing data. Unfortunately, this is uncorrectable since official records of pollutant levels are only available in the manner described above, leaving a significant

Authorized licensed use limited to: DELHI TECHNICAL UNIV. Downloaded on June 15,2022 at 11:26:08 UTC from IEEE Xplore. Restrictions apply.

portion of data out. Each air quality record contains city, date, SO2, PM2.5, PM10, NH3, O3, NO2, and CO, Benzene, AQI_Bucket, Xylene, AQI, Toluene.

We firstly fill the null values present in the city with the city-wise mean and still, there was around 20 per cent of null values present in the dataset. Secondly, we have taken the column-wise mean i.e. (taking the mean of pollutants monthly). At last, to fill the null values in the AQI column we have calculated the subindex of the pollutants and have taken the maximum of all the subindex of SO2, PM2.5, PM10, NH3, O3, NO2, and CO i.e. (the AQI of a particular city at that day). The need to calculate subindex arises as CO is measured in mg/m3 and other pollutants in ug/m3

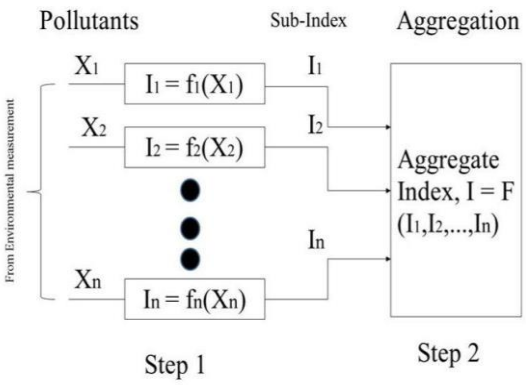

Figure 4: Steps for AQI calculation.

Sub-Index Calculation:

- SO2, PM2.5, PM10, NH3, O3, NO2, and CO are used in the AQI calculation.
- The average value from the previous 24-hours is utilized for PM10, SO2, NH3, PM2.5, and N02, with a minimum of 16 readings.
- The greatest value in the past 8 hours is utilized for CO and O3.
- Based on pre-defined groupings, each measure is turned into a Sub-Index.
- Measures are sometimes unavailable owing to a lack of measuring equipment or data points.
- The highest Sub-Index is the Final AQI, with the requirement that at least one of PM10 and PM2.5, as well as three of the seven, be accessible.

4. *Model Design*

4.1) LSTM

Most of the time series data is univariate, and certain univariate time series forecasting techniques require "standardization". When using neural networks to forecast time series, it's common practice to normalize the data as well. So, we have normalized our data to 0-1 using a min-max scaler.

$$x' = \frac{x - \min(x)}{\max(x) - \min(x)}$$

Fig.5. The formula for feature normalization.

We have used a time series generator to convert univariate (AQI) time-series data into supervised learning. With the help of a time series generator, we have created 24 features. As there are 24 hours in a day. We have used a very basic LSTM model with just 2 layers i.e. (lstm, dense). The activation function used is relu, and during compiling the model we have used adam as an optimization function and mean squared error as our loss function. We have resampled our data to month wise by finding the mean of all days of a particular month of a particular city. After resampling, we have 5 years of data month wise. The first three years of data is used for training purposes and next month's data is used for validation. We have used the same model but with the entire dataset now and predict one year into the future.

Model summary:

Layer (Type)	Output Shape	Param #
lstm_2 (LSTM)	(None , 50)	10400
Dense_2 (Dense)	(None , 1)	51

Table 3. Model Architecture of LSTM.

EXPERIMENTAL RESULT

1) LSTM Model Prediction and Forecasting Result

The RMSE of prediction for one year is 15.45. The below figure is a graph between the value predicted AQI and the actual AQI value. We have averaged out all the city AQI and used it for our training and prediction, so the below graph is between the actual averaged out AQI values vs predicted averaged out values.

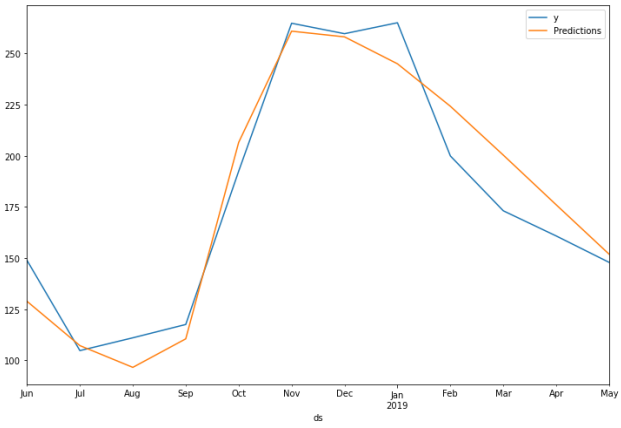

Figure 6: The actual averaged out AQI values vs predicted averaged out values.

This Forecasting of true values: We can see that the prediction is highly optimistic due to COVID-19 which can possibly be better by removing the year 2020 and predicting two years using data before 2020. Forecasting is done from 2020-06-01 to 2021-05-01.

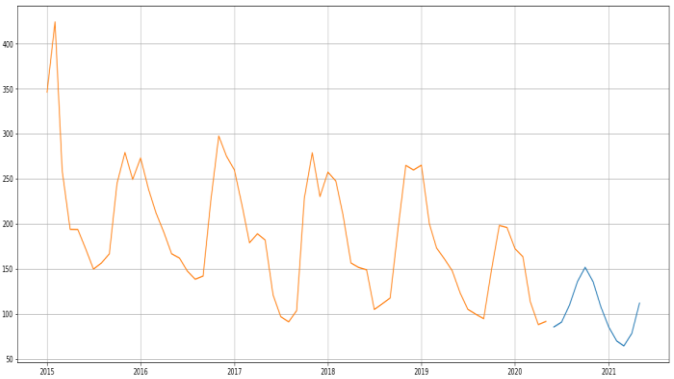

Figure 7. This figure is a pictorial representation of AQI values forecasted.

Authorized licensed use limited to: DELHI TECHNICAL UNIV. Downloaded on June 15,2022 at 11:26:08 UTC from IEEE Xplore. Restrictions apply.

Date	Forecasted AQI
2020-06-01	85.265714
2020-07-01	90.720444
2020-08-01	109.729612
2020-09-01	135.701242
2020-10-01	151.608910
2020-11-01	135.535671
2020-12-01	107.874887
2021-01-01	85.268701
2021-02-01	69.812453
2021-03-01	64.201062
2021-04-01	78.119878
2021-05-01	111.716441

Table 4: Forecasted AQI values of following dates

2) SARIGMA Model Prediction and Forecasting Result

Prediction of the AQI values for the year 2015-2018.

We have used the years 2015-2018(till June) as our train dataset and July-June the next year as our test dataset.

The forecasted AQI values SARIGMA model of the next 12 months is given in the below graph along with the Actual AQI values.

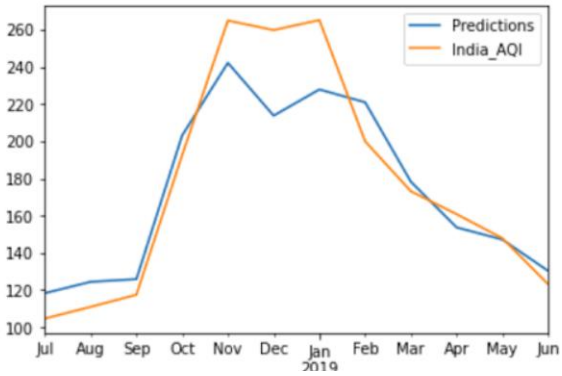

Figure 8: The forecasted AQI vs actual AQI values.

The RMSE result of this prediction is 20.69

Prediction of the AQI values for the year 2019-2020(July-May)

We have used the years 2015-2018(till June) as our train dataset and July-June the next year as our test dataset.

The forecasted AQI values SARIGMA model of the next 12 months is given in the below graph along with the Actual AQI values.

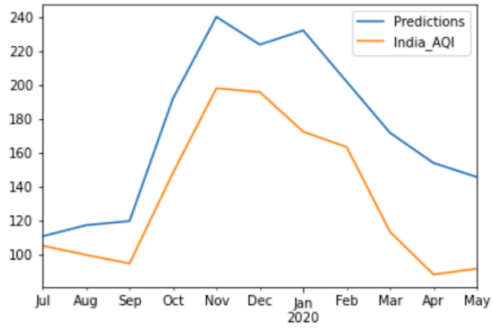

Figure 9: The forecasted AQI vs actual AQI values.

The RMSE result of this prediction is 21.56

Predicting into the future

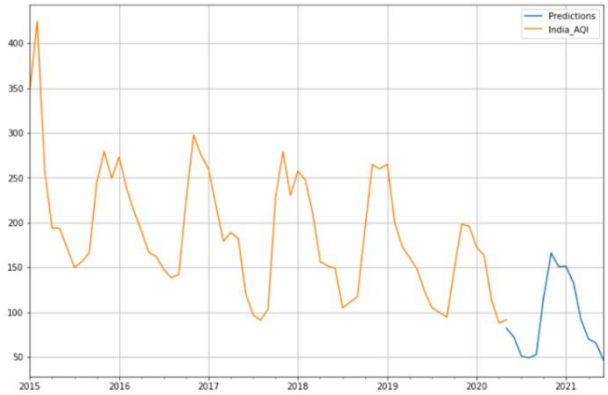

Figure 10: Prediction result for 2020.

This is the plot for the predictions in continuation with 2020 and one thing we note is the highly optimistic prediction.

3) Forecasting result using Facebook Prophet Model.

We have also split 2015-2018(till June) data as our train dataset and July-June the next year as our test dataset and we have predicted the AQI values for 2018-2019 using Facebook Prophet Model.

The below graph contains the prediction result for 2018-2019.

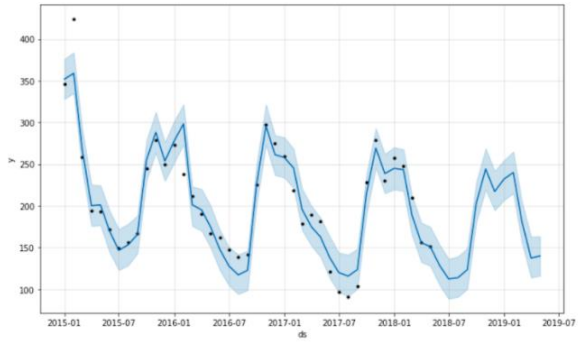

Figure 11: Prediction result for 2018-2019.

Authorized licensed use limited to: DELHI TECHNICAL UNIV. Downloaded on June 15,2022 at 11:26:08 UTC from IEEE Xplore. Restrictions apply.

The RSME result is 24.87 The RMSE value is quite good which indicates that Prophet weighs long past data with more weight.

CONCLUSION

Air pollution is the one of the major problems, which not only affecting our environment but also causing serious health-related issues which leads to lower life expectancy. Many people are struggling everyday and facing this pollution problem in every corner of this world.

This comparison models have been studied and analyzed to find better fit for prediction of Air Quality Index.

After analyzing three major prediction model LSTM, SARIGMA, and Facebook Prophet, we have found that SARIGMA Model is performing better in comparison to another two models. SARIGMA Model is best fit.

REFRENCES

[1] G. Yue, K. Gu and J. Qiao, "Effective and Efficient Photo-Based PM2.5 Concentration Estimation," in IEEE Transactions on Instrumentation and Measurement, vol. 68, no. 10, pp. 3962-3971, Oct. 2019, doi: 10.1109/TIM.2018.2886091.

[2] Ponce de Leon A, Anderson HR, Bland JM, et alEffects of air pollution on daily hospital admissions for respiratory disease in London between 1987-88 and 1991-92. Journal of Epidemiology & Community Health 1996;50:s63-s70.

[3] IEEE Conference on “Computing for Sustainable Global Development New Delhi”, India 31 October 2016 Jagat Sesh Challa, et al.

[4] Acharjya, D. P., & Ahmed, K. (2016). A survey on big data analytics: challenges, open research issues and tools. International Journal of Advanced Computer Science and Applications, 7(2), 511-518.

[5] Qin, D., Yu, J., Zou, G., Yong, R., Zhao, Q., & Zhang, B. (2019). A novel combined prediction scheme based on CNN and LSTM for urban PM 2.5 concentration. IEEE Access, 7, 20050-20059.

[6] Li, S., Song, S., & Fei, X. (2011, June). Spatial characteristics of air pollution in the main city area of Chengdu, China. In 2011 19th International Conference on Geoinformatics (pp. 1-4). IEEE.

[7] Ivanova[1], D., & Elenkov, A. (2019). Big Data Analytics for Air Quality Monitoring Assessment Based on IoT Platform.

[8] Zhang, S., Li, X., Li, Y., & Mei, J. (2018, June). Prediction of urban pm 2.5 concentration based on wavelet neural network. In 2018 Chinese Control And Decision Conference (CCDC) (pp. 5514-5519). IEEE.

[9] Amado, T. M., & Cruz, J. C. D. (2018, October). Development of machine learning-based predictive models for air quality monitoring and characterization. In TENCON 2018-2018 IEEE Region 10 Conference (pp. 0668-0672). IEEE.

[10] Hochreiter, S., & Schmidhuber, J. (1997). Long short-term memory. Neural computation, 9(8), 1735-1780.

[11] Ho, T. K. (1995, August). Random decision forests. In Proceedings of 3rd international conference on document analysis and recognition (Vol. 1, pp. 278-282). IEEE.

[12] Liu, J., Zhang, X. L., Xu, X. F., & Xu, H. H. (2008). Comparison analysis of variation characteristics of SO2, NOx, O3 and PM2. 5 between rural and urban areas, Beijing. Huan Jing ke Xue= Huanjing Kexue, 29(4), 1059-1065.

Authorized licensed use limited to: DELHI TECHNICAL UNIV. Downloaded on June 15,2022 at 11:26:08 UTC from IEEE Xplore. Restrictions apply.

Proceedings of the Sixth International Conference on Trends in Electronics and Informatics (ICOEI 2022)
IEEE Xplore Part Number: CFP22J32-ART; ISBN: 978-1-6654-8328-5

Comparative Study of Supervised Learning Algorithms for Fake News Classification

Tejas Harish Borkar
Department of Computer Science and Engineering
Delhi Technological University
Delhi, India
tejasharishborkar_2k18co373@dtu.ac.in

Tushar Ahuja
Department of Computer Science and Engineering
Delhi Technological University
Delhi, India
tusharahuja_2k18co374@dtu.ac.in

2022 6th International Conference on Trends in Electronics and Informatics (ICOEI) | 978-1-6654-8328-5/22/$31.00 ©2022 IEEE | DOI: 10.1109/ICOEI53556.2022.9777118

***Abstract*— Fake news refers to misleading or false information often presented as news. It is spread to earn advertising revenue when users read them, spread hate, or tarnish the image of a person, group of people, or an organisation. One of the main reasons for fake news is social media. Social media has allowed everyone to post or share whatever they want, which can sometimes create a problem if the shared information isn't verified before sharing. Fake news affects the readers, and the media houses since edited fake images floating around social media tarnish the reputation of the media houses. Therefore, it becomes imperative to resolve the fake news issue as it impacts a lot of stakeholders. Recent techniques used for fake news classification are Naive Bayes, K nearest neighbours, Random forest classifier, Logistic regression, etc. The proposed research study has compared various supervised machine learning models for classifying fake news (hoax news) from legit news.**

Keywords*— *Fake news, Logistic Regression, Naive Bayes, K nearest neighbour, SVM, Random forest.

I. Introduction

Social media can spread the news quickly, and if the information comes out to be fake, it creates a problem since people may panic or be falsely informed. Specifically in India, Whatsapp forwards is one of the leading causes of the spread of fake news. Information on Whatsapp is generally forwarded without any verification, leading to a large scale spread of fake news.

While reading fake news, the readers aren't aware that this news is fake. Therefore, they have false opinions on issues and are often misinformed. Thus, it becomes essential to classify information as counterfeit or genuine as it directly or indirectly affects everyone, even though it is not an easy task to do so.

Our primary objective is to build a machine learning model that can enable us to filter out fake news from a collection of news. This research work has taken a dataset of fake news and authentic/ legit news and combined them to make a new data set. Then, various pre-processing methods are applied to clean and process the data set.

A few pre-processing techniques used are oversampling, checking missing values, checking duplicate entries, removing spaces, links, URLs and all unnecessary data and variables, vectorisation, etc. After the pre-processing operations, we have performed hold out validation to train and test the data and find the performance measures.

To perform Hold out Validation, we divided our data set into two parts: one to train the model and the other to test the model. After splitting the data, we have trained the machine learning model using different supervised learning algorithms separately. We have calculated the performance measures as well. After getting the performance measures of all the algorithms, we have compared and analysed which algorithm gave us the best performance.

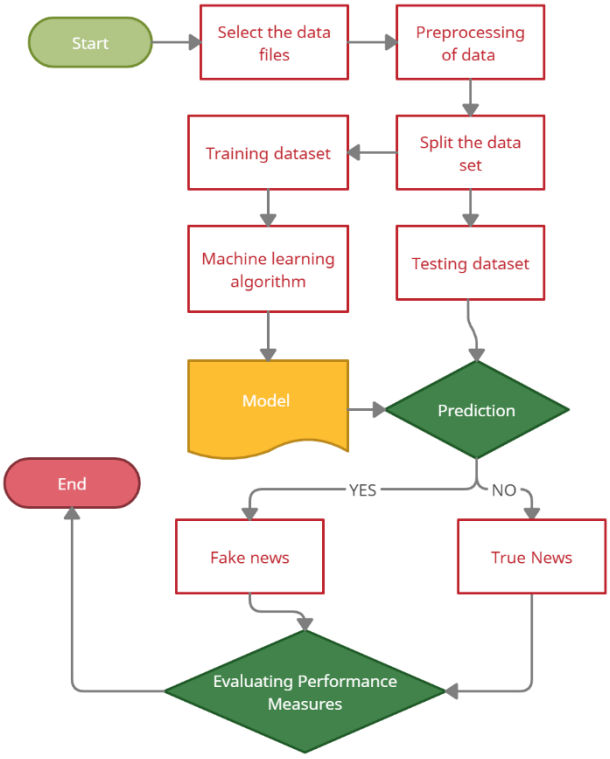

Fig. 1. The sequence of events

II. Literature Review

There are various supervised machine learning algorithms for classifying fake news like Logistic regression, K nearest Neighbours (KNN), Gradient boosting classifier, Naïve Bayes, etc. We analyse these algorithms from various sources and compare their performances. The performance of the algorithms varies with the distribution of the dataset.

There are only two output classes: fake news and non-fake news. Since we have a dataset that contains the output class, we will be analysing supervised algorithms for detection.

Authorized licensed use limited to: DELHI TECHNICAL UNIV. Downloaded on June 03,2022 at 06:31:31 UTC from IEEE Xplore. Restrictions apply.

Mykhailo Granik et al. used the Naive Bayes algorithm [1] on the dataset of Facebook news posts. They achieved an accuracy of 74%, which is acceptable because of the model's simplicity. However, the accuracy of fake news wasn't as good, possibly due to the imbalanced dataset, as less than 5% of its entries were fake news.

An advantage of Naive Bayes is that it is quick and can often be used to solve multi-class prediction problems. One of the issues often associated with Naive Bayes is that it assumes that the predictors are independent. Such a case may not always be valid, and we may get faulty predictions. Another issue is that it needs to use a smoothing technique to overcome the zero-frequency problem.

Dr S. Rama Krishna et al. analyzed the various algorithms [2]. They used the Liar dataset [3] for the analysis and figured out the performances of Logistic Regression, Random Forest, Naive Bayes and Support Vector Machine. They concluded that Random Forest performed the best.

Logistic regression is relatively easy to implement and has a low training time. It is also speedy in classifying unknown records. However, it assumes linearity between dependent and independent variables that may not always be true, and it is also prone to overfitting.

Random forest works well with both continuous and categorical variables and can be used to solve classification and regression problems. It can also handle the situation of missing values and is unaffected by outliers. However, since it is a complex algorithm, it requires a high training time and more resources.

SVM is reasonably accurate when there is a clear margin of separation among the variables. It is also memory efficient. However, it is not suitable for large datasets and when there is noise in the dataset.

Uma Sharma et al. used various machine learning algorithms for fake news detection [4] on the Liar dataset [3]. They analysed Naive Bayes, Logistic regression and Random forest classifiers and compared them. The best performance was given by logistic regression with an accuracy of 65%. This accuracy was further improved by using grid search parameter optimisation, and the accuracy obtained was 75%.

Poddar K et al. used various techniques for fake news detection [5]. The dataset was taken from Kaggle. The Support Vector Machine (SVM) with TF-IDF gave the most accurate prediction among the different techniques used.

Himank Gupta et al. proposed a framework for Real-Time Spam Detection in Twitter [6] on the HSpam dataset [7]. The feature set was divided into three categories, and their results were analysed. Neural networks performed the best in one of the feature sets, whereas random forest performed best in the other. Only SVM could be used in the remaining feature set, so they couldn't make the comparison with the other techniques.

Arush Agarwal et al. used an Ensemble Learning Approach for fake news detection [8]. They made use of ensemble learning so that multiple techniques could be used. The average accuracy score was 85% which was 15% higher than KNN, which performed the worst. The best performance algorithm was LSTM (Long Short Term Memory), with an accuracy of 97%. KNN is relatively easy to implement, and since it is a lazy learner, no training period is required, and new data can be added seamlessly. However, it does not work well with large datasets and is sensitive to noisy data and outliers.

III. Data Preprocessing

A. Introduction

Data preprocessing is the first and most crucial step in developing any machine learning model. If we don't perform data preprocessing, our ML model may not work correctly and give faulty results. Preprocessing of data means processing the data in a particular way to fit fine with the machine learning operation we will perform later on. Data that we get from the real world could contain some flaws like outliers, and it may have redundant values, may have missing values etc. All these problems/concerns could be resolved by using data preprocessing methods. Data preprocessing is a process in which we transform the given data into a usable format that can be understandable by computer and utilised by the machine learning algorithms directly.

B. Steps involved in Data preprocessing

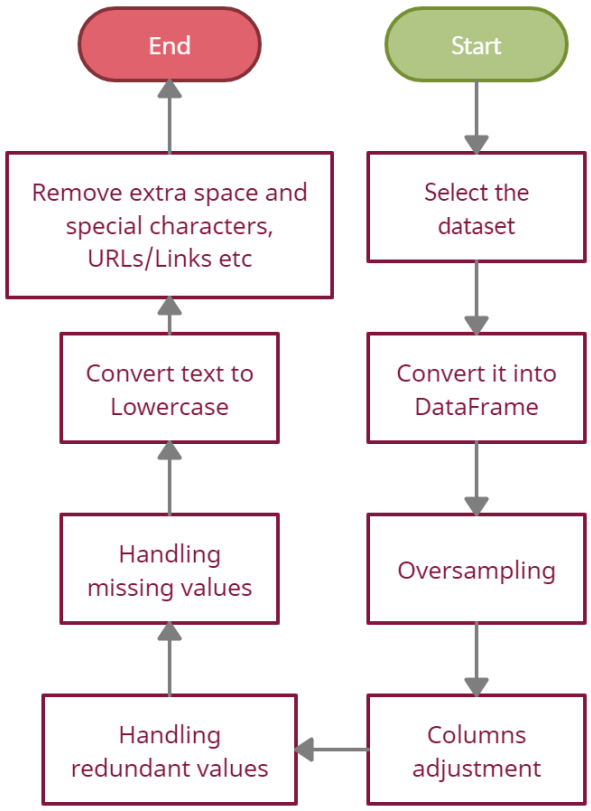

Fig. 2. Steps involved in data preprocessing

1. Importing different Datasets to make a good Dataset: We can find many datasets on kaggle, but all are not that good. A good data set is a dataset used directly to train and test the machine learning model and give good results. In our case, we have imported two data sets, one containing fake news and the other one containing authentic/legit news.

Authorized licensed use limited to: DELHI TECHNICAL UNIV. Downloaded on June 03,2022 at 06:31:31 UTC from IEEE Xplore. Restrictions apply.

So, to make a good data set, we have performed the following steps:

- We have merged both data set into one using python.
- Then we shuffled them so that they would contain data in random order.
- Oversampling: Oversampling is a process to adjust the class distribution in a data set. In other words, it helps to change the ratio between the different classes/categories represented by the dataset. We have dependent variables as 0 (fake news) and 1 (true news). In short, we had to make sure the distribution of legit and fake news in the data set should be equal(approx.). The distribution ratio of 50:50 is perfect, and 40:60 is also acceptable, but 30:70 or worse distribution could cause problems in results as it will be biased to the higher distributed class. In our dataset, the distribution is 45:55, which is acceptable.

2. Data Cleaning: Data cleaning is the process to remove/fixing unnecessary junk data from the data set. The data we get online (ex: kaggle) may contain missing or extreme values. This may cause an unrefined dataset and will result in a faulty model. All these issues can be fixed in the data preprocessing step. The following data cleaning operations are a must for fake news classification:
   - Removal/Addition of unnecessary columns: Data set may contain various columns like title, text, subject, date. But we don't need all the columns. Therefore remove all the unnecessary columns.
   - Handling redundant values: We have deleted the duplicate rows; we keep only a single instance of every message.
   - Handling missing values: We have deleted the rows which contain missing values; if either class is missing or text, we deleted the row from the data set.
   - Convert text to lowercase, then remove extra white spaces and special characters. Also, remove URL/ links as they didn't serve any purpose in our implementation.

3. Creating Test & Training Sets: This is one of the most critical steps in data preprocessing. We have divided the data set into two separate datasets, one serves as a training dataset, and the other part has been used to test the model. Generally, 70-80% of the dataset is used to train, and the remaining 20-30% is used to test models. We have used 75% for training and 25% for testing.

4. Vectorise the training and testing data: Text Vectorisation converts text into numerical representation to process the data and find patterns using machine learning algorithms. To vectorise the text data, we have imported the library function from sklearn.

IV. Classification Models Used

A. *Logistic Regression*

Logistic Regression is a supervised learning algorithm that is majorly used to solve classification problems. It is used to predict binary output based on a set of some independent variables. Since fake news or non-fake news serves as a binary output, this algorithm can be used for our purpose. Logistic Regression is a classification algorithm and thus is used to predict discrete values, whereas Linear Regression is used to predict continuous values. The probability of occurrence of an event is used in Logistic Regression based on which it fits data to the logistic function. It uses the logistic sigmoid function to assign probabilities and thus predict the value of the target variable.

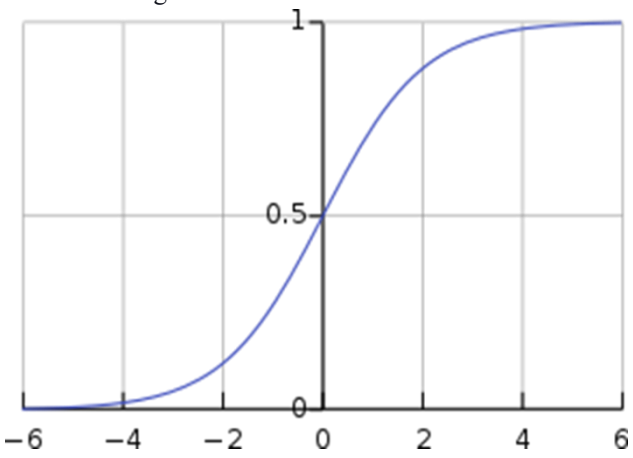

Fig. 3. Sigmoid Function Graph

B. *K Nearest Neighbours (KNN)*

It is a popular supervised learning algorithm used for regression or classification but is mainly used for classification. It is helpful when we have some categories and need to determine the class of a new object. One of the main assumptions is that "similar things exist in close proximity". The factor 'k' is often found out by trial and error method by running the algorithm on various values of 'k'.

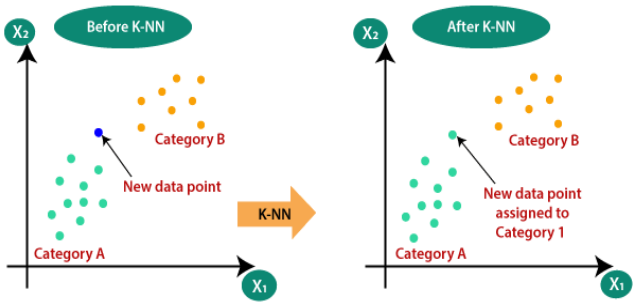

Fig. 4. KNN Example

C. *Gradient Boosting Classifier*

Boosting is an Ensemble Learning technique that combines several weak learners(predictors with poor accuracy) into a strong learner(a model with strong accuracy). Adaptive boosting and gradient boosting are the two most popular boosting techniques. Gradient boosting algorithms can be used for both classification and regression.

Authorized licensed use limited to: DELHI TECHNICAL UNIV. Downloaded on June 03,2022 at 06:31:31 UTC from IEEE Xplore. Restrictions apply.

It uses a cost function that is Mean Square Error in regression problems and Log loss in classification problems.

D. RANDOM FOREST CLASSIFIER

Decision trees are the constituents of the random forest classifier. Decision trees help predict the value of the target variable by learning some training rules. Therefore, it forms a tree that can be used to make decisions at every step and hence helps predict the value of our target variable. The leaf nodes correspond to the class label, and the internal nodes represent the attributes. The comparison starts from the root of the tree and is based on the rules using which the tree is made, we traverse through the tree's branches, and the same process is repeated for the other nodes until we reach a terminal node. Various algorithms such as ID3, C4.5, CART etc., can be used to make a decision tree.

As the name implies, the random forest contains a large number of decision trees. Each tree in the forest is used to predict the value of the target variable. The target variable with the highest number of occurrences is the predicted value of the target variable. An advantage of this is that the constituent trees help prevent their errors, i.e. even if some trees give an incorrect result, the others that are in the majority can correct the overall outcome

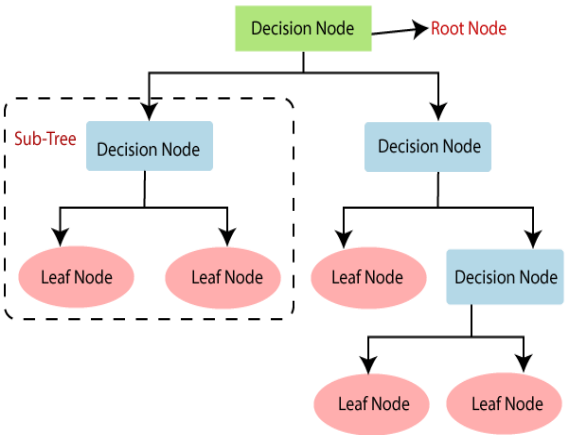

Fig. 5. Decision Tree example

E. NAIVE BAYES

The Naive Bayes algorithm is primarily based on the Bayes theorem and is comparatively easier to build than other algorithms. One of the assumptions that it considers is the independence between predictors. It can be used for large datasets since it is comparatively easier to build.

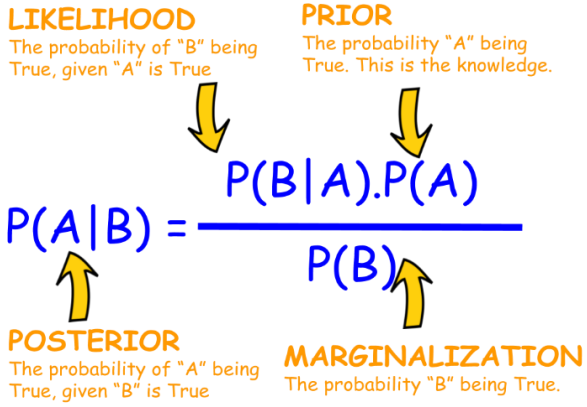

Fig. 6. Bayes Theorem

V. PERFORMANCE MEASURES USED

Performance measures are the measures that help to determine the effectiveness of the machine learning classification model. We have used Accuracy, Recall, Precision, F1 value and Classification error as the performance measures.

To calculate the performance, we need some other values that are popularly showcased in the confusion matrix, which are:

- True-Negative (TN): Total number of truly predicted rows of negative class.
- False-Positive (FP): Total number of falsely predicted rows of the positive class.
- False-Negative (FN): Total number of falsely predicted rows of negative class.
- True-Positive (TP): Total number of truly predicted rows of the positive class.

Accuracy: The ratio of correctly classified news both fake and true over the total classifications.

$$A = (TP+TN)/Total$$
$$\text{Where } Total = (TP+TN+FP+FN)$$

Recall: The ratio of correctly predicted true news over the sum of correctly predicted true news and incorrectly predicted fake news.

$$r = TP / X$$
$$\text{Where } X = (TP+ FN)$$

Precision: The ratio of correctly predicted legit news over the sum of correctly predicted legit news and incorrectly predicted true news.

$$p = TP / (TP+ FP)$$

Classification Error: It is the ratio of incorrectly classified news over the total classification.

$$E = (FP+FN)/Total$$
$$\text{Where } Total = (TP+TN+FP+FN)$$

F1 value: It is equal to twice the division of product recall and precision over the sum of recall and precision.

$$F1\text{-value} = 2*(p.r)/(p+r)$$

F1 value is a F-beta value where beta = 1. The question that arises is why we have chosen the beta = 1, why not other values?

There are some criteria to choose the value of beta in the F-beta score as follows:

1. If FP and FN both are equally important, then we have to use beta = 1
2. If FP is more important than FN, we have to use a beta value between 0 and 1.
3. If FN is more important than FP, we have to use a beta value greater than 1.

Authorized licensed use limited to: DELHI TECHNICAL UNIV. Downloaded on June 03,2022 at 06:31:31 UTC from IEEE Xplore. Restrictions apply.

In the case of Fake News Detection criteria, one follows because both FN and FP are equally important. Therefore, we have chosen beta = 1.

VI. Results

A. Logistic Regression

TABLE I. LOGISTIC REGRESSION PERFORMANCE

True Negative	2496
False Positive	24
False Negative	27
True Positive	2464
Accuracy	0.9898223907403711
Precision	0.9903536977491961
Recall	0.9891609795262947
F1-score	0.988756979313115
Classification Error	0.0101776092596289

B. K Nearest Neighbour(KNN)

To find a suitable value of K, we have iterated from 1 to 40 and calculated the accuracy for each iteration. We also plotted a graph between the accuracy rate and 'k' value as follows:

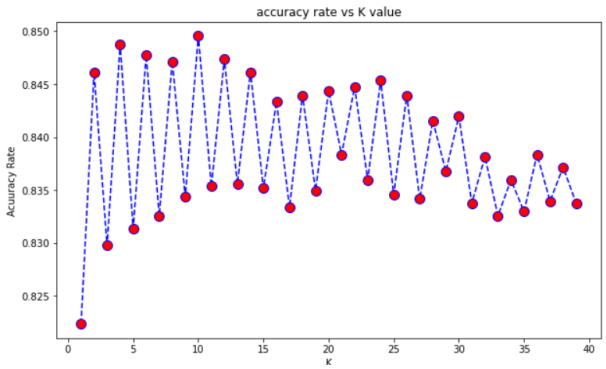

Fig. 7. Comparing accuracies for diff. values of k

As can be observed from the graph, we got the best accuracy at K = 10,

TABLE II. KNN PERFORMANCE

True Negative	2048
False Positive	472
False Negative	248
True Positive	2243
Accuracy	0.8563161045699461
Precision	0.8261510128912444
Recall	0.9004415897230028
F1-score	0.8616980407222435
Classification Error	0.1436838954300539

To improve the performance of KNN to classify fake news, we performed Hyperparameter Tuning using grid-search CV, and we got the best values for hyperparameter as follows:

TABLE III. KNN PERFORMANCE USING HYPERPARAMETER TUNING

True Negative	2193
False Positive	294
False Negative	152
True Positive	2372
Accuracy	0.9109958092197166
Precision	0.8897224306076519
Recall	0.9397781299524565
F1-score	0.9140655105973025
Classification Error	0.0890041907802834

C. Gradient Boosting Classifier

TABLE IV. GRADIENT BOOSTING CLASSIFIER PERFORMANCE

True Negative	2516
False Positive	4
False Negative	9
True Positive	2482
Accuracy	0.997405707443624
Precision	0.998390989541432
Recall	0.9963869931754316
F1-score	0.997387984729757
Classification Error	0.002594292556376

D. Random Forest Classifier

TABLE V. RANDOM FOREST CLASSIFIER PERFORMANCE

True Negative	2496
False Positive	24
False Negative	16
True Positive	2475
Accuracy	0.992017561364997
Precision	0.9903961584633854
Recall	0.9935768767563228
F1-score	0.9919839679358716
Classification Error	0.007982438635003

Authorized licensed use limited to: DELHI TECHNICAL UNIV. Downloaded on June 03,2022 at 06:31:31 UTC from IEEE Xplore. Restrictions apply.

E. Naïve Bayes

TABLE VI. NAIVE BAYES PERFORMANCE

True Negative	2350
False Positive	170
False Negative	133
True Positive	2358
Accuracy	0.9395330273398523
Precision	0.932753164556962
Recall	0.9466077880369329
F1-score	0.939629408248655
Classification Error	0.06046697266

VII. CONCLUSION

We have performed Fake News Detection using five Machine learning algorithms: Logistic Regression, K Nearest Neighbours(KNN), Gradient boosting classifier, Random Forest classifier, and Naive Bayes. We have used Accuracy, Precision, Recall, F1-score and classification error to determine the performance.

The primary performance measure that governs which technique is better is accuracy. So, according to the accuracy, the best performing algorithm was the Gradient Boosting classifier with accuracy = 0.997. The worst performance algorithm was KNN with accuracy = 0.85, further improved to 0.91 by hyper-parameter tuning.

Classification error is proportional to accuracy. Therefore, according to the classification error best performing algorithm is the Gradient Boosting classifier and the worst performance algorithm was KNN.

Apart from accuracy, precision and recall are also essential factors to conclude the performance of any model. Precision tells us about the quality, and recall tells us about the quantity.

If the values of precision and recall are highly distinct from the accuracy, then this means the quality or quantity of the model prediction is not good. Generally, the precision and recall values are good in a balanced data set (45-55% distribution of fake and true news in the data set).

From the above results (in section VI. RESULTS), we can observe that the precision and recall values are around the accuracy value. Therefore, we can conclude that the quality and quantity of the performed algorithms are good.

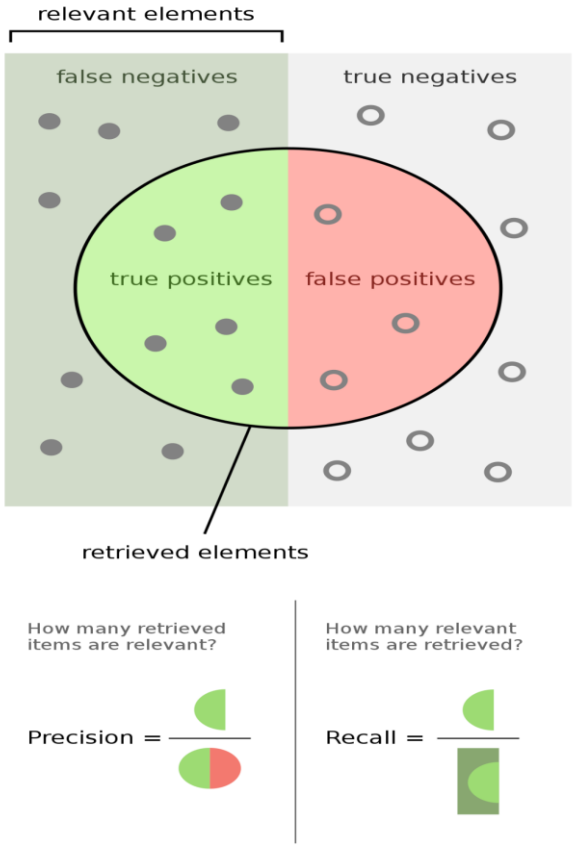

Fig. 8. Precision and Recall

Now talking about the F1 score, the higher the F1 score, the better the algorithm's performance. By definition, the 'F1-score is the harmonic mean of precision and recall", which means that it is accountable for both precision and recall; if the values of accuracy and memory are good, then the F1-score is also good. From the above results section, we can conclude that the F1 score of all the algorithms is good (by good, this means it is not at the extreme ends of accuracy)

Generally, if we have a balanced data set (45-55% distribution of fake and true news in the data set), then our recall, precision and f1 values will be good (by good, this means it is not in extreme ends of accuracy). Therefore, the primary performance measure that governs which technique is better is accuracy.

Therefore, we can conclude that the best performing algorithm was the Gradient Boosting classifier with an accuracy of 0.997. The worst performance algorithm was KNN with accuracy = 0.85, further improved to 0.91 by hyper-parameter tuning. Although accuracy = 0.85 is not bad, this is the lowest accuracy in comparison to others.

Authorized licensed use limited to: DELHI TECHNICAL UNIV. Downloaded on June 03,2022 at 06:31:31 UTC from IEEE Xplore. Restrictions apply.

REFERENCES

1] M. Granik and V. Mesyura, "Fake news detection using naive Bayes classifier," 2017 IEEE First Ukraine Conference on Electrical and Computer Engineering (UKRCON), 2017, pp. 900-903, doi: 10.1109/UKRCON.2017.8100379.

[2] Dr S. Rama Krishna, Dr S. V. Vasantha, K. Mani Deep, 2021, Survey on Fake News Detection using Machine learning Algorithms, INTERNATIONAL JOURNAL OF ENGINEERING RESEARCH & TECHNOLOGY (IJERT) ICACT – 2021 (Volume 09 – Issue 08),

[3] Datasets: Liar dataset source: https://huggingface.co/datasets/liar accessed on:16th Oct 2021 uploaded by: Hugo Abonizio[4] Uma Sharma, Sidarth Saran, Shankar M. Patil, 2021, Fake News Detection using Machine Learning Algorithms, INTERNATIONAL JOURNAL OF ENGINEERING RESEARCH & TECHNOLOGY (IJERT) NTASU – 2020 (Volume 09 – Issue 03),[5] K, P., D, G. & S, U. (2019). Comparison of Various Machine Learning Models for Accurate Detection of Fake News. 2019 Innovations in ower and Advanced Computing Technologies (i-PACT). doi: 10.1109/i-PACT44901.2019.8960044

[6] H. Gupta, M. S. Jamal, S. Madisetty and M. S. Desarkar, "A framework for real-time spam detection in Twitter," 2018 10th International Conference on Communication Systems & Networks (COMSNETS), 2018, pp. 380-383, doi: 10.1109/COMSNETS.2018.8328222.

[7] "HSpam14 Dataset," http://www.ntu.edu.sg/home/axsun/datasets.html, [Online].

[8] A. Agarwal and A. Dixit, "Fake News Detection: An Ensemble Learning Approach," 2020 4th International Conference on Intelligent Computing and Control Systems (ICICCS), 2020, pp. 1178-1183, doi: 10.1109/ICICCS48265.2020.9121030.

[9] Ksieniewicz P., Choraś M., Kozik R., Woźniak M. (2019) Machine Learning Methods for Fake News Classification. In: Yin H., Camacho D., Tino P., Tallón-Ballesteros A., Menezes R., Allmendinger R. (eds) Intelligent Data Engineering and Automated Learning – IDEAL 2019. IDEAL 2019. Lecture Notes in Computer Science, vol 11872. Springer, Cham. https://doi.org/10.1007/978-3-030-33617-2_34

[10] Parikh, Shivam B. and Pradeep K. Atrey. "Media-Rich Fake News Detection: A Survey." 2018 IEEE Conference on Multimedia Information Processing and Retrieval (MIPR) (2018): 436-441.

[11] Stemming. (n.d.) Wikipedia. [Online]. Available: https://en.wikipedia.org/wiki/Stemming. Accessed Oct 2, 2021.

[12] Naive Bayes classifier. (n.d.) Wikipedia. [Online]. Available: https://en.wikipedia.org/wiki/Naive_Bayes_classifier. Accessed Oct. 10, 2021

[13] Helmstetter, S., & Paulheim, H. (2018, August). Weakly supervised learning for fake news detection on Twitter. In 2018 IEEE/ACM International Conference on Advances in Social Networks Analysis and Mining (ASONAM) (pp. 274-277). IEEE.

[14]. Haiden, L., & Althuis, J. (2018). The Definitional Challenges of Fake News.

[15] Scikit-learn 1.0.1: machine learning in python

[16] Tacchini, E., Ballarin, G., Della Vedova, M. L., Moret, S., & de Alfaro, L. (2017). Some like it hoax: Automated fake news detection in social networks. arXiv preprint arXiv:1704.07506.

Authorized licensed use limited to: DELHI TECHNICAL UNIV. Downloaded on June 03,2022 at 06:31:31 UTC from IEEE Xplore. Restrictions apply.

FinTech

MDPI

Article

Comparison between Information Theoretic Measures to Assess Financial Markets

Luckshay Batra and Harish Chander Taneja *

Department of Applied Mathematics, Delhi Technological University, Delhi 110042, India; luckshay25@gmail.com
* Correspondence: hctaneja2629@gmail.com

Abstract: Information theoretic measures were applied to the study of the randomness associations of different financial time series. We studied the level of similarities between information theoretic measures and the various tools of regression analysis, i.e., between Shannon entropy and the total sum of squares of the dependent variable, relative mutual information and coefficients of correlation, conditional entropy and residual sum of squares, etc. We observed that mutual information and its dynamical extensions provide an alternative approach with some advantages to study the association between several international stock indices. Furthermore, mutual information and conditional entropy are relatively efficient compared to the measures of statistical dependence.

Keywords: entropy; conditional entropy; mutual information; financial markets; time series

check for updates

Citation: Batra, L.; Taneja, H.C. Comparison between Information Theoretic Measures to Assess Financial Markets. *FinTech* **2022**, *1*, 137–154. https://doi.org/10.3390/fintech1020011

Academic Editor: David Roubaud

Received: 18 March 2022
Accepted: 17 May 2022
Published: 19 May 2022

Publisher's Note: MDPI stays neutral with regard to jurisdictional claims in published maps and institutional affiliations.

Copyright: © 2022 by the authors. Licensee MDPI, Basel, Switzerland. This article is an open access article distributed under the terms and conditions of the Creative Commons Attribution (CC BY) license (https://creativecommons.org/licenses/by/4.0/).

1. Introduction

Financial markets are dynamic structures which exhibit nonlinear behavior. The correlation structure of time series data for financial securities incorporates important statistics for many real world applications such as portfolio diversification, risk measures, and asset pricing modeling [1,2]. Strict linear correlation studies are likely to neglect important financial system characteristics. Traditionally, non-linear correlations with higher order moments have been studied.

Some researchers considered the information measures theoretic approach to study this statistical dependence because of its potential to identify a stochastic relationship as a whole, including linearity and non-linearity (refer to [3–6]), and so making it a general approach. For example, network statistics based on mutual information can successfully replace statistics based on the coefficient of correlation [7]. Ormos et al. [8] defined continuous entropy as an alternative measure of risk in an asset pricing model. Mercurio et al. [9] introduced a new family of portfolio optimization problems called the return-entropy portfolio optimization (REPO), which simplifies the computation of portfolio entropy using a combinatorial approach. Novais et al. [10] described a new model for portfolio optimization (PO), using entropy and mutual information instead of variance and covariance as measurements of risk.

Ghosh et al. [11] presented a non-parametric estimate of the pricing kernel, extracted using an information-theoretic approach. This approach delivers smaller out-of-sample pricing errors and a better cross-sectional fit than leading factor models. Batra et al. [12] compared the efficiency of the traditional Mean-Variance (MV) portfolio model proposed by Markowitz with the models that incorporate diverse information theoretic measures such as Shannon entropy, Renyi entropy, Tsallis entropy, and two-parameter Varma entropy. Furthermore, they derived risk-neutral density functions of multi-asset to model the price of European options by incorporating a simple constrained minimization of the Kullback measure of relative information to evaluate the explicit solution of this multi-asset option pricing model [13].

In this paper, we propose a way of integrating non-linear dynamics and dependencies in the study of financial markets using several information entropic measures and some dynamical extensions using mutual information, such as the normalized mutual information measure, relative mutual information rate, and variation of information. We show that this approach leads to better results than other studies using a correlation-based approach on the basis of nine international stock indices which are traded continuously over eighteen years, i.e., (2001–2018).

The paper is divided into four sections. In Section 1, we give the theoretical framework of the information measures and methodology used. In Section 2, we describe financial market daily closing price data of some international stock indices with comparative results. In Section 3, we give a detailed comparative study with the help of tables and figures based on our analysis of the several international stock indices networks. In Section 4, we conclude the paper with a discussion.

2. Theoretical Framework: Entropy Measures

2.1. Shannon Entropy

Shannon [14] introduced the concept of entropy in the communication system. For the given probability distribution $p_i = P(X = x_i)$, $i = 1, 2 \ldots, n$ of a random variable X, the Shannon entropy $H(X)$ is given by

$$H(X) = -\sum_{i=1}^{n} p_i log_e p_i \,, \quad 0 \leq p_i \leq 1 \text{ and } \sum_{i=1}^{n} p_i = 1. \tag{1}$$

This entropy has found many applications in various diversified fields specifically as a measure of volatility in financial market [15].

2.2. Joint Entropy

The joint entropy is the uncertainty measure allied with a joint probability distribution of two discrete random variables, say $X = \{x_1, x_2, x_3, \ldots, x_s\}$ and $Y = \{y_1, y_2, y_3, \ldots, y_t\}$, and is defined as

$$H(X, Y) = -\sum_{i=1}^{s} \sum_{j=1}^{t} p_{ij} log_e p_{ij},$$

where $p_{ij} = p(x_i, y_j) = P(X = x_i, Y = y_j)$ is the joint probability density function of random variables X and Y.

2.3. Conditional Entropy

The conditional entropy, also called the equivocation, of the random variable $Y = \{y_1, y_2, y_3, \ldots, y_t\}$ given $X = \{x_1, x_2, x_3, \ldots, x_s\}$ is defined as

$$H(Y|X) = -\sum_{i=1}^{s} \sum_{j=1}^{t} p_{ij} log_e p_{j|i},$$

where $p_{j|i} = p(y_j|x_i) = P(Y = y_j|X = x_i)$ is the conditional probability of the random variable Y given $X = x_i$.

The joint and conditional entropy measures follow some properties as given below:

- $H(Y|X) \leq H(Y)$
- $H(X, Y) \leq H(X) + H(Y)$
- $H(X, Y) = H(X) + H(Y|X) = H(Y) + H(X|Y)$.

2.4. Mutual Information

The mutual information, also called the transinformation, of Y relative to X is defined as:

$$\begin{aligned} I(Y|X) =& H(Y) - H(Y|X) \\ =& H(Y) + H(X) - H(X, Y). \end{aligned}$$

This information measure follows some properties, as given below:

- Non-negative: $I(Y|X) \geq 0$
- Symmetric: $I(Y|X) = I(X|Y)$.

It is easy to see that

$$I(Y|X) = \sum_{i=1}^{s} \sum_{j=1}^{t} p_{ij} \, log_e \frac{p_{ij}}{p_i q_j},$$

where $p_i = P(X = x_i)$ and $q_j = P(Y = y_j)$ are marginal probability distributions of X and Y, respectively; and $p_{ij} = p(x_i, y_j) = P(X = x_i, Y = y_j)$ is the joint probability density function of X and Y.

Next, we can estimate the entropy of a specific stock X from the stock index Y, refer to [16], as

$$H(X) = I(X, Y) + H(X|Y); \tag{2}$$

Further, for Y as independent and X as dependent variables, the total variance of the stock can be subdivided into two parts: the explained sum of squares, i.e., systematic risk and the residual sum of squares, i.e., specific risk.

Next, we summarize some of the extensions of mutual information measure as follows:

2.4.1. Relative Mutual Information

The relative mutual information measure is directly comparable to the coefficient of determination (R^2), because both estimate the proportion of variability demonstrated by an independent variable in the dependent variable [16].

$$RMI_{XY} = \frac{I(X, Y)}{H(Y)}. \tag{3}$$

2.4.2. Normalized Mutual Information

For the two discrete random variables say, X and Y, the normalized mutual information is defined as:

$$NMI_{XY} = \frac{I(X, Y)}{\sqrt{H(X)H(Y)}}. \tag{4}$$

In addition to capturing strong linear relationships, this non-linear approach based on mutual information captures the non-linearity found in the volatile market data which could not be captured by the approach based on correlation coefficient [17].

2.4.3. Global Correlation Coefficient

This standardized measure of mutual information can be used as a predictability measure based on the distribution of empirical probability, and is defined as:

$$\lambda_{XY} = \sqrt{1 - e^{-2I(X,Y)}}. \tag{5}$$

It ranges from 0 to 1 and records the linear as well as the nonlinear dependence between two discrete random variables, say X and Y, and is easily comparable with the linear correlation coefficient [18].

$$\lambda_{XY} = \begin{cases} 0, & \text{if X contains no information on } Y \\ 1, & \text{if there is a perfect relationship between the vectors } X \text{ and } Y. \end{cases} \tag{6}$$

2.5. Variation of Information

This information measure, denoted as VI_{XY}, is a true estimate of distance between two discrete random variables, say X and Y and, as such it obeys the triangle inequality [19]. Furthermore, it is closely related with mutual information measure and is given as

$$\begin{aligned} VI_{XY} =& H(X) + H(Y) - 2I(X,Y) \\ =& H(X,Y) - I(X,Y) \\ =& H(X|Y) + H(Y|X). \end{aligned} \tag{7}$$

It is easy to see that

$$VI_{XY} = \begin{cases} 0, & \text{when } X \text{ is equal to } Y \\ < H(X,Y), & \text{when } X \text{ and } Y \text{ are dependent} \\ H(X,Y), & \text{when } X \text{ and } Y \text{ are independent,} \end{cases} \tag{8}$$

where $H(X)$ is the entropy of the discrete random variable $X = \{x_1, x_2, x_3, \ldots, x_s\}$ and $I(X,Y)$ is mutual information between two discrete random variables $X = \{x_1, x_2, x_3, \ldots, x_s\}$ and $Y = \{y_1, y_2, y_3, \ldots, y_t\}$ and $H(X,Y)$ is the joint entropy of X and Y.

3. Data and Result

The main objective of this paper is to show that information theoretic measures present a decent solution to the problem of dependence in the financial series data. For this purpose, we considered 14 time series comprising the daily closing price of the international stock indices and their selective stocks which were traded continuously between 1 January 2001 and 31 December 2018 (about 4433 observations in each time series).

To apply entropic measures in operation and to find their properties, we obtained daily closing price data over eighteen years of international stock market indices, namely IBOVESPA (Brazil), Hang Seng (Hong Kong), SSE Composite (China), Dow Jones Industrial Average (United States), CAC 40 (France), DAX (France), NASDAQ (United States), Nifty 50 (India) and BSE sensex (India), accessed on 1 August 2020 from in.finance.yahoo.com, the free financial data online platform. Furthermore, we make a comparison of two Indian market indices namely, NIFTY 50 and S&P BSE sensex with their common stocks. During the complete selection process, daily closing price data filtered to select stocks listed in their respective indices and as a result due to inadequate data, five stocks were selected from the study.

Our main emphasis is on determining the dependence level between each stock and its stock index, i.e., to select a stock which is more dependent on its relative index and this has been estimated by the information theoretic measures. Further, to compare two different indices with their stocks and measure their level of dependence, the concept of mutual information is used as analogous to covariance and normalized mutual information is calculated akin to the Pearson's coefficient of correlation.

4. Tables and Figures

Figure 1 presents the allocation of the aforementioned Indian stock indices with their selected stocks. Figure 2 gives the details of the distribution of the aforementioned international stock indices; and Figure 3 gives the nature of indices with their stocks. Next, Figures 4–7 represent the visual comparison of information and statistical measures. Furthermore, in Figures 4 and 5 if we increases bin counts, entropy and TSS measures become inversely symmetric. We have presented equivalence between statistical measures and information theoretic measures, refer to Table 1. From the data given in Tables 2–5, by using statistical software R (RStudio© 2021.09.1, 2009–2021 RStudio, Build 372, PBC, 250 Northern Ave, Boston, MA 02210), we present four correlation matrix plots of above-mentioned international indices with their stocks, refer to Figures 8 and 9.

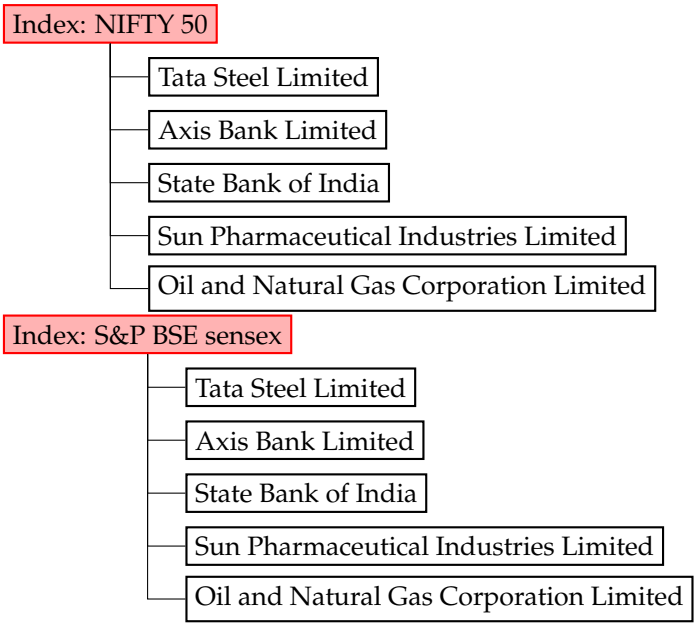

Figure 1. Distribution of Indian market indices with their stocks.

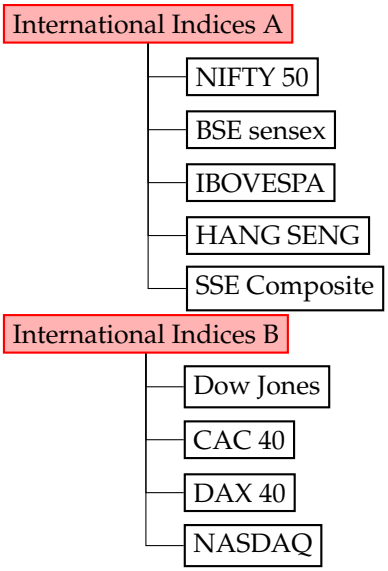

Figure 2. Distribution of International market indices.

Table 1. Equivalences between statistical measures and information theoretic measures.

Information Theoretical Measures	**Statistical Measures**
$H(Y)$ Entropy	(TSS) Total sum of squares
$H(Y\|X)$ Conditional entropy	(RSS) Residual sum of squares
I(X,Y) Mutual information	cov(X,Y) Covariance or (ESS) Explained sum of squares
$NMI_{X,Y}$ Normalized mutual information	R_{XY} Correlation
RMI_{XY} Relative mutual information	R^2_{XY} Coefficient of determination

Table 2. Correlation between NIFTY 50 index and its stocks with R^2 = 0.96765.

	NIFTY 50	SBI	ONGC	TATA STEEL	SUN PHARMA	AXIS BANK
NIFTY 50	1					
SBI	0.91277	1				
ONGC	0.75195	0.87759	1			
TATA STEEL	0.62706	0.70924	0.72980	1		
SUN PHARMA	0.84981	0.74144	0.63281	0.24771	1	
AXIS BANK	0.96812	0.88938	0.68445	0.49662	0.90294	1

Table 3. Correlation between BSE sensex index and its stocks with R^2 = 0.96035.

	BSE Sensex	SBI	ONGC	TATA STEEL	SUN Pharma	AXIS BANK
BSE sensex	1					
SBI	0.90630	1				
ONGC	0.77082	0.85210	1			
TATA STEEL	0.61634	0.69028	0.71104	1		
SUN Pharma	0.84751	0.74785	0.63540	0.23767	1	
AXIS BANK	0.96070	0.88372	0.67863	0.48074	0.90138	1

Table 4. Correlation between International Indices A.

	NIFTY 50	BSE Sensex	IBOVESPA	HANG SENG	SSE COMPOSITE
NIFTY 50	1				
BSE sensex	0.99312	1			
IBOVESPA	0.84651	0.85487	1		
HANG SENG	0.90201	0.91444	0.91677	1	
SSE COMPOSITE	0.62997	0.62134	0.66574	0.72005	1

Table 5. Correlation between International Indices B.

	DOW JONES	CAC 40	DAX	NASDAQ
DOW JONES	1			
CAC 40	0.51827	1		
DAX	0.94938	0.57404	1	
NASDAQ	0.99037	0.46469	0.94892	1

We discussed the choice of bin counts for the nature of calculation of statistical and information theoretic measures, see Tables 6–11. In general, the count of bins should be selected on the basis of availability of the number of observations of time series data. In Tables 6 and 7 we show a count of total number of bins for the indices NIFTY 50 (342 bins) and BSE sensex (341 bins), respetively; we come to a conclusion that BSE sensex is more uncertain stock index as compared to NIFTY 50 and furthermore, Axis bank is the underlying stock which is more dependent compared with other stocks.

Table 6. NIFTY 50 and its stocks.

	Entropy	Conditional Entropy	RSS	Mutual Information	Covariance	TSS/ESS	Normalized Mutual Informaion	Correlation	Relative Mutual Information	R^2	Global Correlation Coefficient	Beta	Joint Entropy	Variation of Information
Number of Bins: 13														
NIFTY 50	2.36540					624,968.00000								
SBI	2.45800	1.19399	525,211.40000	1.17139	14,421.80000	99,756.55000	0.48580	0.39952	0.49522	0.15962	0.95075	0.27691	3.65204	1.57500
ONGC	2.25030	1.27108	611,529.30000	1.09430	9615.42000	13,438.65000	0.47432	0.14664	0.46263	0.02150	0.94229	0.18463	3.52135	1.55790
TATA STEEL	2.31830	1.55828	271,045.30000	0.80710	39,897.10000	353,922.70000	0.34466	0.75253	0.34121	0.56631	0.89495	0.76606	3.87655	1.75198
SUN PHARMA	2.01200	1.24765	311,598.80000	1.11772	70,651.40000	313,369.20000	0.51235	0.70811	0.47253	0.50142	0.94501	1.35658	3.25969	1.46354
AXIS BANK	2.24080	0.95023	311,899.70000	1.41515	50,735.60000	313,068.3	0.61468	0.70777	0.59827	0.50093	0.97005	0.97417	3.19106	1.33263
Number of Bins: 114														
NIFTY 50	4.40485					155446.00000								
SBI	4.51377	2.36359	109,584.07000	2.04125	602.40700	45,861.93000	0.45778	0.54317	0.45222	0.29503	0.99153	0.43791	6.87737	2.19911
ONGC	4.27008	2.54428	154,842.61420	1.86057	90.22120	603.38580	0.42900	0.06230	0.43572	0.00388	0.98782	0.06559	6.81436	2.22571
TATA STEEL	4.42332	2.63715	117,870.67000	1.76769	543.83200	37,575.33000	0.40046	0.49165	0.39963	0.24172	0.98531	0.39533	7.06047	2.30060
SUN PHARMA	4.01116	2.17026	141,939.42000	2.23459	756.63700	13,506.58000	0.53161	0.29476	0.55709	0.08688	0.99425	0.55003	6.18142	1.98666
AXIS BANK	4.22039	2.13511	152,160.01800	2.26973	324.84100	3285.98200	0.52642	0.14539	0.53780	0.02113	0.99464	0.23614	6.35551	2.02133
Number of Bins: 234														
NIFTY 50	5.09440					82294.00000								
SBI	5.19725	2.41142	66,285.66000	2.68298	133.91900	16,008.34000	0.52141	0.44105	0.52665	0.19452	0.99766	0.37916	7.60868	2.21939
ONGC	4.95544	2.66188	81,787.85930	2.43251	29.42920	506.14070	0.48413	0.07842	0.47748	0.00615	0.99613	0.08332	7.61733	2.27701
TATA STEEL	5.12072	1.93975	68,218.60000	2.47435	117.95700	14,075.40000	0.48445	0.41356	0.48569	0.17103	0.99644	0.33397	7.06047	2.14152
SUN PHARMA	4.64187	2.37953	78,821.26900	2.71487	163.41200	3472.73100	0.55828	0.20542	0.53291	0.04219	0.99780	0.46267	7.02140	2.07521
AXIS BANK	4.91521	2.33849	80,765.57500	2.75591	76.24460	1528.42500	0.55074	0.13628	0.54096	0.01857	0.99797	0.21587	7.25371	2.12080
Number of Bins: 342														
NIFTY 50	5.45397					59342.00000								
SBI	5.56269	2.30139	48,867.00000	3.15258	63.97360	10,474.90000	0.57235	0.42014	0.57803	0.17652	0.99908	0.36761	7.86408	2.17059
ONGC	5.32691	2.57858	58,991.00000	2.87539	13.99120	350.64500	0.53346	0.07687	0.52721	0.00591	0.99840	0.08040	7.90540	2.24278
TATA STEEL	5.48573	2.48593	49,847.00000	2.96804	56.51610	9495.09000	0.54262	0.40001	0.54419	0.16001	0.99867	0.32476	7.97166	2.23687
SUN PHARMA	5.00516	2.36412	56,861.00000	3.08985	78.31970	2480.87000	0.59138	0.20447	0.56653	0.04181	0.99896	0.45005	7.36928	2.06867
AXIS BANK	5.27565	2.29104	58,604.00000	3.16292	31.07630	738.05400	0.58965	0.11152	0.57993	0.01244	0.99910	0.17858	7.56670	2.09851
Number of Bins: 494														
NIFTY 50	5.80256					42.468.00000								
SBI	5.90688	2.14323	35.651.97000	3.65933	31.17240	6816.03000	0.62504	0.40062	0.61950	0.16049	0.99966	0.36187	8.05011	2.09542
ONGC	5.67248	2.42322	42,191.98000	3.37934	7.23935	276.02000	0.58902	0.08061	0.59574	0.00649	0.99941	0.08404	8.09570	2.17172
TATA STEEL	5.83876	2.29205	35,612.20000	3.51050	27.99800	6855.81000	0.60311	0.40178	0.60124	0.16143	0.99955	0.32502	8.13082	2.14949
SUN PHARMA	5.32343	2.31891	41,213.97000	3.48364	35.53140	1254.03000	0.62679	0.17183	0.65439	0.02952	0.99952	0.41248	7.64235	2.03929
AXIS BANK	5.61646	2.51435	41,923.79000	3.51050	15.80730	544.21300	0.61493	0.11320	0.62503	0.01281	0.99955	0.18350	8.13082	2.14949
Number of Bins: 1482														
NIFTY 50	6.77728					17,490.00000								
SBI	6.88017	1.43809	15,580.71000	5.33919	3.61783	1909.30000	0.78189	0.33040	0.77602	0.10916	0.99998	0.30635	8.31826	1.72599
ONGC	6.66510	1.67938	17,431.45000	5.09790	0.70358	58.55070	0.75850	0.05785	0.76486	0.00334	0.99998	0.05958	8.34448	1.80182
TATA STEEL	6.81970	1.52493	15,687.37000	5.25235	3.19311	1802.63000	0.77257	0.32103	0.77017	0.10306	0.99998	0.27038	8.34463	1.75848
SUN PHARMA	6.27082	1.85394	17,199.72000	4.92333	3.85145	290.28400	0.75521	0.12882	0.78511	0.01659	0.99997	0.32613	8.12477	1.78925
AXIS BANK	6.58587	1.63262	17,377.21000	5.14466	1.50709	112.79300	0.77005	0.08030	0.78116	0.00644	0.99998	0.12762	8.21849	1.75323

Table 7. BSE sensex and its stocks.

	Entropy	Conditional Entropy	RSS	Mutual Information	Covariance	TSS/ESS	Normalized Mutual Information	Correlation	Relative Mutual Information	R^2	Global Correlation Coefficient	Beta	Joint Entropy	Variation of Information
Number of Bins: 13														
BSE sensex	2.36610					634,618.00000								
SBI	2.45447	1.21135	507,692.90000	1.15475	16,513.00000	126,925.10000	0.47917	0.44721	0.48803	0.20000	0.94900	0.31224	3.66582	1.58463
ONGC	2.24806	1.26131	617,196.60000	1.10479	10970.17000	17,421.43000	0.47902	0.16568	0.46692	0.02745	0.94353	0.20743	3.50937	1.55067
TATA STEEL	2.32674	1.56586	254,483.20000	0.80024	407,79.83000	380,134.80000	0.34105	0.77394	0.33821	0.59899	0.89342	0.77110	3.89260	1.75851
SUN PHARMA	2.00817	1.27706	332,931.90000	1.08904	69,300.58000	301,686.10000	0.49960	0.68947	0.46026	0.47538	0.94166	1.31040	3.28523	1.48195
AXIS BANK	2.22799	1.02924	329,834.50000	1.33686	50,682.83000	304,783.50000	0.58225	0.69301	0.56500	0.48026	0.96488	0.95836	3.25723	1.38577
Number of Bins: 31														
BSE sensex	3.15224					427,756.00000								
SBI	3.28062	1.68710	299,283.30000	1.46514	5517.76700	128,472.70000	0.45560	0.54800	0.46479	0.30034	0.97294	0.38698	4.96772	1.87151
ONGC	3.04249	1.75543	399,161.80000	1.39681	4018.90000	28,594.25000	0.45103	0.25854	0.44311	0.06684	0.96891	0.28185	4.79792	1.84421
TATA STEEL	3.15385	2.01077	306,297.50000	1.14147	6719.06700	121,458.50000	0.36202	0.53286	0.36211	0.28394	0.94763	0.47123	5.16463	2.00578
SUN PHARMA	2.79928	1.57570	197,588.50000	1.57654	182,22.33000	230,167.50000	0.53072	0.73354	0.50013	0.53808	0.97840	1.27799	4.37498	1.67285
AXIS BANK	3.04681	1.42946	203,804.30000	1.72278	12,906.50000	223,951.70000	0.55590	0.72356	0.54652	0.52355	0.98392	0.90517	4.47628	1.65936
Number of Bins: 143														
BSE sensex	4.62278					127,290.00000								
SBI	4.72456	2.42919	101,753.60000	2.19359	347.06340	25,536.36000	0.46937	0.44790	0.47451	0.20061	0.99376	0.38717	7.15375	2.22714
ONGC	4.49114	2.59902	125,777.00000	2.02375	101.78170	1513.03200	0.44414	0.10902	0.43777	0.01188	0.99122	0.11354	7.09017	2.25087
TATA STEEL	4.65221	2.64883	98,543.81000	1.97394	343.30990	28,746.19000	0.42565	0.47521	0.42700	0.22583	0.99030	0.38298	7.30105	2.30805
SUN PHARMA	4.19777	2.23328	118,472.40000	2.38949	472.82390	8817.57300	0.54243	0.26319	0.51689	0.06927	0.99578	0.52746	6.43106	2.01036
AXIS BANK	4.43235	2.24883	124,754.50000	2.37395	207.80280	2535.48800	0.52444	0.14113	0.51353	0.01991	0.99565	0.23181	6.68118	2.07538
Number of Bins: 341														
BSE sensex	5.45260					61,410.00000								
SBI	5.54762	2.31164	51,572.05000	3.14096	63.57059	9837.95000	0.57109	0.40025	0.57604	0.16020	0.99906	0.35196	7.85927	2.17216
ONGC	5.31997	2.56153	61,220.07650	2.89107	11.29412	189.92400	0.53678	0.06097	0.53021	0.00371	0.99845	0.06253	7.88151	2.23393
TATA STEEL	5.49089	2.47744	52,035.55100	2.97515	55.82941	9374.45000	0.54373	0.39070	0.54563	0.15265	0.99869	0.30910	7.96834	2.23454
SUN PHARMA	4.98351	2.34789	58,636.81300	3.10471	86.90882	2773.19000	0.59559	0.21250	0.56939	0.04515	0.99899	0.48117	7.33140	2.05589
AXIS BANK	5.26056	2.28971	60,892.79310	3.16289	26.05882	517.20700	0.59056	0.09177	0.58006	0.00842	0.99910	0.14427	7.55027	2.09460
Number of Bins: 403														
BSE sensex	5.61651					51,504.00000								
SBI	5.70792	2.25205	43,313.94000	3.36446	46.60945	8190.06000	0.59421	0.39877	0.59903	0.15901	0.99940	0.36379	7.95997	2.14371
ONGC	5.47974	2.49112	51,260.09620	3.12538	9.12437	243.90400	0.56336	0.06881	0.55646	0.00473	0.99903	0.07121	7.97086	2.20124
TATA STEEL	5.65151	2.40696	42,810.67900	3.20955	42.28607	8693.32000	0.56967	0.41083	0.57144	0.16878	0.99918	0.33005	8.05847	2.20202
SUN PHARMA	5.14687	2.32651	49,158.15900	3.28999	60.63433	2345.84000	0.61191	0.21341	0.58577	0.04554	0.99930	0.47326	7.47339	2.04533
AXIS BANK	5.41261	2.28429	51,126.86590	3.33221	17.46517	377.13400	0.60436	0.08557	0.59328	0.00732	0.99936	0.13631	7.69691	2.08918

Table 8. International market indices A.

	Entropy	Mutual Information	Correlation	Joint Entropy	Conditional Entropy	Relative Mutual Information
Number of Bins: 31						
NIFTY 50	3.15029					
BSE SNESEX	3.15202	2.11485	0.98778	4.18746	1.03544	0.67095
IBOVESPA	3.22630	1.51731	0.07871	4.85927	1.63298	0.47029
HANG SENG	3.20100	1.37211	−0.12990	4.97918	1.77818	0.42864
SSE COMPOSITE	2.95250	1.11249	0.44629	4.99030	2.03779	0.37679
Number of Bins: 143						
NIFTY 50	4.61974					
BSE SNESEX	4.62246	2.69859	0.95322	6.54361	1.92115	0.58379
IBOVESPA	4.71728	2.15750	0.10364	7.17952	2.46224	0.45736
HANG SENG	4.70464	2.05491	−0.10610	7.26947	2.56483	0.43678
SSE COMPOSITE	4.44981	1.89907	0.38445	7.17049	2.72067	0.42677
Number of Bins: 341						
NIFTY 50	5.45048					
BSE SNESEX	5.45222	3.37328	0.91252	7.52942	2.07720	0.61869
IBOVESPA	5.56159	3.06538	0.08978	7.94668	2.38509	0.55117
HANG SENG	5.54328	2.98039	−0.08060	8.01337	2.47009	0.53765
SSE COMPOSITE	5.28904	2.78918	0.34756	7.95034	2.66130	0.52735
Number of Bins: 403						
NIFTY 50	5.60935					
BSE SNESEX	5.61617	3.55583	0.9062	7.66968	2.05351	0.63314
IBOVESPA	5.72184	3.29735	0.08618	8.03383	2.31199	0.57627
HANG SENG	5.70409	3.20949	−0.08090	8.10395	2.39985	0.56266
SSE COMPOSITE	5.44616	3.02750	0.33483	8.02801	2.58184	0.55589

Table 9. International market indices B.

	Entropy	Mutual Information	Correlation	Joint Entropy	Conditional Entropy	Relative Mutual Information
Number of bins: 16						
DOW JONES	2.39734					
CAC 40	2.59322	0.74548	0.24985	4.24508	1.65186	0.28747
DAX	2.61923	1.23358	0.53358	3.78299	1.16376	0.47097
NASDAQ	2.35936	1.58996	0.76201	3.16674	0.80737	0.67389
Number of bins: 283						
DOW JONES	5.13384					
CAC 40	5.41487	2.42453	0.25323	8.12418	2.70930	0.44775
DAX	5.43041	2.63143	0.35362	7.93282	2.50241	0.48457
NASDAQ	5.14322	2.87793	0.58449	7.39913	2.25591	0.55955
Number of bins: 556						
DOW JONES	5.79039					
CAC 40	6.06928	3.52548	0.22600	8.33420	2.26491	0.58087
DAX	6.08881	3.61385	0.32142	8.26536	2.17654	0.59352
NASDAQ	5.79907	3.58918	0.55368	8.00029	2.20121	0.61892
Number of bins: 1132						
DOW JONES	6.41815					
CAC 40	6.69865	4.72292	0.19908	8.39388	1.69523	0.70505
DAX	6.71238	4.75384	0.28448	8.37669	1.66431	0.70821
NASDAQ	6.42275	4.54329	0.51441	8.29761	1.87486	0.70737

In other words, by observing the Axis bank stock, more information about NIFTY 50 and BSE sensex can be obtained. Furthermore, by observing ONGC stock, remaining uncertainty about the aforementioned indices is greater than other stocks. We have also come to the conclusion that the measure of global correlation coefficient can be useful if a lower count of bins are considered, otherwise this measure gives a similar output to all stock variables. Thus, in this case, the large count of data bins would not be a reasonable choice for comparative analysis of information theoretic measures with statistical measures, as even in very small change in the prices no depth-patterns are to be found. The coefficient of correlation is a long-standing estimator of the degree of statistical dependence; however mutual information has advantages over it. Furthermore, it is evident from

from Tables 7 and 8 that the Shannon entropy, mutual information and the conditional entropy perform well in accordance with the systematic risk and the specific risk derived through the linear market model. Furthermore, from Table 8, as per maximum count of bins (i.e., 403), the index BSE sensex can be used as the appropriate variable for the dependency of the index NIFTY 50.

Furthermore, studies based on other stock market indices and foreign exchange markets can also be carried out to further examine the effectiveness of this approach. One cannot directly visualize dependency of a stock on its index using technical analysis; therefore the investor has to work on theoretical aspects too. In Table 9, as per maximum count of bins (i.e., 1132), the international index DAX can be used as the appropriate variable for the dependency of DOW Jones in comparison of other indices, such as CAC 40 and NASDAQ.

Table 10. Comparison of Shannon entropy and Total sum of square of BSE Sensex stocks.

	BSE SENSEX				
Number of Bins	13	31	143	341	403
Entropy	2.36610	3.15224	4.62278	5.45260	5.61651
TSS	634,618.00000	427,756.00000	127,290.00000	61,410.00000	51,504.00000

Table 11. Comparison of Shannon entropy and Total sum of square of NIFTY 50 stocks.

	NIFTY 50					
Number of Bins	13	114	234	342	494	1482
Entropy	2.36539	4.40485	5.09440	5.45397	5.80256	6.77728
TSS	624,968.00000	155,446.00000	82,294.00000	59,342.00000	42,468.00000	17490.00000

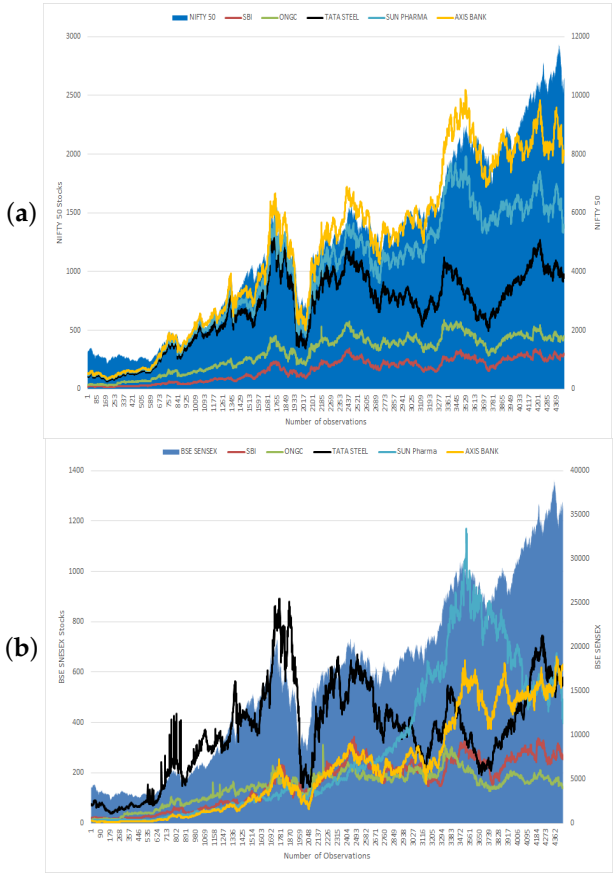

Figure 3. Nature of indices with their stocks. (**a**) NIFTY 50. (**b**) BSE SENSEX.

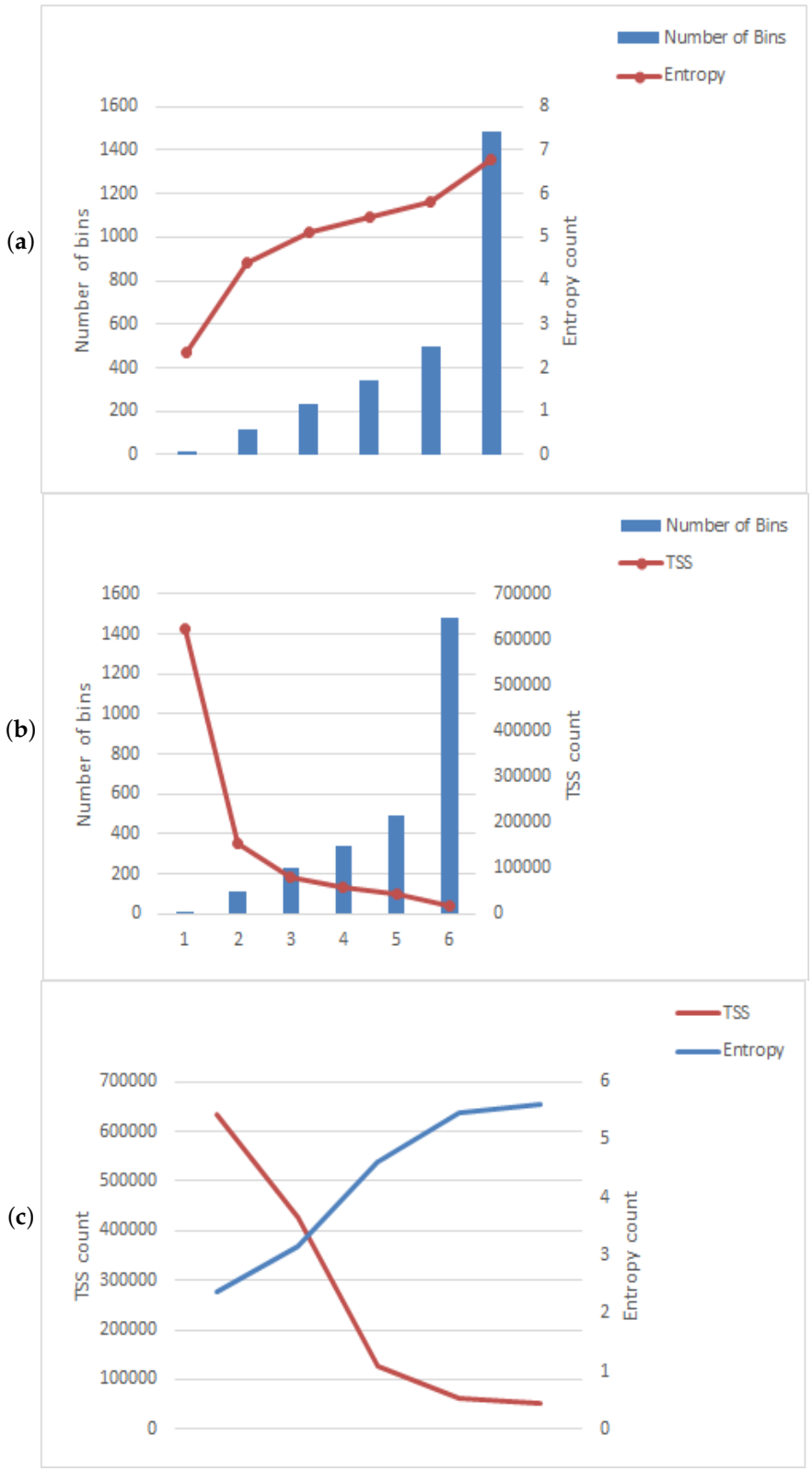

Figure 4. Comparison of Shannon entropy and Total sum of square of BSE sensex stocks. (**a**) Entropy with bins. (**b**) TSS with bins. (**c**) Entropy and TSS.

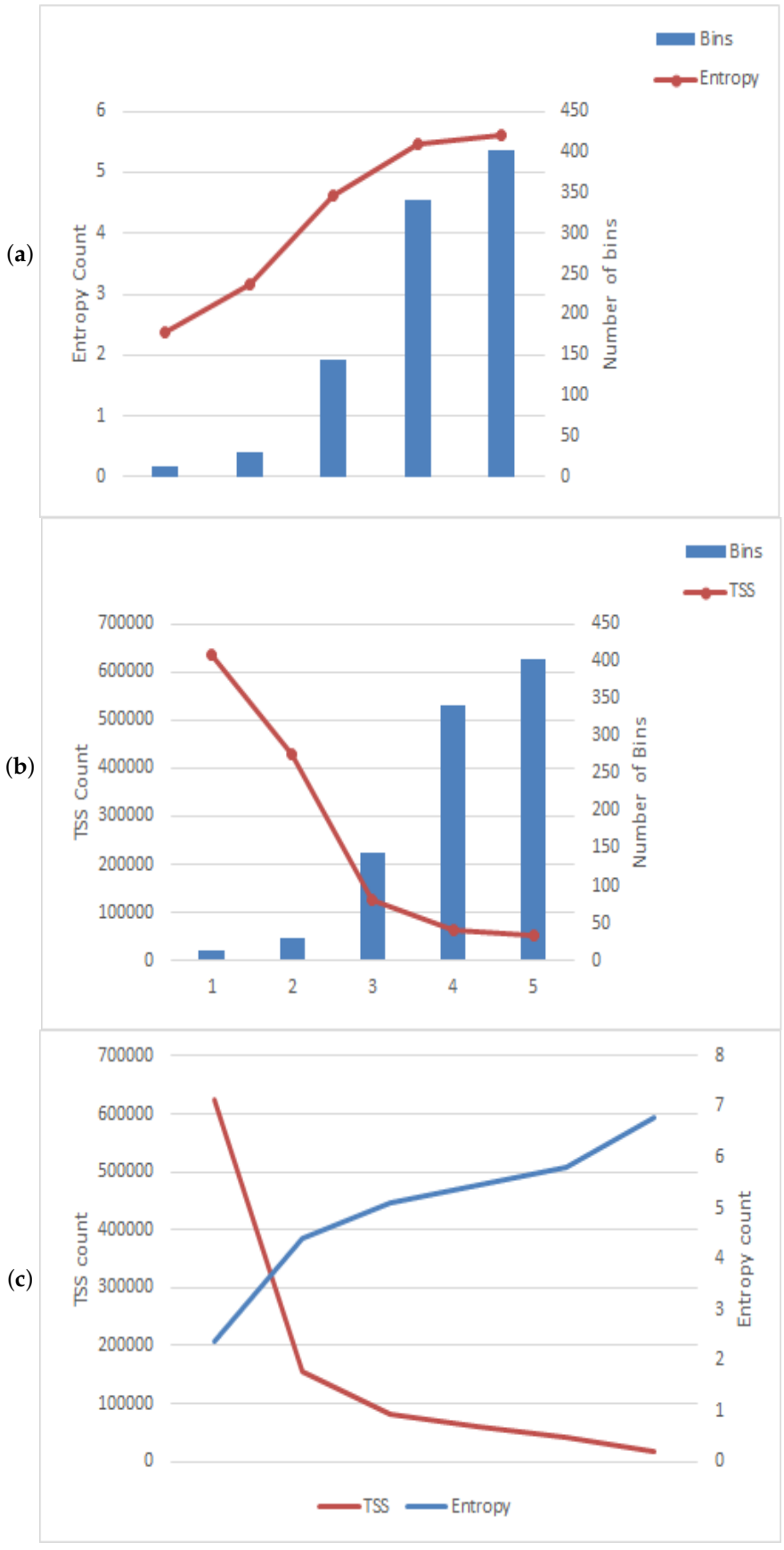

Figure 5. Comparison of Shannon entropy and Total sum of square of NIFTY 50 stocks. (**a**) Entropy with bins. (**b**) TSS with bins. (**c**) Entropy and TSS.

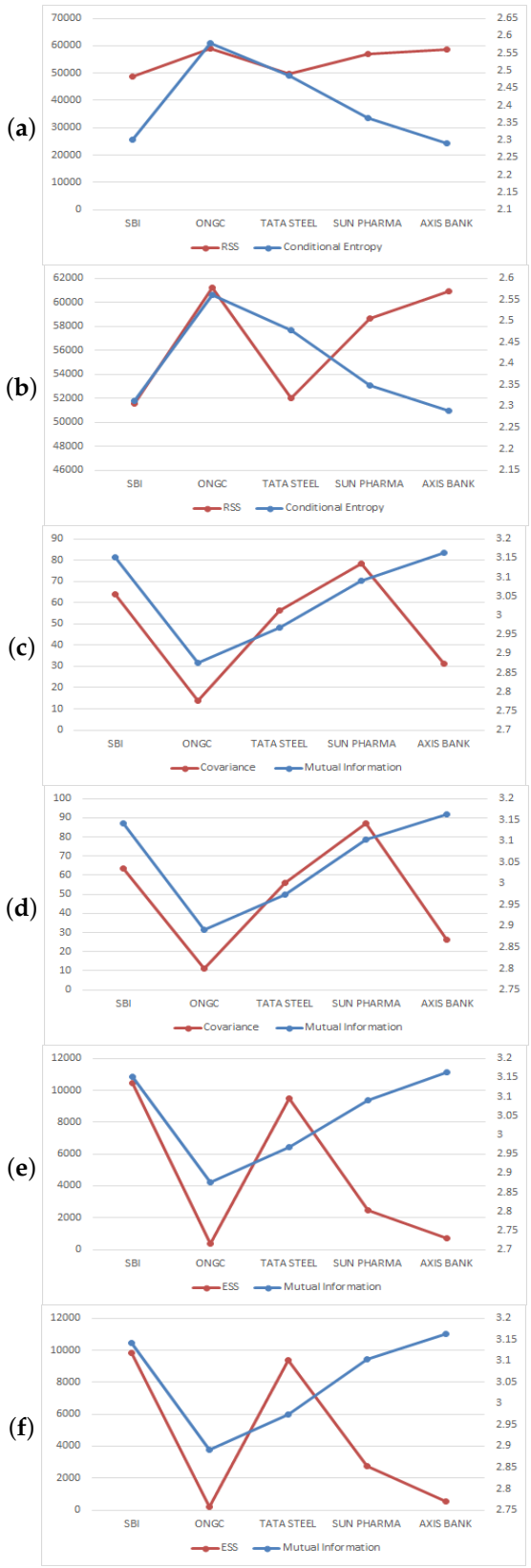

Figure 6. Comparison of information and statistical meaures of NIFTY 50 and BSE sensex stocks. (**a**) Conditional entropy and RSS with Nifty stocks. (**b**) Conditional entropy and RSS with BSE sensex stocks. (**c**) Mutual information and covariance with Nifty stocks. (**d**) Mutual information and covariance with BSE sensex stocks. (**e**) Mutual information and ESS with Nifty stocks. (**f**) Mutual information and ESS with BSE sensex stocks.

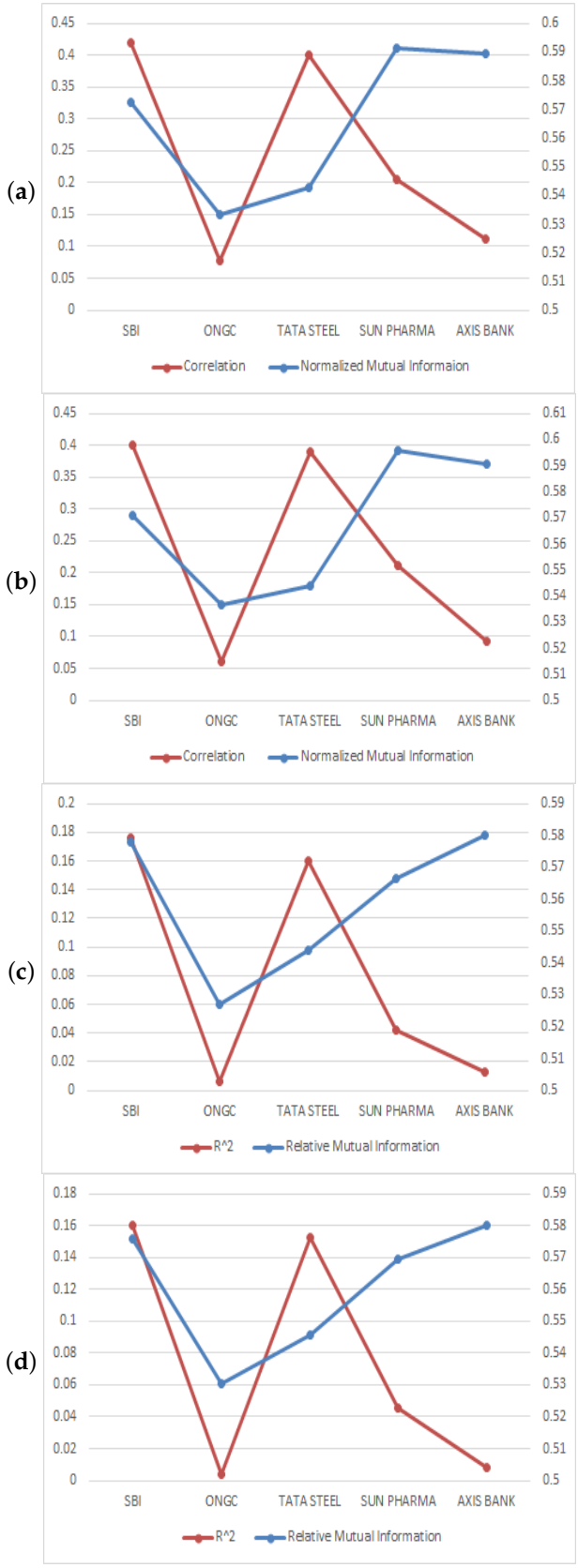

Figure 7. Comparison of information and statistical meaures of NIFTY 50 and BSE sensex stocks. (**a**) Correlation and Normalized mutual information with Nifty stocks. (**b**) Correlation and Normalized mutual information with BSE sensex stocks. (**c**) Relative mutual information and R^2 with Nifty stocks. (**d**) Relative mutual information and R^2 with BSE sensex stocks.

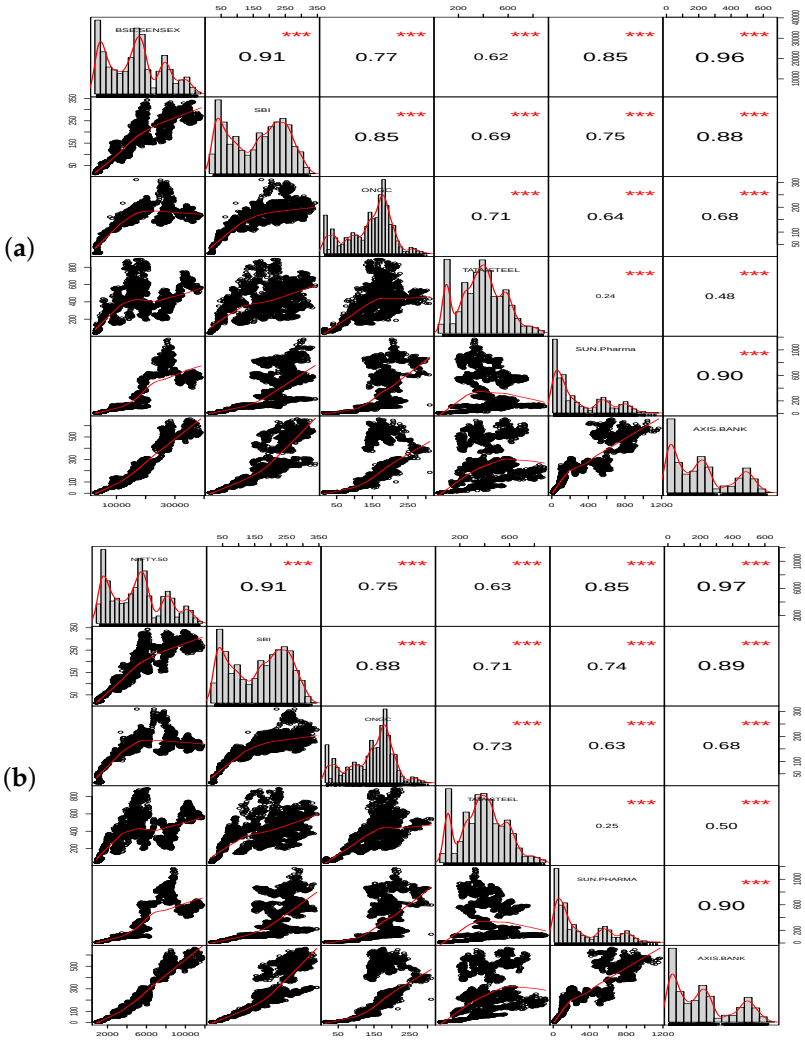

Figure 8. Correlation matrix plot of BSE sensex and Nifty 50 with their stocks SBI, ONGC, Tata Steel, Sun Pharma, and Axis Bank. (**a**) BSE sensex. (**b**) NIFTY 50. The distribution of each stock/index is shown on the diagonal; on the lower diagonal, the bi-variate scatter plots with the fitted higher order degree polynomial are shown and on the upper diagonal, the correlation value plus the significance level (*p*-values: 0.001) as stars ("***").

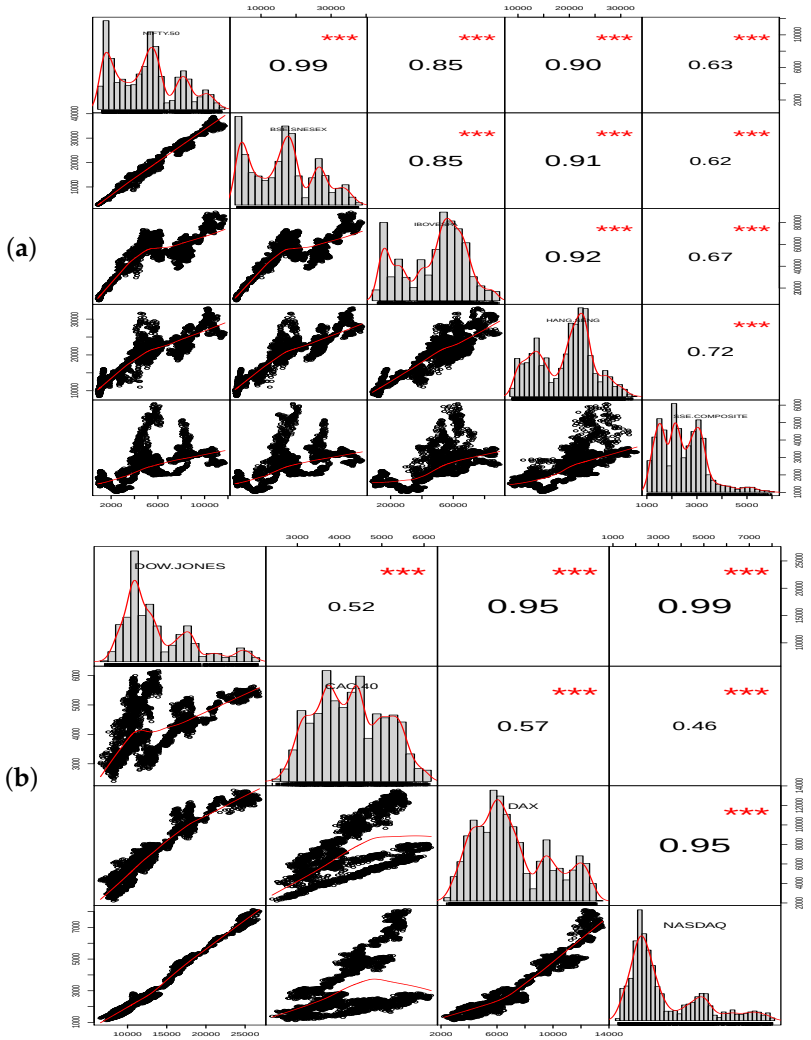

Figure 9. Correlation matrix plot of indices: Nifty 50 with BSE sensex, IBOVESPA, Hang Seng, and SSE Composite and Dow Jones with CAC 40, DAX, and NASDAQ. (**a**) Nifty 50. (**b**) Dow Jones. The distribution of each stock/index is shown on the diagonal; on the lower diagonal, the bi-variate scatter plots with the fitted higher order degree polynomial are shown and on the upper diagonal, the correlation value plus the significance level (*p*-values: 0.001) as stars ("***").

5. Discussion and Conclusions

5.1. Discussion

We find that the information measures such as mutual information is an ideal way to expand the financial networks of stock market indices based on statistical measures, while the measure of variation of information presents a different side of the markets but produces networks with troubling characteristics. The proposed methodology is sensitive to the choice of data bin counts in which the daily closing prices of market data are separated and require a large sample size. Furthermore, the comparison of entropy measures with statistical measures of dependent stock indices, such as Shannon entropy vs. variance of a stock, conditional entropy vs. residual sum of squares, coefficient of determination vs. the relative mutual information rate, and correlation vs. normalized mutual information measures indicate the further existence of non-linear relationships that are not identified by the statistical correlation measure and hence present a different aspect of market analysis.

Information measures such as Shannon entropy and one parametric entropy, such as Renyi and Tsallis entropies, were studied extensively by many researchers for analyzing volatility in financial markets. However, this concept can still be explored further using

various two parametric entropy measures. The non-linear fluctuations in a variety of markets (i.e., stock, future, currency, commodity, and cryptocurrency) require powerful tools such as entropy for extracting information from the market that is otherwise not visible in standard statistical methods. Further, we can extend the information theoretic approach used in this paper to highly volatile financial markets.

5.2. Conclusions

This paper uses information theoretic concepts such as entropy, conditional entropy, and mutual information and their dynamic extensions to analyze the statistical dependence of the financial market. We checked some equivalences between information theoretic measures and statistical measures normally employed to capture the randomness in financial time series. This approach has the ability to check the non-linear dependence of market data without any specific probability distributions. We used different international stock indices to address our problem. Mutual information and conditional entropy were relatively efficient compared to the measures of statistical dependence. From the results obtained, it is inferred that the information theoretic approach observes the dependency effectively and can be considered to be an efficient approach to study financial markets. In addition, these measures can provide some additional information for financial market investors.

Author Contributions: L.B., Conceptualization, Writing—original draft, Methodology, Software. H.C.T., Conceptualization, Supervision, Writing—review & editing. All authors have read and agreed to the published version of the manuscript.

Funding: This research received no external funding.

Institutional Review Board Statement: Not applicable.

Informed Consent Statement: Not applicable.

Data Availability Statement: Not applicable.

Acknowledgments: We thank Junzo Watada for their keen interest in this work, and the reviewers for their valuable comments leading to the improvement of the earlier version of paper.

Conflicts of Interest: The authors declare no conflict of interest.

References

1. Mantegna, R.N. Hierarchical structure in financial markets. *Eur. Phys. J. B Condens. Matter Complex Syst.* **2012**, *11*, 193–197. [CrossRef]
2. Tumminello, M.; Matteo, T.D.; Aste, T; Mantegna, R.N. Correlation based networks of equity returns sampled at different time horizons. *Eur. Phys. J. B* **2007**, *55*, 209–217. [CrossRef]
3. Gulko, L. The entropy theory of stock option pricing. *Int. J. Theor. Appl. Financ.* **1999**, *2*, 331–355. [CrossRef]
4. Taneja, H.C.; Batra, L.; Gaur, P. Entropy as a measure of implied volatility in options market. *AIP Conf. Proc.* **2019**, *2183*, 110005.
5. Batra, L.; Taneja, H.C. Evaluating volatile stock markets using information theoretic measures. *Phys. A Stat. Mech. Its Appl.* **2020**, *537*, 122711. [CrossRef]
6. Darbellay, G.A.; Wuertz, D. The entropy as a tool for analysing statistical dependences in financial time series. *Phys. A Stat. Mech. Appl.* **2000**, *287*, 429–439. [CrossRef]
7. Song, L.; Langfelder, P.; Horvath, S. Comparison of co-expression measures: Mutual information, correlation, and model based indices. *BMC Bioinform.* **2012**, *13*, 328 . [CrossRef] [PubMed]
8. Ormos, M; Zibriczky, D. Entropy-Based Financial Asset Pricing. *PLoS ONE* **2014**, *9*, E115742. [CrossRef] [PubMed]
9. Mercurio, P.J.; Wu, Y; Xie, H. An Entropy-Based Approach to Portfolio Optimization. *Entropy* **2020**, *22*, 332. [CrossRef] [PubMed]
10. Novais, R.G.; Wanke, P.; Antunes, J.; Tan, Y. Portfolio Optimization with a Mean-Entropy-Mutual Information Model. *Entropy* **2022**, *24*, 369. [CrossRef] [PubMed]
11. Ghosh, A.; Julliard, C.; Taylor, A.P. *An Information-Theoretic Asset Pricing Model*; London School of Economics: London, UK, 2016.
12. Batra, L.; Taneja, H.C. Portfolio optimization based on generalized information theoretic measures. *Commun. Stat. Theory Methods* **2020**, 1861294 . [CrossRef]
13. Batra, L.; Taneja, H.C. Approximate-Analytical solution to the information measure's based quanto option pricing model. *Chaos Solitons Fractals* **2021**, *153*, 111493. [CrossRef]
14. Shannon, C.E. A mathematical theory of communication. *Bell Syst. Tech. J.* **1948**, *27*, 379–423. [CrossRef]
15. Zhou, R.; Cai, R.; Tong, G. Applications of entropy in finance: A Review. *Entropy* **2013**, *15*, 4909–4931. [CrossRef]

16. Dionisio, A.; Menezes, R.; Mendes, D.A. Entropy and uncertainty analysis in financial markets. *arXiv* **2007**, arXiv:0709.0668.
17. Guo, X.; Zhang, H.; Tian, T. Development of stock correlation networks using mutual information and financial big data. *PLoS ONE* **2018**, *13*, e0195941. [CrossRef] [PubMed]
18. Soofi, E.S. Information theoretic regression methods. In *Applying Maximum Entropy to Econometric Problems (Advances in Econometrics)*; Emerald Group Publishing Limited: Bingley, UK, 1997; Volume 12, pp. 25–83.
19. Melia, M. Comparing clusterings—An information based distance. *J. Multivar. Anal.* **2007**, *98*, 873–895. [CrossRef]

TechRxiv
Powered by IEEE

Complaint and Severity Identification from Online Financial Content

This paper was downloaded from TechRxiv (https://www.techrxiv.org).

LICENSE

CC BY 4.0

SUBMISSION DATE / POSTED DATE

17-06-2022 / 21-06-2022

CITATION

Bhatia, Rohan; Singh, Apoorva; Saha, Sriparna (2022): Complaint and Severity Identification from Online Financial Content. TechRxiv. Preprint. https://doi.org/10.36227/techrxiv.20087675.v1

DOI

10.36227/techrxiv.20087675.v1

Complaint and Severity Identification from Online Financial Content

Apoorva Singh, Rohan Bhatia, and Sriparna Saha

***Abstract*—The automatic detection of financial complaints can benefit businesses and online merchants. Compared to manually tagged complaints, they can use this information to monitor and address issues and effectively route them to appropriate teams. This can also promote greater transparency and accountability when dealing with consumer financial products and services, strengthening the firm's brand value. In linguistic studies, complaints have been classified into severity categories based on the level of risk the complainant is prepared to accept. Furthermore, since emotions influence every speech act, an individual's emotional state considerably impacts the complaint expression. In this paper, we introduce a Financial Complaints resource, a collection of annotated complaints arising between financial institutions and consumers expressed in English on Twitter. The dataset has been enriched with the associated emotion, sentiment, and complaint severity classes. The dataset comprises 3149 complaint and 3133 non-complaint instances spanning over ten domains (e.g., credit cards, mortgages, etc.). For a comprehensive evaluation of our dataset, we develop a multi-task framework for complaint detection and severity classification with emotion recognition and sentiment classification as the additional tasks and compare it with several existing baselines[1].**

***Index Terms*—Complaint Corpus, Complaint Detection, Complaint Severity Detection, Deep learning, Finance Complaints, Multi-task learning**

I. Introduction

ARTIFICIAL INTELLIGENCE (AI) is transforming how people and organizations access and manage their finances. While the shift from traditional financial services to digital finance was already underway pre-pandemic, the pandemic accelerated the process as stay-at-home requests became the new normal for financial institutions, and customers decided to seek more self-service options. AI and machine learning in finance cover everything from fraud detection to chatbot assistants and task automation. Other than these mainstream applications, addressing digital service complaints could be a significant commercial application for AI in finance. Compared to manually tagged complaints, automated detection of financial complaints pertaining to fraudulent transactions, delayed fund transfers, lousy customer service, etc., could help direct them to appropriate teams. This can further help promote fairness and transparency while dealing with loans, credit cards, and other consumer financial products and services, thus improving customer experience and increasing the organization's brand value.

In linguistics, complaining is defined as an individual's statement of dissatisfaction with an enterprise, commodity, or event [1]. Complaints have been grouped into various degrees of severity based on the emotional intensity of the complaint, the amount of face-threat that the complainer is willing to undertake, and the complaint's motive [2], [3]. The objective of complaining could be to voice dissatisfaction, seek explanations, or both. Identifying complaints and associated severity levels in natural language is crucial for downstream application developers such as customer service chatbots [4] and commercial organizations to improve their customer support capabilities by identifying and resolving complaints [5].

Various social media and microblogging services, such as Twitter[2], Facebook[3], and Tumblr[4], have skyrocketed in popularity in recent years. The reason being all these forums enable effective communication amongst Web users worldwide. These social media sites, which offer millions of messages and information to be exchanged daily, are multifaceted and invaluable resources for investigating and understanding people's perceptions and evaluating the data generated by participants. Among various social media platforms, Twitter is among the most widely used social media services, with engaging individuals, famous events, and intriguing issues. The social aspect of Twitter, combined with its huge volume, has transformed it into a cost-effective data repository for exploring and evaluating activities, conduct, and user opinions. As a result, the crux of this study is analyzing Twitter-based complaints essentially focused on the Financial domain.

The intended content of every speech act is strongly influenced by a user's emotional condition [6]. Emotion detection is far more sophisticated and fine-grained in terms of research than sentiment classification [7]. Emotion provides a deeper understanding of the customer's mind when combined with sentiment. A statement, for example, could entail only a negative sentiment, whereas emotion could be anger or even disgust. The relationship between

Apoorva Singh and Sriparna Saha are with the Department of Computer Science and Engineering, Indian Institute of Technology, Patna, India (e-mail: apoorva_1921cs19@iitp.ac.in).

Rohan Bhatia, is with Delhi Technological University, Delhi, India (e-mail: rohanbhatia_2k19ep079@dtu.ac.in).

[1]The corpus and code will be made publicly available in the camera-ready version.

[2]http://twitter.com/

[3]https://facebook.com/

[4]https://tumblr.com/

emotion and sentiment urges us to examine the sentiment and emotion of customers while studying complaints.

The following are the major contributions of our proposed work:

- We curate a new corpus *Financial Complaints* (*FINCORP*) for aiding complaint identification and complaint severity classification research.
- We perform good quality annotations for the *FINCORP* dataset for solving four tasks: complaint detection, severity level detection, emotion recognition, and sentiment analysis.
- We present a framework for joint learning of (a) binary complaint classification, (b) complaint severity level classification, (c) emotion recognition, and (d) sentiment analysis. Complaint Identification (CI) and Complaint Severity level classification (CS) are the primary tasks in our multi-task framework. In contrast, Emotion Recognition (ER) and Sentiment Analysis (SA) are considered additional tasks. According to experimental results, the proposed approach surpasses the baselines and state-of-the-art approaches.

The rest of the paper is structured as follows. We present a brief overview of the existing literature in Section 2. In Section 3, we go over the specifics of the proposed dataset. In Section 4, we describe our proposed technique for multi-task experiments. The experimental setting and results analysis are covered in Section 5. Finally, we conclude in Section 6 with a discussion on future work prospects.

II. Related Work

This section discusses some of the prior works on the complaint identification task and the publicly available annotated complaint corpora.

A. Complaints in Linguistic Studies

Previous work in linguistics has categorized complaints based on their severity and directness. Complaints can be divided into four fine-grained severity classifications, according to Trosberg [2]: (a) no explicit reproach; (b) disapproval; (c) accusation; and (d) blame. Quite recently, [3] divided complaints into three categories: very direct, moderately direct, and indirect. Clear violations of expectations are referred to as direct complaints (i.e., very direct and moderately direct). On the other hand, indirect complaints do not directly specify or imply a breach of expectations. Furthermore, the contrast between very direct and moderately direct is that the former underlines the obligation of the complaint recipient, while the latter does not.

B. Multi-task Learning

Previous findings [8], [9], [10] have confirmed the efficiency of multi-task systems by simultaneously learning multiple associated tasks. An individual's emotional state and sentiment have a decisive impact on the intended content [6]. Along with sentiment, emotion offers a deeper understanding of the consumer's mindset [11], [8]. The correlation between emotion and sentiment motivates us to consider complainants' sentiment and emotion while analyzing complaints. Moreover, sentiment and emotion play significant roles in human interactions and thereby contribute toward building efficient and versatile artificial intelligence-based systems [7].

Table I
Statistics of the existing and proposed dataset for complaint identification

Dataset	Size	Description
Complaints [12]	3449 instances out of which 1235 are complaints	Sample instances collected from Twitter grouped in nine generic domains.
Product Review [13]	3449 instances out of which 566 are complaints	Product Reviews collected from Amazon and Youtube websites.
FINCORP	6282 instances out of which 3149 are complaints	Sample instances collected from Twitter based on financial product type & concerns.

C. Complaint Identification

Complaint identification on social media is a time-consuming and challenging process that needs identifying complaints from disparate and noisy text samples with character constraints, the use of unpredictable abbreviations, and sarcastic expressions. Text-based complaints have earlier been investigated via semi-supervised strategies, complex feature engineering-based machine learning methods, and deep learning models [14], [12], [15]. In the work [12], authors proposed a logistic regression model with hand-crafted features for detecting complaints. The authors of the work [16] used an ensemble of neural language models enhanced by the usage of transformer networks on a Twitter-based Complaint dataset. In linguistics, complaints were earlier classified based on responsible branch, the level of urgency and the possibility of receiving a response [17], [18], [19].

D. Complaint Datasets

The *Complaints* dataset[5] was published in the work [12]. The authors selected 93 customer service handles from Twitter and sampled original tweets addressed to these accounts. Only tweets that received a response from the customer support accounts were considered. A total of 1971 tweets were collected using this method. Additionally, 1478 tweets were sampled to guarantee a diverse and representative range of tweets. Overall, the

[5]https://github.com/danielpreotiuc/complaints-social-media

Table II
ANNOTATION EXAMPLES FOR EACH COMPLAINT SEVERITY LEVELS

Severity level	Annotation Example
Accusation	I ordered a mattress from your site. Item is missing now. You are doing fraud.
Blame	One payment was made with my consent the another payment seems a fraud transaction gone to an unkown account.
Disapproval	Can't even begin to tell how disappointed I am with crypto market. Lost so much money.
No explicit reproach	I have a problem and need help, support site kept putting me in a loop. Help!

Table III
ANNOTATION EXAMPLES FOR EACH EMOTION CLASS

Emotion	Annotation Example
Anger	Most of the time your ATM machines does not work. Over that you will charge ATM usage charges also! What the hell is your problem?
Disgust	What kind of service is this? Absolutely pathetic and disgusting packaging. I want my money back.
Fear	I am scared due to this pandemic and lockdown will worsen our world economy.
Happiness	I love your mobile app, makes it so easy to do all my payments from one place. Awesome!
Sadness	I am not able to use netbanking and mobile since last evening. When will downtime end?
Surprise	Best investment I've ever made. The knowledge and understanding there is amazing!!
Other	Can we apply debit card in our nearest branch or only in home branch and what documents are required for this purpose?

dataset consists of 2214 non-complaints and 1235 complaints in English. The dataset was grouped into nine domains (i.e., Apparel, Cars, Electronics, Food, Retail, Service, Software, Transport, and Other). Recently in the work [15], authors extended the *Complaints* dataset with the complaint severity classes and analyzed the effect of severity levels on CI.

The *Product Review* corpus[6] [13] is a Hindi language-based product review corpus. This corpus is a collection of product reviews posted on the retail website Amazon[7] and the video-sharing platform, YouTube[8] comment section. The corpus comprises 3711 instances, with 3145 being non-complaints and 566 being complaints. The dataset was further grouped into five domains (i.e., Book, Headphones, Phone, Watch, and Miscellaneous).

[6]https://github.com/MrRaghav/Complaints-mining-from-Hindi-product-reviews/blob/master/amazon-youtube-hindi-complaints-data.xlsx
[7]https://www.amazon.in/
[8]https://www.YouTube.com/

Figure 1. One hundred most frequent words used for expressing complaints by Twitter users.

In this work, we introduce the *Financial Complaints* dataset (*FINCORP*), which unlike the *Complaints* and *Product Review* datasets, is a balanced dataset with nearly equal percentage of complaints (50.13%) and non-complaints (49.87%) samples. Unlike the other two datasets, which contain generic complaints from various domains, our dataset focuses on grievances arising between financial institutions and consumers on the social media network Twitter. Another unique feature of our dataset is that, in addition to the complaint identification axis, we have expanded the dataset on three other closely related axes (severity level classification, sentiment classification, and emotion recognition) to better understand the nuances of the complaint identification task. To the best of our knowledge, this is the first gold standard complaint dataset specifically dealing with Financial complaints.
We create a word cloud to graphically depict the frequency of words that appear more frequently in complaints expressed on Twitter. The more frequently a term occurred in the complaint tweets, the larger the term is in the image. Figure 1 depicts the top 100 terms used by 6282 Twitter users to convey their dissatisfaction. If we observe Figure 1 closely, we will see that Twitter users complain more frequently using key phrases like response, refund, and please, alongside other words like RBI, fraud, and help. Table I shows the details of various existing and proposed CI-related datasets.

III. Corpus Description

The existing complaint datasets [12], [13] constitute only binary-class complaints. To encourage complaint identification and severity prediction research in the financial domain, we curate a *Financial Complaints* dataset (*FINCORP*) labeled with complaint labels, severity classes,

emotion, and sentiment classes. We chose Twitter as the data source as it is a forum that allows for a lot of self-expression, and users can communicate directly with each other or with corporate support handles. Tweets are freely available and are a popular choice for data analysis in various other similar tasks such as sentiment and emotion analysis ([9], [8]), etc. Here, we discuss the details of the FINCORP dataset.

A. Data Collection

Complaints account for a small percentage of all Twitter posts. Many companies employ Twitter to offer customer support and deal with customer complaints. To collect finance-related complaints and opinions from tweets, we use Tweepy[9] library to fetch tweets containing specific keywords and phrases using its *cursor class*. Based on an analysis of previous complaint datasets, we used a combination of keywords such as credit card/ debit card/ net banking/ UPI in combination with transaction failure/ fraud/ no response/ customer support/ complaint, etc., to fetch finance-related complaint tweets. Twitter Developers'[10] account is required to use this library, in which API tokens are provided by Twitter necessary to make the tweepy API object. In order to fetch tweets, queries in the form of strings have to be passed to the cursor object, and tweets containing those strings can be fetched and saved into data structures. We collected 6945 tweets to be considered for annotation using this technique.

Furthermore, we manually sorted the tweets into ten domains (Credit card, Customer service, Debit card, Economy, Financial policies, Investments, Loans, Retail banking, Salary, and Transaction failure) based on the financial product type and concerns expressed. We have done this to enable complaint analysis on a more granular level. In related studies on complaint analysis, tweets and product reviews were similarly sorted based on domains ([12], [13]).

We anonymize all usernames and URLs in the tweet and substitute them using placeholder tokens for preprocessing. Using langid.py ([20]), tweets were filtered for English, and retweets were discarded. The Unicode emojis in the tweets were converted to emoji short text with the help of a Python module called Emoji. The Python library Textblob was used to correct the spellings of many improperly spelled words. We use the NLTK library to remove stopwords and stem the corpus using Snowball Stemmer.

B. Data Annotation

We selected three graduate students[11] who are articulate in English to annotate the tweets with suitable complaint/non-complaint classes, severity levels, as well as emotion and sentiment tags. Before the annotation process began, the guidelines for annotation were provided.

[9]https://www.tweepy.org/
[10]https://developer.twitter.com/
[11]Annotators were recruited from the author's institution.

Table IV
DOMAIN-WISE DATA DISTRIBUTION IN THE *FINCORP* DATASET.

Domain	Non-Complaints	Complaints
Credit card	402	238
Customer service	12	697
Debit card	668	191
Economy	600	4
Financial policies	238	29
Investments	906	70
Loans	102	285
Retail banking	45	303
Salary	28	140
Transaction failure	132	1256
Total	3133	3149

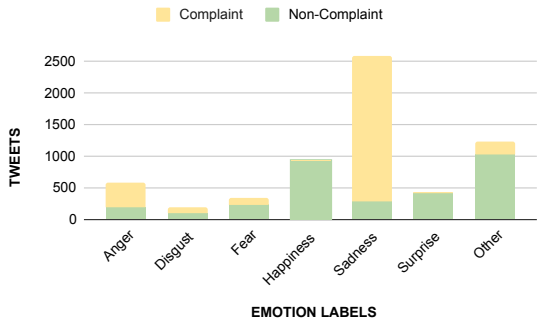

Figure 2. Distribution of emotion labels across *FINCORP* dataset.

Some sample cases outside the corpus were provided to train the annotators for the annotation work.
Annotators were selected using the following criteria:

- They are at least 22 years old and fluent in English (reading, writing, and speaking).
- Prepared to read, interpret, and annotate twitter instances according to the provided guidelines.

A few examples were provided before annotation for complaint severity level, and emotion task annotation as shown in Table II, III, respectively. Initially, we construct a binary annotation task to determine whether or not a tweet involves a complaint. Tweets are most often brief and convey a single idea. As a result, if a tweet includes a single complaint speech act, we consider the overall tweet to be a complaint. We utilize the complaint definition from earlier linguistic research [21] for complaint annotation: *A complaint presents a state of affairs that breaches the writer's clear expectation.*

We utilize the complaint severity levels (*no explicit reproach, disapproval, accusation, and blame*) defined in [2] as it is considered a benchmark in linguistic studies[12]. According to [2], classes are disconnected. In the 'No explicit reproach' class, the reason for the complaint is not specified, and the complaint is not harsh. The 'Disapproval' class conveys clear negative emotions, including discontent, anger, contempt, or disapproval. The primary distinction between 'Accusation' and 'Blame' is that the

[12]We assign a 'No Complaint Severity' class for non-complaint tweets.

Table V
SAMPLE INSTANCES FROM THE *FINCORP* DATASET. COMP: COMPLAINT, NON-COMP: NON-COMPLAINT

Domain	Tweet	Label	Severity	Emotion	Sentiment
Loan	Why is your Panvel branch team not working on disbursing my loan which is approved since Friday?	Comp	Accusation	Sadness	Negative
Transaction Failure	I am not able to do online transaction from my credit card and customer care number also not responding.	Comp	Blame	Sadness	Negative
Credit Card	Rejecting Lost Credit Card Replacement without any valid reason! Using your card service for 10years. Highly disappointed with the way you treated your existing loyal customer.	Comp	Disapproval	Anger	Negative
Debit Card	I've found a Debit Card on my walk. I'd like to report it found. What do I do next?	Comp	No explicit reproach	Other	Neutral
Credit Card	Kpop concert tickets are great for my credit card points I got like $100 off a flight thanks.	Non-Comp	Non-Comp	Happiness	Positive

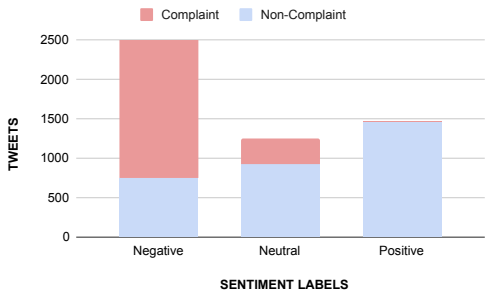

Figure 3. Distribution of sentiment polarities across *FINCORP* dataset

Table VI
DISTRIBUTION OF COMPLAINT INSTANCES ACROSS THE INDIVIDUAL SEVERITY LEVELS.

Severity class	Amount
Accusation	121
Blame	876
Disapproval	604
No explicit reproach	1548
Total	3149

complainant assumes the complainee is responsible for the violation in the latter. For the emotion annotation of the *FINCORP* dataset, we consider Ekman's [22] six basic emotions (*anger, disgust, fear, happiness, sadness, and surprise*). Other than these six basic emotions, we add a category 'Other' to represent such tweets that do not fall under the six emotion classes' scope. For the sentiment annotation, we consider three sentiment classes (*negative, neutral, positive*).
The final complaint, severity level, emotion, and sentiment labels are selected by utilizing the majority voting technique. The final annotated dataset excluded tweets with no common severity level, emotion, or sentiment label.

Finding agreement among the different annotators is vital in any annotation task requiring two or more annotators to obtain a credible annotated dataset. One such metric is Fleiss' kappa [23] score. We computed the Fleiss' kappa score on the annotated dataset to assess inter-rater agreement among the three annotators. We attained agreement scores of 0.83, 0.69, 0.68, and 0.82 on the complaint, severity level, emotion, and sentiment tasks, respectively, indicating that the annotations are of good quality.

C. Statistics

The *FINCORP* dataset comprises 6282 tweets with the corresponding complaint, severity, emotion, and sentiment labels. It consists of 3133 tweets in the non-complaint category (49.87%) and 3149 tweets in the complaint category (50.13%). Distributions of sentiment and emotion labels across the dataset are shown in Figure 2 and 3, respectively. Table IV presents the domain-wise data distribution statistics. Table V shows sample instances along with the corresponding complaint, severity, emotion, and sentiment labels. As can be observed from Figure 3, most of the complaint-type tweets have a negative polarity, with a few being neutral. In the case of emotion labels, most complaint tweets show sadness, and the next significant emotion is anger. The distribution of tweets across complaint severity classes is shown in Table VI.

IV. METHODOLOGY

In this section, we outline our problem and discuss the details of the baselines used for the evaluation of the dataset.

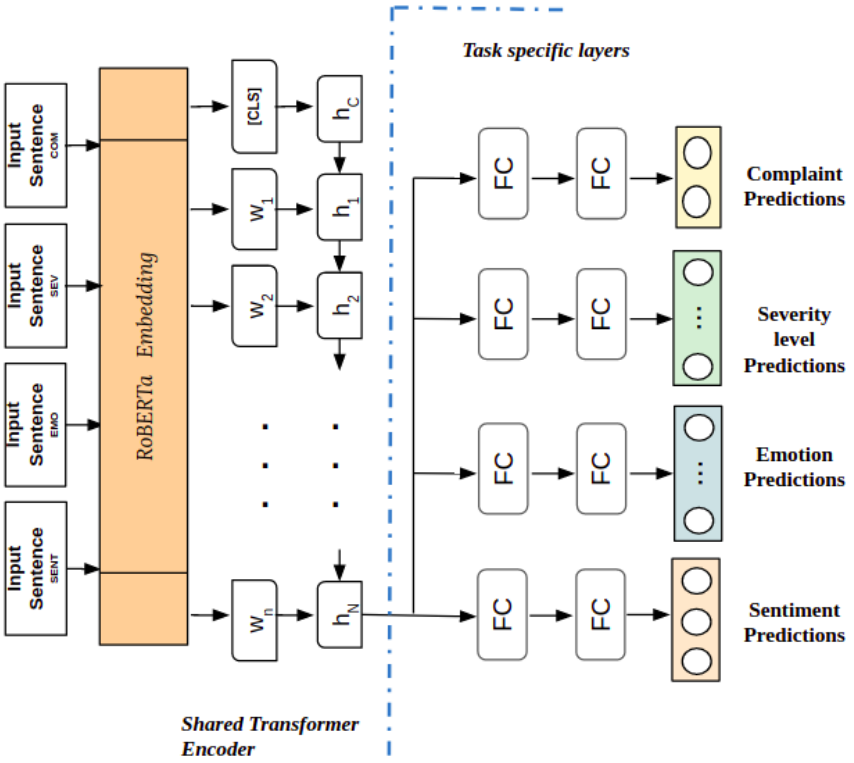

Figure 4. The architectural diagram of Multi-task Learning with RoBERTa (MTL-RoBERTa) framework. FC: Fully connected layers

A. Problem Definition:

We intend to learn four closely related tasks at the same time, including binary complaint identification (main-task), complaint severity prediction (main-task), emotion recognition, and sentiment analysis (auxiliary tasks). Let $(t_{\mathrm{i}}, e_{\mathrm{i}}, s_{\mathrm{i}}, m_{\mathrm{i}}, c_{\mathrm{i}})_{i=1}^{T}$ be a set of T instances where e_{i}, s_{i}, m_{i} and c_{i} represent the matching emotion, sentiment, severity and complaint labels for ${t_{\mathrm{i}}}^{\mathrm{th}}$ tweet, respectively. Here, $t_{\mathrm{i}} \epsilon T$, $e_{\mathrm{i}} \epsilon E$ (emotion classes), $s_{\mathrm{i}} \epsilon S$ (sentiment classes), $m_{\mathrm{i}} \epsilon M$ (severity classes) and $c_{\mathrm{i}} \epsilon C$ (binary complaint classes).

Our multi-task learning framework's objective is to maximize the function f (Eqn 1) that draws a new instance t_{i} to its fitting emotion label e_{i}, sentiment label s_{i}, severity label m_{i} and complaint label c_{i}, simultaneously.

$$argmax(\Pi_{k=0}^{R} P(m_i, s_i, e_i, c_i | t_i; \theta)), \tag{1}$$

where t_i is the input tweet whose complaint label (c_i), severity label (m_i), emotion label (e_i), and sentiment label (s_i) and are to be predicted. θ denotes the model's parameters we aim to optimize.

B. Multi-task learning with RoBERTa (MTL-RoBERTa):

Based on the work in [24], we employ multi-task learning with hard parameter sharing (MTL) to boost the binary complaint classification utilizing severity levels, emotion, and sentiment tasks. MTL with hard parameter sharing comprises a single encoder that is shared and modified by all the tasks and succeeded by task-specific branches. MTL allows two or more tasks to be learned simultaneously by sharing model knowledge and parameters. This boosts the binary complaint classification utilizing severity levels, emotion, and sentiment task features. The overall MTL-RoBERTa framework is shown in Figure 4.

Bidirectional Encoder Representations from Transformers (BERT) is a multi-layer bidirectional transformer encoder [25] based on the original work shown in [26]. It is trained on masked language modeling, which involves arbitrarily masking certain tokens from the input to predict them only based on context. RoBERTa [27] is an extension of BERT that has exhibited enhanced performance on social media analysis tasks [28], [29], by training on more data with varying hyperparameters.

The proposed MTL-RoBERTa model utilizes a single encoder layer that is shared and modified by all four tasks, with independent feed-forward networks for each task. We use the pre-trained RoBERTa model to embed the words of each tweet instance. The embedding representations are then fed to the shared transformer encoder (the 'roberta-base' model supports an inbuilt encoder as an attribute) to generate the instance's latent representation. This representation is then passed in parallel to four fully connected layers (for each of the four tasks), each of which has two hidden layers, to predict the output for each task separately. Each task-specific loss function is assigned a weight by the final loss function to be optimized. Finally, we add four separate output layers with softmax activation functions for binary and multi-class prediction.

Calculation of Loss: The categorical-cross entropy (CE) losses are calculated for the complaint (C), severity (M), emotion (E), and sentiment (S) tasks. Our proposed model's (MTL-RoBERTa) integrated loss function (L) is realized as follows:

$$L = a * L^{\mathrm{C}}{}_{\mathrm{CE}} + b * L^{\mathrm{M}}{}_{\mathrm{CE}} + c * L^{\mathrm{E}}{}_{\mathrm{CE}} + d * L^{\mathrm{S}}{}_{\mathrm{CE}}. \quad (2)$$

To calculate the overall loss, we calculated the weighted sum of the losses from the four tasks. The loss weights indicating the per-task loss-share to the overall loss are determined by the constants a, b, c, and d, which range from 0 to 1.

V. Experiments and Results

This section discusses the result and analysis of various baseline models and our proposed paradigm, as tested on the FINCORP corpus. The dataset and codes will be released publicly via the corresponding repository.

A. Baselines

Since *FINCORP* is a new dataset, for a comprehensive evaluation, we evaluate the dataset on multiple baselines, discussed as follows:

- **Logistic Regression (LR-BOW):** To measure the performance of the deep learning models, we also employ Logistic Regression, a common machine-learning-based classifier that has repeatedly served as a good baseline in many classification tasks. We employ Logistic Regression with standard Bag-of-Words (BOW) for CI and CS tasks.
- **Single-task systems:** For binary complaint identification and complaint severity prediction, we develop a single-task deep learning model based on RoBERTa ($\mathrm{STL_{CI}}$, $\mathrm{STL_{CS}}$).
- **Multi-task system:** Based on existing works in CI, we develop $\mathrm{Baseline_1}$[10] model as the multi-task baseline. $\mathrm{Baseline_1}$ is a shared private multi-task model for simultaneous classification of complaint, emotion, and sentiment tasks. For training the model, the authors employed three different sources of data. We also build an $\mathrm{MTL_{GloVe}}$ model wherein the textual embeddings are generated using the pre-trained GloVe[13] [30]. The word sequence encoder receives the embedding layer's output and analyses it to attain contextual knowledge from the text. The rest of the framework is the same.
- **Ablation models:** To evaluate the influence of complaint severity, emotion, and sentiment prediction on the complaint task independently and in varying combinations, we developed dual-task ($\mathrm{MTL_{CI+ER}}$, $\mathrm{MTL_{CI+SA}}$, $\mathrm{MTL_{CI+CS}}$) and tri-task variants ($\mathrm{MTL_{CI+ER+SA}}$, $\mathrm{MTL_{CI+ER+CS}}$, $\mathrm{MTL_{CI+SA+CS}}$) of our proposed model.

[13]GloVe:urlhttp://nlp.stanford.edu/data/wordvecs/glove.840B.300d.zip

B. Experimental Setup

We employ Python-based libraries to implement our proposed framework as well as the baselines, namely TensorFlow[14], Scikit-learn[15] [31]. The pre-trained model (RoBERTa) is from the open-source library[16] huggingface transformer. We ran all of the experiments on a single NVIDIA GeForce RTX 2080 Ti GPU. We evaluated the predictive performance of the proposed model and the baselines using accuracy and macro-F1 score. We have utilized 60% of the *FINCORP* dataset as training data, 15% for validation, and 25% as testing data for all the experiments. A seed value of 40 was used for a fair assessment of the models, allowing them to encounter the same training and testing data. To effectively employ the GPU, we kept the batch size at 8. We use *Adam* optimizer [32] with a learning rate of lr = 1e-3, lr ϵ {1e-1, 1e-2, 1e-3, 1e-4}. We use the base uncased model for RoBERTa, and fine-tune it with learning rate of lr = 5e-5, lr ϵ {1e-4, 5e-5, 1e-5, 1e-6}. The maximum sentence length is set at 50 characters, which spans 93% of the tweets in the training set. We utilize *ReLU* [33] activation and a *dropout* [34] of 30%, *dropout* ϵ {20%, 30%, 50%}. The output layers for complaint, severity, emotion, and sentiment classification tasks use $Softmax$ activation with 2, 4, 6, and 3 neurons, respectively. To train across all channels, categorical cross-entropy is employed as the loss function. *All of these parameter values were chosen following a thorough sensitivity study.*

C. Results

*1) **Results Discussion:**: Kindly note that the current paper's objective is to boost the efficacy of the CI and CS tasks by utilizing the two secondary tasks (ER and SA). As a result, we present the results and analysis with CI and CS as the primary tasks in all task pairings.*

The classification results from the various experiments are shown in Table VII. It can be observed that combining all associated tasks, such as severity, emotion, and sentiment, improves performance compared to single-task, dual-task, and tri-task variants. This improvement indicates that the proposed model makes effectual usage of interaction between the four tasks. As seen in Table VII, the MTL-RoBERTa model, which includes all four tasks (CI, CS, ER, and SA), beats the single-task complaint and severity variants ($\mathrm{STL_{CI}}$, $\mathrm{STL_{CS}}$). $\mathrm{MTL_{CI+CS}}$ outperforms $\mathrm{MTL_{CI+ER}}$ and $\mathrm{MTL_{CI+SA}}$ in the dual-task variants. This supports our assumption that the complaint severity level information can boost the complaint identification task while simultaneously learning these two tasks. This could also be influenced by the notion that sentiment by itself is usually unable to convey essential details about the complainant's predicament. For instance, negative feelings toward a company or a product

[14]https://www.tensorflow.org/

[15]https://scikit-learn.org/stable/

[16]https://huggingface.co/model and https://tfhub.dev/google/collections/bert/1

Table VII
RESULTS OF THE PROPOSED MODEL AND OTHER BASELINES WITH RESPECT TO MACRO-F1 SCORE AND ACCURACY VALUE FOR CI TASK. BOLD-FACED VALUES INDICATE THE MAXIMUM SCORES ACHIEVED. THE * INDICATES THAT THE RESULTS ARE STATISTICALLY SIGNIFICANT.

Model	Accuracy (%)	F1-score(%)
$SOTA_{CI}$[16]	84.26 ± .15	83.53 ± .03
LR-BOW	67.52 ± .03	64.28 ± .03
$Baseline_1$[10]	82.38 ± 1.02	81.84 ± 1.05
MTL_{GloVe}	80.45 ± 1.03	79.32 ± 1.02
Single-task baseline		
STL_{CI}	81.26 ± 0.03	80.16 ± 0.05
Dual-task baselines		
MTL_{CI+ER}	81.79 ± 1.07	81.54 ± 1.13
MTL_{CI+SA}	80.58 ± 1.12	79.51 ± 1.06
MTL_{CI+CS}	83.87 ± 1.04	83.28 ± 1.07
Tri-task baselines		
$MTL_{CI+ER+SA}$	82.48 ± 1.17	82.14 ± 1.03
$MTL_{CI+ER+CS}$	84.28 ± 1.05	83.54 ± 1.02
$MTL_{CI+SA+CS}$	83.39 ± 1.02	81.89 ± 1.06
Quad-task baseline		
MTL-RoBERTa	**86.33*** ± .03	**85.82*** ± .05

Table VIII
RESULTS OF ALL THE PROPOSED MODEL AND OTHER BASELINES WITH RESPECT TO THE MACRO-F1 SCORE AND ACCURACY VALUE FOR CS TASK. BOLD-FACED VALUES INDICATE THE MAXIMUM SCORES ACHIEVED. THE * INDICATES THAT THE RESULTS ARE STATISTICALLY SIGNIFICANT.

Model	Accuracy (%)	F1-score(%)
$SOTA_{CS}$[15]	65.67 ± .11	64.17 ± .12
LR-BOW	48.52 ± .14	46.28 ± .12
MTL_{GloVe}	60.49 ± 1.03	60.12 ± 0.14
Single-task baseline		
STL_{CS}	57.89 ± 1.04	57.19 ± 1.12
Dual-task baselines		
MTL_{CS+CI}	61.22 ± 1.14	60.08 ± 1.03
MTL_{CS+ER}	58.67 ± 1.02	56.88 ± 1.04
MTL_{CS+SA}	57.88 ± 1.11	57.37 ± 1.03
Tri-task baselines		
$MTL_{CS+ER+SA}$	62.58 ± 1.07	61.74 ± 1.03
$MTL_{CS+ER+CI}$	64.68 ± 1.07	63.14 ± 1.13
$MTL_{CS+SA+CI}$	63.69 ± 1.12	60.19 ± 1.04
Quad-task baseline		
MTL-RoBERTa	**67.89*** ± .15	**66.52*** ± .12

might be influenced by numerous emotions such as anger, sorrow, etc. Consequently, distinct or minor variations in emotion cannot be accurately determined and conveyed solely through sentiment.

Specifically, in the case of tri-task variants, $MTL_{CI+ER+CS}$ outperforms other tri-task baselines with the macro-F1 score of 83.54%. One of the reasons for the inferior results of $MTL_{CI+ER+SA}$ and $MTL_{CI+SA+CS}$ variants could be that the sentiment analysis task does not contribute much to the multi-task architecture as compared to severity and emotion tasks.

In Table VIII, we report the results of the MTL-RoBERTa model for the complaint severity task. Overall, the MTL-RoBERTa model yields the best result with the macro-F1 score of 66.52%. Moreover, of all the baselines, $MTL_{CS+ER+CI}$ outperforms other baselines with the macro-F1 score of 63.14%. This is in line with [2], where the author claims that the way people convey their grievances is linked to their emotional states.
The findings reported here are all statistically significant.[17] *[35]..*

*2) **Comparison with State-of-the-art (SOTA):**:* For single-task CI, we compare the MTL-RoBERTa model to the existing state-of-the-art technique [16]. $SOTA_{CI}$ makes use of a variety of neural language models that are aided by transformer networks. We also compare the results of the MTL-RoBERTa model with those of the existing state-of-the-art approach [15] for single-task CS task. $SOTA_{CS}$ uses a wide range of neural language models with several linguistic features augmented by transformer networks. We re-implement it on the FINCORP dataset and report the results in Table VII and VIII. The MTL-RoBERTa model outperforms the SOTA techniques for complaint identification and severity prediction tasks.

*3) **Qualitative Analysis:**:* Table IX presents a few examples of MTL-RoBERTa and single-task (complaint task) model predictions. Even though the 1st and 2nd cases in Table IX communicate dissatisfaction in a less explicit tone, the MTL-RoBERTa model accurately predicts the examples as complaints. Even though the 3rd and 4th examples are indirect and vague in nature, the MTL_{All} model identifies that there is no violation of trust. These examples highlight the importance of detecting complaints based on severity, emotion, and sentiment knowledge.

*4) **Error Analysis:**:* We examine some of the plausible reasons for the MTL-RoBERTa model's complaint and severity prediction inaccuracies:

- **Elusive Complaints:** Non-complaints are incorrectly predicted when complaints are communicated in an implicit or cryptic manner. One justification for this could be the complainant's lack of explicit accusation or blame. For example, *'Why am I waiting 60mins just so I can ok a debit card transaction!?'*. The predicted class is non-complaint, whereas the instance's actual class is complaint. Unless the tweet does not mention the particular company or use a critical phrase, the model misinterprets it as non-complaint.
- **Neighbouring Severity Level Errors:** Instances that belong to neighboring severity levels tend to be semantically and compositionally similar, sometimes leading to misclassification. For example, *'You are looting consumer's money. It's very disappointing behavior that they didn't refund back failed transaction money even after weeks and their costumer support show us the way to our bank, who doesn't recognize their transaction number.'*; predicted severity level: 'disapproval'. The correct severity level for the preceding example is 'accusation', but due to the presence of negative terms such as *disappointing* which

[17]For the significance test, we utilized the Student's t-test. When testing the null hypothesis, the results are statistically significant (p-value < 0.05).

Table IX
FEW EXAMPLE INSTANCES ALONG-WITH ASSOCIATED PREDICTED LABELS FOR THE BEST PERFORMING MULTI-TASK (MTL-ROBERTA) MODEL AND ITS SINGLE-TASK CI EQUIVALENT. (STL_{CI}).

Sentence	MTL-RoBERTa	STL_{CI}	Actual Label
This has been a great way to spend an afternoon, trying to "chase" down that $832 deposit-student loan funds-that disappeared, then you mysteriously closed the account	Complaint	Non-Complaint	Complaint
I had to report my visa as STOLEN after purchasing from Amazon! Thanks alot. And no proper response from the team.	Complaint	Non-Complaint	Complaint
I actually don't prefer AMEX. A great card but I only use cards that have a zero annual fee. I personally think annual fees on a credit card are ridiculous.	Non-Complaint	Complaint	Non-Complaint
Great job, dude why there's no crypto payment for VIP membership?	Non-Complaint	Complaint	Non-Complaint

usually appear in the 'disapproval' severity class, the proposed model misclassifies it.

- **Satirical Instances:** Instances where the underlying tone is positive or neutral, but the instance is of complaint type, the MTL-RoBERTa model inaccurately predicts such instances as non-complaint. For example, *'Yes, I need to pay a transaction that cannot be done online/over the phone because it exceeds the daily limit.'*. For this instance, the correct class is complaint, but the model predicts it as non-complaint. One reason could be the neutral undertone and the usage of less explicit words to signify complaint.
- **Probing Complaints:** We also identified that the model incorrectly labels cases of weak discontent with a inquiring tone as non-complaints. For example, *'What is this restaurant packaging charges and where is this money going when McDonald's on their website is not charging it?'*. The correct class for the given example is complaint. The model classifies it as non-complaint because there is no clear objection, and the sentence is interrogative. To effectively classify such occurrences, the system requires background information and knowledge about the key aspects of the sentence.

VI. Conclusion

In this work, we have introduced FINCORP, an annotated dataset of complaints originating between financial institutions and consumers on Twitter. We have addressed the task of complaint identification and severity level prediction (primary tasks) jointly using a multi-task framework assisted by emotion and sentiment detection as auxiliary tasks. The paper goes into a detailed description of the dataset and the complete process of creating it. Every instance in the FINCORP dataset has been annotated across four axes: complaint, severity level, emotion, and sentiment classes, resulting in a dataset with a lot of diversity. We evaluated the dataset and reported the findings using several single-task, multi-task and other existing baselines. Given the scarcity of task-specific (complaint identification) data in English and even some low-resource languages, we believe this dataset would add value to social media analytics research and practice.

We plan to expand our work in complaint identification at the sentence level in english as well as code-mixed languages in the future. Furthermore, the annotated corpus can aid research in other emotion and sentiment classifications tasks.

Acknowledgments

This publication is an outcome of the R&D work undertaken in the project under the Visvesvaraya Ph.D. Scheme of Ministry of Electronics & Information Technology, Government of India, being implemented by Digital India Corporation (Formerly Media Lab Asia).

References

[1] E. Olshtain and L. Weinbach, "Complaints: A study of speech act behavior among native and nonnative speakers of hebrew. the prag-matic perspective," 1985.

[2] A. Trosborg, *Interlanguage pragmatics: Requests, complaints, and apologies*. Walter de Gruyter, 2011, vol. 7.

[3] L. N. Kakolaki and M. Shahrokhi, "Gender differences in complaint strategies among iranian upper intermediate efl students," *Studies in English Language Teaching4 (1)*, pp. 1–15, 2016.

[4] A. Xu, Z. Liu, Y. Guo, V. Sinha, and R. Akkiraju, "A new chatbot for customer service on social media," in *Proceedings of the 2017 CHI conference on human factors in computing systems*, 2017, pp. 3506–3510.

[5] G. Van Noort and L. M. Willemsen, "Online damage control: The effects of proactive versus reactive webcare interventions in consumer-generated and brand-generated platforms," *Journal of interactive marketing*, vol. 26, no. 3, pp. 131–140, 2012.

[6] M. Lewis, J. M. Haviland-Jones, and L. F. Barrett, *Handbook of emotions*. Guilford Press, 2010.

[7] A. Kumar, A. Ekbal, D. Kawahra, and S. Kurohashi, "Emotion helps sentiment: A multi-task model for sentiment and emotion analysis," in *2019 International Joint Conference on Neural Networks (IJCNN)*. IEEE, 2019, pp. 1–8.

[8] T. Saha, A. Upadhyaya, S. Saha, and P. Bhattacharyya, "Towards sentiment and emotion aided multi-modal speech act classification in twitter," in *Proceedings of the 2021 Conference of the North American Chapter of the Association for Computational Linguistics: Human Language Technologies*, 2021, pp. 5727–5737.

[9] M. S. Akhtar, A. Ekbal, and E. Cambria, "How intense are you? predicting intensities of emotions and sentiments using stacked ensemble [application notes]," *IEEE Computational Intelligence Magazine*, vol. 15, no. 1, pp. 64–75, 2020.

[10] A. Singh and S. Saha, "Are you really complaining? a multi-task framework for complaint identification, emotion, and sentiment classification," in *International Conference on Document Analysis and Recognition*. Springer, 2021, pp. 715–731.
[11] N. Majumder, S. Poria, D. Hazarika, R. Mihalcea, A. Gelbukh, and E. Cambria, "Dialoguernn: An attentive rnn for emotion detection in conversations," in *Proceedings of the AAAI Conference on Artificial Intelligence*, vol. 33, 2019, pp. 6818–6825.
[12] D. Preotiuc-Pietro, M. Gaman, and N. Aletras, "Automatically identifying complaints in social media," *arXiv preprint arXiv:1906.03890*, 2019.
[13] R. P. Singh, R. Haque, M. Hasanuzzaman, and A. Way, "Identifying complaints from product reviews: A case study on hindi," in *Proceedings of the 17th International Conference on Natural Language Processing (ICON)*, 2020, pp. 108–116.
[14] A. Singh, S. Saha, M. Hasanuzzaman, and A. Jangra, "Identifying complaints based on semi-supervised mincuts," *Expert Systems with Applications*, p. 115668, 2021.
[15] M. Jin and N. Aletras, "Modeling the severity of complaints in social media," in *Proceedings of the 2021 Conference of the North American Chapter of the Association for Computational Linguistics: Human Language Technologies*, 2021, pp. 2264–2274.
[16] ——, "Complaint identification in social media with transformer networks," in *Proceedings of the 28th International Conference on Computational Linguistics*, 2020, pp. 1765–1771.
[17] S. Tjandra, A. A. P. Warsito, and J. P. Sugiono, "Determining citizen complaints to the appropriate government departments using knn algorithm," in *2015 13th International Conference on ICT and Knowledge Engineering (ICT & Knowledge Engineering 2015)*. IEEE, 2015, pp. 1–4.
[18] W. Yang, L. Tan, C. Lu, A. Cui, H. Li, X. Chen, K. Xiong, M. Wang, M. Li, J. Pei *et al.*, "Detecting customer complaint escalation with recurrent neural networks and manually-engineered features," in *Proceedings of the 2019 Conference of the North American Chapter of the Association for Computational Linguistics: Human Language Technologies, Volume 2 (Industry Papers)*, 2019, pp. 56–63.
[19] D. Law, R. Gruss, and A. S. Abrahams, "Automated defect discovery for dishwasher appliances from online consumer reviews," *Expert Systems with Applications*, vol. 67, pp. 84–94, 2017.
[20] M. Lui and T. Baldwin, "langid. py: An off-the-shelf language identification tool," in *Proceedings of the ACL 2012 system demonstrations*, 2012, pp. 25–30.
[21] A. D. Cohen and E. Olshtain, "The production of speech acts by efl learners," *Tesol Quarterly*, vol. 27, no. 1, pp. 33–56, 1993.
[22] P. Ekman, W. V. Friesen, M. O'sullivan, A. Chan, I. Diacoyanni-Tarlatzis, K. Heider, R. Krause, W. A. LeCompte, T. Pitcairn, P. E. Ricci-Bitti *et al.*, "Universals and cultural differences in the judgments of facial expressions of emotion." *Journal of personality and social psychology*, vol. 53, no. 4, p. 712, 1987.
[23] J. L. Fleiss, "Measuring nominal scale agreement among many raters." *Psychological bulletin*, vol. 76, no. 5, p. 378, 1971.
[24] R. Caruana, "Multitask learning," *Machine learning*, vol. 28, no. 1, pp. 41–75, 1997.
[25] J. Devlin, M.-W. Chang, K. Lee, and K. Toutanova, "Bert: Pre-training of deep bidirectional transformers for language understanding," in *Proceedings of the 2019 Conference of the North American Chapter of the Association for Computational Linguistics: Human Language Technologies, Volume 1 (Long and Short Papers)*, 2019, pp. 4171–4186.
[26] A. Vaswani, N. Shazeer, N. Parmar, J. Uszkoreit, L. Jones, A. N. Gomez, Ł. Kaiser, and I. Polosukhin, "Attention is all you need," *Advances in neural information processing systems*, vol. 30, 2017.
[27] Z. Liu, W. Lin, Y. Shi, and J. Zhao, "A robustly optimized bert pre-training approach with post-training," in *China National Conference on Chinese Computational Linguistics*. Springer, 2021, pp. 471–484.
[28] W. Liao, B. Zeng, X. Yin, and P. Wei, "An improved aspect-category sentiment analysis model for text sentiment analysis based on roberta," *Applied Intelligence*, vol. 51, no. 6, pp. 3522–3533, 2021.
[29] Y. Liu, H. Liu, L.-P. Wong, L.-K. Lee, H. Zhang, and T. Hao, "A hybrid neural network rbert-c based on pre-trained roberta and cnn for user intent classification," in *International Conference on Neural Computing for Advanced Applications*. Springer, 2020, pp. 306–319.
[30] J. Pennington, R. Socher, and C. Manning, "Glove: Global vectors for word representation," in *Proceedings of the 2014 conference on empirical methods in natural language processing (EMNLP)*, 2014, pp. 1532–1543.
[31] F. Pedregosa, G. Varoquaux, A. Gramfort, V. Michel, B. Thirion, O. Grisel, M. Blondel, P. Prettenhofer, R. Weiss, V. Dubourg *et al.*, "Scikit-learn: Machine learning in python," *Journal of machine learning research*, vol. 12, no. Oct, pp. 2825–2830, 2011.
[32] D. P. Kingma and J. Ba, "Adam: A method for stochastic optimization," in *3rd International Conference on Learning Representations, ICLR 2015, San Diego, CA, USA, May 7-9, 2015, Conference Track Proceedings*, Y. Bengio and Y. LeCun, Eds., 2015. [Online]. Available: http://arxiv.org/abs/1412.6980
[33] X. Glorot, A. Bordes, and Y. Bengio, "Deep sparse rectifier neural networks," in *Proceedings of the fourteenth international conference on artificial intelligence and statistics*, 2011, pp. 315–323.
[34] N. Srivastava, G. Hinton, A. Krizhevsky, I. Sutskever, and R. Salakhutdinov, "Dropout: a simple way to prevent neural networks from overfitting," *The journal of machine learning research*, vol. 15, no. 1, pp. 1929–1958, 2014.
[35] B. L. Welch, "The generalization of 'student's'problem when several different population varlances are involved," *Biometrika*, vol. 34, no. 1-2, pp. 28–35, 1947.

Apoorva Singh is a research scholar in the Department of Computer Science and Engineering, IIT Patna. She completed her M.Tech from BIT, Mesra in 2016. She has been pursuing research in Text Mining, Information Retrieval and Applications of Federated Learning.

Rohan Bhatia is an undergraduate at Delhi Technical University, Delhi. He is pursuing his B.Tech in Engineering Physics with a minor in Computer Science. His interest lies in Data Science and Quantum Computation.

Dr. Sriparna Saha is currently an Associate Professor in the Department of Computer Science and Engineering, Indian Institute of Technology Patna, India. She is the author of a book published by Springer-Verlag. She has authored or coauthored more than 290 papers. Her current research interests include deep learning, natural language processing, machine learning, information extraction, text mining, bioinformatics and multiobjective optimization. She is involved with different sponsored research projects in the broad areas of Artificial Intelligence and Machine Learning technologies, funded by different Govt. and private agencies.

e-ISSN: 2582-5208
International Research Journal of Modernization in Engineering Technology and Science
(Peer-Reviewed, Open Access, Fully Refereed International Journal)
Volume:04/Issue:05/May-2022 Impact Factor- 6.752 www.irjmets.com

CONCEPT OF GROUP TECHNOLOGY AND IT'S IMPLEMENTATION IN THE FIELD OF MOBILE PRODUCTION SYSTEMS

Dr. Ak Madan[*1], Aditya Atul Gupta[*2], Aman Kumar Kaushik[*3]

[*1]Professor, Department Of Mechanical Engineering, Delhi Technological University, Delhi, India.

[*2,3]Student, Department Of Mechanical Engineering, Delhi Technological University, Delhi, India.

ABSTRACT

In this paper we plan to provide a detailed examination of the group technology (GT) and its implementation goal in the field of cellular manufacturing to achieve a major change in product production. The mobile manufacturing system has been proven to be an important means of collection, production of workshops and further transition to industry and team technology has become an important tool for the development of the mobile manufacturing system. With the basic application of team technology it acts as a traditional concept and still plays an important role in new production concepts such as timely, complete quality management and technologies such as optimized production technologies, integrated computer production in a team production technology concept and we cite other examples to easily understand the concept of team technology by generating basic ideas about GT in the mobile manufacturing sector and decision-making and accountability are highly focused on location, which often results in quality and production improvement.

Keywords: Mobile Production, Traditional Concept, Team Technology, Key Method.

I. INTRODUCTION

Group Technology or GT is a production process in which components with similar geometry, production process and / or functions are integrated together. GT is based on the common principle that many problems are the same and by combining similar problems, a single solution can be found in a collection of problems, thus saving time and effort. A group of similar components is known as a family component and the group of machines used to process each family component is known as a machine cell [1]. This type of production in which the family of a part is produced by a machine cell is known as cell production. In this type of production efficiency has often been increased through the use of GT because the required functions can be closed only in a small cell and thus avoid the need for the transport of processed parts. Cell Production is an example of a workplace design, and has become an integral part of energy-intensive production systems and is based on Group Technology principles, which seek to take full advantage of parallel components, with the same configuration and processing [2]. at the bottom of the factory into independent and multi-skilled teams, or work cells, producing complete products or complex components. Well-trained and versatile cells are more flexible and more responsive than conventional mass production lines, and can handle processes, errors, scheduling, storage, and other productive issues more efficiently and this paper offers some idea of GT concepts for mobile phones. production systems in various manufacturing industries.

II. METHODOLOGY

The method and analysis used in your research work should be documented in this section. A simple strategy you can follow is to use keywords in your topic in the first few sentences.

Increase in Group Technology to Test Products, Components and Assemblies

Unlike Henry Ford, modern manufacturers cannot simply make "any color as long as it is black." Different markets, competition and complex customers have created a variety of confusing products usually with low volume. Many companies have focused on this diversity. Increased inventory, slow product delivery, confusion and declining quality reflect the inability to cope with increasing diversity. Group Technology (GT) breeds this diverse animal. Group Technology evaluates products, components and assemblies. It then integrates the same materials to facilitate design, production, purchase and other business processes. The figures below show that a seemingly randomized group of objects has striking similarities [3]. From this more ever all of the manufacturing and production industries were follow and implement the concept of group technology and they discovered several advantages of GT in their production units.

e-ISSN: 2582-5208
International Research Journal of Modernization in Engineering Technology and Science
(Peer-Reviewed, Open Access, Fully Refereed International Journal)
Volume:04/Issue:05/May-2022 Impact Factor- 6.752 www.irjmets.com

GT Design in Engineering

A typical mechanical designer produces about two different parts a week. So, even a small door designs hundreds of parts each year. Without official methods, designers cannot track drawings. They duplicate or close many of the existing components. Like the Hydra of Greek Mythology, the problem will feed on itself. As more new projects enter the system it becomes more difficult to track and encourage more duplication. GT uses Coding and Classification (C&C) to address this.

GT and other departments

GT produces savings and profits in almost every business environment. It combines functions, tools, gears, tools and schedules into large groups of the same objects to find similar solutions. Purchases can include similar components and benefit from bulk discounts. For unconventional purchased parts, grouping helps providers find savings and lower the price. Accounting is easy in the GT area [4]. Here the costs are collected by the cell and the family rather than by each component. A simple distribution process provides cost accurately between families.

GT and Manufacturing

Group Technology benefits production in many ways. Reduces the number and variety of components. The process planning of the remaining parts is simple and consistent. Computer Aided Process Planning (CAPP) is an important tool for this [5]. It uses code-like similarities to consistently organize, measure and accurately measure costs. It then contributes to the GT production cell. Group Technology Cells reduce Operating Time and Process Internal Process. They simplify schedules, reduce transportation and facilitate surveillance. Some amazing and practical savings come from improved settings and equipment costs. Reduction of set time results in smaller lot sizes and smaller lines which means faster exits, shorter lead times and lower inventory inventory. Sometimes GT eliminates the need for expensive NC equipment. Combined with NC, GT makes it easy to plan, adjust and use tools.

Techniques for Group Techniques

Separation can be done in many ways. 'That ball' and knowledge is enough when the parts are few. Production Flow Analysis looks at current processes and sequences. It combines the parts accordingly [6]. The separation of images helps in designing the design and finding the design. Coding systems vary widely in production, design and purchase but are more expensive due to the work involved in original coding. Production method where similar components are identified and grouped together to achieve their similarity in construction and production The similarity between components allows them to be subdivided into families In each family unit, processing steps are the same Development is usually achieved. by organizing production facilities into productive cells that specialize in producing specific household components.

Family Partition in the GT System

A group of components that have similarities in geometric shapes and sizes, or in the processing step used in their manufacture Part Families are a key element of group technology. There are always differences between the parts in the family but the similarities are so close that the parts can be combined into one family.

Methods of Identifying the Family Part

Visual testing - using the best judgment to combine parts into proper families, based on parts or pictures of parts.

Production flow analysis - using information contained in route pages to categorize.

Segmentation and coding - identifying similarities and differences between components and associating them using a coding system [7].

Three Structures used in Classification and Coding Schemes

Hierarchical structure, known as a mono-code, in which the interpretation of each successive symbol depends on the value of the preceding symbols Chain-type structure, known as a polycode, in which the interpretation of each symbol in the sequence is always the same; it does not depend on the value of preceding symbols Mixed-mode structure, which is a hybrid of the two previous codes.

e-ISSN: 2582-5208
International Research Journal of Modernization in Engineering Technology and Science
(Peer-Reviewed, Open Access, Fully Refereed International Journal)
Volume:04/Issue:05/May-2022 Impact Factor- 6.752 www.irjmets.com

Some of the Important System

Opitz's separation program - University of Aachen in Germany, non-proprietary, type Chain. Brisch System - (Brisch-Birn Inc.), CODE (Production Data System, Inc.), CUTPLAN (Metcut Associates) DCLASS (Brigham Young University), MultiClass (i -OIR: Industrial Research Organization), hierarchical or coding tree structure, Part of Analog System (Lovelace, Lawrence & Co., Inc.).

Production Flow Analysis (PFA) in the Mobile Production System

In Production Flow Analysis the use of the matrix in selecting part numbers and machine numbers for families to collect. In the matriculation below, the columns represent the machines with their numbers and uppercase letters. The lines represent the parts the numbers and their names on the left. If a particular component requires a specific machine, the sequence number is the opposite spreadsheet cell. Sometimes, an "X" just indicates that a particular part needs a particular machine. Many families have "natural sequences." For example "Lathe" usually precedes "Deburr". This natural sequence dominates and forms the basis of the structure of the function cell. You can ignore sequence problems as you develop the PFA matrix. It is difficult to see the order or similarity in the first matrix. Rearranging the lines and columns, as in the second matrix, clearly shows the families of the same parts and the equipment needed to build them. These machines form a function cell [8].

Implementation of Production Flow Analysis (PFA) in the Mobile Production Program

Computer systems are available to use matric but cannot solve the problem of incompatible channels that are often encountered in PFA analysis. Incompatible route means that the same parts use different machines [9]. This happens for a variety of reasons such as: The components usually go into product mixing over a period of many years. Different situations and different planners during this time have come to different route decisions. Energy problems can affect route decisions. For example, machine A will usually be used for a specific task but is heavily loaded so the process planner uses machine B. Different process planners have different backgrounds and different biases. This may lead to different routes in the same section. Analysts encountered inconsistent trends in most PFA analyzes. If product mixing is not very complicated, they can make manual changes. When product mixing is greater than 100 items or more, PFA becomes more complex and Coding & Classification analysis is indicated.

Coding and Production Division

Production coding systems usually have both product information and processing. The analyst works with both If there is a significant conflict in existing processes, the analyst can return to basic factors such as size, shape and material. Parts with the same body parts usually have the same procedures. The coding system allows the analyst to set up a process and combine components into families. The example below shows a small section of the simulation website. Each digit area represents the element of a particular component. For examples the third area shows the completed simulation weight. Each character in the code contains information about the product feature assigned to that digital area. For example, a "1" three-letter space may indicate a completed weight of between 1.0 and 5.0 pounds.

Using Coding and Dividing

Entering Codes of Use and Planning introduces some major challenges that are rarely seen by an inexperienced physician. This is especially true for large databases. However, larger projects have equally large returns [10]. A successful project requires knowledge and judgment in code-building, early coding and family development. It is not the job of an amateur.

Group Technology Work cell Example for Cellular Manufacturing

This cell has the classic U-shape but it does not operate like a Toyota Cell. This cell produces about 85 different turned parts. These are shafts and shafts with integral pinions and/or splines. Arrows show the sequence for three of these many parts. All parts have dedicated carts for handling and storage. They serve as material handling devices, containers and kanban. Perimeter carts are a kanban stockpoint. The internal lot size (transfer batch) is one cart (16 parts). External lot size varies from 16-48 parts in multiples of 16. Work times are highly variable and unbalanced. The hobbing machine (7-1) is extremely slow while the NC lathe is fast. The product mix was carefully selected to include some parts that require hobbing and many others that do not.

e-ISSN: 2582-5208
International Research Journal of Modernization in Engineering Technology and Science
(Peer-Reviewed, Open Access, Fully Refereed International Journal)
Volume:04/Issue:05/May-2022 Impact Factor- 6.752 www.irjmets.com

Operators schedule their work from kanban signals. They must schedule non-hobbed parts immediately after a hobbed part. If they did not, the slow hobber would bring output to a crawl. They may have 2-3 part numbers underway at the same time. Operators stay alert because the variation in cycle time means that machines finish at unforeseen moments. Operators constantly move from one machine to another, loading and unloading. Small queues highlight temporary bottlenecks which get special attention. Some drilling and milling might have been done on the NC lathe using special attachments. But, we chose to make these secondary operations to reduce machine time on the lathe. These operations occur internally to lathe turning and cell output increases as a result. While the whole arrangement may seem like a recipe for chaos, it actually works quite well. It is not nearly as smooth as a classic Toyota cell but it is far better than the genuine chaos of a functional layout. A lot depends on the operators. Here, they were skilled and experienced machinists[9]. With kanban, we knew they could figure out what part to run and this will not give the optimum layout design and arrangement of machines but while we implement the group technology principle by separating the work process in to different cells. Then we have to achieve some improvement in productivity without any queue formation.

Advantages of GT in the field of Mobile Production Systems

There are many benefits to GT in the production of cell phones in the company if used properly. Soon, processes become more balanced and productivity grows because the production area has been redesigned and remodeled. There are other costs for initiating cell phone production, however, in addition to the set-up costs for equipment and suspensions mentioned above. Sometimes different work cells may need the same equipment and tools, which can result in duplication that results in higher equipment investment and reduced machine usage. However, this is a matter of efficiency and can be addressed through the design process. Enable Mobile Production with GT policy may provide Engineering Reduction Costs, Accelerate Product Improvement Improve Cost, Simplify Process Planning, Reduce Operating Costs, Simplify Purchase, Help with Broadcast Map. Savings from GT come in many forms, often invisible. Here are some of the improvements achieved by successful users: • Setting Time ..... 35% -40% • Operating Cost ..... 40% • Inventory. ..... 15% -35% • Throughput Time .... 80% • Purchased Items ..... 15% Group Technology is the most effective way to deal with and variety desired by today's customers and allows for customization of the product through process configuration [11].

Gap In Research

There has been a great deal of work done by various researchers on cell-specific techniques. Most of the published cell phone production activities pay little attention to production planning and cellular production control activities. Many current mobile production apps are operating in the wrong place and their performance can be improved by configuring parameters. But this paper provides some details about the benefits of group technology during product development and there are other strategies discussed above and they do not investigate the impact on different performance measurements if cell / cell size / cell structure varies. . And our vision is largely based on a specific function related to cell formation problems in the group's goal of cellular manufacturing technology to show major changes in automation production in the workplace..

III. CONCLUSION

This study brings attention to the need to design a GT cell production system to make it more efficient as most of it focuses on machine and components in a cell that has a family component. Therefore, there is a great need to develop models to determine the total number of teams and the appropriate production mix under technical and operational barriers in order to effectively operate a mobile production system in order to achieve success in team technology. There is a need to develop more efficient tools enabling manufacturing system designer to achieve optimal solution in reasonable processing time. Also, with the help of the team technology system we have developed a more efficient production system GT application in an advanced production system improves the design and efficiency of the system and the more flexibility and flexibility of a particular production system and integration of system production functions. And our main idea for designing this paper was to produce the beauty of GT in cellular production to reach the limit in the small and large scale process processes.

IV. REFERENCES

[1] Arkat J, Hosseini L and Farahan M H 2011 Minimization of exceptional elements and voids in the cell formation Problem using a multi-objective genetic algorithm. Expert Syst. Appl. 38(8): 9597–9602

[2] BajestaniM A, Rabbani M, Rahimi-Vahed A R and Khoshkhou G B 2009 A Multi- objective scatter search for a dynamic cell formation problem. Comput. Oper. Res. 36(3): 777–794 Burbidge J L 1975 The introduction of group technology, Landon: Heinenan

[3] Boctor F F 1991 A linear formulation of the machinepart cell formation problem. Int. J. Prod. Res. 29(2): 343– 349

[4] Chan W M, Chan C Y and Ip W H 2003 A heuristic Algorithms for Machine Assignment in Cellular Layout. Comput. Ind. Eng. 44(1): 49–73

[5] Chan Felix T S, Lau K W, Chan P L Y and Choy K L 2006 Two-stage approach for machine-part grouping and cell layout problems. Comput. Ind. Eng. 22(3): 217–238

[6] P.K. Arora1,∗, A.Haleem2 and M. K Singh3, Recent development of cellular manufacturing systems, SadhanaVol. 38, Part 3, June 2013, pp. 421–428.c Indian Academy of Sciences.

[7] A. Gunasekaran, S.K.Goyal, I.Vetranan, P.Yli-Olli, An Investigation into Application of Group Technology in Advanced Manufacturing Systems, published in International Journal on Computer Integerated Manufacturing Vol 7,No-4 P.No-,215-228,Aug2013.

[8] Urban Wemmerlöv∗ , Nancy Lea Hyer, Procedures for the Part Family/Machine Group Identification Problem in Cellular Manufacturing, Journal of Operations Management Volume 6, Issue 2, February 2013, Pages 125–147.

[9] Suresh, Nallan C., Kay, John M, Group Technology and Cellular Manufacturing, Journal on A State-of-the-Art Synthesis of Research and Practice, Volume 5, Issue 21, February 2014, Pages 125–129.

2022 IEEE International Conference on Distributed Computing and Electrical Circuits and Electronics (ICDCECE)

Control of DSTATCOM in Distribution Systems by Artificial Intelligence based Controller

1st Pooja Meena
Dept. of Electrical Engineering
Delhi Technological University (DTU)
Delhi, India
poojameena0399@gmail.com

2nd Piyush Dua
Dept. of Electrical Engineering
Delhi Technological University (DTU)
Delhi, India
piyushdua88269@gmail.com

3rd Nilayan Maji
Dept. of Electrical Engineering
Delhi Technological University (DTU)
Delhi, India
nilayan.maji2610@gmail.com

4th Ankita Arora
Dept. of Electrical Engineering
Delhi Technological University (DTU)
Delhi, India
arora.ankita09@gmail.com

***Abstract*—Power quality relevant problems are of most concern nowadays. Reasons behind the problems for the quality of power are the use of non-linear devices. Due to their non-linearity, all these loads cause disturbances in the supply of power services, efficiency of system, power factor decrement etc. In this paper, the SRFT, IRPT, and ANFIS named respectively synchronous reference frame theory, Instantaneous reactive power theory and Adaptive neuro fuzzy inference system-based control algorithms for a three-Phase DSTATCOM are proposed for power Quality improvement in grid connection. The DSTATCOM is basically operated for compensating current harmonics injected in the supply current because of non-linear loads and also used for improvement in power factor, active and reactive balancing of power. The simulation, performance analysis, and comparison are done on MATLAB Simulink software.**

Keywords—DSTATCOM, Power Quality improvement, shunt compensation, Total Harmonic Distortion (THD), SRFT, IRPT, ANFIS.

I. INTRODUCTION

In a power system, a distribution system distributes electrical Power for local use in the area i.e., for end consumers. Power quality is always counts as the most important factor of any power distribution system. Due to the excessive use of power electronics-based devices in a distribution system, power quality issues have substantially increased. Power quality could be defined as the set of limits defined for an electrical parameter of a system so that the entire electrical system operates in the intended way and operates without significant losses [1].

Many power quality problems we face on a daily basis are voltage swell, voltage sag, transients, unbalanced load, harmonics, low power factor etc., that need to be addressed in order to enhance the Power quality of the system. The voltage level is challenged whenever there is an increase in load demand, as it increases the load on the line. In the distribution system as we move away from the source the voltage level decreases due to the occurrence of high losses [2-3]. There are classical methods to deal with power quality problems such as using passive filters consisting of capacitors, inductors and damping resistors, thus providing a simple solution but are large in size and weight placing but when they get tuned with the system resonance, they resonate [4-5].

Therefore, FACTS (Flexible Alternating Current Transmission System) devices such as DSTATCOM are used as they are having technological advantages such as faster response to the changes in the network [6]. The combination of voltage source converter in parallel with the capacitor is called distribution static compensator (DSTATCOM). It provides active power, reactive power balance, improves the power factor to unity and removes the harmonics in the source current [7]. The various algorithms are discussed in literature review such as Legendre-based neural network method [8], LMS-based adaptive control of SPV method [9] Biquad filter [10], cubic Bezier functional expansion-based adaptive filter [11]. The control strategy used for DSTATCOM will affect its efficiency of system.

The main goal of any compensation technique is to have a quick, flexible response and it should be easy to implement. The approval of the result will be based on the IEEE-Grid standards. The THD in source current in grid connected systems should be less than 5% following IEEE-519 standard [12].

The basic premise is to read Power quality problems and their best possible solutions. To achieve this goal, we have implemented three different control strategies for comparative research namely; Synchronous Reference Frame Theory (SRFT), Instantaneous Reactive Power Theory (IRPT) and Adaptive Neuro Fuzzy Inference System (ANFIS) method to achieve power factor correction and THD reduction in the system according to IEEE- Grid Standards [13]. So that same DSTATCOM can be used to deal with the Power quality issues in different situations with non-linear loads in a fragile environment of electrical grid [14]. All results have been interpreted through the simulations that have been performed in MATLAB-SIMULINK (SimPowerSystem) and comparisons has been done to show the effectiveness of the control algorithms used [15].

II. PROPOSED METHODOLOGY

To incorporate DSTATCOM in distribution system, literature research and analysis is done. Both reactive and active power can be injected using DSTATCOM. The active power flow between DSTATCOM and grid depends upon the phase angle differences and the active power flow depends upon the voltage magnitudes difference between the two voltage of grid and DSTATCOM. The active power output of a DSTATCOM will vary proportional to the system voltage

978-1-6654-8316-2/22/$31.00 ©2022 IEEE

Authorized licensed use limited to: DELHI TECHNICAL UNIV. Downloaded on June 22,2022 at 04:51:21 UTC from IEEE Xplore. Restrictions apply.

2022 IEEE International Conference on Distributed Computing and Electrical Circuits and Electronics (ICDCECE) | 978-1-6654-8316-2/22/$31.00 ©2022 IEEE | DOI: 10.1109/ICDCECE53908.2022.9792732

However, DSTATCOM is associated at the point of coupling provides compensating current to improve power factor and provide active power and reactive power balance. Fig. 1. shows a basic control idea for using DSTATCOM in the system.

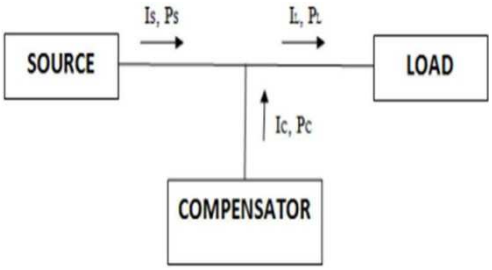

Fig. 1. Basic control idea of implementing DSTATCOM

A. Modelling of DSTATCOM

The DSTATCOM performance depends on the control algorithm used to produce VSC switch signals. DSTATCOM is attached to the grid of the system at PCC using a coupling inductor. It has a control unit and a pulse generation unit for the implementation of control strategy and to provide a gate pulse for VSC respectively. The DSTATCOM control is modelled based on three control strategies to reduce THD as the main goal. The measurements required to use the algorithm are:

- System voltage and current measurements
- Compensating signal calculation
- DC Voltage across Capacitor
- Generation of controlling pulses

B. Steps to activate the operation of DSTATCOM:

- Source voltage amplitude is obtained.
- Reference current are obtained using various algorithms.
- Generated reference current & actual current sensed by sensors are compared to achieve the error signal
- Derived error signal is used for controlling the switching of IGBT of DSTATCOM.
- Thus, bidirectional flow of active power is managed by DSTATCOM.

The modelling of DSTATCOM has been done on MATLAB SIMULINK using SIMSCAPE (SimpowerSystem) toolbox.

III. Control Algorithm

With Power quality compensation, depending on load requirements Power quality compensation is provided to DSTATCOM. DSTATCOM is optimized by a number of algorithms. Here we actually use an algorithm by which we generate data, and use control-based AI (Artificial Intelligence) algorithms to improve results.

A. Synchronous reference frame theory and algorithm (SRFT):

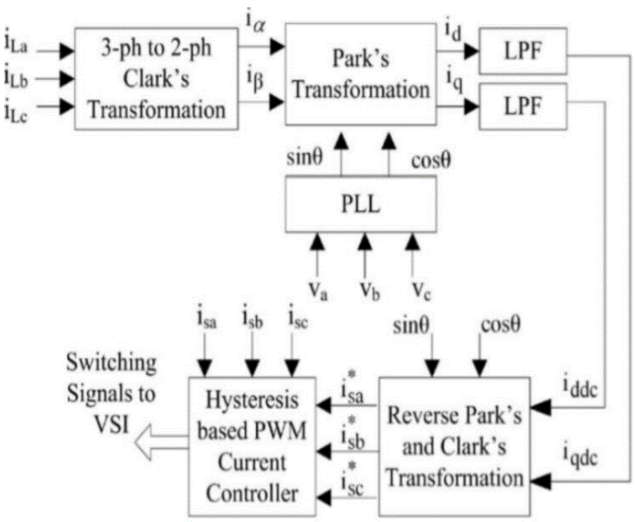

Fig. 2. Schematic chart representation of SRFT algorithm

Since, d-q-based algorithm is also referred as the synchronous reference frame theory algorithm. Clarke conversion is used to convert synchronous reference frame a-b-c load currents into αβ0 currents and further αβ0 into d-q framework using Park Transformation.

After obtaining the required load currents in the d-q frame, the active component is used to produce reference supply currents. The DC link voltage and the reference is compared and passed to PI controller to generate the loss component. The loss component is summed with the active component produce the fundamental component of load current. The fundamental component is called d component. The d-q components are transformed to reference a-b-c source currents called Reverse Park Transformation shown in Fig. 2.

B. Instantaneous Reactive Power Theory (IRPT)

The modeling of IRPT (Instantaneous Reactive Power Theory) algorithm based DSTATCOM is done in this section for calculation of active power to generate reference source current signals discussed in equations from (1) to (9). The Load current signals are converted to two orthogonal rotating vectors (α and β). The IRPT flow diagram representation shown in Fig. 3.

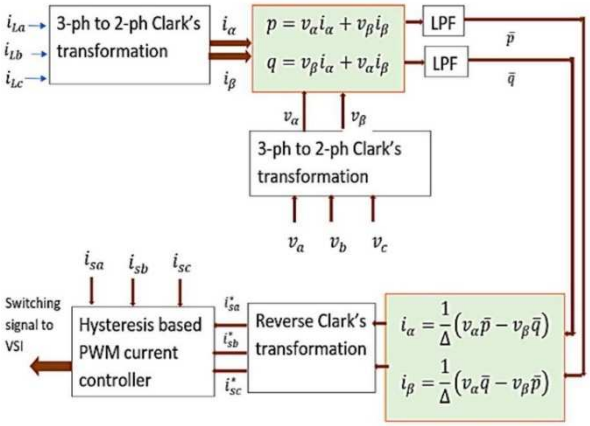

Fig. 3. Scheme chart representation of IRPT algorithm

The three phase voltages are given by

Authorized licensed use limited to: DELHI TECHNICAL UNIV. Downloaded on June 22,2022 at 04:51:21 UTC from IEEE Xplore. Restrictions apply.

$$v_a = v_m \sin \omega t$$

$$v_b = v_m \sin\left(\omega t - \frac{2\pi}{3}\right)$$

$$v_c = v_m \sin\left(\omega t - \frac{4\pi}{3}\right)$$

$$i_{La} = \sum\{ I_{Lan} \sin\{n(\omega t) - \theta_{an}\}$$

$$i_{Lb} = \sum\{ I_{Lbn} \sin\{n(\omega t - 2\pi/3) - \theta_{bn}\}$$

$$i_{Lc} = \sum\{ I_{Lcn} \sin\{n(\omega t - 4\pi/3) - \theta_{cn}\}$$

The three phase voltages are transformed to α-β frame by utilizing Clark's transformation:

$$\begin{bmatrix} v_\alpha \\ v_\beta \end{bmatrix} = \sqrt{\frac{2}{3}} \begin{bmatrix} 1 & -\frac{1}{2} & -\frac{1}{2} \\ 0 & \frac{\sqrt{3}}{2} & -\frac{\sqrt{3}}{2} \end{bmatrix} \begin{bmatrix} v_a \\ v_b \\ v_c \end{bmatrix} \quad (1)$$

$$\begin{bmatrix} i_\alpha \\ i_\beta \end{bmatrix} = \sqrt{\frac{2}{3}} \begin{bmatrix} 1 & -\frac{1}{2} & -\frac{1}{2} \\ 0 & \frac{\sqrt{3}}{2} & -\frac{\sqrt{3}}{2} \end{bmatrix} \begin{bmatrix} i_{La} \\ i_{Lb} \\ i_{Lc} \end{bmatrix} \quad (2)$$

The instantaneous active and reactive power generated are expressed below

$$p = v_\alpha i_\alpha + v_\beta i_\beta \quad (3)$$

$$q = -v_\beta i_\alpha + v_\alpha i_\beta \quad (4)$$

Power and current signals are expressed in matrix form as:

$$\begin{bmatrix} p \\ q \end{bmatrix} = \begin{bmatrix} v_\alpha & v_\beta \\ -v_\beta & v_\alpha \end{bmatrix} \begin{bmatrix} i_\alpha \\ i_\beta \end{bmatrix} \quad (5)$$

$$\begin{bmatrix} i_\alpha \\ i_\beta \end{bmatrix} = \frac{1}{\Delta} \begin{bmatrix} v_\alpha & -v_\beta \\ v_\beta & v_\alpha \end{bmatrix} \begin{bmatrix} p \\ q \end{bmatrix} \quad (6)$$

here,

$$\Delta = Determinant\ is\ expressed\ as\ \sqrt{v_\alpha^2 + v_\beta^2} \quad (7)$$

$$\begin{bmatrix} i_{s\alpha^*} \\ i_{s\beta^*} \end{bmatrix} = \frac{1}{\Delta} \begin{bmatrix} v_\alpha & -v_\beta \\ v_\beta & v_\alpha \end{bmatrix} \begin{bmatrix} \bar{p} \\ 0 \end{bmatrix} \quad (8)$$

Where, $\bar{p}$ is the dc part.

Reference supply current is obtained:

$$\begin{bmatrix} i_{s\alpha}^* \\ i_{sb}^* \\ i_{sc}^* \end{bmatrix} = \sqrt{\frac{2}{3}} \begin{bmatrix} \frac{1}{\sqrt{2}} & 1 & 0 \\ \frac{1}{\sqrt{2}} & \frac{1}{2} & \frac{\sqrt{3}}{2} \\ \frac{1}{\sqrt{2}} & \frac{1}{2} & \frac{\sqrt{3}}{2} \end{bmatrix} \begin{bmatrix} i_{0^*} \\ i_{s\alpha^*} \\ i_{s\beta^*} \end{bmatrix} \quad (9)$$

The achieved reference current in both is compared with the actual source current in the hysteresis current controller to produce switching pulses.

A. Adaptive Neuro Fuzzy Inference System (ANFIS)

The ANFIS is essentially a family of artificial sensory networks that working parallel with the incomprehensible inference systems and incorporate consistent problem-solving artificial intelligence solutions. The common advantage is that ANFIS produces the best learning ability.

The modeling of ANFIS structure as illustrated in Fig. 4 is consist of five layers. Layer 1 accepts three-phase load currents as input and sends the input to layer 2. In Layer 2 the process of fuzzification takes place which makes the crisp values fuzzy. In Layer 3 the matching of output membership function to input membership functions takes place. The Layer 4 called normalization layer, calculates the firing strength of rule corresponding to input and output. Layer 5 called defuzzification layer, is used for converting the crisp values to fuzzy values and gives the desired output load current. The neurons used to train the structure of ANFIS are 10, and triangular input and output membership functions have been used as shown in Fig. 5, Fig. 6, and Fig. 7 respectively. The Training error obtained for 10 epochs is illustrated in Fig. 8.

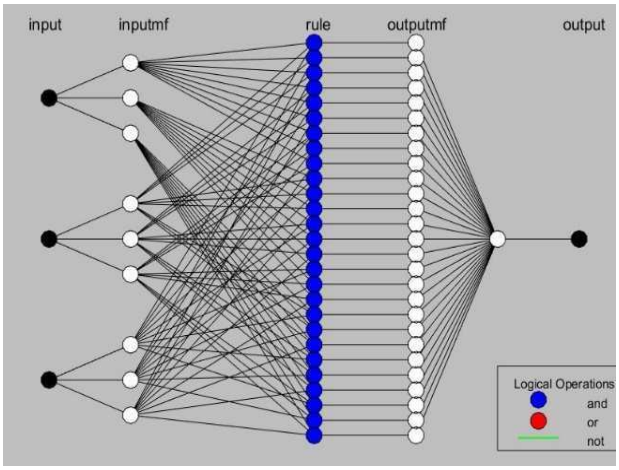

Fig. 4. ANFIS structure

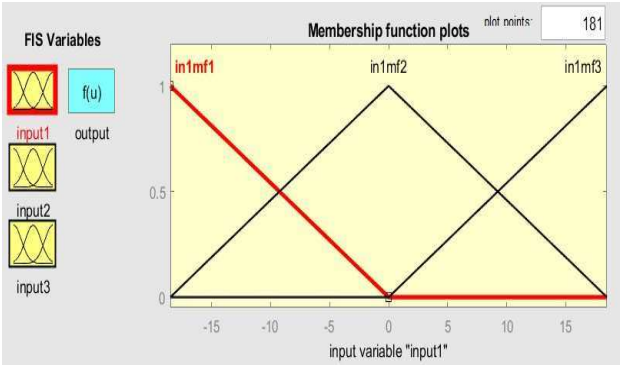

Fig. 5. Membership function plots for input1

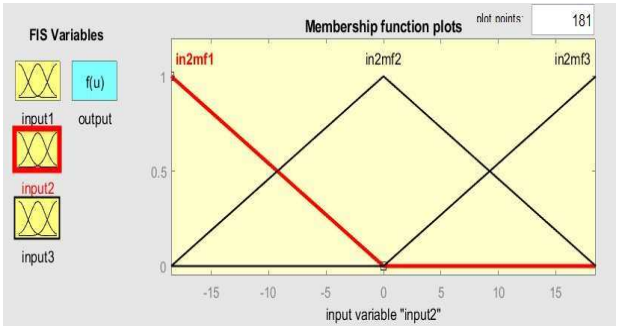

Fig. 6. Membership function plots for input2

Authorized licensed use limited to: DELHI TECHNICAL UNIV. Downloaded on June 22,2022 at 04:51:21 UTC from IEEE Xplore. Restrictions apply.

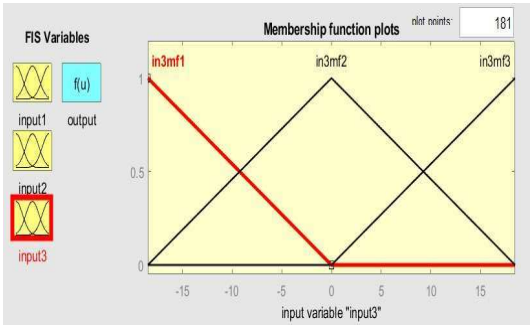

Fig. 7. Membership function plots for input3

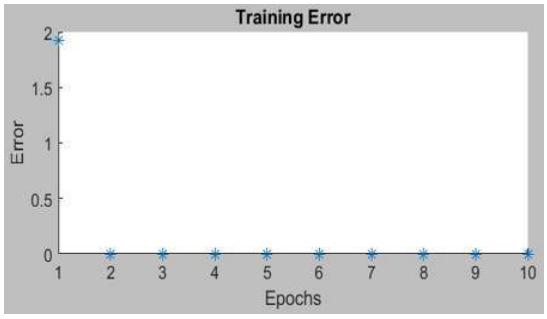

Fig. 8. Training error for 10 epochs

IV. Arrangment of DSTATCOM in MATLAB

The DSTATCOM system complies with the system structure given above in Fig. 1 includes source, load, DSTATCOM, and control blocks. The source part includes the combination of inductance and resistance and load part includes the non-linear load. The non-linear load is designed with the help of diode bridge rectifier. Non-liner load introduces harmonics in source current, algorithms such as SRFT, IRPT and ANFIS helps in cancelling those harmonics, The DSTATCOM coupled at point of common coupling sends the neutralizing current with help of the above algorithms. Table I. illustrates the values of parameters used in simulation. Fig. 9 illustrates the circuit diagram of ANFIS algorithm used. Fig. 10, Fig. 11 and Fig. 12 illustrates the DSTATCOM controlled using SRFT, IRPT and ANFIS.

TABLE I. Simulation Parameter

Sampling Time	5e-06 s
Shunt Capacitor, initial voltage	3000e-06 F, 156 V
Proportional Integral (PI) Controller	0.5, 50
Load Inductor	0.003 H
Supply RMS Voltage	110 V
Supply Impedance	2e-06 H
Shunt Induct	0.002 H

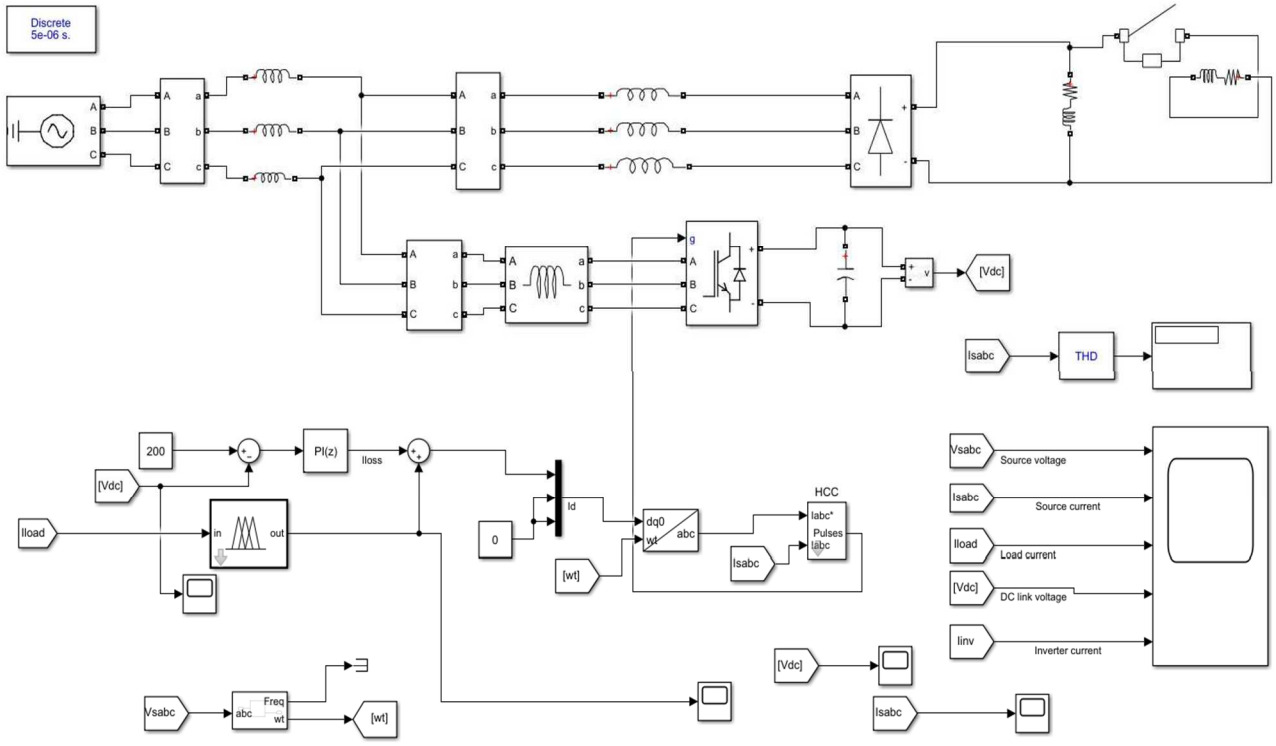

Fig. 9. Control Circuit Diagram of ANFIS Algorithm

V. Results

Simulated a non-linear load, resistance(R) and inductance(L) were 15Ω and $40*10-3H$ respectively along with diode bridge rectifier. The circuit breaker was used to create dynamics in R-L load connected. It was observed that the current load of 10 A was obtained from t = 0 to t = 0.3 s and used to meet the load requirement. It remained sinusoidal and in phase with the voltage. Non-linear load increased at t = 0.3 s, observed that the grid current also increased to meet the increased load demand but remained sinusoidal and balanced. It was also observed that dc link capacitor voltage shows few oscillations during load change but settles down within few cycles.

Fig. 10, Fig. 11, and Fig. 12 shows the supply current ($isabc$), supply voltage ($vsabc$), load current ($ilabc$), dc link capacitor voltage (Vdc), and compensator current ($icabc$), of SRFT, ANFIS and IRPT. Fig. 13. illustrates the Total harmonic distortion of supply current using SRFT algorithm is 2.19%. Fig. 14. illustrates the THD of supply current using

Authorized licensed use limited to: DELHI TECHNICAL UNIV. Downloaded on June 22,2022 at 04:51:21 UTC from IEEE Xplore. Restrictions apply.

IRPT algorithm is 2.14%. Fig. 15. illustrates the THD using the ANFIS algorithm of the supply current is 2.00%.

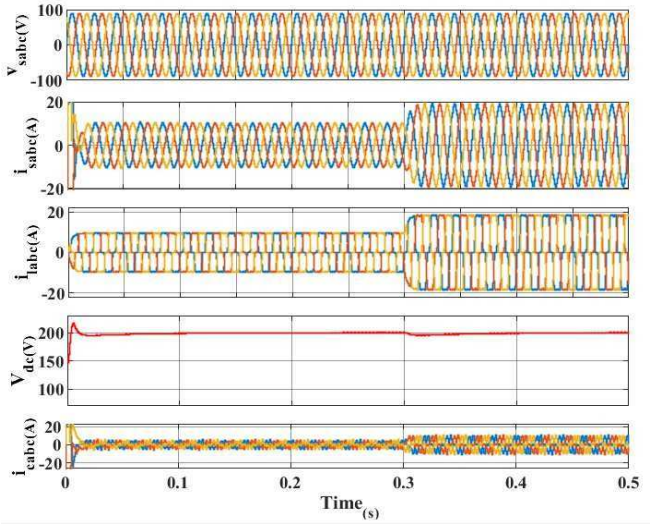

Fig. 10. Waveforms obtained using SRFT controlled algorithm

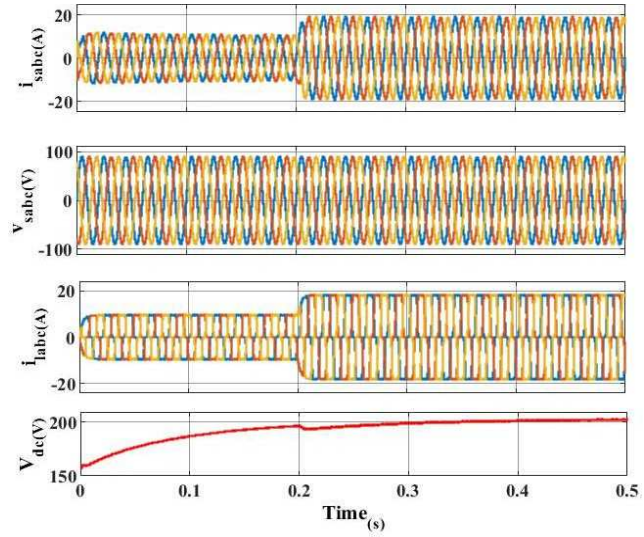

Fig. 11. Waveforms obtained using IRPT controlled algorithm

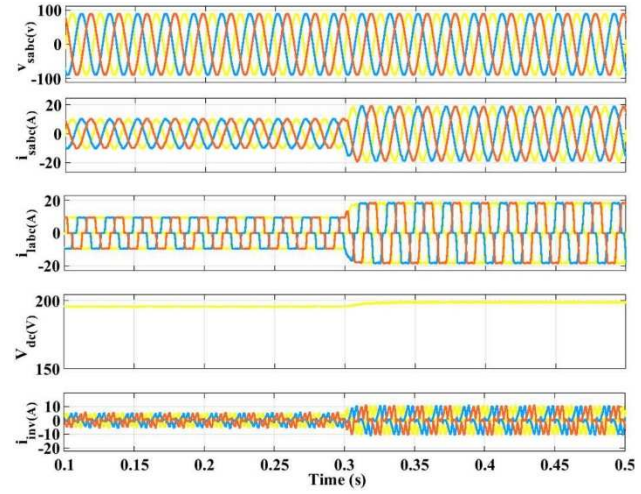

Fig. 12. Waveforms obtained using ANFIS controlled algorithm

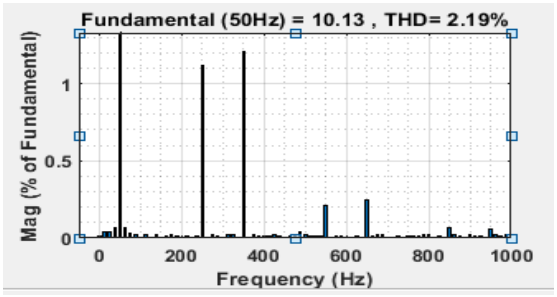

Fig. 13. THD using SRFT algorithm

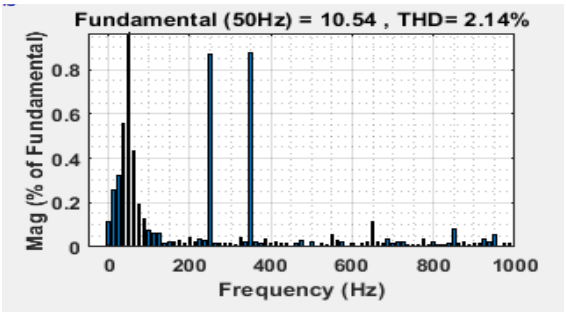

Fig. 14. THD using IRPT algorithm

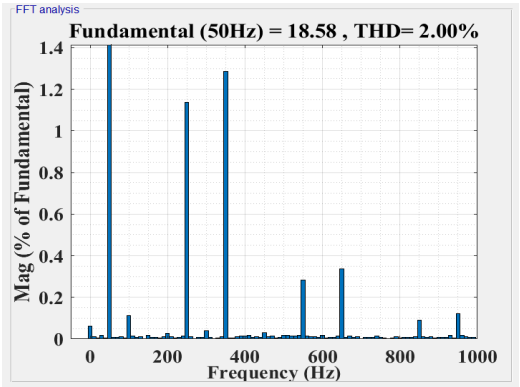

Fig. 15. THD using ANFIS algorithm

VI. Comparision between SRFT, IRPT and ANFIS Control Algorithm

The THD also known as Total Harmonic Distortion, rise time, peak overshoot and convergence rate is used for performance analysis of three control algorithms. The THD is defined as the equivalent RMS voltage of all harmonic frequencies divided by RMS voltage of the fundamental frequency. Since the THD of supply current is calculated using POWERGUI FFT analysis block. The ANFIS control algorithm in comparison to SRFT and IRPT controlled algorithm provides better waveforms as well as low THD. Table II. illustrates the obtained rise time, peak overshoot, THD and convergence rate. The rise time is 0.0058s for SRFT, 0.0059s for IRPT and 0.0060 for ANFIS. Peak overshoot obtained is 1.991% for SRFT, 1.988% for IRPT and 1.9789% for ANFIS as illustrated in Fig. 17 the convergence rate is observed to be high in SRFT and IRPT but low in ANFIS. THD of supply current is 2.19% for SRFT, 2.14% for IRPT and 2.00% for ANFIS. Fig. 16 illustrates SRFT, IRPT and ANFIS of dc link capacitor voltage.

Authorized licensed use limited to: DELHI TECHNICAL UNIV. Downloaded on June 22,2022 at 04:51:21 UTC from IEEE Xplore. Restrictions apply.

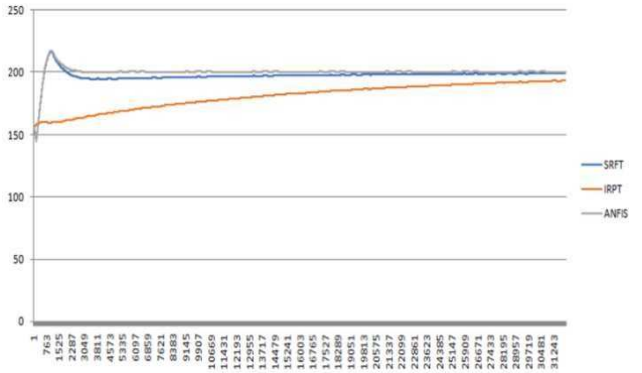

Fig. 16. Comparation analysis of dc link voltage of SRFT, ANFIS and IRPT

TABLE II. COMPARISON RESULTS

DSTATCOM control algorithm	Peak overshoot	Rise time	%THD	Convergence rate
SRFT	1.991%	0.0058	2.19%	High
IRPT	1.988%	0.0059	2.14%	High
ANFIS	1.9789%	0.0060	2.00%	Low

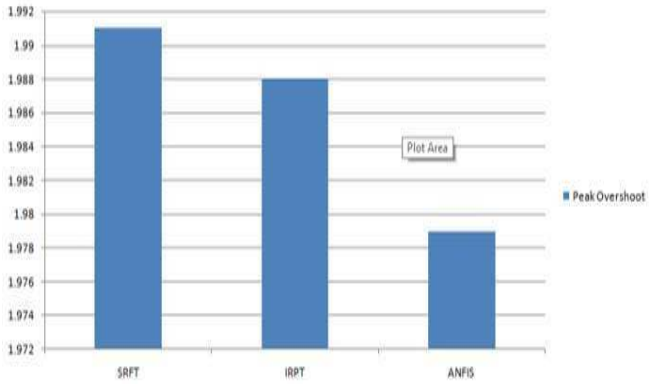

(a)

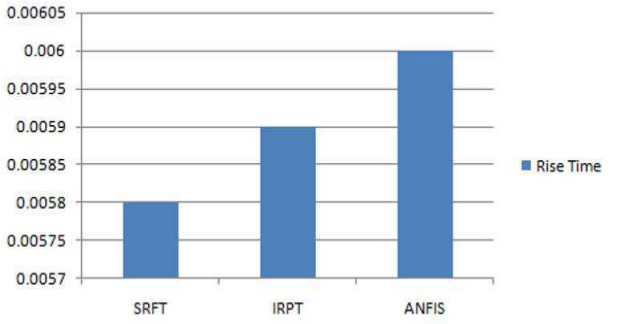

(b)

Fig. 17. Comparative analysis of Peak Overshoot and Rise Time of SRFT, IRPT and ANFIS control algorithm

VII. CONCLUSION

In this paper, we used SRFT, IRPT, and ANFIS based control measures to enhance power quality compensation. The SRFT, IRPT and ANFIS based theory technology has demonstrated satisfactory performance of DSTATCOM. The ANFIS control system shows the improved DSTATCOM performance compared to that SRFT and IRPT strategy. ANFIS-based approach uses both Fuzzy Logic and ANN algorithm also gives high efficiency and low THD in the supply current for varying load conditions. The MATLAB simulation and test results ensure the proper functioning of the specified algorithms.

The simulation outcomes with MATLAB illustrates that ANFIS based DSTATCOM has an immediate response time and accurate compensation. The Performance comparisons of the three control algorithms were performed based on % THD and realized that the Adaptive neural fuzzy based control gives a good result. Therefore, ANFIS has proven to be very effective control DSTATCOM to improve power quality.

REFERENCES

[1] L.H. Tey, P. L. So and Y. C. Chu, "Improved energy quality improvement active shunt filter", in IEEE Transactions on Power Delivery, volume. 20, no. 2, pages 1558-1568, April 2005.

[2] M. Bajaj, M. Pushkarna, A. S. Rana and M. T. Khan, "Improved SRF D-STATCOM-based control algorithm under a random source voltage, "2015 Annual IEEE India Conference (INDICON), 2015.

[3] Arora A, Singh A. Design and analysis of functional link artificial neural network controller for shunt compensation. IET Generation, Transmission & Distribution. 2019 Jun 27;13(11):2280-9.

[4] A. A. Patel and A. A. Patel, "The use of DSTATCOM harmonics elimination and improvement of energy quality, "2017 International Power Conference, Communication, Data Analysis and Software Computing (ICECDS), 2017A.

[5] B. Singh, P. Jayaprakash, D. P. Kothari, A. Chandra and K. A. Haddad, "Extensive DSTATCOM Configuration Study," in IEEE Transactions on Industrial Informatics, vol. 10, no. 2, pp.854-870, May 2014.

[6] B. Singh and J. Solanki, "Comparison of control algorithms of DSTATCOM, "in IEEE Transactions on Industrial Electronics, vol. 56, no. 7, pages 2738-2745, July 2009.

[7] A. Singh and B. Singh, "Energy issues related to distribution integration of energy source into utility grids, "2010 Annual IEEE India Conference (INDICON), 2010.

[8] Arora A, Singh A. Design and implementation of Legendre-based neural network controller in grid-connected PV systems. IET Renewable Power Generation. 2019 Nov 18;13(15):2783-92.

[9] Verma P, Garg R, Mahajan P. Smooth LMS-based adaptive control of SPV system tied to grid for enhanced power quality. IET Power Electronics. 2020 Nov 6;13(15):3456-66.

[10] A. Arora and A. Singh, "Design and Implementation of Biquad Filter for Shunt Compensation under Normal and Distorted Grid Conditions," 2020 IEEE 9th Power India International Conference (PIICON), 2020, pp. 1-6, doi: 10.1109/PIICON49524.2020.9112949.

[11] Arora A, Singh A. Development and performance analysis of cubic Bezier functional expansion-based adaptive filter for grid-interfaced PV system. International Transactions on Electrical Energy Systems. 2021 Oct;31(10):e12840.

[12] B. Singh, A. Chandra and K. Al-Haddad, Energy Quality: Problems with Reduction Strategies, John Wiley and Sons, U.K., 2015.

[13] M. Badoni, A. Singh and B. Singh, "Adaptive Neurofuzzy Inference System Least-Mean-Square-Based Control Algorithm for DSTATCOM, "in IEEE Transactions on Industrial Informatics, vol. 12, no. 2, pages 483-492, April 2016.

[14] S. Sinha and A. Arora, "Comparison of IRPT and ANN based Control Algorithm for Shunt Compensation in Grid Connected Systems," 2021 International Conference on Intelligent Technologies (CONIT), 2021, pp. 1-5, doi: 10.1109/CONIT51480.2021.9498281.

[15] R. Deepak Singh, T. Praveen Kumar, Dr. K. Electrical and Electrical Equipment, Volume 5, NO.7, pages 6493-6501, July 2016.

Authorized licensed use limited to: DELHI TECHNICAL UNIV. Downloaded on June 22,2022 at 04:51:21 UTC from IEEE Xplore. Restrictions apply.

BULMIM Journal of Management & Research (January-June 2022) 7(1): 11–29
DOI: 10.5958/2455-3298.2022.00002.2

Corporate Governance and M&A Performance: A Systematic Review of Literature

Harsh Gautam[1]*, Archana Singh[2] and Girish Chandra Maheshwari[3]*****

[1]Ph.D. Scholar, [2]Associate Professor and Head, [3]Professor, Delhi School of Management, Delhi Technological University, Shahbad Daulatpur, Main Bawana Road, Delhi-110042, India

(*Corresponding author) email id: *harshgautam_phd2k19@dtu.ac.in, **archanasingh@dtu.ac.in, ***gcmaheshwari2004@yahoo.com

Received: 06-08-2021; Accepted: 24-11-2021

www.IndianJournals.com
Members Copy, Not for Commercial Sale
Downloaded From IP - 14.139.251.98 on dated 13-Jun-2022

Abstract

Mergers and Acquisitions are generally undertaken for strategic purposes but from a corporate governance standpoint, they can be regarded as those events that can intensify agency conflicts. Through this study, therefore, an attempt has been made to systematically review the existing literature on the role of various corporate governance attributes in minimizing agency conflicts that may arise during mergers and acquisitions. A sample of 116 research articles was identified that were clustered into three broad themes viz. board structure, ownership structure and compensation structure. The findings of the study shed light on the importance of each of the governance attributes classified under these three themes during mergers & acquisitions. Further, the study also highlights the under-explored areas that future researchers can undertake to contribute to this research stream.

Keywords: Corporate Governance, Board of Directors, Ownership structure, Compensation and mergers & acquisition performance, Literature review

INTRODUCTION

Corporate governance mechanisms such as the board of directors and performance linked-incentive measures exist to minimize agency costs whether arising as a result of a conflict of interest between executives and shareholders or between the dominant and non-dominant shareholders (Rani *et al.*, 2013). To examine their effectiveness, to date a large number of researchers have studied their relationship with firm performance or firm value (Redor, 2015). The basic idea underlying these studies is to empirically establish the causation impact of these governance mechanisms on firm performance or firm value and to identify whether these mechanisms can minimize agency conflicts and maximize firm value. However, despite the proliferation of studies, there is still much debate about the effectiveness of certain corporate governance mechanisms in minimizing agency conflicts as evidenced by the inconclusive findings in the literature (Certo *et al.*, 2008; Daily *et al.*, 2003; Masulis, 2020; Redor, 2015). One significant explanation provided for this is that firm performance or value is influenced by a variety of factors therefore empirically isolating the effect of the governance mechanisms on overall firm performance or value may be difficult (Redor, 2015). Further, (Masulis, 2020) also proposed that if one has to gauge the effectiveness of these governance mechanisms, quasi-experimental studies or studies focusing on specific firm decisions will yield a better picture with more reliable results about their effectiveness. Mergers & Acquisitions (M&A hereafter) can be regarded as one such instance; further, they also represent events where there is a higher likelihood of managers or majority shareholders maximizing their gains (Jeong and Bae, 2013; Demirtas, 2017).

Using the traditional principal-agent model originally conceived by Berle and Means (1932) and conceptualized by Jensen and Meckling (1976) in the form of agency

theory, researchers have put forward several arguments that explain how managers can expropriate wealth from the shareholders during mergers & acquisitions. The empire-building hypothesis implies that managers are empire builders and for solely selfish purposes, they undertake M&A activities (Mueller, 1969). Managers behave this way because some of their private interests can be served by growing company size, such as their desire for status, influence, reputation and higher compensation (Jensen, 1986). Likewise, managerial entrenchment theory implies that acquisitions increase the company's reliance on the managers' talents and expertise, rendering them so indispensable and difficult to substitute that they extract higher compensation from shareholders (Bebchuk and Fried, 2012). Further, (Roll, 1986) put forward the management hubris argument where the executives at the acquiring company think that the target company is undervalued and they can better manage the assets of the target company under their management, therefore, sometimes under this misconception, they tend to overpay for the target firm by overestimating their abilities. Under all these circumstances, acquisitions often destroy, instead of creating value for shareholders, particularly acquiring firm shareholders (Redor, 2015). It is important to note that these claims largely take into account the conflict of interest between bidder firm management and its shareholders. A similar conflict of interest may also arise between target management and its shareholders (Redor, 2015). Though, it is generally argued that target firm shareholders earn significant positive abnormal returns during the takeover process owing to large takeover premiums, however, this may not be the case with the target firm management, including the directors. After the deal completion, they often face the risk of job loss, reduced compensation, status and other perks. Thus, to protect their positions, they may oppose certain acquisitions even if they are beneficial for the shareholders, or alternatively, they may structure the terms of acquisitions in such a way that protects their positions even at the expense of a lower bid premium for the shareholders (Stulz, 1988).

Thus, M&A can be regarded as those events that can create or intensify the interest conflict between managers and shareholders, both in the case of acquiring as well as target firms (Aggarwal *et al.*, 2019; Field and Mkrtchyan, 2017). To mitigate such conflicts and effectively reduce agency costs, corporate governance mechanisms have a vital role to play.

Therefore, in order to understand the role of corporate governance mechanisms in the creation of wealth during M&A, this paper attempts to review the existing research in the area by systematically synthesizing the research articles published between the period 1991 and 2020. The present paper is different from the previous papers in the sense that the previous reviews examining the relationship between these two are often limited in their scope as they generally focused on board-related attributes such as size, independence and duality (Redor, 2015; Sundaram, 2004; Surbhi and Vij, 2018; Varottil, 2012). Though boards of directors are central to corporate governance, there are other mechanisms as well that also helps in resolving the agency conflict whether arising between managers and shareholders or between dominant and non-dominant shareholders. The relevance of the study, therefore, lies in the fact that it has attempted to include other relevant corporate governance mechanisms that are broadly classified into three major themes viz. board structure, ownership structure, compensation structure. The study, therefore, attempts to fill this gap by offering a more comprehensive approach to previous studies by including other corporate governance mechanisms that were not considered in the previous studies.

RESEARCH METHODOLOGY

The study adopts a systematic literature review (SLR) methodology in order to systematically synthesize the existing literature on the relationship between corporate governance and M&A performance. The SLR approach was selected as it not only allows the researchers to consider a large number of articles with various methodological approaches, as opposed to meta-analysis (Pickering and Byrne, 2014), but also can enhance the doubtful quality of the "mass of often-contradictory" evidence, which has made conventional narrative reviews less effective for policy-makers and practitioners (Tranfield *et al.*, 2003). Moreover, the pre-defined eligibility criteria used in SLR help to reduce the researcher's personal biases in the article selection process while at the same time enhancing the objectivity and validity of the results

www.IndianJournals.com
Members Copy, Not for Commercial Sale
Downloaded From IP - 14.139.251.98 on dated 13-Jun-2022

produced (Collins and Fauser, 2005). Therefore, the SLR method can ensure a replicable, transparent and scientific way of conducting reviews (Cook *et al.*, 1997) which may not be possible in the case of traditional narrative reviews. The article selection process has been done by following the Preferred Reporting Items for Systematic Reviews and Meta-Analyses (PRISMA) approach and was adapted from Page *et al.* (2021) and Kolve *et al.* (2019).

Figure 1 illustrates the PRISMA framework indicating the number of articles included and excluded at each individual phase of the entire review phase. The article selection process for the study began by entering the appropriate and relevant keywords such as "corporate governance and M&A performance", "board of directors and mergers and acquisitions", "independent directors and mergers and acquisitions", "board attributes and mergers and acquisitions", "ownership and mergers and acquisitions, "compensation and mergers and acquisitions", "agency conflict and merger and acquisitions" among other relevant search terms. The databases that were used to conduct the search were *Business Source Premium* and *SCOPUS* as they have been used widely in previous review articles. These databases were used to search for all the articles that were published between the period 1991 and 2020. The year 1991 has been taken as the starting point as the issue of corporate governance began to gain traction in the early 90s owing to the major corporate collapses and the subsequent publication of the Cadbury committee report. Using the above-mentioned criteria a total of 6834 articles were identified. These articles were further filtered by applying certain exclusion and inclusion criteria similar to the one followed by (Kolve *et al.*, 2019). *Conceptual articles, editorials, book chapters, conference papers and commentaries* were removed and articles that were published in the English *language and in peer-reviewed academic journals* were considered. After applying the above exclusion criteria 972 articles were identified. These articles were further filtered by applying the relevant *subject area* criteria. Articles that were published in the area of *business and management, accounting, finance, management, business and social sciences* among others were considered. With these filters, 431 articles were found eligible for full-text review. After going through each of these articles, studies that did not present any empirical findings and were duplicative were also removed. Only empirical articles that were focused on non-financial firms were considered. Thus, studies that focused on financial firms such as banks were excluded owing to their different regulatory norms. An iterative snowballing strategy was also used to identify articles from the reference lists of the initially selected articles. This was done to include those articles as well that did not directly match our search terms but were significantly related to our subject area (Hopkinson & Blois, 2014). The final sample for the study consists of 116 research articles that were published between 1991 and 2020.

RESULTS AND ANALYSIS

Descriptive Analysis

Classification based on themes identified

After reviewing the total number of articles, it is observed that these articles could be classified into three broad themes viz. board structure related studies, ownership structure related studies, and compensation structure related studies. The type of corporate governance attributes that have been classified under each of these themes has been illustrated using Figure 2. Under the theme of board structure, attributes such as board size, independence, diversity, busyness, leadership were included. Under the theme of ownership structure, attributes such as equity share ownership by internal members such as CEOs and non-executive directors and by external members such as institutional investors and large block holders were included. Lastly, under the theme of compensation structure, attributes such as type and form of compensation paid to the executives such as CEO and external directors were considered. The studies classified under these three themes have majorly considered the impact of these governance attributes on the performance of the M&A deal both for the target as well as for the acquiring firms.

i. Distribution of articles based on the themes identified

Figure 3, illustrates the number of articles published under each of the themes identified. From Figure 3, it can be observed that the articles are unevenly distributed among each of these themes. A majority number of studies are focused on the attributes related to the board structure. A total of 43 articles were published that have evaluated the

www.IndianJournals.com
Members Copy, Not for Commercial Sale
Downloaded From IP - 14.139.251.98 on dated 13-Jun-2022

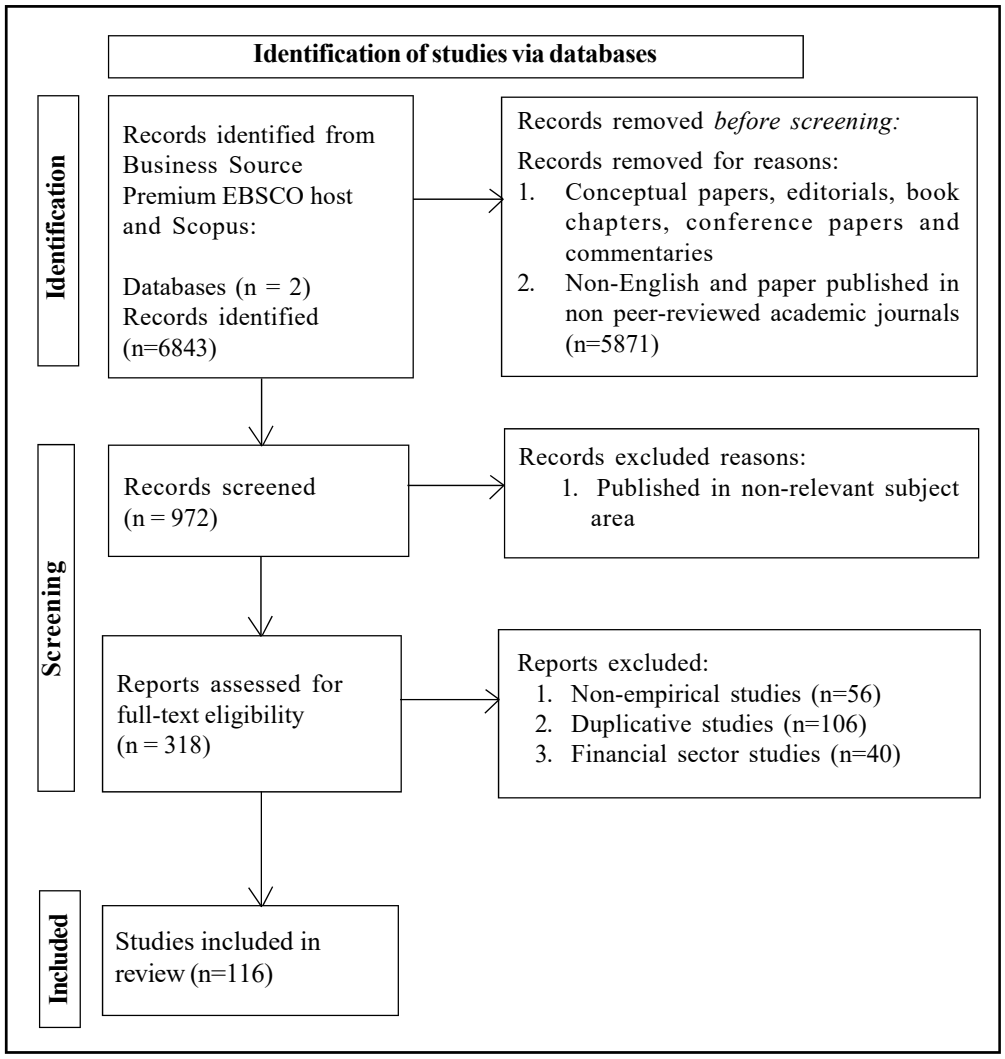

Figure 1: PRISMA flow diagram adapted from Kolve *et al.* (2019) and Page *et al.* (2021)

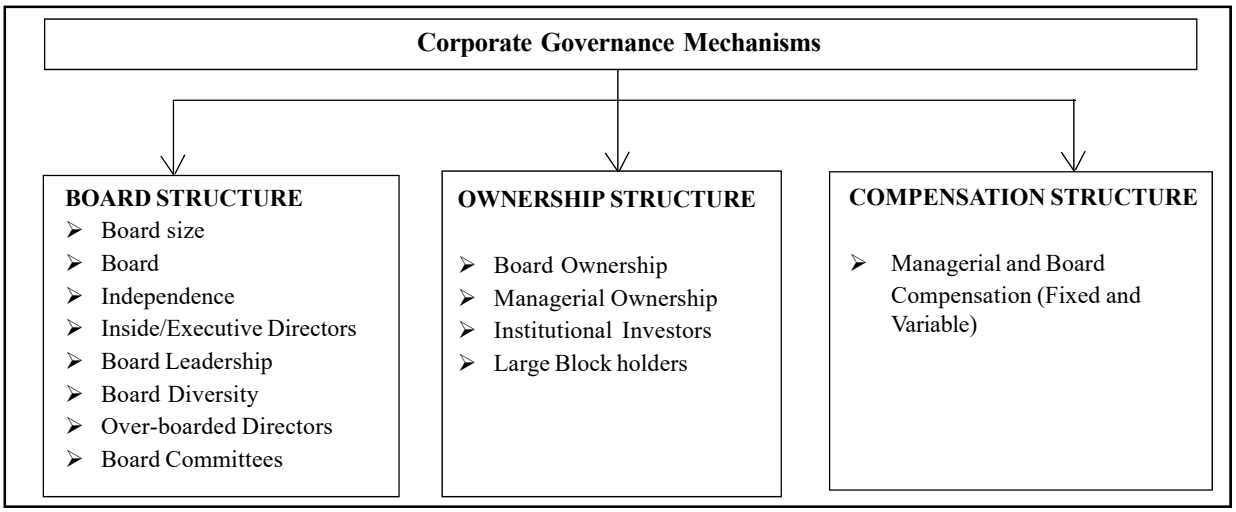

Figure 2: Classification Themes

www.IndianJournals.com
Members Copy, Not for Commercial Sale
Downloaded From IP - 14.139.251.98 on dated 13-Jun-2022

role of board structure on the performance of the M&A deals. The boards of directors are considered as the focal point in the corporate governance framework (Hauser, 2018) as they are entrusted with the paramount task of protecting shareholder's interests and keeping a check on managerial opportunism (Bauguess and Stegemoller, 2008). Therefore, the way the board of a company is structured in terms of its size, independence and leadership among other characteristics will influence its effectiveness. Further, M&A deals are generally approved with the consent of the directors (Demirtas, 2017). This might explain that the majority of the studies are on board structure. As against this, there are 32 articles on the ownership structure of the firm and 16 articles on compensation structure. Further, it is also found that these attributes are not only studied in isolation of each other but there are 25 studies as well that have used a combination of these attributes. A major purpose of such studies is to assess the complementarity or the substitution effects of different governance attributes on M&A performance. Though the number of such studies is still relatively few.

ii. Distribution of articles based on year of publication and country of study

Figure 4 illustrates the number of articles that were published in peer-reviewed academic journals during the period 1991-2020. Further, the figure also shows whether these articles have considered a developed country or a developing country in their analysis or if it is a cross-country study. Table 1 also illustrates the number of articles that were published in each of the individual countries. The Figure 4 shows that overall there is an upward trend in the number of articles that are being published on the relationship between corporate governance and M&As thus indicating a growing interest among the research community, however, it is observed that a large number of these articles have considered a developed country in their analysis, especially the US and UK. Contribution of articles that consider a developing country or cross-countries are still in scarcity. It is important to mention here that firms in developed countries are often characterized by type 1 agency issues owing to dispersed shareholding patterns and professional management (Amar *et al.*, 2011). Thus, the conflicts that occur in such firms are between principal and agents. On the other hand, emerging and developing economies' firms have concentrated shareholdings with the control often residing in the hands of family members or the government (Aggarwal *et al.*, 2019). This leaves important insights into

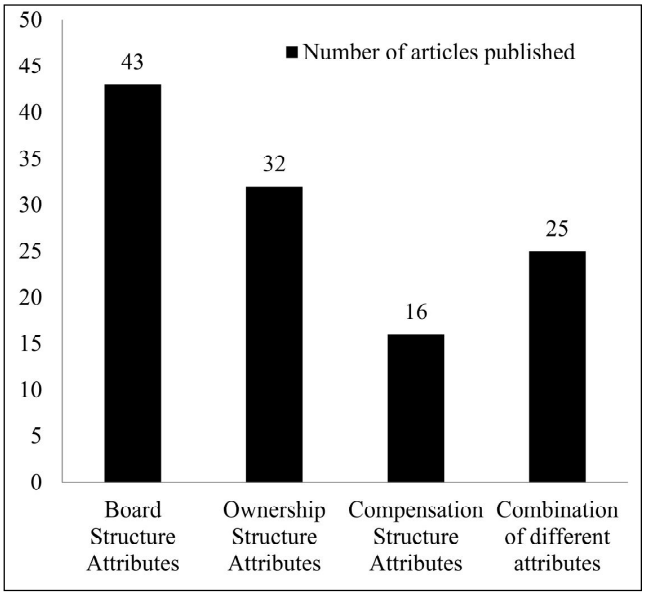

Figure 3: Articles distribution based on themes identified

Table 1: Number of articles published in different countries

Country	Total No. of Articles
United States of America	49
United Kingdom	19
Australia	7
Canada	4
Japan	1
India	6
China	11
Brazil	1
South Africa	2
France	3
The Netherlands	1
Pakistan	1
Korea	1
Vietnam	1
Taiwan	2
Sweden	1
Gulf Countries	1
Cross-Countries	5
Total	**116**

www.IndianJournals.com
Members Copy, Not for Commercial Sale
Downloaded From IP - 14.139.251.98 on dated 13-Jun-2022

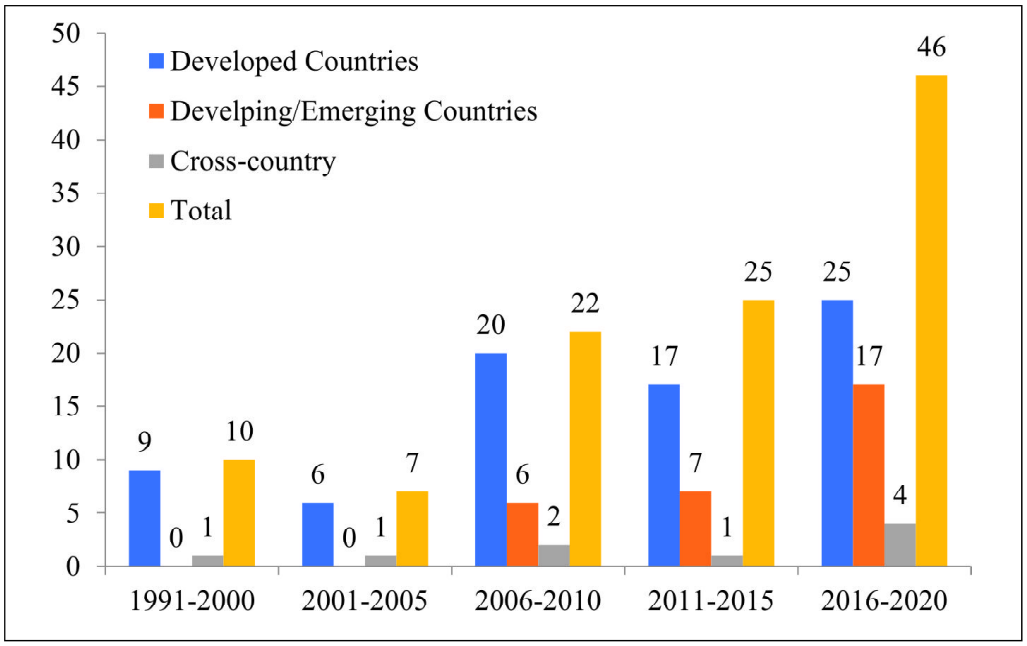

Figure 4: Articles distribution based on country of study

www.IndianJournals.com
Members Copy, Not for Commercial Sale
Downloaded From IP - 14.139.251.98 on dated 13-Jun-2022

the management structure of emerging and developing economies and how the governance mechanisms' functions will function in such economies in the context of M&As. Therefore, it would not be appropriate to generalize the results obtained in the studies of developed country studies to emerging economies.

iii. Distribution of articles based on the focus of study and the performance measures used

Figure 5 and 6 illustrate the number of articles that describe whether the author(s) have focused on acquiring firms or target firms and the performance measures (short-term or long-term measures) they have used to quantify the performance of the M&A deal, respectively. To bring more clarity to the analysis, these figures have also classified these articles based on the country of study as well. These figures reveal three important things, firstly, a major focus in the literature has been on acquiring firms with only a few studies on target firms. A total of 110 articles were published that have considered the acquiring firms in their analysis. Secondly, among these studies, a large number of articles have considered developed economy firms in their analysis (88 articles). Though there are studies on developing countries as well but a shred of startling evidence that is found from the review is that there were no studies on emerging economy target firms during our sample period. Thirdly, it is found that the performance measures used by the author(s) in these studies to quantify M&A deal performance are short-term oriented. It is found that a majority of the studies (85 articles) included in our sample period have short-term performance measures which are generally market-based like cumulative abnormal returns (CAR), cumulative average abnormal returns (CAAR). Long-term performance measures like buy-and-hold abnormal returns (BHAR) or financial performance measures like liquidity ratios, efficiency ratios and profitability ratios that are measured over a long time frame are not used by many author(s) in their studies. Only 25 articles were published in the sample period that used long-term performance measures. Although short-horizon methods offer some insights, however, it has been observed in some empirical studies that investors generally under or overreact to certain corporate events such as M&As (Frazzini, 2006; Ikenberry *et al.*, 1995; Popli *et al.*, 2017). Therefore, changes in stock prices immediately around the deal announcement may not fully absorb the information generated through such actions (Popli *et al.*, 2017). Furthermore, M&As are complex events, using long-term performance measures will more appropriately capture the true value created for shareholders.

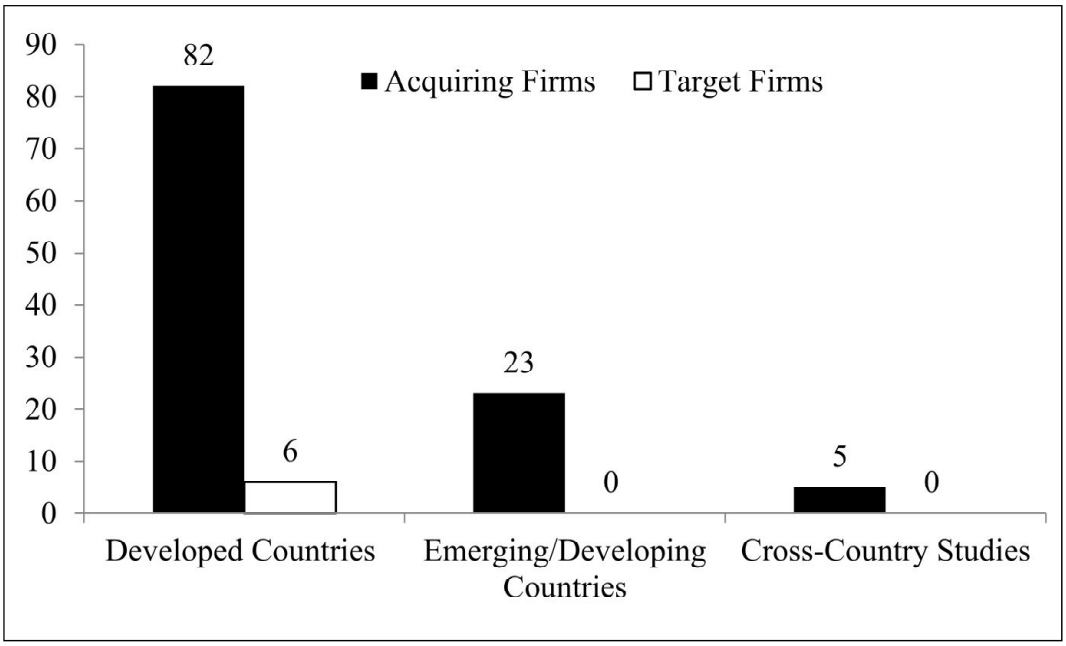

Figure 5: Articles distribution based on the focus of the study

www.IndianJournals.com
Members Copy, Not for Commercial Sale
Downloaded From IP - 14.139.251.98 on dated 13-Jun-2022

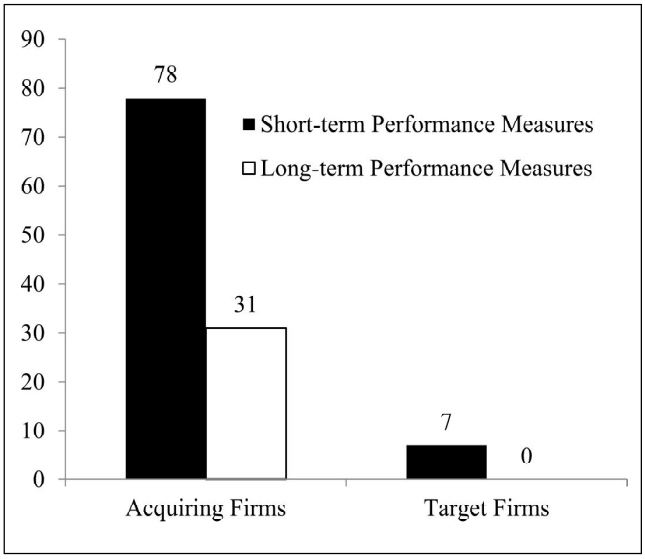

Figure 6: Articles distribution based on performance measure used

Empirical Evidences

The following sections elaborate on the empirical findings of the studies that are included in this review.

Theme 1: Board structure

In the corporate governance literature, the board of directors is considered as a major governance mechanism that oversees managers' conduct. Essentially, the job of the board of directors becomes even more important in the case of an M&As because such deals are approved with the board's consent and they shoulder the accountability for its success or failure (Gaughan, 2013). In the literature, their role has been classified into two categories, one internal where the directors are responsible for monitoring the actions of management and providing suitable advice and counsel on major decisions (Fama, 1980; Jensen, 1986) and second is the external role where the directors through their contacts in the external environment provide access to important resources and information (Pfeffer, 1972). These two primary roles of directors can be drawn from three theoretical perspectives viz. agency perspective, social capital perspective and resource-based view (Figure 7). The agency theory provides that, due to separation of ownership and control, managers do not act in the best interest of the shareholders and maximize their personal gains. Further, with dispersed ownership, it becomes costly for the shareholders to monitor the actions of the managers (Jensen and Meckling, 1976). Therefore, the board of directors is appointed to control the actions of managers, safeguard the shareholder's interest and minimize the agency cost (Turnbull, 2019). According to the resource-based view, the board of directors not only monitor the managers but as a part of strategic leadership offer counsel

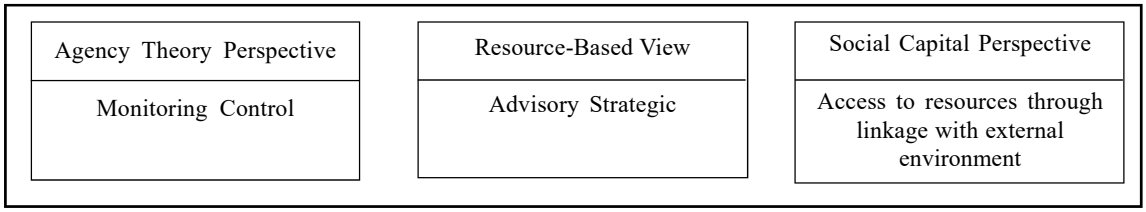

Figure 7: Role of board of directors

and advice to top management on strategic investments (Lorsch and Maclver, 1989), and participate in strategy formulation and implementation (Judge and Zeithaml, 1992). There is also evidence in the literature to support this notion. A survey conducted by Stiles (2001) provides that the board of directors is not only responsible for monitoring the managers but also takes an active part in setting the mission and vision of the company and help the firm deal with the complexity and uncertainty involved in strategic decisions. However, the ability of the directors to offer advice depends to a large extent on their professional expertise and capabilities. The social capital perspective on the other hand focuses on the externally-oriented role that the board of directors performs. It proposes that directors through their contacts and linkages in the external environment obtain critical resources and information which may not be available to the firm otherwise. Such information may enable the management to gain a competitive advantage over its rivals and take actions that can generate positive gains for the shareholders (Huse *et al.*, 2011; Pfeffer, 1972). During an event such as that of M&A, all the three roles discussed above assume special significance.

Within the theme of board structure, seven attributes were identified that are related to the board of directors in terms of their composition, independence, committees, etc. All these attributes have been discussed below:

i. Inside and outside/independent directors

Directors can be broadly classified into two categories viz. inside directors and outside directors, depending on their relationship with the company (Adams *et al.*, 2010). Inside directors are the directors that are engaged in the day-to-day functioning of the firm and have some sought of financial connection with the firm whereas outside directors are the ones without any pecuniary relationship with the firm and are independent of its management (Faleye *et al.*, 2011). It is important to note that such classification of directors was used traditionally, however, now in most countries the term outside directors is rarely used instead outside directors are further divided into two categories viz. non-executive and non-executive independent directors (Sarkar and Sarkar, 2009). E.g. In India there are typically three classes of directors' *viz.* executive directors, non-executive directors and independent directors. In this category, independent directors are the ones who are truly independent who do not hold any kind of direct or indirect financial relationship with the company whereas executive and non-executive directors have some kind of pecuniary relationship with the firm. In this study, we have only considered inside executive directors and independent directors as there were very few studies that have considered non-executive directors separately in their analysis.

Existing studies suggest that a balanced proportion of inside and independent directors is required for a board to be effective in its decision-making. Both inside and independent directors have their own merits and demerits. Studies on board of directors have found that independent directors are considered more effective monitors than inside directors since they are not associated with the firm (Cheng, 2017; Ibrahim and Samad, 2011). There is also evidence that outside directors grill the CEO on important decisions (Byrd and Hickman, 1992). Also, they are more actively involved in making CEO retention decisions (Byrd and Hickman, 1992). Outside directors through their network and social ties in the external environment provide valuable inputs about strategies and practices of other firms (Li and Aguilera, 2008). Drawing from the above arguments it can be inferred that the independent directors are well equipped to perform all the three roles discussed above and having more such directors on board will relate positively to M&A

www.IndianJournals.com
Members Copy, Not for Commercial Sale
Downloaded From IP - 14.139.251.98 on dated 13-Jun-2022

outcomes as they will be more objective in considering the cost and benefits associated with the deal (Byrd and Hickman, 1992). The empirical evidence, however, has presented us with inconclusive findings with Amar *et al.* (2011) and Teti *et al.* (2017) reporting a positive association between acquirer returns and board independence; Byrd and Hickman (1992) and Haqi (2017) reported a non-linear relationship whereas there are other studies as well that found the role of independent directors insignificant during M&A (Masulis *et al.*, 2007; Swanstrom, 2006) Similarly, in the case of target firms, Clarkson *et al.* (2008) reported that an independent board is able to extract a higher bid premium whereas on the contrary Bange and Mazzeo (2004) reported an inverse relationship. These findings suggest that having mostly independent directors on board may not increase the overall board functioning. This is because their task at least in part depends upon the information they receive from the management. Since they are not full-time employees who are actively involved in the regular functioning of the management their actions are dependent upon the information they receive from the management thus there can be situations where it is difficult for them to effectively monitor or give suitable advice to managers, especially during M&As (Duchin *et al.*, 2010). Further, outside directors also hold a number of outside directorships or they themselves may be the CEO of some other firm (Ahn *et al.*, 2010). In such situations, it might become difficult for independent directors to devote sufficient time to the firm in which they are serving as a director making them ineffective monitors.

On the other hand, a board dominated by inside directors is often considered a weak board (Beatty and Zajac, 1990). The inside directors are usually treated as "rubber stamps" (Herman, 1981) or "tools of top management" (Pfeffer, 1972) or "creatures at the will of CEO" (Mace, 1971). These directors often do not question the decisions of the CEO as their compensation and reappointment decision are made by the CEO. However, the authors have argued that having a good proportion of inside directors could be favorable for the firm as they are involved in the regular functioning of the firm and therefore may be able to offer better explanations to the shareholders about the internal operations of the firm (Harris and Shimizu, 2004). There is also evidence that inside executive directors' represents a potential replacement for a bad performing CEO thus forcing the existing CEO to not undertake value-destroying deals (Masulis and Zhang, 2019). Therefore, it is beneficial for firms to have a reasonable proportion of both inside and outside independent directors on board as having only one kind in the majority may not be rewarding. Both have their unique set of skills and functions which is very essential for a sustainable firm.

ii. Size of the board

Another essential factor determining the board's ability to function effectively is the size of the board. Jensen (1993) argues that board oversight and monitoring capabilities are weakened when the number of members on the board reaches seven or eight members, making it easier for the CEO to control the business, implying that larger boards might be ineffective. Empirically Yermack (1996) and Eisenberg *et al.* (1998) proved that firms with smaller board size firms have higher market valuations. They contend that smaller boards are more effective, more unified and monitor the firm better while larger boards result in coordination and communication problems which leads to ineffective decision making.

With regard to M&As, it was found that researchers generally argue in favor of having a large board. Alabdullah *et al.* (2018); Bauguess *et al.* (2009) and Swanstrom, 2006) reported a positive relationship between the two constructs, arguing that firms with larger boards have better tools at their disposal and can contribute additional information about the target firm and its industry. Similarly, Coles *et al.* (2008); Coletta and Roberto (2020) also support the notion of having large boards. They argue that boards not only perform the monitoring function but are also required to offer advice and counsel to the CEO in making important strategic decisions about the firm. Such a role can more appropriately be fulfilled by larger boards. In contrast to the above findings, there are few studies as well that supported the arguments proposed by Yermack (1996) and Eisenberg *et al.* (1998). A negative relationship between board size and short-term abnormal returns around the M&A announcement for acquirer firms was documented by Amar *et al.* (2011), Haqi (2017) and Zelenskaia (2018).

www.IndianJournals.com
Members Copy, Not for Commercial Sale
Downloaded From IP - 14.139.251.98 on dated 13-Jun-2022

iii. Board Leadership

CEO duality refers to a system in which a single person holds the positions of both the Chief executive officer (CEO) and the Chairman of the board (Rechner and Dalton, 1991). In the corporate governance literature, the separation of the two roles is viewed as an indicator of the relative balance of power in the upper echelons of an organization (Musteen *et al.*, 2010). It is often considered that CEO duality is one of the reasons why boards of directors fail in performing their oversight duties (Puni and Anlesinya, 2020). This is because combining both roles will give CEO complete authority over the firm, thus leading to managerial entrenchment (Pham *et al.*, 2015) however, CEO duality is rather a complex issue. Finkelstein and D'aveni (1994) in their study consider CEO duality as a double edge sword. They posit that advocates of agency theory believe that avoiding CEO duality will result in improved monitoring by the board and limit potential managerial entrenchment whereas proponents of organization theory, which focuses on leadership and organizational structure, are of the view that CEO duality strengthens command stability and uniting the two roles would lead to strong leadership, speedy decision-making and send a signal of reassurance to all stakeholders.

Despite its significance, inconclusive evidence has been reported by researchers. Chadam (2018); Haqi (2017) and Teti *et al.* (2017) found an inverse relationship between CEO duality and acquirer returns. Pham *et al.* (2015) found a positive relationship while Amar *et al.* (2011); Liu and Zhao (2012) found no relation between the two constructs. In the case of target firms, Bange and Mazzeo (2004) reported positive gains for target shareholders when both the positions are combined.

iv. Over-boarded directors

Largely, the emphasis of corporate governance literature has been on board independence and board size, but there has increasingly been a movement toward the idea of multiple directorships by the board of directors with a few numbers of studies examining the link between multiple directorships and M&A performance (Ahn *et al.*, 2010; Cotter *et al.*, 1997; Defrancq *et al.*, 2020; Harris and Shimizu, 2004). The relationship between overboarded directors and firm performance in general and M&A performance in specific is not clear and often revolve around two opposing hypotheses viz. reputation hypothesis and busyness hypothesis (Ahn *et al.*, 2010). The reputation hypothesis signifies that these directors are over-committed because they have built their goodwill over time by effectively performing their duties. These directors have a wide network of contacts, are more experienced and therefore they can offer better advice and counsel. Thus such directors are beneficial to the firm as they can prevent value-reducing acquisitions. The number of directorships held by directors is therefore often used as a tool to measure their quality (Chen and Lin, 2010). On the other hand, according to the busyness hypothesis directors holding multiple directorships are too busy to perform their governance duties as a result they may not be able to perform their monitoring functions. This lack of oversight by directors may result in increased agency conflicts as managers may procure private benefits which are against the interest of shareholders. Thus the busyness hypothesis contends that over-committed directors are ineffective monitors. In their study, Defrancq *et al.* (2020) reported that multiple directorships are positively associated with M&A performance, further they also found that for firms with few inside directors on the board, overboarded directors have a significant positive impact on decision making thus acting as a complement for lack of inside directors. Similarly, Cotter *et al.* (1997) found that gains made by target shareholders are more when their board members hold multiple directorships. Thus these studies supported the reputation hypothesis according to which over-boarded boards will perform their governance duties effectively since they do not want to damage their reputation by making bad decisions. On the contrary, there are studies that conclude that when the board becomes too over-boarded the busyness effect will overcome the benefits of reputation effect. Ahn *et al.* (2010) in their study stated a non-linear relation between multiple directorships and abnormal returns made around the M&A announcement suggesting that overboarded directors are beneficial up to a certain threshold limit. When the limit is crossed the directors become too busy to monitor effectively however, the study did not provide the limit up to which it was beneficial for the firm to have directors with multiple directorships.

www.IndianJournals.com
Members Copy, Not for Commercial Sale
Downloaded From IP - 14.139.251.98 on dated 13-Jun-2022

www.IndianJournals.com
Members Copy, Not for Commercial Sale
Downloaded From IP - 14.139.251.98 on dated 13-Jun-2022

v. Board diversity

Apart from the above-discussed attributes, the board's effectiveness can also be influenced by its diverse nature. In line with the resource-based view a more diverse board is expected to have better resources at its disposal and in turn can provide better counsel and advice on major decisions (Ben-Amar *et al.*, 2013).

Chen *et al.* (2014); Levi *et al.* (2014) in their study reported that greater female representation of board is negatively associated with the number of acquisitions undertaken. They also conclude that deal size is also small when there are more females on the board. The study, therefore, points out that having gender-balanced boards results in more comprehensive decision-making at the board level thus lowering the probability of approval. However, it also implies their risk-averse nature. Besides, women directors are also more sincere when it comes to attending meetings about major strategic decisions. Adams and Ferreira (2009) found that women directors generally do not have any attendance issues and are more likely to be present at board meetings. With regard to demographic diversity, Ben-Amar *et al.* (2013) found a U-shaped relationship with acquirer M&A performance indicating that initially as demographic diversity (in terms of experience, culture, and nationality) is introduced there will be a slightly negative impact, however, as it continues to increase it will start improving M&A performance. Ben-Amar *et al.* (2013) assume this to problems related to integration difficulties that could counterbalance the positive effects of demographic diversity. Aggarwal *et al.* (2019) also reported a positive relation between board demographic diversity and M&A performance of acquiring firms, however, this positive relationship was observed only in standalone firms and it was negative for group affiliated firms. Since director-interlocking arrangements are the norm in group-affiliated firms, there may be diversity on paper but effectively these diverse members represent group goals rather than individual firm goals (Aggarwal *et al.*, 2019)

vi. Board committees

Board committees are considered essential corporate governance mechanisms that assist the board of directors in performing their duties and improving information transparency and disclosures (Silvaa *et al.*, 2018). Such committees are important because, as Kesner (1988) and Klein (1998) suggest, committee meetings, and not the board meetings, are where most board activity actually takes place. Silvaa *et al.* (2018) further provide that the formation of such committees offers three vital benefits to the firm *viz.* knowledge specialization, task allocation efficiency and increased accountability of the board to the firm. Among these specialized board committees, audit and nomination and remuneration committees are considered to be the most important ones because of the criticality of their functions. Due to this, several countries such as India, U.S. and U.K. have mandated the formation of these two committees. Deloitte in its report provides that the audit committee has a vital role to play throughout the M&A process, specifically with regards to the risk assessment and financial due diligence (Deloitte, 2014). Kim *et al.* (2014) found that members of the audit and compensation committees with long tenure enable the firm to make better and profitable investment choices and lower excess executive pay. Apart from this, there are other committees as well, such as ethics, strategy, and health committee, etc., that are generally characterized as "less traditional" however, they are still regarded as relevant as they can offer useful perspectives into a firm's actions and priorities (Kolve *et al.*, 2019). Beekun *et al.* (1998) found that firms with strategic planning committees are more likely to focus their efforts on long-term sustainability rather than on achieving short-term financial outcomes. Similarly, Peters and Romi (2014) reported that firms make more environmental disclosures when they constitute an environmental committee; however, the decision to form such committees is generally left to the firms.

Theme: 2 Ownership Structure

Another significant governance mechanism in current literature, which can have a possible effect on the outcome of an M&A transaction, is the ownership structure of the company. Ownership literature typically focuses on two issues. The first issue concerns the ownership of equities by the management Team, CEOs and directors. The second issue focuses on equity ownership by large shareholders and institutional investors.

i. Ownership by board and management

The importance of equity ownership by key executives generally revolves around two contrasting hypotheses viz.

"alignment of interest hypothesis" and "entrenchment hypothesis" (Edmans, 2014; Jensen and Meckling, 1976; Morck *et al.*, 1988). According to the incentive alignment hypothesis, when managers or directors hold large shareholdings in the company, their interest is more in line with that of shareholders, since any loss in equity value will be their loss, therefore they will usually resist value destruction deals in order to preserve their own financial stake in the company (Jensen and Meckling, 1976). On the contrary, entrenchment hypothesis predicts that the positive effect of the alignment of interest hypothesis would vanish at a very high level of ownership stakes. This is so because with substantial ownership managers may effectively control the firm and may indulge in personal-wealth maximizing practices (Morck *et al.*, 1988). The entrenchment argument is often challenged as there may be situations where managers may be entrenched with the firm by the virtue of their status as a founder, personality, or their tenure with the firm even when they hold a low stake in the firm (Morck *et al.*, 1988).

Accordingly, Amar *et al.* (2011); Cotter *et al.* (1997); Yaacob and Alias (2018) conclude that management and board of directors' ownership of equity has a positive impact on the M&A performance of the acquiring firm thus supporting the convergence of interest hypotheses. These researchers are of the opinion that the executives will not indulge in self-interested actions with the financial stake in the company and the board of directors would also have an incentive to monitor management actions as any bad decisions taken would result in a financial loss not only to the shareholders but to them also. Therefore, with a significant ownership stake in the company, the boards are not likely to approve value-reducing deals. In contrast to the above findings, Wright *et al.* (2002) partially supported the entrenchment hypothesis. They contend that at moderate levels of ownership managers may prefer undertaking risks that maximize the value to shareholders, however, as the value of equity ownership raises to very high levels their personal wealth may be concentrated and therefore they prefer to undertake risk-reducing strategies that may not be value-enhancing.

Desai *et al.* (2005) investigated this relationship further by creating two sub-samples of owner-controlled or owner-manager controlled (i.e. family firms) and manager-controlled firms. They found that ownership by outside directors had a significant positive impact only in the case of manager-controlled firms establishing that when the owner controls the firm the impact of ownership by outside directors is not much of value since the ultimate authority to make the decisions is in the hands of owners. Byrd and Hickman (1992) posit that the positive relationship does not hold when the ownership by directors (all three categories viz. independent, outside and inside directors) is used as a continuous variable however when they reassess their result by creating a dummy variable the results were statistically significant implying that benefits of having equity stakes do not vary with the stake itself. Similar results have also been found by Nogueira and Castro (2019) in the case of family-controlled Brazilian firms.

ii. Institutional investors and large blockholders

Researchers have also recognized the role that institutional investors and large shareholders play in monitoring the activities of the managers. The rationale is that such investors have invested large sums of money and have the requisite resources and expertise at their disposal which they can use to monitor the firm. Nesbitt (1994) and Smith (1996) argue that the presence of such investors forces the managers to work in the interest of the shareholders rather than indulging in opportunistic and self-serving behavior. This clearly has potential implications for M&A performance.

Edmans (2014) argues that such investors generally employ two mechanisms to promote good governance i.e. "voice" and "exit". Under the voice channel, these investors can raise concerns about any bad managerial practices at the firm. E.g. These investors can vote against a proposal at shareholder meetings or can put forward a strategic change via public shareholder proposal. Under the exit route, these investors indulge in trading of shares when they believe that their voices are not being given any attention. By selling their large block of shares they can push the stock prices down thus keeping the management under check. Alternatively, only a threat to sell shares can also amplify their influences.

Empirically, Chen and Yur-Austin (2007); Lou *et al.* (2020) in their study reported that stock holdings by institutional

www.IndianJournals.com
Members Copy, Not for Commercial Sale
Downloaded From IP - 14.139.251.98 on dated 13-Jun-2022

investors have a significant and positive impact on M&A outcomes of acquiring firm shareholders, however, the results were positive only for those investors which were independent and that there was no impact for grey institutional investors i.e. those that have potential business ties with the firm. Lou *et al.* (2020) further reported that it is only the foreign institutional investors that actively monitor and not the domestic investors. Further, it has also been argued that the ability of the institutional investors to influence corporate actions such as M&A is partially a function of their size of holdings (Maug, 1998). Larger holdings imply it is better to monitor the management whereas in the case of smaller holdings it is preferable to liquidate holdings if the firm performs poorly (Maug, 1998). Ma (2019) empirically tested this hypothesis and reported that only large institutional investors that have a significant stake in the firm act as active monitors and are positively related to acquisition returns. Similar to institutional investors, block holders also exert significant influence on corporate decision-making activities owing to their large ownership. A shareholder owning at least 5% stake in the company is generally considered as a block holder (Bhagat and Black, 1999). The 'active monitoring hypothesis' as proposed in the studies by Demsetz and Lehn (1985); Shleifer and Vishny (1986) have explained that block holders are considered as active monitors reason being they have invested a large sum of money in the firm and will therefore not want their money to be utilized inefficiently. Thus, the hypothesis argues that with block holders there will be better monitoring and reduced agency cost. Aktas *et al.* (2015); Haqi (2017); Nashier and Gupta (2020) all have reported findings that are consistent with this hypothesis. Even in the case of closely-held firms. Peng and Sauerwald (2013) argues that block holders can provide internal safeguards against the expropriation by controlling shareholders as multiple block holders have the ability to form coalitions and oppose the actions of the controlling shareholder. As against this, some authors are of the view that instead of reducing agency costs such investors can further exacerbate it. Edmans (2014) also posits that such investors may force the management to initiate actions that maximize their personal benefit rather than the firm value such as to buy firms at an inflated price in which they have substantial ownership. Supporting the argument Hardeveld (2017) reported a significant negative relationship between block ownership at 10 per cent and acquirer performance.

Compensation Structure

Corporate governance critics, institutional investors and numerous financial economists have been demanding for a long time that the remuneration paid to executives be related to company results in order to better protect the interests of shareholders (Datta *et al.*, 2001). According to Bebchuk and Fried (2012) not only can the board and ownership structure help balance the interests of shareholders and executives, but the incentives paid to executives and non-executives can also motivate them to make decisions that would optimize company value.

i. Managerial and board compensation

For the compensation paid the executive, researchers general argue that it must not be completely fixed and a major portion of it should be variable by linking it to the firm performance or alternatively, it should an equity-based compensation The rationale behind it is that when the wealth of the executives is linked with the sensitivity of the stock prices they can directly experience the consequences of their actions therefore they are more likely to avoid bad decisions (Guay, 1999). Researchers also argue that such incentive contracts should also be employed to compensate outside directors as well. Deutsch *et al.* (2007) suggest a dual agency model in which they consider both the executives and directors as agents and suggest that not only the incentives of executives but outside director's incentives must also be aligned with that of shareholders. Contracting theory suggests that the sole purpose of compensation contracts is to encourage the agents to take such actions that are most beneficial to the principals (Deutsch *et al.*, 2007). The fundamental argument in the literature when concentrating on management compensation is that it must be linked to firm performance so that the interests of both shareholders and managers are aligned. This is necessary because managers are more concerned about their job security, their risk preferences might not same as shareholders risk preferences therefore, performance-linked compensation is required to motivate them and be less risk-averse than they would be otherwise whereas, in the case of external directors, the protection of jobs by means of the seat on the board may be less relevant because board roles are seldom the sole source of income for them, but external directors worry more about risking

www.IndianJournals.com
Members Copy, Not for Commercial Sale
Downloaded From IP - 14.139.251.98 on dated 13-Jun-2022

their reputations (Certo *et al.*, 2008) and thus require similar incentives (Fich and Shivdasani, 2005).

It is important to note here that directors determine their own compensation and also approve the compensation of executives which is often tied to the size of the firm (Raithatha and Komera, 2016). Given that M&A transactions result in increased firm size, it is highly likely that directors may also become self-interested to maximize their own welfare and approve such transactions even if it is not in the best interest of the shareholders (Amewu and Alagidede, 2019).

Consequently, there is mixed evidence with some arguing in favor of it while others rejecting it. Datta *et al.* (2001); Fich and Shivdasani (2005); Haqi (2017); Mkrtchyan (2013) found support for this hypothesis and provide evidence that the acquiring firm shareholders benefit when compensation is structured in this manner, whereas Amewu and Alagidede (2019); Jiang *et al.* (2020); Masulis *et al.* (2007) reported a negative or no significant association of such contracts with M&A outcomes. Further, researchers posit the even if the compensation to executives is linked to firm performance there might still be chances of shareholders expropriation. Aboody and Kasznik (2000); Byard and Li (2005); Yermack (1997) all have found evidence that options are not granted randomly to executives rather they are timed before or after the announcement of some good or bad news about the company so that they can benefit from the increase or decrease in the share prices. This is referred to as "timing opportunism". Byard and Li (2005) further found evidence that outside directors also receive the options on the same day as the CEO thus suggesting that such form of compensation can undermine the director's independence also. As against this, Bhagat and Bolton (2013) proposed that this issue can be mitigated. They argued that directors should instead be compensated with "restricted equity" where they should not be allowed to sell their stock for a minimum period of time. Bhagat and Bolton (2013) also tested this empirically and found that companies adopting such a method performed much better in future years. Further, they also found that such directors are more likely to initiate disciplinary actions against the CEO when the stock performance deteriorates.

CONCLUDING REMARKS AND AVENUES FOR FUTURE RESEARCH

Through this study, we have attempted to synthesize the existing literature on the influence of corporate governance mechanisms on the M&A outcomes by classifying the governance mechanisms into three broad themes with each consisting of certain sub-themes as well. Our study reveals that this particular strand of literature is clearly evolving, especially in the context of developing and emerging economies. Overall, we found that these mechanisms do have a significant influence on the ultimate M&A outcomes and if implemented effectively they indeed create value for shareholders or at least reduce managerial opportunism to a larger extent.

By reviewing the existing literature we believe that our results shed light on which mechanisms policymakers, regulators and business firms can work upon to further improve their corporate governance framework and in turn can enjoy its associated benefits of increased market value and greater access to capital while at the same also creating value for its shareholders.

Going through this review, we observed that, despite the abundance of literature on corporate governance, there is still some room for work and contributions that can be made by researchers in this particular area. Our analysis revealed that the existing literature is primarily concentrated on three board structure attributes such as its size, independence and leadership. Other important attributes such as board committees and their attributes, outside directorships and diversity have received considerably less attention in the context of M&A. Similarly, more work is also required on the role of institutional investors, block holders and compensation structure of executives and board.

It was also found that the papers are typically more leaned towards the returns generated to shareholders in the short-time frame around the deal announcement however, we still do not know whether such mechanisms also create value for shareholders in the long run as we could find only a few studies that have used long-term measures to evaluate the M&A performance. Similarly, M&A performance is often measured from the perspective of acquiring firm shareholders, whether these mechanisms create value for

www.IndianJournals.com
Members Copy, Not for Commercial Sale
Downloaded From IP - 14.139.251.98 on dated 13-Jun-2022

target firm shareholders or for the combined firm is still an under-explored area. Further, the majority of these mechanisms have been studied in isolation from each other. This might be one of the reasons for inconclusive findings still being reported with no consistent agreement among the researchers about the efficacy of certain of these mechanisms. Future researchers can take up this opportunity to study them together thus shedding light on their complementarity or substitution effects thus offering a more comprehensive view on the topic.

Another related avenue of research whose importance is growing is cross-country studies. As emerging and developing economies have largely adopted these mechanisms from developed nations while ignoring the fact that corporations in both types of countries often do not share the same structural characteristics (Young *et al.*, 2008) undertaking such studies can yield new insights into the related research stream.

www.IndianJournals.com
Members Copy, Not for Commercial Sale
Downloaded From IP - 14.139.251.98 on dated 13-Jun-2022

REFERENCES

Aboody D and Kasznik R, 2000. "CEO stock option awards and the timing of corporate voluntary disclosures", *Journal of Accounting and Economics,* Vol. 29, No. 1, pp. 73–100.

Adams RB and Ferreira D 2009. "Women in the boardroom and their impact on governance and performance", *Journal of Financial Economics,* Vol. 94, No. 2, pp. 291–309.

Adams RB, Hermalin BE and Weisbach MS 2010. "The role of boards of directors in corporate governance: A conceptual framework and survey", *Journal of Economic Literature,* Vol. 48, No. 1, pp. 58–107.

Aggarwal R, Jindal V and Seth R 2019. "Board diversity and firm performance: The role of business group affiliation", *International Business Review,* Vol. 28, No. 6, available at: https://doi.org/10.1016/j.ibusrev.2019.101600.

Ahn S, Jiraporn P and Kim YS, 2010. "Multiple directorships and acquirer returns", *Journal of Banking and Finance, Elsevier B.V.,* Vol. 34, No. 9, pp. 2011–2026.

Aktas N, Croci E and Simsir SA 2015. "Corporate Governance and takeover outcomes", *Corporate Governance: An International Review,* Vol. 24, No. 3, pp. 242–252.

Alabdullah TTY, Ahmed ER and Yahya S, 2018. "The determination of firm performance in emerging nations: Do board size and firm size matter?", *International Academic Journal of Accounting and Financial Management,* Vol. 5, No. 2, pp. 57–66.

Amar W Ben, Boujenoui A and Francoeur C, 2011. "CEO attributes, board composition, and acquirer value creation: A Canadian study", *Canadian Journal of Administrative Sciences,* Vol. 28, No. 4, pp. 480–492.

Amewu G and Alagidede P 2019. "Mergers and executive compensation changes: Evidence from African markets", *Research in International Business and Finance, Elsevier,* Vol. 48, No. 2, pp. 397–419.

Bange MM and Mazzeo MA, 2004. "Board composition, board effectiveness, and the observed form of takeover bids", *Review of Financial Studies,* Vol. 17, No. 4, pp. 1185–1215.

Bauguess S and Stegemoller M 2008. "Protective governance choices and the value of acquisition activity", *Journal of Corporate Finance, Elsevier B.V.,* Vol. 14, No. 5, pp. 550–566.

Bauguess SW, Moeller SB, Schlingemann FP and Zutter CJ 2009. "Ownership structure and target returns", *Journal of Corporate Finance, Elsevier B.V.,* Vol. 15, No. 1, pp. 48–65.

Beatty RP and Zajac EJ 1990. "Top management incentives, monitoring, and risk-bearing: a study of executive compensation, ownership, and board structure in initial public offerings", *Academy of Management Proceedings,* Vol. 19, No. 1, pp. 7–11.

Bebchuk LA and Fried JM, 2012. "Executive compensation as an agency problem", *The Economic Nature of the Firm: A Reader,* Vol. 17, No. 3, pp. 327–345.

Beekun RI, Stedham Y and Young GJ, 1998. "Board characteristics, managerial controls and corporate strategy/ : A study of U.S. hospitals, *Journal of Management,* Vol. 24, No. I, pp. 3–19.

Ben-Amar W, Francoeur C, Hafsi T and Labelle R, 2013. "What makes better boards? A closer look at diversity and ownership", *British Journal of Management,* Vol. 24, No. 1, pp. 85–101.

Berle AA and Means G, 1932. "The modern corporation and private property", Transaction Publishers.

Bhagat BS and Black B, 1999. "The uncertain relationship between board composition and firm performance", *Business Lawyer,* Vol. 54, No. 175, pp. 921–963.

Bhagat S and Bolton B, 2013. "Director ownership, Governance, and performance", *Journal of Financial and Quantitative Analysis,* Vol. 48, No. 1, pp. 105–135.

Byard D and Li Y, 2005. "The impact of directors' option compensation on their independence", *SSRN Electronic Journal,* available at: https://doi.org/10.2139/ssrn.683385.

Byrd JW and Hickman KA 1992. "Do outside directors monitor managers? Evidence from tender offer bid", *Journal of Financial Economics,* Vol. 32, No. 2, pp. 195–221.

Certo ST, Dalton CM, Dalton DR and Lester RH 2008. "Boards of directors' self interest: Expanding for pay in corporate acquisitions?", *Journal of Business Ethics,* Vol. 77, No. 2, pp. 219–230.

Chadam AA, 2018. "Does the structure of the board of directors improve M&A performance?", *International Journal of Synergy and Research,* Vol. 7, p. 15.

Chen CW and Barry Lin J 2010. "Director affiliations and acquisition announcement performance", *Proceedings for the Northeast Region Decision Sciences Institute* (NEDSI), No. March, pp. 361–366.

Chen G, Crossland C and Huang S 2014. "Female board representation and corporate acquisition intensity", *Strategic Management Journal,* available at: https://doi.org/10.1002/smj.2323.

Chen X (Cindy) and Yur-Austin J, 2007. "Re-measuring agency costs: The effectiveness of block holders", *Quarterly Review of Economics and Finance,* Vol. 47, No. 5, pp. 588–601.

Cheng Y, 2017. "Bidder returns and corporate governance: Evidence from China's domestic acquisitions and mergers", *Journal of Accounting & Finance* (2158-3625), Vol. 17, No. 7, pp. 104–139.

Clarkson PM, Craswell A and MacKenzie P, 2008. "The effect of board independence on target shareholder wealth", *Australian Accounting Review,* Vol. 18, No. 2, pp. 135–148.

Coles JL, Daniel ND and Naveen L, 2008. "Boards: Does one size fit all?", *Journal of Financial Economics,* Vol. 87, No. 2, pp. 329–356.

Coletta C and Roberto LA de S, 2020. "Board of directors, performance and firm value in Brazilian listed state-owned enterprises", *Brazilian Review of Finance,* Vol. 18, No. 2, p. 1.

Collins JA and Fauser BCJM, 2005. "Balancing the strengths of systematic and narrative reviews", *Human Reproduction Update,* Vol. 11, No. 2, pp. 103–104.

Cook DJ, Mulrow CD and Haynes RB, 1997. Systematic reviews: Synthesis of best evidence for clinical decisions, pp. 1–8.

Cotter JF, Shivdasani A and Zenner M, 1997. "Do independent directors enhance target shareholder wealth during tender offers?", *Journal of Financial Economics,* Vol. 43, No. 2, pp. 195–218.

Daily CM, Dalton DR and Cannella AA, 2003. "Corporate governance: Decades of dialogue and data", *Academy of Management Review,* Vol. 28 No. 3, pp. 371–382.

Datta S, Iskandar-Datta M and Raman K, 2001. "Executive compensation and corporate acquisition decisions", *Journal of Finance,* Vol. 56 No. 6, pp. 2299–2336.

Defrancq C, Huyghebaert N and Luypaert M, 2020. "Influence of acquirer boards on M&A value creation: Evidence from continental Europe", *Journal of International Financial Management and Accounting,* Vol. 32 No. 1, pp. 21–62.

Deloitte, 2014. "Role of the audit committee in M&A", *Financier Worldwide.*

Demirtas G, 2017. "Board involvement in the M&A negotiation process", *International Review of Financial Analysis,* Vol. 50, pp. 27–43.

Demsetz H and Lehn K, 1985. "The structure of corporate ownership: causes and consequences", *Journal of Political Economy,* Vol. 93 No. 6, pp. 1–439.

Desai A, Kroll M and Wright P, 2005. "Outside board monitoring and the economic outcomes of acquisitions: A test of the substitution hypothesis", *Journal of Business Research,* Vol. 58 No. 7, pp. 926–934.

Deutsch Y, Keil T and Laamanen T, 2007. "Decision making in acquisitions: The effect of outside directors' compensation on acquisition patterns", *Journal of Management,* Vol. 33 No. 1, pp. 30–56.

Duchin R, Matsusaka JG and Ozbas O, 2010. "When are outside directors effective?", *Journal of Financial Economics, Elsevier,* Vol. 96 No. 2, pp. 195–214.

Edmans A, 2014. "Blockholders and corporate governance", *Annual Review of Financial Economics,* Vol. 6, pp. 23–50.

Eisenberg T, Sundgren S and Wells MT, 1998. "Larger board size and decreasing firm value in small firms", *Journal of Financial Economics,* Vol. 48 No. 1, pp. 35–54.

Faleye O, Hoitash R and Hoitash U, 2011. "The costs of intense board monitoring", *Journal of Financial Economics, Elsevier,* Vol. 101 No. 1, pp. 160–181.

Fama E, 1980. "Agency Problems and the Theory of the Firm", *Journal of Political Economy,* Vol. 88 No. 21, pp. 270–282.

Fich EM and Shivdasani A, 2005. "The impact of stock-option compensation for outside directors on firm value", *Journal of Business,* Vol. 78 No. 6, pp. 2229–2254.

Field LC and Mkrtchyan A, 2017. "The effect of director experience on acquisition performance", *Journal of Financial Economics, Elsevier B.V.,* Vol. 123 No. 3, pp. 488–511.

Finkelstein S and D'aveni RA, 1994. "CEO duality as a double-edged sword: how boards of directors balance entrenchment avoidance and unity of command", *Academy of Management Journal,* Vol. 37 No. 5, pp. 1079–1108.

Frazzini A, 2006. "The disposition effect and under-reaction to news", Vol. LXI No. 4, pp. 2017–2046.

Gaughan PA, 2013. "Role of corporate governance in M&A", *Maximizing Corporate Value through Mergers and Acquisitions,* pp. 233–262.

Guay WR, 1999. "The sensitivity of CEO wealth to equity risk: An analysis of the magnitude and determinants", *Corporate Governance and Corporate Finance: A European Perspective,* Vol. 53, pp. 43–71.

Haqi NM, 2017. "Does corporate governance influence merger and acquisition performance?", Erasmus University.

www.IndianJournals.com
Members Copy, Not for Commercial Sale
Downloaded From IP - 14.139.251.98 on dated 13-Jun-2022

Hardeveld M van, 2017. The relationship between ownership concentration and acquirer's performance comparison between the United States and Europe, Radboud University.

Harris IG and Shimizu K, 2004. "Too busy to serve? an examination of the Influence of Overboarded Directors", *Journal of Management Studies,* Vol. 41 No. 5, pp. 775–798.

Hauser R, 2018. "Busy directors and firm performance: Evidence from mergers", *Journal of Financial Economics, Elsevier B.V.,* Vol. 128 No. 1, pp. 16–37.

Herman ES, 1981. Corporate control, corporate power, Cambridge University Press, Cambridge, MA.

Hopkinson GC and Blois K, 2014. "Power-base research in marketing channels: A narrative Review", *International Journal of Management Reviews,* Vol. 16 No. 2, pp. 131–149.

Huse M, Hoskisson R, Zattoni A and Viganò R, 2011. "New perspectives on board research: Changing the research agenda", *Journal of Management and Governance,* Vol. 15 No. 1, pp. 5–28.

Ibrahim H and Samad FA, 2011. "Corporate governance mechanisms and performance of public-listed family-ownership in Malaysia", *International Journal of Economics and Finance,* Vol. 3 No. 1, available at: https://doi.org/10.5539/ijef.v3n1p105.

Ikenberry D, Lakonishok J and Vermaelen T, 1995. "Market underreaction to open market share repurchases", *Journal of Financial Economics,* Vol. 39 No. 2–3, pp. 181–208.

Jensen C and Meckling H, 1976. "Theory of the firm: managerial behavior, agency cost and ownership structure", *Journal of Financial Economics,* Vol. 3, pp. 305–360.

Jensen MC, 1986. "Agency costs of free cash flow, corporate finance, and takeovers", *The American Economic Review,* pp. 11–16.

Jensen MC, 1993. "The modern industrial revolution, exit, and the failure of internal control systems", *The Journal of Finance,* Vol. 48 No. 3, pp. 831–880.

Jeong JW and Bae G, 2013. "Do acquiring firms knowingly pay too much for target firms? Evidence from earnings management in member-firm mergers in Korean business groups", *Asia-Pacific Journal of Accounting and Economics,* Vol. 20 No. 3, pp. 223–251.

Jiang L, Kling G and Bo H, 2020. "Does executive compensation affect firms' acquisition decisions? Evidence from China", *Asia Pacific Business Review, Routledge,* pp. 1–18.

Judge WQ and Zeithaml CP, 1992. "Institutional and strategic choice perspectives on board involvement in the strategic decision process", *The Academy of Management Journal,* Vol. 35 No. 4, pp. 766–794.

Kesner IF, 1988. "Directors' characteristics and committee membership: an investigation of type, occupation, tenure, and gender", *The Academy of Management Journal,* Vol. 31 No. 1, pp. 66–84.

Kim K, Mauldin E and Patro S, 2014. "Outside directors and board advising and monitoring performance", *Journal of Accounting and Economics, Elsevier,* Vol. 57 No. 2–3, pp. 110–131.

Klein A, 1998. "Firm performance and board committee structure", *Journal of Law and Economics,* Vol. XLI.

Kolve DK, Wangrow BD, Barker VL and Schepker JD, 2019, "board committees in corporate governance: A cross-disciplinary review and agenda for future", *Journal of Management Studies,* available at: https://doi.org/10.1111/joms.12444.

Levi M, Li K and Zhang F, 2014. "Director gender and mergers and acquisitions", *Journal of Corporate Finance, Elsevier B.V.,* Vol. 28, pp. 185–200.

Li Y and Aguilera RV, 2008. "Target director turnover in acquisitions: A conceptual framework", *Corporate Governance: An International Review,* Vol. 16 No. 6, pp. 492–503.

Liu J and Zhao L, 2012. "Does corporate governance affect M&A performance?", *Advances in Intelligent and Soft Computing,* Vol. 136 No. 2001, pp. 387–393.

Lorsch JW and Maclver E, 1989. Pawns or potentates: The Reality of America's Corporate Boards, Harvard Business School, available at: https://doi.org/10.5465/ame.1990.4277214.

Lou KR, Lu YK and Shiu CY, 2020. "Monitoring role of institutional investors and acquisition performance: Evidence from East Asian markets", *Pacific Basin Finance Journal, Elsevier B.V.,* Vol. 59, p. 101244.

Ma L, 2019. "The effect of institutional ownership on M&A performance: evidence from China", *Applied Economics Letters, Routledge,* Vol. 27 No. 2, pp. 140–144.

Mace M, 1971. Directors: Myth and Reality, Harvard Business School Press, Boston.

Masulis RW and Zhang EJ, 2019. "How valuable are independent directors? Evidence from external distractions", *Journal of Financial Economics, Elsevier B.V.,* Vol. 132 No. 3, pp. 226–256.

Masulis RW, 2020. "A survey of recent evidence on boards of directors and CEO incentives", *Asia-Pacific Journal of Financial Studies,* Vol. 49 No. 1, pp. 7–35.

Masulis RW, Wang C and Xie F, 2007. "Corporate governance and acquirer returns", *Journal of Finance,* Vol. 62 No. 4, pp. 1851–1889.

Maug E, 1998, Large shareholders as monitors: Is there a trade-off between liquidity and control," *Journal of Finance,* Vol. 53 No. 1, pp. 65–98.

www.IndianJournals.com
Members Copy, Not for Commercial Sale
Downloaded From IP - 14.139.251.98 on dated 13-Jun-2022

Mkrtchyan A, 2013. Essays in Corporate Finance, The Pennsylvania State University, available at: http://ezproxy.auckland.ac.nz/login?url=http://proquest.umi.com/pqdweb?did=1742858191&Fmt=7&clientId=13395&RQT=309&VName=PQD.

Morck R, Shleifer A and Vishny RW, 1988. "Management ownership and market valuation. An empirical analysis", *Journal of Financial Economics,* Vol. 20, No. 2, pp. 293–315.

Mueller DC, 1969. "A Theory of conglomerate mergers", *Quarterly Journal of Economics Turley,* available at: https://doi.org/https://doi.org/10.2307/1885454.

Musteen M, Datta DK and Kemmerer B, 2010. Corporate reputation: Do board characteristics matter?", *British Journal of Management,* Vol. 21, No. 2, pp. 498–510.

Nashier T and Gupta A, 2020. Ownership concentration and firm performance in India", *Global Business Review,* available at: https://doi.org/10.1177/0972150919894395.

Nesbitt SL, 1994. "Long-term rewards from shareholder activism: A study of the CalPERS effect", *Journal of Applied Corporate Finance,* Vol. 6.4, available at: https://doi.org/https://doi.org/10.1111/j.1745-6622.1994.tb00251.x.

Nogueira NV and Castro LRK de, 2019. "Effects of ownership structure on the mergers and acquisitions decisions in Brazilian firms", *RAUSP Management Journal,* Vol. 55 No. 2, pp. 227–245.

Page MJ, McKenzie JE, Bossuyt PM, Boutron I, Hoffmann TC, Mulrow CD, Shamseer L, *et al.* 2021. "The PRISMA 2020 statement: an updated guideline for reporting systematic reviews", *Research Methods & Reporting,* available at: https://doi.org/https://doi.org/10.1136/bmj.n71.

Peng MW and Sauerwald S, 2013. Corporate Governance and Principal–Principal Conflicts", *Oxford Handbooks Online,* available at: https://doi.org/10.1093/oxfordhb/9780199642007.013.0029.

Peters GF and Romi AM, 2014. "Does the voluntary adoption of corporate governance mechanisms improve environmental risk disclosures? Evidence from Greenhouse Gas emission accounting", *Journal of Business Ethics,* available at: https://doi.org/10.1007/s10551-013-1886-9.

Pfeffer J, 1972. "Size and composition of corporate boards of directors: The organization and its environment", *Administrative Science Quarterly,* Vol. 17, No. 2, pp. 53–64.

Pham N, Oh KB and Pech R, 2015. "Mergers and acquisitions: CEO duality, operating performance and stock returns in Vietnam", *Pacific Basin Finance Journal,* Vol. 35, pp. 298–316.

Pickering C and Byrne J, 2014. "The benefits of publishing systematic quantitative literature reviews for PhD candidates and other early-career researchers", *Higher Education Research and Development,* Vol. 33, No. 3, pp. 534–548.

Popli M, Ladkani RM and Gaur AS, 2017. "Business group affiliation and post-acquisition performance: An extended resource-based view", *Journal of Business Research,* Vol. 81, pp. 21–30.

Puni A and Anlesinya A, 2020. "Corporate governance mechanisms and firm performance in a developing country", *International Journal of Law and Management,* Vol. 62, No. 2, pp. 147–169.

Raithatha M and Komera S, 2016. "Executive compensation and firm performance: Evidence from Indian firms", *IIMB Management Review, Elsevier Ltd,* Vol. 28, No. 3, pp. 160–169.

Rani N, Yadav SS and Jain PK, 2013. "Impact of Corporate Governance Score on Abnormal Returns of Mergers and Acquisitions", *Procedia Economics and Finance, Elsevier B.V.,* Vol. 5, No. 13, pp. 637–646.

Rechner PL and Dalton DR, 1991. "CEO duality and organizational performance: A longitudinal analysis", *Strategic Management Journal,* Vol. 12, No. 2, pp. 155–160.

Redor E, 2015. "Board attributes and shareholder wealth in mergers and acquisitions: a survey of the literature", *Journal of Management and Governance, Springer US,* Vol. 20 No. 4, pp. 789–821.

Roll R, 1986. "The hubris hypothesis of corporate takeovers", *The Journal of Business,* Vol. 59 No. 2, p. 197.

Sarkar J and Sarkar S, 2009. "Multiple board appointments and firm performance in emerging economies: Evidence from India", *Pacific Basin Finance Journal, Elsevier B.V.,* Vol. 17, No. 2, pp. 271–293.

Shleifer A and Vishny RW, 1986. Large shareholders and corporate policies", *Review of Financial Studies,* Vol. 94 No. 3, pp. 461–488.

Silvaa A da, Cunha PR da and Teixeira SA, 2018. "Recommendations for audit committees in Brazilian companies", *Journal of Accounting and Organizations,* Vol. 55, No. 47, p. 56.

Smith MP, 1996. "Shareholder activism by institutional investors: Evidence from CalPERS", *Journal of Finance,* Vol. 51, No. 1, pp. 227–252.

Stiles P, 2001. "The impact of board on strategy: An empirical investigation", *Journal of Management Studies,* Vol. 38, No. 5, pp. 627–650.

Stulz RM, 1988. "Managerial control of voting rights: Financing policies and the market for corporate control", *Journal of Financial Economics,* Vol. 20, No. 3, pp. 25–54.

Sundaram AK, 2004. "Mergers and acquisitions and corporate Governance", *Advances in Mergers and Acquisitions,* Vol. 3, No. 4, pp. 193–219.

Surbhi and Vij S, 2018. "The Interface of corporate Governance with M&A: Research themes", *IUP Journal of Business Strategy,* Vol. 15, No. 3, pp. 19–38.

www.IndianJournals.com
Members Copy, Not for Commercial Sale
Downloaded From IP - 14.139.251.98 on dated 13-Jun-2022

Swanstrom M, 2006. "Corporate governance and abnormal returns to acquisitions announcement", *Journal of Business Strategies,* Vol. 32, No. 2, p. 23.

Teti E, Dell' Acqua A, Etro L and Volpe M, 2017. "The impact of board independency, CEO duality and CEO fixed compensation on M&A performance", *Corporate Governance,* Vol. 17, No. 5, pp. 947–971.

Tranfield D, Denyer D and Smart P, 2003. "Towards a methodology for developing evidence-informed management knowledge by means of systematic review", *British Journal of Management,* Vol. 15, No. 2, pp. 20–32.

Turnbull S, 2019. "Corporate governance: Its scope, concerns and theories, Corporate Governance: Values", *Ethics and Leadership,* Vol. 5, No. 4, pp. 415–440.

Varottil U, 2012. Corporate Governance in M&A Transactions", *National Law School of India Review,* Vol. 24, No. 2, p. 23.

Wright P, Kroll M, Lado A and Van Ness B, 2002. "The structure of ownership and corporate acquisition strategies", *Strategic Management Journal,* Vol. 23, No. 1, pp. 41–53.

Xu X, Wang F, Chen X and Yang G, 2021. Does managerial ability matter for cross-border M&As: Evidence from Chinese listed firms", *Journal of Asian Economics, Elsevier Inc.,* Vol. 74, p. 101302.

Yaacob MH and Alias N, 2018. "Ownership structure, types of M&A and long-term performance", *Journal Pengurusan,* Vol. 52, No. 2, pp. 235–244.

Yermack D, 1996. "Higher market valuation of companies with a small board of directors", *Journal of Financial Economics,* Vol. 40, No. 2, pp. 185–211.

Yermack D, 1997. "Good Timing: CEO Stock Option Awards and Company", *News Announcements,* Vol. 12, No. 2, p. 23

Young MN, Peng MW, Ahlstrom D, Bruton GD and Jiang Y, 2008. "Corporate governance in emerging economies: A review of the principal-principal perspective", *Journal of Management Studies,* Vol. 45, No. 1, pp. 196–220.

Zelenskaia V, 2018. Board Structure and M&A Performance: Evidence from China, Saint-Petersburg State University.

How to cite this article: Gautam H, Singh A and Maheshwari GC, 2022. "Corporate Governance and M&A Performance: A Systematic Review of Literature", *BULMIM Journal of Management & Research,* Vol. 7, No. 1, pp. 11-29.

www.IndianJournals.com
Members Copy, Not for Commercial Sale
Downloaded From IP - 14.139.251.98 on dated 13-Jun-2022

2022 6th International Conference on Devices, Circuits and Systems (ICDCS) | 978-1-6654-8094-9/22/$31.00 ©2022 IEEE | DOI: 10.1109/ICDCS54290.2022.9780833

Covid Prevention using machine learning and blockchain technology

Rajat Goel[0000-0003-4708-4590]
Department of Electronics and Communication Engineering
Ajay Kumar Garg Engineering College Ghaziabad(AKGEC)
Ghaziabad, Uttar Pradesh,India
rajatgoel498@gmail.com

Tulika Aggarwal[0000-0003-0091-389X]
Department of Information Technology
Raj Kumar Goel Institute of Technology(RKGIT)
Ghaziabad, Uttar Pradesh,India
tulikaaggarwal07@gmail.com

Kancharla Sai[0000-0002-2561-9390]
Department of Computer Science and Engineering
GIT, GITAM (Deemed to be University)
Visakhapatnam, Andhra Pradesh, India
nikhilmohansai@gmail.com

Naga Devulapalli[0000-0002-9386-3029]
Department of Computer Science and Engineering
GIT, GITAM (Deemed to be University)
Visakhapatnam, Andhra Pradesh, India
devulapallivishal@gmail.com

Venkata Mudunuru[0000-0002-0374-1264]
Department of Computer Science and Engineering
GIT, GITAM (Deemed to be University)
Visakhapatnam, Andhra Pradesh, India
vivekmudunuru210@gmail.com

Ashish Kumar[000-0003-4139-9700]
Department of Information Technology
Delhi Technological University Shabad Daulatpur,Delhi,India
ksndelash@gmail.com

***Abstract*— From 2020, Covid has seen the rise due to flare-up brought about the respiratory infection with high peak of death rate . The unexpected event and uncontrolled overall spread of COVID-19 infection show the impediments of existing medical care frameworks in dealing with general wellbeing crises. In such settings, inventive advances, for example, Block chain and Artificial Intelligence (AI) have arisen as promising answers for battling Covid plague. Specifically, Block chain can battle pandemics by empowering early detection. With the protocols implemented to avoid infections by wearing masks, social distancing with 6m and regular testing and 2 doses of vaccination. In this mask detection, person detection , temperature detection and information tracking with in person contact tracking included and status of health record of a person. With the emerging technologies and advancement of use taken of phones, tracking and controlling of spread of diseases. With the development of the reopening of economic but still Covid wide spread not yet over, Following the protocols is more important for avoiding infection**

Keywords—Deep learning, Single Shot Detection, Face recognition, Block chain.

I. INTRODUCTION

Facial recognition is software used to detect objects and store the information using an algorithm .With the advancement of deep learning and facial recognition
Block chain technologies can be used for digital banking and information speculation to avoid crowded areas and also online block chain recommendation system for marketing and heath record information storage. With the advancement of technology, networks of information are been stored to access with the mobile application. With just a smart phone and mobile application and tracking system Covid infected can be tracked for active movement and health records and with block chain and AI we can avoid implications. . A scope of new advanced advances, for example, Smartphone, Machine learning and computerized reasoning (AI) that utilizes profound learning and huge information examination, has arisen in the previous ten years. These innovations could have significant possible applications and impacts in wellbeing care. The COVID-19 pandemic, which incapacitated admittance to worldwide medical care frameworks through remarkable lockdowns and implemented physical removing, has quickly sped up the improvement of these advanced advances to meet different medical services needs worldwide.3 Coordination of enormous scope tasks, for example, populace level mass screening, fast contact following, production network the board for antibodies and medications, telemedicine discussions, and web based business development has incited the reception of a wide scope of computerized advances. Block chain is a primary advanced innovation that coordinates numerous other such advances In medical care, block chain could fill in as a substitution to customary disseminated data set administration frameworks, which have commonly been client-waiter data sets. Although conventional circulated information base administration frameworks are a laid out stage in medical services frameworks, they have significant constraints, for example, the failure to help distributed information sharing, helplessness to outer foes and the shortfall of a permanent review trail. With its special highlights, like straight forwardness, discernibility, non-disavowal disintermediation, and permanence, block chain might actually resolve these issues, permitting it to convey significant benefits over traditional stages appropriated data set administration frameworks). By consolidating block chain innovation, decentralized medical services information the board framework could be made those directions on-chain occasions and off-chain occasions.

II. METHODOLOGY

The recognition of object is defined in this methodology with face recognition included with the object identification. In this method, there is a classifier which detects the object and it detects scaling of the objects and it identifies the face and identifies the object as human. The input is extracted as input image and then implemented with the test train data and then the classifier with the help of test data stores the image, In this the image size will be reduces to make a impact factor.

A. Input processing

First, the low cost camera or CCTV with higher resolution is used for detection and attached in the highest point for better

Authorized licensed use limited to: DELHI TECHNICAL UNIV. Downloaded on June 06,2022 at 04:25:52 UTC from IEEE Xplore. Restrictions apply.

capture and also calculating the distances between two people and get the best view point for scanning and detection and then the video streaming is taken as the input for the whole framework. In this framework, the image snapshots are taken from the video stream. In this we use Single Shot Methodology.

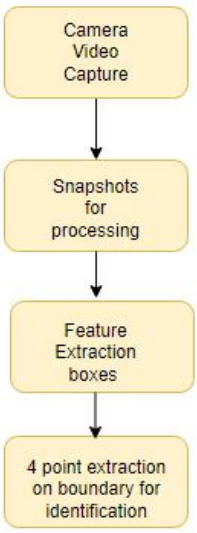

Fig.1.Block Diagram of Capturing a Image.

B. Pre processing of Snip shots of Video streaming.

In this SSD, uses feature extraction boxes instead of CNN method which uses high end embedded system and object proposal method. The image is done to several boxes to equal dimensions in terms of height, width and classifier. In this the boxes are of smaller size and only input snapshot image is as input and implemented in feature mapping system with smaller matrix size of |M|*|N|. It takes consideration of different dimensions and ratios and there are two sets, one is the train set boxes and test set boxes and this approach is just comparative and set boxes and detection. It uses detector and it has 2 comparative matching results one is positive and negative set box.

In this method, it uses higher accurate and prediction train model for different ratios and have faster detector than other methods. It has the ability to detect the object in the video stream input from the camera instantaneously.

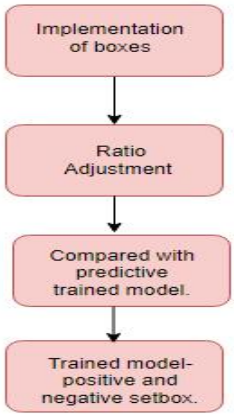

Fig.2.Implementation of Object detection.

C. Classifier

In this Approach, It uses box approach method with 4 points to the captured snapshots of the image and it uses detector and mapping functionality into boxes of needed ratio with 4 points covering the whole object to be detected. With the SSD train data based successful filtering of other boxes we capture the main objects using classifier with the co-ordinates. With the bounding overlap with the prediction elimination which eliminates box overlapping. With the prediction boxes and trained boxed we get the final detection boundary.

After the final image boundary, the classifier compares with train data for detection of the object as human, dog and so on with the accuracy reading. With the SSD it detects with single spot detection with one layer of neutral networks and with the trained model classification is easier to detect.

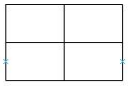

Fig.3 . 4*4 Dimension for image boundary identification.

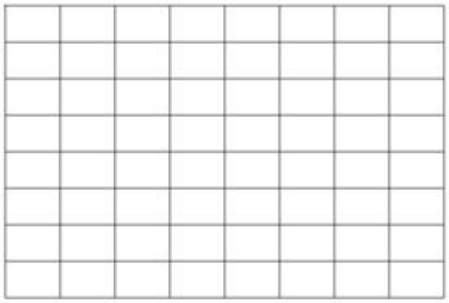

Fig.4. 8*8 Dimension. for image boundary identification.

D. Distances Calcuation

With the deep learning and SSD Algorithm in detecting the objects and computation view for number of persons and the distances between the boundary boxes and walking speed and distances evaluation. With the color distancing with safer distances and color tagging and dark red for unsafe distance and green color and the distances is calculated with the boundary boxes and taken as average and then compared with the stored distance and the two colors are associated with it and then which is used to indicate with green and red band which suggest the safe or not safe indication Distance. With the distances of 6 feet to be safety protocol with the top view estimation with the distance of capturing the image and the top view in the aligns value with the rectangle and parallely computing by scaling factor.

Authorized licensed use limited to: DELHI TECHNICAL UNIV. Downloaded on June 06,2022 at 04:25:52 UTC from IEEE Xplore. Restrictions apply.

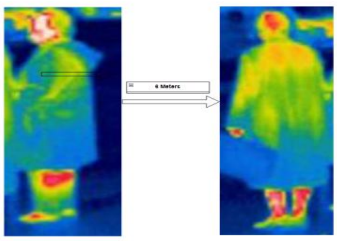

Fig.5.Implementation of Social distancing of 6 meters.

E. Detecting the Face Detector

In this snapshots of video stream for object detection and then use classifier for the detection of face using four points for face detection and then load the image to compare with the index and extract the range of interest of face features and also make use of classifier and detect if the person is wearing mask or not with comparison of trained data image .So two cases are taken into consideration with mask or no mask. In the training model dataset is made into ground two data sets one with mask and another without mask. The class is divided with the face detector with 3 points in the framework.

F. Thermal Scanner for Temperature Measurement

Using the Infrared camera we can measure the temperature of the person like a thermal scanner since use of FLIR camera can identify higher temperature with the screening of the person. With the set temperature the screening of temperature is recorded and then it is compared and if it is higher than the person is recorded and sent to the admin for further processing.

G. Block Chain technology for Covid Prevention.

In this approach, we use network method for tracking information and with the stored information like the health profile from the hospitals and temperature and also Covid vaccination details. From the hospitals and public and private healthcare data is collected and linked to any official record of a person with government identification. With this linkage of network helps in monitoring of infectious patients with tracking of in contact persons and active movement profile locations to prevent spreading of diseases.

With the role of data be linked with the health sectors and linking with a common data base using block chain helps to get track of the simulation of people exposed to covid.

Data privacy and technology implemented through block chain has its benefits for prevention. With the security software, data handling of health records with block chain it provides a platform and infrastructure to observe the covid spread and with the online transaction facilities and secured environments with node network for online transaction.

A technical aspect of monitoring gives the idea of the medical data and to improve the methodology f medical facilities follow up and precautions.

With online documentation and bill payments and ordering of medical facilities may also help to improve the data of the health care and installing a system to verify vaccination and in contact details will help for better health care collaboration with networks.

Tracking of in contact helps with the covid with contact control with mobile tracking system to analyze the quarantine period and keep track of rise of the covid with infection and with the health history kept at record it's easier to treat with any emergency situation .

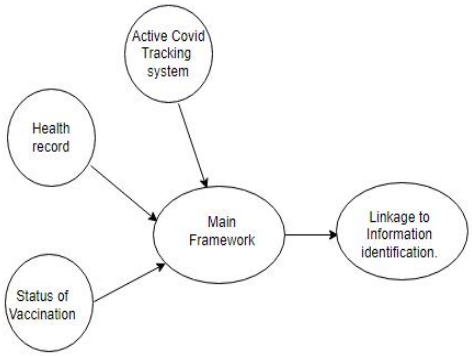

Fig.6.Block Diagram of Block chain networking of information.

IV. CONCLUSION

In the methodology, A automated method approach is taken for the social distancing with face detection and identification and face mask protocol detection included .In this the state implementation rules for wearing masks and following social distances and allowing action against person identification automatically who don't follow the rules and storing the identified image in the database. This allows implementing of low cost solution during the COVID phase and preventing manual work and also it is more efficient than the CNN automated approach and shows more accurate result and amplify with the live online video streaming and a larger database storage which would help for larger population and identification in crowded area with faster accuracy. With the thermal scanning included it is with the best prevention with all the prevention methods included in the automated system. In this method, Block chain technologies is used for the movement of the patients with tracking of the person identification of health track like current COVID status, person in contacts and precautions and distances maintained and his quarantine history and vaccination status. There can be enormous scope execution obstacles to such a framework. One of the significant disadvantages of the framework is that it depends on members claiming and working a cell phone. Notwithstanding the weighty entrance of cell phones lately, member ability to constantly convey a cell phone to move around may not be satisfactory in certain populaces. What's more, the moral what's more philanthropic worries to such an execution will should be inspected preceding an enormous scope carry out. Little pilot preliminaries can help and distinguish member worries in utilizing the innovation.

REFERENCES

[1] R. A. Addi, A. Benksim, M. Amine and M. Cherkaoui, "COVID-19 Outbreak and Perspective in Morocco", Electron J Gen Med., 2020.

[2] C. M. Pulido, B. Villarejo-Carballido, G. Redondo-Sama and A. Gómez, "COVID-19 infodemic: More retweets for science-based information on coronavirus than for false information", International Sociology, vol. 35, no. 4, pp. 377-392, 2020.

Authorized licensed use limited to: DELHI TECHNICAL UNIV. Downloaded on June 06,2022 at 04:25:52 UTC from IEEE Xplore. Restrictions apply.

[3] A. Al-Badia, A. Tarhinia and A. Islam Khan, "Exploring Big Data Governance Frameworks", *Procedia Computer Science*, vol. 141, pp. 271-277, 2018.

[4] S. Saberi, M. Kouhizadeh, J. Sarkis and L. Shen, "Blockchain technology and its relationships to sustainable supply chain management", *International Journal of Production Research*, vol. 57, no. 7, pp. 2117-2135, 2019.

[5] M. Ienca and E. Vayena, On the responsible use of digital data to tackle the COVID-19 pandemic, Zurich, Switzerland:Department of Health Sciences & Technology, Swiss Federal Institute of Technology in Zurich.

[6] P. Brous, M. Janssen and R. Vilminko-Heikkinen, Coordinating Decision-Making in Data Management Activities: A Systematic Review of Data Governance Principles, Electronic Government, pp. 115-125, 2016.

Authorized licensed use limited to: DELHI TECHNICAL UNIV. Downloaded on June 06,2022 at 04:25:52 UTC from IEEE Xplore. Restrictions apply.

Proceedings of the International Conference on Applied Artificial Intelligence and Computing (ICAAIC 2022)
IEEE Xplore Part Number: CFP22BC3-ART; ISBN: 978-1-6654-9710-7

Credit Card Fraud Detection using Deep and Machine Learning

Sahil Negi
Department of Computer Science and Engineering
Delhi Technological University
Delhi, India
sahilnegi_2k18co310@dtu.ac.in

Sudipta Kumar Das
Department of Computer Science and Engineering
Delhi Technological University
Delhi, India
sudiptakumardas_2k18co361@dtu.ac.in

Rigzen Bodh
Department of Computer Science and Engineering
Delhi Technological University
Delhi, India
rigzenbodh_2k18co288@dtu.ac.in

2022 International Conference on Applied Artificial Intelligence and Computing (ICAAIC) | 978-1-6654-9710-7/22/$31.00 ©2022 IEEE | DOI: 10.1109/ICAAIC53929.2022.9792941

***Abstract*— Credit-Card Fraud is indeed a menace in the financial system, with far-reaching consequences. The loss of a credit card or its information is considered Credit Card Fraud. A variety of machine learning techniques can be utilized to detect this fraud. This study demonstrates a variety of classification algorithms. Whether the transaction is a fraud or a real one is difficult to determine without an efficient machine learning algorithm. The models that are utilized in this paper were Logistic Regression, XGBoost, and Multi-Layer Perceptron. Kaggle dataset is used to train and test these models. Accuracy, confusion matrix, Area under ROC Curve, recall, f1 score, and precision were the classification metrics used to judge the performance of the proposed system models. This research work conclude that the Multi-Layer Perceptron [MLP] outperforms XGBoost and Logistic Regression.**

Keywords*— *Under-Sampling, Credit Card Fraud, Logistic Regression, XGBoost, Multi Layer-Perceptron

I. INTRODUCTION

Credit cards are widely used for electronic transactions in both developing and developed countries because they are convenient and simple to use. Online transactions are becoming simple, easy, and convenient since the invention of credit cards. A credit card, on the other hand, offers criminals brand-new scams to use that will ultimately lead to a rise in the number of scams. Cybercriminals are also constantly developing new and innovative methods. Hence, the result is very important to develop a more secure detection system.

We can borrow money if we have a credit card. This money can be put to any of the above uses. Whenever it comes to the card's issuance, the cardholder must reimburse both the original amount borrowed and any additional amount they agreed to pay. Credit Card Fraud can occur for a variety of reasons, including negligence on the part of the card's owner, card information was accidentally leaked, if someone's credit card gets lost or stolen, making a duplicate of a credit card or the owner's email or phone number that is linked to his or her credit card is hijacked.

It's possible that the crime was committed to obtain products without paying money or to obtain an unlawful fund. The explanation for this is that a huge amount of money may be produced in a small period of time without putting oneself in danger, and even catching the criminal will take weeks.

Even when we make transactions over the internet and fraudsters employ phishing techniques to steal our information, we are unaware that our information has been compromised. They only require card data for a few purchases to commit fraud, and the credit card owner may be unaware that his credit card information has been compromised. The expiration date and card number should be kept confidential. However, this is not always in our control.

Information may be disclosed as a result of phishing sites, or the card itself might get stolen or lost. To determine whether or not a transaction is fraudulent, we must first determine the customer's spending behavior using the existing data and then use machine learning to sniff out fraudulent transactions.

Site cloning, cardholder account takeovers, credit card generators, fake cards, and theft via mail are all methods used by online fraudsters. Criminals can also obtain information via cloned websites, also from employees of card issuers[1]. In this case, the detecting procedure has a number of issues. It's difficult to tell the difference between real and fake activities because they appear to be the same. The precision of Credit Card

Authorized licensed use limited to: DELHI TECHNICAL UNIV. Downloaded on June 22,2022 at 04:33:14 UTC from IEEE Xplore. Restrictions apply.

Fraud is also affected by variable selection, different testing, and identification procedures. Due to data changing over time, what appeared to be normal behavior may turn out to be fraudulent behavior in the future [2]. At the same time, many transactions that are similar to one another take place because it is impossible to track each transaction separately. Before fraud can be discovered, it must first be determined. Due to all of these difficulties, it becomes a necessity to develop an effective fraud detection system and understand the challenges [9] that will tell the difference between a valid and a fraudulent transaction. The idea of a system like this is to learn user-specific behavior cards.

In This paper, we have implemented three models namely XGBoost, Logistic Regression, and Multi Layer-Perceptron, and compared these models to find out the best-suited model to detect Credit Card Fraud.

II. Literature Survey

In 2017, [7] have investigated the models of Logistic Regression, k-nearest neighbors algorithm, and Naïve Bayes on a dataset having highly skewed credit card data. They use 30% dataset in testing and 70% dataset in training. It is also found that on a highly imbalanced dataset, hybrid sampling (Under-Sampling and oversampling) greatly improves binary classification performance. Their Comparative study shows that the K-nearest neighbor is the best among the algorithms they compared.

In 2020, [3] have implemented and compared machine learning algorithms like Random Forest and Adaboost. The Adaboost algorithm was designed to optimize the effectiveness of binary classifiers. However, the Adaboost Algorithm is at a disadvantage as it is sensitive to noisy data and to outliers. The F1 Score, accuracy, recall, and precision of the two algorithms were compared. They have also plotted a ROC Curve based on the Confusion Matrix. It was noted that the Adaboost Algorithm had better precision, F1 Score, and recall than Random Forest Algorithm. Hence, it was concluded that the Random Forest Algorithm works better at detecting Credit Card Fraud than the Adaboost Algorithm.

In 2020, [6] have implemented and compared several predictive models like Random Forests, ANN,k-nearest neighbors algorithm, Decision Trees, Gaussian Naive Bayes, Logistic Regression, and SVM. They compared the accuracy of all of these models' results. They discovered that the Artificial Perceptron algorithm delivers the best outcome. They've also shown how crucial feature selection and dataset balancing are in generating meaningful findings.

In 2021, [4] have implemented and compared various machine learning algorithms like Logistic Regression, Random Forest, k-nearest neighbors algorithm, and Decision Tree. Confusion Matrix, precision, and recall were the classification metrics used. Only 492 transactions, or 0.17 percent of the total 264807 transactions, are classified as fraudulent, indicating a very unbalanced dataset. One of the most typical problems encountered while working with credit card transaction databases is class imbalance. In this study, the class imbalance problem is addressed through SMOTE. After examining the machine learning algorithms, our conclusion is that Random Forest is the best classifier. Furthermore, after the problem of class imbalance was addressed, the model's accuracy was found to have improved.

In 2021, [5] have implemented and compared machine learning algorithms like Decision Tree, Logistic regression, Naïve Bayes, and Random Forest. The comparison occurred on the basis of their AUC score, Confusion Matrix, precision, accuracy, F1 score, and recall. Dataset is heavily imbalanced so accuracy is 99.9% for any algorithm. Hence, they have done Under-Sampling. A heat map is used to visualize the correlation between variables. The extreme outliers have been removed. The dataset has been divided into the ratio of 70 to 30, 70% of the time is spent on training and 30% on testing. After comparing the models which had been applied, we have concluded that the best classifier is the Random Forest with 96.77% accuracy, 91.11% recall, 100% precision, 95.34% F1 score, and 95.55% AUC score.

III. METHODOLOGY

Python programming language along with ML and different tools were used in our research to compare various models and propose a credit fraud detection system.

Authorized licensed use limited to: DELHI TECHNICAL UNIV. Downloaded on June 22,2022 at 04:33:14 UTC from IEEE Xplore. Restrictions apply.

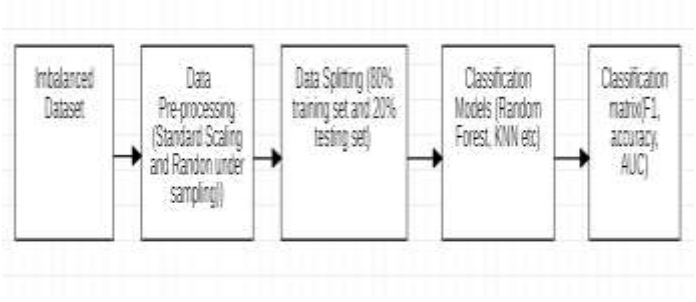

Figure 1: Steps of Methodology

A. Imbalanced Dataset uploading:

Researchers have a considerable hurdle due to the scarcity of credit card databases. The dataset utilized in this work is Credit Card Fraud Detection, which is accessed from the Kaggle dataset. This dataset comprises the transactions done by European cardholders. 284,807 transactions were made in this dataset during the course of two days. Positive instances (fraud cases) make up about 0.172 percent of total transactions. The data is highly imbalanced and slanted in favor of the positive.

In this research, a total of 30 input features are used. The 'Time' class represents the time difference between the current and preceding transactions in seconds. The monetary transaction is represented by the class 'Amount.' Another important feature is 'Class,' which indicates whether or not the transaction is fraudulent. The number 1 denotes a fraudulent transaction, while 0 denotes non-fraudulent transactions.

B. Dataset pre-processing:

Preprocessing[14] of the data is crucial because the distribution ratio of classes has a massive effect on model precision and accuracy. We used Undersampling to sample data. Undersampling is a technique for balancing uneven datasets by retaining all data in the minority class while reducing the size of the majority class.

A basic strategy for deciding which variables in a dataset are the most essential is feature selection. By carefully finding suitable features and removing the less critical things, overfitting, accuracy, and training time can all be reduced. Techniques such as visualization may help with this.

When classification categories are not evenly distributed, machine learning algorithms have difficulty in learning. Given the highly imbalanced nature of the data, some sort of balancing is required so that the model can be effectively trained. We can undersample the majority class, oversample the minority class or adjust the class distribution in a variety of ways, including a combination of the two. In this paper, we have used Feature Scaling. Feature Scaling is a method of bringing the independent features of data into a specified range. It is used to handle highly varying magnitudes, values, or units during data pre-processing. It basically is a very effective technique for rescaling a feature value to give it a distribution with a 0 mean value and 1 variance.

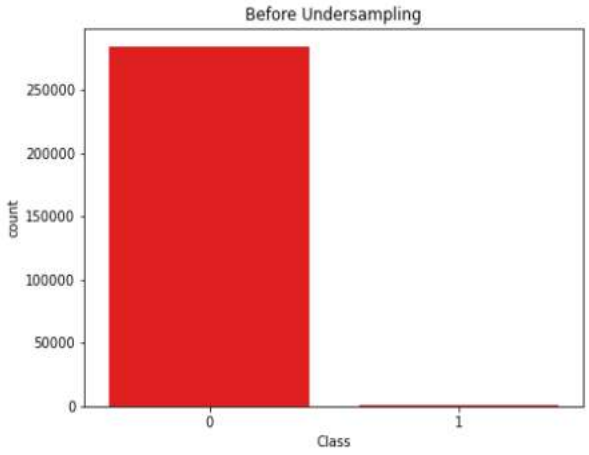

Figure 2: Processing of Data before Undersampling

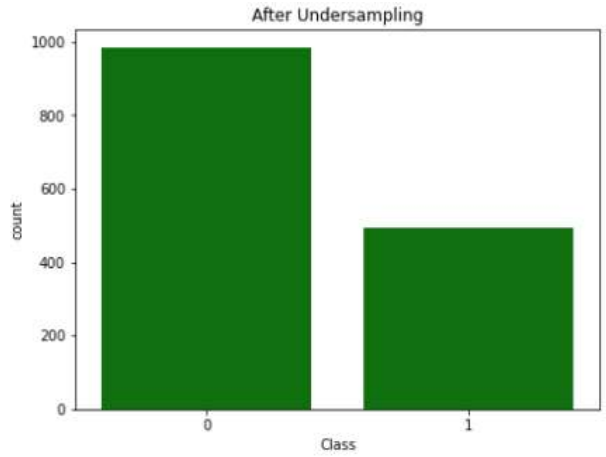

Figure 3: Processing of Data after Undersampling

C. Dataset splitting

When you have a large dataset to work with, a costly model to train, or you need a quick estimate of model performance, the train-test split procedure works best. It is best to use the Scikit-learn machine learning library for the train-test split. We had divided the dataset into two parts: 80% for training and 20% for testing. Following

Authorized licensed use limited to: DELHI TECHNICAL UNIV. Downloaded on June 22,2022 at 04:33:14 UTC from IEEE Xplore. Restrictions apply.

this step, we set the random state to 1, and our dataset is then ready for the machine learning techniques of our choice for the generation of system models.

D. Selecting model and Applying Algorithm

1) Confusion Matrix: The confusion matrix[11] adds to our understanding of our model's performance by displaying information on correctly and incorrectly classified classes, allowing us to spot errors.

a) Accuracy: The percentage of correctly predicted outputs is known as accuracy eq(2).
b) Precision: We can measure the exactness of a model by the number of correctly classified outputs eq(3).
c) Recall The percentage of True Positives that our model correctly identifies eq(4).
d) F1 score: It is the Average of Precision and Recall eq(5).

2) Logistic Regression: It can be used for classification as well as regression, but classification is the most typical use. Although in the terms "regression" and "classification" are incompatible, the focus of logistic regression is on the word "logistic," which refers to the logistic function that performs the classification operation[15] in the algorithm As a consequence, you'll get a binary that represents one of the classes. Also by imposing a decision rule, a probability-predicting regression model can be employed as part of a classifier. With the help of dependent variables, it is possible to predict the output. Binary data can be easily classified with this approach into one of two values: 0 or 1.

$$p = 1/1 + e^{-(a0+a1x1+a2x2+\cdots\ldots+anxn)} \quad \textbf{(1)}$$

The principle of Logistic Regression and how it works is explained in the equation (1) a0, a1…. an are coefficients x1, x2, x3,.....xn are independent variables, and the result is p.

3) XGBoost: XGBoost[13] is a high-performance, high-speed and gradient boosted decision tree implementation. The beauty of this strong algorithm is its scalability, which enables quick learning via distributed and parallel computing while still making effective use of memory.We use XGBoost because it's efficiency is not impacted by integration of data sampling[8]

4) Multi-Layer Perceptron: The collection of more than one layer of artificial neurons or nodes makes up a multi-layer Perceptron. In terms of design, they are quite different. During the early revolution of AI single-layer Perceptrons were useful[10], Today's networks almost all use a multi-layer model. We use this model along with a high-level neural network library [12] because it helps to control model complexity or capacity.

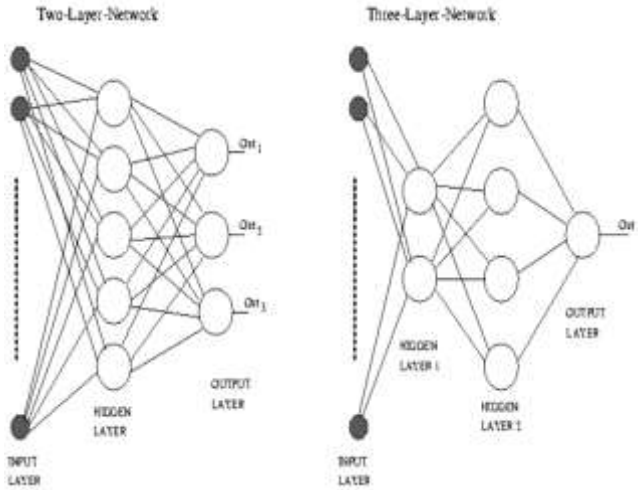

Figure 4: Multilayer Perceptron Architecture

We used the default parameters for all of these classifiers.

5) Evaluation of models performance: After getting the output from every model, we have compared them all by using parameters like F1 score, accuracy, precision, etc.

$$ACCURACY=(TP+TN)/(TP+FP+TN+FN) \quad (2)$$
$$Precision=TP/(FP+TP) \quad (3)$$
$$Recall=TP/(FN+TP) \quad (4)$$
$$F1=2*precision*recall/(recall+precision) \quad (5)$$

From the above equations
True Positive (TP): It is an outcome where the model correctly predicts the positive class.
True Negative (TN): It is an outcome where the model correctly predicts the negative class.
False Positive (FP): It is an outcome where the model incorrectly predicts the positive class.
False Negative (FN): It is an outcome where the model incorrectly predicts the negative class.

Authorized licensed use limited to: DELHI TECHNICAL UNIV. Downloaded on June 22,2022 at 04:33:14 UTC from IEEE Xplore. Restrictions apply.

IV. RESULTS

We have compared different models based on XGBoost, Logistic Regression, and Multi-Layer Perceptron to determine the best model. To evaluate this model, 80% dataset is used for training, and the rest of the dataset, that is 20%, is used for testing. Accuracy, F1 score, Recall, AUC, and Precision were used for evaluating the performance of our models. A Confusion matrix is created to give us a look at the performance of each of our models

A) Logistic Regression

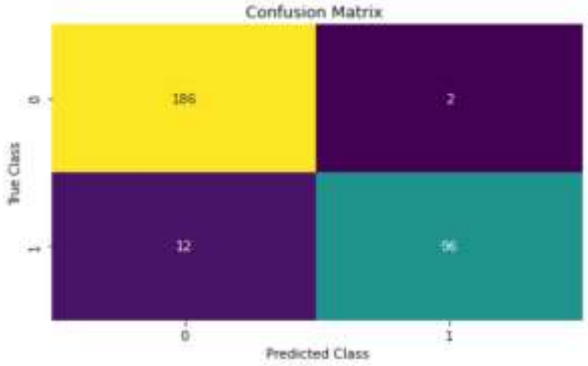

Figure 5: Confusion Matrix of Logistic Regression

In figure 5 the X-Axis represents the Predicted Class and the Y-Axis represents the True Class. The class has a value 1 in case of fraud and 0 otherwise.

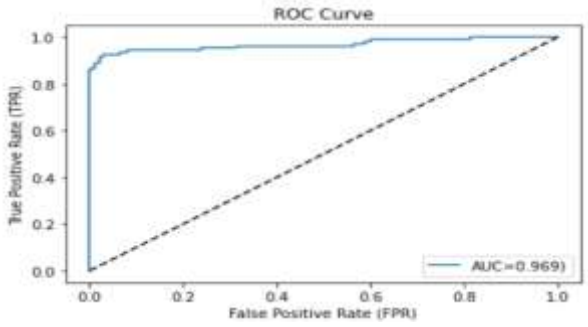

Figure 6: ROC Curve and AUC of Logistic Regression

In figure 6 the X-Axis represents the False Positive Rate and the Y-Axis represents the True Positive Rate. The curve plotted is a Receiver Operating Characteristic curve and AUC stands for Area Under the Curve which shows the performance of a classification model at all classification thresholds.

B) XGBoost

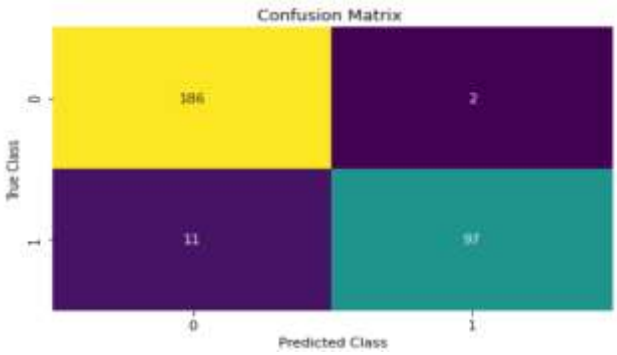

Figure 7: Confusion Matrix of XGBoost

In figure 7 the X-Axis represents the Predicted Class and the Y-Axis represents the True Class. The class has a value of 1 in case of fraud and 0 otherwise.

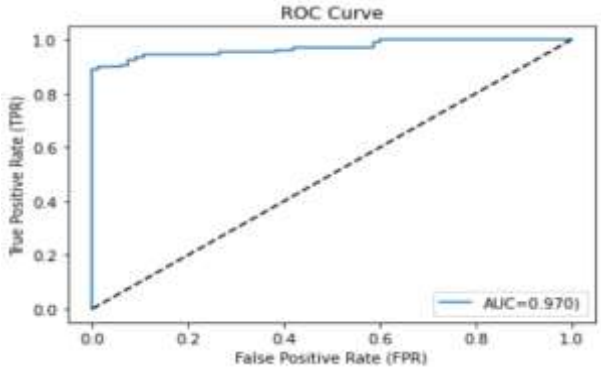

Figure 8: ROC Curve and AUC of XGBoost

In figure 8 the X-Axis represents the False Positive Rate and the Y-Axis represents the True Positive Rate. The curve plotted is a Receiver Operating Characteristic curve and AUC stands for Area Under the Curve which shows the performance of a classification model at all classification thresholds.

Authorized licensed use limited to: DELHI TECHNICAL UNIV. Downloaded on June 22,2022 at 04:33:14 UTC from IEEE Xplore. Restrictions apply.

C) Multi-Layer Perceptron

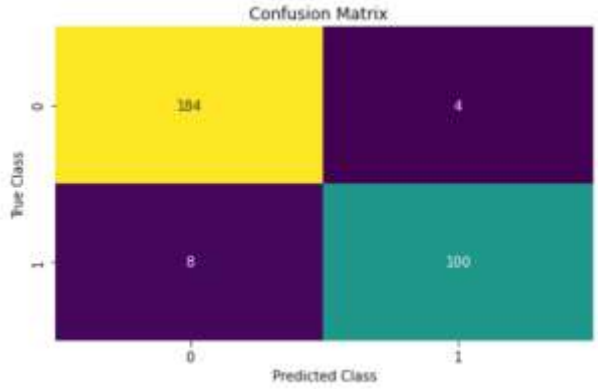

Figure 9: Confusion Matrix of Multi-Layer Perceptron

In figure 9 the X-Axis represents the Predicted Class and the Y-Axis represents the True Class. The class has a value 1 in case of fraud and 0 otherwise.

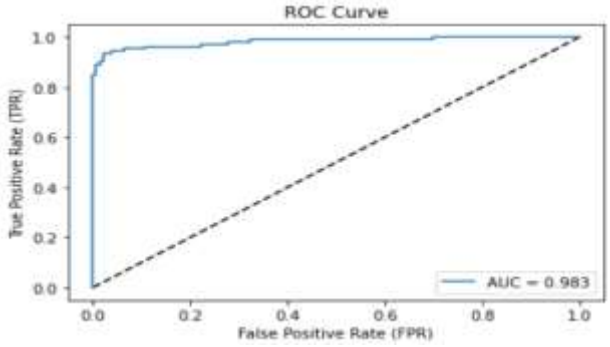

Figure 10: ROC Curve and AUC of Multi-Layer Perceptron

In figure 10 the X-Axis represents the False Positive Rate and the Y-Axis represents the True Positive Rate. The curve plotted is a Receiver Operating Characteristic curve and AUC stands for Area Under the Curve which shows the performance of a classification model at all classification thresholds.

TABLE 1: Comparison of All Three Models

Models Used	Accuracy	Precision	Recall	F1 Score
XGBoost	0.956	0.978	0.898	0.937
Neural Network	0.959	0.962	0.926	0.943
Logistic Regression	0.953	0.980	0.889	0.932

Here, in table 1 we can see that our Perceptron beats the XGBoost and Logistic Regression Algorithms in terms of Accuracy, F1 score, Recall, and AUC while having lower precision. Hence, we can conclude that our *Multi-Layer Perceptron* is better.

V. CONCLUSION

Credit Card Fraud is a serious concern for businesses. Scams of this nature may result in personal losses and substantial financial losses. Due to this, businesses are investing more in the development of new fraud detection and prevention ideas and methods.

A better result could have been obtained by increasing the sample size. The scope of the paper can also be narrowed down by comparing Credit Card Fraud committed in Europe to other continents like Asia and America. Also, the scope of the paper may be limited in comparison to the research work done by more experienced academics.

The study's main goal was to look at a variety of machine learning algorithms (methods for detecting fraud transactions). The comparison revealed that the best result is delivered by Multi-layer Perceptron, i.e. it correctly classifies whether or not a transaction is fraudulent. Various criteria like recall, accuracy, F1 score, and precision were used to establish this. A high recall value is required for this type of challenge.

To improve results, more research into additional machine learning techniques like stacked classifiers and various types of genetic algorithms, as well as careful feature selection, is needed.

Authorized licensed use limited to: DELHI TECHNICAL UNIV. Downloaded on June 22,2022 at 04:33:14 UTC from IEEE Xplore. Restrictions apply.

VI. FUTURE SCOPE

We have currently used Multi-Layer Perceptron, XGBoost, and Logistic Regression. As there is room for improvement in every task and for better Credit Card Fraud detection, we can use more deep learning algorithms.

We can also employ more advanced Multi-Layer Perceptrons for improved performance. There are a lot of Machine Learning algorithms available. Since we could only compare a limited number of algorithms across the scope of this paper, for better comparison more Machine Learning(ML) algorithms can be used. Moreover, the dataset we have used is the European dataset. We can use a dataset from another continent and compare them to observe the similarities and differences in Credit Card Fraud across the world.

VII. REFERENCES

[1] A. A. Akinyelu and A. O. Adewumi, "A survey of machine-learning and nature-inspired based Credit Card Fraud detection techniques," Int. J. Syst. Assur. Eng. Manag., vol. 8, no. 2, pp. 937–953, Nov. 2017.

[2] H. Jaiman, S. Lawte, J. Wosowei, and O. Adepoju, "Comparative Evaluation of Credit Card Fraud Detection Using Machine Learning Techniques," Global Conference for Advancement in Technology, 2019, pp. 1-6.

[3] R Sailusha, V. Gnaneswar, R. Ramesh and G. Ramakoteswara Rao "Credit Card Fraud Detection Using Machine Learning" Proceedings of the International Conference on Intelligent Computing and Control Systems (ICICCS 2020)

[4] A. S. Rathore, A. Kumar, D. Tomar, V. Goyal, K. Sarda, and D. Vij, "Credit Card Fraud Detection using Machine Learning," 10th International Conference on System Modeling & Advancement in Research Trends, pp. 1-5, 2021.

[5] D. Tanous, D. Eswar, G. V. P. Reddy, C. H. V. N. M. Praneeth, A. R. Kumar, and R. R. Subramania, "Credit Card Fraud Detection Using Machine Learning" Proceedings of the Fifth International Conference on Intelligent Computing and Control Systems, 2021, pp. 1-6.

[6] S. K. Pradhan, P. Harish, N. V. K. Rao, M. A. P. Kumar, N. M. Deepika, and P. S. Kumar "Credit Card Fraud Detection Using Artificial Perceptrons and Random Forest Algorithms" Proceedings of the Fifth International Conference on Electronics, Communication and Aerospace Technology, 2021, pp. 1-6.

[7] S. A. Oluwadare, J.A. O. Adetunmbi, and . O. Awoyemi "Credit Card Fraud detection using Machine Learning Techniques: A Comparative Analysis," International Conference on Computing Networking and Informatics, 2017, pp. 1-9.

[8] C. V. Priscilla and D. P. Prabha, "Influence of Optimizing XGBoost to handle Class Imbalance in Credit Card Fraud Detection," 2020 Third International Conference on Smart Systems and Inventive Technology (ICSSIT), 2

[9] S Jain, Y Jain, S Dubey and N Tiwari, "A Comparative Analysis of Various Credit Card Fraud Detection Techniques, Blue Eyes Intelligence Engineering and Sciences Publications 2019\

[10] K. He, X. Zhang, S. Ren, and J. Sun, "Deep residual learning for image recognition," in 2016 IEEE Conference on Computer Vision and Pattern Recognition (CVPR), pp. 770–778, June 2016

[11] J. C. Olivier, B. P. Salmon,, C. P. Schwegmann and W. Kleynhans "Proper comparison among methods using a confusion matrix," 2015 IEEE International Geoscience and Remote Sensing Symposium (IGARSS), 2015, pp. 3057-3060.

[12] N. Hooda and K. Jakhar, "Big Data Deep Learning Framework using Keras: A Case Study of Pneumonia Prediction," 2018 4th International Conference on Computing Communication and Automation (ICCCA), 2018, pp. 1-5.

[13] L. Sun, "Application and Improvement of Xgboost Algorithm Based on Multiple Parameter Optimization Strategy," 2020 5th International Conference on Mechanical, Control and Computer Engineering (ICMCCE), 2020, pp. 1822-1825.

[14] N. Shakhovska, "The method of big data processing," 2017 12th International Scientific and Technical Conference on Computer Sciences and Information Technologies (CSIT), 2017, pp. 122-126,

[15] X. Zou, Y. Hu, Z. Tian, and K. Shen, "Logistic Regression Model Optimization and Case Analysis," 2019 IEEE 7th International Conference on Computer Science and Network Technology (ICCSNT), 2019, pp. 135-139.

Authorized licensed use limited to: DELHI TECHNICAL UNIV. Downloaded on June 22,2022 at 04:33:14 UTC from IEEE Xplore. Restrictions apply.

WWW.IJRPR.COM

International Journal of Research Publication and Reviews

Journal homepage: www.ijrpr.com ISSN 2582-7421

Cryogenic Grinding

Roshan Kumar[1], Sachin Malik[2], Saksham Verma[3] and AK Madan[4]

[1, 2, 3] Student, Mechanical Engineering, Delhi Technological University, New Delhi

[4]Professor, Mechanical Engineering department, Delhi Technological University, New Delhi

ABSTRACT

The Cryogenic grinding answers were used for difficult-to-grind or specialist substances, in particular difficult materials like plastics and rubbers, and so far have no longer been broadly used inside the manufacturing of pharmaceuticals and nutraceuticals.However, in this paper we would love to present a neglect on cryogenic grinding and its utility.

KEYWORDS : Cryogenic grinding,Cryogens,Application

INTRODUCTION

The term “Cryogenics” originates from the Greek phrase because of this creation or production by cold. As fees for strength and uncooked substances upward thrust and subject for the surroundings makes secure waste disposal hard and Costly, useful resource healing becomes a important be counted for nowadays’s commercial enterprise. Cryogenic grinding generation can correctly grind maximum tough materials and can also facilitate Cryogenic recycling of tough composite materials and multi component scrap. The coronary heart of this era is the CRYO-GRIND SYSTEM. It employs a cryogenic technique to embrittle and grind materials to achieve constant particle length for a huge variety of products. The cryogenic system additionally has a unique functionality for recycling difficult to split composite materials.

Cryogenic grinding is a method of powdering herbs at sub-zero temperatures starting from zero to minus 70°F. The herbs are frozen with liquid nitrogen as they're being floor. This method does not harm or modify the chemical composition of the plant in any manner. Normal grinding procedures which do not use a cooling device can attain as much as two hundred°F. These excessive temperatures can reduce unstable additives and heat- touchy parts in herbs. The cryogenic grinding process starts with air-dried herbs, in preference to freeze-dried herbs.

Solid substances are floor or pulverized with the aid of way of hammer mills, attrition mills, granulators or different device. A smaller particle size is normally needed to decorate the further processing of the strong, as in mixing with different materials. A finer particle also allows in melting of rubber and plastics for molding. However, many substances are either very tender or very hard at room temperatures. By cooling to cryogenic temperatures with liquid nitrogen, those can be embrittled and effortlessly fractured into small debris.

A scientifically controlled examine the usage of 4 herbs changed into carried out at Frontier Herbs in the Fall of 1996, evaluating cryogenic grinding techniques with everyday grinding strategies. The herbs examined covered feverfew, goldenseal, valerian and echinacea. In all instances the cryogenically ground herb contained more amounts of the components tested. Feverfew herb showed the greatest distinction, with the cryogenically floor herb containing 21.Eight% higher stages of parthenolide, the primary lively constituent. Valerian root showed an 18.7% increase in valerenic acid while cryogenically floor. Goldenseal root showed a sixteen.Four% boom in berberine and 10.7% boom in hydrastine. Lastly, Echinacea purpurea root confirmed a 12.1% growth in general phenolic content material inside the cryogenically ground root. Test effects had been obtained by means of HPLC (excessive performance liquid chromatography) techniques.

Cryogenic grinding was shown to seriously have an effect on active constituent ranges in herbs. Test results showed a mean boom of 15.6% in materials examined in 4 medicinal herbs once they had been ground cryogenically. The range changed into 10.7% to 21.Eight%, indicating that some herbs are affected more than others by using the temperatures at which they're ground.

APPLICATION OF CRYOGENICS

The most important regions in which cryogenics discover its programs are : -

1. Gas Industry – in air separation. The quantity of production of nitrogen and Oxygen by means of cryogenic separation of air is the essential of the separation of air, refrigeration and separation. In the separation column, the difference in the boiling points of the

components of air is used to split them out.
2. As the source of fuel. For example, the respiration oxygen needed for the pilots of the fighter aircraft is provided via vaporizing liquid oxygen on board. In this manner is a weight reduction of sixty five% and space reduction of 85%.
3. In area studies – as rocket propellant and for area simulation. The maximum crucial advantage of cryogenic fuels is that these have very excessive specific impulse while in comparison to other fuels (particular impulse is kgs of thrust produced in line with kg of propellant consistent with sec). The fee is about 500 for cryogenic fuels while it's about 250 for alcohol oxygen mixture.
4. In biology – for upkeep and in remedy of diseases.
5. In meals enterprise – for meals dealing with and processing.
6. In electronics – both semiconductor and superconductor electronics for higher sign to noise ratio pace and so forth.

CRYOGENIC GRINDING PROCESS

Since nearly all materials embrittle when exposed to bloodless temperatures, cryogenic size reduction utilizes the bloodless strength to be had from liquid nitrogen to cool, embrittle and inert substances prior to and or all through the grinding technique. All substances which because of their unique homes at ambient temperatures are elastic, have low melting factors, include volatile or oily substances, have low combustion temperatures and are touchy to oxygen, are perfect applicants for cryogenic length discount.
Physical residences of liquid nitrogen is produced with the aid of the separation of air into its components in an air separation plant and is shipped in vacuum insulated transport vessels to the quit person in which it's miles saved in a vacuum insulated storage vessel until it's miles used. At atmospheric pressure liquid nitrogen is at a temperature of –320 deg F and possesses a latent strength content of ninety four BTU/LB ensuing in a complete cooling power content material of 179.6 BTU/LB. Nitrogen is a non-flammable, non poisonous and inert fuel which makes up 78.09% of the air we breathe. It has the traits of an inert fuel, except at relatively improved temperatures, and does not shape any compound under normal temperatures and strain. Drawn from the liquid section, nitrogen normally has a purity of ninety nine.998 % with a dew point much less than – 100 deg F and could be very dry.

CRYOGENIC GRINDING TECHNOLOGY

For pulverizing many materials, cryogenic grinding era will increase productiveness and lowers electricity costs. Many elastic or "soft" materials are very hard to pulverize, requiring long cycle times and excessive power consumption. This aggregate decreased productivity and multiplied fees unnecessarily. Cryogenic grinding includes cooling a fabric under its embrittlement temperature with a cryogenic fluid, usually liquid nitrogen or, in sure applications, carbon dioxide.
Probably the greatest benefit provided by cryogenic grinding is the ability to grind "soft" or elastic materials that otherwise could not be ground, or could be ground only with long cycle times and high energy use. By embrittling the material, fine powder or crumb can be obtained easily and with a minimum expenditure of energy. Because embrittled material grinds easily, the throughput for a given mill is substantially increased and less power is used per pound of material ground.In Fig. 1 is a plan of moment situating the work piece during a solitary transformation when in-feed grinding? The apparatus way feed rate is checked t. assuming stipend is taken with specific pieces of the surface, the work piece diminishes and is moved to the directing wheel.
Cryogenic grinding is used for grinding spices, thermoplastics, elastomers, color concentrates, and similar materials. It is also used to recover a variety of scrap materials, such as factory scrap rubber and scrap tires, and to separate the components in composite materials.

ADVANTAGES OF CRYOGRINDING

1. Higher manufacturing price
2. Lower strength intake
three. Finer particle length
four. More uniform particle distribution
5. Lower grinding fee
6. No heat era which is good whilst grinding spices,
pharmaceuticals and scrap plastics
7. Provides an inert ecosystem as a result disposing of the opportunity of
oxidation

APPLICATIONS OF CRYOGENIC GRINDING

CryoGrinding of metallic

Thermoplastics
Adhesives & Waxes
Explosives
Spices
Thermo sets

CONCLUSION

From the evaluate it could be concluded that the cryogenic grinding process produces quite easy fracture surfaces. Little or no warmth is generated in the method. This outcomes in plenty less degradation of the material. Apart from this Fineness and uniform distribution of unique sized particle is met in this manner consistent with requirement; it may be adjusted the usage of suitable configuration of Cryogenic grinders. As the manufacturing is in inert surroundings the cloth is covered from oxidation and rancidity. Comparatively the price of Cryogenic grinding approach is much less and strength intake is reduced. Production charge is likewise advanced.

FUTURE SCOPE

As the cost of raw materials and energy is growing day by day, it's far very vital to use most effective quantity and on the same time get the required satisfactory. By the use of CryoGrinding era these factors can be met correctly. By using this we also can recycle hard and composite materials. It has many massive benefits over traditional grinding. This additionally ends in cost addition to the product. CryoGrinding is economically feasible, if liquid nitrogen prices aren't bold. By adopting CryoGrinding generation the main spice industries of our u . S . Will earn substantial foreign exchange by way of exporting greater cost-added processed spices, in place of exporting complete spices. The method may be without difficulty prolonged to processing of PVC and industrial waste plastics in view of recycling of non-biodegradable materials.

REFERENCES

[1] Rohit Saxena, Cryogenic Grinding: A Physical Technique To Retain Volatile Content In Natural Products, Department of Humanities and Science.
[2] Charles Astafan and Rudi Kohler (October 1995.)Comparison of Scrap Tire Processing Technologies: Ambient Processing vs.Cryogenic Processing,'ACS Rubber Division MeetingCleveland',paper #35
[3] S.S Thipse, Cryogenics, Narosa publication, pp(149-157)
[4] McGraw Hill encyclopedia of science and technology,pp(341-346).

Proceedings of the Sixth International Conference on Trends in Electronics and Informatics (ICOEI 2022)
IEEE Xplore Part Number: CFP22J32-ART; ISBN: 978-1-6654-8328-5

Customer Market Segmentation using Machine Learning Algorithm

Swesh Raj Regmi
Department of Information Technology
Delhi Technological University
Delhi, India
sweshregmi@gmail.com

Jasraj Meena
Department of Information Technology
Delhi Technological University
Delhi, India
jasrajmeena@dtu.ac.in

Utkarsh Kanojia
Department of Information Technology
Delhi Technological University
Delhi, India
utkarshkanojia2001@gmail.com

Vishesh Kant
Department of Information Technology
Delhi Technological University
Delhi, India
vishesh.kant1010@gmail.com

2022 6th International Conference on Trends in Electronics and Informatics (ICOEI) | 978-1-6654-8328-5/22/$31.00 ©2022 IEEE | DOI: 10.1109/ICOEI53556.2022.9777146

***Abstract*—Everything is becoming more mechanized in today's times, especially in this age of data. Data is the world's new electricity. Many firms can benefit from this information in their marketing efforts. Every company wanted to grow and be better than the competition, so they employed innovative ideas and invested in product development, but only to keep their customers and expand their market. Customers are segmented in today's commercial world. They analyze their consumers' behaviors and purchasing patterns and can assist them in generating profit. Customer segmentation refers to the process of categorizing a company's customers into groups based on their commonalities. Client segmentation is the process of determining how to interact with consumers in different groups to amplify the value of each customer to the company. Unsupervised machine learning is used to segment customers. There are many algorithms that can partition customers based on their behavior and other parameters, and our study's main goal is to cluster customers into various clusters based on their behavior patterns. This research study has compared five clustering algorithms and selected the best of them for further research.**

Keywords—Machine Learning, Classification, Clustering, Customer Segmentation, Spending behavior, K-Mean Algorithm.

I. INTRODUCTION

Customers are people who purchase and use the firm's goods. Customers have wants, and they are the ones who ultimately decide whether the company's product meets those demands. Customers represent the company's market share, and sales and profits are generated by them. Customer loyalty to a product or service is advantageous since customers will continue to look for the thing they want [3]. Every business owner must improve the quality of their current offerings as well as client satisfaction. The company's sales and earnings will increase as the number of business customers grows, and vice versa. The technique of dividing a company's customers into groups based on their commonalities is known as customer segmentation. Customer segmentation refers to the process of determining how to interact with consumers in various groups to amplify the value of each customer to the company. Marketers can use customer segmentation to reach out to each consumer in the most efficient way feasible [5-6]. A customer segmentation analysis helps marketers properly identify different groups of customers based on demographic, behavioral, and other aspects by leveraging the large amount of data available on customers (and potential customers). Customer segmentation allows businesses to see what their customers are buying, allowing them to provide better service and boost customer happiness [1]. It also enables companies to identify their potential consumers and refine their marketing methods to increase revenue from them. Because a marketer's goal is to maximize each client's potential (revenue and/or profit), it's vital to anticipate how each marketing activity will influence the customer ahead of time. Clustering has been proved to be a good way to implement consumer segmentation. Clustering, which is the capacity to uncover categories in unlabeled datasets, is an example of unsupervised learning. K-means, hierarchical clustering, DBSCAN clustering, and other approaches are among the clustering methods available. The purpose of this paper is to find consumers that businesses can use to boost profits and grow their enterprises by fulfilling current customer demands and recruiting new customers based on their wants. It's challenging to identify clients and meet their unique requirements [4]. This is owing to the fact that consumers have different expectations, desires, and tastes, among other things. Customer segmentation, rather than a "one-size-fits-all"

Authorized licensed use limited to: DELHI TECHNICAL UNIV. Downloaded on June 03,2022 at 06:28:33 UTC from IEEE Xplore. Restrictions apply.

approach, divides customers into groups with comparable characteristics or behaviors. A marketing approach known as customer segmentation separates a market into homogeneous groups. A multitude of factors influence the data used in the customer segmentation strategy, which divides consumers into categories, including demographical situations, data geographical conditions, economic conditions, and behavioral patterns [2]. Businesses can utilize the customer segmentation technique to make better use of their marketing resources, acquire a competitive and fruitful over their rivals, and display a deeper and clear understanding in client expectations. It also assists a business in increasing marketing efficiency, budgeting for marketing and recognizing the new market abilities and opportunities.

II. LITERATURE REVIEW

Because of the fierce competition in the business world, companies have had to increase their profitability and business throughout time by fulfilling customer requests and attracting new customers depending on their desires. A significant number of papers have been examined in relation to segmenting clients in various areas. A wide range of approaches and objectives have been identified [8]. Methods for producing segmentation predictions appear to be based on the upvote and support of several new recent technologies. The work of customer segmentation within K-Means clustering is presented here. In mega business retail organizations, K-Means Clustering was used to construct client segmentation for focused customer services [12]. Because clients can be classified based on demographics and behaviors, this was the context. For the milk business, customer segmentation was done using K-Means to construct customer profiles and analyze profitability and market segmentation to learn customer preferences. K-Means and decision trees were used as data mining tools in these studies. Bank customers were grouped using K-Means based on their credit payment history and RFM score [11]. To anticipate customer eligibility in credit approval and categorize customer rank, the classification rules were constructed using a decision tree as a classification technique [24]. Customer segmentation was done using K-Means and RFM approaches. In electronic enterprises and fertilizer manufacturer, researchers proposed consumer segmentation utilizing RFM, K-Means, and LEM2 approaches. Decision-makers segment customers using a variety of variables, according to [13]. The easiest and most popular demographic factors for segmentation include age, gender, family, education level, and income. Other important segmentation criteria include socio-cultural, psychographic, geographic, and behavioral variables; [5].

III. METHODOLOGY

A. Clustering

Clustering methods produce clusters that are like one another based on specified characteristics. The similarity is measured by the distance between the objects in space. Clustering is an unsupervised machine learning approach for grouping related occurrences into clusters. Clustering is a way of looking at or assessing data by looking at natural groupings or segments that separate data instances. [7].

B. Dataset

Any clustering algorithm relies heavily on the supplied data. The quality and quantity of available data are the most essential factors. A great amount of data is required to produce the best outcomes, and the lack of data points must be kept to a minimum. In most circumstances, the amount of data is not an issue because corporations today store all types of user and item data in enormous databases. The information we used outlines the spending habits of around 9000 active credit cardholders. The file contains 18 behavioral characteristics at the consumer level [10].

C. Principal Component Analysis

PCA is a commonly used statistical analysis tool. By linearly integrating the characteristics, PCA is utilized to uncover underlying structures (Principal Components) in the data. An orthogonal linear transformation of the original data is defined as PCA. A simple linear translation that preserves the inner product of the vectors is known as an orthogonal linear transformation [9].

D. Algorithms Used

1) K - Means Clustering

K-means is a clustering technique that divides a collection of items into K subgroups or clusters. The algorithm is reliant on a manually entered K value. The K centroids are set to random observations from the dataset as their starting point. K-Means is an approach that is relatively efficient [15]. However, the number of clusters must be specified ahead of time, and the results are sensitive to initialization, frequently terminating at a local optimum. Unfortunately, there is no universal theoretical method for determining the ideal cluster size. Comparing the results of numerous runs with varying k and selecting the best one based on a predetermined criterion is a useful technique. In general, a large k reduces error while also increasing the risk of overfitting [14].

2) Agglomerative Clustering

Flat clustering returns an unstructured collection of clusters in agglomerative clustering; this structure is more revealing. With this clustering process, we don't need to specify the number of clusters ahead of time. [25]. Bottom-up algorithms begin by considering each piece of data as a singleton cluster, then agglomerate

Authorized licensed use limited to: DELHI TECHNICAL UNIV. Downloaded on June 03,2022 at 06:28:33 UTC from IEEE Xplore. Restrictions apply.

pairs of clusters until they are all merged into a single cluster containing all of the data. [20].

3) Spectral Clustering

Spectral Clustering is a new clustering approach that has surpassed various traditional clustering methods in a variety of situations. By considering each data point as a graph node, it transforms the clustering issue into a graph partitioning problem.

4) Gaussian Mixture Model-based clustering

Gaussian Mixture Models (GMMs) assume that there are a finite number of Gaussian distributions, each representing a cluster. As a result, in a Gaussian Mixture Model, data points from a single distribution tend to be clustered together [18].

5) DBSCAN Clustering

The DBSCAN clustering algorithm is based on the concepts of "clusters" and "noise." The basic concept is that the neighborhood of a given radius must have at least a certain number of points for each point of a cluster [17].

E. PROJECT IMPLEMENTATION

1) DATASET FEATURES

CUSTID: Credit Cardholder Identification Number (Categorical)

BALANCE: The amount of money left in their account for purchases.

BALANCE FREQUENCY: Score between 0 and 1 for how frequently the Balance is updated (1 = frequently updated, 0 = not frequently updated) [19].

PURCHASES: The total amount of money spent from the account.

ONE OFF PURCHASES: Purchases made in a single transaction.

INSTALLMENTS PURCHASES: Amount paid in installments.

CASH ADVANCE: The user provides cash in advance.

PURCHASES FREQUENCY: A score between 0 and 1 indicating how frequently purchases are made (1 = frequently purchased, 0 = not commonly purchased).

ONE OFF PURCHASES FREQUENCY: The frequency with which purchases are made in a single transaction (1 = frequently purchased, 0 = not commonly purchased).

PURCHASES INSTALLMENTS FREQUENCY: The frequency with which purchases in installments are made (1 = frequently, 0 = not frequently).

CASH ADVANCE FREQUENCY: The frequency with which purchases in installments are made (1 = frequently, 0 = not frequently).

CASH ADVANCE TRX: Transactions conducted using "Cash in Advance"

PURCHASES TRX: Number of purchase transactions made

CREDIT LIMIT: The user's credit card limit

PAYMENTS: The amount of money paid by the user.

MINIMUM PAYMENTS: The user's minimum payment amount.

PRC FULL PAYMENT: The percentage of the total payment that the user has paid [26].

TENURE: The percentage of the total payment that the user has paid.

For segmentation, we're going to look at a dataset of credit card users. There is no feature about customer labels. That is to say, we do not have information about the qualities of our customers. We're going to try clustering clients using machine learning methods to find similarities. In the new marketing disciplines, customer segmentation plays a crucial role for businesses [16].

The balance rises in lockstep with the credit limit, resulting in a linear connection. The number of "cash in advance" transactions reduces as the number of purchases rises. Purchases, one-time purchases, and instalment purchases are all reduced since the credit amount is low. As a result, our hypothesis from univariate analysis was confirmed. Purchases, including one-time and instalment purchases, are all linearly connected. The "cash in advance" transactions are fewer because the credit balance is low. [27].

IV. RESULT ANALYSIS

To summarize this large amount of data and observe some patterns between variables we plotted the correlation matrix [23]. The correlation between purchases, one-time purchases, and investment purchases is strong. That is to say, the majority of the transactions are one-time purchases. When the sum is large, many don't make complete payments. The frequency of purchases and cash advances are negatively connected. That is, when the frequency of purchases increases, the number of cash payments in advance decreases, and vice versa.

Authorized licensed use limited to: DELHI TECHNICAL UNIV. Downloaded on June 03,2022 at 06:28:33 UTC from IEEE Xplore. Restrictions apply.

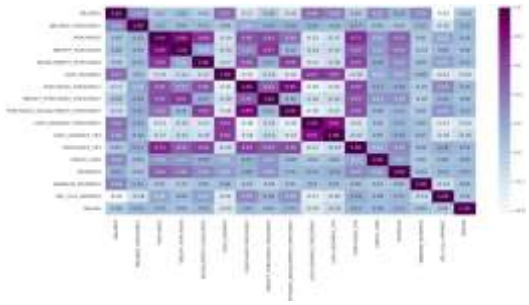

Fig.1 Correlation Matrix

Mean of balance is $1500, 'Balance Frequency' for most customers is updated frequently ~1 For 'PURCHASES_FREQUENCY', there are two distinct group of customers for 'ONEOFF_PURCHASES_FREQUENCY' and 'PURCHASES_INSTALLMENT_FREQUENCY' most users don't do one off purchases or installment purchases frequently. Very small number of customers pay their balance in full 'PRC_FULL_PAYMENT'~0. Credit limit average is around $4500. Most customers are ~11 years tenure. The majority of the data is skewed, thus we'll have to log convert the dataset. Clustering techniques aim to reduce observations by grouping them according to varied criteria, but generally seeking: Greater internal similarity (within groups), Less external similarity (inter groups - external) [21]. These similarities are verified by looking at the distances between observations. These distances can be calculated in different ways, but before presenting some of them, it is important to emphasize that, as they are distance measurements, we can state that this type of analysis is performed on continuous or discrete metric variables. Categorical variables should not be used in these clustering models, but they can help to understand groups of observations after applying them. The choice of the number of clusters can also be done in different ways. Overall, we seek a balance between the incremental gain from increasing the number of clusters and the costs involved (business, processing, marketing, etc.). When this increase in the number of clusters no longer produces such distinct groups (closer, with less variability between them), this is usually where the ideal quantity (candidate) works.

	PCA1	PCA2
0	-2.286545	3.003892
1	1.134734	0.431864
2	-1.458100	-1.493199
3	0.740702	-0.539478
4	0.648369	-1.077164

Table.1 PCA

Most variables have asymmetric distributions with high inflation of zeros and elongated tails. By the characteristic of the base, this is a possible behavior, because they broadly represent the consumption capacity of a population, which follows a similar distribution (the higher the financial capacity, the lower the number of customers). The CREDIT_LIMIT variable, although also asymmetric and elongated, has the lowest coefficient of variation, being an interesting variable to observe regarding the distribution of clusters. The Elbow technique is a tool for evaluating our dataset's clusters and selecting the optimal number of clusters in the dataset. Using this method, we discovered that the best number of clusters for our dataset is four. [28-29].

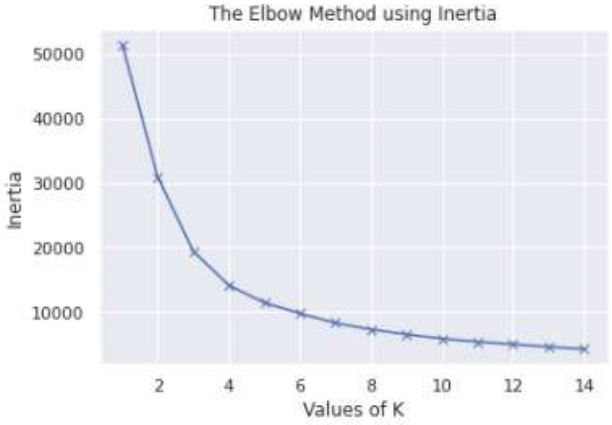

Fig.2 Elbow Method

To obtain a mathematical reference, we will use a function that calculates the distance between the points and the line and returns the greatest distance, which represents the point of greatest inflection. It is important to note, however, that this optimal number of clusters will vary with the maximum number of clusters selected for the calculation [22]. The elbow method brought as an optimal number of clusters 4 groups. This number identifies the point of greatest inflection of the curve. Thus, from this value, the gain of differentiation between groups and proximity within groups becomes smaller and smaller as more groups are created. The silhouette value compares how similar a point is to its own cluster (cohesion) to other clusters (separation).

Authorized licensed use limited to: DELHI TECHNICAL UNIV. Downloaded on June 03,2022 at 06:28:33 UTC from IEEE Xplore. Restrictions apply.

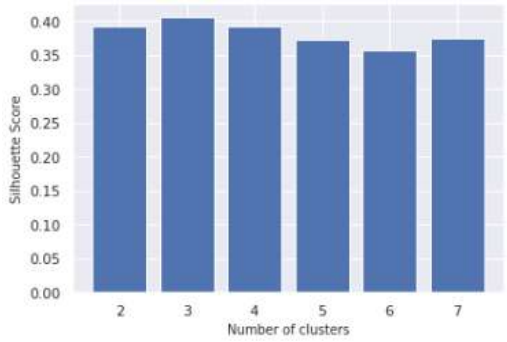

Fig.3 No. of clusters vs silhouette Score

The ideal number of clusters was calculated, and four groups were formed. However, when observing the number of clients per cluster, there is a relatively small number of users in some clusters.

A. K-means Analysis

Fig.4 K -means Algorithm

Clusters created with K-Means must have the same feature size and be spherical or convex in shape. For big datasets, K-means clustering is more efficient, but it is also sensitive to the number of clusters provided. Outliers and noisy datasets don't work well with K-means Clustering.

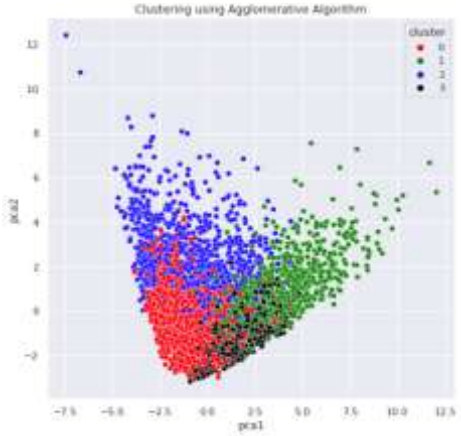

Fig.5 Agglomerative Clustering

The first cluster, as seen in the graph above, is made up of consumers with medium to high credit limits who do not make any transactions. Customers from this segment made up a sizable portion of the total. Regrettably, it does not appear to be appropriate for marketing techniques. Customers in the second cluster have the lowest credit limits and make the smallest purchases, resulting in low payments. Customers in the third cluster are those who spend a lot of money. Their credit limit is variable, ranging from low to large. This category includes a sizable number of customers.

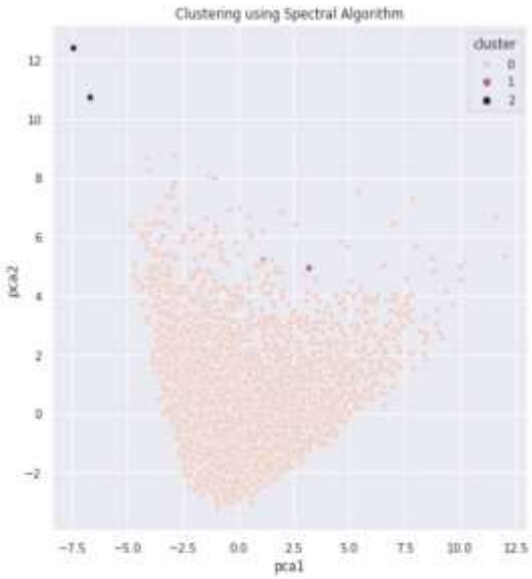

Fig.6 Spectral Clustering

Data points are considered as nodes of a network in spectral clustering. A graph partitioning problem is spectral clustering. The nodes are then transferred to a low-dimensional space where clusters may be readily formed. No assumptions are made regarding the clusters' structure or appearance.

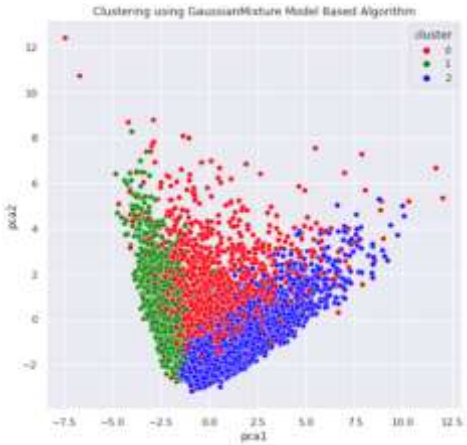

Fig.7 Gaussian Mixture Model-Based Algorithm

Gaussian mixture models, unlike k-means, take variance into account and yield the likelihood that a data point belongs to each of the K clusters.

Authorized licensed use limited to: DELHI TECHNICAL UNIV. Downloaded on June 03,2022 at 06:28:33 UTC from IEEE Xplore. Restrictions apply.

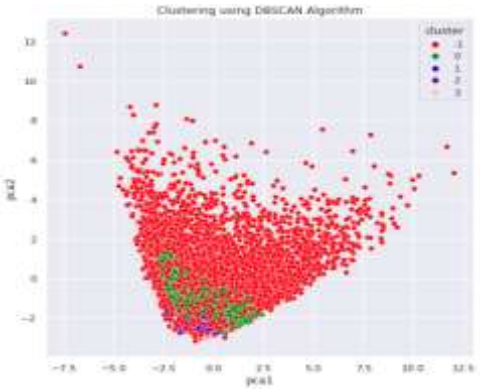

Fig.8 DBSCAN Algorithm

Spatial Clustering of Applications with Noise Using Density. Finds high-density core samples and expands clusters from them. It's ideal for data with clusters of comparable density. Using DBSCAN, arbitrary-shaped clusters can be formed. Here no need to specify the number of clusters manually. When k-means clustering is used instead of alternative clustering algorithms, we can see that all of the data points are clustered nicely with very few errors. In this dataset, we'll cluster using the K-Means model [23].

V. CONCLUSION AND FUTURE WORK

Big data analysis, machine learning, and data mining approaches are all undergoing increasing research. Machines with great computational capacity, such as those provided by cloud computing services like Google Cloud Platform, are becoming more widely available and less expensive. This processing capacity, combined with new advanced machine learning and data analysis tools, works in tandem to help organizations achieve their goals, which include a better understanding of the market and the ability to make decisions based on user data. The substantial rise in marketing services in recent years has provided data analysts new jobs and challenges, necessitating greater time and effort. Sophisticated and intricate analytical approaches that produce useful outcomes for future strategic planning. A client segmentation strategy was provided and assessed. We began by analyzing the dataset and removing the null values that were present. Then, from the columns with approximately 10%, we moved on to detect outliers. Following that, we used clustering methods. After analyzing the clustering models, we chose to go with K-Means and store clusters as a column in our dataset. More clustering techniques should be used to completely comprehend the variety of client roles as well as the number of segments within the customer data. We determined that the K - Means clustering technique is best suited for our dataset based on the visualized results of several clustering algorithms, and we intended to focus our research specifically on K - Means clustering. Finally, clustering isn't limited to consumer segmentation; it may be applied to any segmentation project.

ACKNOWLEDGMENT

The authors are grateful to the Delhi Technological University's central library for providing all of the research lab and resources needed to finish the project and research work. Besides it we are thankful to the Dr. Jasraj Meena for Guiding us in every step for completion of the research work.

REFERENCES

[1] B. K. Shah, A. K. Jaiswal, A. Shroff, A. K. Dixit, O. N. Kushwaha, and N. K. Shah, "Sentiments Detection for Amazon Product Review," *2021 Int. Conf. Comput. Commun. Informatics, ICCCI 2021*, 2021, doi: 10.1109/ICCCI50826.2021.9402414.

[2] E. Y. L. Nandapala and K. P. N. Jayasena, "The practical approach in Customers segmentation by using the K-Means Algorithm," *2020 IEEE 15th Int. Conf. Ind. Inf. Syst. ICIIS 2020 - Proc.*, no. 978, pp. 344–349, 2020, doi: 10.1109/ICIIS51140.2020.9342639.

[3] R. Gupta and C. Pathak, "A machine learning framework for predicting purchase by online customers based on dynamic pricing," *Procedia Comput. Sci.*, vol. 36, no. C, pp. 599–605, 2014, doi: 10.1016/j.procs.2014.09.060.

[4] M. S. Kahreh, M. Tive, A. Babania, and M. Hesan, "Analyzing the Applications of Customer Lifetime Value (CLV) based on Benefit Segmentation for the Banking Sector," *Procedia - Soc. Behav. Sci.*, vol. 109, no. Clv, pp. 590–594, 2014, doi: 10.1016/j.sbspro.2013.12.511.

[5] V. Kedia, S. R. Regmi, K. Jha, A. Bhatia, S. Dugar, and B. K. Shah, "Time Efficient IOS Application for CardioVascular Disease Prediction Using Machine Learning," *Proc. - 5th Int. Conf. Comput. Methodol. Commun. ICCMC 2021*, no. Iccmc, pp. 869–874, 2021, doi: 10.1109/ICCMC51019.2021.9418453.

[6] A. Bhatia, V. Kedia, A. Shroff, M. Kumar, B. K. Shah, and Aryan, "Fake currency detection with machine learning algorithm and image processing," *Proc. - 5th Int. Conf. Intell. Comput. Control Syst. ICICCS 2021*, no. Iciccs, pp. 755–760, 2021, doi: 10.1109/ICICCS51141.2021.9432274.

[7] E. Umuhoza, D. Ntirushwamaboko, J. Awuah, and B. Birir, "Using unsupervised machine learning techniques for behavioral-based credit card users segmentation in Africa," *SAIEE Africa Res. J.*, vol. 111, no. 3, pp. 95–101, 2020, doi: 10.23919/saiee.2020.9142602.

[8] S. Dibb and L. Simkin, "Implementation problems in industrial market segmentation," *Ind. Mark. Manag.*, vol. 23, no. 1, pp. 55–63, 1994, doi: 10.1016/0019-8501(94)90027-2.

[9] M. B. Holbrook and R. M. Schindler, "Market segmentation based on age and attitude toward the past: Concepts, methods, and findings concerning nostalgic influences on customer tastes," *J. Bus. Res.*, vol. 37, no. 1, pp. 27–39, 1996, doi:

Authorized licensed use limited to: DELHI TECHNICAL UNIV. Downloaded on June 03,2022 at 06:28:33 UTC from IEEE Xplore. Restrictions apply.

10.1016/0148-2963(96)00023-9.

[10] G. R. Carini, "Rediscovering market segmentation [5]," *Harv. Bus. Rev.*, vol. 84, no. 6, p. 141, 2006.

[11] S. Wu, W. C. Yau, T. S. Ong, and S. C. Chong, "Integrated Churn Prediction and Customer Segmentation Framework for Telco Business," *IEEE Access*, vol. 9, pp. 62118–62136, 2021, doi: 10.1109/ACCESS.2021.3073776.

[12] B. K. Shah, V. Kedia, and R. K. Jha, "Integrated Vendor-Managed Time Efficient Application to Production of Inventory Systems," *Proc. 6th Int. Conf. Inven. Comput. Technol. ICICT 2021*, pp. 275–280, 2021, doi: 10.1109/ICICT50816.2021.9358504.

[13] S. S. Andaleeb, "Market Segmentation, Targeting and Positioning," *Strateg. Mark. Manag. Asia*, pp. 179–207, 2016, doi: 10.1108/978-1-78635-746-520161006.

[14] W. Xiong, L. Chen, Z. ZhanG, and Z. Qiu, "RFM value and grey relation based customer segmentation model in the logistics market segmentation," *Proc. - Int. Conf. Comput. Sci. Softw. Eng. CSSE 2008*, vol. 5, no. 1, pp. 1298–1301, 2008, doi: 10.1109/CSSE.2008.79.

[15] M. Namvar, M. R. Gholamian, and S. Khakabi, "A two phase clustering method for intelligent customer segmentation," *ISMS 2010 - UKSim/AMSS 1st Int. Conf. Intell. Syst. Model. Simul.*, pp. 215–219, 2010, doi: 10.1109/ISMS.2010.48.

[16] F. M. Epetimehin, "Market Segmentation: A Tool for Improving Customer Satisfaction and Retention in Insurance Service Delivery," *J. Emerg. Trends Econ. Manag. Sci.*, vol. 2, no. 1, pp. 62–67, 2011, [Online]. Available: http://jetems.scholarlinkresearch.com/articles/Market Segmentation.pdf.

[17] K. Torizuka, H. Oi, F. Saitoh, and S. Ishizu, "Benefit Segmentation of Online Customer Reviews Using Random Forest," *IEEE Int. Conf. Ind. Eng. Eng. Manag.*, vol. 2019-Decem, pp. 487–491, 2019, doi: 10.1109/IEEM.2018.8607697.

[18] Y. Liu, S. Ram, R. F. Lusch, and M. Brusco, "Multicriterion market segmentation: A new model, implementation, and evaluation," *Mark. Sci.*, vol. 29, no. 5, pp. 880–894, 2010, doi: 10.1287/mksc.1100.0565.

[19] D. Zakrzewska and J. Murlewski, "Clustering algorithms for bank customer segmentation," *Proc. - 5th Int. Conf. Intell. Syst. Des. Appl. 2005, ISDA '05*, vol. 2005, pp. 197–202, 2005, doi: 10.1109/ISDA.2005.33.

[20] T. Kansal, S. Bahuguna, V. Singh, and T. Choudhury, "Customer Segmentation using K-means Clustering," *Proc. Int. Conf. Comput. Tech. Electron. Mech. Syst. CTEMS 2018*, pp. 135–139, 2018, doi: 10.1109/CTEMS.2018.8769171.

[21] A. S. M. S. Hossain, "Customer segmentation using centroid based and density based clustering algorithms," *3rd Int. Conf. Electr. Inf. Commun. Technol. EICT 2017*, vol. 2018-Janua, no. December, pp. 1–6, 2018, doi: 10.1109/EICT.2017.8275249.

[22] D. Kamthania, A. Pahwa, and S. S. Madhavan, "Market segmentation analysis and visualization using K-mode clustering algorithm for E-commerce business," *J. Comput. Inf. Technol.*, vol. 26, no. 1, pp. 57–68, 2018, doi: 10.20532/cit.2018.1003863.

[23] C. Dullaghan and E. Rozaki, "Integration of Machine Learning Techniques to Evaluate Dynamic Customer Segmentation Analysis for Mobile Customers," *Int. J. Data Min. Knowl. Manag. Process*, vol. 7, no. 1, pp. 13–24, 2017, doi: 10.5121/ijdkp.2017.7102.

[24] S. F. Sabbeh, "Machine-learning techniques for customer retention: A comparative study," *Int. J. Adv. Comput. Sci. Appl.*, vol. 9, no. 2, pp. 273–281, 2018, doi: 10.14569/IJACSA.2018.090238.

[25] P. D. Hung, N. D. Ngoc, and T. D. Hanh, "K-means clustering using R A case study of market segmentation," *ACM Int. Conf. Proceeding Ser.*, pp. 100–104, 2019, doi: 10.1145/3317614.3317626.

[26] P. D. Hung, N. T. Thuy Lien, and N. D. Ngoc, "Customer segmentation using hierarchical agglomerative clustering," *ACM Int. Conf. Proceeding Ser.*, vol. Part F1483, pp. 33–37, 2019, doi: 10.1145/3322645.3322677.

[27] L. Abidar, D. Zaidouni, and A. Ennouaary, "Customer segmentation with machine learning: New strategy for targeted actions," *ACM Int. Conf. Proceeding Ser.*, pp. 221–226, 2020, doi: 10.1145/3419604.3419794.

[28] P. Monil, "Customer Segmentation using Machine Learnin," *Int. J. Res. Appl. Sci. Eng. Technol.*, vol. 8, no. 6, pp. 2104–2108, 2020, doi: 10.22214/ijraset.2020.6344.

[29] M. Meadows and S. Dibb, "Implementing market segmentation strategies in UK personal financial services: Problems and progress," *Serv. Ind. J.*, vol. 18, no. 2, pp. 45–63, 1998, doi: 10.1080/02642069800000018.

Authorized licensed use limited to: DELHI TECHNICAL UNIV. Downloaded on June 03,2022 at 06:28:33 UTC from IEEE Xplore. Restrictions apply.

Research Square

Preprints are preliminary reports that have not undergone peer review.
They should not be considered conclusive, used to inform clinical practice,
or referenced by the media as validated information.

Design and analysis of a compact asymmetrical CPW fed stubs loaded hook-shaped patch antenna for upper 5G- and data collection applications

KARTEEK VISWANADHA (karteekviswanath@gmail.com)
Delhi Technological University

Nallanthighal Srinivasa Raghava
Delhi Technological University Department of Electronics and Communication

Research Article

Keywords: CPW, patch antenna, stubs, multiple, ultra-wideband

Posted Date: June 22nd, 2022

DOI: https://doi.org/10.21203/rs.3.rs-898651/v1

License: This work is licensed under a Creative Commons Attribution 4.0 International License.
Read Full License

Design and analysis of a compact asymmetrical CPW fed stubs loaded hook-shaped patch antenna for upper 5G- and data collection applications.

Karteek Viswanadha
Research Scholar
Delhi Technological University
New Delhi, India
karteekviswanath@gmail.com

N.S.Raghava
Professor
Delhi Technological University
New Delhi, India
nsraghava@dtu.ac.in

Abstract:- In this paper, a 9.5 x 9.5 x 1.524mm^3 asymmetrical CPW fed stub loaded hook-shaped patch antenna is proposed. The proposed antenna is mounted on the partial ground with the dimensions of 4.5 x 9.5 x 0.035mm^3 and is excited by a 50-ohm line. A slot of dimensions 2.5 x 2.5mm^2 is etched on the ground plane to achieve a wideband feature for the proposed patch antenna. The antenna consists of a λ/4 'L' shaped stub and a λ/4 vertical stub attached outside the hook-shaped patch antenna. The hook antenna resonates at 20.6GHz (simulated) and the stubs help the antenna to radiate at multiple frequencies with proper impedance matching. The 'L' shaped stub introduces resonance at 6.96GHz (simulated) and the vertical stub introduces resonance at 11.67GHz (simulated). The proposed antenna has been designed, fabricated, and tested. The measured impedance bandwidth of the ultra-wideband antenna is 33.88GHz (6.12–40GHz). The ultra-wideband feature makes the proposed patch antenna eligible for ultra-wideband and data collection applications. The proposed antenna has gains ranging from 1.1dBi to 5.25dBi. The proposed antenna possesses good radiation features in both E- and H-planes at all the resonant frequencies. Moreover, the proposed antenna is an excellent candidate for Federal Communications Commission (FCC) licensed frequencies, data collection and upper 5G applications. The proposed antenna exhibits better performance compared to the existing ultra-wideband antennas which are discussed in the literature. The measured and simulated results are in acceptable agreement.

Keywords: CPW; patch antenna; stubs; multiple; ultra-wideband.

1. Introduction

Modern-day wireless devices are designed to achieve high data rates with minimum losses. Rapid progress is seen in the development of wideband and ultra-wideband communication systems after the amendment of rules of ultra-wideband transmission and reception by the Federal Communication Commission(FCC) [1]. Design of compact wideband and ultra-wideband antennas poses a challenging task as they have to satisfy specifications such as wider impedance bandwidth, reasonable gain, and ease of fabrication. The above specifications are achieved by CPW-fed antennas. Coplanar waveguide (CPW) feed provides widebandwith, reasonable gains, and low radiation leakages. Also, a small and slotted partial ground plane reduces system complexity and further enhances bandwidth with the decrease in the cross-polarization levels and gain. CPW is superior than conventional microstrip lines. The active and passive devices can easily be mounted on the CPW surfaces.This feature eases the fabrication. CPW lines not only eases the fabrication but also reduce interference and cross-talk.

Various UWB patch antennas [2–24] with different structures for achieving compactness, ultra-wideband have been discussed in the literature. A 75 x 10mm^2 patch antenna covering the entire frequency range from 2.754GHz – 14.656GHz is proposed in [2]. The antenna in [2] antenna consists of a circular ground plane and a patch radiator with having two slits and a folding arm. The antenna further possesses a peak gain of 6dBi. A 25 x 25mm^2 U-shaped slottedcircular patch antenna for ultra-wideband applications is proposed in [3]. The antenna in [3] has a wide bandwidth from 2.9GHz - 20GHz with a peak gain of 12dBi. A 14 x 18mm^2 low-profile fish-shaped antenna for ultra-wideband applications is proposed in [4]. The resonant frequencies in [4] are produced by using a U-shaped slot and stepped arms on the upper patch, as well as a tilt-folded patch feed. The wide bandwidth of 4.21GHz – 21GHz is achieved in [4]. A peak of 9.5dBi is achieved in [4]. A 16 x 25mm^{2}CPW fed ultra-wideband (UWB) antenna with a rectangular notch for wireless area network (WLAN) band that has controllable notched bandwidth and the center frequency is proposed in [5]. The notch characteristics in [5] are achieved by using Electromagnetic Bandgap (EBG) structures. The antenna in [5] has an operational bandwidth of 3.1GHz-12.5GHz. A peak gain of 4.5dBi is achieved in [5]. A 15 x 14.5mm^2 ultra-wideband patch antenna with two rejected bands is proposed in [6]. The antenna in [6] is mounted on the partial ground plane andhas an operational bandwidth of 3.42GHz-11.7GHz. A peak gain of 6dBi is achieved in [6]. A 28 x 29mm^2 patch antenna with a rectangular slotand having the operational bandwidth of 5.73GHz – 10.8GHz is presented in [7]. The antenna in [7] is mounted on the truncated ground plane. The peak gain is 4.5dBi. A 2.4 x 1.8mm^2 ultra-wideband metamaterial loaded patch antenna for C-band applications is proposed in [8]. An impedance bandwidth of 6GHz is observed in [8]. A 40 x 38mm^2 DoubleElliptical Microstrip Patch Antenna (DEMPA) is proposedin [9]. The antenna in [9] has an impedance bandwidth ranging from 3.52GHz-17.17GHz with a peak gain of 5.2dBi. A 40 x 45mm^2 a co-planar waveguide (CPW) fed circular patch antenna with a ground plane reflector by using fractal elements and rectangular defective ground structure (RDGS) technique is proposed in [10]. The antennain [10] has a UWB range from 1.8GHz-11.6GHz. The antenna in [10] has a peak gain of 6.81dBi. A 15 x 20mm^2 UWB patch antenna for S-, C- and X-band applications is developed in [11]. The antenna in [11] is mounted on the partial and notched ground plane. The antenna has the operational bandwidth from 2.8GHz-

12.39GHz with the peak gain being 3.7dBi. A 26 x 30mm^2 compact microstrip patch antenna is proposed in [12]. The antenna in [12] is composed of a wide slot and a Y-shaped microstrip feed line with a pair of inverted-L-shaped notches. The operational frequency range in [12] is 3.09GHz-10.74GHz. A 20 x 20mm^2 patch antenna with an ultra-wide bandwidth from 2.68GHz-16 GHz, and 18.2GHz–20 GHz is proposed in [13]. The antenna in [13] is an elliptical shape antenna loaded with stubs and chamfered ground. The maximum gain observed in [13] is 6.9dBi. A 27.6 x 32mm^2 patch antenna utilizing metamaterial (MTM) double-sided planar periodic structures is proposed in [14]. The antenna in [14] covers an ultra-wide bandwidth from 3.2GHz-23.9GHz with a peak gain of 6.2dBi. An 18 x 12mm^2 compact circular patch antenna for ultra-wideband applications is proposed in [15]. The antenna is mounted on a partial ground plane and possesses an operational bandwidth from 3.26GHz-14.23GHz. The antenna in [15] possesses a peak gain of 3.55dBi. An 18 x 16mm^{2}fractal patch antenna mounted on a partial ground plane and having an impedance bandwidth from 4.8GHz-11.6GHz is proposed in [16]. A peak gain of 5.7dBi is observed in [16]. A 40 x 20mm^2 planar ultra-wideband (UWB) antenna with triple-notched bands using triple-mode stub loaded resonator (SLR) is presented in [17]. The impedance bandwidth of the antenna in [17] is ranging from 2GHz-11GHz with a peak gain of 5.3dBi. A 20 x 20mm^2 patch antenna with partial ground plane and T-shaped strip employed in the ground plane as well as an inverted Ω-and L-shaped slots incorporated within the radiated element is proposed in [18]. An operational bandwidth of 2.39GHz-18GHz excluding notched bands is observed in [18]. A peak gain of 8.71dBi is obtained. A 10.5 x 14mm^{2}slotted patch antenna mounted on the slotted partial ground plane is proposed in [19]. The reconfigurable patch antenna in [19] possesses an impedance bandwidth ranging from 3.1GHz-10.6GHz. A 30 x 27.2mm^2 metamaterial inspired star slot patch antenna for UWB applications is proposed in [20]. The antenna in [20] mounted on the partial ground plane possesses operating bandwidth from 4GHz-16.2GHz with a peak gain of 8.1dBi. A 20 x 16.51mm^2 fractal UWB patch antenna having the operational bandwidth from 4.6GHz-20.4GHz is proposed in [21]. By using triangular and circular slots in the patch and rectangle slot on the trapezoidal ground plane, the antenna in [21] possesses ultra-wide bandwidth. A 5.4 x 4.7mm^2 S-shaped metamaterial ultra-wideband directive patch antenna is proposed in [22]. An impedance bandwidth ranging from 3.8GHz-4.8GHz is achieved along with the peak gain of 6.2dBi. A 30 x 30mm^2 psi-shape patch antenna having an impedance bandwidth ranging from 3.4GHz-12GHz is proposed in [23]. A peak gain of 4.6dBi is observed in [23]. A 25 x 25mm^2 patch antenna is designed in [24]. The antenna is designed to have a frequency range of 3.3GHz-11.43GHz with a peak gain of 1.32dBi.

In this article, a 9.5 x 9.5 x 1.524mm^{3}asymmetrical CPW fed stub loaded hook-shaped patch antenna is presented. The antenna consists of a λ/4 'L' shaped stub and a λ/4 vertical stub attached outside the hook-shaped patch antenna. The hook antenna resonates at 20.6GHz and the stubs help the antenna to radiate at multiple frequencies with proper impedance matching. The 'L' shaped stub introduces resonance at 6.96GHz and the vertical stub introduces resonance at 11.67GHz. The proposed antenna has been designed, fabricated, and tested. The impedance bandwidth of the proposed antenna is 33.8GHz (6.2 – 40GHz). Miniaturization of a CPW-fed patch is usually achieved using metamaterials due to their capability to bend an EM-wave and thereby increasing increasing the wavelength of the later. At the same time, they increase the losses in the patch antenna and thereby deteriorating the gain at the resonant frequencies. It is a complex method to embed micro sized metamaterials inside a millimetre sized substrate and at the same time fabrication machinery is limited. Hence, the stub lines loaded proposed patch antenna serves an alternative to achieve miniaturization without degradation in the performance parameters. The proposed patch antenna occupies less area than the conventional patch antenna which occupies a total area of 16.56 x 12.83mm^2 for the same dielectric constant and thickness. A minimum miniaturization of 55% is achieved without considering the etched area (by the stub lines) on the proposed patch antenna. The main purpose of designing the proposed patch antenna at 6.96GHz, 11.67GHz and 20.6GHz is to make the device suitable for Federal Communications Commission (FCC) licensed spectrum where the user can own the frequency of his choice. The ultra-wideband feature of the proposed patch antenna makes the antenna an eligible candidate for Federal Communications Commission (FCC) licensed frequencies, data collections and upper 5G- applications (25GHz - 39GHz).

The paper consists of four sections. In Sect. 2 the evolution of the proposed antenna structure along with corresponding return loss plots are presented. The detailed parametric analysis is presented in Sect. 3. All the simulated, measured results and comparison table are presented in Sect. 4.

2. Antenna Design

The structure of the proposed hook-shapedpatch antenna with λ/4 vertical and L-shaped stub-lines and the fabricated patch antenna are shown in Figure 1 and 2 respectively. The antenna is printed on one side of a RT/duroid-6202 with a thickness of 1.524 mm, relative permittivity of 2.94 and loss tangent of 0.0015. Initially, a hook patch is excited by a CPW with the feedlength (l_f) of 2.2mm and width (w_f) of 3.81mm.The right coplanar ground plane has alength(l'') of 5mm andwidth(w'') of 3mm. The gap between the feed and the right coplanar ground plane is 0.12mm. The left coplanar ground plane has a length (l') of 2.2mm and width(w') of 3mm. The gap between the feed and the left coplanar ground plane is 0.12mm. The characteristic impedance of the feed of CPW corresponds to 50Ω. The patch possesses low impedance bandwidth. To further increase the impedance bandwidth, the proposed patch is connected to an L-shaped stub of length equal to λ/4 and a vertical stub of length equal to λ/4. The proposed patch antenna is mounted on the ground plane having the dimensions (W_g x L_g x t) of 4.5 x 9.5 x 0.035mm^3. A slot of dimensions 2.5mm x 2.5mm is etched on the ground to further enhance the operational bandwidth of the proposed antenna. The proposed patch antenna is fed with TM_{20} mode. The bandwidth is enhanced by increasing the effective coupling between asymmetric coplanar ground planes and slotted partial ground plane. The effect of the length of the ground plane on the impedance bandwidth of the proposed patch antenna is studied in the further sections.

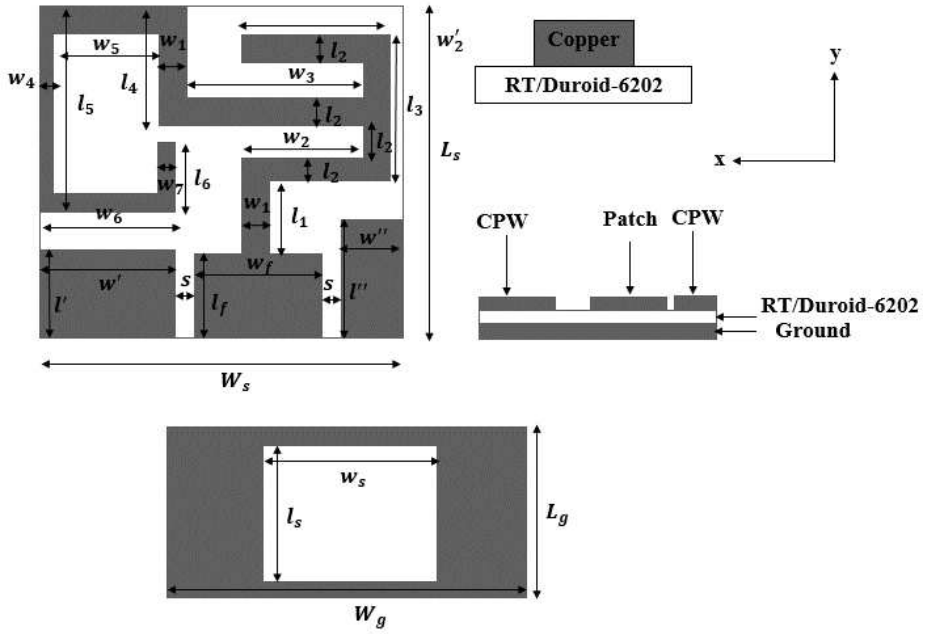

Fig.1.The geometry of the proposed patch antenna

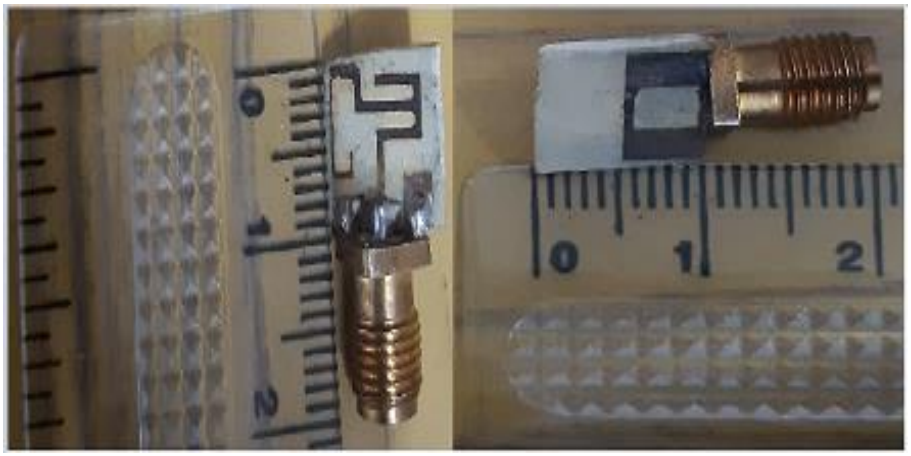

Fig.2 Top and bottom views of the fabricated antenna

Table.1 shows the detailed dimensions of the proposed patch antenna.

TABLE 1 Detailed dimensions of the proposed antenna

Parameter	Value(mm)	Parameter	Value(mm)
L_s	9.5	w_5	1
W_s	9.5	w_6	1
l_1	3	w_7	5.5
l_2	1.5	l_f	2
l_3	5	w_f	3.5
l_4	4	l'	2.5
l_5	6.8	w'	2.75
l_6	2.5	l''	5.75
w_1	1	w''	2.75
w_2	3	L_g	4.5
w_2'	3	W_g	9.5
w_3	4	l_s	2.5
w_4	1	w_s	2.5
		s	0.12

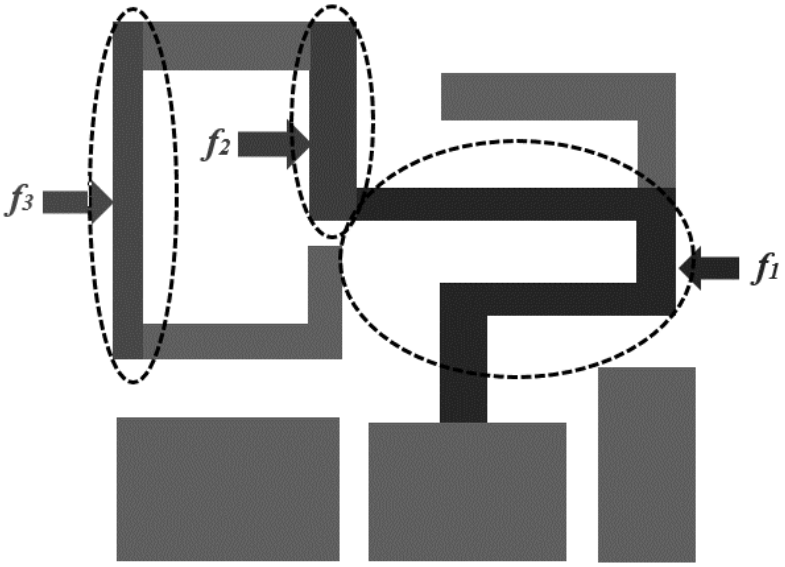

Fig.3. Radiation branches of the proposed patch antenna

Figure.3 shows the radiating branches of the proposed patch antenna.

The resonant frequency of the hook antenna (f_1) [25] is given by:

$$f_1 = \frac{c}{2(l_1+3l_2)\sqrt{\varepsilon_{eff}}} \tag{1}$$

Where, 'c' is the velocity of the light, $'l_1 + 3l_2'$ is the length of the hook portions and $'\varepsilon_{eff}'$ is the effective dielectric constant given by:

$$\varepsilon_{eff} = \frac{\varepsilon_r+1}{2} + \left(\frac{\varepsilon_r-1}{2}\right)\left[\frac{1}{\sqrt{1+\frac{12h}{w}}}\right] \tag{2}$$

Where, $'\varepsilon_r'$ is the relative dielectric constant, 'h' is the thickness of the dielectric, and 'w' is the width of the feed line. The length of the stubs is taken to be quarter wavelength as they provide capacitance and inductance around the resonant frequency. capacitive and inductive impedance around the resonance frequency of the patch and realizes dual-frequency response. Mathematically, the frequency (f_1) at hook antenna resonates is obtained as 19.92GHz and a dip is observed at 20.6GHz in the simulated result of the return loss of the proposed patch antenna. The difference in the mathematical and simulated results is due to the non-consideration of the dielectric and conductor losses.

Similarly, the resonant frequency (f_2) of the vertical stub line is given by:

$$f_2 = \frac{c}{4(l_4)\sqrt{\varepsilon_{eff}}} \tag{3}$$

Mathematically, the frequency at which vertical stub line resonates is obtained as 11.9GHz and a dip is observed at 11.67GHz in the simulated result of the return loss of the proposed patch antenna. The difference in the mathematical and simulated results is due to the non-consideration of the dielectric and conductor losses.

The frequency of the L-shaped strip line is given by:

$$f_3 = \frac{c}{4(l_5)\sqrt{\varepsilon_{eff}}} \tag{4}$$

Mathematically, the frequency at which the L-shaped stub line resonates is obtained as 7.1GHz and a dip is observed at 6.96GHz in the simulated result of the return loss of the proposed patch antenna. The difference in the mathematical and simulated results is due to the non-consideration of the dielectric and conductor losses.

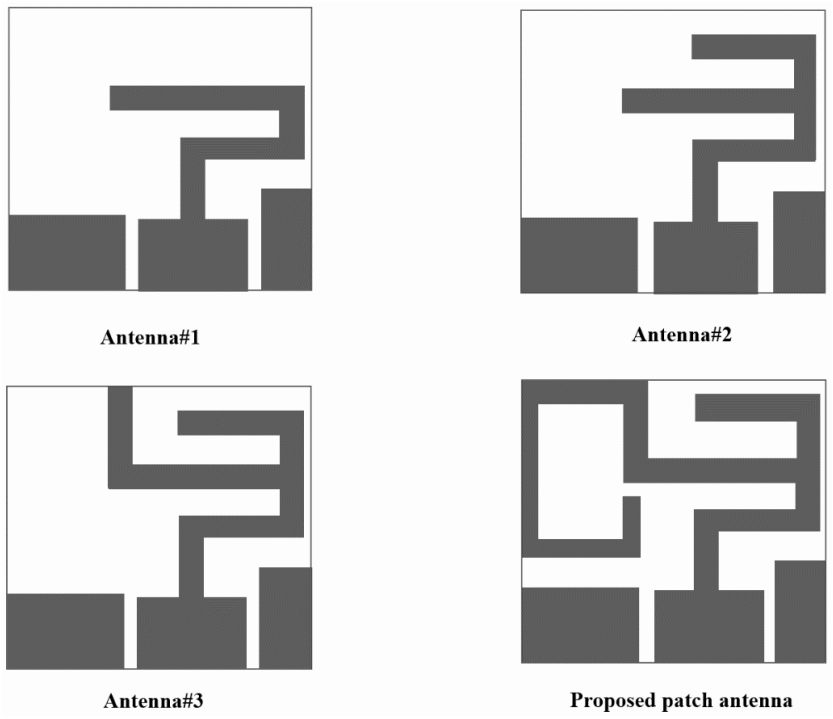

(a)

Figure.4(a) shows the different stages in the evolution of the proposed antenna and the corresponding simulated return losses are shown in Fig. 4(b). The antenna presented in stage 1 of Fig. 4(a) is a basic hook-shaped patch antenna resonating at 20.6GHz as represented by the black curve in figure.4(b). An impedance bandwidth (S11<-10dB) of 5GHzis observed in the frequency ranges of (17.1GHz - 22.1GHz).

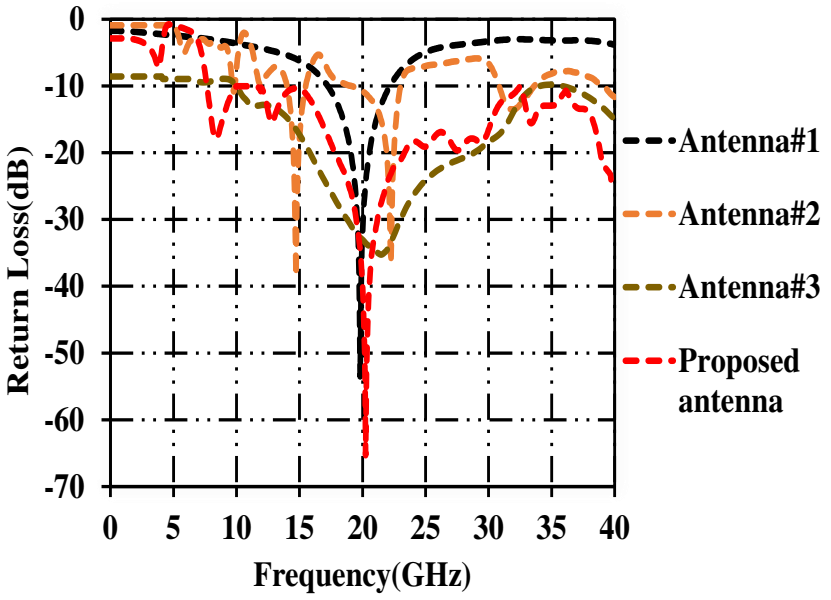

(b)

When a branch is connected on the top of antenna#1, a double hook antenna is evolved as shown in stage#2. Antenna#2 resonates at 11.9GHz,14.5GHz, 22.5GHz, and 32.68GHz with the impedance bandwidths of 123MHz (11.85GHz – 11.95GHz), 1.8GHz (13.6GHz – 15.4GHz), 3.3GHz (19.7GHz – 23GHz), and 3.8GHz (30.71GHz – 34.51GHz) respectively (as represented by the orange curve in figure.4(b)). By adding a vertical stub of quarter-wavelength to antenna#2, antenna#3 is evolved. Antenna#3 resonates at 11.96GHz and 22.12GHz (as represented by the brown curve in figure.4(b)). When the L-shaped stub of quarter wavelength is added to antenna#3, the proposed patch antenna is evolved. The proposed patch antenna resonates at 6.96GHz, 11.67GHz, and 20.6GHz (as represented by the red curve in figure.4(b)). Figure.4(c) shows the variation of the return loss of the proposed antenna with the variation in the length of the ground plane. When the proposed antenna is mounted on the full ground plane, it resonates at 13.1GHz, 14.5GHz, 16.8GHz, 20GHz, 25GHz, and 33.8GHz.

The impedance bandwidth at these resonant frequencies are 312MHz (12.94GHz – 13.25GHz), 306MHz (14.35GHz – 14.65GHz), 518MHz (16.65GHz – 17.16GHz), 258MHz (19.95 - 20.25GHz), 830MHz (24.6GHz – 25.43GHz) and 4.5GHz (31.3GHz-35.8GHz). When the proposed patch antenna is mounted on the partial ground plane with the dimensions of 4.5 x 9.5mm^2, the antenna resonates at 6.86GHz, 11.56GHz, 17.6GHz, 23.8GHz, 32.96GHz. The structure possesses impedance bandwidths of 212MHz (6.71GHz – 6.92GHz), 114Hz (11.51GHz-11.62GHz), and 24.6GHz (15.4GHz – 40GHz). The proposed patch antenna resonates at 6.96GHz, 11.67GHz, and 20.6GHz with an impedance bandwidth of 33.4GHz (6.2GHz – 40GHz).

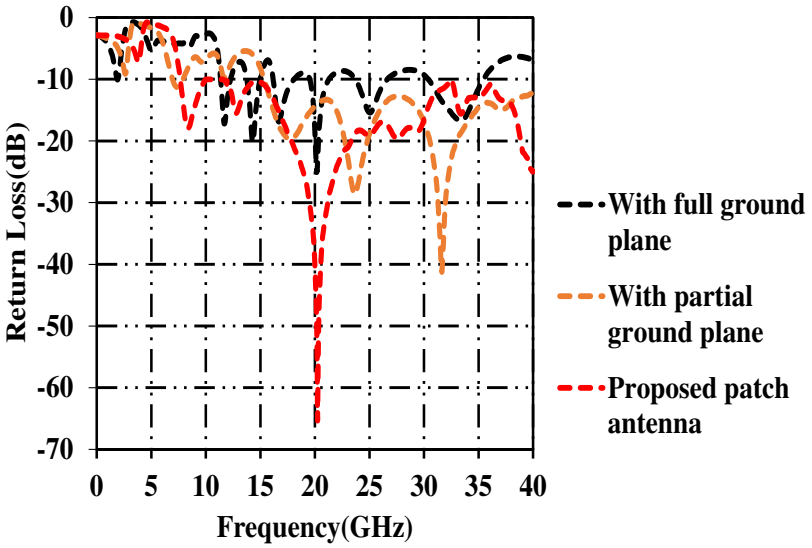

(c)

Fig.4.a. Evolution stages of the proposed antenna. b. Simulated return losses of the evolution stages. c. Variation of return losses of the proposed patch antenna with the length of the ground plane.

3. Parametric analysis

The lengths of the stubs (l_4&l_5) and width of the double hook (w_2') of the proposed antenna play an important role in achieving ultra-wideband characteristics. Figure 5(a),(b), and (c) shows the variation of return loss characteristics of the above parameters keeping the total length of the hook section (l_1+$3l_2$) constant. The length of the vertical stub line (l_4) is varied from 2.5 to 4.5mm. When the length of the vertical stub line(l_4) is 2.5 mm, it resonates at 10.56GHz with a return loss of -20.76dB. When the length of the vertical stub line(l_4) is 3.5mm, it resonates at 11.23GHz with the return loss of -21.1dB at the said frequency. When the length of the vertical stub line (l_4) is 4.5mm, the proposed antenna resonates at 12.52GHz with a return loss of -20.62dB. The variation in the length of the vertical stub line affects the second resonant frequency and variation in the length of the vertical stub line beyond 4.5mm produces unacceptable results. Hence, the length of the vertical stub line is optimized to 4mm.

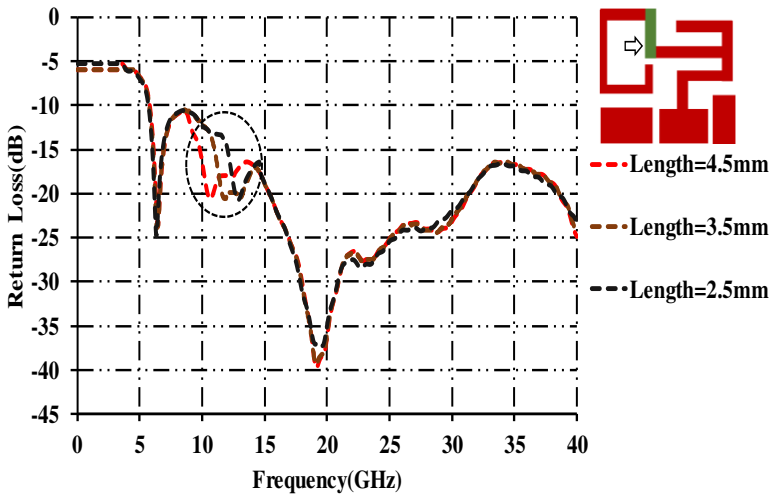

(a)

Figure.5(b) shows the variation of return loss with the length of the L-shaped stub (l_5). When the length of the L-shaped stub (l_5) is 6.5mm, the proposed antenna resonates at 8.15GHz with a return loss of -17.58dB. When the length of the L-shaped stub(l_5) is 7mm, it resonates at 7.32GHz with a return loss of -22.62dB. When the length of the left stub (l_5)is 7.25mm, the proposed patch resonates at 6.21GHz with a return loss of -24.71dB. From the above analysis, it can be confirmed that l_5 is 6.75 mm produces the desired results. It is also found that l_5 shifts the resonant frequency of the hook antenna (22.3GHz, 19.9GHz, and 19.72GHz) due to the strong coupling between the hook antenna and l_5.

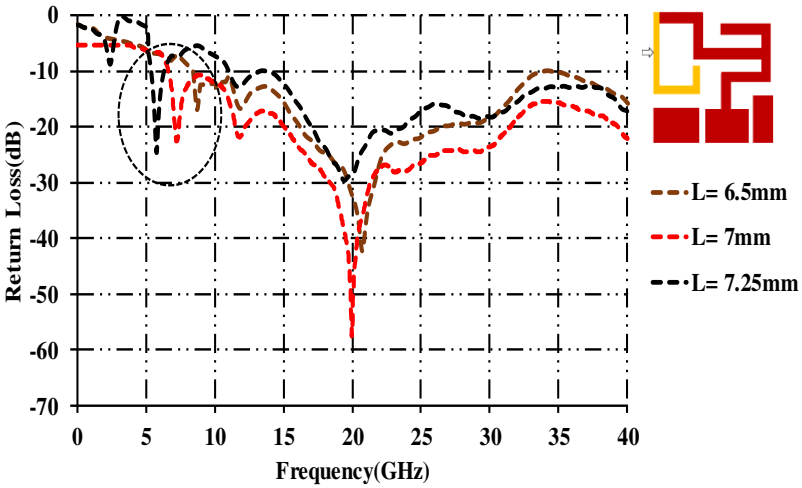

(b)

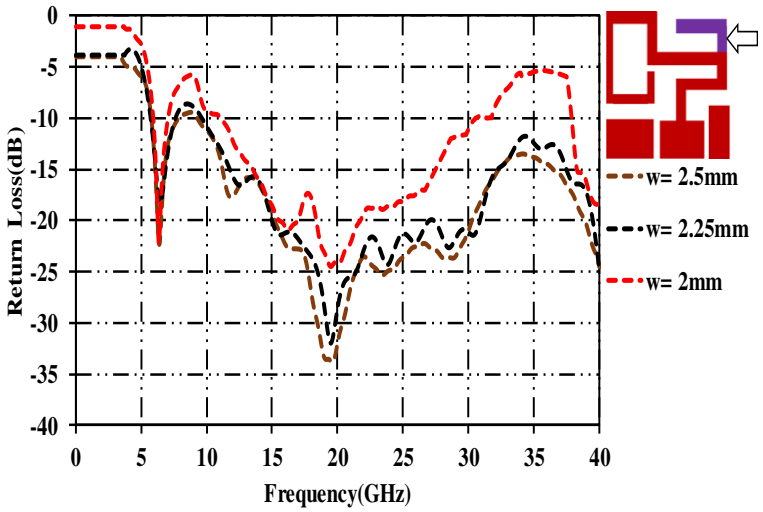

(c)

Fig.5(a). Effect of length of the vertical stub section on the return loss of the proposed patch antenna. (b). Effect of length of the L-shaped stub section on the return loss of the proposed patch antenna. (c). Effect of the width of the upper hook portion on the return loss of the proposed patch antenna

Figure 5(c) shows the return loss characteristics of the proposed antenna for various w_2'values from 2 to 2.5mm. The width of the upper hook (w_2') affects the operational bandwidth of the proposed antenna. When the width of the upper hook (w_2') is 2mm, the proposed antenna possesses a bandwidth of 22.5GHz (10.3GHz- 32.8GHz). When the width of the upper hook (w_2') is 2.25mm, the proposed antenna possesses a bandwidth of 30.7GHz (9.3GHz- 40GHz). When the width of the upper hook (w_2') is 2.5mm, the proposed antenna possesses a bandwidth of 31GHz (9GHz- 40GHz). From the above analysis, it can be confirmed that is $w_2'$is 3mm produces the desired results. A slight shift in the resonant frequency of the hook antenna is due to the couple between $w_2'$and the hook portion.

4. Results and Discussions

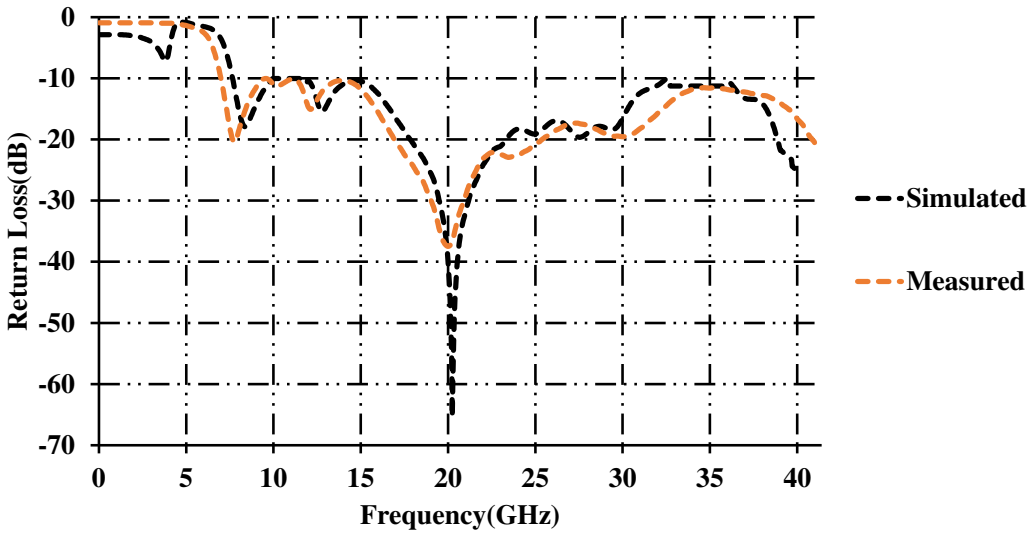

Fig.6. Simulated and measured results of the return loss of the proposed patch antenna

The proposed antenna is designed using the CST Microwave Studio utilizing the Finite Integration Technique (FIT) and fabricated with optimized dimensions. Figure. 6 shows the measured and simulated reflection coefficients of the proposed patch antenna. The measurements have been performed using Rohde & Schwarz vector network analyser. Simulated and measured results are in acceptable agreement. The difference between the measured and simulated results is because of the discontinuities in the substrate, SMA connector quality, and fabrication tolerances. The measured resonant frequencies of the proposed patch antenna are 6.45GHz, 11.12GHz, and 20GHz. Different mesh sizes and slight inaccuracies in the same led to the slight difference in the measured and simulated results. The designed antenna in CST-MWS is fed by lossless wave port with the characteristic impedance of 50ohms in the entire frequency range of 6.2GHz – 40GHz. Current distribution gives a better idea about the resonance behaviour of the proposed patch antenna. Figure.7 shows the surface current distribution of the proposed patch antenna at 6.96GHz, 11.67GHz, and 20.6GHz. The portions on the proposed patch antenna where the current distribution is maximum are observed. From this figure, it is observed that the surface current is maximum along the L-shaped at 6.96GHz and a part of the current is concentrated on the hook antenna and ground plane. At 11.67GHz, the surface current concentrates along with the vertical stub, and a part of the current is concentrated on the hook portion, L-shaped stub, and the ground plane. At 20.6GHz, the current in the vertical stub is distributed towards the hook portion.

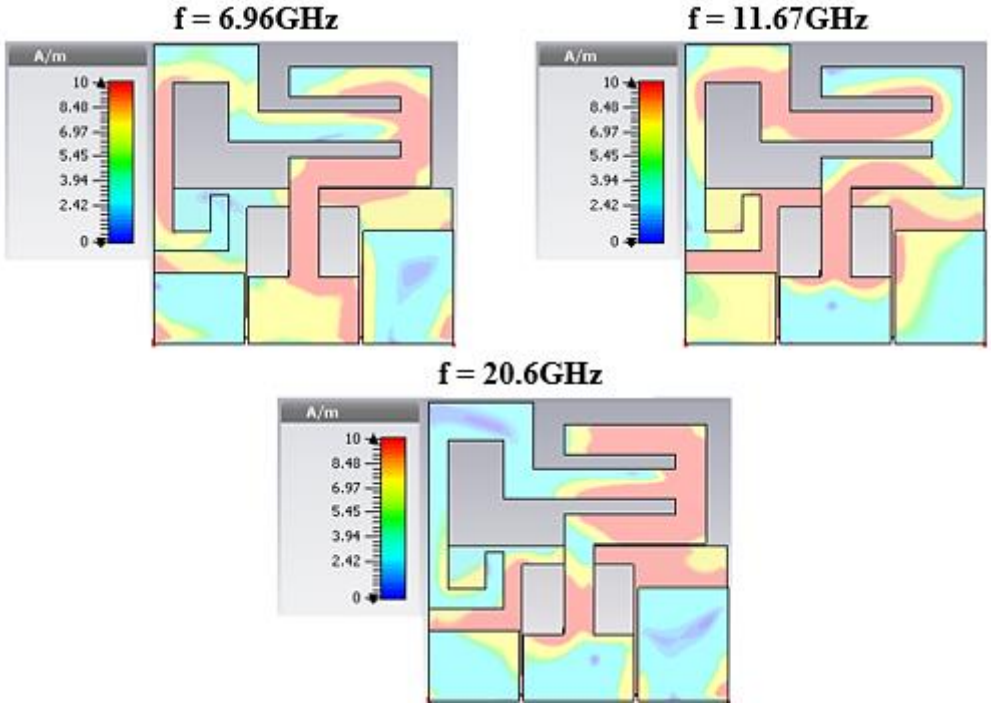

Fig.7. Surface current distributions of the proposed patch antenna at 6.96GHz, 11.67GHz and 20.6GHz

Figure. 8 shows the simulated and measured gains of the proposed patch antenna. Simulated peak gains are varying from 1.21dBi to 5.1dBi in the frequency range of 6.2GHz – 40GHz.

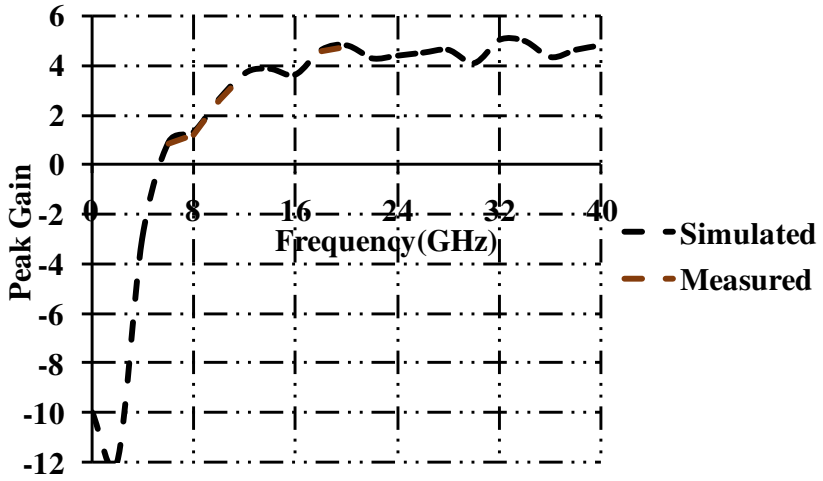

Fig.8. Measured and simulated peak gains of the proposed patch antenna.

The bandwidth of the proposed patch antenna depends on its quality factor (Q). Antenna's radiation Q-factor is the ratio of total Q-factor and the antenna's efficiency (η_{rad}). Thus, decreasing the antenna's Q-factor decreases efficiency and the gain (increasing losses widen the bandwidth). Therefore, the proper trade-off should be maintained between size, bandwidth, and gain in small antennas.

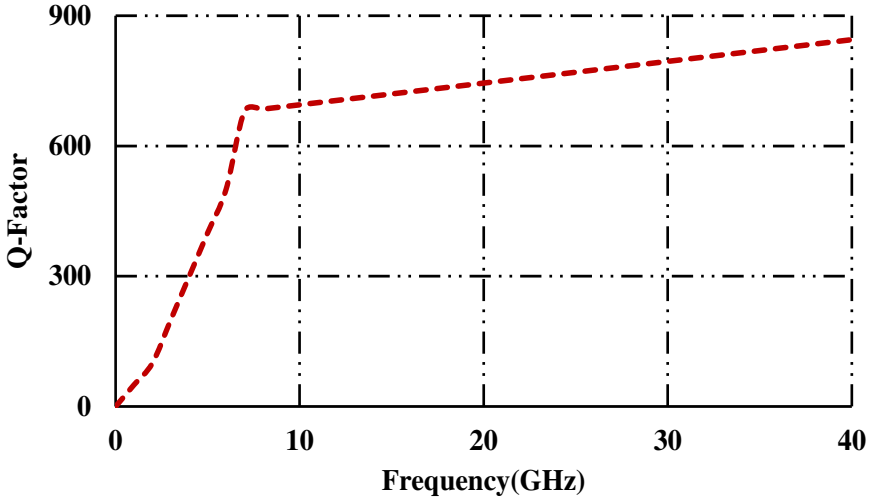

Fig.9. Q-factor of the proposed patch antenna

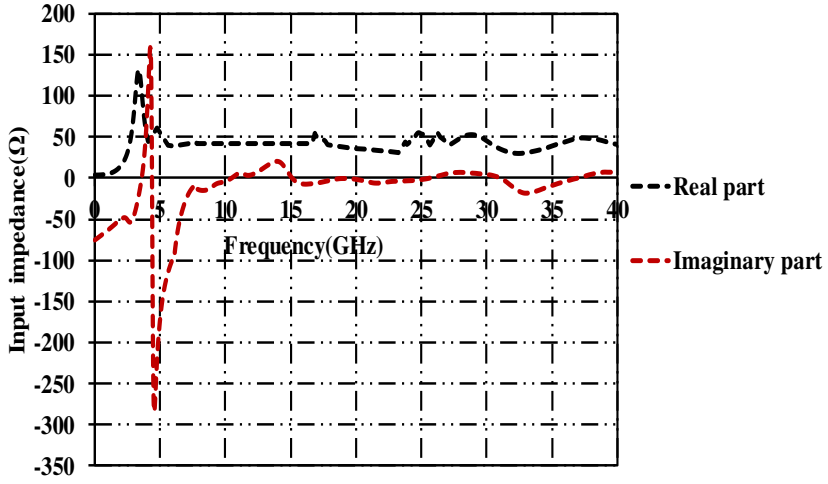

Fig.10. Real and Imaginary parts of the input impedance of the proposed patch antenna

Figure.10 shows the variation of the input impedance with frequency. It can be seen that the simulated values of the real part of the input impedance (shown in the dotted black curve) are around 50Ω in the frequency range of 6.2GHz - 40GHz. The simulated values of the imaginary part of the input impedance (shown in the dotted brown curve) are nearly crossing zero in the frequency range of 6.2GHz – 40GHz. This means that the impedance matching occurs at the desired frequency range. Figure.11 shows the group delay response of the proposed patch antennas in the face to face and side by side positions. Group delay is simulated in CST microwave studio by putting two proposed patch antennas in the face to face and side by side positions. Group delay is an important parameter in designing UWB patch antenna. Proposed antenna is almost stable with the group-delay less than 1ns in the frequency range of 6.2GHz – 40GHz. For distortionless transmission, group delay should be less than 1ns. The group delay (GD) characteristics simply tells the time taken by a signal to travel from transmitter to receiver and it should be proportional to the frequency.

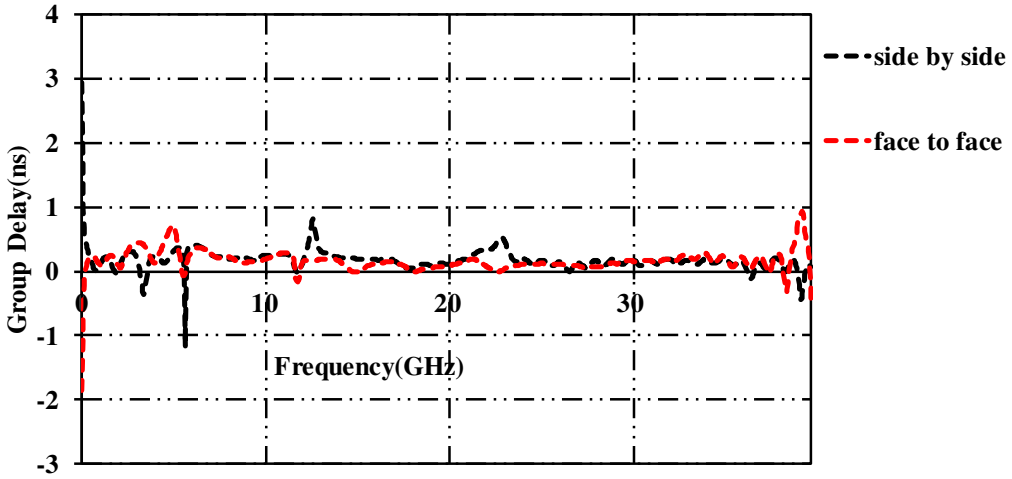

Fig.11.Group delay for face to face and side by side positions

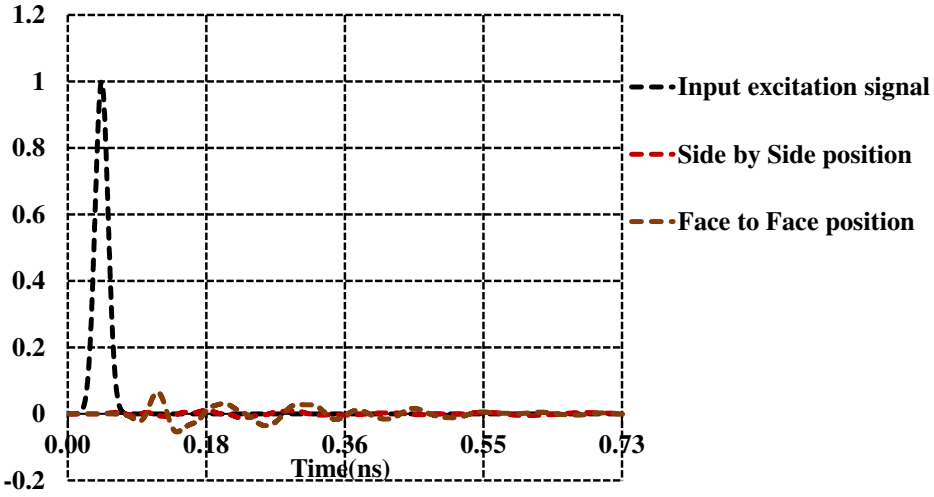

Figure.12. Response of the antennas in side by side and face to face positions.

Figure.12 shows the time domain analysis of antennas in side by side and face to face positions. The analysis is performed by exiting antennas side by side and face to face positions and the corresponding responses are observed. The radiation patterns of the proposed patch antenna are simulated in E-plane and H-plane using CST Microwave Studio and measured in an anechoic chamber utilizing an antenna measurement system as shown in figure.13. The reference antenna used for testing is a double-ridged horn. Figure.14 shows the radiation pattern measurement setup of the proposed patch antenna. The measured radiation patterns of the proposed antenna at 6.45GHz, 11.12GHz, and 20GHz are shown in Figure.14. Both E-plane and H-plane have unidirectional radiation patterns at 6.45GHz, 11.12GHz, and 20GHz. A slight distortion in the radiation pattern at 20GHz is observed due to the common mode currents flowing through the feed line at higher frequencies. The Cross-polarization levels at the desired resonant frequencies are observed to be below -13dB in the main bean direction. Simulated and measured results are found to be in close agreement with a little difference due to measurement and alignment, human error.

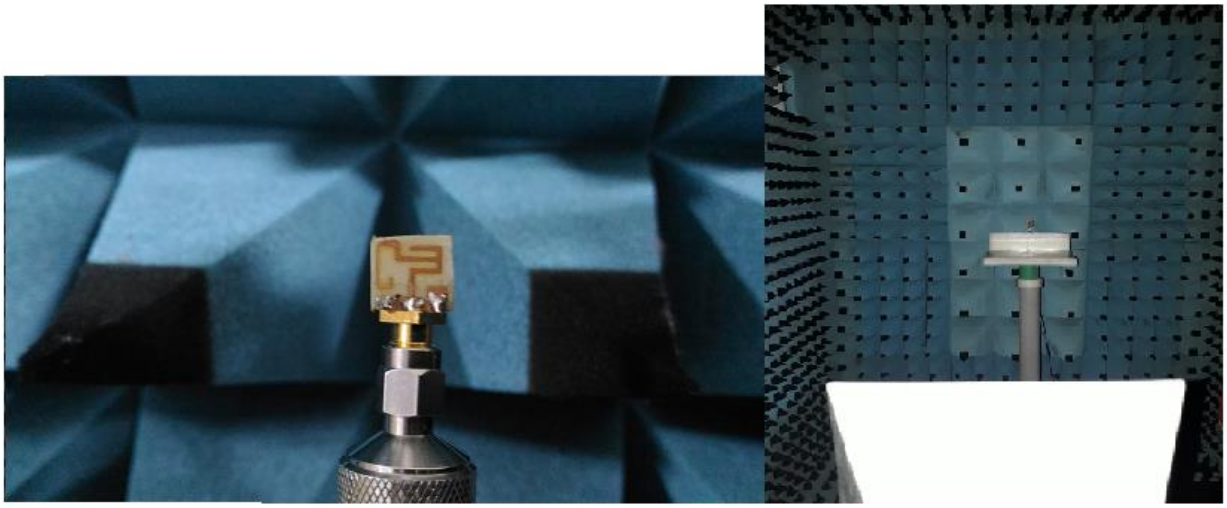

Fig.13. Radiation pattern measurement setup.

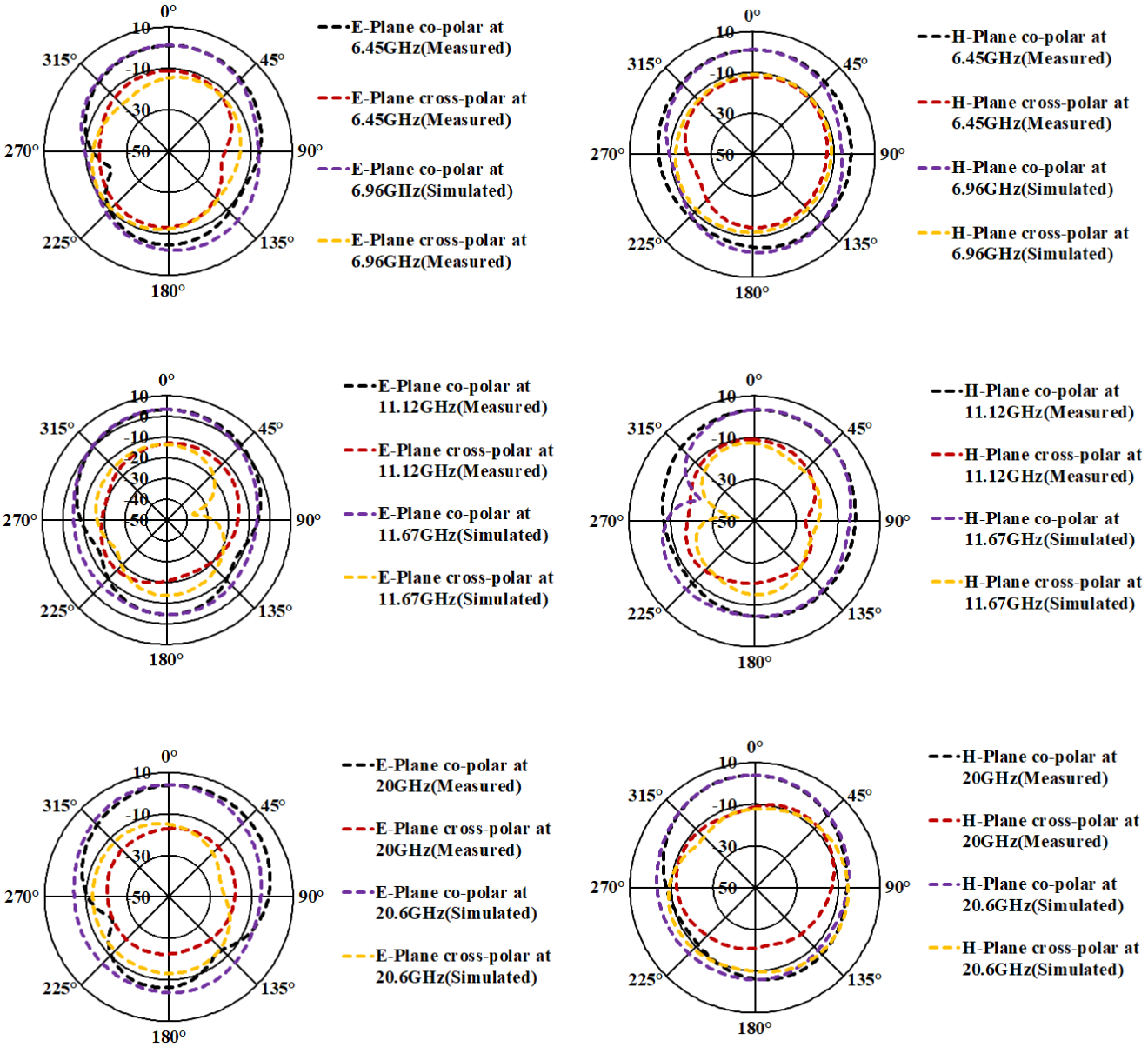

Fig. 14. Measured and simulated radiation patterns of the proposed patch antenna

Table.2 shows the comparison between the existing antennas and the proposed patch antenna. The proposed patch antenna exhibits superior performance over the existing antennas in terms of impedance bandwidth and gain.

TABLE 2 Comparison between the existing antennas and the proposed antenna

Reference	Area (mm^2)	Frequency Range (GHz)	Bandwidth (GHz)	Peak Gain (dBi)
[2]	750	2.754 – 14.656	11.9	6
[3]	625	2.9 - 20	17.1	12
[4]	252	4.28 - 21	16.72	9.5
[5]	400	3.1 – 12.5	9.4	4.5
[6]	217.5	3.42 – 11.7	8.28	6
[7]	812	5.73 -10.8	5.07	4.5
[8]	4.32	2.1 – 8.1	6	Not Mentioned
[9]	115.5	3.52 – 17.17	14.35	5.2
[10]	1800	1.8 – 11.6	9.8	6.8
[11]	300	2.82 – 12.39	9.57	3.7
[12]	780	3.09 – 10.74	7.65	7
[13]	400	2.68 -20	17.32	5.48
[14]	883.2	3.2 – 23.9	20.7	6.2
[15]	196	3.26 – 14.23	10.97	3.55
[16]	288	4.8 – 11.6	6.8	3.63
[17]	800	2 - 11	9	5.3
[18]	400	2.39 -18	15.61	8.7
[19]	147	3.1 -10.6	7.5	Not Mentioned
[20]	847.8	4 -16	12	8.2
[21]	330.2	4.6 -20.4	15.8	Not Mentioned
[22]	25.38	3.8 -4.8	0.9	6.2
[23]	360	3.4 - 12	8.4	4.6
[24]	625	3.3 – 11.43	8.1	1.32
This work	**90.25**	**6.12 - 40**	**33.88**	**5.25**

5. Conclusion

A very compact stubs loaded hook-shaped patch antenna is proposed. The proposed antenna resonates at 6.96GHz, 11.67GHz, and 20.6GHz. Simulated gains of 1.45dBi, 3.72dBi, and 4.82dBi are obtained at 6.96GHz,11.67GHz, and 20.6GHz respectively. Measured gains of 1.3dBi, 3.62dBi, and 4.78dBi are observed at 6.45GHz, 11.12GHz, and 20GHz respectively. The proposed antennas are fabricated on RT/Duroid-6202 substrate and their performances measured. The measured and simulated results of the fabricated antenna show unidirectional in all the planes. The ultra-wide bandwidth and reasonable gain make the proposed antenna suitable for ultra-wideband communications and data collection applications.

Declarations

The research in this manuscript has no funding associated with it. We declare that there is no conflict of interest. The figures of the manuscript are present in https://doi.org/10.6084/m9.figshare.16616269. There is no computer program or code associated with the manuscript. There is no extra material contributed by a researcher/ author included in the manuscript without his/ her consent. The research in the manuscript is solely carried out by us.

References

[1] Archana Agarwal, Manish Kumar, Priyanka Jain, and Shagun Maheshwari, *Ultra-Wideband Tapered Microstrip Antenna with Modified Ground plane*, IEEE-International Conference on Signal processing and Communication (ICSC), 2013, pp.33-35.

[2] Han-UI Bong, Niamat Hussain, Seung-Yeop Rhee, Sang-Keun Gil, and Nam Kim, *Design of an UWB antenna with two slits for 5G/WLANnotched bands*, Microwave and Optical Technology Letters, 61(2019), no.5, 1-6. DOI: 10.1002/mop.31670.

[3] Jiwan Ghimire, and Dong-You Choi, Design of a Compact *Ultrawideband U-Shaped Slot Etched on a Circular Patch Antenna with Notch Band Characteristics for Ultrawideband Applications*, International Journal of Antennas and Propagation, (2019),1-10, https://doi.org/10.1155/2019/8090936.

[4] Bingjie Chen, Xuesong Yang, and Dacheng Hu, *Fish-shaped ultra-wideband patch antenna with tilt-folded patch feed*, IET- Microwaves, Antennas & Propagation,13(2019), no.3,1312-1317.DOI: 10.1049/iet-map.2018.5556.

[5] Abbas.A, Hussain.N, Jeong MJ, Park J, Shin KS, Kim T, and Kim N, *A Rectangular Notch-Band UWB Antenna with Controllable Notched Bandwidth and Centre Frequency*, Sensors,20(2020), no.3,1-11, https://doi.org/10.3390/s20030777.

[6] Noor.M.Awad, and Mohamed.K.Abdelazeez, *Multislot microstrip antenna for ultra-wide band applications*, Journal of King Saud University - Engineering Sciences, 30(2018), no.1,38-45,https://doi.org/10.1016/j.jksues.2015.12.003.

[7] Neeba George, and B.Lethakumary, *A compact microstrip antenna for UWB applications*, Microwave and Optical Technology Letters, 57(2015), no.3,621-624, https://doi.org/10.1002/mop.28910.

[8] ParulDawar, N.S.Raghava, and Asok De, *UWB Metamaterial-Loaded Antenna for C-Band Applications*, International Journal of Antennas and Propagation, (2019), 1-13, https://doi.org/10.1155/2019/6087039.

[9] Jerry.V.Jose, Aruldas.S.Rekh, and Manayanickal J. Jose, *Double-Elliptical Shaped Miniaturized Microstrip Patch Antenna for Ultra-Wide Band Applications*, Progress In Electromagnetics Research C, 97(2019),95-107, DOI: 10.2528/PIERC19092002.

[10] Anurima Majumdar, Sisir.K.Das, and Annapurna Das, *Ultra Wide Band CPW Fed Patch Antenna with Fractal Elements and DGS for Wireless Applications*, Progress in Electromagnetics Research C, 94(2019), 131-144, DOI: 10.2528/PIERC19043001.

[11] Tapesh Bhandari, and Sandeep Baudha, *An UWB Compact Microstrip Antenna for S Band, C Band and X Band Applications*, 12th European Conference on Antennas and Propagation (EuCAP 2018), 2018, pp.1-5.

[12] X.Zhang, Y.-Y.Xia, J.Chen, and W.-T.Li, *Compact microstrip-fed antenna for utra-wideband applications*, Progress In Electromagnetics Research Letters, 6(2009), 11-16,DOI:10.2528/PIERL08111404.

[13] Tale Saeidi, Idris Ismail, Wong Peng Wen, and Adam.R.H.Alhawari, *Ultra-wideband elliptical patch antenna for microwave imaging of wood*, International Journal of Microwave and Wireless Technologies, 11(2019),no.9,948-966,DOI:https://doi.org/10.1017/S1759078719000588.

[14] Ehab K. I. Hamad, and GehadNady, *Bandwidth Extension of Ultra-wideband Microstrip Antenna Using Metamaterial Double-side Planar Periodic Geometry*, RADIOENGINEERING, 28(2019), no.1, 25-32, DOI:10.13164/re.2019.0025.

[15] SoufianLakrit, Hassan Ammor, JaouadTerhzaz, Mohamed Chaïbi, and À. MediavillaSànchez, *A New Compact Small Circular Patch Antenna for UWB Communication*, Journal Communications Software and Systems, 11(2015), no.4,210-214, DOI: http://dx.doi.org/10.24138/jcomss.v11i4.100.

[16] Shereen AbdalkadumShandal, Yaqeen Sabah Mezaal, Mohammed Aboud Kadim, and Mahmood Ferhan Mosleh, *New Compact Wideband Microstrip Antenna for Wireless Applications*, ADVANCED ELECTROMAGNETICS, 7(2018), no.4,85-92, DOI: https://doi.org/10.7716/aem.v7i4.860.

[17] Shicheng Wang, *A New Compact Printed Triple Band-Notched UWB Antenna*, Progress In Electromagnetics Research Letters, 58(2016), 67-72, DOI: 10.2528/PIERL15111302.

[18] E.K.I.Hamad, and N.Mahmoud, *Compact Tri-Band Notched Characteristics UWB Antenna for WiMAX, WLAN and X-Band Applications,* ADVANCED ELECTROMAGNETICS, 6(2017), no.2, 53-58, DOI: https://doi.org/10.7716/aem.v6i2.465.

[19] G.Aishvarya Devi, J.Aarthi, P.Bhargav, Aarthi.J, Pandeeswari.R, Ananda Reddy.M, and Samson Daniel.R, *UWB Frequency Reconfigurable Patch Antenna for Cognitive Radio Applications*, IEEE International Conference on Antenna Innovations & Modern Technologies for Ground, Aircraft and Satellite Applications (IAIM), 2017, pp.1-4.

[20] Hassan Umair, M.Jasim Uddin, M.Habib Ullah, Tarik Bin Abdul Latef, Wan nor Liza Binti Wan Mahadi, and Mohamadariff Bin Othman, "A unique metamaterial inspired star-slot UWB antenna with soft surface ground", Electromagnetics, 40(2020), no.2,152-163, https://doi.org/10.1080/02726343.2019.1710686.

[21] Bo Hu, Feihong Tang, Peng Chen, and Xutao Yu, *Fractal UWB patch antenna with omnidirectional pattern*, Sixth Asia-Pacific Conference on Antennas and Propagation (APCAP), 2017, pp.1-3.

[22] ParulDawar, Asok De, and N.S.Raghava, *S-Shaped Metamaterial Ultra-Wideband Directive Patch Antenna*, Radioelectronics and Communications Systems,61(2018), no.9,394-405,https://doi.org/10.3103/S0735272718090029.

[23] AnithaPeram, A.Subbi Rami Reddy, and M.N.Giri Prasad, *Miniaturized Single Layer Ultra Wide Band (UWB) Patch Antenna Using a Partial Ground Plane*, Wireless Personal Communications,106(2019), no.1, 1-17, DOI: 10.1007/s11277-019-06213-4.

[24] A.P.Padmavathy, and M.Ganesh Madhan, *An improved UWB Patch Antenna Design using Multiple Notches and Finite Ground Plane*, Journal of Microwaves, Optoelectronics and Electromagnetic Applications, 14(2015)no.1, 73-82, https://doi.org/10.1590/2179-10742015v14i1428.

[25] K.Viswanadha, and N.S.Raghava, *Design and Analysis of a Compact Dual-Band Serpentine-Shaped Patch Antenna with Folded Stub Lines for C- and X-Band Applications*, Journal of Communications Technology and Electronics, 65(2020), no.10, 1147-1160. https://doi.org/10.1134/S106422692010006X

Wireless Personal Communications
https://doi.org/10.1007/s11277-022-09867-9

Design and Analysis of Circular Microstrip Patch Antenna for White Space TV Band Application

Richa Sharma[1] · **N. S. Raghava**[1] · **Asok De**[1]

Accepted: 29 May 2022
© The Author(s), under exclusive licence to Springer Science+Business Media, LLC, part of Springer Nature 2022

Abstract
In the presented paper a novel application of microstrip circular patch antenna with three rings on patch is proposed. The novel application of this antenna is to use white space TV (470MHz to 806MHz) band which is totally free as TV communication has been moved from TV band to C-band and Ku-band (satellite TV). The proposed antenna can work in a complete TV band (420MHz to 810MHz). The bandwidth of a circular microstrip patch antenna with the infinite ground plane is 11MHz. To enhance the bandwidth of the antenna infinite ground plane is converted into a finite ground plane. To further enhance the bandwidth three circular rings are etched from the patch. The proposed antenna can use white space TV band frequency with a gain of 1.3dBi and a radiation efficiency of 92 percent.

Keywords Circular microstrip patch antenna (CMPA) · TV band · Satellite TV · Ultra-high frequency (UHF) band

1 Introduction

White Space TV band is the unused TV band frequencies between the used frequencies of very-high and ultra-high frequency spectrum. These unused frequencies are typically referred to as the guard band.In the last years, these guard bands were placed between active TV channels to protect broadcasting interference. The Indian national satellite (INSAT) plays a major role in the development of digital television services in the country. Now satellite television covers 100 percent population and area of the country. Totally 33 satellite television channels that are operating in C-band are digitized.

N. S. Raghava and Asok De these authors contributed equally to this work.

✉ Richa Sharma
richa.sharma70@gmail.com

N. S. Raghava
nsraghava@dtu.ac.in

Asok De
asok.de@gmail.com

[1] ECE, Delhi Technological University, Main Bawana Road, Shahbad Daulatpur, Delhi 110042, India

Published online: 20 June 2022

Direct-to-home (DTH) broadcasting facilities are fascinating others with the launching of premium services like high-definition television services, live streaming, etc. direct to subscriber's premises. Dynamic Ku-band transponders are used to assist DTH television facilities with dish antenna of very small size, all over India. UHF band was reserve for TV services, now television services are shifted from ultra-high frequency (UHF) band to C-band and Ku-band. This band can be used for different applications as it is going to be free. In analog TV communication, 6-8 MHz frequency range is used by each active channel for TV transmission. But, these bands of frequencies that hold different slots in the UHF band ranging from 470-806 MHz are highly under-utilization. In the past years, there have been diverse attempts from industries, academia, and government bodies for accomplishment for finding out the potentials of the white space TV frequencies for several applications including the medical field, internet access, Super Wi-Fi, white space TV spatial-temporal and variations, fragmentation, antenna design, and security [1]. Lower frequencies unused band between TV channels from 470-806 MHz can be used for different applications as these frequencies allow signals to penetrate the objects like walls, trees, etc. better as compared to higher frequencies.

In the UHF band, antenna size will be huge as the size of the antenna is inversely correlated with the frequency of operation. [2]. To reduce the size of the antenna, which has been using for TV signals is to use a microstrip patch antenna. The size of the microstrip patch antenna will be small as compared to the Yagi-Uda antenna, with the disadvantage of a small gain and narrow bandwidth. In literature, various techniques have been defined to increase bandwidth and enhance the gain of the microstrip patch antenna. The bandwidth of the antenna can be expanded by using different techniques in the patch [3–5]. In literature various slots i.e. S-shape slot [6], L-shape slot [7], double U and H slots [8] T-shaped cut, bow-tie slot [9], diagonal edges, rectangular slot [10], single ring, double ring, defected ground structure, a parasitic element with impedance matching network [11], loading of meander line [12], etc. are presented for expanding bandwidth. It detects that the resonant frequency reduces for those designs and finally, the bandwidth acquired is higher than the earlier design due to a change in ground structure. It observed that with the augmentation of new slots on the radiating patch, the bandwidth expands, but radiation efficiency decreases with the augmentation of new slots. So, there is a trade-off lies between radiation efficiency and slots number. The gain of the slot antenna is also insignificant due to lesser radiation efficiency [13]. Selecting an appropriate substrate for microstrip patch antenna manufacturing plays an important role to overcome many limitations of the microstrip antenna such as low gain, narrow bandwidth, and low efficiency without shifting the resonant frequency significantly [14]. White Space TV technology can radiate over 10 kilometers in diameter. This long-distance coverage technology was introducing as Super Wi-Fi because of its wide range and ability to penetrate objects such as walls, trees, and rough terrain. A case study of the availability of white space TV band in Malawi using cost-effective tools had been described with the Z antenna with 99 percent efficiency for rural use [15, 16].

In the present work, a circular microstrip patch antenna (CMSPA) that can operate in the UHF band is proposed. Three circular rings and a finite ground plane are used to cover the complete white space TV frequency range. The principal contributions of the proposed idea are i) The proposed antenna can work in the complete ultra-high frequency television band. ii) To increase the bandwidth of the antenna three circular rings and finite ground planes are introduced in the geometry of the antenna. iii) Radiation efficiency of the presented antenna is 92 percent. iv) The presented antenna has extensive impedance-matching bandwidth.

This paper is arranged into four sections. The design equations are described in the second section of the paper and demonstrating the effect of three circular rings and finite ground plane in the UHF TV band. The effect of etching three circular rings and finite ground on antenna parameters are discussed in the third section of the paper. Simulated results are compared with measured results also in the third section. The findings and observations of the proposed idea are concluded in the final section of the paper. The presented antenna is designed with a finite ground plane to increase the bandwidth.

2 Antenna Design

The conformation of CMSA is manifest in Fig. 1. In a rectangular microstrip patch antenna, the variation of the field beneath the patch is elucidated in terms of sine or cosine functions. Contrasting the field variations for a CMSA are elucidated in terms of the Bessel function. The resonant frequency of a CMSA is calculating using the given formula

$$f_0 = \frac{K_{nm}c}{2\pi a_e \sqrt{\epsilon_e}}, \tag{1}$$

where K_{nm} is the mth root of the derivative of the Bessel function of order n and c is the velocity of light [17]. The a_e and ϵ_e are the effective radius and the effective dielectric constant of the CMSA, respectively. The fringing fields along the circumference of the CMSA

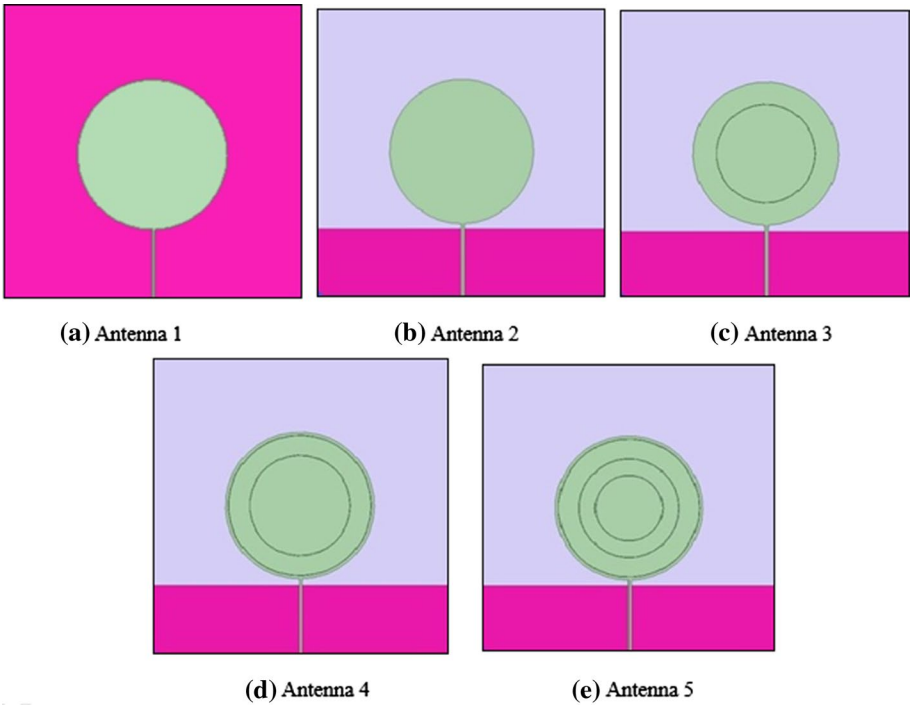

Fig. 1 Evaluation of proposed antenna

are taken into account by replacing the patch radius a by the effective radius a_e given by [18]

$$a_e = \sqrt{a\left[1 + \frac{2h}{\pi a \epsilon_r}\left\{ln\left(\frac{0.5a}{h}\right) + \frac{1}{\sqrt{2}}\epsilon_r + \frac{1}{0.564} + \frac{h}{a}\left(\frac{1}{3.73}\epsilon_r + 1.65\right)\right\}\right]}. \quad (2)$$

The value of ϵ_e is obtained using

$$\epsilon_e = \frac{C(a, h, \epsilon_0\epsilon_r)}{C(a, h, \epsilon_0)}, \quad (3)$$

where $C(a, h, \epsilon_0\epsilon_r)$ and $C(a, h, \epsilon_0)$ are the total capacitance of TM_{11} mode of CMSA with and without a dielectric substrate, respectively [19]. These can be determined by the given equation:

$$C(a, h, \epsilon_0\epsilon_r) = \frac{0.8525\epsilon_0\epsilon_r\pi a^2}{h} + 0.5C_f. \quad (4)$$

Equation (4), is the combination of the main capacitance of the disc and the fringing capacitance [20]. Fringing capacitance is given by the following relation:

$$C_f = 2a\epsilon_0\left[ln\left(\frac{0.5a}{h}\right) + \frac{1}{\sqrt{2}}\epsilon_r + \frac{1}{0.564} + \frac{h}{a}\left(\frac{1}{3.73}\epsilon_r + 1.65\right)\right], \quad (5)$$

where, $C(a, h, \epsilon_0)$ is calculating by putting ϵ_r=1 in equation (4) and (5) [21, 22]. For thin substrates, ϵ_r should be used instead of ϵ_e in equation (1) and for thick substrate $h > 0.05\lambda_0$, ϵ_e should be used.

In this paper, a novel three-ring circular microstrip patch antenna is designed. The substrate plays an important role in providing mechanical strength to the microstrip antenna and the selection of substrate is also very important. It is found that for low-frequency FR4 substrate is good. In the proposed designed FR4 substrate of 346.4mm x 346.4mm dimensions are used. The radius of the patch is calculated for 480MHz frequency as per equation (1) and it comes out to be 86.6mm. Three circular rings of 0.5mm are etched over a circular patch, and the position of the ring is also calculated from equation (1) for 500MHz, 700MHz, and 900MHz respectively from the outer to the inner side of the main patch. The bandwidth of the proposed antenna was enhanced by adding circular rings in the structure, but efficiency gets reduced due to the insertion of circular rings. Microstrip circular patch antenna with FR4 substrate and the infinite ground plane had been designed using equation (1), as shown in Fig. 1. It had been noticed that when the size of the ground is exceeded the patch dimensions by just about six times the substrate thickness all around the boundaries, the results are close to that of the infinite ground plane. For the limited ground plane, the back lobes are appeared in a radiation pattern, whereas for the infinite ground plane, back lobes are missing from the radiation pattern. The antenna presented in (a) of Fig. 1 is a basic antenna of circular shape. From Fig. 2 the impedance bandwidth (S_{11}< -10dB) of basic antenna is 11 MHZ. To enhance the bandwidth of the antenna, the proposed antenna has undergone through 5 stages which are shown in Fig. 1 from (a) to (e).

In Fig. 1(b) infinite ground plane is converted into a finite ground plane to increase bandwidth and the radiation pattern becomes in the figure of eight. Now antenna impedance bandwidth is 390MHz which covers frequencies from 470MHz to 806MHz but return

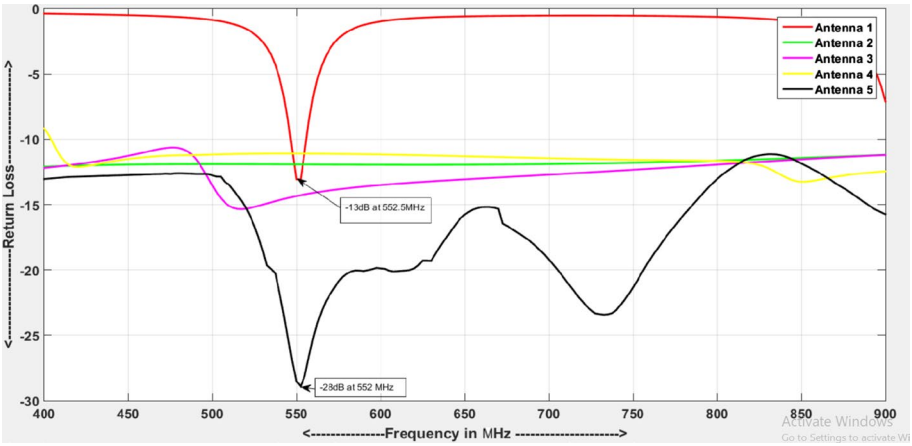

Fig. 2 Return Loss of proposed antenna

loss decreased. In the 3rd stage of the design, as shown in Fig. 1(c) 0.5mm circular ring is removed from the patch at 700MHz frequency. By removing a ring from the patch, return loss has been improved. Similarly, rings 2 and 3 are removed from the main patch at 500 MHz and 900 MHz by calculating the location of the ring from equation (1), as shown in Fig. 1(d) and Fig. 1(e), respectively. The final proposed design is shown in Fig. 1(e). From Fig. 2 it is ascertained that return loss is -28 dB at the resonance frequency of the antenna 5 at about 552 MHz and the impedance bandwidth (S_{11}< -10dB) is 390 MHZ. The gain has been reduced from 5dBi to 1.3dBi due to the introduction of circular ring slots in the designed antenna 5.

3 Results

High-frequency structure simulator (HFSS) is used for designing and simulation of the proposed antenna, which is based on the finite element method (FEM) numerical technique. The final design of the proposed antenna is depicted in Fig. 1.

The comparison of the return loss of all five antennas is presenting in Fig.2. It is cleared from the graph that, as the number of rings on the patch increased from one to three, the return loss is getting improve. In this design the return loss is obtained -28dB at 552MHz. Various parameters of antenna are compared and the result of the comparison is shown in Table 1. Return loss has been improved from -13dB to -28dB. The designed antenna can work in a complete TV band with a gain of 1.3dBi. The total radiation efficiency of the designed antenna is 92 percent which is less than the theoretical value of radiation efficiency of 98 percent, as total radiation efficiency is the product of radiation efficiency and all losses (conduction losses, dielectric losses, and minor impedance mismatch losses).

3.1 Experimental Results

The proposed antenna has been fabricated in Advance Microwave Lab at the Indian Institute of Technology, Roorkee. The designed antenna is manifested in Fig. 3. The fabricated antenna is better in terms of return loss as compared with the simulated design. The return

Table 1 Comparisons of parameters of all five antennas

Parameters	Antenna 1	Antenna 2	Antenna 3	Antenna 4	Antenna 5
Return Loss	−13dB	−11dB	−12dB	−14dB	−28dB
Type	Spot	Broadband	Broadband	Broadband	Broadband
Bandwidth	7MHz	TV Band	TV Band	TV Band	TV Band
Gain	5dBi	1.4dBi	1.33dBi	1.32dBi	1.3dBi
Efficiency	6.8	97	95	94	92
Radiated Power	8.8dBm	29.48dBm	29.45dBm	29.49dBm	29.64dBm

Fig. 3 Fabricated antenna

loss of the manufactured antenna is manifested in Fig. 4. It is observed that the maximum peak of return loss is obtained at 553 MHz i.e. −31dB.

A comparison of measured and simulated return loss is depicted in Fig. 5. Here the variation of 0.54 percent is observed in the measured operating frequency and resonant frequency of the designed antenna. The resonant frequency of the fabricated antenna is 1MHz less than the simulated antenna.

The measured and simulated VSWR is shown in Fig. 6. The bandwidth achieved is 100 percent. The VSWR curve is below 1.2 for frequency range from 400MHz to 900MHz.

The antenna is also tested in Advance Microwave Lab at the Indian Institute of Technology Roorkee. Fig. 7 shows the manufactured antenna in the Anechoic Chamber of IITR.

The simulated and measured gain is shown in Fig. 8. The measured gain is 1.2dBi and the simulated gain is 1.3dBi. The back lobe is present in the gain pattern because of the finite ground plane.

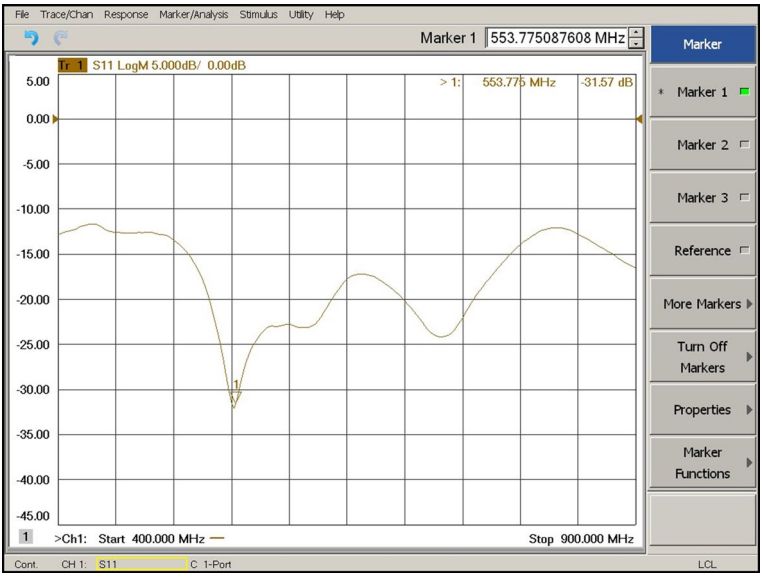

Fig. 4 Measured return loss

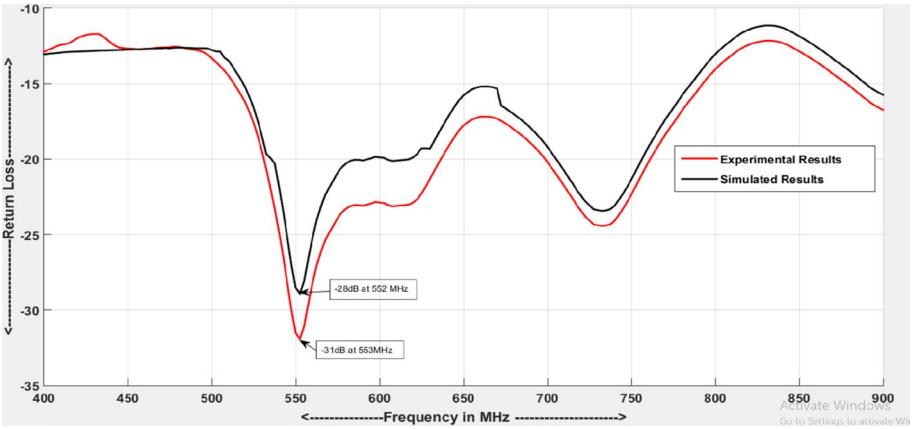

Fig. 5 Experimental and measured results of return loss

The bandwidth and efficiency of the proposed antenna can be compared with the work already published in the white space TV band. It was observed that the proposed antenna is having good bandwidth and efficiency with considerable gain (Table 2).

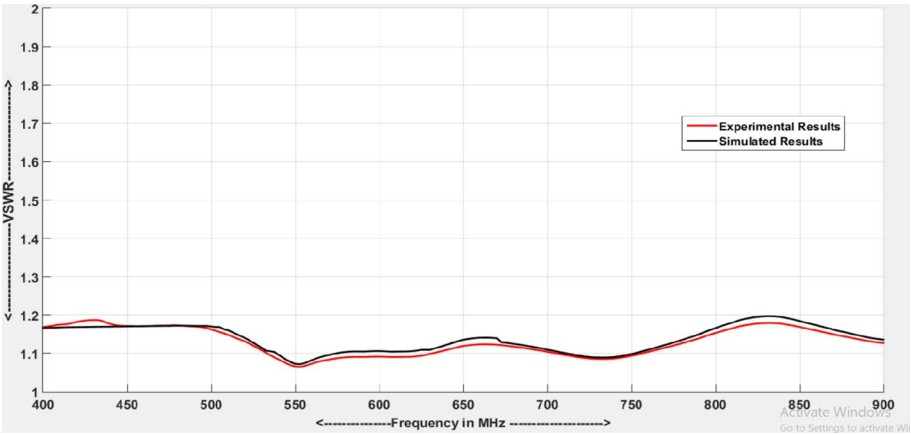

Fig. 6 VSWR of experimental and measured results

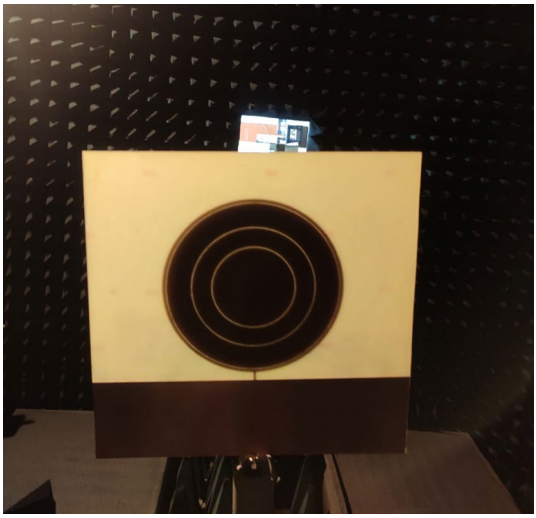

Fig. 7 Fabricated antenna in anechoic chamber

4 Conclusion

The novel circular microstrip patch antenna with three rings cut from the patch is designed and fabricated. The fabricated antenna gives better results as compared to the simulated design in terms of bandwidth and return loss. The deigned antenna is appropriate to use in a TV band with a gain of 1.3dBi and radiation efficiency of 92 percent. The return loss of the antenna is -31dB at 553MHz. The VSWR curve is less than 1.2 throughout the complete band. The bandwidth achieved is 100 percent. The trade-off

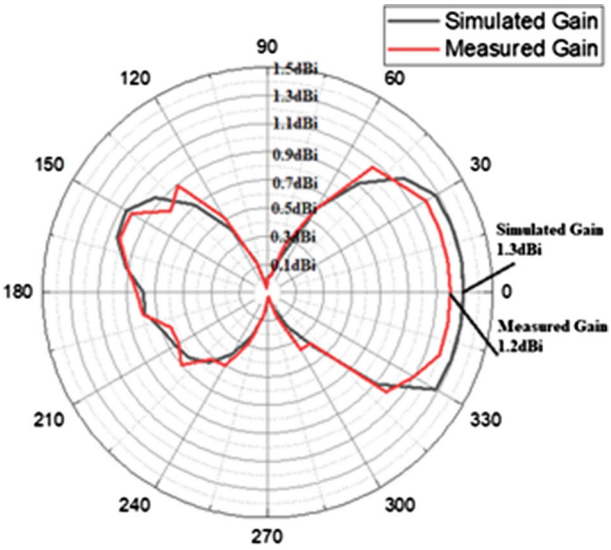

Fig. 8 Measured and simulated gain of proposed antenna

Table 2 Comparison of proposed antenna performance with the published work

Reference	Design	Substrate	Gain	Radiation Efficiency	Bandwidth
Bauer et al. [9]	Bow -Tie	FR4	−2 to 1 dBi	50 percent	470–860 MHz
Wang et al. [11]	Printed Monopole	FR4	1 to 2 dBi	-	460–870 MHz
Darwhekar et al. [12]	Triangular patch	FR4	-	-	470–806 MHz
Pinifolo et al. [15]	Wire Antenna	Copper	1.87 dBi	99.6 percent	13.7 MHz
Vithanawasam et al. [16]	U-Shaped	FR4	1.4 dBi	76.2 percent	474–1212 MHz
Zhang et al. [23]	Circular Patch	Rogers5880	2.5 dBi	-	470–987 MHz
Present Work	CP with rings	FR4	1.3 dBi	92 percent	400–900 MHz

lies between gain and improved bandwidth. The proposed design is suitable to use in the UHF band especially in the TV band.

Author Contributions The principal contributions of the proposed idea are (i) The proposed antenna can work in the complete ultra-high frequency television band. (ii) To increase the bandwidth of antenna three circular rings and finite ground plane are introduced in the geometry of antenna. (iii) Radiation efficiency of presented antenna is 92 percentage. (iv) The presented antenna has an extensive impedance-matching bandwidth.

Funding This paper received no funding.

Availability of data and materials Not Applicable

Code availability Not Applicable

Declarations

Conflict of interest There is no conflict of interest.

Ethics approval Not Applicable

Consent to participate Not Applicable

Consent for publication Not Applicable

References

1. Rahman, M., & Saifullah, A. (2019). A comprehensive survey on networking over TV white spaces. *Pervasive and Mobile Computing, 59*, 101072. https://doi.org/10.1016/jpmcj.2019.101072
2. Sharma, R., Raghava, N. S., and De, A.(2021). Design of compact circular microstrip patch antenna using parasitic patch. In Proceeding of IEEE Convergence in Technology (I2CT), pp. 1-4. https://doi.org/10.1109/i2ct51068.2021.9418104.
3. Chakravarty, T., Roy, S. M., Sanyal, S. K., & De, A. (2005). A novel microstrip patch antenna with large impedance bandwidth in VHF/UHF rang. *Progress in Electromagnetics Research, 54,* 83–93. https://doi.org/10.2528/PIER04102101.
4. Viswanadha, K., & Raghava, N. S. (2020). Design and analysis of a multi-band flower shaped patch antenna for WLAN/WiMAX/ISM band applications. *Wireless Personal Communications, 112*, 863–887. https://doi.org/10.1007/s11277-020-07078-8
5. Dawar, P., Raghava, N. S., & De, A. (2015). A novel metamaterial for miniaturization and multi-resonance in antenna. *Cogent Physics, 2*(1), 1–13. https://doi.org/10.1080/23311940.2015.1123595
6. Patel, J. M., Patel, S. K., & Thakkar, F. N. (2012). Design of S-shaped multiband microstrip patch antenna. *In Proceeding of Nirma University International Conference on Engineering (NUiCONE), 1–3*,. https://doi.org/10.1109/nuicone.2012.6493229
7. Thakur, Shivkant, Vishwakarma, Rajesh Kumar, & Verma, K. K. (2013). L-shaped microstrip antenna for wideband. *In Proceeding of International Conference on Communication Systems and Network Topologies*. https://doi.org/10.1109/icoin.2013.6496337
8. Sharma, Tej Raj, Singh, Arjun, & Saini, Himanshu. (2015). Triple band MSA for WiMAX and WLAN application. *In Proceeding of International Conference on Advances in Computing and Communication Engineering, 214–218*,. https://doi.org/10.1109/icacce.20150.107
9. Bauer, J., and Schühler, M. (2014). Compact wide band antenna for TV White Spaces, In proceeding of 8th European Conference on Antennas and Propagation (EuCAP 2014), 2894-2896. https://doi.org/10.1109/eucap.2014.6902431.
10. Dhande, T. A., Peshwe, P. D., Darwhekar, I. S., and Kothari, A. G. (2019). Wideband patch antenna for cognitive radio applications in TV white space. In Proceedinf of 10th International Conference on Computing, Communication and Networking Technologies (ICCCNT), 1-6. https://doi.org/10.1109/icccnt45670.2019.8944832.
11. Wang, Naizhi, Gao, Yue, & Zeng, Qingsheng. (2017). Compact wideband omnidirectional UHF antenna for TV white space cognitive radio application. *AEU - International Journal of Electronics and Communications, 74*, 158–162. https://doi.org/10.1016/j.aeue.2017.02.011
12. Darwhekar, I. S., Peshwe, P. D., Surender, K., and Kothari, A. G. (2019). Wideband triangular patch antenna for cognitive radio in TV white space. In Proceeding of 2nd International Conference on Innovations in Electronics, Signal Processing and Communication (IESC),115-118. https://doi.org/10.1109/iespc.201908902398.
13. Shah, R., and Prajapati, P. (2017). Slot loaded dielectric resonator antenna for bandwidth enhancement. In Proceeding of IEEE International Conference on Wireless Communications, signal Processing and Networking, (WiSPNET), 647-649. https://doi.org/10.1109/wispnet.2017.8299839.
14. De, Asok, Raghava, N. S., Malhotra, Sagar, Arora, Pushkar, & Bazaz, Rishik. (2010). Effect of different substrates on Compact stacked square Microstrip Antenna. *Journal of Telecommunications, 1*(1), 63–65. https://doi.org/1002.3337v1.
15. Pinifolo, J., Rimer, S., Paul, B., Daka, C., Mikeka, C., & Mlatho, S. (2015). Design of a low cost television White Space Z antenna. *IST-Africa Conference*. https://doi.org/10.1109/istafrica.2015.71905

16. Vithanawasam, Chamath Kalanaka, Then, Yi Lung, & Su, Hieng Tiong. (2020). A review of microstrip antenna designs for TV white space applications. *Indonesian Journal of Electrical Engineering and Computer Science, 19*(2), 855–863. https://doi.org/10.11591/ijeecs.v19.i2
17. Ray, K. P., & Kumar, G. (1999). Determination of the resonant frequency of microstrip antenna. *Microwave Optical Technology Letters, 23*(2), 114–117. https://doi.org/10.1002/(SICI)1098-2760(19991020).
18. Singh, R., De, A., & Yadava, R. S. (1990). Resonant frequency of elliptical microstrip patch radiator. *International Journal of Electronics, 69*(3), 385–388. https://doi.org/10.1080/00207219008920324
19. Kumprasert, N., & Kiranon, W. (1995). Simple and accurate formula for the resonant frequency of the circular micostrip disk antenna. *IEEE Transaction Antenna Propagation, 43*(11), 331–1333. https://doi.org/10.1109/8.475109.
20. Howell, J. O. (1975). Microstrip Antenna. *IEEE Transaction Antenna Propagation, 23,* 90–93.
21. Wolff, I., & Knoppik, N. (1974). Rectangular and circular microstrip disk capacitors and resonators. *IEEE Transaction Microwave Theory Technology, 22,* 857–864. https://doi.org/10.1109/TMTT.1974.1128364.
22. Derneryd, A.G. (1978)Microstrip disc antenna covers multiple frequency, Microwave Journal, pp. 77-79.
23. Zhang, Q., Ma, R., Su, W., & Gao, Y. (2018). Design of a multimode UWB antenna using characteristic mode analysis. *IEEE Transactions on Antennas and Propagation, 66*(7), 3712–3717. https://doi.org/10.1109/tap.2018.2835370.

Publisher's Note Springer Nature remains neutral with regard to jurisdictional claims in published maps and institutional affiliations.

Richa Sharma is presently working as Assistant Professor in Ajay Kumar Garg Engineering College, Ghaziabad, U.P., India. She has received B.Tech and M.Tech in Electronics and Communication Engineering from Sant Longowal Institute of Engineering and Technology (SLIET) in 2009 and 2011 respectively. She has attended/presented more than 10 National/International Conferences. Her area of interest is Antenna, RF & microwave and Data communication.

N. S. Raghava is working as Professor & Head of the Department in Electronics and Communication Engineering Department in Delhi Technological University (Formerly Delhi College of Engineering), New Delhi. His area of specialization is Antenna and Propagation, Microwave Engineering, Digital Communication, Wireless Communication, Cloud Computing, Information Security

Asok De obtained his Bachelor and Master of Engineering with specialization of Electronics and Communication from Jadavpur University Kolkata in 1978 and 1980, respectively. He was awarded Ph.D. degree from Indian Institute of Technology Kharagpur in the year 1986. He joined Delhi University, Delhi, India as Lecturer in the year 1984 and promoted as Reader in the year 1987. In 1991 he joined Kolkata University, Kolkata, India as Reader and subsequently joined Delhi College of Engineering (presently Delhi Technological University), Delhi, India as Professor in the year 1997 and worked as Professor in Electronics and Communication Engineering Department, Head of Computer Engineering and Head of Information Technology. In 2005, he joined Ambedkar Institute of Advanced Communication Technology and Research Delhi as Principal and continued with this position till July 2012. Then he worked as Director of National Institute of Technology Patna from 2012-2017. At that period of time, he also had an additional charge of Director of National Institute of Technology Durgapur, India. His area of interest includes Antennas, Transmission Lines, Microwave Circuits, and Computational Electromagnetics. He has published over more than 120 research articles in international journals and more than 130 research articles in international/national conference proceedings. He is a senior member IEEE (USA), fellow IEI (India), fellow IETE (India), and life member CSI (India).

e-ISSN: 2582-5208
International Research Journal of Modernization in Engineering Technology and Science
(Peer-Reviewed, Open Access, Fully Refereed International Journal)
Volume:04/Issue:05/May-2022 Impact Factor- 6.752 www.irjmets.com

DESIGN AND ANALYSIS OF KINETIC ENERGY RECOVERY SYSTEM FOR BICYCLE

Dr. Ashok Madan[*1], Sarthak Jain[*2], Tushar Gupta[*3], Abhay Singh[*4]

[*1]Professor, Department Of Mechanical Engineering, Delhi Technological University, Delhi, India.

[*2,3,4]Student, Department Of Mechanical Engineering, Delhi Technological University, Delhi, India.

ABSTRACT

The Kinetic Energy Recovery System (KERS) is a braking system that recovers the Kinetic energy of a moving vehicle. This mechanism stores kinetic energy as potential energy and then converts it back to kinetic energy as necessary. When riding a bicycle, it becomes too exhausting to restart after braking. If the bicycle is equipped with a kinetic energy recovery system, the rider will have two different power sources to choose from. When brakes are applied, kinetic energy is squandered because friction at the contact surface converts kinetic energy to heat energy, which then dissipates into the atmosphere owing to thermal radiation.

Vehicles fitted with KERS devices can extract some of their kinetic energy, slowing them down. This is a type of braking where the energy is not squandered but instead stored in a gadget. This potential energy can be transformed back into kinetic energy with the help of a correct mechanism, giving the vehicle an extra boost of power. Various types of available KERS systems are examined in the literature review, and a mechanical-based KERS system is shown to be the best fit for a bicycle. There are two types of mechanical KERS systems: clutch-based and CVT-based K.E. recovery systems. In this project a hybrid of the above two types of KERS systems is designed. Instead of CVT a variable sprocket ratio is used to make the power transmission smoother.

Keywords: Analysis, Investigation, Research.

I. INTRODUCTION

A kinetic energy recovery system abbreviated like KERS is a motor system that restores the kinetic energy of a moving car under the brakes. The energy obtained is stored as potential energy as a reservoir for later use to accelerate. Examples of reservoir batteries with high voltage, flywheels, hydraulic coupling, etc. The choice of water storage area depends largely on the purpose.

In recent days restorative Kinetic power has become an exciting area of research for many. Let's find out first. The absolute power in this universe can be broadly divided into two potential Powers and Kinetic Powers. Potential Energy is the energy the body has because of position or position while Kinetic Energy is the energy the body gains due to its movement. As we know, vision is a related concept as a Kinetic force. For example a car has Kinetic power over the road but respectfully another car at the same speed has no Kinetic power. So when we need to move movement in the body we have to convert a certain amount of potential Kinetic energy. When that body has to rest, that amount of kinetic energy needs to be converted into potential energy. But naturally the kind of power that can exist where Kinetic power is converted is low, in most cases, and very difficult to reuse. To make an example of a car, when we drive a car we burn gasoline and turn the potential fuel of the car into the Kinetic power of the car and when we apply the brakes the kinetic energy converts into heat energy in the brake caliper and eventually gain. scattered in space. If this energy were to be stored it would be used.

There are two types of Kinetic Energy Recovery Systems that have gained popularity in recent days. One is KERS electric and the other is Mechanical KERS. Both have their advantages and disadvantages. The electrical system does not work very well but it can save energy for a long time and give us the ability to trim the torque and rpm output according to our requirement. On the other hand the mechanical system works better (almost twice as much as the previous one) but is prone to decay due to its natural anti-corrosion properties, although very small in number, so it cannot be stored for long. for a long time and should be used for a short time. In the real world we can find many situations where we need to use the Kinetic power acquired during a very short period of recovery and we do not need even a wide range of torque and rpm output as a specific range of torque & rpm combinations fully satisfy our needs. A bicycle is a perfect example of this type. That's why KERS cycling

e-ISSN: 2582-5208
International Research Journal of Modernization in Engineering Technology and Science
(Peer-Reviewed, Open Access, Fully Refereed International Journal)
Volume:04/Issue:05/May-2022 Impact Factor- 6.752 www.irjmets.com

has been selected as a final year project. There has been a lot of work related to this topic but this article still needs further research. During the project the goal will be to design an advanced KERS machine that will improve kinetic storage time and improve system compliance.

II. METHODOLOGY

Solidworks and ANSYS software are used to design and analyze the KERS system. The clutch system has been upgraded and a flexible transmission (instead of CVT) system is used to obtain the best output of the KERS machine. This program has advantages over the above two methods and eliminates their limitations. In this paper the principle of operation, design and production process when this model is discussed in detail.

The advantages of this system are:

1. This is user-friendly.
2. This is less costly.
3. Avoids completely the initial jerk.
4. Avoids the application jerk upto a large extent.
5. Easy to fit.
6. Marketable.
7. Easy to manufacture.

III. FINITE ELEMENT ANALYSIS

A complete feature analysis of the whole component is required in any design process. Everything designed should be considered to be able to take the load you want and maintain the working environment. The product life cycle is an important term coined in this field. FEA helps us identify flaws in our designs. Demonstrates concentration of stress and stress in various desirable areas. It even helps to find the exact safety feature of the component. The best part is that we can change part of the asset and inspect it as many times as we like without losing any raw material. In this project also a comprehensive FEA analysis has been conducted on various components to determine their integrity and sustainability. All the results of those activities are listed below:

Flywheel:

Flywheel is the most rigid component among the components of a KERS system which has the least amount of chance to undergo a failure.

Forces acting on the flywheel:

- Gravitational force
- Rotational inertia force (66.66rps)
- Force due to actuation of clutch (373.4N)
- Supports of the flywheel:
- Bearing support.
- Displacement support

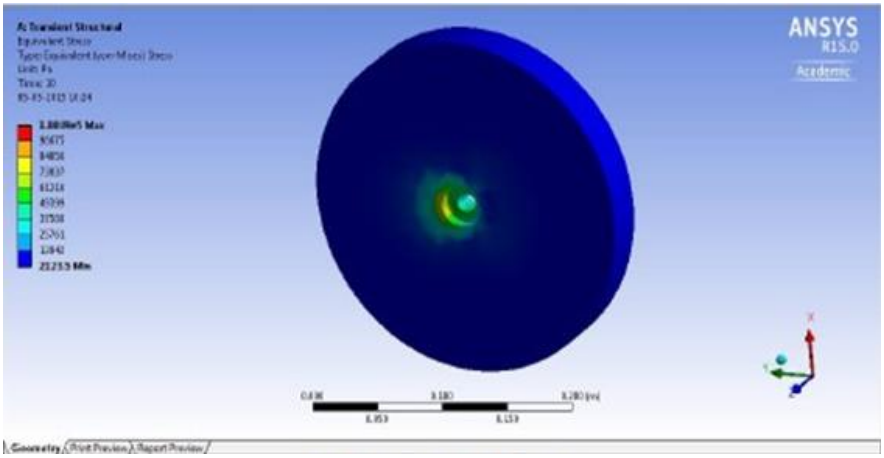

Figure 1: Equivalent stress.

e-ISSN: 2582-5208
International Research Journal of Modernization in Engineering Technology and Science
(Peer-Reviewed, Open Access, Fully Refereed International Journal)
Volume:04/Issue:05/May-2022 Impact Factor- 6.752 www.irjmets.com

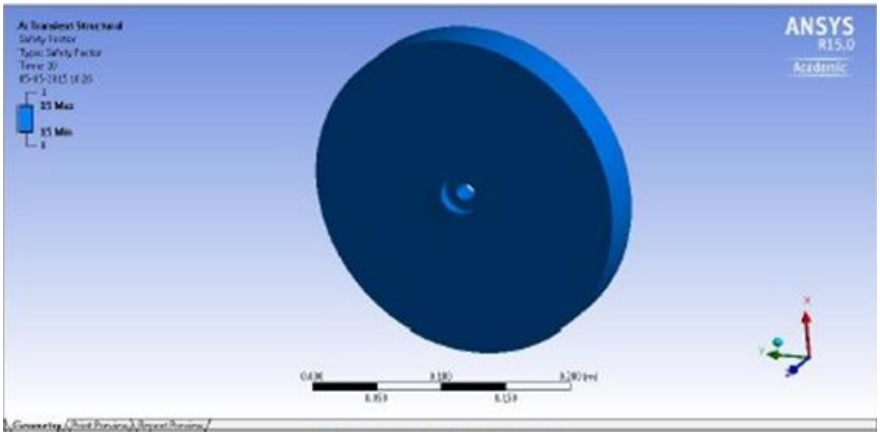

Figure 2: Factor of Safety.

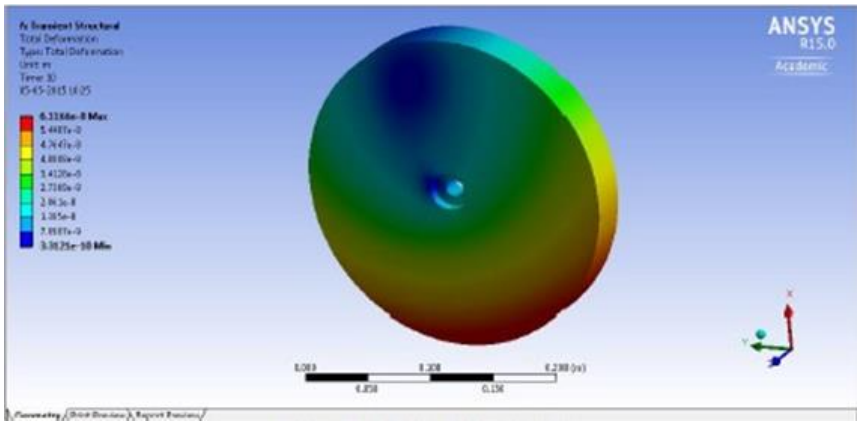

Figure 3: Total Deformation.

From the FEA analysis photos we can see:

Factor of safety of the flywheel = 15.

Maximum equivalent stress = 108.5KPa

Maximum equivalent strain = 1.5e-6

Maximum deflection = 6.1e-8m

The above data show that the design of the flywheel is completely safe.

Clutch:

Clutch is the most vulnerable component of the KERs system. It is exposed to continuous engagement and disengagement with the flywheel.

Force acting on clutch:

Force due to actuation of the clutch

F = 373.4N

Gravitational force

Rotational inertia force

Speed of rotation when the cycle runs at 30Kmph amd the sprocket ratio is

maximum (s=3) $=\omega 2=30\times518\times2\pi\pi D\times s$ = 66.66rad/sec

Torque T = 8.96Nm Supports:

Compression only support

Contact support, no displacement

e-ISSN: 2582-5208
International Research Journal of Modernization in Engineering Technology and Science
(Peer-Reviewed, Open Access, Fully Refereed International Journal)
Volume:04/Issue:05/May-2022 Impact Factor- 6.752 www.irjmets.com

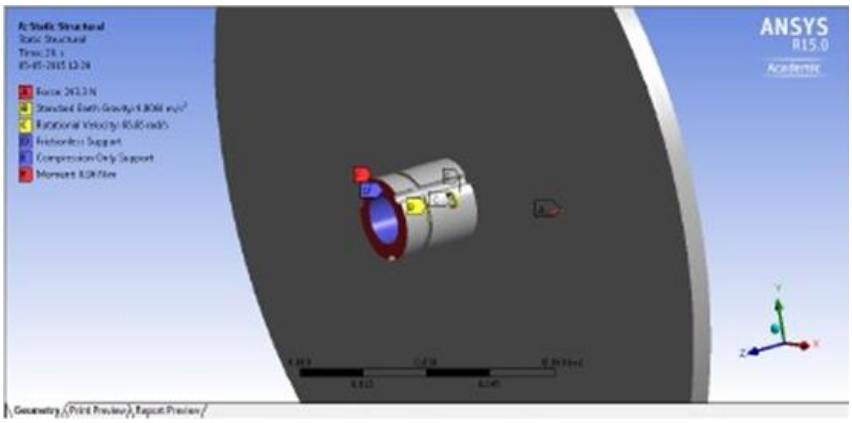

Figure 4: Forces acting.

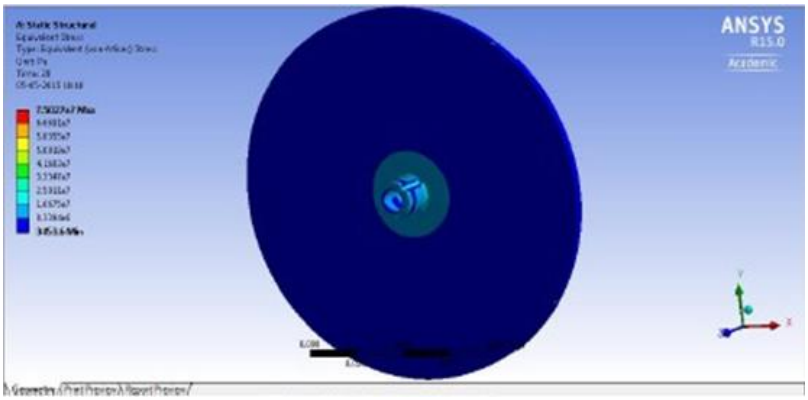

Figure 5: Equivalent stress.

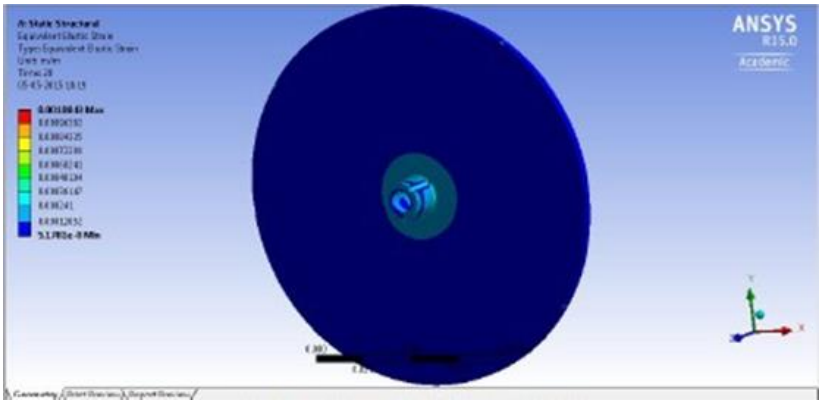

Figure 6: Equivalent elastic strain.

IV. RESULTS AND DISCUSSION

The 3D model of the KERS system is made with great accuracy. The model was modeled on SOLIDWORKS to test its functionality. The analysis of the finished element of the parts is done to assess the durability of the product and the health of the product. Initially all parts were made using aluminum but other components such as front sprocket, clutch drive and central shaft faced failure. So these are reconfigured with minimal modification and using SS304. The clutch also experienced failures initially but its material has not changed as that will increase the weight, instead it is redesigned several times to get a higher quality design with a higher safety feature.

V. CONCLUSION

In this project a KERS flywheel-based system was developed. The product designed for this project is a combination of clutch and CERST-based KERS programs. This program is expected to be cheaper than the KERS based CVT program. Effective and efficient production processes for KERS components were also discovered.

Using FEA analysis the components are inspected and adjusted to avoid failure. This project can guide anyone to customize their KERS cycling system very easily. It has been found that all parts are safe under very poor working conditions. Different types of KERS programs and their applications were also researched. It has been found that the flywheel can be used instead of a battery to store and deliver energy efficiently. Since the use of the flywheel on a bicycle is a new concept, this field has a wide range and a wide range of upcoming launches.

VI. REFERENCES

[1] Sreevalsan S Menon, Sooraj M S, Sanjay Mohan, Rino Disney, Suneeth Sukumaran "Design and Analysis of Kinetic Energy Recovery System in Bicycles" - International Journal of Innovative Research in Science, Engineering and Technology, Vol. 2, Issue 8, August 2013

[2] Kevin Ludlum "Optimizing Flywheel Design for use as a Kinetic Energy Recovery System for a Bicycle", June 2013

[3] Radhika Kapoor, C. Mallika Parveen, Member, IAENG "Comparative Study on Various KERS"- Proceedings of the World Congress on Engineering 2013 Vol III, WCE 2013, July 3 - 5, 2013.

[4] Ricardo Chicurel, "A Compromise Solution for Energy Recovery in Vehicle Braking," Energy, vol.24, pp. 1029-1034, 2009.

[5] Barr A., Veshagh A., "Fuel Economy and Performance Comparison of Alternative Mechanical Hybrid Powertrain Configuration," SAE 2008 World congress, Detroit, USA, 2008.

[6] Brockbank C., Cross D., "mechanical Hybrid System Comprising a Flywheel and CVT for Motorsport & Mainstream Automotive Applications," SAE 2009 World Congress, Detroit, MI, USA, 2009.

[7] Ayad M-Y, Pierfederici S., Raël S., Davat B., "Voltage Regulated Hybrid DC Power Source using Supercapcitors as Energy Storage Device," Energy Covers Manage, 2007.

[8] Ayad M-Y, Becherif M., Henni A., Aboubout, Wack M., Lagroche S., "Passivity –Based Control Applied to DC Hybrid Power Source using Fuel Cell and Supercapacitors," Energy Covers Manage, 2010.

[9] Payman A., Pierfederici S, Meibody-Tabar F., "Energy control of supercapacitor/fuel cell hybrid power source," Energy Convers Manage, 2008.

[10] Uzunoglu M., Alam MS., "Dynamic modeling, design and simulation of a PEM fuel cell/ultra-capacitor hybrid system for vehicular applications," Energy Convers Manage, 2007.

[11] Adib E., Farzanehfard H., "Soft switching bidirectional DC–DC converter for ultracapacitor–batteries interface," Energy Convers Manage, 2009.

[12] Farzanehfard H., Beyragh D.S., Adib E., "A bidirectional soft switched ultracapacitor interface circuit for hybrid electric vehicles," Energy Convers Manage, 2008.

[13] Rufer A., Hotellier D., Barrade P., "A supercapacitor-based energy storage substation for voltage compensation in weak transportation networks," IEEE Trans Power Del, 2004.

[14] Chau K.T., Wong Y.S., Chan C.C., "An overview of energy sources for electric vehicles," Energy Convers Manage, 1999.

[15] Sharma P., Bhatti T.S., "A review on electrochemical double-layer capacitors," Energy Convers Manage, 2010.

[16] L. Guzzella, A. Sciarretta,"Vehicle Propulsion Systems: Introduction to Modeling and Optimization," Springer, 2007.

Research Square

Preprints are preliminary reports that have not undergone peer review.
They should not be considered conclusive, used to inform clinical practice,
or referenced by the media as validated information.

Design and Analysis of wide bandwidth Quad ‘e’ mirror-shaped metamaterial for Wi-Fi and Satellite Applications

Ankit .
Delhi Technological University Department of Applied Physics
Kamal Kishor
Delhi Technological University Department of Applied Physics
Ravindra Kumar Sinha (dr_rk_sinha@yahoo.com)
Delhi Technological University Department of Applied Physics https://orcid.org/0000-0002-3447-412X

Research Article

Keywords: effective medium ratio (EMR), epsilon negative, metamaterial (MTM), negative refraction, negative permeability

Posted Date: June 9th, 2022

DOI: https://doi.org/10.21203/rs.3.rs-1705287/v1

License: This work is licensed under a Creative Commons Attribution 4.0 International License.
Read Full License

Design and Analysis of wide bandwidth Quad ‘e’ mirror-shaped metamaterial for Wi-Fi and Satellite Applications

Ankit, Kamal Kishor and Ravindra Kumar Sinha*

TIFAC- Centre of Relevance and Excellence in Fiber Optics and Optical Communication

Department of Applied Physics, Delhi Technological University, Bawana Road, Delhi-110042, India

*E-mail: dr_rk_sinha@yahoo.com

Abstract

In this paper, we report a novel design of wide bandwidth Quad ‘e’ mirror-shaped metamaterial (MTM) structure for Wi-Fi and Satellite Applications. Further, the geometrical parameters of the copper-based metamaterial on FR- 4 epoxy resin fiber substrate is optimized and analyzed for a triple-band operation in the frequency range of 0.1 GHz-16 GHz. The proposed design exhibits left-handed characteristics over the three (L, C and Ku) frequency bands in microwave regime. The electric field, magnetic field and surface current distribution of the proposed MTM unit has been studied at three resonance frequencies (f_r) namely 1.4 GHz, 5.0 GHz and 14.8 GHz. The effective electromagnetic parameters for the MTM were calculated using the obtained Propagation (transmission and reflection) characteristics. The unit cell provides negative permittivity (ε_r) in the region 0.5-1 GHz and a broad negative permeability (μ_r) in the 9-16 GHz region. The structure exhibits a negative refractive index (η_r) in the region 0.5-1 GHz, 3-3.5 GHz, and 9-12 GHz. The effects of dielectric materials, design parameters, resonator width (w_r), substrate thickness (t_s), middle gap width (r), and the influence of different metal conductors of unit cell on resonance frequencies were also investigated. The proposed design has an unprecedented effective medium ratio (EMR) value of 13.37, implying better effectiveness and compactness of the Quad ‘e’ mirror-shaped metamaterial. The designed structure could be extremely useful for design and development of compact wide bandwidth devices for Wi-Fi and satellite applications.

Keywords: effective medium ratio (EMR), epsilon negative, metamaterial (MTM), negative refraction, negative permeability

1. Introduction

A metamaterial is a combination of two words, “Meta” and “material.” Meta is a Greek word that means something beyond, altered, or changed. These materials derive their properties mainly from their structures rather than their compositions. Metamaterials (MTMs) are artificial composite materials with unique electromagnetic properties which are not found in nature and are made by arranging small metallic resonators periodically (Karaaslan et al. 2017). On a host ground, periodic arrays of metallic and dielectric substances can be used to create a metamaterial structure (Ziolkowski 2006). Victor Veselago first portrayed materials with negative permittivity and permeability in 1968, however, these characteristics were largely ignored until 1999. In 2000, Smith et al. proposed metallic split-ring resonators (SRRs) with dimesnions of the unit cell lesser than the operating wavelength (Smith et al. 2000). They developed a ground-breaking simulated media where the permittivity and permeability are negative, referred to as double-negative (DNG) metamaterial or Left-handed metamaterials (LHM). Metamaterial, which consists of either negative permeability or negative permittivity can be classified as a single negative (SNG) metamaterial (Srinivasan et al. 2019). The spread of metamaterial research, which revealed the MTMs unique characteristics such as negative permittivity (ε), negative permeability (μ) and negative refractive index (n), has led to a wide range of applications in microwave and optical regime such as reconfigurable antenna (Zhang et al. 2019), satellite (Mao et al. 2017), invisibility cloaking (Jing et al. 2020), filters (Ahamed et al. 2020) and superlenses (Lv et al. 2019) etc. MTMs have recently originated with utilization in various frequency bands, as every frequency band has a diverse range of applications. For example, in the microwave region, the L-band covers frequencies between 1-2 GHz with the usage in RADAR and satellite broadcasting applications, the S-band covers frequencies between 2-4 GHz, the C-band covers frequencies between 4-8 GHz with the usage in WIFi applications, the X-band covers frequencies between 8-12 GHz and the Ku-band covers 12.5-18 GHz frequency range with the widely employed in ships for VSAT systems and satellite TV. The Ku-band has the benefit of being less influenced by terrene signals and operating in a range of large frequencies, enabling tiny dish antennas to be used for VSAT applications.

In the recent past, various metamaterial structures such as V-shaped, spider structure, T-shaped, modified H-shaped, H-shaped, I-shaped, asymmetric split ring and circular split ring type structures (Esmail et al. 2022; Fedotov et al. 2007; Hossain et al. 2018; Kishor et al. 2014; Kishor and Sinha 2012a; Kishor and Sinha 2012b; Lahiri et al. 2009; Sureshkumar et al. 2018) have evolved to meet the demands for the design and development of antennas to improve their efficiency for satellite

communication, radar communication and sensor applications. Various studies have been conducted to encounter the demand for improved design of metamaterials exhibiting single, dual, triple, or multi-band operation for satellite applications. Dhouibi et al. introduced a “Z” shaped meta-atom with SNG characteristics for single-band operation with negative permittivity (Dhouibi et al. 2012). In the case of single-sided diamond-shaped left-handed metamaterial, an elevated transmission peak has been suggested but has excessively low Effective medium ratio (EMR) (Urbani 2010). Moniruzzaman et al. suggested a quadband double negative MTM with smaller effective medium ratio for microwave applications, with modest bandwidth at each resonance frequencies (Moniruzzaman et al. 2020). EMR is a significant factor in metamaterial design and indicates the miniaturization of metamaterials for the desired purpose. In 2017, a double C-shaped metamaterial (Faruque et al. 2017) structure was proposed, with a narrow band frequency and EMR equal to 7.44. As a result, a new quad 'e' mirror shaped metamaterial structure has been designed based on triple band applications with wide bandwidth and high EMR value.
This paper reports a new design for triple-band applications (L, C and Ku-band) in the microwave region with a high value of EMR (=13.37) by optimising the design of unit cell. The transmiission parameters were obtained using Finite Element Method (FEM) for the frequency range of 0.1-16 GHz and the obtained results were cross verified using two simulation tools COMSOL Multiphysics and CST microwave studio. The bandwidth of transmission coefficient (S_{21}) using less than -17 dB is 1.49 GHz (0.70-2.19 GHz), 2.22 GHz (4.20-6.42 GHz), and 0.58 GHz (14.41-14.99 GHz) showing wider bandwidth of the proposed structure. The proposed metamaterial structure exhibits negative relative effective permeability characteristics in the X-band and Ku-band and negative refractive index in the region 0.5-1 GHz, 3-3.5 GHz, and 9-12 GHz. In section 2 of the paper, the designning, optimization and simulation of the metamaterial is shown. The parametric studies such as the effects of dielectric materials, resonator width (w_r), FR-4 substrate thickness (t_s), middle gap width (r), and the influence of different metal conductors of unit cell on resonance frequencies is shown in the section 3. The final section, the result and discussion, covers estimation of the scattering parametrs, electromagnetic field distribution, far-field radiation pattern and effective medium ratio of the proposed metamaterial structure. Finally, the proposed quad 'e' mirror-shaped metamaterial achieved the study's aims and can be used for Wi-Fi and wireless communication systems.

2. Design, geometry and simulation of a MTM structure

The proposed MTM unit cell is formed on a low-cost FR-4 epoxy resin fibre dielectric material with a thickness of 0.16 cm and a size of 1.6 cm × 1.6 cm. The permittivity of the dielectric material is 4.3, with a dielctric loss tangent (δ) of 0.025. Because FR-4 has a moisture absorption rate of 0.10%, it is suited for high humidity environments (Bellal Hossain et al. 2022). The MTM unit cell's schematic arrangement is depicted in Fig. 1 (a). The operating frequency in this study was fixed between 0.1-16 GHz. On this substrate, the resonating patch is made up of copper material with a thickness of 0.035 cm and a conductivity of 5.99×10^7 S/m.

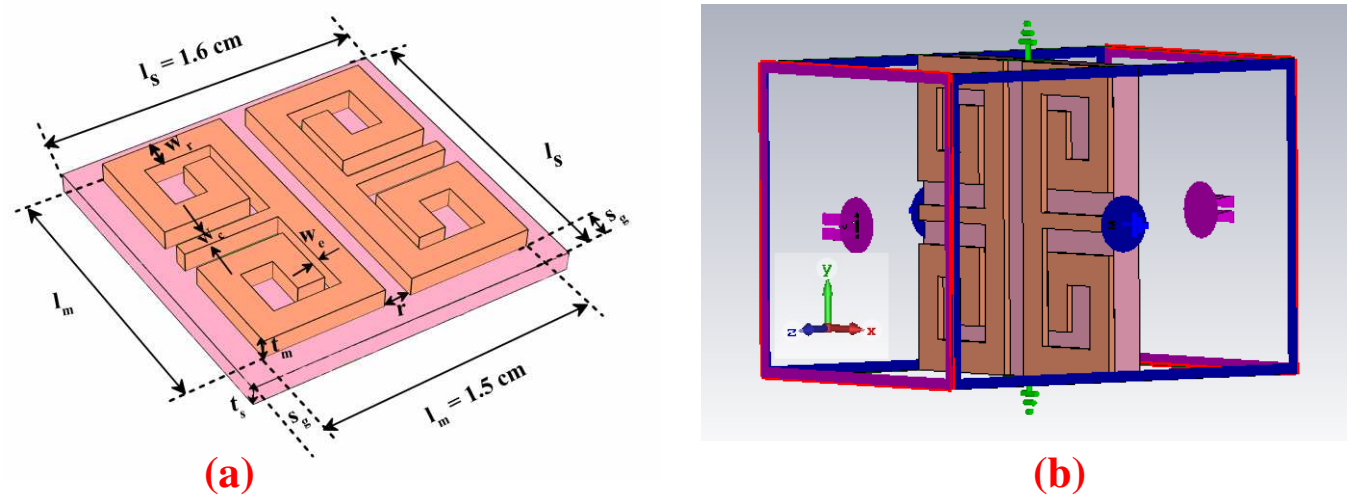

Fig. 1 (a) Designed MTM unit cell structure with geometrical parameters and (b) simulation setup for S_{11} and S_{21} measurement.

The resonating patch is made up of four mirror-shaped quad 'e' structures. Each symmetric structure contains four metallic strips and a vertical rectangular strip connecting two symmetric structures. The split gap between two rectangular shape strip was 0.159 cm that has been determined by numerical simulation performed in COMSOL Multiphysics with Finite element method (FEM) of frequency domain solver which provides a desired resonance. The thickness of the resonator strips is 0.159

cm. The dimensions of the unit cell of quad 'e' based MTM unit cell are shown in Table I. The numerical simulation arrangement is shown in Fig. 1 (b) where electromagnetic plane wave incident normally on a metamaterial unit cell from z-axis. The x-axis and y-axis are used as perfect electric conductor (PEC) and perfect magnetic conductor (PMC) boundary condition, respectively. Two waveguides ports are applied on the resonator from front and back side along positive and negative z-axis alongwith the electric field component in y-axis.

Table I Unit cell's dimension

Parameters	Values (cm)	Description
l_s	1.600	length of substrate
l_m	1.599	length of the material
r	0.159	middle gap
w_c	0.079	width of central line
w_r	0.159	width of resonator
w_e	0.047	width of edge gap
s_g	0.001	$(l_s - l_m)$
t_s	0.160	thickness of substrate
t_m	0.035	thickness of metamaterial

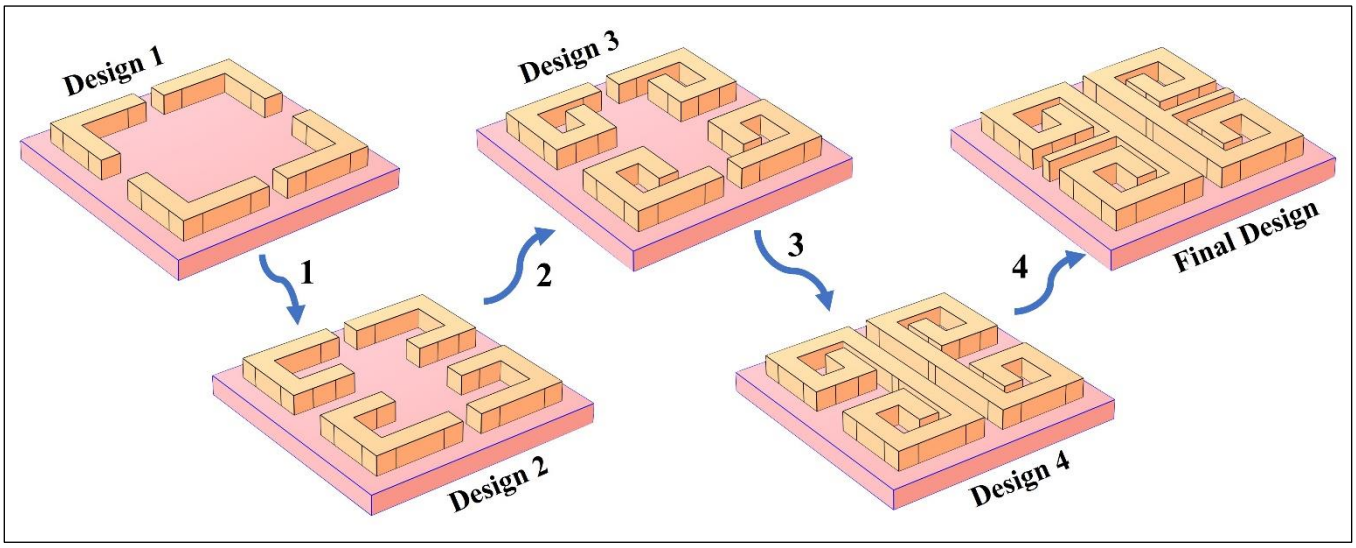

Fig. 2 Design methodology of the proposed structure

The design methodology of the presented structure includes the five design steps of the structure, as shown in Fig. 2. The proposed structure's step-by-step methodology indicates that the quad 'e' structure resonates in triple-band, including the microwave region's L, C and Ku bands (0.1-16 GHz). Design 1 is obtained by combining four outer L-shaped metallic strips at the four corners of the substrate. The resonance frequency of the transmission coefficient is located at 8.5 GHz (Fig. 3 (b)). In design 2, four horizontally metallic wires are connected in the middle edge, and the resonance frequency is situated at 5.8 GHz. In design 3, four more vertical metallic strips are added to the continuity in design 2. Furthermore, this design produces the two resonance frequencies (nearly at 5 GHz and 14.8 GHz) in the desired operating microwave region. Two more vertical metallic strips are joined to the upper end of design 3. Finally, in design 5, two horizontal bars are connected in the middle of design 4 to obtain the resulting quad 'e' shaped metamaterial, observing the triple-band operating resonance frequencies at 1.4 GHz, 5.0 GHz and 14.8 GHz in the microwave region (Fig. 3(b)).

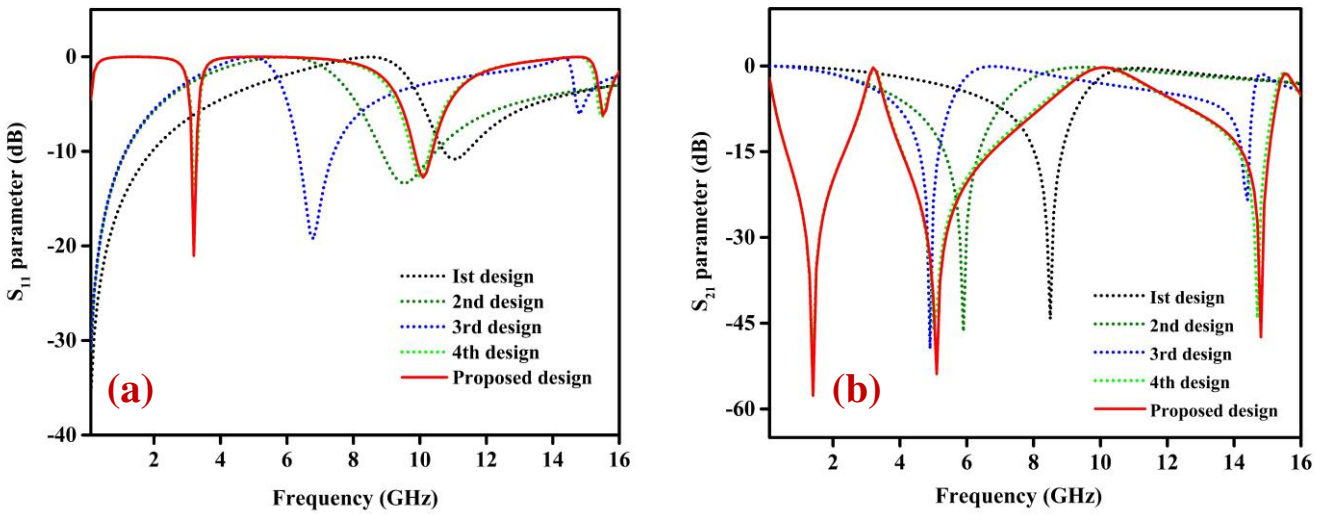

Fig. 3 Response of scattering parameters (a) S_{11} (reflection coefficient) and (b) S_{21} (transmission coeficient) w.r.t incident electromagnetic plane wave frequency

3. Parametric analysis of proposed MTM unit cell structure

3.1. Effect of middle gap width (r) and resonator width (w_r) on resonance frequency

The shift in resonance frequency with the middle gap (r) decreases in a step size of 0.01 cm, as shown in Fig. 4.

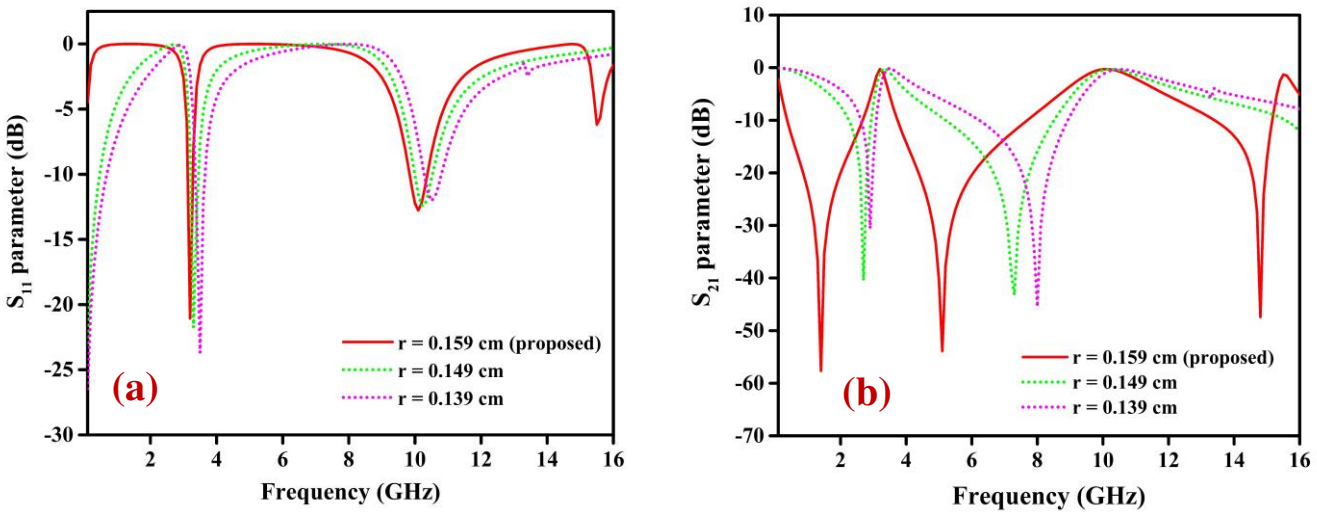

Fig. 4 Scattering parameters response (a) S_{11} (b) S_{21} with the different middle gap width (r)

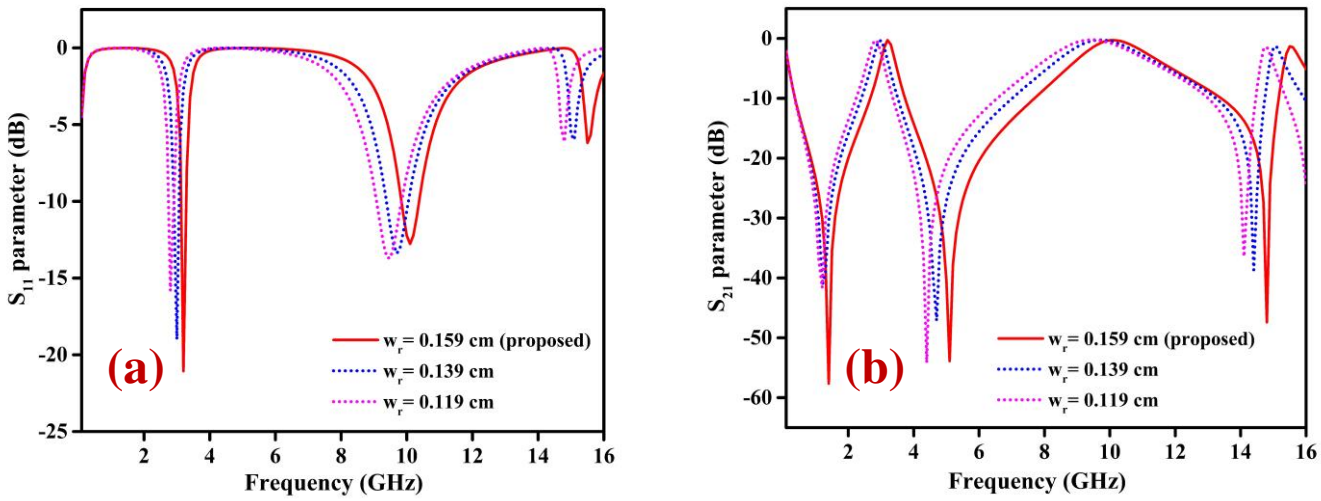

Fig. 5 A plot of scattering parameters response (a) S_{11} (b) S_{21} with the different resonator width (w_r)

The peaks of S_{11} & S_{21} get shifted, showing red-shift, i.e., the higher frequency side, when the middle gap width (r) decreases from 0.16 cm to 0.15 cm. The resonance peaks of S_{21} get reduced to two bands resonance from three bands, further decreasing the middle gap to 0.14 cm, as seen in Fig. 6 (b). The variation of scattering parameters with resonator width (w_r) is also observed and shown in Fig. 5. There is a significant blue shift in a step size of 0.02 cm for both S_{11} and S_{21} parameters with the change of resonator width (w_r). Therefore the designed structure can also be a potential candidate for tunable devices to the appropriate resonance frequency based on the parametric variability (r and w_r).

3.2. Different dielectric material effects on MTM

The impact of modifying the dielectric material on MTM performance was also investigated in the present study. Here we take three Rogers versions (RT 6002, RT 6202, and RT 5880 with FR-4). In the first trial, RT 6002 (lossy) was utilized with a dielectric loss of 0.0012 and an electric permittivity of 2.94, yielding dual resonance frequencies of 1.5 and 5.8 GHz with magnitudes of -45.0 and -48.8 dB, respectively, as shown in Fig. 6. (a). The RT-6202, which has a dielectric loss of 0.0015 and an electric permittivity of 2.9, has dual resonance frequencies of -45.59 and -60.34 dB at 1.5 and 5.8 GHz, respectively. RT 5880 (lossy) has a dielectric loss of 0.0009 and an electric permittivity of 2.2, and also has dual resonance frequencies of -69.07 and -52.04 dB at 1.5 and 6.2 GHz, respectively. Finally, the most commonly used FR-4 (epoxy resin fibre) substrate was chosen, which revealed triple resonances at 1.4, 5.0, and 14.8 GHz with magnitudes of -57.0, -53.8, and -47.4 dB, respectively. Ultimately, due to 5 GHz Wi-Fi applications, the dielectric material for the proposed structure is chosen as FR-4.

3.3. Impact of different metal conductor on resonance frequency

Figure 6 (b) depicts the effect of various metal conductors on resonance frequency. A resonant patch is made up of various conductors such as copper, nickel, gold and platinum. Copper was initially used as a patch to demonstrate triple resonance frequencies of sufficient magnitude and bandwidth. The remaining metals, like platinum, gold and nickel, have the same triple resonance frequencies as copper, although with smaller magnitudes. Consequently, copper has been employed as a resonating patch.

3.4. Impact of the FR-4 substrate thickness (t_s) on metamaterial performance

The substrate material thickness (t_s) is varied from 0.06 to 0.36 cm to analyse its impact on the scattering parameter (S_{21}) performance, as shown in Fig. 6 (c). The decrease in resonance frequency with increase in the substrate thickness is due to the increase in parallel capacitance (Bellal Hossain et al. 2022). The substrate acts as a dielectric medium between the two waveguide ports, due to which at higher frequency values, the shift in resonance frequencies towards lower values is more apparent but low resonance frequency values are not much affected with the substrate thickness. The substrate thickness of 0.16 cm is preferable to others for the proposed metamaterial unit cell due to the requisite resonance frequency depending on the application.

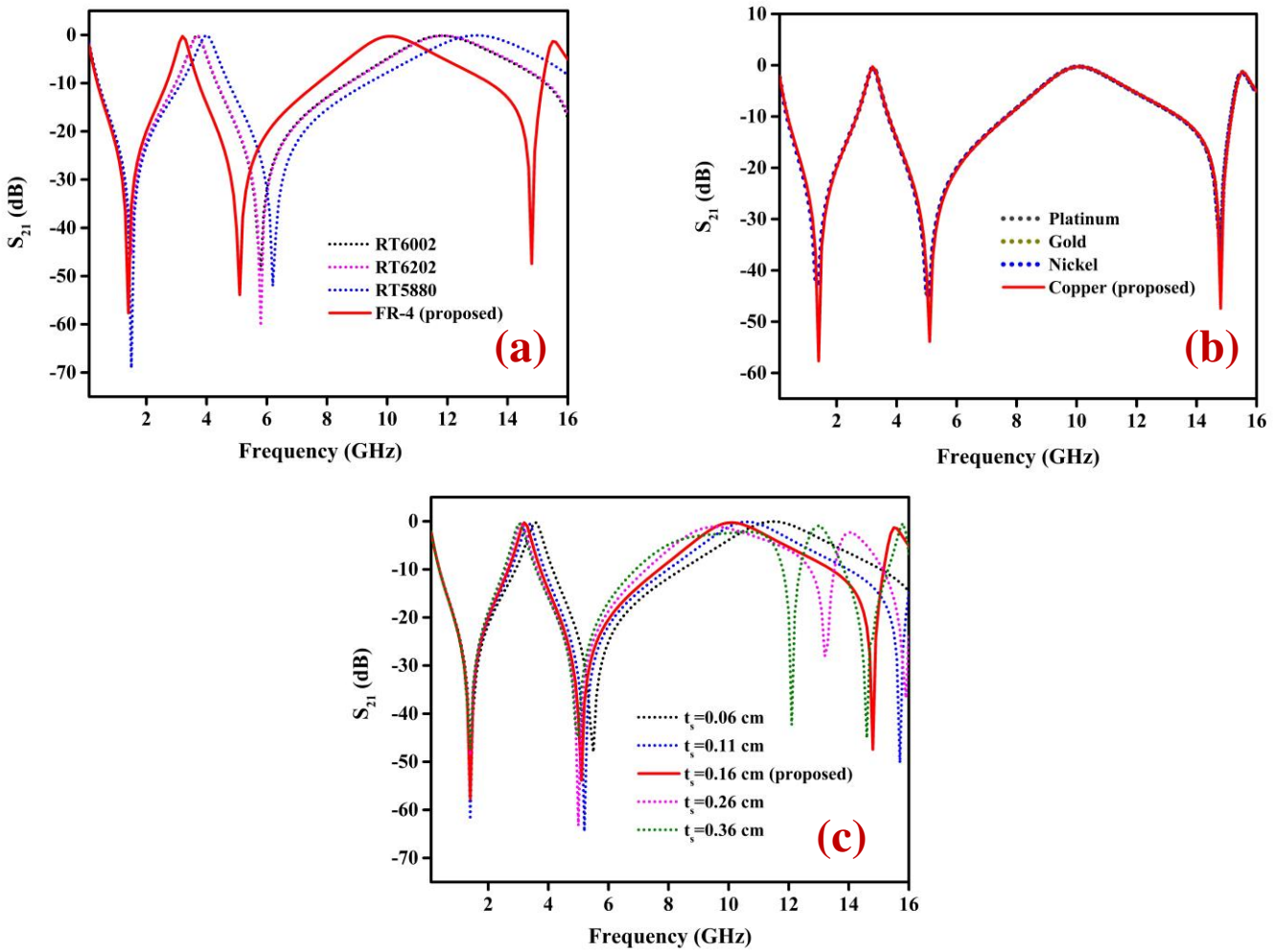

Fig. 6 Variation of transmission coefficient (S_{21}) with the incident wave frequency with the change in (a) different dielectric material, (b) different type of metallic conductor and (c) substrate thickness (t_s) of the designed MTM.

4. Result and Discussion

4.1. Extraction of effective parameters of MTM

The calculation of relative effective permeability (μ_r) and permittivity (ε_r), which are the characteristics of the metamaterials, completely depends on the results of the complex S-parameters. Ziolkowski et al. present a mathematical form of Nicolson-Ross-Wier (NRW), most widely used method of effective parameter extraction in which the transmission coefficient (S_{21}) and the reflection coefficient (S_{11}) obtained from the simulation of a MTM unit cell are used to extract the relative effective permittivity (ε_r), permeability (μ_r), and refractive index (n_r) values (Chen et al. 2004; Islam et al. 2015b; Nicolson and Ross 1970; Rothwell et al. 2016; Smith et al. 2005; Weir 1974; Ziolkowski 2003). For,

$$V_1 = |S_{11}| + |S_{21}| \tag{1}$$

$$V_2 = |S_{21}| - |S_{11}| \tag{2}$$

Eqs. (3) and (4) are used to calculate relative permittivity (ε_r) and relative permeability (μ_r), respectively (Ziolkowski 2003).

$$\varepsilon_r \sim \frac{2}{jk_0 d} \times \frac{(1-V_1)}{(1+V_1)} = \frac{c}{j\pi\nu d} \frac{(1-S_{21}-S_{11})}{(1+S_{21}+S_{11})} \tag{3}$$

$$\mu_r \sim \frac{2}{jk_0 d} \times \frac{(1-V_2)}{(1+V_2)} = \frac{c}{j\pi\nu d} \frac{(1-S_{21}+S_{11})}{(1+S_{21}-S_{11})} \tag{4}$$

Where $k_0 = \frac{2\pi\nu}{c}$, c represents the velocity of light, ν is the incident frequency of electromagnetic wave and d is the thickness of the substrate.

The refractive index (η_r) can be calculated using simplified formula written as (Islam et al. 2015b)-

$$\eta_r = \sqrt{\varepsilon_r \mu_r} = \frac{c}{j\pi\nu d}\sqrt{\left\{\frac{(S_{21}-1)^2-(S_{11})^2}{(S_{21}+1)^2-(S_{11})^2}\right\}} \tag{5}$$

The normalized impedance (Z) can be calculated using the following formula-

$$Z = \sqrt{\frac{(1+S_{11})^2-S_{21}^2}{(1-S_{11})^2-S_{21}^2}} \tag{6}$$

Fig. 7 (a) and (b) represent the comparison of the simulation result of the unit cell's reflection (S_{11}) and transmission coefficient (S_{21}) from two different software.

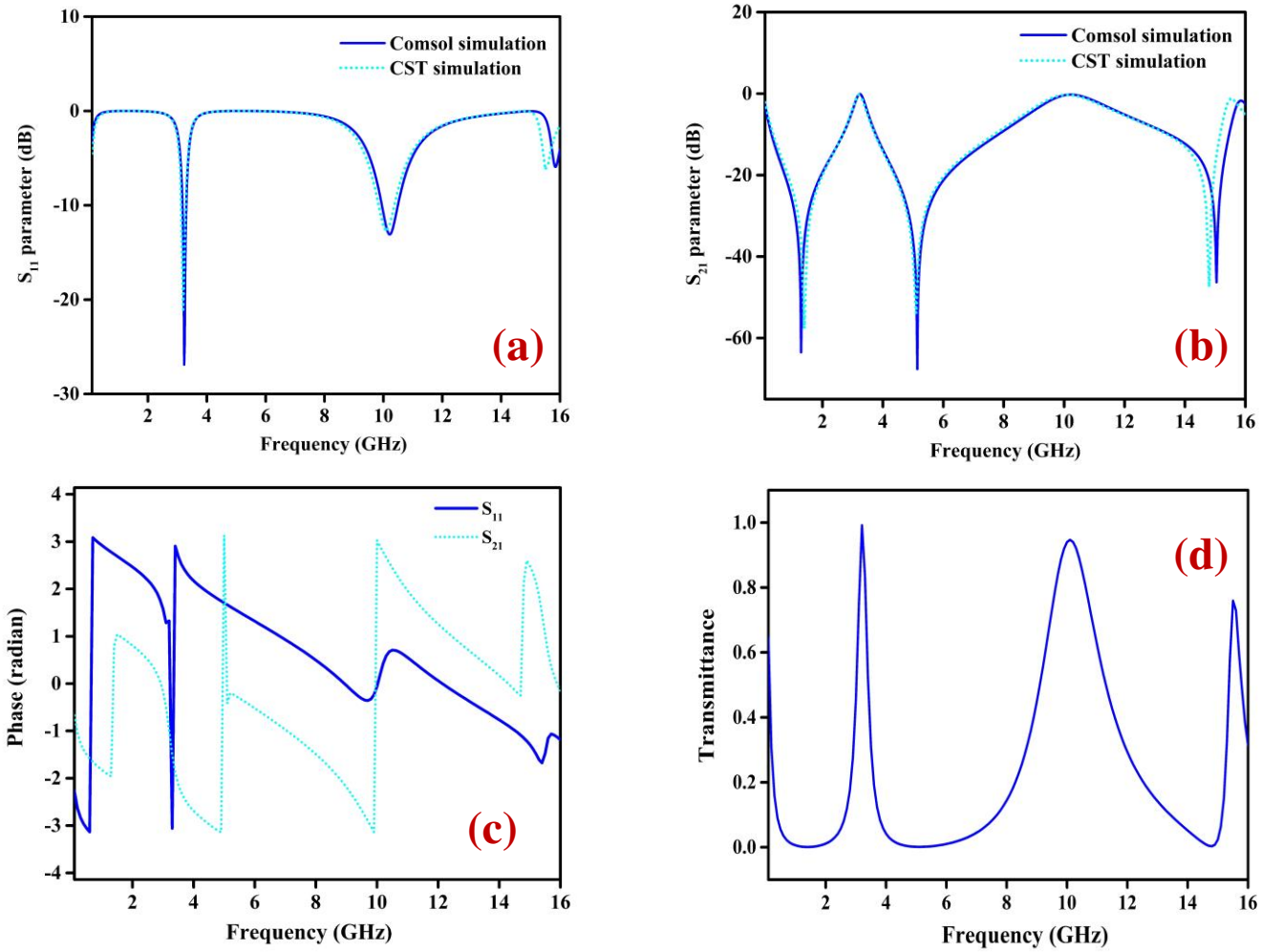

Fig. 7 (a) Reflection coefficient (S_{11}), (b) transmission coefficient (S_{21}) comparison from two simulation software COMSOL and CST Microwave Studio, (c) phase plot of scattering parameters and (d) transmittance plot with the incidence wave frequency of the unit cell of the structure

The scattering parameters (S_{11} and S_{21}) for FR-4 substrate material with wave propagation in the z-axis direction were calculated using COMSOL and CST simulators based on Finite element method (FEM), shown in Fig. 7 (a),(b). For the FR-4 substrate material, the findings from both simulators are quite identical. The S_{21} findings of the unit cell reveal triple resonance frequencies at 1.4, 5.0 and 14.8 GHz with magnitudes of -57.0, -53.8 and -47.4 dB, respectively, using COMSOL simulator.

The CST simulator, on the other hand, shows same resonance frequencies at 1.4, 5.0 and 14.8 GHz with magnitudes of -57.0, -53.9 and -47.7 dB, respectively, shown in Fig. 7 (b). These three findings of resonance frequencies lies within the microwave region, namely 1-2 GHz, 4-6 GHz, and 14-16 GHz, which depict the L-band, C-band, and Ku-band. Using COMSOL simulator, the bandwidth of S_{21} using less than -17 dB is 1.49 GHz (0.70-2.19 GHz), 2.22 GHz (4.20-6.42 GHz), and 0.58 GHz (14.41-14.99 GHz), whereas CST simulator yields 1.54 GHz (0.70-2.25 GHz), 2.27 GHz (4.16-6.44 GHz), and 0.61 GHz (14.38-15.00 GHz). The reflection coefficient (S_{11}) findings of the unit cell reveal triple resonance frequencies at 3.2, 10.2, and 15.8 GHz with magnitudes of -21.06, -13.08, and -5.87 dB, respectively, using COMSOL simulator. however, the CST simulator exposed similar resonance frequencies at 3.2, 10.2, and 15.8 GHz with magnitudes of -21.06, -12.76, and -6.18 dB, respectively, as shown in Fig. 7. (a). Each resonance frequency of S_{11} follows the resonance frequency of S_{21}, as shown in Fig. 7 (a) and (b) from both the simulation. From the above discussion, we can say that the metamaterial unit cell's bandwidth is roughly same in both simulators. However, in wireless communications, bandwidth is a vital element. For satellite and Wi-Fi applications, the proposed MTM design provides ample bandwidth. The comparison of proposed work with published work with effective bandwith is shown in Table 2. The phase plot of scattering parameters (S_{11} and S_{21}) is shown in Fig. 7 (c), which demonstrates that the input wave with the output of reflected and transmitted varies in $-\pi\ to + \pi$ (value $\mp$ 3.14 in plot 4 (c)) with the total phase change is 2π. There is maximum transmittance at the frequency span of 2.5-3.5 GHz, 9.5-10.5 GHz, and 15.5-16 GHz which corresponds to the resonance peaks of the reflection (S_{11}) coefficient (Fig. 7 (a)). The real and imaginary plots of the proposed metamaterials unit cell structure's relative effective permeability, permittivity and refractive index are shown in Fig. 8 (a)-(c).

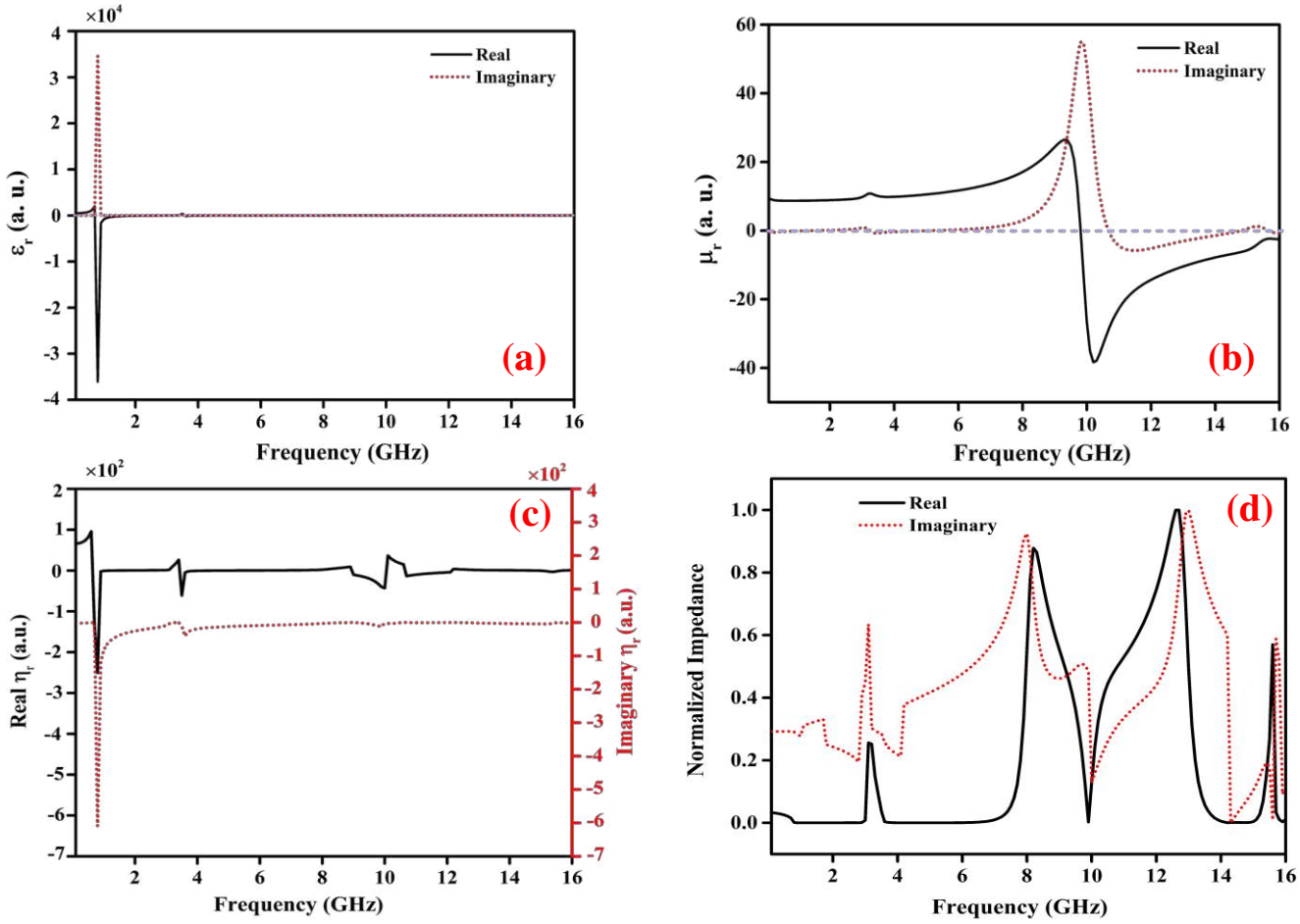

Fig. 8 Variation of (a) relative effective permeability (μ_r), (b) permittivity (ε_r), (c) refractive index (η_r) and (d) normalised impedance (Z) with the frequency of the designed unit cell

Table II Comparison of different Bandwidth of proposed work with the recent papers.

References	Dimension (physical and electrical)	Resonance Frequencies (GHz)	Frequency band	Effective Bandwidth (GHz)
(Hossain et al. 2021)	9×9 mm^2 (0.087λ×0.087λ)	2.896, 8.11, 9.76, 12.48, 13.49	S, X, Ku	0.3, 0.54, 0.59, 0.24, 0.35
(Moniruzzaman et al. 2021)	10×10 mm^2 (0.14λ×0.14λ)	4.20, 10.14, 13.15, 17.1	C, X, Ku	0.72, 1.55, 0.17, 0.24
(Rashedul Islam et al. 2020)	8×8 mm^2 (0.070λ×0.070λ)	2.61, 6.32, 9.29	S, C, X	0.11, 0.79, 0.15
(Islam et al. 2021b)	8×8 mm^2 (0.06λ×0.06λ)	2.48, 4.28, 9.36, 13.7	C, S, X, Ku	0.19, 0.4, 1.3, 0.6
(Islam et al. 2021a)	8×8 mm^2 (0.076λ×0.076λ)	2.86, 5, 8.30	S, C, X	0.11, 0.41, 0.37
(Bellal Hossain et al. 2022)	10×10 mm^2 (0.17λ×0.17λ)	5, 6.88, 8.429	C, X	1.67, 0.52, 0.98
Present work	16×16 mm^2 (0.07λ×0.07λ)	1.4, 5, 14.8	L, C, Ku	1.49, 2.22, 0.58

Relative effective permittivity is negative between 0.5 and 1.5 GHz, while permeability is negative between 9 and 16 GHz for the proposed structure, as evident in Fig. 8 (a), (b). The frequency ranges for which the real part of the negative refractive index has been observed are 0.5-1 GHz, 3.5-4 GHz, and 9-12 GHz, as illustrated in Fig. 8 (c). The graph of normalized impedance against frequency, shown in Fig. 8 (d), demonstrates the positive and real values of the normalized impedance over the whole frequency range. Normalized impedance is detected nearly equal to zero, for instance, 0.045×10^{-3}, 0.118×10^{-3} and 0.615×10^{-3} at the resonance frequency of 1.4, 5.0 and 14.8 GHz, respectively. The smaller values of normalized impedance at resonance frequencies show the passiveness of the proposed metamaterial.

4.2. Analysis of Electromagnetic Fields and Surface current distribution

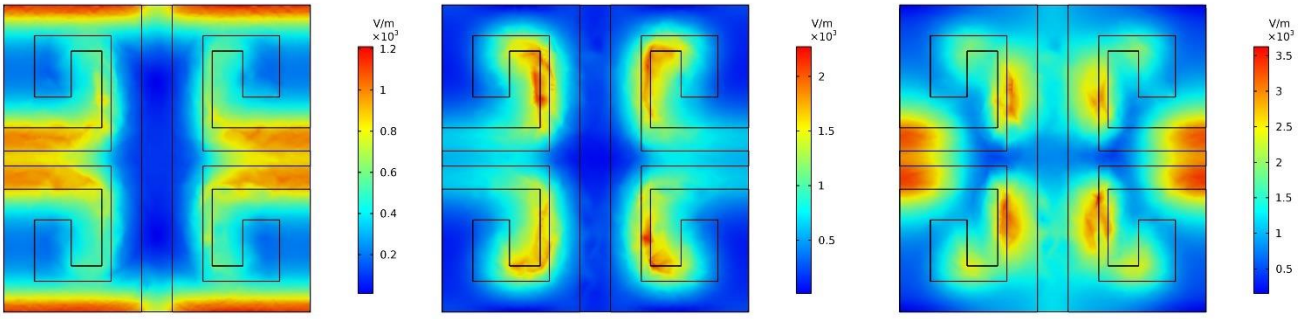

Fig. 9 Electric field distribution at 1.4 GHz, 5.0 GHz, and 14.8 GHz, respectively.

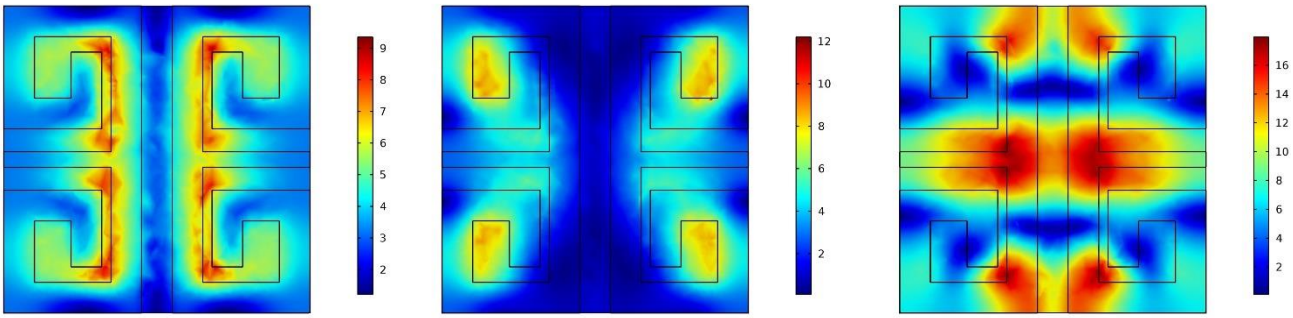

Fig. 10 Magnetic field distribution at 1.4 GHz, 5.0 GHz and 14.8 GHz respectively of quad 'e' shaped structure

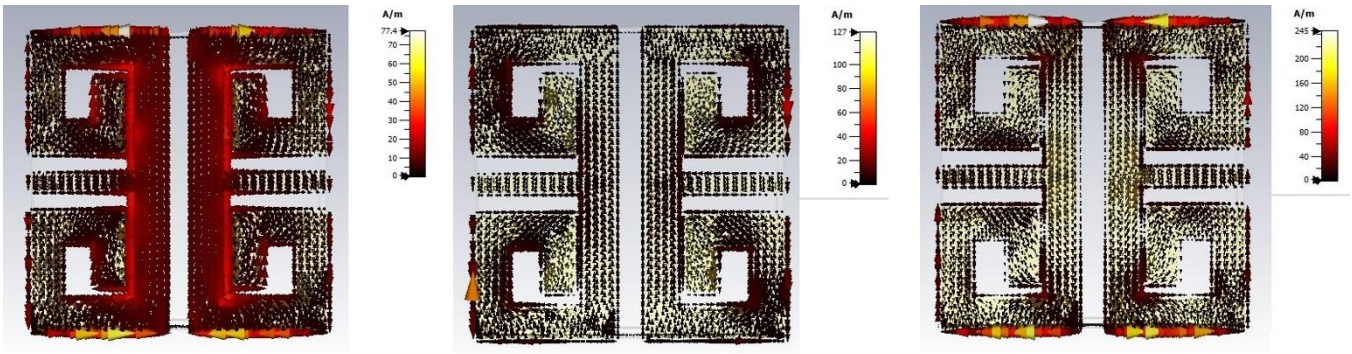

Fig. 11 Surface current distribution at 1.4 GHz, 5.0 GHz and 14.8 GHz respectively of quad 'e' shaped structure

Fig. 9 depicts the electric field at 1.4 GHz, 5.0 GHz, and 14.8 GHz, where the electric field indicates the current density. For 14.8 GHz, the electric field is stronger on both ends of the central line (w_c) separating the structure, whereas, for 1.4 GHz and 5.0 GHz, it is lower on both ends of (w_c). Fig. 10 depicts the magnetic field at 1.4 GHz, 5.0 GHz, and 14.8 GHz. At the higher frequency of 14.8 GHz, the magnetic field in the resonator width (w_r) strip near the middle gap (r) is stronger than at 1.4 GHz and 5.0 GHz. The electric field for 1.4 GHz, 5.0 GHz and 14.8 GHz is shown in Fig. 9, where the electric field represents the current density. Fig. 11 depicts the excitation of the surface current distribution at 1.4 GHz, 5.0 GHz, and 14.8 GHz, with the intensity of the currents represented by different colors. Fig. 11 shows that the current intensity distribution at lower resonance frequencies (1.4 GHz) is greater than at higher resonance frequencies (14.8 GHz). At both resonance frequencies, 1.4 GHz and 14.8 GHz, the current flow in the top resonator strip section is relatively opposite to that in the lower section, with the sole difference being the current distribution. At 14.8 GHz, the current dispersion is lower than at 1.4 GHz. Fig. 12 represents the designed structure's 2-D Far-Field normalized radiation pattern plot.

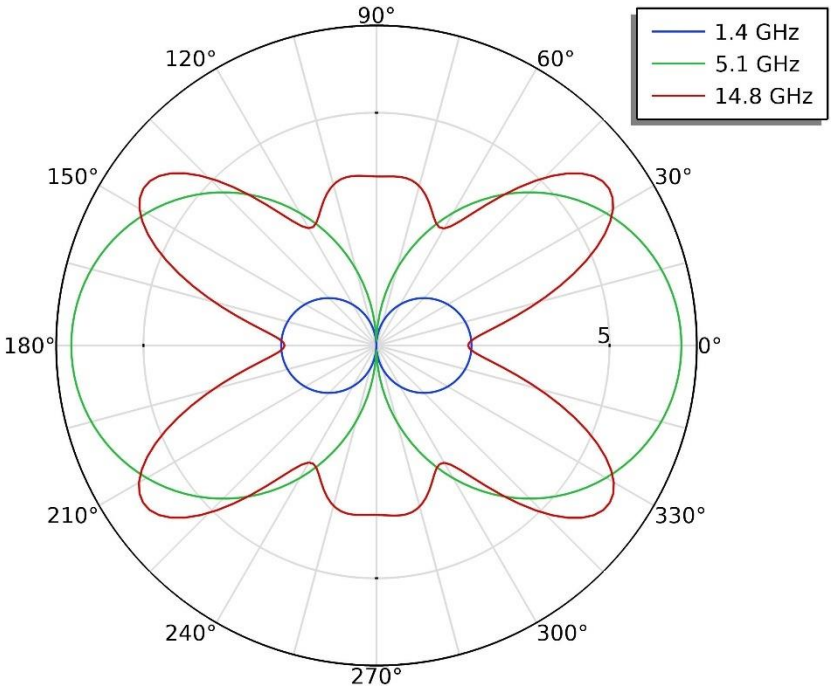

Fig. 12 2-D Far-field normalized radiation pattern

The peaks of the transmission coefficient (S_{21}) are obtained at 1.4 GHz, 5.0 GHz, and 14.8 GHz (Fig. 4(b)). At these frequencies, it is seen from Fig. 12 that the lobe part of the radiation pattern at a higher frequency is multi-directional, and it is distributed symmetrically along the central line, i.e., along the horizontal or vertical corresponding 0^o and 90^o. Also, it is seen that when we move further across higher frequencies, the lobes increase and get bigger.

4.3. Effective Medium Ratio (EMR)

EMR is one of the significant aspects of metamaterial design and development that provides the compactness of the metamaterial. For the designed structure to be considered a metamaterial, the Effective Medium Theory (EMT) is applied according to which unit cell dimension should be less than the operating wavelength (Slovick et al. 2014). It is observed that the dimension of a unit cell is 1.6 cm which is less than the operating wavelength for all three frequency bands. Therefore, EMT becomes applicable, and the structure acquires metamaterial character. It is calculated as follows (Almutairi et al. 2019):

$$\text{EMR} = \frac{\text{Operating Wavelength for the unit cell}}{\text{length of the unit cell}} \tag{4}$$

The EMR of the proposed Quad ‘e' mirror-shaped unit cell is compared with various metamaterial designs reported in recent years in Table III. These designs suffer from significant limitations, such as a reduced EMR and resonant frequency functioning inside the single or double microwave band. The proposed unit cell has a high EMR, compact dimension, and covers all three frequency bands (L, C, Ku) used in satellite and multi-band applications. The EMR of the designed metamaterial is found to be 13.37 for the unit cell (1.6 cm × 1.6 cm × 1.635 cm) in the frequency range 0.1-16 GHz. The compactness of the structure is improved due to the high value of EMR.

Table III. A comparison of the EMR of various metamaterial design

References	The shape of a unit cell	Dimension (cm^2)	Substrate	Bands	No. of Resonant frequency	EMR
(Urbani 2010)	Diamond shape	2.0 × 2.5	FR-4	-	-	1.2

(Karamanos et al. 2012)	Wedge- shaped	0.53 × 0.43	Taconic CER-10	-	-	6.9
(Mallik et al. 2013)	Two rectangular U-shaped	2.0 × 2.5	Glass	-	-	1.99
(Islam et al. 2014)	Split H- shaped	2.0 × 2.0	FR-4	S, C, X, Ku	4	4.32
(Islam et al. 2015a)	Modified SRR & CLS unit cell	0.5 × 0.32	FR-4	-	-	6.38
(Sarkhel et al. 2015)	DBEM (Dual-band electric meta-atom)	0.75 × 0.75	Rogers RT	Dual bands	2	7.14
(Faruque et al. 2017)	Double C- shaped	1.2 × 1.2	FR-4	S, C, X	3	7.44
(Almutairi et al. 2019)	CSRR	0.5 × 0.5	FR-4	C	2	8
(Mohammad Siddiky et al. 2020)	Inverse double C- type	0.9 × 0.9	FR-4	S, C, X, K	5	12.34
Present Work	Proposed metamaterial	1.6 × 1.6	FR-4	L, C, Ku	3	13.37

Conclusion

This paper introduces a new metamaterial structure for triple-band operation with wide bandwidth. The effective propagation characteristics of the proposed structure were investigated over the frequency range of 0.1-16 GHz, and the effective medium parameters were obtained. A high-frequency electromagnetic simulator was used for the design, simulation, and extraction of the metamaterial's S-parameters. The NRW method was used to obtain the metamaterial's effective medium parameters. Analysis of the proposed Quad ‘e’ mirror-shaped metamaterial exhibits a relatively effective negative refractive index for multi-band operations. The CST software was also used to study the scattering parameter results of the unit cell, and the S_{21} results were compared to the findings of the simulator COMSOL software to verify the results. Surface current and electromagnetic field (electric and magnetic field distribution) analysis are used to investigate the MTM phenomenon thoroughly in this paper. The proposed quad 'e' mirror-shaped metamaterial can enhance emerging satellite communications and radar applications with multiband microwave applications, such as gain enhancement of multiband antennas due to its small size, low-cost FR-4 substrate, multiband resonance, high EMR, and wideband characteristics. EMR of the designed structure is 13.37, which specifies that this design is compact and has potential application in the microwave region covering all three frequency bands. Thus, the reported structure can be used in various advanced applications for electromagnetic cloaking, filter design, sensor, detector layout, and antenna with improved features.

Acknowledgments

Authors gratefully acknowledge the initiatives and support from TIFAC-Centre of Relevance and Excellence in Fiber Optics and Optical Communication at Delhi College of Engineering, now DTU, Delhi, under Mission REACH program of Technology Vision-2020, Government of India. One of the authors, Mr. Ankit, would like to acknowledge (i) Delhi Technological University Delhi for financial support in terms of the Research Fellowship and (ii) Mr. Monu Nath Baitha of Yonsei University for giving his help in crucial and critical discussions on this research work.

References

Ahamed, E., Faruque, M.R.I., Alam, M.J., Mansor, M.F. Bin, Islam, M.T.: Digital metamaterial filter for encoding information. Sci. Rep. 10, 3289 (2020). https://doi.org/10.1038/s41598-020-60170-8

Almutairi, A.F., Islam, M.S., Samsuzzaman, M., Islam, M.T., Misran, N., Islam, M.T.: A complementary split ring resonator based metamaterial with effective medium ratio for C-band microwave applications. Results Phys. 15, 102675 (2019). https://doi.org/10.1016/j.rinp.2019.102675

Bellal Hossain, M., Rashed Iqbal Faruque, M., Alshammari, A.S., Tariqul Islam, M.: Wide bandwidth enriched symmetric hexagonal split ring resonator based triple band negative permittivity metamaterial for satellite and Wi-Fi applications. Results Phys. 37, 105511 (2022). https://doi.org/10.1016/j.rinp.2022.105511

Chen, X., Grzegorczyk, T.M., Wu, B.I., Pacheco, J., Kong, J.A.: Robust method to retrieve the constitutive effective parameters of metamaterials. Phys. Rev. E - Stat. Physics, Plasmas, Fluids, Relat. Interdiscip. Top. 70, 7 (2004). https://doi.org/10.1103/PhysRevE.70.016608

Dhouibi, A., Burokur, S.N., de Lustrac, A., Priou, A.: Study and analysis of an electric Z-shaped meta-atom. Adv. Electromagn. 1, 64–70 (2012). https://doi.org/10.7716/aem.v1i2.82

Esmail, B.A.F., Koziel, S., Szczepanski, S.: Overview of Planar Antenna Loading Metamaterials for Gain Performance Enhancement: The Two Decades of Progress. IEEE Access. 10, 27381–27403 (2022). https://doi.org/10.1109/ACCESS.2022.3157634

Faruque, M.R.I., Hossain, M.J., Islam, S.S., Jamlos, M.F. Bin, Islam, M.T.: Design and analysis of a new double C-shaped miniaturized metamaterial for multiband applications. Appl. Phys. A Mater. Sci. Process. 123, 1–8 (2017). https://doi.org/10.1007/s00339-016-0727-y

Fedotov, V.A., Rose, M., Prosvirnin, S.L., Papasimakis, N., Zheludev, N.I.: Sharp trapped-mode resonances in planar metamaterials with a broken structural symmetry. Phys. Rev. Lett. 99, 5–8 (2007). https://doi.org/10.1103/PhysRevLett.99.147401

Hossain, M.B., Faruque, M.R.I., Islam, S.S., Islam, M.T.: Modified double dumbbell-shaped split-ring resonator-based negative permittivity metamaterial for satellite communications with high effective medium ratio. Sci. Rep. 11, 19331 (2021). https://doi.org/10.1038/s41598-021-98703-4

Hossain, T.M., Jamlos, M.F., Jamlos, M.A., Soh, P.J., Islam, M.I., Khan, R.: Modified H-shaped DNG metamaterial for multiband microwave application. Appl. Phys. A Mater. Sci. Process. 124, 1–7 (2018). https://doi.org/10.1007/s00339-018-1593-6

Islam, M.M., Islam, M.T., Samsuzzaman, M., Faruque, M.R.I., Misran, N., Mansor, M.F.: A miniaturized antenna with negative index metamaterial based on modified SRR and CLS unit cell for UWB microwave imaging applications. Materials (Basel). 8, 392–407 (2015)(a). https://doi.org/10.3390/ma8020392

Islam, M.R., Islam, M.T., Soliman, M.S., Baharuddin, M.H., Mat, K., Moubark, A.M., Almalki, S.H.A.: Metamaterial based on an inverse double V loaded complementary square split ring resonator for radar and Wi-Fi applications. Sci. Rep. 11, 21782 (2021)(a). https://doi.org/10.1038/s41598-021-01275-6

Islam, M.T., Moniruzzaman, M., Alam, T., Samsuzzaman, M., Razouqi, Q.A., Almutairi, A.F.: Realization of frequency hopping characteristics of an epsilon negative metamaterial with high effective medium ratio for multiband microwave applications. Sci. Rep. 11, 16898 (2021)(b). https://doi.org/10.1038/s41598-021-96228-4

Islam, S.S., Faruque, M.R.I., Islam, M.T.: A new double negative metamaterial for multi-band microwave applications. Appl. Phys. A. 116, 723–733 (2014). https://doi.org/10.1007/s00339-014-8549-2

Islam, S.S., Faruque, M.R.I., Islam, M.T.: A new direct retrieval method of refractive index for the metamaterial. Curr. Sci. 109, 337–342 (2015)(b). https://doi.org/10.18520/cs/v109/i2/337-342

Jing, X., Feng, D., Tian, Y., Li, M., Chu, C., Li, C., He, Y., Gan, H., Hong, Z.: Design of two invisibility cloaks using transmissive and reflective metamaterial-based multilayer frame microstructures. Opt. Express. 28, 35528 (2020). https://doi.org/10.1364/oe.409137

Karaaslan, M., Bağmancı, M., Ünal, E., Akgol, O., Sabah, C.: Microwave energy harvesting based on metamaterial absorbers with multi-layered square split rings for wireless communications. Opt. Commun. 392, 31–38 (2017). https://doi.org/10.1016/J.OPTCOM.2017.01.043

Karamanos, T.D., Dimitriadis, A.I., Kantartzis, N. V.: Compact double-negative metamaterials based on electric and magnetic resonators. IEEE Antennas Wirel. Propag. Lett. 11, 480–483 (2012). https://doi.org/10.1109/LAWP.2012.2197170

Kishor, K., Baitha, M.N., Sinha, R.K., Lahiri, B.: Tunable negative refractive index metamaterial from V-shaped SRR structure: fabrication and characterization. J. Opt. Soc. Am. B. 31, 1410 (2014). https://doi.org/10.1364/josab.31.001410

Kishor, K., Sinha, R.K.: Design of planar metamaterial optical resonator. 2012 Int. Conf. Fiber Opt. Photonics, PHOTONICS 2012. 8–10 (2012)(a). https://doi.org/10.1364/photonics.2012.m3b.5

Kishor, K., Sinha, R.K.: Design of planar metamaterial optical antenna. Plasmon. Met. Nanostructures Their Opt. Prop. X. 8457, 84572N (2012)(b). https://doi.org/10.1117/12.929581

Lahiri, B., Mcmeekin, S.G., Khokhar, A.Z., De La Rue, R.M., Johnson, N.P.: Asymmetric split ring resonators for organic sensing. Ict. 2009 11th Int. Conf. Transparent Opt. Networks. 17, 1107–1115 (2009). https://doi.org/10.1109/ICTON.2009.5185094

Lv, J., Zhou, M., Gu, Q., Jiang, X., Ying, Y., Si, G.: Metamaterial Lensing Devices. Molecules. 24, 2460 (2019). https://doi.org/10.3390/molecules24132460

Mallik, A., Kundu, S., Goni, M.O.: Design of a novel two-rectangular U-shaped double negative metamaterial. In: 2013 International

Conference on Informatics, Electronics and Vision (ICIEV). pp. 1–6. IEEE (2013)
Mao, C.-X., Gao, S., Wang, Y., Chu, Q.-X., Yang, X.-X.: Dual-Band Circularly Polarized Shared-Aperture Array for C -/ X -Band Satellite Communications. IEEE Trans. Antennas Propag. 65, 5171–5178 (2017). https://doi.org/10.1109/TAP.2017.2740981
Mohammad Siddiky, A., Rashed Iqbal Faruque, M., Tariqul Islam, M., Abdullah, S., Uddin Khandaker, M.: Inverse double-C shaped square split ring resonator based metamaterial with multi-resonant frequencies for satellite band applications. Results Phys. 19, (2020). https://doi.org/10.1016/j.rinp.2020.103454
Moniruzzaman, M., Islam, M.T., Hossain, I., Soliman, M.S., Samsuzzaman, M., Almalki, S.H.A.: Symmetric resonator based tunable epsilon negative near zero index metamaterial with high effective medium ratio for multiband wireless applications. Sci. Rep. 11, 21842 (2021). https://doi.org/10.1038/s41598-021-01266-7
Moniruzzaman, M., Islam, M.T., Muhammad, G., Singh, M.S.J., Samsuzzaman, M.: Quad band metamaterial absorber based on asymmetric circular split ring resonator for multiband microwave applications. Results Phys. 19, 103467 (2020). https://doi.org/10.1016/j.rinp.2020.103467
Nicolson, A.M., Ross, G.F.: Measurement of the Intrinsic Properties of Materials by Time-Domain Techniques. IEEE Trans. Instrum. Meas. 19, 377–382 (1970). https://doi.org/10.1109/TIM.1970.4313932
Rashedul Islam, M., Tariqul Islam, M., Moniruzzaman, M., Samsuzzaman, M., Bais, B., Arshad, H., Muhammad, G.: Square enclosed circle split ring resonator enabled epsilon negative (ENG) near zero index (NZI) metamaterial for gain enhancement of multiband satellite and radar antenna applications. Results Phys. 19, 103556 (2020). https://doi.org/10.1016/j.rinp.2020.103556
Rothwell, E.J., Frasch, J.L., Ellison, S.M., Chahal, P., Ouedraogo, R.O.: Analysis of the Nicolson-Ross-Weir method for characterizing the electromagnetic properties of engineered materials. Prog. Electromagn. Res. 157, 31–47 (2016). https://doi.org/10.2528/PIER16071706
Sarkhel, A., Mitra, D., Paul, S., Chaudhuri, S.R.B.: A compact meta-atom for dual band negative permittivity metamaterial. Microw. Opt. Technol. Lett. 57, 1152–1156 (2015). https://doi.org/10.1002/mop.29041
Slovick, B.A., Yu, Z.G., Krishnamurthy, S.: Generalized effective-medium theory for metamaterials. Phys. Rev. B. 89, 155118 (2014). https://doi.org/10.1103/PhysRevB.89.155118
Smith, D.R., Padilla, W.J., Vier, D.C., Nemat-Nasser, S.C., Schultz, S.: Composite Medium with Simultaneously Negative Permeability and Permittivity. Phys. Rev. Lett. 84, 4184–4187 (2000). https://doi.org/10.1103/PhysRevLett.84.4184
Smith, D.R., Vier, D.C., Koschny, T., Soukoulis, C.M.: Electromagnetic parameter retrieval from inhomogeneous metamaterials. Phys. Rev. E - Stat. Nonlinear, Soft Matter Phys. 71, 1–11 (2005). https://doi.org/10.1103/PhysRevE.71.036617
Srinivasan, K., Ali, N. Ben, Trabelsi, Y., Mani Rajan, M.S., Kanzari, M.: Design of a modified single-negative metamaterial structure for sensing application. Optik (Stuttg). 180, 924–931 (2019). https://doi.org/10.1016/J.IJLEO.2018.12.012
Sureshkumar, S., Anand, P.M.R., Prajapati, A., Sankaran, K.S.: Negative Index Metamaterial Based Dual-Band Microwave Absorber. In: 2018 International Conference on Communication and Signal Processing (ICCSP). pp. 0897–0900. IEEE (2018)
Urbani, F.: Experimental analysis of novel single-sided left-handed metamaterial. IEEE Antennas Wirel. Propag. Lett. 9, 720–723 (2010). https://doi.org/10.1109/LAWP.2010.2058837
Weir, W.B.: Automatic measurement of complex dielectric constant and permeability at microwave frequencies. Proc. IEEE. 62, 33–36 (1974). https://doi.org/10.1109/PROC.1974.9382
Zhang, J., Yan, S., Vandenbosch, G.A.E.: Metamaterial-inspired dual-band frequency-reconfigurable antenna with pattern diversity. Electron. Lett. 55, 573–574 (2019). https://doi.org/10.1049/el.2019.0329
Ziolkowski, R.W.: Design, fabrication, and testing of double negative metamaterials. IEEE Trans. Antennas Propag. 51, 1516–1529 (2003). https://doi.org/10.1109/TAP.2003.813622
Ziolkowski, R.W.: Metamaterial-Based Antennas : Research and Developments. 1267–1275 (2006)

e-ISSN: 2582-5208
International Research Journal of Modernization in Engineering Technology and Science
(Peer-Reviewed, Open Access, Fully Refereed International Journal)
Volume:04/Issue:05/May-2022 Impact Factor- 6.752 www.irjmets.com

DESIGN OF MULTI-PURPOSE DRONE CAPABLE OF SURFICIAL AND AERIAL MOVEMENT

Dr. Ak Madan[*1], Aakash[*2], Abhay Dharia[*3], Aayush Kumar[*4], Abhishek Verma[*5], Ashwin Rao[*6]

[*1]Professor, Department of Mechanical Engineering, Delhi Technological University, Delhi, India.

[*2,3,4,5,6]Student, Department of Mechanical Engineering, Delhi Technological University, Delhi, India.

ABSTRACT

In recent times, drone technology finds a plethora of applications ranging from military to commercial. During the covid pandemic, drones were crucial in assisting individuals and government in various ways to prevent the pandemic from spreading further. Drones were used for a range of purposes, including medical supplies, surveillance, disinfection, infection screening, public awareness, temperature monitoring, and more. Drone technology is capable of carrying out all of these tasks without any human-to-human interaction. With the advancement in science and technology drones will find use in every field. This paper presents the conceptual design of a multipurpose drone which helps in doing surveillance from land as well as air for a proper ariel and landscape view. The drone is capable of travelling up to 20 km having a flight time of about 1hr with a payload capacity of 5kgs.Done the CFD analysis to improvise the aerodynamics and minimize the drag effect on the drone by Rectifying the design.

Keywords: UAV, Drone, Pay Load, CFD, Industry 4.0.

I. INTRODUCTION

A quadcopter, sometimes known as a quadrotor helicopter, is a multirotor helicopter that is lifted and propelled by four rotors. Each of the four arms has an engine and a propeller at the end. Quadcopters are classed as rotorcrafts since they use rotors and vertically phased propellers to produce lift. Pre-programmed missions are another name for this. A quadcopter uses two sets of identical fixed-pitch propellers: two clockwise (CW) in one direction and two counter-clockwise (CCW) in the opposite direction. Its aim is to allow the machine to hover in a stable position. In comparison to most helicopters, this is unusual. The vehicle's motion is controlled by adjusting the rotor discs' rotation rate, which alters the torque load and thrust/lift characteristics. Lift and torque are controlled by varying the RPM unit. For optimal yaw smoothness lift capacity, multirotor with a larger number of blades are envisioned and developed to carry a proportionally heavier payload. Various series may be employed depending on the efficiency necessary for a specific job/task. Drones (unmanned aerial vehicles) are electronic aircraft that may be operated remotely. It can achieve vertical flight with stability and can be utilised for a number of purposes like as live streaming, capturing photographs with a camera, and increasing the performance and lowering the cost of the microcontroller as technology progresses. This will assist the average person in designing their own drone. The primary goal of this project is to stream live and collect photographs. A frame, flight control board, motors, electronic speed controllers, a transmitter, a receiver, Lipo battery, and camera interfaced with the kit are all included in this drone. Drones have the ability to perform a variety of jobs in which people are unable to participate. For example, in numerous sectors, extreme temperature and high altitude monitoring, as well as rescue missions. Drones have four propellers with motors that produce the thrust needed to lift the aircraft. Quad copter is another name for a drone. The quad copter's main operating principle is that two motors revolve in a clockwise manner and the other rotates in an anticlockwise way. This aids the aircraft's vertical ascent. We can access live streaming and image capture during the flight with the help of a camera.

Unmanned aerial vehicles (UAVs) and drones are other terms for unmanned aerial vehicles. Industries are starting to recognise the operational and economic benefits of drone-enabled tasks. The Internet of Things (IoT), Big Data, drones, and other advanced technologies that can be implemented to achieve Industry 4.0 are examples of implementable advanced technologies. The goal of this research is to go over the significant contributions of drones to Industry 4.0.

e-ISSN: 2582-5208
International Research Journal of Modernization in Engineering Technology and Science
(Peer-Reviewed, Open Access, Fully Refereed International Journal)
Volume:04/Issue:05/May-2022 Impact Factor- 6.752 www.irjmets.com

II. METHODOLOGY

SolidWorks software is used to design the following parts:

Spider Base, Spider Top, Spacer, Distribution Board, Spider Arm, Spinner, Fan, Motor, Battery, Electrical Unit 1 and Electrical Unit 2.

- A quadcopter is a device that combines Electronics, Mechanical, and primarily Aviation principles.
- The Quadcopter contains four motors whose rotational speed and direction alter depending on the user's wish to propel the gadget in a specific direction (i.e Takeoff motion, Landing motion, Forward motion, Backward motion, Left motion, Right Motion.)
- Motor rotation varies depending on the sent signal from the 6-Channel transmitter.
- The AT-MEGA 16 chip is used to write the programme.
- The microprocessor sends a signal to the ESCs, which control the motor's speed.

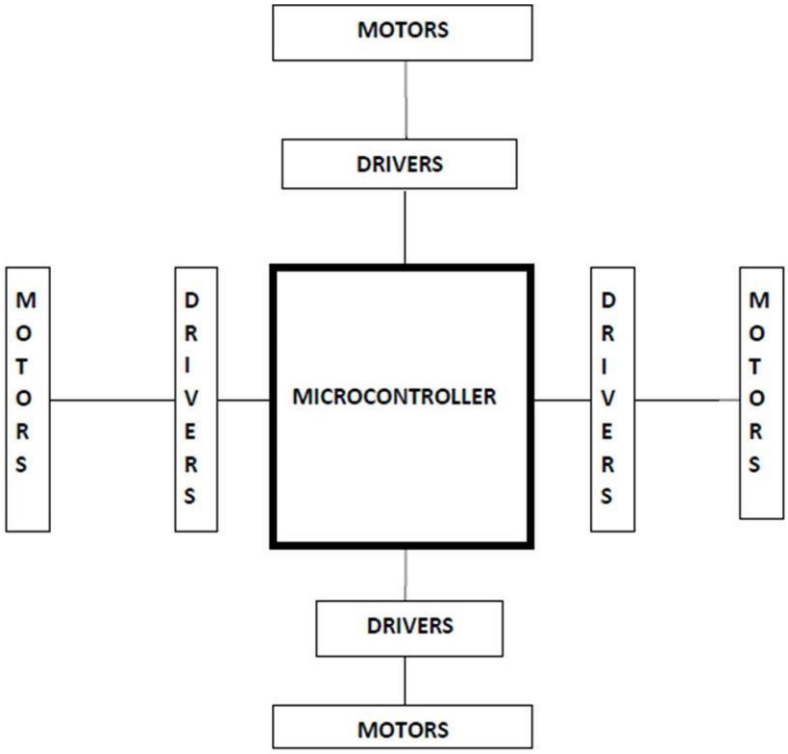

III. MODELING

The fully designed model of Drone in SolidWorks is shown below with various figures showing all possible views.

Figure: Multi-purpose Quadcopter Orthogonal Projection

e-ISSN: 2582-5208
International Research Journal of Modernization in Engineering Technology and Science
(Peer-Reviewed, Open Access, Fully Refereed International Journal)
Volume:04/Issue:05/May-2022 Impact Factor- 6.752 www.irjmets.com

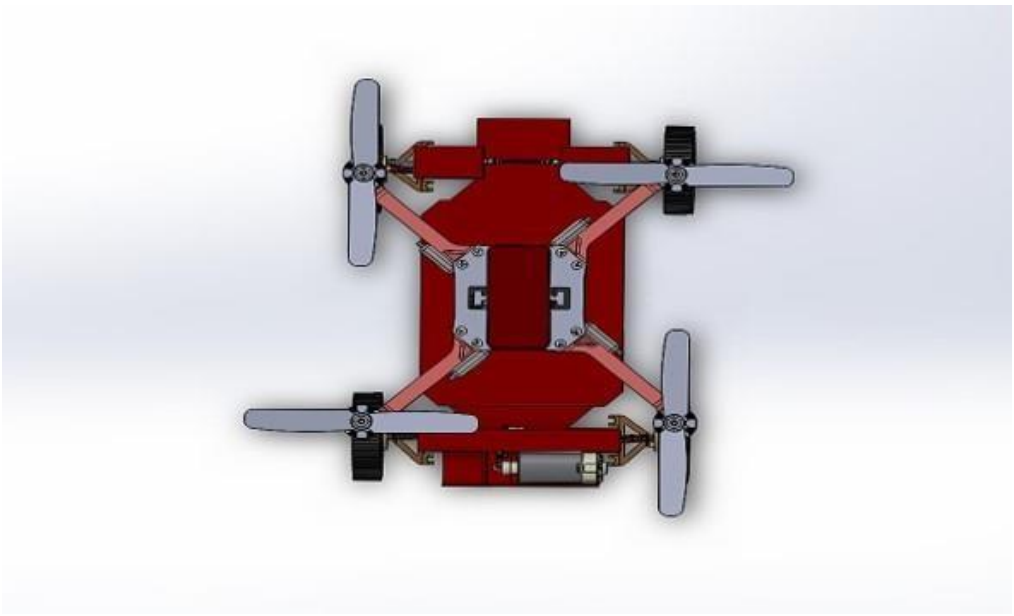

Figure: Multi-purpose Quadcopter from Above

Figure: Multi-purpose Quadcopter from the Side

IV. APPLICATIONS

We presented the conceptual aerodynamic design of a UAV in this article capable of surficial movement.

- Quadcopter - Military and law enforcement agencies use unmanned aerial vehicles for surveillance and reconnaissance, as well as search and rescue missions in urban areas.
- The Aeryon Scout is a small unmanned aerial vehicle (UAV) developed by Aeryon Labs in Canada that can quietly hover in place and use a camera to observe people and things on the ground. According to the company, the device was used in a narcotics bust in Central America, allowing video surveillance of a drug traffickers' hideaway deep in the jungle.
- Use of UAV in a disaster has various advantages: it reduces the time required to find the victims and time needed for further intervention by searching a large area in very less time. It also provides crucial information to rescuers about the path that needs to be taken during rescue operations
- Drones can aid in tracking down illegal activities, monitor fauna, take a count of their population, plan planting of forest cover and furthermore help in assessing the overall situation of a forest protected region.

V. CONCLUSION

We presented the conceptual aerodynamic design of a UAV .The uniqueness of this paper lies in its discussion and exploration of drone capabilities for Industry 4.0. This work helps to build a common foundation for

understanding Industry 4.0 outcomes from a variety of disciplinary perspectives, allowing for more research and development for industrial innovation and technological progress.

VI. REFERENCES

[1] Turkish Naval Research Center Command, Pendik/Istanbul, Turkey #Graduate School of Informatics, Middle East Technical University, Ankara, Turkey !Department of Computer Engineering, Bahçeşehir University, Besiktas/Istanbul, Turkey.

[2] Kardasz P, Doskocz J, Hejduk M, Wiejkut P, Zarzycki H (2016) Drones and Possibilities of Their Using. J Civil Environ Eng 6: 233. doi:10.4172/2165-784X.1000233

[3] M. Hassanalian, A. Abdelkef Department of Mechanical and Aerospace Engineering, New Mexico State University, Las Cruces, NM 88003, USA.

[4] Javaid, M., Khan, I.H., Singh, R.P., Rab, S. and Suman, R. (2022), "Exploring contributions of drones towards Industry 4.0", Industrial Robot, Vol. 49 No. 3, pp. 476-490.

[5] Department of Diagnostics and Allied Health Sciences, Faculty of Health and Life Science, Management and Science University, 40100 Shah Alam, Selangor, Malaysia.

[6] Pravin Ekka Department of Electronics & Communication Vivekananda Institute of Technology, Jaipur, India.

Cluster Computing
https://doi.org/10.1007/s10586-022-03622-2

Detecting malicious transactions in database using hybrid metaheuristic clustering and frequent sequential pattern mining

Rajni Jindal[1] · Indu Singh[1]

Received: 16 August 2021 / Revised: 22 February 2022 / Accepted: 3 May 2022
© The Author(s), under exclusive licence to Springer Science+Business Media, LLC, part of Springer Nature 2022

Abstract
Database systems have become imperative for organisations around the world to store and analyse information. However, as one of the ramifications of a massive surge in cloud-based activities and interactions brought forth by the advent of the internet era, the data is exposed to an audience broader than ever and there are a variety of new challenges putting database security in jeopardy. To be able to address the problem of data security, we propose a unique method for Database Intrusion Detection System build on frequent sequential pattern mining and a modified metaheuristic hybrid clustering of Grey Wolf and Whale optimization algorithm to determine malicious transactions in Role Based Access Control and non-RBAC supervised databases. Our proposed approach extracts data dependency rules from the database logs using CM-SPADE mining algorithm to detect outsider threats. It then assigns role profiles to the users based on the previous user activities using the modified metaheuristic clustering to detect insider threats. Thereby, identifying incoming transactions as malicious by matching the role profile of the user and comparing the adherence of the transaction pattern to the generated dependency rules. To evaluate the efficiency of the model we generated a synthetic dataset including malicious and non-malicious transactions adhering to the TPC-C benchmark, and the findings were encouraging, with levels of accuracy of around 97.8 percent.

Keywords Database intrusion detection · Data dependency rule mining · Frequent sequential pattern mining · Hybrid metaheuristic clustering · Grey wolf optimization · Whale optimization

1 Introduction

In this modern era, data and information have become an indispensable part of any organization, and its importance can be seen in all phases of business activities; from product idealization to realization. According to some estimates, the total data stored across the world across all companies increases twofold in every 1.2 years [1]. This has led to the meteoric rise of database management systems as the main method to process information. With increasingly sensitive data and greater movement of operations online, the concerns for security against malicious attacks is at an all-time high.

Therefore, existing security measures like encryption, auditing, specific user level access and separation of powers have been adopted by numerous organizations to counter external threats. However, these approaches fail to account for malicious insider attacks. Hence, we must come up with novel techniques that are capable of simultaneously handling both outsider as well as insider threats [2]. A number of different measures have been implemented with reference to insider threats and cyber frauds according to the guidance offered in the Computer Emergency Response Team (CERT) Guide to Insider Threats [3]. The effectiveness of these existing systems can be enhanced through various rules, configurations and business processes.

According to the definition provided by CERT [3], an insider threat could be any employee, contractor or business partner that currently has, or in the past had authorized

✉ Indu Singh
indusingh@dtu.ac.in

Rajni Jindal
rajnijindal@dce.ac.in

[1] Delhi Technological University, Delhi, India

Published online: 01 June 2022

access to an organization's database infrastructure, and is willing to misuse this access to undermine the Confidentiality, Integrity or Availability of the organization's data [2]. Therefore, protecting data from unauthorized internal access is integral in maintaining the CIA triad.

The fundamental difficulty in identifying and preventing unauthorized internal access is that these are legitimate users with relevant access rights who are familiar with the internal architecture of the database schema as well as the security mechanisms put in place for its security. Therefore, insider threats can cause considerable damage to the system without being detected for extended periods of time. To maintain the integrity of data in such a complex environment requires high security standards in conjunction with a flexible intrusion detection system that evolves and adapts according to the threats encountered during operation.

In recent times there has been an unprecedented expansion in the usage of networked systems. This has resulted in the exposure of the database to quite a few vulnerabilities and threats. Thus, it is critical to shield the database against not only external malicious attacks but also against breaches of privileges by insiders who abuse the access rights granted to them. An intrusion can be described as any set of activities that make an effort to compromise the integrity, confidentiality or availability of a resource [4]. Although many different methods are used to protect important data under current network conditions, these methods are usually unsuccessful. The solution to recovering lost or damaged data without much difficulty in the event of a computer system getting compromised is early detection [5]. Confidentiality, integrity and availability (CIA) are the three key requirements that must be met for data protection.

One approach to reducing data vulnerability is to employ an Intrusion Detection System (IDS) in vital information systems. The main aim of intrusion detection systems is to identify/catch attacks against networks and information systems. This is because it is quite challenging to bestow information systems that are not only secure but also maintainable for their entire lifespan in such a secure and stable state [6]. Sometimes a fully secure computer system or network is not at all realized. One of the reasons for this could be operational constraints or legacy. Therefore, the job of an intrusion detection system is to track the operation of such systems and diagnose the existence of unsafe conditions. They identify active abuse and attempts by external parties or legitimate users misusing their rights or exploiting vulnerabilities present in the security system.

Preuveneers et al. [7] suggested that the use of federated learning systems for intrusion detection can improve the detection of malicious behavior by joining forces and pooling together monitoring data. Lee et al. [8] suggested Intrusion detection by using data mining techniques. Various sets of data mining algorithms like link analysis, sequential analysis and classification were considered. Barbara et al. [9] have suggested Intrusion detection by building a testbed using data mining techniques. Despite intrusion detection being a well-researched area, not much focus has been given on database intrusion detection. Besides, only two-fold judgment regarding the transaction is provided by existing database intrusion systems i.e. either the transaction is malicious or non-malicious. Although a system of the aforementioned category protects the database against threats satisfactorily, it results in unwanted system overhead and degradation of user experience [10] .

We can classify existing IDS into various categories depending on their properties [6]. The common ones are:

- Host-based Intrusion Detection Systems (HIDS): It monitors not only the incoming network packets but also the central file structure of the information system.
- Network Intrusion Detection Systems (NIDS): It consistently examines the network traffic and also the incoming transactions.

There exist other classifications which depend upon anomaly detection or signature detection and misuse.

- Misuse-based Detection: It identifies potential threats by looking for specific patterns similar to previously known threats. The main disadvantage of misuse-based detection is that it cannot identify new attacks whose patterns are not available.
- Anomaly-based Detection: It can identify and detect novel attacks which were not already known. It uses various machine learning algorithms to create a model which is then used to compare new transactions against that model. This model may suffer from false positives as the attacks are unknown.

For database security, the administrator creates preset roles with specified privileges and permissions, allowing only approved users to access the database using RBAC, or Role Based Access Control [11]. Users are given different levels of access depending on their position within the company. Users are given authority through the job processes and responsibilities that have been assigned to them, rather than directly. Instead of controlling individual user access and privileges, they are centralised across a network and allocated to a set of roles which assures database security.

This technique works by capturing sequences [2] and mining association rules [3] from transaction data, which is then used to identify an incoming transaction as legitimate or malicious. By limiting user activity to certain roles, the NIST model [11] further enhanced the security system's effectiveness. To tackle insider attacks, the RBAC

mechanism is widely being implemented [12]. We propose a novel approach (FPGWWO) which is capable of handling not only external attacks but internal attacks as well. Data dependency rules of the legitimate queries are generated using the frequent sequential pattern mining algorithm CM-SPADE that assists in inspecting the resemblance of the incoming transactions. For calculating the adherence between the incoming intra-transactional query and the set of rules mined we introduce the concept of similarity threshold. This similarity threshold known as Congruity Index is used to classify the incoming transaction as either malicious or non-malicious. To maintain the integrity of the Database Intrusion Detection System (DIDS) from insider attacks, we employ a modified hybrid of grey wolf and whale optimization metaheuristic clustering algorithm (mhGW-WOA). This algorithm takes in the user transactions as a parameter for the objective function and constructs role profiles based on previous user activities.

During the detection phase, a role matcher authenticates role clusters for the incoming transaction. If the role profile is not matched, the transaction is labelled as malicious and aborted. This module renders our approach immune to internal attacks. Subsequently, the transaction is forwarded to the rule validator if the role profile matches, which then compares the incoming query to mined rules produced during the learning phase by computing the similarity threshold, i.e., the "congruity index". Transactions are labelled malicious based on this threshold and an alarm is triggered and the database executes a rollback. Consequently, any external or internal attacks on the system that could lead to alterations will be prohibited.

The major contributions of this work are as follows:

1. *We present a comprehensive DIDS that uses a rule mining module to prevent external threats and a role clustering analyzer to assess transaction validity for preventing insider attacks and detecting intrusions in the database.*
2. *We introduce a "modified hybrid of Grey Wolf Optimizer with Whale Optimisation Algorithm (mhGW-WOA)" to cluster role profiles based on user activity for matching the roles of incoming transactions. We also employ frequent sequential pattern mining technique i.e. CM-SPADE to analyze previous user patterns in the database logs to obtain read and write rules based on the legitimate user access patterns.*
3. *We propose a novel similarity threshold, called the Congruity Index which calculates the adherence between the dependency rules and the extracted transactions. On the basis of this index, the transactions are classified into malicious or non-malicious.*

The remaining paper is organised as follows. Section 2 provides an overview of the related work. The proposed methodology is described in Sect. 3. Section 4 contains the experimental results as well as a comparison to previous methodologies. Finally, in Section 5, we offer our conclusion.

2 Related work

There are various Intrusion Detection System Models [13–15] which have been proposed for detecting intrusions at the network-level and OS-level. However, very few models have been implemented to identify database intrusions. There is a need for database IDSs to ensure three goals [2] :

1. Confidentiality - to protect data against unauthorized exposure.
2. Integrity - to prevent malicious data modifications
3. Availability - to protect against hardware or software failures, as well as malicious data accesses, and to recover from them.

Any set of actions which hamper these goals is termed an intrusion [4]. Since the beginning of the 21st century, concrete progress has been made in IDS[5, 16, 17] for detecting database intrusions with the help of data mining and data dependency rules. D.E. Denning [18] states that on inspection when a system's records are searched for unusual patterns, security violations can be attributed to malicious activity. Their model is based on a rule-based pattern matching system to monitor standard OS operations such as logging in, command and program executions, disk accesses, etc., looking only for deviations in usage. Despite the unique approach, at the local level, the system has great problems due to its weakness for the inadequate resolution of complex procedures. According to research, efforts to identify unauthorized usage of software applications by users [19] using an increasing time frame for user profile training and abstracting into groups of apps reduces the amount of false alarms generated considerably. Cardenas et al. [20] concluded that while control systems are pivotal, they are quite likely to be targeted by skilled and motivated hackers due to increasingly exposed vulnerabilities. In fact, the security mechanism for detecting and finding controlled data changes before hackers compromise the system was clear and in use. Different norms were depicted by Debar et.al. [6], with focus on the internal dynamics of the elements, and their corresponding behaviors and principles. The model aggregated the recommendations of many evaluation indicators to assess the accuracy of efficiency and utilise the chance variation approach in the process. Legitimate users' patterns of access are compared against those kept in a database. Bertino et al. [2] concentrated on access control systems and discussed the major access

control types. Due to the disturbing additions in security dangers and systems administration, Liao et al. [21] established that intrusion detection systems(IDS) have been conclusive and pivotal in the world of computation.

2.1 Data dependency mining

Data dependency mining [22] is highly effective in discovering patterns and dependencies in large data sets. It employs statistical methods to analyse the data sets and detects relationships amongst the attributes. It is immensely useful in data rectification, extracting regularities from datasets and resource filtering. This section reviews some of the related works that delve into the potential of this method in intrusion detection.

As Chen et al. [23] established, data dependency mining is given significant importance in a variety of research fields including, but not limited to, database systems, machine learning, statistics, information management and artificial intelligence. Various state of the art data mining methods are applied to gain insights into user behaviour and access patterns which has enhanced opportunities in diverse fields.

[5, 16] highlighted the use of data dependency mining in detecting database intrusions as opposed to the existing methods that used the operating system log or the application log. Before a given data item is updated, other data items are written or read from the dataset. The model proposed by Hu et al. [16] provides strategies for detecting these data dependencies and employs Petri-Nets to model normal data patterns. They further leveraged this in mining data dependencies [5] from database logs. The transactions that did not meet the criteria for the mined dependencies are flagged as malicious. While the results were promising, they did not take into account the different sensitivities of the attributes of the database.

Srivastava et al. [17] proposed an approach using weighted sequence mining to detect the dependencies that considered the varying sensitivity of the attributes. The algorithm performed better than the previous algorithms in detecting changes in sensitive attributes.

Hashemi et al. [24] furthered the existing approaches by introducing a behaviour similarity criterion to constrain the false positive rate. Besides the transactions that do not satisfy the data dependencies, the transactions which seemed identical to these invalid transactions in the log in this similarity test were also flagged as malicious. The proposed approach detecting anomalies in a time series dataset is able to identify malicious transactions even when they confirmed to data dependency rules, thereby yielding a much better true positive rate.

Rahman et al. [25] worked on an algorithm centred around pattern mining. They used weighted uncertain sequence mining to detect sequences or patterns in uncertain databases. It was effective and efficient in in mining frequent weighted sequences. It is also suitable for real life databases because real world data tends to be uncertain. The main obstacle they encountered was recognising the more significant valid patterns according to their relevance.

Kundu et al. [26] tried to tackle the problem of identification appropriate support and confidence values with attribute dependency mining. They suggested an intrusion detection system that leveraged sequence alignment which allows for a wide range of transactional and profile granularity levels to be selected. It gave more efficient results than the existing methods.

Subudhi et al. [27] introduced an intrusion detection system (IDS) that used OPTICS clustering in conjunction with Ensemble Learning, which included numerous aggregation methods such as Boosting, Bagging, and Stacking, to identify malicious users in a database. They divided intrusion detection into 2 phases, namely, training and testing. In the training phase, the input dataset attributes were preprocessed. Subsequent to that, OPTICS clustering was applied to it to develop behavioural profiles. During the testing phase, a new transaction was reviewed against these profiles to check for conformity. If it turned out to be deviant from the profiles, it was checked for maliciousness by an ensemble learner.

Sallam et al. [28] used an anomaly detection system to discover data aggregation and data updation. Their method involved using a standard table reference rate and retrieving tuples from previous database access logs. In addition, the incoming user requests were evaluated to see if any of them were likely to exceed the regular data access rates.

2.2 Sequence pattern mining

First coined by Agrawal et al. [29], a data mining subdomain, namely, Sequential Pattern Mining (SPM) has extensive applications in the field of database security to detect recurrently occurring sequences, intriguing features and patterns in sequential databases.

Agrawal and Srikant [29] introduced AprioriAll and AprioriSome algorithms. These algorithms can be utilized to extract sequential patterns from a database. Both algorithms grow linearly as the size of the database increases but face the same challenge of determining the support and confidence worths. To overcome these issues, Agrawal and Srikant [30] put-forth a new algorithm which generalizes the SPM algorithm and provides more efficient performance than the Apriori algorithms. In this procedure, the cost or profit of the item that is being used is taken as the weight while also taking into account the unique or distinct sign of all the items in real-time application.

Zaki et al. [31] proposed a novel algorithm called SPADE which divides the original problem into smaller sub-problems using equivalence classes on recurrent sequences. A major advantage is that each equivalence can be analyzed individually and processed in the main-memory. Also, unlike other approaches which take multiple scans, SPADE uses at most three database scans and only one scan if 2-sequence instruction is supported. It outperforms the AprioriAll algorithm by at-least a factor of 2 with 2-sequence instruction support. Similarly, Pei et al. introduced a prefixspan approach [32] with the motive of searching for necessary sequences by looking for the prefix sub-sequences and projecting just their corresponding postfix sub-sequences into projected databases. It also outperforms the Apriori algorithms. However, for large datasets the SPAM algorithm proposed by Ayres et al. [33], which uses a depth-first traversal process coupled with a vertical bit-map representation to store every sequence allowing noteworthy bitmap compression along with an efficient support counting, is considered more efficient. Although, the SPAM algorithm has a major limitation as it consumes more space in comparison to PrefixSpan or SPADE algorithm.

Gomariz et al. [34] developed a new close constraint algorithm called ClaSP which was tested of the gazelle dataset, can be used to mine frequent close sequential pattern utilizing various search-space pruning methods combined with a vertical database layout. Similarly, the CMAP algorithm introduced by Viger et al.[35] is based on the CMAP structure that can be built within a single database scan and utilizes co occurrence-based pruning. It outperforms algorithms like Apriori, SPADE, PrefixSpan, SPAN as well as close-sequential patterns like ClaSP by 8 times post-integration with them. Upon testing on six real-life datasets, it is found that integration with ClaSP and SPADE provides best results.

Lan et al. [36] devised a different method in order to retrieve weighted sequential patterns. Here, the maximum weighted upper bound model was taken into account which resulted in higher accuracy and efficiency for the subsequences. The major disadvantage of this model was its failure to handle the updating or removal of sequences and dynamic addition.

Rahman et al. [25] proposed the concept of pattern mining where sequences are selected, via an algorithm, from uncertain databases with weight restrictions. The main challenge is to distinguish between important and valid patterns based on significance. In 2019 Rahman et al. [37], devised a method to overcome this downside by utilizing weight and support constraints in order to build patterns in uncertain databases.

2.3 Anomaly detection

Chung et al. [38] developed a DEMIDS abuse detection system, customized to relational database systems. DEMIDS creates profiles based on audit records that reflect normal user behavior while dealing with the DBS. Although DEMIDS may be used to identify both intrusion and insider abuse, it focuses on detecting anomalous activity by authorised individuals who misuse their rights. As a result, the system is especially beneficial for internal control.

Spalka et al. [39] presented a framework for database expansion and user interaction with a DBMS, as well as a database misuse detection system. They examine two techniques to handle with database extension, first relying on measured value and another based upon Δ-relations, in a detailed examination, and show that previously conventional statistical functions produce acceptable detection results. These reference data can assist discover a number of abnormalities in primarily developing relationships. Anomaly detection in user interactions relies heavily on reference data.

The Collaborative Adversarial Network (CAN) model, proposed by Alzubi et al. [40], is a collaborative network of generators that is pitted against a discriminator adversarial network.It entails the segmentation of frequent highlights between two phrases and the use of community-oriented learning to traditional ill-disposed and adversarial learning for the extraction of common features which can be used for the calculation of similarity between rules and queries to efficiently detect anomalous transactions.

In order to identify intrusions in databases, Hashemi et al. [24] suggested a data mining technique. This technique is based on (1) mining dependencies, (2) identifying aberrant update trends, and (3) comparing normal transactions. The first and second characteristics are intended to improve the rate of genuine positive detection. The third feature is designed to lower the number of false positives. The proposed approach's main advantages are (1) its ability to identify interruption transactions, (2) its capacity to spot malicious activities, and (3) its potential to classify transactions as regular also when they violate the addiction rules.

Alzubi et. al. [41], proposed a CNN and LSTM based two-layer architecture for image captioning, a custom form of which can be used for the captioning of queries in the form of signals as anomalous or non-anomalous queries.

Kamra et al. [42], suggested a method for identifying unusual access patterns in database management systems. They have created three models, each with a different level of granularity, to describe SQL queries seen in database log files. The FP rate for clustering methods based on k-means

and k-centers is exceptionally low. The FN ratio for k-means was significantly higher than other algorithms. Either of the clustering techniques, the findings for the outlier identification methodology was not particularly outstanding.

For threat detection, Panigrahi et al. [43] developed architecture that employs both intra-transactional and inter-transactional methods. For assessing the transaction provided by a customer, sequence alignment and spatio-temporal outlier identification were used. Transaction was categorised as regular, unusual, or suspicious. Analyses were conducted on a vast number of simulated databases and the simulation produced a TP of approximately 98% and an FP just under 10%. Dempster-Shafer theory assist in True positive and Bayesian learning can aid to minimize the frequency of false alarms even further.

When an application makes a query, The relevant profile and restrictions were compared to the platform's current scenario in the DetAnom identification process[44]. The query was tagged as unusual if there was a difference. The major benefit in this technique was that it doesn't require any prior information of the system nor examples of prospective attacks in order to create system profiles.

Sallam et al. [45] proposed a new technique called DBSAFE for anomaly detection in databases that use the RBAC(role-based access control model). The procedure requires recording training information during either normal operation or by using the audit log. Query features issued by each role are then used to denote the access profiles. Analyzing the syntactic features of queries provides the access patterns. It assumed only one role activated per user. A major extension of the technique was proposed by Sallam et al.[46] which considered common access patterns between the roles. It uses NBC and MLC classifiers for RBAC models and unsupervised anomaly detection when role information is unavailable. However, these alone prove to be insufficient. Therefore, Sallam et al. [47] proposed another extension of his previous work. It uses a three-stage process for collecting profile information. It uses a standard periodicity detection algorithm to detect the frequency corresponding to which queries in logs are regularly issued after which the expected time-interval in which periodic queries are expected to be issued is determined. The final stage recognizes the relationships among periodic queries that are issued together. A query is marked anomalous if it is received at an unexpected time. However, a major limitation of this method is that it is still unable to process aperiodic queries.

Ronao et al. [48] proposed random forest with weighted voting (WRF) and principal component analysis (PCA) as a feature selection approach for detecting database access anomalies, provided that the database employs a role-based access control (RBAC) model. PCA generates uncorrelated and meaningful characteristics while also reducing dimensionality for easier integration with big databases. RF takes advantage of SQL queries' inherent tree-structure syntax, and its weighted voting mechanism reduces false alarms even more.

They suggest utilizing CNN-LSTM neural networks to classify a device's status and authorization by obtaining characteristics from SQL server [49]. CNN derives significant characteristics from queries autonomously, while LSTM analyzes the SQL sequence's temporal features from TPC- E benchmark.The authors also used statistical analysis to determine the features of misclassification data.

2.4 Metaheuristic clustering

Mahalingam et al. [50] suggested a dynamic clustering technique by breaking up the moving object Optimal Background separation using Optimal Weighted Centroid (OWC) - Modified Kernel Fuzzy C Means Algorithm (MKFCM) for information clustering utilizing the OWC (Optimal Weighted Centroid) [50] .The effectiveness of the suggested procedure is inspected with going before procedures k-NN just as MLP concerning precision, f-measure, ROC just as review.The effectiveness of the suggested procedure is inspected with going before procedures k-NN just as MLP concerning precision, f-measure, ROC just as review.

Rathore et al. [51] proposed a hybrid whale and grey wolf optimisation (WGWO)- based bunching component for energy gathering remote sensor organizations (EH-WSNs). The exploitation and investigation abilities of the proposed mixture WGWO approach are a lot higher than the conventional different existing metaheuristic calculations during the assessment of the algorithm.

Ali Akbar et al. [52], proposed a novel artificial neural network(ANN) training algorithm which utilizes the power of invasive weed optimization and differential evolutionary model to find the optimal weights of the ANN. This proposed training mechanism is proven to be more efficient and less error-prone and thus can be utilized as a classifier to detect intrusive transactions in databases.

Rahnema et al. [53] used a hybrid of improved artificial bee colony and whale optimization algorithm for data clustering. This hybrid solves the issue of late convergence and exploration of ABC by using Random Memory and Elite Memory. The former in the ABCWOA algorithm has utilized the search stage as a bait in the whale optimization algorithm whereas the latter is used to increase convergence. This combination performs better than other metaheuristic algorithms.

Aljarah et al. [54], proposed a novel grey-wolf inspired clustering approach and enhanced it using the Tabu Search(TS) algorithm whereas Ghany et al.[55] proposed a

modified Hybrid Whale algorithm with Tabu Search for Data Clustering. In [54], the GWO is used to deal with problems related to clustering while the TS algorithms behaves like a local search hill-climbging algorithm. However, TS accepts non-upgrading solutions to escape from local optima. The main intent behind the hybrid GWOTS is to use the process of adaptive memory in TS for exploring the neighbourhood of each leader before extracting the updated positions of the remaining pack. GWOTS tries to find the optimal solution centroid for each group in such a manner that each member wolf in GWOTS represents a solution containing clusters / groups of centroids. This hybrid approach was run on 15 datasets out of which it showed significantly great results on 8 datasets. Contingent on these outputs, it can be concluded that the effectiveness of the GWOTS is highly competitive and comparatively better than usual methods in most cases. The primary rationale is that it can establish an equilibrium between main exploitative and exploratory trends and in the scenario of finding any high-quality solution; it is locally-informed and aggravates the exploitation around that position, which drives to increase the level of the quality. While in [55], WOA uses optimal solutions to relocate swarm members. In order to overcome this problem, WOA needs to retain multiple optimal solutions within the scope of the solution. While the Tabu Search(TS) algorithm being a meta-heuristic method, uses memory components to exploit and explore search space. They presented WOATS for data clustering in [55], which uses an objective function inspired by partitional clustering to keep clustering solutions of high quality. The efficiency of WOATS is measured using publicly available real-world data sets. These data sets vary in size, from small data sets to large data sets, demonstrating their advantages over a variety of primitive and hybrid swarm intelligence technologies. The results obtained by WOATS are significantly better than other methods, ensuring its effectiveness. Each whale in the group symbolizes a complete solution in WOATS (Group Center). These centers are selected based on the best value of the objective function. WOATS always achieves the best objective function value with the least number of iterations-for all data sets, compared with other methods, WOATS achieves the smallest objective function value with the least number of iterations, and the number of iterations is less than 50. WOATS is designed to pool huge biological data sets based on big data technology.

3 Proposed methodology

We propose a Database Intrusion Detection System (DIDS) that uses rule mining and clustering in the initial training phase and then followed by the classification in the detection phase. The proposed approach FPGWWO mines the read and write dependency rule subsequently followed by the modified Hybrid of GreyWolf Optimizer with Whale Optimisation Algorithm (mhGW-WOA) clustering using the current database logs containing transactional details. The pertinent patterns generated by the algorithm prevents undesirable rules from being created. In the first part of the learning phase, we make use of the CM-Spade [35] algorithm to generate sequential patterns succeeded by generating data dependencies that occur from the preprocessed transaction logs. Classification rules above certain confidence values are generated pertaining to the mined data dependencies. In the second part of the learning phase, role profiles (clusters) are generated from defined parameters after analysis of database logs using (mhGW-WOA) clustering. It is assumed that only legitimate transaction logs and database logs are provided in this phase.

3.1 System architecture

The proposed DIDS functions as a separate unit, enhancing system security without interfering with the database management system (DBMS). The system is designed to identify and abort malicious transactions sent by attackers to the DBMS, which managed to bypass the initial security of the database system. The scenario may arise due to a compromised legitimate account, web portal susceptible to SQL injection, abuse of user privileges [56]. In all these cases, an attacker can access the database by submitting transactions manually or through an application. The architecture of the proposed system (FPGWWO) consists of two modules:

- Learning Phase
- Detection and Classification Phase

3.2 Learning phase

The architecture of the learning phase is represented in Fig. 1. In this phase, the rule generator uses transaction logs to extract data dependencies, and then stores them for resemblance calculations in subsequent stages. While assessing resemblance, database records are also used to analyze user access patterns, and then these patterns are grouped into role profiles. These role profile groups and generated rules are then passed to the discovery phase. The rules and role clusters formed are then used in the detection phase. The learning module has two vital units:

- Rule mining
- mhGW-WOA Clustering

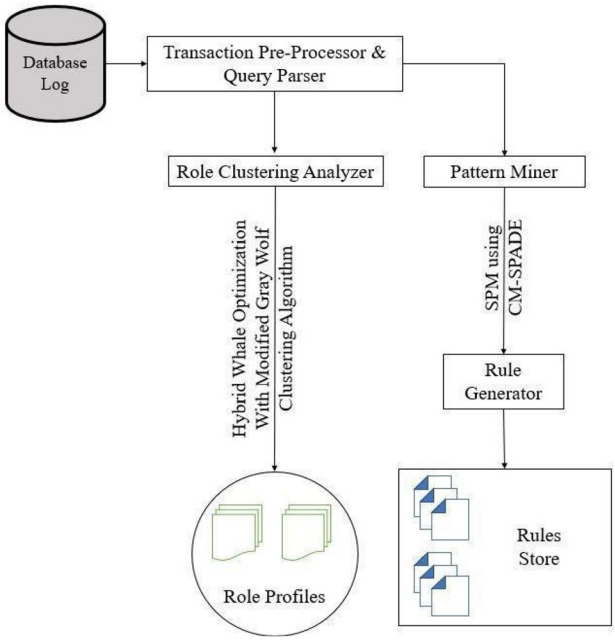

Fig. 1 Learning phase architecture

3.2.1 Rule mining

Rule mining refers to the discovery of patterns that indicate the basic and important characteristics of the database, then preprocess the appropriate pattern derived from the algorithm in a way that excludes the generation of undesired rules. In the first part of the learning phase, we make use of the CM-Spade [35] algorithm to generate sequential patterns succeeded by generating data dependencies that occur from the preprocessed transaction logs. The classification rules that are higher than the defined confidence threshold are generated with respect to the mined data dependencies.

Query parser The SQL queries from the transaction table cannot be categorized as malicious or non-malicious as such. In order for our model to classify the transaction, we use a query parser which takes the SQL queries as input, parses and analyses them to convert to appropriate read and write transaction sequences. Each transaction is assigned a unique transaction ID. The commands are executed for tokens taken from the source token list. If no error occurs when parsing the input into a read-write stream, a parse tree is generated. The generation of the parse tree proceeds recursively until no error occurs while parsing the input into read and write rules.

For example,

Consider a SQL query as:

Account_id = select ID_no from Account where name= 'Alice' and IFSC='ASCR4112';

update Loan set amount=amount + 1500 where Loan_id = Account_id;

Output generated by query parser:

Tid = <R(name), R(IFSC), R(ID_no), W(Account_id), R(Loan_id), R(Account_id), R(amount), W(amount)>

Transaction pre-processor The module specifies the identified transactions in an ideal way. Each transaction can be expressed as a set of queries (select, insert, delete or update). Then, each query can be expressed as a series of operations (read or write) on the item set. The items in the item set are arranged in lexicographic order to avoid multiple representations of the same query.

- Each transaction starts with the beginning transaction and ends with commit/rollback.
- We denote a transaction T as $< q_1, q_2, q_3, \cdots, q_n >$ where $q_i \in Q(s).Q(s)$ is the set of queries.
- We denote a query q_i as $< op_1(D_1), op_2(D_2), op_3(D_3), \cdots, op_n(D_n) >$. Where $op_i \in$ [R,W] and D_i represent an item-set $< d_1, d_2, \cdots, d_k >$ lexicographically sorted.
- Transactions are expressed as queries in order. For each of these queries, the sub-query (if any) is expressed first. Clauses like while, order by, etc. they are evaluated before the SQL statement type (select, update, insert, or delete).

Sequential patterns A sequence is an ordered list of operations. Sequential patterns are those elements that appear multiple times in the same order simultaneously in the data. Data correlation is symbolized as a read stream and a write stream.

Definition 1 (*Transaction*): A transaction is an orderly arrangement of operations performed on a data-base instance, with the user operation denoted by Op ∈ Read, Write. For the transaction to be completed, the operations must be executed in a discrete manner. TIDs are issued to transactions as a unique identifier.

Definition 2 (*Operation O(a)*): O(a) represents the relationship with the action of a data item a. It comprises action to the set Read,Write.

Definition 3 (*Sequence*): It is an ordered set of read, write operations with respect to time, which is defined as: $Seq = \{O_1(a_1), O_2(a_2), \cdots, O_n(a_n)\}$ where Oi ∈ R,W and a_i represent an attribute of a data item. There are two categories of data dependency sequences extracted from transaction logs:

Definition 4 (*Read Sequence RdSq(a)*): For a particular attribute a, read sequence is defined in the format: $RdSq(a) = \{R(a_1), R(a_2), \in, R(a_n), O(a)\}$ where $a_1, a_2, \cdots, an$ are the attributes that are to be read before a transaction performs any operation O ∈ R, W on the attribute a and R(a_j) denotes a quantum unit of read operation performed on a_j.

Table 1 Transactions for Mining Sequential Patterns

Transaction ID	Transaction
20	$<r10, r15, r11, w13, r16, r12, w15, r10, r15, w11, r12, r14, r11, w14>$
21	$<r15, r10, w12, r10, w15, r11, r16, r13, w11>$
22	$<r16, r10, r15, w14, r10, w13>$
23	$<r11, w11, r13, r16, w12, r15, w14, r10, w13>$
24	$<r11, r14, w15>$
25	$<r10, r14, w10, r13, r14, w13>$
26	$<r13, w15>$
27	$<r15, r14, w14, r12, r13, w13, r12, w16>$
28	$<r14, r12, r15, w16>$
29	$<r14, r15, w14, r14, w13>$

Definition 5 (*Write Sequence WrSq*(*a*)): For a particular attribute a, write sequence is defined in the format: $WrSq(a) = \{O(a), W(a_1), W(a_2), \cdots, W(a_n)\}$ where $a_1, a_2, \cdots, a_n$ are the attributes that are to be updated after a transaction performs operations O ∈R, W on the attribute a and W(a_j) denotes a quantum unit of write operation performed on a_j .

Definition 6 (*Sensitive elements*): They are defined as those elements which are either updated in the transaction or belong to restricted access groups. Sensitivity of an element is determined by its weight in the transaction.

Definition 7 (*Confidence*) The confidence of a given sequence (read or write) is the ratio between the weighted count of occurrences of the given sensitive element a_i and the weighted count of occurrences of sensitive element a_i. We have given a formal definition of confidence for a read sequence below. The confidence level for the script sequence is similar.

$$Confidence(RdSq(a_i)) = \frac{CountRdSq(a_i)}{Count(a_i)} \quad (1)$$

Definition 8 (*Read Rules* (*RR*)): For every read sequence $\{R(a_1), R(a_2), \cdots, R(a_n), Op(a)\}$, that is generated using sequential pattern mining, we generate a read rule of the format $<R(a_1), R(a_2), \cdots, R(a_n)> \rightarrow O(a)$, that implies, before a, we must read $a_1, a_2, \cdots, a_n$.

A rule is added to the Read Rules set only if the rule that is generated from the read sequence has a confidence value greater than the minimum confidence provided.

Definition 9 (*Write Rules* (*WR*)): For every write sequence $\{Op(a), W(a_1), W(a_2), \cdots, W(a_n)\}$, that is generated using sequential pattern mining, we generate a write rule of the format $O(a) \rightarrow <W(a_1), W(a_2), \cdots, W(a_n)>$, that implies, after updating a, data items $a_1, a_2, \cdots, a_n$ must be updated during the transactions. A rule is added to the Write Rules set only if the rule that is generated from the write sequence has a confidence value greater than the minimum confidence provided.

Table 1. displays the read and write items in a transaction. Each of these transactions are assigned a unique transaction ID.

Definition 10 (*Prefix*): Given two transactional sequences $a = \{Op_1(it_1), Op_2(it_2), \cdots, Op_n(it_n)\} and b = \{Op_1(it_1), Op_2(it_2), \cdots, Op_m(it_m)\} (m < n)$, sequence b is called a prefix of sequence a $\iff Op_i(it_i) = Op_i o(it_i o) \forall i \in \{1, 2, \cdots, m\}.T$

Rule generator The process of extracting relevant rules from the data mainly involves the extraction of frequent sequence patterns through successive algorithms, because the transactions have previously been processed in an ordered set of queries. For this, we use the CM-SPADE algorithm to extract sequence patterns from the transaction log. CM-SPADE was chosen because it outperforms the most advanced algorithms in mining sequential patterns (GSP, PrefixSpan, SPADE, and SPAM) and closed sequential patterns (ClaSP and CloSpan)[35].

Definition 11 (*Sequential Pattern Mining*):
Consider SDB a sequence database and minsup as threshold. A sequence s is considered a sequential pattern iff supSDB(s) ≥ minsup.

Table 2 displays the number of frequent sequential patterns mined using transaction table (Table 1). Patterns with support value higher than the specified minimum support are added to the set of Sequential Patterns. We have taken minsup = 5.

Table 2 Mined sequential patterns

Sequential patterns
*r*15, *w*14, *w*13
*r*16, *r*15, *r*10
*r*16, *r*15, *w*13
*r*16, *r*15, *w*14

Definition 12 (*Vertical Database Format*): Vertical Format Sequence Database SDB is a database, where each entry represents an item and indicates the sequence list in which the item appears and where it appears [31]. Table 3 shows the vertical representation of the database of Table1.

Definition 13 (*i-extension*): An item q is said to succeed by i-extension to an item j in a sequence $I_1, I_2, \cdots, I_n$ iff j, q $\in I_x$ for an integer x such that $1 \leq$ x $\leq$ p and q $>$ lex j.

Definition 14 (*s-extension*): An item q is said to succeed by s-extension to an item j in a sequence $I_1, I_2, \cdots, I_n$ iff j$\in I_n$ and q$\in I_m$ for some integers n and m such that $1 \leq$ n$<$m $\leq$p.

Definition 15 (*CMAP*): A Co-occurrence MAP (CMAP) is a structure mapping each item q$\in$ I to a set of items succeeding it. We define two $CMAP_s$ named $CMAP_i$ and $CMAP_s$. $CMAP_i$ maps each item q to the set cmi(q) of all items j $\in$ I succeeding q by i-extension in no less than minsup sequences of SDB. $CMAP_s$ maps each item q to the set $cm_s(q)$ of all items j $\in$ I succeedings q by s-extension in no less than minsup sequences of SDB.

The algorithm generates data dependency rules after the generation of frequent sequences which are transformed to read and write sequence. Read rules are denoted in the format: $<R(a_1), R(a_2), \cdots, R(a_n)> \rightarrow O(a)$ which gives the attributes that are to be read before any operation is performed on an attribute a. Write rules are denoted in the format: $O(a) \rightarrow <W(a_1), W(a_2), \cdots, W(a_n)>$ which gives the attributes that are to be updated after any operation is performed on an attribute a. If the confidence value of any read or write rule generated is greater than the minimum confidence provided, it is added to the rule set.

Table 4 shows the number of data dependency rules generated in the set $\in$ Read, Write in accordance to the sequential pattern generated from Table 2. Confidence value for each rule is shown which is maintained above the specified minimum confidence.

Algorithm 1: Dependency Rule Miner

```
Input : DB: Initial Database
        minsup: Minimum Support
Result: R: Set of Sequential Patterns
1  Begin:
2    Scan DB to create Vertical(DB) and identify F
3    the list of frequent items
     Enumerate(F) for each pattern A_i ∈ F do
4      Output A_i.
5      T_i ← φ for each pattern A_j ∈ F, with j ≥ i
       do
6        R ← MergePatterns(A_i, A_j)
7        for each pattern r ∈ R do
8          a ← last element in r
9          if r is i-ext then
10           if sup(CMAP_i ≥ minsup) then
11             T_i ← T_i ∪ {R};
12           else if r is s-ext then
13             if sup(CMAP_s ≥ minsup
                then
14             | T_i ← T_i ∪ {R};
15             else if ∄x : x ∈ cm_i(a) AND
16             ∄x : x ∈ cm_s(a) then
17             | continue;
18             end
19           end
20         end
21       end
22     end
23   end
24 End
```

In line 2 of the algorithm 1 the initial database is scanned to create a vertical representation of the database and identify the list of frequent items F. From line 3 the enumerate function is initialized. From line 3 the loop iterates over each element A_j from frequent list F. In step 6, the T_i is initialized to an empty set. From line 7 a nested for loop iterates over each element A_i from frequent list F with j greater than equal to i. Inside the nested loop pattern, A_i and A_j are merged and saved to variable R in line 8. From line 9 to line 18, the for loop iterates over the merged patterns R and checks if the pattern is either i-ext or s-ext and its support is greater than or equal to the minimum support and adds the respective pattern to T_i. In line 19 the Enumerate function is called recursively with frequent list T_i.

3.2.2 Role clustering analyzer

We use a role clustering method to detect the insider threats which would be otherwise left undetected. In our model (FPGWWO) we use a hybrid meta heuristic clustering algorithm to achieve the same. This hybrid module has two components namely Grey Wolf Optimizer (GWO) and Whale Optimizer (WO).These are defined as follows:

Grey wolf optimizer (GWO) Mirjalili et al. [12] introduced a new method based on swarm intelligence

Table 3 Vertical representation of Table 1

(a) Read rules

*r*10		*r*11		*r*12		*r*13		*r*14		*r*15		*r*16	
TID	Item sets	TID	Item sets	TID	Item sets	TID	Item sets	TID	Item sets	TID	Item sets	TID	Item sets
20	1,8	20	3,13	20	6,11	20		20	12	20	2,9	20	5
21	2,4	21	6	21		21	8	21		21	1	21	7
22	2,5	22		22		22		22		22	3	22	1
23	8	23	1	23		23	3	23		23	6	23	4
24		24	1	24		24		24	2	24		24	
25	1	25		25		25	4	25	2,5	25		25	
26		26		26		26	1	26		26		26	
27		27		27	4,7	27		27	2	27	1	27	
28		28		28	2	28	5	28	1	28	3	28	
29		29		29		29		29	1,4	29	2	29	

(b) Write rules

*w*10		*w*11		*w*12		*w*13		*w*14		*w*15		*w*16	
TID	Item sets	TID	Item sets	TID	Item sets	TID	Item sets	TID	Item sets	TID	Item sets	TID	Item sets
20		20	10	20		20	4	20	14	20	7	20	
21		21	9	21	3	21		21		21	5	21	
22		22		22		22	6	22	4	22		22	
23		23	2	23	5	23	9	23	7	23		23	
24		24		24		24		24		24	3	24	
25	3	25		25		25	6	25		25		25	
26		26		26		26		26		26	2	26	
27		27		27		27	6	27	3	27		27	8
28		28		28		28		28		28		28	4
29		29		29		29	5	29	3	29		29	

Table 4 Data dependency Rules

Sequential Pattern	Data Dependency Rule	Confidence
*r*16, *r*15, *w*14	*r*15, *w*14 → *r*16	60%
*r*16, *r*15, *w*13	*r*15, *w*13 → *r*16	60%
*r*16, *r*15, *w*14	*r*16, *r*15 → *w*14	75%
*r*16, *r*15, *w*13	*r*16, *r*15 → *w*13	75%
*r*16, *r*15, *r*10	*r*10 → *r*16, *r*15	80%
*r*15, *w*14, *w*13	*w*13 → *w*14, *r*15	83%
*r*15, *w*14, *w*13	*w*14, *w*13 → *r*15	100%
*r*16, *r*15, *w*14	*r*16, *w*14 → *r*15	100%
*r*16, *r*15, *r*10	*r*16, *r*15 → *r*10	100%

technology, called the Grey Wolf Optimizer (GWO), inspired from Grey Wolf, and studied its techniques for solving standard and real-life problems. The GWO variants imitate the hunting methods and leadership skills inherited by grey wolves in the wild. In GWO, the population is divided into four groups such as alpha, beta, delta and omega, which are used to mimic the management hierarchy and simulate the leadership hierarchy.

In this section the numerical models of the social chain of command, following, encompassing, and assaulting prey are given. At that point the GWO calculation is laid out.

To numerically display the social order of wolves when planning GWO, people can consider the most suitable arrangement as alpha (α). Therefore, the second and third best arrays are named beta (β) and delta (δ), respectively. The remaining competitor deals are considered Omega (γ). In the GWO calculation, the chasing (improvement) is guided by α, β and δ. x wolves follow these three wolves.

Encircling prey As referenced above, grey wolves encircle prey during the chase.To numerically demonstrate surrounding conduct, the accompanying conditions are proposed:

$$\mathbf{d} = |\mathbf{c}.\mathbf{x}_{p(t)} - \mathbf{x}(t)| \quad (2)$$

$$\mathbf{x}(t+1) = \mathbf{x}_{p(t)} - \mathbf{a}.\mathbf{d} \quad (3)$$

where t represents the current iteration, **a** and **c** are coefficient vectors, x_p is the position vector of the prey and x is the position vector of the grey wolf. The vectors a and c are calculated as follows:

$$\mathbf{a} = 2l.\mathbf{r}_1 \quad (4)$$

$$\mathbf{c} = 2.\mathbf{r}_2 \quad (5)$$

where components of a are linearly decreased from 2 to 0 over the course of iterations and r_1, r_2 are random vectors in [0, 1].

Hunting In order to simulate hunting behavior mathematically, we assume that alpha (α), beta (β), and delta (δ) have a better understanding of the potential location of the prey.The following mathematical equations are developed in this regard: Equation of hunting Cums

$$\mathbf{d}_\alpha = |\mathbf{c}_1.\mathbf{X}_\alpha - \mathbf{x}|, \mathbf{d}_\beta = |\mathbf{c}_1.\mathbf{X}_\beta - \mathbf{x}|, \mathbf{d}_\delta = |\mathbf{c}_1.\mathbf{X}_\delta - \mathbf{x}| \quad (6)$$

$$\mathbf{x}_1 = \mathbf{X}_\alpha - \mathbf{a}_1.(\mathbf{d}_\alpha), \mathbf{x}_2 = \mathbf{X}_\beta - \mathbf{x}_2.(\mathbf{d}_\beta), \mathbf{x}_3 = \mathbf{X}_\delta - \mathbf{a}.(\mathbf{d}_\delta) \quad (7)$$

$$\mathbf{x}(t+1) = \frac{\mathbf{x}_1 + \mathbf{x}_2 + \mathbf{x}_3}{3} \quad (8)$$

Searching for prey and attacking prey A is random value in gap$[-2a, 2a]$.When random value $|A| < 1$, the wolves are forced to attack the prey. Searching for prey is the exploration ability and attacking the prey is the exploitation ability. The arbitrary values of A are utilized to force the search to move away from the prey. When $|A| > 1$, the members of the population are enforced to diverge from the prey.

Attacking prey (exploitation) As referenced above, the grey wolves finish the chase by assaulting the prey when it quits moving. To numerically display moving toward the prey we decline the estimation of $\sim a$. Note that the vacillation scope of $\sim A$ is likewise diminished by $\sim a$. In other words $\sim A$ is an arbitrary incentive in the stretch [2a, 2a] where an is diminished from 2 to 0 throughout emphasess. At the point when irregular estimations of $\sim A$ are in [1, 1], the following situation of a pursuit specialist can be in any position between its present position and the situation of the prey. It shows that $|A| < 1$ powers the wolves to assault towards the prey.

Search for prey (exploration) Grey wolves mostly search as indicated by the situation of the alpha, beta, and delta. They wander from one another to look for prey and unite to assault prey. To numerically show disparity, we use $\sim A$ with random values greater than 1 or less than -1 to oblige the pursuit specialist to wander from the prey.- This emphasizes exploration and permits the GWO algorithm to look universally. It additionally shows that $|A| > 1$ powers the grey wolves to separate from the prey to ideally locate a fitter prey.

Whale optimization algorithm(WOA) The WOA is presented by Mirjalili et al. [12] to take care of the global optimization problem by imitating the conduct of humpback whales. WOA investigations show us two methods through which WOA can be adapted even more . First being the fact that its gradient free mechanism because it has capacity to dodge nearby optima and get global optimal solution. Second, that WOA doesn't require underlying changes in calculations for addressing distinctive improvement issues because it just has two fundamental parameters to be adjusted

- First, it presents all the investigations and explorations for WOA, in which a meta-heuristic hybrid model is used to integrate WOA with different methods to update the presentation of subsequent calculations.
- Second, this work has zeroed out all modification techniques that have been applied to WOA to improve its ability to find the best arrangement.
- Third, we have collected most of the scouting work identified by various applications used in the WOA.

The focus of this research includes several aspects: First, it presents all the investigations and explorations for WOA, in which a meta-heuristic hybrid model is used to integrate WOA with different methods to update the presentation of subsequent calculations. Second, this work has zeroed out all modification techniques that have been applied to WOA to improve its ability to find the best arrangement. Third, we collected most of the scouting work identified by the different applications used in the WOA.

In this section the mathematical model of encircling prey, spiral bubble-net feeding maneuver, and search for prey is first provided. The WOA algorithm is then proposed.

Encircling prey phase Humpback whales can identify the location of their prey and surround them. Since the position of the optimal design in the search space is not known a priori, the WOA algorithm assumes that the current best candidate solution is the target prey or is close to the optimal solution. Once the best search agent is defined, other search agents will try to upgrade their ranking to the best search agent. This behavior is represented by the following equations:

$$\mathbf{D} = |\mathbf{C}.\mathbf{X}_{p(t)} - \mathbf{X}(t)| \quad (9)$$

$$\mathbf{X}(t+1) = \mathbf{X}_{p(t)} - \mathbf{A}.\mathbf{D} \quad (10)$$

where t indicates the current iteration, **A** and **D** are coefficient vectors, X_p is the position vector of the prey, and X indicates the position vector of a whale.

The vectors **A** and **D** are calculated as follows:

$$\mathbf{A} = 2\mathbf{a}.\mathbf{r}_1 - \mathbf{a} \tag{11}$$

$$\mathbf{C} = 2.\mathbf{r}_2 \tag{12}$$

where the components of **a** are linearly decreased from 2 to 0 over the course of iterations and **r1**, **r2** are random vectors in [0,1].]

Bubble-net attacking method (Exploitation Phase) In order to mathematically model the bubble-net behavior of humpback whales, two approaches are designed as follows:

1. **Shrinking encircling mechanism** This behavior is achieved by reducing the value of **a**. Note that the fluctuation range of **A** is also reduced by **a**. In other words, **A** is a random value on the interval [a, a], where a decreases from 2 to 0 during the iteration. Set a random value for **A** to [1,1] and you can define a new location for the search agent at any position between the original agent location and the current best agent location.
2. **Spiral updating position** This approach first calculates the distance between the whale located at (X,Y) and prey located at (X*,Y*). A spiral equation is then created between the position of whale and prey to mimic the helix-shaped movement of humpback whales as follows:

$$\mathbf{X}(t+1) = \mathbf{D}' e^{bt} cos(2\Pi t) + \mathbf{X}^*(t) \tag{13}$$

where $\mathbf{D}' = |\mathbf{X}^*(t) - X(t)|$ and indicates the distance of the i_{th} whale the prey (best solution obtained so far), b is a constant for defining the shape of the logarithmic spiral, and t is a random number in [− 1,1].

Note that the humpback whale swims around its prey in a tight circle while following a spiral path. To simulate this simultaneous behavior, we assumed a 50% probability of choosing between the shrink wrap mechanism or the spiral model to update the position of the whale during the optimization process. The mathematical model is as follows:

$$\mathbf{X}(t+1) = \begin{cases} \mathbf{X}^*(t) + \mathbf{A}.\mathbf{D}, & \text{if } p < 0.5 \\ \mathbf{D}' e^{bt} cos(2\Pi t) + \mathbf{X}^*(t), & \text{if } p \geq 0.5 \end{cases} \tag{14}$$

where p is a random number in [0,1].

In addition to the bubble-net method, the humpback whales search for prey randomly. The mathematical model of the search is as follows:

Search for prey(Exploration Phase) The same method based on the change of the vector **A** can be used to search for prey . In fact, humpback whales randomly search based on each other's location. Therefore, we use **A** with a random values greater than 1 or less than -1 to force the search agent to stay away from the reference whale. Unlike the exploitation phase, we update the position of the search agent in the exploration phase based on the randomly selected search agent instead of the best search agent. This mechanism and $|A| > 1$ emphasize browsing and allow the WOA algorithm to perform a global search. The mathematical model is as follows:

$$\mathbf{D} = |\mathbf{C}.\mathbf{X}_{rand} - \mathbf{X}(t)| \tag{15}$$

$$\mathbf{X}(t+1) = \mathbf{X}_{rand} - \mathbf{AD} \tag{16}$$

where $\mathbf{X}_{rand}$ is a random position vector (a random whale).

Algorithm 2: mhGW-WOA Clustering

```
   Input : Load Database Logs
   Result: Cluster centroids
 1 Begin:
 2   Initialize number of search agents
 3   Initialize each search agent to contain K
       randomly cluster centers
 4   while t < no. of total iterations do
 5     for search agent do
 6       Calculate fitness value for the agent
 7       Update best search agent
 8     end
 9     for search agent do
10       Update a, A, r, c, l, p, b
11     end
12     if p<0.5 then
13       if |a| <1 then
14         D⃗ = |C⃗.X⃗*(t) − X⃗(t)|
15         X⃗(t+1) = X⃗*(t) − A⃗.D⃗
16       else
17         D⃗ = |C⃗.X⃗_rand − X⃗|
18         X⃗(t+1) = X⃗_rand − A⃗.D⃗
19       end
20     else
21       if |a| <1 then
22         D⃗′ = |X⃗*(t) − X⃗(t)|
23         X⃗(t+1) = D⃗′.e^bl. cos(2πl) + X⃗*(t)
24       else
25         Get best 3 positions
26         x[i] = pscores[0][1] + pscores[1][1] +
             pscores[2][1]
27         x[i]/ = 3
28       end
29     end
30   end
31 End
```

Steps 2 and 3 consist of the following tasks: initialising search agent variables. The next five steps entail searching for the most qualified potential agent available.

In step 9, the variables are updated to reflect the new values that have been determined. Using the Whale Optimization Algorithm, we will next update our agents at stages 10 through 20 of the process.

Then, in steps 21 to 24, we use the Modified Grey Wolf Optimization Algorithm to update our agents' information. When compared to previous techniques, this step broadens the scope of the algorithms' learning capabilities.

The algorithm produces the best cluster centres, which will be utilised as the basis for role profiles in the following section. Our clustering method is optimised via hybrid of the Whale Optimization Algorithm and the Grey Wolf Optimization Algorithm, as shown in Fig. 2.

3.3 Detection and classification phase

The learning phase of the algorithm provides the read rules, write rules and the role profiles. Now, these rules and role profile clusters are used to detect any anomalous transaction via the detection phase architecture.

The architecture of the detection phase is shown in Fig. 3. In this detection phase, the current user transaction is first passed through the transaction pre-processor and query parser. Then the anomalies are detected in the current user transactions for each transaction by checking them against the user role profiles through role authenticator and against the sequential rules generated in the learning phase segment, via the rule validator. If a query is found to be malicious, an alarm is triggered. Otherwise the transaction is committed to the database.

The detection phase architecture has 2 levels namely Role Authenticator and Rule Validator, which are described below.

3.3.1 Role authenticator

The role profile clusters generated by the clustering algorithm in the learning phase are matched against the incoming transaction in the database. The role authenticator individually checks all the queries to determine whether they are justified by the role of the user or not, thereby making the intrusion detection model immune against the insider threats as well. If the role profile of an incoming transaction is not matched to the existing profile clusters, the transaction is declared as malicious and aborted, instantaneously. However, if the role profile match is found, the transaction sequence is further checked by the rule validator for classification.

3.3.2 Rule validator

The rule validator identifies whether queries in a single configuration file are executed in an order similar to the order of previously validated queries. The incoming transaction query sequence is compared with read and write rules that are derived from data dependency mining using the CMSPADE algorithm in the learning phase. The input sequence list generated at run time is compared to the data-dependent rules generated for each sensitive element present in the list. Therefore, compliance with each rule is calculated. Now, we need to quantify the rule-based similarity of the two sequence datasets to draw conclusions about the credibility of the incoming transactions. This is done by calculating the similarity, as described in the next section.

3.3.3 Calculating similarity

A 100 point similarity system has been introduced to measure the extent of adherence between transaction and a set of rules mined using the rule mining algorithm. We have four grades of similarity called resemblance (R). Each grade has been allocated points. We try to contain the values of overlap measurement between 0.1 and 0.9 for minimum and maximum adherence respectively.

We define:

$$\mathbf{l} = 0.1 \; and \; \mathbf{h} = 0.9 \tag{17}$$

I ***Grade D resemblance:*** **(10 Points assigned out of 100)**

Grade D resemblance denoted by R4 is the measure of the number of mined rules in our database that have the same element accused in the transaction as in the rules. Let, a : the number of rules that follow this condition. b : the number of rules that do not follow this condition.

$$R_4 = \left[1 + \frac{(a-1)\cdot 1b}{(a+b)} * (h-1)\right] * 10 \tag{18}$$

(Higher weight is assigned to rules that do not follow the required conditions)

II ***Grade C resemblance:*** **(20 Points assigned out of 100)**

This stage considers a subset of rules that belong to set "a" in stage i.e the rules that have common elements as incoming transactions. Let, x : denotes the number of rules that follow the same order as in transactions. *Eg* : TR : R(a)R(b)W(c) *Rule* : R(d)R(a)R(b)W(a)W(c) y : denotes the number of rules that do not follow that condition.

$$R_3 = \left[1 + \frac{(x-1)\cdot 2y}{(x+y)} * (h-1)\right] * 20 \tag{19}$$

III ***Grade B resemblance:*** **(30 Points assigned out of 100)**

This stage considers subsets of stage 2.The set of rules is used i.e those rules that follow the same order as transactions. Let, p : the number of rules that

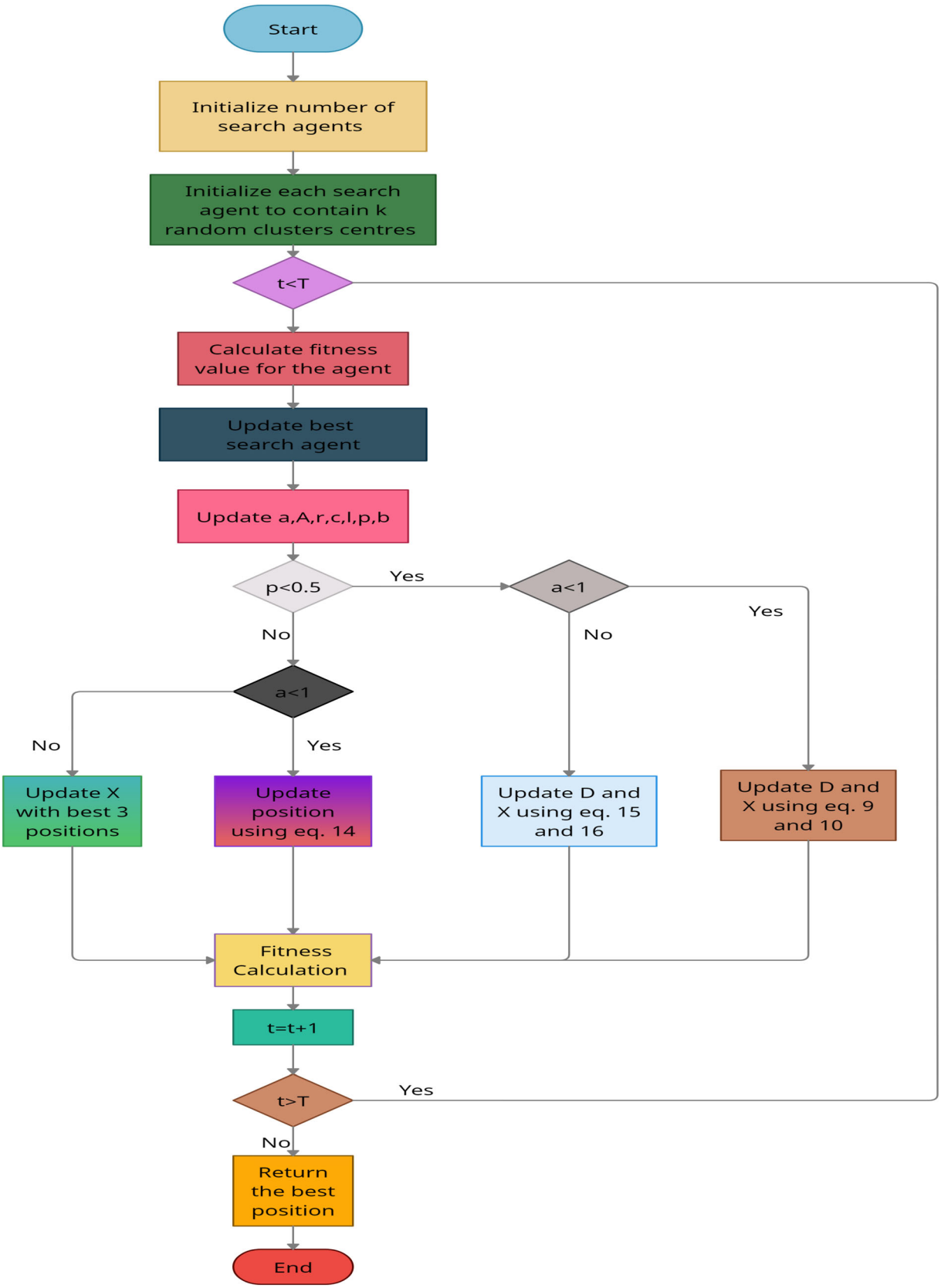

Fig. 2 Flowchart of the mhGW-WOA clustering

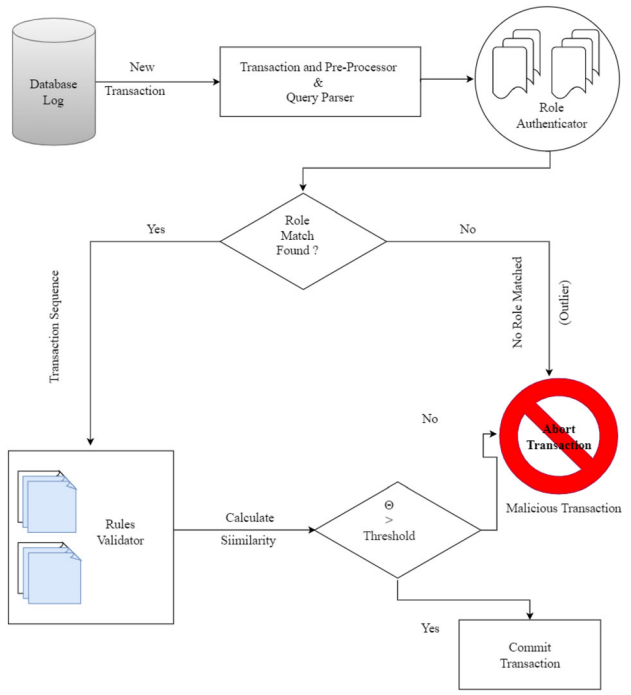

Fig. 3 Detection Phase architecture

contain transactions as a subset i.e all common elements are together as in the transaction. q : the number of elements that do not follow this rule.

$$R_2 = \left[1 + \frac{(p-1)\cdot 25q}{(p+q)} * (h-1)\right] * 30 \quad (20)$$

IV ***Intra-Transaction rules:*** These rules consider a group of transactions that are executed together in a sequential manner. The algorithm used will be similar to the mentioned above. The rule transaction will be considered sequentially in the batches of k $(2 \leq K \leq 5)$. Let, s : number of rules that adhere to the transaction set in exact order. t : number of rules that do not adhere to the transaction set.

(a) ***Grade A_2 resemblance***

This follows the above methods given in the above sections. The batch of size 2 is assigned a high weight and the order should look like: **k=2 12 Points assigned out of 100**

$$R_{12} = \left[1 + \frac{(s-1)\cdot 2t}{(s+t)} * (h-1)\right] * 12 \quad (21)$$

(b) ***Grade A_3 resemblance***

The batch size of 3 will follow the same order as the above subset. It is assigned a lower weight than the A_2 resemblance. But it will have the same multiple of A_2 resemblance as the points assigned to both these resemblances are the same. **k=3 12 Points assigned out of 100**

$$R_{13} = \left[1 + \frac{(s-1)\cdot 1t}{(s+t)} * (h-1)\right] * 12 \quad (22)$$

(c) ***Grade A_4 resemblance***

A_4 resemblance represents a batch with size 4. The order for the A_4 resemblance will be exactly half of that of A_3 resemblance as the points given to the A_4 resemblance is half of it and also the weight assigned to it is the same as that of the previous subset. **k=4 6 Points assigned out of 100**

$$R_{14} = \left[1 + \frac{(s-1)\cdot 1t}{(s+t)} * (h-1)\right] * 6 \quad (23)$$

(d) ***Grade A_5 resemblance***

The A_5 resemblance is for the final batch of size 5. As the A_5 resemblance contains the same points as that of the previous subset, i.e. A_4 resemblance so it will have the same multiple as that of A_4. But the two equations should differ as the weights assigned to A_5 resemblance is the lowest of all the Grade A resemblances. **k=5 6 Points assigned out of 100**

$$R_{15} = \left[1 + \frac{(s-t)}{(s+t)} * (h-1)\right] * 6 \quad (24)$$

Definition 16 (*Congruity Index*) A Congruity Index (Θ) is a similarity threshold defined as the sum of all the grades of similarity (resemblances).

$$\Theta = \sum_{i=1}^{n} R_i$$

where n is the number of grades.

In our case we have four grades namely A,B,C,D with four subgrades for A (A_1, A_2, A_3, A_4) Therefore,

$$\Theta = R_{12} + R_{13} + R_{14} + R_{15} + R_2 + R_3 + R_4 \quad (25)$$

3.3.4 Detection algorithm

In our proposed algorithm 3 we take in the generated rule set, number of clusters, similarity threshold (δ) and the transactions itself. Our main aim is to classify the transaction as either malicious or non-malicious. The algorithm starts with converting the transaction into sequence using the sequence generator. Then in steps 4- 9 we calculate the role similarity of each cluster and store the highest role similarity cluster along with its similarity. We compare that

similarity with that of the threshold, if it's less than the threshold we classify the transaction as malicious and raise an alarm. However if the similarity is greater than the threshold, we pass in the respective rule into the rule authenticator module. This novel module simply calculates the different resemblances (B, C, D, A_1, A_2, A_3, A_4) from step 13-20. We define congruity index (Θ) which would be used to classify the transaction. In steps 22-25 we compare the value of Θ with the δ . If Θ is less than δ then the transaction is declared malicious and if Θ is greater than δ then the transaction is declared non-malicious. Also following this in steps 27–30 if the transaction was malicious the database executes a rollback along with raising an alarm and if the transaction was non-malicious the database commits all the data.

Algorithm 3: Detection Phase

Data : R: Rule Set
K: Number of Clusters
δ: Similarity Threshold
T: Transaction
Result: C:Class (malicious or non-malicious)

1 **During Transaction:**
2 **for** *each of the Query q in TRN* **do**
3 Seq ← SequenceGenerator(q)
4 Max_sim ← ϕ
5 for all $C_k \forall$ Cluster_Centres
6 Temp ← cal_role_sim(q,C_k)
7 **if** *Temp* > *Max_sim* **then**
8 Max_sim ← Temp
9 Max_cluster ← C_k
10 **End If**
11 **end**
12 if($Max_sim < \delta$)
13 **Raise Alarm**
14 **for** *each* ***rule*** *in R* **do**
15 R_4 = GradeD_resemblance(rule, Seq)
16 R_2 = GradeC_resemblance(rule, Seq)
17 R_3 = GradeB_resemblance(rule, Seq)
18 R_{12} = GradeA_2_resemblance(rule, Seq)
19 R_{13} = GradeA_3_resemblance(rule, Seq)
20 R_{14} = GradeA_4_resemblance(rule, Seq)
21 R_{15} = GradeA_5_resemblance(rule, Seq)
22 $\Theta = R_4 + R_3 + R_2 + R_{12} + R_{13} + R_{14} + R_{15}$
23 **if** $\Theta < \delta$ **then**
24 C← malicious
25 **else**
26 C← non-malicious
27 **end**
28 **if** *(C== malicious)* **then**
29 **Rollback – Raise Alarm**
30 **else**
31 commit
32 **end**
33 **end**
34 **End**

4 Experimentation and results

In order to analyze the performance of the proposed methodology (FPGWWO), multiple assessments were performed on a synthetically generated banking databases adhering to the TPC-C benchmark [57]. The database consisted of two types of logs - one with the normal user transactions of various user roles and other which comprised a mixture of normal and malicious user transactions. These two types of logs in the data-base were used to evaluate the performance of our system. In total, 5000 transactions were generated. Precision, recall, and F1-score were the performance measures utilised in the assessment. Precision is defined as the ratio of properly identified malicious transactions, referred to as True Positives (TP), to the total number of transactions classified as malicious from database logs, which includes both False Positives (FP) and True Positives (TP). The ratio of correctly identified malicious transactions, known as True Positives (TP), to the total number of malicious transactions in the database logs, a combination of False Negatives (FN) and True Positives (TP), is defined as recall. High precision and low recall, as well as low precision and high recall, indicate a poor performing model in the situation of an unbalanced dataset. For performance evaluation, the F1-score is employed, which considers both precision and recall. The harmonic mean of precision and recall is defined as the F1-score.

4.1 Generation of synthetic transactions

FPGWWO took into account the fact that no datasets that conformed to our methodology existed, prompting us to employ synthetically created datasets effectively. This dataset comprises two separate modules for the two sorts of transactions that we worked on: malicious transactions generation module and regular transactions generation module, both of which are described and worked on below.

4.2 Generation of malicious transactions

We created two sets of fraudulent transactions to test our technique against a wide range of threats. The attacker may be ignorant of regular database requirements, thus the first batch of transactions was produced at random. This collection is created by randomly changing characteristics of genuine queries that make up normal behaviour, as well as legitimate transactions of each. The second set of transactions were created in such a way that they do not correspond to typical user behaviour and are signs of people attempting transactions that are outside of their scope and authorization.

4.3 Generation of normal transactions

Normal transactions are ones that, at the moment of execution, fulfil data dependencies and user-access patterns. We define a predefined set of SQL queries that comply to the TPC-C benchmark and the schema used to create regular transactions. Individual characteristics are allocated to each user that are within the scope of their access and permissions, and transactions are created based on those attributes, meeting the user-access patterns.

4.4 Evaluation of our approach

The Figs. 4, 5, 6 above depict the variation in precision, recall and F1 Score of the system for threshold value of 50. With change in the number of transactions in the database. It can be inferred from the graph that the value of Precision first increases from 0.785 to 0.855. With an increase in the number of transactions, the value of Recall rises from 0.912 to 0.950. The number of rules created for each transaction grows as the number of transactions grows. As a result, rules will be more matched to the database, and role clustering will be more refined. As a result, the number of false negatives decreases while the number of true positives rises, resulting in an increase in the recall value. Because the F1-score is a harmonic mean of Precision and Recall, it reflects a good balance of precision and recall by continuing to rise between the two values, ranging from 0.845 to 0.882 (Table 5).

Using a threshold value of 60, the Figs. 7, 8, 9 illustrate the variance in accuracy, recall, and F1 Score of the system as a function of the number of transactions in the database. As shown in the graph, the value of Precision begins to rise from 0.772 to 0.818 at the beginning of the study period. Increase in the number of transactions result in an increase in the value of Recall, which rises from 0.921 to 0.938. Increasing the number of transactions leads to an increase in the number of rules that are created for each transaction. As a result, the rules are more matched to the database, and

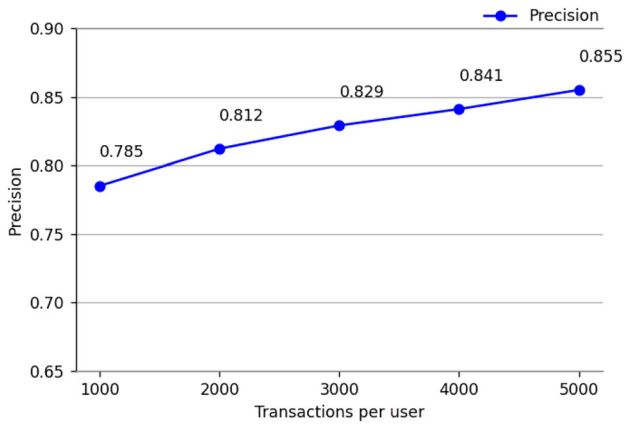

Fig. 4 Variation of precision with number of transactions per user at Threshold 50

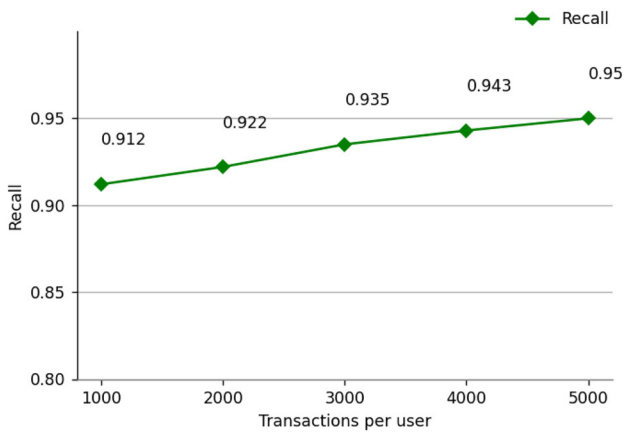

Fig. 5 Variation of recall with number of transactions per user at Threshold 50

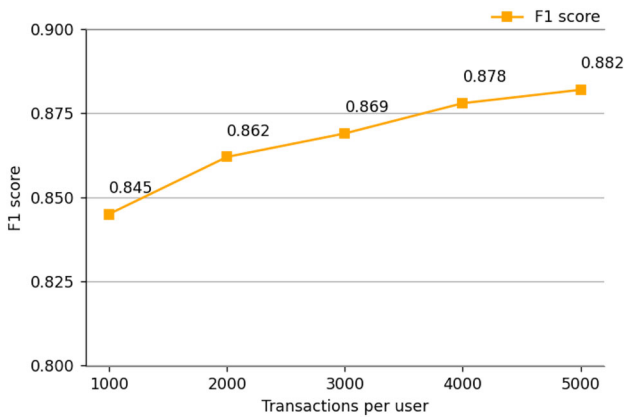

Fig. 6 Variation of F1 score with number of transactions at Threshold 50

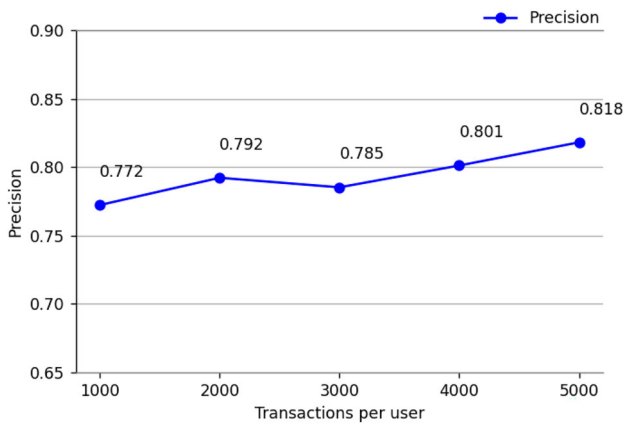

Fig. 7 Variation of Precision with number of transactions per user at Threshold 60

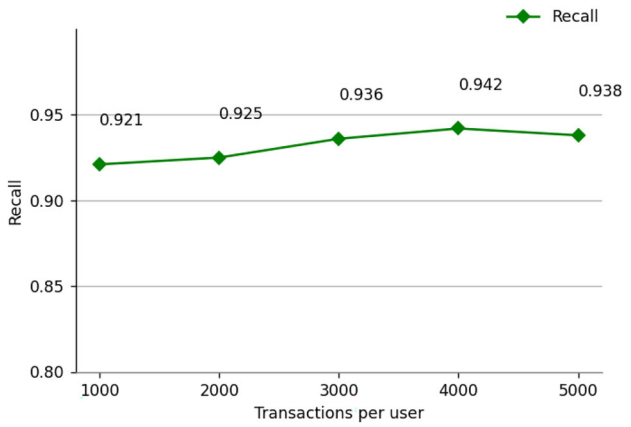

Fig. 8 Variation of Recall with number of transactions per user at Threshold 60

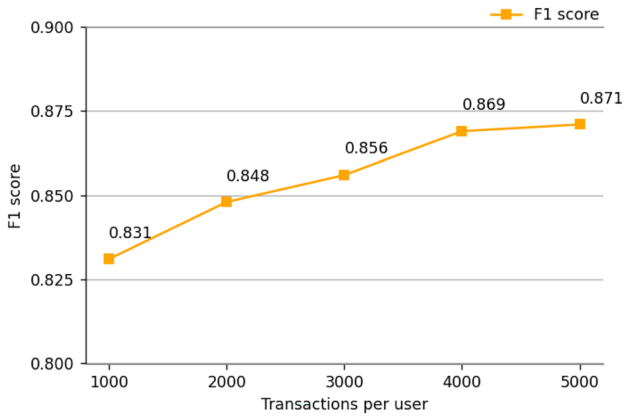

Fig. 9 Variation of F1 score with number of transactions at Threshold 60

the role clustering is more refined as a result of these improvements. Thus, there is a drop in the number of false negatives and an increase in the number of true positives, which leads to an increase in the recall value due to the decrease in false negatives. Here also, the value of F1 Score shows a slight increase from 0.831 to 0.871 (Table 6).

We also assess how well our role clustering algorithm performs. Figure 10 shows the variation of the loss of the clustering algorithm. As observed from the graph, the loss steadily decreases initially and then reaches a stable value and sustains it. Loss value becomes less than half of its initial value which is an impressive improvement and shows the adaptability of the algorithm on the dataset. This behaviour validates that the algorithm is performing good for the study.

Comparative performance of our technique with other eminent authors of this domain has been tabulated below. We have incorporated an approach that examines the intra-transactional queries to deal with the insider threats as well

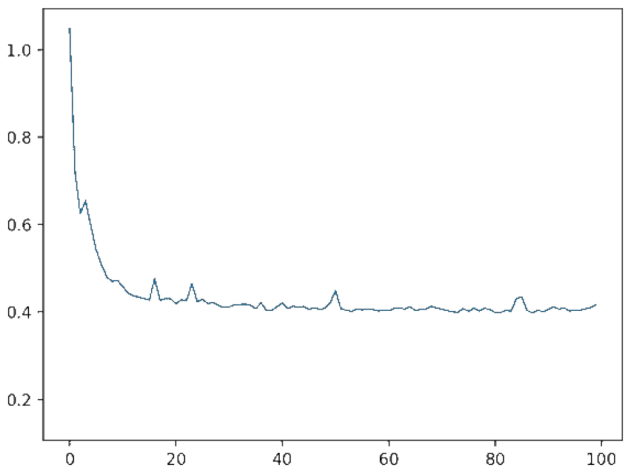

Fig. 10 Loss of mhGW-WOA clustering

Table 5 Precision, recall, F1-score at Threshold 50

Parameter	Threshold = 50				
	Number of transactions				
	1000	2000	3000	4000	5000
Precision	0.785	0.812	0.829	0.841	0.855
Recall	0.912	0.922	0.935	0.943	0.95
F1 Score	0.845	0.862	0.869	0.878	0.882

Table 6 Precision, recall, F1-score at Threshold 60

Parameter	Threshold = 60				
	Number of transactions				
	1000	2000	3000	4000	5000
Precision	0.772	0.792	0.785	0.801	0.818
Recall	0.921	0.925	0.936	0.942	0.938
F1 Score	0.831	0.848	0.856	0.869	0.871

as external threats. We have used algorithms like CM-SPADE and Hybridization of Whale Optimization Algorithm with Modified Grey Wolf clustering Algorithm and a novel approach to similarity calculation. These algorithms have enhanced the performance of our approach as compared to the other state-of-the-art techniques.

Table 7 contrasts the various techniques based on the algorithm used, including but not limited to its ability to avoid intrusion and higher performance on metrics such as precision and recall. On comparing the metrics across different support values for each technique, the maximum values were considered. We observed better performance for our algorithm compared to the alternatives. The critical factor behind the improved performance is the sensitivity

Table 7 Performance Comparison of FPGWWO with state-of-the-art techniques

Author Name	Proposed technique	Use of RBAC	Intrusion detection capabilities	Approach for query evaluation	Detection level	Detection of threats	Detection paradigm	Performance
Hu et al. [5]	Integrated dependency with sequence alignment analysis	No	Partial	Syntax Centric	Transaction level	External and user threats only	Anomaly	Recall = 0.90 Precision = 0.64
Srivastava et al. [17]	Integrated dependency with sequence alignment analysis	No	Partial	Syntax Centric	Transaction level	External and user threats only	Anomaly	Recall = 0.77 Precision = 0. 80
Kamra et al. [42]	Dependency And Relation Analysis	Yes	Yes	Syntax Centric	Transaction level	Insider using RBAC, External using clustering	Anomaly	Recall = 0.63 Precision = 0.77
Hashemi et al. [24]	Temporal Mining	No	Yes	Syntax Centric	Transaction Level	Both external and insider threats	Anomaly analysis of the time series	Recall = 0.90 Precision = 0.75
Kundu et al. [26]	Sequence alignment analysis	No	Partial	Syntax Centric	Transaction level	External and user threats	Anomaly	Precision = 0.945
Panigrahi et al. [43]	User Behavior Mining	Yes	Partial	Syntax Centric	Transaction level	Both External and Insider threats	Both Anomaly detection and misuse detection	Recall = 0.93 Precision = 0.91
Doroudian et al. [58]	Mining dependencies	No	Yes	Syntax Centric	Transaction level	External and user threats	Anomaly and specification based	Recall = 0.89 Precision = 0.91
Ronao and Cho [48]	Weighted Random Forest	Yes	Yes	Syntax Centric	Root level	External and user threats	Anomaly	Recall = 0.95 Precision = 0.89
Sallam et al. [46]	Anomaly Detection using Bayesian Classifier	Yes	Yes	Data and Syntax Centric	RDBMS level	Insider threats	Anomaly	Recall = 0.97 Precision = 0.90
Kim and Cho [49]	CNN - LSTM Neural Network	Yes	Yes	Data Centric	RDBMS level	User threats and Insider threats	Anomaly	Recall = 0.887 Accuracy of 0.933
Seok-Jun et al. [59]	Convolutional Neural-based Learning Classifier	Yes	Yes	Data-Centric	RDBMS level	Insider Threats	Anomaly	Recall = 0.93 Precision = 0.92
FPGWWO (our approach)	Frequent Sequential Pattern Mining and metaheuristic clustering	Yes	Yes	Data and Syntax centric	Transaction level	External and insider threats	Anomaly	Recall = 0.938 Precision = 0.91

of the algorithm to change in user patterns since we consider the relative adherence to data dependencies. This behaviour is expressed by real-world transactions where they never fully comply with data dependencies.

Since our algorithm combines the benefits of anomaly-based and statistical detection methods, we are able to reduce the number of false positives and false negatives errors.

5 Conclusion and future scope

In this study, we have proposed a Database Intrusion Detection System (DIDS) to prevent unauthorised access from changing critical user details. Our method (FPGWWO) can identify threats from both within and outside the system by incorporating a frequent sequential pattern mining algorithm and a hybrid metaheuristic clustering using modified Grey Wolf optimization and Whale Optimization Algorithm (mhGW-WOA).

CM-SPADE is used to mine frequent sequential patterns from database logs to construct read and write rules, which are based on legitimate access patterns. Parallely, the hybrid swarm clustering algorithm (mhGW-WOA) clusters out users based on their role profiles to ensure that each user's role is matched in the current role profiles and determine congruity index.

In terms of computational complexity, storage efficiency, and faster convergence rate, the hybrid of grey wolf and whale optimizers appears to be advantageous, as well as provides increased accuracy in clustering role profiles for user transactions. As a result, when compared to existing state-of-the-art methodologies in the literature, our proposed methodology has a higher overall efficiency. Our future research will focus on improvising ways for integrating user behaviour and other elements of transaction pattern mining utilising more efficient mining algorithms. It would also take into account the limits of the current technique in terms of adding new features and calculating adherence to improve the model's performance.

References

1. Fernández-García, A.J., Iribarne, L., Corral, A., Criado, J., Wang, J.Z.: A flexible data acquisition system for storing the interactions on mashup user interfaces. Comput. Standards Interfaces **59**, 10–34 (2018)
2. Bertino, E., Sandhu, R.: Database security-concepts, approaches, and challenges. IEEE Trans. Depend. Secure Comput. **2**(1), 2–19 (2005)
3. Cappelli, D.M., Moore, A.P., Trzeciak, R.F.: The CERT guide to insider threats: how to prevent, detect, and respond to information technology crimes (Theft, Sabotage, Fraud). Addison-Wesley (2012)
4. Heady, R., Luger, G., Maccabe, A., Servilla, M.: The architecture of a network level intrusion detection system. Tech. rep., Los Alamos National Lab., NM (United States); New Mexico Univ., Albuquerque (1990)
5. Hu, Y., Panda, B.: A data mining approach for database intrusion detection. In: Proceedings of the 2004 ACM symposium on Applied computing, pp. 711–716 (2004)
6. Debar, H., Dacier, M., Wespi, A.: Towards a taxonomy of intrusion-detection systems. Comput. Netw. **31**(8), 805–822 (1999)
7. Preuveneers, D., Rimmer, V., Tsingenopoulos, I., Spooren, J., Joosen, W., Ilie-Zudor, E.: Chained anomaly detection models for federated learning: An intrusion detection case study. Appl. Sci. **8**(12), 2663 (2018). https://doi.org/10.3390/app8122663
8. Lee, W., Stolfo, S.: Data mining approaches for intrusion detection (1998)
9. Barbará, D., Couto, J., Jajodia, S., Wu, N.: Adam: a testbed for exploring the use of data mining in intrusion detection. ACM Sigmod Record **30**(4), 15–24 (2001)
10. Kanoun, W., Cuppens-Boulahia, N., Cuppens, F., Autrel, F.: Advanced reaction using risk assessment in intrusion detection systems. In: International Workshop on Critical Information Infrastructures Security, pp. 58–70. Springer (2007)
11. Sandhu, R., Ferraiolo, D., Kuhn, R., et al.: The nist model for role-based access control: towards a unified standard. In: ACM workshop on Role-based access control, vol. 10 (2000)
12. Mirjalili, S., Lewis, A.: The whale optimization algorithm. Adv. Eng. Softw. **95**, 51–67 (2016)
13. Hoglund, A.J., Hatonen, K., Sorvari, A.S.: A computer host-based user anomaly detection system using the self-organizing map. In: Proceedings of the IEEE-INNS-ENNS International Joint Conference on Neural Networks. IJCNN 2000. Neural Computing: New Challenges and Perspectives for the New Millennium, vol. 5, pp. 411–416. IEEE (2000)
14. Lunt, T.F., Tamaru, A., Gillham, F.: A real-time intrusion-detection expert system (IDES). SRI International, Computer Science Laboratory (1992)
15. Talpade, R., Kim, G., Khurana, S.: Nomad: Traffic-based network monitoring framework for anomaly detection. In: Proceedings IEEE International Symposium on Computers and Communications (Cat. No. PR00250), pp. 442–451. IEEE (1999)
16. Hu, Y., Panda, B.: Identification of malicious transactions in database systems. In: Seventh International Database Engineering and Applications Symposium, 2003. Proceedings., pp. 329–335. IEEE (2003)
17. Srivastava, A., Sural, S., Majumdar, A.K.: Database intrusion detection using weighted sequence mining. J. Comput. **1**(4), 8–17 (2006)
18. Denning, D.E.: An intrusion-detection model. IEEE Trans. Softw. Eng. **2**, 222–232 (1987)
19. Corney, M., Mohay, G., Clark, A.: Detection of anomalies from user profiles generated from system logs. In: Proceedings of the Ninth Australasian Information Security Conference, pp. 23–31. Australian Computer Society (2011)
20. Cárdenas, A.A., Amin, S., Lin, Z.S., Huang, Y.L., Huang, C.Y., Sastry, S.: Attacks against process control systems: risk assessment, detection, and response. In: Proceedings of the 6th ACM symposium on information, computer and communications security, pp. 355–366 (2011)
21. Liao, H.J., Lin, C.H.R., Lin, Y.C., Tung, K.Y.: Intrusion detection system: a comprehensive review. J. Netw. Comput. Appl. **36**(1), 16–24 (2013)
22. Hastie, T., Tibshirani, R., Friedman, J.: Unsupervised learning. In: The elements of statistical learning, pp. 485–585. Springer (2009)
23. Chen, M.S., Han, J., Yu, P.S.: Data mining: an overview from a database perspective. IEEE Trans. Knowledge Data Eng. **8**(6), 866–883 (1996)
24. Hashemi, S., Yang, Y., Zabihzadeh, D., Kangavari, M.: Detecting intrusion transactions in databases using data item dependencies and anomaly analysis. Expert Syst. **25**(5), 460–473 (2008)
25. Rahman, M.M., Ahmed, C.F., Leung, C.K., Pazdor, A.G.: Frequent sequence mining with weight constraints in uncertain databases. In: Proceedings of the 12th international conference on ubiquitous information management and communication, pp. 1–8 (2018)

26. Kundu, A., Sural, S., Majumdar, A.K.: Database intrusion detection using sequence alignment. Int. J. Inform. Security **9**(3), 179–191 (2010)
27. Subudhi, S., Panigrahi, S.: Application of optics and ensemble learning for database intrusion detection. J. King Saud University-Comput. Inform. Sci. (2019)
28. Sallam, A., Bertino, E.: Result-based detection of insider threats to relational databases. In: Proceedings of the ninth ACM conference on data and application security and privacy, pp. 133–143 (2019)
29. Agrawal, R., Srikant, R.: Mining sequential patterns. In: Proceedings of the eleventh international conference on data engineering, pp. 3–14. IEEE (1995)
30. Srikant, R., Agrawal, R.: Mining sequential patterns: Generalizations and performance improvements. In: International conference on extending database technology, pp. 1–17. Springer (1996)
31. Zaki, M.J.: Spade: an efficient algorithm for mining frequent sequences. Mach. Learn. **42**(1), 31–60 (2001)
32. Pei, J., Han, J., Mortazavi-Asl, B., Wang, J., Pinto, H., Chen, Q., Dayal, U., Hsu, M.C.: Mining sequential patterns by pattern-growth: the prefixspan approach. IEEE Trans. Knowledge Data Eng. **16**(11), 1424–1440 (2004)
33. Ayres, J., Flannick, J., Gehrke, J., Yiu, T.: Sequential pattern mining using a bitmap representation. In: Proceedings of the eighth ACM SIGKDD international conference on Knowledge discovery and data mining, pp. 429–435 (2002)
34. Gomariz, A., Campos, M., Marin, R., Goethals, B.: Clasp: An efficient algorithm for mining frequent closed sequences. In: Pacific-Asia Conference on Knowledge Discovery and Data Mining, pp. 50–61. Springer (2013)
35. Fournier-Viger, P., Gomariz, A., Campos, M., Thomas, R.: Fast vertical mining of sequential patterns using co-occurrence information. In: Pacific-Asia Conference on Knowledge Discovery and Data Mining, pp. 40–52. Springer (2014)
36. Lan, G.C., Hong, T.P., Lee, H.Y.: An efficient approach for finding weighted sequential patterns from sequence databases. Appl. Intell. **41**(2), 439–452 (2014)
37. Rahman, M.M., Ahmed, C.F., Leung, C.K.S.: Mining weighted frequent sequences in uncertain databases. Inform. Sci. **479**, 76–100 (2019)
38. Chung, C.Y., Gertz, M., Levitt, K.: Demids: A misuse detection system for database systems. In: Working Conference on Integrity and Internal Control in Information Systems, pp. 159–178. Springer (1999)
39. Spalka, A., Lehnhardt, J.: A comprehensive approach to anomaly detection in relational databases. In: IFIP Annual Conference on Data and Applications Security and Privacy, pp. 207–221. Springer (2005)
40. Alzubi, J.A., Jain, R., Kathuria, A., Khandelwal, A., Saxena, A., Singh, A.: Paraphrase identification using collaborative adversarial networks. J. Intell. Fuzzy Syst. **39**(1), 1021–1032 (2020). https://doi.org/10.3233/JIFS-191933
41. Alzubi, J.A., Jain, R., Nagrath, P., Satapathy, S., Taneja, S., Gupta, P.: Deep image captioning using an ensemble of cnn and lstm based deep neural networks. J. Intell. Fuzzy Syst. **40**(4), 5761–5769 (2021). https://doi.org/10.3233/JIFS-189415
42. Kamra, A., Terzi, E., Bertino, E.: Detecting anomalous access patterns in relational databases. VLDB J. **17**(5), 1063–1077 (2008)
43. Panigrahi, S., Sural, S., Majumdar, A.K.: Two-stage database intrusion detection by combining multiple evidence and belief update. Inform. Syst. Front. **15**(1), 35–53 (2013)
44. Hussain, S.R., Sallam, A.M., Bertino, E.: Detanom: Detecting anomalous database transactions by insiders. In: Proceedings of the 5th ACM Conference on Data and Application Security and Privacy, pp. 25–35 (2015)
45. Sallam, A., Bertino, E., Hussain, S.R., Landers, D., Lefler, R.M., Steiner, D.: Dbsafe-an anomaly detection system to protect databases from exfiltration attempts. IEEE Syst. J. **11**(2), 483–493 (2015)
46. Sallam, A., Fadolalkarim, D., Bertino, E., Xiao, Q.: Data and syntax centric anomaly detection for relational databases. Wiley interdisciplinary reviews: data mining and knowledge discovery **6**(6), 231–239 (2016)
47. Sallam, A., Bertino, E.: Detection of temporal insider threats to relational databases. In: 2017 IEEE 3rd International Conference on Collaboration and Internet Computing (CIC), pp. 406–415. IEEE (2017)
48. Ronao, C.A., Cho, S.B.: Anomalous query access detection in rbac-administered databases with random forest and pca. Inform. Sci. **369**, 238–250 (2016)
49. Kim, T.Y., Cho, S.B.: Cnn-lstm neural networks for anomalous database intrusion detection in rbac-administered model. In: International Conference on Neural Information Processing, pp. 131–139. Springer (2019)
50. Mahalingam, T., Subramoniam, M.: A hybrid gray wolf and genetic whale optimization algorithm for efficient moving object analysis. Multim Tools Appl. **78**(18), 26633–26659 (2019)
51. Rathore, R.S., Sangwan, S., Prakash, S., Adhikari, K., Kharel, R., Cao, Y.: Hybrid wgwo: whale grey wolf optimization-based novel energy-efficient clustering for eh-wsns. EURASIP J. Wireless Commun. Netw. **2020**(1), 1–28 (2020)
52. Movassagh, A.A., Alzubi, J.A., Gheisari, M., Rahimi, M., Mohan, S., Abbasi, A.A., Nabipour, N.: Artificial neural networks training algorithm integrating invasive weed optimization with differential evolutionary model. J. Ambient Intell. Human. Comput. (2021). https://doi.org/10.1007/s12652-020-02623-6
53. Rahnema, N., Gharehchopogh, F.S.: An improved artificial bee colony algorithm based on whale optimization algorithm for data clustering. Multim. Tools Appl. **79**(43), 32169–32194 (2020)
54. Aljarah, I., Mafarja, M., Heidari, A.A., Faris, H., Mirjalili, S.: Clustering analysis using a novel locality-informed grey wolf-inspired clustering approach. Knowledge Inform. Syst. **62**(2), 507–539 (2020)
55. Ghany, K.K.A., AbdelAziz, A.M., Soliman, T.H.A., Sewisy, A.A.E.M.: A hybrid modified step whale optimization algorithm with tabu search for data clustering. Journal of King Saud University-Computer and Information Sciences (2020)
56. Viet, K., Panda, B., Hu, Y.: Detecting collaborative insider attacks in information systems. In: 2012 IEEE International Conference on Systems, Man, and Cybernetics (SMC), pp. 502–507. IEEE (2012)
57. Benchmark, T.C.: (2020). http://www.tpc.org/tpcc/default5.asp
58. Doroudian, M., Shahriari, H.R.: A hybrid approach for database intrusion detection at transaction and inter-transaction levels. In: 2014 6th Conference on Information and Knowledge Technology (IKT), pp. 1–6. IEEE (2014)
59. Bu, S.J., Cho, S.B.: A convolutional neural-based learning classifier system for detecting database intrusion via insider attack. Inform. Sci. **512**, 123–136 (2020)

Publisher's Note Springer Nature remains neutral with regard to jurisdictional claims in published maps and institutional affiliations.

Rajni Jindal is currently Professor in Department of Computer Science & Engineering at Delhi Technological University (erstwhile Delhi College of Engineering). She is working here as faculty for more than 25 years. She completed her PhD (Computer Engineering) from Faculty of Technology, Delhi University in the area of Data Mining. She received her M.E. (Computer Technology & Applications) degree from - Delhi college of Engineering and her Master of Computer Applications (MCA) degree from Jawaharlal Nehru University (JNU), Delhi. Prior to joining teaching she has also worked with Tata Consultancy Services (TCS). She also worked as Professor, Head (IT) and Dean (Research & Collaboration) at IGDTUW for almost three years. She possesses a work experience of more than 25 years in research and academics. Her major areas of interest are Database Systems, Data Mining and Operating systems. She has supervised many M.Tech and 8 Ph.D thesis. She has authored/co-authored more than 160 research papers and articles for various national and international journals/conferences. She has visited and presented papers abroad at places like San Francisco, Las Vegas and Spain. She has completed AICTE sponsored project in the area of education data mining as Co-Principal Investigator. She has authored books on "Data Structures using C" and "Compiler-Construction and Design". Other than organizing various workshops and lectures she successfully organized an IEEE International Conference on Data mining and Intelligent Computing (ICDMIC-2014) held at IGDTUW and another IEEE International Conference on information processing (IICIP 2016) at DTU. She is a life member of professional bodies like CSI, ISTE and Senior member of IEEE, USA

Indu Singh is currently working as Assistant Professor in Computer Science Engineering Department at Delhi Technological University, Delhi, India. Singh has received her B.Tech in 2010 in Computer Science Engineering and M.Tech degree in Information Security from Ambedkar Institute of Advanced Communication Technologies & Research, Govt. of NCT Delhi in 2012. She is currently pursuing her Ph.D in Computer Science Engineering from Delhi Technological University, Delhi with specialisation in Data Mining and Information Security. Her research interests include Database Systems, Data Mining, Information Security, Machine Learning, Fuzzy systems and Swarm Intelligence. She has several papers published in International conferences and Journals of IEEE, Elsevier, Springer and ACM. She has received IEEE Best Paper Award in ICACCI-2016. Singh is also serving as a reviewer for Computers in Biology and Medicine (Elsevier), Soft Computing Journal (Springer), Journal of Ambient Intelligence and humanized computing (Springer) and various International Conferences of Elsevier, Springer and IEEE. She is also a member of IEEE.

Proceedings of the Sixth International Conference on Intelligent Computing and Control Systems (ICICCS 2022)
IEEE Xplore Part Number: CFP22K74-ART; ISBN: 978-1-6654-1035-9

2022 6th International Conference on Intelligent Computing and Control Systems (ICICCS) | 978-1-6654-1035-9/22/$31.00 ©2022 IEEE | DOI: 10.1109/ICICCS53718.2022.9788376

Detection of hatefulness in Memes using unimodal and multimodal techniques

Aruna Bhat
Computer Engineering
Delhi Technological University
Delhi, India
(aruna.bhat@dtu.ac.in)

Vaibhav Varshney
Computer Engineering
Delhi Technological University
Delhi, India
(varshney.vaibhav18@gmail.com)

Varun Bajlotra
Computer Engineering
Delhi Technological University
Delhi, India
(varunbajlotra@gmail.com)

Vishesh Gupta
Computer Engineering
Delhi Technological University
Delhi, India
(vishesh1999gupta@gmail.com)

***Abstract* - Memes have become a common way to spread humor, information, and ideas. However, some objectionable content in memes might transmit hatefulness among people. Identification of hatefulness in memes is thus essential and even challenging as it simultaneously involves analyzing two modes of information. We propose two different methods to classify hateful memes through this research work. The first method focuses on using BERT to improve the efficiency of existing text based models. The second method introduces a novel Multimodal technique which detects objects using pre-trained models like InceptionV3, ResNet50, and Xception and combines the modalities of text and image. The models created are lightweight and perform on par with complex transformer models.**

***Keywords* - Unimodal, Multimodal, Transformers, BERT, InceptionV3, ResNet50, Xception, , AUROC, Linear SVM, Logistic Regression, Sentiment Analysis, Tokenization, OCR**

I. INTRODUCTION

Social Media has rapidly advanced as the prime mode of communication between people. People have been all the more dependent on it since the Covid Era has started. Keeping in mind the dependence of the current generation on social media, the content on social media influences the lives of many people [3]. Social media has provided people a platform where they can showcase their talents and reach out to people all over the world while themselves sitting at home comfortably. It has aided many people to gain recognition and at the same time earn money through their content. Social media is widely used for the purpose of entertainment. One of the major reasons for the rapid growth of social media is the increasing popularity of Memes. Memes basically are motionless images coupled with a caption. New memes are created daily on all social media sites like Instagram, Facebook, WhatsApp, etc. Just like two sides of a coin, there are two aspects of memes. Though most memes are aimed at spreading humour and laughter, there are some which target an individual or a specific section of society and try to demean them [2]. Such memes are very unhealthy and may lead to the deterioration of mental health in people. Memes are distributed over various categories ranging from funny and sarcastic to hateful and offensive.

Memes can be an excellent medium for entertainment and humour. However, a meme which is pleasing and funny to a person can be repulsive for someone else. Some negative elements of the society intentionally create memes to spread hatred towards a person or community. Seeing the growing popularity of memes, even political parties use memes to foster their agenda [1]. These entities do not uphold the principles of integrity and feel free to spread false information regarding their opposition parties and leaders. The memes which misguide people or spread hostility must be banned and removed from all social platforms. Strict actions must be taken against the creators of these memes. Millions of new memes enter social media and it is impossible to identify the hateful memes manually. Therefore there is a need for an automated solution for this task.

II. RELATED WORK

Despite the fact that the Hateful Memes Dataset [14] is one of the first of its sort, there are some other comparable datasets that are available. SemEval-2020 Task 8 (Memotion analysis) [9] entails categorizing various types of sentiments from a collection of 10,000 memes. Reddit Memes Dataset [10] includes 3326 memes, as well as their post ID, image URL, up/downvotes, and other information. It was prepared to estimate the dankness percentage of memes.

With an exponential growth of textual data on the internet in recent years, it has become important to provide precise results to the users. It has always been a challenging task for the researchers to develop an AI model to extract the required information from textual data. In paper [19], authors have

Authorized licensed use limited to: DELHI TECHNICAL UNIV. Downloaded on June 15,2022 at 11:25:13 UTC from IEEE Xplore. Restrictions apply.

discussed an approach of tokenization to reduce the inference time.

Apeksha Aggarwal et al. [1] attempted Sequential and Multimodal Classification on the Hateful Memes Dataset [14]. In the Sequential Approach, they created the image caption using Resnet-152 and LSTM. They used Tesseract API to extract the text and embedded the text using GloVe embeddings. In the Multimodal Approach, they extracted the text features using FastText and used a Neural Network for classification. As they used the traditional GloVe Embeddings, they were only able to achieve a validation accuracy of 0.55 and 0.59 in Text Based and Multimodal respectively.

The authors of [11] employed an image captioning model to capture relevant context from the images and then generate embedding for text and images present in the Hateful Memes Dataset [14] using techniques like tf-idf and DistilBERT. The embedding for the engineered features associated with a meme were then passed on to two different models: gradient-boosted decision tree and LSTM model. The best auroc score achieved was 72.7 on the test data. The performance of their model was slightly compromised due to usage of a faster and less accurate version of BERT i.e. DistilBERT.

Researchers of [17] proposed a DisMultiHate framework for hatefulness detection of memes. They generated disentangled text representation via text encoder and visual representation via Attention-based image encoder and introduced a self-supervised matching loss to constrain the disentangled visual data to be similar to textual data. Their research lacked the use of advanced reasoning modules to classify memes that do not provide a context via image caption.

Classification of Static Visual data is among the most extensively researched disciplines, with a slew of high-level papers published in the last several years. Image processing, Computer vision, and ML are some of the fields that deal with this type of study. Krishna et al. [18] discussed how they investigated Deep convolutional neural networks for classification tasks and used the AlexNet Architecture with CNN to do so. As an outcome, the study's findings were really encouraging, with accuracy on test data of roughly 76.24% on MNIST and CIFAR-100.

The authors of [13] designed a Triplet-Relation network that improves and accounts the multimodal relationship modelling between image and caption. It models the cross-modality relationship between image and textual sentences. They were able to achieve a comparative AUROC score of 74.80 on the hateful memes [14] test data set. Their method was not able to detect text which was not semantically aligned with the images and hence weakened the effectiveness of sentence augmentation and slightly compromised the performance of the model.

The authors of [3] developed a deep learning multimodal method to analyze the use of varied words in different images. However, their dataset was a self-reported dataset which may introduce bias and unobtrusive behavioral measure while categorizing the dataset. For our model we aim at using a dataset developed by researchers at facebook which may be subject to little or almost no bias.

Researchers in [12] have done a comparative analysis of different multimodal architectures for sentiment analysis however, in order to keep a fair baseline for all models they have not performed any hyper parameter optimization which may not give the accurate results for comparison.

III. EXPERIMENTAL DESIGN

A. Dataset

In this implementation, the Hateful Memes [14] dataset has been used, which was constructed by Meta AI. This dataset consists of memes (with text embedded in the images) and text in string format to simplify processing for the programmers. The dataset was launched along with the Hateful Memes Challenge which aimed at making AI a much more effective tool in Hateful Speech Detection. The distribution of hateful and non hateful memes in the dataset is shown in Fig 1. The dataset covers varied hateful memes which discriminate on the basis of race, nationality, religion, caste, gender and sexual orientation.

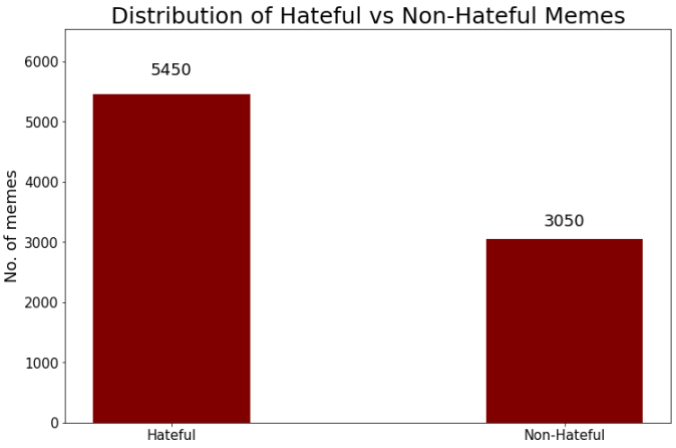

Fig. 1 Distribution of hateful and non-hateful memes

B. Research Variables

It contains over 8500 memes categorised under two binary classes ‘0’ (non-offensive) and ‘1’ (offensive). These memes can be further classified as offensive and benignantly non-offensive.

C. Data Cleaning and Preprocessing

The prime objective of applying a technique in ML is that it must be able to effectively analyse the input's attributes and give

Authorized licensed use limited to: DELHI TECHNICAL UNIV. Downloaded on June 15,2022 at 11:25:13 UTC from IEEE Xplore. Restrictions apply.

accurate and precise results while making predictions. Thus, Data Preprocessing is essential to treat inconsistent data and to make data suitable for the ML algorithm to work upon.

Steps of Pre-processing performed for unimodal analysis:

1) **Lower Casing:** Firstly, the text captions present in the dataset were converted to the lower-case format.
2) **URL Elimination:** In the next step, elimination of URLs was performed using various RegEx expressions.
3) **Removal of Punctuation Marks:** The punctuations present in the text were then removed from the captions.
4) **Tokenization:** The captions were then broken down into meaningful tokens for simplification of further analysis.
5) **Stop Word Elimination:** Words like ("an", "the", "a") were eliminated so as to preserve valuable processing time.
6) **Stemming:** The last step of text preprocessing was to reduce the words to their root format using the Porter Stemmer.

D. Model Development and Validation

The Machine Learning Algorithms are trained and tuned to fit the dataset in the best possible way. The models are validated with the Holdout Validation Technique.

1. Unimodal Approach

The clean text was generated for 8500 images after data pre-processing. At this stage, the text was in sentence form. So, the next step was tokenization of the cleaned text using a tokenizer. To select the best feature extractor, Bag of Words, TF-IDF, FastText, Word2Vec, GloVe, BERT, etc. were analysed [12].

BERT was found to perform the best among all these. Bag of words and TF-IDF representation does not consider the semantic relation between words and the total dimension of the matrix depends on the vocabulary size which can lead to overfitting of the model.

Glove and Word2Vec limit only to the words that are present in the model dictionary and do not take into account the position of the word in the sentence whereas BERT calculates the embedding of a word by considering its index in the sentence and also provides support for word which are not in its vocabulary by using a subword segmentation algorithm called wordpiece.

BERT was chosen as it trains the transformers bidirectionally on large amounts of data and resources. Whereas, other models are either unidirectional, i.e, trained left to right or are sequentially trained from left to right and then from right to left. Moreover, BERT also uses the concept of masked words where it masks 15-20% of the words and tries to predict them using the context of the remaining words. The BERT embedding can be represented as:

$$[s, C] = \text{BERT}([w_{[CLS]}, O]) \quad (1)$$

where $w_{[CLS]} \in R^{|V|}$ represents the one-hot representations of positions of [CLS] tokens, [∘,∘] is used for concatenation, and C denotes the numerical representations of text.

$$C = \{c_j\}_{j=1}^{M} \quad (2)$$

Where $c_j \in R^u$ represents the jth word present in input text O [13].

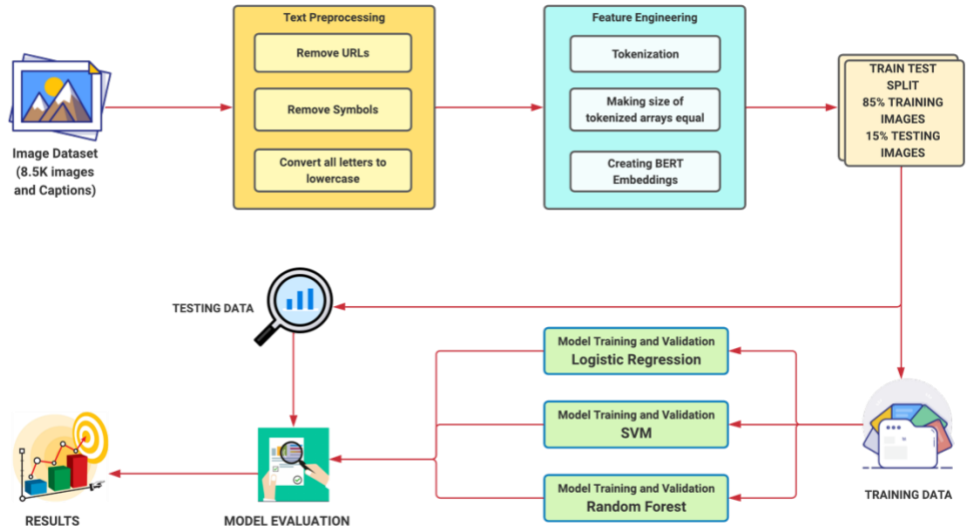

Fig. 2. Model Architecture of Unimodal Approach

Authorized licensed use limited to: DELHI TECHNICAL UNIV. Downloaded on June 15,2022 at 11:25:13 UTC from IEEE Xplore. Restrictions apply.

To generate the BERT embeddings, the clean text was first divided into words and then the words were replaced by their mappings in the tokenizer. CLS tokens were inserted at the beginning of the first sentence of every text caption. SEP tokens were inserted at the end of each sentence. SEP token is used to distinguish between different sentences and the meaning they carry.

After tokenization, the word count of each sentence was calculated and the maximum length of the sentences was stored. For further processing, the size of each tokenized array should be the same. Therefore, zeroes were appended to each array to make the size of each array equal to the maximum length. The attention masks were also calculated.

The Hold-out method is used as the validation technique where the data is split into a train set and a test set. The model was tested on various split percentages like 70% train and 30% test, 90% train and 10% test but the model was either overfitting or underfitting. Model performed the best on the split percentage of 85% training and 15% testing data. The labels of the text were extracted and the dataset was split into train data (85%) and test data (15%). The train data and test data had 7225 and 1275 rows respectively. The training data was used to fit various classification algorithms and the test data was used to find the performance of the models. The architecture of the unimodal approach is depicted clearly in Fig 2.

i. Linear SVM

The Linear SVM model was trained on the training data consisting of 7225 rows. During training, the model tried to find the best hyperplane that can linearly separate the data into two classes.

Fig. 3 and Fig. 4 show the ROC AUC Curve and the Confusion Matrix for Linear SVM.

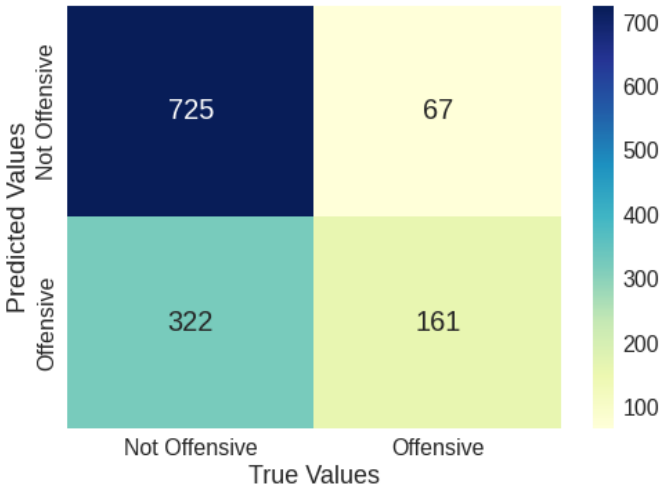

Fig. 3. Confusion Matrix for Linear SVM

To plot the AUC ROC, the True Positive Rate (TPR) and False Positive Rate (FPR) are calculated.

The TPR and FPR need to be calculated for multiple threshold values to get the plotting points for the graph. The FPR and TPR values are plotted on the x-axis and y-axis respectively.

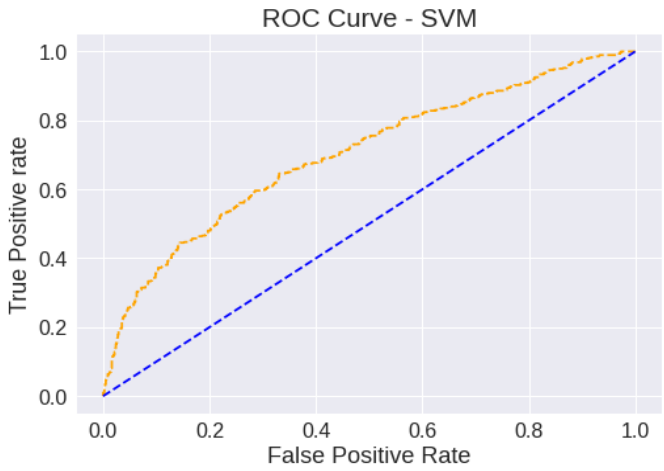

Fig. 4. ROC AUC Curve for Linear SVM

ii. Logistic Regression

Binomial Logistic Regression is a supervised classification algorithm. During training, a threshold value is set for classification and the sigmoid function is used to map the predicted values to their corresponding probabilities. In our model, we want to reduce the number of false negatives, therefore, we have chosen the decision value that has a high value of Recall.

Fig. 5 and Fig. 6 show the ROC AUC Curve and the Confusion Matrix for Logistic Regression.

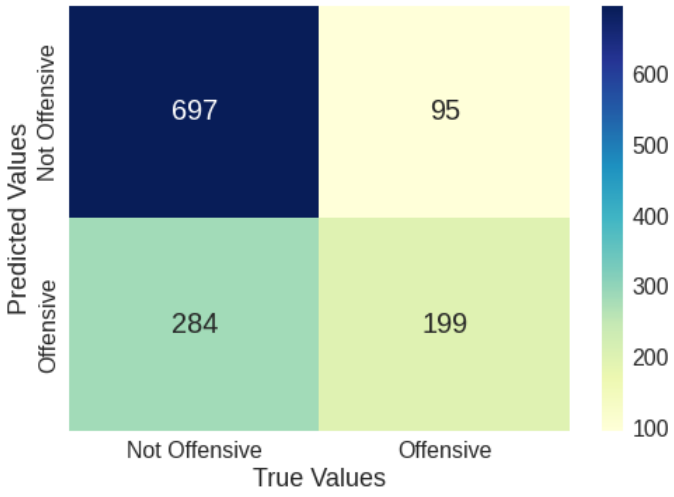

Fig. 5. Confusion Matrix for Logistic Regression

Authorized licensed use limited to: DELHI TECHNICAL UNIV. Downloaded on June 15,2022 at 11:25:13 UTC from IEEE Xplore. Restrictions apply.

Fig. 6. ROC AUC Curve for Logistic Regression

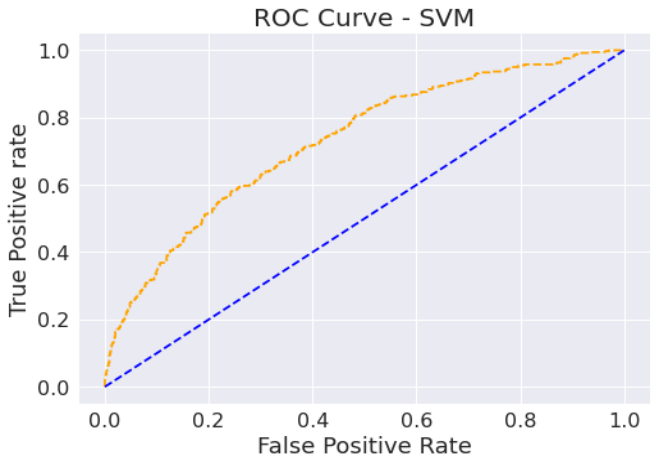

Fig. 8. ROC AUC Curve for InceptionV3 + BERT

2. Multimodal Approach

i) Inception V3

Loading image arrays - Images were pre-processed by resizing them to a dimension of (299 x 299) and then converting images into the array format.

The InceptionV3 model [5], pre-trained on ImageNet was then loaded and object detection was performed using this model. The text obtained through object detection was then combined with the image captions for further text analysis. The concatenated text can be represented as:

$$O = \{o_j\}_{j=1}^{M} \quad (2)$$

where $o_j \in \mathbb{R}^{|V|}$ denotes the one hot vector projection for the j^{th} word that comes in the sentence, M represents the number of words in text and V is the vocabulary[13].

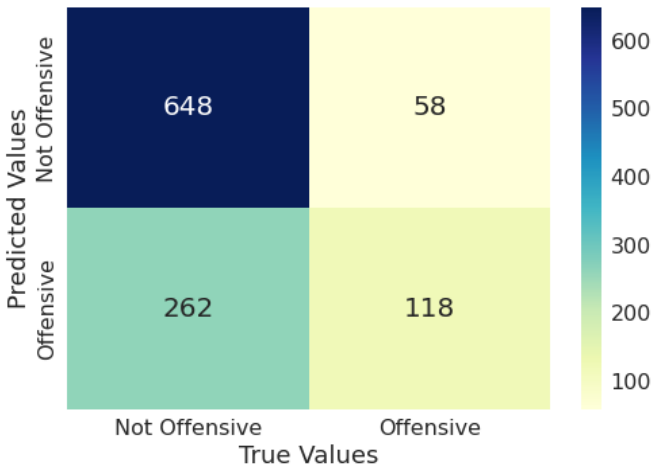

Fig. 7. Confusion Matrix for InceptionV3 + BERT

Fig. 7 and Fig. 8 show the Confusion Matrix and ROC AUC Curve for this model.

ii) ResNet50

Loading image arrays - Images were pre-processed by resizing them to a dimension of (224 x 224) and then converting images into an array format.

The model architecture of ResNet50 [7] and weights pre-trained on the ImageNet database were then loaded, and the process of object identification was performed using this model. The textual data obtained through the image analysis was then integrated with the captions of respective images.

Fig. 9 and Fig. 10 show the Confusion Matrix and ROC AUC Curve for this model

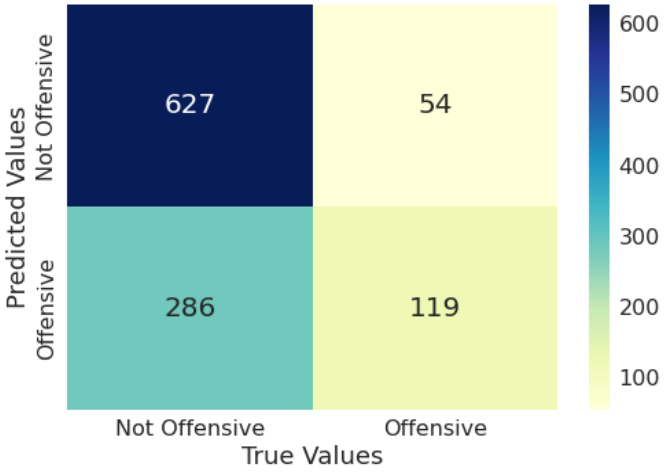

Fig. 9. Confusion Matrix for ResNet50 + BERT

Authorized licensed use limited to: DELHI TECHNICAL UNIV. Downloaded on June 15,2022 at 11:25:13 UTC from IEEE Xplore. Restrictions apply.

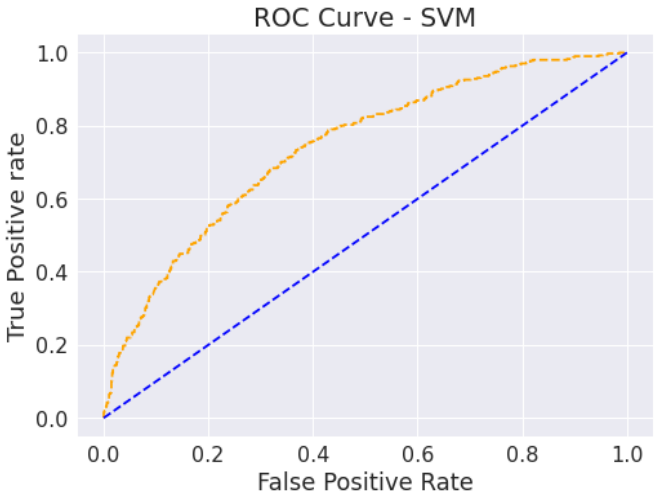

Fig. 10. ROC AUC Curve for ResNet50 + BERT

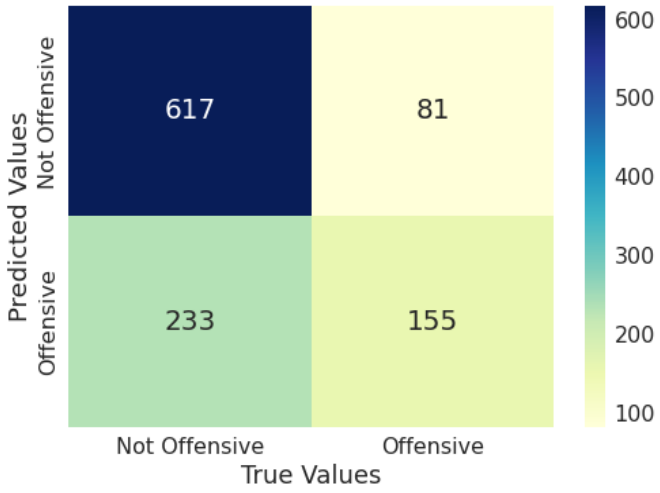

Fig. 11. Confusion Matrix for Xception + BERT

iii) Xception

Loading image arrays - Images were resized to a dimension of (299 x 299) and then converted into array format for image entity detection.

Xception model [6] and its weights pre-trained on the ImageNet data were then loaded, and the image entity classification process was executed. The data thus obtained was amalgamated with the corresponding captions present in the original dataset.

Fig. 11 and Fig. 12 show the Confusion Matrix and ROC AUC Curve for this model

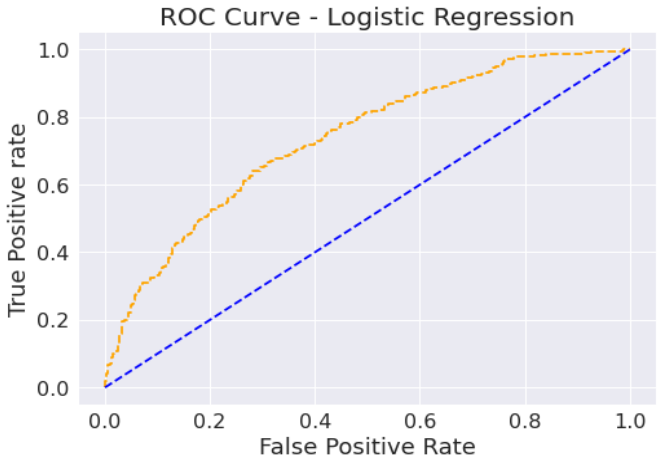

Fig. 12. ROC AUC Curve for Xception + BERT

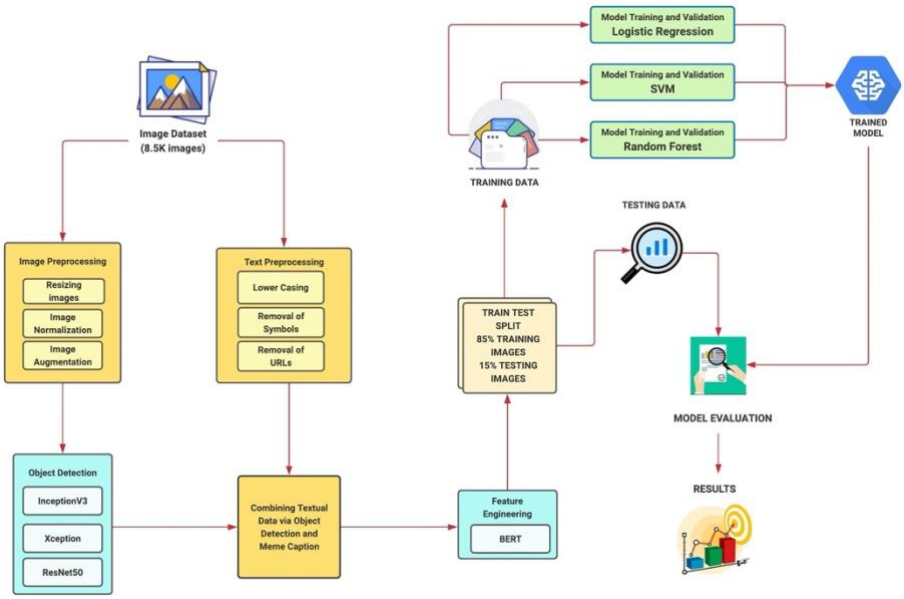

Fig. 13. Model Architecture of Multimodal Approach

Authorized licensed use limited to: DELHI TECHNICAL UNIV. Downloaded on June 15,2022 at 11:25:13 UTC from IEEE Xplore. Restrictions apply.

After the generation of additional textual data through image object detection for each corresponding model, the new captions were cleaned using the same techniques employed in the Unimodal approach and then were fed into the BERT model [2] for the generation of embeddings. The data was divided into two training data (85%) and testing data (15%) for evaluation using various classification models.

The classification models used for evaluation of the multimodal technique were Logistic Regression and Linear Support Vector Machine.

IV. RESULTS AND ANALYSIS

To analyse the performance of the models better, two cases have been taken here. For the first case, we have a meme which has only text and no background image. Here, the prediction is solely based on the textual unimodal approach. To classify accurately, the model must be able to extract the correct textual features and semantic meaning of the text. Our unimodal approach is able to identify multiple explicit words used in Fig. 14 and classifies it as a Hateful meme.

Fig. 14. Meme classified as hateful (Unimodal)

For the second case, we have two memes with the same caption but different image backgrounds. To correctly identify the hatefulness in such images, the multimodal approach should be able to correlate the key features extracted from the text and the image. Our multimodal approach classifies Fig. 15 as non-hateful and Fig. 16 as hateful. Though, the background image in Fig. 16 changes the inference of the meme completely, the multimodal approach is able to correlate the text and image features and make the correct prediction.

Fig. 15. Meme classified as non-hateful (multimodal)

Fig. 16. Meme classified as hateful (multimodal)

The trained models were loaded from the local machine, and were evaluated on the same test dataset on various metrics like Accuracy, Precision, F1 Score, and AUC Score. AUROC score is given by the following formula:

$$\text{AUROC} = \int_{x=0}^{1} TPR(FPR^{-1}(x))dx \qquad (3)$$

The following results were obtained:

	Accuracy(%)	Precision	F1 Score	AUC
Bert + Linear SVM	0.6949	**0.70**	0.67	0.7015
Bert + Logistic Regression	0.7027	0.68	0.68	0.7124
Bert + InceptionV3 (SVM)	0.7053	**0.70**	**0.71**	0.7311
Bert + Resnet50 (SVM)	0.69	0.69	0.65	**0.74**
Bert + Xception (LR)	**0.7108**	**0.70**	0.69	0.7141

Table. 1. Compilation of Model Performance

- Table 1 shows the compiled results from all our models. Our InceptionV3 model gave an AUROC score of 73.11% which might be due to effective utilization of varying convolutional filter sizes in its network which helps it to learn spatial patterns at varying scales in the input data thus helping in overall feature extraction.

- The Resnet50 model gave the best AUROC score of 74% for the dataset. The architecture of ResNet50 uses identity mapping which helps in tackling vanishing gradient problems which might occur due to network gradients becoming very small thus preventing the network weights from changing values during the training of neural networks.

Authorized licensed use limited to: DELHI TECHNICAL UNIV. Downloaded on June 15,2022 at 11:25:13 UTC from IEEE Xplore. Restrictions apply.

- The architecture of Xception is similar to the inception model except that it has a pointwise 1x1 convolution followed by a depth wise separable convolution architecture which makes it easier for the model to learn from training data. Our Xception model gave similar results as the Inception model with an AUROC score of 71.41%.

- Both Linear SVM and Logistic Regression with BERT in unimodal have given almost similar results, but Logistic Regression manages to perform slightly better because data points present around the decision boundary in SVM might depict a false representation of the real decision boundary thus giving margin classifier boundary which may not be true.

- The human experts could achieve an AUROC score of 82.65 and an accuracy of 84.70 [11] which is quite comparable to our best multimodal results considering the limited resources employed for creation of models. Our Multimodal outperforms most of the baseline models created by Facebook [15].

- The BERT text model created outperforms the sequential model [1] as it uses the text generated from image captioning and the existing OCR detected directly for classification through the Neural Networks. It lacks the creation of sentence embeddings and thus might not understand the context of the sentence in a way that transformer models would interpret.

Model	Accuracy	AUROC
Human [11]	84.70	82.65
LSTM w/ BERT features [11]	66.39	72.72
Text based [1]	0.55	-
Multimodal [1]	0.59	-
Sequential [1]	0.64	-
Text BERT [15]	63.60	62.65
ViLBERT [17]	62.2	71.1
Text BERT + Logistic Regression (Ours)	0.7027	0.7124
BERT + ResNet50 (SVM) (Ours)	0.69	0.74
BERT + Xception (LR) (Ours)	0.7108	0.7141

Table 2. Performance of our models compared to other existing models.

- Multimodal approach was able to outperform unimodal but not with a very high margin because it is difficult to get the exact context from the image in a meme and the model might have been extracting features which might not be relevant to the meme thus giving poor results. However, it could be improved by transfer learning and using better image feature extraction models.

V. CONCLUSION AND FUTURE WORK

Memes are nowadays very commonly present on social media platforms. They play a major role in spreading ideas amongst people. It is thus necessary to keep a check on the memes being posted in these social media platforms.

In this paper, we talked about meme sentiment analysis and the importance of classification of memes as offensive or non-offensive. This report presents two techniques to determine offensiveness of memes: 1) Unimodal 2) Multimodal

The unimodal approach employs a BERT model to create embeddings of the textual data and then classification models have been used to evaluate the model. The validation technique used is holdout and the model performs best with Logistic Regression Classifier giving Accuracy of 70.27% and AUC ROC score of 71.24%.

The Multimodal approach using InceptionV3, ResNet50 and Xception pre-trained on ImageNet and BERT model gave an accuracy of 70.53%, 73.11% and 69% respectively and AUC ROC score of 73.11%, 74% and 71.41% respectively.

In future, high level pre-trained Multimodal techniques like VisualBert, Uniter and ResNet151 can be tested on this data. These models require high computation power, therefore, the presence of a powerful GPU is a must. Also the current models can be pre-trained on other existing datasets with the existence of better resources so as to get better performance. These models, when created in future, will be generic and can be used to determine the hatefulness (if present) in Memes. Considering the human accuracy of 84% on the dataset, the results obtained are more than satisfactory.

The limitations of our research work are listed as follows:

- It is often difficult to vectorise our data, i.e. convert textual and visual raw data to numeric form for analysis in Machine Learning

- Sentiment of a meme is subjective from person to person in real-life, hence it becomes even more difficult for a machine to analyse the context of a text.

- Ironies, metaphors and sarcasm in memes are even more difficult to analyse, sometimes even for humans. The models we trained did not take these factors into account.

- It is difficult to classify a meme, there is sometimes a very fine line which separates an offensive and non-offensive meme thus its classification could be difficult.

Authorized licensed use limited to: DELHI TECHNICAL UNIV. Downloaded on June 15,2022 at 11:25:13 UTC from IEEE Xplore. Restrictions apply.

Even though the paper failed to cover up some limitations and problems faced while solving a Meme Analysis problem, the results were fairly decent. The limitations of our research work listed above can be tackled in the future, to get a better comparative study of these classification models.

REFERENCES

[1] Apeksha Aggarwal,1 Vibhav Sharma,1 Anshul Trivedi,1 Mayank Yadav,1 Chirag Agrawal,1 Dilbag Singh,1 Vipul Mishra,1 and Hassène Gritli, Two-Way Feature Extraction Using Sequential and Multimodal Approach for Hateful Meme Classification, vol. 2021, Article ID 5510253, 7 Pages, 2021

[2] Chauhan, Dushyant Singh and S R, Dhanush and Ekbal, Asif and Bhattacharyya, Pushpak, 'All-in-One: A Deep Attentive Multi-task Learning Framework for Humour, Sarcasm, Offensive, Motivation, and Sentiment on Memes', in Proceedings of the 1st Conference of the Asia-Pacific Chapter of the Association for Computational Linguistics,
pages 281–290, December 4 - 7, 2020

[3] Hu, Anthony and Flaxman, Seth, 'Multimodal Sentiment Analysis To Explore the Structure of Emotions', DOI 10.1145/3219819.3219853, july 2018

[4] G.Darshan, K.Deepak, G.Suresh, 'Hateful Meme Detection for Social Media Applications', in International Research Journal of Engineering and Technology (IRJET), vol 8, pages 1606-1609, 2021

[5] Szegedy, C., Vanhoucke, V., Ioffe, S., Shlens, J. and Wojna, Z., 2016. Rethinking the inception architecture for computer vision. In Proceedings of the IEEE conference on computer vision and pattern recognition (pp. 2818-2826).

[6] Chollet, F., 2017. Xception: Deep learning with depthwise separable convolutions. In Proceedings of the IEEE conference on computer vision and pattern recognition (pp. 1251-1258).

[7] He, K., Zhang, X., Ren, S. and Sun, J., 2016. Deep residual learning for image recognition. In Proceedings of the IEEE conference on computer vision and pattern recognition (pp. 770-778).

[8] Devlin, J., Chang, M.W., Lee, K. and Toutanova, K., 2018. Bert: Pre-training of deep bidirectional transformers for language understanding. arXiv preprint arXiv:1810.04805.

[9] Chhavi Sharma, Deepesh Bhageria, William Scott, Srinivas PYKL, Amitava Das, Tanmoy Chakraborty, Viswanath Pulabaigari, and Björn Gambäck. 2020. SemEval2020 Task 8: Memotion Analysis- the Visuo-Lingual Metaphor!. In Proceedings of the Fourteenth Workshop on Semantic Evaluation. International Committee for Computational Linguistics, Barcelona (online), 759–773. https://www.aclweb.org/anthology/2020.semeval-1.99

[10] Goswami, S. (2018, April). Reddit Memes Dataset, Version 3. Retrieved October 20, 2021 from https://www.kaggle.com/sayangoswami/reddit-memes-dataset .

[11] Deshpande, T., & Mani, N. (2021, October). An Interpretable Approach to Hateful Meme Detection. In Proceedings of the 2021 International Conference on Multimodal Interaction (pp. 723-727).

[12] Salminen, J., Hopf, M., Chowdhury, S.A. et al. Developing an online hate classifier for multiple social media platforms. Hum. Cent. Comput. Inf. Sci. 10, 1 (2020). https://doi.org/10.1186/s13673-019-0205-6

[13] Y. Zhou, Z. Chen and H. Yang, "Multimodal Learning For Hateful Memes Detection," 2021 IEEE International Conference on Multimedia & Expo Workshops (ICMEW), 2021, pp. 1-6, doi: 10.1109/ICMEW53276.2021.9455994.

[14] Kiela, Douwe, Hamed Firooz, Aravind Mohan, Vedanuj Goswami, Amanpreet Singh, Pratik Ringshia, and Davide Testuggine. "The Hateful Memes Challenge: Detecting Hate Speech in Multimodal Memes." Advances in Neural Information Processing Systems 33, 14 pages, 2020.

[15] Kiela, D., Firooz, H., Mohan, A., Goswami, V., Singh, A., Fitzpatrick, C. A., ... & Parikh, D. (2021, August). The Hateful Memes Challenge: Competition Report. In NeurIPS 2020 Competition and Demonstration Track (pp. 344-360). PMLR.

[16] Lin, T. Y., Maire, M., Belongie, S., Hays, J., Perona, P., Ramanan, D., ... & Zitnick, C. L. (2014, September). Microsoft coco: Common objects in context. In European conference on computer vision (pp. 740-755). Springer, Cham.

[17] Roy Ka-Wei Lee, Rui Cao, Ziqing Fan, Jing Jiang, and Wen-Haw Chong. 2021. Disentangling Hate in Online Memes. *Proceedings of the 29th ACM International Conference on Multimedia*. Association for Computing Machinery, New York, NY,USA,5138–5147.
DOI:https://doi.org/10.1145/3474085.3475625

[18] M. Krishna, M. Neelima, H. Mane, and V. Matcha, "Image classification using deep learning," International Journal of Engineering & Technology, vol. 7, p. 614, 2018.

[19] P. Viola and M. Jones, "Robust real-time object detection," International Journal of Computer Vision, vol. 4, no. 34–47, p. 4, 2001.

Authorized licensed use limited to: DELHI TECHNICAL UNIV. Downloaded on June 15,2022 at 11:25:13 UTC from IEEE Xplore. Restrictions apply.

2022 IEEE International Conference on Distributed Computing and Electrical Circuits and Electronics (ICDCECE)

Dielectric Insertion effect on Frequency Selective Surfaces for Band Pass Filter design

Sanjeeta Dhegaya
Department of Electronics and Communication Engineering
Delhi Technological University, Rohini
Delhi, India
sanjeeta_2k10spd17@dtu.ac.in

Lavi Tanwar
Department of Electronics and Communication Engineering
Delhi Technological University, Rohini
Delhi, India
lavi.tanwar@dtu.ac.in

2022 IEEE International Conference on Distributed Computing and Electrical Circuits and Electronics (ICDCECE) | 978-1-6654-8316-2/22/$31.00 ©2022 IEEE | DOI: 10.1109/ICDCECE53908.2022.9792715

***Abstract*—One of the major sources of radar cross section (RCS) in the frontal sector is the Radome section of the Aircraft. As Radome is made of dielectric material due to which RCS contribution by the antenna used for the surveillance and communication purpose become highly visible to enemy radar (Surface to air mode) or other enemy aircraft (air to air mode). It allows all EM energy to enter the dielectric radome raising the RCS of aircraft to a high level. To counter this effect, a band pass filter of frequency selective surface is proposed with the dielectric substrate affecting the performance of a filter in the context of resonant frequency, band-width, oblique incident angle and polarization. In view of this, paper on optimization of the dielectric substrate is realized at oblique incidence angle for both TE and TM polarization. Frequency selective surface element and dielectric material are examined through unit cell using floquet boundaries analysis method with the help of 3D EM Computational software. Simulation with a resonant frequency between 8 GHz to 12 GHz is examined with a band-width of more than 1 GHz is modeled. In this paper dielectric layer effect on frequency selective surface element is analyzed keeping in mind the stability of resonant frequency.**

Keywords—Computer Simulated Technology (CST), Dielectric Substrate, Electromagnetic Wave (EM Wave), Equivalent circuit method (ECM), Frequency Selective Surface (FSS), Oblique incidence angle, Radar Cross Section (RCS).

I. INTRODUCTION

Frequency Selective Surface (FSS) is typically periodic element structure and can be used as filters or absorbers [1], as used in traditional methods in circuit theory [2]. There are two main application for the FSS structure. FSS can be used as a spatial frequency filters in radome etc. or absorbing material in application area of stealth platform [3, 4]. Dielectric material play an important role in Frequency Selective Surface (FSS). In paper [5], a new design method was proposed in which the thickness of the 3D band-pass FSS is reduced by folding the substrate, thus provide good filtering for conformal structures. Similarly in [6] the 3D FSS were developed from 2D FSS stacked by coupling it using air. Keeping in view the various conformal FSS structure the paper [7] shows the ultra thin three layer conformal transmit array feed by an horn antenna with various beam of radiation at oblique incident angle.

To make the aircraft stealthy frontal area .i.e. radome play important role which is made of dielectric material [3, 4]. In the area of development of radome, a new hybrid composite sandwich radome was proposed in [8] showing the stack of layers of various material .i.e. E-glass/aramid/polyester face sheets with polyvinyl chloride foam are presented which shows the enhancement of the transmission loss in out of band of desired frequency range and good transmission at resonant frequency. In paper [9], the equivalent circuit design method for band pass FSS and wide band rejection is proposed, while for high angular stability, the composite sandwich structure is proposed in [10] for radome application. Similarly to get low RCS characteristic meta surface is proposed in [11] composed of metal layer and dielectric layer. In paper [3] simulation of the whole computer aided design (CAD) model of the stealth bomber B-2 spirit is shown with and without radar absorbing material (RAM) showing the effectiveness of the RAM in the reduction of RCS.

List of contribution of this paper are:

- Optimization of the dielectric substrate is observed at oblique incidence angle for both TE and TM polarization.
- Frequency selective surface element and dielectric material are examined through unit cell using floquet boundaries analysis method with the help of 3D EM Computational software.
- Dielectric material and thickness effect on unit cell FSS element is analyzed keeping in mind the stability of resonant frequency.

In this paper stability of the resonance frequency is analyzed for X-band application at oblique incidence angle for both polarization in unit cell using floquet port analysis with varying dielectric material property and thickness. Section II tells about the related work done while Section III represents various method of FSS structure design and analysis method. Section IV describes the results obtained and discussion. Section V present the Conclusion.

II. RELATED WORKS

In the previous studies the basic linear dipole slots and patches as shown in Fig. 1 is embedded on single layer dielectric substrate are observed in [12] to understand the frequency pulling effect as per the change in thickness of the dielectric material. In paper [13] the dielectric material is proposed which has both FSS characteristics for achieving the resonant frequency and is ultralight mechanical properties by reducing the density of the material. To optimize the resonant frequency and performance paper [14] is present on tunable FSS in which the sliding 3D-printed inserted dielectric is proposed which behaves as a variable capacitance for tuning the resonant frequency. To enhance the gain in patch antenna, ENZ (epsilon near zero) metamaterial superstrate was proposed in [15] to observe the effect of thickness of multi layer material .i.e. indium antimonide and silicon dioxide. Moving forward for the tri-band pass FSS and miniaturization the paper [16] shows the sandwich dielectric layer between two periodic metallic FSS array .i.e. convoluted structure on top and bottom. Same miniaturized 2.5 D FSS is achieved by

978-1-6654-8316-2/22/$31.00 ©2022 IEEE

Authorized licensed use limited to: DELHI TECHNICAL UNIV. Downloaded on June 22,2022 at 04:51:53 UTC from IEEE Xplore. Restrictions apply.

printing the rectangular spiral FSS elements on both sides of the dielectric are presented in paper [17].

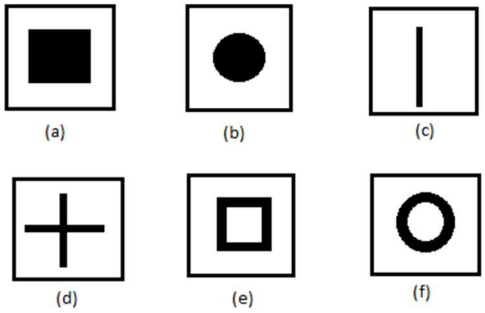

Fig. 1. Various Geometrical Structure of FSS element.

As per the past research the dielectric material and its thickness is present but not shown the effect as an individual, while in this paper a study related to variation of dielectric material property and thickness of a substrate keeping unit cell FSS element constant is analyzed and optimized as per desired resonant frequency. In view of the application area in microwave antenna and radome, the design evolved from simple to the complex geometries [6, 7, 14, 16, 17].

In this paper regular Square Slot FSS element is designed for X-band that is 8 GHz to 12 GHz frequencies. Unit cell FSS is a single layer with a size of $10\ mm \times 10\ mm$. Initially Equivalent circuit model for single layer is presented with the respective equations. FSS layer depicts the filter structure with parallel connection of inductance and capacitance in band-pass filter while dielectric substrate is used as a transmission line response. To stabilize the resonant frequency dielectric substrate is optimized and analyzed to get efficient frequency response in both TE and TM polarization. The reflection and transmission parameter of frequency along with bandwidth is examined in unit cell using floquet port analysis.

III. Methods

Dielectric layer which is the substrate of unit cell FSS element not only provides mechanical strength to the structure but also used for optimization of the resonant frequency keeping FSS element same. FSS element serves as a filter/absorber. Substrate design will have least effect on the performance of the FSS structure [12] but its property shifts the resonant frequency.

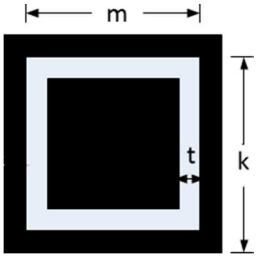

Fig. 2. FSS Structure of Square slot with metallic parts in black colour.

As per the FSS element design, it is a metallic array of patch or slot followed by the thin dielectric as a substrate for providing mechanical strength. There are various method to design based on the efficient use of time and cost. Simulation and verification of the designed FSS are done by two methods: Numerical method [5, 6, 15-17, 23] and Equivalent Circuit Analysis [2, 9, 18-21]. In this paper numerical analysis which is cost effective as it shows the exact replica of the prototype and equivalent circuit analysis which is time efficient are used to obtain the Scattering parameter.

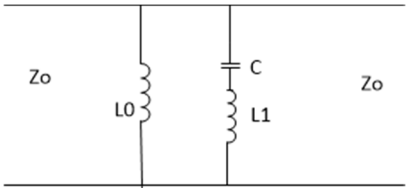

Fig. 3. Equivalent Circuit Model: Square slot shown as shunt LC Circuit.

A. Equivalent Circuit Analysis

There are various method or techniques for design and analysis of the FSS structure, one of which is the equivalent circuit model which results in fast prediction of the results [2, 18, 19]. In some papers [2, 18-21] the FSS behavior is replicated in terms of circuit analysis by showing the design in lumped inductor and capacitors connected in shunt or parallel to get immediate results instead of waiting for full wave simulation results. From paper [22] the equivalent circuit model due to the effect of the shifting of design on double sided FSS is shown. While in paper [23] FSS model is designed using ECM for electromagnetic interference (EMI) shielding application. Equivalent circuit is the method to analyze FSS and can be seen as LC circuit, which is based on the shape of the element. For X-band, square slot band pass filter the equivalent circuit will be a series inductance L1 to capacitor C and because of center patch it is then shunt to an inductance L0. Equivalent circuit and their respective structures are represented in Fig. 3 and Fig. 2. It suggests the designer to adopt the way to meet the required and relevant results. Square slot represent ECM circuit with a shunt LC for frequency response in the required band. In this square slot the inner square patch represents the inductance L1 in (3) with a one side length of m-2t. The square inner patch is in series with the capacitance C in (4), while outer ring of metal which is an inductance L0 in (1) is in shunt with the capacitance, because of the effect of slot. Thus, the equation is evolved and the equivalent circuit is formed where m,k,t,v are the various parameters of the square slot shown in the Fig. 2.

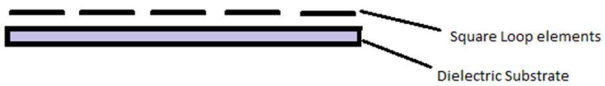

Fig. 4. Geometrical Structure (Side View) with Square slot FSS element and Dielectric Substrate.

$$\frac{X_{L0}}{Z_0} = \omega L0 = cos\theta F(k, v, \lambda, \theta) \tag{1}$$

$$\frac{X_{L1\text{int}}}{Z_0} = \frac{k-2t}{k} cos\theta F\left(k, m-2t, \lambda, \theta\right) \tag{2}$$

$$\frac{X_{L1}}{Z_0} = \omega L1 = \frac{X_{L1\text{int}}}{Z_0} + \frac{t}{m-2t+v}\frac{X_{L0}}{Z_0} \tag{3}$$

$$\frac{B_C}{Y_0} = 4sec\theta F(k, m, \lambda, \theta) \tag{4}$$

Authorized licensed use limited to: DELHI TECHNICAL UNIV. Downloaded on June 22,2022 at 04:51:53 UTC from IEEE Xplore. Restrictions apply.

$$F(k,\omega,\lambda,\theta)=\frac{k}{\lambda}\left[ln\left(cosec\frac{\pi\omega}{2k}\right)+G(k,\omega,\lambda,\theta)\right] \tag{5}$$

$$G(k,\omega,\lambda,\theta)=\frac{1}{2} \times \frac{\left(1-\beta^2\right)^2\left[\left(1-\frac{\beta^2}{4}\right)\left(A_+ + A_-\right)+4\beta^2 A_+ A_-\right]}{\left(1-\frac{\beta^2}{4}\right)+\beta^2\left(1+\frac{\beta^2}{2}-\frac{\beta^4}{8}\right)\left(A_+ + A_-\right)+2\beta^6 A_+ A_-} \tag{6}$$

$$A\pm=\frac{1}{\sqrt{\left[1\pm\frac{2ksin\theta}{\lambda}-\left(\frac{kcos\theta}{\lambda}\right)^2\right]}}-1 \tag{7}$$

$$\beta=\left(sin\frac{\pi\omega}{2k}\right) \tag{8}$$

B. *Numerical Analysis*

Numerical analysis frequency response is analyzed through frequency solver as it can sweep to oblique incidence angle while time domain solver can do analysis at normal incidence only. Before moving to prototype fabrication of the design it is efficient to do simulation. Full wave Computer Simulation Software (CST) is used as a 3D EM analysis tool to design FSS. As Fig. 5 shows, the design of FSS element in CST software while Fig. 4 shows the side view of it. The FSS element is designed based on the circumference of the element which should be effectively one wavelength.

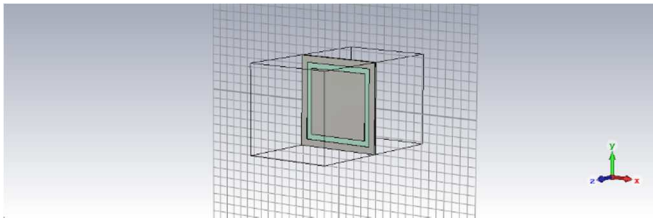

Fig. 5. Geometrical Structure in CST Software (Front view) with Square slot FSS element and Dielectric Substrate.

IV. Results And Discussions

The parameters to be considered during design are the FSS element size and shape. Apart from FSS element, substrate play a vital role in design as it changes the frequency response of FSS. Influence of dielectric layer is analyzed through CEM software. By utilizing the numerical method, accurate data of Scattering parameter that are transmission, reflection coefficients are obtained. Single layer FSS results obtained are illustrated in Fig. 6 to Fig. 13. These figures present the stability of response with change in oblique incidence angle. The dielectric layer property that is epsilon, thickness in Fig. 6 to Fig. 13 shows the shift in the resonant frequency. With respect to oblique measurement the resonant nature and bandwidth remain unaffected.

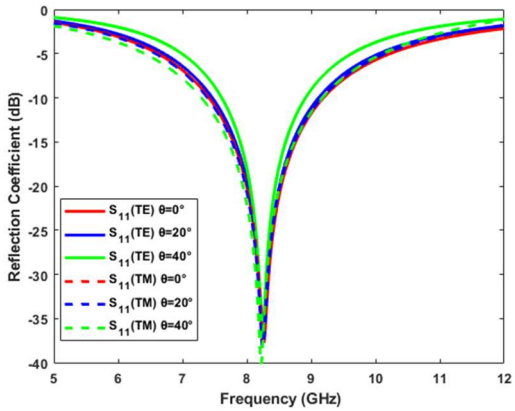

Fig. 6. S-Parameters at Oblique incidence angle, FR-4, thickness=0.50 mm, epsilon=4.3.

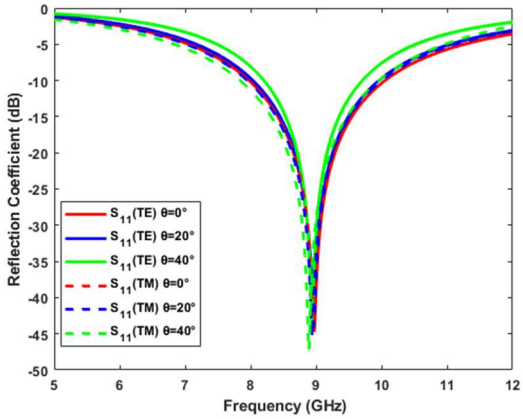

Fig. 7. S-Parameters at Oblique incidence angle, FR-4, thickness=0.30 mm, epsilon=4.3.

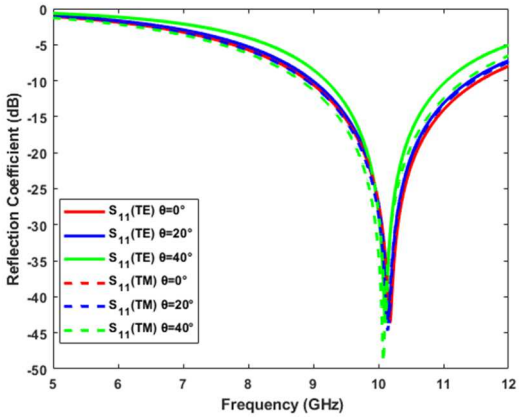

Fig. 8. S-Parameters at Oblique incidence angle, PTFE, thickness=0.50 mm, epsilon=2.1.

As dielectric constant, that is epsilon decreases towards zero the resonant frequency shifts to higher frequency and substrate is behaving like foam structure. The FR4 substrate of high epsilon corresponds resonant frequency response of 7.9 GHz, while with the same configuration PTFE corresponds to 9.4 GHz and RT5880 to 9.5 GHz. If consider the thickness as a feature in every material, the shift of resonant frequency towards high frequency is observed. As

Authorized licensed use limited to: DELHI TECHNICAL UNIV. Downloaded on June 22,2022 at 04:51:53 UTC from IEEE Xplore. Restrictions apply.

the thickness decrease from 0.30 mm to 0.15 mm FR4 substrate resonant frequency move from 7.9 GHz to 8.7 GHz, PTFE from 9.4 GHz to 9.8 GHz and in RT5880 from 9.5 GHz to 9.87 GHz. CEM Simulation results are presented in table I which shows that as the thickness and material properties change the respective behavioural response to Resonant Frequency also changes with slight change in Bandwidth.

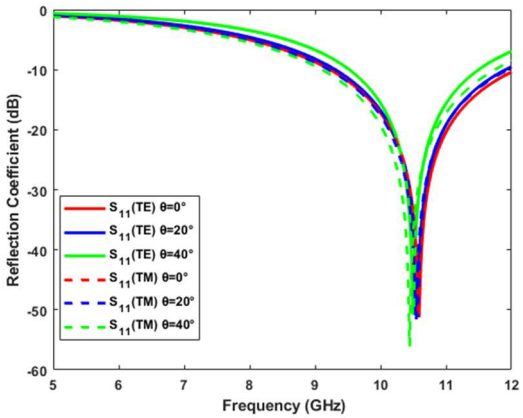

Fig. 9. S-Parameters at Oblique incidence angle, PTFE, thickness=0.30 mm, epsilon=2.1.

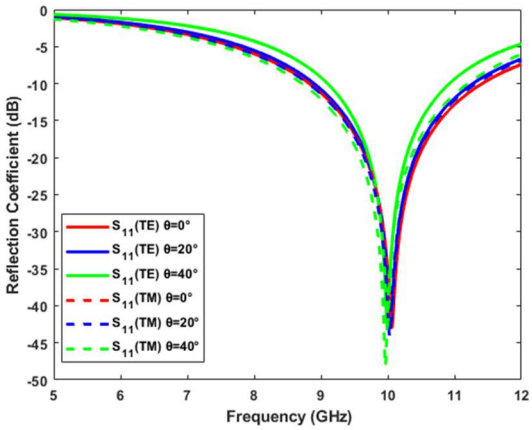

Fig. 10. S-Parameters at Oblique incidence angle, RT5880, thickness=0.50 mm, epsilon=2.0.

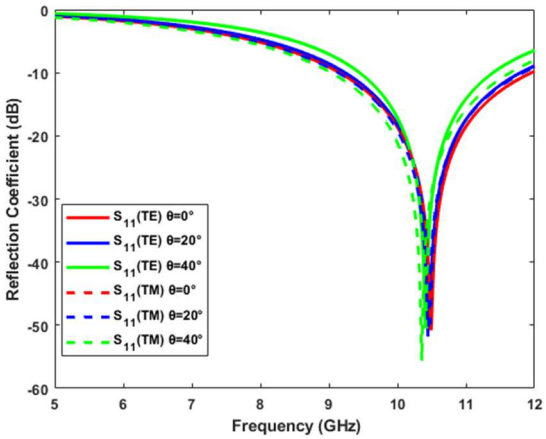

Fig. 11. S-Parameters at Oblique incidence angle, RT5880, thickness=0.30 mm, epsilon=2.0.

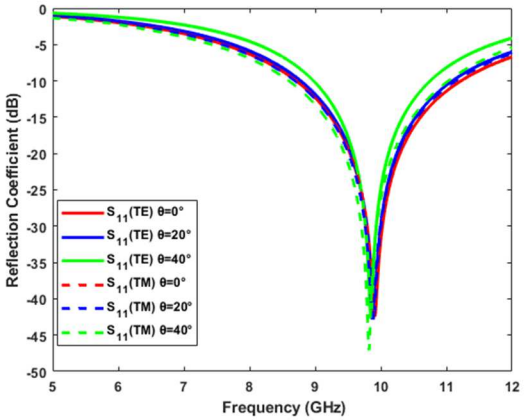

Fig. 12. S-Parameters at Oblique incidence angle, RT5870, thickness=0.50 mm, epsilon=2.33.

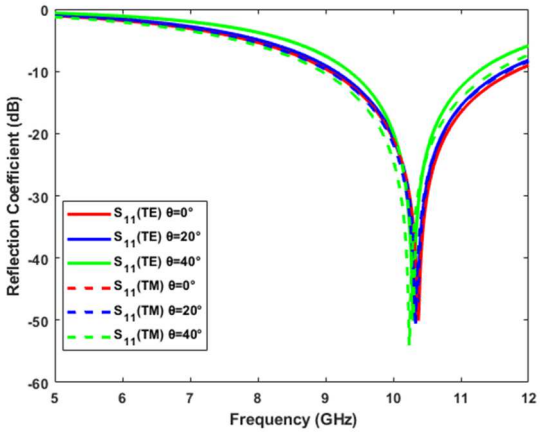

Fig. 13. S-Parameters at Oblique incidence angle, RT5870, thickness=0.30 mm, epsilon=2.33.

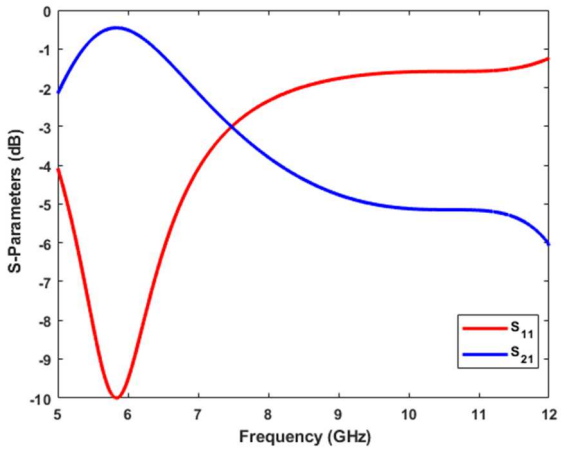

Fig. 14. S-Parameters at Normal incidence angle, FR4, thickness=3.0 mm, epsilon=4.3.

There are some limitation for increase in the thickness of dielectric. As the thickness of the dielectric increase beyond $\lambda/10$ the losses are introduced which are easily visible through the transmission and reflection coefficient plot obtained and shown in Fig. 14. Dielectric Thickness of 3 mm with the same unit cell FSS design does not show any transmission at the desired resonant frequency and the insertion loss is too high with high return loss.

Authorized licensed use limited to: DELHI TECHNICAL UNIV. Downloaded on June 22,2022 at 04:51:53 UTC from IEEE Xplore. Restrictions apply.

V. CONCLUSION

In this paper, Band pass filter is designed keeping in mind the effect of dielectric material on resonant frequency and the oblique incidence angle. The reflection and transmission coefficients are the characteristics of the designed filter which shows significant band-width of 1.20 GHz in X-Band at -10 dB insertion loss. EM simulation is carried out with the result shown in Fig. 6 to Fig. 13. Fig. 6 to Fig. 13 present the stability of response with change in oblique incidence angle while shift in resonant frequency due to the dielectric thickness and material property.

TABLE I. ANALYSIS OF INFLUENCE OF DIELECTRIC MATERIAL AND THICKNESS FOR BOTH TE AND TM POLARIZATION

Material	Thickness(mm)	Dielectric Constant (epsilon)	Resonant Frequency(GHz)
FR4	0.50	4.3	8.26
FR4	0.30	4.3	8.96
PTFE	0.50	2.1	10.12
PTFE	0.30	2.1	10.57
RT5880	0.50	2.0	10.00
RT5880	0.30	2.0	10.48
RT5870	0.50	2.33	9.90
RT5870	0.30	2.33	10.33

It is concluded that the simulation of the simple unit cell FSS element is taken for the analysis of the dielectric layer. It is find through the results shown in table form that apart from the FSS element shape the dielectric layer thickness and material property play a significant role in the shifting of the resonant frequency. So for optimization of the resonant frequency for radome application dielectric layer not only provide mechanical support but also provide aid for tuning the resonant frequency.

There are some limitation for increase in the thickness of dielectric. As the thickness of the dielectric increases beyond $\lambda/10$ the losses are introduced which are easily visible through the scattering parameter shown in Fig. 14. Dielectric Thickness of 3 mm with the same unit cell FSS design is not showing any transmission at the desired resonant frequency and the Insertion loss is too high with high return loss.

In further future work regarding the radome design application, the angular stability for both planar and conformal FSS structure will be observed and the observation will be in terms of gain as a performance parameter simulated with antenna.

REFERENCES

[1] B. A. Munk. Frequency Selective Surfaces: Theory and Design. Hoboken, NJ, USA: Wiley, ISBN 0-471-37047-9, 2000.

[2] F. Costa, A. Monorchio, G. Manara,“ An Overview of Equivalent Circuit Modeling Techniques of Frequency Selective Surfaces and Metasurfaces," Applied Computational Electromagnetics Society Journal, 29(12), 2014.

[3] M. A. Alves, R. J. Port and M. C. Rezende,“ Simulations of the radar cross section of a stealth aircraft," SBMO/IEEE MTT-S International Microwave and Optoelectronics Conference, 409-412, 2007.

[4] V. A. Vincent, C. Kailasanathan, G. Ramesh et al,“ Fabrication and Characterization of Hybrid Natural Fibre-Reinforced Sandwich Composite Radar Wave Absorbing Structure for Stealth Radomes," Transactions on Electrical and Electronic Materials, 22, 794–802, 2021.

[5] A. A. Omar and Z. Shen,“ Thin 3-D Bandpass Frequency-Selective Structure Based on Folded Substrate for Conformal Radome Applications," in IEEE Transactions on Antennas and Propagation, 67(1), 282-290, Jan. 2019.

[6] A. K. Rashid, B. Li, Z. Shen,“ An overview of three-dimensional frequency-selective structures," IEEE Antennas and Propagation Magazine, 56(3), 43–67, 2014.

[7] P. Y. Qin, L. z. Song and Y. J. Guo,“ Beam Steering Conformal Transmitarray Employing Ultra-Thin Triple-Layer Slot Elements," in IEEE Transactions on Antennas and Propagation, 67(8), 5390-5398, Aug. 2019.

[8] H. Rafieipour, A. Setoodeh, A. K. T. Lau,“ Mechanical and electromagnetic behavior of fabricated hybrid composite sandwich radome with a new optimized frequency-selective surface," Composite Structures, 273, 114256, 2021.

[9] N. Liu, X. Sheng, C. Zhang and D. Guo,“ Design and Synthesis of Band-Pass Frequency Selective Surface With Wideband Rejection and Fast Roll-Off Characteristics for Radome Applications," in IEEE Transactions on Antennas and Propagation, 68(4), 2975-2983, April 2020.

[10] N. Liu, X. Sheng, C. Zhang and D. Guo,“ Design of Frequency Selective Surface Structure With High Angular Stability for Radome Application," in IEEE Antennas and Wireless Propagation Letters, 17(1), 138-141, Jan. 2018.

[11] Z. Zhang, X. Cao, H. Yang, T. Li, J. Tian, and J. Gao,“ Novel strategy to design a metasurface with integrated radiation and a broadband low radar cross section," Optical Material Express, 11(11), 3636-3645, 2021.

[12] P. Callaghan, E.A. Parker, R.J. Langley,“ Influence of supporting dielectric layers on the transmission properties of frequency selective surfaces," IEE Proceedings H Microwaves, Antennas and Propagation, 138(5), 448–454, 1991.

[13] L. Li, W. Jiang, J. Wang, H. Ma, and S. Qu,“ Feasible strategy for simultaneously achieving excellent frequency selective characteristic and ultralight mechanical properties," Optics Express 30(3), 4492-4503, Jan. 2022.

[14] S. Qiu, Q. Guo and Z. Li,“ Tunable Frequency Selective Surface Based on a Sliding 3D-Printed Inserted Dielectric," in IEEE Access, 9, 19743-19748, 2021.

[15] C. Cheng, Y. Lu, D. Zhang, F. Ruan, G. Li,“ Gain enhancement of terahertz patch antennas by coating epsilon-near-zero metamaterials," Superlattices and Microstructures, 139, 106390, 2020.

[16] N. Liu, X. Sheng, C. Zhang, J. Fan, D. Guo,“ A Miniaturized Tri-band Frequency Selective Surface Based on Convoluted Design," IEEE Antennas and Wireless Propagation Letters, 16, 2384-2387, 2017.

[17] M. Chaluvadi, V. K. Kanth and K. G. Thomas,“ Design of a Miniaturized 2.5-D Frequency Selective Surface With Angular Incidence and Polarization Stability," in IEEE Transactions on Electromagnetic Compatibility, 62(4), 4, 1068-1075, Aug. 2020.

[18] X. Yuan, H. Mang,“ Design of Multilayer Frequency-Selective Surfaces by Equivalent Circuit Method and Basic Building Blocks," International Journal of Antennas and Propagation, 1–13, 2019.

[19] X. Yao, M. Bai and J. Miao,“ Equivalent Circuit Method for Analyzing Frequency Selective Surface With Ring Patch in Oblique Angles of Incidence," in IEEE Antennas and Wireless Propagation Letters, 10, 820-823, 2011.

[20] A. Firouzfar, M. Afsahi, A. A. Orouji,“ Novel, straightforward procedure to design square loop frequency selective surfaces based on equivalent circuit model," AEU - International Journal of Electronics and Communications, 119, 153164, 2020.

[21] A. Chatterjee, S. K. Parui,“ A triple-layer dual-bandpass frequency selective surface of third order response with equivalent circuit analysis," International Journal of RF and Microwave Computer-Aided Engineering, 30(2), e22047, 2020.

[22] X. Ma, Y. Liu, G. Wan and A. Pan,“ Angularly Stable Frequency-Selective Surface Using Shifted Double-Sided Screens," in IEEE Antennas and Wireless Propagation Letters, 19(7), 1192-1196, July 2020.

[23] V. K. Kanth and S. Raghavan,“ Design and optimization of complementary frequency selective surface using equivalent circuit model for wideband EMI shielding," Journal of Electromagnetic Waves and Applications, 34(1), 51-69, Jan. 2020.

Authorized licensed use limited to: DELHI TECHNICAL UNIV. Downloaded on June 22,2022 at 04:51:53 UTC from IEEE Xplore. Restrictions apply.

Revista Brasileira de Farmacognosia
https://doi.org/10.1007/s43450-022-00262-w

REVIEW

Disease Prevention and Treatment Using β-Carotene: the Ultimate Provitamin A

Raksha Anand[1] · Lalit Mohan[1] · Navneeta Bharadvaja[1]

Received: 17 March 2022 / Accepted: 6 May 2022
© The Author(s) under exclusive licence to Sociedade Brasileira de Farmacognosia 2022

Abstract

Humans being unable to synthesize beta-carotene, the provitamin A, depend on external sources as its supplement. Health benefits and dietary requirements of beta-carotene are interrelated. This orange-red coloured pigment has been enormously examined for its capacity to alleviate several chronic diseases including various types of cancer, cystic fibrosis, as well as COVID-19. However, this class of phytoconstituents has witnessed a broad research gap due to several twin conclusions that have been reported. Natural sources for these compounds along with their extraction methods have been mentioned. The current communication aims at contributing to the global scientific literature on beta-carotene's application in prevention and treatment of lifestyle diseases.

Keywords Lifestyle diseases · Disease prevention · Disease treatment · Phytocompounds · Natural pigment · Antioxidant · Cancer · Cardiovascular diseases

Introduction

Carotenoids are the class of natural pigments belonging to the tetraterpenoids (C_{40} atoms) consisting of a long polyene chain with alternative conjugated double bonds with hefty scientific attention due to their substantial properties. Generally, carotenoids are classified as hydrocarbon carotenes, composed of only carbon and hydrogen (lycopene, alpha-carotene, and β-carotene *etc.*) and oxygenated carotenoids (xanthophylls), which contain an epoxy- (violaxanthin, neoxanthin, fucoxanthin), hydroxy- (lutein and zeaxanthin), keto- (canthaxanthin and astaxanthin), and methoxy- (spirilloxanthin) functional groups (Lakshminarayana et al. 2022). Out of around 600 structurally and functionally diverse natural types, three major provitamin As are the alpha, beta, and gamma isomers. The beta isomers get actively cleaved at the centre in an O_2-dependent manner to produce retinal (Liang et al. 2013; PubChem 2022). Plants and algae are considered the best sources of these bright orange-red coloured pigments, such as β-carotene (**1**). These hydrocarbonated carotenes are fat-soluble and highly hydrophobic due to the conjugated double bonds and central symmetry (Rodriguez-Amaya 2016). These have been reported to be safe for consumption, as nutritional supplements as well as food additives (Akram et al. 2021).

β-Carotene (**1**, $C_{40}H_{56}$) is an oxygen-lacking isoprene-containing compounds, the characteristic colour imparted due to the presence of double bonds (PubChem 2022). Both the ends of the molecule have cyclic rings. During isolation, *cis*-isomers of carotenoids are the most common; however, they readily undergo *cis* ↔ *trans* isomerization in polar environments (Bartalucci et al. 2008). Due to the number of therapeutic and preventive effects that β-carotene offers, it has been recognized as a functional component of food.

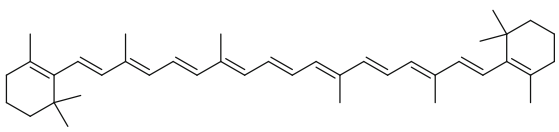

1

Raksha Anand and Lalit Mohan contributed equally to this work.

✉ Navneeta Bharadvaja
navneetab@dce.ac.in

[1] Plant Biotechnology Laboratory, Department of Biotechnology, Delhi Technological University, Delhi, India

Published online: 30 May 2022

Upon oral administration of β-carotene, a hike of up to 60% in serum concentration is reported. It is the *trans*-isomer of β-carotene that is higher in serum than the *cis*-isomer. The concentration of β-carotene is different in parts of the body, being 2.2–122.7 μg/dl in serum, 0.21–6.3 μg/g in the liver, 0.05–1.5 μg/g in the kidney, and 0.05–0.86 μg/g in the lungs (Institute of Medicine 2000). However, the levels of β-carotene do not change in the kidneys, liver, or heart (DrugBank 2022). It is found that the carotenoid content of tissues with a greater number of low-density lipoprotein receptors (LDL-R) is greater, due to non-specific uptake (Maria et al. 2015). The intact β-carotene that is ingested has several metabolic fates to undergo, which are depicted in Fig. 1. However, research states that the lower the concentration of β-carotene, the more biologically effective is the pigment mixture of carotenoids (Lohan et al. 2018).

As per James Olson, the activity of carotenes can be studied better upon the categorization of its properties as, "functions, actions, and associations". The equivalence amongst these three would imply greater confidence in studies (Cooper 2004). Functions would be the indispensable role of β-carotene, to convert into vitamin A. Actions are demonstrations noted upon the administration of β-carotene in clinical subjects, minimized photosensitivity and so on. Associations could be simply understood as the correlation of β-carotene to any medical condition, like cancer or diabetes (Bendich and Olson 1989; Olson 1993; Hercberg 2005; Druesne-Pecollo et al. 2010; Marcelino et al. 2020)

This paper reviews the currently recognized potential of β-carotene in disease treatment and prevention. The carotenoid class of umbrella term nutraceuticals is underrated in the sense of its capabilities due to the literature gap and the research void. These points have been discussed in the paper in brief bringing its unnoticed therapeutic characteristics to light.

Search Strategies

Search keywords associated with β-carotene for various lifestyle disorders like cardiovascular diseases, cancer, COVID-19, and other diseases were used in the following order: β-carotene, sources of β-carotene, extraction technique, cancer, COVID-19, and cardiovascular diseases. The following list of biological databases was used to search the data for writing this article: PubMed, PubMed Central, Google Scholar, Springer, Science Direct, Wiley Online Library, LiebertPub, Nature. A time filter was used to retrieve articles from 2015 to 2021 in PubMed.

Discussion

Physicochemical Properties

β-Carotene, a type of secondary metabolite produced by plants and algae, is a dark red to brown-coloured solid substance. The brightness of the colour depends upon the level of double bond *cis* ↔ *trans* isomerization, as a result of exposure to high temperatures (Bogacz-Radomska and Harasym 2018). The melting point of β-carotene is around 178 °C, having variable solubility in non-polar organic solvents but water-insoluble. The substance is heat-labile and photosensitive, making the storage condition preferably in dark at 4 °C. The lipophilic properties of β-carotene make it localized in lipoproteins and cell membranes. Hence, the extracted β-carotene is also found dissolved in the lipid phase (Bogacz-Radomska and Harasym 2018).

Dietary Requirements

Even being categorized as a micronutrient, due to its requirement in minute amounts as compared to other requirements of

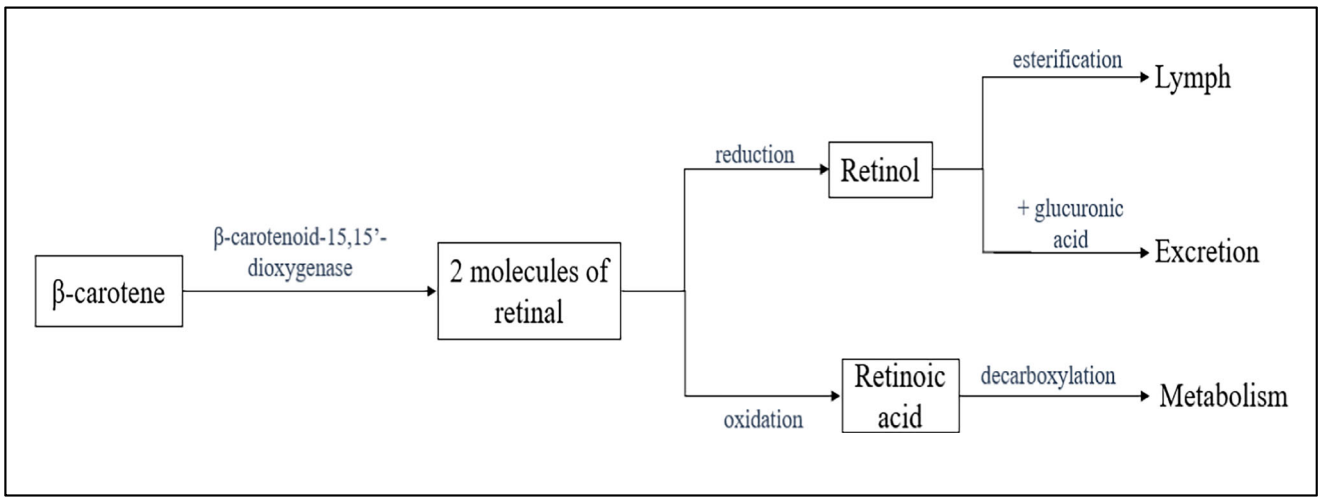

Fig. 1 Fate of ingested β-carotene

the body, β-carotene is considered to be very essential. β-Carotene conversion to vitamin A has moved from 6:1 to the current ratio of 28:1. The reason is the single nucleotide polymorphisms in the β-carotene-15′,15-monooxygenase (BCMO) enzyme, responsible for converting provitamin A into retinol. This means that, in the affected individuals, 28 mg of β-carotene is converted into 1 mg of retinol. This exposes the population to a greater risk of developing vitamin A deficiency and associated disorders, as well as the inability to utilize provitamin A from the diet (Gröber and Holick 2022).

To date, no potential adverse effects of β-carotene consumption have been reported other than 'carotenodermia' which is skin discolouration due to elevated concentrations of carotenoids. β-Carotene did not appear to be mutagenic, carcinogenic, nor teratogenic in any of the assays carried out (Milani et al. 2017; Pham et al. 2014). In fact, no increase in serum retinol level was found even after long-term β-carotene supplementation in people with already adequate levels of vitamin A (Nierenberg et al. 1997). For prolonged serum and tissue accumulation of β-carotene, its administration must be with dietary fats (Kwatra and Modi 2020). However, people who smoke are better not subjected to high supplementations of β-carotene as this might put them at higher risk of lung cancer and an enhanced chance of mortality (Bohn et al. 2019). Most of the absorbed β-carotene is converted by the gut microbes into unknown complex compounds, and the remainder gets excreted. The general absorption, distribution, metabolism, and excretion route of β-carotene in humans is illustrated in Fig. 2.

Sources and Production

Mammals lack the *de novo* carotenoid synthesis capability and hence totally depend on external sources for their supplementation (Huang et al. 2018) (Fig. 3). These yellow-, red-, and orange-coloured pigments are naturally found in algae, higher plants (in fruits and flowers as esters), fungi, and animals as illustrated in Fig. 4 (Rodriguez-Amaya 2016). Even human milk has a carotenoid component, which is easily alterable, depending on the manipulations in the mother's diet (Institute of Medicine 2000). This intake of β-carotenoids is reflected in serum levels which is also an indicator of the health parameters. A natural pigment, so promising, should have been the centre of the bio-pharmaceutical industry. However, it is not. Out of all the β-carotenoids in the market, only 3% of it comprise the bio-synthesized type and the rest comes under the synthetic β-carotene category. There is no strict difference between the function of the two, natural and synthetic. But the latter costs more. Switching to microalgae for β-carotene extraction is both scientifically and economically sensible. A lot of research has been done on the optimization of pigment in various species, along with special extraction techniques for cost-effective and enhanced yields (Marino et al. 2020).

There are several extraction methods of β-carotene, depending upon the source selected. A lot of research is involved in the optimization of pigment production as well as its extraction. From a broader perspective, the extraction methods can be divided into the organic solvent-based, enzymatic method as well as mechanical extraction. Some collaborative

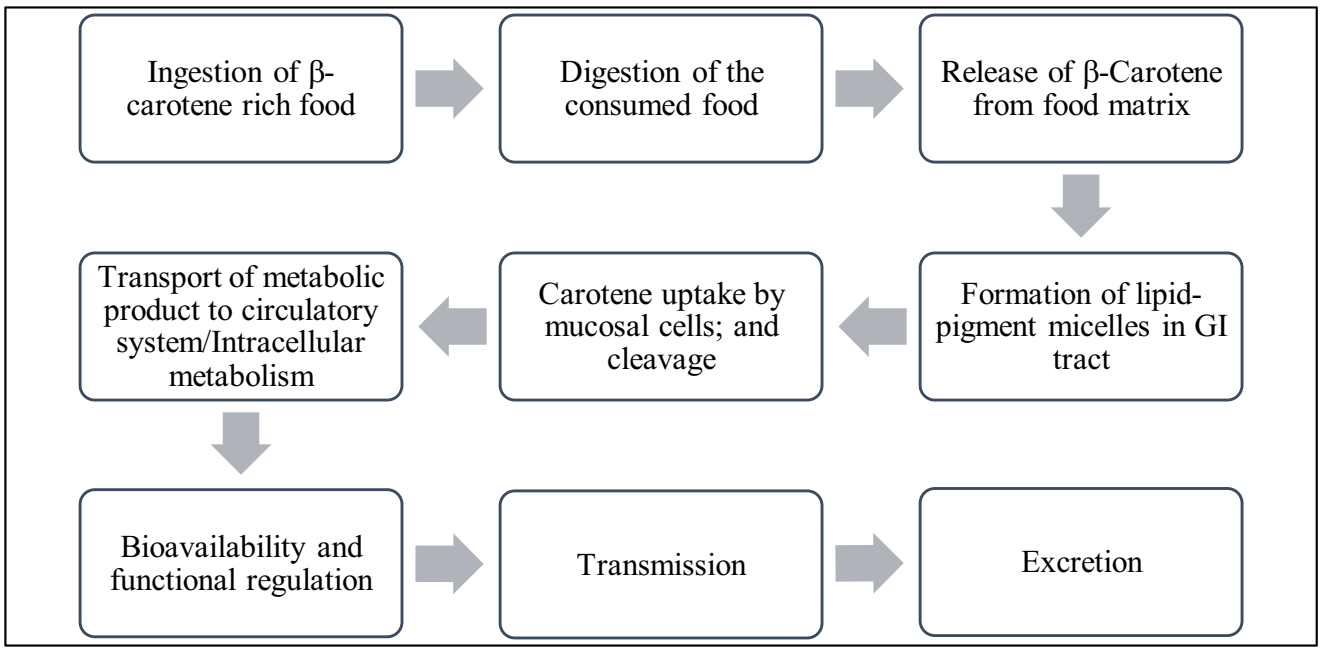

Fig. 2 ADME (absorption, distribution, metabolism and excretion) of β-carotene

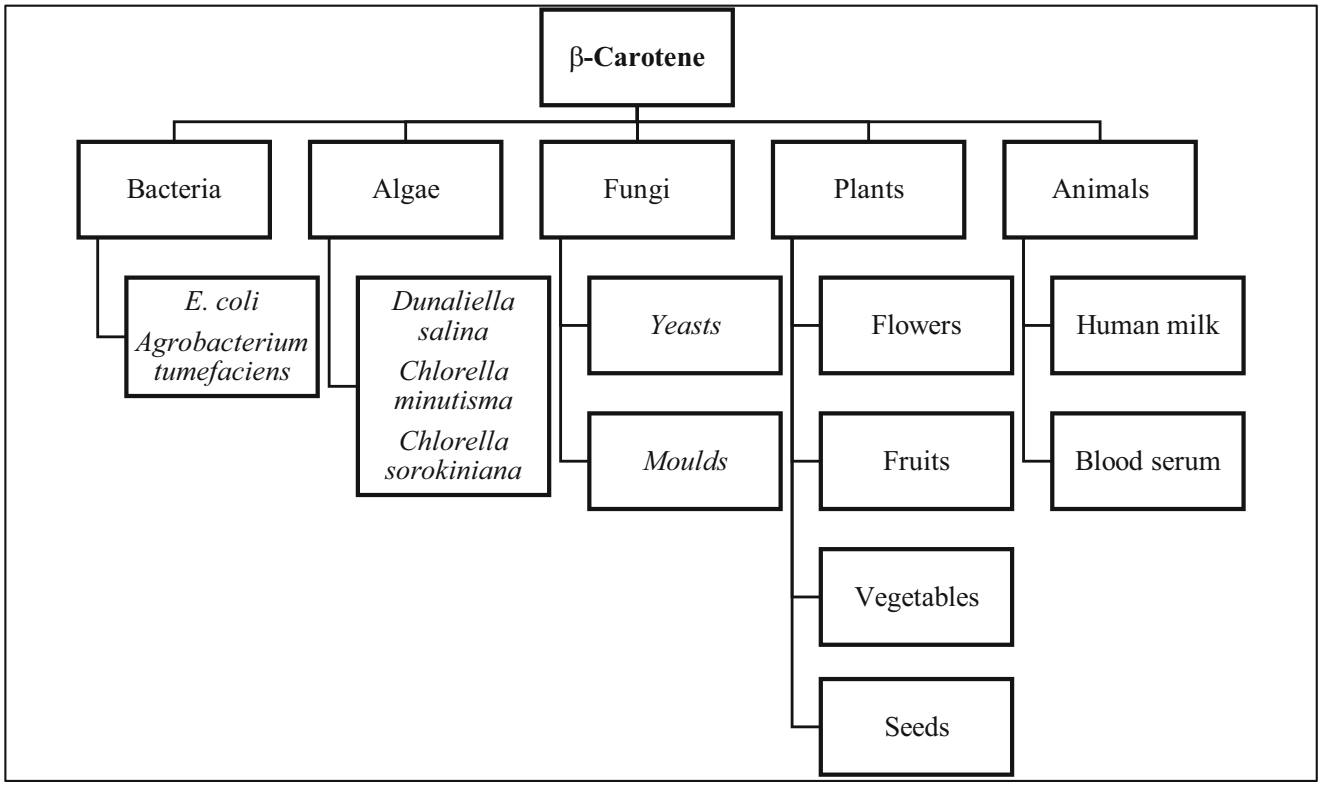

Fig. 3 Different natural sources of β-carotene

extraction techniques also exist which involve clubbing of the existing methods, as well as some innovation (Chen et al. 2021).

Extraction

Solvent-based extraction includes the use of aprotic organic solvents such as hexane, tetrahydrofuran, and acetone for the extraction of β-carotene from algae post- and pre-treatment. These extraction solvents are useful for the extraction of β-carotene from algae, fungi, and plants (Chen et al. 2021). Supercritical fluids reduce the extraction time of β-carotene as well as enhance the efficiency of extraction. Atmospheric liquid extraction with the help of maceration is used for extraction purposes without the use of sophisticated instruments and is simple to carry out. Soxhlet extraction is much simpler and most widely used for the extraction of carotenoids such as β-carotene.

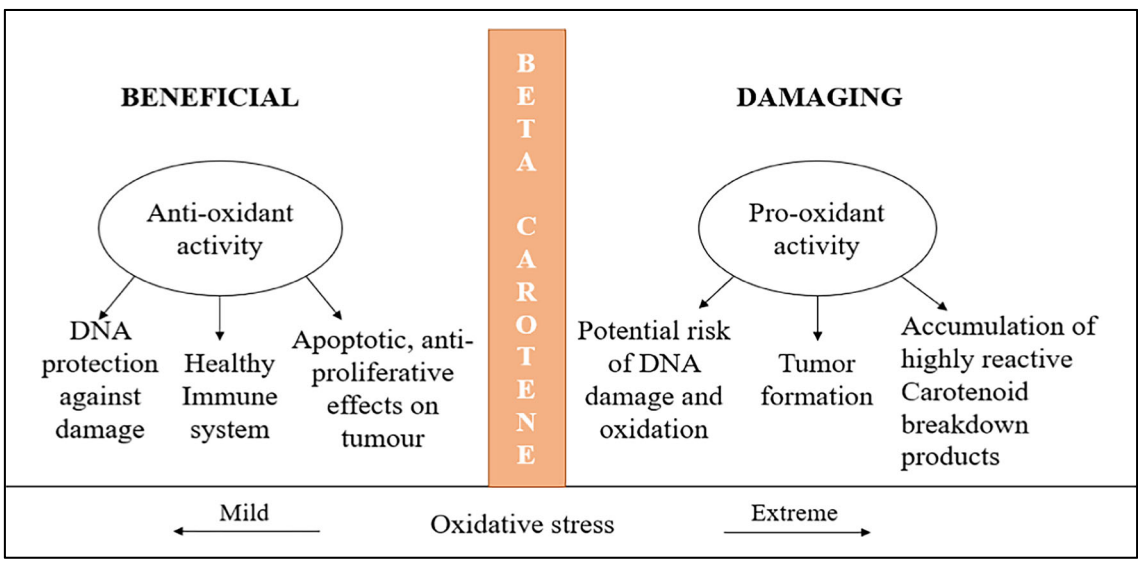

Fig. 4 A representation of the necessary balance of antioxidant properties of β-carotene

This method provides the highest recovery rates and does not require sophisticated instruments. This method uses large amounts of solvents along with the starter material for extraction purposes which makes the extraction procedure highly expensive (Saini and Keum 2018). Supercritical fluids are used for the extraction of β-carotene from plants and algae (Baysal et al. 2000). Various physical methods such as ultrasonic waves, microwave-assisted extraction, pressurized liquid extraction, bead milling, and high-pressure homogenization are also used for the extraction of β-carotene. These methods prevent thermal as well as chemical damage to pigment. This method is used for the extraction of β-carotene from algae, yeast, and plants (Dey and Rathod 2013; Yu and Rupasinghe 2013). There are several enzymatic approaches including pectinolytic and cellulolytic approaches which can be used in combination with other extraction methods for cell disruption and β-carotene extraction. These methods can be used for the extraction of β-carotene from carrots, bagasse, apples, and other juice-extracted leftover (Macedo et al. 2014). The selection of an appropriate method for β-carotene extraction depends upon the efficacy and the targeted purpose (Saini and Keum 2018).

Synthesis

Genetic engineering approaches such as the insertion of functional genes such as *crtI*, *crtE*, *crtY*, and *crtYB* enhance the production of β-carotene and block the expression of repressor genes like *crgA* which blocks the synthesis of β-carotene. These approaches have been applied to red yeast and fungus so far (Zhang et al. 2016; Wu et al. 2020). There are various environmental conditions such as organism-based culture condition, optimization of light intensity, salt stress, pH, and carbon sources that can be optimized for enhanced production of β-carotene. These optimizations have been carried out on microalgae, plants, and fungi for enhanced production of β-carotene (Chen et al. 2021). One of the key methods for enhanced production of β-carotene is the construction of polyene chains using Wittig's reaction, such as two 15 carbons containing phosphonium salt molecule along with one 10 carbons containing dialdehyde molecule, and using Grignard's reaction involving 2 molecules of methanol and diketone (Farfán et al. 2019).

Quantification

The spectrophotometric analysis method is an inexpensive, sensitive, simple, and rapid procedure for the estimation of β-carotene. This method employs the use of smaller amounts of toxic chemical solvent for the analysis of β-carotene. Spectroscopic methods have widely been employed in commercial settings; however, this method faces certain disadvantages such as being applicable for certain food components only (Biswas et al. 2011). Recently, many liquid chromatography (LC) techniques have also been developed for the analysis of β-carotene. Amongst all the LC techniques, high-performance liquid chromatography (HPLC) is the most suitable method for analysis (separation and quantification) of β-carotene. HPLC has a requirement for high sample purification steps for the analysis of β-carotene present in the sample (Olives-Barba et al. 2006). Column chromatography is also one of the most important methods for the separation and detection of various carotenoids including β-carotene. In the case of column chromatography, silicic acid and alumina are used as stationary phases in order to separate different carotenoids from the extracts (Starek et al. 2015; Ganea et al. 2016).

Disease Prevention and Treatment

β-Carotene not only treats or prevents the likeliness of disease development but also improves its prognosis. It has been found to play roles like antioxidant and anti-inflammation, upon administration in varying amounts:

i) In a study, subjects with a generous amount of β-carotene intake, about 12–25 mg/day, reported a decrease in DNA strand breakage, along with a reduction in Cu-induced LDL oxidation. There was also subsequent supplementation of vitamins C and E (Pool-Zobel and Bub 1997; Mosca et al. 1997). An amount of 10 mg/day was reported in increased CuZn-superoxide dismutase activity (Hininger et al. 1997). In subjects with increased oxidative stress, smokers, and sufferers of cystic fibrosis, administered β-carotene resulted in depleted lipid peroxidation as compared to control. The biological markers responded inconsistently when the amounts of β-carotene were higher than 25 mg/day (Institute of Medicine 2000).

ii) *In vitro* studies have demonstrated a stimulation of cellular communication through gap junctions (Sies and Stahl 1997). A study concluded the positive effect of β-carotene leading to increased intercellular communications in rats (Novo et al. 2013).

iii) The degree of conversion of the consumed provitamin A carotenes to retinol is the essential measure to which the deficiency of vitamin A, common in children, can be treatable. This is because vitamin A deficiency is indirectly related to poor immunity of the body, night blindness, and so on. In older men, β-carotene

increased the activity of natural killer cells (Hughes et al. 1997).

iv) There is a contrary association between the pigment levels in serum and systemic inflammation markers like neutrophil to lymphocyte ratio and resistance to insulin as well as dysfunctional beta cells (Huang et al. 2018).

v) The carotenoid-derived metabolites have been found to participate in gene alterations by interactions with nuclear and retinoic acid receptors (Piga et al. 2014).

Various studies have been carried out to identify the actions of β-carotene intake; CARET study was carried out for the prevention of lung cancer using β-carotene along with retinol. The study reported a twin conclusion that daily consumption of 30 mg of β-carotene along with retinol supplementation showed no harm as well as no benefit in preventing lung cancer (NLM NCT00712647 2022). Another study named as ATBC (α-tocopherol, β-carotene cancer prevention) has been carried out to access the incidence rate of cancer and mortality in male smokers using β-carotene and α-tocopherol. The study reported that these compounds can be used as a "chemo-preventive" for lung cancer (NLM NCT00342992 2022; ATBC cancer prevention study group 1994).

Depending upon the extent of oxidative stress in the environment to which the pigment is exposed, the actions can be beneficial or damaging. The accumulation of very reactive products released upon carotenoid breakdown contributes to pro-oxidation. This involves the production of very reactive organic compounds like aldehydes. Such products are termed carotene breakdown products (CBPs) (Siems et al. 2009). A representation of the necessary balance of antioxidant properties of β-carotene is depicted in Fig. 4. Hence, it can be summarized that the pigment offers several therapeutic effects in the context of acting as a provitamin A: antioxidants neutralizing ROS, regulating connexin expression, thus improving communications through gap junctions, activating macrophages, and triggering an immune response (Chen et al. 2021). Various therapeutic effects of β-carotene are recapitulated in Fig. 5. A combination of magnesium along with vitamins having antioxidant properties has been used to treat noise-induced hearing loss (NIHL) in animals, which is assumed to scavenge oxidative radicals produced due to trauma (le Prell et al. 2011; Eroglu and Harrison 2013; Álvarez et al. 2014; Maurya et al. 2021).

Bioavailability and Absorption

The lipophilic β-carotene like all other lipids and lipid-associated compounds is absorbed in the mammalian small intestine for further transport to the peripheral tissues. Despite the presence of β-carotene-cleaving enzymes in the small intestine, about half of the uncleaved β-carotene enters the circulatory system. The readily available provitamin A absorbed by human intestinal epithelia can be estimated by the concentration of intact plasma-β-carotene (Shete and Quadro 2013). The other factors affecting the bioavailability of β-carotene are genetic factors like pigment-cleaving gene polymorphisms and mutations, the type and lipid content of the food and its matrix, its digestibility and interactions, and subjective variations referring to individuals' endogenous digestive enzymes (Reboul 2013).

Lipoproteins and cholesterols facilitate the transport and distribution of the non-polar β-carotenes in the organism. They can be found in the hydrophobic cores of organic compounds like various sub-types of lipoproteins, and cholesteryl-esters (Shete and Quadro 2013). This β-carotene flowing from blood can be taken up by tissues for either storage or metabolism. The most efficient reservoir of β-carotene in the human body is the liver, followed by muscles, kidneys, and skin, as well as glands like adrenal and mammary glands. It has also been found in the placenta and the yolk sac. Hence, it is comparatively very widely distributed in the body as compared to the other classes of carotenoids (Renzi et al. 2012). The cleavage, transport, and distribution of β-carotene in humans are similar to that in ruminants, and hence, they are considered a good study model (Bohn et al. 2019).

Being water-insoluble, the bioavailability of β-carotene through the gastrointestinal tract is very low. Due to its vulnerability to physiochemical degradation during processing, storage, and post-consumption, its protected delivery becomes necessary. Nanotechnology offers better solubility, storage, target delivery, encapsulated protection stability, and dispersion properties to the β-carotene. Some such nano-engineered forms of β-carotene are nanostructure- or solid-lipid-carriers, microemulsions, nano-spheres, and capsules, *inter alia*. The polymer-based and lipid-based delivery systems are the most adopted delivery systems for β-carotene. These nano-engineered pigments have to be targeted to the gastrointestinal tract fluid for them to be absorbed by the enterocytes for subsequent assimilation. For this purpose, micelles and niosomes have been widely exploited. However, the interaction of these nano-pigments with the gastrointestinal tract cells and the environment within must be wisely researched before their incorporation into functional foods.

Cancer

The confirmation of the anti-cancer properties of fruits and vegetables rich in carotenes comes from epidemiological studies. According to the observations, the pigment-rich food preceded the direct intake of supplements in

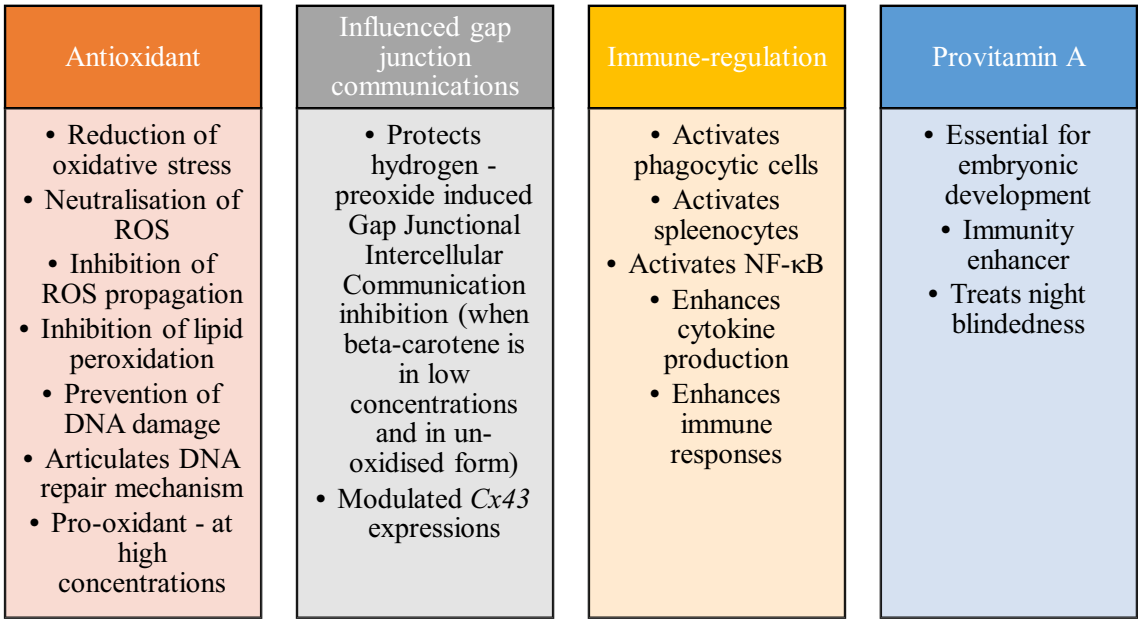

Fig. 5 Therapeutic effects of β-carotene

preference. This protection against cancer that carotene provides is due to metabolisms like singlet-oxygen quenchers, immunity enhancement, intracellular communications through gap junctions, and inhibition of cell division (Cooper 2004).

Communication that is regulated amongst cells means coordination in metabolism and growth. The failed signalling would eventually lead to uncontrolled cell growth and ultimately cancer. Hence, the cell-signalling regulation is another mode of action, through which β-carotene offers anti-cancer properties (Institute of Medicine (US) Panel on Dietary Antioxidants and Related Compounds, 2000). In fact, β-carotene supplementation can be useful in the treatment of site-specific cancers categorized as that of high incidence. For example, gastric cancer, which has complex aetiology has been under research against this natural pigment by many scientists. Varied research methods and subject areas have been used for epidemiological and cohort studies on patients suffering from gastric cancer. Several molecular mechanisms of the pigment are established for the probable result in the treatment of such patients in the past years (Chen et al. 2021). It also exhibits apoptotic as well as anti-proliferative effects on tumour cells (Kacar et al. 2022).

Cardiovascular Diseases

Diet rich in β-carotene has been found to be preventive for heart-related problems (Yang et al. 2022). The pigment is fat-soluble and is transported primarily in low-density lipoproteins (LDL). This association protects LDL from getting oxidized which would otherwise upon oxidation cause atherogenesis. A decrease in the thickness of "intima-media" resembles decreased risk of atherosclerosis, which was a result of increased total carotenoid concentration in serum (Mikkilä et al. 2009; Bhat et al. 2019). There is a lowered risk of CVD and related mortality cases due to the antioxidant effect of β-carotene which modifies the LDL oxidation and peroxidation mechanism (Carroll et al. 2000).

The β-carotene in blood plasma effectively increases the bioavailability of nitrous oxide (NO) along with levels of cyclic guanosine monophosphate (cGMP). This leads to a decline in endothelial cells' NF-κB-dependent molecules responsible for adhesion. The pigment also can enhance drug activity and function in the downregulation of genes that are involved in metabolizing cholesterol. Hence, there is a reduced chance of developing atherogenesis or other cardiac-related issues (Aizawa et al. 2003; Shaish et al. 2006).

COVID-19

Medical professionals confirm that the deficiency of vitamin A is associated with infections of the respiratory tract (Calder 2020). On the other hand, deficiency of vitamin D, due to less exposure to the sun, has been the reason for viral epidemics in winters. Muscogiuri et al. (2020) has described the interrelation of quarantine periods practised during COVID-19 with vitamin deficiency in patients. Doctors recommended strict diets to patients infected with corona virus, inclusive of β-carotene supplementing vegetables and fruits along with those

supplementing vitamin C and other micronutrients. On the other hand, β-carotene due to its antioxidant activity stimulates responses from lymphocytes, interleukin production, and the activity of natural killer cells and, thus, stimulating the overall immune system (Muscogiuri et al. 2020; Gröber and Holick 2022).

Other Diseases

Patients suffering from diseases like cystic fibrosis (CF) and non-CF-associated bronchiectasis have lower levels of plasma-β-carotene as well as vitamin E. They have been found to be disposable to damage by oxidation, which can be prevented by β-carotene supplementation (Çobanogcarlu et al. 2002). The different roles played by β-carotene contribute to different therapeutic effects in the management of several diseases including cancer, cardiovascular disorders, COVID-19, cystic fibrosis, and bronchiectasis. In the case of cancer, β-carotene acts as an antioxidant and anti-inflammatory, enhances immunity, and increases intracellular signalling. In addition to these effects, β-carotene also exhibits anti-apoptotic and anti-progressive effects on tumour (Middha et al. 2019). β-Carotene exhibits antioxidative properties and enhances drug activity in the case of cardiovascular diseases (Huang et al. 2018). In the case of cystic fibrosis, β-carotene helps to reduce the levels of TNF-α (tumour necrosis factor) and helps to increase the levels of vitamin E; also, it acts as an antioxidant (Çobanogcarlu et al. 2002). In bronchiectasis, β-carotene has been reported to reduce the levels of malondialdehydes and also serves as an antioxidant (Çobanogcarlu et al. 2002; Bartoli et al. 2011). In COVID-19 disease, β-carotene has been reported to stimulate cellular immune responses as well as act as an antioxidant (Muscogiuri et al. 2020).

Perspectives and Future Directions

Some of the physiological properties of β-carotene limit its effectiveness. Its poor bioavailability in crystalline form was reported, and is insoluble in water. Hence, its better delivery is obtained in oil/water emulsion, which also imparts the pigment and its stability (Liu et al. 2014). Its sensitivity to heat and light and liability to oxidation are other challenges that need to be addressed. The trend of involving low-on-fat products in food has been adversely affecting the absorption of β-carotene in the body. This might also be the reason for trial results not agreeing with the epidemiological observations. The span of the study and the dosage of β-carotene are all crucial in determining the pigment's disease-preventing potential.

The effect of carotenes on diseases can be studied better by considering the epigenetic factors. The diet pattern is another factor. The complex evidence of research has to be translated into an effective lifestyle and dietary recommendation, to lower the risk of disease development. The existing pattern of public health will then witness a paradigm shift, post-recognition of carotenes not only in disease treatment but also in prevention.

It is important to identify the indicators of carotene adequacy in the system and evaluate them. Such biological markers could be strong evidence of β-carotene intake levels required to prevent diseases. The biomarkers, indicative of disease progression, should be ligand-specific and indicative of β-carotene intake with responsiveness. However, these biomarkers must be validated, engaging a broad range of analogues and subjects.

The biological activity of β-carotene is enhanced in an aqueous solution if it is present in the form of nanoparticles (Rocha et al. 2018). This is where the role of nanotechnology might come. β-Carotene can be applied as nutraceuticals, cosmeceuticals, and pharmaceuticals in the form of emulsions, with improved sensitivity, solubility, and bioavailability (Yuan et al. 2008). There are a lot of prospects for enhanced production of β-carotenoid engaging the technological advancements of genetic engineering and nanotechnology. Regulation of gene expression or transformation of genes involved in β-carotene biosynthesis in some ways is to be listed. Proteins and water-soluble nano-β-carotene particles can offer bioactivity beyond their limitations.

Conclusions

The human body has a very vigilant feedback mechanism that maintains a balance between the serum retinol and β-carotene concentration. When the body gets deficient in vitamin A, the pre-consumed available β-carotene is converted into retinol and the metabolic conversion stops as the levels reach optimum. Until now, no side effects of β-carotene consumption have been reported apart from the harmless skin pigmentation due to overdose. However, some studies suggest post-menopause women are at a higher risk of fractures if having an excess of supplemental vitamin A. This could be simply concluded as making a wise preference of choosing diet-based β-carotene over-supplementation. During the literature survey, it was found that not much work has been carried out on β-carotene in the past two decades. Most of the available research data date back to the mid-90s, which resembles the scientific gap that the carotenoid family has been subjected to.

Acknowledgements The authors would like to acknowledge the Department of Biotechnology, Delhi Technological University, for their constant support.

Author Contribution Conceptualization of the article, editing, and supervision were done by NB. Literature search, data compilation, and writing and editing of the article were done by RA and LM. All authors have read and approved the final submission.

References

Aizawa T, Wei H, Miano JM, Abe J, Berk BC, Yan C (2003) Role of phosphodiesterase 3 in NO/cGMP-mediated anti-inflammatory effects in vascular smooth muscle cells. Circ Res 93:406–413. https://doi.org/10.1161/01.RES.0000091074.33584.F0

Akram S, Mushtaq M, Waheed A (2021) β-Carotene: beyond provitamin A. In: Mushtaq M, Anwar F (eds) A centum of valuable plant bioactives. Academic Pres, London, pp 1–3. https://doi.org/10.1016/B978-0-12-822923-1.00008-X

Álvarez R, Vaz B, Gronemeyer H, de Lera ÁR (2014) Functions, therapeutic applications, and synthesis of retinoids and carotenoids. Chem Rev 114:1–125. https://doi.org/10.1021/cr400126u

ATBC cancer prevention study group (1994) The alpha-tocopherol, beta-carotene lung cancer prevention study: design, methods, participant characteristics, and compliance. Ann Epidemiol 4:1–10. https://doi.org/10.1016/1047-2797(94)90036-1

Bartalucci G, Delroy C, Fisher S, Helliwell M, Liaaen-Jensen S (2008) 13- *cis*-β,β-carotene and 15- *cis*-β,β-carotene. Acta Crystallogr Structure 64:128–131. https://doi.org/10.1107/S0108270108001583

Bartoli ML, Novelli F, Costa F, Malagrinò L, Melosini L, Bacci E, Cianchetti S, Dente FL, di Franco A, Vagaggini B, Paggiaro PL (2011) Malondialdehyde in exhaled breath condensate as a marker of oxidative stress in different pulmonary diseases. Mediat Inflamm 2011:891752. https://doi.org/10.1155/2011/891752

Baysal T, Ersus S, Starmans DAJ (2000) Supercritical CO_2 extraction of β-carotene and lycopene from tomato paste waste. J Agric Food Chem 48:5507–5511. https://doi.org/10.1021/jf000311t

Bendich A, Olson JA (1989) Biological actions of carotenoids. FASEB J 3:1927–1932

Bhat S, Mocciaro G, Ray S (2019) The association of dietary patterns and carotid intima-media thickness: a synthesis of current evidence. Nutr Metab Cardiovasc Dis 29:1273–1287. https://doi.org/10.1016/j.numecd.2019.08.014

Biswas AK, Sahoo J, Chatli MK (2011) A simple UV-Vis spectrophotometric method for determination of β-carotene content in raw carrot, sweet potato and supplemented chicken meat nuggets. LWT - Food Sci Technol 44:1809–1813. https://doi.org/10.1016/j.lwt.2011.03.017

Bogacz-Radomska L, Harasym J (2018) β-Carotene-properties and production methods. Food Qual Saf 2:69–74. https://doi.org/10.1093/fqsafe/fyy004

Bohn T, Desmarchelier C, El SN, Keijer J, van Schothorst E, Rühl R, Borel P (2019) β-Carotene in the human body: metabolic bioactivation pathways – from digestion to tissue distribution and excretion. Proc Nutr Soc 78:68–87. https://doi.org/10.1017/S0029665118002641

Calder PC (2020) Nutrition, immunity and COVID-19. BMJ Nutr Prev & Health 3:74–92. https://doi.org/10.1136/bmjnph-2020-000085

Carroll Y, Corridan B, Morrissey P (2000) Lipoprotein carotenoid profiles and the susceptibility of low-density lipoprotein to oxidative modification in healthy elderly volunteers. Eur J Clin Nutr 54:500–507. https://doi.org/10.1038/sj.ejcn.1601046

Chen Q-H, Wu B-K, Pan D, Sang L-X, Chang B (2021) Beta-carotene and its protective effect on gastric cancer. World J Clin Cases 9:6591–6607. https://doi.org/10.12998/wjcc.v9.i23.6591

Çobanogcarlu N, Özçelik U, Göçmen A, Kiper N, Doğru D (2002) Antioxidant effect of β-carotene in cystic fibrosis and bronchiectasis: clinical and laboratory parameters of a pilot study. Acta Paediatr 91:793–798. https://doi.org/10.1080/08035250213212

Cooper DA (2004) Functions and actions of retinoids and carotenoids: building on the vision of James Allen Olson carotenoids in health and disease: recent Scientific Evaluations, Research Recommendations and the Consumer. J Nutr 134:220S–293S. https://doi.org/10.1093/jn/134.1.220S

Dey S, Rathod VK (2013) Ultrasound assisted extraction of β-carotene from *Spirulina platensis*. Ultrason Sonochem 20:271–276. https://doi.org/10.1016/j.ultsonch.2012.05.010

Druesne-Pecollo N, Latino-Martel P, Norat T, Barrandon E, Bertrais S, Galan P, Hercberg S (2010) Beta-carotene supplementation and cancer risk: a systematic review and metaanalysis of randomized controlled trials. Int J Cancer 127:172–184. https://doi.org/10.1002/ijc.25008

DrugBank (2022) Compound summary for DBAN DB06755, beta-carotene. Retrieved March 14, 2022 from https://go.drugbank.com/drugs/DB06755.

Eroglu A, Harrison EH (2013) Carotenoid metabolism in mammals, including man: formation, occurrence, and function of apocarotenoids. J Lipid Res 54:1719–1730. https://doi.org/10.1194/jlr.R039537

Farfán P, Gómez S, Restrepo A (2019) Dissection of the mechanism of the Wittig reaction. J Org Chem 84:14644–14658. https://doi.org/10.1021/acs.joc.9b02224

Ganea M, Moisa C, Cozma A, Bota S (2016) Determination of carotenoids by thin layer chromatography. Analele Univ din Oradea, Fasc Protecţia Mediu 26:247–252

Gröber U, Holick MF (2022) The coronavirus disease (COVID-19) – a supportive approach with selected micronutrients. Int J Vitam Nutr Res 92:13–34. https://doi.org/10.1024/0300-9831/a000693

Hercberg S (2005) The history of beta-carotene and cancers: from observational to intervention studies. What lessons can be drawn for future research on polyphenols? Am J Clin Nutr 81:218S–222S. https://doi.org/10.1093/ajcn/81.1.218s

Hininger I, Chopra M, Thurnham DI, Laporte F, Richard M-J, Favier A, Roussel A-M (1997) Effect of increased fruit and vegetable intake on the susceptibility of lipoprotein to oxidation in smokers. Eur J Clin Nutr 51:601–606. https://doi.org/10.1038/sj.ejcn.1600451

Huang J, Weinstein SJ, Yu K, Männistö S, Albanes D (2018) Serum beta carotene and overall and cause-specific mortality. Circ Res 123:1339–1349. https://doi.org/10.1161/CIRCRESAHA.118.313409

Hughes DA, Wright AJA, Finglas PM, Peerless ACJ, Bailey AL, Astley SB, Pinder AC, Norwich SS (1997) The effect of 13-carotene supplementation on the immune function of blood monocytes from healthy male nonsmokers. J Lab Clin Med 129:309–317. https://doi.org/10.1016/s0022-2143(97)90179-7

Institute of Medicine (US) Panel on Dietary Antioxidants and Related Compounds (2000) Dietary reference intakes for vitamin C, vitamin E, selenium, and carotenoids. NAP (US), Washington (DC)

Kacar S, Sariisik E, Sahinturk V (2022) Beta-carotene exerted antiproliferative and apoptotic effect on malignant mesothelioma cells. Naunyn-Schmiedeb Arch Pharmacol 395:407–415. https://doi.org/10.1007/s00210-022-02214-6

Kwatra B, Modi R (2020) Therapeutic potentials and applications of folic acid and beta carotene. Int J Sci Res Sci Technol 7:271–282. https://doi.org/10.32628/IJSRST1207481

Lakshminarayana R, Vijay K, Ambedkar R, Ranga Rao A, Ravishankar GA (2022) Biological activities and health benefits of seaweed carotenoids with special reference to fucoxanthin. In: Ranga Rao A, Ravishankar GA (eds) Sustainable global resources of seaweeds Volume 2. Springer, Cham, pp 539–558. https://doi.org/10.1007/978-3-030-92174-3_29

le Prell C, Lindblad A, Ulfendahl M, Green G, Miller J, Johnson A, Skjönsberg Å, Guire K, Campbell KCM (2011) Increased vitamin plasma levels in Swedish military personnel treated with nutrients prior to automatic weapon training. Noise Health 13:432–443. https://doi.org/10.4103/1463-1741.90317

Liang R, Huang Q, Ma J, Shoemaker CF, Zhong F (2013) Effect of relative humidity on the store stability of spray-dried beta-carotene nanoemulsions. Food Hydrocoll 33:225–233. https://doi.org/10.1016/j.foodhyd.2013.03.015

Liu Y, Hou Z, Yang J, Gao Y (2014) Effects of antioxidants on the stability of β-carotene in O/W emulsions stabilized by Gum Arabic. J Food Sci Technol 52:3300–3311. https://doi.org/10.1007/s13197-014-1380-0

Lohan SB, Vitt K, Scholz P, Keck CM, Meinke MC (2018) ROS production and glutathione response in keratinocytes after application of β-carotene and VIS/NIR irradiation. Chem Biol Interact 280:1–7. https://doi.org/10.1016/j.cbi.2017.12.002

Macedo M, Robrigues RDP, Pinto GAS, de Brito ES (2014) Influence of pectinolyttic and cellulotyc enzyme complexes on cashew bagasse maceration in order to obtain carotenoids. J Food Sci Technol 52:3689–3693. https://doi.org/10.1007/s13197-014-1411-x

Marcelino G, Machate DJ, de Freitas KC, Hiane PA, Maldonade IR, Pott A, Asato MA, Candido CJ, Guimarães RCA (2020) β-Carotene: preventive role for type 2 diabetes mellitus and obesity: a review. Molecules 25:5803. https://doi.org/10.3390/molecules25245803

Maria AG, Graziano R, Nicolantonio D (2015) Carotenoids: potential allies of cardiovascular health? Food Nutr Res 59:26762. https://doi.org/10.3402/fnr.v59.26762

Marino T, Casella P, Sangiorgio P, Verardi A, Ferraro A, Hristoforou E, Molino A, Musmarra D (2020) Natural beta-carotene: a microalgae derivate for nutraceutical applications. Chem Eng Trans 79:103–108. https://doi.org/10.3303/CET2079018

Maurya VK, Shakya A, Aggarwal M, Gothandam KM, Bohn T, Pareek S (2021) Fate of β-carotene within loaded delivery systems in food: state of knowledge. Antioxidants 10:426. https://doi.org/10.3390/antiox10030426

Middha P, Weinstein SJ, Männistö S, Albanes D, Mondul AM (2019) β-Carotene supplementation and lung cancer incidence in the alpha-tocopherol, beta-carotene cancer prevention study: the role of tar and nicotine. Nicotine Tob Res 21:1045–1050. https://doi.org/10.1093/ntr/nty115

Mikkilä V, Räsänen L, Laaksonen MML, Juonala M, Viikari J, Pietinen P, Raitakari OT (2009) Long-term dietary patterns and carotid artery intima media thickness: the cardiovascular risk in Young Finns Study. Br J Nutr 102:1507–1512. https://doi.org/10.1017/S000711450999064X

Milani A, Basirnejad M, Shahbazi S, Bolhassani A (2017) Carotenoids: biochemistry, pharmacology and treatment. Br J Pharmacol 174:1290–1324. https://doi.org/10.1111/bph.13625

Mosca L, Rubenfire M, Mandel C, Rock C, Tarshis T, Tsai A, Pearson T (1997) Antioxidant nutrient supplementation reduces the susceptibility of low density lipoprotein to oxidation in patients with coronary artery disease. J Am Coll Cardiol 30:392–399. https://doi.org/10.1016/S0735-1097(97)00188-5

Muscogiuri G, Barrea L, Savastano S, Colao A (2020) Nutritional recommendations for CoVID-19 quarantine. Eur J Clin Nutr 74:850–851. https://doi.org/10.1038/s41430-020-0635-2

Nierenberg DW, Dain BJ, Mott LA, Baron JA, Greenberg ER (1997) Effects of oral supplementation with 3-carotene on serum concentrations of retinol, tocopherol, and five carotenoids. Am J Clin Nutr 66:315–319. https://doi.org/10.1093/ajcn/66.2.315

NLM NCT00342992 Clinicaltrials.gov (2022) Carotene and retinol efficacy trial. [online] Available at: https://clinicaltrials.gov/ct2/show/study/NCT00342992 [Accessed 14 Mar 2022]

NLM NCT00712647 Clinicaltrials.gov (2022) Carotene and retinol efficacy trial. [online] Available at: https://clinicaltrials.gov/ct2/show/study/NCT00712647 [Accessed 14 Mar 2022].

Novo R, Azevedo PS, Minicucci MF, Zornoff LAM, Paiva SAR (2013) Effect of beta-carotene on oxidative stress and expression of cardiac connexin 43. Arq Bras Cardiol 101:233–239. https://doi.org/10.5935/abc.20130160

Olives-Barba AI, Cámara-Hurtado M, Sánchez-Mata MC, Fernández-Ruiz V, López-Sáenz de Tejada M (2006) Application of a UV-vis detection-HPLC method for a rapid determination of lycopene and β-carotene in vegetables. Food Chem 95:328–336. https://doi.org/10.1016/j.foodchem.2005.02.028

Olson JA (1993) Molecular actions of carotenoids. Ann N Y Acad Sci 691:156–166. https://doi.org/10.1111/j.1749-6632.1993.tb26167.x

Pham MA, Byun HG, Kim KD, Lee SM (2014) Effects of dietary carotenoid source and level on growth, skin pigmentation, antioxidant activity and chemical composition of juvenile olive flounder *Paralichthys olivaceus*. Aquaculture 431:65–72. https://doi.org/10.1016/j.aquaculture.2014.04.019

Piga R, van Dartel D, Bunschoten A, van der Stelt I, Keijer J (2014) Role of Frizzled6 in the molecular mechanism of beta-carotene action in the lung. Toxicology 320:67–73. https://doi.org/10.1016/j.tox.2014.03.002

Pool-Zobel BL, Bub A (1997) Consumption of vegetables reduces genetic damage in humans: first results of a human intervention trial with carotenoid-rich foods. Carcinogenesis 18:1847–1850. https://doi.org/10.1093/carcin/18.9.1847

PubChem 2022- National Center for Biotechnology Information (2022) PubChem Compound Summary for CID 5280489, beta-Carotene. Retrieved March 1, 2022 from https://pubchem.ncbi.nlm.nih.gov/compound/beta-Carotene

Reboul E (2013) Absorption of vitamin A and carotenoids by the enterocyte: focus on transport proteins. Nutrients 5:3563–3581. https://doi.org/10.3390/nu5093563

Renzi LM, Hammond BR, Dengler M, Roberts R (2012) The relation between serum lipids and lutein and zeaxanthin in the serum and retina: results from cross-sectional, case-control and case study designs. Lipids Health Dis 11:33. https://doi.org/10.1186/1476-511X-11-33

Rocha F, Yumi Sugahara L, Leimann FV, de Oliveira SM, da Silva BE, Calhelha RC, Barreiro MF, Ferreira ICFR, Porto Ineu R, Gonçalves OH (2018) Nanodispersions of beta-carotene: effects on antioxidant enzymes and cytotoxic properties. Food Funct 9:3698–3706. https://doi.org/10.1039/C8FO00804C

Rodriguez-Amaya DB (2016) Structures and analysis of carotenoid molecules. Subcell Biochem 79:71–108. https://doi.org/10.1007/978-3-319-39126-7_3

Saini RK, Keum Y-S (2018) Carotenoid extraction methods: a review of recent developments. Food Chem 240:90–103. https://doi.org/10.1016/j.foodchem.2017.07.099

Shaish A, Harari A, Hananshvili L, Cohen H, Bitzur R, Luvish T, Ulman E, Golan M, Ben-Amotz A, Gavish D, Rotstein Z, Harats D (2006) 9-*cis* β-Carotene-rich powder of the alga *Dunaliella bardawil* increases plasma HDL-cholesterol in fibrate-treated patients. Atherosclerosis 189:215–221. https://doi.org/10.1016/j.atherosclerosis.2005.12.004

Shete V, Quadro L (2013) Mammalian metabolism of β-carotene: gaps in knowledge. Nutrients 5:4849–4868. https://doi.org/10.3390/nu5124849

Siems W, Salerno C, Crifò C, Sommerburg O, Wiswedel I (2009) β-Carotene degradation products – formation, toxicity and prevention of toxicity. Forum Nutr 61:75–86. https://doi.org/10.1159/000212740

Sies H, Stahl W (1997) Carotenoids and intercellular communication via gap junctions. Int J Vitam Nutr Res. 67:364–367

Starek M, Guja A, Dąbrowska M, Krzek J (2015) Assay of β-carotene in dietary supplements and fruit juices by TLC-densitometry. Food Anal Methods 8:1347–1355. https://doi.org/10.1007/s12161-014-0019-0

Wu Y, Yan P, Li Y, Liu X, Wang Z, Chen T, Zhao X (2020) Enhancing β-carotene production in *Escherichia coli* by perturbing central carbon metabolism and improving the NADPH supply. Front Bioeng Biotechnol 8:585. https://doi.org/10.3389/fbioe.2020.00585

Yang J, Zhang Y, Na X, Zhao A (2022) β-Carotene supplementation and risk of cardiovascular disease: a systematic review and meta-analysis of randomized controlled trials. Nutrients 14:1284. https://doi.org/10.3390/nu14061284

Yu LJ, Rupasinghe HV (2013) Improvement of cloud stability, yield and β-carotene content of carrot juice by process modification. Food Sci Technol Int 19:399–406. https://doi.org/10.1177/1082013212455342

Yuan Y, Gao Y, Mao L, Zhao J (2008) Optimisation of conditions for the preparation of β-carotene nanoemulsions using response surface methodology. Food Chem 107:1300–1306. https://doi.org/10.1016/j.foodchem.2007.09.015

Zhang Y, Navarro E, Cánovas-Márquez JT, Almagro L, Chen H, Chen YQ, Zhang H, Torres-Martínez S, Chen W, Garre V (2016) A new regulatory mechanism controlling carotenogenesis in the fungus *Mucor circinelloides* as a target to generate β-carotene over-producing strains by genetic engineering. Microb Cell Factories 15:99. https://doi.org/10.1186/s12934-016-0493-8

Proceedings of the Sixth International Conference on Intelligent Computing and Control Systems (ICICCS 2022)
IEEE Xplore Part Number: CFP22K74-ART; ISBN: 978-1-6654-1035-9

2022 6th International Conference on Intelligent Computing and Control Systems (ICICCS) | 978-1-6654-1035-9/22/$31.00 ©2022 IEEE | DOI: 10.1109/ICICCS53718.2022.9788129

Dleep Learning based Regularization as defense against Clean Label Targeted Data Poisoning

Anil Singh Parihar
Dept. of Computer Science and Engineering
Delhi Technological University
Delhi, India
parihar.anil@gmail.com

Jushaan Singh Kalra
Dept. of Computer Science and Engineering
Delhi Technological University
Delhi, India
jushaan18@gmail.com

Abhinav Java
Dept. of Computer Science and Engineering
Delhi Technological University
Delhi, India
java.abhinav99@gmail.com

***Abstract*—Adversarial examples are doctored inputs to predictive models intentionally designed with a malicious purpose – to manipulate the inference time outputs of the machine learning system. One such recent threat to Deep Neural Networks is the targeted clean label data poisoning attack, wherein the adversary modifies training samples in the dataset without modifying the original labels. A model trained on these seemingly benign examples is likely to misclassify specific queries to targeted labels. While ample research is ongoing on the ways to generate and attack deep models, there is little work in mitigating such attacks. This research work employs a simpler strategy of making the model robust to poison samples during training and study the effect of regularization techniques on such attacks. Specifically, this research work proposes a strong pruning and autoencoder-based strategies to defend against data poisoning attacks and show its effectiveness on various deep models. The proposed methods reduce attacker efficacy by 23% and can serve as strong baselines for future work on defense against such adversarial attacks.**

***Index Terms*—Adversarial Attacks, Defense, Data Poisoning, Autoencoders, Sparsification, Deep Learning**

I. Introduction

Deep Neural Networks (DNNs) can capture vital statistics from training data samples and achieve impressive performance on several tasks like classification [1], [2], object detection [3], [4], sales prediction [5], text extraction [6], etc. The ability to learn from data through a composition of linear and nonlinear functions is the key reason for the prominence of DNNs in industry and academia. Currently, deep learning is being used for applications like healthcare, business analytics, search engines, facial recognition, driverless cars, among others. However, a consequence of beating state of the art on various benchmarks has inadvertently raised privacy and security concerns due to the critical nature of the applications. A common privacy concern that is the reason for the malfunction of DNNs are Adversarial attacks [7]–[13]. In general, adversarial attacks are designed with a malicious intent whereby an adversary injects doctored inputs to a neural network to make it malfunction. Recently, an attack scheme called

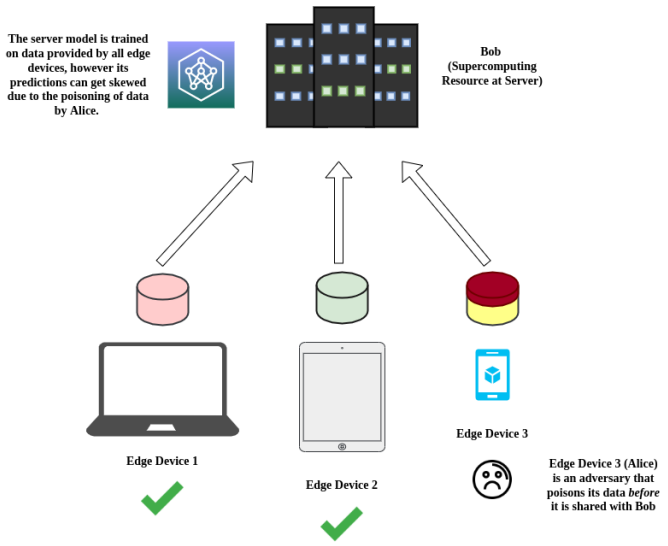

Fig. 1. A malicious adversary can add a small amount of poisoned data to the mix to manipulate the outputs of a larger server model (zoom in for best view).

Clean Label Targeted Data Poisoning [11], [12] (CLTDP) has been proposed. CLTDP shows that practically imperceptible manipulation of a very small percentage of training data can shift the decision boundary of a DNN. In contrast to inference time attacks like FSGM [8], in this attack, the adversary simply injects seemingly harmless examples (poisons) into a training dataset and achieves desired outputs for particular inputs to the model trained on this dataset. MetaPoison [10] shows that their method has an important application in watermarking images; however, they also point out the dangers of such an attack since even a small number of poisoned samples can shift the outcome by a large degree. Server models trained on client data would be particularly vulnerable to such attacks since CLTDP can work with a very small percentage of manipulated training examples. For instance (Fig. 1), consider a large

Authorized licensed use limited to: DELHI TECHNICAL UNIV. Downloaded on June 15,2022 at 11:18:56 UTC from IEEE Xplore. Restrictions apply.

server model (Bob) and several edge devices (Alices) in a distributed learning setting [14]–[16]. Here, Bob is trained on data samples collected by Alices. If a malicious edge device injects unwanted perturbations in the shared data to manipulate the outcome of the server model, it can have several repercussions, especially in domains handling sensitive information like healthcare, politics, law, self-driving vehicles, facial recognition systems, hate speech detection, etc. With large scale models being trained on data from public sources like Twitter, Facebook, etc., it is all the more vital to create defenses against such attacks, to protect sensitive information, including the training data, model architecture, and its biases, enabling the deployment of such models for real-world use without the security concerns that currently exist.

The focus of our work is to mitigate the recently proposed attack scheme, viz Clean Label Targeted Data Poisoning, by making machine learning systems robust to potential vulnerabilities due to the CLTDP attacks. While most predominant methods have made significant strides in coming up with defenses for several types of adversarial attacks like [17]–[19], very little work has been done to mitigate CLTDP attacks. Initial methods [20], [21] mostly attempted to filter poisoned samples by identifying data samples whose features are disjoint from the rest of the data of the same class. Other techniques can broadly be divided into proxy adversarial training based [22] and differential privacy based [23]. These methods have had limited success in terms of both the attacker efficacy-utility trade-off and defense against more recent attack schemes like MetaPoison [10] that don't necessarily rely on feature manipulation for crafting poisons. We posit that a data sanitization strategy can sufficiently reduce the dimensionality of input data, effectively getting rid of the perturbations in the poisoned samples. We show that our regularization strategies are effectively able to mitigate the effects of poisoning; specifically, we are able to achieve a better tradeoff on the MetaPoison attack benchmark. The contributions of the proposed work can be summarized as follows:

1) We formalize the Clean Label Data Poisoning Attack scheme and discuss the existing techniques to prevent these attacks.
2) We design an autoencoder-based regularization technique to sanitize the poisoned data and show that it successfully prevents data poisoning on recent benchmarks.
3) Finally, we also discuss the effects of other regularization techniques like pruning on CLTDP and motivate the need for regularization-based solutions to prevent adversarial attacks.

The remainder of this paper is organized as - In Sec II we discuss the body of literature related to our work; this includes various CLTDP attack schemes (Sec II-A) and the mitigation strategies (Sec II-B). In Sec III-D we present our Autoencoder based regularization for preventing CLTDP attacks along with other strong baselines. Further in Sec IV, we share the experimental setup and the key findings of our work followed by conclusion and future scope in Sec V.

II. Related Work

Neural Networks are vulnerable to attacks after deployment [7]–[13]. This allows adversaries to manipulate outputs based on certain triggers. One of such attacks - the targeted data poisoning is triggered by a specific pre-decided data.

A. Data Poisoning Attacks

There has been an immense amount of work around such "attacks" which can compromise the ability of a model to perform its task. Mostly, literature has focused on evasion attacks, which involve perturbing inputs at inference to get a different prediction from the model. Similar to this, backdoor attacks add a "*keyword*", which can trigger an unexpected output from the attacked model. However, both attacks require control over the data at inference time. Data poisoning, on the other hand, attacks data at training itself and does not require any interference at inference time. In this case, the hacker modifies or replaces some data which is to be used by the model for training. This poisoned data then leads to a compromised training pipeline. Adding this poisoned data is easy, as increasingly data is scraped from the internet by bots and used to train such models. This data could also be poisoned when it is provided by anonymous individuals, such as for Face Identification and recognition systems which are currently being used in industry [24]–[26]. Data poisoning consists of two types - one allowing the change in label as well as training input, while the other, called clean label data poisoning, allows changes in the input but with the label intact. In these attacks, the poisoned data is imperceptible from the unpoisoned one and so is difficult to remove from the training data. Moreover, these changes in the input images cause misclassification at inference time on one target image that is pre-decided. This makes defense against such systems even more difficult. There are various different Clean label data poisoning attacks that have been used against Deep learning models. MetaPoison [10] crafts a poison dataset for this purpose. They find the optimal poison images by a bilevel meta-learning approach. The novelty in this paper is that they approximate the inner optimization loop of the meta-learning pipeline by only running the SGD for K steps in the inner loop and making it tractable. The data is crafted using an adversarial approach. Intriguingly, their poisons do not collide with the target, implying that they employ some other mechanism to achieve the same objective. They do not even reside in the target class distribution, which may render neighborhood conformity tests such as Deep KNN [20] less effective as a defense. They use the CIFAR-10 [27] dataset to check their algorithm in the real world while making use of a wide variety of models such as Resnet 20 [28], VGG19 [29], Alexnet [30], LeNet [31] for poison crafting. They show high accuracy of success in both training from scratch and transfer learning. Similar to MetaPoison, PoisonGAN [32] proposes constructing poisoned data based on regeneration of victim class using GANs. They use this method to attack federated learning systems by updating global parameters using a poisoned model

Authorized licensed use limited to: DELHI TECHNICAL UNIV. Downloaded on June 15,2022 at 11:18:56 UTC from IEEE Xplore. Restrictions apply.

from the client. They use MNIST and CIFAR-10 datasets to show the efficacy of their method against federated systems.

B. Defense against Data Poisoning Attacks

Most defenses work against a particular type of attack and are unable to defend against a wide variety of clean label attacks. Existing literature has broadly approached this problem through adversarial training (De-Pois [22]), differential privacy (DP-Aug [23]), or feature manipulation (Deep KNN [20]). These methods have had limited success in terms of both the privacy-utility trade-off and the range of attacks they can defend against and are mostly reliant on identifying the poisons. Deep KNN [20] assumes that the data poisoning is done through feature manipulation [11] and essentially removes the anomalous samples by finding the samples whose feature space is not with the rest of its class labels. CLP with LGM [21] replaces the softmax activation in the last layer with an LGM loss, building upon a very similar intuition that the features of the poison samples are actually far away than claimed (from the features of other samples of the same class). LGM loss implicitly allows the network to capture the deviation from a gaussian distribution. Both [20] and [22] fail to produce optimal results if the attack scheme is changed to something other than feature collision [11] or convex polytope [33]. DP-Aug [23] argues that mixup augmentations concentrate training data near the center of the ambient unit hypercube and saturates this region of space more densely than the original dataset, leveraging data augmentations through differential privacy they are able to secure the dataset. The key issue with this work remains that these augmentations come at the cost of poor test accuracy. De-Pois [22] uses a more expensive approach of crafting poisons using a cGAN [34] to facilitate data augmentation. However, the metric to identify poisoned samples (the difference between the performance of the mimic model and the original model) is not only computationally expensive but also uninterpretable.

III. Method

In this section, we first mathematically formulate CLTDP attacks, then we present the proposed Autoencoder-based regularization technique along with pruning baseline to mitigate clean label targeted data poisoning.

A. Preliminaries

Clean Label Data Poisoning was introduced by [4]. In this section we will provide the relevant background and related attack schemes. For a given training dataset at the server (Bob), let the client adversary (Alice) manipulate a subset of this dataset as such that:

$$S_{train} = S_p \cup S_c \tag{1}$$

Where S_{train} is the entire training dataset and S_p, S_c are the poisoned subset and clean subset. Note that both the subsets have correct labels in this setting. However, the subset S_c is the perturbed subset that is added maliciously and without the practitioner's (Charlie) knowledge. The poisoned subset consists of:

$$S_c = (\tilde{X}_i, Y_i)_{i=0...(n_p-1)} \tag{2}$$

Where $\tilde{X}_i$ is the perturbed sample injected into the original dataset and Y_i is the corresponding clean label. The number of poisoned samples is denoted by n_p. Let the total dataset size be n_{train}. Then generally $n_p << n_{train}$, making it very hard to filter the data. Furthermore, in this setting the adversary usually targets the misclassification of a particular image to the desired label. For instance, if an adversary wants to maliciously manipulate a traffic camera to not trigger when their face is inputted to this machine learning system, they can change data such that only that one input is misclassified.

In the case of the CIFAR10 dataset this problem can be simplified as follows. A target class L_k where $k \in [0, 9]$ is picked, this is the adversarial label that we want some input query q_j to be misclassified to and j is the actual class of the input query as follows:

$$k = \arg\max\left(f(q_j)\right) \tag{3}$$

Where f is the victim model and $\arg\max$ is taken over the output probabilities to output the predicted class which is k(incorrect) in this case.

$$i = \arg\max f(q_i) \tag{4}$$

When $i \neq j$, the victim model predicts the correct output class i.

For example: A target class can be "*frog*" and a query class can be "*airplane*". With this setup, particular airplanes are likely to be mis-classified as "*frog*".

B. Problem Requirements

We need to modify the victim model f such that it becomes robust to adversarial perturbations during train time. Let f be originally trained as follows:

$$minimize(L_{BCE}(f(X_i, Y_i; \theta))) \tag{5}$$

Where $i \in [0, (n_{train} - 1)]$ and the victim model is parameterized by θ and $(X, Y) \in S_{train(clean)}$. However due to CLTDP, X_i is modified as shown above which changes the decision boundary of f. We therefore reformulate the optimization problem as follows:

$$minimize(L_{BCE}(p(f(S_{train}; f); p))) \tag{6}$$

Where p is an additional learnable model that acts both as a protective model for the victim. We refer to it as a trainable data sanitizer.

C. Mitigating Data Poisoning using Pruning

Neural Networks are highly overparameterized [35] and have abundant unused parameters. Our initial hypothesis was that due to these excessive neurons, the DNN becomes more susceptible to CLTDP attacks. Pruning has shown to be effective against other types of adversarial attacks [36]. Similar to [36], wherein pruning was used to counter inference time

Authorized licensed use limited to: DELHI TECHNICAL UNIV. Downloaded on June 15,2022 at 11:18:56 UTC from IEEE Xplore. Restrictions apply.

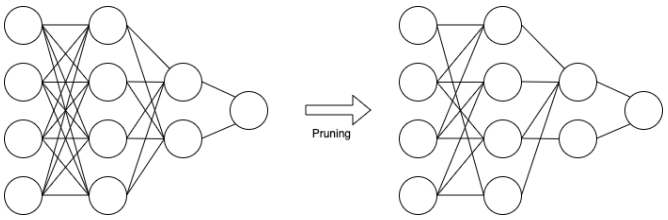

Fig. 2. A pruned DNN, is able to reduce the effectiveness of CLTDP attacks by forcing the network to share neurons to generate a representation of the input making it harder for a small group of adversarial samples to affect its decision boundary.

attack (like the adversary injecting noise during test time), we did global unstructured pruning of a network trained on the poisoned dataset to verify if there is a noticeable performance drop before and after pruning. This is our baseline model and will be used to compare against other pruning strategies. Pruning allows a deep learning practitioner to remove weights/parameters (Fig. 2) from a DNN without affecting its accuracy to a large extent. This helps the practitioner to cut deployment costs by using a smaller model. Furthermore, [37] shows that pruning is an effective regularization method as well. Optimal Brain Damage [38] argues that although the magnitude is a viable metric to judge which neurons to remove, a better method would be to use the double differential as an approximation of saliency (importance). Since then, several works have shown the benefits of both; pruning before and after training, with [39] showing that dynamic pruning followed by fine-tuning can sometimes even help achieve better accuracy. In 2019, [40] gave striking empirical results that training the best-pruned model from scratch (by resetting its weights) is actually the best method to outperform the model's overparameterized (un-pruned) counterpart. Since then, researchers have also shown interesting studies suggesting that finding the best-pruned model (or lottery ticket) is actually similar to Neural Architecture Search (NAS). In order to motivate and explore the impact of pruning on the attack efficacy, we set up a simple baseline with global unstructured pruning. This is the simplest form of pruning that globally removes some percentage of weights based on their L1 distance from zero, i.e., magnitude-based. This pruning is done after training, and the model is not fine-tuned after pruning. (as shown in Fig. 4) This essentially amounts to forcing the network to share neurons to learn a richer representation of the input. Such that, even if a certain group of adversarial examples attempts to skew a subset of weights, the other (pristine) examples preserve their correct representation.

D. Mitigating Data Poisoning using Autoencoders

Machine Learning (ML) practitioners have been using regularization methods to tackle the problem of balancing bias and variance in ML systems. Common regularization methods include Dropout [41], Weight Decay [42], Label Smoothing [43], Pruning [37], etc. In essence, all these methods are designed to prevent overfitting on the training data and improve performance on the test examples. We hypothesize that the

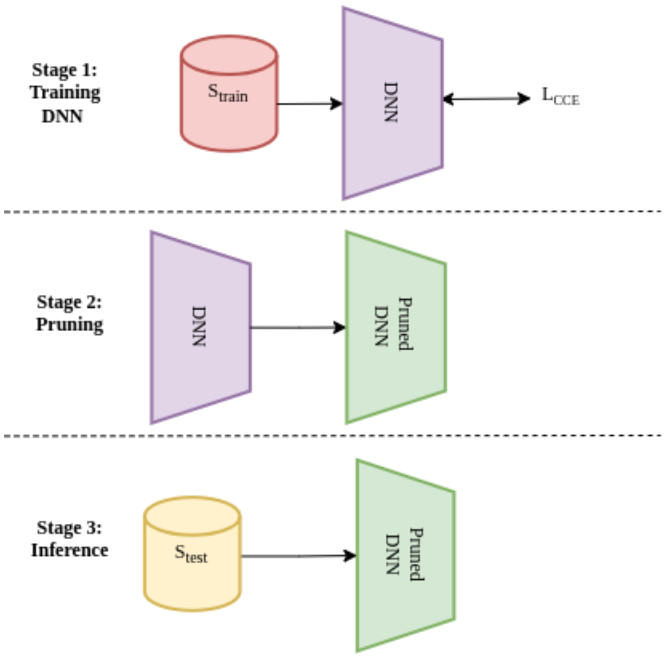

Fig. 3. System Architecture for pruning a neural network

likelihood of a DNN malfunctioning due to CLTDP attack is correlated with the dimensionality of the input training data. We sought to reduce the dimensionality of the input using a convolutional autoencoder in order to decrease the efficacy of the attacker. Specifically, the protective model p in Eq. (6) is an autoencoder [33]. Autoencoders are a class of DNNs that are used to create a more compact representation by adding a bottleneck layer that encodes the most important information needed to recreate the initial representation. (Fig. 4) It is an unsupervised technique that forms the basis of representation learning. An autoencoder can be thought of as an extension to PCA. It reduces dimensions while conserving the non-linearity of the feature space. A simple Mean Squared Error (MSE) loss can be applied between the input and the output to train an autoencoder. The compressed representation will lose the information encoded by the data poisoning attack and thereby act as an unpoisoning step before actually training a network for our original problem statement. The training is divided into two steps. We assume that the data available to the ML practitioner is already poisoned Eq. 1. We use the poisoned data to train an autoencoder p_{AE} in an unsupervised manner in order to capture the compressed representation of the data. The trained autoencoder p_{AE} is then frozen and used as p in Eq. (6) effectively acting as a protective data sanitizer over the victim model. (as shown in Fig. 5)

IV. Experiments

In this section we highlight the experimental details like preparing the proxy poisoned data (Sec. IV-A.), evaluation protocol (Sec. IV-B.), implementation details (Sec. IV-C.) for reproducibility and finally the effectiveness of our method as results (Sec. IV-D.).

Authorized licensed use limited to: DELHI TECHNICAL UNIV. Downloaded on June 15,2022 at 11:18:56 UTC from IEEE Xplore. Restrictions apply.

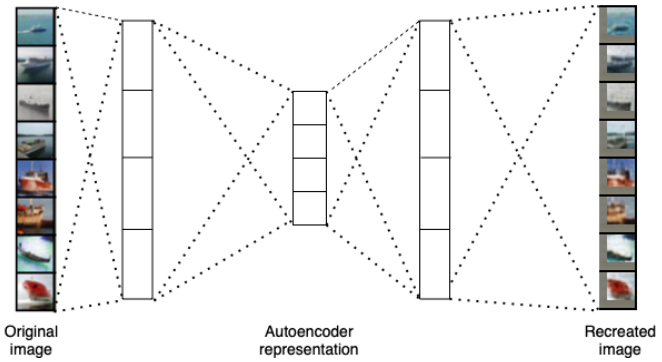

Fig. 4. Autoencoder reduces the dimensionality and is successfully able to sanitize the input data by removing the poisoning artifacts added by a malicious adversary (here Meta Poison [10]).

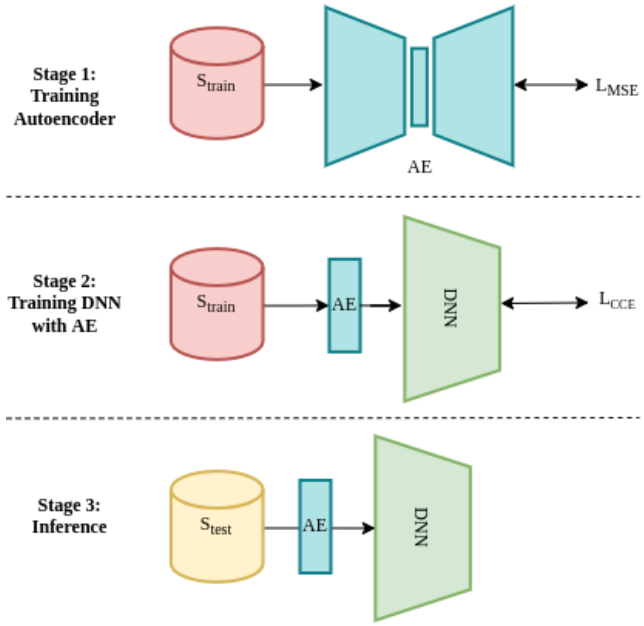

Fig. 5. System architecture for training Neural Networks with Autoencoders.

A. Dataset Preparation

In this section, we describe the preparation of data used for our CLTDP setup. We take MetaPoison [10] to first poison the CIFAR-10 [27] dataset. MetaPoison uses an approximation of a bijective function to find the optimal poison images by a meta-learning approach. However, due to computational constraints, running the bijective function is not feasible. So, the authors approximate the inner optimization loop of the meta-learning pipeline by only running the SGD for K steps in the inner loop and making it not intractable. The data is crafted using an adversarial approach. These slight perturbations in one class of the dataset make the prediction of the target image at inference time incorrect while ensuring that the changed dataset is imperceptible from the original one. Using this methodology, we construct 24 poisoned datasets from the CIFAR-10 dataset. Firstly, these datasets can be classified by choice of poison class and the targeted class. For each of these classes, 12 models were trained.

1) Poison-dog-target-bird
2) Poison-frog-target-plane

In the first case, the model takes a subset of dataset from class dog and perturbs it, such that an image of a specific bird (say parrot) selected from the test dataset predicts the Target label defined while construction. Similarly, we use the same foundations for the construction of the 2^{nd} dataset. For each of the above cases, we can choose a target label. For our purposes we choose 3 labels - plane, cats and frog. Next, we take $50, 500, 1000, 5000$ images to be poisoned for each of the previous cases. Together these created 24 different training configurations. For each of the 24 models trained we prune $10\%, 20\%, 40\%, 60\%, 80\%, 100\%$ of the total neurons, which gives us 144 different models after pruning.

B. Evaluation Method

After training our models, we evaluate the success of our approach using two metrics – defense against CLTDP attack and the validation accuracy of the resulting model. Defense against attacks is measured by calculating the average number of times the adversarial prediction is not equal to the predicted one. The validation accuracy is determined by the average accuracy of all models on the test dataset. These results are shown in Table 1. We can observe the clear trade-off between validation accuracy and successful defense against CLTDP attacks. This is due to the nature of such defenses, they reduce information used by the model, thereby degrading it's overall performance but protecting the model against unexpected attacks. Finding the fine-line between these two trade-offs is a challenging problem that could be explored in future works.

C. Implementation Details

We perform all our experiments on 1 Nvidia Titan RTX GPU using PyTorch [44]. We train the ResNet [28] models for 100 epochs and AlexNet [30] for 25 epochs. The learning rate is 0.001, while a batch size of 64 is maintained. We use the Adam solver [45] in all our experiments.

D. Results

From the results shown in Table 1, we can see that both our strategies tremendously reduce the attacker efficacy. Pruning gives 10% protection against Meta Poison [10] while maintaining a reasonable validation accuracy. Our hypothesis that strong regularization can help defend against such attacks is further validated by the fact that the best performance is on AlexNet which is inherently a smaller architecture. We note that autoencoders as data sanitizers give the best tradeoff in terms of attacker efficacy and validation accuracy of the base model. Since autoencoders offer a direct regularization effect on the data without manipulating the base model, it outperforms pruning by giving a 23% reduction in attacker accuracy.

Authorized licensed use limited to: DELHI TECHNICAL UNIV. Downloaded on June 15,2022 at 11:18:56 UTC from IEEE Xplore. Restrictions apply.

TABLE I
EFFECTS OF PRUNING AND AUTOENCODERS ON POISONING EFFICACY. WHILE META POISON [10] WORKS 50% OF THE TIME, OUR METHOD IS ABLE TO REDUCE ITS EFFICACY BY 23%, MAKING IT MORE ROBUST.

Attack	Model	*Success against poisoning attacks*	*Number of trained models*	*Val accuracy*
MetaPoison	**Average**	49.98%	432	80.03%
	ResNet20	45.14%	144	83.46%
	ResNet32	48.55%	144	83.50%
	AlexNet	56.25%	144	73.29%
MetaPoison + Pruning	**Average**	**59.65%**	**432**	**64.28%**
	ResNet20	55.55%	144	64.51%
	ResNet32	59.51%	144	65.43%
	AlexNet	63.89%	144	62.90%
MetaPoison + Autoencoder	**Average**	**73.61%**	**72**	**61.43%**
	ResNet20	70.83%	24	62.33%
	ResNet32	75%	24	62.20%
	AlexNet	75%	24	59.86%

V. CONCLUSION

The goal of this work was to formalize Clean Label Targeted Data Poisoning and devise strategies to make the existing DNNs more robust to these attacks. Given the ever increasing use of DNNs in critical areas like healthcare, surveillance, etc and the nature of these attacks, it is imperative to protect sensitive data and make models invariant to adversaries. Since predominant works fail to defend against recent attacks (Meta Poison [10]), we design regularization-based techniques that act as generic data sanitizers and strong baselines for a diverse set of models. Our experiments show the effectiveness of the proposed method and pave the way for future research in this domain.

REFERENCES

[1] B. Pandey and N. Garg, "Swarm optimized modular neural network based diagnostic system for breast cancer diagnosis," *Int. J. Soft Comput. Artif. Intell. Appl.(IJSCAI)*, vol. 2, no. 4, pp. 11–20, 2013.

[2] N. A. Mohamad, N. A. Jusoh, Z. Z. Htike, S. L. Win *et al.*, "Bacteria identification from microscopic morphology: a survey," *International Journal on Soft Computing, Artificial Intelligence and Applications (IJSCAI)*, vol. 3, no. 1, pp. 2319–1015, 2014.

[3] S. Mittal, "Unsupervised learning models of invariant features in images: recent developments in multistage architecture approach for object detection," *Int J Soft Comput Artif Intell Appl (IJSCAI)*, vol. 5, no. 2, pp. 63–70, 2016.

[4] J. P. Verma, S. Agrawal, B. Patel, and A. Patel, "Big data analytics: Challenges and applications for text, audio, video, and social media data," *International Journal on Soft Computing, Artificial Intelligence and Applications (IJSCAI)*, vol. 5, no. 1, pp. 41–51, 2016.

[5] A. Massaro, V. Vitti, and A. Galiano, "Model of multiple artificial neural networks oriented on sales prediction and product shelf design," *International Journal on Soft Computing, Artificial Intelligence and Applications (IJSCAI)*, vol. 7, no. 3, pp. 1–19, 2018.

[6] A. Thilagavathy, K. Aarthi, and A. Chilambuchelvan, "Text detection and extraction from videos using ann based network," *International Journal on Soft Computing, Artificial Intelligence and Applications (IJSCAI)*, vol. 1, no. 1, 2012.

[7] I. Goodfellow, J. Pouget-Abadie, M. Mirza, B. Xu, D. Warde-Farley, S. Ozair, A. Courville, and Y. Bengio, "Generative adversarial nets," *Advances in neural information processing systems*, vol. 27, 2014.

[8] I. J. Goodfellow, J. Shlens, and C. Szegedy, "Explaining and harnessing adversarial examples," *arXiv preprint arXiv:1412.6572*, 2014.

[9] S.-M. Moosavi-Dezfooli, A. Fawzi, and P. Frossard, "Deepfool: a simple and accurate method to fool deep neural networks," in *Proceedings of the IEEE conference on computer vision and pattern recognition*, 2016, pp. 2574–2582.

[10] W. R. Huang, J. Geiping, L. Fowl, G. Taylor, and T. Goldstein, "Metapoison: Practical general-purpose clean-label data poisoning," *Advances in Neural Information Processing Systems*, vol. 33, pp. 12 080–12 091, 2020.

[11] A. Shafahi, W. R. Huang, M. Najibi, O. Suciu, C. Studer, T. Dumitras, and T. Goldstein, "Poison frogs! targeted clean-label poisoning attacks on neural networks," *Advances in neural information processing systems*, vol. 31, 2018.

[12] P. W. Koh and P. Liang, "Understanding black-box predictions via influence functions," in *International conference on machine learning*. PMLR, 2017, pp. 1885–1894.

[13] A. Ghiasi, A. Shafahi, and T. Goldstein, "Breaking certified defenses: Semantic adversarial examples with spoofed robustness certificates," *arXiv preprint arXiv:2003.08937*, 2020.

[14] J. Verbraeken, M. Wolting, J. Katzy, J. Kloppenburg, T. Verbelen, and J. S. Rellermeyer, "A survey on distributed machine learning," *ACM Computing Surveys (CSUR)*, vol. 53, no. 2, pp. 1–33, 2020.

[15] J. Konečnỳ, H. B. McMahan, F. X. Yu, P. Richtárik, A. T. Suresh, and D. Bacon, "Federated learning: Strategies for improving communication efficiency," *arXiv preprint arXiv:1610.05492*, 2016.

[16] P. Kairouz, H. B. McMahan, B. Avent, A. Bellet, M. Bennis, A. N. Bhagoji, K. Bonawitz, Z. Charles, G. Cormode, R. Cummings *et al.*, "Advances and open problems in federated learning," *Foundations and Trends® in Machine Learning*, vol. 14, no. 1–2, pp. 1–210, 2021.

[17] K. Ren, T. Zheng, Z. Qin, and X. Liu, "Adversarial attacks and defenses in deep learning," *Engineering*, vol. 6, no. 3, pp. 346–360, 2020.

[18] F. Boenisch, P. Sperl, and K. Böttinger, "Gradient masking and the underestimated robustness threats of differential privacy in deep learning," *arXiv preprint arXiv:2105.07985*, 2021.

[19] B. Lindqvist and R. Izmailov, "Minimax defense against gradient-based adversarial attacks," *arXiv preprint arXiv:2002.01256*, 2020.

[20] N. Peri, N. Gupta, W. R. Huang, L. Fowl, C. Zhu, S. Feizi, T. Goldstein, and J. P. Dickerson, "Deep k-nn defense against clean-label data poisoning attacks," in *European Conference on Computer Vision*. Springer, 2020, pp. 55–70.

[21] M. Yaseen, M. Aadil, and M. Sargsyan, "Preventing clean label poisoning using gaussian mixture loss," *arXiv preprint arXiv:2003.00798*, 2020.

[22] J. Chen, X. Zhang, R. Zhang, C. Wang, and L. Liu, "De-pois: An attack-agnostic defense against data poisoning attacks," *IEEE Transactions on Information Forensics and Security*, vol. 16, pp. 3412–3425, 2021.

[23] E. Borgnia, J. Geiping, V. Cherepanova, L. Fowl, A. Gupta, A. Ghiasi, F. Huang, M. Goldblum, and T. Goldstein, "Dp-instahide: Provably defusing poisoning and backdoor attacks with differentially private data augmentations," *arXiv preprint arXiv:2103.02079*, 2021.

[24] F. Schroff, D. Kalenichenko, and J. Philbin, "Facenet: A unified embedding for face recognition and clustering," in *Proceedings of the IEEE conference on computer vision and pattern recognition*, 2015, pp. 815–823.

[25] J. Deng, J. Guo, N. Xue, and S. Zafeiriou, "Arcface: Additive angular margin loss for deep face recognition," in *Proceedings of the IEEE/CVF conference on computer vision and pattern recognition*, 2019, pp. 4690–4699.

[26] Y. Sun, C. Cheng, Y. Zhang, C. Zhang, L. Zheng, Z. Wang, and Y. Wei, "Circle loss: A unified perspective of pair similarity optimization," in *Proceedings of the IEEE/CVF Conference on Computer Vision and Pattern Recognition*, 2020, pp. 6398–6407.

[27] A. Krizhevsky, G. Hinton *et al.*, "Learning multiple layers of features from tiny images," 2009.

[28] K. He, X. Zhang, S. Ren, and J. Sun, "Deep residual learning for image recognition," in *Proceedings of the IEEE conference on computer vision and pattern recognition*, 2016, pp. 770–778.

[29] J. Verbraeken, M. Wolting, J. Katzy, J. Kloppenburg, T. Verbelen, and J. S. Rellermeyer, "A survey on distributed machine learning," *ACM Computing Surveys (CSUR)*, vol. 53, no. 2, pp. 1–33, 2020.

[30] A. Krizhevsky, I. Sutskever, and G. E. Hinton, "Imagenet classification with deep convolutional neural networks," *Advances in neural information processing systems*, vol. 25, 2012.

[31] R. Zaheer and H. Shaziya, "Gpu-based empirical evaluation of activation functions in convolutional neural networks," in *2018 2nd International*

Authorized licensed use limited to: DELHI TECHNICAL UNIV. Downloaded on June 15,2022 at 11:18:56 UTC from IEEE Xplore. Restrictions apply.

Conference on Inventive Systems and Control (ICISC). IEEE, 2018, pp. 769–773.

[32] J. Zhang, B. Chen, X. Cheng, H. T. T. Binh, and S. Yu, "Poisongan: Generative poisoning attacks against federated learning in edge computing systems," *IEEE Internet of Things Journal*, vol. 8, no. 5, pp. 3310–3322, 2020.

[33] C. Zhu, W. R. Huang, H. Li, G. Taylor, C. Studer, and T. Goldstein, "Transferable clean-label poisoning attacks on deep neural nets," in *International Conference on Machine Learning*. PMLR, 2019, pp. 7614–7623.

[34] M. Mirza and S. Osindero, "Conditional generative adversarial nets," *arXiv preprint arXiv:1411.1784*, 2014.

[35] K. A. Sankararaman, S. De, Z. Xu, W. R. Huang, and T. Goldstein, "The impact of neural network overparameterization on gradient confusion and stochastic gradient descent," in *International conference on machine learning*. PMLR, 2020, pp. 8469–8479.

[36] X. Yuan, P. He, Q. Zhu, and X. Li, "Adversarial examples: Attacks and defenses for deep learning," *IEEE transactions on neural networks and learning systems*, vol. 30, no. 9, pp. 2805–2824, 2019.

[37] H. Wang, C. Qin, Y. Zhang, and Y. Fu, "Neural pruning via growing regularization," *arXiv preprint arXiv:2012.09243*, 2020.

[38] Y. LeCun, J. Denker, and S. Solla, "Optimal brain damage," *Advances in neural information processing systems*, vol. 2, 1989.

[39] S. Han, J. Pool, J. Tran, and W. Dally, "Learning both weights and connections for efficient neural network," *Advances in neural information processing systems*, vol. 28, 2015.

[40] J. Frankle and M. Carbin, "The lottery ticket hypothesis: Finding sparse, trainable neural networks," *arXiv preprint arXiv:1803.03635*, 2018.

[41] N. Srivastava, G. Hinton, A. Krizhevsky, I. Sutskever, and R. Salakhutdinov, "Dropout: a simple way to prevent neural networks from overfitting," *The journal of machine learning research*, vol. 15, no. 1, pp. 1929–1958, 2014.

[42] A. Krogh and J. Hertz, "A simple weight decay can improve generalization," *Advances in neural information processing systems*, vol. 4, 1991.

[43] R. Müller, S. Kornblith, and G. E. Hinton, "When does label smoothing help?" *Advances in neural information processing systems*, vol. 32, 2019.

[44] A. Paszke, S. Gross, F. Massa, A. Lerer, J. Bradbury, G. Chanan, T. Killeen, Z. Lin, N. Gimelshein, L. Antiga *et al.*, "Pytorch: An imperative style, high-performance deep learning library," *Advances in neural information processing systems*, vol. 32, 2019.

[45] D. P. Kingma and J. Ba, "Adam: A method for stochastic optimization," *arXiv preprint arXiv:1412.6980*, 2014.

Authorized licensed use limited to: DELHI TECHNICAL UNIV. Downloaded on June 15,2022 at 11:18:56 UTC from IEEE Xplore. Restrictions apply.

Proceedings of the Sixth International Conference on Trends in Electronics and Informatics (ICOEI 2022)
IEEE Xplore Part Number: CFP22J32-ART; ISBN: 978-1-6654-8328-5

Driver Drowsiness Detection System using Convolutional Neural Network

1st Mohammad Elham Walizad
Department of Software Engineering
Delhi Technological University
New Delhi, India
md.elham_2k18se080@dtu.ac.in

2nd Mehreen Hurroo
Department of Software Engineering)
Delhi Technological University)
New Delhi, India
mehreenhurroo_2k18se081@dtu.ac.in

3rd Divyashikha Sethia
Department of Software Engineering
Delhi Technological University
New Delhi, India
divyashikhasethia@dtu.ac.in

2022 6th International Conference on Trends in Electronics and Informatics (ICOEI) | 978-1-6654-8328-5/22/$31.00 ©2022 IEEE | DOI: 10.1109/ICOEI53556.2022.9777182

***Abstract*—Driver drowsiness is a condition that impairs judgment. Many accidents have occurred due to sleepy drivers behind the wheel. Multiple studies require drivers to wear health sensors to gather useful physiological health data. This technique is intrusive and makes the driver feel uneasy while driving. Also, this method is less successful since the sensors must remain in specific positions for reliable results. Accurate detection of tiredness and prevention of a potential mishap on the road is a tedious and practically impossible process. Hence this paper proposes to build a driver sleepiness detection system utilizing a behavioral approach to warn drivers before an accident occurs. This system can help reduce traffic accidents and save the lives of drivers. This work trains a Convolutional Neural Network and uses it to assess whether the driver's eyes are closed or open. The dataset comprises images acquired from a large portion of the MRL eye dataset. Before training, the proposed model processes the images in the dataset using computer vision techniques such as edge detection, grayscale conversion, and dilation. The Google MediaPipe Face mesh model is then used to track facial landmarks from video frames in real-time. The eyes region is retrieved, processed, and fed to the proposed trained model for prediction. The model detects drowsiness and alarms the driver to take safety measures. This paper proposes and implements a CNN model that achieves an overall accuracy of 95%, outperforming all previous studies on drowsiness detection.**

***Index Terms*—Convolutional Neural Network, Drowsy, Mediapipe, MRL eye dataset;**

I. Introduction

Every day, hundreds of individuals fall prey to vehicle accidents. Some are wounded and disabled, while others die, leaving their loved ones behind to mourn their loss. Road accidents have indeed become a significant problem in the world. The National Highway Traffic Safety Administration implies that drowsy driving is responsible for 100,000 police-reported crashes each year, resulting in more than 1,550 deaths, 71,000 injuries, and $12.5 billion in monetary damages [1]. In a study conducted by the transport research wing of the ministry of road transport and Highway, 151,113 persons lost their lives in 480,652 road crashes across India in 2019; this makes 414 per day or 17 per hour [2]. It is important to note that the leading causes of every accident or crash may be humans, insufficient road infrastructure, or vehicles. Human-related errors are predominant among these critical factors, and they are as follows: checking phones and texts, driving when drunk, inadequate sleep, shifting time zones, and being under medication. Drivers lose control of their car whenever these situations arise and consequently risk an accident. As per a study conducted at AIIMS Neurology India [18], about 20% of road fatalities victims had a sleep disorder, and over 23% of truckers are overly tired. Owing to a driver shortage on the market, rental businesses overworked truck drivers with inflexible work schedules, increasing fatigue and lowering rest periods. These drowsy individuals are more likely to face fatal road accidents.

As well stipulated by Desiderius Erasmus, "Prevention is better than cure," traffic safety is critical and must be tackled at the earliest to prevent further road accidents. As a solution, this paper proposes a Convolutional Neural Network-based intelligent driver sleepiness detection system. Three approaches are usually applied to detect driver's fatigue. They are the vehicular-based approach, the Physiological approach, and the Behavioural approach. A vehicular-based system scrutinizes factors such as lane position, lane deviation angle, speed of and distance between vehicles, force applied on the pedal, and steering wheel angular [3], [11]. The physiological-based approach relies on health-related factors such as heartbeat, blood pressure, and temperature. Lastly, the behavioral system uses equipment to detect movement of the eyes, mouth, frequency of blinks, and other indicators. It is the most extensively used and highly accepted method for detecting sleepiness.

This paper uses the images from a considerable portion of the MRL dataset from Kaggle [19], [20]. They are processed and analyzed for sleepiness detection using Computer vision techniques. The proposed model trains a Convolutional Neural Network to build a real-time prediction model. The base model proposed by Suresh et al. [16] trains a CNN model on the same dataset and utilizes the Haar cascades algorithm to detect eye blinking. It achieves an accuracy of 86 percent. The primary contribution of this paper is to improve the accuracy for a better drowsiness prediction model. The proposed model conducts noise removal, Canny edge detection, and dilation of the images in the pre-processing step before training the CNN model. This work also uses the Google Media Pipe library's face-mesh model instead of Haar cascade to track the face and eye landmarks over all the continuous frames in real-time. In this context, the model extracts the eye's region of interest and processes it using the OpenCV python library. The processed

Authorized licensed use limited to: DELHI TECHNICAL UNIV. Downloaded on June 03,2022 at 06:32:55 UTC from IEEE Xplore. Restrictions apply.

images are input to the proposed trained CNN model. It detects critical features of the eyes and predicts whether or not the subject is sleeping. The proposed model monitors closed eye frequency and sets a score. When the frequency exceeds the score, an alarm is sound to wake the driver.

The rest of the paper is structured as follows: Section 2 contains the literature review. Section 3 elaborates on our overall system proposal and explains the processes involved. Section 4 discusses the experimental outcomes. Finally, section 5 summarises the article with a conclusion and future work.

II. Literature Review

In [4], the authors have merged two different systems, each using different approaches in one robust integrated system. They have applied a behavioral technique in the first one. A face landmark algorithm detected facial features like the eye, mouth, and nose. Coordinates on each region of the face helped trace those features. Then, the Euclidean distance method used the coordinates on the eye region to get the eyelid segment. Whenever the EAR was less than 0.25 and number frames more than 30, the system activated a voice speaker to awaken the driver, and at the same time, it sent an emergency mail to an authorized person. The second approach was vehicular-based, where they used a crash sensor connected to an IoT module to detect impacts of collision and generate information on the driver's location. These data were saved in a database and retrieved when the driver met an accident. The nearest clinics or an authorized person received an emergency message along with the information of the collision detection system. The recipients then tool the necessary steps to handle the situation.

The authors in [5] focused on the health-related aspects of driver drowsiness. They used a heartbeat sensor to monitor the heart's rhythms, a temperature sensor to determine the level of moisture and the climate condition in the car, and an alcohol sensor to detect if a driver has consumed alcohol. When the camera connected to Raspberry Pi detected closure of the eyes for longer than 5 seconds, a buzzer was turned on. The system sent data from the sensors and the driver's location to a colleague. A speed limiter is integrated into the system to forcefully decrease the driver's speed in emergencies.

The authors of [14] employed the Haar Cascade approach in conjunction with a mean shift to determine the peak or center of gravity of data distribution, OpenCV's Hough circle to locate pupils, and Canny edge detection to select the picture boundary. These approaches significantly enhance system performance. The system also incorporated a carbon dioxide sensor chip in the design and voice recognition technology that used the speech to text, allowing the driver to play music or call someone.

Some researchers have also created mobile applications since smartphones are more convenient, less complicated, and less expensive. The authors in [6] developed a driver sleepiness detection application for Android. Before driving, the driver did a physiological analysis by placing his finger on the camera's surface. The system analyzed the bloodstream beneath the skin, and the inbuilt app calculated the average of the beats per minute in just 14 seconds. To know whether the driver is potentially drowsy, the authors determined a threshold. A pulse rate of fewer than 80 beats per minute suggested that the driver is inebriated. In contrast, more than 100 beats per minute heart rate indicated that the motorist had just completed a vigorous activity. Implementation of facial analysis required the use of Google FACE API. It recognized face traits and followed landmarks. Authors employed smile detection instead of yawning detection because the Google API does not acknowledge yawning. The output was drowsy if the driver yawned twice in 10 seconds. The application also had an emergency button to call someone in a crash. The authors compared the physiological result, the behavioral method, and the physiological and behavioral approaches. The accuracy rose to 93.3 percent when using both approaches, compared to 88.5 percent for only the physiological method.

Warwick et al. [10] used a bio harness three sensors, a wearable biosensor, to collect driver physiological data such as accelerometers, activity, heart rate, posture, and breathing rate. The driver delivered the data to a mobile application by waving the sensor close to his chest. A filtering algorithm was applied to the data to reduce noise in muscle movement or other interference. FFT transforms precompiled pulse heart and respiration frequency-time information to their frequency response. The data obtained was then classified into 'drowsy' or 'awake' states using a neural network classification method.

Riztiane et al. [13] created an Android-based application that captured the driver's face and removed the region of interest, the eyes, in the case of driver sleepiness detection. A threshold was specified to determine the darkest area of the picture (pupil). When the eyes are closed, the value dropped from 5 to 0, allowing for speedier drowsiness detection. When the driver blinks for more than 0.6 seconds, the system checks the heart rate value. A driver used an Android wear OS. It kept track of the heartbeat and provided pulse data to the mobile application. Three states, namely alert, sleepy, and sleeping, were set to identify the condition based on heart rate value. The authors tested the system successfully by adjusting the distance and positioning the camera's angle from the driver. The system collected the average heartbeat in various situations to calculate the percentage at which the heart rate lowers from each state. The optimal angle is between 30 and 60 degrees, with a distance of 20 to 50 centimeters perpendicular to the face, and the decrease percentage between alert and sleepy conditions is 20

Using the Morphological face recognition idea and the FLANN (Fast Library for Approximate Nearest Neighbor) method, [12] developed a system that recognizes faces and eyes. A buzzer warns the driver when the eyes are not open for an extended period. If the latter still does not respond, the system can halt the vehicle.

Researchers have executed the drowsiness detection system using various strategies. Sensors, mobile applications, and hybrid techniques have all been employed by some. While others solely base their studies on behavioral analysis, [7]

Authorized licensed use limited to: DELHI TECHNICAL UNIV. Downloaded on June 03,2022 at 06:32:55 UTC from IEEE Xplore. Restrictions apply.

developed a method for detecting the eyes based on a histogram of directed gradient characteristics. The performance of HOG against skin color, light, and scale variations justifies its use. The distribution of intensity gradients determines the parts of a picture. The feature vectors acquired are sent into a feed-forward back propagation neural network, which classifies them and assigns a 1 to all open eyes and a 0 to all bleary eyes. It is worth noting that the authors compared the performance of the NN classifier with SVM. On a vast dataset of 3600 samples, NN provides an accuracy of 94.2% and SVM,94.7%. Perclos, the eye closure duration, and the percentage of overhead (PEROH) were all computed after categorization. To determine alert or not, fuzzy logic combines these three metrics. The if-THEN RULES create the fuzzy expert system.

Deep learning model compression models were presented in [9] to address run-time problems, decrease complexity, and save money. Their research focuses on condensing a large baseline model into a small, deployable model for an embedded board. There were three models: baseline-4, baseline-2, and compressed-2 models. The authors chose faster RCNN with VGG-16 and AlexNetarchitectures as benchmarks for comparison analysis. The overall accuracy was 89.5%.

In [11], Hussein et al. utilized the Viola-Jones approach to identify the facial area from a camera picture. The authors discovered two techniques for detecting the eye region: an appearance-based method and a feature-based process. Their first model used eight Fourier coefficients, the second model five Fourier coefficients and five texture features, the third model five wavelet coefficients and five texture features, and the fourth model used method three coupled with identified feature-based features such as circularity and black ratio. All models employed SVM, with model 4 achieving the most remarkable accuracy of 91.3 percent.

In [15], the Raspberry Pi Camera and raspberry Pi module, and the Haar cascade classifier determined the amount of sleepiness in drivers. The authors used the frequency of head tilting and eye blinking to detect whether a diver was sleepy. 99.59 percent was the accuracy achieved after testing on ten subjects.

In [16], the authors have employed the viola-jones technique to detect the face and eye region. They trained a convolutional neural network with images from the MRL eye dataset from Kaggle [19], [20]. An alarm turns on when the system detects drowsiness in a continuous frame. They achieved an accuracy of 86.05%. This paper improves the accuracy score for the drowsiness detection using the MRL eye dataset from Kaggle [19].

For facial analysis and tracking down facial locations, Gupta et al. [17] have used the Histogram Oriented Gradient feature descriptor. First, the machine learning model, Support Vector Machine, determines whether the item in front of the camera is a face. The system will calculate the Eye Aspect Ratio and Mouth Aspect Ratio for a certain number of frames. It is worth noting that they have also considered the number of hours a person has been driving, and the threshold values for the eyes and mouth are adjusted correspondingly. The system resets and executes again to match the new driver's data whenever a new face is detected. The accuracy achieved was 90%.

Hashmi et al. [21] used a camera module to gather streaming data continually. The camera transfers this data to a Raspberry Pi board, which is processed to yield the appropriate parameters like facial points with Haar cascade and compute the eye aspect ratio. If it is smaller than the threshold set, the system triggers an alarm to inform the driver. The work by [22] suggested combining the Viola-Jones approach, Histogram equalization, Canny Edge detection, the Circular Hough Transform (CHT), and the percentage of eyelid closure (PERCLOS) technique. With 50 samples, this suggested method obtained 92.5 percent accuracy in detecting eyes open photos and 86.65 percent accuracy in detecting eyes close images. In real-time video processing, it obtained 90 percent accuracy during the day and 86 percent accuracy at night.

Systems which use a vehicular approach are non-invasive and give almost exact findings. However, the shape of the road can be problematic and might occasionally activate the alarm system unnecessarily. The driver's driving style must be learned and modeled for the system to be efficient. Micro sleeping, which is most common on straight roadways, is undetectable. Works that employ IoT modules and sensors provide the most precise drowsiness findings. However, it necessitates the installation of numerous electrodes on the head, chest, and face, which is inconvenient and uncomfortable for a driver. Users must properly position the devices to get accurate results. Many researchers also use face detection algorithms in the behavioral approach. These algorithms are OpenCV Haar Cascade, Dlib HOG, and OpenCV deep learning. This method of detecting drowsiness may be affected by the position of the face, day and night time, and whether the user is wearing glasses or not.

III. Proposed system

The goal of this paper is to design a successful Convolutional Neural Network classification model. It must properly recognize the state of the eye and promptly declare whether the driver is drowsy or alert. Figure 1 depicts a high-level operating schema of the system. The proposed method performs data processing on the images of the MRL eye dataset from Kaggle [19]. It extracts features and trains a CNN model for classification. The model is evaluated and used to predict drowsiness from real-time video frames. At this stage, we use the Mediapipe framework to extract the eye area and input it into our trained CNN model. The trained CNN model removes and predicts the ocular characteristics. Finally, the system computes the score to determine whether or not the person is sleepy. An alarm is activated if the individual is detected to be asleep. The five stages involved in the suggested model are:

1) Dataset Description
2) Data pre-processing
3) Feature Extraction
4) CNN model

Authorized licensed use limited to: DELHI TECHNICAL UNIV. Downloaded on June 03,2022 at 06:32:55 UTC from IEEE Xplore. Restrictions apply.

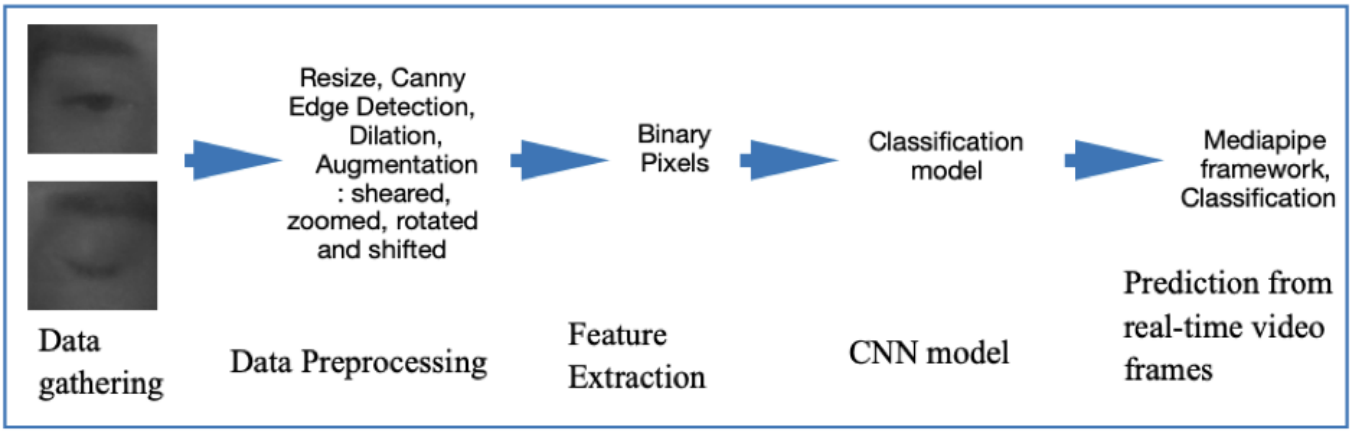

Fig. 1. Proposed System

5) Classifying and Predicting from video frames

A. Dataset Description

This paper uses an open-sourced dataset of 48000 eye images from the MRL eye dataset from Kaggle [19]. These images originate from a substantial component of the MRL eye dataset, having 84989 eye pictures [20]. The collection from Kaggle comprises low and high-quality infrared photos acquired in various lighting circumstances and multiple instruments. It involves 37 participants, 33 males, and four females. Some are wearing glasses, while others are not. The dataset has two states: closed and opened eyes. The images in the dataset are in the ratio of 70:20:10 for training, testing, and validation.

B. Data pre Processing

- **Image Resize**

The images are initially of varying sizes. They must be resized to a particular dimension of 100 by 100 pixels for consistency.

- **Canny Edge Detection**

Canny Edge Detection is a well-known approach for identifying borders of objects and areas in images. We may learn about an image's internal frame by inspecting its edges. John F. Canny created this technique in 1986. His technique is still helpful in various computer vision applications today. The images in our dataset are in grayscale. The two-color channels present in the white and black images have pixel values ranging from 0 to 255. However, to detect edges, the colorspace information is not required. Therefore, we maintain the images as grayscale only. The first step is to blur the images with a 3x3 Gaussian filter. Blurring evens out the intensity variations around the edges, making it simpler to spot the image's prominent edge structure. The photos will be free of noise as a result of this. Moreover, this is an essential step because edge detection is prone to noise. The second step determines the intensity gradient by applying a Sobel kernel horizontally(Gx) and vertically (Gy) across the images. Equations (1) and (2) show the kernels used in x-direction and y-direction for Sobel Edge Detection. In order to compute the estimates of the derivatives, these two kernels convolve with the original picture. Positive and negative coefficients present in the kernels imply that the final picture will have positive and negative values. The gradient approximations supplied by Gx and Gy are combined in (3) to obtain the gradient magnitude at each pixel in the picture. Equation 4 computes the gradient's direction.

Following noise reduction and calculation of the intensity gradient, we move to a phase that discards undesired pixels. This phase compares the value of each pixel in the image. If the current pixel's gradient magnitude is more significant than its neighbors, it is left untouched. Else, it is assigned the value of zero.

The last phase of Canny Edge Detection determines whether edges are indeed edges or not. By comparing the gradient magnitude to two thresholds values set, one higher than the other, edges and non-edges are detectable. If the gradient value falls within these two threshold values or exceeds the more significant threshold value, its corresponding pixels are edges. However, the pixels are omitted from the final edge map when the gradient magnitude value is less than the smaller threshold value. Cv.Canny() is the function used in OpenCV to determine edges. It combines all of the above techniques. It takes five parameters. The first one is the image, second and third are the minimum and maximum threshold values. In the third parameter, we put the size of the kernel used for Sobel edge detection. By default, it is 3. The last parameter is by default false and uses equation (3) to calculate the edge gradient.

$$Gx = \begin{bmatrix} -1 & 0 & 1 \\ -2 & 0 & 2 \\ -1 & 0 & 1 \end{bmatrix} \tag{1}$$

$$Gy = \begin{bmatrix} 1 & 2 & 1 \\ 0 & 0 & 0 \\ -1 & -2 & -1 \end{bmatrix} \tag{2}$$

Authorized licensed use limited to: DELHI TECHNICAL UNIV. Downloaded on June 03,2022 at 06:32:55 UTC from IEEE Xplore. Restrictions apply.

$$EdgeGradient(G) = |Gx| + |Gy| \tag{3}$$

$$\theta = \tan^{-1}\left(\frac{Gx}{Gy}\right) \tag{4}$$

- **Dilation**

The dilation process dilates the edges of the images. It augments the region in the white of the images.

- **Image Augmentation**

This technique creates new versions of existing images. This work utilizes the Keras ImageDataGenerator function. Distortions, vertical and horizontal flips, rotations, scaling, blurring, and noise are all possible augmentation techniques. Our training data undergoes rescaling of 1./255. Thoe model also rotates to a scale of 10 and shifts to 0.1 both horizontally and vertically. It sets the shear parameter to 0.1 and the zooming magnitude to 0.2. The test and validation images undergoes a rescale of 1. /255. These images are input to the convolution neural network.

C. Feature Extraction

The most crucial step of processing images is to extract critical features. Photos in the dataset use much space as they include many data. Feature extraction assists us in solving this challenge by automatically decreasing the data after the model has extracted the essential characteristics. It also helps to keep the classifier's accuracy and lowers its complexity. In our situation, the system discovered the binary pixels of the photographs to be significant. By resizing the images to 100 by 100 pixels, the model can get enough characteristics to categorize the eye conditions effectively. We have 10000 features generated by multiplying 100 by 100 pixels.

D. System Architecture

A Convolutional neural network is helpful to recognize patterns. It uses a concept similar to multilayer perceptron, optimized for low processing needs. Like any other neural network, CNN comprises three layers: Input, Output, and Hidden. It is good to note that the hidden layer is formed by several convolutional, fully connected, and normalizing layers. The pooling and convolutional layers consolidate features acquired in preceding layers while also receding the size of these layers by making the most of a sensory domain. Dropout layers help avert overfitting, and our CNN model includes it too.

- **Proposed CNN model**

The model proposed model has many layers, as shown in Fig. 2. The first convolution layer has an input shape of 100x100x1. Thus images of 100 by 100 pixels with the grayscale color format are loaded. Our architecture has three convolutional layers. Each of which is succeeded by a pooling layer. The last pooling layer is, in turn, followed by a flatten layer and a dropout layer positioned between two ultimately linked hidden layers.

1) *The Convolutional Layers*: The model has three levels of convolution, each followed by pooling. Because images get into the model through the first Convolution layer, we can refer to it as the input layer. The first and second convolutional layers comprise 32 filters, having a filter shape of three by three and a default stride dimension of one. However, the last layer, in turn, employs 64 filters, with a filter dimension of 3x3 and a stride value of one. The convolution layers compute the dot product of the image pixel and the filter values. This stage captures essential information from the input picture for subsequent processing.
2) *The Pooling Layers:* The model adds a pooling layer per convolutional layer. Performing max-pooling operation was successful with a two by two kernel shape. It works by taking the maximum 2x2 area in the input's deep frame.
3) *The Dropout Layer*: Linking the output layer and the concealed layer was a dropout layer. In complex and sophisticated models, we utilize dropout layers to reduce overfitting. It boosts the performance of neural networks in supervised learning applications. Its value might range between 0 and 1. Our model provided the best results when the ratio was 0.3. This value signifies that the learning model discards 30% of the nodes to minimize overfitting.
4) *The Hidden Layers:* Two hidden, fully connected layers were there in the model. The first layer consisted of 128 nodes, whereas the second layer had two nodes as the output layer. The model performed classification across two classes.
5) *The Activation Functions:* Rectified Linear Unit is the activation function utilized in the convolution layers. For negative numbers, the ReLu function yields a value of 0, and positive values return their value only. The model also applied the reLu activation function in the first wholly linked hidden layer and Softmax in the last layer. It gives distributed probability for each class.
6) *The Loss function and Metric:* The loss function and metrics are critical for assessing and interpreting the model's performance. We set their values at the time of compilation. The proposed model's loss function is the categorical cross-entropy which computes the cross-entropy loss between the observed and expected output. As for the model's metric is accuracy, the fraction of the projected result that corresponds to the actual result.
7) *The Optimizer:* The model's basic optimizer is Adam. Adam takes the most delicate traits of algorithms like AdaGrad to devise an optimization process that tackles noise issues with sparse gradients. Adam is uncomplicated to set up and works well for most situations. Fig. 2 summarises the implemented model.

E. Classifying and predicting the final output:

In real-time, a web camera captures the eye of the driver. Google Mediapipe detects the eye from each frame in the

Authorized licensed use limited to: DELHI TECHNICAL UNIV. Downloaded on June 03,2022 at 06:32:55 UTC from IEEE Xplore. Restrictions apply.

```
Model: "sequential_1"
_________________________________________________________________
 Layer (type)                Output Shape              Param #
=================================================================
 conv2d_3 (Conv2D)           (None, 98, 98, 32)        320

 max_pooling2d_3 (MaxPooling  (None, 49, 49, 32)       0
 2D)

 conv2d_4 (Conv2D)           (None, 47, 47, 32)        9248

 max_pooling2d_4 (MaxPooling  (None, 23, 23, 32)       0
 2D)

 conv2d_5 (Conv2D)           (None, 21, 21, 64)        18496

 max_pooling2d_5 (MaxPooling  (None, 10, 10, 64)       0
 2D)

 flatten_1 (Flatten)         (None, 6400)              0

 dense_2 (Dense)             (None, 128)               819328

 dropout_1 (Dropout)         (None, 128)               0

 dense_3 (Dense)             (None, 2)                 258

=================================================================
Total params: 847,650
Trainable params: 847,650
Non-trainable params: 0
_________________________________________________________________
```

Fig. 2. Model Summary

video stream and sends it to our trained CNN model for prediction.

1) Mediapipe framework:
   Google introduced MediaPipe in the year 2019. It is a framework for developing cross-platform multimodal applied machine learning pipelines, and it is fast, robust, and reliable. Google MediaPipe's face detection model bases itself on BlazeFace, which is light, GPU- friendly, and performs well. It is capable of determining more characteristics than Dlib's model. That is indeed 468 3-dimensional points on any frame. It works by detecting the face and tracking the landmarks on the face. This paper uses MediaPipe to extract eye key points that MediaPipe already provides by customizing source code. It tracks down the eyes in real-time video streams.
2) Classifications:
   With the critical points obtained from Mediapipe, we draw a bounding box on the region of the eye. This region is cropped and sent for processing, feature extraction, and classification. Our trained CNN model predicts whether eyes are closed or open. We note the number of times eyes were closed in each frame. If the score exceeds 15, the motorist is considered sleepy, and an alarm is triggered to wake the motorist. Figure 3 is a flowchart that shows the outline used in the prediction part.

IV. RESULTS AND DISCUSSIONS

The model trains on a considerable portion of the MRL eye dataset obtained from Kaggle. We evaluate the model for each of the states present in the dataset. We have used a total of

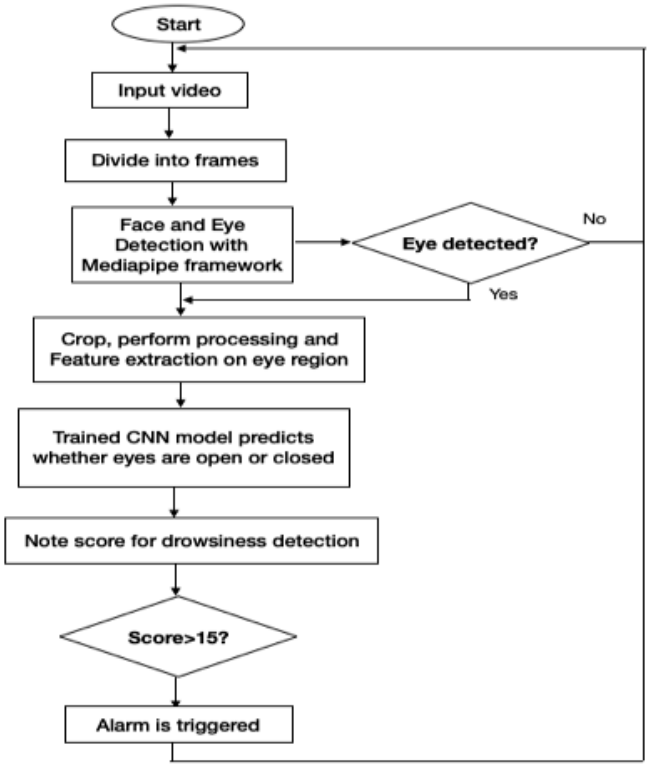

Fig. 3. Pseudocode of algorithm used in the prediction part

48000 images. The images in the dataset are in the ratio of 70:20:10 for training, testing, and validation. An image can be either closed or open eyes.

When the model predicts, it gives a multi-dimensional array of values. The inner arrays belong to the categories (closed or open) present in the model. Any category with the most significant number will be the predicted category. The CNN model gave an accuracy of 95%. Table 1 illustrates the accuracy, recall, and F-measures for each category. Table 2 also depicts the confusion Matrix.

TABLE I
ACCURACY OF THE MODEL

	precision	recall	f1-score	support
Closed_eyes	0.92	0.98	0.95	4800
Open_eyes	0.98	0.92	0.94	4800
accuracy			0.95	9600
macro avg	0.95	0.95	0.95	9600
weighted avg	0.95	0.95	0.95	9600

TABLE II
CONFUSION MATRIX

n=9600	Predicted: Closed Eyes	Predicted: Open Eyes	
Actual: Closed Eyes	4691	109	4800
Actual: Open Eyes	408	4392	4800

Authorized licensed use limited to: DELHI TECHNICAL UNIV. Downloaded on June 03,2022 at 06:32:55 UTC from IEEE Xplore. Restrictions apply.

A. Comparative Study

The work depicted in [16] is the baseline for assessing the performance of our technique. The model produced in this study minimizes the difficulties indicated in [16]—we address deficiencies to the best of our technological skills. Table 3 reveals a quick comparison of the performance of both models. An examination of the study published by authors Suresh et al. [16] used the same MRL dataset from Kaggle and trained a CNN model. Computer vision techniques performed were only limited to grayscale conversion and image resize. Augmentation operations were also not performed on the dataset. In the prediction part, Haar-cascades with Adaboost training extract the region of interest and send it to the model for classification. Our proposed study caters explicitly to these matters such that it aims to achieve better accuracy than the one in [16]. We performed noise removal and Canny edge detection followed by dilation on the images to make the system more robust. The degree of randomness is increased by rescaling, shearing, rotating, and zooming the data. Our CNN model achieved a better accuracy value. The Mediapipe framework is preferred over Haar Cascades to extract the eye area in the prediction stage. The Haar cascade tends to be slower and is prone to predicting false positives.

TABLE III
PERFORMANCE COMPARISON

Performance metrics	**Model Performance(%)**	
	Proposed model	Suresh et al. [16]
Accuracy	95	86

V. CONCLUSION & FUTURE WORK

This research provides a Convolution Neural Network model equipped with thorough architecture, layout, and execution for drowsiness detection based on the eye condition. Images have undergone image resize and augmentation, Canny edge detection, noise removal, and dilation before training the model. The Mediapipe framework extracts the eye region in real-time for prediction. An alarm is sound when the system detects drowsiness in 15 continuous frames. CNN is quite complex and often uses the metric of accuracy to evaluate performance. Our CNN model attained an accuracy of 95 percent. This accuracy score improves the base model [16], having an accuracy of only 86 percent.

In terms of the project's future scope, the Internet of Things (IoT) components like Arduino-Uno, along with sensors such as alcohol and pulse, can be incorporated to get the driver's health-related factors. A model based on the ResNet architecture can be worked upon to examine the capacities of convolutional networks and more profound layers to create a more refined and more robust-performing prototype. The implemented model can also be experimented on massive datasets with more eye condition samples to show model generalizability.

REFERENCES

[1] American Trauma Society, National Trauma Awareness Month 2015, https://www.amtrauma.org/page/NTAM2015?&hhsearchterms=%22drowsy+and+statistics%22
[2] Megha.Sood, India had most deaths in road accidents in, 2019. Hindustan Times, https://www.hindustantimes.- com/mumbai-news/ india-had-most-deaths-in-road-accidents-in-2019-report/story-pikRXxsS4hpt- NVvf6J2g9O.html
[3] G. Zhenhai, L. DinhDat, H. Hongyu, Y. Ziwen and W. Xinyu, "Driver Drowsiness Detection Based on Time Series Analysis of Steering Wheel Angular Velocity," 2017 9th International Conference on Measuring Technolo- gy and Mechatronics Automation (ICMTMA), 2017, pp. 99-101, doi: 10.1109/ICMTMA.2017.0031
[4] Anil Kumar Biswal, Debabrata Singh, Binod Kumar Pattanayak, Debabrata Samanta, Ming-Hour Yang, "IoT- Based Smart Alert System for Drowsy Driver Detection", Wireless Communications and Mobile Computing, vol. 2021, Article ID 6627217, 13 pages, 2021.
[5] Sathish Kumar. R; Nivedha. K; Anitha. K; Jayaprakash. D. "IOT Based Driver Drowsiness Detection and Health Monitoring System". European Journal of Molecular & Clinical Medicine, 7, 9, 2020, 1581-1590. doi: https://doi.org10.31838/ejmcm.07.09.173.
[6] Rajkumarsingh, B., & Totah, D.. (2021). Drowsiness Detection using Android Application and Mobile Vision Face API. R&D Journal, 37, 26-34
[7] O. Rigane, K. Abbes, C. Abdelmoula and M. Masmoudi, "A Fuzzy Based Method for Driver Drowsiness De- tection," 2017 IEEE/ACS 14th International Conference on Computer Systems and Applications (AICCSA), 2017, pp. 143-147, doi: 10.1109/AICCSA.2017.131
[8] Mainak Das, "Sleep testing can reduce sleep disor- der related road accidents in India", 2021. Available: https://auto.hindustantimes.com/auto/news/sleep-testing-can-reduce- sleep-disorder-related-road-accidents-in-india-41620010214153.html.
[9] B. Reddy, Y. Kim, S. Yun, C. Seo and J. Jang, "Real-Time Driver Drowsiness Detection for Embedded System Using Model Compression of Deep Neural Networks," 2017 IEEE Conference on Computer Vision and Pattern Recognition Workshops (CVPRW), 2017, pp. 438-445, doi: 10.1109/CVPRW.2017.59.
[10] B. Warwick, N. Symons, X. Chen and K. Xiong, "Detecting Driver Drowsiness Using Wireless Wearables," 2015 IEEE 12th International Conference on Mobile Ad Hoc and Sensor Systems, 2015, pp. 585-588, doi: 10.1109/MASS.2015.22.
[11] W. Hussein and M. S. A. El-Seoud, "Improved Driver Drowsiness Detection Model Using Relevant Eye Im- age's Features," 2017 European Conference on Electrical Engineering and Computer Science (EECS), 2017, pp. 261-265, doi: 10.1109/EECS.2017.55.
[12] Sasikala, R., S. Suresh, J. Chandramohan and M. Valanrajkumar. "Driver Drowsiness Detection System using Image Processing Technique by the Human Visual System." (2018).
[13] A. Riztiane, D. H. Hareva, D. Stefani and S. Lukas, "Driver Drowsiness Detection Using Visual Information On Android Device," 2017 International Conference on Soft Computing, Intelligent System and Information Technology (ICSIIT), 2017, pp. 283-287, doi: 10.1109/ICSIIT.2017.20.
[14] Jang, S.-W.; Ahn, B. Implementation of Detection System for Drowsy Driving Prevention Using Image Recognition and IoT. Sustainability 2020, 12, 3037. https://doi.org/10.3390/su12073037
[15] O. Khunpisuth, T. Chotchinasri, V. Koschakosai and N. Hnoohom, "Driver Drowsiness Detection Using Eye- Closeness Detection," 2016 12th International Conference on Signal-Image Technology & Internet-Based Systems (SITIS), 2016, pp. 661-668, doi: 10.1109/SITIS.2016.110.
[16] Y. Suresh, R. Khandelwal, M. Nikitha, M. Fayaz and V. Soudhri, "Driver Drowsiness Detection using Deep Learning," 2021 2nd International Conference on Smart Electronics and Communication (ICOSEC), 2021, pp. 1526-1531, doi: 10.1109/ICOSEC51865.2021.9591957.
[17] "Gupta, I., Garg, N., Aggarwal, A., Nepalia, N., & Verma, B. (2018, August). Real-time driver's drowsiness monitoring based on dynamically varying threshold. In 2018 Eleventh International Conference on Contemporary Computing (IC3) (pp. 1-6). IEEE"
[18] Mainak Das, "Sleep testing can reduce sleep disor- der related road accidents in India", 2021. Available: https://auto.hindustantimes.com/

Authorized licensed use limited to: DELHI TECHNICAL UNIV. Downloaded on June 03,2022 at 06:32:55 UTC from IEEE Xplore. Restrictions apply.

auto/news/sleep-testing-can-reduce- sleep-disorder-related-road-accidents-in-india-41620010214153.html-[Accessed: 24-Jun-2021]

[19] Kutay Kutlu, “Drowsiness Detection”, Version-2, 2021 [Online] Available: https://www.kaggle.com/kutaykutlu/drowsiness-detection [Accessed:20-Dec-2021].

[20] Radovan Fusek, “MRL eye dataset”. Available: http://mrl.cs.vsb.cz/eyedataset [Accessed: 20-Dec-2021].

[21] Hashmi, Md Farukh, N. Kusuma Priya, S. Surya Reddy, G. Vakula, and D. Usha. ”Drowsiness Detection System Using Raspberry Pi and OpenCV.” In International Conference on Mobile Computing and Sustainable Informatics, pp. 661-671. Springer, Cham, 2020.

[22] Lim, Teik Jin, Hung Yang Leong, Jia Yew Pang, and Mohd Rizon Mohamed Juhari. ”Eye Fatigue Algorithm for Driver Drowsiness Detection System.” In International Conference on Image Processing and Capsule Networks, pp. 638-652. Springer, Cham, 2020.

Authorized licensed use limited to: DELHI TECHNICAL UNIV. Downloaded on June 03,2022 at 06:32:55 UTC from IEEE Xplore. Restrictions apply.

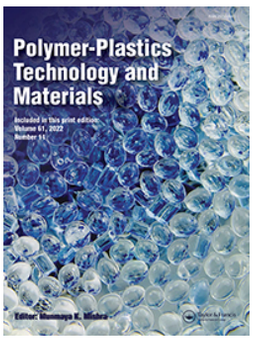

Polymer-Plastics Technology and Materials

ISSN: (Print) (Online) Journal homepage: https://www.tandfonline.com/loi/lpte21

Effect of post-treatment methods and nanoparticles on the conformation of silk fibroin and their impact on electrical properties

Reetu Yadav & Roli Purwar

To cite this article: Reetu Yadav & Roli Purwar (2022): Effect of post-treatment methods and nanoparticles on the conformation of silk fibroin and their impact on electrical properties, Polymer-Plastics Technology and Materials, DOI: 10.1080/25740881.2022.2089576

To link to this article: https://doi.org/10.1080/25740881.2022.2089576

Published online: 14 Jun 2022.

Submit your article to this journal

Article views: 5

View related articles

View Crossmark data

Full Terms & Conditions of access and use can be found at
https://www.tandfonline.com/action/journalInformation?journalCode=lpte21

POLYMER-PLASTICS TECHNOLOGY AND MATERIALS
https://doi.org/10.1080/25740881.2022.2089576

Taylor & Francis
Taylor & Francis Group

RESEARCH ARTICLE

Check for updates

Effect of post-treatment methods and nanoparticles on the conformation of silk fibroin and their impact on electrical properties

Reetu Yadav and Roli Purwar

Discipline of Polymer Science and Chemical Technology, Department of Applied Chemistry, Delhi Technological University, Delhi, India

ABSTRACT

This paper investigates the effect of different plasticizers (glycerol and dextrose), post-treatment methods, and metal oxide nanoparticles, i.e. zinc oxide and copper oxide on the structural properties of silk fibroin films and their effect on electrical properties, i.e. dielectric strength. Structural properties of the silk fibroin films have been evaluated using Fourier transform infrared spectroscopy and X-ray diffraction technique. It was found that plasticizers and post-treatment applied on the regenerated silk fibroin films have impacted the β-sheet conformation significantly. The dielectric strength of the silk fibroin films was measured using the parallel plate capacitor method and an interrelation with structural properties was observed. Nanoparticles have been introduced into the silk fibroin films as a progressive method to impart substantial effect on the dielectric strength of the silk fibroin films. However, an unexpected change in dielectric strength has been obtained. The mechanism behind the change in dielectric strength has been explored in this work.

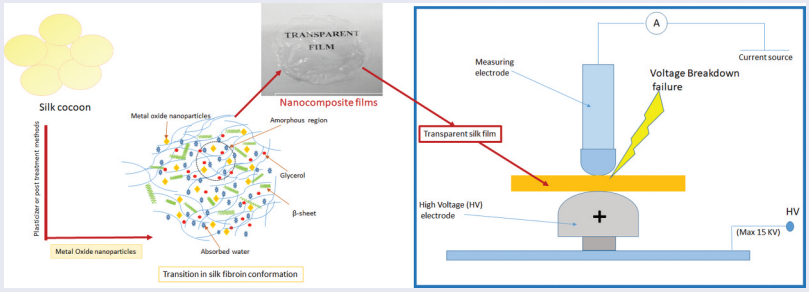

ARTICLE HISTORY
Received 7 December 2021
Revised 11 April 2022
Accepted 9 June 2022

KEYWORDS
Silk fibroin; nanocomposite; dielectric strength; zinc oxide; copper oxide

1. Introduction

The persistent increase in usage of polymer-based materials in abundant electronics applications prevailing for the demand of studying their electrical properties concerning their molecular structure.[1–3] The presence of a low concentration of free charges in the polymers classified them majorly as insulating material. To study the electrical performance of polymer, one of the key component properties to be explored is dielectric behavior[3–5] It involves dielectric strength, dielectric constant, dielectric loss, capacitance, impedance, and bulk resistance. Dielectric strength is found to be an intrinsic property of the material which dominates the design rules of dielectric material that involves dielectric thickness, energy density, molecular composition, and the processing method.[1] To increase the dielectric strength, dielectric constant, and energy density in a dielectric material, it is suggested to be converted in nano dimension either by changing the thickness of the dielectric material in the nanometer or by adding a nanofiller in polymers to fabricate a nanocomposite known as nanodielectrics. These alterations bring change in the molecular property of the material which in turn affects the dielectric behavior.[6–8]

The effort to build thin dielectric films cannot be always suitable for capacitor technology as thinner material exhibit more surface defects such as dimples, contamination, roughness, pits, wrinkles, and variable thickness which can lead to local plasma erosion could result in wide distribution of dielectric strength which affects the overall property of a dielectric.[9–11] The choice of dielectric material for high-performance capacitors involves minimal processing and excellent properties like optimum dielectric strength, lower dielectric loss, no harmful solvents, heat shrinkage, film-forming ability,

CONTACT Roli Purwar roli.purwar@dtu.ac.in Discipline of Polymer Science and Chemical Technology, Department of Applied Chemistry, Delhi Technological University, Delhi, India

© 2022 Taylor & Francis

and self-clearing capability.[12–15] Few commercial high-temperature films such as poly tetra fluoro ethylene (PTFE), polyetherimide (PEI), polyethylene naphthalate (PEN), fluorene polyester (FPE), and polyimide (PI) have these properties but are way expensive.[1,14,16,17]

Polymer used as dielectric material possesses a more complicated mechanism for dielectric strength due to its constituents, chemical structure, surface imperfection, interfaces, structure irregularities, crystallinity, crystal size, molecular motion, thermal, and electrical conductivity.[18] Dielectric breakdown due to degradation mechanism involves oxygen mitigation, water trees, and electrical trees occur during long voltage endurance.[18] Charge trap is one of the key elements to occur voltage breakdown in polymeric dielectric material as it can cause space charge accumulation by delaying the charge transportation which is one of the mechanisms that clench in polymeric materials. These charge traps are influenced by interfaces such as amorphous or intermediate phases which significantly affect the dielectric strength.[1,19] Many methods have been adopted to bring change in the dielectric strength of the polymer but adding inorganic nanoparticles into the polymer matrix is one of the generic methods to do that. As nanoparticles can alter the composite structure and properties which can prevent the space charge accumulation in the nanocomposite volume, thus increasing the dielectric strength.[20–22] Nanoparticles with low electrical conductivity and high thermal conductivity with better dispersion appear to be more desirable for the achievement of high dielectric strength in polymeric nanocomposite-based nanodielectrics. For better dispersion, a lower concentration of nanoparticles is required affecting the translational region of the nanoparticles which in turn affect the dielectric strength.[23] Incorporation of conductive nanoparticles like silver, palladium, zinc oxide, titanium dioxide, copper oxide, and other semiconductor particles in polymers has opted as an unconventional method because it forms conducting-insulating interfaces that act as electrical charge traps that delay the charge transport and obstruct the formation of conducting pathway in the nanocomposites.[24–31] However, it needs a careful inspection to understand up to which loading of these nanoparticles could give benefit to increment in dielectric strength rather than decreasing the surface resistivity and make nanocomposite more conductive.

Biomaterial is no wonder taking the place of conventional polymers in electronic devices due to its sustainability. Among so many biomaterials, silk fibroin is seeking the attention of researchers to be used in electronics applications.[32–34] Recently, silk fibroin has been used as dielectric material in many thin-film transistors due to its structure and properties like solution processability, flexibility, optical transparency, thermal stability, biodegradability, and biocompatibility.[35–38] Silk fibroin is composed of β-sheet crystalline domains and amorphous regions which are affected by many factors such as processing method, solvent, post-treatment, plasticizer, and ionic impurity. Moreover, its structural-molecular property affects the dielectric behavior significantly reported in the literature.[2,39] Dickerson et al. have reported that the dielectric strength of silk fibroin-based dielectric film is interrelated to the β-sheet crystals.[2] Thus, to bring the change in dielectric behavior of silk fibroin, we need to play with the β-sheet structure of the silk fibroins. Water has a significant effect on the structure of the silk fibroins as it induces β-sheet formation via helix–helix interactions. Amorphous regions of silk fibroin were plasticized via water molecules known as bound water that disrupts the intermolecular cohesive forces between silk fibroin chains, leading to an increase of steric hindrance between the chains which enhances the chain movements in amorphous regions, thus inducing β-sheet crystallization in silk fibroin.[40,41] The addition of plasticizer brings a similar effect as it is associated with moisture which affects the amorphous region of the silk fibroin.

In this work, silk fibroin films have been prepared using two different plasticizers such as dextrose and glycerol and two post-treatment methods have been opted for instance water annealing and coagulation process to bring the β-sheet structure formation in silk fibroin chains. The water annealing method is a safe post-treatment to bring conformational transition in silk fibroin chains from random coil to β-sheet structure as it does not change the physiochemical structure of silk fibroin.[42] Alcohol solvent is used in the coagulation process of silk fibroin films to impart change in the structure of silk fibroin films.[43]

The addition of conductive nanoparticles zinc oxide (n-type) and copper oxide (p-type), as they play a noteworthy role in dielectric strength, has been opted to fetch change in structure and dielectric properties of silk fibroin nanocomposite. Till now there is no such work has been reported that explores the dielectric behavior of silk fibroin films using conductive nanoparticles, i.e. ZnO and CuO. In this article, the mechanism behind the change in the dielectric strength of silk fibroin upon conformational transition has been explored.

2. Experimental

2.1. Materials

Silk fibroin (*Bombyx mori*) silkworm (multivoltine) were supplied from Central Sericultural Research and Training Institute, Mysore, India. Glycerol

(99.5 percentage purity) was supplied from Thermos Fisher Scientific India Pvt. Ltd. Dextrose was procured from Methanol (AR) and formic acid (AR) 98 percentage purity were obtained from Avontar performance materials India Ltd. Zinc oxide nanopowder (Type I) (Average particle size: 30 nm) and Copper oxide nanopowder (Average particle size: 40 nm) were supplied from Sisco Research Laboratories Pvt. Ltd. Milli-Q water was used in the coagulation process and water annealing process.

2.2. Fabrication of Silk fibroin/metal oxide nanocomposite films

Silk fibroin (SF) was degummed according to previously reported procedures.[44] The obtained silk fibroins were rinsed 3–4 times in hot water (2 liters) for 30 minutes and dried overnight in an oven at 70°C. Silk fibroin was then cut into small pieces and dissolved in formic acid solution at room temperature by continuous stirring for 3–4 hours. The final concentration of silk fibroin was kept at 10 wt. % (w/v) in the solution. Films were fabricated on a Petri dish (PET) through solvent casting in the desired thickness of 30 µm and films were dried overnight. Dried films immersed in 100% methanol for 4 hours followed by 80% methanol (24 hours) for coagulation process. The coagulated films were then kept for water annealing (15 mins). After that, films were stored in a refrigerator at 4°C.

In the case of nanocomposite films, metal oxide nanoparticles and plasticizers were added into the formic acid with different concentrations and then sonicated for more than 30 mins for complete dispersion then silk fibroin is added and stirred for 3–4 hours. And then, casting, drying, and post-treatment method has been opted. In Scheme 1, the degumming and fabrication process of the silk fibroin nanocomposite films has been presented. The thicknesses of films (30 µm, 50 µm, 70 µm, 100 µm, 200 µm) were measured by using the digital thickness Gauge micrometer of MGW Precision OMC25 (LC 0.001 mm). A detailed description of the concentration of plasticizers, metal oxide nanoparticles, applied post-treatment method, and involved time duration has been mentioned in Table 1 with the abbreviation of the samples.

2.3. Characterization of silk fibroin/metal oxide nanocomposite films

The absorption spectra of silk fibroin films were obtained through Fourier transform infrared (FTIR) spectroscopy using an ATR plate. Spectra were recorded in the range of 400–4000 cm-1 by using Bruker, Tensor 37 model, India. Wide-angle X-ray diffraction (XRD) was used to calculate the chemical composition and crystallinity of silk fibroin and nanocomposite films. XRD spectra were obtained from 5° to 50° angle by PANalytical, X'Pert PRO model,

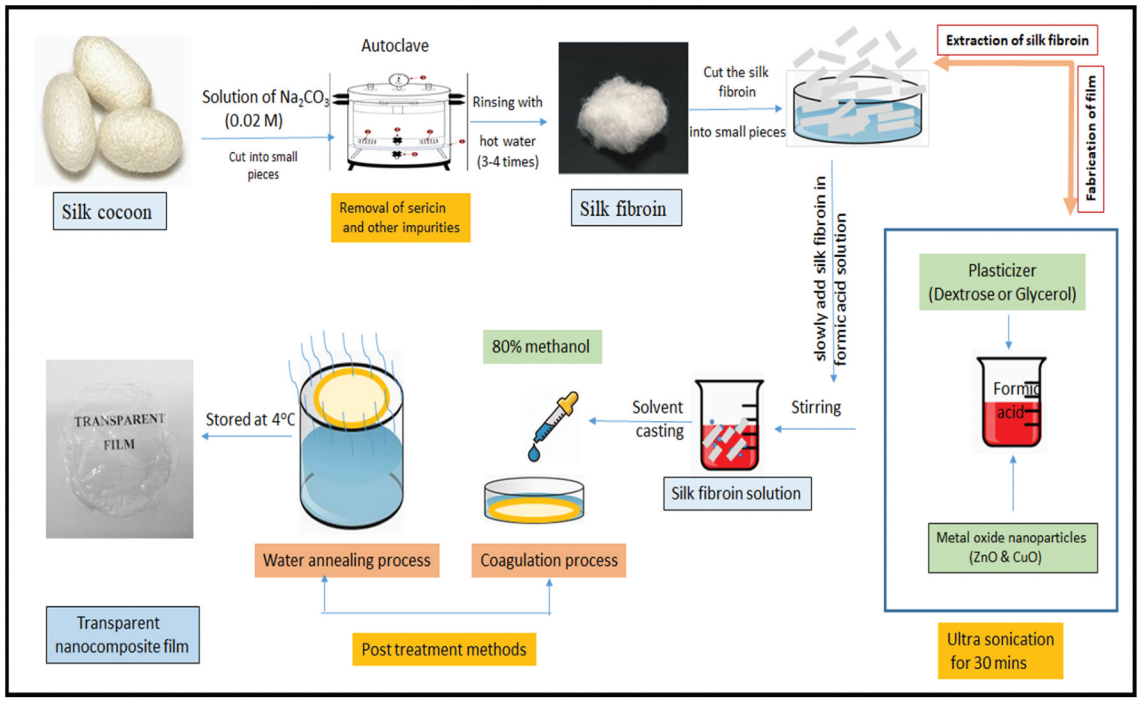

Scheme 1. Degumming of silk fibroin and fabrication process of transparent silk fibroin nanocomposite films.

Table 1. Fabrication process and post-treatment methods applied on films with their respective abbreviations.

Sample code	Fabrication and post treatment conditions
SF	No post-treatment was involved. The pure silk fibroin film is air-dried only.
SFM	Silk fibroin film is air-dried and then coagulated with methanol solvent to induce crystallization.
SFMD	Dextrose (15% w/v) has been added into the silk fibroin solution as a plasticizer to induce flexibility in the films. After air dry, methanol solvent has been used for the coagulation process to induce crystallinity in the films.
SFMG	Glycerol (15% w/v) act as a plasticizer has been added in the silk fibroin solution to induce flexibility then coagulation process has been applied similarly as mentioned above further water annealing process has been added for long lasting flexibility.
SFMG/ZnO (0.1), (0.25), (0.5), (0.75), (1)	Zinc oxide (0.1, 0.25, 0.5, 0.75, and 1% w/w) as nanofiller and Glycerol (15percentage w/v) as plasticizer added in the silk fibroin solution. Coagulation process has been involved using methanol solvent after air drying of films and then water annealing of the films.
SFMG/CuO (0.1), (0.25), (0.5), (0.75), (1)	Copper oxide (0.1, 0.25, 0.5, 0.75, and 1% w/w) as nanofiller and Glycerol (15% w/v) as plasticizer added in the silk fibroin solution. Similar coagulation process and water annealing process has been used as mentioned above.

Netherlands. To elucidate the secondary structure, β-sheet content, and crystallinity percentage in the regenerated silk fibroin films, the deconvolution method was applied to the absorption spectra and XRD spectra. Deconvolution was carried out using Peak Fit. The numbers and positions of peaks were defined from the results of second derivatives spectra and fixed during the deconvolution process and data minimized by the chi-squared criterion. The Gaussian model with integral type was applied for the band shape and bandwidth to adjust by the origin pro 9.0 software.[45]

The crystallinity percentage of the films was measured by Herman's formula as a similar method is adopted by R.R. Naik et al.[2] Briefly, the degree of crystallinity (Xc) of the polymers or polymer nanocomposites was calculated from the ratio of areas under the crystalline peaks and using the relation[46]:

$$\mathrm{Xc}(\%) = \frac{\mathrm{Ac}}{(\mathrm{Ac} + \mathrm{Aa})} \times 100 \qquad (1)$$

Where, A_c and A_a are the areas of crystalline and amorphous regions in the samples, respectively.

The surface morphology of the fabricated pure silk fibroin and nanocomposite films was characterized by using the Field Emission Scanning Electron Microscope (FESEM) at a high vacuum accelerated voltage of 15kV. FESEM images were acquired by JEOL Model JSM-7900 F prime with oxford EDS system, Netherland. The vacuum dried samples were sputter-coated with platinum before mounting on the sample holder of the FESEM-EDS instrument.

Dielectric strength of the silk fibroin films was analyzed by using the parallel plate capacitor method. The samples were prepared in the form of a circle with a diameter of 3 cm and placed between the two electrodes and voltage was applied to 15 kV with the speed of 1 kV/min. As the films were sparked upon the applied voltage, breakdown voltage was noted. Dielectric strength is defined as the maximum potential gradient to which a material can be subjected without insulating breakdown. The dielectric strength of the film was evaluated using the following formula.[2]

$$Dielectric\ Strength\ (v/um) = \frac{Breakdown\ Voltage(V)}{Thickness\ of\ the\ film(um)}$$

3. Result and discussions

3.1. Structure properties of silk fibroin films

To understand the structure-property of the silk fibroin films quantitatively, FTIR and XRD characterization are shown in Figure 1a–b, respectively. These spectra have been used to calculate the β-sheet content percentage and crystallinity percentage, and data are presented in Table 2. Silk fibroin is composed of amino acids such as glycine, alanine, serine in a sequence of Gly-Ser-Gly-Ala -Gly-Ala that propagate beta-pleated sheets via hydrogen bonding to form crystallites.[47] In FTIR spectra sharp peaks at 1618 cm^{-1}, 1512 cm^{-1}, and 1229 cm^{-1} were observed and assigned as Amide I (1618–1650 cm^{-1}), Amide II (1520–1540 cm^{-1}), and Amide III (1200–1350 cm^{-1}) absorption band, respectively.[45,48] The peptide carbonyl stretch represents the secondary structure of silk fibroin shown by the Amide I band which is used to calculate the β-sheet content of the films. The β-sheet content percentage from FTIR has been calculated by deconvolution method using Gaussian peak fit and the graphs are shown in Figure 2. In the Amide I region 1616 cm^{-1} is assigned as β-sheet conformation while other regions were overlapped by the peaks of a random coil, α-helical conformation (1638–1662 cm^{-1}) and β turns conformation (1690–1700 cm^{-1}) shown in Figure 2.

It was observed that SF film has shown the lowest β-sheet content percentage, as the film was air-dried and no other method has been applied to induce conformational transition while SFM film treated with methanol solvent during the coagulation process has shown an increase in β-sheet percentage

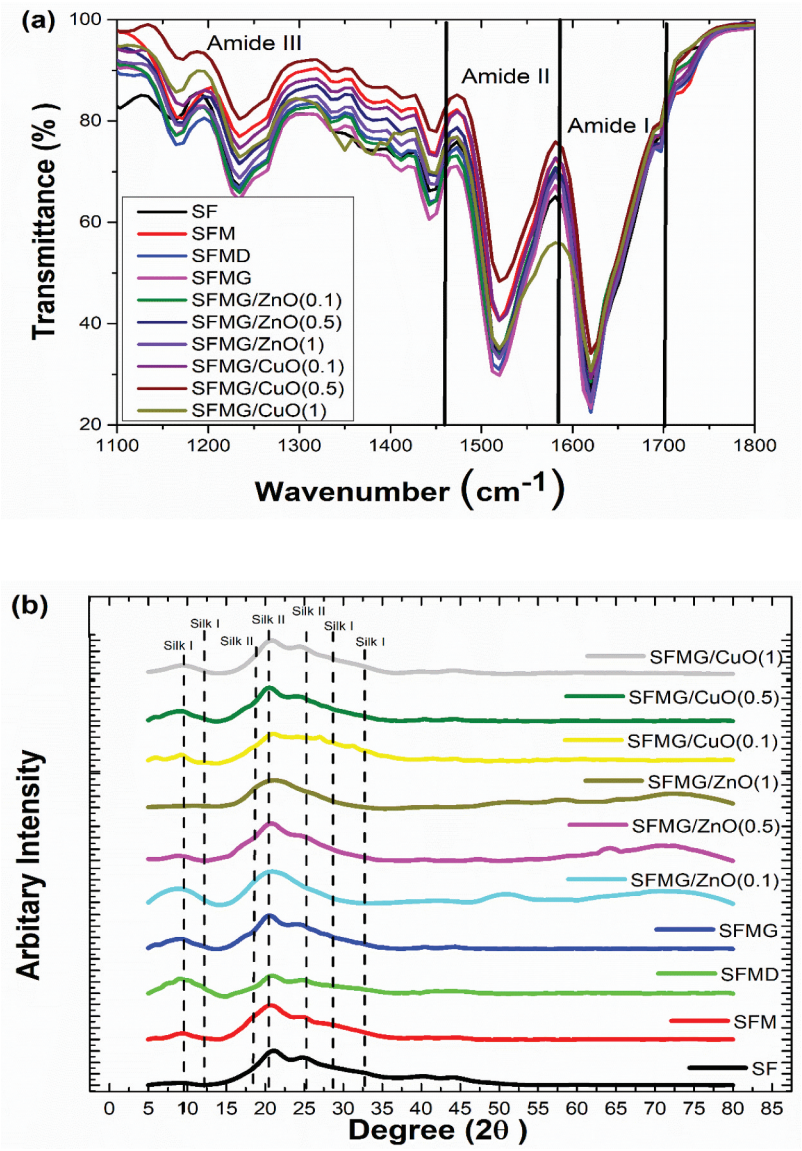

Figure 1. (**a**) FTIR spectra (**b**) XRD spectra showing the amide peaks and silk I & II structures, respectively, of the silk fibroin samples.

significantly as alcohol solvent absorbs water from the silk fibroin molecules and enhances the interaction of hydrophobic amino acids, increasing the crystalline domains and thus inducing the β-sheet formation.[43]

Table 2. β-sheet content and crystallinity percentage of silk fibroin films measured by FTIR and XRD.

Sample	β sheet (%)	Crystallinity (%)
SF	28.3	24.8
SFM	32.8	27.3
SFMD	39.7	34.9
SFMG	48.4	44.7
SFMG/ZnO(0.1)	48.1	43.1
SFMG/ZnO(0.5)	34.6	31.8
SFMG/ZnO(1)	29.5	26.4
SFMG/CuO(0.1)	47.3	44.2
SFMG/CuO(0.5)	45.8	42.9
SFMG/CuO(1)	34.7	29.3

It was observed that as the plasticizer, dextrose is added into the silk fibroin matrix, i.e. SFMD film, β-sheet content increased due to water plasticization effect. The water annealing method also works synergistically as observed by an increase in β-sheet content in the SFMG film incorporated with glycerol plasticizer compared to SFMD film due to the formation of hydrogen bonding via alpha-helix structures. However, nanoparticles were affecting the β-sheet structures adversely. The incorporation of metal oxide nanoparticles in the silk fibroin matrix reduced the β-sheet content in the nanocomposites films (SFMG/ZnO and SFMG/CuO) found to be more amorphous. As the concentration of zinc oxide and copper oxide increased more amorphous structures have been formed in the silk fibroin matrix. This

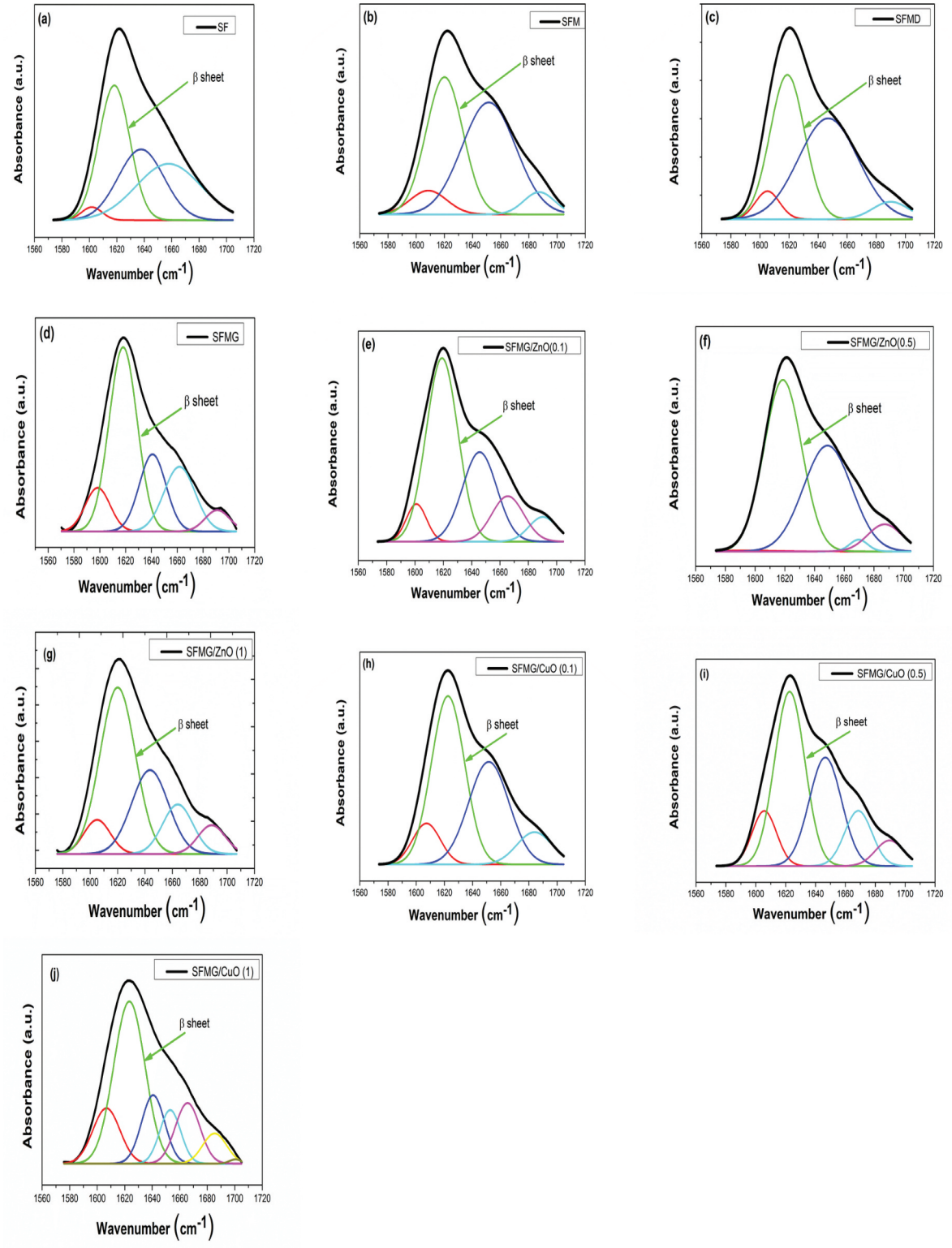

Figure 2. Deconvolution results of amide I region of regenerated silk fibroin films denoting β-sheet structure.

suggests that metal oxide nanoparticles might have behaved as a chaotropic agent in the silk fibroin which disturbs the ordered structure in the silk fibroin so that plasticizer and other post-treatment methods are also not able to bring the conformational transition in the nanocomposite films.

Furthermore, structural studies of regenerated silk fibroin films were supported by XRD studies. Here, to understand the secondary structure of silk fibroin, Silk I and Silk II notation has been used. Silk I denotes the metastable zigzag amorphous conformation due to the presence of random coil and alpha-helix structures while silk II denotes the β-sheet and β-turn structures where β-turn can be formed due to the close packing of loose structures and β-sheet formed by orderly arranged anti-parallel β-sheet conformation.[49,50] Sharp peaks observed at 9°, 12.2°, 20°, 24.9°, 27.8°, and 32° represents the Silk I structures while the sharp peak at 18.9°, 20.6°, and 25.8° identified as Silk II structure.[2] By using the deconvolution method in the range of 5°–50°, evaluation of the crystalline percentage has been done and the graphs are shown in Figure 3. It was observed that all regenerated silk fibroin films contain a mixture of silk I and silk II structures. However, their quantitative analysis has differences and crystallinity percentage has been mentioned in Table 2. It shows that regenerated silk fibroin film (SF) has the lowest crystallinity percentage and found a resemblance with FTIR data. Similarly, methanol-treated films (SFM and SFMD) have shown an increment in crystallinity due to the formation of β-sheet crystalline structures on dehydration of polypeptide chains. However, water vapor annealed films have shown more increment in crystallinity as these absorbed water during the process reduces the hydrogen bonds between the β-sheet conformation in the crystalline region of regenerated silk fibroins.[51] These water vapors are capable of inducing the conformational transition of silk fibroin from random coil to β-sheet structure as found to be a huge increment in crystallinity percentage in SFMG film compared to SFMD film as both the films have plasticizer. It was observed that the degree of crystallinity decreases with the loading of the zinc oxide and copper oxide in the silk fibroin which is consistent with FTIR data presented in Table 2. As the concentration of nanoparticles increased crystallinity percentage decreased simultaneously. The reason behind it might be the high surface area of nanoparticles, affecting the motion of protein chains which results in nanoconfined crystallization of silk fibroin and hence more amorphous, similarly explained by Y. Zang et al. for SF/GO and SF/TiO_2 that loading of nanofiller leads to decrements in crystallinity.[52,53] In Figure 4, a schematic diagram has been presented to make it comprehensible that shows the conformational transition in secondary structure occurred in the regenerated silk fibroin films influenced by alcohol solvent, absorbed water molecules, plasticizers, and nanoparticles.

3.2. Morphology of silk fibroin films

In Figure 5, Field Emission Scanning Electron Microscopy (FESEM) images have been presented to show the surface morphology of the regenerated silk fibroin films at 100 nm level, influenced by alcohol solvent, absorbed water molecules, plasticizers, and nanoparticles. To analyze the homogeneity and morphology of the nanocomposite films, FESEM-EDS studies were carried out. It was observed that pure silk fibroin film (SF) had a smooth surface (Figure 5(a)) while SFM, SFMG, and SFMD have rough surfaces because of regeneration and surface etching due to methanol treatment during the coagulation process (Figure 5b–d). The effect of post-treatment methods is identifiable on the surface of the regenerated silk fibroin films.[2] SFMG/ZnO (Figure 5e–g) and SFMD/CuO (Figure 5h–j) nanocomposite films showed uniformly dispersed nanoparticles in the silk fibroin matrix. However, at a higher concentration of nanoparticles in the regenerated silk fibroin films some agglomeration of nanoparticles was observed and the size of agglomerates was found to be lower than 100 nm. The altered morphology of films indicates the formation of nanocomposites with a homogeneous surface.

3.3. Dielectric strength of silk fibroin films

Dielectric strength of silk fibroin films has been evaluated by placing the film sample with a varying thickness (30 μm, 50 μm, 70 μm, 100 μm, 200 μm) between the two electrodes and voltage with the speed of 1KV/min has been applied to calculate the dielectric strength of these dielectric films. In Figure 6 the effect of film thickness, plasticizer, post-treatment, and metal oxide nanoparticles on the dielectric strength of silk fibroin have been shown. An inversely proportional relationship between the film thickness and the dielectric strength of the silk fibroin has been observed for all the samples. It was observed that only air-dried sample, SF has shown the lowest dielectric strength and methanol treated film SFM has shown the slight increase in the dielectric strength while SFMG film sample contains plasticizer, i.e. glycerol, treated with methanol solvent, and water annealing process as post-treatment method has shown the highest breakdown strength. Also, the SFMD sample has shown a high dielectric strength. As the nanoparticles were added into the silk fibroin matrix,

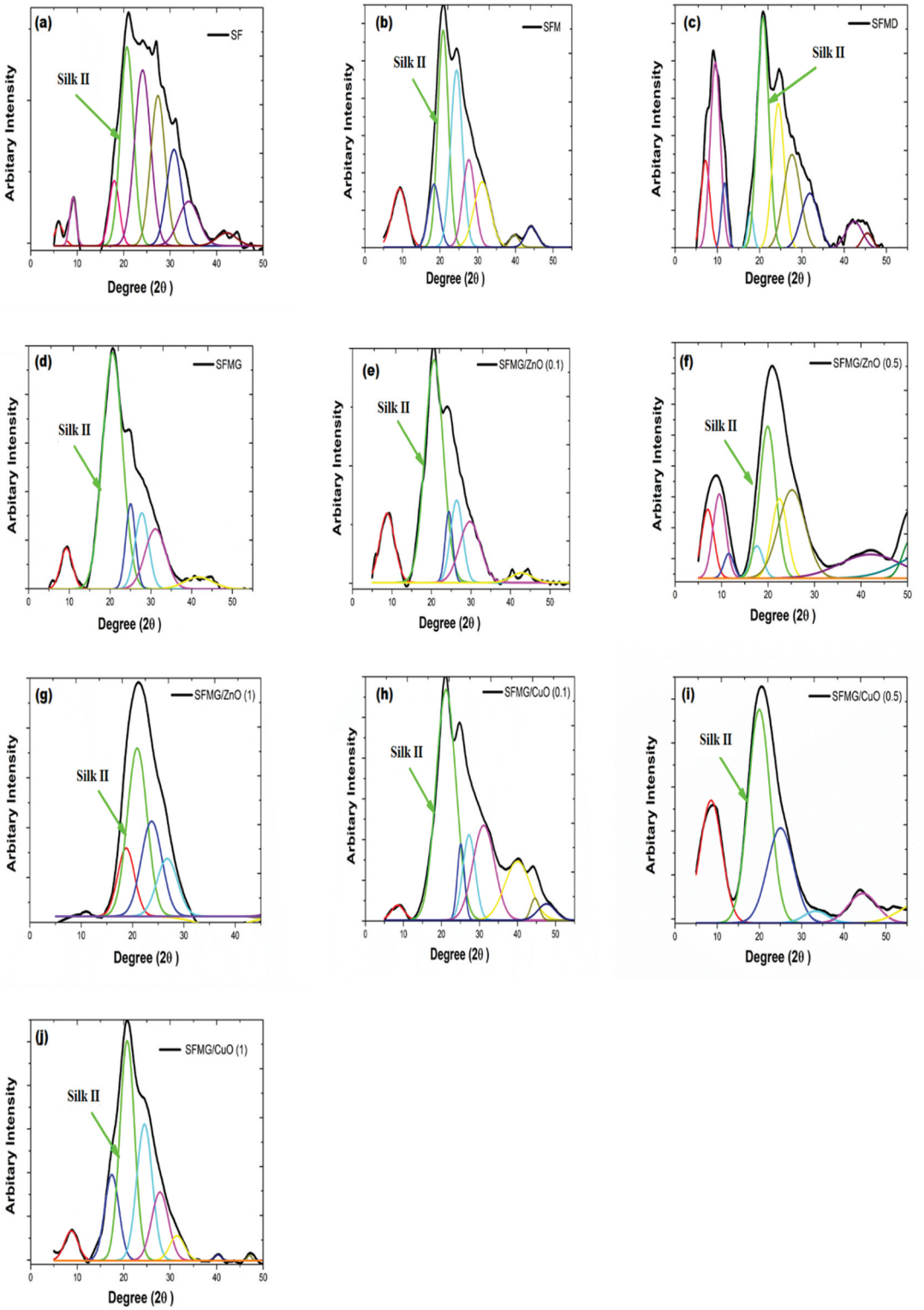

Figure 3. Multi peak fit diagram of regenerated silk fibroin films from 5–50° angle denoting the silk II structure peak measured by XRD.

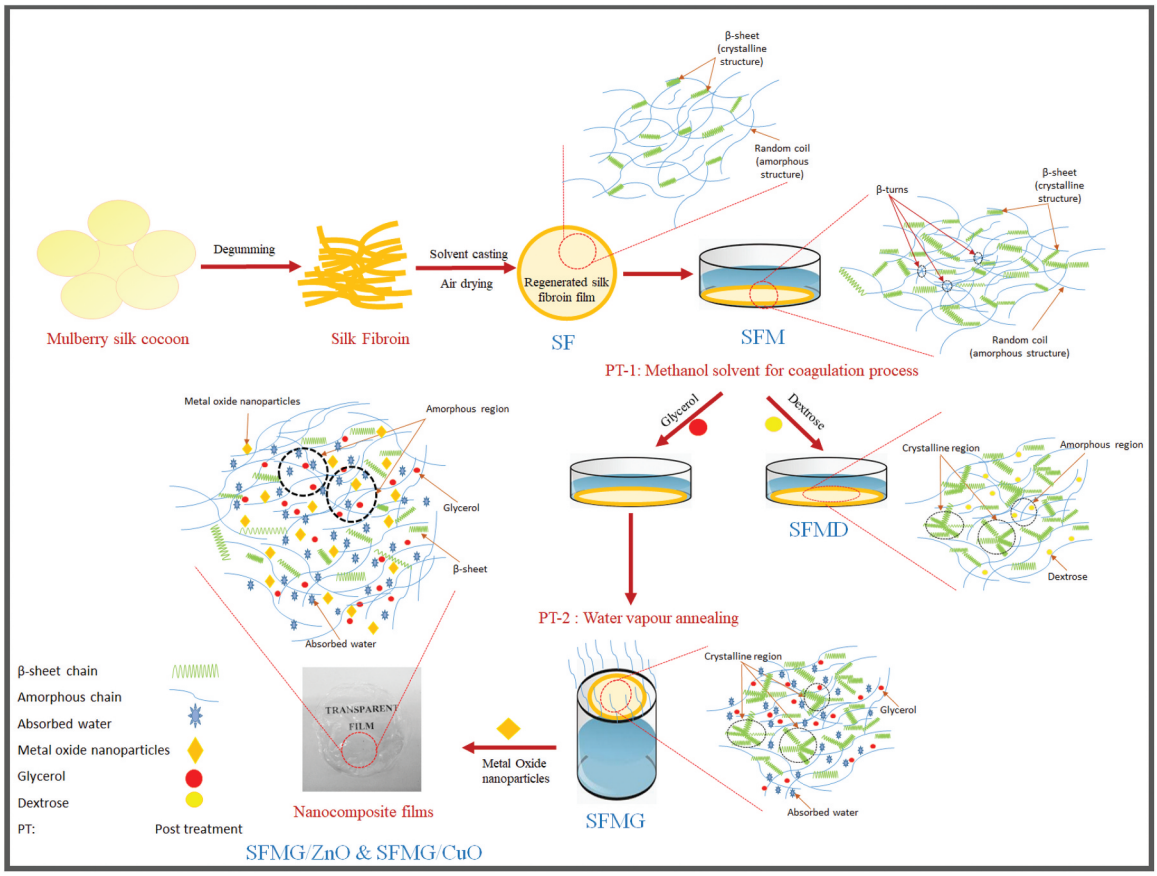

Figure 4. Schematic diagram to show the conformational transition in the secondary structure of the silk fibroin influenced by post-treatment methods, plasticizers, and metal oxide nanoparticles.

nanocomposite films have shown a decrement in dielectric strength; however, it is still greater than the naive SF sample. SFMG/CuO films have shown higher dielectric strength as compared to SFMG/ZnO films. The intrinsic dielectric behavior of copper oxide played a significant role here.

The effect of the concentration of zinc oxide nanoparticles and copper oxide nanoparticles on the dielectric strength of silk fibroin films at different film thicknesses (30 μm, 50 μm, 70 μm, 100 μm, 200 μm) has been presented in Figures 7 and 8, respectively, and the Weibull probability distribution of these dielectric strengths has been presented in Figure 9. As the concentration of nanoparticles (ZnO and CuO) increases in the silk fibroin matrix, dielectric strength is found to be decreased significantly at lower thickness while at higher thickness slight decrement is observed. The addition of nanoparticles in silk fibroin has been considered to bring a positive upshot on dielectric strength but contrary, it adversely affects the structural properties of silk fibroin matrix which hindered the efficacy of nanoparticles.

3.4. Interrelation between structure of silk fibroin and dielectric properties

The protein conformation plays a critical role in the dielectric properties of silk fibroin. β-sheet structures and the amorphous region of silk fibroin are closely related to the dielectric strength of the silk fibroin films as reported in the literature.[2] These β-sheet structures may obstruct the flow of charge carriers to delay the conduction, hence increasing the dielectric strength. The addition of metal oxide nanoparticles bought more amorphous regions in the silk fibroin matrix rather than conformational transition from random coil to β-sheet structures despite post-treatment methods applied to these nanocomposite films as shown by FTIR and XRD results. Ideally, these nanoparticles could be bought with more charge traps in silk fibroin matrix due to conducting-insulating interface that delays the charge transport.[21,22] However, the hydroxyl groups of silk fibroin and metal oxide nanoparticles have formed a charge transfer complex which reduces the barrier height between the tapping sites and provides a charge tunneling in the nanocomposites. This

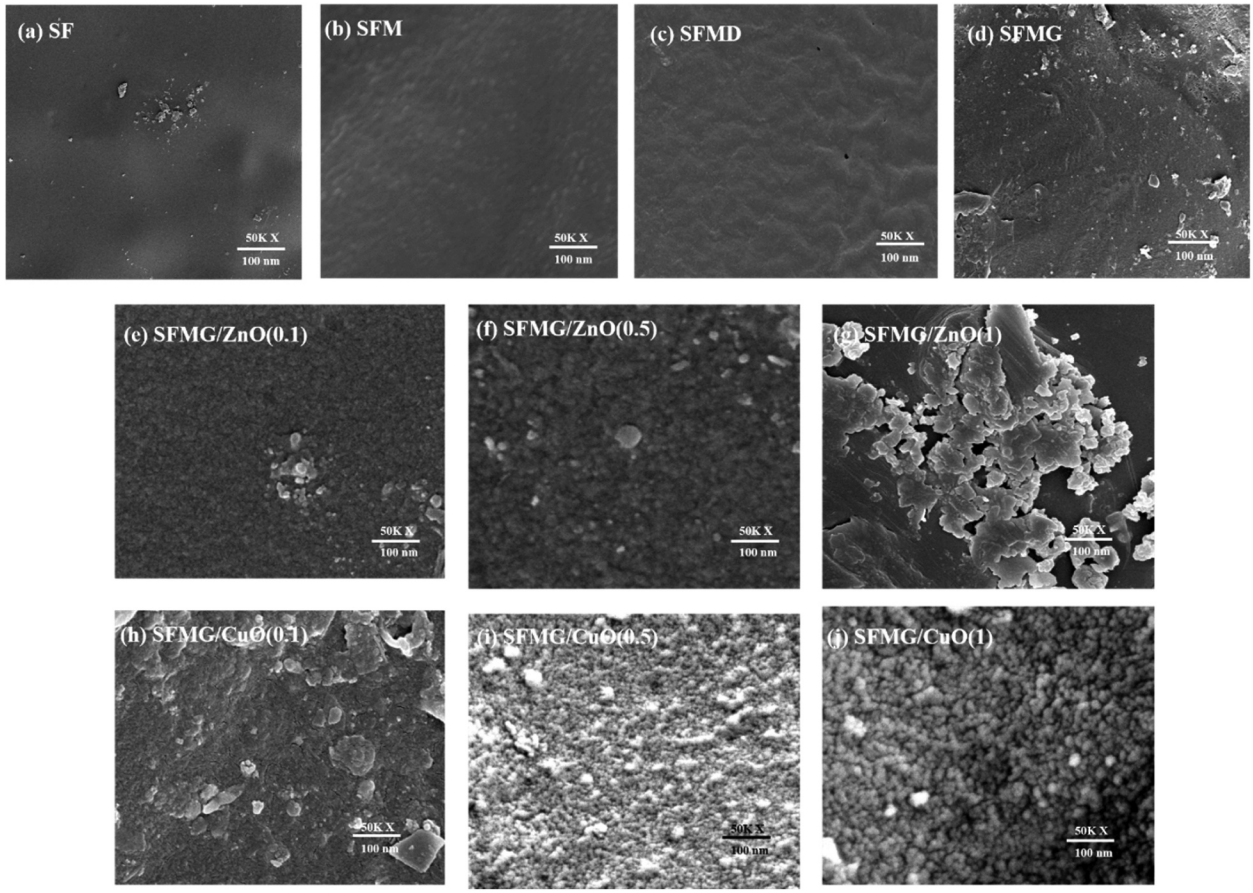

Figure 5. Field Emission Scanning Electron Microscopy (FESEM) images of the regenerated silk fibroin films influenced by alcohol solvent, absorbed water molecules, plasticizers, and nanoparticles.

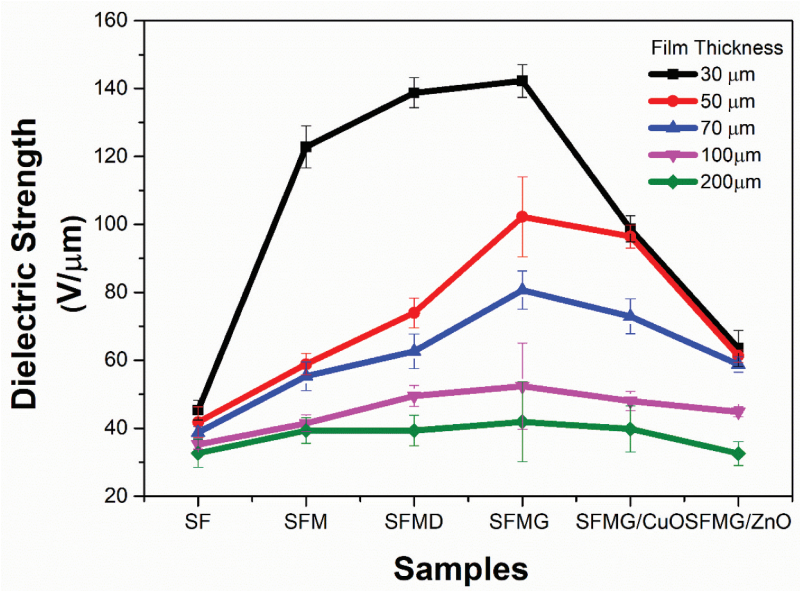

Figure 6. Effect of post-treatment methods, plasticizer, film thickness, and metal oxide nanoparticles on the dielectric strength of the silk fibroin films.

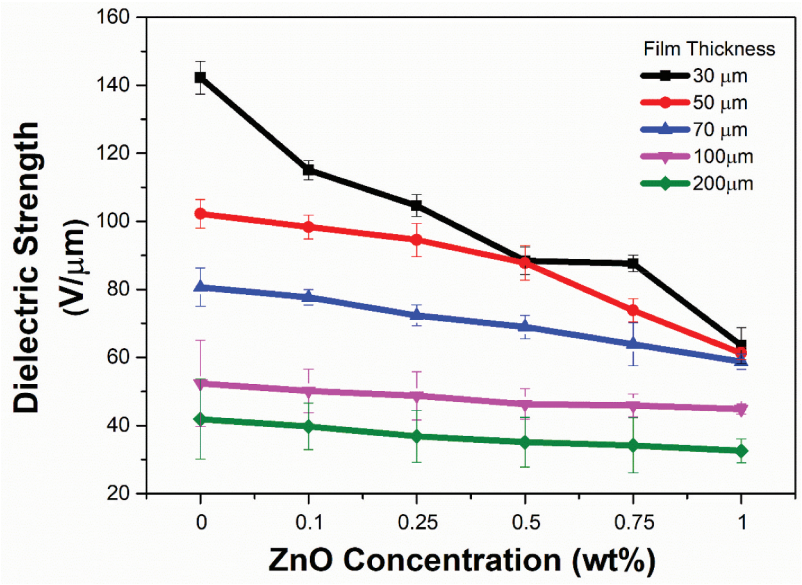

Figure 7. Effect of concentration of zinc oxide nanoparticles and film thickness on the dielectric strength of silk fibroin nanocomposite films.

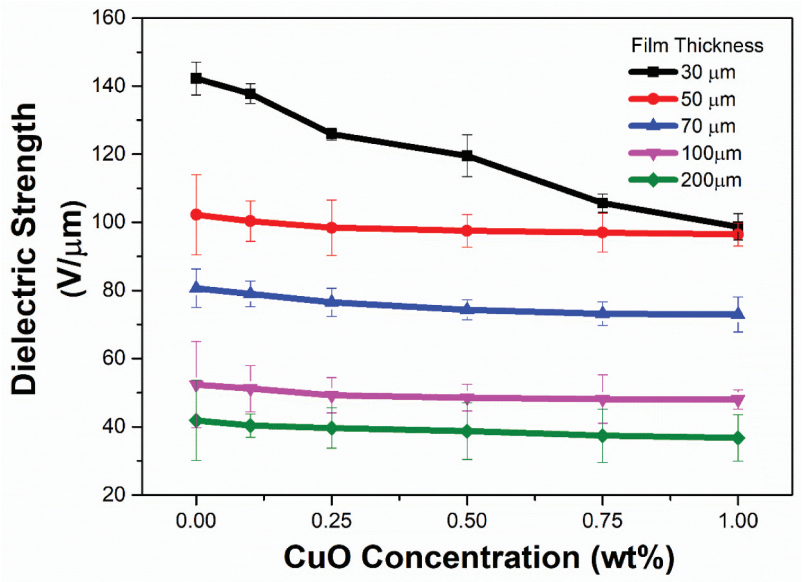

Figure 8. Effect of concentration of copper oxide nanoparticles and film thickness on the dielectric strength of silk fibroin nanocomposite films.

creates a conducting pathway through the amorphous region of silk fibroin and thus charge flows via the charge hopping mechanism in the silk fibroin matrix without much delay thus lowering the dielectric strength. The creation of conducting pathways in the silk fibroin is presented schematically in Figure 10. A conductivity study of these nanocomposites films has been reported in our previous study in which increment in concentration of nanoparticles bought the high conductivity at various film thicknesses (Data is presented in Table 3) and supports the aforementioned mechanism.[54]

In the highly crystalline films formed charge traps accumulate the space charge due to the intermediate phase, i.e. the β-sheet crystalline region in silk fibroin thus delays the charge transition and causes high dielectric strength. Water annealing process has bought more significance in terms of conformational transition by pre-

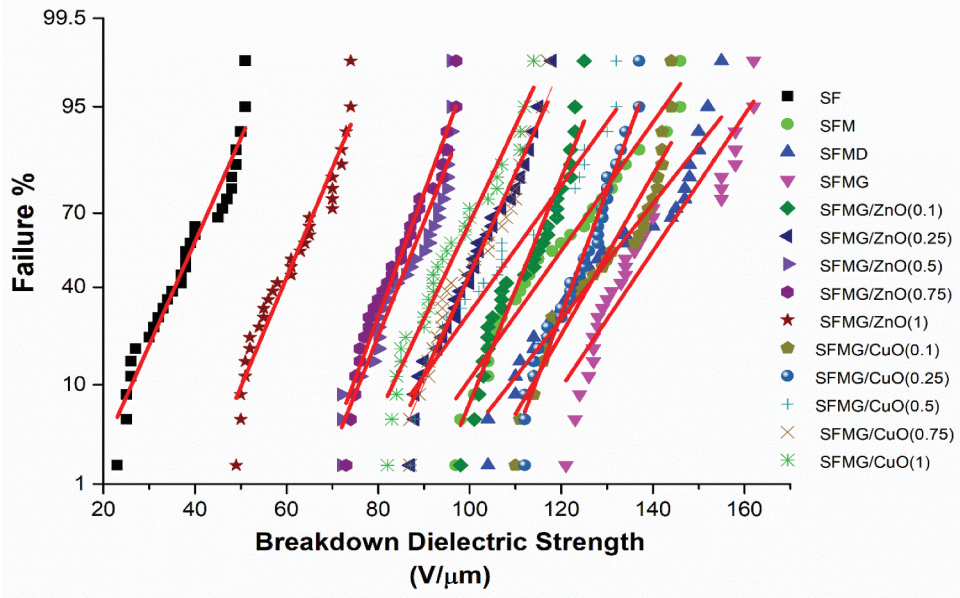

Figure 9. Weibull distribution of probability of dielectric strength of silk fibroin samples after applying the voltage.

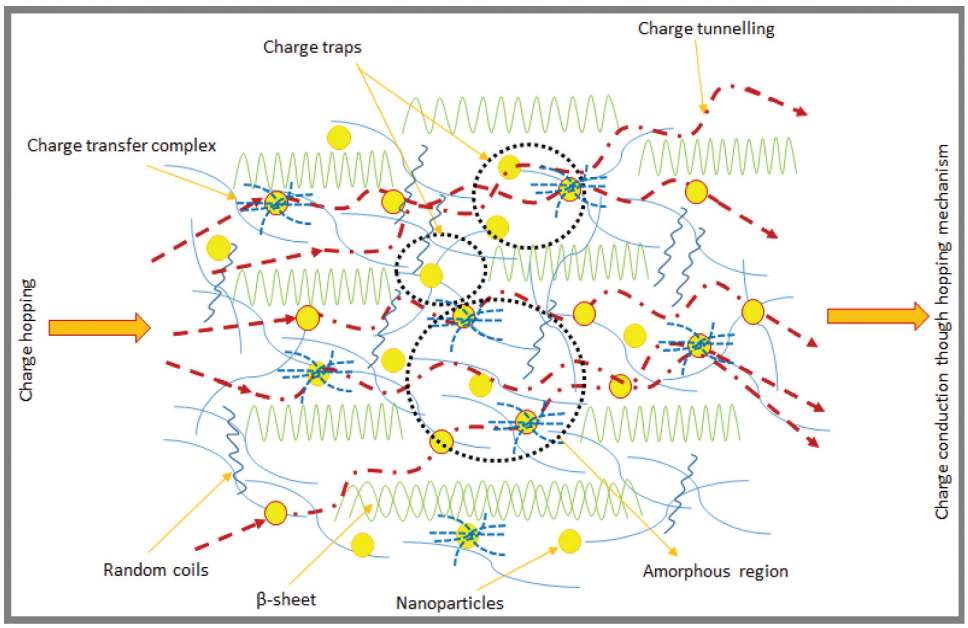

Figure 10. Schematic diagram of charge hopping mechanism for the conduction of charge carriers through the amorphous region of the silk fibroin matrix.

Table 3. Electrical properties of silk fibroin nanocomposites incorporated with zinc oxide and copper oxide nanoparticles.

Electrical conductivity ($S.cm^{-1}$)					
	Film thickness				
Silk nanocomposite films	30 μm	50 μm	70 μm	100 μm	200 μm
SFMG	32.3 ± 0.6	33.3 ± 0.9	34.1 ± 0.1	34.6 ± 0.2	35.6 ± 0.3
SFMG/ZnO(0.1)	113.2 ± 0.3	91.4 ± 0.2	85.4 ± 0.3	69.1 ± 0.9	53.6 ± 0.2
SFMG/ZnO(0.25)	243.7 ± 0.5	213.8 ± 0.5	121.5 ± 0.6	109.2 ± 0.6	89.5 ± 0.7
SFMG/ZnO(0.5)	632.8 ± 0.2	413.6 ± 0.2	226.4 ± 0.4	128.4 ± 0.7	103.5 ± 0.1
SFMG/ZnO(0.75)	1023.4 ± 0.4	745.8 ± 0.7	407.8 ± 0.7	218.3 ± 0.1	201.3 ± 0.3
SFMG/ZnO(1)	963.3 ± 0.3	634.7 ± 0.9	412.8 ± 0.3	223.5 ± 0.3	207.6 ± 04
SFMG/CuO(0.1)	43.8 ± 0.9	48.5 ± 0.1	54.2 ± 0.9	61.7 ± 0.2	69.3 ± 0.1
SFMG/CuO(0.25)	187.3 ± 0.6	178.4 ± 0.3	106.2 ± 0.4	85.2 ± 0.9	71.3 ± 0.3
SFMG/CuO(0.5)	548.2 ± 0.5	365.7 ± 0.8	132.7 ± 0.8	103.2 ± 0.6	93.7 ± 0.5
SFMG/CuO(0.75)	974.5 ± 0.1	712.4 ± 0.3	213.9 ± 0.1	107.4 ± 0.3	98.3 ± 0.7
SFMG/CuO(1)	589.3 ± 0.2	412.7 ± 0.6	225.4 ± 0.3	112.6 ± 0.4	102.3 ± 0.5

venting the formation of hydrogen bonds between the β-sheet in crystalline region and enhance the crystallization via alpha helix structures as observed in degree of crystallinity of SFMG film which in turn resulted in higher dielectric strength. Therefore, as the β-sheet content or degree of crystallinity increases in the silk fibroin films, dielectric strength increases, whereas, more the amorphous region present in the silk fibroin lesser will be the dielectric strength of the films as observed by the nanocomposite films (SFMG/ZnO and SFMG/CuO).

4. Conclusion

Methanol-treated silk fibroin films have shown increment in β-sheet structures observed by both FTIR and XRD results. Plasticizers seek to take benefit from the water annealing process by procuring bound water in the silk fibroin matrix; thus, an increase in β-sheet content and crystallinity percentage has been observed in SFMG film. The addition of metal oxide nanoparticles decreased the crystalline region in the silk fibroin matrix as observed in SFMG/ZnO and SFMG/CuO nanocomposite films. It was observed that the β-sheet conformation of silk fibroin helps in obstructing the flow of charge carriers to delay the charge transportation which helps in increment of dielectric strength of the films. However, as the concentration of metal oxide nanoparticles increases in silk fibroin, a decrement in dielectric strength was observed. Thus, a hypothesis about introducing conductive nanoparticles in silk fibroin to increase dielectric strength in nanocomposite films to form a nanodielectric has fallen to bits and in fact, it seems that the addition of such conductive nanoparticles brings conductivity in silk fibroin films. A mechanism of the formation of the charge-transfer complex that causes the charge tunneling in silk fibroin was proposed which overpowers the charge traps formed by nanoparticles in the matrix.

Acknowledgments

The authors thank for the financial support by Science & Engineering Research Board (SERB), Department of Science and Technology (DST), Govt. of India (EMR/2017/002833).

Disclosure statement

No potential conflict of interest was reported by the authors.

Funding

This work was supported by the Science and Engineering Research Board [EMR/2017/002833].

Notes on contributors

Reetu Yadav, a senior research scholar in Department of applied Chemistry, Delhi Technological University. Qualifications: Ph D, M.Sc., B. Sc. I am a disciplined and passionate researcher in the field of Polymer Technology to carry out comprehensive research and development in silk fibroin for electronic applications. The focal aim of my work is the fabrication of silk fibroin based nanocomposite solutions, films, gels, and nanofibers using latest techniques and methods such as electrospinning and soft freezing method by incorporating metal oxide nanoparticles with different concentration and thickness of film & fiber to study the rheological, structural, morphological, thermal, electronics, dielectrics, and optical properties for optoelectronics applications.

Dr. Roli Purwar, Professor, Department of Applied Chemistry, Discipline of Polymer and Chemical Technology, Delhi Technological University. Qualifications Ph D, M.Tech, B.E. Areas of Interest: Fibre Technology, Polymer Processing, Medical Textiles, Polymer nanocomposites, Nanofibrous membranes, Dope Dyeing Specialization: Biopolymers, Polymeric membranes, Ecofriendly Processing of Textiles, Natural Materials and their Application, Medical Textiles, Effluent Treatment

References

[1] Tan, D. Q. The Search for Enhanced Dielectric Strength of Polymer-Based Dielectrics: A Focused Review on Polymer Nanocomposites. *J. Appl. Polym. Sci.* 2020, *137*(33), 1–32. DOI: 10.1002/app.49379.

[2] Dickerson, M. B.; Fillery, S. P.; Koerner, H.; Singh, K. M.; Martinick, K.; Drummy, L. F.; Durstock, M. F.; Vaia, R. A.; Omenetto, F. G.; Kaplan, D. L., et al. Dielectric Breakdown Strength of Regenerated Silk Fibroin Films as a Function of Protein Conformation. *Biomacromolecules*.2013, *14*(10), 3509–3514. DOI: 10.1021/bm4008452.

[3] Ceres, B. V.; Schultz, J. M. Dependence of Electrical Breakdown on Spherulite Size in Isotactic Polypropylene. *J. Appl. Polym. Sci.* 1984, *29*(12), 4183–4197. DOI: 10.1002/app.1984.070291248.

[4] Cheng, Y.; Yu, G.; Duan, Z. Effect of Different Size ZnO Particle Doping on Dielectric Properties of Polyethylene Composites. *J. Nanomater.* 2019, *2019*, 1–11. DOI: 10.1155/2019/9481415.

[5] Devikala, S.; Kamaraj, P.; Arthanareeswari, M. AC Conductivity Studies of PMMA/TiO2 Composites. *Mater. Today Proc.* 2018, *5*(2), 8678–8682. DOI: 10.1016/j.matpr.2017.12.293.

[6] Li, S.; Yin, G.; Chen, G.; Li, J.; Bai, S.; Zhong, L.; Zhang, Y.; Lei, Q. Short-Term Breakdown and Long-Term Failure in Nanodielectrics: A Review. *IEEE Trans. Dielectr. Electr. Insul.* 2010, *17*(5), 1523–1535. DOI:10.1109/TDEI.2010.5595554.

[7] Cao, Y.; Irwin, P. C. Younsi, K. The Future of Nanodielectrics in the Electrical Power Industry. *IEEE Trans. Dielectr. Electr. Insul.* 2004, *11*(5), 797–807. DOI:10.1109/TDEI.2004.1349785.

[8] Nelson, J. K.; Fothergill, J. C.; Dissado, L. A.; Peasgood, W. Towards an Understanding of Nanometric Dielectrics. *Conf. Electr. Insul. Dielectr. Phenom. (CEIDP), Annu. Rep.* 2002, 295–298. DOI: 10.1109/ceidp.2002.1048793.

[9] Narumanchi, S.; Bennion, K.; Devoto, D.; Moreno, G.; Rugh, J.; Waye, S. *Advanced Power Electronics and Electric Motors Annual Report - 2013. National Renewable Energy Lab*, 2015.

[10] Neusel, C.; Jelitto, H.; Schneider, G. A. Electrical Conduction Mechanism in Bulk Ceramic Insulators at High Voltages until Dielectric Breakdown. *J. Appl. Phys.* 2015, *117*(15), 154902. DOI: 10.1063/1.4917208.

[11] Baniecki, J. D.; Shioga, T.; Kurihara, K.; Kamehara, N. Investigation of the Importance of Interface and Bulk Limited Transport Mechanisms on the Leakage Current of High Dielectric Constant Thin Film Capacitors. *J. Appl. Phys.* 2003, *94*(10), 6741–6748. DOI: 10.1063/1.1620377.

[12] Lanter, W. C.; Kosai, H.; Bixel, T.; Tolson, B. A.; Stricker, J.; Scofield, J.; Brar, N.; Ray, B. Capacitor Characterization Study for a High Power, High Frequency Converter Application. *Int. Conf. Exhib. High Temp. Electron.* 2010, *2010*, 174–181. DOI: 10.4071/hitec-jstricker-wa11.

[13] Dang, Z. M.; Yuan, J. K.; Yao, S. H.; Liao, R. J. Flexible Nanodielectric Materials with High Permittivity for Power Energy Storage. *Adv. Mater.* 2013, *25*(44), 6334–6365. DOI: 10.1002/adma.201301752.

[14] Tan, D. Q. Review of Polymer-Based Nanodielectric Exploration and Film Scale-Up for Advanced Capacitors. *Adv. Funct. Mater.* 2020, *30*(18), 1–23. DOI: 10.1002/adfm.201808567.

[15] Zhou, Z.; Carr, J.; Mackey, M.; Yin, K.; Schuele, D.; Zhu, L.; Baer, E. Interphase/Interface Modification on the Dielectric Properties of Polycarbonate/Poly (Vinylidene Fluoride-Co-Hexafluoropropylene) Multilayer Films for High-Energy Density Capacitors. *J. Polym. Sci. Part B Polym. Phys.* 2013, *51*(12), 978–991. DOI: 10.1002/polb.23296.

[16] Pfeiffenberger, N.; Milandou, F.; Niemeyer, M.; Sugawara, T.; Sanner, M.; Mahood, J. High Temperature Dielectric Polyetherimide Film Development. *IEEE Trans. Dielectr. Electr. Insul.* 2018, *25*(1), 120–126. DOI:10.1109/TDEI.2018.006806.

[17] Kerwien, C. M.; Malandro, D. L.; Broomall, J. R. Large Area DC Dielectric Breakdown Voltage Measurement of BOPP and PTFE Thin Films. *Annu. Rep. - Conf. Electr. Insul. Dielectr. Phenomena*. 2016, *2016*, 486–489. DOI: 10.1109/CEIDP.2016.7785688.

[18] Kasap, S. O. *Principles of Electronic Materials and Devices*, 4th ed; McGraw-Hill Education: New York, 2018; pp 1369.

[19] Huang, X.; Jiang, P.; Tanaka, T. A Review of Dielectric Polymer Composites with High Thermal Conductivity. *IEEE Electr. Insul. Mag.* 2011, *27*(4), 8–16. DOI:10.1109/MEI.2011.5954064.

[20] Uehara, H.; Montanari, G. C.; Chen, Q.; Li, Z.; Cao, Y. Comparison of Space Charge Behavior in XLPE and EPR with Thermal Gradient. *Proc. 2016 IEEE Int. Conf. Dielectr. ICD 2016*. 2016, *1*, 143–146. DOI: 10.1109/ICD.2016.7547564.

[21] Tanaka, T.; Montanari, G. C.; Mülhaupt, R. Polymer Nanocomposites as Dielectrics and Electrical Insulation- Perspectives for Processing Technologies, Material Characterization and Future Applications. *IEEE Trans. Dielectr. Electr. Insul.* 2004, *11*(5), 763–784. DOI:10.1109/TDEI.2004.1349782.

[22] Tuncer, E.; Sauers, I.; James, D. R.; Ellis, A. R.; Paranthaman, M. P.; Goyal, A.; More, K. L. Enhancement of Dielectric Strength in Nanocomposites. *Nanotechnology*. 2007, *18*(32), 325704. DOI: 10.1088/0957-4484/18/32/325704.

[23] Li, S.; Min, D.; Wang, W.; Chen, G. Modelling of Dielectric Breakdown through Charge Dynamics for Polymer Nanocomposites. *IEEE Trans. Dielectr. Electr. Insul.* 2016, *23*(6), 3476–3485. DOI:10.1109/TDEI.2016.006051.

[24] Lei, T.; Xue, Q.; Chu, L.; Han, Z.; Sun, J.; Xia, F.; Zhang, Z.; Guo, Q. Excellent Dielectric Properties of Polymer Composites Based on Core-Shell Structured Carbon/Silica Nanohybrid. *Appl. Phys. Lett.* 2013, *103*(1), 0–4. DOI: 10.1063/1.4813086.

[25] Shen, Y.; Lin, Y.; Nan, C. W. Interfacial Effect on Dielectric Properties of Polymer Nanocomposites Filled with Core/Shell-Structured Particles. *Adv. Funct. Mater.* 2007, *17*(14), 2405–2410. DOI: 10.1002/adfm.200700200.

[26] Jung, H. M.; Kang, J. H.; Yang, S. Y.; Won, J. C.; Kim, Y. S. Barium Titanate Nanoparticles with Diblock Copolymer Shielding Layers for High-Energy Density Nanocomposites. *Chem. Mater.* 2010, *22*(2), 450–456. DOI: 10.1021/cm9030254.

[27] Xu, J.; Wong, C. P. Low-Loss Percolative Dielectric Composite. *Appl. Phys. Lett.* 2005, *87*(8), 1–4. DOI: 10.1063/1.2032597.

[28] Yu, L.; Skov, A. L. ZnO as a Cheap and Effective Filler for High Breakdown Strength Elastomers. *RSC Adv.* 2017, *7*(72), 45784–45791. DOI: 10.1039/c7ra09479e.

[29] Wang, F. F.; Yan, D. D.; Su, Y.; Lu, Y. F.; Xia, X. F.; Huang, H. M. Research on the Dielectric Properties of Nano-ZnO/Silicone Rubber Composites. *IOP Conf. Ser. Mater. Sci. Eng.* 2017, *231*(1), 012060. DOI: 10.1088/1757-899X/231/1/012060.

[30] Deepti, K. R.; Karthikeyan, B. Frequency and Temperature Dependent Dielectric Properties of CuO-Polyvinyl Alcohol Polymer Films. *2012 Int. Conf. Emerg. Electron.* 2012, (1), 10–13. DOI: 10.1109/ICEmElec.2012.6636259.

[31] Putjuso, T.; Sangarun, P. In Fl Uence of Annealing on the Giant Dielectric Properties of CuO Ceramics Prepared by a Simple PVA Sol-Gel. *Asia-Pacific J. Sci. Technol.* 2012, *17*(2), 203–210.

[32] Wang, C.; Xia, K.; Zhang, Y.; Kaplan, D. L. Silk-Based Advanced Materials for Soft Electronics. *Acc. Chem. Res.* 2019, *52*(10), 2916–2927. DOI: 10.1021/acs.accounts.9b00333.

[33] Sun, Q.; Qian, B.; Uto, K.; Chen, J.; Liu, X., and Minari, T. . In *Biosensors and Bioelectronics,* Prof. Dr. Man Bock Gu (Ed), 2018; pp 237–251. doi:10.1016/j.bios.2018.08.018.

[34] Koh, L. D.; Yeo, J.; Lee, Y. Y.; Ong, Q.; Han, M.; Tee, B. C. K. Advancing the Frontiers of Silk Fibroin Protein-Based Materials for Futuristic Electronics and Clinical Wound-Healing (Invited Review). In *Materials Science and Engineering C*, Elsevier Ltd, 2018; pp 151–172. doi:10.1016/j.msec.2018.01.007.

[35] Lee, J. H.; Kwak, H. W.; Park, M. H.; Hwang, J.; Kim, J. W.; Jang, H. W.; Jin, H. J.; Lee, W. H. Understanding Hydroscopic Properties of Silk Fibroin and Its Use as a Gate-Dielectric in Organic Field-Effect Transistors. *Org. Electron.* 2018, *59*(May), 213–219. DOI: 10.1016/j.orgel.2018.05.012.

[36] Luo, Y.; Pei, Y.; Feng, X.; Zhang, H.; Lu, B.; Wang, L. Silk Fibroin Based Transparent and Wearable Humidity Sensor for Ultra-Sensitive Respiration Monitoring. *Mater. Lett.* 2020, *260*, 126945. DOI: 10.1016/j.matlet.2019.126945.

[37] Fan, S. N.; Zhang, Y.; Huang, X. Y.; Geng, L. H.; Shao, H. L.; Hu, X. C., and Zhang, Y. P. Silk Materials for Medical, Electronic and Optical Applications. In *Science China Technological Sciences,* TongYi ZHANG (Ed), Springer Verlag, 2019; pp 903–918. doi:10.1007/s11431-018-9403-8.

[38] Lu, Z.; Zhang, H.; Mao, C.; Li, C. M. Silk Fabric-Based Wearable Thermoelectric Generator for Energy Harvesting from the Human Body. *Appl. Energy.* 2016, *164*, 57–63. DOI: 10.1016/j.apenergy.2015.11.038.

[39] Shivananda, C. S.; Lakshmeesha Rao, B. Structural, Thermal and Electrical Properties of Silk Fibroin–Silver Nanoparticles Composite Films. *J. Mater. Sci. Mater. Electron.* 2020, *31*(1), 41–51. DOI: 10.1007/s10854-019-00786-3.

[40] Wang, Y.; Ma, R.; Hu, K.; Kim, S.; Fang, G.; Shao, Z.; Tsukruk, V. V. Dramatic Enhancement of Graphene Oxide/Silk Nanocomposite Membranes: Increasing Toughness, Strength, and Young's Modulus via Annealing of Interfacial Structures. *ACS Appl. Mater. Interfaces.* 2016, *8*(37), 24962–24973. DOI: 10.1021/acsami.6b08610.

[41] Johari, N.; Moroni, L.; Samadikuchaksaraei, A. Tuning the Conformation and Mechanical Properties of Silk Fibroin Hydrogels. *Eur. Polym. J.* 2020, *134*(June), 109842. DOI: 10.1016/j.eurpolymj.2020.109842.

[42] Min, B. M.; Jeong, L.; Lee, K. Y.; Park, W. H. Regenerated Silk Fibroin Nanofibers: Water Vapor-Induced Structural Changes and Their Effects on the Behavior of Normal Human Cells. *Macromol. Biosci.* 2006, *6*(4), 285–292. DOI: 10.1002/mabi.200500246.

[43] Kaewpirom, S.; Boonsang, S. Influence of Alcohol Treatments on Properties of Silk-Fibroin-Based Films for Highly Optically Transparent Coating Applications. *RSC Adv.* 2020, *10*(27), 15913–15923. DOI: 10.1039/d0ra02634d.

[44] Srivastava, C. M.; Purwar, R.; Kannaujia, R.; Sharma, D. Flexible Silk Fibroin Films for Wound Dressing. *Fibers Polym.* 2015, *16*(5), 1020–1030. DOI: 10.1007/s12221-015-1020-y.

[45] Ling, S.; Qi, Z.; Knight, D. P.; Shao, Z.; Chen, X. Synchrotron FTIR Microspectroscopy of Single Natural Silk Fibers. *Biomacromolecules.* 2011, *12*(9), 3344–3349. DOI: 10.1021/bm2006032.

[46] Hermans, P. H.; Weidinger, A. Quantitative X-Ray Investigations on the Crystallinity of Cellulose Fibers. A Background Analysis. *J. Appl. Phys.* 1948, *19*(5), 491–506. DOI: 10.1063/1.1698162.

[47] Zafar, M. S.; Belton, D. J.; Hanby, B.; Kaplan, D. L.; Perry, C. C. Functional Material Features of Bombyx Mori Silk Light versus Heavy Chain Proteins. *Biomacromolecules.* 2015, *16*(2), 606–614. DOI: 10.1021/bm501667j.

[48] Kong, J.; Yu, S. Fourier Transform Infrared Spectroscopic Analysis of Protein Secondary Structures. *Acta Biochim. Biophys. Sin.* 2007, *39*(8), 549–559. DOI: 10.1111/j.1745-7270.2007.00320.x.

[49] Qi, Y.; Wang, H.; Wei, K.; Yang, Y.; Zheng, R. Y.; Kim, I. S.; Zhang, K. Q. A Review of Structure Construction of Silk Fibroin Biomaterials from Single Structures to Multi-Level Structures. *Int. J. Mol. Sci.* 2017, *18*(3), 237. DOI: 10.3390/ijms18030237.

[50] Dubey, P.; Murab, S.; Karmakar, S.; Chowdhury, P. K.; Ghosh, S. Modulation of Self-Assembly Process of Fibroin: An Insight for Regulating the Conformation of Silk Biomaterials. *Biomacromolecules.* 2015, *16*(12), 3936–3944. DOI: 10.1021/acs.biomac.5b01258.

[51] Cheng, Y.; Koh, L. D.; Li, D.; Ji, B.; Han, M. Y.; Zhang, Y. W. On the Strength of β-sheet Crystallites of Bombyx Mori Silk Fibroin. *J. R. Soc. Interface*. 2014, *11*(96), 20140305. DOI: 10.1098/rsif.2014.0305.

[52] Zhang, C.; Zhang, Y.; Shao, H.; Hu, X. Hybrid Silk Fibers Dry-Spun from Regenerated Silk Fibroin/Graphene Oxide Aqueous Solutions. *ACS Appl. Mater. Interfaces*. 2016, *8*(5), 3349–3358. DOI: 10.1021/acsami.5b11245.

[53] Pan, H.; Zhang, Y.; Shao, H.; Hu, X.; Li, X.; Tian, F.; Wang, J. Nanoconfined Crystallites Toughen Artificial Silk. *J. Mater. Chem. B*. 2014, *2*(10), 1408–1414. DOI: 10.1039/c3tb21148g.

[54] Yadav, R.; Purwar, R. Tailoring of Electrical and Optical Properties of Regenerated Silk Fibroin Films with Metal Oxides. *J. Mater. Sci. Mater. Electron*. 2020, *31*, 17784–17797. DOI: 10.1007/s10854-020-04332-4.

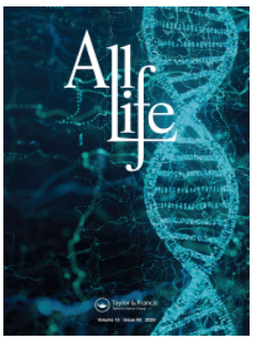

All Life

ISSN: (Print) (Online) Journal homepage: https://www.tandfonline.com/loi/tfls21

Electromyography data recorded from orbicularis oculi muscle during a novel grasping pilot study

Mohd Rizwan Jafar

To cite this article: Mohd Rizwan Jafar (2022) Electromyography data recorded from orbicularis oculi muscle during a novel grasping pilot study, All Life, 15:1, 678-683, DOI: 10.1080/26895293.2022.2079731

To link to this article: https://doi.org/10.1080/26895293.2022.2079731

© 2022 The Author(s). Published by Informa UK Limited, trading as Taylor & Francis Group.

Published online: 06 Jun 2022.

Submit your article to this journal

Article views: 41

View related articles

View Crossmark data

Full Terms & Conditions of access and use can be found at
https://www.tandfonline.com/action/journalInformation?journalCode=tfls21

ALL LIFE
2022, VOL. 15, NO. 1, 678–683
https://doi.org/10.1080/26895293.2022.2079731

Taylor & Francis
Taylor & Francis Group

DATA NOTE

OPEN ACCESS Check for updates

Electromyography data recorded from orbicularis oculi muscle during a novel grasping pilot study

Mohd Rizwan Jafar

Department of Mechanical Engineering, Delhi Technological University, Delhi, India

ABSTRACT

Developing assistive devices for quadriplegic people is very difficult because there are only a few ways in which we can take control commands from the patients. The challenge is to fulfill all the functional and non-functional requirements of the patients using those limited control commands. It is reported in the published literature that the abandonment rate of already available assistive devices is very high. We require more and more research in this domain so that we can develop more effective devices and control algorithms. One hindrance in the development of these devices and control algorithms is the limited access to machines to receive required data from the patients to control assistive devices. In this research, we have proposed a novel way to control assistive devices and presented data for the development of the algorithm too. We recorded the data from the orbicularis oculi muscle from 5 healthy volunteers. Volunteers included 3 males and 2 females, aged 29.5 ± 2.1 years. The recording was done with the help of the RMS Salus 2c EMG machine.

ARTICLE HISTORY
Received 7 September 2021
Accepted 2 May 2022

Introduction

Quadriplegia is a condition in which a person cannot move his arms and legs. The general cause of this condition is an injury to the spinal cord. Published literature reports an average of 500,000 fresh cases of quadriplegia annually (Mathur et al. 2015).

Although the situation of spinal cord injuries is terrible for all the patients, it is worse for the patients of poor countries. Most patients suffering from quadriplegia in poor countries are industrial laborers having an average family monthly income of $15 or less. Published survey report's that about 50% of the patients suffering from this condition are from nuclear families (Mathur et al. 2015; Bian et al. 2016; O'Bard et al. 2017). Another important takeaway from these surveys is that most of the patients, i.e. (80–90%) are male. Hence, in many cases, the caregiver is a woman. Keeping the fact in mind that a quadriplegic patient depends on caregivers for all of its needs, it becomes very difficult for a caregiver to attend to all the needs of the patient. An assistive device/self-help device that can address some of the functional and non-functional requirements of these patients can make the task of caregiver easy.

It has been reported in the literature that the abandonment rate of already available assistive devices for quadriplegic people is very high. Major reasons for the abandonment are the cost of the device, the device not addressing the actual issues, and the patient's inability to accept the technology (Jiang et al. 2018; Jafar and Nagesh 2020). It has been reported that there is a vast gap between the requirements of the quadriplegic subject and the solutions available for them in the published literature (Ruíz-Serrano et al. 2013; Chowdhury et al. 2018; Jiang et al. 2018; Jafar and Nagesh 2020).

We conducted a literature review to find the current state-of-the-art in the development of assistive devices for quadriplegic people. We did a search using keywords ('Self-help devices' OR 'Assistive Devices' OR 'Assistive Product' OR 'Assistive Technology') AND 'Quadriplegia' in Science Direct, Pubmed, IEEE Xplore digital library, and Web of Science databases. Original articles, technical and case studies, conference articles, and literature reviews published between 2014and 2019 were used for the study. The research group published the detailed review in the cited article (Jafar and Nagesh 2021). From the review of the literature,

CONTACT Mohd Rizwan Jafar mohdrizwan_phd2k16@dtu.ac.in Department of Mechanical Engineering, Delhi Technological University, Bawana Road, Delhi 110042, India

© 2022 The Author(s). Published by Informa UK Limited, trading as Taylor & Francis Group.
This is an Open Access article distributed under the terms of the Creative Commons Attribution-NonCommercial License (http://creativecommons.org/licenses/by-nc/4.0/), which permits unrestricted non-commercial use, distribution, and reproduction in any medium, provided the original work is properly cited.

we can categorize Assistive devices which work on physiology-based signals in the following categories.

Electroencephalography (EEG) Based devices: EEG-based Self-help devices (SHD) use signals generated in the brain. To use these signals, to develop SHD, we need to classify them efficiently. But the classification of these signals is very difficult due to low spatial resolution (AL-Rousan and Assaleh 2011; Khalid et al. 2015). There is a lot of noise present in these signals too, which makes it difficult to classify them. We can increase the classification accuracy by placing electrodes strategically in specific locations. This will help us in extracting multiple signals simultaneously and using a combination of patterns to identify a specific task (Squires et al. 2013; Schmalfuß et al. 2016). But placing these electrodes in these strategic locations is a challenge, as a minor change in position can have a tremendous impact on classification algorithms.

Voice recognition-based SHD: These kinds of devices use voice-based instructions to receive commands. We use these devices in smart homes to control electronic devices (Laumann et al. 2015; Jiang et al. 2018; Jafar and Nagesh 2021), Voice-controlled smart wheelchairs (Nam et al. 2014; Schmalfuß et al. 2016; Jafar and Nagesh 2021). The challenges with these devices are that the environmental conditions significantly affect classification accuracy. Misinterpreted commands can lead to sudden changes in velocity, the direction of the wheelchair, which can cause injury or frustration in these people (Hakonen et al. 2015; Jiang et al. 2018).

Tongue movement-based devices: These devices track the movement of the tongue and, based on these movements, SHD is controlled. They use external devices placed inside the mouth, which causes lots of speech and hygiene-related problems (Linskell and Bouamrane 2012). It has been reported that implantable tongue motion tracking devices can cause infections and other complications in subjects (26).

Electromyography (EMG) based devices: They are the devices that record the electrical signals generated when a muscle contracts. They have a better signal-to-noise (SNR) ratio as compared to the other type of physiological signals. They require less user attention as compared to the other type of signals (Nam et al. 2014; Hakonen et al. 2015). They are less affected by environmental noise. Although these signals have lots of advantages, they have some disadvantages too. All quadriplegic persons can't use them, as their application is limited to the physical condition of the subject. It is a challenge to identify multiple tasks while single commands can be identified easily.

We can conclude from the review that EMG-based devices are the best choice for developing self-help devices if the number of commands required to operate SHD is less. As these devices require voluntary control of muscles, for quadriplegic people only a limited amount of muscles can be used to generate the control signal as they cannot move their body below their neck. One muscle that is the best candidate to be used to control SHD by these people is the orbicularis oculi muscle.

In this paper, we have presented the recorded EMG signals which can operate an Assistive Device. With the help of this dataset, researchers can develop algorithms to operate assistive devices which can be operated by voluntary eye blinks. The researchers can also use this data to improve the currently available algorithms, which can address the unmet function and non-functional requirements of the users in a more efficient way.

Theory

The motor components of our nervous system control and execute the motor functions (movements) of our body. We have two types of motor components in our body.

Visceral Motor System
Somatic motor system

The Visceral motor system handles the involuntary control of muscles, while the somatic motor system handles voluntary control muscles. Hence, if a user wants to control a self-help device with the help of the movement of muscles, then the somatic motor system is the best candidate for that. We showed the motor components in Figure 1.

In this study, we aim to get control signals from a quadriplegic person. As a quadriplegic person in most cases can only move their body above the neck, we chose EMG signals generated during eye-blinks to receive control commands from the patient as they are less affected by environmental noise, they have a better signal-to-noise ratio and require less user attention.

Mechanism of Eyeblink: The eye blink occurs when the eyelid opens and closes. The following muscles control the movement of the eyelid.

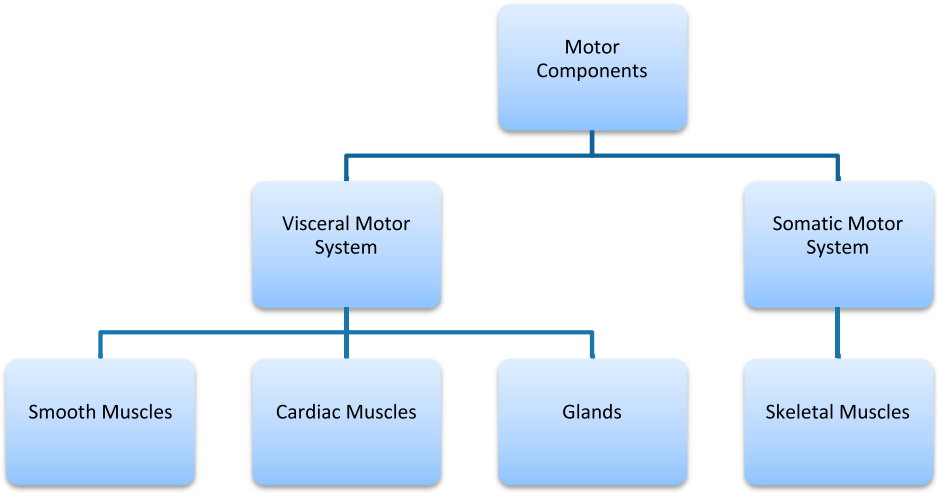

Figure 1. Motor components.

- Levator palpebrae superioris muscle
- Muller's muscle
- Frontalis muscle
- Orbicularis oculi muscle

For the opening of the eyelid, the Levator palpebrae superioris muscle is majorly responsible, with minor contributions from the muller's muscle and frontalis muscle, while for the closing of eyelid orbicularis oculi muscle is responsible.

Orbicularis oculi muscle has two major parts:

- Orbital part
- Palpebral part

The orbital part of the orbicularis oculi muscle is responsible for the voluntary closure of the eyelid while the palpebral part of the orbicularis oculi muscle does the involuntary closure. In this study, we have placed electrodes on the orbital part of the orbicularis oculi muscle to record EMG during eye voluntary closure of the eyelid.

Methods

Inclusion and exclusion criterion

Inclusion

(1) Volunteers with ability to understand the research requirements, signed informed consent form and consent to any restrictions applicable during the study.
(2) The age of volunteers was above 18.
(3) Volunteers who were completely healthy based on a medical assessment.

Exclusion

(1) Volunteers with visual impairment
(2) Volunteers with hearing Impairment

Experiment scenario

Following strategy was followed to perform the grasping operation

Step 1. The subjects were asked to view a computer screen where images of different hand configurations were flashed in a loop.
Step 2. Subjects were asked to blink voluntarily whenever the image of their choice was flashed.
Step 3. Whenever a blink was detected, an audio message was played asking if you wanted to do the selected grasp.
Step 4. The subject was again asked to confirm by blinking, if blink was detected wrongly then the subject was asked to do nothing.
Step 5. If the subject confirms the grasp selection then commands were sent to the actuator.
Step 6. If no grasp was detected till the end of the loop then the loop was re-initiated (Figure 2)

Recording of data

In this study, we have placed electrodes on the orbital part of the orbicularis oculi muscle to record EMG during voluntary closure of the eyelid.

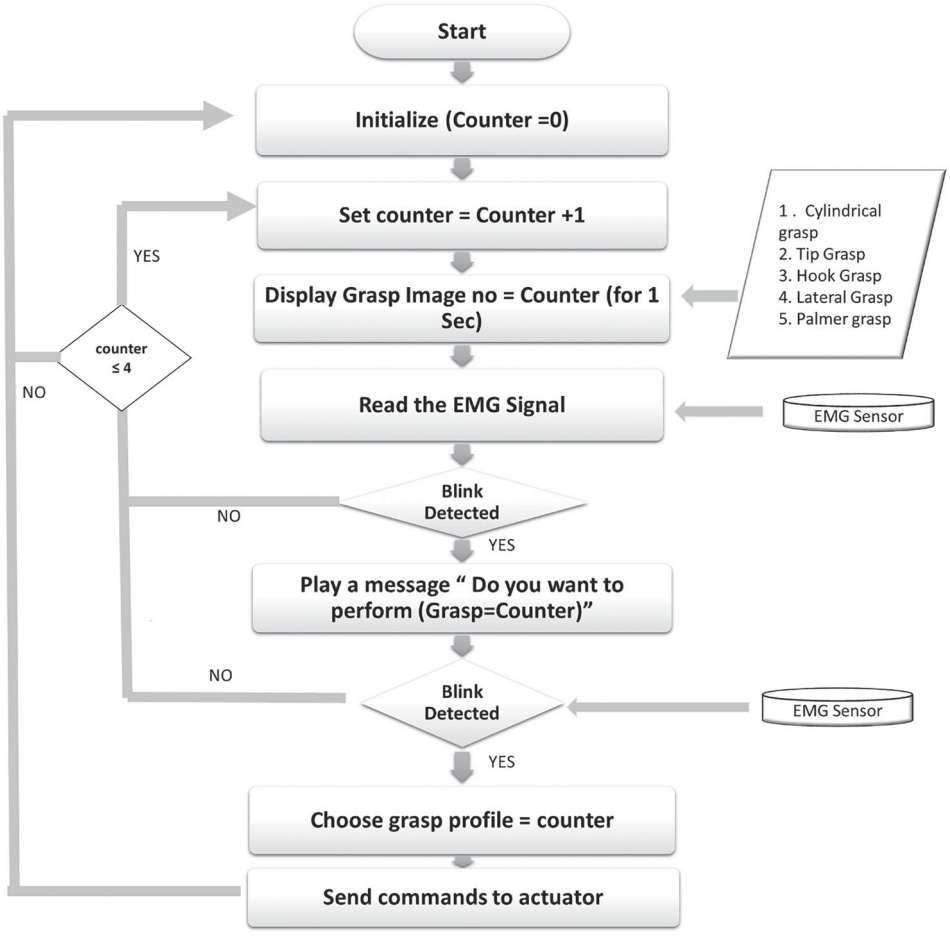

Figure 2. Grasp selection experiment.

We recorded surface EMG from the orbital part of the orbicularis oculi muscle of 5 healthy subjects. Subjects included 3 males and 2 females, age 29.5 ± 2.1 years. We recorded each subject 2 times a day for two days. The recording period was chosen randomly from 9 am to 5:30 pm. Each session was not less than 4 h apart.

The recording was done with the help of the RMS Salus 2C EMG machine, provided by RECORDERS & MEDICARE SYSTEMS PVT. LTD., India. Recording software was RMS EMG Salus V.7.7.1. The study was approved by the Ethical Committee of the Delhi Technological University, Delhi and all participants provided informed consent before their participation. We have shown the details of the experiment in Figure 3.

Table 1. Results of grasping experiment.

S. No	Participant 1	Participant 2	Participant 3	Participant 4	Participant 5
Trial 1	Yes	No	Yes	No	No
Trial 2	Yes	No	No	No	Yes
Trial 3	Yes	No	No	No	Yes
Trial 4	Yes	No	Yes	Yes	No
Trial 5	Yes	Yes	Yes	Yes	Yes
Trial 6	Yes	No	Yes	No	Yes
Trial 7	No	Yes	Yes	No	Yes
Trial 8	No	Yes	No	Yes	Yes
Trial 9	Yes	Yes	Yes	No	Yes
Trial 10	Yes	Yes	Yes	Yes	Yes
Trial 11	Yes	Yes	Yes	Yes	Yes
Trial 12	Yes	Yes	Yes	Yes	No
Trial 13	Yes	Yes	Yes	Yes	Yes
Trial 14	Yes	Yes	No	Yes	Yes
Trial 15	Yes	Yes	Yes	Yes	Yes
Trial 16	No	Yes	Yes	Yes	Yes

Results

In each recording session, 4 trials were recorded. Each day, recording was conducted in 2 sessions. As we did the recording for 2 days, hence total of 16 trials were recorded. We have shown the results of the experiment in Table 1, where yes represents a trial where grasp was done successfully, while no represents the trial where grasp was not performed successfully.

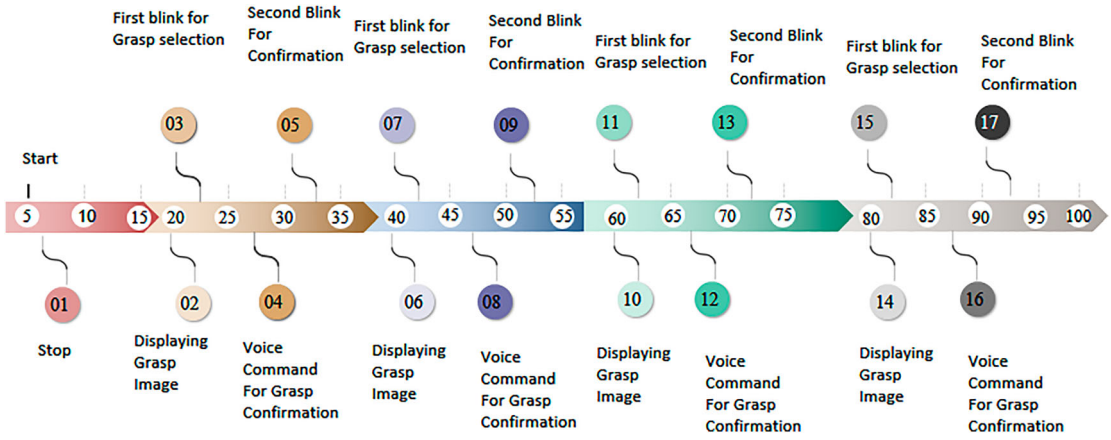

Figure 3. Signal recording trial timeline.

Author contribution

Jafar, Mohd Rizwan contributed to conception and design of the research, acquisition of data, analysis and interpretation of data, drafting the manuscript, revision of the manuscript for important intellectual content. All authors read and approved the final manuscript.

Disclosure statement

No potential conflict of interest was reported by the author(s).

Data availability statement

'The data that support the findings of this study are openly available in Mendeley Data [Jafar, Mohd Rizwan. 2022. EMG Data from Eyeblinks. Mendeley Data, V2. DOI:10.17632/nm535v73jj.2] at https://data.mendeley.com/datasets/nm535v73jj/2.

ORCID

Mohd Rizwan Jafar http://orcid.org/0000-0001-5048-6756

References

AL-Rousan M, Assaleh K. 2011. A wavelet- and neural network-based voice system for a smart wheelchair control. J Franklin Inst. 348(1):90–100. DOI:10.1016/j.jfranklin.2009.02.005.

Bian Z, Hou J, Chau L, Magnenat-Thalmann N. 2016. Facial position and expression-based human–computer interface for persons with tetraplegia. IEEE J Biomed Health Inform. 20(3):915–924. DOI:10.1109/JBHI.2015.2412125.

Chowdhury MR, Mollah MN, Raihan M, Ahmed AS, Halim MA, Hossain MS. 2018. Designing a cost effective prototype of an automated wheelchair based on EOG (electrooculography).

Hakonen M, Piitulainen H, Visala A. 2015. Current state of digital signal processing in myoelectric interfaces and related applications. Biomed Signal Process Control. 18:334–359. DOI:10.1016/j.bspc.2015.02.009.

Jafar MR, Nagesh D. 2020. Classification of mental tasks by using statistical process control and artificial neural networks. Eur J Mol Clin Med. 7(8):3085–3093. https://ejmcm.com/article_4823.html.

Jafar MR, Nagesh DS. 2021. Literature review on assistive devices available for people with quadriplegia: Indian context. Disabil Rehabil Assist Technol. DOI:10.1080/17483107.2021.1938708.

Jiang H, Duerstock BS, Wachs JP. 2018. Variability analysis on gestures for people with quadriplegia. IEEE Trans Cybern. 48(1):346–356. DOI:10.1109/TCYB.2016.2635481.

Khalid U, Conti GE, Erlandson RF, Ellis RD, Brown V, Pandya AK. 2015. Voice-activated lightweight reacher to assist with upper extremity movement limitations: a case study. Assist Technol Off J RESNA. 27(2):112–120. DOI:10.1080/10400435.2014.970676.

Laumann A, Holbrook J, Minocha J, Rowles D, Nardone B, West D, Kim J, Bruce J, Roth E, Ghovanloo M. 2015. Safety and efficacy of medically performed tongue piercing in people with tetraplegia for use with tongue-operated assistive technology. Top Spinal Cord Inj Rehabil. 21(1):61–76. DOI:10.1310/sci2101-61.

Linskell J, Bouamrane M-M. 2012. Assisted-living spaces for end-users with complex needs: a proposed implementation and delivery model. Health Informatics J. 18(3):159–170. DOI:10.1177/1460458212441474.

Mathur N, Jain S, Kumar N, Srivastava A, Purohit N, Patni A. 2015. Spinal cord injury: scenario in an Indian state. Spinal Cord. 53(5):349–352. DOI:10.1038/sc.2014.153.

Nam Y, Koo B, Cichocki A, Choi S. 2014. GOM-face: GKP, EOG, and EMG-based multimodal interface with application to humanoid robot control. IEEE Trans Biomed Eng. 61(2):453–462. DOI:10.1109/TBME.2013.2280900.

O'Bard B, Larson A, Herrera J, Nega D, George K. 2017. Electrooculography based iOS controller for individuals with quadriplegia or neurodegenerative disease. In: 2017 IEEE international conference on healthcare informatics (ICHI), August. p. 101–106. DOI:10.1109/ICHI.2017.90.

Ruíz-Serrano A, Posada-Gómez R, Sibaja AM, Rodríguez GA, Gonzalez-Sanchez BE, Sandoval-Gonzalez OO. 2013.

Development of a dual control system applied to a smart wheelchair, using magnetic and speech control. Procedia Technol. 7:158–165. DOI:10.1016/j.protcy.2013.04.020.

Schmalfuß L, Rupp R, Tuga MR, Kogut A, Hewitt M, Meincke J, Klinker F, Duttenhoefer W, Eck U, Mikut R, Reischl M. 2016. Steer by ear: myoelectric auricular control of powered wheelchairs for individuals with spinal cord injury. Restor Neurol Neurosci. 34(1):79–95. DOI:10.3233/RNN-150579.

Squires LA, Rush F, Hopkinson A, Val M. 2013. The physical and psychological impact of using a computer-based environmental control system: a case study. Disabil Rehabil Assist Technol. 8(5):434–443. DOI:10.3109/17483107.2012.749427.

Research Square

Preprints are preliminary reports that have not undergone peer review.
They should not be considered conclusive, used to inform clinical practice,
or referenced by the media as validated information.

Energy efficient cluster-based routing protocol for Wireless Sensor Network using Nature Inspired Mechanism

Rashmi Mishra (dtuphd.rashmi@gmail.com)
Delhi Technological University https://orcid.org/0000-0003-0015-8732
Rajesh K. Yadav
Delhi Technological University Department of Computer Engineering

Research Article

Keywords: Wireless Sensor Networks, Energy Efficiency, Throughput, Delay, Nature Inspired Algorithm

Posted Date: June 13th, 2022

DOI: https://doi.org/10.21203/rs.3.rs-1618701/v1

License: This work is licensed under a Creative Commons Attribution 4.0 International License.
Read Full License

Energy efficient cluster-based routing protocol for Wireless Sensor Network using Nature Inspired Algorithm

[1]Rashmi Mishra, [2]Rajesh K. Yadav
[1]Ph.D. Scholar
[1-2]Delhi Technological University, Delhi, India

Abstract:

WSN consist of tiny sensors which are distributed over the entire network having capabilities of sensing the data, processing it and convey it from one node to another node. The purpose of the study is to minimize the power utilization per round and elevate the network lifespan. In the present case, the nature inspired mechanisms are used to minimize the power utilization of the network. In the proposed study Butterfly Optimization Mechanism is used to choose the optimum quantity of CH from the dense nodes. The parameter is to be considered for the choosing of the CH is the remaining power of the node, interspace from the other nodes in the network, interspace from the BS, node centrality and node degree. The PSO is used to form the CH by choosing certain parameters such as interspace from the CH and the BS. The path is choosing by means of the Ant Colony Optimization (ACO) Mechanism. The route is optimized by the interspace, node degree and the choose remaining power. The inclusive performance of the projected protocol is measured in terms of stability period, quantity of active nodes, data acknowledged by the BS and the overall power utilization of the network. The results of the put redirect methodology are correlated with the extant mechanisms such as LEACH, DEEC, DDEEC, EDEEC [50-53] and also correlated with the swarm mechanisms such as CRHS, BERA, FUCHAR, ALOC, CPSO, FLION. This review will help investigators to discover the applications in this arena.

Keyword: Wireless Sensor Networks, Energy Efficiency, Throughput, Delay, Nature Inspired Algorithm

1. INTRODUCATION

With concern of Wireless Sensor networks lifespan, nature-inspired mechanisms are evolving as an appropriate technique. For increasing the lifespan of the network or in order to decrease sensing the unnecessary data by the battery-driven sensors, optimal network scope plays an important role. To sense and store the actual data from the nature, the large quantity of geographically distributed sensors communicated along the wireless means, it is formally known as Wireless Sensor networks (WSNs) [1]. Sensors are operating like repeater as they will accept the data, convert the analogue to digital form and redirect the data to the other nodes, CH and the sink. The BS will collect the data, analyze it and take decision as per the application. There are various parameters on which WSN architecture is depend such as fault tolerance (sensor node will redirect the packet and acknowledged the packet if some of the sensors get drained), scalability (how network will work if sensors will be added or removed), stability, power efficiency. These sensors are battery powered. So, after some time, the power of the sensors will get depleted and it affects the entire lifespan of the network. The purpose of the study is to maximize the network lifespan by increasing the quantity of nodes per round, data send to the BS and the optimal quantity of CH choosing. In the extant case, optimal network scope, clustering mechanism and the path choosing are mostly used in the WSNs to elevate the lifespan of the network.

WSN consist of tiny sensors which are distributed over the entire network having capabilities of sensing the data, processing it and convey it from one node to another node. These sensors sense the nature, evaluate, send and accept it. Military, weather forecasting, industrial area, medical services, agriculture or many other applications use the WSN for the data transmission. Sensors are limited battery powered and very compact in size. Once, sensors are placed in the harsh and no-man nature, these sensors will be used in the adequate way because it cannot be replaced and charged. Nodes drain their power in two ways such as sensing the natural data and conveying the data to the BS [2-10]. Most of the work has been done to maximize the entire lifespan of the network by saving the power of the sensors. Liank et al. [11] has put redirect the mechanism named as Huang mechanism, aims is to balance the power utilization in the entire network by using optimal choosing of clusters in the entire network. But the restriction of this mechanism is, it is very complex and if in case the data size of the packet is large then it may block the channel. In contract, Cardei et al. [12] have put redirect TianD mechanism, in which sensors nodes are arranged in disjoint set form to cover the maximal range. As compare to the Hunag mechanism, TianD mechanism is less complex in nature. However, the mechanism will not able to find the duplicate nodes and data in the nature.

2. LITERATURE SURVEY

The challenges faced by the wireless sensor network are power constraint, correct detection of data, and non-duplicate data, the sensors need to be placed in such a way that they in appropriate interspace from each other but considering the uncovered area which leads to the scope hole or blind area problem. For the above stated problem, Wang et al. [13] has put redirect a mechanism named as Scope Configuration Protocol. The protocol is well suited for the nature where the quantity of sensors is less or significant. After the literature survey, the two problems have been observed, i.e., power depletion of the sensors and the sensor node scope problem and there exit aback-and-forth between these two problems. In the literature, may authors have put redirect

the solution for the individual problem but not provide collectively. After the survey, keeping the extant problems, we have collectively considered the problem and put redirect the multi-purpose optimization mechanism. There are various mechanisms are published in the literature for the WSN by using nature-inspired mechanisms [14-18]. There are multiples mechanisms put redirect by the authors to cover the optimal scope in WSN [19-21]. In [19], Metaheuristics for the deployment problem of WSN: A review, discuss ethe various types of issues while deploying the sensors in the nature by using nature-inspired mechanisms. In [20], Optimal sensor network layout using multi-purpose metaheuristics, author equated the three protocols and highlights the problem associated with mechanisms in terms of optimal scope. In [21], Transmutative intelligence in wireless sensor network: routing, clustering, lateralization and scope., have discussed the genetic, transmutative and theoretical, mathematical and practical applications of the cluster formation, optimal scope of the network and the lateralization problem in WSNs. Other challenges faced by the WSN is insufficient power of the sensors which leads to the network failure [14-17]. So, the main dissimilarity between the WSN and the other network is, WSN is oversensitive and vulnerable to the power. So, the optimal utilization of power mechanism is the esteem necessity for the wireless sensor network [20]. Nature-inspired mechanism is best suited for cluster formation and choosing the best path will elevate the life of sensors along which the we can elevate the entire lifespan, stability period and scalability of the network [21-23]. A cluster having CH who communicate with the other CHs in the network. Most of the power is consumed when the data is transfer in between the CHs and the BS. To turn down the power utilization in the clustered wireless sensor network, routing mechanism is used in between the CHs and the BS [24-27]. However, none of the mechanisms deliver serious effects of the problem in the wireless sensor network to cover the optimal solution. The purpose of the paper is to turn down the power utilization of the network during the data transmission by literature survey of recent clustering and routing mechanisms. We have also briefed the nature-inspired mechanisms and their applications used in the wireless sensor networks in terms of capacity, robustness, self-adaptability. We have also discussed the strengths and weaknesses of the work done by the different researchers in section 3. The optimization mechanism is segregated into three types such as model based, simulator based, mechanism based. Mechanism based is further bifurcate two parts such as deterministic and stochastic mechanism. Stochastic mechanism is further bifurcate two parts heuristic and meta-heuristic. The meta-heuristic mechanism which is further bifurcate four parts i.e., human inspired, geography inspired, physics inspired and bio-inspired. Bio-inspired mechanism is further bifurcate three parts transmutative, swarm based and plant based [62-64]. Furthermore, there are more than thirty swarm based optimization is put redirect by the researchers. The swarm-based mechanism is used in wireless sensor network to resolve many extant problems such as to upgrade the power efficiency of the network, to elevate the network lifespan, to maximize the packet delivery ratio in the network. The conventional routing protocols are inefficient to upgrade the power constrain of the wireless sensor network. So, to upgrade the power constrain of the network, researchers used the efficient clustering and routing protocols by the use of swarm-based approach. As per the research, the Ant Colony Optimization [28] is used to upgrade the power efficiency of the network and one of the efficient mechanisms for routing. A review chronology of the research is shown in the fig 1. The review is done on the basis of paper publication in the area of power efficiency, security based, delay, error free protocol and the cluster-based. The most of the paper were based on the cluster formation and based on the power efficiency upgradient of the network [65-70].

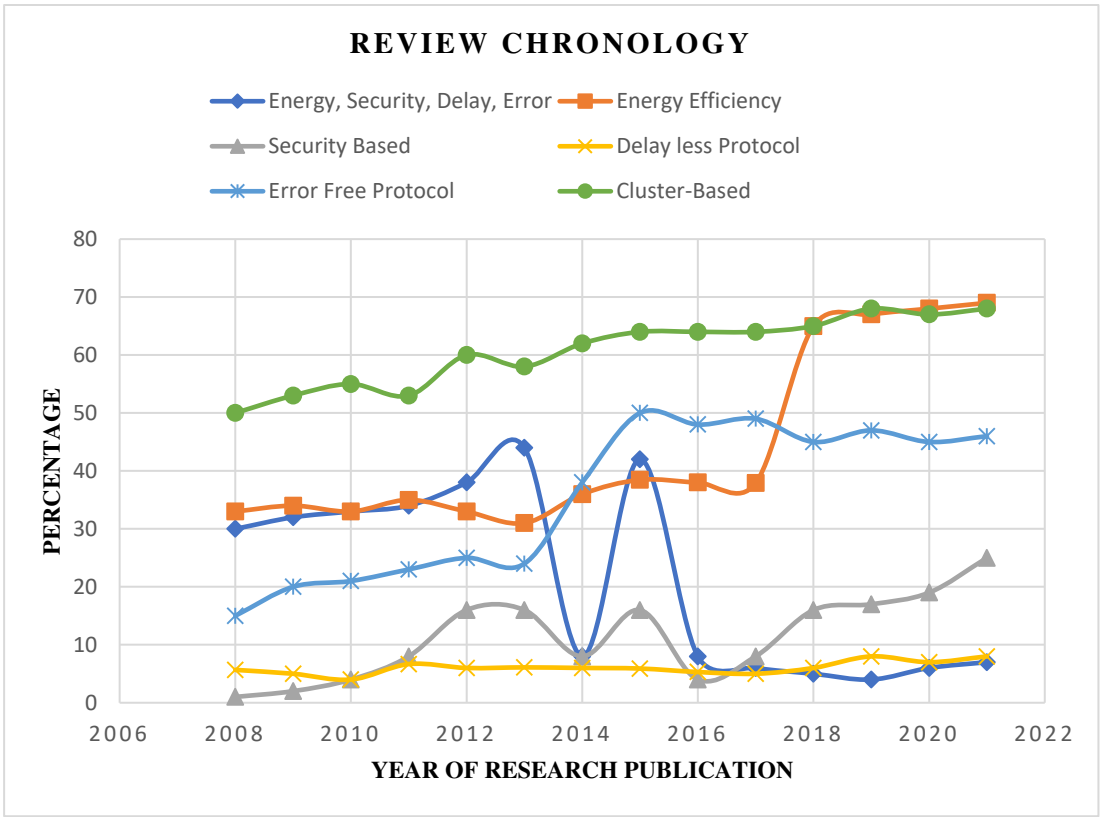

Fig 1: Review Chronology

2.1 Classical approaches

In 2002, LEACH was habituated by W. Heinzelman, the sensors choose their CH and form a cluster. CH collect all the data form the nodes and send the data to the BS. The elected CH will lose their power very fast. In 2017, Wang et al. put redirect a mechanism named as LEACH-impt [48]. Is LEACH-impt the communication follows the inter-cluster routing. The route is choosing on the basis of quantity of hops per path, path remaining power, power utilization per round. The overall performance of LEACH-impt in terms of power efficiency is upgraded but due to arbitrarily choosing of CH and changes in topology, the data loss is high.

Haseeb et al. put redirect a mechanism named as WECRR (Weighted Power-Efficient Clustering with Robust Routing protocol. In WECRR [47], the CH is choosing on the basis of deterministic strategy. Secondly, the routing decision is taken based on multi-facet factors such as traffic density, remaining power and packet error ratio. Furthermore, the route maintenance and load distribution among the nodes are upgraded by the protocol. But the restriction of the put redirect mechanism is that, the interspace between the node and the BS is not considered by the protocol. Again, Haseeb et al. has put redirect a mechanism named as AECR (Aware Cluster Based Routing) [45]. The CH choosing is based on the node density and the position of the node. The advantages of the mechanism are it turn downs the cluster overhead and communication cost and it mainly focus on the power of the node. The disadvantage of the mechanism is that it doesn't focus on interspace between the nodes [28].

Hang and Zhang put redirect a mechanism named as WPO-EECRP [47]. In this protocol, the CH is choosing on the basis of remaining power, interspace from the node, interspace from node to BS and the cluster density. The mechanism works well when there is adjacent quantity of nodes are present in between the CH and BS and it will elevate the power utilization of the network.

2.2 Optimizations in WSNs using Swarm Intelligence

An optimization is achieved by designing a model, by using a simulation and by designing a mechanism. A detailed taxonomy of the swarm-based optimization used in WSNs is shown in Fig 2. The swarm-based mechanism is bifurcate two parts such as local search (deterministic) and global search (stochastic). Local search provides the theoretical assumption about the formulated problems, provide the analytical properties [71-72]. Guarantee of reaching the global minimum and at least a local minimum, whereas global search provides the guarantee in terms of probability. However global search is much faster than the local search. Additionally, the global search method is further classified into two parts: heuristic mechanism is problem-dependent mechanism and meta-heuristic mechanisms is problem-independent. Both the mechanism is used to speed up the process of finding the global optimum solution where the finding the solution is difficult. Because the heuristic mechanisms are based on the adaptive and greedy approach, therefore they are more prone to get stuck at local optima which result to fail to obtain global optima [29]. However, meta-heuristic is non-adaptive and non-greedy approach and able to find the global solution. The meta-heuristic mechanism is also known as nature-inspired mechanism. The nature inspired mechanism is further bifurcate four parts: bio-inspired, physics inspired, geography inspired and human inspired [30-37]. The bio-inspired mechanism is bifurcate three parts: transmutative, swarm based and plant based. Because the nature inspired mechanisms, most of the mechanisms are inspired by the biological system. Therefore, most of the parts of the nature inspired mechanisms are based on the bio-inspired mechanism. The transmutative mechanism is based on the Darwin's principle of choosing whereas the swam is based on the collective intelligence [38].

Fig 2: Taxonomy of the Swarm-Based Optimization

As per the research the most popular mechanism used for the CH choosing is butterfly optimization mechanism, for the cluster formation particle swarm optimization mechanism is popular and for the efficient route choosing the ant colony optimization mechanism is used by the researchers to upgrade the power efficiency of the wireless sensor network [73]. The ant colony optimization mechanism works with other popular mechanisms to upgrade the power efficiency of the network such as fuzzy logic [39]. Xie et al [41]. put redirect a mechanism based on the ACO for wireless sensor network named as Type-2 Mamdnai Fuzzy Logic System. The route in between the CHs is chooses on the basis of Ant Colony Optimization and the CH choosing is based on the remaining power, interspace to the BS and quantity of nearest nodes. The CHs choose all the statistics from the nodes and send it to the BS. Arjunan and Sujatha put redirect a mechanism-based o the fuzzy logic to develop the inadequate clusters and the routes were chooses using Ant Colony Optimization technique. The CHs are chooses on the basis of remaining power, node degree, interspace from the BS, node centrality and interspace from the nearest nodes [40]. The mechanism is well suited to maintain the lifespan of the network [74]. Trend of the literature Fig 3. shows that ACO, PSO and BOA is used by the

many researchers to optimize the extant problem in wireless sensor network such as optimal route choosing, optimal quantity of CH choosing per round, optimal quantity of nodes is chooses per round and elevate the packet transmission in between the CH and the BS [42][51].

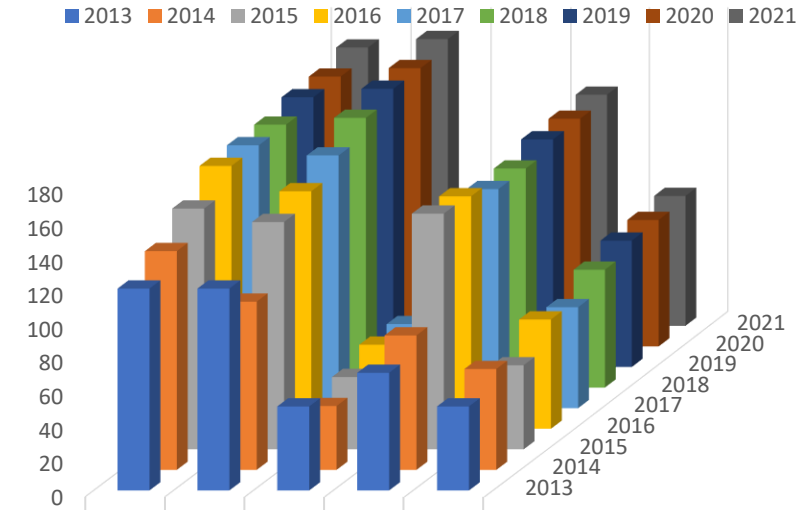

	PSO	ACO	FA	BOA	ABC
2013	120	120	50	70	50
2014	130	100	38	80	60
2015	143	135	43	140	50
2016	156	141	50	138	65
2017	156	150	50	130	60
2018	156	160	50	130	70
2019	160	165	50	135	75
2020	160	165	50	135	75
2021	165	170	52	137	77

Fig 3: Trends of the mechanism

3. WSN AND OPTIMIZATIONS

The main issues related to the wireless senor network is categories into three main sections such as power efficiency, Quality of service and the security. The optimization mechanisms are used in wireless sensor network to solve the extant problem i.e., optimal scope of the sensors, data aggregation, power efficient clustering and routing and the sensor lateralization. There is a correlation in between all the stated problems such as if we go for the service quality then we have to trade off with the lifespan of the network. Same follow with the security, for achieving the security, again we have to trade off with the lifespan of the network. If we address the problem individually, many loopholes exit and will never solved. So, to discover balanced wireless sensor network, we have to build the optimized mechanism which can handle all the problems simultaneously. The solution of the problem is to create a multi-purpose function and optimize the mechanism by using appropriate optimizer mechanism. For choosing the appropriate mechanisms, various factors have been considered such as problem type, time constraint, availability of resources, accuracy desired. To achieve the better performance of the network, the researchers have used many approaches in nature inspired mechanisms such as, classical approaches [28-32] and swarm intelligence-based approaches [33-43]. There are various types of mechanisms present in the literature focused on the different types of problem faced by the wireless sensor networks named as Optimal Scope, Data Aggregation, Power Efficient Clustering, Power Efficient Routing mechanisms, Sensor lateralization [75-76]. Table 1 shows the detailed survey of the extant mechanism in terms of the various parameters such as Power Efficiency, Latency, along put, Scalability, Connectivity, Load Balancing, Packet Loss Ratio, Reliability, Complexity.

Table 1: Survey of the extant mechanism with various parameters

S.No	Mechanism	Abb.	Authors	Year	Best For	Power Efficiency	Latency	Throughput	Scalability	Connectivity	Load Balancing	Packet loss rate	Reliability	Complexity
1	Ant Colony Optimization	ACO	Dorigo	1992	Path choosing, routing	H	S	H	H	M	M	M	M	M

2	Particle Swarm Mechanism	PSO	Kennedy and Eberhart	1995	Cluster, path choosing, gives optimum results in less parameters	L	S	M	H	N/A	S	H	M	S
3	Artificial Fist Swarm Mechanism	AFSA	Li et al.	2002	Cluster formation	L	M	S	H	M	M	H	M	M
4	Bacterial Foraging Optimization Mechanism	BFOA	Passion	2002	CH choosing, routing	M	M	S	M	M	S	S	M	M
5	Glowworm Swarm Optimization	GWO	Krishnanad and Ghose	2005	Path choosing, routing	H	S	S	M	M	M	M	S	M
6	Cat Swarm Optimization	CSA	Chu et al.	2006	Find best location for the near sink node, choose CH, Perform well with K-mean Clustering	L	M	M	M	S	M	M	S	M
7	Artificial Bee Colony	ABC	Karaboga and Basturk	2007	Cluster formation, CH choosing	M	S	M	M	M	S	M	L	M
8	Cuckoo Search	CS	Yang and Deb	2009	Cluster formation, CH choosing	M	S	M	M	M	S	S	M	S
9	Bat Mechanism	BA	Yang	2010	Node lateralization	M	S	M	M	M	M	M	M	M
10	Firefly Mechanism	FA	Yang	2010	Clustering, Node lateralization	M	S	M	M	M	S	M	S	M
11	Krill Herd Mechanism	KH	Gandomi and Alavi	2012	Finding the interspace	L	S	S	M	S	M	M	M	M
12	Dolphin Enholocation	DE	Kaveh and Farhoudi	2013	CH choosing, Security needs to be considered	M	S	M	M	M	M	M	M	H
13	Chicken Swarm Optimization	CSO	Meng et al.	2014	CH choosing	M	M	S	H	M	S	M	M	M
14	Grey Wolf Optimizer	GWO	Mirjalili et al.	2014	Network scope optimization, CH CHOOSING	H	M	M	H	M	M	M	M	H
15	Ant Lion Optimizer	ALO	Mirjalili	2015	Scope, connection, the network-longevity and minimized power utilization.	H	M	M	M	M	M	M	M	H
16	Dragonfly Mechanism	DA	Mirjalili	2015	lateralizationproblem	L	S	M	M	M	M	M	M	M
17	Whale Optimization Mechanism	WOA	Mirjalili and Lewis	2016	CH Choosing	M	S	M	M	M	M	M	M	M
18	Crow Search Mechanism	CSA	Lalireza Askarzadeh	2016	CH choosing, Work with few parameters	H	S	M	M	M	M	M	S	S
19	Grasshopper Optimization Mechanism	GOA	Saremi et al.	2017	Network lifespan, end-to-end delay, best with ABC	M	S	M	M	M	M	M	M	M
20	Butterfly-inspired Mechanism	BOA	Qi et al.	2017	Node lateralisation, cluster formation	S	M	M	M	S	S	S	M	M

21	Salp Swarm Mechanism	SSA	Mirjalili et al.	2017	Node lateralisation	S	M	M	M	S	S	S	S	M
22	Equilibrium Optimizer	EO	Faramarzi et al.	2019	Routing, Load Balancing, Clustering	M	M	H	M	M	M	M	M	H
23	Bald Eagle Search	BES	Alsattar et al.	2019	Latest Technology, Literature not available									
24	Harris Hawks Optimization	HHO	Heidari et al.	2019										
25	Nuclear Reaction Optimization	NRO	Wei et al.	2019										
26	Border Collie Optimization	BCO	Dutta et al.	2020										

3.1 Optimal Scope in WSN

Optimal Scope of sensors in the wireless sensor network is very essential part of the network to elevate the network lifespan. Scope of the area in such a way that it targets the entire area with minimum quantity of senor nodes. The key parameter of choosing the area is to choose the shape of the test area. In the extant literature, there are various shape available such as irregular, solid structure, hexagonal shape or the circular shape. In the figure, we show the four two-dimensional geometrical-based sensing shapes [54-57]. In the present case, the outline of the test area is uneven and multifaceted due to territory properties and solid shape. However, the hexagonal or a circular shape is use for the computational and conceptual ease. In general, hexagonal shape is applied or used by the researchers/industry experts because of its flexible and overlapping feature. Though, the circular shape is more pronoun because of its low complexity. The restriction is remunerated by growing the radius of the circle. Due to elevate in the radius of the circle, another problem comes into picture that is duplicate data sensed by the sensor. As more duplicate data is sensed by the sensor, there will more power utilization [58-60]. We can turn down the problem by enhancing the single purpose optimization problem into multi-purpose problems by choosing the other parameters.

3.2 Power efficient clustering and routing in wireless sensor network

As wireless sensor network is composed of the sensors which are inbuilt with the battery for shorter duration. These batteries are not be recharged, so the need of the power efficient networks is of the utmost importance in the extant case [61]. The sensors dissipate their power by sensing the data from the nature and send it to the BS by using multi-hop communication. For reducing the power utilization of the nodes, first clusters are formed, secondly CHs are chooses based on the remaining power, and thirdly, the path is chooses for the data transmission using optimum routing techniques. In the given domain, the problem faced by the networks are:

- The choosing of the CH having high power and choosing of routing path from each round.
- Maximization of network lifespan and packet delivery ratio to the BS.
- Interspace from the sensor node to the CH and CH to the BS should be minimized.

4 PROBLEM STATEMENT

The problem faced by the WSN are: To find the appropriate purpose function to preserve or creating the power efficient network. For remaining power, weighted power-efficient clustering with robust routing for wireless sensor network [44], and Aware cluster-based routing [45] is put redirect. The overall power of the network is preserved by considering the power as well as interspace. In clustering and routing in wireless sensor using harmony search mechanism [46], the lifespan is affected by the quantity of member nodes in of the CH. In energy efficient clustering routing protocol [47] based on parameters optimization in WSN, the information communication from Cluster Head to the Base Station also affects the network lifespan. The Ant colony optimization generate the packet loss due to the proactive and reactive mechanisms. The solution of the above mentioned to create a mechanism focused on the power of the node and the interspace of the node to the CH and from CH to the BS. The best path choosing will be implemented by multi-purpose function. And the packet drop ratio is minimized by the considering the power of each node. For creating the purpose function, one need to consider the remaining power, interspace from the node to the CH and from CH to the BS. Therefore, it will work in the small as well as large network.

4.1 Preliminaries

This section describes the network and power model as well as describe the PSO (Particle Swarm Optimization) is used to formulate the clusters, BOA (Butterfly Optimization) technique for finding the CH, ACO (Ant Colony Optimization) technique for finding the route from the source to the sink.

4.1.1 Network model

- Sensors are arbitrarily deployed in the network, later they are constant in nature.

- BS receives the data such as remaining power of the node, interspace from the sensors from all the sensors in the nature.
- To configure the network model of wireless sensor network, all the knob are comparable to each other in terms of original energy and the dispensation period.
- The interspace amongst the sensor knob to the Cluster Head and from Cluster Head to the BS is intended grounded on the Euclidean interspace.
- Clusters are formed using Cluster formation mechanism, then CHs are chooses using choosing mechanism. Then the routing mechanism is used to find the route from source to the sink.

4.1.2 Energy Model

Given in the research, a elementary radio model (1st order) is measured to compute the power of the nodes. For conveying the l bits from the source to the sink over the interspace d is calculated by using the equation 1 and 2 respectively:

$$E_{TX}(l,d) = \begin{cases} LE_{elec} + LEfsd^2 & if\ d < do \\ LE_{elec} + LEmpd^4 & if\ d \geq do \end{cases} \quad (1)$$

Where LE_{elec} is the power used to run the converter (ETX) or (ERX) and the threshold value is d_0. For the experimental survey, free space and multi-path models is expressed as E_{fs} and E_{mp} . These values are depended on the converter amplifier model. Where d0 is expressed as

$$d_0 = \sqrt{\frac{E_{fs}}{E_{mp}}} \quad (2)$$

5 PUT REDIRECT METHOD

The put redirect model has three mechanisms: First is used to form clusters, second is used to choose the CH by considering the remaining power and the interspace from the sensors and other one is used to find the path or route over the entire network. The PSO is used to form the cluster, BOA is used to find the optimum quantity of CHs in each round and ACO is used to find the route from the source to the sink or from CH to the BS. The entire process is described in the figure 4.

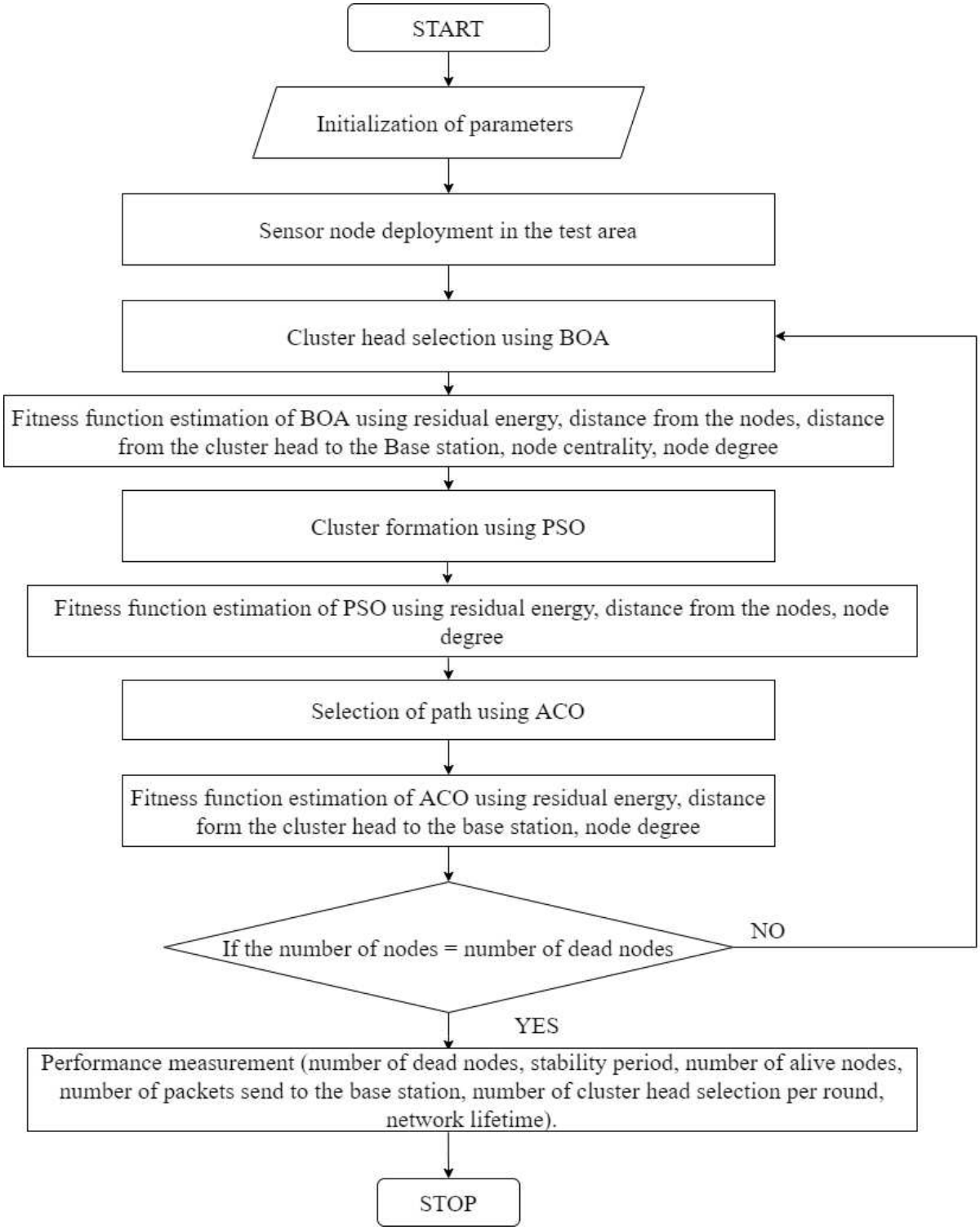

Fig 4: Flow Chart

6.1 CH choosing using BOA

BOA (Butterfly Optimization Mechanism) is introduced in 2019 by Sankalap Arora [50]. The mechanism shows the butterfly food search and its mating behavior. In general, butterflies are fascinated to every last one along the cologne of other apprehensions. The crusade of butterfly is moreover in haphazard way or in the way of the other butterflies who produces the stronger cologne. The purpose function is used to compute the inducement strength. The butterfly optimization mechanism chooses the ideal quantity of CH using the certain parameter: node notch, node uniqueness, interspace to its nearest, interspace between the Base Station to the Cluster Head and the remaining power of the sensors. The author use algorithm proposed by Prachi M. et al. [30]. The steps of the algorithm are as follows:

Node degree: It is defined as the quantity of sensors connect to the Cluster Head. The Cluster Head with the less quantity of knob are chooses as CH with the higher quantity of connected sensors deplete their power fast. The degree of the node is calculated as sum of power of all the sensors belongs to the CH. The weight value for the purpose function is 0.1.

$$ND = \sum_{i=1}^{m} I_i \tag{3}$$

Node centrality: It is defined as how much a node is halfway situated from the nearest nodes. The weight value for the purpose function is 0.1 and it is calculated by using the eq:

$$C_n = \sum_{i=m}^{m} \frac{\sqrt{\frac{\sum_{j \in n} dist^2(i,j)}{n(i)}}}{Network\ dimension} \tag{4}$$

where n(i) quantity of nearest node to the CH i.

Remaining Power of the node: The node with the higher remaining power will become the CH because the CH need to perform the various task such as aggregate the data, remove the duplicate data, data transmission to the BS. The weight value for the purpose function is 0.3. Thus, the node with higher remaining power will chose as the CH and the remaining power is calculated as:

$$R_e = \sum_{i=1}^{m} \frac{1}{E_{CHi}} \tag{5}$$

where the remaining power of the ith CH is E_{CHi}.

Interspace between the sensors: It is defined as the interspace from the sensors to the CH and from nearest sensors with in the cluster. Lesser the interspace, less power will be consumed in the transmission. The weight value for the purpose function is 0.2. Thus, the interspace is calculated by using the formula:

$$Dij = \sum_{i=1}^{m} \left(\sum_{j=1}^{Ii} dis(s_j, CH_i)/I_i \right) \tag{6}$$

where $dis(s_j, CH_i)$ is interspace from sensor node to the CH and $I_i$shows the ith sensor node within the cluster.

Interspace from the CH and BS: It shows the interspace from the from the CH to the BS. If the CH is far away from the BS, then it consumes more power for the data transmission. So, the nodes near to the BS is used to convey the data to the BS. The weight value for the purpose function is 0.25. The purpose function used to calculate the interspace from the BS to the CH is calculated as:

$$D_{CH-BS} = \sum_{i=i}^{m} dis(CH_j, BS) \tag{7}$$

So, the single purpose function to find the CH from the set of nodes is calculated as

$$F = \alpha_1 ND + \alpha_2 C_n + \alpha_3 R_e + \alpha_4 D_{ij} + \alpha_5 D_{CH-BS} \tag{8}$$

Mechanism

CH choosing using BOA

1. Fitness function derivation using $F = \alpha_1 ND + \alpha_2 C_n + \alpha_3 R_e + \alpha_4 D_{ij} + \alpha_5 D_{CH-BS}$
2. Generate a preliminary populace of butterflies.
3. Prepare impetus strength (I) at node I which is intended by f(xi)
4. Prepare shift possibility, sensor modality and power exponent.
5. For j=max quantity of reiterations
6. For every butterfly in populace
7. Calculate cologne $f = cI^a$
8. End for
9. Identify the optimum butterfly populace
10. For every butterfly in populace
11. Generate a arbitrary quantity r from [0,1]
12. If arbitrary quantity < population
13. $x_i^{t+1} = x_i^t + (r^2 \times g^* - x_i^t) \times f_i$ where f_i is butterfly fragrance, $g^*$is current iteration.
14. $else$
15. Move arbitrarily $x_i^{t+1} = x_i^t + (r^2 \times x_j^t - x_k^t) \times f_i$
16. End if
17. End for

18. Update the value of energy proponent
19. End for
20. Optimal quantity of CH chooses from the population.

6.2 Cluster formation using PSO

PSO is one of the oldest mechanisms is the nature inspired mechanism used by the researchers to find the optimum results in the WSN. The mechanism is put redirect by the Kennedy and Eberhart in 1995. The mechanism is inspired by the social behavior of the bird flocking of fish schooling. It is an effective method to solve the clustering problem in WSN. On the basis of centralized clustering, the clusters are formed by the BS. For this, BS sends the data collection message to all the sensors in the nature. After receiving the data, nodes send the data to the BS such as node id, location (interspace from the BS in and position), power loss and power loss ratio (velocity), and current power to send BS. Then BS initiates the clustering process steps as follows.

Function: PSO-Cluster formation

Initialize the optimization problem and mechanism, parameters.

1. for i=1 to the particle size do
2. Initialize Xi within the search range of (Xmin,Xmax) arbitrarily;
3. Initialize Vi within the velocity range of (Vmin,Vmax) arbitrarily;
4. pi=xi
5. end for
6. Evaluate each particle **// fitness value= a$\frac{\sum_{i=0}^{n} d(current\ node, member\ node\ i)}{n} + b\frac{\sum_{i=0}^{n} E(member\ i)}{E(existing\ node)} + (1 - a - b)\frac{1}{number\ of\ nodes\ exist\ in\ the\ current\ node}$ where a & b is normalized values and n shows the quantity of nodes in the cluster
7. Identify the best position Ps;

//Loop:

8. While (Stop criterion is not satisfied & t < maximum iteration times) do
9. for i=1 to the particle size do
10. $V_i^{t+1} = \boldsymbol{\omega} V_i^t + c_1 r_1 (P_i^t - X_i^t) + c_2 r_2 (P_g^t - X_i^t)$
11. $X_i^{t+1} = X_i^t + V_i^{t+1}$
12. $P_i^{t+1} = P_i^t$
13. Evaluate fitness value
14. If fitness (P_i^{t+1}) < fitness (X_i^{t+1});
15. Update (P_i^{t+1});
16. End if
17. If fitness (P_g^{t+1}) < fitness (P_i^{t+1}) then
18. Update (P_g^{t+1});
19. End if
20. End for
21. End While

6.3 Routing Mechanism using ACO

Ant Colony Optimization is a metaheuristic mechanism inspired by the performance of the ants. Commonly, ACO applied on the discrete problems. ACO is used to find the shortest path from source node to the destination node by the use of graph in which the ant colony (nodes associated with the CH) is represented as a node and the L represent the link in between the nodes with different weights. In the initial phase, the weight of the link is calculated as the actual interspace in between the nodes by using arbitrarily quantity which is calculated by the mathematical formula. The disadvantage of ACO mechanism, i.e., undefined conjunction is overcome by improving the ACO in terms of remaining power, interspace from the destination and the knob degree. The route-finding procedure by using ACO is as follows:

1. In the formed CH, the ants are situated in every cluster. CH will create the way from the Cluster Head to the destination (BS). These routes data are known as redirect data.

2. Based on the probability matrix, the redirect containers are arbitrarily converted to the following CH. The redirect program packet is conveyed to the next CH until the packet is acknowledged by the BS.
3. The redirect packet will maintain the local data base about the visited CH, remaining power of the nodes and the CH (Remaining power of the nodes are calculated as the quantity of data conveyed along the network), interspace from the CH to the BS and the node degree.
4. The redirect data base is used to create the backward data base or backward packet. We need to create the backward packet because to extend the path until the packet reaches to the BS. The backward packet path is same as the path followed by the redirect packet.
5. The pheromone level of the link is updated by the remaining power, interspace to the BS and the node degree.
6. The next node for the transmission is chooses on the basis of **equation no. 9** which shows the chance of selecting the knob j as the subsequent knob i by means of ant k.

$$P_{ij}^{k}(t) = \begin{cases} \frac{[\tau_{ij}(t)]^{\alpha}[\eta_{ij}]^{\beta}}{\sum_{l\in \mathrm{N}_k}[\tau_{ij}(t)]^{\alpha}[\eta_{ij}]^{\beta}} & if\ j \in \mathrm{N}_k \\ 0 & otherwise \end{cases} \quad (9)$$

Where, the heuristic value and pheromone intensity are represented as η_{ij} and τ_{ij} respectively. To control the relative importance of the both the values, parameter α and β is used. Submission of nodes who has not visited yet is represented asN_k. Base on the data stored in the routing table by the CH, the heuristic and pheromone intensity are updated. Both the values are updated by the following formulas:

$$\eta_{ij} = \frac{1}{d_{CH}} \quad (10)$$

And $$\tau_{ij} = (1-\rho)\tau_{ij}^{old} + \sum_{k=1}^{m} \Delta\, \tau_{ij}^{k} \quad (11)$$

Where, d_{CH} shows the interspace from the CH, m shows the quantity of ants initialized and the pheromone deterioration quantity is shown as$\rho\epsilon[0,1]$. Where $\Delta\tau_{ij}^{k}$ is calculated as:

$$\Delta\tau_{ij}^{k} = \int \frac{Q}{c_k} \quad if\ the\ k^{th}\ ant\ traversed\ link\ (i,j), otherwise\ 0 \quad (12)$$

Where the value of Q is constant and the route cost is found by the ant is calculated asc_k.

$$c_k = \boldsymbol{\varphi}_1 E_r + \boldsymbol{\varphi}_2 d_{CH,BS} + \boldsymbol{\varphi}_3 N_D \quad (13)$$

Where the weighted values of$\boldsymbol{\varphi}_1$,$\boldsymbol{\varphi}_2$, $\boldsymbol{\varphi}_3$ are 0.5,0.3 and 0.2. For the successful communication, remaining power of the nodes should be considered as the priority because the node failure me leads to the communication failure. After that, to obtained the shortest interspace in between the CH and the BS is considered as the second priority because it consumes the minimum power or we can say that the power utilization is low in order to find the shortest interspace as compare to maintain the remaining power of the sensors. Lastly, we consider the node degree as a third priority, in which we choose the next CH as a hop having lesser quantity of member nodes. To find the route in between the source node to the destination node following steps need to be followed:

Routing Steps using ACO

1) Initialize pheromone exponential weight and heuristic exponential weight.
2) Generate the initial population of the ants.
3) for j=higher level of the iterations.
4) for each ant in the population.
5) Repeat the steps until kth ant complete its journey to the final destination.
6) Choose the successive ant using equation 9.
7) Update the pheromone using equation 11.
8) End for
9) Update the best solution.
10) End for
11) Output is the optimal route from source to the BS.

6.4 Cluster maintenance

In the literature survey present, the cluster preservation phase is one of the most significant stages to stable the load amongst the clusters. The cluster closer to the BS drain their power so fast because of the traffic of inter cluster. So, the preservation of

the cluster is important factor to turn down the problem of knob disaster. Node failure mains to the network failure and maintenance of the cluster leads to the maximization of the lifespan of the cluster or the entire network. In the put redirect mechanism, if the power of the CHs drains to the below the threshold value, the butter fly optimization mechanism is used to initialized the cluster, partial swarm optimization mechanism is used to elect the CH and then ant colony optimization mechanism is used to find the optimised path in amongst the knob to the Cluster Head and Cluster Head to the BS to maximize the network lifespan. Furthermore, it leads to the maximize the quantity of data conveyed to the BS.

7. Performance Measurement

The performance of the put redirect mechanism is measured by considering various factors such as:

Number of active nodes: The quantity of active nodes elevates the lifespan of the network. It describes as the quantity of active nodes in the network.

Dead nodes: The stability period of the network is calculated till the first node die. The network life time will decree when the quantity of dead nodes will elevate per round.

Data send to the BS

Along put: quantity of bits conveyed to the BS and it will measure in quantity of bits conveyed per second.

Stability period: It is measured along at what round the first node die, quantity of rounds when half of the nodes die in the network

Power utilization in each round: The total power utilization is calculated by the power loss of each node in the network.

Packet Drop Ratio: Quantity of data lost during the transmission from node to the CH and from CH to the BS.

Congestion in the network: It is calculated as quantity of acknowledged data by the BS to the quantity of produced data by the nodes in the network.

8. Simulation Setup

The put redirect power efficient protocol is implemented and tested on the MATLAB. The reason for using MATLAB is that it is very appropriate for the data survey and gives mathematical operations. There are 300 devices arbitrarily positioned in the test reason of 200 m x 200 m. The first order radio model for the power efficiency is considered for analysing the put redirect model with the extant model. The simulation parameters used for the examination purpose is shown in table 2. The purpose of the put redirect mechanism is to turn down the power utilization in wireless sensor networks. SO, to achieve the object, author used the BOA for the CH choosing, PSO is used for the cluster formation process and ACO is used for the routing process.

Table 2: Simulation Parameter

Parameters	Value
Network Field	(200,200)
Quantity of nodes	500
Packet Size	4000 Bits
Eelec	50nJ/bit
Efs	10nJ/bit/m2
Eamp	0.0013pJ/bit/m4
EDA	5nJ/bit/signal
Do (Threshold Interspace)	70 m
Eo (Original power of the normal nodes)	0.5J

Parameter that are considered for the butterfly optimization algorithm are: population size considered as 200, switch probability has taken as 0.8, power exponent considered as 0.1 and sensor mobility is considered as 0.01. Now for the cluster formation, the parameters considered as Quantity of Particles, Number of of iterations, Inertia Weight, Local Weight (c1), Local Weight (c2), Fitness are as 200, 100, 0.8, 1.49, 1.49, Predication accuracy. For the optimal route consideration, the parameters chosen as Quantity of ants, Pheromone exponential weight, Experiential exponential weight, Disappearance rate are as 200, 1,1,0.1.

Fig 5: Illustration of Case 1.

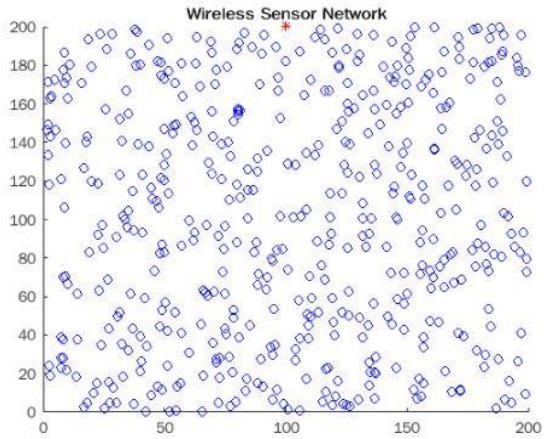

Fig 6: Illustration of Case 2.

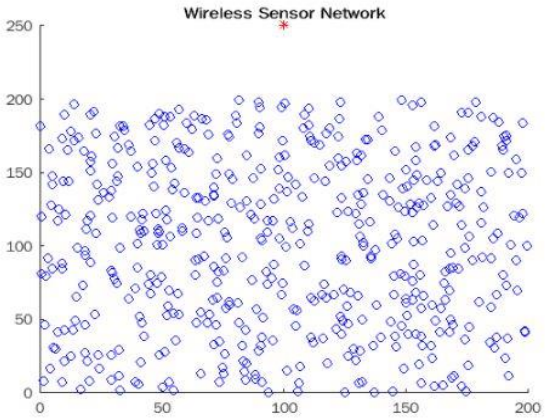

Fig 7: Illustration of Case 3.

The put redirect mechanism is validated in 3 cases.

Case 1: In the 1st case, the Base Station is placed at the centre of the test area (100,100) which is used to analyses the shorter interspace communication.

Case 2: In the 2nd case, the Base Station is placed at the last area which is in the range of the sensing reason (100,200). It is used to analyse the means range communication.

Case 3: In the 3rd case, the Base Station is placed at the outer area (100,250), which is situated far away from the examination zone. This case is used to analyse the extended rang communication.

8.1 Performance evaluation in terms of active nodes: The quantity of active nodes in put redirect mechanism is correlated with the LEACH, DEEC, EDEEC, DDEEC for 500 nodes in different cases such as in the 1st case, the BS is placed at the centre of the test area (250,250) which is used to analyses the shorter interspace communication, in the 2nd case, the BS is placed at the last area which is in the range of the sensing reason (100,250). It is used to analyse the means range communication, in the 3rd case, the BS is placed at the outer area (100,550), which is situated

far-off from the test area. This case is castoff to analyse the long rang communication. The put redirect mechanism prolongs the network lifespan as compare to the other protocols.

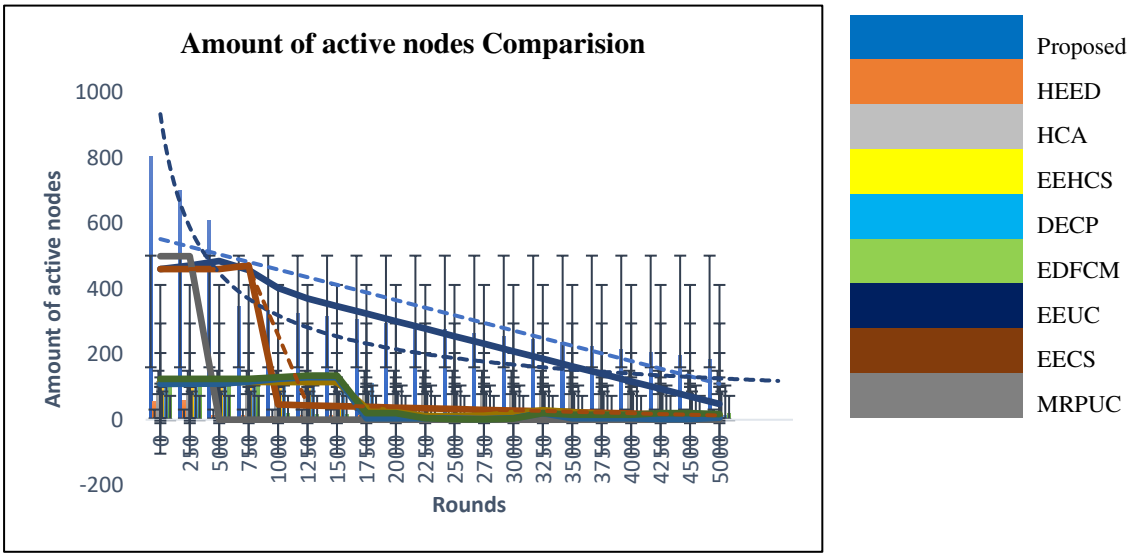

Fig 8: Number of Active Nodes

8.2 Performance evaluation in terms of stability period: The stability period is measured till the round when 1st node dies after the certain quantity of iterations. Fig 9 shows the quantity of dead nodes in the case 1, fig 10 shows the quantity of dead nodes for the case 2 and the fig 11 shows the quantity of death node for the case 3.

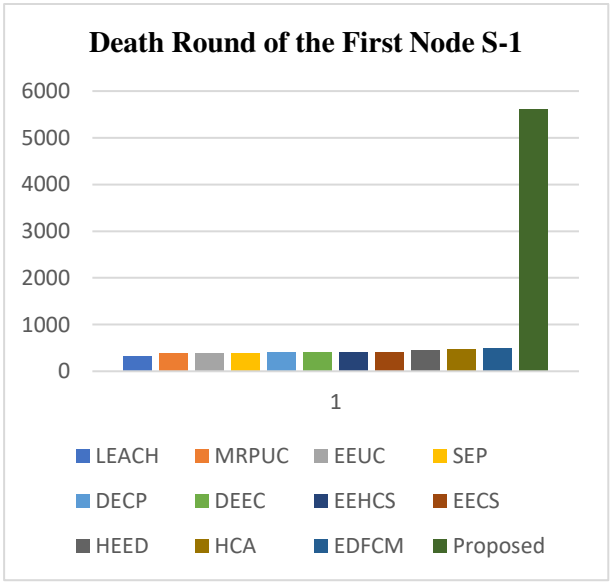

Fig 9: For the case 1

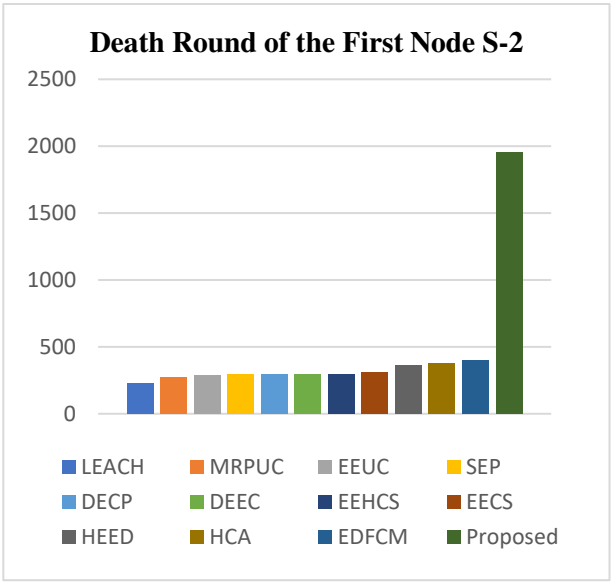

Fig 10: For the case 2

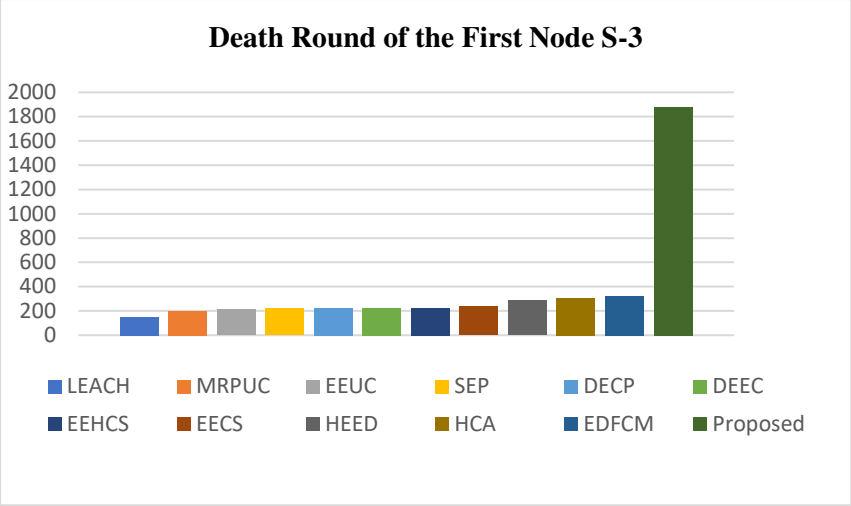

Fig 11: For the case 3

8.3 Performance evaluation of average power utilization: The performance evaluation of average power utilization of the put redirect mechanism is correlated with the extant mechanisms like LEACH, DEEC, MEEDEEC, SEP, EDEEC, DDEEC is shown in the figure 12. The power utilization is calculated when the BS is situated in centre of the region (100,250) and second comparison is based when the BS is situated far away from the BS (100,250) respectively. As per the result obtained from the mechanism, it is clearly shown that the put redirect mechanism gives higher power efficiency as compare to the LEACH and other mentioned protocols. The put redirect mechanism gives the higher power efficiency because it considers the optimal quantity of CH choosing per round, it includes the interspace while choosing the CH and optimal route when sending the data from one node to the other node. The reason behind the higher power utilization is that LEACH choose the CH arbitrarily and use single hop transmission whereas DEEC does not consider the interspace during CH choosing. The overall comparison in terms of remaining power of the put redirect mechanism with the extant mechanism is shown in the table 6.

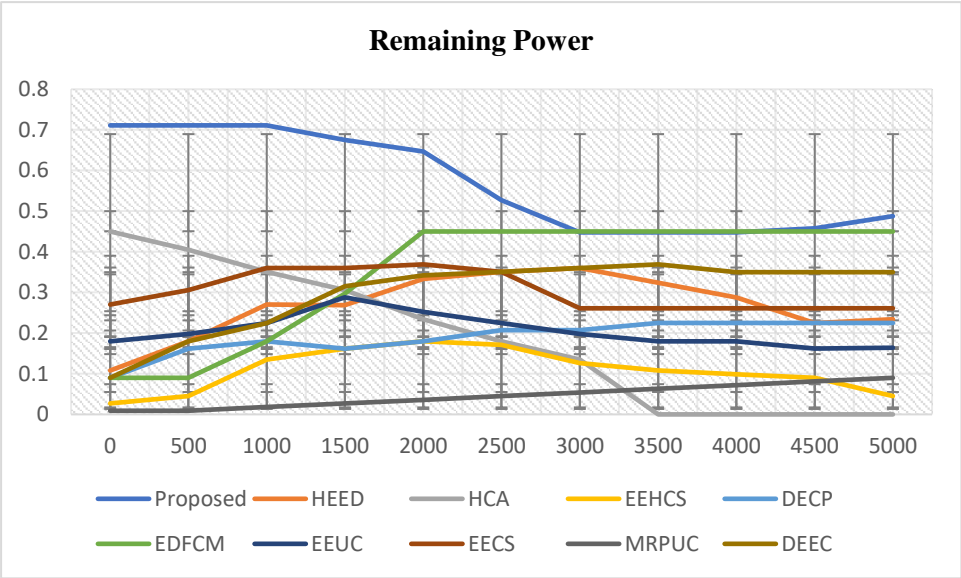

Fig 12: Remaining power

Table 6: Comparison of the remaining power of the extant mechanism with the put redirect mechanism

Rounds	Put redirect	HEED	HCA	EEHCS	DECP	EDFCM	EEUC	EECS	MRPUC	DEEC
0	0.711	0.108	0.45	0.027	0.09	0.09	0.18	0.27	0.009	0.09
500	0.711	0.18	0.405	0.045	0.162	0.09	0.198	0.306	0.009	0.18

1000	0.711	0.27	0.351	0.135	0.18	0.18	0.225	0.36	0.018	0.225
1500	0.675	0.2691	0.306	0.162	0.162	0.297	0.288	0.36	0.027	0.315
2000	0.64675	0.333	0.234	0.18	0.18	0.45	0.252	0.369	0.036	0.342
2500	0.52735	0.351	0.18	0.171	0.207	0.45	0.225	0.351	0.045	0.35091
3000	0.44775	0.36	0.135	0.126	0.207	0.45	0.198	0.261	0.054	0.36
3500	0.44775	0.324	0	0.108	0.225	0.45	0.18	0.261	0.063	0.369
4000	0.44775	0.288	0	0.099	0.225	0.45	0.18	0.261	0.072	0.349992
4500	0.4577	0.225	0	0.09	0.225	0.45	0.162	0.261	0.081	0.349992
5000	0.48755	0.234	0	0.045	0.225	0.45	0.1638	0.261	0.09	0.349992

8.4 Performance evaluation based on the packet transmission to the BS: The put redirect mechanism gives the higher packet acknowledged by the BS is that, the fitness functions of BOA, PSO and ACO reserve the power utilization of the nodes due to which leads to elevate the quantity of active nodes in the network along which the data packet will be conveyed to the BS. The fitness function chosen for the CH choosing and route choosing, it helps to minimize the overhead in the routing process due to which a smaller quantity of nodes dies in each round during the data transmission and it leads to the higher quantity of data acknowledged by the BS. In the extant mechanism, the inappropriate quantity of CH choosing and routing overhead, the lesser quantity of data is conveyed to the BS. Fig 13 shows the quantity of data acknowledged by the BS if there are 250 nodes are present in the case and Fig 14 shows the quantity of data acknowledged by the BS if there are 150 nodes are present in the case.

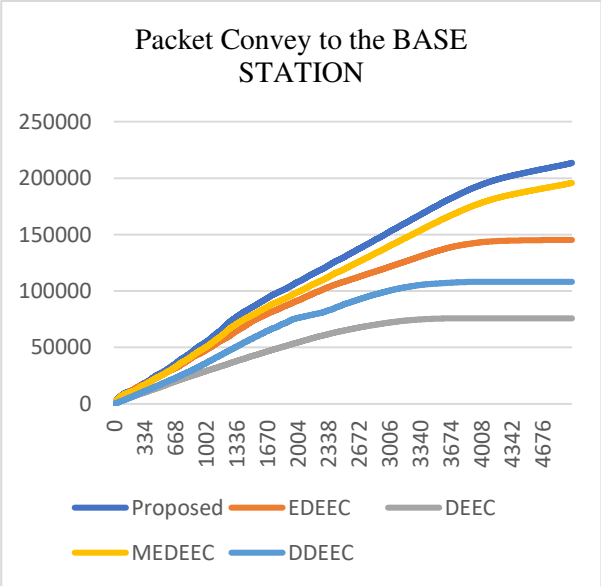

Fig 13: For the 250 Nodes

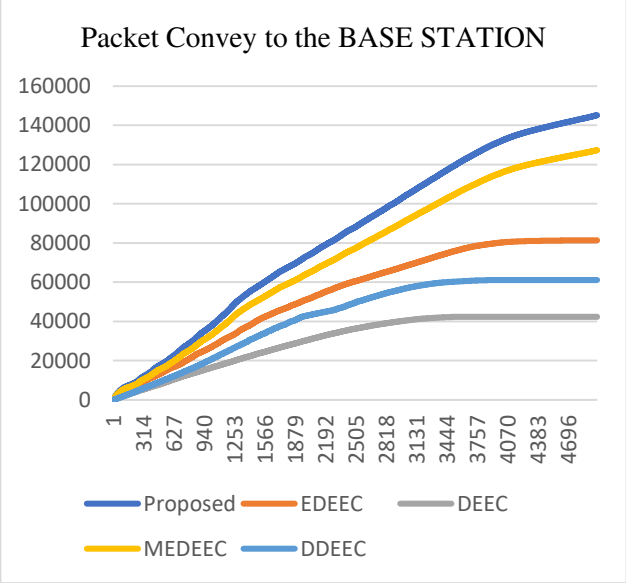

Fig 14: For the 150 Nodes

8.5 Performance evaluation of throughput: The inappropriate choosing of CH in the extant mechanism is the main reason for the higher power utilization in the data transmission. The put redirect mechanism chooses the CH and the route in the efficient way due to which higher data are conveyed to the BS and achieve the efficiency. The comparison of put redirect mechanism is correlated with the extant mechanism.

8.6 Performance evaluation of the network lifespan: Network lifespan is totally dependent on the remaining power of the nodes and the lifespan of the network got exhausted when entire node will lose their power. The network lifespan of the entire network is correlated when the first node die, half of the nodes die and last node die in the network. It is well said by the researchers that the demise of the 1st node in the network doesn't disturb the network execution but the system performance is affected when half of the node die in certain rounds or in the data transmission. Furthermore, the entire network gets drained when all the nodes die. So, to upgrade the network lifespan, the optimal quantity of CH choosing per round and chosen of optimal path from node to BS is mandatory requirement in the present case.

8.7 Comparative survey of the put redirect procedure with further cluster-based routing mechanisms

The comparative survey of the put redirect mechanism is correlated with some extant mechanism is shown in the figure 15. Table 7 shows the Comparative survey of Delay, Packet Drop Ratio, Throughput to the BS with the extant routing protocol.

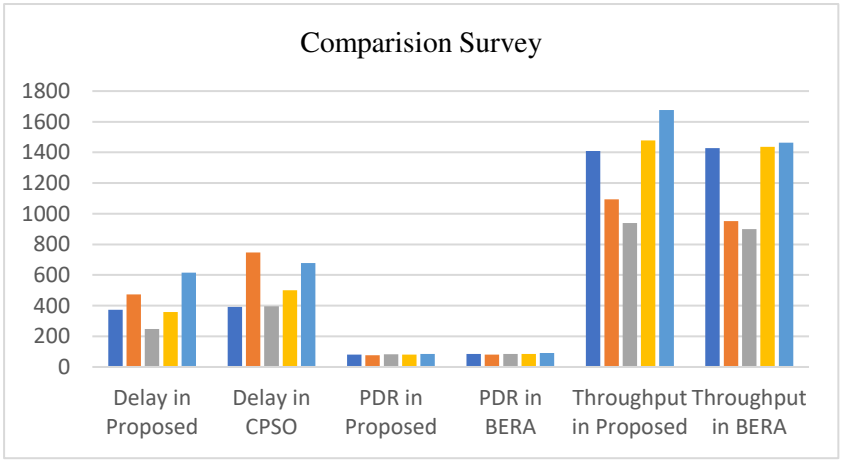

Fig 15: Comparison survey with CPSO, BERA

Table 7: Comparative survey of Delay, Packet Drop Ratio, Throughput to the BS with the extant routing protocol

	Delay		PDR		Throughput	
Nodes	Put redirect	CPSO	Put redirect	BERA	Put redirect	BERA
50	373.82	391	81.8197	84.0419	1409.99	1427.34
100	473.45	746.97	76.6302	80.0872	1094.45	951.33
150	248	395.48	82.5347	84.9127	940.1	899.76
225	359	501.48	80.4411	83.9704	1477.54	1436.96
315	616.1	677.81	85.1583	90.3678	1677.48	1463.59

	Delay		PDR		Throughput	
Nodes	Put redirect	FUCHAR	Put redirect	FUCHAR	Put redirect	FUCHAR
50	467.57	465.57	79.2301	83.1894	1415.3	1409.87
100	517.78	515.78	79.8012	81.1282	989.09	952.42
150	444.22	442.22	83.2691	84.238	989.44	937.5
225	696.14	694.14	85.7013	88.1779	1563.04	1502.28
315	539.6	537.6	90.044	91.5886	1475.36	1383.06

9. Conclusion

In the extant case of Wireless Sensor Network, the power utilization of the network is very high due to which the network lifespan gets turn down. So, to upgrade the network lifespan author focus on the following parameters such as optimal quantity of CH choosing par round, quantity of cluster formation and the optimal route choosing. The author uses the BOA, PSO and ACO to turn down the power utilization per round and elevate the network lifespan. The BOA mechanism is used to choose the CH, the fitness function was used with consideration of five parameters such as remaining power of the node, interspace from the nodes and the BS, node centrality and the node degree to turn down the CH choosing per round. The PSO is used to form the cluster by using certain parameters such as interspace to the CH and the BS. The ACO is used to find the best route from source to the destination by considering

following parameters such as interspace to the neighbour node, remaining power of the nodes and the node degree. The performance of the put redirect mechanism was measured in three different cases in which the BS was situated at different positions. The put redirect mechanisms were correlated with the extant mechanism and result shows that the put redirect mechanism gives the higher result in terms of stability period.

Authors' contributions RM and RKY contributed to collecting related literature and implementing the mechanism.

Funding "Not applicable"

Declarations

Conflict of Interests The authors declare that there is no conflict of interests regarding the publication of this paper.

Consent for publication "Not applicable"

References

[1]. K. Sohrabi, J. Gao, V. Ailawadhi, G.J. Pottie, Protocols for self-organization of a wireless sensor network, IEEE Pers. Commun. 7 (5) (2000) 16–27.
[2]. A. Singh, V. Kotiyal, S. Sharma, J. Nagar, C.C. Lee, A machine learning approach to predict the average localisation error with applications to wireless sensor networks, IEEE Access 8 (2020) 208253–208263.
[3]. I.F. Akyildiz, W. Su, Y. Sankarasubramaniam, E. Cayirci, Wireless sensor networks: A survey, Comput. Netw. 38 (4) (2002) 393–422.
[4]. L. Borges, F.J. Velez, A.S. Lebres, Survey on the characterization and classification of wireless sensor network applications, IEEE Commun. Surv. Tutor. 16 (4) (2014) 1860–1890.
[5]. S. Lu, X. Huang, L. Cui, Z. Zhao, D. Li, Design and implementation of an ASIC-based sensor device for wsn applications, IEEE Trans. Consum. Electron. 55 (4) (2009) 1959–1967.
[6]. S. Sharma, J. Singh, R. Kumar, A. Singh, Throughput-save ratio optimiza- tion in wireless powered communication systems, in: 2017 International Conference on Information, Communication, Instrumentation and Control (ICICIC), 2017, pp. 1–6, http://dx.doi.org/10.1109/ICOMICON.2017. 8279031.
[7]. R. Kumar, A. Singh, Throughput optimization for wireless information and power transfer in communication network, in: 2018 Conference on Signal Processing and Communication Engineering Systems (SPACES), 2018, pp. 1–5, http://dx.doi.org/10.1109/SPACES.2018.8316303.
[8]. J. Yick, B. Mukherjee, D. Ghosal, Wireless sensor network survey, Comput. Netw. 52 (12) (2008) 2292–2330.
[9]. M. Imran, H. Hasbullah, A.M. Said, Personality wireless sensor networks (pwsns), 2012, CoRR abs/1212.5543.
[10]. S. Sharma, R. Kumar, A. Singh, J. Singh, Wireless information and power transfer using single and multiple path relays, Int. J. Commun. Syst. 33 (14) (2020) e4464.
[11]. Daji, H., Jinping, Z., & Jilan, S. (2003). Practical implementation of Hilbert-Huang transform mechanism. ACTA OCEANOLOGICA SINICA-ENGLISH EDITION-, 22(1), 1-14.
[12]. Cardei, M., Du, DZ. Improving Wireless Sensor Network Lifespan through Power Aware Organization. Wireless Netw 11, 333–340 (2005). https://doi.org/10.1007/s11276-005-6615-6
[13]. Huang R., Chen Z. and Xu G.2010 International Conference on Communications, Circuits and Systems (ICCCAS), IEEE (2010), pp. 103-107
[14]. Y. Liang, H. Yu, Power adaptive cluster-head selection for wireless sensor networks, in: Sixth International Conference on Parallel and Distributed Computing Applications and Technologies (PDCAT'05), 2005, pp. 634–638, http://dx.doi.org/10.1109/PDCAT.2005.134.
[15]. M. Cardei, D.-Z. Du, Improving wireless sensor network lifespan through power aware organization, Wirel. Netw. 11 (3) (2005) 333–340.
[16]. X. Wang, G. Xing, Y. Zhang, C. Lu, R. Pless, C. Gill, Integrated scope and connectivity configuration in wireless sensor networks, in: Proceedings of the 1st International Conference on Embedded Networked Sensor Systems, in: SenSys '03, ACM, New York, NY, USA, 2003, pp. 28–39, http://dx.doi.org/10.1145/958491.958496, URL: http://doi.acm.org/10. 1145/958491.958496.
[17]. C.-W. Tsai, T.-P. Hong, G.-N. Shiu, Metaheuristics for the lifespan of wsn: A review, IEEE Sens. J. 16 (9) (2016) 2812–2831.
[18]. S.J. Nanda, G. Panda, A survey on nature inspired metaheuristic mechanisms for partitional clustering, Swarm Evol. Comput. 16 (2014) 1–18.
[19]. M. Iqbal, M. Naeem, A. Anpalagan, A. Ahmed, M. Azam, Wireless sensor network optimization: Multi-purpose paradigm, Sensors 15 (7) (2015) 17572–17620.

[20]. O. Demigha, W.-K. Hidouci, T. Ahmed, On power efficiency in collaborative target tracking in wireless sensor network: A review, IEEE Commun. Surv. Tutor. 15 (3) (2012) 1210–1222.
[21]. R.V. Kulkarni, A. Forster, G.K. Venayagamoorthy, Computational intelligence in wireless sensor networks: A survey, IEEE Commun. Surv. Tutor. 13 (1) (2010) 68–96.
[22]. C.-W. Tsai, P.-W. Tsai, J.-S. Pan, H.-C. Chao, Metaheuristics for the deployment problem of wsn: A review, Microprocess. Microsyst. 39 (8) (2015) 1305–1317.
[23]. G. Molina, E. Alba, E.-G. Talbi, Optimal sensor network layout using multi-purpose metaheuristics., J. UCS 14 (15) (2008) 2549–2565.
[24]. A.J. Al-Mousawi, Transmutative intelligence in wireless sensor network: routing, clustering, localization and scope, Wirel. Netw. 26 (8) (2019) 1–27.
[25]. J. Grefenstette, Optimization of control parameters for genetic mechanisms, IEEE Trans. Syst. Man Cybern. 16 (1) (1986) 122–128.
[26]. Y. Sun, W. Dong, Y. Chen, An improved routing mechanism based on ant colony optimization in wireless sensor networks, IEEE Commun. Lett. 21 (6) (2017) 1317–1320.
[27]. A. Mehrotra, K.K. Singh, P. Khandelwal, An unsupervised change detection technique based on ant colony optimization, in: 2014 International Conference on Computing for Sustainable Global Development (INDIACom), 2014, pp. 408–411, http://dx.doi.org/10.1109/IndiaCom.2014.6828169.
[28]. S. Arjunan, P. Sujatha, Lifespan maximization of wireless sensor network using fuzzy based unequal clustering and ACO based routing hybrid protocol, Applied Intelligence 48 (8) (2018) 2229–2246.
[29]. Z.X. Wang, M. Zhang, X. Gao, W. Wang, X. Li, A clustering WSN routing protocol based on node power and multipath, Cluster Comput. (2017) 1–13.
[30]. Prachi Maheshwari, Ajay K. Sharma, Karan Verma, "Power efficient cluster-based routing protocol for WSN using butterfly optimization mechanism and ant colony optimization", Ad Hoc Networks, Volume 110, 2021, 102317, ISSN 1570-8705, https://doi.org/10.1016/j.adhoc.2020.102317.
[31]. J. Tian, M. Gao, G. Ge, Wireless sensor network node optimal scope based on improved genetic mechanism and binary ant colony mechanism, EURASIP J. Wireless Commun. Networking 2016 (1) (2016) 104.
[32]. M. Yazdani, F. Jolai, Lion optimization mechanism (loa): a nature-inspired metaheuristic mechanism, J. Comput. Des. Eng. 3 (1) (2016) 24–36.
[33]. G. Han, H. Xu, T.Q. Duong, J. Jiang, T. Hara, Localization mechanisms of wireless sensor networks: a survey, Telecommun. Syst. 52 (4) (2013) 2419–2436.
[34]. B. Xing, W.-J. Gao, Innovative computational intelligence: a rough guide to 134 clever mechanisms, in: Intelligent Systems Reference Library, Springer, 2014, pp. 1–451.
[35]. F. Campelo, C. Aranha, R. Koot, Transmutative computation bestiary, 2019, URL: https://github.com/fcampelo/EC-Bestiary (accessed November 1, 2020).
[36]. A. Tzanetos, I. Fister Jr, G. Dounias, A comprehensive informationbase of nature-inspired mechanisms, Information Brief (2020) 105792.
[37]. F. Tao, Y. Laili, L. Zhang, Brief history and overview of intelligent optimization mechanisms, in: Configurable Intelligent Optimization Mechanism, Springer, 2015, pp. 3–33.
[38]. D. Pham, D. Karaboga, Intelligent Optimisation Techniques: Genetic Mechanisms, Tabu Search, Simulated Annealing and Neural Networks, Springer Science & Business Media, 2012.19
[39]. T. M. Behera, S. K. Mohapatra, U. C. Samal, M. S. Khan, M. Daneshmand and A. H. Gandomi, "I-SEP: An Improved Routing Protocol for Heterogeneous WSN for IoT-Based Environmental Monitoring," in IEEE Internet of Things Journal, vol. 7, no. 1, pp. 710-717, Jan. 2020, doi: 10.1109/JIOT.2019.2940988.
[40]. Vinitha, M.S.S Rukmini, International Journal of Pure and Applied Mathematics Volume 118 No. 11 2018, 725-732 ISSN: 1311-8080 (printed version); ISSN: 1314-3395 (on-line version) url: http://www.ijpam.eu doi: 10.12732/ijpam.v118i11.93.
[41]. Xie, B., & Wang, C. (2017). An Improved Distributed Power Efficient Clustering Mechanism for Heterogeneous WSNs. 2017 IEEE Wireless Communications and Networking Conference (WCNC). doi:10.1109/wcnc.2017.7925670.
[42]. M.T. Mekonnen, K.N. Rao, Cluster optimization based on metaheuristic mechanisms in wireless sensor networks, Wireless Personal Communications 97 (2) (2017) 2633–2647.
[43]. Anamika Chauhan and Amit Kaushik, "TADEEC: Threshold Sensitive Advanced Distributed Power Efficient Clustering Routing Protocol for Wireless Sensor Networks," International Journal of Computer Applications (0975 – 8887), Volume 96 No.23 June 2014.
[44]. K. Haseeb, K.A. Bakar, A. Ahmed, T. Darwish, I. Ahmed, WECRR: weighted powerefficient clustering with robust routing for wireless sensor networks, Wireless Personal Communications 97 (1) (2017) 695–721.
[45]. . Haseeb, K.A. Bakar, A.H. Abdullah, T. Darwish, Adaptive power aware clusterbased routing protocol for wireless sensor networks, Wireless Networks 23 (6) (2017) 1953–1966.
[46]. P. Lalwani, S. Das, H. Banka, C. Kumar, CRHS: clustering and routing in wireless sensor networks using harmony search mechanism, Neural Computing and Applications 30 (2) (2018) 639–659.
[47]. G. Han, L. Zhang, WPO-EECRP: power-Efficient Clustering Routing Protocol Based on Weighting and Parameter Optimization in WSN, Wireless Personal Communications 98 (1) (2018) 1171–1205.

[48]. Z.X. Wang, M. Zhang, X. Gao, W. Wang, X. Li, A clustering WSN routing protocol based on node power and multipath, Cluster Comput. (2017) 1–13.
[49]. N. Javaid, T. N. Qureshi, A.H. Khan, A. Iqbal, E. Akhtar and M. Ishfaq (2013), "EDDEEC: Enhanced Developed Distributed Power-Efficient Clustering for Heterogeneous Wireless Sensor Networks", ELSEVIER, Procedia Computer Science 00, 2013, pp 1-6.
[50]. M. Y. Khan, N. Javaid, M. A. Khan,"Hybrid DEEC: Towards Efficient Power Utilization in Wireless Sensor Networks", Published in World Applied Science Journal (ISI Indexed), 2013.
[51]. S. Arora, S. Singh, Butterfly optimization mechanism: a novel approach for global optimization, Soft comput. 23 (3) (2019) 715–734
[52]. Saini, Parul, and Ajay K. Sharma. "E-DEEC-enhanced distributed power efficient clustering scheme for heterogeneous WSN." Parallel Distributed and Grid Computing (PDGC), 2010 1st International Conference on. IEEE, 2010.
[53]. Elbhiri, Brahim, et al. "Developed Distributed Power-Efficient Clustering (DDEEC) for heterogeneous wireless sensor networks." I/V Communications and Mobile Network (ISVC), 2010 5th International Symposium on.IEEE, 2010.
[54]. J. Luo, J. Hu, D. Wu and R. Li, "Opportunistic Routing Mechanism for Relay Node Selection in Wireless Sensor Networks," in IEEE Transactions on Industrial Informatics, vol. 11, no. 1, pp. 112-121, Feb. 2015, doi: 10.1109/TII.2014.2374071.
[55]. Cui, Z., Xue, F., Zhang, S., Cai, X., Cao, Y., Zhang, W., & Chen, J. (2020). A Hybrid BlockChain-Based Identity Authentication Scheme for Multi-WSN. IEEE Transactions on Services Computing, 1–1. doi:10.1109/tsc.2020.2964537.
[56]. Sabir Hussain Awan, et al.," BlockChain with IoT, an Emergent Routing Scheme for Smart Agriculture", 2020 (IJACSA) International Journal of Advanced Computer Science and Applications, Vol. 11, No. 4,pp.420-429, 2020.
[57]. A. Gambhir, A. Payal, and R. Arya, "Performance analysis of artificial bee colony optimization-based clustering protocol in various scenarios of WSN," Procedia Computer Science, vol. 132, pp. 183–188, 2018.
[58]. L. Feng, H. Zhang, L. Lou and Y. Chen, "A Blockchain-Based Collocation Storage Architecture for Information Security Process Platform of WSN," 2018 IEEE 22nd International Conference on Computer Supported Cooperative Work in Design ((CSCWD)), Nanjing, 2018, pp. 75-80, doi: 10.1109/CSCWD.2018.8465319.
[59]. F. Engmann, F. A. Katsriku, J. Abdulai, K. S. Adu-Manu, and F. K. Banaseka, "Prolonging the Lifespan of Wireless Sensor Networks: A Review of Current Techniques," Wireless Communications and Mobile Computing, vol. 2018, pp. 1–23, 2018.
[60]. M. K. Khan, M. Shiraz, K. Z. Ghafoor, S. Khan, A. S. Sadiq, and G. Ahmed, "EE-MRP: Power-Efficient Multistage Routing Protocol for Wireless Sensor Networks," Wireless Communications and Mobile Computing, vol. 2018, 2018.
[61]. C. Xu, Z. Xiong, G. Zhao and S. Yu, "An Power-Efficient Region Source Routing Protocol for Lifespan Maximization in WSN," in IEEE Access, vol. 7, pp. 135277-135289, 2019, doi: 10.1109/ACCESS.2019.2942321.
[62]. 20. M. Sheik Dawood, S. Sakena Benazer, S.K. Vijaya Saravanan, V. Karthik, Power efficient distance based clustering protocol for heterogeneous wireless sensor networks, Elsevier, Materials Today: Proceedings,2020,ISSN 2214- 7853,chttps://doi.org/10.1016/j.matpr.2020.11.339.
[63]. Mehta, D., & Saxena, S. (2020). MCH-EOR: Multi-purpose Cluster Head based Power-aware Optimized Routing Mechanism in Wireless Sensor Networks. Sustainable Computing: Informatics and Systems, 100406. doi:10.1016/j.suscom.2020.100406.
[64]. Hussien, Abdelazim & Amin, Mohamed & Wang, Mingjing & Liang, Guoxi & Alsanad, Ahmed & Gumaei, Abdu & Chen, Huiling. (2020). Crow Search Mechanism: Theory, Recent Advances, and Applications. IEEE Access. 10.1109/ACCESS.2020.3024108.
[65]. Kaushik, A., Indu, S., & Gupta, D. (2019). A Grey Wolf Optimization Approach for Improving the Performance of Wireless Sensor Networks. Wireless Personal Communications. doi:10.1007/s11277-019-06223-2
[66]. Yu Xiuwu, Liu Qin, Liu Yong, Hu Mufang, Zhang Ke, Xiao Renrong, Uneven clustering routing mechanism based on glowworm swarm optimization, Ad Hoc Networks, Volume 93,2019, 101923, ISSN 1570-8705, https://doi.org/10.1016/j.adhoc.2019.101923.
[67]. Mahesh, N., Vijayachitra, S. DECSA: hybrid dolphin echolocation and crow search optimization for cluster-based power-aware routing in WSN. Neural Comput & Applic 31, 47–62 (2019). https://doi.org/10.1007/s00521-018-3637-4
[68]. Y. Lin, J. Zhang, H.S.-H. Chung, Wai Hung Ip, Yun Li, Yu.-Hui. Shi, An ant colony optimization approach for maximizing the lifespan of heterogeneous wireless sensor networks, IEEE Trans. Syst. Man. Cybernet., 42 (3) (2012), pp. 408-420
[69]. Cui, Z., Xue, F., Zhang, S., Cai, X., Cao, Y., Zhang, W., & Chen, J. (2020). A Hybrid BlockChain-Based Identity Authentication Scheme for Multi-WSN. IEEE Transactions on Services Computing, 1–1. doi:10.1109/tsc.2020.2964537
[70]. Lazrag, H., Chehri, A., Saadane, R., & Rahmani, M. D. (2020). Efficient and secure routing protocol based on Blockchain approach for wireless sensor networks. Concurrency and Computation: Practice and Experience, John Wiley & Sons, Ltd. doi:10.1002/cpe.6144

[71]. She, W., Liu, Q., Tian, Z., Chen, J., Wang, B., & Liu, W. (2019). Blockchain Trust Model for Malicious Node Detection in Wireless Sensor Networks. IEEE Access, 1–1. doi:10.1109/access.2019.2902811

[72]. Liu, Y., Dong, M., Ota, K., & Liu, A. (2016). ActiveTrust: Secure and Trustable Routing in Wireless Sensor Networks. IEEE Transactions on Information Forensics and Security, 11(9), 2013–2027. doi:10.1109/tifs.2016.2570740

[73]. Belkasmi, M., Ben-Othman, J., Li, C., & Essaaidi, M. (Eds.). (2020). Advanced Communication Systems and Information Security. Communications in Computer and Information Science. doi:10.1007/978-3-030-61143-9

[74]. M. Sheik Dawood, S. Sakena Benazer, S.K. Vijaya Saravanan, V. Karthik,Power efficient distance based clustering protocol for heterogeneous wireless sensor networks, Materials Today: Proceedings, 2020, ISSN 2214-7853, https://doi.org/10.1016/j.matpr.2020.11.339.

[75]. D. Yi, H. Yang, HEER – A delay-aware and power-efficient routing protocol for wireless sensor networks, Computer Networks, Volume 104, 2016, Pages 155-173, ISSN 1389-1286, https://doi.org/10.1016/j.comnet.2016.04.022.

[76]. H. Mostafaei, "Power-Efficient Mechanism for Reliable Routing of Wireless Sensor Networks," in IEEE Transactions on Industrial Electronics, vol. 66, no. 7, pp. 5567-5575, July 2019, doi: 10.1109/TIE.2018.2869345.

Proceedings of the Sixth International Conference on Trends in Electronics and Informatics (ICOEI 2022)
IEEE Xplore Part Number: CFP22J32-ART; ISBN: 978-1-6654-8328-5

Enhancing Spam Detection on SMS performance using several Machine Learning Classification Models

Tarandeep Singh
Department of Computer Science and Engineering
Delhi Technological University
Delhi, India
tarandeepsingh_2k18co372@dtu.ac.in

Tushar Anupam Kumar
Department of Computer Science and Engineering
Delhi Technological University
Delhi, India
tusharanupamkumar_2k18co375@dtu.ac.in

Prashant Giridhar Shambharkar
Department of Computer Science and Engineering
Delhi Technological University
Delhi, India
prashant.shambharkar@dtu.ac.in

***Abstract*— The Short Message Service (SMS) is swiftly turning into the most stable and secured mode of interaction because of its wide-ranging global coverage, reliability, dependability, and power efficiency. Because A2P messaging is more secure in comparison to P2P messaging, anybody can send a message, which leads to an attack. Spammers make use of this opportunity to spread harmful information, participate in disruptive behaviour, and harass others. In our work, we used machine learning classifiers for instance Multinomial-Naive-Bayes algorithm, Support-Vector-Machine models (SVM), Logistic-Regression, and Decision Trees to detect SMS spam from a dataset of nearly six thousand messages, taking into account combinations of Term-Frequency-Inverse-Document-Frequency (TF–IDF) and Count-Vectorization features to investigate the trade off between F1-score, accuracy -score, and computing time. Following that, we conducted a comparison study of the accuracy of various models for spam detection in order to determine the most accurate model that can be employed in this situation.**

Keywords*— *Spam detection; SVM; TF-IDF; Naive Bayes; Logistic Regression; Stemming; Lemmatization

I. Introduction

SMS (short message service) is referred to as a text-based communication system that enables the process of exchanging short text messages allowing mobile phone users to communicate. (often exceeding 160 letters in 7-bit) with others. Along with its widespread utilisation and appeal as the primary means of communication, it is also used for commercial goals for example advertising and also fraud by a large number of people. In China, the SMS fee is well under $ 0.001, that is the major cause of escalating SMS spam. Furthermore, this number exceeds the amount of email spam, according to the major security agency situated in Korea also called KISA. For instance, Every week, US mobile users get more than 1 billion SMS spam, and Chinese mobile users receive more than 8 billion SMS spam. There is a quick fix solution that can be utilised to address the issues mentioned above. It's done by categorising and filtering SMS messages. Some of the most prevalent text classification algorithms include decision-trees, Naive-Bayes, rule-induction, neural-networks, nearest neighbours, and SVMs

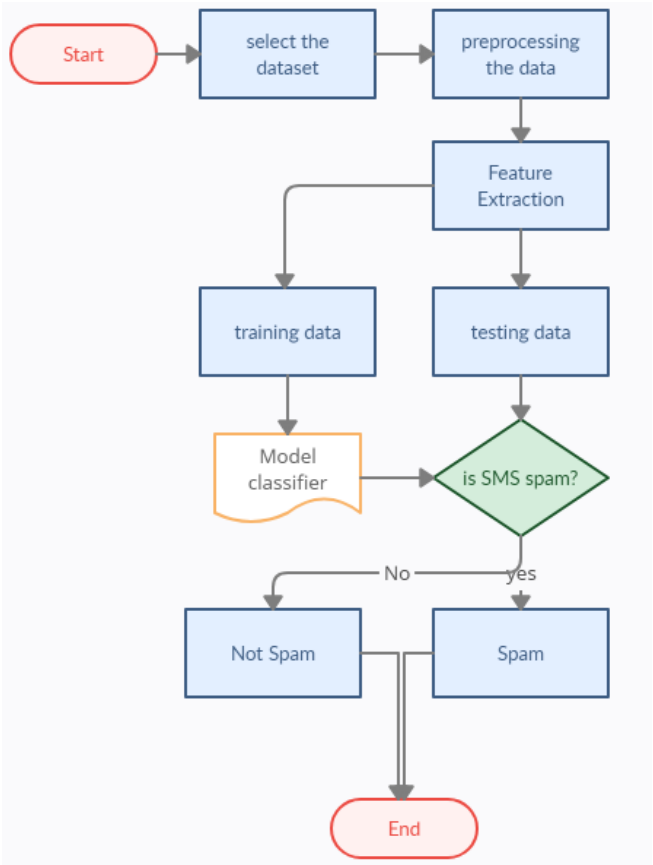

Fig. 1. Sequence of Events

II. Literature Review

There are various supervised machine learning algorithms available for classifying spam messages like Multinomial-Naive-Bayes algorithm, Support-Vector Machine models, Logistic-Regression, Decision Trees etc. We perform an analysis of these algorithms from various sources and measure their performances. We noticed that the performance of the algorithms varies with the distribution of the dataset.

Here we have two output classes, a message can belong to the spam class or the ham class(not spam). Since we have a dataset that contains the output class, we will be analysing various algorithms for detection.

2022 6th International Conference on Trends in Electronics and Informatics (ICOEI) | 978-1-6654-8328-5/22/$31.00 ©2022 IEEE | DOI: 10.1109/ICOEI53556.2022.9777157

Authorized licensed use limited to: DELHI TECHNICAL UNIV. Downloaded on June 03,2022 at 06:35:34 UTC from IEEE Xplore. Restrictions apply.

Delvia Arifin et al. [1] attempted to improve SMS spam filtering effectiveness by using data mining methods such as FP growth and naïve bayes classifier to assess whether an SMS belongs to the spam class or the ham class. The dataset they have used is SMS spam collection v.1. They got extremely excellent results, with an overall accuracy of 98 and 0.025 percent better than without employing the FP-growth.

Dedeturk et al. [2] analyzed various existing models and algorithms for sms spam detection and then came up with a strategy that merged an artificial bee colony algorithm with an LR classification model, which, when compared, clearly surpassed other models if we consider the accuracy of the models.

Gangavarapu et al. [3] Their suggested strategy and model yielded a 99 percent overall accuracy in this study. They did so by inventing a method for extracting email content and behavior-based characteristics, as well as identifying features that are beneficial in detecting UBEs and selecting the most discriminating feature set.

Li et al. [4] researched and proposed an approach considering into account two big challenges that we face in anti-spam softwares that is adversarial actions taken by spammers and the scalability of the data. Their approach was based on graph convolutional networks. To capture the local as well as the global context of a message, they used a heterogeneous and homogeneous graph in their method. This software is live and deployed at a company called Xianyu.

Shirani-Mehr et al. investigated and compared the outcomes of numerous machine learning techniques[5]. As per simulation findings, the optimal models for SMS spam detection are multinomial naive Bayes with the assistance of Laplace smoothing and SVM incorporating a linear kernel. In the original publication referencing this dataset, the top classifier uses SVM as the learning method and achieves an overall accuracy of 97.64 percent.

Traditional SMS filters, Qian et al. realised, are essentially text-based filtering, and they discussed its shortcomings in their study[6]. Spam and online content screening are becoming more commonly used as a consequence of sophisticated data mining technologies (Decision Tree, ID3 algorithm) and their spam messages. This article reviewed and highlighted a number of technological challenges that need greater study and development, such as dealing with content-based filtering, which requires a more efficient method.

Delany et al. looked at the present state of SMS spam filtering and discussed a number of different ways that have been developed and tested[7]. Machine learning algorithms have been demonstrated to be effective for SMS spam classification utilising a number of data sets, with reported accuracies of up to 97 percent, according to several studies. Non-content approaches such as social network analysis and recognising SMS submission patterns have also been discovered.

Almeida et al. introduced a new mobile phone spam collection, which is the biggest we've seen thus far, as well as data on the suggested corpus, such as token frequencies[8]. It also examined the outcomes of many well-known machine learning algorithms, finding that SVM outperforms other classifiers and so serves as a strong baseline for future comparison.

It has lately become possible to get to the base of the factor that drives client turnover via extensive research in the field of Artificial Intelligence. Kumar et al.[14] propose a practical solution to the difficult problem of predicting customer churn by combining a telecommunications data set with Artificial Neural Networks to identify the factors that influence customer churn and optimising the alternatives by experimenting with different activation functions.

III. Dataset

The SMS Spam Dataset, produced by UCI Machine Learning, was used in our work. It is available publicly on Kaggle and can be downloaded. The dataset acquired from Corpus SMS is used to assess the SMS detection system developed in this work's capacity. Containing SMS Spam Collection v.1, after combining and merging various SMS spam datasets, a total of more than five thousand SMS were received, with more than four thousand ham SMS and approximately one thousand spam SMS.

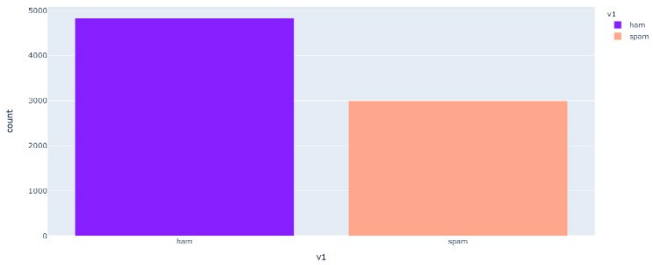

Fig. 2. Distribution of Dataset

IV. Data Preprocessing

A. Introduction

Preprocessing the data is the initial stage. To make the procedure easier, the data used for training is preprocessed and also the testing part is done independently. Preprocessing is done at the start of the process, prior to both the testing and the training.

B. Steps involved in Data preprocessing

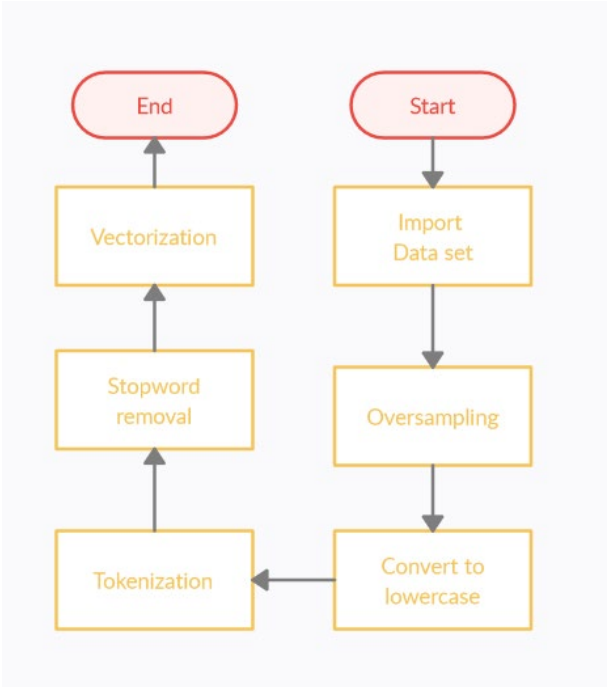

Fig. 3. Steps involved in data preprocessing

Authorized licensed use limited to: DELHI TECHNICAL UNIV. Downloaded on June 03,2022 at 06:35:34 UTC from IEEE Xplore. Restrictions apply.

The steps and operations involved in preprocessing are as follows:

1. Converting to lowercase and then erasing letters: To homogenise the data, all text is transformed to lowercase and any letters other than numbers, punctuation, or letters are deleted.

2. Dividing a huge text content into smaller chunks: Prior to proceeding to the following steps, the token procedure is used to divide the string down into tokens or individual words, making the token search process easier.

3. Stopword Removal: Stop words are common in phrases. (for example, "the," "a," "an," or "in") that a search engine has been set to ignore while indexing and obtaining search query results. To remove the texts that are grouped into the stopwords, the word dictionary corresponding strategy is utilised, which makes use of stopwords lists from the Natural Language Toolkit package.

4. Vectorization: To make the corpus of documents more computer-friendly, they must first be translated into a numerical format. There are a number of methods for doing so, but in our work, we'll focus on Vector Space models, sometimes known as Bag-of-Words (BoW) models. To address this, here we have employed the scikit-learn library and it consists of tools for the most prevalent techniques of extracting numerical information from text, including

   - Tokenizing employs punctuation and white spaces as token-separators, for example, and assigning an integer id to each potential token.
   - Weighting along with normalisation of the tokens of decreasing importance that occur in the bulk of dataset document contents.
   - Maintaining a count of how many times the given tokens emerged in each doc's examples.

   The following is how characteristics and examples are defined in this scheme:
   1. The number of times each token's frequency (normalised or unnormalized) is considered a characteristic.
   2. A multivariate sample is a vector that comprises all of the token's frequencies for a certain text.

V. Feature Extraction

A. CountVectorizer & PorterStemmer

Stemming is the way of creating morphological variations of a word. It was discovered that many of the terms in the dataset include affixes, necessitating the process of performing stemming in order to convert such words back to their root and original form. Its purpose is to eliminate the differences between words that ought to have the same definition but may have distinct appends. Porter's Stemmer algorithm was employed in this process. It was one of the most widely utilised stemming techniques when it was first created in 1980. We have used porterstemmer. It is a technique used for removing morphological and inflexional endings which occur often from English words developed by Martin Porter. It's most commonly used in the normalisation process, which is most of the time done when we are constructing Information Retrieval systems.

This stemmer is well-known for its efficiency and convenience of use. Porter Stemmer's principal uses are data mining and information retrieval.
The porter's stemmer algorithm is used in this process, which is based on Martin Porter's paper "An algorithm for suffix stripping."

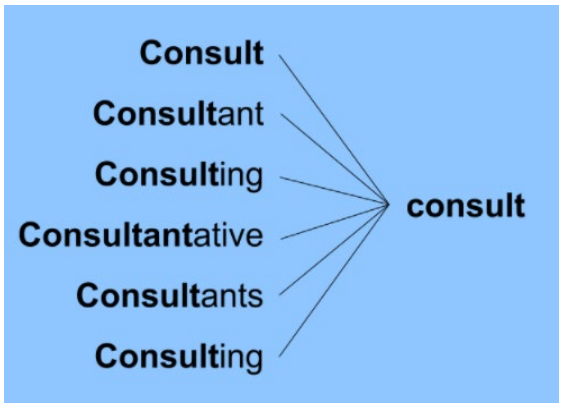

Fig. 4. Stemming example

Machines are unable to understand characters and words. As a consequence, while working with text data, we must represent it mathematically in order for the computer to comprehend it. Countvectorizer is a method for the conversion of text to the numbers data that we can deal with. It takes the data and turns it into a sparse matrix containing the words and their counts. CountVectorizer takes the text input and changes it to a vector based on how many times each phrase has emerged in the text. When we have a huge number of similar messages, this is really handy. (in our example, an SMS dataset) and want to turn each word into a vector. The CountVectorizer also has parameter max features, which select the words/features/terms that occur the most frequently. In our case, we set max features to 5000, which means it will select the 5000 most common words in the data.

B. TFIDF Vectorizer & WordNetLemmatizer

Lemmatization is the process of eliminating infectional terminologies and restoring the origin or lexical form of the words, referred to as the lemma, employing a vocabulary and intrinsic study of words. Stemming may only yield s when confronted with the token saw, but lemmatization might well attempt in returning of saw or saw according to whether the provided token was employed as a noun or a verb. Lemmatization and stemming vary in that stemming compress the act of deriving co-related words, whereas lemmatization breaks down a lemma's multiple inflectional forms. Linguistic handling for lemmatization and stemming is usually performed as a distinct plug-in module to the indexing technique, and there are a no. of commercial and open-source choices to choose from.

The full-form called for TF-IDF is "term frequency-inverse document frequency," which signifies that the allocation of

Authorized licensed use limited to: DELHI TECHNICAL UNIV. Downloaded on June 03,2022 at 06:35:34 UTC from IEEE Xplore. Restrictions apply.

weights for each of the tokens is based not exclusively on its provided repetition in document examples, but additionally on how recurring those words are throughout the given corpora. The idea is to use TF-IDF to score the relative value of words.

Term Frequency (TF)
The no. of time for a word to occur in a text division by the overall no. of words present in the documentation examples. The frequency of words in each text is different.

$$tf_{i,j} = \frac{n_{i,j}}{\sum_k n_{i,j}} \quad (1)$$

Now it's time to compute the IDF.

Inverse-Data-Frequency (or IDF for short)
The logarithm of the total number of document examples divided by the overall no. of documents with the phrase w Inverse data frequency overall texts in the corpus determines the weight of odd terms.

$$idf(w) = log(\frac{N}{df_t}) \quad (2)$$

The lower a word's IDF value, the less unique it is to any given document.
Finally, The TF-IDF is just the TF multiplied by the IDF

$$w_{i,j} = tf_{i,j} \times \log\left(\frac{N}{df_i}\right) \quad (3)$$

The lower the score for a term, the more frequent it is across papers, and the higher the score for a word that is unique to our initial document. The word counts, IDF, and TF-IDF values are all computed at once with the TF-IDF vectorizer. The TF-IDF Vectorizer considers a word's whole document weightage. It aids us in dealing with the most often used phrases. We can punish them if we use it. The word counts are weighted by a measure of how often they appear in the documents in TF-IDF Vectorizer.

VI. Classification Models Used

A. LOGISTIC REGRESSION

Logistic regression is among the most basic classification algorithms used for Machine-Learning. It's a statistically set strategy for estimating binary-classes. And the goal variable and result are asymmetric. Only two classes are conceivable in a dichotomous system. It computes the chance of an event occurring, for example, in our scenario an SMS might be spam or ham. For logistic-regression, the variable which is dependent is known to be a binary variable with data labelled as 0 (failure, no, etc) and 1 (success, yes, etc.). The given logistic-regression model is used to predict P(Y=1) like a function for X.
The logistic regression method is a simple and quick way to analyse data, and the findings are transparent and straightforward. We need to labelize SMS as spam or ham in our case, despite the fact that it's only a binary classification strategy.

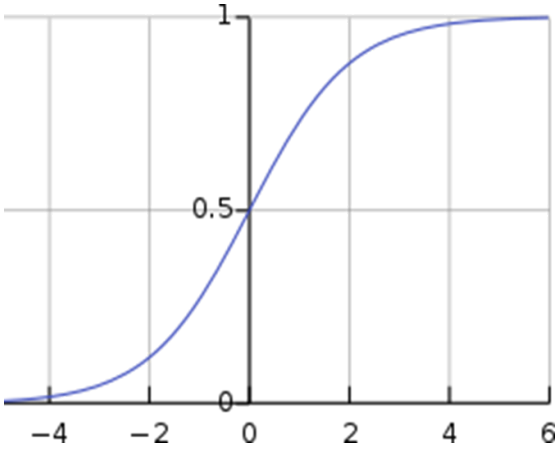

Fig. 5. Sigmoid Function Graph

B. SUPPORT VECTOR MACHINES

Support vector machines are potent data categorization tools. They give two-category points to non-overlapping half-spaces in the initial input-space among the task for linear-classifier, or even a high dimension feature-map for the non-linear classifier.

The task of an SVM(Support Vector Machines) is to generate a particular surface of decision with a hyperplane that maximises the margin-of-distinction around negative and positive samples. A systematic technique in statistical learning theory is used to obtain this desirable attribute. It employs a strategy of structural risk minimization in particular. The generalisation error rate is bounded by the mathematical notion of Vapnik-Chervonenkis dimensionality, according to those theories. The VC dimension is reduced by constructing optimal hyperplanes.

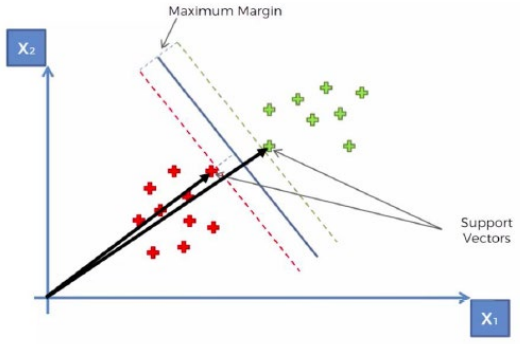

Fig. 6. Maximum Margin hyperplane

C. MULTINOMIAL NAÏVE BAYES

For binary/multiclass classification by using the distinct features, the Naive Bayes classifiers are appropriate (for example: word quantity of text data recognition). For fractional-counts like TF-IDF(term frequency-inverse data frequency), on the other hand, may operate in practice.

The Naive Bayes technique is helpful to collect probabilistic learning in Natural Language Processing. This program determines the tag associated with a text, like SMS or an email or a fake newspaper story, while making use of the Bayes theorem. It determines the likelihood of each and every tag for a given data sample and returns the tag with the greatest probability.

Authorized licensed use limited to: DELHI TECHNICAL UNIV. Downloaded on June 03,2022 at 06:35:34 UTC from IEEE Xplore. Restrictions apply.

A multinomial Naive Bayes classifier is composed of a number of algorithms that all share one characteristic: each and every feature categorised is unassociated to the others. The existence or lack of one attribute has no effect on the presence or disappearance of the other.

Thomas Bayes discovered the Bayes theorem which determines the likelihood of an occurrence happening as a result of previous awareness of the conditions surrounding the event. It is built on the current formula below.

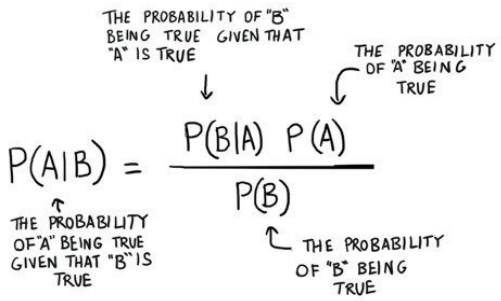

(4)

This algorithm aids in determining the likelihood of tags embedded in the text Multinomial Naive Bayes (NB) is straightforward to implement since all we have to do is compute the probability. It may also be used to anticipate real-time applications, such as our SMS spam detection.

D. DECISION TREE

The prominent iterative Dichotomiser 3 (ID3) technique created by Ross Quinlan to build the decision tree utilising entropy and information gain was described in this research effort. The information gain is utilised to compute entropy by dividing the SMS sample by some attributes, whereas the entropy analyses the adulteration of a random corpus of SMS samples. Entropy is determined using Eq. below, assuming we have an SMS dataset E with classifications CJ:

$$\text{entropy}\,(E)\sum_{j=1}^{|c|}\Pr(c_j)\log_2\Pr(C_j) \tag{5}$$

Eq represents the connection between entropy and information gain. below, where entropy is present The estimated entropy of Feature Fi is Ai(E), which is used to categorise SMS texts as spam or legitimate.

$$\text{gain}\,(E,\ F_i) = \text{entropy}(D) - \text{entropy}_{Fi}(E) \tag{6}$$

The resulting SMS(spam/ham) dataset provides the greatest information gain and so the impurity (sms comprise both spam and ham) of the dataset is decreased by dividing the sms dataset according to least entropy. After the tree is formed using the training sms dataset, the dataset may be tested using the decision tree method. The sms dataset that is being tested is processed in the tree using certain predetermined rules till it reaches a leaf node. The tested data is then given the label from the leaf node

A theoretical tree is shown below that explains how the decision tree algorithm does its spam filtering activity. The letter F stands for the characteristics or phrases in the text message. The letter V represents the values or word frequencies of some of the words in the SMS message. The letter C represents the labels, which are either spam or ham.

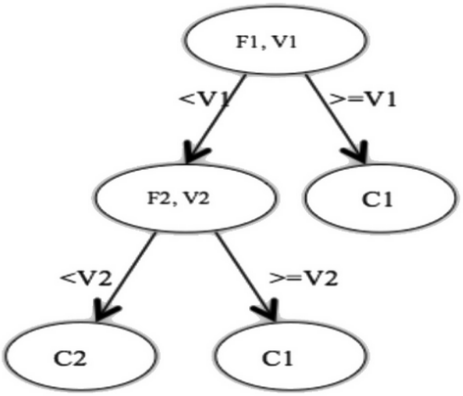

Fig. 7. Decision Tree Algorithm for sms spam filtering

VII. PERFORMANCE MEASURES USED

Performance measures are the measures that help to determine the efficacy of the machine learning classification model. We have used Accuracy, Recall, Precision and F1 score value as the performance measures.

To calculate the performance, we need some other values that are popularly showcased in the confusion matrix, which are:

- True-Negative (TN): Total number of truly predicted rows of negative class.
- False-Positive (FP): Total number of falsely predicted rows of the positive class.
- False-Negative (FN): Total number of falsely predicted rows of negative class.
- True-Positive (TP): Total number of truly predicted rows of the positive class.

Accuracy: The ratio of correctly classified SMS both spam and ham over the total classifications.

$$A = (TP+TN)/\text{Total} \tag{7}$$
$$\text{Where Total} = (TP+TN+FP+FN)$$

Recall: The ratio of correctly predicted spam SMS over the sum of correctly predicted spam SMS and incorrectly predicted ham SMS.

$$r = TP / X \tag{8}$$
$$\text{Where } X = (TP+ FN)$$

Precision: The ratio of correctly predicted spam SMS over the sum of correctly predicted spam SMS and incorrectly predicted spam SMS.

$$p = TP / (TP+ FP) \tag{9}$$

F1 value: It is equal to twice the division of product recall and precision over the sum of recall and precision.

$$\text{F1-value} = 2*(p.r)/(p+r) \tag{10}$$

Authorized licensed use limited to: DELHI TECHNICAL UNIV. Downloaded on June 03,2022 at 06:35:34 UTC from IEEE Xplore. Restrictions apply.

VIII. RESULTS

To make a comparison of the project's algorithms, this work makes use of performance assessment metrics such as precision, accuracy, and f-measure to assess performance. Table 1 & 2 shows the summarised performance of ML algorithms.

PorterStemmer with countVectorizer:

Performance parameter	Logistic Regression	Multinomial NB	Support Vector Machine	Decision Tree (ID3 algo)
True Negative	994	965	983	934
False Positive	08	37	19	68
False Negative	53	70	41	46
True Positive	509	492	521	516
Accuracy	0.9865	0.9856	0.9874	0.9739
Precision	0.99	0.93	0.98	0.94
Recall	0.90	0.96	0.92	0.86
F1-score	0.95	0.95	0.95	0.90

Table 1: PorterStemmer with countVectorizer output

Lemmatizer with Tf Idf Vectorizer :

Performance parameter	Logistic Regression	Multinomial NB	Support Vector Machine	Decision Tree (ID3 algo)
True Negative	991	975	988	952
False Positive	11	27	14	50
False Negative	77	71	49	48
True Positive	485	491	513	514
Accuracy	0.9641	0.9748	0.9847	0.9704
Precision	0.97	0.99	0.99	0.91
Recall	0.74	0.81	0.89	0.86
F1-score	0.84	0.89	0.94	0.88

Table 2: Lemmatizer with Tf Idf Vectorizer output

IX. CONCLUSION

We have performed Spam Detection on SMS using four Machine learning classification algorithms in this paper: Decision Trees(ID3 algorithm), Logistic Regression, Multinomial Naive Bayes and Support Vector Machines. We have used Accuracy, Precision, Recall and F1-score to determine our performance and capabilities.

The primary performance measure that governs which technique is better is accuracy. So according to accuracy the best results were obtained by linear SVM (countVectorizer), which beat all other techniques tested. It has a 98.7 % accuracy_scores rate. Given how difficult it is for categorising mobile phone communications, this is a fantastic accomplishment. However, the findings show that the four countVectorizer methods performed similarly, with no statistically significant differences. They all achieved a 97 percent accuracy rate, which is a pretty good baseline in this situation. As a consequence of the obtained findings, we can confidently state that the linear SVM (for both countVectorizer and Tf-IDF) provides the greatest baseline performance for future comparison.

In this work report, we looked at machine learning techniques and how they may be used for spam filtering. The avant garde in terms of algorithms for identifying communications as ham or spam is addressed. Several academics' efforts to use machine learning classifiers to combat spam were highlighted. Spam communications have evolved over time to bypass filters, which has been studied. The fundamental structure of email spam filters was explored, as well as the principles behind spam email filtering. The study looked at some of the publicly accessible performance measures and datasets that may have guided to assess the spam filters' efficacy .The snags of efficiently using machine learning algorithms dealing with spam/ham threat have been acknowledged, and relative assessments of ML approaches were undertaken on the basis of information readily available in the literature.

REFERENCES

[1] D. Delvia Arifin, Shaufiah and M. A. Bijaksana, "Enhancing spam detection on mobile phone Short Message Service (SMS) performance using FP-growth and Naive Bayes Classifier," 2016 IEEE Asia Pacific Conference on Wireless and Mobile (APWiMob), 2016, pp. 80-84, doi: 10.1109/APWiMob.2016.7811442.

[2] Dedeturk, B. K., & Akay, B. (2020). Spam filtering using a logistic regression model trained by an artificial bee colony algorithm. *Applied Soft Computing*, *91*, 106229.

[3] Gangavarapu, T., Jaidhar, C. D., & Chanduka, B. (2020). Applicability of machine learning in spam and phishing email filtering: review and approaches. *Artificial Intelligence Review*, *53*(7), 5019-5081.

[4] Li, A., Qin, Z., Liu, R., Yang, Y., & Li, D. (2019, November). Spam review detection with graph convolutional networks. In *Proceedings of the*

Authorized licensed use limited to: DELHI TECHNICAL UNIV. Downloaded on June 03,2022 at 06:35:34 UTC from IEEE Xplore. Restrictions apply.

28th ACM International Conference on Information and Knowledge Management (pp. 2703-2711).
[5] Shirani-Mehr, Houshmand. "SMS spam detection using machine learning approach." (2013): 1-4.
[6] Qian, Wang, Han Xue, and Wang Xiaoyu. "Studying of classifying junk messages based on the data mining." Management and Service Science, 2009. MASS'09. International Conference on. IEEE, 2009.
[7] Delany, Sarah Jane, Mark Buckley, and Derek Greene. "SMS spam filtering: Methods and data." Expert Systems with Applications 39.10 (2012)
[8] Almeida, Tiago A., José María G. Hidalgo, and Akebo Yamakami. "Contributions to the study of SMS spam filtering: new collection and results." Proceedings of the 11th ACM symposium on Document engineering. 2011
[9] Srinivasan, S., Ravi, V., Alazab, M., Ketha, S., Al-Zoubi, A. M., & Kotti Padannayil, S. (2021). Spam emails detection based on distributed word embedding with deep learning. In Machine intelligence and big data analytics for cybersecurity applications (pp. 161-189). Springer, Cham.
[10] Asghar, M. Z., Ullah, A., Ahmad, S., & Khan, A. (2020). Opinion spam detection framework using hybrid classification scheme. Soft computing, 24(5), 3475-3498
[11] Han, Jiawei, Micheline Kamber, and Jian Pei. Data mining: concepts and techniques 3rd Edition. Morgan Kaufmann Publishers, 2013
[12] "Natural language toolkit": https://www.nltk.org/
[13] "Sms spam collection dataset": https://www.kaggle.com/uciml/sms-spam-collection-dataset/
[14] Kumar, S., Kumar, M. (2019). Predicting Customer Churn Using Artificial Neural Network. In: Macintyre, J., Iliadis, L., Maglogiannis, I., Jayne, C. (eds) Engineering Applications of Neural Networks. EANN 2019. Communications in Computer and Information Science, vol 1000. Springer, Cham.
[15] Hamdan, Yasir Babiker. "Construction of Statistical SVM based Recognition Model for Handwritten Character Recognition." Journal of Information Technology 3, no. 02(2021): 92-107.
[16] Tripathi, Milan. "Sentiment Analysis of Nepali COVID19 Tweets Using NB, SVM AND LSTM." Journal of Artificial Intelligence 3, no. 03 (2021): 151-168.

Authorized licensed use limited to: DELHI TECHNICAL UNIV. Downloaded on June 03,2022 at 06:35:34 UTC from IEEE Xplore. Restrictions apply.

ACADEMIA
Accelerating the world's research.

Environmental Management in the World's Largest Mass Gathering Kumbh Mela 2019 at Confluence of River Ganga and ...

ayushi raghav

International Journal of Innovative Research in Information Security

Cite this paper

Downloaded from Academia.edu

Get the citation in MLA, APA, or Chicago styles

Related papers

Download a PDF Pack of the best related papers

SIMULATION OF ATMOSPHERIC POLLUTANTS DISPERSION IN AN URBAN ENVIRONMENT
IJIRIS Journal Division, Vinay Prabhakar

ASSESSMENT OF PRACTICES AND CHALLENGES RELATED TO HIV STATUS DISCLOSURE TO MINORS A...
IJIRIS Journal Division, Fredrick Wekesa Wanyonyi,, Joyce Owino, Elizabeth Role

SWARM INTELLIGENCE TECHNIQUES WITH CONSCIOUSNESS AND COMMONSENSE IN ARTIFICIAL ECO...
IJIRIS Journal Division

International Journal of Innovative Research in Information Security (IJIRIS) ISSN: 2349-7017
Issue 04, Volume 7 (April 2020) www.ijiris.com

ENVIRONMENTAL MANAGEMENT IN THE WORLD'S LARGEST MASS GATHERING KUMBH MELA 2019 AT CONFLUENCE OF RIVER GANGA AND YAMUNA AT PRAYAGRAJ, INDIA

Ayushi Raghav
Department of Environmental Engineering, Delhi Technological University, Delhi, India
ayushiraghav96@gmail.com
S.K Singh
Department of Environmental Engineering, Delhi Technological University, Delhi, India
sksinghdce@gmail.com
Twinkle Bhatia
Department of Environmental Engineering, Delhi Technological University, Delhi, India
twinklekiet93@gmail.com

Manuscript History
Number: **IJIRIS/RS/Vol.07/Issue04/APIS10080**
Received: 02, April 2020
Final Correction: 10, April 2020
Final Accepted: 12, April 2020
Published: **April 2020**
Citation: Ayushi, Singh & Twinkle (2020). Environmental Management in the World's Largest Mass Gathering Kumbh Mela 2019 at Confluence of river Ganga and Muna at Prayagraj, India. International Journal of Innovative Research in Information Security, Volume VII, 25-35. **doi://10.26562/IRJCS.2020.APIS10080**
Editor: Dr.A.Arul L.S, Chief Editor, IJIRIS, AM Publications, India
Copyright: **©2020 This is an open access article distributed under the terms of the Creative Commons Attribution License, Which Permits unrestricted use, distribution, and reproduction in any medium, provided the original author and source are credited**

Abstract: Mass gathering events is very common in India due to which there have been various instances which has made certain negative impact on our environment. Kumbh Mela is one of the largest mass gathering event on the earth. It is one of the most important and sacred festival which is celebrated four times in 12 years on the banks of river Ganga (Haridwar), river Shipra (Ujjain) . River Godavari (Nashik) , and at the confluence of rivers the Ganges, the Yamuna, and the mythical Sarasvati(Prayagraj). This time it has taken place at Prayagraj. This paper studies the water and Sanitation management and impact on the environment before and after Kumbh Mela 2019 at Prayagraj with the help of relevant data of that event collected. Moreover, it discusses what steps have been taken by the government to curb the ill effects of the place of event to be held with the implementation of new technologies like Geo-tubes and Bio-Remediation. The study shows that there were proper arrangements for the Sanitation with use of 1.22 lakhs Eco-toilets along with 20,000 dustbins. Moreover, solid waste was properly managed at most of the locations with the help of Tipper vehicles which carried the solid waste to the treatment plants. Several new STPs were installed to manage the waste generated.
Keywords: Kumbh Mela; Sanitation; Waste Management; Water Supply and its Quality and Water Pollution;

I. INTRODUCTION

A mass-gathering event abbreviated as MG is usually defined as the assemblage of people in large numbers at a particular location for some purpose (WHO, 2015). Kumbh Mela, the holy event of India is one of the largest congregations in the pilgrimage world of faith to bath at Sangam, Prayagraj. Approximately 12 crore visitors from 75 nationalities were present of this mammoth event to be held from January 15th to March 4th, 2019. The observance site rotate between pilgrimage places located on four sacred rivers on the bank of river Ganga at Haridwar , on the bank of river Shipra at Ujjain, on the bank of river Godavari at Nashik as well as on the Sangam of the rivers Ganges, the Yamuna, and the mythological Sarasvati at Prayagraj (Singh & Bisht, 2014). In addition, a Great Kumbh Mela festival is celebrated in every 144 years at Prayagraj.

© 2014- 20, IJIRIS- All Rights Reserved

Kumbh mela 2019 has covered an area of around 45 km .Many people take a holy dip in rivers during special occasions including Makar Sankaranti, Purnima , Amavasya , Ganaga Dashara, Deepawali,, etc. as a symbol of faith. Such mass bathing events greatly affect the health of the river with respect to water pollution. The main aim of the study is to manage the mass gathering and to find out the measures taken to treat the solid waste generated during the Kumbh Mela 2019 held at Prayagraj. This paper discusses the water, sanitation, and hygiene components at the Kumbh Mela, In this study, various water quality parameters before, during and after the Mela dates are taken into consideration. The chosen parameters describe the designated best use for river waters. Central Pollution Control Board (CPCB), India, has given the definition of Designated Best Use (DBU) of rivers and the evaluated parameters were compared with their standard values to estimate the quality of the river during the mass gathering.

Fig 1: Kumbh Mela 2019 at Prayag Arial View

II. THE KUMBH MELA 2019 AT PRAYAG

Kumbh Mela, 2019 was held at Triveni Sangam in Prayagraj(previously known as Allahabad), Uttar Pradesh, India , starting from January 15th to March 4th 2019. Pilgrimage from all over the world has visited the Kumbh 2019 to be a part of this religious festival.

2.1 GEOGRAPHICAL LOCATION OF PRAYAGRAJ2019

Prayagraj lies in the southern Uttar Pradesh and stands at the Sangam of the river Ganges, Yamuna and the mythological river Sarasvati. It covers an area of 70.5 km^2 (27.22 sq miles). Prayagraj lies in the humid subtropical climate zone. It exhibit hot dry summer season from April to June, cool dry winter season from December to February as well as warm humid monsoon season from July to September. It is well connected to other parts of country by road, rail and by air facilities (Singh & Bisht, 2014).

2.2 MAKING OF KUMBH 2019

The pilgrims from around the globe assemble on the below mentioned dates in table 1 to take a holy dip on the occasion of Kumbh Mela. The approximate visitors were estimated on these dates of Shahi Snan.

Table 1: Important Bathing Dates and Approximate Visitors

S.No	Occasion	Date	Approx. Crowd (in lakhs)
1	Makar Sankranti	15.01.19	140
2	Paush Purnima	21.01.19	35
3	Mauni Amavasya	04.02.19	181
4	Basant Panchami	10.02.19	125
5	Maghi Purnima	19.02.19	120
6	Maha Shivratri	04.03.19	110

Praygraj is well connected to other parts of the country by road, train and air. The airport is located at Bamrauli, away from city center. The city has four major railway stations namely Prayag Station, Allahabad Junction, City Station at Rambagh and Daraganj Station. During the Allahabad Kumbh Mela, inland waterways have been used for transportation of pilgrims as well as tourists between Varanasi and Allahabad, a distance of 60 km. The government has also set up four floating terminals, one each at Sujawan Ghat, Kila Ghat, Naini Bridge and Saraswati Ghat. Additionally, two vessels - SL Kamla and CL Kasturba as small boats were also deployed for pilgrim movement. Special trains were being run by the Indian Railways to Prayagraj during the Allahabad Kumbh Mela. Similarly, several new flights have been operational from January 13 to March 30. Facilities were provided to ensure that no problems occur during the stay of pilgrims for 55 day Kumbh Mela.

© 2014- 20, IJIRIS- All Rights Reserved

Table 2: Facilities provided in Kumbh Mela 2019

S.No	Services Provided	Numbers
1	Toilets	1,22,000
2	Dustbins	20,000
3	Tent City	4200 Premium beds
4	Electricity	40,700 L.E.D Lights
5	Drinking Water	200 Water ATMs

Source: Kumbh Mela Official Website

2.3. TREATMENT OF DRAINS DISCHARGING INTO RIVER GANGA

National Mission for Clean Ganga (NMCG) , State Mission for Clean Ganga (SMCG) and Government of Uttar Pradesh supported the treatment of drains projects in UP from December 2018 in light of Kumbh 2019. A total of 152 drains were being treated through different technologies which were polluting discharging wastewater into river Ganga and polluting it. At Prayag, drains treated were namely Amitabh Bacchan Culvert- Salori Nala, Mawaiya Nala, Old GT Road Nala, Rajapur Nala etc for reducing the pollution of river Ganga at Sangam area.

Table 3: Technology used for treatment of Drains

S.No	Number of Drains treated	Technology Used for Treatment
1	05	Modular Technology(Geo Bag)
2	06	NEERI Technology(Natural Attenuation based treatment Technology)
3	141	Bio- Remediation

Table 4: Performance monitoring parameters for treatment of drains decided by NMCG, New Delhi

S.No	Parameters	Permitted Value
1	BOD(mg/ l)	<= 30mg/ l or 40% reduction in Initial value of BOD
2	COD (mg/ l)	<=100mg/ l or 40% reduction in Initial value of COD
3	TSS(mg/ l)	<=100mg/ l or 40% reduction in Initial value of TSS
4	pH	6.5 – 9.0
5	Fecal Coliform	2500 MPN/ 100 ml

Table 5: Analysis of Parameters between Inlet and Outlet samples collected from the drains treated by CSIR-NEERI

Parameters	Inlet Samples	Outlet Samples	Percent Reduction
pH	7.27	7.29	-0.275
DO(mg/ L)	9.27	9.76	-5.258
TSS(mg/ L)	233.3	91.0	60.99
BOD(mg/ L)	63.5	27.8	56.22
COD(mg/ L)	332.7	100.7	69.73
Total Coliforms(MPN/ 100ml)	69472.7	55154	20.61
Fecal Coliforms(MPN/ 100ml)	31064.8	21559.5	30.59

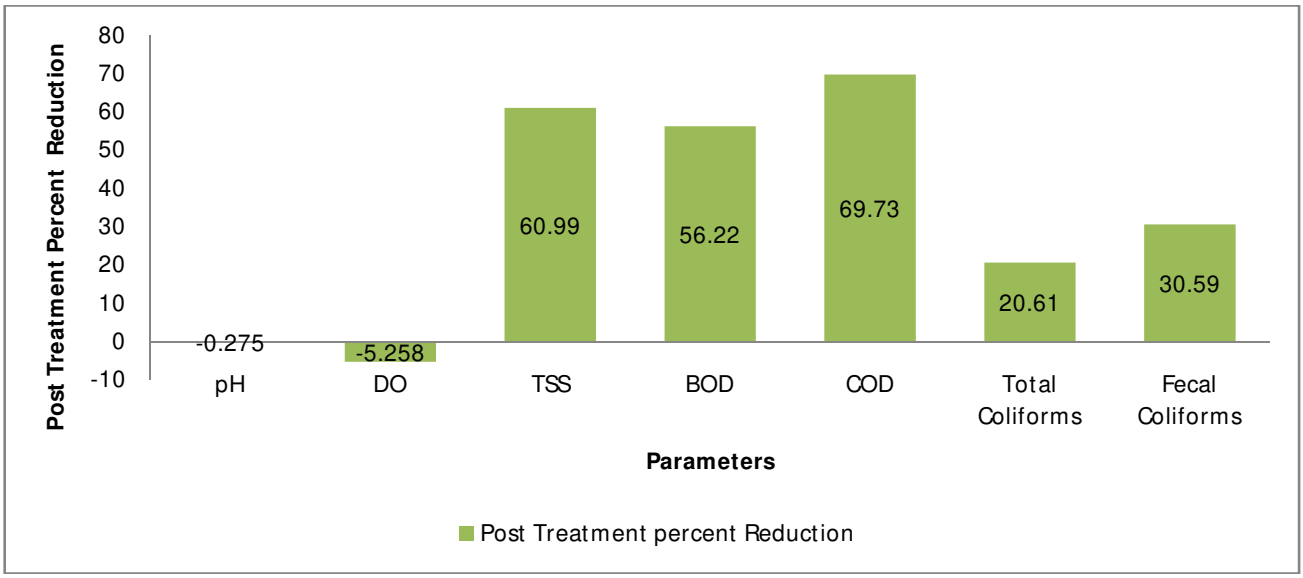

Fig 2: Graphical Representation of post treatment reduction in tested parameters

© 2014- 20, IJIRIS- All Rights Reserved

In Fig 2, pH and D.O have negative values for post treatment percent reduction. Increment in DO values at outlet give a positive sign of treatment given to the drains.

2.4. INTRODUCTION OF NEW TECHNOLOGIES

Modular technologies like bioremediation and geo-bag modular STP is also used for making clean Kumbh. Collaboration has been done with the National Environmental Engineering Research Institute (NEERI) in treating the influents at some drains. It was expected that the effluents that enter in the Ganga from these drains are treated up to the level of less than 30 Biological Oxygen Demand (BOD).

2.4.1. Bioremediation: It is a process in which living organisms are used such as micro organisms to rectify contaminants from water. It was used to achieve some of the below mentioned objectives-

- Reduction of B.O.D or C.O.D or T.S.S of the waste water of drains.
- To increase the dissolved oxygen of the flowing waste water of drains.
- Reduction of the Organic Build up or Sludge in the drains's bottom.
- To maintain the physical appearance of the waste water.

2.4.2. Geo-bag or Nonwoven Geotextile bag- This new system has been extensively used in the Kumbh Festival at Prayagraj , wherein approximately 69 MLD of wastewater was subjected to treatment through geosynthetic dewatering tubes with remarkable results. It is made out of porous synthetic fabric stitched from three sides and is open from one side. It is filled with soil and is installed at the river bank or near sea shores. It helps in protecting rivers and other water bodies from erosion by developing an embankment and by filtering sludge from the wastewater. Since this system does not require any elaborate civil construction, the deploying time is very less. In fact, a 30 MLD set up in Mawaiya during the Kumbh Mela was set up in 13 days, without any civil construction.

2.4.3. Natural Attenuation Based treatment Technology-Natural attenuation is a treatment technology for the contaminants and it also used for reducing the concentration and mass of petroleum hydrocarbons .It is adopted for the protection of human health as well as the environment from their adverse effects. It is a combination of physical, chemical, or biological processes. It is a natural technique to reduce the concentration of contaminants, mobility, mass, volume, toxicity in groundwater or soil. Most prominent disadvantage of this treatment technology is that it takes a longer duration to obtain the remediation objectives as compared to other remediation techniques.

III. RIVER WATER QUALITY AT PRAYAG DURING KUMBH 2019

In India, water quality is affected by disposal of treated and untreated sewage and industrial runoff into rivers. Upstream from the location of kumbh and its bathing sites which includes large number of factories including leather tanneries, runoff from the agricultural farms, and small towns that continuously discharge waste directly into the Ganga (Vortmann, & Balsari, Satchit & Holman, Susan & Greenough, (2015)). Sangam is among the top four highly polluted stretches in the longest Indian River, Ganga. The Central Pollution Control Board (CPCB) has recognized the water of river Ganga in Prayagraj as "Not Satisfactory". The main reason of water pollution in this city is lack of sewage system. According to the Namami Ganga Project reports, 70% of the pollution of river is due to sewage, 20% is due to industrial waste and only 10% is due to non-point sources like throwing of garbage, open defecation.

Table 6: Primary Water Quality Standards for Bathing (CPCB)

S.No	Parameter	Permissible Range
1	pH range	6.5-8.5
2	Dissolved Oxygen	4.0 mg/ l or 50% saturation value whichever is higher.
3	Color And Odor	No noticeable color.
4	Floating Matter	Nothing Obnoxious
5	Fecal Coliform	100/ 100 ml(MPN)
6	Biochemical Oxygen Demand(3 days at 27ºC)	3 mg/ l

The quality of river was monitored regularly at monthly interval. The quality of river Ganga in Allahabad before, during and after the Kumbh Mela is tabulated below:

Fig 2: Graphical Representation of post treatment reduction in tested parameters

Parameters	Dec 2018		Jan 2019		Feb 2019		Mar 2019	
	u/ s	d/ s	u/ s	d/ s	u/ s	d/ s	u/ s	d/ s
D.O(mg/ L)	8.8	9.0	11.9	10.9	10.4	9.8	8.7	8.3
B.O.D(mg/ L)	3.2	3.4	3.0	2.8	3.1	3.4	3.0	3.3
Total Coliform(MPN/ 100ml)	22000	21000	17000	20000	14000	17000	16000	20000
Fecal Coliform(MPN/ 100ml)	13000	11000	9300	11000	7800	9300	9200	11000

© 2014- 20, IJIRIS- All Rights Reserved

It can be seen from the Fig 3 and 4 that before the start of the Kumbh the quality of water was not satisfactory. In December 2018, the Total Coliform and the Fecal Coliform (MPN/100ml) were decreasing towards the downstream of the region indicating that steps were taken to improve the quality of River at Prayag. The river water can be considered suitable for bathing if the DO is more than 5 mg/l and BOD level is less than 3 mg/l, as per CPCB. For January month the BOD level was quite satisfactory for bathing, but for February and March months the B.O.D values were exceeding the permissible values, because of the important bathing events as Mauni Amavaysa, Basant Panchami, Maghi Purnima and Maha Shivratri. But for each month during Kumbh (January-March) the Total coliform and Fecal Coliform (MPN/100ml) were increasing towards downstream of the region. It shows that the quality of river was degrading during the Kumbh.

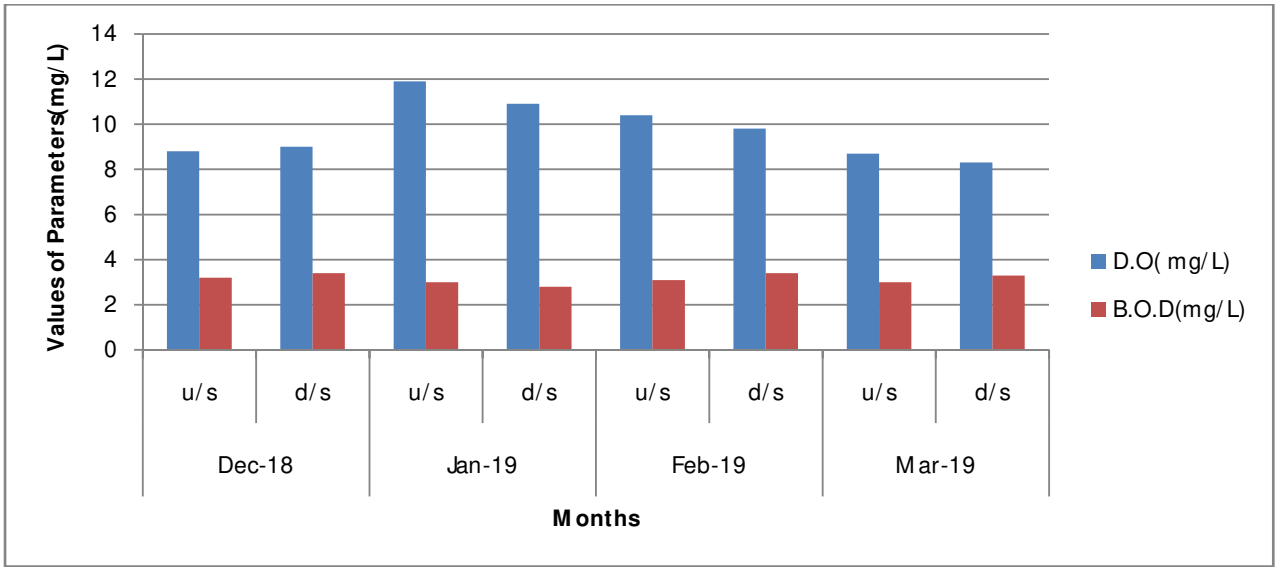

Fig 3: Variation of D.O and B.O.D from December 2018 to March 2019 at Prayagraj

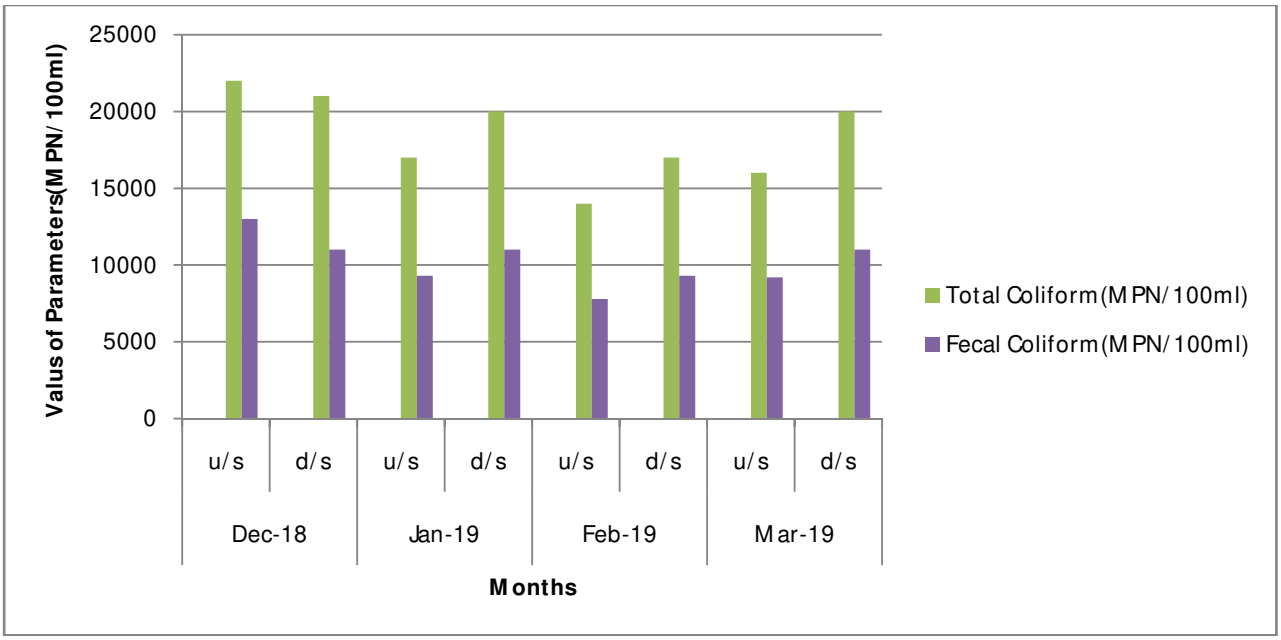

Fig 4: Variation of Total Coliform and Fecal Coliform from December 2018 to March 2019 at Prayagraj

The Government of Uttar Pradesh had ordered to shutdown leather factories in the cities lying upstream to the Prayagraj like Unnao and Kanpur from December 15th to March 15th so that clean water can be provided to devotees participated in the Kumbh 2019 at Prayag (The Financial Express,2019,Jan 2).

The river water was monitored by Uttar Pradesh Pollution Control Board (UPPCB) before and just after the first day of Shahi Snan during Kumbh and the result is tabulated as below.

© 2014- 20, IJIRIS- All Rights Reserved

Table 8: Quality of River at Different Monitoring Stations, Prayag (UPPCB)

Name of the station	Distance from Sangam	Date of monitoring	BOD (mg/l)	DO (mg/l)
Sangam	0	8-1-2019	3.2	12.4
Sangam	0	15-1-2019	3.0	10.6
Rasulabadghat	10 km upstream	8-1-2019	3.8	12.5
Rasulabadghat	10 km upstream	15-1-2019	3.1	12.4
Shastri bridge	2 km upstream	8-1-2019	3.4	12.3
Saraswati ghat	2 km downstream	8-1-2019	2.7	9.8
Saraswati ghat	2 km downstream	15-1-2019	2.5	9.6
Chhatnag ghat	5 km downstream	8-1-2019	3.7	10.5
Chhatnag ghat	5 km downstream	15-1-2019	2.9	10.5

IV. CHALLENGES IN ORGANISATION OF KUMBH MELA 2019

Each of the below issues is quite important regarding the environmental approach of event management. These issues are studied in detail. Following were the challenges faced in the organization of Kumbh Mela 2019 at Prayag:

i. Drinking water supply
ii. Sanitation
iii. Solid Waste Management
iv. Sewerage
v. Public Health Hazards
vi. Failure of Modern Technologies used

4.1. DRINKING WATER SUPPLY

All water supplies for human consumption should follow the Guidelines of World Health Organization (WHO) on Drinking Water Quality (WHO, 2015) as mentioned in Table 9.

Table 9: WHO guidelines on Drinking Water Standards

Parameters	Highest Desirable	Maximum Desirable
pH	7.0-8.5	6.5-9.2
Turbidity	5.0 JTU	25.0 JTU
Taste and Odour	Nothing	Disaggreable
Total Solids	500 mg/L	1500 mg/L
Coliform count in the water entering the distribution system	Zero in any sample of 100 mL	Zero in any sample of 100 mL

The National Green Tribunal (NGT) had directed the Uttar Pradesh and Uttarakhand Pollution Control Boards to display the quality of water of the river Ganga at all important locations on monthly basis, to indicate whether the river water is fit for drinking (Sandrp 2019). The UP government have taken responsibilities for supplying drinking water to the attendees at Kumbh Mela, 2019 by providing 5,000 stand posts, about 800 km pipeline. Moreover, 200 water ATM's based on reverse osmosis (RO) technique as well as 150 water tankers had been made in use for Kumbh Mela. Also, about 100 hand pumps had been installed so that there is no scarcity of water in the mass gathering at Prayagraj. 8,000 cusecs of clean water was released before every Shahi Snan to ensure clean water during the entire Kumbh Mela. Building materials company HIL Ltd., a CK Birla Group, with its roofing solutions brand Charminar had installed numerous water kiosks to serve clean drinking water to the devotees at Kumbh Mela, Prayagraj (The Hindu Business Line, 2019,Jan 31)

4.2. SANITATION

The Kumbh Mela organized in 2013 had faced a lot of waste generation, people were forced to defecate in open areas putting their lives in danger. That's why Cleanliness and proper Sanitation was given the top priority in Kumbh Mela 2019. The campaign used during the Kumbh Mela 2019 was "Swachh Kumbh". The campaign combines the messages of cleanliness and Clean Ganga and commitment of Swachhta. The Sanitation activities involves installation of about 1.2 Lakh eco-toilets with proper management and disposal of waste, placement of about 15000 Manpower so to keep the streets and Mela area clean. It also includes the installation of about 20,000 dustbins for solid waste collection (Kumbh Mela official website). The Global Interfaith WASH Alliance (GIWA) and UN's Water Supply and Sanitation Collaborative Council (WSSCC) were also present in the Kumbh Mela. They were involved in spreading awareness about the role of clean water, hygiene and sanitation in supporting human health and enhancing prospects for a better healthy life (*WSSCC*, 2019).

© 2014- 20, IJIRIS- All Rights Reserved

Table 10: Sanitation facilities provided at the Kumbh Mela 2019

S.No	Facilities provided	Numbers
1	Community toilets	62,500
	Urinals	20,000
	Institutional	40,000
	Total	1,25,000
2	Dustbins	20,000
3	Swachhagrahis	15,00
4	Night Sweepers	9000
5	Tipper Vehicles	120
6	Compactors	40

Fig 5: Ecofriendly toilets at Kumbh Mela 2019, Prayagraj

4.3. SOLID WASTE MANAGEMENT

Efforts were made to reduce the generation of waste during the mass gathering in Kumbh Mela 2019 held at Prayag by setting up of more than 1.22 Lakhs of eco-toilets. Manpower was also enforced to take care of waste lying on the roads. According to a report by Centre for Science and Environment (CSE), New Delhi, the amount of waste generated during the 55 day long Kumbh was about 18 times more than what the district produces daily. The existing sewage treatment capacity of the district was about 254 Million Litres per Day was not able to treat half of the generated waste. This result in lying of the waste at the banks of river Ganga, thus making it more polluted (Down To Earth's,2019, May 16-31).

More effects are:

i. The trash was left unattended on the roads which would attract files.
ii. Animals can swallow plastics putting their life in Danger.
iii. Waste Discharged in the river would lower its DO level thus making the existence of aquatic life difficult (Singh & Bisht ,2014)

Fig 6: Garbage left at Sangam after the Kumbh Mela at Prayag

© 2014- 20, IJIRIS- All Rights Reserved

The Jal Board deputed 46 engineers, one to monitor each of the 46 drains in order to curb the muck entering the river. The engineers appointed were given the task to report the condition of the drains, ensure sample collection and update the findings to the Ganga Pollution Control Unit in real time. They are also required to report the volume of sludge added by the drain into the Ganga and the technology used to clean the drain water. Real-time pictures of the drain are also supposed to be shared regularly. The unsegregated solid waste was dumped into Baswar treatment plant which was not operational since September (2018). On the other hand, the waste which was untreated was directly falling into the nearby streams, which ultimately flows into the Ganga. The plant was receiving around 600 tons of waste per day when it had been assigned to treat only 400 tons per day, and was, therefore, unable to treat all the waste (IANS, 2019).

4.4. SEWERAGE SYSTEM

With a view of organizing a huge mass gathering in Kumbh Mela, three new Sewage Treatment Plants were setup at:

Table 11: Establishment of 3 New STPs

S.No	Locations of New STPs	Capacity(in MLD)
1	Naini	42
2	Phaphamau	14
3	Jhunsi	16

These projects were established to prevent 7.8 crore litres per day of sewage from flowing untreated waste directly into River Ganga. Out of the total waste generated during the Kumbh Mela, 2000 Metric Tons of waste was transported to a STP located at Baswar village and dumped it in the premises of a non-functional Sewage Management Plant. The Baswar STP has been non-operational since September 2018. All the five machines installed to treat solid waste were non-functional (IANS, 2019). According to the reports of NGT, despite of installment of new Sewage Treatment Plants (STPs), large number of existing plants (STPs) were overflowing in Prayagraj and as a result, they were sending untreated waste directly into the Ganga, making it unfit even for bathing. The Sewage Treatment Plant (STP) located at Rajapur was receiving excess sewage than the installed capacity. But it was capable of treating only half of the waste with the help of geotube technology and the remaining half was being allowed to enter the Ganga without treatment. In the Mawaiya Nala, the untreated water from the drain was directly entering the Ganga because it had a bypass.

4.5. PUBLIC HEALTH HAZARDS

Mass gathering poses a risk to public health. Therefore, it is important to prevent or minimize the risk of poor health for the devotees. The type of planning for mass gathering is mainly dependent on the event conducted along with the risk assessments as well as with the help of resources available. Unfortunately, efficient methods to control and mitigate health risks are proven to be inadequate on execution to such mass gathering events, especially on such a large scale (Sharma et.al, 2019). A analysis of 10 years of public health safety in India shows that around 540 injured casualties along with 936 dead occurred in 27 traditional mass gathering events (Sanyal et.al ,2011).

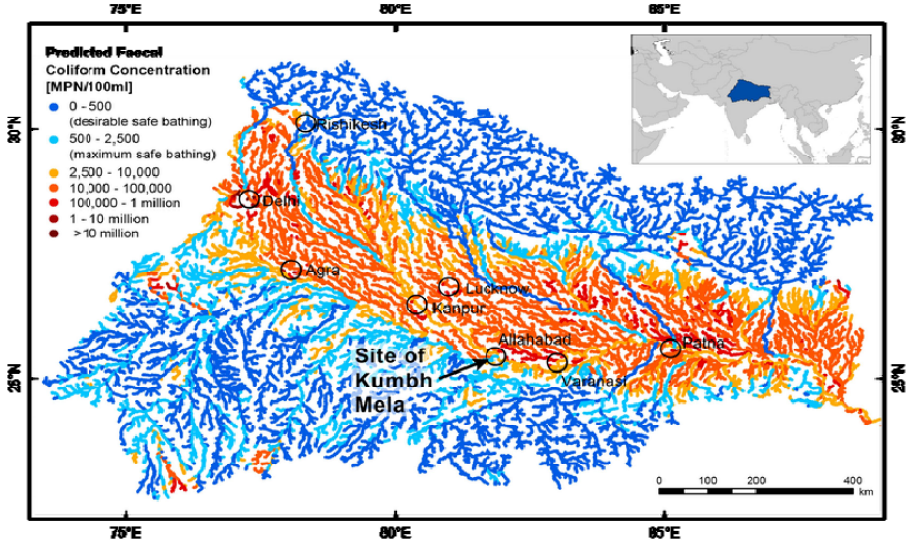

Fig 7: Predicted sewage pollution across the Ganges catchment including Allahabad – (Milledge et al., 2018)

In Kumbh mela 2019, the main risk to attendees and the residents of the area was through presence of Faecal coliform in the river Ganga. These bacteria enter rivers through disposal of untreated sewerage and through open defecation activities. Total coliforms abbreviated as TC is a biological parameter which measures quality of water, given by the Central Pollution Control Board (CPCB) for organized outdoor bathing. Its maximum permissible limit is 500 MPN/ 100 ml (MPN = most probable number).

© 2014- 20, IJIRIS- All Rights Reserved

The Total coliform count in January in the river Ganga at Prayagraj was found out to be around 20,000 MPN/ 100 ml and 17,000 MPN/ 100 ml downstream and upstream respectively, which was around 40 times more than the maximum permissible limit. The high numbers of faecal coliform indicate that the pathogens are present in water, usually contributed through excreta of human and animals. Their presence can cause water borne diseases such as diarrhea ("*Hindustan Times*, 2018, March 28).

4.6. FAILURE OF MODERN TECHNOLOGIES USED

Modern technologies like Bioremediation, Non-woven geobags or geotubes are used to reduce the discharge of waste into the river. But to some extent only they were effective. National Green Tribunal (NGT) stated that the use of Geotubes were completely waste of money. The technology involves treatment of waste water with the help of activated carbon and polymers. It is introduced inside 50 meter or 25 meter bags commonly known as Geotubes, where waste is filtered with the help of membranes. Then the solid waste gets collected inside these bags. But the Activated carbon and polymer reduces odor only, they didn't reduce the dissolved BOD of the waste. Moreover, the installation of Geotube technology is done at only five out of the 85 drains flowing into the Ganga and even at installed stations they treat only some portion of the waste and the rest is discharged into the river untreated ("Item No. 06 Court No. 1 PRINCIPAL BENCH, NEW DELHI NCR ...").

V. MEARSURS AND INNOVATIVE TECHNOLOGIES WHICH CAN BE USED TO PREVENT POLLUTION DURING KUMBH MELA

There are so many innovative technologies which are introduced to treat the commercial, residential as well as industrial wastewater and solid waste so as to make the environment pollution free. In such mass gatherings, pollution such as air pollution, water pollution, soil pollution as well as noise pollution are very common. To rectify such issues, various emerging and innovative technologies can be opted for the event of Kumbh at Haridwar which would be effective and inexpensive at the same time.Various measures and technologies include:

5.1. VERMIFILTERATION

Vermifilter is a biofilter which removes contaminates in the waste water using Earthworms. It is very similar to a trickling filter. The earthworms secrete certain kind of enzymes from their gut and digest the microbial biomass as a result of which the organic matter is converted into humus and can be used to improve soil fertility. The wastewater gets purified and is discharged as effluent passing though the Vermi bed containing worms. This technology is cheap, requires less space and has low maintenance. It can be used at nearby treatment plants to decontaminate waste water.

5.2. PHYTOREMEDIATION

Phytoremediation is a technique of removing contaminants from the wastewater using living green plants. It is a low cost, natural technique which uses solar energy. Removal of contaminants from surface water, groundwater as well as from soil can be done. It is a technology which is environmentally sound for prevention and control of pollution. Plants like *Jetropha Curcas*, *Ficus Microcarpa*, *Alyssum Lesbiacum*, *Arabidopsis Halleri* etc can be used to remove contaminants specially metals from the wastewater. This technology can be installed at the banks of the River at suitable distance.

5.3. SEGREAGATION OF WASTE AT SOURCE

Solid waste generation in such mass gatherings are so much that it sometimes become very difficult to manage the waste and thus pollution occurs along with several diseases. People do a lot of littering on such mass events like polyethene bags, rags, garlands, leftover food etc, and to curb such issues, dustbins should be provided at various locations. Each spot should have two dustbins (one green for biodegradable waste and one blue for non-biodegradable waste) so that the waste gets separated at source only. To make the people aware of following the rule of throwing the waste in bins, certain public awareness posters can be made and announcements can be made at regular basis.

5.4. MEASURES TO CONTROL AIR POLLUTION

Several people visit the Kumbh by their own transportation, which leads to air pollution. Therefore, to prevent air pollution, battery cars can be used to avoid fuel burning. Use of Carpool by the attendees is another option to control air pollution. Also, more and more trees can be planted to maintain the beauty of Kumbh Mela.

VI. CONCLUSION

India is well known for its rich culture and traditions. So many festivals are celebrated in our country and Kumbh Mela is no less than a festival here. Kumbh Mela had been a bench mark to other countries and is always a success at all 4 sacred places Haridwar, Ujjain, Nasik and Prayag. Kumbh mela is the assemblage of millions of people on the banks of rivers Ganga, Godavari, Shipra and Confluence of Ganga, Yamuna and Mythological Sawarsati. People gather from all round the globe to participate and witness the stream of knowledge, religion and spirituality. The Kumbh Mela organized at Prayagraj, 2019 was based on the theme "Swachh Kumbh for a Swachh Bharat".

© 2014- 20, IJIRIS- All Rights Reserved

Arrangements such as Eco-toilets, Drinking water ATMs, tents, installation of dustbins, establishment of new sewage treatment plant (STPs), renovation of already installed STPs, various swachhagirhis were deployed in order to regulate the waste generated during the Kumbh Mela. UP Govt. along with CPCB has monitored the Ganga basin before, during and after the Kumbh to analyze the water quality and to conclude whether the efforts made were up to the point or not. New techniques like Bio-remediation, Geotubes and Natural Attenuation based treatment technologies are also used to prevent the solid waste being discharged into the river, but they were partially effective. Three Sewage Treatment Plants were also installed and several existing Sewage Treatment Plants were upgraded in order to ensure a clean Kumbh. Sanitation was given a top priority and to ensure that approximate 1.22 lakhs eco-toilets were installed, to avoid open-defecation.

REFERENCES

1. Central Pollution Control Board (2019). E-Governance, viewed 01st December 2019. Available at: http://www.cpcb.nic.in/.
2. Down to Earth (2019).“Faith to Filth: Thanks to Kumbh, Prayagraj Sinks in Solid Waste.”, viewed 2nd December 2019. Available at: https://www.downtoearth.org.in/news/pollution/faith-to-filth-thanks-to-kumbh-prayagraj-sinks-in-solid-waste-64579.
3. Ganga River Monitoring Portal –UPPCB (2019).“Prayagraj Kumbh.” Viewed 5th December 2019. Available at: http://kumbh.upecp.in/.
4. Hindustan Times (2018). “Bathing in Ganga Can Expose People to High Levels of Faecal Coliform Bacteria.”, viewed 05th December 2019. Available at: https://www.hindustantimes.com/india-news/bathing-in-ganga-can-expose-people-to-high-levels-of-faecal-coliform-bacteria/story-UZILeZk6eNGjI9OWh22L0H.html.
5. IANS (2019). “Prayagraj 'On Verge of Epidemic' as 2000 Tones of Kumbh Garbage Pile Up.” Viewed 15th December 2019. Available at: https://weather.com/en-IN/india/pollution/news/2019-05-21-prayagraj-kumbh-mela-garbage-pollution-health
6. Item No. 06 Court No. 1 PRINCIPAL BENCH, NEW DELHI NCR. , Viewed 15th December 2019. Available at: http://www.indiaenvironmentportal.org.in/files/file/Kumbh_Mela_industrial_pollution_NGT_Order_Ganga.pdf.
7. Milledge, David (2019). “Why over 350 Million People in the Ganges Catchment Live near Rivers Too Polluted for Bathing” viewed 5th December 2019. Available at: https://medium.com/@d.g.milledge/why-over-350-million-people-in-the-ganges-catchment-live-near-rivers-too-polluted-for-bathing-or-2eefd145087e.
8. National Mission for Clean Ganga, et al..” National Mission for Clean Ganga(NMCG),Ministry of Jal Shakti, Department of Water Resources, River Development & Ganga Rejuvenation, Government of India, https://nmcg.nic.in/.
9. SANDRP (2019). “DRP News Bulletin 18 March 2019: Citizens Act on Worsening Water Pollution.”, viewed 2nd December 2019. Available at: https://sandrp.in/2019/03/18/drp-news-bulleting-18-march-2019-citizens-act-on-worsening-water-pollution
10. Sanyal S, Madan A. (P2-39) Public Health Safety for Traditional MGs in India: A 10-Year Analysis. Prehosp Disaster Med. 2011;26(S1):s156.
11. Sharma, U., Desikachari, B. R., & Sarma, S. (2019). Protocol for development of a risk assessment tool for planning and management of religious mass-gathering events of India—a health system-strengthening initiative. Pilot and Feasibility Studies, 5(1). doi:10.1186/s40814-019-0464-z
12. Singh, S, and Anshika Bisht. “‘Environmental Management in Mass Gatherings: A Case Study of Maha Kumbh Mela 2013 at Prayag, India.’.” International Journal Of Innovative Research in Science & Technology, vol. 1, no. 7, 2014, pp. 107–115., http://www.ijirst.org/articles/IJIRSTV1I7017.pdf
13. The Financial Express (2019) “Kumbh Mela 2019: Pilgrims to Get Cleaner Ganga Water as UP Govt Orders Shutdown of Tanneries.” Viewed 1st December 2019. Available at: https://www.financialexpress.com/india-news/kumbh-mela-2019-pilgrims-to-get-cleaner-ganga-water-as-up-govt-orders-shutdown-of-tanneries/1421399/.
14. The Hindu Business Line (2019). Bureau, Our. “HIL's Charminar Installs Water Kiosks at Kumbh Mela 2019, viewed 15th December 2019. Available at: https://www.thehindubusinessline.com/news/hils-charminar-installs-water-kiosks-at-kumbh-mela-2019/article26139194.ece.
15. Vortmann, M., Balsari, S., Holman, S.R., & Greenough, P.G. (2015). Water, Sanitation, and Hygiene at the World’s Largest Mass Gathering. *Current Infectious Disease Reports, 17*, pp. 1-7.
16. World Health Organization (2015). “Guidelines for Drinking-Water Quality, Fourth Edition.” , viewed 01st December 2019 . Available at: https://www.who.int/water_sanitation_health/water-quality/guidelines/en/
17. World Health Organization. Public health for MGs: key considerations. Geneva: WHO; 2015
18. WSSCC (2019) “WSSCC and GIWA Spread the Word on Sanitation and Water at Kumbh Mela.”, viewed 5th December 2019. Available at: https://www.wsscc.org/2019/01/25/wsscc-and-giwa-spread-the-word-on-sanitation-and-water-at-kumbha-mela/.

© 2014- 20, IJIRIS- All Rights Reserved

Environmental Science and Pollution Research
https://doi.org/10.1007/s11356-022-21493-3

RESEARCH ARTICLE

Evaluation of water quality using water quality index, synthetic pollution index, and GIS technique: a case study of the river Gomti, Lucknow, India

Amit Krishan[1] · Anwar Khursheed[2,3] · Rajeev Kumar Mishra[1]

Received: 1 February 2022 / Accepted: 12 June 2022
© The Author(s), under exclusive licence to Springer-Verlag GmbH Germany, part of Springer Nature 2022

Abstract
The river Gomti, one of India's most polluted rivers, passing through Lucknow, Uttar Pradesh, India, has been selected for this study. An attempt has been made to assess its water quality status by combining the water quality index (WQI) and synthetic pollution index (SPI). Further, the data integration with the geographic information system (GIS) along with twelve water quality parameters for the seven sampling stations (S1 to S7) over 5 years (2013–2017) has been performed. The study area showed a variation of WQI from 78.993 to 249.388 and SPI from 0.868 to 2.096 in 5 years. The map interpolated through GIS revealed that the WQI falls into the category of severely polluted (76–100) and unsuitable for human consumption (> 100), while SPI lies in the category of moderately polluted (0.5–1.0) and severally polluted (1.0–3.0). The BOD and COD were found to significantly influence the WQI and SPI scores. With the constant release of waste effluents into the river, all selected parameters increased from S1 to S7. Based on the study, effective wastewater management is immediately required to improve water quality and support any sustainable river restoration plan.

Keywords Gomti river · Water quality index (WQI) · Synthetic pollution index (SPI) · Water quality · Interpolation technique · Lucknow · Water pollution

Introduction

The river Gomti is a significant tributary of the river Ganga, running only in Uttar Pradesh (UP), India, in the northern section of the nation. The river begins in UP near Pilibhit town around 50 km south of Himalayan foothills, at a natural reservoir called Fulhar lake, Madhotanda (at an elevation of about 200 m; 28°13′40″ N and 80°10′70″ E), and flows for about 960 km through the Indo-Gangetic alluvial region before its merger with the river Ganga near Kaithighat, Varanasi. The river drains a catchment area of 30,437 km^2 (Abeysingha et al. 2020). The principal tributaries of the Gomti river are the Kathna, Sarayan, Reth, Luni, Kalyani, and Sai rivers. The catchment's topography is undulating, with steep hills near the basin's upstream end and elevations ranging from 58 to 238 m above mean sea level. The basin's climate varies between semi-arid and sub-humid tropical. The basin gets yearly rainfall ranging from 850 to 1100 mm, with the southwest monsoon accounting for roughly 75% of total annual rainfall from June to September (Abeysingha et al. 2016). The Gomti river has a slow flow for the whole year, except during the monsoon season when excessive rainfall creates a 20 to 50 fold increase in its average discharge (Abeysingha et al. 2015). Many urban and rural agglomerations in eastern UP, India, rely on the Gomti river for water (Gupta et al. 2014). The pressure on the Gomti river basin has increased due to rising population and expanding agricultural operations, resulting in significant changes in its natural status (Khan et al. 2020). The river's water

Responsible Editor: Xianliang Yi

✉ Rajeev Kumar Mishra
rajeevkumarmishra@dtu.ac.in

Amit Krishan
krishan001amit@gmail.com

Anwar Khursheed
akhursheedalig@gmail.com

[1] Department of Environmental Engineering, Delhi Technological University, Delhi 110042, India

[2] Department of Civil Engineering, King Saud University, PO Box 800, Riyadh 11421, Saudi Arabia

[3] Department of Civil Engineering, Z. H. College of Engineering & Technology, AMU, Aligarh 202002, India

Published online: 23 June 2022

quality has deteriorated dramatically because of anthropogenic activities such as sewage, untreated industrial effluent discharge, large-scale idol immersion, and the dumping of dead bodies. The Gomti river receives approximately 865 MLD wastewater from 68 major drains, mainly from 8 major towns located in the catchment of the river, namely, Sitapur, Sandila, Lucknow, Barabanki, Jagdishpur, Sultanpur, Jaunpur, and Kerakat (Jaunpur). Treated effluent from 30 water-polluting industries, mainly sugar, distillery, electroplating, textile, and slaughter house industries, is discharged through 10 drains located in the Gomti river (UPPCB (Uttar Pradesh Pollution Control Board) 2019). Despite the severe load of pollution levels, untreated water is being used for various purposes, posing a health risk (Jaiswal et al. 2019). As a result, water quality evaluation is critical as the first stage in raising public awareness and assisting planners and government officials in conserving and managing water bodies (Iqbal et al. 2019).

Rivers are one of the most important sources of freshwater for human survival around the world. River water is a major source of drinking water as well as other uses such as agriculture, industry, and many other recreational activities (Krishan et al. 2022). In its most basic form, assessing water quality through quantifying multiple physicochemical characteristics is extremely difficult to comprehend and scarcely portrays the actual condition. As a result, an evaluation tool is needed to objectively combine all the factors in order to portray water quality as a single numerical number (Mishra and Kumar 2021). The water quality index is the most commonly used indexing technique for water quality analysis, combining all parameters and comparing them with water quality standards (government's regulations) to protect human health (Ewaid et al. 2020; Nong et al. 2020). Horton (1965) developed it and used arithmetic weighting with multiplicative variables (Naubi et al. 2016; Shah and Joshi 2017; Bora and Goswami 2017; Dutta et al. 2018a, b; Sener et al. 2017; Iqbal et al. 2019; Aliyu et al. 2019; Lkr et al. 2020; Khan et al. 2020; Roy et al. 2021; Ali et al. 2021). Over the years, many changes have been made in response to user feedback. Many new indices have been created, including the National Sanitation Foundation-WQI (NSFWQI), Oregon Water Quality Index, Canadian Council of Ministers of the Environment-WQI (CCME-WQI), Overall Index of Pollution (OIP), British Columbia Water Quality Index (BCWQI), WQI by Bhargava, and so on (Uddin et al. 2021). These indices have been used to evaluate the water quality of India's river system (Shah and Joshi 2017; Bora and Goswami 2017; Dutta et al. 2018a, b; Iqbal et al. 2019; Lkr et al. 2020; Khan et al. 2020, 2021; Roy et al. 2021; Ali et al. 2021).

The synthetic pollution index (SPI), another innovative instrument, was also investigated in this work to confirm the level of pollution indicated by WQI. Ma et al. (2009) developed it to analyze the influence of contaminants on water quality, and it was afterward utilized in numerous researches owing to its easiness (Solangi et al. 2018; Hui et al. 2020; Sunar et al. 2020; Ali et al. 2021).

Despite the fact that the above-mentioned indices indicate water quality, they do not create a real perception of the quality. As a result, the data set integration with a geographic information system (GIS) helps communicate the real status of the river Gomti's water quality to the stakeholders, namely, public and policymakers. The resulting study output will be more accessible and understandable to policymakers and the general population (Ali et al. 2021).

The river Gomti's once-pristine status has deteriorated significantly, as evidenced by its ranking as one of India's most polluted rivers (Khan et al. 2020). Various studies have been conducted to analyze the river Gomti's water quality (Dutta et al. 2018a, b; Goel et al. 2018; Iqbal et al. 2019; Khan et al. 2020, 2021). However, the combined use of SPI, WQI, and integration with GIS to assess the Gomti river's water quality has not been used by researchers. This is a pioneer study to analyze the river water quality using these integrated methodologies in the specified stretch of the river Gomti in Lucknow, UP (India), based on monitoring data collected from the Uttar Pradesh Pollution Control Board (UPPCB), Lucknow, from 2013 to 2017. The results were confirmed by a good linkage between WQI and SPI, which authenticates the water's suitability for drinking, irrigation, and other uses. This baseline study of water quality along a defined length of the Gomti river may aid policymakers in developing appropriate management methods for river pollution abatement.

Materials and methods

Details of the study area

The study is being carried out along the Gomti river in Lucknow. Lucknow, the capital of UP (India), is situated between the latitudes of 26.30° and 27.10° N and the longitudes of 80.30° and 81.13° E on the central Gangetic plain (Fig. 1).

A humid subtropical climate prevails in the city, with a cold, dry winter (December to February) and a scorching summer (April to June). The temperature ranged from 48.90 °C in the summer to 1.67 °C in the winter. The city gets roughly 900 mm of yearly rainfall from July to September, largely from the southwest monsoon. The elevation of the city ranges between 100 and 130 m above sea level, with a typical eastward slope (Khan et al. 2020). The Gomti river approaches Lucknow, where it meanders, after flowing around 240 km from its source. Water is pumped from the river Gomti at Gaughat Pumping Station for the public water supply as it approaches Lucknow. The river Gomti separates

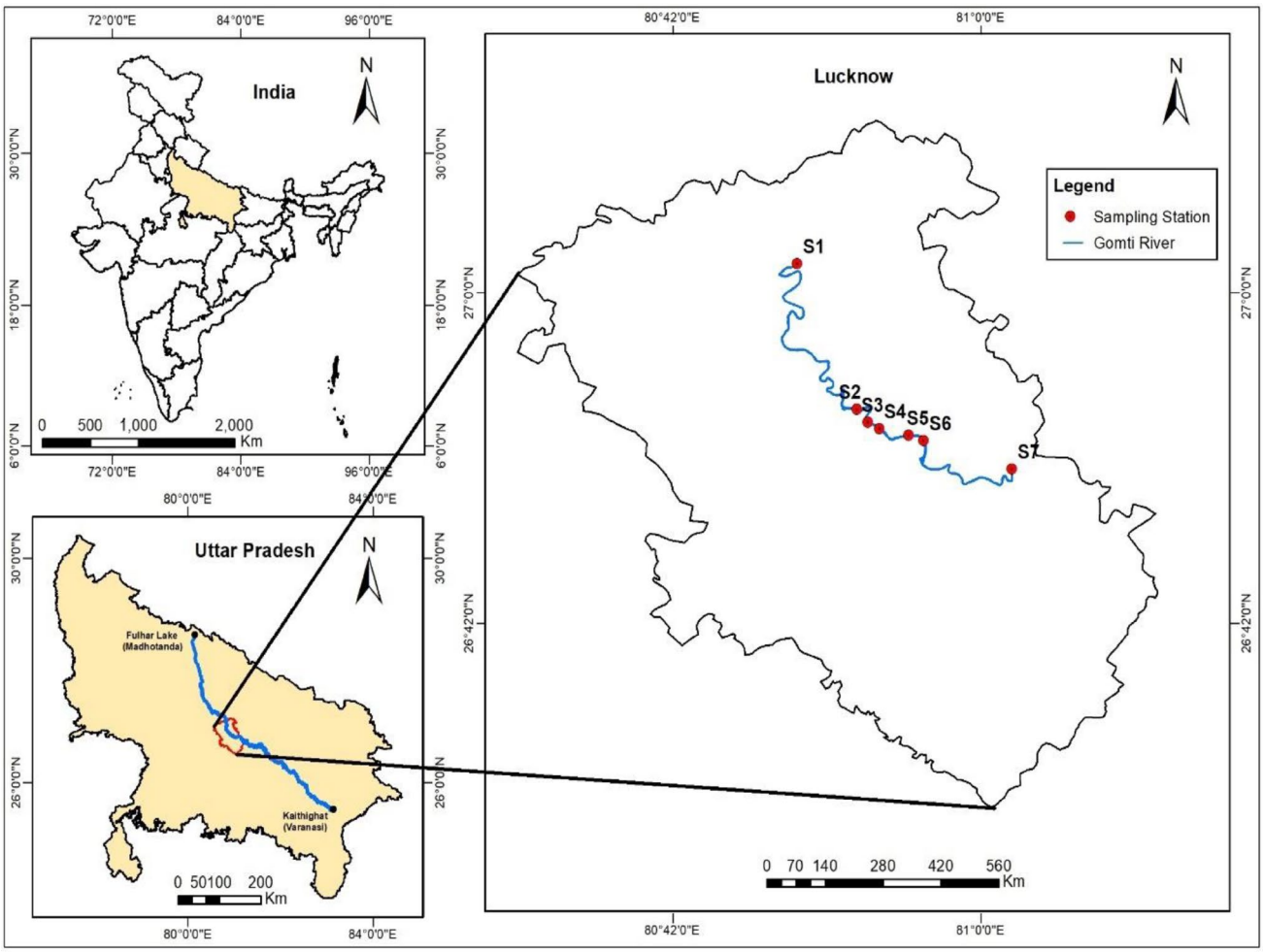

Fig. 1 Map showing sampling stations in the river Gomti of Lucknow city

Lucknow into cis and trans portions along its passage. There are 28 city drains in the Lucknow region that discharges untreated sewage water into the river, severely contaminating it. Out of them, 14 are located in the Cis-Gomti area, i.e., the southern part of the city, and 14 are located in the Trans-Gomti area, i.e., the northern half. Some of these drains are very large, carrying up to 78 MLD of sewage, while others are smaller, carrying only 0.5 MLD of sewage (Tangri et al. 2018). The Gomti Barrage, located near Lucknow city at the river's downstream end, impounds the river and turns it into a stagnant lake.

During the lean rainfall season, the available discharge in the Gomti river near Lucknow city is around 500 MLD, but the discharge is around 55,000 MLD during the monsoon season. During the majority of the year, the discharge averages around 1500 MLD (Dutta et al. 2011). Due to low water discharge, the post-monsoon season is related to the river's depositional phase. The urban core covers roughly 250 km^2 of land, and continuously, it is growing at an exponential rate. Lucknow is one of the country's fastest growing cities, with a projected population of 4.7 million in 2031 from 2.8 million in 2011 (LDA, Lucknow Master Plan 2031 2016), and the inhabitants of Lucknow use this stretch as their principal supply of drinking water. To protect human health, water quality assessments and documentation of management procedures are essential.

Sampling and data collection

The UPPCB is in charge of monitoring the water quality along the Gomti river in Lucknow. For this study, a total of seven sampling locations were selected, all of which were deliberately decided by the UPPCB for effective river monitoring (Table 1).

Therefore, physicochemical monitoring data from 2013 to 2017 was taken from the UPPCB database. Water samples were collected on a monthly basis from all seven sampling stations in Lucknow, and the raw data used for the study was derived from this information. These data set were evaluated using WQI and SPI to determine the river water's

Table 1 Location of the sampling station and their geo-coordinates of Gomti river at Lucknow district

Sampling station	Station code	Landmark of sampling location	Latitude	Longitude	Elevation	Distance between sampling stations
Station 1	S1	Manjhi Ghat	27°01′37.10″N	80°50′19.20″E	111 m	0
Station 2	S2	U/S water intake	26°53′14.58″N	80°53′59.86″E	111 m	32.5 km
Station 3	S3	Kuriyaghat	26°52′29.30″N	80°54′42.14″E	102 m	3.2 km
Station 4	S4	Downstream Mohan Meakins	26°52′07.67″N	80°55′25.46″E	109 m	1.4 km
Station 5	S5	Nishat Ganj, bridge	26°51′44.19″N	80°57′11.94″E	112 m	3.5 km
Station 6	S6	U/S Barrage	26°51′25.22″N	80°58′07.32″E	110 m	1.8 km
Station 7	S7	D/S of STP Nala Bharwara junction	26°49′47.34″N	81° 3′35.56″E	108 m	16.0 km

acceptability for drinking and irrigation as well as other uses. These indices were calculated mathematically using different physicochemical parameters, namely, pH (units), temperature (°C), electrical conductivity (µS/cm), total dissolved solids (mg/l), total alkalinity (mg/l, $CaCO_3$), total hardness (mg/l, $CaCO_3$), calcium (mg/l), magnesium (mg/l), chloride (mg/l), dissolved oxygen (mg/l), biochemical oxygen demand (mg/l), and chemical oxygen demand (mg/l).

Water quality indices

WQIs provide a broad picture of water's appropriateness for diverse uses. However, defining river water quality by a single metric is difficult. The WQI and the SPI, on the other hand, are regarded to be very effective and efficient techniques for assessing water quality (Ali et al. 2021). Many academics, water managers, and scientists worldwide are currently using these indexes.

Arithmetic WQI

The current study assessed water quality using an arithmetic WQI method first introduced by Horton (1965), improved by Brown et al. (1970), and later by Cude (2001). The weighted arithmetic WQI can be used to evaluate the acceptability of Gomti river water for drinking and irrigation, as well as other applications. The WQI was calculated using the following three equations:

$$Q = \frac{(Vo - Vi)}{(Vs - Vi)} \times 100 \tag{1}$$

where Qi, Vo, Vi, and Vs are the ith parameter's subindex, observed value, ideal value, and standard value, respectively. The optimum values for pH and DO were set to 7 and 14.6 mg/l, respectively, while Vi was set to zero for all other parameters:

$$Wi = \frac{K}{Vs} \tag{2}$$

where Wi is the ith parameter's unit weightage, which was calculated as an inversely proportional value to the Bureau of Indian Standards (BIS) (2012)/WHO (2011) standard value (Vs) for each of the observed physicochemical parameters. For all of the reported physicochemical parameters, however, K is a constant taken as unity. Then, using Eq. (3), a WQI based on a simple arithmetic average was developed:

$$WQI = \sum_{i=1}^{n} \frac{WiQi}{\sum_{i=1}^{n} Wi} \tag{3}$$

Table 2 summarizes the calculations of unit weightage (Wi) based on the constant (K) and standard values (Vs). The water quality grading is summarized in Table 3 (Brown et al. 1972) based on the computed WQI.

Synthetic pollution index

The SPI was used to determine the appropriateness of the Gomti river's water quality. The following three relationships were used to create the index. The constant of proportionality (K) was determined in the first phase using the following method:

$$K = \frac{1}{\left(\sum_{i=1}^{n} \frac{1}{Si}\right)} \tag{4}$$

The ith parameter's standard level is Si, and the number of parameters is n. The weight coefficient (Wi) was computed in the second stage using the following method:

$$Wi = \frac{K}{Vs} \tag{5}$$

Finally, the SPI was computed using the following approach:

$$SPI = \sum_{i=1}^{n} \frac{Ci}{Si} \times Wi \tag{6}$$

Table 2 Abbreviation, unit weightage (*Wi*) of different parameters, and their standards used for WQI and SPI determination

S. No	Parameter	Abbreviation	Standard value (*Vi*)	Unit weightage (*Wi*)
1	Temperature	T	40	0.034435
2	pH	pH	6.5–8.5	0.183655
3	Electrical conductivity	EC	300	0.004591
4	Total dissolved solids	TDS	500	0.002755
5	Total alkalinity (as $CaCO_3$)	TA	120	0.011478
6	Total hardness (as $CaCO_3$)	TH	300	0.004591
7	Calcium	Ca^{++}	75	0.018365
8	Magnesium	Mg^{++}	30	0.045914
9	Chloride	Cl^{-}	250	0.005510
10	Dissolved oxygen	DO	5	0.275482
11	Biochemical oxygen demand	BOD	5	0.275482
12	Chemical oxygen demand	COD	10	0.137741

Table 3 WQI and SPI range, status, and possible usage of water sample

WQI range	SPI range	Water classification	Probable usage
0–25	< 0.2	Suitable for drinking	Drinking, irrigation, and industrial purpose
26–50	0.2–0.5	Slightly polluted	Drinking, irrigation, and industrial purpose
51–75	0.5–1.0	Moderately polluted	Irrigation and industrial purpose
76–100	1.0–3.0	Severally polluted	For irrigation purpose
> 100	> 3.0	Unsuitable for human consumption	Proper treatment required for any kind of usage

where *Ci* denotes the concentration recorded for each physicochemical water quality parameter that has been determined. Water quality is divided into five groups based on the SPI (Solangi et al. 2018) determined levels, as shown in Table 3.

Geospatial assessment

Integration of the WQI and SPI data collection with GIS can help display the water quality state of the river Gomti in Lucknow (UP) to policymakers or stakeholders clearly and understandably (Tiwari et al. 2015). The spatial interpolation is accomplished using the spatial analyst tool's inverse distance weighted (IDW) interpolation approach in ArcGIS 10.4. IDW uses a weighted distance between measured and unknown sites to forecast their respective values. The weights are inversely proportional to the distance measured from the power value, *p*. In this study, parameter *p* is set to 2, which is the default number for the ArcGIS platform. IDW's mathematical formula for predicting an unknown value (Ali et al. 2021) is as follows:

$$Zp = \frac{\sum_{i=0}^{n} \frac{z_i}{d_i^p}}{\sum_{i=0}^{n} \frac{1}{d_i^p}} \tag{7}$$

where *Zp* is the value of an unknown point, *di* is the distance from the known point, *Zi* is the measured location's value, and *p* is the chosen exponent.

Statistical analysis

For each physicochemical parameter, WQI and SPI, fundamental statistics as a minimum, maximum, mean, mode, median, and standard deviation were determined. The correlation coefficient analysis, in general, is based on the methodical calculation of several parameters. The correlation coefficient is mostly associated with two different variables; one is clearly dependent. To find the correlation coefficient between distinct parameters, the Pearson's correlation approach has been utilized. A strong connection is shown by the correlation coefficient values of + 1 and − 1 among the variables, and the absence of a variable association is indicated by a correlation coefficient value of "0" or near "0". A correlation

coefficient of 0.7 or above is considered a strong positive correlation, while a correlation coefficient of 0.5 to 0.7 is considered a moderate positive correlation. (Karunanidhi et al. 2021). MS Excel 2016 has been used to calculate the minimum, maximum, mean, mode, median, standard deviation, and Perason's correlation (Sharma et al. 2020).

Results and discussions

Physicochemical analysis

The statistical overview of the chosen water quality parameters at seven sampling stations of the river Gomti during the study period (2013–2017) is presented in Table 4.

Temperature is extremely essential in a riverine system and impacts aquatic life. Temperature affects dissolved oxygen, salt solubility, physicochemical characteristics, and biodegradation rate. A temperature change, for example, can stimulate photosynthesis in water plants (Rao and Rao 2010). All of the sampling stations (S1–S7) had temperatures ranging from 15.3 to 34 °C, which is well within the WHO's recommended range (Fig. S1). The highest and lowest temperatures were noted during the study period in June and January, respectively. Sharma et al. (2020) observed a similar value and trend in the Yamuna river. Water temperatures usually fluctuate with air temperature on a daily and seasonal basis. Surface water bodies can buffer water temperature, but due to aquatic organisms' limited temperature tolerance, even small changes in water temperature can significantly impact river ecosystems. High sewage flows and religious rituals along the riverbank significantly impact river water temperature (Singh et al. 2018; Tyagi et al. 2013).

The pH value is crucial for aquatic environments, affecting animal and plant toxicity. The pH of a water sample indicates its acidity and basicity in general (Yang et al. 2007). All of the sampling stations (S1–S7) recorded pH values ranging from 6.89–8.59, 6.89–8.86, 7.11–8.59, 7.23–8.59, and 7.23–8.89 for 2013, 2014, 2015, 2016, and 2017 respectively. According to Bureau of Indian Standards (BIS (2012), the permissible pH range is 6.5–8.5. The pH of the Gomti river water ranged from 6.89 to 8.89, indicating that it is either mildly acidic or alkaline. The pH of the Gomti river was found in the range of 6.22 to 8.6 (Iqbal et al. 2019). During the study period, the pH value increases from S1 to S7 (Fig. S2). In natural waters, the stability of carbonate–bicarbonate–carbon dioxide is the regulating factor of pH. The discharge of wastewater, including soaps and detergents, might result in the alkaline nature of the river water (Khan et al. 2016).

The measurement of electric current carrying capacity and dissolved ions in a water sample is called electrical conductivity EC. In this study at S1, S2, S3, S4, S5, S6 and S7, the EC was found to be in the range of 172.0–560.2 µS/cm, 180.8–582.4 µS/cm, 201.0–772.5 µS/cm, 212.0–795.6 µS/cm, 224.6–858.5 µS/cm, 221.6–882.6 µS/cm, and 240.6–984.2 µS/cm respectively, while the Bureau of Indian Standards (BIS (2012) standard is 300 µS/cm. The EC values at station S1 are relatively low in this study. This could be owing to the land cover pattern here, which is semi-green, resulting in reduced topsoil erosion (Shah and Joshi 2017). The summer season is when the EC values at stations S6 and S7 are at their highest. This could be attributed to sewage discharges and anthropogenic activities near these stations' riverbanks. The sampling stations in the downstream region have greater EC values than those in the upstream (Fig. S3). Iqbal et al. (2019) found that the river Gomti has the same value and trend.

The measuring of dissolved particles in a water sample using direct measurement is known as TDS. During the study period from 2013 to 2017, TDS concentrations ranged as 112.0–332.0 mg/l, 118.0–346.0 mg/l, 128.0–482.0 mg/l, 136.0–496.0 mg/l, 152.0–538.0 mg/l, 160.0–554.0 mg/l, and 172–616 mg/l at S1, S2, S3, S4, S5, S6, and S7 respectively. TDS concentrations were under the desired range of 500 mg/l at S1, S2, S3, and S4 but exceeded it at S5, S6, and S7, according to the Bureau of Indian Standards (BIS) (2012). The lowest TDS was found at S1, while the highest was found at S7 (Fig. S4). Areas with high population density result in the release of significant amounts of solid waste, domestic wastewater discharge, encroachment, and sewage, resulting in a gradual increase from S1 to S7 (Iqbal et al. 2019). Unfortunately, the rivers are considered to be the best place to dump garbage, yet it has been proven to be a big load there, increasing TDS in the water and causing unsanitary conditions, as well as health issues in the form of waterborne communicable diseases (Kharake and Raut 2021).

Total alkalinity (TA) is found in water due to various hydroxides, bicarbonates, and carbonates, and it refers to an aqueous solution's ability to neutralize acids. During the study period, the TA values for the selected sampling stations ranged from 142 to 316 mg/l. For the years 2013, 2014, 2015, 2016, and 2017, the average values of TA were 236.05 ± 39.92 mg/l, 241.64 ± 38.16 mg/l, 247.90 ± 27.10 mg/l, 237.62 ± 36.34 mg/l, and 244.81 ± 32.50 mg/l, respectively. The average value of TA was found to be greater than 200 mg/l as per Bureau of Indian Standards (BIS) (2012) at all sampling stations during the study period. TA was determined to be lowest during the rainy season at S1 (142 mg/l) and highest during the summer season at S7 (316 mg/l) (Fig. S5). Iqbal et al. (2019) found a similar value and trend in the Gomti river. This could be due to freshwater entry into the river system in the monsoon season, producing dilution (Kamboj and Kamboj 2019).

Table 4 Location-wise statistics of physicochemical parameters, WQI, and SPI

	T	pH	EC	TDS	TA	TH	Ca^{++}	Mg^{++}	Cl^{-}	DO	BOD	COD	WQI	SPI
S1														
Minimum	15.300	7.200	172.000	112.000	142.000	120.000	24.700	12.480	8.000	2.800	2.300	12.400	78.993	0.868
Maximum	33.800	8.890	560.200	332.000	252.000	236.000	49.600	29.280	17.000	11.400	11.000	18.400	175.607	1.277
Mean	26.850	8.223	384.468	231.367	216.200	196.767	39.998	23.078	13.050	6.809	4.188	14.887	120.805	1.112
Mode	30.000	8.290	388.400	233.000	228.000	206.000	40.800	23.520	13.000	6.900	3.000	14.800	115.980	1.103
Median	30.000	8.290	388.400	233.000	228.000	206.000	40.800	23.520	13.000	6.900	3.000	14.800	115.980	1.103
Standard deviation	5.515	0.357	93.795	47.207	30.066	30.161	6.513	3.974	1.731	2.572	2.572	1.141	22.898	0.104
S2														
Minimum	15.400	7.170	180.800	118.000	148.000	128.000	25.500	13.440	11.000	2.900	3.100	13.600	83.701	0.908
Maximum	33.800	8.580	582.400	346.000	264.000	244.000	49.600	30.240	19.000	10.900	4.200	24.800	148.227	1.312
Mean	26.910	8.124	397.095	240.833	224.200	202.700	41.318	23.880	14.533	7.262	3.412	18.993	117.519	1.151
Mode	18.000	8.540	348.000	192.000	236.000	232.000	49.600	25.920	14.000	6.500	3.300	17.600	138.472	1.171
Median	30.000	8.210	413.800	240.000	236.000	212.000	41.600	24.240	14.000	6.700	3.300	18.800	116.119	1.149
Standard deviation	5.510	0.323	98.924	49.839	29.335	31.704	6.535	4.059	1.864	2.132	0.242	2.193	14.401	0.111
S3														
Minimum	15.500	7.110	201.000	128.000	156.000	134.000	27.100	14.400	12.000	0.700	3.600	18.800	92.860	0.987
Maximum	33.900	8.380	772.500	482.000	272.000	256.000	53.600	32.160	22.000	9.500	9.000	44.800	184.851	1.465
Mean	27.032	7.874	450.825	274.233	233.467	211.967	43.052	25.024	16.717	5.020	5.193	28.140	137.620	1.250
Mode	30.300	7.820	364.000	270.000	258.000	236.000	49.600	26.880	15.000	3.500	4.000	28.800	151.860	1.242
Median	30.100	7.825	440.400	255.000	244.000	220.000	44.000	25.680	16.000	5.050	4.600	27.400	139.182	1.242
Standard deviation	5.526	0.286	147.983	84.811	30.567	31.897	6.524	4.291	2.394	2.408	1.492	5.944	21.425	0.103
S4														
Minimum	15.500	7.040	212.000	136.000	162.000	140.000	28.500	15.360	13.000	1.300	4.500	24.400	102.993	1.070
Maximum	33.900	8.260	795.600	496.000	278.000	262.000	55.200	32.640	24.000	8.400	10.000	47.600	196.601	1.601
Mean	27.065	7.800	469.442	286.533	240.333	218.800	44.582	25.733	18.417	4.363	6.385	34.487	152.334	1.367
Mode	30.300	7.710	388.000	232.000	252.000	244.000	50.400	28.320	20.000	4.200	6.000	35.200	166.865	1.367
Median	30.050	7.765	454.450	266.000	252.000	228.000	46.400	25.920	18.000	4.200	6.000	35.200	152.138	1.372
Standard deviation	5.557	0.252	148.765	85.766	30.751	32.136	6.840	4.231	2.586	1.744	1.478	5.490	20.724	0.109
S5														
Minimum	15.600	7.000	224.600	152.000	168.000	148.000	30.300	16.320	14.000	1.100	6.000	31.200	123.345	1.254
Maximum	34.000	8.150	858.500	538.000	286.000	274.000	56.000	33.600	27.000	6.000	11.500	56.400	220.987	1.859
Mean	27.150	7.701	496.187	304.767	250.033	228.467	46.385	26.959	21.333	3.020	8.372	43.740	176.660	1.532
Mode	30.300	7.690	426.000	274.000	268.000	254.000	53.600	28.320	24.000	3.200	8.500	44.800	199.724	1.648
Median	30.200	7.695	474.600	282.000	260.000	238.000	47.200	27.360	21.000	2.800	8.500	44.800	178.082	1.513
Standard deviation	5.537	0.225	155.839	88.703	30.875	32.252	6.893	4.230	2.927	1.193	1.490	6.219	21.831	0.141
S6														
Minimum	15.600	6.950	221.600	160.000	172.000	156.000	31.100	16.800	15.000	0.600	6.500	35.600	132.492	1.338

Table 4 (continued)

	T	pH	EC	TDS	TA	TH	Ca^{++}	Mg^{++}	Cl^-	DO	BOD	COD	WQI	SPI
Maximum	34.000	8.090	882.600	554.000	298.000	282.000	59.200	34.560	29.000	5.100	12.500	60.800	228.687	2.020
Mean	27.175	7.642	512.500	316.467	256.700	235.867	48.078	27.680	23.333	2.448	9.768	50.120	192.489	1.662
Mode	30.300	7.620	456.000	290.000	282.000	258.000	56.000	28.320	25.000	3.000	10.000	51.600	192.447	1.664
Median	30.200	7.640	489.100	293.000	266.000	244.000	48.800	28.320	23.000	2.100	10.000	49.600	193.320	1.648
Standard deviation	5.535	0.218	158.382	89.237	31.586	32.238	7.225	4.227	3.229	1.122	1.530	6.099	21.546	0.148
S7														
Minimum	15.700	6.890	240.600	172.000	186.000	170.000	34.200	18.720	18.000	0.300	8.500	48.400	154.655	1.513
Maximum	34.000	7.820	984.200	616.000	316.000	294.000	64.000	36.000	33.000	3.800	18.600	70.800	249.388	2.177
Mean	27.272	7.479	559.402	343.733	270.300	248.233	50.370	29.303	27.183	1.522	12.477	61.793	221.123	1.927
Mode	30.800	7.430	489.000	342.000	296.000	258.000	56.000	30.240	29.000	1.000	13.000	63.600	246.520	2.096
Median	30.300	7.500	513.500	314.000	278.000	258.000	52.000	29.040	28.000	1.200	13.000	63.600	227.607	1.950
Standard deviation	5.522	0.191	179.190	99.631	32.154	32.942	7.116	4.432	3.442	0.862	1.695	6.182	21.754	0.149

In river water, dissolved calcium and magnesium ions contribute the most to total hardness (TH) concentration and other divalent cations in terms of mg/l as $CaCO_3$. The surrounding rocks of the water bodies give the majority of their source (Lkr et al. 2020). The highest TH values were 294, 294, 276, 282, and 292 mg/l observed at S7, and the lowest TH values were 120, 120, 176, 132, and 128 mg/l recorded at S1 during the study period. TH concentrations were significantly below the recommended limit of 300 mg/l (Bureau of Indian Standards (BIS) 2012). According to the TH values, the Gomti river water is classified as moderately hard to hard water (Bora and Goswami 2017). During the study period, Ca^{++} concentrations varied between 24.7–49.6 mg/l, 25.5–49.6 mg/l, 27.1–53.6 mg/l, 28.5–55.2 mg/l, 30.3–56.0 mg/l, 31.1–59.2 mg/l, and 34.2–64.0 mg/l at S1, S2, S3, S4, S5, S6, and S7 respectively, with the maximum and minimum values of 64.0 mg/l at S7 and 24.7 mg/l at S1. The temperature rise, drop in water levels, and accumulation of other household garbage may have contributed to its higher concentration (Lkr et al. 2020). Mg^{++} in natural water is due to the chemistry of the river bedrock's geological makeup. At sampling stations, Mg^{++} concentrations were recorded as 12.48–35.52 mg/l in 2013, 12.48–36.00 mg/l in 2014, 19.68–32.12 mg/l in 2015, 16.80–35.52 mg/l in 2016, and 16.70–36.0 mg/l in 2017. The maximum Mg^{++} concentration was 36.0 mg/l at S7, while the minimum Mg^{++} concentration was 12.48 mg/l at S1. At all sampling stations, the Ca^{++} concentrations were well within the prescribed limit of 75 mg/l (Bureau of Indian Standards (BIS) 2012), but the Mg^{++} concentrations were significantly over the permissible limit of 30 mg/l (Bureau of Indian Standards (BIS) 2012) except S1. The measured values of TH, Ca^{++}, and Mg^{++} increased from S1 to S7 during the study period (Fig. S6, Fig. S7, and Fig. S8).

Cl^- is an important water quality parameter that is found naturally in the form of NaCl, KCl, and $CaCl_2$. Multiple sources of Cl^- include leaching from different rocks through the weathering process, surface runoff from inorganic fertilized agricultural areas, irrigation outflow, animal feed, and a variety of other sources (Bora and Goswami 2017). The average Cl^- concentration for the selected water samples during 2013, 2014, 2015, 2016, and 2017 was 1032 mg/l, 11–32 mg/l, 10–31 mg/l, 11–33 mg/l, and 8–33 mg/l respectively. The detected Cl^- values were substantially below Bureau of Indian Standards (BIS) (2012) recommended limit of 250 mg/l. During the study period, the maximum and minimum Cl^- concentrations were 8 and 33 mg/l at S1 and S7, respectively, which demonstrates that the measured Cl^- values increased from S1 to S7 over the study period (Fig. S9).

Water bodies have varying levels of dissolved oxygen (DO), which is the total amount of oxygen dissolved in them. The DO concentration is determined by the physical,

chemical, and biological activity of the water body. In water pollution control, DO estimation is critical. According to the Bureau of Indian Standards (BIS) (2012), a DO level of 5 mg/l is considered ideal for maintaining aquatic life. A water sample is considered polluted when the DO concentration is below the optimum range (Bora and Goswami 2017). During the study period, the DO values at S1, S2, S3, S4, S5, S6, and S7 were 2.8–11.4 mg/l, 2.9–10.9 mg/l, 0.7–9.5 mg/l, 1.3–8.4 mg/l, 1.1–6.0 mg/l, 0.6–5.1 mg/l, and 0.3–3.8 mg/l, respectively (Fig. S10). During the summer and lean rainfall periods, the minimum value observed at all sample stations was well below the recommended range (5 mg/l). The presence of high organic load and discharges by the drains as well as religious ritual activities along the river bank caused present trends of DO depletion at most sampling stations. The stream's temperature raised in the summer. The solubility of oxygen in water reduces as the temperature increases. The metabolism, development, and reproduction of bacteria involved in the decomposition of organic materials in water are also affected by temperature. As the temperature increases, it slows down biological activity and biodegradation rate. As a result, the oxygen requirement in the water increases (Shah and Joshi 2017).

BOD is the amount of total oxygen required by aerobic microorganisms to oxidize the biodegradable organic wastes in a waterbody. As a result, BOD is a measure of organic pollution, with greater readings indicating higher amounts (Bora and Goswami 2017). BOD levels more than 5 mg/l are unfavorable. During this study, the BOD values in river water ranged from 2.3–11.0 mg/l to 3.1–4.2 mg/l, 3.6–9.0 mg/l, 4.5–10.0 mg/l, 6.0–11.5 mg/l, 6.5–12.5 mg/l, and 8.5–18.6 mg/l at S1, S2, S3, S4, S5, S6, and S7, respectively (Fig. S11). According to Bureau of Indian Standards (BIS) (2012), the maximum BOD value observed at all sampling stations during the study period was unacceptable, and it increased from S1 to S7. A high value in each sampling station suggests that irreversible damage has occurred due to untreated organic waste discharge and religious ceremonial activities near the riverbank. Depletion of DO, increased TDS, high quantum discharge, and insufficient water flow may all contribute to an increase in BOD in river water bodies, with rubbish mounds along the river as well as the dead bodies of humans and animals also adding to this occurrence (Singh et al. 2018).

COD is a valuable tool to determine contamination level by measuring nearly total organic matter in sewage and industrial waste. COD levels in the river were measured at S1, S2, S3, S4, S5, S6, and S7 and varied from 12.4–18.4 mg/l to 13.6–24.8 mg/l, 18.8–44.8 mg/l, 24.4–47.6 mg/l, 31.2–56.4 mg/l, 35.6–60.8 mg/l, and 48.4–70.8 mg/l, respectively. S7 had the highest COD of 70.8 mg/l, while S1 had the lowest, 12.4 mg/l exceeding the maximum permitted limit (10 mg/l) during the study period (WHO 2011). Current trends in the increase of BOD and COD and decrease in DO concentrations were observed in the downstream (S7), which contained higher organic wastes. Untreated industrial and municipal wastes and religious ritual activities along the riverbank contributed significantly to inorganic and organic carbon, raising BOD and COD and decreasing DO (Fig. S10, Fig. S11, and Fig. S12).

Correlation analysis

Table 5 shows the Pearson's correlation matrix used to find connections between the 12 water quality parameters of the Gomti river collected from 2013 to 2017.

DO was found to have a high inverse significant association with BOD and COD, which could be due to aerobic species consuming DO during organics assimilation in polluted water (Singh et al. 2018). The amount of oxygen dissolved in water was positively correlated with pH and negatively correlated with chloride (Cl^-), implying that pH could play a role. According to the findings, water samples with a slightly higher pH had higher amounts of DO, which resulted in a lower bacterial count (Dutta et al. 2018b). The negative relationship between temperature and DO may be due to the fact that large concentrations of oxygen dissolve more readily in cooler water (Jaiswal et al. 2019). TDS had a high positive

Table 5 Pearson's correlation matrix between the physicochemical parameters of the Gomti river

	T	pH	EC	TDS	TA	TH	Ca^{++}	Mg^{++}	Cl^-	DO	BOD	COD
T	**1.00**											
pH	-0.22	**1.00**										
EC	0.03	-0.12	**1.00**									
TDS	0.08	-0.18	**0.97**	**1.00**								
TA	-0.23	0.03	0.62	0.59	**1.00**							
TH	-0.19	0.04	0.64	0.61	**0.98**	**1.00**						
Ca^{++}	-0.21	0.04	0.57	0.50	**0.93**	**0.94**	**1.00**					
Mg^{++}	-0.16	0.03	0.63	0.64	**0.91**	**0.95**	**0.79**	**1.00**				
Cl^-	0.08	-0.48	0.55	0.56	0.62	0.61	0.58	0.58	**1.00**			
DO	-0.31	0.68	-0.38	-0.42	-0.37	-0.38	-0.33	-0.37	**-0.71**	**1.00**		
BOD	0.06	-0.56	0.50	0.55	0.55	0.53	0.47	0.52	**0.85**	**-0.83**	**1.00**	
COD	0.10	-0.62	0.49	0.54	0.60	0.59	0.54	0.58	**0.91**	**-0.79**	**0.92**	**1.00**

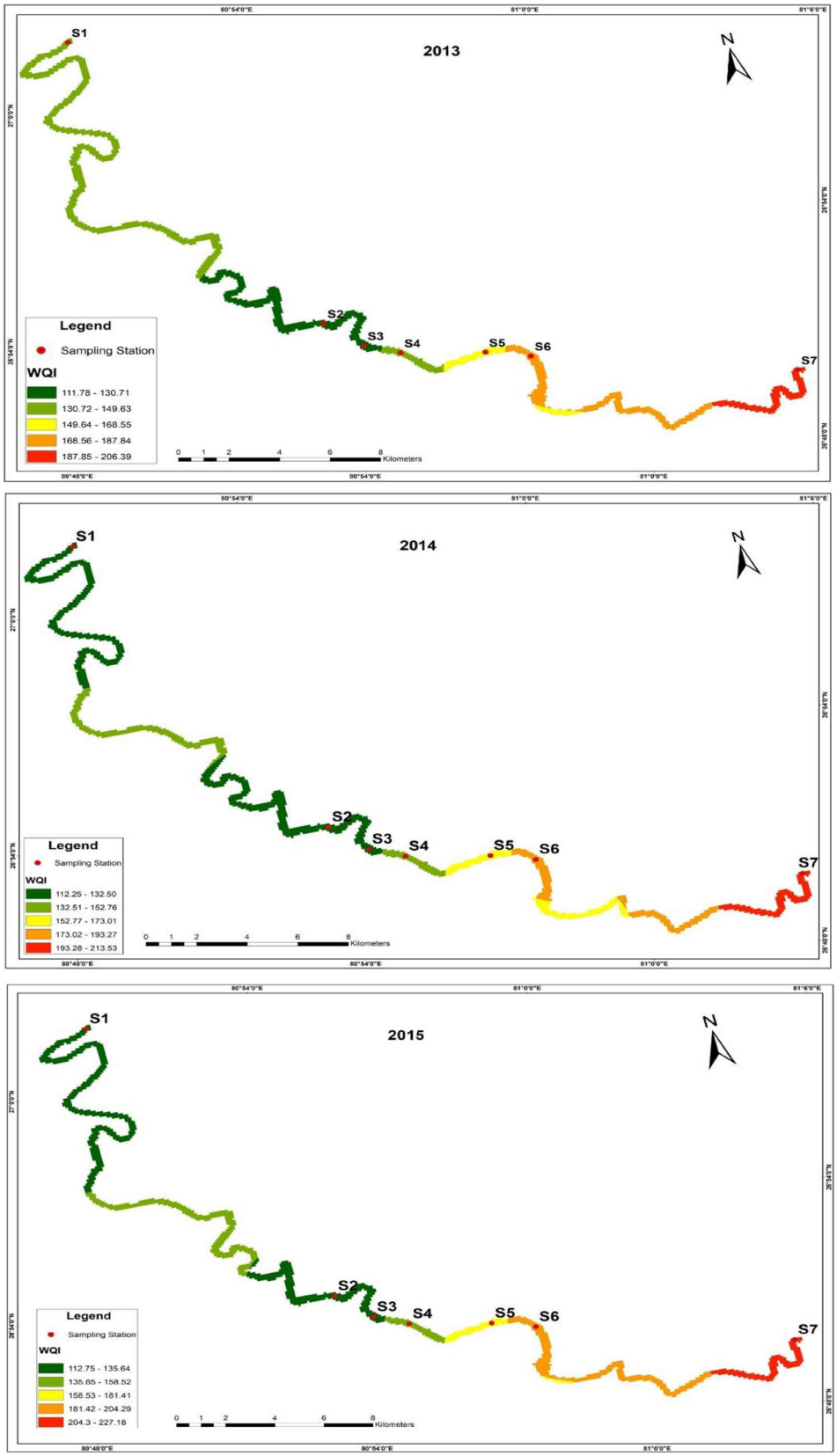

Fig. 2 WQI of the river Gomti for suitability assessment (2013–2017)

Fig. 2 (continued)

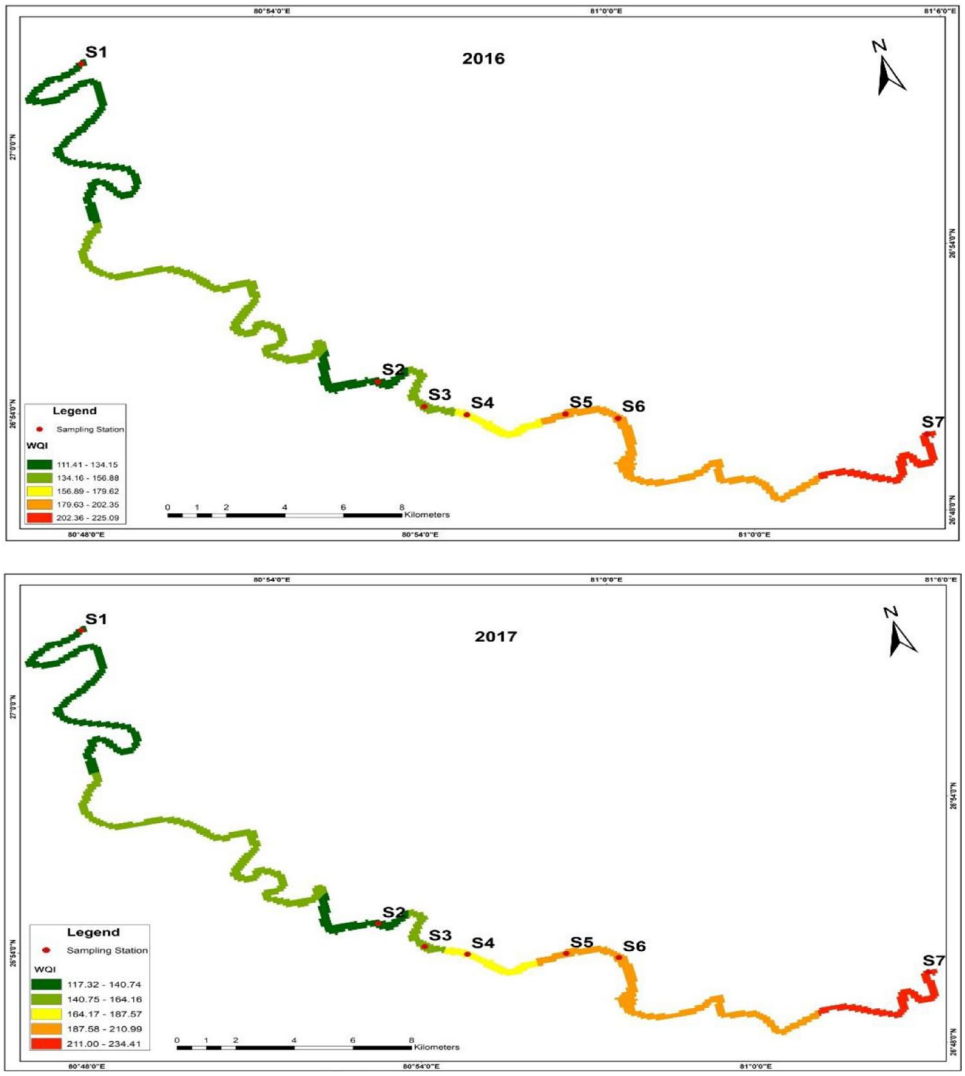

correlation with EC and a moderate positive correlation with TA, TH, Ca^{++}, Mg^{++}, Cl^{-}, BOD, and COD. TDS, TA, TH, Ca^{++}, Mg^{++}, and Cl^{-} were all substantially correlated with EC, indicating that EC has the greatest impact on conductivity. Furthermore, the significant correlation between ionic charges could be linked to the river basin's geochemical composition. Ca^{++} and Mg^{++} had a strong positive correlation with TH and TA but only a moderate positive correlation with Cl^{-}, indicating that Ca^{++} and Mg^{++} were mostly present as chloride salts (Jaiswal et al. 2019).

Water quality assessment through WQI and SPI

For the given stretch of the river Gomti in Lucknow, WQI was analyzed for 5 years in a row (2013–2017). The WQI (Fig. 2) and SPI (Fig. 3) values were interpolated using IDW geostatistics in ArcGIS for enhanced interpretability. The WQI of the Gomti river section from S1 to S7 was 83.701–246.520 in 2013, 78.993–242.570 in 2014, 88.073–246.566 in 2015, 88.073–246.520 in 2016, and 95.539–249.388 in 2017. The WQI was determined to be in the range of severally contaminated (76–100) to unsuitable for human consumption (> 100) during the study period. SPI results were similar, ranging from 0.868–2.096 in 2013, 0.868–2.109 in 2014, 1.023–2.096 in 2015, 0.973–2.096 in 2016, and 0.973–2.177 in 2017, indicating that the river stretch was determined to be moderately polluted (0.5–1.0) to severally polluted (1.0–3.0).

Throughout the study period, the WQI and SPI values indicated a varied pattern of changes in all sampling stations with different years. The WQI of the river in this study suggests that it is in danger of losing its water quality because of the regular discharge of effluents from diverse manmade sources into it, which necessitates suitable treatment for any use. As the river enters the city at S2 and goes through S3, S4, S5, and S6, the WQI deteriorates to the worst category at S7, as depicted in Fig. 4. It occurred

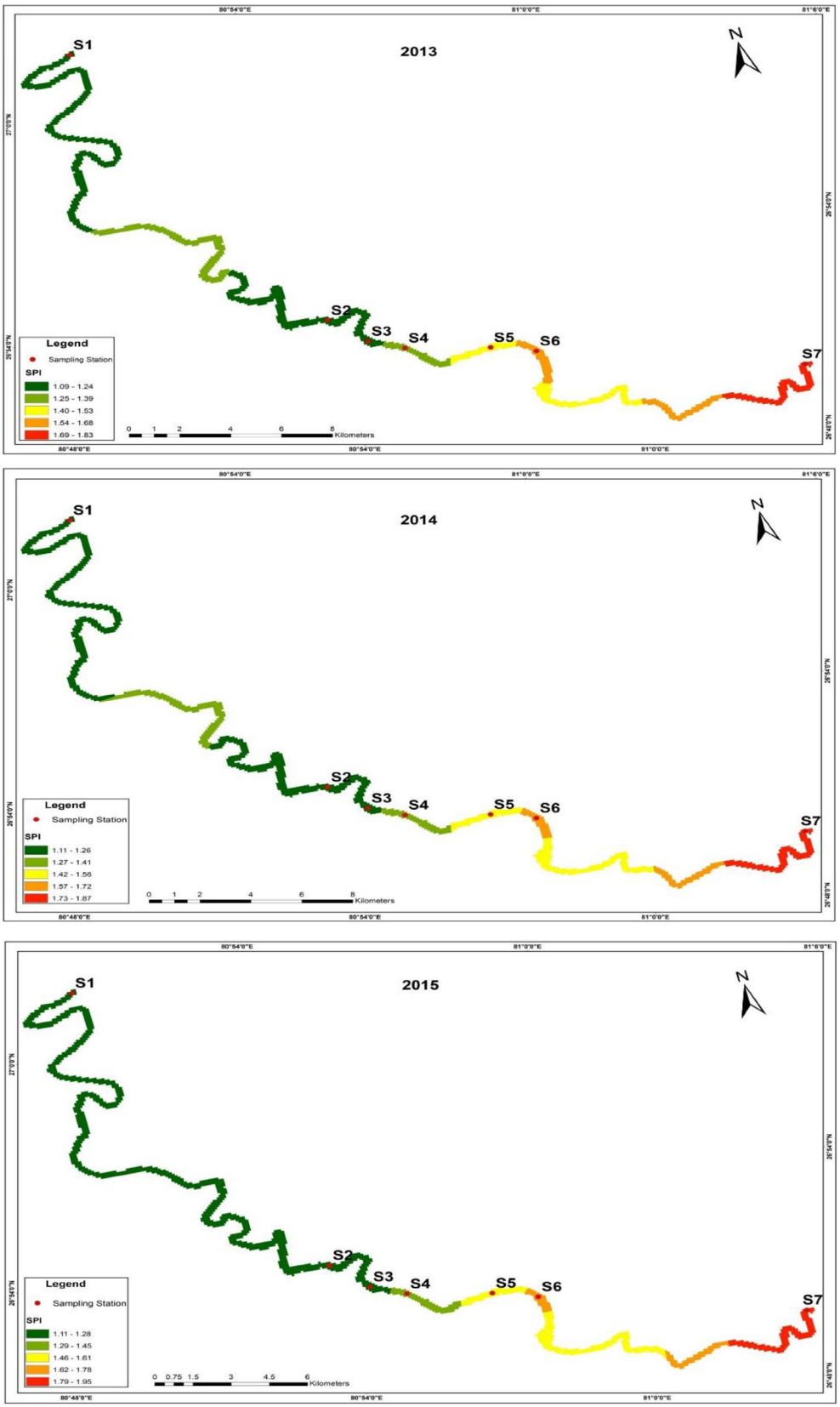

Fig. 3 SPI of the river Gomti for suitability assessment (2013–2017)

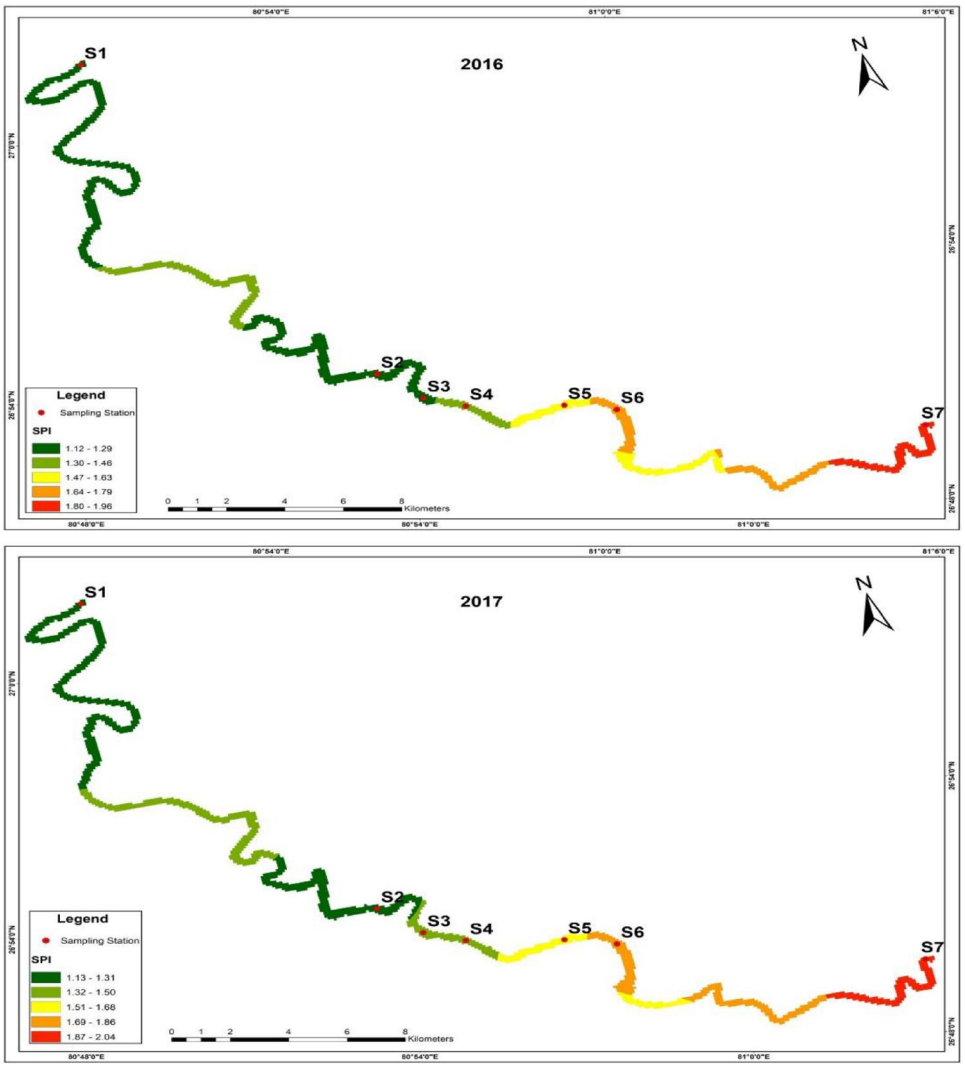

Fig. 3 (continued)

due to the concentration of domestic, municipal, and industrial effluents in this area. As seen in Fig. 5, SPI followed the same pattern as WQI, with values increasing from S1 (upstream) to S7 (downstream). Iqbal et al. (2019) reported a similar observation in their study of the river Gomti (UP) water quality assessment, where water samples indicated an increasing pollution trend further downstream.

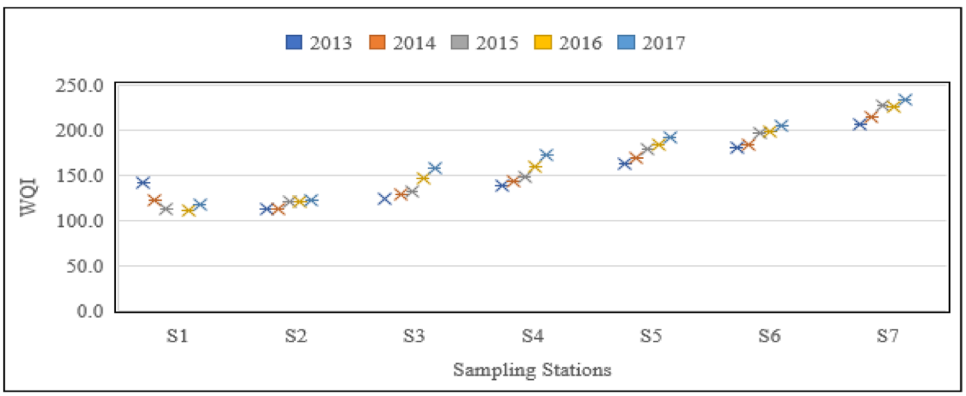

Fig. 4 Variation in WQI at sampling stations of the river Gomti

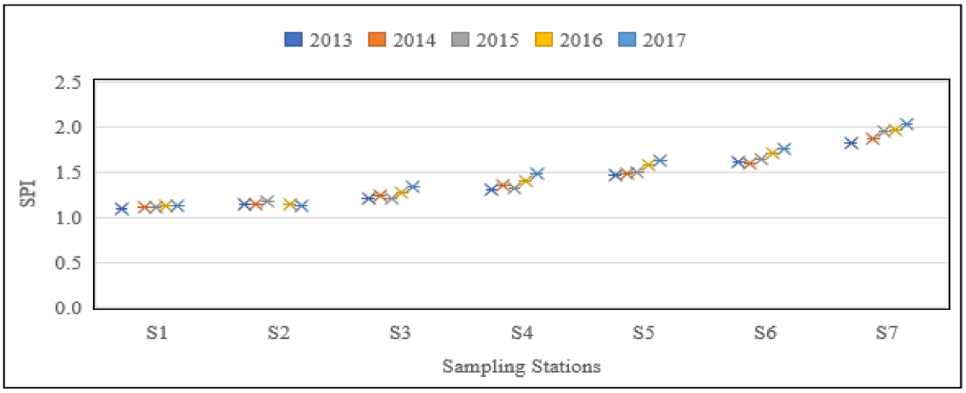

Fig. 5 Variation in SPI at sampling stations of the river Gomti

Conclusions

This study constitutes water quality assessment of the stretch of river Gomti, Lucknow (UP), one of the most polluted rivers in India. This study represents the combined application of WQI and SPI and further integrates the data set with GIS to conveniently depict the water quality status. Twelve water quality parameters data have been collected from the UPPCB, Lucknow (UP), for the seven sampling stations (S1 to S7) from 2013 to 2017. The WQI of the Gomti river section from S1 to S7 was 83.701–246.520 in 2013, 78.993–242.570 in 2014, 88.073–246.566 in 2015, 88.073–246.520 in 2016, and 95.539–249.388 in 2017, and the similar result was found for SPI, ranging from 0.868–2.096 in 2013, 0.868–2.109 in 2014, 1.023–2.096 in 2015, 0.973–2.096 in 2016, and 0.973–2.177 in 2017. BOD and COD were found to significantly influence the WQI and SPI scores of the twelve parameters.

The study concludes that WQI falls into either severally polluted (76–100) or unsuitable for human consumption (> 100), while SPI lies in the category of moderately polluted (0.5–1.0) to severally polluted (1.0–3.0). Most of the EC, TDS, TA, BOD, COD, and DO values did not fall under the permissible limit in the river Gomti. All selected physicochemical parameters increased from S1 to S7, which may be due to the repetitive discharge of waste effluents by various discharges pouring directly into the river by many manmade sources, surface runoff, and uncontrolled dumping of solid waste with a very low rate of dilution. The WQI and SPI of the river Gomti show variation at its entry in the city and when it leaves the city, as the index worsens to a marginal value as it travels through the city premises, which gives the impression that pollution is ascribed to various sources. Effective wastewater treatment measures for the polluting sources are urgently required to augment water quality and support any sustainable plan for river restoration.

Supplementary Information The online version contains supplementary material available at https://doi.org/10.1007/s11356-022-21493-3.

Acknowledgements The authors are incredibly grateful to Uttar Pradesh Pollution Control Board (UPPCB), Lucknow, India (http://www.uppcb.com), for providing the physiochemical water quality data of the Gomti river to carry out this study and the Environmental Engineering Department, Delhi Technological University, Delhi (India), for encouraging to conduct this research and providing all the facility to compile this work.

Author contribution Conceptualization, methodology, formal analysis and investigation, and draft preparation, Amit Krishan; investigation, supervision, and review and editing, Rajeev Kumar Mishra; resources, data curation, and review and editing, Anwar Khursheed.

Data availability The data used in the current study have been taken from UPPCB (Uttar Pradesh Pollution Control Board), Lucknow, India.

Declarations

Ethics approval This article does not contain any studies with human participants or animals performed by any of the authors.

Consent for publication The authors confirm that the final version of the manuscript has been reviewed, approved, and consented for publication by all authors.

Competing interests The authors declare no competing interests.

References

Abeysingha NS, Islam A, Singh M (2020) Assessment of climate change impact on flow regimes over the Gomti river basin under IPCC AR5 climate change scenarios. J Water Clim Chang 11:303–326. https://doi.org/10.2166/wcc.2018.039

Abeysingha NS, Singh M, Sehgal VK, Khanna M, Pathak H (2016) Analysis of trends in stream flow and its linkages with rainfall and anthropogenic factors in Gomti river basin of North India. Theor Appl Climatol 123:785–799. https://doi.org/10.1007/s00704-015-1390-5

Abeysingha NS, Singh M, Sehgal VK, Khanna M, Pathak H, Jayakody P, Srinivasan R (2015) Assessment of water yield and evapotranspiration over 1985 to 2010 in the Gomti river basin in India using the SWAT model. Curr Sci 108:2202–2212

Aliyu GA, Jamil NRB, Adam MB, Zulkeflee Z (2019) Assessment of Guinea Savanna River system to evaluate water quality and

water monitoring networks. Glob J Environ Sci Manag 5:345–356. https://doi.org/10.22034/GJESM.2019.03.07

Ali SY, Sunar S, Saha P, Mukherjee P, Saha S, Dutta S (2021) Drinking water quality assessment of river Ganga in West Bengal, India through integrated statistical and GIS techniques. Water Sci Technol 84:2997–3017. https://doi.org/10.2166/wst.2021.293

Bora M, Goswami DC (2017) Water quality assessment in terms of water quality index (WQI): case study of the Kolong River, Assam, India. Appl Water Sci 7:3125–3135. https://doi.org/10.1007/s13201-016-0451-y

Brown RM, McClelIand NI, Deininger RA, O'Connor MF (1972) A water quality index—crashing the physiological barrier. Indic Environ Qual 1:173–182

Brown RM, McClelIand NI, Deininger RA, Tozer RG (1970) A water quality index—do we dare? Water Sew Works 117:339–343

Bureau of Indian Standards (BIS) (2012) Indian standard (10500: 2012) drinking water - specification (Second Revision), New Delhi, India.

Cude C (2001) Oregon water quality index: a tool for evaluating water quality management effectiveness. J Am Water Res Assoc 37:125–137. https://doi.org/10.1111/j.1752-1688.2001.tb05480.x

Dutta S, Dwivedi A, Kumar MS (2018a) Use of water quality index and multivariate statistical techniques for the assessment of spatial variations in water quality of a small river. Environ Monit Assess 190:718. https://doi.org/10.1007/s10661-018-7100-x

Dutta V, Sharma U, Iqbal K, Kumar R, Pathak AK (2018b) Impact of river channelization and river front development on fluvial habitat: evidence from Gomti River, a tributary of Ganges, India. Environ Sustain 1:167–184. https://doi.org/10.1007/s42398-018-0016-0

Dutta V, Srivastava RK, Yunus M, Ahmad S, Pathak VV, Rai A, Prasad N (2011) Restoration plan of Gomti river with designated best use classification of surface water quality based on river expedition, monitoring and quality assessment. Earth Sci India 4:80–104

Ewaid SH, Abed SA, Al-Ansari N, Salih RM (2020) Development and evaluation of a water quality index for the Iraqi rivers. Hydrology 7:67. https://doi.org/10.3390/hydrology7030067

Goel P, Saxena A, Singh DS, Verma D (2018) Impact of rapid urbanization on water quality index in groundwater fed Gomati river, Lucknow, India. Curr Sci 114:650–654. https://doi.org/10.18520/cs/v114/i03/650-654

Gupta KS, Chabukdhara M, Kumar P, Singh J, Bux F (2014) Evaluation of ecological risk of metal contamination in river Gomti, India: a biomonitoring approach. Ecotoxicol Environ Saf 110:49–55. https://doi.org/10.1016/j.ecoenv.2014.08.008

Horton RK (1965) An index number system for rating water quality. J Water Pollut Control Fed 3:300–306

Hui T, Jizhong D, Qifa S, Qiang L, Zhuang K, Hongtao J (2020) Using the water quality index (WQI), and the synthetic pollution index (SPI) to evaluate the groundwater quality for drinking purpose in Hailun, China. Sains Malaysiana 49:2383–2401. https://doi.org/10.17576/jsm-2020-4910-05

Iqbal K, Ahmad S, Dutta V (2019) Pollution mapping in the urban segment of a tropical river: is water quality index (WQI) enough for a nutrient-polluted river? Appl Water Sci 9:197. https://doi.org/10.1007/s13201-019-1083-9

Jaiswal M, Hussain J, Gupta SK, Nasr M, Nema AK (2019) Comprehensive evaluation of water quality status for entire stretch of Yamuna River India. Environ Monit Assess 191:208. https://doi.org/10.1007/s13201-019-1083-9

Kamboj N, Kamboj V (2019) Water quality assessment using overall index of pollution in riverbed-mining area of Ganga-River Haridwar, India. Water Sci 33:65–74. https://doi.org/10.1080/11104929.2019.1626631

Karunanidhi D, Aravinthasamy P, Subramani T, Muthusankar G (2021) Revealing drinking water quality issues and possible health risks based on water quality index (WQI) method in the Shanmuganadhi River basin of South India. Environ Geochem Health 43:931–948. https://doi.org/10.1007/s10653-020-00613-3

Khan R, Saxena A, Shukla S (2020) Evaluation of heavy metal pollution for River Gomti, in parts of Ganga Alluvial Plain India. SN Appl Sci 2:1451. https://doi.org/10.1007/s42452-020-03233-9

Khan R, Saxena A, Shukla S, Sekar S, Goel P (2021) Effect of COVID-19 lockdown on the water quality index of River Gomti, India, with potential hazard of faecal-oral transmission. Environ Sci Pollut Res 28:33021–33029. https://doi.org/10.1007/s11356-021-13096-1

Khan MYA, Khan B, Chakrapani GJ (2016) Assessment of spatial variations in water quality of Garra River at Shahjahanpur, Ganga Basin. India Arab J Geosci 9:516. https://doi.org/10.1007/s12517-016-2551-2

Kharake AC, Raut VS (2021) An assessment of water quality index of Godavari river water in Nashik city Maharashtra. Appl Water Sci 11:101. https://doi.org/10.1007/s13201-021-01432-2

Krishan A, Mishra RK, Khursheed A (2022) Assessment of water quality using water quality index: a case study of the River Gomti Lucknow, Uttar Pradesh, India. Urban Water J. https://doi.org/10.1080/1573062X.2022.2032210

LDA, Lucknow Master Plan 2031 (2016) Lucknow Development Authority. Uttar Pradesh, India

Lkr A, Singh MR, Puro N (2020) Assessment of water quality status of Doyang River, Nagaland, India, using water quality index. Appl Water Sci 10:46. https://doi.org/10.1007/s13201-019-1133-3

Ma J, Ding Z, Wei G, Zhao H, Huang T (2009) Sources of water pollution and evolution of water quality in the Wuwei basin of Shiyang river, Northwest China. J Environ Manage 90:1168–1177. https://doi.org/10.1016/j.jenvman.2008.05.007

Mishra S, Kumar A (2021) Estimation of physicochemical characteristics and associated metal contamination risk in the Narmada River. India Environ Eng Res 26:190521. https://doi.org/10.4491/eer.2019.521

Naubi I, Zardari NH, Shirazi SM, Ibrahim NFB, Baloo L (2016) Effectiveness of water quality index for monitoring Malaysian river water quality. Pol J Environ Stud 25:231–239. https://doi.org/10.15244/pjoes/60109

Nong X, Shao D, Zhong H, Liang J (2020) Evaluation of water quality in the South-to-North Water Diversion Project of China using the water quality index (WQI) method. Water Res 178:115781. https://doi.org/10.1016/j.watres.2020.115781

Rao GS, Rao GN (2010) Study of groundwater quality in Greater Visakhapatnam City, Andhra Pradesh (India). J Environ Sci Eng 52:137–146

Roy M, Shamim F, Chatterjee S (2021) Evaluation of physicochemical and biological parameters on the water quality of Shilabati River, West Bengal, India. Water Sci 35:71–81. https://doi.org/10.1080/23570008.2021.1928902

Sener S, Sener E, Davraz A (2017) Evaluation of water quality using water quality index (WQI) method and GIS in Aksu River (SW-Turkey). Sci Total Environ 584–585:131–144. https://doi.org/10.1016/j.scitotenv.2017.01.102

Shah KA, Joshi GS (2017) Evaluation of water quality index for River Sabarmati, Gujarat, India. Appl Water Sci 7:1349–1358. https://doi.org/10.1007/s13201-015-0318-7

Sharma R, Kumar R, Satapathy SC, Al-Ansari N, Singh KK, Mahapatra RP, Agarwal AK, Le HV, Pham BT (2020) Analysis of water pollution using different physicochemical parameters: a study of Yamuna River. Front Environ Sci 8:581591. https://doi.org/10.3389/fenvs.2020.581591

Singh AN, Shivastava R, Mohan D, Kumar P (2018) Assessment of spatial and temporal variations in water quality dynamics of River

Ganga in Varanasi. Pollution 4:239–250. https://doi.org/10.22059/POLL.2017.240626.310

Solangi GS, Siyal AA, Babar MM, Siyal P (2018) Evaluation of surface water quality using the water quality index (WQI) and the synthetic pollution index (SPI): a case study of Indus Delta region of Pakistan. Desalin Water Treat 118:39–48. https://doi.org/10.5004/dwt.2018.22407

Sunar S, Tripathi OP, Mishra BP (2020) Water quality and pollution indices application in monitoring water quality of Serlui river impacted by Serlui-B dam, Mizoram, North East India. Curr Sci 119:1685–1689. https://doi.org/10.18520/cs/v119/i10/1685-1689

Tangri AK, Kumar D, Singh DS, Dubey CA (2018) The Gomati river: lifeline of central Ganga plain. Springer, Singapore, pp 135–150. https://doi.org/10.1007/978-981-10-2984-4_11

Tiwari AK, De Maio M, Singh PK, Mahato MK (2015) Evaluation of surface water quality by using GIS and a heavy metal pollution index (HPI) model in a coal mining area, India. Bull Environ Contam Toxicol 95:304–310. https://doi.org/10.1007/s00128-015-1558-9

Tyagi VK, Bhatia A, Gaur RZ, Khan AA, Ali M, Khursheed A, Kazmi AA, Lo SL (2013) Impairment in water quality of Ganges River and consequential health risks on account of mass ritualistic bathing. Desalin Water Treat 51(10–12):2121–2129. https://doi.org/10.1080/19443994.2013.734677

Uddin MG, Nash S, Olbert IA (2021) A review of water quality index models and their use for assessing surface water quality. Ecol Indic 122:107218. https://doi.org/10.1016/j.ecolind.2020.107218

UPPCB (Uttar Pradesh Pollution Control Board) (2019) Action plan for restoration of polluted stretch of river Gomti from Sitapur to Kaithi (District Ghazipur), UPPCB, Lucknow, India.

WHO (2011) Guidelines for drinking water quality, 4th edn. World Health Organization, Geneva, Switzerland

Yang HJ, Shen ZM, Zhang JP, Wang WH (2007) Water quality characteristics along the course of the Huangpu River (China). J Environ Sci 19:1193–1198. https://doi.org/10.1016/S1001-0742(07)60195-8

Publisher's note Springer Nature remains neutral with regard to jurisdictional claims in published maps and institutional affiliations.

The current issue and full text archive of this journal is available on Emerald Insight at:
https://www.emerald.com/insight/0957-4093.htm

Exploring relationships between service quality dimensions and customers satisfaction: empirical study in context to Indian logistics service providers

Received 30 August 2021
Revised 16 April 2022
Accepted 22 May 2022

Anchal Gupta
Lal Bahadur Shastri Institute of Management, Delhi, India
Rajesh Kumar Singh
Management Development Institute, Gurgaon, India
K. Mathiyazhagan
Thiagarajar School of Management, Madurai, India
Pradeep Kumar Suri
Delhi School of Management, Delhi Technological University, Delhi, India, and
Yogesh K. Dwivedi
School of Management, Swansea University, Wales, UK and Department of Management, Symbiosis Institute of Business Management, Pune & Symbiosis International (Deemed University), Pune, India

Abstract

Purpose – This study aims to identify service quality dimensions for logistics service providers (LSPs) and to examine their relationships with customer satisfaction and customer loyalty.

Design/methodology/approach – Service quality dimensions are identified from vast literature review. Customers who take services from LSPs were surveyed to collect data on basis of developed survey instrument. Structural Equation Modelling (SEM) is applied to test the proposed research hypotheses.

Findings – The study shows that all the five service quality constructs, i.e. "Operational Quality", "Resource Quality", "Information Quality", "Personnel Contact Quality" and "Customization and Innovation Quality" have direct relationship with customer satisfaction. They also have indirect relationship with customer loyalty, implying the full mediation of customer satisfaction.

Practical implications – The results of the study suggest that the logistics service quality (LSQ) can be measured multi-dimensionally. It provides clear implications to LSPs for improvement of service quality. The present research work is expected to be useful for both, logistics service providers and the customer organizations, which take services from LSPs. LSPs can develop strategies to improve their service quality on basis of findings from this study.

Originality/value – The present research will help in extending the existing literature on service quality in context to LSPs.

Keywords Logistics service providers, Service quality, Customer satisfaction, Structural equation modelling

Paper type Research paper

1. Introduction

In changing business environment, supply chains can take competitive advantage by building organization's competence and fulfilling dynamic customer needs (Mishra *et al.*,

Authors would like to express sincere thanks to editor and reviewers for giving valuable inputs/ suggestions on this study.

The International Journal of Logistics Management
© Emerald Publishing Limited
0957-4093
DOI 10.1108/IJLM-02-2022-0084

2021). It is increasingly evident that the organizations can achieve competitive success and effective performance through their well-established supply chain processes and logistical activities (Baral *et al.*, 2021). To meet the dynamic requirements of organizations, logistics service providers (LSPs) are focusing largely on service quality. Customer expectations and subsequent identification of factors for logistics service quality (LSQ) frameworks are important with respect to developing nations (Grant *et al.*, 2014; Vu *et al.*, 2020). In emerging economies like India, logistics sector performance has become extremely crucial due to increased opportunities through e-commerce businesses (Gupta and Singh, 2020). Moreover, Make-in-India project has opened new initiatives for manufacturing sector and calls for better logistics support and performance. In fact, the South-Asian countries have become dependent on India for meeting their local demands which further expects LSPs to be strengthened to meet global standards (Gupta *et al.*, 2021). In order to grab these opportunities, it is important for LSPs to understand and identify the service quality dimensions for delivering quality and satisfactorily services.

In literature, many LSQ frameworks are available but most of the LSQ frameworks are inclined towards developed countries (Juga *et al.*, 2010; Vu *et al.*, 2020). Parasuraman *et al.* (1985) has explored the importance of factors affecting service quality which impact initial customer perceptions and ultimately affect the customer satisfaction. Several researchers extended Parasuraman's work and contributed in LSQ scale development and measurement of LSQ, for instance, Mentzer *et al.* (1999) extended the Service Quality (SERVQUAL) concept in logistics sector in US aiming to identify the important dimensions for evaluating LSQ. The authors have identified nine dimensions (information quality, ordering procedures, order release quantities, timeliness, order accuracy, order quality, order condition, order discrepancy handling and personnel contact quality) to measure customer perceptions for service quality of LSPs. Juga *et al.* (2010) investigated the role of LSQ in customer satisfaction and loyalty in context to Finland. However, studies related to service quality of logistics sector for developing countries like India remain are limited.

Therefore, we have chosen to conduct an exploratory empirical study for LSPs in India for three reasons. First, logistics sector in India is booming with its current 14% contribution to Gross Domestic Product (GDP) and worth United States (US) $ 160 billion. It is expected to grow at a Compounded Annual Growth Rate (CAGR) of 10 percent to US$215 billion by 2023 (Sudan and Taggar, 2021). Secondly, India's logistics sector needs to grab upcoming opportunities due to increased businesses from e-commerce markets, Make-in-India initiative and demands from South-Asian countries. Thirdly, due to varied infrastructural requirements of India, the existing frameworks cannot fit directly and need suitable frameworks. Gupta *et al.* (2018a) observed that Indian logistics sector is still fragmented and only partially capable of meeting customer needs. Further, rigid government policies and lack of effective strategies may make Indian logistics sector less competitive in global market. However, information technology is taking place at various levels of transportation, warehousing and other processes but still several service quality issues are required to address.

So, in order to enhance the level of service quality and for better customer satisfaction, customized service quality framework is required to meet the specific requirements of Indian market. Therefore, our study addresses gaps in understanding the importance of LSQ expectations and perceptions among Indian customers. To build a LSQ framework in the Indian context, this study aims to identify the important LSQ dimensions of LSPs. It further tries to determine impact of LSQ on customer satisfaction and loyalty. Therefore, to bridge existing research gaps and to extend the logistics literature, we will answer the following research questions in this study:

RQ1. What are the critical service quality dimensions of LSPs in the Indian market?

RQ2. How service quality dimensions are related with customer satisfaction?

To answer the proposed questions, the literature related to service quality factors and frameworks for LSPs are reviewed in Section 2. The third section consists of development of research hypotheses. In Section 4, the research methodology section includes research process, questionnaire development and data collection procedures. Section 5 details our findings from empirical analysis. Finally, the sixth section has discussion of the data analysis results and the last section concludes the study with future scope of the research work.

2. Literature review

In this study, the authors initiate the literature review by discussing the origins of customer service quality in general and in Supply Chain Management (SCM) and logistics specifically. For an organization, quality services imply as how well the organizations perform its operations to serve their customers. Suppliers have also set their own service quality specifications to achieve the performance level as per their capabilities (Thai, 2013). However, in 1980s, services marketing being the first in literature which was explored with the customer perspectives. Two primary approaches were widely used to measure the service quality-subjective and objective. The first one is mainly applicable when organizations have mentioned their specifications for assessing the services whereas latter is mainly emphasized on comparing customers' expectations before taking services and customer perceptions during and after taking services, which works as per the framework given by Parasuraman *et al.* (1985).

Parasuraman *et al.* (1985) SERVQUAL framework explored the service quality by determining the gaps between customer expectations and perceptions from the services acquired. However, SERVQUAL model is widely applied and explored by many researchers but, it has been also criticized by researchers for taking customer expectations and perceptions altogether. Consequently, Cronin and Taylor (1992) introduced Service Performance (SERVPERF) model by considering consumer perceptions only. Parasuraman's framework is further expanded by supply chain and logistics researchers and several studies in similar lines have been conducted in developed countries, as for example, Mentzer *et al.* (2001), Rafiq and Jaafar (2007), Grant *et al.* (2014), Le *et al.* (2020), adapted by Parasuraman's conceptual and generic model of service quality.

The basic requirement for LSPs is to understand the customer expectations from the service provided. The customer expectations can be built based on communication with previous users, received in the form of reviews on websites and word-of-mouth from their past experiences. Then, these customer expectations can be converted into definite service specifications. LSPs can design and execute their services as per identified service specifications. The purpose is to understand and meet the customer expectations up to the possible extent. But still few gaps between phases may occur on how well the ideas are transformed into actual operations. In past studies, the frameworks developed not only measure the service quality but also analyze the service quality gaps to meet customer expectations (Figure 1). LSQ issues are identified to fulfill service quality gaps and the corresponding LSQ frameworks are discussed in literature and subsequently in next section.

2.1 Logistics service quality (LSQ)

To measure LSQ, several researchers explored physical logistics operations with dimensions of timeliness, availability and condition (Mentzer *et al.*, 2001). Stock and Lambert (1992) considered 13 constructs for developing a world class LSQ for four industry sectors (furniture, plastics resins, imaging products and video tapes). Seth *et al.* (2006) explored the supply chain service quality framework and considered bi-directional gaps between supplier and firm, firm and distributor and distributor and customer. Mentzer *et al.* (2001) introduced a LSQ framework with nine service quality dimensions which is further adopted by Rafiq and

Jaafar (2007) to examine the perceptions of LSPs customers. Grant (2004) also extended Mentzer's model with the addition of customer service experience and satisfaction as output attributes. Juga *et al.* (2010) has also extended LSQ and satisfaction towards customer loyalty specifically in outsourcing relationships.

Tian *et al.* (2008) developed a service quality model to establish association between 3PL and customer organizations by considering trust as an important parameter for study. Huang *et al.* (2014) studied about the service quality of logistics while delivering orders of online retail purchasing in Taiwan and developed a model with 7 constructs and 15 dimensions. The synthesis of recent literature conducted for LSQ in different countries are given in Table 1.

In literature, the recent studies conducted for other countries have provided in-depth insights for LSQ dimensions considered for framework development as discussed in Table 1. However, the literature related to development of LSQ frameworks specifically in context to India is very limited which gives huge scope of studying further LSQ literature in context to India.

Most past studies in context to Indian literature highlighted the service quality issue of LSPs with different perspective. For example, Seth *et al.* (2006) developed conceptual model for measuring service quality by analyzing bi-directional gaps among supplier and focal firm, focal firm and distributor, and distributor and customer. Gupta and Singh (2020) identified 17 service quality attributes and 5C's (Commitment, Competence, Communication, Creativity and Customization, and Coordination and Collaboration) for measuring sustainable service quality by using multi-criteria decision-making approach. However, these studies are not directly measuring the impact of LSQ on customer

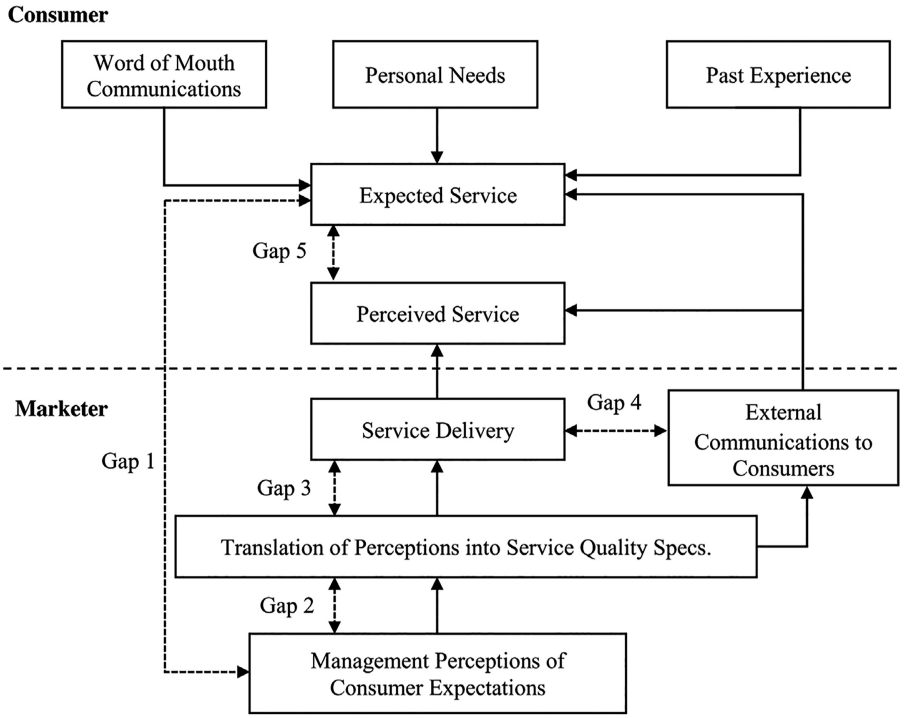

Figure 1.
Model of service quality gaps

Source(s): Adapted from Parasuraman *et al.* (1985)

Year	Authors	Sample	Dimensions	Comments
1989	Mentzer, Gomes and Krapfel	US	3 (Availability, timeliness and quality)	Discussed the role of physical distribution service in the marketing. Early development of LSQ concept. Focused mainly on service outcomes
1997	Beinstock, Mentzer and Bird	–	1 (Physical distribution and service quality (PDSQ)-timeliness, availability and condition	PDSQ is second order construct measuring physical distribution of goods and measuring service quality on timeliness, availability and condition
2001	Mentzer, Flint and Hult	US	9 (Personnel contact quality; order release quantities; information quality; ordering procedures; order accuracy; order condition; order quality; order discrepancy handling and timeliness)	Most popular model for measuring LSQ. Two constructs (information quality and ordering procedures) consist of only two items whereas minimum of three items are required for identification unless the scale is correlated with another construct. However, the validation of model remains untested in the context of LSPs
2003	Stank	US	3 (Relational performance, operational performance and cost performance) – 8 items and customer satisfaction, loyalty and market share	Emphasized on measuring LSPs' performance and its impact on market share. However, the results of market share are not validated and subjective
2006	Davis and Mentzer	North America	2 (Operational quality, relational quality) and satisfaction and loyalty	Operational quality implies the operations performed by LSPs for delivering consistent quality and efficiency; relational quality implies understanding of customer's needs and expectations to provide quality services to them efficiently
2007	Rafiq and Jafaar	UK	Same as Mentzer *et al.* (2001)	The limitations with Mentzer *et al.* (2001) were improved by adding more items to 'information quality' and 'ordering procedures' construct. Also tested and validate the Mentzer's model
2010	Juga *et al.* (2010)	Finland	3 (Operational service quality, personal service quality and technical service quality) – 13 items and customer satisfaction and loyalty	The number of items considered in constructs (operations service quality, technical service quality and customer satisfaction) is less than 3. So, this arises the question on the validity of the framework

(*continued*)

Table 1.
Synthesis of recent literature on logistics service quality

Year	Authors	Sample	Dimensions	Comments
2013	Thai	Singapore	7 (Personnel contact quality, information quality, order handling quality, physical distribution service quality, timeliness, image and social responsibility) and 32 items	Empirical based study by taking inputs from 86 LSPs and 85 customers. The research work is limited only to develop measurement model which can be extended further by linking with customer satisfaction or LSPs performance as a future scope
2014	Grant and Philipp	Europe	40 variables for LSQ and loyalty and 10 items of customer satisfaction	B2C LSQ framework developed for European retail markets
2018	Hüseyinoğlu, Sorkun and Börühan	Turkey	Relational LSQ, Operational LSQ, Omni channel Capability, Channel consistency, Cross-channel and social media	Developed framework and found positive impact of operational LSQ on omni channel capabilities
2020	Le, Nguyen and Truong	Vietnam	5 (Empathy, Reliability, assurance, Responsiveness and tangibles) and Customer Satisfaction	Adopted SERVQUAL model for measuring port logistics service quality. Under tangibles, technological advancement component is considered which is found to be important factor impacting customer satisfaction
2020	Uvet	US	Personnel Contact quality, Timeliness, order condition, order discrepancy handling, operational information quality and customer satisfaction and 19 items	Adopted Mentzer's framework with minor modifications. Considered operational information sharing as item first time for measuring customer satisfaction
2021	Vasic *et al.* (2021)	Serbia	8 (Availability, delivery time, shipping costs, delivery reliability, product quality and condition, consumer complaints and return policy, information quality, and e-customers' perception and satisfaction), with 31 items	Developed a framework for measuring LSQ affecting customer satisfaction in e-commerce. Results indicated that all the LSQ constructs have a significant positive impact on the perception and satisfaction of e-customers

Table 1.

satisfaction and loyalty in India. This paves the way for exploring further and develop a framework for suffice the purpose.

From the literature over the past 20 years about the LSQ issues, we have identified LSQ dimensions as discussed in Table 2.

After identifying LSQ dimensions from literature, a theoretical framework has been developed to establish relationship among LSQ constructs, customer satisfaction and customer loyalty as shown in Figure 2.

3. Research hypotheses

In this section, the authors have built a theoretical framework, as shown in Figure 2, to develop three research hypotheses (H1 to H3). Seven constructs have been developed based on literature review. Operational quality, Resources quality, Information Quality,

S.No	Service quality dimensions	Description	Key sources
1	Right	Delivers the right product to the right place	Gupta *et al.* (2021), Gupta and Singh (2020), Le *et al.* (2020), Buldeo Rai *et al.* (2019), Awasthi *et al.* (2018), Gupta *et al.* (2018b), Yeung *et al.* (2012), Stank *et al.* (2003), Mentzer *et al.* (2001), Franceschini and Rafele (2000)
2	Capacity	Having sufficient temporary or permanent storage capacity	Gupta and Singh (2020), Le *et al.* (2020), Buldeo Rai *et al.* (2019), Du and Han (2018), Gupta *et al.* (2018a), Jothimani and Sarmah (2014), Bouzaabia *et al.* (2013), Juga *et al.* (2010), Farmer (1988)
3	Promised	Delivers the promised services without failure	Le *et al.* (2020), Prakash (2019), Awasthi *et al.* (2018), Gupta *et al.* (2018a), Jothimani and Sarmah (2014), Juga *et al.* (2010), Davis and Mentzer (2006), Franceschini and Rafele (2000)
4	Loss	Delivers goods without loss or damage	Jothimani and Sarmah (2014), Juga *et al.* (2010), Huang *et al.* (2009), Thai (2008), Stank *et al.* (2003), Mentzer *et al.* (2001), Parasuraman *et al.* (1985, 1988)
5	Doc	Handles trade documents effectively	Gupta and Singh (2020), Prakash (2019), Awasthi *et al.* (2018), Gupta *et al.* (2018b), Thai (2008)
6	Prompt	Gives prompt services	Buldeo Rai *et al.* (2019), Du and Han (2018), Gupta *et al.* (2018b), Zailani *et al.* (2018), Jothimani and Sarmah (2014), Yeung *et al.* (2012), Ghobadian *et al.* (1994)
7	Inventory	Gives adequate importance to your inventory controls	Gupta *et al.* (2021), Buldeo Rai *et al.* (2019), Zailani *et al.* (2018), Gupta *et al.* (2018a)
8	Time	Delivers goods on scheduled date/ time	Juga *et al.* (2010), Rafiq and Jaafar, (2007), Mentzer *et al.* (2001)
9	Consistency	Shows consistency in services	Le *et al.* (2020), Vu *et al.* (2020), Gupta *et al.* (2018b), Yumurtacı Huseyinoglu *et al.* (2018), Huo *et al.* (2008), Parasuraman *et al.* (1985)
10	Fleet	Availability of fleet and physical facility	Awasthi *et al.* (2018), Gupta *et al.* (2018a), Yeo *et al.* (2015), Hamdan and Rogers (2008), Thai (2008), Ghobadian *et al.* (1994), Farmer (1988) Parasuraman *et al.* (1985)
11	Workforce	Availability of adequate workforce	Gupta and Singh (2020), Juga *et al.* (2010), Hamdan and Rogers (2008), Thai (2008)
12	Financial	Financial stability	Ozbekler and Ozturkoglu (2020), Awasthi *et al.* (2018), Gupta *et al.* (2018b), Jothimani and Sarmah (2014), Yeung *et al.* (2012), Huo *et al.* (2008), Stank *et al.* (2003)
13	Network	Geographical reach and network coverage	Gupta *et al.* (2021), Gupta and Singh (2020), Gupta *et al.* (2018a)
14	Modern	Fleet and physical facility are modern and always function properly	Le *et al.* (2020), Yeo *et al.* (2015), Thai (2008)
15	Infra	Adequate, maintained and updated Information technology (IT) infrastructure	Gupta and Singh (2020), Prakash (2019), Mathauer and Hofmann (2019), Juga *et al.* (2010), Hamdan and Rogers (2008)

(*continued*)

Table 2.
Service quality dimensions

S.No	Service quality dimensions	Description	Key sources
16	Equipment	Availability of physical equipment like Pallets, trolleys, forklifts etc.	Le *et al.* (2020), Ozbekler and Ozturkoglu (2020), Vu *et al.* (2020), Yeo *et al.* (2015)
17	Reverse	Manages reverse logistics	Gupta and Singh (2020)
18	Complete	Information communicated by logistics service provider is complete	Vu *et al.* (2020), Juga *et al.* (2010), Saura *et al.* (2008), Mentzer *et al.* (2001), Ghobadian *et al.* (1994), Farmer (1988), Parasuraman *et al.* (1985)
19	Timely	Information communicated by the logistics service provider is timely	Le *et al.* (2020), Gupta *et al.* (2018a), Juga *et al.* (2010), Saura *et al.* (2008), Mentzer *et al.* (2001)
20	Accurate	Information communicated by logistics service provider is accurate	Yumurtacı Huseyinoglu *et al.* (2018), Mentzer *et al.* (2001), Ghobadian *et al.* (1994), Farmer (1988), Parasuraman *et al.* (1985)
21	Adequate	Information communicated by logistics service provider is adequate	Zailani *et al.* (2018), Thai (2013), Saura *et al.* (2008), Mentzer *et al.* (2001)
22	Credible	Information communicated by logistics service provider is credible	Le *et al.* (2020), Vu *et al.* (2020), Gupta *et al.* (2018a), Yumurtacı Huseyinoglu *et al.* (2018), Juga *et al.* (2010), Rafiq and Jaafar (2007), Mentzer *et al.* (2001)
23	Tracking	Tracking and tracing of shipments	Mathauer and Hofmann (2019), Takele (2019), Gupta *et al.* (2018a)
24	Application	Application of IT and Electronic Data Interchange (EDI) in customer service	Gupta and Singh (2020), Huma *et al.* (2020), Gupta *et al.* (2018b)
25	Confidence	Maintains confidentiality in all operations	Gupta and Singh (2020), Shin *et al.* (2018), Jothimani and Sarmah (2014), Farmer (1988)
26	Effort	Makes an effort to understand my situation	Takele (2019), Yumurtacı Huseyinoglu *et al.* (2018), Parasuraman *et al.* (1988)
27	Courteous	Maintains courteous behavior while dealing	Wetzel and Hofmann (2020), Le *et al.* (2020), Parasuraman *et al.* (1985), Ghobadian *et al.* (1994)
28	Access	Easily accessible when needed	Wetzel and Hofmann (2020), Takele (2019), Juga *et al.* (2010), Ghobadian *et al.* (1994), Parasuraman *et al.* (1985)
29	Queries	Handles queries and complaints effectively	Awasthi *et al.* (2018), Gupta *et al.* (2018b), Mentzer *et al.* (1999, 2001), Farmer (1988)
30	Experience	Product knowledge and experience of the logistics service provider is adequate	Vu *et al.* (2020), Wetzel and Hofmann (2020), Juga *et al.* (2010), Mentzer *et al.* (2001)
31	Attitude	Shows a positive attitude while dealings	Vu *et al.* (2020), Gupta *et al.* (2018b), Rafiq and Jaafar (2007), Mentzer *et al.* (2001), Farmer (1988)
32	Mutual	Builds mutual relationship and trust	Huma *et al.* (2020), Shin *et al.* (2018), Thai (2013)
33	Creativity	Shows creativity in its methods of operations	Gupta and Singh (2020), Shin *et al.* (2018), Yeung *et al.* (2012)
34	New ways	Seeks out new ways to do things	Gupta and Singh (2020), Huang *et al.* (2014), Naim *et al.* (2010)

Table 2. (*continued*)

Service quality dimensions for LSPs

S.No	Service quality dimensions	Description	Key sources
35	First	My logistics service provider is often the first to initiate with new services	Huma *et al.* (2020), Mathauer and Hofmann (2019)
36	Environment	Shows concern towards the environment	Gupta and Singh (2020), Naim *et al.* (2010), Huang *et al.* (2014)
37	Specific	Offers me services that satisfy my specific needs	Gupta and Singh (2020), Vu *et al.* (2020), Yeung *et al.* (2012), Stank *et al.* (2003), Parasuraman *et al.* (1985), Ghobadian *et al.* (1994)
38	Changing	Accommodates my changing and urgent requirements	Takele (2019), Yumurtacı Huseyinoglu *et al.* (2018), Jothimani and Sarmah (2014), Huo *et al.* (2008), Farmer (1988)
39	Ideas	Tries out new ideas frequently	Cichosz *et al.* (2020), Gupta *et al.* (2018a), Huo *et al.* (2008), Farmer (1988)

Table 2.

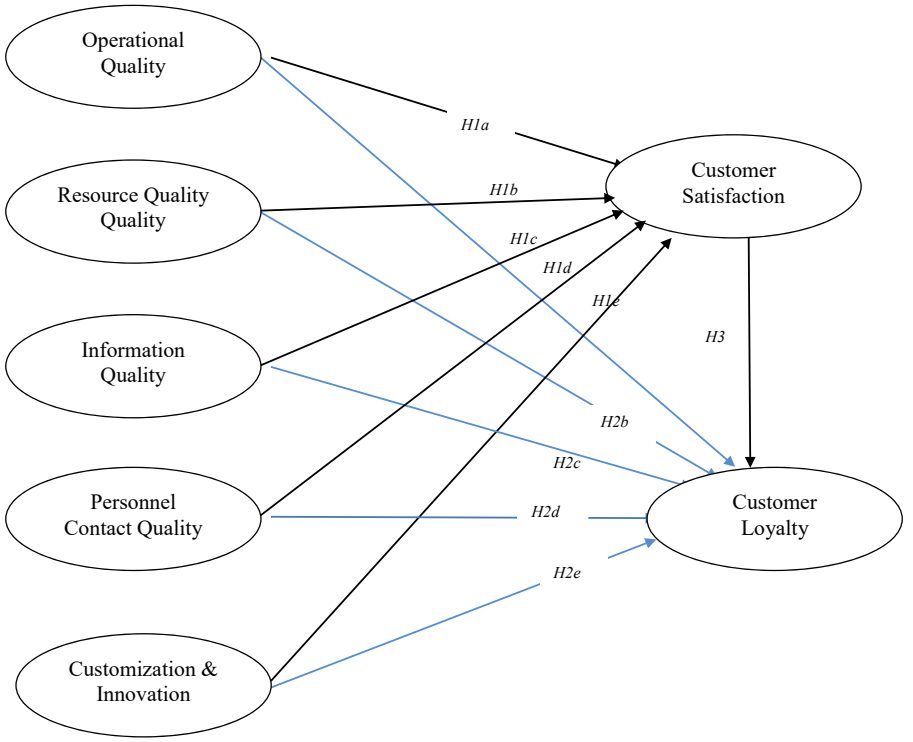

Figure 2.
Theoretical framework for logistics service quality (LSQ)

Personnel contact quality, Customization and innovation in services are taken as constructs. We have tested relationship of these Service Quality (SQ) constructs with customer satisfaction and customer loyalty has been tested. Uvet (2020) has developed LSQ framework by considering five constructs: personnel contact quality, timeliness,

order condition, order discrepancy handling and operational information sharing and tested research hypotheses for establishing significant relationships with customer satisfaction. The significant relationship of operational service quality with customer loyalty specifically for developing country has already explored in literature (Huma *et al.*, 2020). SERVQUAL framework has been expanded for measuring service quality in the port logistics industry and resources quality (technical infrastructure and tangibles) is found to be most significant factor responsible for enhancing service quality and ultimately satisfies customer (Le *et al.*, 2020). However, Sorkun *et al.* (2020) had examined operational LSQ as a mediating role when omni channel capabilities leads to customer satisfaction. Fernandes *et al.* (2018) considered LSQ into mediating role between logistics capabilities and customer satisfaction. However, in this research work, customer satisfaction would be in mediating role between LSQ and customer loyalty.

3.1 Logistics service quality and customer satisfaction

Many authors have related service quality and customers satisfaction as synonymous but theoretically, both are distinct concepts and delivery of quality services will increase customer satisfaction from services (Sureshchandar *et al.*, 2002; Saura *et al.*, 2008; Uvet, 2020). The customer satisfaction level from logistics can be measured on various parameters. The consumer's satisfaction depends on both, internal and external environmental factors. Many authors considered performance measures to ensure customer satisfaction whereas some have defined and focused on internal factors of LSPs to deliver satisfactory services to consumers (Mentzer *et al.*, 1999; Huo *et al.*, 2008). Numerous findings strongly support that the improvements done in LSQ by LSPs results in increasing customer satisfaction (Daugherty *et al.*, 1996; Gaudenzi *et al.*, 2021).

The theoretical idea is that the "operational quality" of services provided by LSPs plays a major role in providing satisfactory services to the customer. The delivery of shipments on promised time at the right time without any failure or loss, efficient inventory management, appropriate capacity allocations and handling documents safely will help in improving the operational service quality which will further result in more satisfied customers. The "Resource Quality" component is defined by the availability of fleet and physical facility, adequate workforce, financial stability, geographical reach, adequate and maintained IT infrastructure, use of modern fleet and manages reverse logistics and impacts satisfaction level of customers. The "Information Quality" component is defined by the information communicated by LSP to the customers must be complete, timely, accurate, adequate and credible. The customer wants to be updated with each transaction of their shipments, their exact location and the time of delivery or delay if any. The quality of information communicated through either offline or online mode helps in satisfying the customer urgent requirements. The "Personnel Contact Quality" component is defined by the effort made by personnel to understand the situation, maintains courteous behavior, maintains confidentiality, easily accessible, handles queries and complaints effectively and has adequate product knowledge and experience. The satisfaction of customer from logistics services also accounts for the behavior and attention of personnel of LSP. The "Customization and Innovation Quality" component is defined by offering services to satisfy specific and urgent requirements, shows creativity in its methods of operations, shows concern toward the environment, seek out new ways to do things and initiate new services. LSPs must fulfill customer's specific or customized requirements to satisfy them and to establish a strong relationship for business continuity. First hypothesis of study is as follows:

H1. Logistics quality (As per following dimensions) has significant impact on customer satisfaction (a) Operations quality, (b) Resource quality, (c) Information quality, (d) Personnel contact quality and (e) Customization and innovation quality.

3.2 Logistics service quality and customer loyalty

Loyalty is usually measured in terms of repurchasing the same product, increase sales from other products and recommend the service providers to other business partners (Oliver, 1999). Several authors have discussed the concept of loyalty in logistics (Saura *et al.*, 2008; Bouzaabia *et al.*, 2013). Past studies showed that LSPs capabilities affect the firm performance directly which becomes the main reason for loyalty of customers (Esper *et al.*, 2007; Cho *et al.*, 2008). Many authors proved the link between service quality and customer loyalty with mediating effect of customer satisfaction (Caruana, 2002; Saura *et al.*, 2008).

In this study, further, the relationship among LSQ and customer loyalty has been tested. LSPs believe in improvement of LSQ in form of operational, resources, information, personnel and customization and innovation and may show more commitment and loyalty towards the LSPs. LSPs have perception that if they invest more in assets like infrastructure, manpower and network extension, etc. and provide timely and accurate information then the quality of services can be improved, and it may impact on customer loyalty. The courteous behavior of LSPs may impact continuity and outsourcing of more activities by the customers. LSPs can also modify their processes to provide customized and innovative services to enhance customer loyalty. Second hypothesis of study is as follows:

H2. Logistics quality (As per following dimensions) has significant impact on customer loyalty (a) Operations quality, (b) Resource quality, (c) Information quality, (d) Personnel contact quality, (e) Customization and innovation quality.

3.3 Customer satisfaction and customer loyalty

The literature suggested a strong link between customer satisfaction and loyalty (Saura *et al.*, 2008; Juga *et al.*, 2010; Bouzaabia *et al.*, 2013; Huang *et al.*, 2014). The satisfied customers usually preferred to repeat the same service provider with expectation of same level of services as they had experienced in the past (Stank *et al.*, 2003). Good feedback about LSQ is a significant indication of increase in future sales and shows customer loyalty towards LSPs (Grant *et al.*, 2014). Huang *et al.* (2014) established the relationship among the LSQ, customer satisfaction and loyalty. Bouzaabia *et al.* (2013) explored LSQ as relational LSQ and Operation LSQ with data set of two countries like Romania and Tunisia. In the literature, various researchers have already established this relationship (Juga *et al.*, 2010; Izogo and Ogba, 2015). This implies that the satisfied customers from LSQ would like to continue or outsource more activities to the same service provider. Satisfied customers may also like to recommend the LSPs to their business partners. LSPs can deliver better services to provide more satisfaction to customers which in turn, results in long term commitment of the customers. Therefore, a hypothesis is proposed that customer satisfaction has significant impact on customer loyalty.

H3. Customer Satisfaction has Significant Impact on Customer Loyalty

4. Research methodology

In this section, both qualitative and quantitative approaches through focused group discussions, direct interviews and survey analysis have been used. The entire research process framework is shown in Figure 3.

With the limitation of time and resources, the authors used their own synthesis from literature about the related studies, theories, the frameworks and scales along with focused group discussions for measuring the quality of services, customer satisfaction and loyalty. In the first step, the authors synthesized and adopted the scale from past studies and modified the scale to draft suitable questionnaire for the survey. Each factor is analyzed thoroughly in order to avoid any problems like unclear questions, unconstructive questions, vague or ambiguous questions, restricted language and misplaced modifiers etc. At the preliminary

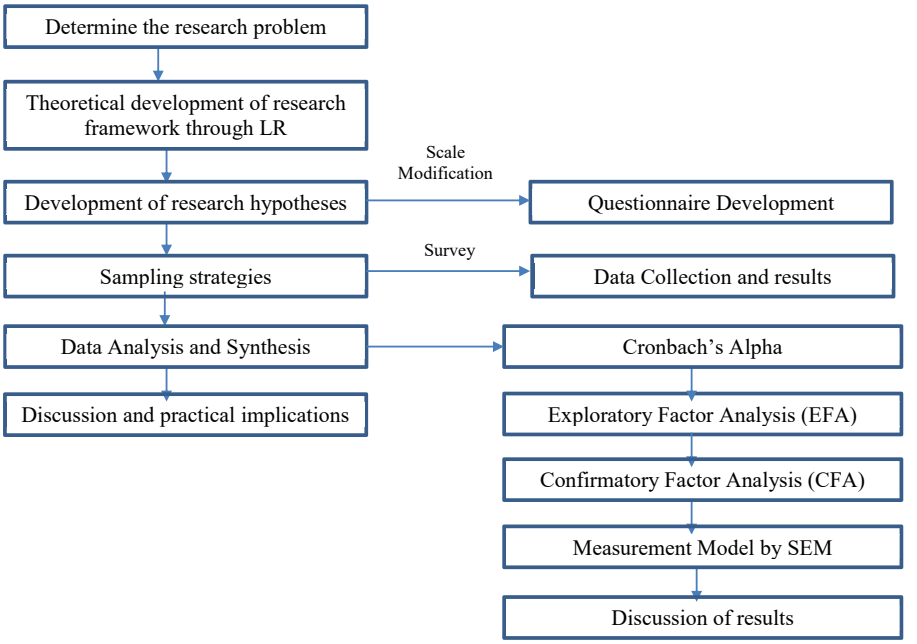

Figure 3.
The research process framework

stage, four to five rounds of focused group discussions were conducted with industry experts to modify and rewording of questions in the questionnaire so that it meets the purpose of the study. Some of the questions were revised in the questionnaire to make it more respondent-friendly and to align the same with Indian cultural context during focused group discussions. The pilot test was administered to 100 respondents (employees working in operations or supply chain department of various Indian organizations and taking services from LSPs). Initially, the questionnaire had 52 questions and after focused group discussions, revisions had been made and the final questionnaire had 58 questions (Annexure). Therefore, at this stage of pilot testing, only internal reliability test like Cronbach's alpha (0.948 > 0.5) was calculated to check the internal consistency, which was acceptable. All the modifications suggested by experts in the questionnaire have been done and form the final scale.

4.1 Questionnaire development and data collection

In this study, the scale measurement is adapted from previous studies and modified after vetting through Indian industry experts to make them relevant in Indian context (Mentzer *et al.*, 2001; Rafiq and Jaafar, 2007; Juga *et al.*, 2010). The existing scales have been modified extensively by adding resource quality and customization and innovation quality constructs. The authors realized after focused group discussions with experts that infrastructure, resources and customization capabilities are specifically important while developing LSQ scale for country like India. Please refer Annexure for literature of constructs and corresponding variables for developing scales of measurement.

In this research work, the authors have used snowball sampling for data collection. In snowball sampling, primary data source nominates other potential data sources for participating in the survey. It is completely based on referrals and known as chain-referral sampling method. In this study, snowball sampling is appropriate sampling technique in order to collect data from the customers of LSPswith the limitation of time, budget and resources.

The final questionnaire for survey included 39 service quality dimensions for LSQ and 9 factors for customer satisfaction and loyalty. So, the minimum sample size is $n \geq 5 * 48 = 240$ samples. Therefore, 240 valid survey responses are required to ensure accuracy of the research work. In this study, 800 questionnaires have been circulated through both offline and online mode. Out of 800 responses, 294 survey responses are collected. There were 24 incomplete and unengaged responses out of 294 responses. Therefore, 24 responses were eliminated from the entire data set and finally, 270 responses were left for further analysis. The respondents are the representatives of the companies which directly takes services from the Indian LSPs.

5. Data analysis

Here, the authors have done detailed data analysis using SPSS (Graphics version 22) and AMOS (Graphics version 22). In this section, the sample composition, scale reliability results, exploratory and confirmatory factor analysis (CFA) along with hypothesis testing are discussed. The mediating effect of customer satisfaction is further tested.

5.1 Sample composition

In this study, the questionnaire had ten demographic questions. The analysis on sample composition on the demographic questions like name, designation, organization, overall experience, annual turnover of the organization, number of employees in the organization, industry sector to which respondent's organization belongs, services taking from LSPs and current LSPs etc. are discussed in Table 3.

S. No	Research sample	*N*	Percentage
1	*Type of business*		
	Auto-Components	59	21.8
	Automobile	29	10.7
	Consumer Durables	20	7.4
	Electronics	25	9.2
	Fast Moving Consumer Goods (FMCG)	22	8.1
	Pharmaceuticals	22	8.1
	Retail	15	5.56
	Others	78	28.8
2	*Services taking from LSPs*		
	Transportation	72	26.7
	Transportation and warehousing	28	10.4
	Warehousing	20	7.4
	All the above	150	55.5
3	*Annual turnover*		
	Less than 5 crores	27	10
	5–50 crores	38	14
	51–100 crores	62	23
	More than 100 crores	143	53
4	*Number of employees*		
	1–100	51	19
	101–500	30	11
	501–1,000	54	20
	More than 1,000	135	50
5	*Overall experience of respondents*		
	0–2 years	89	33
	2–5 years	30	11
	5–10 years	84	31
	More than 10 years	67	25

Table 3. Descriptive analysis of research sample

5.2 Scale reliability results

In this study, the Cronbach's alpha value is 0.946 for the entire data set, which is greater than 0.7 for a reliable multi-item scale. Validity can be defined as the extent to which the data collection method measures accurately what it is intended to measure (Saunders *et al.*, 2011). Different types of validity can be checked to ensure the results obtained from the designated test. In this research, the content validity of the instrument has been ensured by identifying all the service quality dimensions from the literature review and questionnaire was thoroughly reviewed by industry professionals. The verification of the reliability of the LSQ dimensions, customer satisfaction and customer loyalty are summarized as below in Table 4:

The Cronbach alpha values for all constructs are in the desired level. The coefficients of the item-total correlation total variables are accepted for all the constructs. As a result, the variables of all scales meet the criteria and can be processed for exploratory factor analysis (EFA).

5.3 Exploratory factor analysis (EFA)

The overall LSQ scales are grouped under one factor and its variables scales are grouped under five factors. The EFA results are obtained using Varimax rotation method. The results of EFA for LSQ scale and its variables are shown in Table 5. The prior tests Kaiser – Meyer – Olkin (KMO) test and Bartlett's test of Sphericity conducted to check the appropriateness of the respondent data for EFA; the KMO value of 0.930, which is more than the suggested value of 0.7 (Field, 2009). The value of Bartlett's test of Sphericity is also significant ($p = 0.000$) for factor analysis as the desired value should be $p < 0.05$.

Five factors were extracted with Eigen values greater than 1.0 (2.553). Factor loadings are found by Principal Component Analysis (PCA) method and Varimax rotation method. The factor loadings for each item were received and determine the contribution of each item in establishing the factors. The factor loadings more than ±0.6 are practically significant and depict the strong correlation among item and the corresponding factor. In our case, the factor structure was established but some factor loadings were less than 0.6 (Table 5). Those items are the candidate for deletion to make the factor structure more robust. To make the framework more robust, six variables are deleted from the data based on observations made by using EFA resulting in 5 factors with 33 observation variables. Further, the revised data is used for CFA to establish the scale validity.

The customer satisfaction scale and customer loyalty scale are grouped under one group respectively and EFA results are obtained using Varimax rotation approach (Table 6). The Bartlett test results in significant values of Bartletts of sphericity ($p = 0.000$) and KMO value = 0.765 > 0.7 shows that factor analysis is appropriate for customer satisfaction. Similarly, KMO value = 0.876 > 0.7 and significant value of Bartlett test for customer loyalty. EFA of customer satisfaction is grouped under one factor with PCA and Varimax rotation method. Eigen values are found to be greater than 1 (1.675) which meets all the requirements. The factor loadings of all the five constructs are more than 0.6 so they are appropriate and

Table 4. Cronbach's alpha value of constructs

Constructs	Number of items	Cronbach alpha	Item-total-correlation
Operational quality (OQ)	8	0.971	0.675
Resources quality (RQ)	7	0.978	0.824
Information quality (IQ)	7	0.944	0.638
Personnel contact quality (PCQ)	5	0.972	0.972
Customization and innovation quality (CIQ)	6	0.970	0.970
Customer satisfaction (CS)	5	0.966	0.966
Customer loyalty (CL)	4	0.952	0.952

Kaiser-Meyer-Olkin measure of sampling adequacy					0.930
Bartlett's test of Sphericity			Approx. Chi-Square		16247.547
			Df		1,128
			Sig		0.000
Variables	Components				
	1	2	3	4	5
Right	0.903				
Capacity	0.871				
Promised	0.868				
Loss	0.867				
Doc	0.864				
Prompt	0.855				
Inventory	0.852				
Time	0.832				
Fleet		0.919			
Workforce		0.908			
Financial		0.900			
Network		0.900			
Modern		0.896			
ITinfra		0.866			
Reverse		0.851			
Complete			0.840		
Timely			0.814		
Accurate			0.801		
Adequate			0.799		
Credible			0.795		
Tracking			0.767		
Application			0.749		
Equipment			0.548		
Mutual			0.533		
Consistency			0.522		
Attitude			0.509		
Ideas			0.467		
Confidence				0.503	
Effort				0.923	
Courteous				0.923	
Access				0.918	
Queries				0.899	
Experience				0.891	
Creativity					0.936
Newways					0.933
First					0.915
Environment					0.901
Specific					0.885
Changing					0.881

Table 5.
EFA results of logistics service quality and its variables

used for further analysis. The EFA results for customer loyalty are also meeting the desired requirements and factor loadings are found to be more than 0.6. All the 4 variables are grouped under customer loyalty and considered for further analysis by CFA.

5.4 Confirmatory factor analysis (CFA)

In our measurement model, all seven constructs are having more than three items. In this study, the measurement model has 7 constructs in which 5 constructs are exogenous

Kaiser-Meyer-Olkin measure of sampling adequacy		Customer satisfaction	Customer loyalty
		0.765	0.876
Bartlett's test of sphericity	Approx. Chi-Square	247.547	256.843
	Df	6	6
	Sig	0.000	0.000

Variables	Component	
Satisoverall	0.774	
Satisprocess	0.760	
Satisfleet	0.758	
Satismgmt	0.754	
Delight	0.743	
Committed		0.873
Outsource		0.854
Recommend		0.823
Continue		0.807

Table 6.
EFA results of customer satisfaction and customer loyalty

variables, whereas 2 constructs are endogenous variables. Following tests are performed for assessing the measurement model.

Composite Reliability (CR) – It measures the reliability of the constructs in the measurement model. In this research, all the CR values are greater than 0.70 and hence we can conclude that all the constructs in the measurement model have good reliability (Table 7).

Convergent Validity – It defines the extent to which all the items converge to a specific component. All the significant factor loadings are more than 0.50. This clearly indicates that all the items are adequate and converging to their corresponding constructs. The two more conditions that are AVE > 0.50 and CR > AVE. also need to satisfy in order to have convergent validity (Hair *et al.*, 2010; Xu *et al.*, 2013). These values are also meeting the criteria and shown in Table 7.

Discriminant Validity – It shows the extent to which inter-correlation among constructs should be minimum (Le *et al.*, 2020). Hair *et al.* (2010) suggested two methods for measuring discriminant validity. Second, Average Variances Extracted (AVE) is calculated for all constructs as a summary indicator of convergence. AVE should be higher than 0.5 to suggest adequate validity of the model. In order to have discriminant validity, AVE should be higher than the Maximum Shared Variance (MSV) and Average Shared Variance (ASV). All the CR, AVE, MSV and ASV values are meeting the desired criteria. Therefore, there is no issue of validity in CFA. The results of discriminant validity are also shown in Table 8.

S. No	Constructs	Composite reliability	Average variance extracted	Maximum shared variance	Average shared variance
1	Operational quality (OQ)	0.938	0.807	0.233	0.120
2	Resources quality (RQ)	0.945	0.865	0.270	0.119
3	Information quality (IQ)	0.913	0.717	0.309	0.169
4	Personnel contact quality	0.932	0.847	0.132	0.058
5	Customization and innovation quality (CIQ)	0.936	0.840	0.138	0.050
6	Customer satisfaction (CS)	0.934	0.854	0.335	0.228
7	Customer loyalty (CL)	0.908	0.841	0.335	0.140

Table 7.
Reliability and Item loadings of Measurement Model

The results shown in Figure 4 show that the model has $\chi^2 = 1674.914$ with 796 df (Degree of Freedom).; $\chi^2/df = 2.104 < 5$, p-value = 0.000 (<0.005) which satisfies the criteria (Hooper *et al.*, 2008). The other indices used to measure the goodness of fit are Comparative Fit Index (CFI) = 0.951 > 0.95, Tucker Lewis Index (TLI) = 0.936 > 0.9 and Normed Fit Index (NFI) = 0.894 > 0.9 (slightly lesser value than desired) etc. whereas badness of fit is usually measured by Root Mean Square of Error Approximation (RMSEA) = 0.064 (<0.09) are appropriate fit. Therefore, the measurement model represents an acceptable model fit.

Constructs	CL	OQ	IQ	PCQ	CS	CI	RS
CL	*0.917*						
OQ	0.379	*0.899*					
IQ	0.441	0.483	*0.847*				
PCQ	0.269	0.196	0.297	*0.920*			
CS	0.579	0.477	0.556	0.364	*0.924*		
CI	0.247	0.183	0.270	0.075	0.372	*0.916*	
RS	0.329	0.363	0.416	0.246	0.520	0.200	*0.930*

Table 8.
Results of discriminant validity test (Fornell–Larcker criterion)

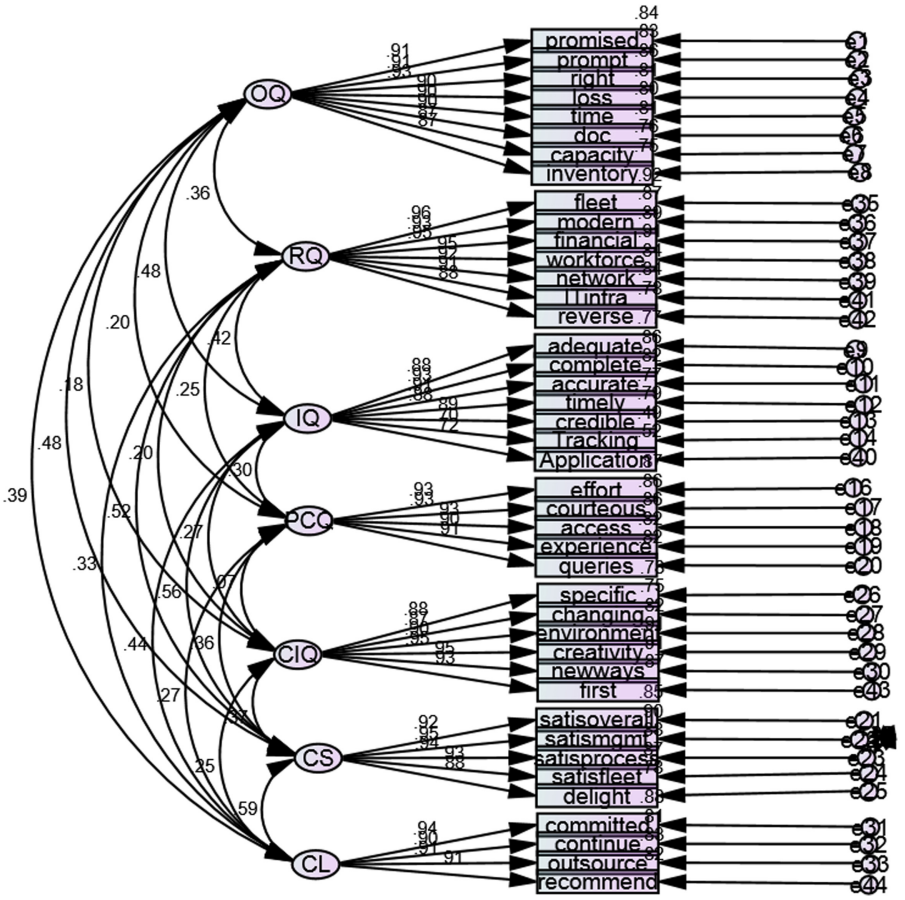

Figure 4.
Confirmatory factor analysis (CFA)

Based on above analysis, it can be summarized that the research model has achieved the convergent and discriminant validity.

5.5 Hypotheses testing

The Structural Equation Modelling (SEM) is applied for testing the research model and processed using Amos Graphics Version 22. In this research, the measurement model will be accepted without any modification to the items incorporated in the respective constructs. Before establishing a structural model, the specifications as the dependent (endogenous) or independent (exogenous) constructs must be done. In the structural model (Figure 5), the relationship between endogenous and exogenous variables has been established.

The structural model will assist in analyzing and testing all proposed hypothesis at 5% significant level. The results of the structural model show that six out of eleven hypotheses, i.e. H1a, H1b, H1c, H1d, H1e and H3 were supported at $p < 0.05$ significance level. Five out of

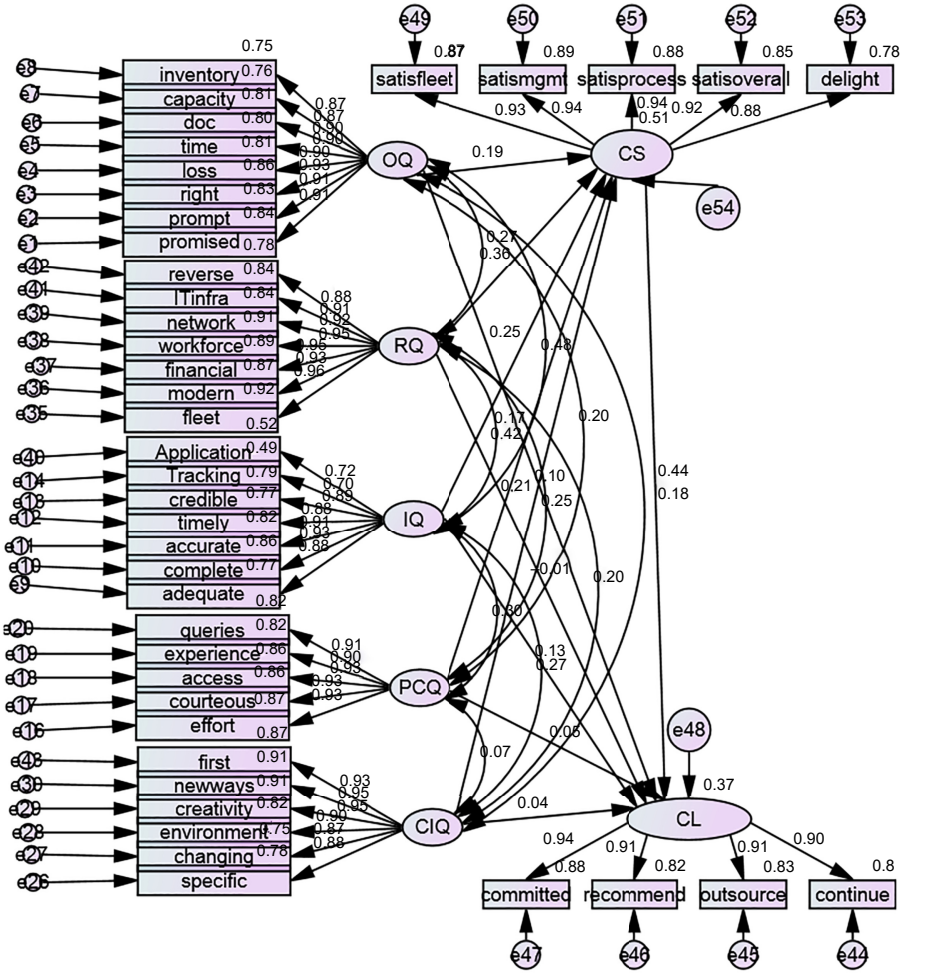

Figure 5.
Structural model

eleven hypotheses were not supported at p-value exceeds 0.05. Table 9 represents the p-values for all the constructs and corresponding hypothesis.

5.6 Testing of customer satisfaction construct as a mediator variable

In this research, the authors identified the re-specification of the model and checked for the mediating effect of customer satisfaction with all exogenous and endogenous variables. A mediating component in SEM is one which comes between two other constructs (one is the exogenous construct and other is the endogenous construct) in the structural model (Chauhan and Jaiswal, 2016).

Firstly, the direct effect of the independent variable and the dependent variable is checked in absence of mediator variable (Baron and Kenny, 1986). In this case, the direct effect of all endogenous variables on an endogenous variable (customer loyalty) is checked and the effects were captured and noted in Table 10 with a column named "Direct without mediator". Further, Customer Satisfaction (CS) is again added to the structural model and the analysis results are observed and pen down in the third column of Table 10 under the

Hypotheses	Estimates (β)	Unstandardized Regression Weights	S.E	CR	p-value	Remarks
H1a: OQ → CS	0.190	0.189	0.053	3.542	***	Supported
H1b: RQ → CS	0.265	0.205	0.040	5.101	***	Supported
H1c: IQ → CS	0.248	0.269	0.063	4.276	***	Supported
H1d: PCQ → CS	0.171	0.143	0.040	3.533	***	Supported
H1e: CIQ → CS	0.205	0.168	0.039	4.279	***	Supported
H2a: OQ → CL	0.102	0.098	0.060	1.639	0.101	Not Supported
H2b: RQ → CL	−0.013	−0.010	0.046	−0.213	0.831	Not Supported
H2c: IQ → CL	0.127	0.135	0.072	1.885	0.059	Not Supported
H2d: PCQ → CL	0.053	0.043	0.046	0.944	0.345	Not Supported
H2e: CIQ → CL	0.035	0.028	0.044	0.638	0.524	Not Supported
H3: CS→ CL	0.443	0.432	0.074	5.832	***	Supported

Note(s): ***Significant at $p < 0.005$ and S.E. – Standard Error; C.R. – Estimate/S.E

Table 9. Structural model results

Hypotheses	Relationship	Direct without mediator	Direct with mediator	Indirect effects	Decision
H4a	OQ → CS → CL	0.186 (0.004)	0.102 (0.223)	0.084 (0.004)	Full Mediation
H4b	RQ → CS → CL	0.104 (0.003)	−0.13 (0.826)	0.117 (0.001)	Full Mediation
H4c	IQ → CS → CL	0.236 (0.000)	0.127 (0.124)	0.110 (0.000)	Full Mediation
H4d	PCQ → CS → CL	0.129 (0.027)	0.053 (0.444)	0.076 (0.001)	Full Mediation
H4e	CIQ → CS → CL	0.126 (0.028)	0.035 (0.595)	0.091 (0.001)	Full Mediation

Table 10. Testing of mediation

column name "Direct with mediator". Baron and Kenny (1986) suggested that these analysis outcomes can lead to three results, that is, no mediation, partial mediation and full mediation. If the relationship of the independent variable with the dependent variable becomes insignificant in presence of the mediator variable, then the effects of the independent variable are said to be completely or fully mediated by the mediator. If all the conditions met, the relationship of independent variables remains significant with the dependent variable in presence of the mediator, then the effects of the independent variable are said to be "partially" mediated by the mediator. If any of the conditions are not satisfied, then there is no mediation.

To test the mediating effect, the following hypotheses are developed.

H4. Customer satisfaction (As per following dimensions) has mediating effect on customer loyalty (a) Operations quality, (b) Resource quality, (c) Information quality, (d) Personnel contact quality and (e) Customization and innovation quality.

Results were captured for "direct without mediator", "direct with mediator", "indirect effects" and noted down in Table 10. The effect of no mediation, partial and full mediation was also observed. Results shows that all LSQ constructs are not directly impacting customer loyalty but mediating fully through customer satisfaction.

6. Discussion

It is observed that the LSQ of Indian LSPs is directly affected by five LSQ constructs, i.e. operational quality, resources quality, information quality, personnel contact quality and customization and innovation quality at 5% level of significance. Hypotheses are tested and analyzed based on responses obtained through a structured questionnaire. At the initial stage, the pilot testing was conducted with data of 100 respondents and Cronbach alpha value is found to be highly significant. Finally, 270 data points out of 294 are found to be relevant for conducting detailed analysis and testing of the proposed framework by using SPSS 22 and AMOS 22. In this study, the Cronbach alpha value for the entire data set is found to be 0.946 which is greater than the minimum threshold of 0.7. Then, EFA technique has been used to reduce data initially and to eliminate less important items from the study. Based on EFA, 5 items out of 48 items are omitted due to low factor loadings (<0.6). After EFA, CFA test was applied to confirm the proposed framework. In CFA, the values of CR, AVE, ASV and MSV had been found and all the values were coming significant and meeting their desired criteria. The CFA provides a measurement model of LSQ based on goodness of model fit. Further, this measurement model was converted into a structural model by using SEM and the structural relationship among all constructs as dependent and independent variables had been established.

Research hypotheses for testing the significant impact of LSQ constructs on customer satisfaction have been developed and tested (H1a–e). Results shown in Table 9 clearly indicate the positive impact of all LSQ constructs on customer satisfaction which implies that customers highly appreciate the quality of logistics services received from Indian LSPs. Regarding Operational quality and personnel contact quality, the results are somewhat like those reported by Juga *et al.* (2010). Yeo *et al.* (2015) reported the significant relationship between resource quality and customer satisfaction. Information quality construct makes significant impact on customer satisfaction. It is also highlighted by Rafiq and Jaafar (2007) in literature. Gupta and Singh (2021) have also recommended use of emerging technologies for improving information quality in logistics sector. However, this framework included customization and innovation quality as one of the constructs of LSQ framework which has significant impact but with lower value as compared to other constructs.

The research hypotheses (H2a–e) for testing impact of all LSQ constructs on customer loyalty has been developed and tested. Results show indirect relationship between LSQ and customer loyalty as their corresponding hypotheses (H2a, H2b, H2c, H2d and H2e) are rejected. In past studies, on the contrary, Jang *et al.* (2013) demonstrated the high level of logistics services can be responsible for attaining higher levels of shipper's loyalty whereas Juga *et al.* (2010) found the significant relationship between service quality and customer loyalty. On similar lines, Huma *et al.* (2020) supported our research results by reporting the significant impact of relational quality over operational quality on customer loyalty and Cotarelo *et al.* (2021) highlighted that none of the construct has no significant influence on loyalty in the scenarios considered in the study. Moreover, research hypothesis (H3) has been developed to test the impact of customer satisfaction on customer loyalty. Findings show that the customers satisfied from service quality of Indian LSPs and is directly impacted the customer loyalty with 5% level of significance and 95% confidence level (H3 is accepted). Results supporting the association between constructs are strong which implies customer loyalty can be nurtured by satisfying customers through providing quality services. Extensive past literature supports this hypothesis, for instance, Juga *et al.* (2010) proved the satisfaction-loyal model in logistics outsourcing; Cotarelo *et al.* (2021) explored the positive relationship between customer satisfaction and loyalty in omni channel environment.

Research hypotheses are developed to test the mediating effect of customer satisfaction on customer loyalty (H4a-e). Results indicated full mediation of all LSQ constructs on customer loyalty through customer satisfaction with acceptance of hypotheses (H4a, H4b, H4c, H4d and H4e) at 5% level of significance and 95% confidence level. This means that all the service quality constructs have indirect impact on customer loyalty and first, LSQ constructs play significant role in customer satisfaction then further loyalty can be impacted. In literature, most of the studies resulted in similar manner while testing the moderation effect of customer satisfaction with customer loyalty (Saura *et al.*, 2008; Juga *et al.*, 2010).

7. Implications of the study

7.1 Theoretical implications

The most important contribution of this research work is extension to the present literature specifically in context of India. The LSQ model is a good fit to the requirements of Indian markets and can provide insights to improve the quality of services of Indian LSPs. Study has identified resource quality and information quality as the most influential factors of LSQ, while others are customization and innovation quality, operational quality and personnel contact quality. This implies that the customers using logistics services are concerned most about resources availability of LSPs reflected by the dedicated workforce in dealing customer issues, particularly the infrastructural and fleet management, geographical coverage and equipment handling. Additionally, the valid effect of resource quality highlights the importance of investment on technology and infrastructure in enhancing service quality. It has been also observed that the degree of accurate and complete information available to customers will help them to track the real time situation.

The results of the study suggest a comprehensive framework for LSQ. This framework will help professionals to understand the factors which affect service quality of Indian LSPs. In the era of online retail and e-commerce businesses, LSPs can use proposed framework to develop strategies to improve their performance by understanding their strengths and weaknesses.

7.2 Managerial implications for LSPs

The LSQ framework has given a solution to the LSPs to improve on their processes for providing better satisfaction to their customers. The study has brought many managerial insights for LSPs for strengthening their weak areas and improving business excellence. Findings imply that for operations quality, firstly, LSPs should emphasis on delivery-oriented processes and must ensure on-delivery on time, reliable and safe shipments with efficient capacity and inventory management and proper documentation. Secondly, forming a uniform code of conduct and benchmarking service quality can be set as a base for annual performance assessment of LSPs and can be spread as managerial solution for achieving quality targets. Thirdly, LSPs should continuously streamline their procedures of customs clearance, intra-port movements and door to door delivery at competitive charges.

For the resource quality, firstly, LSPs should emphasize on enhancing and expanding the existing infrastructure and transport capacity by taking support from waterways to avoid traffic jams on roads and delayed consignments through railways. Secondly, warehouse capabilities need to be expanded. Moreover, LSPs should procure modern and high performing equipment to manage transportation and warehouses operations efficiently. Additionally, the old and malfunctioning machines need to be replaced from time to time to ensure smooth and uninterrupted workflow. Thirdly, LSPs need to devise policies for recruiting talented and young employees for effective service quality and for understanding customer requirements. LSPs can develop short term training programs for their existing manpower in order to improve staff expertise, communication competence and problem -solving skills.

Regarding the information quality, firstly, LSPs should adopt latest technologies for tracing and tracking the shipments on real time basis. Secondly, the privacy and security of shared information across entire supply chain is crucial to manage efficiently. Thirdly, LSPs should create a platform for customers where they can give their feedback about logistics services and suggest solutions for unsatisfied responses. Regarding the personnel contact quality, firstly, LSPs should devise policies for complaints and query handling with proper solutions. Therefore, these policies will assist LSPs to resolve issues quickly and provide the appropriate support system to customers. Secondly, LSPs should hire experienced and dedicated personnel to strengthen their processes to deal with requirements of developed countries. Thirdly, LSPs can provide better access to customers by creating more lines to operate especially in case of urgency.

Regarding the customization and innovation quality, firstly, LSPs should expand value-added services such as sorting, labelling, binning, kitting and packaging. Secondly, LSPs should strengthen collaborative ties with national and international logistics players to learn their advanced technologies and utilize them for enhancing LSQ. Thirdly, rewarding policy can be commensurate for encouraging employees to suggest creative and innovative solutions to the existing logistics problems.

7.3 Conclusion, limitations and future scope

In this study, we have tried to identify major LSQ constructs and respective dimensions. Study also tries to analyze relationships of these constructs with customer satisfaction and loyalty. Operations quality, resources quality, information quality, personnel contact quality, customization and innovation quality are major constructs considered for the study. To test and validate the proposed framework, the data was collected through questionnaire-based survey. The demographic data of respondents is analyzed using descriptive analysis. EFA technique has been used to eliminate less important items from the study and CFA test is applied to confirm the proposed scale. Further, the structural model is developed by using SEM and the structural relationships among all constructs have been explored. The findings

indicate the impact of all LSQ dimensions on customer satisfaction directly whereas customer loyalty has indirect effect.

This research has got some limitations. Despite considerable efforts put by the authors in collecting the data, responses were not uniformly distributed across all regions. Although the measurement models are found to be statistically fit by SEM, the present study can be attempted with a larger sample size. More dimensions related to sustainable operations and digitization can be also added to extend this study in context to digital and circular economy. Empirical studies can be further carried out to analyze relationships among new constructs. Study may be further extended in context to different sectors and countries also.

References

Awasthi, A., Sayyadi, R. and Khabbazian, A. (2018), "A combined approach integrating gap analysis, QFD and AHP for improving logistics service quality", *International Journal of Logistics Systems and Management*, Vol. 29 No. 2, pp. 190-214.

Baral, M.M., Singh, R.K. and Kazançoğlu, Y. (2021), "Analysis of factors impacting survivability of sustainable supply chain during COVID-19 pandemic: an empirical study in the context of SMEs", *The International Journal of Logistics Management*, Vol. ahead-of-print No. ahead-of-print, doi: 10.1108/IJLM-04-2021-0198.

Baron, R.M. and Kenny, D.A. (1986), "The moderator-mediator variable distinction in social psychological research: conceptual, strategic, and statistical considerations", *Journal of Personality and Social Psychology*, Vol. 51 No. 6, pp. 1173-1182.

Bellingkrodt, S. and Wallenburg, C.M. (2015), "The role of customer relations for innovativeness and customer satisfaction: a comparison of service industries", *The International Journal of Logistics Management*, Vol. 26 No. 2, pp. 254-274, doi: 10.1108/IJLM-06-2012-0038.

Bouzaabia, R., Bouzaabia, O. and Capatina, A. (2013), "Retail Logistics service quality: a cross-cultural survey on customer perceptions", *International Journal of Retail and Distribution Management*, Vol. 41 No. 8, pp. 627-647.

Buldeo Rai, H., Verlinde, S., Macharis, C., Schoutteet, P. and Vanhaverbeke, L. (2019), "Logistics outsourcing in omnichannel retail: State of practice and service recommendations", *International Journal of Physical Distribution and Logistics Management*, Vol. 49 No. 3, pp. 267-286, doi: 10.1108/IJPDLM-02-2018-0092.

Caruana, A. (2002), "Service loyalty: the effects of service quality and the mediating role of customer satisfaction", *European Journal of Marketing*, Vol. 36 Nos 7/8, pp. 811-828.

Chauhan, S. and Jaiswal, M. (2016), "Determinants of acceptance of ERP software training in business schools: empirical investigation using UTAUT model", *The International Journal of Management Education*, Vol. 14 No. 3, pp. 248-262.

Cho, J., Ozment, J. and Sink, H. (2008), "Logistics capability, logistics outsourcing and firm performance in an e-commerce market", *International Journal of Physical Distribution and Logistics Management*, Vol. 38 No. 5, pp. 336-359.

Chu, Z. and Wang, Q. (2012), "Drivers of relationship quality in logistics outsourcing in China", *Journal of Supply Chain Management*, Vol. 48 No. 3, pp. 78-96.

Cichosz, M., Wallenburg, C.M. and Knemeyer, A.M. (2020), "Digital transformation at logistics service providers: barriers, success factors and leading practices", *The International Journal of Logistics Management*, Vol. 31 No. 2, pp. 209-238, doi: 10.1108/IJLM-08-2019-0229.

Coelho, P.S. and Henseler, J. (2012), "Creating customer loyalty through service customization", *European Journal of Marketing*, Vol. 46 Nos 3/4, pp. 331-356.

Cotarelo, M., Calderón, H. and Fayos, T. (2021), "A further approach in omnichannel LSQ, satisfaction and customer loyalty", *International Journal of Retail and Distribution Management*, Vol. 49 No. 8, pp. 1133-1153, doi: 10.1108/IJRDM-01-2020-0013.

Cronin, J.J. and Taylor, S.A. (1992), "Measuring service quality: a reexamination and extension", *Journal of Marketing*, Vol. 56, pp. 55-68.

Daugherty, P.J., Ellinger, A.E. and Gustin, C.M. (1996), "Integrated logistics: achieving logistics performance improvements", *Supply Chain Management*, Vol. 1 No. 3, pp. 25-33, doi: 10.1108/13598549610155297.

Davis, B.R. and Mentzer, J.T. (2006), "Logistics service driven loyalty: an exploratory study", *Journal of Business Logistics*, Vol. 27 No. 2, pp. 53-73.

Du, N. and Han, Q. (2018), "Pricing and service quality guarantee decisions in logistics service supply chain with fairness concern", *Asia-Pacific Journal of Operational Research*, Vol. 35 No. 5, 1850036.

Esper, T.L., Fugate, B.S. and Davis-Sramek, B. (2007), "Logistics learning capability: sustaining the competitive advantage gained through logistics leverage", *Journal of Business Logistics*, Vol. 28 No. 2, pp. 57-82.

Farmer, J.H. (1988), "A Conceptual Model of service quality", *International Journal of Operations and Production Management*, Vol. 8 No. 6, pp. 19-29.

Fernandes, D.W., Moori, R.G. and Filho, V.A.V. (2018), "Logistic service quality as a mediator between logistics capabilities and customer satisfaction", *Revista de Gestão*, Vol. 25 No. 4, pp. 358-372, doi: 10.1108/REGE-01-2018-0015.

Field, A. (2009), *Discovering Statistics Using SPSS: Book Plus Code for E Version of Text*, SAGE Publications, London, p. 896.

Flint, D.J., Larsson, E., Gammelgaard, B. and Mentzer, J.T. (2005), "Logistics innovation: a customer value-oriented social process", *Journal of Business Logistics*, Vol. 26 No. 1, pp. 113-147.

Franceschini, F. and Rafele, C. (2000), "Quality evaluation in logistic services", *International Journal of Agile Management Systems*, Vol. 2 No. 1, pp. 49-54, doi: 10.1108/14654650010312589.

Gaudenzi, B., Confente, I. and Russo, I. (2021), "Logistics service quality and customer satisfaction in B2B relationships: a qualitative comparative analysis approach", *The TQM Journal*, Vol. 33 No. 1, pp. 125-140, doi: 10.1108/TQM-04-2020-0088.

Ghobadian, A., Speller, S. and Jones, M. (1994), "Service quality", *International Journal of Quality and Reliability Management*, Vol. 11 No. 9, pp. 43-66.

Grant, D.B. (2004), "UK and US management styles in logistics: different strokes for different folks?", *International Journal of Logistics Research and Applications*, Vol. 7 No. 3, pp. 181-197.

Grant, D., Juntunen, J., Juga, J. and Juntunen, M. (2014), "Investigating brand equity of third-party service providers", *Journal of Services Marketing*, Vol. 28 No. 3, pp. 214-222.

Gronroos, C. (1984), "A service quality model and its marketing implications", *European Journal of Marketing*, Vol. 18 No. 4, pp. 36-44.

Gupta, A. and Singh, R.K. (2020), "Managing operations by a logistics company for sustainable service quality: Indian perspective", *Management of Environmental Quality*, Vol. 31 No. 5, pp. 1309-1327, doi: 10.1108/MEQ-11-2019-0246.

Gupta, A. and Singh, R.K. (2021), "Applications of emerging technologies in logistics sector for achieving circular economy goals during COVID 19 pandemic: analysis of critical success factors", *International Journal of Logistics Research and Applications*, pp. 1-22.

Gupta, A., Singh, R.K. and Suri, P.K. (2018a), "Sustainable service quality management by logistics service providers: an Indian perspective", *Global Business Review*, Vol. 19, 3_suppl, pp. S130-S150.

Gupta, A., Singh, R.K. and Suri, P.K. (2018b), "Prioritizing critical success factors for sustainable service quality management by logistics service providers", *Vision*, Vol. 22 No. 3, pp. 295-305.

Gupta, A., Singh, R.K. and Mangla, S.K. (2021), "Evaluation of logistics providers for sustainable service quality: analytics based decision making framework", *Annals of Operations Research*, pp. 1-48.

Hair, J.F., Ortinau, D.J. and Harrison, D.E. (2010), *Essentials of Marketing Research*, Vol. 2, McGraw-Hill/Irwin, New York, NY.

Hamdan, A. and Rogers, K.J. (2008), "Evaluating the efficiency of 3PL logistics operations", *International Journal of Production Economics*, Vol. 113 No. 1, pp. 235-244.

Hooper, D., Coughlan, J. and Mullen, M. (2008), "Evaluating model fit: a synthesis of the structural equation modelling literature", *7th European Conference on Research Methodology for Business and Management Studies*, pp. 195-200.

Hu, M., Huang, F., Hou, H., Chen, Y. and Bulysheva, L. (2016), "Customized logistics service and online shoppers' satisfaction: an empirical study", *Internet Research*, Vol. 26 No. 2, pp. 484-497, doi: 10.1108/IntR-11-2014-0295.

Huang, Y.K., Kuo, Y.W. and Xu, S.W. (2009), "Applying importance-performance analysis to evaluate logistics service quality for online shopping among retailing delivery", *International Journal of Electronic Business Management*, Vol. 7 No. 2.

Huang, C.C., Yen, S.W., Liu, C.Y. and Chang, T.P. (2014), "The relationship among brand equity, customer satisfaction, and brand resonance to repurchase intention of cultural and creative industries in Taiwan", *International Journal of Organizational Innovation*, Vol. 6 No. 3, p. 106.

Huma, S., Ahmed, W., Ikram, M. and Khawaja, M.I. (2020), "The effect of logistics service quality on customer loyalty: case of logistics service industry", *South Asian Journal of Business Studies*, Vol. 9 No. 1, pp. 43-61, doi: 10.1108/SAJBS-10-2018-0114.

Huo, B., Selen, W., Hoi Yan Yeung, J. and Zhao, X. (2008), "Understanding drivers of performance in the 3PL industry in Hong Kong", *International Journal of Operations and Production Management*, Vol. 28 No. 8, pp. 772-800.

Iacobucci, D., Ostrom, A. and Grayson, K. (1995), "Distinguishing service quality and customer satisfaction: the voice of the consumer", *Journal of Consumer Psychology*, Vol. 4 No. 3, pp. 277-303.

Izogo, E.E. and Ogba, I.-E. (2015), "Service quality, customer satisfaction and loyalty in automobile repair services sector", *International Journal of Quality and Reliability Management*, Vol. 32 No. 3, pp. 250-269, doi: 10.1108/IJQRM-05-2013-0075.

Jang, H.M., Marlow, P.B. and Mitroussi, K. (2013), "The effect of logistics service quality on customer loyalty through relationship quality in the container shipping context", *Transportation Journal*, Vol. 52 No. 4, pp. 493-521.

Jothimani, D. and Sarmah, S.P. (2014), "Supply chain performance measurement for third party logistics", *Benchmarking: An International Journal*, Vol. 21 No. 6, pp. 944-963.

Juga, J., Juntunen, J. and Grant, D.B. (2010), "Service quality and its relation to satisfaction and loyalty in logistics outsourcing relationships", *Managing Service Quality*, Vol. 2 No. 6, pp. 496-510.

Le, D.N., Nguyen, H.T. and Truong, P.H. (2020), "Port logistics service quality and customer satisfaction: empirical evidence from Vietnam", *The Asian Journal of Shipping and Logistics*, Vol. 36 No. 2, pp. 89-103.

Mathauer, M. and Hofmann, E. (2019), "Technology adoption by logistics service providers", *International Journal of Physical Distribution and Logistics Management*, Vol. 49 No. 4, pp. 416-434, doi: 10.1108/IJPDLM-02-2019-0064.

Mentzer, J.T., Flint, D.J. and Kent, J.L. (1999), "Developing a logistics service quality scale", *Journal of Business Logistics*, Vol. 20 No. 1.

Mentzer, J.T., Flint, D.J. and Hult, G.T.M. (2001), "Logistics service quality as a segment-customized process", *Journal of Marketing*, Vol. 65 No. 4, pp. 82-104.

Mishra, R., Singh, R.K. and Subramanian, N. (2021), "Impact of disruptions in agri-food supply chain due to COVID-19 pandemic: contextualised resilience framework to achieve operational excellence", *The International Journal of Logistics Management*, Vol. ahead-of-print No. ahead-of-print, doi: 10.1108/IJLM-01-2021-0043.

Naim, M., Aryee, G. and Potter, A. (2010), "Determining a logistics provider's flexibility capability", *International Journal of Production Economies*, Vol. 127, pp. 39-45.

Oliver, R.L. (1999), "Whence consumer loyalty?", *Journal of Marketing*, Vol. 63, 4_suppl1, pp. 33-44.

Ozbekler, T.M. and Ozturkoglu, Y. (2020), "Analysing the importance of sustainability-oriented service quality in competition environment", *Business Strategy and the Environment*, Vol. 29 No. 3, pp. 1504-1516.

Panayides, P.M. and So, M. (2005), "Logistics service provider–client relationships", *Transportation Research Part E: Logistics and Transportation Review*, Vol. 41 No. 3, pp. 179-200.

Parasuraman, A., Zeithaml, V.A. and Berry, L.L. (1985), "A conceptual model of service quality and its implications for future research", *Journal of Marketing*, Vol. 49 No. 3, pp. 41-50.

Parasuraman, A., Zeithaml, V.A. and Berry, L.L. (1988), "SERVQUAL: a Multiple-Item Scale for measuring consumer perceptions of service quality", *Journal of Retailing*, Vol. 64 No. 1, pp. 12-37.

Prakash, G. (2019), "Understanding service quality: insights from the literature", *Journal of Advances in Management Research*, Vol. 16 No. 1, pp. 64-90, doi: 10.1108/JAMR-01-2018-0008.

Rafiq, M. and Jaafar, H.S. (2007), "Measuring customers' perceptions of logistics service quality of 3pl service providers", *Journal of Business Logistics*, Vol. 28 No. 2, pp. 159-175.

Saunders, R., Jacobvitz, D., Zaccagnino, M., Beverung, L.M. and Hazen, N. (2011), "Pathways to earned-security: the role of alternative support figures", *Attachment and Human Development*, Vol. 13 No. 4, pp. 403-420.

Saura, G.I., Servera Frances, D., Berenguer Contri, G. and Fuentes Blasco, M. (2008), "Logistics service quality: a new way to loyalty", *Industrial Management and Data Systems*, Vol. 108 No. 5, pp. 650-668.

Seth, N., Deshmukh, S.G. and Vrat, P. (2006), "A framework for measurement of quality of service in supply chains", *Supply Chain Management: An International Journal*, Vol. 11 No. 1, pp. 82-94.

Shin, Y., Thai, V. and Yuen, K.F. (2018), "The impact of supply chain relationship quality on performance in the maritime logistics industry in light of firm characteristics", *The International Journal of Logistics Management*, Vol. 29 No. 3, pp. 1077-1097, doi: 10.1108/IJLM-10-2016-0227.

Simon, A. and Honore PetnjiYaya, L. (2012), "Improving innovation and customer satisfaction through systems integration", *Industrial Management and Data Systems*, Vol. 112 No. 7, pp. 1026-1043.

Sorkun, M.F., Yumurtacı Hüseyinoğlu, I.O. and Boruhan, G. (2020), "Omni-channel capability and customer satisfaction: mediating roles of flexibility and operational logistics service quality", *International Journal of Retail and Distribution Management*, Vol. 48 No. 6, pp. 629-648, doi: 10.1108/IJRDM-07-2019-0235.

Stank, T.P., Goldsby, T.J., Vickery, S.K. and Savitskie, K. (2003), "Logistics service performance: estimating its influence on market share", *Journal of Business Logistics*, Vol. 24 No. 1, pp. 27-55.

Stock, J.R. and Lambert, D.M. (1992), "Becoming a", *The International Journal of Logistics Management*, Vol. 3 No. 1, pp. 73-81.

Sudan, T. and Taggar, R. (2021), "Recovering supply chain disruptions in post-COVID-19 pandemic through transport intelligence and logistics systems: India's experiences and policy options", *Frontiers in Future Transportation*, Vol. 7.

Sureshchandar, G.S., Rajendran, C. and Anantharaman, R.N. (2002), "The relationship between service quality and customer satisfaction – a factor specific approach", *Journal of Services Marketing*, Vol. 16 No. 4, pp. 363-379.

Takele, T.B. (2019), "The relevance of coordinated regional trade logistics for the implementation of regional free trade area of Africa", *Journal of Transport and Supply Chain Management*, Vol. 13 No. 1, pp. 1-11.

Thai, V.V. (2008), "Service quality in maritime transport: conceptual model and empirical evidence", *Asia Pacific Journal of Marketing and Logistics*, Vol. 20 No. 4, pp. 493-518.

Thai, V.V. (2013), "Logistics service quality: a conceptual model and empirical evidence", *International Journal of Logistics Research and Applications*, Vol. 16 No. 2, pp. 114-131.

Tian, Y., Lai, F. and Daniel, F. (2008), "An examination of the nature of trust in logistics outsourcing relationship: empirical evidence from China", *Industrial Management and Data Systems*, Vol. 108 No. 3, pp. 346-367.

Uvet, H. (2020), "Importance of logistics service quality in customer satisfaction: an empirical study", *Operations and Supply Chain Management: An International Journal*, Vol. 13 No. 1, pp. 1-10.

Vasić, N., Kilibarda, M., Andrejić, M. and Jović, S. (2021), "Satisfaction is a function of users of logistics services in e-commerce", *Technology Analysis and Strategic Management*, Vol. 33 No. 7, pp. 813-828.

Victorino, L., Verma, R., Plaschka, G. and Dev, C. (2005), "Service innovation and customer choices in the hospitality industry", *Managing Service Quality: An International Journal*, Vol. 15 No. 6, pp. 555-576, doi: 10.1108/09604520510634023.

Vu, T.P., Grant, D.B. and Menachof, D.A. (2020), "Exploring logistics service quality in Hai Phong, Vietnam", *The Asian Journal of Shipping and Logistics*, Vol. 36 No. 2, pp. 54-64.

Wetzel, P. and Hofmann, E. (2020), "Toward a multi-sided model of service quality for logistics service providers", *Administrative Sciences*, Vol. 10 No. 4, p. 79.

Xu, F., Michael, K. and Chen, X. (2013), "Factors affecting privacy disclosure on social network sites: an integrated model", *Electronic Commerce Research*, Vol. 13 No. 2, pp. 151-168.

Yeo, G.T., Thai, V.V. and Roh, S.Y. (2015), "An analysis of port service quality and customer satisfaction: the case of Korean container ports", *The Asian Journal of Shipping and Logistics*, Vol. 31 No. 4, pp. 437-447.

Yeung, K., Zhou, H., Yeung, A.C. and Cheng, T.C.E. (2012), "The impact of third-party logistics providers' capabilities on exporters' performance", *International Journal of Production Economics*, Vol. 135 No. 2, pp. 741-753.

Yumurtacı Huseyinoglu, I.Ö., Sorkun, M.F. and Börühan, G. (2018), "Revealing the impact of operational logistics service quality on omni-channel capability", *Asia Pacific Journal of Marketing and Logistics*, Vol. 30 No. 5, pp. 1200-1221, doi: 10.1108/APJML-08-2017-0169.

Zailani, S., Jafarzadeh, S., Iranmanesh, M., Nikbin, D. and Selim, N.I.I. (2018), "Halal logistics service quality: conceptual model and empirical evidence", *British Food Journal*, Vol. 120 No. 11, pp. 2599-2614, doi: 10.1108/BFJ-07-2017-0412.

Further reading

Economictimes, available at: https://economictimes.indiatimes.com/small-biz/sme-sector/strong-logistics-infrastructure-has-to-be-the-fuel-for-manufacturing-growth-in-india/articleshow/66664013.cms?from=mdr (accessed 28 January 2022).

Kilibarda, M., Nikolicic, S. and Andrejic, M. (2016), "Measurement of logistics service quality in freight forwarding companies: a case study of the Serbian market", *The International Journal of Logistics Management*, Vol. 27 No. 3, pp. 770-794, doi: 10.1108/IJLM-04-2014-0063.

Mentzer, J.T., Gomes, R. and Krapfel, R.E. (1989), "Physical distribution service: a fundamental marketing concept?", *Journal of the Academy of Marketing Science*, Vol. 17 No. 1, pp. 53-62.

Parasuraman, A., Berry, L.L. and Zeithaml, V.A. (1991), "Refinement and reassessment of the SERVQUAL scale", *Journal of Retailing*, Vol. 67 No. 4, p. 420.

Annexure

Table A1.
Scale of "Operational quality" adopted/ modified from literature

S.No	Construct	Service quality dimensions	Description	References (scale adapted/ modified)
1	Operational quality	Right	Delivers the right product to the right place	Bouzaabia *et al.* (2013), Juga *et al.* (2010), Davis and Mentzer (2006), Gronroos (1984)
		Capacity	Having sufficient temporary or permanent storage capacity	
		Promised	Delivers the promised services without failure	
		Loss	Delivers goods without loss or damage	
		Doc	Handles trade documents effectively	
		Prompt	Gives prompt services	

Table A2.
Scale of "Resources quality" adopted/ modified from literature

S.No	Construct	Service quality dimensions	Description	References (scale adapted/modified)
2	Resources quality	Fleet	Availability of fleet and physical facility	Yeo *et al.* (2015), Thai (2008)
		Workforce	Availability of adequate workforce	
		Financial	Financial stability	
		Network	Geographical reach and network coverage	
		Modern	Fleet and physical facility are modern and always function properly	
		Infra	Adequate, maintained and updated Information Technology (IT) infrastructure	
		Equipment	Availability of physical equipment like Pallets, trolleys, forklifts etc.	
		Reverse	Manages reverse logistics	

S.No	Construct	Service quality dimensions	Description	References (scale adapted/ modified)
3	Information quality	Complete	Information communicated by logistics service provider is complete	Thai (2013), Huang *et al.* (2009), Saura *et al.* (2008), Rafiq and Jaafar (2007), Mentzer *et al.* (2001)
		Timely	Information communicated by the logistics service provider is timely	
		Accurate	Information communicated by logistics service provider is accurate	
		Adequate	Information communicated by logistics service provider is adequate	
		Credible	Information communicated by logistics service provider is credible	
		Tracking	Tracking and tracing of shipments	
		Application	Application of IT and EDI in customer service	

Table A3.
Scale of "Information quality" adopted/ modified from literature

S.No	Construct	Service quality dimensions	Description	References (scale adapted/ modified)
4	Personnel contact quality	Confidence	Maintains confidentiality in all operations	Saura *et al.* (2008), Rafiq and Jaafar (2007), Mentzer *et al.* (2001)
		Effort	Makes an effort to understand my situation	
		Courteous	Maintains courteous behavior while dealing	
		Access	Easily accessible when needed	
		Queries	Handles queries and complaints effectively	
		Experience	Product knowledge and experience of the logistics service provider is adequate	
		Attitude	Shows a positive attitude while dealings	
		Mutual	Builds mutual relationship and trust	

Table A4.
Scale of "Personnel contact quality" adopted/modified from literature

No	Construct	Service quality dimensions	Description	References (scale adapted/ modified)
5	Customization	Creativity	Shows creativity in its methods of operations	Hu *et al.* (2016), Coelho and Henseler (2012), Iacobucci *et al.* (1995)
		New ways	Seeks out new ways to do things	
		First	My logistics service provider is often the first to initiate with new services	
		Environment	Shows concern towards the environment	
		Specific	Offers me services that satisfy my specific needs	
		Changing	Accommodates my changing and urgent requirements	
		Ideas	Tries out new ideas frequently	
	Innovation			Bellingkrodt and Wallenburg (2015), Simon and Honore PetnjiYaya (2012), Panayides and So (2005), Flint *et al.* (2005) Victorino *et al.* (2005)
	Customization and Innovation			

Table A5.
Scale of "Customization and innovation quality" adopted/modified from literature

S.No	Construct	Service quality dimensions	Description	References (scale adapted/ modified)
6	Customer satisfaction	Satisoverall	We are satisfied with the overall service quality of the logistics service providers	Yeo *et al.* (2015), Chu and Wang (2012), Juga *et al.* (2010), Saura *et al.* (2008), Tian *et al.* (2008), Stank *et al.* (2003), Mentzer *et al.* (2001)
		Satisprocess	We are satisfied with the processes or operations of the logistics service providers	
		Satisfleet	We are satisfied with the fleet, facilities and physical infrastructure of the logistics service providers	
		Satismgmt	We are satisfied with the management and employees of the logistics service providers	
		Delight	We are delighted with our relationship with the logistics service provider	

Table A6.
Scale of "Customer satisfaction" adopted/ modified from literature

S.No	Construct	Service quality dimensions	Description	References (scale adapted/ modified)
3	Customer loyalty	Committed	We are committed to the relationship with logistics service providers	Juga *et al.* (2010), Saura *et al.* (2008), Tian *et al.* (2008), Stank *et al.* (2003)
		Outsource	We will outsource more activities to our logistics service providers in the coming years	
		Recommend	We are likely to recommend our logistics service providers to other organizations	
		Continue	We will continue the relationship with our present logistics service providers as long as possible	
		Committed	We are committed to the relationship with logistics service providers	

Table A7.
Scale of "Customer loyalty" adopted/ modified from literature

About the authors

Dr. Anchal Gupta is Assistant Professor in Apeejay School of Management, Delhi, India. Her interest is in Supply Chain Management, Logistics Management and Service Quality Management. She has published research papers in journals such as *International Journal of Productivity and Performance Management*, *Management of Environment Quality, Global Business Review* etc.

Dr. Rajesh Kumar Singh is Professor in Operations Management Area at Management Development Institute (MDI), Gurgaon, India. His areas of interest include Supply chain management, Industry 4.0, Circular Economy. Currently he is serving as Associate Editor to *International Journal of Consumer Studies* (Wiley) and *International Journal of Global Business and Competitiveness* (Springer). He is also in Editorial Board of *Journal of Supply Chain Management Systems*, *Operations Management Research Journal*, *Journal of Asia Business Studies* and *Vision-The Journal of Business Perspective*. He has also worked as Guest Editor for special issues of Resources, Conservation and Recycling, Sustainable Production and Consumption, Competitiveness Review, *Journal of Modelling in Management*, Administrative Sciences, *Global Journal of Operations and Strategic Sourcing* etc. He has published research papers in reputed international/national journals and conferences. He has published papers in journals such as *Annals of Operations Research, Resources, Conservation and Recycling, Journal of Cleaner Production, Production planning and Control, International Journal of Production Research, Applied Soft Computing, Clean Technologies and Environmental Policy, Industrial Management and Data Systems, Singapore Management Review, International Journal of Productivity and Performance Management, Benchmarking: An International Journal, Journal of Modelling in Management, Competitiveness Review: An International Business Journal.*

Dr. K. Mathiyazhagan working as a chairperson – Research Centre/ Associate Professor, Thaigarajar School of Management, Madurai, Tamil Nadu. He is an associate editor in *Management Decision* (Emerald) impact factor 4.9 and Environment, *Development and Sustainability Journal* – Springer with an impact factor of 3.2 and has more than 3,000 research citations. Editing special issues in *Journal of Business Logistics (JBL), International Journal of Physical Distribution and Logistics Management (IJPDLM), International Journal of Logistics Management (IJLM), Sustainable Production and Consumption* (Elsevier), *Socio-Economic Planning Science* (Elsevier). His publications are in *IJPE, IJPR, PPC, IEEE TEM, JCP, RCR, IJAMT* etc. Also, he is an editorial member in many reputed journals. One of his papers was awarded as Excellence Citation Award by Emerald Publisher Ltd. In addition, he is editing international books on Blockchain and Lean-Green and Society 4.0 in Elsevier, Taylor and Francis, Springer publishers. He is a visiting faculty at the University of Rome Tor Vergata, Italy. Active reviewer of more than thirty reputed international journals and organized two international conferences and workshops. Received best reviewer certificate from reputed journals. He supervised more than 10 undergraduate and 3 postgraduate and 3 PhD scholars. Edited many international conference

proceedings in springer's publisher. His research interest is Green Supply Chain Management; Sustainable Supply Chain Management; Multi-Criteria Decision Making; Third Party Logistic Provider; Sustainable Lean Manufacturing, Public Distribution System; Lean Six Sigma. He is having more than 10 years of research and teaching experience. K. Mathiyazhagan is the corresponding author and can be contacted at: madii1984@yahoo.com

Dr. Pradeep Kumar Suri is serving as a Professor in the Delhi School of Management, Delhi Technological University (DTU). He is originally from the 1986 batch of the Indian Statistical Service. Prior to joining the DTU in 2012, he served as Senior Technical Director at the National Informatics Centre (NIC), Government of India. He joined NIC during 1993, where he served in different capacities during the life cycle of several ICT-based projects in the agriculture and allied sectors. In particular, He has been the NIC National Co-ordinator for establishing Agriculture Marketing Information System Network (AGMARKNET) linking about 3,000 agriculture produce wholesale markets in India. The system has created opportunities for developing ICT enabled supply chains for various agricultural commodities. He is PhD in Management from IIT Delhi. He has publications in both national and international journals and providing consultancy support to Government and UN FAO.

Dr. Yogesh K. Dwivedi is a Professor of Digital Marketing and Innovation and Founding Director of the Emerging Markets Research Centre (EMaRC) at the School of Management, Swansea University, Wales, UK. Professor Dwivedi is also currently leading the *International Journal of Information Management* as its Editor-in-Chief. His research interests are at the interface of Information Systems (IS) and Marketing, focusing on issues related to consumer adoption and diffusion of emerging digital innovations, digital government, and digital and social media marketing particularly in the context of emerging markets. Professor Dwivedi has published more than 300 articles in a range of leading academic journals and conferences that are widely cited (more than 28 thousand times as per Google Scholar). He was recently named on the annual Highly Cited Researchers™ 2020 list from Clarivate Analytics. Professor Dwivedi is an Associate Editor of the *Journal of Business Research*, *European Journal of Marketing*, *Government Information Quarterly* and *International Journal of Electronic Government Research*, and Senior Editor of the *Journal of Electronic Commerce Research*. More information about Professor Dwivedi can be found at: http://www.swansea.ac.uk/staff/som/academic-staff/y.k.dwivedi/.

For instructions on how to order reprints of this article, please visit our website:
www.emeraldgrouppublishing.com/licensing/reprints.htm
Or contact us for further details: **permissions@emeraldinsight.com**

Hindawi
Advances in Materials Science and Engineering
Volume 2022, Article ID 7860273, 22 pages
https://doi.org/10.1155/2022/7860273

Research Article

Factors Influencing Piezoelectric Response of Horizontally and Vertically Embedded PZT Patch in Confined Granular Fills

Nisha Kumari [1] **and Ashutosh Trivedi** [2]

[1]*Research Scholar, Civil Engineering Department, Delhi Technological University, Delhi-110042, India*
[2]*Civil Engineering Department, Delhi Technological University, Delhi-11042, India*

Correspondence should be addressed to Nisha Kumari; nishasoni.ce@gmail.com

Received 7 March 2022; Revised 14 May 2022; Accepted 27 May 2022; Published 16 June 2022

Academic Editor: Wen-Shao Chang

Copyright © 2022 Nisha Kumari and Ashutosh Trivedi. This is an open access article distributed under the Creative Commons Attribution License, which permits unrestricted use, distribution, and reproduction in any medium, provided the original work is properly cited.

The energy harvesting from ambient vibrations in the confined granular fill along the expressways and highways is a prospective power source for varied engineering applications. This paper presents the study of charge density, voltage output, and power from the *PZT* (lead zirconate titanate) patches embedded in dynamically loaded confined granular fill. The effect of the alignment of *PZT* patches, thickness ratio, material properties of the confined granular fill, and retaining structure on the voltage output is investigated. It provides the scope for the evaluation of voltage output directly from the stress-strain response, position of the *PZT* patch, and the engineering properties of the confined granular fill. The alignment of *PZT* patches in the horizontal and vertical directions has been examined analytically to optimize voltage outputs. The results indicate that the modulus ratio of the material, alignment of *PZT* patches, and gradation of infill material significantly affect the voltage generation. A relationship for voltage and power output has been proposed for a set of engineering applications. The observed voltage output is found appropriate for wide-ranging implements classified as low- (LRA), medium- (MRA), and high- (HRA) resistance applications. It is proposed to be up-scaled using multiple patches embedded throughout the confined granular fill and pavements subjected to continuous dynamic loads.

1. Introduction

The dynamically loaded transportation infrastructures find a unique application for energy harvesting and structural health monitoring due to the profound developments in sensor technology. This energy can be captured using a suitable mechanism for various micro- and macro-engineering operations, including electrical devices and transportation as a renewable energy system [1]. The piezoelectric material provides higher energy density and flexibility in being integrated into a system than the electromagnetic and electrostatic units [2, 3]. Many researchers [4–6] have analysed the effectiveness of embedded *PZT* (lead zirconate titanate) patches for energy harvesting and health monitoring structures.

Many studies [7–9] considered vibration-based energy harvesting using piezoelectric material for civil infrastructure systems due to dynamic loads of traffic movements. An analytical expression has been proposed for a small *PZT* patch attached to the surface of a bridge structure. The Hamiltonian principle was considered to account for all the vibration modes of the structure and pointed out that the surface strain fluctuations influence voltage output [10]. The electrical energy generation was investigated in a prestressed tuneable piezoelectric beam harvester from a bridge's vibrations under ambient loading conditions [11]. They concluded that the maximum power generation from the *PZT* patch is a function of the excitation frequency of the dynamic loads. Experimental validation for a rail bridge in their operational condition for energy harvesting from the random vibrations of the built infrastructure within the laboratory environment was presented where the theoretical predictions were less than the experimental output [12]. The feasibility of energy harvesting from friction-induced vibration was associated with stronger vibrations [13]. A few researchers [14, 15] have analysed the performance and

structural response of the pavement with an embedded piezoelectric energy harvester. The structural response of the asphalt pavement embedded with a piezoelectric energy harvester (PEH) provided a couple of optimization solutions for design [16]. Table 1 presents a brief review of specific power production capabilities of alternative energy harvesting sources, including *PZT* patches. It shows the vast potential of *PZT* patches for various micro- and macro-engineering operations.

Few investigators performed field observation for the piezoelectric cantilever installed above the pavement and embedded underground [17]. They found that a significant amount of electrical energy is generated from the embedded piezoelectric cantilever. The stress on the surface influences the piezoelectric effect of the PZT patches. The voltage polarization of the *PZT* patch is significantly affected by its embedment depth and orientation. It was found that the vertical compressive stress is decreased when depth is increased effectively [18]. The performance of the *PZT* patches for energy harvesting from the pavement combines the stiffness and load pattern. Comparing the impact of the dynamic loads, the influence of the pavement thickness on the power generation is negligible [19].

The literature review indicates that the application of piezoelectric material in civil structures is an abundant source of energy. The existing experimental and numerical analysis usually focuses on the methods of piezoelectric energy from various structural elements, namely beams, bridges, roads, and rail tracks. By contrast, there are no significant studies on the stress response of confined granular fill on power generation due to vibrations. The *PZT* patches embedded in the pavement undergo reversal in the voltage polarity for both horizontal and vertical faces [18]. Therefore, the piezoelectric power output is not necessarily higher for the stronger vibrations. The power output depends on the magnitude of strain generation due to vertical and horizontal vibrations. From previous analytical studies [18, 38], it appears that the resultant vertical stresses and horizontal stresses are affected by the placement of the *PZT* patch on the retaining face compared to the horizontal pavement structure. Similar observations were made [39] for the increasing depth of embedment of the *PZT* patch. The analytical study helps us to identify the set of design parameters that can improve the efficiency of the piezoelectric energy output. The efficiency of charge output depends upon the magnitude of the force excitation, the material characteristics, and the electromechanical coupling of the piezoelectric material structure [40, 41]. The piezoelectric response of the *PZT* patch can be optimized by changing the mechanical properties through variation in the modulus [42].

The objective of this study is a parametric investigation of the factors influencing the piezoelectric voltage generation considering the installation position of the *PZT* patch, and geometric and mechanical properties of the embedded *PZT* patch in confined granular fill. The confined granular fill is contained by the pavement and the retaining structure. The confined granular fill experiences vibrations due to dynamic loads. The strain fluctuation is absorbed by the *PZT* patch, which polarized and induced a voltage. This deformation per unit length is analysed by the stress-strain response of the confined granular fill due to the ambient vibration. The deformation of the *PZT* patch is used to calculate the charge density and voltage output. The model that consists of confined granular fill with embedded *PZT* patches is analysed theoretically. The electromechanical process is used to convert mechanical energy into electrical energy. The charge density and voltage output from the *PZT* patch are discussed with a focus on the influence of the embedded position, piezoelectric properties, geometric properties of the *PZT* patch, and confined granular fill.

The present study evaluates the charge density and voltage output over the permittivity, placement of the *PZT* patch, depth of embedment, and geometric properties of the retaining structure. Figure 1 shows a flow chart of the conversion of mechanical energy into electrical energy from the confined granular fill. The mechanical vibration of dynamic loads for energy harvesting consists of a loading system, which transfers the vibration waves through the mechanical units. The mechanical unit comprises a pavement with a *PZT* patch embedded horizontally and vertically over the granular fill retained by a retaining wall. Besides the energy generation, the influence of the material properties on the polarization of the *PZT* patch is a vital engineering parameter influencing charge density.

The results show the geometric properties of the retaining structure and mounted position of the *PZT* patch on the transformation of mechanical into electrical energy through the change in charge density and voltage output. It has been demonstrated that the piezoelectric response of a *PZT* patch embedded in the confined granular fill can be tuned through the changes in its thickness and stiffness. A comparison of output voltage among the hard, semihard, and soft *PZT* patches based on piezoelectric material properties has been made. Based on the theoretical analysis, the influence of different alignments and stiffness of the *PZT* patch on the output energy is captured.

2. Engineering Properties of *PZT* Patches

When piezoelectric materials are subjected to mechanical stress, electrical energy generated in proportion to that stress is known as the direct piezoelectric effect. The direct effect occurs through the compression of piezoelectric material, as shown in Figure 2. D_3 is the electric displacement on the *PZT* patch, E_3 is the electric field in direction-3, d_{31} is the piezoelectric strain coefficient in mode 31, ε_{33}^{T} represents the permittivity of the material in the direction-33 under conditions of constant mechanical stress ($\varepsilon_{33}^{T=0}$ corresponds to free permittivity), and σ_{PZT} is stress in the *PZT* layer.

Piezoelectric energy output is commonly based on two coupling modes: 33-mode and 31-mode, as shown in Figures 3–4. The coupling mode defines the capability of piezoelectric material to transform mechanical energy into electrical energy. Figure 3 shows a 33-mode *PZT* patch where the external stress direction generated an electric field in the same direction. Figure 4 shows 31-mode where the applied

Table 1: Energy output capacities of varied system configurations.

System configuration	Energy output	Estimated cost
Typically a dynamic loading from the busy expressway[a]	188 kW	\$0.08-\$0.18/kWh
PZT system paved in roadway section with very high traffic volume[b]	4.04 MWh	\$1.77/kWh
Fan-typed windmill using induced resonance[c]	613 μW	—
Piezoelectric cantilever embedded in small fan windmill[d]	363 μW	—
Aero-elastic energy harvesting using the piezoelectric transducer from wind tunnel[e]	27mw	—
Dynamic loading from the ocean waves[f]	60–180mw	—
Hydraulic pressure in the hydraulic systems[g]	1.2 mW	—
High-rise buildings due to wind and earthquake[h]	432.21 MW	—
Building due to pedestrian traffic[i]	1.1 MWh	\$3850/per tile
A vibration-based system installed on bridge cable[j]	35.67 mW	\$80-\$85/kWh
Electromagnetic energy harvester from low-frequency mechanical vibrations[k]	554.7 μW	—
Electromagnetic generator utilized the low ambient vibrations[l]	46 μW	—
Oscillation motion of human body and vibration of machines[m]	95 mW	—
Power generation utilizing the vibration of moving cars[n]	3.9 mW	—
Pavement system supported by solar panels[o]	1718 MW	\$0.05-\$0.075/kWh
PV panels mounted 33-bus distribution network[p]	14 KW	—
Households and village power stations[q]	200–2500 W	\$10-\$12/W
Photovoltaic noise barriers with motorways and railway tracks[r]	800 MWh	—

[a]Hill et al. [20]; [b]Guo and Lu [21]; [c]Yang et al. [22]; [d]Rezaei-Hosseinabadi et al. [23]; [e]Sousa et al. [24]; [f]Murray and Rastegar [25]; [g]Cunefare et al. [26]; [h]Xie et al. [27]; [i]Li and Strezov [28]; [j]Kim et al. [29]; [k]Zorlu et al. [30]; [l]Beeby et al. [31]; [m]Sasaki et al. [32]; [n]Glynne-Jones et al. [33]; [o]Wang et al. [34]; [p]Jiang et al. [35]; [q]Zahedi [36]; [r]Nordmann et al. [37].

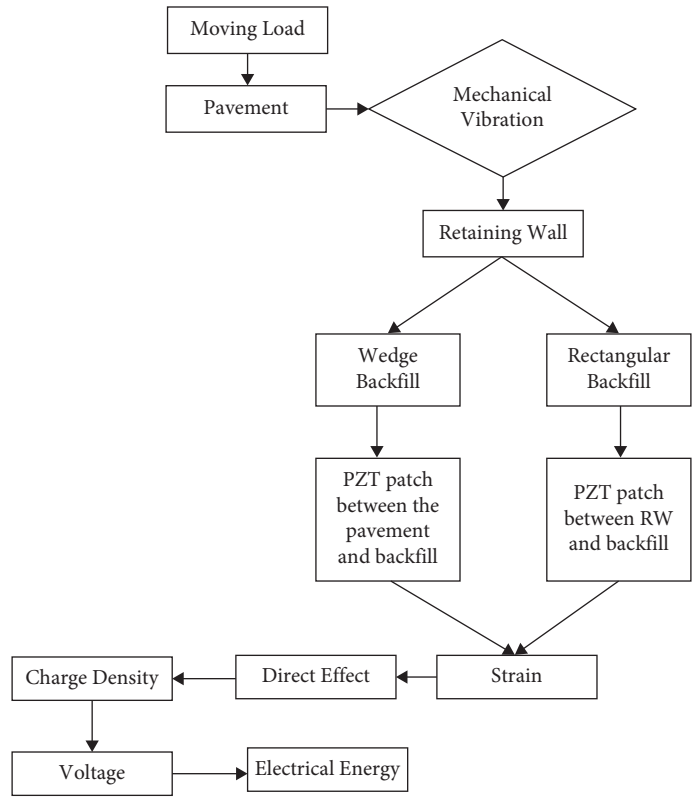

Figure 1: Flow chart for electromechanical energy output from mechanical vibrations.

stress is axial and perpendicular to the direction of the electric field.

The parameters influencing the voltage output from the PZT patches are relative permittivity ($\varepsilon_{33}^{T}/\varepsilon_o$) (here, ε_0 refers to the absolute permittivity of the vacuum), piezoelectric strain constant (d), polarization ratio (d_{31}/ε_{33}), and piezoelectric voltage coefficient (g). The charge density of the PZT patch is the most important consideration when choosing a piezoelectric material for energy harvesting. The product of the effective piezoelectric strain constant (d) and the effective piezoelectric voltage constant (g) determines the magnitude of the charge density [44]. The *PZT* material considerations are classified as the hard, semihard, and soft *PZT* patches, as shown in Table 2. The piezoelectric material considerations

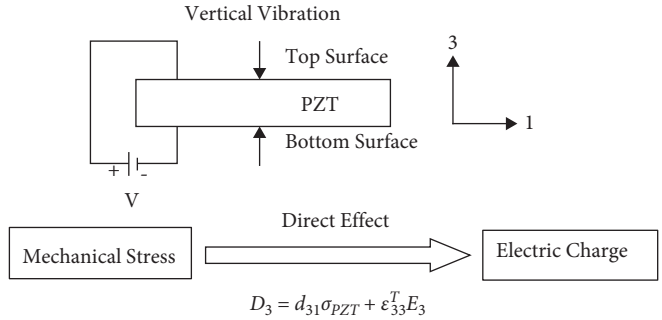

Figure 2: Flow chart for the generation of electric charge due to mechanical vibrations.

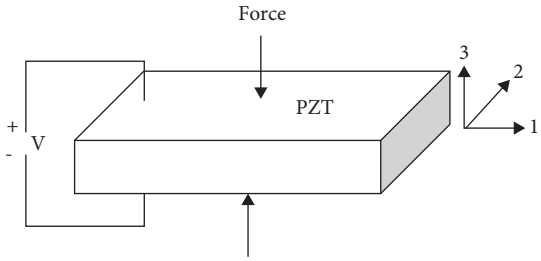

Figure 3: Mode of operation for the PZT patch (33-mode).

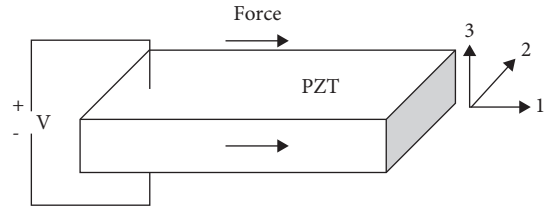

Figure 4: Mode of operation for the PZT patch (31-mode).

for engineering applications include piezoelectric strain constant, piezoelectric voltage constant, and mechanical quality factor (Q). The relative permittivity of the selected *PZT* patches (Table 2) was 1250, 1450, and 2400, while the polarization ratio was 0.112, 0.114, and 0.087, respectively. The polarization ratio is defined as the ratio of piezoelectric strain constant and relative permittivity.

2.1. Stress-Strain and Charge Density. The stress-strain response of the *PZT* patch embedded in the confined granular fill has been obtained in terms of charge density and voltage using a systematic numerical approach. The position of the *PZT* patch and its geometric properties influences the magnitude of deformation as described in the following sections.

2.2. Stress-Strain Behaviour. The stress-strain behaviour of the *PZT* patch has been considered for horizontal and vertical alignments. Initially, a *PZT* patch is horizontally and vertically embedded in the confined granular fill (Figure 5(a)). It has been assumed that the neutral plane of the *PZT* patch does not coincide with the geometrical centre of the fill. There is a negligible shear movement or separation among the retaining structure, *PZT* patch, and granular fill. The retaining structure is considered flexible and elastically constrained at the base. The shape of the useful part of the granular fill is considered a triangular wedge as shown in Figure 5(b). The vibrating system consists of a wall of height H, length L (such that $L = 1$), and backfill of thickness h_R. The thickness of *PZT* patch is h_p. As the result of the vibration, the stresses are generated in the pavement, granular fill, and *PZT* patch.

The deformation in the horizontally embedded *PZT* patch is a function of *PZT* material properties, bending moment, the width of backfill, modulus ratio, and thickness ratio (Appendix A). The strain in the horizontally embedded *PZT* patch [45] is expressed as

$$\varepsilon_{HE} = f\left(M, b_S, E_s, h_R, \mu, n\right) = \frac{36M}{b_S E_S h_R^2}\left[\frac{(1+\mu)(1+\mu n)}{3\mu^5 n^3 + 6\mu^4 n^2 + 5\mu^3 n + \mu^2 n^2 + \mu^2 + 4\mu n + 2}\right]. \quad (1)$$

The stress in the horizontally embedded patch is a function of strain and modulus of the *PZT* and is expressed as

$$\sigma_{HE} = \varepsilon_{HE} * E_P = \frac{36M}{b_S h_R^2}\left[\frac{n(1+\mu)(1+\mu n)}{3\mu^5 n^3 + 6\mu^4 n^2 + 5\mu^3 n + \mu^2 n^2 + \mu^2 + 4\mu n + 2}\right], \quad (2)$$

Table 2: Engineering properties of piezoelectric patches.

Engineering properties	Symbol	Hard patch; PZT-141	Semihard; PZT-155	Soft patch; PZT-151
Density (kg/m^3)	ρ	7800	7800	7800
Modulus of PZT patch (GPa)	E_P	81	63	60
Relative permittivity[a]	$\varepsilon_{33}^T/\varepsilon_o$	1250	1450	2400
Dielectric loss factor[a]	tan δ	5×10^{-3}	20×10^{-3}	20×10^{-3}
Piezoelectric strain constant[a] (C/N)	d_{31}	-140×10^{-12}	-165×10^{-12}	-210×10^{-12}
	d_{33}	310×10^{-12}	360×10^{-12}	500×10^{-12}
Piezoelectric voltage coefficient[a] (Vm/N)	g_{31}	-13.1×10^{-3}	12.9×10^{-3}	-11.5×10^{-3}
	g_{33}	29×10^{-3}	27×10^{-3}	22×10^{-3}
Polarization ratio[b]	d_{31}/ε_{33}	0.112	0.114	0.087

[a]Physik Instrumente GmbH [43]; [b]present work.

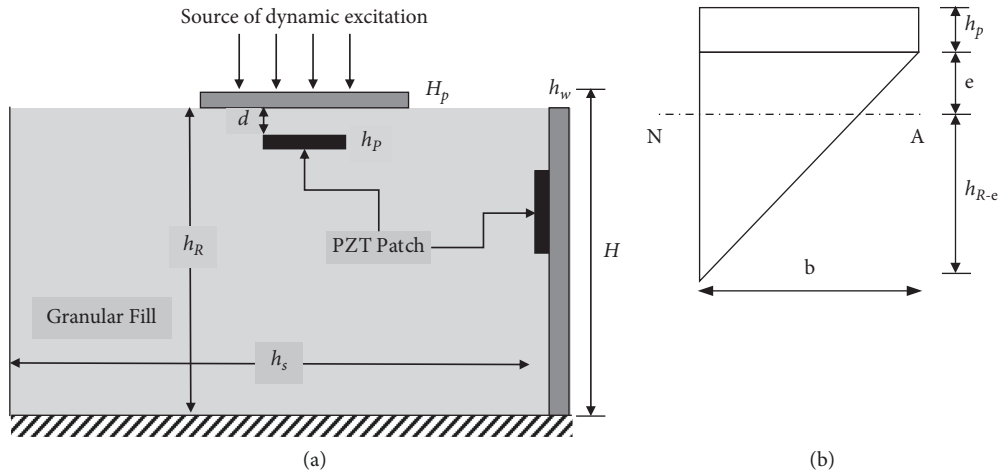

Figure 5: (a) PZT patch of the thickness (h_P) horizontally and vertically embedded in the confined granular fill of thickness (h_R) retained by retaining structure of height (H). (b) Cross section of the triangular wedge with PZT patch.

where ε_{HE} and σ_{HE} are the strain and the stress in a horizontally embedded *PZT* patch. E_S and E_P are Young's modulus of backfill and PZT patch, respectively; μ is the ratio of the thickness of the *PZT* patch to the backfill h_P/h_R; and n is the ratio of the modulus of the *PZT* patch to the backfill (E_P/E_R), and M is the bending moment *PZT* patch.

The strain in the vertically embedded *PZT* patch is the function of bending moment, the height of the retaining structure, modulus ratio, height of the backfill, and thickness ratio [46] is expressed as

$$\varepsilon_{VE} = \int (M, H, h_S, a, b, \mu, n) = \frac{36M}{E_s H h_s^2}\left[\frac{\left(3\mu + 2 - 12a^2b\mu^2n\right)[24\mu n(a+b)+1]}{\left[3n\mu^3\left(1+ba^3\right)+1\right][24\mu n(a+b)+1]^2 + 18\left(3\mu+2-12a^2b\mu^2n\right)[2\mu n(1+ab)+1]}\right]. \tag{3}$$

Similarly, the stress for vertically embedded *PZT* patch between the granular fill and retaining wall is expressed as

$$\sigma_{VE} = \varepsilon_{VE} * E_P = \frac{36nM}{Hh_s^2}\left[\frac{\left(3\mu + 2 - 12a^2b\mu^2n\right)[24\mu n(a+b)+1]}{\left[3n\mu^3\left(1+ba^3\right)+1\right][24\mu n(a+b)+1]^2 + 18\left(3\mu+2-12a^2b\mu^2n\right)[2\mu n(1+ab)+1]}\right], \tag{4}$$

where ε_{VE} and σ_{VE} are the strain and stress in vertically embedded *PZT* patch, a is the thickness ratio of retaining wall and *PZT* patch (h_w/h_P), and b is the modulus ratio of retaining wall and *PZT* patch (E_w/E_P).

2.3. Charge Density for the Horizontally Embedded PZT Patch. The charge density equations for the hard, semihard, and soft *PZT* patches embedded horizontally have been derived from the stress-strain relationship of the *PZT* patch subject to vibrations in the confined granular fill. A single layer of *PZT* patch horizontally embedded between the pavement and the granular fill is shown in Figure 5(a). The deflection induces curvature in the triangular wedge at an arbitrary point on the neutral axis due to bending. The power output and the dynamic response of the piezoelectric system entirely depend on the coupling mode of the PZT patch. The researchers [47, 48] have identified that the natural way of excitation of retaining structure is in d_{31} mode. Therefore, the d_{31} mode has been chosen in the present work for analysis. For the so configured system, the tensorial representation of the piezoelectric constitutive equation [49] gives the electric displacement as

$$D_3 = d_{31}\sigma_{PZT} + \varepsilon_{33}^{T} E_3. \tag{5}$$

The stress generated in the *PZT* patch due to the dynamic loads on the confined granular fill changes the polarization and the displacement on the upper and lower surface of the *PZT* patch. As there is no external electric source ($E_3 = 0$), the electric displacement in the *PZT* patch is expressed as

$$D_3 = d_{31}\sigma_{PZT}. \tag{6}$$

The charge density function at the top and bottom surfaces of the horizontally embedded *PZT* patch is expressed as

$$\rho_{\mathrm{THE}} = D_3\left(Z, h_p + \frac{h_R}{3}\right), \tag{7}$$

$$\rho_{\mathrm{BHE}} = D_3\left(Z, h_P\right), \tag{8}$$

where ρ_{THE} and ρ_{BHE} are charge density functions at the top and bottom surfaces of the horizontally embedded *PZT* patch, respectively, and D_3 is electric displacement according to the piezoelectric coupling constitutive equation, and Z is the thickness direction coordinate from the neutral plane as shown in Figure 5(b).

From equations (6) and (7), the charge density is expressed as

$$Q_{\mathrm{THE}} = d_{31}\int_0^{(h_P+(h_R/3))} \sigma_B \mathrm{d}z, \tag{9}$$

$$Q_{\mathrm{THE}} = \frac{12 d_{31} M}{b h_R}\left[\frac{n(1+\mu)(1+\mu n)(3\mu+1)}{3\mu^5 n^3 + 6\mu^4 n^2 + 5\mu^3 n + \mu^2 n^2 + \mu^2 + 4\mu n + 2}\right], \tag{10}$$

$$Q_{\mathrm{BHE}} = -d_{31}\int_0^{(h_p)} \sigma_B \mathrm{d}z, \tag{11}$$

$$Q_{\mathrm{BHE}} = \frac{-12 d_{31} M}{b h_R}\left[\frac{n\mu(1+\mu)(1+\mu n)}{3\mu^5 n^3 + 6\mu^4 n^2 + 5\mu^3 n + \mu^2 n^2 + \mu^2 + 4\mu n + 2}\right]. \tag{12}$$

The negative sign represents the opposite charge of the top surface, while Q_{THE} and Q_{BHE} are the charge density at the top and bottom surfaces of the horizontally embedded *PZT* patch, respectively.

2.4. Charge Density for the Vertically Embedded PZT Patch. The charge density determines the dipole mobility of the charges on the *PZT* surface and affects the efficiency of power generation. The charge density function at the top and bottom surfaces of the vertically embedded *PZT* patch is expressed as

$$\rho_{TVE} = D_3\left(Z, h_p + e\right), \tag{13}$$

where e is the distance between the bottom surface of *PZT* and the centre of gravity of the granular backfill, and is expressed as

$$e = \frac{h_P\left[6a + 1 - 6a^2\right]}{18a + 12}, \tag{14}$$

$$\rho_{BVE} = D_3\left(Z, h_p\right), \tag{15}$$

where ρ_{TVE} and ρ_{BVE} are the charge density function at the top and bottom surfaces of the vertically embedded *PZT* patch in the confined granular fill, h_p is the thickness of the *PZT* patch, a is the thickness ratio of the retaining wall and the *PZT* patch (h_w/h_P), D_3 is electric displacement according to the constitutive equation of the piezoelectric coupling, Z is the thickness direction coordinate from the neutral plane, and e is the distance between the neutral plane and bottom surface of the *PZT* patch as shown in Figure 5(b).

The charge density (equations (13) and (14)) is expressed as

$$Q_{\mathrm{TVE}} = d_{31}\int_{0}^{(h_P+e)} \sigma_E \mathrm{d}z, \tag{16}$$

$$Q_{TVE} = \frac{36d_{31}nM}{hah_s}\left[\frac{\left(3\mu+2-12a^2b\mu^2n\right)(24\mu n(a+b)+1)\left(6a+1-6a^2\right)}{(18a+12)\left[\left(3n\mu^2\left(1+ba^3\right)+1\right)(24\mu n(a+b)+1)^2+18\left(3\mu+2-12a^2b\mu^2n\right)(2\mu a(1+ab)+1)\right]}\right], \tag{17}$$

$$Q_{\mathrm{BVE}} = -d_{31}\int_{0}^{(e)} \sigma_E \mathrm{d}z, \tag{18}$$

$$Q_{\mathrm{BVE}} = \frac{-36d_{31}nM}{hah_s}\left[\frac{\left(3\mu+2-12a^2b\mu^2n\right)(24\mu n(a+b)+1)\left(6a^2+12a+11\right)}{(18a+12)\left[\left(3n\mu^2\left(1+ba^3\right)+1\right)(24\mu n(a+b)+1)^2+18\left(3\mu+2-12a^2b\mu^2n\right)(2\mu a(1+ab)+1)\right]}\right]. \tag{19}$$

Q_{TVE} and Q_{BVE} are the generated charge density at the top and bottom surfaces of the vertically embedded *PZT* patch, respectively.

2.5. Voltage Output for Horizontally and Vertically Embedded PZT Patches. Due to the phase difference, the charge developed at the opposite side of the *PZT* patch is collected by a separate electrode so that charge cancellation due to the phase difference in the electric displacement is prevented.

Since the charge quantity of the top and bottom surfaces is not the same, the voltage between the two poles is expressed as

$$V = \int_{e}^{(h_P+e)} E(x,z)\mathrm{d}z, \tag{20}$$

$$E = \frac{d_{31}\sigma_P}{\varepsilon_{33}}. \tag{21}$$

where V is the voltage between the top and bottom surfaces of the PZT patch due to vibration of the system, E is the equivalent electric field intensity, σ_P is stress in the PZT patch, and $\varepsilon_{33}^T/\varepsilon_o$ is relative permittivity. For a horizontally embedded PZT patch, the voltage output between the top and bottom surfaces of the PZT patch is expressed as

$$V_{HE} = \frac{h_R^2 d_{31}E_P\mu(3\mu+2)}{12\varepsilon_{33}\rho}, \tag{22}$$

$$V_{HE} = \frac{3Md_{31}}{b\varepsilon_{33}}\left[\frac{n\mu(1+\mu)(1+\mu n)(2+3\mu)}{3\mu^5n^3+6\mu^4n^2+5\mu^3n+\mu^2n^2+\mu^2+4\mu n+2}\right], \tag{23}$$

where V_{HE} is the voltage output for a horizontally embedded *PZT* patch in confined granular fill, d_{31} is the piezoelectric strain constant for 31-mode, and E_P is the elastic modulus of the *PZT* patch. Similarly, for a vertically embedded *PZT* patch, the voltage output between the top and bottom surfaces of the *PZT* patch is expressed as

$$V_{VE} = \frac{h_P^2 d_{31}\varepsilon_o E_P\mu^2\left(-6a^2+15a+13\right)}{2\varepsilon_{33}\rho(18a+12)}, \tag{24}$$

$$V_{VE} = \frac{18n\varepsilon_o Md_{31}}{H\varepsilon_{33}}\left[\frac{\mu^2\left(3\mu+2-12a^2b\mu^2n\right)(24\mu n(a+b)+1)\left(-6a^2+15a+13\right)}{18a+12\left[\left(3n\mu^3\left(1+ba^3\right)+1\right)(24\mu n(a+b)+1)^2+18\left(3\mu+2-12a^2b\mu^2n\right)(2\mu n(1+ab)+1)\right]}\right], \tag{25}$$

where V_{VE} is the voltage output of vertically embedded *PZT* patch, H is the height of the retaining structure, a and b denote the thickness ratio of retaining wall with *PZT* patch and the modulus ratio of retaining wall with *PZT* patch, respectively.

3. Results and Discussion

This section provides the stress-response results on power generation from the ambient vibration in retaining the structure of height *(H)* with horizontally and vertically embedded *PZT* patches. The charge density and voltage output are obtained, which are significantly affected by the

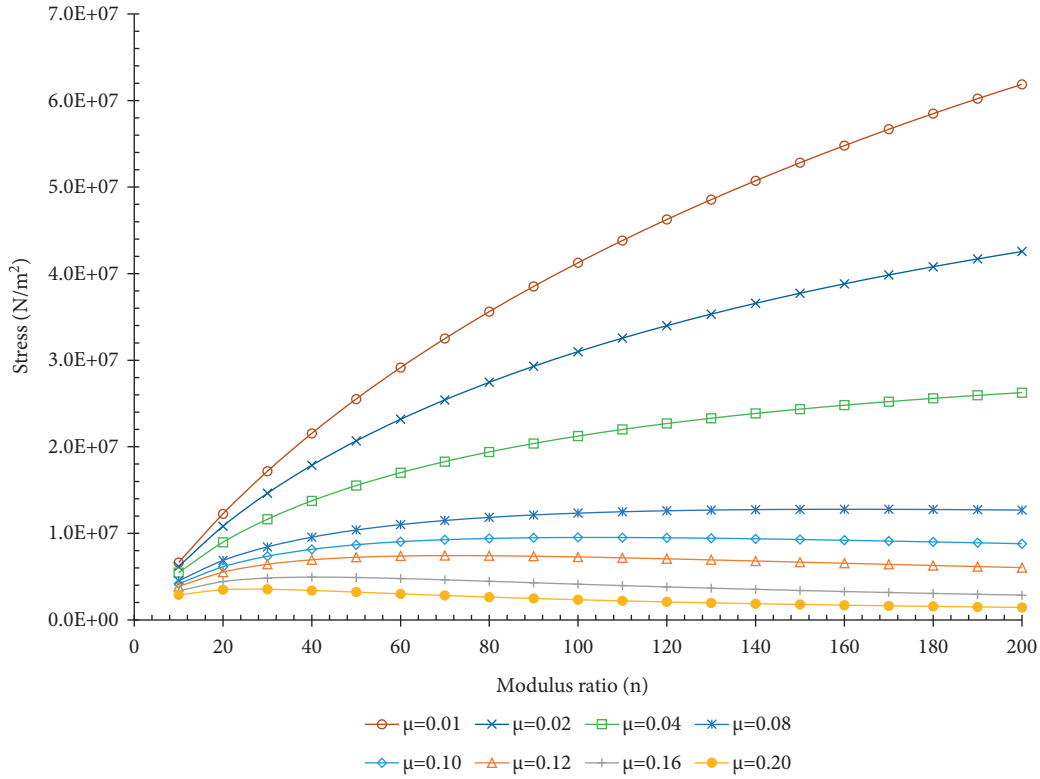

FIGURE 6: Stress variation with modulus ratio for the horizontally embedded PZT patch in confined granular fill computed for modulus ratio, the thickness of the backfill, the width of retaining structure, and thickness ratio.

stress state of the *PZT* patch. The stress-strain response of horizontally and vertically embedded *PZT* patches is analysed using equations (1)–(4). The effects of stiffness, polarization per unit permittivity, and geometric properties of the *PZT* patch have been obtained by equations (5)–(25). It is considered difficult to embed the *PZT* on the upper surface of the pavement (environmental, abrasion, and iteration effects). Therefore, it is recommended to embed the *PZT* at depth (d). Accordingly, the stiffness of the base course layer has been considered as 1–4 GPa [39]. The resilient modulus of hardened concrete is reported in the range of 10–30 GPa, while that of aggregate is between 45 and 85 GPa. Hence, the range of values (1–5 GPa), which are well below the hardened concrete, is used in this study.

The strain on the *PZT* patch is evaluated for varying thickness of the granular backfill. The comparative analysis is shown for varied piezoelectric materials, namely hard *(H)*, semihard *(SH)*, and soft *(S)* patches. To perform the technical analysis, the most commonly used parameters of the *PZT* patches, namely the relative permittivity ($\varepsilon_{33}^{T}/\varepsilon_o$), piezoelectric strain constant (d), piezoelectric voltage coefficient (g), and polarization ratio, are considered as mentioned in Table 2. The modulus of the *PZT* material varies with the temperature and thickness of the material. The researchers [50, 51] suggested that piezoelectric material has a stiffness of the order of 50–90 GPa. Therefore, to analyse the effect of the modulus ratio, the modulus of the hard, semihard, and soft *PZT* patch has been taken as 81, 63, and 60 GPa, respectively. The charge density and voltage output have been analysed for hard, semihard, and soft *PZT* patches.

4. Effect of Stiffness of Confined Granular Fill, Retaining Structure, and PZT Patch

The stiffness is the function of the geometry and the thickness of the material. The stress-strain response has been analysed by considering equations (2)–(4). Figure 6 shows the stress variation of the horizontally embedded *PZT* patch for varying thickness ratios considered in the range of $0.01 \le \mu \le 0.20$. The *PZT* patches are commercially available in a range of thicknesses from 0.20 to 20 mm (piezoelectric ceramic product 2011). The thickness ratio range is selected to capture the effect of the thickness of the *PZT* patch and granular fill. The thickness of the *PZT* patch was kept 10 mm while that of granular fill was 5–100 cm leading to a thickness ratio of 0.01 to 0.20.

From equation (16), it is observed that charge density is directly proportioned to the stress. Thus, the phenomenon indicates that the thickness of the retaining structure is a vital parameter for voltage output. Similarly, Figure 7 shows the stress response for the vertically embedded PZT patch for thickness ratio in the range of $0.01 \le \mu \le 0.20$. The negative values show the change in the nature of the stress. The change in sign indicates the compression and tension response of the stress. When a thin *PZT* patch has been embedded vertically, then the stress shows the opposite trend. It shows that the thickness of the surrounded granular

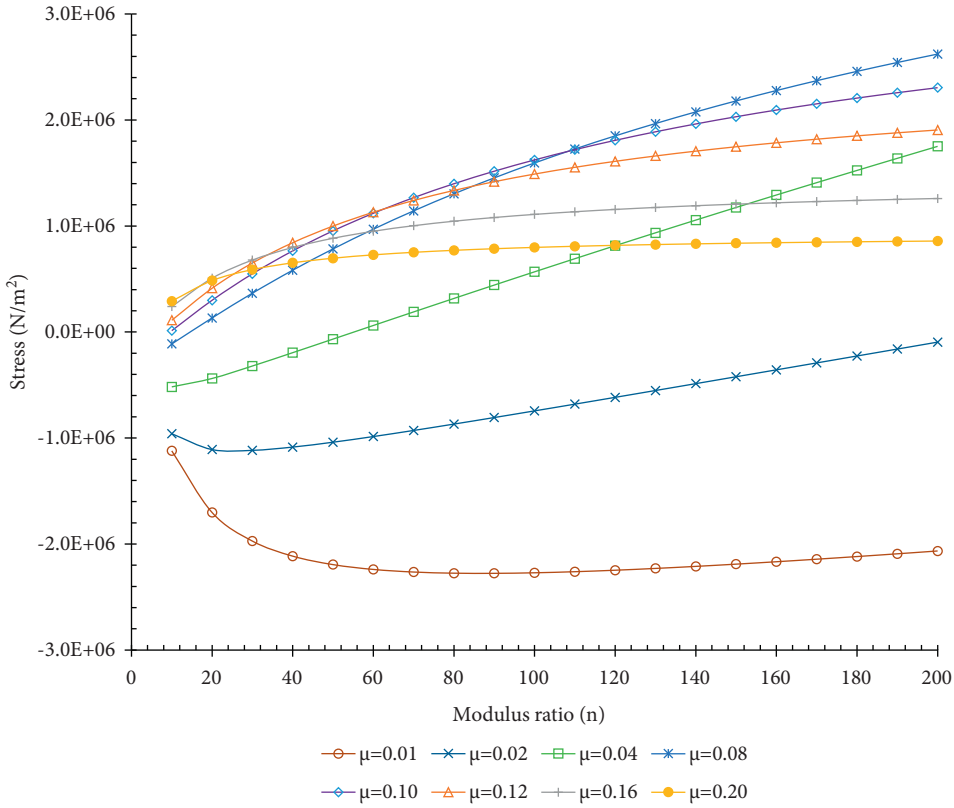

Figure 7: Stress variation with modulus ratio for the vertically embedded PZT patch in the confined granular fill computed for modulus ratio, the width of backfill, the width of retaining structure, and thickness ratio.

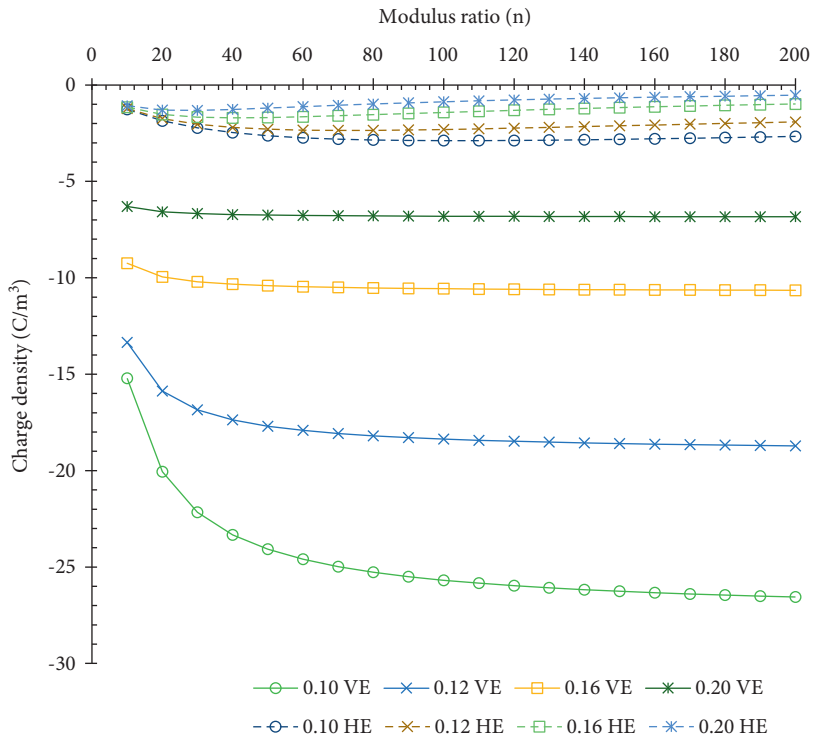

Figure 8: Charge density computed for retaining structure of unit width, piezoelectric strain, modulus ratio, and thickness ratio on the top surface of the horizontally and vertically embedded hard *PZT* patch in the confined granular fill.

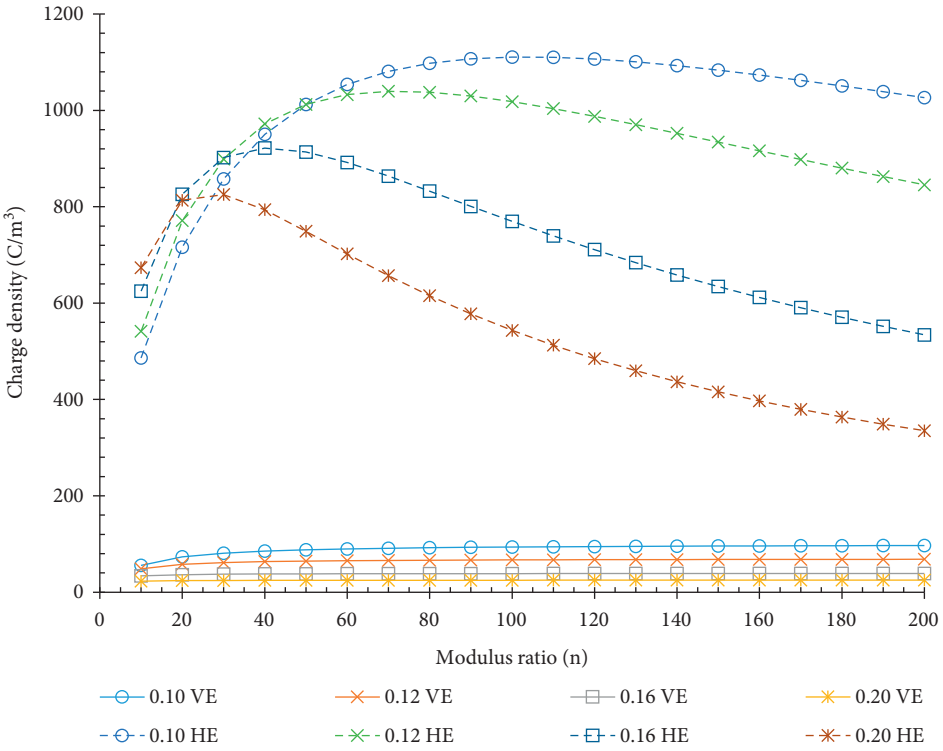

Figure 9: Charge density computed for retaining structure of unit width, piezoelectric strain, modulus ratio, and thickness ratio on the bottom surface of the horizontally and vertically embedded hard *PZT* patch in the confined granular fill.

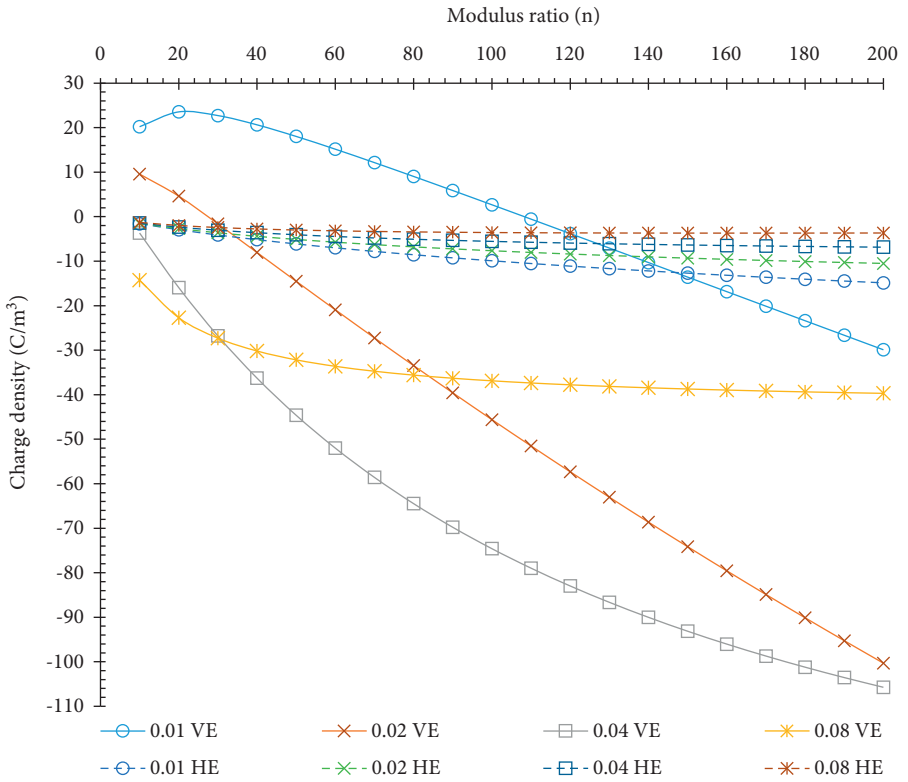

Figure 10: Charge density computed for retaining structure of unit width, piezoelectric strain, modulus ratio, and thickness ratio on the top surface of the horizontally embedded and from for vertically embedded hard *PZT* patch in the confined granular fill.

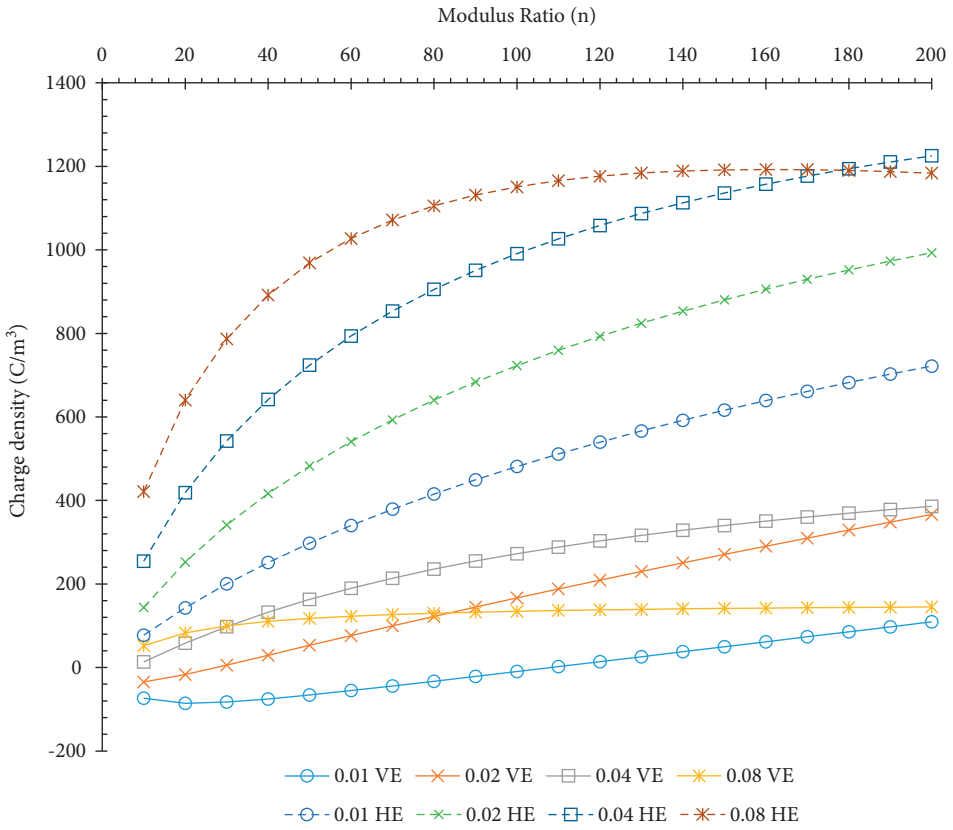

FIGURE 11: Charge density computed for retaining structure of unit width, piezoelectric strain, modulus ratio, and thickness ratio on the bottom surface of the horizontally and vertically embedded hard *PZT* patch in the confined granular fill.

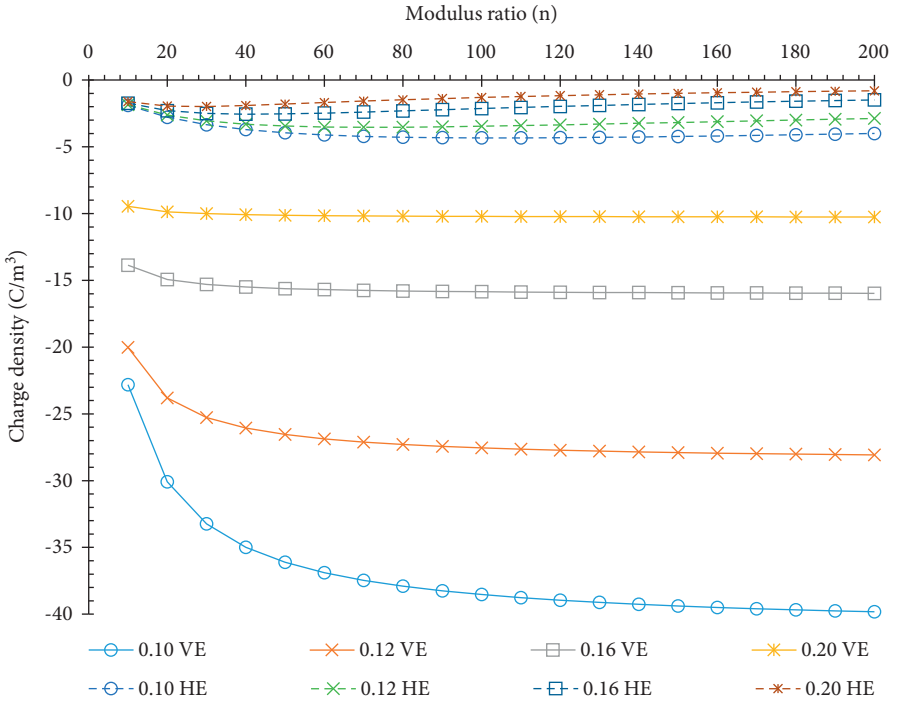

FIGURE 12: Charge density computed for retaining structure of unit width, piezoelectric strain, modulus ratio, and thickness ratio on the top surface of the horizontally and vertically embedded soft *PZT* patch in the confined granular fill.

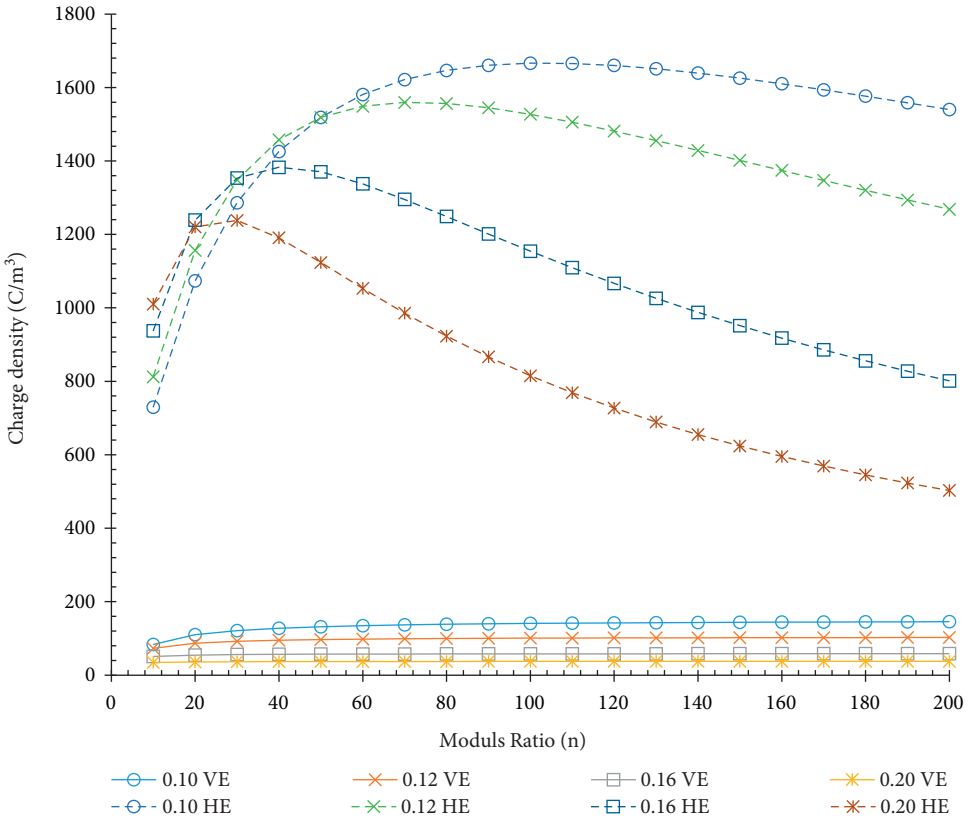

Figure 13: Charge density computed for retaining structure of unit width, piezoelectric strain, modulus ratio, and thickness ratio on the bottom surface of the horizontally and vertically embedded soft *PZT* patch in the confined granular fill.

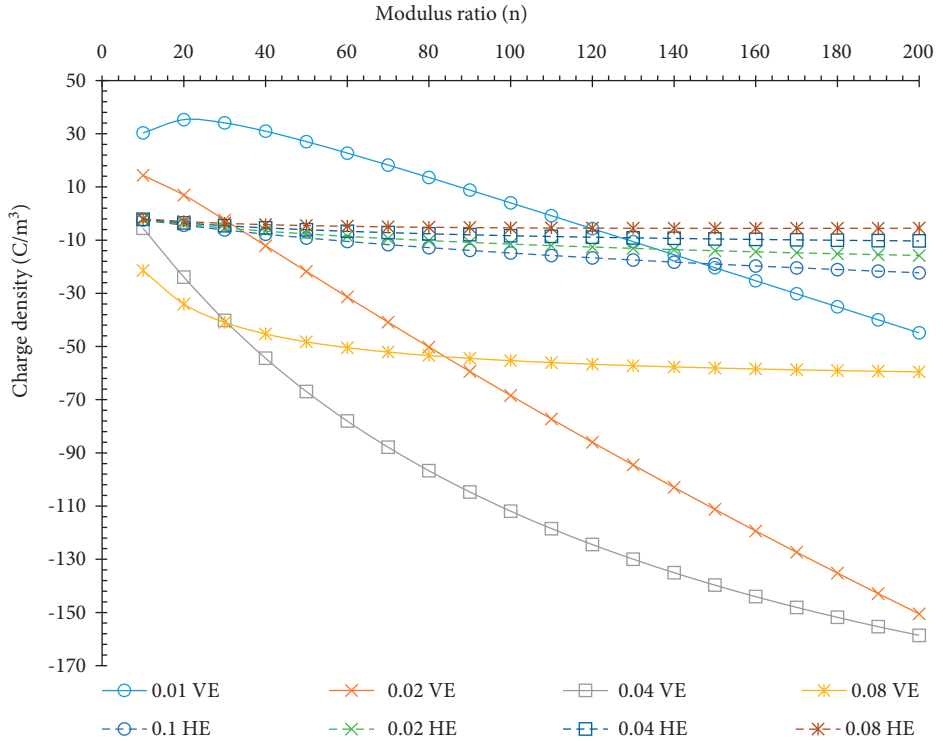

Figure 14: Charge density computed for retaining structure of unit width, piezoelectric strain, modulus ratio, and thickness ratio on the top surface of the horizontally and vertically embedded soft *PZT* patch in the confined granular fill.

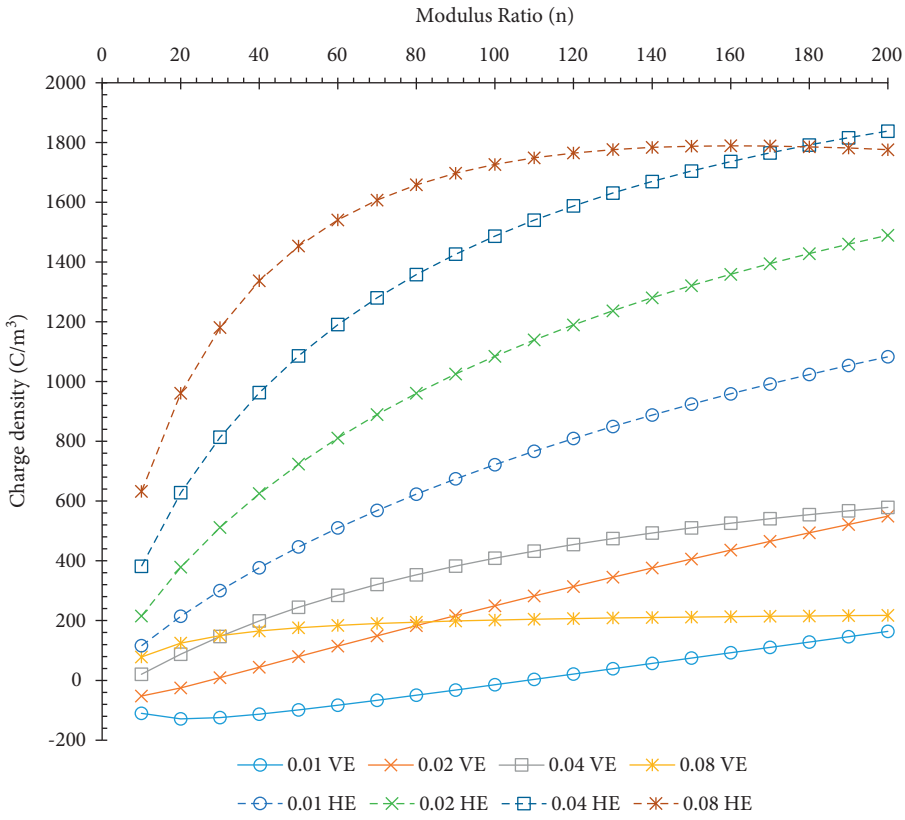

FIGURE 15: Charge density computed for retaining structure of unit width, piezoelectric strain, modulus ratio, and thickness ratio on the bottom surface of the horizontally and vertically embedded soft *PZT* patch in the confined granular fill.

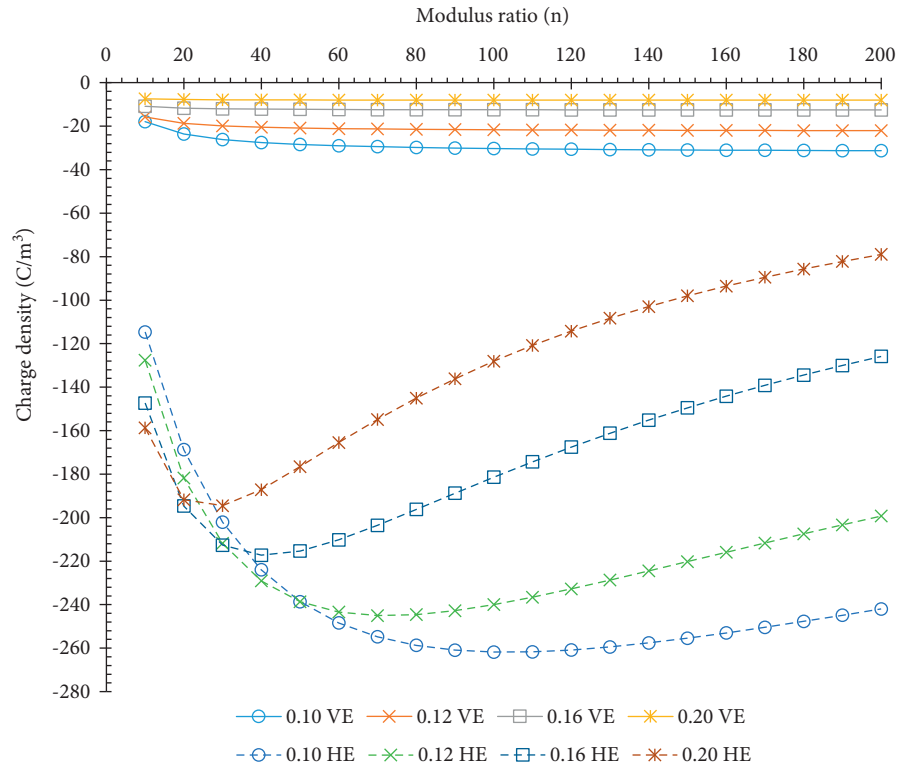

FIGURE 16: Charge density computed for retaining structure of unit width, piezoelectric strain, modulus ratio, and thickness ratio on the top surface of the horizontally and vertically embedded semihard *PZT* patch in the confined granular fill.

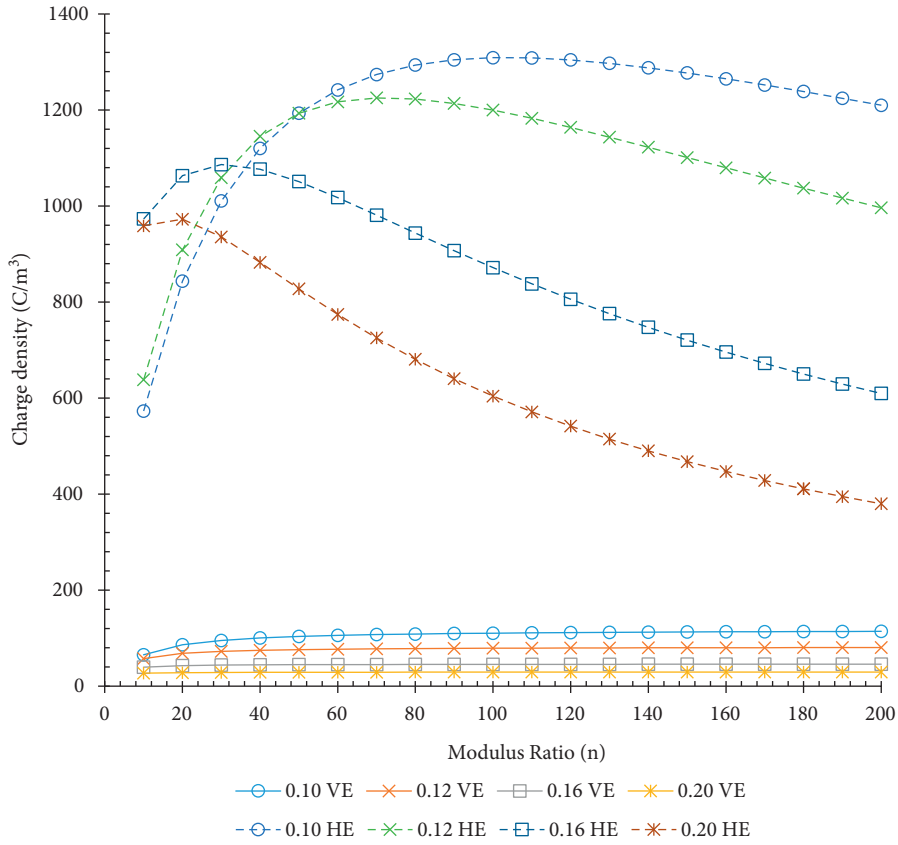

Figure 17: Charge density computed for retaining structure of unit width, piezoelectric strain, modulus ratio, and thickness ratio on the top surface of the horizontally and vertically embedded semihard *PZT* patch in the confined granular fill.

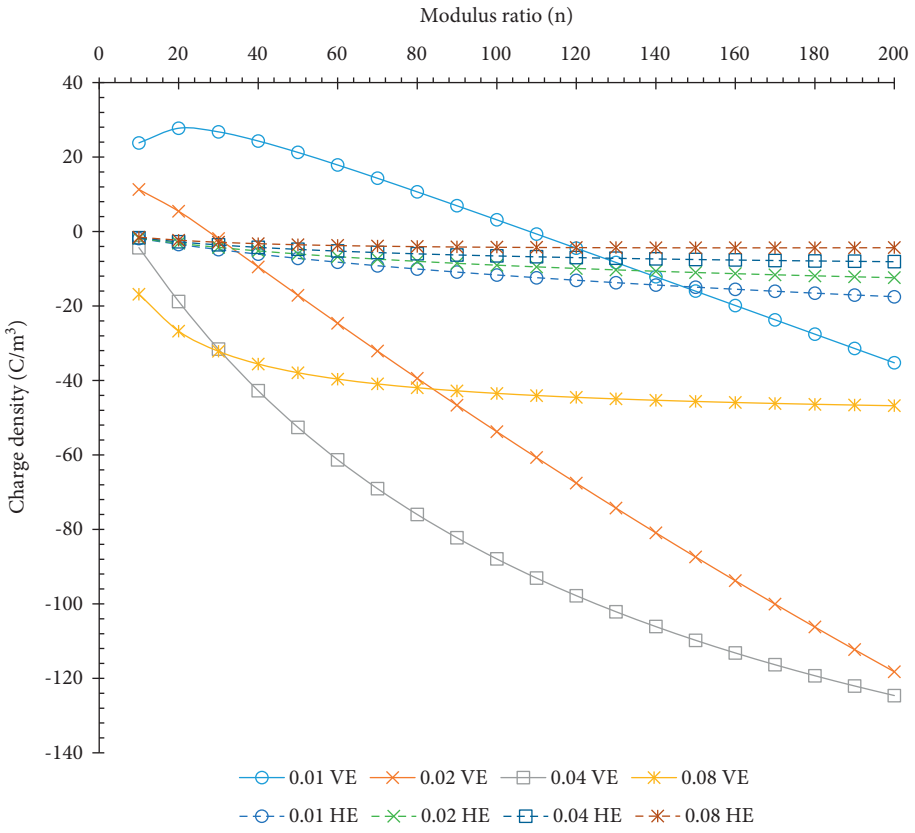

Figure 18: Charge density computed for retaining structure of unit width, piezoelectric strain, modulus ratio, and thickness ratio on the top surface of the horizontally and vertically embedded semihard *PZT* patch in the confined granular fill.

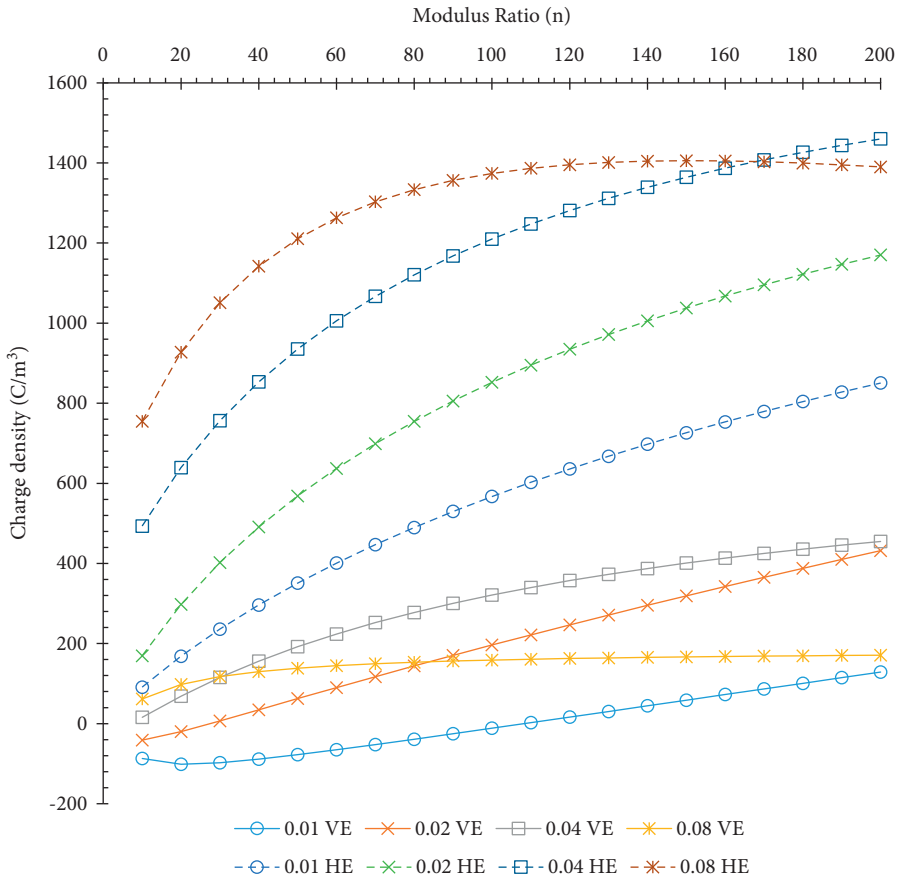

Figure 19: Charge density computed for retaining structure of unit width, piezoelectric strain, modulus ratio, and thickness ratio on the bottom surface of the horizontally and vertically embedded semihard *PZT* patch in the confined granular fill.

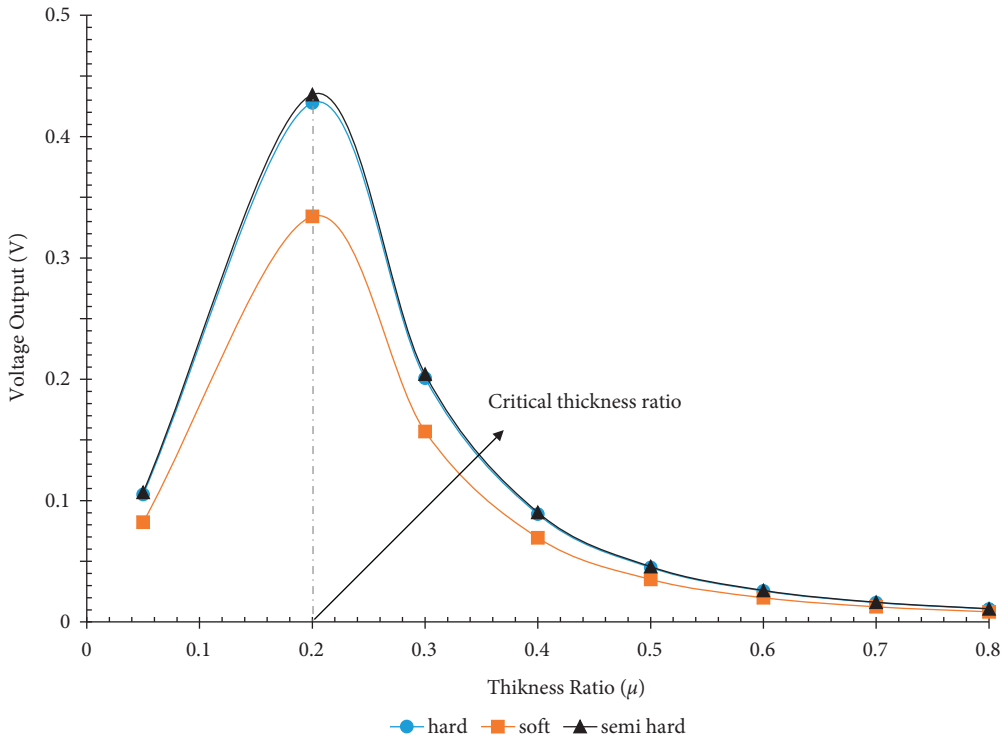

Figure 20: Voltage output computed for the retaining structure, piezoelectric strain constant, polarization ratio (0.112, 0.087, and 0.114), and thickness ratio of horizontally embedded hard, semihard, and soft PZT patch in the confined granular fill.

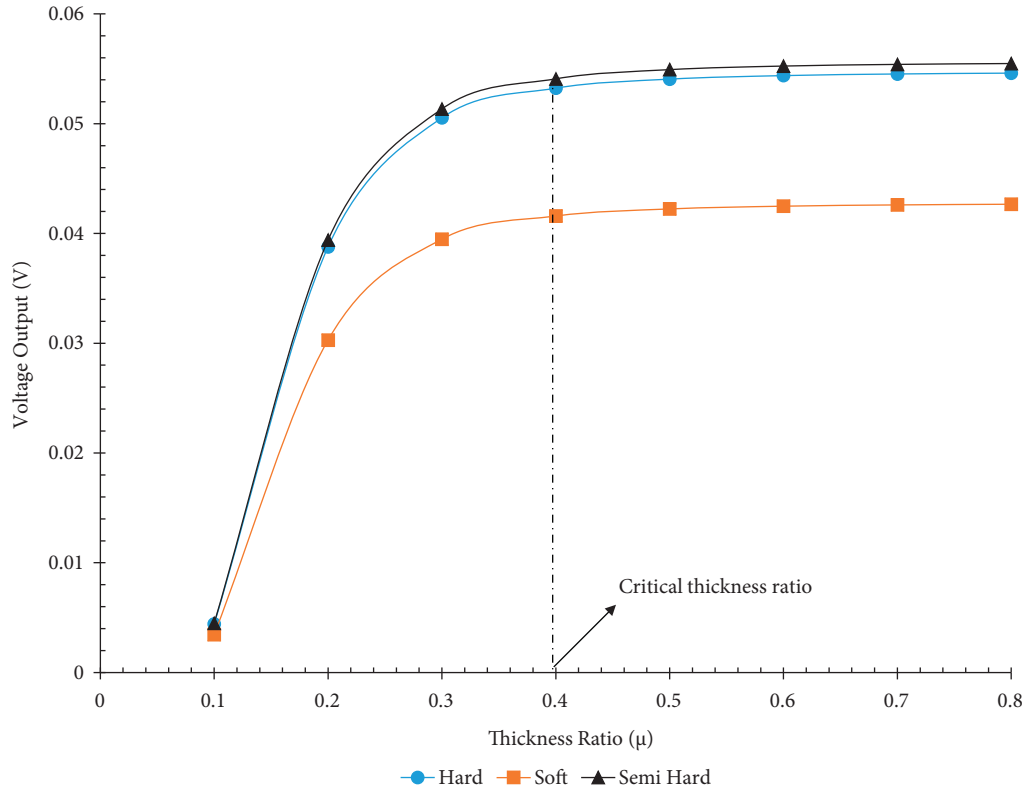

Figure 21: Voltage output computed for the retaining structure, piezoelectric strain constant, polarization ratio (0.112, 0.087, and 0.114) and thickness ratio of vertically embedded hard, semihard, and soft PZT patch in the confined granular fill.

fill affects the average stress in the *PZT* patch. This curve trend owes to the change in the distance between the centroid of the *PZT* patch and the neutral surface. Suppose the thickness ratio is reduced to 0.01. In that case, the maximum stress in the horizontally embedded *PZT* patch is more than five times higher than vertically embedded *PZT* patch. It has been observed that the thickness and material of the wall also affect the strain and stress behaviour of the confined granular fill (equation (4)).

4.1. Charge Density on Hard, Semihard, and Soft PZT Patches. A comparative study is presented for the hard (*H*), semihard (*SH*), and soft (*S*) *PZT* patches to capture the effect of geometric and mechanical parameters on the charge density on the *PZT* patch. The dominant parameters for the analysis are the installation position of the *PZT* patch, the thickness, and the modulus of the backfill material. The engineering properties of the *PZT* patch are shown in Table 2. As a result of the embedment of the *PZT* patch between the pavement and the granular material, the charge is induced on the top and on the bottom surface of the *PZT* patch. The difference between the positive and negative charges is proportional to the energy produced.

Figure 5(a) shows a physical model of the horizontally and vertically embedded *PZT* patch in the confined granular fill. The vibration in the backfill material deforms the horizontal embedded *PZT* patch. The piezoelectric phenomenon generates charge density on the surface of the *PZT* patch. Figures 8–19 show the variation of the charge density for the thickness ratios (μ) in the range of 0.10–0.20. Due to a small polarization ratio (0.114), the lowest charge is generated on the hard *PZT* patch as shown in Figures 8–11. The maximum charge is generated on the semihard (SH) patch as shown in Figures 16–19. Therefore, a semihard *PZT* patch is recommended as an effective piezoelectric material. The results also indicate that the energy efficiency of the output voltage is low for the loose granular fills.

For the vertically embedded *PZT* patch, the maximum charge is generated on the soft *PZT* patch as shown in Figures 12–15. For the thickness ratios (μ) in the range of 0.10–0.20, the results show that the total charge induced on the horizontally embedded *PZT* patch is higher than the vertically embedded patch. It indicates that the geometric parameters, modulus of granular fill, and wall significantly affect the charge density on the top and the bottom surface of the *PZT* patch (equations (17)–(19)).

Table 3 presents the maximum charge density on the top and bottom surfaces of the *PZT* patches for thickness ratios in the range of 0.01–0.08 and 0.10–0.20 based on the alignment of a patch.

4.2. Comparative Analysis of Voltage Output. In this section, the voltage output from different *PZT* patches is analysed by considering the variation of the stress-strain response (equations (20)–(25)). The key parameters influencing voltage output are the polarization, alignment of the *PZT*

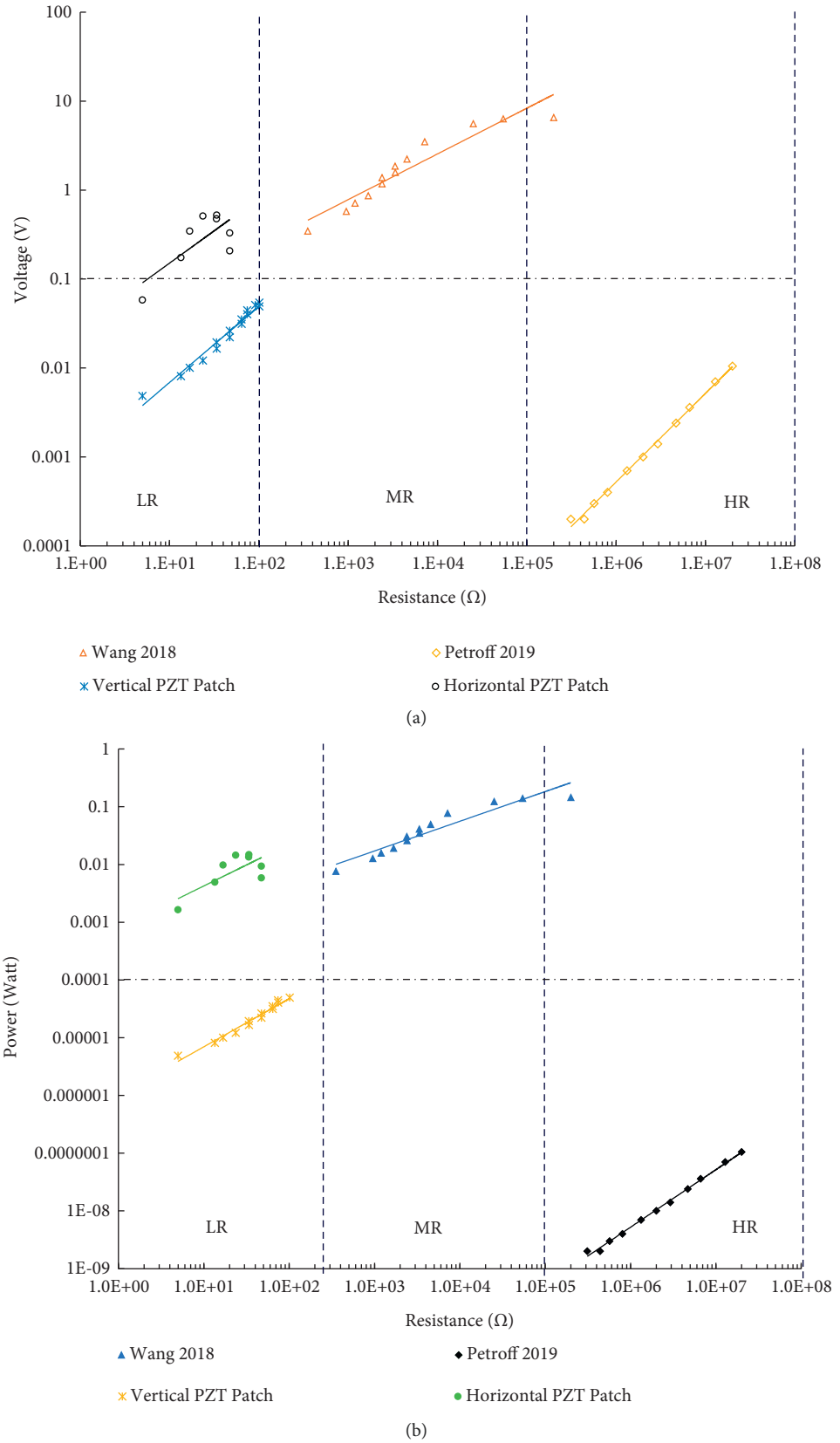

Figure 22: (a) The output voltage for different external resistances for high, medium, and low resistance applications. (b) Power output for different external resistances for high-, medium-, and low-resistance applications.

Table 3: Charge density for confined granular fill with PZT patches.

Alignment of the PZT patch	Maximum charge density at the top surface (Coulombs/m^2)						Maximum charge density at the bottom surface (Coulombs/m^2)					
	H	SH	S	H	SH	S	H	SH	S	H	SH	S
	$0.10 \le \mu \le 0.20$			$0.01 \le \mu \le 0.08$			$0.10 \le \mu \le 0.20$			$0.01 \le \mu \le 0.08$		
Horizontal PZT	−26	−256	−5	−12	−15	−20	0	0	0	0	0	0
	0	0	0	0	0	0	+1080	+1300	+1680	+1200	+1480	+1700
Vertical PZT	−3	−30	−40	−104	−125	−166	0	0	0	+280	-100	+480
	0	0	0	+25	+30	+38	+100	+150	+200	-100	+360	-160

Table 4: Voltage output for various PZT patches.

Type of the PZT patch	Maximum voltage output for horizontally embedded PZT patch (Volt)	Maximum voltage output for vertically embedded PZT patch (Volt)	Difference (%)
Hard (H)	0.44	0.05	159.18
Semihard (SH)	0.56	0.06	161.29
Soft (S)	0.33	0.04	156.75

Table 5: Classification of *PZT* applications for output voltage and resistance.

Description	ξ	η	Output voltage (Volt)	Resistance (Ω)	Classification
A flexible piezoelectric energy harvester[a]	5E-10	0.996	10^{-4}–10^{-1}	10^{8}–10^{5}	High-resistance applications (HRA)
A two-degree freedom system with the piezoelectric element[b]	0.0224	0.514	10^{-1}–10^{1}	10^{5}–10^{2}	Medium-resistance applications (MRA)
Horizontally embedded PZT patch[c]	0.001	0.8561	10^{-1}–1	10^{2}–1	Low-resistance applications (LRA)
Vertically embedded PZT patch[d]	0.0282	0.7274	10^{-3}–10^{-1}	10^{2}–1	Low-resistance applications (LRA)

[a]Petroff et al. [42]; [b]Wang et al. [13]; [c, d]present study.

patch, thickness ratio, and material properties. The polarization of the *PZT* patch depends on the piezoelectric strain and the relative permittivity of the *PZT* material. The comparison of the voltage output of the hard, semihard, and soft PZT patches is shown in Figures 20 and 21. As the thickness of the retaining wall increases, the voltage output increases up to a critical thickness ratio. A critical thickness ratio is defined as a ratio of the thickness of the granular fill to that of *PZT* patch at which the maximum energy is harvested.

Figures 20–21 show a graphical representation of the voltage output at various thickness ratios. The semihard *PZT* patch shows the highest voltage output due to the highest polarization ratio of 0.114. At the critical thickness ratios of 0.2 and 0.4, the maximum voltage is obtained for horizontally and vertically aligned patches, respectively, as shown in Table 4. The maximum voltage output observed for horizontally embedded patches is 0.44, 0.56, and 0.33 volt. Similarly, for vertically embedded *PZT* patch voltage output is 0.05, 0.06, and 0.04 volt for hard, semihard, and soft *PZT* patches, respectively. The variation in output voltage indicates that interaction between the *PZT* patch and the retaining wall strongly influences the energy output from the confined granular fill.

4.3. Effect of External Resistance on Power Output of the PZT Patch. This section shows the effect of external resistance on the voltage and power output of the *PZT* patch as per its alignment in the granular fill. Figure 22(a) shows the magnitude of voltage output for the different external resistances. The magnitude of voltage increases logarithmically until a peak voltage of 56 mV for the horizontally embedded *PZT* patch and 6 μV for the vertically embedded *PZT* patch. The magnitude of the voltage output from experimental data from Wang et al. [13] and Petroff et al. [42] is appropriate for MRA and HRA, respectively. Eq. (26) shows a generalized relationship for the output voltage based upon a set of design parameters considered by the present study. An empirical relationship of output voltage for high, medium, and low resistance applications for varying design parameters is expressed as

$$V = \xi R^{\eta}. \tag{26}$$

The variables ξ and η depend upon the design parameters, namely polarization, modulus ratio, position of the *PZT* patch, strain, geometrical, and engineering properties of the confined granular fill and retaining structure. The response of the *PZT* patch can be optimized by changing the design parameters and mechanical properties. Table 5 shows

the classification of the application of *PZT* patches based on the voltage output for external resistance. Based on the range of external resistance, the applications of *PZT* patches are classified as low resistance, medium resistance, and high resistance applications.

Figure 22(b) illustrates the magnitude of the power of the present work, and experiment results from the literature are plotted with high medium and low resistance applications. The higher power output is observed for the horizontally embedded *PZT* patch for the same range of the external resistance. The alignment of the *PZT* patch significantly affects the voltage and power output due to the vertical and lateral vibrations due to dynamic loads.

5. Conclusion

A quantitative estimate of piezoelectric voltage output depends upon the stress-strain response of confined granular fill, retaining structure, and *PZT* patches. The stress distribution in the embedded *PZT* patch is affected by the alignment, thickness, and modulus of the material. Three types of PZT patches, namely hard, semihard, and soft *PZT* patches, have been considered to evaluate charge density and voltage output. The conclusions of this study are summarized as follows:

(i) The charge density is significantly affected by the parameters, namely modulus ratio, the magnitude of strain, placement of *PZT* patch, relative permittivity, and polarization of the *PZT* patch.

(ii) Once the *PZT* patches are embedded horizontally, the maximum charge density is observed to be more than three times compared to the vertically embedded *PZT* patches for a set of numerical parameters.

(iii) The maximum voltage output was obtained for the thickness ratio of 0.2–0.6. The voltage output for the horizontally and vertically embedded hard, semihard, and soft PZT patches is obtained in the range of 0.01–0.5 volts and 0.001–0.06 volts, respectively.

(iv) The magnitude of voltage increases logarithmically until a peak voltage of 56 mV for the horizontally embedded *PZT* patch and 6 μV for the vertically embedded *PZT* patch.

(v) A relationship for voltage and power output has been proposed for wide-ranging engineering implements classified as low (LRA), medium (MRA), and high (HRA) resistance applications.

This study considers a comprehensive set of design parameters for selecting *PZT* patches for the voltage output. It provides a framework for evaluating power outputs from confined granular fill and improving the conversion efficiency from the strain fluctuations, polarization per unit permittivity, and geometric properties, which play a significant role in the structural health monitoring of the pavement and retaining structures. The observed voltage output is found appropriate for wide-ranging resistance applications. It is proposed to be up-scaled using multiple patches embedded throughout the confined granular fill subjected to continuous dynamic loads.

Abbreviations

PZT:	Lead zirconate titanate
ε_{HE}:	Strain in horizontally embedded PZT patch
σ_{PZT}:	The stress in the PZT patch
σ_{HE}:	Stress in horizontally embedded PZT patch
ε_{VE}:	Strain in vertically embedded PZT patch
ρ_{Top}, ρ_{Bottom}:	Charge density at the top and bottom surfaces of the *PZT* patch, respectively
$\rho_{\text{THE}}, \rho_{\text{BHE}}$:	Charge density at the top and bottom surfaces of the horizontally embedded PZT patch, respectively
Q_{Top}, Q_{Bottom}:	Charge quantity at the top and bottom surfaces of the PZT patch, respectively
$Q_{\text{THE}}, Q_{\text{BHE}}$:	Charge quantity at the top and bottom surfaces of the horizontally embedded PZT patch, respectively
$\rho_{\text{TVE}}, \rho_{\text{BVE}}$:	Charge density function at the top and bottom surfaces of the vertically embedded PZT patch, respectively
$Q_{\text{TVE}}, Q_{\text{BVE}}$:	Charge quantity at the top and bottom surfaces of the vertically embedded PZT patch, respectively
h_w:	Thickness of the wall
μ:	Thickness ratio of PZT patch and backfill (h_P/h_R)
a:	The thickness ratio of the retaining wall and PZT patch (h_w/h_P)
b:	The modulus ratio of retaining wall and PZT patch (E_w/E_P)
$D3$:	Electric displacement
$\varepsilon_{33}^T/\varepsilon_o$:	Relative permittivity
ε_0:	The absolute permittivity of the vacuum
ε_{33}^T:	The permittivity of the material in direction-33 under constant stress
$\varepsilon_{33}^{T=0}$:	The free permittivity of the material in direction-33 under no stress
d31:	Piezoelectric strain constant in the mode 31
d33:	Piezoelectric strain constant in the mode 33
d:	Depth of embedment of PZT patch
z:	The thickness direction coordinate from the neutral plane
e:	Distance between the neutral axis and lower surface of the PZT patch
E:	Equivalent electric field intensity
K:	Constant of proportionality
VE:	Subscript for vertically embedded patch
HE:	Subscript for horizontally embedded patch
EP:	Modulus of the PZT patch
EW:	Modulus of the retaining wall
H:	Height of the retaining structure
L:	Length of the retaining structure
hP:	Thickness of the PZT patch
hR:	Thickness of the granular backfill
n :	Modulus ratio of *PZT* patch and backfill (E_P/E_R)

V_{HE}: The voltage output for horizontally embedded *PZT* patch

V_{VE}: The voltage output for vertically embedded PZT patch

Appendix

Derivation of Equations for Stress Strain, Charge Density, and Voltage Output of *PZT* Patch

Stress-Strain Analysis for PZT Patch. The stress of confined granular fill is a product of the strain and Young's modulus of the material of the layer. The strain in *PZT* and granular fill depends on the location of the neutral surface [52] of the composite structure; thus, the magnitude of stress strain is expressed as

$$\sigma_z = E_i \varepsilon_z, \varepsilon_z = \frac{z}{R}. \tag{A.1}$$

The relation between the radius of curvature due to small deformation in the layer and stress is expressed as

$$\frac{1}{R} = \frac{M}{EI}, M = -\iint_A z\sigma \, dA, I = \iint_A z^2 \mathrm{d}A, \tag{A.2}$$

where I is the moment of inertia of the composite structure with *PZT* patches and M is the bending moment.

The moment of inertia of the retaining structure is expressed as a composite beam [52]. From equations (A.1) and (A.2), the strain is expressed as

$$\varepsilon_z = \frac{M_z z}{E_i I}. \tag{A.3}$$

The average strain in the middle surface of the vertically embedded *PZT* patch is expressed as

$$\varepsilon_{VE} = \frac{M\left(\overline{z} - z_p\right)}{E_p I_p + E_R I_R + E_w I_w}, \tag{A.4}$$

where $\overline{z} = \sum A_i z_i / \sum A_i$, and $E_w = bE_p$, $h_w = ah_p$, and the neutral surface location of the confined granular fill and retaining structure is expressed as

$$\left(\overline{z} - z_p\right) = \frac{h_s\left(3\mu + 2 - 12a^2 b\mu^2 n\right)}{24\mu n(ab+1) + 1}, \tag{A.5}$$

$$\varepsilon_{VE} = \frac{M}{E_s H}\left[\frac{\left(\overline{z} - z_p\right)}{\left\{nh_p^3/12\left(1 + ba^3\right) + h_s^3/36\right\} + \left(\overline{z} - z_p\right)^2\left\{nh_p(1+ab) + h_s/2\right\}}\right], \tag{A.6}$$

where μ is the ratio of the thickness of *PZT* to the backfill (h_P/h_R), n is the ratio of the modulus of the *PZT* patch and the backfill (E_P/E_R), a is the thickness ratio of retaining wall and *PZT* patch (h_w/h_P), and b is the modulus ratio of retaining wall and *PZT* patch (E_w/E_P).

From equations (A.1) and (A.6), the total stress on the *PZT* patch is expressed as

$$\sigma_{VE} = \frac{ME_p}{E_s H}\left[\frac{\left(\overline{z} - z_p\right)}{\left\{nh_p^3/12\left(1 + ba^3\right) + h_s^3/36\right\} + \left(\overline{z} - z_p\right)^2\left\{nh_p(1+ab) + h_s/2\right\}}\right]. \tag{A.7}$$

Similarly, the average strain can be calculated for the horizontal embedded *PZT* patch.

Charge Density and Voltage. The electromechanical piezoelectric coupling constitutive equation [49] is expressed as

$$D_3 = d_{31}\sigma_{PZT} + \varepsilon_{33}^T E_3. \tag{A.8}$$

According to the stress relationship equation (A.1), the piezoelectric coupling constitutive equation, when the external applied electrical energy is zero ($E_3 = 0$), the lateral electric displacement of the top and bottom surfaces of the *PZT* patch [53], the charge density is expressed as

$$\rho_{\mathrm{Top}} = D_3\left(x, e + h_P\right) = d_{31}\sigma_{PZT}, \tag{A.9}$$

where h_P is the thickness of the *PZT* patch, e is the distance between the neutral plane and interface of the *PZT* patch and granular fill, d_{31} is the piezoelectric strain constant, and σ_{PZT} is average stress on the surface of the *PZT* patch (equation (A.1)). The total quantity of the charge on the top surface of the *PZT* patch has been evaluated by integrating equation (A.2) as

$$Q_{\mathrm{Top}} = \int_0^L bD_3\left(x, e + h_P\right)\mathrm{d}x. \tag{A.10}$$

Similarly, the charge density (equation (A.4)) and total charge quantity on the bottom surface (equation (A.5)) are expressed as

$$\rho_{\text{Bottom}} = -D_3(x,e) = d_{31}\sigma_{PZT}. \tag{A.11}$$

$$Q_{\text{Bottom}} = \int_0^L bD_3(x,e)\mathrm{d}x. \tag{A.12}$$

Thus, by calculating the total charge quantity due to stress on the surface of the *PZT* patch, the open-circuit voltage between the top and bottom surfaces is expressed as

$$V = \int_e^{e+\delta} E(x,z)\mathrm{d}z = \frac{1/2h_P\left(\left|Q_{\text{Top}}\right| + \left|Q_{\text{Bottom}}\right|\right)}{bL\left(\varepsilon_{33}^T/\varepsilon_o\right)}. \tag{A.13}$$

where $\varepsilon_{33}^T/\varepsilon_o$ is the relative permittivity of the piezoelectric material.

Data Availability

All data, models, and code generated or used during the study are included within the article.

Conflicts of Interest

The authors declare that they have no conflicts of interest.

Acknowledgments

The financial support received under the research project entitled "Energy Harvesting through Mechanical Vibrations Generated in Retaining Structure" (grant: F. No. DTU/IRD/619/2105) of Delhi Technological University, Delhi, is thankfully acknowledged.

References

[1] A. García-Olivares, J. Solé, and O. Osychenko, "Transportation in a 100% renewable energy system," *Energy Conversion and Management*, vol. 158, pp. 266–285, 2018.

[2] S. R. Anton and H. A. Sodano, "A review of power harvesting using piezoelectric materials (2003-2006)," *Smart Materials and Structures*, vol. 16, no. 3, pp. R1–R21, 2007.

[3] V. Singh, D. Meena, H. Sharma, A. Trivedi, and B. Singh, "Investigating the role of chalcogen atom in the piezoelectric performance of PVDF/TMDCs based flexible nanogenerator," *Energy*, vol. 239, Article ID 122125, 2022.

[4] S. D. Bahador and Y. Yaowen, "Monitoring hydration of concrete with piezoelectric transducers," in *Proceedings of the 35th Conference on Our World in Concrete & Structures*, Singapore, October 2010.

[5] B. Xu, T. Zhang, G. Song, and H. Gu, "Active interface debonding detection of a concrete-filled steel tube with piezoelectric technologies using wavelet packet analysis," *Mechanical Systems and Signal Processing*, vol. 36, no. 1, pp. 7–17, 2013.

[6] D. Xu, S. Banerjee, Y. Wang, S. Huang, and X. Cheng, "Temperature and loading effects of embedded smart piezoelectric sensor for health monitoring of concrete structures," *Construction and Building Materials*, vol. 76, pp. 187–193, 2015.

[7] A. Erturk and D. J. Inman, "On mechanical modeling of cantilevered piezoelectric vibration energy harvesters," *Journal of Intelligent Material Systems and Structures*, vol. 19, no. 11, pp. 1311–1325, 2008.

[8] H. A. Sodano, D. J. Inman, and G. Park, "A review of power harvesting from vibration using piezoelectric materials," *The Shock and Vibration Digest*, vol. 36, no. 3, pp. 197–205, 2004.

[9] S. P. Beeby, M. J. Tudor, and N. M. White, "Energy harvesting vibration sources for microsystems applications," *Measurement Science and Technology*, vol. 17, no. 12, pp. R175–R195, 2006.

[10] A. Erturk, "Piezoelectric energy harvesting for civil infrastructure system applications: moving loads and surface strain fluctuations," *Journal of Intelligent Material Systems and Structures*, vol. 22, no. 17, pp. 1959–1973, 2011.

[11] M. Rhimi and N. Lajnef, "Tunable energy harvesting from ambient vibrations in civil structures," *Journal of Energy Engineering*, vol. 138, no. 4, pp. 185–193, 2012.

[12] P. Cahill, A. Mathewson, and V. Pakrashi, "Experimental validation of piezoelectric energy-harvesting device for built infrastructure applications," *Journal of Bridge Engineering*, vol. 23, no. 8, Article ID 04018056, 2018.

[13] D. W. Wang, J. L. Mo, X. F. Wang, H. Ouyang, and Z. R. Zhou, "Experimental and numerical investigations of the piezoelectric energy harvesting via friction-induced vibration," *Energy Conversion and Management*, vol. 171, pp. 1134–1149, 2018.

[14] H. Roshani, P. Jagtap, S. Dessouky, A. Montoya, and A. T. Papagiannakis, "Theoretical and experimental evaluation of two roadway piezoelectric-based energy-harvesting prototypes," *Journal of Materials in Civil Engineering*, vol. 30, no. 2, Article ID 04017264, 2017.

[15] F. Chen, R. Balieu, E. Córdoba, and N. Kringos, "Towards an understanding of the structural performance of future electrified roads: a finite element simulation study," *International Journal of Pavement Engineering*, vol. 20, no. 2, pp. 204–215, 2019.

[16] P. Liu, Q. Zhao, H. Yang et al., "Numerical study on influence of piezoelectric energy harvester on asphalt pavement structural responses," *Journal of Materials in Civil Engineering*, vol. 31, Article ID 04019008, 2019.

[17] L. Guo and Q. Lu, "Modeling a new energy harvesting pavement system with experimental verification," *Applied Energy*, vol. 208, pp. 1071–1082, 2017.

[18] H. Yang, Q. Zhao, X. Guo, W. Zhang, P. Liu, and L. Wang, "Numerical analysis of signal response characteristic of piezoelectric energy harvesters embedded in pavement," *Materials*, vol. 13, no. 12, p. 2770, 2020.

[19] H. Roshani and S. Dessouky, "Feasibility Study to Harvest Electric Power from Highway Pavements Using Laboratory Investigation," *Department of Civil and Environmental Engineering University of Texas at San Antonio*, 2015.

[20] D. Hill, A. Agrawal, and N. Tong, *Assessment of Piezoelectric Materials for Roadway Energy Harvesting, Report Prepared by DNV KEMA Energy and Sustainability Inc. For the California Energy Commission*, KEMA, Mumbai, 2013.

[21] L. Guo and Q. Lu, "Potentials of piezoelectric and thermoelectric technologies for harvesting energy from pavements," *Renewable and Sustainable Energy Reviews*, vol. 72, pp. 761–773, 2017.

[22] Y. Yang, Q. Shen, J. Jin, Y. Wang, W. Qian, and D. Yuan, "Rotational piezoelectric wind energy harvesting using

impact-induced resonance," *Applied Physics Letters*, vol. 105, no. 5, Article ID 053901, 2014.

[23] N. Rezaei-Hosseinabadi, A. Tabesh, R. Dehghani, and A. Aghili, "An efficient piezoelectric windmill topology for energy harvesting from low-speed air flows," *IEEE Ind. Electron. Mag.*vol. 62, no. 6, pp. 3576–3583, 2014.

[24] V. C. Sousa, M. de M Anicézio, C. De Marqui, and A. Erturk, "Enhanced aeroelastic energy harvesting by exploiting combined nonlinearities: theory and experiment," *Smart Materials and Structures*, vol. 20, no. 9, Article ID 094007, 2011.

[25] R. Murray and J. Rastegar, "Novel two-stage piezoelectric-based ocean wave energy harvesters for moored or unmoored buoys," *Int. Soc. Opt. Eng.*vol. 7288, Article ID 72880E, 2009.

[26] K. A. Cunefare, E. A. Skow, A. Erturk, J. Savor, N. Verma, and M. R. Cacan, "Energy harvesting fro m hydraulic pressure fluctuations," *Smart Materials and Structures*, vol. 22, no. 2, Article ID 025036, 2013.

[27] X. D. Xie, Q. Wang, and S. J. Wang, "Energy harvesting from high-rise buildings by a piezoelectric harvester device," *Energy*, vol. 93, pp. 1345–1352, 2015.

[28] X. Li and V. Strezov, "Modelling piezoelectric energy harvesting potential in an educational building," *Energy Conversion and Management*, vol. 85, pp. 435–442, 2014.

[29] S. W. Kim, B. G. Jeon, N. S. Kim, and J. C. Park, "Vision-based monitoring system for evaluating cable tensile forces on a cable-stayed bridge," *Structural Health Monitoring*, vol. 12, no. 5-6, pp. 440–456, 2013.

[30] Ö. Zorlu, E. T. Topal, and H. Külah, "A vibration-based electromagnetic energy harvester using mechanical frequency up-conversion method," *IEEE Sensors Journal*, vol. 11, no. 2, pp. 481–488, 2010.

[31] S. P. Beeby, R. N. Torah, M. J. Tudor et al., "A micro electromagnetic generator for vibration energy harvesting," *Journal of Micromechanics and Microengineering*, vol. 17, no. 7, pp. 1257–1265, 2007.

[32] K. Sasaki, Y. Osaki, J. Okazaki, H. Hosaka, and K. Itao, "Vibration-based automatic power-generation system," *Microsystem Technologies*, vol. 11, no. 8, pp. 965–969, 2005.

[33] P. Glynne-Jones, M. J. Tudor, S. P. Beeby, and N. M. White, "An electromagnetic, vibration-powered generator for intelligent sensor systems," *Sensors Actuators, A Phys.*vol. 110, no. 1-3, pp. 344–349, 2004.

[34] H. Wang, A. Jasim, and X. Chen, "Energy harvesting technologies in roadway and bridge for different applications–A comprehensive review," *Applied Energy*, vol. 212, pp. 1083–1094, 2018.

[35] Z. Jiang, J. Cai, and P. S. Moses, "Smoothing control of solar photovoltaic generation using building thermal loads," *Applied Energy*, vol. 277, Article ID 115523, 2020.

[36] A. Zahedi, "Solar photovoltaic (PV) energy; latest developments in the building integrated and hybrid PV systems," *Renewable Energy*, vol. 31, no. 5, pp. 711–718, 2006.

[37] T. Nordmann, A. Froelich, A. Goetzberger et al., "The potential of PV noise barrier technology in Europe," in *Sixteenth European Photovoltaic Solar Energy Conference*, pp. 2912–2916, Routledge, Milton Park, Abingdon-on-Thames, 2020.

[38] F. Chen, N. Taylor, R. Balieu, and N. Kringos, "Dynamic application of the Inductive Power Transfer (IPT) systems in an electrified road: dielectric power loss due to pavement materials," *Construction and Building Materials*, vol. 147, pp. 9–16, 2017.

[39] H. Zhao, J. Ling, and J. Yu, "A comparative analysis of piezoelectric transducers for harvesting energy from asphalt pavement," *Journal of the Ceramic Society of Japan*, vol. 120, no. 1404, pp. 317–323, 2012.

[40] X. Ren, "Large electric-field-induced strain in ferroelectric crystals by point-defect-mediated reversible domain switching," *Nature Materials*, vol. 3, no. 2, pp. 91–94, 2004.

[41] B. Singh, D. Varandani, and B. R. Mehta, "Effect of conductive atomic force microscope tip loading force on tip-sample interface electronic characteristics: unipolar to bipolar resistive switching transition," *Applied Physics Letters*, vol. 103, no. 5, Article ID 051604, 2013.

[42] C. A. Petroff, T. F. Bina, and G. R. Hutchison, "Highly tunable molecularly doped flexible poly(dimethylsiloxane) foam piezoelectric energy harvesters," *ACS Applied Energy Materials*, vol. 2, no. 9, pp. 6484–6489, 2019.

[43] Physik Instrumente (Pi) GmbH, "Co. KG," *CAT 125E R3 Piezoelectric Ceramic Products*, Karlsruhe, Germany, 2011.

[44] R. A. Islam and S. Priya, "Realization of high-energy density polycrystalline piezoelectric ceramics," *Applied Physics Letters*, vol. 88, no. 3, Article ID 032903, 2006.

[45] N. Kumari and A. Trivedi, "Application of semi-active control strategy for the wall retaining granular fills," *Springer Series in Geomechanics and Geoengineering*, vol. 13, pp. 978–982, 2018.

[46] N. Kumari and A. Trivedi, "Vibration control of flexible retention systems," *Lecture Notes in Civil Engineering*, Springer, no. 56, , pp. 529–539, Singapore, 2020.

[47] G. Park, T. Rosing, M. D. Todd, C. R. Farrar, and W. Hodgkiss, "Energy harvesting for structural health monitoring sensor networks," *Journal of Infrastructure Systems*, vol. 14, no. 1, pp. 64–79, 2008.

[48] L. Mateu and F. Moll, "Review of energy harvesting techniques and applications for microelectronics," *VLSI Circuits and Systems II*, vol. 5837, pp. 359–374, 2005.

[49] A. Meitzler, H. Tiersten, A. Warner, D. Berlincourt, G. Couqin, and F. Welsh, *IEEE Standard on Piezoelectricity*, pp. 176–1987, IEEE Ultrasonics, Ferroelectrics, and Frequency Control Society, Metropolitan Area, France, 1988.

[50] Y. Amini, M. Heshmati, P. Fatehi, and S. E. Habibi, "Energy harvesting from vibrations of a functionally graded beam due to moving loads and moving masses," *Journal of Engineering Mechanics*, vol. 143, no. 9, Article ID 04017063, 2017.

[51] I. Chopra, "Review of state of art of smart structures and integrated systems," *AIAA Journal*, vol. 40, no. 11, pp. 2145–2187, 2002.

[52] M. Kerboua, M. Benguediab, A. A.Megnounif, K. H. Benrahou, and F. Kaoulala, "Semi active control of civil structures, analytical and numerical studies," *Physics Procedia*, vol. 55, pp. 301–306, 2014.

[53] G. Zhang, S. Gao, and H. Liu, "A utility piezoelectric energy harvester with low frequency and high-output voltage: theoretical model, experimental verification and energy storage," *AIP Advances*, vol. 6, no. 9, Article ID 095208, 2016.

Journal of Energy Storage 52 (2022) 105002

Contents lists available at ScienceDirect

Journal of Energy Storage

journal homepage: www.elsevier.com/locate/est

Research Paper

Financial feasibility of concentrated solar power with and without sensible heat storage in hot and dry Indian climate

Naman Goyal [a], Akshansh Aggarwal [a], Anil Kumar [a,b,*]

[a] Department of Mechanical Engineering, Delhi Technological University, Delhi 110 042, India
[b] Centre for Energy and Environment, Delhi Technological University, Delhi 110 042, India

ARTICLE INFO

Keywords:
Financial feasibility
Concentrated solar power
Thermal energy storage
Net present value
Hot and dry climate
System Advisor Model

ABSTRACT

The present work assesses the economic feasibility of Concentrated Solar Power plants employing 3 different technologies – PTC, SPT and LFR with two different plant capacities of 50 MW and 100 MW for Jodhpur (annual average DNI of 2237 kWh/m^2). CSP plants are economically analysed both with and without thermal energy storage system (8 h of storage). System Advisor Model (SAM) software has been used for the study employing the recent regulatory policies as provided by the Central Electricity Regulatory Commission (CERC) in 2016. Financial parameters, namely Net Present Value (NPV), Discounted Payback Period (DPP), Payback Period (PBP), and Levelized cost of electricity (LCOE), have been calculated to get a crude economic comparison of the plants taken under consideration. CUF and annual generation of all the plants were observed to have increased when fitted with thermal storage. Highest NPV is 6940. 4 million ₹ (93.55 million $) for a 50 MW PTC plant with storage while the lowest LCOE calculated is 9.27 ₹ (0.125 $)/kWh for a 50 MW LFR plant without thermal storage. Findings of this study would enable an appropriate selection and installation of a solar project for the country's hot and dry climatic regions. Applied assessment methods can also aid the investors and decision-makers in better understanding the upcoming CSP projects' financial viability beforehand.

1. Introduction

Energy is often referred to as the currency for development and technology. Global energy demand has shown unprecedented growth in past decade, led by the developing countries. The rise in demand reflects rapid industrialization, increasing populations, global economic expansion, and urbanization [1]. However, due to health crises caused by Covid-19 in recent years, a decline of 3.8% in global energy demand was observed during the first quarter of 2020. As per data analysis done by the International Energy Agency (IEA), countries that imposed a full lockdown experienced a mean decline of 25% in energy demand per week, while the nations imposing the partial lockdowns showed an average decline of 18%. Even though other energy sources showed a decline in demand, Renewables sources of energy were the only ones that displayed growth in demand due to the priority dispatch and the larger installed capacity [2]. Renewable energy posted 2019 as another year of record-breaking, as the installed power capacity displayed a growth exceeding 200 gigawatts (GW). Investments and capacity installations spread continuously throughout all the corners of world. The demand for renewables is further expected to increase majorly due to the

Abbreviations: °C, degree Celsius; Al, aluminium; BCR, benefit-cost ratio; C_{an}, CSP power plant's annual cash flow.; CERC, Central Electricity Regulatory Commission; CF_{csp}, capacity factor; CI, cash inflow; CI_y, cash inflow of yth year; CLFR, compact linear Fresnel reflector; CO, cash outflow; CRF, capital recovery factor; CSP, concentrated solar power; Cu, copper; CWET, Centre for Wind Energy Technology; C_y, operation and maintenance cost; d, discount rate; DNI, direct normal irradiance; DPBP, discounted payback period; Fe, iron; GHI, Global Horizontal Irradiance; GW, gigawatts; HFC, heliostat field collectors; HTF, heat transfer fluid; IEA, International Energy Agency; IMD, India Meteorological Department; IRR, internal rate of return; kWh/m^2, kilowatt-hour per square meter; LCOE, levelized cost of energy; LFR, linear Fresnel reflectors; LFRS, linear Fresnel reflector with storage; MNRE, Ministry of New and Renewable Energy; NASA – POWER, National Aeronautics and Space Administration – Prediction of Worldwide Energy Resources; NPV, net present value; NREL, National Renewable Energy Laboratory; NREL-SEC, National Renewable Energy Laboratory – Solar Energy Centre; PCM, phase change materials; P_{csp}, CSP plant's net capacity; PDC, parabolic dish collectors; PM KUSUM, Pradhan Mantri Kisan Urja Suraksha Evam Utthaan Mahabhiyaan; PTC, parabolic trough collectors; PTCS, parabolic trough collector with storage; PV, photovoltaic; R&D, research and development; SAM, System Advisor Model; SPT, solar power towers; SPTS, solar power tower with storage; TEA, techno-economic analysis; TES, thermal energy storage; TWh/year, terawatt-hour per square meter; UCE_y, unit cost of electricity in the yth year; USD, United States dollar.

* Corresponding author at: Department of Mechanical Engineering, Delhi Technological University, Delhi 110 042, India.
E-mail address: anilkumar76@dtu.ac.in (A. Kumar).

https://doi.org/10.1016/j.est.2022.105002
Received 7 September 2021; Received in revised form 17 May 2022; Accepted 27 May 2022
Available online 2 June 2022
2352-152X/© 2022 Elsevier Ltd. All rights reserved.

low operation costs. Latest capacity growth and few new projects which will come online in the coming years would also boost the output [3]. Among all the options in renewable energy sources, solar energy has shown significant growth and contribution to meeting global energy demand. Solar energy can be converted into useful energy via the Photovoltaic (PV) system, which utilizes incident light energy from the sun and the Concentrated Solar Power (CSP) system, which converts absorbed thermal energy from the concentrated incident rays into electricity. Awan [4] did a comparative analysis between 100 MW CSP and PV. Plants employing PV system have better economic performance, while those using CSP systems displayed better technical performance. However, CSP trumps PV when two systems are compared in terms of holistic sustainability. Marcin et al. [5] found that making PV cells consume far more energy than what the cells could generate, which from a global perspective indicated a negative balance. Even the disposal of these cells causes adverse effects on the environment. This marks CSP as the better route towards a sustainable solar powered future. Heavy investments have been made internationally in developing these technologies. Installation of commercial systems has been done since 2005. However, still lack sufficient experience to transform CSP into a reliable, low-cost source of electricity.

1.1. CSP technologies

The various technologies adopted are yet to be optimized technically and economically [6]. The most widely used and researched technologies are the following: parabolic dish collectors (PDC), linear Fresnel reflectors (LFR), solar power towers (SPT), and parabolic trough collectors (PTC) [7]. Their construction and work are depicted in Fig. 1.

Recently an advanced design for LFR technology has been developed. It is called a compact linear Fresnel reflector (CLFR). CFLR prevails over PTC in area requirements using 2 parallel reflectors for each row of mirrors. Advanced design of CFLR requires less area to attain a given power output comparatively [8]. PDCs, in comparison to their peers, possess bulky designs and are expensive. These factors make PDCs less favourable for medium to large scale applications (50 MW plants and above CSP technology has captured global interest as a solution to meet the energy demands of the growing population [9].

Technologies mentioned in Fig. 1 are further combined with TES systems to overcome inconsistent solar energy supply. Thermal Energy Storage (TES) systems can be classified into 3 categories based on the thermal principles used. These are namely: 1) Sensible Heat Storage (SHS) 2) Latent Heat Storage (LHS) [10] 3) Thermochemical Heat Storage (TCS). The most practically advanced are the sensible heat-based TES, while the latter two are still under research [11,12]. SHS based TES employing two tanks has been considered with molten salt as

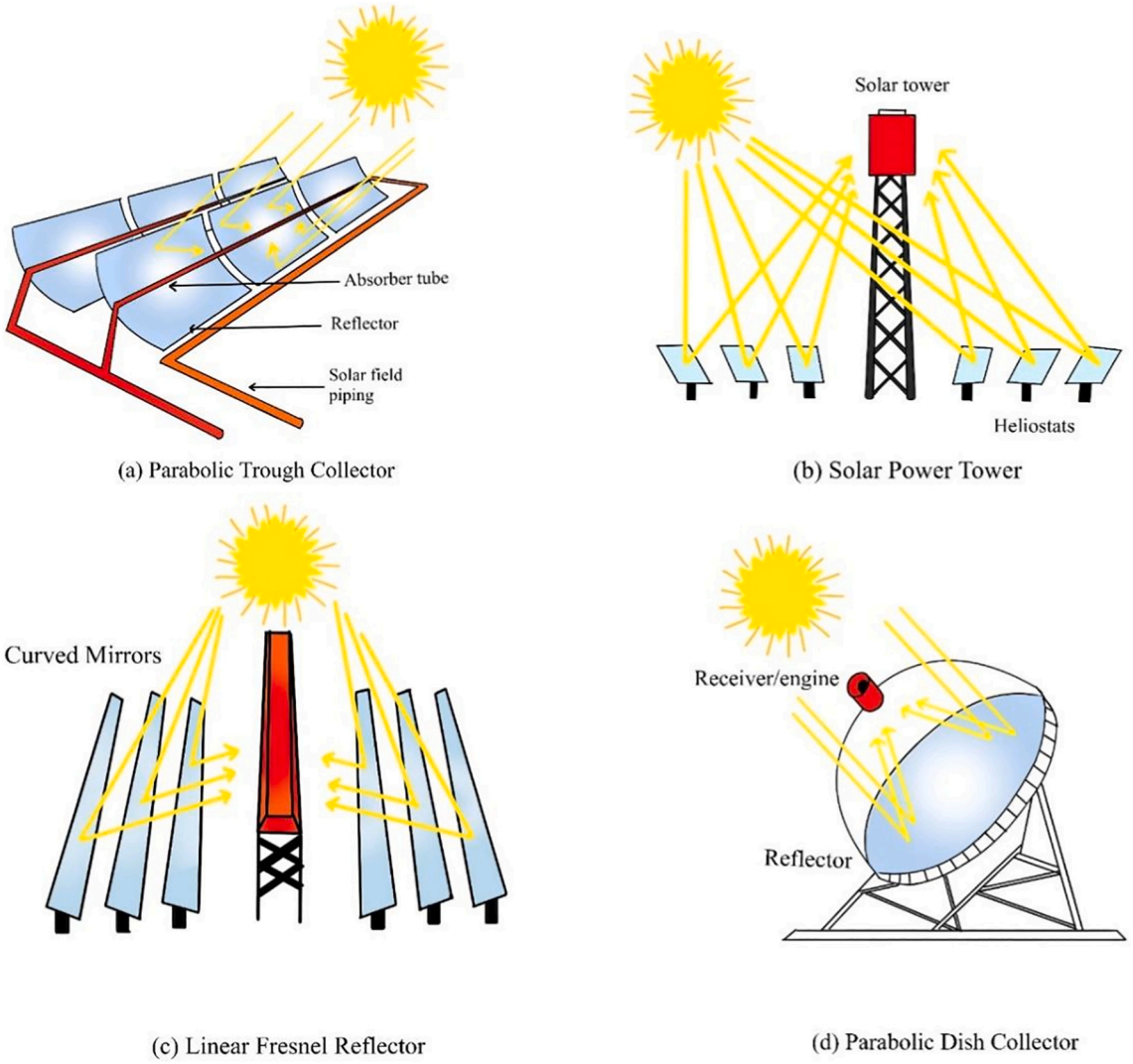

Fig. 1. Most developed CSP technologies.

the storage material [13].

In 2019, the CSP capacity on a global level grew 11% to 6.2GW, as 600 MW of capacity came online. Even though growth was far lower than the average annual increase of 24% as seen in past decade, continue spread of CSP into new markets was also seen, including Kuwait, Israel and France. Few new plants were also brought into service by China and South Africa. [3]. Electricity generated by a CSP plant depends on the amount of solar radiation received normally per unit area by a surface, also known as direct normal irradiance (DNI). A threshold of around 6 kWh/m^2 of DNI is required to produce enough electricity economically [7,14].

1.2. CSP economics

To analyse the feasibility of a renewable energy source from the perspective of a region, one needs to exercise Techno-Economic Analysis (TEA) of the source under consideration. For a CSP system, TEA theory, when applied, enables the decision-maker to carry out the necessary tasks like 1) economic feasibility analysis, 2) Lifetime analysis of the cash flows related to the system, 3) Application and scales assessment, and 4) Assessment on the basic economic utility evaluation of different technologies. Numerous works related to techno-economic analysis of CSP plants concerning the financial viability of such systems have been published. Islam et al. [15] conducted TEA for all three CSP technologies, namely: PTC, SPT, and LFR for Malaysia, analysing PBP, NPV, profitability index and IRR. Their study found that the most feasible technology for Malaysia is PTC. Shaifee et al. [16] also performed lifetime cost analysis of CSP technologies for Tucson city in Arizona USA, to estimate their profitability. The researchers used the following financial parameters LCOE, BCR, DPBP, IRR and NPV, to assess CSP's economic performance. After finding PTC as the most viable technology, they also performed a sensitivity analysis to identify crucial factors affecting the CSP technologies' economic performance. The increment in plant power output and the investment tax credit were the most significant factors. Another cost-benefit analysis for CSP technologies was performed by Yang et al. [17] and confirmed that even though initial cost and annual electricity generation have notable impacts on the economic performance of CSP technologies, the effects of maintenance and operation costs and loan interest rate on the cost cannot be ignored. Furthermore, the economic assessment of CSP plants was reviewed by Dowling et al. [18]. Most of the research focused on LCOE does not heed advanced features of the upcoming technologies; economic incentives underestimate energy storage and flexibility. Meanwhile, the works employing NPV and return on investment, the ratio of net profit and invested cost, are more in line with the investment parameters utilized by potential investors [19]. Hence, LCOE on its own is insufficient to compare different CSP technologies. A broader TEA is required to accommodate the comparable benefits of the CSP technologies. Various studies related to TES systems working in conjunction with CSP systems have also been conducted [10,13]. Hernandez-Moro and Martínez-Duart [20] estimated the capital costs of CSP systems with and without TES. Capital cost without thermal storage is 4.2 $/W, while the plant, including TES of 7.5 h of storage, costs 8.6 $/W. Luca et al. carried out a simulation wherein the researchers assessed the performance and estimated the cost of 50 MW CSP plants with solar multiple (with values in the range 1–3) along with TES capacity (0–24 h of storage) approximated that for solar multiple of 2 that has been used. Levelized cost of energy for CPS plants with storage is least among 16 h, 12 h, and 8 h of thermal energy storage [21]. 8 h of sensible thermal energy storage has been incorporated, and LCOE is the lowest [22].

Feldman et al. compared solar power using thermal storage and photovoltaic using electrochemical energy storage and indicated that CSP is cheaper than PV in terms of LCOE for longer storage duration [23]. At the end of year 2019, 21 GWh of thermal energy storage (TES) was operational with CSP plants across five continents. Almost every commercial CSP developed by the end of 2019, located in Asia, the Middle East, and Latin America, includes TES. Investment in concentrating solar thermal power (CSP) capacity reached USD 4.6 billion, an increase of 256% from 2018. [3]. Among the various available options for TES systems, most of the operational plants around the globe employ sensible heat based thermal storage as it is most widely preferred and currently matured for practical use [24]. Thus, the study uses a two-tank sensible heat storage system [11].

Many works involving a financial assessment of CSP plants have been carried out when it comes to India. A decade ago, Purohit and Purohit [25] performed a study regarding the techno-economic assessment of CSP generation in India. Approximated calculation of financial parameters and simulation were performed. CSP plants located in Spain, namely: PS-10 and ANDASOL-1 were considered base models. Plants were based on PTC technology but had capacity. PS-10 has a capacity of 11 MW, while ANDASOL-1 was a 50 MW power plant. The financial parametric data estimated were converted into INR from EURO directly without moderations. Bishoyi and Sudhakar performed a simulation and modeling of 100 MW PTC and LFR based CSP plants in Rajasthan, hot and dry climatic region with an annual DNI of 2248.17 kWh/m^2/year. Hitech Solar Salt was used as the HTF used because of its excellent performance. PTC plant with 6 h of TES had a plant efficiency of 21%, while LFR based plant with the same hours of storage exhibited 18.3% efficiency. [26,27]. Kumar et al. studied financial viability of CSP technologies of 50 MW capacity plant in 10 different locations with diverse climatic conditions of India. Jodhpur, a city in India's hot and dry climatic region, is the most suitable site for installing CSP plants. In the study, authors used guidelines laid in 2016 by CERC [28,29]. NPV, LCOE, PBP, DPP, and CRF were used to estimate and compare the viability of plants in a particular region.

1.3. Objectives of the research

Literature on CSP financial viability is abundant; however, no latest work presents a more in-depth analysis of CSP plants with storage in India and compares these with those without storage. The present work presents a detailed analysis of the economic assessment of 3 CSP technologies, namely SPT, PTC, and LFR, in India's hot and dry climatic region, taking Jodhpur as the city of reference. Numerous economic parameters like PBP, LCOE, NPV, and DPP based on the latest fiscal guidelines laid by CERC-2016 were considered for economic analysis. It is a comprehensive analysis of plants of two capacities 50 MW and 100 MW, for the region for each kind of technology with and without TES system. Research aims to light the financial viability of CSP systems in the country and enable policy and decision-makers to look towards this sustainable green means of energy generation as a viable option for futuristic energy-related projects. The findings of the present study can be adopted for all the country's hot and dry climatic regions.

2. Installation of CSP system in India

As per the 2017 report of the World Resource Institute [30,31], India contributes about 6.65% to the total carbon emission accounted globally. The country ranked 4th after China (26.83%), the USA (14.36%), and the EU (9.66%). As per a prediction made by the World Energy Council, the global electricity demand will hit its maxima by 2030. After China, India is the second-largest consumer of coal globally and imported around 213 million tons of coal in 2017–2018, as per the Centre for Monitoring Indian Economy report. Presently, around 74% of the country's energy demand is fulfilled by oil and coal [32,33]. There is an urgent need for alternative renewable sources of generation in the country. MNRE launched a scheme, Pradhan Mantri Kisan Urja Suraksha Evam Utthaan Mahabhiyaan (PM KUSUM), intending to increase solar and other renewable capacities by 25,750 MW by the end of 2022. For this, the scheme has received total central financial support of Rs. 34,422 Crore (46.4 billion $). Financial support provided includes the service charges to be paid to the implementing agencies [34]. Financial

budget of 2020–21 of the country expanded the scheme wherein 2 million farmers were to be given funds to install stand-alone solar pumps [35].

Clean and green energy is often economical and less hazardous. By the end of the year 2022, India aims to reach the goal of 175 GW being produced by renewable energy sources, comprising 60 GW produced by wind power, 10 GW generated by bio-power, 100 GW contributed by solar energy (40 GW from rooftop solar and remaining 60 GW from CSP), and 5 GW from small hydropower plants [36]. At present, India has 5 operational plants, namely viz. National Solar thermal power facility (1 MW, PTC, Haryana), Godawari Solar project (50 MW, PTC, Rajasthan), ACME solar tower (2.5 MW, SPT, Rajasthan), Megha solar plant (50 MW, PTC, Andhra Pradesh) and the largest among them all the Dhursar (125 MW, LFR, Rajasthan). Besides these, 5 other CSP initiatives are still under development in Uttar Pradesh, Gujrat and Rajasthan states. Total energy generation capacity of the plants is 300 MW [37,38]. India's northwestern regions hold a huge potential of about 1800 kWh/m^2 for CSP systems that are feasible for installing CSP technologies. Although, the tropical regions with high diffuse fractions, such as setups, are not economical [37]. To enable a good installation rate of CSP projects in India, the country still needs to win over several hurdles like unskilled labour, improper maintenance, non-supportive policies, and expensive finance.

3. Methodology

For this paper, 3 kinds of CSP based technologies have been considered, namely: Solar Power Tower (SPT), Parabolic Trough Collector (PTC), and Linear Fresnel Reflector (LFR). All three technologies were analysed with and without thermal energy storage. Direct Normal Irradiance (DNI) data has been collected for Jodhpur from Ministry of New and Renewable Energy (MNRE), India. Simulation has been carried out for each CSP technology of 2 different capacities: 50 MW and 100 MW. Thus, encapsulating the assessment for 12 different plant setups in the city of Jodhpur, India. Numerous software is available in the market for simulating CSP projects, like SAM, GateCycle, STEAM PRO, FLUENT and AEETES. Among the most recommended and widely used simulation software is the System Advisor Model (SAM). SAM's software development and data accuracy are managed by the NREL [39,40]. Due to high preference and better accuracy of results, SAM has been selected for the present study [41].

3.1. Location selection

India being a tropical- temperate country, possess numerous climatic regions which are usually categorized as follows: 1) Temperate- towards the northern plains, 2) Cold spanning over the entire northern borders inclusive of the Himalayas, 3) Hot and Dry – comprising of the northwestern Thar desert region of the country, 4) Composite – covering the

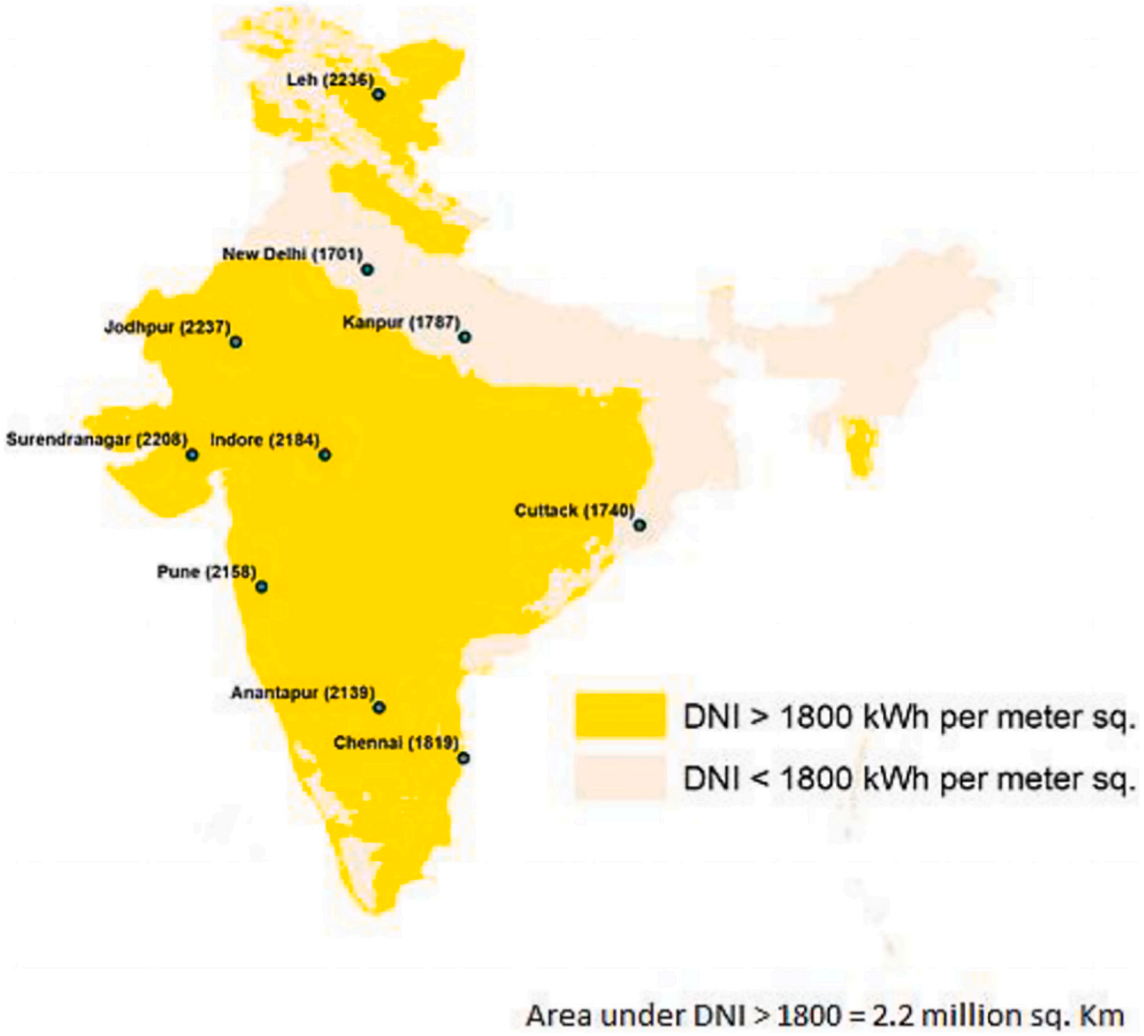

Fig. 2. DNI readings (in kWh/m^2) of different cities in India [28].

Deccan region of the country and, 5) Warm and Humid- the eastern and western coasts of the country. Among all these, the Hot and dry climate shows high DNI values, as illustrated in Fig. 2. The present work has considered Jodhpur, a city located in the Rajasthan state with an average annual DNI of 2237 kWh/m^2 [28].

3.2. Solar radiation data

Solar radiation data for India can be obtained from numerous sources. A few most used sources are- India Meteorological Department (IMD), NASA – POWER, Centre for Wind Energy Technology (CWET), Solar GIS, PVGIS, and Meteonorm. Most of the sources mentioned above comprise similar datasets. However, DNI value in these datasets is variable even for the same geographical location [42,43]. Solar radiation data has been taken from NREL-SEC because of its compatibility with SAM and access to accurate analysis. NREL-SEC is the data developed by the NREL, in association with – MNRE India. These datasets comprise Global Horizontal Irradiance (GHI) and Direct Normal Irradiance (DNI) in months and years. The data set has been created using satellite data collected on an hourly basis from January 2000 to December 2014. With a spatial resolution of 10 km × 10 km, the datasets cover the entire country while keeping accuracy of 15%. MNRE website facilitates the NREL-SEC solar radiation data of India [25,39]. Jodhpur's annual DNI data has been provided in Appendix.

3.3. Thermal storage selection

TES systems are broadly categorized into 3 categories, namely: 1) Thermochemical TES systems [44], 2) Latent heat TES systems [45], and 3) Sensible heat TES system [46]. Fig. 3 illustrates the interrelation between energy density and technical maturity while plotting the working temperature against the various storage mechanisms in use [47]. Sensible heat-based systems are much more mature in technological development and practical use than other TES systems (Fig. 3). Two tank concepts are most widely used in sensible heat-based TES systems. It is more advantageous than the single volume regenerative type storage because its power requirement is externally met rather than within the storage volume [48,49]. In addition to the two tanks, a thermal reaction (for thermochemical heat) or a heat exchanger (for sensible heat storage) can be developed to meet the thermal power. Henceforth, the concept of two tanks enables the decoupling of the thermal power (additional external component) and the thermal capacity (stored in two tanks) [50]. Fig. 4 illustrates the two-tank direct active systems used in the simulation. Thus, in the present study, two tank sensible heat TES systems are considered along with CSP

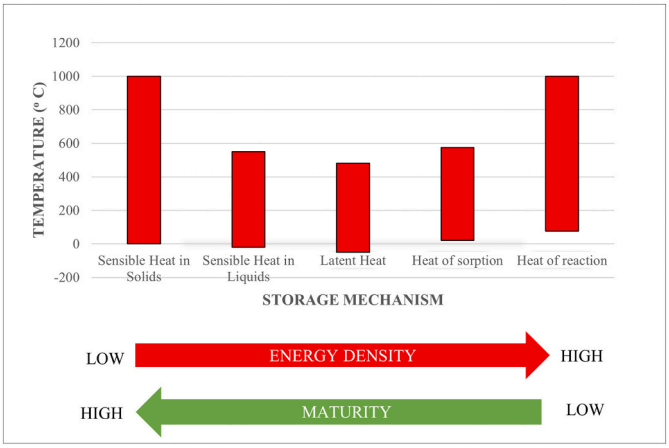

Fig. 3. Thermal energy storage working temperature, the mechanism employed and interrelation between energy density and level of technical maturity [47].

technologies with 8 h of storage. To account for the storage costs, operation, maintenance, and capital costs after summation have been increased by 11.73%. [51–54].

3.4. Annual energy generation

Annual Electricity Generation is calculated as [25]:

$$Annual\ Energy\ Output = 8760 \times CF_{CSP} \times P_{CSP} \quad (1)$$

where, Capacity Factor is represented by CF_{csp} and Net Capacity of CSP plant is given by $P_{csp.}$ However, for using the above equation of annual energy output, CF_{csp} is needed; for specific technology and specific location, it is not available, and as of now, calculation of CF_{csp} of a plant can't be done by any method.

Another method to calculate the Annual Electricity Generation of a CSP plant of a particular location is simulation. Usually, the solar radiation data is fetched from NREL-SEC in two formats: annually and monthly; NASA – ASDC refers to the average ambient temperature of the month [55]. GHI data on hourly basis, dry bulb temperature, DNI, dew point temperature are used while carrying out the simulation and wind speed data sets are taken from PVsyst (V.6.83). Simulation in PVsyst is performed over a whole year in hourly steps. NASA – ASDC and NREL-SEC do not provide meteorological and solar radiation data for such time resolution. Therefore, for such an analysis generating hourly data becomes necessary. Common software that can generate values on hourly basis for the meteorological data is PVsyst [56]. Hourly meteorological data needs to be imported into SAM (V.2020.2.29). The simulation of the CSP plant in SAM requires Typical Meteorological Year 3 (TMY3) data files which are location specific. If not getting a TMY3 file on SAM resources, another method to generate TMY3 file is by using a software called Meteonorm V7.3, which contains 8760 h of temperature and various meteorologic data parameters for the location being selected [57]. 50 MW and 100 MW CSP plants have been simulated for Jodhpur for 3 CSP technologies viz (Table 1). PTC, SPT, and LFR for both the cases with and without storage. CERC (2016) (Table 3) was referred for additional input parameters used in SAM. CSP plant specific details are mentioned in Table 2 [43].

3.5. Financial evaluation

There are numerous economic factors on which the feasibility of a power plant depends. To evaluate financial viability analysis for CSP plants, the following factors are considered: Payback Period (PBP), Levelized Cost of Electricity (LCOE), Net Present Value (NPV), Discounted Payback Period (DPP), and Capital Recovery Factor (CRF) [25,58–63].

3.5.1. Levelized cost of electricity (LCOE)

Refers to cost incurred per unit of electricity generated, taken over a given life period of the power plant. LCOE is majorly used in comparison with other methods of generating electricity. Lower value of LCOE signifies that the technique used for electricity generation is more viable when compared to a technique having greater LCOE values. LCOE is estimated from Eq. (2) [43].

$$LCOE = \sum_{y=1}^{t_{csp}} \frac{UCE_y}{(1+d)^y} \times CRF \quad (2)$$

UCE_y in the above equation is the Unit Cost of Electricity in the y^{th} Year, which is given in Eq. (3) [43].

$$UCE_y = \frac{Total\ annual\ cost\ in\ the\ yth\ year}{Total\ energy\ generation\ in\ yth\ year} \quad (3)$$

Following 5 expenses, when combined, account for the total annual cost of a CSP plant in a given y^{th} year: (1.) interest on the working capital, (2.) return on equity, (3.) interest on loan taken, (4.) principal

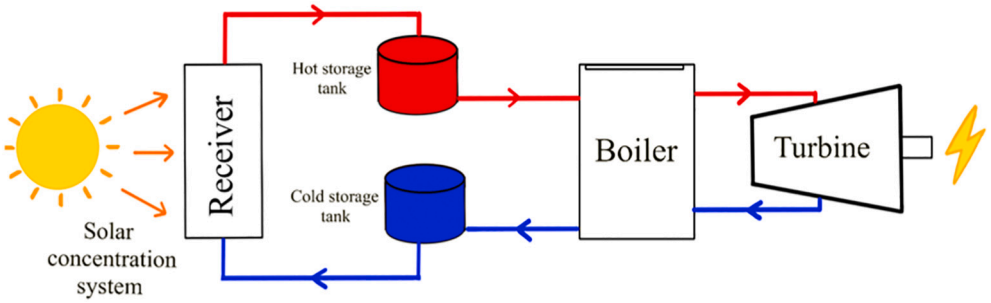

Fig. 4. Two tank direct active system.

Table 1
Specification of CSP plants considered for the evaluation based on three technologies (SAM, 2021).

Parameter	Parabolic trough collector	Solar power tower	Linear Fresnel reflector	Parabolic trough collector	Solar power tower	Linear Fresnel reflector
Net capacity (MW)	50	50	50	100	100	100
Collector	Solargenix SGX – 1	Heliostats	Fresnel mirrors	Solargenix SGX – 1	Heliostats	Fresnel mirrors
Receiver	Schott PTR 70	External	Cavity	Schott PTR 70	External	Cavity
Heat transfer fluid	Therminol VP - 1	Molten Salt	Therminol VP – 1	Therminol VP - 1	Molten Salt	Therminol VP - 1
Design inlet temperature (°C)	293	350	230	293	350	230
Design outlet temperature (°C)	391	574	420	391	574	420
Solar multiple	2	2	2	2	2	2
Irradiation at design (W/m^2)	950	950	950	950	950	950
Land area (km^2)	1.81	3.46	0.80	3.61	6.317	1.58
Power cycle	Steam Rankine	Steam Rankine	Steam Rankine	Steam Rankine	Steam Rankine	Steam Rankine
Storage system configuration	Two-tank	Two-tank	Two-tank	Two-tank	Two-tank	Two-tank
Full load hours of storage (h)	8	8	8	8	8	8
Storage material used	Hitech Solar Salt	Molten Salt	Hitech Solar Salt	Hitech Solar Salt	Molten Salt	Hitech Solar Salt

Table 2
Financial parameters of the CSP plants for the location Jodhpur, India.

CSP technology	Capacity (MW)	Annual generation (MWh/yr)	CUF	Hours of storage	LCOE (₹($)/kWh)	Payback period (years)	Discounted payback period (years)	Net present value (₹($) in millions)
Linear Fresnel reflector	50	105,208	0.24	0	9.27 (0.125)	0	7.07	2541.39 (34.25)
Linear Fresnel reflector	100	204,332	0.23	0	9.54 (0.128)	0	7.46	4465.43 (60.19)
Linear Fresnel reflector	50	107,706	0.25	8	10.33 (0.139)	3.6	8.72	1584.44 (21.35)
Linear Fresnel reflector	100	209,879	0.24	8	10.63 (0.143)	5.65	9.27	2551.52 (34.39)
Parabolic trough collector	50	109,668	0.25	0	10.19 (0.137)	3.33	8.4	1788.83 (24.11)
Parabolic trough collector	100	219,215	0.25	0	10.19 (0.137)	3.36	8.41	3566.48 (48.07)
Parabolic trough collector	50	114,977	0.26	8	11.35 (0.152)	10.9	10.57	6940.4 (93.55)
Parabolic trough collector	100	232,280	0.27	8	11.35 (0.152)	10.96	10.58	1369.6 (18.46)
Solar power tower	50	135,719	0.22	0	10.12 (0.136)	3.75	8.23	2293.98 (30.92)
Solar power tower	100	212,141	0.24	0	12.87 (0.173)	17.17	14.11	−1441.21 (−19.42)
Solar power tower	50	154,920	0.25	8	11.27 (0.151)	10.86	10.2	944.02 (12.72)
Solar power tower	100	251,641	0.29	8	14.35 (0.193)	More than 25 years	19.98	(−55.82) −4141.14

amount of loan, and (5.) operation and maintenance.

Eq. (4) represents the Capital Recovery Factor (CRF) [64].

$$CRF = \frac{d(1+d)^{t_{csp}}}{(1+d)^{t_{csp}} - 1} \quad (4)$$

Here, d is discount rate, t_{csp} is useful life of a CSP plant.

3.5.2. Payback period (PBP)

Time required to reach Breakeven point or the time needed to recover the invested capital. The Payback Period is mentioned by Eq. (5) [58]:

Table 3
Financial parameters and conditions (CERC 2016).

Parameter	Description
Useful life (t_{csp})	25 Years
Capital cost (per MW)	₹ 102 million ($1.375 million) for LFR ₹ 152 million ($2.048 million) for SPT ₹ 120 million ($1.618 million) for PTC
Debt to equity ratio	70% Debt and 30% Equity
Period of loan repayment	12 years
Interest rate on loan	12.76%
Depreciation rate	For the initial 12 years – 5.83%, from 13th year onwards – 1.54%
Return on equity	20% (for the initial 10 years), 24% (from 11th year onwards)
Discount rate (d)	10.70%
O&M expenses (C_y)	₹ 1.87 Million ($0.025 million)
O&M expenses escalation	5.72%
Working capital	O&M expenses (of 1 month) + 15% O&M expenses + revenue from 2 months of electricity sale
Interest on working capital	13.26%
Levelized tariff rate	₹ 12.08/Unit (0.16 $/Unit)

1 INR = 0.0134800229 USD (as on 2021-27-06 20:08 UTC).

$$Payback\ Period = T_1 - 1 + \frac{\left|\sum_{y=1}^{T_1-1}(CI-CO)_y\right|}{(CI-CO)_{T_1}} \quad (5)$$

Here, cash inflow is represented by CI; basically, it is the revenue which is collected in the y^{th} year from electricity generation, CO represents cash outflow, the total annual cost incurred in y^{th} year is referred to as cash outflow, project year y is represented by T_y and $y = T_0 + 1, \ldots T$.

3.5.3. Discounted payback period (DPP)

Time incurred in recovering the capital investment using the data given by government of India on subsidised discount rate is referred to as discounted payback period. DPP of an investment in CSP plant, estimated from Eq. (6) [25]:

$$DPP_{CSP} = \left[\frac{lnln\left(CI_y - C_y\right) - lnln\left\{\left(CI_y - C_y\right) - dC_{CSP}\right\}}{lnln\left(1+d\right)}\right] \quad (6)$$

Here, operation and maintenance cost of y^{th} year is given by C_y, cash inflow of y^{th} year is presented by CI_y, and C_{CSP} represents the initial investment(capital) used in CSP system.

3.5.4. Net present value (NPV)

It is a profitability measuring tool in which we discount the cash flows of future years to get the present value of these cash flows and then add them to the given present value of the investment. Both the revenue and cost of investment are taken into account while calculating NPV. While interpreting the economic feasibility of a CSP plant compared to other factors, NPV is given the highest priority compared to other factors included in decision making. NPV of a CSP plant is determined by Eq. (7) [62]:

$$NPV = \sum_{y=1}^{t_{CSP}} \frac{C_{an}}{(1+d)^y} \quad (7)$$

Here, average rate of discount (d) is used in calculating the NPV.

If the value of NPV > 0 then this is considered an economically feasible investment.

if NPV < 0 it is considered an infeasible economic investment.

For the given CSP plant annual cash flows are presented by: C_{an}.

4. Results and discussions

After successful simulation in SAM, Annual electricity generation and Capacity Utilization Factor for each CSP technology were obtained. The generated results were then used in conjunction with the CERC 2016 guidelines [29] to estimate the parameters: Net present Value, Discounted payback period, Payback period and Levelized Cost of Electricity for each CSP technology with and without storage. All of these findings have been consolidated in Table 4. Figs. 5–9 illustrate all the parameters mentioned in Table 4 of each plant taken under consideration. 50 MW are mid-size plants, whereas the 100 MW plants lie in large-size plants [65]. The inclusion of storage along with these has shown significant effects on all parameters of a plant type. Result section

Table 4
Simulation results for CSP technologies of 50 MW and 100 MW capacities both with and without storage.

Plant technology	Plant capacity (MW)	Storage (hours)	Annual electricity generation (MWh/ yr)	CUF	LCOE (₹/kWh) ($/kWh)	NPV (million ₹) (million $)	Payback period (years)	Discounted payback period (years)
LFR	50	0	105,208	0.24	9.27 (0.125)	2541.39 (34.25)	0	7.07
PTC	50	0	109,668	0.25	10.19 (0.137)	1788.83 (24.11)	3.33	8.4
SPT	50	0	135,719	0.22	10.12 (0.136)	2293.98 (30.92)	3.75	8.23
LFR	100	0	204,332	0.23	9.54 (0.128)	4465.43 (60.19)	0	7.46
PTC	100	0	219,215	0.25	10.19 (0.137)	3566.48 (48.07)	3.36	8.41
SPT	100	0	212,141	0.24	12.87 (0.173)	−1441.21 (−19.42)	17.17	14.11
LFR	50	8	107,706	0.25	10.33 (0.139)	1584.44 (21.35)	3.6	8.72
PTC	50	8	114,977	0.26	11.35 (0.152)	6940.40 (93.55)	10.9	10.57
SPT	50	8	154,920	0.25	11.27 (0.151)	944.02 (12.72)	10.86	10.2
LFR	100	8	209,879	0.24	10.63 (0.143)	2551.52 (34.39)	5.65	9.27
PTC	100	8	232,280	0.27	11.35 (0.152)	1369.60 (18.46)	10.96	10.58
SPT	100	8	251,641	0.29	14.35 (0.193)	−4141.14 (−55.82)	25	19.98

1 INR = 0.0134800229 USD (as on 2021-27-06 20:08 UTC)

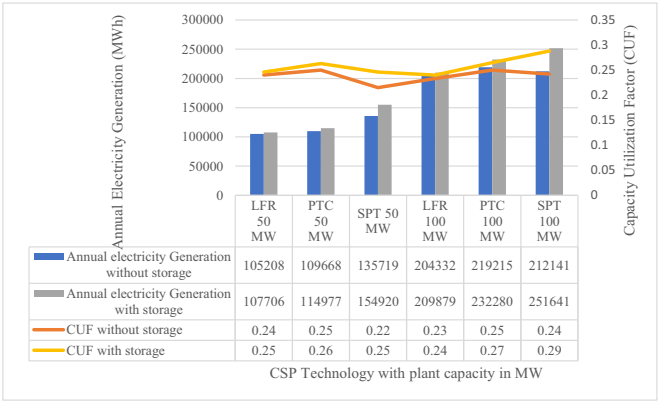

	LFR 50 MW	PTC 50 MW	SPT 50 MW	LFR 100 MW	PTC 100 MW	SPT 100 MW
Annual electricity Generation without storage	105208	109668	135719	204332	219215	212141
Annual electricity Generation with storage	107706	114977	154920	209879	232280	251641
CUF without storage	0.24	0.25	0.22	0.23	0.25	0.24
CUF with storage	0.25	0.26	0.25	0.24	0.27	0.29

Fig. 5. Annual Electricity Generation and CUF of CSP Plants without and with Thermal Energy Storage.

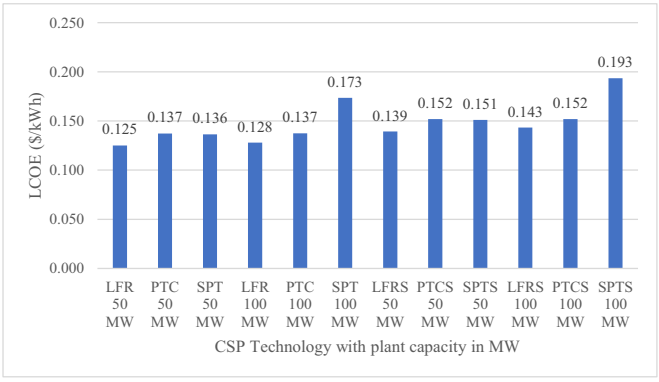

Fig. 6. LCOE ($/kWh) comparison of different CSP plants.

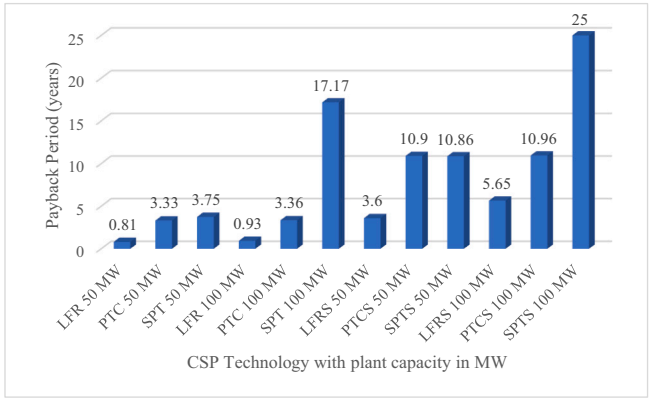

Fig. 7. Payback Period (years) comparison of different CSP plants.

has been presented in 4 parts. It has been divided based on capacity of the plant and presence of TES. Such segregation has been made to enable better decision-making under a broader category.

4.1. 50 MW without storage

The range of annual electricity generation for 50 MW capacity plants having 0 h of storage is 105–135 GWh/yr (Fig. 5). LFR has generated the lowest output and the highest one belongs to the SPT technology plant type. This difference in generation is due to the larger area occupied by SPT than LFR, enabling SPT to concentrate more solar radiation per metre square. PTC produces an annual electricity generation of 109

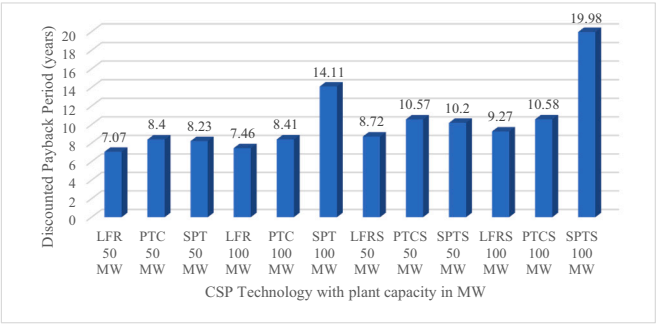

Fig. 8. Discounted Payback Period (years) comparison of different CSP plants.

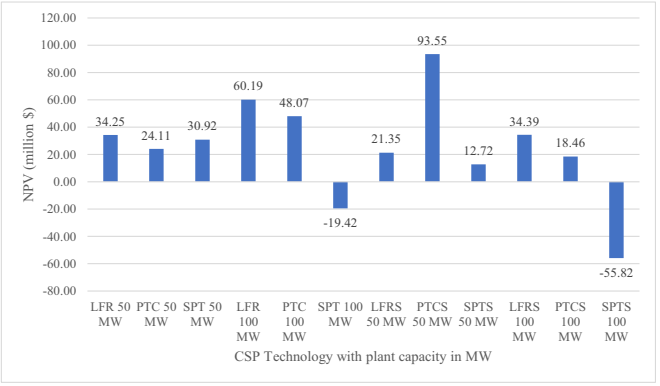

Fig. 9. NPV (million $) comparison of different CSP plants.

GWh/yr, and exhibits a higher value of CUF (0.25) than the other two. When compared in terms of financial parameters, PTC plant, even though with maximum value of CUF, has the highest LCOE of 10.19 ₹ (0.137$/kWh) (Fig. 6), lowest NPV of 1788.83 million ₹ (24.11 million $) (Fig. 9). Payback period and discounted payback period of the PTC are also the longest among all others. LFR has the least LCOE that, is 9.27 ₹/kWh (0.125$/kWh) with a minimum payback period of <1 year (Fig. 7) and has the highest NPV of 2541.39 million ₹ (34,25 million $). Hence if a person has decided not to invest additional capital in storage system and requires a 50 MW plant, LFR 50 MW would be the right way to go about it. Meanwhile, PTC is the least obvious choice. Irrespective of high CUF, PTC standing last indicates that a plant working more optimally may not always be the best economical choice.

4.2. 50 MW plant with storage

Addition of thermal energy storage of 8 h and the technologies has shown significant changes in all the plant parameters. Range of annual electricity generation for this storage-equipped 50 MW plant type category is 107–155 GWh/yr. (Fig. 5). Inclusion of storage also increased the capacity utilization for each CSP technology. The increased numbers prove that TES increases plant efficiency while reducing the energy supply-demand issue. On studying the financial parameters, LFR has minimum LCOE 10.33 ₹/kWh (0.139$/kWh) (Fig. 6). LFR also has a minimum payback and discounted payback period of 3.6 years (Fig. 7) and 8.72 years (Fig. 8), respectively. NPV of this plant is 1584.44 million ₹ (21.35 million $) (Fig. 9). Even though PTC has slightly higher LCOE in comparison to LFR but has a significant difference in NPV, for this category of plant setup PTC has the highest NPV of 6940.4 million ₹ (93.55 million $). This eye-catching result has some disadvantages, including longer payback periods of 10.9 years and a discounted payback period of 10.57 years. However, in cases where energy generation overpowers the financial aspects of plant, SPT is the

best alternative by producing a humongous annual electricity generation of 154,920 MWh/yr. (Fig. 5). If given a choice between a 50 MW plant with or without storage, it seems clear that the plants without storage are much cheaper than their counterparts utilizing TES. Nevertheless, when one considers the plant's capacity to power a larger town or city for longer durations, the need resolved by TES based plants easily overpowers the cost incurred.

4.3. 100 MW without storage

100 MW capacity CSP plants fall in the range of large size plants. With doubled capacity than 50 MW category, the parametric findings of these plants are on a completely different scale. In this category, plants have a massive range of annual electricity generation that is 204–219 GWh/yr even without additional TES systems (Fig. 5). An interesting point to note for this category is that PTC has outperformed SPT in annual generation. However, the comparison of CUF remains the same, with PTC leading the group with a capacity utilization factor of 0.25. This indicates that when expanded on a larger scale, the optimal play of PTC having higher CUF finally compensates for it having a reduced area size as compared to SPT. LFR outperforms other plants in every aspect. It has a maximum NPV of 4465.43 million ₹ (60.19 million$) (Fig. 9), lowest LCOE 9.54 ₹/kWh (0.12$/kWh) (Fig. 6) and payback period of <1 year (Fig. 7). Although LFR's annual generation is lower than the other two, the difference in the values isn't considerable to overpower the financial profitability of the same. The difference in LFR's such optimum financial profitability is due to its lower area of utilization which again bodes well for the state/city as a lesser area is needed for plant development.

4.4. 100 MW plant with storage

Annual electricity generation of 100 MW capacity plants considerably increases by great values with 8 h of storage. These plants can produce 209–251 GWh/yr of electricity annually (Fig. 5), which is enormous. In terms of CUF, this category of plants exhibits the highest values compared to its peers, with 100 MW SPT with storage having the maximum CUF of 0.29. This can be attributed to SPT's larger area of utilization that adds to better usage of plant resources when considered for a larger capacity. The same also makes the plant very capital expensive too. Thus, financially LFR and PTC display promising results, and SPT displays the contrary results by giving negative NPV. LFR has lower LCOE of 10.63 ₹ /kWh (0.14$/kWh) (Fig. 6) and payback period of 5.65 years (Fig. 7). LFR also has highest NPV of 2551.52 million ₹ (34.39 million $) (Fig. 9). If annual generation is the primary selection parameter, PTC plant type is the most suitable since SPT with negative NPV is no longer a viable option.

5. Conclusions

The study's results and findings are presented in 4 broad major categories, divided based on plant capacity and hours of storage. Significant conclusions of the study are as follows:

- Inclusion of 8 h of storage impact economics of the plants. Electricity generation (annual) also increases significantly and improves the capacity utilization factor. However, it increases the overall expenses of the setup by 11.73%, which can hinder the viability of projects with low funds.
- Solar power tower (SPT) technology produces the highest annual electricity for all the plant categories except the plants with 100 MW capacity and no storage. Here PTC overpowers the SPT's generation by 7 GWh/yr.
- Both 100 MW, SPT plants with and without storage, have negative NPV of −4141.14 million ₹ (−55.82 million $) and −1441.21 million ₹ (−19.42 million $), respectively. Thus, neither of them is financially viable and is disregarded as promising plant setups.
- Payback period for 100 MW SPT with storage exceeds 25 years. Hence, even in a significant future timeline, plant will never even payback the invested capital, let alone generate profit.
- In the 50 MW category, PTC with 8 h of storage seems to be the preferable option due to its decent annual power generation of 114,977 MWh/yr compared to others. It also possesses a maximum CUF of 26%. Major criterion of this plant being preferable is its highest NPV of 6940.4 million ₹ (99.55 million $).
- LFR based plants of 50 MW and 100 MW with no storage show an interesting result. Both plants have a payback period of less than a year. This indicates that these will generate energy with profit even before completing the first year of installation.
- CUF of plants with storage is always more than CUF of plants without storage. Even the annual electricity generation of plants with storage show an increase compared to the plants without it.
- LFR 50 MW with no storage has the lowest LCOE of 9.27 ₹/kWh (0.125 $/kWh) and discounted payback period of 7.07 years.

6. Recommendations for further work

Overall, the positive values of NPV complemented by high values of annual electricity generation and CUF indicate the presence of unexplored potential of solar power extraction in India's hot and dry climatic regions. The present study has covered medium to large plant capacities and has presented an in-depth study of the financial viability of such projects in the region. The addition of TES is beneficial for a CSP system. It ensures a constant supply of energy an increment in overall efficiency of plant and an increase in effectiveness. Findings of the study can fuel further region-specific research and development of state of art CSP plants and systems in India. This comprehensive analysis can also be a guide to conducting similar studies in other possible country regions.

CRediT authorship contribution statement

Naman Goyal: Formal analysis, Visualization, Writing – original draft; **Akshansh Aggarwal:** Data curation, Methodology, Investigation; **Anil Kumar:** Conceptualization, Project administration, Resources, Supervision, Writing – review & editing

Declaration of competing interest

Authors declare that they have no known competing financial interests or personal relationships that could have appeared to influence the work reported in this paper.

Acknowledgments

Authors are highly thankful to Centre for Energy and Environment, Delhi Technological University, for providing the basic infrastructure for compiling this work. This research did not receive any specific grant from funding agencies in the public, commercial, or not-for-profit sectors.

Appendix

The TMY data files for Jodhpur.
https://drive.google.com/drive/folders/1hWSENDcD7-dMwtt21hPgSbFkgjGJJ1kF?usp=sharing

References

[1] Abdalla Mahmoud Alim, Imad Alsyouf, Development of renewable energy in the GCC region: status and challenges, Int.J.Energy Sector Manag. (2020), https://doi.org/10.1108/IJESM-07-2019-0012.

[2] IEA, Global Energy Review 2020, IEA, Paris, 2020 https://www.iea.org/reports/global-energy-review-2020.
[3] REN21, Renewables 2020 Global Status Report (Paris: REN21 Secretariat), 2020. ISBN 978-3-948393-00-7.
[4] A.B. Awan, Comparative analysis of 100 MW concentrated solar power plant and photovoltaic plant, in: 5th International Conference on Energy, Environment And Sustainable Development (EESD-2018), 2019, https://doi.org/10.1063/1.5115363.
[5] M. Landrat, K. Pikoń, M. Bogacka, Harmful environmental impact of the production process of photovoltaic panels—a review, in: K. Mudryk, S. Werle (Eds.), Renewable Energy Sources: Engineering, Technology, Innovation, Springer Proceedings in Energy, Springer, Cham, 2018, https://doi.org/10.1007/978-3-319-72371-6_34.
[6] Ahmad Alalewi, Project: Concentrated Solar Power (CSP). https://www.researchgate.net/publication/262178578_Concentrated_Solar_Power_CSP, 2014.
[7] H.L. Zhang, et al., Concentrated solar power plants: review and design methodology, Renew. Sustain. Energy Rev. 22 (2013) 466–481, https://doi.org/10.1016/j.rser.2013.01.032.
[8] H.L. Zhang, J. Baeyens, J. Degrève, G. Cacères, Concentrated solar power plants: review and design methodology, Renew. Sustain. Energy Rev. 22 (2013) 466–481, https://doi.org/10.1016/j.rser.2013.01.032.
[9] Anil Kumar, Om Prakash, Akarshi Dube, A review on technology and promotional initiatives for concentrated solar power in world, Int.J.Ambient Energy 39 (2018) 297–316, https://doi.org/10.1080/01430750.2017.1298058.
[10] Cristina Prieto, Luisa F. Cabeza, Thermal energy storage with phase change materials in solar power plants. Economic analysis, J. Energy Storage 43 (2021), 103184, https://doi.org/10.1016/j.est.2021.103184.
[11] Akshansh Aggarwal, Naman Goyal, Anil Kumar, Thermal characteristics of sensible heat storage materials applicable for concentrated solar power systems, Mater. Today: Proc. 47 (2021) 5812–5817, https://doi.org/10.1016/j.matpr.2021.04.174.
[12] Zhiwen Ma, Patrick Davenport, Ruichong Zhang, Design analysis of a particle-based thermal energy storage system for concentrating solar power or grid energy storage, J.Energy Storage 29 (2020), 101382, https://doi.org/10.1016/j.est.2020.101382.
[13] Huili Zhang, Thermal energy storage: recent developments and practical aspects, Prog. Energy Combust. Sci. 53 (2016) 1–40, https://doi.org/10.1016/j.pecs.2015.10.003.
[14] Jordan Macknick, Ted Quinby, Emmet Caulfield, Margot Gerritsen, Jay Diffendorfer, Seth Haines, Geospatial Optimization of Siting Large-scale Solar Projects, NREL/TP-6A50-61375, National Renewable Energy Lab (NREL), Golden, CO (United States), 2014, https://doi.org/10.2172/1126849.
[15] Islam Tasbirul Md, Nazmul Huda, R. Saidur, Current energy mix and techno-economic analysis of concentrating solar power (CSP) technologies in Malaysia, Renew. Energy 140 (2019) 789–806.
[16] M. Shafiee, A. Alghamdi, C. Sansom, P. Hart, A. Encinas-Oropesa, A through-life cost analysis model to support investment decision-making in concentrated solar power projects, Energies 13 (7) (2020) 1553, https://doi.org/10.3390/en13071553.
[17] Shuxia Yang, Xianguo Zhu, Weishang Guo, Cost-benefit analysis for the concentrated solar power in China, J. Electr. Comput. Eng. vol. 2018 (2018), 4063691, https://doi.org/10.1155/2018/4063691, 11 pages.
[18] A.W. Dowling, T. Zheng, V.M. Zavala, Economic assessment of concentrated solar power technologies: a review, Renew. Sustain. Energy Rev. 72 (2017) 1019–1032, https://doi.org/10.1016/j.rser.2017.01.006.
[19] K. Reddy, G. Veershetty, Viability analysis of solar parabolic dish stand-alone power plant for Indian conditions, Appl. Energy 102 (2013) 908–922, https://doi.org/10.1016/j.apenergy.2012.09.034.
[20] J. Hernández-Moro, J. Martínez-Duart, Analytical model for solar PV and CSP electricity costs: present LCOE values and their future evolution, Renew. Sustain. Energy Rev. 20 (2013) 119–132, https://doi.org/10.1016/j.rser.2012.11.082.
[21] F.D. Luca, V. Ferraro, V. Marinelli, On the performance of CSP oil-cooled plants, with and without heat storage in tanks of molten salts, Energy 83 (2015) 230–239, https://doi.org/10.1016/j.energy.2015.02.017.
[22] J. Jorgenson, P. Denholm, M. Mehos, C. Turchi, Estimating the Performance And Economic Value of Multiple Concentrating Solar Power Technologies in a Production Cost Model, National Renewable Energy Laboratory, Golden, CO, 2013. NREL/TP-6A20-58645.
[23] David Feldman , Robert Margolis , Paul Denholm Joseph Stekli . Exploring the Potential Competitiveness of Utility-Scale Photovoltaics plus Batteries with Concentrating Solar Power, 2015–2030. United States: N. p., 2016. Web. doi: 10.2172/1321487.
[24] NREL website. https://solarpaces.nrel.gov/, 2020 (accessed 10-06-2021).
[25] I. Purohit, P. Purohit, Techno-economic evaluation of concentrating solar power generation in India, Energy Policy 38 (2010) 3015–3029, https://doi.org/10.1016/j.enpol.2010.01.04.
[26] Deepak Bishoyi K. Sudhakar , Modeling and performance simulation of 100MW PTC based solar thermal power plant in Udaipur India, Case Studies in Thermal Engineering, doi:10.1016/j.csite.2017.05.005.
[27] D. Bishoyi, K. Sudhakar, Modeling and performance simulation of 100 MW LFR based solar thermal power plant in Udaipur India, Resour.Efficient Technol. 3 (4) (2017) 365–377, https://doi.org/10.1016/j.reffit.2017.02.002.
[28] Sankalp Kumar, Aviral Agarwal, Anil Kumar, Financial viability assessment of concentrated solar power technologies under Indian climatic conditions, Sustain. Energy Technol.Assess. 43 (2021), 100928, https://doi.org/10.1016/j.seta.2020.100928.
[29] CERC, Tariff Order 2016-17, Central Electricity Regulatory Commission (CERC), Government of India, New Delhi, Petition No. SM/03/2016 (Suo-Motu), 2016.
[30] Canadian environmental sustainability indicators, Global greenhouse gas emissions, Available at, http://www.ec.gc.ca/indicateurs-indicators/54C061B5-44F7-4A93-A3EC-5F8B253A7235/GlobalGHGEmissions_EN.pdf, 2017. (Accessed 24 May 2021).
[31] D. Pappas, Energy and industrial growth in India: the next emissions superpower? Energy Procedia 105 (2017) 3656–3662.
[32] World energy scenarios composing energy futures to 2050, World Energy Council, 2013 (Last accessed on 24 May 2021), https://www.worldenergy.org/wp-content/uploads/2013/09/World-Energy-Scenarios_Composing-energy-futures-to-2050_Full-report.pdf.
[33] M. Blondeel, T. Van de Graaf, Toward a global coal mining moratorium? A comparative analysis of coal mining policies in the USA, China,India and Australia, Clim. Chang. 150 (1–2) (2018) 89–101.
[34] Ministry of New and Renewable Energy, Government of India. https://mnre.gov.in/solar/schemes. (Accessed 25 May 2021).
[35] Union budget 2020-21. https://www.indiabudget.gov.in/budget2020-21/index.php. (Accessed 24 May 2021).
[36] MNRE, Annual report 2018-19. https://mnre.gov.in/img/documents/uploads/file_f-1608040317211.pdf, 2018-19 https://www.iea.org/reports/global-energy-review-2020.
[37] A. Kumar, O. Prakash, A. Dube, A review on progress of concentrated solar power in India, Renew. Sustain. Energy Rev. 79 (2017) 304–307, https://doi.org/10.1016/j.rser.2017.05.086.
[38] Concentrating Solar Power Projects in India | Concentrating Solar Power Projects, solarpaces.nrel.gov/by-country/IN.
[39] Solar Energy Centre, Ministry of New and Renewable Energy, Government of India. https://mnre.gov.in/india-solar-resource-maps. (Accessed 2 August 2019).
[40] NREL Data: India Direct Normal & Global Horizontal Irradiance Solar Resources. https://data.nrel.gov/submissions/43. (Accessed 24 May 2021).
[41] Alberto Boretti, Stefania Castelletto, High-temperature molten-salt thermal energy storage and advanced-ultra-supercritical power cycles, J.Energy Storage 42 (2021), 103143, https://doi.org/10.1016/j.est.2021.103143.
[42] Ministry of Power, Energy Conservation Building Code, Government of India, ECBC, 2017.
[43] C. Sharma, A.K. Sharma, I. Purohit, S.C. Mullick, T.C. Kandpal, Comparison of solar radiation data sources for design and performance appraisal of CSP systems in India, Int. J. Ambient Energy 39 (2017) 594–605, https://doi.org/10.1080/01430750.2017.1324813.
[44] Ugo Pelay, Dynamic modeling and simulation of a concentrating solar power plant integrated with a thermochemical energy storage system, J. Energy Storage 28 (2020), 101164, https://doi.org/10.1016/j.est.2019.101164.
[45] Abhishek Anand, Cycle test stability and corrosion evaluation of phase change materials used in thermal energy storage systems, J. Energy Storage 39 (2021), 102664, https://doi.org/10.1016/j.est.2021.102664.
[46] S. Vijayan, et al., Experimental and thermal performance investigations on sensible storage based solar air heater, J.Energy Storage 31 (2020), 101620, https://doi.org/10.1016/j.est.2020.101620.
[47] Thomas Bauer Wolf-Dieter Steinmann Doerte Laing Rainer Tamme . Thermal energy storage materials and systems. Annual Review of Heat Transfer, Vol. 15, p.131-177. doi:10.1615/AnnualRevHeatTransfer.2012004651.
[48] S. Riahi, M. Liu, R. Jacob, M. Belusko, F. Bruno, Assessment of exergy delivery of thermal energy storage systems for CSP plants: cascade PCMs, graphite-PCMs and two-tank sensible heat storage systems, Sustain.Energy Technol.Assess. 42 (2020), 100823, https://doi.org/10.1016/j.seta.2020.100823.
[49] Perapong Tekasakul, Anil Kumar, Chalad Yuenyao, Pairoj Kirirat, Gumpon Prateepchaikul, Assessment of sensible heat storage and fuel utilization efficiency enhancement in rubber sheet drying, J.Energy Storage 10 (2017) 67–74, https://doi.org/10.1016/j.est.2017.01.002.
[50] S.N. Nyamsi, M. Lototskyy, I. Tolj, Optimal design of combined two-tank latent and metal hydrides-based thermochemical heat storage systems for high-temperature waste heat recovery, Energies 13 (2020) 4216, https://doi.org/10.3390/en13164216.
[51] F. De Luca, V. Ferraro, V. Marinelli, On the performance of CSP oil-cooled plants, with and without heat storage in tanks of molten salts, Energy 83 (2015) 230–239, https://doi.org/10.1016/j.energy.2015.02.017.
[52] Renewable energy cost analysis - concentrating solar power. https://irena.org/publications/2012/Jun/Renewable-Energy-Cost-Analysis—Concentrating-Solar-Power.
[53] IRENA, Renewable Power Generation Costs in 2019, International Renewable Energy Agency, Abu Dhabi, 2020.
[54] Concentrated solar power: technology brief. https://www.irena.org/publications/2013/Jan/Concentrated-Solar-Power.
[55] ASDC, NASA. NASA. https://eosweb.larc.nasa.gov/. (Accessed 24 May 2021).
[56] Home. PVSyst. https://www.pvsyst.com/. (Accessed 24 May 2021), 11 pages.
[57] Typical meteorological year – an overview | ScienceDirect Topics. https://www.sciencedirect.com/topics/engineering/typical-meteorological-year. (Accessed 24 May 2021).
[58] M.T. Islam, N. Huda, R. Saidur, Current energy mix and techno-economic analysis of concentrating solar power (CSP) technologies in Malaysia, Renew. Energy 140 (2019) 789–806, https://doi.org/10.1016/j.renene.2019.03.107.
[59] N. Gakkhar, M. Soni, Techno-economic parametric assessment of CSP power generations technologies in India, Energy Procedia 54 (2014) 152–160, https://doi.org/10.1016/j.egypro.2014.07.258.

[60] G.S. Miguel, B. Corona, Economic viability of concentrated solar power under different regulatory frameworks in Spain, Renew. Sustain. Energy Rev. 91 (2018) 205–218, https://doi.org/10.1016/j.rser.2018.03.017.
[61] A. Khellaf, Overview of economic viability and social impact of renewable energy deployment in Africa, in: Springer Proceedings in Energy Africa-EU Renewable Energy Research And Innovation Symposium 2018 (RERIS 2018), 2018, pp. 59–70, https://doi.org/10.1007/978-3-319-93438-9_5.
[62] A.B. Awan, M. Zubair, R. Praveen, A.R. Bhatti, Design and comparative analysis of photovoltaic and parabolic trough based CSP plants, Sol. Energy 183 (2019) 551–565, https://doi.org/10.1016/j.solener.2019.03.037.
[63] B. Duquette, T. Otanicar, Comparative economic analysis of concentrating solar technologies, J. Sol. Energy Eng. 135 (2012), https://doi.org/10.1115/1.4007936.
[64] G. Iaquaniello, W. Montanari, A. Salladini, Standalone CSP-DG system for electrification of remote areas and desalinated water supply, Sol. Energy 157 (2017) 1056–1063, https://doi.org/10.1016/j.solener.2017.09.026.
[65] A.R. Devidas, M.V. Ramesh, Wireless smart grid design for monitoring and optimizing electric transmission in India, in: 2010 Fourth International Conference on Sensor Technologies And Applications, 2010, https://doi.org/10.1109/sensorcomm.2010.100.

Proceedings of the International Conference on Applied Artificial Intelligence and Computing (ICAAIC 2022)
IEEE Xplore Part Number: CFP22BC3-ART; ISBN: 978-1-6654-9710-7

GenGen: Analysing the Performance of Transformer-based Encoder-Decoder in a General Natural Language Generation Paradigm

1st Angad Sethi
Computer Science Department
Delhi Technological University
Delhi, India
angadsethi_2k18co066@dtu.ac.in

2nd Aman Kumar Gond
Computer Science Department
Delhi Technological University
Delhi, India
amankumargond_2k18co053@dtu.ac.in

3rd Abhishek Kumar Singh
Computer Science Department
Delhi Technological University
Delhi, India
abhishekkumarsingh_2k18co021@dtu.ac.in

4th Prashant Giridhar Shambharkar
Computer Science Department
Delhi Technological University
Delhi, India
prashant.shambharkar@dtu.ac.in

2022 International Conference on Applied Artificial Intelligence and Computing (ICAAIC) | 978-1-6654-9710-7/22/$31.00 ©2022 IEEE | DOI: 10.1109/ICAAIC53929.2022.9793209

***Abstract*—The Natural Language Processing [NLP] community has branched off in different directions, making windfall gains within each individual task but relatively slow progress in a general paradigm. In this paper, we attempt a comprehensive analysis of the performance of transformer-based encoder-decoder setups, when both individually and jointly trained on tasks spread across four domains – question answering, natural language inference, sentiment analysis and summarisation. The proposed model is trained both separately and jointly on these tasks, experimenting with varied training strategies. The results of our experiments will highlight the downsides like decreased performance, and upsides, such as performance gains of upto 114% on the MultiNLI dataset when jointly trained. We prove that the model accumulates generalised knowledge, which is applicable to language in general, as opposed to specific tasks. Also, this research work tests the zero-shot capabilities of the proposed model in unseen domains for achieving a EM score of 66.490 without any fine-tuning and an EM score of 86.324 with fine-tuning on the SNLI dataset.**

***Index Terms*—Natural Language Processing, Transformers, Language Models, Generalised Models, Seq2Seq**

I. Introduction

Transformers [1] have taken the natural language generation and understanding community by storm; quickly becoming the de-facto architecture for a wide variety of tasks: machine translation, summarisation, and comprehension. In their landmark paper, 'Attention is All You Need' [1], Vaswani *et al.* proposed an encoder-decoder based architecture, which entailed stacked transformer blocks for the encoder and stacked transformer blocks with cross-attention layers for the decoder. They also displayed the tremendous potential and unparalleled performance of this setup, and also laid the groundwork for future experiment.

Building upon the success of transformers, Devlin *et al.* in yet another breakthrough paper 'BERT: Pre-training of Deep Bidirectional Transformers for Language Understanding' [2], showed the benefit of pre-training a transformer based architecture, minus the decoder half. By pre-training the encoder half on objectives pertaining to masked language modelling and next sentence prediction, the Bi-Directional Encoder Representation from Transformers, (or BERT, its well known moniker) and then fine-tuning the model on downstream tasks for relatively less time, Devlin *et al.* were able to achieve state-of-the-art results on almost all natural language understanding tasks [2]. This spurred on a variety of efforts committed to solving these tasks, each unique in their own way but geared towards NLU : ALBERT [3], DeBERTa [4], DistilBERT [5], FlauBERT [6], GPT-2, GPT-3 [7], RoBERTa [8]. This accelerated pace in the NLU community have rather left the trusty Seq2Seq [9]–[12] model in the lurch.

In recent times, the original transformer encoder-decoder architecture seems to have found champions in T5 [13] and BART [14]. A driving philosophy for these novel inventions seems to be exploiting the flexibility these setups allow: the output vocabulary is no longer limited to the tokens in the input sequence which signals a tremendous potential for performance. Elaborating, the "answer" to a "question" no longer needs to come from the "question" or the "context" it can come from a pre-determined, external vocabulary. The single biggest advantage of this is that it removes the need for custom neural network heads: a single model can be trained across a range of tasks, without any architecture changes. BERT [2] models had traditionally been disadvantaged because of this fine tuning on x different tasks required x different heads; making it unsuitable for a general paradigm.

Despite this, T5 [13] and BART [14] are not truly 'generalisable'. In the results reported for both setups, metrics are reported for a task x and a task y, but only when the model was fine-tuned on tasks x and y respectively. Rudimentarily, the performance of a model trained on x and x has neither

Authorized licensed use limited to: DELHI TECHNICAL UNIV. Downloaded on June 22,2022 at 04:33:52 UTC from IEEE Xplore. Restrictions apply.

been reported nor been analysed. This has seriously hindered the invention of models in a general paradigm; a model that is trained on a subset of tasks before it is tested. Depending on the intricacies of the setup, a model trained on a range of task might benefit from the combined knowledge or suffer from catastrophic forgetting.

We attempt to explore these very intricacies in this paper. We rewind back to the time of 'Attention is All You Need' [1] and choose a transformer-based encoder-decoder architecture. We train this model, and its variations, on four separate tasks: **Stanford Question Answering Dataset (SQuAD)** [15], **Multi-Genre Natural Language Inference (MultiNLI)** [16], **CNN / DailyMail Summarisation Dataset (CNN/DM)** [17], [18], and **Stanford Sentiment Treebank (SST)** [19]. **We train our model both separately on each task and on all four tasks together, and report results for each scenario.** Since in generalised setups, there are a lot of moving parts, so we also experiment with training strategies too, namely Round-Robin and Anti-Curriculum Learning [20]. With this paper, we hope researchers gain some insight into the limits and capabilities of a transformer operating in the general paradigm. This work also aims to encourage work in general context, which brings us closer to real-world conditions, as opposed to ladder climbing and metric chasing in specific niche domains.

II. Related Works

A. General Natural Language Generation

There has been enormous amount of work in the natural language processing community involving transformers. However, we won't be covering works related to the inner workings of transformers, but the reader can refer to other resources to gain a deeper understanding of transformers and pre-trained language models.

We instead focus on works related to the general ability of language models across distinct NLP/NLG tasks and their performance in a truly general paradigm. True generalisability implies the attempt to solve talks across a variety of tasks, by attempting to learn the intricacies and patterns of *all of them*. That is, at no point, do we segregate training examples, and as thus, the learning entity is unaware of the task it is solving, resorting to a more expansive understanding of natural language. "The Natural Language Decathlon: Multitask Learning as Question Answering" [21] by McCann *et al.* is one such work, which focuses solely on the discovery and working of truly generalisable language models, capable of understanding tasks from unique genres.

In "The Natural Language Decathlon: Multitask Learning as Question Answering" [21] McCann *et al.* propose a benchmark, a yardstick for truly generalisable models. In this benchmark, they assemble a set of ten tasks, namely: question answering, machine translation, summarization, natural language inference, sentiment analysis, semantic role labeling, relation extraction, goal-oriented dialogue, semantic parsing, and commonsense pronoun resolution. Each example in these datasets is framed as a $(context, question, answer)$ tuple and the model is then asked to answer the given question based on the context. This approach has been borrowed from Kumar *et al.* [22]. McCann *et al.* even come up with a Multitasking Question Answering Network (MQAN) that is trained on all ten tasks simultaneously and then evaluated on all tasks separately. The model is judged on the basis of DecaScore, which is the sum of all metrics computed during evaluation. The reported performance of the MQAN is reported in table I.

TABLE I: Reported Performance of the MQAN on DecaNLP [21]

Task	MQAN (Sampling+ CoVe)	MQAN (QA-first+ CoVe)	MQAN (QA-first)	Seq2 Seq
SQuAD	77.0	75.5	74.4	47.5
IWSLT	21.4	18.9	18.6	14.2
CNN/DM	24.4	24.4	24.3	25.7
MNLI	74.0	73.6	71.5	60.9
SST	86.5	86.4	87.4	85.9
QA-SRL	80.9	80.8	78.4	68.7
QA-ZRE	40.9	37.4	37.6	28.5
WOZ	84.8	85.8	84.8	84.0
WikiSQL	70.2	68.5	64.8	45.8
MWSC	48.8	48.8	45.8	52.4
	609.0	**599.9**	**590.5**	**513.6**

The MQAN, despite coming around the time of transformers, made sparing use of transformer layers, choosing instead a dated LSTM framework. Richard Socher, a co-author, substantiated this choice by stating the volatility of transformer layers, which made training atrociously hard owing to the unstable gradient changes given the different genres it was expected to learn from.

B. Transformer-based Encoder-Decoder Architectures

Encoder-decoder architecture have risen from their grave, resuscitated by the woks of Lewis *et al.* [14], Raffel *et al.* [13], Zhang *et al.* [23], Zaheer *et al.* [24], Yan *et al.* [25]. Their crawling development has not been without reason though. Pre-trained language models come with the baggage of billions of parameters, placing their pre-training in the ballpark of only large organizations [26]. Stack two such models together, as is done in encoder-decoder setups, and the training costs skyrocket. In "Leveraging Pre-trained Checkpoints for Sequence Generation Tasks", [26] Rothe *et al.* propose a cheaper and faster alternative: warm starting with public checkpoints.

In "Leveraging Pre-trained Checkpoints for Sequence Generation Tasks" [26], Rothe *et al.* provide an answer to the question: what is the best way to leverage publicly available pre-trained checkpoints for warm starting sequence-to-sequence generation models. They run experiments on a wide variety of pre-trained checkpoints and use a suite of five tasks to evaluate the performance. While most of their tasks are significantly different from ours, there is one overlapping task: the CNN/DM dataset. We list the results of their experiments on the CNN/DM dataset in table II. *It is necessary to note that their results are markedly different from ours, since their*

Authorized licensed use limited to: DELHI TECHNICAL UNIV. Downloaded on June 22,2022 at 04:33:52 UTC from IEEE Xplore. Restrictions apply.

experiments focus on solving singular tasks rather than trying to solve them in a general paradigm.

TABLE II: Results of Experiments - CNN/DM Dataset

Model Type	ROUGE-1	ROUGE-2	ROUGE-L
RND2RND	35.77	14.00	32.96
BERT2RND	38.74	17.76	35.95
RND2BERT	36.65	15.55	33.97
BERT2BERT	39.02	17.84	36.29
BERTSHARE	39.09	18.10	36.33
ROBERTASHARE	**40.10**	**18.95**	**37.39**
GPT	37.26	15.83	34.47
RND2GPT	32.08	8.81	29.03
BERT2GPT	25.20	4.96	22.99
ROBERTA2GPT	36.35	14.72	33.79

While Rothe *et al.* were the first to fine tune the encoder-decoder tack on publicly available checkpoints, theirs isn't the first attempt to leverage pre-training on the encoder-decoder stack. Ramachandran *et al.* [27] improve BLEU scores on newtest2014 and ROUGE Scores on CNN/DailyMail [17], [18] by using a language model to pre-train the encoder and decoder of an RNN Seq2Seq model. UniLM by Dong *et al.* [28] is another attempt at the same concept and seeks to unify sequence to sequence language modeling. Lample and Conneau [29] pre-train their model using auto-regressive language modeling like GPT, masked language modeling like BERT [2], and a third new objective called translation language modeling.

III. Tasks

To train the model across a genre of tasks, we needed to choose a common way of denoting the training examples of all four datasets. For this purpose, we have chosen to frame each training example as a Question-Answer pair, similar to McCann *et al.* in [21].

These are the tasks that have been implemented and incorporated throughout our paper. This section not only includes description of each individual task but also details the way we process and train them.

A. Stanford Question Answering Dataset (SQuAD)

SQuAD [15] has quickly gained recognition as the yardstick for machine comprehension-centred models. SQuAD already consists of question and answers, so we use the questions, contexts, and answers as-is. Each question is paired with a context. The answer to each question is always a span from the context and doesn't include any word from an external vocabulary. Each question is guaranteed to have an answer. Table III consists of details of the dataset and the splits.

TABLE III: SQuAD 1.1 - Dataset Description

	Training	Validation
No. of Samples	87599	10570
Avg. Len. of Questions	10.39	10.25
Avg. Len. of Answers	3.16	3.01
Avg. Len. of Context	119.76	123.93

Wherever we mention the SQuAD task, this is how we process and evaluate the dataset:

- Each training data point in the dataset is framed by concatenating the context and question, separated by a separator token, a special token meant to signify the separation of two sentences. In our case this token is $[SEP]$.
- We then tokenise the context-question pair using a pre-trained tokeniser, pulled from HuggingFace [30] and compatible with our encoder's vocabulary. If the number of tokens in the tokenised and concatenated context and question exceeds 512, we truncate it. If it is shorter, we pad it with a special token $[PAD]$.
- The answer is processed in an almost similar fashion. We tokenise each answer using a pre-trained tokeniser pulled from HuggingFace [30], but it has to be compatible with our decoder instead. If the number of tokens are greater than 50, we truncate it. If it is shorter, we pad it with a special token $[PAD]$.
- **This task is evaluated using the Normalized F1 (NF1) metric which strips texts of punctuation and articles before computing the F1 score.** To compute NF1, we utilise the predicted answer and the provided answer. We then remove all punctuation and articles, and tokenise each answer separately. The metric is computed on the basis of number of common words between the two sets of tokens. **Precision** is the ratio of number of shared tokens to the number of tokens in the predicted answer. **Recall** is the ratio of number of shared tokens to the number of tokens in the provided answer. Then, we calculate NF1 as stated in equation 1.

$$NF1 = \frac{2}{\frac{1}{precision} + \frac{1}{recall}} \tag{1}$$

B. Multi-Genre Natural Language Inference (MultiNLI)

MultiNLI [16] is a crowd-sourced corpus of sentence pairs annotated with textual entailment information. The number of example is detailed below in table IV.

TABLE IV: MultiNLI - Dataset Description

	Training	Validation
No. of Samples	392702	19647
Avg. Len. of Premise	10.549	10.657
Avg. Len. of Hypotheses	11.256	10.584

Each text pair consists of a premise and hypothesis. For a human annotator, given the premise, they are expected to answer the following question: *'Is the given hypothesis an entailment, contradiction or natural in context of the given premise?'*

The context for this task is framed as **'Premise-{premise}'** and the question is framed as **'Hypothesis-{hypothesis}:–entailment, neutral, or contradiction?'**

- We process the question and context as discussed in subsection III-A.

Authorized licensed use limited to: DELHI TECHNICAL UNIV. Downloaded on June 22,2022 at 04:33:52 UTC from IEEE Xplore. Restrictions apply.

- The answer for each context-question pair is a single word and is always one of the following: entailment, neutral, or contradiction, so there is no need for truncation.
- **This task is evaluated using the Exact Match (EM) metric which awards full points for an exact match and 0 in all other cases.**

C. CNN / DailyMail Summarisation Dataset (CNN/DM)

CNN/DailyMail [17], [18] is a dataset containing over 300 thousand news articles. Each news article is accompanied by a short highlight written by the original author that is also treated like a summary. That is, for each training example we have an article and its summary. All articles have been extracted from news-sharing websites, in this case, the CNN and DailyMail news agencies.

A random article from the dataset reads as "(CNN) – An American woman died aboard a cruise ship that docked at Rio de Janeiro on Tuesday, the same ship on which 86 passengers previously fell ill, according to the state-run Brazilian news agency, Agencia Brasil. The American tourist died aboard the MS Veendam, owned by cruise operator Holland America. Federal Police told Agencia Brasil that forensic doctors were investigating her death. The ship's doctors told police that the woman was elderly and suffered from diabetes and hypertension, according the agency. The other passengers came down with diarrhea prior to her death during an earlier part of the trip, the ship's doctors said. The Veendam left New York 36 days ago for a South America tour."

Its corresponding summary is "The elderly woman who died suffered from diabetes and hypertension, ship's doctors say. Previously, 86 passengers had fallen ill on the ship, Agencia Brasil says." It includes all the essential details from the article: elderly woman's death, her medical history, history of previous passengers, name of the source.

Due to the auto-encoder nature of our model, we are only able to perform abstractive summarisation, which involves generating spans of novel text, as opposed to extractive summarisation, which involves extracting spans of text from the article. The details of this dataset are included in table V. We also include lengths of articles to emphasise the fact that these are some of the longest articles this model is expected to solve or summarise.

TABLE V: CNN/DM - Dataset Description

	Training	Validation
No. of Samples	287113	13368
Avg. Len. of Articles	781.65	765.85
Avg. Len. of Summaries	56.36	54.55

Unlike SQuAD and MultiNLI, the question for each training data point in our example remains the same – "What is the summary?".

- To form the input to the encoder, we concatenate the article and question, separated by a special $[SEP]$ token. Any input longer than 512 tokens is truncated and inputs shorted that 512 tokens are padded.
- The answer is considered to be the highlight which accompanies each article. We tokenize each answer with a pre-trained tokeniser compatible with our decoder setup. Even though the mean token length is 58, we keep the output length fixed at 60, to maintain coherence with our other tokens. This means we pad each summary so that they are all 60 tokens long.
- This task is evaluated by an average of ROUGE-1, ROUGE-2 and ROUGE-N [31].

D. Stanford Sentiment Treebank (SST)

The Stanford Sentiment Tree Bank [19] is used to evaluate a model's capacity to analyse the sentiment of a given statement [32], [33]. SST consists of movie reviews with the corresponding sentiment: positive, negative and neutral. The model is then expected to predict the sentiment by analyzing just the statement.

The model is provided with a movie review, and expected to provide a single word detailing the underlying sentiment. This task is effective as it tests the model's capacity to understand the deep-rooted semantics of the English language. For example, a review reads as "A thunderous ride at first, quiet cadences of pure finesse are few and far between; their shortage dilutes the potency of otherwise respectable action." If the model was simply establishing a mapping between the input and output via a cursory function such as the number of positive words, this review would be classified as 'positive'. However, a native speaker would disagree, and classify this review as 'negative' which is the correct answer in this case. By providing this task to the model, we test the limits of its understanding of the English language while simultaneously checking whether it is establishing a superficial correlation between the 'question' and the 'answer', or a deep-rooted one.

The statistics of this dataset are listed in table VI.

TABLE VI: SST - Dataset Description

	Training	Validation
No. of Samples	8544	1101
Avg. Len. of Reviews	19.32	19.18

For our purpose, the question for each example in the training data set is "Is this positive, negative or neutral?". We keep the movie review as-is.

- We concatenate the question with the review, separated by a $[SEP]$ token.
- The answer for each example is always one of the following: positive, negative, neutral.
- We also tokenise the answer using a pre-trained tokeniser compatible with our decoder. Even though the answer is always 1 token long, we set the output length to 60, to maintain uniformity with the other tasks.
- **This task is evaluated using the Exact Match (EM) metric which awards full points for an exact match and 0 in all other cases.**

It is interesting to note that even though this task can be solved by approaching it as a classification problem, we don't,

Authorized licensed use limited to: DELHI TECHNICAL UNIV. Downloaded on June 22,2022 at 04:33:52 UTC from IEEE Xplore. Restrictions apply.

or more appropriately, can't do that. The model is expected to generate the answer just like it does for summaries.

Why did we choose only these datasets? To truly test the general ability of our model, it was clear to us from the onset that we would require tasks from diverse genres. Based on this thinking, these tasks were cherry-picked.

1) **SQuAD** [15] is purely a question-answering dataset. The questions vary according to the context and solving this task depends on the model's ability to understand both the question and the context. Additionally, the answer to each question in this dataset comes from the context as is; there is no need to generate novel text.
2) **MultiNLI** [16] is a task that requires the model to understand the relationship between two sentences, which is always one of the three given categories. In essence, this is a classification task and the model is forced to find the answer within the question itself. The model is penalized for erroneous words generated.
3) **CNN/DM** [17], [18] is a summarisation dataset. It tests the model's ability to understand a large body of text and generate a summary. This dataset exposes the model to some of the largest texts it has even seen. Moreover, the answer, almost always, includes novel vocabulary. Thus the model's generative capabilities are tested too.
4) **SST** [19] is a sentiment classification task. The model needs to predict the sentiment of just the one sentence, without considering any other text. The answer too belongs to one of three categories, and the model is penalized for generating a word not belonging to this set.

This creates a perfect balance of classification and generative abilities, cherry-picking tasks that test varied facets of the model's capabilities.

IV. The Model

All our experiments utilize just one model : **the encoder-decoder setup described by Vaswani *et al.* in [1]**. We will not include an exhaustive description of that setup here, but instead point the reader to some excellent resources such as Jay Alammar's 'The Illustrated Transformer'. [1]

In "Leveraging Pre-trained Checkpoints for Sequence Generation Tasks" [26], Rothe *et al.* highlight the huge training costs and time associated with training such a setup from scratch, i.e. starting with completely random parameters and then learning them. They instead propose a cheaper and more efficient alternative: warm starting encoder-decoder with publicly available checkpoints.

A. Warm-Starting the Encoder

Warm-starting typically implies using weights pre-trained on some other task for use on a related or unrelated task. Let us take the example of a BERT [2] encoder to better understand this.

[1] https://jalammar.github.io/illustrated-transformer/

Starting from a BERT [2] encoder utilized with random parameters, if we were to warm-start it with a publicly available checkpoint, it would start by copying every weight layer from the checkpoint to the corresponding layer in the encoder setup. Any layer which was missing in the checkpoint would then be randomly initialized.

B. The BERT Encoder

BERT [2] stands for Bidirectional Encoder Representations from Transformers. Essentially the BERT model consists of stacked bidirectional transformer [1] blocks. BERT is an encoder-only architecture; it encodes the input into an encoded representation, but the representation is not suitable for immediate decoding. However, the reason for BERT's superior performance is not limited to its architecture, it is also because of the pre-training routine put forward by Devlin *et al.* in [2]. They put forward two pre-training objectives:

1) Masked Language Modelling: In this pre-training task, certain tokens in a sentence are removed (masked) and the model is expected to predict these tokens, by inferring the context from its neighbouring tokens. To achieve this, Devlin *et al.* train the encoder-only model on the BooksCorpus dataset [34] and English Wikipedia. Masked language modelling is able to overcome the limitations of the traditional one-way language modelling: that is from left-to-right or right-to-left. In unidirectional language modelling, the model is only ever exposed to context from one side: the left or the right. In BERT, the model benefits from bidirectional context, which enables better and more robust training.

2) Next Sentence Prediction: In Next Sentence Prediction (NSP), each training example consists of two sentences, Sentence A and Sentence B. The model is provided with both sentences and expected to answer the question, "Should sentence B come after sentence A?". This is a classification task, and the model approaches it that way, using a special $[CLS]$ token to classify sentence B into two categories: 'next' and 'not next'.

By pre-training the stacked transformer block on these two objectives, BERT is able to amass a wealth of knowledge from the pre-training corpora that can be further fine-tuned on any downstream task, as is done by Devlin *et al.* in [2].

C. Warm-Starting the Decoder

The decoder is warm started just like the encoder. Once the decoder is warm-started, we add in cross-attention layers, which have been randomly utilized to better tie it with the warm starting encoder.

Rothe *et al.* [26] run a multitude of experiments using the warm-started encoder-decoder setup and are able to achieve remarkable performance: sometimes surpassing encoder-decoder trained from scratch. This success could be attributed to the generic and vast amounts of knowledge pre-trained checkpoints have already amassed. It is easier, cheaper and more efficient to train a model with some knowledge than the one with none.

Authorized licensed use limited to: DELHI TECHNICAL UNIV. Downloaded on June 22,2022 at 04:33:52 UTC from IEEE Xplore. Restrictions apply.

Following in Rothe *et al.*'s footsteps, we use a similar technique for all our experiments. We use the encoder-decoder setup described by Vaswani *et al.*. We warm-start the encoder with the **bert-base-uncased** checkpoint available here [2]. We choose the **bert-base-uncased** checkpoint because it includes the weight maps of an encoder-only setup (BERT [2]) pre-trained on a colossal language modeling dataset. This makes it uniquely suitable for its use as an encoder checkpoint. There are multiple other options such as RoBERTa [8] and DeBERTa [4] but we are limited by both time and computational infrastructure. We leave these experiments to future researchers.

For the decoder-half, we choose the GPT2 checkpoint because it includes the weight maps of a decoder-only setup (GPT2) pre-trained on a huge language modelling dataset, available here [3]. This makes it uniquely suitable for its use a decoder checkpoint. There are, once again, multiple checkpoints, but we leave these for future researchers The cross attention layers that are typical of the encoder decoder setup are introduced in the decoder, and are randomly utilized.

It is important to note that to prevent the decoder from seeing the token it is expected to predict (which would make it a trivial exercise), the output sequence is shifted to the right by one place and during the time of generation all tokens to the right of the current position are masked. This prevents pollution of the encoder states.

V. Training

All of our models are trained on a single Nvidia Tesla P-100 GPU. The batch size for all experiments is 8, the number of the input tokens is limited to 512 and the number of output tokens at 60. We utilize an AdaFactor [35] optimizer with a learning rate of 10^{-4}, and perform a linear warm-up over 10000 steps. We also report training times in section VI.

For our joint training on all four tasks, we utilize only two training strategies and compare their results:

A. Round-Robin Training

In this training strategy, the model is trained on each task in a circular fashion. This means that the model is first trained on task A for one epoch, then on task B, then task C, then task D, then again A. This type of strategy doesn't take into account the difficulty of the training examples in each task.

B. Anti-Curriculum Training

In very simple words, anti-curriculum training [20] involves training on 'tough' tasks before training on 'easy' ones. "Tough" tasks are tasks that requires twice the number of iterations of "easy" tasks. In "The Natural Language Decathlon: Multitask Learning as Question Answering" [21] McCann *et al.* demonstrate a significant boost in performance when their model was trained on SQuAD before it shifted to fully joint training.

[2]https://huggingface.co/bert-base-uncased
[3]https://huggingface.co/gpt2

Due to limited computational resources, we are able to experiment with just these two strategies but leave further experiments to future researchers.

Our cost function for training the models is a simple Cross-Entropy Loss Function averaged over all time-steps.

VI. Results

We present the results of all our experiments in table VII. We also report training times for each experiment.

In single task training, we train our encoder-decoder model warm-started with the BERT [2] checkpoint for the encoder-half, and GPT2 checkpoint for the decoder-half, individually on each task. The tasks aren't mixed and only one task is chosen at a time. Evaluation is performed on the validation set of the same task.

In multi-task training, we train our encoder-decoder model warm-started with the BERT [2] checkpoint for the encoder-half, and GPT2 checkpoint for the decoder-half, jointly on all tasks. As far as the model is concerned, it is unaware of the current task. We only include the metadata of the task for evaluating.

Overall, the performance of the encoder-decoder model trained jointly on all tasks is less than its corresponding individual variation. This is expected, since in a generalized setup a model is expected to learn four tasks together as opposed to an individualized setup where it is expected to learn about just one task. What is interesting to note is that the disparity in performance is not significantly high. For SQuAD [15], for example, the model fine-tuned specifically achieves an NF1 of **62.999** while the generalised setup achieves an NF1 of **56.342**. This shows that even though there is a significant more amount of learning to be performed, and ample chance of catastrophic forgetting, the model is able to keep up, showing that transformers can be applied to a generalized paradigm too.

Even though there are four tasks in the generalized setup, the model never confuses any task i.e. when an example from the Stanford Sentiment Treebank [19] shows up, the model knows it must predict a single word – positive, negative, or neutral, and when an example from the Stanford Question Answering Dataset [15] shows up, it must predict an answer from the context given. This revelation is corroborated by McCann *et al.*'s findings in [21], where their model never mistakes the task it must solve for; even when languages other than English are involved.

The most startling revelation in the joint training experiment is the windfall gain we accumulated while training and validating the Multi-Genre Natural Language Inference task [16]. Individual training is only able to achieve an EM of **35.461**, but when we train jointly on all four tasks, we are able to achieve an EM of **76.144**. That implies a gain of **114.72%**. This task serves as an indicator of the potential of generalized encoder-decoder models. Tasks that were "too tough" to solve on their own, become easier to solve with the combined knowledge of the other three tasks. It also means that the system is able to accumulate knowledge from the

Authorized licensed use limited to: DELHI TECHNICAL UNIV. Downloaded on June 22,2022 at 04:33:52 UTC from IEEE Xplore. Restrictions apply.

TABLE VII: Results

	Single Task		**Multi-Task Training**			
			Round-Robin		**Anti-Curriculum**	
Dataset	Metric Value	Training Time	Metric Value	Training Time	Metric Value	Training Time
SQuAD	62.999 (NF1)	18 hours	56.342 (NF1)	40 hours	47.56 (NF1)	40 hours
SST	82.652 (EM)	4 hours	78.565 (EM)		73.842 (EM)	
CNN/DM	26.444 (ROUGE-AVG)	24 hours	23.996 (ROUGE-AVG)		20.93 (ROUGE-AVG)	
MultiNLI	35.461 (EM)	14 hours	76.144 (EM)		73.842 (EM)	
-	-	**60 hours**	**235.047**	**40 hours**	**216.174**	**40 hours**

other three tasks, and utilize that knowledge in the fourth task. This knowledge is thus generalized and applies to language in general, dispelling the theory that the model gains just task-aware knowledge.

Jump-starting on the SQuAD [15] task, that is training on the SQuAD task before resorting to joint training doesn't yield high dividends. Training for longer times might yield better results, but we leave these experiments for future researchers.

A. Zero-Shot Adaptation

A generalized setup also enables us to add more tasks to our repertoire without a change in model architecture or parameters. Since out list of tasks includes MultiNLI [16], it is only natural to validate performance on the SNLI [36] dataset.

The encoder-decoder model trained jointly on all four tasks achieves an exact match score of **66.490** without any fine-tuning. This bolsters the claim of generalizability for such models and also proves its efficacy on zero-shot adaptations of tasks. The model is able to utilize its knowledge towards tasks that it has never seen before, giving reasonable results without any fine-tuning. This proves that models emerging in a general paradigm are more suited to zero-shot task learnings.

As is evident from figure 1b, the training of a model that has been trained on all four tasks detailed in section III, achieves almost zero validation loss just as it begins training, as opposed to the model which is trained from scratch on this task, which starts off at a validation loss of almost 12. This proves the benefits of transfer learning: the model benefits greatly from the knowledge gathered over the four tasks. The system is not only able to converge faster, but experiences windfall gains early in the training as is evident in figure 1a. Before the first step, the model which is pre-trained on four tasks achieves an EM score of **66.490**, while the model which has not been pre-trained starts off at almost 0. This makes the jointly-trained model a great asset: new tasks can be added both with and without further fine-tuning. Thus, the model benefits greatly in a general paradigm: adding new tasks is easy, requires less training, and achieves greater performance within the same time frame than models trained individually.

Fine-tuning too has dramatic effects. Fine-tuning a pre-trained model boosts the EM score on SNLI [36] to **86.324**, which implies that models containing a vast amount of knowledge are few-shot learners [7].

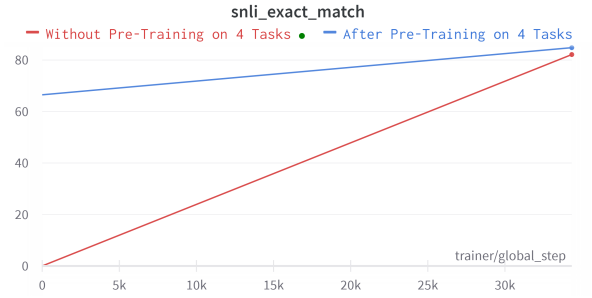

(a) Exact Match Over Time

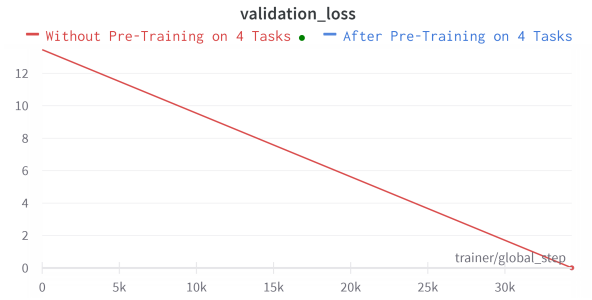

(b) Validation Loss Over Time

Fig. 1: Results of Zero-Shot Adaptation to SNLI Experiments

VII. Conclusion

We explored and analysed the performance of transformer-based encoder-decoder setups in a general natural-language generation paradigm. We displayed results of our experiments, which proved that the benefits of jointly training on natural language generation tasks far supersedes the downside of catastrophic forgetting. In fact, we make windfall gains on the MultiNLI [16] task achieving a boost of **114%** as compared to the individually trained models. Anti-curriculum training [20] doesn't hurt performance but doesn't boost it either. Jointly-trained models also show tremendous potential in zero-shot adaptations of tasks, proving their efficacy in never-before seen domains. Our experiments achieved an EM of **66.490** on the SNLI [36] task without any fine-tuning and an EM of **86.324** with fine-tuning, showing the benefits of transfer learning. Overall, GenGen presents a comprehensive analysis of encoder-decoder models in a general paradigm and tests the extents of their capabilities in both known and unknown domains.

Authorized licensed use limited to: DELHI TECHNICAL UNIV. Downloaded on June 22,2022 at 04:33:52 UTC from IEEE Xplore. Restrictions apply.

REFERENCES

[1] A. Vaswani, N. Shazeer, N. Parmar, J. Uszkoreit, L. Jones, A. N. Gomez, L. Kaiser, and I. Polosukhin, "Attention is all you need," 2017.

[2] J. Devlin, M.-W. Chang, K. Lee, and K. Toutanova, "Bert: Pre-training of deep bidirectional transformers for language understanding," 2019.

[3] Z. Lan, M. Chen, S. Goodman, K. Gimpel, P. Sharma, and R. Soricut, "ALBERT: A lite BERT for self-supervised learning of language representations," *CoRR*, vol. abs/1909.11942, 2019. [Online]. Available: http://arxiv.org/abs/1909.11942

[4] P. He, X. Liu, J. Gao, and W. Chen, "Deberta: Decoding-enhanced BERT with disentangled attention," *CoRR*, vol. abs/2006.03654, 2020. [Online]. Available: https://arxiv.org/abs/2006.03654

[5] V. Sanh, L. Debut, J. Chaumond, and T. Wolf, "Distilbert, a distilled version of BERT: smaller, faster, cheaper and lighter," *CoRR*, vol. abs/1910.01108, 2019. [Online]. Available: http://arxiv.org/abs/1910.01108

[6] H. Le, L. Vial, J. Frej, V. Segonne, M. Coavoux, B. Lecouteux, A. Allauzen, B. Crabbé, L. Besacier, and D. Schwab, "Flaubert: Unsupervised language model pre-training for french," *CoRR*, vol. abs/1912.05372, 2019. [Online]. Available: http://arxiv.org/abs/1912.05372

[7] T. B. Brown, B. Mann, N. Ryder, M. Subbiah, J. Kaplan, P. Dhariwal, A. Neelakantan, P. Shyam, G. Sastry, A. Askell, S. Agarwal, A. Herbert-Voss, G. Krueger, T. Henighan, R. Child, A. Ramesh, D. M. Ziegler, J. Wu, C. Winter, C. Hesse, M. Chen, E. Sigler, M. Litwin, S. Gray, B. Chess, J. Clark, C. Berner, S. McCandlish, A. Radford, I. Sutskever, and D. Amodei, "Language models are few-shot learners," *CoRR*, vol. abs/2005.14165, 2020. [Online]. Available: https://arxiv.org/abs/2005.14165

[8] Y. Liu, M. Ott, N. Goyal, J. Du, M. Joshi, D. Chen, O. Levy, M. Lewis, L. Zettlemoyer, and V. Stoyanov, "Roberta: A robustly optimized BERT pretraining approach," *CoRR*, vol. abs/1907.11692, 2019. [Online]. Available: http://arxiv.org/abs/1907.11692

[9] I. Sutskever, O. Vinyals, and Q. V. Le, "Sequence to sequence learning with neural networks," *CoRR*, vol. abs/1409.3215, 2014. [Online]. Available: http://arxiv.org/abs/1409.3215

[10] ——, "Sequence to sequence learning with neural networks," *CoRR*, vol. abs/1409.3215, 2014. [Online]. Available: http://arxiv.org/abs/1409.3215

[11] D. Bahdanau, K. Cho, and Y. Bengio, "Neural machine translation by jointly learning to align and translate," in *3rd International Conference on Learning Representations, ICLR 2015, San Diego, CA, USA, May 7-9, 2015, Conference Track Proceedings*, Y. Bengio and Y. LeCun, Eds., 2015. [Online]. Available: http://arxiv.org/abs/1409.0473

[12] M. Luong, H. Pham, and C. D. Manning, "Effective approaches to attention-based neural machine translation," *CoRR*, vol. abs/1508.04025, 2015. [Online]. Available: http://arxiv.org/abs/1508.04025

[13] C. Raffel, N. Shazeer, A. Roberts, K. Lee, S. Narang, M. Matena, Y. Zhou, W. Li, and P. J. Liu, "Exploring the limits of transfer learning with a unified text-to-text transformer," *CoRR*, vol. abs/1910.10683, 2019. [Online]. Available: http://arxiv.org/abs/1910.10683

[14] M. Lewis, Y. Liu, N. Goyal, M. Ghazvininejad, A. Mohamed, O. Levy, V. Stoyanov, and L. Zettlemoyer, "BART: denoising sequence-to-sequence pre-training for natural language generation, translation, and comprehension," *CoRR*, vol. abs/1910.13461, 2019. [Online]. Available: http://arxiv.org/abs/1910.13461

[15] P. Rajpurkar, J. Zhang, K. Lopyrev, and P. Liang, "Squad: 100, 000+ questions for machine comprehension of text," *CoRR*, vol. abs/1606.05250, 2016. [Online]. Available: http://arxiv.org/abs/1606.05250

[16] A. Williams, N. Nangia, and S. Bowman, "A broad-coverage challenge corpus for sentence understanding through inference," in *Proceedings of the 2018 Conference of the North American Chapter of the Association for Computational Linguistics: Human Language Technologies, Volume 1 (Long Papers)*. Association for Computational Linguistics, 2018, pp. 1112–1122. [Online]. Available: http://aclweb.org/anthology/N18-1101

[17] K. M. Hermann, T. Kociský, E. Grefenstette, L. Espeholt, W. Kay, M. Suleyman, and P. Blunsom, "Teaching machines to read and comprehend," *CoRR*, vol. abs/1506.03340, 2015. [Online]. Available: http://arxiv.org/abs/1506.03340

[18] R. Nallapati, B. Zhou, C. dos Santos, Ç. Gulçehre, and B. Xiang, "Abstractive text summarization using sequence-to-sequence RNNs and beyond," in *Proceedings of The 20th SIGNLL Conference on Computational Natural Language Learning*. Berlin, Germany: Association for Computational Linguistics, Aug. 2016, pp. 280–290. [Online]. Available: https://aclanthology.org/K16-1028

[19] R. Socher, A. Perelygin, J. Wu, J. Chuang, C. D. Manning, A. Ng, and C. Potts, "Recursive deep models for semantic compositionality over a sentiment treebank," in *Proceedings of the 2013 Conference on Empirical Methods in Natural Language Processing*. Seattle, Washington, USA: Association for Computational Linguistics, Oct. 2013, pp. 1631–1642. [Online]. Available: https://aclanthology.org/D13-1170

[20] Y. Bengio, J. Louradour, R. Collobert, and J. Weston, "Curriculum learning," in *Proceedings of the 26th Annual International Conference on Machine Learning*, ser. ICML '09. New York, NY, USA: Association for Computing Machinery, 2009, p. 41–48. [Online]. Available: https://doi.org/10.1145/1553374.1553380

[21] B. McCann, N. S. Keskar, C. Xiong, and R. Socher, "The natural language decathlon: Multitask learning as question answering," *CoRR*, vol. abs/1806.08730, 2018. [Online]. Available: http://arxiv.org/abs/1806.08730

[22] A. Kumar, O. Irsoy, J. Su, J. Bradbury, R. English, B. Pierce, P. Ondruska, I. Gulrajani, and R. Socher, "Ask me anything: Dynamic memory networks for natural language processing," *CoRR*, vol. abs/1506.07285, 2015. [Online]. Available: http://arxiv.org/abs/1506.07285

[23] J. Zhang, Y. Zhao, M. Saleh, and P. J. Liu, "PEGASUS: pre-training with extracted gap-sentences for abstractive summarization," *CoRR*, vol. abs/1912.08777, 2019. [Online]. Available: http://arxiv.org/abs/1912.08777

[24] M. Zaheer, G. Guruganesh, A. Dubey, J. Ainslie, C. Alberti, S. Ontañón, P. Pham, A. Ravula, Q. Wang, L. Yang, and A. Ahmed, "Big bird: Transformers for longer sequences," *CoRR*, vol. abs/2007.14062, 2020. [Online]. Available: https://arxiv.org/abs/2007.14062

[25] Y. Yan, W. Qi, Y. Gong, D. Liu, N. Duan, J. Chen, R. Zhang, and M. Zhou, "Prophetnet: Predicting future n-gram for sequence-to-sequence pre-training," *CoRR*, vol. abs/2001.04063, 2020. [Online]. Available: https://arxiv.org/abs/2001.04063

[26] S. Rothe, S. Narayan, and A. Severyn, "Leveraging pre-trained checkpoints for sequence generation tasks," *CoRR*, vol. abs/1907.12461, 2019. [Online]. Available: http://arxiv.org/abs/1907.12461

[27] P. Ramachandran, P. J. Liu, and Q. V. Le, "Unsupervised pretraining for sequence to sequence learning," *CoRR*, vol. abs/1611.02683, 2016. [Online]. Available: http://arxiv.org/abs/1611.02683

[28] L. Dong, N. Yang, W. Wang, F. Wei, X. Liu, Y. Wang, J. Gao, M. Zhou, and H. Hon, "Unified language model pre-training for natural language understanding and generation," *CoRR*, vol. abs/1905.03197, 2019. [Online]. Available: http://arxiv.org/abs/1905.03197

[29] G. Lample and A. Conneau, "Cross-lingual language model pretraining," *CoRR*, vol. abs/1901.07291, 2019. [Online]. Available: http://arxiv.org/abs/1901.07291

[30] T. Wolf, L. Debut, V. Sanh, J. Chaumond, C. Delangue, A. Moi, P. Cistac, C. Ma, Y. Jernite, J. Plu, C. Xu, T. Le Scao, S. Gugger, M. Drame, Q. Lhoest, and A. M. Rush, "Transformers: State-of-the-Art Natural Language Processing." Association for Computational Linguistics, 10 2020, pp. 38–45. [Online]. Available: https://www.aclweb.org/anthology/2020.emnlp-demos.6

[31] C.-Y. Lin, "ROUGE: A package for automatic evaluation of summaries," in *Text Summarization Branches Out*. Barcelona, Spain: Association for Computational Linguistics, Jul. 2004, pp. 74–81. [Online]. Available: https://aclanthology.org/W04-1013

[32] P. P. A., "Performance evaluation and comparison using deep learning techniques in sentiment analysis," *June 2021*, vol. 3, no. 2, pp. 123–134, Jul. 2021. [Online]. Available: https://doi.org/10.36548/jscp.2021.2.006

[33] D. A. Sungheetha and D. R. S. R, "TransCapsule model for sentiment classification," *September 2020*, vol. 2, no. 3, pp. 163–169, Jul. 2020. [Online]. Available: https://doi.org/10.36548/jaicn.2020.3.003

[34] Y. Zhu, R. Kiros, R. S. Zemel, R. Salakhutdinov, R. Urtasun, A. Torralba, and S. Fidler, "Aligning books and movies: Towards story-like visual explanations by watching movies and reading books," *CoRR*, vol. abs/1506.06724, 2015. [Online]. Available: http://arxiv.org/abs/1506.06724

[35] N. Shazeer and M. Stern, "Adafactor: Adaptive learning rates with sublinear memory cost," *CoRR*, vol. abs/1804.04235, 2018. [Online]. Available: http://arxiv.org/abs/1804.04235

[36] S. R. Bowman, G. Angeli, C. Potts, and C. D. Manning, "A large annotated corpus for learning natural language inference," *CoRR*, vol.

Authorized licensed use limited to: DELHI TECHNICAL UNIV. Downloaded on June 22,2022 at 04:33:52 UTC from IEEE Xplore. Restrictions apply.

abs/1508.05326, 2015. [Online]. Available: http://arxiv.org/abs/1508.05326

Authorized licensed use limited to: DELHI TECHNICAL UNIV. Downloaded on June 22,2022 at 04:33:52 UTC from IEEE Xplore. Restrictions apply.

Int J Syst Assur Eng Manag
https://doi.org/10.1007/s13198-022-01666-6

ORIGINAL ARTICLE

iCACD: an intelligent deep learning model to categorise current affairs news article for efficient journalistic process

Sachin Kumar[1] · Shivam Panwar[1] · Jagvinder Singh[2] · Anuj Kumar Sharma[3] · Zairu Nisha[4]

Received: 3 February 2022 / Revised: 3 February 2022 / Accepted: 30 March 2022
© The Author(s) under exclusive licence to The Society for Reliability Engineering, Quality and Operations Management (SREQOM), India and The Division of Operation and Maintenance, Lulea University of Technology, Sweden 2022

Abstract In the present-day technology-driven world, information reaching at the individual's doorstep sometimes becomes complex, haphazard and difficult to classify to get the insights. The endpoint consumer of the information requires processed information which is contextually suited to their needs, interests and is properly formatted and categorised. Interests and need-based categorization of news and stories would enable the user beforehand to further evaluate information deeply. For instances, the type current affairs related issues and news to read or not to read. This research work proposes an advanced current affairs classification model based on deep learning approaches called Intelligent Current Affairs Classification Using Deep Learning (iCACD). The proposed model is better than already proposed models based on machine learning approached which have been compared on accuracy and performance criteria. The proposed model is better in the following ways. Firstly, It is based on advanced deep neural network architecture. Secondly, the model advances the work to include both headline and body of the information/news articles rather than only processing headlines. Thirdly, A detailed comparative analysis and discussion on accuracy and performance with other machine leaning models have also been presented.

Keywords Current affairs · News articles · Machine learning · Deep learning · Accuracy · Efficiency · Text classification

✉ Jagvinder Singh
jagvinder.singh@gmail.com

Sachin Kumar
officialid.sachin@gmail.com; skumar@cic.du.ac.in

Shivam Panwar
shivam140128@one.ducic.ac.in

Anuj Kumar Sharma
anujsharma1920@gmail.com

Zairu Nisha
zairunisha@gmail.com

[1] Cluster Innovation Centre, University of Delhi, New Delhi, Delhi, India

[2] School of Management and Entrepreneurship, Delhi Technological University, New Delhi, Delhi, India

[3] Dept of Mathematics, Shyamlal College, University of Delhi, New Delhi, Delhi, India

[4] Ramanujan College, University of Delhi, New Delhi, Delhi, India

1 Introduction

Recent technological advancements in ICT and its associated domains have significantly remodelled our life. Now, our digital footprints have information about our interests and needs (Golder and Macy 2014). Moreover, Data obtained through platforms recording our activities and decision over the digital space have helped the companies to cater to the demand and satisfy our needs using technologies such as big data, artificial inelegance etc (Youyou et al. 2015). Data-driven intelligence has transformed our life decision making systems in several ways starting from career guidance, sleep help app, health informatics, intelligent transportation and weather reporting and in many more ways (Foster and Tom 2013). Our daily life goes in reading and writing important information depending on our personal interests. More often we feel the need to

Published online: 12 June 2022

intelligent assistant to get the text and information classified as per our interests and present to us in processed format (Altınel and Ganiz 2018). In this direction, Intelligent data-driven models can also be modelled and developed to satisfy the needs and requirements of users, readers or the followers of current affairs and news articles. News and media organisations have also maintained their website disseminating current affairs and important information to the users or citizens efficiently and productively (Mark 2019). They also are in need to make the news processing and publishing process efficient by incorporating the automated and intelligent processes to classify the articles they are getting from authors as this needs a manual process to read and then classify the story to place in the correct news item category (Kumar et al. 2021). The news life cycle consists of the phases such as the collection of a news story in an unformatted manner, processing the news that are unformatted and uncontext, decision making to place and categorise the news article based on the quality and other parameters and publication and dissemination. The present-day media industry and its stakeholders are competing to be first in breaking the news with a high level of accuracy and efficiency in publishing and dissemination. This requires an efficient, effective, intelligent solutions to be deployed in the news article processing phase of news life cycle system (Chaker 2016). In this situation, some level of feature selection, feature generation techniques and processing with machine learning or deep learning method can be helpful. There are many areas where artificial intelligence and machine learning approaches (Longo et al. 2020) have been used such as smart cities (Allam and Dhunny 2019). They have been used on energy and building domain to predict energy load (Kumar et al. 2016), temperature prediction (Sachin et al. 2018) and energy performance and indoor temperature prediction (Kumar et al. 2019), occupancy detection (Kumar et al. 2020), intelligent transportation (Sachin et al. 2018) and intelligent health systems development too (Kumar et al. 2018). The proposed deep learning model is designed to automate intelligently, some of the hectic and time-consuming processes such as news categorisation at primary level with a new type of information and labels. As per the previous works and feedback from stakeholders, the news processing tasks including the classification requires a lot of human effort of reading the article, asking the author itself to classify the articles and their place in the news portals. The volume of the articles, their quality and complexity of classification necessitates the efficient system automating this process for the news agencies. It will also benefit users to access news of interest in a more efficient manner. Some of the works have proposed models for the classification and processing of the articles based on many rigid mathematical and statistical systems (Wang et al. 2016). The models have not been able to produce good results as they took limited data such as only headlines to classify the articles (Kanan and Fox 2016). Such approaches suffer from truncating the information ingrained at the initial stage that could have been useful in a later stage of classification and news placement. Such models are not even suitable for real-world situations as they suffer from over fitting. The proposed model iCACD(intelligent Current Affairs Classification Using Deep Learning) has further improved the existing work in term of accuracy. This work facilitates current affairs based news article intelligent processing to help the users, writers, editors and news organisation and other stakeholders to accurately label the current affairs related information and news articles very effectively and efficiently in terms of human and computational resources (Zubiaga et al. 2011). The proposed model has incorporated improvements such as reading the whole article, not just headline and extracts meaningful relationships between words to label an article into one of the appropriate categories (Morales et al. 2012). Fundamentally, the research paper proposes the following improvements and findings.

1. Firstly, it designs the experiment using the complete current affairs related text and news articles (titles and news story) to have an improvement over previous work.
2. Secondly, It proposes intelligent iCACD model to effectively classify the news articles with highest probability of falling into one of the news categories.
3. Thirdly, it performs current affairs and news classification and comparison on the newly developed data set among other machine learning and deep learning models.

This research article is organised in the following manner. Section 2 describes the literature. Section 3 explain the artificial intelligence approaches. Section 4 describes the research methodology and purposed model. Section 5 arranges results and discusses the results in detail. Section 6 concludes the paper.

2 Literature survey

Text classification and processing is a sub domain of in Natural Language Processing(NLP) which have wide applications in a real-world and present-day data-driven society. Initially, work started for the processing only which later on get transformed to get deep insights using intelligent techniques such as sentiment analysis and high-frequency words. Previous work in the literature has used rigid mathematical equation-based processing techniques (Chiranjib 2019). Critically analysing, it has been observed

that such methods and approaches fall short of performing the desired task of sentiment analysis, text categorization and to further policy decisions in a real-world environment (Manoochehr et al. 2013). Over this development, probabilistic and statistical methods were developed catering to the processing of the data on a limited scale. With the advent of databases and web-based applications and huge data generation required to have more accurate and efficient methods to accurately analyses and categorise the text in dynamic categories of the text on a real-time basis. Such a conducive environment helped Artificial Intelligence(AI) based approaches to perform well as the environment of large datasets and high computational power has been made available and gained prominent space. Artificial Intelligence approaches have been very effective in several domains of real life (Azizi 2019). Talking specifically in text classification, Some of the specific and very relevant work has been presented in the following discussions. Initially, the method used the text without doing any feature selection and extraction methods to get the designed analysis and categorisation. Jones (1972) proposed the idea of converting textual data into features using term frequency and inverse document frequency. This set the foundation for other research work to apply different type of algorithms, for instance, Bayesian algorithms (Kibriya et al. 2004) and Support Vector Machine (SVM) (Joachims 1998). In one of the studies by Kanan and Fox (2016), applied P-S Temmer and machine learning approaches for tailored article classification and demonstrated good appreciative results. Scharkow et al did the thematic content analysis on german online news (Michael 2013). Laila (2009) used an N-gram frequency with machine learning for Arabic text. Haruechaiyasak et al. (2008) implemented browsing based text categorization. Kadhim (2019) and (Aggarwal and Zhai 2012) have surveyed the domain of text classification based on machine learning. Some of the researchers have applied text classification on clinical text too (Garla and Brandt 2012). Figueiredo et al used Word co-occurrence features for the text classification (Figueiredo et al. 2011). Prasetijo et al developed a hoax detection system using SVM and SGD on Indonesian text (Prasetijo et al. 2017). Ahmed et al applied text classification techniques to detect opinion and fake news (Hadeer et al. 2018) Classification approaches based on Artificial Neural Network (ANNs) have good performance with non-sequential data but since they don't use the sequential relationship in textual data, they were not effective in text classification. Later on this ability to use sequential relationship is explored by recurrent neural networks (RNNs). The idea of word embedding was implemented by Mikolov et al. (2013). Researchers worked over RNNs and proposed a powerful deep architecture approach Long Short Terms Memory(LSTM) which have ruled the NLP horizon. Later on (Vaswani et al. 2017) proposed a specialised transformers architecture. These are attention-based encoder-decoder models primarily designed for sequential data processing. These don't suffer from long term dependencies and vanishing gradient issue. This architecture was used by Devlin et al. (2018). They proposed a new method of training transformer-based language models. This broke many states of the art results in NLP. Researchers from CMU and Google proposed another language model in the form of BERT which have been demonstrating the good results in text classification tasks (Yang et al. 2019). This set the stage that deep learning based model involving inherent features selection and relationship development can provide better accuracy and performance than machine learning approaches.

3 Artificial intelligence approaches

There are several AI approaches which have been developed and have been implemented in different domains depending of their suitability. Our experiment have used some of them and their foundational understating and mathematical formulations are following.

3.1 Machine learning approaches

Random forest(RF) as the name suggests is a forest of trees (Ho 1998). It is a bagging algorithm which constructs multiple trees and averages out their probability to get the final result. It is based on the philosophy of collective intelligence. Hundred people's decision is better than one, so hundred trees are better than one. It's a fairly simple yet powerful algorithm. It reduces the over fitting done by the single decision tree. Other machine learning methods such as Support Vector Machine(SVM) is a linear model for classification and regression problems (Corinna and Vladimir 1995). It can solve linear and non-linear problems. The idea of SVM is simple: The algorithm tries to create a hyperplane which separates the data into classes. For n-dimensional data, it finds an 'n-1' dimensional hyperplane or simply a decision boundary. Data points falling on the same side of the hyperplane are classified in the same class. SVM finds this hyperplane using the property that it should maximize the distance or margin between two classes. For a plane, it's hyperplane is a line whereas for a 3D data, it's hyperplane is a plane. Another machine learning approach, Multinomial Naive Bayes(MNB) is a probabilistic classification model which works by using Bayes theorem (Rennie et al. 2003). It works by assuming features are independent of each other, which is rarely the case. Let's say we want to classify type of tree based on three features such as length of leaves, height of tree, diameter of tree. It

will assume each of these features as being independent of each other in final classification of type of tree. Kibriya et al. (2004) explained the effectiveness of Bayesian algorithms in text classification in their work. Given a feature vector $X = (X1, X2, \ldots, X_n)$ and a class variable C_k, we need to find the probability of class C_k given X. We need to do this for all classes.

$$P(C_k|X) = \frac{P(X|C_k)P(C_k)}{P(X)} \, for \, k = 1, 2, \ldots, K.. \tag{1}$$

$P(X|C_k)$ can be written as

$$P(X|C_k) = P(x_1, \ldots, x_n|C_k) = \prod_{P(x_i|C_k)} \tag{2}$$

Equation 2 means we need to take a product for each individual feature where the class of document is k. This is because we assumed the features to be independent of each other. We will calculate $P(Ck|X)$for each category for a given document and return the class with the highest probability. This is a fairly simple algorithm and works when data is less and can be used as a baseline model for future models. It has a very less training time and doesn't need much data for training.

3.2 Deep learning approaches

In the AI domain, new subset of DL have emerged which have been performing well on the more data set with higher accuracy. More specifically, our problem is of the text classification. Text or sequential data has the special property that all the text is spatially related to each other. We as humans, derive the meaning of sentences based on the order of words in them. There is some sequence in them which helps us to understand their meaning. This spatially is not explored by the machine learning methods mentioned above. Each algorithm assumes the words are independent of each other. Consider, for instance, apple, mango, and tea are not different for machine learning algorithms. It is not the case in the actual scenario as we know apple and mango are more close to each other. If words are represented as vectors, and these vectors are representative of the spatial relationship between word on the n-dimensional plane, then we could exploit the relationship between words. Word vectors precisely do this. While processing some textual information, we understand each word based on previous words understanding. We keep some information about previous words to process and derive meaning from the given word. Traditional Neural networks don't work in this manner. They don't keep the context from previous words. This issue was addressed by Sepp and Jürgen (1997). He proposed using a Long short term memory(LSTM) algorithm, a variant of Recurrent neural networks(RNN). LSTM networks are able to process information sequentially and keep longer contexts in their memory. Bidirectional Encoder Representations from Transformers(BERT) in 2018 was released by Vaswani et al. (2017). They introduced an attention based encoder-decoder architecture dispensing recurrent and convolutional networks. This architecture was named as transformer.The Encoder is on the left and the Decoder is on the right in the image below. Both Encoder and Decoder are composed of modules that can be stacked on top of each other multiple times, which is described by Nx. BERT is a transformer based model of learning language representations. It is a bidirectional transformer pre-trained model developed using a combination of two tasks namely: masked language modeling objective and next sentence prediction on a large corpus. It has achieved state of the art results on various NLP tasks. We can use the language representation learned by Bert to fine tune our task. It doesn't suffer with problems of vanishing gradient and context remembering issues making it suitable for our long articles. Bert comes in various flavors such as Bert base uncased, Bert base cased, Bert large uncased and so on. It depends on the task whether we want to choose an uncased or cased model. We can also choose Bert's large variant but that would mean too much utilisation of resources. Based on our task we found certain parameters to give better results. Another DL method used is XLNet (Yang et al. 2019). Conceptually, XLNet is a method of learning language representations using an auto regressive pre-training method. The model is itself pretty similar to the Bert model, only difference being training objective. It has been fine tuned XLNet for our news classification task. Similar to BERT, XLNet too comes in various flavors such as XLNet large cased, XLNet large uncased and so on. Xlnet base cased was found to give the best results.

4 Proposed experimentation and iCACD model

The proposed experiment design is as follows. News or current affairs text classification is one of the variations of text classification applied on news articles, blogs, political text, tweets and so on.

4.1 Data processing

For the classification purpose first, it needs to be formulated in the form of a mathematical format suitable for AI approaches. More specifically, Let's suppose that $D = \{d_1, d_2 \ldots d_N\}$ is a collection of all the desired news or current affairs articles and articles are correspondingly labelled and represented with set $L = \{L_1, L_1, \ldots L_N\}$. Here N represents the total number of documents in the data set. As per the research objective, the research work has to

develop a novel classifier to put the documents in their correct categories defined by labels. More specifically, Any coming article,d would be classified into one of the categories defined in L. In our case these labels were spread across nine categories namely:(1) Business & Economy, (2)Education & Career, (3) Entertainment, (4)Food & Health, (5) International, (6) Others (7) Politics & Governance (8)Science & Technology and (9)Sports represented respectively by $L_1, L_2 \ldots L_9$. In the name of machine learning models, six algorithms based models have been developed namely, SVM, MNB, RF, LSTM, BERT and XLNet. Developing a new classifier is an iterative process. It is primarily distributed into five steps: Obtaining the dataset, analysing/cleaning the data, modelling the data, analysing model and it's predictions, deploying the model in the real world. All these steps are iterative, as soon as data keeps on arriving, we keep on performing these steps to model or train the data. The best classifiers are one which correctly labelled the current affairs text in the classification process and ensures that the model does not learn the wrong mapping from input space to output vector. Certain balance in data set needs to be maintained to prevent models from overfitting. The ML classification life cycle involves some steps and challenges associated with them. Modelling itself presents certain challenges. For machine learning algorithms, Documents first need to be converted into vectors. To be able to improve the classification accuracy, relationship and meaning between the words in the text need to be part of the proposed models. This incorporation needs our data as sequential data and feeds it into deep learning models. News articles are often very long texts, many deep learning algorithms suffer from vanishing gradient issues in longer texts. Data have been collected from the standard website of the news portals labelled into nine categories. There is a total of approximately 1800 current affairs in the British English language. Data is available at Git Hub repository(https://github.com/sachinblessed95/Current-Affairs-Stories-and-Article-Data-Set). The data related information has been provided in Table 1. For model training, data is segmented into 75:25 train and test split respectively. We stratified data based on label column to ensure the same division in train and test set. We can see that the data distribution is balanced. First step for any machine learning approach is text cleaning. Figure 1 displays the whole proposed model. After the cleaning, data is formatted and structured into the features by converting them into vectors. The cleaned text documents are processed through Tf-IDf vectorisation process. For each algorithm firstly, the most suitable Tf-IDf parameters are found followed by those parameters, text data sets converted into their vectorized representation. The proposed model uses GridSearch() method to find the optimal parameters. For each ML Model, TF-IDf parameters have been arranged in the Table 3.

Table 1 Category wise training and testing data distribution

Category	Training count	Testing count
Business and economy	160	40
Education and career	160	40
Entertainment	159	40
Food and health	160	40
Others	160	40
Politics and governance	160	34
Science and technology	156	40
Sports	156	40
International	160	40

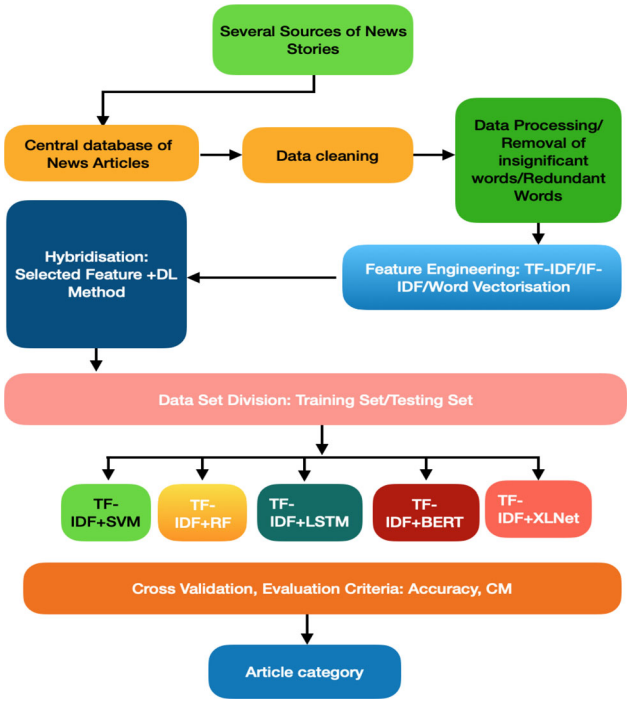

Fig. 1 ICACD: proposed model

5 Result analysis and discussion

The experiment results have been discussed in details with their implications and improvements over the previous works. ML model based on Tf-IDf and RF results are shown with confusion matrix for each classes of current affairs text or news articles. Confusion matrix gives clear picture of how each document has been classified with properly and not properly. Table 2 provides the accuracy or all the models for the comparison. Table 4 provides

Table 2 Models wise accuracy and time efficiency

Models	Accuracy	Time (In Sec)
TF-IDF+RF (Kumar et al. 2021)	81.83	3.0
TF-IDF+SVM (Kumar et al. 2021)	85.62	5.0
LSTM	81.63	342 (On Tesla K80 GPU)
Prop. iCACD-BERT	85.78	6600 (On Tesla K80 GPU)
XLNet	83.43	7200 (On Tesla K80 GPU)

precision of the each model for the article classification task. Table 5 gives recall information of the classification. Table 6 give details of models F-Score for the classification task. Table 2 also lists the running time of the proposed models for each algorithms. Now the results are discussed taking proposed models one by one. With the proposed model based on $TF - IDF + RF$, results are shown in Fig. 2. The $TF - IDF + RF$ model have two parameter set for the results obtained. One of the $TF - IDF + RF$ and Other for RF. RF parameters are maximum depth=8, minimum sample leaf=1 and estimator count=500. With these parameters, TF-IDF setting are as following-Max DIF=0.5, Maximum features=40,000, Norm=L2. This $TF - IDF + RF$ proposed model gives 81.83 percent results. Best classification results are for sports category of current affairs and news articles while model perform worst for the other category of news articles followed by science and technology. With the similar parameter setting of TF-IDF, Model $TF - IDF + SVM$ results are shown in Fig. 3. SVM parameter applied are arc C=3, gamma=auto depreciated, decision function=orr, degree=3. $TF - IDF + SVM$ gives 85.62 percent accuracy in article classification

Table 3 Model Parameter setting comparison

Serial No	Machine learning model	Parameter settings	TFIDF parameter	Accuracy
1	TF-IDF+RF (Kumar et al. 2021)	max depth=8, max features='log2', max leaf nodes=None, min impurity decrease=0.0, min samples leaf=1, min samples split=2, min weight fraction leaf=0.0, n estimators=500	analyzer='word', binary=False, decode error='strict', lowercase=True, max df=0.5, max features=40000, min df=1, ngram range=(1, 2), norm='l2', preprocessor=None,smooth idf=True, stop words=None,tokenizer=None, use idf=True, vocabulary=None	81.83
2	TF-IDF+SVM (Kumar et al. 2021)	C=3, class weight=None, decision function shape='ovr', degree=3, gamma='auto deprecated', kernel='linear', max iter=-1, probability=False	analyzer='word', binary=False, decode error='strict', lowercase=True, max df=0.5, max features=40000, min df=1, ngram range=(1, 2), norm='l2', preprocessor=None,smooth idf=True, stop words=None, tokenizer=None, use idf=True, vocabulary=None	85.62
3	BERT	Word length: 200, Optimizer: Adam, Epochs:12, Word embedding dimensions:300, LSTM output cells: 64, Pooling strategy: MaxPooling		85.78
4	XLnet	XLNet base cased, batch size:8, sequence length:512, learning rate:2e-5, optimizer:Adam, epochs:11		83.43

Table 4 Model and current affairs category wise precision analysis

News category	TF-IDF+RF	TF-IDF+SVM	LSTM	BERT	XLNet
Business & economy	0.609375	0.900000	0.921053	0.894737	0.853659
Education & career	0.714286	0.725490	0.717391	0.864865	0.888889
Entertainment	0.800000	0.711538	0.795455	0.857143	0.829268
Food & Health	0.815789	0.864865	0.900000	0.942857	0.944444
International	0.861111	0.888889	0.738095	0.837209	0.875000
Others	0.823529	0.680000	0.444444	0.705882	0.575758
Politics & governance	0.774194	0.794118	0.645161	0.800000	0.756757
Science & technology	0.733333	0.717949	0.681818	0.755102	0.729167
Sports	0.909091	1.000000	0.952381	1.000000	0.951220

Table 5 Model and current affairs category wise recall analysis

News category	TF-IDF+RF	TF-IDF+SVM	LSTM	BERT	XLNet
Business & Economy	0.975000	0.850000	0.875000	0.850000	0.875000
Education & Career	0.875000	0.850000	0.825000	0.800000	0.800000
Entertainment	0.900000	0.900000	0.897436	0.923077	0.871795
Food & Health	0.775000	0.700000	0.675000	0.825000	0.850000
International	0.775000	0.825000	0.775000	0.900000	0.875000
Others	0.350000	0.625000	0.400000	0.600000	0.475000
Politics & Governance	0.705882	0.735294	0.588235	0.823529	0.823529
Science & Technology	0.550000	0.825000	0.750000	0.925000	0.875000
Sports	1.000000	1.000000	1.000000	1.000000	0.975000

Table 6 Model and current affairs category wise F-Score analysis

News category	TF-IDF+RF	TF-IDF+SVM	LSTM	BERT	XLNet
Business & Economy	0.750000	0.860759	0.897436	0.871795	0.864198
Education & Career	0.786517	0.860759	0.767442	0.831169	0.842105
Entertainment	0.847059	0.867470	0.843373	0.888889	0.850000
Food & Health	0.794872	0.788732	0.771429	0.880000	0.894737
International	0.815789	0.835443	0.756098	0.867470	0.875000
Others	0.491228	0.617284	0.421053	0.648649	0.520548
Politics & Governance	0.738462	0.781250	0.615385	0.811594	0.788732
Science & Technology	0.628571	0.725275	0.714286	0.831461	0.795455
Sports	0.952381	0.987654	0.975610	1.000000	0.962963

tasks including the best classification of sports related news stories and worst accuracy on others and politics and governance.

Coming to the DL based model LSTM, Confusion matrix is shown in Fig. 4. This model gives accuracy of 81.63 percent. This accuracy is achieved by following parameters:-Optimise='adam', epochs=12, word embedding dimension=300, LSTM output cells 64 and pooling strategy is maximum pooling. Here also similar trend of the results for each news article is observed with good level of accuracy in sports category and worst in others category. Figure 5 displays confusion matrix for the BERT model. This model gives accuracy of the classification 85.78 percent which is the highest achieved accuracy. The same trend is observed in sports category of articles and other category articles. Figure 6 displays confusion matrix for the XL-net with the parameters values such as batch size=8, sequence length=512, learning rate=2e-5, optimiser='adam' and epochs =11. XLnet based model reports accuracy of 83.43 percent. XLNet model performed also similarly the best for sports news articles and worst for other categories. It is observed that in traditional machine learning approaches, SVM performed the best on the test data with the highest accuracy. There are certain reasons for SVM outperforming it's machine learning counterpart such as high dimensional input space, few irrelevant features, document vectors are sparse. Most text categorization problems are linearly separable. These factors enable

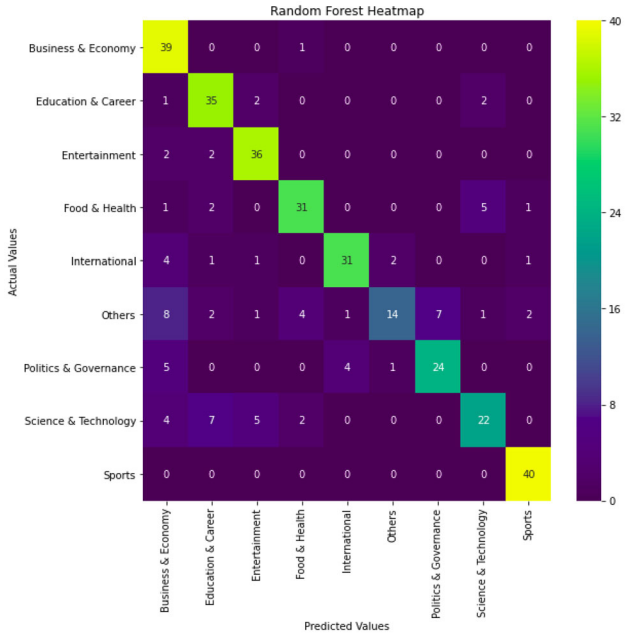

(a) TF-IDF+RF

Fig. 2 Confusion matrix for TF-IDF+RF

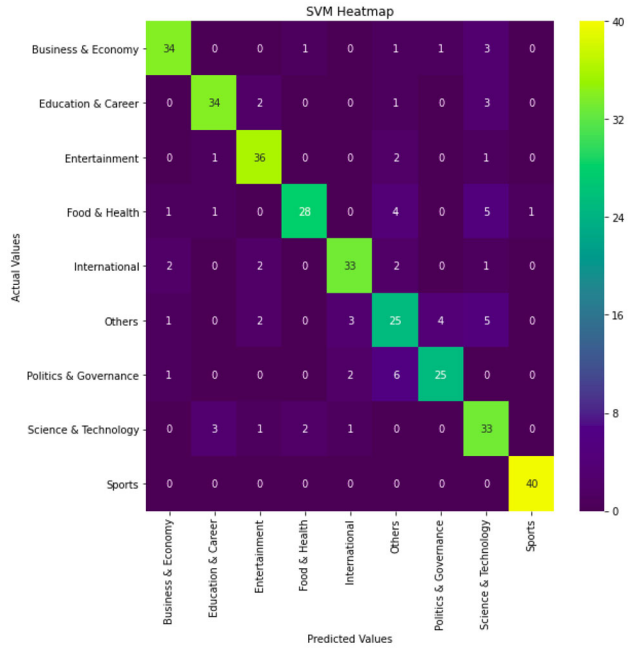

(a) TF-IDF+SVM

Fig. 3 Confusion matrix for TF-IDF+SVM

SVM to excel during text classification problems. LSTM didn't work that well in this case. Firstly, the quantity of data is very less. We just have around 1400 labeled examples. Secondly, the data set news articles are very long each approximately of 200 word length news articles.

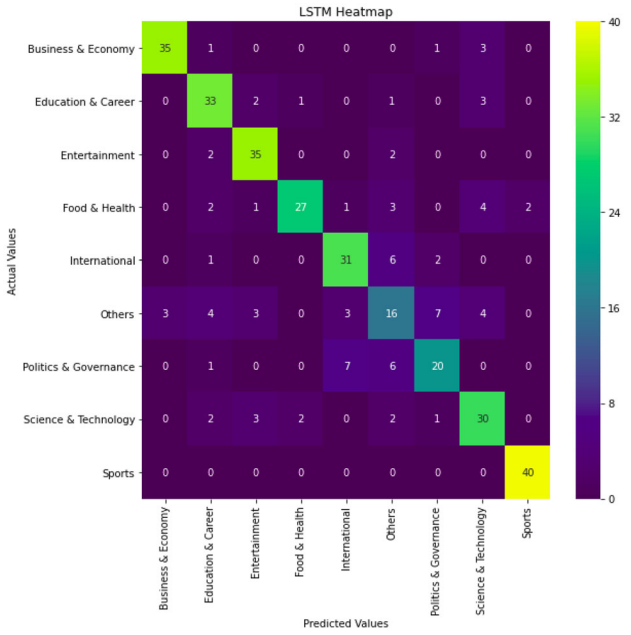

(a) TF-IDF+LSTM model

Fig. 4 Confusion matrix for TF-IDF+LSTM model

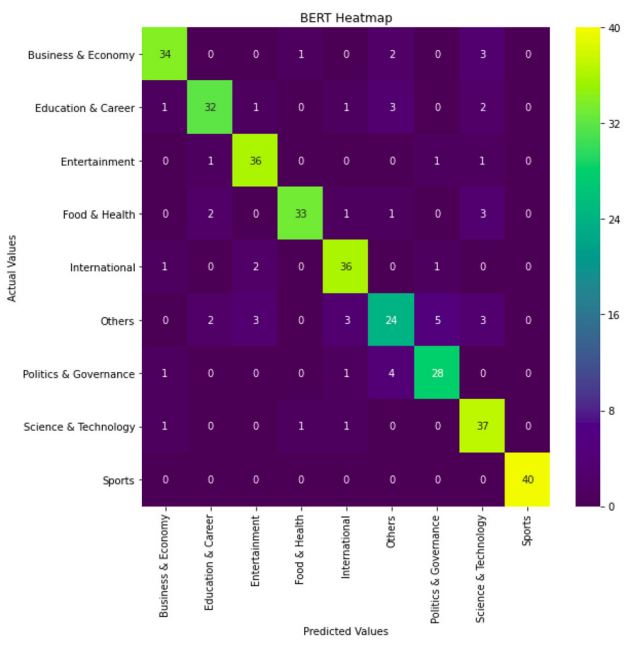

(a) BERT model

Fig. 5 Confusion matrix for BERT model

Model LSTM might suffer from vanishing gradient issues. BERT significantly outperformed all other methods.

There are multiple reasons which led to BERT outperforming all other methods. Primarily, first reason is that BERT's pretrained model. Articles were mainly in English

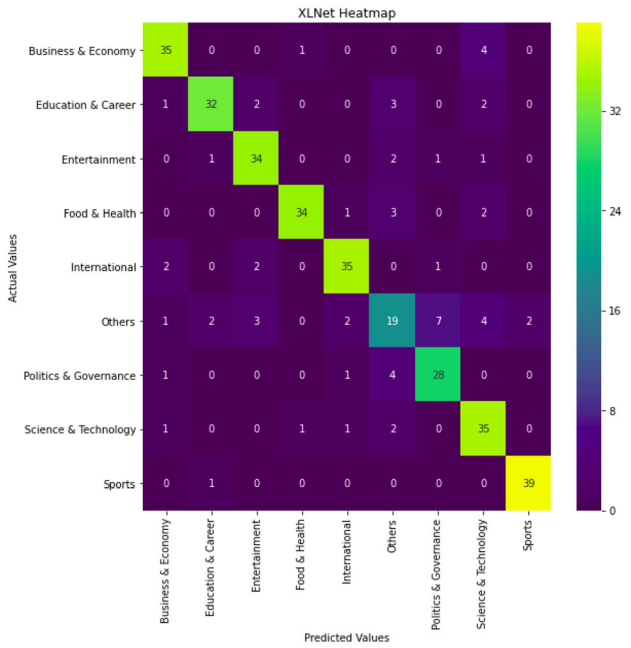

(a) XLNet model

Fig. 6 Confusion matrix for XLNet model

and BERT has been trained on English corpus. Another reason is that BERT doesn't suffer from vanishing gradient issue in longer sentences. It's ability to handle longer sentences helped to improve the result. XLNet outperformed all other approaches except BERT. Various algorithms have been evaluated on accuracy. They have also been analysed on class wise precision, recall and F1-score. All the results have been shown below in tabular form. For any algorithm to go into production, precision is an important metric. The precision implies that for any class C_i, how many examples predicted as C_i actually belongs to C_i. Models must not send wrong news classification. Precision is a very important metric in news or current affairs classification as per the user needs. Class wise precision for each model have been presented in Table 4. It is observed that BERT has the highest precision values amongst all the algorithms for majority of classes. Category 'Others' and 'Science Technology' have the lowest precision rate amongst most of the classes. Even in these less precise classes Bert is performing exceptionally well except in category 'others' by random forest. Recall is an equally important metric for any classification. For any category C_i, Model should recall all the examples belonging to C_i (Table 5). It is observed that recall have mixed results for various categories. Certain models have best recall for certain classes.

But on an average BERT has the best recall score amongst all the categories. Just like precision, class 'others' have the lowest recall. In classification tasks, precision is more important than recall and vice-versa. But in news classification both are important. F1-scores is the metric which captures both of them as displayed in Table 6. BERT has significantly outperformed all other algorithms for majority of classes followed by XLNet. The ability of transformer based models to capture the semantics of longer texts helped them in outperforming other Models. Observing scientifically, All models have easily classified the best possible way 'Sports' Categories current affairs articles while suffer in case of 'Others' and Science and technology articles. The probable reason is that Sports category have words in the articles which are unique than other categories so their identification becomes easy. In case of 'Other' category, it is observed that news articles are of some mixed type having some common key words which make the modeler confuse in labeling them. Running time of Models have also been presented for the classification tasks with Table 2. Ml based models such as RF, SVM, MNB are highly efficiency but their classification accuracy is not acceptable level. While the DL based model, BERT is the best performer but the all models takes more time than ML based models. Among DL models, LSTM is one of the best performer follower by BERT and than XLNet.

6 Conclusion

In this research work, Current affairs news article text or news stories have been classified using intelligent model based on deep learning. The proposed model can be deployed for News editors, media organisation, reviewers and Current affairs news readers to make the task of sorting and categorisation of news article smooth and efficient. The two types of approaches have been proposed. ML models such as TF-IDF+RF, TF-IDF+SVM and DL models such as BERT, LSTM, XLNet have been proposed on newly created data set to develop the best model for the real world deployment. Based on various metrics such as Accuracy, Precision and Recall, transformer based models like BERT with 85.00 percent accuracy and XLNet with 82.43 percent accuracy performed better than that of DL and ML based models. Amongst machine learning approaches, TF-IDF+SVM gave promising results with 81.35 percent accuracy. It was observed that DL model were taking more time as they are based on deep architecture but giving better results on selected criteria. In this model, categories can be dynamically increased or decreased as per the requirements. In the future, the present work can be extend by improving the DL models, improving features selection and feature generation stage in the over all design of the experiment.

Funding There is no funding received for this research work.

Declarations

Conflict of interest There is no conflict of interest in this work

References

Aggarwal CC, Zhai CX (2012) A survey of text classification algorithms. Mining text data. Springer, Berlin, pp 163–222

Allam Z, Dhunny ZA (2019) On big data, artificial intelligence and smart cities. Cities 89:80–91

Altınel B, Ganiz MC (2018) Semantic text classification: a survey of past and recent advances. Inf Process Manag 54(6):1129–1153

Azizi A (2019) Applications of artificial intelligence techniques in industry 4.0. Springer, Berlin

Chaker M (2016) Transgressing media boundaries: news creation and dissemination in a globalized world. Mediterr J Soc Sci 7(5):272–272

Chiranjib S (2019) Survey of deep learning and architectures for visual captioning-transitioning between media and natural languages. Multimedia Tools Appl 78(22):32187–32237

Corinna C, Vladimir V (1995) Support-vector networks. Mach Learn 20(3):273–297

De Morales GF, Gionis A, Lucchese C (2012) From chatter to headlines: harnessing the real-time web for personalized news recommendation. In: Proceedings of the fifth ACM international conference on Web search and data mining, pp 153–162

Devlin J, Chang M-W, Lee K, Toutanova K (2018) Bert: pre-training of deep bidirectional transformers for language understanding. arXiv preprint arXiv:1810.04805

Figueiredo F, Rocha L, Couto T, Salles T, Gonçalves MA, Meira W Jr (2011) Word co-occurrence features for text classification. Inf Syst 36(5):843–858

Foster P, Tom F (2013) Data science and its relationship to big data and data-driven decision making. Big data 1(1):51–59

Garla VN, Brandt C (2012) Ontology-guided feature engineering for clinical text classification. J Biomed Inf 45(5):992–998

Golder SA, Macy MW (2014) Digital footprints: opportunities and challenges for online social research. Ann Rev Sociol 40:129–152

Hadeer A, Issa T, Sherif S (2018) Detecting opinion spams and fake news using text classification. Secur Privacy 1(1):e9

Haruechaiyasak C, Jitkrittum W, Sangkeettrakarn C, Damrongrat C (2008) Implementing news article category browsing based on text categorization technique. In: 2008 IEEE/WIC/ACM International Conference on Web Intelligence and Intelligent Agent Technology, volume 3, pp 143–146. IEEE

Ho TK (1998) The random subspace method for constructing decision forests. IEEE Trans Pattern Anal Mach Intell 20(8):832–844

Joachims T (1998) Text categorization with support vector machines: learning with many relevant features. In: European conference on machine learning, pp 137–142. Springer

Jones KS (1972) A statistical interpretation of term specificity and its application in retrieval. J Doc 2:1789

Kadhim AI (2019) Survey on supervised machine learning techniques for automatic text classification. Artif Intell Rev 52(1):273–292

Kanan T, Fox EA (2016) Automated arabic text classification with p-s temmer, machine learning, and a tailored news article taxonomy. J Am Soc Inf Sci 67(11):2667–2683

Kibriya AM, Frank E, Pfahringer B, Holmes G (2004) Multinomial naive bayes for text categorization revisited. In: Australasian joint conference on artificial intelligence, pp 488–499. Springer

Kumar S, Pal SK, Singh R (2019) A novel hybrid model based on particle swarm optimisation and extreme learning machine for short-term temperature prediction using ambient sensors. Sustain Cities Soc 2:15589

Kumar S, Pal SK, Singh R (2016) Intelligent energy conservation: Indoor temperature forecasting with extreme learning machine. In: Proceedings of intelligent systems technologies and applications 2016, vol 2, pp 977–988. Springer Switzerland

Kumar S, Sharma A, Reddy BK, Sachan S, Jain V, Singh J (2021) An intelligent model based on integrated inverse document frequency and multinomial naive bayes for current affairs news categorisation. In: International journal of system assurance engineering and management, pp 1–15

Kumar S, Singh J, Singh O (2020) Ensemble-based extreme learning machine model for occupancy detection with ambient attributes. In: International journal of system assurance engineering and management, pp 1–11

Kumar S, Singh R, Pal SK (2018) A conceptual architectural design for intelligent health information system: case study on India. In: Proceedings in business and economics, quality, vol 1. IT and business operations, Springer, Singapore, pp 1–15

Laila K (2009) A machine learning approach for Arabic text classification using n-gram frequency statistics. J Inf 3(1):72–77

Longo L, Goebel R, Lecue F, Kieseberg P, Holzinger A (2020) Explainable artificial intelligence: concepts, applications, research challenges and visions. In: International cross-domain conference for machine learning and knowledge extraction, pp 1–16. Springer

Manoochehr G, James S, David Z (2013) Twitter brand sentiment analysis: a hybrid system using n-gram analysis and dynamic artificial neural network. Expert Syst Appl 40(16):6266–6282

Mark B (2019) Social network sites and acquiring current affairs knowledge: the impact of twitter and facebook usage on learning about the news. J Inf Technol Politics 16(1):36–51

Michael S (2013) Thematic content analysis using supervised machine learning: an empirical evaluation using German online news. Qual Quan 47(2):761–773

Mikolov T, Sutskever I, Chen K, Corrado GS, Dean J (2013) Distributed representations of words and phrases and their compositionality. In: Advances in neural information processing systems, pp 3111–3119

Prasetijo AB, Isnanto RR, Eridani D, Soetrisno YAA, Arfan M, Sofwan A (2017) Hoax detection system on indonesian news sites based on text classification using svm and sgd. In: 2017 4th international conference on information technology, computer, and electrical engineering (ICITACEE), pp 45–49. IEEE

Rennie J, Shih L, Teevan J, Karger D (2003) Tackling the poor assumptions of naive bayes classifiers (pdf). ICML. Accessed 10 Feb 2017

Sachin K, Anushtha K, Arjun S (2018) Predictive analysis of alertness related features for driver drowsiness detection. Adv Intell Syst Comput 736:368–377

Sachin K, Saibal P, Rampal S (2018) Intra elm variants ensemble based model to predict energy performance in residential buildings. Sustain Energy Grids Netw 16:177–187

Sepp H, Jürgen S (1997) Long short-term memory. Neural Comput 9(8):1735–1780

Vaswani A, Shazeer N, Parmar N, Uszkoreit J, Jones L, Gomez AN, Kaiser Ł, Polosukhin I (2017) Attention is all you need. In: Advances in neural information processing systems, pp 5998–6008

Wang J, Zhang J, Zhao J (2016) Texture classification using scattering statistical and cooccurrence features. Math Problems Eng 2:158

Yang Z, Dai Z, Yang Y, Carbonell J, Salakhutdinov RR, Le Quoc V (2019) Xlnet: generalized autoregressive pretraining for

language understanding. In: Advances in neural information processing systems, pp 5753–5763
Youyou W, Michal K, David S (2015) Computer-based personality judgments are more accurate than those made by humans. Proc Natl Acad Sci 112(4):1036–1040
Zubiaga A, Spina D, Fresno Víctor, MR (2011) Classifying trending topics: a typology of conversation triggers on twitter. In: Proceedings of the 20th ACM international conference on Information and knowledge management, pp 2461–2464

Publisher's Note Springer Nature remains neutral with regard to jurisdictional claims in published maps and institutional affiliations.

Proceedings of the Sixth International Conference on Trends in Electronics and Informatics (ICOEI 2022)
IEEE Xplore Part Number: CFP22J32-ART; ISBN: 978-1-6654-8328-5

Importance of Human Gait Analysis in Biometric Recognition using Machine Learning: A Review

Shipra Shand
Department of Software Engineering
Delhi Technological University
New Delhi, India
meetshipra43@gmail.com

Rahul
Department of Software Engineering
Delhi Technological University
New Delhi, India
rahul@dtu.ac.in

2022 6th International Conference on Trends in Electronics and Informatics (ICOEI) | 978-1-6654-8328-5/22/$31.00 ©2022 IEEE | DOI: 10.1109/ICOEI53556.2022.9776760

***Abstract*—When it comes to protecting consumers from security breaches, biometric recognition has proven to be a highly attractive approach. Biometric gait recognition is a popular issue in biometric research right now. The importance of biometric user recognition based on gait, which is more productive as compared to a number of other biometric traits, is discussed in this study. Various studies have been considered for various processes that have been employed in the past years for human gait analysis and biometric recognition via gait. The introduction of new technology brings with it new obstacles. Similarly, there are several obstacles or hurdles in gait analysis, which are explored in this article. This research study has also examined and studied numerous machine-learning algorithms, such as supervised-machine-learning, reinforcement-learning, etc., and concluded which are the most effective machine algorithms for this goal.**

Keywords—Human Gait Analysis (HGA), Machine Learning (ML), Biometric Recognition (BR).

I. INTRODUCTION

There is an incredible amount of data available now because of the internet. The goal of creating a user-friendly, customer-focused workplace, with secured data is rapidly being realized in today's society[41]. Each new fantasy brings the fear of a system security breach, allowing the system to be misused. One of the most crucial parts of security is identification. One of the approaches that can be used to identify a person is biometrics. The use of biometrics has proven to be a huge success in helping to avoid security breaches. Biometric solutions are becoming more popular as a reliable & effectual method of verifying identification. Fingerprint recognition, for example, is used to distinguish people based on their fingerprints [30]. Aside from fingerprints, other biometrics include ear, vein, retina, & gait recognition [3]. These types of biometrics help to fulfill individualistic features. On the other hand, HGA is designed to obtain individualistic as well as anatomical characteristics that are more stable than the aforementioned. Furthermore, unlike other biometrics, this can be obtained without the consent of the individual. Because of HGA's effectiveness, it has been shown to protect against intimidation. For all of these reasons, it's critical that we think about HGA for biometric recognition.

HGA is a rigorous research of animal mobility, most likely human motion, applying technology assisting eye & brain observers. In gait recognition, a person's actual movement is recognized. Human Gait Analysis helps in giving quantitative information in terms of supporting to prescribe of some treatments including that also help in assessing its possible outcome. In addition, on a basic pattern, this gait analysis is utilized in identifying several inefficiencies in human movements, with or without any kind of injury. This gait analysis supports identifying postural or else movement-focused issues that can create dysfunctions [26]. Moreover, it can be stated that this gait analysis in current times is utilized for several reasons not just for injury-oriented purposes. In the current scenario, gait analysis is emerging as a necessary parameter that might support personal identification while some forensic examinations.

Gait analysis is a biometric method for identifying biological as well as behavioral characteristics [4]. Gait differs from other biometrics in many ways. The most enticing feature of gait as a biometric characteristic is its inconspicuousness, allowing it to be gathered without the subject's agreement. Different patterns of sensors have been basically used in order to capture the numerous signals that characterize people's gait analysis, including their own walking patterns [28]. Gait analysis is equally necessary these days, and it is used in several sectors to gain a better understanding of human body language [23]. At the time of evaluating a person's running and walking, it can be easily identified that each person's different movements can be determined by determining basic gait patterns. In order to proceed with gait analysis techniques, gaining a better understanding of the machine and the procedure of utilizing those machines is equally important [21]. With the support of improved utilization of techniques, data collection has become simpler in unique corrections. comprising business, security, and medicine. In terms of prediction, ML is considered to be an advanced technique [42]. Gait recognition is the technique of recognizing a person based on their distinct walking style. This biometric feature is thought to be extremely

Authorized licensed use limited to: DELHI TECHNICAL UNIV. Downloaded on June 03,2022 at 06:37:39 UTC from IEEE Xplore. Restrictions apply.

accurate and trustworthy, making it a useful tool for security and surveillance.

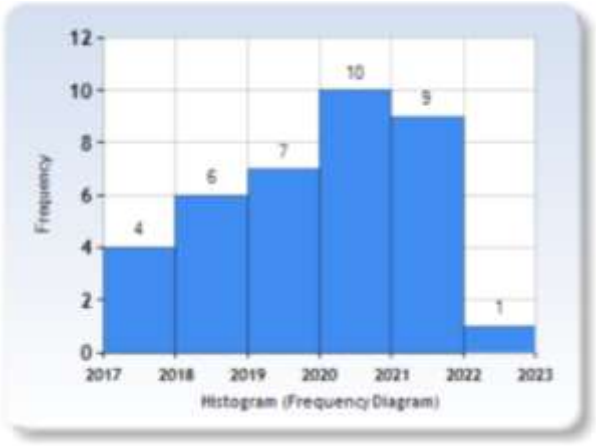

Fig. 1. Shows a graph of the number of papers studied over time.

ML can be considered as the process of automation that helps in studying the function and structures that might be learned along with that create calculations depending upon the provided data[2]. The importance of biometric user recognition based on gait, which can be combined with a variety of other biometric features, as well as ML, which allows multiple people to provide a massive amount of data to a computer-based algorithm, which then evaluates the data and makes data-driven judgments and recommendations, is discussed in this paper. Combining ML with BR could be a viable technique to make evaluation and analysis easier [23].

II. RELATED WORK

In their work, Zhang, Huanghe, Yi Guo, and Damiano Zanotto[6] , they provide an unique two-step calibration approach that use regression models to derive reliable estimations of critical stride-to-stride gait parameters using custom-engineered instrumented insoles while performing walking and running activities. As a result of the results, both SS or GN linear machine learning regression models (SVR) increased precision though demonstrating stronger interrater & test-retest consistency than linear models.

Castro, Francisco Manuel, et al.[8] performed a rigorous experimental assessment of planned-CNN planning on stimulating TUM-GAID dataset, which was used in their research. As shown in the findings, employing spatiotemporal cuboids of optical flow as input data for CNN enables for cutting edge gait detection and identification outcomes by an image resolution 8 times under before published outcomes (i.e. 80 x 60 pixels).

In their paper, Kececi, Aybuke[2], and colleagues worked with HugaDB, an open source database. Running, sitting, walking, and standing are just a few of the human behaviors that are combined in this database. The data were obtained utilizing a body SN comprising 6 inertial sensors on the thighs, shins, & feet.In this investigation, the Random Forest classifier was above 99% accurate.

Table 1. summarises the papers that were reviewed. It includes the names of the authors, the year of publication, the dataset that was used, the algorithms employed, and the three types of gait approaches (MV, FS, and WS). Where MV indicates that gait data was gathered using a video camera, and FS and WS indicate that data was collected using sensors. The only difference between FS and WS is that the sensor in WS is attached to the item, whereas the sensor in FS is attached to the floor. [4]

TABLE I. CONCISE SUMMARY OF PAPERS STUDIED

Author	Year of Publication	Algorithm Used	Dataset Used	Gait Method Used	Remarks
Munif, and Ausif Mahmood. [34]	2017	Deep CNN	CasiaB	MV	Subspace-learning-methods were avoided.
Yu, Shiqi, et al.[35]	2017	Auto-Encoders	SZUR GB-D, CasiaB	MV and FS	Recognition rates of 97.58%, 72.14% and 45.45% achieved on different walking angles.
Pradeep Kumar [31]	2018	LTSM, 3D-CNN, GA, GWO	Video taken as input.	MV	Achieved accuracy of 91.3%
Mehmood, A., Khan, M.A., Sharif, M. *et al.* [36]	2018	CNN, OAMSVM	CasiaB	MV	94.3%,93.8% and 94.7% was achieved at different angles.
Arshad, H., Khan, M.A., Sharif, M. et al. [37]	2019	QDoND, Bayesian with Binomial Distribution	AVA MVG, CASIA A, CASIA B and CASIA C	MV	100%,98.8%, 87.7%, and 91.6% were the accuracy found on different datasets respectively.
Wang, Fangzheng, Lei Yan, and Jiang Xiao. [39]	2019	SVM, BP, RBF	5 persons gait data was conside-red	WS	SVM gave an accuracy of 96.5%.
Arshad, Habiba, et al.[38]	2020	D-CNN, FEcS	AVAMVG gait, CASIA A,B and C.	MV	99.8, 99.7, 93.3 and 92.2%, were the accuracies of the respective datasets

Authorized licensed use limited to: DELHI TECHNICAL UNIV. Downloaded on June 03,2022 at 06:37:39 UTC from IEEE Xplore. Restrictions apply.

Liao, Rijun, et al. [33]	2020	PoseGait, CNN	CASIA B, CASIA E	MV	Results are equivalent to certain cutting- edge appearance-based approaches.
Saleem, Faizan, et al. [40]	2021	Inception-ResNet-V2 and NASNet Mobile, MDeSF	CASIA B	MV	Accuracy of 89% was achieved.
Aydemir, Emrah, et al.[32]	2021	DT ,SVM, KNN,LD, SD.	Noisy and clean audio as input.		98% and 94.9% respectively for both types of datasets.

III. METHODOLOGY

A. Human Gait Analysis System

Gait analysis can be considered as systematic research of animal locomotion, more particularly research of human motion, utilizing eyes including brain observers that are increased through instrumentation [4][5]. In addition, the instrumentation is for calculating human body activities, physical mechanics including activities of muscles. Gait recognition is mainly concentrated upon the work of human identification through utilizing analyzing people at a gap cantered upon the style that those people walk. Gait analysis is utilized to critically identify any human being's movement that is in relation to abnormalities, inefficiency, or other pain at the time any human being walks or runs [7]. In addition, gait analysis is utilized in terms of assessing including that treatment towards individuals along with conditions that are affecting their capability to walk [11]. It is mainly utilized in sports biometrics in terms of supporting athletes to run more productively. Moreover, gait analysis helps in identifying posture-oriented or else movement-oriented issues in human beings with numerous injuries. Gait analysis can be considered as kinematic with that kinetic evaluation of locomotion has generally been executed in gait labs, and with the involvement of optoelectronic or optical cameras in a provided recording volume. It is basically, the force plates lying in the pathway in terms of allowing joint moment estimations.

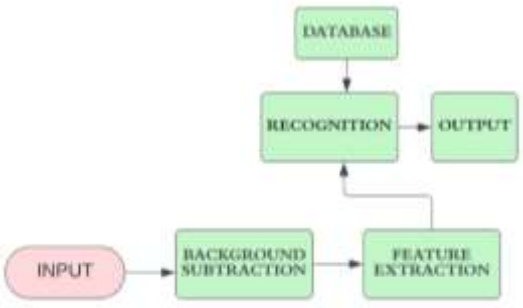

Fig 2. General Gait Recognition System

According to the articles chosen for this study, the majority of the writers used CASIA-B datasets. Many factors are taken into account when performing gait analysis. Various walking circumstances, walking styles, accessories utilized, viewing angles, and many more are some of the elements that are gathered and taken into consideration in variations of CASIA datasets. All of these aspects aid in the analysis of human gait[45].

B. Machine Learning-Based Human Gait Analysis System

In the health sector, machine learning has proven to be beneficial because it can forecast diseases [43]. In order to critically utilize this gait analysis system, it is obvious to gain a critical understanding including that knowledge of machine learning [13]. It is because without utilizing proper equipment it is not possible to identify human body language. Different varieties of sensors are generally utilized in terms of capturing the several signals that characterize the human being's gait and walking. These comprise gyroscopic sensors, accelerometers, force sensors, magnetometers, goniometers, electromyography, and active markers including the extensometer.

For the purpose of doing human beings' gait analysis, several types of equipment have been used therefore; experts need to have the required understanding of machine learning procedures [9]. The four phases of gait recognition using ML are depicted in Figure 4. They are data acquisition, which collects human gait data, feature representation, which extracts gait features from gait data, dimensionality reduction, which reduces information from a high-dimensional space to a low-dimensional space, and classification, which detects human gait [25]. Different types of approaches are generally used for the purpose of recognition including that for doing analysis of human gait and these approaches are floor sensors, image processing, and sensors that have been placed in the human body parts. The three types of machine learning that can be utilized for Human-Gait-Analysis are SL, USL, and RL.

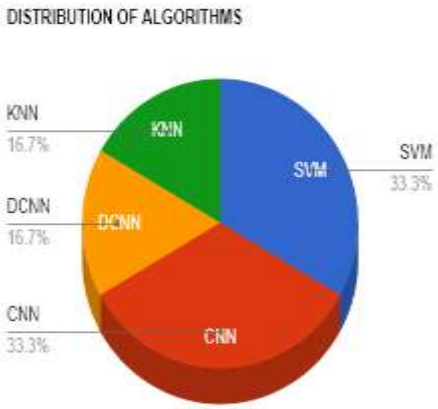

Fig.3. depicts the algorithm distribution and percentages employed.

Authorized licensed use limited to: DELHI TECHNICAL UNIV. Downloaded on June 03,2022 at 06:37:39 UTC from IEEE Xplore. Restrictions apply.

Fig.4. Overview of human gait recognition using ML [25].

The majority of authors take the approach indicated in figure 4. Starting with step length, walking speed, viewing angles, stride length, and cadence, a general HGA system captures all the physiological features. These attributes are attained through a variety of physical activities that the individual must engage in. Walking, running, standing, and other activities are among them. Different sorts of sensors are being employed to collect data while performing these actions. Some sensors, such as those found in shoes, are directly attached to the body. These sensors are known as MR or motion recording sensors, and they are worn. Sensors that are mounted on the floor are another option. When the person steps on them, the data is collected. Some data is also gathered through the use of videos. Now that all of the data has been collected, it is pre-processed and the most essential features are extracted, which is a crucial step. They are then fed in order to be classified. There are a number of well-known classifiers that have provided better-than-average accuracy. However, we discovered that neural networks were commonly employed for this purpose by several of the writers in a previous survey. Different authors have utilized different parameters to calculate the accuracy of the presented models, including precision, recall, loss functions, MAR, MAE, and so on. All of these variables contribute to determining the magnitude of the inaccuracy and the accuracy of the proposed models. The accuracy of various models ranged from 95 to 100 percent on average.

C. In Biometrics Recognition, The Importance Of Human Gait Analysis

In its most basic form, biometric authentication is the process by which an individual's physical and behavioral features may be authenticated and painstakingly documented; numerous authentication-related methods have been created over the last few years. One of the strategies suggested is human gait-oriented recognition, which may be used in conjunction with other techniques. The purpose of this research is to examine machine learning-related strategies for numerous users' authentication on a particular database that is a human person and is associated with the collection of gait data for analysis, which includes activity recognition [13]. These activities have been recorded and analyzed in a variety of datasets, with the majority of them consisting of running, walking, sitting, and standing activities [2]. These datasets are now available in video or image format. To feed these into the computer, we must first convert them to binary [44]. It can then be utilized for additional processing. Human biomechanics, which includes gait formation, may be seen as an intrinsic part of one's daily life experience. It is possible that the explanation of this gait analysis will be problematic due to the large number of interdependent factors that have been estimated, as well as the large number of interconnected relationships that were estimated. It is possible that the addition of ML with biomechanics will be a capable option in order to ease assessment and analysis[28]. It may also be determined that regulating techniques for gait rehabilitation are superior when compared to other machine-learning approaches and neural networks because of their capacity to capture the variety of participants' variability.

Gait analysis might be defined as a set of some movements of the limbs that, mainly in a cyclic manner, provide an allowance for the locomotion of several humans [16]. The most basic practice of some gait-related assessments consists of a specialist easily observing the human's walking pattern, including looking at some indicators such as gait-focused speed, stride length, or else speed. Machine learning provides an allowance to several users in terms of feeding a computer-based algorithm an enormous estimation of data, including that of having the computer evaluate and make data-driven decisions as well as recommendations. Therefore, in terms of recognizing any human being's gait-related analysis [25], it is necessary to gain some knowledge about computers and machine learning in order to proceed with the algorithm process. In this case, appropriate training is the major integral part of this machine learning and it is important to select features as well as hyperparameters meticulously.

Now we'll talk about some of the issues that are causing this system to lack. The first problem that this system faces is one of recognition. When it comes to recognizing certain factors, there are a few things to keep in mind. Brightness, inspection margins, and nearby habitat are examples of external elements. The physical condition of the person in question is an intrinsic aspect that is regarded an impediment. Furthermore, obtaining the data of those who have taken advantage of the single-viewpoint concession is a major challenge. Single-point concession or recognition is commonly employed in the current situation. As a result, incorporating other points of view continues to be difficult. Labeled data is currently commonly utilized for classification, although locating labeled data is not always possible. Furthermore, gait analysis necessitates a large amount of data for recognition, which is a problem. For this aim, all of these considerations present a substantial challenge. However, as technology advances, appropriate solutions for tackling these difficulties are being created.

IV. CONCLUSION AND FUTURE WORK

Human biomechanics, which includes gait formation, can be thought of as an integral component of one's everyday existence. Due to the huge number of interdependent components that have been estimated, as well as the vast number of interrelated interactions that have been calculated, it is probable that explaining this gait analysis will be difficult. It's feasible that combining machine learning with biomechanics may be a viable solution for easing examination and analysis[28].In order to critically use this gait analysis system, it is obvious to gain a critical understanding including that knowledge of machine learning. It is because without utilizing proper equipment it is not possible to identify the human body. In addition to this, gait analysis of any human being naturally supports diagnosing problems that are increasing the pain along with that also implementing and evaluating

Authorized licensed use limited to: DELHI TECHNICAL UNIV. Downloaded on June 03,2022 at 06:37:39 UTC from IEEE Xplore. Restrictions apply.

some treatments in order to correct some abnormalities[11]. Human beings' gait analysis can be considered as systematic research of animal locomotion, and particularly research of people's motion through utilizing eye & observers of brain[5]. Human gait analysis supports in providing quantitative information in order to support in terms of prescribing some treatments along with that in support in assessing its possible result. As a result, we can deduce that human gait analysis is crucial for biometric recognition. It is now clear that ML is playing a important role in the procedure of gait analysis and ML is in three varieties that are reinforcement learning; supervised learning including that unsupervised learning that helps in the procedure of gait analysis[2]. We will attempt to address and eliminate the issues that the suggested approach entails in future work. The discussed techniques can be used in future projects, and we will endeavour to apply them in order to obtain more accurate results.

REFERENCES

[1] Smith, Andrew W, and Del P Wong. "Sagittal and Frontal Plane Gait Initiation Kinetics in Healthy, Young Subjects." Journal of human kinetics vol. 67 85-100. 5 Jul. 2019, doi:10.2478/hukin-2018-0087.

[2] Kececi, Aybuke, et al. "Implementation of machine learning algorithms for gait recognition." Engineering Science and Technology, an International Journal 23.4 (2020): 931-937.

[3] Tripathi, K. P. "A comparative study of biometric technologies with reference to human interface." International Journal of Computer Applications 14.5 (2011): 10-15.

[4] Gupta, Nishtha. "Biometric System using Gait Feature Analysis and Comparison.". International Journal of Engineering Research & Technology (IJERT),ISSN: 2278-0181,IJERT V6IS050195,Vol. 6 Issue 05, May - 2017.

[5] Sharma, Oshin, and Sk Bansal. "Gait Recognition System for Human Identification Using BPNN Classifier." International Journal of Innovative Technology and Exploring Engineering 3.1 (2013): 217-220.

[6] Zhang, Huanghe, Yi Guo, and Damiano Zanotto. "Accurate ambulatory gait analysis in walking and running using machine learning models." IEEE Transactions on Neural Systems and Rehabilitation Engineering 28.1 (2019): 191-202.

[7] Aha, David W., Dennis Kibler, and Marc K. Albert. "Instance-based learning algorithms." Machine learning 6.1 (1991): 37-66.

[8] Castro, Francisco Manuel, et al. "Automatic learning of gait signatures for people identification." International work-conference on artificial neural networks. Springer, Cham, 2017.

[9] Lai, Daniel TH, et al. "Automatic recognition of gait patterns exhibiting patellofemoral pain syndrome using a support vector machine approach." IEEE Transactions on Information Technology in Biomedicine 13.5 (2009): 810-817.

[10] Khera, Preeti, and Neelesh Kumar. "Role of machine learning in gait analysis: a review." Journal of Medical Engineering & Technology 44.8 (2020): 441-467.

[11] Abdulhay, Enas, et al. "Gait and tremor investigation using machine learning techniques for the diagnosis of Parkinson disease." Future Generation Computer Systems 83 (2018): 366-373.

[12] Klöpfer-Krämer, Isabella, et al. "Gait analysis–Available platforms for outcome assessment." Injury 51 (2020): S90-S96.

[13] Cho, Jae-sung, et al. "Scoliosis screening through a machine learning based gait analysis test." International Journal of Precision Engineering and Manufacturing 19.12 (2018): 1861-1872.

[14] Zhang, Zixuan, et al. "Deep learning-enabled triboelectric smart socks for IoT-based gait analysis and VR applications." npj Flexible Electronics 4.1 (2020): 1-12.

[15] Lemoyne, Robert, and Timothy Mastroianni. "Classification of software control architectures for a powered prosthesis through conventional gait analysis using machine learning applications." Journal of Mechanics in Medicine and Biology 19.06 (2019): 1950044.

[16] Júnior, Ivair Matias, et al. "Effective parameters for gait analysis in experimental models for evaluating peripheral nerve injuries in rats." Neurospine 16.2 (2019): 305.

[17] Caldas, Rafael, et al. "Adaptive predictive systems applied to gait analysis: A systematic review." Gait & Posture 77 (2020): 75-82.

[18] Guffanti, Diego, Alberto Brunete, and Miguel Hernando. "Development and validation of a ROS-based mobile robotic platform for human gait analysis applications." Robotics and Autonomous Systems 145 (2021): 103869.

[19] Figueiredo, Joana, Cristina P. Santos, and Juan C. Moreno. "Automatic recognition of gait patterns in human motor disorders using machine learning: A review." Medical engineering & physics 53 (2018): 1-12.

[20] Zelik, Karl E., and Eric C. Honert. "Ankle and foot power in gait analysis: Implications for science, technology and clinical assessment." Journal of Biomechanics 75 (2018): 1-12.

[21] Celik, Yunus, et al. "Gait analysis in neurological populations: Progression in the use of wearables." Medical Engineering & Physics 87 (2021): 9-29.

[22] Han, Jinguang, and Bir Bhanu. "Individual recognition using gait energy image." IEEE transactions on pattern analysis and machine intelligence 28.2 (2005): 316-322.

[23] Sharma, Sanjeev, Ritu Tiwari, and Vikas Singh. "Identification of people using gait biometrics." International journal of machine learning and computing 1.4 (2011): 409.

[24] Isaac, Ebenezer RHP, et al. "Trait of gait: A survey on gait biometrics." arXiv preprint arXiv:1903.10744 (2019).

[25] Wan, Changsheng, Li Wang, and Vir V. Phoha, eds. "A survey on gait recognition." ACM Computing Surveys (CSUR) 51.5 (2018): 1-35.

[26] Mukaino, Masahiko, et al. "Clinical-oriented three-dimensional gait analysis method for evaluating gait disorder." JoVE (Journal of Visualized Experiments) 133 (2018): e57063.

[27] Garofalo, Pietro. Development of motion analysis protocols based on inertial sensors. Diss. University of Bologna, Italy, 2010.

[28] Akhtaruzzaman, M. D., Amir Akramin Shafie, and Md Raisuddin Khan. "Gait analysis: Systems, technologies, and importance." Journal of Mechanics in Medicine and Biology 16.07 (2016): 1630003.

[29] Yang, Wencheng, et al. "Security and accuracy of fingerprint-based biometrics: A review." Symmetry 11.2 (2019): 141.

[30] Hassan, Bilal, Ebroul Izquierdo, and Tomas Piatrik. "Soft biometrics: a survey." Multimedia Tools and Applications (2021): 1-44.

[31] P. Kumar, S. Mukherjee, R. Saini, P. Kaushik, P. P. Roy and D. P. Dogra, "Multimodal Gait Recognition With Inertial Sensor Data and Video Using Evolutionary Algorithm," in IEEE Transactions on Fuzzy Systems, vol. 27, no. 5, pp. 956-965, May 2019, doi: 10.1109/TFUZZ.2018.2870590.

[32] Aydemir, Emrah, et al. "A novel biometric recognition method based on multi kernelled bijection octal pattern using gait sound." Applied Acoustics 173 (2021): 107701.

[33] Liao, Rijun, et al. "A model-based gait recognition method with body pose and human prior knowledge." Pattern Recognition 98 (2020): 107069.

[34] Alotaibi, Munif, and Ausif Mahmood. "Improved gait recognition based on specialized deep convolutional neural network." Computer Vision and Image Understanding 164 (2017): 103-110.

[35] Yu, Shiqi, et al. "Invariant feature extraction for gait recognition using only one uniform model." Neurocomputing 239 (2017): 81-93.

[36] Mehmood, A., Khan, M.A., Sharif, M. et al. Prosperous Human Gait Recognition: an end-to-end system based on pre-trained CNN features selection. Multimed Tools Appl (2020). https://doi.org/10.1007/s11042-020-08928-0.

[37] Arshad, H., Khan, M.A., Sharif, M. et al. Multi-level features fusion and selection for human gait recognition: an optimized framework of Bayesian model and binomial distribution. Int. J. Mach. Learn. & Cyber. 10,3601–3618(2019).https://doi.org/10.1007/s13042-019-00947-0.

Authorized licensed use limited to: DELHI TECHNICAL UNIV. Downloaded on June 03,2022 at 06:37:39 UTC from IEEE Xplore. Restrictions apply.

[38] Arshad, Habiba, et al. "A multilevel paradigm for deep convolutional neural network features selection with an application to human gait recognition." Expert Systems (2020): e12541.

[39] Wang, Fangzheng, Lei Yan, and Jiang Xiao. "Human gait recognition system based on support vector machine algorithm and using wearable sensors." Sensors and Materials 31.4 (2019): 1335-1349.

[40] Saleem, Faizan, et al. "Human gait recognition: A single stream optimal deep learning features fusion." Sensors 21.22 (2021): 7584.

[41] Rahul, S. Adhikari and Monika, "NLP based Machine Learning Approaches for Text Summarization," 2020 Fourth International Conference on Computing Methodologies and Communication (ICCMC), 2020, pp. 535-538, doi: 10.1109/ICCMC48092.2020.ICCMC-00099.

[42] Rahul, Rauniyar K., Khan J.A., Monika A. (2021) Review of Different Machine Learning Techniques for Stock Market Prediction. In: Suma V., Chen J.IZ., Baig Z., Wang H. (eds) Inventive Systems and Control. Lecture Notes in Networks and Systems, vol 204. Springer,Singapore.https ://doi.org/10.1007/978-981-16-1395-1_53.

[43] Rahul, Monika, Ray P., Kharke R.B., Chauhan S.S. (2021) Cardiovascular Disease Classification Using Different Algorithms. In: Ranganathan G., Chen J., Rocha Á. (eds) Inventive Communication and Computational Technologies. Lecture Notes in Networks and Systems, vol 145.Springer,Singapore.https://doi.org/10.1007/978-981-15-7345-3_16.

[44] Rahul, H. Kajla, J. Hooda and G. Saini, "Classification of Online Toxic Comments Using Machine Learning Algorithms," 2020 4th International Conference on Intelligent Computing and Control Systems (ICICCS), 2020, pp. 1119-1123, doi: 10.1109/ICICCS48265.2020.9120939.

[45] Sepas-Moghaddam, Alireza, and Ali Etemad. "Deep gait recognition: A survey." *IEEE Transactions on Pattern Analysis and Machine Intelligence* (2022).

[46] Mugunthan, S. R., and T. Vijayakumar. "Design of improved version of sigmoidal function with biases for classification task in ELM domain." *Journal of Soft Computing Paradigm (JSCP)* 3.02 (2021): 70-82.

[47] Manoharan, J. Samuel. "Study of variants of Extreme Learning Machine (ELM) brands and its performance measure on classification algorithm." *Journal of Soft Computing Paradigm (JSCP)* 3.02 (2021): 83-95.

Authorized licensed use limited to: DELHI TECHNICAL UNIV. Downloaded on June 03,2022 at 06:37:39 UTC from IEEE Xplore. Restrictions apply.

ISSN No:-2456-2165

Industrial AI in Manufacturing

Amulya Tiwari[1],Tanishk Verma[2], Dr. A.K Madan[3]

[1, 2]Student, [3] Professor
Department of Mechanical Engineering,
Delhi Technological University, Delhi, Delhi, India

Abstract:- Engineering expertise and the digitization of all business operations are the important factors in today's industrial firms' success. The engineer's design process and expertise are highly personal, and rule-based procedure explanations are almost always difficult and/or time-consuming. As a result, passing on existing information to new engineers, particularly training effort, is very challenging. Another issue is the lack of an overview of the company's existing components. Multiple designs and engineers spend their valuable time as a result of this. The goal of this approach is to use machine learning techniques to extract information from current CAD models and codify it. Furthermore, proper categorization and similarity analysis should reveal existing components rapidly.For this, an AI-based support system will be developed. Engineers merely need to adjust the parameters of the proposed components based on the application. The assistant should then be able to recommend an appropriate next design step based on the existing CAD data and design history. As a result, current CAD models' implicit empirical knowledge supports production-friendly design and the avoidance of design errors.

I. INTRODUCTION

The level of innovation in an organisation determines its success.

- This entails product and service innovation as well as internal value stream design for each market offering. As a result, an industrial firm's primary competences are product creation and manufacturing procedures. Relevant efforts are being made to improve production and logistical systems, as well as internal organisational processes, through digitalization. Individual product design knowledge, individual ties to product characteristics, and historical knowledge of similar product generations, in particular, hold a lot of promise for improving the product development and the design process.
- Transparency: This article discusses methods for achieving the needed transparency, as well as automated design possibilities based on individual preferences and previous product generations. An AI-based approach is a must because of the goal of transferring large inconsistent datasets and such support systems to different product categories.

II. STATE OF THE ART

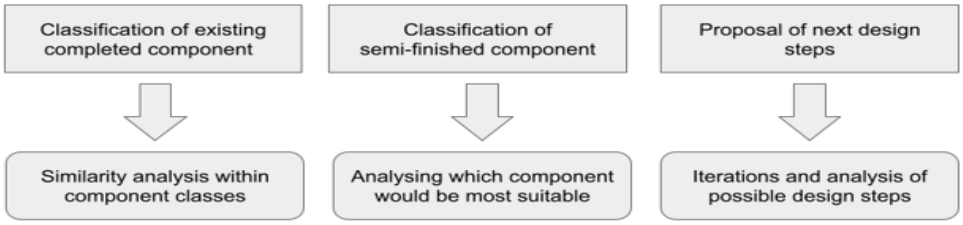

Here we see the development steps of the approach.
The existing database is categorized to enable the designer to find the most suitable part for his purpose. In a next step, components currently in process are classified in order to propose already existing, similar components to the designer. In the last step, the explicit next x design steps are suggested, which are then on the order of case-by-case are measured on the assigned parameters. Component class instance includes lid, housing, process connectors etc.

Fig. 1

Because it is not strictly defined according to predefined standards, the design process is very individualised and empirical. This frequently necessitates tacit and unformalized experience. A non-automated system model for product feature ideas based on product-generated data is another option. The current AI-based CAD model processing approach focuses more on categorization problems. The degree of automation can be used to distinguish these approaches. On the one hand, it encodes specific model features using hand-crafted descriptors and processes them using machine learning techniques. A CAD model, for example, is grouped initially using the kmeans technique. These clusters can then be used for classification in the second stage.

On the other hand, there is a method that can learn the traits to consider automatically from the incoming data. The multi-view method generates 3D photos components from many angles. For image processing, standard CNNs are used to classify the images. The main idea is to forecast the class based on the angle of view used to make the image. It is based on the object's approximation through the cubic lattice. A 3D convolution kernel categorises CNN-generated voxel structures, just like pixels. The coordinates of randomly distributed points in the volume or on the surface of the model are used as input to the CNN in the

ISSN No:-2456-2165

point cloud-based technique.The classification result should be unaffected by the sequence in which the points are entered. An edge-constrained convolution technique is other option. Specific signals are allocated to vertices in this method based on adjacent vertices and input edges. The convolutional layer's local characteristics are detected by clustering points or vertices that are spatially adjacent to one other, both in a point cloud and a graph-based approach. There are several techniques of comparing 3D model similarities. Feature vectors are the most frequently utilised method. The distance between the vectors determines the similarity of the 3D model described by these vectors. The actual design process and implementation, on the other hand, is left to the designer and his expertise. Therefore, this paper develops a way to formalize existing knowledge to pass it on to inexperienced designers and to use it to support repetitive activities not requiring creativity

III. METHODOLOGY

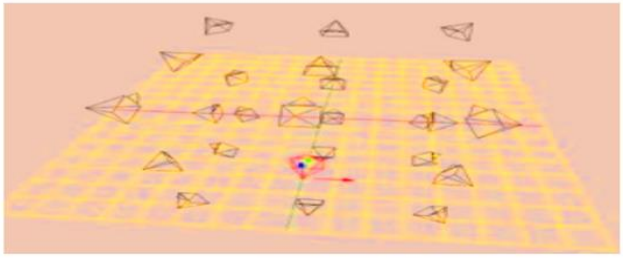

Alignment of the 26 perspectives regarding the basis (red)

Fig. 2

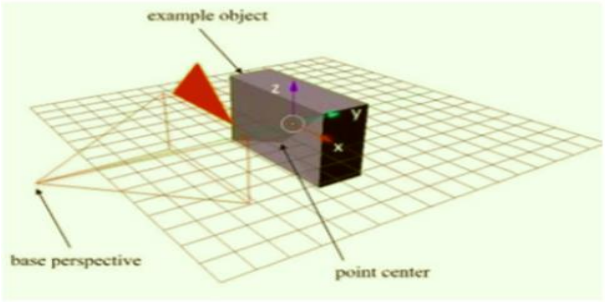

Alignment by standard orientation

Fig. 3

As shown in Figure 1, the examined design aid can be divided into three development stages of increasing complexity. The method is first applied to individual components, which are referred to as components in the following. The goal is to apply the method to assemblies as well. Individual components are represented by 3D CAD models, which serve as the foundation for the developed approach's input and output. A classification of the different product groups is required in order to locate already existing, highly comparable CAD models in a company's data base. Following that, semi-finished component classification must be developed in order to offer relevant, previously existing CAD models to the designer during the design process based on the design phases already completed. On the one hand, the appropriate category must be anticipated, and on the other, the class's most likely related component(s) must be provided. It is now no more an issue of complete pieces in the last stages of development, but of appropriate future design steps. The goal is to make the approach as clear as possible to the designer, including the adaption of case-specific parameters to the respective design steps.

A. Considered database and information content:

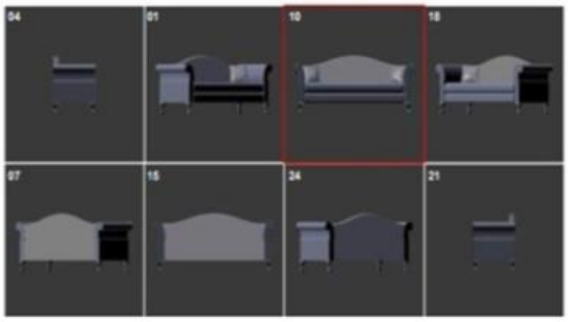

Sample perspectives of object

Fig. 4

Understanding the 3D data and how it can be stored is necessary for applying machine learning to 3D models. There are two main formats here: boundary representation (B-Rep), which stores the body's surfaces, and constructive solid geometry (CSG), which stores the body as a collection of basic bodies (e.g., cuboids, cylinders). Internally, most commercial CAD software uses a CSG-based storage format. Individual steps taken by a user to design a basic body are recorded, including parameterized dimensions. The parameterization allows for changes to the fundamental body to be made afterwards. The so-called PART (.prt) format, which is used in the approach proposed in this work, is a very frequently used format.This file format provides information on the design process, which is represented in the so-called structure tree, in addition to geometric information (also model tree or element tree). It contains the individual design steps, sometimes known as features (such as drilling), as well as the parameterization for each (e.g., diameter of the drilling). The structure tree can be used to extract and codify the technique of expert designers when designing pieces of a specific class from already existing CAD models. The structural tree can be read out in the form of an XML file, for example. B-Rep formats, on the other hand, are designed for file exchange between different CAD systems, but information about the design process is lost during conversion. From this file format, information regarding only shape can be extracted.

B. Classification of components:

Because existing CAD models in a company are frequently kept in an unstructured state, they must first be assigned to component classes. The categorization was done within the scope of this project using the Multiview approach, which is only based on shape information. The smallest bounding box of the 3D objects is used to determine the standard orientation. The concept to note here is that objects of the same class have identical length,

ISSN No:-2456-2165

width, and height proportions. A standard orientation can be found by rotating and displacing the smallest bounding box according to some specified rules.Following that, virtual cameras can generate the corresponding photos of the 3D object from the defined views. The standard orientation is defined by five criteria:

- The centre of the bounding box lies in the origin of the coordinate system,
- the basic perspective shows the largest side surface of the box,
- the longest side of the box is parallel to the x-axis, the point centre of the polygon mesh representing the 3D object has a
- yvalue and a
- zvalue less than or equal to 0.

A sofa is represented in Fig. 4 with photographs of the base perspective (framed in red) and the seven additional perspectives all positioned in the same plane. Finally, these images are fed into CNNs that are viewpoint specific. The images of two opposing perspectives are summed for this purpose, resulting in only 13 CNNs for the 26 perspectives. The input data is then classified by each CNN based on the two picture views. The probabilities for each perspective specific CNN are added together for the final classification of the item, and the object is allocated to the class which has the highest probability.During the design phase, classification of semifinished components is required in order to offer to the design engineer equivalent existing, very similar parts. A semifinished part is one that is currently being manufactured. From the current state of the design process, numerous classes may be appropriate. The more complex your design is, the easier it will be components categorization. This classification is accomplished in the developed approach by training the current approach in other semi-finished items. A CAD model's intermediate status is usually not saved separately in the company's database and must be produced intentionally.To achieve this, either remove the structure tree's features one by one or save the CAD model's intermediate status. The design assistant may see what type of part the designer is designing, search for very similar parts in the existing CAD model, and communicate with the designer by being able to categorise semi-finished pieces as the designer works. To whom the first draught of completed parts is provided. Make case-specific adjustments as needed.

C. Proposal of next design steps:

You must first classify the semi-finished items to ascertain what type of component is there before proposing the next explicit design step. After you've defined the component class, you can use the design process to suggest the next design step. The structure tree is extracted from all existing CAD models of the appropriate class to understand the steps specific to this component class. Appropriate ML methods (such as Random Forest) are trained to uncover common design trends using these structure trees. The construction assistant's job is to present a variety of options. It also indicates the likelihood that the assistant will accept the recommendation in order to maintain adequate traceability.By simply suggesting the next step, the designer can make adjustments as soon as needed. Finally, the next proposed procedure is based on these adjustments.

IV. CASE STUDY

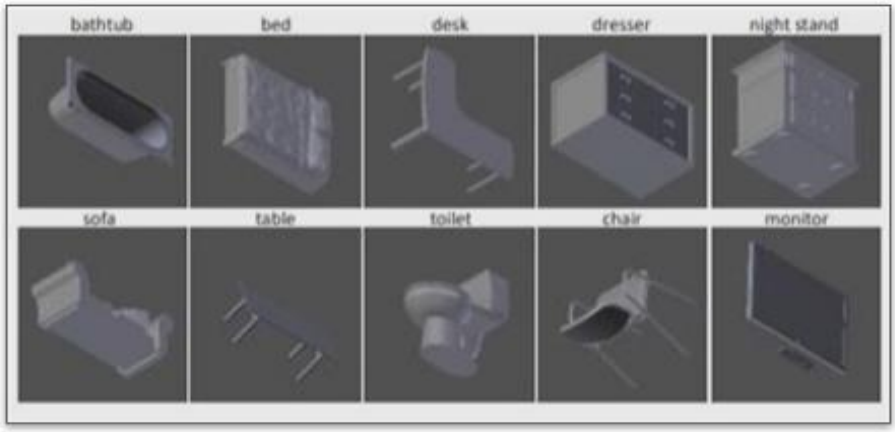

3D models of 10 different categories from ModelNet10
fig 5

Fig. 5

Figure 5 shows the ModelNet10 database, which has 4899 3D models of various furniture in ten different categories. As a result, the classification process entails categorising models into ten separate groups. First, only one perspective photos were used to evaluate the three distinct CNN architectures. One architecture is based on the Alex Net architecture, another is based on the modified VGG-16 network, and the third is a custom configuration. The self-developed architecture is shown in Figure 6. The names and parameters of the layers are contained in the rounded rectangles; for example, the first convolutional layer uses 32 kernels of size 3x3 and the Rectified Linear Unit (ReLU) as an activation function.The input and output formats of the layers are indicated by the names on the

arrows, for example, the input picture is 256x256 pixels with three channels. Despite the high number of factors, the performance of the displayed architecture is betterthan the other two, which is why the results for this architecture are presented. The accuracy of the look at information is 80.0 percent when snap photos are taken from a single perspective. One reason for the latter architectures' worse overall performance is that they were meant to differentiate a somewhat wider range of learning.

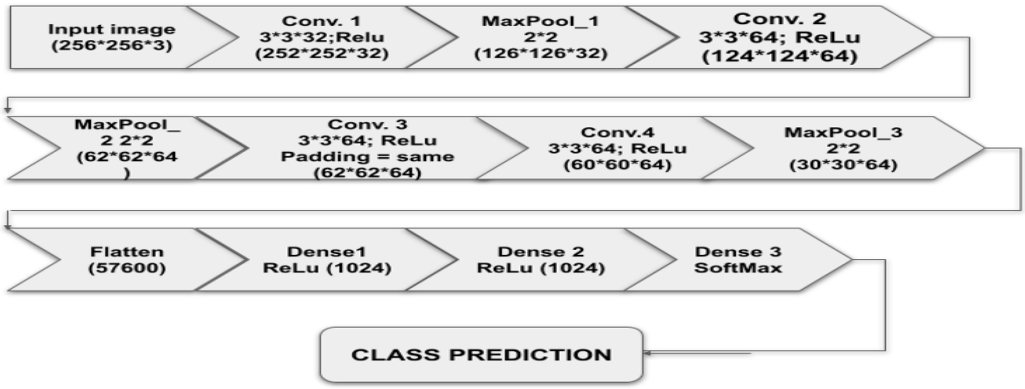

Architecture of CNN

Fig. 6

The self-advanced structure became widely used for all different viewpoint-precise CNNs as a result of the effects received for snap photos from a single perspective. As shown in Fig. 6, each of those CNNs was configured. Depending on the perspective, the accuracy of man or woman views ranged between 68.4 percent and 84.0 percent. A final check accuracy of 88.4 percent was achieved by merging the individual projections and averaging over all perspective-precise magnificence predictions. The accuracy of the man or woman views, as well as the overall accuracy after taking all views into account (crimson x), are displayed for each item.The general impacts for all views are shown in Fig. 8 as a confusion matrix. For instance, most effective 58 percent of desks are correctly classified as such, but a large minority are misclassified as sofas. One reason for this is because items from distinct lessons appear to be extremely similar from certain perspectives (e.g., the rectangular base of a settee or desk). As a result, it becomes clear that analysing the items' field of vision alone may not be adequate; their shape should also be considered. Graph-primarily based approaches can be appropriate for this, and they should be considered in comparable projects.The objective is to base the category on actual CAD data from a business dimension generating provider that is available in PART format. Following that, the form tree is extracted from those CAD fashions, and the layout assistant's actions are followed.

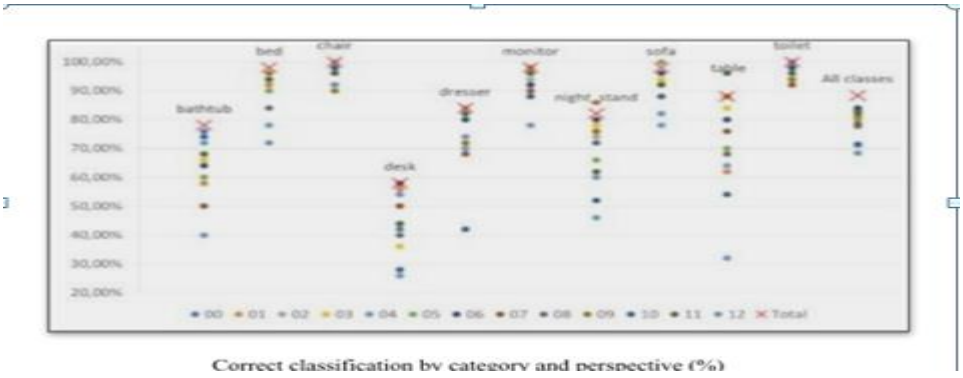

Correct classification by category and perspective (%)

Fig. 7

V. CONCLUSION AND OUTLOOK

Based on appropriate machine learning approaches, this research presents a three-step methodology for a CAD design assistance. The support system can only classify components in the form of 3D CAD models which are in the early stages of development. For this goal, an original method is described that translates 3D models into a standard orientation before generating 2D photos from diverse views.As shown in a case study, those perspective-specific images are finally used as input for CNN classification. Additional CNN architectures should be examined in future study, especially those having fewer parameters. Other approaches, such as graph-based approaches, should also be investigated to better map the component's structural architecture. The classification of semi-finished components is examined in the approach's next development step, so that existing, very similar components can be proposed to the designer during the design process. Using appropriate machine learning methods, a general approach or design pattern for each

class is learned from the design history stored in the CAD models in the final development step.

	bathtub	bed	chair	desk	dresser	monitor	night stand	sofa	table	toilet
bathtub	78	0	0	0	0	0	0	0	0	0
bed	8	98	0	2	0	2	0	2	0	0
chair	0	0	100	8	0	0	0	0	0	0
desk	2	0	0	58	2	0	0	0	12	0
dresser	0	0	0	2	84	0	16	0	0	0
monitor	2	2	0	0	0	98	0	0	0	0
night stand	2	0	0	4	10	0	82	0	0	0
sofa	8	0	0	18	2	0	0	98	0	0
table	0	0	0	16	0	0	2	0	88	0
toilet	0	0	0	2	2	0	0	0	9	100

Confusion matrix with actual classes*predicted classes. The proportion per class identified correctly is displayed

Fig. 8

REFERENCES

[1.] Srinivasan, S., Pauwels, K., Silva-Risso, J., Hanssens, D.M., 2009. Product Innovations, Advertising, and Stock Returns. Journal of Marketing 73 (1), 24–43.

[2.] Negri, E., Fumagalli, L., Macchi, M., 2017. A Review of the Roles of Digital Twin in CPS-based Production Systems. Procedia Manufacturing 11, 939–948.

[3.] Albers, A., Haug, F., Fahl, J., Hirschter, T., Reinemann, J., Rapp, S., 2018 - 2018. Customer-Oriented Product Development: Supporting the Development of the Complete Vehicle through the Systematic Use of Engineering Generations, in: 2018 IEEE International Systems Engineering Symposium (ISSE). 2018 IEEE International Systems Engineering Symposium (ISSE), Rome. 01.10.2018 - 03.10.2018. IEEE, pp. 1–8.

[4.] VDI, 1993. Systematic approach to the development and design of technical systems and products.

[5.] Albers, A., Bernijazov, R., Kaiser, L., Dumitrescu, R., 2018. Internet of Things Canvas for Ideation in Model-Based Product Generation Planning, in: 2018 13th System of Systems Engineering Conference (SoSE). June 19-22, 2018, Sorbonne université, campus Pierre et Marie Curie, Paris, France. 2018 13th Annual Conference on System of Systems Engineering (SoSE), Paris. 6/19/2018 - 6/22/2018. IEEE, Piscataway, NJ, pp. 327–334.

[6.] Su, H., Maji, S., Kalogerakis, E., Learned-Miller, E., 2015. Multi-view Convolutional Neural Networks for 3D Shape Recognition, in: 2015 IEEE International Conference on Computer Vision. 11-18 December 2015, Santiago, Chile : proceedings. 2015 IEEE International Conference on Computer Vision (ICCV), Santiago, Chile. 12/7/2015 - 12/13/2015. IEEE, Piscataway, NJ, pp. 945–953.

[7.] SIMUFORUM® Search Solutions GmbH. https://www.simuform.com/. Accessed 12 June 2019.

[8.] Kanezaki, A., Matsushita, Y., Nishida, Y., 2016. Rotation Net: Joint Object Categorization and Pose Estimation Using Multiviews from Unsupervised Viewpoints, 24 pp. http://arxiv.org/pdf/1603.06208v4.

[9.] Sedaghat, N., Zolfaghari, M., Amiri, E., Brox, T. Orientation-boosted Voxel Nets for 3D Object Recognition, in: Procedings of the British Machine Vision Conference 2017. British Machine Vision Conference 2017, London, UK. British Machine Vision Association. [10] Charles, R.Q., Su, H., Kaichun, M., Guibas, L.J., 2017. PointNet: Deep Learning on Point Sets for 3D Classification and Segmentation, in: 30th IEEE Conference on Computer Vision and Pattern Recognition. CVPR 2017 : 21-26 July 2016, Honolulu, Hawaii : proceedings. 2017 IEEE Conference on Computer Vision and Pattern Recognition (CVPR), Honolulu, HI. 7/21/2017 - 7/26/2017. IEEE, Piscataway, NJ, pp. 77–85.

[10.] Charles Ruizhongtai Qi, Li Yi, Hao Su, Leonidas J. Guibas, 2017. PointNet++: Deep Hierarchical Feature Learning on Point Sets in a Metric Space, in: NIPS.

[11.] Simonovsky, M., Komodakis, N., 2017. Dynamic Edge-Conditioned Filters in Convolutional Neural Networks on Graphs. http://arxiv.org/pdf/1704.02901v3.

[12.] Wu, Z., Song, S., Khosla, A., Yu, F., Zhang, L., Tang, X., Xiao, J., 2015. 3D ShapeNets: A deep representation for volumetric shapes, in: 2015 IEEE Conference on Computer Vision and Pattern Recognition (CVPR). - 12 June 2015, Boston, MA. 2015 IEEE Conference on Computer Vision and Pattern Recognition (CVPR), Boston, MA, USA. 6/7/2015 - 6/12/2015. IEEE, Piscataway, NJ, pp. 1912–1920.

[13.] Defferrard, M., Bresson, X., Vandergheynst, P., 2016. Convolutional Neural Networks on Graphs with Fast Localized Spectral Filtering.

[14.] Zehtaban, L., Elazhary, O., Roller, D., 2016. A framework for similarity recognition of CAD models. Journal of Computational Design and Engineering 3 (3), 274–285.

[15.] Hong, T., Lee, K., Kim, S., 2006. Similarity comparison of mechanical parts to reuse existing designs. Computer-Aided Design 38 (9), 973–984.

[16.] Huang, J., You, S., 2012. Point cloud matching based on 3D self-similarity, in: IEEE Computer Society Conference on Computer Vision and Pattern Recognition workshops (CVPRW), 2012. 16 - 21 June 2012, Providence, RI, USA. 2012 IEEE Computer Society Conference on Computer Vision and Pattern Recognition Workshops (CVPR Workshops), Providence, RI, USA. 6/16/2012 - 6/21/2012. IEEE, Piscataway, NJ, pp. 41–48.

[17.] Lima, J.P.S.d.M., Teichrieb, V., 2016. An Efficient Global Point Cloud Descriptor for Object Recognition and Pose Estimation, in: 2016 29th SIBGRAPI Conference on Graphics, Patterns and Images - SIBGRAPI 2016. São José dos Campos, Sao Paulo, Brazil, 4-7 October 2016 : proceedings. 2016 29th SIBGRAPI Conference on Graphics, Patterns and Images (SIBGRAPI), Sao Paulo, Brazil. 10/4/2016 - 10/7/2016. IEEE, Piscataway, NJ, pp. 56–63.

[18.] Zhong, Y., 2009. Intrinsic shape signatures: A shape descriptor for 3D object recognition, in: IEEE 12th International Conference on Computer Vision workshops (ICCV workshops), 2009. Kyoto, Japan, 27 September - 4 October 2009. 2009 IEEE 12th International

[19.] Conference on Computer Vision Workshops, ICCV Workshops, Kyoto, Japan. 9/27/2009 - 10/4/2009. IEEE, Piscataway, NJ, pp. 689–696.

[20.] Roj, R., 2016. Eine Methode für eineautomatisierteInformationsextraktionausgroßen CAD-DatenbeständenzurBauteilsuche und Klassifikation. Dissertation, Wuppertal. [21] Krizhevsky, A., Sutskever, I., Hinton, G.E., 2017. ImageNet classification with deep convolutional neural networks. Commun. ACM 60 (6), 84–90. [22] Simonyan, K., Zisserman, A., 2014. Very Deep Convolutional Networks

e-ISSN: 2582-5208
International Research Journal of Modernization in Engineering Technology and Science
(Peer-Reviewed, Open Access, Fully Refereed International Journal)
Volume:04/Issue:05/May-2022 Impact Factor- 6.752 www.irjmets.com

INDUSTRY 4.0: IMPACT ON FUTURE OF WORK

Aman Jha*1, Dr. Ashok Madan*2

*1,2Department of Mechanical Engineering Delhi Technological University, Delhi-110042

ABSTRACT

One of the most significant predictors of industrial revolutions (IR) has been technological advancements that enhance manufacturing processes. Industries have recently reached a point where production technologies indicate a new IR, Industry 4.0. It is set to not only improve industrial processes but also bring about changes in economic, environmental, and social aspects. Factors such as employment and the future of work are at the forefront of these changes. While some argue that the shift to Industry 4.0 can lead to unemployment as many jobs will be replaced by automation and robotics, others believe that overall employment rates will be higher as new job opportunities will emerge. Nonetheless, its impacts on myriad occupations remain uncertain. This study presents a literature review highlighting. According to the findings of the literature review, it, on one hand, will increase the demand for higher-level jobs which shows higher demand for labor with advanced qualifications as well as updated skillsets. Whereas on the other hand, the destruction of low-level jobs which can be easily replaced by automation is inevitable.

Keywords: Industry 4.0, technological advancements, Employment strategies

I. INTRODUCTION

In our ever-developing world, we now can see a significant change in how the fundamental transformation of the economy is taking place. For businesses to prevail and gain a competitive advantage, they must invest in continuous technological advancements. All around the past incidents, actors in various industries have always strived to meet changing consumer wants, resulting in the inevitability of continual technological improvement. The example of previous industrial revolutions might be used to study this technological advancement. The third and fourth IR saw the most significant technological and labor market changes, with CCA (computer-controlled automation) being supplanted by the fourth IR's digitalization, in which technologies interacted autonomously along the value chain. Many scholars have previously looked at the impact of digitalization along with automation and robotics as well as the use of virtual autonomous systems on the workforce [1–3], which has grown significantly as a result of the pandemic.

The IR may be viewed as a sequence of technical breakthroughs that improve the manufacturing process. The first industrial revolution, in this sense, began with the use of water and the power of steam in manufacturing. After that, the introduction of the assembly line and electricity use in manufacturing. The third one began with the switch to computer and automation technologies in the manufacturing process. The next one, often known as Industry 4.0, is the most recent stage at which production technologies have arrived. Quantum computing, artificial intelligence, synthetic biology, nanotechnology, as well as industrial robots are all examples of current technologies.

Automation and digitalization, according to research on the subject, are two of the most critical concerns in the job market today. [6], as a result of the technology revolution, considerable job shifts, robotics' replacement of human labor, employees, firms must adapt to shifting circumstances, and social and economic consequences. Although digitalization and the employment of industrial robots are becoming more common, the depth of their impacts on persons and professions, as well as their general appeal, are disputed. [7,8]. According to most research, massive advancements throughout the world affect millions of individuals [2,9,10]. Approximately 1.4 million industrial robots may be used in various job processes, with that number expected to increase by up to 13% every year. As per the World Bank report, the proportion of jobs threatened by I4.0 technologies in India is 69 percent year-on-year (Business Today, 2017).

The IR, in truth, entails considerably more than technological improvements. Every industrial revolution, in this spirit, ushers in both anticipated and unplanned changes in social, economic, environmental, and political systems (Hinton, 2018). Without a question, the skill mix required by Industry 4.0 and the future of work is at the top of the list of expected changes. Also, in the next 10 to twenty years, low-skill and routine employment are

e-ISSN: 2582-5208
International Research Journal of Modernization in Engineering Technology and Science
(Peer-Reviewed, Open Access, Fully Refereed International Journal)
Volume:04/Issue:05/May-2022 Impact Factor- 6.752 www.irjmets.com

more likely to be substituted or replaced by automation and robots, and lower-skilled persons face a larger risk of being jobless or underemployed if active and passive employment strategies are not integrated.

On the one hand, these robots will be able to repeat jobs with more accuracy and speed than humans, making them a more efficient labor replacement (BRICS Business Council, 2017: 5). However, if the changeover to Industry 4.0 is successful, a reduction in workload by hand and a shift to more gratifying jobs for workers could have a significant beneficial impact. According to the IFR, robots are more of a replacement for labor activities than for work. Robots provide improved opportunities for workers to participate in greater, relatively high, and professional jobs. However, Industry 4.0's influence on the future of work is yet unknown, and its success or failure is closely related to the labor market and the interaction between employees, unions, businesses, and government agencies. The goal of this research is to give a survey of the literature discussing the potential impact of Industry 4.o on employment and the future scope of the workplace.

II. LITERATURE REVIEW

Employee demand and supply influence labor market dynamics. In this vein, the impact of Industry 4.0 on technology, production, and organizational structure is projected to have an impact on the future workforce and employment. Changes in markets and technological progress are continually transforming industries throughout economies, as well as jobs. Schumpeter used the phrase "creative destruction" to describe the normal circulation process in capitalist economies. (Schumpeter, 1942: 82–85). Most jobs that have historically been done by humans will be completed by robots and automation technologies. Furthermore, old industries will be obliterated through creative destruction, while new ones will emerge that are more likely technologically arduous. Lastly, as a result of the shift to a technology-intensive industry, the overall economy will hit a "tipping point.". Companies will prefer to use automation and robots in production rather than human labor. In this regard, the World Economic Forum (WEF) predicts that total task hours completed by automation, which are currently at 29% across 12 industries, would climb to 58 percent by 2022 (WEF, 2018: viii). The key question here is how will the transition to Industry 4.0 affect unemployment and the changing nature of work? Academic and institutional debates on this topic are still occurring between two opposing viewpoints. According to pessimists, Industry 4.0 may result in massive job losses if increasingly smart technologies and robotics displace many current employees. Optimists claim that Industry 4.O will expand employment by creating new jobs and disciplines. (BRICS Business Council, 2017: 5-6).

Technological developments in robotics and automation will result in net job losses or reduced compensation as labor is finally replaced by automation and robots. They predict administrative and routine jobs with low and moderate skill levels positions. For 702 specified occupations in the United States, Frey and Osborne (2017) investigated the link between computerization and probability, earnings, and educational attainment. To do so, they classified jobs based on their potential for computerization, estimating that roughly 47 percent of total employment in the United States belongs to the high-risk group. Furthermore, researchers from the Mannheim Centre for European Economic Research (ZEW) found that 42 percent of employment in Germany was in high danger owing to automation, and the probability of automation For individuals with primary or elementary education, the percentage rises to 80% and degree reduce their risk to 18 percent. When it comes to income levels, the likelihood of automation decreases as income rises. (Schroeder, 2016:4). Furthermore, Deloitte (2014) anticipated that in the next 15 years, roughly 35 percent of occupations in the United Kingdom would be made redundant by new technology. According to the World Bank predictions (2016), automation and robotics will dispense with 66.6 percent of present manual occupations in developing countries. According to McKinsey (2015),

automation may replace 45 percent of existing jobs which are human-performed work, and 5% of full-time occupations might be fully replaced by technology. The impact of Industry 4.0 on the workplace is intimately linked to worker skill levels and whether a task is a routine type or others. The majority of research agrees that Industry 4.O will have less impact on high-skilled personnel. Some studies indicate that lower-skilled employees would suffer disproportionately, while others believe that the people with medium skills will suffer disproportionately.

e-ISSN: 2582-5208
International Research Journal of Modernization in Engineering Technology and Science
(Peer-Reviewed, Open Access, Fully Refereed International Journal)
Volume:04/Issue:05/May-2022 Impact Factor- 6.752 www.irjmets.com

In contrast, many predict that the shift to Industry 4.0 will boost job prospects, particularly in the fields of mathematics, architecture, and computer science. In the past, technical advancements were thought to have had a favorable impact on people's jobs. The Internet cost 500,000 french people their jobs while creating 1.2 million new ones in the last 15 years. The enforcement of enhanced productivity throughout the industry's value chain, enabled by Industry 4.0 technology, might offer new employment opportunities for selected industries in response to rising demand. To meet these problems, lower and middle-skilled workers' skills might be updated. Traditional financial sector jobs including, banking, legal assistance, and accountancy will be radically modified and substituted by Blockchain (BC) technologies. Furthermore, this technology also has the potential to produce new occupations, such as internet of things developers and Blockchain developers. The implementation of Industry 4. zero will necessitate the hiring of multi-professional employees. The way artworks are displayed within cyber-bodily machine technology may alter dramatically. New qualifications and skill sets would be required for new jobs with superior capabilities generated as a result of Industry 4. zero. Management and communication skills are far more likely to develop their significance in this context. Personnel is expected to have technical competencies, IT security expertise, system understanding, coding competencies, cutting-edge knowledge, and media competencies. (Sony & Naik,2019b)

According to Martin Ford (2009), technology reduces certain employment in some places, but where it promotes economic growth and creativity, new entrepreneurs emerge, new products and services are expanded, and new jobs are produced. He predicts that a job will appear. According to the Boston Consulting Group, relying on Industry 4.0 technology might result in over 100,000 new engineering and construction employment by 2024. Industry 4.0 adoption, according to some analysts, will not result in employment losses, even if it does not result in net job creation. In this sense, they predict that Industry 4.0 will enhance worker productivity and productivity. Low-wage employment is rapidly vanishing. However, as the demand for high-quality items grows, more employment for highly skilled persons will be created. As a result, the increase in high-skill occupations more than compensates for the loss of low-skill ones. According to the World Economic Forum, the percentage of emerging occupations in total employment will increment from 16%-27% by 2022, while the share of decreasing occupations would decrease from 31%-21%. 980,000 jobs will be lost, according to the WEF, resulting in a 1.74 million rise in employment.

Industry 4.0 will need the employment of multi-skilled individuals. The way artworks are shown may alter dramatically as a result of cyber-bodily machine technology. New qualifications and skill sets would be required for new employment with better capabilities established as a result of Industry 4.0. In this context, self-organization, governance, teamwork, and communication skills are far more likely to grow in importance. Personnel must possess cutting-edge knowledge, technological skills, system comprehension, media skills, coding skills, and IT security competence. The following methodological qualities are demanded of personnel: creativity, entrepreneurial thinking, problem-solving, war-solving, decision-making, analytical competencies, studies competencies, and performance orientation. Intercultural competence, language competencies, communication competencies, networking competencies, and teamwork, Some of the social skills expected in Industry 4 are the capacity to compromise and collaborate, the ability to convey information, and managerial competence. Adaptability and ambiguity are two words that come to mind when thinking about flexibility and Tolerance, learning drive, the capacity to work under pressure, a long-term perspective, and compliance are some of the personal qualities demanded of the employee. It's possible that finding someone with those skills may be difficult. Furthermore, educating current employees to acquire such competencies may necessitate strategic education modules and packages to minimize costs, as employee churn may be substantial. As per our consideration, the need for highly qualified individuals will grow, making it tough to meet the needs of businesses.

The relevance of programming skills and information technology will grow in terms of employability, according to Boston Consulting Group. Furthermore, companies will enlist human resources who have essential qualities and skill-sets, reconstruct the infrastructure of the organization and train new managers with new management techniques to improve more efficiency of the organization's assets. (Kergroach, 2017: 8). In the coming future, expertise in ICT and decision-making skills, and imaginativeness will be the most valuable capabilities that employers are seeking. ICT, big data, and cyber-security expertise will become the top vocations in industrialized

e-ISSN: 2582-5208
International Research Journal of Modernization in Engineering Technology and Science
(Peer-Reviewed, Open Access, Fully Refereed International Journal)
Volume:04/Issue:05/May-2022 Impact Factor- 6.752 www.irjmets.com

economies' labor markets (Davies, 2015: 6). According to the World Economic Forum, jobs that heavily rely on technology, such as Data Scientist and Data Analyst, Software Developer, Application Developer, and E-commerce and Social Media Specialists, will be significantly more in demand by 2022. (WEF). Customer service representatives, sales representatives, and marketing executives, as well as training and development professionals, people and culture specialists, organizational development specialists, and innovation managers, are more likely to expand. In addition, new competencies and skill sets required by Industry 4.0 will necessitate changes in the educational backgrounds, and also research and skills training. In this vein, educational systems need to focus on not only establishing core STEM (science, technology, engineering, and mathematics) education, but also on improving human skills including compassion, and critical thinking or systematic thinking which machines will be unable to fulfill. Additionally, The increased use of Industry 4.0 Jobs may be transferred from developing to developed nations as a result of technology in developed countries that demand specialized expertise. It's due to the fact that the labor cost of the industry will be diminished in developing countries. In comparison to developing countries and developed countries, the life qualities in developed countries will be much better for employees. Thus, it is a factor in transferring jobs to developed countries which will help industries in developed countries reduce their labor cost too.

According to the Labour Bureau's employment and joblessness in India survey (2015–2016), high-skilled and average-skilled individuals accounted for 14 percent of total workers, whereas the majority of the workforce (86 percent) are employed in unskilled or low-skilled positions. High- and medium-skilled occupations, it is believed, need complex analytical and management abilities and are hence less affected by automation. Managers, experts, technologists, and associate professionals are among the highest-paid occupations. Nonetheless, a large number of positions are now available in the information technology (IT), electronics and communication (EC), manufacturing, business, and financial sectors, all of which have a high risk of being automated. This organized-sector automation of middle-skilled jobs is likely to have an impact on low-skilled workers' migration to higher-skilled and higher-paying jobs. Low-skilled and unskilled employment, on the other hand, require operational skills as well as frequent or manual operations that can be easily automated with emerging technology. Employment with minimum or less wage includes clerical assistance, service and sales workers, crafts and allied trades, maintenance workers and manufacturing line keepers, armed forces positions, labor, domestic servants, building caretakers, porters, and garbage collectors. For example, these essential jobs employ half of all present workers. As there is a large number of people employed in low-skilled professions, India is particularly vulnerable to the effects of automation or 4.0 technologies.

Researchers believe that IR 4.0 is additional seemingly to alter well the character of jobs, future geographical points, and labor force. A large number of existing occupations are being replaced by a new category of employment. On the contrary, with a transition to Industry 4.0, the necessity for skillful staff can increase whereas demand for the low and average-skilled staff can fall. For instance, jobs requiring a low level of social interaction, creativity, quality, and quickness area unit additional seemingly become automatic. Also, routine jobs that need measure, processing, pattern recognition, or manipulation are way more susceptible to computerization and automation. Furthermore, automated systems and robotics may progressively displace workers, widening the skills gap. Digitalization and computerization are two terms that are used interchangeably. In this aspect, the proof shows that computers may supplement non-routine psychological feature activities. Technical advancements resulting from IR 4.0 are likely to eliminate not only regular job, but also high skilled jobs are required like pattern recognition and psychological feature non-routine duties. In addition, they said about computerization and robotics which can replace millions of occupations performed by toil all over industries. As a result, Industry 4.0 may exacerbate labor market inequities, with low-skilled/low-paid workers facing even more tough circumstances. The World Health Organization discovered that intelligent and cyber-physical systems would disproportionately displace those who added lower-skill jobs involving basic and repetitive activities when they studied the effects of this revolution on operational, indirect, and management tasks and activities. Martin Ford (2009) used a scenario to anticipate how cyber-physical systems and technology might affect employability and job structure. He (2009) predicted that computer science, machine learning, and packaging automation applications would predominantly serve the demands of low-wage, uneducated workers, and that computers would increasingly perform the majority of occupations that require extensive coaching and

e-ISSN: 2582-5208
International Research Journal of Modernization in Engineering Technology and Science
(Peer-Reviewed, Open Access, Fully Refereed International Journal)
Volume:04/Issue:05/May-2022 Impact Factor- 6.752 www.irjmets.com

training.

Based on current patterns and earlier industrial revolution teachings, it's plausible to expect a personnel disruption as a result of this industrial revolution. The potency and production of each historical period increased. Automation solutions have become more affordable and effective as a result of recent technological advancements. Potentially leading to the "technological unemployment" that John Maynard Keynes predicted. According to this idea, technological developments will be able to substitute human employment faster than we can create new ones.

Many authors stand by the disappearance of jobs and also the decrease in human work, however, their estimated dissent in terms of the extent and speed of the negative effects. Today, five-hundredths of all tasks are often machine-controlled with on-the-market technologies. Only a small percentage of employment (less than 5%) have duties that cannot be automated at all; in the meantime, technology frequently replaces the tierce of tasks in the hour of work. Technological breakthroughs will almost certainly cause some jobs to go in the short term, but the structural state looks to be strong, despite the fact that advancements will have major effects on both low- and high-skilled workers. Different analytical articles, on the other hand, identify favorable developments related to the unfolding of automation. According to the study, maintaining human property 2021, 13, 7703 nine of nineteen health might provide a higher profit over time. The advantages of automation include the elimination of risky jobs, lower costs, greater quality, increased safety, and environmentally friendly solutions. Personnel automation, according to certain viewpoints, would assist people rather than damage them since robots will take over tasks that are potentially hazardous or toxic for humans, such as attachment or car paint. On the other side, technology solutions may improve some vocations or activities, such as employing video games for teaching to eliminate the chance of accidents, or imposing sensor-driven internal control on production lines to replace a dull work.

Existing writing on acts of Industry 4.0 on HR and corporate association features that collaboration, interdisciplinary engagement, and collaborator networks are certain to grow in importance. Also, with Industry 4.0, it is expected that work-life flexibility, as well as interest in and programming talents, would increase. Moreover, there is a growing interest in innovation-related and non-mental dedicated talents.(World Economic Forum'18) Capabilities in ICT, large data, and cyber security Office and administrative, transmission and coordinated aspects, Blockchain designers, IoT modelers, and mental PC engineers are all examples of people who work in this field. It can get help with accounting, banking, and even legal matters. Electricity-powered machines and equipment Thanks to changes in job positions and accompanying structures, the textile, clothing, and footwear industries, Agriculture 321, are more inventive and evolving than at any other moment in recent memory. This interaction drives steadily improves the requirement for new kinds of instruction and preparation. Likewise, the chances of lack of employment will undeniably be more ascent for individuals without word-related training. The justification for this, innovative change is that I4.0 will request fresh prerequisites for content and cycles of utilization as well as essential capabilities & skills. Furthermore, the authors observed that there is a negative connection between compensation and instructive accomplishment and the likelihood of computerization. Their discoveries infer that as innovation advances, low-talented specialists should move to undertakings requiring inventive and social knowledge and gain new imaginative and interactive abilities. In such a manner, coordinating re-preparing projects to help to acquire new abilities is so basic for laborers at high-risk.

It has been encountering progress from the workforce to mechanical technology and mechanization in numerous enterprises. Low-skilled laborers are, without a question, the most vulnerable category. Laborers who are skilled in using Industry 4.0 technologies may gain greater autonomy and be assigned more interesting or less stressful work. Electrical apparatuses and gadgets, material, dress, and footwear businesses happen among the most touchy enterprises concerning mechanical technology and computerization. For the authors, most specialists in the assistance area who connect with transportation and coordinated operations, workplace and authoritative help, as well as workers' underway works, could be subbed via mechanization and robots somewhat soon. The other area impacted by Industry 4.0, especially in created nations, is agribusiness. For instance, it is normal that 223,000 positions in horticulture, ranger service, hunting, and fishing will be lost in the USA by 2022. The

individuals who go against this view contend that it is probably not going to dispose of all positions in those areas where innovation substitutes for work.

Regarding good work, with the use of Industry 4.0 advancements underway, positions will be isolated into more modest parts to help worldwide and computerized creation. Additionally, new positions made by Industry 4.0 might be in non-standard structures, for example, part-time, brief, ready to come in case of an emergency, and so forth instead of the standard everyday work models. In this context, the World Economic Forum predicted that by 2022, robotization will result in a reduction in the workforce in routine jobs. Subsequently, the number of laborers connecting with non-standard positions might increment and the eventual fate of work might turn into a more divided structure that an individual needs to work on more than one task to make up for money from their normal work. Furthermore, non-standard occupations with little pay and no social insurance or security, as well as "the gig economy" 2 with issues such as a lack of bartering power and legal certainty, are predicted to become more common sooner rather than later.

III. CONCLUSION

The main motivation for our analysis is to provide literature on the possible positive and on adverse scenarios of Industry 4.0 on utilization and the upcoming work. On the one hand, optimists are excited about the potential for economic development owing to technological improvement, which may result in a significant reduction in working time and a significant increase in leisure time. Pessimists, on the contrary, are concerned about the loss of some employment in industries, as well as the low pay that comes with automation's efficiency, because they feel that job losses will primarily impact low and middle-skilled uninteresting occupations. According to most of the studies done on the subject; it is well understood that new technology does not eliminate existing jobs, but rather generates new ones. As a result, a large market of specialty jobs is growing, ready to be exploited, with new technologies in full swing. However, this process of job creation and elimination doesn't happen overnight, rather takes place over a longer period.

Again, despite the ongoing debate on the work subsequently, it seems that the future of work remains ambivalent. The aspects that certainly are higher education and skills are more likely to be required for the new jobs that will be innovated soon. If we further add, these jobs will be made up of non-standard standards, and provide more fragmented jobs, requiring a person to perform more than one work. As a result, the likelihood of future unemployment will soar. Industry 4.0 job-skill standards should be included in the employment strategy.

The expectations mentioned above demand, the development of employment and skill development policies. Governments should take proactive steps, invest in high-intensity infrastructure and construction, and encourage micro-entrepreneurship models and start-ups. It is important for job-skill criteria for Industry 4.0 should be built into the employment policy. It is worth noting that the current educational curriculum should be redesigned based on basic STEM education, with an emphasis on human competence such as creativity, critical thinking, and empathy. Furthermore, sufficient passive employment rules should be developed to ensure unavoidable costs are minimized and shared evenly, as Industry 4.0 will offer new job opportunities as well as dangers of less utilization of manpower. This entire process can be viewed positively; not only does it open up a wide range of opportunities for a more dignified existence, but it is also an unavoidable element of competition, lowering marginal costs, and job losses can be minimized with proper employment policies and skill training programs.

IV. REFERENCES

[1]. Balliester, T. and Elsheikhi, A., (2018), "The Future of Work: A Literature Review", ILO Research Department, Working Paper No. 29.

[2]. BRICS Business Council (2017), "Skill development for Industry 4.0", A White Paper by BRICS Skill Development Working Group, BRICS Business Council, India Group. Online available at http://www.globalskillsummit.com/ Whitepaper-Summary.pdf (Accessed on 11.06.2019

[3]. Bonekamp, L. & Sure, M., (2015), "Consequences of Industry 4.0 on Human Labour and Work Organisation", Journal of Business and Media Psychology 6, Issue 1, 33-40, available at www.journalbmp.de

[4]. Cambridge Dictionary (2019), available online at https://dictionary.cambridge.org/ (Accessed on 11.06.2019)

[5]. The Future of Jobs and the Fourth Industrial Revolution: Business as Usual for Unusual Business (worldbank.org)

[6]. Davies, R., (2015), "Industry 4.0 Digitalisation for productivity and growth", Briefing, European Parliamentary Research Service.

[7]. Flynn, J., Dance, S. and Schaefer, D., (2017), "Industry 4.0 and its Potential Impact on Employment Demographics in the UK", 15th International Conference on Manufacturing Research, University of Greenwich, London, UK

[8]. Frazer, J., (2019), "How The Gig Economy Is Reshaping Careers For The Next Generation", *Forbes*, available online at *https://www.forbes.com/sites/johnfrazer1/2019/02/15/how-the- gig-economy-is- reshaping-careers-for-the-next-generation/#75fdf06649ad.* (Accessed on 11.06.2019).

[9]. Ford, M., (2009), The Lights in the Tunnel: Automation, Accelerating Technology and the Economy of the Future, USA: Acculant Publishing.

[10]. Hinton, S., (2018), "How The Fourth Industrial Revolution Is Impacting The Future of Work", Forbes, available online at https://www.forbes.com/sites/theyec/2018/10/19/how-the-fourth- industrial-revolution-is-impacting-the-future-of-work/#62c9f90a65a7. (Accessed on 11.06.2019).

[11]. Kergroach, S., (2017), "Industry 4.0: New Challenges and Opportunities for the Labour Market",

[12]. Foresight and STI Governance, vol. 11, no 4: 6–8. DOI: 10.17323/2500-2597.2017.4.6.8.

[13]. Kusmin, K. L. (n.d). "Information Society Approaches and ICT processes Industry 4.0", IFI8101, available online at http://www.tlu.ee/~pnormak/ISA/Analytical articles/2-Industry

[14]. 4.0 - Kusmin.pdf. (Accessed on 11.06.2019).

[15]. Makhoul, F. (2018), "Industry 4.0 – How it will shape the Future of Work", available online at https://www.linkedin.com/pulse/industry-40-how-shape-future-work-feras-makhoul. (Accessed on 11.06.2019).

[16]. Morrar, R., Arman, H. and Mousa, S., (2017), "The Fourth Industrial Revolution (Industry 4.0): A Social Innovation Perspective", Technology Innovation Management Review, Vol. 7, Issue 11: 12-20.

[17]. Riminucci, M., (2018), "Industry 4.0 and Human Resources Development: A View from Japan",

[18]. E-Journal of International and Comparative LABOUR STUDIES, Volume 7, No. 1: 1-16.

[19]. Schroeder, W., (2016), "Germany's Industry 4.0 Strategy Rhine capitalism in the age of digitalization", Friedrich-Ebert-Stiftung, London, The United Kingdom.

[20]. Schumpeter, J. A., (1942), "The Process of Creative Destruction", In Capitalism, Socialism and Democracy, Ch. 7, New York, Harper: 82–85

[21]. Sun, M., (2018), "The Impacts of the Fourth Industrial Revolution on Jobs and the Future of the Third Sector", NICVA, available online at http://www.nicva.org/sites/default/files/d7content/attachments-articles/the_impact_of_the_4th_industrial_revolution_on_jobs_and_the_sector.pdf. (Accessed on 11.06.2019).

[22]. World Economic Forum (WEF) (2018), The Future of Jobs Report 2018, Centre for the New Economy and Society, Geneva, Switzerland.

[23]. Zheng, P., Wang, H., Sang, Z. et al. (2018), "Smart Manufacturing Systems for Industry 4.0: Conceptual Framework, Scenarios, and Future Perspectives", Frontiers of Mechanical Engineering, Vol: 13, Issue:2: 137-150, DOI: 10.1007/s11465-018-0499-5.4

Trans Indian Inst Met
https://doi.org/10.1007/s12666-022-02655-w

ORIGINAL ARTICLE

Influence of Nano-Sized Al_2O_3 Nanoparticles and Multipass FSW on Microstructure and Mechanical Characteristics of Dissimilar Welded Joints of AA6061 and AA5083

Preety Rani[1] · **Radhey Shyam Mishra**[1]

Received: 8 February 2022 / Accepted: 30 May 2022
© The Indian Institute of Metals - IIM 2022

Abstract The present research fabricated a dissimilar friction stir welded joints of AA6161 and AA5083 by incorporating Nano-sized Al_2O_3 nanoparticles. The effect of multipass friction stir welding (FSW) on the dispersion pattern of Al_2O_3 nanoparticles and the impact of particles' dispersion on microstructure and various mechanical characteristics was investigated. The results demonstrated that multi-pass FSW had significant impacts on the Al_2O_3 nanoparticles' distribution. Furthermore, the dispersion pattern of Al_2O_3 nanoparticles in the stir zone strongly influenced the microstructure and mechanical characteristics. The results obtained from mechanical testing after a microstructural study corroborate multi-pass FSW. Tensile strength, strain rate, and micro-hardness of the Al_2O_3 reinforced joints of AA6061/AA5083 were improved after implementing multipass FSW. The improvement in the mechanical characteristics was observed via higher grain refinement by pinning effect and dynamic recrystallization by Al_2O_3 nanoparticles. The tensile strength after one, two and three FSW passes were observed to be 227.3, 257.4 and 272.7 MPa, with a % strain of 24.4, 26.8 and 30.7, respectively. Furthermore, the hardness value after 1 pass, 2 pass, and 3 pass FSW were 127.1, 136.4 and 145.7 HV, respectively.

Keywords Multipass FSW · Microhardness · Microstructure · Tensile strength · Reinforcement particles

✉ Preety Rani
preetyhmritm@gmail.com

[1] Department of Mechanical Engineering, Delhi Technological University, Delhi, India

1 Introduction

Aluminum and its alloys are well recognized for being the most extensively used materials for structural components in almost all industrial domains, including aircraft, defense marine, automotive etc. [1, 2]. The joining of dissimilar alloys improves structural design flexibility and extend their uses [3]. Many fusion and solid-state welding approaches have been used to investigate the welding of different aluminum alloys [4–6]. But, due to the increased propensity for intermetallic compounds, larger residual stress, solidification cracking, and evaporation of alloying elements are caused by high heat input. For joining dissimilar materials, several solid-state welding approaches, including explosive welding, diffusion welding and ultrasonic welding, are considered as suitable substitutes for fusion welding. However, these techniques' applicability is limited by high implementation costs, dimensional constraints, and significant energy usage [7]. The FSW process is extensively employed to weld dissimilar alloys because of its, low cost, good weld quality and low energy consumption [8]. Various researchers have successfully used FSW to weld dissimilar aluminum alloys [9–11]. Reinforcement particles-based metal-matrix composites (MMCs) are extensively utilized to develop surface composites using friction stir processing (FSP) for improving surface and mechanical characteristics, including hardness, strength, corrosive, and wear resistance [12–14]. This is due to the reinforcing particles' outstanding mechanical and physical properties, including high hardness, high strength to weight ratio, and superior corrosion and wear resistance [15]. The enhancement in mechanical strength of these MMCs is considerably affected by the concentration and size (nano/micro) of reinforcing particles [16]. Nano-composites are

Published online: 24 June 2022

more difficult to fabricate than micro-composites because uniform dispersion of nanoparticles is difficult to accomplish in the base metal matrix using powder metallurgy and molten metal processing methods [17]. These methods cause mechanical characteristics to deteriorate owing to the production of unsuitable secondary phases [18]. FSW has also been effectively used to fabricate reinforcement particles-based MMCs because of its solid-state joining nature and eliminating undesirable secondary phases. Therefore, FSW has been successfully used to a variety of aluminum alloys for the fabrication of reinforcement particles-based MMCs such as, AA7005 + Al_2O_3 [19], AA6061 + TiC [20], AA6061 + Al_2O_3 [21], AA5083/AA7075 + Al_2O_3 [22]. The dispersion pattern of reinforcing particles in the metal matrix of the base material is mainly influenced by the number of FSW passes compared to process parameters [23]. Increased tool rotational speed (TRS), especially at higher welding speed (WS), produce defects in the aluminum matrix composites. Increased FSP passes result in homogenous core and fine Al_2O_3 reinforcement particle's dispersion in the stir zone (SZ) [24]. The inclusion of Al_2O_3 reinforcement particles in AA2024 considerably reduces the grain size of the FSPed specimens and enhances the tensile strength up to 71% [25]. Adding Al_2O_3 to the aluminum matrix composite increases its wear and hardness properties. Except for regaining the HAZ's hardness value, heat-treating the surface composite has no favorable effect on the wear and hardness values [26]. The aluminum surface hybrid composite was fabricated by mixing two nanoparticles, Al_2O_3 and Ti_3AlC_2, and observed the maximum wear and tensile properties compared to the base metal [27, 28]. However, the influence of reinforced metal-matrix and multi-pass FSW on the weld quality of dissimilar aluminum alloys has never been examined by the researchers in the available literature. Therefore, this study fabricated a reinforced FSWed joint of AA6061 and AA5083 using Al_2O_3 nanoparticles. The influence of multi-pass FSW and reinforcement of Al_2O_3 nanoparticles on the microstructural and mechanical behavior of dissimilar FSWed joints of AA6061 and AA5083 was studied.

2 Materials and method

Base metals AA6061 and AA5083 of dimensions 150×40×6 mm were used for multi-pass FSW. The optical microscope (OM), field-emission scanning electron microscopy (FESEM), and energy dispersive spectroscopy (EDX) was employed to analyze the material characterization of the welded joints of dissimilar aluminum alloys of AA5083 and AA6061. Nanoparticles Al_2O_3 (50–70 nm) were employed as reinforcement particles (RPs). The SEM and EDX images of Al_2O_3 nanoparticles (np-Al_2O_3) are shown in Fig. 1. The groove was created on the adjoining faces of both the plates. The details of groove dimension are shown in Fig. 2. Before welding, the grooves were cleaned with CH_3COCH_3. Thereafter, the grooves were filled manually by Al_2O_3 and ethanol of 99% purity. While welding dissimilar metal alloys, the location of base plates is critical. Therefore, the AA5083 plate was positioned on the retreating side and AA6061 plates on advancing side during the welding process [29, 30]. A numeric controlled FSW machine was utilized for the experimentation. The base plates of AA5083 and AA6061 were clamped to prevent them from abutting during welding, as shown in Fig. 2b. A pinless tool of H13 tool steel diameter of 20 mm was used at 950 rpm, 30 mm/min, and 1° tool tilt angle to cover the groove. The FSW tool consisting of a threaded pin and H13 tool-steel (hardness-465 HV) was employed.

The dimensional characteristics of the tool are delineated in Fig. 2c. The FSW was performed at a constant TRS of 950 rpm, WS of 30 mm/min with a tilt angle of 1°. A number of preliminary trials were used to determine the parameters. The reinforcement condition of np-Al_2O_3 and the FSP passes are illustrated in Table 1. The FSWed specimens, after implementation of a different number of FSW passes and reinforcement conditions, are depicted in Fig. 3. CNC

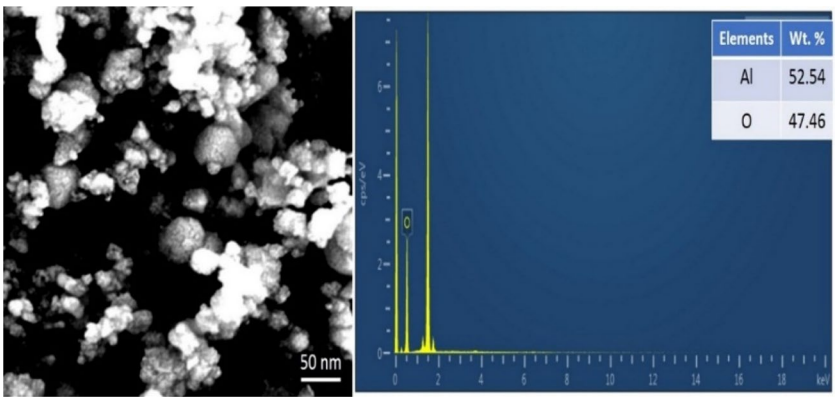

Fig. 1 **a**, **b** FESEM image and EDS elemental characterization of Al_2O_3 nanoparticles

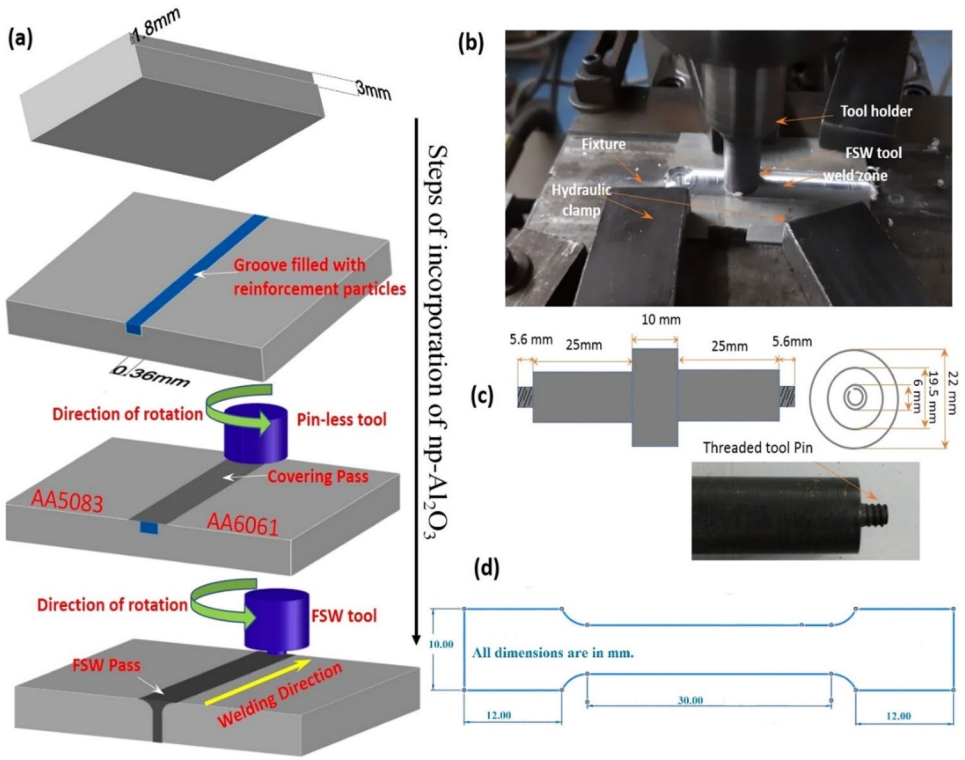

Fig. 2 **a** Steps of FSW experimentation incorporated with Al_2O_3 nanoparticles, **b** FSW Set-up, **c** Tool used for multi-pass FSW, **d** Dimensions of tensile specimen (ASTM- E8 standard)

Table 1 Process parameters of FSWed samples

S/No	TRS (RPM)	WS (mm/min)	Number of FSW passes	Reinforcement condition
1	950	30	One-pass (1P)	Without np-Al_2O_3
2	950	30	One-pass (1P)	With np-Al_2O_3
3	950	30	Two-pass (2P)	With np-Al_2O_3
4	950	30	Three-pass (3P)	With np-Al_2O_3

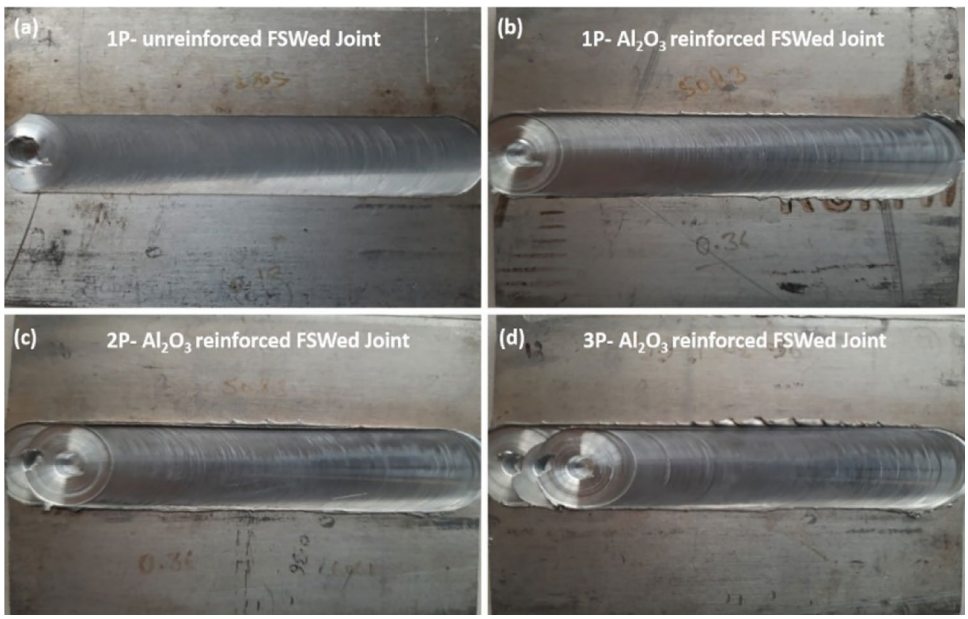

Fig. 3 Images of various FSWed specimens

wire-cut EDM was used to extrude the samples for further testing from the FSWed joints. The tensile test samples were extruded according to ASTM E-8 specifications, as delineated in Fig. 2d. A Vickers microhardness machine (Model: XHVT-1000Z) was used on the perpendicular surface to the weld line at a load to measure the micro-hardness of 200 gm for a dwell duration of 10 s. To analyze the profile of micro-hardness variation, the indentation was performed with a spacing of 1 mm. The samples for microstructure evolution were polished using different emery papers with increasing grades of 100 to 2000 grade. After polishing, the samples were etched in a solution containing: 9 ml of HCL, 5 ml of HNO3, 3 ml of HF and 5 ml of H2O for about 10 s. OM (Olympus, Model: GX41), FESEM (Jeol, Model: JSM-7620Plus) and EDS (Oxford Instrument, Model:51-ADD0076) were employed for microstructure evolution.

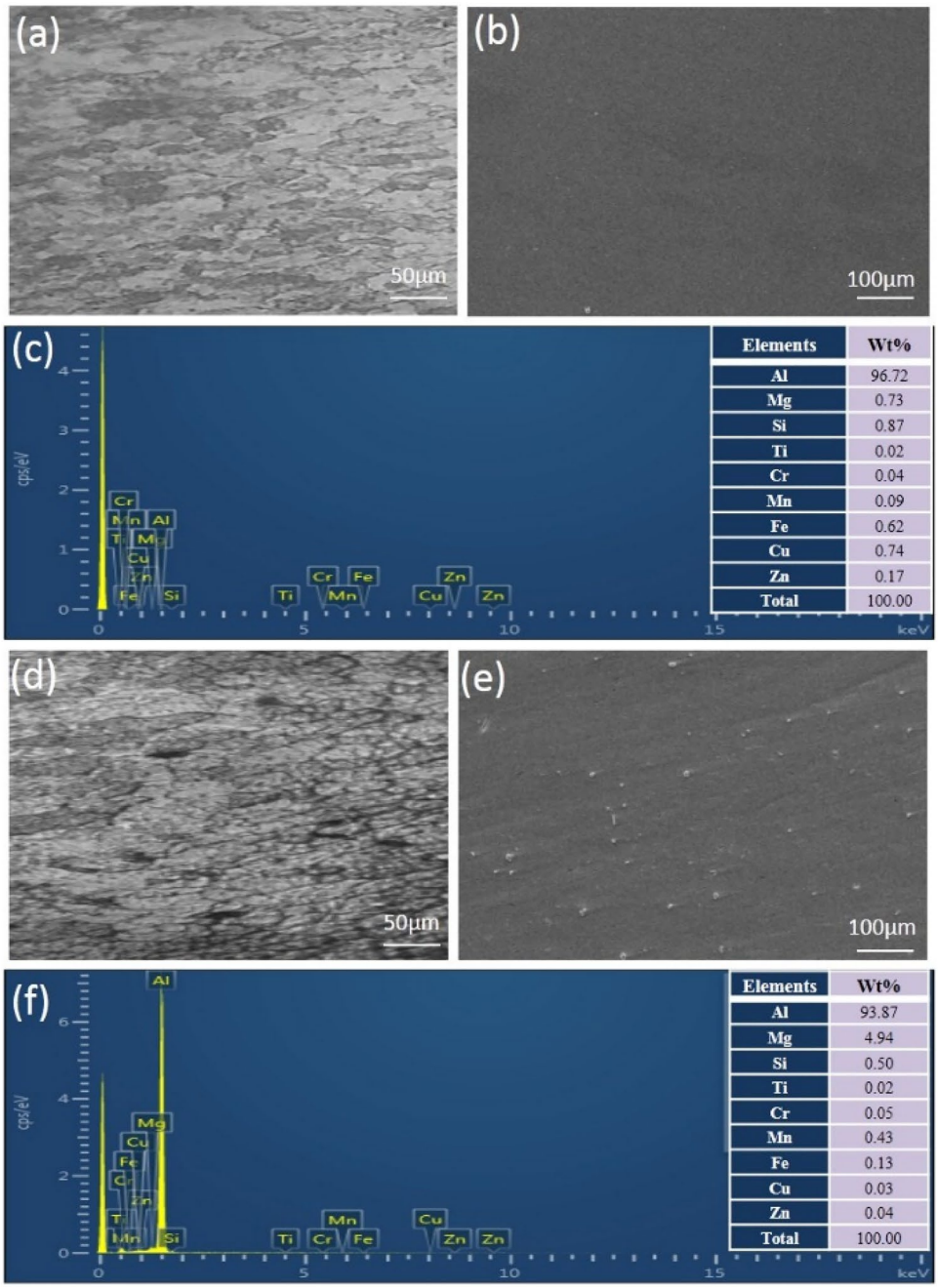

Fig. 4 OM micrograph, FESEM images and EDS elemental characterization **a**, **b**, **c** AA6061, **d**, **e**, **f** AA5083

3 Results and Discussion

3.1 Microstructural Observation

Figure 4a and d demonstrate the optical microstructure (OM) of the base metal of AA6061 and AA5083 with an average grain size of − 37 µm and − 41 µm, respectively. The average grain size was analyzed by ImageJ software. Due to DRX and SPD (severe plastic deformation), the welded region of AA6061 and AA5083 after FSW was refined in the heat-affected zone (HAZ), thermos-mechanical affected zone (TMAZ) and SZ [31]. When the number of passes with nanoparticles was introduced, the grain structure in the SZ refined even further [32].

The microstructure is the most significant factor in the tensile strength of an unreinforced FSWed joint. Other factors that influence the tensile properties of the multi-pass FSW joints include the RPs size, the bonding quality between the RPs and the matrix, the RPs dispersion pattern, and the location produced by the matrix's unequal coefficient of thermal expansion [33]. After FSW, the stretched microstructure of AA6061 and AA5083 was turned into a fine and equiaxed grain structure in the SZ. The DRX, annealing effect, and the influence of the dispersion pattern of RPs in the SZ contribute to grain refining during FSW. These phenomena compete for dominance, and the dominant factors define the grain size. The SPD at high temperatures causes DRX, resulting in converting high angle to low angle boundaries and the nucleation of new grain structures at preferential places, reducing the grain size. A high TRS and low WS cause annealing, which accelerates coarsening and grain growth [34]. The RPs behave as barriers to grain boundaries in the SZ and prevent grain expansion [35].

Consequently, the DRX and the influence of the dispersion pattern of RPs (np-Al_2O_3) are the dominating factors in the grain size reduction at 950 rpm of TRS and 30 mm/min of WS. Due to the absence of np-Al_2O_3 in unreinforced FSWed joints, only the effect of DRX is prominent and decreases the grain size. However, in np-Al_2O_3 reinforced FSW joints, the impact of np-Al_2O_3 and DRX both dominate the grain size reduction [36].

Figure 5 depicts the FESEM images of all the FSWed joints. Figure 5a illustrates the micrograph of the 1P-unreinforced FSWed joint. In contrast, Fig. 5b–d depicts micrographs of reinforced joints subjected to multi-pass FSW. The SZ of the 1P-unreinforced FSWed joint (Fig. 5a) demonstrated appropriate intermixing of both the alloys without any defect. Figure 5b–d shows the SZ of multi-pass reinforced FSWed joints and confirms the RPs dispersion pattern. The clustering of np-Al_2O_3 was detected in the SZ of the 1P-reinforced FSWed joint, as depicted in Fig. 5b. Therefore, it was evident that 1P-FSW was not sufficient for the uniform dispersion of the np-Al_2O_3 due to asymmetrical material flow [37].

The clustering of np-Al_2O_3 was found to be absent after 2P-FSW, and the moderate distribution of nanoparticles, including the particle rich area and particle less area, was perceived, as depicted in Fig. 5c. The dispersion of np-$Al_2O_3$was more pronounced and uniform after implementing 3P-FSW, as delineated in Fig. 5d. Therefore, it is

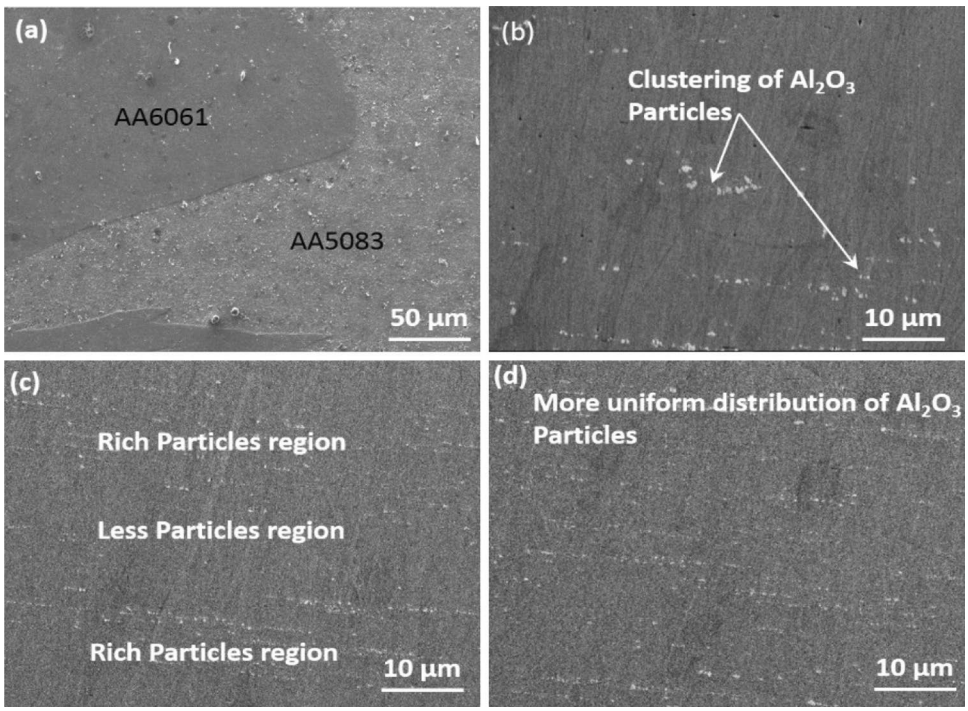

Fig. 5 FESEM micrograph **a** 1P- unreinforced FSWed joint, **b–d** np-Al_2O_3 reinforced FSWed joint, **b** 1P, **c** 2P, **d** 3P

evident in Fig. 5b–d that the distribution of nanoparticles was enhanced by breaking the clusters of np-Al_2O_3 on increasing the FSW passes from 1 to 3P. Thus, the FSW passes from 1 to 3P reduced grain size due to uniform dissemination of np-Al_2O_3 nanoparticles that resulted in high dislocation and enhanced dynamic recovery and DRX [38]. As a result of the pinning effect and DRX generated by the uniform dispersion of np-Al_2O_3, the OM images suggests that equiaxed and fine grain structure were observed. The peaks of the EDX data for the single-pass unreinforced FSWed joint and three passes reinforced FSWed joint are shown in Fig. 6. The EDX image also demonstrated that the SZ of the third pass reinforced FSWed joints had 4.11% oxygen. These findings illustrate the inclusion of np-Al_2O_3 to the SZ by FSW. The existence of equiaxed and refined grains in the stir zone in all three FSP passes could be attributed to the DRX generated by a combination of tool-driven heat generation and plastic deformation [39, 40]. The precipitates and solute pinning effect, also known as the Zener Pinning effect, may well be accountable for grain refinement in the SZ of the FSPed samples. The grain refinement was hampered by the clustered free, more uniformly distributed dispersed precipitates, and fine grain size was perceived in the SZ. A continuous type of strain was seen during multipass FSP, resulting in the breaking of elongated and coarse grains, considerably reducing the grain structure of the parent metal. The multipass FSP enhanced the fine grains structure and DRX mechanism [41].

3.2 Grains Structure Characterizations

Figure 7 reveals the microstructure of 1P unreinforced and multipass np-Al_2O_3 reinforced FSWed joints. The grain size of AA6061 and AA5083 was perceived as 38 µm and 42 µm respectively. Due to DRX and strong plastic deformation, the SZ of single-pass unreinforced FSW comprised fine recrystallized grains of 17 µm (Fig. 7a). With a granular size of 10.4 µm, the grain structure of the single-pass reinforced FSWed joints was observed to be more refined (Fig. 7b). As the FSW passes increased from 1 to 3, the grain size became even more distorted. This was due to np- Al_2O_3 in the stir zone, despite all FSWed joints having the same welding conditions. When dislocations accumulated due to RPs during plastic deformation, particle-induced nucleation-based DRX was conceivable [42]. Therefore, the grain size of the np-Al_2O_3 reinforced FSWed joints after the second pass and third pass was perceived as 3.9 µm and 2.8 µm, respectively (Fig. 7c, d). So, it could be concluded that incorporating np-Al_2O_3 with multipass FSW reduced the grain size of the SZ.

3.3 Effect of Multi-pass FSW/np-Al_2O_3 on Mechanical Behavior

3.3.1 Influence of Multi-Pass FSW/np-Al_2O_3 on UTS

The UTS of the single-pass unreinforced FSWed joint was less than the parent materials due to softening of the aluminum metal matrix [43], as shown in Table 2. In contrast, the UTS of a single-pass FSWed joint with reinforced

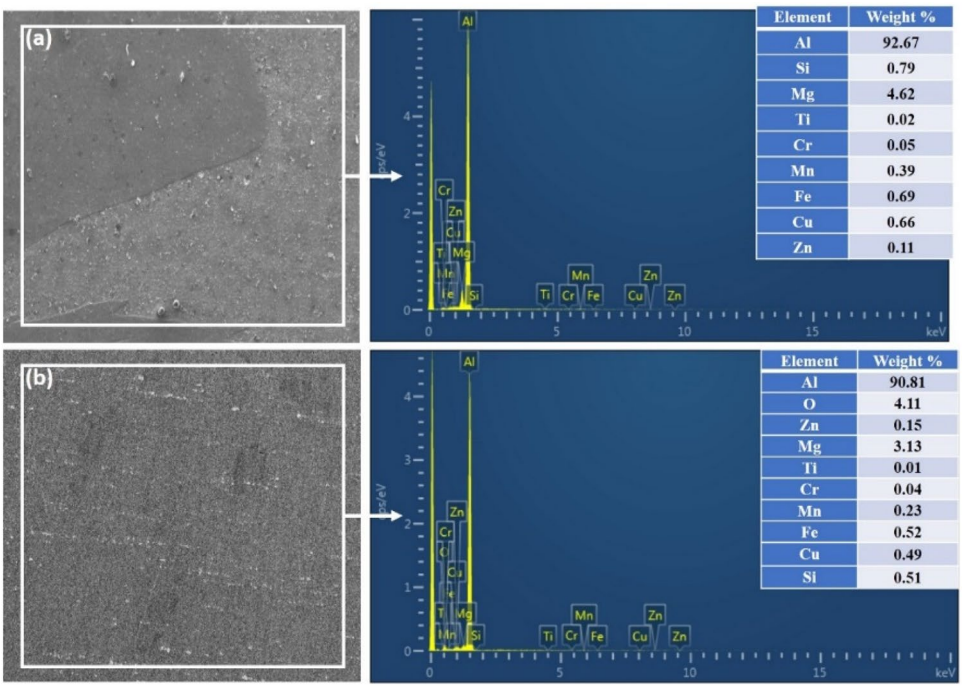

Fig. 6 EDS peaks of FSWed joints, **a** 1P-unreinforced FSWed joint, **b** 3P-reinforced FSWed joint

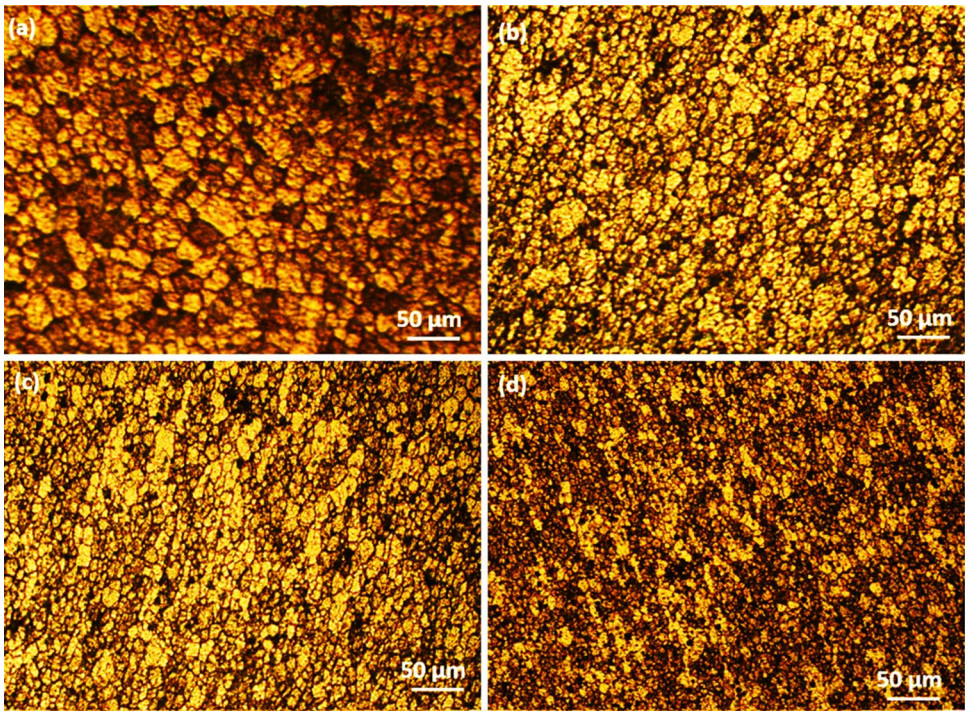

Fig. 7 Grain structure macrographs, **a** 1P-unreinforced FSWed joint, **b–d** np-Al_2O_3 reinforced FSWed joint, **b** 1P, **c** 2P, **d** 3P

Table 2 UTS, strain rate and hardness value of multipass FSWed joints

FSW conditions	UTS (MPa)	Joint's efficiency (%)	Strain rate	Hardness(HV)
1P-unreinforced FSW	205.8	71.32	20.7	108.5
1P-reinforced FSW	227.3	78.38	24.4	127.1
2P-reinforced FSW	257.4	88.76	26.8	136.4
3P-reinforced FSW	272.7	94.03	30.7	145.7

particles Al_2O_3 was more significant than the single-pass FSWed joint without reinforced particles. The UTS of FSWed joints with nanoparticles was influenced by bonding strength between RPs and metal matrix, dislocation density, and grain size [44]. Increasing the FSW passes from 1 to 3P improved the distribution of RPs in the stir zone. Further, uniform distribution of nanoparticles provides higher obstacles to preventing grain growth and reducing grain sizes [45]. The mean UTSs of AA6061and AA5083 were 310 and 290 MPa, respectively. Furthermore, the % strain was found to be 21.9 and 20, respectively. The reinforced FSWed joint's tensile properties improved compared to the unreinforced FSWed joint after implementing multi-pass FSW. Consequently, the 3P-reinforced FSWed joint revealed the highest UTS of 272.7 MPa, nearly 94% of as-received AA5083. These results agree with Jamalian et al. [46]. The enhanced strain rate of reinforced FSWed after 1P, 2P, and 3P FSW was 24.4, 26.8, and 30.7, respectively. Figure 8 depicts the stress–strain diagrams of all the tensile specimens of FSWed joints. The enhancement of the UTS of three-pass FSP in comparison to base metal can be ascribed to the following

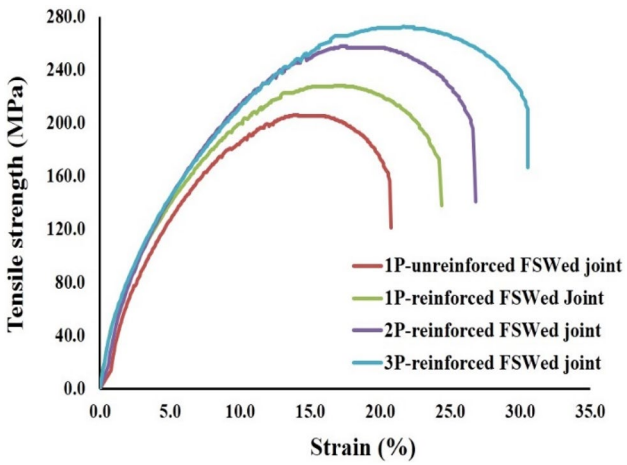

Fig. 8 True stress strain diagram of multipass FSWed joints of AA6061 and AA5083

reasons: (1) as per the Hall–Petch relationship, the three-pass FSP led to the grains refinement, which enhanced the UTS. (2) Difference in thermal expansion coefficient: further dislocations were created due to the difference in thermal expansion coefficient of the base metals and precipitates, which hindered dislocation's free movement, resulting in enhancement of the UTS. (3) Shear drag mechanism: the interface between base metals and precipitates was clean without any defect in 3 passes FSP, which implied good bonding between the base metals and precipitates, improving UTS. (4) Orowan strengthening: the nanoparticles and some precipitates were uniformly distributed in the stir zone, which may obstruct the dislocation movement due to the pinning effect leading to enhancement of the hardness values.

3.3.2 Fractography

The dimples in the multipass fractured specimens were observed in the range of 0.54–12.5 µm. one pass FSP samples formed relatively small and large circular honeycomb dimples, indicating the heterogeneity of the material structure. In contrast, the conglomerates of dimples on the ridges covered with fine or small dimples with a size of 0.7 µm to 2.4 µm were observed in the three-pass FSP. The shapes and sizes of the dimples were directly proportional to precipitates and the grain sizes in the various zones and ductilities [47]. The large and deeper dimples were observed in the area where the grain size and precipitates were larger. Small dimples associated with ductile fracture [48, 49] were observed in the three-pass FSP.

Figure 9 reveals the fractography images of reinforced and unreinforced FSWed joints specimens; all the samples were broken in the HAZ region on the AA5083 side due to low hardness. The fractured surface revealed a dimple-like structure, indicating a ductile failure mode during tensile loading. Furthermore, the unreinforced FSWed joint's fractured surface shows large and deep dimples (Fig. 9a). While small and tiny dimples were observed in the broken surface micrograph of 1P np-Al_2O_3 reinforced the FSWed joint (Fig. 9b) in comparison with the 1P-unreinforced joint, big and small dimples (Fig. 9c) in the second pass were observed due to rich and fewer nanoparticles regions as revealed by FESEM micrograph (Fig. 5c). The dimple size was found to further decreases after three FSP passes, as illustrated in Fig. 9d.

3.3.3 Effect of Multipass FSW/np-Al_2O_3 on Micro-hardness

The dissimilarity of the hardness value of the FSWed joints of AA5083 and AA6061 might be associated with the microstructure of the various welded zone. The variation in the microhardness values reveals the non-homogeneity of the grain size. The particle density, grain size, temperature distribution, and strain rate dominate the hardness values [50]. The increase in temperature caused a decrease in the

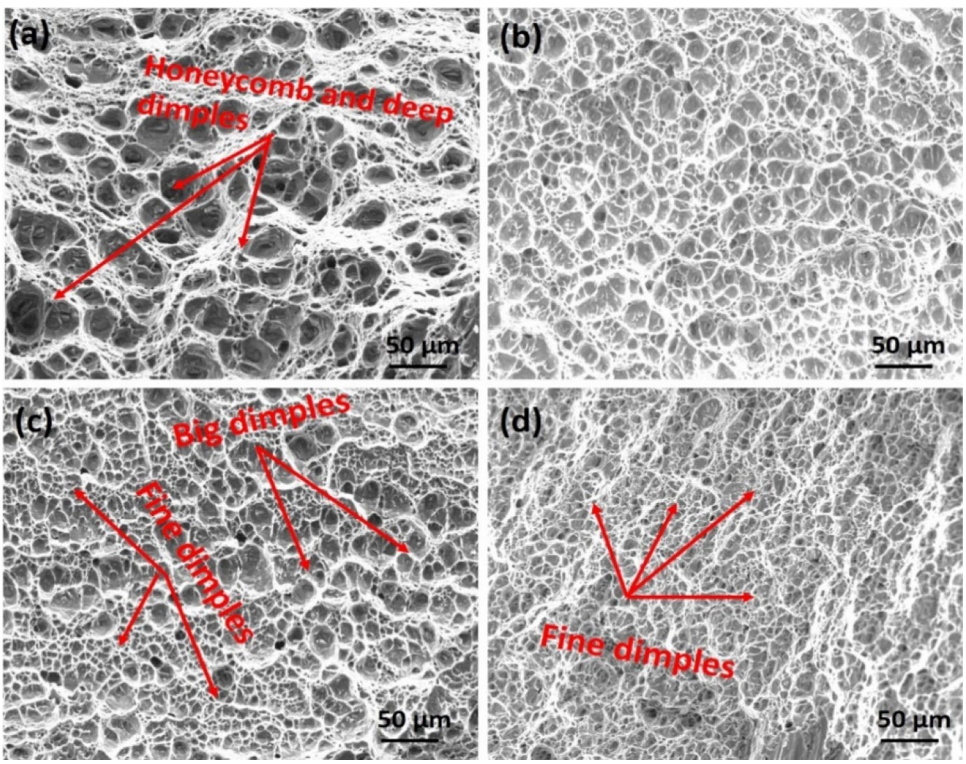

Fig. 9 Fractured surfaces morphology; **a** 1P-unreinforced FSWed joint; **b–d** np-Al_2O_3 reinforced FSWed joint, **b** 1P, **c** 2P, **d** 3P

Table 3 Micro-hardness range of each zone

Position	AA5083	HAZ	TMAZ	SZ	TMAZ	HAZ	AA6061
Hardness range (HV)	85–89	68–73	90–110	121–149	97–119	77–95	95–102

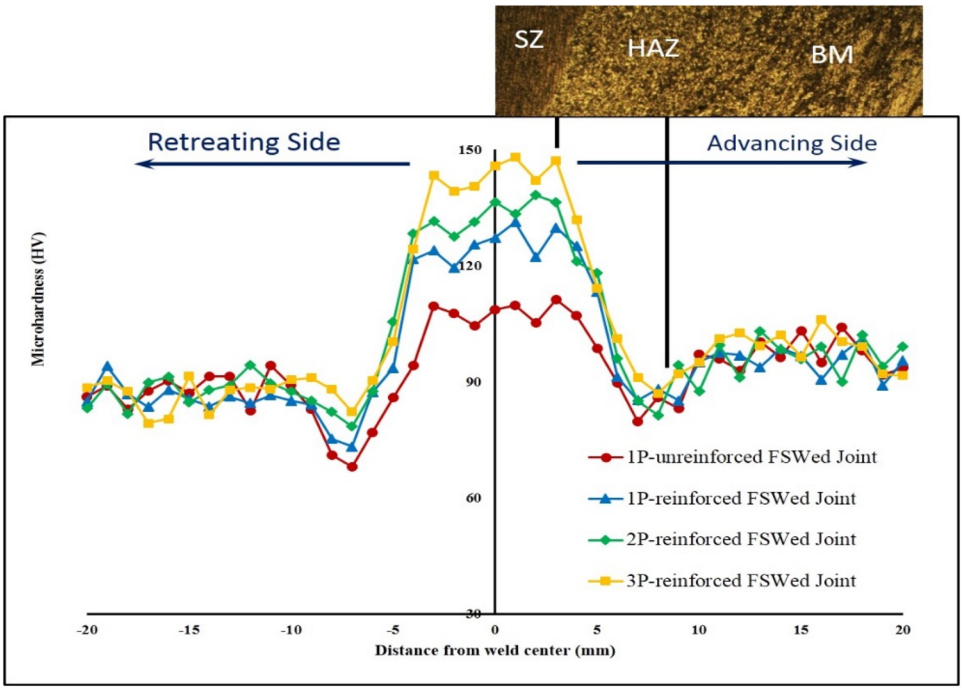

Fig. 10 Micro-hardness variation of Various FSWed joints

hardness and strain hardening in the SZ due to insufficient material flow produced by the rotating tool [51]. Table 3 also summarizes the variation of micro-hardness results in the welded region. The hardness variation profile of the aluminum metal composite is depicted in Fig. 10. The hardness value of the AA6061 and AA5083 was found as 98 HV and 85 HV, respectively. The hardness value of single-pass FSP without reinforcement was more significant than the parent metals. This may be attributed to grain refinement via DRX.

Conversely, the hardness value of a single-pass FSWed joint with nanoparticles was perceived to be higher than that of a single-pass FSWed joint without nanoparticles. The hardness value of multipass FSWed joints could be ascribed to grain refinement, presence of np- Al_2O_3, heat input and dislocation density [52, 53]. The microhardness after 1P, 2P and 3P-reinforced FSWed joint was observed as 127.1, 136.4 and 145.7 HV, respectively. Thus, the 3P-reinforced FSWed joint exhibited the highest hardness value of 145. HV due to the uniform distribution of np-Al_2O_3 in the stir zone.

4 Conclusions

In this work, single pass unreinforced and multipass Al_2O_3 reinforced FSWed joints of AA6061 and AA5083 were successfully fabricated and the following conclusions were obtained.

- The reinforced FSWed joint's tensile properties improved compared to the unreinforced FSWed joint after implementing multi-pass FSW. Consequently, the 3P-reinforced FSWed joint revealed the highest UTS of 272.7 MPa, nearly 94% of as-received AA5083.
- When dislocations accumulated due to RPs during plastic deformation, particle-induced nucleation-based DRX was conceivable. Therefore, the grain size of the np-Al_2O_3 reinforced FSWed joints after the second pass and third pass was perceived as 3.9 µm and 2.8 µm, respectively.
- The microhardness after 1P, 2P and 3P-reinforced FSWed joint was observed as 127.1, 136.4 and 145.7 HV, respectively. Thus, the 3P-reinforced FSWed joint exhibited the highest hardness value of 145.7 HV due to the uniform dispersion of np-Al_2O_3 in the stir zone.
- The dimples in the multipass fractured specimens observed were from 0.54 to 12.5 µm. one pass FSP samples formed relatively small and large circular honeycomb dimples, indicating the heterogeneity of the material structure. The conglomerates of dimples on

the ridges covered with fine or small dimples with sizes varying from 0.7 µm to 2.4 µm were observed in the three-pass FSP.

References

1. Mishra, RS, Ma, ZY. Material Science and Engineering R 2005; 50: 1.
2. Husain Mehdi, Mishra, RS. Proceedings of the Institution of Mechanical Engineers, Part L: Journal of Materials: Design and Applications 2021; 11: 2531.
3. Liu L, Ren D, Liu F (2014) Mater (Basel) 7:3735.
4. Husain Mehdi, R.S. Mishra, Journal of Achievements in Materials and Manufacturing Engineering, 77, 31, (2016).
5. D. Akbari, M. Farahani, and N. Soltani, J. Strain Anal. Eng. Des., vol.47, pp. 73, 2012
6. Husain Mehdi, R.S. Mishra, Investigation of mechanical properties and heat transfer of welded joint of AA6061 and AA7075 using TIG+FSP welding approach, Journal of Advanced Joining Processes, 1, 100003, (2020) https://doi.org/10.1016/j.jajp.2020.100003.
7. A.Nait Salah, M. Kaddami, Husain Mehdi, Turkish Journal of Computer and Mathematics Education, 12, 1051 (2021).
8. H. Mohammadzadeh Jamalian, M. Farahani, M. K. Besharati Givi, M. Aghaei Vafaei. Int J Adv Manuf Technol, In Press, 2015.
9. Husain Mehdi, R.S. Mishra, Advances in Materials and Processing Technologies, 2020, https://doi.org/10.1080/2374068X.2020.1829952.
10. S. Jain, N. Sharma, and R. Gupta, Dissimilar alloys (AA6082/AA5083) joining by FSW and parametric optimization using Taguchi, grey relational and weight method Engineering Solid Mechanics, pp. 51–66, 2018.
11. Husain Mehdi, R.S. Mishra, Defence Technology, 17 (3), 715–727 (2021). https://doi.org/10.1016/j.dt.2020.04.014
12. Saini, N., Pandey, C., Thapliyal, S. et al. Silicon 10, 1979(2018).
13. Rejil CM, Dinaharan I, Vijay SJ, Murugan N. Mater Sci Eng A, 2012; 552: 336
14. Liu, F., Li, Y., Sun, Z., Ji, Y. Journal of Materials Research and Technology, Volume 11,2021,Pages 1019.
15. K.K. Chawla, Composite Materials: Science and Engineering, Springer Science & Business Media, Heidelberg, NY, 2012.
16. J. Kaczmar, K. Pietrzak, W. Wlosinski, The production and application of metal matrix composite materials, J. Mater. Process. Technol. 106 (1) (2000) 58–67.
17. S.C. Tjong, Novel nanoparticle-reinforced metal matrix composites with enhanced mechanical properties, Adv. Eng. Mater. 9 (8) (2007) 639–652.
18. M. Gupta, F.A. Mohamed, E.J. Lavernia, Solidification behaviour of Al-Li-SiCp MMCs processed using variable co-deposition of multi-phase materials, Mater. Manuf. Process. 5 (2) (1990) 165–196.
19. Ceschini L, Boromei I, Minak G, Morri A, Tarterini F. Compos Sci Technol 2007;67:605.
20. S. Gopalakrishnan, N. Murugan, Prediction of the tensile strength of friction stir welded aluminium matrix TiCp particulate reinforced composite, Mater. Des. 32 (2011) 462–467.
21. T. Singh, S. K. Tiwari, and D. K. Shukla, Friction-stir welding of AA6061-T6: The effects of Al2O3 nano-particles addition Results in Materials, p. 100005, Aug. 2019, doi: https://doi.org/10.1016/j.rinma.2019.100005.
22. M. Saeidi, M. Barmouz, and M. K. B. Givi, Investigation on AA5083/AA7075+Al2O3 Joint Fabricated by Friction Stir Welding: Characterizing Microstructure, Corrosion and Toughness Behavior. Materials Research, no. 6, pp. 1156–1162, Dec. 2015.
23. Husain Mehdi, R.S. Mishra, Journal of Adhesion Science and Technology, 2021, https://doi.org/10.1080/01694243.2021.1964846.
24. Essam Moustafa, Effect of Multi-Pass Friction Stir Processing on Mechanical Properties for AA2024/Al2O3 Nanocomposites, Materials, 10 (9), 1053-1069, 2017.
25. W. Hoziefa, S. Toschi, M.M.Z. Ahmed, Al. Morri, A.A. Mahdy, M.M. El-Sayed Seleman, I. El-Mahallawi, L. Ceschini, A. Atlam, Materials & Design Volume 106, 273, 2016.
26. Haddad, A., Benamor, A., Chiker, N. *et al.* Effect of heat treatment on microstructure and tribological behavior of friction stir processed Al_2O_3-reinforced AA2024-T351 matrix. *Int J Adv Manuf Technol* **115,** 1671–1681 (2021). https://doi.org/https://doi.org/10.1007/s00170-021-07237-6
27. Ahmadifard, S., Shahin, N., Vakili-Azghandi, M. et al. Microstructure, mechanical, and tribological properties of Al7075-T6/Ti3AlC2/Al2O3 surface hybrid nanocomposite produced by friction stir processing: A comparison of hybrid ratio. Int J Adv Manuf Technol 118, 2205–2220 (2022). https://doi.org/https://doi.org/10.1007/s00170-021-07997-1.
28. H. Eskandari, R. Taheri, F. Khodabakhshi, Friction-stir processing of an AA8026-TiB2-Al2O3 hybrid nanocomposite: Microstructural developments and mechanical properties, Materials Science and Engineering: A Volume 660, 13 April 2016, 84-96.
29. Shigematsu, I., Kwon, YJ., Suzuki, K. et al. Joining of 5083 and 6061 aluminum alloys by friction stir welding. Journal of Materials Science Letters 22, 353–356 (2003).
30. Ghaffarpour M, Kazemi M, Mohammadi Sefat MJ, Aziz A, Dehghani K. Evaluation of dissimilar joints properties of 5083-H12 and 6061-T6 aluminum alloys produced by tungsten inert gas and friction stir welding. Proceedings of the Institution of Mechanical Engineers, Part L: Journal of Materials: Design and Applications. 2017;231(3):297-308.
31. Jain, S., & Mishra, R. S. (2021). Proceedings of the Institution of Mechanical Engineers, Part E: Journal of Process Mechanical Engineering.
32. El-Rayes, MM, El-Danaf, EA. The influence of multi-pass friction stir processing on the microstructural and mechanical properties of Aluminum Alloy 6082. Journal of Materials Processing Technology, Volume 212, Issue 5, 2012, Pages 1157-1168.
33. Husain Mehdi, R.S. Mishra, SN Applied Science, 1, 712 (2019). https://doi.org/10.1007/s42452-019-0712-0.
34. A.Nait Salaha, Husain Mehdi, Arshad Mehmood, Abdul Wahab Hashmid, Chandrabhanu Malla, Ravi Kumar, Materials Today: Proceedings, 56, 1675, 2021, https://doi.org/10.1016/j.matpr.2021.10.288.
35. Sun YF, Fujii H. The effect of SiC particles on the microstructure and mechanical properties of friction stir welded pure copper joints. Mater Sci Eng A. 2011; 528: 5470–5.
36. Husain Mehdi, Arshad Mehmood, Ajay Chinchkar, Abdul Wahab Hashmi, Chandrabhanu Malla, Prabhujit Mohapatra, Optimization of process parameters on the mechanical properties of AA6061/Al2O3 nanocomposites fabricated by multi-pass friction stir processing, Materials Today: Proceedings, 56 (4), 1995-2003, 2021, https://doi.org/https://doi.org/10.1016/j.matpr.2021.11.333.
37. Sarkari Khorrami, M.; Kazeminezhad, M.; Kokabi, A.H. Materials Science and Engineering: A, 602 (2014), 110.
38. Mehdi, H, Mishra, RS. Effect of Friction Stir Processing on Mechanical Properties and Wear Resistance of Tungsten Inert Gas

Welded Joint of Dissimilar Aluminum Alloys. Journal of Material Engineering and Performance 2021; 30: 1926–1937.
39. N. Kumbhar, S. Sahoo, I. Samajdar, G. Dey, K. Bhanumurthy, Microstructure and microtextural studies of friction stir welded aluminium alloy 5052, Materials & Design 32(3) (2011) 1657-1666.
40. Husain Mehdi, R.S. Mishra, Advances in Industrial and Manufacturing Engineering, 3, 100062 (2021). https://doi.org/10.1016/j.aime.2021.100062
41. Abdellah Nait Salah, Sipokazi Mabuwa, Husain Mehdi, Velaphi Msomi, Mohammed Kaddami, Prabhujit Mohapatra, Silicon (2022). https://doi.org/10.1007/s12633-022-01717-4.
42. Srivastava, M, Rathee, S, Siddiquee, AN, et al. Investigation on the Effects of Silicon Carbide and Cooling Medium during Multi-Pass FSP of Al-Mg/ SiC Surface Composites. Silicon 2019; 11: 2149–2157.
43. Srivatsan T, Narendra N, Troxell J. Tensile deformation and fracture behavior of an oxide dispersion strengthened copper alloy. Mater Des 2000; 21:191–8.
44. Sharma, DK, Patel, V, Badheka, V, et al. Fabrication of hybrid surface composites AA6061/(B 4 C+MoS) via friction stir processing. J. Tribology 2019; 141: 52201–52210.
45. Lloyd, DJ. Particle reinforced aluminum and magnesium matrix composites. International Materials Reviews 1994; 39: 1.
46. Jamalian, HM, Ramezani, H, Ghobadi, H, Ansari, M, Yari, S, Givi, MKB, Processing–structure–property correlation in nano-SiC-reinforced friction stir welded aluminum joints, Journal of Manufacturing Processes, Volume 21,2016,Pages 180-189.
47. Husain Mehdi, R.S. Mishra, Microstructure, and Analysis, 9, 403 (2020). https://doi.org/10.1007/s13632-020-00640-7
48. Husain Mehdi, R.S. Mishra, Transactions of the Indian Institute of Metals, 73, 1773 (2020). https://doi.org/10.1007/s12666-020-01994-w
49. Kumar, KS, Murigendrappa, SM, Kumar, H. Journal of Materials Research 2019; 455.
50. Hashmi, A.W., Mehdi, H., Mabuwa, S. et al. Influence of FSP Parameters on Wear and Microstructural Characterization of Dissimilar TIG Welded Joints with Si-rich Filler Metal. Silicon (2022). https://doi.org/https://doi.org/10.1007/s12633-022-01848-8
51. Hashmi, A.W., Mehdi, H., Mishra, R.S. et al. Mechanical Properties and Microstructure Evolution of AA6082/Sic Nanocomposite Processed by Multi-Pass FSP. Transactions of the Indian Institute of Metals, (2022). https://doi.org/https://doi.org/10.1007/s12666-022-02582-w.
52. Ebrahimzadeh, V, Paidar, M, Safarkhanian, MA, et al. Orbital friction stir lap welding of AA5456-H321/AA5456-O aluminum alloys under varied parameters. Int. J. Adv. Manuf. Technol 2018. 96: 1237–1254.
53. McNelley TR, Swaminathan S, Su JQ. Recrystallization mechanisms during friction stir welding/processing of aluminum alloys. Scr Mater 2008; 58: 349–54.

Publisher's Note Springer Nature remains neutral with regard to jurisdictional claims in published maps and institutional affiliations.

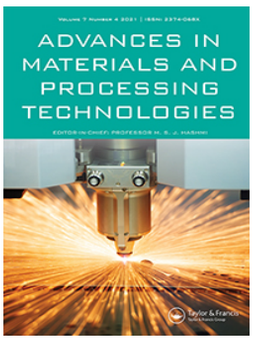

Advances in Materials and Processing Technologies

ISSN: (Print) (Online) Journal homepage: https://www.tandfonline.com/loi/tmpt20

Influence of process parameters in synergic MIG welding of 304L stainless steel using response surface methodology

Shanti Lal Meena, Ravi Butola, Muhsin Ahmad Khan, R.S Walia & Qasim Murtaza

To cite this article: Shanti Lal Meena, Ravi Butola, Muhsin Ahmad Khan, R.S Walia & Qasim Murtaza (2022): Influence of process parameters in synergic MIG welding of 304L stainless steel using response surface methodology, Advances in Materials and Processing Technologies, DOI: 10.1080/2374068X.2022.2091090

To link to this article: https://doi.org/10.1080/2374068X.2022.2091090

Published online: 22 Jun 2022.

Submit your article to this journal

Article views: 25

View related articles

View Crossmark data

Full Terms & Conditions of access and use can be found at
https://www.tandfonline.com/action/journalInformation?journalCode=tmpt20

ADVANCES IN MATERIALS AND PROCESSING TECHNOLOGIES
https://doi.org/10.1080/2374068X.2022.2091090

Taylor & Francis
Taylor & Francis Group

Check for updates

Influence of process parameters in synergic MIG welding of 304L stainless steel using response surface methodology

Shanti Lal Meena[a], Ravi Butola[b], Muhsin Ahmad Khan[b], R.S Walia[c] and Qasim Murtaza[b]

[a]Department of Mechanical Engg, Rajasthan Technical University, India; [b]Department Mechanical Engineering, Delhi Technological University, India; [c]Department of Industrial and Production Engineering, Punjab Engineering College, Chandigarh, India

ABSTRACT

Welding is a fabrication process used for joining two metals or non-metals by producing coalescence between them. However, welding process is destructive in nature. Therefore, impact of processing parameters on bead characteristics has drawn the interest of researchers around the globe. The complexity in analysis of bead characteristics lies in the fact that there are usually several parameters that interact with one another and therefore it is difficult to determine the dominant factor. The present research work attempts to address this issue through statistical analysis. The research work describes the optimisation of experimental observations made on stainless steel plate through bead-on-plate technique using RSM, an attempt was made to correlate the observed values with the input process variables. It was found that RSM was an effective tool for predicting output values for the corresponding input, which was justified from the residual graphs. In addition, interaction of input variables could also be analysed through this technique, thereby proving the viability of RSM for weld bead analysis.

ARTICLE HISTORY
Accepted 12 June 2022

KEYWORDS
MIG welding; response surface methodology; stainless steel

1. Introduction

Gas Metal Arc Welding (GMAW) is a type of welding method in which heat is generated by generating an arc across the non-consumable electrode and workpiece gap. The arc is shielded with an inert gas to prevent the inclusion of impurities [1]. GMAW is suitable for welding aluminium, bronze and copper, as well as welding steels as well by using active gases instead of inert gases [2]. In addition to the techniques economic advantage [3], a major advantage of GMAW lies in the fact that it can be used to create small welds in all positions. Though widely used, one critical disadvantage of GMAW is the process's low deposition efficiency. In addition, the torch's proximity to the weld region requirement also contributes to the complexity and skill requirement. This demands for a system or an approach that bridges these operational gaps and enhance the overall efficiency of the process in terms of cost, resource utilisation and quality of the project.

CONTACT Ravi Butola ravibutola33855@gmail.com Department Mechanical Engineering, Delhi Technological University, New Delhi 110042, India.

© 2022 Informa UK Limited, trading as Taylor & Francis Group

Synergic metal inert gas (MIG) welding, a type of GMAW welding process, is a welding system that utilises pulse and spray transfer and uses apparatus that is controlled by a range of microprocessors. This computerised control helps the welder in determining optimised current values, the voltage, wire feed speed and create a good quality weld. Parameters such as number of pulsations, base current and the form can be controlled by the welding equipment [4]. Input variables are critical as they not only determine the bead geometric characteristics but also determine the material properties. It is imperative that better equipment can definitely help tune the process and output, however, a more economical approach can be developed through statistical analysis which will probably not require large initial equipment costs.

Gunaraj and Murugan [5] evaluated the parameters of submerged arc welding (SAW) and evaluated the dependency of the area of the heat affected zone (HAZ) on these parameters for various low carbon steel joint types. By keeping the heat input constant, it was found that, area of the HAZ was lesser for the bead-on-joint. A similar trend was observed with the SAW parameters HAZ area for both cases. Murugan et al. [6] developed relations between bead geometry and welding parameters using RSM. The study was performed for automated SAW used to deposit stainless steel into structure steel. Murugan and Parmar [6] carried out the same study for gas metal arc welding [7]. Ribeiro et al. [8] used RSM in conjuncture with global criterion method to optimise operational parameters of resistance spot welding (RSW). The optimisation was carried out for 22MnB5 steel on welding parameters such as the effective welding time, welding current, the quenching and the upslope time. Subsequent to the removal of the coating, it was found that nugget width and cross-sectional area were maximised. In addition, maximisation was also observed in joint characteristics such as strength efficiency and penetration. Koleva [9] utilised RSM to develop relations between performance characteristics and operational parameters for Electron Beam Welding (EBW) of austenitic stainless steel. Statistical analysis techniques were proposed for the prediction of optimal conditions to obtain desired welding seams. Liu et al. [10] used RSM to optimise the weld seam width and lap-shear force of a DP780 steel to Al5052 joint. Mathematical models were developed to relate the operational parameters with the responses. It was found that the models were effective for predicting the weld seam and lap shear force.

An integrated approach that analyzes the impact of processing variables on bead geometric descriptors using 5 level full factorial central composite design and use of regression analysis to formulate mathematical models for predicting and studying the bead characteristics/properties of the MIG welded sample is hardly found in any literature. The present research work attempts to address this issue. This research work describes the optimisation of experimental observations made on stainless steel plate through bead-on-plate technique using RSM. The metallurgical aspects of the welded metal were also studied and an attempt was made to correlate the observed values with the input process variables.

2. Experimental procedure

The weld beads were deposited on the stainless steel workpiece using the bead on plate process. Plate thickness, gas flow rate, travel speed, and current were chosen as the five parameters. Five levels of RSM necessitated the computation of 30 orders, which necessitated the cutting out of 30 separate plates.

After the plates were cut out, each one was welded using individual parameters with a 1.2 mm diameter 304 L filler material, in the form of a wire through 20 mm contact tip separation. At five different flow rates, a mixture of carbon dioxide and argon was used as a shielding agent. Synergic MIG technique was used for the bead on plate strategy using a reversed polarity DC power source (DCEP- direct current electrode positive). The welded samples are shown in Figure 1.

True response function f is unknown in most RSM [11–13] problems. A low order polynomial is usually selected to for the approximation of the response function. A first-order model (linear function) can be defined as:

$$y = b_0 + b_1 x_1 + b_2 x_2 + e \tag{1}$$

For curved responses, higher degree polynomials should be chosen for approximation. A function with 2 variables is called a second-order model:

$$y = b_0 + b_1 + b_2 + b_{11} x^2{}_{11} + b_{22} x^2{}_{22} + b_{12} x_{12} + e \tag{2}$$

In practice, all RSM situations use one of these models or a combination of the two [14].

Data should be collected through an effective experiment design model for the proper approximation of true response function. Method of least squares is then used, once the approximation is complete after data acquisition. Fitted surface technique is then used for response surface analysis. This is accomplished through the employment of a Box-Wilson Central Composite Design [15]. Four independently controllable process parameters were identified based on their own effect on weld bead geometry, ease of control, and ability to be maintained at the desired level, namely the welding current (A), travel speed (S), gas flow rate (GFR), and plate thickness (T) at constant nozzle to plate distance. Bead height (H), bead width (W), and bead penetration (P) were the weld bead geometry parameters chosen for this study (P). Trial runs were undertaken by adjusting process parameters one at

Figure 1. Welded samples.

Table 1. Design parameters and their limits.

	LEVELS				
PARAMETERS USED	1 (−2)	2 (−1)	3 (0)	4 (1)	5 (2)
Plate thickness (mm)	3	6	8	12	15
Gas flow rate (lit/min.)	8	10	13	15	18
Current (A)	166	200	241	275	316
Travel speed (cm/min.)	27	32	37	42	47

a time. The operational range was determined by previous research articles. The numbers +2 and 2 were employed to represent the extremes. The following relationship can be used to calculate the coded values for intermediate values [16].

$$X_i = \frac{2[2X - (X_{max} + X_{min})]}{(X_{max} - X_{\min})} \tag{3}$$

Where Xi represents the value of a X, and X is a variable value that lies between the extremes X_{min} and X_{max}. Table 1 lists the selected process parameters, as well as their upper and lower limits, notations, and units.

A fully rotatable four factor-five level matrix was developed for this study with alpha value equal to two. Coded conditions used for developing matrix are shown in Table 1. The first 16 conditions were formulated as per 2^4 factorial design. The ideal design for a first order model or a first order plus two factor interaction model is indicated by these factorial points. The next eight conditions are referred to as star points, while the last six are referred to as centre points.

3. Results and discussion

3.1. Summary

A summary of results has been described in Table 2. The calculation of regression coefficients was carried out using Design Expert 8.5.0 and the model was verified by analysis of variance (ANOVA) technique [17,18]. For this analysis, confidence interval of 95% has been taken.

For 30 test scenarios, it is discovered that the best fit line deviates slightly from the ideal y = x line in all cases. Furthermore, the predicted values are discovered to be close to the goal values. Figure 2 shows the comparison of the residuals and run order for reinforcement height plots.

Table 2. Design summary.

Response	Units	Obs	Analysis	Min.	Max.	Mean	Std Dev.	Ratio	Model
H	mm	30	polynomial	2.86	3.78	3.395	0.2365	1.321	Quadratic
W	mm	30	polynomial	6.55	10.22	8.020	1.0716	1.560	Quadratic
P	mm	30	polynomial	1.46	2.48	1.957	0.2460	1.698	Quadratic

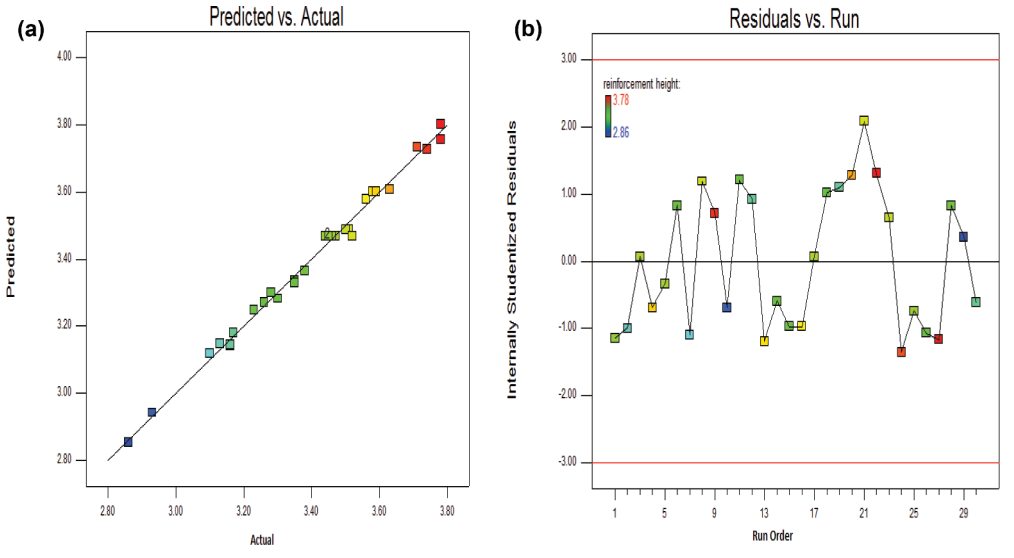

Figure 2. (a) Predicted vs Actual values; (b) Residual graph for reinforcement height analysis.

3.2. Effects of process parameters on reinforcement height

Increase of reinforcement heights is observed as the value of current A is increased. It is imperative that the greatest increase in reinforcement height is at 316 A (+2 level current). Since, power per unit length is increased due to the increase in current, larger volume of base metal is melted, ultimately causing the height to increase. In addition, positive coefficient of A value also explain the direct relationship between current value and reinforcement height. In addition, for all values from −2 to 2 levels, the reinforcement height reduces as the travel speed increases as seen in Figure 3. This is because as the torch travel speed is raised, the power per unit length of the weld bead decreases. Gas flow rate affects weld bead characteristics through its dynamic effect on the molten metal being deposited on the plate. By increasing the gas flow rate, greater force acts on the walls of the bead thus creating a force acting inwards which yields in a greater height. Whereas, increasing the plate thickness results in higher reinforcement height due to reduced heat dispersion capacity.

From ANOVA analysis –

$$\begin{aligned}\textbf{Reinforcement height} = {} & +3.46833 - 0.11458(T) + 0.023750(G) - 0.020417(S) \\ & + 0.11458(I) - 0.16312(T*G) + 0.033125(T*S) \\ & - 0.08187(T*I) + 0.079375(G*S) - 0.11062(G*I) \\ & + 0.010625(S*I) - 0.023854T^2 - 0.037604G^2 \\ & - 0.045104S^2 + 0.014896(I)^2 \end{aligned} \quad (4)$$

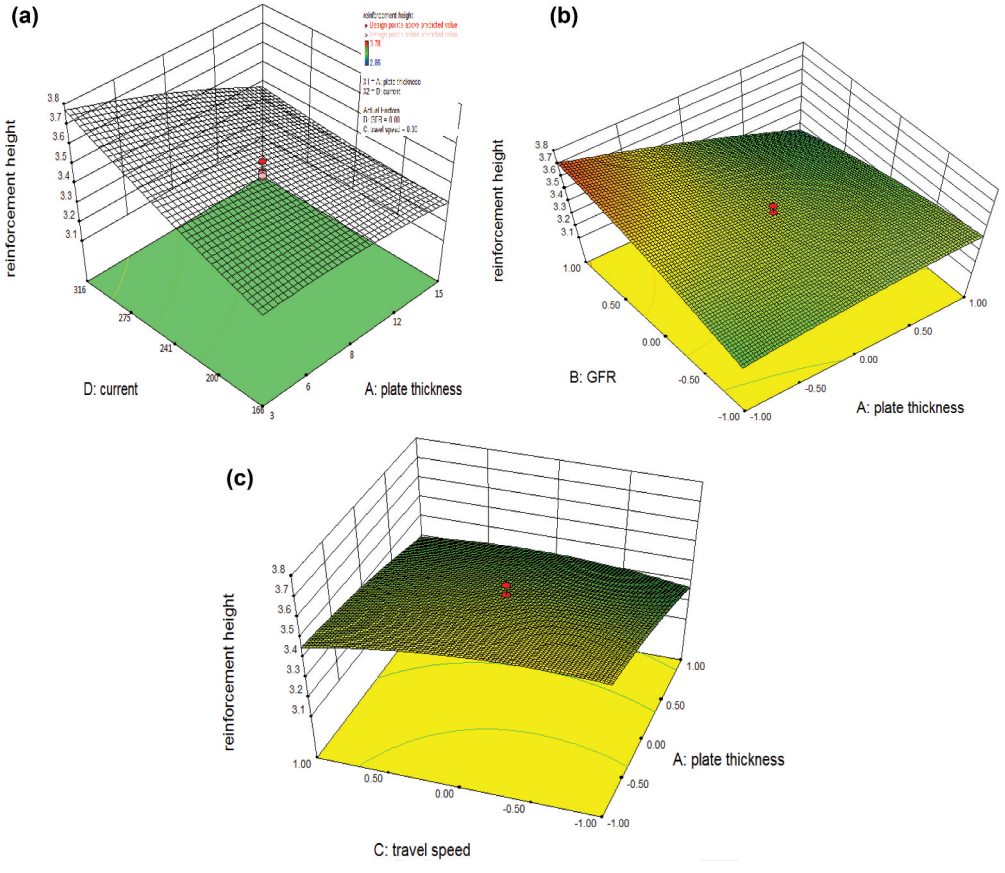

Figure 3. Surface and contour plots showing interaction effect of (a) I and T; (b) GFR and T; (c) S and T on H.

The relation between reinforcement height and welding parameters shows that increase in plate thickness causes a decrease in reinforcement height, higher GFR results in incremented heights, higher travel speeds result in smaller heights and higher current results in greater reinforcement height. This is mainly associated with the heat transfer characteristics under the specified operational parameters.

3.3. Effects of process parameters on bead width

The bead width varies from 6.55 mm to 10.22 mm at various welding parameters i.e. plate thickness, GFR, Travel speed and current. The width increased form 7.76 mm to 9.82 mm when current increased from low level to high level. It is also observed that by increasing the travel speed results in a steady decrease of bead width. From ANOVA analysis

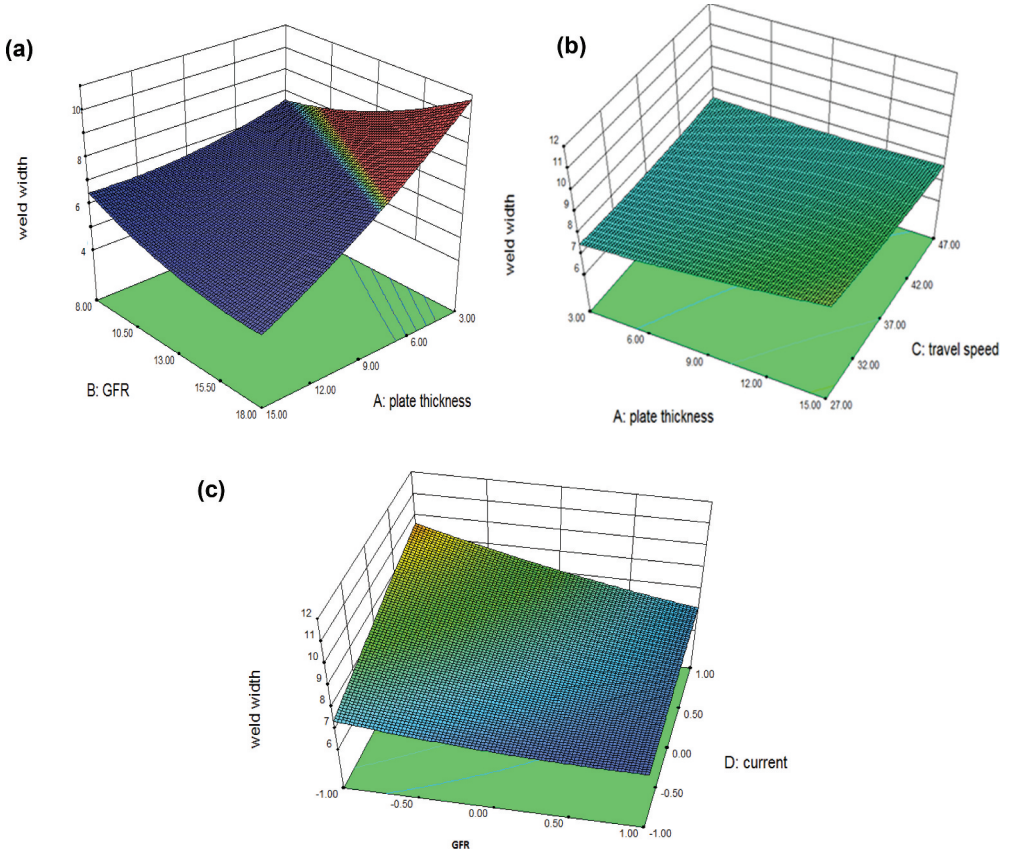

Figure 4. Surface and contour plots showing interaction effect of (a) T and GFR on W; (b) S and T on W; (c) G and I on W.

$$\begin{aligned}\textbf{Weld width} = {} & + 7.71833 + 0.38542 * T - 0.77042 * G - 0.24792 * S \\ & + 0.12625 * I - 0.38437T * G - 0.27187T * S - 0.08562T * I \\ & - 0.043125\, G * S - 0.44937\, G * I + 0.5506S * I + 0.098229T^2 \\ & + 0.20573G^2 + 0.12448S^2 - 0.050521(I)^2 \end{aligned} \quad (5)$$

The relation between reinforcement width and welding parameters shows that increase in plate thickness causes the width to increase, increase in GFR causes the width to decrease, increasing the travel speed results smaller width, increase in current results in greater width. From Figure 4, it can be seen that increasing the current (at all levels) while the travel speed decreases, results in incremented bead width. Therefore, it can be concluded that effect of travel speed and current oppose each other. It has already been discussed that increasing the travel speed results in decremented bead width values. This is due to the fact that by increasing the travel speed, lesser thermal energy is imparted to the base metal and lower amount of filler material is deposited and the bigger weld bead is obtained and vice versa. Increasing the plate thickness also results in smaller bead widths. A similar trend is observed by increasing the GFR. As discussed in the previous section, increasing GFR results in a greater force which acts on the bead wall that results in lower width.

3.4. Effect of process parameters in penetration depth

From ANOVA analysis, following relationship was determined –

$$\begin{aligned}\textbf{Depth of penetration} = &+ 1.91 + 0.075 * T - 0.031 * G - 0.14 * S + 0.020 * I \\ &+ 0.043 * T * G - 0.050\ T * S - 0.080 T * I + 0.081 G * S \\ &- 0.066 G * I + 0.16 S * I + 0.055 T^2 + 0.073 G^2 - 0.037 S^2 \\ &- 0.028 I^2 \end{aligned} \quad (6)$$

The relation between reinforcement width and welding parameters shows that travel speed has detrimental effect on bead characteristics and by increasing the current, rate of increase in penetration depth becomes steel as compared to reinforcement height. From Figure 5, it can be seen that travel speed has detrimental effect on bead characteristics. This is because when the torch travel speed is increased it results in the decrease of power per unit length of the weld bead. In addition, the distance covered by the torch is also greater, which results in lower deposition rates, ultimately hindering penetration.

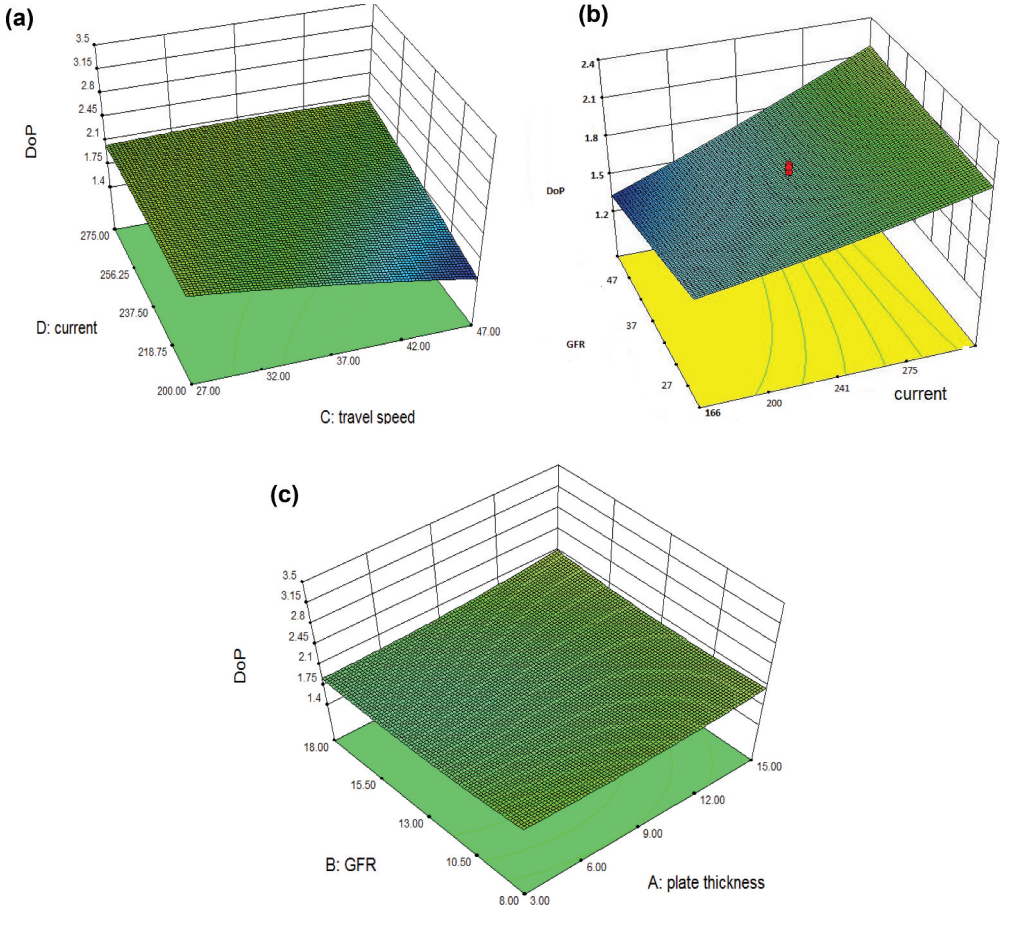

Figure 5. Surface and contour plots showing interaction effect of (a) I and GFR; (b) S and I; (c) GFR and T on P.

However, by increasing the current, rate of increase in penetration depth becomes steel as compared to reinforcement height. This is brought by higher volume of melted base metal which occurs due increase in current density and power per unit length. By increasing the gas flow rate, greater penetration depths can be obtained. However, it can be done so upto an optimum value where maximum penetration depth is obtained. After that, decrease in penetration depth can be observed.

4. Conclusions

The study was carried out successfully through the RSM approach. This enabled the formation of surface plots which could help determine the exact optimised values for the desired welds. From the results, the conclusions were drawn:

(1) The models developed have been verified by ANOVA and can be used for predicting characteristics of bead geometry. The mathematical models show fair degree of accuracy in predicting the bead geometry feature The relationships display linear behaviour and can be used to predict optimum values for specific dimensions.
(2) Increasing the current resulted in higher order values of the output parameters under investigation. By increasing the current, heat supplied is increased which results in the deposition of greater volume of filler material. It can be noted that current is mainly associated with volume of metal deposited and does not have a strong effect on shaping of the bead.
(3) Increasing the traverse speed resulted in poor bead dimensions due to a decrease in heat transferred per unit length. This resulted in lower heat transfer to weld pool which resulted in lower order bead dimensions. It can thus be noted that traverse speed has dominant effect of bead shaping.
(4) GFR also had crucial impact on bead characteristics whose effect was mainly dynamic in nature. Increasing the rate resulted in the exertion of a greater force. In addition, increasing GFR had a detrimental impact on process heat transfer characteristics and therefore is ultimately a limiting parameter. Like traverse speed, GFR also plays a crucial role in bead dimensioning.
(5) Effect of plate thickness is associated with heat dispersive capabilities of that plate. By increasing the thickness, it can be seen that heat dispersion reduces and higher order dimensions are obtained as the weld pool is able to retain the heat. Lower plate thickness permits greater heat dispersion rates which ultimately reduces overall dimensions of the bead.

Disclosure statement

No potential conflict of interest was reported by the author(s).

ORCID

Ravi Butola http://orcid.org/0000-0002-6581-4131
Qasim Murtaza http://orcid.org/0000-0001-8784-2304

References

[1] Karadeniz E, Ozsarac U, Yildiz C. The effect of process parameters on penetration in gas metal arc welding process. Mater Des. 2007;28(2):649–656.

[2] Suban M, Tusek J. Methods for the determination of arc stability. J Mater Process Technol. 2003;143-144:430–437.

[3] Rathinasuriyan C, Kumar VSS, V S. Mechanical and metallurgical properties of GTAW, GMAW and FSW lap joints on AA6061-T6 Alloy. Adv Mater Process Technol. 2021;1–17. DOI:10.1080/2374068x.2021.1946322

[4] Misra RK, Porwal R, Saxena KK, et al. Effect of post weld heat treatment on mechanical properties of MIG welded mild steel. Adv Mater Process Technol. 2021;1–15. DOI:10.1080/2374068x.2021.1934644

[5] Gunaraj V, Murugan N. Prediction and comparison of the area of the heat-affected zone for the bead-on-plate and bead-on-joint in submerged arc welding of pipes. Journal of Materials Processing Technology. 1999;95(1–3):246–261.

[6] Murugan N, Parmar RS, Sud SK. Effect of submerged arc process variables on dilution and bead geometry in single wire surfacing. Journal of Material Processing and Technology. 1999;371:767–780.

[7] Murugan N, Parmar RS. Effect of MIG process parameters on the geometry of the bead in the automatic surfacing of stainless steel. Journal of Material Processing and Technology. 1994;41(4):381–398.

[8] Ribeiro R, Romão EL, Luz E, et al. Optimization of the resistance spot welding process of 22MnB5-galvannealed steel using response surface methodology and global criterion method based on principal components analysis. Metals. 2020;10(10):1338.

[9] Koleva E. Electron beam weld parameters and thermal efficiency improvement. Vacuum. 2005;77(4):413–421.

[10] Liu G, Gao X, Peng C, et al. Optimization of laser welding of DP780 to Al5052 joints for weld width and lap-shear force using response surface methodology. Opt Laser Technol. 2020;126:1–8. 18.

[11] Tyagi L, Butola R, Kem L, et al. Comparative analysis of response surface methodology and artificial neural network on the wear properties of surface Composite fabricated by friction Stir processing. Journal of Bio- and Tribo-Corrosion. 2021;7(2). DOI: 10.1007/s40735-020-00469-1.

[12] Meena SL, Butola R, Murtaza Q, et al. Metallurgical Investigations of Microstructure and Micro hardness across the various zones in Synergic MIG Welding of Stainless steel. Mater Today Proc. 2017;4(8):8240–8249.

[13] Butola R, Singari RM, Murtaza Q, et al. Comparison of response surface methodology with artificial neural network for prediction of the tensile properties of friction stir-processed surface composites. Proc Inst Mech Eng Part E. 2022;236(1):126–137.

[14] Srivastava S, Garg R. Process parameter optimization of gas metal arc welding on IS: 2062 mild steel using response surface methodology. J Manuf Processes. 2017;25:296–305.

[15] Wagner JR, Mount EM, Giles HF. 25 - design of experiments. Extrusion (Second Edition) ed. Norwich, NY: William Andrew Publishing; 2014. p. 291–308.

[16] Butola R, Meena SL, Kumar J. Effect of welding parameters on microhardness of synergic MIG welding of 304L austenitic steel. Int J Mech Eng Technol. 2013;4(3):337–343.

[17] Shahi AS, Pandey S. Modelling of the effects of welding conditions on dilution of stainless steel claddings produced by gas metal Arc welding procedures. J Mater Process Technol. 2008;196(1–3):339–344.

[18] Parappagoudar MB, Pratihar DK, Datta GL. Non-linear modelling using central composite design to predict green sand mould properties. Proc Inst Mech Eng Part B. 2007;221(5):881–895.

Proceedings of the International Conference on Applied Artificial Intelligence and Computing (ICAAIC 2022)
IEEE Xplore Part Number: CFP22BC3-ART; ISBN: 978-1-6654-9710-7

License Plate Image Super Resolution Using Generative Adversarial Network(GAN)

Bickey Kumar Shah
Department of Computer Engineering
Delhi Technological University
Delhi, India
Bickeyshah721@gmail.com

Anshul Yadav
Department of Computer Engineering
Delhi Technological University
Delhi, India
raoanshul294@gmail.com

Ashutosh Kumar Dixit
Department of Computer Engineering
Delhi Technological University
Delhi, India
adixit.ashu@gmail.com

2022 International Conference on Applied Artificial Intelligence and Computing (ICAAIC) | 978-1-6654-9710-7/22/$31.00 ©2022 IEEE | DOI: 10.1109/ICAAIC53929.2022.9792759

***Abstract*—Super resolution of images in the field of Computer Vision is a widely used for the conversion of images into high resolution without the loss of pixel data into the images. Due to fast movement of vehicles and low quality of camera the image cannot be verified easily so, the techniques of Generative Adversarial network have been applied for the Super resolution of license plate Images which works to recover the loss data of license plate images without loss of pixel data. Earlier, mean square error (MSE) and peak signal to noise ratio (PSNR) was used as content loss to minimize the error but at optimal minimization the images get over smoothen and pixel data were lost. This paper has proposed and applied VGG-19 as pretrained neural network along with MSE and PSNR to minimize the content loss which overall optimizes the perpetual loss, and over smoothness of the images gets controlled which saves pixel data. Later, the pre-trained neural network is integrated with Generative Adversarial Network [GAN] of discriminator and generator to produce high resolution images. Taking the PSNR as an evaluation metrices for the images, it increases from 26.184 to 28.696 and accuracy from 58% to 84%.**

Keywords—Super Resolution, Generator, Discriminator, Peak signal to noise ratio, VGG-19

I. INTRODUCTION

The field of Image processing and computer Vision has taken a core place in the field of engineering and technology. Super resolution of images has been developed very much is very short period. The Computational work and Complexity of the work as compared to past years has been developed a lot with a great efficiency. Algorithms are being developed day by day with some greater value and efficiency on a particular time series [4]. The application observed in the era and as expected to grow in the coming years things are going to change more drastically. Super Resolution a very well-known domain of computer vision where we try to retrieve fine texture details to make high resolution images from given low resolution images. Super Resolution of an image can be done using various methods, including bicubic interpolation, convolution neural networks. The interpolation technique uses pre-known pixel values to estimate values for generated pixels. The CNN techniques include SRGAN and Super Resolution using Residual Network which gives better ratio of peak signal with respect to noise which we call as PSNR metrics. Better result is obtained by PSNR as compared to interpolation techniques [19]. An SRGAN comprises of two parts or models, the generator which has the generating image's function and discriminator which has discriminating image's function. Generator model is used to create Super Resolution images while the discriminator model classifies the image as a real High-Resolution image or generated Super Resolution image. The two models compete to get better in their respective works [6]. The Super resolution over a license plate image is like SRGAN as they have a similar Generative model. In the GAN model of License plate images, loss function has two components, adversarial loss and perceptual loss [20]. The perceptual loss pushes our model to produce Super Resolution images which are more feature wise inclined to High-Resolution images. Super resolution of images with GAN network is useful in research field for the field of computer vision that has been considered for gaining the unknown and useful information in the field of medical imaging, space technology, industry world, surveillance and security and is applicable for building different new technology in the field of image analysis. This learning gives great inspiration, different applications based on Image super-resolution has been studied through researchers and scientist across the world, The traditional method was inappropriate and thus, the sequential progress and technologies used in the super-resolution of images inspires more, earlier we used deep networks i.e., CNN, Resnet and then we proceed to GAN with Concepts of Residual blocks and Skip Connections. The idea and sentiments used by researchers and scientists for the formation of architectures and then results obtained on the sample images have a proper frequency match that inspires to learn and implement these techniques with novelty fill of interest and enthusiasm. In this project, we plan to dive deep into the approaches and the various technologies that tackle Super-Resolution using GAN to learn more about the key areas that affect it. The major problem with Super Resolution is the missing fine texture details in the output image [5]. Also, the unavailability of a uniform metric to gauge the performance of the super-resolved image poses a challenge. Many approaches discussed in the report have created their own version of models and loss function for the same and we aim to compare their advantages and disadvantages, to ultimately get a measure of the key methodologies used in the domain of super-resolution images [18].

II. LITERATURE SURVEY

In this section the survey of the past works over the super resolution of images is developed. Researchers tried to overcome the problem of missing texture details in SR photos in license plate when done at a large upscale factor [29]. As the main target of other algorithms remained to minimize MSE loss to increase Peak signal to noise ratio (PSNR), that makes the overall super-resolution photos smooth but lacks fine texture details. But it was shown that it's not necessary that an image with high PSNR will give high texture details. Researchers aims to enhance the

Authorized licensed use limited to: DELHI TECHNICAL UNIV. Downloaded on June 22,2022 at 04:34:35 UTC from IEEE Xplore. Restrictions apply.

existing SRGAN by carefully analyzing all components of network architecture, including generative model, discriminative model, and loss function. In brief, the author introduces the Residual in Residual block (RRDB) in the generator, Relativistic Discriminator [31]. The existing method used per pixel loss to train the optimized SR methods researcher observed it by using for pretraining model to conclude high-level feature to calculate loss between two images. Earlier, authors have combined per pixel loss and perpetual loss to train feedforward neural networks [32]. Along with optimization in the loss function, there are some optimizations in feedforward networks for image generation [30]. Through this survey we have carefully compared the various approaches that have been undertaken, solving the given problem of super resolution of single image. "GAN" is a broad topic that encompasses different methodologies and definitions which are used to detect the texture qualities of the output super-resolution photo [33]. The resolution of image is enhanced based on Residual network, Residual-in-Residual network, Adversarial Multi-Path Residual Network and Generative Adversarial using Multiple Cycle to Cycle Networks. In depth analysis of each of these methods throws light on the areas for improvement of the problem statement "Super resolution Images" [2].

III. METHODOLOGY

This section deals with the tools and concepts of the stacks and technology used for the Super resolution of images of License plate images.

A. Datasets

The datasets used for the research work was obtained from the Chinese datasets which contains numerous sets of license plate images for carrying out the training of model and applying the relevant technical stacks of Computer vision for image super resolution out of which it contains total of 2362 training images, 5000 testing images and 1890 validation images [14-17].

B. Data Preprocessing

This section discusses the preprocessing of the datasets which includes the filtering of the images and obtaining the new cycle images from the datasets required for the model generation. The task of preprocessing is carried out with the extraction of image coordinates from the file path implementing a particular constant of image mean and image deviation. The images are then cropped to obtain a particular image reliable for model preparation. The large image plates are discarded and finally the images which are suitable for training is fixed as a particular dataset [26-27].

C. Generative Adverserial Network (GAN)

A generative adversarial network is a machine learning algorithm that uses input data in an unsupervised modelling challenge to uncover and learn patterns in data [25]. It does it in such a way that the model may be utilized to create new plausible cases from the original data [13].

$$minG\ maxD\ V\ (D,\ G) = Ex{\sim}Pdata(x)\ [logD(x)] + Ez{\sim}Pz(z)\ [log\ (1 - D(G(z)))] \quad \ldots\ldots\ldots\ldots\ (1)$$

E[x] is expectation value overall P data set
D(X) represents output of discriminator
G(X) represents output of Generator

A GAN comprises two parts or models, named the discriminator after the generator. This generator is to create enhanced output while the classification model classifies the newly created output. The two models are trained such that they are adversarial and until the discriminator model is accepted almost in half the instances, as it implies that the output given by the generator model creates correct examples [1].

1) Generator

The generator part of GAN generates the data which helps the discriminator part to learn and classify its output data as real data. The figure 1 shows the architecture of generator of the GAN. One convolutional layer extracts high frequency information, followed by eight residual blocks in the generator network [28]. Each residual block is made up of two convolutional layers with a kernel size of 33 and 64 feature maps, with the activation function being ParametricReLU. In the system the generator coefficient i.e., learning rate of generator is taken as 1e-4.

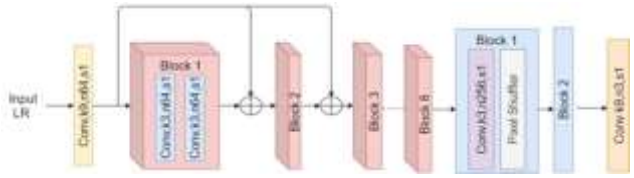

Fig.1` Generator Architecture, where s is the stride k is the kernel size, and n is the output feature maps

2) Discriminator

The main task of Discriminator is classifying the real data from the data created by generator. The Discriminator Part of GAN is tightly integrated to the generator part as to perform the min-max operation and discriminates well between the real obtained images and ground truth images. The discriminator network begins with a single convolutional layer of kernel size 3X3 and a leaky ReLU activation function of factor 0.2, followed by seven blocks. Figure.2 shows the discriminator network [3].

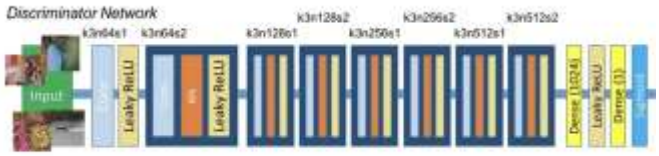

Fig.2 Discriminator network

D. Loss Function

Loss function consider a texture gradient loss L_{teg}, a content loss L_{co}, and loss named adversarial network gradient L_{adg}

$$L_{all} = L_{co} + \alpha L_{teg} + \beta L_{adg} \quad \ldots\ldots\ldots\ldots\ (2)$$

1) Content loss

Content Loss on output Image Lco: Its goal is to increase the mathematical quality of SR photos by lowering the L1

Authorized licensed use limited to: DELHI TECHNICAL UNIV. Downloaded on June 22,2022 at 04:34:35 UTC from IEEE Xplore. Restrictions apply.

factor in the error in between produced SR photos and genuine HR images, that may be expressed as

$$Lco = 1\ N \sum N\ i = 1\ |li - l\hat{}i\ |\ldots\ldots\ldots\ldots \quad (3)$$

For the license plate super resolution, the content loss is the sum of alpha times perceptual loss and mean absolute error (MAE) where alpha is 0.1.

2) Texture Gradient Loss Lteg

It concentrates on gradients of the photos to learn the optimized SR photos with higher objective and perceptual quality. It reduces the gradient error between the produced SR picture and the real Higher resolution Photos, which is be written as

$$Lteg = 1\ N \sum N\ i = 1\ |Sobel(li) - Sobel\ (l\hat{}i)\ |\ldots\ldots\ldots \quad (4)$$

3) Perceptual Loss

Perceptual loss is closer to human visual perception. Perceptual loss rather than focusing on pixel-wise loss calculates the loss of feature in SR photos from HR photos. Perceptual loss with reference to the paper is the distance Euclidean in space or MS distance between the output of the map of features of the i_{th} layer of VGG network Φi[23-24].

E. Residual in Residual Dense block (RRDB) Architecture

This Architecture is introduced without the use of batch normalization which helps the discriminator to find the relative realness of the image instead of absolute value. This architecture provides the improved accuracy with increase in the performance of the computational complexity in different evaluation metrices like PSNR [9-10].

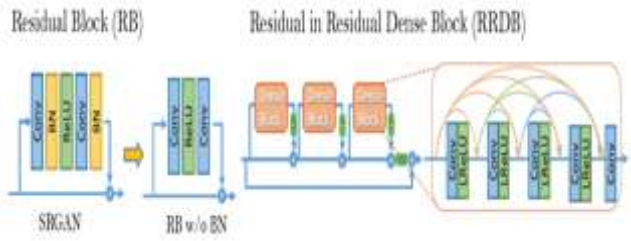

Fig.3 RRDB architecture

We preserve Super resolution using GAN's high-level architecture design and utilize a new basic block called RRDB, as shown in the figure.3. The proposed RRDB uses a deeper and more complicated structure than the original residual block in SRGAN, based on the notion that extra layers and connections may always improve performance. The primary channel uses dense blocks, which allows the network capacity to grow because of the dense connections [22].

F. Model Training

The training of the model with the basic algorithmic and neural network implementations has been carried out using TensorFlow [8].

IV. RESULT ANALYSIS

This section discusses the result obtained for the license plate image super resolution using GAN. The super resolution of license plate has different parts on which the work has been carried out starting from data preprocessing to building the neural network and Architecture of GAN, implementing residual in residual dense block, optimizing the loss function by adding the VGG-19 Pretrained network, model training and then obtaining a high-resolution images of license plate with optimized and efficient evaluation metrices called PSNR. The result has been calculated and measured over 2 different factors, initially the results were carried out over bicubic interpolation and then adding VGG-19 loss function to the MSE loss to create a whole optimized perceptual loss [11-12]. The images obtained through bicubic interpolation was enlarge and sharp which has sometimes higher and sometimes lower PSNR values which was not able to identify the pixel data and the data were lost. While Applying GAN without VGG-19 Network it was seen that the result obtained through the sum of MSE loss and perceptual loss as a content loss, the value of PSNR was very high as a result due to high PSNR value and low MSE the obtained images were over smoothened and due to over smoothness of the images, the pixel data was lost which was not very much efficient. After applying VGG-19 loss to content loss, the PSNR value was optimized, and pixel data were not lost. The adding of VGG-19 to Content loss with MSE was seen to be the best optimized result in all the cases on which the experiment was performed [21].

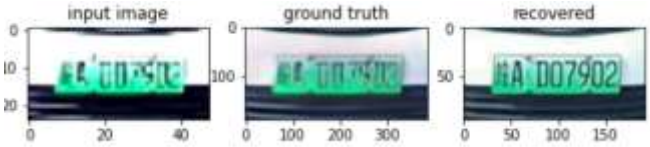

Fig.4 High resolution images obtained with VGG-19 loss

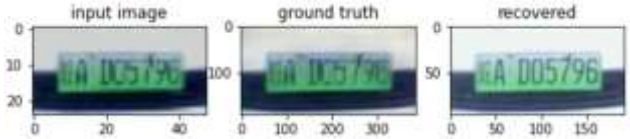

Fig.5 HR images obtained with VGG-19 Loss

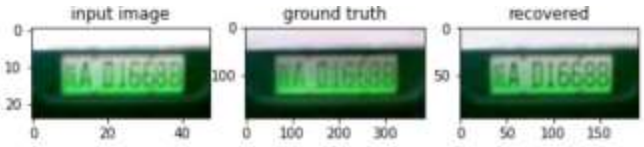

Fig.6 HR images obtained with VGG-19 Loss better than ground truth image

Now, taking the values of the evaluation metrices i.e., PSNR and SSIM with bicubic interpolation, vgg-19 network and tabulating them in Table.1

	Bicubic interpolation	Without VGG-19 approach	With VGG-19 approach
PSNR	22.187	26.184	28.696
SSIM	0.914	0.958	0.984

Table.1 Evaluation metrices

Authorized licensed use limited to: DELHI TECHNICAL UNIV. Downloaded on June 22,2022 at 04:34:35 UTC from IEEE Xplore. Restrictions apply.

V. CONCLUSION AND FUTURE WORK

In this paper, we discussed the License plate super resolution system (LPR). The application developed has a significant contribution to modern world and technology. License plate super resolution results over the algorithms implemented in this paper gives accurate results and is satisfactory but it can be more optimized as per time complexity series using Cycle to cycle GAN architecture for Super resolution of images and even Hyper parameter can be used to stable the learning rate of generator and discriminator of the GAN's Network which will yield efficient and optimized values in evaluation Metrices. This algorithm of cycle-to-cycle implementation is slight complex to implement, and researchers are working on to develop the efficient and reliable algorithms to get access to more advanced field of super resolution of images in the field of computer vision [7].

ACKNOWLEDGMENT

The Authors are indebted to the central library of Delhi Technological University for providing all the lab access and research materials for Successfully Completing the research works. Besides it, we are thankful to our Mentor Minni Jain for helping us in each and all cases and steps for Completing the research work.

REFERENCES

[1] H. Seibel, S. Goldenstein, and A. Rocha, "Eyes on the Target: Super-Resolution and License-Plate Recognition in Low-Quality Surveillance Videos," *IEEE Access*, vol. 5, pp. 20020–20035, 2017, doi: 10.1109/ACCESS.2017.2737418.

[2] L. Mallikarachchi and A. Dharmaratne, "Super resolution to identify license plate numbers in low resolution videos," *ACM Int. Conf. Proceeding Ser.*, vol. 2014-Augus, no. August, pp. 220–223, 2014, doi: 10.1145/2636240.2636867.

[3] A. Hamdi, Y. K. Chan, and V. C. Koo, "A New Image Enhancement and Super Resolution technique for license plate recognition," *Heliyon*, vol. 7, no. 11, pp. 12–13, 2021, doi: 10.1016/j.heliyon.2021.e08341.

[4] Y. Lee, J. Yun, Y. Hong, J. Lee, and M. Jeon, "Accurate License Plate Recognition and Super-Resolution Using a Generative Adversarial Networks on Traffic Surveillance Video," *2018 IEEE Int. Conf. Consum. Electron. - Asia, ICCE-Asia 2018*, pp. 16–19, 2018, doi: 10.1109/ICCE-ASIA.2018.8552121.

[5] Y. Lee, J. Jun, Y. Hong, and M. Jeon, "Practical license plate recognition in unconstrained surveillance systems with adversarial super-resolution," *VISIGRAPP 2019 - Proc. 14th Int. Jt. Conf. Comput. Vision, Imaging Comput. Graph. Theory Appl.*, vol. 5, pp. 68–76, 2019, doi: 10.5220/0007378300680076.

[6] V. Vasek, V. Franc, and M. Urban, "License plate recognition and super-resolution from low-resolution videos by convolutional neural networks," *Br. Mach. Vis. Conf. 2018, BMVC 2018*, pp. 1–12, 2019.

[7] X. Chen and C. Qi, "A super-resolution method for recognition of license plate character using LBP and RBF," *IEEE Int. Work. Mach. Learn. Signal Process.*, pp. 0–4, 2011, doi: 10.1109/MLSP.2011.6064550.

[8] W. Lina and L. Ying, "A license plate super-resolution reconstruction algorithm based on manifold learning," *Proc. - 17th IEEE Int. Conf. Comput. Sci. Eng. CSE 2014, Jointly with 13th IEEE Int. Conf. Ubiquitous Comput. Commun. IUCC 2014, 13th Int. Symp. Pervasive Syst.* , pp. 1855–1859, 2015, doi: 10.1109/CSE.2014.340.

[9] A. N. Vicente and H. Pedrini, "A learning-based single-image super-resolution method for very low quality license plate images," *2016 IEEE Int. Conf. Syst. Man, Cybern. SMC 2016 - Conf. Proc.*, pp. 515–520, 2017, doi: 10.1109/SMC.2016.7844291.

[10] "SEMANTIC SUPER-RESOLUTION FOR EXTREMELY LOW-RESOLUTION VEHICLE LICENSE PLATE The Chinese University of Hong Kong Department of Electrical and Electronic Engineering , University of Surrey , U . K .," pp. 3772–3776, 2019.

[11] W. Zeng and X. Lu, "A generalized DAMRF image modeling for superresolution of license plates," *IEEE Trans. Intell. Transp. Syst.*, vol. 13, no. 2, pp. 828–837, 2012, doi: 10.1109/TITS.2011.2180714.

[12] W. Liu, X. Liu, H. Ma, and P. Cheng, "Beyond human-level license plate super-resolution with progressive vehicle search and domain priori GAN," *MM 2017 - Proc. 2017 ACM Multimed. Conf.*, pp. 1618–1626, 2017, doi: 10.1145/3123266.3123422.

[13] M. Zhang, W. Liu, and H. Ma, "JOINT LICENSE PLATE SUPER-RESOLUTION AND RECOGNITION IN ONE MULTI-TASK GAN FRAMEWORK Minghui Zhang , Wu Liu , Huadong Ma Beijing Key Lab of Intelligent Telecommunication Software and Multimedia , Beijing University of Posts and Telecommunications , Beijin," *2018 IEEE Int. Conf. Acoust. Speech Signal Process.*, pp. 1443–1447, 2018.

[14] Z. Li, G. Han, S. Xiao, and X. Chen, "MAP-based single-frame super-resolution image reconstruction for license plate recognition," *Proc. - 2009 Int. Conf. Comput. Intell. Softw. Eng. CiSE 2009*, pp. 0–4, 2009, doi: 10.1109/CISE.2009.5366989.

[15] H. Sun, L. Luo, W. Zhou, and L. Luo, "Location and super-resolution enhancement of license plates based on video sequences," *2009 1st Int. Conf. Inf. Sci. Eng. ICISE 2009*, no. 1, pp. 1319–1322, 2009, doi: 10.1109/ICISE.2009.722.

[16] Y. Yang, P. Bi, and Y. Liu, "License Plate Image Super-Resolution Based on Convolutional Neural Network," *2018 3rd IEEE Int. Conf. Image, Vis. Comput. ICIVC 2018*, pp. 723–727, 2018, doi: 10.1109/ICIVC.2018.8492768.

[17] J. Du, Q. Liu, and K. Chen, "License plate super-resolution reconstruction based on improved ESPCN network," *Proc. 2019 IEEE 3rd Adv. Inf. Manag. Commun. Electron. Autom. Control Conf.*

Authorized licensed use limited to: DELHI TECHNICAL UNIV. Downloaded on June 22,2022 at 04:34:35 UTC from IEEE Xplore. Restrictions apply.

IMCEC 2019, no. Imcec, pp. 122–125, 2019, doi: 10.1109/IMCEC46724.2019.8984050.

[18] J. Yuan, S. D. Du, and X. Zhu, "Fast super-resolution for license plate image reconstruction," *Proc. - Int. Conf. Pattern Recognit.*, pp. 8–11, 2008, doi: 10.1109/icpr.2008.4760990.

[19] F. Shi, J. Yuan, and X. Zhu, "Fast super-resolution reconstruction for video-based pattern recognition," *Proc. - 4th Int. Conf. Nat. Comput. ICNC 2008*, vol. 4, no. 22, pp. 135–139, 2008, doi: 10.1109/ICNC.2008.553.

[20] C. H. Chuang, L. W. Tsai, M. S. Deng, J. W. Hsieh, and K. C. Fan, "Vehicle licence plate recognition using super-resolution technique," *11th IEEE Int. Conf. Adv. Video Signal-Based Surveillance, AVSS 2014*, pp. 411–416, 2014, doi: 10.1109/AVSS.2014.6918703.

[21] M. Ghoneim, M. Rehan, and H. Othman, "Using super resolution to enhance license plates recognition accuracy," *Proc. ICCES 2017 12th Int. Conf. Comput. Eng. Syst.*, vol. 2018-Janua, pp. 515–518, 2018, doi: 10.1109/ICCES.2017.8275361.

[22] Y. Xue, W. Deng, D. Zhou, and H. Zhang, "Single image super resolution for license plate," *Proc. - 2010 6th Int. Conf. Nat. Comput. ICNC 2010*, vol. 2, no. Icnc, pp. 586–588, 2010, doi: 10.1109/ICNC.2010.5583108.

[23] S. Lee, J. H. Kim, and J. P. Heo, "Super-resolution of license plate images via character-based perceptual loss," *Proc. - 2020 IEEE Int. Conf. Big Data Smart Comput. BigComp 2020*, pp. 560–563, 2020, doi: 10.1109/BigComp48618.2020.000-1.

[24] J. Leinonen, D. Nerini, and A. Berne, "Stochastic Super-Resolution for Downscaling Time-Evolving Atmospheric Fields With a Generative Adversarial Network," *IEEE Trans. Geosci. Remote Sens.*, vol. 59, no. 9, pp. 7211–7223, 2020, doi: 10.1109/tgrs.2020.3032790.

[25] X. Zhu, L. Zhang, L. Zhang, X. Liu, Y. Shen, and S. Zhao, "Generative Adversarial Network-based Image Super-Resolution with a Novel Quality Loss," *Proc. - 2019 Int. Symp. Intell. Signal Process. Commun. Syst. ISPACS 2019*, vol. 2, no. 5, pp. 1–2, 2019, doi: 10.1109/ISPACS48206.2019.8986250.

[26] S. M. Learning, J. Cai, H. Han, S. Shan, and S. Member, "FCSR-GAN : Joint Face Completion and," *IEEE Trans. Biometrics, Behav. Identity Sci.*, vol. PP, no. 2, p. 1, 2019.

[27] Y. Zhang, S. Liu, C. Dong, X. Zhang, and Y. Yuan, "Multiple cycle-in-cycle generative adversarial networks for unsupervised image super-resolution," *IEEE Trans. Image Process.*, vol. 29, pp. 1101–1112, 2020, doi: 10.1109/TIP.2019.2938347.

[28] L. Xia, J. Zhu, and Z. Yu, "Real-World Person Re-Identification via Super-Resolution and Semi-Supervised Methods," *IEEE Access*, vol. 9, pp. 35834–35845, 2021, doi: 10.1109/ACCESS.2021.3063000.

[29] A. Lucas, S. Lopez-Tapia, R. Molina, and A. K. Katsaggelos, "Generative Adversarial Networks and Perceptual Losses for Video Super-Resolution," *IEEE Trans. Image Process.*, vol. 28, no. 7, pp. 3312–3327, 2019, doi: 10.1109/TIP.2019.2895768.

[30] S. H. Nam, Y. H. Kim, N. Q. Truong, J. Choi, and K. R. Park, "Age Estimation by Super-Resolution Reconstruction Based on Adversarial Networks," *IEEE Access*, vol. 8, pp. 17103–17120, 2020, doi: 10.1109/ACCESS.2020.2967800.

[31] C. Wang, Y. Zhang, Y. Zhang, R. Tian, and M. Ding, "Mars image super-resolution based on generative adversarial network," *IEEE Access*, vol. 9, pp. 108889–108898, 2021, doi: 10.1109/ACCESS.2021.3101858.

[32] Q. Wang, Q. Gao, L. Wu, G. Sun, and L. Jiao, "Adversarial Multi-Path Residual Network for Image Super-Resolution," *IEEE Trans. Image Process.*, vol. 30, pp. 6648–6658, 2021, doi: 10.1109/TIP.2021.3096089.

[33] M. Adil, S. Mamoon, A. Zakir, M. A. Manzoor, and Z. Lian, "Multi scale-adaptive super-resolution person re-identification using GAN," *IEEE Access*, vol. 8, pp. 177351–177362, 2020, doi: 10.1109/ACCESS.2020.3023594.

Authorized licensed use limited to: DELHI TECHNICAL UNIV. Downloaded on June 22,2022 at 04:34:35 UTC from IEEE Xplore. Restrictions apply.

The current issue and full text archive of this journal is available on Emerald Insight at:
https://www.emerald.com/insight/1463-5771.htm

Managing resilience of micro, small and medium enterprises (MSMEs) during COVID-19: analysis of barriers

Anchal Gupta
Lal Bahadur Shastri Institute of Management, New Delhi, India, and
Rajesh Kumar Singh
Management Development Institute, Gurugram, India

Received 21 November 2021
Revised 28 March 2022
Accepted 10 May 2022

Abstract

Purpose – Micro, small and medium enterprises (MSMEs) are facing major difficulties with working capital, need of digitalisation and lack of skilled workforce during this crisis situation. Managing resilience post pandemic is again a huge challenge for MSMEs. Therefore, the main objective of the study is to identify the critical barriers for recovery of MSMEs from the pandemic outbreak and recommending potential solutions for avoiding vulnerabilities.

Design/methodology/approach – The most significant barriers, which will impact MSMEs resilience issues are extracted from vast literature review, discussed with nine experts from MSMEs and further categorised into organisational, operational and technical barriers. Best–worst method (BWM) has been used to find the importance rating of barriers for developing resilience in MSMEs.

Findings – It can be observed that the organisational barriers (0.507) are the most significant, followed by operational barriers (0.300) and then, technological barriers (0.192). Liquidity crunch and inadequate technical skills of employees are the most significant barriers for MSMEs resilience during COVID-19, whereas fluctuation in input cost, unavailability of containers on time and decreased process efficiency are the least significant barriers for recovering MSMEs post COVID-19.

Practical implications – Findings imply that MSMEs should try to overcome major barriers such as resource constraints, lack of skills and knowledge and inefficient inventory planning.

Originality/value – Findings of study will be of immense use for MSMEs in efficient management of operations and in developing resilience during uncertain business environment.

Keywords MSMEs, Resilience, Barriers, COVID-19, Best–worst method

Paper type Research paper

1. Introduction

Due to the global COVID-19 pandemic, the world has witnessed severe losses impacting lifestyle, businesses and economy. This seems to be the largest health crisis which brought production, consumption and distribution to the halt (Haleem *et al.*, 2020; Khurana *et al.*, 2021). Due to increased uncertainties, the economy of affected countries has slowed down and stock exchanges have started showing negative responses. COVID-19 has impacted all organisations irrespective of their size but micro, small and medium enterprises (MSMEs) have got impacted the most particularly in developing countries like India. During COVID-19, organisations are struggling with increased interest rates, unemployment and sluggish economic growth. During this time, government major focus had been to safeguard the population from health crisis and to provide relief to the sufferers (Kumar and Nayar, 2021). But to stimulate the long-term economy growth, it is very important to give immediate attention to the viability of MSMEs (Lal *et al.*, 2020; Sahoo and Ashwani, 2020). MSMEs contribute to the economic growth of all countries. Their role in developing countries like India is more significant as their contribution is 30% to GDP (Singh *et al.*, 2022).

Benchmarking: An International Journal
© Emerald Publishing Limited
1463-5771
DOI 10.1108/BIJ-11-2021-0700

MSMEs have developed gradually over the decades and now contributing towards production, processing, preservation and import–export activities of commodities. In India, there are around 6.33 crores MSMEs in which 6.30 crores (99.4%) are micro enterprises, 3.31 lakhs (0.52%) are medium enterprises and 5,000 (0.007%) are small-sized enterprises approximately and employing around 124 million people (Lal *et al.*, 2020). In India, MSMEs contribute 30% to the GDP and is accountable for around 50% of the total exports (Chaudhary *et al.*, 2020; Mahajan, 2020). As per the micro, small and medium enterprises development (MSMED Act 2020, the government facilitates MSMEs with funds and subsidies in processes for their growth, development and promotion (India-MSME annual report, 2020–21). Despite of government support, many challenges such as infrastructural bottlenecks, lack of technology implementation, risk in capital investment and delayed payments, etc. create hindrance in the growth of the industry. Moreover, the COVID-19 disturbed the microeconomic cycle resulting in revenue losses, business disruptions and threat of permanent shutdown (Farooque *et al.*, 2019; Ivanov and Dolgui, 2020).

To sustain in uncertain business environment, it is felt that MSMEs should develop long-term strategies for being resilient (Sopha *et al.*, 2022). MSMEs should identify ways for strengthening the foundation for long-term competitiveness (Singh *et al.*, 2021). In literature, many researchers have discussed the problems faced by organisations after COVID-19 outbreak (Chaudhary *et al.*, 2020); supply chain challenges (Paul *et al.*, 2021); impact of pandemic on small and medium enterprises (Mahajan, 2020); disruptions in business (Sahoo and Ashwani, 2020) and resilience strategies and policies for overcoming its impact (Khurana *et al.*, 2021). But in context to MSMEs, there are very limited studies for analysing resilience after COVID-19 outbreak. There is huge opportunity to explore the challenges in implementing the resilience strategies for MSMEs. Therefore, to bridge the existing research gaps in context to analysis of barriers for resilience of MSMEs post COVID-19, the following research objectives (RO) are proposed as part of this study.

RO1. To identify the major barriers that MSMEs are facing for being resilient post COVID-19 outbreak.

RO2. To prioritise the identified barriers from strategic perspective.

RO3. To understand the major operational areas, where MSMEs should focus for being resilient during uncertain business environment.

The rest of this paper is organised as follows. Section 2 reviews the literature on impact of COVID-19 on MSMEs, and identification of barriers for being resilient. Section 3 describes the research methodology. Sections 4, 5 and 6 deal with the results, discussion and implications of the study respectively. Section 7 presents the recommendations to industry practitioners and Sections 8 and 9 conclude the study along with directions for future research.

2. Literature review

Coronavirus is a contagious disease firstly identified in Wuhan, China in December 2019 (WHO Novel Coronavirus Report-1, 2020). This disease spread worldwide and impacted people adversely and continuously disrupted global value chains, financial markets and production network. As per data, around 81% people had developed mild and moderate symptoms including breathing problems and loss of smell and taste, whereas 14% people had severe symptoms (more than 50% lung infected, pneumonia) and 5% people had developed critical symptoms including respiratory failure and multiorgan dysfunction (CDC, 2020). It did not only affect the health but also impacted the entire world economy (Baldwin and Di Mauro, 2020; Ciotti *et al.*, 2020; Xu *et al.*, 2020). The complete lockdown severely affected both the demand and supply side which directly impacted the economic development

of the nation. The business cycles were affected severely resulting into a global recession of historic proportions (Roy *et al.*, 2021). According to literature, India experienced steep decline in economic growth, being among the 15 most affected economies (Koshle *et al.*, 2020). In the beginning of 2020, the COVID-19 outbreak has hampered the production and sales to a big extent which directly affected the MSMEs performance and resulted in huge revenue losses (Sahoo and Ashwani, 2020). MSMEs have been affected disproportionately by COVID-19 due to sudden change in demand and supply, supply chain disruptions and financial implications (Spicer, 2020). Many micro-, small- and medium-sized enterprises could not survive due to financial losses, reduced workforce and inventory disruptions. Several large enterprises have also faced difficulties in existence and business continuity. This pandemic has questioned many organisations for their readiness to deal with vulnerability and possible solutions to handle global disruptions (Singh *et al.*, 2021). MSMEs also need to develop strategies for post COVID-19 resilience in their business processes for surviving in uncertain business environment (Khurana *et al.*, 2021; Baral *et al.*, 2021). Although, the government is also trying to make conditions better by providing direct or indirect support wherever possible but Indian MSMEs need a system to recover from negative disturbances and strengthening their business processes to survive during COVID-19 (Elavarasan and Pugazhendhi, 2020). It will require improvements and innovations in existing processes and shared responsibility of all the stakeholders to build more resilient business operations.

In order to achieve resilient processes, MSMEs require to re-analyse their performance metrics and implement solutions for achieving new benchmarks. Proactive and reactive policies can be formulated to improve business performances (Baah *et al.*, 2021). The risk mitigation strategies can be developed to reduce the chances of failure by adopting proactive policies (Botzen *et al.*, 2021). Reactive policies not only minimise the impact but also ensure recovery for disease outbreaks, earthquake and unpredictable events (Dohale *et al.*, 2022). Formulating these recovery strategies will help MSMEs to return to normal operational processes (Mukherjee *et al.*, 2020). There is very less literature available on how the organisations can recover quickly from epidemic or pandemic outbreaks (Clarke and Boersma, 2017; Mishra *et al.*, 2021a). Organisations face many barriers while formulating resilience strategies. Resource constraints (Gupta and Singh, 2020), limited funds (Sipahi, 2020), backlog and overstock issues (Mishra *et al.*, 2021b), and supply chain disruptions (Li and Zobel, 2020) further weakened the implementation of resilience strategies.

In previous studies, there are limited studies which explore barriers in implementing resilience strategies for MSMEs post COVID-19. Most of the studies focus on the impact of COVID-19 and developing recovery models for various industrial sectors including MSMEs (Chaudhary *et al.*, 2020; Lal *et al.*, 2020; Mahajan, 2020; Shahed *et al.*, 2021; Paul *et al.*, 2021). It is very important to identify potential challenges in developing and formulating recovery models and policies for MSMEs. There is further need to find and implement solutions to overcome the identified barriers for resilient strategies.

Few recent studies have highlighted some challenges, along with other outcomes for recovering the MSMEs from the pandemic. According to these studies, the challenges can create hurdles in recovering business and global economy in both short and long term (Clarke and Boersma, 2017; Ivanov and Dolgui, 2020). From the literature review and discussion with industry experts, some barriers have been identified. The barriers are further categorised into three categories – organisational, operational and technological. These barriers are discussed in the following subsections.

2.1 Organisational barriers

Several organisational barriers create hindrances in recovering MSMEs post COVID-19. Past studies consider different organisational barriers in resilience of MSMEs, including those related to

decreased demand and lack of funds. The major barrier faced by MSMEs COVID-19 had been liquidity crunch due to cash shortage (Mahajan, 2020; Sahoo and Ashwani, 2020; Tripathy and Bisoyi, 2021). During COVID-19 outbreak, many employees lost their jobs and struggled with their livelihood (Nicola *et al.*, 2020). This resulted in reduced purchasing power of people which further impacted the decreased consumption of goods (Laing, 2020; Khurana *et al.*, 2021; Mishra *et al.*, 2021b; Shen *et al.*, 2020). Millions of contractual or daily wages labour are migrated due to unemployment to their villages and towns. A big challenge is to bring them back by providing assurance of jobs, food security, health and safety (Jha and Kumar, 2020; Sinha, 2021). There is need to establish resilient systems to provide security and safety to migrant workers (Khanna, 2020). MSMEs also need to manage the fluctuations in input cost, procurement cost, transportation and inventory cost while formulating resilience strategies (Bansal, 2021; Mishra *et al.*, 2021a). MSMEs are facing difficulties in making payments of their fixed expenses (electricity, logistics, rent and interest) (Tripathy and Bisoyi, 2021). It is very important to overcome these organisational barriers to improve the conditions of MSMEs post COVID-19 in India.

2.2 Operational barriers

Operational barriers severely impact resilience of MSMEs. The major issue being faced by MSMEs during COVID-19 is unavailability of skilled workforce due to labour migration (Khanna, 2020; Lal *et al.*, 2020; Gupta *et al.*, 2022). Most of MSMEs are labour intensive and have suffered problems during COVID-19. Many small, micro and medium organisations have shut down their operations temporarily during lockdown (Clarke and Boersma, 2017). Resilience policies are required to restart the production processes. The major reasons behind slowdown of production processes are unavailability of raw material on time along with huge logistics cost (Sen, 2020; Singh *et al.*, 2021). Unavailability of fleet and containers have also resulted in mismatch of demand and supply of goods (Cui *et al.*, 2019; Lalon, 2020; Karmaker *et al.*, 2021). These disturbances in production also affected inventory and raw material cost. Shortages of essential items impacted inventory maintenance costs for MSMEs (Yadav *et al.*, 2020; Mahmud *et al.*, 2021). There is need to revise the processes for improving process efficiencies (Singh *et al.*, 2021). Before building improvement plans, these operational barriers need to rectify in order to smoothen the business operations of MSMEs.

2.3 Technological barriers

Current literature suggests a number of technology related barriers, such as lack of IT infrastructure and preparedness to adopt and process operations digitally. Due to physical limitations during Covid, most of the business operations are either converted to online or automation (Gupta and Singh, 2021). The unavailability of adequate IT infrastructure with MSMEs and lack of preparation for adoption is found to be one of the crucial barriers (Leite *et al.*, 2020; Khurana *et al.*, 2021; Sharma *et al.*, 2021). Digitalisation of all offline processes is also a big challenge for organisations and inadequate technical skills of employees make adoption of new changes more difficult (Javaid *et al.*, 2020; Gupta *et al.*, 2022; Sharma *et al.*, 2021). MSMEs also face difficulty with inadequate forecasting capabilities due to their limited use of digital technologies which further affect their manufacturing and inventory imbalances (Sahoo and Ashwani, 2020; Bai *et al.*, 2021). MSMEs need to use more flexible systems for enhancing manufacturing performance (Singh, 2019).

All the identified major barriers and sub-barriers are summarised in Table 1.

3. Research methodology

In this study, the barriers for MSMEs resilience are identified from literature review and finalised after discussion with industry experts. Although many multi-criteria decision-

S.N.	Barrier's category	Sub-barriers	Codes	References
1	Organisational (OG)	Liquidity crunch	OG1	Mahajan (2020), Sahoo and Ashwani (2020), Tripathy and Bisoyi (2021)
		Decreased consumption and purchasing power of people	OG2	Laing (2020), Khurana *et al.* (2021), Mishra *et al.* (2021b)
		Migration of contractual/daily wages labour	OG3	Jha and Kumar, 2020, Khanna (2020), Misra and Gupta (2021)
		Fluctuation in input cost	OG4	Bansal (2021), Mishra *et al.* (2021a)
		Difficulty in managing fixed expenses	OG5	Tripathy and Bisoyi (2021)
2	Operational (OP)	Unavailability of skilled workforce	OP1	Khanna (2020), Gupta *et al.* (2022)
		Production shut down due to lockdown	OP2	Clarke and Boersma (2017), Sen (2020), Singh *et al.* (2021)
		Unavailability of raw material on time	OP3	Cui *et al.* (2019), Lalon (2020), Karmaker *et al.* (2021)
		Unavailability of containers on time	OP4	Cui *et al.* (2019), Lalon (2020), Karmaker *et al.* (2021)
		High logistic/transportation cost	OP5	Clarke and Boersma (2017), Sen (2020), Singh *et al.* (2021)
		Stocking up of unessential items resulting in huge inventory and maintenance cost	OP6	Yadav *et al.* (2020), Mahmud *et al.* (2021)
		Decreased process efficiency	OP7	Kaushik *et al.* (2012)
3	Technological (T)	Lack of IT infrastructure and preparedness	T1	Leite *et al.* (2020), Sharma *et al.* (2021) Khurana *et al.* (2021)
		Lack of process digitalisation	T2	Javaid *et al.* (2020), Gupta *et al.* (2022), Sharma *et al.* (2021)
		Inadequate technical skills of employees	T3	Javaid *et al.* (2020), Gupta *et al.* (2022), Sharma *et al.* (2021)
		Inadequate forecasting capability	T4	Gupta and Singh (2021), Sahoo and Ashwani (2020), Bai *et al.* (2021)

Table 1.
Barriers and sub-barriers for developing resilience

making (MCDM) techniques are explored and applied in literature but best–worst method (BWM) is preferred over other MCDM techniques for two reasons. (1) simultaneous best and worst values are calculated to avoid biasedness in pairwise comparison (2) the outcomes are more structured, reliable and consistent (Rezaei, 2015; Ahmadi *et al.*, 2017; Liu *et al.*, 2021). BWM is found to be more suitable and has been applied in this study to rank the identified barriers. BWM performs significantly better than analytical hierarchy process (AHP) in terms of less data requirement over pair-wise comparison matrix needed for AHP. BWM has been introduced to reduce the inconsistency among pairwise comparisons which makes result more reliable and consistent (Liu *et al.*, 2021). Similarly, other MCDM techniques are mostly based on full pair-wise comparison matrix which are not data efficient, whereas BWM uses single vector concept for the input data which makes method data efficient. For collecting more data, there is need to ask lots of questions from decision makers which can create inconsistency and confusion of the decision maker. BWM can give the better solution as two specific reference criteria (or factors) are considered simultaneously for taking inputs from decision makers. The decision makers give their inputs in identifying best (most crucial) and worst (least crucial) factors and compare them with other factors in pairwise comparison

matrices. The method is found to be very simple and easy to compute and gives reliable results which increases its popularity among other MCDM techniques. BWM requires less comparison data and performs significantly better on many evaluation criteria which makes it most suitable for present study. The research methodology followed in this study is discussed in Figure 1. Rezaei (2015) proposed BWM to solve MCDM problems. BWM works effectively by taking inputs from many decision makers simultaneously. In literature, BWM has been applied for prioritising several management fields such as establishing resilience in agri-food supply chains (Kumar and Singh, 2021), collaboration barriers in SMEs (Mahmud *et al.*, 2021), critical success factors for I4.0 and circular economy in logistics sector (Gupta *et al.*, 2022), supply chain resilience challenges (Paul *et al.*, 2021), risk mitigation strategies (Wang *et al.*, 2020), sustainable supply chain (Rezaei *et al.*, 2018) etc.

The steps of BWM method are as follows (Rezaei, 2015; Rezaei *et al.*, 2016).

Step 1: Firstly, identify resilience barriers from review of literature and then discuss with decision makers. "n" decision criteria (barriers) are taken as (B_1, B_2, B_3 . . .. .B_n).

Step 2: Best (most crucial) and worst (least crucial) barriers are determined by decision makers, out of all identified barriers in Step 1.

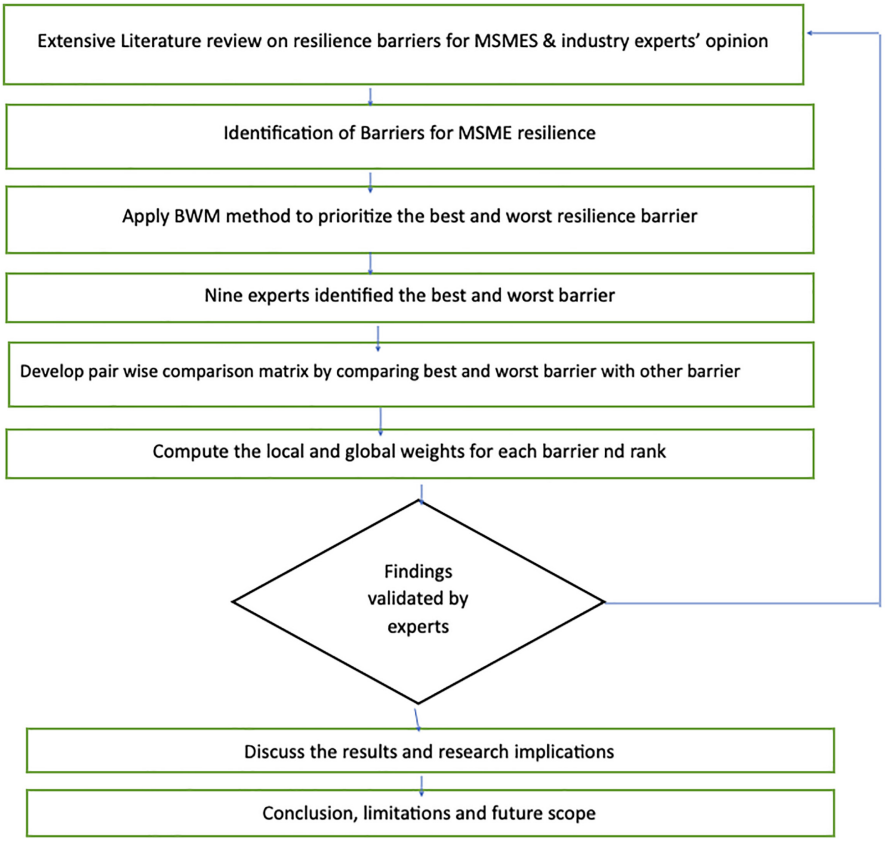

Figure 1.
Research methodology

Step 3: The decision maker assist in comparing best barrier with other barriers by creating a vector Best-to-Others (BO) using 1–9 scale (Table 2).

In Table 2, 1 represents equal importance with other criteria and 9 represents absolutely important than other criteria.

The BO vector can be written as

$$X_S = (X_{S1}, X_{S2}, \ldots, X_{Sn}), \tag{1}$$

where X_{sj} denotes the importance of Best Criterion B with criterion j.

Step 4: Further, worst barrier is compared with other barriers by creating a vector Others-to-Worst (WO) using 1–9 scale as discussed in Table 2. The WO vector can be written as

$$XO = (X_{1O}, X_{2O}, \ldots\ldots\ldots, X_{nO}) \tag{2}$$

where X_{jO} denotes the importance of j criterion over worst criterion O.

Step 5: The optimal weights (W_1*,W_2*, …., W_n*) of the decision criteria (barriers) are evaluated to minimise the maximum absolute differences for all j over the following set:

$$\left\{\left|W_B - x_{sj\ W_j}\right|,\ \left|W_j - x_{jo W_w}\right|\right\}$$

A min–max model is formulated as follows

$$Min\max j\left\{\left|W_B - x_{sj\ W_j}\right|,\ \left|W_j - x_{jo W_w}\right|\right\},$$

subject to,

$$\sum_j Wj = 1,$$

$$Wj \geq 0 \ \text{ for all } \ j \tag{3}$$

Equation (3) can be changed into linear programming problem as follows:

$$Min\ \ \xi^L,$$

$$\text{Subject to } \left|W_B - x_{sj\ W_j}\right| \leq \xi^L \text{ for all } j,$$

$$\left|W_j - x_{jo\ W_w}\right| \leq \xi^L \text{ for all } j,$$

$$\sum_j Wj = 1,$$

Value	Scale
1	Equal Importance
2	Somewhat between Equal and Moderate
3	Moderately more important than
4	Somewhat between Moderate and Strong
5	Strongly more important than other
6	Somewhat between Strong and Very strong
7	Very strongly important than other
8	Somewhat between Very strong and Absolute
9	Absolutely more important than other

Table 2. Scale used for comparison (Rezaei, 2015)

$$Wj \geq 0 \text{ for all } j \tag{4}$$

By solving above model (4), the objective function ξ^L and the optimal weights for each criteria can be calculated. The lower value of objective function is found to be more consistent and vice-versa.

4. Results

BWM is used to rank the barriers for recovery of MSMEs post COVID-19 outbreak. In this method, the best (most crucial) and worst (least crucial) barriers are identified in each category (organisational, operational and technological) with the help of decision-makers' inputs. A team of nine industry experts from India has been considered for taking inputs for this study. Nine decision makers gave their inputs to prioritise different barriers by BWM. The decision makers are experts with experience of more than eight years and working in MSMEs sectors. However, the number of experts (9) considered for this study is quite small for unbiased judgement but in literature, some past similar studies have been conducted by considering inputs from less number (<9) of decision makers (Rezaei *et al.*, 2016; Gupta and Singh, 2021; Wankhede and Vinodh, 2021). The details of decision makers are mentioned in Table 3. The decision makers are contacted through both online and offline mode. For offline, the authors visited to corresponding organisations to meet decision makers and to take their desired inputs. Data collection has been done through semi-structured interviews and in-depth discussions on resilience barriers with experts.

The best and worst value of each barrier with respect to other barriers has to be chosen by decision makers as per their perceptions from the scales mentioned in Table 2. The pairwise comparison matrix for best barrier in all categories and then best barrier with other barriers is developed by taking decision-makers' opinion. Further, as discussed in Step 3, BO (Best-to-Others) vectors for each category are developed and results are discussed in Tables 4–7. Similarly, OW (Others-to-Worst) vectors for each category are developed and results are discussed in Tables 8–11. Nine experts assisted us in finding relative weights in this analysis using BWM. The weights for the barriers are calculated after developing BO and OW vectors. By using equation (4), a linear programming model has been formulated to calculate the weights. Further, the optimal value of objective function is also evaluated. The consistency ratio is also computed to check the consistency of data, as per the scale given by Rezaei (2015)

Table 3. Demographics of decision makers

S.No	Decision maker	Designation	Organisation	Sector	Experience (in years)
1	DM1	Manager	Khadi Village Industries Commission (KVIC)	Khadi and Hosiery Products	10
2	DM2	Senior Manager	Vishal Bearings Ltd	Auto-components	12
3	DM3	Area head	Bombay Industries	Leather Industries	8
4	DM4	Assistant General Manager	GI Exports and Imports	Coir Industry	15
5	DM5	Manufacturer	Starware Ceramics Ltd	Ceramics	9
6	DM6	Senior Manager	National Agro Industries	Agro Technology	11
7	DM7	Owner	Paxshell Private Limited	Packaging and Paper	10
8	DM8	Manager	B.M. Engineering and Constructions	Construction and Real Estate	8
9	DM9	Senior Manager	Siri Logistics	Travel and Tourism	12

Decision Maker(s)	Best (most important) barrier	Organisational (OG)	Operational(OP)	Organisational (OG)	Technological (T)
1	Organisational (OG)	1	2	1	6
2	Operational (OP)	2	1	2	7
3	Organisational (OG)	1	3	1	6
4	Organisational (OG)	1	5	1	2
5	Operational (OP)	4	1	4	7
6	Technological (T)	3	6	3	1
7	Operational (OP)	2	1	2	8
8	Organisational (OG)	1	6	1	7
9	Organisational (OG)	1	4	1	6

Table 4.
BO vectors for three categories of the resilience barriers for MSMEs

as shown in Table 12. The value of consistency index is closer to zero implies high consistency of data. Consistency Ratio (CR) = ξ^*/Consistency Index (CI). The results are found to be consistent as all the Consistency Ratio (CR) values within the range. The local weights have been already calculated in above tables. Further, the global weights for each category and for each barrier is evaluated for prioritising the barriers on the basis of ranks. The results will help to identify the most and least crucial barrier so that mitigation strategies can be developed accordingly. The results are discussed in Table 17.

In Tables 13–17, the weights for all the major categories and barriers are calculated.

5. Discussion

In the study, the three major categories of barriers (organisational, operational and technological) are considered crucial for managing MSMEs resilience during COVID pandemic. The results in Table 17 clearly indicate that the organisational barriers (OG) (0.507) are most crucial, followed by operational barriers (OP) (0.300) and then, technological barriers (*T*) (0.192). MSMEs face most difficult hindrances at organisational levels during pandemic. MSMEs are expected to revise their organisational processes as per the available resources. The organisations are not ready for these sudden changes and require proper strategies to come out from the crisis situation. After understanding organisational barriers, it is important to understand operational barriers for MSMEs to recover from pandemic outbreak. MSMEs need to optimise resources to smoothen up their disturbed production processes. Proper planning is required to rectify operational issues which occur during pandemic and to improve operational efficiency of MSMEs. The technological barriers are found to be least critical barriers while recovering MSMEs.

Under organisational category, the liquidity crunch (OG1) is found to be the most crucial barrier, which need to be overcome on priority, whereas fluctuation in input cost (OG4) is considered to be least important. The fluctuations in cost is a temporary change due to pandemic thereby the experts feel this barrier is less crucial. Under operational category, production shut down due to lockdown (OP2) is very critical barrier. The shutting down of production facilities brought everything to standstill. So, this calls for an urgent action to rectify this barrier. Stocking up of unessential items (OP6) is found to be less critical under operations category. It is obvious that when the production processes will come back to their original pace then inventory management with accurate forecasting can be managed

Table 5.
BO vectors for operational category of resilience barriers

Decision maker	Best (most important)	Unavailability of skilled workforce (OP1)	Production shut down due to lockdown (OP2)	Unavailability of raw material on time (OP3)	Unavailability of containers on time (OP4)	High logistic/ transportation cost (OP5)	Stocking up of unessential items resulting in huge inventory and maintenance cost (OP6)	Decreased process efficiency (OP7)
1	OP2	2	1	4	6	5	8	7
2	OP3	3	2	1	6	4	7	5
3	OP2	4	1	2	5	3	5	7
4	OP1	1	2	3	4	5	7	6
5	OP2	2	1	4	7	3	8	6
6	OP4	2	2	3	1	4	7	5
7	OP1	1	3	4	7	3	6	7
8	OP5	3	2	3	5	1	7	6
9	OP3	3	2	1	6	4	8	7

Decision maker	Best (most important)	Liquidity crunch (OG1)	Decreased consumption and purchasing power of people (OG2)	Migration of contractual/ daily wages labour (OG3)	Fluctuation in input cost (OG4)	Difficulty in managing fixed expenses (OG5)
1	OG3	2	3	1	7	4
2	OG1	1	4	2	8	6
3	OG2	3	1	5	7	4
4	OG1	1	3	2	7	5
5	OG3	2	3	1	8	7
6	OG1	1	2	4	6	5
7	OG5	2	4	3	7	1
8	OG1	1	4	2	8	5
9	OG2	3	1	4	6	7

Table 6. BO vectors for organisational category of resilience barriers

Decision maker	Best (most important)	Lack of IT infrastructure and preparedness (T1)	Lack of process digitalisation (T2)	Inadequate technical skills of employees (T3)	Inadequate forecasting capability (T4)
1	T2	2	1	7	5
2	T4	3	2	5	1
3	T1	1	2	6	4
4	T2	2	1	6	5
5	T4	4	3	6	1
6	T1	1	3	4	7
7	T1	1	2	7	5
8	T2	2	1	8	4
9	T2	3	1	7	5

Table 7. BO vectors for technological category of resilience barriers

Decision maker	1	2	3	4	5	6	7	8	9
Worst (least important) Barrier	T	T	T	OP	T	OP	T	T	OP
Organisational (OG)	5	3	8	6	3	4	6	7	5
Operational (OP)	3	5	4	1	8	1	8	4	1
Technological (T)	1	1	1	4	1	8	1	1	3

Table 8. OW vectors for three categories of the resilience barriers for MSMEs

Decision maker	1	2	3	4	5	6	7	8	9
Worst (least important) Barrier	OG4	OG2	OG4	OG5	OG4	OG4	OG5	OG2	OG4
Liquidity crunch (OG1)	8	7	7	8	6	5	8	7	8
Decreased consumption and purchasing power of people(OG2)	5	1	6	4	7	8	5	1	5
Migration of contractual/daily wages labour (OG3)	7	6	8	7	5	4	6	6	7
Fluctuation in input cost (OG4)	1	4	1	2	1	1	3	4	1
Difficulty in managing fixed expenses (OG5)	3	2	3	1	3	2	1	2	4

Table 9. OW vectors for organisational category of resilience barriers

Decision maker	1	2	3	4	5	6	7	8	9
Worst (least important) CSF	OP6	OP7	OP6	OP6	OP7	OP6	OP4	OP7	OP4
Unavailability of skilled workforce (OP1)	8	7	7	5	8	7	7	4	7
Production shut down due to lockdown (OP2)	4	4	3	8	4	5	5	5	4
Unavailability of raw material on time (OP3)	5	3	2	3	4	4	4	3	5
Unavailability of containers on time (OP4)	3	3	4	5	3	3	1	6	1
High logistic/transportation cost (OP1)	7	4	2	3	3	8	4	4	7
Stocking up of unessential items resulting in huge inventory and maintenance cost (OP6)	1	7	1	1	5	1	3	4	6
Decreased process efficiency (OP7)	3	1	5	4	1	3	3	1	4

Table 10. OW vectors for operational category of resilience barriers

Decision maker	1	2	3	4	5	6	7	8	9
Worst (least important)	T3	T4	T3	T4	T3	T3	T1	T4	T3
Lack of IT infrastructure and preparedness (T1)	7	5	6	5	7	7	1	6	8
Lack of process digitalisation (T2)	8	7	7	8	8	8	3	7	7
Inadequate technical skills of employees (T3)	1	2	1	3	1	1	5	2	1
Inadequate forecasting capability (T4)	3	1	2	1	3	3	7	1	3

Table 11. OW vectors for technological category of resilience barriers

X_{BW}	1	2	3	4	5	6	7	8	9
Consistency Index	0.00	0.44	1.00	1.63	2.30	3.00	3.73	4.47	5.23

Source(s): Rezaei (2015)

Table 12. Consistency index

efficiently. Under technological category, lack of process digitalisation (T2) and inadequate technical skills of employees (T3) found to be most and least crucial barrier respectively. Digitalisation of processes is very important for MSMEs to recover from COVID and they need to train their manpower to make them ready for automated systems.

It has been observed from the results shown in Table 17 that "liquidity crunch (OG1)" (0.167) is the most crucial barrier for MSME resilience during COVID-19. This pandemic slows down the MSME growth, thereby bringing businesses to the situation of cash dry and decreasing profits (Mahajan, 2020). Frequent order cancellations, delay in payments and less affordability of services and deliverables by customers impacted revenues and profit badly (Lal *et al.*, 2020; Saini, 2020). Credit cycle has also got impacted, which further leads to shortages in working capital and future expansion investments. Therefore, to manage pending bills and smooth credit terms, "access to finance" is the major area of concern for MSMEs. MSMEs need to make efficient use of scarce resources for future investments for speedy recovery. After handling financial crunch, the MSMEs need to show their concern towards the second most crucial barrier "Inadequate technical skills of employees (T3)" (0.0163). In this pandemic outbreak, the employees face a transition phase and need to shift from manual processes to online digital processes. However, the manpower has inadequate technical skills to adopt and implement changes in their operations and processes (Gupta *et al.*, 2022; Paul *et al.*, 2021). The gap needs to be bridged by conducting appropriate trainings for MSMEs employees and make them ready for handling automated processes.

"Stocking up of unessential items resulting in huge inventory and maintenance cost (OP6)" is the third crucial barrier for recovering MSMEs post COVID-19. MSMEs cannot predict the exact demand and supply requirements due to impact of virus outbreak. As a result, due to uncertain demand shocks and inflations, there is a shortage of essential items, whereas unessential items are unnecessarily piled up in factories and warehouses. MSMEs need to deal with holding and maintenance cost of unsold inventories along with the liquidity issues of the working capital. The fourth most crucial barrier for resilience MSME from pandemic is "Migration of contractual/daily wages labour (OG3)". Loss of jobs and un-paid or low paid salaries are the main reasons for migrating the contractual or daily wage labour to their native places. Millions of labour migrates from urban areas to rural areas which has made adverse effect on several businesses such as construction (38 million), domestic work (21 million), textile (12 million) and transportation, agriculture, manufacturing and mining (Chaudhary *et al.*, 2020; Sahoo and Ashwani, 2020). MSMEs require their entire workforce back to restart their production facilities and distribution. This is found to be one of the crucial barriers, which need to addressed to recover MSMEs from COVID. Decreased consumption and purchasing power of people (OG2) is the fifth rank barrier. During pandemic, either people received less salaries or they have lost jobs. It reduced the purchasing capacity of consumers which further resulted into few orders and decreased consumption of goods (Laing, 2020;

	Optimal weights of resilience barriers				
Decision maker	Operational(OP)	Organisational (OG)	Technological (T)	Ksi*	CR
1	0.361	0.528	0.111	0.194	0.06481
2	0.250	0.583	0.167	0.917	0.24576
3	0.308	0.615	0.077	0.308	0.06883
4	0.100	0.575	0.325	0.075	0.025
5	0.712	0.197	0.091	0.076	0.01695
6	0.091	0.255	0.655	0.109	0.02441
7	0.600	0.333	0.067	0.067	0.01491
8	0.156	0.760	0.083	0.177	0.01787
9	0.125	0.719	0.156	0.219	0.05982
Average	0.300	0.507	0.192	0.238	0.0195

Table 13. Optimal weights for three categories of resilience barriers

	Optimal weights of organisational barriers						
Decision maker	Liquidity crunch (OG1)	Decreased consumption and purchasing power of people (OG2)	Migration of contractual/ daily wages labour (OG3)	Fluctuation in input cost (OG4)	Difficulty in managing fixed expenses (OG5)	Ksi*	CR
1	0.253	0.169	0.407	0.044	0.127	0.099	0.0431
2	0.442	0.065	0.312	0.078	0.104	0.182	0.0791
3	0.217	0.449	0.130	0.041	0.163	0.201	0.0874
4	0.414	0.181	0.271	0.077	0.057	0.128	0.0558
5	0.280	0.187	0.403	0.049	0.080	0.157	0.0684
6	0.414	0.280	0.140	0.053	0.112	0.147	0.0639
7	0.292	0.069	0.194	0.083	0.361	0.222	0.0966
8	0.435	0.145	0.290	0.072	0.058	0.145	0.0630
9	0.222	0.464	0.166	0.053	0.095	0.201	0.0876
Average	0.330	0.223	0.257	0.061	0.129	0.165	0.0716

Table 14. Optimal weights for organisational category of resilience barriers

Table 15.
Optimal weights for operational category of resilience barriers

	Optimal weights of operational barriers								
Decision maker	Unavailability of skilled workforce (OP1)	Production shut down due to lockdown (OP2)	Unavailability of raw material on time (OP3)	Unavailability of containers on time (OP4)	High logistic/ transportation cost (OP5)	Stocking up of unessential items resulting in huge inventory and maintenance cost (OP6)	Decreased process efficiency (OP7)	Ksi*	CR
1	0.251	0.329	0.125	0.084	0.100	0.039	0.072	0.173	0.046
2	0.160	0.240	0.295	0.080	0.120	0.069	0.036	0.186	0.050
3	0.116	0.295	0.233	0.093	0.155	0.041	0.067	0.171	0.046
4	0.323	0.219	0.146	0.109	0.088	0.042	0.073	0.115	0.031
5	0.236	0.320	0.118	0.067	0.157	0.059	0.042	0.152	0.041
6	0.202	0.202	0.134	0.249	0.101	0.032	0.081	0.154	0.041
7	0.389	0.154	0.115	0.045	0.154	0.077	0.066	0.072	0.019
8	0.147	0.220	0.147	0.088	0.297	0.063	0.039	0.143	0.038
9	0.158	0.237	0.324	0.035	0.119	0.059	0.068	0.150	0.040
Average	0.220	0.246	0.182	0.095	0.143	0.053	0.060	0.146	0.039

Decision maker	Optimal weights of technological barriers				Ksi*	CR
	Lack of IT infrastructure and preparedness (T1)	Lack of process digitalisation (T2)	Inadequate technical skills of employees (T3)	Inadequate forecasting capability (T4)		
1	0.307	0.512	0.058	0.123	0.102	0.063
2	0.212	0.318	0.076	0.394	0.242	0.149
3	0.481	0.333	0.111	0.074	0.185	0.114
4	0.314	0.505	0.105	0.076	0.124	0.076
5	0.192	0.256	0.067	0.485	0.283	0.174
6	0.544	0.272	0.068	0.117	0.272	0.167
7	0.151	0.504	0.144	0.201	0.856	0.525
8	0.333	0.500	0.083	0.083	0.167	0.102
9	0.245	0.554	0.053	0.147	0.181	0.111
Average	0.309	0.417	0.085	0.189	0.268	0.164

Table 16. Optimal weights for technological category of resilience barriers

Khurana *et al.*, 2021). MSMEs face difficulties in forecasting the accurate demands and meeting the demands by managing inventory imbalances (Mishra *et al.*, 2021a). For rapid recovery, MSMEs need to understand the purchasing pattern of consumers and require to design appropriate action plans to meet the changed needs of the consumers. The barrier "Lack of process digitalisation (T2)" is found on sixth position while ranking all the identified barriers. MSMEs are not prepared to shift to digitalisation due to lack of technological systems and methods at their work place. Work from home is also not an easy and feasible option for several MSMEs. The new technologies are either unavailable or inaccessible which creates difficulty in changing work processes digitally (Saini, 2020). Even in the recovery phase, the organisations are looking forward to hybrid (online and offline) mode collectively to process their operations but MSMEs need to find solutions to deal with changed environment of automation. "Production shut down due to lockdown (OP2)" is found to be the seventh important barrier, which is faced by MSMEs in the recovery phase. During lockdown, scarce availability of raw materials and daily wages labour brought MSMEs production facilities to be halt. After pandemic, MSMEs have to reactive to disruptions so that they can restart their operations with the same scale. MSMEs need to analyse the available data and develop resilience strategies for vulnerability (Kaviani *et al.*, 2020).

The eighth and ninth barriers are "unavailability of skilled workforce (OP1)" and "difficulty in managing fixed expenses (OG5)". During lockdown, the migration of contractual and daily wage workers is more frequent. Therefore, getting the skilled workers for routine tasks is becoming difficult. MSMEs face the huge challenge of availability of limited workforce, and then order fulfilment with them. This definitely impacts their businesses in form of loss of customer and ultimately loss in revenue. Not only this, the fixed expenses, rent, employee salaries and the utility bills have to be paid by MSMEs even in the situation of COVID. In the current scenario, it is very important for businesses to develop potential to reduce risks, disruptions and chances of failure which will help them in recovering from identified barriers (Machado *et al.*, 2019).

The tenth important barrier for resilience of MSME's is "Lack of IT infrastructure and preparedness (T1)". In post COVID-19 environment, MSMEs are struggling for survival and looking for alternative solutions for business continuity (Ivanov, 2019). To come out of this crisis situation, the technological development is the best possible solution (Gupta *et al.*, 2022). In the recovery phase, MSMEs need to prepare technical systems and make their manpower ready for automation. "Unavailability of raw materials on time (OP3)" is found to be eleventh crucial barrier. The pandemic has led to sudden increase in demand of all essential items and

Categories. Weights	Resilience barriers	Local weight	Local ranking	Global weight	Global ranking
Organisational (OG) 0.507	Liquidity crunch (OG1)	0.330	1	0.167	1
	Decreased consumption and purchasing power of people (OG2)	0.223	3	0.113	5
	Migration of contractual/daily wages labour (OG3)	0.257	2	0.130	4
	Fluctuation in input cost (OG4)	0.061	5	0.031	14
	Difficulty in managing fixed expenses (OG5)	0.129	4	0.065	9
Operational (OP) 0.300	Unavailability of skilled workforce (OP1)	0.220	2	0.066	8
	Production shut down due to lockdown (OP2)	0.246	1	0.074	7
	Unavailability of raw material on time (OP3)	0.182	3	0.055	11
	Unavailability of containers on time (OP4)	0.095	5	0.028	15
	High logistic/transportation cost (OP5)	0.143	4	0.043	12
	Stocking up of unessential items resulting in huge inventory and maintenance cost (OP6)	0.053	7	0.0160	3
	Decreased process efficiency (OP7)	0.060	6	0.018	16
Technological (T) 0.192	Lack of IT infrastructure and preparedness (T1)	0.309	2	0.059	10
	Lack of process digitalisation (T2)	0.417	1	0.080	6
	Inadequate technical skills of employees (T3)	0.085	4	0.0163	2
	Inadequate forecasting capability (T4)	0.189	3	0.036	13

Table 17. Local and global ranking of the resilience barriers for implementing strategies

stoppage of all non-essential items resulting in supply side disruptions which further transgressed into a demand shock (Lal *et al.*, 2020). Indian MSMEs largely depend upon other countries for sourcing of raw materials and during pandemic, the connectivity with other countries becomes questionable. Moreover, the logistics and supply chain practices within the nation have disrupted badly and the cost of transportation also becomes unaffordable. Now, post COVID-19, MSMEs need to explore all possible alternate options of sourcing and strengthen their supply chains to handle crisis situations.

The next crucial barrier is "Inadequate forecasting capability(T4)". With rising uncertainties, the MSMEs are required to equip with forecasting tools to monitor the changing demand patterns and improve business performance while recovering from COVID. Fluctuation in input cost (OG4), Unavailability of containers on time (OP4) and Decreased process efficiency (OP7) are the least important barriers for recovering MSMEs post COVID-19. Once major barriers got rectified, then these barriers can be easily handled. When the working environment will become more favourable then the barriers like variation in cost of inputs and unavailability of containers can be solved to a big extent. The processes and systems of MSMEs will come back to same position which will automatically improve the performance and efficiency of business processes. MSMEs need to develop systems for constant monitoring and relief strategies to deal with unseen disturbances.

6. Managerial implications of the study

Findings of this study may help MSMEs professionals and the government in planning and implementing resilience strategies for business continuity in the post COVID-19 era. To overcome the recovery challenges, the decision makers need to revise their investment policies for smooth flow of cash and redesign their production operations for meeting unseen disruptions. MSMEs are looking forward to technological advancements and skilled workforce to overcome the recovery challenges during uncertainties caused by COVID outbreak. In this study, all the important barriers for successful recovery of MSMEs from pandemic have been identified and the MSMEs need to develop new strategies at organisational, operational and technological level to come out of the crisis situation. The prioritisation of the critical barriers will assist the government and decision makers in framing an action plan to improve the disruptions caused. Findings can be useful for MSME's senior management in understanding the hierarchy of critical resilience barriers on the basis of their importance ranking. The results of the study can be helpful to understand the criticalities of the hurdles in recovering MSMEs and the professionals can use these results for preparing themselves to deal with these uncertain and unexpected risks.

7. Conclusion

This study provides a holistic view of MSMEs resilience challenges after the pandemic outbreak. Most of the literature emphasises on investigating and analysing the impacts of pandemic on businesses but in this study, we have tried to analyse major barriers for MSMEs to be resilient. The authors have identified the critical resilience barriers for MSMEs from literature review and experts opinion and categorised them into organisational, operational and technological categories. The importance rating of these barriers has been done using BWM by taking inputs from the experts. Liquidity crunch, inadequate technical skills of employees, stocking up of unessential items resulting in huge inventory and maintenance cost, migration of contractual/daily wages labour, and decreased consumption and purchasing power of people are the first five most significant and critical barriers in recovering of MSMEs after pandemic. On the same lines, high transportation cost, inadequate forecasting capability, fluctuation in input cost, unavailability of containers on time and decreased process efficiency are found to be least critical barriers based on the importance ranking.

8. Limitations and future scope of the study

In spite of significant findings and recommendations for MSMEs resilience, study has got some limitations. Firstly, only nine industry experts have been considered for study which is comparatively less. However, few past studies conducted similar studies with lesser number of experts than considered for this study (Rezaei *et al.*, 2016; Gupta and Singh, 2021; Wankhede and Vinodh, 2021) but on the contrary, in literature, it has been evident that many past studies have considered larger number of experts for unbiased judgements (Ahmadi *et al.*, 2017; Moktadir *et al.*, 2020) . Secondly, the findings of the study cannot be generalised as the opinion may vary within experts. The authors believe that the study will help MSMEs to become more stronger. As the study is done in India, therefore, findings cannot be generalised for all countries. Therefore, this gives an opportunity to extend this work for other countries and further, comparison of findings can be done for developed and developing countries. Few case studies and real-life illustrations on MSMEs can be carried out to identify and understand the resilience issues in the post COVID-19 era. Proposed study can be further validated by empirical analysis and results can be used by decision makers for strategy formulation for improving business performance. As formulation and implementation of

resilience strategies specifically for MSMEs is highly unexplored area. Therefore, the researchers may propose strategic framework for MSMEs by overcoming recovering challenges in present uncertain business environment post COVID-19 pandemic.

9. Recommendations to industry practitioners

Based on findings of this study, the following recommendations can be suggested to MSME practitioners so that the barriers for achieving resilience can be handled smoothly:

(1) MSMEs need to revise investment and credit policies for smooth liquidity flow and managing fixed expenses. The benefits from government schemes such as MUDRA, Aadhar and Mobile, Jandhan etc. along with recently announced collateral free loans can be taken by MSMEs for tackling financial implications. MSMEs can also get support from government for deferment of utility payments or partially paying for property taxes, rent and other basic utilities

(2) MSMEs can make alternate plans for utilising their existing production facilities and distribution. In order to survive, MSMEs may switch to other businesses such as manufacturing of PPE, masks, COVID-19 testing kits, medical equipments and sanitizers. The government can provide support to these leading MSMEs by providing market access, financial support and making infrastructure highly economical.

(3) MSMEs need to be more digitalised to deal with current market requirements. MSMEs need to develop technical infrastructure and ensure manpower readiness for digitalisation by providing proper trainings and guidance.

(4) MSMEs in manufacturing goods can emphasis more on domestic sourcing rather than fully global sourcing to ensure sufficient availability of raw material and other supplies.

(5) MSMEs can plan proper inventory management for segregating goods into essential and unessential items. ABC analysis can be applied to segregate the inventory items.

(6) MSMEs can devise new strategies for contractual and daily wage labour to increase in daily wages and assurance of job security. Moreover, MSMEs can take support from government for the provision of wage support or subsidy package for paying wages and retaining employees as the government itself directed all employers for continue paying wages without any deductions or stipulations.

(7) MSMEs should develop risk mitigation strategies and alternative plans to avoid sudden breakdown and disruptions.

(8) MSMEs can understand consumer demand patterns through accurate forecasts and analyse the data to evaluate the purchasing power of consumers and plan accordingly.

(9) MSMEs dealing with logistics should develop long-term plan in alignment with government policies and future plans.

(10) MSMEs must ready with contingency plans to deal with continuous changing market requirements.

MSMEs can follow these recommendations to deal with resilient barriers and recovering from issues arises during and post COVID-19.

References

Ahmadi, H.B., Kusi-Sarpong, S. and Rezaei, J. (2017), "Assessing the social sustainability of supply chains using Best Worst Method", *Resources, Conservation and Recycling*, Vol. 126, pp. 99-106.

Baah, C., Opoku-Agyeman, D., Acquah, I.S.K., Issau, K. and Abdoulaye, F.A.M. (2021), "Understanding the influence of environmental production practices on firm performance: a proactive versus reactive approach", *Journal of Manufacturing Technology Management*, Vol. 32 No. 2, pp. 266-289, doi: 10.1108/JMTM-05-2020-0195.

Bai, C., Quayson, M. and Sarkis, J. (2021), "COVID-19 pandemic digitization lessons for sustainable development of micro-and small-enterprises", *Sustainable Production and Consumption*, Vol. 27, pp. 1989-2001.

Bansal, P. (2021), "Government strategies to minimize the COVID-19 fallout on MSMEs in India", *Handbook of Research on Sustaining SMEs and Entrepreneurial Innovation in the Post-COVID-19 Era*, IGI Global, pp. 173-190.

Baldwin, R. and Di Mauro, B.W. (2020), *Economics in the Time of COVID-19: A New eBook*, VOX CEPR Policy Portal, pp. 2-3.

Baral, M.M., Singh, R.K. and Kazançoğlu, Y. (2021), "Analysis of factors impacting survivability of sustainable supply chain during COVID-19 pandemic: an empirical study in the context of SMEs", *The International Journal of Logistics Management*, Vol. ahead-of-print No. ahead-of-print, doi: 10.1108/IJLM-04-2021-0198.

Botzen, W., Duijndam, S. and van Beukering, P. (2021), "Lessons for climate policy from behavioral biases towards COVID-19 and climate change risks", *World Development*, Vol. 137, 105214.

CDC (2020)"Interim Clinical Guidance for Management of Patients with Confirmed Coronavirus Disease (COVID-19)", *U.S. Centers for Disease Control and Prevention (CDC)*, 6 April 2020 Archived from the original on 2 March 2020 (accessed 19 April 2020).

Chaudhary, M., Sodani, P.R. and Das, S. (2020), "Effect of COVID-19 on economy in India: some reflections for policy and programme", *Journal of Health Management*, Vol. 22 No. 2, pp. 169-180.

Ciotti, M., Ciccozzi, M., Terrinoni, A., Jiang, W.C., Wang, C.B. and Bernardini, S. (2020), "The COVID-19 pandemic", *Critical Reviews in Clinical Laboratory Sciences*, Vol. 57 No. 6, pp. 365-388.

Clarke, T. and Boersma, M. (2017), "The governance of global value chains: unresolved human rights, environmental and ethical dilemmas in the apple supply chain", *Journal of Business Ethics*, Vol. 143 No. 1, pp. 111-131.

Cui, L., Chan, H.K., Zhou, Y., Dai, J. and Lim, J.J. (2019), "Exploring critical factors of green business failure based on Grey-Decision Making Trial and Evaluation Laboratory (DEMATEL)", *Journal of Business Research*, Vol. 98, pp. 450-461.

Dohale, V., Ambilkar, P., Gunasekaran, A. and Verma, P. (2022), "Supply chain risk mitigation strategies during COVID-19: exploratory cases of 'make-to-order' handloom saree apparel industries", *International Journal of Physical Distribution and Logistics Management*, Vol. 52 No. 2, pp. 109-129, doi: 10.1108/IJPDLM-12-2020-0450.

Elavarasan, R.M. and Pugazhendhi, R. (2020), "Restructured society and environment: a review on potential technological strategies to control the COVID-19 pandemic", *Science of The Total Environment*, Vol. 725, 138858.

Farooque, M., Zhang, A., Thürer, M., Qu, T. and Huisingh, D. (2019), "Circular supply chain management: a definition and structured literature review", *Journal of Cleaner Production*, Vol. 228, pp. 882-900.

Gupta, A. and Singh, R.K. (2020), "Managing operations by a logistics company for sustainable service quality: Indian perspective", *Management of Environmental Quality*, Vol. 31 No. 5, pp. 1309-1327, doi: 10.1108/MEQ-11-2019-0246 (In press).

Gupta, A. and Singh, R.K. (2021), "Applications of emerging technologies in logistics sector for achieving circular economy goals during COVID 19 pandemic: analysis of critical success factors", *International Journal of Logistics Research and Applications*, pp. 1-22.

Gupta, A., Singh, R.K. and Gupta, S. (2022), "Developing human resource for the digitization of logistics operations: readiness index framework", *International Journal of Manpower*, Vol. 43 No. 2, pp. 355-379, doi: 10.1108/IJM-03-2021-0175.

Haleem, A., Javaid, M., Vaishya, R. and Deshmukh, S.G. (2020), "Areas of academic research with the impact of COVID-19", *The American Journal of Emergency Medicine*, Vol. 38 No. 7, pp. 1524-1526.

India MSME annual report (2020-21), available at: https://msme.gov.in/sites/default/files/MSME-ANNUAL-REPORT-ENGLISH%202020-21.pdf (accessed 20 February, 2022).

Ivanov, D. (2019), "Disruption tails and revival policies: a simulation analysis of supply chain design and production-ordering systems in the recovery and post-disruption periods", *Computers and Industrial Engineering*, Vol. 127, pp. 558-570.

Ivanov, D. and Dolgui, A. (2020), "Viability of intertwined supply networks: extending the supply chain resilience angles towards survivability. A position paper motivated by COVID-19 outbreak", *International Journal of Production Research*, Vol. 58 No. 10, pp. 2904-2915.

Javaid, M., Haleem, A., Vaishya, R., Bahl, S., Suman, R. and Vaish, A. (2020), "Industry 4.0 technologies and their applications in fighting COVID-19 pandemic", *Diabetes and Metabolic Syndrome: Clinical Research and Reviews*, Vol. 14 No. 4, pp. 419-422.

Jha, S.K. and Kumar, A. (2020), "Revitalizing MSME sector in India: challenges and the road ahead", *Journal of Politics and Governance*, Vol. 8 No. 5, pp. 4-10.

Karmaker, C.L., Ahmed, T., Ahmed, S., Ali, S.M., Moktadir, M.A. and Kabir, G. (2021), "Improving supply chain sustainability in the context of COVID-19 pandemic in an emerging economy: exploring drivers using an integrated model", *Sustainable Production and Consumption*, Vol. 26, pp. 411-427.

Kaushik, P., Khanduja, D., Mittal, K. and Jaglan, P. (2012), "A case study: application of Six Sigma methodology in a small and medium-sized manufacturing enterprise", *The TQM Journal*, Vol. 24 No. 1, pp. 4-16, doi: 10.1108/17542731211191186.

Kaviani, M.A., Tavana, M., Kowsari, F. and Rezapour, R. (2020), "Supply chain resilience: a benchmarking model for vulnerability and capability assessment in the automotive industry", *Benchmarking: An International Journal*, Vol. 27 No. 6, pp. 1929-1949.

Khanna, A. (2020), "Impact of migration of labour force due to global COVID-19 pandemic with reference to India", *Journal of Health Management*, Vol. 22 No. 2, pp. 181-191.

Khurana, S., Haleem, A., Luthra, S., Huisingh, D. and Mannan, B. (2021), "Now is the time to press the reset button: helping India's companies to become more resilient and effective in overcoming the impacts of COVID-19, climate changes and other crises", *Journal of Cleaner Production*, Vol. 280, 124466.

Koshle, H., Kaur, R. and Basista, R. (2020), "Breakdown of business and workers in India: impact of corona virus", available at: SSRN 3557544.

Kumar, A. and Nayar, K.R. (2021), "COVID 19 and its mental health consequences", *Journal of Mental Health*, Vol. 30 No. 1, pp. 1-2.

Kumar, P. and Singh, R.K. (2021), "Strategic framework for developing resilience in Agri-Food Supply Chains during COVID 19 pandemic", *International Journal of Logistics Research and Applications*, pp. 1-24, doi: 10.1080/13675567.2021.1908524.

Laing, T. (2020), "The economic impact of the Coronavirus 2019 (Covid-2019): implications for the mining industry", *The Extractive Industries and Society*, Vol. 7 No. 2, pp. 580-582.

Lal, B.S., Sachdeva, P. and Simran, T.M. (2020), "Impact of Covid-19 on micro small and medium enterprises (MSMEs): an overview", *International Journal of Multidisciplinary Research and Development*, Vol. 7 No. 12, pp. 5-12.

Lalon, R.M. (2020), "COVID-19 vs Bangladesh: is it possible to recover the impending economic distress amid this pandemic?", *Journal of Economics and Business*, Vol. 3 No. 2, pp. 825-836.

Leite, H., Lindsay, C. and Kumar, M. (2020), "COVID-19 outbreak: implications on healthcare operations", *The TQM Journal*, Vol. 33 No. 1, pp. 247-256.

Li, Y. and Zobel, C.W. (2020), "Exploring supply chain network resilience in the presence of the ripple effect", *International Journal of Production Economics*, Vol. 228, pp. 1-13.

Liu, P., Zhu, B. and Wang, P. (2021), "A weighting model based on best–worst method and its application for environmental performance evaluation", *Applied Soft Computing*, Vol. 103, 107168.

Machado, M.C., Telles, R., Sampaio, P., Queiroz, M.M. and Fernandes, A.C. (2019), "Performance measurement for supply chain management and quality management integration: a systematic literature review", *Benchmarking: An International Journal*, Vol. 27 No. 7, pp. 2130-2147.

Mahajan, Y. (2020), "Study of impact of coronavirus pandemic on small and medium enterprises (SME's) in India", *GIS Science Journal*, Vol. 7 No. 9, pp. 1-6.

Mahmud, A., Ding, D. and Hasan, M.M. (2021), "Corporate social responsibility: business responses to Coronavirus (COVID-19) pandemic", *SAGE Open*, Vol. 11 No. 1, 2158244020988710.

Mishra, M.N., Mohan, A. and Sarkar, A. (2021a), "Role of lean six sigma in the Indian MSMEs during COVID-19", *International Journal of Lean Six Sigma*, Vol. 12 No. 4, pp. 697-717, doi: 10.1108/IJLSS-10-2020-0176.

Mishra, R., Singh, R.K. and Subramanian, N. (2021b), "Impact of disruptions in agri-food supply chain due to COVID-19 pandemic: contextualised resilience framework to achieve operational excellence", *The International Journal of Logistics Management*, Vol. ahead-of-print No. ahead-of-print, doi: 10.1108/IJLM-01-2021-0043.

Misra, P. and Gupta, J. (2021), "Impact of COVID 19 on Indian migrant workers: decoding Twitter data by Text mining", *The Indian Journal of Labour Economics*, Vol. 64 No. 3, pp. 731-747.

Moktadir, M.A., Kumar, A., Ali, S.M., Paul, S.K., Sultana, R. and Rezaei, J. (2020), "Critical success factors for a circular economy: implications for business strategy and the environment", *Business Strategy and the Environment*, Vol. 29 No. 8, pp. 3611-3635.

Mukherjee, M., Chatterjee, R., Khanna, B.K., Dhillon, P.P.S., Kumar, A., Bajwa, S., ... and Shaw, R. (2020), "Ecosystem-centric business continuity planning (eco-centric BCP): a post COVID19 new normal", *Progress in Disaster Science*, Vol. 7, pp. 100-117.

Nicola, M., Alsafi, Z., Sohrabi, C., Kerwan, A., Al-Jabir, A., Iosifidis, C., ... and Agha, R. (2020), "The socio-economic implications of the coronavirus pandemic (COVID-19): a review", *International Journal of Surgery*, Vol. 78, pp. 185-193.

Paul, S.K., Chowdhury, P., Moktadir, M.A. and Lau, K.H. (2021), "Supply chain recovery challenges in the wake of COVID-19 pandemic", *Journal of Business Research*, Vol. 136, pp. 316-329.

Rezaei, J. (2015), "Best-worst multi-criteria decision-making method", *Omega*, Vol. 53, pp. 49-57, doi: 10.1016/j.omega.2014.11.009.

Rezaei, J., Nispeling, T., Sarkis, J. and Tavasszy, L. (2016), "A supplier selection life cycle approach integrating traditional and environmental criteria using the best worst method", *Journal of Cleaner Production*, Vol. 135, pp. 577-588.

Rezaei, J., van Roekel, W.S. and Tavasszy, L. (2018), "Measuring the relative importance of the logistics performance index indicators using Best Worst Method", *Transport Policy*, Vol. 68, pp. 158-169.

Roy, A., Singh, A.K., Mishra, S., Chinnadurai, A., Mitra, A. and Bakshi, O. (2021), "Mental health implications of COVID-19 pandemic and its response in India", *The International Journal of Social Psychiatry*, Vol. 67 No. 5, p. 587.

Sahoo, P. and Ashwani (2020), "COVID-19 and Indian economy: impact on growth, manufacturing, trade and MSME sector", *Global Business Review*, Vol. 21 No. 5, pp. 1159-1183.

Saini, R. (2020), "COVID-19 and MSMEs", *International Journal of Professional Development*, July-December, Vol. 9 No. 2, pp. 30-35.

Sen, S. (2020), "The unprecedented pandemic 'COVID-19' effect on the apparel workers by shivering the apparel supply chain", *Journal of Textile and Apparel, Technology and Management*, Vol. 11 No. 3, pp. 1-20.

Shahed, K.S., Azeem, A., Ali, S.M. and Moktadir, M.A. (2021), "A supply chain disruption risk mitigation model to manage COVID-19 pandemic risk", *Environmental Science and Pollution Research*, pp. 1-16.

Sharma, A., Borah, S.B. and Moses, A.C. (2021), "Responses to COVID-19: the role of governance, healthcare infrastructure, and learning from past pandemics", *Journal of Business Research*, Vol. 122 No. 102, pp. 597-607.

Shen, H., Fu, M., Pan, H., Yu, Z. and Chen, Y. (2020), "The impact of the COVID-19 pandemic on firm performance", *Emerging Markets Finance and Trade*, Vol. 56 No. 10, pp. 2213-2230.

Singh, D. (2019), "Implementation of technology innovation in MSMEs in India: case study in select firms from Northern region", *Journal of Science and Technology Policy Management*, Vol. 10 No. 3, pp. 769-792.

Singh, S., Chamola, P., Kumar, V., Verma, P. and Makkar, N. (2022), "Explaining the revival strategies of Indian MSMEs to mitigate the effects of COVID-19 outbreak", *Benchmarking: An International Journal*. doi: 10.1108/BIJ-08-2021-0497.

Singh, S., Kumar, R., Panchal, R. and Tiwari, M.K. (2021), "Impact of COVID-19 on logistics systems and disruptions in food supply chain", *International Journal of Production Research*, Vol. 59 No. 7, pp. 1993-2008.

Sinha, D. (2021), "Hunger and food security in the times of Covid-19", *Journal of Social and Economic Development*, Vol. 23 No. 2, pp. 320-331.

Sipahi, E. (2020), "COVID 19 and MSMEs: a revival framework", *Research Journal in Advanced Humanities*, Vol. 1 No. 2, pp. 7-21.

Sopha, B.M., Arvianto, A. and Tjahjono, B. (2022), "Survival strategies of traditional retailers during the COVID-19 pandemic: some insights from a developing country", *Journal of Industrial Engineering and Management*, Vol. 15 No. 2, pp. 185-201.

Spicer, A. (2020), "Organizational culture and COVID-19", *Journal of Management Studies*, Vol. 57 No. 8, pp. 1737-1740.

Tripathy, S. and Bisoyi, T. (2021), "Detrimental impact of COVID-19 pandemic on micro, small and medium enterprises in India", *Jharkhand Journal of Development and Management Studies*, Vol. 19 No. 1, pp. 8651-8660.

Wang, F., Wang, J., Ren, J., Li, Z., Nie, X., Tan, R.R. and Jia, X. (2020), "Continuous improvement strategies for environmental risk mitigation in chemical plants", *Resources, Conservation and Recycling*, Vol. 160, 104885, doi: 10.1016/j.resconrec.2020.104885.

Wankhede, V.A. and Vinodh, S. (2021), "Analysis of industry 4.0 challenges using best worst method: a case study", *Computers and Industrial Engineering*, Vol. 159, 107487.

World Health Organization, Novel Coronavirus, situation Report 1 (2020), available at: https://www.who.int/docs/default-source/coronaviruse/situation-reports/20200121-sitrep-1-2019-ncov.pdf (accessed 25 February, 2022).

Xu, Z., Elomri, A., Kerbache, L. and El Omri, A. (2020), "Impacts of COVID-19 on global supply chains: facts and perspectives", *IEEE Engineering Management Review*, Vol. 48 No. 3, pp. 153-166.

Yadav, N., Shankar, R. and Singh, S.P. (2020), "Impact of Industry4.0/ICTs, Lean Six Sigma and quality management systems on organisational performance", *The TQM Journal*, Vol. 32 No. 4, pp. 815-835, doi: 10.1108/TQM-10-2019-0251.

About the authors

Dr. Anchal Gupta has done PhD in supply chain and logistics from Delhi Technological University. Her interest is in Supply Chain Management, Logistics Management and Service Quality Management. She has published many research papers in reputed national and international journals and conferences. Anchal Gupta is the corresponding author and can be contacted at: anchal.gupta1503@gmail.com

Dr. Rajesh Kumar Singh is a Professor in Operations Management area at Management Development Institute, Gurugram, India. His areas of interest include Supply Chain Management, Small Business Management and Quality Management. He has published around 125 research papers in reputed international/national journals and conferences. His papers have appeared in journals such as Journal of Cleaner Production, Resources Conservation and Recycling, Production Planning and Control, Journal of Industrial and Production Engg, Industrial management and Data Systems, Singapore Management Review, International Journal of Productivity and Performance Management, Benchmarking: An International Journal, Journal of Modelling in Management, Competitiveness Review, Global Journal of Flexible Systems and Management, Journal of Advances in Management Research, International Journals of Productivity and Quality Management, International Journal of Services and Operations Management, Management Research Review, IIMB Management Review, etc.

For instructions on how to order reprints of this article, please visit our website:
www.emeraldgrouppublishing.com/licensing/reprints.htm
Or contact us for further details: **permissions@emeraldinsight.com**

Maneuvering Control of Autonomous Underwater Vehicle (AUV) by Simulated Annealing and Moth Flame Optimization Tuned Controllers

Sudarshan K.Valluru
Center for Control of Dynamical Systems and Computation
Dept. of Electrical Engineering
Delhi Technological University
Delhi-110042, India
sudarshan_valluru@dce.ac.in

Hitesh Thareja
Center for Control of Dynamical Systems and Computation
Dept. of Electrical Engineering
Delhi Technological University
Delhi-110042, India
hiteshthareja_2k18ee084@dtu.ac.in

2022 International Conference on Electronic Systems and Intelligent Computing (ICESIC) | 978-1-6654-8385-8/22/$31.00 ©2022 IEEE | DOI: 10.1109/ICESIC53714.2022.9783493

***Abstract*—This paper emphasizes maneuvering control of Autonomous Underwater Vehicle (AUV) with the help of Linear-Proportional Integral Derivative (L-PID) and Fractional Order PID (FOPID) controllers. The values of the gain parameters of L-PID (K_p, K_i, K_d) and FOPID ($K_p, K_i, K_d, \lambda, \mu$) are tuned by Simulated Annealing (SA) and Moth Flame optimization (MFO) techniques. The performance of both the controllers is compared and the better algorithm to tune the parameters of the controllers is determined. A step function is applied to the system's input to test the AUV, and the corresponding response to the input function is examined. The transient parameters of the AUV, such as rise time, settling time, overshoot, and performance index ITAE were calculated and compared. The investigatory results show that both the algorithms used to tune the FOPID controller accurately steer the AUV. Also, the MFO tuned FOPID controller is more efficient than the SA tuned FOPID controller.**

Keywords— AUV, LPID, FOPID, Moth-flame Optimization, Simulated Annealing

I. INTRODUCTION

Autonomous Underwater Vehicle is a system that can accomplish many tasks under the water. The vehicle proves to be an instrumental technology for various departments concerning military operations, commercial and research purposes, etc. In the deep sea, AUV proves to help gather information about the environment where human reach is difficult. It enables the vehicle to be controlled in harsh surroundings without any human interference. The robust control of the AUV is difficult due to the more subsystems embedded into it. The six degrees of freedom (DoF) ensure the consistency of the vehicle. A pictorial representation of the AUV[1] is depicted in Fig.1, and the notations [2] are given in Table. I. The AUV is a quite complex system, due to the natural and unexpected disturbances in the water, thereby the maneuvering control of AUV becomes a complex task, yet.

To resolve this complex task, researchers have tried many intelligent techniques[3], [4] to control the AUV under natural and unexpected disturbances more precisely. But, it seems that controlling an AUV with controllers like PD, PID[5] is a more straightforward approach with satisfactory results. Additionally, this type of scheme appears to be an easy-to-use application for linearized systems. In contrast, however, PID controllers[6] suffer from tedious calculations during changes in system parameters due to the occurrence of natural perturbations. Many research papers have also been proposed in the literature for the application and control of the system, using the LPID and FOPID controllers. Such controllers are also required to control many other real-time systems, such as tracking and control of the helicopter[7], cart pendulum[8], and Ball beam[9] benchmarked systems.

For the robust control of an AUV, this experimental study formulates LPID and FOPID controllers that are effectively tuned using a bio-inspired meta-heuristic optimization algorithm named the Moth-Flame Optimization (MFO) and Simulated Annealing (SA). The performance of the FOPID controller is found to be superior to that of the LPID controller, and the MFO algorithm is found to be more reliable than the SA algorithm in maneuvering control of the AUV.

The arrangement of the topics in this paper is AUV system is analytically modelled in Section II. After that, Section III contains the design of LPID and FOPID controllers. Section IV involves designing and implementing LPID and FOPID controllers using MFO and SA algorithms. After that, section V shows the experimental results and responses obtained. Finally, section VI ends with the conclusion.

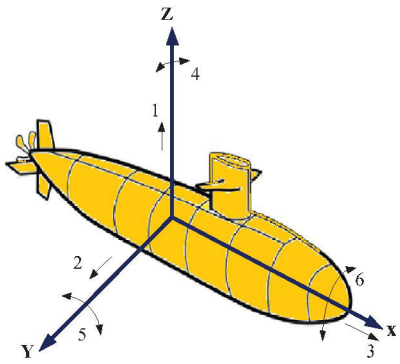

Fig1. Six DOF of an AUV

TABLE I. NOTATIONS OF AUV

Direction Of Motion	*Force & Moment*	*Fixed Earth Frame (Position)*	*Fixed-Body Frame(velocity)*
Surge (Motion along $X-axis$)	X	x	u
Sway Motion along $Y-axis$)	Y	y	v
Heave (Motion along $Z-axis$)	Z	z	w
Roll (Rotation along $X-axis$)	K	Φ	p
Pitch (Rotation along $Y-axis$)	M	θ	q
Yaw (Rotation along $Z-axis$)	N	Ψ	r

Authorized licensed use limited to: DELHI TECHNICAL UNIV. Downloaded on June 07,2022 at 09:58:25 UTC from IEEE Xplore. Restrictions apply.

II. AUV MODELLING

The first step in analyzing the AUV is calculating the transfer function and stability. The transfer function would then be used to design the controllers for maneuvering control of the AUV. The system's transfer function provides us information about the yaw angle, the deflection parameter, and a relation between the above parameters.

Thus, an AUV's mathematical modelling is proceeded by examining two separate reference frames, known as the earth-fixed and body-fixed frames of reference. AUV coordinates are defined by considering the three axes perpendicular to each other, starting at an arbitrary location. The X-axis shows a movement direction, while Y-axis corresponds to the orthogonal direction and Z-axis depicts the depth. Equations (1) and (2) describe the velocity vector (ν) and position vector (η) of an AUV respectively.

$$\nu = [u \quad v \quad w \quad p \quad q \quad r]^T \tag{1}$$
$$\eta = [x \quad y \quad z \quad \phi \quad \theta \quad \Psi]^T \tag{2}$$

On simplifying the equations (1) and (2) in the pure steering plane and considering the origin of the body-fixed frame to synchronize with the center of gravity:

$$m(v + mu_o\dot{r}) = \sum Y \tag{3}$$
$$I_Z\dot{r} = \sum N \tag{4}$$

The surge speed (u_0) value is assumed, and the value has been set at 0.75 m/s. To simplify our calculations, it considered that pitch and roll angles to be minimal and thus can be neglected:

$$\Psi = \frac{\sin\phi}{\cos\theta}q + \frac{\cos\phi}{\cos\theta}r \approx r \tag{5}$$

Equation (6) can be deduced in the matrix form by rewriting the equations from (1) to (5).

$$\begin{bmatrix} m - Y_{\dot{v}} & -Y_{\dot{r}} & 0 \\ -N_{\dot{v}} & I_{ZZ} - N_{\dot{r}} & 0 \\ 0 & 0 & 1 \end{bmatrix} \begin{bmatrix} \dot{v} \\ \dot{r} \\ \dot{\psi} \end{bmatrix} + \begin{bmatrix} -Y_v & -Y_r + mv_o & 0 \\ -N_v & -N_r & 0 \\ 0 & -1 & 0 \end{bmatrix} \begin{bmatrix} v \\ r \\ \Psi \end{bmatrix} = \begin{bmatrix} Y_{\delta i} \\ N_{\delta i} \\ 0 \end{bmatrix} \delta_r \tag{6}$$

Values of the corresponding parameters of the AUV[10] are substituted in the above equation to get the state equations (7) to (9)

$$\dot{x}(t) = Cx(t) + Du(t) \tag{7}$$

Where

$$C = \begin{bmatrix} -0.114 & -0.2647 & 0 \\ 0.0225 & -0.2331 & 0 \\ 0 & 1 & 0 \end{bmatrix}$$

$$D = [0.0211 \quad -0.0258 \quad 0]\,T$$

$$U = \delta_r \tag{8}$$

Equation (9) shows the association of the yaw angle (ψ) for the rudder deflection (δ_r).

$$\frac{\Psi(s)}{\delta_r(s)} = \frac{-0.0258s - 0.0024}{s^3 + 0.3445s^2 + 0.0319s} \tag{9}$$

which is used for designing controllers for the AUV.

III. DESIGN OF CONTROLLERS FOR AUV

This section is dedicated to designing the controllers for efficient controlling of the AUV. The two controllers proposed to control the AUV are LPID and FOPID controllers.

A. LPID CONTROLLER

The AUV maneuvering control LPID is a conventional control scheme based on the three control parameters (k_p, k_i, k_d). The equation for LPID controller with unity feedback is depicted as equations (10), (11), and (12).

$$c(t) = k_p e(t) + k_i D^{-1} e(t) + k_d D e(t) \tag{10}$$

$$U(s) = \frac{c(s)}{e(s)} = k_p + k_i s^{-1} + k_d s \tag{11}$$

$$1 + G(s)U(s) = 0 \tag{12}$$

After obtaining the feedback equation, the next task is to find the optimal gains of the three parameters of the LPID controller (k_p, k_i, k_d). This is achieved by optimizing the characteristic equation, thus minimizing the error based on ITAE- Integral of the Time multiplied by Absolute Error.

$$\text{ITAE} = \int_0^t t|e(t)|dt \tag{13}$$

The schematic diagram of MFO/SA tuned LPID Controlled AUV is shown in Fig.2.

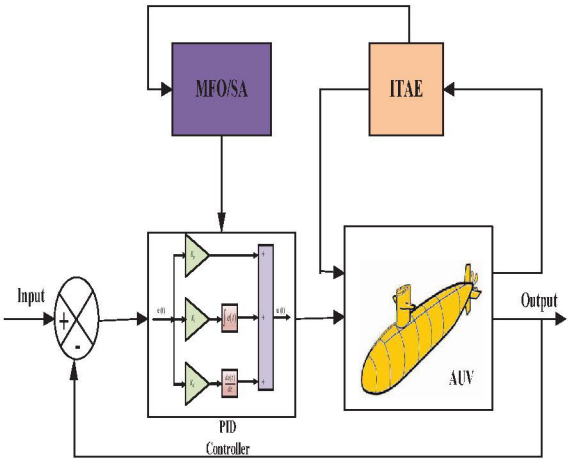

Fig.2. Schematic diagram of the feedback system of LPID on AUV

B. FOPID CONTROLLER

FOPID is another type of controller under the PID family which consists of five controlling parameters (k_p, k_i, k_d, λ, μ), thus, the AUV response is more accurate than the LPID controller. The characteristic equation of a FOPID controller[11] and the unity feedback system using the controller are shown in equations (14) and (15).

$$U(s) = \frac{c(s)}{e(s)} = k_p + k_i s^{-\lambda} + k_d s^{\mu} \tag{14}$$

$$1 + G(s)U(s) = 0 \tag{15}$$

Authorized licensed use limited to: DELHI TECHNICAL UNIV. Downloaded on June 07,2022 at 09:58:25 UTC from IEEE Xplore. Restrictions apply.

The MFO/SA tuned FOPID for AUV is shown in Fig. 3.

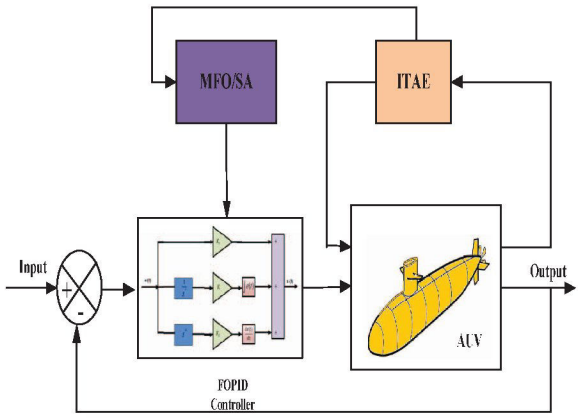

Fig.3. Block Diagram of the feedback system of FOPID on AUV

IV. IMPLEMENTATION OF SA AND MFO FOR TUNING THE CONTROLLERS

Tuning is defined as obtaining the controller's parameters to precisely controlling our system. LPID and FOPID controllers can be very useful in controlling the dynamical systems, but the tuning of these controllers requires several iterations and computational techniques to achieve our desired result. They also need constant adjustment of the control approach to avoid the system's stagnant reaction.

Various types of algorithms can be used to optimize the controller efficiently. One class of the algorithm based on bio-inspired techniques is discussed. The bio-inspired algorithms can be used to minimize the struggles in the tedious tuning of the controllers and achieve the desired results.

A. Simulated Annealing Tuned Controllers

One of the most extensively utilized approaches for solving the challenges of dynamical systems is Simulated Annealing. This simulated annealing[12] method is inspired by the response of the actual scenario in the heating environment and is based on statistical mechanics theories. A material kept in a heating environment is allowed to cool very slowly in steps till it reaches a state of lowest energy or optimized state.

The pseudocode of the SA algorithm to tune the gain parameters of LPID/FOPID controllers is :

Step 1: The gain parameters of an LPID/FOPID controller have fixed ranges defined by an objective function $f(x) = [K_p, K_i, K_d]^T or\ [K_p, K_i, K_d, \lambda, \mu]^T$

Step 2: Consider a temperature (t_0) at the beginning

Step 3: Initially, s_i is taken as the state of the system

Step 4: The lowest energy or optimal state is represented by s_{opt}

Step 5: At the beginning of the process set t as t_o and s_{opt} as s_i

Step 6: ***for*** $t = 1$ to t_{max} **do**

Assign s_{opt+1} to adjacent/nearest(s_{opt})

Change ΔE to ($f(s_{opt+1})$-$f(s_{opt})$)

if $min\ (1, e^{-\Delta E/t}) \geq$ random (0,1) ***then***

Update s_{opt} to s_{opt+1}

end if

update the value of t with the temperature schedule (t)

end for

Step 7: The final optimized state can be presented as output.

The gain coefficients for LPID controller Kp, Ki, and Kd derived with the help of SA techniques are -19.9298, -4.9419, and -41.25, respectively, and the gain coefficients for FOPID controller Kp, Ki, Kd, λ, μ obtained using the SA method are -18.296, -1.9659, -41.7380, 0.9187 and 1.0219 respectively. Simulated Annealing is an efficient algorithm even though it exhibits a significant disadvantage during iterations in course of minimizing the cost function (ITAE). Still, in some cases, the values of parameters also get accepted where the cost function 'ITAE' increases instead of decreasing. This number of cases occurs with a probability denoted by p called the transition probability. To overcome this disadvantage, MFO is implemented to realize the AUV more efficiently.

B. Moths Flame Optimization Algorithm tuned Controllers

MFO is a newly designed mechanism based on the nature of the movement of moths. It uses the principle of population search to find the optimized solution of a cost function. This bio-inspired optimization technique is exceptionally adaptable and may be used to identify the best answer to various real-world issues. Mirjalili [13] introduced the moth–flame optimization (MFO) approach. It starts by randomly producing moths inside the solution zone using a transverse orientation, as illustrated in Fig.4.

Fig.4 Traversal of Moth

The value of the fitness function for each moth is then computed, and flame tags the ideal spot. The moths' locations are then updated on the spiral movement function to achieve appropriate positions ordered according to a flame. The current acceptable locations of individuals are updated, and the previous actions are replicated. The process continues for a defined value of iteration.

There are three main postulates in the MFO algorithm. These are discussed below:

Authorized licensed use limited to: DELHI TECHNICAL UNIV. Downloaded on June 07,2022 at 09:58:25 UTC from IEEE Xplore. Restrictions apply.

1. Population Initiation:

It is assumed that the moths have the freedom to fly in all dimensions. It is represented by the matrix form in equation(16).

$$B = \begin{bmatrix} b_{1,1} & b_{1,2} & \cdots & \cdots & b_{1,d} \\ b_{2,1} & \cdots & \cdots & \cdots & b_{2,d} \\ \vdots & \vdots & \vdots & \vdots & \vdots \\ b_{x,1} & b_{x,2} & \cdots & \cdots & b_{x,d} \end{bmatrix} \quad (16)$$

x denotes the number of moths

The number of dimensions is denoted by d . These dimensions remain in the region of solution.

Following is an array that shows the fitness function at each step:

$$OB = \begin{bmatrix} OB_1 \\ OB_2 \\ \vdots \\ OB_x \end{bmatrix} \quad (17)$$

The d-dimensional space contains the flames that are represented by the following matrix:

$$F = \begin{bmatrix} F_{1,1} & F_{1,2} & \cdots & \cdots & F_{1,d} \\ F_{2,1} & \cdots & \cdots & \cdots & F_{2,d} \\ \vdots & \vdots & \vdots & \vdots & \vdots \\ F_{x,1} & F_{x,2} & \cdots & \cdots & F_{x,d} \end{bmatrix} \quad (18)$$

$$OF = \begin{bmatrix} OF_1 \\ OF_2 \\ \vdots \\ OF_x \end{bmatrix} \quad (19)$$

Moths and flames are the solutions. Each iteration handles and updates the main distinction between moth and flames. Moths are the actual searching agents that travel about the search area. Flames are the best places for moths that have been discovered so far.

2. Updation in the Position of Moths:

The below three steps of the algorithm helps us to find the global value of a problem.

MFO=(I,P,T) (20)

In the equation(20), I denote the initial moth in the population arbitrarily. $I: \phi \rightarrow \{B, OB\}$ .The movement of moths within the constrained area is denoted by, $P: B \rightarrow B$.

To end the process, a criterion is to be mentioned, denoted by $T: B \rightarrow true, false$

The equation (21) explains function I, which applies random distribution.

$$\mathrm{M(c, d)} = \big(ub(\mathrm{c}) - lb(\mathrm{d})\big) * \mathrm{rand}(\cdot) + lb(c) \quad (21)$$

Where lb , ub are upper bound and lower bound respectively. When using a logarithmic spiral, there are three things to keep in mind are:

- The spiral must commence with the moth as its beginning point.
- The spiral's final point must be at the flame position.
- The range variation of the spiral should not go beyond our search space.

$$S(B_c, F_d) = D_c \cdot e^{bt} \cdot \cos(2\Pi t) + F_d \quad (22)$$

D_c denotes the region between c^{th} moth and d^{th} flame.

$$Dc = |Fd - Bc| \quad (23)$$

The shape of the logarithmic spiral is described by Bp. Also, t represents a random value within the range $[r, 1]$. Close to the flame, the spiral motion balances exploitation and exploration. The variable r has a range [-1, 2] during the iterations in the algorithm. It is termed the convergence constant. Fig.5 shows a pictorial view of the facts mentioned above.

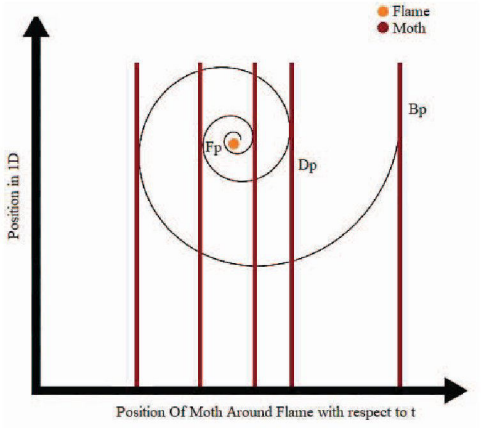

Fig.5. Logarithmic spiral shape

3. Flame Updation

Moth locations are modified at n various locations around the search zone, limiting the best solutions. As a result, using the equation (24), reducing the flames resolves the conflict:

$$flame\ no. = round\left(N - l * \frac{N-1}{T}\right) \quad (24)$$

Total flames are represented by N

Present iteration is represented l

Total iterations are represented by T

The mathematical analysis of the MFO in the form of pseudocode is:

Step 1: Range for control parameters is assigned as

$$f(x) = [K_p, K_i, K_d]^t or\ [K_p, K_i, K_d, \lambda, \mu]^t$$

Step 2: The population of Moth-Flame is defined

Step 3: Moth B's position is initialized randomly

Step 4: **for** $p = 1\ to\ n$ **do**

Evaluate the value of fitness function F

end for

Step 5: i=iterations

While I <=total i **do**

Eq. (23) is used to update flames

OB = Fitness Func(B);

if i == 1

F = sort(B);

OF = sort (OB);

else

F = sort (B_{t-1}, B_t);

OF = sort (B_{t-1}, B_t);

end

Step 6: **for** $p = 1: n$

for $q = 1: d$

The values of r and t are updated

Eq. (22) can be used to find the value of D

Eq. (21) is used to update $S(p, q)$

end

end

Authorized licensed use limited to: DELHI TECHNICAL UNIV. Downloaded on June 07,2022 at 09:58:25 UTC from IEEE Xplore. Restrictions apply.

Step 7: Finally, obtained the minimized cost function with efficiently tuned parameters

The parameters obtained after tuning the controllers with the MFO algorithm for LPID, the gain parameters K_p, K_i, and K_d are calculated as -15.5343, -0.025, and -38.93, respectively. For the FOPID controller, the gain parameters K_p, K_i K_d, λ, and μ are calculated as -13.5283, -0.0261, -40.225, 0.4405, and 0.9987, respectively.

V. Simulation and Results

The unit step is provided to the AUV controlled by the LPID and FOPID controllers. The response of the AUV is recorded to compare the performance of controllers.

The tuned controller's response for SA-LPID and SA-FOPID is shown in Fig.6. Whereas MFO-LPID, and MFO-FOPID controllers for AUV maneuvering control is shown in Fig.7. Also, a comparative depiction between MFO tuned FOPID and SA tuned FOPID is represented in Fig.8.

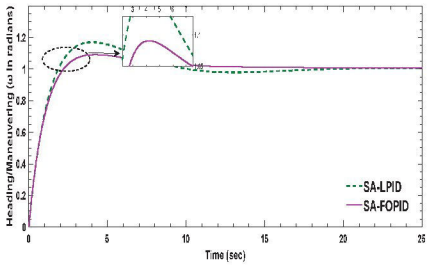

Fig.6 Response for SA tuned FOPID and LPID controllers

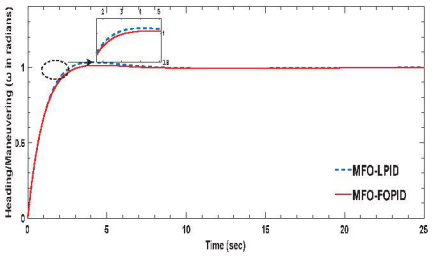

Fig.7. Response for MFO tuned FOPID and LPID controllers

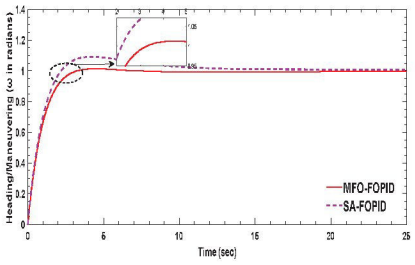

Fig.8. Response for MFO and SA tuned FOPID controllers

Table II represents SA tuned gain values for LPID and FOPID controlled AUV. Table III depicts MFO tuned gain parameters of LPID and FOPID controllers.

TABLE II. SA TUNED GAIN COEFFICIENTS

Gain Coefficients using SA algorithm		
Parameters	***LPID***	***FOPID***
K_p	-19.9298	-18.2960
K_i	-4.9419	-1.9659
K_d	-41.25	-41.7380
λ	-	0.9187
μ	-	1.0219

TABLE III. MFO TUNED GAIN COEFFICIENTS

Gain Coefficients using MFO algorithm		
Parameters	***LPID***	***FOPID***
K_p	-15.5343	-13.5283
K_i	-0.025	-0.0261
K_d	-38.93	-40.2255
λ	-	0.4405
μ	-	0.9987

The transient characteristics of the LPID controller with the utilization of MFO and SA are compared in Table IV.

TABLE IV. TUNED CONTROLLER TRANSIENT PERFORMANCE

ITAE				
Controller	***LPID***		***FOPID***	
Tuning Algorithm	***SA***	***MFO***	***SA***	***MFO***
Rise Time(Sec)	1.3813	1.7334	1.5418	1.834
%Overshoot	16.9740	3.1643	8.885	1.264
Settling Time(Sec)	14.1150	5.61	10.5802	2.7768
ITAE	3.24	2.72	2.06	1.67

Table IV shows that when the AUV is controlled by the FOPID controller using a particular algorithm has much better performance than the LPID controller. In addition to this, it also observed that MFO tuned FOPID controller shows superior performance than SA tuned FOPID controller.

VI. CONCLUSION

This paper intends to provide an insight into the comparison of the two controllers used to control the movement of a vehicle under the water-AUV. To achieve robust control of the system, two algorithms have been implemented. The first algorithm is known as Moth-Flame Optimization, inspired by the movement of moths, and another algorithm based on quantum physics called Simulated Annealing. These two algorithms are used to obtain the gain coefficients of the controllers to stabilize the steering management of the AUV. The step responses of the FOPID and LPID controller are compared. It turns out that the response obtained for the FOPID controller is superior to the LPID controller in terms of overshoot, rise time, settling time and ITAE. Furthermore, we also observe that MFO tuned FOPID controller has better results than SA tuned FOPID controller.

Authorized licensed use limited to: DELHI TECHNICAL UNIV. Downloaded on June 07,2022 at 09:58:25 UTC from IEEE Xplore. Restrictions apply.

REFERENCES

[1] S. K. Valluru and H. Thareja, "Evaluation of moth-flame optimization, genetic and simulated annealing tuned PID controller for steering control of autonomous uthe nderwater vehicle," in *IEEE International IOT, Electronics and Mechatronics Conference,* 2021, pp. 1–6.

[2] B. Jalving, "The NDRE-AUV Flight Control System," *IEEE Journal of Oceanic Engineering*, vol. 19, no. 4, pp. 497–501, 2007.

[3] A. J. Healey and D. Lienard, "Multivariable Sliding-Mode Control for Autonomous Diving and Steering of Unmanned Underwater Vehicles," *IEEE Journal of Oceanic Engineering*, vol. 18, no. 3, pp. 327–339, 1993.

[4] G. V Lakhekar, L. M. Waghmare, and P. G. Jadhav, "Robust Diving Motion Control of an Autonomous Underwater Vehicle Using Adaptive Neuro-Fuzzy Sliding Mode Technique," *IEEE Access*, vol. 8, pp. 109891–109904, 2020.

[5] Q. Chen, T. Chen, and Y. Zhang, "Research of GA-based PID for AUV motion control," in *2009 IEEE International Conference on Mechatronics and Automation, ICMA 2009*, 2009, pp. 4446–4451.

[6] K. H. Ang, G. Chong, and Y. Li, "PID Control System Analysis , Design , and Technology," *IEEE Transactions on Control Systems Technology*, vol. 13, no. 4, pp. 559–576, 2005.

[7] Sudarshan.K.Valluru, R. Kumar, and R. Kumar, "Design and Implementation of L-PID and IO-PID Controllers for Twin Rotor MIMO System," in *IEEE International Conference on Power Electronics, Control and Automation (ICPECA)*, 2019, pp. 1–5.

[8] S. K. Valluru and M. Singh, "Stabilization of Nonlinear Inverted Pendulum System Using MOGA and APSO Tuned Nonlinear PID Controller," *Cogent Engineering*, vol. 4, no. 1, pp. 1–15, 2017.

[9] S. K. Valluru, M. Singh, and S. Singh, "Prototype Design and Analysis of Controllers for One Dimensional Ball and Beam System," in *1st IEEE International Conference on Power Electronics. Intelligent Control and Energy Systems*, 2016, pp. 1–6.

[10] C. W. Chen, J. S. Kouh, and J. F. Tsai, "Modeling and simulation of an AUV simulator with guidance system," *IEEE Journal of Oceanic Engineering*, vol. 38, no. 2, pp. 211–225, 2013.

[11] J. Wan, B. He, D. Wang, T. Yan, and Y. Shen, "Fractional-order PID motion control for AUV using cloud-model-based quantum genetic algorithm," *IEEE Access*, vol. 7, pp. 124828–124843, 2019.

[12] C. Yu, A. A. Heidari, and H. Chen, "A quantum-behaved simulated annealing algorithm-based moth-flame optimization method," *Applied Mathematical Modelling*, vol. 87, pp. 1–19, 2020.

[13] S. Mirjalili, "Moth-flame optimization algorithm: A novel nature-inspired heuristic paradigm," *Knowledge-Based Systems*, vol. 89, pp. 228–249, 2015.

Authorized licensed use limited to: DELHI TECHNICAL UNIV. Downloaded on June 07,2022 at 09:58:25 UTC from IEEE Xplore. Restrictions apply.

Research Square

Preprints are preliminary reports that have not undergone peer review.
They should not be considered conclusive, used to inform clinical practice,
or referenced by the media as validated information.

Mapping of glacial lakes and glacial lake outburst flood in Kinnaur district, Himachal Pradesh using remote sensing and GIS

Gopinadh Rongali (gopinadh01@gmail.com)
Multidisciplinary Centre for Geoinformatics, Delhi Technological University
K. C. Tiwari
Multidisciplinary Centre for Geoinformatics, Delhi Technological University
Poonam Vishwas
Multidisciplinary Centre for Geoinformatics, Delhi Technological University

Research Article

Keywords: Glacial lake outburst floods (GLOFs), GIS, Remote Sensing, NDWI, LULC, NDSI

Posted Date: June 13th, 2022

DOI: https://doi.org/10.21203/rs.3.rs-1729005/v1

License: This work is licensed under a Creative Commons Attribution 4.0 International License.
Read Full License

Abstract

Glacial lake outburst floods (GLOFs) are a severe and escalating threat to livelihoods and infrastructure in high-mountain areas around the world. To implement a first-order assessment of GLOF risk across the Kinnaur district of Himachal Pradesh (HP), we combine modelling approaches that capture both current and future potential for GLOF triggering, quantification of affected downstream areas, and assessment of the underlying societal vulnerability to such climate-related disasters. As a result, the assessment takes into account both current glacial lakes and future lakes predicted to occur as glaciers retreat. Current hazard, vulnerability, and exposure indices are combined to indicate various risk 'hotspots,' demonstrating that high GLOF risk might occur well downstream from the glaciated headwaters where threats arise in some cases. Landsat images for the years 1989, 1998, 2008 and 2018 were used to map glacier lakes. Cartosat DEM (30 m) was used for computing topographic information including maximum, minimum, mean elevation, slope, and aspect. ArcGIS 10.8 was used to generate other characteristics such as area, slope, aspect, and drainage network. The maximum likelihood classification (MLC) algorithm was used to create the land use and land cover (LULC) maps using the supervised classification technique. To augment the findings, the study also uses the indices i.e. NDSI, NDWI, NDPI. based on the data a total of 39 glacial lakes were identified of which 10 lakes were found dangerous lakes having area > 0.1 Km^2 Trans-national GLOFs originating in China's upper Satluj River Basin, in particular, pose a threat to eastern HP's downstream territories. In the future deglaciated scenario, most administrative units are expected to have a large increase in GLOF danger levels as lakes grow closer to steep headwalls, where impacts from falling ice and rock could trigger outburst occurrences. Strengthening resilience and capacities to lower the current GLOF risk will be a critical first step toward adjusting to future problems in such situations.

1. Introduction

The Indian Himalayan Region (IHR) is experiencing tremendous challenges in dealing with the negative effects of climate change. The IHR, like many other mountain regions around the world, is particularly vulnerable to changes in global climate, both physically and societally. The retreat of mountain glaciers and the rise of massive glacial lakes are two of the most visible and dynamic effects of climate change in this environment (Bolch et al. 2012). The potential hazards from glacial lake outburst floods (GLOFs) are thus growing over time, in conjunction with altered stability of adjacent rock and ice walls (Schaub et al. 2013; Clague and O'Connor 2014; Deline et al. 2014). With residential, tourism, and especially hydroelectric infrastructure extending higher into alpine valleys and human demand on limited hydrological resources increasing, there is a compelling need for enhanced application of GLOF risk reduction techniques within climate adaptation planning (Khanal et al. 2015). GLOFs are the abrupt release of a water reservoir that has formed beneath, on the side, in front of, within, or on the surface of a glacier, and related dam constructions can be made of ice, moraine, or bedrock. With projected warming and continuous loss of alpine glaciers (Church et al. 2013), attention has recently switched away from monitoring and assessing existing outburst concerns and toward predicting where new, possibly problematic lakes will arise in the future. Such lakes will emerge mostly in depressions in the exposed

glacier bed (Frey et al. 2010) and will be blocked by bedrock or moraine, depending on the glacier type, erosional features, and pace of retreat (Linsbauer et al. 2016).

To unveil the process and mechanism of GLOFs for hazard assessment, mitigation, and risk management, a database of GLOF incidents assembled from current literature is required. From literature, media reports, and remote sensing data, GLOF incidents have been documented in the Bhutan Himalayas, Tibet, China (Liu et al. 2013; Yao et al. 2012), Nepali Himalayas (Bajracharya et al. 2007; ICIMOD, 2011), and Indian Himalayas (Durga Rao et al. 2014; Das et al. 2015). However, because most GLOFs occurred in remote and sparsely populated areas, poor data availability or quality can lead to significant misunderstandings, particularly for GLOFs that occurred before the advent of satellite remote sensing.

Satellite remote sensing, particularly the use of optical images such as Landsat imagery with archived records dating back to 1972, is an excellent modern technique for monitoring and analyzing previous GLOFs in less accessible high mountain areas. Geomorphic evidence, such as a V-shaped trench, massive debris deposits, and paleo river beds, has been used in conjunction with remote sensing data to identify previous outburst occurrences. These traits, on the other hand, could develop in other cryo-hydrologic events besides GLOFs. As a result, caution is advised when relying solely on satellite data to detect a GLOF incident. A more rigorous method for GLOF verifications is the use of multiple sources of evidence, such as historical documents, field surveys, long-term satellite observations, and high-resolution image archives (e.g., Google Earth), to better reveal the hydrogeomorphic processes induced by various GLOF incidents across the Himalayas (Nie et al. 2018).

The present study therefore, is an attempt to map and monitor glacier lakes in Kinnaur district of Himachal Pradesh making use of satellites data. In addition of our analysis addresses the future threats of GLOFs in line with other climate risks (e.g. fluvial floods or droughts) for which policymakers require and demand best available knowledge on expected changes over the next decades to century.

2. Study Area

Kinnaur is located in the northeast corner of Himachal Pradesh, bordering Tibet to the east, and is about 235 kilometers from the state capital, Shimla. It has three high mountain ranges, the Zanskar, the Himalayas, and the Sutlej, Spiti, and Baspa valleys, as well as their tributaries. Thick timber, orchards, pastures, and hamlets cover the hills. A natural rock Shivling may be seen at the summit of Kinnaur Kailash mountain (Shiva lingam). Outsiders were allowed into the district in 1989. The old Hindustan-Tibet Road travels through the Kinnaur valley, following the Sutlej River's bank, before entering Tibet at the Shipki La Mountain. Kinnaur, after Solan in Himachal Pradesh, is the second richest district in terms of per capita income.

3. Data Used

High-resolution satellite imagery and a digital elevation model were employed as remote sensing datasets in this study. The research used Landsat-7 and Landsat-8 data to analyze glacier lakes for the years, 1989, 1998,2008,2018. Images with a maximum of 10% cloud cover and the least amount of snow cover from October to November were chosen by comparing all available datasets for this investigation. The USGS website (https://earthexplorer.usgs.gov) has been used to download a total of 12 Landsat images. October (11 scenes) and November (11 scenes) were the months for which Landsat images were used. The also uses the Carotsat Digital elevation model (30 m) for topographic information. Google Earth images were also used for carrying out manual checking and analysis.

Table 1
List of satellite data used in the study

Sensor	Acquisition date	Resolution
Landsat-8 OLI	08th March 2018	30 m
	5th December 1989	
Landsat 4–5 TM	1st March 1998	30 m
	13th April 2008	
Cartosat DEM	29th April 2015	30 m

4. Methodology

For spatial and temporal analysis of snow cover and glacier lake, Landsat TM were used primarily. Then image pre-processing of Landsat TM i.e. Geometric and Radiometric correction was performed using ERDAS IMAGINE software and mosaic all the images to cover the whole scene of the study area. The study area was subset using ArcGIS10.4. Then using of it performed some indices like NDSI, NDWI, and NDPI. Then used for analysing and finding the results. Cartosat DEM was used for relief analysis of the study area. Land Use and Land cover also prepared using Landsat TM using maximum likelihood supervised technique.

4.1 Normalized difference water index (NDWI)

The study of temporal variation in the lake region has been carried out using satellite images. Landsat images have been used classification and change detection using Normalized Difference Water Index (NDWI). The NDWI (McFeeters, 1996) has been calculated as:

$$\text{NDWI} = \frac{GREEN - NIR}{GREEN + NIR} \quad (1)$$

4.2 Normalized Difference Snow Index (NDSI)

The thresholding of normalized difference snow index (NDSI) image and time-intensive manual delineation is generally known to be most accurate (Paul 2002). NDSI is generally used for snow cover

mapping using satellite data (Hall et al. 1995). NDSI uses high and low reflectance of snow in visible (green) and short-wave infrared region, respectively, and it can also delineate and map snow in mountain shadows (Kulkarni et al. 2001). NDSI is used to mask the glaciated region:

$$\text{NDSI} = \frac{Green - SWIR}{Green + SWIR} \quad (2)$$

Where, SWIR = Short Wave Infra-Red

4.3 Normalised Difference Pond Index (NDPI)

Normalised Difference Pond Index (NDPI) was applied to identify and to see the change in the nature of these lakes.

$$\text{NDPI} = \frac{Green - SWIR}{Green + SWIR} \quad (3)$$

NDSI used for demarcation of snow covered area using threshold value of 0.4. From NDVI and NDWI, taking some samples for demarcation of lakes of the study area. Then calculated the area and using area calculated the volume of the glacial lakes. According the larger volumes of lakes more the dangerous. So, in this way, the glacier lakes were detected and validate through high resolution google earth images.

5. Results And Discussion

In this present study, the four land use and land cover map was prepared since 1989, 1998, 2008 and 2018 respectively. The purpose of land use and land cover was for analyzing the changes and findings glacier lake. For this maximum likelihood supervised technique was used in ERDAS Imagine software. Further these were classified into six categories i.e. Glacier, forest, Scrubland, wasteland, waterbody and agriculture respectively. Most of the area was covered from glaciers in all maps of year1989, 1998, 2008 and 2018. As seen these figures, we found that snow coverage was less in in the year 1989 than 1998 and also less in area of waste land but the after 10 year and snow coverage decreased continuously and waste land also increased. The river path was also wide in the map of 2018.

Mapping of glaciers is an important part of the glacial lake hazard assessment as their position with respect to lakes, their slope and surface area play an important part in assessing glacial lake hazard. Remote sensing is, in general, the only possible method for mapping and monitoring these glaciers.

Clean ice glaciers can be mapped using NDSI but many glaciers in the Himalayas are characteristically debris covered. Manual delineation is, in general, still possible because the glacier boundary exhibits differences in illumination caused by its shape. A threshold of 0.4 was used here to map the glacier. All the values laid above this threshold came into Glacier and below came under non-snow cover. Here the figure shows the snow coverage was lager in the year 1998 and lesser in the year of 2018.

As far as glacial lakes are concerned Normalized Difference Water index (NDWI= (NIR -Blue) / (NIR + Blue). The combination of digital satellite data and the Digital Elevation Model (DEM) of the area was

also used for better and more accurate results for the inventory of glaciers and glacial lakes. Ground truthing were done to rectify the errors while identifying the exact location of glaciers and glacial lakes through google earth.

The Samples of lake pixels were taken from the known glacial lakes and water body. From the NDWI and NDPI images of range between − 1 to + 1. From the collected samples mean value were calculated for water body. The calculated mean value were taken as threshold to demarcate glacial lake features from the other features. The gray scale threshold was used to segment an input into two classes – one for those pixels having values below an analyst defined gray level and one for those above this value. The calculated threshold value for NDWI and NDPI combine indices is -0.69. On screen digitisation were performed on reclassified image to extract the areal extent of each and every glacial lake lying in district of Kinnaur district. A total of 39 glacial lakes were identified in this district lying 1200–6,300 m in altitude. The total area of the lakes in the district is around 4.02 sq km.

5.1 Identification of potentially dangerous lakes

For selecting potentially dangerous lakes, following parameters have been used.

(1) Lakes of area smaller than 0.1 km^2 have been considered as harmless owing to the less volume of water contained by it (area and volume are empirically related by Huggel's formulae).

The lake volume; $V = 0.104\ A^{1.42}$ (4)

(2) Lakes which are still attached to or are near to the parent glaciers or at the snout of the glaciers are considered as more dangerous as they are capable of expanding. In general, lakes which are isolated are stagnant, do not expand and pipe their volume of water in most of the cases rather than bursting. For this purpose, overlay analysis has been carried out to check the position of the lakes with respect to glaciers.

(3) Lakes were also checked for the steep slopes around them (which can cause influx into them). Conditions of the thick or thin were estimated from the visual interpretation and distance calculations using high-resolution satellite imagery on Google Earth.

5.2 Identification of the most vulnerable lake

Now, for the final GLOF modelling, the most dangerous lake was to be selected. For the selection of the most dangerous lake, volume is generally considered as the single most important factor, and the largest lake is generally selected. Here, in this study, four main factors have been considered for selecting the most dangerous lake:

Table 2
Area, volume and distance from outlet of the selected potentially dangerous lakes

Lake no.	Area	Volume	Distance from Outlet (m)
9	0.76	0.07	65.23
17	0.20	0.01	60.32
21	0.11	0.0045	78.21
24	0.13	0.0057	39.91
26	0.21	0.113	87.25
34	0.10	0.0039	73.32
31	0.11	0.0045	34.74
33	0.10	0.0039	46.32
36	0.33	0.0215	76.67
37	0.29	0.017	53.67

5.3 Validation of the findings

Validation of Glacier lake were done through high resolution google earth images. The Landsat-based glacier lake maps were evaluated by comparing them to the glacial lake outlines that were manually scanned from Google Earth pictures. The discrepancy in image collection date between Landsat and Google Earth photos was no more than five days to guarantee the trustworthiness of the assessment findings due to the changeable nature of certain glacial lake conditions and the surrounding environment. For all lake and land pixels combined, commission and omission errors were determined. A small percentage inaccuracy in the water and land classifications indicates that the categorization is correct.

6. Conclusion

Traditional field studies would not have been able to document lakes that have evolved at higher altitudes without the use of GIS and remote sensing technology. The findings of a comprehensive satellite image analysis shed light on the origins of these lakes. In total of 39 glacial lakes, 10 lakes were found dangerous lakes having area > 0.1 Km^2 were shown in the table in Kinnaur district of HP. The formation and expansion of glacial lakes were in concert with the climatic change (increase in temperature and decrease in precipitation) induced glacier retreat in Kinnaur district. The rate of growth of glacial lakes varied inversely with the proximity to the parent glacier, closer the glacial lake to mother glacier higher was its growth rate. Hence, glacier meltwater flowing into the lakes is the main source of water to the areal expansion of lakes in the region. As a consequence of the continuous expansion of lakes and glacier retreat, GLOF is an emerging threat in Kinnaur district.

Declarations

Acknowledgements

The authors are grateful to the NASA for making the Landsat and ASTER GDEM datasets freely available under the umbrella of USGS web server. The present work was financially supported by the National Mission on Himalayan Studies (NMHS), MoES & CC, India under the Himalayan Research Fellowship (HRF) program.

Disclosure statement

No potential conflict of interest was reported by the author(s).

Compliance with ethical standards

The author declares that no copyright norms have been violated, and the study has no conflict of interest.

References

1. Bajracharya, S., Mool, P. and Shrestha, B. (2007). Impact of Climate Change on Himalayan Glaciers and Glacial Lakes. Kathmandu: International Centre for Integrated Mountain Development (ICIMOD) and United Nations Environment Programme Regional Office Asia and the Pacific (UNEP/ROAP).
2. Bolch, T., Kulkarni, A., Kääb, A., Huggel, C., Paul, F., Cogley, J. G., Frey, H., Kargel, J.S., Fujita, K., Scheel, M. and Bajracharya, S., & Stoffel, M. (2012). The state and fate of Himalayan glaciers. *Science*, *336*(6079), 310-314.
3. Church, J. A., Clark, P. U., Cazenave, A., Gregory, J. M., Jevrejeva, S., Levermann, A., Merrifield, M.A., Milne, G.A., Nerem, R.S., Nunn, P.D., & Unnikrishnan, A. S. (2013). Sea Level Change In Stocker TF et al.(Eds.), Climate Change 2013: The Physical Science Basis. Contribution of Working Group I to the Fifth Assessment Report of the Intergovernmental Panel on Climate Change. Cambridge, United Kingdom and New York, NY.
4. Clague JJ, O'Connor JE (2014) Glacier-related outburst floods. In: Haeberli W, Whiteman C (eds) Snow and ice-related hazards, risks, and disasters. Elsevier, Amsterdam.
5. Das, S., Kar, N. S., and Bandyopadhyay, S. (2015). Glacial lake outburst flood at Kedarnath, Indian Himalaya: a study using digital elevation models and satellite images. Nat. Hazards 77, 769–786. doi: 10.1007/s11069-015- 1629-6.
6. Deline P, Gruber S, Delaloye R, Fischer L, Geertsema M, Giardino M, Hasler A, Kirkbride M, Krautblatter M, Magnin F, McColl S, Ravanel L, Schoeneich P (2014) Ice loss and slope stability in high-mountain regions. In: Haeberli W, Whiteman C (eds) Snow and ice-related hazards, risks, and disasters. Elsevier, Saint Louis.
7. Durga Rao, K. H. V., Rao, V., Dadhwal, V., and Diwakar, P. (2014). Kedarnath flash floods: a hydrological and hydraulic simulation study. Curr. Sci. 106, 598–603.

8. Frey H, Haeberli W, Linsbauer A, Huggel C, Paul F (2010) A multi-level strategy for anticipating future glacier lake formation and associated hazard potentials. Nat Hazards Earth Syst Sci 10:339–352.
9. Hall, D. K., Foster, J. L., Chien, J. Y., & Riggs, G. A. (1995). Determination of actual snow-covered area using Landsat TM and digital elevation model data in Glacier National Park, Montana. *Polar Record*, *31*(177), 191-198.
10. ICIMOD (2011) Glacial lakes and glacial lake outburst floods in Nepal. *International Centre for Integrated Mountain Development (ICIMOD)*, Kathmandu
11. Khanal NR, Mool PK, Shrestha AB, Rasul G, Ghimire PK, Shrestha RB, Joshi SP (2015) A comprehensive approach and methods for glacial lake outburst flood risk assessment, with examples from Nepal and the transboundary area. Int J Water Resour Dev 31:219–237.
12. Linsbauer A, Frey H, Haeberli W, Machguth H, Azam MF, Allen S (2016) Modelling glacier-bed overdeepenings and possible future lakes for the glaciers in the Himalaya-Karakoram region. Ann Glaciol 57:119–130.
13. Liu J-J, Tang C, Cheng Z-L (2013) The two main mechanisms of Glacier Lake Outburst Flood in Tibet, China. J Mt Sci 10:239–248.
14. McFeeters, S. K. (1996). The use of the normalized difference water index (NDWI) in the delineation of open water features. Int. J. Remote Sens. 17, 1425–1432.
15. Nie, Y., Liu, Q., Wang, J., Zhang, Y., Sheng, Y., and Liu, S. (2018) An inventory of historical glacial lake outburst floods in the Himalayas based on remote sensing observations and geomorphological analysis, Geomorphology, 308, 91–106.
16. Paul, F., Kääb, A., Maisch, M., Kellenberger, T., & Haeberli, W. (2002). The new remote-sensing-derived Swiss glacier inventory: I. Methods. *Annals of Glaciology*, *34*, 355-361.
17. Schaub Y, Haeberli W, Huggel C, Ku¨nzler M, Bru¨ndl M (2013) Landslides and new lakes in deglaciating areas: a risk management framework. In: Margottini C, Canuti P, Sassa K (eds) Landslide science and practice. Springer, Heidelberg, pp 31–38.
18. Yao, X., Liu, S., Sun, M., Wei, J., and Guo, W. (2012) Volume calculation and analysis of the changes in moraine-dammed lakes in the north Himalaya: a case study of Longbasaba lake, J. Glaciol., 58, 753–760.

Figures

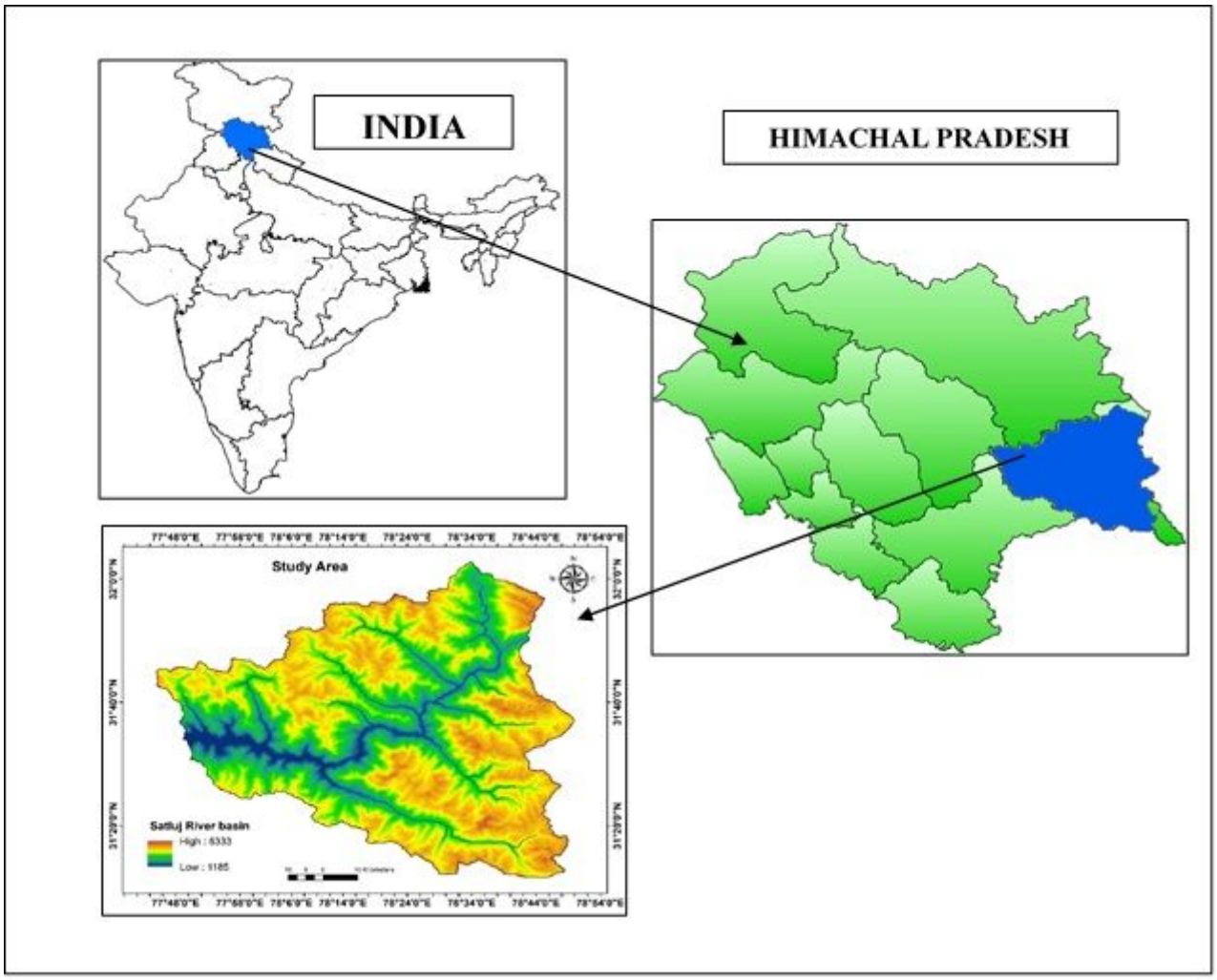

Figure 1

Location map showing Kinnuar, Himachal Pradesh

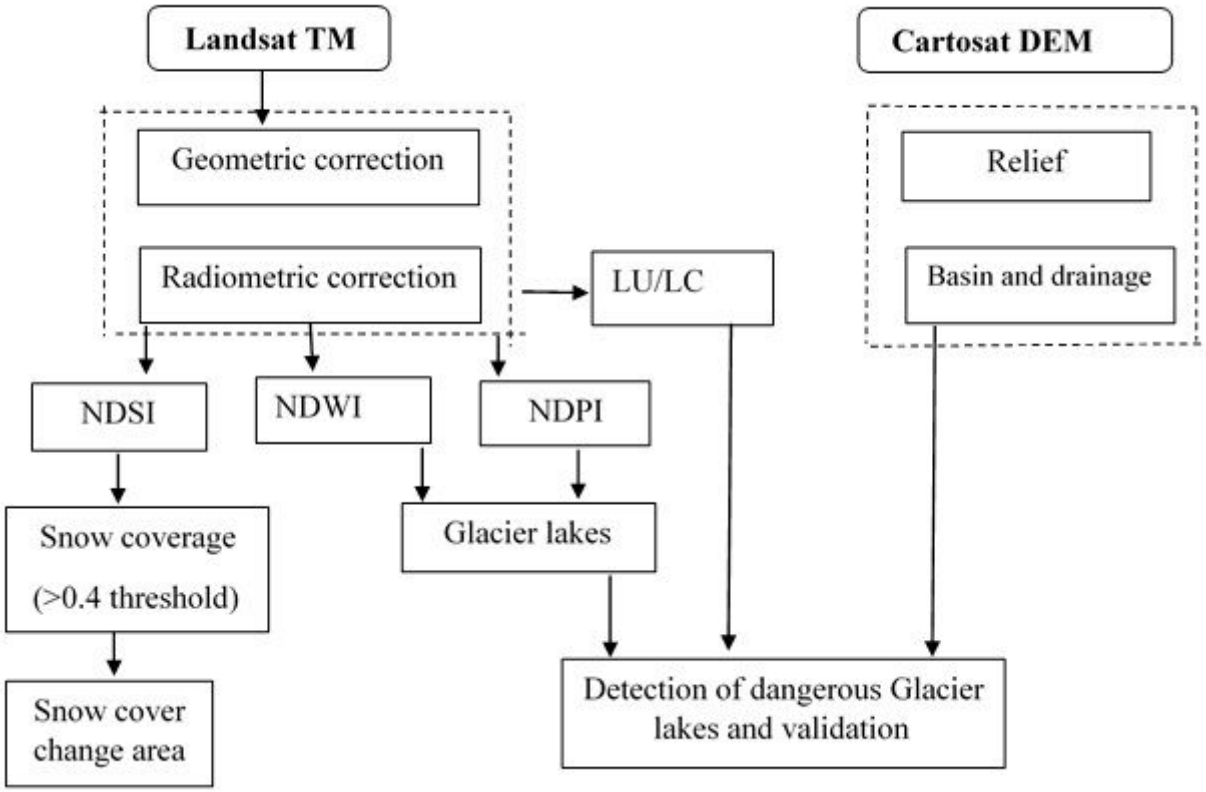

Figure 2

Methodological framework of the study

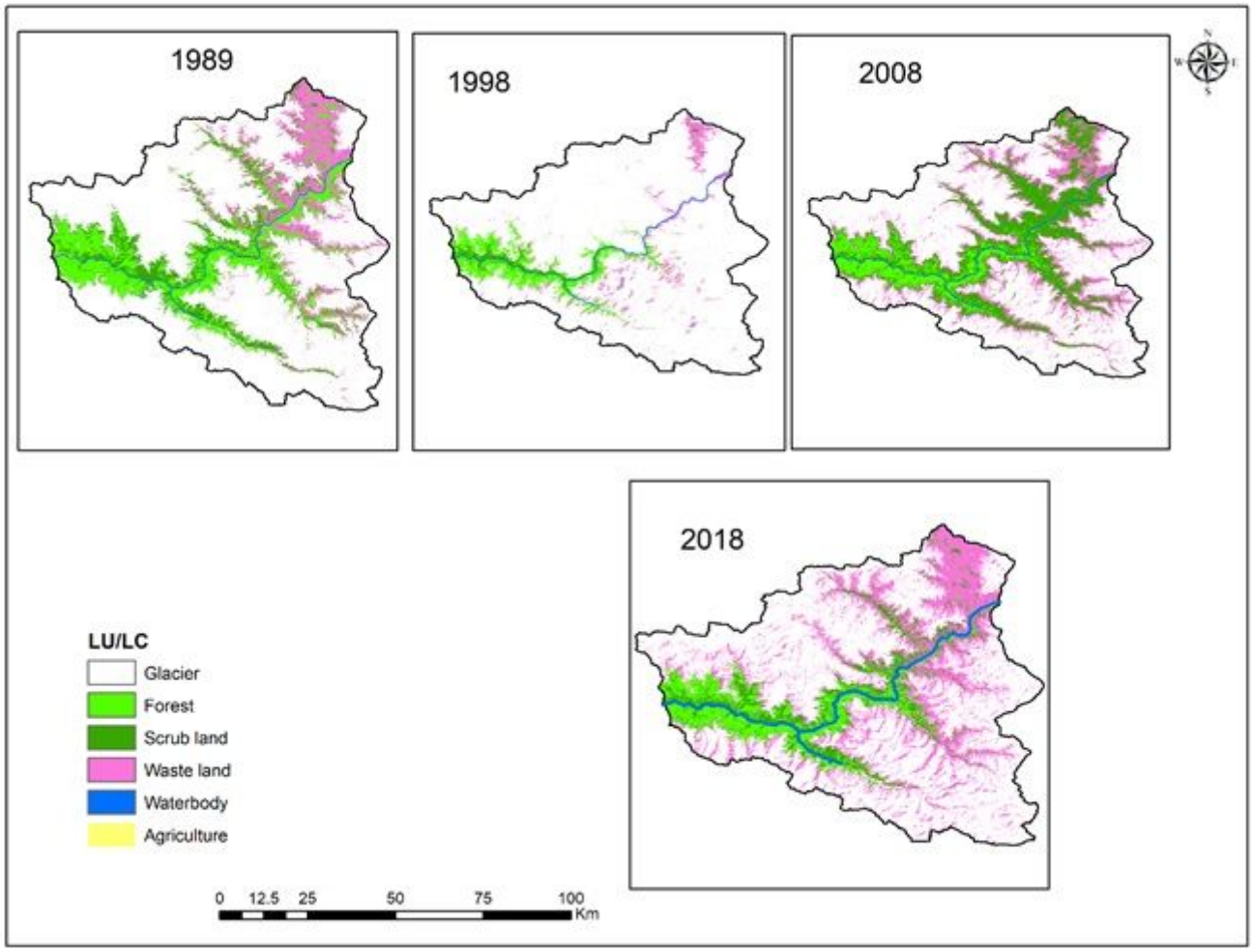

Figure 3

Land use and Land cover area pattern of the study area

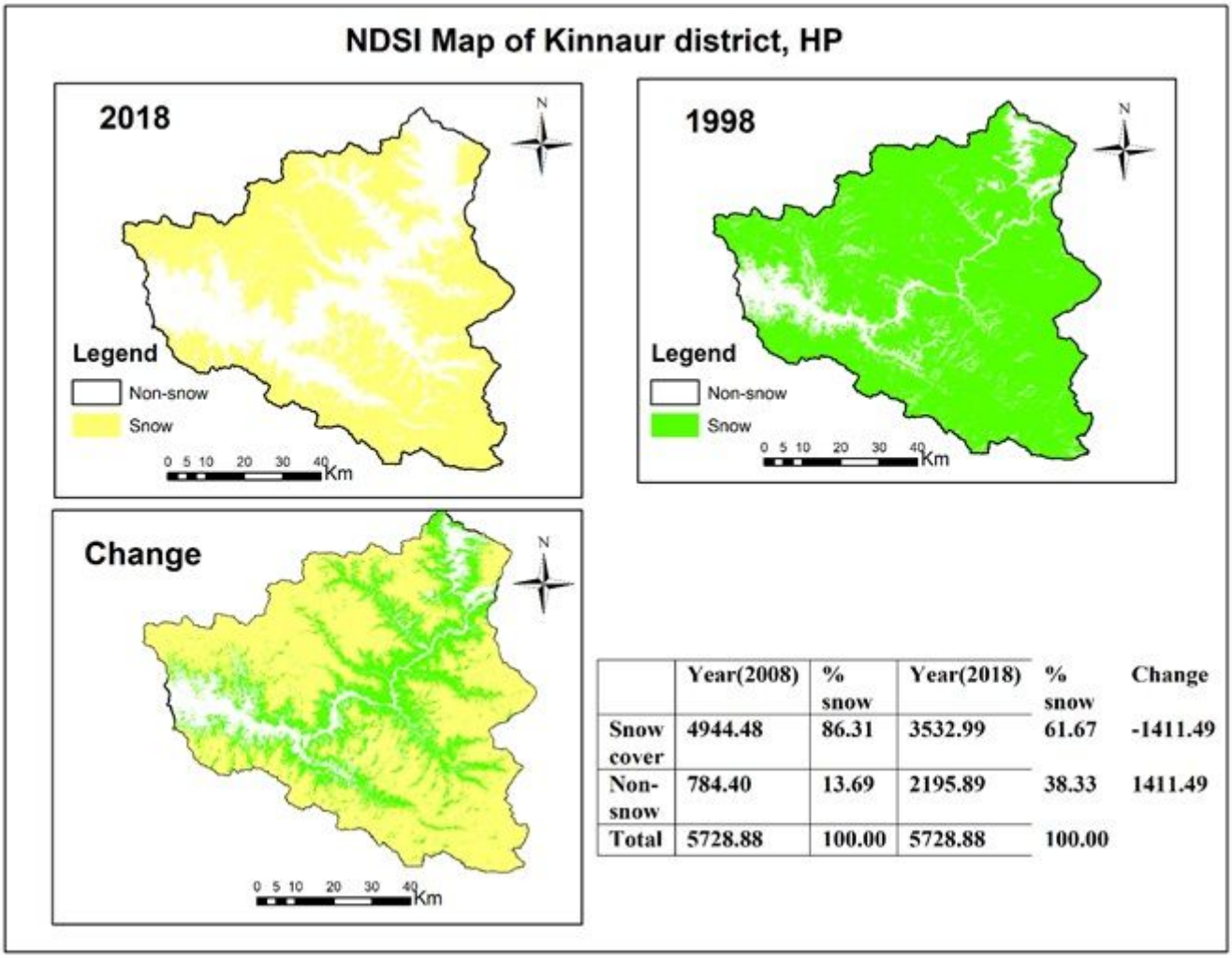

	Year(2008)	% snow	Year(2018)	% snow	Change
Snow cover	4944.48	86.31	3532.99	61.67	-1411.49
Non-snow	784.40	13.69	2195.89	38.33	1411.49
Total	5728.88	100.00	5728.88	100.00	

Figure 4

Spatio - temporal pattern of NDSI in Study area

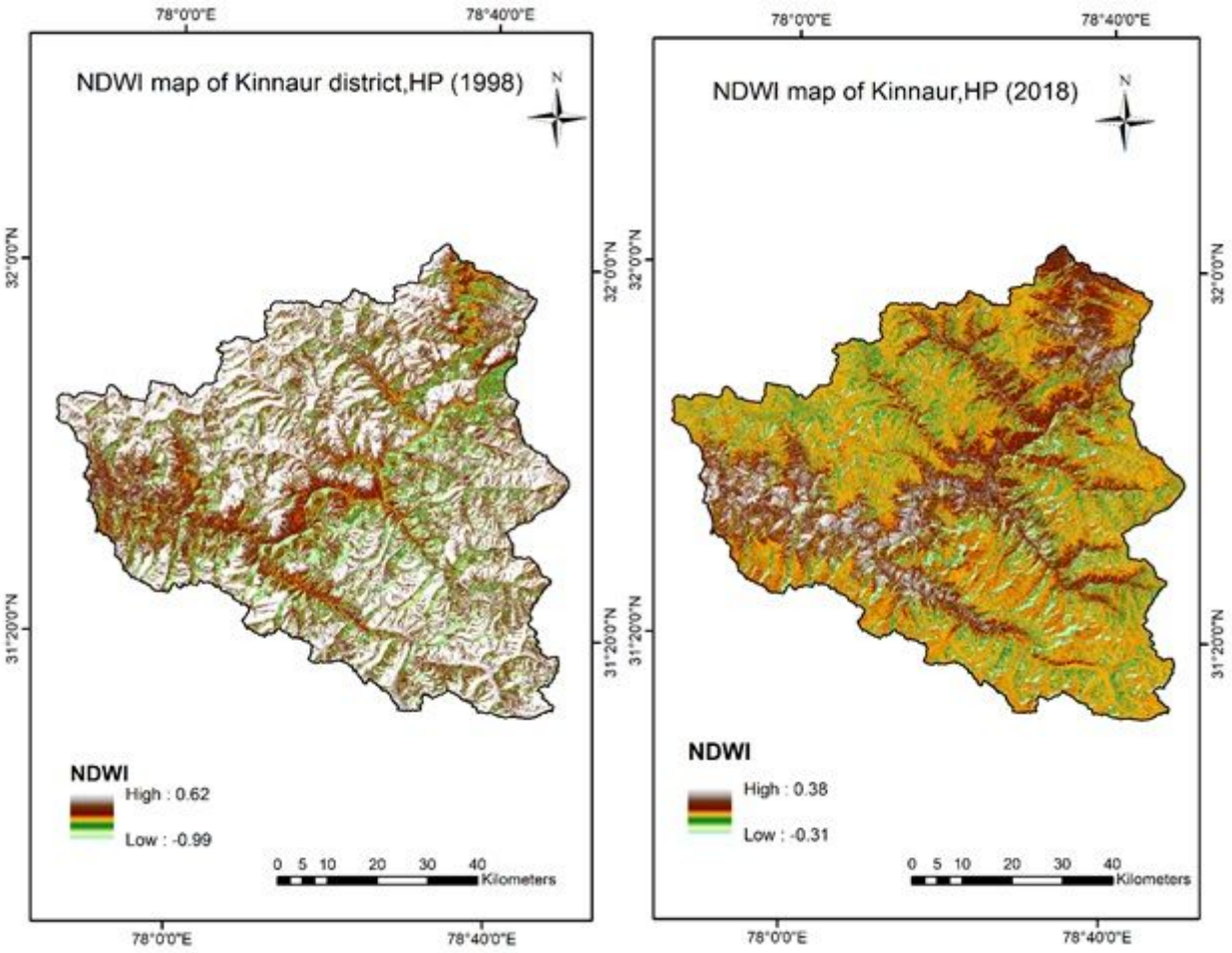

Figure 5

Spatio-Temporal pattern of NDWI in the study area

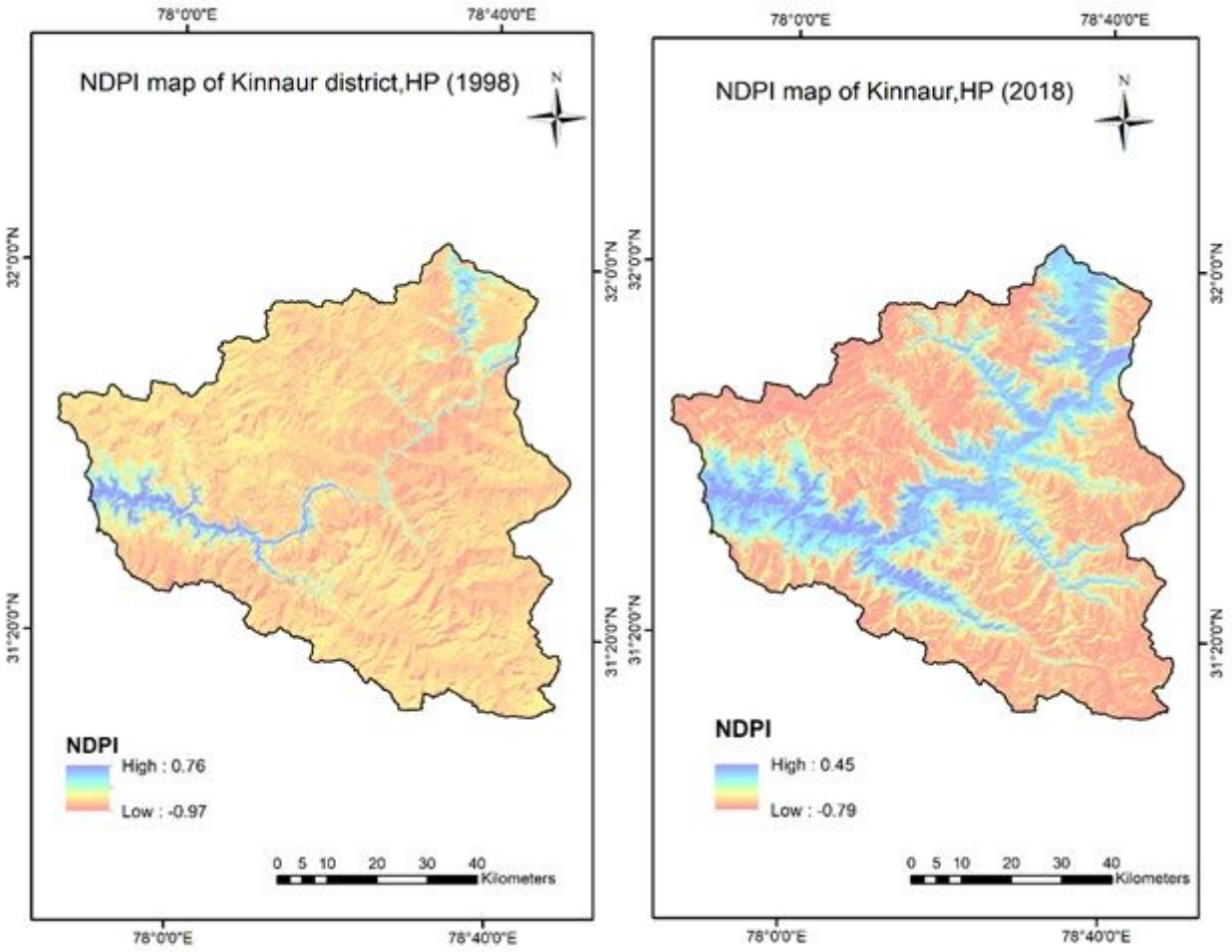

Figure 6

spatio-temporal pattern of NDPI in the study area

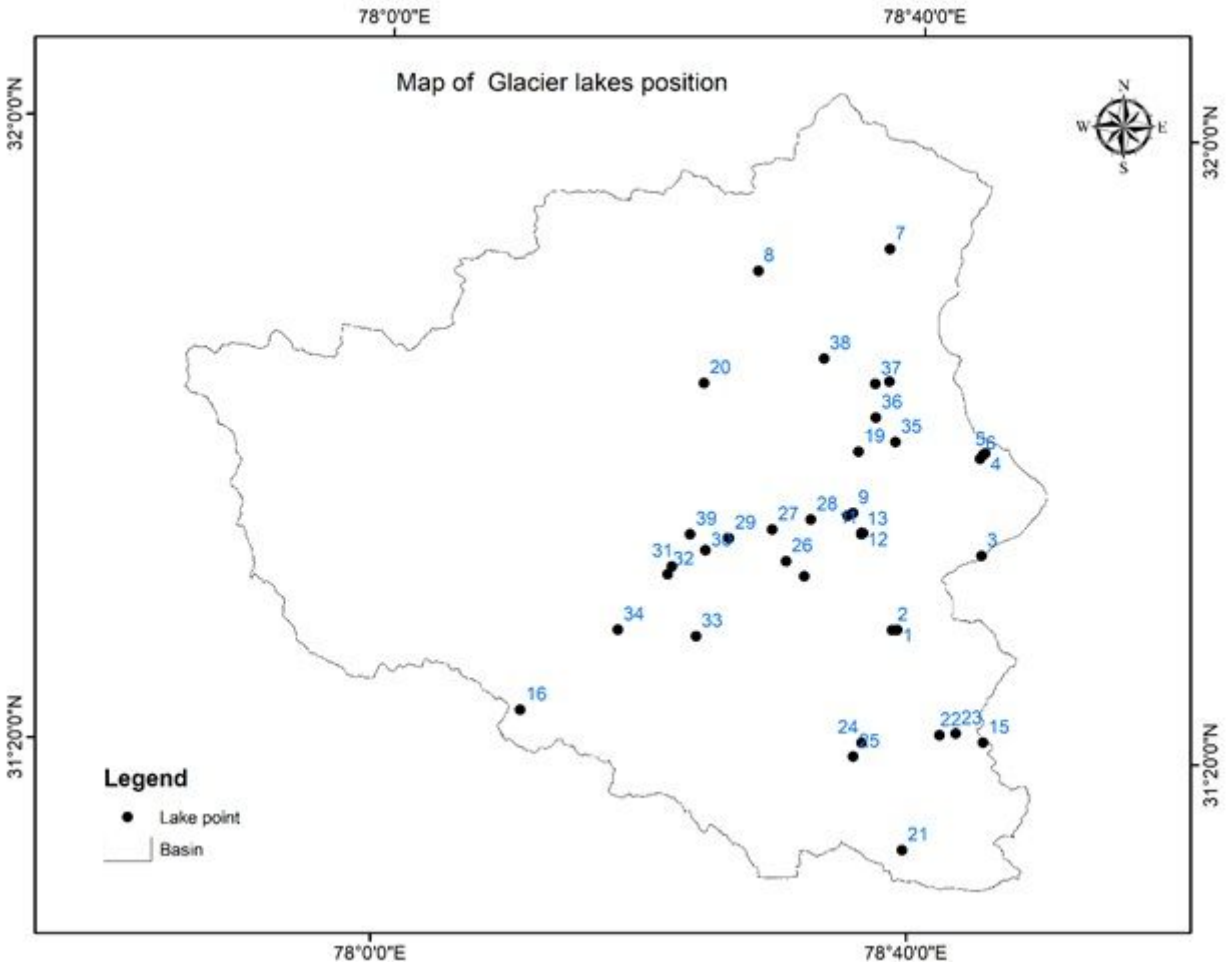

Figure 7

Location of vulnerable lakes in the study area

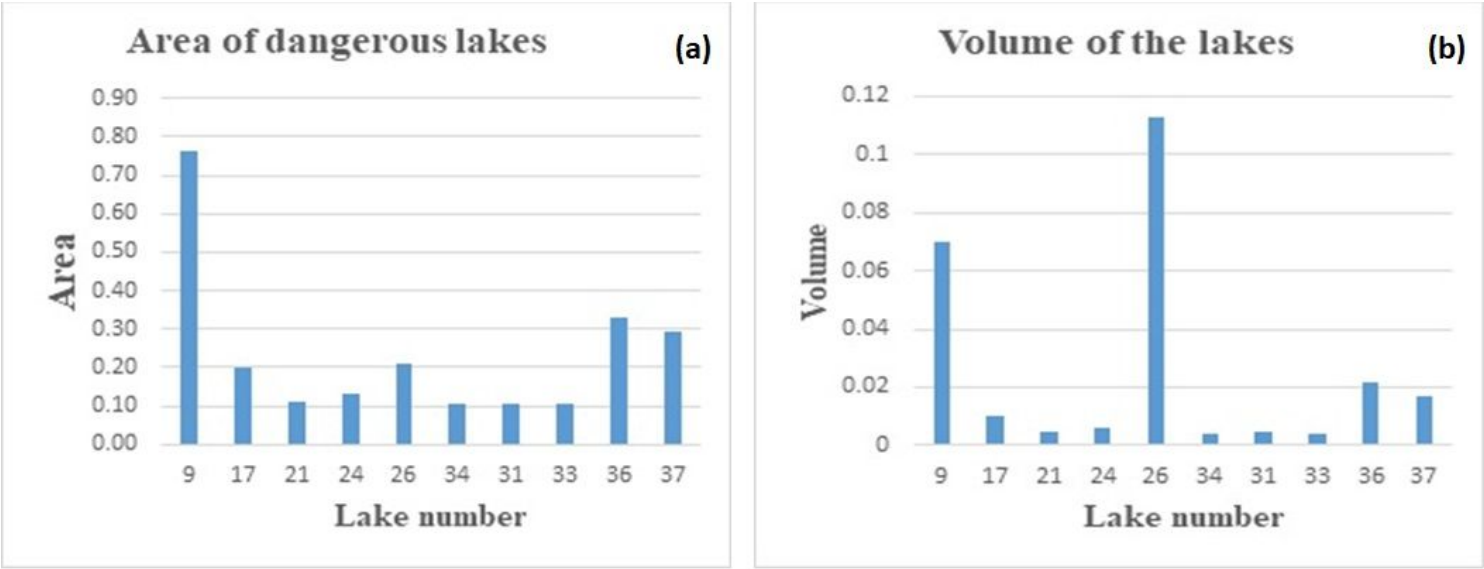

Figure 8

Area (a), Volume (b) of the vulnerable lakes in the study area

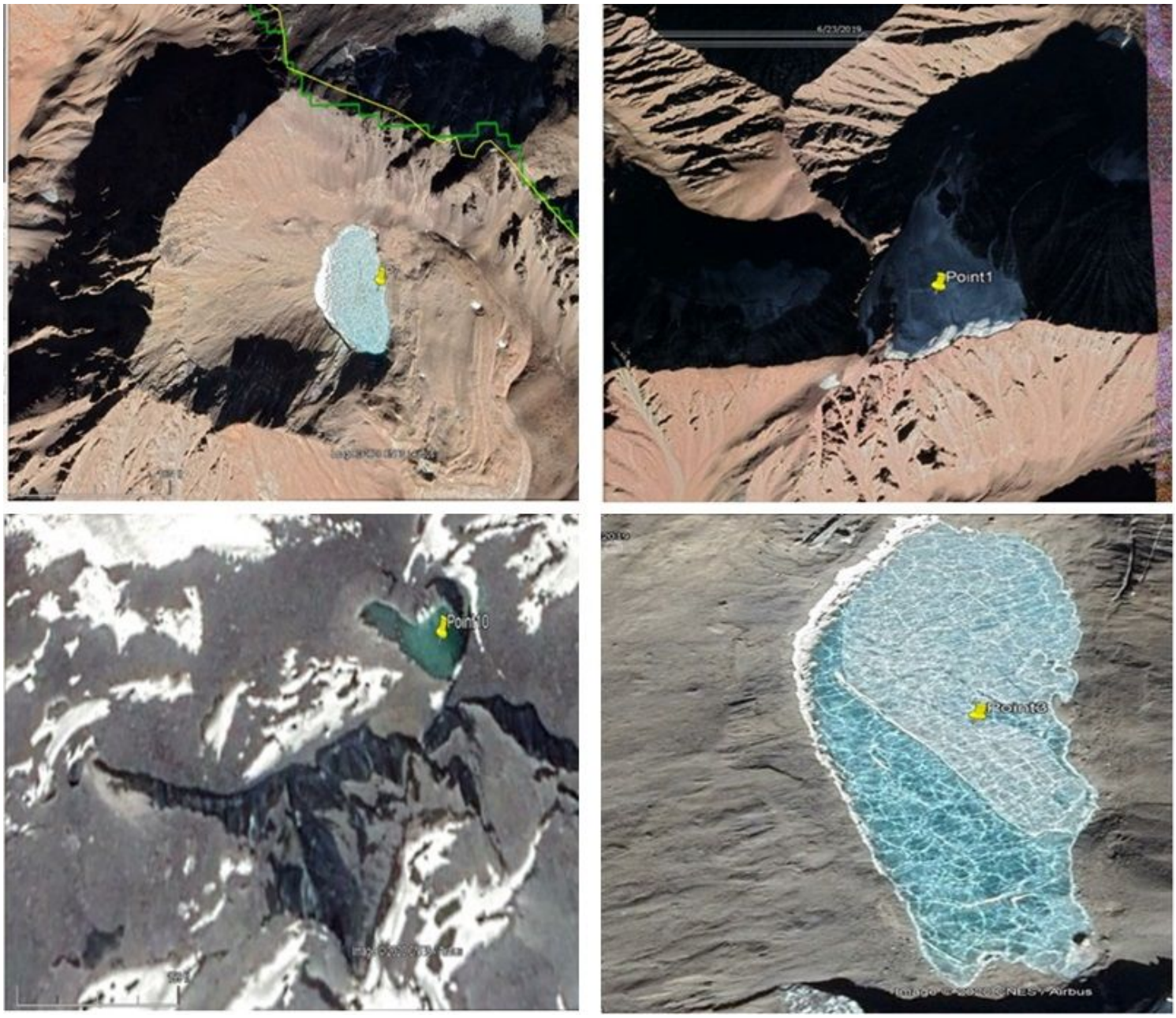

Figure 9

Validation of the vulnerable lakes with google earth images in the study area

International Journal of Research in Engineering and Innovation (IJREI)
journal home page: http://www.ijrei.com
ISSN (Online): 2456-6934

Modeling of variable speed compressor vapour compression refrigeration system using ecofriendly refrigerants and nano refrigerants and water cooled condenser-evaporator with experimental validation

Radhey Shyam Mishra

Department of Mechanical Engineering, Production & Industrial engineering and Automobiles Engineering
Delhi Technological University, Delhi 110042
E Mail-rsmishradtu@gmail.com, rsmishra@dce.ac.in , rsmishra@dtu.ac.in

Abstract

Lots of researches have been done and going on based on the performance evaluation of various metallic/ nonmetallic nanoparticle suspended into the conventional fluid to enhance the heat transfer property of base fluid. Also some theoretical analysis of suspension of nanoparticle Al_2O_3 in conventional refrigerant. On the other hand the performance of vapour compression cycle based chiller facility using nano refrigerant yet to be analyzed with different type, concentration and diameter of nanoparticle. Such as TiO_2, CuO nanoparticle suspension into conventional refrigerant with different concentration and diameter have been analyzed by several investigators and also effect of variation of concentration and nanoparticle diameter on the first and second law performance of vapour compression refrigeration system is presented. The effect of changing input parameter of VCRS using nano refrigerant also affecting significantly the evaporative heat transfer coefficient and very little condor heat transfer coefficient. The idea of Suspension nanoparticle into conventional refrigerant and theoretical analysis of VCRS using nano-refrigerant is proposed after going through extensive literature review presented in this paper.
© 2017 ijrei.com. All rights reserved
Keywords: VCRS, First & Second Law Performance, Nano Materials, Energy-Exergy Analysis

1. Introduction

Theoretical and experimental investigation of refrigeration systems based on first law and second law analysis using refrigerants.is carried out. Chopra, [1] investigated the exergy analysis of vapour compression refrigeration system with R134a R407Cand R410A. In their study they have calculated the effect of varying evaporator temperature of the C.O.P. of VCS for different types of ecofriendly refrigerant and also the effect of varying evaporator temperature on the exergetic efficiency of VCS. Chopra [2] developed a computational model for computing a coefficient of performance (COP), energy destruction, exergetic efficiency and energy defects for R502, R404A, and R507A of detailed energy analysis on actual vapor compression refrigeration cycle. It has been done for evaporator and condenser temperature in the range of 50^0C to 0^0C and 40^0C to 55^0 C respectively. He found that R507A is better substitute to R502 than R404A. The efficiency defects in condenser are highest and lowest in liquid vapour heat exchanger for the refrigerants considered. Choi, S. U. S, [3] investigated thermal properties and rheological behavior of water based Al_2O_3 nano fluid as a heat transfer fluid and found that Thermal conductivity and convective heat transfer of nano fluid increases as mass concentration of nano fluid increases. Jwo et.al, [4] presented the Effect of different nano particle shapes on shell and tube heat exchanger using different baffle angles and operated with nano fluid, in his study he has analyze the effect of nanoparticle volume fraction on overall heat transfer coefficient and entropy generation & heat transfer rate and found that as well as we increase the volume fraction of nano particle the overall heat transfer coefficient generation & heat transfer rate increases and

Corresponding Author: Radhey Shyam. Mishra
Email rsmishra@dtu.ac.in

entropy generation decreases. Simulation result has been plotted for the same. Lee K, Hwang [5] in his experimental measured on heat transfer coefficient using Al_2O_3 /water nano fluid in an air finned heat exchanger concluded the overall heat transfer coefficient of Fe_2O_3/water nano fluids in compact air cooled heat exchanger using LMTD technique under laminar flow regime. Joaquin Navarro, Francisco, Angel, [6] carried out thermal modelling analysis of vapour compression refrigeration system and found that the influence of an internal heat exchanger on the performance of a vapour compression system using R1234yf as replacement for R134a and compare the energy performance of vapour compression system using ecofriendly refrigerants,R134a and R1234yf, and found that the presence of an internal heat exchanger results, reductions in cooling capacity and COP between 6 and 13% , when R134a is replaced by the R1234yf. Although the presence of an Internal heat exchanger reductions between 2 and 6%. Murshed S. M. S., K. C. Leong, and C. Yang [7] in this study Comparison of convective heat transfer coefficient and friction factor of TiO_2 nano fluid flow in tube with twisted tape inserts' determined the heat transfer coefficient and friction factor of TiO_2/water nano fluid up to 3.0% volume concentration at an average temperature of 30°C and a significant enhancement of 23.2 % in heat transfer coefficient is observed at 1.0% concentration for flow in tube. An increase in the nanofluid concentration to 3.0% decreased heat transfer coefficient to value lower than water for flow in tube and with tape inserts. A thermal system with tape inserts of twist ration 15 and 1.0% TiO_2 concentration gives maximum advantage ratio, if pressure drop is considered along with enhancement in heat transfer coefficient. Hao Peng et.al [8] in his study on Heat transfer and flow characteristics of Al_2O_3 water nanofluid in a double tube heat exchanger and evaluated that the viscosity, relative viscosity of nano fluid at different mass fraction and sizes of nano particles and found that viscosity, Nusselt no. increases as mass fraction and size of nano particles. And observed that the, for a given refrigerating mass faction of nanoparticles, viscosity, Nusselt no. Reynolds No. increase of base fluid. Henderson et al. [9] evaluated the performance parameters of a vapour compression refrigeration system with different lubricants including nano lubricants and concluded that (i) R134a refrigerant and mineral oil mixture with nano particles worked normally (ii) Freezing capacity of the refrigeration system is higher (iii) The power consumption of the compressor reduces by 25% when the nano lubricant (iv) The coefficient of performance of the refrigeration system also increases by 33% with nano refrigerant (v) the energy enhancement factor in the evaporator is 1.53. Juan Carlos et al [10] investigated the use of nano fluids as secondary coolants in vapor compression refrigeration systems using different nanoparticles (Cu, Al_2O_3, CuO and TiO_2) for different volume fraction and particle diameters. Simulation results have shown that, for a given refrigerating capacity, evaporator area and refrigerant-side pressure drop are reduced when: (i) the volume fraction of nanoparticles increase; (ii) the diameter of nanoparticles decrease. Also, nano fluid side pressure drop and, consequently, pumping power, increase with nanoparticle volume fraction and decrease with nanoparticle size. Henderson et al. [9] Measured enhanced thermal conductivity of Cu-water Nano fluid using secondary circuit of evaporator and observed that the rate of heat transfer is increases with increasing flow rate and also its concentration. By nanoparticle dispersed into de-ionized base fluid a better enhancement is achieved. Xuan Y [10]. Investigated the nanoparticle collision and deposition in the surface investigated the base fluid should possess high prandle number, and get enhanced heat transfer rate by minimize particle-particle and particle-wall collision. Viscous dissipation effect is important of narrow channel, because Nusselt number high for high aspect ratio channel. Wang RX, Xie HB [11] studied experimentally the heat transfer coefficient and friction factor of a nano fluid consisting of water and 0.2 vol. % TiO_2 flowing a double pipe heat exchanger. They investigated the effects of the flow Reynolds number and the temperature of the nano fluid and the temperature and flow rate of the heating fluid on the heat transfer coefficient and flow characteristics. Their results showed that the convective heat transfer coefficient of nano fluid is slightly higher than that of the base liquid by about 6 -11%. The heat transfer coefficient of the nano fluid increased with an increase in the mass flow rate of the hot water and nano fluid.

Lee K, Hwang YJ, [12] Studied about the relation between thermal resistance-size of nanoparticle and found that the thermal resistance is directly proportional to the size of the nanoparticle. The maximum reduction of thermal resistance by using 10 nm sized particles, because particle size is increasing the wall temperature also increases. Due to sized particle suitable for enhanced heat transfer rate. Thermal resistance is decreases with increasing heat and concentration of Nano particle.

Murshed S. M. [13] numerically studied heat transfer characteristics of double-tube helical heat exchangers using nano fluids under laminar flow conditions. CuO and TiO_2 nano particles with diameters of 24 nm dispersed in water with volume concentrations of 0.5–3 vol. % were used as the working fluid. The overall heat transfer coefficient ratio was higher at higher nanoparticle concentrations. In other words, the overall heat transfer coefficient ratio was higher when the probability of collision between nanoparticles and the wall of the heat exchanger were increased under higher concentration, confirming that nano fluids. Wen, D., and Y. Ding (2004) [13] investigated convective heat transfer co efficient of diamond based Nano fluid by using heat tube apparatus and showed the heat transfer coefficient is increases with increasing concentration and Reynolds number of Nano fluid. I.M. Mahbubul, A. Saadah [14] investigated heat transfer enhancement and flow characteristic of Al2O3-Water Nano fluid using micro channel heat sink. The dimension of test section is 5x5 mm and 50W heat is

applied and found heat transfer is enhanced at high Reynolds number and high concentration of Nano fluid, because at high Reynolds number wall temperature is decreases and pressure drop is increased. Y. He, [15] investigated the thermal performance of air-water heat exchanger using TiO_2Nano fluid. And found that the heat transfer coefficient is increases with increasing Reynolds number at constant volume of friction up to 0.6%. D.P. Kulkarni [16] investigated heat transfer and fluid dynamic performance of nano fluids of silicon dioxide (SiO2) nanoparticles suspended in a 60:40 (% by weight) ethylene glycol and water (EG/water) mixture and observed increase in heat transfer coefficient due to nano fluids for various volume concentrations and loss in pressure was observed with increasing nanoparticle volume concentration. S.Z. Heris, et.al. [17] investigated the flow and heat transfer characteristic of spiral pipe heat exchanger using different type of Nano fluid with different concentration as Al_2O_3 water, TiO_2-water, CuO-water Nano fluid with 1%, 1% and 3% concentration respectively. And observed that the heat transfer enhanced 28% at 0.8% concentration of Nano fluid, due to, increased shear stress of Nano fluid. Bobbo S. et.al, [18] Investigated the friction factor and heat transfer rate of CuO Water and Al_2O_3 water and observed that the increase of Nusselt number with increasing the Reynolds number and concentration decreases the friction factor of Nano fluid. As compared the CuO-water and better enhancement as Al_2O_3 water Nano fluids by using CuO-water Nano fluid. Mishra [19-20] observed the overall heat transfer coefficient of nano fluids increases significantly with prandle number. For both nano fluids the overall heat transfer coefficient increases with nanoparticle concentration compared to the base fluid. The experimental results for the Nusselt number of Al_2O_3/water and TiO_2/water nano fluids and Results show that at 0.5 vol. % of Al_2O_3. Nano particles and at 0.3 vol. % of TiO_2 nanoparticles. Considerable enhancement in convective heat transfer coefficient of the nano fluids as compared to the base fluid, ranging from 2% to 50%. Moreover, the results indicated that with increasing nanoparticles concentration and nano fluid temperature, the convective heat transfer coefficient of nano fluid increases. The Nano fluid shows greater heat transfer coefficient compare with water and increase the inlet liquid temperature decreases the overall heat transfer coefficient. The increasing mass flow rate of brine increases Re and overall heat transfer coefficient.

2. Result and Discussion

The main heading should be A computational program has been developed to solve nonlinear equation of vapour compression refrigeration cycle by considering same performance parameter of the VCRS model (i.e. variation of mass flow rate of brine from 0.006 kg/sec to 0.010 kg/sec for fixing 0.008 condenser water flow rate , mass flow rate of water in condenser from 0.006 to 0.010kg/sec by fixing 0.008 kg/sec of brine mass flow rate at pressure of 2 bars , with 0.000010 m nano particle size mixed in the brine water, the theoretical analysis has been done using EES software for nano fluid (nanoparticle mixed with R718) flowing in secondary circuit and eco friendly refrigerant in primary circuit of VCRS and results are given below.

Table 1 shows the enhancement in C.O.P using different R-404a ecofriendly refrigerant of VCRS and maximum COP is found 14.8% using Cuo nano particles 10.7% using TiO2 and 11.5% using Al_2O_3 for 5% of Volume Fraction (ϕ). Although by varying Volume Fraction (ϕ) the first law performance is increased from 3.8% to 11.5% using Al_2O_3 and 2.6% to 10.5% and 5.2% to 14.8% using Cuo nano materials as compared without nano particles mixed in the brine water flowing in the secondary circuit of evaporator

Table 1: Enhancement in C.O.P using different nano refrigerant of Vapour compression Refrigeration System [21]

Refrigerant		R404a	
Nano particle	Volume Fraction (ϕ)	C.O.P.	% Enhancement
	0	2.379	-
Al_2O_3.	0.01	2.47	3.8%
	0.02	2.524	6.1%
	0.03	2.536	6.6%
	0.04	2.558	7.5%
	0.05	2.653	11.5%
TiO_2	0.01	2.44	2.6%
	0.02	2.498	5.0%
	0.03	2.548	7.1%
	0.04	2.594	9.0%
	0.05	2.634	10.7%
CuO	0.01	2.502	5.2%
	0.02	2.572	8.1%
	0.03	2.63	10.6%
	0.04	2.683	12.8%
	0.05	2.73	14.8%

Table 2 shows the enhancement in C.O.P using different R-407c ecofriendly refrigerant of VCRS and maximum COP is found 14.8% using CuO nano particles 10.7% using TiO_2 and 11.5% using Al_2O_3 for 5% of Volume Fraction (ϕ). Although by varying Volume Fraction (ϕ) the first law performance is increased from 2.9% to 9.4% using TiO_2 and 3.2% to 9.9% Al_2O_3 and 4.4% to 12.1% using Cuo nano materials as compared without nano particles mixed in the brine water flowing in these condary circuit of evaporator.

Table: 2 Enhancement in second law using different nano refrigerant of Vapour compression Refrigeration System [21]

Refrigerant		R407C	
Nano particle	Volume Fraction (ϕ)	C.O.P.	% Enhancement
	0	2.556	-
Al_2O_3	0.01	2.637	3.2%
	0.02	2.702	5.7%
	0.03	2.755	7.8%
	0.04	2.787	9.0%
	0.05	2.808	9.9%
TiO_2	0.01	2.629	2.9%
	0.02	2.685	5.0%
	0.03	2.733	6.9%
	0.04	2.765	8.2%
	0.05	2.795	9.4%
CuO	0.01	2.669	4.4%
	0.02	2.748	7.5%
	0.03	2.806	9.8%
	0.04	2.842	11.2%
	0.05	2.864	12.1%

Table 3 shows experimentally the enhancement in C.O.P using different R-404a ecofriendly refrigerant of VCRS and maximum COP is found 3.817 using CuO and 3.691 using TiO_2 and 3.748 using Al_2O_3. Similarly as volume fraction (ϕ) is increased the first law performance is increased maximum using R134a and minimum as using ecofriendly refrigerant R404a. The % improvement is found in Table-4 from 21.3% in case of Volume Fraction (ϕ) is 1% to 35.4% using R-134a and CuO as nano material and 16.6% to 30.9 % using TiO_2 and 22.8% to 32.9% using Al_2O_3.

Table: 3 Enhancement in C.O.P using different nano refrigerant of Vapour Compression Refrigeration System [22]

Refrigerant		R134a	R404A	R407c
Nano particle	Volume Fraction (ϕ)	C.O.P.	C.O.P.	C.O.P.
	0	2.82	2.379	2.556
CuO	0.01	3.421	2.47	2.637
	0.02	3.604	2.524	2.702
	0.03	3.701	2.536	2.755
	0.04	3.717	2.558	2.787
	0.05	3.817	2.653	2.808
TiO_2	0.01	3.287	2.44	2.629
	0.02	3.488	2.498	2.685
	0.03	3.603	2.548	2.733
	0.04	3.666	2.594	2.765
	0.05	3.691	2.634	2.795
Al_2O_3	0.01	3.464	2.502	2.669
	0.02	3.616	2.572	2.748
	0.03	3.681	2.63	2.806
	0.04	3.725	2.683	2.842
	0.05	3.748	2.73	2.864

Table-4, showing the enhancement in first law efficiency in terms of COP using different ecofriendly refrigerants of Vapour Compression Refrigeration System and maximum COP is found 14.8% using ecofriendly R404a refrigerant and Cuo nano particles, 10.7% using TiO_2 and 11.5% using Al_2O_3 for 5% of Volume Fraction (ϕ). Although by varying Volume Fraction (ϕ) the first law performance is increased from 3.2% to 9.9% using ecofriendly R407c refrigerant and Cuo nano particles and from 2.9% to 9.4% using R407c and TiO_2 as nano particles and 3.2% to 9.9% Al_2O_3 as compared to without nano particles mixed in the brine water flowing in these condary circuit of evaporator

Table: 4 Show % enhancement in C.O.P using different nanorefrigerant of Vapour Compression Refrigeration System [23]

Refrigerant		R134a	R404A	R407c
Nano particle	Volume Fraction (ϕ)	% Enhancement	% Enhancement	% Enhancement
	0	-	-	-
CuO	0.01	21.3%	3.8%	3.2%
	0.02	27.8%	6.1%	5.7%
	0.03	31.2%	6.6%	7.8%
	0.04	31.8%	7.5%	9.0%
	0.05	35.4%	11.5%	9.9%
TiO_2	0.01	16.6%	2.6%	2.9%
	0.02	23.7%	5.0%	5.0%
	0.03	27.8%	7.1%	6.9%
	0.04	30.0%	9.0%	8.2%
	0.05	30.9%	10.7%	9.4%
Al_2O_3	0.01	22.8%	5.2%	4.4%
	0.02	28.2%	8.1%	7.5%
	0.03	30.5%	10.6%	9.8%
	0.04	32.1%	12.8%	11.2%
	0.05	32.9%	14.8%	12.1%

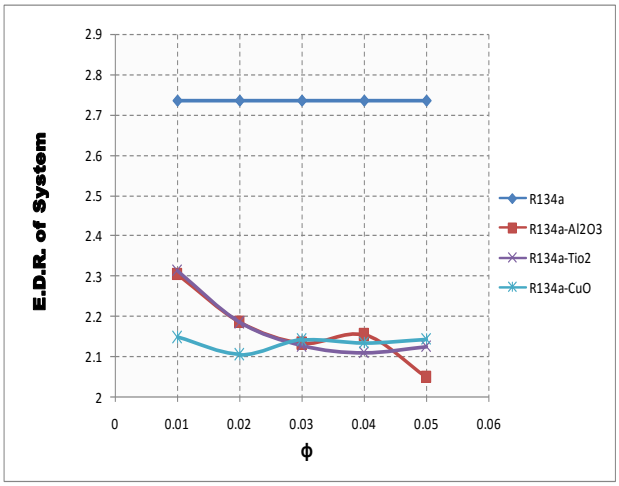

Figure: 1 Variation of Exergy destruction ratio with volume fraction (ϕ) of Vapour Compression Refrigeration System with R134a using different nano particles [24]

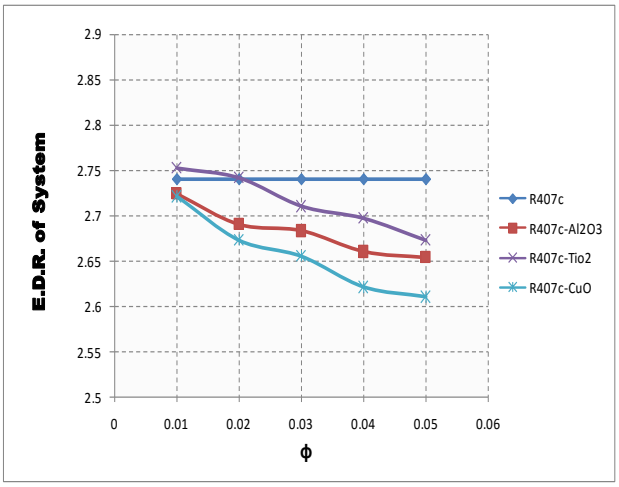

Figure: 2 Variation of Exergy Destruction ratio with volume fraction (ϕ) of Vapour Compression Refrigeration System with R407c using different nano particles [24]

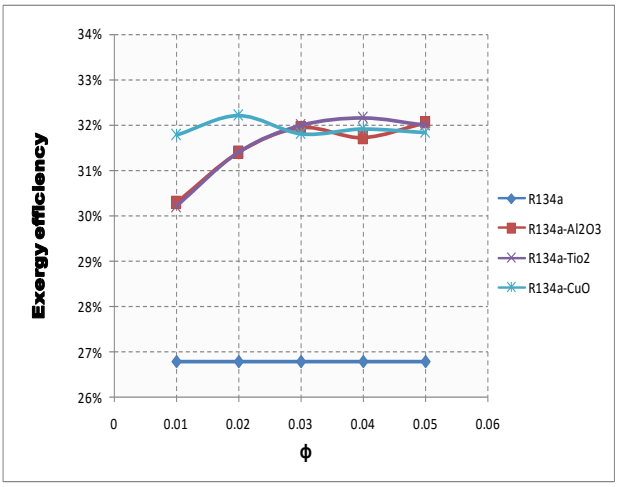

Figure: 4 Variation of Exergy Efficiency with volume fraction (ϕ) of Vapour Compression Refrigeration System with R134a using different nano particles [25]

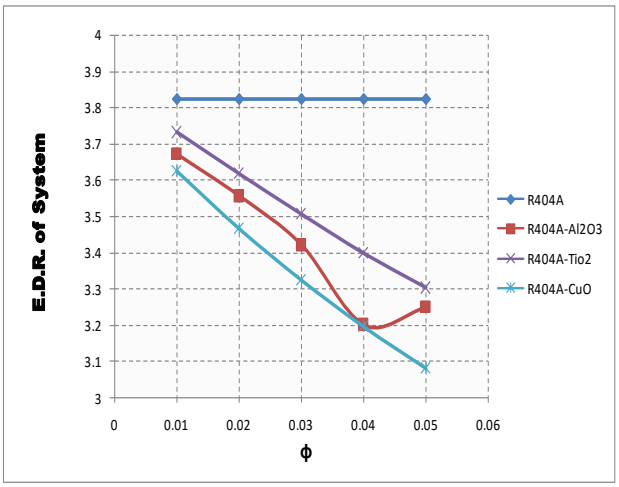

Figure: 3 Variation of Exergy destruction ratio with volume fraction (ϕ) of VCRS with R404A using different nano particles [24]

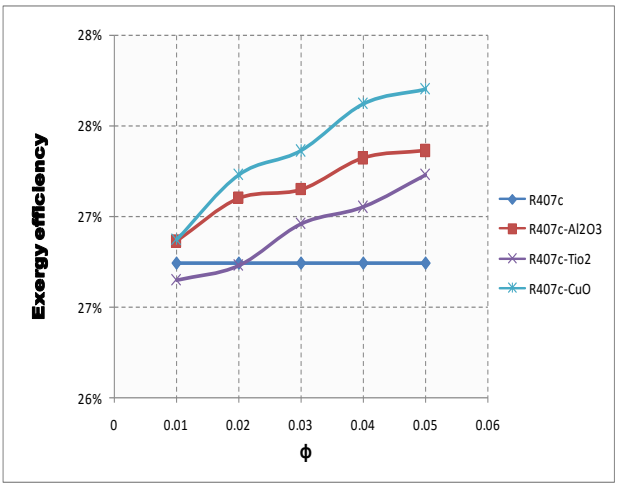

Figure: 5 Variation of Exergy Efficiency with volume fraction (ϕ) of Vapour Compression Refrigeration System with R407c using different nano particles [25]

Fig 1-3 shows that the Exergy .Destruction Ratio (EDR) of VCRS (i.e. which is a ratio of exergy losses in the system to the exergy of output is decreasing as volume fraction ratio is increasing) and will reduce by using nano fluid (nanoparticle based nano refrigerant) and thus improving second law efficiency

The Effect of nanoparticle volume fraction (ϕ) on the second law efficient using R134a as ecofriendly refrigerants in primary circuit of evaporator and with three type of nano materials of 0.000010(m) diameter is shown in Fig-4. As volume fraction Ratio is increasing from 0.01 to 0.05, the exergetic efficiency is increased.

Similarly The Effect of nanoparticle volume fraction (ϕ) on the second law efficiency using R407c and R404a as ecofriendly refrigerants in primary circuit of evaporator and with three type of nano materials of 0.000010(m) diameter is shown in Fig-5-6 respectively. As volume fraction Ratio is increasing from 0.01 to 0.05, the exergetic efficiency is also increasing sharply. The similar trend is also observed in case of using nano materials.

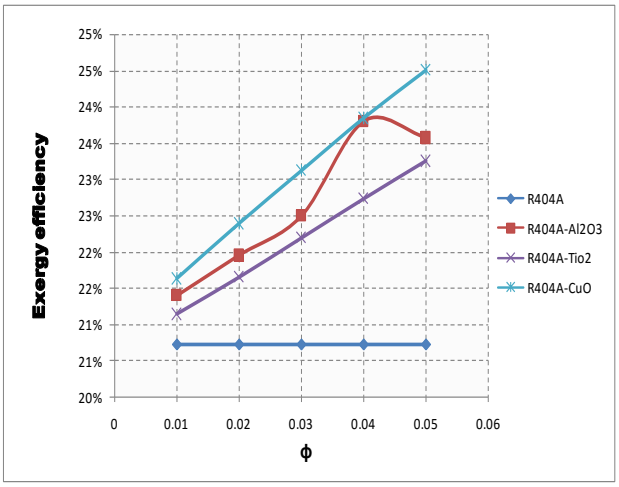

Figure: 6 Variation of Exergy Efficiency with volume fraction (ϕ) of Vapour Compression Refrigeration System with R404A using different nano particles [25]

It was observed that the 2nd Law efficiency will increase by using nano refrigerant. The 2nd law efficiency of vapour compression refrigeration system using nano refrigerant R134a/CuO is much higher than the other nano refrigerant having value approx 32%. A computational program has been developed to solve nonlinear equation of vapour compression refrigeration cycle Considering same geometric parameter of the VCRS model theoretical analysis has been done using EES software for nano fluid (nanoparticle mixed with R718) flowing in secondary circuit and eco friendly refrigerant in primary circuit of VCRS and Theoretical result of eight different ecofriendly refrigerants and using Al_2O_3 at 5 vol % nano fluid in secondary circuit as obtained from model is shown in Table-5.

Table 5 Enhancement in C.O.P in Vapour Compression Refrigeration System using Al_2O_3at 5 vol % nano fluid in Secondary circuit [26]

For Al_2O_3at volume fraction of 5 vol %		
Refrigerant	First law efficiency C.O.P.	% Improvement in first law efficiency (C.O.P.)
R134a	3.406	17.98%
R404A	3.0635	16.00%
R407c	3.110488	17.20%
R-152a	3.4102	18.00%
R-600	3.3402	17.20%
R-600a	3.466	19.90%
R-125	3.033016	14.80%
R-290	3.54312	19.70%

3. Conclusions

The research work presented in this thesis work following conclusion have been drawn.

1. Use of nanoparticles enhances thermal performance of vapour compression refrigeration system from 8 to 35 % using nano refrigerant in primary circuit.
2. Use of nanoparticles enhances the thermal performance of vapour compression refrigeration system from 7 to 19 % using nano fluid in secondary circuit.
3. Maximum enhancement in performance was observed using R134a/ Al_2O_3 nano refrigerant in primary circuit and water in secondary circuit of VCRS.
4. Lowest enhancement in performance was observed using R404Aa/TiO_2 nano refrigerant in primary circuit and water in secondary circuit of VCRS.

References

[1] Kapil Chopra .V.Sahni and R.S Mishra (2013)*Energetic and Exergetic Based Comparison Multiple Evaporators with Compound Compression and Flash Intercooler with Individual or Multiple Throttle Valves International Journal of Advance Research & Innovations (IJARI-Vol-1) ISSN No: 2347-3258, pp-73-81.

[2] Kapil Chopra .V.Sahni .R.S Mishra*(2014) "Thermodynamic Analysis of Multiple evaporators vapour compression Refrigeration Systems with R-410a, R290, R1234yf, R502, R404a, R152a and R134a " International Journal of Air conditioning and Refrigeration (Ms. No: IJACR-D-13-00043R1) , Paper Vol-22 No-1, 145-158.

[3] Choi, S. U. S. (1995). Enhancing thermal conductivity of fluids with nanoparticles, in *Developments and Applications of Non-Newtonian Flows* FED–31/MD-66:99–105.

[4] Jwo et.al, 2009. Effect of nano lubricant on the performance of Hydrocarbon refrigerant system. J. Vac. Sci. Techno. B, Vol.27, No. 3, pp. 1473-1477.

[5] K.S. Hwang, S.P. Jang, S. U. S. Choi, (2009) Flow and convective heat transfer characteristics of water-based Al_2O_3 nanofluids in fully developed laminar flow regime, Int. J. Heat Mass Transf. 52 193-199.

[6] Joaquin Navarro, Francisco, Angel, (2013). Experimental analysis of internal heat exchanger influence on vapour compression system performance working with R1234yf as drop in replacement of R134a. Applied thermal Engineering, 59, 153-161.

[7] Murshed S. M. S., K. C. Leong, and C. Yang (2005). Enhanced thermal conductivity of TiO_2-water based nanofluids, *Int. J. Therm. Sci.*, 44: 367–373.

[8] Hao Peng et.al., (2010). Nucleate pool boiling heat transfer characteristics of refrigerant/oil mixture with diamond nano parti cles. International Journal of Refrigeration, Vol.33, pp. 347-358.

[9] Henderson et al. (2010) Experimental analysis on the flow boiling heat transfer of R134a based nanofluids in a horizontal tube. IJHMT , Vol. 53, pp. 944-951.

[10] Xuan, Y., and Q. Li (2003). Investigation on convective heat transfer and flow features of nanofluids, *J. Heat Transfer*, 125: 151–155.

[11] Wang RX, et.al. [2003.] A refrigerating system using HFC134a and mineral lubricant appended with N- TiO_2(R) as working Fluids. In: Proceedings of the 4th international symposium on HAVC, Tsinghua University.

[12] Lee K, Hwang YJ, [2009]Performance evaluation of nano-lubricants of fullerene nanoparticles in refrigeration mineral oil. Curr Appl Phys;9:128–131.

[13] Wien, D., and Y. Ding (2004). Experimental investigation into convective heat transfer of nanofluids at the entrance region under laminar flow conditions, *Int. J. Heat Mass Transfer*, 47: 5181–5188.

[14] I.M. Mahbubul , A.Saadah (2015) Thermal performance analysis of Al_2O_3 R134a nanorefrigerant , international journal of heat and mass transfer 85 1034-1040.

[15] Y. He, (2007) Heat transfer and flow behavior of aqueous suspensions of TiO_2 nanoparticles (nanofluids) flowing upward through a vertical pipe, Int. J. Heat Mass Transf. 50 2272-2281.

[16] D.P. Kulkarni, (2008) Convective heat transfer and fluid dynamic characteristics of SiO_2-ethylene glycol/water nanofluid, Heat Transf. Eng. 29 (12) 1027-1035.

[17] S.Z. Heris, S.G. Etemad, M.N. Esfahany(2006), Experimental investigation of Al_2O_3 nanofluids laminar flow convective heat transfer, Int. Commun. Heat Mass Transf. 33 529535.

[18] Bobbo S. et.al, (2010). Influence of nanoparticles dispersion in POE oils on lubricity and R134a solubility. International Journal of Refrigeration, Vol.33, pp. 1180-1186.

[19] Lee K, Hwang YJ, Cheong S, Kwon L, Kim S, Lee J. Performance evaluation of nano-lubricants of fullerene nanoparticles in refrigeration mineral oil. Curr Appl Phys 2009;9:128–131.

[20] R.S. Mishra (2015) Irreversibility Reduction in Vapour Compression Refrigeration Systems Using Al_2O_3 Nano Material Mixed in R718 as Secondary Fluid s" International journal of Advance Research and Innovation Vol-3, Issue 2 (June-2015), pp. 321-327.

[21] R. S. Mishra (2015) "Performance Evaluation of Ecofriendly Refrigerants in the Low Temperature Circuit in Terms of First Law and Second Law Efficiency of Three Stages Cascade Vapour Compression Refrigeration of Biomedical Applications" International journal of Advance Research and Innovation Vol-3, Issue 2 (June-2015), pp. 332-339.

[22] R.S.Mishra (2015) Methods for Improving Thermodynamic Performance of Vapour Compression Refrigeration Systems Using Nano Mixed Ecofriendly Refrigerants in Primary Circuit and Comparsion with Nano Particles Mixed Wih R718 Used in Secondary Evaporator Circuit and Ecofriendly Refrigerants in Primary Circuit for Reducing Global Warming and Ozone Depletion, International journal of Advance Research and Innovation Vol-3, Issue 2 (June-2015), pp. 433-439.

[23] R. S. Mishra(2015) Modeling of Natural Convection Non Reversible Single Pass Pressurized and Non Pressurized Solar Hot Water Systems for Domestic Applications" International journal of Advance Research and Innovation , ISSN. No:2347 – 3258, Vol-3, Issue 3 (Sept-2015), pp. 451- 458.

[24] R. S. Mishra(2015) " Energy-Exergy Performance Comparison of Vapour Compression Refrigeration Systems using Three Nano Materials Mixed in R718 in the Secondry Fluid and Ecofriendly Refrigerants in the Primary Circuit and Direct Mixing of nano Materials in the Refrigerants" International journal of Advance Research and Innovation Vol-3, Issue 3 (Sept-2015), pp. 471-477.

[25] R. S. Mishra(2015) "Vapour Compression Refrigeration Technology for Sustainable Development" International journal of Advance Research and Innovation Vol-3, Issue 4 (Dec-2015)

[26] R. S. Mishra (2015) Thermodynamic performance comparison using HFO-1234yf and hfo-1234ze in the high temperature cascade refrigeration systems and ecofriendly refrigerants in low temperature applications, International journal of Advance Research and Innovation Vol-3, Issue 4 (Dec-2015).

[27] R. S. Mishra(2015) Energy-exergy performance comparison of vapour compression refrigeration systems using three nano materials mixed in r718 as secondry fluid and r-1234yf and r-1234ze ecofriendly refrigerants in the primary circuit International journal of Advance Research and Innovation Vol-3, Issue 2 (June-2015), pp. 321-327

[28] R.S. Mishra (2013) "Irriversibility Analysis of Multi-Evaporators Vapour Compression Refrigeration Systems Using New and Refrigerants: R134a, R290, R600, R600a, R1234yf,R502, R404a and R152a and R12, R502" International Journal of Advance Research & Innovations International Journal of Advance Research & Innovations (IJARI-Vol-1) , ISSN No: 2347-3258 , PP-180-193.

ISSN: 0974-5823 Vol. 7 No. 4 April, 2022

International Journal of Mechanical Engineering

Multi-label Classification Methods and Challenges

Raghav Agrawal[1], Rohit Sah[2]

[1,2]Department of Applied Mathematics, Delhi Technological University, Delhi, India

Abstract

Conventional classification problems usually deal with classification of a single label from one or more (single-label) classes or two or more (multi-class) classes. But when an instance can be associated with multiple classes simultaneously, it is known as Multi-label Classification. With more and more use of machine learning algorithms in the real world applications, the need for multi-label classification has also arisen. This has caused in development of a range of multi-label classification algorithms.Keeping this in mind, with this study we aim to give an overview label classification algorithms. Our goal is to provide a comprehensive study of challenges faced during the training of classifier.

Keywords–Algorithm Adaptation,Dimensionality Reduction, Label Drifting,Multi-label, Problem Transformation

1. INTRODUCTION

Multi-label classification is the problem where each instance may be associated with multiple labels. The problem of single-label classification is the one where each instance is associated with a single label selected from a finite set of labels. When there are at least two labels in the label set for single-label classification, it is known as multi-class classification. It can be said that multi-label classification is a generalization of multi-class classification wherein there is no limitation to the number of labels which are selected for an instance and instead it produces a ranking for the labels.

Nowadays, with most of the people having access to the internet, everyone has a different profile on the internet which is used for showing relevant ads and targeting on social media. These user or customer profiles are made with the help of multi-label classification. For example, if an iPhone user is also a cricket fan, he can be targeted with ads of iPhone accessories with cricket players on it.

Multi-label classification can be divided mainly into two categories:

(a) Algorithm Adaptation Methods
(b) Problem Transformation Methods

The major challenges of classifier training discussed are:

a) Dimensionality
b) Label Drifting
c) Label Imbalance
d) Data cleaning
e) Label dependency
f) Label Uncertainty

The mounting number of labels and interdependencies among them make multi-label problems difficult to resolve. Therefore, there is a pressing need to comprehend and handle this issue. This paper talks about different algorithm adaptation and problem transformation methods. It further talks about usual challenges faced when doing multi-label classification and also tried to bring light to some related research.

2. MULTI-LABEL LEARNING METHODS

With so many technological developments in the recent years. Multi-label classification can be done using many methods. They can be divided mainly into two categories:

(a) Algorithm Adaptation Methods: An adaptation of existing single-label methods.

(b) Problem Transformation Methods: A conversion of multi-label problems to one or more single label problems.

2.1 Algorithm Adaptation Methods

Algorithm Adaptation methods are multi-label methods that tailor already known algorithms for the task of multi-label learning.

2.1.1 Decision Trees

Multi-label C4.5 (ML-C4.5) [1] is a variation of famous C4.5 algorithm. This was done by modifying formula for calculating entropy. This is done by calculating sum of entropy of the labels recursively. This uses the concept of hierarchical multi-label classification.

2.1.2 Boosting

This refers to tree-based boosting, which is based on ADABOOST. ADABOOST.MH and ADABOOST.MR [2] are extensions of ADABOOST for multi-label learning. ADABOOST.MR finds a hypothesis to rank the labels at top, while ADABOOST.MH minimizes hamming loss. Its goal is to improve loss functions, but it is prone to noisy data.

2.1.3 Lazy Learning

Many methods exist which are based on k-Nearest Neighbor (i.e. Lazy Learning). ML-kNN [3] is an extension of kNN for multi-label data. It is based on maximum a posteriori principle. This method follows the concept of error function in backpropagation.

2.1.4 Support Vector Machines

This a ranking approach [4] used for multi-label learning that is based on SVMs. Their cost function is average fraction of incorrectly ordered pairs of labels. It uses a maximum margin ranking strategy. MLTSVM [5] is a recently proposed algorithm which uses a nonparallel hyperplane.

2.2 Problem Transformation Methods

Problem transformation methods are multi-label methods that aim to convert multi-label problems to one or more single-label problems. Since, there exists a lot of machine learning algorithms for single-label problems. Finally, the results of single-label problems are again transformed to multi-label.

2.2.1 Binary Relevance

Binary Relevance (BR) [6] is a type of problem transformation algorithm. It considers prediction of each label as an independent binary classification task. It is a one-against-all strategy. Thus, BR builds binary classifiers, one for each different label. This method also has a shortcoming as it doesn't consider correlation amongst the labels.

2.2.2 Label Power-set

Label Power-set is to group label sets into single-labels to form single-label problems. The set of single-labels represent different label subsets from multi-label representation. This gets rid of the problem of label independency in binary relevance method. Calibrated Label Ranking (CLR) [7] is based on popular pair-wise method for multi-label classification.All classifiers are trained using first label instances as positive example and second label's as negative. Majority voting algorithm is instinctively used to combine the classifiers.

2.2.3 PT Methods

To demonstrate we will use Table 1 as dataset. It consists of four instances and four labels.

TABLE 1 Multi-label Dataset

Instance	L1	L2	L3	L4
1	X			X
2			X	X
3	X			
4		X	X	

Two simple problem transformations methods convert the learning problem into single-label classification problems [8]. The first one is PT1 in which one of the labels is randomly selected in a multiple label instance and the rest are discarded (shown in Table 2) and the second one is PT2 in which it drops every instance of the dataset which is multi-label (shown in Table 3). Both of these reject a lot of information and hence, affects the accuracy of the result.

TABLE 2 Transformed Dataset after PT1

Instance	L1	L2	L3	L4
1	X			X
2				X
3	X			
4		X		

TABLE 3 Transformed Dataset after PT2

Instance	L1	L2	L3	L4
3	X			

The third method, PT3, takes the relationship of the labels into consideration. It uses each set of label as a single label as shown in Table 4. It has been used by [8] and [9] in the past.

TABLE 4 Transformed Dataset after PT3

Instance	L1	L1 ∧ L4	L3 ∧ L4	L2 ∧ L3
1		X		
2			X	
3	X			
4				X

The fourth method, PT4, considers binary classifier for each label. This transforms the original dataset into multiple datasets that have all the instances of the original dataset.

TABLE 5 Transformed Dataset after PT4

Instance	L1	¬L1
1	X	
2		X
3	X	
4		X

Instance	L2	¬L2
1		X
2		X
3		X
4	X	

Instance	L3	¬L3
1		X
2	X	
3		X
4	X	

Instance	L4	¬L4
1	X	
2	X	
3		X
4		X

Another problem transformation method, PT5, converts an instance to multiple instances with same instance and different labels[10]. This uses a distribution classifier that outputs a distribution for all labels.

TABLE 6 Transformed Dataset after PT5

Instance	Label
1	L1
1	L4
2	L3
2	L4
3	L1
4	L2
4	L3

3. CHALLENGES

With continuous development in the field of multi-label methods, various problems are arising. Numerous solutions have been proposed which are based on assumptions. The nature of the dataset also contributes to the accuracy of the result. The major challenges faced are listed below.

3.1 Dimensionality

Dimensionality represents the number of features in a dataset.Dimensionality Reduction [11] aims to remove insignificant features for a clearer and better understanding of the data. This allows us to accentuate more relevant features of the data. There are many unsupervised methods for reducing dimensionality of high-dimensional data. These include Principal Component Analysis (PCA), Linear Discriminant Analysis (LDA), Support Vector Machines (SVM), Singular Value Decomposition (SVD), Independent Component Analysis (ICA), etc. A drawback of unsupervised methods is that they ignore information in labels.

3.2 Data Cleaning

There are a number of concerns that need to be addressed during the data cleaning. For example, data of job searchers, who are requested to mention their talents in a job recruitment application. Regardless of which domain their skills pertain to, every seeker enters them. Text analytics, tokenization, stemming, and stop word removal are required for this type of multi-label data. This can lead to the loss of crucial information and a reduction in data quality.

3.3 Label Dependency

When the data has a lot of labels, investigating correlations between labels may help to minimize complexity. Mainly, two types of multi-label data dependence have been recognized [12]. Conditional label dependency represents the likeliness of labels to occur together given the features of an instance. Unconditional (or marginal) label dependency represents the likeliness of labels to occur together independent of an instance. Since, multi-label classifier process multiple labels simultaneously, it affects the performance of classifier and introduces loss. A way to minimize loss by linking label dependencies [12] has been proposed.

3.4 Label Uncertainty

There is a lot of uncertainty in labels in real-world applications. For example, in a database which stores different skills of users, every user can have a different set of skills which can result into creation of multiple new labels. The major challenge is the preprocessing and categorization for each new label.

3.5 Drifting

Learning algorithms are usually used in dynamic environments in real world where the data is continuously growing. In such a case, the target concept changes over time, this is known as drifting. According to [13], drifting is one of the biggest challenges for a classifier.A method for drift detection in multi-label data streams using label grouping andentropy has been proposed by [14].

3.6 Data Imbalance

Data Imbalance is a common problem in which some labels with lesser frequency have higher importance than the labels which have lower frequency. This has a great effect on the performance of the classifier. An approach was proposed by [15] to solve this, in which they were able to reduce hamming loss but not completely eliminate it. In real world, most of such data is gathered by sensors, on which substantial research is going on to tackle these challenges.

4. CURRENT TRENDS

4.1 Active Learning

Labelling multi-label data manually is a time-consuming, impractical and laborious task. Active learning is a type of learning in which training dataset is kept to minimum and only valuable data points are selected. By this, it intends to reduce label cost and efforts.Mainly, active learning is used single label problems. Such a system consists of a teacher (or oracle), which is the source of data, and a learner. There are mainly three active learning methods:

a) Membership query synthesis
b) Pool-based sampling
c) Stream-based selective sampling.

4.2 Multi-view Multi-label Learning

Multi-view multi-label dataset has instances with multiple views and multiple labels. Since there is lot of multi-label data easily accessible, it needs to be analyzed from using different views for best analysis. Multi-view learning methods [16] can be generally classified into three major categories:

a) Co-training
b) Subspace Learning
c) Multiple Kernel Learning

5. CONCLUSION

In this paper, we discussed several multi-label classification methods. The general challenges faced in a scenario of multi-label classification are also discussed in detail. We also highlighted the new methods which are becoming a need now for superior analysis in multi-label classification. The classification of data can become convoluted in real world application since the data is imbalanced and incomplete. Dimensionality reduction is also a very challenging task for large dataset.

REFERENCES

[1] A. Clare and R. King, "Knowledge Discovery in Multi-label Phenotype Data", Principles of Data Mining and Knowledge Discovery, pp. 42-53, 2001. Available: 10.1007/3-540-44794-6_4.

[2] R. Schapire and Y. Singer, Machine Learning, vol. 39, no. 23, pp. 135-168, 2000. Available: 10.1023/a:1007649029923.

[3] M. Zhang and Z. Zhou, "ML-KNN: A lazy learning approach to multi-label learning", Pattern Recognition, vol. 40, no. 7, pp. 2038-2048, 2007. Available: 10.1016/j.patcog.2006.12.019.

[4] "A kernel method for multi-labelled classification", Advances in Neural Information Processing Systems 14, 2002. Available: 10.7551/mitpress/1120.003.0092.

[5] W. Chen, Y. Shao, C. Li and N. Deng, "MLTSVM: A novel twin support vector machine to multi-label learning", Pattern Recognition, vol. 52, pp. 61-74, 2016. Available: 10.1016/j.patcog.2015.10.008.

[6] G. Tsoumakas and I. Katakis, "Multi-Label Classification", International Journal of Data Warehousing and Mining, vol. 3, no. 3, pp. 1-13, 2007. Available: 10.4018/jdwm.2007070101.

[7] S. Park and J. Fürnkranz, "Efficient Pairwise Classification", Machine Learning: ECML 2007, pp. 658-665, 2007. Available: 10.1007/978-3-540-74958-5_65.

[8] M. Boutell, J. Luo, X. Shen and C. Brown, "Learning multi-label scene classification", Pattern Recognition, vol. 37, no. 9, pp. 1757-1771, 2004. Available: 10.1016/j.patcog.2004.03.009.

[9] S. Diplaris, G. Tsoumakas, P. Mitkas and I. Vlahavas, "Protein Classification with Multiple Algorithms", Advances in Informatics, pp. 448-456, 2005. Available: 10.1007/11573036_42.

[10] G. Tsoumakas and I. Katakis, "Multi-Label Classification", International Journal of Data Warehousing and Mining, vol. 3, no. 3, pp. 1-13, 2007. Available: 10.4018/jdwm.2007070101.

[11] W. Siblini, P. Kuntz and F. Meyer, "A Review on Dimensionality Reduction for Multi-label Classification", IEEE Transactions on Knowledge and Data Engineering, pp. 1-1, 2019. Available: 10.1109/tkde.2019.2940014.

[12] K. Dembczyński, W. Waegeman, W. Cheng and E. Hüllermeier, "On label dependence and loss minimization in multi-label classification", Machine Learning, vol. 88, no. 1-2, pp. 5-45, 2012. Available: 10.1007/s10994-012-5285-8.

[13] E. Spyromitros-Xioufis, M. Spiliopoulou, G. Tsoumakas and I. Vlahavas, "Dealing with concept drift and class imbalance in multi-label stream classification", in IJCAI'11: Proceedings of the Twenty-Second international joint conference on Artificial Intelligence, 2011, pp. 1583-1588.

[14] Z. Shi, Y. Wen, C. Feng and H. Zhao, "Drift Detection for Multi-label Data Streams Based on Label Grouping and Entropy", 2014 IEEE International Conference on Data Mining Workshop, 2014. Available: 10.1109/icdmw.2014.92.

[15] L. Li and H. Wang, "Towards Label Imbalance in Multi-label Classification with Many Labels", 2016. Available: https://arxiv.org/abs/1604.01304. .

[16] P. Pant, A. SaiSabitha, T. Choudhury and P. Dhingra, "Multi-label Classification Trending Challenges and Approaches", Advances in Intelligent Systems and Computing, pp. 433-444, 2018. Available: 10.1007/978-981-13-2285-3_51.

Hindawi
Mathematical Problems in Engineering
Volume 2022, Article ID 5348017, 22 pages
https://doi.org/10.1155/2022/5348017

Research Article

Optimal Sizing of Hybrid Energy System Using Random Exploratory Search-Centred Harris Hawks Optimizer with Improved Exploitation Capability

Priyanka Anand,[1] **Vikram Kumar Kamboj**,[2,3] **Muhannad Alaraj**,[4] **Mohammad Rizwan**,[5] **and Isaka J. Mwakitalima**[6]

[1]*Department of Electronics and Communication Engineering, Bhagat Phool Singh Mahila Vishwavidyalaya, Khanpur Kalan, Sonipat 131305, India*
[2]*School of Electronics and Electrical Engineering, Lovely Professional University, Phagwara, Punjab 144402, India*
[3]*Schulich School of Engineering, University of Calgary, Alberta, Canada*
[4]*Department of Electrical Engineering, College of Engineering, Qassim University, Buraydah 52571, Qassim, Saudi Arabia*
[5]*Department of Electrical Engineering, Delhi Technological University, Delhi 10042, India*
[6]*Department of Electrical and Power Engineering, College of Engineering and Technology, Mbeya University of Science and Technology (MUST), 131 Mbeya, Tanzania*

Correspondence should be addressed to Isaka J. Mwakitalima; mwakitalimaisaka0@gmail.com

Received 23 August 2021; Revised 6 April 2022; Accepted 7 April 2022; Published 30 May 2022

Academic Editor: Raffaele Carli

Copyright © 2022 Priyanka Anand et al. This is an open access article distributed under the Creative Commons Attribution License, which permits unrestricted use, distribution, and reproduction in any medium, provided the original work is properly cited.

Due to the depletion of traditional energy resources, emissions of greenhouse gases, climate change, etc., renewable energy resources (RER) based power generation is becoming the main source of the present and future power sector. The major RERs, including solar, wind, and small hydro, may provide reliable and sustainable solutions in the smart grid environment. Solar and wind energy-based power generation is more prevalent but varies in nature and is not even very predictable very efficiently. Therefore, it has become necessary to integrate two or more RER and develop a hybrid energy system (HES). The HESs provide a cost-effective and reliable power supply with reduced and/or almost negligible greenhouse gas emissions as well. Due to economic and power reliability concerns, the optimal sizing of components is necessary for the development of an optimum HES. In recent years, metaheuristic evolutionary algorithms have been widely used for optimal sizing of HES. Harris hawk's optimizer (HHO) is a recently devised metaheuristics search method that has the ability to discover global minima and maxima. However, due to its weak exploitation capacity, the basic HHO algorithm's local search is pretty slow and has a slow rate of convergence. Thus, to boost the exploitation phase of HHO, a new approach, random exploratory search centered Harris hawk's optimizer (hHHO-ES), has been developed in the present work for optimal sizing of HES. The suggested approach is validated and compared to existing optimization approaches for a variety of well-known benchmark functions, including unimodal, multimodal, and fixed dimensions. Following this, it is used to develop HES, which will be capable of providing power to remote areas where grid supply is scarce. The objective function is formulated using net present cost (NPC) as a prime function under a set of constraints such as bounds of system components and reliability. The obtained results are compared with those from harmony search (HS) and particle swarm optimization (PSO) and found to be better.

1. Introduction

Reliable and sustainable power generation plays a vital role in the power sector and economy of any nation, particularly developing countries like India. Furthermore, the sustainable power sector is necessary for the survival of modern society in terms of improving socio-economic growth, increasing comfort levels, and essential services for humanity

like health care and sanitation. It has been stated that the shortage of energy that is ubiquitous in many developing nations, particularly in India, is heavily indicative of poor socio-economic development. This is often prevalent in rural areas of the country. In this regard, renewable energy resources (RER) are becoming popular around the world for various reasons, like depleting conventional sources of energy, environmental concerns, etc. Furthermore, RER will provide versatility in the power sector [1–3].

RER offers several advantages, but they also have some drawbacks. The fundamental downside of these resources, particularly wind and solar, is that they are unpredictable and intermittent. The most viable response to this challenge is a hybrid energy system (HES), which is a system that combines multiple RER to improve system efficiency and energy balance in off-grid or grid-linked scenarios [4–6]. Because solar irradiation and wind speed are affected by weather conditions, off-grid solar or wind-based HES typically require a storage device like a battery as well as a backup supply. Despite the benefits of HES, the current cost of these systems limits their widespread implementation. As a result, significant attempts are being made to lower the cost of HES through optimal design, particularly optimal component sizing [7–11], and a few of them are outlined in the forthcoming paragraphs.

Sen and Bhattacharyya have proposed the best HES involving RER such as solar photovoltaic (SPV), bio-diesel, wind, and small-scale hydropower to serve Palari village's electricity needs in Chhattisgarh, India. A comparison of off-grid and grid extension was made by employing hybrid optimization of multiple energy resources (HOMER). In terms of cost-effectiveness and environmental sustainability, the off-grid HES was shown to be more acceptable [12]. Khan et al. used HOMER to investigate several configurations of the SPV/wind/diesel generator (DG)/battery HES for communication applications in Punjab, India. The SPV/wind/DG/battery HES was found to be the most economical, with the lowest cost of energy (CoE) across several configurations [13]. Dhass and Harikrishnan examined the HES of SPV/wind/biomass for rural electrification in terms of life cycle cost [14]. Ho et al. used RER containing solar and biomass resources to create a self-sustaining tiny town. A mixed-integer linear programming-based approach has been created to design HESs [15]. Garrido et al. applied HOMER to analyse the performance of a SPV/biomass HES in Nampula, Mozambique, using cashew shell as a fuel source. It was revealed that the proposed system had a lower CoE than the SPV-DG and the traditional DG. The proposed system had a CoE of \$0.33/kWh [16].

Sharafi and Mekkawy employed particle swarm optimization (PSO) for optimising HES, including the wind turbine, SPV panel, DG, fuel cell (FC), battery, electrolyser, and hydrogen tank. An approach based on e-constraint was used to reduce the total cost of the system, fuel emissions, and unmet load. A sensitivity analysis has been performed to assess the sensitivity of the outcomes to the input parameters. The total cost of the system is more affected by the amount of CO_2 that can be released than by other factors [17]. Optimal sizing of a grid-linked SPV/wind/DG/battery HES has been carried out by Ogunjuyigbe et al. using a genetic algorithm (GA) to meet the demand for electricity in a residential building. In this work, the multiobjective problem is addressed using two objectives: life cycle cost and emissions. Several configurations of system components were examined, and it was found that the configuration SPV/wind/DG/battery is the most suitable for supplying the load [18]. Nadjemi et al. proposed an optimal design of grid-connected HES using SPV, wind and battery using the cuckoo search (CS) approach. The multiobjective problem is addressed according to the cost and environmental objectives. It is revealed that the price of electricity has a massive effect on reducing costs [19]. Eteiba et al. have explored the feasibility of renewable energy-based HES of SPV/biomass/battery bank to generate a small village's needed electricity. Four specific metaheuristic methods have been used to achieve optimum sizing. It has been found that, among the other examined algorithms, the firefly algorithm (FA) achieved the minimum execution time with the greatest performance [20]. Sufyan et al. also proposed FA for optimising an isolated microgrid's economic scheduling and battery capacity. The proposed method was also compared with artificial bee colony (ABC), harmony search (HS), and PSO and observed to have a 50% decline in operating cost [21].

Khiareddine et al. performed the techno-economic analysis of an off-grid system consisting of SPV, wind, and hydrogen with battery. Achieved results show the significant role of integrating RER in minimising the cost of the system. It has also been revealed that the utilisation of hydrogen chain increases the life of the battery [22]. Jamshidi and Askarzadeh carried out the multiobjective design of HES using SPV, FC, and DG to electrify the off-grid community in the existence of load, operating reserve, and solar energy inconsistencies. The multiobjective crow search algorithm (MOCSA) was applied to minimise the system cost and loss of power supply probability (LPSP). The influence of various parameters, such as cost of FC system equipment, fuel price, and cost of emissions, on the sizing results was explored. It is observed that integrating hydrogen energy technology decreases the system cost [23]. Jiang et al. proposed a strategy for energy management and sizing of the system components for hybrid power systems using FC, battery, and supercapacitor. To achieve the goal, algorithms have been proposed for achieving it at a cost. It is observed that optimal strategies greatly minimise energy consumption along with battery and FC deterioration [24].

To optimise the size of an off-grid HES consisting of a collection of SPVs, FC, and DG, as well as electrolyzers and hydrogen tanks, Ghaffaria and Askarzadeh devised an upgraded crow search algorithm (CSA). Total net present cost (NPC) was considered as a prime function minimised by the constraints of renewable energy penetration and LPSP. It has been observed that the CSAadaptive-AP provides more accurate results than the original CSA, PSO, and GA [25]. Tong et al. applied the salp swarm algorithm (SSA) to optimise the size of grid-linked HES associated with a pumped-storage system. Various configurations of HES have been examined and found to be the optimal solution.

The results revealed that the power exchange with the grid can be minimised by HES [26]. Sanjay et al. used the PSO and biogeography-based optimization (BBO) to optimise the size of HES both with and without the load shifting procedure. The HES, which consists of SPV, microhydro (MHP), and storage batteries, is thought to meet the needs of distant populations in India's western Himalayas. The accuracy and utility of the proposed method were demonstrated by testing the outcomes of these algorithms with HOMER [27].

Alturki et al. were the first to use the supply-demand-based optimization (SDO) approach to tackle the challenge of designing an ideal HES with SPV, wind turbines, batteries, and DGs to meet the load requirements of an off-grid community in Saudi Arabia. Three HES situations were investigated in this study, and the most effective option was discovered in terms of maximising HES reliability while lowering costs. In addition, the GA, PSO, grey wolf optimization (GWO), big-bang-big-crunch (BBBC) algorithm, flower pollination algorithm (FPA), and grasshopper optimization algorithm (GOA) were used to make a comparison in order to assess the performance of the SDO approach for the optimal design issue with the goal of optimising dependability while lowering costs. The optimization results show that the suggested SDO method outperforms other algorithms in terms of performance [28]. Alturki and Awwad built and optimised a stand-alone SPV/wind turbine/biomass/pump hydrostorage HES based on techno-economic and environmental criteria to meet electrical load demand while minimising CoE. The whale optimization algorithm (WOA), PSO, and FA, are three distinct optimization techniques proposed in this work for sizing and decreasing the CoE. The results of these algorithms are compared to see which is the most efficient, and the one with the lowest CoE is picked using statistical analysis. According to the findings, the suggested SPV/wind turbine/biomass/pump hydrostorage HES is both ecologically and economically feasible. Meanwhile, the findings showed that, when compared to other current systems, a pump-hydro energy storage system might enhance the use of RER [29].

A modified cuckoo search (MCS) optimization technique is proposed by Eltamaly and Alotaibi for sizing HES components in view of minimising the CoE and loss of load probability (LOLP). The suggested MCS is compared to ten benchmarking optimization approaches. According to the results of this study, the MCS is more accurate and takes less time to do than other systems [30]. Eltamaly et al. optimise a reverse osmosis desalination system powered by a RER to provide a source of pure water to Arar City, Saudi Arabia. Wind turbines, SPVs, batteries, and a water tank, as well as their control systems and power conditioners, are all included in the planned HES. For this problem, the bat algorithm (BA), PSO, and social mimic optimization (SMO) were employed as optimization strategies and compared. When compared to these optimization techniques, the results from the suggested system demonstrated the efficacy of using an RER for ingesting a reverse osmosis desalination power plant in Arar city, as well as the fact that the BA provides the most optimal results with the lowest execution time [31]. Eltamaly et al. use three distinct optimization strategies to size the HES depending on technological and economic goals using the unique demand response (DR) method. The results revealed that the BA is the quickest and also the most trustworthy way to find the lowest cost and best component size. It does this in just five iterations, whereas the PSO and SMO take eight and forty-five iterations, respectively [32].

According to the above listed literature, researchers applied either software tools or traditional optimization approaches for performance evaluation. However, as compared to other existing optimization methods, software tools have severe drawbacks, including single function minimization, inflexible, black box coding, and demand more computational effort. Several works in HESs, however, have been recognized, in which many researchers have offered various conventional and evolutionary strategies to achieve the optimal size of the components used in HESs. Many studies have been carried out by employing traditional methodologies like graphical construction, iterative, linear programming, and the trade off approach [33–36]. The dilemma with traditional methods is that they generally trap in local minima. Numerous metaheuristic evolutionary algorithms, such as the GA, PSO, HS, simulated annealing (SA), ant colony optimization (ACO), bacterial foraging algorithm (BFA), artificial bee swarm optimization (ABSO), mine blast algorithm (MBA), BBO, GWO, and others, have been deployed in various HESs to address these challenges. In recent years, a new trend has emerged in which investigators have begun to use metaheuristic evolutionary algorithms to determine the optimal sizing of HESs [37–42].

Optimization is a vast field of research and is progressing at a breakneck pace. Researchers are continuously working on a variety of problems, implementing various types of new optimization approaches on a lot of issues and are obtaining promising results. The work is lucrative because it allows you to see the most recent algorithms, as well as algorithms in hybrid form, to minimise any types of drawbacks in the present. Several innovative optimization approaches have been devised over the last few decades to increase system performance with multiple motives. The search strategy, which comprises intensification (exploitation stage) and diversification (exploration stage), is a common element of these metaheuristics algorithms. Local minima stagnation, on the other hand, is a key flaw in these heuristic methods, culminating in premature convergence.

A Harris hawk's optimizer (HHO) metaheuristics search method invented by Heidari *et al.* has the ability to seek the maxima as well as minima in a global region [43]. However, due to its weak exploitation capacity, the basic HHO algorithm's local search is slow and has a sluggish convergence rate. The exploitation stage of HHO has been improved in the present work by developing a hybrid version of the HHO using the random exploratory search (RES) algorithm, which is called the hybrid Harris hawk's random exploratory search algorithm (hHHO-RES).

HHO's key feature is that it uses four tactics to imitate collective hunting: encircling, surprise pouch, and soft and harsh besiege. HHO is a rapid, simple, and effective

approach for solving complicated optimization problems such as continuous, discrete, and unconstrained and constraint issues. The main benefits of HHO are its ease of use, capacity to safely escape local minima stasis, better performance, operational flexibility, and ease of adaptation [44,45]. However, there are some limitations to HHO that go along with all of these benefits. The risk of being caught in local minima while tackling optimization-related problems in large multimodal as well as composition optimization issues, failure to maintain a healthy balance between local and global search, and feeble performance in multidimensional problems are the significant drawbacks. This is in conformity with the results of Heidari et al. [43], who found that HHO performs poorly in a few multimodal as well as unimodal benchmark functions under certain conditions.

Nonetheless, because no single strategy is enough to solve all types of optimization-related problems, the No Free Lunch theorem leads to additional refinement and improvements. Multiple HHO variants have been devised by researchers in a short period of time and have found wide applications in tackling optimization-related problems in a variety of disciplines, including engineering design, drug design, manufacturing problems, image segmentation, pattern recognition, networking, and power quality. Several new HHO optimizer variations have been developed recently. These hybrid variations are used to handle a variety of optimization-related problems, including both global and numerical optimization. One of the hybrid forms of HHO is the intensified Harris hawk's optimizer (IHHO) [46], which is utilised to tackle many sorts of interdisciplinary engineering design challenges. The HHO-IGWO optimizer is a version of the HHO optimizer. It has been evaluated on CEC2005 benchmarks [47], and quasireflected HHO is used to solve optimization problems throughout the global search area [48]. In addition, the dynamic HHO in combination with the mutation mechanism [49] is taken into account to tackle optimization-related challenges in a variety of domains.

It has been revealed from the literature that the conventional HHO has poor exploration search capability and lacks exploration of local search space [43]. Thus, to step up the global search process of the current HHO and to keep the local search space, the devised algorithm in the present work aims to boost the exploitation process of the current optimizer. Taking into account the efficacy of metaheuristics algorithms and the limitations of conventional HHO, the hybrid version of the HHO is therefore developed using the random exploratory search (RES) algorithm and is called the hybrid Harris hawk's random exploratory search (hHHO-RES) algorithm.

The aim of the present work is to provide a new approach based on a nature-inspired hybrid optimization technique, hHHO-RES. The key idea of the proposed optimization approach is inspired by the cooperative natural behaviour of the brainiest birds, called Harris hawk's, who escape or resist the nature of their prey (rabbits). The proposed approach is validated for various well-known standard benchmarks, namely, unimodal, multimodal, and fixed dimensions, and also compared with existing optimization approaches. Thereafter, it is used for the optimal sizing and development of HES, which would be able to provide rural areas with electricity where grid supply is rarely available. Depending on the availability of RERs, multiple models of grid-extension and off-grid modes have been chosen to electrify the selected areas. Consequently, the size of selected models of HES is obtained using the newly developed hHHO-RES algorithm, which finds the optimal one for the selected region. Moreover, the obtained results are compared with the PSO and HS approaches and found to be more accurate.

2. Study Area Description

In this paper, the study area includes 533 families from the community of villages located in Sonipat, Haryana, India, which is geographically situated at 77.02° E and 28.98 °N coordinates [50]. Owing to temperature fluctuations throughout the year having an impact on energy consumption, three seasons of four months each have been considered in the present study. The summer season (SS) runs from April to July. The moderate season (MS) involves August to November, while December to March encompasses the winter season (WS). The study area's daily energy requirements during the SS, MS, and WS were estimated at 2997.58 kWh/day, 2357.98 kWh/day, and 1286.149 kWh/day, respectively. The annual energy requirement for the selected site is computed as 809002.4 kWh/year. Furthermore, based on the data obtained, the potential of RER like solar irradiation, biogas, and biomass has been evaluated. The mean solar irradiation of this area has been measured to be 5.26 kWh/m^2/day. The identified region has been calculated to have 820.24 m^3/day of biogas through cattle dung and 470.19 of biomass in tons/year via crop residues.

3. Model of HES Components

The present work focuses on the optimum design of the HES that integrates the energies of a set of SPV panels, biomass, and biogas, as shown in Figure 1. In order to design and size HES, each component must be formulated mathematically. Therefore, the mathematical expressions are outlined as follows.

3.1. SPV. The actual power output of SPV (P_{SP} (t)) is determined as [5]

$$P_{SP} = (t) = S_{RP} \times L_P \times \left(\frac{Q_H(t)}{Q_S}\right)\left(1 + \chi\left(T_{C1} - T_{TC}\right)\right). \quad (1)$$

In the above equation, the rated capacity of the SPV panel under standard operating conditions (STC) is defined by S_{RP}; SPV panel loss factor is indicated by L_P; solar irradiation is defined by $Q_H(t)$; solar irradiation is represented by Q_S under STC; SPV cell temperature is marked by T_{Cl}; SPV cell temperature is denoted by T_{TC} under STC; and χ defines temperature coefficient.

3.2. Biomass Generator. The biomass generator power output at hour t (P_{BMS} (t)) is calculated as [51]

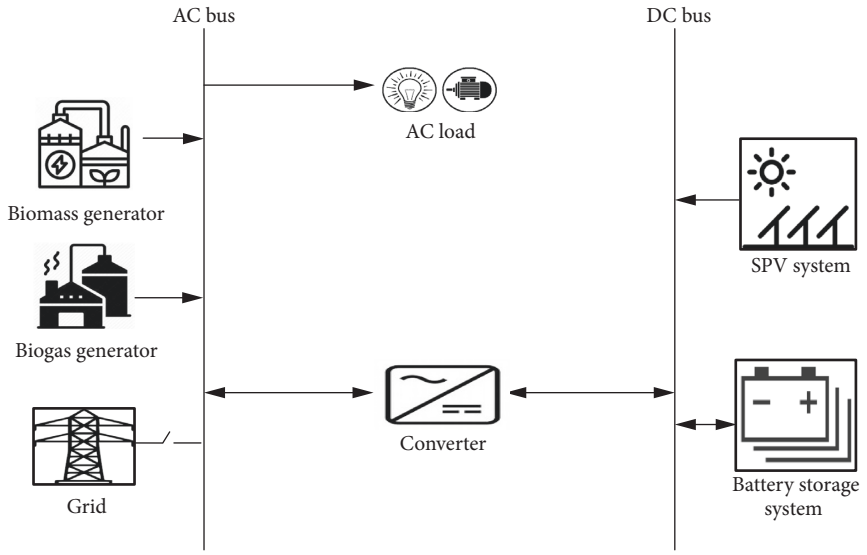

Figure 1: Schematic diagram of the proposed HES.

$$P_{BMS} = \frac{C_{BM} \times A_{BM} \times \eta_{MS} \times 1000}{365 \times H_{OG} \times 860}, \quad (2)$$

where C_{BM} denotes calorific value of biomass; A_{BM} indicates biomass availability; η_{MS} defines biomass system conversion efficiency; and $\mathrm{H_{OM}}$ is the number of biomass generator operational hours per day.

3.3. Biogas. The biogas generator power output ($\mathrm{P_{BGS}}$ (t)) is evaluated using the following equation [5]:

$$P_{\mathrm{BGS}} = \frac{C_{\mathrm{BG}} \times A_{\mathrm{BG}} \times \eta_{\mathrm{GS}}}{H_{\mathrm{OG}} \times 860}. \quad (3)$$

where $\mathrm{C_{BG}}$ describes calorific value of biogas; A_{BG} is biogas availability in a day; η_{GS} defines overall efficiency of converting biogas to electricity generation; and $\mathrm{H_{OG}}$ is biogas generator operational hours in a day.

3.4. Battery. The battery runs in one of two states: charging or discharging, depending on the amount of energy produced and consumed. In the charging state, the amount of electricity generated by RER exceeds the amount of electricity required by the hourly load demand. During the discharging stage, on the other hand, the hourly load demand exceeds the amount of electricity generated by RER. The battery capacity at hour t has been calculated using (4)–(7) when the battery is in the charging and discharging states [51]:

$$E^{\mathrm{d}}_{\mathrm{Bt}}(\mathrm{t}) = E^{d}_{\mathrm{Bt}}(t-1) + \left[E_{E_{\mathrm{BMS}}}(t) + E_{E_{\mathrm{BGS}}}(t) + E^{d}_{E_{\mathrm{SPS}}}(t)\right] \times \eta_{\mathrm{CH}}, \quad (4)$$

where $E^{d}_{\mathrm{Bt}}(t)$ signifies the amount of energy stored in the battery. In this equation, $E^{d}_{\mathrm{ESPS}}(t)$, $E_{\mathrm{EBGS}}(t)$, and $E_{\mathrm{EBMS}}(t)$ represent the excess energy generated by SPV, biogas, and biomass generator, respectively, after fulfilling the electrical load demand and η_{CH} indicates the battery charging efficiency.

$$E^{d}_{\mathrm{Bt}}(t) = (1-\gamma) \times E^{d}_{\mathrm{Bt}}(t-1) - E_{\mathrm{ND}}(t), \quad (5)$$

$$E_{\mathrm{ND}}(t) = \frac{E_{\mathrm{NTDM}}(t)}{\eta_{\mathrm{INV}} \times \eta_{\mathrm{DCH}}}, \quad (6)$$

where γ is the self-discharging rate in view of battery at hour t; $E_{\mathrm{ND}}(t)$ defines total electrical energy demand; η_{DCH} and η_{INV} represents discharging efficiency of battery and inverter efficiency, respectively; $\mathrm{E_{NTDM}}$ (t) denotes energy demand not met out by RER; and $\mathrm{E_{DMD}}$ (t) is hourly load demand.

$$E_{\mathrm{NTDM}}(t) = E_{\mathrm{DMD}} - \left[E_{\mathrm{BMS}}(t) + E_{\mathrm{BGS}}(t) + E^{d}_{\mathrm{SPS}}(t) \times \eta_{\mathrm{INV}}\right]. \quad (7)$$

3.5. Grid. In grid-connected HES, the grid may operate in two modes. In the first mode, it can supply deficit electricity to HES in case RER, along with the battery, is not able to meet the demand. Mathematically, grid energy purchased can be modelled as [51]

$$E_{\mathrm{PG}}(t) = E_{\mathrm{DMD}}(t) - E_{\mathrm{BMS}}(t) + E_{\mathrm{BGS}}(t) + E^{d}_{\mathrm{SPS}}(t) + \left(E^{t}_{\mathrm{Bt}}(t) + \left(E^{t}_{\mathrm{Bt}}(t) - E_{\mathrm{Btmin}} \times \eta_{\mathrm{INV}}\right)\right], \quad (8)$$

where $\mathrm{E_{PG}}$ (t) denotes the energy purchased grid and $\mathrm{E_{Btmin}}$ is minimum battery storage capacity.

$$E_{\mathrm{SG}}(t) = \left[E_{\mathrm{BMS}}(t) - E_{\mathrm{BGS}}(t) + \left[E^{d}_{\mathrm{SPVS}}(t) + E_{\mathrm{Btmax}}(t) - E^{d}_{\mathrm{Bat}}(t) \times \eta_{\mathrm{INV}}\right]\right] E_{\mathrm{DMD}}(t), \quad (9)$$

where $\mathrm{E_{SG}}$ (t) symbolizes the additional energy required, which must be sold to the grid. The term $\mathrm{E_{Btmax}}$ refers to the maximum battery storage capability.

4. Optimization Framework

The framework for optimization leads to the formulation of the objective function with constraints. The objective

function has been perceived to be to minimise the total NPC of the HES. The formulated objective function is optimised for the design of HES underneath the constraints of battery storage capability limits, lower and upper boundaries, and unmet load.

4.1. Objective Function. The total NPC has been used as an economic indicator for HES sizing. It consists of all expenditures that arise over the system's life span, including net present capital cost (C_{NV}), operation and maintenance (O&M) cost (OM_{NV}), replacement cost (RP_{NV}), fuel cost (F_{NV}), cost of electricity purchased through the utility grid (C_{PG}), and generated revenue in terms of salvage value (SV_{NV}) and selling electricity price to the power grid (C_{SG}) represented by the following equation:

$$\mathrm{NPC} = C_{\mathrm{NV}} + \mathrm{RP}_{\mathrm{NV}} + \mathrm{OM}_{\mathrm{NV}} - \mathrm{SV}_{\mathrm{NV}} + F_{\mathrm{NV}} + C_{\mathrm{PG}} - C_{\mathrm{SG}}. \quad (10)$$

4.1.1. C_{NV}. C_{NV} involves the net present capital cost within each component of HES and may be determined as [51]

$$C_{\mathrm{NV}} = \left(\left(N_{\mathrm{SP}} \times P_{\mathrm{Pnl}} \times \Psi_{\mathrm{SP}}\right) + \left(\Psi_{\mathrm{BG}} \times P_{\mathrm{BGS}}\right)\left(\Psi_{\mathrm{BM}} \times P_{\mathrm{BMS}}\right) + \left(\Psi_{\mathrm{Bt}} \times N_{\mathrm{Bt}}\right) + \left(\Psi_{\mathrm{INV}} \times P_{\mathrm{INV}}\right)\right). \quad (11)$$

In the above (11), the number of SPV panel and battery are indicated by N_{SP} and N_{Bt}, respectively; The power of the individual SPV panel is symbolized by P_{pnl}. The power output of biogas, biomass generator, and inverter are denoted by P_{BGS}, $P_{BMS,}$ and P_{INV}, respectively. The initial cost in view of SPV panel, biogas generator, biomass generator, inverter and battery is represented by $\Psi_{SP,}$ $\Psi_{BG,}$ $\Psi_{BM,}$ Ψ_{INV}, and Ψ_{Bt}, respectively.

4.1.2. OM_{NV}. $\mathrm{OM}_{\mathrm{NV}}$ of HES comprises the total O&M costs of each and every component over the course of the year and has been determined by (12) as [51]

$$\mathrm{OM}_{\mathrm{NV}} = \left(\left(\varpi_{\mathrm{SP}} \times P_{\mathrm{Pnl}} \times N_{\mathrm{SP}}\right) + \left(\varpi_{\mathrm{FBM}} \times P_{\mathrm{BMS}} + \varpi_{\mathrm{VBM}} \times P^{\mathrm{W}}_{\mathrm{ABM}}\right) + \left(\varpi_{\mathrm{FBG}} \times P_{\mathrm{BGS}} + \varpi_{\mathrm{VBG}} \times P^{\mathrm{W}}_{\mathrm{ABG}}\right) + \left(\varpi_{\mathrm{Bt}} \times N_{\mathrm{Bt}}\right) + \left(\varpi_{\mathrm{INV}} \times N_{\mathrm{INV}}\right)\right) \times \sum_{i=1}^{\mu} \left(\frac{1+\zeta}{1+R}\right)^{i}. \quad (12)$$

The yearly O&M costs of SPV panel, battery, and inverter are designated by ϖ_{SP}, ϖ_{Bt}, and ϖ_{INV}, respectively. The biogas and biomass generators' annual fixed O&M costs are denoted by ϖ_{FBG} and ϖ_{FBM}, respectively, while the variable O&M costs of the same generators are indicated by ϖ_{VBG} and ϖ_{VBM}, respectively. The biomass and biogas generator yearly working power is represented by the symbols $P^{W}{}_{ABM}$ and $P^{W}{}_{ABG}$ in the above equation. An escalation rate of HES components is ζ. Interest rate and project lifespan are defined by R and μ, respectively.

4.1.3. RP_{NV}. This present research discusses the lifespan of SPV, biomass, and biogas, which are considered the project life (25 years). As a result, there is no requirement for replacing these components, and the cost to replace these components is not factored into the NPC calculation. However, the battery and inverter lifespans are chosen as five and ten years, respectively, which is lower than the project life (25 years). Hence, the battery and inverter need to be replaced four and two times, respectively, in the whole lifetime of the project, and extra investment because of replacement cost is required that can be evaluated as

$$\mathrm{RP}_{\mathrm{NV}} = \left(\Psi_{\mathrm{Bt}} \times N_{\mathrm{Bt}} \times \sum_{i=5,10,15,20} \left(\frac{1+\zeta_{\mathrm{Bt}}}{1+R}\right)^{i}\right) + \left(\Psi_{\mathrm{INV}} \times P_{\mathrm{INV}} \times \sum_{i=10,20} \left(\frac{1+\zeta_{\mathrm{INV}}}{1+R}\right)^{i}\right). \quad (13)$$

4.1.4. F_{NV}. In the considered system, fuels contain crop residues (biomass) and cattle dung (biogas) that have been utilised in the biomass and biogas generators, respectively. For this reason, F_{NV} has been determined by considering the cost of biomass and cattle dung and is expressed by [51]

$$F_{\mathrm{NV}} = \left(\left(\xi_{\mathrm{BG}} \times F_{\mathrm{BGR}}\right) + \left(\xi_{\mathrm{BM}} \times F_{\mathrm{BMR}}\right)\right) \times \sum_{i=10,20} \left(\frac{1+\zeta}{1+\mathrm{R}}\right)^{i}. \quad (14)$$

In the above stated (14), the biomass and biogas fuel cost is denoted by ξ_{BM} and ξ_{BG}, respectively. The annual biomass and biogas demands are represented by F_{BMR} and F_{BGR}, respectively.

4.1.5. SV_{NV}. $\mathrm{SV}_{\mathrm{NV}}$ includes the resale value of HES components after the project lifecycle and has been computed using the following equation:

$$\mathrm{SV}_{\mathrm{NV}} = \left(\left(\varepsilon_{\mathrm{Bt}} \times \mathrm{N}_{\mathrm{SP}} \times \mathrm{P}_{\mathrm{Pnl}}\right) + \left(\varepsilon_{\mathrm{BM}} \times \mathrm{P}_{\mathrm{BMS}}\right) + \left(\varepsilon_{\mathrm{BG}} \times \mathrm{P}_{\mathrm{BGS}}\right) + \left(\varepsilon_{\mathrm{Bt}} \times \mathrm{N}_{\mathrm{Bt}}\right) + \left(\varepsilon_{\mathrm{INV}} \times \mathrm{P}_{\mathrm{INV}}\right)\right) \times \left(\frac{1+\lambda}{1+\mathrm{R}}\right)^{\mathrm{u}}. \quad (15)$$

The resale price of each component of HES is denoted by $\varepsilon_{SP,}$ $\varepsilon_{BM,}$ $\varepsilon_{BG,}$ ε_{Bt}, and ε_{INV}, respectively. Inflation rate is symbolized by λ in the above equation.

4.1.6. C_{PG} and C_{SG}. In the grid-connected mode, C_{PG} and C_{SG} have been calculated using the (16) and (17) as follows [51]:

$$C_{\mathrm{PG}} = \theta_P \times E_{\mathrm{PG}} \times \sum_{I=1} \left(\frac{1+\lambda}{1+R}\right)^{i}, \quad (16)$$

$$C_{\mathrm{SG}} = \theta_S \times E_{\mathrm{SG}} \times \sum_{I=1} \left(\frac{1+\lambda}{1+R}\right)^{i}, \quad (17)$$

where θ_S and θ_P indicates the cost per unit of selling and buying power to and from the power grid.

Finally, the cost of energy (CoE) is evaluated as

$$\text{CoE} = \frac{\text{NPC} \times C_{\text{RS}}}{E_{\text{DMD}} + E_{\text{SG}}}. \tag{18}$$

The capital recovery factor is denoted by C_{RS} in the above equation and can be calculated using the following equation:

$$C_{\text{RS}} = \frac{R(1+R)^R}{R(1+R)^u - 1}. \tag{19}$$

4.2. Design Constraints. In the present research, the selected objective function has been optimised under constraints described as follows.

4.3. HES Component Limits. In the present research, the size of the SPV panel, battery, biomass, and biogas generator may vary to fulfil the demand of the load. Hence, the generator limits of system components can be defined as

$$\begin{aligned} N_{\text{SP}} &= \text{integer}, \quad N_{\text{SP}}^{\text{Min}} \le N_{\text{SP}} \le N_{\text{SP}}^{\text{Max}}, \\ N_{\text{Bt}} &= \text{integer}, \quad N_{\text{Bt}}^{\text{Min}} \le N_{\text{Bt}} \le N_{\text{Bt}}^{\text{Max}}, \\ P_{\text{BGS}} &= \text{integer}, \quad P_{\text{BGS}}^{\text{Min}} \le P_{\text{BGS}} \le P_{\text{BGS}}^{\text{Max}}, \\ P_{\text{BMS}} &= \text{integer}, \quad P_{\text{BMS}}^{\text{Min}} \le P_{\text{BMS}} \le P_{\text{BMS}}^{\text{Max}}. \end{aligned} \tag{20}$$

4.4. Battery Storage Capacity Boundaries. For running a battery in a safer mode, the lower and upper boundaries of the battery storage system are considered and described as

$$E_{\text{Btmin}} \le E_{\text{Bt}} \le E_{\text{Btmax}}. \tag{21}$$

4.5. Unmet Load. Unmet load has been considered as being one of the constraints under this work. It is interpreted as the unserved load divided by the total load in one year and is estimated as [5]

$$\text{unmet load} = \sum_{t=1}^{t=8760} \frac{\text{Unserved load in one year}}{\text{total load in one year}}. \tag{22}$$

5. Proposed Methodology: hHHO-RES Optimizer

The HHO is inspired by the Harris Hawk bird. The Harris Hawks are sophisticated raptors that can be seen in Mexico and the United States. Hawks used to hunt in groups to ensure their survival. The hunting procedure entails their natural capacity to communicate among group members in order to encircle and attack with a huge number of soft and hard besiegement. If the target manages to flee throughout this procedure, the hawks will regroup and launch another attack. In the meantime, each hawk may switch spots. Finally, the tired victim runs out of energy and is attacked by the hawks. The seized prey is divided evenly among the members of the group. If there is any leftover food, the hawks carry it to their nest for the young hawks [52]. In this procedure, each matching approach has a probability based on the locations of the family associates and the prey, which is usually a rabbit. Despite a reasonable convergence rate, HHO struggles to locate the best optimal solution. Thus, to improve the exploitation phase and to avoid local optima, it needs to be upgraded with a RES optimizer. So, in the suggested research, the RES algorithm is used to make the hybrid variation of HHO, which is called the hybrid Harris hawks random exploratory search (hHHO-RES) algorithm.

In the present work, first, the HHO mechanism and its appliances are considered. Firstly, consider the normal strategy of hunting for Harris hawks, i.e., hawks identify the prey (rabbits) and then track the rabbit using their eyes. The hawks' eyes are dominant, through which the rabbit cannot easily realise the strategy. Furthermore, the behaviour of the Harris hawk bird in terms of four main strategies is described as follows [46].

5.1. Cooperative Behaviour and Chasing Style of Harris Hawks. The first tactic refers to the Harris hawks' hunting style. Hawks use this method to find and follow their prey, and the victim is not aware of it.

5.2. Nature Inspired including Soft Encircle with Hard Encircle of Harris Hawks. After spotting the victim, the hawks' natural instinct is to launch a surprise assault. After that, the prey tries to flee the situation. As a result, there are a variety of hunting and evasion strategies for the recognized target that can be used in real-life circumstances. The mathematical representations of these tactics are shown underneath. After locating the target in the first stage, Harris hawks use soft and hard encircles to attack the prey in any situation. A variety of soft and hard ways are used by the hawks to get close to their prey, depending on the animal's evasion skills and energy level.

5.3. Advanced Fast Dives: Soft Encircle of Harris Hawks. This procedure employs the levy flight (here abbreviated as L_{F} in (32)) concept. The movements of the leapfrog and the escape pattern of the prey are depicted mathematically using this approach. This method makes it simple to detect the prey's current activities and escape patterns. The main movements of the detected prey's escaping nature are zigzagged in this technique. Harris hawks make quick dives around the prey they have found and then try to move and change their positions to match the prey's directions and escape moves.

5.4. Advanced Fast Dives: Hard Encircle of Harris Hawks. In this situation, the identified prey lacks adequate energy to flee, so the Harris hawks' hard encircle tactic is interpreted before attacking the detected prey. Hawks try to get closer to their prey at this point.

Based on the behaviour of Harris hawks, the mathematical equations are formulated.

The equal coincidental chance for every strategy of balance is based upon the position of additional family members who are nearer to them. For the attacking time and here, the rabbit is considered as prey, which is shown by (23). As such, a consideration where a <0.5 for balancing strategy to maintain the random position is shown by (24), where $a \geq 0.5$ and the average position of hawks can be calculated from (25).

$$\mathrm{HH}(\mathrm{iteration}+1) = \{\mathrm{HH}_{\mathrm{rand}}(\mathrm{iteration}) - S_1 \times \mathrm{absHH}_{\mathrm{rand}}(\mathrm{iteration}) - 2 \times S_2 \times \mathrm{HH}(\mathrm{iteration})\}; \quad a \geq 0.5, \tag{23}$$

$$\mathrm{HH}(\mathrm{iteration}+1) = \left\{\mathrm{HH}_{\mathrm{rabit}}(\mathrm{iteration}) - \mathrm{HH}_m(\mathrm{iteration}) - S_3 \times \left(\mathrm{LOW}_{\mathrm{boundary}} + S_4 \times \left(\mathrm{UP}_{\mathrm{boundary}} - \mathrm{LOW}_{\mathrm{boundary}}\right)\right)\right\}; \quad a < 0.5, \tag{24}$$

$$\mathrm{HH}(\mathrm{iteration}+1) = \frac{1}{N}\sum_{i=1}^{N} \mathrm{HH}_{\mathrm{i}}(\mathrm{iteration}+1), \tag{25}$$

where S_1, S_2, S_3, and S_4 lie in the range of 0 and 1, which is improved for each iteration. HH (iteration +1) is signified as the rabbit's location and $\mathrm{HH}_{\mathrm{rand}}$ is denoted as random number of Harris hawks bird. N is taken as the entire number of the hawks.

The escape performance reduces rabbit energy. Thus, the equation constructed based on the performance of the energy of the rabbit is as follows:

$$\mathrm{ER} = 2 \times \mathrm{ER}_{\mathrm{O}} \times \left(1 - \frac{\mathrm{iteration}}{\mathrm{iteration}_{\max}}\right), \tag{26}$$

where ER is the escaping energy of a rabbit, ER_0 is the preliminary state of the energy, and $\mathrm{iteration}_{\max}$ is denoted as the maximum number of iterations.

$$\begin{aligned}\mathrm{HH}(\mathrm{iteration}+1) = {} & \Delta\mathrm{HH}(\mathrm{iteration}) - \mathrm{ER} \\ & \times \mathrm{abs}\left(\mathrm{J} \times \mathrm{HH}_{\mathrm{rabit}}(\mathrm{iteration})\right. \\ & \left. - \mathrm{HH}(\mathrm{iteration})\right),\end{aligned} \tag{27}$$

where J is taken as indication parameter.

$$\Delta\mathrm{HH}(\mathrm{iteration}) = \left(\mathrm{HH}_{\mathrm{rabit}}(\mathrm{iteration}) - \mathrm{HH}(\mathrm{iteration})\right). \tag{28}$$

From the above equations, the alteration between the number of iterations constructed upon the present locations and the vector constructed upon that location of the victim prey, i.e., rabbit, is defined. The levy strategy, L_{F} (d) conception, is applied to HHO optimization, which helps us to comprehend the scientific model of the strategy for leapfrog arrangements as well as the patterns of escaping the rabbit or fleeing prey.

$$\begin{aligned}\mathrm{HH}(\mathrm{iteration}+1) = {} & \mathrm{HH}_{\mathrm{rabit}}(\mathrm{iteration}) \\ & - \mathrm{ER} \times \mathrm{abs}\left(\Delta\mathrm{HH}(\mathrm{iteration}),\right.\end{aligned} \tag{29}$$

$$\begin{aligned}P = {} & \mathrm{HH}_{\mathrm{rabit}}(\mathrm{iteration}) \\ & - \mathrm{ER} \times \mathrm{abs}\left(J \times \mathrm{HH}_{\mathrm{rabit}}(\mathrm{iteration})\right. \\ & \left. - \mathrm{HH}(\mathrm{iteration}),\right.\end{aligned} \tag{30}$$

$$V = P + Z_s \times L_F(d), \tag{31}$$

where d = dimension of the problem and Z_{S} = random vector is by size 1xd.

Thus, for superior performance in the phase of the soft encircle, the hawk bird can choose their subsequent movement, i.e., P. Here, P is based on a rule given in the (30). Based on the L_{F} (d) pattern, it established to follow the specified rule in the

$$L_F(x) = 0.01\left(\frac{\vartheta \times \sigma}{|\nu|^{1/\beta}}\right), \tag{32}$$

$$\sigma = \left(\frac{\Gamma(1+\beta) \times \mathrm{Sin}(\pi\beta/2)}{\Gamma(1+\beta/2) + \beta \times 2(\beta - 1/2)}\right)^{1/\beta}, \tag{33}$$

where ϑ, σ are signified as such kinds of values are random in manner in between (0, 1) and β is denoted as default constant which is taken as 1.5.

In the hHHO-RES algorithm, the position vector HH (iteration + 1) is disturbed by Δ_i and new position vector HH [(iteration + 1) + Δ_i] and HH [(iteration + 1) − Δ_i] has been obtained. The variation of the parameter Δ_i is considered randomly within the local search space for exploiting the search space in a better way.

Fitness resolution $f^{+} \leftarrow f[\mathrm{HH}(\mathrm{iteration}+1) + \Delta_i]$ and $f^{-} \leftarrow f[\mathrm{HH}(\mathrm{iteration}+1) - \Delta_i]$ is considered with earlier fitness resolution $f \leftarrow f[\mathrm{HH}(\mathrm{iteration}+1)]$, and ultimate fitness is estimated taking minimum values using equation $f_{\mathrm{final}} \leftarrow \min(f^{+}, f^{-}, f)$

Therefore, counting all, real as well as the ultimate approach for upgrading the real position of hawks for soft encircle can be accomplished through (34) and (35) as

$$\mathrm{HH}(\mathrm{iteration}+1) = \begin{cases} P; & \text{if } F(\mathrm{P}) < F(\mathrm{HH}(\mathrm{iteration})), \\ V; & \text{if } F(\mathrm{V}) < F(\mathrm{HH}(\mathrm{iteration})). \end{cases} \tag{34}$$

$$\begin{aligned}\mathrm{P} = {} & \mathrm{HH}_{\mathrm{rabit}}(\mathrm{iteration}) \\ & - \mathrm{ER} \times \mathrm{abs}\left(J * \mathrm{HH}_{\mathrm{rabit}}(\mathrm{iteration})\right. \\ & \left. - \mathrm{HH}_m(\mathrm{iteration}),\right.\end{aligned} \tag{35}$$

$$V = P + Z_S \times L_F(d). \tag{36}$$

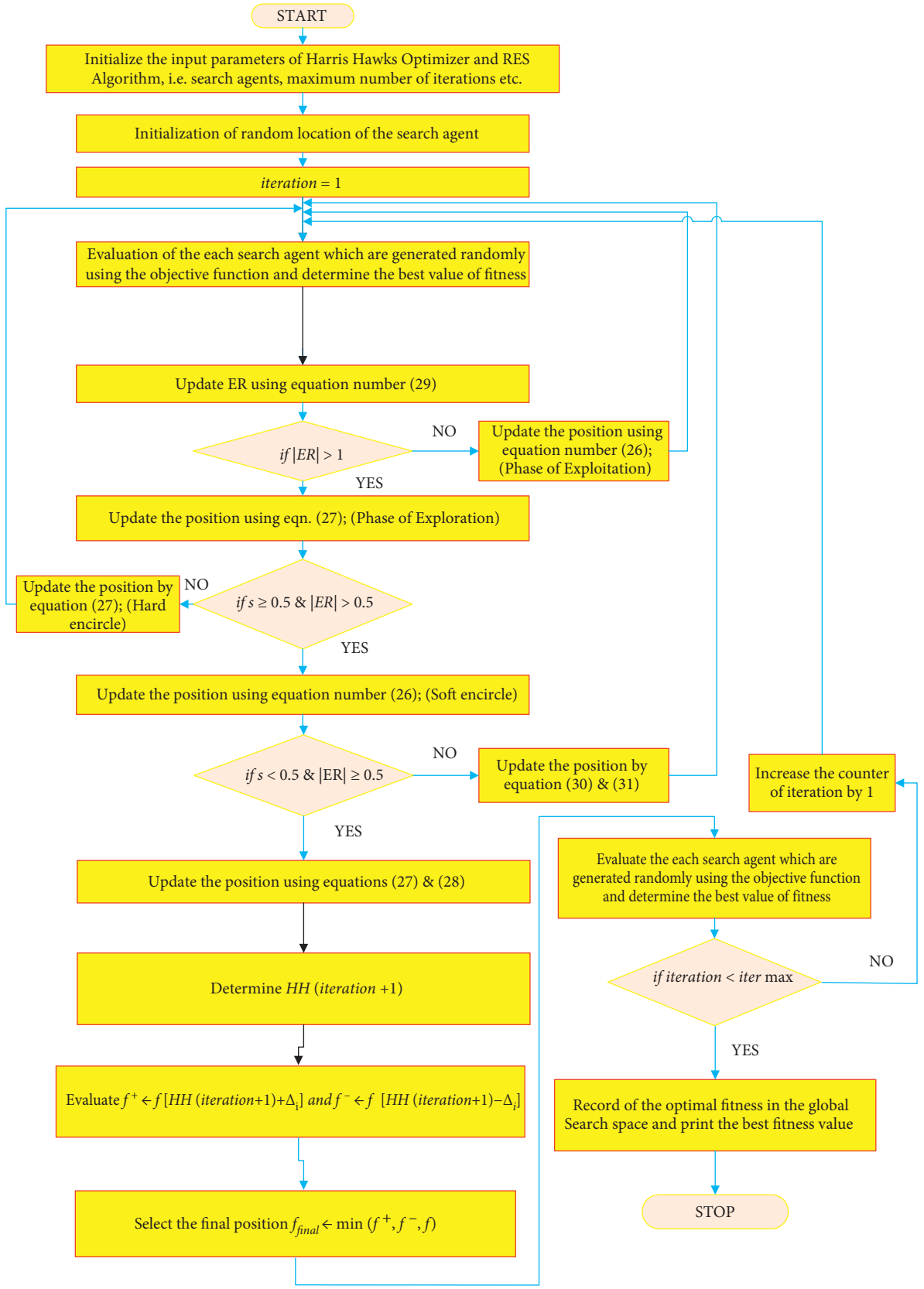

Figure 2: Flowchart of Proposed hHHO-RES.

Input: size of the population is considered as N and max. Number of iterations is $\text{iteration}_{\max}$
Output: the position of prey, i.e. rabbit &fitness value
Initialization of random population $\text{HH}_i\,(i = 1, 2, 3, \ldots, N)$
  While (iteration < $\text{iteration}_{\max}$)
    Design of the fitness value used for hawks bird
    Parameter set as $\text{HH}_{\text{rabbit}}$ for the best location of rabbit (prey)
      for each hawks bird, i.e., (HH_i)
        Do update energy at primary condition ER_O
        If $|\text{ER}| \geq 1$, then
        Position vector updated using $\text{ER} = 2 \times \text{ER}_0 \times (1 - \text{iteration}/\text{iteration}_{\max})$, i.e., phase of exploration
        else if $a \geq 0.5$ then
      $\text{HH}\,(\text{iteration} + 1) = \{\text{HH}_{\text{rand}}\,(\text{iteration}) - s_1 \times abs\,(\text{HH}_{\text{rand}}\,(\text{iteration}) - 2 \times s_2 \times \text{HH}\,(\text{iteration}))\}$
      else if $a < 0.5$ then
$\text{HH}\,(\text{iteration} + 1) = \{(\text{HH}_{\text{rabbit}}\,(\text{iteration}) - \text{HH}_m\,(\text{iteration})) - s_3 \times (\text{LOW}_{\text{Boundary}} + s_4 \times (\text{UP}_{\text{Boundary}} - \text{LOW}_{\text{Boundary}}))\}$
        If $|\text{ER}| < 1$ then do phase of exploitations
        $\text{HH}\,(\text{iteration} + 1) = \Delta\text{HH}\,(\text{iteration}) - \text{ER} \times abs\,(\text{JHH}_{\text{rabbit}}\,(\text{iteration}) - \text{HH}\,(\text{iteration}))$
          If $(s \geq 0.5)$ and $|\text{ER}| \geq 0.5$ then do the phase of soft encircle
            Position vector restructured through $\Delta\text{HH}\,(\text{iteration}) = (\text{HH}_{\text{rabbit}}\,(\text{iteration}) - \text{HH}\,(\text{iteration}))$
              else if $(s \geq 0.5)$ and $|\text{ER}| < 0.5$ then do the phase of hard encircle
                  Position vector restructured using
              $\text{HH}\,(\text{iteration} + 1) = \text{HH}_{\text{rabbit}}\,(\text{iteration}) - \text{ER} \times abs\,(\Delta H\,(\text{iteration}))$
              else if $(s < 0.5)$ and $|\text{ER}| \geq 0.5$ then do the phase of soft encircle with progressive
            Fast dives
            Position vector restructured through
            $P = \text{HH}_{\text{rabbit}}\,(\text{iteration}) - \text{ER} \times abs\,(\text{JHH}_{\text{rabbit}}\,(\text{iteration}) - \text{HH}\,(\text{iteration}))$
          else if $(s < 0.5)$ and $|\text{ER}| < 0.5$ then do the phase of hard encircle with progressive
        Fast dives
      Position vector restructured by
      $\text{HH}\,(\text{iteration} + 1) = \Delta\text{HH}\,(\text{iteration}) - \text{ER} \times abs\,(\text{JHH}_{\text{rabbit}}\,(\text{iteration}) - \text{HH}\,(\text{iteration}))$
Using RES optimizer, the position vector $\text{HH}\,(\text{iteration} + 1)$ is disturbed by Δ_i
New positions vector $\text{HH}\,[(\text{iteration} + 1) + \Delta_i]$ and $\text{HH}\,[(\text{iteration} + 1) - \Delta_i]$ has been obtained
The fitness resolution $f^+ \leftarrow f\,[\text{HH}\,(\text{iteration} + 1) + \Delta_i]$ and $f^- \leftarrow f\,[\text{HH}\,(\text{iteration} + 1) - \Delta_i]$ are considered with earlier fitness resolution $f \leftarrow f\,[\text{HH}\,(\text{iteration} + 1)]$
Ultimate fitness are estimated taking minimum values using equation $f_{\text{final}} \leftarrow \min\,(f^+, f^-, f)]$
End all process

Algorithm 1: Pseudocode of proposed hHHO-RES algorithm

where $\text{HH}_{\text{m}}\,(\text{iteration})$ can take from (25).

To solve the optimization problem, some constants and parameters are needed. The required parameters are added in the proposed work are, such as scaling parameter and crossover probability will be within 0.5, inertia factor will be 0.2, teaching factor is 1,0, convergence constant is [0,0] and spiral factor is [-1,-1], loudness is 0.5, pulse rate is 0.5, and frequency parameter including minimum and maximum frequency is taken as 0 and 2, respectively; probability switch must be 0.8. Habitat modification probability is 1, immigration probability limit is [0.1], mutation probability is taken as 0.005, and step size is taken as 1.

Further, the algorithm steps for hHHO-RES optimizer are as follows:

Step 1: initialize the inputs, size of the population is considered as N and max. Number of iterations is $\text{iteration}_{\max}$.

Step 2: need to find the best position of the prey, i.e., rabbit and the fitness value and initialization of random population $\text{HH}_i\,(i = 1, 2, 3, \ldots, N)$.

Step 3: while (iteration < $\text{iteration}_{\max}$), design of the fitness value for Harris hawks and the parameter set as $\text{HH}_{\text{rabbit}}$ the best location of the prey, i.e., rabbit.

Step 4: for each Harris hawks (HH_i).

Step 5: do update energy at the primary condition ER_{O}.

Step 6: if $|\text{ER}| \geq 1$, then position vector updated using $\text{ER} = 2 \times \text{ER}_0 \times (1 - \text{iteration}/\text{iteration}_{\max})$, i.e., phase of exploration, else if $a \geq 0.5$, then

$\text{HH}\,(\text{iteration} + 1) = \{\text{HH}_{\text{rand}}(\text{iteration}) - s_1 \times abs\,(\text{HH}_{\text{rand}}\,(\text{iteration}) - 2 \times s_2 \times \text{HH}\,(\text{iteration}))\}$, else if $a < 0.5$, then

$\text{HH}\,(\text{iteration} + 1) = \{\text{HH}_{\text{rabbit}}\,(\text{iteration}) - \text{HH}_m\,(\text{iteration}) - s_3 \times (\text{LOW}_{\text{Boundary}} + s_4 \times (\text{UP}_{\text{Boundary}} - \text{LOW}_{\text{Boundary}}))\}$ Step 7: if $|\text{ER}| < 1$, then phase of exploitation occurred.

$\text{HH}\,(\text{iteration} + 1) = \Delta\text{HH}\,(\text{iteration}) - \text{ER} \times abs\,(\text{JHH}_{\text{rabbit}}\,(\text{iteration}) - \text{HH}\,(\text{iteration}))$.

Step 8: if $(s \geq 0.5)$ and $|\text{ER}| \geq 0.5$ then soft encircle occurred

Table 1: Unimodal standard benchmarks.

Functions	Dimensions	Range	$f_{\min}$
$F_1(U) = \sum_{\dot{m}=1}^{z} U_m^2$	30	[−100, 100]	0
$F_2(U) = \sum_{\dot{m}=1}^{z} \lvert U_m\rvert + \prod_{m=1}^{z} \lvert U_m\rvert$	30	[−10,10]	0
$F_3(U) = \sum_{\dot{m}=1}^{z} (\sum_{n-1}^{m} U_n)^2$	30	[−100, 100]	0
$F_4(U) = \max_m\{\lvert U_m\rvert, 1 \le m \le z\}$	30	[−100, 100]	0
$F_5(U) = \sum_{\dot{m}=1}^{z-1} [100(U_{m+1} - 1 - U_m^2)^2 + (U_m - 1)^2]$	30	[−38, 38]	0
$F_6(U) = \sum_{\dot{m}=1}^{z} ([U_m + 0.5])^2$	30	[−100, 100]	0
$F_7(U) = \sum_{\dot{m}=1}^{z} mU_m^4 + \text{random}[0,1]$	30	[−1.28, 1.28]	0

Table 2: Multimodal standard benchmarks.

Functions	Dimension	Range	$f_{\min}$
$F_8(U) = \sum_{\dot{m}=1}^{z} -U_m \sin(\sqrt{\lvert U_m\rvert})$	30	[−500, 500]	−418.982
$F_9(U) = \sum_{\dot{m}=1}^{z} [U_m^2 - 10\cos(2\pi U_m) + 10]$	30	[−5.12, 5.12]	0
$F_{10}(U) = -20\exp(-0.2\sqrt{(1/z\sum_{\dot{m}=1}^{z} U_m^2)}) - \exp 1/z\sum_{\dot{m}=1}^{z}\cos(2\pi U_m) + 20 + d$	30	[−32, 32]	0
$F_{11}(U) = 1 + \sum_{\dot{m}=1}^{z} U_m^2/4000 - \Pi_{m=1}^{z}\cos U_m/\sqrt{m}$	30	[−600, 600]	0
$F_{12}(U) = \pi/z\{10\ \sin(\pi\tau_1) + \sum_{\dot{m}=1}^{z-1}(\tau_m - 1)^2[1 + 10\sin^2(\pi\tau_{m+1})] + (\tau_z - 1)^2\}$ $+ \sum_{\dot{m}=1}^{z} g(U_m, 10, 100, 4),\ \tau_m = 1 + U_m + 1/4$ $g(U_m, b, x, i) = \begin{cases} x(U_m - b)^i U_m > b, \\ 0 - b < U_m < b, \\ x(-U_m - b)^i U_m < -b, \end{cases}$	30	[−50, 50]	0
$F_{13}(U) = 0.1\{\sin^2(3\pi U_m) + \sum_{\dot{m}=1}^{z}(U_m - 1)^2[1 + \sin^2(3\pi U_m + 1)] + (x_z - 1)^2[1 + \sin^2(2\pi U_m)]\}$ $+ \sum_{\dot{m}=1}^{z} g(U_m 5, 100, 4)$	30	[−50, 50]	0

Table 3: Fixed dimension standard benchmarks.

Functions	Dimension	Range	$f_{\min}$
$F_{14}(U) = [1/500 + \sum_{\dot{n}=1}^{2} 5(1/n + \sum_{\dot{m}=1}^{z}(U_m - b_{mn})6)]^1$	2	[−65.536, 65.536]	1
$F_{15}(U) = \sum_{\dot{m}=1}^{11}[b_m - U_1(a_m^2 + a_m\eta_2)/a_m^2 + a_m\eta_3 + \eta_4]^2$	4	[−5, 5]	0.00030
$F_{16}(U) = 4U_1^2 - 2.1U_1^4 + 1/3U_1^6 + U_1U_2 - 4U_2^2 + 4U_2^4$	2	[−5, 5]	−1.0316
$F_{17}(U) = (U_2 - 5.1/4\pi 2U_1^2 + 5/\pi U_1 - 6)^2 + 10(1 - 1/8\pi)\cos U_1 + 10$	2	[−5, 5]	0.398
$F18(U) = [1 + (U1 + U2 + 1)21(9 - 14U1 + 3U21 - 14U2 + 6U1U2 + 3U22)]$ $\times[30 + (2U1 - 3U2)2\,x(18 - 32U1 + 12U21 + 48U2 - 36U1U2 + 27U22)]$	2	[−2,2]	3
$F_{19}(U) = -\sum_{\dot{m}=1}^{4} d_m \exp(-\sum_{\dot{n}=1}^{3} U_{mn}(U_m - q_{mn})^2)^2)$	3	[1, 3]	−3.32
$F_{20}(U) = -\sum_{\dot{m}=1}^{4} d_m \exp(-\sum_{\dot{n}=1}^{6} U_{mn}(U_m - q_{mn})^2)$	6	[0, 1]	−3.32
$F_{21}(U) = -\sum_{\dot{m}=1}^{5}[(U - b_m)(U - b_m)_T + d_m]^{-1}$	4	[0, 10]	−10.1532
$F_{22}(U) = -\sum_{\dot{m}=1}^{4}[(U - b_m)(U - b_m)_T + d_m]^{-1}$	4	[0, 10]	−10.4028
$F_{23}(U) = -\sum_{\dot{m}=1}^{7}[(U - b_m)(U - b_m)_T + d_m]^{-1}$	4	[0, 10]	−10.5363

Table 4: Statistical and hypothetical test result in view of unimodal benchmarks by the hHHO-RES approach.

Functions	Mean	SD	Best	Worst	Median	p value
F_1	$1.79672E-95$	$9.03E-95$	$2.2262E-120$	$4.94116E-94$	$9.152E-105$	$1.734E-06$
F_2	$1.39556E-51$	$4.277E-51$	$1.81668E-56$	$1.79123E-50$	$1.0014E-53$	$1.734E-06$
F_3	$2.69946E-75$	$1.446E-74$	$8.906E-102$	$7.92614E-74$	$6.0026E-85$	$1.734E-06$
F_4	$1.19818E-49$	$3.752E-49$	$2.88272E-60$	$1.93948E-48$	$3.8302E-52$	$1.734E-06$
F_5	0.004344402	0.0057405	$4.38987E-05$	0.025296502	0.00252563	$1.734E-06$
F_6	0.000197648	0.0003509	$2.94818E-07$	0.001754092	$5.3867E-05$	$1.734E-06$
F_7	0.000248711	0.0003242	$4.84758E-06$	0.00147427	0.00013667	$1.734E-06$

Table 5: Statistical and hypothetical test result in view of multimodal benchmarks by the hHHO-RES approach.

Functions	Mean	SD	Best	Worst	Median	p value
F_8	−12569.23959	0.18307213	−12569.48662	−12568.93169	−12569.19403	$1.7344E-06$
F_9	0	0	0	0	0	1
F_{10}	$8.88178E-16$	0	$8.88178E-16$	$8.88178E-16$	$8.88178E-16$	$4.32046E-08$
F_{11}	0	0	0	0	0	1
F_{12}	$1.42119E-05$	$1.853E-05$	$6.06594E-08$	$6.56599E-05$	$7.01747E-06$	$1.7344E-06$
F_{13}	$9.91151E-05$	0.00015148	$8.23616E-09$	0.000531648	$2.30969E-05$	$1.7344E-06$

Table 6: Statistical and hypothetical test results in view of fixed dimension benchmarks by the hHHO-RES algorithm.

Functions	Mean	SD	Best	Worst	Median	p value
F_{15}	0.000346352	$3.28017E-05$	0.000307988	0.000454895	0.00034178	$1.734E-06$
F_{16}	−1.031628451	$1.29894E-08$	−1.031628453	−1.031628382	−1.031628453	$1.734E-06$
F_{18}	3.000000979	$3.23036E-06$	3	3.000012844	3.000000023	$1.734E-06$
F_{20}	−3.086651553	0.091761153	−3.236498312	−2.814621525	−3.092425922	$1.734E-06$
F_{21}	−7.219196247	2.220066434	−10.07568334	−5.048431651	−6.84997893	$1.734E-06$
F_{22}	−6.146328648	1.967379234	−10.16209669	−5.047223357	−5.086311231	$1.734E-06$
F_{23}	−6.787325891	2.265291538	−10.3684221	−4.955074036	−5.128053641	$1.734E-06$

Position vector updated by $\Delta HH(\text{iteration}) = (HH_{\text{rabbit}}(\text{iteration}) - HH(\text{iteration}))$.

Step 9: else if $(s \geq 0.5)$ and $|ER| < 0.5$ then hard encircle occurred.

Position vector updated using $\Delta HH(\text{iteration}+1) = HH_{\text{rabbit}}(\text{iteration}) - ER \times abs(\Delta HH(\text{iteration}))$.

Step 10: else if $(s < 0.5)$ and $|ER| \geq 0.5$, then soft encircle with advanced fast dives occurred.

Position vector update by $P = HH_{\text{rabbit}}(\text{iteration})ER \times abs(JHH_{\text{rabbit}} - HH(\text{iteration}))$.

Step 11: else if $(s < 0.5)$ and $|ER| < 0.5$, then hard encircle with advanced fast dives happened.

Position vector updated. $HH(\text{iteration}+1) = \Delta HH(\text{iteration}) - ER \times abs(JHH_{\text{rabbit}}(\text{iteration}) - HH(\text{iteration}))$.

Step 12: end all loops.

Step 13: in the hHHO-RES algorithm, the position vector $HH(\text{iteration}+1)$ is disturbed by Δ_i and new position vector $HH[(\text{iteration}+1)+\Delta_i]$ and $HH[(\text{iteration}+1)-\Delta_i]$ has been obtained.

Step 14: the variation of the parameter Δ_i is considered randomly within the local search space for exploiting the search space in a better way.

Step15: fitness resolution $f^+ \leftarrow f[HH(\text{iteration}+1)+\Delta_i]$ and $f^- \leftarrow f[HH(\text{iteration}+1)-\Delta_i]$ are considered with earlier fitness resolution $f \leftarrow f[HH(\text{iteration}+1)]$ and ultimate fitness are estimated taking minimum values using equation $f_{\text{final}} \leftarrow \min(f^+, f^-, f)$.

Step 16: end the process.

The flowchart along with the pseudocode for the proposed hHHO-RES is demonstrated in Figure 2 and algorithm 1, respectively.

6. Test Systems

A well-studied set of different variations of standard benchmarks [53, 54] is considered to verify the effectiveness of the suggested hHHO-RES optimizer. The standard benchmarks are composed of three types of major functions, i.e., unimodal, multimodal, and fixed dimension functions. Each standard benchmark has its own mathematical expressions, which are mentioned in Table 1–3. To check the effectiveness of these standard functions, 30 trail runs are taken into consideration. The numbers of the search agents are taken as 30 for the entire analysis of this research work. The total number of iterations is taken as 500 for this research work. the suggested hHHO-RES optimizer has been developed, and it was tested upon Intel ® Core TM, i7-5600 cpu@2.60 GHz.

7. Result and Discussion

In this research work, firstly, hHHO-RES, a new hybrid metaheuristics optimization approach, is developed to handle the problem of sizing HES components while reducing cost and For statistical analysis, the me maximising reliability. To demonstrate the effectiveness of the proposed optimization approach, it is initially tested on standard benchmark functions. Then, the performance of the suggested optimizer has also compared to that of other existing optimization approaches such as fast evolutionary programming (FEP), gravitational search algorithm (GSA), GA, GWO, CS, binary dragonfly algorithm (BDA), dragonfly algorithm (DA), FPA, ant lion optimizer (ALO), GOA, multiverse optimizer (MVO), WOA, binary gravitational search algorithm (BGSA), (SSA), Binary particle swarm optimization (BPSO), states of matter search (SMS), HHO, differential evolution (DE), sine-cosine

Table 7: Result of several optimization approaches in view of unimodal functions.

Function	Metric	Algorithms					
		Fast evolutionary programming (FEP) [54]	Gravitational search algorithm (GSA) [55]	GA [56]	GWO [57]	CS [58]	Binary dragonfly algorithm (BDA) [59]
F_1	Mean	0.001	0	0.119	0	0.007	0.282
	SD	0	0	0.126	0	0	0.418
F_2	Mean	0.008	0.056	0.145	0	0.212	0.059
	SD	0.001	0.194	0.053	0.029	0.04	0.069
F_3	Mean	0.016	896.535	0.139	0	0.247	14.2
	SD	0.014	318.956	0.121	79.15	0.021	22.7
F_4	Mean	0.3	7.355	0.158	0	0	0.248
	SD	0.5	1.741	0.862	1.315	0	0.331
F_5	Mean	5.06	67.543	0.714	26.813	0.007	23.6
	SD	5.87	62.225	0.973	69.905	0.007	34.7
F_6	Mean	0	0	0.168	0.817	0	0.095
	SD	0	0	0.869	0	0	0.13
F_7	Mean	-12600	-2820	-2090	-6120	-2090	-924
	SD	52.6	493	2.47	-4090	0.008	65.7
		Dragonfly algorithm (DA) [59]	FPA [60]	Ant lion optimizer (ALO) [61]	GOA [62]	Multi-verse optimizer (MVO) [63]	WOA [64]
F_1	Mean	0	0	0	0	2.086	0
	SD	0	0	0	0	0.649	0
F_2	Mean	0	0.001	0	0.002	15.925	0
	SD	0	0	0	0.001	44.746	0
F_3	Mean	0	0	0	0.001	453.2	0
	SD	0.003	0	0	0.02	177.097	0
F_4	Mean	0.001	0.004	0	0	3.123	0.073
	SD	0.003	0.002	0	0	1.583	0.397
F_5	Mean	7.6	0.781	0.347	0	1272.13	27.866
	SD	6.79	0.367	0.11	0	1479.477	0.764
F_6	Mean	0	0	0	0	2.295	3.116
	SD	0	0	0	0	0.631	0.532
F_7	Mean	-2860	-1840	-1610	1	-11700	-5080
	SD	384	50.4	314	0	937	696
		Binary gravitational search algorithm (BGSA) [65]	(SSA) [66]	Binary particle swarm optimization (BPSO) [67]	States of matter search (SMS) [68]	HHO	**hHHO-RES**
F1	Mean	83	0	5.59	0.0057	$1.72E-96$	$\mathbf{1.79672E-95}$
	SD	49.8	0	1.98	0.015	$3.95E-97$	$\mathbf{9.03E-95}$
F2	Mean	1.19	0.227	0.196	0.007	$6.98E-51$	$\mathbf{1.39556E-51}$
	SD	0.228	1	0.053	0.002	$1.56E-51$	$\mathbf{4.277E-51}$
F3	Mean	456	0	15.5	0.96	$1.05E-62$	$\mathbf{2.69946E-75}$
	SD	272	0	13.7	0.823	$1.92E-63$	$\mathbf{1.446E-74}$
F4	Mean	7.37	0	1.9	0.277	$5.01E-47$	$\mathbf{1.19818E-49}$
	SD	2.21	0.656	0.484	0.006	$1.02E-47$	$\mathbf{3.752E-49}$
F5	Mean	3100	0	86.4	0.085	$1.87E-02$	**0.004344402**
	SD	2930	0	65.8	0.14	$1.32E-02$	**0.0057405**
F6	Mean	107	0	6.98	0.125	$1.56E-04$	**0.000197648**
	SD	77.5	0	3.85	0.085	$1.15E-04$	**0.0003509**
F7	Mean	-861	0.056	-989	-4.21	$1.07E-04$	**0.000248711**
	SD	80.6	0.809	16.7	0	$1.40E-04$	**0.0003242**

algorithm (SCA), moth flame optimization (MFO). Thereafter, the hHHO-RES is used to optimise the sizing and design of HES, including various RER, in order to meet the energy demand of the chosen area. In this case, different models of off-grid and grid-connected HES were looked at, and the best one has been found. With a view to validate the findings, the HS and PSO algorithms have also been used to get optimization results for the selected HES models.

7.1. Testing of Benchmark Functions. The proposed hHHO-RES is tested for standard benchmark functions such as unimodal F_1 to F_7, multimodal F_8 to F_{13}, and benchmark

Table 8: Result of several optimization approaches in view of multimodal function.

Function	Metric	Algorithms						
		FEP [54]	GSA [55]	GA [56]	GWO [57]	CS [58]	Differential evolution (DE) [69]	Sine-cosine algorithm (SCA) [70]
F_8	Mean	−12554.50	−2821.07	−2.090 $E+03$	−6.123 $E+224$	-5.19 $E+01$	−11080.10	1.000$E+00$
	SD	52.60	493.04	2.470 $E+00$	−4087.44	1.76 $E+01$	574.70	3.600$E-03$
F_9	Mean	0.05	25.97	6.590$E-01$	0.310521	1.51 $E+01$	69.20	0.000$E+00$
	SD	0.01	7.47	8.160$E-01$	47.35612	1.25 $E+00$	38.80	7.300$E-01$
F_{10}	Mean	0.02	0.06	9.560$E-01$	1.06E−13	3.29$E-02$	0.00	3.800$E-01$
	SD	0	0.24	8.080$E-01$	0.077835	7.93$E-03$	0.00	1.000$E+00$
F_{11}	Mean	0.02	27.70	4.880$E-01$	0.004485	4.29$E-05$	0.00	0.000$E+00$
	SD	0.02	5.04	2.180$E-01$	0.006659	2.00$E-05$	0.00	5.100$E-03$
F_{12}	Mean	0	1.80	1.110$E-01$	0.053438	5.57$E-05$	0.00	0.000$E+00$
	SD	0	0.95	2.150$E-03$	0.654464	4.96$E-05$	0.00	0.000$E+00$
F_{13}	Mean	0	8.90	1.290$E-01$	0.654464	8.19$E-03$	0.00	0.000$E+00$
	SD	0	7.13	6.890$E-02$	0.004474	6.74$E-03$	0.00	0.000$E+00$
		SSA [66]	ALO [61]	Moth flame optimization (MFO) [71]	MVO [63]	DA [59]	HHO	**hHHO-RES**
F_8	Mean	5.570$E-02$	−1.61 $E+03$	−8.500$E+03$	−1.170 $E+04$	−2.860$E+03$	−1.25 $E+04$	**-12569.23959**
	SD	8.090$E-01$	3.14 $E+02$	7.260$E+02$	9.370 $E+02$	3.840$E+02$	1.47 $E+02$	**0.18307213**
F_9	Mean	0.000 $E+00$	7.71$E-06$	8.460$E+01$	1.180 $E+02$	1.600$E+01$	0.00 $E+00$	**0**
	SD	0.000 $E+00$	8.45$E-06$	1.620$E+01$	3.930 $E+01$	9.480 $E+00$	0.00 $E+00$	**0**
F_{10}	Mean	1.950$E-01$	3.73$E-15$	1.260$E+00$	4.070 $E+00$	2.310$E-01$	8.88E−16	**8.88178$E-16$**
	SD	1.530$E-01$	1.50$E-15$	7.300$E-01$	5.500 $E+00$	4.870$E-01$	4.01E−31	**0**
F_{11}	Mean	0.000 $E+00$	1.86$E-02$	1.910$E-02$	9.400$E-01$	1.930$E-01$	0.00$E+00$	**0**
	SD	6.510$E-02$	9.55$E-03$	2.170$E-02$	6.000$E-02$	7.350$E-02$	0.00$E+00$	**0**
F_{12}	Mean	1.420$E-01$	9.75$E-12$	8.940$E-01$	2.460 $E+00$	3.110$E-02$	2.08$E-06$	**1.42119$E-05$**
	SD	5.570$E-01$	9.33$E-12$	8.810$E-01$	7.900$E-01$	9.830$E-02$	1.19$E-05$	**1.853$E-05$**
F_{13}	Mean	8.320$E-02$	2.00$E-11$	1.160$E-01$	2.200$E-01$	2.200$E-03$	1.57$E-04$	**9.91151$E-05$**
	SD	7.060$E-01$	1.13$E-11$	1.930$E-01$	9.000$E-02$	4.630$E-03$	2.15$E-04$	**0.00015148**

Table 9: Result of several optimization approaches in view of fixed dimension function.

<!-Col Count:8->Function	Metric	Algorithms					
		FEP [54]	GSA [55]	GWO [56]	DE [57]	HHO	**hHHO−RES**
F_{15}	Mean	0	0	0	0	3.10E−04	**0.000346352**
	SD	0	0	0	0	1.97E−04	**3.28017$E-05$**
F_{16}	Mean	−1.03	−1.03	−1.03	−1.03	−1.03 $E+00$	**−1.031628451**
	SD	0	0	−1.03	0	6.78E−16	**1.29894$E-08$**
F_{18}	Mean	3.02	3	3	3	3.0 $E+00$	**3.000000979**
	SD	0.11	0	3	0	0.00	**3.23036$E-06$**
F_{20}	Mean	−3.27	−3.32	−3.29	–	−3.322	**−3.086651553**
	SD	0.06	0.02	−3.25	–	0.137406	**0.091761153**
F_{21}	Mean	−5.52	−5.96	−10.15	−10.15	−10.1451	**−7.219196247**
	SD	1.59	3.74	−9.14	0	0.885673	**2.220066434**
F_{22}	Mean	−5.53	−9.68	−10.4	−10.4	−10.40	**−6.146328648**
	SD	2.12	2.01	−8.58	0	1.3523	**1.967379234**
F_{23}	Mean	−6.57	−10.54	−10.53	−10.54	−10.5364	**−6.787325891**
	SD	3.14	0	−8.56	0	0.927655	**2.265291538**

problems of fixed dimensions by considering 30 trial runs and 500 iterations. The statistical test including standard deviation (SD), mean value, best, worst values and median, and hypothetical test involving p value was calculated for each function and demonstrated in Tables 4–6.

For statistical analysis, the mean value, SD, median value, and best and worst values have been taken into consideration. From Table 4, it reveals that the mean value of each unimodal function is near zero, which shows it matches the null hypothesis. Furthermore, it is found that the mean value for F_1 is $1.79672E-95$, which is better than F_2 to F_7. Furthermore, Table 5 shows the statistical analysis of multimodal standard benchmarks. These functions start from F_8 to F_{13}. The dimensions and range of each benchmark are different as shown in Table 2. As for some functions, the ranges are between −ve and for some benchmarks, they are

Table 10: Execution time of standard benchmark functions using hHHO-RES.

Methods	hHHO-RES		
Benchmark functions	Best value (seconds)	Mean value (seconds)	Worst value (seconds)
F_1	0.0468	0.08229	0.2656
F_2	0.0468	0.07760	0.187
F_3	0.218	0.24427	0.2968
F_4	0.0468	0.05989	0.12
F_5	0.06	0.08177	0.1093
F_6	0.0468	0.06145	0.093
F_7	0.12	0.1583	0.2656
F_8	0.062	0.0838	0.1093
F_9	0.0468	0.0682	0.093
F_{10}	0.062	0.0770	0.218
F_{11}	0.0781	0.0880	0.1093
F_{12}	0.281	0.3088	0.5
F_{13}	0.281	0.3192	0.43
F_{14}	0.5	0.5421	0.62
F_{15}	0.0468	0.0567	0.1406
F_{16}	0.0468	0.0557	0.0781
F_{17}	0.031	0.0651	0.18
F_{18}	0.031	0.0520	0.093
F_{19}	0.0468	0.0604	0.0781
F_{20}	0.0468	0.0645	0.093
F_{21}	0.062	0.0713	0.093
F_{22}	0.062	0.0838	0.1093
F_{23}	0.0781	0.0973	0.125

Table 11: Economical indices of different components of HES.

System	Capital cost ($)	O&M cost ($)	Salvage value ($)	Fuel cost
SPV system (0.235 kW)	166.4	3.328	16.64	—
Biomass generator(1 kW)	895.267	44.763	268.58	13$/ton
Biogas generator(1 kW)	572	28.6	171.6	6.93 $/ton

between +ve values. So, the outputs of some benchmarks are negative, while few are positive in nature. For F_9 and F_{11}, the proposed optimizer is performing perfectly as the output is 0, which accepts its null hypothesis. Furthermore, the statistical analysis of fixed-dimension functions is given in Table 6. The range of F_{16} is in −ve, so the output of the benchmarks F_{16}, F_{20}, F_{21}, F_{22}, and F_{23} is in −ve for mean value, best, worst value, and median value.

The p value is one of the most important tests that approaches testing for hypothesis to calculate the probability of whether for that problem there is evidence to discard the null hypothesis. Also, the null hypothesis is identified as a conjecture that can initially claim a population as well as data-generating procedure. In the case of an alternative hypothesis, whether population parameters differ from the value of population parameters stated in that conjecture. In the case of practices, the significant levels are stated in advance to define the small number of p values that must be rejected as null hypothesis. This is done because of the different researcher's usages of their different levels of significance when observing questions. Someone may sometimes face difficulties comparing the results or outcome from the groups of different kinds of tests. The p value helps to provide solutions to these types of problems. The null hypothesis and alternative hypothesis are the most commonly used hypothesis. From Tables 4–6, it is observed that the p value for unimodal and fixed dimension benchmarks is $1.7344E-06$ and for multimodal functions it is $1.7344E-06$ for F_8, F_{12}, and F_{13}; 1 for F_9 and F_{11}; and $4.32046E-08$ for F_{10}, which successfully indicates its null hypothesis.

Furthermore, in view of evaluating the performance, the proposed hHHO-RES is compared with the other existing optimizers in view of unimodal, multimodal, and fixed dimension functions and demonstrated in Tables 7–9. The mean value and the value of SD have been taken into consideration to make comparison with other optimization approaches.

While analysing the output of the proposed hHHO-RES optimizer in the case of unimodal functions, as shown in Table 7, it is clear that, in most cases, the proposed hHHO-RES optimizer outperforms the other existing optimizers. In the case of multimodal functions, as seen in Table 8, the output of hHHO-RES for standard functions F_9, F_{10}, F_{11}, and F_{12} surpasses the other optimizers since its output is 0, proving the null hypothesis. Furthermore, the parameter ranges for F_{16} and F_{20} to F_{23} are all negative, resulting in the output also being negative, as illustrated in Table 9. In a nutshell, it is experimentally revealed that the output of the suggested hHHO-RES performs better than other existing

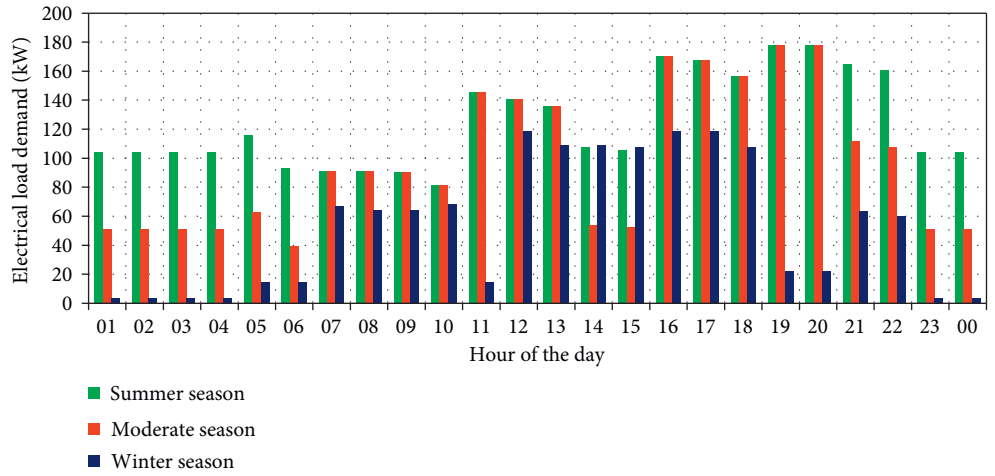

Figure 3: Seasonal hourly load demand of the selected site.

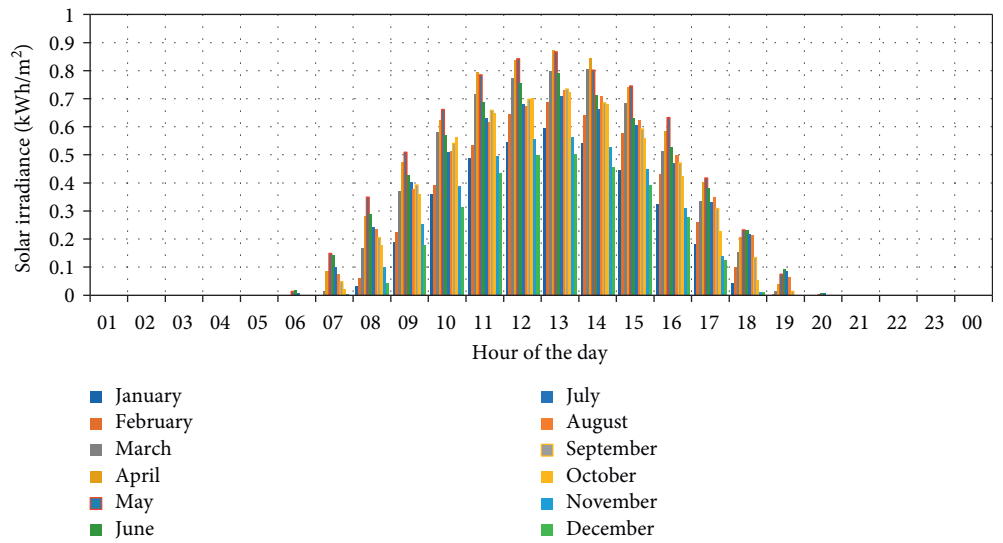

Figure 4: Monthly average solar energy for the study area [72].

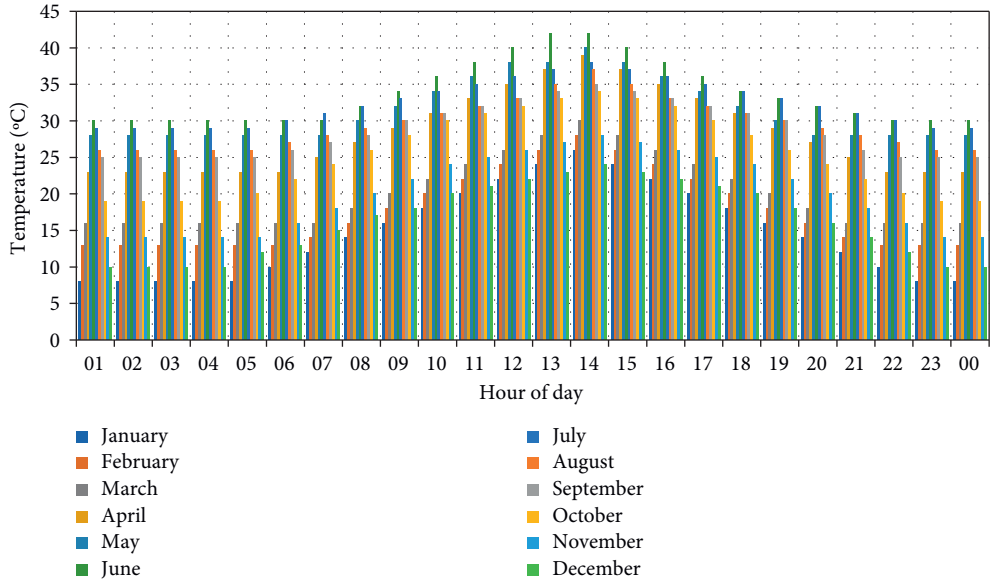

Figure 5: Mean air temperature for a study area [72].

Table 12: Biogas and biomass generator scheduling for the selected region.

Bio-generator	SS	MS	WS
Biogas generator	01.00 to 05.00	01.00 to 05.00	17.00 to 19.00
Biomass generator	18.00 to 24.00	16.00 to 24.00	20.00 to 22.00

Table 13: Result of off-grid models using hHHO-RES algorithm for 0% unmet load.

Model	Algorithm	N_{SP}	N_{Bt}	P_{SP} (kW)	E_{Bt} (kWh)	P_{BMS} (kW)	P_{BGS} (kW)	NPC (10^5 \$)	CoE (\$/kWh)
M_{11}	hHHO-RES	903	278	212.21	667.2	174	-	7.81	0.115
	HS	461	636	108.34	1526.4	255	-	13.03	0.191
	PSO	894	280	210.09	672	176	-	7.88	0.116
M_{12}	hHHO-RES	991	217	232.89	520.8	-	165	7.96	0.117
	HS	577	510	135.60	1224	-	302	14.80	0.217
	PSOdsb	962	235	226.07	564	-	168	8.20	0.120
M_{13}	hHHO-RES	974	278	228.89	667.2	182	142	9.96	0.146
	HS	804	356	188.94	854.4	179	216	11.95	0.175
	PSO	902	316	211.97	758.4	235	94	10.55	0.155

Table 14: Result of grid-linked model using different algorithms for 0% unmet load.

Algorithm	N_{SP}	N_{Bt}	P_{SP} (kW)	P_{BMS} (kW)	P_{BGS} (kW)	E_{Bt} (kWh)	NPC (10^5\$)	CoE (\$/kWh)
hHHO-RES	1000	11	235	56	11	26.4	5.50	0.076
HS	963	23	226.305	41	98	55.2	6.00	0.081
PSO	858	34	201.63	87	5	81.6	6.12	0.088

Table 15: Comparative analysis of algorithms for the best model.

Algorithm	NPC (\$)	CoE (\$/kWh)	Best	Means	Worst	SD
hHHO-RES	5.50	0.076	600870.3	653231.4	946238.3	112877.1
HS	6.00	0.081	607875.2	628041	687766.6	20059.17
PSO	6.12	0.088	627390.3	816840.2	1087709	121326.9

optimizers in most cases. Furthermore, the simulation time for standard benchmark functions using hHHO-RES is presented in Table 10.

7.2. Optimal Sizing and Designing of HES for the Selected Area. After successfully testing the performance of the proposed hHHO-RES in the present research, the optimal sizing and designing of HES, including various RER, were obtained for fulfilling the energy demand for the selected area because of minimising NPC. First of all, three models of off-grid HES have been considered in the present study as follows:

(a) Model M_{11} : SPV/biomass with battery

(b) Model M_{12} : SPV/biogas with battery

(c) Model M_{13} : SPV/biomass/biogas with battery

The proposed hHHO-RES algorithm has been applied to optimise the above-stated models. The optimization results for the same models of off-grid HES have also been obtained from HS and PSO algorithms to validate the results. Furthermore, the grid-linked SPV/biomass/biogas with battery model of HES has also been optimised using the same algorithms. Finally, the results obtained from the above-stated off-grid models were compared with the grid-linked model, and the most optimal solution was found. The optimization results have been obtained based on several techno-economic indices as listed in Table 11 [51]. Besides, the hourly electrical load demand, solar irradiation, and air temperature of the selected site have been shown in Figures 3–5 [5, 72]. Also, biogenerators have been scheduled to operate at peak load hours during each season and are shown in Table 12.

The annual real interest, escalation, and inflation rates are set at 0.11, 0.05, and 0.075, respectively. The hourly simulation for all the selected models has been performed in MATLAB for one year using hHHO-RES, HS, and PSO algorithms. The parameters of the hHHO-RES, HS, and PSO algorithms are set as follows: hHHO-RES: iteration (max) = 150, Run-30; HS: iteration (max) = 150; harmony memory size = 4; harmony memory consideration rate = 0.95; pitch adjustment rate = 0.1; maximum pitch adjustment rate = 1; minimum pitch adjustment rate = 0.1; PSO: $m = 4$, learning coefficient (L_{C1}, L_{C2}) = 2, population size = 30, and iteration (max) = 150. The optimization results obtained after hourly

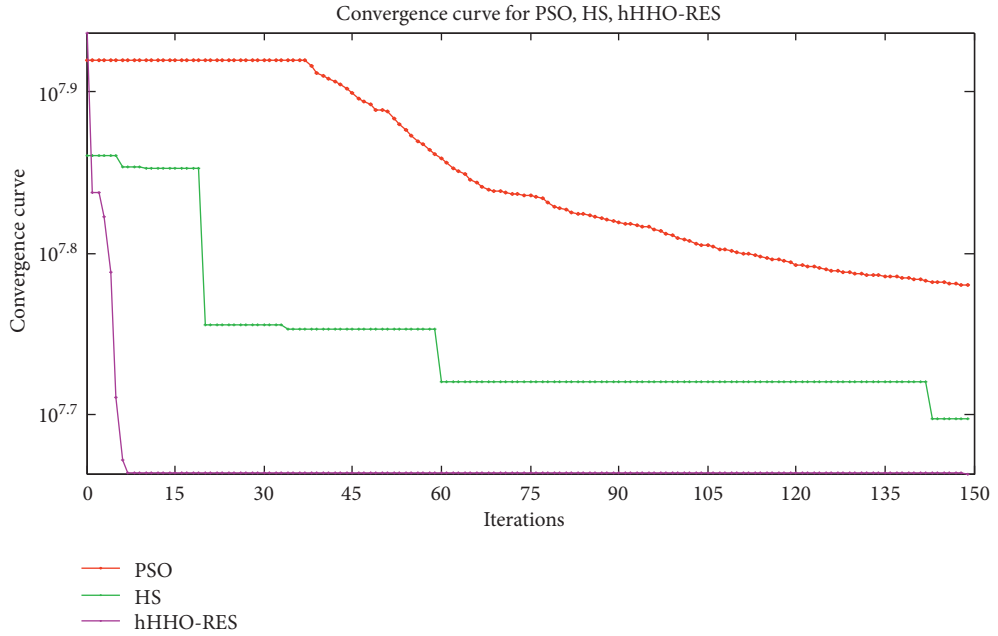

Figure 6: Convergence curve of PSO, HS, and hHHO-RES in view of NPC.

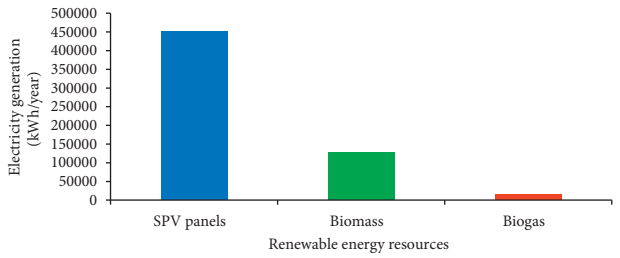

Figure 7: Share of RER in yearly electricity generation.

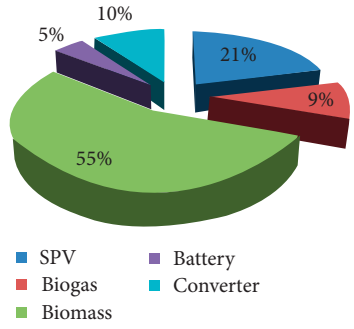

Figure 8: Bifurcation of NPC in view of HES components.

Table 16: Costwise bifurcation of NPC.

S. No.	Cost/revenue	Value ($)
1	C_{NV}	108441.1
2	OM_{NV}	90153.33
3	F_{NV}	38190.67
4	SV_{NV}	8508.933
5	C_{SG}	50912
6	C_{PG}	372973.3

Table 17: Seasonal grid energy purchases and sales.

Season	Electricity purchase from the grid (kWh)	Electricity sold to the grid (kWh)
SS	170270	21278
MS	111980	14004
WS	45314	13159
Total (kWh/year)	327565	48441

simulation for selected off-grid models along with their size are listed in Table 13.

It is noticed from Table 13 that the proposed hHHO-RES algorithm gives the least NPC with the minimum CoE of model M_{11}. The hHHO-RES algorithm estimates 212.21 (903 no.s) kW SPV, 174 kW biomass, and 667.2 (278 no.) kWh of battery storage with an NPC of $\$7.81 * 10^5$ that results from a CoE of 0.115 \$/kWh. Furthermore, the optimization result obtained using the above-stated algorithms for grid-linked HES is illustrated in Table 14.

While comparing Tables 13 and 14, it is found that the grid-linked HES has the least NPC of $\$5.50 * 10^5$ and a CoE of 0.076 \$/kWh. Moreover, the grid-linked HES has the fewest batteries among the selected models of HES. Based on the acquired results, the grid-linked HES is proposed to be the most optimal solution for the selected area. The optimum size of the proposed system components is found as the biogas and biomass generators of 11 kW and 56 kW, respectively, the SPV system of 235 kW with a battery storage of 26.4 kWh, and the converter of 100 kW. It is also inferred that the performance of the proposed algorithm is better in

comparison with HS and PSO. Furthermore, in Table 15, several other parameters are also measured and compared, and it is apparent that hHHO-RES performs better. Likewise, the PSO, HS, and hHHO-RES convergence curve for NPC is graphed in Figure 6.

While carefully examining the results of all algorithms, it is observed that the hHHO-RES converges completely and gives the optimal solution before 10 iterations. However, HS and PSO are given constant values after 140 iterations. Furthermore, the significant parameters related to the suggested grid-connected HES are analysed and demonstrated in the following paragraphs.

The share of each RER in yearly electricity generation by the proposed HES is given in Figure 7. It reveals that the maximum share of electricity generation comes from SPV panels of 450500 kWh/year, followed by biomass and biogas of 127325 kWh/year and 15830 kWh/year, respectively.

The costwise bifurcation of NPC in view of different types of costs and revenues is shown in Table 16.

It is revealed that the purchasing cost of electricity is the highest of all. Also, the bifurcation of NPC in view of system components is presented in Figure 8 and found that biomass has the maximum share of 55% compared to SPV, converter, biogas, and battery of 21%, 10%, 9%, and 5%, respectively.

The input and output power of the battery are estimated as 78011 kWh/year and 334450 kWh/year, respectively, in a year. Furthermore, the yearly electricity purchased and sold to the utility grid in each season is presented in Table 17.

It has been witnessed that the major electricity has been purchased in the SS due to higher demand. On the contrary, the grid purchases and sales are less in the WS as compared to other seasons due to less energy demand.

8. Conclusion

In this research, optimum design and sizing of RER based on HES for remote locations in Haryana state (India) has been carried out using a newly devised hHHO-RES algorithm. Various developed models are analysed and compared using the hHHO-RES algorithm in off-grid and grid-linked scenarios. The grid-linked model composed of SPV/biomass/biogas with battery has been proven to be the most optimum for the area of study. The optimum size of the HES in the grid scenario for the research area is determined based on simulation on hourly basis as 235 kW SPV array, 11 kW biogas, 56 kW biomass, a 26.4 kWh battery bank, and a 100 kW converter. The estimated total NPC and CoE are $\$5.50 * 105$ and \$0.076/kWh, respectively.

Furthermore, the exploitation phase of the existing HHO is upgraded effectively using the RES algorithm, and the developed algorithm (hHHO-RES) is tested for standard benchmarks. It is observed that the proposed hybrid optimizer approves its efficacy in the field of nature-inspired and metaheuristic algorithms.

Abbreviations

ABC: Artificial bee colony
ABSO: Artificial bee swarm optimization
ACO: Ant colony optimization
ALO: Ant lion optimizer
BA: Bat algorithm
BBO: Biogeography-based optimization
BBBC: Big-Bang-Big-Crunch
BDA: Binary dragonfly algorithm
BFA: Bacterial foraging algorithm
BPSO: Binary particle swarm optimization
CoE: Cost of energy
CS: Cuckoo search
CSA: Crow search algorithm
DA: Dragonfly algorithm
DE: Differential evolution
DG: Diesel generator
DR: Demand response
FA: Firefly algorithm
FC: Fuel cell
FEP: Fast evolutionary programming
FPA: Flower pollination algorithm
GA: Genetic algorithm
GOA: Grasshopper optimization algorithm
GSA: Gravitational search algorithm
GWO: Grey wolf optimization
HES: Hybrid energy system
HHO: Harris hawk's optimizer
HHHO-RES: Random exploratory search centered Harris hawks optimizer
HS: Harmony search
HHO: Harris hawk's optimizer
HOMER: Hybrid optimization of multiple energy resources
LOLP: Loss of load probability
LPSP: Loss of power supply probability
MBA: Mine blast algorithm
MCS: Modified cuckoo search
MFO: Moth flame optimization
MHP: Microhydro
MOCSA: Multiobjective crow search algorithm
MS: Moderate season
NPC: Net present cost
PSO: Particle swarm optimization
RER: Renewable energy resources
RES: Random exploratory search
SA: Simulated annealing
SCA: Sine-cosine algorithm
SD: Standard deviation
SDO: Supply-demand-based optimization
SMO: Social mimic optimization
SMS: States of matter search
SPV: Solar photovoltaic
SS: Summer season
SSA: Salp swarm algorithm
WOA: Whale optimization algorithm
WS: Winter season.

Data Availability

Hourly load demand, biogas, and biomass related data have been collected locally. The solar irradiance and ambient temperature data have been collected from an open-source platforms.

Conflicts of Interest

The authors declare that they have no conflicts of interest.

References

[1] D. Akinyele, "Techno-economic design and performance analysis of nanogrid systems for households in energy-poor villages," *Sustainable Cities and Society*, vol. 34, pp. 335–357, 2017.

[2] P. Anand, S. K. Bath, and M. Rizwan, "Renewable energy-based hybrid model for rural electrification," *International Journal of Energy Technology and Policy*, vol. 15, no. 1, pp. 86–113, 2019.

[3] A. Razmjoo and A. Davarpanah, "Developing various hybrid energy systems for residential application as an appropriate and reliable way to achieve Energy sustainability," *Energy Sources, Part A: Recovery, Utilization, and Environmental Effects*, vol. 41, no. 10, pp. 1180–1193, 2019.

[4] S. Jamshidi, K. Pourhossein, and M. Asadi, "Size estimation of wind/solar hybrid renewable energy systems without detailed wind and irradiation data: a feasibility study," *Energy Conversion and Management*, vol. 234, Article ID 1139, 2021.

[5] P. Anand, M. Rizwan, and S. K. Bath, "Sizing of renewable energy based hybrid system for rural electrification using grey wolf optimisation approach," *IET Energy Systems Integration*, vol. 1, no. 3, pp. 158–172, 2019.

[6] J. Lian, Y. Zhang, C. Ma, Y. Yang, and E. Chaima, "A review on recent sizing methodologies of hybrid renewable energy systems," *Energy Conversion and Management*, vol. 199, Article ID 112027, 2019.

[7] T. Ma and M. S. Javed, "Integrated sizing of hybrid PV-wind-battery system for remote island considering the saturation of each renewable energy resource," *Energy Conversion and Management*, vol. 182, pp. 178–190, 2019.

[8] M. D. A. Al-falahi, S. D. G. Jayasinghe, and H. Enshaei, "A review on recent size optimization methodologies for standalone solar and wind hybrid renewable energy system," *Energy Conversion and Management*, vol. 143, pp. 252–274, 2017.

[9] O. Ekren and B. Y. Ekren, "Size optimization of a PV/wind hybrid energy conversion system with battery storage using simulated annealing," *Applied Energy*, vol. 87, no. 2, pp. 592–598, 2010.

[10] A. Chauhan, S. Upadhyay, M. T. Khan, S. M. S. Hussain, and T. S. Ustun, "Performance investigation of a solar photovoltaic/diesel generator based hybrid system with cycle charging strategy using BBO algorithm," *Sustainability*, vol. 13, no. 14, pp. 8048–8118, 2021.

[11] A. Maleki and A. Askarzadeh, "Artificial bee swarm optimization for optimum sizing of a stand-alone PV/WT/FC hybrid system considering LPSP concept," *Solar Energy*, vol. 107, pp. 227–235, 2014.

[12] R. Sen and S. C. Bhattacharyya, "Off-grid electricity generation with renewable energy technologies in India: an application of homer," *Renewable Energy*, vol. 62, pp. 388–398, 2014.

[13] M. J. Khan, A. K. Yadav, and L. Mathew, "Techno economic feasibility analysis of different combinations of PV-Wind-Diesel-Battery hybrid system for telecommunication applications in different cities of Punjab, India," *Renewable and Sustainable Energy Reviews*, vol. 76, pp. 577–607, 2017.

[14] A. D. Dhass and S. Harikrishnan, "Cost effective hybrid energy system employing solar-wind-biomass resources for rural electrification," *International Journal of Renewable Energy Resources*, vol. 3, no. 1, pp. 222–229, 2013.

[15] W. S. Ho, H. Hashim, and J. S. Lim, "Integrated biomass and solar town concept for a smart eco-village in Iskandar Malaysia (IM)," *Renewable Energy*, vol. 69, pp. 190–201, 2014.

[16] H. Garrido, V. Vendeirinho, and M. C. Brito, "Feasibility of KUDURA hybrid generation system in Mozambique: sensitivity study of the small-scale PV-biomass and PV-diesel power generation hybrid system," *Renewable Energy*, vol. 92, pp. 47–57, 2016.

[17] M. Sharafi and T. Y. ELMekkawy, "Multi-objective optimal design of hybrid renewable energy systems using PSO-simulation based approach," *Renewable Energy*, vol. 68, pp. 67–79, 2014.

[18] A. S. O. Ogunjuyigbe, T. R. Ayodele, and O. A. Akinola, "Optimal allocation and sizing of PV/Wind/Split-diesel/Battery hybrid energy system for minimizing life cycle cost carbon emission and dump energy of remote residential building," *Applied Energy*, vol. 171, pp. 153–171, 2016.

[19] O. Nadjemi, T. Nacer, A. Hamidat, and H. Salhi, "Optimal hybrid PV/wind energy system sizing: application of cuckoo search algorithm for Algerian dairy farms," *Renewable and Sustainable Energy Reviews*, vol. 70, pp. 1352–1365, 2017.

[20] M. B. Eteiba, S. Barakat, M. M. Samy, and W. I. Wahba, "Optimization of an off-grid PV/Biomass hybrid system with different battery technologies," *Sustainable Cities and Society*, vol. 40, pp. 713–727, 2018.

[21] M. Sufyan, N. Abd Rahim, C. Tan, M. A. Muhammad, and S. R. Sheikh Raihan, "Optimal sizing and energy scheduling of isolated microgrid considering the battery lifetime degradation," *PLoS One*, vol. 14, no. 2, Article ID e0211642, 2019.

[22] A. Khiareddine, C. Ben Salah, D. Rekioua, and M. F. Mimouni, "Sizing methodology for hybrid photovoltaic/wind/hydrogen/battery integrated to energy management strategy for pumping system," *Energy*, vol. 153, pp. 743–762, 2018.

[23] M. Jamshidi and A. Askarzadeh, "Techno-economic analysis and size optimization of an off-grid hybrid photovoltaic, fuel cell and diesel generator system," *Sustainable Cities and Society*, vol. 44, pp. 310–320, 2019.

[24] H. Jiang, L. Xu, J. Li, Z. Hu, and M. Ouyang, "Energy management and component sizing for a fuel cell/battery/supercapacitor hybrid powertrain based on two-dimensional optimization algorithms," *Energy*, vol. 177, pp. 386–396, 2019.

[25] A. Ghaffari and A. Askarzadeh, "Design optimization of a hybrid system subject to reliability level and renewable energy penetration," *Energy*, vol. 193, Article ID 116754, 2020.

[26] T. Wu, H. Zhang, and L. Shang, "Optimal sizing of a grid-connected hybrid renewable energy systems considering hydroelectric storage," *Energy Sources, Part A: Recovery, Utilization, and Environmental Effects*, vol. 42, pp. 1–17, 2020.

[27] S. Kumar, T. Kaur, S. Upadhyay, V. Sharma, and D. Vatsal, "Optimal sizing of stand alone hybrid renewable energy system with load shifting," *Energy Sources, Part A: Recovery, Utilization, and Environmental Effects*, vol. 42, pp. 1–20, 2020.

[28] F. A. Alturki, A. A. Al-Shamma'a, H. M. H. Farh, and K. AlSharabi, "Optimal sizing of autonomous hybrid energy

system using supply-demand-based optimization algorithm," *International Journal of Energy Research*, vol. 45, no. 1, pp. 605–625, 2020.

[29] F. A. Alturki and E. M. Awwad, "Sizing and cost minimization of standalone hybrid WT/PV/Biomass/Pump-hydro storag*E* – based energy systems," *Energies*, vol. 14, no. 489, pp. 1–20, 2021.

[30] A. M. Eltamaly and M. A. Alotaibi, "Novel fuzzy-swarm optimization for sizing of hybrid energy systems applying smart grid concepts," *IEEE Access*, vol. 9, Article ID 93650, 2021.

[31] A. M. Eltamaly, E. Ali, M. Bumazza, S. Mulyono, and M. Yasin, "Optimal design of hybrid renewable energy system for a reverse osmosis desalination system in Arar, Saudi Arabia," *Arabian Journal for Science and Engineering*, vol. 46, no. 10, pp. 9879–9897, 2021.

[32] A. M. Eltamaly, M. A. Alotaibi, A. I. Alolah, and M. A. Ahmed, "A novel demand response strategy for sizing of hybrid energy system with smart grid concepts," *IEEE Access*, vol. 9, Article ID 20294, 2021.

[33] B. S. Borowy and Z. M. Salameh, "Methodology for optimally sizing the combination of a battery bank and PV array in a wind/PV hybrid system," *IEEE Transactions on Energy Conversion*, vol. 11, no. 2, pp. 367–375, 1996.

[34] S. Diaf, D. Diaf, M. Belhamel, M. Haddadi, and A. Louche, "A methodology for optimal sizing of autonomous hybrid PV/wind system," *Energy Policy*, vol. 35, no. 11, pp. 5708–5718, 2007.

[35] R. Chedid and S. Rahman, "Unit sizing and control of hybrid wind-solar power systems," *IEEE Transactions on Energy Conversion*, vol. 12, no. 1, pp. 79–85, 1997.

[36] E. S. Gavanidous and A. G. Bakirtzis, "Design of a stand alone system with renewable energy sources using trade off methods," *IEEE Transactions on Energy Conversion*, vol. 7, no. 1, pp. 42–48, 1992.

[37] A. E. S. A. Nafeh, "Optimal economical sizing of a PV-wind hybrid energy system using genetic algorithm," *International Journal of Green Energy*, vol. 8, no. 1, pp. 25–43, 2011.

[38] S. Upadhyay and M. P. Sharma, "Development of hybrid energy system with cycle charging strategy using particle swarm optimization for a remote area in India," *Renewable Energy*, vol. 77, pp. 586–598, 2015.

[39] A. Heydari and A. Askarzadeh, "Optimization of a biomass-based photovoltaic power plant for an off-grid application subject to loss of power supply probability concept," *Applied Energy*, vol. 165, pp. 601–611, 2016.

[40] R. Kumar, R. A. Gupta, and A. K. Bansal, "Economic analysis and power management of a stand-alone wind/photovoltaic hybrid energy system using biogeography based optimization algorithm," *Swarm and Evolutionary Computation*, vol. 8, pp. 33–43, 2013.

[41] A. Maleki and F. Pourfayaz, "Sizing of stand-alone photovoltaic/wind/diesel system with battery and fuel cell storage devices by harmony search algorithm," *Journal of Energy Storage*, vol. 2, pp. 30–42, 2015.

[42] A. Fathy, "A reliable methodology based on mine blast optimization algorithm for optimal sizing of hybrid PV-wind-FC system for remote area in Egypt," *Renewable Energy*, vol. 95, no. 562, pp. 367–380, 2016.

[43] A. A. Heidari, S. Mirjalili, H. Faris, I. Aljarah, M. Mafarja, and H. Chen, "Harris Hawks optimization: algorithm and applications," *Future Generation Computer Systems*, vol. 97, pp. 849–872, 2019.

[44] H. M. Alabool, D. Alarabiat, L. Abualigah, and A. A. Heidari, "Harris hawks optimization: a comprehensive review of recent variants and applications," *Neural Computing & Applications*, vol. 33, no. 15, pp. 8939–8980, 2021.

[45] A. M. Helmi, R. Carli, M. Dotoli, and H. S. Ramadan, "Efficient and sustainable reconfiguration of distribution networks via metaheuristic optimization," *IEEE Transactions on Automation Science and Engineering*, vol. 19, no. 1, pp. 82–98, 2022.

[46] V. K. Kamboj, A. Nandi, A. Bhadoria, and S. Sehgal, "An intensify Harris Hawks optimizer for numerical and engineering optimization problems," *Applied Soft Computing*, vol. 89, Article ID 106018, 2020.

[47] D. Dhawale and V. K. Kamboj, "hHHO-IGWO,A new hybrid harris hawks optimizer for solving global optimization problems," in *Proceedings of the 2020 International Conference on ComputationAutomation and Knowledge Management (ICCAKM)*, pp. 9-10, Dubai, UAE, January 2020.

[48] Q. Fan, Z. Chen, and Z. Xia, "A novel quasi-reflected Harris hawks optimization algorithm for global optimization problems," *Soft Computing*, vol. 24, no. 19, Article ID 14843, 2020.

[49] H. Jia, C. Lang, D. Oliva, W. Song, and X. Peng, "Dynamic harris hawks optimization with mutation mechanism for satellite image segmentation," *Remote Sensing*, vol. 11, no. 12, pp. 1421–1435, 2019.

[50] "Description of Sonipat District," 2021, http://www.sonipat.nic.in/.

[51] P. Anand, S. K. Bath, and M. Rizwan, "Size optimisation of RES-based grid connected hybrid power system using harmony search algorithm," *International Journal of Energy Technology and Policy*, vol. 16, no. 3, pp. 238–276, 2020.

[52] J. C. Bednarz, "Cooperative hunting harris' hawks (p," *Science*, vol. 239, no. 4847, pp. 1525–1527, 1988.

[53] J. G. Digalakis and K. G. Margaritis, "On benchmarking functions for genetic algorithms," *International Journal of Computer Mathematics*, vol. 77, no. 4, pp. 481–506, 2001.

[54] X. Xin Yao, Y. Yong Liu, and G. Guangming Lin, "Evolutionary programming made faster," *IEEE Transactions on Evolutionary Computation*, vol. 3, no. 2, pp. 82–102, 1999.

[55] E. Rashedi, H. Nezamabadi-Pour, and S. Saryazdi, "GSA: a gravitational search algorithm," *Information Sciences*, vol. 179, no. 13, pp. 2232–2248, 2009.

[56] H. John, "Adaptation in Natural and Artificial Systems: An Introductory Analysis with Applications to Biology, Control, and Artificial Intelligence," *Computing and Processing*, MIT Press, Cambridge, 1992.

[57] S. Mirjalili, S. M. Mirjalili, and A. Lewis, "Grey wolf optimizer," *Advances in Engineering Software*, vol. 69, pp. 46–61, 2014.

[58] X. S. Yang and S. Deb, "Cuckoo Search via Lévy Flights," in *Proceedings of the 2009 World Congress on Nature & Biologically Inspired Computing(NaBIC)*, pp. 210–214, IEEE, Coimbatore, India, December 2009.

[59] S Mirjalili, "Dragonfly algorithm: a new meta-heuristic optimization technique for solving singl*E* – objective, discrete and multi-objective problems," *Neural Computing & Applications*, vol. 27, no. 4, pp. 1053–1073, 2016.

[60] X.-S. Yang, M. Karamanoglu, and X. He, "Flower pollination algorithm: a novel approach for multiobjective optimization," *Engineering Optimization*, vol. 46, no. 9, pp. 1222–1237, 2014.

[61] S. Mirjalili, "The ant lion optimizer," *Advances in Engineering Software*, vol. 83, pp. 80–98, 2015.

[62] S. Saremi, S. Mirjalili, and A. Lewis, "Grasshopper optimisation algorithm: theory and application," *Advances in Engineering Software*, vol. 105, pp. 30–47, 2017.
[63] S. Mirjalili, S. M. Mirjalili, and A. Hatamlou, "Multi-verse optimizer: a natur*E* – inspired algorithm for global optimization," *Neural Computing & Applications*, vol. 27, no. 2, pp. 495–513, 2016.
[64] S. Mirjalili and A. Lewis, "The whale optimization algorithm," *Advances in Engineering Software*, vol. 95, pp. 51–67, 2016.
[65] E. Rashedi, H. Nezamabadi-Pour, and S. Saryazdi, "BGSA: binary gravitational search algorithm," *Natural Computing*, vol. 9, no. 3, pp. 727–745, 2010.
[66] S. Mirjalili, A. H Gandomi, S. Z. Mirjalili, S. Saremi, H. Faris, and S. M. Mirjalili, "Salp Swarm Algorithm: a bio-inspired optimizer for engineering design problems," *Advances in Engineering Software*, vol. 114, pp. 163–191, 2017.
[67] J. Kennedy and R. C. Eberhart, "A discrete binary version of the particle swarm algorithm," in *Proceedings of the 1997 IEEE International Conference on Systems, Man, and Cybernetics. Computational Cybernetics and Simulation*, pp. 4104–4108, FL, USA, October 1997.
[68] E. Cuevas, A. Echavarría, and M. A. Ramírez-Ortegón, "An optimization algorithm inspired by the States of Matter that improves the balance between exploration and exploitation," *Applied Intelligence*, vol. 40, no. 2, pp. 256–272, 2014.
[69] R. Storn and K. Price "Differential evolution-a simple and efficient heuristic for global optimization over continuous spaces," *Journal of Global Optimization*, vol. 11, no. 4, pp. 341–359, 1997.
[70] S. Mirjalili, "SCA: a Sine Cosine Algorithm for solving optimization problems," *KnowledgE – Based Systems*, vol. 96, pp. 120–133, 2016.
[71] S. Mirjalili, "Moth-flame optimization algorithm: a novel natur*E* – inspired heuristic paradigm," *KnowledgE – Based Systems*, vol. 89, pp. 228–249, 2015.
[72] "Solar Irradiation and Air temperature of study area: NASA," *Surface Meteorology and Solar Energy: A Renewable Energy Resource Website*, https://asdc.larc.nasa.gov, 2021.

ResearchGate

See discussions, stats, and author profiles for this publication at: https://www.researchgate.net/publication/361021781

OTA Based Fractional-Order Oscillator With Controlled Phase Difference

Conference Paper · June 2022

CITATIONS
0

READS
43

3 authors:

Garima Varshney
Delhi Technological University
12 PUBLICATIONS **11** CITATIONS
SEE PROFILE

Neeta Pandey
Delhi Technological University
312 PUBLICATIONS **1,834** CITATIONS
SEE PROFILE

Rajeshwari Pandey
Delhi Technological University
108 PUBLICATIONS **874** CITATIONS
SEE PROFILE

Some of the authors of this publication are also working on these related projects:

for teaching View project

Ph.D. work View project

All content following this page was uploaded by Garima Varshney on 02 June 2022.

The user has requested enhancement of the downloaded file.

OTA Based Fractional-Order Oscillator With Controlled Phase Difference

Garima varshney
ECE department
Delhi Technological University
New Delhi,India
gvarshn1@gmail.com

Neeta Pandey
ECE department
Delhi Technological University
New Delhi,India
neetapandey@dce.ac.in

Rajeshwari Pandey
ECE department
Delhi Technological University
New Delhi,India
rpandey@dce.ac.in

***Abstract*—In this manuscript, a new fractional-order (FO) oscillator is proposed, which employs two fractional-order capacitors (FOC) and two operational trans-conductance amplifiers (OTA). The difference of phase between two output voltages of FO oscillator can be independently controlled. Sensitivity of frequency of oscillations with respect to different circuit parameters is drafted mathematically. The functionality of the proposed structure is confirmed through SPICE simulations with 180nm CMOS technology model parameters and stability of the same is confirmed through pole plot in W-plane using *forlocus* function of MATLAB. Corner analysis and Monte-Carlo analysis are also carried out to illustrate the robustness of the proposed FO oscillator.**

***Index Terms*—Independent phase control, fractional-order oscillator, stability analysis, sensitivity, OTA, corner analysis, Monte-Carlo analysis.**

I. Introduction

The inherent ability of fractional-order calculus to provide increased accuracy in the depiction of a real-time phenomenon than those based on conventional integer-order techniques makes it more resourceful, hence the applications of fractional-order calculus are rising at an exponential rate [1]. Fractional-order circuits are found in numerous areas of science and engineering, for example electrical engineering [2], control systems [2]- [3], electronics and analog signal processing [2], biomedical [5]- [6], communication and image encryption [7]- [8]. Thus, an enormous horizon for research lies in the fractional-order domain at the integrative level.

Oscillators are the most commonly used electronic circuits in the analog signal processing domain. Various applications of oscillators are signal transmission, reception, jamming [9]. Researchers are integrating the notion of fractional-order concepts in oscillator designing; these kinds of oscillators are recognized as fractional-order (FO) oscillators.

In [10], the FO oscillator was first substantiated using the well-known oscillator Wein oscillator. In [11]- [12], the Barkhausen condition for FO oscillator was formulated and verified via Wien oscillators, Colpitts oscillator and LC tank resonator. Based upon different analog building blocks (ABB) various fractional-order oscillators were introduced in literature, for example operational transresistance amplifier (OTRA), differential voltage current conveyor (DVCC), current-controlled current follower transconductance amplifier (CCCFTA), MOS-RC, operational transconductance amplifier (OTA) and differential difference current conveyor (DDCC) based FO oscillators are discussed in [13]- [18] respectively. Stability analysis on some oscillator circuits appeared in [19]- [20]. Oscillation frequency of FO oscillator depends upon the circuit components used as well as the order of fractional-order elements, hence the frequency of oscillation of FO oscillator has extra degree of freedom and enhanced controllability over classical integer-order one.

Further, controllability of phase difference between the output voltages of an oscillator is an added advantage as this quality can be utilized in communication systems to design phase arrays, biomedical devices to diagnose Alzheimer and many more.

A summary of FO oscillators with independent phase and frequency control [16], [18], [21] based upon active and passive components count, %THD and power consumption is given in Table I and following are the observations:

- MOS transistors [16], differential difference current conveyor (DDCC) [18] and current feedback operational amplifier (CFOA) [21] based FOOs are reported in respective references.
- All of these FO oscillators employ 2 or more than ABBs.
- All FO oscillators with independent phase and frequency control, available in open literature, require resistor or floating FOC.

It is apparent from Table I that limited research is available for oscillators with independent phase and frequency control in fractional-domain which are resistor-less and use all grounded FOCs. In view of these issues the objectives of the proposed work are below:

- Independent phase and frequency control.
- Resistor-less FO oscillator with all grounded FOCs.
- Lesser number of components count with better performance.

The proposed FO oscillator provides independent control over the phase difference and frequency with minimum components count i.e. only two OTAs and two grounded FOCs.

The rest of the manuscript is organized as follows: Section 2 gives basic idea of FO oscillators and Section 3 deals with the design and implementation of the proposed circuit. Section

978-1-6654-8485-5/22/$31.00 ©2022 IEEE

4 talks about simulation results with corner and Monte-Carlo analysis followed by the concluding remarks in Section 5.

TABLE I
COMPARISON FOR DIFFERENT PARAMETERS OF PROPOSED FO OSCILLATOR

Ref.	ABBs used (count)	Components count (R/FOC)	%THD	Power consumed
[16]	MOS(12)	1/2	3.02	7.7mW
[18]	DDCC(2)	2/2	2.82	4.3mW
[21]	CFOA(3)	5/3	3.96	18.2mW
Proposed	**OTA(2)**	**0/2**	**1.60**	**0.58mW**

II. PRELIMINARIES

A. OTA

The OTA processes the difference of input voltages and provides current at low impedance output node. The block diagram of OTA appears in Fig.1 and the input-output port relationship is given by (1).

$$I_o = g_m(V_p - V_n) \tag{1}$$

where g_m is depending upon bias current I_b and called as transconductance gain of OTA. The dependence of g_m upon I_b is presented in (2)

$$g_m = \sqrt{\mu_n C_{ox} \frac{W}{L} I_b} \tag{2}$$

The symbols used in (2) have their usual meaning.

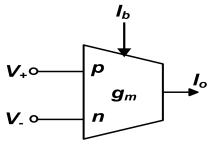

Fig. 1. Block diagram of dual-output OTA

B. Basic of FO oscillator

A linear fractional-order circuit with two fractional-order elements having fractional-order as α and β can be represented as (3) and the characteristics equation for this system is given in (4) :

$$\begin{bmatrix} D^\alpha x_1 \\ D^\beta x_2 \end{bmatrix} = \begin{bmatrix} a_{11} & a_{12} \\ a_{21} & a_{22} \end{bmatrix} \begin{bmatrix} x_1 \\ x_2 \end{bmatrix} \tag{3}$$

$$s^{\alpha+\beta} - a_{11}s^\beta - a_{22}s^\alpha + |A| = 0 \tag{4}$$

here $|A| = (a_{11}a_{22} - a_{12}a_{21})$ is the determinant of the system matrix.

The Barkhausen criterion is not sufficient but necessary condition for the sustained oscillations in a fractional-order oscillatory system [11]. Therefore, to make sure that the imaginary conjugate poles exist on $\pm j\omega$ axis, it is assumed that the imaginary conjugate poles are already on $\pm j\omega$ axis and they must satisfy the characteristics equation for a particular frequency of oscillation (ω_0) of the oscillatory system. As a consequence, in complex s-plane, the pair of poles must occur at $\pm j\omega_0$ and both poles must satisfy the characteristics equation. Hence putting $+j\omega_0$ and $-j\omega_0$ in (4) gives (5).

$$(+j\omega_0)^{\alpha+\beta} - (+j\omega_0)^\alpha a_{22} - (+j\omega_0)^\beta a_{11} + |A| = 0 \tag{5a}$$

$$(-j\omega_0)^{\alpha+\beta} - (-j\omega_0)^\alpha a_{22} + (-j\omega_0)^\beta a_{11} + |A| = 0 \tag{5b}$$

By solving (5), the conditions of oscillation and frequency of oscillation can be calculated.

III. PROPOSED FO OSCILLATOR

The proposed circuit to realize FO oscillator using OTA is shown in Fig. 2, it employs two OTAs and two FOCs ($C_\alpha,\ C_\beta$) with fractional-order α and β. By doing routine analysis, the voltage relation and characteristic equation of the proposed FO oscillator is shown as in (6) and (7) respectively:

$$\begin{bmatrix} D^\alpha V_{O1} \\ D^\beta V_{O2} \end{bmatrix} = \begin{bmatrix} \frac{g_{m1}}{C_\alpha} & -\frac{g_{m1}}{C_\alpha} \\ \frac{g_{m2}}{C_\beta} & 0 \end{bmatrix} \begin{bmatrix} V_{O1} \\ V_{O2} \end{bmatrix} \tag{6}$$

$$s^{\alpha+\beta} - s^\beta \frac{g_{m1}}{C_\alpha} + \frac{g_{m1}g_{m2}}{C_\alpha C_\beta} = 0 \tag{7}$$

The pair of poles must occur at $\pm j\omega_0$ and both poles must

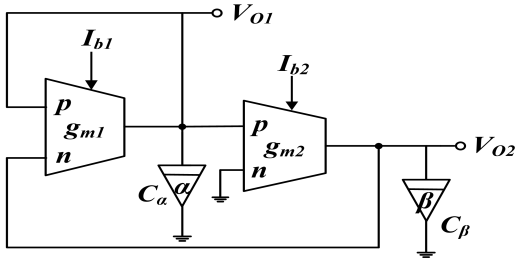

Fig. 2. Proposed fractional-order oscillator realization using OTA

satisfy characteristics equation to necessitate oscillations as discussed in subsection IIB. Hence putting $+j\omega_0$ and $-j\omega_0$ in (7) and separating its real and imaginary parts gives (8).

$$\omega_0^{\alpha+\beta}\ cos\frac{(\alpha+\beta)\pi}{2} - \frac{g_{m1}}{C_\alpha}\omega_0^\beta\ cos\frac{\beta\pi}{2} + \frac{g_{m1}g_{m2}}{C_\alpha C_\beta} = 0 \tag{8a}$$

$$\omega_0^{\alpha+\beta}\ sin\frac{(\alpha+\beta)\pi}{2} - \frac{g_{m1}}{C_\alpha}\omega_0^\beta\ sin\frac{\beta\pi}{2} = 0 \tag{8b}$$

By solving (8b) , the frequency of oscillation (ω_0) is calculated as:

$$\omega_0 = \left[\frac{g_{m1}\ sin\frac{\beta\pi}{2}}{C_\alpha\ sin\frac{(\alpha+\beta)\pi}{2}}\right]^{\frac{1}{\alpha}} \tag{9}$$

The condition for sustained oscillations can be obtained by putting the value of ω_0 from (9) into (8a) and is given as below:

$$g_{m1} = \left[\frac{C_\alpha\ sin\frac{(\alpha+\beta)\pi}{2}}{sin\frac{\beta\pi}{2}}\right]\left[\frac{g_{m2}}{C_\beta\left(cos\frac{\beta\pi}{2} - \frac{sin\frac{\beta\pi}{2}}{tan\frac{\alpha+\beta\pi}{2}}\right)}\right]^{\frac{\alpha}{\beta}} \tag{10}$$

Further, the output terminals' voltage (V_{O1} and V_{O2}) of the proposed FO oscillator are linked as $\frac{V_{O1}}{V_{O2}} = \frac{s^\beta C_\beta}{g_{m2}}$, which

suggests that $\angle V_{O1} - \angle V_{O2}$ equals to $\frac{\beta\pi}{2}$, i.e. the phase difference between two voltages depends only upon the order of the corresponding FOC and can be controlled independently. In FO oscillators, generally the condition of oscillation and frequency of oscillation are not independent of each other, since the condition of oscillation is derived from the frequency of oscillation itself.

A. Stability analysis

The stability of any fractional-order system is determined by mapping s-plane into W-plane for any value of $\alpha = \frac{p}{q}$ where p and q are positive integers and $q \neq 0$ [22]. Let take $W = s^{\frac{1}{q}}$, the $\pm j\omega$ axes (i.e. $|\theta_s| = \frac{\pi}{2}$) in the s-plane are mapped onto the lines $|\theta_W| = \frac{\pi}{2q}$ and the negative axis (i.e. $\theta_s = \pi$) of s-plane onto the line $|\theta_W| = \frac{\pi}{q}$, as shown in Fig. 3. The unstable region (i.e. $|\theta_s| < \frac{\pi}{2}$) and stable regions (i.e. $\frac{\pi}{2} < |\theta_s| < \pi$) in the s-plane transform into $|\theta_W| < \frac{\pi}{2q}$ and $\frac{\pi}{2q} < |\theta_W| < \frac{\pi}{q}$ respectively. Therefore, the system will be stable if and only if all roots in the W-plane lie in the region $|\theta_W| > \frac{\pi}{2q}$ and will oscillate if at least one root lies on the lines $|\theta_W| = \frac{\pi}{2q}$ while all other roots are in the stable region.

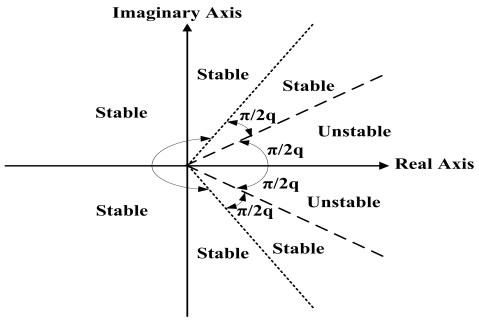

Fig. 3. Stability regions in W-plane

B. Sensitivity analysis

In this subsection, the sensitivity of frequency of oscillation of proposed FO oscillator with respect to various circuit components (i.e. C_α, C_β, g_{m1} and g_{m2}) has been derived mathematically and displayed below:

$$|S_{g_{m1}}^{\omega_0}| = |S_{C_\alpha}^{\omega_0}| = \frac{1}{\alpha}$$

$$|S_{g_{m2}}^{\omega_0}| = |S_{C_\beta}^{\omega_0}| = 0$$

From the above equations of sensitivity, it is clear that the proposed FO oscillator is more sensitive towards lower values of the fractional-order α. As the value of fractional-order α approaches unity the sensitivity also becomes one.

IV. SPICE Simulation Results

To demonstrate the functionality of the proposed FO oscillator, SPICE is used with 180nm CMOS technology model parameters. The OTA provided in [23] is used, for quick reference Fig. 4(a) is showing CMOS structure of the OTA, the W/L ratios of the transistors M_{3-4} are taken as $5.76/0.72$, $M_{1,2,5,7}$ are $2.16/0.72$ and $M_{6,8}$ are $1.44/0.72$. The supply voltages are used as $\pm 1.5V$. The proposed FO oscillator uses FOCs approximated through RC ladder network method reported in [24]. The constructed RC network is shown in Fig. 4(b).

First of all, β is chosen as 0.5/0.8 to make phase difference

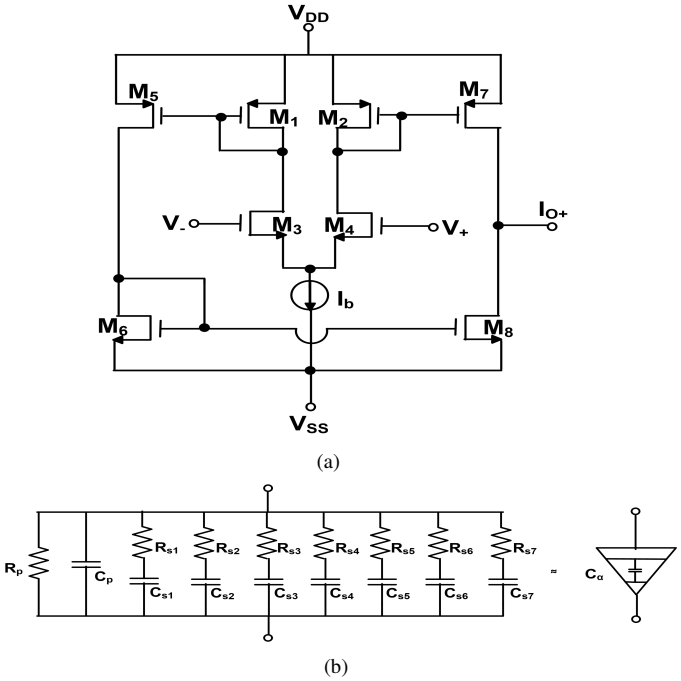

Fig. 4. Sructures used for simulation (a) OTA's CMOS structure [23] (b) RC network to realize FOC [24]

between two output voltages equals to $45°/72°$. Now by choosing C_α=$1\mu\mho/s^\alpha$, C_β=$2\mu\mho/s^\beta$ and g_{m1}=100μA/V the value of g_{m2} to satisfy condition of oscillations is calculated as 100μA/V for α=β=0.5 while for α=β=0.8, choosing C_α=C_β=$1\mu\mho/s^\alpha$ and g_{m1}=155.26μA/V gives the value of g_{m2} to satisfy condition of oscillations as 406.42μA/V. The transient response and frequency spectrum for both the cases of the proposed FO oscillator are shown in Fig.5. The simulated and theoretical frequency of oscillation are 727.08Hz and 795.7Hz respectively for α=β=0.5 whereas the same are 154.4Hz and 159.15Hz respectively for α=β=0.8, the error between simulated and theoretical values of frequency of oscillation lies within 9%. The transient response of V_{O1} and V_{O2} is shown in Fig. 6, which verifies the phase difference between the two voltages is $46°$ for α=β=0.5 and $71.2°$ for α=β=0.8 with an error of 2.22% and 1.15% for α=β=0.5 and 0.8 respectively from the theoretical phase difference.

The pole plot for specified simulation settings (i.e. α=β=0.5) is acquired through *forlocus* function of MATLAB [25] for k=1 and m=2 and appears in Fig. 7. The roots lie on the line $|\theta_W| = \frac{\pi}{2m}$ or in stable region, so the proposed FO oscillator does not show unstable behavior.

Additionally, to check the robustness of the proposed FO

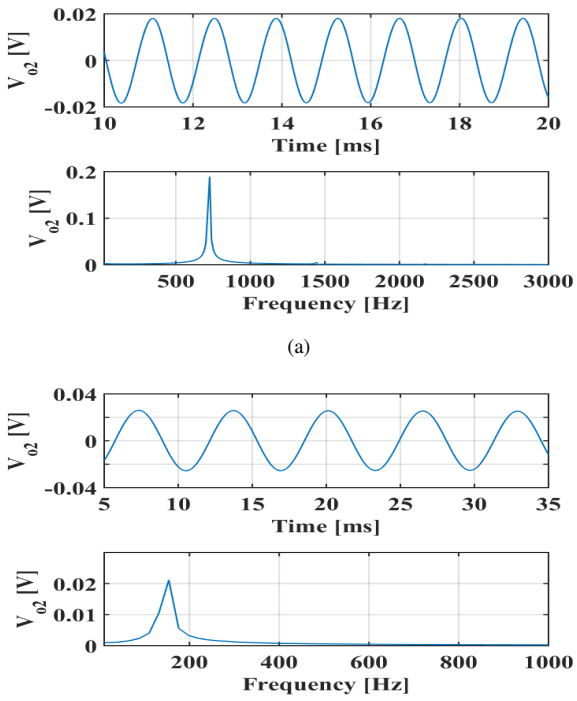

(a)

(b)

Fig. 5. Proposed FO oscillator's transient response and frequency spectrum for (a) α=β=0.5 (b) α=β=0.8

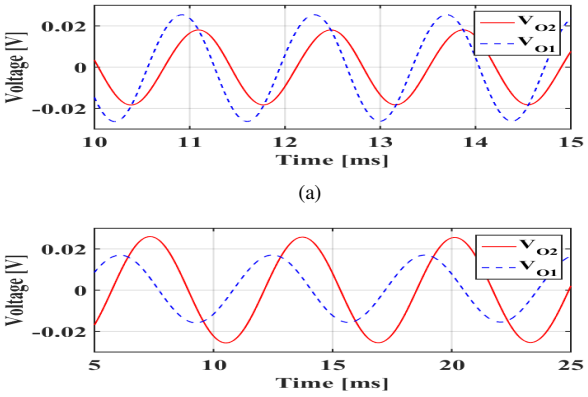

(a)

(b)

Fig. 6. Transient response of V_{O1} and V_{O2} (a) α=β=0.5 (b) α=β=0.8

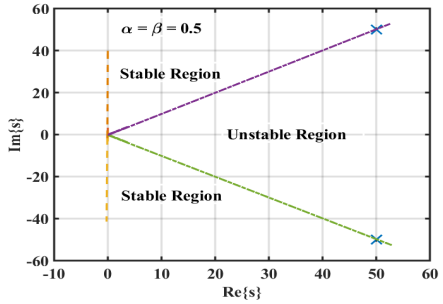

Fig. 7. Proposed FO oscillator's pole plot in W-plane for $\alpha = \beta = 0.5$

oscillator for the random variation in process variable during fabrication, it is examined at all process corners i.e. fast fast (ff), slow slow (ss), slow fast (sf), fast slow (fs) and typical typical (tt) for the same simulation settings for α=β=0.5. Table II contains frequency of oscillation (f_0) and $\%$ error for all five corner points from $'tt'$ corner point and it appears that the $\%$ error lies within 5%, which corroborates robustness of the proposed FO oscillator for given corners.

TABLE II
f_0 AND $\%$ ERROR FOR ALL FIVE PROCESS CORNERS

	tt	**ss**	**ff**	**fs**	**sf**
f_0 (Hz)	727.08	698.25	760.33	717.29	721.18
$\%$ error from $'tt'$ corner	–	3.96$\%$	4.60$\%$	1.35$\%$	0.81$\%$

To get further impression on the sensitivity of the proposed FO oscillator with respect to FOC, Monte-Carlo analysis is carried out on 250 random samples with $\pm5\%$ tolerance and uniform Gaussian distribution of passive components which are used to realize FOCs (i.e. C_α and C_β) for α=β=0.5 case. The distribution of frequency of oscillation (f_0) for 250 samples is shown in Fig. 8. The entire data range lies in between 4 times the standard deviation and the mean is matched with the corresponding f_0 within $\pm0.5\%$ error, this shows the validity of proposed FO oscillator's for the random variation in FOC's value.

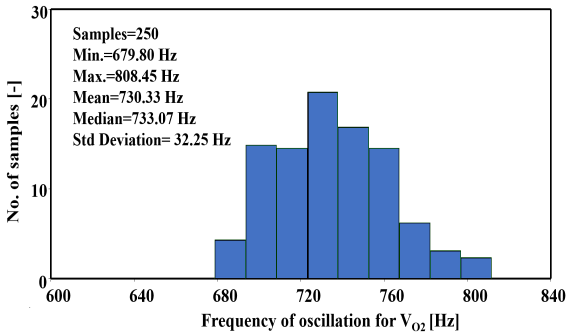

Fig. 8. Histogram of f_0 for the variation of C_α on 250 samples

V. Conclusion

In this work, a new FO oscillator has been proposed with 2 OTAs and 2 FOCs. The phase difference between two outputs of FO oscillator can be controlled independently and has been verified. The functionality of the proposed structure has been confirmed through SPICE simulations with 180nm CMOS technology model parameters. Stability of the proposed FO oscillator has been verified through pole plot in W-plane using *forlocus* function of MATLAB. Sensitivity of frequency of oscillation with respect to various circuit parameters has been derived mathematically and found smaller for higher values of fractional-order α. Corner analysis and Monte-Carlo analysis has been carried out and robustness of the proposed FO oscillator has been proved.

REFERENCES

[1] L. Debnath, "Recent applications of fractional calculus to science and engineering," Int. J. Math. Math. Sci., vol. 54, 2003, pp. 3413–3442.

[2] S. Das and I. Pan, "Fractional order signal processing—introductory concepts and applications," In: Springer Briefs in Applied Sciences and Technology, 2012.

[3] L. Dorcak, J. Valsa, E. Gonzalez, J. Terpak, I. Petras and L. Pivka, "Analogue realization of fractional-order dynamical systems," Entropy, vol. 15, no. 10, 2013, pp. 4199–4214.

[4] I. Podlubny, I. Petras, B.M. Vinagre, P.O. Leary, and L. Dorcak, "Analogue realizations of fractional-order controllers," Nonlinear Dyn., vol. 29, no. 4, 2012, pp. 281–296.

[5] P. Bertsias, M. Mohsen, L.A. Said, A.S. Elwakil, C. Psychalinos and A.G. Radwan, "Design and Implementation of an Optimized Artificial Human Eardrum Model," Circuits Syst Signal Process, vol. 39, 2020, pp. 3219–3233.

[6] G. Tsirimokou, C. Psychalinos and A. Elwakil, "Design of CMOS analog integrated fractional-order circuits: applications in medicine and biology," Springer, 2017.

[7] E. Tlelo-Cuautle, A.D. Pano-Azucena, O. Guillén Fernández and A. Silva-Juárez, "Analog/Digital Implementation of Fractional Order Chaotic Circuits and Applications," Springer, 2020.

[8] W.S. Sayed and A.G. Radwan, "Generalized Switched Synchronization and Dependent Image Encryption Using Dynamically Rotating Fractional-Order Chaotic Systems," AEU-International Journal of Electronics and Communications, vol. 127, 2020, DOI: 10.1016/j.aeue.2020.153268

[9] S. Minaei and O. Cicekogl, "New current-mode integrator and all-pass section without external passive elements and their application to design a dual-mode quadrature oscillator," Frequenz, vol. 57, 2013, pp. 1–2.

[10] W. Ahmad, R. El-Khazali and A. S. Elwakil. "Fractional-order Wien-bridge oscillator," Electronics Letters vol. 37, no. 18, 2001, pp. 1110-1112.

[11] A.G. Radwan, A.S. Elwakil and A.M. Soliman, "Fractional-order sinusoidal oscillators: design procedure and practical examples," IEEE Transactions on Circuits and Systems I: Regular Papers, vol. 55, no. 7, 2008, pp. 2051–2063, DOI:10.1109/TCSI.2008.918196

[12] A. G. Radwan, A. M. Soliman and A. S. Elwakil, "Design equations for fractional-order sinusoidal oscillators: four practical design examples," International Journal of Circuit Theory and Applications, vol. 36, 2008, pp. 473–492.

[13] L. A. Said, A. G. Radwan, A. H. Madian and A. M. Soliman, "Fractional order oscillators based on operational transresistance amplifiers," AEU-International Journal of Electronics and Communications, vol. 69, no. 7, 2015, pp. 988–1003.

[14] D. Kubánek, F. Khateb, G. Tsirimokou and C. Psychalinos, "Practical design and evaluation of fractional-order oscillator using differential voltage current conveyors," Circuits, Systems, and Signal Processing, vol. 35, no. 6, 2016, pp. 2003-2016.

[15] T. Comedang and P. Intani, "Current-controlled CFTA based fractional order quadrature oscillators," Circuits and Systems, vol. 7, no. 13, 2016, pp. 4201–4212.

[16] A. Kartci, N. Herencsar, J. Koton and C. Psychalinos, "Compact MOS-RC Voltage-Mode Fractional-Order Oscillator Design," in

[17] A. Pradhan, and R. K. Sharma, "Generalised Fractional-Order Oscillators using OTA," In 2018 5th International Conference on Signal Processing and Integrated Networks (SPIN), 2018, pp. 402-406.

[18] S. K. Mishra, M. Gupta and D. K. Upadhyay, "Design and implementation of DDCC-based fractional-order oscillator," International Journal of Electronics, vol. 106, no. 4, 2019, pp.581-598.

[19] L. A. Said, O. Elwy and A. H. Madian, "Stability analysis of fractional-order Colpitts oscillators," Analog Integr. Circuits Signal Process., vol. 101, 2019, pp. 267–279, DOI:10.1007/s10470-019-01501-2.

[20] A. Radwan, "Stability analysis of the fractional-order $RL_\beta C_\alpha$ circuit," Journal of Fractional Calculus and Applications, vol. 3, no. 1, 2012, pp. 1–15.

[21] L.A. Said, A.G. Radwan, A.H. Madian and A.M. Soliman, "Three fractional-order-capacitors-based oscillators with controllable phase and frequency," J. Circuits Syst. Comput., vol. 26, no. 10, 2017, pp. 1750160.

[22] Radwan, A. G.; Soliman, A. M.; Elwakil, A. S.; Sedeek, A.: On the stability of linear systems with fractional-order elements, Chaos, Solitons and Fractals, 40(5), 2317-2328 (2009).

[23] J. Ramirez-Angulo, M. Robinson and E. Sanchez-Sinecio, "Current modde continuous-time filters:Two design approaches," IEEE Transactions on Circuits and Systems II: Analog and Digital Signal Processing, vol. 39, no. 6, 1992, pp. 337-341, doi: 10.1109/82.145290.

[24] J. Valsa, P. Dvorak and M. Friedl, "Network model of the CPE," Radioengineering, Vol. 20, no. 3, 2011, pp. 619–26.

[25] Z. Li, "Fractional order root locus," (online-Matlab Central) http://www.mathworks.com/ matlabcentral/fileexchange/50458, 2015.

View publication stats

Eur. Phys. J. Plus (2022) 137:633
https://doi.org/10.1140/epjp/s13360-022-02841-1

THE EUROPEAN PHYSICAL JOURNAL PLUS

Regular Article

Pressure-induced topological phase transition in XMR material YbAs: a first-principles study

Mukhtiyar Singh[1,a], **Ramesh Kumar**[1], **Ramesh K. Bibiyan**[2]

[1] Department of Applied Physics, Delhi Technological University, New Delhi, Delhi 110042, India
[2] Department of Physics, Guru Jambheshwar University of Science & Technology, Hisar 125001, India

Received: 22 February 2022 / Accepted: 16 May 2022
© The Author(s), under exclusive licence to Società Italiana di Fisica and Springer-Verlag GmbH Germany, part of Springer Nature 2022

Abstract Many rare-earth monopnictides having extremely large magnetoresistance (XMR) show topologically non-trivial nature under applied hydrostatic pressure. We find that YbAs which show XMR effect, is stable in rocksalt structure (*NaCl-type*) for entire studied pressure range (0–40 GPa). The structural phase transition to *CsCl-type* structure takes place at 67 GPa which is in fine agreement with previous experimental study. We also verify its dynamical stability from phonon dispersion spectrum. This material undergoes topological phase transition (trivial to non-trivial) under applied hydrostatic pressure of 6 GPa and retains this non-trivial nature up to 39.5 GPa without breaking any symmetry. This quantum phase transition is associated with spin–orbit coupling effect. We find the band inversions near the Fermi level at X and Γ point at 6 GPa and 39.5 GPa, respectively, and verified the same with the help of band parities.

1 Introduction

Topological phases of matter [1–3] with unusual behaviour have fundamentally changed the understanding of condensed matter physics. The trend of discoveries in last decade has established a connection between topology and band structure in crystalline materials [4–6]. Existence of conducting gapless $(d-1)$-dimensional boundary states with d-dimensional bulk insulator in a crystalline material makes it topological insulator (TI). Recently, it is found that existence of gapless surface states in semimetals makes them topologically non-trivial [7]. These can be categorized mainly as Dirac, Weyl and nodal-line semimetals [8]. The presence of point or line nodes in three-dimensional momentum space of non-trivial semimetal separates it from trivial semimetals. The formation of these nodes takes place when two distinct bands touch near fermi surface and can be described with the help of massless two-component Dirac (Weyl) Hamiltonian in momentum space [9, 10]. Gapless electronic excitation in these non-trivial semimetals is protected by both topology and crystal symmetry [7, 9, 11]. Another class of semimetals which can be characterized by a non-trivial Z_2 invariant (i.e. shows band inversion), although they do not possess any bulk bandgap, are called Z_2 topological semimetals [12]. Rare earth-based monopnictides fit into this category of semimetals [13, 14]. This new class of quantum materials having non-trivial topologies with phenomenon including fermionic excitation, spin textures, etc., found a vast application in the field of spintronics, quantum computing, superconductivity, and thermoelectric [3, 15, 16].

The rare earth monopnictide LnPn (Ln: rare earth element; Pn: As, Sb, Bi) have shown the signature of topological states. These compounds exist in simple rocksalt face-centred cubic structures (except YbBi) [14]. In LnPn (Ln = Ce, Pr, Sm, Gd, Yb; Pn = Sb, Bi), topological band inversion fades away as the atomic number increases from Ce to Yb and finally, SmSb and DyBi become topologically trivial [14]. It has been found that LaBi show topological band inversion under ambient conditions, whereas LaAs [12] and LaSb [17] show inversion under applied external pressure. Recently, the extreme magnetoresistance (XMR) has been found in some trivial semimetals [18–20]. The origin of XMR which is quadratic function of magnetic field can be understood by electron–hole compensation mechanism [18, 21–23] and topological symmetry protection [24, 25]. The electron–hole compensation mechanism approach is quite mature, whereas relation between XMR and topological symmetry protection is not reached to an agreement yet [26]. It has been observed that topological protection restricts the backscattering at zero magnetic field, but increase in external magnetic field breaks the symmetry protection that give rise to XMR [24, 25]. The rare earth monopnictides like LaSb, LaBi [18], LaAs [20], TmSb [19], TaAs [27], NbAs [28] which possess XMR are also have been shown to become non-trivial under applied external pressure [12, 14, 17, 26, 29].

YbAs also belongs to rare earth monopicnide family and has been experimentally reported as topologically trivial semimetal under ambient condition of pressure and showing XMR with existence of electron and hole pockets on Fermi surface observed at low temperature [30]. Due to its crystal similarity with other topological trivial semimetals, YbAs can be an ideal candidate to explore topological phase transition with spin–orbit coupling (SOC). As the electronic correlation in As is less than the Sb and Bi,

[a] emails: msphysik09@gmail.com; mukhtiyarsingh@dtu.ac.in (corresponding author)

Published online: 28 May 2022

so weak SOC prevails in YbAs compound [30]. But it is well known that extent of SOC can be increased by applied magnetic field [31], chemical doping or alloy composition or by applying pressure or strain [12, 14, 17, 26, 29]. Amongst these, external pressure can be an influential approach which leads to a defect free environment [12, 14, 17, 26, 29]. So, in this article, we address the topological phase transition of ytterbium monoarsenide (YbAs) under external hydrostatic pressure. Band inversions under SOC are verified with Z_2 topological invariants which are calculated from parity table of wavefunctions on high symmetry points under varying pressure values.

2 Computational details

We were used first-principles electronic structure calculation method based on density functional theory (DFT) [32, 33] as implemented in VASP code [34] with projector augmented wave (PAW) formalism [35]. To include the exchange–correlation potential, generalised gradient approximation (GGA) of Perdew–Burke–Ernzerhof (PBE) [36] formulation was used. The PAW potentials used in this calculation have nine valence electrons for Yb, i.e. $5p^6 5d^1 6s^2$, and five valence electrons for As, i.e. $4s^2 4p^3$, respectively. All the calculations were performed assuming that $4f$ electrons of Yb are well localized [14, 30]. The plane wave basis set cut-off kinetic energy was 380 eV. For the rocksalt primitive unit cell which contain single formula unit, a k-mesh of $13 \times 13 \times 13$ for the Brillion zone (BZ) sampling was used. Gaussian smearing was used for Fermi level broadening with width 0.001 eV. Internal atomic positions and the lattice parameters were relaxed fully at different applied external hydrostatic pressures. All atoms were relaxed until the forces between them became smaller than 0.001 eV/Å. After the relaxed crystal structures were achieved at different applied pressures, the SOC effect was incorporated for further study of electronic structures. To confirm the dynamical stability of structures at different applied pressure, phonon dispersion calculations were also performed using PHONOPY code [37]. The Z_2 topological invariants at all time reversal invariant momenta (TRIM) points in the BZ were calculated by parities of all filled states, i.e. for valence band as per Kane and Mele criterion [2, 38].

3 Results and discussion

At ambient pressure, YbAs has *NaCl-type* rocksalt structure (space group No. 225) with Yb atom at (0.5, 0.5, 0.5) and As atom at (0, 0, 0) as shown in Fig. 1a. We have considered primitive unit cell to avoid band folding. The optimized lattice parameter of *NaCl-type* structure is 5.722 Å which is in good agreement with previous studies [39–41] as compared in Table 1.

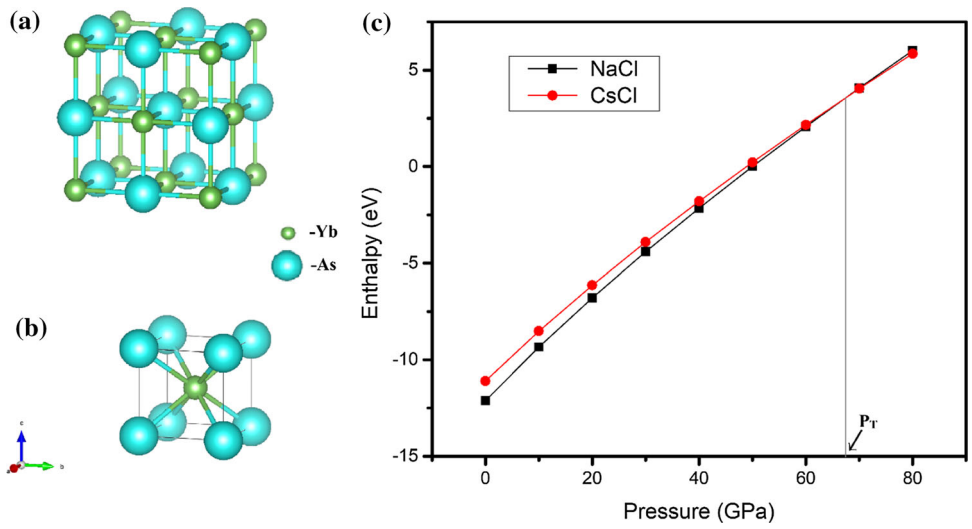

Fig. 1 Crystal structure of YbAs **a** *NaCl-type* and **b** *CsCl -type* and **c** enthalpies of YbAs in *NaCl-type* and *CsCl-type* structures as a function of applied hydrostatic pressure. SPT takes place at P_T = 67 GPa

Table 1 Comparison of lattice constant and structural phase transition pressure with previous experimental and theoretical studies

YbAs	Previous experimental study	Previous theoretical study	Present study
Lattice parameter, a (Å)	5.708 [39] 5.6976 [40]	5.7796 [41]	5.722
Structural phase transition (SPT) pressure (GPa)	52 [39]	20 [41] 95 [42]	67

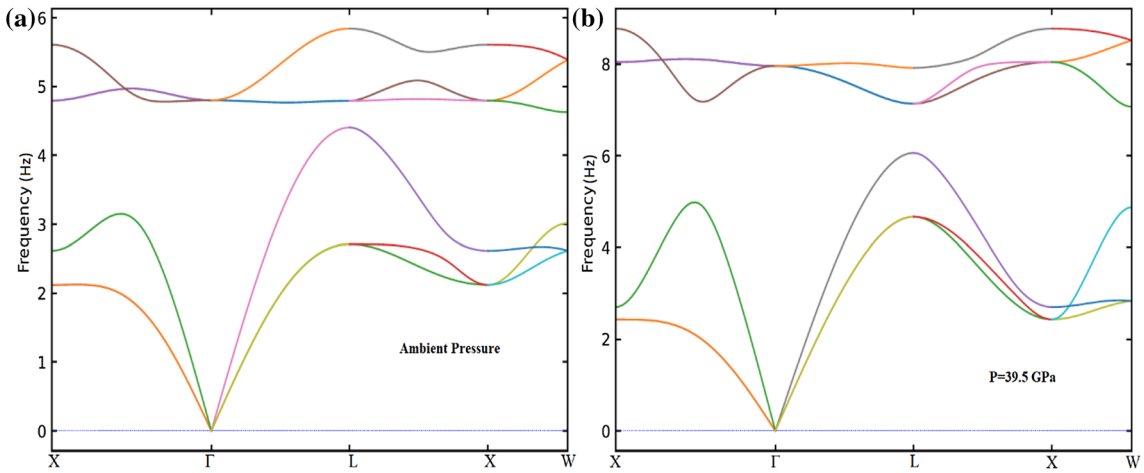

Fig. 2 Phonon dispersion spectrum along high symmetry points of YbAs **a** at ambient pressure, **b** at $P = 39.5$ GPa

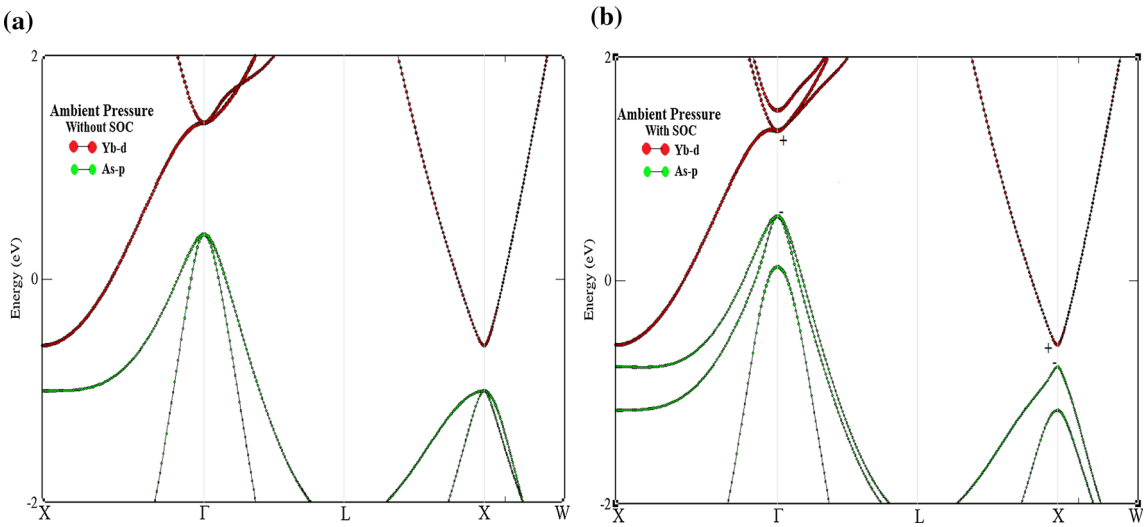

Fig. 3 Band structure of YbAs in *NaCl-type* structure **a** without SOC, **b** with SOC at ambient pressure. The Fermi level is set to 0 eV

Before investigating topological phase in YbAs with the effect of external hydrostatic pressure, we have checked the stability of the crystal structure as a function of pressure. YbAs get transformed into *CsCl-type* structure (Fig. 1b) under applied external pressure [39, 41, 42]. To investigate the structural phase transition (SPT) of YbAs under applied external pressure, we have analysed the pressure-dependent enthalpies for YbAs in *NaCl* and *CsCl-type* structures (Fig. 1c). The structure which has lower enthalpy, $H = E + PV$ where E denotes the total energy of structure, P is applied pressure and V is the volume of the unit cell, is more stable. At ambient pressure, *NaCl-type* structure is more stable as its enthalpy is lower than *CsCl-type* structure. But with the increase in pressure, enthalpy of both *NaCl* and *CsCl-type* structures increases gradually, but this increase is more prevalent in *NaCl-type* structure and at ~ 67 GPa crossover from *NaCl-type* structure to *CsCl-type* structure takes place (Fig. 1c).

This value of pressure (phase transition pressure, P_T) corresponds to SPT in YbAs. SPT pressure calculated in this study is relatively closer to the available experimental value as shown in Table 1. Further, the dynamical stability of *NaCl-type* structure is verified from its phonon dispersion spectrum under ambient pressure and applied pressure of 39.5 GPa as shown in Fig. 2.

As we have determined the stable crystal structure of YbAs, now we can study the effect of pressure on band structure. The band structure of YbAs at ambient pressure along high symmetry points using PBE is shown in Fig. 3. Band structure plotting is done along a specific path, i.e. X to Γ, Γ to L, L to X and X to W, because it contains the Time Reversal Invariant Momenta (TRIM) points in the BZ (X, Γ and L are TRIM points).

This is also important to note that we are interested in band structure for topological phase transition which do not consider time reversal variant points. Near the fermi level, there is small overlapping between valance and conduction bands, which shows YbAs is of semimetallic nature [30]. We have plotted the projected density of states (PDOS) or atom-resolved density of states of YbAs (Fig. 4) to understand the semimetallic nature of this system. The very feeble DOS at Fermi level established its semimetallic nature. It can be seen from the figure that the main contribution in the valence band is from *p-states* of As (as all states of *p-orbital*

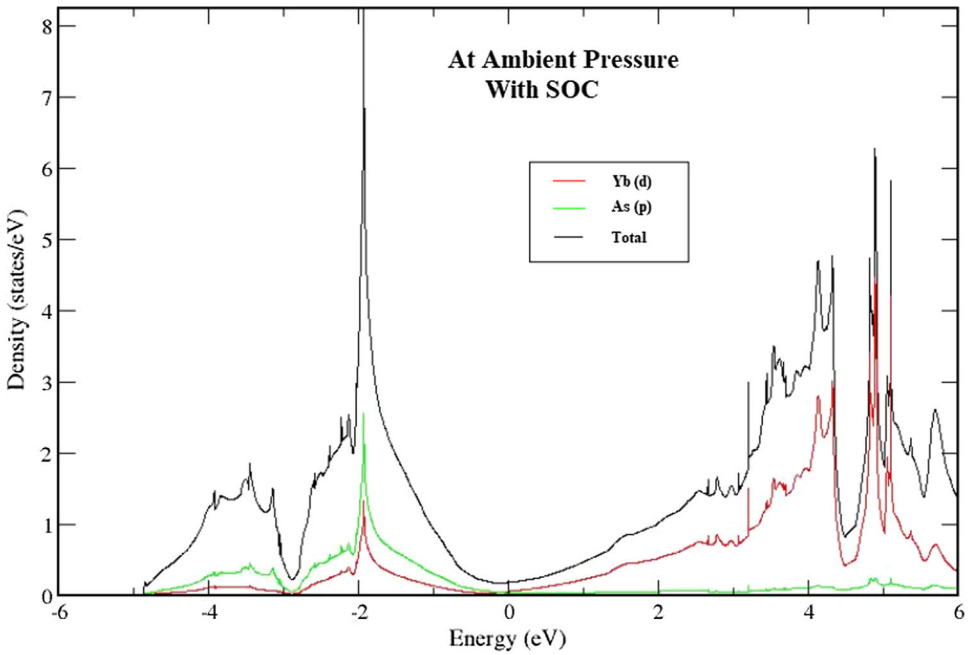

Fig. 4 Projected density of state (PDOS) of YbAs at ambient pressure

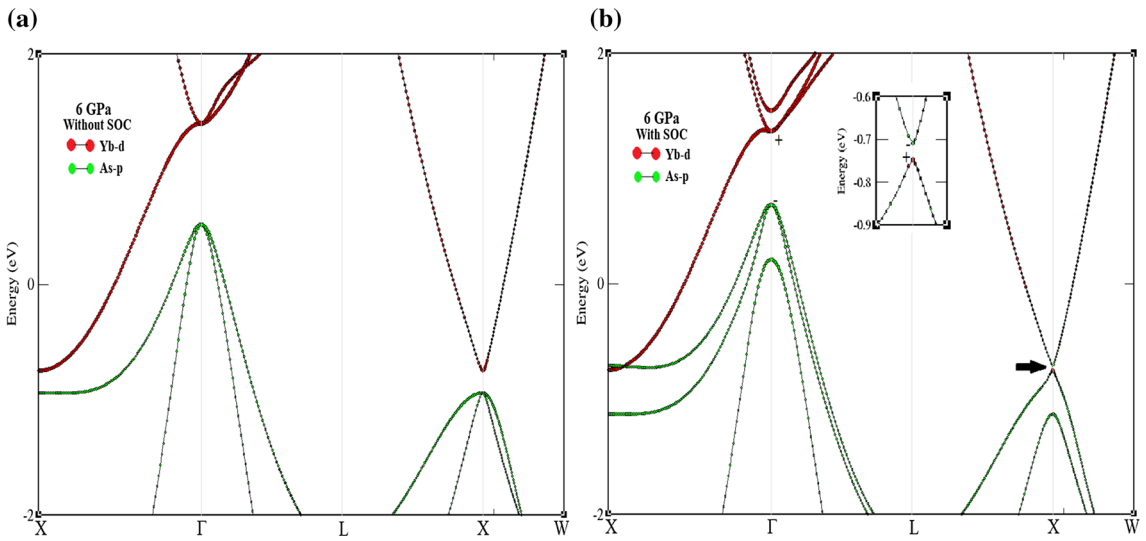

Fig. 5 Band structure of YbAs in *NaCl-type* structure **a** without SOC, **b** with SOC at 6 GPa pressure. The Fermi level is set to 0 eV

is half-filled) with relatively smaller weight of *Yb-d* states (only one state in *d-orbital* is filled). However, in the conduction band this trend gets reversed with Yb-d states dominating here (four out of five *d-orbitals* are empty) over *As-p* states.

It can be observed from Fig. 3 that *d-orbital* of Yb and *p-orbital* of As mainly contributed near the fermi level and also no band inversion can be seen near the fermi level which shows YbAs is topologically trivial semimetal. Experimental study using angle-resolved photoemission spectroscopy (ARPES) measurement [30] has also verified that there is no band inversion in YbAs at ambient pressure around X and Γ points. Hence, our study has predicted the true state of YbAs at this pressure.

In order to study the topological quantum phase transition in YbAs semimetal, we increased the external hydrostatic pressure within the limit of SPT. Figure 1c also shows that neither NaCl-*type* nor *CsCl-type* structure is stable after ~ 45 GPa (enthalpy greater than equal to 0), so we restricted our investigation up to 40 GPa. The band structures of YbAs at various applied pressures with and without SOC are depicted in Figs. 5 and 6. Under the effect of external pressure, lattice parameter of YbAs gets changed and consequently the width between bands also changes without altering any charge neutrality or composition of the system.

To find the signature of quantum phase transition, we checked the band inversion on all the TRIM points. We found that from 0 to 5 GPa, there is no adiabatic change in band structure of YbAs and it remains in trivial state. As we raise pressure from 5 to 6 GPa, we found a band inversion on X point (marked with bold arrow) as shown in Fig. 5b. This inversion is attributed to the enhanced SOC due to applied hydrostatic pressure. At X point YbAs has C_{4v} double group in rocksalt structure [17]. This implies that YbAs

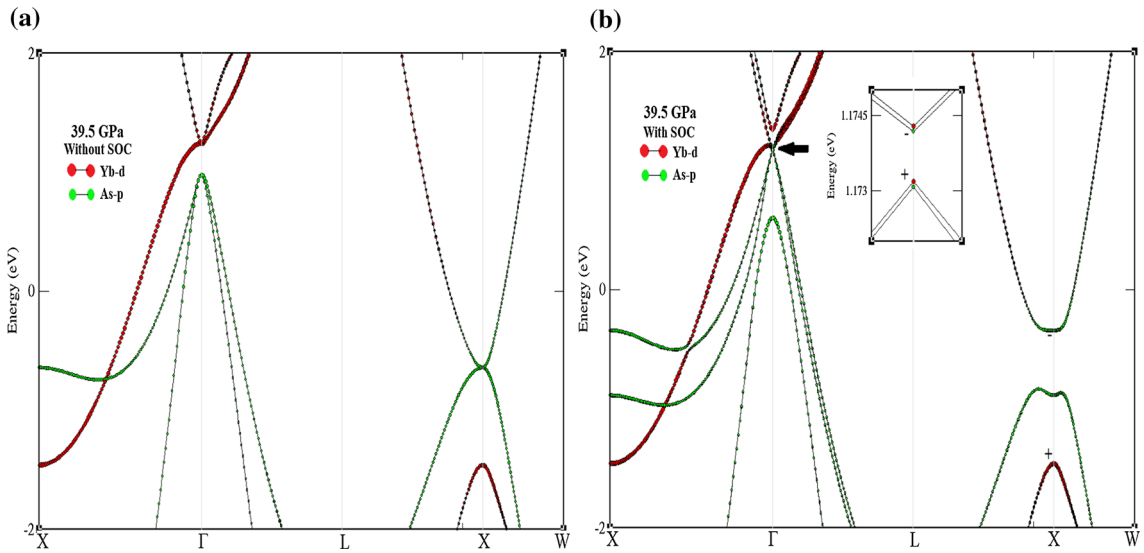

Fig. 6 Band structure of YbAs in *NaCl-type* structure **a** without SOC, **b** with SOC at 39.5 GPa pressure. The Fermi level is set to 0 eV

Table 2 Parities of all the occupied bands at TRIM points of first BZ of YbAs in the *NaCl-type* structure under ambient pressure condition

Band no.	*L*	*L*	*L*	*L*	*Γ*	*X*	*X*	*X*	Total
1	+	+	+	+	−	−	−	−	+
3	+	+	+	+	−	−	−	−	+
5	+	+	+	+	−	−	−	−	+
7	+	+	+	+	+	+	+	+	+
9	−	−	−	−	−	−	−	−	+
11	−	−	−	−	−	−	−	−	+
13	−	−	−	−	−	−	−	−	+
Total	−	−	−	−	+	+	+	+	(+)

YbAs is topologically trivial at ambient condition

Table 3 Parities of all the occupied bands at TRIM points of first BZ of YbAs in the *NaCl-type* structure under 6 GPa

Band no.	*L*	*L*	*L*	*L*	*Γ*	*X*	*X*	*X*	Total
1	+	+	+	+	−	−	−	−	+
3	+	+	+	+	−	−	−	−	+
5	+	+	+	+	−	−	−	−	+
7	+	+	+	+	+	+	+	+	+
9	−	−	−	−	−	−	−	−	+
11	−	−	−	−	−	−	−	−	+
13	−	−	−	−	−	+	+	+	−
Total	−	−	−	−	+	−	−	−	(−)

YbAs is topologically non-trivial due to odd number of inversions at 6 GPa pressure

has both space inversion and time reversal symmetries. To further verify this quantum phase change, we have also evaluated the parity of the bands near the fermi level at *X* point. Table 2 shows the band parities at ambient pressure, whereas Table 3 depicts the same at 6 GPa. It can be seen that with applied hydrostatic pressure (6 GPa), the parities get switched near Fermi level. This switching of band parities justified our claim of band inversion. The opening of band gap at *X* point after inversion (inset of Fig. 5b) suggests that YbAs is not Dirac semimetal. A band inversion at *X* points and opposite parities on all three equivalent *X* points in BZ (Tables 2, 3) indicate that YbAs may be a topological insulator described on curved fermi surface [17].

As we increase the pressure beyond 6 GPa, the single inversion holds up to 39 GPa, i.e. YbAs remains in topologically non-trivial state in pressure range from 6 to 39 GPa which can also be verified from change in parity (Table 3). But when we further increased the pressure from 39 to 39.5 GPa, we found that one more band inversion take place at *Γ* high symmetry point as shown in Fig. 6 (marked with bold arrow) and parity also switched (Tables 3, 4). Both the inversion exists within the limit of structural phase transition pressure ~ 67 GPa and below the 40 GPa pressure up to which stable *NaCl-type* structure exists as shown in Fig. 1.

At ambient pressure (Fig. 3) near the Fermi level, the valence band and conduction band of YbAs are dominated mainly by *p-orbital* of As and *d-orbital* of Yb, respectively, but at 6 GPa of applied pressure, a small contribution of *d-orbital* of Yb in valance

Table 4 Parities of all the occupied bands at TRIM points of first BZ of YbAs in the *NaCl-type* structure under 39.5 GPa

Band no.	L	L	L	L	Γ	X	X	X	Total
1	+	+	+	+	−	−	−	−	+
3	+	+	+	+	−	−	−	−	+
5	+	+	+	+	−	−	−	−	+
7	+	+	+	+	+	+	+	+	+
9	−	−	−	−	−	−	−	−	+
11	−	−	−	−	−	+	+	+	−
13	−	−	−	−	+	−	−	−	−
Total	−	−	−	−	−	−	−	−	(+)

YbAs is topologically trivial due to even number of inversions at 39.5 GPa pressure

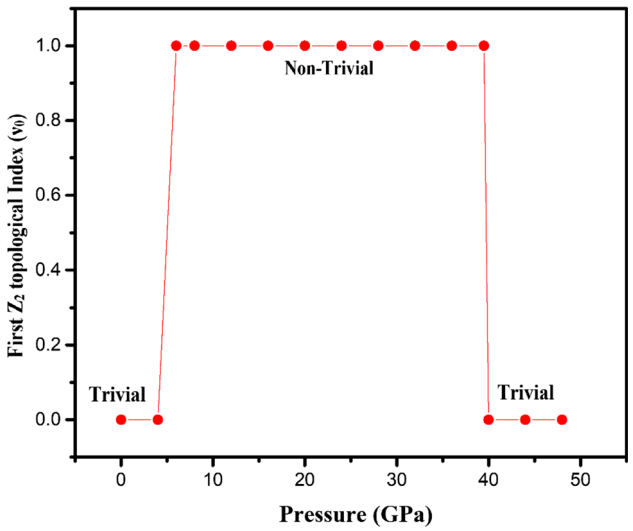

Fig. 7 First Z_2 topological index (ν_0) as a function of applied hydrostatic pressure in YbAs

band and *p-orbital* of As in conduction band can be observed at X point near fermi level (Fig. 5). The same inverted contribution can also be seen at Γ point at 39.5 GPa pressure (Fig. 6). Even number of band inversion at 39.5 GPa shows that it may be weak topological phase or topologically trivial semimetal [2, 38].

Further, to verify the non-trivial topological phase of YbAs with applied hydrostatic pressure, we have calculated Z_2 topological invariants as discussed by Kane and Mele [2, 38]. For three-dimensional system, eight different possible TRIM points exist which can be given as:

$$G_{i=(m_1m_2m_3)} = (m_1a_1 + m_2a_2 + m_3a_3)/2 \tag{1}$$

where $m_j = 0, 1$ and a_1, a_2, a_3 are the reciprocal primitive lattice vectors. An adiabatic transformation in band structure will change the sign of parity, and this change can be identified by four Z_2 indices.

For a 3D system having inversion and time-reversal symmetries, four Z_2 topological invariants, i.e. ν_0; (ν_1, ν_2, ν_3), exist. These indices can be calculated by the following relationship between parity and Z_2 indices:

$$(-1)^{\nu_0} = \prod_{m_j=0,1} \delta_{m_1m_2m_3} \tag{2}$$

$$(-1)^{\nu_{i=1,2,3}} = \prod_{m_{j\neq i}=0,1\&m_i=1} \delta_{m_1m_2m_3} \tag{3}$$

where first Z_2 index will define the class of topological material and $\delta_{m_1m_2m_3}$ is the product of all the occupied bands at selected TRIM point. $\nu_0 = 1$ states that the system is in strong topological phase, and $\nu_0 = 0$ states that system is either in weak topological state or topologically trivial. Further, to differentiate between weak and trivial topological state, other three indices (ν_1, ν_2, ν_3) can be helpful. Parity details for YbAs under ambient condition, 6 GPa and 39.5 GPa hydrostatic pressure, are summarised in Tables 2, 3 and 4, respectively.

As YbAs holds both time reversal symmetry and space-inversion symmetry, so Z_2 topological invariants can be calculated using parities of all occupied bands at TRIM points [2, 38]. As discussed earlier, there is no band inversion at ambient pressure so when we calculate ν_0 at this pressure from Eq. (2), we get zero which shows that it is topologically trivial. But when we increased pressure to 6 GPa, a band inversion can be observed at X point and also switch of parity in Table 3 indicates that $\nu_0 = 1$ which exhibits that YbAs is in topologically non-trivial phase. Further increase in pressure, from 6 to 39.5 GPa, leads to two band inversions presents at

X as well as Γ high symmetry point. At this pressure, there is another switch in parity of the system as shown in Table 4 indicating topologically weak or trivial condition. Now, to ensure this, we further calculated other Z_2 indices (ν_1, ν_2, ν_3) using Eq. (3). From Table 4, we can observe that parities at all four L and three X TRIM points are the same. This results in other three Z_2 indices (ν_1, ν_2, ν_3) as (0, 0, 0) indicating that system is topologically trivial at 39.5 GPa hydrostatic pressure.

The variation of ν_0 with applied external hydrostatic pressure is shown in Fig. 7. Magnetotransport measurements in YbAs have shown XMR effect [30], which depends on mobility and carrier concentration in the system. Applied pressure increases the overlapping of valance and conduction band of YbAs, which increases the carrier concentration, and hence, it may increase the XMR effect. The evolution of XMR can be explained as a function of applied pressure as mobility of charge carrier increases. This evolution can only be verified experimentally. Topological quantum phase transition study in YbAs with applied pressure can provide a platform to study the role of topology in XMR effect.

4 Conclusion

First-principles-based electronic structure calculations of XMR material YbAs have been carried out within GGA-PBE approximation to understand the topological phase transition. First of all, we have analysed the structural stability of this material and found that it is stable in *NaCl-type* structure up to ~ 45 GPa and a structural phase transition to *CsCl-type* occurs at 67 GPa which in fine agreement to the corresponding experimental value, but both structures are unstable at this pressure. The dynamical stability (up to 39.5 GPa) of the material is also verified with the help of phonon dispersion spectrum. This material is topologically trivial at ambient pressure and undergoes the first topological phase transition at 6 GPa of applied hydrostatic pressure with spin–orbit coupling. This non-trivial nature holds up to 39 GPa, after which it became topologically trivial again. Interchange of orbital contribution in bands near the Fermi level conforms the band inversion with applied pressure. Switching of band parities near the Fermi level conforms the adiabatic transformation in band structure which took place under hydrostatic pressure of 6 GPa and 39.5 GPa. The topological phase transition has been further verified by calculation of Z_2 indices or Z_2 topological invariants. The product of parities of all occupied bands shows that the value of topological invariant ν_0 changes from 0 to 1 at 6 GPa pressure and then again from 1 to 0 at 39.5 GPa. This suggests that YbAs is topologically non-trivial for aforementioned pressure range. The XMR effect in YbAs may be explained on the basis of topological non-trivial nature of YbAs, and it may hold a relationship between topology and XMR effects in material.

Acknowledgements One of the authors (Ramesh Kumar) would like to thank Council of Scientific and Industrial Research (CSIR), Delhi, for financial support.

Declarations

Conflict of interest The authors declare that they have no conflict of interest.

References

1. C.L. Kane, E.J. Mele, Z_2 topological order and the quantum spin hall effect. Phys. Rev. Lett. **95**, 146802 (2005). https://doi.org/10.1103/PhysRevLett.95.146802
2. L. Fu, C.L. Kane, E.J. Mele, Topological insulators in three dimensions. Phys. Rev. Lett. **98**, 106803 (2007). https://doi.org/10.1103/PhysRevLett.98.106803
3. J.E. Moore, The birth of topological insulators. Nature **464**, 194 (2010). https://doi.org/10.1038/nature08916
4. M.Z. Hasan, C.L. Kane, Colloquium: topological insulators. Rev. Mod. Phys. **82**, 3045 (2010). https://doi.org/10.1103/RevModPhys.82.3045
5. M.Z. Hasan, J.E. Moore, Three-dimensional topological insulators. Annu. Rev. Condens. Matter Phys. **2**, 55 (2011). https://doi.org/10.1146/annurev-conmatphys-062910-140432
6. M.Z. Hasan, S.-Y. Xu, M. Neupane, in *Topological Insulators: Fundamentals and Perspectives*, 1st edn., ed. by F. Ortmann, S. Roche, S.O. Valenzuela (Wiley-VCH Verlag GmbH & Co. KGaA, Weinheim, 2015), pp. 55–100
7. A.A. Burkov, Topological semimetals. Nat. Mater. **15**, 1145 (2016). https://doi.org/10.1038/nmat4788
8. H. Gao, J.W.F. Venderbos, Y. Kim, A.M. Rappe, Topological semimetals from first principles. Annu. Rev. Mater. Res. **49**, 153 (2019). https://doi.org/10.1146/annurev-matsci-070218
9. N.P. Armitage, E.J. Mele, A. Vishwanath, Weyl and Dirac semimetals in three-dimensional solids. RMP **90**, 015001 (2018). https://doi.org/10.1103/RevModPhys.90.015001
10. A.A. Burkov, M.D. Hook, L. Balents, Topological nodal semimetals. Phys. Rev. B **84**, 235126 (2011). https://doi.org/10.1103/PhysRevB.84.235126
11. B. Yan, C. Felser, Topological materials: Weyl semimetals. Annu. Rev. Condens. Matter Phys. **8**, 337 (2017). https://doi.org/10.1146/annurev-conmatphys
12. S. Khalid, F.P. Sabino, A. Janotti, Topological phase transition in LaAs under pressure. Phys. Rev. B **98**, 220102(R) (2018). https://doi.org/10.1103/PhysRevB.98.220102
13. R. Lou, B.-B. Fu, Q.N. Xu, P.-J. Guo, L.-Y. Kong, L.-K. Zeng, J.-Z. Ma, P. Richard, C. Fang, Y.-B. Huang, S.-S. Sun, Q. Wang, L. Wang, Y.-G. Shi, H.C. Lei, K. Liu, H.M. Weng, T. Qian, H. Ding, S.-C. Wang, Evidence of topological insulator state in the semimetal LaBi. Phys. Rev. B **95**, 115140 (2017). https://doi.org/10.1103/PhysRevB.95.115140

14. X. Duan, F. Wu, J. Chen, P. Zhang, Y. Liu, H. Yuan, C. Cao, Tunable electronic structure and topological properties of LnPn (Ln = Ce, Pr, Sm, Gd, Yb; Pn = Sb, Bi). Commun. Phys. **1**, 71 (2018). https://doi.org/10.1038/s42005-018-0074-8
15. M. He, H. Sun, Q.L. He, Topological insulator: spintronics and quantum computations. Front. Phys. **14**, 4 (2019). https://doi.org/10.1007/s11467-019-0893-4
16. Y. Fan, K.L. Wang, Spintronics based on topological insulators. SPIN **6**, 2 (2016). https://doi.org/10.1142/S2010324716400014
17. P.J. Guo, H.-C. Yang, K. Liu, Z.Y. Lu, Theoretical study of the pressure-induced topological phase transition in LaSb. Phys. Rev. B **96**, 081112(R) (2017). https://doi.org/10.1103/PhysRevB.96.081112
18. P.J. Guo, H.-C. Yang, B.-J. Zhang, K. Liu, Z.-Y. Lu, Charge compensation in extremely large magnetoresistance materials LaSb and LaBi revealed by first-principles calculations. Phys. Rev. B **93**, 235142 (2016). https://doi.org/10.1103/PhysRevB.93.235142
19. Y.-Y. Wang, H. Zhang, X.-Q. Lu, L.L. Sun, S. Xu, Z.-Y. Lu, K. Liu, S. Zhou, T.-L. Xia, Extremely large magnetoresistance and electronic structure of TmSb. Phys. Rev. B **97**, 085135 (2018). https://doi.org/10.1103/PhysRevB.97.085137
20. H.Y. Yang, T. Nummy, H. Li, S. Jaszewski, M. Abramchuk, D.S. Dessau, F. Tafti, Extreme magnetoresistance in the topologically trivial lanthanum monopnictide LaAs. Phys. Rev. B **96**, 235128 (2017). https://doi.org/10.1103/PhysRevB.96.235128
21. O. Pavlosiuk, P. Swatek, D. Kaczorowski, P. Wiśniewski, Magnetoresistance in LuBi and YBi semimetals due to nearly perfect carrier compensation. Phys. Rev. B **97**, 235132 (2018). https://doi.org/10.1103/PhysRevB.97.235132
22. Y. Sun, S.C. Wu, B. Yan, Topological surface states and Fermi arcs of the noncentrosymmetric Weyl semimetals TaAs, TaP, NbAs, and NbP. Phys. Rev. B **92**, 115428 (2015). https://doi.org/10.1103/PhysRevB.92.115428
23. M.N. Ali, J. Xiong, S. Flynn, J. Tao, Q.D. Gibson, L.M. Schoop, T. Liang, N. Haldolaarachchige, M. Hirschberger, N.P. Ong, R.J. Cava, Large, non-saturating magnetoresistance in WTe_2. Nature **514**, 205 (2014). https://doi.org/10.1038/nature13763
24. J. Jiang, F. Tang, X.C. Pan, H.M. Liu, X.H. Niu, Y.X. Wang, D.F. Xu, H.F. Yang, B.P. Xie, F.Q. Song, P. Dudin, T.K. Kim, M. Hoesch, P.K. Das, I. Vobornik, X.G. Wan, D.L. Feng, Signature of strong spin–orbital coupling in the large nonsaturating magnetoresistance material WTe_2. Phys. Rev. Lett. **115**, 166601 (2015). https://doi.org/10.1103/PhysRevLett.115.166601
25. T. Liang, Q. Gibson, M.N. Ali, M. Liu, R.J. Cava, N.P. Ong, Ultrahigh mobility and giant magnetoresistance in the Dirac semimetal Cd_3As_2. Nat. Mater. **14**, 280 (2015). https://doi.org/10.1038/nmat4143
26. P. Wadhwa, S. Kumar, A. Shukla, R. Kumar, First principles investigation of topological phase in XMR material TmSb under hydrostatic pressure. J. Phys. Condens. Matter **31**, 335401 (2019). https://doi.org/10.1088/1361-648X/ab1f5b
27. X. Huang, L. Zhao, Y. Long, P. Wang, D. Chen, Z. Yang, H. Liang, M. Xue, H. Weng, Z. Fang, X. Dai, G. Chen, Observation of the chiral-anomaly-induced negative magnetoresistance in 3D Weyl semimetal TaAs. Phys. Rev. X **5**, 031023 (2015). https://doi.org/10.1103/PhysRevX.5.031023
28. N.J. Ghimire, Y. Luo, M. Neupane, D.J. Williams, E.D. Bauer, F. Ronning, Magnetotransport of single crystalline NbAs. J. Phys. Condens. Matter **27**, 152201 (2015). https://doi.org/10.1088/0953-8984/27/15/152201
29. P. Barone, T. Rauch, D.D. Sante, J. Henk, I. Mertig, S. Picozzi, Pressure-induced topological phase transitions in rocksalt chalcogenides. Phys. Rev. B **88**, 045207 (2013). https://doi.org/10.1103/PhysRevB.88.045207
30. W. Xie, Y. Wu, F. Du, A. Wang, H. Su, Y. Chen, Z.Y. Nie, S.-K. Mo, M. Smidman, C. Cao, Y. Liu, T. Takabatake, H.Q. Yuan, Magnetotransport and electronic structure of the antiferromagnetic semimetal YbAs. Phys. Rev. B **101**, 085132 (2020). https://doi.org/10.1103/PhysRevB.101.085132
31. E. Cheng, W. Xia, X. Shi, C. Wang, C. Xi, S. Xu, D.C. Peets, L. Wang, H. Su, L. Pi, W. Ren, X. Wang, N. Yu, Y. Chen, W. Zhao, Z. Liu, Y. Guo, S. Li, Magnetism-induced topological transition in $EuAs_3$ (2020). http://arxiv.org/abs/2006.16045
32. P. Hohenberg, W. Kohn, Inhomogeneous electron gas. Phys. Rev. **136**(3B), B864–B871 (1964). https://doi.org/10.1103/PhysRev.136.B864
33. W. Kohn, L.J. Sham, Self-consistent equations including exchange and correlation effects. Phys. Rev. **140**(4A), A1133–A1138 (1995). https://doi.org/10.1103/PhysRev.140.A1133
34. G. Kresse, J. Furthmüller, Efficient iterative schemes for ab initio total-energy calculations using a plane-wave basis set. Phys. Rev. B **54**, 16 (1996). https://doi.org/10.1103/PhysRevB.54.11169
35. G. Kresse, D. Joubert, From ultrasoft pseudopotentials to the projector augmented-wave method. Phys. Rev. B **59**, 3 (1999). https://doi.org/10.1103/PhysRevB.59.1758
36. J.P. Perdew, K. Burke, M. Ernzerhof, Generalized gradient approximation made simple. Phys. Rev. B **77**, 18 (1996). https://doi.org/10.1103/PhysRevLett.77.3865
37. A. Togo, I. Tanaka, First principles phonon calculations in materials science. Scr. Mater. **108**, 1 (2015). https://doi.org/10.1016/j.scriptamat.2015.07.021
38. L. Fu, C.L. Kane, Topological insulators with inversion symmetry. Phys. Rev. **76**, 045302 (2007). https://doi.org/10.1103/PhysRevB.76.045302
39. J. Hayashi, I. Shirotani, T. Adachi, O. Shimomura, T. Kikegawa, Phase transitions of YbX (X = P, As and Sb) with a NaCl-type structure at high pressures. Philos. Mag. Lett. **84**, 3663 (2004). https://doi.org/10.1080/14786430412331284469
40. L. Degiorgi, S. Teraoka, G. Compagnini, P. Wachter, Optical and Raman investigation of Yb pnictide compounds. Phys. Rev. B **47**, 10 (1992). https://doi.org/10.1103/PhysRevB.47.5715
41. B. Winkler, V. Milman, Revised prediction of B1 to B2 phase transition pressures in YbN, YbP and YbAs. Z. Kristallogr. Cryst. Mater. **220**, 700 (2005). https://doi.org/10.1524/zkri.220.8.700.67080
42. P.K. Jha, S.P. Sanyal, Pressure–volume relation and pressure induced structural phase transformation in ytterbium pnictides. Phys. Stat. Sol. (b) **205**, 465 (1998). https://doi.org/10.1002/(sici)1521-3951(199802)205:2%3c465::aid-pssb465%3e3.0.co;2-i

Proceedings of the Sixth International Conference on Intelligent Computing and Control Systems (ICICCS 2022)
IEEE Xplore Part Number: CFP22K74-ART; ISBN: 978-1-6654-1035-9

2022 6th International Conference on Intelligent Computing and Control Systems (ICICCS) | 978-1-6654-1035-9/22/$31.00 ©2022 IEEE | DOI: 10.1109/ICICCS53718.2022.9788204

Real Time Drowsiness Detection System based on ResNet-50

Ankit Kumar Yadav
Dept. of Software Engineering
Delhi Technological University
Delhi, India
aky29feb@gmail.com

Ankit
Dept. of Software Engineering
Delhi Technological University
Delhi, India
ankit99145@gmail.com

Dr. Abhilasha Sharma
Dept. of Software Engineering
Delhi Technological University
Delhi, India
abhi16.sharma@gmail.com

Abstract—**The staggeringly high frequency of traffic/road accidents is well-known. Drowsy driving, which is the risky combination of driving with sleepiness or weariness, is one of the leading causes of such accidents i.e., roughly 100,000 crashes, or about 9.5 percent of all crashes, according to the National Safety Council (NSC). A driver's fatigue can have multiple causes such as lack of sleep, long journey, restlessness, alcohol consumption and mental pressure. Early study in this domain includes detecting the same using Machine learning and multi-layer perceptron. This paper proposes a model with increased accuracy, where the cameras are used to capture the facial landmarks. To make it easier to predict drowsiness, those images are made to go through a Convolutional Neural Network (CNN). To proceed, they are collected and thoroughly analyzed for the driver's head and facial expressions in drowsy conditions. Then, using the ResNet-50 transfer learning neural network model, datasets are built and a system to detect and classify drowsiness is developed. Finally, the experiment's conclusion validates the proposed model's efficacy. The proposed model shows an accuracy of 0.9860.**

Keywords— **CNN(Convolutional Neural Network), Resnet-50, Drowsiness Detection.**

I. INTRODUCTION

The number of death cases all around the world have ten common reasons, and road traffic accidents are one of those, according to the WHO (World Health Organization). The driver is the main cause of these failures. Driver fatigue can be caused by a variety of factors, including lack of sleep, driving long distances, anxiety, excessive drinking, and psychological stress. Therefore, driver drowsiness monitoring can be a practical way to avoid crashes. This will not only increase road safety, but can also help in improving the efficiency of ADAS, which stands for advanced driver assistance systems, while also helping with the better performance of DMS, i.e., driver monitoring systems. Fatigue detectors fall into three categories: vehicle-based, signal-based, and face-based. Changes in steering angle (), acceleration and lateral position are used to assess vehicle-specific fatigue. However, these methods are too slow to work in real time. Signal-based methods are used to determine drowsiness as a psychophysiological characteristic. In recent years, many studies have been conducted based on this approach. The main physiological signs utilized and assessed were electroencephalogram (EEG), electrocardiogram (EOG), electrocardiogram (ECG) of autonomic sensory system action, skin temperature (ST), skin electrical reaction (SSR), and electromyography (EMG). This approach can negatively affect driving, so you should consider compulsive car thieves. Approaches that are totally face-based are less expensive and easier to use than other available options, since they can assess and analyze the targets in real time. Also, they accomplish this task, without using any invasive instruments.Our model has many purposes in our genuine like giving continuous tiredness criticism to the driver if drier establishes to be lazy it alert him/her to take a rest or a break, giving execution input to an exhaustion the board program, and additionally. giving administrative consistence data to requirement authorities.

II. RELATED WORK

The Rateb Jabbar et al. [2] proposed another way to deal with realtime laziness recognition. It utilizes a profound learning strategy that turns out great with all Android applications and is incredibly exact, at 80%. Packing strong base models into lighter variants was a major aspect of their responsibilities. For their work, an insignificant organization structure was planned, that depended on identifying central issues in the facial region to decide whether the driver is sluggish.

Kamel Barkaoui et al. [3] They zeroed in on auto analysts and producers. As indicated by this article, microsleep and sluggishness recognition is finished utilizing neural network-based strategies. For their task, AI was utilized, with multi-facet perceptrons so they could recognize the sleepiness. The facial acknowledgment focuses caught by the camera were made to go through a CNN, which helped in further developing exactness. H. 83%. This work depends on Convolutional Neural Networks (CNN) and AI, a constant tiredness discovery framework for implanted frameworks and Android gadgets.

Sri Krishna H V et al. [4] for constant tiredness discovery, proposed undertaking of perceiving a driver's face utilizing the Dlib library and applying countless tourist spots to the whole driver's face. Tourist spots on the driver's face is

Authorized licensed use limited to: DELHI TECHNICAL UNIV. Downloaded on June 15,2022 at 11:20:49 UTC from IEEE Xplore. Restrictions apply.

utilized to check assuming that the driver's eyes were open or shut, and assuming the driver was yawning, and distinguished driver exhaustion.

Maryam Hashemi et al.. [5] likewise proposed working with a convolutional neural organization (CNN). Its principle objective is a constant weakness location application that incorporates high precision and fast. For these two objectives, three organizations have been presented as potential eye condition arrangement organizations. One is a completely planned neural organization (FDNN) and the other is move learning at VGG16 and VGG19 and the extra plan layer (TLVGG). Moreover, datasets have been proposed to prepare the model to work on the exactness of eye conclusion assessment and lessen computational intricacy.

Shuailei Ma et al. [6] To tackle the normal issue of distinguishing driver weakness, they utilized exchange learning hypothesis and the Resnet 18 model. These characterize the key exhaustion qualities of the three drivers and make a framework to catch them. Subsequent to making the dataset, a framework to decide exhaustion attributes in light of the Resnet18 move learning neural organization model is assembled. The exactness they accomplished was 98.05%, which was extremely amazing.

Table 1. Comparison between the common areas of related works and their architecture-based.

Reference	Models used	based on	Accuracy (%)
[2]	EEG,ECG,EOG and CNN	Eye	80
[3]	CNN and Facial Landmark Detection (D2CNN-FLD)	Eye	83
[4]	Dlib Library	Eye and Yawning	-
[5]	CNN, FD-NN, VGG16 and VGG19	Eye	98.15
[6]	CNN and Resnet - 18	Eye, Head position	98.05

There are a few limitations found in recently proposed work, some of them have moderate precision , a few necessities obtrusive instruments to be set up to run the model and to find the ideal outcome yet a considerable lot of them utilized Convolutional Neural Network (CNN). Already work incorporates help of VGG16 , VGG19 and ResNet-18 yet as displayed in Table 3 their top-1 error and top-5 error rate is extremely high in analyse of ResNet-50 that are utilized in our proposed work. This is one of the impediments that our work is winning.

III. PROPOSED WORK

The model take the catch picture from the camera, in the wake of tolerating the picture the got RGB frame is first different into 24x24 pixel size grayscale picture. As illustrated in figure 1, The aftereffect of this stage is input into our prepared RESNET-50 model that will give score based on eyes status(i.e., assuming close score will expanded by 1 else score will be 0) in the event that the score is more noteworthy than aur equivalent to 15, alert will blare, that will illuminate driver.

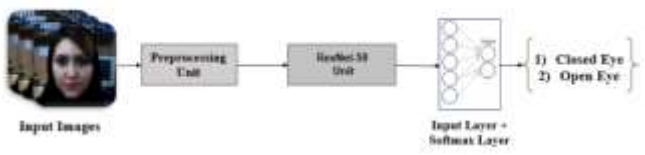

Fig. 1 Structure of transfer learning ResNet-50.

A. Region of interest

Accepts a picture as a contribution from the camera. I made a boundless circle that catches each edge. When the casing is recovered, it tracks down the eye region, sets it up, and sends it to the organization. Figure 2 shows the system proposed in this segment. The caught RGB outline is first changed over to grayscale. To decide the eye attachment, you first need to actually look at the size of the headbox. The Viola and Jones procedure is utilized for head and face acknowledgment. This relapse tree AI framework was prepared utilizing the iBUG300W perspective dataset. The high recognition precision in various head presents recognizes this methodology from different methodologies. The ROI will be cut when it arrives at the milestone of the eye. Because of facial deviation, just one eye should be assessed to distinguish tiredness. This technique essentially lessens the time it takes to identify something. You ought to pick the camera eye front since it contains more data and has a lower blunder rate. This system achieves this by computing the distance between the right and left edges of the right and passed on eyes and contrasting them with figure out which distance is reasonable for managing. To address the trouble of lighting conditions, histogram is utilized evening out to address eye contrast. This system works on the precision of the eye closeness discovery strategy. After amendment and recognition, the adjusted eye is shipped off the organization.

Fig. 2 Proposed structure for Region of Interest Selection.

B. Dataset

The dataset used to prepare our model is taken from kaggle.com. The dataset comprises of around 48,898 pictures of 37 distinct people (33 men and 4 ladies), around 24,300 pictures of open eye and 24,598 of close eye. The dataset that

Authorized licensed use limited to: DELHI TECHNICAL UNIV. Downloaded on June 15,2022 at 11:20:49 UTC from IEEE Xplore. Restrictions apply.

has been utilized, contains both high, as well as low goal of infrared pictures. All caught in different lighting conditions and by various devices. The pictures gained by three separate sensors are remembered for the dataset (Intel RealSense RS 300 sensor with 640 x 480 goal, IDS Imaging sensor with 1280 x 1024 goal, and Aptina sensor with 752 x 480 resolution).This dataset's solidarity is that it considers different eye conditions. The data gained from different distances pivots and points, permitting the driver to move all the more uninhibitedly. Drivers who use glasses and the people who don't are both reviewed. A ring of eyeglasses separated into a thick ring and a slender ring. There are two kinds of data. The principle bunch thinks about what the driver's head resembles with various eye pivots. The information gathered while turning the driver's head will be utilized in the subsequent classification, however provided that it is inside the permitted range. H. The camera caught the side view. The subsequent class incorporates the techniques as per the innovation for datasets of the eye with sideways perspectives. The organization in this model is prepared at the same time utilizing straight and askew perspectives.

Table 2. Number of Images in Dataset

Total Number	Closed Eye and Look Ahead	Open Eye and look Ahead	Closed Eye and Turned Head	Open Eye and Turned Head
48898	20400	18900	4198	5400

Fig. 3 Illustration of Closed Eye (the First and Second Row), Open Left Eye (the Third and Fourth Row) Samples from our Dataset.

Fig. 4 Display of Straight Head for Closed Eye (the First and Second Row) and Open Eye (the Third and Fourth Row) from our Dataset.

C. Architecture design

The ResNet 50 model had a top-1 error pace of 20.47 percent and top-5 error pace of 5.25 percent on the ImageNet approval set, which was very great. Likewise, network with bigger number of layers can be prepared effectively without expanding the preparation mistake rate. The 50-layer ResNet accomplishes a presentation of 3.8 Bn of FLOPS.

Table 3. Comparison between the top 1 error and top -5 error of various methods.

Methods	Top-1 error	Top-5 error
VGG [41] (ILSVRC'14)	-	8.43
GoogLeNet [44] (ILSVRC'14)	-	7.89
VGG [41] (v5)	24.4	7.1
PRELU-net [13]	21.59	5.71
BN-inception [16]	21.99	5.81
ResNet-34 B	21.84	5.71
ResNet-34 C	21.53	5.60
ResNet-50	20.74	5.25

Number As the establishment for PC vision applications, ResNet (Residual Networks) is the neural organization that is frequently utilized. In this model, ResNet-50 is used for our organization architecture. ResNet-50 has five levels of its own convolution and personality block. Every convolution block has three convolution layers, and every character block has three convolution layers. The ResNet-50 has around 24 million teachable boundaries. ResNet50 comprises of 48 Convolution layers, 1 MaxPool layer, and 1 Average Pool layer in a ResNet variety. It contains 3.8×10^9 drifting point tasks.

Table 4. ResNet – 50 architecture layers.

Layer name	Output size	50-layer
Conv 1	112 x 112	7 x 7, 64, stride 2
Conv 2_x	56 x 56	3 x 3 max Pool, stride 2 $\begin{bmatrix} 1\,x\,1, & 64 \\ 3\,x\,3, & 64 \\ 1\,x\,1, & 256 \end{bmatrix}$ X 3

Authorized licensed use limited to: DELHI TECHNICAL UNIV. Downloaded on June 15,2022 at 11:20:49 UTC from IEEE Xplore. Restrictions apply.

Conv 3_x	28 x 28	$\begin{bmatrix} 1\,x\,1, & 128 \\ 3\,x\,3, & 128 \\ 1\,x\,1, & 512 \end{bmatrix}$ X 4
Conv 4_x	14 x 14	$\begin{bmatrix} 1\,x\,1, & 256 \\ 3\,x\,3, & 256 \\ 1\,x\,1, & 1024 \end{bmatrix}$ X 6
Conv 5_x	7 x 7	$\begin{bmatrix} 1\,x\,1, & 512 \\ 3\,x\,3, & 512 \\ 1\,x\,1, & 2048 \end{bmatrix}$ X 3
	1 x 1	Average pool, 1000-d fc, SoftMax
FLOPs	-	3.8×10^9

The ResNet-50 design contains:-

1) One layer from a convolution with a part size of 7 * 7 and 64 unmistakable portions, all with a step of size 2 is considered.

2) Now from that point forward, there's greatest pooling with a step size of 2.

3) There is a 1 * 1,64 part in the following convolution, trailed by a 3 * 3,64 piece, lastly a 1 * 1,256 bit. These three layers are rehashed multiple times altogether, giving us 9 layers in this stage.

4) Following there is a part of 1 * 1,128, trailed by a portion of 3 * 3,128, lastly a bit of 1 * 1,512. This stage was performed multiple times, providing us with an aggregate of 12 layers.

5) Then there's a 1 * 1,256 portion, trailed by 3 * 3,256 and 1 * 1,1024 pieces, which are rehashed multiple times for a sum of 18 layers.

6) Then a 1 * 1,512 portion was added, trailed by two additional 3 * 3,512 and 1 * 1,2048 pieces, for a sum of nine layers.

7) After that, a normal pool is run and wrapped up with a completely connected layer with 1000 hubs, trailed by a softmax work, giving us one layer.

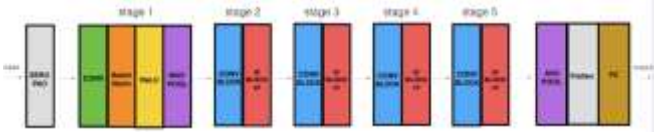

Fig. 5 Architecture layer of ResNet – 50

D. Decision Making

In the last advance of location, images at a pace of 6 edges each second are caught. Figure 6 shows the design of conclusion eye identification. Assuming the organization accepts that the likelihood of closeness of eye is more than 50 % for over 2 seconds (i.e for 15 frames).A hazard is thought of and an advance notice voice caution is given to the driver. As indicated by the consequences of the trials, a solid individual's squinting time is somewhere in the range of 100 and 400 milliseconds. Subsequently, shut eyes that stay longer than one second are an indication of fatigue. To restrict our calculation's misleading adverse outcome, to sound the caution assuming that the eyelids are shut for more than equivalent to 2.5 seconds is opted. Identification shows laziness since six casings each second, or 15 casings of shut eye are processed.

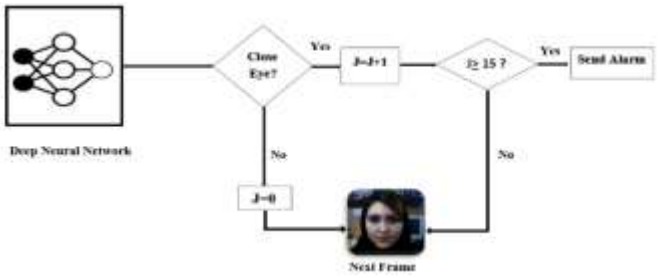

Fig. 6 Framework of Close Eye Detection.

IV. Result And Discussion

A. Accuracy Evaluation

The dataset, which was utilized to assess the model, includes static depictions of the eye taken under different lighting situations, with unmistakable student directions and various eye ascribes. In the preparation cycle, the eye is parted into 2 gatherings (open and shut notwithstanding assuming that it is correct or left eye). A driver sluggishness recognition framework utilizes this ROI, which is characterized via milestone areas. The train and approval information in the dataset are involved to contrast our organizations with other proposed examinations on the grounds that past work in this field had just utilized train and approval information. Cross entropy and stochastic angle plunge were chosen as enhancers and misfortune capacities. The learning rate was set at 0.01 percent, with 70% of the information being used for preparing and the rest of approval. The ResNet-50 yield .0986 precision on ROI pictures, as per the exactness and Area Under Curve (AUC) of organizations on the dataset introduced in Table 5.

Utilizing a stochastic inclination plummet streamlining agent with a learning pace of 0.01 and a cross-entropy misfortune work, the dataset was separated into three organizations. The dataset was parted into 3 sections: 80% of it was made of preparation information, 10% utilized for approval, while the excess 10% was made of trying information. The measurements show that the picked convolutional neural organization technique and arrange engineering can satisfactorily fulfill the exactness boundary. As displayed in Table 5, CNN has the most noteworthy precision. The FD-True NN's Positive (TP), False Positive (FP), True Negative (TN), False Negative (FN), review, and

Authorized licensed use limited to: DELHI TECHNICAL UNIV. Downloaded on June 15,2022 at 11:20:49 UTC from IEEE Xplore. Restrictions apply.

accuracy are completely estimated in True Positive (TP), False Positive (FP), True Negative (TN), False Negative (FN). The precision of discovery in the dataset with ResNet-50 is higher than different organizations, as shown by the discoveries of this section. Each strategy's exactness and AUC are definite in Table 6 . It very well may be shown that among the proposed networks as a whole, the proposed ResNet-50 has the most elevated precision and AUC.

Table 5. Precision and Recall in CNN and ResNet-50 for our Dataset.

Total No. of Test	TP	FP	TN	FN	Precision	Recall
9780	4995	59	4632	94	98.69%	97.62 %

Table 6. Comparison of Accuracy and AUC among the proposed Net-works and Other Methods on the Kaggle Dataset.

Research	Method	Accuracy (%)	AUC (%)
Pan [34]	Cas-Adaboost(W=3)	88.8	-
Song [20]	HPOG + LTP +Gabor(s)	95.91	89.22
Song [20]	MultiHPOG+LTP+Gabor	96.83	99.27
Song [20]	MultiHPOG+LTP+Gabor	96.40	96.67
Zhao [21]	DNN	94.45	97.91
Zhao [21]	DCNN	95.79	98.15
Zhao [21]	DINN	97.20	99.29
Our	CNN and ResNet-50	98.60	98.78

B. *Limitation and Implementation*

As per the creators, the proposed calculations offer high precision and modest handling costs. There is a compromise, be that as it may, among dataset and exactness. More profound organizations perform better and require huge datasets in light of the fact that they have more secret layers and boundaries. Subsequently, there is a trade between the quantity of FD-NN boundaries and the quantity of information focuses introduced. Moreover, during information gathering, a wide scope of visual attributes ought to be assessed. Nature of light, the morals of the driver, the camera's point and area, mugginess, facial attributes, and eyewear are only a couple of models. The creators picked the most fundamental factors since it was difficult to think about every one of them. In reality, nonetheless, erasing different boundaries affects the result. Besides, from a mental viewpoint, nodding off comprises of a few phases that can't be separated into two classifications. At the point when rest a twofold situation is considered, it is alluded to an estimation of transitional levels that impact execution, in actuality. The improvement of a counterfeit neural organization requires superior execution equipment. The most notable equipment stages for neural organization structures are FPGA and GPU. Many elements, including power, effectiveness, and adaptability of the framework, should be considered while picking a stage. Since there are sufficient stages for building counterfeit neural organizations on ready GPUs, the writers accept that numerous preconfigured durable goods with GPU, like cell phones and tablets, may be utilized for arrangement.

Fig. 7 Model demonstration - I (Close eye detected, score increased).

Here exhibition of our model , when eyes are shut score will continue to increment displayed in figure 7 score is equivalents to 3 no alarm sound is there, when eyes will get open score will become 0 displayed in figure 8 score is equivalents to 0, additionally when eyes are shut for all the more then couple of moments and score will arrive at 15 or past that caution will begin ringing or our model will caution the driver about the sleepiness and prompt him/her to enjoy some time off or take a rest as displayed in figure 9 score is equivalents to 23 and ready sound is begun and red imprint around the screen is showed.

Authorized licensed use limited to: DELHI TECHNICAL UNIV. Downloaded on June 15,2022 at 11:20:49 UTC from IEEE Xplore. Restrictions apply.

Fig. 8 Model demonstration - II (Open eye detected, score equals to 0).

Fig. 9 Model demonstration - III (Close eye detected, score exceeds 15, alarm beeps).

V. CONCLUSION AND FUTURE WORK

Recognizable proof of sleepiness is urgent for safe driving, and this paper proposed an original technique for limiting tiredness related impacts. The framework catches a surge of casings in the primary stage, and milestone focuses are utilized in the preprocessing unit to get to ROI in the subsequent stage. After this, the eye region is picked, and the preprocessing unit picks the camera's eye front. The picture is then changed over to grayscale and the visual differentiation is changed. At long last, the picture is diminished to a 24 x 24 pixel size. The result of this stage is input into an organization that recognizes eye states. An alert will be sent to the driver assuming the organization identifies that the driver's eye is shut for in excess of 15 back to back pictures.

The lengthy dataset enjoys the benefit of representing the sideways view, permitting the framework to work in a bigger scope of scenarios. Additionally three organizations are made for recognizing sluggishness relying upon eye state, which would upgrade precision and cut down on calculation time. Three unique organizations are shown, and precision and different boundaries are contrasted with figure out which organization is the most dependable. The CNN network has a 98.15 percent precision and a 99.8 percent AUC, as indicated by the aftereffects of the trials. The CNN network is additionally reasonable for ongoing applications; eye state order takes just 1.4 milliseconds. To additionally continue with our examination, zero on investigating yawning is intended, as that is likewise a decent component to consider for laziness. It tends to be recognized utilizing mouth tourist spots. Since the differentiations between various degrees of weakness are so fine, an alternate degree of tiredness can be broke down without being in two situations, which would be more mind boggling.

REFERENCES

1. National Safety Council(NSC) https://www.bankrate.com/insurance/car/drowsy-driving-statistics/
2. Rateb Jabbar, Khalifa Al-Khalifa, Mohamed Kharbeche, Wael Alhajyaseen, Mohsen Jafari, Shan Jiang: (5 Nov 2018) Real-time Driver Drowsiness Detection for Android Application Using Deep Neural Networks Techniques.
3. Kamel Barkaoui, Rateb Jabbar, Mohammed Shinoy, Mohamed Kharbeche, Khalifa Al-Khalifa, Moez Krichen: (17 Jan 2020) Driver Drowsiness Detection Model Using Convolutional Neural Networks Techniques for Android Application.
4. Sri Krishna H V, Tarun Srinivas, Kedarnath R Gubbi, Vijay Kumar S.: REAL-TIME DROWSINESS DETECTION (RTD2) (HUST Journal 2021).
5. Maryam Hashemi, Alireza Mirrashid, Aliasghar Beheshti Shirazi: (15 Jan 2020) Driver Safety Development Real Time Driver Drowsiness Detection System Based on Convolutional Neural Network.
6. Shuailei Ma, Tingxuan Huang, Xiaojie Sun, Ying Wei: Driver Drowsiness Detection Based On ResNet-18 And Transfer Learning (2021 33rd Chinese Control and Decision Conference (CCDC)).
7. Thomas Kundinger, Nikoletta Sofra, Andreas Riener : 2020, Assessment of the Potential of Wrist-Worn Wearable Sensors for Driver Drowsiness Detection, Sensors.
8. Kartik Mutya, Jayesh Shah, Anthony D. McDonald, Jaycelyn Jefferson: 2019, Proceedings of the Human Factors and Ergonomics Society Annual Meeting.
9. Driver Drowsiness Detection Model - Archive ouverte HAL https://hal.archives-ouvertes.fr/hal-02479367/document ,last accessed 2022/01/28.
10. Aliasghar Beheshti Shirazi's lab - ResearchGate https://www.researchgate.net/lab/Aliasghar-Beheshti-Shirazi-Lab last accessed 2022/01/28.
11. Driver Safety Development Real Time Driver Drowsiness ... https://arxiv.org/abs/2001.05137 last accessed 2022/01/27.
12. Paper tables with annotated results for Driver Safety ... https://paperswithcode.com/paper/deep-learning-based-driver-distraction-and/review/ last accessed 2022/01/29.
13. Rateb Jabbar, Khalifa Al-Khalifa, Mohamed Kharbeche, Wael Alhajyaseen, Mohsen Jafari, Shan Jian: 2018 Real-time Driver Drowsiness Detection for Android Application Using Deep Neural Networks Techniques, Procedia Computer Science.
14. Jing-Ming Guo, Herleevandi Markoni: 2018 Driver drowsiness detection using hybrid convolutional neural network and long short-term memory, Multimedia Tools and Applications.

Authorized licensed use limited to: DELHI TECHNICAL UNIV. Downloaded on June 15,2022 at 11:20:49 UTC from IEEE Xplore. Restrictions apply.

15. Muhammad Rizwan Ullah, Muhammad Aslam, Muhammad Imran Ullah, Martinez-Enriquez Ana Maria: Driver's Drowsiness Detection Through Computer Vision.

16. Muhammad Zeeshan Baig,Manolya Kavakli: 2019, A Survey on Psycho-Physiological Analysis & Measurement Methods in Multimodal Systems, Multimodal Technologies and Interaction.

17. Laiali Al Mazaydeh, Khaled Elleithy, Miad Faezipour: 2012, Detection of obstructive sleep apnea through ECG signal features, 2012 IEEE International Conference on Electro/Information Technology.

18. Massimiliano de Zambotti, John Trinder, Alessandro Silvani, Ian M. Colrain, Fiona C. Baker: 2018, Dynamic coupling between the central and autonomic nervous systems during sleep, Neuroscience & Biobehavioral Reviews.

19. Polysomnographic Technique: 1994, An Overview Sharon A. Keenan Sleep Disorders Medicine.

20. Real-time Driver Drowsiness Detection for Android - arXiv https://arxiv.org/pdf/1811.01627 last accessed 2022/01/28.

21. Driver Distraction And Drowsiness Detection Based ... - SID.ir https://www.sid.ir/en/journal/ViewPaper.aspx?id=807570 last accessed 2022/01/28.

22. REAL-TIME DROWSINESS DETECTION (RTD2) - Papers ... https://paperswithcode.com/paper/real-time-drowsiness-detection-rtd2 last accessed 2022/01/28.

23. Intelligent Technologies and Applications Communications in Computer and Information Science, 2020.

24. Sukrit Mehta, Sharad Dadhich, Sahil Gumber, Arpita Jadhav Bhatt: 2019, Real-Time Driver Drowsiness Detection System Using Eye Aspect Ratio and Eye Closure Ratio, SSRN Electronic Journal .

25. Sergio Cerutti, Anna M. Bianchi, Harald Reiter: 2006, Analysis of sleep and stress profiles from biomedical signal processing in wearable devices, 2006 International Conference of the IEEE Engineering in Medicine and Biology Society.

26. Understanding and Coding a ResNet in Keras - Towards Data ... https://towardsdatascience.com/understanding-and-coding-a-resnet-in-keras-446d7ff84d33 last accessed 2022/01/28.

27. Real-Time Driver Drowsiness Detection System Based on ... https://www.semanticscholar.org/paper/9b5ef0ddbd913d966b7e313489bfaa43f283c2e6 last accessed 2022/01/28.

Authorized licensed use limited to: DELHI TECHNICAL UNIV. Downloaded on June 15,2022 at 11:20:49 UTC from IEEE Xplore. Restrictions apply.

Bull. Mater. Sci. (2022) 45:109
https://doi.org/10.1007/s12034-022-02680-x
© Indian Academy of Sciences

Recent advancements over a decade for organic light-emitting diodes: from structural diversity, role of layers, colour emission, material classification, performance improvement, fabrication to applications

SUGANDHA YADAV[1], POORNIMA MITTAL[1,*] and SHUBHAM NEGI[2]
[1]Department of Electronic and Communication Engineering, Delhi Technological University, New Delhi 110042, India
[2]Department of Electronics and Communication Engineering, Tula's Institute, Dehradun 248197, India
*Author for correspondence (poornimamittal@dtu.ac.in)

MS received 11 October 2021; accepted 24 January 2022

Abstract. Organic light-emitting diode (OLED) is an emerging technology of organic electronics that exhibits an assortment of salient and attractive features like self-emitting ability, great flexibility, true dark tone, transparency and many more. Along with display applications, OLEDs are prudent for light detection-based applications. Enormous research work has been reported to refine the OLED technology in terms of structures, materials, performance parameters, lifetime and applications. There is a vast scope for developing white OLED devices for utilization in solid-state lighting applications. This review paper summarizes recent advancements in different aspects for OLEDs over the last decade. The main focus is to diversify different multilayer structures of OLEDs highlighting the role and significance of charge injection, charge transport, emission and blocking layers. Also, a timeline analysis for characteristics parameters, layer-wise materials and fabrication techniques is presented. Further, different performance improvement techniques based on layers, parameters and colour emission are demonstrated. This article also illustrates prudent applications based on organic thin-film transistor-driven OLED, sensors, military and healthcare. Some challenges and reliability issues are also discussed with a scope for future work for OLED.

Keywords. Active-matrix OLED (AMOLED); healthcare; military; organic light-emitting diode (OLED); sensors.

1. Introduction

In inorganic electronics, the integrated circuits can be made only on single crystals of semiconductors using high-temperature processing steps. Monolithic integration of components on other substrates like plastic, glass, etc. is not possible [1]. On the other hand, the properties of organic semiconductors are driven by the properties of molecules [2]. There is always a major scope of amending the properties of semiconductors by altering the molecular structure.

In 1950, electroluminescence was first observed in organic materials by giving high voltage in the air to acridine orange [3]. Further, the need for electrode contact was explained by Martin Pope in NY University in 1960 [4]. They developed the Ohmic dark-injecting electrode. First DC electroluminescence under vacuum was noticed on the crystal of anthracene in 1965. Therefore, electroluminescence in anthracene was observed through hole and electron double injection recombination in Canada [3]. They discussed about electron excitation between graphite molecules and anthracene particles at contacts. The first polymer light-emitting diode was reported in 1987 using a novel two-layer structure having electron and hole transporting layers for the recombination. This resulted in light emission between organic layers. Thereafter in 1990, a green light-emitting polymer device was produced at the Cavendish Laboratory, Cambridge [3].

Organic semiconductors are molecular in nature where molecules are carried together by weak Van der Waals forces. Because of this property, semiconductors can be vaporized at very low temperatures to develop thin films. Additional to small molecules (SMs), polymers also belong to the organic semiconductors class, as these are soluble in common solvents such as xylene or chloroform and their films can be formed by simple spin-coating techniques. The organic semiconductors are not crystalline in nature and can be fabricated at very low temperatures. Due to this nature, organic devices like OLED, transistors, solar cells, etc. can be fabricated not only on inexpensive glass but also paper, plastic and fabric as these devices contain great flexibility.

Organic light-emitting diode (OLED) has been considered as one of the most promising techniques in display technology, as it is providing a new dimension to the display technology. There are many advantages of OLED over

Published online: 23 June 2022

conventional display technologies, such as better display quality, flexible displays, wide viewing angle, varieties of colours, etc. These devices are thinner and lighter, also the fabrication process is less complicated in comparison with inorganic technology. Besides this, other benefits of organic LEDs include lower power consumption, higher contrast ratio, faster response time and better environmental stability.

This article thoroughly discusses a timeline progress of the OLED at various technology nodes. The analysis is done based on working principles, performance parameters, various applications, fabrication techniques, materials for different layers and their imperative usage. Additionally, reliability issues, research challenges and future scope are discussed.

2. OLED and its working principle

Organic LED is a semiconducting device that consists of an emissive layer and conducting layer as shown in figure 1. These layers are sandwiched between the electrodes named anode and cathode and placed on a substrate. The layers are made of organic materials and are very thin, about 200 times smaller than a human hair (less than 500 nm) [5]. A bright light is generated when an electrical current is applied. This technology utilizes carbon-based molecules that play an important role to produce light. The brightness and colour of light can be controlled by enhancing the properties of the materials. The OLED displays provide a bright and clear picture quality with a wider viewing angle. These devices are more energy efficient because OLED displays do not require backlighting, as these devices are self-luminous.

The working of the OLED is due to the recombination of electrons and holes. The complete process of light emission includes (1) injection of charge carriers, (2) transportation of charge carriers, (3) recombination of charge carriers and (4) light emission. First of all, the electrons and holes are inserted into the LUMO and HOMO level from the cathode and anode, respectively [6]. These energy levels act like conduction and valence bands, respectively. The work function difference between the electrode and organic semiconductor plays a very important role in the injection of the charge carrier. After the insertion of charge carriers, these are transmitted in the organic semiconductor for the recombination process [7]. Thereafter, within the emissive layer, the recombination occurs. The recombination process results in the generation of energy in the form of photons and light is produced [8]. The process of recombination should take place within the emissive layer.

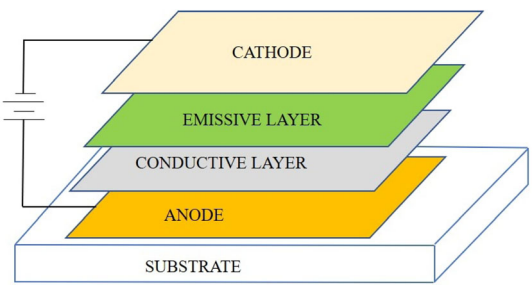

Figure 1. The basic structure of OLED.

Practically, due to mobility difference, recombination does not happen within the emissive layer [9]. Because the desired result is that, every electron that is injected into the organic layer from the cathode must form exciton with the one hole that is injected from the anode. So, to get 100% efficiency, there should be no electron that goes from cathode to anode without forming the exciton. For this purpose, the charge balance should be right in order to get good exciton formation. But normally for the organic materials, the hole's mobility is more than the electron. Due to this, all the recombination occurs close to the cathode only because of the mobility difference of charge carriers. This is the problem as these excitons are quenched because of the proximity to the cathode. Therefore, it is required that the mobility of these two charge carriers should match.

This can be done by incorporating some more layers into the OLED structure, such as transport, injection and blocking layer [10,11]. These layers also overcome the problem of mismatch in energy level between LUMO and the cathode work function (ϕ_b) and HOMO and the anode work function (ϕ_a). Figure 2a and b shows the energy band diagram for both basic structure and multi-layered structure, respectively. In the basic structure of OLED depicted in figure 2a, the emissive layer requires to maintain high quantum efficiency, mobility and better hole and electron injection. But, most of the materials could not meet this demand. Therefore, multi-layered device architecture is utilized (figure 2b) to improve these parameters. There should not be a large mismatch in energy levels, otherwise, device performance will get poorer due to low charge carrier injection [12]. It is possible to reduce the energy barrier for charge injection by incorporating such layers between the emissive layer and the electrodes. The presence of an electron transport layer dramatically lowers the hole current in the OLED due to band offset and increases electron mobility.

The electron and hole transport layers are utilized for the higher recombination of the charge carriers. But due to the energy barrier between these layers and electrodes, charge carriers are not significantly inserted into the device [13]. To overcome this issue, electron and hole injection layers (EIL/HIL) are introduced. These layers aid in injecting the charge carriers and transporting these into the device. An intermediate energy level is established between HOMO/LUMO and the work function of the electrode to reduce the energy barrier. Due to the higher mobility, holes move faster than electrons and reach the emissive layer too early [14]. Thus, recombination does not occur properly. To

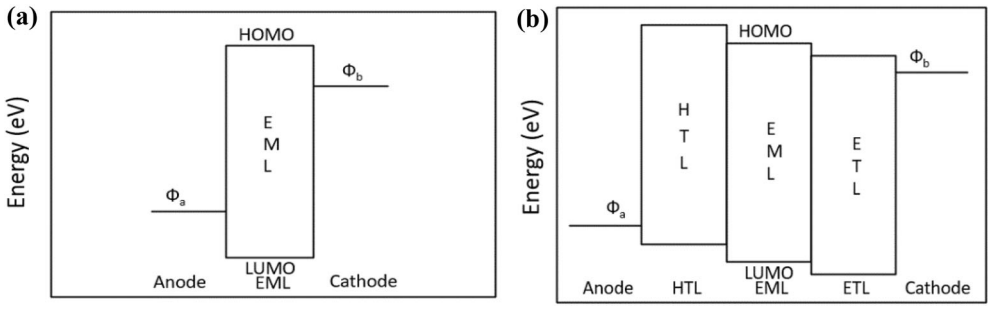

Figure 2. Energy band diagram of (**a**) single-layered and (**b**) multi-layered OLEDs.

restrict the movement of holes and match the mobility with electrons, the hole blocking layer is incorporated.

In figure 3, it can be seen that electrons from cathode are inserted towards the emissive layer via electron injection and transport layers. Similarly, holes are introduced to the device from the anode side. Holes travels from hole injections layer to emissive layer via hole transport layer. But further movement of holes towards the electron transport layer is blocked. These electrons and holes recombine in the emissive layer and produce energy in the form of photons. In addition to the above-mentioned layers, some more novel layers are added to the basic structure to enhance the performance of OLED devices. These layers include mixed interlayer [15], charge generation layer [16], spacer layers [17], etc.

3. Characteristics parameters

Highly efficient displays can be achieved in addition to great flexibility and large-area fabrication by enhancing characteristics parameters of OLED devices. Many characteristics parameters highlight the performance of organic LEDs, such as (1) luminance, (2) current density, (3) current efficiency, (4) power efficiency, etc. These parameters are defined in the following sections.

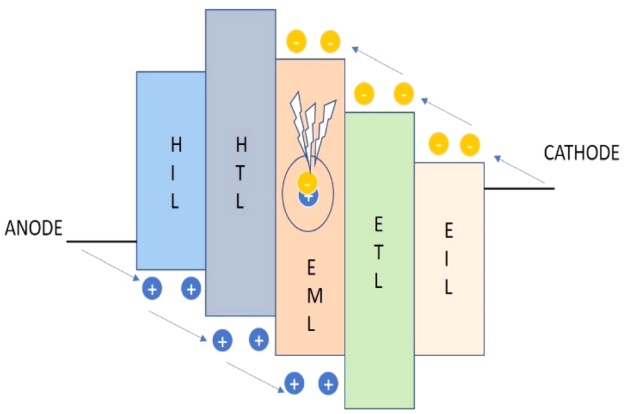

Figure 3. The multi-layered structure of OLED.

3.1 *Luminescence*

The general property of light emission by a substance without any heat is known as luminescence. Also, the intensity of light emitted per unit area is defined as luminescence [18]. It is known that many semiconductors absorb energy in some form that may be photon absorption, electron bombardment, the introduction of the currents, etc. This energy is re-emitted in the form of electromagnetic radiation in the visible region of the spectrum. Luminescence is a two-step process, one is the excitation of the system and the other is the subsequent emission of the photons. In the case of OLED, luminescence depends mostly on the type of organic material, the colour of light emitted, the supply voltage, etc. This parameter is the major requirement for OLED devices as it is a light-emitting device itself.

Some of the notable work in recent times are discussed now. In 2014, Chen *et al* [19] proposed two tailored luminogens having tetraphenylethene (TPE), diphenylamino and dimesitylboryl as a π-conjugated linkage, electron donor and electron acceptor, correspondingly and achieved luminescence of 49,993 cd m^{-2}. Thereafter, in 2015, Gomez *et al* [18] reported adenine as a HIL. The maximum luminescence was obtained as 45,000 cd m^{-2} on glass, which is increased by 4 times as compared to the previous device (12,500 cd m^{-2}) fabricated in the paper. Also on cellulose, it improved from 2000 to 8400 cd m^{-2}.

In 2018, Zhuo *et al* [20] designed a white OLED and gained the maximum luminescence of 9296 cd m^{-2} with R G B in the double light-emitting layer, which was 2 times of B-O WOLED constructed using the same materials. Furthermore in 2020, Klein *et al* [21] utilized Cu(I) and Ag(I) complexes with a new type of tridentate N,P,P-ligand and achieved luminance of 10,000 cd m^{-2} for green OLED based on compound 8 having 2 wt% concentration. This luminescence is the maximum as compared with other devices having 4 and 8 wt% concentrations. Moreover in 2020, Zheng *et al* [22] utilized a host material, i.e., 3,5-bis(N-carbazolyl)benzene into organic layers to enhance the efficiency of inkjet-printed blue OLED. With this material,

luminescence was improved by 5 times and achieved as 3743 cd m^{-2}.

Figure 4 highlights the data of five devices (D1, D2, D3, D4 and D5) [19,21,23–25] in terms of luminescence and external quantum efficiency (EQE). It can be noticed that the maximum luminescence is exhibited as 92,455 cd m^{-2} by device D5. This device was fabricated by Lu *et al* [25] in 2021 using two green chiral iridium(III) isomers. The device D1 is also showing very good luminescence of 49,993 cd m^{-2}. It is constructed by Chen *et al* [19] in 2014. They synthesized two thermally stable TPE derivatives (TPE-NB and TPE-PNPB) carrying diphenylamino and dimesitylboryl as electron donors and acceptors.

3.2 *Efficiency*

The efficiency can be defined in terms of many parameters such as current, power and EQE. The current efficiency is expressed as the ratio of luminescence over current density. This parameter plays a very important role to inspect the performance of OLED devices. Various researchers have worked to improve the current efficiency. In 2011, Chen *et al* [16] utilized a heterojunction organic bipolar charge injection layer by blending zinc phthalocyanine: fullerene (ZnPc:C_{60}). The device showed current efficiency of 36.5 cd A^{-1}, which is enhanced by 2.4 times as compared with the single-unit device that exhibited 15.2 cd A^{-1} efficiency at the same current density of 20 mA cm^{-2}. Afterwards in 2018, Zhuo *et al* [20] fabricated a double light-emitting layer utilizing red-green emitting light. The device exhibited 10 times higher current efficiency, i.e., 10.17 cd A^{-1}. Additionally, in 2018, Wang *et al* [26] incorporated two host type materials N,N′-diphenyl-N,N'-bis(1-naphthylphenyl)-1,1'-biphenyl-4,4'-diamine (NPB) and 4,4′,4″-tri(N-carbazolyl)triphenylamine (TCTA) to design a double-emissive layer and showed current efficiency as 42.3 cd A^{-1}. Thereafter, in 2020, Mohan *et al* [27] added CuI as dopants into CuPC to improve hole transport layer and achieved current efficiency as 70 cd A^{-1}. Afterwards, in 2021, Lu *et al* [25] fabricated some conventional devices using chiral complexes as dopants. In this research, the peak current efficiency was attained as 105.6 cd A^{-1}.

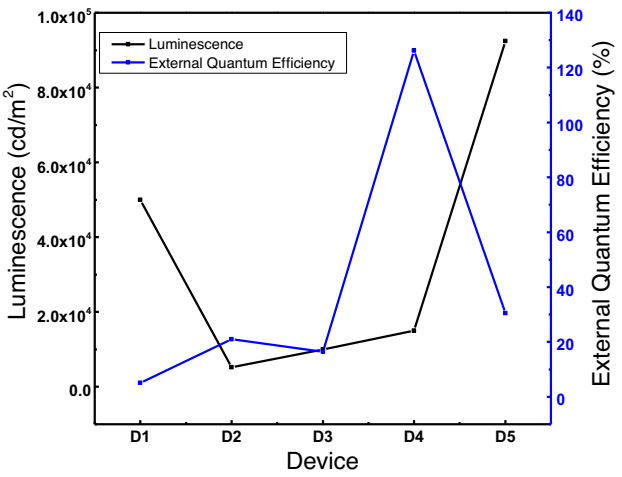

Figure 4. Comparison of luminescence and external quantum efficiency.

The next sub-category of efficiency is power efficiency. It is described as the ratio luminous flux with respect to the power consumption of organic LED. This parameter is also known as luminous efficacy. A lot of research work has been investigated to enhance power efficiency. In 2018, Xi *et al* [28] reported a white OLED having high power efficiency of 31.0 lm W^{-1}. It was the maximum efficiency achieved at that time. Then in 2019, Han *et al* [29] developed a purely blue colour TADF (thermally activated delayed fluorescence) device using a fused B-N emitter. This device showed a very good power efficiency of 33.3 lm W^{-1}. Afterwards, in 2020, Han *et al* [30] presented an internal light extraction layer for white OLED with a high refractive index. The device showed 93.2 lm W^{-1}. Moreover, in 2021, Cui *et al* [31] employed emission layers with different substrate temperatures (from 30 to 100°C) to the OLED devices. The peak power efficiency was exhibited as 68.9 lm W^{-1} at 60°C.

Another important sub-parameter of this category is external quantum efficiency (EQE). The ratio of the number of photons that are emitted by the organic LED with respect to the total electrons is described as EQE. This parameter is improved using various methods by the researchers. In 2012, Park *et al* [32] incorporated a novel highly twisted material using anthracene with xylene. The EQE was obtained using this material as 5.26%. Thereafter, in 2016, Rajamalli *et al* [33] utilized blue TADF emitters BPy-pC, BPy-pTC, BPy-p2C and BPy-p3C. The device using BPy-p3C dopant showed a maximum EQE of 23.9%. This value was almost 6 times higher than the EQE of a device having BPy-pC dopant. Moreover in 2019, Yang *et al* [34] constructed a donor−acceptor type TADF emitter with a large rigid phenanthro[4,5-abc] phenazine-11,12-dicarbonitrile as an acceptor unit and a triphenylamine (TPA) as a donor moiety. In this article, efforts have been made to enhance the performance of DR/NIR (deep-red/near-infrared) OLED devices. The maximum EQE of DR and NIR devices are achieved as 20.2 and 16.4%, correspondingly.

In 2020, Han *et al* [30] reported an extremely high efficiency of 103% by using a light extraction layer with a high refractive index. Additionally, in 2021, Lu *et al* [25] developed a pair of chiral green Ir(III) containing dual stereochiral centres and achieved a maximum EQE of 30.5%. In this article, the work has been done to overcome the challenges of CP-OLEDs (circularly polarized-organic LED) using chiral emitters, which provide high phosphorescence quantum yields and circularly polarized

Table 1. Comparison of the essential parameters.

Year	Ref.	Luminescence (cd m^{-2})	External quantum efficiency (%)
2021	[35]	9156	—
2021	[25]	92,455	30.5
2021	[31]	32,710	18.9
2021	[36]	—	25.5
2020	[24]	15,000	126.2
2020	[37]	1031	9.3
2020	[21]	10,000	16.4
2020	[22]	3743	5.03
2020	[23]	5200	21.0
2019	[34]	1273	20.2
2018	[20]	9296	4.09
2018	[26]	5000	30.3
2017	[38]	100	9.4
2016	[39]	5219	2.39
2015	[40]	—	2.56
2014	[19]	49,993	5.12

luminescence property. Table 1 shows comparison of the recent work of luminescence and external quantum efficiency.

In the graph mentioned above (figure 4), the peak EQE is achieved as 126.2% by device D4. This device (white OLED) was constructed in 2020 by Huang *et al* [24] utilizing an exciplex host and a blue-red unit based on a TADF blue emitter. In addition to this, devices D2 and D5 also show better performance as compared to D1 and D3 in terms of EQE.

4. Structural diversity for oled

Apart from materials, device structure also plays a very important role to improve the performance of OLED devices. Various diverse structures like top-emitting OLED, foldable OLED and transparent OLED are proposed to fabricate a better organic LED device in terms of efficiency, current density, durability, etc. [41]. There are numerous structural modifications related to the OLED. However, here the latest structural modifications are discussed.

4.1 *Top-emitting OLED*

Top-emitting organic LEDs (TEOLEDs) are utilized in active-matrix OLEDs because thin-film transistors can be implanted under these OLEDs [42]. Also, it becomes easy to fabricate the complicated pixel without reducing the aperture ratio. These OLEDs are very well fitted for microdisplay applications. The former structure with indium-tin oxide (ITO) as the anode is preferred in most of the fabricated TEOLED. These OLEDs are applicable in smart cards such as credit cards and debit cards.

Figure 5 highlights the three different structures of OLED such as (a) top emission, (b) inverted top emission and (c) bottom emission. The comparison can be easily done by analysing these structures. In TEOLED, two highly reflective contacts are utilized; one is at bottom of the structure and the other (semi-transparent contact) is established at top of the organic layers. The top-emitting OLEDs show strong microcavity effects because of the reflective contacts at both sides (bottom and top) [43]. The top-emitting OLED (TEOLED) can be connected in both ways like it can make contact with anode as a bottom-emitting OLED as well as it can have cathode in contact with the substrate as an inverted mode as shown in figure 3c. In the bottom emitting organic LED, light is emitted via transparent bottom contact of ITO (tin-doped indium oxide).

Many researchers have investigated the TEOLEDs to enhance the performance. In 2017, Qu *et al* [44] demonstrated high-efficiency light extraction for TEOLED. There is a transparent conductive oxide in top-emitting OLED on the surface of a non-diffractive, reflecting metal-coated scattering grid situated below the organic active layer. The EQE was improved from 20 to 30% for green phosphorescent OLED devices with or without reflecting grid structures. Further, Liu *et al* [45] in 2018 used mixed interlayer of poly(9-vinylcarbazole) (PVK) and poly[(9, 9-dioctylfluorenyl-2, 7-diyl)-co-(4, 4′-(N-(4-secbutylphenyl) diphenylamine)) (TFB) between emitting layer and the PEDOT:PSS layer to significantly improve the hole injection from PEDOT:PSS.

4.2 *Foldable OLED*

OLEDs open up opportunities to create flexible devices. For the fabrication of foldable OLED, a very flexible substrate is used. For damage control, strong materials are utilized in these OLEDs. The merits of these devices include high contrast images, faster response time and crisper resolution for flexible display devices. The applications of foldable organic OLEDs are big screen curved televisions, GPS devices, mobile phones, etc.

Figure 6 illustrates the top view of the prototype model. If the scan drivers having high resistance to bending are placed on both sides of the display, then the display can be bent parallel to FPC (flexible printed circuit) and IC area. The FPC and IC should not be placed in the display area to avoid the breakage of FPC and ICs due to bending stress.

Noteworthy efforts have been made to improve the performance of foldable OLEDs. In 2015, Takahashi *et al* [46] designed a 13.3-inch 8k4k 664-ppi high-resolution foldable organic LED display using crystalline oxide semiconductor FETs. In this design, there were three transistors and one capacitor for each pixel circuit. Also, it consists of one

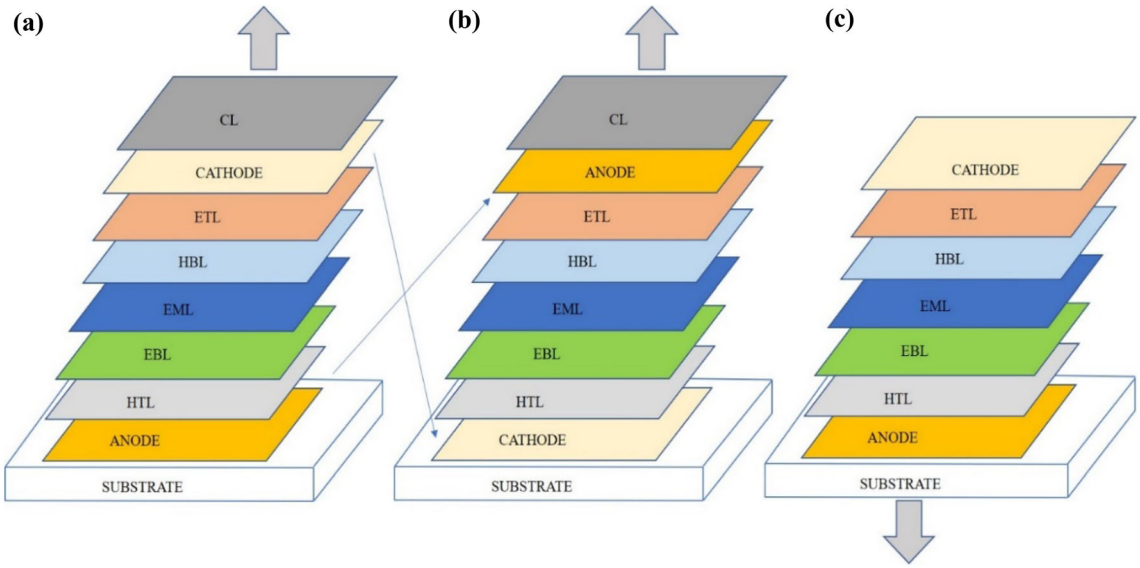

Figure 5. (**a**) Top emission, (**b**) inverted top emission and (**c**) bottom emission OLED.

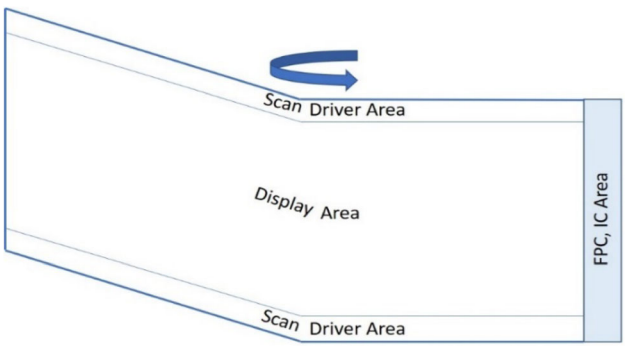

Figure 6. Top view of a prototype model of foldable OLED.

external circuit that rectifies pixel current. Afterwards, Watanabe *et al* [47] fabricated an 8.67-inch foldable display having an in-cell touch sensor. Here, sensor electrodes are designed in a display counter substrate which was utilized to obtain lower parasitic capacitance. The OLED and sensors can be worked appropriately even after 10^5 folding operations including 5 mm as the radius of curvature.

In 2019, De Dieu *et al* [49] proposed a 3D touch sensor technology. It included pressure-sensitive adhesive and a transparent P(VDF-TrFE) layer to permit high-resolution static and dynamic pressure sensing. This technology also detects types of touching objects besides multitouches and pressures. Moreover in 2020, Zhang *et al* [50] developed a 17.3-inch WQHD foldable active-matrix OLED display with 10-bit depth. Table 2 highlights the specification comparison of three foldable display devices D_6, D_7 and D_8 on the basis of screen size, driving method, number of effective pixels, pixel pitch and density, source driver and aperture ratio.

Figure 7 is depicting the comparison of specifications of three foldable displays D6, D7 and D8 in terms of screen size, pixel density and aperture ratio.

4.3 *Transparent OLED*

As the name suggests, these OLEDs are transparent. One can see through these devices as in active mode photon particles can travel in both directions. The technology used in these OLEDs is PMOLED/AMOLED. These devices exhibit good contrast even in bright sunlight. The organic devices can be utilized in smart windows, laptops, mobile phones, etc. [51].

Figure 8 represents the architecture where the see-through image of a transparent OLED is taken. To determine the display region for the calculation of diffraction lens aperture DL, background distance D1 and viewer distance D2 are considered. The researchers' Qin *et al* [51] reported the diffraction calculation. The display region was calculated as a circle where the diameter was obtained by $DL \times D1/(D1 + D2)$. The architecture was constructed by using a camera (Canon 550D) having pixel size of 4.30 μm and 50 mm lens. The transparent OLED display of 9 inches was considered. Also, to illuminate the background, D65 standard source was used. In this pixel structure, the aperture ratio was 62.1%.

Some research work to improve the transparent display is discussed here. In 2016, Qin *et al* [51] proposed a calculation method for accurate simulation of blurred see-through images for transparent organic LED display. Error in terms of MTF (Modulation Transfer Function) and pattern's characteristics were only 5.7 and 5.6%, respectively, between calculated and actual images. Then, in 2017, Shu *et al* [52] introduced ITO-free, inkjet-printed transparent organic LED. High emission brightness in a voltage pulsed driving mode on PEDOT:PSS and ITO were obtained as 16,000 and 50,000 cd m^{-2}, correspondingly. Afterwards, Tsai *et al* [53] reported a flexible T-OLED (transparent-OLED) having FlexUP^{TM} technology. To improve the

Table 2. Specification comparison of foldable displays.

Device	D6 [46]	D7 [47]	D8 [48]
Screen	13.3 inches	8.67 inches	13.3 inches
Driving method	Active matrix	Active matrix	Active matrix
Number of effective pixels	4320×RGB×7680	1080×RGBY×1920	4320×RGB×7680
Pixel pitch	12.75 μm×RGB×38.25 μm	0.100 × 0.100 mm	12.75 μm×RGB×38.25 μm
Pixel density	664 ppi	254 ppi	664 ppi
Aperture ratio	40.1%	46.0%	44.3%
Pixel arrangement	RGB stripe	RGBY checker	RGB stripe
Source driver	COG (chip on glass)	COF (chip on film)	COF (chip on film)
Scan driver	Integrated	Integrated	Integrated

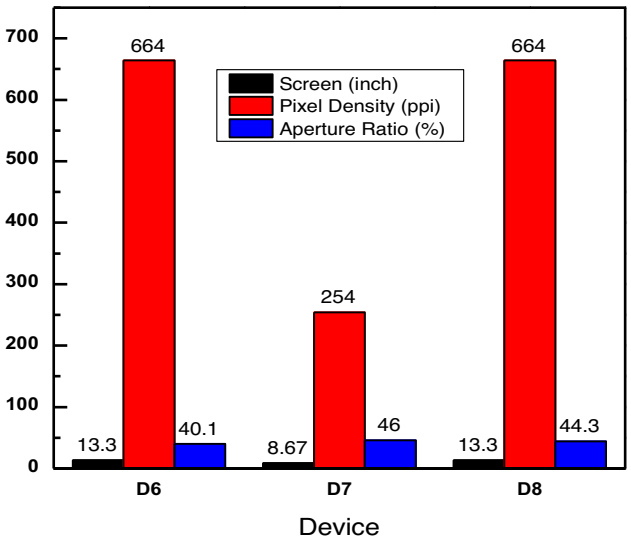

Figure 7. Column graph comparison of foldable displays specification.

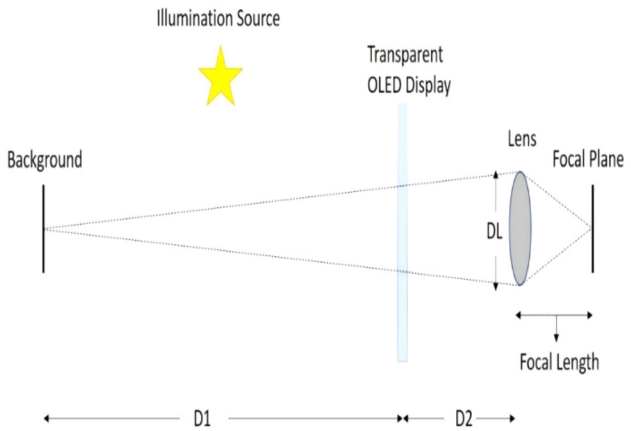

Figure 8. The architecture of transparent OLED.

ambient contrast ratio a flexible electrochromic shutter was placed behind the transparent OLED as a light-blocking layer. Total transmittance of T-OLED/electrochromic was achieved as 54.2%. Moreover in 2020, Song *et al* [54] demonstrated a highly reliable and transparent cathode for T-OLED applications. Silver (Ag) and aluminium (Al) metals were utilized for the fabrication of cathode by thermal evaporation. The current efficiencies of T-OLED were calculated as 18 and 36 cd A^{-1} emission from top and bottom sides, respectively.

5. Categorization of layers based on materials

The OLED is a multi-layered structure as it contains a series of stacked layers such as cathode, EIL/HIL, electron/hole transport layer, emissive layer, block layer and anode. In this section, some significant key layers will be discussed which play a very important role to improve the performance parameters of OLED. For each layer, some specific materials are opted to enhance the properties (electronics/structural) of organic LED. To achieve the advancement in OLED devices, optimization is done within charge transport/injection layers and in the quantum efficiency of the emissive layer.

5.1 *Electron/hole injection layer*

Generally, it becomes difficult to transport/inject an adequate amount of charge carriers due to the energy barrier between electrodes and the layers. To overcome this, charge injection layers are incorporated for the insertion of the charge carriers into the device. As a result, these layers reduce the energy barrier between HOMO/LUMO and the work function of the electrodes. Table 3 represents the comparison of different materials and thickness of layer for injection layer.

Various methods have been proposed to improve the carrier injection layer. In 2015, Gomez and Steckl [18] fabricated an OLED device and achieve high-performance parameters by replacing the common substrate and HIL with cellulose and DNA nucleobase adenine. The HIL material that is utilized contains a wide energy level range. This material improved the luminance and emission efficiency five times and provided the maximum values of

Table 3. Material and thickness for injection layer.

Year	Ref.	Material		Thickness (EIL, HIL)
		Electron injection layer (EIL)	Hole injection layer (HIL)	
2021	[57]	—	PEDOT:PSS/MoS_2	40 nm
2020	[58]	—	Li:NiO_x	—
2019	[59]	PEDOT:PSS (poly(3,4-ethylenedioxythiophene): poly(styrenesulphonate))	—	—
2018	[60]	MoO_x	—	—
2017	[61]	ZnO	—	—
2017	[62]	—	PEDOT:PSS and MoO_x	—
2016	[56]	Polyethylenimine	—	10 nm
2016	[63]	1,4,5,8,9,11-hexaazatriphenylenehexacarbonitrile (HAT-CN)	—	10 nm
2015	[55]	poly[(9,9-bis(3′-(N,N-dimethylamino) propyl)-2,7-fluorene)-alt-2,7-(9,9-dioctylfluorene)] (PF-NR2) and poly[9,9-bis (6′-(N,N-diethylamino)hexyl)-fluorene-alt-9,9-bis (3-ethyl(oxetane-3-ethyoxy)-hexyl)-fluorene] (PFN-OX)	—	–, 7 nm
2015	[18]	—	Adenine	10 nm
2010	[64]	MoO_3	—	8 nm
2010	[65]	3% F4-TCNQ-doped 2TNATA and 2T-NATA	—	—

8400 cd m^{-2} and 14 cd A^{-1}, respectively. Additionally, Zhong *et al* [55] fabricated organic LEDs using aliphatic amine groups materials, such as poly[9,9-bis(6′-(N,N-diethylamino)hexyl)-fluorene-alt-9,9-bis(3-ethyl(oxetane-3-ethyoxy)-hexyl)-fluorene] (PFN-OX) and poly[(9,9-bis(3′-(N,N-dimethylamino)propyl)-2,7-fluorene)-alt-2,7-(9,9-dioctylfluorene)] (PF-NR_2). These materials trap a large number of holes during the working of OLED, hence providing excellent electron injection by reducing electron tunnelling distance. Afterwards, in 2016, Stolz *et al* [56] proposed an OLED that comprises polyethylenimine as an EIL. The maximum current density is obtained as 20 mA cm^{-2}, also the lifetime of the device is increased by 1000 h.

In 2017, Zheng *et al* [62] utilized the combination of PEDOT:PSS and MoO_x (molybdenum oxide) as a HIL. This material helps provide improved surface work function and enhanced hole injection capacity. With better durability, the parameters such as maximum EQE and radiance are calculated as 4.4% and 12.2 mW cm^{-2}. Thereafter, in 2020 Wang *et al* [58] reported a novel material, Li-doped nickel oxide (Li:NiO_x) as HIL. The OLED exhibited excellent performance having maximum current efficiency, power efficiency, low turn-on voltage and EQE of 55.8 cd A^{-1}, 57.2 lm W^{-1}, 3.1 V and 17.1%, correspondingly. Moreover in 2021, a hybrid material, i.e., PEDOT: PSS/MoS_2 (metal sulphide) quantum dots were proposed by Zhu *et al* [57] for HIL. The OLED device having this material showed 28% improvement in current efficiency as compared to the device having a single PEDOT: PSS HIL. The maximum current efficiency was recorded as 72.7 cd A^{-1}.

5.2 *Electron/hole transport layer*

These layers are deposited within the OLED structure for the transportation of the charge carriers in the same manner as EIL/HIL are placed to diminish the energy level difference between HOMO/LUMO and the work function of the electrodes. In 2016, Dong *et al* [66] proposed a methodology to investigate the degradation of hole transport materials via laser deposition ionization-time of flight (LDI-TOF) of unaged and aged organic LED devices and DFT calculation of bond dissociation energies. It is reported that due instability of radical cation, TAPC is not considered a robust hole transport material for OLEDs. Table 4 depicts the comparison of different materials and thickness of layers for the transport layer.

A lot of research work has been reported in order to enhance the transport layer. In 2018, Lu *et al* [67] reported a genetic algorithm to study the combination of molecular materials to design high-performance OLED devices. It is investigated that pyridine-based central core with acridine-based fragments are excellent molecules for host molecules, as these molecules contain good energy alignment with common electrode materials. Also, weak electron-donating groups such as xylene and naphthalene-based fragments are suggested for electron transport materials and acridine and

Table 4. Material and thickness for transport layer.

Year	Ref.	Material		Thickness (ETL, HTL)
		Electron transport layer (ETL)	Hole transport layer (HTL)	
2020	[69]	TiO_2-doped TPBi (2,2′,2″-(1,3,5-benzinetriyl)-tris(1-phenyl-1-H-benzimidazole))	—	35 nm
2020	[70]	CBP	—	
2020	[71]	—	N, N'-bis-(1-4 naphthyl)-N, N′-diphenyl-1,1′-biphenyl-4,4′-iamine (NPB)	25 nm
2019	[68]	—	MoO_3	105 nm
2019	[59]	—	N,N-bis(4-(6-((3-ethyloxetan-3-yl) methoxy)hexyloxy)phenyl)-3,5-di(9H-carbazol-9-yl)benzenamine (Oxe-DCDPA))	
2018	[72]	TPBi	NPB (N,N′-diphenyl-N,N′-bis(1-napthyl)-1,1′-biphenyl-4,4′-diamine)	NA, 10 nm
2018	[73]	BPen (bathophenanthroline)	NPB	65, 50 nm
2018	[60]	—	NPB	55 nm
2018	[20]	TPBi	NPB	15 nm, 25 nm
2014	[74]	TPBi	TCTA-doped NPB	—
2012	[75]	Alq_3 and BPhen	NPB	—
2012	[76]	BmPyPb	—	—
2011	[77]	Alq_3	NPB	—
2010	[65]	Alq_3 and PyPySPyPy (1:1200 ratio)	NPB	—

triphenylamine-based fragments are good options for hole transport materials because of their strong electron-donating property.

Additionally, in 2019, Tsai *et al* [59] proposed a novel high triplet energy and cross-linkable hole transporting material, i.e., N,N-bis(4-(6-((3-ethyloxetan-3-yl)methoxy)hexyloxy)phenyl)-3,5-di(9H-carbazol-9-yl)benzenamine (Oxe-DCDPA)) for HTL. The highest EQE/luminous efficiency (EQE/ηL) among the reported devices with double HTLs are recorded as 27.2%/83.8 cd A^{-1} and 30.8%/111.9 cd A^{-1} for bluish-green emission and green emission, correspondingly. Moreover, Zhang *et al* [68] introduced an ultra-thick (105 nm) inorganic MoO_3 layer as HTL. A highly stable hybrid OLED (HyOLED) was prepared to utilize this HTL layer. This device achieved excellent hole mobility and efficient hole injection, which resulted in a low turn-on voltage of 2.65 V. Also, the HyOLED device exhibited maximum current efficiency and power efficiency as 60.87 cd A^{-1} and 58.84 lm W^{-1}, respectively.

In 2020, Nagar *et al* [69] proposed a high-performance OLED device by utilizing TiO_2 (titanium oxide)-doped TPBi (2,2′,2″-(1,3,5-benzinetriyl)-tris(1-phenyl-1-H-benzimidazole)) as an ETL. The device showed good properties for yellow emission and outstanding electron mobility. The performance parameter such as maximum current efficiency, power efficacy and EQE were achieved as 53.9 cd A^{-1}, 56.1 lw W^{-1} and 15.5%, respectively.

5.3 *Emissive layer*

This layer plays a major role in OLED devices as the main function of OLED, i.e., production of light occurs here. In this layer, the recombination process takes place which results in massive emissions. The colour of light/emission mostly depends on the properties of materials. A lot of research work has been done for better and long-lasting emissions. Table 5 outlines the comparison of different materials and thickness of layer for emissive layer. In 2011, Kim *et al* [78] fabricated a high-efficiency OLED which contained the sandwiching of ambipolar blends of electron and hole transport polymer hosts doped with a green-emitting iridium complex between a vacuum-deposited ETL and photo-crosslinked HTL. This device exhibited a maximum EQE of 13.6% and luminous efficiency of 44.6 cd A^{-1}. Then, Zhao *et al* [79] in 2012, utilized a double emissive layer structure in blue/orange complementary white OLED that resulted in improved spectral density and better luminance of 20,000 cd m^{-2}. Afterwards, in 2013, Erickson and Holmes [80] proposed an approach for determining the location and spatial extent of the exciton recombination area in an organic LED. The calculation of the exciton density profile was obtained by incorporating a thin strip into the EML.

In 2015, Yoo *et al* [87] designed a PHOLED (blue phosphorescent OLED) with the addition of double dopants FIr_6 and FIrpic in the emissive layer. Luminous efficiency is achieved as 24.8 cd A^{-1} having dopant ratio 8% FIrpic:4% FIr_6 in EML. Also, efficiency roll-off was enhanced up to 20% in comparison with single dopants FIr_6 and FIrpic. Additionally, in 2018, Singh *et al* [84] presented a high-quality blue emission OLED device having single emissive layer. This device is hazard free and exhibited EQE and current efficiency of 24.5% and 24.9 cd A^{-1}, respectively, at 100 cd m^{-2}. Moreover, in 2019, Nayak and Choudhary [83] investigated electrical and optical properties of PMMA (polymethyl methacrylate), ZnS and PMMA-ZnS and

Table 5. Material and thickness for emissive layer.

Year	Ref.	Material for emissive layer (EML)	Thickness of layer
2021	[81]	Alq_3	50 nm
2020	[82]	BEPP (bis(2-(2-hydroxyphenyl)-pyridine) beryllium and TCTA: Ir(ppy)3	—
2019	[83]	PMMA:ZnS	40 nm
2018	[84]	FIrpic, Ir(ppy)3, $Ir(piq)_2(acac)$	—
2018	[60]	Alq_3	25 nm
2018	[72]	CBP and $Irppy_3$	15 nm
2017	[85]	$TCTA:(Irmppy)_3$	30 nm
2014	[74]	SSM-doped DSA-Ph	20 nm
2013	[80]	TCTA:BPhen:Ir(ppy)3	100 nm
2012	[76]	DCzPPy:bt2Iracac	20 nm
2012	[75]	Alq_3 (for phosphorescence) and $Ir(ppy)_3$-doped CBP (for fluorescence)	20, 20 nm
2011	[86]	4-Hydroxy-8-methyl-1,5-naphthyridine aluminium chelate (AlmND3)	50 nm
2011	[78]	Bis-oxadiazole polymer, PVK and $Ir(pppy)_3$	40 nm
2010	[65]	TBADN and DSA-ph	—

concluded that PMMA-ZnS nanocomposite is suitable to be utilized as an emissive layer in organic LEDs. The colour purity and decay time were obtained as ∼34.08% and ∼4.8413 ns, correspondingly having an improved current density of ∼249%. Additionally, Sharma and Das [82] in 2020, reported a highly efficient, having double emissive layer OLED device that showed EQE of 39%.

5.4 *Blocking layer*

Charge blocking layers are incorporated to oppose the movement of charge carriers. Generally, the mobility of hole is higher than electrons. This results in the early arrival of holes to the emissive layer as compared to electrons. Due to this, the recombination rate decreases in emissive layer. So, to overcome this, hole blocking layers are introduced to block the hole carriers. Similarly, electron blocking layers can be utilized. These layers are beneficial for enhancing the efficiency of the organic LED through promoting electron/hole recombination. Table 6 illustrates the comparison of different materials and thickness of layer for emissive layer.

Several researchers have done investigations to enhance the blocking layer for a higher recombination rate. In 2015, Seo *et al* [88] designed an acridine-derived compound 9,9-dimethyl-10-(9-phenyl-9H-carbazol-3-yl)-9,10-dihydroacridine (PCZAC) that is applicable as an exciton blocking layer for blue phosphorous OLEDs. This compound exhibited high glass transition temperature and triplet energy as 101°C and 2.99 eV, respectively, hence improving the efficiency and lifetime. Afterwards, in 2016, Fujimoto *et al* [63] utilized 2,4,6-tris(biphenyl-3-yl)-1,3,5-triazine (T2T) as a hole blocking layer, which improved the lifetime nine times. Additionally, Tan *et al* [89] reported a versatile electron transport/hole blocking material, i.e., 3-(m-diphenylphosphinylphenyl)-1,10-phenanthroline (Phen-m-PhDPO), which provides high power efficiency. The maximum power efficiency was achieved as 41 lm W^{-1} in green PHOLED.

In 2017, Wei *et al* [90] presented a new material, phenanthroline-derivative Phen-DFP by adding 3-(3,5-bis(2,4-difluorophenyl)phenyl)phenyl with 1,10-phenanthroline. This material contains a high glass transition (T_g) of 95°C, as well as the luminous and power efficiency, are calculated as 16 cd A^{-1} and 13 lm W^{-1}, correspondingly. Moreover in 2018, Jang *et al* [91] synthesized two new hole blocking materials, pPPyrPB (1,3,5-tri(mpyrid-2-yl-phenyl)benzene) and mPyrPPB (1,3,5-tris(3-(3-(pyridine-3-yl)phenyl)phenyl)benzene) for high-performance blue phosphorescent OLEDs having T_g value of 137 and 118°C, respectively. The performance parameters, such as current efficiency, EQE and power efficiency in case of mPyrPPB are obtained as 36.7 cd A^{-1}, 16.4% and 13.4 lm W^{-1}, correspondingly.

In 2019, Soman and Unni [92] investigated the effect of different electron blocking layer like N,N'-Bis(naphthalene-1-yl)-N,N′-bis(phenyl)-benzidine (NPB), Tris(4-carbazoyl-9-ylphenyl)amine(TCTA) and Di-[4-(N,N-di-p-tolyl-amino)-phenyl]cyclohexane (TAPC). Among these materials, it was noticed that TCTA was blocking the electrons very effectively and enhanced the recombination rate in a better way as compared to other mentioned materials. The luminance was recorded as 1000 cd m^{-2} with the 27.8% improvement in EQE in comparison with NPB. Furthermore, in 2021, Bachelet *et al* [81] reported two molecules, 2,2′,2"-(1,3,5-benzinetriyl)-tris(1-phenyl-1-H-benzimidazole) (TPBi) and 2,9-dimethyl-4,7-diphenyl-1,10-phenanthroline (BCP) that were utilized to decouple the efficacy of hole blocking from electron injection and transport layer. The optical performance was improved effectively.

6. Fabrication for OLED

Nowadays, the main concern is to fabricate organic devices with less complexity. The energy level of compounds should be matched while fabricating the device [93]. There are some steps to fabricate the OLED discussed below that help keep the device more flexible, durable and secure from moisture as organic devices are sensitive to water.

6.1 *Fabrication steps*

In this section, the fabrication steps from the substrate to a complete device are discussed. Generally, four steps are included during the fabrication process of the OLED device.

6.1a *Substrate cleaning*: This is the very first process where the substrate is loaded in to the cleaning rack. Afterwards, this loaded substrate rack is placed in a breaker and drowned in the water with 10% solution of NaOH. Next, sonication process is utilized to remove the photoresist. After sonicating, the process substrate is rinsed using water to remove the photoresist. To ensure that the photoresist is removed completely from the substrate, it is again drenched into the fresh solution of NaOH in water for the same duration. The time duration is dependent on the temperature and ultrasonic bath used. Again, after sonication, the substrate was rinsed with water thoroughly.

6.1b *Applying active layer*: This layer can be applied either in a glovebox or in the air. Good even coverage can be achievable by pipetting 20 µl of the solution on a substrate that spins at 2000 rpm. The spinning should continue until the substrate dries. Finally, at the end of the aperture, the substrate is placed down in the evaporation shadow mask with a cathode strip. This cathode strip should be properly cleaned before using.

6.1c *Cathode evaporation*: Generally, 100 nm aluminium is evaporated at the rate of ∼1.5 A s^{-1}, but cathodes having a lower thickness of around 50 nm have also been used with

Table 6. Material and thickness for blocking layer.

Year	Ref.	Material		Thickness (EBL, HBL)
		Electron blocking layer (EBL)	Hole blocking layer (HBL)	
2021	[81]	—	2,2′, 2″-(1,3,5-benzinetriyl)-tris (1-phenyl-1-H-benzimidazole) (TPBi) and 2,9-dimethyl-4,7-diphenyl-1, 10-phenanthroline (BCP)	10, 10 nm
2019	[92]	Tris (4-carbazoyl-9-ylphenyl)amine (TCTA)	—	—
2018	[73]	—	1-(2,5-dimethyl-4-(1-pyrenyl)phenyl)pyrene (DMPPP)	10 nm
2018	[91]	—	mPyrPPB	25 nm
2018	[72]	TCTA	—	5 nm
2018	[60]	—	BPhen (bathophenanthroline)	
2017	[90]	—	Phen-DFP	150 nm
2016	[63]	—	2,4,6-tris(biphenyl-3-yl)-1,3,5-triazine (T2T)	10 nm
2016	[89]	3-(m-diphenylphosphinylphenyl)-1, 10-phenanthroline (Phen-m-PhDPO)		10 nm
2015	[88]	—	9,9-dimethyl-10-(9-phenyl-9H-carbazol-3-yl)-9,10-dihydroacridine (PCZAC)	10 nm

the same initial performances. Also, calcium evaporation is least preferable as it melts at low temperatures. Although using glovebox it can be used effectively.

6.1d *Encapsulation*: This process protects the device against degradation by moisture and oxygen after taking out the device from the glovebox. The glass welding technology is utilized for this purpose for long life.

6.2 *Fabrication techniques*

Some traditional techniques like physical vapour deposition and spin coating have contributed to a very great extent for manufacturing OLED devices. But the recent trend demands some versatile and low-cost techniques such as inkjet printing, screen printing, etc. Unlike vacuum deposition and spin coating, the screen printing process permits an excellent reduction in the use of materials as materials are only needed for printed areas [94]. Also, this technique is quite faster as compared to other techniques. First of all, substrate (flexible/non-flexible) is placed. After the substrate deposition, an anode layer is fabricated using thermal evaporation/solutions processing techniques based on material. Next, organic layers are deposited. The fabrication of organic layers is done in two different ways based on the type of organic materials whether it is conducting polymers [95] or SMs [96]. For SM, thermal vacuum evaporation techniques are utilized as organic molecules are suitable for heating processes in the vacuum chamber. On the other hand, solution processing techniques like inkjet printing, drop-casting, spin coating, etc. are used for conducting polymers. There are few widely used techniques explained in details below.

6.2a *Thermal vacuum evaporation*: The process is mainly utilized for making displays using SMs [97]. In this process, the material is permitted for the evaporation and condensation process until it is fabricated on the substrate as thin films. To avoid the interaction between atmospheric molecules and vapour, molecules are heated up under a vacuum around 10^{-5} to 10^{-7} Torr. The morphology of the substrate is influenced by the average energy (in order of kT) that reaches the substrate surface. This technique is not suitable for conducting polymers, as conjugated polymer's structure exhibits high conductance. Also, a higher temperature may damage these polymers.

6.2b *Physical vacuum deposition*: This technique is very suitable for inorganic materials as well as organic materials. Multi-layered OLED structures can easily be deposited using this process [98]. For future development of organic devices, physical vacuum deposition is one of the indispensable techniques. The materials are heated to evaporation and condensed onto the substrate as depicted in figure 9. Even nanometre ranges of thickness can be achieved by this method under a high vacuum. The steps involved in this process are:

- Formation of an evaporant from the source material
- Transfer the evaporant from source to substrate
- Condensation of the evaporant to form thin film onto the substrate

The process of physical vacuum deposition is quite convenient to provide the path for achieving high chemical purity, deposition of very thin layers and good adhesive quality between substrate and thin films.

6.2c *Solution processing*: These techniques are quite beneficial for low cost and large-area fabrication. Many processes are utilized using solution technique such as spin coating, inkjet printing, screen printing, etc. These processes are explained in detail below.

- Spin coating: Soluble polymers are deposited using spin coating in monochrome displays. Uniform deposition of emissive material in the form of drop occurs on the flat substrate and further it is rotated at high-speed multiple times until it gets the desired thickness, as shown in figure 10. In this process, the carrier material is evaporated at a faster rate and this results in a uniform deposition of the film. The parameters such as spin time, fume extraction, speed of spin coater, temperature, fluids volatility and viscosity are greatly responsible for the thickness of the film.

The spin-coating process has been investigated by many researchers to improve organic devices. In 2012, Hyun *et al* [99] demonstrated a method for corrugated structure using spin coating process to improve light extraction of organic LEDs. The performance parameters were controlled by mixing the ratio of solution of SiO_2 and TiO_x and varying the speed of the spin-coating process. Afterwards, Yuan *et al* [100] proposed a low-cost simple spin-coating method to form distributed embossed structures produced by Al_2O_3 nanospheres. The performance parameters such as maximum current efficiency, power efficiency and EQE are achieved as 52.1 cd A^{-1}, 32.7 lm W^{-1} and 20.9%, respectively. Moreover, in 2020, Juhari *et al* [101] analysed the electrical and structural properties of ITO/PEDOT: PSS/MEH doped PEIE organic LED using spin-coating technique.

- Inkjet printing: OLED materials are sprayed out through inkjet head on the substrate in a similar manner as paper printing is done. This process is applicable for large devices as large films can be printed [102]. High resolution, easy multi-layered deposition, cost-effective process are the main advantages of this printing process. Better sealing methods are advisable in inkjet printing as OLED devices can interact with moisture that may degrade the performance of organic devices. Figure 11 highlights the inkjet printing steps.

The improvement in OLED devices by utilizing inkjet printing process has been reported by many researchers. In 2019, Xing *et al* [103] proposed a high-luminance phosphorescent inkjet printing organic OLED having hole transporting material m-MTDATA (4,40,400-tris[3-methylphenyl(phenyl)amino]-triphenylamine). The OLED exhibited maximum luminance of 13240 cd m^{-2}. Furthermore, in 2020, Zheng *et al* [22] proposed a highly efficient blue OLED based on inkjet printing having a novel host material 3,5-bis(N-carbazolyl)benzene (mCP) into the emissive layer. In this device, the brightness uniformity is obtained as 92.7%, which is sufficient for the realization of highly efficient large-area organic LEDs using inkjet printing. Additionally, Hu *et al* [104] utilized inkjet printing method to demonstrate a novel display based on blue OLED and green and red quantum dots CCL (colour conversion layers). The inkjet method in this report provided a cost-effective display for quantum dots applications.

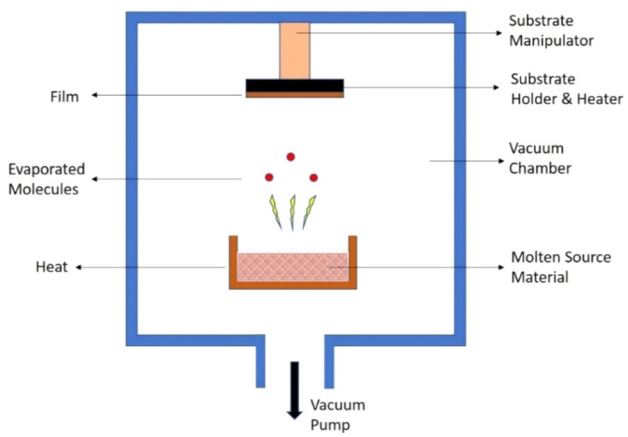

Figure 9. The physical vacuum deposition process.

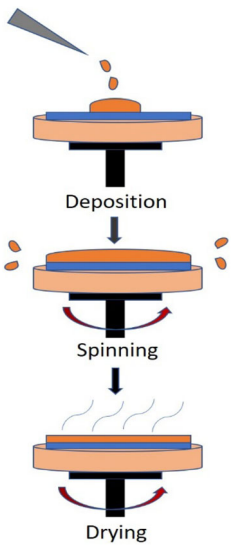

Figure 10. Spin-coating process.

- Screen printing: This process is executed in such a way that a screen mask is utilized to squeeze the ink to get print patterns. Further, these patterns are situated on the substrate. Screen printing is widely applicable in commercial usage of printed circuit boards, active polymer layers and electrode printing. To avoid screen blockage, particle size should be large enough. This process requires less use of materials, as they are directed onto substrate at a faster rate as compared to inkjet printing. In 2017, Preinfalk *et al* [105] discussed a cost-effective screen printing method that was utilized for the deposition of high-refractive index scattering polymer:TiO_2-nanoparticle mixture onto a large area. In this research, luminous efficacy was increased up to 56%. Additionally, in 2019, Wan *et al* [106] developed a printable mesoscopic perovskite solar cell containing a triple-layer scaffold of TiO_2/ZrO_2/carbon. The screen-printing process was used for the deposition of scaffold, which resulted in low-cost photovoltaics.

7. Performance improving techniques for OLED

There are many key factors like material of layer, the colour of emission (white, red, blue, etc.), performance parameters, etc. that are very important to improve the performance of organic LEDs. In this section, some improvement techniques are highlighted based on these mentioned factors.

7.1 *Based on layer*

Addition of some specific layers like hole/electron injection layer, hole/electron transport layer, blocking layer to a simple basic single-layer structure makes an OLED very efficient and improves the parameters, such as luminance, current density, quantum efficiency, etc. Table 7 shows the improvement based on these layers.

Enormous work has been done in respect of layers to improve the OLED structures. In 2010, Lu *et al* [65] utilized different combinations of 2T-NATA (4,4′,4″-tris(N-(2-naphthyl)-Nphenylamino) triphenylamine) and F4-TCNQ (tetrafluorotetracyanoquinodimethane) as HTL and HIL. This results in improved power efficiency, i.e., 22% in doped devices. Also, this device exhibits a better life as compared with undoped devices. Later in 2018, Zheng *et al* [60] studied MoO_x as a hole injection material in the solution phase. In this research, power efficiency and luminescence are enhanced by 1.8 times and 83.7%, correspondingly. Thereafter in 2020, Mohan *et al* [27] used copper iodide into copper(II) phthalocyanine HTL and fabricated the OLED device. The device showed excellent improvement in performance parameters, such as 32% in EQE, 33.3% in power efficiency and 34.6% in current efficiency. Additionally, in 2021, Zhu *et al* [57] utilized HIL of hybrid poly(3,4-ethylenedioxythiophene)/poly(styrenesulphonate) (PEDOT:PSS)/QDs to design organic LED and achieved very good luminescence of 49,005 along with other parameters, such as power and current efficiency as 45.6 lm W^{-1} and 72.7 cd A^{-1}, respectively. The hybrid HIL provides better carrier injection, higher luminescence and lower turn-on voltage, which results in highly efficient OLED devices.

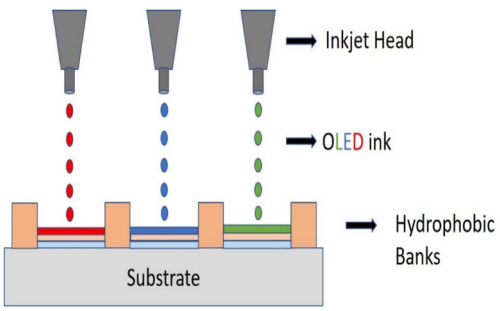

Figure 11. Inkjet printing process.

7.2 *Based on characteristics parameters*

To highlight the performance of organic LED, there are some characteristic parameters, such as luminescence, current efficiency, power efficiency, EQE, etc. These parameters are well defined already in Section 3. Table 8 illustrates the research work of many researchers to improve these performance parameters. Some of the noteworthy research work is discussed here. In 2014, Guo *et al* [40] designed an ultraviolet-emitting EL (electroluminescent) device with

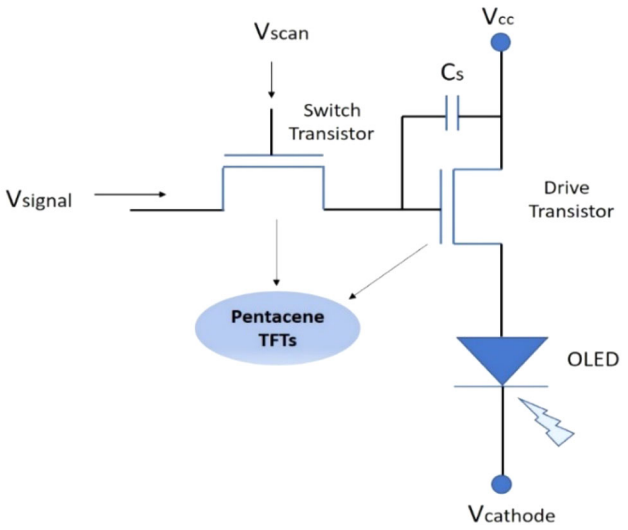

Figure 12. OTFT-driven full-colour AMOLED pixel circuit (C1).

Table 7. Improving techniques based on layer.

Year	Ref.	Techniques	Outcomes
2021	[57]	Designed a highly efficient green OLED with hybrid poly (3,4-ethylenedioxythiophene)/poly(styrenesulphonate) (PEDOT:PSS)/QDs HIL	• luminescence = 49,005 cd m^{-2} • Current efficiency = 72.7 cd A^{-1} • Power efficiency = 45.6 lm W^{-1} • The current efficiency is increased by 28.2% as compared with single (PEDOT:PSS) HIL
2020	[107]	Gate tunable OLED is analysed with electron transport layer (4,4′-bis(N-carbazolyl)-1,1'biphenyl) and hole-blocking layer (1,3,5-tris[(3-pyridyl)-phen-3-yl]benzene))	• Low current density leakage = 0.01 mA cm^{-2} • Saturated on-current density = ~0.01 cd m^{-2} • Low off luminescence = 100 cd m^{-2}
2020	[27]	Incorporated CuI as dopants into CuPC hole transport layer	• Higher performance was achieved by doping CuI into CuPC for OLED devices as compared to the PEDOT: PSS as hole transport layer • Current efficiency = 70 cd A^{-1} • Power efficiency = 74.1 lm W^{-1} • External quantum efficiency = 18.5%
2018	[57]	Modified the thickness of electron transport layer	• External quantum efficiency = 23.4% at 1000 cd m^{-2}
2018	[72]	Utilized a guest-host structure to control the charge carrier transport layer	• Current density ↑ • HTM current and charge density are improved by two orders of magnitude
2018	[108]	Fabricated mixed HTL by mixing the cross-linkable SM HTL with polymer HTL	• Highly uniform crosslinked HTL films are fabricated with peak-to-peak roughness values (10.1 nm) • OLED stability ↑
2015	[18]	Utilized adenine as hole injection layer	• Challenges for charge injection are overcome by utilizing adenine as HIL on gold • Luminescence and emission efficiency are increased up to five times • Luminescence and emission efficiency on glass = 45,000 cd m^{-2} and 32 cd A^{-1} • Luminescense and emission efficiency on cellulose = 8400 cd m^{-2} and 1432 cd A^{-1}
2011	[109]	Improving hole injection and transport layer using Fe_3O_4 as a P-dopant	• OLED is doped in two different hosts of NPB and m-MTDATA • The current density, luminescence and power efficiency are significantly improved as compared to undoped devices

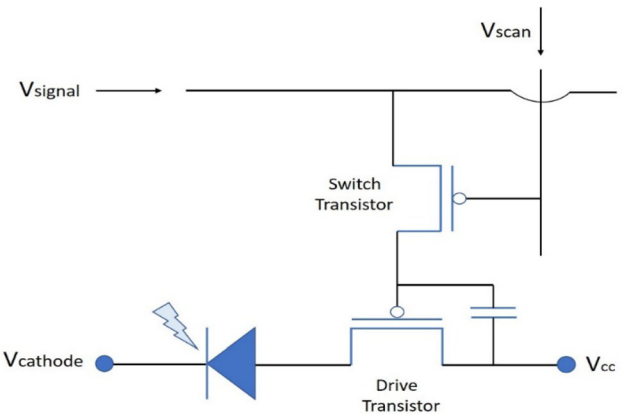

Figure 13. OTFT-driven AMOLED pixel circuit (C2).

star-shaped materials (SSM) using carbazole/arylamine backbone. This report concluded the performance parameter as current efficiency of 10.37 cd A^{-1}, power efficiency of 8.69 lm W^{-1} and EQE of 2.56%. This research provides a method to fabricate highly efficient and pure blue OLED by considering SSM as a host material. Thereafter, in 2018, Xi *et al* [28] reported highly efficient white OLED using energy transfer from host to orange dopant. The parameter such as current efficiency, power efficiency and EQE are obtained as 35.3 cd A^{-1}, 31.0 lm W^{-1} and 18.7%, respectively. These parameters were reported with the highest values as compared with the devices of that time.

In 2020, Han *et al* [30] fabricated an internal light extraction layer with high-refractive index material for blue OLED. The reported device exhibited excellent performance as power efficiency and EQE are concluded as 93.2 lm W^{-1} and 103%, correspondingly. Recently, in 2021, Vasilopoulou *et al* [111] focused on hole transport interlayer having low triplet energy and by utilizing this layer they fabricated blue TADF OLED with high luminescence of 49,530 cd m^{-2} and below bandgap turn-on voltage of 2.5 V.

7.3 *Improving techniques based on colour emission*

In this sub-section, different materials are investigated for the utilization of emissive layers to emit white and blue colours of light.

7.3a *In terms of blue OLED*: Three main colours red, blue and green are required for white lighting and full-colour display. Lot of research work is being done for RGB emitters in recent times [113,114]. On the other hand, it is quite difficult to produce high-performance blue emissions due to the wide bandgap that makes it complicated to insert charges into blue emitters. The electro-luminescence performance and other parameters of blue emitters are needed to be improved. The comparison of improvement techniques on basis of blue OLED is depicted in table 9.

There is a major scope of improvement in the field of blue OLEDs. The electro-luminescence performance and other parameters of blue emitters are needed to be improved. For thermally activated delayed fluorescence OLED, in 2017, Nakao *et al* [119] designed blue pyrimidine emitters. In the article, the nitrogen effect is analysed on the photophysical properties. Also, the EQE is calculated as 25%. The performance parameters exhibited in this article contained the best results as compared with other devices of that time for TADF organic LEDs. In 2018, Yang *et al* [118] fabricated a deep-blue HLCT using triphenylbenzene. The maximum exciton utilizing the efficiency of Cz-TPB and CzPh-TPB are achieved as 86 and 85%, respectively. The report added new possibilities for developing highly efficient, low-cost deep-blue materials with hybrid local and charge transfer emitters.

In 2020, Han *et al* [117] varied the alkyl substituent of acridine to adjust the energy levels and using this, five blue thermally activated delayed fluorescence emitters DAc-C1-DAc-C5 are designed. The maximum EQE in this report is obtained as 24.1% based on DAc-C2 OLED, which is 1.42 times more than the DAc-C2-based device that showed the EQE of 17%. Also, high-photoluminescence quantum is achieved between 75 and 85%. Recently in 2021, Chan *et al* [116] investigated the methods to overcome the challenges of blue OLEDs, such as efficiency, lifetime and colour purity. They designed a pure-blue OLED with a high EQE of 32% and narrow emission. The technology is based on a two-unit stacked tandem hyperfluorescence OLED.

7.3b *In terms of white OLED*: White inorganic LEDs are being utilized commercially for general purposes like indoor and outdoor lighting and automotive lighting, etc. For back-lights in flat panel displays, white organic LED are used as a low-cost alternative [39]. White OLED can be designed as flexible panels having superior white colour balance and wide viewing angles. There are many approaches to fabricate white SSL (solid-state lighting) devices, such as (1) combining a single chip emitting UV light absorbed in the LED package by three RGB (red, green and blue) phosphors and re-emitted as a white light spectrum, (2) combining a yellow phosphor and a blue LED pumped from the blue light of the LED and (3) three different LED chips producing different wavelengths (RGB) individually to simulate the RGB colour model.

Table 10 shows the improvement techniques reported by different researchers in terms of white OLED. In 2016, Chen *et al* [123] designed white OLED using the dip-coating technique with an emission area of 72 × 72 mm^2. The dip-coating process is useful for removing the material pile-up near the metal grids, which results in uniform light emission across the whole panel. Non-uniformity is reduced from 49 to 15% by decreasing the speed withdrawal speed from 1 to 0.06 mm s^{-1}. Furthermore, in 2020, a high-performance white OLED is reported by Huang *et al* [24] using a blue-red unit based on a TADF and a phosphorescent yellow-red unit. The

Table 8. Improving techniques based on the performance parameter.

Year	Ref.	Technique	Parametric improvement
2022	[110]	Designed and synthesized two small cross-linkable TADF: DV-2CzBN and DV-2CzTBN	• Current efficiency = 25.1 cd A^{-1} • Power efficiency = 19.6 lm W^{-1} • EQE = 11.4%
2021	[111]	Fabricated blue TADF organic LED using low triplet energy hole transporting interlayer with high mobility	• Luminescence = 49,530 cd m^{-2} • Current efficiency = 72.2 cd A^{-1} • Power efficiency = 87.2 lm W^{-1} • EQE = 41.2%
2020	[22]	Fabricated inkjet printed blue OLED using 3,5-bis(N-carbazolyl)benzene as a host material	• Luminescence = 3743 cd m^{-2} • EQE = 5.03%
2020	[30]	Designed an internal light extraction layer using high-refractive index material for white organic LED	• Power efficiency = 93.2 lm W^{-1} • EQE = 103%
2018	[20]	Constructed double light-emitting layer using red-green emitting light originated from host of tris-(8-hydroxyquinolinato) aluminium (Alq_3) to guest of 4-(dicyanomethylene)-2-tert-butyl-6-(1,1,7,7-tetramethyljulolidin-4-yl-vinyl)−4*H*-pyran (DCJTB)	• Luminescence: 9296 cdm^{-2} • Current efficiency: 10.17 cd A^{--} • Power efficiency: 5.80 lm W^{-1} • EQE: 4.09%
2018	[28]	Fabricated highly efficient warm white organic LED by energy transfer from exciplex host to orange dopant	• Current efficiency: 35.3 cd A^{-1} • Power efficiency: 31.0 lm W^{-1} • EQE: 18.7%
2016	[39]	Applied a benzene-benzothiadiazole-benzene core-based new triaryl molecule in a white OLED device	• Luminescence: 5219 cd m^{-2} • Current efficiency: 6.5 cd A^{-1} • Power efficiency: 2.60 lm W^{-1} EQE: 2.39%
2014	[40]	Fabricated a near ultraviolet-emitting electroluminescent device using star-shaped material (SSM) having carbazole/arylamine backbone	• Current efficiency: 10.37 cd A^{-1} • Power efficiency: 8.69 lm W^{-1} • EQE: 2.56%
2014	[19]	Synthesized two-tailored luminogens (TPE-NB and TPE-PNPB) consisting of tetraphenylethene (TPE), diphenylamino, and dimesitylboryl as a π-conjugated linkage, electron donor, and electron acceptor, respectively	• Luminescence: 49993 cd m^{-2} • Current efficiency: 15.7 cd A^{-1} • Power efficiency: 12.9 lm W^{-1} • EQE: 5.12%
2011	[112]	The utilized sandblasting process to roughening white OLED surface to improve the performance	• Luminous efficiency: 20 cd A^{-1} • EQE: 11.6%

performance parameters such as luminous efficacy and EQE are achieved as 150.7 lm W^{-1} and 126.2%, respectively. Also, the device showed a colour rendering index near to 80 at luminescence of 1000 cd m^{-2} with a lifetime of 12,600 h. The lifetime was enhanced by 3 times as compared with the conventional hybrid tandem white OLED.

Recently in 2021, Lee [35] designed a white organic LED utilizing a single host of bis(1-phenylisoquinoline)(acetylacetonate) iridium(III) and 1,3-bis(9-carbazolyl)benzene with iridium(III) bis[(4,6-difluorophenyl) pyridinato-N,C2′]picolinate as red and blue phosphorescent, respectively. In this report, luminescence is improved from 265 to 9156 cd m^{-2} as well as decay time is analysed to observe the emission mechanism utilizing transient photoluminescence and electro-luminescence technique.

8. Different applications for OLED

Organic electronics is still a young technology that provides various applications in terms of organic thin-film transistor (OTFT)-driven OLED, sensors [125], military, healthcare, etc. It was a real challenge to replace inorganic devices with organic ones. The properties like flexibility, large-area fabrication, transparency, wider viewing angle, etc. made organic devices compete with conventional devices. There are some applications of OLEDs from various categories that are discussed in this section.

8.1 *OTFT-driven OLED device*

Organic TFT-driven OLED are great choices in terms of excellent performance and large-area fabrication. Additionally, a backplane based on OTFT can be utilized in fabricating at low temperatures. Therefore, the various flexible substrate can be applied to the backplane. Also, a low-temperature process leads to lower energy consumption while fabrication. These OTFT-driven OLED devices contain super flexible properties, which can be wrapped around. Due to the great mechanical flexibility, the light weighted, thinner, form factor enhanced, mechanical-shock resistant electronic devices can be achieved.

Various researchers have explored OTFT-driven organic LEDs. In 2009, Katsuhara *et al* [126] fabricated a full-

Table 9. Improving techniques on the basis of blue OLED.

Year	Ref.	Technique	Observation
2021	[115]	Designed and synthesized a novel deep-blue fluorescent material 2,6-di-tert-butyl-1,5-bis-(3,5-di-tert-butyl-phenyl)-naphthalene $N(dtb)_4$	• External quantum efficiency = 7.8% • Current efficiency = 11.52 cd A^{-1} • Power efficiency = 10.33 lm W^{-1}
2021	[116]	Designed a pure blue hyperfluorescence OLED	• External quantum efficiency = 32% • Good stability of 18 hours at an initial luminance of 1000 cd m^{-2} • Narrow emission
2020	[117]	Five blue thermally activated delayed fluorescence emitters by varying the alkyl substituent of acridine to adjust the energy levels	• High-photoluminescence quantum yields between 75 and 85% • Maximum external quantum efficiency (EQE) = 24.1%
2020	[22]	Fabricated inkjet-printed blue OLED using 3,5-bis(N-carbazolyl)benzene as a host material	• External quantum efficiency = 5.03% • Luminescence = 3743 cd m^{-2}
2018	[118]	Designed and synthesized a deep-blue hybrid local and charge transfer (HLCT) based on triphenylbenzene	• The maximum exciton utilizing the efficiency of CzPh-TPB and Cz-TPB are obtained as 85 and 86%, correspondingly.
2017	[119]	Developed blue pyrimidine emitters for thermally activated delayed fluorescence (TADF) OLED	• The effect of nitrogen is investigated on the photophysical properties • The external quantum efficiency is obtained as 25%
2016	[33]	Synthesized blue TADF emitters BPy-pC, BPy-pTC, BPy-p2C and BPy-p3C using carbazolyl, t-butyl carbazolyl, dicarbazolyl and tercarbazolyl as an electron-donating unit and 4-benzoylpyridine as electron-accepting unit, respectively	• The single triplet energy gap (ΔE_{ST}) is reduced from 0.29 to 0.05 eV • EQE = 23.9%
2012	[32]	Synthesized new rigid and highly twisted materials made of anthracene with xylene as the core unit	• Using BDNA non-doped devices exhibited a maximum EQE of 5.26%

Table 10. Improving techniques based on white OLED.

Year	Ref.	Technique	Observation
2022	[120]	Designed low voltage, high luminance, top emitting, three-wavelength WOLED	• Luminescence = 170,000 cd m^{-2} • Color gamut = 136% (as compared to sRGB)
2021	[121]	Fabricated high-efficiency fluorescent dual-wavelength white OLED	• Luminescence = 21,070 cd m^{-2} • Current efficiency = 18.09 cd A^{-1} • Power efficiency = 8.77 lm W^{-1}
2021	[35]	Fabricated white OLED using a single host of bis(1-phenylisoquinoline) (acetylacetonate) iridium(III) and 1,3-bis(9-carbazolyl)benzene with iridium(III) bis[(4,6-difluorophenyl) pyridinato-N,C2′]picolinate as red and blue phosphorescent, correspondingly	• Luminescence = 9156 cd m^{-2} • The decay time of excitons is also calculated to observe the emission mechanism using electroluminescence and transient photoluminescence technique
2020	[30]	Designed an internal light extraction layer using high-refractive index material for white organic LED	• The maximum EQE without and with light extraction structure is obtained as 35.6 and 103%, respectively • Power efficiencies without and with light extraction are calculated as 26.5 and 93.2 lm W^{-1} at 100 cd m^{-2}, respectively
2020	[24]	Demonstrated highly efficient WOLED fabricated with a blue-red unit based on a TADF and a phosphorescent yellow-red unit using an exciplex host based on a modified hybrid tandem structure	• Luminous efficacy = 150.7 lm W^{-1} • EQE = 126.2% • The colour rendering index = 80 at 1000 cd m^{-2} • The T50 lifetime = 12,600 h at 1000 cd m^{-2}
2018	[28]	Fabricated highly efficient warm white organic LED by energy transfer from exciplex host to orange dopant	• EQE = 18.7% • Power efficiency = 31.0 lm W^{-1} • Current efficiency = 35.3 cd A^{-1} • Very low efficiency roll-off is exhibited.
2016	[122]	To improve the optical power of red colour, quantum dot nanocrystals dispersed in photoresist film is applied to WOLED	• 40.2% enhancement in optical power is noticed in white OLED using quantum dot dispersed PR film
2016	[123]	Designed WOLED-based large area lighting panels using the dip-coating process in the air having an emission area of 72 × 72 mm^2	• Non-uniformity of the film decreases from 49 to 15% on reducing the withdrawal speed from 1 to 0.06 mm s^{-1}. • The uniformity of dip-coated film is improved by adding a buffer zone to the panel
2016	[39]	Applied a benzene-benzothiadiazole-benzene core-based new triaryl molecule in a white OLED device	• The maximum brightness = 5219 cd m^{-2} • Current = 6.5 cd A^{-1} • The device also exhibited good colour quality with C.I.E. coordinates of (0.38, 0.45) and 4500 K colour temperature
2014	[124]	Synthesized WOLED based on the temperature-sensitive β-diketonate complex of molecular formula $[Eu_{0.45}Tb_{0.55}(btfa)_3$ (4,4′-bpy)(EtOH)] ($btfa^-$, 4,4,4-trifluoro-l-phenyl-1,3-butanedionate; 4,4′-bpy, 4,4′-dipyri-dyl; EtOH, ethanol)	• The emission colour coordinates are varying from (0.521, 0.443) to (0.658, 0.335) by changing the temperature from 11 to 298 K

colour AMOLED display on a flexible substrate driven by OTFT based on pentacene. This OTFT-driven OLED is made by a scalable manufacturing process. High electrical and environmental stability is achieved by the fabricated panel. Figure 12 depicts the pixel circuit for this configuration.

In the circuit, two pentacene-based transistors and one capacitor were utilized. The operating frequency of this pixel circuit is 60 Hz. The voltage swing is 12 V of the signal. The two other potentials V_{cc} and V_{cath} are applied in a way that $V_{cc} - V_{cath} = 20$ V. The scan voltage is 30 V. Some specifications of this device such as pixel size, resolution, display size and peak luminescence are obtained as 318 × 318 μm, 80 ppi (pixel per inch), diagonally 2.5 inch and 150 cd m^{-2}, correspondingly.

In 2011, Noda *et al* [127] reported an OTFT-driven AMOLED display that is rollable and 80 μm thick. Organic TFT with PXX (*peri*-xanthnoxanthene) derivative (a newly developed organic semiconductor) is used, which leads to the improvement in subthreshold swing and field-effect mobility as compared with pentacene TFT. The picture quality and initial properties of this display do not vary even after having 1000 cycles of roll up and release test having a radius of 4 mm. The circuit diagram of the pixel panel is shown in figure 13 for this OTFT-driven organic LED.

This circuit contains one capacitor and two organic transistors, one is switching and the other is a driving transistor based on PXX derivative. The designed circuit operates at the frame rate of 60 Hz. The other parameter of the device, such as pixel size, display size, resolution and peak luminescence, are obtained as 210 × 210 μm, 4.1 inch wide, 121 ppi, 100 cd m^{-2}.

In 2016, Kim and Song [128] reported AMOLED display devices. This device is fabricated on polyethylene fabric substrate. A TIPS pentacene-based OTFT is utilized as a driving device for the organic LED. One capacitor, one OLED and two OTFTs are applied to the pixel circuit (figure 14). The major requirement is to produce high luminance at low voltage, and low I_{off} and small V_{on} are also essential as well for low voltage operations of OLED and OTFT. This pixel circuit fulfils all the requirements needed for high-performance OTFT-driven device. Both OTFTs exhibited the mobilities as 0.23 and 0.34 cm^2 V^{-1} and the luminescence of OLED is recorded as 64.459 cd m^{-2}. The other specifications like pixel pitch, aperture ratio, resolution and display size is calculated as 1.5 ×1.5 mm, 22%, 32 × 32 and 2.7 inches, respectively.

Table 11 depicts the performance comparison of three different OTFT-driven active-matrix OLEDs C_1, C_2 and C_3 based on pixel size, display size, resolution, luminescence, contrast ratio, signal voltage and thickness.

8.2 *Sensors*

Tremendous research work has been done in terms of organic LED fabrication, which leads to many sensor applications. In 2011, Kim *et al* [129] reported a highly sensitive ultrathin active-matrix OLED device with the property of capacitive touch sensors. The capacitive change and internal electric field distribution based on Q3D extractor model are investigated to obtain the desired application. The malfunction-free signals are verified by electrostatic simulations for capacitive touch sensors of 4-inch diagonal size. In this report, the touch sensor device of thickness 1.2 mm is developed to be operable at low temperature (200°C).

A chemical imaging sensor was developed with organic LED as a light source by Miyamoto *et al* [130] in 2012. This semiconductor-based sensor is used to recognize the two-dimensional distribution of specific molecules in a solution. The researchers studied pH sensitivity, generated photocurrent waveform and current–voltage characteristics. The size of the fabricated device is comparatively small due to the avoidance of complicated optics and mechanisms.

The researchers Watanabe and group [131] fabricated an 8.76-inch diagonal sized in-call touch sensor using a foldable OLED device. The properties of this device remain the same even after 105 folding operations having a radius of 5 mm. To obtain lower parasitic capacitance, metal-mesh sensor electrodes are utilized. The OLED specifications used to fabricate this sensor like pixel size, aperture ratio, pixel density, number of effective pixels are 0.100 × 0.100 mm, 46%, 254 ppi, 1080 × RGBY × 1920, respectively. Also, the number of sensor units and sensor unit pitch is specified as 27 (T)×48 (R) and 4.00 × 4.00 mm, correspondingly.

In 2019, for the detection of ovarian cancer, an OLED-based light sensor is reported by Negi *et al* [132]. One multi-layered OLED and one triple hole block layer are used for detection of light and source of light, respectively, in this report. Also, dual-gate organic TFT is utilized as a driving transistor for the triple hole block layer. The DG-OTFT exhibits 18% better performance as compared to single gate TFT. The cathode current at an incident wavelength of 440 and 420 nm is concluded as 13 and 29 mA in multi-layered OLED.

8.3 *Health-care applications*

The organic LED has contributed to many medical applications such as cancer detection, health monitoring, chronic optogenetic applications, etc. Some of the applications are listed in table 12.

8.4 *Military applications*

Along with sensors, healthcare, OTFT applications, the organic LED is suitable for some military applications as well. Barre *et al* [137] presented some applications for military purposes, such as assistant gunner display, night

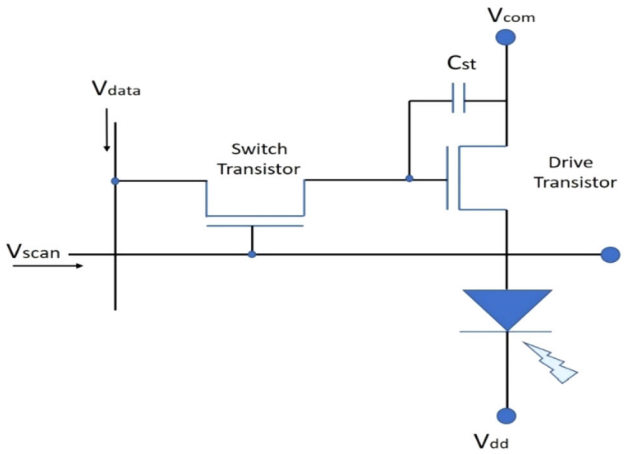

Figure 14. OTFT-driven AMOLED pixel circuit (C3).

vision goggles and vision enhancement systems. The researchers Trakalo and Lorimer [138] implemented OLED that is applicable in three military display devices. These devices are OLED DDACT, OLED AGD (assistant gunner display) and polymer-OLED AGD. In this article, optical and environmental testing of these devices is described. Afterwards, in 2012, Sarma [139] reported some high-performance applications that are utilized in the military and aerospace.

Figure 15 illustrates the applications of different categories like OTFT-driven OLED, sensors, military and healthcare. As shown in the figure, there are three OTFT-driven AMOLED displays discussed in this section. Various sensor-based applications are also reported here as an in-call touch sensor, capacitive touch sensor, chemical imaging sensor, light sensor, etc. Furthermore, health-care applications include ovarian cancer detection, mental health disorder treatment, circulating cancer biomarkers detection, health monitoring application and many more. Apart from these categories, there are some military applications such as assistant gunner display, vision enhancement system, night vision goggles, etc.

9. Reliability issues for OLED

Organic light-emitting diodes have been examined widely to implement various potential display applications. The quality of OLED devices has been refined during the last two decades. But under some conditions, OLED devices suffer from early failure due to the sudden change/increment in current, which causes a major loss of light [140]. Also, there are some other challenges in these devices like prevention of breakage by bending, moisture protection in the air, durability, high cost, etc. Degradation and instability of organic devices have become major concerns nowadays [141]. Many researchers are investigating the organic LEDs rigorously to overcome these issues [142–144].

Basically, unreliable OLEDs exhibit some characteristics such as current noise spectrum with $1/f^{3/2}$ and $1/f^{\gamma}$ proportionalities and high DC leakage current, where γ varies from 0.9 to 1.6. To make the device reliable and overcome these issues, Rocha *et al* [140] in 2013 proposed a diagnostic tool for reliability. Furthermore, in 2015, Jimbo *et al* [145] proposed an OLED device that was completely coated with AlO_x (aluminium oxide) by ALD (atomic layer deposition) to enhance the mechanical durability and reliability. In this research, some tests were performed to check the reliability of having AlO_x coating on the device such as pencil hardness test, repetitive bending test and high humidity and temperature preservation test. The device was working properly for up to 500 h at 65°C, exhibited pencil hardness of 4H and survived to 100,000 repetitive bending with 4 mm curvature radius.

In 2018, Shin *et al* [146] utilized IGZO TFTs in an OLED panel to improve reliability. The device achieved a lifetime of upto 60,000 h and was implemented to 55-inch UHD, 55-inch FHD and 65-inch UHD OLED displays and enhanced cost-competitiveness of organic LEDs as compared to LCDs. Thereafter in 2019, Huang *et al* [147] proposed a 55-inch 4K UHD organic LED display, which comprised high-reliability image sticking. To achieve a reliable device, optimization of oxygen in IGZO layer was performed as well as the excess oxygen of the gate insulator layer was decreased.

Table 11. Performance comparison of OTFT-driven AMOLEDs.

Device	C_1 [126]	C_2 [127]	C_3 [128]
Pixel size	318 μm × 318 μm	210 μm × 210 μm	1.5 mm× 1.5 mm
Display size	2.5 inch	4.1 inch	2.7 inch
Resolution	80 ppi	121 ppi	32 × 32
Peak luminescence	150 cd m^{-2}	100 cd m^{-2}	64,459 cd m^{-2}
Contrast ratio	—	>1000:1	—
Scan voltage	30 Vp-p	20 Vp-p	—
Signal voltage	12 Vp-p	<10 Vp-p	—
Thickness	0.4 μm	80 μm	30 μm

Table 12. Organic LEDs based healthcare applications.

Year	Ref.	Technology	Observations	Application
2019	[132]	Analysed the change in wavelength of light using urine sample of the human using two organic OLED.	Cathode currents: 13 mA at 440 nm wavelength 29 mA at 420 wavelength	Ovarian cancer detection
2016	[133]	Utilized a drug-free non-invasive optogenetics-based therapy	Obtained ten times greater instantaneous blue light intensity, i.e., 1 mW mm^{-2} at a maximum bias voltage of 13 V	Treatment of mental health disorder and chronic inflammatory disease
2016	[134]	Combined flat-panel organic LED technology with protein microarray technology	—	Circulating cancer biomarkers detection
2014	[135]	Developed an amber marker light panel	—	Lighting panels for health-care applications
2010	[136]	Realized a WSG (wireless sensor gateway) within the wireless sensor network	—	Health monitoring (recording of bio-signals such as pulse wave, body weight, electrocardiogram)

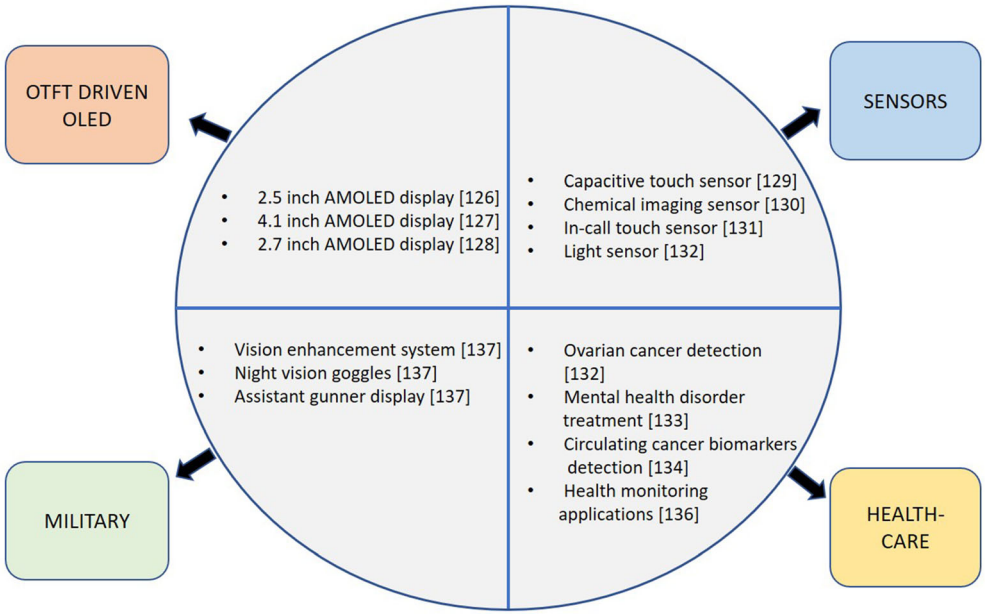

Figure 15. OLED applications based on different categories.

10. Future scope

Organic LEDs have proven their superiority over conventional LEDs in terms of solution processability, flexibility, low thickness, lightweight and low-cost manufacturing. However, there is still a very large scope to improve many parameters like material properties, efficiency, lifetime, resistivity, current density, etc. The requirement of the utilization of 100% excitons after the recombination of charge carriers have attracted researchers to devote their efforts to enhance the performance of these devices. Recently, TADF OLEDs have emerged as a great alternative to phosphorescent OLEDs, as these devices can exhibit 100% internal quantum efficiency. TADF devices contain purely organic materials hence becomes inexpensive and provide a large number of design opportunities. But there is scope of improvement in terms of lifetime and colour purity. A lot of research work is being done in the direction to improve TADF devices.

On the other hand, red, green and orange OLEDs have achieved already very high EQE in previous years. However, blue OLEDs still lag in stability and efficiency. Though significant progress has already been made to achieve high performance and long lifetime blue OLEDs, this field is still available as one of the hot research projects in OLED technology. The blue TADF emitters can be utilized to achieve highly efficient blue OLEDs. The reverse intersystem crossing-based technology is used in blue TADF emitters to achieve high luminescence by harvesting both singlet and triplet excitons for the emission of light.

Although a remarkable development has been made in lighting and display devices, there are still massive challenges to having a long lifespan, high efficiency and high visual quality. In the past few years, sunlight-style and candlelight-style OLEDs have received attention, as these devices contain attractive features like energy-saving, eco-friendly, roll-to-roll fabrication, low cost and blue hazard-free emission. Another parameter that plays an important role to improve the performance of OLEDs is EQE. EQE depends on the product of internal quantum efficiency and extraction efficiency. If the photons developed in the active region can exit from the epitaxial layer, extraction efficiency can be enhanced; hence, quantum efficiency can be improved as well. But blue wavelength is less sensitive to the human eye as compared to green or red. This results in less efficiency and higher barrier, which creates hurdles to improve quantum efficiency in some cases.

11. Conclusion

This research article illustrates a deep review of OLED of the last decade in terms of working, types, materials, fabrication, improvements techniques, reliability and applications. Having various advantages over inorganic LEDs, there is still large scope of improvements in some parameters of OLEDs like EQE, light extraction efficiency, lifetime, cost, etc. This article shows various methods to enhance these parameters. Various fabrication techniques like physical vapour deposition, screen printing, spin casting and inkjet printing are discussed as well. Additionally, improvement methods being executed in the last 10 years are highlighted based on different layers, such as HIL/EIL, HTL/ETL, an emissive layer, blocking layer, on the basis of colour of emission (white and blue) and characteristics parameters. Also, rigorous efforts are made to demonstrate

the reliability concern and application of different fields like sensors, OTFT-driven organic LEDs, healthcare and military.

References

[1] Pal N S, Kumar B and Mittal P 2021 *Semiconductors.* **55** 618
[2] Mittal P 2021 *J. Soc. Inf. Disp.* **1** 17
[3] Sain N, Sharma D and Choudhary P 2020 *Int. J. Eng. Appl. Sci. Technol.* **11** 587
[4] Pope M, Kallmann HP and Magnante PJ 1963 *J. Chem. Phys.* **38** 2042
[5] Patel B N and Prajapati M M 2014 *Int. J. Sci. Res. Publ.* **4** 1
[6] Geffroy B, Le Roy P and Prat C 2006 *Polym. Int.* **55** 572
[7] Malliaras G G and Scott J C 1999 *J. Appl. Phys.* **85** 7426
[8] Gupta D, Katiyar M and Gupta D 2009 *Org. Electron.* **10** 775
[9] Dodabalapur A 1997 *Solid State Commun.* **102** 259
[10] Negi S, Mittal P and Kumar B 2019 IET Circuits. *Devices Syst.* **13** 1255
[11] Fujikawa H, Ishii M, Tokito S and Taga Y 2000 *MRS Online Proceedings Library* **621** Q3.4.1
[12] Kulkarni A P, Tonzola C J, Babel A and Jenekhe S A 2004 *Chem. Mater.* **16** 4556
[13] Ammermann D, Bohler A, Dirr S, Johannes H H and Kowalsky W 1996 *Int. J. Electron. Commun.* **50** 327
[14] Hung L S, Tang C W, Mason M G, Raychaudhuri P and Madathil J 2001 *Appl. Phys. Lett.* **78** 544
[15] Gao C H, Shi X B, Zhou D Y, Zhang L, Wang Z K and Liao L S 2013 *Int. J. Photoenergy* **2013** 1
[16] Chen Y, Chen J, Ma D, Yan D, Wang L and Zhu F 2011 *Appl. Phys. Lett.* **98** 114
[17] Kim Y M, Lee J W, Jung J H, Paek K K, Sung M Y, Kim J K *et al* 2006 *IEEE Electron Device Lett.* **27** 558
[18] Gomez E F and Steckl A J 2015 *ACS Photonics* **3** 439
[19] Chen L, Jiang Y, Nie H, Hu R, Kwok H S, Huang F *et al* 2014 *ACS Appl. Mater. Interfaces* **6** 17215
[20] Zhou N, Wang S, Xiao Y and Li X 2018 *J. Lumin.* **196** 40
[21] Klein M, Rau N, Wende M, Sundermeyer J, Cheng G, Che C M *et al* 2020 *Chem. Mater.* **32** 10365
[22] Zheng X, Liu Y, Zhu Y, Ma F, Feng C, Yu Y *et al* 2020 *Opt. Mater.* **101** 109755
[23] Zheng X, Huang R, Zhong C, Xie G, Ning W and Huang M 2020 *Adv. Sci.* **7** 1902087
[24] Huang C, Zhang Y, Zhou J, Sun S, Luo W, He W *et al* 2020 *Adv. Opt. Mater.* **8** 2000727
[25] Lu G, Wu Z G, Wu R, Cao X, Zhou L, Zheng Y X *et al* 2021 *Adv. Funct. Mater.* **31** 2102898
[26] Wang Y, Wang W, Huang Z, Wang H, Zhao J, Yu J *et al* 2018 *J. Mater. Chem. C* **6** 7042
[27] Mohan V, Gautam A K, Choudhary S D, Bee M M, Puviarasi R, Saranya S *et al* 2020 *IEEE Trans. Nanotechnol.* **19** 699
[28] Xi Z, Zhao B, Chen L, Li W, Wang H, Liu X *et al* 2018 *Org. Electron.* **57** 21
[29] Han S H, Jeong J H, Yoo J W and Lee J Y 2019 *J. Mater. Chem. C* **7** 3082
[30] Han K H, Kim K, Han Y, Kim Y D, Lim H, Huh D *et al* 2020 *Adv. Mater. Interfaces* **7** 1901509
[31] Cui D, Wang S, Li S, Liu Y, Du H, Du Q *et al* 2021 *J. Mater. Sci. Mater.* **32** 12075
[32] Park H, Lee J, Kang I, Chu H Y, Lee J I, Kwon S K *et al* 2012 *J. Mater. Chem.* **22** 2695
[33] Rajamalli P, Senthilkumar N, Gandeepan P, Ren-Wu C C, Lin H W and Cheng C H 2016 *ACS Appl. Mater. Interfaces* **8** 27026
[34] Yang T, Liang B, Cheng Z, Li C, Lu G and Wang Y 2019 *J. Phys. Chem. C* **123** 18585
[35] Lee H 2021 *Curr. Appl. Phys.* **21** 116
[36] Wang Y F, Li M, Teng J M, Zhou H Y and Chen C F 2021 *Adv. Funct. Mater.* **31** 2106418
[37] Luo Y, Li S, Zhao Y, Li C, Pang Z, Huang Y *et al* 2020 *Adv. Mater.* **32** 2001248
[38] Albrecht K, Matsuoka K, Yokoyama D, Sakai Y, Nakayama A and Fujita K 2017 *ChemComm.* **53** 2439
[39] Angioni E, Chapran M, Ivaniuk K, Kostiv N, Cherpak V, Stakhira P *et al* 2016 *J. Mater. Chem. C* **4** 3851
[40] Guo K, Zhang J, Xu T, Gao X and Wei B 2014 *JDT* **10** 642
[41] Negi S, Mittal P and Kumar B 2020 *J. Electron. Mater.* **49** 4610
[42] Wu Z, Guo H and Wang J 2007 *Microelectron. J.* **38** 686
[43] Dong C, Fu X, Amoah S, Rozelle A, Shin D H, Salehi A *et al* 2019 *J. Soc. Inf. Disp.* **8** 469
[44] Qu Y, Coburn C, Fan D and Forrest S R 2017 *ACS Photonics* **4** 363
[45] Liu Y, Wei X, Li Z, Liu J, Wang R, Hu X *et al* 2018 *ACS Appl. Energy Mater.* **2** 543
[46] Takahashi K, Sato T, Yamamoto R, Shishido H, Isa T, Eguchi S *et al* 2015 *Dig. Tech. Pap. SID Int. Symp.* **46** 250
[47] Watanabe K, Iwaki Y, Uchida Y, Nakamura D, Ikeda H, Miyake H *et al* 2015 *Dig. Tech. Pap. SID Int. Symp.* **46** 246
[48] Idojiri S, Ohno M, Takeshima K, Yasumoto S, Sato M and Sakamoto N 2015 *Dig. Tech. Pap. SID Int. Symp.* **46** 8
[49] De Dieu B, Mugiraneza J, Maruyama T, Yamamoto T and Sugita Y 2019 *Dig. Tech. Pap. SID Int. Symp.* **50** 608
[50] Zhang B, Qi P, Yang Z, Lai Z, Wang Z, Li S *et al* 2020 *Dig. Tech. Pap. SID Int. Symp.* **51** 1836
[51] Qin Z, Yeh Y W, Tsai Y H, Cheng W Y, Huang Y P and Shieh H P D *Dig. Tech. Pap. SID Int. Symp.* **47** 393
[52] Shu Z, Beckert E, Eberhardt R and Tünnermann A 2017 *J. Mater. Chem. C* **44** 11590
[53] Tsai Y H, Wu Y L, Liou W T, Kung Y R, Huang Y H and Lee K C 2017 *Dig. Tech. Pap. SID Int. Symp.* **48** 2021
[54] Song M G, Kim K S, Yang H I, Kim S K, Kim J H, Han C W *et al* 2020 *Org. Electron.* **76** 105418
[55] Zhong Z, Hu Z, Jiang Z, Wang J, Chen Y, Song C *et al* 2015 *Adv. Electron. Mater.* **3** 1400014
[56] Stolz S, Zhang Y, Lemmer U, Hernandez-Sosa G and Aziz H 2017 *ACS Appl. Mater. Interfaces* **3** 2776
[57] Zhu W, Ding K, Yi C, Chen R, Wei B, Huang L *et al* 2021 *Front. Chem.* **9** 1
[58] Wang M, Zhu W, Yin Z, Huang L and Li J 2020 *Org. Electron.* **85** 105823
[59] Tsai K W, Hung M K, Mao Y H and Chen S A 2019 *Adv. Funct. Mater.* **15** 1901025
[60] Zheng Q, Qu D, Zhang Y, Li W, Xiong J, Cai P *et al* 2018 *Opt. Laser Technol.* **101** 85
[61] Dong D, Wang Y, Ian L, Feng D, Wang H and He G 2017 *Phys. Status Solidi A* **12** 1700583
[62] Zheng Q, You F, Xu J, Xiong J, Xue X, Cai P *et al* 2017 *Org. Electron.* **46** 7

[63] Fujimoto H, Yahiro M, Yukiwaki S, Kusuhara K, Nakamura N, Suekane T *et al* 2016 *Appl. Phys. Lett.* **24** 243302
[64] Wang Q, Deng Z, Chen J and Ma D 2010 *IEEE Trans. Electron Device* **9** 2221
[65] Lu L, Yu J N, Long L, Yu F F, Zhang J H, Zhang H *et al* 2010 *Phys. Status Solidi A* **208** 2321
[66] Dong S C, Xu L and Tang C W 2017 *Org. Electron.* **42** 379
[67] Lu S Y, Mukhopadhyay S, Froese R and Zimmerman P M 2018 *J. Chem. Inf. Model.* **12** 2440
[68] Zhang J, Zhang X, Feng H, Yu Z, Zhang J, Liu S *et al* 2019 *J. Mater. Chem. C* **7** 1991
[69] Nagar M R, Shahnawaz Yadav R A K, Lin J T and Jou J H 2020 *ACS Appl. Electron. Mater.* **2** 1545
[70] Li H and Lili Z 2020 *ACS Appl. Electron. Mater.* **2** 885
[71] Huang F, Liu H, Sun W, Li X and Wang S 2020 *J. Mater. Chem. C* **8** 9184
[72] Lee W H, Kim D H, Jesuraj P J, Hafeez H, Lee J C, Choi D K *et al* 2018 *Mater. Res. Express* **5** 076201
[73] Chen C H, Tierce N T, Leung M K, Chiu T L, Lin C F, Bardeen C J *et al* 2018 *Adv. Mater.* **30** 1804850
[74] Guo K, Zhang J, Xu T, Gao X and Wei B 2014 *J. Display Technol.* **10** 642
[75] Yun C, Cho H, Koh T W, Kim J H, Kim J W, Park Y *et al* 2011 *IEEE Trans. Electron Devices* **59** 159
[76] Huh J W, Moon J, Lee J W, Cho D H, Shin J W, Han J H *et al* 2011 *IEEE Photonics J.* **4** 39
[77] Zhang X W, Liu L M, Li J, Zhang L, Jiang X Y, Zhang Z L *et al* 2011 *J. Display Technol.* **7** 515
[78] Kim S J, Zhang Y, Zuniga C, Barlow S, Marder S R and Kippelen B 2011 *Org. Electron.* **12** 492
[79] Zhao Y, Zhu L, Chen J and Ma D 2012 *Org. Electron.* **13** 1340
[80] Erickson N C and Holmes R J 2013 *Adv. Funct. Mater.* **23** 5190
[81] Bachelet A, Chabot M, Ablat A, Takimiya K, Hirsch L and Abbas M 2021 *Org. Electron.* **88** 106024
[82] Sharma A and Das T D 2020 *Optik*. **221** 165350
[83] Nayak D and Choudhary R B 2019 *Opt. Mater.* **91** 470
[84] Singh M, Jou J H, Sahoo S, Sujith S S, He Z K, Krucaite G *et al* 2018 *Sci. Rep.* **8** 1
[85] Olivier S, Ishow E, Della-Gatta S M and Maindron T 2017 *Org. Electron.* **49** 24
[86] Lee C C, Yuan C H, Liu S W and Shih Y S 2011 *J. Display Technol.* **7** 454
[87] Yoo S I, Yoon J A, Kim N H, Kim J W, Kang J S, Moon C B *et al* 2015 *J. Lumin.* **160** 346
[88] Seo J A, Jeon S K, Gong M S, Lee J Y, Noh C H and Kim S H 2015 *J. Mater. Chem. C.* **3** 4640
[89] Tan W Y, Zou J H, Gao D Y, Liu J Z, Chen N N and Zhu X H 2016 *Adv. Electron. Mater.* **2** 1600101
[90] Wei X F, Tan W Y, Zou J H, Guo Q X, Gao D Y, Ma D G *et al* 2017 *J. Mater. Chem. C* **5** 2329
[91] Jang S, Han S H, Lee J Y and Lee Y 2018 *Synth. Met.* **239** 43
[92] Soman A and Unni K N 2019 *EPJ Appl. Phys.* **86** 10201
[93] Pardo D A, Jabbour G E and Peyghambarian N 2000 *Adv. Mater.* **12** 1249
[94] Kalyani N T and Dhoble S J 2015 *Renew. Sust. Energ. Rev.* **44** 319
[95] Yoshioka Y and Jabbour G E 2006 *Synth. Met.* **156** 779
[96] Derue L, Olivier S, Tondelier D, Maindron T, Geffroy B and Ishow E 2016 *ACS Appl. Mater.* **8** 16207
[97] Burrows P E, Forrest S R, Sapochak L S, Schwartz J, Fenter P and Buma T 1995 *J. Cryst. Growth* **156** 91
[98] Ummartyotin S, Juntaro J, Wu C, Sain M and Manuspiya H 2011 *J. Nanomater.* **2011**
[99] Hyun W J, Im S H, Park O O and Chin B D 2012 *Org. Electron.* **13** 579
[100] Yuan S, Hao Y, Miao Y, Sun Q, Li Z, Cui Y *et al* 2017 *RSC Adv.* **7** 43987
[101] Juhari N, Shukri N I A, Sabani N, Shaari S, Ahmad M F and Zakaria N F 2020 *In AIP Conf. Proc.* **2203** 020046
[102] Chen H C, Kung C P, Houng W G, Peng Y R, Hsien Y M, Chou C C *et al* 2009 *IEEE/OSA J. Display Technol.* **5** 216
[103] Xing X, Lin T, Hu Y X, Sun Y L, Mu W Y, Du Z Z *et al* 2019 *Mod. Phys. Lett. B* **33** 1950149
[104] Hu Z, Yin Y, Ali M U, Peng W, Zhang S, Li D *et al* 2020 *Nanoscale* **12** 2103
[105] Preinfalk J B, Eiselt T, Wehlus T, Rohnacher V, Hanemann T, Gomard G *et al* 2017 *ACS Photonics* **4** 928
[106] Wan Z, Xu M, Fu Z, Li D, Mei A, Hu Y *et al* 2019 *Front. Optoelectron.* **12** 344
[107] Li H and Zhou L 2020 *ACS Appl. Electron. Mater.* **2** 885
[108] Lee J, Kim G, Shin D K, Seo Y, Kim K and Park J 2018 *IEEE Trans. Electron Devices* **65** 3311
[109] Zhang D D, Feng J, Chen L, Wang H, Liu Y F, Jin Y *et al* 2011 *IEEE J. Quantum Electron.* **47** 591
[110] Sun K, Tian W, Ge C, Gu F, Zhou Y, Wang W *et al* 2022 *Org. Electron.* **101** 106417
[111] Vasilopoulou M, Yusoff M, Daboczi M, Conforto J, Gavim A E X and da Silva W J 2021 *Nat. Commun.* **12** 1
[112] Zhou J, Ai N, Wang L, Zheng H, Luo C, Jiang Z *et al* 2011 *Org. Electron.* **12** 648
[113] Wahyuningrum D and Alni A 2015 *Procedia Chem.* **16** 586
[114] Triboni E R, Fernandes M R, Garcia J R, Carreira M C, Berlinck R G D S, Filho P B *et al* 2015 *Univ. Sci.* **9** 579
[115] Wei B, Xu H, Zhao N, Gao X, Ye Y, Wang Y *et al* 2021 *J. Ind. Eng. Chem.* **102** 44
[116] Chan C Y, Tanaka M, Lee Y T, Wong Y W, Nakanotani H, Hatakeyama T *et al* 2021 *Nat. Photonics* **15** 203
[117] Han M, Chen Y, Xie Y, Zhang F, Li X, Huang A *et al* 2020 *Cell Rep.* **1** 100252
[118] Yang J, Guo Q, Wang J, Ren Z, Chen J, Peng Q *et al* 2018 *Adv. Opt. Mater.* **6** 1800342
[119] Nakao K, Sasabe H, Komatsu R, Hayasaka Y, Ohsawa T and Kido J 2017 *Adv. Opt. Mater.* **5** 1600843
[120] Lee S J, Kang C M, Shin J W, Ahn D H, Joo C W, Cho H *et al* 2022 *J. Ind. Eng. Chem.* **105** 132
[121] Yang S H and Huang T L 2021 *Opt. Mater.* **111** 110725
[122] Kim H J, Shin M H, Hong H G, Song B S, Kim S K, Koo W H *et al* 2015 *J. Display Technol.* **12** 526
[123] Chen Y, Wang J, Zhong Z, Jiang Z, Song C, Hu Z *et al* 2016 *Org. Electron.* **37** 458
[124] Lima P P, Paz F A A, Brites C D S, Quirino W G, Legnani C, e Silva M C *et al* 2014 *Org. Electron.* **15** 798
[125] Shin D, Kim Y, Chang N and Pedram M 2013 IEEE Trans. *Comput. Aided Des. Integr. Circuits Syst.* **32** 1017
[126] Katsuhara M, Yagi I, Yumoto A, Noda M, Hirai N, Yasuda R *et al* 2009 *In Organic Field-Effect Transistors VIII*, *International Society for Optics and Photonics* **7417** 74170
[127] Noda M, Obayashi N, Katsuhara M, Yumoto A, Ushikura S, Yasuda R *et al* 2011 *J. Soc. Inf. Disp.* **19** 316
[128] Kim J S and Song C K 2016 *Org. Electron.* **30** 45

[129] Kim S, Choi W, Rim W, Chun Y, Shim H, Kwon H *et al* 2011 *IEEE Trans. Electron. Dev.* **58** 3609
[130] Miyamoto K I, Kaneko K, Matsuo A, Wagner T, Kanoh S I, Schöning M J *et al Sens. Actuators B Chem.* **170** 82
[131] Watanabe K, Iwaki Y, Uchida Y, Nakamura D, Ikeda H, Miyake H *et al Dig. Tech. Pap. SID Int. Symp.* **46** 246
[132] Negi S, Mittal P, Kumar B and Juneja P K 2019 *Microelectron. Eng.* **218** 111154
[133] Smith J, Shah A, Lee Y K, O'Brien B, Kullman D, Sridharan A *et al* 2016 *Electron. Lett.* **52** 900
[134] Katchman B A, Smith J T, Obahiagbon U, Kesiraju S, Lee Y K, O'Brien B *et al* 2016 *Sci. Rep.* **6** 1
[135] Hamer J, Boroson M, Kondakova M, Spindler J and Majka D 2014 *Dig. Tech. Pap. SID Int. Symp.* **45** 754
[136] Becher K, Figueiredo C P, Mühle C, Ruff R, Mendes P M and Hoffmann K P 2010 in *2010 Annu. Int. Conf. IEEE Eng. Med. Biol.* p 374
[137] Barre F, Chiquard A, Faure S, Landais L and Patry P 2005 in *Building European OLED Infrastructure, International Society for Optics and Photonics* **5961** 596109
[138] Trakalo M and Lorimer S 2008 in *Display Technologies and Applications for Defense, Security, and Avionics II, International Society for Optics and Photonics* **6956** 69560
[139] Sarma K R 2012 in *Head-and Helmet-Mounted Displays XVII; and Display Technologies and Applications for Defense, Security, and Avionics VI*, *International Society for Optics and Photonics* **8383** 83830
[140] Rocha P R, Vandamme L K J, Meskers S C J, Gomes H L, De Leeuw D M and Van De Weijer P 2013 in *2013 22nd International Conference on Noise and Fluctuations (ICNF)* p 1
[141] Mittal P, Yadav S and Negi S 2021 *Mater. Sci. Semicond Process* **133** 105975
[142] Negi S, Mittal P and Kumar B 2020 *J. Soc. Inf. Disp.* **22** 956
[143] Negi S, Mittal P and Kumar B 2021 *IEEE Trans. Circuits Syst. I Regul. Pap.* **68** 3254
[144] Negi S, Mittal P and Kumar B 2018 *Microsyst. Technol.* **24** 4981
[145] Jimbo Y, Tamatsukuri Y, Ito M, Yokoyama K, Hirakata Y and Yamazaki S 2015 *J. Soc. Inf. Disp.* **23** 313
[146] Shin H J, Takasugi S, Choi W S, Chang M K, Choi J Y, Jeon S K *et al* 2018 *Dig. Tech. Pap. SID Int. Symp.* **49** 358
[147] Huang Y, Cheng J, Fang J, Ding L, Zhao C, Zhou B *et al* 2019 *Dig. Tech. Pap. SID Int. Symp.* **50** 44

Neural Computing and Applications
https://doi.org/10.1007/s00521-022-07425-9

S.I. : NEURAL COMPUTING FOR IOT BASED INTELLIGENT HEALTHCARE SYSTEMS

Recognition of multi-cognitive tasks from EEG signals using EMD methods

Akshansh Gupta[1] · Dhirendra Kumar[2] · Hanuman Verma[3] · M. Tanveer[4] · Andreu Perez Javier[5,6] · Chin-Teng Lin[7] · Mukesh Prasad[7]

Received: 16 April 2021 / Accepted: 10 May 2022
© The Author(s) 2022

Abstract
Mental task classification (MTC), based on the electroencephalography (EEG) signals is a demanding brain–computer interface (BCI). It is independent of all types of muscular activity. MTC-based BCI systems are capable to identify cognitive activity of human. The success of BCI system depends upon the efficient feature representation from raw EEG signals for classification of mental activities. This paper mainly presents on a novel feature representation (formation of most informative features) of the EEG signal for the both, binary as well as multi MTC, using a combination of some statistical, uncertainty and memory- based coefficient. In this work, the feature formation is carried out in the two stages. In the first stage, the signal is split into different oscillatory functions with the help of three well-known empirical mode decomposition (EMD) algorithms, and a new set of eight parameters (features) are calculated from the oscillatory function in the second stage of feature vector construction. Support vector machine (SVM) is used to classify the feature vectors obtained corresponding to the different mental tasks. This study consists the problem formulation of two variants of MTC; two-class and multi-class MTC. The suggested scheme outperforms the existing work for the both types of mental tasks classification.

Keywords Brain–computer interface · Mental tasks classification · Feature extraction · EMD Algorithms · Parameters

1 Introduction

Human brains are capable to accomplish two or more different cognitive activities simultaneously. These activities can be termed as mental tasks. In BCI scientific domain, the majority of the research actions have been augmented to differentiate between two diverse mental tasks at a given time. It is pointed out the researchers that the capability of human mind is to perform more two action simultaneously [35]. Also, a handful studies deal with multi-mental task classification [1, 13, 30, 36, 41, 45]. Thus, it is essential requirement of a system that can segregate more than two cognitive activities at a given instance of time, can be termed as multi-mental task classification system. It becomes more harder to classify a test sample correctly when number of classes increases in a given dataset. Also, the computational efforts to solve the multi-class problem are larger than a binary class problem as it involves the learning of several hyperplanes for classification model. The electroencephalograph (EEG) technology is dominant invigilating techniques to capture brain activity corresponding to a given mental task. The EEG signals, in its raw form cannot, give significant feature for distinguishing among different brain activity. Thus, from these arguments, classification of both types mental tasks classification is presumed to be a challenging problem.

In literature, numerous systems of working for the feature representation (feature extraction) from the EEG signals have been studied and suggested for BCI researches [3]. The feature extraction methods can be clustered into these major domains: (i) temporal [44]; (ii) frequency (spectral) domain; and (iii) hybrid of temporal and frequency domain methods; (iv) band power [28] and (v) through principle component analysis and linear discriminant analysis [14].

Extended author information available on the last page of the article

Published online: 13 June 2022

To describe accurate and precise time information of the neuro-physiological signal, methods in the temporal domain adapt predominantly approach. The changes information, of the signal with respect to the time, are designated by the extracted features. In the temporal domain, the amplitude of the signal or statistical measures like absolute mean, standard deviation and kurtosis of the signal are explored to represent EEG signal [4, 21, 32, 40]. There is a set of explicit oscillations functions in the EEG signal, which can be termed as rhythms. Commensurate with distinct mental tasks, different rhythms are allies to these EEG signals [6, 27, 29, 37, 38]. Hence, frequency information which is embedded in the signal can be used as a feature of the signal and utilized to characterize the signal more accurately. Power spectral analysis (density) is more powerful technique in BCI research community to extract accurate frequency content features and produces high-frequency resolution [36]. The phase synchronization between EEG signals in a same frequency has been also used as feature descriptors [2]. However, the neuro-physiological signals utilize in BCI contain distinct virtues in the both temporal and frequency domain. The variation in frequency contents of the EEG signal with respect to time demonstrates that the nature of EEG signal is non-stationary. Short-time Fourier transform and wavelet transform are widely used methods to extract the both frequency and temporal information-based features from the non-stationary signal. Such methods can detect abrupt temporal variations in the EEG signal. The wavelet transform (WT) [9, 31] is a useful technique by which analysis of both time and frequency contents of the signal can be analyzed simultaneously. WT is utilized in analysis of EEG signals in the fields of motor imagery and epileptic seizures, [4, 8, 22, 34], brain disorders, [20], classification of human emotions [33] and non-motor imagery [5]. However, WT uses some fixed basis functions which make it non-adaptive [23] to the signal to be processed. Another method for analyzing signals like EEG is empirical mode decomposition (EMD)[23], which is a data-dependent approach. This method is self-adaptive according to the signal to be processed unlike to WT, where a fixed set of basis functions is used. The signals are decomposed into finite set of low and high components by EMD, also known as intrinsic mode functions (IMFs) or modes. The EMD and its many variant like multi-EMD (MEMD) confers proper analysis of EEG signal having muscle artifacts [7]. The EMD method has been used to extract representative data for BCI [11, 18, 25] to classify mental task. In this paper, the following novelties are presented:

1. This is very first comprehensive study of three different types of *EMD* algorithm for binary as well as multi cognitive task recognition system.
2. A new parameter named as *Husrt Exponent* is investigated first time for cognitive task recognition system.

Rest of the paper is organized as follows: Section 2 glimpses brief overview of EMD algorithm and its variants. Section 3 elucidates the description of proposed approach. Data, experimental setup and result are discussed in Section 4, and finally, Section 5 mark-outs the conclusion.

2 Empirical mode decomposition and its variants

The brief description of the variants of EMD is discussed below.

2.1 Empirical mode decomposition (EMD)

The non-stationary and nonlinear signal can be proper investigated with the help of empirical mode decomposition (EMD) by breaking the signal into a series of its different endogenous oscillation components, which is also known as intrinsic mode function (IMF). A continuous function would be an IMF under the following circumstances [23]:

1. The difference between extrema and zero crossings of the function must be at most one.
2. At a given point, the mean value of the envelope defined by the local maxima and local minima.

To be stationary Gaussian process for a signal, the requirement of narrow band is fulfilled by first condition. To abstain instantaneous frequency from unwanted fluctuations induced by asymmetric wave forms, second condition comes in the picture. The first four IMFs on EEG segment are shown Fig. 1 obtained using EMD algorithm. From Fig. 1, it can be noted that these IMFs can characterize the signal well. Thus, a signal $x(m)$, can be expressed as:

$$x(m) = \sum_{j=1}^{k} IMF_j + r_k \tag{1}$$

According to [23], the stopping criteria in T steps to further produce IMFs on the basis of standard deviation are defined as

$$SD_i = \sum_{t=0}^{T} \frac{|IMF_{i+1}(t) - IMF_i(t)|^2}{IMF_i(t)^2} \tag{2}$$

There will be no decomposition in the signal, when the value of *SDs* reaches smaller than predefined value.

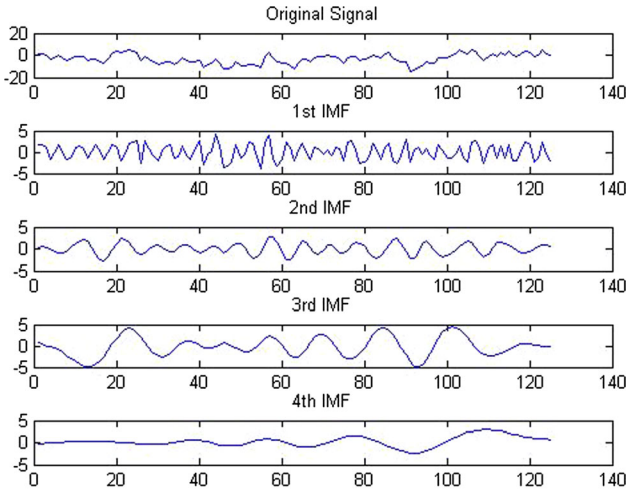

Fig. 1 IMF plot obtained for a given EEG signal

2.2 Ensemble empirical mode decomposition (EEMD)

The major drawback of EMD algorithm is the frequent mode mixing. This problem arises when a different scale of signal is contained by a single IMF or distinct IMFs produces a single scale of signal. To alleviate the problem of scale separation, [42] has suggested a noise-embedded data analysis method, called ensemble empirical mode decomposition (EEMD). EEMD defines exact IMF ingredients as the average of an ensemble of the trails which consists of signal plus white noise with finite amplitude [42]. Thus, the signal $x(m)$ in i^{th} trial after adding white noise can be represented as

$$x^i(m) = x(m) + a_0 w^i(n), \text{ for } i = 1, \ldots l \tag{3}$$

where $w^i(n)$ is the white noise in i^{th} trial with unit variance and a_0 amplitude. For each $i = 1, 2 \ldots l$, the IMF_k^i is calculated with different realization of white noise with the signal obtained using Equation 3. The average k^{th} $\overline{IMF}_k$ can be defined as

$$\overline{IMF}_k = \frac{1}{l}\sum_{i=1}^{l} IMF_k^i \tag{4}$$

where l is number of white noise realizations.

In this work, parameter values of a_0 and l have been empirically determined. The distinctive concepts of EEMD are as follows:

1. The ensemble mean neutralizes effect of added collection of white noises; thus, the mixture of the signal and white noises contains only signal.
2. To explore all feasible solution, it is essential to ensemble white noise of finite amplitude with signal.
3. To obtain true and physically meaningful IMFs from EMD, it is necessary to add noise to the signal.

2.3 Complete ensemble empirical mode decomposition with adaptive noise (CEEMDAN)

The mode mixing problem of the original EMD algorithm is successfully alleviated by EEMD with adding white noise into the signal, but this also leads to a problem that noise is not fully segregated from the signal and the resultant different IMFs may contain mixture of noise and signal. To resolve this problem, [39] have proposed CEEMDAN algorithm that provides good spectral separation of the modes. Hence, it gives an exact reconstruction of the original signal with a lower computational cost.

The first residue can be calculated as:

$$r_1(m) = x(m) - \overline{IMF_1} \tag{5}$$

where $\overline{IMF_1}$ is the first average *IMF* obtained by EEMD. The second average *IMF* can be found as:

$$\overline{IMF} = \frac{1}{l}\sum_{i=1}^{l} E_1\left(r_1(m) + a_0 E_1\left(w^i(m)\right)\right) \tag{6}$$

After finding k^{th} residue, for $k = 2, \ldots, K$, the $k+1$ average *IMF* can be defined as:

$$\overline{IMF}_{k+1} = \frac{1}{l}\sum_{i=1}^{l} E_1\left(r_k(m) + a_k E_k\left(w^i(m)\right)\right) \tag{7}$$

where $E_k(.)$ is an operator to extract k^{th} *IMF* from given signal by EMD algorithm and amplitude a_k allows to select the SNR at each stage. Detailed description can be found in [39].

3 Proposed approach

The proposed method involves the extraction of features with the application of the EMD algorithms separately from the raw EEG data in the very first stage. In second stage, these decomposed EEG signals are encoded with the help of parametric feature transformation using information feature to represent them compactly which leads to dimensionality reduction of the features via encoding with the help of statistical features as every signal or data have the distinguishable property in terms of a set of statistical parameters associated with the signal or data [19]. It may be possible that the two signals have same value associated with one or more statistical parameter. In this work, these eight parameters are selected empirically as discussed below in subsection.

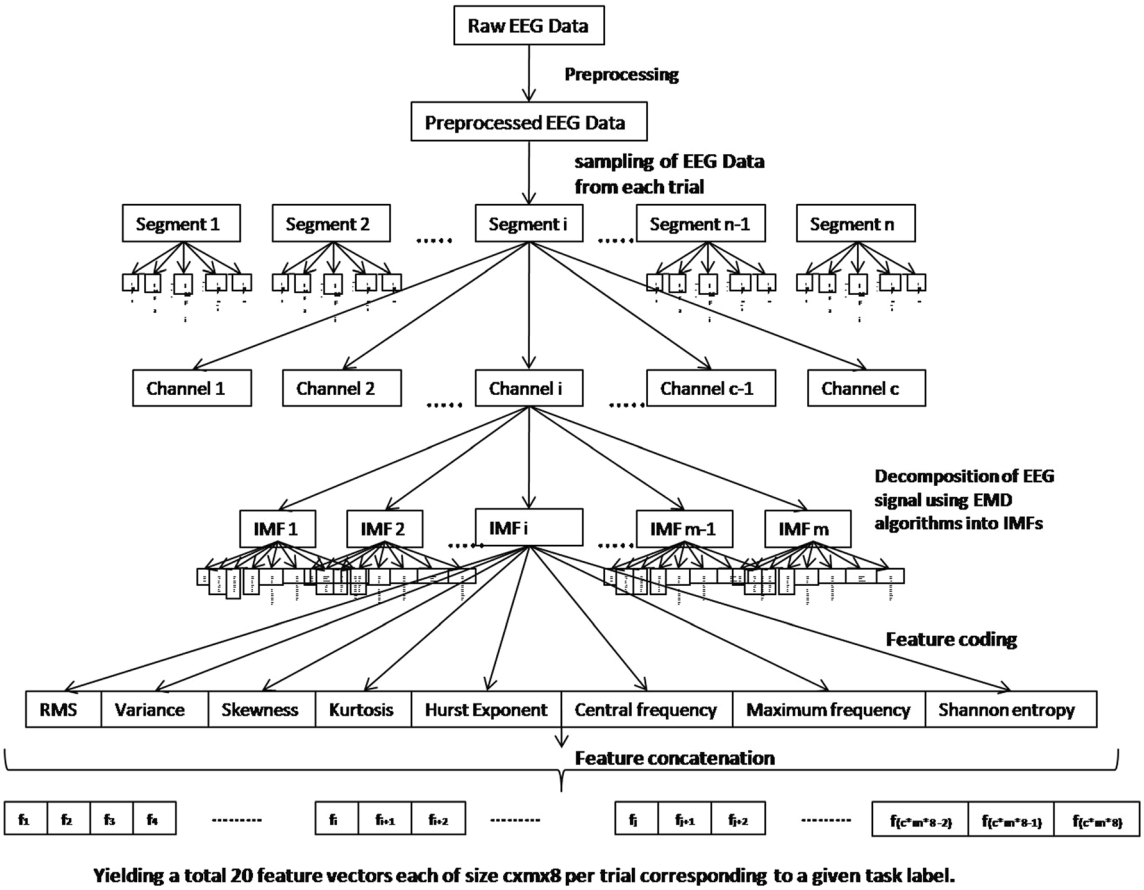

Fig. 2 Schematic flowchart of the proposed model for mental task classification

3.1 Information feature

Extraction of useful information from the data is one of the crucial tasks. Statistical and uncertainty parameters have capability to produce good amount of information along with the interpretation from raw data obtained from instruments [43]. We have extracted following parameters:

- Root mean square
- Variance
- Skewness
- Kurtosis
- Shannon entropy
- Central frequency
- Maximum frequency
- Hurst exponent [24]

In this study, we have formulated a problem for the multi-mental task classification as well as binary mental task classification with the help of EEG signals. Classification of these EEG signals can only be done if an efficient feature representation for signals obtained. Further the obtained features vector is used for classification of these signals. In order to develop a classification model for multi-class problem, one versus rest approach-based support vector machine (SVM) is incorporated as a multi-mental task classifier to build the decision model. The overall flowchart of proposed model is shown in Fig. 2.

4 Experimental setup and result

4.1 Dataset

For mental task, classification experiments were performed on a publicly available EEG dataset. This dataset consists the recordings of EEG signals using seven electrode channels (namely C3, C4, P3, P4, O1, O2 and EOG) of different lobes of the brain (central, parietal, occipital and near the eyes) from seven subjects with the recording protocols described below. Each subject was asked to perform five different mental tasks as: *Baseline task* (relax: *B*); mental *Letter Composing task* (*L*); non-trivial *Mathematical task* (*M*); *Visualizing Counting* (*C*) of numbers written on a blackboard and *Geometric Figure Rotation* (*R*) task. Each of the recording session consists of five trials of each of the five mental tasks. Each trial is of 10 second

Table 1 Data description

Subject	Tasks	Trial
1	Baseline (Relax); letter composing	10
2		5
3	Visual counting; mathematics	10
4		10
5	Geometric rotation	15
6		10
7		5

duration recorded with a sampling frequency of 250 Hz, which resulted in 2500 samples points per trial. We have utilized data of all subjects except Subject 4, due to some missing and incomplete information [15]. Detailed explanation can be found in the work of [26][1] and Table 1. Six electrodes placed on the scalp at C3, C4, P3, P4, O1 and O2 are used for extracting the feature for mental task classification as EOG gives the only artifact.

4.2 Constructing feature vector

For feature construction, the data of each task of each subject is sampled into half-second segments, yielding 20 segments (signal) per trial for each subject as some researchers have done [36]. The complete pipeline for constructing the feature vector from each subject using all trial corresponding to each mental task labels (B, L, M, C and R) is described below:

1. The EEG signal corresponding to each task of a given subject is sampled into half-second segments, yielding 20 segments (signal) per trial per channel.
2. In this way, corresponding to each channel, each of the 20 segments is used to generate the IMFs using EMD algorithms. First 4 IMFs are used for further analysis as it captures enough information to represent the signal.
3. To represent each of these IMFs per segment per channel compactly, eight statistical or uncertainty parameters (QM, Variance, Skewness, Kurtosis, Hurst Exponent [24], Shannon Entropy, Central Frequency, Maximum Frequency) are calculated for a given subject. Some of these parameters represent linear characteristics of the EEG signal, and other represent nonlinear properties of EEG [12, 17, 18]. In this work, the parameters are selected empirically as every signal or data has the distinguishable property regarding a particular set of statistical parameters associated with the signal or data as shown in Fig. 3.
4. Hence, final feature vector obtained after concatenation of features from six channels contains 192 parameters (4 IMFs corresponding to each segment $\times$ 8 parameters corresponding to each IMFs $\times$ 6 channels) for each task labels for a given subject.

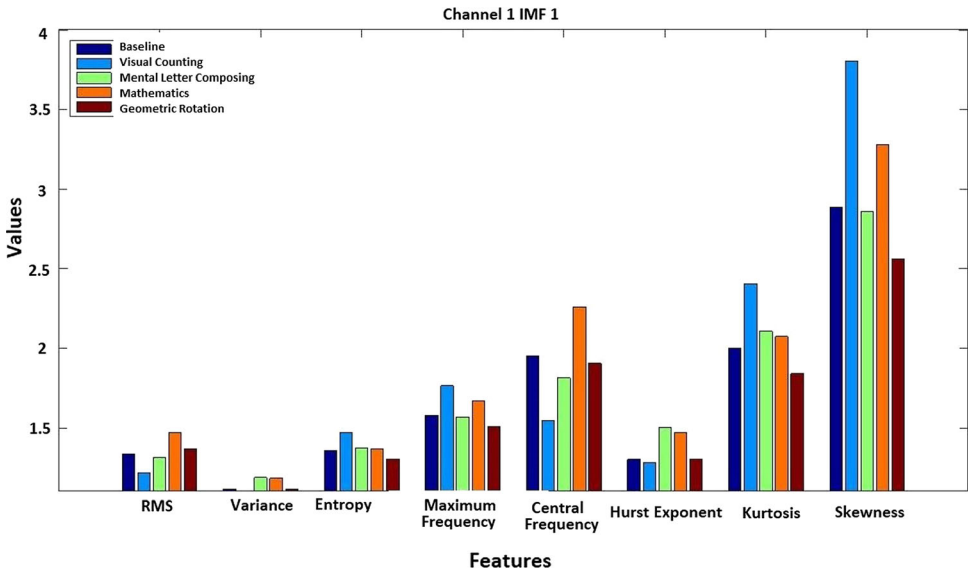

Fig. 3 Eight features obtained corresponding to all five mental tasks for channel 1 from IMF 1 using EEMD method for Subject 1

[1] http://www.cs.colostate.edu/eeg/main/data/1989_Keirn_and_Aunon

Table 2 Comparison table of classification performance for binary mental task classification for Subject 1 and Subject 2

TASKs		Accuracy			Sensitivity			Specificity			Kappa		
		EMD	EEMD	CEEMDAN	EMD	EEMD	CEEMDAN	EMD	EEMD	CEEMDAN	EMD	EEMD	CEEMDAN
Sub1	MR	0.9775	0.9773	0.9818	0.9975	1.0000	0.9985	0.9575	0.9545	0.9650	0.9550	0.9545	0.9635
	BC	0.9233	0.9375	0.9313	0.9560	0.9250	0.9390	0.8905	0.9500	0.9235	0.8465	0.8750	0.8625
	BL	0.8435	0.8648	0.8620	0.8495	0.9010	0.9020	0.8375	0.8285	0.8220	0.6870	0.7295	0.7240
	BM	0.9293	0.9323	0.9225	0.8985	0.9100	0.9010	0.9600	0.9545	0.9440	0.8585	0.8645	0.8450
	BR	0.9678	0.9683	0.9760	0.9885	0.9800	0.9815	0.9470	0.9565	0.9705	0.9355	0.9365	0.9520
	CL	0.6845	0.7130	0.7253	0.8035	0.7905	0.8225	0.5655	0.6355	0.6280	0.3690	0.4270	0.4505
	CM	0.9650	0.9663	0.9703	0.9775	0.9845	0.9885	0.9525	0.9480	0.9520	0.9300	0.9325	0.9405
	CR	0.7465	0.7660	0.7810	0.7120	0.7515	0.7525	0.7810	0.7805	0.8095	0.4930	0.5320	0.5620
	LM	0.9825	0.9825	0.9743	0.9660	0.9680	0.9710	0.9990	0.9970	0.9775	0.9650	0.9650	0.9485
	LR	0.8698	0.8700	0.8748	0.8695	0.8700	0.8780	0.8700	0.8700	0.8715	0.7395	0.7400	0.7495
Sub2	MR	0.8835	0.9015	0.9060	0.9040	0.9480	0.9610	0.8630	0.8550	0.8510	0.7670	0.8030	0.8120
	BC	0.7774	0.9085	0.9005	0.7620	0.9280	0.9180	0.7944	0.8890	0.8830	0.5549	0.8170	0.8010
	BL	0.6585	0.7155	0.7130	0.6250	0.7640	0.7320	0.6920	0.6670	0.6940	0.3302	0.4310	0.4279
	BM	0.8740	0.8895	0.9050	0.8610	0.8870	0.9190	0.8870	0.8920	0.8910	0.7480	0.7790	0.8100
	BR	0.9835	0.9820	0.9920	0.9950	0.9900	0.9980	0.9720	0.9740	0.9860	0.9670	0.9640	0.9840
	CL	0.7779	0.8850	0.8380	0.7766	0.9080	0.8170	0.7798	0.8620	0.8590	0.5555	0.7700	0.6760
	CM	0.8305	0.8690	0.8720	0.8338	0.8570	0.8600	0.8269	0.8810	0.8840	0.6617	0.7380	0.7440
	CR	0.9021	0.9535	0.9515	0.9072	0.9680	0.9450	0.8964	0.9390	0.9580	0.8034	0.9070	0.9030
	LM	0.9215	0.9430	0.9345	0.9290	0.9480	0.9600	0.9140	0.9380	0.9090	0.8430	0.8860	0.8690
	LR	0.9765	0.9895	0.9970	0.9990	1.0000	1.0000	0.9540	0.9790	0.9940	0.9530	0.9790	0.9940

Table 3 Comparison table of classification performance for binary mental task classification for Subject 3 and Subject 5

TASKs		Accuracy			Sensitivity			Specificity			Kappa		
		EMD	EEMD	CEEMDAN	EMD	EEMD	CEEMDAN	EMD	EEMD	CEEMDAN	EMD	EEMD	CEEMDAN
Sub3	MR	0.6750	0.6258	0.6450	0.6800	0.6500	0.6810	0.6700	0.6015	0.6090	0.3500	0.2561	0.2910
	BC	0.7235	0.7233	0.7273	0.7795	0.7625	0.7265	0.6675	0.6840	0.7280	0.4470	0.4465	0.4545
	BL	0.7750	0.7953	0.7893	0.8000	0.7865	0.7635	0.7500	0.8040	0.8150	0.5500	0.5905	0.5785
	BM	0.7645	0.8033	0.8063	0.7260	0.7745	0.7630	0.8030	0.8320	0.8495	0.5290	0.6065	0.6125
	BR	0.6605	0.6870	0.6773	0.7040	0.6740	0.6020	0.6170	0.7000	0.7525	0.3210	0.3740	0.3545
	CL	0.8415	0.8503	0.8523	0.8020	0.8395	0.8115	0.8810	0.8610	0.8930	0.6830	0.7005	0.7045
	CM	0.6685	0.6563	0.6763	0.6400	0.6025	0.6420	0.6970	0.7100	0.7105	0.3370	0.3144	0.3525
	CR	0.5835	0.6060	0.6170	0.5380	0.5560	0.5460	0.6290	0.6560	0.6880	0.1830	0.2206	0.2360
	LM	0.8158	0.8288	0.8138	0.8370	0.8525	0.8445	0.7945	0.8050	0.7830	0.6315	0.6575	0.6275
	LR	0.7560	0.7750	0.7383	0.8115	0.8470	0.8535	0.7005	0.7030	0.6230	0.5120	0.5500	0.4765
Sub5	MR	0.7940	0.8020	0.8138	0.8023	0.8343	0.8550	0.7857	0.7697	0.7727	0.5880	0.6040	0.6277
	BC	0.6520	0.9743	0.6738	0.6577	0.9687	0.7350	0.6463	0.9800	0.6127	0.3040	0.9487	0.3477
	BL	0.7057	0.9638	0.7277	0.7133	0.9537	0.7227	0.6980	0.9740	0.7327	0.4113	0.9277	0.4553
	BM	0.7085	0.9717	0.7355	0.7280	0.9643	0.7857	0.6890	0.9790	0.6853	0.4170	0.9433	0.4710
	BR	0.7592	0.9688	0.7813	0.7307	0.9567	0.7647	0.7877	0.9810	0.7980	0.5183	0.9377	0.5627
	CL	0.7155	0.7420	0.7588	0.7500	0.7717	0.7590	0.6810	0.7123	0.7587	0.4310	0.4840	0.5177
	CM	0.6557	0.6550	0.6877	0.6993	0.6927	0.6987	0.6120	0.6173	0.6767	0.3113	0.3100	0.3753
	CR	0.7878	0.7905	0.8053	0.8200	0.8530	0.8477	0.7557	0.7280	0.7630	0.5757	0.5810	0.6107
	LM	0.6955	0.6760	0.7083	0.6760	0.6863	0.6580	0.7150	0.6657	0.7587	0.3910	0.3527	0.4167
	LR	0.8790	0.8862	0.8817	0.9157	0.9407	0.9300	0.8423	0.8317	0.8333	0.7580	0.7723	0.7633

4.3 Result

The performance of the EMD and its variant has been evaluated in terms of various classification performance measures such as accuracy, sensitivity, specificity and kappa statistics, achieved by the SVM classifier with one versus all approach. Grid search is used to find optimal choice of regularization parameters. To check the efficacy of the proposed method, we have formulated three type of multi-mental task classification problems, viz. three class, four class, and five class as well as binary mental task classification.

Binary class problem

We have used binary combination of these tasks as BC, BL, BM, BR, CL, CM, CR, LM, LR and MR in this work.

Three-class problem

In this problem, we have formed three-class mental tasks problems by choosing three different mental tasks at a time from given five mental tasks. There are ten different triplet mental task combinations for forming three-class problem given as BCL, BCM, BCR, BLM, BLR, BMR, CLM, CLR, CMR and LMR.

Four class problem

Construction of four mental task classification problem has been done by choosing four tasks at a time from the given five tasks. There are five different four class problems namely BCLM, BCLR, BCMR, BLMR and CLMR.

Five-class problem

For the formation of the five mental task classification problem, we have taken all five mental tasks at a time. Thus, we have the five-class mental tasks classification problem as BCLMR.

Tables 2, 3, 4 show classification performance for binary mental task for all subjects. Similarly from Tables 5, 6, 7 for three class, Tables 8, 9 for four class and Table 10 for five-class mental task classification problem. From these tables, we can observe following:

- For binary mental task classification problem, majority of tasks combination on the ground of accuracy parameter CEEMDAN outperforms among three chosen algorithms for Subject 1, Subject 3,and Subject 6 and EEMD performs best among three algorithms for Subject 7, and EEMD and CEEMDAN equally perform for Subject 2, and Subject 5.
- The performance of EEMD is the best among three algorithms for Subject 3, Subject 5, Subject 7 and CEEMDAN performs best for Subject 1, Subject 2 and the performance of both EEMD and CEEMDAN is same for Subject 5, on the basis of sensitivity parameter for the binary mental task classification problem.

Table 4 Comparison table of classification for binary mental task classification for Subject 6 and Subject 7

TASKs		Accuracy			Sensitivity			Specificity			Kappa		
		EMD	EEMD	CEEMDAN	EMD	EEMD	CEEMDAN	EMD	EEMD	CEEMDAN	EMD	EEMD	CEEMDAN
Sub6	MR	0.8455	0.8773	0.8880	0.8895	0.8845	0.8785	0.8015	0.8700	0.8975	0.6910	0.7545	0.7760
	BC	0.8680	0.8985	0.9063	0.8895	0.9135	0.9250	0.8465	0.8835	0.8875	0.7360	0.7970	0.8125
	BL	0.6733	0.7103	0.7310	0.7785	0.7695	0.7345	0.5680	0.6510	0.7275	0.3465	0.4205	0.4620
	BM	0.8925	0.9423	0.9435	0.8840	0.9525	0.9485	0.9010	0.9320	0.9385	0.7850	0.8845	0.8870
	BR	0.8860	0.9398	0.9408	0.9080	0.9665	0.9605	0.8640	0.9130	0.9210	0.7720	0.8795	0.8815
	CL	0.7803	0.8245	0.8503	0.8110	0.8425	0.8630	0.7495	0.8065	0.8375	0.5605	0.6490	0.7005
	CM	0.9878	0.9943	0.9968	0.9875	0.9935	0.9950	0.9880	0.9950	0.9985	0.9755	0.9885	0.9935
	CR	0.8718	0.9200	0.9058	0.8990	0.9325	0.9145	0.8445	0.9075	0.8970	0.7435	0.8400	0.8115
	LM	0.8725	0.9175	0.9210	0.8400	0.9230	0.9110	0.9050	0.9120	0.9310	0.7450	0.8350	0.8420
	LR	0.8113	0.8903	0.8995	0.7970	0.8715	0.8830	0.8255	0.9090	0.9160	0.6225	0.7805	0.7990
Sub7	MR	0.8225	0.8750	0.8430	0.7760	0.8520	0.8090	0.8690	0.8980	0.8770	0.6450	0.7500	0.6860
	BC	0.8447	0.9165	0.8830	0.8490	0.9080	0.8410	0.8400	0.9250	0.9250	0.6889	0.8330	0.7660
	BL	0.7700	0.8270	0.8100	0.8320	0.8900	0.8700	0.7080	0.7640	0.7500	0.5400	0.6540	0.6200
	BM	0.9210	0.9680	0.9190	0.9080	0.9910	0.9100	0.9340	0.9450	0.9280	0.8420	0.9360	0.8380
	BR	0.9905	0.9880	0.9825	0.9960	1.0000	0.9950	0.9850	0.9760	0.9700	0.9810	0.9760	0.9650
	CL	0.9216	0.9190	0.9140	0.9566	0.9820	0.9970	0.8848	0.8560	0.8310	0.8424	0.8380	0.8280
	CM	0.9326	0.9640	0.9530	0.9427	0.9630	0.9370	0.9220	0.9650	0.9690	0.8648	0.9280	0.9060
	CR	0.9932	0.9855	0.9850	1.0000	0.9910	1.0000	0.9861	0.9800	0.9700	0.9863	0.9710	0.9700
	LM	0.9895	0.9830	0.9875	0.9950	0.9770	0.9800	0.9840	0.9890	0.9950	0.9790	0.9660	0.9750
	LR	0.9945	1.0000	0.9950	0.9990	1.0000	1.0000	0.9900	1.0000	0.9900	0.9890	1.0000	0.9900

Table 5 Comparison table of classification for three class mental task classification for Subject 1 and Subject 2

TASKs		Accuracy			Sensitivity			Specificity			Kappa		
		EMD	EEMD	CEEMDAN	EMD	EEMD	CEEMDAN	EMD	EEMD	CEEMDAN	EMD	EEMD	CEEMDAN
Sub1	LMR	0.8792	0.8832	0.8832	0.8792	0.8832	0.8832	0.9396	0.9416	0.9416	0.7281	0.7371	0.7371
	BCL	0.6167	0.6515	0.6458	0.6167	0.6515	0.6458	0.8083	0.8258	0.8229	0.1512	0.2192	0.2063
	BCM	0.8738	0.8775	0.8663	0.8738	0.8775	0.8663	0.9369	0.9388	0.9332	0.7161	0.7244	0.6993
	BCR	0.7682	0.8070	0.8090	0.7682	0.8070	0.8090	0.8841	0.9035	0.9045	0.4784	0.5658	0.5703
	BLM	0.8122	0.8405	0.8342	0.8122	0.8405	0.8342	0.9061	0.9203	0.9171	0.5774	0.6411	0.6269
	BLR	0.7467	0.7785	0.7763	0.7467	0.7785	0.7763	0.8733	0.8893	0.8882	0.4300	0.5016	0.4968
	BMR	0.9253	0.9300	0.9260	0.9253	0.9300	0.9260	0.9627	0.9650	0.9630	0.8320	0.8425	0.8335
	CLM	0.7500	0.7778	0.7762	0.7500	0.7778	0.7762	0.8750	0.8889	0.8881	0.4375	0.5001	0.4964
	CLR	0.6225	0.6665	0.6642	0.6225	0.6665	0.6642	0.8113	0.8333	0.8321	0.1630	0.2522	0.2466
	CMR	0.8007	0.8265	0.8332	0.8007	0.8265	0.8332	0.9003	0.9133	0.9166	0.5515	0.6096	0.6246
Sub2	LMR	0.8407	0.8837	0.8770	0.8407	0.8837	0.8770	0.9203	0.9418	0.9385	0.6415	0.7383	0.7233
	BCL	0.5934	0.6857	0.6777	0.5923	0.6857	0.6777	0.7965	0.8428	0.8388	0.1535	0.3030	0.2876
	BCM	0.7241	0.8230	0.8287	0.7276	0.8230	0.8287	0.8628	0.9115	0.9143	0.3829	0.6018	0.6145
	BCR	0.7421	0.8363	0.8120	0.7469	0.8363	0.8120	0.8707	0.9182	0.9060	0.4215	0.6318	0.5770
	BLM	0.6687	0.6827	0.6867	0.6687	0.6827	0.6867	0.8343	0.8413	0.8433	0.2657	0.2940	0.3030
	BLR	0.7117	0.7607	0.7500	0.7117	0.7607	0.7500	0.8558	0.8803	0.8750	0.3536	0.4615	0.4375
	BMR	0.8290	0.8317	0.8597	0.8290	0.8317	0.8597	0.9145	0.9158	0.9298	0.6153	0.6213	0.6843
	CLM	0.7403	0.8127	0.7873	0.7437	0.8127	0.7873	0.8702	0.9063	0.8937	0.4158	0.5785	0.5215
	CLR	0.7383	0.8153	0.7630	0.7440	0.8153	0.7630	0.8691	0.9077	0.8815	0.4111	0.5845	0.4668
	CMR	0.7945	0.8187	0.8490	0.7969	0.8187	0.8490	0.8969	0.9093	0.9245	0.5392	0.5920	0.6603

Table 6 Comparison table of classification for three class mental task classification for Subject 3 and Subject 5

TASKs		Accuracy			Sensitivity			Specificity			Kappa		
		EMD	EEMD	CEEMDAN	EMD	EEMD	CEEMDAN	EMD	EEMD	CEEMDAN	EMD	EEMD	CEE MDAN
Sub3	LMR	0.6015	0.5818	0.5752	0.6015	0.5818	0.5752	0.8008	0.7909	0.7876	0.1304	0.0987	0.1080
	BCL	0.6672	0.6917	0.6938	0.6672	0.6917	0.6938	0.8336	0.8458	0.8469	0.2542	0.3067	0.3111
	BCM	0.5680	0.5798	0.5827	0.5680	0.5798	0.5827	0.7840	0.7899	0.7913	0.1149	0.1133	0.1171
	BCR	0.5105	0.5393	0.5265	0.5105	0.5393	0.5265	0.7553	0.7697	0.7633	0.1182	0.0994	0.0913
	BLM	0.6687	0.7107	0.6995	0.6687	0.7107	0.6995	0.8343	0.8553	0.8498	0.2571	0.3490	0.3249
	BLR	0.6198	0.6498	0.6445	0.6198	0.6498	0.6445	0.8099	0.8249	0.8223	0.1604	0.2197	0.2057
	BMR	0.5607	0.5618	0.5718	0.5607	0.5618	0.5718	0.7803	0.7809	0.7859	0.0963	0.0983	0.1016
	CLM	0.6260	0.6250	0.6213	0.6260	0.6250	0.6213	0.8130	0.8125	0.8107	0.1720	0.1744	0.1669
	CLR	0.5662	0.5957	0.5885	0.5662	0.5957	0.5885	0.7831	0.7978	0.7943	0.0897	0.1259	0.1026
	CMR	0.4907	0.4688	0.4927	0.4907	0.4688	0.4927	0.7453	0.7344	0.7463	0.1388	0.1696	0.1339
Sub5	LMR	0.6461	0.6374	0.6589	0.6461	0.6374	0.6589	0.8231	0.8187	0.8294	0.2070	0.1852	0.2325
	BCL	0.5497	0.7792	0.5452	0.5497	0.7792	0.5452	0.7748	0.8896	0.7726	0.0828	0.5033	0.0812
	BCM	0.5216	0.7376	0.5341	0.5216	0.7376	0.5341	0.7608	0.8688	0.7671	0.0880	0.4095	0.0861
	BCR	0.5934	0.8251	0.6132	0.5934	0.8251	0.6132	0.7967	0.9126	0.8066	0.1033	0.6065	0.1413
	BLM	0.5383	0.7622	0.5497	0.5383	0.7622	0.5497	0.7692	0.8811	0.7748	0.0800	0.4650	0.0774
	BLR	0.6620	0.8792	0.6592	0.6620	0.8792	0.6592	0.8310	0.9396	0.8296	0.2419	0.7283	0.2333
	BMR	0.6512	0.8344	0.6713	0.6512	0.8344	0.6713	0.8256	0.9172	0.8357	0.2195	0.6275	0.2610
	CLM	0.5134	0.5166	0.5472	0.5134	0.5166	0.5472	0.7567	0.7583	0.7736	0.1074	0.1003	0.0663
	CLR	0.6503	0.6557	0.6763	0.6503	0.6557	0.6763	0.8252	0.8278	0.8382	0.2171	0.2253	0.2718
	CMR	0.5862	0.5980	0.6036	0.5862	0.5980	0.6036	0.7931	0.7990	0.8018	0.0997	0.1184	0.1177

- As per specificity parameter, CEEMDAN performs best for Subject 2, Subject 3, Subject 6 and EEMD is best for Subject 7, EMD and CEEMDAN equally perform for subject 1, and EEMD and CEEMDAN perform same for Subject 5 for binary mental task classification problem.
- Analysis based on Kappa measure shows that CEEMDAN gives best performance for Subject 1, Subject 3, Subject 6, and EEMD gives best performance for Subject 7, and the equally perform by EEMD and CEEMDAN for Subject 2, Subject 5 for the binary mental task classification problem.
- As per accuracy, sensitivity and specificity parameters concern, EEMD performs best among three algorithms for Subject 1, Subject 2, Subject 5 and Subject 7 for ternary mental task classification. The performance of CEEMDAN is superior or equal than other two algorithms for Subject 3 and Subject 6.
- For the KAPPA parameter, EEMD is best choice among three chosen algorithms for Subject 1, 2, 3, 5 and 7.
- For quaternary mental task classification problem, EEMD achieve highest classification performance among three selected algorithms for Subject 1, 2, 5, and 7, for performance measures accuracy, sensitivity and specificity. It is also observed for these parameters EMD and CEEMD are equally perform for Subject 3.
- For kappa performance measure, the three algorithms compete each other.
- For mental task classification problem with five tasks, EEMD is the best for all performance parameters except kappa measure. EMD is the best choice for kappa measures for five-class mental task classification.

Further average value of performance measures is obtained over all the subject. Tables 11, 12, 13 and 14 show the comparison table of classification performance for binary mental task classification, three-class mental task classification, four class mental task classification and five-class mental task classification over all the subjects, respectively. It can be noted from these tables that the EEMD method performed well in comparison with EMD and CEEMD methods in terms of aforementioned performance measures except kappa index. CEEMD performs well than other two methods in terms of kappa index for some combinations of the tasks for the different type of class combinations of the mental task.

4.4 Comparison of the proposed model for multi-mental task classification problem

In this subsection, we have discussed and compared the proposed approach with the work of [45] for multi-mental task classification in Table 15.

Table 7 Comparison table of classification for three class mental task classification for Subject 6 and Subject 7

TASKs		Accuracy			Sensitivity			Specificity			Kappa		
		EMD	EEMD	CEEMDAN	EMD	EEMD	CEEMDAN	EMD	EEMD	CEEMDAN	EMD	EEMD	CEEMDAN
Sub6	LMR	0.7212	0.8160	0.8288	0.7212	0.8160	0.8288	0.8606	0.9080	0.9144	0.3729	0.5860	0.6149
	BCL	0.6435	0.6920	0.6930	0.6435	0.6920	0.6930	0.8218	0.8460	0.8465	0.2013	0.3070	0.3093
	BCM	0.8202	0.8788	0.8722	0.8202	0.8788	0.8722	0.9101	0.9394	0.9361	0.5954	0.7274	0.7124
	BCR	0.7630	0.8362	0.8435	0.7630	0.8362	0.8435	0.8815	0.9181	0.9218	0.4668	0.6314	0.6479
	BLM	0.6672	0.7572	0.7630	0.6672	0.7572	0.7630	0.8336	0.8786	0.8815	0.2561	0.4536	0.4668
	BLR	0.6628	0.7328	0.7283	0.6628	0.7328	0.7283	0.8314	0.8664	0.8642	0.2489	0.3989	0.3888
	BMR	0.7632	0.8515	0.8453	0.7632	0.8515	0.8453	0.8816	0.9258	0.9227	0.4671	0.6659	0.6520
	CLM	0.7500	0.8162	0.8230	0.7500	0.8162	0.8230	0.8750	0.9081	0.9115	0.4375	0.5864	0.6018
	CLR	0.7102	0.8047	0.7957	0.7102	0.8047	0.7957	0.8551	0.9023	0.8978	0.3479	0.5605	0.5403
	CMR	0.7867	0.8602	0.8575	0.7867	0.8602	0.8575	0.8933	0.9301	0.9288	0.5200	0.6854	0.6794
Sub7	LMR	0.8383	0.8600	0.8523	0.8383	0.8600	0.8523	0.9192	0.9300	0.9262	0.6363	0.6850	0.6678
	BCL	0.7024	0.7850	0.7750	0.7070	0.7850	0.7750	0.8518	0.8925	0.8875	0.3323	0.5163	0.4947
	BCM	0.8341	0.8800	0.8493	0.8368	0.8800	0.8493	0.9171	0.9400	0.9247	0.6268	0.7300	0.6610
	BCR	0.8348	0.9017	0.8853	0.8385	0.9017	0.8853	0.9162	0.9508	0.9427	0.6284	0.7788	0.7420
	BLM	0.7863	0.8347	0.8293	0.7863	0.8347	0.8293	0.8932	0.9173	0.9147	0.5193	0.6280	0.6160
	BLR	0.8253	0.8547	0.8743	0.8253	0.8547	0.8743	0.9127	0.9273	0.9372	0.6070	0.6730	0.7173
	BMR	0.8097	0.8410	0.8033	0.8097	0.8410	0.8033	0.9048	0.9205	0.9017	0.5718	0.6423	0.5575
	CLM	0.8600	0.9200	0.8937	0.8624	0.9200	0.8937	0.9300	0.9600	0.9468	0.6850	0.8200	0.7608
	CLR	0.8683	0.9080	0.9063	0.8714	0.9080	0.9063	0.9335	0.9540	0.9532	0.7036	0.7930	0.7893
	CMR	0.8093	0.8603	0.8543	0.8127	0.8603	0.8543	0.9054	0.9302	0.9272	0.5709	0.6858	0.6723

Table 8 Comparison table of classification for four class mental task classification for Subject 1 Subject and Subject 3

TASKs		Accuracy			Sensitivity			Specificity			Kappa		
		EMD	EEMD	CEEMDAN	EMD	EEMD	CEEMDAN	EMD	EEMD	CEEMDAN	EMD	EEMD	CEEMDAN
sub1	BCLM	0.6503	0.6954	0.6763	0.6503	0.6954	0.6763	0.8834	0.8985	0.8921	0.1076	0.1922	0.1469
	BCLR	0.6680	0.7140	0.6923	0.6680	0.7140	0.6923	0.8893	0.9047	0.8974	0.1319	0.2398	0.1913
	BCMR	0.7496	0.7736	0.7748	0.7496	0.7736	0.7748	0.9165	0.9245	0.9249	0.3323	0.3963	0.3993
	BLMR	0.7648	0.7860	0.7805	0.7648	0.7860	0.7805	0.9216	0.9287	0.9268	0.3727	0.4293	0.4147
	CLMR	0.5650	0.6166	0.6055	0.5650	0.6166	0.6055	0.8550	0.8722	0.8685	0.1385	0.0912	0.0876
sub2	BCLM	0.5728	0.6505	0.6373	0.5796	0.6505	0.6373	0.8580	0.8835	0.8791	0.1540	0.1391	0.1519
	BCLR	0.6821	0.7595	0.7413	0.6868	0.7595	0.7413	0.8943	0.9198	0.9138	0.1779	0.3587	0.3100
	BCMR	0.6508	0.6873	0.6970	0.6508	0.6873	0.6970	0.8836	0.8958	0.8990	0.1360	0.2084	0.2289
	BLMR	0.6772	0.7580	0.7690	0.6824	0.7580	0.7690	0.8925	0.9193	0.9230	0.1777	0.3547	0.3840
	CLMR	0.5859	0.6560	0.6425	0.5942	0.6560	0.6425	0.8619	0.8853	0.8808	0.1325	0.1379	0.1313
sub3	BCLM	0.5518	0.5711	0.5536	0.5518	0.5711	0.5536	0.8506	0.8570	0.8512	0.1604	0.1349	0.1564
	BCLR	0.4819	0.4685	0.4791	0.4819	0.4685	0.4791	0.8273	0.8228	0.8264	0.2696	0.2884	0.2730
	BCMR	0.5336	0.5425	0.5448	0.5336	0.5425	0.5448	0.8445	0.8475	0.8483	0.1939	0.1748	0.1717
	BLMR	0.4576	0.4516	0.4564	0.4576	0.4516	0.4564	0.8192	0.8172	0.8188	0.3026	0.3115	0.3049
	CLMR	0.4864	0.5276	0.5300	0.4864	0.5276	0.5300	0.8288	0.8425	0.8433	0.2630	0.1975	0.1969

Table 9 Comparison table of classification performance for four class mental task classification for Subject 5,Subject 6andSubject 7

TASKs		Accuracy			Sensitivity			Specificity			Kappa		
		EMD	EEMD	CEEMDAN	EMD	EEMD	CEEMDAN	EMD	EEMD	CEEMDAN	EMD	EEMD	CEEMDAN
sub5	BCLM	0.4330	0.5968	0.4313	0.4330	0.5968	0.4313	0.8110	0.8656	0.8104	0.3357	0.0829	0.3371
	BCLR	0.4955	0.5051	0.5163	0.4955	0.5051	0.5163	0.8318	0.8350	0.8388	0.2528	0.2364	0.2194
	BCMR	0.5348	0.6925	0.5192	0.5348	0.6925	0.5192	0.8449	0.8975	0.8397	0.1889	0.1818	0.2148
	BLMR	0.4936	0.6499	0.5075	0.4936	0.6499	0.5075	0.8312	0.8833	0.8358	0.2545	0.0882	0.2327
	CLMR	0.5259	0.7013	0.5245	0.5259	0.7013	0.5245	0.8420	0.9004	0.8415	0.2051	0.2033	0.2091
sub6	BCLM	0.6300	0.7108	0.7066	0.6300	0.7108	0.7066	0.8767	0.9036	0.9022	0.0678	0.2300	0.2183
	BCLR	0.6446	0.7593	0.7598	0.6446	0.7593	0.7598	0.8815	0.9198	0.9199	0.0942	0.3580	0.3593
	BCMR	0.6095	0.7128	0.7205	0.6095	0.7128	0.7205	0.8698	0.9043	0.9068	0.0982	0.2347	0.2566
	BLMR	0.7101	0.7900	0.7916	0.7101	0.7900	0.7916	0.9034	0.9300	0.9305	0.2270	0.4400	0.4443
	CLMR	0.6090	0.6840	0.6728	0.6090	0.6840	0.6728	0.8697	0.8947	0.8909	0.0936	0.1701	0.1474
sub7	BCLM	0.7092	0.7855	0.7490	0.7149	0.7855	0.7490	0.9031	0.9285	0.9163	0.2383	0.4280	0.3429
	BCLR	0.7697	0.8363	0.8098	0.7741	0.8363	0.8098	0.9237	0.9454	0.9366	0.3870	0.5633	0.4927
	BCMR	0.7200	0.7820	0.7653	0.7200	0.7820	0.7653	0.9067	0.9273	0.9218	0.2598	0.4187	0.3740
	BLMR	0.7464	0.7970	0.7665	0.7508	0.7970	0.7665	0.9158	0.9323	0.9222	0.3271	0.4587	0.3786
	CLMR	0.7113	0.8053	0.7940	0.7171	0.8053	0.7940	0.9034	0.9351	0.9313	0.2454	0.4807	0.4507

Table 10 Comparison table of classification performance for five-class mental task classification for all subjects

	Accuracy			Sensitivity			Specificity			Kappa		
	EMD	EEMD	CEEMDAN	EMD	EEMD	CEEMDAN	EMD	EEMD	CEEMDAN	EMD	EEMD	CEEMDAN
Sub1	0.5960	0.6523	0.6385	0.5960	0.6523	0.6385	0.8990	0.9131	0.9096	0.2046	0.1112	0.1211
Sub2	0.5671	0.6300	0.6292	0.5732	0.6300	0.6292	0.8919	0.9075	0.9073	0.2497	0.1649	0.1485
Sub3	0.4453	0.4469	0.4693	0.4453	0.4469	0.4693	0.8613	0.8617	0.8673	0.4192	0.4172	0.3933
Sub5	0.4795	0.6204	0.4845	0.4072	0.5396	0.4194	0.8579	0.8943	0.8598	0.3830	0.1530	0.3762
Sub6	0.5747	0.6747	0.6781	0.5747	0.6747	0.6781	0.8937	0.9187	0.9195	0.2409	0.0864	0.0841
Sub7	0.6641	0.7426	0.7140	0.6696	0.7426	0.7140	0.9161	0.9356	0.9285	0.1333	0.2202	0.1658

Table 11 Comparison table of classification performance for binary mental task classification over all the subjects

Tasks	Accuracy			Sensitivity			Specificity			Kappa		
	EMD	EEMD	CEEMD	EMD	EEMD	CEEMD	EMD	EEMD	CEEMD	EMD	EEMD	CEEMD
MR	0.8330	0.8431	0.8463	0.8416	0.8615	0.8638	0.8244	0.8248	0.8287	0.6660	0.6870	0.6927
BC	0.7981	0.8931	0.8370	0.8156	0.9009	0.8474	0.7809	0.8853	0.8266	0.5962	0.7862	0.6740
BL	0.7377	0.8128	0.7722	0.7664	0.8441	0.7874	0.7089	0.7814	0.7569	0.4775	0.6255	0.5446
BM	0.8483	0.9178	0.8720	0.8343	0.9132	0.8712	0.8623	0.9224	0.8727	0.6966	0.8356	0.7439
BR	0.8746	0.9223	0.8916	0.8870	0.9279	0.8836	0.8621	0.9168	0.8997	0.7491	0.8446	0.7833
CL	0.7869	0.8223	0.8231	0.8166	0.8557	0.8450	0.7569	0.7889	0.8012	0.5736	0.6447	0.6462
CM	0.8400	0.8508	0.8593	0.8468	0.8489	0.8535	0.8331	0.8527	0.8651	0.6800	0.7019	0.7186
CR	0.8141	0.8369	0.8409	0.8127	0.8420	0.8343	0.8155	0.8318	0.8476	0.6308	0.6753	0.6822
LM	0.8795	0.8885	0.8899	0.8738	0.8925	0.8874	0.8853	0.8844	0.8924	0.7591	0.7770	0.7798
LR	0.8812	0.9018	0.8977	0.8986	0.9215	0.9241	0.8637	0.8821	0.8713	0.7623	0.8036	0.7954

Table 12 Comparison table of classification performance for three-class mental task classification over all the subjects

Tasks	Accuracy			Sensitivity			Specificity			Kappa		
	EMD	EEMD	CEEMD	EMD	EEMD	CEEMD	EMD	EEMD	CEEMD	EMD	EEMD	CEEMD
LMR	0.7545	0.7770	0.7792	0.7545	0.7770	0.7792	0.8772	0.8885	0.8896	0.4527	0.5050	0.5139
BCL	0.6288	0.7142	0.6718	0.6294	0.7142	0.6718	0.8145	0.8571	0.8359	0.1959	0.3592	0.2817
BCM	0.7236	0.7961	0.7555	0.7247	0.7961	0.7555	0.8619	0.8981	0.8778	0.4207	0.5510	0.4817
BCR	0.7020	0.7909	0.7483	0.7034	0.7909	0.7483	0.8507	0.8955	0.8741	0.3694	0.5523	0.4616
BLM	0.6902	0.7646	0.7271	0.6902	0.7646	0.7271	0.8451	0.8823	0.8635	0.3259	0.4718	0.4025
BLR	0.7047	0.7760	0.7388	0.7047	0.7760	0.7388	0.8524	0.8880	0.8694	0.3403	0.4972	0.4132
BMR	0.7565	0.8084	0.7796	0.7565	0.8084	0.7796	0.8783	0.9042	0.8898	0.4670	0.5830	0.5150
CLM	0.7066	0.7447	0.7415	0.7076	0.7447	0.7415	0.8533	0.8724	0.8707	0.3759	0.4600	0.4356
CLR	0.6926	0.7410	0.7323	0.6941	0.7410	0.7323	0.8462	0.8705	0.8662	0.3221	0.4236	0.4029
CMR	0.7113	0.7388	0.7484	0.7123	0.7388	0.7484	0.8557	0.8694	0.8742	0.4034	0.4768	0.4814

In Table 15, methods A, B and C are the schemes used by [45] based on asymmetry ratio for calculation of a different number of frequency band powers using 75-dimensional, 90-dimensional and the 42-dimensional feature vector, respectively. From this Table, it is clear that our approach for creating features vectors outperforms regarding average classification accuracy for all the three subjects for all the multi-mental tasks classification problem.

Table 13 Comparison table of classification performance for four class mental task classification over all the subjects

Tasks	Accuracy			Sensitivity			Specificity			Kappa		
	EMD	EEMD	CEEMD	EMD	EEMD	CEEMD	EMD	EEMD	CEEMD	EMD	EEMD	CEEMD
BCLM	0.5912	0.6683	0.6257	0.5933	0.6683	0.6257	0.8638	0.8894	0.8752	0.1773	0.2012	0.2256
BCLR	0.6236	0.6738	0.6664	0.6251	0.6738	0.6664	0.8747	0.8913	0.8888	0.2189	0.3408	0.3076
BCMR	0.6331	0.6984	0.6702	0.6331	0.6984	0.6702	0.8777	0.8995	0.8901	0.2015	0.2691	0.2742
BLMR	0.6416	0.7054	0.6786	0.6432	0.7054	0.6786	0.8806	0.9018	0.8929	0.2769	0.3471	0.3599
CLMR	0.5806	0.6651	0.6282	0.5829	0.6651	0.6282	0.8601	0.8884	0.8761	0.1797	0.2134	0.2038

Table 14 Comparison table of classification performance for five-class mental task classification over all the subjects

Tasks	Accuracy			Sensitivity			Specificity			Kappa		
	EMD	EEMD	CEEMD	EMD	EEMD	CEEMD	EMD	EEMD	CEEMD	EMD	EEMD	CEEMD
BCLMR	0.5544	0.6278	0.6023	0.5443	0.6144	0.5914	0.8867	0.9052	0.8987	0.2718	0.1922	0.2148

Table 15 Comparison table of classification accuracy achieved for multi-mental task classification of the work of [45] with proposed approach

	Two-class classification			Three-class classification			Four-class classification			Five-class classification		
	A	B	C	A	B	C	A	B	C	A	B	C
S1	77.60	**85.90**	83.80	63.90	**75.30**	70.90	54.40	**66.60**	60.50	47.60	**60.40**	55.40
S2	62.90	**67.50**	66.20	46.50	**53.80**	47.90	37.90	**45.40**	38.30	31.90	**39.90**	33.60
S3	69.40	**72.50**	71.50	54.10	**59.40**	57.00	45.30	**52.10**	49.80	39.30	**46.30**	43.70
	Scheme1	Scheme2	Scheme3	Scheme1	Scheme2	Scheme3	Scheme1	Scheme2	Scheme3	Scheme1	Scheme2	Scheme3
S1	**88.90**	**89.78**	**89.99**	77.95	**80.39**	80.14	67.95	**71.71**	70.59	59.60	**65.23**	63.85
S2	85.85	**90.37**	90.10	73.83	**79.50**	78.91	63.37	**70.23**	69.74	56.71	**63.00**	62.92
S3	72.64	**73.51**	73.43	58.79	**60.05**	59.97	50.23	51.23	**51.28**	44.53	44.69	**46.93**

The bold value indicates the best classification accuracy among the three schemes for subjects S1, S2, and S3. A, B, and C are the proposed schemes in [45], whereas Scheme 1 (EMD), Scheme 2 (EEMD), and Scheme 3 (CEEMD) are the proposed schemes in this paper

Table 16 Average Rankings of the algorithms

Algorithm	Ranking			
Method	Binary class	Three class	Four class	Five class
EMD	3.00	3.00	3.00	2.93
EEMD	**1.03**	**1.01**	**1.03**	**1.17**
CEEMDAN	1.97	1.99	1.97	1.90

The bold value indicates the highest average Friedman ranking among the three proposed schemes in this paper, lowest value denotes the highest

4.5 Discussion

Since EEG signal has nonlinear and non-stationary property, thus there is a need for an algorithm which can capture such properties of the signal. EMD is such an algorithm which can capture tempo-spectral information of the signal. After decomposing the signal into high- and low-frequency components, it is important to extract some statistical and uncertainty parameters from this decomposed signal for compact representation regarding features which can help in differentiating one mental state to another. Also, there is two improved version of EMD algorithm named as EEMD and CEEMDAN algorithm, which can capture tempo-spectral information even from noise assisted signal.

4.6 Statistical test

We have utilized a two-way, nonparametric statistical test known as Friedman test [10, 16] to find out the significant difference among these three EMD methods for EEG signal. Table 16 shows the average Friedman ranking of the methods for different combination of metal tasks classification problem, which shows that EEMD method outperforms among three methods for all the possible metal tasks classification problem.

Table 17 Adjusted p-values

Class combinations	Algorithm	unadjusted p	p_{Bonf}	p_{Holm}	p_{Hoch}	p_{Homm}
Binary class	EMD	4.16E-44	8.33E-44	8.33E-44	8.33E-44	8.33E-44
	CEEMDAN	2.99E-11	5.99E-11	2.99E-11	2.99E-11	2.99E-11
Three class	EMD	5.69E-45	1.14E-44	1.14E-44	1.14E-44	1.14E-44
	CEEMDAN	4.22E-12	8.44E-12	4.22E-12	4.22E-12	4.22E-12
Four class	EMD	4.16E-44	8.33E-44	8.33E-44	8.33E-44	8.33E-44
	CEEMDAN	2.99E-11	5.99E-11	2.99E-11	2.99E-11	2.99E-11
Five class	EMD	1.49E-35	2.97E-35	2.97E-35	2.97E-35	2.97E-35
	CEEMDAN	2.44E-7	4.89E-7	2.44E-7	2.44E-7	2.44E-7

The performance of different EMD methods (in this work) is studied to control method, i.e., best performer from the Friedman's ranking (which is EEMD). The test statistics for the comparison of m^{th} method to n^{th} method, z, is given as

$$z = \frac{R_m - R_n}{\sqrt{\frac{k(k+1)}{6N}}} \tag{8}$$

where R_m and R_n are the average ranking of the methods, k and N are the number of methods (algorithms) and experiments, respectively. However, these p values so obtained are not suitable for comparison with the control method. Instead, adjusted p values [10] are computed which take into account the error accumulated and provide the correct correlation. For this, a set of post hoc procedures is defined and adjusted p values are computed. For pair-wise comparisons, the widely used post hoc methods to obtain adjusted p values are [10]: Bonferroni–Dunn, Holm, Hochberg and Hommel procedures. Table 17 shows the various value of adjusted p values obtained from methods mentioned above. From this Table, it is clear that there is a statistical difference between EEMD and other two methods.

5 Conclusion

Classification of electroencephalograph (EEG) signal for designing brain–computer interface systems requires detailed analysis of the signal, i.e., intrinsic properties related to the signal such as temporal-spectral virtue of a signal. This work has presented a comprehensive study of the three variants of empirical mode decomposition (EMD) algorithms to find intrinsic characteristics of the EEG signal for mental task classification problem. EMD and its variants are very useful for extracting the EEG signal's intrinsic properties, as these algorithms can capture non-stationary and nonlinear properties of the signal. After decomposing the signal through the EMDs algorithms, 8 parameters, using statistical properties, uncertainty virtues and structural relationship of the decomposed signal, were calculated from each segment of the decomposed signal to form the feature vector from the signal for further classification. For developing the classification model from the extracted features, we have utilized support vector machine (SVM) and several performance measures are utilized to validate the model on test sets for mental task classification problem. Experimental results showed that Ensemble EMD (EEMD) algorithm performs best among the three chosen EMD algorithms as the number of the mental task grows. Further, statistical analysis is also conducted to investigate whether three EMD algorithms were statistically different or not for MTC.

In future work, we would explore more advanced decomposition methods for extracting the efficient features from the EEG signal to improve the classification accuracy for metal task classification problem. Further to reduce the dimensionality, feature selection approaches can be investigated to improve time complexity of learning the MTC classification model. It is also interesting to examine some new set of parameters associated with the signals, which can help distinguish different mental states more accurately. It will also be interesting to see whether deep learning architecture will be suitable for MTC or not.

Acknowledgements This work is the part of the research work [19], digital version of which is available online at biorxiv.org https://www.biorxiv.org/content/early/2017/04/26/076646.

Funding Open Access funding enabled and organized by CAUL and its Member Institutions.

Declarations

Conflict of Interest The authors declare that they have no conflict of interest.

Informed Consent Informed consent was not required, as no humans or animals were involve.

Human and Animal Rights This article does not contain any studies with animals or humans performed by any of the authors.

Open Access This article is licensed under a Creative Commons Attribution 4.0 International License, which permits use, sharing, adaptation, distribution and reproduction in any medium or format, as long as you give appropriate credit to the original author(s) and the source, provide a link to the Creative Commons licence, and indicate if changes were made. The images or other third party material in this article are included in the article's Creative Commons licence, unless indicated otherwise in a credit line to the material. If material is not included in the article's Creative Commons licence and your intended use is not permitted by statutory regulation or exceeds the permitted use, you will need to obtain permission directly from the copyright holder. To view a copy of this licence, visit http://creativecommons.org/licenses/by/4.0/.

References

1. Anderson C, Forney E, Hains D, Natarajan A (2011) Reliable identification of mental tasks using time-embedded eeg and sequential evidence accumulation. J Neural Eng 8(2):025023
2. Andreu-Perez J, Cao F, Hagras H, Yang GZ (2016) A self-adaptive online brain machine interface of a humanoid robot through a general type-2 fuzzy inference system. IEEE Trans Fuzzy Syst 26(1):101–116
3. Bashashati A, Fatourechi M, Ward RK, Birch GE (2007) A survey of signal processing algorithms in brain-computer interfaces based on electrical brain signals. J Neural Eng 4(2):R32
4. Bostanov V (2004) Bci competition 2003-data sets ib and iib: feature extraction from event-related brain potentials with the continuous wavelet transform and the t-value scalogram. Biomed Eng IEEE Trans 51(6):1057–1061
5. Cabrera AF, Farina D, Dremstrup K (2010) Comparison of feature selection and classification methods for a brain-computer interface driven by non-motor imagery. Med and Biol Eng and Comput 48(2):123–132
6. Canolty RT, Knight RT (2010) The functional role of cross-frequency coupling. Trends Cogn Sci 14(11):506–515
7. Chen X, Xu X, Liu A, McKeown MJ, Wang ZJ (2017) The use of multivariate emd and cca for denoising muscle artifacts from few-channel eeg recordings. IEEE Trans Instrum Meas 67(2):359–370
8. Cvetkovic D, Übeyli ED, Cosic I (2008) Wavelet transform feature extraction from human ppg, ecg, and eeg signal responses to elf pemf exposures: a pilot study. Digit Sigl Process 18(5):861–874
9. Daubechies I (1990) The wavelet transform, time-frequency localization and signal analysis. Inform Theory, IEEE Trans 36(5):961–1005
10. Derrac J, García S, Molina D, Herrera F (2011) A practical tutorial on the use of nonparametric statistical tests as a methodology for comparing evolutionary and swarm intelligence algorithms. Swarm Evol Comput 1(1):3–18
11. Diez PF, Mut V, Laciar E, Torres A, Avila E (2009a) Application of the empirical mode decomposition to the extraction of features from eeg signals for mental task classification. In: Engineering in medicine and biology society, 2009. EMBC 2009. Annual international conference of the IEEE, IEEE, pp 2579–2582
12. Diez PF, Torres A, Avila E, Laciar E, Mut V (2009) Classification of mental tasks using different spectral estimation methods. INTECH Open Access Publisher, USA
13. Donoghue JP (2002) Connecting cortex to machines: recent advances in brain interfaces. Nat Neurosci 5:1085–1088
14. Duan L, Bao M, Cui S, Qiao Y, Miao J (2017) Motor imagery eeg classification based on kernel hierarchical extreme learning machine. Cogn Comput 9(6):758–765
15. Faradji F, Ward RK, Birch GE (2009) Plausibility assessment of a 2-state self-paced mental task-based bci using the no-control performance analysis. J Neurosci Method 180(2):330–339
16. Friedman M (1937) The use of ranks to avoid the assumption of normality implicit in the analysis of variance. J Am Stat Assoc 32(200):675–701
17. Gupta A, Agrawal R (2012) Relevant feature selection from eeg signal for mental task classification. In: Advances in knowledge discovery and data mining. Springer
18. Gupta A, Agrawal R, Kaur B (2015) Performance enhancement of mental task classification using eeg signal: a study of multivariate feature selection methods. Soft Comput 19(10):2799–2812
19. Gupta A, Kumar D, Chakraborti A, Sharma K (2017) Performance evaluation of empirical mode decomposition algorithms for mental task classification. bioRxiv https://doi.org/10.1101/076646
20. Hazarika N, Chen JZ, Tsoi AC, Sergejew A (1997) Classification of eeg signals using the wavelet transform. Sig Process 59(1):61–72
21. Hjorth B (1970) Eeg analysis based on time domain properties. Electroencephalogr Clin Neurophysiol 29(3):306–310
22. Hsu WY, Sun YN (2009) Eeg-based motor imagery analysis using weighted wavelet transform features. J Neurosci Method 176(2):310–318
23. Huang NE, Shen Z, Long SR, Wu MC, Shih HH, Zheng Q, Yen NC, Tung CC, Liu HH (1998) The empirical mode decomposition and the hilbert spectrum for nonlinear and non-stationary time series analysis. Proc Royal Soc London Ser Mathemat Phys Eng Sci 454(1971):903–995
24. Hurst HE (1951) Long-term storage capacity of reservoirs. Trans Amer Soc Civil Eng 116:770–808
25. Kaleem MF, Sugavaneswaran L, Guergachi A, Krishnan S (2010) Application of empirical mode decomposition and teager energy operator to eeg signals for mental task classification. In: Engineering in medicine and biology society (EMBC), 2010 Annual international conference of the IEEE, IEEE, pp 4590–4593
26. Keirn ZA, Aunon JI (1990) A new mode of communication between man and his surroundings. Biomed Eng, IEEE Trans 37(12):1209–1214
27. Keren AS, Yuval-Greenberg S, Deouell LY (2010) Saccadic spike potentials in gamma-band eeg: characterization, detection and suppression. Neuroimage 49(3):2248–2263
28. Kirar JS, Agrawal R (2017) Composite kernel support vector machine based performance enhancement of brain computer interface in conjunction with spatial filter. Biomed Signal Process Control 33:151–160
29. Klimesch W (2012) Alpha-band oscillations, attention, and controlled access to stored information. Trends Cogn Sci 16(12):606–617
30. Li X, Chen X, Yan Y, Wei W, Wang ZJ (2014) Classification of eeg signals using a multiple kernel learning support vector machine. Sensors 14(7):12784–12802
31. Mallat SG (1989) A theory for multiresolution signal decomposition: the wavelet representation. Pattern Anal Mach Intell IEEE Trans 11(7):674–693
32. Motamedi-Fakhr S, Moshrefi-Torbati M, Hill M, Hill CM, White PR (2014) Signal processing techniques applied to human sleep eeg signals-a review. Biomed Signal Process Control 10:21–33
33. Murugappan M, Ramachandran N, Sazali Y et al (2010) Classification of human emotion from eeg using discrete wavelet transform. J Biomed Sci Eng 3(04):390
34. Ocak H (2009) Automatic detection of epileptic seizures in eeg using discrete wavelet transform and approximate entropy. Expert Syst Appl 36(2):2027–2036

35. Ong YS, Gupta A (2016) Evolutionary multitasking: a computer science view of cognitive multitasking. Cogn Comput 8(2):125–142
36. Palaniappan R, Paramesran R, Nishida S, Saiwaki N (2002) A new brain-computer interface design using fuzzy artmap. Neural Syst Rehabil Eng, IEEE Trans 10(3):140–148
37. Pfurtscheller G, Da Silva FL (1999) Event-related eeg/meg synchronization and desynchronization: basic principles. Clin Neurophysiol 110(11):1842–1857
38. Sauseng P, Griesmayr B, Freunberger R, Klimesch W (2010) Control mechanisms in working memory: a possible function of eeg theta oscillations. Neurosci and Biobehav Rev 34(7):1015–1022
39. Torres ME, Colominas MA, Schlotthauer G, Flandrin P (2011) (2011) A complete ensemble empirical mode decomposition with adaptive noise. Acoustics, speech and signal processing (ICASSP). IEEE international conference on, IEEE, pp 4144–4147
40. Vidaurre C, Krämer N, Blankertz B, Schlögl A (2009) Time domain parameters as a feature for eeg-based brain-computer interfaces. Neural Netw 22(9):1313–1319
41. Wang D, Miao D, Blohm G (2012) Multi-class motor imagery eeg decoding for brain-computer interfaces. Front Neurosci 6:151
42. Wu Z, Huang NE (2009) Ensemble empirical mode decomposition: a noise-assisted data analysis method. Adv Adapt Data Anal 1(01):1–41
43. Yan R, Gao RX (2011) An introduction to complexity measure: non-linear statistical parameters in measurements: Part 35 in a series of tutorials on instrumentation and measurement. IEEE Instrument and Measure Magazine 14(5):27–35
44. Yang Y, Bloch I, Chevallier S, Wiart J (2016) Subject-specific channel selection using time information for motor imagery brain-computer interfaces. Cogn Comput 8(3):505–518
45. Zhang L, He W, He C, Wang P (2010) Improving mental task classification by adding high frequency band information. J Med Syst 34(1):51–60

Publisher's Note Springer Nature remains neutral with regard to jurisdictional claims in published maps and institutional affiliations.

Authors and Affiliations

Akshansh Gupta[1] · Dhirendra Kumar[2] · Hanuman Verma[3] · M. Tanveer[4] · Andreu Perez Javier[5,6] · Chin-Teng Lin[7] · Mukesh Prasad[7]

✉ Mukesh Prasad
mukesh.prasad@uts.edu.au

Akshansh Gupta
akshanshgupta@ceeri.res.in

Dhirendra Kumar
dhirendrakumar@dtu.ac.in

Hanuman Verma
hv4231@gmail.com

M. Tanveer
mtanveer@iiti.ac.in

Andreu Perez Javier
javier.andreu@imperial.ac.uk

Chin-Teng Lin
Chin-Teng.Lin@uts.edu.au

[1] Central Electronics Engineering Research Institute, Pilani, Rajasthan, India

[2] Department of Applied Mathematics, Delhi Technological University, Delhi, India

[3] Department of Mathematics, Bareilly College, Bareilly, Uttar Pradesh, India

[4] Discipline of Mathematics, Indian Institute of Technology Indore, Indore, India

[5] School of Computer Science and Electronic Engineering, University of Essex, Colchester, United Kingdom

[6] Department of Surgery and Cancer, Faculty of Medicine, Imperial College London, London, United Kingdom

[7] Australian Artificial Intelligence Institute, School of Computer Science, University of Technology Sydney, Sydney, Australia

ResearchGate

See discussions, stats, and author profiles for this publication at: https://www.researchgate.net/publication/360933614

Residual stress investigation in the metallic coating approach of micro-sized particles on the substrate: cold spray additive manufacturing

Article *in* Advances in Materials and Processing Technologies · May 2022

DOI: 10.1080/2374068X.2022.2079250

CITATIONS
0

READS
41

6 authors, including:

Abdul Faheem
Aligarh Muslim University
9 PUBLICATIONS **8** CITATIONS
SEE PROFILE

Ankit Tyagi
SGT University
29 PUBLICATIONS **210** CITATIONS
SEE PROFILE

Faisal Hasan
Aligarh Muslim University
80 PUBLICATIONS **524** CITATIONS
SEE PROFILE

Abid Ali Khan
Aligarh Muslim University
103 PUBLICATIONS **436** CITATIONS
SEE PROFILE

Some of the authors of this publication are also working on these related projects:

conjugate heat transfer within cavity View project

Part family formation in RMS View project

All content following this page was uploaded by Abdul Faheem on 30 May 2022.

The user has requested enhancement of the downloaded file.

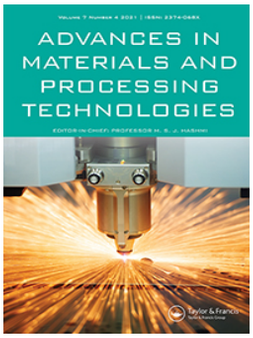

Taylor & Francis
Taylor & Francis Group

Advances in Materials and Processing Technologies

ISSN: (Print) (Online) Journal homepage: https://www.tandfonline.com/loi/tmpt20

Residual stress investigation in the metallic coating approach of micro-sized particles on the substrate: cold spray additive manufacturing

Abdul Faheem, Ankit Tyagi, Faisal Hasan, Abid Ali Khan, Qasim Murtaza & Kuldeep K Saxena

To cite this article: Abdul Faheem, Ankit Tyagi, Faisal Hasan, Abid Ali Khan, Qasim Murtaza & Kuldeep K Saxena (2022): Residual stress investigation in the metallic coating approach of micro-sized particles on the substrate: cold spray additive manufacturing, Advances in Materials and Processing Technologies, DOI: 10.1080/2374068X.2022.2079250

To link to this article: https://doi.org/10.1080/2374068X.2022.2079250

Published online: 29 May 2022.

Submit your article to this journal

View related articles

View Crossmark data

Full Terms & Conditions of access and use can be found at
https://www.tandfonline.com/action/journalInformation?journalCode=tmpt20

ADVANCES IN MATERIALS AND PROCESSING TECHNOLOGIES
https://doi.org/10.1080/2374068X.2022.2079250

Taylor & Francis
Taylor & Francis Group

Check for updates

Residual stress investigation in the metallic coating approach of micro-sized particles on the substrate: cold spray additive manufacturing

Abdul Faheem [a], Ankit Tyagi [b], Faisal Hasan [c], Abid Ali Khan [c], Qasim Murtaza [d] and Kuldeep K Saxena [e]

[a]Mechanical Engineering Section, University Polytechnic, Aligarh Muslim University, Aligarh, India; [b]Department of Mechanical Engineering, SGT University, India; [c]Department of Mechanical Engineering, ZHCET, Aligarh Muslim University, Aligarh, India; [d]Department of Mechanical Engineering, Delhi Technological University, New Delhi, India; [e]Department of Mechanical Engineering, GLA University, Mathura, India

ABSTRACT

Recently, copper and its alloys have been widely used as coating materials due to their high applications in industries and the medical sector. Meanwhile, it is necessary to investigate several stresses induced in such coatings, especially residual stress (RS). Furthermore, this RS can influence the integrity of a coating or repair. The RS is favourable for fatigue life, fatigue strength and resistance to crack under environmental assistance. Meanwhile, the cold spray additive manufacturing approach (CSAM) has been widely adopted for successful metallic coating. The deposition phenomenon is due to the high-velocity impact with a high strain rate that introduces different stresses in the coating and substrate. In this study, both experimental and numerical approaches were adopted to investigate the RS in coating. A finite element approach called Abaqus/Explicit has been used to validate the residual stress under high-velocity impact. The experimental techniques, i.e. X-ray diffraction, scanning electron microscopy, Debye-Scherrer μ-X360n analyser have used to investigate the deposition of cold spray. Numerical output gives minute deviation of RS from the experimental one. It has been found that sufficient RS is induced to enhance the coating life used for several engineering and medical aspects along with improved fatigue life and strength.

ARTICLE HISTORY
Accepted 13 May 2022

KEYWORDS
CSAM; residual stress; X-ray; SEM; FEM

1. Introduction

The stress that remains within a material after removing an external load is called residual stress, or that remains in a body when it is in equilibrium with its surroundings. It is a significant component of the selection of manufacturing methodology. Prolonging the life of ageing for structural materials is a major global challenge as fatigue is one of the most significant aspects of structural failures in several engineering applications. Improving fatigue strength in structural materials

CONTACT Qasim Murtaza qasimmurtaza@dce.ac.in Department of Mechanical Engineering, Delhi Technological University, New Delhi 110042, India

© 2022 Informa UK Limited, trading as Taylor & Francis Group

has become a critical and effective area for researchers. A strategy for increasing the life of a fatigue strength material is to reinforce the material surface with high velocities of the particles under cold spray additive manufacturing techniques (CSAM). It is a solid-state process in which small-sized micro/nanoparticles are impacted on the surface and joined by using the high velocity of particle impact [1,2]. This high speed, approximately in the range of 300 to 1250 m/s, is generated by using the de-Laval supersonic nozzle. RS is induced within the component in every manufacturing process due to the high plastic deformation [3–5]. Cold gas additive manufacturing (CSAM) is a novel manufacturing process used to deposit a metallic, non-metallic, and polymer coating on the surface or substrate. The CSAM is a solid-state metal coating technology that has recently been applied to fabricate and repair damaged components. The arrangement of the supersonic nozzle, gas chamber and powder preheating device is shown in Figure 1.

In comparison with fusion-based additive manufacturing processes, CSAM has been shown to retain the original properties, produce oxide-free deposits, and not adversely influence the substrate material during manufacturing [6–9]. The properties of this metallic coating are strongly built upon the grain size, orientation values of stress and strain; furthermore, these affect the manufacturing parameters. The specific feature of the cold spray is the minimal residual stress or compressive residual stress developed in the coating or film zone [10–13]. This compressive feature of the RS is essential for fatigue life and fatigue strength, cohesive strength, adhesive strength and resistance to crack under environmental assistance. Due to the peening and annealing effect and intense plastic deformation, the grain and grain boundary also refined [14–17]. The bonding mechanism in the coating is defined with the help of the critical velocity and mechanical and thermal properties of the particle and substrate [18–24]. Different investigations evaluated the fatigue behaviour of materials under CSAM by considering several factors, i.e. bonding strength and grain refinement, induced residual stress, the properties, quality of coating and surface roughness value. Different surfaces of the materials in public places are contaminated and deteriorate after a certain time.

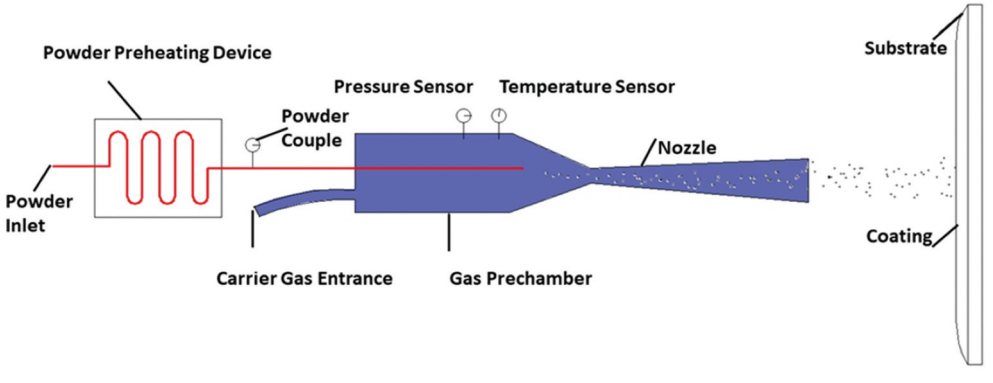

Figure 1. Schematic diagram of cold spray additive manufacturing.

Moreover, there is a high risk of microorganism transmission in places, i.e. hospitals, public transportation and so on. By consideration, the surfaces of the materials are coated with copper and its alloys. We know that this highly conductive and ductile material releases its ions that kill the bacteria or other microorganisms. Yildrim et al. [25] studied the single-particle impact using the FEM approach and investigated the distribution of RS. Arabgol et al. [26] figure out how different parameters, i.e. coating thickness, affect the build-up of residual stress when copper particle coating is done on the steel substrate. Seraj et al. [27] investigated that the effect of preheating or pre-treatment on the substrate influences the RS developed during the deposition of aluminium (Al), copper (Cu) and titanium (Ti) particles. Luzin et al. [28] investigated by creating a coating of Cu and Al and measured RS with a technique called neutron diffraction. Ghelichi et al. showed that fatigue strength improved by up to 30% in the case of Al7075 coating. Li et al. [29] tried to solve the RS distribution by using a finite element methodology with the Eulerian approach. Furthermore, their work is also extended up to single and multi-particle impact. Bobzin et al. [30] studied the comparison of Residual Stress with X-ray Stress Analysis and the hole drilling method. It has been found that residual micro-stresses for a coarse-grained material are within the state of biaxial stress. Oviedo et al. [31] studied parametric research with the physical parameters over peening phenomenon, thermal stress, and residual stress. The parameters, i.e. particle velocity, temperature and morphology, help to obtain the required residual stress in the coating. However, more research is still needed in the residual stress measurement in the metallic, composites and polymeric coating. This study tried to fill the gap between medical and industrial aspects, i.e. metallic coating in mild steel substrate. Meanwhile, experimental approach and numerical investigation (using the FEM tool with Abaqus/Explicit) for residual stress measurement are presented. Micro-sized copper particles have been used as the coating material for the same substrate. The numerical modelling was interpreted with the help of a constitutive model called the Johnson-Cook plasticity model. This study also focused on the distribution of RS induced by the high-velocity impact of the particles under cold spray additive manufacturing approach

2. Experimental procedure

In this investigation, copper particles are accelerated with the velocity of 500 m/s through the supersonic nozzle on the mild steel substrate. Since, every material has some critical velocity that should be achieved or needs to be found to obtain material deposition on the substrate. Otherwise, the particle will rebound after striking from the surface. As far as this study is concerned, copper particle has a critical velocity of 500 m/s obtained experimentally, which is mandatory for successful coating on the substrate. Furthermore, both the particle and substrate are at the temperature through the analysis. To investigate RS, μ-X360n portable X-ray residual stress analyser by the Pulstec Industrial Cooperation Limited has been used. The Debye Scherrer ring gives the pattern of residual stress measurement, as shown in Figure 2. The μ-X360n analyser is a compact, high precision device based on the cosine-alpha method, as shown in Figure 3, used for the residual stress measurement. The injection parameters under this study have been displayed in Table 1.

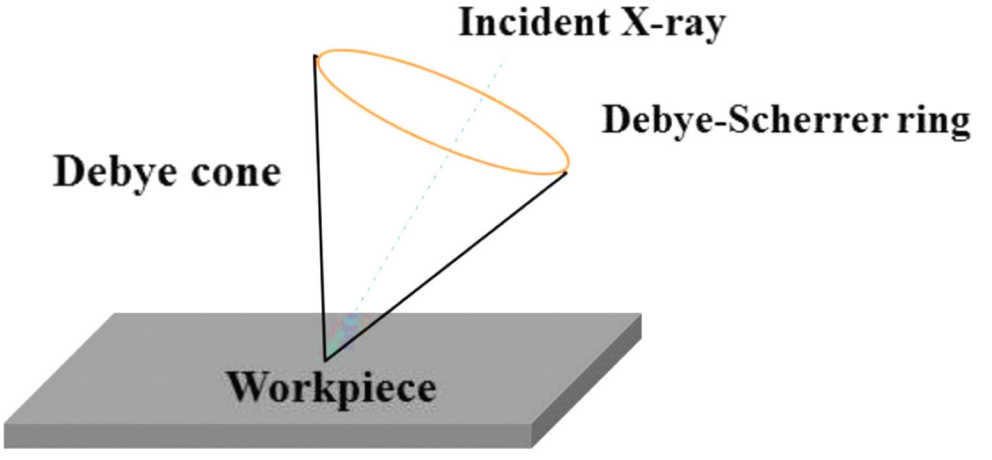

Figure 2. Measurement approach of residual stress.

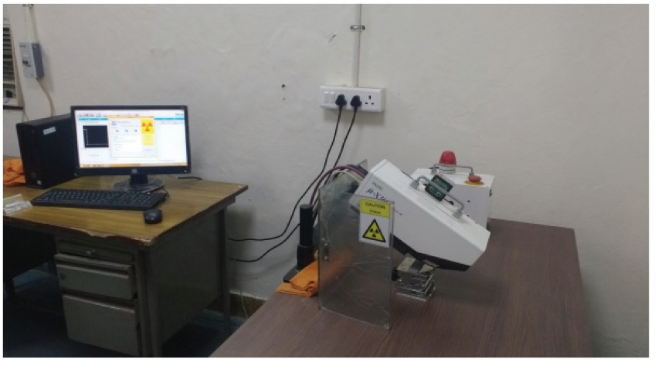

Figure 3. μ-X360n setup for residual stress measurement.

Table 1. Injection parameters for the CSAM.

Gas inlet pressure (bar)	Injection pressure (bar)	Gas inlet temperature (K)	Particle injection temperature (K)	Ambient pressure (bar)
25	27	300	300	1

During residual stress measurement by x-ray diffraction, the residual strain present in the crystal lattice is measured, and the cause of the strain called is calculated by assuming a linear elastic distortion of the lattice. This method is a unique way to determine residual stress at the microscopic and macroscopic levels. The Scherrer formula for the particle size is given by Equation (1): Where k, λ, β are the shape factor, X-ray wavelength and full width half maximum, respectively [32]. However, Bragg's law can also calculate the RS: $2d\sin\theta = n\lambda$, where d is the interplanar spacing.

$$D = \frac{k\lambda}{\beta cos\theta} \tag{1}$$

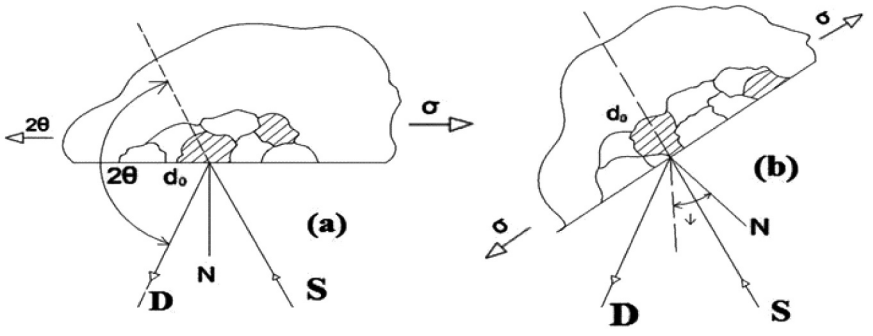

Figure 4. Principle of X-ray diffraction (a) orientation of object surface (Ψ) = 0 and (b) Ψ at some certain angle.

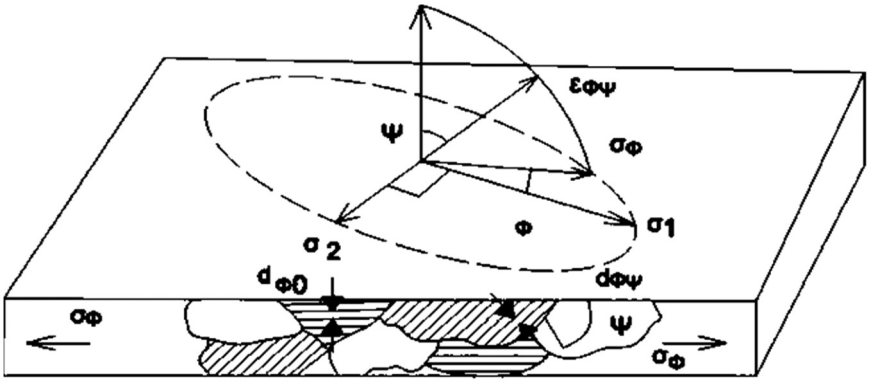

Figure 5. Elastic model of the plane stress.

In Figure 4, D is the X-ray detector, S represents the X-ray source, and N is normal to the surface. Figure 5 shows the representation of plane stress. σ_1 and σ_2 are the principle stresses and σ_Φ is the surface stress [33]. The value of strain in Φ and Ψ directions is shown in Equation (2).

The strain ($\epsilon_{\Phi\Psi}$) in the direction of Φ and Ψ is given by

$$\in_{\Phi\Psi} = \left[\frac{1+\vartheta}{E}\left(\sigma_1\alpha_1^2 + \sigma_2\alpha_2^2\right)\right] - \left[\frac{\vartheta}{E}(\sigma_1 + \sigma_2)\right] \tag{2}$$

where E is the Young's elasticity, ν is the Poisson's ratio, and α_1 and α_2 are the cosine angles of the strain vector. This study showed the impact of copper particles on the mild steel substrate. The XRD technique showed the surface metallic coating of copper microsized particles confirmed by the JCPDS reference number 00–004-0836. Furthermore, a scanning electron microscope (SEM) from Jeol Ltd. at the university's sophisticated instrument facility, Aligarh Muslim University, Aligarh, India, was used to examine the surface and cross-section morphologies of the deformed particle and substrate. A critical velocity of roughly 500 m/s was achieved for inert gas-atomised copper powder with particle sizes ranging from 10 to 20 μm. Throat to the exit, the downstream length was 100 mm. Meanwhile, the Cu powders, shower and spray conditions were 2.7

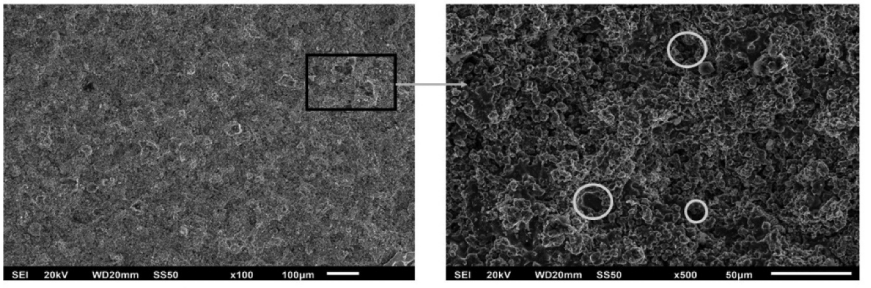

Figure 6. (a) SEM of the copper coating (b) Magnified view of copper coating with small pits.

MPa injection pressure, nitrogen as a carrier gas, and a temperature of 27°C. The distance between the nozzle exit and the substrate surface was 20 mm. Figure 6 shows the copper coating under high-velocity impact. As shown in Figure 6(b), a few small pits circled in the coating indicate minute surface irregularities in the roughness of copper coatings on mild steel substrates.

3. Numerical methodology with constitutive model

A numerical methodology is a vital tool that anticipates the analysis to be challenging with the experimental approach. Generally, for finite element methodology (FEM), commercially accessible software Abaqus/Explicit is used. In this tool, there are two approaches: (1) Lagrangian method and (2) Eulerian method. The Lagrangian method is used in this study to predict adhesive bonding between particles and substrates. The model chosen for the plastic deformation of metal is the Johnson-Cook plasticity model [34]. Since the high-velocity particle is accelerated through the D-Laval nozzle, resulting in high plastic deformation of the particle and substrate. The Johnson Cook plasticity model is well adopted under such high plastic deformation of the material. The yield flow stress ($\bar{\sigma}$) of the material is given by Equation (3):

$$\bar{\sigma} = \left(A + B \in_p^n\right)(1 + C ln \in^*)(1 - (T^*)^m) \tag{3}$$

$$T^* \equiv \left\{ \begin{array}{c} 0 \; for \; T < T_{trans} \\ \frac{T - T_{Trans}}{T_m - T_{trans}} \; for \; T_{trans} \leq T \leq T_m \\ 1 \; for \; T > T_m \end{array} \right\} \tag{4}$$

where A, B, C, n and m are the yield stress, work hardening parameter, dimensionless strain rate parameter, power exponent and thermal softening, respectively. T^* is the homologous temperature, and T, T_m and T_{trans} are the normal temperatures, melting point, and transition temperature, respectively, as in Equation (4). The damage parameter ω for the failure criteria is expressed as:

$$\omega = \sum^{\frac{\Delta \bar{\varepsilon}^p}{\bar{\varepsilon}_f^p}} \tag{5}$$

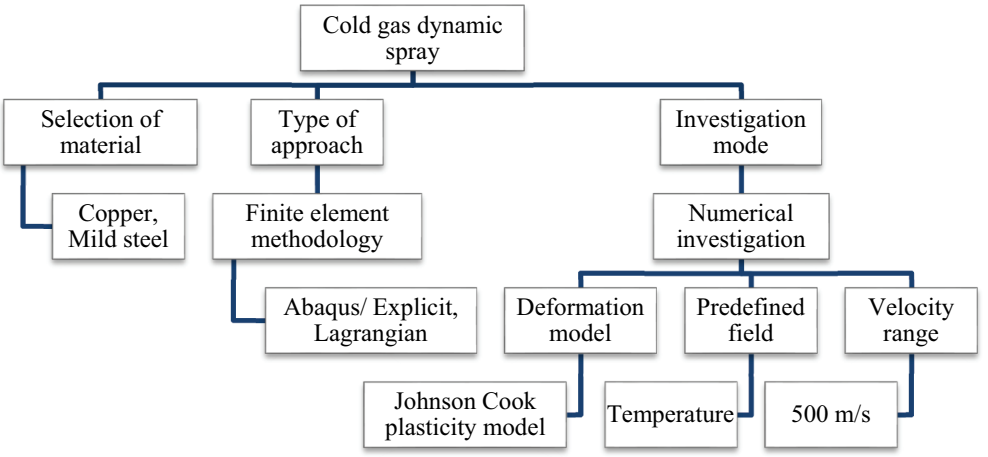

Figure 7. Flow chart of cold spray under numerical modelling.

Table 2. Thermal and mechanical properties of copper material.

Material	Cu	Mild steel
Density (kg/m^3)	8960	7870
Heat capacity(J/kgK)	383	481
Thermal conductivity (W/mK)	386	46
Young's modulus (GPa)	124	200.1
Poisson's ratio	0.34	0.30
A (MPa)	90	532
B (MPa)	292	229
N	0.31	0.3024
C	0.025	0.0274
M	1.09	1
Melting point (K)	1356	1793
Reference temperature (K)	298	298
Reference strain rate (s^{-1})	1	1

$$\bar{\varepsilon}_f^P = \left[D_1 + D_2 exp\left(D_3 \frac{p}{q}\right)\right]\left[1 + D_4 ln\left(\frac{\varepsilon^p}{\varepsilon_0}\right)\right]\left[1 + D_5\left(\frac{T - T_{ref}}{T_m - T_{ref}}\right)^m\right] \quad (6)$$

The Johnson Cook failure model depends on the value of the equivalent plastic strain (PEEQ), and failure occurs when the value of ω exceeds 1. Here $\Delta\bar{\varepsilon}^p$ and $\bar{\varepsilon}_f^p$ are the steps of equivalent plastic strain and stress at failure point mentioned in Equation (5) and (6), D_1 to D_5 are the failure parameters [35]. The material model is implemented with a particle size (d_p) having a range of 10–20 micrometre (μm). The flow chart of numerical modelling has been shown in Figure 7, which depicts the overall parameter for the study. In the numerical investigation, copper is used as material for the particle and mild steel for the substrate during cold spraying. Meshing size is a crucial factor in finding the numerical approach accurate result. Different meshing sizes have been taken for analysis in this study, but the optimum meshing size is approximate as $d_p/40$. Different thermal and mechanical properties of copper used in the investigation have been listed in Table 2.

4. Results and discussions

In this investigation, high-velocity copper particles are impacted on the mild steel substrate. The copper particles having a range of 10–20 μm are impacted on the substrate at a velocity of 500 m/s. Under this high velocity, a tremendous amount of compressive stress is induced in the coating as well as in the substrate. When the micro-sized particles come out of the de-Laval nozzle, impact onto the substrate intense plastic deformation occurred and a uniform coating formed; however, the effect of high-velocity benefits residual stress distribution. To ensure the successful deposition of micro-sized metallic particles, x-ray diffraction provides a pattern of copper that ensures Cu coating onto the substrate, as shown in Figure 8.

The copper coating onto a mild steel substrate has been clearly indicated in Figure 9 under cold spray technology. Meanwhile, coating thickness and interface have depicted the successful coating phenomenon. Furthermore, the interface between substrate and copper coating through cold spray helped to understand the optimum thickness of the coating. Sufficient velocity (500 m/s) is required to achieve the optimal plastic deformation. The scanning electron microscopy gave sufficient characterisation output, as shown in Figure 9(a–c) that showed the significant plastic deformation of the Cu particles to achieve the successful coating.

The Debye-Sherrer approach has been used to analyse residual stress under the high-velocity impact. The two- and three-dimension Debye rings showed the pattern of induced residual stress. When the X-ray is incident at an angle of 35 degrees through the μ-360 n portable analyser, the Debye ring showed the optimal amount of residual stress as in Figure 10. In Figure 11, the peak and valley in the

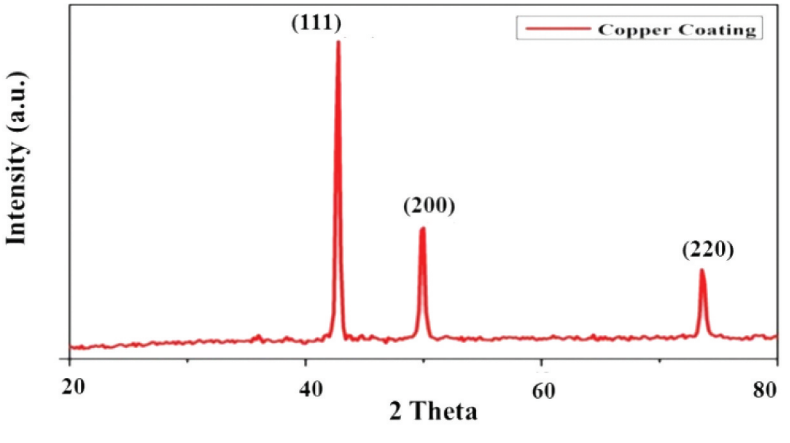

Figure 8. XRD pattern for copper coating.

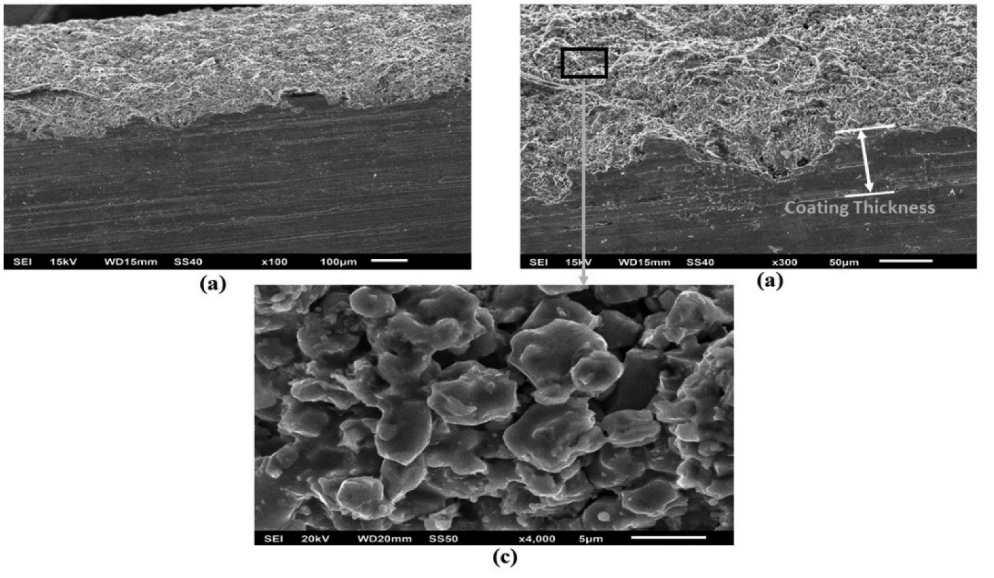

Figure 9. (a) Side view of copper Coating (b) Copper coating thickness (c) Plastically deformed copper particles.

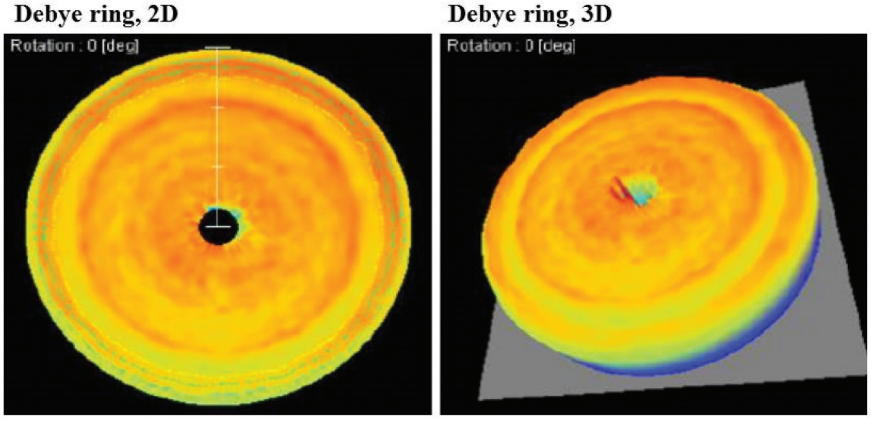

Figure 10. 2&3 Dimension Debye-Scherrer rings for residual stress measurement.

different coating locations depict the average value of RS. The greater the distortion value, the greater the RS, and hence the fatigue strength. Figure 12 depicts the copper coating's distortion rings and temperature profiles.

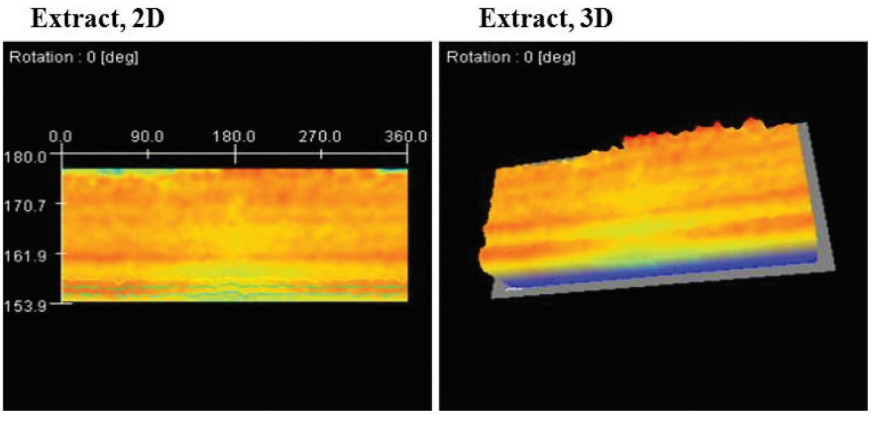

Figure 11. 2&3 Dimension extract for residual stress measurement with 360°.

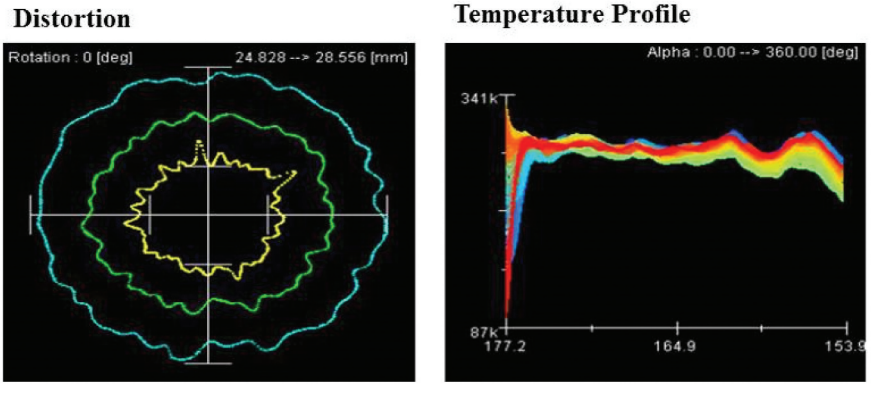

Figure 12. Distortion rings with temperature profile.

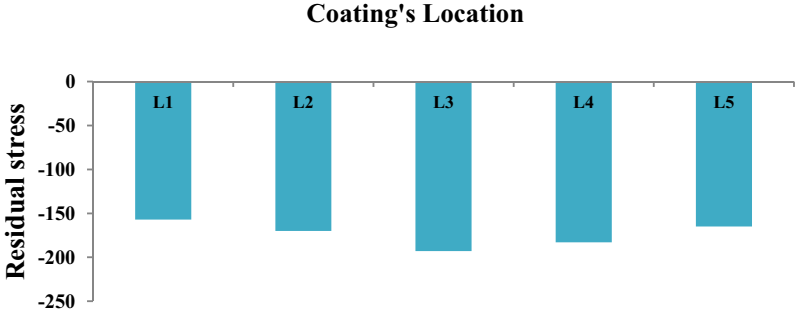

Figure 13. Residual stress vs Different coating's location.

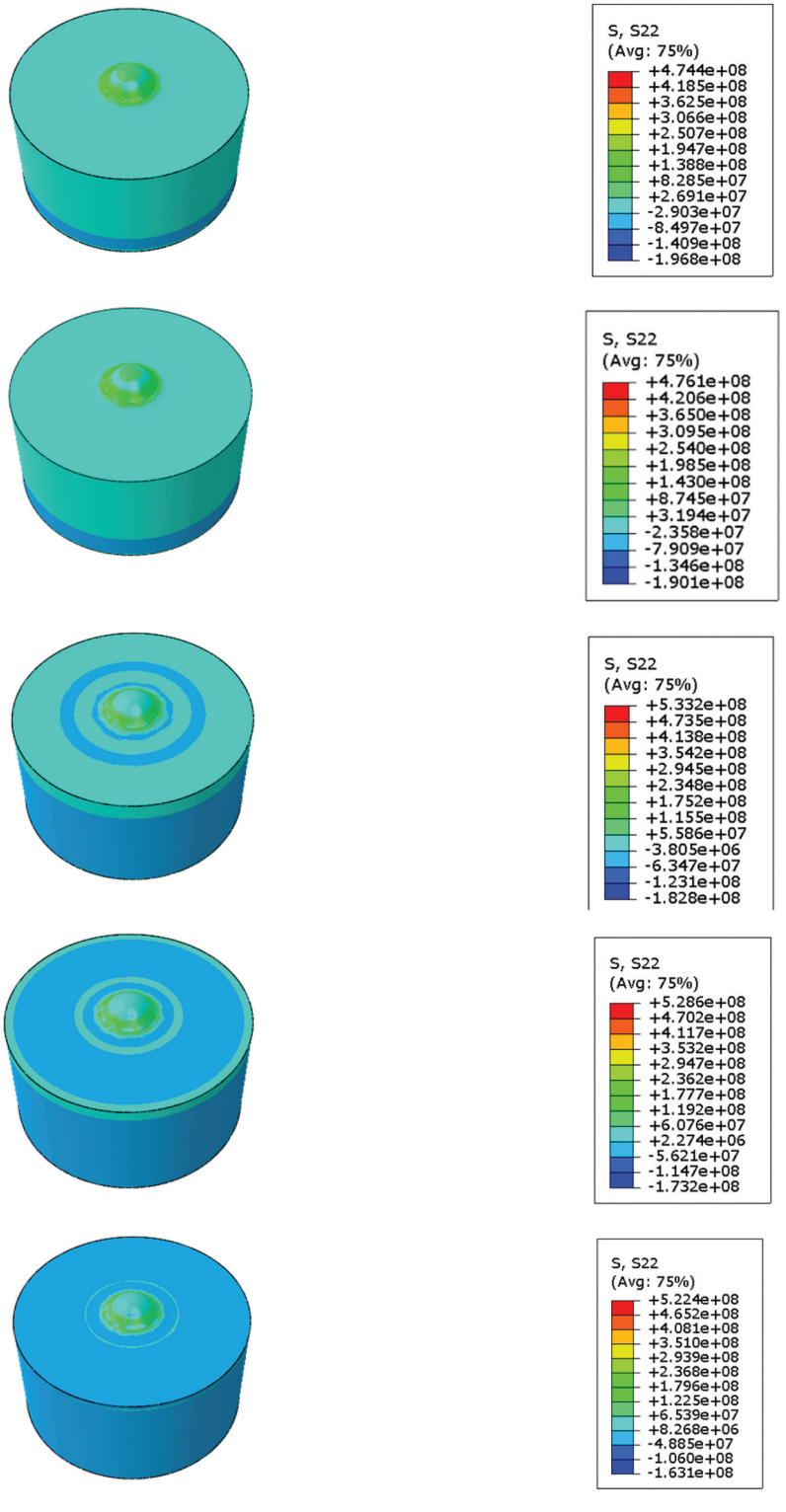

Figure 14. Residual stress values at different coating's location.

In this study, different zones have been selected to investigate the distribution of compressive RS. A uniform distribution of RS throughout the coating is required to improve the fatigue life and strength, cohesive and adhesive strength, and crack resistance. As a result, in several locations, the RS values lie between −150 and −180 MPa, as shown in Figure 13.

Residual stress measurement with the numerical tool can be solved with the help of two analyses: (1) by visualising pressure stress (S), i.e. positive and negative values denote tensile stress and compressive stress, respectively, and (2) by normal stress (S22). Furthermore, the numerical method validates the experimental findings of the residual stress analysis. In Figure 14, the RS values with a velocity of 500 m/s impact the substrate by considering the different elements at the periphery of the contour zone.

In this numerical investigation, the step time should be considered about 1 ns for the completion of impact and plastic deformation of the particle and substrate for the successful completion of the metallic coating. In Figures 15 and 16, the variation of residual stress corresponds to step time; moreover, its value is in the range of negative 150–200 MPa. It has been estimated that there is 7% deviation in the experimental and numerical findings of the RS. The numerical results showed minute variation in output with experimental one. When the high velocity of metallic particles strikes on the MS substrate, a tremendous amount of temperature is generated as shown in Figure 17 due to intense plastic deformation of substrate and particles. Furthermore, for a better understanding of the deformation, Figure 18 shows the variation from step time up to the full deformation of the particle under the high-velocity cold spray additive manufacturing approach.

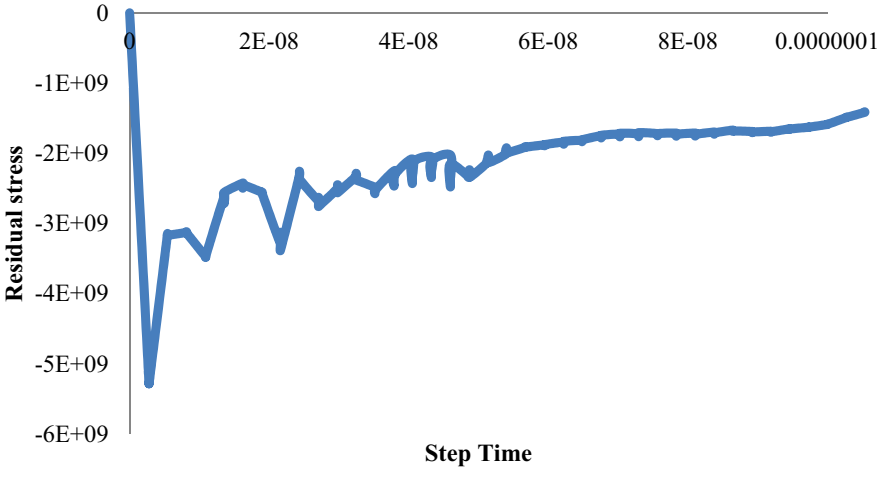

Figure 15. Residual stress vs Step time under numerical investigation.

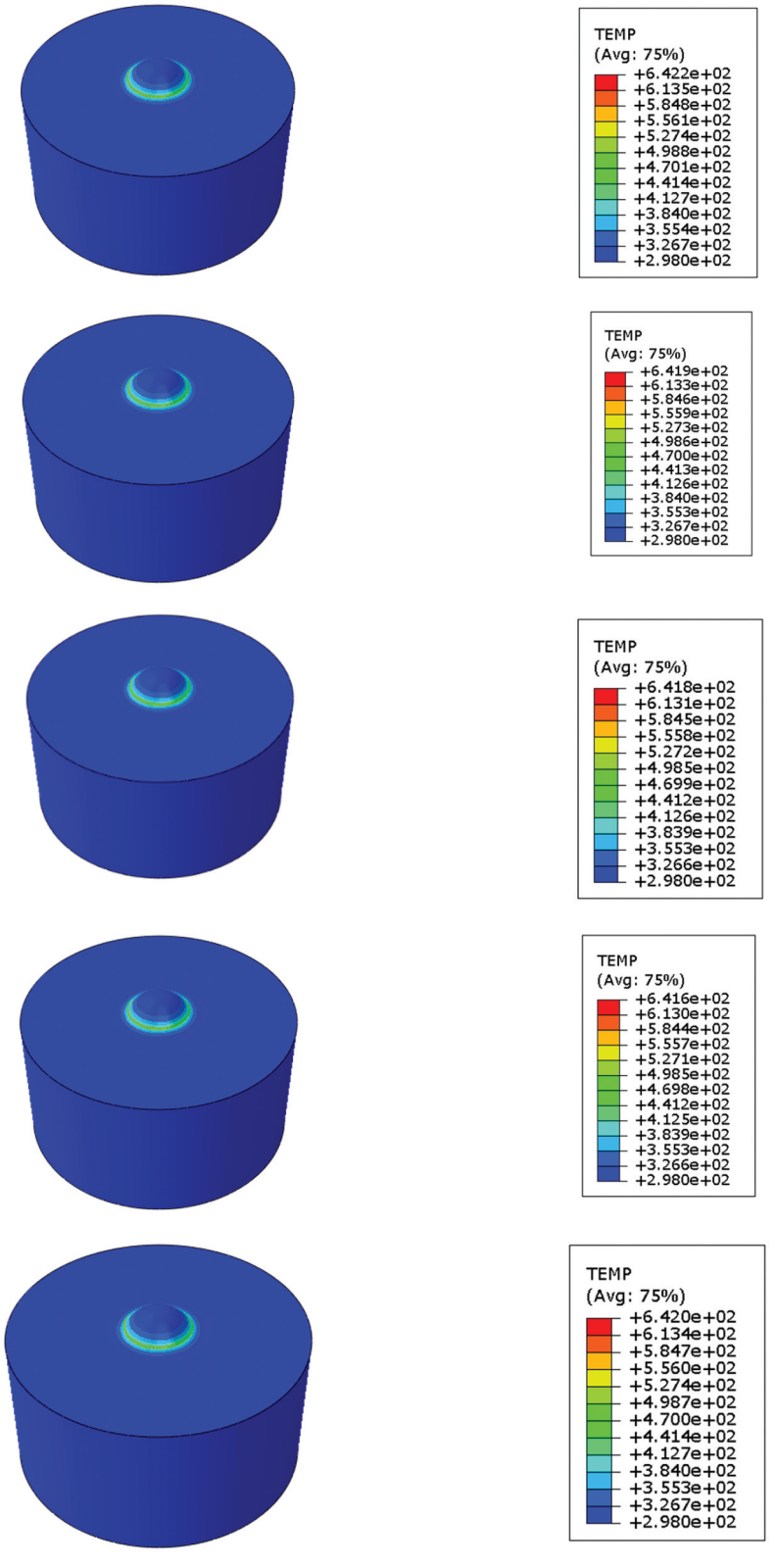

Figure 16. Residual stress value at the peripheral location of the coating.

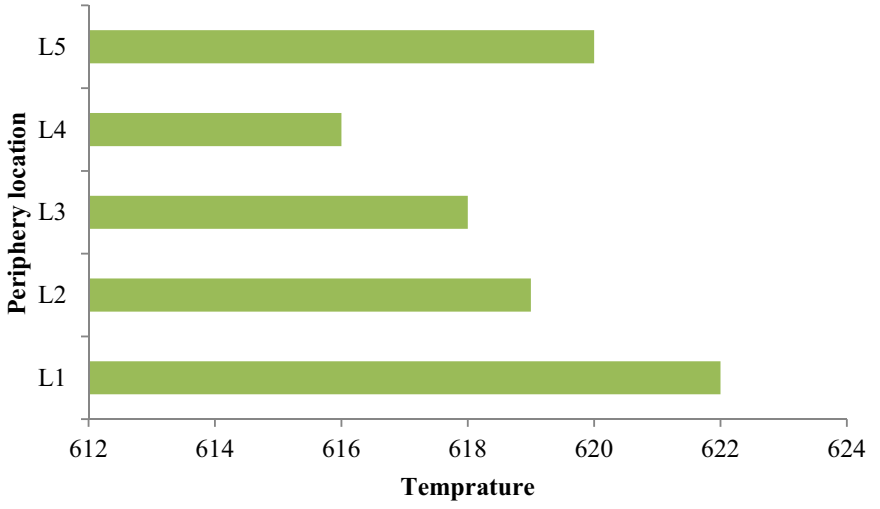

Figure 17. Temperature variation under numerical approach.

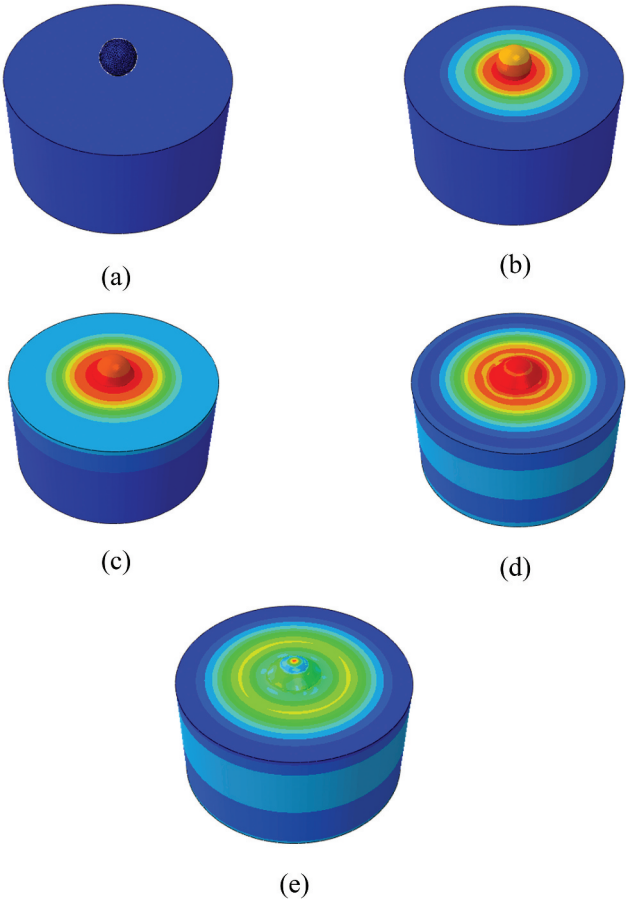

Figure 18. Variation of contour under different ranges of step time.

5. Conclusions

Analysis under the experimental and FEM approach easily allows us to better understand the distribution of residual stress in the coating and substrate.

(1) This study contributed to the domain of micro-sized particles with high-velocity impact, as well as successful coating onto the substrate. The induced residual stress due to high velocity helped fatigue life and strength.
(2) The distortion and Debye's ring depict the actuation of residual stress in the coating under cold spray additive manufacturing technology. To understand the uniform distribution of residual stress different locations have been selected and resulted in evenness in the values.
(3) The characterisation approach of XRD and SEM showed the significant Cu coating onto the MS substrate. Meanwhile, interface and coating thickness have clearly been shown through SEM. In addition, the substantial value of residual stress has been investigated for the longer life of the coating used for several industrial and medical purposes.
(4) Furthermore, plastic deformation and jetting formation have also been studied that define the interface bonding between the particle/substrate and particle/particle. These findings are favourable for the manufacturing criteria precisely to fatigue life and strength and resistance to crack under environmental assistance.

Disclosure statement

No potential conflict of interest was reported by the author(s).

ORCID

Abdul Faheem http://orcid.org/0000-0002-8502-935X
Faisal Hasan http://orcid.org/0000-0002-9901-890X
Abid Ali Khan http://orcid.org/0000-0002-9325-6640
Qasim Murtaza http://orcid.org/0000-0001-8784-2304
Kuldeep K Saxena http://orcid.org/0000-0003-4064-5113

References

[1] Assadi H, Ga F, Stoltenhoff T, et al. Bonding mechanism in cold gas spraying. Acta Mater. 2003;51:4379–4394.
[2] Bae G, Xiong Y, Kumar S, et al. General aspects of interface bonding in kinetic sprayed coatings. Acta Mater. 2008;56:4858–4868.
[3] Cavaliere P, . Processing parameters affecting cold spray coatings performances. Int J Adv Manufact Technol. 2014;71:263–277. DOI:10.1007/s00170-013-5465-0. https://link.springer.com/article/10.1007/s00170-013-5465-0
[4] Zhou X, Wu X, Wang J, et al. Numerical investigation of the rebounding and the deposition behavior of particles during cold spraying. Acta Metall Sin. 2011. DOI:10.11890/1006-7191-111-43.

[5] Murtaza Q, Stokes J, Ardhaoui M, et al. Experimental analysis of spray dryer used in hydroxyapatite thermal spray powder. J Therm Spray Technol. 2012;21:963–974.
[6] Yin S, Wang X, Suo X, et al. Deposition behavior of thermally softened copper particles in cold spraying. Acta Mater. 2013;61:5105–5118.
[7] Saleh M, Luzin V, Spencer K, et al. Analysis of the residual stress and bonding mechanism in the cold spray technique using experimental and numerical methods. Surf Coat Technol. 2014;252:15–28.
[8] Tan AWY, Sun W, Phang YP, et al. Effects of traverse scanning speed of spray nozzle on the microstructure and mechanical properties of cold-sprayed Ti6Al4V coatings. J Therm Spray Technol. 2017;26:1484–1497.
[9] Faheem A, Tyagi A, Pandey SM, et al. A sustainable ecofriendly additive manufacturing approach of repairing and coating on the substrate: cold spray. Australian J Mech Eng. 2022;1–18. DOI:10.1080/14484846.2021.2023379.
[10] Seraj RA, Abdollah-Zadeh A, Assadi H, et al. Effect of substrate on the properties of cold sprayed coating of WC-10Ni. Adv Mater Process Technol. 2020. DOI:10.1080/2374068X.2020.1794228.
[11] Katarkar AS, Pingale AD, Belgamwar SU, et al. Fabrication of Cu@G composite coatings and their pool boiling performance with R-134a and R-1234yf. Adv Mater Process Technol. 2022. DOI:10.1080/2374068X.2022.2033046.
[12] Fayomi OSI, Sode AA, Anyanwu BU, et al. Experimental studies and influence of process factor on zinc-nickel based coating on mild steel. Adv Mater Process Technol. 2021. DOI:10.1080/2374068X.2021.1896863.
[13] Lunt AJG, Baimpas N, Salvati E, et al. A state-of-the-art review of micron-scale spatially resolved residual stress analysis by FIB-DIC ring-core milling and other techniques. J Strain Anal Eng. 2015;50:1–19.
[14] Yeom H, Dabney T, Johnson G, et al. Improving deposition efficiency in cold spraying chromium coatings by powder annealing. Int J Adv Manufact Technol. 2019;100:1373–1382.
[15] Song X, Xie M, Hofmann F, et al. Residual stresses in linear friction welding of aluminium alloys. Mater Des. 2013;50:360–369.
[16] Khodabakhshi F, Marzbanrad B, Jahed H, et al. Interfacial bonding mechanisms between aluminum and titanium during cold gas spraying followed by friction-stir modification. App Surf Sci. 2018;462:739–752.
[17] Sirvent P, Garrido MA, Múnez CJ, et al. Effect of higher deposition temperatures on the microstructure and mechanical properties of Al 2024 cold sprayed coatings. Surf Coat Technol. 2018;337:461–470.
[18] King PC, Bae G, Zahiri SH, et al. An Experimental and Finite Element Study of cold spray copper impact onto two aluminum substrates. J Therm Spray Technol. 2010;19:620–634.
[19] Moridi A, Azadi M, Farrahi GH, et al. Surface & coatings technology thermo-mechanical stress analysis of thermal barrier coating system considering thickness and roughness effects. Surf Coat Technol. 2014;243:91–99.
[20] Faheem A, Hasan F, Murtaza Q, et al. Material perspective and deformation pattern of micro-sized metallic particle using cold gas dynamic spray. In: Narayanan R, Joshi S, Dixit U, editors. Advances in computational methods in manufacturing. Lecture notes on multidisciplinary industrial engineering. Singapore: Springer; 2019. 978-981-32-9071-6. DOI:10.1007/978-981-32-9072-3_34.
[21] Kikuchi S, Hirota Y, Komotori J, et al. Effects of particle size for peening on microstructural changes in steel. J Jpn Soc Abras Technol. 2010;54:720–724.
[22] Hassani M, Veysset D, Nelson KA, et al. In-Situ observations of single micro-particle impact bonding. Scr Mater. 2018;145:9–13.
[23] Shayegan G, Mahmoudi H, Ghelichi R, et al. Residual stress induced by cold spray coating of magnesium AZ31B extrusion. Mater Des. 2014;60:72–84.

[24] Suhonen T, Varis T, Dosta S, et al. Residual stress development in cold sprayed Al, Cu and Ti coatings. Acta Mater. 2013;61:6329–6337.
[25] Yildirim B, Muftu S, Gouldstone A, et al. Modeling of high velocity impact of spherical particles. Wear. 2011;270(9):703–713.
[26] Arabgol Z, Assadi H, Schmidt T, et al. Analysis of thermal history and residual stress in cold-sprayed coatings. J Therm Spray Technol. 2014;23:84–90.
[27] Seraj RA, Zahed AA, Assadi H, et al. Effect of substrate on the properties of cold sprayed coating of WC-10Ni. Adv Mater Process Technol. 2020;14. DOI:10.1080/2374068X.2020.1794228.
[28] Luzin V, Spencer K, Zhang MX, et al. residual stress and thermo-mechanical properties of cold spray metal coatings. Acta Mater. 2011;59:1259–1270.
[29] Li W, Yang K, Zhang D, et al. Residual stress analysis of cold-sprayed copper coatings by numerical simulation. J Therm Spray Technol. 2016;25:131–142.
[30] Bobzin K, Wietheger W, Knoch MA, et al. Comparison of residual stress measurements conducted by X ray stress analysis and incremental hole drilling method. J Therm Spray Tech. 2020;29:1218–1228.
[31] Oviedo F, Valarezo A, et al. Residual stress in high-velocity impact coatings: parametric finite element analysis approach. J Therm Spray Tech. 2020;29:1268–1288. DOI:10.1007/s11666-020-01026-5.
[32] Scherrer P, Gottingen NGW. Bestimmung der Größe und der inneren Struktur von Kolloidteilchen mittels Röntgenstrahlen. Math-Pys Kl. 1918;2:96–100. http://eudml.org/doc/59018
[33] Prevéy PS. X-ray diffraction residual stress techniques. In: Metals handbook metals park: American Society for Metals. 1986;380–392. 978-1-62708-178-8. DOI:10.31399/asm.hb.v10.9781627081788.
[34] Johnson GR. Prog Astronaut Aeronaut 1993, pp. 155:165.
[35] Lin E, Chen Q, Ozdemir OC, et al. Effects of interface bonding on the residual stresses in cold- sprayed Al-6061: a numerical investigation. J Therm Spray Technol. 2018;28:472–483.

View publication stats

Proceedings of the Sixth International Conference on Intelligent Computing and Control Systems (ICICCS 2022)
IEEE Xplore Part Number: CFP22K74-ART; ISBN: 978-1-6654-1035-9

Review based on Variations of DBSCAN algorithms

Ankit Bhardwaj
Student
Dept. of Software Engineering,
Delhi Technological University,
Shahbad Daulatpur Village,
Rohini, Delhi, 110042.
ankitbhardwaj_2k18se022@dtu.ac.in

Ankit Pandey
Student
Dept. of Software Engineering,
Delhi Technological University,
Shahbad Daulatpur Village,
Rohini, Delhi, 110042.
ankitpandey_2k18se025@dtu.ac.in

Sonika Dahiya
Assistant Professor
Dept. of Software Engineering,
Delhi Technological University,
Shahbad Daulatpur Village,
Rohini, Delhi, 110042.
sonika.dahiya@dtu.ac.in

2022 6th International Conference on Intelligent Computing and Control Systems (ICICCS) | 978-1-6654-1035-9/22/$31.00 ©2022 IEEE | DOI: 10.1109/ICICCS53718.2022.9788463

Abstract— **Clustering is among the most broadly used algorithms that works by separating the data points into many different groups (clusters) having similar data points and properties. Density Based Spatial Clustering of Applications with noise (DBSCAN) is one such clustering algorithm used for identifying distinctive clusters in the given dataset. The algorithm works on a dataset which has noise and outliers, clusters of various sizes and shapes are discovered in a large dataset. DBSCAN has certain issues when it comes to the time complexity ($O(n^2)$) of the algorithms and also it produces incorrect results when the database is large and that too with varied densities. In order to overcome these limitations one needs certain variations or improvements. In this paper a review of some of the variations of this algorithm that have been modified or those which have a high efficiency on varied densities have been presented. Eight variations have been discussed in this report, after which it was concluded that these variations are better performing than the conventional DBSCAN algorithms.**

Keywords—Density based spatial clustering of applications with noise, clustering, machine learning

I.INTRODUCTION

One of the major part of data analytics is data mining. This uses analytics techniques in order to find important information in the dataset. Data mining finds its application in in planning various business strategies, artificial intelligence, healthcare, cybersecurity, fraud detection and so on. There are four major steps in data mining: data gathering, preparation, mining the data and the interpretation with analysis of data.

One of the majorly used data mining techniques is data clustering. In clustering data grouping is done in a particular way so that the data points with similar points are usually grouped together. So one can say that clustering works by finding the similarities and dissimilarities in data points. Clustering techniques find its application in many fields that may include bio informatics, pattern recognition, social network analysis, image processing, healthcare etc.

There are many clustering techniques like k-means. k-Means finds clusters of only spherical shapes, it also requires an input (number of number of cluster) to the algorithm. Drawback of k-means is that it's both space and time complexities is $O(n^2)$, therefore not suitable for large dataset. Hierarchical clustering methods, single linkage methods, CURE, BIRCH also some of the clustering algorithms. But, DBSCAN is one which is mostly used as it handles noise and outliers quite easily.

One of the pioneers of clustering-based techniques is the DBSCAN algorithm but it has certain limitations. This algorithm has quadratic time complexity with given data size. Spatial index structures like R-trees can be used to reduce the time complexity of the algorithm when working on large datasets. But then also this algorithm cannot be applied efficiently for datasets having higher dimensions. The objective in this paper is to study various variations of DBSCAN algorithms and then compared them on various parameters like time complexity, noise removal, input parameters, output etc.

Motivation

The DBSCAN algorithm is one the most widely used clustering algorithms but it also has certain limitations. These are, but not limited to:

a. Higher time complexity.
b. Does not work well in case of high dimensional dataset.
c. Difficulty in choosing the threshold ε when data and scales are not well understood.
d. The algorithm is not entirely deterministic.

These are reasons which call for improvements in the existing conventional DBSCAN algorithm. In the last decade many such variations have been introduced by various scholars all over the world which helps in overcoming these limitations. In this report review of a few such variations of the algorithms was done and then they were compared on the basis of certain parameters.

II. DBSCAN ALGORITHM

Density based spatial clustering of applications with noise is among the density-based clustering algorithms which is used mainly for clustering data of any shape where there is a presence of noises and outliers in the background for a big dataset. The DBSCAN algorithm has the following key advantages over the other clustering algorithms such as hierarchical and partitioning clustering algorithms.

Authorized licensed use limited to: DELHI TECHNICAL UNIV. Downloaded on June 15,2022 at 11:28:24 UTC from IEEE Xplore. Restrictions apply.

1. Even in the presence of outliers and noises this algorithm works successfully. In the presence of noise, this algorithm gives much better results when compared with other algorithms ,making DBSCAN an useful algorithm.
2. This algorithm can work for any arbitrary shapes whether it is spherical or convex based shapes as DBSCAN can properly detect the noise present in given dataset. Hierarchical and partitioning clustering algorithms fail in this. This distinguishes it from k-means and other clustering techniques.

The main principle of this algorithm is that if a point is close to many points present in a cluster then that point also belongs to that cluster. Fig1. denotes the comparison between DBSCAN and K-Means. Another salient feature of the DBSCAN algorithm over the K-means algorithm is that one need not to pre specify the value of k which is number of clusters, so that the numbers of clusters can be anything depending upon the dataset. This makes it even more effective.

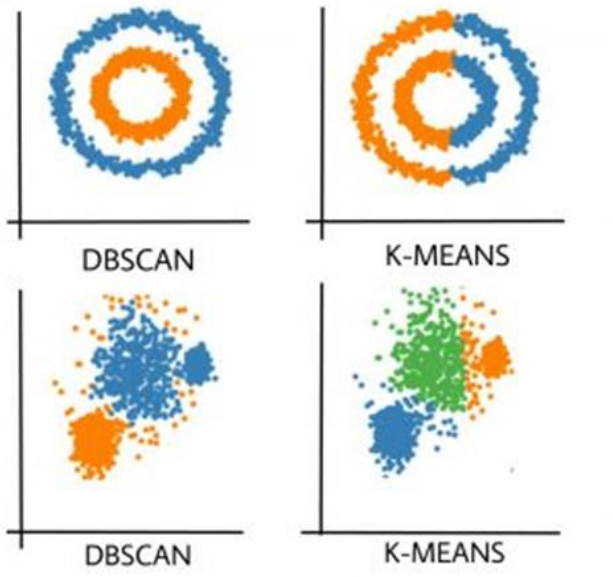

Fig. 1. DBSCAN vs k-means

The DBSCAN algorithm mainly uses two parameters-

1. eps (ε): It acts like a radius of the cluster that any point within the circumference of the circle made by this radius would be counted as a part of cluster and anything that is outside of it would be treated as outliers. This value needs to be considered carefully otherwise it may lead to loss of certain data points.

2. minPts: There should be a threshold i.e. in order to be considered dense there should be certain number of minimum points in that area. minPts can be decided from the number of dimensions (D) present in our the dataset since minPts>=D+1. If dataset is larger, larger value of minPts is chosen. Fig 2.shows the DBSCAN graph.

One mainly gets 3 types of points when the DBSCAN algorithm on any given dataset is completed:-

1. Core- Core is the point around which one can make different clusters and within the r distance of radius there would be at least k number of points.
2. Border- Border is the boundary point that would be having at least one core point at a distance of radius r.
3. Noise- If a point is neither a border point not a core point. In distance of radius r, it has less than k points.

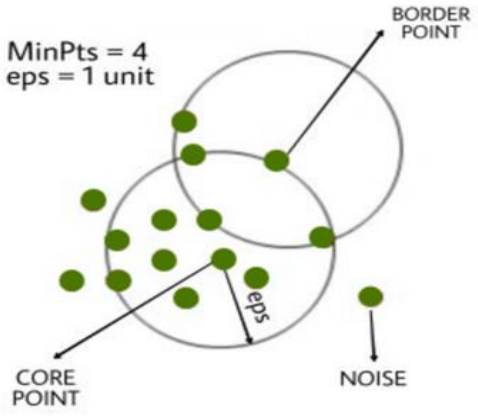

Fig. 2. About Dbscan

The steps of DBSCAN algorithm are following -

1. The working of this algorithm is in this way that it arbitrarily picks up a point in the database till the time until all the points are visited.
2. All these points are considered to belong to the same cluster if there are at least 'minpoint' points of 'ε' to the point.
3. By repeating the neighbourhood computation for each surrounding point in recursive fashion, clusters are being enlarged.
4. The minpts can be computed by using a number of dimensions of a data MinPts>=D+1.
5. Fig 3. Shows DBSCAN result.

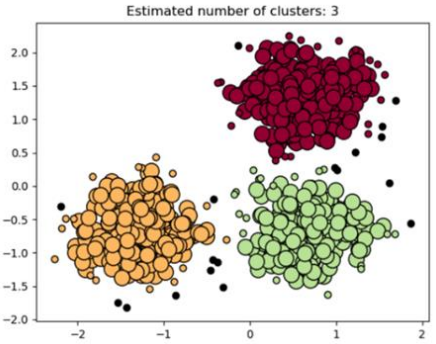

Fig. 3. DBSCAN result

Authorized licensed use limited to: DELHI TECHNICAL UNIV. Downloaded on June 15,2022 at 11:28:24 UTC from IEEE Xplore. Restrictions apply.

III. VARIATIONS OF DBSCAN

A. DBSCAN WITH K-Nearest Neighbour(KNN)

DBSCAN suffers from the drawback of dependence on user-defined parameters, in the referenced paper had a method that uses the information of k-nearest neighbors to achieve clustering method free of input parameters. In this variation of DBSCAN the results of two separate approaches have been combined. [1] The first one is usual DBSCAN algorithm and another is graph-theoretic concept of searching strongly connected components in a penalized knn graph. Because both the methods work in a sequential order, they can be combined.

The combined approach combines the benefits of both methods while also allowing for the proven and time-tested practical execution of both. As a result, the idea offers a viable and practical alternative for clustering in the presence of arbitrary shaped clusters. In this algorithm basically each cluster is constructed one at a time. The size of a cluster is increased until it reaches its peak, after which it is removed from the dataset. The remaining dataset is analyzed once again in order to find a peak or kernel. When a peak or kernel is found, concepts of density are utilized to build the cluster around it. In Fig 4. we have made the comparison between two sets of DBSCAN.

This gives a clustering method based on density with benefit of both the algorithm where user is not required to decide the values of parameters. The parameters which were to be used by knn graph formation and DBSCAN are not calculated by the proposed rules of method.

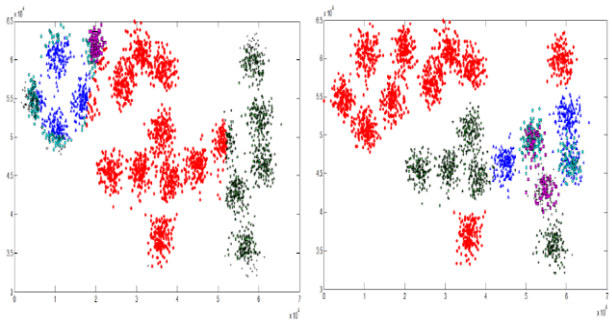

Fig. 4. Comparision of DSets-DBSCAN and KNN-DBSCAN

B. DBSCAN WITH PSO

The clusters which are formed by DBSCAN algorithm are heavily dependent on input variables (Minpoints and epsilon) that the user must provide. In DBSCAN with Particle Swarm Optimization (PSO) it automatically computes these values and finds the spatial hotspots. It is inspired from nature like group behavior of birds and fishes and simulate the behavior of natural things to solve complex algorithmic problems. [2] In this paper 6 artificial datasets are used to evaluate the accuracy of PSO based DBSCAN technique. Table 1 shows results on artificial datasets. The achieved purity for all the datasets were approximately between 76 percent and 100 percent as can be seen in the table.

.

TABLE I. RESULTS WHEN WORKED ON ARTIFICIAL DATASETS

S No.	Dataset	MinPoints	Epsilon	Purity (%)
1	[12]	4	1.7	76.6
2	[13]	10	15.48	99.8
3	[14]	3	1.5	97.4
4	[15] DS1	6	0.5	100
5	[15] DS2	3	0.941	100
6	[15] DS3	10	0.1504	99.5

This method can be further extended to find the spatio-temporal hotspots in other fields like earthquake zoning, medical specialty, epidemiology, and criminology etc.

C. DBSCAN WITH REVERSE KNN

In this variation of DBSCAN with adaptive parameter k-RNN (k- Repetitive Nearest Neighbor) ARKNN-DBSCAN clusters can be easily identified and separated using the correlation through reverse knn of observation. [3] This algorithm is more accurate than DBSCAN using adaptive parameter. In this variation, core point is searched by giving a query of different number of k-RNN in the dataset, the k nearest neighbors of the core points is expanded into the clusters. The correlation between the parameter k and the generated cluster is used to find k value with optimal solution. The advantages of this algorithm are that in this algorithm there is no need to input parameter that helps to boost the robustness of algorithm. Table II shows the comparison between clustering algorithms. There are few limitations to this algorithm as well i.e., this algorithm is inefficient on large scale datasets. Four different datasets were chosen and F-score was used to measure the accuracy of clustering. One can clearly infer from results that the accuracy of AKRNN-DBSCAN is higher than other algorithms.

TABLE II. CLUSTERING ALGORITHM COMPARISON

Datasets	Clusters	Observations	Algorithms	F-score
Aggregation	7	788	I-DBSCAN	0.9246
			AF-DBSCAN	0.9655
			AKRNN-DBSCAN	0.9833
Compound	6	399	I-DBSCAN	0.8561
			AF-DBSCAN	0.8251
			AKRNN-DBSCAN	0.9013
R15	15	600	I-DBSCAN	0.8908
			AF-DBSCAN	0.8207
			AKRNN-DBSCAN	0.9286
Iris	3	150	I-DBSCAN	0.8626
			AF-DBSCAN	0.8339
			AKRNN-DBSCAN	0.9325

Authorized licensed use limited to: DELHI TECHNICAL UNIV. Downloaded on June 15,2022 at 11:28:24 UTC from IEEE Xplore. Restrictions apply.

D. .DBSCAN clustering algorithm by accelerating neighbor searching using Groups method

GDBSCAN is also one of the density-based clustering algorithms whose performance is better than the conventional DBSCAN. In this an efficient graph-based structure is used once entire dataset is scanned two times. Fig 5. In this algorithm the process of finding the nearest neighbor is improved by using the group method. This algorithm involves two phases:

1. Finding the set of groups by using group algorithm on entire dataset.
2. Running conventional DBSCAN algorithm on desired groups.

This includes a master-slave pattern where each vertex (Group) is represented by master and slave is the Eps-neighborhood pattern of master. [4]This method is also parameter free and thus requires no input from user.

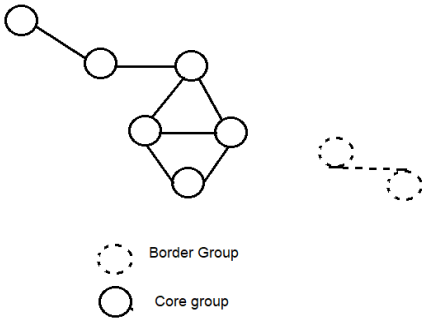

Fig. 5. Groups obtained as disconnected graphs

Each pattern is searched, if distance between master pattern and taken pattern<=Eps then the pattern is taken into to the group, if this distance is =Eps, taken pattern is not assigned any group and is then processed during next iteration. Fig 6. If the distance is >2Eps new group is created with the pattern as master pattern. In the second iteration if distance <=Eps, pattern is assigned to that group otherwise new group with it as master pattern is created.

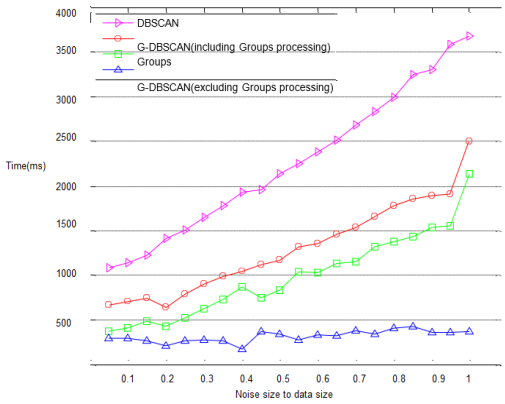

Fig. 6. Comparison of running time of DBSCAN and G DBSCAN with noise

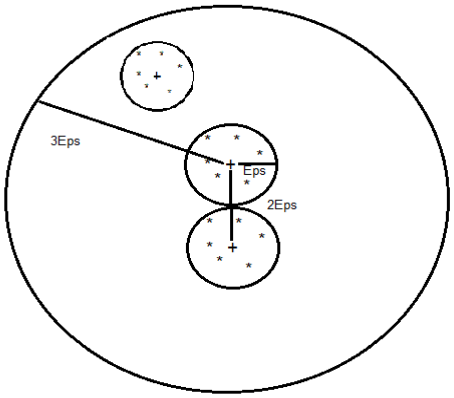

Fig. 7. Groups with its reachable groups

Advantages of this algorithm:

1. Does not require input from user.
2. Handles noise effectively
3. Ensures that the space search is small area.
4. Performance: Algorithm has O(n+nd) time complexity, where d is maximum number of distance computations.
5. GDBSCAN speeds up the neighbour search operation in clustering since GDBSCAN improves the execution speed of DBSCAN. It ensures that for any given pattern neighbour searching does moves to points that are beyond 5 times eps.
6. No user input is required.
7. Groups method is much more stable when compared with the indexed based structures.

Fig 7 shows groups with its reachable groups

Application areas: *Bioinformatics, pattern recognition, image analysis etc*.

E. DBSCAN by parallelizing K Dimensional Tree (KD-Tree) using Spark

KD-Tree helps to reduce the search time in DBSCAN algorithm. In a normal binary tree, there is only one key while in KD Tree there are k keys and it cycles through each key in successive levels.
In a KD Tree, Left subtree<parent<right subtree
Spark: [5] It's an open-source platform that is used for data computing, analytics etc. It has much better speed, fault tolerance, scalability etc. when compared to other platforms.
Amazon Web Services (AWS): It's a cloud computing platform used by many companies worldwide. In Fig 8 and Fig 9 we compares DBSCAN using KD Tree with and without spark.
Euclidean distance is taken as a measure of similarity among different points. The spark framework is used to construct the KD tree in parallel way. After that in order to avoid inter-executer communication KD Tree is propagated through accumulator. A hypersphere is drawn of radius Eps around

Authorized licensed use limited to: DELHI TECHNICAL UNIV. Downloaded on June 15,2022 at 11:28:24 UTC from IEEE Xplore. Restrictions apply.

data point. this is done in order to check if other points fall within hypersphere or not.

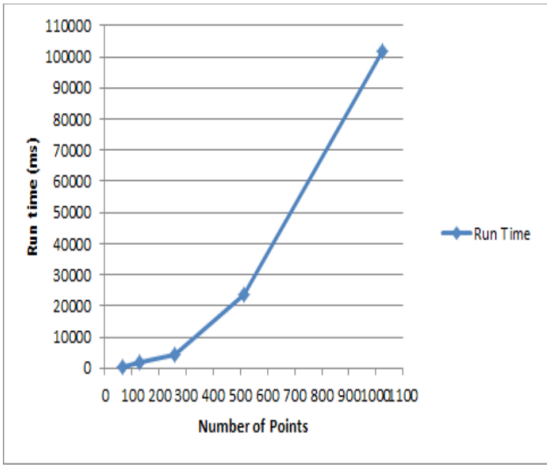

Fig. 8. DBSCAN using KD tree without spark

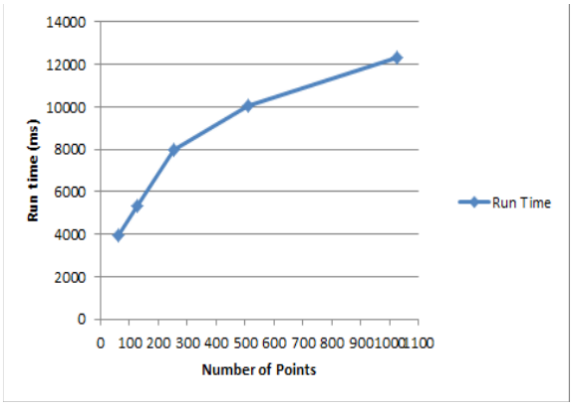

Fig. 9. DBSCAN using KD tree with spark

The result analysis of this variation of algorithm was done using 2 criteria, according to dimensions and according to number of points. The figures show the analysis in accordance to the number of points.

Advantages:

1. This method is superior to existing DBSCAN parallelization methods.
2. Algorithm has efficient clustering in multi-dimensional dataset.
3. More efficient in removing noise.

Application areas: big data applications, fraud detection, social media analytics etc.

F. The Combination Synthetic Minority Oversampling Technique (SMOTE) and DBSCAN

This algorithm involves SMOTE technique along with DBSCAN algorithm in order to improve the predictive performance of imbalanced data. The k fold cross validation technique is used for training and testing the datasets. Then for data preprocessing, there are 5 cases: SMOTE, DBSM, DBSCAN, SMOTE+Tomek Links, Tomek Links. So, there are 5 sampling methods and 6 training datasets.

Then a decision mode tree is constructed from each training data set. The models are then evaluated in order to find the classification performance on the same set.

The DBSM algorithm successfully handled the imbalance problem. [6] The performance of F measure was improved because of the effectiveness of DBSCAN algorithm. This variation is not that efficient in regards to time complexity but by using this varied density clusters on 2D data are identified easily. Its time complexity is same as that of conventional DBSCAN. This algorithm does require input parameters from the user.

TABLE III. IMPROVED PERFORMANCE OF DBSCAN ALGORITHM

Dataset Name	Original	SMOTE	TL	SM+TL	DBSCAN
glass!	31.49%	3.29%	3.92%	1.55%	7.41%
WISCOSID	0.72%	0.51%	-1.44%	-1.44%	-0.18%
glassO	1.14%	0.00%	2.23%	4.83%	1.88%
yeast!	8.56%	8.87%	4.10%	1.55%	8.64%
haberman	62.62%	24.42%	6.45%	-3.75%	38.10%
vehicle2	1.14%	0.39%	1.10%	1.01%	1.13%
vehicle!	20.66%	9.36%	12.04%	13.85%	3.91%
new-thyroid I	9.27%	0.29%	9.75%	3.49%	7.33%
new-thyroid2	7.47%	8.57%	16.23%	8.57%	7.23%
ecoli2	9.70%	4.29%	-0.35%	-2.50%	1.17%
glass6	12.95%	15.96%	1.21%	3.79%	11.12%
yeast3	6.67%	1.38%	4.19%	-0.37%	3.58%

The experiment involved rebalancing 12 datasets using 5 resampling techniques and using the decision tree algorithm the models were constructed. In the result this variation of DBSCAN algorithm successfully handled the imbalance problem

The effectiveness of this variation of DBSCAN algorithm is reflected in improved F-measure (62.62). With this variation the effectiveness of conventional DBSCAN algorithm improved. Table III shows the improved performance of DBSCAN algorithm.

Advantages:

1. Reduced time complexity than the DBSCAN algorithm.
2. Handles the class imbalance problem.
3. This algorithm is more effective and has much better performance.

Authorized licensed use limited to: DELHI TECHNICAL UNIV. Downloaded on June 15,2022 at 11:28:24 UTC from IEEE Xplore. Restrictions apply.

G. Fast Density based clustering algorithms

The aim of FDBSCAN algorithm is to increase the performance and bring the time complexity to linear. Major advantage of using FDBSCAN is that points are calculated only once because it in this labelling is maintained with the help of indexing. Even if datasets have dense region, the FDBSCAN works fine. [7] The eps value determines the number and shape of clusters. In the runtime complexity of FDBSCAN α 1/ Eps value. The problem with this algorithm is that in this varied density clusters in not addressed.

H. Varied DBSCAN

In data mining finding the sparse clusters is also necessary but conventional DBSCAN only finds the dense clusters. In DBSCAN the cluster density is dependent upon the Eps value. [8] In order to calculate different densities varied density method measures different values of Eps. In VDBSCAN algorithm the distances of each point from their Kth nearest neighbor are computed and then the points are plotted according to the K-distance. New value of Eps is indicated by sharp change in k-distance value. After all this, Normal DBSCAN algorithm is implemented for given value of Eps. This variation is not that sufficient in regards to time complexity but by using this varied density clusters on 2D data are identified easily. Its time complexity is same as that of conventional DBSCAN. This algorithm does require input parameters from the user.

IV. PARAMETRES

All of the solutions for improving the DBSCAN algorithm with various drawbacks are evaluated on certain parameters in order to compare and evaluate these algorithms.

A. Problem to overcome: Gives the scope of improvement in original DBSCAN with the new variation.
B. Dataset used: Either synthetic or real-world dataset is used.
C. Time complexity: This parameter compares the complexity of variation.
D. Input parameters: These are the parameters on which input is given to the variations and then compared with DBSCAN.
E. Output: It shows if result is same as that of the conventional DBSCAN.
F. Noise removal: One of the DBSCAN's key advantages is noise reduction which is analysed in each technique

TABLE IV. IMPROVED PERFORMANCE OF DBSCAN ALGORITHM

S no.	Algorithm	Problem to overcome	Dataset Used	Time Complexity	Input parameters	Output	Noise Removal
1	DBSCAN with KNN	To achieve a parameter free clustering technique	Synthetic	Reduced	Same as DBSCAN	Separation of clusters to more extent	Clusters of outer regions are fully free from noise
2	DBSCAN with PSO	To automatically compute the value of minpts and ε	Same	Same	Same as DBSCAN	Purity value is in a range	Same as DBSCAN
3	DBSCAN with Reverse KNN	To effectively identify and separate clusters with different densities without input parameters	Synthetic	Reduced	No inputs required	Accuracy is higher measured by f score	Same as DBSCAN
4	DBSCAN Clustering algorithm by accelerating neighbor searching using groups method	Time complexity and low accuracy	Synthetic	Reduced O(n+p)	No inputs required	Better and stable results	Handled noise effectively
5	DBSCAN by parallelizing KD Tree using Spark	Time complexity and inefficient clustering in multidimension	Synthetic	Reduced	Same as DBSCAN	Efficient clustering in multidimension	More efficient in removing noise
6	Combination of DBSCAN and SMOTE for imbalance data classification	Class imbalance problem	Real (from KEEL)	Reduced	Amount of synthetic samples and number of nearest neighbors	More effective and improved performance	Same as DBSCAN
7	Fast Density based clustering algorithm	Complexity	Synthetic	Reduced to Linear	Same as DBSCAN	Better than DBSCAN	At final stage
8	Varied DBSCAN	Varied Density	Synthetic	Same	Predefined K-distance	Better identified varied density	At final stage

Authorized licensed use limited to: DELHI TECHNICAL UNIV. Downloaded on June 15,2022 at 11:28:24 UTC from IEEE Xplore. Restrictions apply.

V. CONCLUSION

In this paper the review work of various variations of DBSCAN algorithms has been presented. There are few limitations of this algorithm and many variations have been proposed to overcome these limitations from time to time. After reviewing various variations conclusion was made that these variations were improvements of the conventional algorithms in some or the other way. These variations were also compared on the basis of certain parameters. Some were improvements in time complexity, some were related to parameters and some were related to noise removal. In a few variations the effect of increasing dimensionality was addressed to a certain extent but in some this issue remained. Table IV denotes the final comparison between all our variations on the given parameters. Some variations also addressed the class imbalance problem. However despite the advantages over the conventional algorithm, each variation has its own limitation. So the type of variation to be chosen for a practical purpose depends upon the application area and also on what parameter is more desirable.

REFERENCES

[1] Sharma, Ankush, and Amit Sharma. "KNN-DBSCAN: Using k-nearest neighbor information for parameter-free density based clustering." 2017 International Conference on Intelligent Computing, Instrumentation and Control Technologies (ICICICT). IEEE, 2017.

[2] Wadhwa, Ankita, and Manish K. Thakur. "Modified DBSCAN Using Particle Swarm Optimization for Spatial Hotspot Identification." 2018 Eleventh International Conference on Contemporary Computing (IC3). IEEE, 2018.

[3] Pei, Pengyu, Dong Zhang, and Feng Guo. "A density-based clustering algorithm using adaptive parameter k-reverse nearest neighbor." 2019 IEEE International Conference on Power, Intelligent Computing and Systems (ICPICS). IEEE, 2019.

[4] Sanguanmak, Yotsathon, and Anantaporn Hanskunatai. "DBSM: The combination of DBSCAN and SMOTE for imbalanced data classification." 2016 13th International Joint Conference on Computer Science and Software Engineering (JCSSE). IEEE, 2016.

[5] Shibla, T. P., and KB Shibu Kumar. "Improving efficiency of DBSCAN by parallelizing kd-tree using spark." 2018 Second International Conference on Intelligent Computing and Control Systems (ICICCS). IEEE, 2018.

[6] Kumar, K. Mahesh, and A. Rama Mohan Reddy. "A fast DBSCAN clustering algorithm by accelerating neighbor searching using Groups method." Pattern Recognition 58 (2016): 39-48.

[7] Rodriguez, Alex, and Alessandro Laio. "Clustering by fast search and find of density peaks." science 344.6191 (2014): 1492-1496.

[8] Liu, Rui, Hong Wang, and Xiaomei Yu. "Shared-nearest-neighbor-based clustering by fast search and find of density peaks." Information Sciences 450 (2018): 200-226.

[9] Mehmood, Rashid, et al. "Clustering by fast search and find of density peaks via heat diffusion." Neurocomputing 208 (2016): 210-217.

[10] Wang, Shuliang, et al. "Clustering by fast search and find of density peaks with data field." Chinese Journal of Electronics 25.3 (2016): 397-402.

[11] Jahirabadkar, Sunita, and Parag Kulkarni. "Algorithm to determine ε-distance parameter in density based clustering." Expert systems with applications 41.6 (2014): 2939-2946.

[12] Jain, Anil K., M. Narasimha Murty, and Patrick J. Flynn. "Data clustering: a review." *ACM computing surveys (CSUR)* 31.3 (1999): 264-323.

[13] Jahirabadkar, Sunita, and Parag Kulkarni. "Algorithm to determine ε-distance parameter in density based clustering." *Expert systems with applications* 41.6 (2014): 2939-2946.

[14] Zhou, Z. P., et al. "An improved adaptive and fast AF-DBSCAN clustering algorithm." *CAAI Trans. Intell. Syst* 11 (2016): 93-98.

[15] Zhao, Liangbin, Guoyou Shi, and Jiaxuan Yang. "An adaptive hierarchical clustering method for ship trajectory data based on DBSCAN algorithm." 2017 IEEE 2nd International Conference on Big Data Analysis (ICBDA). IEEE, 2017.

[16] Ozkok, Fatma Ozge, and Mete Celik. "A new approach to determine Eps parameter of DBSCAN algorithm." *International Journal of Intelligent Systems and Applications in Engineering* 5.4 (2017): 247-251.

[17] Xie, Ningwei, et al. "Adaptive DBSCAN algorithm based on sample density gradient." Journal of Physics: Conference Series. Vol. 1229. No. 1. IOP Publishing, 2019.

[18] Tang, Xun, et al. "Significant linear hotspot discovery." IEEE Transactions on Big Data 3.2 (2017): 140-153.

[19] Tang, Xun, et al. "Significant linear hotspot discovery." *IEEE Transactions on Big Data* 3.2 (2017): 140-153.

[20] Louhichi, Soumaya, Mariem Gzara, and Hanène Ben Abdallah. "A density based algorithm for discovering clusters with varied density." *2014 world congress on computer applications and information systems (wccais)*. IEEE, 2014.

Authorized licensed use limited to: DELHI TECHNICAL UNIV. Downloaded on June 15,2022 at 11:28:24 UTC from IEEE Xplore. Restrictions apply.

WWW.IJRPR.COM

International Journal of Research Publication and Reviews

Journal homepage: www.ijrpr.com ISSN 2582-7421

Review of development and advancement in Flexible Manufacturing System

Ritvik Maliya[1], Rohan Gupta[2], Ak Madan[3]

[1]Student, Dept. of Mechanical Engineering, Delhi Technological University, Delhi
[2]Student, Dept. of Mechanical Engineering, Delhi Technological University, Delhi
[3]Associate professor, Dept. of Mechanical Engineering, Delhi Technological University, Delhi

A B S T R A C T

Flexible manufacturing system consists of Computer numeric Control (CNC) machine tools, interconnected by material handling and storage system. It has ability to change and adjust itself according to the market demands. FMS is really useful in industry but it is not enough to deal with modern problems. This leads to development of new technologies like Reconfigurable Manufacturing System (RMS). Its software and hardware are of modular structure. Different modules can be added, removed and switched according to the requirement. Implementation of AI can also be helpful to deal with many complicated processes in manufacturing. We can upload our data on a cloud and use this data to remove defected parts in future.

Keywords:Flexible Manufacturing System, Reconfigurable Manufacturing System.

1. INTRODUCTION

Flexible manufacturing system is manufacturing system with highly automated machine cells. It contains multiple interconnected workstations (CNC machines) by automated material handling and storage systems. All of these components are controlled by computer with the help of computer-controlled system.

Features of Flexible Manufacturing System

1. A Flexible Manufacturing System is different from an automated production line due to its ability to process different product style at once.
2. Flexible Manufacturing System gives us flexibility in changing production time in order to fulfil the demand of different products.
3. It has capability of producing large number of similar parts at low cost.
4. It can produce different part without major retooling.

2. COMPONENTS OF FMS

1) Workstations - They are CNC machine tools that performs different machining operations on the workpiece. First our workpiece reaches to the machining centers. Then it is loaded and unloaded to different Machine tools to perform different operations with the help of Load and Unload stations. After this all the parts are assembled and send to inspection stations.

2) Automated Material Handling and Storage system

They are used to transport unfinished and unassembled parts between the processing stations and storage system. The parts can be moved randomly and independently between the work stations and can also be stored temporarily in the storage system.

3) Computer Control System

It helps in controlling all the components of FMS like workstations and the material handling system. It can also control the system performance and can report it to the users.

3. RECONFIGURABLE MANUFACTURING SYSTEM

Rms was developed by the university of michigan college of engineering's research centre. A reconfigurable manufacturing system (rms) is a system used by manufacturers that emphasizes the importance of being able to change rapidly in short time. It can change its productivity capacity and functionality according to the changes in market demand. Rms has a modular structure in software and hardware. We can add, remove and switch these modules to make the changes in our system. Due to a sudden change in the market, the fms are forced to change their production to mass production that affects the optimization of the inventory but the reconfigurable manufacturing system changes in response, allowing the company to produce goods or products in an efficient manner.

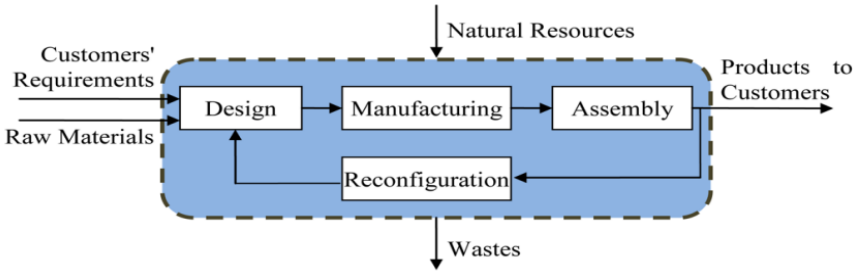

4. CHARACTERISTIC OF RMS

1) modularity – machines, tools and other items in rms are present in modules. They can be integrated, removed and switched according to the requirement.

2) integrability – different modules can be integrated in an rms at both machine and system levels.

3) customization - rms is flexible enough to upgrade and add new modules.

4) scalability – rms can rearrange itself to add new products.

5) convertibility – rms can change its design to suit a new production line.

6) diagnosability – rms has the ability to detect the defects and errors in the system.

4. IMPLEMENTATION OF ARTIFICIAL INTELLIGENCE IN FMS

There are two major categories in Manufacturing. First is Continuous manufacturing and second is Discrete manufacturing. Now we will focus on a mathematical model of discrete manufacturing. It consists of three stages including part design, process design, process execution.

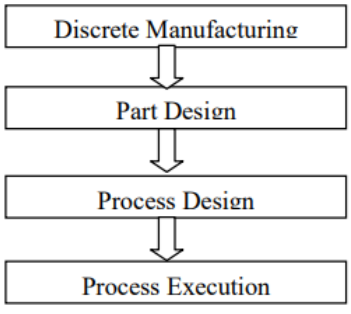

Part Design - The first stage is a conceptual and contains many constraints. The product planning function gives the request for particular set of functions like product performance level and its selling price in the marketplace. Management function contains design and development.

Process Design- this stage is similar to part design, except that it focuses more on designing process. It also contains many important constraints like the production facilities and the inventory of tools, parts and materials.

Process Execution- As our product is designed completely, next we have to execute the process. In the first step of process execution, all the raw materials and tools and parts are brought together with CNC machines. The second step in Process Execution includes assembly of products with the help of sensor-based robots. After this our product goes for finishing, inspecting, testing and finally gets stored in the storage system.

REFERENCES

Arvind Kaushal, Ajay Vardhan, R. S. Rajput, "Flexible Manufacturing System A Modern Approach To Manufacturing Technology", International Refereed Journal of Engineering and Science, Vol. 05, Issue: 4 (April 2016), pp.16-23.

Ravi Kumar, Arun Kumar, Sumit Kumar, "Review of Trends and development in flexible and reconfigurable manufacturing systems", International ResearchJournal of Engineering and Technology, Vol. 05 Issue. 04 | Apr-2018: pp. 2047-2052.

Amar Kumar Das, Manas Ranjan Das, "Role of Artificial Intelligence in Flexible Manufacturing Process - A Review", International Research Journal of Engineering and Technology, Vol. 05 Issue. 11, Nov. 2018, pp.1788-1790.

Kashif Mahmood, Tatjana Karaulov, Tauno Otto, Eduard Shevtshenko, "Performance Analysis of a Flexible Manufacturing System (FMS)", ELSEVIER B.V. (2017), pp. 424-429.

Proceedings of the Sixth International Conference on Trends in Electronics and Informatics (ICOEI 2022)
IEEE Xplore Part Number: CFP22J32-ART; ISBN: 978-1-6654-8328-5

Sentiment Analysis on Online Reviews using Machine Learning and NLTK

Shailender Kumar
Department of Computer Engineering
Delhi Technological University
Delhi, India
shailenderkumar@dce.ac.in

Nazir Ahmad Jailani
Department of Computer Engineering
Delhi Technological University
Delhi, India
nazirahmadjailani35@gmail.com

Abhinav Raj Singh
Department of Computer Engineering
Delhi Technological Univerity
Delhi, India
nav.abhi.raj@gmail.com

Shubham Panchal
Department of Computer Engineering
Delhi Technological University
Delhi, India
impanchals@gmail.com

2022 6th International Conference on Trends in Electronics and Informatics (ICOEI) | 978-1-6654-8328-5/22/$31.00 ©2022 IEEE | DOI: 10.1109/ICOEI53556.2022.9776850

Abstract— **Advancement in technology paved the way to the new era where machines play great role. Machines make decisions and understand us based on our behaviors and can be trained by data to learn and provide a good accuracy in analyzing business data insights, recommending of goods. The sentiment analysis determines the product effectiveness felt to the customers or public in terms of ratings. The analysis is carried out on modern data science tool and technologies. The machine learning and natural language processing tools and algorithms determines the sentiment classifications either in positive, negative, or neutral class. The accusation of data, through preprocessing and feature extraction in supervised form has been analyzed for the accuracy enhancement on a particular set of algorithms and NLTK tools. The pre architecture was designed and the data sets were then implemented for the effective results and accuracy. In this paper, different machine learning algorithms are applied with natural language kit tools for extraction of features, and it is concluded that logistic regression works best with accuracy of 80% and rest algorithms have less accuracy as compared to logistic regression.**

Keywords—Machine learning, Linear Regression, k nearest neighbors, Data Preprocessing, Principal Component Analysis

I. INTRODUCTION

Machine learning is the trending area in last decades and is widening day after day. Technology is evolving and enhancing that significantly shows their necessity in business, advertisements, and many more areas [6]. It is a trend because it provides companies a view of insights in customer behavior and operational business models and recognize the patterns in business. All of today's successful companies, such as google, Uber, Ola, Amazon, Facebook, utilizes machine learning and natural language Processings for the sentiment analysis over their products or feedbacks. Most of the companies, influencers, politicians, government officials, sports stars, and film artists generally express their thought on twitter on daily basis and sentiment analysis on these data can help them assess what the public thinks about them or their products or services in case of companies. Sentiment Analysis has become of importance in nowadays time as getting to know the opinion of the public has a lot to do so that improvement can be done where public figures and feel they are lacking. Sentiment Analysis is a technique through which we try to find out what a sentence or word indicates. It is of extreme use to understand the thought, emotions, feelings that the sentence is describing [10]. Twitter is a very popular microblogging platform; anyone can express their opinions and thought freely on twitter due to which large number of data are generated every day and analyzing on these data helps to identify the sentiment of tweets. Bringing the thoughts and feedback to a machine level and giving another interface for a global word value detection, sentiment Analysis has come to play a big role in today's time as getting to know the opinion of the public has a lot to do so that improvement can be done where public figures feel they are lacking. Some other features in twitter or online products review contains URL, #, @, numbers which usually have no benefit and add noise into the tweet, so they are supposed to be pre-processed because it brings ineffectiveness in the implemented stack and technology. Which methods of pre-processing are more useful have been discussed? When we are classifying online products review based on various sentiments into classes then we need to take care as to how many classes are required will it be beneficial to have more classes or having a smaller number of classes will improve accuracy. We have seen that in detail as well. Most of the techniques in sentiment analysis use nominal class data labels but they have problems in pattern recognition in ordinal scale so to better it we have done ordinal regression. We perform ordinal regression on our dataset and check which classifier method is the best [7-8].

II. LITERATURE SURVEY

Most of the current approaches deal with reducing the amount of noise in the tweets or reviews with the intention being to increase the performance in the

Authorized licensed use limited to: DELHI TECHNICAL UNIV. Downloaded on June 03,2022 at 06:28:58 UTC from IEEE Xplore. Restrictions apply.

process also improving the speed It has been reported that the vocabulary has been reduced to 62 percent experiments have shown that accuracy rises after removal of stop words and expanding of acronyms [12]. A study was conducted wherein the use of six different stop words are done. It was seen whether these top words any the effects of various methods have like stemming and lemmatization are applied and then by using two different feature models the effect on the performance is analyzed. Generally, there has not been much thought given to having more number classes, researchers have given more focus to the content of tweets, but now since very established methods are present focus has shifted on a greater number of classes recently [11]. Most of the advanced work in case of deciding number of classes has been to increase the degrees of positive and negative. There are recent works that have classified reader emotions into several categories these have been done on newspaper headlines. Sentiment classification and extracted more than one sentiment class for twitter extraction. Recommendation of emoticons is one field where multi class classification has been seen to be useful [9].

III. METHODOLOGY

The sentiments detection procedures can be categorized into different sections based and theories based on the understanding and implementations [16]. This is very initial topic for the understanding of Machine learning algorithms and these problems can also be solved using higher and enhanced ML algorithms using Deep learning and Natural Language processing. The basic flow chart of the methodology of Sentiment detection can be seen in the fig.1

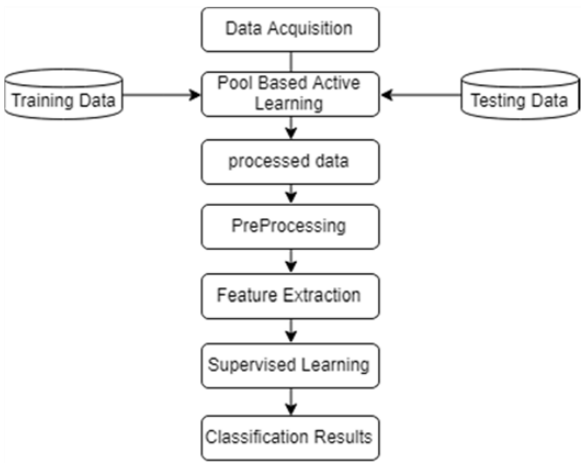

Fig.1 flowchart of sentiment detection

Fig.1 shows that how data is preprocessed through training and testing the data and then following the process of features extraction followed by supervised learning experience and then processing classification results.

A. Datasets

The datasets obtained here is from the Kaggle environment. A lot of datasets are present for the deep sentiment analysis. The datasets are in the form of Amazon product review for sentiments analysis, twitter review for sentiment analysis. We generated a common dataset of online reviews from different datasets in CSV form from scratch with the common features for the Sentiment detection for the online reviews. The datasets contain the review of mobile electronic products, tweets, and amazon products review. This is newly designed datasets with combination of 3 different datasets.

B. Data Preprocessing

Since the dataset contains some impurities that some information is missing and even some data of a particular row and column are missing [13]. To make the datasets pure and complete for efficient execution of algorithms the preprocessing task is carried out. The preprocessing task not just only involves the methods of data cleaning. All the different natural language processing tools to be performed over datasets is the part of data preprocessing. The data preprocessing task involves data cleaning, tokenization, removing stop words and POS tagging [15].

1) Tokenization

After the cleaning of data, the newly designed datasets become efficient for execution of the algorithms and tools of natural language processing. The initial task after data cleaning is tokenization which tokenize all the reviews. During the tokenization the reviews are broken into tokens and their frequency is measured. All the words of a sentences are treated as token and then frequency of each word is measured and stored for the future reference. The full stops and the punctuation marks are removed during the process of tokenization and all the words of uppercases are converted to lower cases to bring the uniformity in the system i.e., the system gets easy to access words in the binary form. Tokenization is one of the most useful steps for the proceedings of sentiment analysis [14].

2) Removing stop words

Those words that doesn't play role for the sentiments of a particular words like is, an, the, it is called as the stop words. These words only occupy spaces in the large scale which declines the algorithms efficiency. So, these words should be removed. Depending on the language and script different country has different stop words, all of them are ejected from the system of the data to bring the efficiency over the algorithms applied [17].

Authorized licensed use limited to: DELHI TECHNICAL UNIV. Downloaded on June 03,2022 at 06:28:58 UTC from IEEE Xplore. Restrictions apply.

3) Pos tagging

When another NLTK tool fails to capture the appropriate functioning and structure of the sentences then the part of speech helps to overcome the situation and give the accurate structure over the sentences. This is used to avoid the wrong meaning given by the bags of words. The 8 parts of speech are highly recognized and maintained in the pos tagging tool to overcome the different meaning given by the sentences. The part of speech taggers functions this task of pos tagging [2].

C. Features Extraction

Features extraction is the important part of the methodology which works on the extracting the essential features of the preprocessed data for the sentiment detection of the reviews [3].

The proposed algorithms of the features extraction of sentiment analysis on products with the preprocessing part is given in fig.2

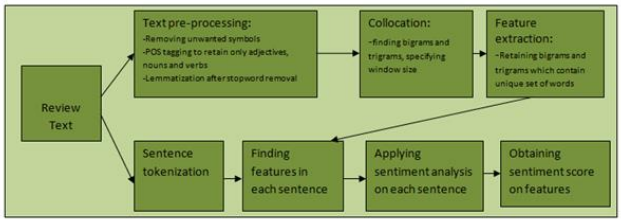

Fig.2 features extraction algorithm

When the similar text results into the closer vector then the vector X must be derived in such a way that all the textual results formed should be applicable to all the linguistic properties in the text [5].

1) Bag of words

The bag of words is used for the information retrieval in the natural language processing. It is generally used for the documentation in the field. In sentiment analysis, bag of words is considered as a group of words that gives a definite meaning, sometime the meanings can sense in two ways so, to enhance this lagging properties we generally update bag of words with pos tagging to give a single definite meaning. In these cases, the frequency of the words doesn't get involved into the double direction of meaning. The Pos tagger handles and gives direction for a single meaning for a particular frequency of words. The bag of words involves two cases, the vocabulary of known words and the measure of presence of the known words [20].

2) Tf-Idf

It gives the numerical and statistic valves of the frequency of the words in the corpus [30]. The meaning is term frequency-inverse documentary function. The function has two major tasks i.e., to count the number of frequencies of word that appears in the corpus and number of times the word appears in the documents [21]. It aims to find the probability of appearance of the word in the given document.

$$TF(w_i, r_j) = \frac{\text{No. of times } w_i \text{ occurs in } r_j}{\text{Total no. of words in } r_j}$$

Fig.3 Probability of word in document

Similarly, Idf which is inverse document frequency provides that how much the word is common and rare in the documents and what information it can provide [4].

3) Word2Vec

Word embedding is generally the vectorize for representation of the words. It helps in bringing the relation between the words of different features which might represent different sentiments in the given documents. Word embedding converts all the data or token of words into array and matrix form that can be easily mapped with other words and nearest relations can be figured out into binary systems of the computer [31]. It closely helps to differentiate between the category of the words in terms of sentiments that whether the word is positive, negative, or neutral [18].

D. Algorithms for proposed approach

Algorithms for the proposed sentiment analysis task over different machine algorithm applied and NLTK tools processed over the datasets can be seen in the fig.4. It shows the common method through which accuracy is obtained the different machine learning algorithms [19]. The machine learning algorithms applied in the task are Decision tree classifier, random forest classifier, linear support vector machine, multinomial naïve and logistic regression.

```
INPUT:
LABELLED DATA=LABELLED DATA OBTAINED AFTER
ACTIVE LEARNING PROCESS.

OUTPUT:
ACCURACY OF CLASSIFIERS.
PRECISION, RECALL, F-1 MEASURE FOR POSITIVE AND
DECEPTIVE VALUES.
//PRODUCT REVIEW POLARITY ACCURACY
    LOAD LABELLED DATA POSITIVE & NEGATIVE
    PRE-PROCESS LABELLED DATA
    FOR EVERY X= {X1,...Xn} IN LABELLED DATA
    EXTRACT FEATURE (Xi)
    CROSSES VALIDATE INTO TRAINING & TESTING
    SET
    CLASSIFIER. TRAIN ()
    ACCURACY= CLASSIFIER. ACCURACY ()
    MAJORITY VOTING(ACCURACY) USING VOTE
    CLASSIFIER
    SHOW RESULT (ACCURACY, PRECISION,
    RECALL, F1MEASURE) 10.END
EXTRACT FEATURE(TEXT) RETURN N-GRAM FEATURE
MAJORITY VOTING(ACCURACY) RETURNS HIGHEST
ACCURACY
```

Fig.4 Preprocessing and Feature extraction algorithm

IV. Evaluation Measures

This section Discusses the algorithms used and the measures taken into the account for the accuracy

Authorized licensed use limited to: DELHI TECHNICAL UNIV. Downloaded on June 03,2022 at 06:28:58 UTC from IEEE Xplore. Restrictions apply.

calculation. This section briefly discusses all the machine learning algorithms and the formulation part for accuracy measure [1].
Before the formulation part there are some terns to be mentioned.

- TP (True Positive) which represents numbers of the data correctly classified in the corpus or documents
- FP (False Positive) which represents numbers of correct data misclassified in the corpus or the documents
- FN (False Negative) which represents numbers of incorrect data classified as correct in the documents or the corpus
- TN (True Negative) which represents numbers of incorrect data classified in the document or corpus

A. Decision tree classifier

It is a supervised learning method that is used for both classification and regression problem solving. It is generally based on the binary system. The decision tree is based on the CART algorithm which is tree-based graph algorithm [24].

B. Random forest classifier

The random forest classifier is commonly based on the ensemble learning concept that helps in solving the complex supervised learning problems and it is also the result of multiple classifiers. The higher the trees numbers in the greater will be the efficiency and helps in preventing the problem of overfitting [22].

C. Linear support Vector Machine

Support vector Machine is one of the methods for the calculation of supervised learning problems. It works for both classification and regression problem. The main aim of the support vector machine is to create a boundary point that divides n dimensional space into the class so that we can put a new data easily into the future in a correct category26].

D. MultinomialNB

It is suitable for a classification type problem and discrete problem features. The distribution generally requires only an integer count but the fractional counts like tf-idf can also work.

E. Logistic Regression

It is very popular machine learning algorithm which is used for calculating the categorical values of the supervised learning data. It is generally used for calculating dependent variable of one category if reference to the independent variable of the same category. It gives the probability values which always lies in between 1 and 0.

F. Precision

It calculates that how exact the classifier is, the documents returned are correct to what extent. A less false positives means a higher precision while false positive means a lower precision. (P) is the ratio of numbers of instance correctly classified from total. It can be formularized as:

$$P = \frac{TP}{TP+FP}$$

G. Recall

It measures the classifiers sensitivity. Among the returns data how many of them are positively returned. Higher recall means less false negatives [23]. It is the ratio of number of instances accurately classified to the total number of predicted instances. This can be formularized as-

$$R = \frac{TP}{TP+FN}$$

H. F1-Score

Combining precision and recall produces single metrics known as F-measure, and that is the weighted harmonic mean of precision and recall [28]. It can be formularized as –

$$F = \frac{2P.R}{P+R}$$

I. Accuracy

It predicts how often the classifier makes the correct prediction. Accuracy is the ratio between the number of correct predictions and the total number of predictions [27].

$$Accuracy = \frac{Correct\ Prediction}{Total\ data\ points}$$

V. RESULT ANALYSIS

In this study, we have used five different machine leaning algorithm to perform sentiment analysis of twitter data. These algorithms are Decision Tree, Random Forest, Support vector machine, multinominal naive bayes and logistic regression. Experiment is performed using scikit learn and open source of machine learning library [26]. Twitter dataset was available in the Kaggle and was collected from there. This dataset undergoes various steps like pre-processing, then feature extraction to collect relevant features and then the model was trained, and finally different machine learning algorithm was applied to check the best algorithm for this dataset.

	Precision	Recall	F1-score	Support
negative	0.79	0.80	0.80	1858
neutral	0.47	0.41	0.44	652

Authorized licensed use limited to: DELHI TECHNICAL UNIV. Downloaded on June 03,2022 at 06:28:58 UTC from IEEE Xplore. Restrictions apply.

positive	0.55	0.61	0.58	418
accuracy			0.69	2928
Macro avg	0.60	0.61	0.60	2928
Weighted avg	0.68	0.69	0.68	2928

Table.1 Accuracy of Decision Tree classifier

Table.1 shows the accuracy of decision tree classifier which results 0.69 and its not really the good and much accurate as per the presence of current mathematical and computational power. Other algorithms can give more accurate result as compared to this method.

.

	Precision	Recall	F1-score	Support
negative	0.91	0.82	0.86	2094
neutral	0.45	0.57	0.50	459
positive	0.60	0.73	0.66	375
accuracy			0.77	2928
Macro avg	0.65	0.70	0.67	2928
Weighted avg	0.79	0.77	0.78	2928

Table.2 Accuracy of Random Forest Classifier

Table.2 shows the accuracy of Random Forest classifier which brings the accuracy of 0.77 which is better than Decision tree classifier but can be optimized more and can give more good results with other methods of machine learning algorithms.

	Precision	Recall	F1-score	Support
negative	0.86	0.85	0.86	1901
neutral	0.56	0.57	0.56	572
positive	0.70	0.71	0.70	455
accuracy			0.77	2928
Macro avg	0.60	0.61	0.60	2928
Weighted avg	0.78	0.77	0.77	2928

Table.3 Accuracy of LinearSVC

Figure.3 shows the accuracy of 0.77 which is like the random forest classifier and this algorithm is more accurate as compared to decision tree classifier.

	Precision	Recall	F1-score	Support
negative	0.96	0.79	0.86	2297
neutral	0.40	0.69	0.50	333
positive	0.54	0.84	0.66	298
accuracy			0.78	2928
Macro avg	0.63	0.77	0.68	2928
Weighted avg	0.85	0.78	0.80	2928

Table.4 Accuracy of MultinomialNB

Table.4 shows the accuracy of MultinomialNB which is 0.78 and is slightly more accurate as compared to Decision tree classifier, random forest tree and support vector machine.

	Precision	Recall	F1-score	Support
negative	0.89	0.86	0.87	1965
neutral	0.58	0.61	0.60	546
positive	0.70	0.77	0.73	417
accuracy			0.80	2928
Macro avg	0.72	0.75	0.73	2928
Weighted avg	0.80	0.80	0.80	2928

Table.5 Accuracy of Logistic Regression

Table.5 shows the accuracy of logistic regression which is much accurate as compared to rest of the algorithm. As per the system this is the best and optimized ML algorithms as compared to others.

Different Machine learning algorithms has been applied for the prediction of sentiments on online products review. Among all the algorithms tested, Logistic regression has been found to be most efficient with efficiency and accuracy of 80%. The accuracy of the data varies according to the hardware effects too. So, the result of the data can vary according to the hardware conditions too [29].

VI. Conclusion and Future work

In sentiment analysis we realized the importance of pre-processing and it is must to also understand the fact that using which preprocessing method is essential which can be ignored and what is the priority order of the various pre-processing methods. The usage and importance of these techniques are now clear and can be used appropriately as and when desired. We realized that having a greater number of classes can be both beneficial as well as detrimental depending on the cause of doing the analysis and application. Hence, after looking at the study the stakeholders should take a call. We finally conclude by saying that even though accuracy might reduce its good to have a way to have all the sentiments present in a piece of document

Authorized licensed use limited to: DELHI TECHNICAL UNIV. Downloaded on June 03,2022 at 06:28:58 UTC from IEEE Xplore. Restrictions apply.

available with us. The sentiment analysis is not limited to machine learning algorithms. The advancement of Computer science and data science has brought a lot of new tools and technologies through which better accuracy can be gained in optimized manner. The concept of natural language Processings and hyperparameter tuning works well to classify the sentiments of tweet or feedback of online products. Highly advanced mathematical and computation features of Computer and machines can be used to classify the sentiments in easier way with higher accuracy.

ACKNOWLEDGMENT

The Authors are indebted to the central library of Delhi Technological University for providing all the access to the research materials and lab equipment's for smooth functioning and Successful competition of the research work. Besides it we are thankful and grateful to professor Shailender Kumar for helping, guiding, and mentoring in each step throughout the project work.

REFERENCES

[1] 2009 Go, Huang, & Bhayani, "Twitter Sentiment Analysis (final project results)," *J. Inform.*, 2009.

[2] M. Kamyab, R. Tao, M. H. Mohammadi, and A. Rasool, "Sentiment analysis on Twitter: A text mining approach to the Afghanistan status reviews," *ACM Int. Conf. Proceeding Ser.*, vol. 9, no. 4, pp. 14–19, 2018, doi: 10.1145/3293663.3293687.

[3] A. Abbasi, A. Hassan, and M. Dhar, "Benchmarking twitter sentiment analysis tools," *Proc. 9th Int. Conf. Lang. Resour. Eval. Lr. 2014*, pp. 823–829, 2014.

[4] H. Thakkar and D. Patel, "Approaches for Sentiment Analysis on Twitter: A State-of-Art study," 2015, [Online]. Available: http://arxiv.org/abs/1512.01043.

[5] V. A. and S. S. Sonawane, "Sentiment Analysis of Twitter Data: A Survey of Techniques," *Int. J. Comput. Appl.*, vol. 139, no. 11, pp. 5–15, 2016, doi: 10.5120/ijca2016908625.

[6] J. Carlos, D. Santos, and O. Violante, "Twitter sentiment analysis with deep neural networks," *Proc. 38th Int. ACM SIGIR Conf. Res. Dev. Inf. Retr.*, pp. 959–962, 2016.

[7] A. Giachanou and F. Crestani, "Like it or not: A survey of Twitter sentiment analysis methods," *ACM Comput. Surv.*, vol. 49, no. 2, 2016, doi: 10.1145/2938640.

[8] D. Zimbra, A. Abbasi, D. Zeng, and H. Chen, "The state-of-the-art in twitter sentiment analysis: A review and benchmark evaluation," *ACM Trans. Manag. Inf. Syst.*, vol. 9, no. 2, 2018, doi: 10.1145/3185045.

[9] H. K. M and K. Rahamathulla, "Resolution," no. Icicct, pp. 17–19, 2017.

[10] S. Bhuta, U. Doshi, A. Doshi, and M. Narvekar, "A review of techniques for sentiment analysis of Twitter data," *Proc. 2014 Int. Conf. Issues Challenges Intell. Comput. Tech. ICICT 2014*, pp. 583–591, 2014, doi: 10.1109/ICICICT.2014.6781346.

[11] R. Nithish, S. Sabarish, M. N. Kishen, A. M. Abirami, and A. Askarunisa, "An ontology based sentiment analysis for mobile products using tweets," *2013 5th Int. Conf. Adv. Comput. ICoAC 2013*, pp. 342–347, 2014, doi: 10.1109/ICoAC.2013.6921974.

[12] A. S. Bickey Kumar Shah, Vansh Kedia, Rohan Raut, Sakil Ansari, "Evaluation and Comparative Study of Edge Detection Techniques," *IOSR J. Comput. Eng. e*, vol. 22, no. 5, pp. 06–15, 2020, doi: 10.9790/0661-2205030615.

[13] Z. Jianqiang and G. Xiaolin, "Comparison research on text pre-processing methods on twitter sentiment analysis," *IEEE Access*, vol. 5, pp. 2870–2879, 2017, doi: 10.1109/ACCESS.2017.2672677.

[14] Z. Jianqiang, G. Xiaolin, and Z. Xuejun, "Deep Convolution Neural Networks for Twitter Sentiment Analysis," *IEEE Access*, vol. 6, pp. 23253–23260, 2018, doi: 10.1109/ACCESS.2017.2776930.

[15] B. K. Shah, A. Kumar, and A. Kumar, "Dog breed classifier for facial recognition using convolutional neural networks," *Proc. 3rd Int. Conf. Intell. Sustain. Syst. ICISS 2020*, pp. 508–513, 2020, doi: 10.1109/ICISS49785.2020.9315871.

[16] A. Bhatia, V. Kedia, A. Shroff, M. Kumar, B. K. Shah, and Aryan, "Fake currency detection with machine learning algorithm and image processing," *Proc. - 5th Int. Conf. Intell. Comput. Control Syst. ICICCS 2021*, no. Iciccs, pp. 755–760, 2021, doi: 10.1109/ICICCS51141.2021.9432274.

[17] A. Goel and A. Mittal, "Stock prediction using twitter sentiment analysis. Standford University, CS229," *Cs229.Stanford.Edu*, no. December, pp. 1–5, 2012, [Online]. Available: http://cs229.stanford.edu/proj2011/GoelMittal-StockMarketPredictionUsingTwitterSentimentAnalysis.pdf.

[18] L. Zhang, R. Ghosh, M. Dekhil, M. Hsu, and B. Liu, "Combining lexicon-based and learning-based methods for twitter sentiment analysis," *HP Lab. Tech. Rep.*, no. 89, 2011.

[19] B. K. Shah, V. Kedia, and R. K. Jha, "Integrated Vendor-Managed Time Efficient Application to Production of Inventory Systems," *Proc. 6th Int. Conf. Inven. Comput. Technol. ICICT 2021*, pp. 275–280, 2021, doi: 10.1109/ICICT50816.2021.9358504.

[20] A. Shroff, B. K. Shah, A. Jha, A. K. Jaiswal, P. Sapra, and M. Kumar, "Multiplex Regulation System with Personalised Recommendation Using ML," *Proc. 5th Int. Conf. Trends Electron. Informatics, ICOEI 2021*, pp. 1567–1573, 2021, doi: 10.1109/ICOEI51242.2021.9453005.

[21] H. Wang, D. Can, A. Kazemzadeh, F. Bar, and S. Narayanan, "A System for Real-time Twitter Sentiment Analysis of 2012 U.S. Presidential Election Cycle," *Proc. 50th Annu. Meet. Assoc. Comput. Linguist.*, no. July, pp. 115–120, 2012, doi: 10.1145/1935826.1935854.

[22] H. Saif, Y. He, and H. Alani, "Semantic sentiment analysis of twitter," *Lect. Notes Comput. Sci. (including Subser. Lect. Notes Artif. Intell. Lect. Notes Bioinformatics)*, vol. 7649 LNCS, no. PART 1, pp. 508–524, 2012, doi: 10.1007/978-3-642-35176-1_32.

[23] A. Shelar and C. Y. Huang, "Sentiment analysis of twitter data," *Proc. - 2018 Int. Conf. Comput. Sci. Comput. Intell. CSCI 2018*, pp. 1301–1302, 2018, doi: 10.1109/CSCI46756.2018.00252.

[24] V. S. Pagolu, K. N. Reddy, G. Panda, and B. Majhi, "Sentiment analysis of Twitter data for predicting stock market movements," *Int. Conf. Signal Process. Commun. Power Embed. Syst. SCOPES 2016 - Proc.*, pp. 1345–1350, 2017, doi: 10.1109/SCOPES.2016.7955659.

[25] T. U. Haque, N. N. Saber, and F. M. Shah, "Sentiment analysis on large scale Amazon product reviews," *2018 IEEE Int. Conf. Innov. Res. Dev. ICIRD 2018*, no. May, pp. 1–6, 2018, doi: 10.1109/ICIRD.2018.8376299.

Authorized licensed use limited to: DELHI TECHNICAL UNIV. Downloaded on June 03,2022 at 06:28:58 UTC from IEEE Xplore. Restrictions apply.

[26] B. K. Shah, A. K. Jaiswal, A. Shroff, A. K. Dixit, O. N. Kushwaha, and N. K. Shah, "Sentiments Detection for Amazon Product Review," *2021 Int. Conf. Comput. Commun. Informatics, ICCCI 2021*, 2021, doi: 10.1109/ICCCI50826.2021.9402414.

[27] M. Kumar, A. Bhatia, P. Gupta, K. Jha, R. K. Jha, and B. K. Shah, "S IGN L ANGUAGE A LPHABET R ECOGNITION U SING," 2021, no. Iciccs, pp. 1859–1865.

[28] V. Kedia, A. Bhatia, S. R. Regmi, S. Dugar, K. Jha, and B. K. Shah, "Time Efficient IOS Application For CardioVascular Disease Prediction Using Machine Learning," no. Iccmc, pp. 869–874, 2021.

[29] P. VEDURUMUDI, "Twitter Sentiment Analysis," *i-manager's J. Comput. Sci.*, vol. 8, no. 4, p. 1, 2021, doi: 10.26634/jcom.8.4.18269.

[30] A. Roy and M. Ojha, "Twitter sentiment analysis using deep learning models," *2020 IEEE 17th India Counc. Int. Conf. INDICON 2020*, pp. 18–21, 2020, doi: 10.1109/INDICON49873.2020.9342279.

[31] A. Srivastava, V. Singh, and G. S. Drall, "Sentiment analysis of twitter data: A hybrid approach," *Int. J. Healthc. Inf. Syst. Informatics*, vol. 14, no. 2, pp. 1–16, 2019, doi: 10.4018/IJHISI.2019040101.

Authorized licensed use limited to: DELHI TECHNICAL UNIV. Downloaded on June 03,2022 at 06:28:58 UTC from IEEE Xplore. Restrictions apply.

Vilnius University Press

Contents lists available at Vilnius University Press

Organizations and Markets in Emerging Economies
2022, vol. 13, no. 1(25), pp. 209–237

ISSN 2029-4581 eISSN 2345-0037
DOI: https://doi.org/10.15388/omee.2022.13.77

Smart Beta Investing: An Alternative Investment Paradigm in Emerging Indian Equity Market

Reema Monga

University School of Management and Entrepreneurship
Delhi Technological University, India
https://orcid.org/0000-0001-9619-0205
reemamonga23@gmail.com

Deepti Aggrawal (corresponding author)

University School of Management and Entrepreneurship
Delhi Technological University, India
https://orcid.org/0000-0003-1899-1570
deeptiaggrawal@dtu.ac.in

Jagvinder Singh

University School of Management and Entrepreneurship
Delhi Technological University, India
https://orcid.org/ 0000-0002-4558-5220
jagvinder.singh@dtu.ac.in

Abstract. *This paper fundamentally looks at the novel concept of Smart Beta investing in constructing a more efficient and well-diversified alternative investment. Smart beta has been a popular investment philosophy, although emerging countries have been slower to adopt and execute it.*

In this way, the study investigates the existence, performance, and robustness of smart beta strategies in a divergent financial market. Moreover, it is an initial attempt to integrate the framework of stock selection and stock weighting to construct and test smart beta strategies against the traditional Indian market benchmark (S&P BSE 500). The findings show that smart beta investing results in a better risk-return profile on an absolute and risk-adjusted basis. Furthermore, the results demonstrate the

Received: 9/9/2021. **Accepted:** 10/1/2022
Copyright © 2022 Reema Monga, Deepti Aggrawal, Jagvinder Singh. Published by Vilnius University Press. This is an Open Access article distributed under the terms of the Creative Commons Attribution Licence, which permits unrestricted use, distribution, and reproduction in any medium, provided the original author and source are credited.

consistency and robustness of smart beta strategies in different market conditions and display their outperformance even in bearish market conditions.
Keywords: *active and passive investment, factor exposure, idiosyncratic risk, Indian equity market, innovative investment, risk parity, smart beta investing*

1. Introduction

Since the introduction of the Capital Asset Pricing Model (CAPM) in 1960, the investment community has depended on the traditional capitalization-weighted indices or CAPM for asset allocations models. Based on the seminal work of Markowitz (1952), investors are just required to hold a 'cap-weighted market portfolio,' which is considered a mean-variance optimal. It has been presumed that investment in a market portfolio could be the optimum solution to generate a risk premium. However, in the subsequent years, numerous researchers (Basu, 1977; Fama & French, 1993, 1996; Jegadeesh & Titman, 1993; Zhang, 2005; Hou et al., 2015) found alternative risk factor-exposures that yielded surplus returns. Empirical analysis has additionally examined that portfolios having alternative risk factors can create superior returns compared with the traditional market portfolios, indicating that these market indices are not mean-variance efficient. As a result, it is imperative to construct well-diversified and mean-variance optimal portfolios apart from the conventional market portfolio.

An intensifying community of professional investors observed that the criticisms of traditional indices tend to center on areas such as concentration, high degree of volatility, absence of mean-reversion, and others (Russo, 2014). At the individual stock level, concentration refers to a couple of organizations having a large index weight, exposing asset holders to stock-specific risk. It is also evident from numerous nations that only a few names accounted for a significant portion of the market index, i. e., the highly concentrated index (Malevergne et al., 2009; Russo, 2014). Another potential flaw of the cap-weighted market index is that it imposes a return drag on portfolios, making it sub-optimal compared to the non-cap-weighted indices (Treynor, 2005; Hsu, 2006; Arnott & Hsu, 2008). Empirical evidence also proposes that cap-weighted market indices are neither diversified nor proficient, resulting in poor-risk adjusted returns (Ferson et al., 1987; Haugen & Baker, 1991; Grinold, 1992; Centineo & Centineo, 2017).

In light of the fluctuations in the traditional index and the impact of inefficient stock markets, investors have started looking for transparent and rule-based indices that apply non-market-cap weighting schemes. These alternative weighted portfolios are termed by the expressions "advanced beta," "smart beta," "alternative beta," "factor investing," and "alternative risk premium" and more (Kudohet al., 2015; Blitz, 2016). The objective of these strategies is to alleviate the inherent frailty of traditional market indices, i. e., "overweighting overpriced stocks and underweighting underpriced

stocks." In other words, this relatively new approach to equity investing is prompted to address these shortcomings (heavy concentration and unfavorable factor exposures) of conventional market indices. Thus, smart beta indices aim to gain advantages from rewarded risk premia factors while diversifying unrewarded risks by using broadened weighting schemes.

This paper contributes to the growing literature by unveiling the existence and effective execution of smart beta strategies in an emerging financial market. The Indian stock market is the world's sixth-largest stock market, with a market capitalization of USD 3.46 trillion (Bloomberg, 2021). It is an attractive emerging market for FIIs and other global portfolio investors because of its size, foreign interest, growth potential, market capitalization, and stable macroeconomic climate. During 2019, the foreign portfolio investors (FPIs) owned around 29% of the Indian equities. Interestingly, among emerging markets, FII inflows into the Indian stock market were the highest for the year 2020. India remains a popular investment destination with substantial foreign portfolio investment, considering the high growth rates and opportunities. For instance, in 2020–2021, the total net investment of these FPIs reached a new height of approximately USD 555 billion. Also, it is the world's third-largest economy, with a PPP-adjusted GDP of USD 10.21 trillion (World Bank, 2021). Therefore, it is worthwhile to devise innovative indexing strategies in the context of the emerging Indian equity market. Considering the sample of the S&P BSE 500 index from July 1, 2003 to June 30, 2020, we construct smart beta strategies by implementing six well-documented factor exposures (such as value, size, investment, momentum, profitability, and low volatility) across three diverse weighting schemes (Risk parity, Factor Weighting, and Equal Weighting).

In line with the idea, the following research questions are proposed to be addressed in this study. First, will factor-based smart beta strategies outperform the traditional cap-weighted market index in the context of an emerging economy? Second, does the application of a specific weighting approach enhance portfolio diversification? Furthermore, the study offers criteria of stock selection with related attributes. It also deals with different portfolio weighting schemes that ought to assess the robustness and add diversification benefits across the selected stocks. Then, it offers a design of a sound integrated approach for the proper execution of the optimal smart beta investment. Finally, the study provides a more comprehensive performance analysis, including factor risk decomposition and performance sensitivity to different market conditions.

The rest of the article is organized into seven sections: Section 2 delves into the relevant literature. Section 3 outlines the research framework for the factor exposures across different portfolio weighting schemes. In Section 4, we provide details of the data used. Section 5 exhibits comparisons based on empirical outcomes for different smart beta strategies. Section 6 presents the conclusion of the study. Finally, Section 7 discusses the implications and future scope.

2. Literature Review

2.1 Overview of Smart Beta Investing

Smart beta is a novel investing ideology that integrates underlying factors such as size, low risk, profitability, value, investment, and momentum (Basu, 1977; Banz, 1981; Jegadeesh & Titman, 1993; Fama & French, 1996, 2012, 2015; Frazzini & Pedersen, 2014). These funds are often expressed as "the vehicle to deliver factor investing" (BlackRock). In other words, smart beta strategies aim to outperform traditional passive indices by introducing a factor-based investment ideology. Ang et al. (2009) analyzed that factor-driven smart beta strategies are intensifying because they are based on well-founded risk factors that substantially improve risk-adjusted performance. They documented that this relatively new indexing approach focuses on capturing exposure to various robust risk premia factors that have been extensively used in actively managed portfolios.

Cakici et al. (2013) examined factor indices of value and momentum in 18 emerging markets, including Eastern Europe, Asia, and Latin America. The authors found substantial evidence for the value and the momentum effects in all emerging economies except in Eastern Europe from January 1990 to December 2011. Amenc et al. (2014) evaluated the smart beta indices of momentum, value, mid-cap, and low volatility. They found a substantial annual outperformance ranging from 2.92% to 4.96%, even after considering high transaction costs. Arnott and Kose (2014) defined smart beta as a "category of valuation-indifferent strategies that consciously and deliberately break the link between the price of an asset and its weight in the portfolio, seeking to earn an excess return over cap-weighted benchmark by no longer weighing assets proportional to their popularity, while retaining most of the positive attributes of passive indexing."

Jacobs and Levy (2014) stated that smart beta investing incorporates the concept of both active and passive investing. They argued that these strategies are centered on a rule-based ideology that weights equities differently from the traditional cap-weighting methodologies. Bender and Wang (2015) examined five-factor strategies from 1993 to 2013 and found that all of them outperformed the MSCI cap-weighted index. Blitz (2016) evaluated the effectiveness of smart beta strategies across two weighting methodologies and concluded that these portfolios consistently beat the cap-weighted index over the study period of 1990–2015. Hanauer and Linhart (2015) examined three factors: value, size, and momentum for 21 emerging and 24 developed countries over July 1996 to June 2012. They documented a strong value effect and a considerable but less significant momentum effect. Furthermore, they found that the value component is more prevalent in emerging economies than in developed markets.

Kahnand Lemmon (2016) observed that smart beta products deliver abnormal returns more cost-effectively and transparently than actively managed products. Agarwalla et al. (2017) examined value, size, and momentum factors in the Indian stock market

over the study period of 1994 to 2017. They concluded that momentum and value are viable investments, but the size component does not outperform the market portfolio in the Indian equity market. Angelidis and Tessaromatis (2017) analyzed four factors portfolios: value, low-risk, small-cap, and momentum for 23 developed and 21 emerging economies from 1980 to 2015. They found that factor portfolios exhibited superior Sharpe ratios and, in most situations, statistically significant returns when compared to world market portfolios. The authors also broadened the research by creating global factor portfolios that included emerging economies and found evidence of improved factor return efficiency.

Bender et al. (2018) tested the five advanced beta strategies: value, profitability, investment, size, and momentum from 1963 to 2015 and reported that all these strategies delivered more excess returns than the cap-weighted market index. Martellini and Milhau (2018) evaluated the six fundamental lead factors from 1970–2015. They identified that these strategies outperformed the traditional index in terms of Sharpe ratio and could diversify the unrewarded risks. In the Korean Stock Market, between 2004 and 2020, Kim (2021) presented a comprehensive examination of five factors: value, size, profitability, low risk, and momentum. The results show that all factors outperformed the market index, with the size factor generating the highest return. Monga et al. (2021) evaluated optimization-based alternative indexing strategies in the emerging Indian equity market from April 2004 to March 2020. They found evidence of extensive outperformance and increased diversification for optimized strategies compared to the standard market index. Silvasti et al. (2021) tested smart beta strategies based on momentum, value, and low beta from December 1991 to January 2019. They noted that these strategies outperformed the Nordic equity market, with momentum and low beta having the highest alpha and Shape ratio.

Empirically, there is substantial evidence regarding the effectiveness of smart beta strategies. However, the literature is mainly limited to the U.S. and other mature markets. In a growing market like India, these investing strategies may or may not be effective. Therefore, given the paucity of such empirical evidence, the current study focuses on the construction, execution, and performance of the smart beta investment in the scarcely researched emerging Indian equity market.

2.2 Theoretical Framework of Factor Exposures

Our study incorporates six factor-based smart beta exposures: value, investment, profitability, size, momentum, and low volatility. Exclusively, all these factors are broadly esteemed in the academic literature (Jagadeesh & Titman, 1993; Fama & French, 1996, 2012; Frazzini & Pedersen, 2014; Hou et al., 2015). The persistence and robustness of the factor exposures are presented as follows:

Value Factor: This factor measures how well value stocks (those with low valuation) outperform growth stocks. For the most part, value investing has been examined by the

most prominent researchers (Basu, 1977; Chan et al., 1991; Zhang, 2005). They found an affirmative association between stocks with low prices and their fundamentals, such as book value, dividends, sales, and earnings. The theoretical rationale for the value premium is intuitive, i. e., value firms carry a higher level of risk because they are more vulnerable to economic shocks during times of financial distress and hence demand a substantial risk premium (Fama & French, 1996; Zhang, 2005). Another strand of research for the value premium has been studied in the context of behavioral biases. Investors tend to extrapolate "growth stocks with past positive news" and "overreact to past negative news about value stocks," resulting in higher returns for value stocks (Lakonishok et al., 1994).

Investment Factor: This fundamental factor exhibits inclination towards lower investment strategies over higher investment ones. Li and Zhang (2010) and Hou et al. (2015) examined "investment" as a relatively more recent asset pricing factor in the q-theory of investment. They found that the rationale behind low investment frictions is characterized by a larger asset size, greater sales growth, higher cash flows, lower debt-to-asset ratio, and higher dividend payout ratio. Similarly, Fama and French (2015) investigated the difference between conservative and aggressive levels of investment and concluded that lower investment levels are associated with higher anticipated returns.

Profitability Factor: Researchers are increasingly emphasizing the "profitability factor" in addition to the conventional value, size, and momentum factors. This factor targets to capture the "quality factor" premium by purchasing "High-profit" companies and evading "Low-profit" companies. The academic explanation for the profitability premium can be explained using a rational risk-based "q-theory of investment" (Hou et al., 2015). Unlike traditional criteria that rely on market price, profitability indicators are solely based on accounting data. For instance, Novy-Marx (2013)used the gross profit margin for measuring profitability. Fama and French (2015) considered operating profit as a dimension of profitability in their five-factor model. Hou et al. (2015) illustrated this factor by the Return on Equity (ROE).

Size Factor: This factor has more exposure to smaller companies and less correspondence to the larger companies. Size as a factor was originated by Banz (1981) to target that smaller companies capture relative returns corresponding to the larger ones. Various theories explain the rationale for the outperformance of small size effect. For instance, Fama and French (1993, 2012) proposed that small caps exposed to undiversifiable risk result in a higher premium. Other studies, in particular, argued that smaller companies are associated with financial distress, low dividends (Chan & Chen, 1991), lower liquidity (Amihud, 2002), information uncertainty (Zhang, 2006), and thus offer superior returns.

Momentum Factor: It suggests that stocks with stronger past performance substantially outperform those with lower past performance. Jegadeesh and Titman (1993) observed that buying past outperformers and selling past underperformers generated extensive "abnormal" returns from 1965–1989 in the U.S. stock market. Similarly, Fama

and French (2012) discovered strong persistence of momentum returns from 1989 to 2011. They also considered "momentum" as a robust and persistent factor that was not captured by either value or size effect. The most widely cited theories underlying this premium are all behavioral (Hong et al., 2000). Evidently, the theories around the momentum effect have been developed in the context of investor behavior, i. e., their over-reaction or under-reaction to new information (such as corporate results or dividend announcements). Another possible reason could be herding behavior, which occurs when profit-seeking investors create a feedback system that causes prices to drift away from fundamentals (Dasgupta et al., 2011).

Low Volatility Factor: The "low volatility" premium measures the outperformance of low volatility stocks over highly volatile stocks. Blitzand Vliet (2007) and Hsu et al. (2015) examined the low-volatility effect and found that low-risk stocks substantially outperformed the market benchmark. The low volatility anomaly and its persistence may be explained by a variety of cognitive and behavioral factors. One of the first explanations is the "lottery effect," which refers to an investor's readiness to pay a higher price for a slight chance of making a significant profit, even when the chances of losing are much higher than winning (Baker et al., 2011). Other behavioral explanations include investors being leverage-constrained and seeking substantial returns in highly volatile stocks (Frazzini & Pedersen, 2014). Also, investors have a natural tendency to overestimate the performance of a few "well-publicized high-riskier stocks" and hence overpay in the hope of owning the enormous returns.

3. Research Framework

The study involves an integrated approach to the construction of smart beta strategies. First, it includes the stock selection criterion by six well-documented factor exposures and then employs three distinct weighting schemes to allocate these selected stocks.

3.1 Factor Selection

The first stage in constructing smart beta strategies is determining well-acknowledged factor exposures for selecting the stocks. To construct portfolios, we used a set of factor attributes and selected stocks according to the accompanying determination rules (see Table 1).

The details of the construction of factor portfolios are as follows:

Value Factor: Stocks are sorted by their high to low B/M ratio, and after that, Top 50% are selected to explore the value tilt.

Investment Factor: First, stocks are arranged as per the two-year growth rate of total assets. Afterward, the stocks from the bottom 50% are selected to get the exposure of low investment.

Table 1

Methodology for Construction of Portfolios Based on Factor Exposures

Factor	Measure	Signal	Supporting Literature
Value (HML)	Book-to-Market Ratio (B/M)	High	Cakici et al. (2013); Hsu et al. (2015); Blitz (2016); Hu et al. (2019)
Investment (INV)	The two-year growth rate of Total asset	Low	Hou et al. (2015); Blitz (2016); Bender et al. (2018)
Profitability (PROF)	Return On Equity	High	Hou et al. (2015); Hsu et al. (2015)
Size (SMB)	Log value of Market Capitalization	Small	Cakici et al. (2013); Hanauer and Linhart (2015); Hou et al. (2015); Bender et al. (2018)
Momentum (MOM)	Stock return over 12-months, minus the last month's return	High	Hanauer and Linhart (2015); Blitz (2016); Agarwalla et al. (2017)
Low Volatility (LVOL)	The standard deviation of returns over the most recent 104 weeks	Low	Hsu et al. (2015); Centineo and Centineo (2017)

Profitability Factor: To explore this strategy, Top 50% of stocks are picked up as per the ROE signal.

Size Factor: The bottom 50% of stocks are selected as per the log value of market capitalization.

Momentum Factor: This strategy looks into the Top 50% of stocks based on the returns over 12 months, skipping the most recent month.

Low volatility: This tilt utilizes the standard deviation of stock returns in the course of the most recent 104 weeks. Afterward, the Bottom 50% of stocks is selected as per this criterion.

3.2 Description of the Weighting Schemes

After selecting appropriate factor exposures, the next significant move is to choose the diversified portfolio weighting methodologies. In other words, stock weighting plays a vital role in evaluating the performance, consistency, and robustness of smart beta strategies. As a result, we tested the portfolios by implementing the following three notable and effectual types of weighting schemes:

Risk Parity Weighting (RP): It is recognized as the "Diversified Risk-Weighted" strategy based on the phenomenon that each stock has an equivalent risk contribution to the portfolio. It is assumed that the strategy attempts to reduce risk concentrations by allocating large weights to less risky stocks while moving away from riskier stocks. This method is used as a proxy for Inverse Volatility Strategy, and thereby weights are

inversely proportional to the stock's volatility (Chaves et al., 2011; Russo, 2014). It is determined as per Equation (1):

$$W_i = \frac{\sigma_i^{-1}}{\sum_{i=1}^{n} \sigma_i^{-1}} \quad (1)$$

where w_i represents the weight of i^{th} stock; n is the number of stocks; σ_i stands for i^{th} stock's volatility.

Factor Weighting (FW): This strategy follows a methodology that ranks stocks based on their factor criteria. For instance, the B/M ratio is used to capture value tilt. Likewise, other factors are formulated as per the desired measurement criteria (see Table 1). Following that, the strategy assigns Z-scores to all the stocks with desired factor attributes. Consequently, the calculated Z-factor scores are then transformed into Standardized factor scores (S-factor scores) by normalizing them between 0 and 1 (refer to Appendix 1). Finally, to calculate stock weights, a common practice is adopted by various factor index providers, i. e., to adjust market cap-weight to the normalized S-factor scores. Hence, the final weights are calculated as per Equation (2):

$$W_i = \frac{S_i \times MC_i}{\sum_{i=1}^{n} S_i \times MC_i} \quad (2)$$

where S_i is the standardized factor score of i^{th} stock, and MC_i is the market cap-weight of i^{th} stock.

Equal Weighting (EW): It is perceived as a "Maximum Deconcentration" strategy and has only one parameter: the number of stocks. This approach gives each stock the same weight, thereby avoiding the large-cap tendency while also taking advantage of smaller companies. It is utilized as a proxy for the diversified weighting plan (Chaves et al., 2011; Amenc et al., 2017). Equation (3) is used to determine the weights:

$$W_i = \frac{1}{n} \quad (3)$$

where n is the number of stocks.

3.3 Integrated Framework for Constructing Smart Beta Strategies

The next major step is to apply an integrated framework, i. e., an approach that links factor-based stock selection and diversified weighting schemes. As a result, our analysis integrates different stock selection and stock weighting methodologies for constructing smart beta strategies (see Figure 1).

Figure 1

Integrated Framework for Construction of Smart Beta Strategies

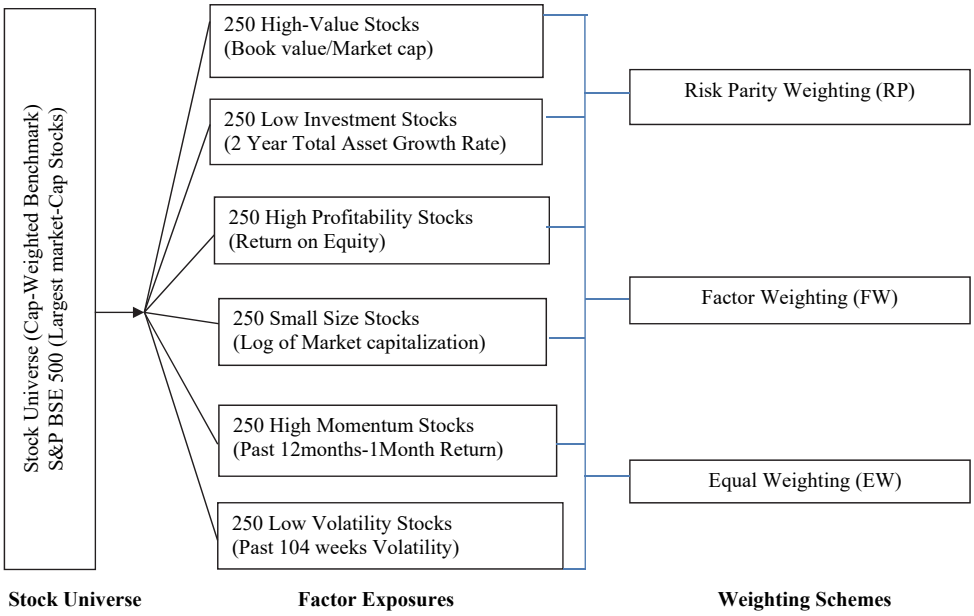

Figure 1 gives an outline of the smart beta strategies for the study. First, we selected S&P BSE 500 stock universe to construct smart beta strategies. Following that, we developed portfolios that comprise value, investment, profitability, size, momentum, and low volatility. Afterward, to add diversification, we applied different weighting allocation schemes to these selected stocks.

4. Data

The entire set of strategies is applied to S&P BSE 500 Stock universe from July 1, 2003 to June 30, 2020. The logical rationale for using this data period is that Indian stock markets underwent numerous structural and economic downturns, including financial crisis of 2007–08, demonetization in 2016, implementation of GST (Goods and Services Tax) in 2017, and recently, the COVID-19 pandemic. In other words, the selected sample period with 204 monthly observations encompasses both bull and bear market circumstances. As a result, the study uses the approach of Fuller and Goldstein (2011), which divides the entire sample period into two sub-periods, bull and bear. The bull sample includes 126 monthly observations, i. e., the period of positive market returns, while the bear sample has 78 months, which corresponds to the period of negative market returns. Such analysis is significant for investors who want to understand how their

portfolio performs in various market conditions and how that behavior contributes to their overall portfolio performance.

All the factors strategies are re-balanced annually, except momentum, which is re-balanced semi-annually. Apart from that, we obtained the weights from the smart beta strategies, retained the portfolio till the following re-balancing period, and accounted for their monthly performance. The entire set of relevant data is collected using the Bloomberg database.

5. Empirical Results and Discussion

The considered smart beta strategies incorporate six factor-exposures across three weighting schemes. Each portfolio is measured from July 1, 2003 to June 30, 2020, and is compared with the Indian Market Index S&P BSE 500.

Table 2

Absolute Performance of Smart Beta Strategies

Panel A: Value Strategy				
	RP	FW	EW	BSE500
Monthly Return	1.58 (0.04)	1.60 (0.12)	1.90 (1.15)	1.57
Volatility	7.99	9.20	9.07	7.07
Sharpe ratio	0.13 (-0.54)	0.11 (-0.48)	0.15 (0.19)	0.14
Maximum Drawdown	26.78	30.34	29.88	27.11
Downside Risk	4.24	4.83	4.70	3.99
Sortino Ratio	0.24 (-0.54)	0.22 (-0.48)	0.29 (0.76)	0.25

Panel B: Investment Strategy				
	RP	FW	EW	BSE500
Monthly Return	1.71 (0.72)	2.02* (2.09)	2.13* (2.39)	1.57
Volatility	6.85	8.03	8.16	7.07
Sharpe ratio	0.17* (2.12)	0.18* (3.16)	0.19* (3.35)	0.14
Maximum Drawdown	22.62	27.41	26.98	27.11
Downside Risk	3.59	4.16	4.19	3.99
Sortino Ratio	0.32* (2.35)	0.35* (7.89)	0.38* (8.72)	0.25

Panel C: Profitability Strategy				
	RP	FW	EW	BSE500
Monthly Return	2.53* (5.41)	3.04* (9.50)	3.13* (9.49)	1.57
Volatility	5.92	6.80	7.03	7.07
Sharpe ratio	0.33* (2.74)	0.36* (5.37)	0.37* (6.57)	0.14
Maximum Drawdown	19.53	22.86	23.07	27.11
Downside Risk	3.06	3.44	3.52	3.99
Sortino Ratio	0.64* (5.63)	0.72* (11.46)	0.73* (13.70)	0.25

Panel D: Size Strategy				
	RP	FW	EW	BSE500
Monthly Return	2.30* (2.62)	2.86* (3.88)	3.01* (4.33)	1.57
Volatility	7.89	9.05	9.12	7.07
Sharpe ratio	0.22* (10.67)	0.25* (3.35)	0.27* (4.06)	0.14
Maximum Drawdown	24.49	28.86	28.56	27.11
Downside Risk	3.97	4.43	4.42	3.99
Sortino Ratio	0.44* (12.46)	0.52* (8.23)	0.55* (9.36)	0.25

Panel E: Momentum Strategy				
	RP	FW	EW	BSE500
Monthly Return	2.44* (4.05)	2.93* (6.08)	2.98* (6.05)	1.57
Volatility	6.58	7.59	7.79	7.07
Sharpe ratio	0.29* (3.19)	0.31* (11.4)	0.31* (15.54)	0.14
Maximum Drawdown	22.10	25.63	26.61	27.11
Downside Risk	3.36	3.79	3.86	3.99
Sortino Ratio	0.56* (6.60)	0.62* (14.82)	0.63* (15.22)	0.25

Panel F: Low Volatility Strategy				
	RP	FW	EW	BSE500
Monthly Return	1.70* (2.13)	1.89* (2.39)	1.94* (3.81)	1.57
Volatility	5.33	5.87	6.11	7.07
Sharpe ratio	0.21* (2.09)	0.23* (2.42)	0.24* (2.79)	0.14
Maximum Drawdown	18.51	20.99	21.37	27.11
Downside Risk	2.88	3.14	3.24	3.99
Sortino Ratio	0.40* (2.21)	0.42* (2.68)	0.43* (3.22)	0.25

Note. Authors'calculation based on monthly total returns from July 1, 2003 to June 30, 2020. The cap-weighted index is represented by the S&P BSE 500. The risk-free rate is calculated using the yield on 91 days Treasury bills. The computed results are reported in percentages except for the Sharpe and Sortino ratios. The t-statistics are presented in parentheses, and (*) values are significant at the 5% level.

Table 2 summarizes the absolute performance statistics of the smart beta strategies over the study period. The results demonstrate that smart beta portfolios outperformed the market index, which is consistent with previous studies (Bender & Wang, 2015; Blitz, 2016; Bender et al., 2018; Kim, 2021). It is noteworthy that smart beta strategies have led to statistically significant higher returns, superior Sharpe, and Sortino ratios than the S&P BSE 500 index. However, we have found no robust value effect in recent years. This result aligns with Hillard and Zhang (2015) and Hu et al. (2019). Particularly, profitability and low volatility are optimal strategies with higher returns and lower volatility than the market index. It is also evident that the EW portfolio delivers comparatively good risk-adjusted performance, i. e., beat other portfolios in terms of monthly return, the Sharpe ratio, and the Sortino ratio. These results where EW portfolios outperformed are consistent with DeMiguel et al.(2009), Malladi and Fabozzi(2017) and more recently, Bermejo et al. (2021).

The RP portfolios hold the lowest volatility, which is consistent with the rationale of risk-minimization strategies (Chaves et al., 2011). At the same time, for the other attributes, e. g., Maximum Drawdown and Downside risk, RP portfolios are clearly at an advantage compared to other stock weighting schemes. Typically, Panel C, E, and F of Table 2 show that profitability, momentum, and low volatility have maximum drawdown generally around 18.51% to 26.61% as compared to 27.11% for the S&P BSE 500 and downside risk ranging between 2.88% to 3.86% as contrasted to 3.99% for the market index. These attributes show lower levels of underperformance for smart beta strategies than the traditional market index.

Table 3

Relative Risk/Return Profile of Smart Beta Strategies

Panel A: Value Strategy			
	RP	FW	EW
Relative Return	0.01	0.03	0.33
Tracking Error	3.13	3.87	3.81
Information Ratio	0.003	0.008	0.09
Maximum Relative Drawdown	12.17	10.44	10.26
Extreme Relative Returns (5^{th} %ile)	-4.61	-5.28	-5.10
Extreme Tracking Error (95^{th} %ile)	4.84	5.84	6.16

Panel B: Investment Strategy			
	RP	FW	EW
Relative Return	0.14	0.45	0.56
Tracking Error	2.64	2.91	3.15
Information Ratio	0.05	0.15	0.18
Maximum Relative Drawdown	12.95	10.99	11.47
Extreme Relative Returns (5^{th} %ile)	-3.65	-3.96	-4.30
Extreme Tracking Error (95^{th} %ile)	4.75	5.48	6.10

Panel C: Profitability Strategy			
	RP	FW	EW
Relative Return	0.96	1.47	1.56
Tracking Error	2.38	2.08	2.17
Information Ratio	0.40	0.71	0.72
Maximum Relative Drawdown	9.17	5.39	5.30
Extreme Relative Returns (5^{th} %ile)	-2.61	-1.83	-1.76
Extreme Tracking Error (95^{th} %ile)	4.62	5.03	5.27

Panel D: Size Strategy			
	RP	FW	EW
Relative Return	0.73	1.29	1.44
Tracking Error	3.73	4.46	4.45
Information Ratio	0.20	0.29	0.32
Maximum Relative Drawdown	12.17	11.19	9.42
Extreme Relative Returns (5^{th} %ile)	-4.58	-4.60	-4.59
Extreme Tracking Error (95^{th} %ile)	7.46	9.68	10.02

Panel E: Momentum Strategy			
	RP	FW	EW
Relative Return	0.87	1.36	1.41
Tracking Error	2.89	3.00	3.13
Information Ratio	0.30	0.45	0.45
Maximum Relative Drawdown	9.35	7.41	8.41
Extreme Relative Returns (5^{th} %ile)	-3.62	-3.15	-3.39
Extreme Tracking Error (95^{th} %ile)	5.26	6.20	6.33

Panel F: Low Volatility Strategy			
	RP	FW	EW
Relative Return	0.13	0.32	0.37
Tracking Error	2.73	2.35	2.36
Information Ratio	0.05	0.14	0.16
Maximum Relative Drawdown	11.66	11.22	10.67
Extreme Relative Returns (5^{th} %ile)	-3.97	-3.60	-3.43
Extreme Tracking Error (95^{th} %ile)	3.88	3.43	3.60

Note. Relative returns are the excess return of the factor strategy over the benchmark (S&P BSE 500 index). All results are reported per month and in percentages except for the information ratio.

The results presented in Table 3 measure the relative risk-return performance of these diverse portfolios. An examination of relative performance shows that the smart beta strategies outperformed the standard index, with monthly excess returns ranging from 0.01% and 1.56%. It is noted that the EW portfolios generate the highest excess returns, which is not surprising as Table 2 displays an identical pattern for the absolute returns. From Table 3, we find that EW portfolios also lead to superior risk-adjusted performance, i. e., information ratio.

Furthermore, it is interesting to examine the tracking error (the volatility of excess returns) for the factor strategies across different weighting schemes. By comparison, the RP weighted portfolios have the lowest tracking error to the S&P BSE 500 in four out of 6 cases. On the other hand, the FW portfolios deliver a lower tracking error in profitability and low volatility. Finally, Panel C of Table 3 displays that the profitability strategy generates the highest relative return and is accompanied by the lowest tracking error, resulting in the highest information ratio. However, value strategy (Table 3, Panel A) gives the lowest excess return compared to other strategies.

Table 4

Robustness of Smart Beta Strategies: Under Bullish and Bearish Market Conditions

Panel A: Value Strategy			
	RP	FW	EW
Upside Participation	1.06	1.20	1.27
Downside Participation	1.27	1.48	1.36
Average Participation	1.17	1.34	1.32
Participation Advantage	-0.21	-0.28	-0.09

Panel B: Investment Strategy			
	RP	FW	EW
Upside Participation	1.04	1.22	1.26
Downside Participation	0.96	1.10	1.10
Average Participation	1.00	1.16	1.18
Participation Advantage	0.08	0.12	0.16

Panel C: Profitability Strategy			
	RP	FW	EW
Upside Participation	1.20	1.41	1.42
Downside Participation	0.53	0.53	0.54
Average Participation	0.87	0.97	0.98
Participation Advantage	0.67	0.88	0.88

Panel D: Size Strategy			
	RP	FW	EW
Upside Participation	1.30	1.54	1.59
Downside Participation	1.03	1.08	1.06
Average Participation	1.17	1.31	1.33
Participation Advantage	0.27	0.46	0.53

Panel E: Momentum Strategy			
	RP	FW	EW
Upside Participation	1.23	1.44	1.47
Downside Participation	0.68	0.73	0.75
Average Participation	0.96	1.09	1.11
Participation Advantage	0.55	0.71	0.72

Panel F: Low Volatility Strategy			
	RP	FW	EW
Upside Participation	0.93	1.02	1.06
Downside Participation	0.67	0.75	0.78
Average Participation	0.80	0.89	0.92
Participation Advantage	0.26	0.27	0.28

Note. In upside participation, the bull market corresponds to the positive market returns, while in downside participation, months with negative returns comprise bear markets.

Besides examining the attributes of return and volatility for different portfolios, our approach includes other parameters that are also valuable for analyzing the consistency and robustness of these strategies. Furthermore, previous literature (Fuller & Goldstein, 2011; Amenc et al., 2014; Monga et al., 2021) suggested separating bull and bear phases when analyzing conditional performance. In light of this, we used the method proposed by Qian (2015) to evaluate a portfolio's ability to capture upside returns while limiting downside risk. As a result, we computed upside and downside participation ratios (refer to Appendix 1) to evaluate whether the performance of smart beta strategies is persistent across different market environments. Following that, we calculated the participation advantage and average participation. Interestingly, participation advantage measures the difference between the upside and downside participation ratios and demonstrates the strategy's effectiveness to create value over the entire market cycle.

A strategy with a positive participation advantage is considered better than the one with negative participation because a strategy with a positive advantage gives "upside participation and downside protection" (Qian, 2015). In comparison, the average participation indicates whether the portfolio is cyclical or defensive. A portfolio can be classified as cyclical when its accumulating benefits arise in the period when the market is up. Conversely, the strategy accruing with substantial benefits when the market is down is considered a defensive one. The convention is that if the average participation value is greater than one, the strategy is cyclical, and if that value is less than one, it turns to be defensive. However, with the average value of 1, the portfolio is termed as neutral, i. e., neither cyclical nor defensive (Sorensen et al., 2018).

To test this empirically, we evaluated the performance patterns of smart beta strategies over different market cycles (Table 4). From the results obtained, the EW approach is progressively preferred as it has the highest participation advantage and thus gives the maximum upside participation and downside protection. The outcome also illustrates that profitability, momentum, and size strategies show relatively high participation advantages and provide more opportunities over the cycle. In comparison to this, other strategies substantially have low participation advantages. Moreover, according to the average participation, low volatility and profitability strategies are more defensive and

pay off more when the market is down. As a result, the present study shows ample evidence that these strategies are consistent, robust, and outperforming irrespective of the market conditions. The results achieved are aligned with Amenc et al. (2014), Sorensen et al. (2018), and Bermejo et al. (2021).

Table 5

Measures of Diversification and Active Risk

Panel A: Value Strategy			
	RP	FW	EW
Effective No. of Stocks	151	157	250
GLR Measure (%)	38.29	39.80	37.66
Active Factor Risk (%)	3.07	3.81	3.75
Idiosyncratic Risk (%)	1.56	1.61	1.60
Residual Sharpe ratio	0.18	0.27	0.31

Panel B: Investment Strategy			
	RP	FW	EW
Effective No. of Stocks	146	164	250
GLR Measure (%)	32.75	33.34	33.44
Active Factor Risk (%)	2.59	2.87	3.10
Idiosyncratic Risk (%)	1.39	1.48	1.48
Residual Sharpe ratio	0.36	0.45	0.47

Panel C: Profitability Strategy			
	RP	FW	EW
Effective No. of Stocks	139	147	250
GLR Measure (%)	29.18	28.45	28.94
Active Factor Risk (%)	2.32	2.04	2.14
Idiosyncratic Risk (%)	1.37	1.49	1.55
Residual Sharpe ratio	0.45	0.47	0.48

Panel D: Size Strategy			
	RP	FW	EW
Effective No. of Stocks	144	168	250
GLR Measure (%)	33.71	32.13	32.01
Active Factor Risk (%)	3.65	4.39	4.38
Idiosyncratic Risk (%)	1.55	1.51	1.52
Residual Sharpe ratio	0.28	0.42	0.45

Panel E: Momentum Strategy			
	RP	FW	EW
Effective No. of Stocks	158	155	250
GLR Measure (%)	30.24	24.53	25.81
Active Factor Risk (%)	2.82	2.94	3.07
Idiosyncratic Risk (%)	1.46	1.51	1.47
Residual Sharpe ratio	0.49	0.37	0.41

Panel F: Low Volatility Strategy			
	RP	FW	EW
Effective No. of Stocks	163	164	250
GLR Measure (%)	31.83	34.03	34.23
Active Factor Risk (%)	2.65	2.29	2.29
Idiosyncratic Risk (%)	1.35	1.38	1.43
Residual Sharpe ratio	0.38	0.43	0.44

To quantify the properties of diversification, we calculated ENS and GLR (Goetzmann et al., 2005; Amenc et al., 2017), as shown in Table 5. The results illustrate that the RP weighting leads to a concentrated index implying a low number of effective constituents, while EW portfolios have considerably higher ENS. Besides this, the findings show that GLR measures for all the smart beta strategies range from 24.53% to 39.80% compared to the 41.33% GLR for the traditional counterpart (BSE S&P 500). The higher GLR suggests that the traditional index accounts for high correlation across stocks and therefore gives sufficient evidence that it is not well diversified. The findings support previous results (Amenc et al., 2014, 2017).

Furthermore, we tested a multi-factor regression model (Equation 4) to examine the two components of active risk, i. e., factor and idiosyncratic risk. Active factor risk is calculated as the square root of the product of R^2 and TE^2, (i. e., R-Squared and Tracking error Squared), whereas the idiosyncratic risk measures the standard deviation of residuals.

$$\begin{aligned} R_P - R_F = {} & \alpha + B1\left(R_M - R_F\right) + B2\left(\mathrm{SMB}\right) + B3\left(\mathrm{HML}\right) \\ & + B4\left(\mathrm{MOM}\right) + B5\left(\mathrm{LVOL}\right) + B6\left(\mathrm{INV}\right) + B7\left(\mathrm{PROF}\right) + \varepsilon \end{aligned} \quad (4)$$

where R_P represents factor portfolio return, R_M stands for the market return, and R_F denotes the risk-free rate.

An essential feature of Table 5 is that the profitability factor has the lowest factor risk, while the low volatility strategy has the lowest idiosyncratic risk. The rationale for low idiosyncratic risk for this strategy is that it accounts for volatility and, therefore, eliminates risk concentration. Furthermore, the findings show that EW portfolios have a predominant residual Sharpe ratio (alpha return per unit of idiosyncratic risk). More specifically,

Panel C of Table 5 shows that the profitability factor in the EW approach has the highest residual Sharpe ratio, implying the highest idiosyncratic risk-adjusted return.

Table 6

Exposure of Smart Beta Strategies: A Multi-Factor Regression Approach

Panel A: Value Strategy			
	RP	FW	EW
Alpha (%)	0.28	0.43*	0.49*
Market Beta	0.85*	0.89*	0.89*
SMB Beta	0.28*	0.21*	0.29*
HML Beta	0.25*	0.34*	0.29*
MOM Beta	0.02	0.02	0.02
LVOL Beta	-0.08*	-0.20*	-0.19*
INV Beta	0.07	0.10	0.07
PROF Beta	-0.06	-0.08	-0.06
R-Squared (%)	96.23	96.97	96.93
Factor Intensity	0.48	0.39	0.42
Relative Return/Factor Intensity (%)	0.02	0.08	0.79

Panel B: Investment Strategy			
	RP	FW	EW
Alpha (%)	0.50*	0.67*	0.70*
Market Beta	0.84*	0.92*	0.91*
SMB Beta	0.31*	0.27*	0.32*
HML Beta	0.04	0.04	0.06
MOM Beta	0.02	0.01	0.02
LVOL Beta	0.02	-0.09*	-0.10*
INV Beta	0.28*	0.35*	0.35*
PROF Beta	-0.05	-0.06	-0.05
R-Squared (%)	95.93	96.63	96.74
Factor Intensity	0.62	0.52	0.60
Relative Return/Factor Intensity (%)	0.23	0.87	0.93

Panel C: Profitability Strategy			
	RP	FW	EW
Alpha (%)	0.61*	0.70*	0.74*
Market Beta	0.86*	0.94*	0.93*
SMB Beta	0.30*	0.28*	0.31*
HML Beta	0.00	0.01	0.03
MOM Beta	0.04	0.02	0.02
LVOL Beta	0.05	-0.05	-0.07

INV Beta	0.08	0.09	0.05
PROF Beta	0.22*	0.33*	0.30*
R-Squared (%)	94.67	95.57	95.18
Factor Intensity	0.69	0.68	0.64
Relative Return/Factor Intensity (%)	1.39	2.18	2.44

Panel D: Size Strategy			
	RP	FW	EW
Alpha (%)	0.44*	0.63*	0.68*
Market Beta	0.87*	0.92*	0.92*
SMB Beta	0.63*	0.72*	0.71*
HML Beta	0.08	0.06	0.07
MOM Beta	0.04	0.04	0.05*
LVOL Beta	0.00	-0.09*	-0.12*
INV Beta	0.06	0.05	0.02
PROF Beta	-0.01	-0.03	-0.01
R-Squared (%)	96.16	97.26	97.23
Factor Intensity	0.80	0.75	0.72
Relative Return/Factor Intensity (%)	0.91	1.72	2.00

Panel E: Momentum Strategy			
	RP	FW	EW
Alpha (%)	0.72*	0.56*	0.60*
Market Beta	0.85*	0.87*	0.89*
SMB Beta	0.35*	0.25*	0.32*
HML Beta	0.11*	-0.06	0.03
MOM Beta	0.33*	0.38*	0.39*
LVOL Beta	0.01	-0.19*	-0.18*
INV Beta	0.07	0.09	0.05
PROF Beta	0.04	-0.05	0.00
R-Squared (%)	95.16	96.06	96.48
Factor Intensity	0.91	0.42	0.61
Relative Return/Factor Intensity (%)	0.96	3.24	2.31

Panel F: Low Volatility Strategy			
	RP	FW	EW
Alpha (%)	0.51*	0.59*	0.63*
Market Beta	0.80*	0.89*	0.89*
SMB Beta	0.29*	0.29*	0.32*
HML Beta	0.00	-0.02	0.00
MOM Beta	0.04*	0.05*	0.03

LVOL Beta	0.18*	0.18*	0.16*
INV Beta	0.02	0.06	0.01
PROF Beta	-0.02	-0.02	-0.04
R-Squared (%)	93.72	94.56	94.45
Factor Intensity	0.51	0.54	0.48
Relative Return/Factor Intensity (%)	0.25	0.59	0.77

Note. The market factor represents the excess return of the cap-weighted benchmark over the risk-free rate. For the regression part, factor portfolios are created by providing equal weight to the top and bottom three deciles of stocks. Factor intensity is the total of all betas, excluding market beta. Relative return to factor intensity is a proportion of relative return over per unit of factor intensity. The results are based on 204 monthly return observations. (*) value corresponds to the regression coefficients (beta(s) and alpha(s)) that are significant at 5% level.

We used a seven-factor regression model to examine the role of factors in smart beta strategies (Equation 4). Table 6 demonstrates positive and statistically significant monthly alpha ranges from 0.43% and 0.74%. In particular, EW portfolios have the highest monthly alpha, generally around 0.49% to 0.74% in five out of 6 cases, with momentum being the only exception. Table 6 also provides notable insights into the assessment of factor exposures. For example, the SMB varies between 0.21 and 0.72, i. e., positive and substantial across all strategies. Also, exposure to low volatility (LVOL) is significant for the larger part of the strategies; however, the magnitude is not as extraordinary as its worth in terms of the size factor.

Moreover, our analysis extends the outcome for other strategies as well. For example, the investment strategy leads to significant INV factor loadings for RP, FW, and EW as 0.28, 0.35, and 0.35, respectively. Besides, the high profitability strategy has a significant PROF beta of 0.22, 0.33, and 0.30 for the three weighting schemes. In this way, it shows sufficient evidence on different exposures for the smart beta strategies.

Finally, we looked at the statistics of Relative Return to factor intensity, which depicts how efficiently the factor intensity is employed (Amenc et al., 2017). By comparison, EW portfolios have the highest relative return to factor intensity, with momentum being the exception. The highest relative return to factor intensity ratio indicates that the EW portfolios effectively used various factor exposures to generate excess returns. Conversely, the RP portfolios have the lowest relative return to factor intensity, implying that they are unable to efficiently bring their factor exposure.

6. Concluding Remarks

Investors in emerging markets are exposed to higher risk in comparison with the developed markets. However, increment in risk exposure prompts more chances for proficient investors in these emergent markets. Earlier studies by Salomons and Grootveld (2003), Kohers et al. (2006), and Chen (2018) found that the developed and emerging econo-

mies contrast to a certain extent, inclusive of the evolution of capital markets, regulatory framework, international diversification, integration of stock market, and others.

The criticism for market cap indices is the starting point for the development of new indexing opportunities. In pursuit of this, researchers have developed various innovative investment styles that offer outperformance over time. Evidently, smart beta as an investment philosophy has rapidly evolved in financial markets and gained popularity worldwide. Numerous studies have already been performed to determine the efficacy of smart beta strategies in developed markets, while the research on emergent markets is limited. With this gap, we conducted an empirical analysis of popular smart beta strategies to affirm their existence and potential execution in the under-researched emerging Indian stock market.

To the extent of the authors' best information, this study is an initial attempt to integrate the framework of factor-based stock selection with the diversified weighting strategies in the Indian context. Our motivation is to assess smart beta investing as an alternative investment compared to the traditional Indian market index. As a result, we implemented six-factor exposures across three weighting schemes to proxy distinctive investment approaches and examined their return-risk characteristics. The results indicate that the smart beta strategies consistently outperformed the market benchmark in terms of higher returns, superior Shape ratio, improved information ratio, lower drawdown, better diversification, and downside protection. This analysis recommends that smart beta investing has extensively led to robust outperformance resulting in a better risk-return profile in terms of absolute and risk-adjusted basis (Amenc et al., 2014; Bender et al., 2018; Sorensen et al., 2018; Bermejo et al., 2021).

Moreover, the study provides valuable insights into the factor exposures and highlight that the profitability strategy has provided the best risk-return profile (higher returns and lower drawdown) among the other strategies analyzed. The other noteworthy point is that profitability and low volatility are strategies that report stability and robust results even in bearish market conditions. Thus, it is evident that these factor-based strategies can effectively diversify investment portfolios across different market situations.

Overall, the empirical results illustrate that the Equal Weighting (EW) approach is progressively compelling due to its potential to generate higher excess returns, superior information ratio, high and significant alpha, enhanced relative factor intensity, maximum downside protection, and better diversification. These findings, however, are consistent with other notable studies (DeMiguel et al., 2009; Chaves et al., 2011; Blitz, 2016; Malladi & Fabozzi, 2017). The results are particularly significant because most of the asset management benchmarks are focused on cap-weighting. Furthermore, EW indices also provide increased portfolio diversification by allowing for a higher percentage of investment in mid-cap or small-cap stocks.

The advantage of equal weighting is that EW indices implicitly adopt a "contrarian investment approach," as they instinctively re-balance away from the overvalued stocks.

As a result, the EW approach can withstand price fluctuations because of its simplicity, maximum diversification, and improved performance. RP weighting, however, has an essential consideration in building risk-balanced portfolios (Chaves et al., 2011). In conclusion, the findings of this study support the widely held belief that smart beta investing "reduces unrewarded risk, promotes diversification and increases risk-adjusted performance" compared to a cap-weighted market index. To summarize, the study suggests that market participants may consider the diverse range of smart beta strategies that best suit their risk appetite.

7. Implications and Future Scope

Smart beta investing is a major development in the field of index investing. In general, it provides researchers, practitioners, and investors' communities with new investment opportunities. These novel strategies enable various market participants to access the returns and risks of a specific investment style through a more transparent and standardized investment product. Moreover, it is gaining widespread popularity for several reasons. First, implementing smart beta strategies generates value additions in terms of improved diversification, drawdown management, and the ability to conduct a better strategic allocation.

Second, this innovative strategy aims to incorporate the advantages of active and passive investment strategies. These strategies can be considered active investing because they harvest "risk premia factors" at a lower cost, and therefore, potentially result in better solutions than conventional cap-weighted indices. Simultaneously, these strategies also have the same characteristics as passive investing, most notably by their transparency and rule-based systematic approach. Third, in the asset management industry, smart beta investing helps numerous portfolio analysts and fund managers to gain exposure to a range of investment styles, thereby achieving the objective of diversification and return enhancement.

In addition, the findings of the study opened up further prospects for the policymakers, index providers, equity analysts, asset managers, and investors to target alternative investments, such as smart beta exchange-traded funds (ETF) and other diversified funds, which could potentially improve the returns. We are optimistic that this framework enhances financial research towards the viability and future advancement of smart beta strategies. It keeps growing popularity, but despite this, we advise various market participants to understand the attributes of these strategies, know about the costs associated with smart beta investing, and vigilantly consider which set of investment styles is best lined up with their investment values and goals.

For future studies, one area of research could be the adoption of smart beta investing in different asset classes and other emerging markets. Further, it is highly encouraged to investigate the risk-return analysis for different multi-factor portfolios. It would likewise be interesting to see the top-down and bottom-up approaches for constructing

smart beta strategies; moreover, considering new dimensions of smart beta investing such as consolidating the ESG factor with other robust factors could be a significant and novel criterion for further research.

Appendix 1
Description of the Measures

Sharpe ratio: It is a ratio of the portfolio's excess return over the risk-free rate to the standard deviation. It is calculated using the formula:

$$\text{Sharpe Ratio} = \frac{R_p - R_F}{\sigma_p} \tag{5}$$

where R_P represents the average return of the portfolio, R_F denotes the risk-free rate, and σ_P stands for the standard deviation of the portfolio.

Sortino ratio: It measures the portfolio's return over the risk-free rate in terms of downside deviation. It is calculated using the following Equation:

$$\text{Sortino Ratio} = \frac{R_p - R_F}{\sigma_{Downside}} \tag{6}$$

where $\sigma_{Downside}$ is the Standard deviation of negative returns.

Tracking error (active risk): It is the standard deviation of the dispersion of a portfolio's excess return to its benchmark. It is computed using Equation 7:

$$\text{Tracking Error} = \sigma(R_p - R_B) \tag{7}$$

Information ratio: It is a ratio of the portfolio's excess return over the benchmark to its active risk (tracking error). It is calculated using Equation 8:

$$\text{Information Ratio} = \frac{R_p - R_B}{\text{Tracking Error}} \tag{8}$$

Upside participation ratio: It is the portfolio's average return over the benchmark's average return in the period when the benchmark index is positive, i. e., the bullish period.

$$\text{Upside Participation}\left(\text{P}_+\right) = \frac{R_S}{R_B}, \quad R_B > 0 \tag{9}$$

where R_s represents the average return of the strategy, R_B denotes the return of the market benchmark.

Downside participation ratio: It measures the portfolio's average return over the benchmark during the period when the benchmark index is negative (i. e., bearish period).

$$\text{Downside Participation}\left(\text{P}_-\right) = \frac{R_S}{R_B}, \quad R_B < 0 \tag{10}$$

Participation advantage: It measures the difference between the upside and downside participation ratios. It is calculated using Equation 11:

$$\text{Participation Advantage} = \text{P}_+ - \text{P}_- \tag{11}$$

Average Participation: It is calculated as the average of the upside and downside participation ratios. The following formula is used to determine it:

$$\text{Average Participation} = \frac{P_+ + P_-}{2} \tag{12}$$

Effective number of stocks (ENS): It is a widely used indicator of portfolio concentration and is calculated as the inverse of the total sum of squared portfolio weights, i. e., the Herfindahl index.

$$\text{ENS} = \frac{1}{\sum_{i=1}^{N} w_i^2} \tag{13}$$

were w_i represents the weight of i^{th} stock; n is the number of stocks.

GLR measure: It is the proportion of the portfolio's variance to the total weighted variance of its stock constituents. It is calculated using Equation 14:

$$\text{GLR Measure} = \frac{Var\left(R_p\right)}{\sum_{i=1}^{N} w_i \times Var\left(R_i\right)} \tag{14}$$

Standardized Factor-scores (S-Scores): Using the CDF (cumulative distribution function), the Z-factor scores are converted into S-scores by normalizing them between 0 and 1.

$$\text{S-Scores } (S_i) = \frac{1}{\sqrt{2\pi}} \int_{-\infty}^{Z_i} e^{\frac{-x^2}{2}}\, dx \tag{15}$$

References

Agarwalla, S. K., Jacob, J., &Varma, J. R. (2017). Size, value, and momentum in Indian equities. *Vikalpa*, *42*(4), 211–219. https://doi.org/10.1177/0256090917733848

Amenc, N., Ducoulombier, F., Esakia, M., Goltz, F., & Sivasubramanian, S. (2017). Accounting for Cross-Factor Interactions in Multi-factor Portfolios without Sacrificing Diversification and Risk Control. *The Journal of Portfolio Management*, *43*(5), 99–114. https://doi.org/10.3905/jpm.2017.43.5.099

Amenc, N., Goltz, F., Lodh, A.,& Martellini, L. (2014). Towards Smart Equity Factor Indices: Harvesting Risk Premia without Taking Unrewarded Risks. *The Journal of Portfolio Management*, *40*(4), 106–122. https://doi.org/10.3905/jpm.2014.40.4.106

Amihud, Y. (2002). Illiquidity and stock returns: cross-section and time-series effects. *Journal of Financial Markets*, *5*(1), 31–56. https://doi.org/10.1016/S1386-4181(01)00024-6

Ang, A., Goetzmann, W. N., & Schaefer, S. (2009). *Evaluation of Active Management of the Norwegian Government Pension Fund–Global*. Retrieved from: https://www0.gsb.columbia.edu/faculty/aang/papers/report%20Norway.pdf

Angelidis, T., &Tessaromatis, N. (2017). Global Equity Country Allocation: An Application of Factor Investing. *Financial Analysts Journal*, *73*(4), 55–73. https://doi.org/10.2469/faj.v73.n4.7

Arnott, R. D., &Kose, E. (2014). What "Smart Beta" Means to Us. *Research Affiliates Fundamentals*, 61–74. Retrieved from: https://www.researchaffiliates.com/en_us/publications/articles/292_what_smart_beta_means_to_us.html.

Arnott, R. D., &Hsu, J. (2008). Noise, CAPM and the Size and Value Effects. *Journal of Investment Management*, *6*(1), 1–11. Available at: https://www.researchaffiliates.com/documents/

JOIM_First_Quarter_2008_Noise_CAPM_and_the_Size_and_Value_Effects.pdf

Baker, M., Bradley, B., &Wurgler, J. (2011). Benchmarks as limits to arbitrage: Understanding the low-volatility anomaly. *Financial Analysts Journal*, *67*(1), 40–54. https://doi.org/10.2469/faj.v67.n1.4

Banz, R. W. (1981). The relationship between return and market value of common stocks. *Journal of Financial Economics*, *9*(1), 3–18. https://doi.org/10.1016/0304-405X(81)90018-0

Basu, S. (1977). Investment Performance of Common Stocks in Relation to their Price-Earnings Ratios: A Test of the Efficient Market Hypothesis. *The Journal of Finance*, *32*(3), 663–682. https://doi.org/10.1111/j.1540-6261.1977.tb01979.x

Bender, J., Sun, X., Thomas, R., &Zdorovtsov, V. (2018).The promises and pitfalls of factor timing. *The Journal of Portfolio Management*, *44*(4), 79–92. https://doi.org/10.3905/jpm.2018.44.4.079

Bender, J., & Wang, T. (2015). Tilted and Anti-Tilted Portfolios: A Coherent Framework for Advanced Beta Portfolio Construction. *The Journal of Index Investing*, *6*(1), 51–64. https://doi.org/10.3905/jii.2015.6.1.051

Bermejo, R., Figuerola-Ferretti, I., Hevia, T., & Santos, A. (2021). Factor investing: A stock selection methodology for the European equity market. *Heliyon*, e08168. https://doi.org/10.1016/j.heliyon.2021.e08168

BlackRock. *Factor-based investing*. Retrieved from: https://www.blackrock.com/institutions/en-au/investment-capabilities-and-solutions/smart-beta

Blitz, D. (2016). Factor investing with smart beta indices. *The Journal of Index Investing*, *7*(3), 43–48. https://doi.org/10.3905/jii.2016.7.3.043

Blitz, D. C., &Van Vliet, P. (2007). The Volatility Effect. *The Journal of Portfolio Management*, *34*(1), 102–113. https://doi.org/10.3905/jpm.2007.698039

Bloomberg (2021). Retrieved from: https://www.bloomberg.com/news/articles/2021-10-11/roaring-india-stock-market-on-track-to-overtake-u-k-s-in-value

Cakici, N., Fabozzi, F. J., & Tan, S. (2013). Size, value, and momentum in emerging market stock returns. *Emerging Markets Review, 16*, 46–65. https://doi.org/10.1016/j.ememar.2013.03.001

Centineo, S., &Centineo, S. (2017). Investment innovation trends: Factor-based investing. *Serbian Journal of Management*, *12*(1), 65–75. https://doi.org/10.5937/sjm12-10764

Chan, K. C., & Chen, N. F. (1991). Structural and return characteristics of small and large firms. *The Journal of Finance*, *46*(4), 1467–1484. https://doi.org/10.1111/j.1540-6261.1991.tb04626.x

Chan, L. K., Hamao, Y., & Lakonishok, J. (1991). Fundamentals and Stock Returns in Japan. *The Journal of Finance*, *46*(5), 1739–1764. https://doi.org/10.1111/j.1540-6261.1991.tb04642.x

Chaves, D., Hsu, J., Li, F., & Shakernia, O. (2011). Risk parity portfolio vs. other asset allocation heuristic portfolios. *The Journal of Investing*, *20*(1), 108–118. https://doi.org/10.3905/joi.2011.20.1.108

Chen, P. (2018). Understanding international stock market comovements: A comparison of developed and emerging markets. *International Review of Economics & Finance*, *56*, 451–464. https://doi.org/10.1016/j.iref.2017.12.004

Dasgupta, A., Prat, A., & Verardo, M. (2011). The price impact of institutional herding. *The Review of Financial Studies*, *24*(3), 892–925. https://doi.org/10.1093/rfs/hhq137

DeMiguel, V., Garlappi, L., & Uppal, R. (2009). Optimal versus naive diversification: How inefficient is the 1/N portfolio strategy? *The Review of Financial Studies*, *22*(5), 1915–1953. https://doi.org/10.1093/rfs/hhm075

Fama, E. F., & French, K. R. (1993). Common risk factors in the returns on stocks and bonds. *Journal of Financial Economics*, *33*(1), 3–56. https://doi.org/10.1016/0304-405X(93)90023-5

Fama, E. F., & French, K. R. (1996). Multi-factor explanations of asset pricing anomalies. *The Journal of Finance, 51*(1), 55–84. https://doi.org/10.1111/j.1540-6261.1996.tb05202.x

Fama, E. F., & French, K. R. (2012). Size, value, and momentum in international stock returns. *Journal of Financial Economics*, *105*(3), 457–472. https://doi.org/10.1016/j.jfineco.2012.05.011

Fama, E. F., & French, K. R. (2015). A five-factor asset pricing model. *Journal of Financial Economics*, *116*(1), 1–22. https://doi.org/10.1016/j.jfineco.2014.10.010

Ferson, W. E., Kandel, S. & Stambaugh, R. F. (1987). Tests of Asset Pricing with Time-Varying Expected Risk Premiums and Market Betas. *The Journal of Finance, 42*(2), 201–220. https://doi.org/10.1111/j.1540-6261.1987.tb02564.x

Frazzini, A., & Pedersen, L. H. (2014). Betting against beta. *Journal of Financial Economics*, *111*(1), 1–25. https://doi.org/10.1016/j.jfineco.2013.10.005

Fuller, K. P., & Goldstein, M. A. (2011). Do dividends matter more in declining markets?. *Journal of Corporate Finance*, *17*(3), 457–473. https://doi.org/10.1016/j.jcorpfin.2011.01.001

Goetzmann, W. N., Li, L., & Rouwenhorst, K. G. (2005). Long-Term Global Market Correlations.*The Journal of Business, 78*(1), 1–38. http://dx.doi.org/10.1086/426518

Grinold, R. (1992). Are Benchmark Portfolios Efficient? *The Journal of Portfolio Management*, *19*(1), 34–40. https://doi.org/10.3905/jpm.1992.34

Hanauer, M. X., & Linhart, M. (2015). Size, value, and momentum in emerging market stock returns: Integrated or segmented pricing?. *Asia-Pacific Journal of Financial Studies, 44*(2), 175–214. https://doi.org/10.1111/ajfs.12086

Haugen, R. A., & Baker, N. L. (1991). The efficient market inefficiency of capitalization-weighted stock portfolios. *The Journal of Portfolio Management, 17*(3), 35–40. https://doi.org/10.3905/jpm.1991.409335

Hilliard, J., & Zhang, H. (2015). Size and price-to-book effects: Evidence from the Chinese stock markets. *Pacific-Basin Finance Journal, 32*, 40-55. https://doi.org/10.1016/j.pacfin.2015.02.003

Hong, H., Lim, T., & Stein, J. C. (2000). Bad news travels slowly: Size, analyst coverage, and the profitability of momentum strategies. *The Journal of Finance, 55*(1), 265–295. https://doi.org/10.1111/0022-1082.00206

Hou, K., Xue, C., & Zhang, L. (2015). Digesting anomalies: An investment approach. *The Review of Financial Studies*, *28*(3), 650–705. https://doi.org/10.1093/rfs/hhu068

Hsu, J. C. (2006). Cap-weighted portfolios are sub-optimal portfolios. *Journal of Investment Management, 4*(3), 1–10. Retrieved from: https://www.researchaffiliates.com/documents/JOIM_Third_Quarter_2006_Cap-Weighted_Portfolios_are_Sub-Optimal_Portfolios.pdf

Hsu, J., Kalesnik, V., & Viswanathan, V. (2015). A Framework for Assessing Factors and Implementing Smart Beta Strategies. *The Journal of Index Investing, 6*(1), 89–97. https://doi.org/10.3905/jii.2015.6.1.089

Hu, G. X., Chen, C., Shao, Y., & Wang, J. (2019). Fama–French in China: Size and value factors in Chinese stock returns. *International Review of Finance*, *19*(1), 3–44. https://doi.org/10.1111/irfi.12177

Jacobs, B. I., & Levy, K. N. (2014). Smart Beta versus Smart Alpha. *The Journal of Portfolio Management, 40*(4), 4–7. https://doi.org/10.3905/jpm.2014.40.4.004

Jegadeesh, N., & Titman, S. (1993). Returns to Buying Winners and Selling Losers: Implications for Stock Market Efficiency. *The Journal of Finance, 48*(1), 65–91. https://doi.org/10.1111/j.1540-6261.1993.tb04702.x

Kahn, R. N., & Lemmon, M. (2016). The Asset Manager's Dilemma: How Smart Beta Is Disrupting the Investment Management Industry. *Financial Analysts Journal, 72*(1), 15–20. https://doi.org/10.2469/faj.v72.n1.1

Kim, S. (2021). Enhanced factor investing in the Korean stock market. *Pacific-Basin Finance Journal*, *67*, 101558. https://doi.org/10.1016/j.pacfin.2021.101558

Kohers, G., Kohers, N., & Kohers, T. (2006). The risk and return characteristics of developed and emerging stock markets: The recent evidence. *Applied Economics Letters*, *13*(11), 737–743. https://doi.org/10.1080/13504850500407210

Kudoh, H., Miazzi, A., & Yamada, T. (2015). The Low-Correlation Enhancement: How to Make Alternative Beta Smarter. *The Journal of Investing*, *24*(4), 81–91. https://doi.org/10.3905/joi.2015.24.4.081

Lakonishok, J., Shleifer, A., & Vishny, R. W. (1994). Contrarian investment, extrapolation, and risk. *The Journal of Finance*, *49*(5), 1541–1578. https://doi.org/10.1111/j.1540-6261.1994.tb04772.x

Li, D., & Zhang, L. (2010). Does q-theory with investment frictions explain anomalies in the cross section of returns?. *Journal of Financial Economics*, *98*(2), 297–314. https://doi.org/10.1016/j.jfineco.2010.06.001

Malevergne, Y., Santa-Clara, P., & Sornette, D. (2009). Professor Zipf Goes to Wall Street. NBER Working Paper, *National Bureau of Economic Research*. https://doi.org/10.3386/w15295

Malladi, R., & Fabozzi, F. J. (2017). Equal-weighted strategy: Why it outperforms value-weighted strategies? Theory and evidence. *Journal of Asset Management*, *18*(3), 188–208. 10.1057/s41260-016-0033-4

Markowitz, H. (1952). Portfolio Selection. *The Journal of Finance*, *7*(1), 77–91. https://doi.org/10.1111/j.1540-6261.1952.tb01525.x

Martellini, L. & Milhau, V. (2018). *Smart Beta and Beyond: Maximising the Benefits of Factor Investing*. Available at: https://risk.edhec.edu/sites/risk/files/edhec_publication_smart_beta_and_beyond_1.pdf

Monga, R., Aggrawal, D., & Singh, J. (2021). Exploring new frontiers in indexing strategies: an optimization-based risk-efficient solution. *International Journal of System Assurance Engineering and Management*, 1–13. https://doi.org/10.1007/s13198-021-01138-3

Novy-Marx, R. (2013). The other side of value: The gross profitability premium. *Journal of Financial Economics*, *108*(1), 1–28. https://doi.org/10.1016/j.jfineco.2013.01.003

Qian, E. (2015). On the Holy Grail of "Upside Participation and Downside Protection". *The Journal of Portfolio Management*, *41*(2), 11–22. https://doi.org/10.3905/jpm.2015.41.2.011

Russo, A. (2014).*Understanding Smart Beta: Beyond Diversification and Low Risk Investing.* Available at: https://silo.tips/download/understanding-smart-beta-beyond-diversification-and-low-risk-investing

Salomons, R., & Grootveld, H. (2003). The equity risk premium: Emerging vs. developed markets. *Emerging Markets Review*, *4*(2), 121–144. https://doi.org/10.1016/S1566-0141(03)00024-4

Silvasti, V., Grobys, K., & Äijö, J. (2021). Is smart beta investing profitable? Evidence from the Nordic stock market. *Applied Economics*, *53*(16), 1826–1839. https://doi.org/10.1080/00036846.2020.1853669

Sorensen, E., Barnes, M., Alonso, N., & Qian, E. (2018). Not All Factor Exposures Are Created Equal. *The Journal of Portfolio Management*, *44*(4), 39–45. https://doi.org/10.3905/jpm.2018.44.4.039

Treynor, J. (2005). Why Market-Valuation-Indifferent Indexing Works. *Financial Analysts Journal*, *61*(5), 65–69. https://doi.org/10.2469/faj.v61.n5.2757

World Bank (2021). Retrieved from: https://www.worldbank.org/en/country/india

Zhang, L. (2005). The value premium. *The Journal of Finance*, *60*(1), 67–103. https://doi.org/10.1111/j.1540-6261.2005.00725.x

Zhang, X. F. (2006). Information uncertainty and stock returns. *The Journal of Finance*, *61*(1), 105–137. https://doi.org/10.1111/j.1540-6261.2006.00831.x

Proceedings of the Sixth International Conference on Intelligent Computing and Control Systems (ICICCS 2022)
IEEE Xplore Part Number: CFP22K74-ART; ISBN: 978-1-6654-1035-9

2022 6th International Conference on Intelligent Computing and Control Systems (ICICCS) | 978-1-6654-1035-9/22/$31.00 ©2022 IEEE | DOI: 10.1109/ICICCS53718.2022.9788196

Software Change Prediction using Ensemble Learning on Object Oriented Metrics

Nikhil Khanna
Software Engineering Department
Delhi Technological University
New Delhi, India
nikhilkhanna_2k18se088@dtu.ac.in

Ojas Agarwal
Software Engineering Department
Delhi Technological University
New Delhi, India
ojasagarwal_2k18se091@dtu.ac.in

Rahul
Software Engineering Department
Delhi Technological University
New Delhi, India
rahul@dtu.ac.in

Abstract— In order to reduce developers' time testing the defects in software, this research work has come up with an ensemble learning approach using various machine learning and deep learning classifiers. This empirical study starts with the data collection process. Own dataset has been created by using Understand tool and further it will be applied over sampling techniques. The data set has a binary class output, and thus by applying data over sampling techniques, the number of instances of both classes remain comparable. After that various classifiers are trained with the entire training data set. After this step, the proposed model will predict the outcome that these classifiers would create using the training set and compare them with the actual values of the training dependent variable. After this the information that claim which of the classifiers were able to correctly predict the outcome will be given a data point. After that the neural networks will be trained for each of the classifiers with input variables as training independent variables and output variables as the previously recorded data as to whether a classifier correctly classifies a data point or not. This predicting network would tell us whether the classifier corresponding to that particular network would correctly classify a particular data point or not. To predict the outcome of any new data point, it will be fed to the predicting network and find which classifier would correctly predict the outcome and the aggregated result of the selected classifiers would be reported.

Keywords—Ensemble Learning, Object Oriented Metrics, Software change prediction, Adaptive Network, Machine Learning classifiers, Neural Network

I. INTRODUCTION

During the life cycle of a software, testing plays a very crucial role and cannot be underestimated. Moreover, this can take up a lot of resources due to its importance. Thus, it is highly required to formulate new ways to reduce the time and resources needed for testing and that was the motivation behind this empirical study that are conducted.

This research work has used own data set for training and testing the model. The data set is created by using Understand Tool, which generated Object Oriented Metrics for the classes from the given source code.

Data imbalance was a major issue encountered while working with this data set and it was resolved by applying outlier detection on the majority class and reducing its count to a comparable number as that of the minority class. This helped the model in getting a better understanding of the data set and this also helped in getting rid of a lot of the noise in the data set

The classifiers that we have used for our model are as follows -

1. Artificial Neural Network (ANN)
2. Decision Tree (DT)
3. Support Vector Machine (SVM)
4. K Nearest Neighbours (KNN)
5. Gaussian Naive Bayes (NB)
6. Random forest

The adaptive technique we use, selects only those classifiers for aggregation that are likely to give correct outcomes. This in turn gives a better result than basic ensemble [1] techniques. This adaptive model also has a better score than most of the machine learning [2] techniques.

The metrics used to analyse and compare the performance for our model are -

1. Area under ROC curve (AUC)
2. Precision

AUC - Area under the Receiver Operating Characteristics (ROC) curve. AUC represents separability. It tells us how well can a model distinguish between classes, i.e., classify 0's as 0's and 1's as 1's. This measure is widely popular and is a better metric than accuracy (which is widely used too even though it has been discredited as a good metric).

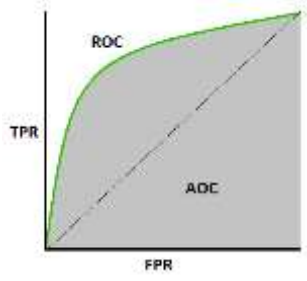

Fig 1 – Area Under ROC curve

Authorized licensed use limited to: DELHI TECHNICAL UNIV. Downloaded on June 15,2022 at 11:21:55 UTC from IEEE Xplore. Restrictions apply.

Precision - Precision is another important metric that reports the ratio of number of true positives to total predicted positives (the sum of number of true positives and number of false positives). It informs as to how many of the reported positive values were actually positive. It tells how precise a model is.

$$Precision = \frac{True\ Positive}{True\ Positive + False\ Positive}$$

An ensemble learning model usually consists of 3 stages -

1. Data collection and Pre-processing
2. Training the classifiers and prediction networks
3. Aggregation of the outcomes

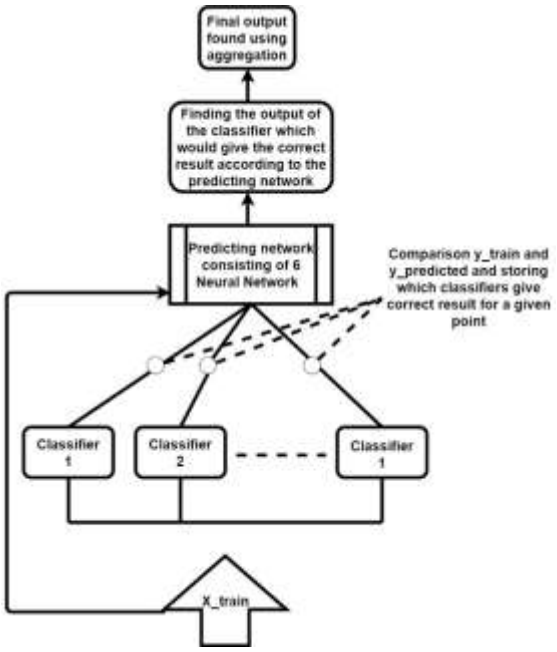

Fig 2 – Architecture of the Model

Let us talk about each of these 3 steps in detail in the following sections.

II. DATA COLLECTION

A. Data Elicitation

The very first step of the study started with data elicitation which means gathering of data from the source. It started by downloading the source code of various applications of android framework for 2 versions, i.e. Android 5.0(Lollipop) and Android 6.0(Marshmallow) from the AOSP[3] github repository which is a mirror of the google git[4] repository. All the Java and CPP files were downloaded and the XML files were not used for the study

B. Extraction of Object-Oriented Metrics

This step was rather a very crucial step in the Data collection process. All the Java and CPP files for both the versions were then subjected to the Understand™ Tool and Object Oriented (OO) Metrics were extracted. The following OO metrics were extracted -

1) AvgCyclomatic
2) CountClassBase
3) CountClassCoupled
4) CountClassDerived
5) CountDeclInstanceMethod
6) CountDeclInstanceVariable
7) CountDeclMethodAll
8) CountDeclMethod
9) CountDeclMethodPublic
10) CountLineCode
11) MaxInheritanceTree
12) PercentLackOfCohesion

These metrics served as the attributes OR independent variables for the data set.

Malhotra *et al.* [5] demonstrate the reason for selecting these OO Metrics in great detail. Singh *et al* [6] also give valid reasons to select these metrics

C. Comparison of the two Versions

Finally, these OO metrics for both the versions were compared. For the classes that had the same OO metrics, no change was reported and for the classes that had a difference in the OO metrics meant there was a change in the 2 subsequent versions of the same class, and thus change was reported. This was finally stored in a CSV file and the data set was finally completed

This concluded the Data collection part, next the study moved onto Data Pre-processing the mainly included handling Data imbalance using Outlier Detection

D. Handling Data Imbalance

The initial data set had a distribution of 32% positive outcome class (Change) and 68% negative outcome class (No Change). This was leading to unfavourable results and low model performance. On inspection, it revealed that the data set had a lot of noise and included instances that did not represent a class thus having outlier characteristics. On applying Outlier Detection on the negative outcome class, a lot of the noise was removed and thus brought the distribution down to 49% positive outcome class (Change) and 51 % negative outcome class (No Change), thus leading to better results and model performance [7].

Authorized licensed use limited to: DELHI TECHNICAL UNIV. Downloaded on June 15,2022 at 11:21:55 UTC from IEEE Xplore. Restrictions apply.

III. TRAINING THE CLASSIFIERS AND PREDICTION NETWORK

This part of the study is the most critical part and needs to be elaborated properly which will be done in the following subsections

A. Selection of Classifiers

This part of the study started with selection of Machine Learning and Deep learning Classifiers. The following classifiers were selected for the model-

ANN, DT, SVM, KNN, NB, Random Forest

There was a reason behind selecting these classifiers, they were not selected at random. These 6 classifiers cover a range of Machine learning classifiers, having different learning quirks. They help in universalizing the results.

B. Training Classifiers

Moving onto the next step of the study, the classifiers were trained using the training data (X_train & y_train).

In this next step of Software Change Prediction [6], we predicted the outcome of X_train over these 6 trained classifiers and stored the output and compared it with y_train. The reason behind doing this step was to find out, for a given data point, which all classifiers were able to correctly predict the outcome. If a classifier was able to correctly predict the outcome, then for that particular data point, it was marked as 1, if not then 0. For future reference, they'll be referred to as comparison matrices

C. Building the Prediction Network

The next part of the study enlightens us about the architecture of the Adaptive Predictive Network which is used to find which all classifiers would be able to correctly predict the outcome for a new data point.

Let's us have a look at the architecture of the Network

As we can see from the above image, the network is a combination of Dense layers and Batch Normalization layers. Batch normalization layers are added to optimize the model. The number of hidden nodes and number of hidden layers was decided by hit and trial and it was concluded after a certain point adding more layers or nodes does not improve performance.

For the Adaptive Predicting Network [8], 6 such networks were built, one for each of the classifiers as seen in Fig 2. The independent variable for these networks remained the same. i.e., X_train but as for the dependent variable, the comparison matrices were used. What this means is that these networks were predicting whether for a particular data point, would the corresponding classifier give a correct output or not. These 6 networks combine to give the Adaptive Predicting Network.

```
Model: "sequential_8"
_________________________________________________________________
Layer (type)                 Output Shape              Param #
=================================================================
dense_48 (Dense)             (None, 64)                832
_________________________________________________________________
batch_normalization_40 (Batc (None, 64)                256
_________________________________________________________________
dense_49 (Dense)             (None, 128)               8320
_________________________________________________________________
batch_normalization_41 (Batc (None, 128)               512
_________________________________________________________________
dense_50 (Dense)             (None, 128)               16512
_________________________________________________________________
batch_normalization_42 (Batc (None, 128)               512
_________________________________________________________________
dense_51 (Dense)             (None, 128)               16512
_________________________________________________________________
batch_normalization_43 (Batc (None, 128)               512
_________________________________________________________________
dense_52 (Dense)             (None, 32)                4128
_________________________________________________________________
batch_normalization_44 (Batc (None, 32)                128
_________________________________________________________________
dense_53 (Dense)             (None, 2)                 66
=================================================================
Total params: 48,290
Trainable params: 47,330
Non-trainable params: 960
_________________________________________________________________
```

Fig 3 – Layers of the Neural Networks in the Adaptive Network

The Network is adaptive, because it dynamically decides which all classifiers would be used in the aggregation process

After training the Adaptive Predictive Network, we input the test data i.e. X_test to it and then apply aggregation to the output from all the dynamically selected classifiers. Next Section talks about the aggregation process

IV. AGGREGATION OF THE OUTCOME

Various studies in the past such as Chandra *et al* [9] have used an aggregation technique called majority voting, while other studies such as Magnus *et al* [10] have used aggregation techniques such as Bayesian model averaging (BMA) and a new method called weighted-average least squares (WALS).

In this study, since the outcome is binary (0 and 1) different techniques such as majority voting, averaging, median voting would all yield the same result and thus we simply resort to majority voting [9], which is a very commonly used aggregation technique when it comes to ensemble learning models.

After the Adaptive Predicting Network reported which, all classifiers were likely to give the correct result, the results of all the said classifiers aggregated their result using majority voting.

Majority voting is as simple as it sounds. The class which holds the majority amongst the outcomes of the classifiers is declared at the reported outcome. In this study as well, the outcomes of the selected classifiers were subjected to this combination technique and the final outcome was reported for all the instances in the test set. Now at times a distinctive condition arises, that is when the

Authorized licensed use limited to: DELHI TECHNICAL UNIV. Downloaded on June 15,2022 at 11:21:55 UTC from IEEE Xplore. Restrictions apply.

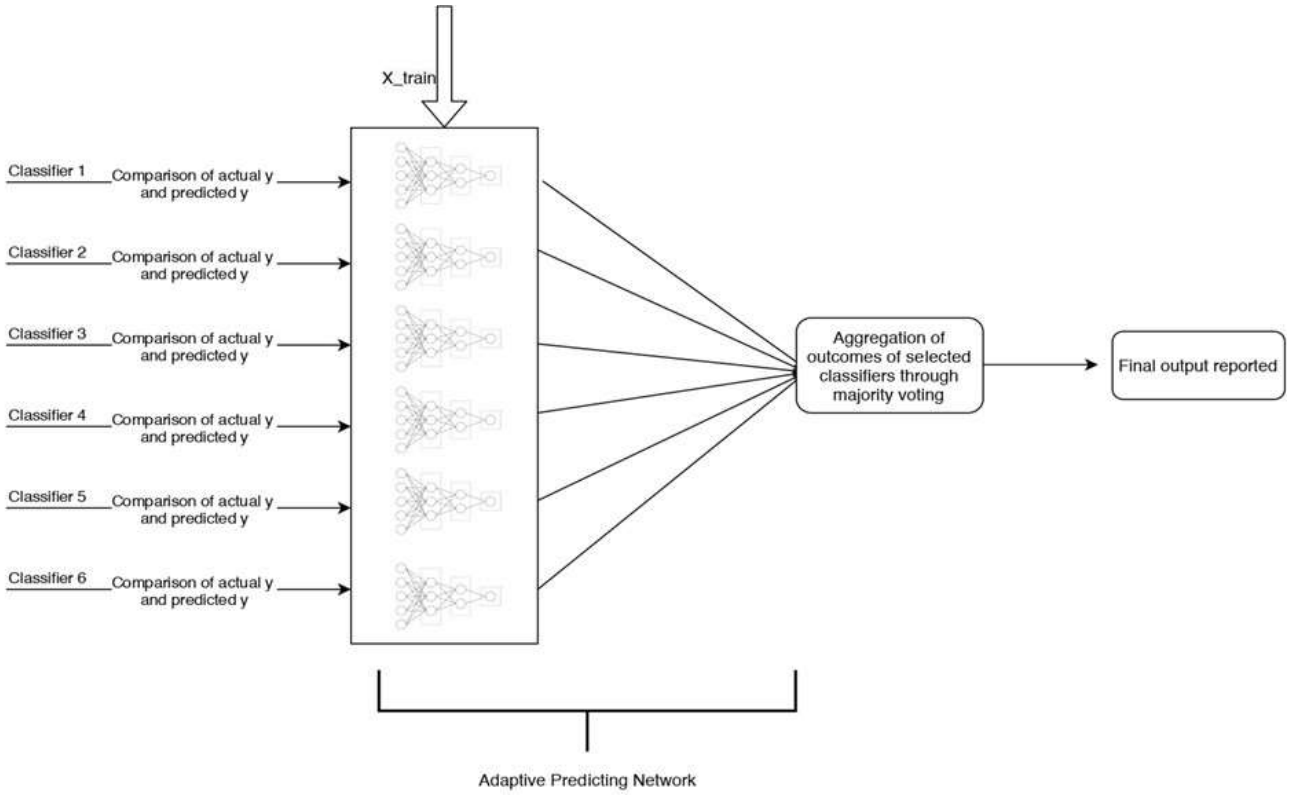

Fig 4 – Architecture of the Adaptive Predictive Network

situation of a tie occurs. In such a situation, the number of 1's is equal to the number of 0's. i.e., both the labels are in equal numbers. In such a situation, researchers such as Chaouiya *et al* [11] have used a random integer generator in the past. Kokkinos *et al* [12] used the properties of SoftMax function in the case of Neural Network to break the ties.

In this study, we simply omitted the outcome of the first reported classifier and since the remaining would obviously have a majority thus it would end up breaking the tie. Random Integer Generator also tried to break the tie but it gave similar results to the one used.

V. ANALYSIS AND RESULT

The results achieved by individual classifiers can be clearly seen in Table 1

Table 1 – Comparison of metrics of Ensemble Model and Individual Classifiers

	AUC	PRECISION
Ensemble Model	0.9418	0.9949
ANN	0.9360	0.9940
Decision Tree	0.9216	0.9326
Logistic Regression	0.9246	0.9797

A. AUC Score

AUC - ROC curve is a measure of performance for classification problems. AUC [13] represents degree or measure of separability. It tells how much a model is capable of differentiating between classes. Higher the AUC, better the model is at predicting 0s as 0s and 1s as 1s.

As we can clearly infer from the above table, the model created in this empirical study gave an AUC score

Authorized licensed use limited to: DELHI TECHNICAL UNIV. Downloaded on June 15,2022 at 11:21:55 UTC from IEEE Xplore. Restrictions apply.

of 0.9418 which was more than that of any other individual classifier.

ANN gave an AUC score of 0.9360 which was as close any Machine learning algorithm got to the score of our model

Other Machine Learning algorithms were only able to achieve scores close to 92%

B. Precision

Precision [14] is another important metric to find the performance of a model

It informs as to how many of the reported positive values were actually positive. It tells how precise a model is.

This model stood out even in its Precision Score. With a precision score of 0.9949, it was higher than that of ANN which was just shy by 0.0009. Other classifiers scored relatively low for this metric with a score of 0.9326 for DT and 0.9797 for Logistic Regression

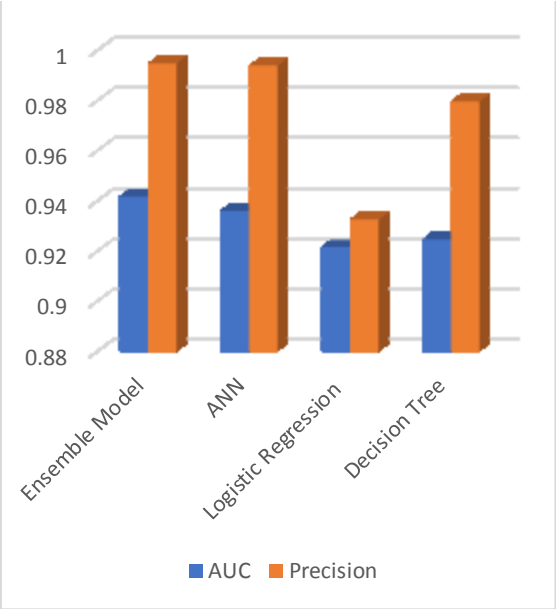

Fig 5 – Graphical Representation for comparison of metrics of Ensemble Model and Individual Classifiers

VI. CONCLUSION

We conducted an empirical study to formulate and build a model to find classes in a software prone to change so as to reduce the time and resources needed by the Testing phase in the life cycle model.

By the end of the study, we were able to achieve a model with performance metrics better than any of the best stand-alone models.

We were able to create an Ensemble Technique that was able to detect the proneness of a class to change based on its Object-Oriented Metrics.

We were able to create a model that was unique to the contemporary work done in Ensemble Learning due to the adaptive nature of the classifier selection process.

We applied majority voting in our aggregation process as due to the binary nature of output classes, all techniques yielded the same result

Finally, we recorded the performance metrics of our model as AUC score and Precision, which outperformed other stand-alone models

VII. REFERENCES

1. Zhou, ZH. (2021). Ensemble Learning. In: Machine Learning. Springer, Singapore.
2. Rahul, Priyansh Kedia, Subrat Sarangi & Monika (2020) Analysis of machine learning models for malware detection, Journal of Discrete Mathematical Sciences and Cryptography, 23:2, 395-407, DOI: 10.1080/09720529.2020.1721870
3. AOSP git repository - https://github.com/aosp-mirror
4. Google git repository- https://android.googlesource.com/platform/
5. K.K.Aggarwal, Yogesh Singh, Arvinder Kaur, Ruchika Malhotra, "Empirical Study of Object-Oriented Metrics ," in JOURNAL OF OBJECT TECHNOLOGY, vol. V, ETH Zurich, Chair of Software Engineering ©JOT, 2006.
6. Yogesh Singh, Arvinder Kaur, Ruchika Malhotra, "Empirical validation of object-oriented metrics for predicting fault proneness models," in Springer Science + Business Media,in July 2009
7. S. Yadav and G. P. Bhole, "Handling Imbalanced Dataset Classification in Machine Learning," 2020 IEEE Pune Section International Conference (PuneCon), 2020, pp. 38-43, doi: 10.1109/PuneCon50868.2020.9362471.
8. A. Lipnickas , J. Korbicz ,"Adaptive Selection of Neural Networks for a Committee Decision", IEEE International Workshop on Intelligent Data Acquisition and Advanced Computing System: Technology and Applications. Luiv. Ukraine (2003)
9. Tej Bahadur Chandra, Kesari Verma, Bikesh Kumar Singh, Deepak Jain, Satyabhuwan Singh Netam, Coronavirus disease (COVID-19) detection in Chest X-Ray images using majority voting based classifier ensemble, Expert Systems with Applications, Volume 165, 2021, 113909, ISSN 0957-4174,
10. De Luca, Giuseppe & Magnus, Jan. (2011). Bayesian Model Averaging and Weighted Average Least Squares: Equivariance, Stability, and Numerical Issues. Stata Journal. 11. 518-544. 10.2139/ssrn.1894610.
11. Chaouiya, C., Ourrad, O., & Lima, R. (2013). "Majority Rules with Random Tie-Breaking in Boolean Gene Regulatory Networks". PLoS ONE, 8(7).
12. Yiannis Kokkinos & Konstantinos G. Margaritis, "Breaking Ties of Plurality Voting in Ensembles of Distributed Neural Network Classifiers Using Soft Max Accumulations", IFIP International Conference on Artificial Intelligence Applications and Innovations (2014)
13. Wu, Shaomin & Flach, Peter. (2005). A scored AUC Metric for Classifier Evaluation and Selection.
14. Anwyl-Irvine, A., Dalmaijer, E.S., Hodges, N. *et al.* Realistic precision and accuracy of online experiment platforms, web browsers, and devices. *Behav Res* **53,** 1407–1425 (2021).

Authorized licensed use limited to: DELHI TECHNICAL UNIV. Downloaded on June 15,2022 at 11:21:55 UTC from IEEE Xplore. Restrictions apply.

WWW.IJRPR.COM

International Journal of Research Publication and Reviews

Journal homepage: www.ijrpr.com ISSN 2582-7421

STUDY OF FAVORABLE SURFACE ROUGHNESS IN MILLING MACHINE AND ITS OPTIMIZATION

Dr. A.K. Madan, R. Maheshwari, R.R. Thakur

Dept. of Mechanical Engineering, Delhi Technological University

ABSTRACT

Milling process is used to remove material with the help of a rotating cutter. This process of machining is generally used by the industries, and by cutting away the material which is unnecessary. The aim of this paper is to get optimum surface roughness, by identifying certain parameters of the machine. Surface roughness is defined as the fine irregularities of surface texture. Also surface roughness takes place due to the tool chip interface and feed marks in machining process. The quality of surface plays an important role in evaluating productivity of machine tool and machined parts. Several parameters of milling process are there like speed of cutting, feed rate, cutting depth, rate of material removal (MRR) etc. which play a crucial role in surface roughness. A suitable method of optimization is needed to find optimum value of parameters for cutting and minimizing surface roughness. Taguchi method will be used in this report for finding optimum roughness and Taguchi's orthogonal array should be used to determine the parameter's settings. ANOVA will be used for result analysis.

1. INTRODUCTION

Milling is a metal removal operation. In milling operation metallic particles are removed by means of a rotating multipoint cutter which is geared up on the Arbor of the milling system. The types of features are fashioned through milling machine on an element by means of cutting away the unwanted material. Milling machine is having certain essential components, which can be its column, saddle, base, table, knee, arbour, over-arm and spindle. In milling process, positive elements perform a very crucial position inclusive of work-piece, fixture, and cutter which are wished in milling system. The work held in a fixture, connected to a table of milling device. Three table moves are possible in a Milling machine i.e., crosswise, vertical, and longitudinal however rotational or swivel movement are also located with respect to the table in some cases. In improving manner of Milling, a completely essential function is performed by the first-class of surface. The fatigue energy, corrosion resistance, or creep life is improved by way of a good surface. Surface roughness impacts some of practical attributes of components, which include, friction among contacted parts, parts wearing, mirrored image of light transmission of warmth, distributing capability and lubricant holding a, capability of load bearing, coating or fatigue resisting and so on. consequently, the chosen of procedures should be right all through the operation and the preferred completed floor is exact. for maximum floor roughness, Taguchi method can be used to optimize the manner parameter.

Taguchi technique: To optimize parameters of a procedure and improve the additives satisfactory, which can be synthetic Taguchi approach is used which is absolutely statistical approach. Taguchi and Konishi have advanced the Taguchi method. by and large To enhancing the manufactured goods (development of manufacturing method) pleasant, Taguchi approach was advanced. At a later level its software of this technique turned into multiplied to diverse other engineering fields, like Biotechnology etc. Taguchi's efforts were stated statisticians in particular inside the improvement of designs for studying variant. favoured results are successfully carried out through cautious choice of manipulate elements and divide them into manage and noise elements. manage elements need to be decided on that it eliminates the impact of noise issue. proper manage elements are recognised via Taguchi method and surest effects of the system are attain by this approach. To behaviour a hard and fast of experiments orthogonal array (OA) are selected. To statistics and expect the satisfactory of additives produced, outcomes of these experiments are used.

ANOVA: The assessment of reaction significance in percent (%) for every parameter of orthogonal array, evaluation of variance (ANOVA) is used. it's miles used to quantify and identify the source of consequences of different trial from specific trial runs (i.e. one-of-a-kind reducing parameters). The ANOVA is basically a way in which the variations most of the extraordinary agencies are tested. to begin with Prof. R.A. Fisher turned into the person who use this time period and later it was evolved through Prof. Snedecor and lots of others. The primary property of ANOVA is that the entire sum of the squares (total version) is identical to the sum of the SS (sum of the squares of the deviations) of all condition parameters and the errors components.

2. LITERATURE REVIEW

Raj R.A. et al. focused on the usage of Taguchi method and ANOVA to analyze and optimize the turning operation to improve the quality of the finished product. The material used here for the processes is AISI 1045 steel and the tool used here is a coated cemented carbide tool.

Herein, various parameters like the maximum material removal rate (MRR) and minimum surface roughness were taken into account to arrive at a definite conclusion. Since the above-mentioned parameters are derived from values like spindle speed, feed rate and depth of cut, these values had to be calculated and recorded as shown in Table No. 1 and Table No. 2, for surface roughness and MRR respectively.

Usage of the CNC lathe machine pushed them to calculate the S/N ratio (signal/noise ratio) which is defined as a value which compares the level of a desired signal to the level of background noise. Here, the reason we use the S/N ratio is because we want to compare two different types of values-controllable and uncontrollable values. The controllable value here would be signal and the uncontrollable one would be the background noise. Since we need to minimize the surface roughness and maximize the material removal rate, Smaller-the-Better is used for surface roughness and Bigger-the-Better is used for material removal rate. The formula used for S/N ratio is:

$$\eta = -10\log [1/n (\sum Yi^2)]$$

The last step of Taguchi parameter design is to verify and predict the improvement of response (surface roughness) using optimum methods (combination of cutting parameters). The predicted optimal value (η_{opt}) can be calculated by:

$$\eta_{opt} = m + \sum_{j=1}^{n} [(m_{i,j})_{\max} - m]$$

In the end, the future scope was discussed wherein, it was suggested that instead of using only 3 parameters, one can enhance the accuracy by taking more parameters into account, such as, nose radius, cutting conditions etc.

Ribeiro João focused on the usage of L9 orthogonal array in the Taguchi method to optimize the CNC end milling operation which is carried out by ANOVA analysis identify the significant factors affecting the surface roughness. The study was carried-out by machining a hardened steel block (steel 1.2738) with tungsten carbide coated tools. Here, three levels of the cutting parameters selected for this study are shown in Table 1. The experimental design for the three cutting parameters using the L9 orthogonal array is presented in Table 2 and Table 3 tells us about the chemical composition of the workpiece i.e., steel 1.2738. The roughness was measured along of cylinder axial direction and in three equi-distance orientations separate by 120º angle (P1,P2, P3) as shown in figure. the Table 4 is presented the average of the surface roughness measurements in the three directions (Ra_P1, Ra_P2, Ra_P3) and the computed signal-to-noise S/N by using the formula: -

$$\eta = -10\log [1/n (\sum Yi^2)]$$

The Taguchi analysis procedure can be described in four steps. In the first, is implemented the evaluation signal-to- noise ratio and allows to define the level of variation for each parameter. This is followed by a comparison of arithmetic mean surface roughness among all the tests. The third is based on analysis of variance, which is used to define the influence of each parameter. Fig. 3 shows the S/N ratio response graph for Ra. One gets a high S/N ratio for smaller variance of surface roughness around the desired value. Nevertheless, the relative importance among the milling parameters for the surface roughness still required to be identified so optimal combinations of the milling parameter levels can be determine more accurately using an ANOVA analysis.

The experimental results confirm the prior parameter design for the optimal cutting parameters with the multiple performance characteristics in milling operations. The optimal solution for minimizing the surface roughness value is A3B1C3 i.e., cutting speed of 250 m/min, the feed rate of 0.075 mm/t and the depth of cut of 0.312 mm leading to average surface roughness of 1.662 μm. Therefore, radial depth of cut is the most significant factor of surface roughness with contribution of approximately 64%.

Verma Narendra Kumar et al. focused on the analysis and optimization methods of different milling parameters using the Taguchi method and ANOVA (Analysis of Variance). The material used here for the processes is EN8 steel. The machine used here was the universal milling machine with maximum spindle speed 1440 rpm and 25 kw drive motor without using cutting fluids.

It is important to know about the material on which the experiments are being performed, so in Table 1 and Table 2, we can see the chemical composition and mechanical properties of EN8 steel. Values like cutting speed, feed rate and depth of cut as shown in Table 3 and Table 4 were observed in order to calculate the material removal rate and the surface roughness.

With the help of Minitab 15, main effects plot for S/N ratios were plotted, from which, it was deduced which factor has a higher impact on the surface roughness of the finished product. The higher the deviation/lesser the angle between the two lines of the graph, more will it affect the surface roughness. Here, X axis represents change in level of the variable and y axis represents the change in the resultant response. From the graphs, it is clearly visible that the

feed rate has the lowest deviation in its graphs and thus has the highest significance in terms of surface roughness.

Also, in the main effects plots, if the line for a particular parameter is near horizontal, then the parameter has no significant effect. On the other hand, a parameter for which the line has the highest inclination will have the most significant effect.

Another important parameter to know exactly about the predictions made by the Taguchi method is the S/N ratio (signal/noise). It gives insight and contributes as a significant factor while calculating the surface roughness and is observed and calculated in Table 5.

ANOVA is another method which is employed for knowing about the surface roughness and is calculated in Table 6 using parameters like DOF (Degree of Freedom), S (sum of square), V (Variance) F (variance ratio) and P (significant factor).

In the end, various conclusions were drawn out from the experiments like the different values of parameters from which low surface roughness is obtained and which operations on the milling machine can provide the best accuracy on the workpiece made out of EN8 steel.

Thakre Avinash A. et al. focused on the usage of Taguchi method and ANOVA to analyze and optimize the turning operation to improve the quality of the finished product on a CNC turning machine. The material used here for the processes is AISI 1045 steel and the tool used here is a coated cemented carbide tool. The orthogonal array, signal to noise ratio (S/N) and analysis of variance were employed to find the maximum material removal rate (MRR) and minimum surface roughness. Table 1 here focuses on the factor and levels for selected machining parameters which are to be used in the Taguchi orthogonal array. Here since the L9 orthogonal array is used, there are 4 different factors which are considered and each factor is assigned 3 different levels. A new factor is taken into account here, known as coolant flow which is measured in lit/min. When the experiments were conducted on Agni, BMV45 TC24 with FANUC controller, several graphs of surface roughness and waviness profiles were obtained which help in finding the S/N ratio for each of the levels of the considered factors.

The quality characteristic for surface roughness is smaller-the-better for which equation 1 is used to calculate the signal to noise ratios (η) where yi is the value of quality characteristics at ith experiment, n is number of runs for an experiment. The experimental data for surface roughness and calculated signal- to-noise ratio for all nine combinations are shown in table 2.

After making the table for the orthogonal array, wherein the S/N ratio was calculated using the provided parameters with the help of Minitab 15, graphs pertaining to the main effects plot for S/N ratio with respect to surface roughness were plotted.

From the graphs, the researcher concluded that the optimal solution for minimizing the surface roughness value is A3 B1 C2 D2 i.e., spindle speed of 2500 rpm, feed of 800 mm/min, 0.8 mm depth of cut, 30 lit/ min coolant flow. The surface roughness value for this combination was found to be 0.357µm. With the help of Taguchi method, it was concluded that coolant flow was observed to be the main controller of the surface roughness with a contribution of approximately 60%. The second most important factor was found to be spindle speed with a contribution of approximately 22%.

Sumesh A.S. et al. focused on the optimization of drilling parameters using the Taguchi technique to obtain minimum surface roughness (Ra) and usage of L9 orthogonal array on a radial drilling machine to conduct a number of drilling experiments. The machine used here was Radial Drilling Machine. However, various parameters like the maximum material removal rate (MRR) and minimum surface roughness were considered to arrive at a definite conclusion. The material used here is Cast Iron and the tool used is made up of HSS- High Speed Steel. The basic composition of HSS is 18% W, 4% Cr, 1%V, 0.7% C and rest Fe. Table 1 shows the chemical composition of the type of cast iron used. We have used Surftest to measure to measure the shape or form of components. A profile measurement device is usually based on a tactile measurement principle. With the help of Taguchi method, we have experimentally concluded the data as shown in table 3. One repetition for each of 9 trials was completed to measure Signal to Noise ratio (S/N ratio) given in Table 4 as shown.

From these tables researcher concluded that the optimal solution for minimizing the surface roughness value is A1 B1 C1 i.e., spindle speed of 80 rpm, feed rate 0.1 mm/rev and 4mm drill diameter. The surface roughness value and S/N ratio of the combination are 0.665 µm and 3.54 respectively. It is found that the drill diameter is the most significant factor for determining surface roughness and its contribution to surface roughness is 38.3%. But another control parameter had a great impact on determining the surface roughness which is feed rate contributing approximately 34% to the result.

3. CONCLUSION

The common factors which were used by majority of the researchers were-

- Cutting speed
- Feed rate
- Depth of cut

Out of all these 3 factors, the major share of the controlling factors for surface roughness turns out to be cutting speed. Also, from this review we can conclude that any further research in this area will revolve more around these 3 selected parameters.

REFERENCES

[1] Raj R. A., Parun T., Sivaraj K. and Kannan T.T.M. (2013). Optimization of milling parameter of EN8 using Taguchi Methodology. International Journal of Mechanical Engineering and Robotics Research, 2, 202-208

[2] Ribeiro João, Lopes Hernâni, Queij Luis and Figueired Daniel (2016). Optimization of Cutting Parameters to Minimize the Surface Roughness in the End Milling Process Using the Taguchi Method. Periodica Polytechnica Mechanical Engineering, 61(1), 30-35

[3] Verma Narendra Kumar and Sikarwar Ajeet Singh (2015). Optimizing Turning Process by Taguchi Method under Various Machining Parameters. International Research Journal of Engineering and Technology (IRJET), 2(6), 307-312

[4] Sumesh A.S. and Melvin Eldho Shibu (2016). Optimization Of Drilling Parameters for Minimum Surface Roughness Using Taguchi Method. IOSR Journal of Mechanical and Civil Engineering (IOSR-JMCE), 12-20

[5] Thakre Avinash A. (2013). Optimization of Milling Parameters for Minimizing Surface Roughness Using Taguchi ‘s Approach. International Journal of Emerging Technology and Advanced Engineering, 3(6), 226-230

International Journal of Engineering Applied Sciences and Technology, 2022
Vol. 6, Issue 12, ISSN No. 2455-2143, Pages 181-184
Published Online April 2022 in IJEAST (http://www.ijeast.com)

STUDY THE SLIDER CRANK MECHANISM

Chander Mohan Aggarwal*1, Bhavya Dhanwaria*2,Ashish Kudiyal*3,
1, 2, 3*under graduate student,
Department of Mechanical Engineering, Delhi Technological University,Delhi,India

Dr.Sushila Rani*4
4*Assistant Professor,
Department of Mechanical Engineering, Delhi Technological University, Delhi,India

***Abstract*—The Slider crank mechanism is a specific barlink configuration that exhibits simultaneous rotation and rectilinear motion. This mechanism is often used to study the kinematics of machines and dynamic forces. The position, speed, acceleration and recoil generated by the sliding shaft mechanism during**

Where,
'R' is the crank length
L>R+E
operation can be determined analytically. The mechanism is capable of operating in balanced and unbalanced configurations so that the magnitude of the shaking force can be compared.

***Keywords*—Crank, Slider, Inversion, Mechanism, Rotary.**

I. INTRODUCTION

A Slider crank mechanism is an arrangement of mechanical components designed to convert reciprocating motion into rotary motion, as in reciprocating piston engines, or it is used to convert rotary motion into linear motion as in reciprocating pump. The internal combustion engine is a common example of this mechanism, where combustion in a cylinder creates pressure that drives a piston. The rectilinear motion of the piston is converted to rotation at the crank by a mutual connection, called the connecting rod. When the hand wheel geometry for cesto convert rectilinear motion into rotary motion, a recoil force is generated and applied to the crank box. Shaking forces cause vibrations that reduce engine function.

The Slider crank mechanism is used to convert rotary motion into reciprocating motion using as lewing bearing beam, connecting rod and sliding body. In this example, as of t body is used for the connecting rod. The sliding mass is not allowed to rotate and rotary joints are used to connect the bodies. While each body has six degrees of freedom in space, the kinetic conditions lead to one degree of freedom for the whole system.

A crank and slide mechanism converts the circular motion of the crank into the linear motion of the sliding body. For the crank to rotate completely, the condition L > R + E must be satisfied where R is the length of the crank, 'L' is the length of the link connecting the crank and the slider, and 'E' is the degree slider deflection. It has three rotary joints and one prismatic joint. The total distance traveled by the slider between its two extreme positions is called the path length. The kinematic reverse of the sliding crank mechanisms produces a normal quick turn mechanism.

A.INDENTATIONS AND EQUATIONS

In order for the crank to rotate fully the following condition must be satisfied,
'L' is the length of the link connecting crank & slider
'E' is the offset of the slider between its two extreme positions
i.e. Path length.

II. INVERSIONS OF SLIDER CRANK MECHANISM

Different mechanisms are obtained when we fix different links of akinetic chain and this phenomen on is called mechanism inversion. The sliding crank mechanism has the following in versions:

A. First Inversion

This inversion is obtained when link 1 is fixed and links 2and4 are made the crank and the slider respectively.

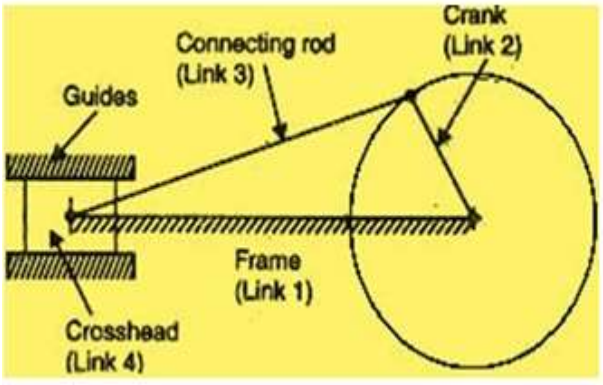

Fig.1: Reciprocating Engine

International Journal of Engineering Applied Sciences and Technology, 2022
Vol. 6, Issue 12, ISSN No. 2455-2143, Pages 181-184
Published Online April 2022 in IJEAST (http://www.ijeast.com)

Application: C commonly used in I.C. engines, steam engines and reciprocating compressor mechanism.

B. Second Inversion

Fixing link 2 of a slider mechanism gives a second inversion. The rotary engine mechanism or gnome engine is the application of the second inversion. It is a rotary cylinder V –type internal combustion engine used as an aero engine. The rotary engine has generally seven cylinders in one plane. The crank (link 2) is fixed and all the connecting rods from the pistons are connected to this link. In this mechanism when the pistons reciprocate in the cylinders, the whole assembly of cylinders, pistons and connecting rods rotate about the axis O,

where the entire mechanical power developed, is obtained in the form of rotation of the crank shaft.

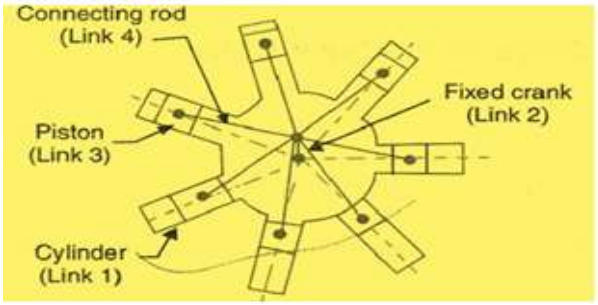

Fig.2: Rotary Engine

Application: Rotary engine mechanism orgnome engine

C. Third Inversion

By fixing the link 3 (connecting rod) of the slider crank mechanism we can obtain third inversion. It is used in hoisting engine mechanism and also in toys. In hoisting purposes, its main advantages lie in its compactness of construction as it allows simple method of supplying steam to the cylinder.

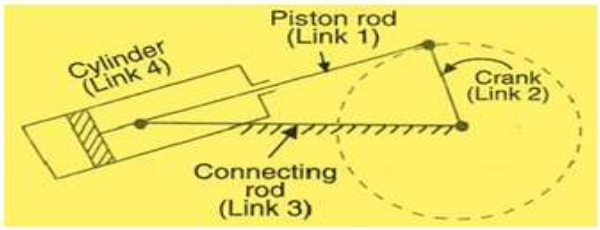

Fig.3: Oscillating Engine

Application: It is used in hoisting engine mechanism and also in toys.

D. Fourth Inversion

By fixing the link 4 of the slider crank mechanism we canobtain the fourth inversion of slider crank. Fixing the slider means that the slider should be fixed in position and also should be fixed in respect to rotation. In this case, the cylinder will have to be slotted to give passage to piston pin of connecting rod as the cylinder slides over the piston. Due to this difficulty, the shapes of the cylinder and piston are exchanged as shown in figure below.

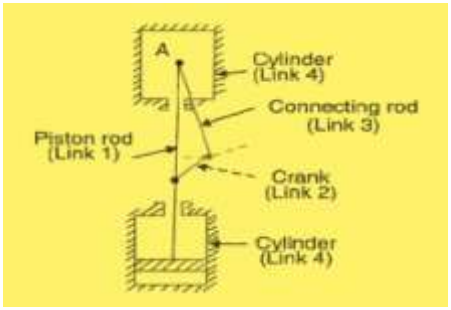

Fig.4: Hand Pump Application: handpump.

III. DESIGNING USING 3DS OF TWARES

For better understanding and to know how these inversions actually take placed, we designed the slider crank mechanism model on 3d software like Solid works and Auto desk 360 Fusion.

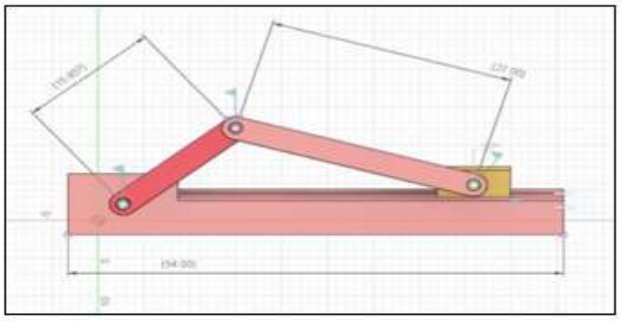

Fig.5:3 Dmodel of Slider Crank

And then by fixing each of the component we obtain different motions.

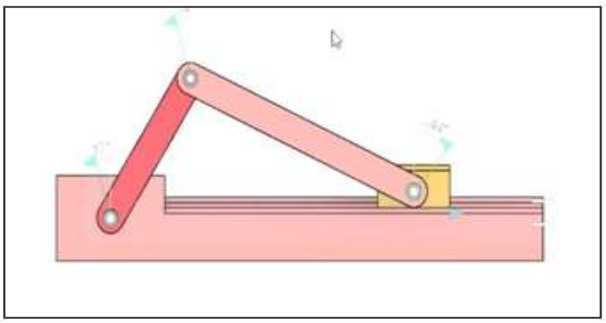

International Journal of Engineering Applied Sciences and Technology, 2022
Vol. 6, Issue 12, ISSN No. 2455-2143, Pages 181-184
Published Online April 2022 in IJEAST (http://www.ijeast.com)

IV. OBSERVATION AND RESULT

Inversion	**Observation**
1st Inversion: Ground Link Fixed	Connecting rodoscillates, crank rotates, And slider reciprocates.
2nd Inversion: Crank Fixed	The ground and Connecting rod rotate about their joints on the crank, and Slider reciprocates.
3rd Inversion: Connecting Rod Fixed	Link 2 acts as crank and link 4 oscillates.
4th Inversion: Slider Fixed	Link 1is reciprocating where as link 3is Oscillating about its pivot on the slider.

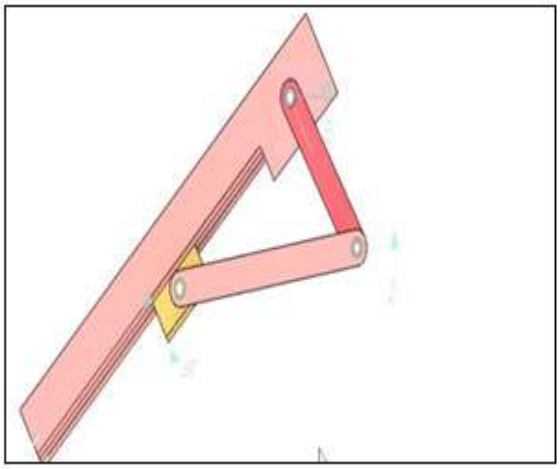

b.

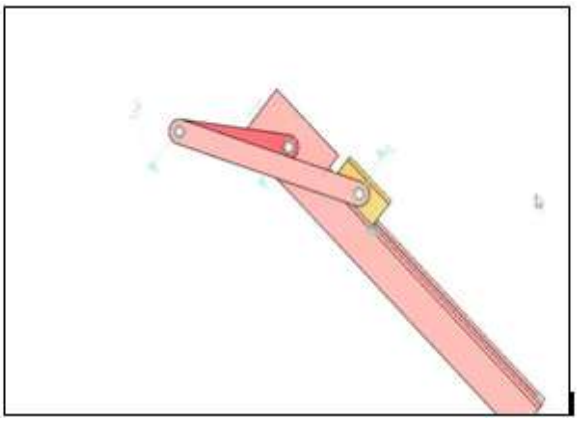

c.

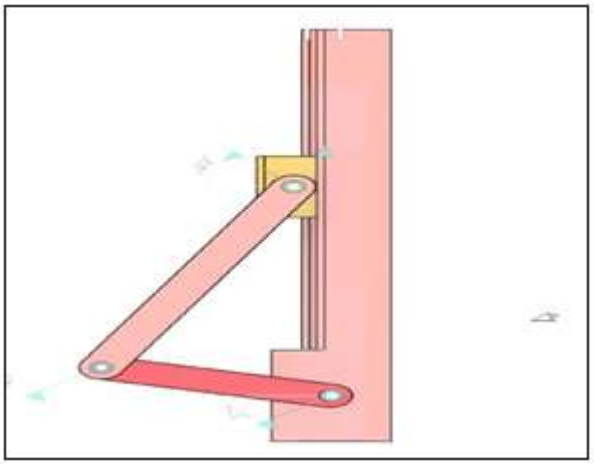

d.

Fig.6.(a)1st Inversion (b)2nd Inversion (c) 3rd Inversion (d) 4th Inversion

IV. CONCLUSION

The dynamic behaviour of a slider-crank mechanism with a flexible connecting rod is investigated. Slider-crank mechanism converts rotary motion into reciprocating motion by means of a rotating driving beam, a connection rod & sliding body. The use of this mechanism in the wide range of machines like pumps and compressors is observed.

V. ACKNOWLEDGEMENTS

We would like to express our gratitude to all those who provided help and cooperation in various ways at the different stages for this research project. Also, we would like to express our sincere appreciation to our teacher Prof. Sushila Rani. Also, we would like to thank our friends and special thanks to Abhishek Kishore for motivating us.

VI. REFERENCE

[1] Erik, Oberg. Machinery's Hand book Tool box Edition. Diss. Industrial Press, 2008.
[2] Norton, Robert L. Design of machinery: an introduction to the synthesis and analysis of mechanisms and machines.WCB McGraw-Hill, 1999.
[3] Norton, Robort L. Machine Design: An Integrated Approach, 2/E. Pearson Education India,2000.
[4] Verburg, Elmer. Elmer's Engines. Old Orchard Pub. Service, 1988.
[5] B.V. Viscomi, R.S. Arye, Nonlinear dynamic response of elastic slider-crank mechanism, ASME Journal of Engineering for Industry93(1971)251–262.
[6] R.F. Fung, Dynamic response of the flexible connecting rod of a slider-crank mechanism with time-dependent boundary effect, Computer & Structure 63 (1) (1997) 79–90.

[7] R.F. Fung, F.J. Lin, J.S. Huang, Y.C. Wang, Application of sliding mode control with alow-pass filter to the constantly rotating slider-crank mechanism, The Japan Society of Mechanical Engineers C 40 (4) (1997) 717–722.

[8] F.J. Lin, R.F. Fung, Y.S. Lin, Adaptive control of slider-crank mechanism motion: simulation and experiments, International Journal of System Science 28 (12) (1997)1227–1238.

[9] J.H.Holl and, Adaptation in Natural and Artificial Systems, The University of Michigan Press, Ann Arbor, MI, 1975.

[10] D.E.Goldberg, Genetic Algorithms in Search, Optimization and Machine Learning, Addison-Wesley, Reading, MA,1989.

[11] K.F.Man,K.S.Tang, S.Kwong, Genetic algorithms: concepts and applications, IEEE Transactions on Industrial Electronics 43(5)(1996) 519–534.

[12] R.L.Haupt, S.E.Haupt, Practical Genetic Algorithms, Wiley Inter science, New York, 1998.

[13] A.A. Adewuya, New Methods in Genetic Search with Real-valued Chromosomes, Master's Thesis, Massachusetts Institute of Technology, Cambridge, 1996.

[14] J.W.Kim, S.W.Kim, P.G.Park, T.J.Park, On the similarities between binary-coded GA and real-coded GA in wide search space, in: IEEE Evolutionary Computation, CEC'02.Proceedings of the 2002 Congress,2002,pp. 681–686.

[15] P.C. Krause, Analysis of Electric Machinery, McGraw-Hill, New York, 1986

ResearchGate

See discussions, stats, and author profiles for this publication at: https://www.researchgate.net/publication/360716422

Technical Analysis of Power Generation using Vertical Axis Wind Turbines on Metro Tracks

Conference Paper · March 2022

DOI: 10.17605/OSF.IO/8NHYG

CITATIONS
0

READS
12

3 authors, including:

Md ZIA Arzoo
Delhi Technological University
5 PUBLICATIONS **0** CITATIONS
SEE PROFILE

Mozammil Hassan
Delhi Technological University
7 PUBLICATIONS **0** CITATIONS
SEE PROFILE

Some of the authors of this publication are also working on these related projects:

Recent Advancements in Supply Chain Management View project

Customer Relationship Management of Different Companies View project

All content following this page was uploaded by Mozammil Hassan on 19 May 2022.

The user has requested enhancement of the downloaded file.

International Journal of Mechanical Engineering and Technology (IJMET)
Volume 13, Issue 3, March 2022, pp. 1-7. Article ID: IJMET_13_03_001
Available online at https://iaeme.com/Home/issue/IJMET?Volume=13&Issue=3
ISSN Print: 0976-6340 and ISSN Online: 0976-6359
DOI: https://doi.org/10.17605/OSF.IO/8NHYG
© **IAEME** Publication

TECHNICAL ANALYSIS OF POWER GENERATION USING VERTICAL AXIS WIND TURBINES ON METRO TRACKS

MD Zia Arzoo[1], Mozammil Hassan[2], David Simeon[3], Dr. Pushpendra Singh[4]
[1,2,3,4] Department of Mechanical Engineering, Delhi Technological University, New Delhi, India

ABSTRACT

People all over the world are turning to clean and green renewable energy sources to minimize their reliance on fossil fuels and other non-renewable energy sources for electricity generation. Wind is one such resource that, when used instead of fossil-fuel-generated power, can minimize harmful environmental emissions. The idea is to use the high wind speeds produced when a metro train enters a platform and convert it into electrical energy using Vertical Axis Wind turbines. This wind energy which is available abundantly throughout the large circuit of Delhi Metro, which would otherwise go to waste, can be utilized to create and supplement the nation's growing demand for clean, green, and affordable electricity, as well as to help the economy. In this paper we will be discussing the design of our Vertical Axis Wind Turbine which we will be installing at the ends of the metro platform and analyze how much power can be generated.

Keywords: Non-renewable Energy, Vertical Axis Wind Turbine, Wind Energy, Turbine, Tip Speed Ratio, Betz limit.

Cite this Article: MD Zia Arzoo, Mozammil Hassan, David Simeon and Pushpendra Singh, Technical Analysis of Power Generation using Vertical Axis Wind Turbines on Metro Tracks, *International Journal of Mechanical Engineering and Technology (IJMET)*, 13(3), 2022, pp.1-7.
https://iaeme.com/Home/issue/IJMET?Volume=13&Issue=3

1. INTRODUCTION

It is widely acknowledged that the world's resources are rapidly decreasing. This has sparked interest in renewable energy sources that are long-term, safe, and non-polluting, such as wind energy. Wind energy is unquestionably one of the cleanest ways to generate electricity from a renewable source. There has been an increase in interest in renewable energy resources in recent decades.

Wind energy, unlike other renewable energy sources, has become competitive with conventional power generating sources, and as a result, the use of wind turbine generators is growing at the fastest rate of any other renewable energy source. The wind blowing through

underground metro stations is one source of wind energy. We get a strong blast of wind here every now and then. The pressure differential at the tunnel's ends, caused by the high-speed metro trains, causes this tremendous wind current. The kinetic energy of the generated wind is high, and it may be transformed into a useful amount of electrical energy using a wind turbine. Wind turbines transform kinetic energy in the wind into rotational energy, which is ultimately converted into electrical energy. As a result, knowing the predicted power and energy production of each wind turbine is critical for determining its economic viability. The type of wind turbine to be used for optimal power output is also determined by a number of factors. A wind turbine should always capture the maximum amount of power from the wind, with energy generation exceeding energy loss due to air drag.

Windmills with a horizontal axis of rotation and those with a vertical axis of rotation have been designed to exploit this natural resource. The first type is currently the most common, but a growing market requires machines with a wide range of capabilities to suit a wide range of needs [4]. Newer and updated technology, as well as lowering costs for components like permanent magnets, along with the unique ability of Vertical axis wind turbines to function when others fail, have reduced the mistreatment of the design of Vertical Axis Wind Turbines. In today's markets, these turbines offer a considerable competitive advantage. [1]. One of the most common VAWTs is the Darrieus wind turbine. This turbine has prompted new study into VAWTs in the aim of increasing efficiency. [3]

2. METHODOLOGY

In underground metro stations, high speed winds are produced when a metro train is about to enter the platform. There can be flow of wind throughout the time when the train is far from the platform because of various factors like pressure and temperature difference. But the high speed winds produced before the train enters is mainly due to the so-called piston effect, which refers to the airflow created by a vehicle as it passes through a tunnel. Trains are speeding through the tunnels, pushing air out in front of them onto the platform- which spreads forward as far as it can -and creates suction by drawing air into the tunnel behind them.

These high speed winds can be utilized to produce electrical energy by placing wind turbines in the vicinity of the metro tracks. Vertical Axis WInd turbines are more feasible in this situation due to various reasons. VAWTs have fewer parts and when scaled down, have much lesser maintenance requirements as compared to Horizontal Axis wind turbines. Also as there is minimum space in the underground metro to place the turbine, VAWTs are a better option as they can be very compact.

After our research and analysis of wind profiles across metro tracks, we came up with positioning our wind turbine at the terminal points of metro stations due to the fact that there will be no role of air drag towards our metro due to the wind turbine because those are the stoppage points and due to breaking there is already a huge loss of energy so as per our research we can use this energy for the generation of electricity.[5]

3. DISCUSSION

3.1 Modeling of Wind Turbine

As talked earlier we have chosen a quiet revolution wind turbines it the best model of VAWT right now the various advantages that it provides are: (1) It has a compact, easy to integrate design (2) the unique aeroelastic design of blade catches the turbulent wind and sheds noise by absorbing vibration (3) It has in-built safety mechanism and power can be regulated alongside a design life of more than 30 years with these turbines finally the operating wind speed is between 1.5m/s to 20m/s which is the working range for our project.

The various design specifications were taken keeping in mind the spacing around metro tracks and are listed below:

Table 1 Specifications of Turbine

Height of the Turbine	700mm
Diameter of Turbine	748mm
Width of Turbine Blade	144mm
Helix Angle	120deg

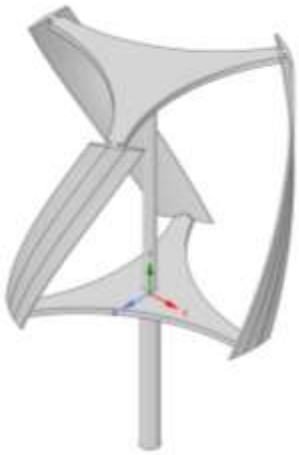

Figure 1 Turbine Model

3.2 Material Selection

We have also done comparative research between various materials used to make wind turbines. We came up with the result of using E-carbon (230Gpa). Carbon fibers are fibers which by weight contain 90-100 % carbon. These are made by polymeric precursor materials like cellulose, polyacrylonitrile (PAN), polyvinyl chloride and pitch. Through a sequence of heating and tensioning operations, these precursors are transformed into carbon fibers. Carbon fibers are extremely thin filaments (diameter about 5-10).

Table 2 Comparison of mechanical properties of steel materials and carbon fibers

Material Type		**Density ρ (kg/m^3)**	**Tensile Strength σ_u(GPa)**	**Elastic Modulus E(GPa)**	**Breaking Length σ_u/(ρg)(km)**
Steel	**Wire**	7850	1.77	210	23
	S355	7850	0.50	210	6
Carbon Fiber	**Standard**	1760	3.35	230	205
	High Strength	1820	7.06	294	396
	High Modulus	1870	3.45	441	188

All carbon fibers have higher tensile strengths than steel materials, as demonstrated in Table 2, yet their densities are substantially lower. The breaking length is a useful metric for demonstrating a material's high strength and lightweight properties. It is computed using σu/(σg), g being the gravity constant 9.8 m/s^2, and can be defined as the maximum length of a hanging bar which can suspend on its own weight. If we compare the breaking lengths of carbon fibers and steel materials, the former has 10 times more breaking length than the later as seen in the table [7].

Also the result of our three analyses i.e., static structural and modal concluded that carbon fiber is much better than other materials in regards to stresses and strains and it is also much lighter along with very less deformation which gives it a major advantage.[6]

4. THEORETICAL CALCULATIONS AND POWER GENERATION

4.1 Wind Profile Across Metro Tracks

We measured wind velocities across various metro stations on various lines using an anemometer. We noticed that the average velocity at the terminals of the metro stations which were above ground when the train is just about to enter was around 1 - 1.5 m/s and maximum going upto 2 m/s. Whereas in the underground stations we could see much higher values averaging 4-5 m/s also for a longer duration of about 30 seconds.

The maximum results we found were on the yellow line so we stuck to that and took readings for three stations i.e Hauz Khas, INA and Chawri Bazar over the span of 30 days. We measured maximum speeds of 7m/s on some days. And the data is given in the below table:

Table 3 Wind Velocities at Each Stations

Day	**Wind Velocity (m/s) for 30 seconds**		
	Hauz Khas	**INA**	**Chawri Bazar**
1	3.2	4.6	4.4
2	3.1	4.8	4.3
3	3.4	4.7	4.1
4	3.2	4.6	3.5
5	3.6	5.1	4
6	3.4	4.6	4
7	3.6	4.7	4
8	3	4.8	3.6
9	3.6	5.2	3.7
10	3.1	4.6	3.8
11	3.6	5.2	4
12	3.6	5	4.3
13	3.3	4.7	4
14	3.2	5.1	4
15	3.5	5	3.9

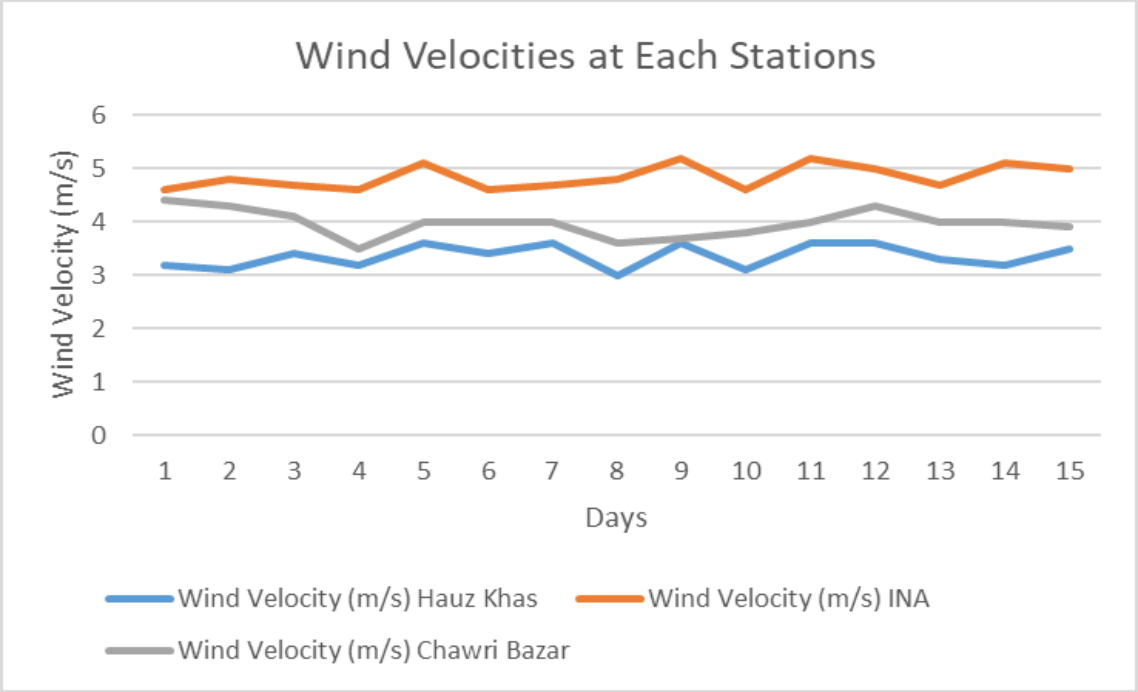

Figure 2 Wind velocities at Each Stations

4.2 Theoretical Calculations

Albert Betz, a physicist from Germany, discovered that the maximum percentage of kinetic energy from the wind that can be converted into mechanical energy is 59.3%. This limit is given the name Betz Limit. This is the maximum power coefficient for any wind turbine.

Gorlov helical turbines have tip speed ratios ranging from 2-2.5 according to all resources used with the exception of Shiono et al., who found the range to be just below 1 to 2.5"[2]. Ignoring the lower range and considering the tip speed ratio of 2-2.5, we can calculate the possible angular velocities of the turbine using the following equation:

$\lambda = Vr \times \omega$

Where:

λ: Tip speed ratio

ω: Angular velocity

V: Average air velocity

r: Turbine radius

After rearranging the above equation:

$\omega = \lambda \times V$

The torque can also be calculated using the below equations:

$T = (1/2 \times Cp \times \rho \times A \times V\text{^}3)/\omega$

A: $Area = L \times d$

ρ: Air density

Cp: Power coefficient

ω: Angular velocity

V: Wind velocity

4.3 Power Generation

The power of the turbine can be calculated using equation:

$Pflow = 1/2 \times \rho \times A \times V\text{^}3$

Power of turbine = Pflow x Cp

Where: Cp = efficiency coefficient of turbine.

We calculated power generated at each of the three stations, Hauz Khas, INA and Chawri Bazar over the span of 15 days.

When we consider the yellow metro line, the average duration between trains is 5 minute. So in an hour, on average, 12 trains would pass through the station. Since these average winds are calculated for 30 seconds when each train passes, the total time in an hour the turbine would get this wind is 30*12 = 360 seconds.

So in the below table we have calculated the power in unit of kWh

Table 4 Power produced in kWh at each station

Power (kWh)		
Hauz Khas	**INA**	**Chawri Bazar**
1.74	5.18	4.54
1.59	5.89	4.23
2.09	5.53	3.67
1.74	5.18	2.28
2.48	7.06	3.41
2.09	5.18	3.41
2.48	5.53	3.41
1.44	5.89	2.48
2.48	7.49	2.70
1.59	5.18	2.92
2.48	7.49	3.41
2.48	6.66	4.23
1.91	5.53	3.41
1.74	7.06	3.41
2.28	6.66	3.16

The below table approximately gives the total power produced per day on average in the span of 15 days. Practically, the power produced in INA per day could supply the electrical needs of 20 houses in Delhi as the average power consumption in Delhi per household is 8-10 units per day.

Table 5 Total power production

Station	Hauz Khas	INA	Chawri Bazar
Average kWh per 15 days	2.04	6.10	3.38
Total Power produced per Day by single turbine(kWh)	34.68	103.7	57.46
Total Power produced at a Station per day(2 turbines)(kWh)	69.36	207.4	114.92

5. CONCLUSION

In our work we have shown in detail the scope of using vertical axis wind turbines to produce electricity from the wind generated in metro stations. We calculated the wind speed in three underground metro stations (Hauz Khas, INA and Chawri bazar) when the train is about to enter the platform. By installing two turbines at each end of the metro platform on either side where the train enters, we have calculated the power that can be produced in kWh. The results were positive with the best results found in INA where the average daily power that can be produced was found out to be 207 kWh. This power from one station per one day, considering the average daily consumption of a household in Delhi, can supply the electricity needs of upto 20 houses in Delhi.

If these turbines are installed in each underground station of the very large metro circuit of Delhi, a large amount of wind energy can be utilized and converted into electrical energy. This energy can also be used for the needs of the Delhi Metro. Therefore the above research can help upcoming researchers to go further in this domain and also it showcases how wind energy can be the part of the sustainable future that we seek.

REFERENCES

[1] Cheng, Q., Liu, X., Ji, H., Kim, K. and Yang, B., 2017. Aerodynamic Analysis of a Helical Vertical Axis Wind Turbine. Energies, 10(4), p.575.

[2] Sritram, P., Treedet, W. and Suntivarakorn, R., 2015. Effect of turbine materials on power generation efficiency from free water vortex hydro power plant. IOP Conference Series: Materials Science and Engineering, 103, p.012018.

[3] Micha Premkumar, T., Mohan, T., Seralathan, S. and Sudheer Kumar, A., 2015. Design and Performance Prediction of Low-Cost Vertical Axis Wind Turbine. Applied Mechanics and Materials, 813-814, pp.1070-1074.

[4] M. Saad, M., 2014. Comparison of Horizontal Axis Wind Turbines and Vertical Axis Wind Turbines. IOSR Journal of Engineering, 4(8), pp.27-30. .

[5] Patwal, S., 2022. Feasibility Study of Conversion of Wind Energy to Electrical Energy at Delhi Metro Stations using Light Rotor Turbines. IJSRD

[6] International Journal of Mechanical Engineering and Technology (IJMET), 2022. COMPARATIVE ANALYSIS OF VERTICAL AXIS WIND TURBINE: CARBON FIBER VS STRUCTURAL STEEL.

[7] Liu, Y., Zwingmann, B. and Schlaich, M., 2015. Carbon Fiber Reinforced Polymer for Cable Structures—A Review. Polymers, 7(10), pp.2078-2099.

View publication stats

Nature Environment and Pollution Technology
An International Quarterly Scientific Journal

p-ISSN: 0972-6268
(Print copies up to 2016)
e-ISSN: 2395-3454

Vol. 21 | No. 2 | pp. 643-650 | 2022

Review Research Paper

https://doi.org/10.46488/NEPT.2022.v21i02.023

Open Access Journal

Toxicity and Challenges of Nanomaterials and Their Impact on the Environment

Sakshi Awasthi and Jai Gopal Sharma†
Department of Biotechnology, Delhi Technological University, Delhi, India
†Corresponding author: Jai Gopal Sharma, Sharmajaigopal@dce.ac.in

Nat. Env. & Poll. Tech.
Website: www.neptjournal.com

Received: 07-06-2021
Revised: 04-07-2021
Accepted: 14-07-2021

Key Words:
Nanomaterials
Toxicity
Environmental impacts
Potential risk

ABSTRACT

Nanomaterials (NMs) are those tiny materials that range from 1-100 nm. These materials show different characteristics in their physical and chemical forms in comparison to their bulk form. The use of nanomaterials is increasing day by day because of their enormous capabilities in the health sector as well as in other industries. There are currently few, if any, actual protocols for the disposal and characterization of these nanomaterials, which results in environmental toxicity. Heavy use of chemicals in the testing of nanomaterials has resulted in polluting our entire ecosystem. Inconsistent results of nanomaterial show that it is challenging to reduce the toxicity generated by it. In this review, we discuss the administration and use of nanomaterials in the agribusiness sector, in food, and, most importantly, in the environment, for purposes of protecting our plants and crops, dealing with incurable diseases, developing new tastes and textures in the food sector, sensations, identifying pathogenic organisms, and distribution systems where these minute particles can wreak havoc. Despite the potential benefits of nanomaterials, their unintentional harm to the environment and, in some cases, our health is making further development difficult. This article discusses the toxicity of nanomaterials and how they damage our environment, as well as the obstacles that come with overcoming them.

INTRODUCTION

Nanotechnology is an amalgamation of nano-sized (very minute size 1-100 nm) structured materials, analytical tools at the nanoscale, and nano-devices, into biological sciences for the development of new biomaterials and toolkits as well as for understanding life science. It's designed to help minimize man's impact on the environment by incorporating more sensible, effective, and low-cost modifications (Pathakoti et al. 2018). Despite ongoing progress in nanotechnology and nanomaterial discovery, understanding and knowledge on the possible effects of nanomaterials on health and the environment are still inadequate (Hutchison 2016). As nanomaterial is not easy to be analyzed after release into the environment, they can result in numerous types of atmospheric problems unless a proper curative plan is not executed. Engineered nanomaterials are generally manufactured with specific sizes and for specific purposes (Iavicoli et al. 2014). They are designed as their characteristic properties like physical and chemical attributes are different compared to their bulk conventional parts. Various types of nanomaterials find application in providing significant benefits to the environment. Furthermore, most nanomaterials have been discovered to have potential hazardous impacts on the environment, the most prevalent of which being nano plastics, which heavily pollute the ecosystem (Rai et al. 2020).

Plastic plays an important part in our general life. Plastic is known as polythene in the common language. Because of its lower cost and affordability, it is one of the most usable products in the modern era (Awoyera & Adesina 2020). However, it contributes to a large amount of pollution because of its non-degradable nature (Da Costa et al. 2016). It is further divided into subcategories like low-density polyethylene (LDPE) and high-density polyethylene (HDPE). Microplastics, which turn into nanoparticles of plastic over a long period of natural disintegration, are common contaminants that threaten our ecosystem and humans (Baztan et al. 2018). Microplastics are major prey for animals because they assume microplastics are their source of food, such as marine food, salt, and bottled water, as well as inhalation from the air and other surroundings.

Nano plastic has a unique property that depicts a high surface-to-volume ratio, which affects its degradation process. A high surface-to-volume ratio is a defining feature of nanotechnology (Bhushan 2017). This characteristic makes nanoparticles or plastic more harmful to the environment. Proper assessment should be done on nanomaterials that generate enough harm during the manufacturing process (Lee et al. 2013). Green nanotechnology is now seen to have the potential to reduce adverse environmental impact as well as harm to human health. Nano plastic agglomerates with chemicals and heavy metals via weaker links such as wander

walls bonds, according to research (Herbort et al. 2018). As a result, when nanoparticles of plastic are moved from one compartment of the environment to another, harmful chemicals are released, making it impossible for marine species to survive (Del Saz-Salazar et al. 2009).

TOXICOLOGY OF NANOMATERIALS

The branch of science that deals with the adverse effect of physical, chemical, and biological materials on living cells or living organisms, is called toxicology (Liu & Yu 2011). Nanotoxicology is a rapidly developing field in today's era (Khan & Shanker 2015). Despite the fact that nanoparticles (NPs) are always present in nature, major advances in their field of research have been made in bioremediation (Cecchin et al. 2017), paints (Goesmann & Feldmann 2010), coatings (Fierascu et al. 2019), electronics (Cardoso et al. 2018), fuel catalysts, water treatment (Kumar et al. 2014), and almost everywhere in human society (López-Serrano et al. 2014). Nanomaterials drugs offer a great advantage over general pharmaceutical formulations because of their clump-free, stable, and water-soluble properties (Malekhosseini et al. 2019). Especially nano plastics can cause more harm to biota than other micro and macro plastic because of their small size (Strungaru et al. 2019). It is a fact that plastic particles in the nano range are able to penetrate cell membranes (Bouwmeester et al. 2015). Aromatic hydrocarbons, polychlorinated biphenyls, and other additives exacerbate the impact of these chemicals on living beings. Nanoplastics can operate as pathogenic vectors for chemical and biological pollutants, causing poisoning in animals and humans (Jiang et al. 2020). Nanoparticle exposure in the environment and surroundings is shown in Fig1.

There are different ways by which microplastic and nano plastics enter our ecosystem. The direct way in which contamination is caused is through the application of plastic mulch in agricultural soils greenhouse buildings matter, raw material, and soil condition improver (Steinmetz et al. 2016). Because of their minute size, many nano plastics are retained in wastewater treatment reactors after being processed in a wastewater treatment facility, and the remainder ends up in generated sludge (Egirani et al. 2020).

Parameters that can affect the toxicity of nanoparticles: Various factors decide the fate of nanoparticles in the environment (Sajid et al. 2015). The morphology of the engineered nanoparticle is affected by the synthesis methods used and the changes in the synthesis procedure (Patra & Baek 2014). The composition of nano-sized particles stems from physical, chemical, mechanical, and biological processes. The physical process comprises the synthesis of the nanoparticles by different techniques like lithographic, ball milling, etching, and sputtering techniques, which focus on the breakdown of larger molecules into a material of suitable functional and morphological characteristics. The buildup of nanoparticles from non-complex molecular structures is done by the chemical process. These methods comprise deposition by chemical vaporization, condensation of atomic and molecular structures, spray with laser heating at controlled temperature conditions, and aerosol formation. There is a limited scien-

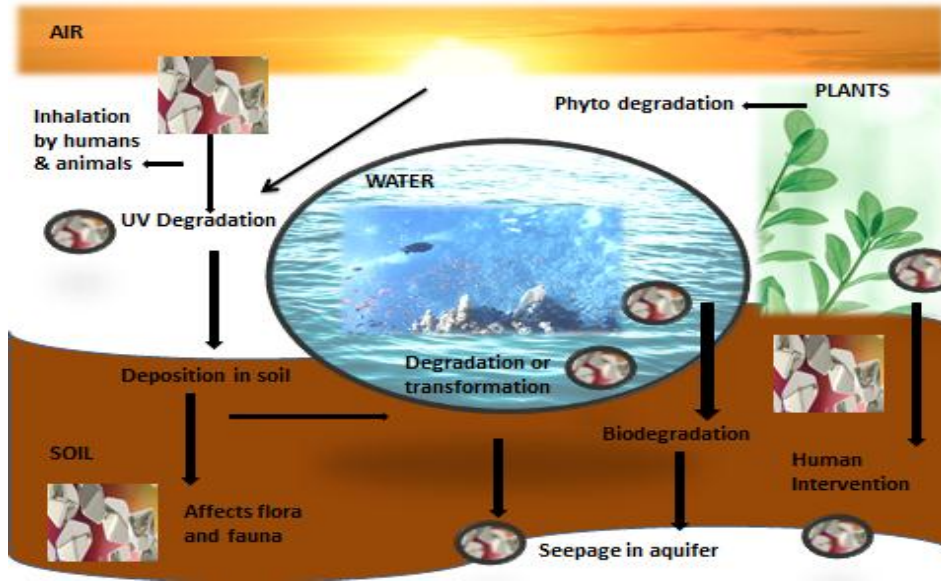

Fig. 1: Exposure of nanoparticles on animal health and environment.

tific understanding of reaction mechanisms and modeling characteristics associated with this factor mentioned below.

1. Size
2. Composition
3. Solubility and crystalline structure
4. Charge with surface characteristics
5. Attached functional groups
6. Agglomeration with impurities and porosity can potentially affect the total removal yield of the nanomaterial from the environmental contaminants (Das et al. 2018).

SOURCES OF NANOMATERIALS

Nanomaterials present in our environment come either from natural processes like volcanic explosions, forest fires, erosion of different soils, clay minerals, and dust storms (Bakshi et al. 2015) or from different anthropogenic activities including fossil fuel burning, mining, automobile traffic, and nanomaterial production, and wastewater release from industries (Kabir et al. 2018). Hydrophobicity, chemical, and physical resistance are the reasons, nanoparticle transports from one place to the other (Kettler et al. 2014). Our clothing, which is made of polyester, nylon, and acrylic fibers, is washed and laundered in wastewater treatment plants (Tiwari et al. 2020). Nanoparticles remain in the environment even after multiple treatments due to their small size and higher resistance power (Zhang 2015). Cosmetic products such as shampoos, soaps, and scrubs release high concentrations of nanoparticles because of the microbeads used and their fragmentation (Lehner et al. 2019). Even plastic tea bags which we use on daily basis in large amounts could release billions of nanoparticles (Auclair et al. 2020). Sources and applications of nanoparticles are compiled below in (Table 1).

Table 1: Sources of nanoparticles in the environment.

S. No.	Types	Applications	References
1	Natural	Volcanic eruption Forest fire Dust storm Soil erosion	(Strambeanu et al. 2015)
2	Intentional or engineered	Drug delivery Engineered nanomaterial Groundwater remediation Biomedical engineering Biosensors	(Sun et al. 2014)
3	Unintentional or incidental	Welding Vehicle exhaust Industrial processes Fuel burning Mining	(Hochella et al. 2019)

NANOMATERIALS OF DIFFERENT SUBSTANCES AND THEIR TOXICITY

Various types of nanomaterials are being used in everyday life including zinc oxide nanoparticles (ZnONPs), silica nanoparticles (SiO_2NPs), titanium dioxide nanoparticles (TiO_2NPs), silver nanoparticles (Ag-NPs), gold NPs (AuNPs), and polymeric nanoparticles (PNPs) (Sajid et al. 2015). Generally, these nanoparticles are for the drug delivery system in various parts of the body (Bharti et al. 2015). All interactions with harmful toxicological effects are caused by changes in the physicochemical and systemic properties of man-made nanoparticles (Gatoo et al. 2014).

ZnO nanoparticles (ZnO NP): Various types of cosmetics as sunscreens, food supplements like additives and color, pigments, and biosensors contain zinc oxide nanoparticles (ZnONPs) (Mirzaei & Darroudi 2017). The toxic effect of ZnO is seen in animal models and humans (Valdiglesias et al. 2013). Cytotoxicity and genotoxicity of ZnONPs have been studied in vitro as well as in vivo (Ng et al. 2017). Depending on the duration or dose, these ZnONPs have lower cell viability. Studies have found dose-dependent hepatotoxicity as well as an increase in oxidative stress because of increased levels of malondialdehyde (MDA) and decreased enzyme activity in the liver (Zhang 2015).

TiO_2 nanoparticles(TiO_2 NPs): TiO_2 is commonly used in beauty and skincare items as a pigment, a binder, and a UV absorber (Torbati & Javanbakht 2020). TiO_2 allows artificial medical implants and bone. Some scientists found the toxicity of TiO_2 nanoparticles through skin penetration in mice and skin of porcine post chronic exposure (Adachi et al. 2010). Other studies have observed in vitro cytotoxicity and genotoxicity of TiO_2NPs in different cell lines, in plants, and model organisms such as mice and zebra fishes (Bennett et al. 2012).

Silica nanoparticles(SiO_2 NPs): For a long time, the indefinite form of silica has been used as a food ingredient (Peters et al. 2012). The main purpose of SiO_2 nanoparticles in the food industry is to overcome flow or caking in powdered products. SiO_2 also have been used as a carrier of flavors as well as a thickener in paste-like substances (Guo et al. 2018). It is sometimes used to clear different beverages and lessen foaming. Various studies have reported the toxicity of SiO_2 nanoparticles as food additives on human gastrointestinal cells, thus enforcing their safety as food additives (Go et al. 2017). Scientists have also demonstrated that oral and intravenous administration of SiO_2 nanoparticles has a negative impact on biodistribution, excretion, and toxicity (Khlebtsov & Dykman 2011).

Silver nanoparticles (Ag-NPs): Silver is well known for its antibacterial potential. Researchers found that silver has been used as a healing agent for a long time (Peng et al. 2012). To increase and use its potential, a silver particle (Ag) is used as a nanoparticle. Ag nanoparticles have been found to exhibit antiviral and antibacterial activities. Another application of silver-containing resin is to fill cavities and cover dental teeth, as well as in medical applications. In mice, researchers confirmed that ammonia and PVPs (polyvidone stabilized Ag nanoparticles) are non-cytotoxic at lower quantities (Saqib & Rahim 2016). Some researchers observed adverse effects of AgNPs on human cells and demonstrated that their cytotoxic and genotoxic effects act as a useful tool to control desirable angiogenesis which means the formation of new blood cells in an uncontrollable way (Gupta & Xie 2018).

Gold nanoparticles (Au-NPs): Gold nanoparticles are used to cap bio-functional moieties that have considerable biological activity, such as peptides and carbohydrates, to control and monitor various cell processes (Zhang et al. 2020). The application of AuNPs is also found in diagnosis due to their light returning ability and surface. Due to their significant potential in therapeutic and diagnostic purposes, AuNPs find great application in understanding toxic effects (Khan et al. 2014). Scientists studied the toxicity of AuNPs on immune dendrites that were obtained from mice bone marrow cells (Zhang et al. 2019).

TYPES OF NANOMATERIALS AND THEIR IMPACT ON THE ENVIRONMENT

Different categories of nanomaterials, classification and their structure are given in Table 2.

Nanomaterials then further classified according to their dimensions are -

- Zero-dimension (0D)
- One-dimension (1D)
- Two-dimensions (2D)
- Three-dimensions (3D).

Major counts of nano-particles are zero dimensions that include nanomaterial in the range of 1-100 nm. Unit dimension nanomaterials contain a thin needle or rod like-structure measure of 100 nm-10 μm and include nanotubes, nanorods, and nanowires (Ghassan et al. 2019). Two Dimensions nanomaterial comprises plate-like shapes including Nanocoatings, nanofilms, and nanolayers. 3D nanomaterials possess random dimensions and multilayer nano-crystalline structure (Yang et al. 2011)**.** These nanomaterials usually include bulk powders, nanowire bundles, multi-nano layers, nanoparticles dispersions, and nanotubes (Saleem & Zaidi 2020).

ENVIRONMENTAL IMPACT OF NANOPARTICLES

Nanomaterial is generally released in the environment as waste from industries, directly into the land, water, air, soil through the remediation of contaminated fields. As technology advances, nanoparticles behave differently in different compartments of the environment.

Nanoparticle in the air: Nanoparticles present in the atmosphere can cover large distances from the point of their delivery or release, thus causing unmanageable exposure to humans as well as eco-toxicological effects on marine or terrestrial life (Ghadimi et al. 2020). The nanoparticles present in the terrestrial ecosystem spread rarely due to their immobile nature, yet they can travel into the human digestive system by gulping and swallowing or even contact with the skin (Berkowitz et al. 2014).

Nanoparticle in the soil: Nanoparticles can enter soils directly through pesticides and fertilizers, or indirectly through land and wastewater treatment materials such as sludges or biosolids (Courtois et al. 2020). Fertilizers are used to increase the productivity of the soil. Contrary outcomes of nanoparticles on biogeochemical cycles like in the nitrogen cycle have been found in some studies.

CHALLENGES ASSOCIATED WITH ENVIRONMENT TOXICOLOGY OF NANOMATERIAL

Analysis and assessments of different nanomaterials are limited due to a lack of knowledge and research in this field, as well as some inadequacies in regulating the spread of contamination by nanoparticles (Lai et al. 2018).

- Hazard and exposure evaluation- Hindrance in evaluating hazards posed by nanomaterials is a major issue due to the lack of standard protocols and methods to resolve them (Weinberg et al. 2011)
- Lack of informative data in the composition and profile of nanomaterials results in fewer testings and monitoring of facts for various NMs (Lead et al. 2018).
- Still, no methodology is available to recognize and identify the exposure of ENMs

CONCLUSION

Nanotechnology has gained significant importance in recent years owing to its widespread application and novelty. Although the majority of nanoparticles are utilized for a wide range of applications, their potential toxic hazards and consequences remain a major constraint to their advantage. The potential negative impacts of nanomaterials and nanoparticles in the environment have been studied by various researchers but major toxic effects of these NMs in the environment

Table 2: Types of nanomaterials.

Sr. No.	Type	Characteristics	Structure	References
1	Fullerenes	Interconnected carbon atoms Withstanding with extreme heat, still can regain its original shape. As hard or harder than diamond	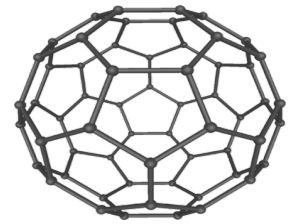	(Castro et al. 2017)
2	Carbon-based	Single-walled or multiple walls 20 nm diameter E.g. Carbon nanotube	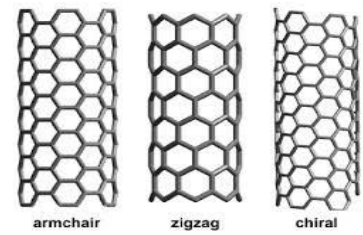	(Xin et al. 2019)
3	Inorganic	Pure metals or various inorganic products alloys Nanoscale distinguishes them from bulk material Display unique mechanical, electrical properties $CaCO_3$, SiO_2, AlOH, $SrCO_3$, TiO_2	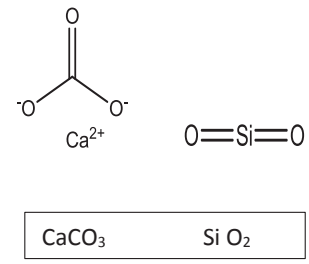	(Wu 2017)
4	Organic	Contain both soluble and insoluble particles. Display catalytic properties not found in bulk material counterpart. Help drugs pass the blood-brain barrier.	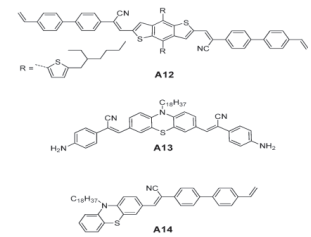	(Lombardo et al. 2020)
5	Nanocapsules, nanoshells	Composed of insoluble organic polymers (methacrylic acid and PEG) Can bypass the digestive tract and act as pharmacologic vectors directly in the intestine.	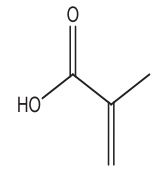	(Bollhorst et al. 2017)
6	Quantum dots	Nanocrystals, artificial atom,1-10 nm in diameter Semiconductors, metal insulators, Magnetic matter or metallic oxides Fluorescent probe CdSe core with ZnS shell	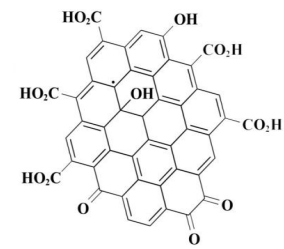	(Yan et al. 2019)

along with adverse consequences on human health is a major cause of concern in coming years. Currently, current investigations using practical methodologies have proven the interactions of nanomaterials with various air surfaces, particularly plastics, restricting their bioavailability, reactivity, and toxicity, posing a risk to the environment. Despite increasing nanotechnology usage in industries, their ecological impacts are still in their infancy to combat them. The nature and composition of various nanomaterials used in fertilizers, and pesticides are often unclear, their utilization is widespread to cause contamination in soil and terrestrial habitat of plants as well.

Continued scientific input and knowledge are required to overcome the toxicological impacts of nanoparticles on the ecosystem and the environment. The long-term sustainability and prolonged exposure of nanoparticles in the environment require proper implementation and judicious regulations to combat toxic impacts. Assessment, risk, and evaluation of nanoparticles to understand potential toxicological impacts caused by them necessitated scientific understanding to learn their fate and action in the surrounding.

REFERENCES

Adachi, K., Yamada, N., Yamamoto, K., Yoshida, Y. and Yamamoto, O. 2010. In vivo effect of industrial titanium dioxide nanoparticles experimentally exposed to hairless rat skin. Nanotoxicology, 4: 296-306. https://doi.org/10.3109/17435391003793095

Auclair, J., Peyrot, C., Wilkinson, K.J. and Gagné, F. 2020. Biophysical effects of polystyrene nanoparticles on Elliptio complanata mussels. Environ. Sci. Pollut. Res., 27: 25093-25102. https://doi.org/10.1007/s11356-020-08920-z

Awoyera, P.O. and Adesina, A. 2020. Plastic wastes to construction products: Status, limitations, and future perspective. Case Stud. Constr. Mater., 12: e00330. https://doi.org/10.1016/j.cscm.2020.e00330

Bakshi, S., He, Z.L. and Harris, W.G. 2015. Natural nanoparticles: Implications for the environment and human health. Crit. Rev. Environ. Sci. Technol., 45: 861-904. https://doi.org/10.1080/10643389.2014.921975

Baztan, J., Bergmann, M., Carrasco, A., Fossi, M.C., Jorgensen, B., Miguelez, A., Pahl, S., Thompson, R.C. and Vanderlinden, J.P. 2018. MICRO 2018 Fate and Impact of Microplastics: Knowledge, Actions and Solutions. Lanzarote, MICRO, pp. 414.

Bennett, S.W., Zhou, D., Mielke, R. and Keller, A.A. 2012. Photoinduced disaggregation of TiO2 nanoparticles enables transdermal penetration. PLOS One, 7: e48719. https://doi.org/10.1371/journal.pone.0048719

Berkowitz, B., Dror, I. and Yaron, B. 2014. Inorganic and Organometallic Compounds. In Berkowitz, B., Dror, I. and Yaron, B. (eds.), Contaminant Geochemistry: Interactions and Transport in the Subsurface Environment. Springer, Berlin, Heidelberg, pp. 53-77. https://doi.org/10.1007/978-3-642-54777-5_3

Bharti, C., Nagaich, U., Pal, A.K. and Gulati, N. 2015. Mesoporous silica nanoparticles in target drug delivery system: A review. Int. J. Pharm. Investig., 5: 124-133. https://doi.org/10.4103/2230-973X.160844

Bhushan, B. 2017. Springer Handbook of Nanotechnology. Springer, New York.

Bollhorst, T., Rezwan, K. and Maas, M. 2017. Colloidal capsules: nano- and microcapsules with colloidal particle shells. Chem. Soc. Rev., 46: 2091-2126. https://doi.org/10.1039/C6CS00632A.

Bouwmeester, H., Hollman, P.C.H. and Peters, R.J.B. 2015. Potential health impact of environmentally released micro- and nano plastics in the human food production chain: Experiences from nanotoxicology. Environ. Sci. Technol., 49: 8932–8947. https://doi.org/10.1021/acs.est.5b01090

Cardoso, V.F., Francesko, A., Ribeiro, C., Bañobre-López, M., Martins, P. and Lanceros-Mendez, S. 2018. Advances in magnetic nanoparticles for biomedical applications. Adv. Healthc. Mater., 7: 1700845. https://doi.org/10.1002/adhm.201700845

Castro, E., Garcia, A.H., Zavala, G. and Echegoyen, L. 2017. Fullerenes in biology and medicine. J. Mater. Chem. B, 5: 6523-6535. https://doi.org/10.1039/C7TB00855D

Cecchin, I., Reddy, K.R., Thomé, A., Tessaro, E.F. and Schnaid, F. 2017. Nanobioremediation: Integration of nanoparticles and bioremediation for sustainable remediation of chlorinated organic contaminants in soils. Int. Biodeterior. Biodegrad. Environ. Biotechnol. Sust. Develop., 119: 419-428. https://doi.org/10.1016/j.ibiod.2016.09.027

Courtois, P., Rorat, A., Lemiere, S., Guyoneaud, R., Attard, E., Longepierre, M., Rigal, F., Levard, C., Chaurand, P., Grosser, A., Grobelak, A., Kacprzak, M., Lors, C., Richaume, A. and Vandenbulcke, F. 2020. Medium-term effects of Ag supplied directly or via sewage sludge to an agricultural soil on Eisenia fetida earthworm and soil microbial communities. Chemosphere, 171: 128761. https://doi.org/10.1016/j.chemosphere.2020.128761

Da Costa, J.P., Santos, P.S.M., Duarte, A.C. and Rocha-Santos, T. 2016. (Nano)plastics in the environment: Sources, fates, and effects. Sci. Total Environ., 566: 15-26. https://doi.org/10.1016/j.scitotenv.2016.05.041

Das, S., Chakraborty, J., Chatterjee, S. and Kumar, H. 2018. Prospects of biosynthesized nanomaterials for the remediation of organic and inorganic environmental contaminants. Environ. Sci. Nanotechnol., 5: 2784-2808. https://doi.org/10.1039/C8EN00799C

Del Saz-Salazar, S., Hernández-Sancho, F. and Sala-Garrido, R. 2009. The social benefits of restoring water quality in the context of the water framework directive: A comparison of willingness to pay and willingness to accept. Sci. Total Environ., 407: 4574-4583. https://doi.org/10.1016/j.scitotenv.2009.05.010

Egirani, D., Shehata, N. and Khedr, M. 2020. A review of nanomaterials in agriculture and allied sectors: Preparation, characterization, applications, opportunities, and challenges. Materials, 2: 0421-0432. https://doi.org/10.33263/Materials23.421432

Fierascu, R.C., Ortan, A., Avramescu, S.M. and Fierascu, I. 2019. Phyto-nanocatalysts: Green synthesis, characterization, and applications. Molecules, 24: 3418. https://doi.org/10.3390/molecules24193418

Gatoo, M.A., Naseem, S., Arfat, M.Y., Mahmood Dar, A., Qasim, K. and Zubair, S. 2014. Physicochemical properties of nanomaterials: Implication in associated toxic manifestations [WWW Document]. BioMed Res. Int., 48: 842. https://doi.org/10.1155/2014/498420

Ghadimi, M., Zangenehtabar, S. and Homaeigohar, S. 2020. An overview of the water remediation potential of nanomaterials and their ecotoxicological impacts. Water, 12: 1150. https://doi.org/10.3390/w12041150

Ghassan, A.A., Mijan, N.A. and Taufiq-Yap, Y.H. 2019. Nanomaterials: An overview of nanorods synthesis and optimization. Nanorods nanocomposites. https://doi.org/10.5772/intechopen.84550

Go, M.R., Bae, S.H., Kim, H.J., Yu, J. and Choi, S.J. 2017. Interactions between food additive silica nanoparticles and food matrices. Front. Microbiol., 8: 101. https://doi.org/10.3389/fmicb.2017.01013

Goesmann, H. and Feldmann, C. 2010. Nanoparticulate functional materials. Angew. Chem. Int. Ed., 49: 1362-1395. https://doi.org/10.1002/anie.200903053

Guo, Z., Martucci, N.J., Liu, Y., Yoo, E., Tako, E. and Mahler, G.J. 2018. Silicon dioxide nanoparticle exposure affects small intestine function in an in vitro model. Nanotoxicology, 12: 485-508. https://doi.org/10.1080/17435390.2018.1463407.

Gupta, R. and Xie, H. 2018. Nanoparticles in daily life: Applications, toxicity, and regulations. J. Environ. Pathol. Toxicol. Oncol., 37: 615. https://doi.org/10.1615/JEnvironPatholToxicolOncol.2018026009.

Herbort, A.F., Sturm, M.T., Fiedler, S., Abkai, G. and Schuhen, K. 2018. Alkoxy-silyl induced agglomeration: A new approach for the sustainable removal of microplastic from aquatic systems. J. Polym. Environ., 26: 4258-4270. https://doi.org/10.1007/s10924-018-1287-3

Hochella, M.F., Mogk, D.W., Ranville, J., Allen, I.C., Luther, G.W., Marr, L.C., McGrail, B.P., Murayama, M., Qafoku, N.P., Rosso, K.M., Sahai, N., Schroeder, P.A., Vikesland, P., Westerhoff, P. and Yang, Y. 2019. Natural, incidental, and engineered nanomaterials and their impacts on the Earth system. Science, 363: 8299. https://doi.org/10.1126/science.aau8299

Hutchison, J.E. 2016. The road to sustainable nanotechnology: Challenges, progress, and opportunities. ACS Sustain. Chem. Eng., 4: 5907-5914. https://doi.org/10.1021/acssuschemeng.6b02121

Iavicoli, I., Leso, V., Ricciardi, W., Hodson, L.L. and Hoover, M.D. 2014. Opportunities and challenges of nanotechnology in the green economy. Environ. Health, 13: 78. https://doi.org/10.1186/1476-069X-13-78

Jiang, B., Kauffman, A.E., Li, L., McFee, W., Cai, B., Weinstein, J., Lead, J.R., Chatterjee, S., Scott, G.I. and Xiao, S. 2020. Health impacts of environmental contamination of micro- and nano plastics: a review. Environ. Health Prev. Med., 25: 29. https://doi.org/10.1186/s12199-020-00870-9

Kabir, E., Kumar, V., Kim, K.H., Yip, A.C.K. and Sohn, J.R. 2018. Environmental impacts of nanomaterials. J. Environ. Manag., 225: 261-271. https://doi.org/10.1016/j.jenvman.2018.07.087

Kettler, K., Veltman, K., Meent, D., Wezel, A. and Hendriks, A.J. 2014. Cellular uptake of nanoparticles as determined by particle properties, experimental conditions, and cell type. Environ. Toxicol. Chem., 33: 481-492. https://doi.org/10.1002/etc.2470

Khan, A.K., Rashid, R., Murtaza and G., Zahra, A. 2014. Gold nanoparticles: Synthesis and applications in drug delivery. Trop. J. Pharm. Res., 13: 1169-1177. https://doi.org/10.4314/tjpr.v13i7.23

Khan, H.A. and Shanker, R. 2015. Toxicity of nanomaterials. BioMed Res. Int., 2015: 521014

Khlebtsov, N. and Dykman, L. 2011. Biodistribution and toxicity of engineered gold nanoparticles: A review of in vitro and in vivo studies. Chem. Soc. Rev., 40: 1647-1671. https://doi.org/10.1039/C0CS00018C

Kumar, S., Ahlawat, W., Bhanjana, G., Heydarifard, S., Nazhad, M.M. and Dilbaghi, N. 2014. Nanotechnology-based water treatment strategies. J. Nanosci. Nanotechnol., 14: 1838-1858. https://doi.org/10.1166/jnn.2014.9050

Lai, R.W.S., Yeung, K.W.Y., Yung, M.M.N., Djuriši-, A.B., Giesy, J.P. and Leung, K.M.Y. 2018. Regulation of engineered nanomaterials: Current challenges, insights and future directions. Environ. Sci. Pollut. Res., 25: 3060-3077. https://doi.org/10.1007/s11356-017-9489-0

Lead, J.R., Batley, G.E., Alvarez, P.J.J., Croteau, M.N., Handy, R.D., McLaughlin, M.J., Judy, J.D. and Schirmer, K. 2018. Nanomaterials in the environment: Behavior, fate, bioavailability, and effects—An updated review. Environ. Toxicol. Chem., 37: 2029-2063. https://doi.org/10.1002/etc.4147

Lee, K.W., Shim, W.J., Kwon, O.Y. and Kang, J.H. 2013. Size-dependent effects of micro polystyrene particles in the marine Copepod Tigriopus japonicus. Environ. Sci. Technol., 47: 11278-11283. https://doi.org/10.1021/es401932b

Lehner, R., Weder, C., Petri-Fink, A. and Rothen-Rutishauser, B. 2019. The emergence of nano plastic in the environment and its possible impact on human health. Environ. Sci. Technol., 53: 1748-1765. https://doi.org/10.1021/acs.est.8b05512

Liu, C.H. and Yu, X. 2011. Silver nanowire-based transparent, flexible, and conductive thin film. Nanosci. Res. Lett., 6: 75. https://doi.org/10.1186/1556-276X-6-75

Lombardo, D., Calandra, P., Pasqua, L. and Magazù, S. 2020. Self-assembly of organic nanomaterials and biomaterials: The bottom-up approach for functional nanostructures formation and advanced applications. Materials, 13: 1048. https://doi.org/10.3390/ma13051048

López-Serrano, A., Muñoz Olivas, R., Sanz Landaluze, J. and Cámara, C. 2014. Nanoparticles: A global vision. Anal. Methods, 6: 38-56. https://doi.org/10.1039/C3AY40517F

Malekhosseini, P., Alami, M., Khomeiri, M., Esteghlal, S., Nekoei, A.R. and Hosseini, S.M.H. 2019. Development of casein-based nanoencapsulation systems for delivery of epigallocatechin gallate and folic acid. Food Sci. Nutr., 7: 519-527. https://doi.org/10.1002/fsn3.827

Mirzaei, H. and Darroudi, M. 2017. Zinc oxide nanoparticles: Biological synthesis and biomedical applications. Ceram. Int., 43: 907-914. https://doi.org/10.1016/j.ceramint.2016.10.051

Mukherjee, A., Majumdar, S., Servin, A.D., Pagano, L., Dhankher, O.P. and White, J.C. 2016. Carbon nanomaterials in agriculture: A critical review. Front. Plant Sci., 7: 172. https://doi.org/10.3389/fpls.2016.00172

Ng, C.T., Yong, L.Q., Hande, M.P., Ong, C.N., Yu, L.E., Bay, B.H. and Baeg, G.H. 2017. Zinc oxide nanoparticles exhibit cytotoxicity and genotoxicity through oxidative stress responses in human lung fibroblasts and drosophila melanogaster. Int. J. Nanomed., 12: 1621-1637. https://doi.org/10.2147/IJN.S124403

Pathakoti, K., Manubolu, M. and Hwang, H.M. 2018. Nanotechnology Applications for Environmental Industry. In Mustansar Hussain, C. (ed.), Handbook of Nanomaterials for Industrial Applications, Micro and Nano Technologies. Elsevier, Netherlands, pp. 894-907. https://doi.org/10.1016/B978-0-12-813351-4.00050-X

Patra, J.K. and Baek, K.H. 2014. Green nanobiotechnology: Factors affecting synthesis and characterization techniques [WWW Document]. J. Nanomater., 11: 155. https://doi.org/10.1155/2014/417305

Peng, J.J.Y., Botelho, M.G. and Matinlinna, J.P. 2012. Silver compounds used in dentistry for caries management: A review. J. Dent., 40: 531-541. https://doi.org/10.1016/j.jdent.2012.03.009

Peters, R., Kramer, E., Oomen, A.G., Herrera Rivera, Z.E., Oegema, G., Tromp, P.C., Fokkink, R., Rietveld, A., Marvin, H.J.P., Weigel, S., Peijnenburg, A.A.C.M. and Bouwmeester, H. 2012. Presence of nano-sized silica during in vitro digestion of foods containing silica as a food additive. ACS Nano, 6: 2441-2451. https://doi.org/10.1021/nn204728k

Rai, P.K., Lee, J., Brown, R.J.C. and Kim, K.H. 2020. Micro- and nano-plastic pollution: Behavior, microbial ecology, and remediation technologies. J. Clean. Prod., 2020: 125240. https://doi.org/10.1016/j.jclepro.2020.125240

Sajid, M., Ilyas, M., Basheer, C., Tariq, M., Daud, M., Baig, N. and Shehzad, F. 2015. Impact of nanoparticles on human and environment: Review of toxicity factors, exposures, control strategies, and prospects. Environ. Sci. Pollut. Res., 22: 4122-4143. https://doi.org/10.1007/s11356-014-3994-1

Saleem, H. and Zaidi, S.J. 2020. Recent developments in the application of nanomaterials in agroecosystems. Nanomaterials, 10: 2411. https://doi.org/10.3390/nano10122411

Saqib, N. and Rahim, M. 2016. Toxicity of silver nanoparticles. Madridge J. Nanotechnol. Nanosci., 1: 1-2.

Steinmetz, Z., Wollmann, C., Schaefer, M., Buchmann, C., David, J., Tröger, J., Muñoz, K., Frör, O. and Schaumann, G.E. 2016. Plastic mulching in agriculture: Trading short-term agronomic benefits for long-term soil degradation? Sci. Total Environ., 550: 690-705. https://doi.org/10.1016/j.scitotenv.2016.01.153

Strambeanu, N., Demetrovici, L. and Dragos, D. 2015. Anthropogenic Sources of Nanoparticles. In Lungu, M., Neculae, A., Bunoiu, M. and Biris, C. (eds.), Nanoparticles' Promises and Risks: Characterization, Manipulation, and Potential Hazards to Humanity and the Environment. Springer International Publishing, Cham, pp. 21-54. https://doi.org/10.1007/978-3-319-11728-7_3

Strungaru, S.A., Jijie, R., Nicoara, M., Plavan, G. and Faggio, C. 2019. Micro- (nano) plastics in freshwater ecosystems: Abundance, toxicological

impact, and quantification methodology. TrAC Trends Anal. Chem., 110: 116-128. https://doi.org/10.1016/j.trac.2018.10.025

Sun, T.Y., Gottschalk, F., Hungerbühler, K. and Nowack, B. 2014. Comprehensive probabilistic modeling of environmental emissions of engineered nanomaterials. Environ. Pollut., 185: 69-76. https://doi.org/10.1016/j.envpol.2013.10.004

Tiwari, N., Santhiya, D. and Sharma, J.G. 2020. Microbial remediation of micro-nano plastics: Current knowledge and future trends. Environ. Pollut., 265: 115044. https://doi.org/10.1016/j.envpol.2020.115044

Torbati, T.V. and Javanbakht, V. 2020. Fabrication of TiO2/Zn2TiO4/Ag nanocomposite for synergic effects of UV radiation protection and antibacterial activity in sunscreen. Colloids Surf. B Biointerf., 187: 110652. https://doi.org/10.1016/j.colsurfb.2019.110652

Valdiglesias, V., Costa, C., Kiliç, G., Costa, S., Pásaro, E., Laffon, B. and Teixeira, J.P. 2013. Neuronal cytotoxicity and genotoxicity induced by zinc oxide nanoparticles. Environ. Int., 55: 92-100. https://doi.org/10.1016/j.envint.2013.02.013

Weinberg, H., Galyean, A. and Leopold, M. 2011. Evaluating engineered nanoparticles in natural waters: Characterization, analysis, and risks of nanomaterials in environmental and food samples. TrAC Trends Anal. Chem., 30, 72-83. https://doi.org/10.1016/j.trac.2010.09.006

Wu, W. 2017. Inorganic nanomaterials for printed electronics: A review. Nanoscale, 9: 7342-7372. https://doi.org/10.1039/C7NR01604B

Xin, Q., Shah, H., Nawaz, A., Xie, W., Akram, M.Z., Batool, A., Tian, L., Jan, S.U., Boddula, R., Guo, B., Liu, Q. and Gong, J.R. 2019. Antibacterial Carbon-Based Nanomaterials. Adv. Mater., 31: 1804838. https://doi.org/10.1002/adma.201804838

Yan, Y., Gong, J., Chen, J., Zeng, Z., Huang, W., Pu, K., Liu, J. and Chen, P. 2019. Recent advances on graphene quantum dots: From chemistry and physics to applications. Adv. Mater., 31: 1808283. https://doi.org/10.1002/adma.201808283

Yang, M., Chen, J., Cao, W., Ding, L., Ng, K.K., Jin, H., Zhang, Z. and Zheng, G. 2011. Attenuation of nontargeted cell-kill using a high-density lipoprotein-mimicking peptide–phospholipid nano scaffold. Nanomed. 6, 631-641. https://doi.org/10.2217/nnm.11.10

Zhang, D., Wu, T., Qin, X., Qiao, Q., Shang, L., Song, Q., Yang, C., and Zhang, Z. 2019. Intracellularly generated immunological gold nanoparticles for combinatorial photothermal therapy and immunotherapy against the tumor. Nano Lett., 19: 6635-6646. https://doi.org/10.1021/acs.nanolett.9b02903

Zhang, X. 2015. Gold nanoparticles: Recent advances in biomedical applications. Cell Biochem. Biophys., 72: 771-775. https://doi.org/10.1007/s12013-015-0529-4

Zhang, Y.M., Liu, Y.H. and Liu, Y. 2020. Cyclodextrin-based multi stimuli-responsive supramolecular assemblies and their biological functions. Adv. Mater., 32: 1806158. https://doi.org/10.1002/adma.201806158

Journal Pre-proof

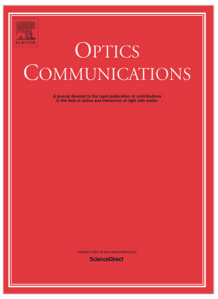

Ultrasensitive dual-band terahertz metasurface sensor based on all InSb resonator

Pooja Agarwal, Kamal Kishor, Ravindra Kumar Sinha

PII: S0030-4018(22)00438-2
DOI: https://doi.org/10.1016/j.optcom.2022.128667
Reference: OPTICS 128667

To appear in: *Optics Communications*

Received date : 19 April 2022
Revised date : 4 June 2022
Accepted date : 16 June 2022

Please cite this article as: P. Agarwal, K. Kishor and R.K. Sinha, Ultrasensitive dual-band terahertz metasurface sensor based on all InSb resonator, *Optics Communications* (2022), doi: https://doi.org/10.1016/j.optcom.2022.128667.

This is a PDF file of an article that has undergone enhancements after acceptance, such as the addition of a cover page and metadata, and formatting for readability, but it is not yet the definitive version of record. This version will undergo additional copyediting, typesetting and review before it is published in its final form, but we are providing this version to give early visibility of the article. Please note that, during the production process, errors may be discovered which could affect the content, and all legal disclaimers that apply to the journal pertain.

© 2022 Published by Elsevier B.V.

Journal Pre-proof

Revised manuscript PV-1587R1

Click here to view linked References

Ultrasensitive Dual-Band Terahertz Metasurface Sensor Based on All InSb Resonator

Pooja Agarwal[1,3], Kamal Kishor[1], and Ravindra Kumar Sinha[1,2*]

[1]TIFAC-Centre of Relevance & Excellence in Fiber Optics & Optical Communications, Applied Physics Department, Delhi Technological University (Formerly Delhi College of Engineering), Bawana Road, Delhi 110 042, India

[2]Gautam Buddha University, Greater NOIDA, Gautam Budh Nagar, Uttar Pradesh-201312, India

[3]University Department of Physics, Lalit Narayan Mithila University, Kameshwaranagar, Darbhanga, Bihar- 846004, India.

* Corresponding author: dr_rk_sinha@yahoo.com

Abstract

Terahertz (THz) metasurface sensors have recently received considerable attention. We report an ultrasensitive dual-band metasurface (DBM) sensor in this work. The reported DBM sensor is a micro-rod periodic structure based on all InSb semiconducting material. The DBM is realized for the dual-band resonance behaviour at 1.911 THz and 1.985 THz. The corresponding Q factor for the DBM sensor is obtained at the higher side, around 174.36 and 181.11 at room temperature (T = 300 K). The geometrical parameters dependency for the resonance frequency of the proposed DBM is analysed and reported. Further, the refractive index sensitivity is observed by varying the surrounding's refractive index from 1.00 to 1.05 (aqueous glucose solution). It is reported that, at room temperature, the proposed DBM sensor shows a sensitivity of 1800 GHz/RIU and 1900 GHz/RIU at the corresponding resonance frequencies 1.911 THz and 1.985 THz respectively. The temperature sensitivity of the proposed DBM is also explored and reported. Furthermore, the figure of merit (FOM) of the proposed DBM sensor is 164 and 173 respectively at corresponding resonance frequencies. So, the reported DBM structure could also find potential applications in the THz region as sensors, detectors, and other optoelectronic devices.

Keywords: THz Metasurface, Sensor, Dual-band, and Absorber

1. Introduction

Waves in the THz range, which are between microwaves and infrared, offer certain unique imaging benefits [1]. In addition to complementing or enhancing conventional solutions, THz radiation offers a number of benefits for sensing applications [2]. In contrast to X-rays, THz waves are non-ionizing and do not harm biological tissue, a vital aspect for health applications and bio-detection in general [3]. Another advantage of THz imaging over microwaves or ultrasound is that it has a higher spatial resolution. Electromagnetic (EM) metamaterial perfect absorbers (MPAs), operated in THz frequency region, have attracted researcher's attention for its numerous applications in sensing, imaging, thermal emitters, and stealth technology [4–11]. After first ever perfect metamaterial absorber introduced by Landy et al. in 2008, there are many different metal-dielectric-metal (MDM) layered or multi-layered structures has been reported for ideal absorbers[12]. The three-layered or multi-layered MDM nano-structures found as the most investigated MPA design. Now a days, several researchers are focussed and working on improving the absorption capacity of MPAs to develop the THz sensing devices [5,13–15]. However, the biggest constraint in the development of MPA-based optoelectronic devices is its complex structure which is difficult to construct, high fabrication cost and low sensitivity.

Metasurfaces, a type of metamaterial made up of patterned sub-wavelength periodic resonator structures, have advantages such as a greater quality factor, a lower profile, and a lower thickness [16,17]. Because of its quasi two-dimensional (quasi-2D) planar property, metasurface patterned structure could be utilized to build miniaturised and integrated THz devices [18–20]. An initial idea for improving interaction of THz waves with

analytes is to develop a metasurface with a large local electromagnetic field enhancement in order to detect trace amounts of analytes in the THz region [21]. Localized electric and magnetic resonances result from the collective excitation of subwavelength metamaterial and plasmonic structures, providing a better framework for electromagnetic sensing [22].

Several THz sensor based on metasurface absorbers (MSAs) have recently been extensively explored for a wide range of applications and it has been demonstrated that high sensing performance may be achieved with a comparatively simple geometric structural design [19,20], [23–25][26][27]. High sensitivity is desirable in sensing because it allows for the detection of more subtle changes in the analyte. Limited sensitivity and complicated fabrication procedures still remain a barrier in sensing applications. As a result, designing a high-performance tunable sensor with a simple structure and enhanced sensitivity is highly desirable. F. Chen et al. suggested a narrow-band MSA based hybrid sensor with maximum sensitivity of 960 GHz/RIU that can be used as a temperature and a RI sensor [23]. Y. Cheng et al. also demonstrated a sensor based on narrow-band MSA using all-dielectric InSb with maximum sensitivity of 1043.3 GHz/RIU [24].

In contrast of these previous study, we designed and analysed a DBM sensor based on all Indium Antimonide (InSb) that can work as a sensor in the THz frequency region for refractive index (RI) and temperature sensing. The proposed DBM structure shows 98% absorbance at 1.911 THz and a 91% absorbance at 1.985 THz at room temperature (300 K). By analysing the distribution of electric field in unit cell structure, the physical mechanism of the proposed DBM has been quantitatively depicted. The Q factors corresponding to the first and second resonance frequencies are 174.36 and 181.11 respectively. Furthermore, modifying geometric parameters can be used to tune the absorption properties. The proposed DBM offers sensitivity of 1800 GHz/RIU and 1900 GHz/RIU respectively when used as RI sensor and it can also be worked as temperature sensor with sensitivity 5.5 GHz/K and 7.5 GHz/K. Due to extraordinary sensing performance and high Q value, DBM sensor is believed to have lot of potential in chemical and biological sensing applications.

2. DBM Design and Modelling

Designing and modelling has been done by using finite element method (FEM) @COMSOL Multiphysics. The schematic diagram of proposed DBM sensor has been illustrated in Fig. 1. It is made up of InSb semiconductor material, acting as a surface plasmonic resonator unit. The corresponding unit cell of DBM having periodic structure in both x-axis and y-axis directions, is depicted in Fig.1(b). The optimized structural parameters of unit cell of DBM are as follows: $p_x = p_y = 150\ \mu m$, $h = 100\ \mu m$, $r = 20\ \mu m$ and $t_s = 60\ \mu m$.

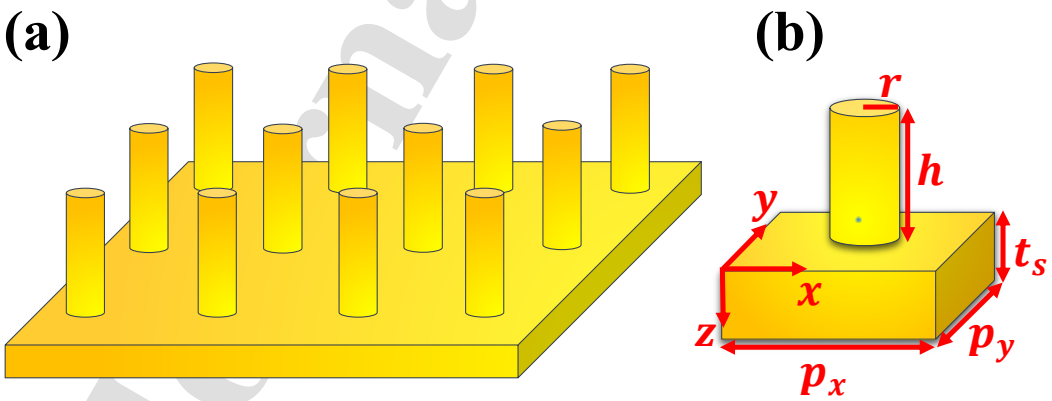

Fig.1: Schematic representation of all InSb based dual-band metasurface (DBM) sensor. (a) Two-dimensional(2D) periodic array carved from an InSb substrate, (b) Unit cell structure.

Journal Pre-proof

Generally, semiconductor materials such as graphene, InSb and Si has the ability to tune the carrier density and the permittivity. This makes them an adequate choice for tunable metamaterial devices in THz region [28–30]. The InSb is a promising active plasmonic material and widely known for its high carrier concentration, high electron mobility and narrow band gap [31][32]. Since proposed DBM's structure can support localized surface plasmon resonance mode and surface plasmon polariton (SPP) in THz radiation, it might be a sustainable choice for plasmonic devices. The permittivity ε(ω) of InSb is complex and dispersive in nature, which can be defined by the Drude's model [31,33][34]:

$$\varepsilon(\omega) = \varepsilon_\infty - \frac{{\omega_p}^2}{\omega^2 + i\gamma\omega} \quad (1)$$

where ω is angular frequency, $\varepsilon_\infty = 15.6$ is the dielectric constant at high frequency and $\gamma = 0.1\pi$ THz is damping constant. The absorption losses of plasmonic material and plasmonic resonance linewidth are determined by damping constant. Further, the plasma frequency is defined as $\omega_p = \sqrt{Ne^2/\varepsilon_0 m^*}$, in which N is the intrinsic carrier density, e is the charge of electron, ε_0 is the permittivity of free space and m^* represent the effective mass of free carriers.

The intrinsic carrier density generally described by the formula $N = 5.76 \times 10^{20} T^{1.5} e^{-0.13/k_B T}$, where k_B is the Boltzmann constant and T is the temperature in Kelvin [34][35]. Hence, it is possible to tune the complex permittivity $\varepsilon(\omega)$ of the InSb by varying the temperature. Thus, it is expected that variation of temperature may result in the tunability of the absorption properties of proposed DBM. In addition, we can believe that the proposed DBM sensor has a better analyte infiltration and diffusion effect.

While analysing, the proposed DBM sensor's structure is illuminated at normal incidence by linearly polarized plane wave, propagating along z- axis direction. Additionally, the periodic boundary conditions were employed along both x-axis and y-axis directions. The absorbance of proposed DBM is evaluated using the given expression:

$$A(\omega) = 1 - R(\omega) - T(\omega) = 1 - |S_{11}(\omega)|^2 - |S_{21}(\omega)|^2 \quad (2)$$

where $S_{11}(\omega)$ and $S_{21}(\omega)$ represents the reflection and transmission coefficient respectively.

3. Results and Discussion

3.1 DBM Structure Simulation Study

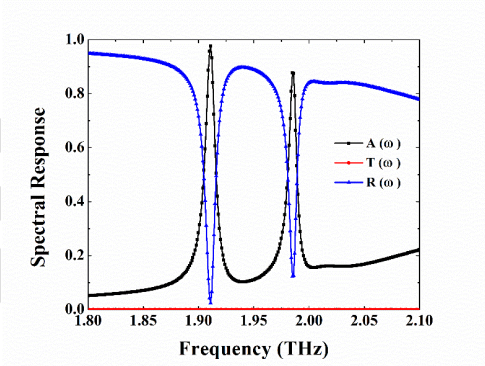

Fig. 2: Simulated spectra in terms of Reflectance R(ω), Transmittance T(ω) and Absorbance A(ω) as a function of frequency ω.

Journal Pre-proof

The reflectance, transmittance and absorbance spectra of the proposed DBM has been illustrated in Fig. 2. As shown in Fig. 2, the proposed DBM has two characteristic resonance modes at frequencies of $f_1 = 1.911$ THz and $f_2 = 1.985$ THz. At these resonances, the absorbance is about 98% and 91% respectively. The transmittance is found zero in the interested frequency range of 1.8 – 2.1 THz. Furthermore, the full width at half maximum (FWHM) of the both resonance frequency peak is 0.01096 THz and the corresponding *Q*-factor is about 174.36 and 181.11, respectively. Due to its high Q-factor and narrow bandwidth, the proposed DBM sensor will offer more potential sensing applications. When the RI value of the metasurface's surrounding media is slightly changed, the ability to detect variations in resonance frequency is considerably improved.

To understand the formation mechanism of absorption peaks of proposed DBM, the distribution of electric field at temperature 300 K has been studied. The electric field distributions at unit cell have been shown in Fig. 3. It has been observed that, the normalized field distribution corresponding to two resonance frequency peaks are different (Fig. 3). The advantage of the InSb micro-rod structure is that, in addition to the electric field it can also couple directly with the magnetic field of the normal incident wave. As shown in Fig. 3(a), at resonance frequency f_1 =1.911 THz, the electric field is accumulated on the upper edges of microrods and for the second resonance frequency f_2 = 1.985 THz, a strong field is visible around the cylinder base (Fig. 3(b)).

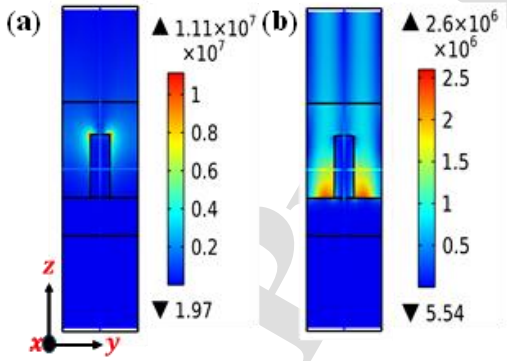

Fig.3: Distributions of the electric field |E| (in the y-z plane) of (a) f_1 =1.911 THz and (b) f_2 =1.985 THz.

The field distribution indicates the accumulation of negative charges and positive charges near InSb micro-rod structure and attribute that the excitation of surface plasmon polariton (SPP) resonance mode is the main cause of absorption. The field enhancement effect of SPPs results in an increase in the absorption of proposed DBMs [36].

3.2 DBM Structure Tunability

The SPP from any system is strongly depends on the various physical properties of the material and/or geometrical parameters of the structure [37]. As metasurface consists of subwavelength structure, the tiny change in dimension of the structure results in change in its collective effective response. The impact of geometrical parameters on the resonance properties of the proposed DBM is investigated. Due to its simple design, only two geometric parameters of the InSb micro-rod are taken under consideration: the radius (r) and the height (h) of the cylinder. The variation in the height and radius of the cylinder of the presented DBM supports the tunability of the SPP based resonance frequency (Fig. 4). The radius (r) of the InSb micro-rod structure gradually increases from 18 μm to 23 μm in the steps of 1 μm.

From Fig. 4(a), a simultaneous red shift for the first resonance peak and blue shift for the second resonance peak has been observed. The resonance frequency peaks represent the resonant modes. Different origin of two resonant modes shows the different behaviour of resonance frequency shift when radius is increased. The

first resonant mode at lower frequency, which is appearance of fundamental mode, is expressed on the basis of LC model based on the equivalent circuit theory [38,39][40].

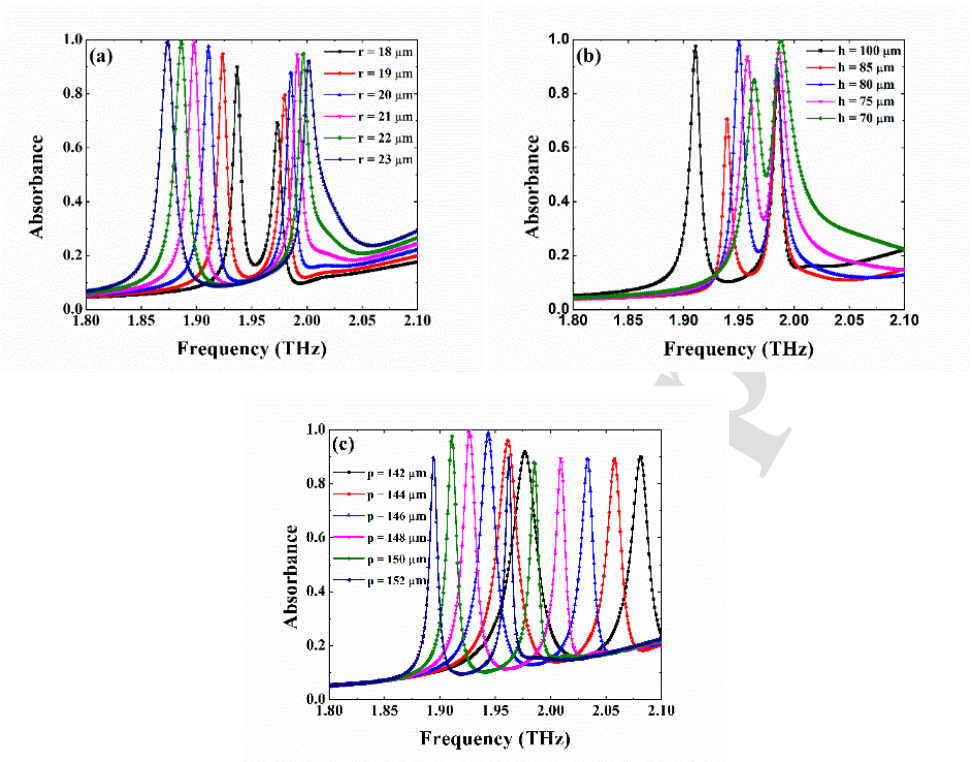

Fig.4: The simulated absorption spectra for the varying (a) radius (r) and (b) height (h) of the micro-rod and (c) period of the of proposed metasurface at 300 K.

By considering LC model, the resonance frequency of DBM is calculated by the given expression [41,42]:

$$f_0 = \frac{1}{2\pi\sqrt{LC}} = \frac{c}{\pi r\sqrt{ABh\varepsilon_r}} \tag{3}$$

where $L = \frac{A\mu_0 dh}{2}$ is equivalent inductance, $C = \frac{B\varepsilon_0\varepsilon_r r^2}{2d}$ is equivalent capacitance, r is the radius and h is the height of resonator structure, A and B are numerical factors, c is the speed of light in free space, d is the distance between adjacent micro-rod, ε_r is the relative dielectric constant of the surrounding environment. When the relative dielectric constant of the surrounding environment and the geometry of resonator structure change, the resonance frequency of proposed DBM sensor will get affected. Obviously, when radius r increases, the distance between adjacent micro-rod decreases and the equivalent capacitance C increases resulting in red-shift of first resonance frequency peak as shown in Fig. 4(a). However, for the second resonant mode at higher frequency, a minor blue shift arises due to near field coupling between air and resonator structure.

The Fig. 4(b) shows the resonance behaviour of the proposed DBM structure with different heights of micro-rod (h = 100 μm, 85 μm, 80 μm, 75 μm, 70 μm). In this case, both resonance frequencies are red shifted

Journal Pre-proof

with increasing h , this is due to increase of equivalent inductance L when height h is increased as confirmed by the LC model.

The resonance behaviour of proposed DBM with respect to the period variation is shown in Fig. 4(c). The shifting of peaks with the variation of a period can be explained by using LC model. When the period decreased, the gap between adjacent unit cells will increase and then the capacitance between adjacent unit cells will decrease. So, the resonance frequency will shift towards a higher value [43,44]. When the period increases, the interference between unit cells will decrease and so the radiation loss will decrease. Thus, FWHM will decrease. The lower value of FWHM is required for high sensing devices, therefore, optimized value for the period of DBM is taken as 150 μm.

3.3 DBM as Temperature Sensor

As complex permittivity of InSb vary with changing the temperature, it is also possible to alter the resonance properties of the DBM by changing the external environment temperature. Thus, the proposed DBM can be served as temperature sensor. Fig. 5(a) gives the absorbance of the suggested DBM under different external surrounding temperatures (T = 290 K, 292 K, 294 K, 296 K, 298 K, 300 K). It has been observed that as the temperature rises, the both resonance frequencies exhibit an obvious blue shift, which is due to the inverse relationship between InSb permittivity and temperature.

In order to evaluate the temperature sensing performance of the proposed DBM, we have defined temperature sensitivity as [45,46] $S = \Delta f / \Delta T$, where Δf is the resonance frequency shift and ΔT is the environment temperature variation corresponding to frequency shift per temperature unit (GHz/K). In Fig. 5(b), it is shown by solid fitted line that there is linear relation between resonance frequency of the DBM and external environment temperature. Further, it has been observed that the resonance frequency is shifted towards higher value with increasing the temperature which is caused by change of permittivity of InSb with temperature. It should also be noticed that the linearly fitted temperature sensitivity of proposed DBM is about 5.5 GHz/K and 7.5 GHz/K corresponding to resonance frequencies 1.911 THz and 1.985 THz respectively. This temperature sensitivity is primarily caused by effective excitations of the SPP resonance mode. Thus, it could be served as dual-band temperature sensor.

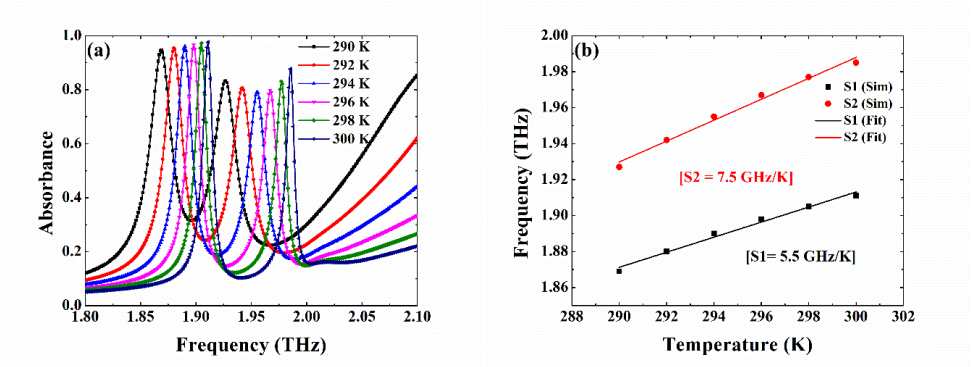

Fig.5: (a) The simulated absorption spectra of the proposed DBM for the varying external environment temperatures. (b) Fitting curve (solid line) and resonance frequencies variation (black and red symbols) with respect to external environment temperatures.

Journal Pre-proof

3.4 DBM as Refractive Index Sensor

In the following section, the variation of absorption spectra with respect to different RI values have been investigated to calculate the RI sensitivity. To analyse the RI sensing properties, glucose aqueous solution is employed as the analyte and air is used as the reference, both of which can diffuse completely in the surroundings of proposed DBM. The RI sensing performance of the proposed DBM is shown below in the Fig. 6(b).

The sensitivity (S_R) and figure of merit (FOM) are two key indicator of sensing performance which are defined as [14,47,48]

$$S_R = \frac{\Delta f}{\Delta n} \qquad FOM = \frac{S_R}{FWHM} \tag{4}$$

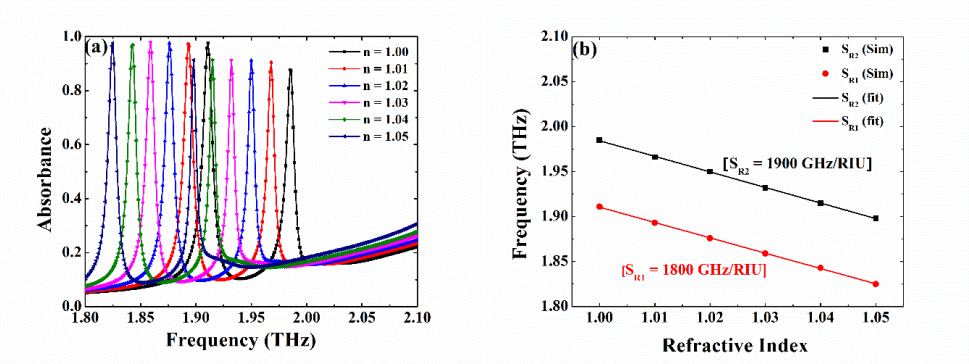

Fig.6: (a) Absorption spectra of the proposed DBM sensor using different RI values of the surrounding analyte. (b)The variation of simulated resonance frequency (square and circle symbols) and linear fitting (solid line) with different RI values of the surrounding analyte at 300 K.

From Fig. 6(a) it has been observed that when refractive index of surrounding analyte varies from 1.00 to 1.05, there is a red shift in absorption spectra. Fig. 6(b) illustrate the relationship between resonance frequency shift Δf and the change of RI values Δn of the analyte. Also, the resonance frequency of the suggested DBM decreases linearly with the increase of RI value of the analyte. Furthermore, it is also clarified that the bulk sensitivity S_{R1} and S_{R2} corresponding to the first and second resonance peak is about 1800 GHz/RIU and 1900 GHz/RIU respectively, which is obviously superior to the previously reported metasurface sensors [49][23][24][50]. Since FWHM of the proposed DBM is about 0.01096 THz, the FOM is about 164 and 173 corresponding to first and second resonance frequency respectively. Therefore, it could be believed that proposed DBM sensor provides a high RI sensitivity in the THz region.

In the presence of modern advance fabrication technology, one can have an on-demand response from the structural material. The proposed DBM sensor can be realized experimentally with electron beam lithography (EBL). EBL is one of the most sophisticated fabrication methods as it has the advantage of high resolution with high positioning accuracy [51].

4. Conclusion

A simple and effective design of ultrasensitive DBM sensor based on InSb micro-rod structure has been presented. It can be used as a temperature and RI sensor simultaneously. The results show that the proposed DBM has an absorbance of 98% and 91% at resonance frequencies of 1.911 THz and 1.985 THz respectively under room temperature. The corresponding Q factor is about 174.36 and 181.11. The electric field distribution generated from the simulation study is suggesting that the principal causes of absorption are intrinsic dielectric

Journal Pre-proof

loss of the structural InSb material and the excitation of SPP resonance mode. Furthermore, the change of geometric parameters of the InSb micro-rod structure has been shown to have a significant impact on the absorption performance of the proposed DBM sensor. The designed DBM is extremely sensitive to both the temperature and RI value of the surrounding. The proposed DBM can reach a sensitivity of about 5.5 GHz/K and 7.5 GHz/K respectively when it used as a temperature sensor. When the proposed DBM used as RI sensor it may achieve a high sensitivity of 1800 GHz/RIU and 1900 GHz/RIU respectively and corresponding FOM of about 164 and 173 can also be acquired. The presented study could be an alternative strategy for developing high-quality multi-function sensors for medical diagnostics, detection and biochemical sensing, owing to its high sensing performance.

Acknowledgments

Authors gratefully acknowledge the initiatives and support from TIFAC-Centre of Relevance and Excellence in Fiber Optics and Optical Communication at Delhi College of Engineering, now DTU, Delhi, under Mission REACH program of Technology Vision-2020, Government of India. One of the authors, Ms. Pooja Agarwal, would like to acknowledge, Dr. Yogita Kalra, DTU Delhi and Mr. Monu Nath Baitha of Yonsei University for valuable discussions on this research work.

Conflict of Interest

The authors have no conflicts of interest to disclose.

Data Availability

The data that support the findings of this study are available from the corresponding authors upon reasonable request.

References:

[1] M. Tonouchi, Cutting-edge terahertz technology, Nat. Photonics 2007 12. 1 (2007) 97–105. https://doi.org/10.1038/nphoton.2007.3.

[2] E. MacPherson, G.P. Gallerano, G.S. Park, H. Hintzsche, G.J. Wilmink, Guest editorial: Terahertz imaging and spectroscopy for biology and biomedicine, IEEE J. Biomed. Heal. Informatics. 17 (2013) 765–767. https://doi.org/10.1109/JBHI.2013.2257333.

[3] M. Beruete, I. Jáuregui-López, Terahertz Sensing Based on Metasurfaces, Adv. Opt. Mater. 8 (2020) 1–26. https://doi.org/10.1002/adom.201900721.

[4] N. Shankhwar, Y. Kalra, R.K. Sinha, LiTaO3 based metamaterial perfect absorber for terahertz spectrum, Superlattices Microstruct. 111 (2017) 754–759. https://doi.org/10.1016/J.SPMI.2017.07.034.

[5] B.X. Wang, Y. He, P. Lou, W. Xing, Design of a dual-band terahertz metamaterial absorber using two identical square patches for sensing application, Nanoscale Adv. 2 (2020) 763–769. https://doi.org/10.1039/C9NA00770A.

[6] Y. Cheng, H. Luo, F.U. Chen, R. Gong, Triple narrow-band plasmonic perfect absorber for refractive index sensing applications of optical frequency, OSA Contin. Vol. 2, Issue 7, Pp. 2113-2122. 2 (2019) 2113–2122. https://doi.org/10.1364/OSAC.2.002113.

[7] T. Chen, S. Li, H. Sun, Metamaterials Application in Sensing, Sensors 2012, Vol. 12, Pages 2742-2765. 12 (2012) 2742–2765. https://doi.org/10.3390/S120302742.

[8] A.A. Jamali, B. Witzigmann, Plasmonic Perfect Absorbers for Biosensing Applications, Plasmon. 2014 96. 9 (2014) 1265–1270. https://doi.org/10.1007/S11468-014-9740-1.

[9] I.E. Carranza, J.P. Grant, J. Gough, D. Cumming, Terahertz metamaterial absorbers implemented in CMOS technology for imaging applications: Scaling to large format focal plane arrays, IEEE J. Sel. Top. Quantum Electron. 23 (2017). https://doi.org/10.1109/JSTQE.2016.2630307.

[10] N. Liu, M. Mesch, T. Weiss, M. Hentschel, H. Giessen, Infrared perfect absorber and its application as plasmonic sensor, Nano Lett. 10 (2010) 2342–2348. https://doi.org/10.1021/NL9041033.

[11] X. Liu, T. Tyler, T. Starr, A.F. Starr, N.M. Jokerst, W.J. Padilla, Taming the blackbody with infrared metamaterials as selective thermal emitters, Phys. Rev. Lett. 107 (2011) 045901. https://doi.org/10.1103/PHYSREVLETT.107.045901/FIGURES/5/MEDIUM.

[12] N.I. Landy, S. Sajuyigbe, J.J. Mock, D.R. Smith, W.J. Padilla, Perfect metamaterial absorber, Phys. Rev. Lett. 100 (2008) 207402. https://doi.org/10.1103/PHYSREVLETT.100.207402/FIGURES/5/MEDIUM.

[13] H. Zhou, C. Yang, D. Hu, D. Li, X. Hui, F. Zhang, M. Chen, X. Mu, Terahertz biosensing based on bi-layer metamaterial absorbers toward ultra-high sensitivity and simple fabrication, Appl. Phys. Lett. 115 (2019) 143507. https://doi.org/10.1063/1.5111584.

Journal Pre-proof

[14] R. Yahiaoui, S. Tan, L. Cong, R. Singh, F. Yan, W. Zhang, Multispectral terahertz sensing with highly flexible ultrathin metamaterial absorber, J. Appl. Phys. 118 (2015) 083103. https://doi.org/10.1063/1.4929449.

[15] M. Aslinezhad, High sensitivity refractive index and temperature sensor based on semiconductor metamaterial perfect absorber in the terahertz band, Opt. Commun. 463 (2020) 125411. https://doi.org/10.1016/J.OPTCOM.2020.125411.

[16] H. Cai, S. Chen, C. Zou, Q. Huang, Y. Liu, X. Hu, Z. Fu, Y. Zhao, H. He, Y. Lu, Multifunctional Hybrid Metasurfaces for Dynamic Tuning of Terahertz Waves, Adv. Opt. Mater. 6 (2018) 1800257. https://doi.org/10.1002/ADOM.201800257.

[17] N. Yu, F. Aieta, P. Genevet, M.A. Kats, Z. Gaburro, F. Capasso, A broadband, background-free quarter-wave plate based on plasmonic metasurfaces, Nano Lett. 12 (2012) 6328–6333. https://doi.org/10.1021/NL303445U/SUPPL_FILE/NL303445U_SI_001.PDF.

[18] J.Y. Suen, K. Fan, W.J. Padilla, X. Liu, All-dielectric metasurface absorbers for uncooled terahertz imaging, Opt. Vol. 4, Issue 6, Pp. 601-604. 4 (2017) 601–604. https://doi.org/10.1364/OPTICA.4.000601.

[19] I. V. Shadrivov, K. Fan, W.J. Padilla, X. Liu, Experimental realization of a terahertz all-dielectric metasurface absorber, Opt. Express, Vol. 25, Issue 1, Pp. 191-201. 25 (2017) 191–201. https://doi.org/10.1364/OE.25.000191.

[20] M.A. Cole, D.A. Powell, I. V. Shadrivov, Strong terahertz absorption in all-dielectric Huygens' metasurfaces, Nanotechnology. 27 (2016) 424003. https://doi.org/10.1088/0957-4484/27/42/424003.

[21] X. Zhang, Z. Tian, W. Yue, J. Gu, S. Zhang, J. Han, W. Zhang, Broadband Terahertz Wave Deflection Based on C-shape Complex Metamaterials with Phase Discontinuities, Adv. Mater. 25 (2013) 4567–4572. https://doi.org/10.1002/ADMA.201204850.

[22] K.A. Willets, R.P. Van Duyne, Localized Surface Plasmon Resonance Spectroscopy and Sensing, Http://Dx.Doi.Org/10.1146/Annurev.Physchem.58.032806.104607. 58 (2007) 267–297. https://doi.org/10.1146/ANNUREV.PHYSCHEM.58.032806.104607.

[23] F. Chen, Y. Cheng, H. Luo, Temperature Tunable Narrow-Band Terahertz Metasurface Absorber Based on InSb Micro-Cylinder Arrays for Enhanced Sensing Application, IEEE Access. 8 (2020) 82981–82988. https://doi.org/10.1109/ACCESS.2020.2991331.

[24] Y. Cheng, Z. Li, Z. Cheng, Terahertz perfect absorber based on InSb metasurface for both temperature and refractive index sensing, Opt. Mater. (Amst). 117 (2021). https://doi.org/10.1016/j.optmat.2021.111129.

[25] H. Luo, X. Wang, H. Qian, Tunable terahertz dual-band perfect absorber based on the combined InSb resonator structures for temperature sensing, J. Opt. Soc. Am. B. 38 (2021) 2638. https://doi.org/10.1364/josab.433122.

[26] S.-X. Xia, X. Zhai, L.-L. Wang, S.-C. Wen, Plasmonically induced transparency in double-layered graphene nanoribbons, Photonics Res. 6 (2018) 692. https://doi.org/10.1364/prj.6.000692.

[27] J. Guan, S. Xia, Z. Zhang, J. Wu, H. Meng, J. Yue, X. Zhai, L. Wang, S. Wen, Two Switchable Plasmonically Induced Transparency Effects in a System with Distinct Graphene Resonators, Nanoscale Res. Lett. 15 (2020) 1–13. https://doi.org/10.1186/s11671-020-03374-1.

[28] T. Wang, Y. Zhang, Y. Zhang, H. Zhang, M. Cao, M. Cao, Dual-controlled switchable broadband terahertz absorber based on a graphene-vanadium dioxide metamaterial, Opt. Mater. Express, Vol. 10, Issue 2, Pp. 369-386. 10 (2020) 369–386. https://doi.org/10.1364/OME.383008.

[29] X. Zhao, Y. Wang, J. Schalch, G. Duan, K. Cremin, J. Zhang, C. Chen, R.D. Averitt, X. Zhang, Optically Modulated Ultra-Broadband All-Silicon Metamaterial Terahertz Absorbers, ACS Photonics. 6 (2019) 830–837. https://doi.org/10.1021/ACSPHOTONICS.8B01644/SUPPL_FILE/PH8B01644_SI_001.PDF.

[30] H. Zou, Y. Cheng, Design of a six-band terahertz metamaterial absorber for temperature sensing application, Opt. Mater. (Amst). 88 (2019) 674–679. https://doi.org/10.1364/OSAC.2.002113.

[31] M. Oszwałldowski, M. Zimpel, Temperature dependence of intrinsic carrier concentration and density of states effective mass of heavy holes in InSb, J. Phys. Chem. Solids. 49 (1988) 1179–1185. https://doi.org/10.1016/0022-3697(88)90173-4.

[32] W. Li, D. Kuang, F. Fan, S. Chang, L. Lin, Subwavelength B-shaped metallic hole array terahertz filter with InSb bar as thermally tunable structure, Appl. Opt. Vol. 51, Issue 29, Pp. 7098-7102. 51 (2012) 7098–7102. https://doi.org/10.1364/AO.51.007098.

[33] J. Zhu, J. Han, Z. Tian, J. Gu, Z. Chen, W. Zhang, Thermal broadband tunable Terahertz metamaterials, Opt. Commun. 12 (2011) 3129–3133. https://doi.org/10.1016/J.OPTCOM.2011.02.038.

[34] P. Halevi, F. Ramos-Mendieta, Tunable Photonic Crystals with Semiconducting Constituents, Phys. Rev. Lett. 85 (2000) 1875. https://doi.org/10.1103/PhysRevLett.85.1875.

[35] R.W. Cunningham, J.B. Gruber, Intrinsic concentration and heavy-hole mass in InSb, J. Appl. Phys. 41 (1970) 1804–1809. https://doi.org/10.1063/1.1659107.

[36] F. Qin, Z. Chen, X. Chen, Z. Yi, W. Yao, T. Duan, P. Wu, H. Yang, G. Li, Y. Yi, A Tunable Triple-Band Near-Infrared Metamaterial Absorber Based on Au Nano-Cuboids Array, Nanomaterials. 10 (2020) 207. https://doi.org/10.3390/NANO10020207.

[37] H. Raether, G. Hohler, E.A. Niekisch, Surface Plasmons on Smooth and Rough Surfaces and on Gratings, Springer Tracts Mod. Phys. 111 (1988) 136. https://doi.org/10.1007/BFB0048317.

[38] K.R. Carver, J.W. Mink, Microstrip Antenna Technology, IEEE Trans. Antennas Propag. 29 (1981) 2–24. https://doi.org/10.1109/TAP.1981.1142523.

[39] N. Engheta, Circuits with Light at Nanoscales: Optical Nanocircuits Inspired by Metamaterials, Science (80-.). 317 (2007) 1698–1702. https://doi.org/10.1126/SCIENCE.1133268.

[40] L.P. Wang, Z.M. Zhang, Resonance transmission or absorption in deep gratings explained by magnetic polaritons, Appl. Phys. Lett. 95 (2009) 111904. https://doi.org/10.1063/1.3226661.

[41] W.J. Padilla, A.J. Taylor, C. Highstrete, M. Lee, R.D. Averitt, Dynamical electric and magnetic metamaterial response at terahertz frequencies, Phys. Rev. Lett. 96 (2006) 107401. https://doi.org/10.1103/PHYSREVLETT.96.107401/FIGURES/3/MEDIUM.

[42] Y. Cheng, Y. Nie, R. Gong, A polarization-insensitive and omnidirectional broadband terahertz metamaterial absorber based on coplanar multi-squares films, Opt. Laser Technol. 48 (2013) 415–421. https://doi.org/10.1016/J.OPTLASTEC.2012.11.016.

[43] B.X. Wang, X. Zhai, G.Z. Wang, W.Q. Huang, L.L. Wang, A novel dual-band terahertz metamaterial absorber for a sensor application, J. Appl. Phys. 117 (2015) 014504. https://doi.org/10.1063/1.4905261.

[44] Z. Ma, F. Ding, Ultra-broadband metamaterial absorber in terahertz regime, 11 (2014) AF4A.25. https://doi.org/10.1364/acpc.2012.af4a.25.

[45] H. Luo, Y. Cheng, Thermally tunable terahertz metasurface absorber based on all dielectric indium antimonide resonator structure, Opt. Mater. (Amst). 102 (2020) 109801. https://doi.org/10.1016/J.OPTMAT.2020.109801.

[46] W. Li, Y. Cheng, Dual-band tunable terahertz perfect metamaterial absorber based on strontium titanate (STO) resonator structure, Opt. Commun. 462 (2020) 125265. https://doi.org/10.1016/J.OPTCOM.2020.125265.

[47] P. Rodríguez-Ulibarri, S.A. Kuznetsov, M. Beruete, Wide angle terahertz sensing with a cross-dipole frequency selective surface, Appl. Phys. Lett. 108 (2016) 111104. https://doi.org/10.1063/1.4944326.

Journal Pre-proof

[48] R. Singh, W. Cao, I. Al-Naib, L. Cong, W. Withayachumnankul, W. Zhang, Ultrasensitive terahertz sensing with high-Q Fano resonances in metasurfaces, Appl. Phys. Lett. 105 (2014) 171101. https://doi.org/10.1063/1.4895595.

[49] L. Zhu, L. Zhu, H. Li, L. Dong, L. Dong, W. Zhou, M. Rong, X. Zhang, J. Guo, Dual-band electromagnetically induced transparency (EIT) terahertz metamaterial sensor, Opt. Mater. Express, Vol. 11, Issue 7, Pp. 2109-2121. 11 (2021) 2109–2121. https://doi.org/10.1364/OME.425126.

[50] K. Zhang, T. Ma, J. Liu, X. Tian, J. Zhu, C. Tan, Dynamically tunable and polarization-insensitive dual-band terahertz metamaterial absorber based on TiNi shape memory alloy films, Results Phys. 23 (2021) 104001. https://doi.org/10.1016/j.rinp.2021.104001.

[51] H. Mei, W. Yang, D. Yang, L. Yao, Y. Yao, C. Chen, L. Cheng, Metamaterial absorbers towards broadband, polarization insensitivity and tunability, Opt. Laser Technol. 147 (2022). https://doi.org/10.1016/j.optlastec.2021.107627.

Journal Pre-proof

Journal Pre-proof

Highlights

- Terahertz (THz) metasurface sensors have recently received considerable attention due to its sensing applications.
- A dual-band metasurface (DBM) sensor has been proposed based on all Indium Antimonide (InSb) that can simultaneously work as a temperature and refractive index (RI) sensor in the THz region.
- The proposed DBM shows high Q factor of 174.36 and 181.11 corresponding to the resonance frequencies 1.911 THz and 1.985 THz respectively.
- The sensitivity is 1800 GHz/RIU and 1900 GHz/RIU respectively when it is used as refractive index sensor. Due to extraordinary sensing performance and high Q value, dual-band sensor could be believed to have great potential application in chemical and biological sensing related areas.
- The proposed simple and effective design of ultrasensitive DBM sensor could be an alternative strategy for developing high-quality multi-function sensors for medical diagnostics, detection and biochemical sensing.

Journal Pre-proof

Journal Pre-proof

Declaration of interests

☒ The authors declare that they have no known competing financial interests or personal relationships that could have appeared to influence the work reported in this paper.

☐The authors declare the following financial interests/personal relationships which may be considered as potential competing interests:

Journal Pre-proof

Proceedings of the Sixth International Conference on Intelligent Computing and Control Systems (ICICCS 2022)
IEEE Xplore Part Number: CFP22K74-ART; ISBN: 978-1-6654-1035-9

2022 6th International Conference on Intelligent Computing and Control Systems (ICICCS) | 978-1-6654-1035-9/22/$31.00 ©2022 IEEE | DOI: 10.1109/ICICCS53718.2022.9788330

Underwater Image Enhancement with Feature Preservation using Generative Adversarial Networks (UIEFP GAN)

Dr. Aruna Bhat
Delhi Technological University
New Delhi, India
aruna.bhat@dtu.ac.in

Yogesh Narang
Delhi Technological University
New Delhi, India
yogeshnarang_2k18co407@dtu.ac.in

Yogesh Goyal
Delhi Technological University
New Delhi, India
yogeshgoyal_2k18co406@dtu.ac.in

Abstract* - *Exploration of the ocean's resources has recently been of significant importance on the world stage as it facilitates functioning in various domains including marine biology, marine archaeology, AUV navigation etc. However, a major problem is that underwater images are usually of sub-optimal quality, having traits such as low brightness, low contrast, high noise and the image is usually blurry with an uneven color composition. This paper presents a GAN based model to perform enhancement on underwater images. The proposed UIEFP GAN model has been inspired by the pix2pix GAN architecture, wherein a patchGAN based discriminator and a encoder-decoder network based generator are used. An enhanced loss function is also proposed to train the network, that focusses on both, local and global feature preservation during image enhancement. The EUVP dataset has been used for training the model.

Keywords* - *Underwater Image Enhancement, Pix2Pix GAN, PatchGAN, Encoder Decoder Network

I. INTRODUCTION

Ocean Exploration is of extreme importance because it supports various research domains such as marine biology, underwater navigation, underwater resource exploration, etc. A major problem with underwater exploration is the fact that images or video recorded underwater is usually of sub-optimal quality. Underwater images usually suffer some of the following traits - low or uneven brightness, extremely low contrast, and high noise in the image. This makes raw underwater images non-ideal for high level computer vision tasks that rely on data comprising of these images. For certain underwater image enhancement situations, like underwater navigation for AUVs, the time frame for enhancement is critical, and requires real time enhancement as discussed in [1].

Previously, researchers have made a lot of effort in developing algorithms and models for enhancing underwater pictures. This enhancement is usually used in the pre-processing stage for major machine learning tasks such as image detection in underwater video clips, autonomous underwater navigation and so on. Hence, it is of extreme importance in developing a pipeline or model for enhancing underwater image or video content. The aim is to reverse the effect of color casts and scattering of light in water - resulting in a much more appealing image that is better suited for high-level vision tasks.

In this text, we have proposed a conditional GAN based model that is used to enhance underwater images. The model has been inspired by the pix2pix GAN architecture and has been trained on the EUVP dataset of over 20K images. The proposed UIEFP GAN model, a fully-convolutional conditional GAN, is able to remove noise from the input images, remove color casts and tints, and also reverses the effects of inconsistent light diffusion to a great extent. The resulting image is much more suited for higher-level computer vision tasks. The generator of the model takes a sub-optimal degraded low quality image as input and returns a much higher quality image. We also propose a more comprehensive loss function that preserves both global and local features during image regeneration. The model is trained on the paired EUVP dataset and generates enhanced versions of underwater images which are sharper, and void of green and blue color casts.

1. Problems with Underwater Images

This section covers the problems that persist in traditional underwater images in detail.

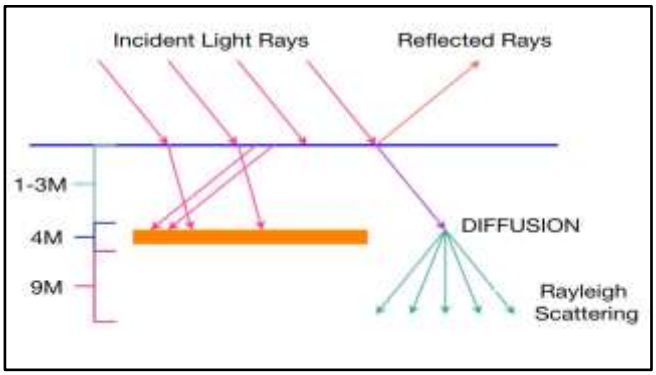

Fig. 1. Diffusion and crinkle patterns [4]

Despite using very high quality cameras, underwater images are of sub-optimal quality because of low visibility, light scattering, light reflection, uneven illumination and light absorption [2] [3]. While capturing underwater images, sea structure greatly affects the intensity of light reflection, since the amount of light absorbed results either in diffusion or crinkle patterns as shown in Fig 1.

Authorized licensed use limited to: DELHI TECHNICAL UNIV. Downloaded on June 15,2022 at 11:26:56 UTC from IEEE Xplore. Restrictions apply.

Density of water inside the sea is considered to be 700-900 times denser as compared to the density of water in air, which leads to another major problem that persists in underwater images. So, the amount of light entering water at a given depth is inversely proportional to the depth of sea which results in darker and dull images as the depth of sea increases. Even the intensity of different colors fade away depending on the depth of sea and color wavelength. For example, yellow color mostly disappears near 9-18m of sea depth.

II. RELATED WORK

The following section covers a brief overview of various studies and techniques that are used for enhancing underwater image and video content. The techniques for enhancement can be categorized as Model Free Methods like dehazing techniques and Model Based Methods like WaterGAN, UGAN etc as described by N.Singh and A.Bhat [11].

2. A. Dehazing Techniques

Dehazing is extremely important for underwater images since a majority of underwater images are hazy in nature. Hazing takes place because of small floating particles that are present in the ocean which causes uneven scattering of light. Dehazing plays a crucial role in situations where images are highly degraded because of unavoidable environmental conditions.

A CycleGAN based approach has been proposed by Lu et al. [5] (MCycleGAN). This technique uses a dark channel prior (DCP) [6] to get information related to the depth parameters in the image. This technique is adaptive in nature and works so well because it accounts for the fact that every image present in a dataset may be clicked from a different depth. This approach also proposed a unique multi-scale similarity index to improve underwater image enhancement.

3. B. Histogram Manipulation for Contrast Enhancement

Histogram manipulation proposed in [7] by Simon et al. offers a unique method for contrast enhancement in degraded images. This is performed by manipulating the histogram of the input image, resulting in an image where much finer details can also be recognized.

The proposed method is an extensive one that performs white balancing, sharpening, histogram equalization, gamma correction, CLAHE, followed by fusion from two different channels in the pipeline resulting in the output image.

White balancing is done to remove color casts in underwater images, as it is usually noticed that underwater images tend to have a greenish or bluish tint to them because other components in light are absorbed more as compared to the bluish wavelengths. The image further undergoes sharpening, luminance enhancement, and histogram linearisation.

Weight maps are generated for the images received from the two different channels and undergo fusion to form the output image. The fusion process is based on the Laplacian Pyramid, where the images undergo multiple passes and upsampling in each layer resulting in an overall enhanced image which is a summation of the contribution of each level.

4. C. WaterGAN

WaterGAN is a generative adversarial network proposed by Jie et al. [8] that is aimed at generating realistic underwater images. The proposed model is trained on images captured in air along with their depth information and is aimed at correcting the color distribution of these images.

The proposed pipeline first generates real-world in-air images with their corresponding depth maps and uses it as an input to a two-part machine learning model which is then used for correcting the color distribution in underwater images. WaterGAN has been trained on an unpaired dataset wherein the problem statement is treated as an unsupervised learning problem.

The discriminator network in WaterGAN uses a CNN based model. The initial size for the images in the discriminator is 48 * 64 * 3. The input goes through multiple convolutional layers where the input is downsampled by a factor of 2 on each layer. The kernel size used in the discriminator is 5 X 5. The output layer in the discriminator uses sigmoid activation and outputs either of the classification labels - Real or Synthetic.

The color restoration portion of the pipeline uses encoder-decoder networks that are employed for dense learning as used in SegNet along with a new upsampling layer in the network. The depth estimation portion of the pipeline takes an image of resolution 56 X 56 X 3 and produces a relative depth map of 56 X 56 X 1 dimension which is later upsampled to 480 * 480 and acts as an input for the color correction phase.

The first half of the pipeline accounts for relative depth estimation in the images, and the second part of the pipeline is a novel color correction system that also accounts for different water columns in a specific location. The model pipeline also uses a skipping layer approach to upsample the image before the final output - resulting in a 512 * 512 image.

5. D. UGAN (Underwater GAN)

UGAN is a GAN based model proposed by Cameron et al. [9] that uses a two step approach to first generate data using a cycleGAN and then trains a fully convolutional GAN to restore and enhance underwater images.

Uniquely, UGAN proposes the use of a cycleGAN as a model for distortion, with the aim of generating a paired dataset of images. If a cycleGAN is trained on a paired dataset, representing degraded and enhanced images, the model is capable of performing the process of transfer of style between images belonging to different domains. Similarly, if we give a clear image to a cycleGAN, it can learn to distort the image, with the end result being the generation of a paired dataset that is later used for image enhancement. This is possible purely because when a cycleGan is learning the mapping $\boldsymbol{F: A \rightarrow B}$, it also learns a mapping $\boldsymbol{G: B \rightarrow A}$.

The generator in UGAN is a convolutional encoder-decoder network inspired by Phillip et al, [10]. The generator uses an encoder to downsample the image via lower-dimensional embeddings which is later upsample by the decoder to reconstruct an image of a much higher quality as compared to the input image. Contrary to previous approaches, UGAN uses

Authorized licensed use limited to: DELHI TECHNICAL UNIV. Downloaded on June 15,2022 at 11:26:56 UTC from IEEE Xplore. Restrictions apply.

a discriminator which is modeled as a PatchGAN [10] that performs on the level of image patches and not on the image as a whole.

UGAN performs the task of color recovery and correction extremely well as shown in the above diagram. Moreover, in comparison to traditional cycleGANs, the proposed model provides results that are superior in terms of color correction, image sharpening and dehazing.

6. *E. UWGAN (Underwater GAN) - Multiscale Dense GAN*

UWGAN addresses the problem of distortion of color and uneven color distribution, fuzz notices in underwater images. The proposed model presents a multi-scale dense block in the generator, where residual learning boosts the performance of the model producing higher quality upgraded images.

The discriminator in the proposed model uses lightweight spectral normalization to stabilize its training. The paper also proposes a deep residual framework for a better optimisation process for the networks. The generator model employs dense blocks for better feature propagation throughout the model.

The proposed model's performance is measured using UIQM and UISM, and the results denote a superior performance as compared to other generative models such as UGAN[9] and CycleGAN.

III. EXPERIMENTAL DESIGN

7. *A. Dataset*

The dataset used for our research purposes is the EUVP (Enhancing Underwater Visual Perception) dataset [12] which contains over 20K underwater images categorized as low/distorted quality and superior/high quality images. The distinction between the images and their enhanced counterparts was based on different image properties including the color, texture, sharpness and contrast.

The dataset is divided into two parts. One part contains around 12K paired underwater images. Each pair consists of a blurry image along with its enhanced version which has the potential to be used for supervised image conversion and translation tasks, such as image translation using Pix2PixGAN. Sample paired images from the dataset are shown in Fig 2. Second part contains around 8K unpaired underwater images which can be used for unsupervised image translation or conversion tasks, such as image translation using CycleGAN.

The paired dataset was created by the original authors by taking high quality real world images during ocean exploration and distorting these images for generating their distorted counterparts using a CycleGAN based model.

Fig. 2. Sample Paired Images from the "EUVP" Dataset

8. *B. Architecture*

Given a paired dataset of images, containing a list of degraded poor quality images, say A, and corresponding high-quality images, say B, the task at hand is to develop a GAN based model that learns the mapping $F: A \rightarrow B$, such that the model is able to perform image enhancement on underwater images.

We propose a GAN-based (UIEFP GAN) model where the generator in the model learns this mapping by being trained adversarially in a repeated min-max game with the discriminator while also preserving the global features in the image as well as the local features.

The proposed pipeline consists of the generator and the discriminator, that are trained together using the paired EUVP dataset. The model has been inspired by U-Net [13] and Pix2Pix [14].

The model is trained in the following manner. Inside the training loop iterating on the dataset, firstly the generator is given a set of distorted images and it generates its counterparts. The discriminator network is then trained on these pairs of images. In the second half of the training loop, the generator is trained such that it tries to minimize the loss that denotes the error between the image it generates and the target image. While calculating the error between the generated and target image, we use the loss function proposed below in the text.

9. *The Generator*

As mentioned above, the generator architecture is inspired from U-Net [13] and uses an encoder-decoder network containing skip connections as depicted in Fig 3.

Authorized licensed use limited to: DELHI TECHNICAL UNIV. Downloaded on June 15,2022 at 11:26:56 UTC from IEEE Xplore. Restrictions apply.

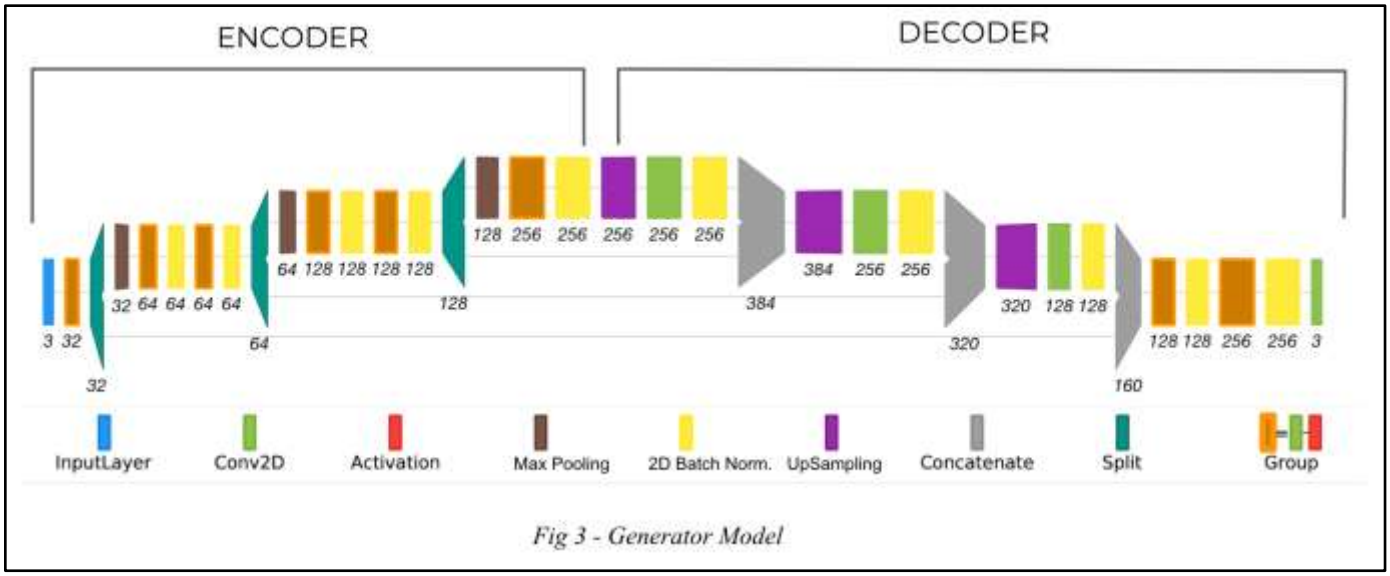

Fig 3 - Generator Model

The architecture comprises of an encoder network which is fully convolutional due to the absence of any fully connected layers. The input to the encoder is a 256 X 256 X 3 image and the network learns over 256 feature maps of size 32 X 32. Each convolutional layer in the encoder network uses a 3X3 or 4X4 filter, stride of size [1,1], a 'relu' activation layer followed by a batch normalization layer. Since stride of only [1,1] is used, the network also consists of 3 MaxPooling layers of pool size [2,2] after every second conv2D layer to downsample the image.

The decoder part of the network utilizes the feature maps generated by the encoder and also utilizes skip connections which have been shown to be very effective. The decoder consists of five convolution layers (d1-d5) where d1-d3 use skip connections from the encoder. The convolutional layers in the decoded upsample the image by a factor of two at three consecutive layers, wherein the final layer in the decoder returns a 256 X 256 X 3 image which is a superior counterpart of the input image.

10. The Discriminator

The discriminator is inspired from the Pix2Pix GAN [14] and uses a Patch GAN architecture, as shown in Fig 4. PatchGAN distributes the image into patches of fixed sizes. This discriminator assumes that pixels present in separate patches are independent of each other and the model discriminates only on information present at the patch level.

PatchGAN architecture maps a 256 X 256 input image to an N X N vector of outputs V, where V[i][j] depicts whether the [i][j]th patch of the image is real or fake.

PatchGAN works for this use-case because it helps to discriminate based on features such as style and local-texture. This model is much more efficient as it discriminates on patch level and thus also extremely efficient as compared to a discriminator that discriminates on the image as a whole.

The discriminator has 4 convolutional layers which convert the input to a 16 X 16 output matrix that signifies average validity as given by the model. Every convolution layer has filters of size 3 X 3 with a [2,2] stride followed by activation(relu) and batch normalization.

11. Loss Function

The Loss function used in the proposed model is a variation of the Wasserstein Loss that also accounts for local feature preservation in the model. The loss function that ensures global similarity of images is the Wasserstein loss given by-

$$GlobalLoss\,(D) = D(B) - D(G(A)) \quad (1)$$

where A represents the input image dataset, B represents the target dataset, D(x) represents the discriminator's output for input x, G(x) represents the output of the generator with input x.

The proposed model adds another portion to this loss function that preserves local features as well. This is done using the help of the VGG-19 pre-trained network where we use the output from a layer of the pre-trained model, which helps us in deriving a feature matrix from the image.

Authorized licensed use limited to: DELHI TECHNICAL UNIV. Downloaded on June 15,2022 at 11:26:56 UTC from IEEE Xplore. Restrictions apply.

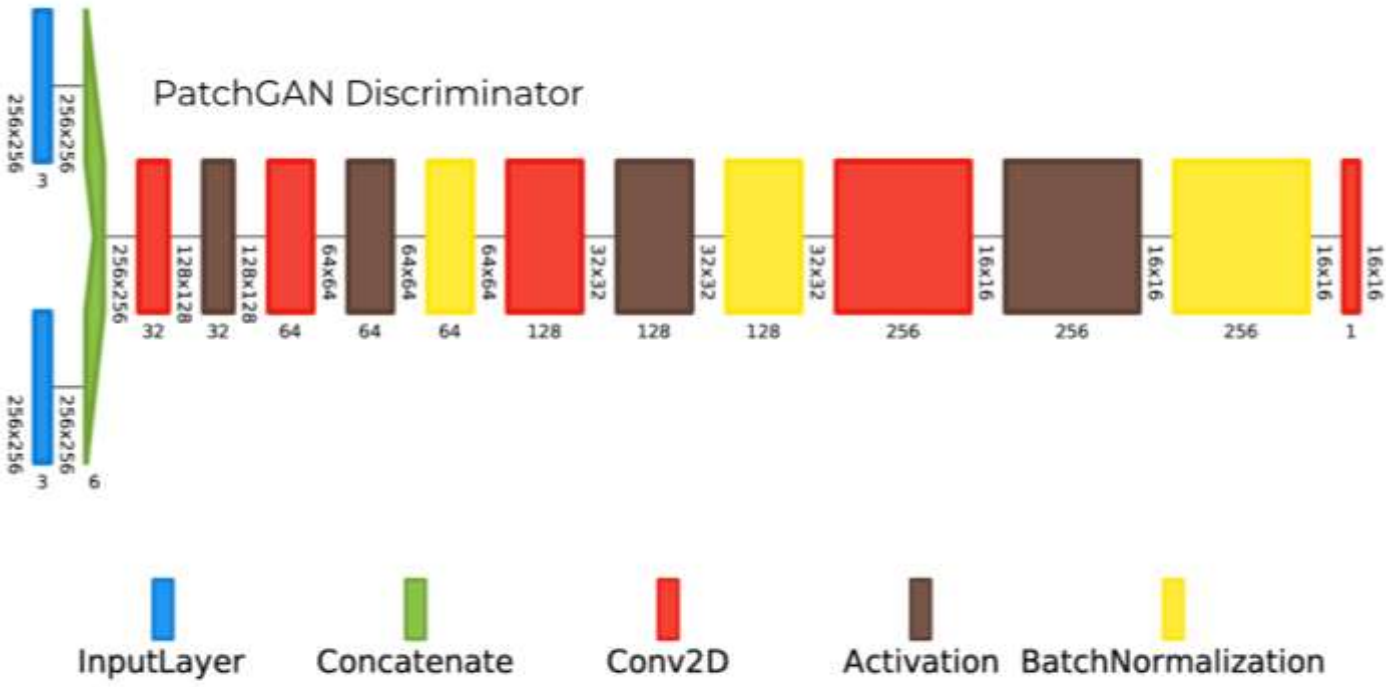

Fig 4 - Discriminator Model

We have proposed a new technique for the calculation of loss function as follows -

12. Calculation of Total Loss

global_loss = $D(B) - D(G(A))$

features_target = V(B)
features_gen = V(G(A))
features_difference = features_target - features_gen
feature_preservation_loss = mse(features_difference)

total_loss =
0.5*global_loss + 0.5*feature_preservation_loss

where A represents the input image dataset, B represents the target dataset, G(x) represents the output from the generator with input x and V(x) represents the output from the VGG-19 layer that represents the feature matrix

The total loss is given by a summation of the global loss and the feature preservation loss where the discriminator tries to maximize this and the generator tries to minimize this loss.

This loss helps in preserving local features in the following manner. The output matrices derived from the pre-trained network represent feature-matrices for both the generated and target images. The feature preservation loss in the total loss is given by taking the mean squared error on the difference of these two matrices. This essentially translates to minimizing the difference of features between the target and generated images.

After analyzing the performance on various hyperparameters, the best results were obtained with the following parameters. We trained the model for 100 epochs with a batch size of 4 and used the Adam optimizer with learning rate as 0.0004 and beta_1 as 0.5 .

13. C. Evaluation Metrics

To evaluate the proposed UIEFP GAN model, we used the following two quantitative evaluation metrics.

14. Structural Similarity Index Measure - SSIM

The SSIM is an evaluation method to compare and measure the resemblance between paired images. SSIM works under a condition that the quality of image being measured is done with respect to an enhanced quality image.

SSIM measures image quality based on these important properties - Contrast, Luminance and Structure of the image.

SSIM index is calculated as follows :

$$SSIM(x,y) = \frac{(2\mu_x\mu_y + C_1)(2\sigma_{xy} + C_2)}{(\mu_x^2 + \mu_y^2 + C_1)(\sigma_x^2 + \sigma_y^2 + C_2)} \quad (2)$$

where, μx and μy are the respective mean, σ2x and σ2y are the respective variance, σxy denotes the covariance between x and y. C1 and C2 are constants with values C1 = (255 × 0.01)2 and C2 = (255 × 0.03)2 respectively.

Authorized licensed use limited to: DELHI TECHNICAL UNIV. Downloaded on June 15,2022 at 11:26:56 UTC from IEEE Xplore. Restrictions apply.

15. Peak Signal-to-Noise Ratio - PSNR

PSNR compares image quality of generated image and original image based on Mean Squared Error (MSE). PSNR is a logarithmic entity represented on the decibel(dB) scale. PSNR is calculated as follows :

$$PSNR(x,y) = 10log_{10}[255^2/MSE(x,y)] \quad (3)$$

where, x is the generated image, y is the original image and MSE(x,y) is Mean Squared Error between them.

IV. RESULTS AND ANALYSIS

Training the proposed UIEFP GAN model on the EUVP paired dataset on over 100 epochs produces the results as depicted in Fig 5. As per observation, the input's quality is drastically enhanced in the produced output exhibiting much better sharpness and white balance. The output is also void of green and blue color casts that dominate the input image.

Fig. 5. Results of the trained model – The left portion of each image represents the input image(underwater), and the right portion represents the enhanced version produced by the generator.

A comparison on the evaluation of the model is done based on the SSIM and PSNR values as shown in Table 1. We analyzed the performance of our algorithm using SSIM and PSNR values, by looping over the test set of over 250 images, calculating the metric values and then the mean and standard deviation for these distributions. As observed from the table below, the model performs better as compared to the existing models on the basis of PSNR value and second-best on the basis of the SSIM value.

TABLE I. COMPARISON OF PROPOSED UIEFP GAN MODEL WITH EXISTING UNDERWATER IMAGE ENHANCEMENT TECHNIQUES BASED ON SSIM AND PSNR

Model	*SSIM (G(a),b) Input: 0.62 ± 0.075 (Mean ± S.D)*	*PSNR (G(a),b) Input: 17.27 ± 2.88 (Mean ± S.D)*
Uw-HL	0.7722 ± 0.066	18.85 ± 1.76
Mband-EN	0.4565 ± 0.097	12.11 ± 2.55
Res-WGAN	0.5762 ± 0.014	16.46 ± 1.80
Res-GAN	0.4685 ± 0.122	14.75 ± 2.22
LS-GAN	0.6725 ± 0.062	17.83 ± 2.88
Pix2Pix	0.7081 ± 0.069	20.27 ± 2.66
UGAN-P	0.6685 ± 0.075	19.59 ± 2.54
CycleGAN	0.6400 ± 0.080	17.14 ± 2.65
UIEFP GAN*	0.8218 ± 0.0409	**22.3884 ± 2.258**
FUnIE-GAN	**0.8876 ± 0.068**	21.92 ± 1.07

a.

V. CONCLUSION & FUTURE WORK

The model performs better as compared to the existing models on the basis of PSNR value and second-best on the basis of the SSIM value.

For the future scope of the project, we plan on using the unpaired samples of the EUVP dataset and develop a cycleGAN model that is capable of performing image translation on underwater images.

Future scope of the project also includes research on whether the same model can be trained to generate images of variable or dynamic resolutions and not just a fixed pre-decided resolution.

To improve the clarity of the images produced by the proposed model, we plan on incorporating a super-resolution GAN which has the capabilities of increasing the resolution while maintaining the integrity of the image.

We also plan on comparing existing models with our proposed model using the evaluation metrics mentioned above, so as to be able to compare and determine the performance of the proposed model.

REFERENCES

[1] A. Bhat, A. Tyagi, A. Verdhan and V. Verma, "Fast Under Water Image Enhancement for Real Time Applications," 2021 6th International Conference for Convergence in Technology (I2CT), 2021, pp. 1-8, doi: 10.1109/I2CT51068.2021.9417963.

[2] Md Jahidul Islam, Youya Xia, & Junaed Sattar. (2020), "Fast Underwater Image Enhancement for Improved Visual Perception".

[3] Iqbal, Kashif & Abdul Salam, Rosalina & Azam, Osman & Talib, Abdullah. (2007), "Underwater Image Enhancement Using an Integrated Colour Model. IAENG International Journal of Computer Science".

[4] Cherian, A.K.; Poovammal, E.; Philip, N.S.; Ramana, K.; Singh, S.; Ra, I.-H, "Deep Learning Based Filtering Algorithm for Noise Removal in Underwater Images. Water 2021, 13, 2742".

Authorized licensed use limited to: DELHI TECHNICAL UNIV. Downloaded on June 15,2022 at 11:26:56 UTC from IEEE Xplore. Restrictions apply.

[5] Jingyu Lu, Na Li, Shaoyong Zhang, Zhibin Yu, Haiyong Zheng, Bing Zheng "Multi-scale adversarial network for underwater image restoration", Optics & Laser Technology Volume 110, 2019.

[6] Kaiming He, Jian Sun and Xiaoou Tang, "Single image haze removal using dark channel prior," 2009 IEEE Conference on Computer Vision and Pattern Recognition, 2009, pp. 1956-1963, doi: 10.1109/CVPR.2009.5206515.

[7] Sangeetha Mohan, Philomina Simon, "Underwater Image Enhancement based on Histogram Manipulation and Multiscale Fusion, Procedia Computer Science".

[8] J. Li, K. A. Skinner, R. M. Eustice and M. Johnson-Roberson, "WaterGAN: Unsupervised Generative Network to Enable Real-Time Color Correction of Monocular Underwater Images," in IEEE Robotics and Automation Letters, vol. 3, no. 1, pp. 387-394, Jan. 2018, doi: 10.1109/LRA.2017.2730363.

[9] Cameron Fabbri, Md Jahidul Islam, Junaed Sattar, "Enhancing Underwater Imagery using Generative Adversarial Networks".

[10] Phillip Isola, Jun-Yan Zhu, Tinghui Zhou, Alexei A. Efros, "Image-to-Image Translation with Conditional Adversarial Networks".

[11] N. Singh and A. Bhat, "A Detailed Understanding of Underwater Image Enhancement using Deep Learning," 2021 5th International Conference on Information Systems and Computer Networks (ISCON), 2021, pp. 1-6, doi: 10.1109/ISCON52037.2021.9702312.

[12] http://irvlab.cs.umn.edu/resources/euvp-dataset

[13] Ronneberger O., Fischer P., Brox T. (2015) "U-Net: Convolutional Networks for Biomedical Image Segmentation". In: Navab N., Hornegger J., Wells W., Frangi A. (eds) Medical Image Computing and Computer-Assisted Intervention – MICCAI 2015. MICCAI 2015. Lecture Notes in Computer Science, vol 9351. Springer, Cham.

[14] Phillip Isola, Jun-Yan Zhu, Tinghui Zhou, Alexei A. Efros. "Image-to-Image Translation with Conditional Adversarial Networks".

[15] Tesfamikael, Hadish Habte, Adam Fray, Israel Mengsteab, Adonay Semere, and Zebib Amanuel. "Simulation of Eye Tracking Control based Electric Wheelchair Construction by Image Segmentation Algorithm." Journal of Innovative Image Processing (JIIP) 3, no. 01 (2021): 21-35.

[16] Vijayakumar, T. "Synthesis of Palm Print in Feature Fusion Techniques for Multimodal Biometric Recognition System Online Signature." Journal of Innovative Image Processing (JIIP) 3, no. 02 (2021): 131-143.

Authorized licensed use limited to: DELHI TECHNICAL UNIV. Downloaded on June 15,2022 at 11:26:56 UTC from IEEE Xplore. Restrictions apply.

Proceedings of the International Conference on Applied Artificial Intelligence and Computing (ICAAIC 2022)
IEEE Xplore Part Number: CFP22BC3-ART; ISBN: 978-1-6654-9710-7

Using AI to Improve India's Logistic Conditions

1st Sanskar Jethi
Delhi Technological University,
Bawana Road, Delhi - 110042

2nd Madhav Rathi
Delhi Technological University,
Bawana Road, Delhi - 110042

3rd Dhiraj Kumar Pal
Delhi Technological University,
Bawana Road, Delhi - 110042

2022 International Conference on Applied Artificial Intelligence and Computing (ICAAIC) | 978-1-6654-9710-7/22/$31.00 ©2022 IEEE | DOI: 10.1109/ICAAIC53929.2022.9792780

***Abstract*—The Logistics Performance Index (LPI) is an interactive benchmarking tool created by the World Bank released every 2 years to help countries identify the challenges and opportunities they face in their performance on trade logistics and what they can do to improve their performance. India's ranking is dropping with every release. In this paper, we analyze some of the major existing Artificial Intelligence-based solutions and provide one of our own.**

***Index Terms*—Artificial intelligence(AI), Logistics Performance Index(LPI), World Bank, benchmarking.**

I. Introduction

The Logistics Performance Index is represented by the World Bank as expected. The LPI relies upon a general audit of accomplices on the ground giving contribution on the logistics "kind attitude" of the countries where they work and those with which they trade. They join all around data on the countries in which they work with taught abstract examinations in regards to various countries where they trade and have knowledge into the overall logistics environment.

Logistics is a $4.3 trillion industry all around. It is the groundwork of the trade, and incredible logistics can diminish trade expenses and influence countries to fight around the world. Getting logistics right, suggests further developing establishment, capacities, customs and rules, approaches and organization to the right degree.

The logistics performance (LPI) is the weighted regular of the nation scores on the six key angles:

INDIA	LPI Rank	LPI Score	Customs	Infrastructure	International Shipments	Logistics competence	Tracking & Tracing	Timeliness
2018	44 ↓	3.18 ↓	2.96 ↓	2.91 ↓	3.21 ↓	3.13 ↓	3.32 ↓	3.5 ↓
2016	35	3.42	3.17	3.34	3.36	3.39	3.52	3.74
Ref #1 Rank 2018								
Germany	1	4.2	4.09	4.37	3.86	4.31	4.24	4.39

Fig. 1. LPI Comparison Parameters

India is competing with the world in this industry. We will analyze the current methods being used in the world and will discuss our solution to bring India at par with the world and help it climb the Logistic Ladder.

- The proficiency of the clearance interaction (i.e; speed, straightforwardness and consistency of conventions) by line control organizations, including customs.
- Quality of exchange and transport-related foundation (e.g., ports, rail lines, streets, data innovation).
- The simplicity of organizing competitively estimated shipments.
- Skill and nature of logistics administrations (e.g., transport administrators, customs merchants).
- Capacity to track and follow transfers.
- The practicality of shipments in arriving at the objective inside the booked or expected conveyance time.

II. METHODOLOGIES

A. Understanding Artificial Intelligence

AI is the designing and framing of intelligent agents that enter precepts from the environment and take supervision that affect the environment, and these are some general use cases of Artificial Intelligence in the industry.
Artificial intelligence has acquired huge ground in a long time since it was set up as an order. Lately, AI types of progress have animated, maintained by advancement in AI, similarly as redesigns in figuring power, data accumulating, and exchange organizations.
For the reason for this note, we follow the definition and depiction of essential, progressed, and self-sufficient man-made consciousness that was advanced in EM Compass Note 69.
This moreover suggests that AI isn't one sort of machine or robot, yet a movement of approaches, procedures, and developments that show shrewd lead by separating their environmental factors and taking actions with a degree of independence to achieve express centres that can work on various strategies for transport.

B. AI Use Cases in Advanced Economies

In advanced economies, there are a few vehicle sub-areas in which AI is as of now having a huge effect. Urban mobility: Small-scale self-ruling transport preliminaries have been executed the world over, in spots as assorted as Finland, Singapore, and China. Self-governing transports are as of now operational in Norway, Sweden, and France. One model is Olli, a self-driving electric transport by Local Motors, an American organization controlled by IBM Watson. Olli is the principal AV to utilize IBM's Watson and its Internet of Things information base to dissect the encompassing traffic and settle on choices dependent on that information. Other than driving itself, Olli likewise furnishes its travelers with café and climate data. Olli has been tested in a few U.S. urban communities.

Authorized licensed use limited to: DELHI TECHNICAL UNIV. Downloaded on June 22,2022 at 04:44:57 UTC from IEEE Xplore. Restrictions apply.

Ride-hailing and sharing stage Uber utilizes AI for driver and ride-coordinating, course advancement, and driver onboarding.

- Traffic management tasks: Numerous AI estimations are proper to handling complex issues, for instance, those introduced by traffic movement, and they are being used all over. One model is SurTrac from Rapid Flow Technologies, a Carnegie Mellon University side venture, which gives deals with serious consequences regarding sharp traffic light controls. It has made traffic streams at an association of nine traffic lights in three critical roads in Pittsburgh. Quick Flow reduced travel times by more than 25% overall and stand by times declined by an ordinary of 40% during the fundamental. It also decreased comes by 30% and outpourings by 20%.
- Logistics: Trucking is a vital objective for AI intercessions, with load conveyance as an expected early space for selection of AV innovation across the world. In 2015, Uber purchased driverless innovation firm Otto, and after a year it finished the principal self-governing truck conveyance conveying 50,000 jars of Budweiser lager over a distance of 120 miles from Fort Collins to Colorado Springs. Set up players like Volvo, just as trucking firms like Starsky, are likewise trying their own models.
- Railways: GE transportation has made intelligent developments to work on the adequacy of their trains. The splendid freight trains are outfitted with sensors that assemble data and feed it into an AI application. The application separates the data and encourages consistent dynamic. In Europe, 250 trains from freight carrier Deutsche Bahn Cargo have been retrofitted with GE's show of the board programming to screen brake execution, motor temperature, and various circumstances to expect upkeep. The framework is more accurate considering the way that it benefits from persistent data on the trains' circumstances instead of set estimations like the distance voyaged. The astute trains were represented to have diminished train disappointment rates by 25% in Deutsche Bahn's pilot adventure.
- Marine: Autonomous boats are one obvious usage of AI in the transport area. Transport affiliations like Nippon Yusen and Rolls-Royce's marine activity (at this point Kongsberg) are endeavouring their models, the rest of which sincerely endeavoured an independent boat in Finland in 2018. Be that as it may, AI besides gives the occasion to streamline affiliations and courses, which could lessen fuel expenses and spreads. In 2018, Hong Kong-based transportation line OOCL cooperated with Microsoft's AI research fixation to further develop their affiliation works out, a 15-week exertion that made save resources of $10 million reliably for OOCL.

That very year, the American affiliation Sea Machines Robotics worked with the world's most noteworthy transportation affiliation, Maersk, to introduce AI situational care improvement on Maersk's ice-class compartment vessels. This meant the headliner when PC vision, Light Detection and Ranging (LiDAR), and information advancements were utilized on a working boat. Ocean Machines ensures its upgrades can diminish useful expenses by 40%.

C. Investment Opportunities

E-coordinations is the most promising zone for guaranteed venture openings that include AI applications in EMs. Helpless streets, problematic truck usage, questionable following and steering, just as an absence of straightforwardness in payload development, all upset the proficiency of customary coordinations. A large group of new start-ups have been using innovation, including AI, to help tackle the productivity and unwavering quality issues that the customary coordinations industry faces, acquainting information investigation and streamlining with lower costs.

Known as e-logistics organizations, the administrations these new businesses spend significant time in will quite often fall into three classifications:

- Transportation information empowering agents, which give stage as-an assistance contributions to further develop transportation/area administrations.
- Long stretch/between city transportation, which normally This appropriation may be reused for noncommercial purposes if the source is alluded to as IFC, a person from the World Bank Group. 6 total drivers and transporters to work with the development of merchandise across urban areas through an advanced stage.
- Last mile/intercity transportation, which total neighborhood conveyance drivers and SMEs/web based business organizations for last-mile conveyance arrangements inside urban areas. More than $4.2 billion has been put into the worldwide e-coordinations area as of December 2017.

Artificial intelligence is helping fuel the accomplishment of e-coordinations suppliers in developing business sectors. Starting around 2015, IFC has put resources into nine e-coordinations organizations across China, India, Brazil, Sri Lanka, and Africa. Dispatched in 2015, Shadowfax, an IFC investee, is an Indian last-mile express coordinations fire up that incorporates web based business organizations' internet based conveyances through its accomplices, the drivers. A main player in the space, Shadowfax is functional in 80 urban areas and administrates enormous corporate customers across the food, staple, design, and buyer durables ventures, for the most part using motorbikes. To control its conveyance stage, Shadowfax utilizes an AI-driven arrangement named Frodo to smooth out transport courses. "Frodo chooses, for instance, which assistant would have the choice to go and the best course for the rider," the association's VP said for the current year.

AI is furthermore joined into the estimation so Frodo tracks data centers, advantageousness, and driver execution to continue to update routes.43 In 2019, IFC put $4 million in Shadowfax as an element of a Series C round to help the association with developing metropolitan regions and customers.

Authorized licensed use limited to: DELHI TECHNICAL UNIV. Downloaded on June 22,2022 at 04:44:57 UTC from IEEE Xplore. Restrictions apply.

Players like these utilize astonishing AI advancement and asset light strategies to give e-coordinations organization to enormous clients in the messed up and separated coordinations region in Indian region that is needed to create at a form yearly improvement speed of 10.5 percent in the accompanying two years. This is essential, as India, which has acquired a ton of ground toward diminishing coordinations costs lately, still spends some place in the scope of 13 and 14 percent of GDP on coordinations.

Loggi, another IFC investee organization and one of Brazil's most current unicorns, is a coordination fire up that interfaces dispatches to clients that need express last-mile conveyance administrations. The organization as of now utilizes an application to associate bike conveyance drivers and its customers in different areas. To support its extension throughout the following five years, the organization is hoping to use AI and enormous information to upgrade conveyance courses and idleness. Keeping that in mind, the organization is investigating pulling in a group of programmers.IFC has put over $9 million in Loggi since 2017. Despite the fact that not carefully AI, interests in enormous information and digitization all more comprehensively structure the structure squares of AI innovation. New businesses and developing organizations that digitize quicker and have more tech-empowered plans of action will have the information important to convey AI to enhance their dependability, consistency, and proficiency. China's Uber-for-trucks startup Full Truck Alliance, an IFC investor, gathers information from its transporters on conveyance and dependability and uses that data to offer auxiliary types of assistance, for example, credit lines to its clients close by accomplices. Full Truck Alliance additionally supports productivity by coordinating trucks, burdens, and drivers, and causing them to discover corner stores. The organization creates income from enrollment charges from organizations that utilize the framework for long stretch administrations, just as drivers' delivery expenses, thruway cost card tops off, and fuel buys. In 2018, Full Truck Alliance additionally put resources into plus.ai, a driverless truck fire up situated in California that can evaluate how to send driverless innovation on long stretch courses in China. In 2016, IFC contributed value to help the organization's development on the planet's biggest coordinations market. This permitted IFC to partake in a creative organization that is improving productivity in a divided industry.

The applications for AI in urban mobility are extensive. The opportunity is because of a blend of components: urbanization, attention to ecological sustainability, and developing mechanization in agricultural nations, which prompts blockage. The rising power of the sharing economy is another donor. Ride-hailing or ride-sharing administrations empower drivers to get to riders through a computerized stage that additionally encourages portable cash instalments. A few models in agricultural nations incorporate Swvl, an Egyptian start up that empowers riders heading a similar course to share fixed course transport excursions, and Didi, the Chinese ride-hailing administration. These can be useful in streamlining usage of resources where they are restricted in EMs, and increment the nature of available transportation administrations. While AVs may effectively be conveyed in developing economies, EM nations may need to wait before they can exploit this innovation completely. KPMG's Autonomous Vehicle Readiness Index, which estimates 25 nations' degrees of readiness for self-sufficient vehicle appropriation, just incorporates five creating economies: China, Russia, Mexico, India, and Brazil. They keep four spots on the rundown, aside from China, which positions above Hungary, at number 21 out of 25.46 This is halfway on the grounds that a portion of these nations, including Brazil and Mexico, don't have numerous local organizations dealing with AVs right now. A few investigations show Level 4 or 5 AVs might be financially available during the 2020s, yet their organization will be restricted by cost and execution. During the 2040s, roughly 40% of vehicle travel could be self-governing in developing economies.47 Some EMs, including India and China, may see quicker selection than others.

D. Solutions that should be Employed By India

Traffic Management: In Bengaluru, India, where gridlocks are normal, Siemens Mobility constructed a checking framework that utilizes AI through traffic cameras that identify vehicles and ascertain thickness of traffic out and about, and afterward changes traffic signals dependent on ongoing street congestion. Alibaba, China's online business monster, dispatched "City Brain" to limit street clog, using information from traffic signals, CCTV cameras, and video acknowledgment to make ideas for traffic stream the executives.

India's coordinations and network foundation battles to stay up with the country's needs, making a drag on seriousness and development possibilities. Nonetheless, we are getting a ton of help and there is a beam of expectation for what's to come.

The World Bank Group upholds the public authority of India's endeavors to further develop availability in three regions creating a transportation framework by working on public and public expressway frameworks, expanding multi-modular vehicle improvement including rail routes and streams, and helping to foster coordination production network foundation. The IFC assembles private area passage into waterway transport and considers interests in transportation framework projects including air terminals, port terminals, streets and different resources.

Trucking: Transition Auto and Fisheyebox, two Indian coordinations associations are using wise driving advancement to send independent trucks on Indian roads this year. The trucks were viably attempted at Level 4 of autonomy, which suggests they can work under select conditions without human input.36 (Automation in vehicles is assessed on a standard six-level arrangement framework where Level 0 involves no motorization and Level 5 is full computerization).

Authorized licensed use limited to: DELHI TECHNICAL UNIV. Downloaded on June 22,2022 at 04:44:57 UTC from IEEE Xplore. Restrictions apply.

We must continue this upward trajectory and aspire to be amongst the top 5 nations in logistics in the world. This leap will require us to focus and implement solutions along 5 priority areas which will have the largest impact and where we are lagging currently:

- Seamless movement of freight: To achieve this we need : a) simplification and automation of regulatory processes, and
  b) integration amongst the various government departments providing speedy clearances to reduce the waiting hours. This would help prevent multiple enroute checks and inspection of goods by different agencies, which leads to inefficiencies in transit. A certification by one agency can be done and made available live to other agencies for their verification.
- Reliability in logistics through technology adoption and automation: To ensure faster, reliable delivery of goods we need the ability to track and trace consignments live and this can be brought by having mandatory track and trace facility for each and every freight under movement. This is possible if each and every vehicle is equipped with sensors for location tracking.
- Move existing paper systems digital platforms: Highly critical to achieve the objective of efficiency and seamless freight movement. With E-waybill we have started the journey of 3 Deloitte Report – Logistics ease across different states Page 4 of 9 paperless supply chains and same should be extended to e-POD (electronic - Proof of delivery) immediately to unblock the credit trapped due to non-availability of POD instantly.
- Availability of trained manpower (truck drivers, loaders): Making their life human by giving them clean and maintained facilities in transit and at warehouses; making truck driving a viable job by bringing dignity to the profession and integrating truck drivers back into the society.
- Compliance with safety standards: Government should also bring mandatory norms to bring the reforms targeting high driver comfort and safety in the long haul trucking equipment. Make installation of advanced driver assistance systems and safety sensors mandatory in the vehicles. India should lead the logistics revolution to make goods transportation faster, digital, safer and human over the next decade.

E. Aviation

There are openings for AI advances in rambles, with numerous applications for conveyances, everything being equal, and types. In India, a Gurgaon based startup Zomato banded together with the Indian government to dispatch India's first business drone conveyance administration, flying food and every day supplies by air quicker than transport on wheels.Amazon, is fostering a robot equipped for conveying 20 tons of freight and flying as much as 7,500 kilometers. Shrewd air terminal applications are likewise accessible, for example, the drive in Chinese air terminals to utilize clever route frameworks furnished with facial acknowledgment and huge information investigation for a paperless and more effective experience.

Based on the following sub criterion, these solutions can be implemented to improve India's Logistical Conditions:

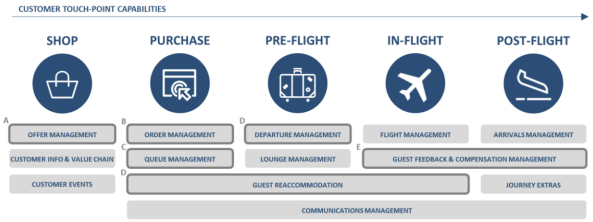

Fig. 2. Customer Touch-Point Enablers

- Intelligent Bot Era: The inquiry and booking experience to become as simple as having a conversation.
- Dynamic Resource Allocation: Queues minimized by predictive analytics, dynamic asset, distribution and traveller warning.
- Personalized Fulfillment: Utilizing information and AI to all the more likely serve the client during the satisfaction stage.
- Disruption Damage Control: Artificial Intelligence can possibly consider endless elements and propose the most ideal choice.
- Complaints Claims Management: Artificial Intelligence can independently deal with client solicitations, grievances and cases, guaranteeing consistency to guidelines (for example EU261), advancing aircraft assets, limiting manual endeavours, pay expenses, and loss of client dependability.

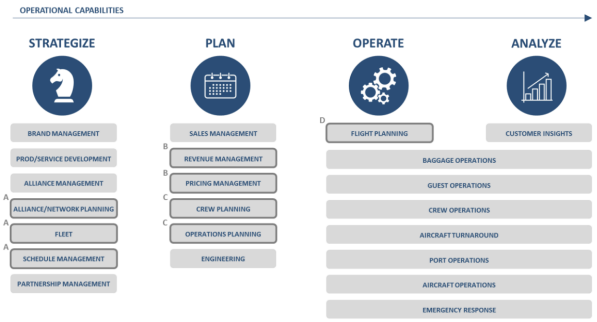

Fig. 3. Operational Enablers

- Prediction: With AI, strategic and functional business choices can be delineated with an exact expectation of result and effect. A wide range of variables are considered in blend with verifiable information to foster expectations.
- Correlations of data: With the wealth of data, the test is by and by how to draw benefits from it without the need to spend tremendous proportions of resources on data assessment. Artificial Intelligence has the ability to bring unstructured data and find associations and models

Authorized licensed use limited to: DELHI TECHNICAL UNIV. Downloaded on June 22,2022 at 04:44:57 UTC from IEEE Xplore. Restrictions apply.

between even evidently detached things, for instance, client direct and its impact on changes.

- Agile and adaptable: Operations can be intended to perfection, notwithstanding, there are generally things that disturb the arrangement and now and again require a rethinking exercise. AI empowers operations to rapidly and productively rethink if there should arise an occurrence of interruptions, taking recorded and continuous information into the record to adjust the new arrangement.
- Machine learning: AI strategies permit the computer to change its calculation in view of past information, and have the option to gain from "encounters".

Fig. 4. Support and Management Enablers

To Support and the board Business capacities, the accompanying AI empowering agents have been recognized:

- A) Value Chain Risk Management: Value chain accomplices (for instance travel organizers, traders) reveal aircrafts to external dangers that can be perceived and administered by AI. Models join Defaults additionally, portion deception.
- B) Asset Protection: Artificial Intelligence can help airlines with their resources (for example aircraft) following the status, area and other resource credits, distinguishing oddities and creating suggested activities.
- C) Maintenance Safety Checks: Complex safety management exercises require refined furthermore, versatile preparation and booking considering numerous boundaries. Simulated intelligence can uphold such exercises.
- D) Supply Chain Risk Management: Supply chain accomplices (for example makes, fuel providers) open carrier to outer dangers that can be identified and made do with the utilization of AI. Models include Fuel supply risk identification; Fuel cost vacillations; Aircraft conveyance delays.

F. Logistics:

Established players can likewise bridle the advantages of AI in their activities. Blume Global, an Indian AI Logistic organization, is utilizing AI to smooth out the worldwide traditions and burdening process by characterizing and arranging items for import and product by material, size, and weight, just as coordinating with them with their related duties.

The following solutions are on the brink of the horizon in terms of their acceptance and can help the Logistical Conditions vastly:

- Automated Warehouses: Dispersion focus robotization frameworks allow an opportunity to defeat a ton of routine tasks. The primary development used in these frameworks is PC vision that can perceive and help with straightening out the stock. Another promising use case is free quality control.

  For instance, Ocado is a corner store arranged in the United Kingdom. It has cultivated a robotized stockroom. The system relies upon a robot called a 'hive-grid machine.' This robot can execute 65,000 orders every week. 'Hive-network machines' essential task is to move, sort, and lift things inside the stockroom. Ocado's automated stockroom radically cuts work and the best an open door for orders to be executed.
- Autonomous Vehicles: Distribution centre automation systems give a chance to overcome a great deal of routine assignments. The main innovation utilized in these systems is PC vision that can recognize and assist with getting sorted out the stock. Another promising use case is independent quality control.
- Demand Prediction: One essential business need affecting most associations is the need to expect the number of arrangements and items it needs in future. Running almost out of stock means lost bargains, lost pay, and habitually lost clients who could flee to a competitor's thing.
  Artificial Intelligence gives various estimations that can predict designs. As demonstrated by Deloitte, generally speaking, these estimations can predict results better contrasted with human subject matter experts.
- Smart Roads: Another Artificial Intelligence use case in coordination is splendid roads. Examples of this advancement fuse streets with daylight based chargers constrained by LED lights. Sun-fueled chargers assist with conveying the power while LED lights are used to alert drivers about the road conditions. Likewise, daylight fueled chargers hold the road back from being subtle in winter. Another application is fiber optic sensors that can identify traffic volumes and models and prepared drivers to road conditions ahead. They can in like manner recognize when vehicles leave the road or are engaged with accidents, and caution the appropriate emergency organizations and subject matter experts. This makes for faster transports and safer road conditions.

Incorporated Roadways association has made the Smart Pavement system. It would connect the vehicles be able to all outfit the drivers with genuine information about setbacks, gridlocks, and so forth The Colorado Department of Transportation began actually testing the system in 2018.

III. RESULT

In its report, the World Bank expressed: "In the course of recent years, major league salary nations, a large portion of which are in Europe, involved the best 10 situations in the LPI rankings. To be expected, since these nations customarily have been predominant in the inventory network industry. "The synthesis of the 15 best-performing nations

Authorized licensed use limited to: DELHI TECHNICAL UNIV. Downloaded on June 22,2022 at 04:44:57 UTC from IEEE Xplore. Restrictions apply.

has not essentially changed by the same token. However, it merits significant enhancements in the LPI scores of Japan, Denmark, the United Arab Emirates, and New Zealand since 2012."

Below is a plot showing variation of LPI index year-wise of India, Japan and Germany:

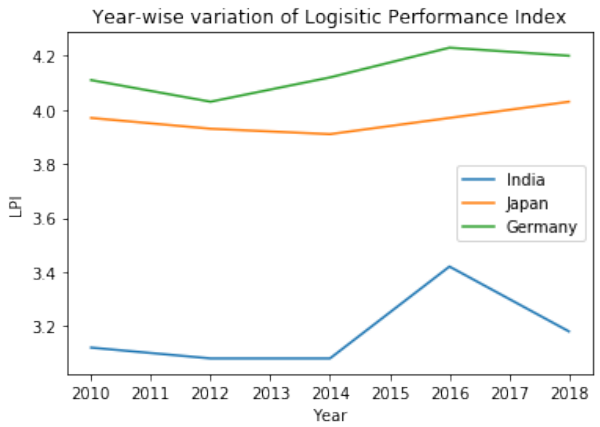

Fig. 5. Year Wise variation of Logistic Performance Index

LPI index of India can be improved by employing the aforementioned machine learning techniques and we can see the LPI index of India improve drastically.

In 2018, just about 6,000 nation appraisals were made by logistics experts. The World Bank said that the report gives new bits of knowledge on network protection dangers in logistics and the utilization of electronic exchanging stages by shippers.

IV. CONCLUSION

Man-made insight holds the assurance of altogether extending value and efficiency in a couple of regions, including transport, and these movements are not in some faraway future; they are happening now. Man-made knowledge is at this point helping with making transport safer, more strong and capable, and cleaner. A couple of utilizations join robots for quick life-saving clinical transports in Sub-Saharan Africa, wise traffic structures that decline blockage and releases in India, and driverless vehicles that van cargo between individuals who cause it and the people who to get it in China. With the phenomenal potential to construct capability and practicality, among various benefits, comes a huge gathering of monetary, institutional, and political hardships that ought to be addressed to ensure that the countries and their occupants would be generally ready to equip the power of AI for money related improvement and shared flourishing.

REFERENCES

[1] "Logistics Performance Index (LPI)." 2017. Gica.global. December 5, 2017. https://www.gica.global/activity/logistics-performance-index-lpi.
[2] Wikipedia Contributors. 2019. "Logistics." Wikipedia. Wikimedia Foundation. April 14, 2019. https://en.wikipedia.org/wiki/Logistics.
[3] Tedder, Michael, and Robert Lawy. 2009. "The Pursuit of 'Excellence': Mentoring in Further Education Initial Teacher Training in England." Journal of Vocational Education and Training 61 (4): 413–29. https://eric.ed.gov/?id=EJ870805.
[4] "India's Mission to Mars : A Feather in the Cap or a Waste of Money?" n.d. Www.careerride.com. Accessed April 14, 2022. https://www.careerride.com/view.aspx?id=12245.
[5] "Tech World Congress 2021 — India Electronics Week IoTShow.in." n.d. Tech World Congress. Accessed April 14, 2022. https://www.indiatechnologyweek.com/wp-content/uploads/2020/07/ANAY-Artifical.
[6] Conde, Maria, and Ian Twinn. 2019. "How Artificial Intelligence Is Making Transport Safer, Cleaner, More Reliable and Efficient in Emerging Markets." https://www.ifc.org/wps/wcm/connect/7c21eaf5-7d18-43b7-bce1-864e3e42de2b/EMCompass-Note-75-AI-making-transport-safer-in-Emerging-Markets.pdf?MOD=AJPERESCVID=mV7VCeN.
[7] Kapoor, Ajay. 2020. "AI Technology Is Making Us Safer: Is That So?" Medium. October 12, 2020. https://chatbotsjournal.com/ai-technology-is-making-us-safer-is-that-so-5f1db27b440a.
[8] "Germany Retains Top Spot in Global Performance Index by World Bank." 2018. Air Cargo News. July 24, 2018. https://www.aircargonews.net/freight-forwarder/germany-retains-top-spot-in-global-performance-index-by-world-bank/.
[9] Wang, Yue. n.d. "China's Uber-like Trucking Startup Mints the Country's Latest Billionaire." Forbes. Accessed April 14, 2022. https://www.forbes.com/sites/ywang/2021/06/17/chinas-uber-like-trucking-startup-mints-the-countrys-latest-billionaire/.
[10] University, Carnegie Mellon. n.d. "Surtrac Allows Traffic to Move at the Speed of Technology - News - Carnegie Mellon University." Www.cmu.edu. Accessed April 14, 2022. https://www.cmu.edu/news/stories/archives/2019/october/traffic-moves-at-speed-of-technology.html.
[11] "What Is an Automated Ocado CFC?" n.d. Ocado Group. https://www.ocadogroup.com/about-us/what-we-do/automated-ocado-customer-fulfilment-centre.
[12] Lewis, Karen. 2016. "Olli: Artificial Intelligence for the Real World of Connected Commuting." Internet of Things Blog. September 5, 2016. https://www.ibm.com/blogs/internet-of-things/olli-ai/.
[13] Budweiser makes first driverless shipment using Uber's Otto in 2022 — Budweiser, Self driving, Fort collins. (n.d.). Pinterest. Retrieved April 14, 2022, from https://www.pinterest.com/pin/budweiser-makes-first-driverless-shipment-using-ubers-otto-in-2022–304626362304317014/
[14] "On the Right Track: Software Is Helping Make European Trains Smarter — GE News." n.d. Www.ge.com. Accessed April 14, 2022. https://www.ge.com/news/reports/right-track-software-helping-make-european-trains-smarter.
[15] Threlfall, Richard. 2020. "Autonomous Vehicles Readiness Index (AVRI) - KPMG Global." KPMG. August 31, 2020. https://home.kpmg/xx/en/home/insights/2020/06/autonomous-vehicles-readiness-index.html.

Authorized licensed use limited to: DELHI TECHNICAL UNIV. Downloaded on June 22,2022 at 04:44:57 UTC from IEEE Xplore. Restrictions apply.

Proceedings of the International Conference on Applied Artificial Intelligence and Computing (ICAAIC 2022)
IEEE Xplore Part Number: CFP22BC3-ART; ISBN: 978-1-6654-9710-7

VLSI Layout: Concept to Realization

Malti Bansal*, Riyanshi Arora, Ritvik Bharti
Department of Electronics and Communication Engineering,
Delhi Technological University (DTU), Delhi-110042, India
*maltibansal@gmail.com

Abstract— Very large-scale integration, commonly referred to as VLSI, means a process in which an integrated chip is made by merging myriads of Metal Oxide Semiconductor transistors. An example of VLSI device is a microprocessor. In India, VLSI and EDA occupy the largest segment of the Indian semiconductor design industry. While VLSI industry is large in Bangalore, Noida is in charge of the largest EDA operations in India. There are various devices and memories which are used to control a system. For example: Random Access Memory, Central Processing Unit, and, Read Only Memory and various other devices. What VLSI does is that it allows us to integrate all these different parts in just one single chip. This paper presents the development of VLSI, its applications, implementation and recent developments in the technology of Very Large-Scale Integration abbreviated as VLSI. The paper is divided into further sections as Introduction of VLSI, History and development of VLSI, VLSI Design/Layout flow, VLSI Layout styles, Current research to make VLSI more effective, Advantages and Disadvantages of VLSI, Uses of VLSI etc.

Keywords— Very Large-Scale Integration, VLSI, design, layout, chip, CMOS, Mosfet, Integrated Circuits, ICs.

I. INTRODUCTION

The devices that we see in our daily life are very compact but their internal design structure is quite complex. This compact structure that we commend is truly an end product of human being and its quest to make devices simpler and better day by day. Now these devices are made simpler by incorporating various parts of a working system into just one single chip by designing it into a complex way but making the working of electronic or nano electronic devices faster, quintessential and faultless. This incorporation of different functional units or memories such as CPU, RAM (known as Random Access Memory) and ROM with many other units is done through a process called Very Large-Scale Integration or VLSI. As the name suggests, VLSI designing means designing the circuit in such a manner that myriads of transistors are incorporated in a single chip. In other words, Very Large-Scale Integration refers to the procedure of fabricating an Integrated Circuit (I.C.). Prior to the development of the VLSI technology, almost all of the integrated circuits performed just some limited functions. But after the development of this VLSI technology, integrated circuit can almost perform any number of functions the fabricator wants the circuit to perform.

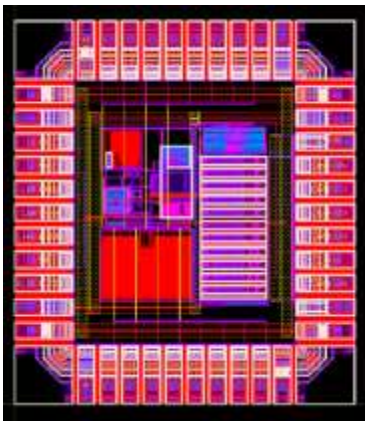

Fig.1: A typical example of VLSI layout
(Reproduced from [1])

II. HISTORY OF VLSI LAYOUT

In the year 1948, researcher and engineer Jack Kilby fabricated the very first integrated circuit or I.C. He invented a flip flop by utilizing two (2) transistors. Jack Kilby worked in Texas Instruments. In today's world, the processors manufactured by INTEL use more than four (4) billion transistors in just one single chip. The advancement and growth rate of this industry is still at the peaks [2]. A decade later, Jack Kilby grasped the prospects of miniaturizing the transistors if many transistors could be constructed on a piece of semiconductor element Silicon (Si) [2]. As a result, Kilby built the first integrated circuit at Texas Instruments and won the Nobel Prize for the same in the year 2000. By the decade if 1960s, Metal Oxide Semiconductor Field Effect Transistors came into picture. Their mass production began in the following decade. MOSFETs are divided broadly into two categories- NMOS and PMOS. The advantage of using MOSFETs in the field of VLSI is that they almost draw zero amount of sway current when they are not in use. In the year 1963, an American electrical engineer named Frank Wanlass fabricated the very first logic gates with MOSFETs. His blueprint used both types of transistors i.e., nMOS as well as pMOS. As a result, these transistors received the name Complementary Metal Oxide Semiconductor transistor which was abbreviated as CMOS.

2022 International Conference on Applied Artificial Intelligence and Computing (ICAAIC) | 978-1-6654-9710-7/22/$31.00 ©2022 IEEE | DOI: 10.1109/ICAAIC53929.2022.9792835

Authorized licensed use limited to: DELHI TECHNICAL UNIV. Downloaded on June 22,2022 at 04:48:34 UTC from IEEE Xplore. Restrictions apply.

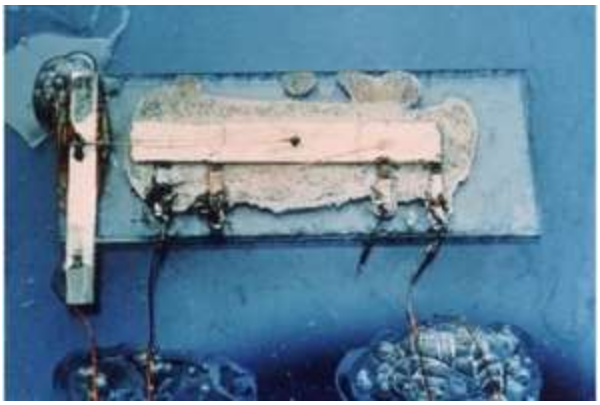

Fig.2: The chip that changed the world- The first Integrated Circuit (Reproduced from [3])

In the early days only pMOS was used due to which the circuits then made had poor productivity and accuracy. It was then in 1970s that the use of nMOS transistors in integrated circuits came into existence. It was first used by Carver Mead-a researcher and scientist at Caltech. He is also known as one of the fathers of VLSI layouts. While the nMOS cooperation was more reasonable than CMOS, nMOS rationale entryways actually burned-through power while inactive. Power use transformed into a critical issue during the 1980s as innumerable semiconductors were composed onto a single fail horrendously. CMOS measures were generally embraced and have basically traded nMOS and bipolar cycles for virtually all computerized rationale applications. In the year 1965, the scientist and researcher Mr. Gordon Moore observed that graphing the quantity of semiconductors which can be fabricated in the most economical way on a chip gave results which were in favour of advancing the transistor technology. When those results were graphed on a semilogarithmic axes, they formed a linear graph. This was later popularly known as Moore's law and it has become an inalienable outcome. Moore's Law is followed principally by downsizing the measurements of semiconductors. It can also be followed by constructing somewhat bigger chips (but to a lesser extent). The extent of incorporation of chips has been delegated limited scope, medium-scale, huge scope, and very large-scale which are popularly known as 1. Small Scale Integration which is abbreviated as SSI, 2.Large Scale Integration, abbreviated as LSI, 3. Very Large-Scale Integration, abridged as VLSI. The circuits which use Small Scale Integration technology (For example: Plessey SL201 and the 7404 inverter) utilize fewer than ten logic gates where each logic gate utilizes approximately six (6) transistors. The circuits which are integrated on a medium scale utilize up to one thousand gates. An example of medium scale integrated circuit is the 74161 counter. If the circuits are integrated on a large scale, it was seen that they used nearly 10,000 logic gates. Now, with the advancement in technology, it became evident that if this level of advancement continued, novel names had to be devised which would create more complexity in understanding technology. Hence the terminology, Very Large-Scale Integration was introduced for integrated circuits or ICs. This term was introduced in the 1980s and has been used to describe ICs since then. An analogy of Moore's law was introduced and named as Dennars's Scaling Law. This law stated that when transistors' size become small i.e., when they shrink, their speed of working increases. They also consume less energy and their manufacturing costs decrease. Each transistor manufacturing company needs to keep up with its rival companies. Therefore, they need to make most efficient designs of transistors as per size and power or energy consumption. Therefore, Moore's law has been used in these designs and thus has turned into a "self-fulfilling prophecy" [2]. But, these transistors also have a limit beyond which their size cannot be reduced. It is understood that transistor size scaling has to stop one day because the size of transistors cannot be made less than that of an atom. Therefore, the use of Dennars' scaling has been reduced and after the forty-five nanometre i.e., 45 nm generation of transistors, fabricators are making compromises between improving force and improving deferral. Although, in the year 2009, it was hypothesized that the use of law given by Moore would continue for yet another decade and in today's world, there are still researches going on in order to make transistors and hence the VLSI layouts and technology more and more advanced and diverse in order to minimize the size of electronic and nano electronic devices and hence make life easier. Table I displays the major breakthroughs and complexities whose introduction led to the development of VLSI.

Table I

ERA (number of logic blocks per chip)	Year	Complexity
Single transistor	1959	less than 1
Unit logic (one gate)	1960	1
Multi-function	1962	2-4
Complex function	1964	5-20
Medium Scale Integration	1967	20-200(MSI)
Large Scale Integration	1972	200-2000(LSI)
Very Large Scale Integration	1978	2000-20000(VLSI)
Ultra Large Scale Integration	1989	20000-? (ULSI)

III. DESIGN FLOW OF VLSI

The designing procedure of a Very Large-Scale integrated chip often change naturally at different levels. It begins with a given set of arrangement of pre-requisites. Those requirements are kept into considerations and a basic circuit is fabricated. It is then tested in various scenarios as per the requirement specified. At the point when necessities are not met, development ought to be improved [4]. In the event that such upgrades don't happen or are costly, an audit of the necessities and an effective evaluation will be thought of. Advanced VLSI configuration is frequently divided into five degrees of deliberations. These five deliberations/abstractions are 1. ARCHITECTURE OUTLINE, 2. MICROARCHITECTURE OUTLINE, 3. LOGIC OUTLINE/DESIGN, 4. CIRCUIT OUTINE/DESIGN and at the last, 5. PHYSICAL OUTLINE. Architecture depicts the elements of the framework. Microarchitecture clarifies the construction of the division into useful registers and units. Logic portrays how the effective sections are manufactured. Circuit configuration/outlining depicts how semiconductors are utilized to execute the rationale i.e., logic. The actual plan i.e., the physical design depicts the format of the chip. For better understanding of the VLSI layout process, a

Authorized licensed use limited to: DELHI TECHNICAL UNIV. Downloaded on June 22,2022 at 04:48:34 UTC from IEEE Xplore. Restrictions apply.

professor named D. Gajski gave a chart popularly known as Gajski-Kuhn Y chart which is depicted in Fig.3.

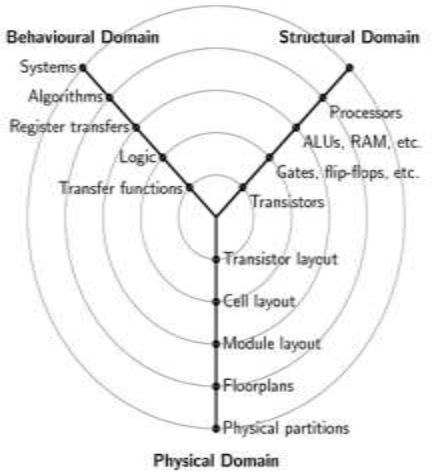

Fig.3: D.Gajski Y chart
(Reproduced from [5])

The lines that are akong the radius in the above defined image depict three (3) variant domains of designs. These domains are specified as- Structural domain, Physical domain and Behavorial domain. These areas can be utilized to depict the plan of practically any curio and accordingly structure an overall scientific classification for portraying the plan interaction. These domains are explained as follows:

A. Behavioural domain

In this space, the conduct of the element can be demonstrated utilizing procedural code which can address the circuit at a more elevated level of reflection. In this area the principal pecking order is a framework where the conduct of the engineering is defined. Then a bunch of calculations which can also be called as algorithms should be characterized for handling the various boundaries and a bunch of flowcharts. The third step is RTL i.e., Register Transfer Language, where the coding should be done and afterwards the rationale level i.e., the logic, where we are worried about 0 and 1 level is defined, succeeding which the transfer function is characterized [6].

B. Structural Domain

The essential space depicts the interconnection of modules critical to achieve an explicit lead. Now, if we take the following example: At the most elevated extent, a generator (touch tone type) may include a keyboard, fragment of a tone generator, cells, a loud speaker, and a sound enhancer. Finally, at subordinate level of consideration, the individual input path and the semiconductor junction that is expected to compose a tone generator is displayed.

C. Physical Domain

This kind of domain is also termed as geometrical domain/geometry. As the name suggests, this kind of domain is more considered with the physical structure of the Very Large-Scale integrated chip. Suppose, we are given a particular level of abstract entity. Now, to achieve that level of physical entity, we need its physical description. The physical domain gives us that description which we require to make that chip up to that level of abstract entity. It has various steps in its procedure. Those are: Defining a Transistor layout, defining a Cell layout, Defining the outline of the module, working on floorplans and finally describing the physical partitions. If any step of the above-mentioned fabrication process is missed, it may lead to incorrect design of the integrated circuit and hence it would result in its improper functioning. The designing process of a very large-scale integrated IC chip has two major parts i.e., the front-end designing process and the back-end designing process. The front design has been discussed in the starting of this section and it is achieved using HDLs i.e. Hardware Description Languages. There are many hardware description languages such as VHDL i.e., VHSIC Hardware Description Language, Verilog, System Verilog etc. The backend development of hardware consists of various steps (which are followed in the correct procedure) such as: "Wafer Processing, Lithography, Etching, Ion Implantation, Metallization and Assembly and Packaging" [7]. This complex process is made easier using a technique called "Divide and Conquer" [8]. In this technique, the circuit is divided into modules. Then each module is further divided into sub-modules and then the same process is repeated with each sub-module. This process is repeated until the whole circuit i.e., the chip is divided into a simple design to be examined and tested for working and logic implementation. The flowchart in Fig. 4 depicts the workflow of VLSI Layout/Design in a simple way for better understanding. The last step, i.e., the layout testing is a very crucial, If the fabricated chip is not tested, it may lead to inaccuracies in result, exorbitant re-designing and other problems. This may also lead to a delay in the time in order to market the chip.

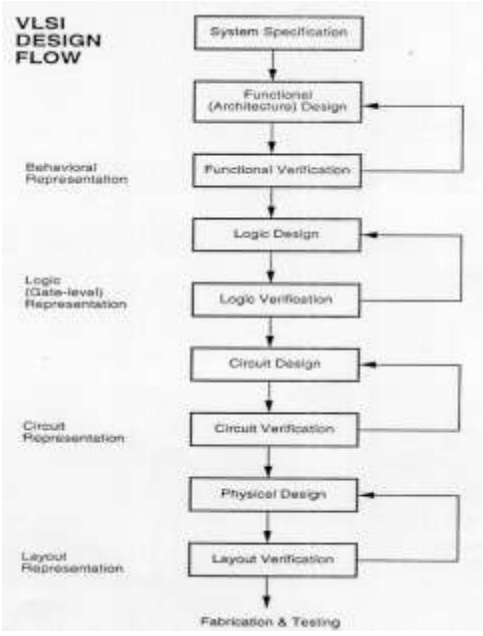

Fig. 4: Flowchart for VLSI layout and fabrication
(Reproduced from [9])

IV. VLSI LAYOUT STYLES

In the process of fabrication of Very Large-Scale integrated chips, various design styles are used. Some of the examples of such designs are as follows: 1. Field Programmable Gate Arrays i.e., FPGAs, 2. Standard Cell Based design, 3. Gate Array design and, 4. Full Custom design etc. Each plan style has its own benefits and weaknesses. Accordingly, a

Authorized licensed use limited to: DELHI TECHNICAL UNIV. Downloaded on June 22,2022 at 04:48:34 UTC from IEEE Xplore. Restrictions apply.

legitimate decision must be made by engineers/fabricators to give the usefulness requiring little effort and minimal cost. The following section briefs about each of the four layouts.

A. *Field Programmable Gate Arrays:*

At its centre, an FPGA is a variety of interconnected computerized subcircuits that execute regular capacities while likewise offering significant degrees of adaptability. Field Programmable Gate Arrays are a portion of the new moving zones of VLSI. Completely created FPGA chips containing a huge number of rationale doors or, with interlinks that can be programmed, are accessible to customers through their customization program to inform the usability required. This plan style gives a way for quick and speedy prototyping and for practical chip plan, particularly for low-volume applications. A commonplace field programmable entryway exhibit chip comprises of input-output supports, a variety of configurable rationale/logic blocks abridged as CLB, and programmable interlinked structures. The benefits of FPGA are exceptionally short pivot time and no actual assembling needed for tweaking it. The impediment is regular cost of these type of chips is normally more than other acknowledgment options. Today, FPGAs are used as a VLSI layout for image processing [10], rake receivers [11] etc.

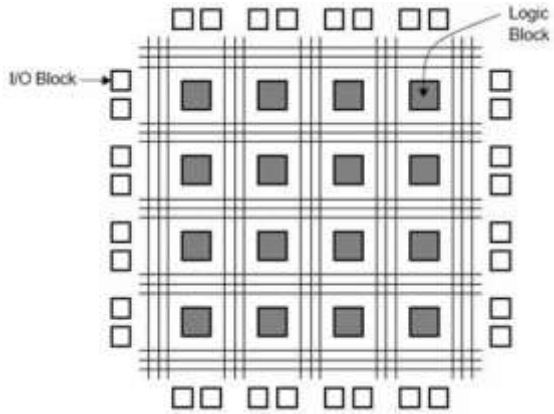

Fig. 5: An FPGA used in VLSI
(Reproduced from [10])

B. *Gate Array Design*

A gate array is a pre-gathered silicon chip with most semiconductors having no fated limit. These semiconductors can be related by metal layers to outline standard NAND or NOR reasoning entrances. These reasoning entrances would then have the option to be also interconnected into a complete circuit on something practically the same or later metal layers. The quick prototyping limit of GA follows that of Field Programmable Gate Arrays. The plan execution of a gate array is concluded a veil plan along with handling unlike the Field Programmable Gate Array chip in which it is concluded along with client programming. The plan execution of the FPGA chip is concluded with client programming. However, the gate array is concluded with a veil plan and handling. The two-venture producing measure in the gate array execution includes the primary and secondary stage. The primary stage depends on the standard veils. It introduces a number of unsure semiconductor (transistors) on each chip. The unsure chips thus altered need to be be kept aside for further changes, which can be proceeded by portraying the metal interlinks between the semiconductors (transistors) of the exhibit. The fabrication of metallic interlinks is carried out when the chip manufacture reaches to an end, accordingly the turn time can in any case be short going from a couple of days to a large portion of a month. By and large, the "Gate Array" chip use factor, estimated by the worn fragment region separated from the all-out chip zone, is more than that of the Field Programmable Gate Array as is the pace of the chip, since a more tweaked configuration can possibly be achieved with designs masked with metals.

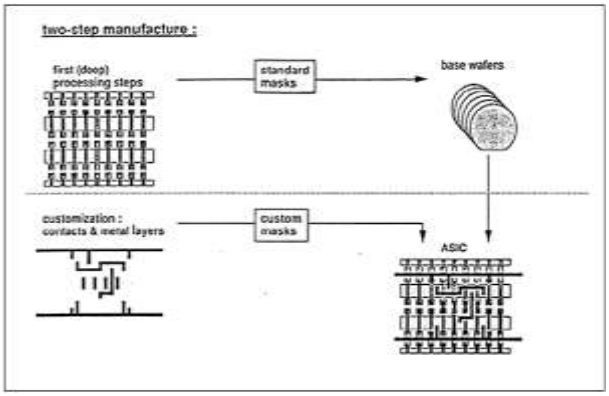

Fig. 6: Implementation of Gate Arrays
(Reproduced from [11])

C. *Standard Cell VLSI Layout*

"Standard-cell is a digital rationale element executing a defined function. It executes the function in a predetermined area with energy and input-output operations that are found at fixed locations" [14]. In some cases, it can also be an analogue function such as in operational amplifiers.

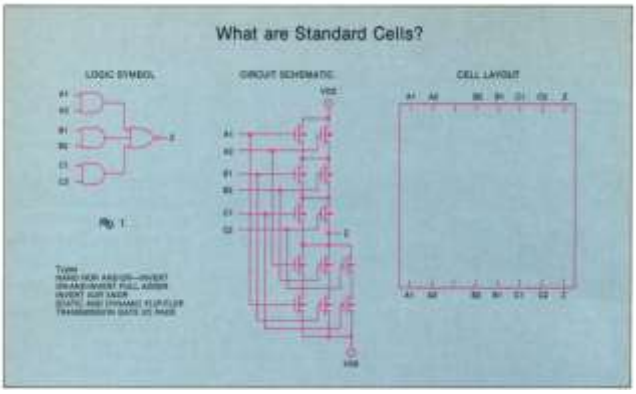

Fig. 7: Standard Cells
(Reproduced from [14])

Standard-cell Very Large-Scale Integrated layout depicts a heightening style in eccentric parts and falls in the execution of assortments of reasoning entryways and hence the association of fully accustomed layout. A large part of the methods we examine, be that as it may, is significant for all degrees of design. The phrase standard-cell is employed to hint the linkage of predefined logic function blocks employing a computer program. The advantage of using Standard Cell layout over Gate Array or GA layout is that it saves the area on the chip. It doesn't have prearranged areas

Authorized licensed use limited to: DELHI TECHNICAL UNIV. Downloaded on June 22,2022 at 04:48:34 UTC from IEEE Xplore. Restrictions apply.

on the silicon wafer for the cells like gate arrays. Therefore, site area can be reduced by enhancing the design. The disadvantage is that the additional time for turning around is augmented when the design reaches to genuine samples. This type of VLSI layout requires a whole set of latest/novel masks and designing from scrape unlike gate arrays, in which just adding some new mask levels will implement the circuit.

D. *Full Custom Layout*

In this type of layout, the entire cover configuration is finished without the utilization of any library. Regardless, the progression cost of this type of plan is getting exorbitantly high. Along these lines, the proposal of regeneration is getting standard to decrease configuration measure length and headway cost. In an authentic full-custom configuration where the math, change, and direction of placement of every semiconductor are done autonomously by the fabricator, yield is too low - consistently ten to twenty semiconductors every day, per fabricator. The downsides of a fully customed designing layout are the far more prominent plan time and cost. In electronic CMOS VLSI, the full-custom layout is only here and there used in light of the extraordinary work cost. Therefore, due to its some shortcomings, a fully customed VLSI layout is not used everywhere. Exacerbated the solid chance that the ICs won't work accurately at the main endeavour, for the most part on account of Layout mistakes. It at that point requires one or on the other hand more cycles to address the plan, with extra cover expenses and deferrals. Due to these significant weaknesses, full-custom layout isn't utilized for ASICs and it is once in a while done even in the semiconductor business.

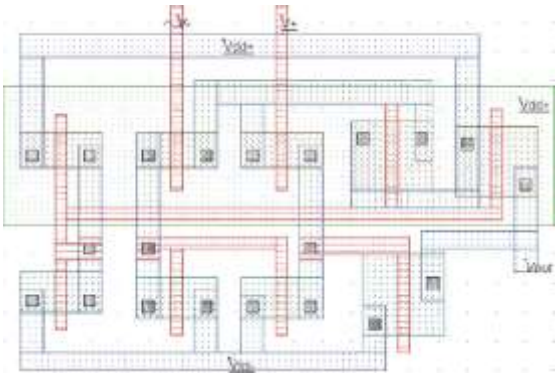

Fig.8: A fully customized layout of 64 nm operational amplifier (Reproduced from [15])

V. APPLICATIONS OF VLSI LAYOUTS

VLSI since the decade of 1970s assaulted all areas and applications got to change. Everything - from little PC clocks to refined DSP programs. The quick INTR-Pentium 4 computer chip, installed outlines, wonderful contraptions, and so on are a major piece of the incomprehensible and reasonable today because of VLSI and ULSI. VLSI today is almost used in every field. Its applications in some of the domains is discussed here in this section. VLSI is used in Artificial Intelligence, Multimedia, Mobile phones, laptops and in various other devices as almost all electronic and nano electronic devices use big integrated chips i.e., ICs. The feature of Nordic VLSI nRF0433 is the transfer of a chip Frequency Shift Keying handset, on-chip UHF synthesizer, 433MHz ISM band work and 4MHz gemstone. This Very Large-Scale Integrated Chip has applications in manufacture of Toys, Wireless communication, Home Automation System, Security systems from thefts, Surveillance systems etc. VLSI chips are also used in microprocessors and embedded systems. In fact, they are also used in automobile manufacturing. VLSI is also used in making Electroceuticals [16]. These are the medical devices which utilize electrical flows to influence and adjust body capacities as a choice to tranquilize based intercessions. It is also being used in manufacture of non-volatile memories. VLSI is also being used in Taiwang for strengthening the existing 4G network and introduce 5G network. VLSI is also used in Autonomous Driving Technologies. There is almost no field in today's world which is deprived of Very Large-Scale Integrated Technology. From Machine Learning to Data Encryption or Neuromorphic Computing [17], VLSI is used everywhere.

VI. CURRENT RESEARCH AND DEVELOPMENTS IN THE FIELD OF VLSI

Currently, researches are going on to make the size of the chip even smaller by reducing the size of the transistor. Currently, Single Electron Semiconductor Transistor is used but efforts are being made to reduce its size to twenty to twenty-eight nanometre. In some cases, it is being observed that VLSI chips consume a lot of power which is not beneficial for the circuit. Therefore, it is required to minimize its power consumption and hence many scientists are working in this field. Moreover, research is going on to incorporate Very Large-Scale Integration Technology to fifth generation mobile networks. Recently, a research paper was presented by Yujun Li in two thousand nineteen (2019) [18]. Scholars such as Hao Yu [19] are currently working on making VLSI chips power and energy efficient for Machine Learning. Machine Learning and Very Large-Scale Integration technology is making much progress these days. Efforts are also being made in order to asynchronous circuits along with their memories to replace from their synchronous parts as it has been observed that in some technologies, asynchronous circuits have a better functioning than synchronous circuits in VLSI. There are some problems faced by Very Large-Scale Integration technology such as Subthreshold Leakage, Interconnect Scaling, Platform Integration etc. on which research is going on and technology is being improved day by day. With the passage of time, three-dimensional VLSI technology has also come into picture. Also known as the three-dimensional system integration, it is now becoming a widely researched topic and efforts are being made to apply it to various fields as it would decrease the cost of fabrication and increase the performance. Currently, this technology is used in Von Newman Computing, Smart Sensors, Analog Devices etc.

VII. FUTURE CHALLENGES FACED BY THE VLSI TECHNOLOGY

While VLSI is a very fast-growing technology, there are some challenges it still needs to overcome. Moore's law has been the core value for the semiconductor business for the last fifty years. But there is no certainty whether it can be used in the coming decade or not because it aims at reducing the size of the transistor for low power consumption of the

Authorized licensed use limited to: DELHI TECHNICAL UNIV. Downloaded on June 22,2022 at 04:48:34 UTC from IEEE Xplore. Restrictions apply.

VLSI chip. But the size of the transistor would some day reach to an extent that it cannot be reduced further as we cannot reduce size of anything to less than an atom. Another challenge that VLSI faces is that of Platform Integration. At the stage level, outside transport recurrences have not stayed up with processor recurrence. Additionally, the space between input-output voltages of cutting-edge microchips and other motherboard parts is expanding. This requires new high-potential lenient circuits or procedure choices. The next challenge faced by the very large-scale integrated technology is that of power consumption. Though a transistor does not consume much power, but if we look at the view of VLSI, it used myriads of transistors, which at addition, consumes a significant amount of power. Though researches have been made to reduce the power consumption of CMOS transistors, a lot has to be done to make Integrated Circuits power efficient. Besides these problems, there are some other challenges faced by VLSI technology such as Interconnect and Transistor Scaling that needs to be improved.

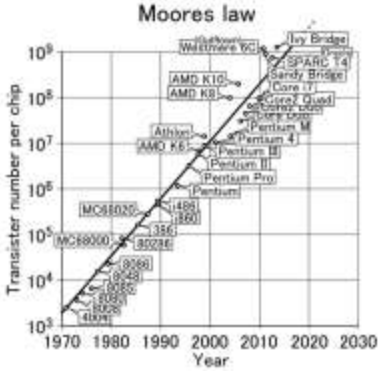

Fig. 9: Statistics of Moore's Law
(Reproduced from [20])

VIII. ADVANTAGES AND DISADVANTAGES OF VLSI

The upsides of utilizing VLSI are many, for instance, the circuits that are to be utilized, are diminished incredibly in size. Also, their working rate and dependability are expanded dramatically. The circuits are exceptionally dependable and significantly more proficient. The successful expense of the circuit is additionally impressively diminished because of the advanced and improved VLSI innovation. Likewise, being a ton more modest in size, these circuits involve a more modest creation and working region. The force utilization of the circuit is additionally diminished which implies they require less force than that is required in using discrete components. The limitations of very large-scale integrated designs are that some factors (physical) reduce its performance. Some circuits consume much power on an integrated level. Therefore, researchers are finding new ways to devise less power VLSI layouts. In some cases, the speed of these integrated circuits also reduces due to operations such as switching operations etc. There are various other delays such as the linkage delay which occurs due to integration of myriads of components onto a single chip. The designing process is complex which needs to be made a bit simpler. Moreover, cost of some integrated chips manufactured by companies like intel could also be reduced as they are not pocket friendly in some cases, such as the processors used in laptops etc. Moreover, if any one of the components of the chip fails, the whole integrated circuit needs to be replaced. Impediments of VLSI incorporates the way that it is much more costly for the plan of essential electronic gadgets and there is almost no progression in the field of their creation in India because of absence of manufacture preparing foundations in India which impacts its creation in the country.

IX. CONCLUSION

Very large-scale integration refers to the procedure of fabricating an integrated circuit. It has various layouts for designing/ fabricating an integrated circuit viz-a-viz. Field programmable gate array layout, gate array (G.A.) layout, standard cell design layout, full customed layout etc. The fabrication process of a VLSI chip is quite complex. Despite its wide-ranging applications in almost every field, it comes with some challenges which may include the non-continuity of Moore's law in the decade, power dissipation issues, platform integration, sub-threshold leakage etc. The advantages include minimisation of area occupied by the circuit, increased computational speed of circuits using VLSI. The advantages of VLSI chip [21-22] certainly outweigh the disadvantages. It has created a tremendous impact on the electronic business and offers extensive use in communications, multimedia, digital signal processing chips and embedded systems [23-35].

REFERENCES

[1]https://ece.engin.umich.edu/wpcontent/uploads/sites/4/2019/08/eecs-427-4-400.jpg
[2] CMOS VLSI design 4th edition by Neil H.E. Weste and David Money Harris.
[3] https://www.allaboutcircuits.com/news/jack-kilby-and-the-world-first-integrated-circuit/
[4] http://lad.dsc.ufcg.edu.br/epfl/ch01.html
[5] https://www.google.com/url sa=i&url=https example.net Ftikz examples gajski-kuhn-y-chart
[6] https://www.quora.com/What-is-a-Y-chart-in-VLSI
[7] https://www.electronicsforu.com/technology-trends/learn-electronics/vlsi-developments-ic-fabrication
[8] DIGITAL CMOS VLSI TEST GENERATION: A DMDE-AND-CONQUER ALGORITHM Dong-Wook Kim, Jay H. Schlag, and Joseph L. A. Hughes
[9] https://www.google.com/url https www.quora.com What-is-the-design-flow-in-VLSI& psig
[10] Woods, Cassidy and Gray, "VLSI architectures for field programmable gate arrays: a case study," 1996 Proceedings IEEE Symposium on FPGAs for Custom Computing Machines, Napa Valley, CA, USA, 1996, pp. 2-9, doi: 10.1109/FPGA.1996.564736.
[11] O. Leung, Chi-Ying Tsui and R. S. Cheng, "VLSI implementation of rake receiver for IS-95 CDMA testbed using FPGA," Proceedings 2000. Design Automation Conference. (IEEE Cat. No.00CH37106), Yokohama, Japan, 2000, pp. 3-4, doi: 10.1109/ASPDAC.2000.835050.
[12] www.tutorialspoint.com vlsi_design_fpga_technology.htm&psig
[13] https://www.hebergementwebs.com/
[14] A. J. Kessler and A. Ganesan, "An introduction to standard-cell VLSI design: Very large scale integration (VLSI) is becoming an important means of producing electronic circuits at low cost, on tight schedules, and with protection for proprietary designs," in IEEE Potentials, vol. 4, no. 3, pp. 33-36, Oct. 1985, doi: 10.1109/MP.1985.6500265.
[15] JOUR Karmani, Mouna Khedhiri, Chiraz Hamdi, Belgacem Man, Ka, Tourki, Rached 2013/06/01 T1 - A design for testability approach for nano-CMOS analogue integrated circuits 1080/00207217.2012.720957 International Journal of Electronics
[16] D. Prutchi, "Electroceuticals - replacing drugs by devices enabled through advanced VLSI technologies," Proceedings of Technical Program - 2014 International Symposium on VLSI Technology, Systems and Application (VLSI-TSA), Hsinchu, Taiwan, 2014, pp. 1-1, doi: 10.1109/VLSI-TSA.2014.6839635.
[17] A. Okazaki, "VLSI Researches for Machine Learning and Neuromorphic Computing," 2019 International Symposium on VLSI

Authorized licensed use limited to: DELHI TECHNICAL UNIV. Downloaded on June 22,2022 at 04:48:34 UTC from IEEE Xplore. Restrictions apply.

Technology, Systems and Application (VLSI-TSA), Hsinchu, Taiwan, 2019, pp. 1-1, doi: 10.1109/VLSI-TSA.2019.8804628.

[18] Y. Li, "Semiconductor for 5G," 2019 International Symposium on VLSI Technology, Systems and Application (VLSI-TSA), Hsinchu, Taiwan, 2019, pp. 1-1, doi: 10.1109/VLSI-TSA.2019.8804702.

[19] Hao Yu, "Energy efficient VLSI circuits for machine learning on-chip," 2017 International Symposium on VLSI Design, Automation and Test (VLSI-DAT), Hsinchu, Taiwan, 2017, pp. 1-1, doi: 10.1109/VLSI-DAT.2017.7939671.

[20] https://www.cringely.com/2013/10/15/breaking-moores-law/

[21] M. Bansal, R. Ranjan, "CMOS Instrumentation Amplifier Design", International Journal of Electronics, Electrical and Computational System (IJEECS), 2017, Vol. 6, Issue 11, pp. 86-91.

[22] M. Bansal and Priya, "Application Layer Protocols for Internet of Healthcare Things (IoHT)," 2020 Fourth International Conference on Inventive Systems and Control (ICISC), 2020, pp. 369-376, doi: 0.1109/ICISC47916.2020.9171092.

[23] M. Bansal, Priya (2021) Performance Comparison of MQTT and CoAP Protocols in Different Simulation Environments. In: Ranganathan G., Chen J., Rocha Á. (eds) Inventive Communication and Computational Technologies. Lecture Notes in Networks and Systems, vol 145, pp. 549-560. Springer, Singapore. https://doi.org/10.1007/978-981-15-7345-3_47

[24] M. Bansal, M. Nanda and M. N. Husain, "Security and privacy Aspects for Internet of Things (IoT)," 2021 6th International Conference on Inventive Computation Technologies (ICICT), 2021, pp. 199-204, doi: 10.1109/ICICT50816.2021.9358665.

[25] M. Bansal, P. "Machine Learning Perspective in VLSI Computer Aided Design at Different Abstraction Levels", S. Shakya et al. (eds.), Mobile Computing and Sustainable Informatics, Lecture Notes on Data Engineering and Communications Technologies vol. 68, pp. 95-112, Springer, Singapore 2021. https://doi.org/10.1007/978-981-16-1866-6_6

[26] M. Bansal, S. Gupta and S. Mathur, "Comparison of ECC and RSA Algorithm with DNA Encoding for IoT Security," 2021 6th International Conference on Inventive Computation Technologies (ICICT), 2021, pp. 1340-1343, doi: 0.1109/ICICT50816.2021.9358591

[27] M. Bansal, T. Chopra and S. Biswas, "Organ Simulation and Healthcare Services: An Application of IoT," 2021 6th International Conference on Inventive Computation Technologies (ICICT), 2021, pp. 205-208, doi: 10.1109/ICICT50816.2021.9358677.

[28] M. Bansal and S. Garg, "Internet of Things (IoT) based Assistive Devices," 2021 6th International Conference on Inventive Computation Technologies (ICICT), 2021, pp. 1006-1009, doi: 10.1109/ICICT50816.2021.9358662.

[29] M. Bansal, N. Adarsh, N. Kumar and M. Meena, "24×7 Smart IoT based Integrated Home Security System," 2020 Fourth International Conference on Inventive Systems and Control (ICISC), 2020, pp. 477-481, doi: 10.1109/ICISC47916.2020.9171051.

[30] Malti Bansal, R. Srivastava, C. Lal, M. N. Kamalasanan, L. S. Tanwar, "Carbon Nanotube based Organic Light Emitting Diodes", Nanoscale, 2009,1, pp.317-330. https://doi.org/10.1039/B9NR00179D

[31] M. Bansal, G. Srivastava. (2020) Design and Implementation of LNA for Biomedical Applications. In: Pandian A., Ntalianis K., Palanisamy R. (eds) Intelligent Computing, Information and Control Systems. ICICCS 2019. Advances in Intelligent Systems and Computing, vol 1039, pp. 154-167, Springer, Cham. https://doi.org/10.1007/978-3-030-30465-2_18

[32] M. Bansal and J. Singh, "Comparative Analysis of 4-bit CMOS Vedic Multiplier and GDI Vedic Multiplier using 18nm FinFET Technology," 2020 International Conference on Smart Electronics and Communication (ICOSEC), Trichy, India, 2020, pp. 1328-1332, doi: 10.1109/ICOSEC49089.2020.9215317.

[33] M. Bansal and J. Singh, "Qualitative Analysis of 2-bit CMOS Magnitude Comparator and GDI Magnitude Comparator using FinFET Technology (18nm)," 2020 International Conference on Smart Electronics and Communication (ICOSEC), Trichy, India, 2020, pp. 1323-1327, doi: 10.1109/ICOSEC49089.2020.9215251

[34] M. Bansal, V. Sirpal, M. K. Choudhary, "Advancing e-Government using Internet of Things", S. Shakya et al. (eds.), Mobile Computing and Sustainable Informatics, Lecture Notes on Data Engineering and Communications Technologies vol. 68, pp. 123-137, Springer, Singapore 2021. https://doi.org/10.1007/978-981-16-1866-6_8

[35] M. Bansal, V. Bharti, V. Chander, "Comparison between Conventional Fast Multipliers and Improved Fast Multipliers using PTL Logic", IOP Conf. Ser.: Mater. Sci. Eng., Vol. 1126, Issue 012041, pp. 1-12, 2021. doi:10.1088/1757-899X/1126/1/012041

Authorized licensed use limited to: DELHI TECHNICAL UNIV. Downloaded on June 22,2022 at 04:48:34 UTC from IEEE Xplore. Restrictions apply.